

# ULTRASONOGRAPHY IN OBSTETRICS AND GYNECOLOGY

## CALLEN



FIFTH  
EDITION

SAUNDERS  
ELSEVIER



ULTRASONOGRAPHY  
IN OBSTETRICS AND  
GYNECOLOGY



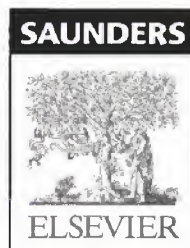


# ULTRASONOGRAPHY IN OBSTETRICS AND GYNECOLOGY

5TH EDITION

**PETER W. CALLEN, MD**

Professor of Radiology, Obstetrics, Gynecology,  
and Reproductive Sciences  
Department of Radiology  
University of California School of Medicine  
San Francisco, California



**All rights reserved.** No part of this publication may be reproduced or transmitted in any form or by any means, electronic or mechanical, including photocopying, recording, or any information storage and retrieval system, without permission in writing from the publisher.

Permissions may be sought directly from Elsevier's Health Sciences Rights Department in Philadelphia, PA, USA: phone: (+1) 215 239 3804, fax: (+1) 215 239 3805, e-mail: [healthpermissions@elsevier.com](mailto:healthpermissions@elsevier.com). You may also complete your request on-line via the Elsevier homepage (<http://www.elsevier.com>), by selecting 'Customer Support' and then 'Obtaining Permissions'.

**Notice**

Knowledge and best practice in this field are constantly changing. As new research and experience broaden our knowledge, changes in practice, treatment and drug therapy may become necessary or appropriate. Readers are advised to check the most current information provided (i) on procedures featured or (ii) by the manufacturer of each product to be administered, to verify the recommended dose or formula, the method and duration of administration, and contraindications. It is the responsibility of the practitioner, relying on their own experience and knowledge of the patient, to make diagnoses, to determine dosages and the best treatment for each individual patient, and to take all appropriate safety precautions. To the fullest extent of the law, neither the Publisher nor the Editors assumes any liability for any injury and/or damage to persons or property arising out or related to any use of the material contained in this book.

The Publisher

Previous editions copyrighted 2000, 1994, 1988, 1983 by Elsevier, Inc.

**Library of Congress Cataloging-in-Publication Data (in PHL)**

Ultrasonography in obstetrics and gynecology / [edited by] Peter W. Callen. — 5th ed. p. ; cm.

Includes bibliographical references and index.

ISBN 1-4160-3264-9

1. Ultrasonics in obstetrics. 2. Generative organs, Female—Ultrasonic imaging.

I. Callen, Peter W. [DNLM: 1. Obstetrics. 2. Fetal Diseases—diagnosis. 3. Fetal Monitoring.

4. Genital Diseases, Female—diagnosis. 5. Ultrasonography, Prenatal.

WQ 100 U47 2007]

RG527.5.U48U47 2007

618.2'07543—dc22 2006030673

*Publishing Director:* Judith Fletcher  
*Developmental Editor:* Martha Limbach  
*Project Manager:* Mary B. Stermel  
*Design Direction:* Gene Harris  
*Marketing Manager:* Catalina Nolte

Working together to grow  
libraries in developing countries

[www.elsevier.com](http://www.elsevier.com) | [www.bookaid.org](http://www.bookaid.org) | [www.sabre.org](http://www.sabre.org)

ELSEVIER

BOOK AID  
International

Sabre Foundation



*To*  
*Mom and Dad,*  
*Karen, Melanie, Brooke, Andy and Daniel*





# CONTRIBUTORS

**Alfred Z. Abuhamad, MD**

Mason C. Andrews Professor and Chairman, Department of Obstetrics and Gynecology, Eastern Virginia Medical School; Department of Obstetrics and Gynecology, Sentara Norfolk General Hospital, Norfolk, Virginia  
*The Role of Doppler Ultrasound in Obstetrics*

**Fred E. Avni, MD, PhD**

Professor of Radiology, Free University of Brussels (ULB); Chief, Department of Medical Imaging, University Clinics of Brussels - Erasme Hospital, Brussels, Belgium  
*The Fetal Genitourinary Tract*

**Robert H. Ball, MD**

Associate Professor, Departments of Obstetrics, Gynecology and Reproductive Sciences and Radiology, University of California, San Francisco, San Francisco, California; Department of Maternal-Fetal Medicine, St. Mark's Hospital, Salt Lake City, Utah; Director, Fetal Therapy Initiative, Hospital Corporation of America, Nashville, Tennessee  
*The Prenatal Management of the Fetus With a Correctable Defect*

**George Bega, MD**

Assistant Professor of Obstetrics and Gynecology, and Director, 3D/4D Education and Research Program, Division of Maternal-Fetal Medicine, Department of Obstetrics and Gynecology, Thomas Jefferson University, Philadelphia, Pennsylvania  
*Ultrasound Evaluation of the Cervix*

**Beryl R. Benacerraf, MD**

Clinical Professor, Departments of Radiology and Obstetrics, Gynecology and Reproductive Sciences, Harvard Medical School; Radiologist, Department of Radiology, Brigham and Women's Hospital; Editor in Chief, Journal of Ultrasound in Medicine, American Institute of Ultrasound in Medicine, Boston, Massachusetts  
*The Role of Three-Dimensional Ultrasound in the Evaluation of the Fetus*

**Carol B. Benson, MD**

Professor of Radiology, Department of Radiology, Harvard Medical School; Director of Ultrasound, and Co-Director of High Risk Obstetrical Ultrasound, Department of Radiology, Brigham and Women's Hospital, Boston, Massachusetts  
*Ultrasound Evaluation During the First Trimester of Pregnancy*

**Vincenzo Berghella, MD**

Professor, Obstetrics and Gynecology, and Director, Maternal-Fetal Medicine Division, Department of Obstetrics and Gynecology, Thomas Jefferson University; Department of Obstetrics and Gynecology, Thomas Jefferson University Hospital, Philadelphia, Pennsylvania  
*Ultrasound Evaluation of the Cervix*

**Shraga Blazer, MD**

Clinical Associate Professor, Department of Pediatrics, Faculty of Medicine, Technion – Israel Institute of Technology; Director of Neonatology, Department of Neonatology, Rambam Medical Center, Haifa, Israel  
*The Gastrointestinal Tract and Abdominal Wall*

**Adam F. Borgida, MD**

Associate Professor, Department of Obstetrics and Gynecology, University of Connecticut School of Medicine, Farmington; Attending Perinatologist, Department of Obstetrics and Gynecology, Hartford Hospital, Hartford, Connecticut  
*Ultrasound Evaluation of Multiple Pregnancies*

**Moshe Bronshtein, MD**

Senior Sonologist, Department of Obstetrics and Gynecology, Rambam Medical Center; Director, Alkol Institute of Ultrasound in Obstetrics and Gynecology, Haifa, Israel  
*The Gastrointestinal Tract and Abdominal Wall*

**Peter W. Callen, MD**

Professor of Radiology, Obstetrics, Gynecology, and Reproductive Sciences, Department of Radiology, University of California School of Medicine, San Francisco, California  
*The Obstetric Ultrasound Examination; Amniotic Fluid Volume: Its Role in Fetal Health and Disease; Ultrasound Evaluation of the Adnexa (Ovary and Fallopian Tubes); Artifacts, Pitfalls, and Normal Variants*

**Marie Cassart, MD, PhD**

Pediatric Radiologist, Department of Medical Imaging, Erasme Hospital, Brussels, Belgium  
*The Fetal Genitourinary Tract*

**Martin R. Chavez, MD**

Assistant Professor, Division of Maternal-Fetal Medicine, Department of Obstetrics and Gynecology, University of Medicine and Dentistry of New Jersey – Robert Wood Johnson Medical School, New Brunswick, New Jersey  
*Antepartum Fetal Assessment by Ultrasonography: The Fetal Biophysical Profile*

**Titia E. Cohen-Overbeek, MD**

Senior Physician, Prenatal Medicine, Division of Prenatal Medicine, Department of Obstetrics and Gynecology, Erasmus Medical Center, Rotterdam, The Netherlands  
*Ultrasound Evaluation of the Fetal Thorax*

**Sidney M. Dashefsky, MD**

Assistant Professor of Radiology, University of Manitoba, Section of Diagnostic Ultrasound, Health Sciences Centre, Winnipeg, Manitoba, Canada  
*Normal Anatomy of the Female Pelvis and Transvaginal Sonography*

**Jan Deprest, MD, PhD**

Professor in Obstetrics and Gynecology, and Head, Research Invasive Fetal Therapy, Woman and Child, Division Woman, Katholieke Universiteit Leuven; Unit Fetal Diagnosis and Therapy, Department of Obstetrics and Gynecology, University Hospitals Leuven, Leuven, Belgium

*The Prenatal Management of the Fetus With a Correctable Defect*

**James F. X. Egan, MD**

Professor and Chairman, Department of Obstetrics and Gynecology, University of Connecticut Health Center, Farmington; Attending Obstetrician-Gynecologist, Department of Obstetrics and Gynecology, John Dempsey Hospital, University of Connecticut Health Center, Farmington, New Britain General Hospital, New Britain, and Hartford Hospital, Hartford, Connecticut

*Ultrasound Evaluation of Multiple Pregnancies*

**Jimmy Espinoza, MD**

Assistant Professor, Department of Obstetrics and Gynecology, Perinatology Research Branch, Intramural Division, NICHD/NIH/DHHS, Wayne State University/Hutzel Women's Hospital, Detroit, Michigan

*The Fetal Musculoskeletal System*

**Danielle Eurin, MD**

Hospital, Department of Pediatric and Fetal Imaging, Charles Nicolle, Rouen, France

*The Fetal Genitourinary Tract*

**Vickie A. Feldstein, MD**

Professor of Clinical Radiology, Obstetrics, Gynecology and Reproductive Sciences, Department of Radiology, University of California School of Medicine, San Francisco, California

*Ultrasound Evaluation of Normal Fetal Anatomy; Ultrasound Evaluation of the Placenta and Umbilical Cord*

**Roy A. Filly, MD**

Professor Emeritus of Radiology, Surgery, and Obstetrics, Gynecology, and Reproductive Sciences, and Co-Founder, Fetal Treatment Program, University of California, San Francisco, San Francisco, California

*Ultrasound Evaluation of Fetal Biometry and Normal and Abnormal Fetal Growth; Ultrasound Evaluation of Normal Fetal Anatomy*

**Mary C. Frates, MD**

Associate Professor of Radiology, Harvard Medical School; Assistant Director, Ultrasound, and Director, Fellowships Programs, Department of Radiology, Brigham and Women's Hospital, Boston, Massachusetts

*Ultrasound Evaluation During the First Trimester of Pregnancy*

**Henry L. Galan, MD**

Associate Professor, and Chief of Maternal-Fetal Medicine, Department of Obstetrics and Gynecology, University of Colorado and Denver Health Sciences Center, and University of Colorado Hospital, Denver, Colorado

*Ultrasound Evaluation of Fetal Biometry and Normal and Abnormal Fetal Growth*

**Steven R. Goldstein, MD**

Professor of Obstetrics and Gynecology, Department of Obstetrics and Gynecology, New York University School

of Medicine, and New York University Medical Center, New York, New York

*Abnormal Uterine Bleeding: The Role of Ultrasound*

**Luís F. Gonçalves, MD**

Assistant Professor of Obstetrics and Gynecology Obstetrics and Gynecology, Wayne State University and Director of Prenatal Diagnosis Perinatology Research Branch, NICHD/NIH/DHHS, Detroit, Michigan

*The Fetal Musculoskeletal System*

**Francesca Gotsch, MD**

Research Fellow, Perinatology Research Branch, Intramural Division, NICHD/NIH/DHHS, Detroit, Michigan

*The Fetal Musculoskeletal System*

**Roberta Granese, MD**

Obstetrician and Gynaecologist, Department of Obstetrics and Gynaecology, University Hospital "G.Martino", Messina, Italy

*Fetal Syndromes*

**Michelle Hall, MD**

Associate Professor, Department of Pediatric Nephrology, Erasme Hospital, Brussels, Belgium

*The Fetal Genitourinary Tract*

**Robert D. Harris, MD**

Professor of Radiology and Obstetrics and Gynecology, Dartmouth Medical School, Hanover; Director of Ultrasound and Research, Department of Radiology, Dartmouth-Hitchcock Medical Center, Lebanon, New Hampshire

*Ultrasound Evaluation of the Placenta and Umbilical Cord*

**Sandra Silva Herbst, MD, RDMS**

Assistant Doctor of the Fetal Medicine Unit, Department of Obstetrics and Gynecology, Santa Casa de Misericórdia de São Paulo, São Paulo, Brazil

*Fetal Syndromes*

**Susan C. Holt, MD**

Assistant Professor, Department of Radiology, University of Manitoba; Staff Radiologist, Department of Radiology, Health Sciences Center, Winnipeg, Manitoba, Canada

*Normal Anatomy of the Female Pelvis and Transvaginal Sonography*

**Edgar Jaeggi, MD**

Associate Professor, Department of Pediatrics, University of Toronto; Head of Fetal Cardiology, Division of Cardiology, Staff Cardiologist, Division of Cardiology, and Associate Scientist, Research Institute, The Hospital for Sick Children, Toronto, Ontario, Canada

*Ultrasound Evaluation of the Fetal Heart*

**Philippe Jeanty, MD, PhD**

Chief Fetustician, Inner Vision Women's Ultrasound, Nashville, Tennessee

*Fetal Syndromes*

**Juan Pedro Kusanovic, MD**

Research Associate, Perinatology Research Branch, NICHD/NIH/DHHS, Detroit, Michigan

*The Fetal Musculoskeletal System*



**Faye C. Laing, MD**

Professor of Radiology, Harvard University; Division of  
Ultrasound, Department of Radiology, Brigham and  
Women's Hospital, Boston, Massachusetts  
*Ultrasound Evaluation During the First Trimester of  
Pregnancy*

**Jacqueline A. M. Laudy, MD, PhD**

Department of Obstetrics and Gynaecology; Erasmus  
Medical Center, Rotterdam, the Netherlands  
*Ultrasound Evaluation of the Fetal Thorax*

**Juliana M. Leite, MD**

TheFetus.net  
*Fetal Syndromes*

**Clifford S. Levi, MD**

Professor, Department of Radiology, University of  
Manitoba; Section Head, Diagnostic Ultrasound,  
Department of Diagnostic Imaging, Health Sciences  
Centre, Winnipeg, Manitoba, Canada  
*Normal Anatomy of the Female Pelvis and Transvaginal  
Sonography*

**Deborah Levine, MD**

Associate Professor, Department of Radiology, Harvard  
Medical School; Associate Chief of Academic Affairs,  
Co-Chief of Ultrasound, and Director of  
Obstetrics/Gynecology Ultrasound, Department of  
Radiology, Beth Israel Deaconess Medical Center,  
Boston, Massachusetts  
*The Role of Computed Tomography and Magnetic Resonance Imaging in  
Obstetrics; Ectopic Pregnancy*

**Edward A. Lyons, MD**

Professor of Radiology, Obstetrics and Gynecology and  
Anatomy, Department of Radiology, University of  
Manitoba; Department of Radiology, Health Sciences  
Center, Winnipeg, Manitoba, Canada  
*Normal Anatomy of the Female Pelvis and Transvaginal  
Sonography*

**Geoffrey A. Machin, MD, PhD**

Emeritus, Professor of Pathology, University of Alberta,  
Edmonton, Alberta, CANADA  
*Ultrasound Evaluation of the Placenta and Umbilical Cord*

**Fergal D. Malone, MD, FACOG, FRCPI**

Professor and Chairman, Department of Obstetrics and  
Gynaecology, Royal College of Surgeons in Ireland;  
Department of Obstetrics and Gynaecology, The  
Rotunda Hospital, Dublin, Ireland  
*First Trimester Screening for Aneuploidy*

**Anne Massez, MD**

Assistant Professor of Radiology, Department of Medical  
Imaging, Erasme Hospital, Brussels, Belgium  
*The Fetal Genitourinary Tract*

**Brigitte Maugey-Laulom, MD**

Praticien Hospitalier Enseignant, Universite Bordeaux 2  
Victor Segalen; Praticien Hospitalier, Unite d'Imagerie  
de la Femme Service du Pr JF Chateil, Chu Pellegrin  
Tripode, Bordeaux, France  
*The Fetal Genitourinary Tract*

**Ellen B. Mendelson, MD, FACR**

Professor of Radiology, Department of Radiology, Feinberg  
School of Medicine, Northwestern University; Section  
Chief, Breast and Women's Imaging, Department of  
Radiology, Northwestern Memorial Hospital, Chicago,  
Illinois  
*Ultrasound of the Breast*

**Kenneth J. Moise, Jr., MD**

Professor of Obstetrics and Gynecology, Department of  
Obstetrics and Gynecology, Baylor College of Medicine,  
Houston, Texas  
*Ultrasound Evaluation of Hydrops Fetalis*

**Mary E. Norton, MD**

Director, Prenatal Diagnostic Center, and Director, Division  
of Perinatal Medicine and Genetics, Department of  
Obstetrics, Gynecology and Reproductive Sciences,  
Radiology and Pediatrics, University of California,  
San Francisco, School of Medicine, San Francisco,  
California  
*Genetics and Prenatal Diagnosis*

**Yinka Oyelese, MD**

Assistant Professor, Division of Maternal-Fetal Medicine,  
Department of Obstetrics, Gynecology and Reproductive  
Sciences, University of Medicine and Dentistry of  
New Jersey – Robert Wood Johnson Medical School,  
New Brunswick, New Jersey  
*Antepartum Fetal Assessment by Ultrasonography: The Fetal Biophysical  
Profile*

**Santosh Pandipati, MD**

Clinical Instructor-Fellow, Maternal-Fetal Medicine,  
Department of Obstetrics and Gynecology,  
University of Colorado Health Sciences Center;  
Department of Obstetrics and Gynecology,  
University of Colorado Hospital, Denver, Colorado  
*Ultrasound Evaluation of Fetal Biometry and Normal and Abnormal  
Fetal Growth*

**Antonella Perolo, MD**

Consultant, Department of Obstetrics and  
Gynecology, Università degli Studi di Bologna,  
Bologna, Italy  
*Ultrasound Evaluation of the Fetal Face and Neck*

**Roger A. Pierson, MS, PhD**

Professor, Department of Obstetrics, Gynecology  
and Reproductive Sciences, University of  
Saskatchewan; Department of Obstetrics,  
Gynecology and Reproductive Sciences,  
Royal University Hospital, Saskatoon,  
Saskatchewan, Canada  
*Ultrasonographic Imaging in Infertility*

**Gianluigi Pilu, MD**

Associate Professor of Obstetrics and Gynecology,  
Department of Obstetrics and Gynecology,  
Università degli Studi di Bologna, Bologna, Italy  
*Ultrasound Evaluation of the Fetal Neural Axis: Ultrasound Evaluation  
of the Fetal Face and Neck*

**Liina Pöder, MD**

Assistant Professor of Clinical Radiology, Department of Radiology, University of California, San Francisco, San Francisco, California

*Ultrasound Evaluation of the Uterus*

**Aliya Qayyum, MD, MBBS**

Associate Professor of Radiology, Department of Radiology, University of California, San Francisco, and University of California, San Francisco, Medical Center, San Francisco, California

*The Role of Magnetic Resonance Imaging in the Evaluation of Gynecologic Disease*

**Roberto Romero, MD**

Professor, Center for Molecular Medicine and Genetics, Wayne State University School of Medicine, Detroit, Michigan; Chief, Perinatology Research Branch, and Program Director for Obstetrics and Perinatology, National Institute of Child Health and Human Development, and Department of Health and Human Services, National Institutes of Health, Bethesda, Maryland, and Detroit, Michigan

*The Fetal Musculoskeletal System*

**Neil J. Sebire, MB, MD, DRCOG, MRCPATH**

Consultant Pathologist, Trophoblastic Disease Unit, Charing Cross Hospital, London, United Kingdom

*Gestational Trophoblastic Neoplasia*

**Maria Segata, MD**

Fellow, Department of Obstetrics and Gynecology, Università degli Studi di Bologna, Bologna, Italy

*Ultrasound Evaluation of the Fetal Face and Neck*

**Lil Valentin, MD, PhD**

Professor, Department of Clinical Sciences Malmö, Lund University; Consultant, Department of Obstetrics and Gynecology, Malmö University Hospital, Malmö, Sweden

*Ultrasound Evaluation of the Adnexa (Ovary and Fallopian Tubes)*

**Anthony M. Vintzileos, MD**

Professor and Chair, Department of Obstetrics, Gynecology and Reproductive Sciences, University of Medicine and Dentistry of New Jersey – Robert Wood Johnson Medical

School; Chief, Department of Obstetrics and Gynecology, Robert Wood Johnson University Hospital, New Brunswick, New Jersey

*The Second Trimester Genetic Sonogram; Antepartum Fetal Assessment by Ultrasonography: The Fetal Biophysical Profile*

**Antonio C. Westphalen, MD**

Assistant Professor, Department of Radiology, University of California, San Francisco, San Francisco, California

*The Role of Magnetic Resonance Imaging in the Evaluation of Gynecologic Disease*

**Juriy W. Wladimiroff, MD, PhD, FRCOG**

Professor Emeritus, Department of Obstetrics and Gynaecology, Erasmus Medical Center, Rotterdam, The Netherlands

*Ultrasound Evaluation of the Fetal Thorax*

**Lami Yeo, MD**

Associate Professor of Obstetrics and Gynecology, Division of Maternal-Fetal Medicine, Department of Obstetrics, Gynecology and Reproductive Sciences, University of Medicine and Dentistry of New Jersey – Robert Wood Johnson Medical School; Director of Perinatal Ultrasound, and Director of Fetal Cardiovascular Unit, Division of Maternal-Fetal Medicine, Department of Obstetrics, Gynecology and Reproductive Sciences, Robert Wood Johnson University Hospital, New Brunswick, New Jersey

*The Second Trimester Genetic Sonogram*

**Shi-Joon Yoo, MD, FRCPC**

Professor, Departments of Medical Imaging and Paediatrics, University of Toronto; Section Head, Cardiac Imaging, Department of Diagnostic Imaging, The Hospital for Sick Children, Toronto, Ontario, Canada

*Ultrasound Evaluation of the Fetal Heart*

**Etan Z. Zimmer, MD**

Clinical Associate Professor, Department of Obstetrics and Gynecology, Faculty of Medicine, Technion – Israel Institute of Technology; Director of Obstetrics, Department of Obstetrics and Gynecology, Rambam Medical Center, Haifa, Israel

*The Gastrointestinal Tract and Abdominal Wall*

# PREFACE

This textbook began nearly twenty-six years ago as a Radiologic Clinics of North America edition with the same title. That edition of nearly 400 pages which had state of the art images now *pales* in comparison to the high-resolution images and information presented in the current text of well over 1200 pages. It has been nearly 8 years since the last edition of this textbook. I am often asked why I wait so long to update this book. The answer is quite straightforward. I have waited until technological advances and our knowledge of imaging the obstetric and gynecologic patient had increased sufficiently to warrant a new edition. Nearly two-thirds of the chapters in this textbook are written by new authors and the remaining chapters have been significantly revised. In keeping with previous editions, I have engaged authors who are experts in their respective fields, whose writing style is authoritative and clear. While I have tried to meticulously edit this text, I made no attempt to insure that there was a uniformity of opinion with controversial issues. I believe that it is useful to read differing opinions on a subject and ultimately decide what works best in your practice. Many readers have asked for a more complete textbook in the field of women's imaging rather than a pure ultrasound text. As such, there are chapters on computed tomography, magnetic resonance imaging and for the first time, a chapter on breast ultrasound. I have tried to make sure that the information in each chapter would appeal to both the neophyte in sonographic imaging as well as the *seasoned* expert who uses this textbook as a reference. As such, chapters

can be read in their entirety from beginning to end or used as a reference text. In addition to the numerous tables and figures in each chapter, an extensive appendix is available for reference. Likewise, in addition to the high-quality sonographic images, there are numerous color medical illustrations throughout the text that will help make specific concepts clear.

There are numerous individuals for whom thanks is due. To begin, the authors did a marvelous job of producing authoritative and clear chapters in a timely fashion. The staff at Elsevier, including Martha Limbach and Todd Hummel, in particular, made this a pleasant and painless process. Dr. James Cooper did a wonderful job in providing beautiful and clear medical illustrations for this text. I am thankful to my colleagues, sonographers and trainees who have provided me with helpful suggestions over the years. Importantly, I am grateful for the support of my family who tolerated an endless stream of papers and books scattered throughout the house and a husband and father who was at the computer late at night and early in the morning. My wife Karen was a source of encouragement, support and as a practicing physician herself, aided in my understanding of obstetric and gynecologic issues. Last, I am grateful to you the readers who have given me so much pleasure in your enthusiasm about understanding the field I have come to love.

PETER W. CALLEN, MD





# CONTENTS

## SECTION I. Obstetric Ultrasound

1. **The Obstetric Ultrasound Examination** 3  
Peter W. Callen, MD
2. **Genetics and Prenatal Diagnosis** 26  
Mary E. Norton, MD
3. **First Trimester Screening for Aneuploidy** 60  
Fergal D. Malone, MD, FACOG, FRCPI
4. **The Second Trimester Genetic Sonogram** 70  
Lami Yeo, MD and Anthony M. Vintzileos, MD
5. **Fetal Syndromes** 112  
Juliana M. Leite, MD, Roberta Granese, MD,  
Philippe Jeanty, MD, PhD, and Sandra Silva Herbst, MD
6. **Ultrasound Evaluation During the First Trimester of Pregnancy** 181  
Faye C. Laing, MD, Mary C. Frates, MD, and  
Carol B. Benson, MD
7. **Ultrasound Evaluation of Fetal Biometry and Normal and Abnormal Fetal Growth** 225  
Henry L. Galan, MD, Santosh Pandipati, MD, and  
Roy A. Filly, MD
8. **Ultrasound Evaluation of Multiple Pregnancies** 266  
James F. X. Egan, MD and Adam F. Borgida, MD
9. **Ultrasound Evaluation of Normal Fetal Anatomy** 297  
Roy A. Filly, MD and Vickie A. Feldstein, MD
10. **Ultrasound Evaluation of the Fetal Neural Axis** 363  
Gianluigi Pilu, MD
11. **Ultrasound Evaluation of the Fetal Face and Neck** 392  
Gianluigi Pilu, MD, Maria Segata, MD, and  
Antonella Perolo, MD
12. **The Fetal Musculoskeletal System** 419  
Luís F. Gonçalves, MD, Juan Pedro Kusanovic, MD,  
Francesca Gotsch, MD, Jimmy Espinoza, MD, and  
Roberto Romero, MD
13. **Ultrasound Evaluation of the Fetal Thorax** 493  
Juriy W. Wladimiroff, MD, PhD, FRCOG, Titia E.  
Cohen-Overbeck, MD, and Jacqueline A. M. Laudy, MD, PhD
14. **Ultrasound Evaluation of the Fetal Heart** 511  
Shi-Joon Yoo, MD, FRCPC and Edgar Jaeggi, MD
15. **The Gastrointestinal Tract and Abdominal Wall** 587  
Moshe Bronshtein, MD, Shraga Blazer, MD, and  
Etan Z. Zimmer, MD
16. **The Fetal Genitourinary Tract** 640  
Fred E. Avni, MD, PhD, Brigitte Maugey-Laulom, MD,  
Marie Cassart, MD, PhD, Danielle Eurin, MD, Anne Masscz,  
MD, and Michelle Hall, MD
17. **Ultrasound Evaluation of Hydrops Fetalis** 676  
Kenneth J. Moise, Jr., MD
18. **Ultrasound Evaluation of the Cervix** 698  
Vincenzo Berghella, MD and George Bcga, MD
19. **Ultrasound Evaluation of the Placenta and Umbilical Cord** 721  
Vickie A. Feldstein, MD, Robert D. Harris, MD, and  
Geoffrey A. Machin, MD, PhD

20. **Amniotic Fluid Volume: Its Role in Fetal Health and Disease** 758  
Peter W. Callen, MD
21. **Antepartum Fetal Assessment by Ultrasonography: The Fetal Biophysical Profile** 780  
Martin R. Chavez, MD, Yinka Oyelese, MD, and  
Anthony M. Vintzileos, MD
22. **The Role of Doppler Ultrasound in Obstetrics** 794  
Alfred Z. Abuhamad, MD
23. **The Role of Computed Tomography and Magnetic Resonance Imaging in Obstetrics** 808  
Deborah Levine, MD
24. **The Role of Three-Dimensional Ultrasound in the Evaluation of the Fetus** 830  
Beryl R. Benacerraf, MD
25. **The Prenatal Management of the Fetus With a Correctable Defect** 867  
Robert H. Ball, MD and Jan Deprest, MD, PhD

## SECTION II. Gynecologic Ultrasound

26. **Normal Anatomy of the Female Pelvis and Transvaginal Sonography** 887  
Clifford S. Levi, MD, Edward A. Lyons, MD, Susan C. Holt, MD,  
and Sidney M. Dashchfsky, MD
27. **Ultrasound Evaluation of the Uterus** 919  
Liina Pöder, MD
28. **Abnormal Uterine Bleeding: The Role of Ultrasound** 942  
Steven R. Goldstein, MD
29. **Gestational Trophoblastic Neoplasia** 951  
Neil J. Sebire, MB, MD
30. **Ultrasound Evaluation of the Adnexa (Ovary and Fallopian Tubes)** 968  
Lil Valentin, MD, PhD and Peter W. Callen, MD
31. **Ultrasonographic Imaging in Infertility** 986  
Roger A. Pierson, MS, PhD
32. **Ectopic Pregnancy** 1020  
Deborah Levine, MD
33. **The Role of Magnetic Resonance Imaging in the Evaluation of Gynecologic Disease** 1048  
Antonio C. Westphalen, MD and Aliya Qayyum, MD, MBBS
34. **Ultrasound of the Breast** 1077  
Ellen B. Mendelson, MD, FACR
35. **Artifacts, Pitfalls, and Normal Variants** 1098  
Peter W. Callen, MD

### Appendix A

Measurements Frequently Used to Estimate Gestational Age and Fetal Biometry 1159

### Appendix B

Measurements Used in Assessing Fetal Weight, Growth, and Body Proportions 1174

### Appendix C

Measurements for Amniotic Fluid Assessment 1181

<b>Appendix D</b>		<b>Appendix I</b>
Fetal Doppler Assessment (Noncardiac) <i>1184</i>		Medications and Reported Associated Malformations <i>1202</i>
<b>Appendix E</b>		<b>Appendix J</b>
Doppler of the Middle Cerebral Artery to Assess Fetal Anemia <i>1188</i>		Estimated Radiation Exposure to the Fetus during Radiographic Examinations <i>1205</i>
<b>Appendix F</b>		<b>Appendix K</b>
Fetal Cardiac Measurements and Doppler Assessment <i>1189</i>		MR Imaging Protocol for Pregnant Patients with Acute Right Lower Quadrant Pain <i>1206</i>
<b>Appendix G</b>		
Sonographic Detection of Chromosomal Abnormalities <i>1198</i>		<b>Index</b> <i>1207</i>
<b>Appendix H</b>		
Normal Measurements of the Uterus and Ovaries <i>1201</i>		



# OBSTETRIC ULTRASOUND

## Section Contents

The Obstetric Ultrasound Examination .....	3	The Gastrointestinal Tract and Abdominal	
Genetics and Prenatal Diagnosis .....	26	Wall .....	587
First Trimester Screening for Aneuploidy .....	60	The Fetal Genitourinary Tract .....	640
The Second Trimester Genetic Sonogram .....	70	Ultrasound Evaluation of Hydrops Fetalis .....	676
Fetal Syndromes .....	112	Ultrasound Evaluation of the Cervix .....	698
Ultrasound Evaluation During the First Trimester of		Ultrasound Evaluation of the Placenta and	
Pregnancy .....	181	Umbilical Cord .....	721
Ultrasound Evaluation of Fetal Biometry and Normal		Amniotic Fluid Volume: Its Role in Fetal Health	
and Abnormal Fetal Growth .....	225	and Disease .....	758
Ultrasound Evaluation of Multiple Pregnancies ..	266	Antepartum Fetal Assessment by Ultrasonography:	
Ultrasound Evaluation of Normal Fetal		The Fetal Biophysical Profile .....	780
Anatomy .....	297	The Role of Doppler Ultrasound in Obstetrics ....	794
Ultrasound Evaluation of the Fetal Neural Axis ..	363	The Role of Computed Tomography and Magnetic	
Ultrasound Evaluation of the of the Fetal Face		Resonance Imaging in Obstetrics .....	808
and Neck .....	392	The Role of Three-Dimensional Ultrasound in the	
The Fetal Musculoskeletal System .....	419	Evaluation of the Fetus .....	830
Ultrasound Evaluation of the Fetal Thorax .....	493	The Prenatal Management of the Fetus With a	
Ultrasound Evaluation of the Fetal Heart .....	511	Corretable Defect .....	867





# THE OBSTETRIC ULTRASOUND EXAMINATION

Peter W. Callen, MD

## Safety of Ultrasound Examination

### Indications for Obstetric Ultrasound Examination

### Who Should Perform the Ultrasound Examination and How Should it be Performed?

Terminology  
Ultrasound Lexicon

### The Guidelines

### Ultrasound Equipment and Documentation

### The First Trimester Ultrasound Examination

Identification of an Intrauterine Pregnancy  
Embryonic/Fetal Number  
Estimating Gestational Age  
Morphologic Abnormalities  
Placenta  
Uterus and Adnexa

## The Second and Third Trimester Ultrasound Examinations

Fetal Number and Fetal Life  
Fetal Position  
Assigning Gestational Age and Weight  
Amniotic Fluid Volume  
Amniotic Fluid Volume in Multiple Gestations  
The Placenta  
Fetal Malformations  
Uterus and Adnexa  
Verbiage Used in the AIUM/ACR/ACOG Guidelines  
Interpretation of the Ultrasound Examination  
Reporting of Ultrasound Results  
Discussing the Examination With the Patient

## Evaluating the Obstetric-Gynecologic Ultrasound Literature

## Malpractice and the Obstetric Ultrasound Examination

## Conclusion

It has now been nearly 4 decades since sonography was first used to evaluate the obstetric patient. At first, the questions this modality sought to answer were basic: Is there a pregnancy? Is the fetus alive? Is there a singleton or a twin gestation? What is the location of the placenta? What is the gestational age? Probably, few envisioned that the day would come when ultrasonography would be used to answer questions as to the presence of subtle anatomic defects such as cleft lip or palate or suggest the presence of a chromosomal abnormality. Likewise, at its inception, it was difficult to convince clinicians as to the usefulness of this new diagnostic modality. Now, it is not unusual for a patient to have one or even several ultrasound examinations during her pregnancy. The recent technologic advances in ultrasound imaging, the use of high frequency transvaginal probes, and the potential for chromosomal screening in early pregnancy (e.g., nuchal translucency) have only magnified the interest in the use of sonographic imaging in the obstetric patient.

Since the last edition of this textbook, there have been dramatic advances in ultrasound technology, including improved spatial and contrast resolution, three-dimensional and four-dimensional imaging, harmonic imaging, new and improved ultrasound scanning probes, and improved digital review workstations, to name a few. Likewise, our knowledge of normal fetal anatomy and pathology, and the pathophysiology of disease have increased substantially. The Internet has made communication among researchers easier. Likewise, there have been many collaborative studies

and refinements of the guidelines for the performance of the obstetric ultrasound examination. However, there are still differences in the approach to the obstetric ultrasound examination from one group to the next. Some very basic issues such as what constitutes a basic ultrasound examination, what structures should be evaluated, the timing of the examination, who should perform and interpret the examination, how safe is ultrasound, how should it be recorded and documented, how should it be reported, and last, how should the patient be told the results of the examination are often hotly debated. These issues are addressed later in the text and some of them discussed here.

## SAFETY OF ULTRASOUND EXAMINATION

It was not long after the inception of ultrasound imaging that questions were raised as to the safety of this new modality. Despite numerous claims of the safety of ultrasound to the mother and fetus, there have been a number of studies noting possible adverse effects of diagnostic ultrasound to the developing fetus. These studies have focused primarily on thermal and cavitation mechanisms, leading to possible injuries to the developing fetus.<sup>1-5</sup>

Absorption of the ultrasound wave's energy by soft tissue and bone, and its conversion to heat are measured by the thermal index. A thermal index of 1 means an increase of 1 degree centigrade. Several studies have suggested a general



threshold of temperature elevation of 1.5 to 2° C above maternal core temperature before any evidence of a developmental effect occurs. With modern ultrasound machines, there is only a negligible rise in temperature, usually less than 1° C. The World Federation for Ultrasound in Medicine and Biology<sup>6</sup> has stated that "a diagnostic exposure that produces a maximum in situ temperature rise of not more than 1.5 degrees C above normal physiological levels may be used without reservation on thermal grounds." In addition, they stated that "a diagnostic exposure that elevates embryonic and fetal in situ temperature above 41 degrees C for 5 minutes should be considered potentially hazardous."<sup>6</sup> As a result of these conclusions, it is unlikely that there is a deleterious effect of ultrasound in the first trimester during embryogenesis with routine grayscale ultrasound.

However, when Doppler ultrasound is used during the first trimester, it is likely that temperatures above 1.5° C may occur.<sup>1</sup> Studies of the effect of Doppler on soft tissues adjacent to bone and nerve conductance demonstrated a significant rise in temperature when the ultrasound Doppler beam was held for more than 30 seconds.<sup>1,7</sup> The European Federation for Societies in Medicine and Biology in 1998 concluded that "until further scientific information is available, investigations using pulsed or color Doppler should be carried out with careful control for output levels."<sup>1,8</sup>

Although the potential for embryonic effects from Doppler imaging exists, there is little evidence that ultrasound is teratogenic. As stated in a recent editorial on the subject, "Many of the studies to date have shown the embryo to be remarkably resilient to ultrasound exposure. Logic would suggest that Doppler techniques should not affect the embryo if the pulses are applied at a low level."<sup>9</sup> A study of animals by Zhu et al<sup>10</sup> examined the genetic effect of diagnostic color Doppler sonography. The researchers insonated pregnant rats with diagnostic levels of color Doppler ultrasound energy and studied the cell cycles of newborn rats by flow cytometry and factorial analysis. They found that the deoxyribonucleic acid content was not affected in any phase of the cell cycle in newborn rats by any of the different insonation times and frequencies.

Cavitation involves the occurrence of gaseous bubble formation in an air-water interface.<sup>1</sup> The concern is that stress from the fluid adjacent to the gaseous body during the process of cavitation may disrupt cell membranes.<sup>1,11</sup> Cavitation has been difficult to document in mammalian fetuses, because, for the most part, there is not an air-water interface, which is needed for the cavitation mechanism.<sup>1</sup>

A number of studies have evaluated the effect of prenatal ultrasound on neonatal and infant outcome in animal models. Although some studies have documented lower birth weights, shorter heights, and lowered white blood cell counts in neonates that were scanned in utero compared with controls, the size differences disappeared when studied after 3 months. In addition, hematologic parameters normalized by this time.<sup>12</sup> Neurodevelopmental studies revealed no significant differences in motor or cognitive tasks, or in learning skills.<sup>1,12</sup> Studies evaluating the human fetus and neonate have reached similar conclusions. Studies have found either no difference in birth weights between exposed and nonexposed fetuses, or a difference that although present at birth, was not present at 6 to 7 years of age.<sup>13,14</sup>

The information on an association between ultrasound and congenital malformations is limited. Studies evaluating chromosomal aberration and ultrasound exposure have demonstrated little or no change.<sup>1,10,15</sup>

The major difficulties with the studies investigating a possible deleterious effect of diagnostic ultrasound evaluation are threefold: (1) experimental ultrasound exposure levels or time of exposure often far exceeded those that are normally used diagnostically; (2) the systems used to show ultrasound effect (plants, cell culture, laboratory animals) may not be applicable to humans; and (3) many studies that have demonstrated adverse effects in vitro have not been reproducible.<sup>16</sup>

A recent study evaluating the effect of diagnostic ultrasound on neuronal migration in mice, once again, raised much attention in the media.<sup>17</sup> Although this is an interesting study in mice, for the reasons stated earlier, it has little to no applicability in humans. There are two major criticisms of this study. Although the study did use commercially available equipment in which only slightly greater ultrasound frequency than normal was used (6.7 MHz versus 3.5–5.0 MHz), the fixed duration of exposure far exceeded what would be normally be used. The study did not demonstrate statistically significant abnormal results until 30 minutes of exposure (2 × 15 minutes). More than 10 years ago, when a sonologist wished to determine that an embryo was nonviable, the recommended evaluation of the embryo was 3 minutes of observation, demonstrating no evidence of embryonic or cardiac activity. Two minutes of evaluation, let alone 3 minutes, seemed like an eternity, and most examiners, in my experience, stopped after 1 minute. In the slightly older embryo and early fetus, greater than 5 to 10 minutes of sustained evaluation of the fetal brain would be excessive. In most cases, the transducer would be moving around the brain rather than being fixed during the examination. The second criticism relates to the timing of embryology and the size of the mouse and human brain. As stated by the authors of this study: "The duration of neuronal production and the migratory phase of cortical neurons in the human fetus lasts approximately 18 times longer than in mice (between 6 and 24 weeks of gestation, with the peak occurring between 11 and 15 weeks), compared with the duration of only approximately 1 week (between E11 and E18) in a mouse."<sup>17–19</sup> Thus an exposure of 30 minutes represents a much smaller time dedicated to the development of the cerebral cortex in the human than in the mouse, and thus could have a lesser overall effect, making human corticogenesis less vulnerable to ultrasound waves."

The American Institute of Ultrasound in Medicine (AIUM) statement on the clinical safety of diagnostic ultrasound reiterates previous findings that no confirmed bioeffects caused by exposure at intensities typical of present diagnostic instruments have ever been reported in patients or instrument operators.<sup>20</sup> This statement acknowledges the possibility that bioeffects may be identified in the future but emphasizes the current data indicating that the benefits of the prudent use of diagnostic sonography outweigh the risks, if any.<sup>20,21</sup> As stated by Kremkau,<sup>22</sup> "even if this risk is so minimal that it is difficult to identify, prudent practice dictates that routine measures be implemented to minimize the risk while obtaining the necessary information to achieve the diagnostic benefit. This is the ALARA (as



low as reasonably achievable) principle of prudent scanning” (Fig. 1-1).

The sonographer’s knowledge of ultrasound and its safety is crucial to the safe implementation of this modality. Merritt, in an editorial, summarized it best: “In view of the rapid growth of sonography and its proliferation into the hands of minimally trained clinicians, it is likely that more patients are harmed each day by misdiagnosis resulting from improper indications, poor examination technique, and errors in interpretation than from all bioeffects.”<sup>21</sup>

INDICATIONS FOR OBSTETRIC ULTRASOUND EXAMINATION

In some countries, as many as 90% to 100% of women seeking obstetric care have at least one ultrasound examination during pregnancy.<sup>23,24</sup> In Glasgow, Scotland, where routine scanning is employed, the average number of scans per pregnancy is 2.8.<sup>25</sup> In Germany, three ultrasound scans (weeks 9–12, 19–22, and 29–32) are routinely performed during pregnancy.<sup>26</sup>

If ultrasound evaluation is relatively safe and noninvasive, and has the potential for yielding important diagnostic information, then why not use this modality in every pregnant patient? As one might imagine, there is much controversy over this single issue.

In countries where routine prenatal ultrasound examination is practiced, investigators have noted that ultrasound scanning is beneficial in detecting congenital malformations, in diagnosing twins and placenta previa, and in identifying patients at risk for postmaturity and intrauterine growth restriction.<sup>24,27</sup> Although these observations are clearly important, the major question still unanswered is whether patient outcome is significantly improved by screening ultrasound examinations. In one study in which the routine use of prenatal ultrasound examination was evaluated, researchers found no benefit from the routine use of “office ultrasound.”<sup>28</sup> Most important errors of gestational age and most twin pregnancies were suspected clinically and diagnosed by an indicated, as opposed to a screening, ultrasound examination.<sup>28</sup> In one of the largest studies of its kind, the RADIUS (Routine Antenatal Diagnostic Imaging with Ultrasound) study evaluated over 15,000 low-risk patients in an attempt to determine the efficacy of screening ultrasounds on perinatal outcome.<sup>29</sup> Low-risk patients were randomly assigned to have either two screening sonograms (at 15 to 22 weeks and 31 to 35 weeks) or conventional obstetric care with ultrasound used only when believed to be clinically necessary. The conclusion of the study was that screening ultrasound examinations did not improve perinatal outcome and were of no clinically significant benefit. The results of the RADIUS study documented a low detection rate for anomalous fetuses (35% in the screened group versus 11% in the nonscreened group) as well as a low abortion rate (9 abortions for anomalies among 7685 fetuses in the screened group, whereas four pregnancies were terminated for fetal anomalies detected among 7596 control subjects).<sup>30</sup> Likewise, many similar studies evaluating the efficacy of screening ultrasound examination have also examined the sensitivity of ultrasound assessment for the detection of congenital anomalies.<sup>31</sup> These studies have demonstrated that in a low-risk population the sensitivity is low, varying from 17% to 35%, whereas the specificity is quite high at 99%.<sup>32,33</sup> When targeted examinations of a high-risk population are performed, the sensitivity is significantly improved, to greater than 90%.<sup>34,35</sup> The major criticisms of the RADIUS and other similar studies have been the low anomaly detection and abortion rates as compared with European studies and those from other countries (Tables 1-1 and 1-2).

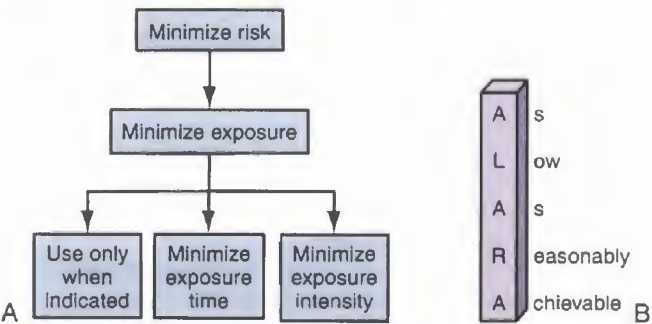


FIGURE 1-1. Minimizing risk by minimizing exposure (A) is the cornerstone of the ALARA principle (B). (From Kremkau FW [ed]: *Diagnostic Ultrasound: Principles and Instruments*, 7th ed. Philadelphia, WB Saunders, 2006.)

Table 1-1 Prevalence of Fetal Anomalies in Published Studies*				
Study Name	Country	No. of Pregnancies Screened	No. of Anomalies in Population Screened	Prevalence of Anomalies Per 1000 Screened
Brocks and Bang <sup>80</sup>	Denmark	14,297	81†	5.67
Levi et al <sup>81</sup>	Belgium	16,072	259†	25.95
RADIUS <sup>29,30</sup>	United States	7765	187†	23.10
Helsinki trial <sup>82,83</sup>	Finland	4073	45†	11.05
Luck <sup>84</sup>	United Kingdom	8523	67†	7.86
Shirley et al <sup>85</sup>	United Kingdom	6183	84†	14.39
Roberts et al <sup>86</sup>	New Zealand	12,909	249†	19.29
Chitty et al <sup>87</sup>	United Kingdom	8432	125†	14.82
Anderson et al <sup>88</sup>	New Zealand	7880	157†	19.80

\*Sonograms performed before 24 weeks' gestation in all series except Roberts et al.<sup>82</sup>  
†88 cases of renal dilation have been deducted from the author's published figure.  
From Anderson N, Boswell O, Duff G: Prenatal sonography for the detection of fetal anomalies: Results of a prospective study and comparison with prior series. *AJR Am J Roentgenol* 165:943, 1995.

**Table 1-2** Detection Rate of Fetal Anomalies Before 24 Weeks' Gestation Compared With Published Studies

Study Name	No. of Anomalies in Population	No. of Anomalies Detected	Percent of Anomalies Detected	Detection Rate per 1000 Screened
Brocks and Bang <sup>80</sup>	81	44	54.3	3.08
Levi et al <sup>81</sup>	259	54	20.8	3.36
RADIUS <sup>29,90</sup>	187	31	16.6	3.97
Helsinki trial <sup>81,83</sup>	45	18	40.9	4.42
Luck <sup>84</sup>	67	41	61.2	4.81
Shirley et al <sup>85</sup>	84	51	60.7	8.25
Roberts et al <sup>86</sup>	218	96	44.0	8.45
Chitty et al <sup>87</sup>	125	93	74.4	11.03
Anderson et al <sup>88</sup>	157	93	60.0	11.80

From Anderson N, Boswell O, Duff G: Prenatal sonography for the detection of fetal anomalies: Results of a prospective study and comparison with prior series. *AJR Am J Roentgenol* 165:943, 1995.

Possible explanations for the variance in the detection rate of anomalous fetuses may include (1) differences in neonatal assessment, (2) differences in the definition of a major anomaly, (3) a differing risk status of the population, (4) differences in what is considered a routine or standard sonogram, and (5) the expertise of the examiner.<sup>36</sup>

Even if one concludes that screening ultrasound examinations are a worthwhile endeavor, two major issues must still be addressed. First, the cost of such an undertaking would be large. With approximately 4 million deliveries in the United States annually, the cost of screening every woman, at a conservative estimate of \$200 per examination, would be \$800 million. If one adds the additional cost for multiple examinations, the added health care costs would be more than \$1 billion. Two major arguments are often put forth to counter the concern over cost of screening ultrasound. First, a significant number of patients in public clinics will be found to be at high risk and, thus, will likely require sonographic evaluation in any event. This number may be as high as 40% to 60% of patients. Second, a major criticism of the cost issue relates to the cost of care for nonaborted anomalous fetuses. It has been argued that if the birth of a child with spina bifida, hypoplastic left heart, or trisomy 21 were prevented, the cost savings would pay for the screening of the entire low-risk population in an area.<sup>36</sup> In addition to the discussions regarding cost, an argument could be made regarding quality of life and the benefit to the pregnant woman gained from a normal ultrasound.

The second issue involves the persons who perform the screening examinations. Many believe the best solution would be to have virtually any sonologist or sonographer do the screening, as long as he or she would willingly refer all questionable abnormalities to more experienced persons. Although that might conceivably alleviate the problem with the false-positive examination, it would not address the issues of missing an abnormality due to examiner inexperience and a large number of unnecessary "second look" examinations.

As a result of the explosion in the number of ultrasound examinations, several persons and organizations began the process of developing a consensus of indications for the performance of the ultrasound examination. In 1983 to 1984, a panel from the National Institutes of Health convened and, after obtaining input from a number of experienced

sonologists, developed a list of indications for obstetric and gynecologic ultrasound evaluation.<sup>37</sup>

- Estimation of gestational age by ultrasound evaluation for confirmation of clinical dating for patients who are to undergo elective repeat cesarean delivery, induction of labor, or elective termination of pregnancy.
- Evaluation of fetal growth (when the patient has an identified etiology for uteroplacental insufficiency, such as severe preeclampsia, chronic hypertension, chronic significant renal disease, or severe diabetes mellitus, or for other medical complications of pregnancy when fetal malnutrition, i.e., intrauterine growth restriction or macrosomia, is suspected).
- Vaginal bleeding of undetermined etiology in pregnancy.
- Determination of fetal presentation when the presenting part cannot be adequately assessed in labor.
- Suspected multiple gestation.
- Adjunct to amniocentesis (chorionic villus sampling).
- Significant uterine size/clinical dates discrepancy.
- Pelvic mass detected clinically.
- Suspected hydatidiform mole.
- Adjunct to cervical cerclage.
- Suspected ectopic pregnancy.
- Adjunct to special procedures.
- Suspected fetal death.
- Suspected uterine abnormality.
- Intrauterine contraceptive device localization.
- Ovarian follicle development surveillance.
- Biophysical profile for fetal well-being (after 28 weeks' gestation).
- Observation of intrapartum events (e.g., version/extraction of second twin, manual removal of placenta).
- Suspected polyhydramnios or oligohydramnios.
- Suspected abruptio placentae.
- Adjunct to external version from breech to vertex presentation.
- Estimation of fetal weight and/or presentation in premature rupture of membranes or premature labor.
- Abnormal serum (alpha-fetoprotein [AFP] value for clinical gestational age when drawn).
- Follow-up observation of identified fetal anomaly.
- History of previous congenital anomaly.



- Serial evaluation of fetal growth in multiple gestations.
- Estimation of gestational age in late registrants for prenatal care.

Although there may be some exceptions, this list serves as a useful guideline for referral for ultrasound evaluation in the obstetric and gynecologic patient.

## WHO SHOULD PERFORM THE ULTRASOUND EXAMINATION AND HOW SHOULD IT BE PERFORMED?

Theoretically, the answer to who should perform the ultrasound examination should be extremely easy. In fact, it is one of the most controversial issues relating to the ultrasound examination. The answer should be that only those persons who have had adequate training (including didactic as well as supervised "hands-on" experience) should perform and interpret an ultrasound examination.

More than 20 years ago, the Joint Task Group on Training for Diagnosis in Obstetrical and Gynecologic Ultrasound developed guidelines for the postresident physician who completed residency programs in either radiology or obstetrics and gynecology that did not provide formal training in obstetric and gynecologic ultrasound evaluation.<sup>38</sup> These guidelines included a recommendation of a minimum of 3 months' experience in obstetric and gynecologic ultrasound evaluation. In addition, it was recommended that this training include 1 month of supervised and documented training in an established ultrasound facility. Such training should include basic physics, technique, performance, and interpretation. In addition, the physician should obtain 2 months of practical experience (at least 200 examinations) before offering services as a physician competent in diagnostic ultrasound examination.<sup>38</sup> There is no reason to believe that in the subsequent 20 years, with the increased complexity of this field, that these guidelines should be anything but more stringent.

The "turf" battles between radiologists and obstetricians as to who should perform the examination are unfortunate. As long as the examining physician is adequately trained and performs the minimum standard obstetrical ultrasound examination, as per the guidelines of the American College of Radiology (ACR), AIUM, and American College of Obstetricians and Gynecologists (ACOG), the specialty of the examiner does not matter.<sup>39,40</sup> I, however, do not believe in the practice of self-referral. Self-referral examinations tend to be performed more and more frequently,<sup>41</sup> and are often less "complete" and of a lower quality than when they are performed by a dedicated ultrasound practitioner. Except in localities where there are no diagnostic ultrasound specialists, patients should be referred to practitioners whose major practice is daily ultrasonography. The potential issues of inconvenience and difficulty in scheduling examinations will undoubtedly always be remedied by practicing sonologists eager for referrals.

Although the previous list of clinical indications addresses the circumstances in which the ultrasound examination should be performed, it does not address the problem of how the examination is performed. In the early 1980s, it became clear that obstetric ultrasound studies were being performed by a variety of persons with disparate levels of training and

that the examinations were different from practitioner to practitioner. There was concern that as the number of examinations was dramatically increasing, their quality was decreasing. In an attempt to address this problem, the ACR Commission on Ultrasound, with minor modification by the AIUM, developed guidelines to serve as a standard for the performance of the obstetric ultrasound examination.<sup>42</sup> These guidelines have been modified slightly several times, the latest in 2003.<sup>43</sup> Although there may be sonologists who exceed these guidelines, the guidelines serve as a minimum standard for all practitioners of obstetric ultrasonography.<sup>44</sup> In a similar fashion, the ACOG published a technical bulletin in 1988, which was revised in 1993, with very similar standards.<sup>40,45</sup>

Before discussing the performance of the ultrasound examination, it is necessary to describe the terminology that is used to describe the examination performed in obstetrical ultrasound.

## Terminology

The latest classification<sup>43</sup> of fetal sonographic examinations by the AIUM, ACR, and ACOG groups the examinations into four major categories: (A) The First Trimester Ultrasound Examination, (B) The Standard Second or Third Trimester Examination, (C) The Limited Examination, and (D) Specialized Examinations. It seems as if the major confusion of what name to call these examinations is centered on categories B and D.

The *standard second and third trimester obstetric examination* is often referred to as a *routine examination*, *basic examination*, *Level 1 examination*, or *complete ultrasound examination*. Although some of these terms are acceptable, some further clarification of the Level 1 and 2 examinations is necessary. These terms, describing sonographic examinations, were developed in the late 1970s to further evaluate patients in whom elevated levels of alpha fetoprotein (AFP) were detected when testing for neural tube defects. Level 1 sonograms were performed largely to detect obstetric problems that result in elevated maternal serum AFP levels (twins, erroneously dated pregnancies, fetal demise). Level 2 sonograms were performed to identify the fetal abnormalities (open neural tube defects, abdominal wall defects) that these programs were designed to detect.<sup>46</sup> It is important to note that while those individuals performing Level 2 examinations are usually proficient in evaluating patients for congenital anomalies, it does not connote that the level 1 examiner is unskilled.<sup>46</sup> In an excellent editorial on the subject, Filly<sup>46</sup> notes that unfortunately some examiners have chosen to use the term "Level 1" as a shield for incompetency. As he states, the Level 1 sonogram is not defined by the technical capability of the examiner, nor by the cost of the sonographic instrumentation employed. In fact, the Level 1 exam "requires a high degree of competency and is for all intents and purposes the standard 2nd or 3rd trimester obstetric sonographic examination as described in the AIUM/ACR/ACOG guidelines" recently published in 2003.<sup>43</sup>

The *specialized examination* is often referred to as the *Level 2 examination* or *survey examination* or *targeted examination*. As the AIUM/ACR/ACOG guidelines state, this is a detailed anatomic examination that is performed when an anomaly is suspected on the basis of history, biochemical abnormalities,



or the results of either a limited or standard examination previously performed.<sup>43</sup>

The individuals performing the sonographic examination are referred to as either *sonographers* or *sonologists*. Traditionally, the technical component and initial production of images has been the responsibility of the sonographer (nonphysician), and the professional component and interpretation of images has been the responsibility of the sonologist (physician). The degree of collaboration between the two and their degree of involvement in the ultrasound examination varies from locality to locality. In many parts of the world, examinations are performed predominantly by physicians. Although the contribution of sonographers to the ultrasound examination is invaluable, it should be remembered as stated by the AIUM, "Ultrasound studies shall be supervised and interpreted by a physician with training and experience in the specific area of sonography. Findings must be recorded and results communicated in a timely fashion to the health care provider responsible for care. Although a sonographer may play a critical role in extracting the information essential to deriving a diagnosis, the rendering of the final diagnosis of ultrasound studies represents the practice of medicine, and, therefore, is the responsibility of the supervising physician."<sup>47</sup>

Perhaps the least controversial aspect of this discussion should be who should interpret the ultrasound examination. This, I believe, is straightforward. Only those with adequate training in a conventional training programs (e.g., residency) in which there are didactic lectures, hands-on scanning, and physician supervision in the performance and interpretation of cases should be performing and interpreting ultrasound. Training by manufacturer's training specialists or 1- to 2-week mini courses does not constitute adequate training in ultrasound.

## Ultrasound Lexicon

There are undoubtedly hundreds of terms that are used in obstetrics and ultrasonography that are either incorrect or confusing. Many of these terms are addressed later in this chapter and in other chapters in this text. Two areas in which terminology is often either misused or misunderstood in obstetric ultrasonography are fetal life and age. The term *viability* is defined as the ability to survive in the extrauterine environment. Even in cases of very late third trimester examinations, this statement cannot be used with complete certainty. I prefer to state that the embryo or fetus is *living*, if that is the case, and use the term *nonviable* for those embryos or fetuses that either are dead or are not capable of living in the extrauterine environment. Early pregnancy failure is another, perhaps even better, way of communicating this information.

The second often-confusing term is *gestational age*. Taken as it sounds, this term would seem to imply the actual age of the fetus from conception to the present. In fact, this term, which is widely used by obstetricians and sonologists, is most often meant to be synonymous with *menstrual age*. *Menstrual age* refers to the length of time calculated from the first day of the last normal menstrual period to the point at which the pregnancy is being assessed. The true age of the embryo or fetus, *fetal age*, is rarely known accurately unless the patient has had assisted fertilization or has extremely regular menstrual periods and the day of conception is known. Some

examiners subtract 2 weeks from the menstrual age to arrive at the *fetal age*.

In this text, the terms *gestational age* and *menstrual age* are used interchangeably. The important point for any examiner to remember is not which term is necessarily preferable but rather that the person interpreting the examination and the physician who ordered the examination both use the same terminology.

Another often-misused term is *fetal pole*. This is a term that should be abandoned. It is most often used to describe the presence of the *embryo* in the early first trimester sonogram. The embryonic period lasts until the end of the 10th menstrual week; during this time the developing conceptus should be referred to as the embryo.

## THE GUIDELINES

In 2003 the *Practice Guideline for the Performance of an Antepartum Obstetric Ultrasound Examination* was developed by the AIUM in collaboration with the ACR and the ACOG.<sup>43</sup> These are a modification of previously developed guidelines which first were published in 1986. This guideline is often referred to as the AIUM guidelines or the *guidelines*. The actual ACR/AIUM/ACOG guidelines are presented in Table 1-3. What follows is my own bias as to what constitutes an appropriate ultrasound examination. In some respects, this is an expansion of the guidelines previously mentioned. Because this multi-author text is essentially a detailed review of the obstetric ultrasound examination, I recognize that my viewpoint in this chapter and those of the authors of the subsequent chapters may differ.

## ULTRASOUND EQUIPMENT AND DOCUMENTATION

It seems that there will always be differences of opinion as to which ultrasound machines produce the best images. With the present state of ultrasound technology, these differences are often subjective, particularly when discussing state-of-the-art machines. Most ultrasound machines use phased-array real-time technology. Three-dimensional/four-dimensional ultrasound technology is still in its infancy, and its role in the ultrasound examination is increasing but still needs to be evaluated.

An often controversial issue is *which* transducer should be used for the ultrasound examination. The answer is as many transducers as are necessary should be used to answer the question for which the patient is referred. There is a misconception that the newest transducer introduced by a manufacturer may be the only one that is needed. When sector and, ultimately, transvaginal probes were first introduced, many practitioners believed that these transducers alone could be used for the entire examination. Many learned that using only a single transducer restricts the field of view or visualization of detail, making diagnosis more difficult.

The most common transducers, which are the workhorses of the ultrasound laboratory, are a linear array, a sector transducer (3 to 5 MHz), and a transvaginal probe (5 to 10 MHz). The higher frequency transducers are most useful in achieving high-resolution scans, particularly in the near-field, and the lower frequency transducers are useful in



**Table 1-3 Guidelines for Performance of the Antepartum Obstetric Ultrasound Examination**

The following are proposed guidelines for the antepartum obstetrical ultrasound examination. The document consists of five parts:

Part I: Specification of Examination

Part IV: Fetal Safety

Part II: Documentation

Part V: Quality Control and Improvement, Safety, Infection

Part III: Equipment Specifications

Control, and Patient Education Concerns

The clinical aspects of this guideline (Specifications of the Examination, and Equipment Specifications) were developed collaboratively by the American Institute of Ultrasound in Medicine (AIUM), the American College of Radiology (ACR), and the American College of Obstetricians and Gynecologists (ACOG). Recommendations for physician requirements, procedure documentation, and quality control vary among these organizations and are addressed by each separately.

This guideline has been developed for use by practitioners performing obstetric sonographic studies. Fetal sonography should be performed only when there is a valid medical reason, and the lowest possible ultrasonic exposure settings should be used to gain the necessary diagnostic information. A limited examination may be performed in clinical emergencies or for a limited purpose, such as evaluation. Of fetal or embryonic cardiac activity, fetal position, or amniotic fluid volume. A limited follow-up examination may be appropriate for reevaluation of fetal size or interval growth or to reevaluate abnormalities previously noted if a complete prior examination is on record.

While this guideline describes the key elements of standard sonographic examinations in the first trimester and second and third trimesters, a more detailed anatomic examination of the fetus may be necessary in some cases, such as when an abnormality is found or suspected on the standard examination or in pregnancies at high risk for fetal anomalies. In some cases, other specialized examinations may be necessary as well.

While it is not possible to detect all structural congenital anomalies with diagnostic ultrasound, adherence to the following guidelines will maximize the possibility of detecting many fetal abnormalities.

#### Part I

##### Specifications of the Examination

##### A. First Trimester Ultrasound Examination

##### 1. Indications

A sonographic examination can be of benefit in many circumstances in the first trimester of pregnancy, including, but not limited to, the following indications:

- To confirm the presence of an intrauterine pregnancy.
- To evaluate a suspected ectopic pregnancy.
- To define the cause of vaginal bleeding.
- To evaluate pelvic pain.
- To estimate gestational (menstrual) age.
- To diagnose or evaluate multiple gestations.
- To confirm cardiac activity.
- As an adjunct to chorionic villus sampling, embryo transfer, and localization and removal of an intrauterine device (IUD).
- To evaluate maternal pelvic masses and/or uterine abnormalities.
- To evaluate suspected hydatidiform mole.

##### Comment

A limited examination may be performed to evaluate interval growth, estimate amniotic fluid volume, evaluate the cervix, and assess the presence of cardiac activity.

##### 2. Imaging parameters

##### Overall Comment

Scanning in the first trimester may be performed either transabdominally or transvaginally. If a transabdominal examination is not definitive, a transvaginal scan or transperineal scan should be performed whenever possible.

- The uterus and adnexa should be evaluated for the presence of a gestational sac. If a gestational sac is seen, its location should be documented. The gestational sac should be evaluated for the presence or absence of a yolk sac or embryo, and the crown-rump length should be recorded, when possible.

##### Comment

The crown rump length is a more accurate indicator of gestational age than is mean gestational sac diameter. However, the mean gestational sac diameter should be recorded when an embryo is not identified.

Caution should be used in making the presumptive diagnosis of a gestational sac in the absence of a definite embryo or yolk sac. Without these findings, an intrauterine fluid collection could represent a pseudogestational sac associated with an ectopic pregnancy.

- Presence or absence of cardiac activity should be reported.

##### Comment

With transvaginal scans, cardiac motion is usually observed when the embryo is 5 mm or greater in length. If an embryo less than 5 mm in length is seen without cardiac activity, an additional scan at a later time may be needed to document cardiac activity.

- Fetal number should be reported.



**Table 1-3** Guidelines for Performance of the Antepartum Obstetric Ultrasound Examination—cont'd**Comment**

Amnionicity and chorionicity should be documented for all multiple pregnancies when possible.

- d. Evaluation of the uterus, adnexal structures, and cul-de-sac should be performed.

**Comment**

Presence, location, and size of leiomyomata and adnexal masses should be recorded. The cul-de-sac should be scanned for the presence or absence of fluid.

## B. Second- and Third-Trimester Examination

### 1. Indications

Sonography can be of benefit in many situations in the second and third trimesters, including, but not limited to, the following circumstances: (adapted from National Institutes of Health. Diagnostic Ultrasound Imaging in Pregnancy: Report of a Consensus. NIH Publication 84-667. Washington, DC: US Government Printing Office; 1984).

- a. Estimation of gestational age.
- b. Evaluation of fetal growth.
- c. Vaginal bleeding.
- d. Abdominal/pelvic pain.
- e. Incompetent cervix.
- f. Determination of fetal presentation.
- g. Suspected multiple gestation.
- h. Adjunct to amniocentesis.
- i. Significant discrepancy between uterine size and clinical dates.
- j. Pelvic mass.
- k. Suspected hydatidiform mole.
- l. Adjunct to cervical cerclage placement.
- m. Suspected ectopic pregnancy.
- n. Suspected fetal death.
- o. Suspected uterine abnormality.
- p. Evaluation of fetal well-being.
- q. Suspected amniotic fluid abnormalities.
- r. Suspected placental abruption.
- s. Adjunct to external cephalic version.
- t. Premature rupture of membranes and/or premature labor.
- u. Abnormal biochemical markers.
- v. Follow-up evaluation of a fetal anomaly.
- w. Follow-up evaluation of placental location for suspected placenta previa.
- x. History of previous congenital anomaly.
- y. Evaluation of fetal condition in late registrants for prenatal care.

In certain clinical circumstances, a more detailed examination of fetal anatomy may be indicated.

### 2. Imaging parameters for a standard fetal examination

- a. Fetal cardiac activity, number, and presentation should be reported.

**Comment**

Abnormal heart rate and/or rhythm should be reported.

Multiple pregnancies require the documentation of additional information: chorionicity, amnionicity, comparison of fetal sizes, estimation of amniotic fluid volume (increased, decreased, or normal) on each side of the membrane, and fetal genitalia (when visualized).

- b. A qualitative or semiquantitative estimate of amniotic fluid volume should be reported.

**Comment**

Although it is acceptable for experienced examiners to qualitatively estimate amniotic fluid volume, semiquantitative methods also have been described for this purpose (e.g., amniotic fluid index, single deepest pocket, 2-diameter pocket).

- c. The placental location, appearance, and relationship to the internal cervical os should be recorded. The umbilical cord should be imaged, and the number of vessels in the cord should be evaluated when possible.

**Comment**

It is recognized that apparent placental position early in pregnancy may not correlate well with its location at the time of delivery.

Transabdominal, transperineal, or transvaginal views may be helpful in visualizing the internal cervical os and its relationship to the placenta.

Transvaginal or transperineal ultrasound may be considered if the cervix appears shortened or if the patient complains of regular uterine contractions.

- d. Gestational age assessment

First trimester crown-rump measurement is the most accurate means for sonographic dating of pregnancy. Beyond this period, a variety of sonographic parameters, such as biparietal diameter, abdominal circumference, and femoral diaphysis

**Table 1-3** Guidelines for Performance of the Antepartum Obstetric Ultrasound Examination—cont'd

length, can be used to estimate gestational age. The variability of gestational age estimations, however, increases with advancing pregnancy. Significant discrepancies between gestational age and fetal measurements may suggest the possibility of fetal growth abnormality, intrauterine growth restriction, or macrosomia.

- i. Biparietal diameter is measured at the level of the thalami and cavum septi pellucidi. The cerebellar hemispheres should not be visible in this scanning plane. The measurement is taken from the outer edge of the proximal skull to the inner edge of the distal skull.

**Comment**

The head shape may be flattened (dolichocephaly) or rounded (brachycephaly) as a normal variant. Under these circumstances, certain variants of normal fetal head development may make measurement of the head circumference more reliable than biparietal diameter for estimating gestational age.

- ii. Head circumference is measured at the same level as the biparietal diameter, around the outer perimeter of the calvarium. This measurement is not affected by head shape.
- iii. Femoral diaphysis length can be reliably used after 14 weeks' gestational age. The long axis of the femur shaft is most accurately measured with the beam of isonation being perpendicular to the shaft, excluding the distal femoral epiphysis.
- iv. Abdominal circumference should be determined at the skin line on a true transverse view at the level of the junction of the umbilical vein, portal sinus, and fetal stomach, when visible.

**Comment**

Abdominal circumference measurement is used with other biometric parameters to estimate fetal weight and may allow detection of intrauterine growth restriction or macrosomia.

- e. Fetal weight estimation

Fetal weight can be estimated by obtaining measurements, such as the biparietal diameter, head circumference, abdominal circumference, and femoral diaphysis length. Results from various prediction models can be compared to fetal weight percentiles from published nomograms.

**Comment**

If previous studies have been performed, interval measurement changes should also be evaluated for growth. Scans for growth evaluation typically can be performed at least 3 weeks apart. A shorter scan interval may result in confusion as to whether anatomic changes truly are due to growth as opposed to variations in the measurement technique itself. Currently, even the best fetal weight prediction methods can yield errors as high as  $\pm 15\%$ . This variability can be influenced by factors such as the nature of the patient population, the number and types of anatomic parameters being measured, technical factors that affect the resolution of ultrasound images, and the weight range being studied.

- f. Maternal anatomy

Evaluation of the uterus and adnexal structures should be performed.

**Comment**

This will allow recognition of incidental findings of potential clinical significance. The presence, location, and size of leiomyomata and adnexal masses should be recorded. It is frequently not possible to image the normal maternal ovaries during the second and third trimesters.

- g. Fetal anatomic survey

Fetal anatomy, as described in this document, may adequately be assessed by ultrasound after approximately 18 weeks' gestational age. It may be possible to document normal structures before this time, although some structures can be difficult to visualize due to fetal size, position, movement, abdominal scars, and increased maternal wall thickness. A second- or third-trimester scan may pose technical limitations for an anatomic evaluation due to imaging artifacts from acoustic shadowing. When this occurs, the report of the sonographic examination should document the nature of this technical limitation. A follow-up examination may be helpful.

The following areas of assessment represent the essential elements of a standard examination of fetal anatomy. A more detailed fetal anatomic examination may be necessary if an abnormality or suspected abnormality is found on the standard examination.

- i. Head and neck

- Cerebellum
- Choroid plexus
- Cisterna magna
- Lateral cerebral ventricles
- Midline falx
- Cavum septi pellucidi

- ii. Chest

The basic cardiac examination includes a 4-chamber view of the fetal heart.

If technically feasible, an extended basic cardiac examination can also be attempted to evaluate both outflow tracts.

- iii. Abdomen

- Stomach (presence, size, and situs)
- Kidneys
- Bladder
- Umbilical cord insertion site into the fetal abdomen
- Umbilical cord vessel number



**Table 1-3** Guidelines for Performance of the Antepartum Obstetric Ultrasound Examination—cont'd

- iv. Spine  
Cervical, thoracic, lumbar, and sacral spine
- v. Extremities  
Legs and arms (presence or absence)
- vi. Gender  
Medically indicated in low-risk pregnancies only for evaluation of multiple gestations.

**Part II****Documentation**

Adequate documentation of the study is essential for high-quality patient care. This should include a permanent record of the sonographic images, incorporating whenever possible the measurement parameters and anatomic findings proposed in this document. Images should be appropriately labeled with the examination date, patient identification, and, if appropriate, image orientation. A written report of the sonographic findings should be included in the patient's medical record.

Reporting should be in accordance with the *AIUM Standard for Documentation of an Ultrasound Examination*.

**Part III****Equipment Specifications**

These studies should be conducted with real-time scanners, using a transabdominal and/or transvaginal approach. A transducer of appropriate frequency should be used.

**Comment**

Real-time sonography is necessary to confirm the presence of fetal life through observation of cardiac activity and active movement.

The choice of transducer frequency is a trade-off between beam penetration and resolution with modern equipment, 3- to 5-MHz abdominal transducers allow sufficient penetration in most patients while providing adequate resolution. A lower-frequency transducer (2 to 2.25 MHz) may be needed to provide adequate penetration for abdominal imaging in an obese patient. During early pregnancy, a 5-MHz abdominal transducer or a 5- to 10-MHz or greater vaginal transducer may provide superior resolution while still allowing adequate penetration.

**Part IV****Fetal Safety**

Diagnostic ultrasound studies of the fetus are generally considered to be safe during pregnancy. This diagnostic procedure should be performed only when there is a valid medical indication, and the lowest possible ultrasonic exposure setting should be used to gain the necessary diagnostic information under the as low as reasonably achievable (ALARA) principle.

The promotion, selling, or leasing of ultrasound equipment for making "keepsake fetal videos" is considered by the US Food and Drug Administration to be an unapproved use of a medical device. Use of a diagnostic ultrasound system for these purposes, without a physician's order, may be in violation of state laws or regulations.

**Part V****Quality Control and Improvement, Safety, Infection Control, and Patient Education Concerns**

Policies and procedures related to quality, patient education, infection control, and safety should be developed and implemented in accordance with the *AIUM Standards and Guidelines for the Accreditation of Ultrasound Practices*. Equipment performance monitoring should be in accordance with the *AIUM Standards and Guidelines for the Accreditation of Ultrasound Practices*.

Modified from Guideline for the antepartum obstetrical ultrasound examination. *J Ultrasound Med* 22:116, 2003.

those circumstances in which increased penetration of the sound beam is necessary. Variations of transducer technology include convex linear transducers and multifrequency probes as well as probes allowing harmonic and three-dimensional imaging and Doppler flow imaging.

Whatever technology is used, the examination should be documented in some form of hard copy. The purpose of documentation is twofold. First, the identification of normal structures is important so they can be viewed retrospectively and compared with later images if pathologic processes are ultimately demonstrated. Second, if a pathologic problem is identified, it can be shown to referring examiners, who will be doing further examinations.

Initially, laboratories used rapid-process film of the Polaroid type for hard copy documentation. The cost and difficulty of mounting these images made this method impractical. Many laboratories then turned to multiformat

cameras that used radiographic film. These cameras added some flexibility but were not without their own problems, including the inconsistency and downtime of these cameras, as well as the added complication of processing time and materials. Some laboratories have chosen videotape as a means of documentation to obviate some of these difficulties. The difficulty with this methodology is the time required to view and compare individual planes of section, particularly when pathologic processes are demonstrated. In the past decade, many imaging centers have implemented picture archiving and communication systems (PACS). These systems allow for the storage of digital ultrasound images on computers and transmission of complete studies to computer workstations for viewing and interpretation. The quality of the images is excellent with these systems. The savings in film costs and development times often compensate for the cost of computer reviewing stations. Likewise, digital images



can be also transmitted to remote locations (telemedicine) for review and consultation.<sup>48</sup>

In addition to the hard copy film, or digitally stored images, a written report of the ultrasound examination should be included in the patient's medical record. When significant pathologic processes are present, the referring physician should be notified immediately before the patient leaves the examination area. This immediate communication should occur not only in cases of fetal malformations but also in cases of oligohydramnios, diminished fetal movement, and macrosomia. Physician notification should be documented.

## THE FIRST TRIMESTER ULTRASOUND EXAMINATION

### Identification of an Intrauterine Pregnancy

Patients referred for first trimester ultrasound evaluation often have vaginal bleeding, which raises the question of an ectopic pregnancy or a threatened abortion. The primary goal of ultrasound evaluation in the first trimester is to determine whether the pregnancy is intrauterine and whether the embryo is living. With present-day equipment, particularly transvaginal transducers, both of these tasks should be readily accomplished at very early stages of gestation. The same care taken in concluding that a pregnancy in the second or third trimester has a lethal malformation should be applied in deciding that an early pregnancy is nonviable. If there is reasonable doubt about embryonic life, a repeat examination in as few as 7 to 10 days will invariably make the conclusion unequivocal.

### Embryonic/Fetal Number

There is no question that, with a careful examination, the true number of embryos can be accurately determined in the first trimester. The literature has emphasized that it is important not to overestimate the number of developing gestations by misinterpreting findings such as a "double sac sign," fluid in the uterine cavity, the yolk sac, or the presence of the amnion as evidence of multiple sacs or embryos and thus multiple gestations. However, the examiner may be just as likely to underestimate the number of developing gestations and embryos if a thorough evaluation of the gestational sac is not made for all embryos.<sup>49</sup> It is my experience that when multiple gestations are missed using ultrasound assessment, it is usually from a less than optimal first trimester examination. The head (crown) of one embryo may be added to the body (rump) of an adjacent embryo and measured as a singleton. This misdiagnosis, of course, occurs only in monochorionic gestations. It is for these reasons that some investigators prefer that if one ultrasound examination is to be done concentrating on fetal number, it should be done in the early to middle second trimester of pregnancy.

### Estimating Gestational Age

The subject of estimating gestational age is covered in detail in Chapter 7. Some estimate of gestational age should be

made when an ultrasound examination is performed in the first trimester. The two most common methods of gestational age estimation are mean gestational sac diameter and crown rump length. For many years, the crown rump length has been acclaimed as the most reliable method of estimating gestational age in utero. The crown rump length is a highly accurate method of estimating gestational age using ultrasound evaluation (accuracy 3 to 7 days). Other measurements, such as the head circumference or femur length, performed in the second trimester, are nearly as accurate and have the added benefit of allowing one to assess fetal morphology to a better advantage in a larger fetus. I believe that the first trimester ultrasound examination should not be done for the sole purpose of obtaining more accurate measurements if there is not a clinical reason why it cannot be done in the second trimester. Clinical indications such as correct estimation of the gestational age to know when to administer other subsequent tests such as maternal serum screening and amniocentesis are examples.

### Morphologic Abnormalities

Since the advent of transvaginal ultrasound transducers, there have appeared numerous reports documenting morphologic abnormalities detected in the embryonic stage in the first trimester. Abnormalities involving virtually every organ system have been reported. In light of these reports, I am frequently asked when is the earliest time that a particular abnormality can be detected. My reply is often that although early detection of a morphologic abnormality is useful, the confident unequivocal detection of an abnormality is even more important. Unless one is extremely confident of the existence of an abnormality in the first trimester, a follow-up examination should be performed.

Although there are a number of investigators who advocate earlier scanning of pregnancies for abnormalities, there are few who believe this should occur in the first trimester. One should beware of four potential pitfalls in diagnosis in the first trimester: (1) the normal extra-abdominal position of the embryonic intestine simulating an abdominal wall defect, (2) the prominence of the developing cerebral vesicles (rhombencephalon), (3) the potential false-negative diagnosis of anencephaly, and (4) the false-positive diagnosis of cerebellar vermian and callosal abnormalities due to these structures not being fully developed at an early gestational age.<sup>50-52</sup>

### Placenta

In very early pregnancies, it may be difficult to ascertain the site of the developing placenta. If, however, the examiner can confidently identify the site of placentation, either anterior or posterior, this information should be documented. There are a number of cases in which the early first trimester ultrasound examination is the only examination obtained during pregnancy. Later in pregnancy, if either an amniocentesis or a cesarean section is planned and no ultrasound equipment is available, it would be helpful to know the location of the placental site from an earlier examination.



## Uterus and Adnexa

The maternal uterus should be examined carefully for evidence of uterine abnormalities, particularly in high-risk patients. Late in pregnancy, these anomalies may be extremely difficult to detect. If uterine myomas are detected, their size, site, and relationship to the cervix should be recorded. It should be remembered that transient myometrial contractions may simulate myomas.

The adnexa should be carefully searched for the presence of cysts as well as ovarian neoplasms, both benign and malignant. Again, later in pregnancy, as the adnexal areas are displaced superiorly, they may be extremely difficult to evaluate adequately.

## THE SECOND AND THIRD TRIMESTER ULTRASOUND EXAMINATIONS

### Fetal Number and Fetal Life

Although evaluating the number of fetuses may be difficult during early pregnancy, it should be extremely easy and accurate in the second and third trimesters. The increased perinatal morbidity and mortality of multiple gestations make it mandatory that a “surprise twin” at delivery be a rare event in any patient who has had a second or third trimester ultrasound examination. The major potential error in determining the number of fetuses is one of underestimation. This mistake, when made, is likely due to either not evaluating the fundal region or not making sure that the fetal head is associated with its body rather than that of a twin. When a multiple gestation is identified, it is important to determine, if possible, the number of placentas and the number of gestational sacs (the chorionicity and amnionicity).

In the ultrasound report, a statement should be made that the fetus was living, if this was the case, by virtue of cardiac motion being identified. In the past, the diagnosis of fetal death was made when there was absence of cardiac motion for at least 2 to 3 minutes, confirmed by more than one examiner. With the improvements in resolution and the availability of transvaginal scanners, this is rarely necessary. However if there is any doubt about fetal life a confirmatory exam at a later date or by another examiner should take place. The lack of fetal motion should not be interpreted as representing fetal death. Slow fetal heart rates often portend a poor prognosis; however, this observation alone should not be considered evidence of a nonviable pregnancy. The author has seen several cases of fetal heart rates less than 80 bpm that have resulted in normal outcomes, followed into childhood.

### Fetal Position

Once fetal life and number have been identified, then the fetal lie and presenting part must be determined. Fetal lie refers to the relationship of the long axis of the fetus to the long axis of the uterus. Presentation defines the presenting fetal part closest to the cervix. The most common fetal lie is longitudinal, and the most common presenting part is the fetal head. Fetal lies or presentations other than these are referred to as malpresentations. Their significance lies in increased perinatal morbidity during delivery.

The advent of real-time ultrasound evaluation has placed an additional demand on the sonographer. If the sonologist interpreting the scans has not performed the examination, he or she must be able to deduce the lie and presentation from several images rather than from a single one. This may be done only by understanding the normal fetal anatomy and applying it to the scanning position (Figs. 1-2 and 1-3). Likewise, some congenital anomalies (e.g., dextrocardia, abnormal right-sided abdominal cystic mass) are recognized only fortuitously if a structure is identified as abnormal by virtue of its abnormal position related to the lie and presentation of the fetus.

As mentioned previously, the most common presenting part is the fetal head (cephalic presentation). (I prefer the term *cephalic* rather than *vertex* because the latter term may also be used to describe a location on the fetal head.) When the head is adjacent to the lower uterine segment, it is likely that the fetus is in cephalic presentation; however, one must see all images before coming to that conclusion. The fetal body may also be low in the uterus with the fetal head, and thus, the fetus would be in a transverse lie rather than in a cephalic presentation.

Fetal malpresentations require that the sonographer extend the examination to answer two additional questions important to the referring obstetrician. First, what specifically is the presenting part (i.e., foot, buttocks in the case of a breech presentation, or shoulder in the case of a fetus in transverse lie) (Figs. 1-4 and 1-5)? Second, is there an associated fetal malformation or placental abnormality that may be causally related to the abnormal lie?<sup>33</sup>

## Assigning Gestational Age and Weight

The assignment of gestational age and weight is covered in detail in Chapter 7. It is important to remember several concepts when assigning gestational age using ultrasonography. First, measurements made early in pregnancy, for the most part, are more accurate than those made near term. In most cases, the measurements of the fetal head, body, and femur will be concordant of one another, within a week in the early to mid second trimester. This is not often true in the late third trimester, when the femur may lag behind the other measurements. In the early to mid second trimester if the femur or the head measurements are greater than one week *less* than the other measurements, this should raise a red flag to alert one to the possibility of either short-limbed bone dysplasia, trisomy 21 or microcephaly. Follow-up in these cases is indicated. Second, pathologic states should be taken into consideration when deciding which body parts to use in assigning gestational age or weight. Most ultrasound machines allow the user to eliminate from the gestational age calculation those body parts that are abnormal. The abdominal circumference measurement is likely to be inaccurate in the presence of fetal ascites, and the femur length measurement is unreliable in fetuses with short-limbed dwarfism. Third, every obstetric ultrasound report should relate the calculated sonographic age to the patient's menstrual age. Because menstrual histories are frequently inaccurate, there is often a tendency to not believe any woman's menstrual history in deference to the calculated sonographic age. In doing so, however, one runs the risk of assigning an earlier gestational age to a fetus that

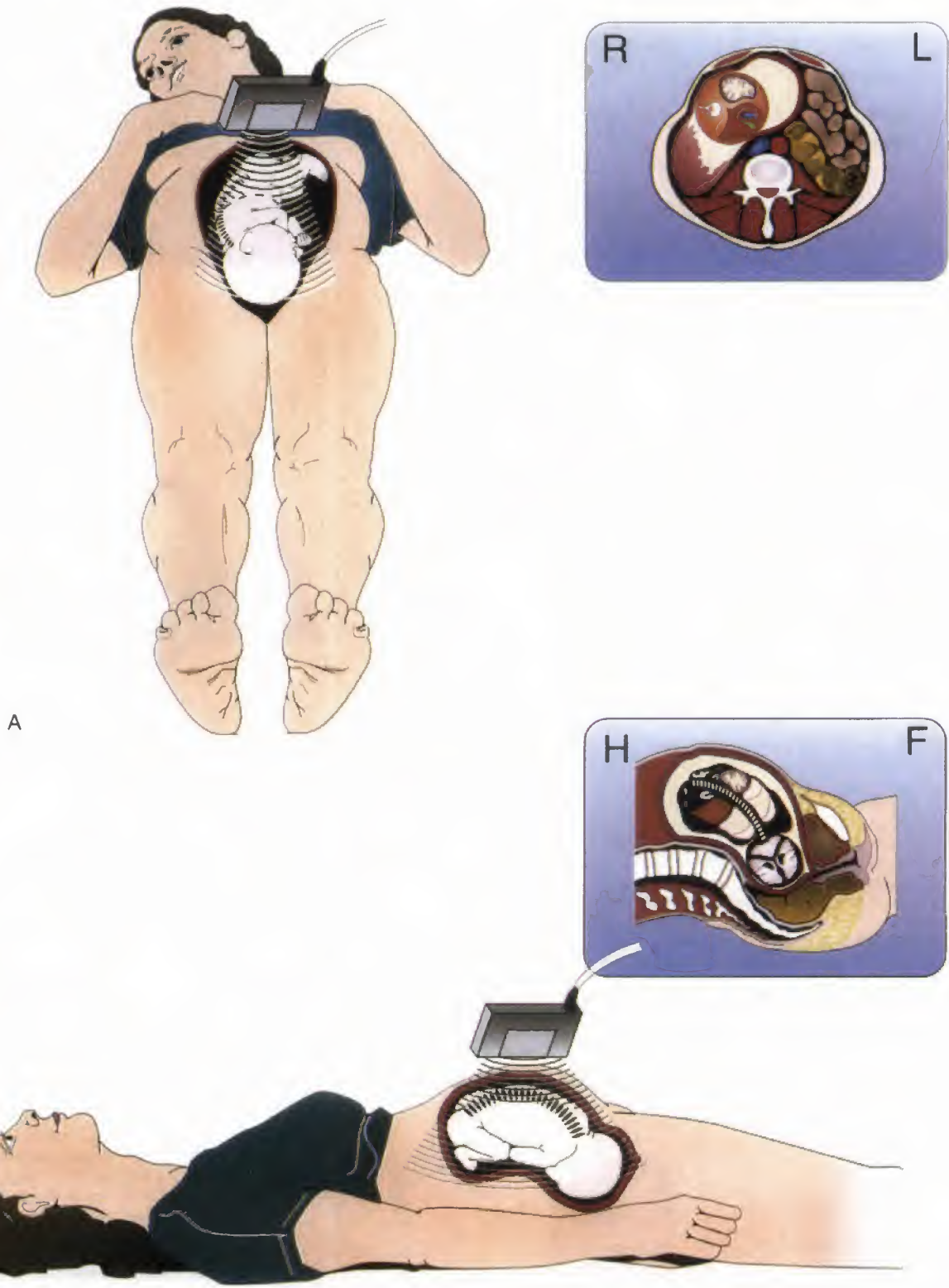


**FIGURE 1-2.** A. Illustration of a transverse plane of section of the gravid uterus. The fetus is in cephalic presentation, so this scan transects the fetal abdomen transversely. B. Longitudinal plane of section of the same fetus. These images are viewed with the maternal head to the left of the recorded image.



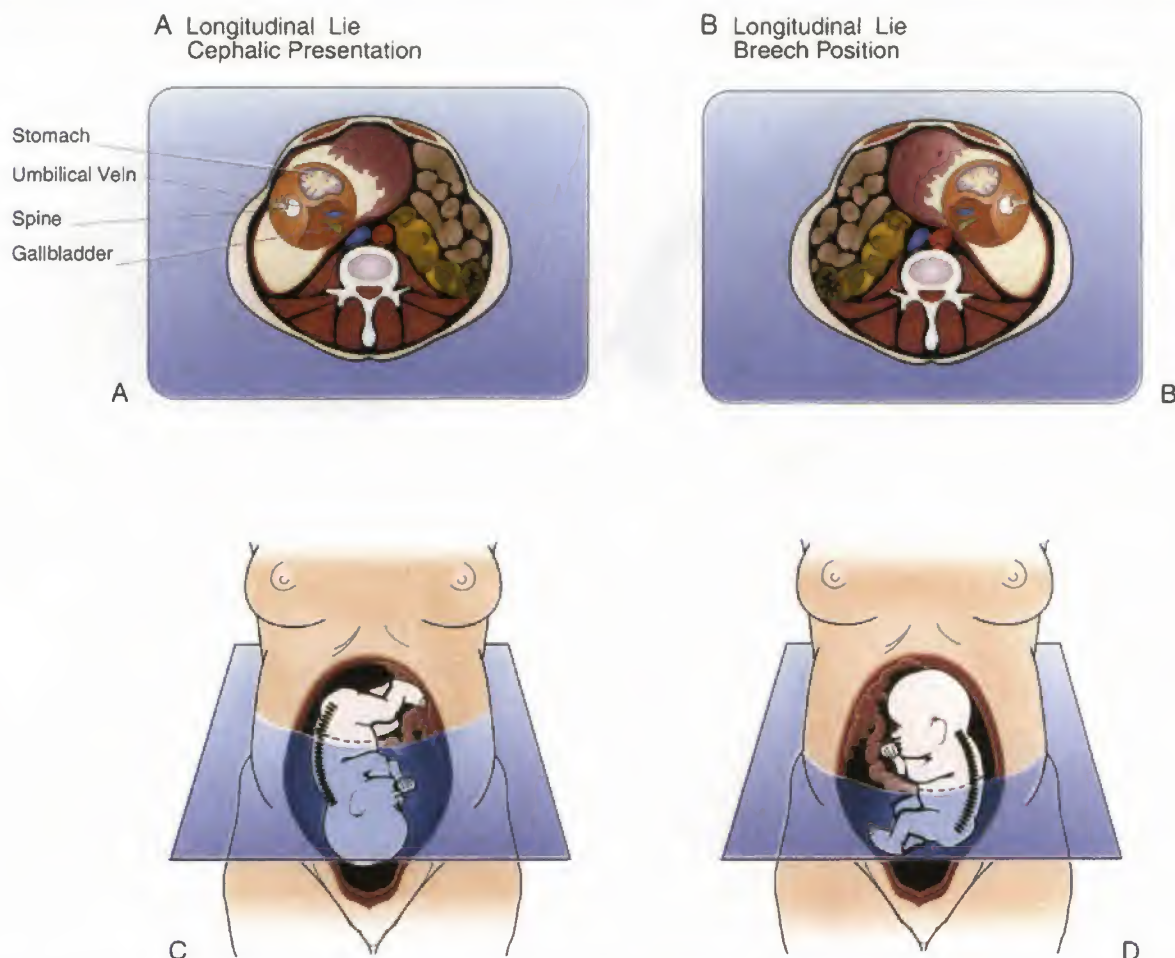


**FIGURE 1-3.** Knowledge of the plane of section across the maternal abdomen (longitudinal or transverse) as well as the position of the fetal spine and left-sided (stomach) and right-sided (gallbladder) structures can be used to determine the fetal lie and presenting part. *A.* This transverse scan of the gravid uterus demonstrates the fetal spine on the maternal right with the fetus lying with its right side down (stomach anterior, gallbladder posterior). Because these images are viewed looking up from the patient's feet, the fetus must be in a longitudinal lie and cephalic presentation. *B.* When the gravid uterus is scanned transversely and the fetal spine is on the maternal left, with the right side down, the fetus is in a longitudinal lie and breech presentation. *C.* When a longitudinal plane of section demonstrates the fetal body to be transected transversely and the fetal spine is nearest the lower uterine segment with the fetal right-side down, the fetus is in a transverse lie with the fetal head on the maternal left. *D.* When a longitudinal plane of section demonstrates the fetal body to be transected transversely and the fetal spine is nearest the uterine fundus with the fetal right-side down, the fetus is in a transverse lie with the fetal head on the maternal right. Although real-time scanning of the gravid uterus quickly allows the observer to determine fetal lie and presentation, this maneuver of identifying specific right- and left-sided structures within the fetal body forces one to determine fetal position accurately and identify normal and pathologic fetal anatomy.

## Breech Presentation



**FIGURE 1-4.** Illustration of the types of breech presentation. In a frank breech presentation (the most common), the thighs are flexed at the hips with the legs and knees extended. In complete breech (the least common), the thighs are flexed at the hips, and there is flexion of the knees as well. One or both hips and knees are extended in the footling breech. The risk of cord prolapse is greatest with a footling breech and least with a frank breech. (Illustration copyright © 2006 Nucleus Medical Art. All rights reserved. [www.nucleusinc.com](http://www.nucleusinc.com).)





**FIGURE 1-5.** Longitudinal scan of a footling breech presentation. In this scan, the leg (arrow) and foot extend into the lower uterine segment and cervix.

is in fact older but growth restricted. Likewise, there is the possibility of assigning an earlier gestational age to a pregnancy that is post term, placing the fetus at risk for fetal postmaturity syndrome or in utero death. Fourth, the calculated fetal weight should be stated not only in grams but also as a percentile based on the patient's menstrual age. Again, if the patient's menstrual dates are inaccurate, the obstetrician can make the decision not to become alarmed at a reported low-weight percentile. This is far better than misinterpreting a growth-restricted fetus as normal by relating only the estimated weight to the ultrasound-determined age. (Remember that although the formulas are different for the calculations of fetal age and weight, they are based upon the same biometric measurements and when compared to one another will often be near the 50%.) Fifth, if there has been a previous ultrasound examination, there should be some statement in the report as to whether the fetal growth has been normal or abnormal. Finally, sonograms attempting to assess normal or abnormal interval growth should have an interval of no less than 2 weeks. It may be difficult to determine whether there has been a growth abnormality versus a measurement error if scans are done with a shorter interval.

## Amniotic Fluid Volume

During the past several years, there has been tremendous interest in the role of amniotic fluid in fetal development and well-being. Although there is relatively good agreement on the significance of extremes of amniotic fluid volume, there is controversy over the methodology used to make the diagnosis of either too much or too little amniotic fluid. I believe that although the diagnosis of oligohydramnios and polyhydramnios can be learned initially by objective measurements, ultimately the diagnosis of extremes of amniotic fluid volume should best be made subjectively. The difficulty with objective measurements is that they are often too stringent and often do not take gestational age into account. The ability to assess amniotic fluid volume subjectively at different stages of gestation is readily learned and should not be difficult for most examiners. Two points should be remembered

when assessing amniotic fluid volume. First, amniotic fluid volume is large compared with fetal volume at early stages of gestation and should not be misinterpreted as polyhydramnios. Conversely, in term patients, the normal volume of amniotic fluid is quite small so that only small pockets may be seen. Second, patients who are obese often *appear* to have less than normal volumes of amniotic fluid. This may be due in part to scattering of sound with resultant artifactual echoes within the amniotic fluid.

In making the diagnosis of oligohydramnios, one should remember two points. First, because, in most cases, this will imply the likelihood of a fetal renal malformation or severe growth restriction in the absence of ruptured membranes, this diagnosis should only be made when there is almost no amniotic fluid. An exception to this is when there is a small amount of fluid in an early or mid-second trimester examination (when normally large amounts of amniotic fluid would be anticipated). Second, because of the association of severe diminution of amniotic fluid in a compromised fetus and ultimate fetal demise, the obstetrician should be alerted immediately if this diagnosis is made, before the patient leaves the ultrasound evaluation area.

The diagnosis of polyhydramnios, although seeming to be less serious, in many cases may in fact be associated with significant complications to the mother and fetus. In the mother, preterm labor and ruptured membranes may occur as a result of polyhydramnios, and in the fetus, fetal anomalies may be present. Although many cases of polyhydramnios ultimately result in a normal fetus, the high number of anomalous fetuses with this condition reported in the literature should alert the sonographer to perform a thorough evaluation when this diagnosis is suggested.<sup>53-55</sup>

## Amniotic Fluid Volume in Multiple Gestations

If one looks at a list of causes of polyhydramnios in many obstetric texts, multiple gestations will most likely appear. Although increased amniotic fluid volume may appear in twin gestations, in most cases the cause is some abnormality of pregnancy.<sup>56</sup> Many of these cases are due to the twin transfusion syndrome.<sup>57</sup>

## The Placenta

As mentioned earlier, whenever the placenta is identified in pregnancy, its position and relationship to the cervix should be noted in the interpretation. The literature has emphasized the large number of false-positive diagnoses of placenta previa that are made either early in pregnancy or in the presence of an overdistended urinary bladder.<sup>58,59</sup> Although this is true, one must not be lulled into a sense of security in thinking that all low-lying placentas will "go away" and be clinically unimportant. If the placenta is low lying during a second trimester examination, every effort should be made to answer the question as to whether there is or is not a placenta previa, often using transvaginal examination. A diagnosis of possible placenta previa may subject the patient to significant life-style restrictions that would not occur if there were not a placenta previa. However, if after a variety of maneuvers and transducers (Trendelenburg position, emptying the bladder, translabial or transvaginal scanning)



one is still unsure about the relationship of the edge of the placenta to the cervical os, the placenta should be interpreted as low lying, and that a placenta previa cannot be excluded. Therefore, these patients will be followed more closely. I prefer to report the distance from the inferior edge of the placenta to the internal cervical os rather than relying on terms that may have differing meanings (e.g., marginal placenta).

Abruptio placentae is a diagnosis that is often difficult to make using ultrasonography. One should remember that the myometrium and its vessels, as well as a transient myometrial contraction, may simulate a hematoma and that these potential false-positive diagnoses should be avoided. Because most clinicians are aware that abruptio placentae is a difficult diagnosis, they often refer patients for ultrasound evaluation to exclude a placenta previa rather than to specifically view the abruption. Patients with a true placental abruption may not ever be seen in the ultrasound laboratory and go straight to labor and delivery.

Vasa previa, which is a variation of umbilical cord anatomy rather than a placental abnormality, is a serious and often overlooked condition. This occurs when fetal vessels cross the internal cervical os in an attempt to reach the main substance of the placenta. This can result in fetal exsanguination during delivery and should be suspected in cases of a velamentous cord insertion or a succenturiate lobe of the placenta.

## Fetal Malformations

The subject of fetal malformations is among the most emotionally charged issues that either the parents or diagnostician may have to face. It is of interest that this subject is dominant in parents' minds during the sonographic examination despite the indications or presonographic counseling they might have received. An interesting study by Eurenus et al<sup>60</sup> evaluated 303 pregnant women and their partners in an attempt to evaluate prescan counseling and the provision of information and their expectations before and experiences during and after a second trimester routine ultrasound scan. Although the information given before the scan clearly stated that the main purposes of the scan were dating and detection of multiple gestations, 89% of the women and 84% of the men thought that the purpose of the scanning was to detect anomalies. "The foremost parental concern is that the baby is healthy and has no malformations, and in spite of the information that 'some serious malformations may be detected,' many think that the scan is a procedure for detection of fetal malformations and a kind of health declaration."<sup>60</sup>

During the past 10 years, ultrasound evaluation has undergone a transformation that has allowed us to answer not only the basic question as to whether the patient is pregnant but also whether a fetal anomaly is present. As smaller and smaller sized abnormalities are identified, the question now becomes what degree of assurance should a patient expect from a report that no anomaly was seen during a routine ultrasound examination. This is a complex issue. The large number of anatomic structures that can be detected by ultrasound studies have necessitated that anomaly detection, by and large, be a *targeted* examination. To examine every patient for all anomalies would be highly impractical.

Fortunately, most *major* anomalies are detected as part of a routine evaluation with several minor modifications.

Major congenital malformations are diagnosed in 4% to 8% of infants during the first year of life.<sup>26</sup> Congenital malformations are the single leading cause of infant mortality in the United States, accounting for more than 21% of all infant deaths.<sup>26</sup> In the United States, it has been estimated that 100,000 to 150,000 children are born each year with major congenital malformations, and approximately 8000 of these babies die before completing their first year of life.<sup>26</sup> Children with congenital malformations account for approximately 30% of pediatric admissions, and the total cost of health care is estimated at more than \$1.4 billion annually.<sup>26,61,62</sup>

As was mentioned in the discussion of the first trimester ultrasound examination, fetal anomalies have been described in virtually every organ system at almost every gestational age. There is much controversy as to when a comprehensive scan of a pregnancy should occur. There has been a desire from many to accomplish this task at a time just before an amniocentesis (14 to 16 weeks) or even earlier, at the time of nuchal translucency measurement.<sup>63</sup> In particular, three advantages have often been cited: (1) transient abnormalities such as an increased nuchal translucency and echogenic bowel (which may serve as markers for chromosomal and structural abnormalities) may disappear if scanning first occurs after 16 weeks<sup>64</sup>; (2) structures such as the fetal hands may be more readily seen, particularly with fingers extended, than later in pregnancy<sup>64</sup>; and (3) if necessary, termination may be easier to accomplish and less dangerous than later in gestation.<sup>64</sup> Although it is true that many morphologic abnormalities will be detected particularly when using a transvaginal probe, certain abnormalities of the face, heart, and skeleton will not be detected at early gestational ages. Likewise, certain embryologic developmental stages, such as the development of the cerebellar vermis and corpus callosum, are not complete until the mid to late second trimester. If one has the economic luxury of performing several sonographic examinations during pregnancy, a scan at 11 to 16 weeks' gestation, followed by a scan at 22 to 24 weeks' gestation might be ideal. It is certainly not unreasonable to exclude gross and potentially lethal abnormalities during the time of the nuchal translucency scan. This would obviously affect the timing of the next scan. However, it is my recommendation that if a single ultrasound or a targeted (level 2) examination is performed, it should be done at a gestational age of 20 weeks. The reason for this is that the fetus will be of a sufficient size to exclude most abnormalities and still allow time for a follow-up examination, if necessary. I have frequently noted that abnormalities that were not seen at 16 to 18 weeks' gestational age became apparent at 19 to 20 weeks. The slight loss of accuracy in assigning gestational age at this time is well worth the gain in visibility of fetal anatomy and pathology.

The patient and the referring obstetrician should be made aware that during the standard ultrasound examination, although many abnormalities may be detected fortuitously, more subtle lesions are likely to be detected only when the fetus is known to be at risk for a specific malformation. Anatomic malformations are likely to grow during pregnancy just as the fetus does; a defect seen at birth may have been too small to be detected earlier in pregnancy. Some



lesions, such as duodenal atresia and heterozygous achondroplasia may not manifest until late in the second trimester. Finally, it is important for sonologists to know the limits of their expertise. If a malformation is suspected and the examiner has had little experience with the abnormality in question, the case should be referred to a more experienced examiner. Only in this way will patients be served best.

## Uterus and Adnexa

Evaluation of the uterus and adnexa becomes more difficult the later in gestation the examination occurs. The most common abnormalities that are likely to be detected are uterine myomas. As stated earlier, it is important to measure the size of the myoma, record the location of the myoma, and define the relationship of the myoma to the cervix. If ovarian abnormalities are suspected and not seen, patients should have a postpartum examination.

## Verbiage Used in the AIUM/ACR/ACOG Guidelines

The committees and individual members of the AIUM, ACR, and ACOG who helped develop the guidelines described earlier did a remarkable job. It is not easy producing a document such as this that will be widely applicable to ultrasound practitioners. There are a few areas where I believe the choice of words were not clear and would like to give my own suggestion for interpretation. The reader should read the editorial addressing this subject concerning two of the points raised in the guidelines.<sup>63</sup>

It is understandable that the guidelines attempted to give the practitioner a wide latitude in requirements for the obstetric ultrasound examination. They attempted to take into account the differences in maternal and fetal anatomy from one patient to the next as well as technical limitations at times. There are a number of instances in which the guidelines state that a structure or structures should be imaged. Unfortunately, additional wording is added that states "when possible" or "can also be attempted" or "when technically feasible." As stated in the editorial mentioned earlier, "One could reasonably state that any of the views defined in the guidelines can only be obtained "if technically feasible." Indeed, the introduction to "Fetal Anatomic Survey" states that one may anticipate technical limitations: "... some structures can be difficult to visualize due to fetal size, position, movement, abdominal scars, and increased maternal wall thickness."<sup>65</sup> Adding these additional words, mentioned earlier, gives the examiner a "way out" to not examine important fetal or maternal anatomy. This occurs in discussion of the first trimester, when these modifying statements are made with respect to the cervix and amnionity and chorionicity in multiple gestations. I do not know of a reason why the cervix cannot be assessed in the first trimester in any patient using a variety of methods available. Perhaps the only time that chorionicity and amnionity can best be assessed is actually in the first trimester of pregnancy. Although the differentiation of mono- from diamniotic twins may be difficult, there is no reason I can think of as to why chorionicity cannot be determined at this time. The same holds true for visualizing the cardiac outflow tracts in the second and third trimester. There is no question that demon-

strating the outflow tracts has a definite learning curve that one needs to conquer. However once learned, the outflow tracts should be demonstrated in more than 90% of patients.<sup>66</sup> In the extremities section, the legs and arms are mentioned. Medically, this would mean only the tibia/fibula and the humerus. I believe the intent was for the femur, humerus, tibia, fibula, radius, and ulna to be evaluated.

The gender was stated as, "Medically indicated in low-risk pregnancies only for evaluation of multiple gestations." I think I know the intent but I would have stated it differently. I would have said that gender should be demonstrated in singleton gestations when medically indicated for diagnosis and counseling. Examples of this type of indication would include hemophilia or distal urinary obstruction, attempting to differentiate [posterior urethra valves [predominantly male disorder] from a cloacal abnormality [predominantly female disorder]]. As for multiple gestations, there are many that would take issue with saying that any multiple pregnancy is low risk. It should have been stated that when chorionicity is difficult to determine in multiple gestation pregnancies, gender determination, when different between the twins, will be helpful in excluding monochorionicity.

For weight determination, a statement is made that "Currently, even the best fetal weight prediction methods can yield errors as high as  $\pm 15\%$ ." Although I agree with this in concept, I would not have put, what appears to be, an upper limit on errors in weight estimation. This seems to imply that numbers greater than this would be below the standard of care. Particularly in macrosomic fetuses, I have seen errors as high as 25% to 30% from what seemed to be reasonable biometry.

A statement regarding technical difficulties reads: "A second- or third-trimester scan may pose technical limitations for an anatomic evaluation due to imaging artifacts from acoustic shadowing. When this occurs, the report of the sonographic examination should document the nature of this technical limitation. A follow-up examination may be helpful." Although I fully understand this limitation, which all of us have encountered, the recommendation is problematic. There are certain anatomic structures or situations in which the anatomy *has* to be imaged or an abnormality reported. The statement "follow-up examination *may* be helpful" is unacceptable. I have seen far too many cases in which the brain or cardiac anatomy were not well seen due to technical limitations. The referring obstetrician did not read the report until the next patient visit. By the time the patient came back for re-evaluation, it was 25 weeks or beyond, precluding the option for termination of an abnormality, if desired. If the brain, heart, or kidneys and bladder (in the presence of oligohydramnios) are not seen, the patient should be seen later that day or the next morning, and only then should the final report be sent. If the structure is still not seen, the referring obstetrician should be notified and the conversation documented.

## Interpretation of the Ultrasound Examination

This is, of course, the focus of the remainder of this book; however, I would like to make several comments. Although the subspecialty of obstetric ultrasound seems to attract new biometric applications daily, I have never been much of an



advocate of the sole use of measurements to achieve a diagnosis. It seems that every day I read in a journal that someone has developed a new chart for the measurement of a fetal anatomic structure. I fully recognize that there are many measurements that are necessary for accurate ultrasound interpretation; fetal biometry for size and weight, cervical length, and fetal ventricular size, to name a few. For many of the abnormalities that can be recognized sonographically, I would prefer that the sonologist give more credence to his or her subjective eye than to a measurement when images or individual structures “just don’t seem right.” Although a measurement may appear to be within normal limits, there are times when subjectivity, in my opinion, wins out. It is acceptable to say that despite an amniotic fluid index of 6, that there is oligohydramnios or that the fetal bowel appears dilated without an objective measurement of the bowel lumen.

Another pitfall is making a measurement of an anatomic structure and not interpreting the significance of the measurement. For example, some ultrasound laboratories believe that adding numerous measurements, for example, transcerebellar, renal, or intraorbital measurements, in addition to standard biometry (biparietal diameter [BPD], head circumference [HC], abdominal circumference [AC], femur length [FL]) will make the examination *more* complete. Although I will not argue the necessity of doing these additional measurements, what is puzzling is that often the interpreter of the examination will not check these measurements against standard tables or nomograms to determine if they are normal or abnormal. In my mind, this is a serious mistake.

Without launching into a discussion of statistics, it is enough to say that no measurement will likely be 100% accurate without false-positive or false-negative results. There are some situations in which false-positive results may be acceptable (e.g., screening examinations for a serious abnormality). Every practitioner abhors the notion of being labeled an “over-reader” of examinations. I have two suggestions: (1) consult with the referring clinician regarding the importance of a specific diagnosis. Ask him or her whether the goal is to not miss any patients with a condition (thus, resulting in more potential false-positive results), which may mean additional testing or intervention, or whether they wish fewer false-positive results and thus risk missing the detection of an abnormality in some patients. With this in mind, one can set the threshold level for the test, either lower or higher. (2) If the sonologist is calling a referring clinician four to six times a week with a suspected abnormality (e.g., pelviectasis, echogenic bowel, and so on), one should perhaps reevaluate the criteria for defining something as abnormal. However, if one calls a referring physician once every 2 to 4 weeks when one is “bothered” by a finding and wishes to call attention to it, one should not feel as if he or she is “over-calling” an abnormality. Likewise, one should not be embarrassed about calling the referring physician about a concern that something might be abnormal even if it ultimately proves to be normal. Only in this way will patients best be served.

## Reporting of Ultrasound Results

One would anticipate that this might be the least contentious topic when discussing the obstetric ultrasound examination.

However, it is controversial. In concert with recommendations by various organizations, for example, AIUM, ACR, ACOG, a written report should be produced at the completion of the ultrasound examination and should be placed in the patient’s medical records. As the electronic medical record becomes a reality, this report may of course be digital. A number of reporting packages (technologies) have been developed to make reporting easier: these include but are not limited to: obstetric worksheets or checklists, computer templates or canned reports, computer voice recognition, digital transcription systems accessed by telephone or computer and traditional voice dictation that is typed by transcriptionists (on site or remotely). All of these methods have the potential for producing an accurate and readable report. However, in my own experience, the easier the reporting method, the more likely that observations made during the examination will *not* be conveyed accurately. Too often, I have observed sonographers and sonologists finish an examination and quickly enter checks into boxes on a worksheet indicating that a particular structure was observed or was normal. It is inconceivable to me, watching the speed with which the worksheet is completed, that they ever asked themselves the question, did I *really* see those structures. Although it is becoming antiquated, conventional dictation systems that require the examiner to pick up the recording device and say “the following structures were seen. . .” or some similar device or mechanism, seem to have a better chance of succeeding in conveying accurate information.

I have mixed emotions about templates that contain standard paragraphs such as: the following structures were seen: “lateral ventricles, cerebellum, and so on.” Although this information may be necessary for reimbursement purposes I have yet to see a sonologist or referring physician who ever reads these paragraphs. They also have the potential to be confusing when abnormalities are detected, particularly if the paragraph ends with “. . . and these structures were normal.” If one does not alter the paragraph, the referring physician will read in this standard paragraph a sentence that says: “the fetal kidneys were normal” and in the next paragraph a sentence that reads “bilateral fetal hydronephrosis was seen.”

It is my practice and recommendation that when fetal abnormalities are detected, the referring physician should be contacted in person or by telephone and the discussion should be documented in the report.

A question often raised is what to do when a structure normally seen on routine (basic) sonograms (and listed in the guidelines) is not seen. Or, what to do when one identifies a structure that has an unusual appearance that one suspects is probably normal. Often, it is assumed that failure to see a structure or structures are secondary to technical limitations, such as shadowing or poor fetal position or fetal physiology (the fetus just urinated or fluid in the stomach passed into the duodenum). If the examination is performed in the early second trimester, the patient should return within 2 to 4 weeks for another evaluation. As was mentioned earlier, if a structure in question relates to the heart or brain or kidneys and bladder (when oligohydramnios is present), the study should be considered *incomplete* and should *not* be reported until the structure is seen either later that day or the next morning. If a follow-up examination is warranted, the



referring physician should be contacted and the conversation documented. The rationale for these recommendations is the concern that adequate follow-up and evaluation will not occur, or if they do occur, they will not be performed in a timely fashion. Statements indicating "clinical correlation recommended" are appropriate when the abnormality seen needs to be correlated with patient's medical condition, laboratory tests, family history and the patient's age, but not when an isolated abnormality is seen (dilated bowel loop).

## Discussing the Examination With the Patient

This topic is also controversial. The patient obviously wants to know that the fetus is healthy and to know the results at the time of the examination. As a general rule, the referring obstetrician knows the patient best and also often has important information about the patient's menstrual history, family history, laboratory values, and emotional state. Thus, the patient's primary physician is often better able to explain the results to the patient and to counsel her effectively. In cases of suspected morphologic or genetic abnormalities, the advice of a reproductive geneticist or perinatologist may prove invaluable. There are situations when the sonologist is asked by the referring obstetrician to explain the results to the patient. As is discussed later, often the first words that are said to the patient are the things that she remembers. Despite what is said later, it may be difficult to undo what was said initially. It is appropriate to say that the interpreter needs to evaluate all of the images together and possibly compare them with old studies. At that time, the final report will be generated.

Counseling is often straightforward if the case is normal or when the diagnosis is unequivocally lethal (anencephaly).<sup>67</sup> It becomes more complex in cases in which the outcome is less than 100% certain (e.g., mild isolated ventriculomegaly). It is important not to insert our own bias and values about raising children with disabilities. One cannot assume that if a serious malformation is detected that a patient will desire an abortion rather than to deliver a baby with disabilities. In some cases, the person informing the patient of the results is uncertain of the significance of the findings,<sup>67-69</sup> and the first information the patient hears may be unclear or misleading. This may color how patients perceive later information and may result in dissatisfaction with the bearer of the news.<sup>67,69</sup>

It is often assumed that women weigh equally the risk of delivering a baby with a congenital abnormality versus a procedure-related pregnancy loss (amniocentesis). In fact, studies have demonstrated that most women see the long-term consequences of raising a disabled child as *worse* than a miscarriage, although women vary widely in this regard.<sup>68</sup> It is important to remember that we do not know better than our patients what is best for them. Our challenge is to help them reach a decision that is best for them given their particular background, experience, and values.

Even when precise and correct information is transmitted in a counseling session, it may not be interpreted with the same intended meaning by the patient. Certain words tend to have more serious and worse connotations to the patient than alternative words.<sup>69</sup> The words *rare* abnormality are often interpreted as serious (even if it is a mild abnormality). The word *abnormality* is often interpreted as worse than a

*variation of normal*. Likewise, technical genetic words often have a worse connotation. Trisomy sounds worse to most patients than an extra chromosome.<sup>69</sup> Choroid plexus cysts (CPCs) and echogenic intracardiac foci (EIF) are discussed in Chapter 4. One should be aware that even if the sonologist firmly believes that the finding of an isolated CPC or an EIF is likely a normal variant and of no consequence, the fact that these structures are in the brain and heart are no small matter. The fact that there may not be a significant increased risk in that individual patient based on other findings and the abnormality is of small size may not alleviate the patient's anxiety once she is told of these findings.

There has been much debate regarding whether physicians should disclose that an isolated sonographic *soft marker* for a chromosomal abnormality has been detected in a fetus in the absence of other risk factors for aneuploidy.<sup>70-72</sup> A recent study by Lee et al<sup>73</sup> found that the detection and communication of isolated aneuploidy markers (choroid plexus cysts, echogenic intracardiac foci, renal pyelectasis, echogenic bowel) is associated with increased maternal anxiety and unnecessary amniocentesis. Their conclusion: "given the amount of maternal anxiety generated with detection of aneuploidy markers, serious consideration should be given to offering pre- and post-ultrasound genetic counseling or otherwise, nothing should be mentioned about ultrasound markers that may be normal variants in patients who have no other risk factors for aneuploidy."<sup>73</sup>

The likelihood of having a normal child when an abnormality is detected is almost always received more favorably by the family than being told of the small percentage of having an abnormal child when an abnormality is detected. (A 99% chance of normal sounds less worrying than 1% chance of abnormal.) When risk is given as a proportion, it often sounds worse than when it is given as a rate (1/X sounds worse than X%).<sup>69</sup> One should be aware, that a large portion of the public lacks functional knowledge of fractions, large numbers, or percentages.<sup>74,75</sup> In one study,<sup>78</sup> a third of adult women with less than a college education did not recognize that 1/1000 is less than 1%. It is interesting that although in most medical specialties, risk or prognosis is given as a percentage, for example, 10% chance of a cure or bad outcome, in prenatal genetic counseling, risk is often given as a proportion, which most patients do not fully understand. In a study by Grimes et al,<sup>74</sup> women of varying ages, education, and language were asked to identify which proportion of bladder infection was higher: 1 in 384 or 1 in 112 persons. The same women were then asked to identify which rate of infection was higher: 2.6 per 1000 women or 8.9 per 1000 women. Overall, 73% correctly identified the higher risk in rate format (X/1000), in contrast with 56% who correctly answered the same question framed as proportions (1/X).<sup>74</sup> Clearly, women understood rates better than proportions.

Perhaps the most important point of this discussion is what to do when a slight variation of normal or an unusual finding is seen. The first answer would be to consult your colleagues. If that does not answer the question, then one should discuss the case further with more experienced experts, for example, perinatologists or geneticists, or refer the patient to a university or specialty center. In some cases, one will simply need to report that there is a finding and that you are



**Table 1-4** Evaluating the Literature

Abstract
What are the objectives, findings, and conclusions of the study?
Introduction
What is the purpose of the diagnostic test?
Materials and Methods
How are the patients selected?
Are they representative of those who are ordinarily tested?
How is the test(s) performed and interpreted?
Are the interpretation criteria well defined and reproducible?
What is the gold standard for diagnosis? Is it appropriate?
Are the sonologists blinded from the final diagnosis and is the final diagnostician (pathologist) blinded from sonographic interpretation?
Is the gold standard applied uniformly?
In a comparison study, are the tests evaluated fairly?
Results
How is the accuracy reported?
Are spectrum of disease and important covariates, such as comorbidity, age, sex, and body habitus, accounted for in tabular presentation of data?
Is the statistical analysis clearly described and appropriate?
Discussion
Are the deficiencies in the methodology of accuracy assessment acknowledged and discussed?
Are other relevant factors, such as disease prevalence, therapeutic effectiveness, and cost, adequately accounted for in the clinical recommendations?

From Black WC: How to evaluate the radiology literature. *AJR Am J Roentgenol* 154:17, 1990.

uncertain of the significance. When the physician feels pressure to always give a black and white, or normal or abnormal answer without honest indecisiveness, this approach does a disservice to the patient.

## EVALUATING THE OBSTETRIC-GYNECOLOGIC ULTRASOUND LITERATURE

Whereas this text serves as a reference to many, as an aid to ongoing clinical problems, new and useful clinical information is reported constantly in the medical literature. It is appropriate that the reader keep current with new advances. It is also important to be vigilant for poorly constructed studies and conclusions. Although virtually every report will have some mention of the sensitivity and specificity of a new test, this is only a small part of an adequate analysis of the utility of a new technique. There are a number of areas that should be considered when evaluating a new report in the literature; these areas are outlined in Table 1-4.<sup>77</sup> Perhaps the most common error is that authors do not state the

prevalence of "disease or abnormality" in their population or that readers do not take this into account when applying the report to their own practice. This also holds true for both equipment and techniques used for analysis.

When the authors discuss a new technique or potentially helpful finding, it is invariably depicted in their first figure, "Figure 1." If after looking at Figure 1 in the new publication, as well as its legend and text description, the reader does not understand what is being demonstrated, the publication is likely to be of little value in clinical practice.

## MALPRACTICE AND THE OBSTETRIC ULTRASOUND EXAMINATION

It is likely that each person reading this text has been touched in some way by the present malpractice crisis. For most of us, this crisis has resulted in increased costs of goods and services, and for some, it has meant being the defendant in a malpractice suit.

Data on the number of claims of malpractice and their settlements are difficult to obtain. In one report, Sanders<sup>78</sup> reported malpractice claims in diagnostic ultrasonography in 228 cases. Obstetric ultrasound examinations represented the majority (78%) of the cases.

Some of the more common reasons for the initiation of malpractice suits (whether legitimate or not) include the following:

- Unreasonable expectations of the ultrasound examination on the part of the patient and the referring physician.
- Physician performing the examination has inadequate training or equipment.
- Failure to seek consultation in difficult cases.
- Inadequate or incomplete study.
- Misinterpretation of the ultrasound examination (resulting in the inability to terminate before the legal state limit, a wrongful termination, or pre- or post-term delivery).
- Poor communication with referring clinicians (improper wording, lack of timely communication).
- Failure to maintain ultrasound equipment.
- Failure to supervise personnel adequately.

It is my desire that this text, through the education process of the sonographer and sonologist, will help alleviate errors in diagnosis and thus reduce the number of these cases. Unfortunately, despite the best medical care, some malpractice suits are brought against physicians.

## CONCLUSION

The appeal of the ultrasound examination is that it is a noninvasive, safe procedure that has a high degree of patient acceptance and can yield a wealth of information. It is always a delight to examine the obstetric patient and reassure her about her pregnancy, when appropriate.

When a pathologic process is first identified, the role of the sonologist is that of a detective who attempts to piece together all of the information to arrive at the correct diagnosis (Fig. 1-6). Although discovering a pathologic process is always disconcerting, the sonologist can be a counselor to the patient and the clinician, and help guide them to appropriate management decisions. However, there are times when an abnormality is strongly suspected but it may be

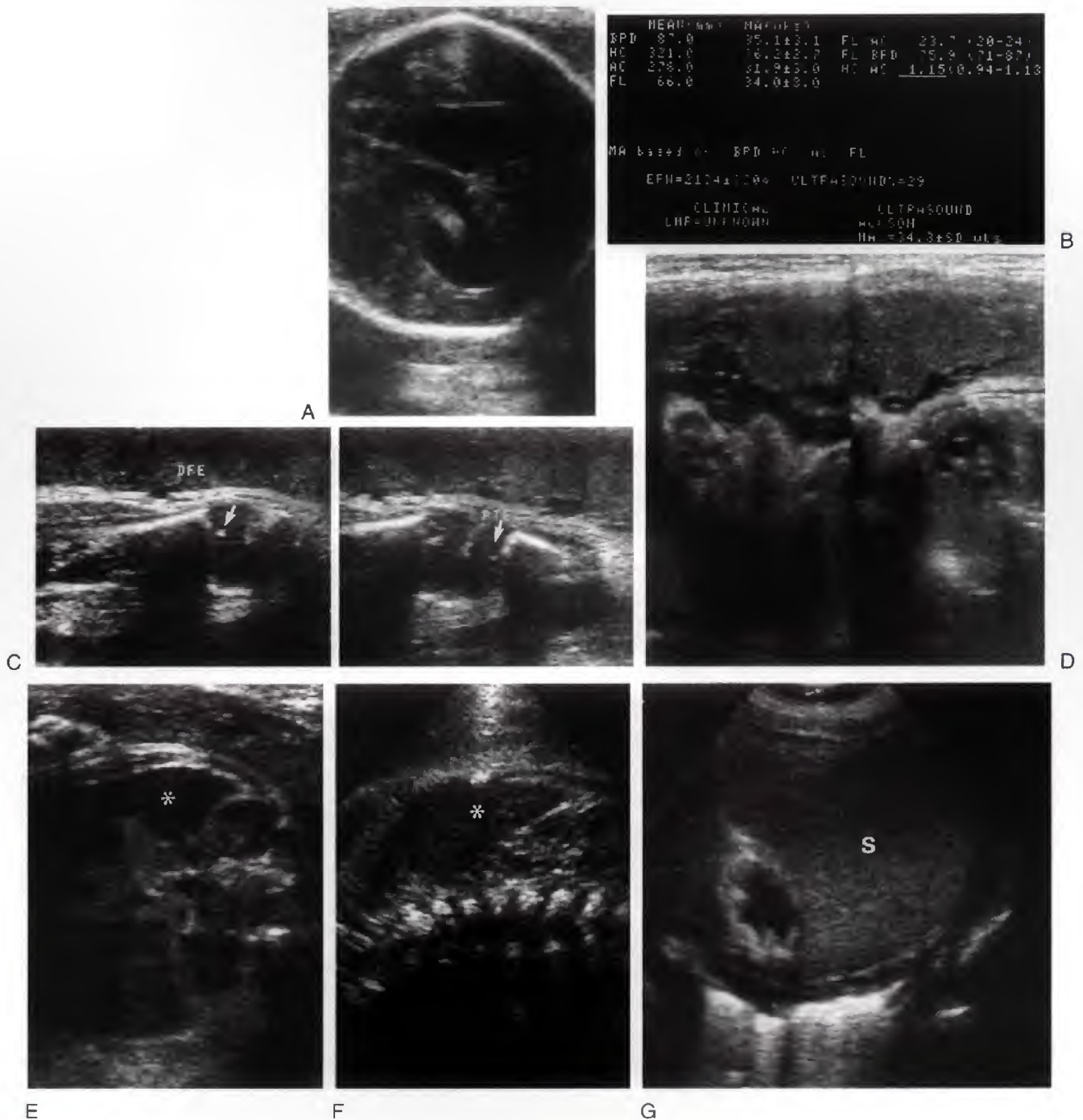


**FIGURE 1-6.** This is an excellent example of how observation of all of the sonographic signs allows one to arrive at the correct diagnosis. The patient was referred because a cyst was seen in the fetal head on initial sonographic scanning. *A*. Slightly angled transverse axial scan of the fetal head demonstrates moderate ventriculomegaly. (The dilated ventricles were what were incorrectly interpreted as a fetal intracranial cyst.) *B*. The ultrasound "worksheet" reveals measurements of the fetal head (biparietal diameter [BPD]), head circumference (HC), abdomen (abdominal circumference [AC]), and femur (femur length [FL]) that are all different from one another. The main differential at this point is that either the head is enlarged and the femur and abdomen more correctly represent the gestational age, or that the head measurements are normal and the fetal abdomen is small from growth restriction. One might assume that the head measurements are abnormally large owing to the ventricular dilation. In fact, the fetal head does not usually enlarge until the ventricular dilation is significantly more pronounced.<sup>79</sup> *C*. The next step would be to evaluate the epiphyseal ossification centers. In this fetus, both the distal femoral epiphyseal (DFE) and proximal tibial epiphyseal (PTE) centers (arrows) show calcification, indicating a fetus with a likely minimum gestational age of 34 to 35 weeks. *D*. These joined dual images of the long axis of the uterus demonstrate little amniotic fluid. The information from images *C* and *D* would seem to indicate that this fetus is likely of 34 to 35 weeks' gestation with a small abdomen (31 weeks' gestation), little amniotic fluid, and probable growth restriction. *E* and *F*. Transverse and coronal planes of section of the fetal abdomen show an enlarged spleen (\*). *G*. A postnatal sonogram confirms the splenomegaly (S). At birth, the neonate was growth restricted, and antibody titers confirmed the diagnosis of cytomegalovirus infection.



equivocal or may not fit into a specific category. Under these circumstances, the best pathway for the sonologist to follow is to do a follow-up examination and seek consultation. If time does not allow a follow-up examination, then the sonologist should communicate to the referring physician and the patient that a definitive answer is not possible and that decisions will have to be made with less-than-perfect information.

I am hopeful that this text will serve two purposes: to educate and to excite. If those reading this text maintain the same enthusiasm for obstetric and gynecologic sonography that I have, I will have fulfilled my goal.

## References

- Hershkovitz R, Sheiner E, Mazor M: Ultrasound in obstetrics: a review of safety. *Eur J Obstet Gynecol Reprod Biol* 101:15, 2002.
- Cavicchi TJ, O'Brien WD Jr: Heat generated by ultrasound in an absorbing medium. *J Acoust Soc Am* 76:1244, 1984.
- Nyborg WL, Steele RB: Temperature elevation in a beam of ultrasound. *Ultrasound Med Biol* 9:611, 1983.
- Flynn HC: Physics of acoustic cavitation in liquids. In Mason WP (ed): *Physical Acoustics*, Vol 1B. New York, Academic Press, 1964.
- Child SZ, Hartman CL, Schery LA, et al: Lung damage from exposure to pulsed ultrasound. *Ultrasound Med Biol* 16:817, 1990.
- Barnett SB: Recommendation on the safe use of ultrasound. Paper presented at Proceedings of the Symposium on Safety of Ultrasound in Medicine, WFUMB (World Federation for Ultrasound in Medicine and Biology), 1998.
- Barnett SB, Rott HD, ter Haar GR, et al: The sensitivity of biological tissue to ultrasound. *Ultrasound Med Biol* 23:805, 1997.
- Rott HD: Clinical Safety Statement for Diagnostic Ultrasound. Tours, France, European Federation for Societies for Ultrasound in Medicine and Biology, 1998.
- Kossoff G: Contentious issues in safety of diagnostic ultrasound. *Ultrasound Obstet Gynecol* 10:151, 1997.
- Zhu J, Lin J, Zhu Z, et al: Effects of diagnostic levels of color Doppler ultrasound energy on the cell cycle of newborn rats. *J Ultrasound Med* 18:257, 1999.
- O'Brien WD Jr: Ultrasound bioeffect issues related to obstetric sonography and related issues of the output display standard. In Fleischer AC, Manning FA, Jeanty P, et al (eds): *Sonography in Obstetrics and Gynecology, Principles and Practice*. New York, McGraw Hill, 1996, pp 17-33.
- Tarantal AF, Hendrickx AG: Evaluation of the bioeffects of prenatal ultrasound exposure in the cynomolgus macaque (*Macaca fascicularis*): II. Growth and behavior during the first year. *Teratology* 39:149, 1989.
- Lyons EA, Dyke C, Toms M, et al: In utero exposure to diagnostic ultrasound: a 6-year follow-up. *Radiology* 166:687, 1988.
- Stark CR, Orleans M, Haverkamp AD, et al: Short- and long-term risks after exposure to diagnostic ultrasound in utero. *Obstet Gynecol* 63:194, 1984.
- Lele PP: No chromosomal damage from ultrasound. *N Engl J Med* 287:254, 1972.
- Reece EA, Assimakopoulos E, Zheng XZ, et al: The safety of obstetric ultrasonography: concern for the fetus. *Obstet Gynecol* 76:139, 1990.
- Ang ES Jr, Gluncic V, Duque A, et al: Prenatal exposure to ultrasound waves impacts neuronal migration in mice. *Proc Natl Acad Sci U S A* 103:12903, 2006.
- Sidman RL, Rakic P: Neuronal migration, with special reference to developing human brain: a review. *Brain Res* 62:1, 1973.
- Letinic K, Zoncu R, Rakic P: Origin of GABAergic neurons in the human neocortex. *Nature* 417:645, 2002.
- Bioeffects considerations for the safety of diagnostic ultrasound. American Institute of Ultrasound in Medicine. Bioeffects Committee. *J Ultrasound Med* 7:S1, 1988.
- Merritt CR: Ultrasound safety: what are the issues? *Radiology* 173:304, 1989.
- Kremkau FW: *Diagnostic Ultrasound: Principles and Practice*, 7th ed. Philadelphia, WB Saunders, 2006.
- Report of the Royal College of Obstetricians and Gynaecologists' Working Party on Routine Ultrasound Examination in Pregnancy. London, 1984.
- Eik-Nes SH, Okland O, Aure JC, et al: Ultrasound screening in pregnancy: a randomised controlled trial. *Lancet* 1:1347, 1984.
- Whitfield CR: The routine ultrasound scan in all pregnancies. World Society of Perinatal Medicine Meeting, Washington, DC, 1984.
- Queisser-Luft A, Stopfkuchen H, Stolz G, et al: Prenatal diagnosis of major malformations: quality control of routine ultrasound examinations based on a five-year study of 20,248 newborn fetuses and infants. *Prenat Diagn* 18:567, 1998.
- Persson PH, Kullander S: Long-term experience of general ultrasound screening in pregnancy. *Am J Obstet Gynecol* 146:942, 1983.
- Ewigman B, LeFevre M, Hesser J: A randomized trial of routine prenatal ultrasound. *Obstet Gynecol* 76:189, 1990.
- Ewigman BG, Crane JP, Frigoletto FD, et al: Effect of prenatal ultrasound screening on perinatal outcome. RADIUS Study Group. *N Engl J Med* 329:821, 1993.
- Crane JP, LeFevre ML, Winborn RC, et al: A randomized trial of prenatal ultrasonographic screening: impact on the detection, management, and outcome of anomalous fetuses. The RADIUS Study Group. *Am J Obstet Gynecol* 171:392, 1994.
- Pitkin RM: Screening and detection of congenital malformation. *Am J Obstet Gynecol* 164:1045, 1991.
- Levi S, Crouzet P, Schaaps JP, et al: Ultrasound screening for fetal malformations. *Lancet* 1:678, 1989.
- Li TC, Greenes RA, Weisberg M, et al: Data assessing the usefulness of screening obstetrical ultrasonography for detecting fetal and placental abnormalities in uncomplicated pregnancy: effects of screening a low-risk population. *Med Decis Making* 8:48, 1988.
- Manchester DK, Pretorius DH, Avery C, et al: Accuracy of ultrasound diagnoses in pregnancies complicated by suspected fetal anomalies. *Prenat Diagn* 8:109, 1988.
- Sabbagha RE, Sheikh Z, Tamura RK, et al: Predictive value, sensitivity, and specificity of ultrasonic targeted imaging for fetal anomalies in gravid women at high risk for birth defects. *Am J Obstet Gynecol* 152:822, 1985.
- VanDorsten JP, Hulsey TC, Newman RB, et al: Fetal anomaly detection by second-trimester ultrasonography in a tertiary center. *Am J Obstet Gynecol* 178:742, 1998.
- The Use of Diagnostic Ultrasound Imaging in Pregnancy, NIH Publication number 84667. US Department of Health and Human Services PHS, National Institute of Health. Washington, D.C., U.S. Government Printing Office, 1984.
- American Institute for Ultrasound in Medicine: Joint Task Group on Training for Diagnosis in Obstetrical and Gynecologic Ultrasound, American Institute for Ultrasound in Medicine: Guidelines for minimum postresidency training in obstetrical and gynecological ultrasound. *J Ultrasound Med* 1:R40, 1982.
- American Institute for Ultrasound in Medicine: Guidelines for the performance of the antepartum obstetrical ultrasound examination. *J Ultrasound Med* 15:185, 1996.
- Ultrasonography in pregnancy. ACOG Technical Bulletin Number 187—December 1993. *Int J Gynaecol Obstet* 44:173, 1994.
- Hillman BJ, Joseph CA, Mabry MR, et al: Frequency and costs of diagnostic imaging in office practice—a comparison of self-referring and radiologist-referring physicians. *N Engl J Med* 323:1604, 1990.
- Leopold GR: Antepartum obstetrical ultrasound examination guidelines. *J Ultrasound Med* 5:241, 1986.
- AIUM Practice Guideline for the performance of an antepartum obstetrical ultrasound examination. *J Ultrasound Med* 22:1116, 2003.
- Leopold GR: Responsibilities associated with obstetric sonography. *AJR Am J Roentgenol* 153:1255, 1989.
- Hobbins JC: Ultrasound in Pregnancy: ACOG Bulletin no. 116. Washington, DC, American College of Obstetricians and Gynecologists, 1998.
- Filly RA: Level 1, level 2, level 3 obstetric sonography: I'll see your level and raise you one. *Radiology* 172:312, 1989.
- American Institute of Ultrasound in Medicine: AIUM Official Statement—Interpretation of Ultrasound Examinations Approved March 26, 1997; revised June 22, 2005.
- Malone FD, Nores JA, Athanassiou A, et al: Validation of fetal telemedicine as a new obstetric imaging technique. *Am J Obstet Gynecol* 177:626, 1997.



49. Doubilet PM, Benson CB: "Appearing twin": undercounting of multiple gestations on early first trimester sonograms. *J Ultrasound Med* 17:199; quiz 205, 1998.
50. Goldstein RB, Filly RA, Callen PW: Sonography of anencephaly: pitfalls in early diagnosis. *J Clin Ultrasound* 17:397, 1989.
51. Hertzberg BS, Bowie JD, Carroll BS, et al: Normal sonographic appearance of the fetal neck late in the first trimester: the pseudo-membrane. *Radiology* 171:427, 1989.
52. Schmidt W, Yarkoni S, Crelin ES, et al: Sonographic visualization of physiologic anterior abdominal wall hernia in the first trimester. *Obstet Gynecol* 69:911, 1987.
53. Neilson DR: Management of the large breech infant. A survey of 203 cases from Emanuel Hospital. *Am J Obstet Gynecol* 107:345, 1970.
54. Barkin SZ, Pretorius DH, Beckett MK, et al: Severe polyhydramnios: incidence of anomalies. *AJR Am J Roentgenol* 148:155, 1987.
55. Sivit CJ, Hill MC, Larsen JW, et al: Second-trimester polyhydramnios: evaluation with US. *Radiology* 165:467, 1987.
56. Hashimoto B, Callen PW, Filly RA, et al: Ultrasound evaluation of polyhydramnios and twin pregnancy. *Am J Obstet Gynecol* 154:1069, 1986.
57. Mahony BS, Filly RA, Callen PW: Amnionicity and chorionicity in twin pregnancies: prediction using ultrasound. *Radiology* 155:205, 1985.
58. Laing FC: Placenta previa: avoiding false-negative diagnoses. *J Clin Ultrasound* 9:109, 1981.
59. Zemlyn S: The effect of the urinary bladder in obstetrical sonography. *Radiology* 128:169, 1978.
60. Eurenius K, Axelsson O, Gallstedt-Fransson I, et al: Perception of information, expectations and experiences among women and their partners attending a second-trimester routine ultrasound scan. *Ultrasound Obstet Gynecol* 9:86, 1997.
61. Sever L, Lynberg MC, Edmonds LD: The impact of congenital malformations on public health. *Teratology* 48:547, 1993.
62. Lynberg MC, Edmonds LD: Surveillance of birth defects. In Halperin W, Baker EL, Monson RR (eds): *Public Health Surveillance of Birth Defects*. New York, Van Nostrand Reinhold, 1992, pp 155-177.
63. Timor-Tritsch IE: As technology evolves, so should its application: shortcomings of the "18-week anatomy scan." *J Ultrasound Med* 25:423, 2006.
64. Bronshtein M, Zimmer EZ: Prenatal ultrasound examinations: for whom, by whom, what, when and how many? *Ultrasound Obstet Gynecol* 10:1, 1997.
65. Schreckengost JL, Filly RA: The new obstetric ultrasound guidelines: some concerns. *J Ultrasound Med* 24:1752, 2005.
66. Vetraino IM, Lee W, Bronsteen RA, et al: Sonographic evaluation of the ventricular cardiac outflow tracts. *J Ultrasound Med* 24:566, 2005.
67. Norton M: Personal Communication. 2006.
68. Kuppermann M, Feeny D, Gates E, et al: Preferences of women facing a prenatal diagnostic choice: long-term outcomes matter most. *Prenat Diagn* 19:711, 1999.
69. Abramsky L, Fletcher O: Interpreting information: what is said, what is heard—a questionnaire study of health professionals and members of the public. *Prenat Diagn* 22:1188, 2002.
70. Filly RA, Benacerraf BR, Nyberg DA, et al: Choroid plexus cyst and echogenic intracardiac focus in women at low risk for chromosomal anomalies. *J Ultrasound Med* 23:447, 2004.
71. Doubilet PM, Copel JA, Benson CB, et al: Choroid plexus cyst and echogenic intracardiac focus in women at low risk for chromosomal anomalies: the obligation to inform the mother. *J Ultrasound Med* 23:883, 2004.
72. Filly RA: Echogenic intracardiac foci and choroid plexus cysts. *J Ultrasound Med* 23:1135; author reply 1138, 2004.
73. Lee MJ, Roman AS, Lusskin S, et al: Maternal anxiety and ultrasound markers for aneuploidy in a multiethnic population. *Prenat Diagn* 27:40, 2007.
74. Grimes DA, Snively GR: Patients' understanding of medical risks: implications for genetic counseling. *Obstet Gynecol* 93:910, 1999.
75. Shaw NJ, Dear PR: How do parents of babies interpret qualitative expressions of probability? *Arch Dis Child* 65:520, 1990.
76. Shiloh S, Sagi M: Effect of framing on the perception of genetic recurrence risks. *Am J Med Genet* 33:130, 1989.
77. Black WC: How to evaluate radiology literature. *Am J Roentgenol* 154:17, 1990.
78. Sanders RC: The effect of the malpractice crisis on obstetrical and gynecological ultrasound. In Chervenak F (ed): *Textbook of Obstetrical and Gynecological Ultrasound*. Boston, Little, Brown & Co., 1993, pp 263-276.
79. Callen PW, Chooljian D: The effect of ventricular dilatation upon biometry of the fetal head. *J Ultrasound Med* 5:17, 1986.
80. Brocks V, Bang J: Routine examination by ultrasound for the detection of fetal malformations in a low risk population. *Fetal Diagn Ther* 6:37, 1991.
81. Levi S, Hyjazi Y, Schaapst JP, et al: Sensitivity and specificity of routine antenatal screening for congenital anomalies by ultrasound: the Belgian Multicentric Study. *Ultrasound Obstet Gynecol* 1:102, 1991.
82. Romero R: Routine obstetric ultrasound. *Ultrasound Obstet Gynecol* 3:303, 1993.
83. Saari-Kemppainen A, Karjalainen O, Ylostalo P, et al: Ultrasound screening and perinatal mortality: controlled trial of systematic one-stage screening in pregnancy. The Helsinki Ultrasound Trial. *Lancet* 336:387, 1990.
84. Luck CA: Value of routine ultrasound scanning at 19 weeks: a four year study of 8849 deliveries. *Br Med J* 304:1474, 1992.
85. Shirley IM, Bottomley F, Robinson VP: Routine radiographer screening for fetal abnormalities by ultrasound in an unselected low risk population. *Br J Radiol* 65:564, 1992.
86. Roberts AB, Hampton E, Wilson N: Ultrasound detection of fetal structural abnormalities in Auckland 1988-9. *N Z Med J* 106:441, 1993.
87. Chitty LS, Hunt GH, Moore J, et al: Effectiveness of routine ultrasonography in detecting fetal structural abnormalities in a low risk population. *Br Med J* 303:1165, 1991.
88. Anderson N, Boswell O, Duff G: Prenatal sonography for the detection of fetal anomalies: results of a prospective study and comparison with prior series. *AJR Am J Roentgenol* 165:943, 1995.

# GENETICS AND PRENATAL DIAGNOSIS

Mary E. Norton, MD

## Introduction

Genetics and Birth Defects

Developmental Disorders: Causes, Mechanisms, and Patterns

## Chromosomal Defects

Abnormalities of Chromosome Number

*Trisomy 21*

*Trisomy 18*

*Trisomy 13*

*Sex Chromosome Aneuploidy*

*Turner Syndrome*

*Klinefelter Syndrome*

*47,XXX and 47,YYY*

*Polyploidy*

Abnormalities of Chromosome Structure

Other Types of Chromosomal Rearrangements

## Single Gene Disorders

Autosomal-Dominant Inheritance

*Penetrance and Expression*

Autosomal-Recessive Disorders

X-Linked Inheritance

Imprinting and Other Novel Genetic Mechanisms

Structural Birth Defects with Complex Inheritance

Syndromes Due to Disordered Function of Specific Developmental Genes

## Teratology

Recognized Teratogenic Agents

Maternal Infections

Medications

Physical Factors

*Radiation*

*Temperature Extremes*

Maternal Factors

Mechanical Factors

## Genetic Screening in Pregnancy

Carrier (Heterozygote) Screening

*Techniques for Carrier Testing*

*Tay-Sachs Disease*

*Cystic Fibrosis*

*Cystic Fibrosis and Echogenic Fetal Bowel*

## Population-based Prenatal Screening for Birth Defects

Alpha-Fetoprotein

Prenatal Screening for Open NTDs

Follow-Up When MSAFP Is Elevated

Other Abnormalities and Elevated AFP

Elevated AFAFP

Biochemical Markers and Fetal Chromosomal Abnormalities

Screening Programs for Fetal Aneuploidy

Trisomy 18 Detection

Prenatal Screening in Multiple Gestations

Controversy of Maternal Age Screening

Third-Trimester Pregnancy Complications after Abnormal Serum Screening

Low Estriol

## Genetic Counseling and Prenatal Diagnostic Testing

Genetic Counseling

## Prenatal Diagnosis

Genetic Counseling Before Prenatal Diagnostic Procedures

Techniques for Prenatal Diagnosis

*Amniocentesis*

*Chorionic Villus Sampling*

Multiple Gestations

*Postprocedural Loss Rates in Multiple Gestations*

*Selective Termination of Multifetal Pregnancies*

Fetal Blood Sampling and Other Fetal Tissue Biopsy

## Prenatal Testing for Congenital Malformations

Techniques of Genetic Analysis

Chromosome Identification

Fluorescence In Situ Hybridization

Molecular Techniques for DNA Analysis

## Future Directions in Genetic Analysis

Quantitative Fluorescent PCR and Comparative Genomic Hybridization

Free Fetal DNA



## INTRODUCTION

Genetic diseases are often perceived as so rare that the average practitioner will seldom encounter them. However, our increasing knowledge and technologic advances in prenatal diagnosis have demonstrated that this is far from the case. The availability of prenatal diagnosis for a wide range of disorders continues to increase with advances in other areas of genetics. In addition, progress has been made in population screening tests to identify couples who carry a genetic disorder. These improvements in prenatal screening and diagnosis mean that many more at-risk couples are able to have unaffected children. In addition to reproductive choice, carrier screening and fetal diagnostic testing afford the important opportunity for preparation of the family and the delivery site for the birth of a fetus with a known genetic disorder.

Ultrasound plays a central role in the provision of prenatal screening and diagnosis. Not only is ultrasound key to guiding prenatal diagnostic procedures, but integration of a genetics-based prenatal diagnosis program has been shown to increase the accuracy of diagnosis when compared to ultrasound alone.<sup>1</sup> This chapter includes a discussion of genetics, with an emphasis on recent advances relevant to prenatal diagnosis and a description of current strategies for genetic testing, and discusses how genetic screening and sonography together contribute to the provision of accurate and precise prenatal diagnosis.

## Genetics and Birth Defects

According to most studies, 2% to 3% of living newborns have a congenital malformation.<sup>2</sup> When considering birth defects noted in the first years of life, this incidence is nearly doubled. With the decline in infant mortality in the United States from infection and malnutrition, congenital malformations are now a leading cause of infant mortality (>20%) and responsible for greater than 30% of intensive care nursery admissions.<sup>3</sup> Congenital defects range from enzyme deficiencies caused by single gene defects to complex associations of structural defects. The continuum between purely biochemical abnormalities and structural birth defects includes disorders of structure, function, metabolism, and behavior.

Birth defects result from the interaction between the genetic makeup of the embryo and the environment in which it develops. The basic developmental information is encoded in genes, but the genotype is subjected to environmental influences that can impact the observed phenotype. In some cases, the genetic information is expressed regardless of environment, whereas in others, environmental causes interfere with normal development despite a normal genotype. Although some processes are primarily environmental and others primarily genetic, the distinctions between the two are not perfect.

Despite considerable advances and research over past several decades, the cause of more than half of human congenital abnormalities remains unknown. Of those with a recognized cause, approximately 15% to 20% are autosomal genetic diseases and 20% are cytogenetic in origin. Less than 1% of anomalies are thought to occur owing to teratogenic medications. Some of the remaining defects are associated

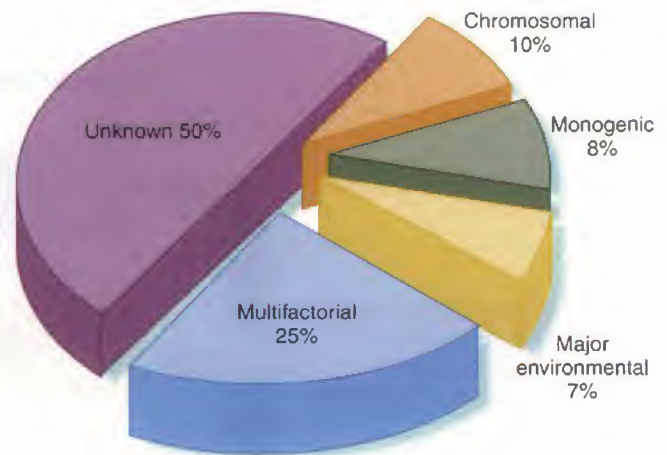


**FIGURE 2-1.** Prevalence of genetic diseases in the population. (Reproduced with permission from Carlson BM: *Human Embryology and Developmental Biology*, 3rd ed. Philadelphia, Mosby/Elsevier, 2004.)

with other environmental exposures during pregnancy including infectious agents (3%), maternal disease states (4%), mechanical problems (1% to 2%), irradiation, and unknown environmental causes. The remainder are of unknown or complex etiology (multifactorial, polygenic, spontaneous errors of development and synergistic interactions of teratogens) (Fig. 2-1).<sup>3,4</sup>

## Developmental Disorders: Causes, Mechanisms, and Patterns

Errors in morphogenesis are often classified by dysmorphologists according to the underlying pathogenesis (Fig. 2-2). *Malformations* are defects in the structure of an organ resulting from a specific primary abnormality of development, such as a congenital heart or neural tube defect (NTD). A *malformation syndrome* is the occurrence together of several such defects, for example, the presence of a congenital heart defect, central nervous defect, and clefting due to trisomy 13. A *malformation sequence* occurs when the primary malformation results in additional defects, such as a foot deformity and hydrocephalus secondary to spina bifida. *Deformations* are abnormalities of form, shape, or position caused by mechanical forces such as intrauterine molding or constraint. Factors leading to deformations may be extrinsic (for example, oligohydramnios owing to ruptured membranes) or intrinsic (for example, oligohydramnios owing to renal agenesis). Deformations may also occur postnatally; for example, an infant may develop a flat head owing to sleeping in one position. A *disruption* is a morphologic defect that results from breakdown of previously normal tissue. Disruptions can be due to extrinsic forces, internal interferences with a developmental process, or vascular insults. Examples of disruptions include amputations owing to amniotic bands, and gastroschisis and pencephaly, both thought to result from in utero vascular insults.

A *sequence* is a pattern of multiple abnormalities resulting from a single primary anomaly or mechanical factor; it may be a malformation, deformation, or disruption. An example is Potter sequence, in which oligohydramnios from any



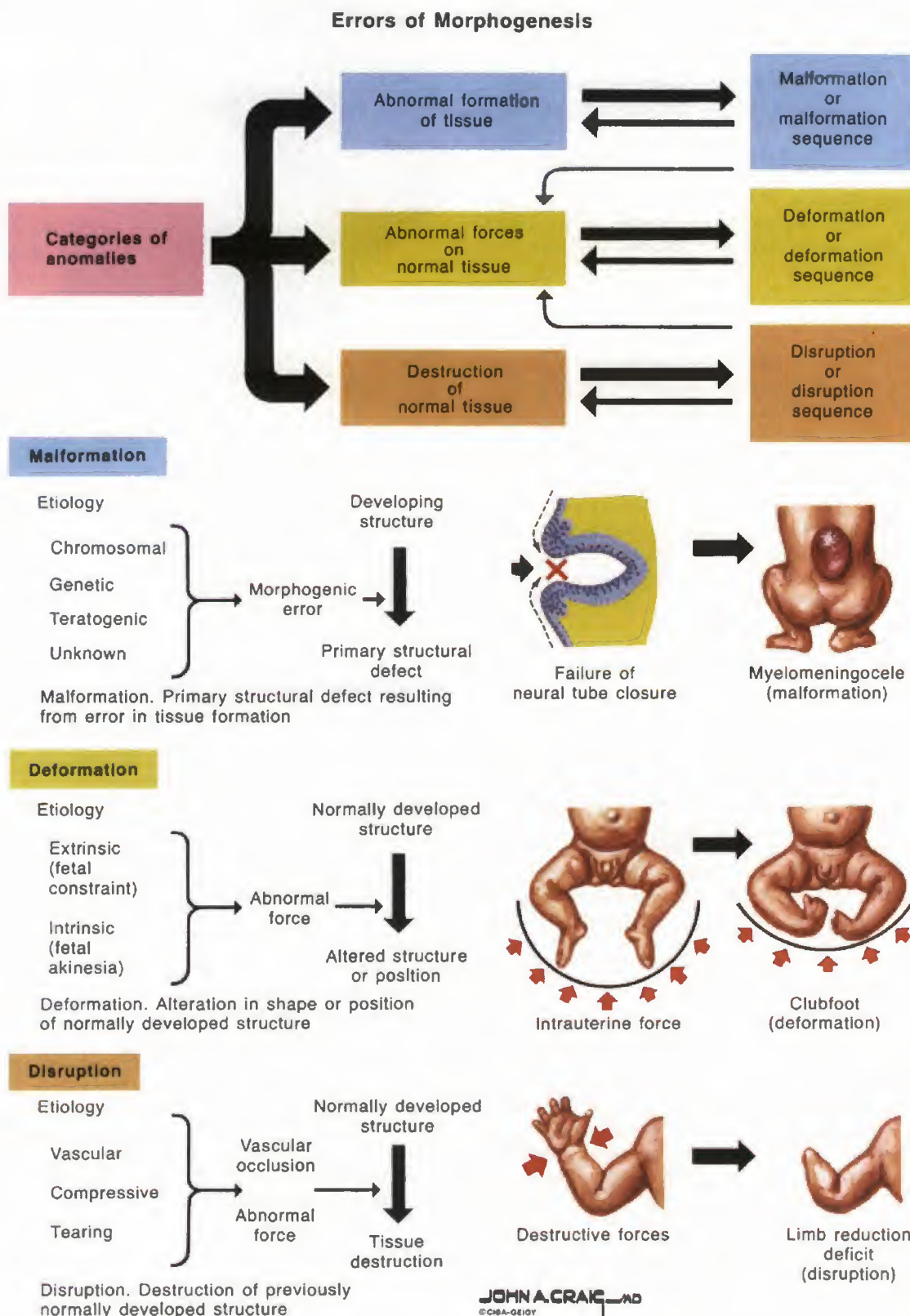


**FIGURE 2-2.** Errors of morphogenesis. (Reproduced with permission from Nyhan WL: *Structural Abnormalities: Clinical Symposia*. CIBA-GEIGY, Vol. 42, No. 2, 1990, Plate 1.)

**Table 2-1****Chromosome Abnormalities in Unselected Newborns**

Abnormality	Frequency (Per 1000 Births)
All	9.1
Autosomal trisomies	1.4
Balanced autosomal rearrangement	5.2
Unbalanced autosomal abnormalities	0.6
Sex chromosome abnormalities	
In phenotypic males	1.2
In phenotypic females	0.75

From Jacobs PA, Browne C, Gregson N, et al: Estimates of the frequency of chromosome abnormalities detectable in unselected newborns using moderate levels of banding. *J Med Genet* 29:103, 1992.

cause leads to similar features of fetal compression: characteristic facial features and abnormal positioning of the hands and feet. A *syndrome* is a pattern of multiple abnormalities known to have a common, specific cause. An example is Down syndrome (DS), which is caused by the presence of an extra copy of chromosome 21. Finally, the term *association* is used to identify the occurrence of two or more features more commonly than expected by chance alone but for which no etiology has been demonstrated. A common example is VATER (Vertebral, Anal, Tracheo-Esophageal, and Renal anomalies) association. This term does not imply a specific diagnosis but rather prompts the search for specific other defects when one component of the association is identified.

## CHROMOSOMAL DEFECTS

Chromosomal abnormalities occur in approximately 0.9% of newborns (Table 2-1), and it is estimated that at least 10% to 15% of conceptions are chromosomally abnormal. Chromosome abnormalities are the leading cause of pregnancy loss, and at least 95% of chromosomally abnormal conceptions are lost before term. Abnormalities seen in abortuses differ from those seen in liveborn infants. This is because the most severe chromosome abnormalities result in early arrest of development, whereas less severe abnormalities yield more mild phenotypes that allow survival until later in pregnancy or even live birth. The most common abnormalities seen in first trimester spontaneous abortions are 45,X and 47,+16 (trisomy 16). Trisomy 16 is never seen in live births, whereas less than 1% of conceptions with 45,X survive until term.

Chromosome abnormalities can be either numeric or structural. They can involve one or more autosomes, sex chromosomes, or both simultaneously. Aneuploidy refers to the presence of an abnormal number of chromosomes, and is almost always associated with abnormalities of physical and/or cognitive development. Translocations, the exchange of segments between nonhomologous chromosomes, are relatively common, and can be balanced, in which the appropriate amount of chromosomal material is present but rearranged, or unbalanced, in which some chromosomal material is gained or lost. Polyploidy, in which there is one or more entire extra set(s) of chromosomes, occurs but is much less common.

**Table 2-2****Risk of Chromosomal Abnormalities in Liveborn Infants**

Maternal Age (years)	Risk for Down Syndrome	Total Risk for Chromosomal Abnormalities*
20	1/1,667	1/526
21	1/1,667	1/526
22	1/1,429	1/500
23	1/1,429	1/500
24	1/1,250	1/476
25	1/1,250	1/476
26	1/1,176	1/476
27	1/1,111	1/455
28	1/1,053	1/435
29	1/1,000	1/417
30	1/952	1/384
31	1/909	1/384
32	1/769	1/323
33	1/625	1/286
34	1/500	1/238
35	1/385	1/192
36	1/294	1/156
37	1/227	1/127
38	1/175	1/102
39	1/137	1/83
40	1/106	1/66
41	1/82	1/53
42	1/64	1/42
43	1/50	1/33
44	1/38	1/26
45	1/30	1/21
46	1/23	1/16
47	1/18	1/13
48	1/14	1/10
49	1/11	1/8

\*47, xxx excluded for ages 20 to 32 (data not available). Modified from the following sources: Hook EB, Cross PK, Schreinemachers DM: Chromosomal abnormality rates at amniocentesis and in live-born infants. *JAMA* 249:2034, 1983 (ages 33-49); Hook EB: Rates of chromosomal abnormalities at different maternal ages. *Obstet Gynecol* 58:282, 1981.

## Abnormalities of Chromosome Number

Aneuploidy is the most common clinically significant type of human chromosomal abnormality, and it occurs in 3% to 4% of recognized pregnancies. The risk of trisomy increases with advancing maternal age (Tables 2-2 and 2-3). Both trisomy, the presence of three copies of an individual chromosome, and monosomy, the presence of a single copy of a chromosome, typically have significant phenotypic consequences. Monosomy is seen less frequently than trisomy because this situation is generally not compatible with life. Trisomy or monosomy for any chromosome can theoretically occur, but in practice, some are seen much more frequently than others (Table 2-4). This is because most aneuploidies are incompatible with life, and aneuploid embryos spontaneously abort very early in gestation. Some chromosome abnormalities, for example, trisomy 8, are seen at birth only in mosaic form and the full trisomy is likely lethal.



**Table 2-3** Prevalence of Trisomy 21 by Maternal Age and Gestational Age

Maternal Age (years)	Gestational Age (weeks)					
	10	12	14	16	20	40
20	1/983	1/1,068	1/1,140	1/1,200	1/1,295	1/1,527
25	1/870	1/946	1/1,009	1/1,062	1/1,147	1/1,352
30	1/576	1/626	1/668	1/703	1/759	1/895
31	1/500	1/543	1/580	1/610	1/658	1/776
32	1/424	1/461	1/492	1/518	1/559	1/659
33	1/352	1/383	1/409	1/430	1/464	1/547
34	1/287	1/312	1/333	1/350	1/378	1/446
35	1/229	1/249	1/266	1/280	1/302	1/356
36	1/180	1/196	1/209	1/220	1/238	1/280
37	1/140	1/152	1/163	1/171	1/185	1/218
38	1/108	1/117	1/125	1/131	1/142	1/167
39	1/82	1/89	1/95	1/100	1/108	1/128
40	1/62	1/68	1/72	1/76	1/82	1/97
41	1/47	1/51	1/54	1/57	1/62	1/73
42	1/35	1/38	1/41	1/43	1/46	1/55
43	1/26	1/29	1/30	1/32	1/35	1/41
44	1/20	1/21	1/23	1/24	1/26	1/30
45	1/15	1/16	1/17	1/18	1/19	1/23

From Snijders RJM, Sundberg K, Holzgreve Hency WG, Nicolaides KH: Maternal age- and gestation-specific risk for trisomy 21. *Ultrasound Obstet Gynecol* 13:167, 1999.

**Table 2-4** Population Frequency of Specific Chromosomal Disorders

	Per 1000 Live Births*
Trisomy 21	1.5
Trisomy 18	0.12
Trisomy 13	0.07
47XXY (Klinefelter syndrome)	1.5
45X (Turner syndrome)	0.4
XXY syndrome	1.5
XXX syndrome	0.65

From Harper PS: *Practical Genetic Counseling*, 6th ed. London, Arnold Publishers, 2004. p 66.

\*Births of appropriate sex only for sex chromosomal abnormalities.

### Trisomy 21

The most common aneuploidy detected at birth is trisomy 21, which occurs in approximately 1/700 live births. Trisomy 21 is the basis for 95% of cases of DS (the remainder are owing to translocations involving chromosome 21). Individuals with DS have a characteristic phenotype that includes distinctive facial features, short stature, brachycephaly, a flat occiput, a short neck with redundant skin on the nape, short broad hands, and hypotonia. Other significant problems in individuals with DS include mental retardation, recurrent respiratory infections, and leukemia. Congenital heart defects are present in about 30%, and duodenal atresia and tracheoesophageal fistulas are also common.

The recurrence risk of trisomy 21 (or other autosomal trisomies) is approximately 1% after one such child is born to a couple. Although often requested, there is no indication

for parental chromosomal evaluation after the birth of a child with trisomy 21 (or other straightforward trisomy). The recurrence risk is somewhat higher in younger women, and only slightly increased over the age related risk in women older than 35. A history of DS elsewhere in the family does not increase the risk of having a child with a chromosome abnormality, provided there is no familial translocation.

### Trisomy 18

Trisomy 18 occurs in about 1/8000 births but is much more common at conception, with about 95% of such cases resulting in spontaneous abortion or stillbirth. As with trisomy 13, postnatal survival is poor, and the majority of patients die in early infancy. Characteristic findings include cardiac malformations, severe mental retardation, growth restriction, a prominent occiput, small mandible, short sternum, clenched hands, and rocker-bottom feet. Prenatally, about 25% of fetuses with trisomy 18 have choroid plexus cysts. As is discussed later, fetuses with trisomy 18 have a characteristic pattern on biochemical screening, which has a relatively high sensitivity for this disorder.

### Trisomy 13

Trisomy 13 syndrome is much less common and more severe than DS. It occurs in about 1/20,000 live births, and most children with this condition die in early infancy. The phenotype includes severe central nervous system malformations, such as holoprosencephaly, severe mental retardation, growth restriction, cleft lip and palate, microphthalmia, polydactyly, clenched hands with overlapping digits, congenital heart defects, and renal abnormalities such as polycystic kidneys.

**Table 2-5 Clinical Features of Sex Chromosome Disorders**

Features	Klinefelter	XYY	Turner	Triple X
Karyotype	47XXY	47XYY	45X	47XXX
Phenotypic sex	Men	Men	Women	Women
Gonads	Atrophic testes	Normal	Streak ovaries	Normal
Fertility	No	Normal	No	Normal
Intelligence	Normal/slightly low	Usually normal	Usually normal	Usually reduced
Behavioral problems	Sometimes	Sometimes	Minimal	Sometimes
Other features	Hypogonadism	Tall, acne	Short, webbed neck, coarctation	Few

From Harper PS: *Practical Genetic Counseling*, 6th ed. London, Arnold Publishers, 2004, p 69.

### Sex Chromosome Aneuploidy

Among live births, about 1/400 men and 1/650 women have some form of sex chromosome aneuploidy. The consequences of this class of chromosome abnormalities in general are less severe than those of autosomal aneuploidies (Table 2-5).

#### Turner Syndrome

Although monosomy for an entire chromosome is almost always lethal, an important exception is monosomy X (45,X), which results in Turner syndrome. Turner syndrome is estimated to occur in 1% to 2% of all conceptions, but most are lost prenatally, resulting in a frequency of 1/2000 to 1/3000 live births. Turner syndrome causes a characteristic phenotype, which includes short stature, ovarian dysgenesis with failure to develop secondary sexual characteristics, and infertility, as well as physical features such as a webbed neck, peripheral lymphedema at birth, congenital heart defects, and renal abnormalities. Prenatally, fetuses with Turner syndrome typically have an increased nuchal translucency or cystic hygroma, lymphangiectasia, structural renal abnormalities, and congenital heart defects, particularly left-sided obstructive lesions such as coarctation of the aorta. Women with Turner syndrome usually have normal intelligence, although they may have specific learning disabilities.

The types of specific chromosomal abnormalities seen in women with Turner syndrome are quite variable. Only about 50% of patients have a straightforward 45,X karyotype. Approximately 30% to 40% of cases involve mosaicism, most commonly 45,X/46,XX or 45,X/46,XY. Patients with a Y chromosome may have ambiguous genitalia and are at risk for development of gonadoblastoma in their dysgenetic gonads. Structural abnormalities of the X chromosome are seen in 10% to 20% of cases and also often involve mosaicism. The fact that these patients have more than one cell line can account for variability in phenotype of women affected with Turner syndrome.

#### Klinefelter Syndrome

Klinefelter syndrome occurs in about 1/1000 male births and is a common cause of primary hypogonadism. Men with Klinefelter syndrome tend to be tall, with long arms and legs. They have small testes and are sterile owing to atrophy of the seminiferous tubules. Gynecomastia occurs in

about 30%. There is an increased risk for learning disabilities, with IQ typically about 10 to 15 points below that of unaffected siblings, although men with Klinefelter syndrome are not typically mentally retarded. Because the disorder is often subtle, men are often first diagnosed in infertility clinics.

#### 47,XXX and 47,XYY

The 47,XXX karyotype occurs in about 1/1000 women. Overt physical abnormalities are not associated with this disorder, but these women can have learning disabilities or mild mental retardation. Men with a 47,XYY karyotype tend to be tall, with mild learning disabilities and IQ 10 to 15 points lower than that of their siblings. The condition is not associated with structural birth defects, but these boys may have behavioral problems. Individuals with increasing numbers of X chromosomes (that is, 48,XXXX or 48,XXXY) have also been described. The degree of mental deficiency and physical abnormalities tend to increase with each additional X chromosome.

#### Polyploidy

In polyploidy (that is, triploidy and tetraploidy) there are one or more extra sets of chromosomes. A triploid cell has 69 chromosomes (one extra set), and a tetraploid cell has 92 chromosomes (two extra sets). Both triploidy and tetraploidy have been seen in fetuses, although they are lethal and rarely reported in live births. Of those fetuses with triploidy who have been liveborn, there are no reported survivors beyond 10.5 months. Congenital abnormalities seen in triploidy include micrognathia, prominent forehead, dysplastic cranial bones, low-set malformed ears, microphthalmia, hypertelorism, cleft lip and palate, macroglossia, omphalocele, syndactyly, and asymmetric development.

The extra chromosome set in triploid pregnancies can be of either maternal or paternal origin. Maternally derived triploidy results from fertilization of a diploid ovum by a haploid sperm and can result in a XXX or XXY karyotype. Paternally derived triploidy can result from fertilization of a haploid ovum by either a diploid sperm, or by two haploid sperm and can result in a XXX, XXY, or XYY karyotype.

The phenotype of triploid pregnancy has been reported to depend on the parental source of the extra chromosome set. Triploids with an extra set of paternal chromosomes have a well-formed fetus with an abnormal placenta and



**Table 2-6** Some Distinctive Cytogenetic Syndromes

Karyotype	Syndrome	Features
4p-	Wolf-Hirschhorn	Characteristic faces, frontal bossing, microcephaly, hypospadias
5p-	Cri-du-chat	Hypertelorism, characteristic cry
Trisomy 8 mosaic		Craniofacial dysmorphism, agenesis of corpus callosum
Tetrasomy 12p	Pallister-Killian	Characteristic faces, diaphragmatic hernia
18p-		
18q-		Genital anomalies
22q+	Cat eye	Coloboma, anorectal atresia

Reproduced with permission from Harper PS: Practical Genetic Counseling, 6th ed. London, Arnold Publishers, 2004, p 74.

often result in partial hydatidiform moles. Those with an extra set of maternal chromosomes usually have a small, growth-restricted fetus and a small, noncystic placenta.<sup>5-7</sup>

### Abnormalities of Chromosome Structure

There are many types of abnormalities of chromosome structure, but all generally result from chromosome breakage, followed by recombination in an abnormal configuration. Overall, structural chromosome abnormalities occur in about 1/375 newborns. *Reciprocal translocations* involve an exchange of segments between nonhomologous chromosomes. These rearrangements are relatively common, and can be balanced (that is, the appropriate amount of chromosomal material is present) typically resulting in a normal outcome, or unbalanced, in which some chromosomal material is gained or lost, therefore resulting in an abnormal outcome. There is an increased risk of unbalanced rearrangements in the offspring of people who carry balanced translocations, thereby leading to decreased fertility and an increased risk of offspring with birth defects.

A *Robertsonian translocation* occurs when the long arms of two acrocentric chromosomes (chromosomes 13, 14, 15, 21, 22) are fused and the corresponding two short arms are lost. Because the short arms of these chromosomes do not contain essential genetic material (they are made up of multiple copies of genes for ribosomal RNA), this does not result in an abnormal phenotype. Offspring of individuals with a Robertsonian translocation can, however, inherit either a missing or extra long arm of the chromosomes involved in the fusion event, resulting in a trisomy for that chromosome arm. The most common Robertsonian translocation involves chromosomes 14 and 21, and is responsible for about 5% of cases of DS. The recurrence of translocation DS depends on whether the translocation was inherited from a carrier parent. In 75% of cases, the translocation is *de novo*, and the recurrence risk is very low (<1%). If the translocation was inherited from a parent who carries a 14;21 balanced translocation, there is a 10% chance of recurrence if the mother is the carrier, and about a 2% chance if the father is the carrier.

When a balanced translocation or other rearrangement is identified in a fetus at the time of prenatal diagnosis, testing of the parents is recommended. If the translocation is inherited from a phenotypically normal parent, the fetus would be predicted to be normal. If a reciprocal translocation occurs as a *de novo* event, there is approximately a

**Table 2-7** Common Microdeletion Syndromes

Syndrome	Location	Frequency
Prader Willi	15q	1/25,000
Angelman	15q	1/30,000
Velocardiofacial	22q	1/3,000
Smith-Magenis	17q	1/25,000
Williams	7q	1/10,000
Alagille	20p	1/70,000
Rubenstein-Taybi	16p	1/100,000
WAGR	11p	1/40,000
Miller Dieker	17p	1/85,000
Wolf-Hirschhorn	4p	1/50,000
Cri-du-chat	5p	1/35,000
Retinoblastoma	13q	1/23,000

doubling of the background risk of phenotypic abnormality. This is thought to be due to subtle, undetected chromosomal imbalance, or disruption of genes at the breakpoint(s).

### Other Types of Chromosomal Rearrangements

In addition to translocations, there are several other types of unbalanced chromosomal rearrangements. These include deletions, which occur with the loss of a chromosome segment, resulting in partial monosomy (Table 2-6). Some deletions are too small to be seen through routine karyotyping, and require specialized techniques such as fluorescence in situ hybridization (FISH) to be detected. Such deletions can involve many genes, and are responsible for a number of clinically distinct microdeletion syndromes (often referred to as 'contiguous gene deletion syndromes') (Table 2-7). One of the most common is the 22q microdeletion syndrome, which occurs in about 1/4000 live births. The 22q microdeletion is a relatively common cause of congenital heart defects, particularly conotruncal abnormalities, such as truncus arteriosus and tetralogy of Fallot. It has recently been recognized that small subtelomere deletions are responsible for some cases (approximately 5%) of otherwise unexplained mental retardation. This recognition is important, because a high percentage of such deletions have been demonstrated to be familial.<sup>8,9</sup> Duplications of a chromosome segment also occur, resulting in partial trisomy. Marker chromosomes are small, additional chromosomes, often unidentified. These



are also known as supernumerary chromosomes or extra structurally abnormal chromosomes (ESACs). Some marker chromosomes contain little more than centromeric heterochromatin and are not significant, whereas others contain material from a chromosome arm and can cause an abnormal phenotype. Other structural rearrangements include ring chromosomes, paracentric and pericentric inversions, and isochromosomes, that are chromosomes that contain two copies of one arm (either the p or q arm) and no copies of the other.

## SINGLE GENE DISORDERS

Many important genetic diseases occur as the result of a mutation at a single gene. The 2006 edition of *Online Mendelian Inheritance in Man* (OMIM) lists more than 13,000 known single gene traits in humans. Of these, more than 12,000 are on autosomes and 655 are on the X chromosome.<sup>10</sup> Many have been mapped to specific chromosome locations, cloned, and sequenced.

Gregor Mendel first described the principles of segregation and independent assortment of genes in his well-known experiments with garden peas. This work led to the classic descriptions of autosomal-dominant (AD) and autosomal-recessive (AR) inheritance. Classically, AD inheritance refers to conditions in which one allele asserts its effect in both the homozygous and heterozygous form, whereas AR inheritance requires mutations at both alleles. X-linked inheritance occurs with conditions encoded on the X chromosome, and it may be either recessive or dominant.

The completion of the human genome project in 2003 was an epic chapter in laying the foundation for the study, diagnosis, and treatment of human genes and genetic disease. Although the human genome has now been sequenced, we still do not know how most genes work in either health or disease. We have gained an increased appreciation, however, for the complexity of human genetics. Relevant to clinical genetics, we have greatly increased our understanding of genetic heterogeneity, and the less than clear-cut association of one gene with one disorder. We now understand that mutations at more than one gene locus can lead to the same phenotype, and that multiple different phenotypes can result from mutations in the same locus. Phenotypes also result from the interaction of genotype with the environment (including other genes), and there are numerous phenomena that our advances in genetic technology have uncovered that make genetics far more fascinating, if far more complex.

## Autosomal-Dominant Inheritance

In AD inheritance, affected individuals are heterozygous for an abnormal allele, that they transmit to 50% of their offspring, independent of gender. Overall, approximately 1/200 individuals is affected with an AD condition, although any individual condition is typically rare. Matings between two individuals affected with the same AD condition are relatively uncommon, and homozygotes for AD conditions are rare. The exception to this occurs with disorders in which there may be cultural or social reasons that affected individuals may preferentially mate, as with achondroplasia. The homozygous state is often more severe (that is, familial hypercholesterolemia) or lethal (achondroplasia), although

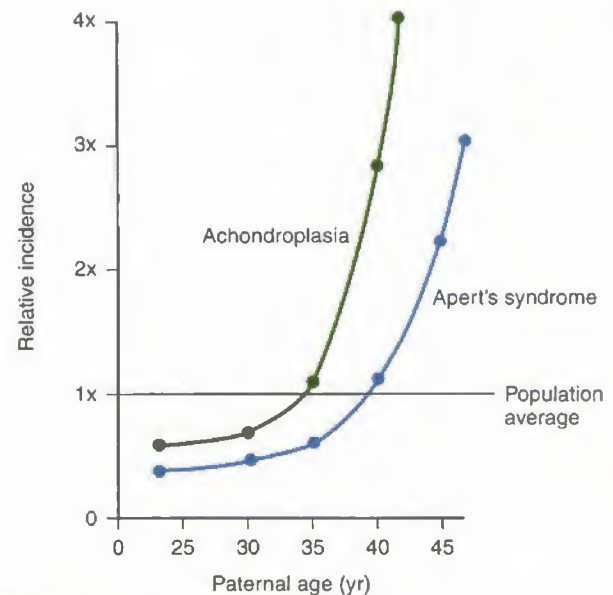


**FIGURE 2-3.** Paternal age and risk of autosomal-dominant disorders. (Modified from Carlson BM: *Human Embryology and Developmental Biology*, 3rd ed. Philadelphia, Mosby/Elsevier, 2004.)

in some cases homozygotes may have same phenotype as heterozygotes (for example, Huntington disease). In couples with same AD disorder, such as achondroplasia, 25% of pregnancies will be affected with the homozygous, lethal form, 50% with heterozygous achondroplasia, and 25% of offspring will be normal.

In theory, AD inheritance is straightforward, but in actuality, there are numerous factors affecting gene expression that can make evaluation of such cases extremely complex. Counseling of families regarding AD disorders requires consideration of mechanisms such as the rate of new mutation, mosaicism, conditions with late or variable age of onset, incomplete penetrance, and variation in expressivity.

AD disorders may be inherited from an affected parent, or may result from a new mutation. Most cases of achondroplasia result from new mutations, as do about half of cases of neurofibromatosis. Paternal age has a demonstrable effect on the rate of such new mutations (Fig. 2-3). If a disorder occurs owing to a new mutation, the risk of recurrence in a sibling is generally very low. However, an individual may be mosaic for an AD mutation, meaning that there are cells of more than one genetic constitution present. In this case, all or part of a person's germline may be affected, whereas the somatic cells are not and, therefore, the individual is asymptomatic. If germline mosaicism is present, an apparently unaffected individual will have an increased risk of having affected offspring. Germline mosaicism has been demonstrated in as many as 6% of cases of the perinatal lethal disorder osteogenesis imperfecta type II, as well as in X-linked disorders such as Duchenne muscular dystrophy and hemophilia A. For practical purposes, it is reasonable to consider a recurrence risk of about 1% to be likely for any apparent new dominant mutation, unless more specific estimates are available.<sup>11</sup>



## Penetrance and Expression

Further complicating recurrence risk counseling and clinical evaluation of AD disorders are the phenomena of penetrance and variable expression. A given individual may have a disease genotype but may not express the phenotype if a disorder is not 100% penetrant, as is the case with retinoblastoma, which affects only about 90% of individuals who inherit the causative mutation. Age is also an important consideration, because a disorder such as polycystic kidney disease is about 80% to 90% penetrant by 20 years of age and nearly 100% penetrant by 30 years of age but only with careful imaging of the kidneys.<sup>12</sup> A disorder may also demonstrate variable expression between affected individuals. Although disorders such as achondroplasia are expressed with little variation, most AD conditions demonstrate variation in clinical severity, even within a family. Targeted physical examinations, radiologic investigation, and other studies may be required to identify features of a disorder; neurofibromatosis (NF) and tuberous sclerosis are notable examples. Essentially all individuals inheriting the NF gene have some clinical symptoms, although they may range from mild skin manifestations to multiple debilitating neurofibromas. An important consideration is that those individuals who reproduce tend to be the least severely affected, and therefore such a disorder is likely to be more severe, on average, in the child than in the parents. Expression may be affected by environmental effects, modifier genes, somatic mutation (for example, with retinoblastoma), genomic imprinting, anticipation, and allelic heterogeneity. Some of these mechanisms are discussed in more detail later.

## Autosomal-Recessive Disorders

AR disorders are classically described as those for which two gene mutations must be present for the disorder to manifest. Such disorders occur most commonly in persons whose healthy parents carry the same recessive gene. The recurrence risk to such carrier parents is 25% in each pregnancy, and these disorders most commonly occur with no prior family history. Carriers are much more common than affected individuals, and the disorders typically cluster in sibships but not in prior generations. Unless there is consanguinity or the disorder is particularly common, the risk to other relatives (for example, half-sibs and children of healthy sibs) is generally low. Consanguinity increases the risk of having offspring with AR disorders. The increased risk to parents who are first cousins to have a child with a major genetic or congenital abnormality is about 6%, or twice the background rate.

Again, with advances in genetics, the exceptions to the traditional rules of AR inheritance are increasingly evident. It is now appreciated that carriers of many of these conditions may have subtle symptoms. Examples of this are cystic fibrosis (CF), in which male carriers may have infertility owing to congenital bilateral absence of the vas deferens (CBAVD). Sickle cell carriers may suffer splenic infarct at high altitudes and are at increased risk for urinary tract infection in pregnancy.

AR disorders demonstrate much less variation in expression, and lack of penetrance is rarely encountered, so counseling is more straightforward with these conditions. Genetic heterogeneity due to more than one causative locus, or multiple alleles at a single locus, is the major cause of

variation in severity of a single disorder. This is important in CF, which is the most common AR condition in the white population and a focus of prenatal screening programs, as described later.

## X-Linked Inheritance

X-linked disorders can be recessive, dominant, or dominant with lethality in men. Most X-linked conditions are recessive, and are traditionally thought of as affecting only men, who have unaffected carrier mothers. As with AD inheritance, some cases occur owing to new mutations, and paternal age has been shown to increase the risk of producing daughters who carry X-linked disorders. Because women carry two X chromosomes whereas men carry only one, one X chromosome is randomly inactivated early in embryonic development, thereby allowing women to produce X-linked gene products in the same quantities as men (Lyon hypothesis). The XIST gene in the X inactivation center is responsible, through methylation, for X inactivation. X inactivation is incomplete, however, which is why individuals with abnormal numbers of X chromosomes are abnormal. And because X inactivation is random, some female heterozygote carriers of X-linked disorders will inactivate primarily their X chromosomes carrying the normal allele, and therefore be symptomatic due to skewed X inactivation. This occurs in hemophilia A, in which some carriers can have a mild bleeding disorder owing to reduced levels of factor VIII. Such affected women have symptoms that are usually, but not always, milder than their male counterparts.

X-linked dominant disorders are less common than X-linked recessive diseases, and some such conditions are lethal in men. Examples include Rett syndrome, incontinenti pigmenti, and Aicardi syndrome. Aicardi syndrome is a rare disorder primarily of the CNS, including agenesis of the corpus callosum, microphthalmia, and infantile spasms. Evaluation of gender can be helpful if such a condition is suspected, because identification of female gender would support this diagnosis. When an affected child with such a condition is born to healthy parents, this is likely owing to a new mutation and the recurrence risk is low.

With isolated X-linked recessive disorders, it is important, but often difficult, to determine if an isolated case represents a new mutation or if the mother is a carrier. When molecular diagnosis or other methods of carrier detection are available, the situation can be clarified. However, such tests are not available for all conditions, and risks must often be empirically determined based on pedigree analysis and consideration of other factors such as the number of unaffected men in the pedigree. An example is demonstrated in Figure 2-4, which represents an isolated case of a lethal, X-linked disorder (for example, Duchenne muscular dystrophy) in a family. If the case is due to a new mutation in the affected boy (III-1), there is no increase in recurrence risk for his sister (III-2) or her children. If the case is due to a new mutation in his mother (II-1), then his sister (III-2) has a 50% risk of being a carrier, but his aunt (II-2) does not. Finally, if the grandmother (I-1) is a carrier, then II-2 has a 50% risk of being a carrier, and his female cousin (III-3) has a 25% chance of being a carrier.

*Fragile X syndrome*, the most common inherited form of mental retardation, is an important disorder that has been

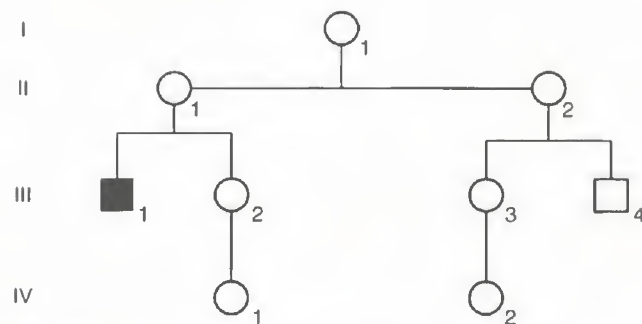
described as X-linked semi-dominant. Fragile X syndrome is characterized by mental retardation, behavioral difficulties, and specific dysmorphic features. The condition affects men (approximately 1/4000) more commonly and more severely than women, and it has a complicated inheritance pattern. Carriers have an intermediate number of trinucleotide (CGG) repeats in the 5' untranslated region of the gene (premutation) that can increase during oogenesis to a larger number of repeats (full mutation) (Fig. 2-5). Full-mutation men have moderate to severe mental retardation and behavior problems, such as autism, whereas women are

affected by a much more variable phenotype, ranging from normal to as severe as affected men. Premutation female carriers have a relatively high rate of premature menopause (15% to 25%), whereas male premutation carriers can have a tremor ataxia condition with an onset later in life.<sup>13,14</sup>

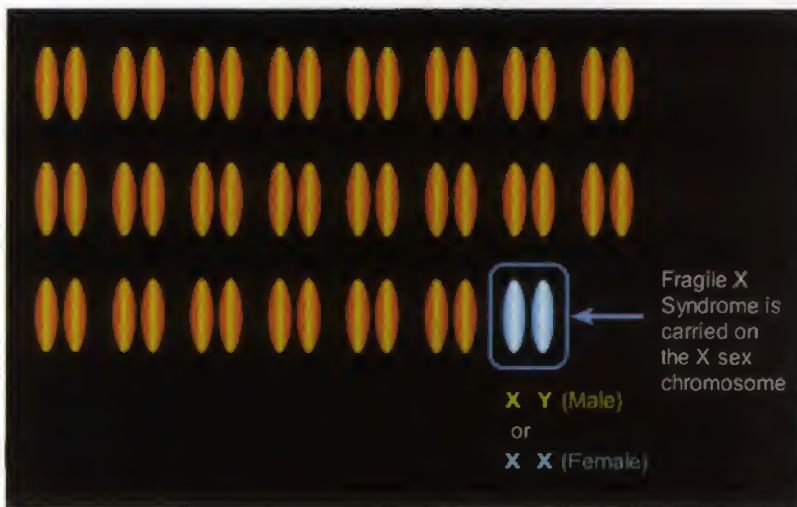
## Imprinting and Other Novel Genetic Mechanisms

Some genetic mutations have been noted to have a very different effect depending on the parent of origin, a phenomenon known as genetic imprinting. Imprinting is probably caused and controlled by differential methylation, with the imprints laid down during very early embryogenesis (Fig. 2-6). A number of genetic disorders, including Prader Willi Syndrome (PWS) and Beckwith Weidemann syndrome (BWS), occur owing to abnormalities of imprinted genes. With PWS, the disorder occurs when both copies of the SNRPN gene, on chromosome 15, are maternally inherited, and no paternal copy is present. Several recent reports have indicated a possible association of imprinting disorders with in vitro fertilization (IVF). An excess number of cases of Beckwith Weidemann syndrome has been reported in the offspring of children conceived with IVF, but the magnitude of this association is, at present, uncertain.<sup>15</sup>

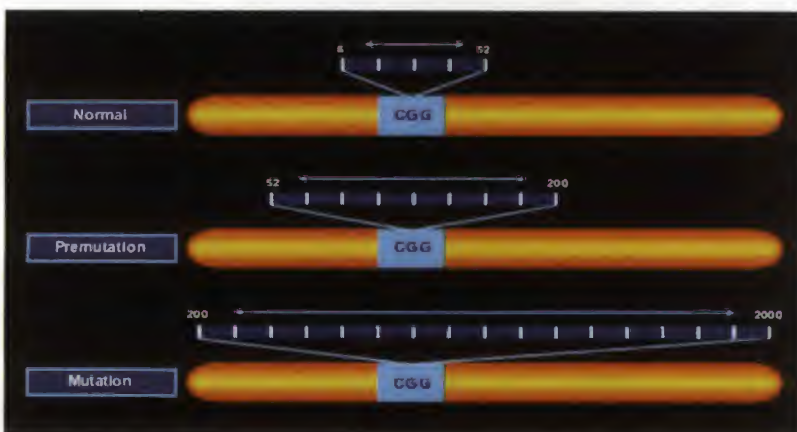
Another novel genetic mechanism, long appreciated clinically but only understood on a molecular level in the last



**FIGURE 2-4.** Pedigree of an isolated case of a lethal X-linked disorder (for example, Duchenne muscular dystrophy). See text for risk estimation discussion.



**FIGURE 2-5.** Fragile X syndrome. A. Fragile X syndrome is carried on the X sex chromosome. B. In Fragile X syndrome there is an expansion of the CGG trinucleotide repeats. The effect of this expanded trinucleotide repeat is methylation of essential proteins. (Images designed by Don Bailey, RTI International, and rendered by the Publications Unit of the FPG Child Development Institute, University of North Carolina at Chapel Hill. Reprinted by permission of the author.)





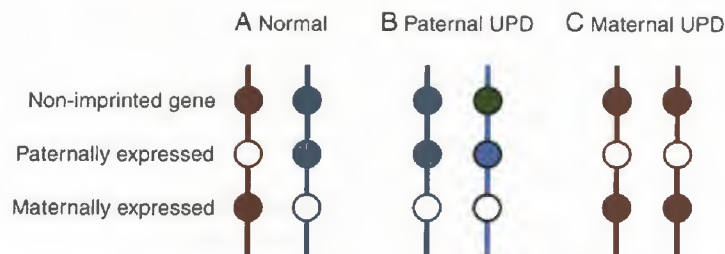


**FIGURE 2-6.** Genomic imprinting and uniparental disomy (UPD). Schematic of a hypothetical chromosome pair representing genomic imprinting. The maternal chromosome is indicated by the red line, and the paternal copy by the blue line. Genes are represented by circles, colored circles indicate genes that are expressed, and the white circles represent genes that are inactive. The green circles are genes that are not imprinted, whereas red circles indicate genes in which only the maternal copy is active and the blue circles genes in which only the paternal copy is active. *A*, Normal state, with one chromosome inherited from each parent. The non-imprinted gene is expressed from both parents, whereas only one copy of the red or blue (imprinted) gene is expressed. *B*, Paternal UPD. With two copies of the paternal chromosome present, there is a double dose of the paternally expressed (blue) gene, and absence of expression of the maternally expressed gene. *C*, Maternal UPD. There is an absence of paternally expressed gene product (blue) and a double dose of the maternally expressed products (red).

**Table 2-8 Mitochondrial Disorders**

Leber's optic atrophy
MELAS (mitochondrial encephalopathy with lactic acidosis and stroke-like episodes)
MERFF (myoclonic epilepsy with ragged red fibers)
Kearns-Sayre syndrome
Pearson syndrome (lactic acidosis, pancreatic insufficiency, pancytopenia)
Deafness (antibiotic-induced and other forms of progressive nerve deafness)
Various other central nervous system degenerations
Diabetes mellitus (some forms)

decade, is known as anticipation. Anticipation refers to the increasing severity of a genetic disorder in successive generations. This occurs in disorders that result from disruption of genes owing to expansion of trinucleotide repeat number, with increasing numbers of repeats being added on through each subsequent generation. Anticipation had been noted clinically in disorders such as Fragile X syndrome, before the basis was understood, and also occurs in other trinucleotide repeat diseases, including myotonic dystrophy, and Huntington disease.

Mitochondria, which produce adenosine triphosphate (ATP), have their own unique DNA. Our mitochondria are all maternally inherited and have a high mutation rate. Many mitochondrial diseases have now been identified, and they are most commonly maternally inherited. Typical symptoms include neuromuscular abnormalities, such as loss of motor control, muscle weakness and pain, gastrointestinal disorders and swallowing difficulties, poor growth, cardiac disease, liver disease, diabetes, respiratory complications, seizures, visual/hearing problems, lactic acidosis, developmental delays, and susceptibility to infection (Tables 2-8 and 2-9).

### Structural Birth Defects with Complex Inheritance

Most common congenital malformations, including NTDs, cleft lip and palate, and congenital heart defects, have an

**Table 2-9 Factors Underlying Variation in Mendelian Disorders**

Factor	Effect
Genomic imprinting	Phenotype varies according to parent of origin
Anticipation due to unstable DNA	More severe phenotype with successive generations
Mosaicism	Mild or nonpenetrant phenotype
Modifying alleles	Influence of unaffected parent
Somatic mutation also required	Variable penetrance of familial cancers

**Table 2-10 Multifactorial Inheritance: Factors Increasing Risk to Relatives**

Close relationship to proband
High heritability of disorder
Proband or more rarely affected gender
Severe or early onset disease in proband
Multiple family members affected

increased risk of recurrence in families. A small percentage of such defects have a specific cause, such as single gene disorders, chromosomal abnormalities, or teratogens. Most, however, are isolated defects that result from complex interactions between a number of factors, including genotype at one or more loci, and a variety of environmental exposures that trigger, accelerate or exacerbate the disorder. Therefore, occurrence does not match simple mendelian inheritance but is complex and multifactorial. Recurrence risk of such disorders is increased by the presence of more than one affected relative, a severe or early onset form of disease, an affected person of less common sex (in disorders in which persons of one gender are more likely to be affected), high heritability of the disorder, and consanguineous parentage (Table 2-10).

NTDs have long been thought to follow a typical complex inheritance pattern determined by multiple genetic and



environmental factors. Therefore, it was a remarkable discovery that the single greatest factor in causing NTD is a deficiency of maternal serum folic acid, which accounts for about 70% of these birth defects. Antiepileptic agents, such as valproate and carbamazepime are thought to increase the risk of NTD by interfering with folate metabolism. The risk of NTD is inversely correlated with maternal serum folic acid levels in pregnancy, with a threshold of 200 µg/L, below which the risk is very significant.<sup>16</sup> Folic acid levels are strongly influenced by dietary intake and can become depressed during pregnancy even with normal dietary intake. The impact of folic acid deficiency is exacerbated by a genetic variant of the enzyme 5,10-methylenetetrahydrofolate reductase (MTHFR), which catalyzes the conversion of 5,10-methylenetetrahydrofolate into 5-methyltetrahydrofolate, the major circulating form of folate. The C677T allele of the MTHFR gene causes an enzymatic dysfunction that results in mild homocystinemia in people whose folate status is not optimal. Mothers of infants with NTD are twice as likely to be homozygous for the mutant allele, although it is so common in many populations that up to 15% are homozygous. Because MTHFR mutations are not present in the mothers of all children with NTD, it appears that other genetic factors or dietary deficiency alone can also cause NTD. Folic acid supplementation has been shown to decrease the risk of NTD by 80%.<sup>17</sup> Public health initiatives to educate reproductive age women about the importance of folate, and fortification of the food supply (cereals and breads) with folic acid have been instituted in the United States for the purpose of decreasing the incidence of NTD.

### Syndromes Due to Disordered Function of Specific Developmental Genes

Identification of the specific genes involved in individual malformation syndromes is a rapidly developing area of medical genetics. Many specific developmental genes have been identified, and they can provide the possibility of early prenatal diagnosis for some of these conditions. Because many developmental genes are conserved between species, discoveries in experimental models have led to important discoveries in human counterparts. Interestingly, many genes involved in developmental defects are proving to be important in neoplasia as well (Table 2-11).

### TERATOLOGY

One of the first milestones in human teratology occurred in 1941, when an Australian named Norman Gregg noted the association between first trimester maternal rubella infection and serious birth defects.<sup>18</sup> Twenty years later, the thalidomide disaster sensitized the medical community to the risks of medications in pregnancy. Thalidomide, a very effective sedative, was widely used for several years in West Germany, Australia, and other countries until the association of prenatal exposure with phocomelia and amelia was recognized. Following the recognition of the potent teratogenicity of this drug, intense investigations into the safety of various medications in pregnancy heralded the modern age of teratology.

Embryos are more susceptible to teratogenic agents at specific critical periods of development (Fig. 2-7). The pre-organogenetic phase, from conception until somite formation,

is known as the all or none period, when insults to the embryo are likely to result in either death of the conceptus and miscarriage (or resorption) or in intact survival.<sup>19</sup> At this stage, the embryo is undifferentiated, and repair and recovery are possible through multiplication of the still totipotent cells to replace those that have been lost. Exposure of embryos to teratogens during the presomitic stage usually does not cause congenital malformations,<sup>20</sup> unless the agent persists in the body beyond this period.

The embryonic period, between weeks 3 and 8 postconception, is the period when the basic steps in organogenesis occur. This is the period of maximum sensitivity to teratogenicity because tissues are differentiating rapidly and damage to them becomes irreparable. Exposure to teratogenic agents during this period has the greatest likelihood of causing a structural anomaly. Because teratogens are capable of affecting many organ systems, the pattern of anomalies produced depends upon which systems are differentiating at the time of teratogenic exposure. In general, organs that form first tend to be sensitive earlier, and very complex organs tend to have prolonged periods of high susceptibility to disruption.

The fetal phase, from the end of the embryonic stage to term, is the period when growth and functional maturation of organs and already-formed systems occur. Exposure to teratogens in this period will mainly affect fetal growth, or the size or function of a specific organ. The brain in particular may be functionally affected almost throughout the entire pregnancy. Teratogens rarely cause gross structural anomalies during this time.<sup>21</sup>

### Recognized Teratogenic Agents

A large number of environmental factors have been reported to be associated with birth defects. These include chemical teratogens, including medications, hormones, maternal infections, and nutritional factors. Although the list of medications suspected of teratogenicity is long, relatively

**Table 2-11**

#### The Molecular Basis of Some Congenital Malformations

Disorder	Gene
Apert syndrome	Fibroblast growth factor
Campomelic dysplasia	SOX9 (SRY-related developmental gene)
Hirschsprung's disease	RET oncogene (also involved in MEN2)
Holt-Oram syndrome	Specific gene, 12q (transcription factor)
Opitz syndrome (X-linked)	MID 1 (midline developmental gene)
Rubenstein-Taybi syndrome	CREB binding protein (16p)
Seathre-Chotzen craniosynostosis	TWIST (Drosophila homologue)
Thanatophoric dysplasia	Fibroblast growth factor (FGFR3)
Treacher-Collins syndrome	Specific gene 5q (function unknown)
Waardenburg syndrome	PAX3 (mouse homologue)



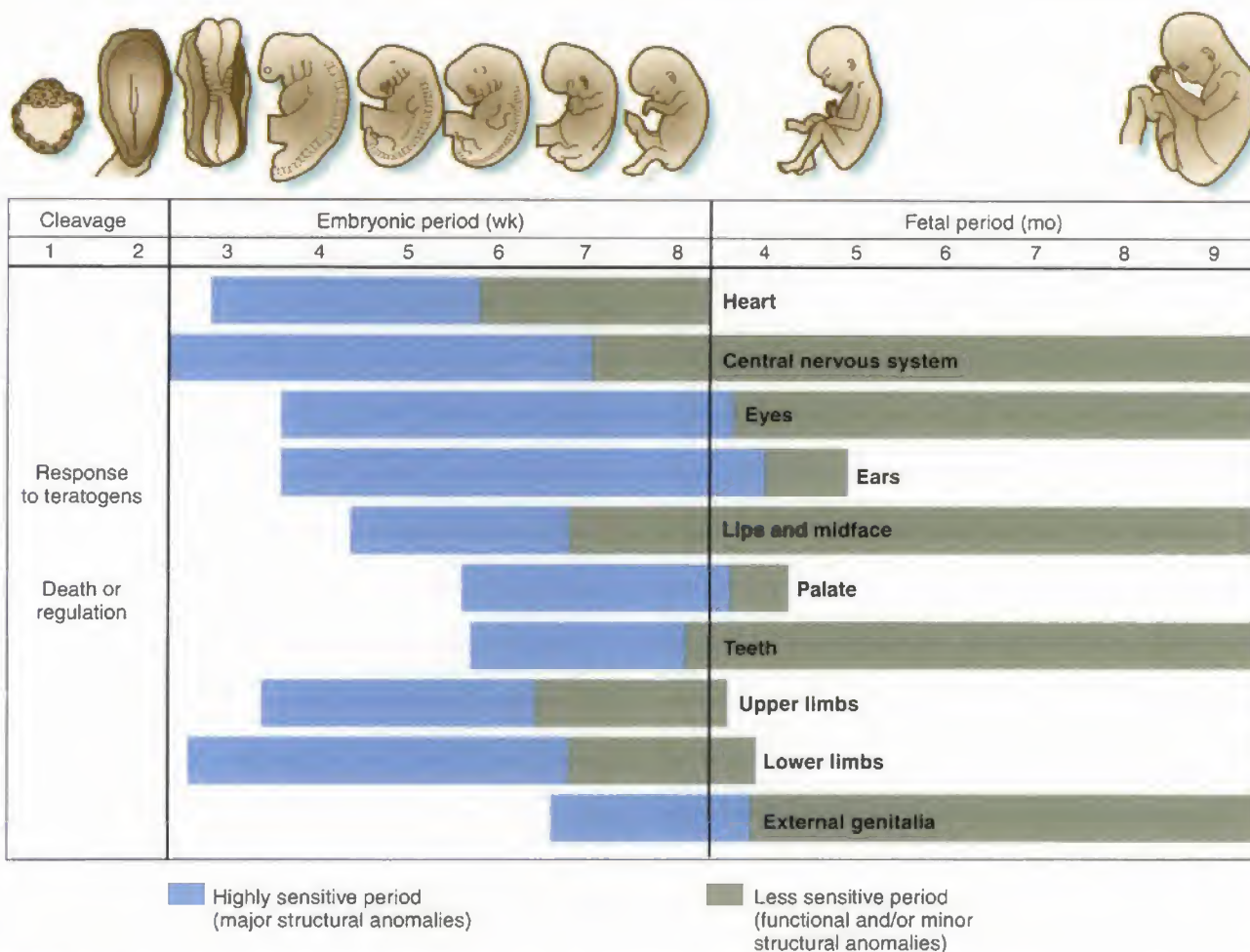


**FIGURE 2-7.** Periods and degrees of susceptibility of embryonic organs to teratogens. (Reproduced with permission from Carlson BM: *Human Embryology and Developmental Biology*, 3rd ed. Philadelphia, Mosby/Elsevier, 2004.)

few agents have been demonstrated to unquestionably cause birth defects in humans (Table 2-12). There are cases in which these medications must still be used during pregnancy, as the benefit outweighs the risk they impose. Often, maternal uncontrolled diseases are more harmful to the fetus than the administered drug.

## Maternal Infections

The incidence of intrauterine infections ranges between 3% and 15%. Rubella was one of the first infectious agents recognized to cause birth defects in humans, and previously one of the most common. Today, because of effective immunization programs against rubella, the most common infection is that apparently caused by cytomegalovirus.

Intrauterine infections with long-term fetal sequelae may be viral, parasitic, or bacterial (see Table 2-12). Most common intrauterine infections are viral, although toxoplasmosis is caused by a protozoan (*Toxoplasma gondii*), and syphilis by a spirochete (*Treponema pallidum*). The timing of maternal infection can influence both the severity and likelihood of fetal infection. Rubella causes a high percentage of malformations in the first trimester, whereas toxoplasmosis

causes fetal infection more commonly in the third trimester, but with more severe consequences if contracted earlier.

Infection of the fetus may occur owing to hematogenous spread through the placental barrier or via ascending infection through the fetal membranes with direct contamination of the amniotic fluid. With intrauterine infections with cytomegalovirus and toxoplasmosis, specific clinical manifestations are seen only rarely in the mother. Cases of suspected intrauterine infections can be evaluated by measuring serum levels of maternal specific antibodies, but the significance of antibody levels is often uncertain. Moreover, a rise in levels of maternal antibodies is diagnostic for maternal, but not necessarily for fetal infection. To diagnose fetal infection, the infective agent should be identified in the amniotic fluid by culture or polymerase chain reaction (PCR), or by specific immunoglobulin M (IgM) in fetal blood. At birth, specific cord blood IgM or typical clinical findings (or both) are the most relevant diagnostic tools.

## Medications

Although many medications have been suspected of being human teratogens, there are only a relatively small number

**Table 2-12** Proven Teratogenic Agents in Humans

Ace inhibitors	CNS defects, congenital heart defects (first-trimester exposure)
Alcohol	Renal failure, skull hypoplasia (second-trimester exposure) Fetal Alcohol Syndrome: intrauterine growth retardation, microcephaly, developmental delay, characteristic facies, CHD, cleft palate
Carbamazepine	Neural tube defects, similar features to fetal hydantoin syndrome
Chemotherapeutic agents	Miscarriage, various malformations
Cocaine	Abruptio placenta, prematurity, fetal loss, decreased birth weight, microcephaly, limb defects, urinary tract anomalies, and poor neurodevelopmental performance.
Coumarin anticoagulants	Fetal warfarin syndrome: hypoplasia and calcific stippling of the epiphyses, intrauterine growth retardation, developmental delay, central nervous system damage, eye defects, hearing loss
Diethylstilbestrol	Clear cell adenocarcinoma, benign adenosis of the vagina, female genital structural changes (cervix/uterus)
Folic acid antagonists	Fetal aminopterin syndrome: central nervous system defects (hydrocephalus, meningomyelocele), facial anomalies (cleft palate, high-arched palate, micrognathia, ocular hypertelorism, external ear anomalies), abnormal cranial ossification, abnormalities of first branchial arch derivatives, intrauterine growth retardation, mental retardation
Heavy metal (lead, mercury)	
Hydantoin	Fetal hydantoin syndrome: craniofacial dysmorphism (wide anterior fontanelle, ocular hypertelorism, meiotic ridge, broad depressed nasal bridge, short anteverted nose, bowed upper lip, cleft lip, cleft palate), hypoplasia of the distal phalanges, nail hypoplasia growth retardation, mental deficiency, cardiac defects
Isotretinoin	Retinoic acid embryopathy: craniofacial anomalies (microtia or anotia, accessory parietal sutures, narrow sloping forehead, micrognathia, flat nasal bridge, cleft lip and palate, and ocular hypertelorism), cardiac defects (primarily conotruncal malformations), abnormalities in thymic development, and alterations in central nervous system development
Lithium	Cardiac defects, especially Ebstein anomaly
Misoprostol	Limb defects, Moebius sequence
Organic mercury	Mental retardation, cerebral atrophy, spasticity, blindness
Sodium iodide (I131)	Ablation of fetal thyroid gland
Thalidomide	Limb reduction defects, phocomelia, polydactyly, syndactyly, oligodactyly, defects of the external ears, facial capillary hemangiomas, palsies of cranial nerves VI or VII, cardiovascular defects, agenesis of kidneys, spleen, gallbladder and appendix, atresia or stenosis of esophagus, duodenum and anus
Trimethadione	Fetal trimethadione syndrome: characteristic craniofacial anomalies, growth retardation, delayed psychomotor development, clefting and congenital heart defects
Valproate	Neural tube defects, fetal valproate syndrome: narrow bifrontal diameter, high forehead, epicanthal folds, infraorbital creases, telecanthus, low nasal bridge, short nose with anteverted nares, midfacial hypoplasia, long philtrum, thin vermilion border, small mouth, cardiovascular defects, long fingers and toes, hyperconvex fingernails, and cleft lip
Intrauterine infections	
Cytomegalovirus	Cytomegalic inclusion disease: intrauterine growth retardation, microcephaly, chorioretinitis, seizures, blindness, optic atrophy. Neonatal hepatosplenomegaly, jaundice and thrombocytopenia
Rubella	Spontaneous abortion, congenital rubella syndrome: heart disease, deafness, cataracts, intrauterine growth retardation, encephalitis, abnormal long bones. Neonatal hepatosplenomegaly, obstructive jaundice and thrombocytopenic purpura, mental retardation, neurologic deficits, and behavioral abnormalities.
Syphilis	Congenital malformations, prematurity, stillbirth, hepatosplenomegaly, osteochondritis or periostitis, jaundice, petechiae or purpuric skin lesions, lymphadenopathy, hydrops, edema, ascites, rhinitis, pneumonia, myocarditis, nephrosis, and bulbar pseudo paralysis.
Toxoplasmosis	Encephalitis, hydrocephalus, intracranial calcifications, chorioretinitis, erythroblastosis, anemia, jaundice, hepatosplenomegaly, glomerulitis, myocarditis, and myositis. Central nervous system damage, seizures, mental retardation, cerebral palsy, deafness, and blindness.
Varicella-zoster virus	Skin lesions, fetal growth retardation, limb hypoplasia brain and eye defects, cerebral and cerebellar atrophy, seizures, developmental delay, and nerve palsies

CHD, congestive heart disease; CNS, central nervous system.

The above table represents selected medications and their possible associations with fetal structural abnormalities. Many of the listed associations are based on isolated case reports that have appeared in the medical literature for which the association is unproven; or in animal studies where the dosage of medication far exceeded the normal clinical amount normally used. It is likely that in many cases the reported association was coincidental to, rather than resultant from, the medication. *This table is not intended for patient counseling regarding the likelihood of fetal malformations or abnormalities.* This table should be used by the sonologist/sonographer as a guide to evaluate specific organ systems in addition to a thorough sonographic examination. In all cases of suspected teratogenic effects a reproductive geneticist or teratologist and the drug manufacturer should be consulted.

Reproduced with permission from Diav-Citrin O, Ornoy A: Adverse environment and prevention of early pregnancy disorders. *Early Pregnancy* 4:5. 2000.

Modified from Briggs GG, Freeman RK, Yaffe SJ: *Drugs in Pregnancy and Lactation*, 5th ed. Philadelphia, Lippincott Williams & Wilkins, 1998.



for which there is convincing evidence linking the substance directly to congenital malformations in humans. Testing drugs for teratogenicity is difficult, because agents may cause a high incidence of severe defects in animals but may not cause malformations in other species or in humans (for example, cortisone causes cleft palate in mice but not humans). Conversely, thalidomide is a tragic example of an agent that is highly teratogenic in humans but not in commonly studied laboratory rodents.

## Physical Factors

### Radiation

Ionizing radiation is a potent teratogen, with the response dependent on the dose as well as the gestational age at which the embryo/fetus is irradiated. Experience with the Japanese atomic bomb survivors as well as women treated with therapeutic radiation in pregnancy provides evidence of the damaging effects of large doses of ionizing radiation in humans. In contrast, there is no evidence that radiation exposure at typical diagnostic levels (a few millirads) poses a significant threat to the embryo, and noncancer health effects are not evident for fetal doses of less than 5 rads. Ionizing radiation at high doses (> 5 to 10 rads) can cause a variety of anomalies in various organ systems. The most prominent radiation-associated abnormalities are defects in the CNS, ranging from NTD to functional disorders, such as mental retardation.<sup>22</sup> For fetuses exposed between 8 to 15 weeks' gestation, atomic bomb survivor data indicate that the decline in IQ score is approximately 25 to 31 points per 100 rads, at doses above 10 rads. At 16 to 25 weeks' gestation, the average IQ loss is approximately 13 to 21 points per 100 rads, at doses above 70 rads. After 26 weeks, at doses above 100 rads, the risks for stillbirth and neonatal death increases.<sup>22,23</sup>

There appears to be a slightly increased risk of childhood cancer with radiation doses to the fetus of greater than 1 rad. There is no evidence that this effect is dependent on gestational age. The absolute risk for fatal cancer at 0 to 15 years of age after prenatal radiation exposure has been estimated to be 0.006% per 100 mrad. For an entire lifespan, this risk is about 0.015% per 100 mrad.<sup>23</sup>

### Temperature Extremes

In animals, excessive core body temperatures have been documented to cause malformations; NTD are among the most frequently reported. In humans, data are inconclusive and often conflicting. A large review and meta-analysis, published in 2005, reported an odds ratio of 1.9 for NTD associated with maternal hyperthermia, and the authors concluded that maternal hyperthermia in early pregnancy appears to be a human teratogen.<sup>24</sup> Other large trials have confirmed the association with NTDs and other birth defects, which has been reported with maternal fever as well as the use of devices such as hot tubs and saunas.<sup>25,26</sup>

### Maternal Factors

A number of maternal illnesses and metabolic disorders have been implicated in the genesis of congenital mal-

formations. Maternal diabetes is strongly associated with congenital malformations, with the risk to the embryo directly related to the degree of maternal glucose control.<sup>27,28</sup> The most common abnormalities include congenital heart defects and NTD, whereas caudal regression is rare but of greatly increased frequency in infants of diabetic mothers. The phenotype of the infant of diabetic mothers also includes macrosomia, polyhydramnios, and stillbirth, with hypoglycemia and erythroblastosis common neonatal complications. Untreated maternal phenylketonuria is also a potent teratogen and results in microcephaly, mental retardation, congenital heart defects, and low birth weight. Risks to the fetus are related to the level of maternal phenylalanine and almost entirely eliminated with maternal dietary management and avoidance of phenylalanine in the diet of affected women during pregnancy.<sup>29</sup>

### Mechanical Factors

Mechanical disruption can result in a number of recognizable and characteristic sequence disorders. Often, the underlying cause is less important than the common disruption pathway. Potter sequence, for example, results from early, longstanding oligohydramnios of any cause, and consists of pulmonary hypoplasia, clubfeet, congenital hip dislocation, low-set ears, micrognathia, and flattened faces. This same phenotype can result from different causes of absent amniotic fluid, including bilateral renal agenesis and early rupture of the amniotic membrane.

## GENETIC SCREENING IN PREGNANCY

Screening is currently recommended in pregnancy for a number of genetic (single gene or Mendelian) disorders, chromosomal abnormalities, and structural birth defects in the fetus. Screening for single gene defects is offered to essentially all patients, although the precise tests offered vary according to ethnic background. Screening for chromosomal abnormalities is also recommended for all patients, with an overwhelming array of sonographic and biochemical options now available for carrying out such screening. Screening for structural birth defects, such as NTD, may involve maternal biochemical screening as well as ultrasound.

### Carrier (Heterozygote) Screening

The main purpose of carrier screening in pregnancy is to identify individuals who are themselves healthy, but are at risk of having children with a genetic disorder. The majority of disorders in this category are AR diseases, in which both parents must be carriers of the gene, but typically are unaffected. In the majority of cases, there is no family history of the disorder.

It is generally agreed that the following criteria should be met for heterozygote-screening programs to be effective: (1) disorder of sufficient severity to warrant screening, (2) high frequency of carriers in the screened population, (3) availability of an inexpensive and dependable test with low false-negative and false-positive results, (4) access to genetic counseling for couples identified as heterozygotes, (5) availability of prenatal diagnosis, (6) acceptance and voluntary participation by the population targeted for screening.



**Table 2-13****Genetic Screening Tests Currently Recommended by Ethnic Group**

Ethnic Group	Disorders Tested	Test
Ashkenazi Jews	Tay Sachs disease	DNA, enzyme (hexosaminidase-A levels)
	Canavan disease	DNA
	Cystic fibrosis	DNA
	Familial dysautonomia	DNA
	Cystic fibrosis	DNA
Caucasians	Cystic fibrosis	DNA
Africans, African Americans	Sickle-cell anemia	
	Beta thalassemia	MCV, hemoglobin electrophoresis
Southeast Asians	Alpha thalassemia	MCV
Mediterraneans	Beta thalassemia	MCV
Middle Eastern	Hemoglobinopathies	MCV, hemoglobin electrophoresis

MCV, mean corpuscular volume.

Table 2-13 lists the inherited disorders for which carrier screening is currently recommended. There are many other disorders for which screening is available and frequently performed. These include Fragile X syndrome, as well as extensive panels of diseases more common in the Ashkenazi Jewish population. As more genetic tests become available, clinicians and policy groups are faced with the challenge of deciding which tests should be offered for general screening.

### Techniques for Carrier Testing

Carrier screening can be performed by biochemical tests that differentiate carriers from noncarriers of a disorder (for example, serum enzyme concentration or activity; low mean corpuscular volume in thalassemia carriers), or by DNA tests that can detect genetic mutations associated with a given disease. In some disorders (for example, Tay-Sachs disease), both biochemical and DNA screening are readily available and either can be used.

Because DNA-based screening tests generally look only at a set of the most common genetic mutations, not all carriers will be detected by a given screening test. Individuals with other mutations not included in the screening panel will not be detected. In some disorders, screening is more effective in a particular ethnic group in which a limited number of disease-causing gene mutations are seen. For example, DNA screening for CF is sensitive in the Ashkenazi Jewish population, in which greater than 95% of carriers can be detected because the majority of disease-causing mutations in this population are known. However, in Asian or black populations, fewer disease-causing mutations are known, therefore fewer carriers of Asian or black descent will be identified by the current CF DNA test. Therefore, it is important to remember that although a negative carrier test lowers the chance that an individual is a carrier, it does not rule it out (Table 2-14).

### Tay-Sachs Disease

Carrier screening for Tay-Sachs disease in the Ashkenazi Jewish population has been done on a massive scale since

**Table 2-14****Cystic Fibrosis Carrier Frequency and Detection Rates by Ethnic Group**

Group	Incidence	Carrier risk	Detection Rate
Ashkenazi jews	1/3,300	1/29	97%
Europeans	1/3,300	1/29	80%
Hispanics	1/8,464	1/46	57%
African-American	1/17,000	1/62	69%
Asian-American	1/32,400	1/90	~30%

1969. Screening, followed by prenatal diagnosis when indicated, has resulted in a dramatic decrease in the incidence of Tay Sachs disease in the Jewish population.<sup>29</sup> A number of practical, social, and ethical complexities have also been identified in this prototypic population-based effort.<sup>30</sup> More than 100 mutations in the hexosaminidase A gene (the TSD locus) have been identified to date. Some are associated with later onset or more chronic forms of neuronal storage disease. Two mutations cause a carrier-like pseudodeficiency when enzymatic testing is used (false-positive results). Educational and counseling components must be provided both before and after screening. Issues of privacy and confidentiality of test results must be addressed. In certain cultures, insurability and employment may be involved. The public perception of the biomedical community as advocates for wide-scale testing and screening may be interpreted, in some systems, as conflicts of interest on the part of entrepreneurial scientists, clinicians, and institutions.<sup>31</sup>

In part because of this history of success with TSD screening, and in part because of cultural isolation, an increased number of tests for genetic disorders have been proposed for testing of the Ashkenazi Jewish population. Some of these tests have become routine, whereas others are provided through commercial laboratories that offer an extensive Ashkenazi Jewish panel.

### Cystic Fibrosis

CF is the most common severe AR disease affecting white children, with an incidence of 1/2500 to 5000 corresponding to a carrier frequency of 1/25 to 35. The disease is characterized by chronic pulmonary obstruction and infection, and by digestive disorders such as pancreatic insufficiency. It is caused by mutations in the gene that encodes the CF transmembrane receptor protein. Since the gene was cloned in 1989, more than 1000 mutations have been identified. The variety of mutations have ethnic and geographic variation, as well as a wide range of phenotypic variation, from those causing classical, severe CF (such as the common delta F508 mutation) to those that may have subtle or no clinical manifestations. Studies of clinical phenotype in correlation with CFTR genotype have revealed a very complex relationship demonstrating that some phenotypic features are closely determined by the underlying mutations, whereas others are modulated by modifier genes, epigenetic mechanisms, and environment.

Genetic testing is used to confirm a clinical diagnosis of CF and can be used for infants with meconium ileus, for carrier detection in individuals with positive family history and partners of proven CF carriers, and for prenatal





**FIGURE 2-8.** Hyperechogenic bowel (arrow) in a fetus with cystic fibrosis.

diagnostic testing if both parents are carriers. Since 2001, the American College of Obstetricians and Gynecologists and the American College of Medical Genetics have recommended that screening for CF should be offered to women at higher risk of having children with CF (e.g., Caucasians) and should be made available to couples in other racial and ethnic groups who are at lower risk and in whom the test may be less sensitive. They also recommend that people with a family history of CF or a partner with CF be offered testing.<sup>32</sup> Implementing this recommendation is complex and therefore, somewhat controversial. The complexity arises in part because the incidence of CF varies in people of different ethnic groups. It is most common in Ashkenazi Jewish and Northern European populations, in which 1/29 is a carrier, but is far less common in Hispanic, black, and Asian-American persons. Furthermore, as mentioned earlier, the detection rate varies greatly between ethnic groups because not all alleles are known for each population. Most laboratories test for the most common mutations present in the population; in the United States this typically involves screening for the 25 to 32 mutations most common in the European population. Genetic counseling is particularly important in order to explain the limitations of testing (that is, not all carriers will be detected), especially for couples in which one or both partners is a carrier or has a positive family history and/or is of nonwhite ancestry.

### **Cystic Fibrosis and Echogenic Fetal Bowel**

Fetal echogenic bowel (EB), defined as bowel with sonographic density equal to or greater than that of surrounding bone, is diagnosed in 0.2% to 1.8% of fetuses during routine ultrasound examination in the second trimester of pregnancy. This increased echogenicity has been associated with chromosomal abnormalities, congenital infections, intestinal obstruction, and CF (Fig. 2-8).<sup>33</sup> In the case of CF, it is hypothesized that the malfunctioning CFTR protein leads to dehydration of mucous secretions, which become viscous and obstruct the bowel lumen, leading to meconium ileus.

The risk for CF with EB has been extensively studied and reported to have a wide range from 0% to 33%.<sup>34</sup> This range could result from differences in ascertainment, CF prevalence, and mutation detection rates.

Because of the complexities and limitations of screening, testing for CF in cases of EB is often not straightforward. In cases of EB and two CF mutations in the fetus, the diagnosis is certain. In cases of EB with no fetal mutations, the risk of CF becomes exceedingly low. However, when the fetus with EB is found to carry one identified CF mutation, the risk of CF is increased but the diagnosis cannot be determined with certainty before birth with current techniques. Given the relatively high CF carrier frequency, this situation is not rare. The precise risk of CF depends on the frequency of CF in EB cases, the frequency of CF in the population studied, and the screening detection rate. It has been estimated at about 9%<sup>35,36</sup> based on a 2% CF frequency in EB cases, a 4% CF carrier frequency and a 90% mutation detection rate. Therefore, screening of a parent with negative results can decrease, but not eliminate entirely, the risk for CF in the offspring. Depending on the clinical situation (family history, presence or absence of echogenic bowel, and carrier state of the other parent), the interpretation of risk to a given fetus can become quite complex. Various techniques to determine risk in different scenarios have been determined.<sup>37</sup>

## **POPULATION-BASED PRENATAL SCREENING FOR BIRTH DEFECTS**

### **Alpha-Fetoprotein**

Population-based prenatal screening began in the late 1970s with the use of maternal serum alpha-fetoprotein (AFP) measurements to identify women at increased risk of carrying a fetus with an open NTD. AFP is the major serum protein early in fetal life.<sup>38</sup> This oncofetal protein is produced initially by the yolk sac and, after involution of this structure in early pregnancy, by the fetal liver. There are relatively little published data on the biologic activities of AFP during fetal development. AFP is present in amniotic fluid initially through diffusion across immature skin, and later through the kidneys and fetal urination. Amniotic fluid AFP is swallowed by the fetus and recirculates, with eventual degradation by the fetal liver. Minute amounts of AFP are present in maternal serum through diffusion across the placenta and amnion. Nonpregnant women have levels of AFP that are barely detectable (1 u/L), whereas normal median levels at 16 to 18 weeks of gestation range from 18 to 40 u/L. When the fetal serum level is 2 million u/L, the corresponding amniotic fluid AFP (AFAFP) is 20,000 u/L, and the maternal serum level is 20 u/L.<sup>39</sup>

Fetal plasma and amniotic fluid levels of AFP peak in the midtrimester of pregnancy, whereas maternal serum AFP (MSAFP) continues to increase until 28 to 32 weeks of gestation (Fig. 2-9). The discrepancy between amniotic fluid and maternal serum levels of AFP is not completely understood, but may be due to the rapidly expanding placental and amniotic interfaces.

In the fetus with a defect such as anencephaly or spina bifida, AFP enters the amniotic fluid in increased amounts, leading to higher levels in the maternal serum as well. Levels of AFP are elevated in amniotic fluid and maternal serum

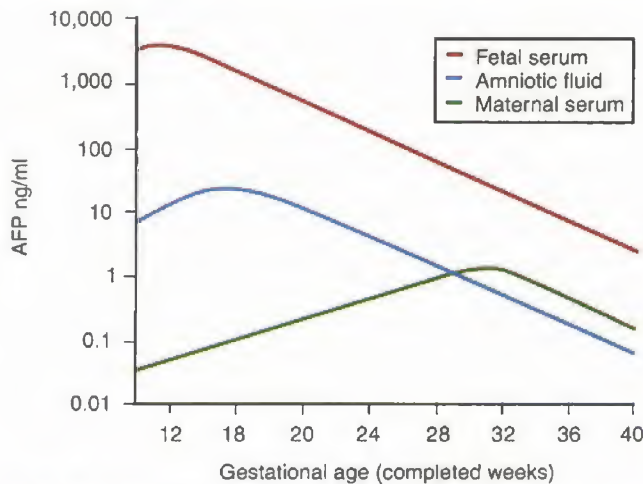


**FIGURE 2-9.** Mean concentrations of alpha-fetoprotein in maternal serum, amniotic fluid, and fetal serum. (Redrawn from Haddow JE: *Prenatal screening for open neural tube defects, Down's syndrome, and other major fetal disorders*. *Semin Perinatol* 14:488, 1990.)

only when such lesions are open, that is, when the neural tissue is exposed or covered by only a thin membrane. When NTD are skin covered, AFP does not escape from the fetal circulation, and such defects are generally not detected by maternal serum AFP (MSAFP). Whereas essentially 100% of anencephaly lesions are open, approximately 20% of spina bifida cases are skin covered, as are 82% of encephaloceles.<sup>39</sup> Discussions of the sensitivity and specificity of AFP testing are generally restricted to open lesions, because it is assumed that closed lesions will not be detected.

### Prenatal Screening for Open NTDs

Because more than 80% of infants with NTD are born into families with no prior history of the disorder, MSAFP screening has become an important public health program. In laboratories providing AFP screening, results are expressed as multiples of the median (MoM). This provides less interlaboratory variation, which can be considerable, as well as a way to report results across a range of gestational ages. The distribution of MSAFP is log gaussian, with median values of 1.0 for normal pregnancies, 3.8 for pregnancies with open spina bifida, and 6.5 for pregnancies affected with anencephaly (Fig. 2-10).<sup>39</sup> There is significant overlap between affected and unaffected pregnancies, and choosing an MSAFP cutoff requires consideration of both detection rates and false-positive rates. The two most commonly used cutoffs for MSAFP are 2.0 and 2.5 MoM. Using either cutoff level, the detection rate for anencephaly is 95% or higher. The detection rate for spina bifida is between 75% and 90% using a cutoff of 2.0 MoM, and between 65% and 80% using 2.5 MoM. False-positive rates are 2% to 5% and 1% to 3%, respectively.<sup>39</sup> Encephaloceles are a less frequent cause of an elevated MSAFP, owing to both a lower incidence and a higher frequency of closed lesions. Given the extent of overlap between affected and unaffected pregnancies, it is not possible to detect all cases of open spina bifida with MSAFP screening and, likewise, most cases reported to be in need of further evaluation will ultimately be determined to be normal.

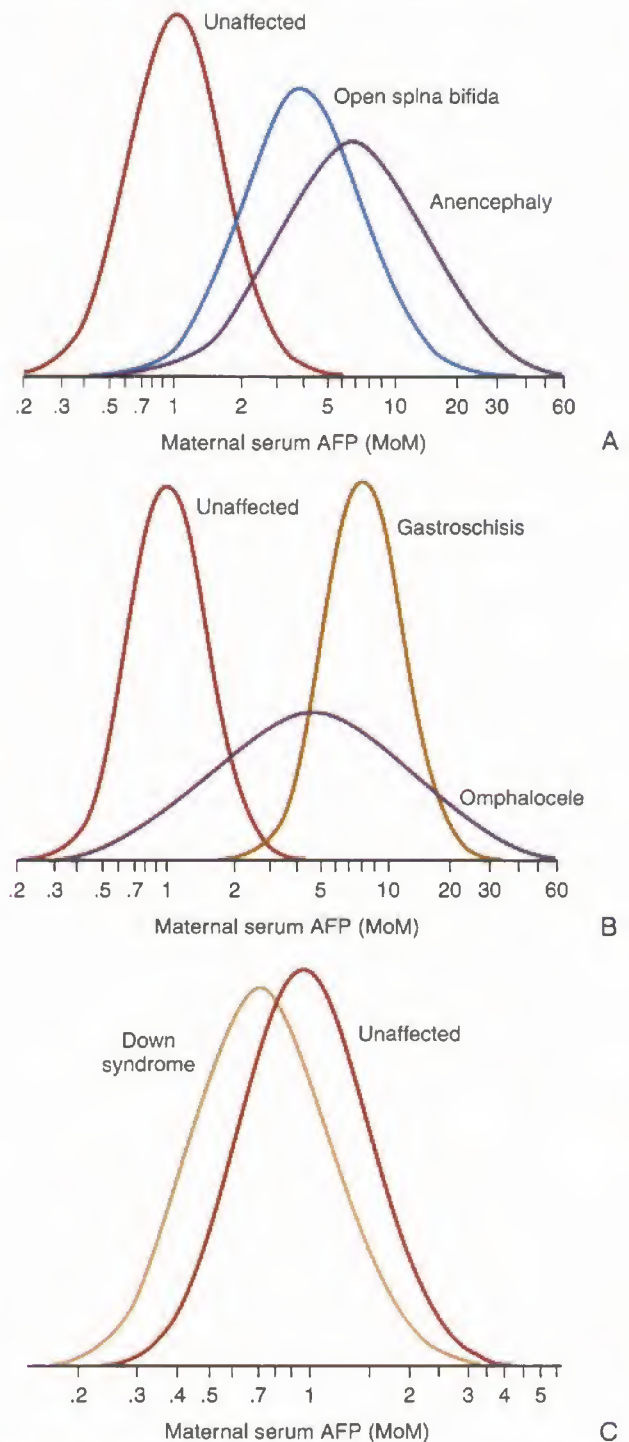


**FIGURE 2-10.** A. Distribution of second trimester maternal serum alpha-fetoprotein levels (MSAFP) in unaffected pregnancies and those affected by open spina bifida and anencephaly. The median for open spina bifida is 3.8 multiples of the median (MoM) and for anencephaly is 6.5 MoM. B. Distribution of second trimester MSAFP levels in unaffected pregnancies and those affected by gastroschisis and omphalocele. The median for gastroschisis pregnancies is 7.0 MoM and for omphalocele is 4.1 MoM. C. Distribution of second trimester MSAFP levels in unaffected pregnancies and those affected by Down syndrome. The median alpha-fetoprotein value is 0.75 MoM, and extensive overlap occurs between the affected and unaffected populations. (A, B, and C redrawn from Haddow JE: *Prenatal screening for open neural tube defects, Down's syndrome, and other major fetal disorders*. *Semin Perinatol* 14:488, 1990.)



As discussed previously, AFP levels vary with gestational age. The optimal time for serum NTD screening is 16 to 18 weeks of gestation. Before 16 weeks, there is more overlap between affected and unaffected pregnancies. Whereas last menstrual period (LMP) dating is sufficiently accurate for NTD screening, sonographic dating is more accurate and its use improves sensitivity and specificity of screening. In addition, because second trimester biparietal diameter measurements are usually smaller in fetuses with spina bifida, the MSAFP will appear higher, and this artifact improves the detection rate for this lesion. Other sonographic measurements (for example, crownrump length or composite biometry) can reliably date the pregnancy but do not have this unique advantage of BPD dating. Therefore, in the second trimester, ultrasound dating based on BPD alone is recommended for pregnancies at 14 weeks of gestation or later for the purposes of AFP screening. Most laboratories have separate sets of distribution parameters for ultrasound versus LMP-dated pregnancies.

There are several factors other than gestational age that affect MSAFP levels, including maternal weight,<sup>40</sup> race,<sup>41,42</sup> insulin-dependent diabetes mellitus (IDDM),<sup>43,44</sup> and the number of fetuses. Studies have also suggested that second trimester MSAFP is consistently elevated after first trimester transabdominal multifetal pregnancy reduction (MFPR), and should not be performed in this setting.<sup>45</sup> Because larger maternal size results in greater dilution of fetally derived AFP, obese women have lower levels of MSAFP. Black and Asian women have levels that are 10% to 15% higher than nonblacks, and insulin-dependent diabetic women have levels that are lower than the general population. Whereas the relationship between AFP and IDDM has long been appreciated, the magnitude of the association has been disputed.<sup>46</sup> Initially, it was felt that AFP levels were 60% to 70% of controls. Later, with correction for age, race, and weight, this was adjusted to 80%.<sup>47</sup> The physiologic basis for this lower value is unclear. There appears to be an association between the degree of glucose control, as determined by measurements of glycosylated hemoglobin, and MSAFP.<sup>48,49</sup> Recent data indicates that perhaps the adjustment in IDDM pregnancies is no longer appropriate.<sup>47</sup> It is possible that better laboratory methods, improved diabetic surveillance and control, and better weight adjusted MoM may have resulted in IDDM values closer to controls. Some correction is still appropriate, although this is less than in the past.

Each of these factors is taken into account in the calculation of risk. Although other factors, such as maternal smoking,<sup>50,51</sup> and IVF<sup>52,53</sup> have a small impact on levels of MSAFP and other biochemical markers, these differences are not of sufficient magnitude to warrant correction.

### Follow-Up When MSAFP Is Elevated

When the MSAFP level is near the cutoff (either 2.0 or 2.5 MoM), the accuracy of dating is assessed. If dating based on LMP was used for the original calculation, an ultrasound should be performed to confirm dating and rule out multiple gestations and fetal demise, both of which can cause an elevated MSAFP. Each program determines the discrepancy in dating at which recalculation is performed, generally between 7 and 14 days.

If the screening ultrasound does not identify an etiology for the increased MSAFP, further assessment with more sophisticated sonography and amniocentesis is indicated. The sensitivity of ultrasound for the detection of NTD and other significant structural abnormalities associated with increased MSAFP has been reported to be as high as 94% to 100%.<sup>54</sup> A recent study in fact indicated that ultrasound alone is more sensitive than MSAFP for the initial detection of NTD; this varies with the experience and expertise of the ultrasound examiner.<sup>55</sup> Ultrasound is less expensive than amniocentesis and does not carry the risk of pregnancy loss.

Amniocentesis allows for measurement of both AFP and acetylcholinesterase (AChE) in the amniotic fluid. In some programs, AChE is only measured when the AFAFP is greater than 2.0 MoM, an approach that provides the best balance between sensitivity and specificity.<sup>56</sup> Occasionally, AChE is done when there is an increased prior risk (for example, elevated MSAFP, abnormal ultrasound, or a positive family history). Measurement of AFAFP and AChE has a 97% detection rate for NTD, with a false positive rate of 0.5%.<sup>57</sup> Although there are many disorders that can result in an elevated AFAFP, AChE is more specific to neural tissue. Detection of AChE in the amniotic fluid generally indicates that an open NTD is present, although a positive AChE has also been reported with omphalocele, gastroschisis, cystic hygroma, fetal skin lesions, and fetal hydrops.<sup>58,59</sup>

A major cause of borderline amniotic fluid AFP elevations and false-positive AChE results is contamination of the sample with fetal blood. Fetal blood AFP levels are more than 100 times higher than AF levels. False-positive AChE results occur in about 2% of visibly blood-stained samples and 0.2% of samples that are not visibly blood stained. Testing for the presence of fetal hemoglobin is indicated for samples with elevated AFAFP, visible red blood cell contamination, and certain other indications (for example, unexplained elevated MSAFP, reddish AF). The false-positive rate of AChE when early amniocentesis is performed (between 10 and 15 weeks), is four times higher than with amniocentesis at 15 weeks or beyond.<sup>60</sup>

One study comparing strategies for evaluation of elevated MSAFP indicated that a program using targeted ultrasound and an MSAFP cutoff of 2.0 MoM would detect 90/110 structurally abnormal fetuses in a cohort of 100,000 hypothetical singleton pregnancies, without iatrogenic fetal loss, at a cost of \$5700 per anomalous fetus. The authors contrast this with a strategy of amniocentesis with karyotyping for MSAFP of 2.5 MoM or greater, which would detect 15 additional abnormal fetuses (including some chromosome abnormalities), but with nine iatrogenic fetal losses and an incremental cost of \$46,100 per anomalous fetus.<sup>61</sup>

Several investigators have reported an association between elevated MSAFP and an increased risk of fetal aneuploidy, an additional argument for amniocentesis. These studies have estimated the prevalence of clinically significant aneuploidy in this setting at 1%, with approximately 55% of these being autosomal aneuploidies and 45% sex chromosomal abnormalities.<sup>62,63</sup>

### Other Abnormalities and Elevated AFP

An elevated MSAFP can be associated with fetal defects other than NTDs (see Fig. 2-10, Table 2-15). Such disorders



**Table 2-15** Causes of an Elevated MSAFP

Multiple gestation
Fetal demise
Fetal-maternal hemorrhage
Placental abnormalities
Uterine abnormalities
Maternal ovarian or hepatic tumors
Fetal congenital defects
Neural tube defects
Spina bifida
Anencephaly
Encephalocele
Open ventral wall defects
Omphalocele
Gastroschisis
Congenital nephrosis
Triploidy
Bilateral renal agenesis
Congenital skin disorders
Epidemolysis bullosa
Aplasia cutis
Autosomal recessive polycystic kidney disease
Sacroccygeal teratoma
Cystic adenomatoid malformation of the lung

MSAFP, maternal serum alpha-fetoprotein.

include other open fetal defects, such as omphalocele and gastroschisis. In addition, some fetal skin disorders allow increased diffusion of AFP into the amniotic fluid, resulting in an elevated MSAFP. Congenital nephrosis can cause extremely high levels of AFP owing to fetal proteinuria and is suspected with a normal ultrasound and markedly elevated MSAFP (often >10 MoM). This AR disorder results in renal failure early in life, and children often die in infancy or early childhood. It is relatively rare except in Finland, where the reported incidence of 1/2600 live births makes the disease a primary focus of AFP screening program. DNA testing for Finnish nephrosis is now available, although it is of less use in families not of Finnish descent.<sup>39,64,65</sup>

## Elevated AFAFP

A number of studies have addressed the risk of an abnormality when an elevated AFAFP is detected. In one study of 85,000 consecutive samples from the California state screening program, 2.2% had an AFAFP greater than 2.0 MoM. One half measured 2.0 to 2.4 MoM, and 93% of these had a normal outcome. Sixty-seven percent of those with higher levels had abnormalities. With a positive AChE, the chance of an abnormal fetus was 67% for levels between 2.0 and 2.4 MoM and 99% at greater than 5.0 MoM. After a normal ultrasound and karyotype, the risk for a fetal abnormality was 1% for AFAFP measuring 2.0 to 2.4 MoM and 3% for higher levels.<sup>66</sup> Like MSAFP, an unexplained AFAFP has also been associated with preeclampsia and preterm delivery.<sup>67</sup>

**Table 2-16**

Pattern of Results Seen with Expanded AFP Screening in Fetal Disorders

	AFP	uE <sub>3</sub>	hCG	Inhibin A
Open NTD	↑	No Change	No Change	No Change
Down syndrome	↓	↓	↑	↑
Trisomy 18	↑	↓	↓	No Change

AFP, alpha-fetoprotein; hCG, human chorionic gonadotropin; NTD, neural tube disorders; uE<sub>3</sub>, unconjugated estriol.

## Biochemical Markers and Fetal Chromosomal Abnormalities

Shortly after the introduction of MSAFP screening for NTD, it was recognized that fetuses with DS had a lower mean MSAFP in the second trimester, estimated at 0.74 MoM.<sup>68,69</sup> Subsequent investigations have reported that maternal serum, amniotic fluid,<sup>69</sup> and fetal cord serum<sup>70</sup> levels of AFP are all lower in pregnancies in which the fetus has DS. This may be owing to either decreased production of AFP by the fetal liver or more rapid removal of AFP from the fetal circulation.<sup>71</sup>

A number of other biochemical markers have also been studied for use in aneuploidy screening. Although some of these markers have not been found to be useful, unconjugated estriol (uE<sub>3</sub>),<sup>72</sup> human chorionic gonadotropin (hCG)<sup>73</sup> and dimeric inhibin A<sup>74-76</sup> all add sensitivity and specificity to second trimester biochemical screening for DS. Like AFP, uE<sub>3</sub> is 25 to 30% lower in DS pregnancy, whereas hCG and inhibin A are both increased with a median value about twice that of normal controls (Table 2-16).<sup>71</sup>

E<sub>3</sub> is a steroid hormone that is produced by the syncytiotrophoblast. Biosynthesis of estriol requires dehydroepiandrosterone sulfate (DHEAS) production by the fetal adrenal gland and subsequent conversion of DHEAS to 16 $\alpha$ -OH-DHEAS in the fetal liver. In the placenta, 16 $\alpha$ -OH-DHEAS is then deconjugated by a sulfatase and the resulting molecule aromatized to yield unconjugated estriol. Fetal disorders that affect the precursors or enzymes involved in this pathway may impact uE<sub>3</sub> levels in maternal screening and can be detected with second trimester multiple marker screening (see later).

HCG is secreted by the syncytiotrophoblast. Other placental secretory products such as progesterone, human placental lactogen (hPL) and pregnancy-specific beta-glycoprotein are higher in maternal samples from DS pregnancies. This finding suggests a hypersecretory or immature placenta as a characteristic of fetal DS.<sup>73,77</sup>

## Screening Programs for Fetal Aneuploidy

Because AFP, uE<sub>3</sub>, hCG, and inhibin A are all independent of maternal age and only weakly correlated with each other, they can be used in combination to estimate fetal DS risk. In the second trimester, screening for DS now most commonly involves either triple marker screening with MSAFP, uE<sub>3</sub> and hCG, or quad screening with those three markers plus inhibin A.<sup>76,78</sup>



**Table 2-17****Screen-Positive Rate of Down Syndrome Screening Test at Different Risk Cutoff**

Down Syndrome Test	Dating Method	1/190	1/270
Triple	US	3.8%	5.7%
	LMP	5.3%	7.4%
	Combined	4.4%	6.3%
Quad	US	3.2%	4.7%
	LMP	4.6%	6.2%
	Combined	3.7%	5.3%

LMP, last menstrual period.

From Knight GJ, Palomaki GE: Epidemiologic monitoring of prenatal screening for neural tube defects and Down syndrome. *Clin Lab Med* 23:531, 2003

In addition to using different combinations of markers for screening, laboratories use different risk cutoff levels. As with many screening tests, a trade-off is made between detection of the disorder and the number of individuals with a screen positive result. Table 2-17 summarizes the relationship between DS risk cutoff, triple marker versus quad screening, and method of dating. In the United States, many laboratories use the triple test, and a cutoff equal to the risk of a 35-year-old. At this risk cutoff, the triple test yields a screen positive rate of 7.4% with LMP dating, with a detection rate (DR) of 70% to 75% (all ages). Some laboratories choose a risk cutoff to provide a false positive rate (FPR) of 5%. This rate occurs at a screening cutoff of 1/190 and is associated with a DR of 60% to 65%. With the addition of inhibin A and use of quad screening, at a cutoff of 1/270, the DR increases to 80% and the positive rate decreases to 6.2% with LMP dating.<sup>79</sup>

### Trisomy 18 Detection

In pregnancies in which the fetus is affected with trisomy 18, the levels of AFP, uE<sub>3</sub>, and hCG are all decreased, with median values of 0.6, 0.5, and 0.3 MoM, respectively. Inhibin A does not contribute to the detection of trisomy 18 and is not included in the screening algorithm. Use of a protocol evaluating this characteristic pattern is associated with an 80% detection rate for trisomy 18, while identifying only 0.5% of women as high risk.<sup>80</sup>

### Prenatal Screening in Multiple Gestations

A number of complexities arise in the screening of twin pregnancies. First, serum markers are approximately, but not exactly, twice those found in singleton pregnancies. Second, a single maternal serum value is used to provide information about multiple fetuses. In discordant cases, the normal cotwin will mask the abnormal marker production associated with the affected twin. Third, with monozygotic twins, both are most commonly either affected or unaffected, whereas with dizygous twins, the risk of DS is independent. Although ultrasound determination of monochorionicity is diagnostic of monozygosity, with same-gender dichorionic pregnancies, zygoty is uncertain. Because nuchal trans-

lucency screening in the first trimester is able to evaluate each fetus individually, this may be the most useful screen for multiple pregnancies.

Although some data are available on serum screening with twins, the distributions of serum markers in twins with DS are not known with any degree of certainty.<sup>81,82</sup> Risk estimates in twins are calculated to classify twins as screen positive or screen negative in a way that ensures a false-positive rate similar to that in singletons. It is generally assumed that the detection rate for chromosomal abnormalities in twin pregnancies is lower than that in singletons, and the predicted detection rate for a 5% false-positive rate is only 47%.<sup>83</sup> However, these assumptions are theoretical rather than based on reliable observations. In high-order multiple gestations, biochemical screening is generally not possible, and again, nuchal translucency is the most useful (or only) option in such cases. Large studies are needed to determine the optimum screening method in multiple pregnancies.

### Controversy of Maternal Age Screening

Maternal age has historically been the most frequent method for identifying women at increased risk for fetal chromosome abnormalities, and determining who should be offered prenatal diagnostic testing. Risk is commonly expressed in two ways, either as risk of delivering a child with DS, or the risk of diagnosing DS in midtrimester, at the time of amniocentesis. This distinction is important, because 25% of affected fetuses are spontaneously lost between midtrimester and term. Thus, the risk of carrying a fetus with DS at 35 years of age is 1/270 in the second trimester, but 1/384 at term. On average, the risk of DS in women older than 35 years of age is about 1/150 in the midtrimester. As maternal age increases, the chance of delivering a child with DS increases from about 1/1000 at 30 years of age, to almost 1/400 at 35 years of age, and 1/100 at 40 years of age (see Table 2-4).<sup>84</sup> Paternal age does not affect aneuploidy risk. This clinical observation is consistent with studies demonstrating that greater than 90% of trisomy 21 results from nondisjunction in the oocyte, most commonly during meiosis I.<sup>85</sup>

Because of the association of advancing maternal age with DS (and other chromosome abnormalities), prenatal diagnosis has been offered to women 35 years of age or older for many years. At 35 years of age, the chance of identifying a fetus with DS approximately equals the chance of miscarriage due to the amniocentesis procedure. It is in part for this reason that testing has traditionally been offered at this point. With advances in screening, a risk threshold comparable to the risk of an unscreened woman 35 years of age continues to be used as the cutoff to recommend diagnostic testing. For many women, however, the decision to undergo amniocentesis is difficult, because not all women weigh the risks equally. For some, the possibility of miscarriage is far more of a concern than the possibility of having a child with DS. For others, concerns over caring for a child with disabilities may be more serious.<sup>86</sup>

Age-based guidelines for offering of prenatal diagnosis have remained largely unaltered despite improvements and availability of second trimester maternal serum screening, the widespread use of ultrasound to identify findings associated

with fetal aneuploidy, demonstrated performance of first trimester screening and the potential for combinations of these approaches.<sup>87</sup> As improvements in screening have provided much better risk estimates than are available using age alone, more and more women 35 years of age and older are electing to have screening prior to making a decision regarding amniocentesis. However, numerous recent editorials have questioned whether the use of maternal age as a sole criterion for aneuploidy risk assessment remains justified.<sup>88</sup>

All patients considering prenatal diagnosis should undergo genetic counseling to discuss the options available and the risks, benefits, and limitations of each testing choice.

### **Third-Trimester Pregnancy Complications after Abnormal Serum Screening**

Extreme marker levels, both low and high, have also been associated with third-trimester pregnancy complications such as hypertensive disorders, intrauterine growth restriction, and preterm birth. Most cases, however, are not due to fetal or maternal pathology and ultimately result in a normal outcome.

Numerous studies have demonstrated that women with elevated levels of MSAFP have an increased risk of complications, such as spontaneous abortion, small-for-gestational age infants, pregnancy-associated hypertensive disorders, and preterm delivery. The magnitude of risk increases with increasing maternal serum levels, from a risk of 19% with levels of 2.5 to 2.9 MoM, to 67% with an MSAFP of greater than 6.0 MoM.<sup>89</sup>

In cases of unexplained increased MSAFP, increased transplacental transfer is responsible for the elevated value. Such increased transfer occurs with various placental abnormalities, and these same placental abnormalities later result in perinatal complications. Abnormalities such as placental accreta, increta, and percreta have also been reported with an elevated AFP,<sup>90</sup> and uterine anomalies have been reported to be 22 times more common in these patients, as well.<sup>91</sup> Because of the very large concentration gradient between fetal and maternal serum levels of AFP, even a slight compromise in uteroplacental integrity will allow detectably increased transport of AFP across the placenta.

Other biochemical markers and combinations of markers have also been studied with respect to adverse outcome in late pregnancy. Elevated hCG in particular has been associated with an increased risk of intrauterine growth restriction, hypertension/preeclampsia, fetal malformations, chromosomal abnormalities, and adverse perinatal outcome. As with MSAFP, the highest levels of hCG are associated with the highest risk of poor outcome.<sup>92</sup> Both singleton and twin pregnancies with elevated hCG and AFP have been associated with adverse obstetric outcomes.<sup>93-95</sup>

The recently completed FASTER trial was a large prospective trial of biochemical screening for chromosomal abnormalities that included comprehensive pregnancy outcome data. This study of over 38,000 women identified numerous associations between serum markers and adverse outcomes. There was a relatively low, but often significant

risk of having an obstetric complication if a patient had a single abnormal marker. However, the risk of having an adverse outcome increased significantly if a patient had two or more abnormal markers.<sup>96</sup>

Another study compared the risks of adverse outcome in women with unexplained elevated hCG or AFP, and whether these risks vary by prepregnancy risk status (medical or previous obstetric complications). These investigators found that abnormal serum screening was independently associated with preeclampsia, intrauterine growth restriction, fetal death, and preterm birth in both high- and low-risk women.<sup>97</sup> In patients with intrauterine growth restriction (IUGR), those who also had elevated hCG or decreased uE<sub>3</sub> were associated with an increased risk of adverse outcome as compared with patients with IUGR and normal markers.<sup>98</sup>

Optimal management of the patients with unexplained abnormal biochemical screening, however, remains controversial. Overall, many experts have concluded that, apart from the six- to seven-fold increased risk when both AFP and hCG are elevated, the clinical utility of differences in one marker are probably poor.<sup>99</sup>

### **Low Estriol**

Women with low estriol (<0.75 MoM) have also been found to have an increased risk of adverse outcome, including IUGR, oligohydramnios, and delivery of small-for-gestational-age infants, a risk that seems independent of elevated hCG or AFP.<sup>100</sup> About 0.27% of women will have a very low uE<sub>3</sub> (<0.15 MoM), a finding that has been associated with a number of metabolic and genetic disorders including Smith-Lemli-Opitz syndrome (SLO), steroid sulfatase deficiency, Kallman syndrome, congenital adrenal hyperplasia, and other disorders associated with adrenal dysfunction. SLO is an AR disorder that results in multiple malformations, including congenital heart defects, mental retardation, and ambiguous genitalia in men. Because the primary abnormality involves cholesterol biosynthesis, a lack of cholesterol precursors from the fetus render the placenta unable to produce uE<sub>3</sub>.<sup>101</sup> Prenatal diagnosis is possible through detection of elevated levels of 7-OH-dehydrocholesterol in amniotic fluid or maternal urine.<sup>102</sup> Some screening programs, including the expanded AFP program in the state of California, provide evaluation of risk for SLO.<sup>103-106</sup> Although detection of SLO has proved rare in such programs, patients identified at increased risk for SLO have been found to have a very high risk of various adverse perinatal outcomes of greater than 50%.<sup>104</sup>

The other, more common cause of very low estriol is the presence of X-linked steroid sulfatase in the fetus. Lack of this enzyme in the placenta also results in the inability to produce unconjugated estriol. This disorder is an X-linked condition leading to ichthyosis as the primary symptom in offspring, and a careful family history will often reveal symptoms in a previously undiagnosed male relative (grandfather or brother). The diagnosis can be confirmed through molecular testing for the causative microdeletion on amniotic fluid. Although the disorder is relatively mild, prenatal diagnosis can reassure the family and physician that another, more serious condition is not present.<sup>106-108</sup>



**Table 2-18****Common Indications for Genetic Counseling**

Previous child with multiple congenital abnormalities, mental retardation, or isolated birth defect
Family history of a hereditary condition, such as cystic fibrosis
Prenatal diagnosis for maternal 35 years of age or older
Follow up of abnormal prenatal screening tests (triple screen, nuchal translucency, etc.)
Ultrasound detection of fetal structural abnormalities
Consanguinity
Teratogen exposure, such as medications, alcohol, occupational chemicals
Recurrent pregnancy loss or infertility
Parent with structural chromosome abnormality
Previous child with chromosome abnormality
Newly diagnosed abnormality or genetic condition
Referral for genetic testing, including testing for cancer susceptibility and late onset disorders
Follow up for a positive screening test, such as the phenylketonuria test in a newborn or the Tay-Sachs carrier test in an adult of reproductive age

## GENETIC COUNSELING AND PRENATAL DIAGNOSTIC TESTING

### Genetic Counseling

Clinical genetics is the discipline that is concerned with the diagnosis and management of the medical, social, and psychological aspects of hereditary disease. Often, people seeking genetic counseling are parents of a child with a potential or known genetic condition. Others who seek genetic counseling include adults with an abnormality or a family history of an abnormality. Genetic counseling is also an integral part of genetic testing and screening programs, including prenatal testing. (Table 2-18).

The process of genetic evaluation involves several components: validation of the diagnosis, obtaining the family history, estimation of the risk of recurrence, helping the family to reach decisions and take appropriate action, and followup. An important part of genetic counseling involves understanding of the family history. Couples referred for prenatal testing for one indication will frequently have other risk factors identified. Generally, patients are not told what decisions to make with regard to testing and management options but, instead, are provided information and support. This approach, referred to as *nondirective counseling*, has been adopted widely as the standard in this field.

A family may be referred to the medical genetics unit for diagnosis, if this has not been made previously, or for prenatal testing if a diagnosis is known in the family and the pregnant woman may be at risk. The precise diagnosis must be certain in order to provide accurate prenatal diagnostic testing. The inheritance pattern must be known to provide correct risk figures, as some disorders may have different patterns of inheritance in different families.

Making a precise diagnosis may have enormous implications for counseling a family. For example, if a prior male fetus was diagnosed with hydrocephalus and the pregnancy terminated, a recurrence risk of 5% in future pregnancies

would generally be quoted. Ultrasound would be offered for prenatal diagnosis, although in some cases, ventriculomegaly may not manifest until late in pregnancy. On the other hand, more thorough evaluation of the prior fetus may have resulted in a diagnosis of X-linked aqueductal stenosis with identification of a mutation in the *L1CAM* (cell-adhesion molecule) gene. In such cases, testing of the mother is possible to determine if she is a carrier. If so, the recurrence risk is 50% for male offspring and very small for female offspring (although 50% of her daughters would also be carriers). CVS at 10 weeks would be possible for prenatal diagnosis if a molecular mutation were identified. The spectrum of the disorder includes boys with mental retardation but without hydrocephalus, so ultrasound would not be adequate for ruling out a recurrence of this condition.

### PRENATAL DIAGNOSIS

For many families seeking genetic counseling, a major goal is learning the risk for heritable disease in their children and the options that are available for avoiding having an affected child. The principal goal of prenatal diagnosis is to supply at-risk families with information so they can make informed choices during pregnancy. The potential benefits of prenatal diagnosis include: (1) providing reassurance to at-risk families when the results are normal, (2) providing risk information to couples who would not have a child without such reassurance, (3) allowing couples to prepare for the birth of an affected child, (4) allowing medical providers to plan for the delivery and postnatal care of an affected infant, (5) providing risk information to couples for whom termination of an affected pregnancy is an option.

Prenatal diagnosis is typically performed early in pregnancy, at a time when termination of an affected fetus can be performed safely. For many families, even if termination of pregnancy is not an acceptable option, prenatal diagnosis can help them prepare mentally, emotionally, and financially, and seek support systems before the baby arrives. For most disorders, the chance of a normal, unaffected child outweighs the risk of birth defects, and prenatal genetic tests will reassure couples they will *not* have a child with a specific disease. In counseling patients, it is important to remember that in many cases, genetic testing of the parents will indicate that there is little or no genetic risk to their offspring, and prenatal diagnosis is not necessary.

Although prenatal diagnosis with termination of affected fetuses is one option for preventing the recurrence of a genetic disorder in a family, it is by no means a universal solution. There are many disorders for which prenatal diagnosis is not possible, and for many parents termination is not an acceptable option, even if prenatal diagnosis is available. Other measures for avoiding recurrence of a genetic disorder include avoiding childbirth through contraception or sterilization; adoption; sperm or ovum donation; or preimplantation genetic diagnosis (PGD) on embryos obtained through IVF (see below).

### Genetic Counseling Before Prenatal Diagnostic Procedures

Parents considering prenatal diagnosis need information that will allow them to understand their situation and give



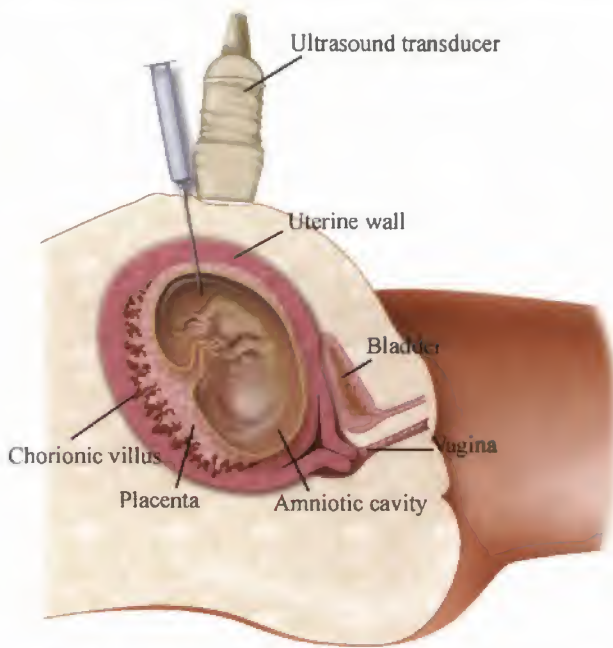


**FIGURE 2-11.** Amniocentesis needle is positioned in the amniotic cavity under ultrasound guidance. (Illustration by James A. Cooper, MD, San Diego, CA.)

(or withhold) consent for the prenatal diagnostic procedures. Genetic counseling before such procedures usually addresses the following: (1) the chance that the fetus will be affected, (2) the nature and consequences of the disorder, (3) the risks and limitations of the procedures being performed, (4) the time required before a report of the test results can be issued, (5) the possibility of complications of the procedures such as a failed attempt to obtain a sufficient, testable sample, or inconclusive results. Options for dealing with abnormal results are usually discussed, and it is emphasized that undertaking prenatal diagnosis in no way obligates the parents to terminate a pregnancy if an abnormality is discovered.

## Techniques for Prenatal Diagnosis

### Amniocentesis

In amniocentesis, a sample of amniotic fluid (typically 20 mL) is removed by inserting a 20- or 22-gauge spinal needle through the maternal abdomen and uterine wall into the amniotic cavity under ultrasound guidance (Fig. 2-11). Amniotic fluid contains desquamated fetal cells that can be cultured and karyotyped, or used for a variety of metabolic assays or DNA extraction if a specific indication is present. Amniotic fluid AFP levels are also routinely measured.

The major complication of amniocentesis is the risk of miscarriage (above the 2% to 3% risk for any pregnancy at this gestational age). Miscarriage risk of midtrimester amniocentesis at 15 to 20 weeks gestation is typically quoted at 0.5%, or 1/200, although the origin of this commonly quote number is obscure. The only randomized trial that has been performed in low-risk patients was in the United Kingdom in 1986; this study demonstrated a 1% procedure

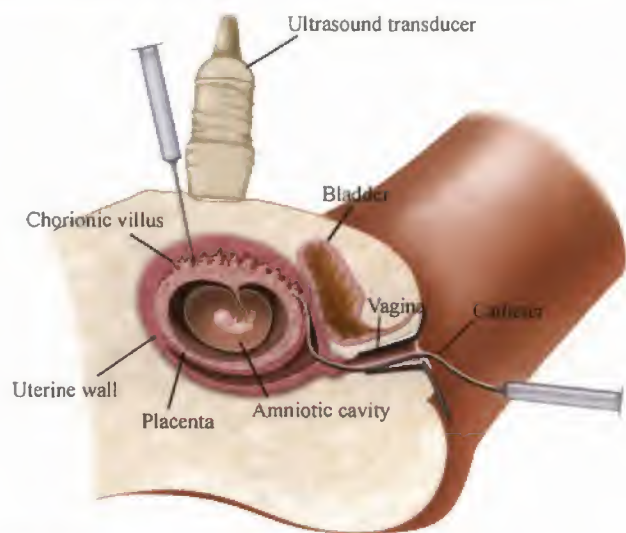


**FIGURE 2-12.** Chorionic villus sampling. Either chorionic villus catheter or sampling needle is placed into the developing placenta under continuous ultrasound guidance. (Illustration by James A. Cooper, MD, San Diego, CA.)

related loss rate.<sup>109,110</sup> More recent data indicate that the risk may be substantially lower.<sup>111,112</sup> Leakage of amniotic fluid following amniocentesis is not uncommon but typically resolves without long-term sequelae. Needle-associated injury to the fetus is rare.

Amniocentesis is typically performed at 15 to 20 weeks' gestation. The volume of amniotic fluid at 15 menstrual weeks is 125 mL, and increases 50 mL/wk for the next 13 weeks.<sup>113</sup> In an attempt to provide earlier results, the feasibility and safety of amniocentesis as early as 11 weeks' gestation has also been investigated. Results of a large, multicenter randomized trial of early (11 0/7 to 13 6/7 weeks) versus midtrimester (15 0/7 to 16 6/7 weeks) amniocentesis revealed a significantly increased loss rate in the early amniocentesis group (7.6% versus 5.9%). In addition, there was a significantly increased incidence of talipes equinovarus in the early amniocentesis group (1.3% versus 0.1%). Thus, it appears that early amniocentesis does carry an increased risk compared with midtrimester amniocentesis, and this procedure is infrequently performed.<sup>114</sup>

### Chorionic Villus Sampling

In chorionic villus sampling (CVS), a biopsy of the developing placenta is performed at 10-13 weeks' gestation (Fig. 2-12). The primary advantage of CVS is that it can be performed earlier in gestation, which allows a decreased period of anxiety for patients at risk. Early results also permit first trimester termination, a safer and more readily available procedure than abortion in the second trimester. Indications for CVS are generally the same as for amniocentesis, although AFP levels cannot be assessed on chorionic villi. Therefore, women who undergo CVS require NTD screening with either maternal serum AFP measurement or ultrasound later in pregnancy.

There are two commonly used approaches to CVS, transcervical and transabdominal. Both are performed under ultrasound guidance, which is used to document fetal life,



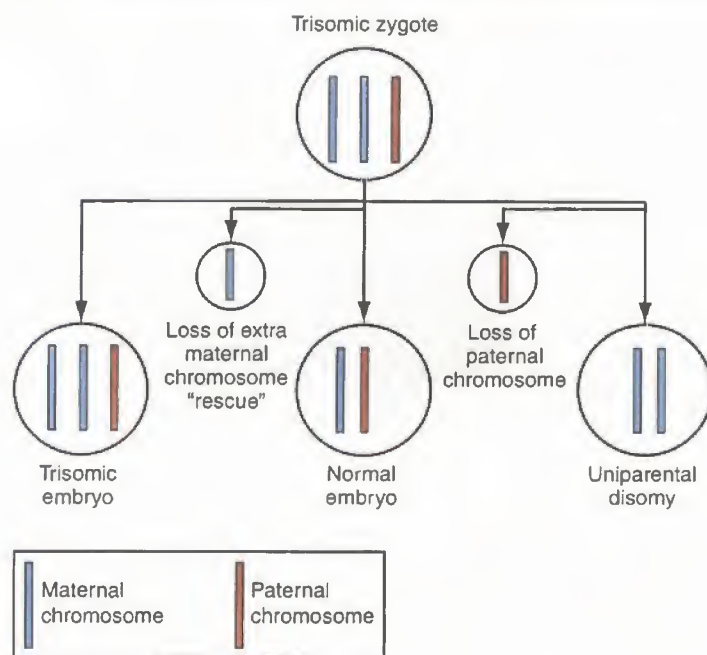


**FIGURE 2-13.** Trisomy rescue and uniparental disomy. Diploid ovum is fertilized by a normal, haploid sperm, resulting in a trisomic zygote. The cells multiple and divide, and one cell reverts to a diploid state owing to anaphase lag. This may happen owing to loss of either of the maternal chromosomes, or of the paternal chromosome. If one of the maternal chromosomes is lost, the resulting cell or cells will be normal. If the paternal chromosome is lost, the cells will be diploid but uniparental disomy will result.

gestational age, fetal number, localization of the trophoblast, and determination of the best approach and sampling path. With transcervical CVS, the patient is placed in the dorsal lithotomy position, a speculum inserted, and the vagina and cervix prepared with iodine antiseptic. A 16 g polyethylene catheter with a flexible, stainless steel obturator is inserted through the cervix and into the developing placenta. With a transabdominal approach, a 20-gauge needle is inserted into the placenta in a fashion similar to amniocentesis. In either approach, a 20-mL syringe is used to apply negative pressure and obtain a sample.

The risks of CVS were compared with those of amniocentesis in several trials performed shortly after introduction of the technique in the 1980s. A U.S. collaborative study demonstrated a loss rate 0.8% higher than that of mid-trimester amniocentesis, a difference that was not statistically significant.<sup>115</sup> A Canadian trial also demonstrated a non-significant increase in losses of 0.6% above amniocentesis (Canadian).<sup>116</sup> Since the completion of these trials over 20 years ago, experience has resulted in a decrease in the loss rates of both procedures. A recent study completed at the University of California San Francisco concluded that the decrease in risk of CVS-related losses has been greater than with amniocentesis. This has resulted in closing of the gap in risk and we now quote comparable rates of miscarriage following CVS or amniocentesis in our center.<sup>112</sup> However, CVS has a long learning curve and the risks are very provider dependent, therefore this equivalent loss rate may not be generalizable to all centers and providers.<sup>117</sup>

One important characteristic of CVS is the risk of confined placental mosaicism, which occurs in 1% to 2% of cases. Confined placental mosaicism (CPM) represents a discrepancy between the chromosomal makeup of the placenta and the fetus, and is diagnosed when a mixture of trisomic and normal cells are detected by CVS, whereas only normal cells are found on a subsequent amniocentesis or in the infant at birth. Most commonly, CPM represents a

trisomic cell line present only in the placenta with a normal diploid chromosome complement in the fetus.<sup>118</sup> However, the fetus is truly mosaic in about 10% of cases,<sup>119</sup> although the risk is somewhat dependent on the specific trisomy identified.<sup>120</sup> Although some cases of CPM are associated with poor placental function and perinatal complications such as IUGR and maternal hypertension, most commonly the outcome is normal.

CPM can arise following so-called trisomy rescue of an originally trisomic conception (Fig. 2-13). When this occurs, the fetus may be disomic but have uniparental disomy (UPD), a condition in which both chromosomes were inherited from the same parent. For example, if an embryo has trisomy 15 due to maternal nondisjunction, one or more cells in the inner cell mass, destined to become the fetus, may be 'rescued' by loss of one chromosome 15. If by chance the paternal copy is lost, there will be a normal chromosome number in the fetus, but maternal UPD 15. Trisomy rescue and UPD can potentially involve any chromosome, but if imprinted genes are present on the particular chromosome involved, this may have consequences for the fetus. Maternal UPD 15 is a cause of PWS, a condition characterized by mental retardation, obesity, and hypogonadism. Therefore, testing for UPD is indicated as a follow up to CPM detected by CVS when a chromosome containing known imprinted genes is involved (chromosomes 7, 11, 14, and 15). If the chromosome involved in the original trisomy does not contain imprinted genes, no phenotypic outcome for the fetus is suspected.

In the early 1990s, there were a number of reports of fetal limb reduction defects following CVS.<sup>121,122</sup> The procedures in the affected infants were largely performed between 55 and 66 days of gestation, and subsequent studies indicated that early gestational age (<10 completed weeks) at sampling increased the risk for this complication. After much investigation, including a large study of more than 140,000 cases of CVS submitted to the World Health Organization

registry, it was concluded that there is no increased risk of limb reduction defects following CVS performed at greater than 10 weeks gestation.<sup>123</sup>

## Multiple Gestations

If a twin gestation is present, the risk of a chromosome abnormality is increased as compared with a singleton pregnancy. The chance that one or both fetuses will have a chromosome abnormality is dependent on the zygosity. There are three possibilities that would result in either one or both twins being affected: (1) dizygotic twins with one fetus affected, (2) dizygotic twins with both fetuses affected, and (3) monozygotic twins with both fetuses affected. Postzygotic errors can also result in discordant karyotypes in monozygotic twins, although this is rare. Using existing tables of estimated risks of chromosomal abnormalities in singleton gestations and mathematically derived formulas, age-related risks of chromosomal abnormalities in twin gestations have been determined. According to these calculations, a patient 31 years of age or older with a twin gestation has a risk of a chromosome abnormality in at least one of her twins equivalent to that of a 35-year-old woman with a singleton.<sup>124</sup> Prenatal genetic testing should therefore be offered to women with twins at a younger age than the traditional 35 years of age.

Knowledge of chorionicity is critical when performing invasive procedures in multiple gestations. This is best determined by ultrasound in the first trimester, at which time the determination of chorionicity is highly accurate.<sup>125</sup> Prenatal diagnosis in monochorionic pregnancies theoretically requires only one sample, because the fetuses should be chromosomally identical. However, there is a small chance of postzygotic mutations leading to discordant karyotype, or of incorrect assignment of chorionicity. For this reason, both twins are typically sampled.

Both CVS and amniocentesis are used in sampling multiple gestations. The technique for amniocentesis involves visualizing the dividing membrane and identifying an amniotic fluid pocket in each sac. In order to be certain that each amniotic sac is sampled, 0.5 mL of indigo carmine dye is instilled after removal of fluid from the first sac. Aspiration of clear fluid from the second sac ensures proper placement. Indigo carmine has not been associated with risks to the fetus, whereas methylene blue dye should not be used owing to reports of fetal hemolysis, bowel atresias, and fetal demise when injected intraamniotically.<sup>126-128</sup> A single-needle insertion technique for amniocentesis has also been reported, with puncture of the dividing membrane to access the second sac.<sup>129</sup> This raises potential for admixture of samples with mosaic results, as well as disruption of the intertwin membrane. Reports of fetal abnormalities in twin gestations following rupture of the membrane,<sup>130</sup> and concern for creating an iatrogenic monoamniotic twin pregnancy with potential for umbilical cord entanglement, are also concerns.

With CVS, the procedure requires careful sonographic determination of placentation, because dye studies to mark the sample are not possible. Placing the tip of the aspiration device (catheter or needle) near the cord insertion can minimize the possibility of sampling the same fetus twice. A risk of less than 2% of sampling error has been reported with CVS in multiple gestations.<sup>131</sup>

With either CVS or amniocentesis, detailed description of the relative locations of the fetuses and placentas is important, particularly if discordant karyotypes are present and selective termination is to be considered. Noting any structural abnormalities or other findings that can differentiate the fetuses is also helpful.

## Postprocedural Loss Rates in Multiple Gestations

Although genetic amniocentesis is frequently performed in multiple gestations, smaller numbers limit the availability of data regarding postprocedural losses in multiple gestations following either amniocentesis or CVS. A number of studies have been performed to assess fetal loss rate following amniocentesis in twins. The quoted range of loss rates of 2.7% to 8.1% is comparable to the 6% background loss rate of twins reported by Yaron et al.<sup>131,132</sup> Whereas some studies do suggest a higher postprocedural loss rate in twin pregnancies when compared with singletons, not all account for the higher background loss rate of twins. Further study is needed to evaluate the risk associated with multifetal amniocentesis.

With CVS, even more limited data are available to determine the safety and accuracy of this procedure in multiple gestations. Reported pregnancy loss rates in the largest recent trials reported in the literature range from 0.6% to 4.0%, again comparing favorably with the 6% background loss rate reported for twin pregnancies.<sup>131-135</sup>

The choice as to whether to perform amniocentesis or CVS in a multiple pregnancy depends on many factors, such as the likelihood of proceeding to multifetal pregnancy reduction, the gestational age at presentation, the experience of the operator, and the technical difficulties of the specific case, including maternal body habitus and relative positions of the gestational sacs and placentas. Several studies have shown that CVS, in the hands of experienced operators, is at least as safe as second trimester amniocentesis for prenatal diagnosis in multiple pregnancies with loss rates comparable to control twins.<sup>131-135</sup>

## Selective Termination of Multifetal Pregnancies

The finding of a single affected fetus in a multiple gestation can present a complex counseling situation. Management options include termination of the entire pregnancy, continuation of the pregnancy, or selective termination. Selective termination in a dichorionic twin pregnancy can be performed with fetal intracardiac injection of potassium chloride. Such an approach is effective, but carries a loss rate of 4% to 12% for the remaining fetus or fetuses, depending on the gestational age of the pregnancy, starting number of fetuses and location of the affected fetus.<sup>136,137</sup> If the pregnancy is monochorionic, but discordant for a chromosomal or structural abnormality, the ubiquitous presence of intertwin anastomoses makes intracardiac injection unsafe for the normal twin. If selective termination is desired in this situation, umbilical cord occlusion using laser, ligation, or bipolar coagulation is the only option. Little data exist as to risks to the pregnancy and the remaining twin if this approach is chosen.



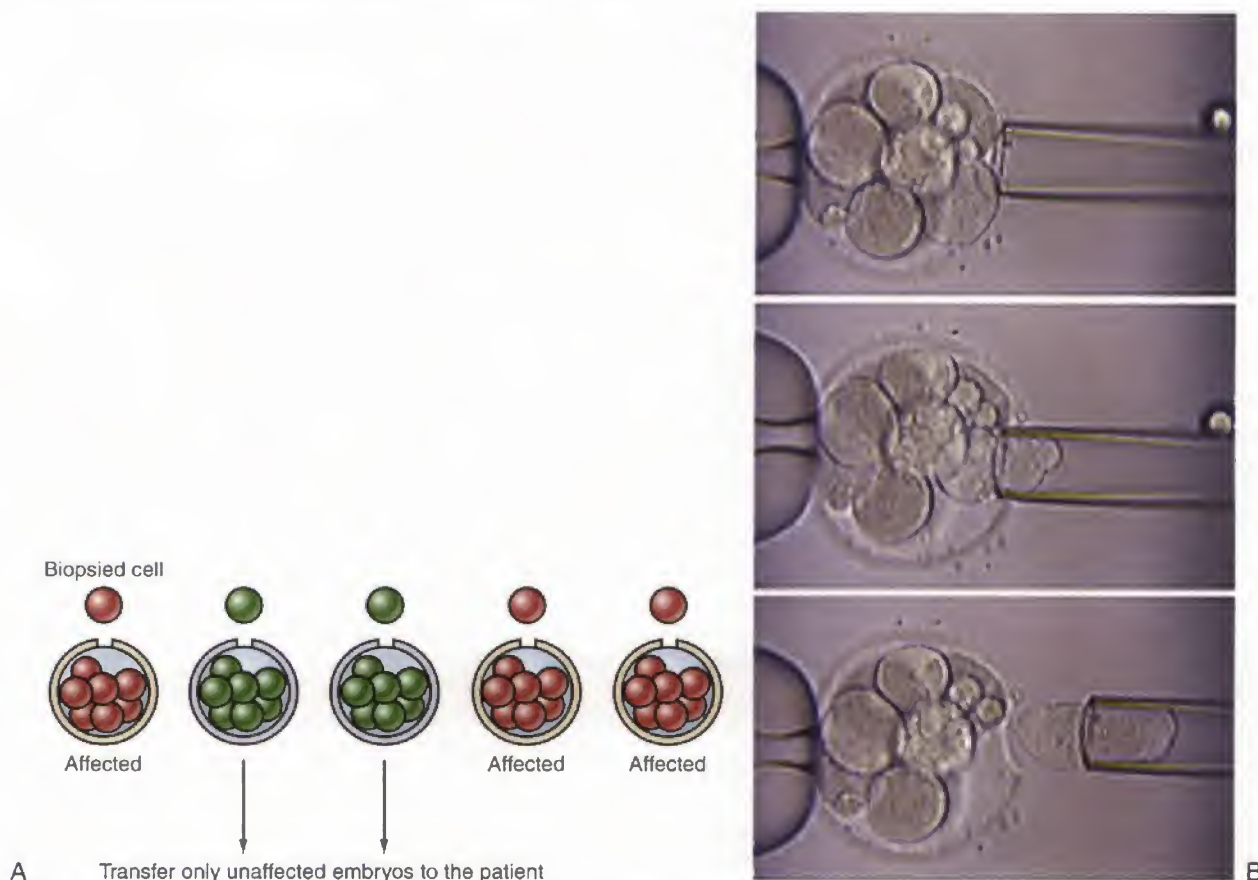


**FIGURE 2-14.** A and B. Preimplantation genetic diagnosis. Technique of preimplantation genetic diagnosis. IVF is used to create embryos. One or two cells are removed for genetic analysis, and unaffected embryos are transferred to the uterus. IVF, in vitro fertilization.

## Fetal Blood Sampling and Other Fetal Tissue Biopsy

Although there are theoretically many indications for accessing the fetal circulation directly, advances in molecular genetic technology have greatly decreased the need for percutaneous umbilical blood sampling (PUBS) as well as for performing biopsy of tissues such as fetal muscle, skin or liver. PUBS has also frequently been used to obtain fetal blood for rapid karyotyping but again, the availability of FISH to detect the most common trisomies has decreased the need for this technique. Disorders such as hemophilia, hemoglobinopathies, immunodeficiencies, and diseases expressed in muscle, skin, and liver that have, in the past, required direct biochemical evaluation of fetal tissue can now commonly be detected through DNA mutation analysis on amniocytes or chorionic villi.

At present, PUBS is most commonly used in the evaluation and treatment of fetal isoimmunization, when a need for in utero transfusion is suspected. When this procedure is performed, it is done under continuous ultrasound guidance. The umbilical cord insertion into the placenta is identified; this is the optimal area for sampling because the cord is fixed at this location. The cord insertion into the fetus, or a free loop of cord can also be accessed, however, this may be more difficult owing to movement of the cord and fetus. The mother may be given parenteral sedation both for her

comfort and to decrease fetal movement. Intramuscular or intravascular injection of curare or Pavulon is also occasionally used to eliminate fetal movement, although the long-term effects of fetal paralysis are unknown.<sup>138,139</sup>

Once the optimal site for accessing the cord has been identified, the maternal abdomen is prepped and draped, and the insertion site is infiltrated with a local anesthetic. Under ultrasound guidance, a 20- or 22-gauge spinal needle is advanced into the umbilical vein. Samples of fetal blood are aspirated into heparinized syringes.

PGD is a prenatal testing technique whereby early embryos, conceived through IVF, undergo genetic testing while being cultured in vitro, before reimplantation in the uterus (Fig. 2-14). Only those embryos with normal results are transferred. This technique can be used to test for most genetic disorders in which a mutation has been identified, and can be helpful for couples at high risk of having a fetus affected by a genetic disease for whom termination of a fetus after CVS or amniocentesis is not an option. PGD is also used to select aneuploid embryos in couples with recurrent pregnancy failure suspected to be owing to recurrent aneuploidy, carriers of balanced translocations, and to optimize IVF efficiency especially in cases of recurrent IVF failure.<sup>140</sup> A surprisingly high percentage of embryos have been found to be aneuploid and/or mosaic in such cases, and it is not clear that biopsy of one or even two cells is

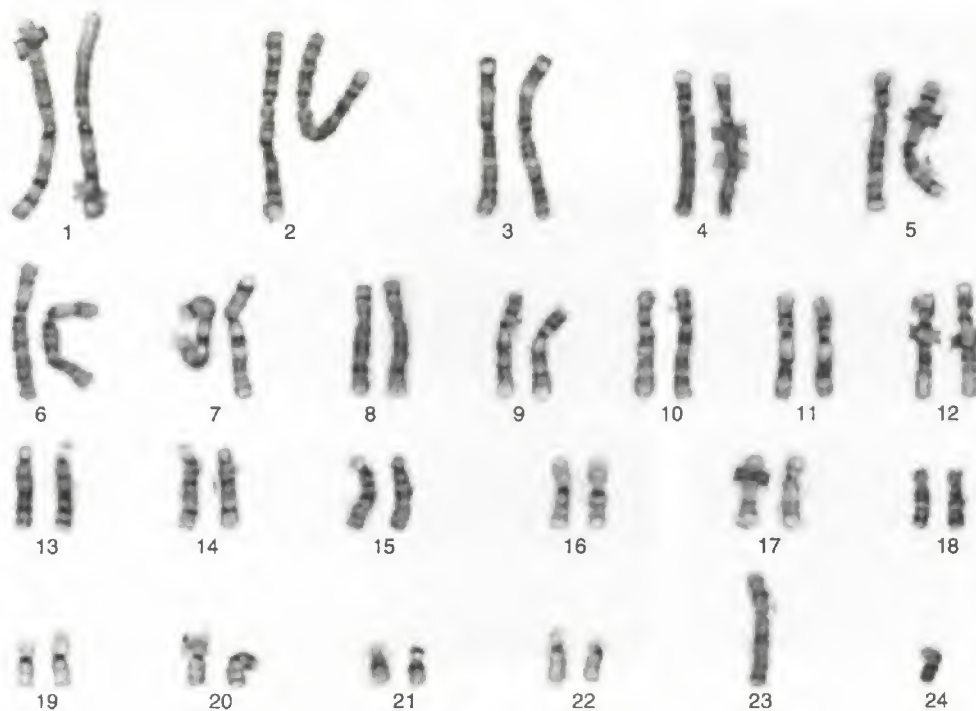


**FIGURE 2-15.** G-banded male karyotype.

indicative of the chromosomal make up of the entire embryo.<sup>141</sup> The utility of PGD for such cases has not been demonstrated in large controlled series.

Because the genetic testing done in cases of PGD must be performed using just one or two cells from these early embryos, with a very rapid turnaround time (generally less than 24 hours), the technique is complex and errors can occur. The rate of error is generally quoted as less than 5%,<sup>142</sup> and it is recommended that CVS or amniocentesis be used to confirm results from PGD. Again, large studies to determine the accuracy and efficacy of PGD are clearly needed.<sup>143</sup>

## PRENATAL TESTING FOR CONGENITAL MALFORMATIONS

Anomalies such as NTD, cleft lip and palate, and congenital heart defects usually occur as multifactorial traits, caused by an interaction of multiple genes with environmental factors. Because these disorders have an elevated risk of recurrence in families, prenatal testing is often requested. Owing to their complex genetic causes, congenital malformations cannot be identified by amniocentesis or CVS. In most cases, prenatal testing consists of detailed ultrasound evaluation aimed at the detection or elucidation of specific fetal birth defects.

As in all other areas of medicine, providing appropriate information and treatment relies on a correct diagnosis. In the prenatal diagnosis of congenital disorders, providing prognostic information or evaluating a possible recurrence in a future pregnancy relies first and foremost on ensuring the correct diagnosis of the original affected child (or other relative). Whereas many congenital malformations are isolated traits, they can also occur as part of a syndrome, in

which a pattern of malformations and features result from a single etiology. The etiology of a syndrome can involve an entire chromosome (that is, trisomy), deletion of a small chromosome region, or a single gene mutation. Often the other features of the syndrome cannot be detected by ultrasound, and therefore careful counseling of the family, as well as consideration of other testing, is important.

As an example, a congenital heart defect (CHD) identified on prenatal ultrasound is commonly an isolated finding. However, it may occur as part of a syndrome in which other abnormalities, such as mental retardation, are present. CHDs are heterogeneous in etiology, caused in some cases by a single gene or chromosomal mechanism, and in others by teratogens such as rubella infection or poorly controlled maternal diabetes. The cause in most cases is unknown, and the majority are believed to be multifactorial in origin. First-degree relatives have an increased recurrence risk of 2% to 4%. Prenatal ultrasound (echocardiography) is typically offered to couples with a strong family history or a previous fetus with CHD. In cases in which a CHD is unexpectedly detected by ultrasound, amniocentesis is offered to test for chromosome abnormalities, which underlie 10% to 15% of fetal CHD. Amniocentesis can also test for genetic abnormalities that increase the risk of CHD. For example, CHD is associated with a relatively common microdeletion on chromosome 22 (22q.11) that can be detected through the use of FISH on fetal tissue obtained by amniocentesis (Fig. 2-15). This microdeletion is associated with a spectrum of outcomes, including DiGeorge sequence and velocardiofacial syndrome. Chromosome abnormalities or deletions have important genetic counseling implications, because a child with such an abnormality typically has other physical and developmental problems, in addition to the heart defect.



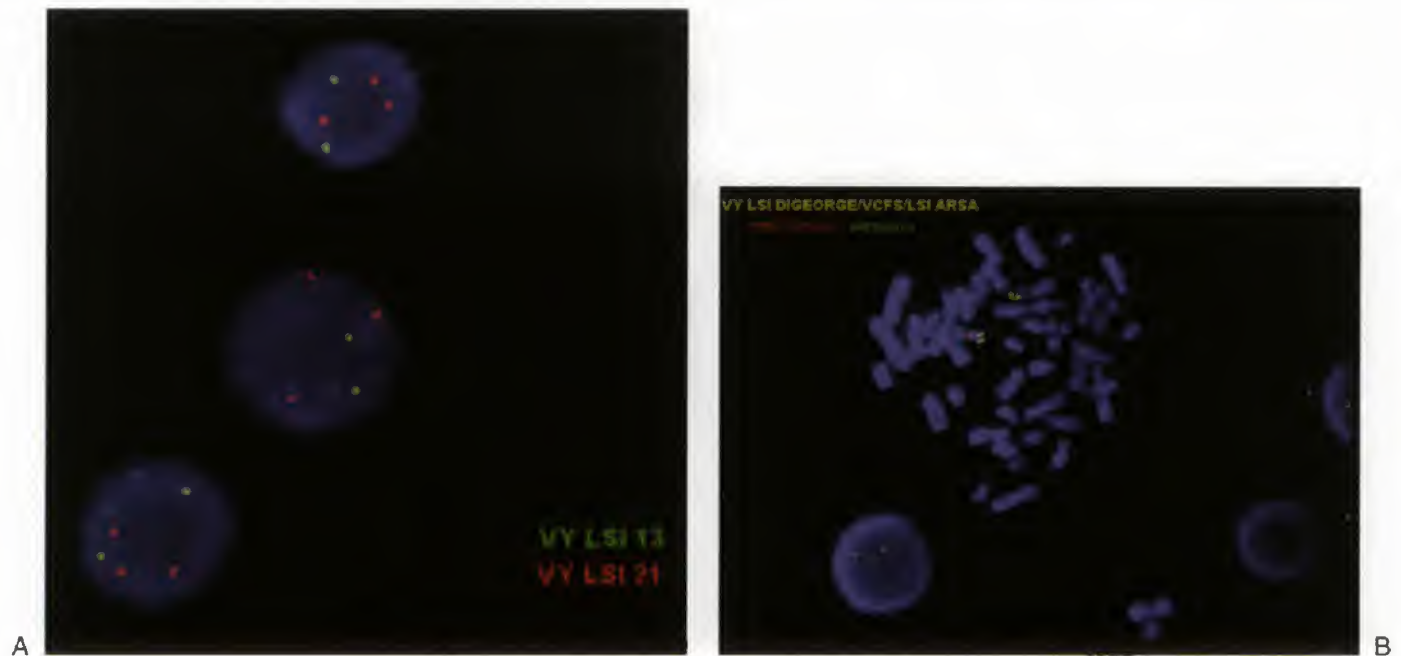


**FIGURE 2-16.** A. Fluorescence in situ hybridization in interphase cells. Probes to chromosome 21 (test) are red, and to chromosome 13 (control) are green. Presence of three red signals indicates the presence of trisomy 21. B. Fluorescence in situ hybridization in metaphase cell. Probes to chromosome 22q11 (test) are red, and to 22q13 (control) are green. Presence of a single red signal indicates a 22q11 deletion and the presence of DiGeorge syndrome.

## Techniques of Genetic Analysis

Over the past 2 decades, advances in genetics have included increases in our understanding of novel genetic mechanisms. Much of this increased understanding has come about because of improvements in genetic technology, allowing more detailed investigation of genes, mechanisms of mutation and genetic variation in the population. As these techniques are used and investigated, an increasing number of clinically available tests are offered, with more and more being applicable to and useful for evaluation of the fetus.

### Chromosome Identification

Standard prenatal diagnosis involves evaluation of the individual chromosomes making up the fetal karyotype. Giemsa staining, which produces a specific banding pattern called G banding, is the technique most widely used in clinical cytogenetics laboratories for chromosome analysis. Each chromosome stains in a characteristic pattern of light and dark bands (see Fig. 2-15). In an internationally accepted system of chromosome classification, the dark and light bands on each chromosome are numbered. This numbering system allows the location of any particular band and its involvement in any chromosome abnormality to be described unambiguously and precisely.

### Fluorescence In Situ Hybridization

FISH is a technique that allows visualization of a small chromosomal region, generally too small to be seen with karyotyping. FISH can also be used for rapid chromosome identification, because it can be performed on interphase

cells and, therefore, culturing is not required for analysis. FISH is carried out by using a small fragment of DNA (called a DNA probe) with the same nucleotide sequence as the stretch of chromosomal DNA of interest. The DNA probe is covalently attached to a fluorescent label, hybridized with metaphase, prophase or interphase chromosomes and then visualized under a fluorescence microscope. FISH is used to determine whether a small portion of a chromosome (too small to be seen on the karyotype) is deleted and to identify translocations and marker chromosomes. It is also used to identify pieces of chromosomal material that are too small or too ambiguous to be localized by banding techniques. Normally, a probe will hybridize in two places, reflecting the presence of two homologous chromosomes. If a probe from the chromosome segment in question hybridizes to only one of the patient's chromosomes, then the patient is likely to have a deletion on the other. Excess chromosomal material can also be detected with FISH, in which case the probe will hybridize in more than two places. As a rapid assessment for trisomy (or other aneuploidy), interphase cells can be analyzed with FISH probes that hybridize to centromeric regions of specific chromosomes, thereby allowing a fast count of the copy number of a specific chromosome (for example, 21 to rule out DS) (Fig. 2-16).

### Molecular Techniques for DNA Analysis

It is surprisingly easy to isolate pure DNA, which is generally very stable when compared with enzymes and other molecules. DNA can be extracted from any cell type that has a nucleus, including white blood cells, buccal cells, amniocytes, chorionic villi, and skin fibroblasts. The DNA is

essentially the same regardless of the tissue of origin. PCR can be used to amplify very small quantities of DNA, allowing small samples to be used for the detection of specific mutations.

Genetic mutations generally occur due to point mutations, deletions, or duplications. PCR and southern blotting are commonly used techniques for identification of genetic mutations in DNA samples. Automated techniques of DNA sequencing are also available; such sequencing was used to complete the human genome project in 2003. Use of sequencing in clinical practice is complicated by the potential for identification of previously undescribed mutations of uncertain clinical significance.

Whether a defect is a deletion or a point mutation, its identification allows a specific test to be applied to at-risk relatives or for prenatal diagnosis. In cases in which the condition has been mapped but the gene itself remains unknown, or a specific mutation has not been identified, linked DNA markers can be used in some cases to follow the gene through the family and compare affected and unaffected individuals. Such analysis is limited in its accuracy by the potential for recombination between the marker and the mutation, the potential for genetic heterogeneity, and the possibility that informative markers will not be identified in the family. With either direct mutation analysis or linkage, it is critical that firm proof of the diagnosis exists, and that the mutation identified is known to be causative. In addition, detection of a mutation in a person (or fetus) at risk does not make a diagnosis of a clinical disorder and all the previously described caveats are critical to accurate diagnosis and management of genetic disorders, particularly in the prenatal setting.

## FUTURE DIRECTIONS IN GENETIC ANALYSIS

### Quantitative Fluorescent PCR and Comparative Genomic Hybridization

Other new techniques for molecular evaluation of the genome, such as quantitative fluorescent PCR and comparative genomic hybridization (CGH), have been recently developed and introduced into clinical use. Such techniques are being increasingly used for prenatal evaluation of chromosomes and chromosome abnormalities in the fetus.<sup>145,146</sup> Quantitative fluorescent PCR (QF-PCR) assays are based on the amplification of DNA sequences unique for each chromosome pair and have been developed to establish the number of specific chromosomes present in a cell. These tests amplify small tandem repeat or microsatellite markers with quantification of the products. QF-PCR can quickly identify aneuploidy and is used in some centers as an alternative to FISH for the rapid prenatal detection of aneuploidies involving chromosomes 21, 18, and 13, and the sex chromosomes.<sup>147,148</sup>

CGH is a technique whereby DNA from a test subject is hybridized together with control DNA. Differential labeling of the test versus control DNA allows comparative analysis of copy number, thus screening for decrease or increase in copy number across the genome. CGH is now most commonly performed using microarrays, or slides to which

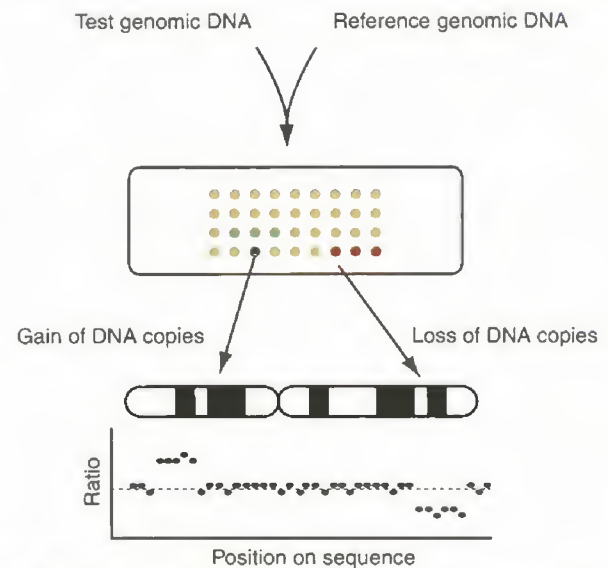


**FIGURE 2-17.** Array CGH technique. CGH, comparative genomic hybridization. DNA to be tested is labeled green, and control, reference DNA red. Labeled DNA is hybridized to a microarray contained hundreds to thousands of DNA clones, and copy number analyzed for each clone. The ratio of test to reference DNA at each clone is indicated on the graph. Increase in ratio of test DNA indicates duplication or trisomy, and decrease in ratio indicates deletion or monosomy for each clone.

the labeled control DNA has been applied. Test DNA is then hybridized and computer analysis done to identify ratios at each individual probe. In simplistic terms, array CGH provides the ability to perform multiple FISH analyses simultaneously. Originally developed primarily for use in cancer, array CGH has great utility in constitutional and prenatal cases, in which features suggest a chromosomal abnormality but are not specific enough to indicate a single FISH analysis (Figs. 2-17 and 2-18).<sup>149</sup>

### Free Fetal DNA

Whereas methods for analysis of intact fetal cells continue to improve, approaches to noninvasive methods of obtaining fetal samples continue to be pursued.<sup>150</sup> In 1998, Lo et al demonstrated that cell-free fetal DNA is present in plasma from healthy pregnant women.<sup>151</sup> Surprisingly high concentrations of fetal DNA, nearly 5% of total maternal DNA, were detected in plasma of pregnant women, using quantification through PCR. That cell-free fetal DNA is consistently detected in maternal blood during pregnancy raises diagnostic potential.<sup>152,153</sup>

Initial diagnostic application of cell-free DNA involved detection of fetuses that had inherited a mutant allele from an affected father. If the father has a DNA sequence that the mother lacks, presence of that sequence in maternal blood must be of fetal origin; thus, the fetus has inherited the mutant paternal allele. Detection of a paternally transmitted AD trait (that is, a fetus with hemoglobin Lepore disease) was reported initially by Camaschella et al.<sup>154</sup> Analysis of cell-free DNA has also been applied to managing Rh(D) isoimmunization. Presence of the *D* allele in maternal blood of Rh-negative women can be detected and has been used to



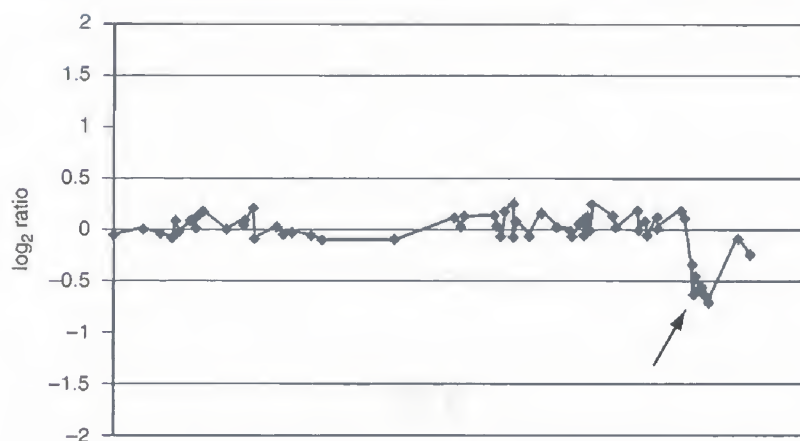


**FIGURE 2-18.** Array comparative genomic hybridization result demonstrating a deletion in chromosome 16q. A decrease in ratio indicated by the arrow is diagnostic of a deletion corresponding to several clones. The most distal clones are present, indicating that this is an interstitial deletion. Karyotype has reported a terminal deletion, and array comparative genomic hybridization was able to clarify the precise deletion more accurately.

determine whether the fetus has inherited the *D* allele from its father and is at risk for hemolytic disease.<sup>155–157</sup>

Analysis of cell-free fetal DNA has other clinical applications. Total cell-free fetal DNA levels are increased two-fold when the fetus has trisomy 21, even though the fetal DNA need not be derived from a gene locus on chromosome 21.<sup>158</sup> Cell-free fetal DNA could thus serve as an additional (and perhaps independent) maternal serum analyte for aneuploidy screening. Active investigation is ongoing into these and other noninvasive strategies for diagnosis and management of fetal disorders.<sup>155</sup>

## References

- Evans MI, Hume RF Jr, Johnson MP, et al: Integration of genetics and ultrasonography in prenatal diagnosis: Just looking is not enough. *Am J Obstet Gynecol* 174:1925, 1996.
- Heinonen OP, Sloane D, Shapiro S: Birth defects and drugs in pregnancy. Littleton, MA, Publishing Sciences Group, 1977.
- Carlson BM (ed): Human Embryology and Developmental Biology, 3rd ed. St. Louis, Mosby, 2004.
- Schardein JL: Chemically Induced Birth Defects, 2nd ed. New York, Marcel-Dekker, 1993, p 2.
- Zaragoza MV, Surti U, Redline RW, et al: Parental origin and phenotype of triploidy in spontaneous abortions: Predominance of diandry and association with the partial hydatidiform mole. *Am J Hum Genet* 66:1807, 2000.
- Redline RW, Hassold T, Zaragoza MV: Prevalence of the partial molar phenotype in triploidy of maternal and paternal origin. *Hum Pathol* 29:505, 1998.
- McFadden DE, Kalousek DK: Two different phenotypes of fetuses with chromosomal triploidy: Correlation with parental origin of the extra haploid set. *Am J Med Genet* 38:535, 1991.
- Yu S, Baker E, Hinton L, et al: Frequency of truly cryptic subtelomere abnormalities—a study of 534 patients and literature review. *Clin Genet* 68:436, 2005.
- Knight SJ, Regan R, Nicod A, et al: Subtle chromosomal rearrangements in children with unexplained mental retardation. *Lancet* 354:1676, 1999.
- Online Mendelian Inheritance in Man, OMIM (TM). McKusick-Nathans Institute for Genetic Medicine, Johns Hopkins University (Baltimore, MD) and National Center for Biotechnology Information, National Library of Medicine (Bethesda, MD), 7/9/2006. World Wide Web URL: <http://www.ncbi.nlm.nih.gov/omim/>.
- Harper PS (ed): Practical Genetic Counseling, 6th ed. London, Arnold Press, 2004.
- Ravine D, Gibson RN, Walker RG, et al: Evaluation of ultrasonographic diagnostic criteria for autosomal dominant polycystic kidney disease. *Lancet* 343:824, 1994.
- Allingham-Hawkins DJ, Babul-Hirji R, Chitayat D, et al: Fragile X premutation is a significant risk factor for premature ovarian failure: The International Collaborative POF in Fragile X study. Preliminary data. *Am J Med Genet* 83:322, 1999.
- Schwartz CE, Dean J, Howard-Peebles PN, et al: Obstetrical and gynecological complications in fragile X carriers: A multicenter study. *Am J Med Genet* 51:400, 1994.
- Allen C, Reardon W: Assisted reproduction technology and defects of genomic imprinting. *BJOG* 112:1589, 2005.
- Nussbaum RL, McInnes RR, Willard HF (eds): Thompson and Thompson Genetics in Medicine, 6th ed. Philadelphia: WB Saunders, 2001, p 306.
- Bradley LA, Palomaki GE, McDowell GA: ONTD Working Group; ACMG Laboratory Quality Assurance Committee. Technical standards and guidelines: prenatal screening for open neural tube defects. *Genet Med* 7:355, 2005.
- Gregg NM: Congenital cataract following German measles in the mother. 1941. *Aust N Z J Ophthalmol* 19:267, 1991.
- Fabro S, Scialli AR: Drug and chemical action in pregnancy. New York, Marcel-Dekker, 1986, p 239.
- Moore KL, Persaud TVN: The Developing Human: Clinically Oriented Embryology, 6th ed. Philadelphia: WB Saunders, 1998.
- Diav-Citrin O, Ornoy A: Adverse Environment and Prevention of Early Pregnancy Disorders. Early Pregnancy: Biology and Medicine (vol. 4), Cherry Hill, NJ, Sisp Publications, p 5, 2000.
- Prenatal Radiation Exposure: A Fact Sheet for Physicians (CDC): <http://www.bt.cdc.gov/radiation/prenatalphysician.asp>
- Schull WJ: Effects of Atomic Radiation, A Half-Century of Studies From Hiroshima and Nagasaki. New York: Wiley-Liss & Sons, 1995.
- Moretti ME, Bar-Oz B, Fried S, Koren G: Maternal hyperthermia and the risk for neural tube defects in offspring: Systematic review and meta-analysis. *Epidemiology* 16:216, 2005.
- Acs N, Banhid F, Puho EH, Czeizel AE: Acute respiratory infections during pregnancy and congenital abnormalities: a population-based case-control study. *Congenit Anom (Kyoto)* 46:86, 2006.
- Suarez L, Felkner M, Hendricks K: The effect of fever, febrile illnesses, and heat exposures on the risk of neural tube defects in a Texas-Mexico border population. *Birth Defects Res A Clin Mol Teratol* 70:815, 2004.
- Wender-Ozegowska E, Wroblewska K, Zawiejska A, et al: Threshold values of maternal blood glucose in early diabetic pregnancy—prediction of fetal malformations. *Acta Obstet Gynecol Scand* 84:17, 2005.
- Temple R, Aldridge V, Greenwood R, et al: Association between outcome of pregnancy and glycaemic control in early pregnancy in type 1 diabetes: population based study. *BMJ* 325:1275, 2002.
- Levy HL: Historical background for the maternal PKU syndrome. *Pediatrics* 112:1516, 2003.
- Kaback M: Population-based genetic screening for reproductive counseling: the Tay-Sachs disease model. *European Journal of Pediatrics* 159:S192, 2000.
- Kaback M, Lim-Steele J, Dabholkar D, et al: Tay-Sachs disease—Carrier screening, prenatal diagnosis, and the molecular era. *An*



- international perspective, 1970 to 1993. The International TSD Data Collection Network. *JAMA* 270:2307, 1993.
32. Committee on Genetics, American College of Obstetricians and Gynecologists. Committee Opinion. Number 325, December 2005. Update on carrier screening for cystic fibrosis. *Obstet Gynecol* 106:1465, 2005.
  33. Berlin BM, Norton ME, Sugarman EA, et al: Cystic fibrosis and chromosome abnormalities associated with echogenic fetal bowel. *Obstet Gynecol* 94:135, 1999.
  34. Scotet V, De Brackeleer M, Audrezet MP, et al: Prenatal detection of cystic fibrosis by ultrasonography: a retrospective study of more than 346,000 pregnancies. *J Med Genet* 39:443, 2002.
  35. Bosco AF, Norton ME, Lieberman E: Predicting the risk of cystic fibrosis with echogenic fetal bowel and one cystic fibrosis mutation. *Obstet Gynecol* 94:1020, 1999.
  36. Hodge SE, Lebo RV, Yesley AR, et al: Calculating posterior cystic fibrosis risk with echogenic bowel and one characterized cystic fibrosis mutation: avoiding pitfalls in the risk calculations. *Am J Med Genet* 82:329, 1999.
  37. Ogino S, Wilson RB, Grody WW: Bayesian risk assessment for autosomal recessive diseases: fetal echogenic bowel with one or no detectable CFTR mutation. *J Med Genet* 41:e70, 2004.
  38. Bergstrand CG, Czar B: Demonstration of a new protein fraction in serum from the human fetus. *Scand J Clin Lab* 8:174, 1956.
  39. Haddow JE: Prenatal screening for open neural tube defects, Down's syndrome, and other major fetal disorders. *Semin Perinatol* 14:488, 1990.
  40. Haddow JE, Knight GJ, Kloza EM: Relation between maternal weight and serum alpha-fetoprotein concentration during the second trimester. *Clin Chem* 27:133, 1981.
  41. Johnson AM: Racial differences in MSAFP screening. In Jizciewski GH, Porter IH (eds): *Alpha-Fetoprotein and Congenital Disorders*. New York: Academic Press, 1985.
  42. O'Brien JE, Drugan A, Chervenak F: Maternal serum alpha-fetoprotein screening: The need to use race/ethnic specific medians in Asians. *Fetal Diagn Ther* 8:367, 1993.
  43. Wald NJ, Cuckle HS, Boreham J, et al: Maternal serum alpha-fetoprotein and diabetes mellitus. *Br J Obstet Gynaecol* 86:101, 1979.
  44. Huttly W, Rudnicka A, Wald NJ: Second trimester prenatal screening markers for Down syndrome in women with insulin-dependent diabetes mellitus. *Prenat Diagn* 24:804, 2004.
  45. Lynch L, Berkowitz RL: Maternal serum alpha-fetoprotein and coagulation profiles after multifetal pregnancy reduction. *Am J Obstet Gynecol* 169:987, 1993.
  46. Evans MI, Harrison HH, O'Brien JE, et al: Correction for insulin-dependent diabetes in maternal serum alpha-fetoprotein testing has outlived its usefulness. *Am J Obstet Gynecol* 187:1084, 2002.
  47. Bradley LA, Palomaki GE, McDowell GA: ONTD Working Group; ACMG Laboratory Quality Assurance Committee. Technical standards and guidelines: prenatal screening for open neural tube defects. *Genet Med* 7:355, 2005.
  48. Baumgarten A, Reece EA, Davis N, et al: A reassessment of maternal serum alpha-fetoprotein in diabetic pregnancy. *Eur J Obstet Gynecol Reprod Biol* 28:289, 1988.
  49. Baumgarten A, Robinson J: Prospective study of an inverse relationship between maternal glycosylated hemoglobin and serum alpha-fetoprotein concentrations in pregnant women with diabetes. *Am J Obstet Gynecol* 159:77, 1988.
  50. Palomaki GE, Knight GJ, Haddow JE, et al: Cigarette-smoking and levels of maternal serum alpha-fetoprotein, unconjugated estriol, and hCG: Impact on Down syndrome screening. *Obstet Gynecol* 81:675, 1993.
  51. Rudnicka AR, Wald NJ, Huttly W, Hackshaw AK: Influence of maternal smoking on the birth prevalence of Down syndrome and on second trimester screening performance. *Prenat Diagn* 22:893, 2002.
  52. Muller F, Dreux S, Lemeur A, et al: Medically assisted reproduction and second-trimester maternal serum marker screening for Down syndrome. *Prenat Diagn* 23:1073, 2003.
  53. Lambert-Messerlian G, Dugoff L, Vidaver J, et al: First- and second-trimester Down syndrome screening markers in pregnancies achieved through assisted reproductive technologies (ART): a FASTER trial study. *Prenat Diagn* 26:672, 2006.
  54. Nadel AS, Green JK, Holmes LB, et al: Absence of need for amniocentesis in patients with elevated levels of maternal serum alpha-fetoprotein and normal ultrasonographic examinations. *N Engl J Med* 323:557, 1990.
  55. Norem CT, Schoen EJ, Walton DL, et al: Routine ultrasonography compared with maternal serum alpha-fetoprotein for neural tube defect screening. *Obstet Gynecol* 106:747, 2005.
  56. Wald N, Cuckle H, Nanchahal K: Amniotic fluid acetylcholinesterase measurement in the prenatal diagnosis of open neural tube defects. Second report of the Collaborative Acetylcholinesterase Study. *Prenat Diagn* 9:813, 1989.
  57. Milunsky A, Sapirstein VS: Prenatal diagnosis of open neural tube defects using the amniotic fluid acetylcholinesterase assay. *Obstet Gynecol* 59:1, 1982.
  58. Mirlesse V, Duguy N, Cynober E, et al: Alphafoetoprotein and acetylcholinesterase in amniotic fluid as a factor suggesting fetal skin and nerve lesions in a case of congenital varicella syndrome. *Prenat Diagn* 24:498, 2004.
  59. Kelly JC, Petrocik E, Wassman ER: Amniotic fluid acetylcholinesterase ratios in prenatal diagnosis of fetal abnormalities. *Am J Obstet Gynecol* 161:703, 1989.
  60. Drugan A, Snyer FN, Greb A, et al: Amniotic fluid alpha-fetoprotein and acetylcholinesterase in early genetic amniocentesis. *Obstet Gynecol* 72:35, 1988.
  61. Nadel AS, Norton ME, Wilkins-Haug L: Cost-effectiveness of strategies used in the evaluation of pregnancies complicated by elevated maternal serum alpha-fetoprotein levels. *Obstet Gynecol* 89:660, 1997.
  62. Feuchtbaum LB, Cunningham G, Waller DK, et al: Fetal karyotyping for chromosome abnormalities after unexplained maternal serum alpha-fetoprotein screening. *Obstet Gynecol* 86:248, 1995.
  63. Megerian G, Godmilow L, Donnemfeld A: Ultrasound-adjusted risk and spectrum of fetal chromosomal abnormality in women with elevated maternal serum alpha-fetoprotein. *Obstet Gynecol* 85:952, 1995.
  64. Ryyanen M, Seppala M, Kuusela P, et al: Antenatal screening for congenital nephrosis in Finland by maternal serum alpha-fetoprotein. *Br J Obstet Gynaecol* 90:437, 1983.
  65. Kallinen J, Heinonen S, Ryyanen M, et al: Antenatal genetic screening for congenital nephrosis. *Prenat Diagn* 21:81, 2001.
  66. Crandall BF, Matsumoto M: Risks associated with an elevated amniotic fluid alpha-fetoprotein level. *Am J Med Genet* 39:64, 1991.
  67. Wenstrom KD, Owen J, Davis RO, et al: Prognostic significance of unexplained elevated amniotic fluid alpha-fetoprotein. *Obstet Gynecol* 87:213, 1996.
  68. Wald NJ, Cuckle HS: Biochemical screening. In Brock DJH, Rodeck CH, Ferguson-Smith MA (eds): *Prenatal Diagnosis and Screening*. Edinburgh, Churchill Livingstone, 1992, p 556.
  69. Merkatz IR, Nitowsky HM, Macri JN, et al: An association between low maternal serum alpha-fetoprotein and fetal chromosome abnormalities. *Am J Obstet Gynecol* 148:886, 1984.
  70. Cuckle HS, Wald NJ, Lindenbaum RH: Cord serum alpha-fetoprotein and Down syndrome. *Br J Obstet Gynaecol* 93:407, 1986.
  71. Wald NJ, Cuckle HS, Densem JW, et al: Maternal serum screening for Down syndrome in early pregnancy. *Br Med J* 297:297, 1988.
  72. Jorgensen PL, Trolle D: Low urinary oestriol excretion during pregnancy in women giving birth to infants with Down syndrome. *Lancet* 2:782, 1972.
  73. Bogart MH, Pandian MR, Jones OW: Abnormal maternal serum chorionic gonadotropin levels in pregnancies with fetal chromosome abnormalities. *Prenat Diagn* 7:623, 1987.
  74. Lambert-Messerlian GM, Canick JA, Palomaki GE, et al: Second trimester levels of maternal serum inhibin A, total inhibin, alpha inhibin precursor, and activin in Down syndrome pregnancy. *J Med Screening* 3:58, 1996.
  75. Wallace EM, Swanston IA, McNeilly AS, et al: Second trimester screening for Down syndrome using maternal serum dimeric inhibin A. *Clin Endocrinol* 44:17, 1996.
  76. Malone FD, Canick JA, Ball RH, et al: First- and second-trimester evaluation of risk (FASTER) research consortium. First-trimester or second-trimester screening, or both, for Down's syndrome. *N Engl J Med* 353:2001, 2005.
  77. Knight GJ, Palomaki GE, Haddow JE, et al: Maternal serum levels of placental products hCG, hPL, Sp1 and progesterone are all elevated in cases of fetal Down syndrome. *Am J Hum Genet* 45:A263, 1989.
  78. Canick JA, MacRae AR: Second trimester serum markers. *Semin Perinatol* 29:203, 2005.
  79. Knight GJ, Palomaki GE: Epidemiologic monitoring of prenatal screening for neural tube defects and Down syndrome. *Clin Lab Med* 23:531, 2003.



80. Palomaki GE, Knight CJ, Haddow JE, et al: Prospective trial of a screening protocol to identify trisomy 18 using maternal serum alpha-fetoprotein, unconjugated estriol, and human chorionic gonadotropin. *Prenat Diagn* 49(suppl):227, 1991.
81. Bush MC, Malone FD: Down syndrome screening in twins. *Clin Perinatol* 32:373-86, 2005.
82. Neveux LM, Palomaki GE, Knight CJ, Haddow JE: Multiple marker screening for Down syndrome in twin pregnancies. *Prenat Diagn* 16:29, 1996.
83. Cuckle H: Down's syndrome screening in twins. *J Med Screen* 5:3, 1998.
84. Savva GM, Morris JK, Mutton DE, Alberman E: Maternal age-specific fetal loss rates in Down syndrome pregnancies. *Prenat Diagn* 26:499, 2006.
85. Antonarakis SE: Parental origin of the extra chromosome in trisomy 21 as indicated by analysis of DNA polymorphisms. *Down Syndrome Collaborative Group. N Engl J Med* 324:872, 1991.
86. Kuppermann M, Nease RF, Learman LA, et al: Procedure-related miscarriages and Down syndrome-affected births: implications for prenatal testing based on women's preferences. *Obstet Gynecol* 96:511, 2000.
87. Benn PA, Fang M, Egan JF: Trends in the use of second trimester maternal serum screening from 1991 to 2003. *Genet Med* 7:328, 2005.
88. Ferguson-Smith M, Aitken D, Arbuzova S, et al: Down syndrome screening: a position statement from the scientific committee of the international Down syndrome screening group, 2004. Available at <http://www.leeds.ac.uk/idsg/position%20statement.htm>.
89. Robinson L, Grau P, Crandall BF: Pregnancy outcomes after increasing levels of maternal serum alpha-fetoprotein. *Obstet Gynecol* 74:17, 1989.
90. Zelop C, Nadel AS, Frigoletto F, et al: Placenta accreta, percreta and increta: A cause of increased maternal serum alpha-fetoprotein. *Obstet Gynecol* 80:693, 1992.
91. Heinonen S, Ryyanen M, Kirkinen P, et al: Uterine malformation: A cause of elevated maternal serum alpha-fetoprotein concentrations. *Prenat Diagn* 16:635, 1996.
92. Palacio M, Jauniaux E, Kingdom J, et al: Perinatal outcome in pregnancies with a positive serum screening for Down's syndrome due to elevated levels of free beta-human chorionic gonadotropin. *Ultrasound Obstet Gynecol* 13:58, 1999.
93. Lepage N, Chitayat D, Kingdom J, Huang T: Association between second-trimester isolated high maternal serum maternal serum human chorionic gonadotropin levels and obstetric complications in singleton and twin pregnancies. *Am J Obstet Gynecol* 188:1354, 2003.
94. Onderoglu LS, Kabukcu A: Elevated second trimester human chorionic gonadotropin level associated with adverse pregnancy outcome. *Int J Gynaecol Obstet* 56:245, 1997.
95. Duric K, Skrablin S, Lesin J, et al: Second trimester total human chorionic gonadotropin, alpha-fetoprotein and unconjugated estriol in predicting pregnancy complications other than fetal aneuploidy. *Eur J Obstet Gynecol Reprod Biol* 110:12, 2003.
96. Dugoff L, Hobbins JC, Malone FD, et al: FASTER Trial Research Consortium. Quad screen as a predictor of adverse pregnancy outcome. *Obstet Gynecol* 106:260, 2005.
97. Chandra S, Scott H, Dodds L, et al: Unexplained elevated maternal serum alpha-fetoprotein and/or human chorionic gonadotropin and the risk of adverse outcomes. *Am J Obstet Gynecol* 189:775, 2003.
98. Ilagan JC, Stamilio DM, Ural SH, et al: Abnormal multiple marker screens are associated with adverse perinatal outcomes in cases of intrauterine growth restriction. *Am J Obstet Gynecol* 191:1465, 2004.
99. Spencer K: Second-trimester prenatal screening for Down syndrome and the relationship of maternal serum biochemical markers to pregnancy complications with adverse outcome. *Prenat Diagn* 20:652, 2000.
100. Kowalczyk TD, Cabaniss ML, Cusmano L: Association of low unconjugated estriol in the second trimester and adverse pregnancy outcome. *Obstet Gynecol* 91:396, 1998.
101. Kelley RI: Inborn errors of cholesterol biosynthesis. *Adv Pediatr* 47:1, 2000.
102. Kratz LE, Kelley RI: Prenatal diagnosis of the RSH/Smith-Lemli-Opitz syndrome. *Am J Med Genet* 82:376, 1999.
103. Palomaki GE, Bradley LA, Knight CJ, et al: Assigning risk for Smith-Lemli-Opitz syndrome as part of second trimester screening for Down's syndrome. *J Med Screen* 9:43, 2002.
104. Craig WY, Haddow JE, Palomaki GE, et al: Identifying Smith-Lemli-Opitz syndrome in conjunction with prenatal screening for Down syndrome. *Prenat Diagn* 26:842, 2006.
105. Shinawi M, Szabo S, Popek E, et al: Recognition of Smith-Lemli-Opitz syndrome (RSH) in the fetus: utility of ultrasonography and biochemical analysis in pregnancies with low maternal serum estriol. *Am J Med Genet* 138:56, 2005.
106. Schoen E, Norem C, O'Keefe J, et al: Maternal serum unconjugated estriol as a predictor for Smith-Lemli-Opitz syndrome and other fetal conditions. *Obstet Gynecol* 102:167, 2003.
107. Kashork CD, Sutton VR, Fonda Allen JS, et al: Low or absent unconjugated estriol in pregnancy: an indicator for steroid sulfatase deficiency detectable by fluorescence in situ hybridization and biochemical analysis. *Prenat Diagn* 22:1028, 2002.
108. Bradley LA, Canick JA, Palomaki GE, Haddow JE: Undetectable maternal serum unconjugated estriol levels in the second trimester: risk of perinatal complications associated with placental sulfatase deficiency. *Am J Obstet Gynecol* 176:531, 1997.
109. Seeds JW: Diagnostic mid-trimester amniocentesis: How safe? *Am J Obstet Gynecol* 191:607, 2004.
110. Tabor A, Philip J, Madsen M, et al: Randomised controlled trial of genetic amniocentesis in 4606 low-risk women. *Lancet* 1:1287, 1986.
111. Simpson JL: Choosing the best prenatal screening protocol. *N Engl J Med* 353:2068, 2005.
112. Caughey AB, Hopkins LH, Norton ME: Chorionic villus sampling compared with amniocentesis and the difference in the rate of pregnancy loss. *Obstet Gynecol* 108:612, 2006.
113. Fuchs F: Volume of amniotic fluid at various stages of pregnancy. *Clin Obstet Gynecol* 9:449, 1966.
114. The Canadian Early and Mid-trimester Amniocentesis Trial (CEMAT) Group: Randomised trial to assess safety and fetal outcome of early and midtrimester amniocentesis. *Lancet* 351:242, 1998.
115. Rhoads GG, Jackson LG, Schlesselman SE, et al: The safety and efficacy of chorionic villus sampling for early prenatal diagnosis of cytogenetic abnormalities. *N Engl J Med* 320:609, 1989.
116. Canadian Collaborative CVS-Amniocentesis Clinical Trial Group: Multicentre randomised clinical trial of chorion villus sampling and amniocentesis. First report. *Lancet* 1:1, 1989.
117. Wijnberger LD, van der Schouw YT, Christiaens GC: Learning in medicine: Chorionic villus sampling. *Prenat Diagn* 20:241, 2000.
118. Robinson WP, Barrett IJ, Bernard L, et al: Meiotic origin of trisomy in confined placental mosaicism is correlated with presence of fetal uniparental disomy, high levels of trisomy in trophoblast, and increased risk of fetal intrauterine growth restriction. *Am J Hum Genet* 60:917, 1997.
119. Phillips OP, Tharapel AT, Lerner JL, et al: Risk of fetal mosaicism when placental mosaicism is diagnosed by chorionic villus sampling. *Am J Obstet Gynecol* 174:850, 1996.
120. Goldberg JD, Wohlferd MM: Incidence and outcome of chromosomal mosaicism found at the time of chorionic villus sampling. *Am J Obstet Gynecol* 176:1349, 1997.
121. Firth HV, Boyd PA, Chamberlain P, et al: Severe limb abnormalities after chorion villus sampling at 56-66 days' gestation. *Lancet* 1:762, 1991.
122. Hsieh FJ, Shyu MK, Sheu BC, et al: Limb defects after chorionic villus sampling. *Obstet Gynecol* 85:84, 1995.
123. Froster UG, Jackson L: Limb defects and chorionic villus sampling: Results from an international registry, 1992-94. *Lancet* 347:489, 1996.
124. Rodis JF, Egan JGX, Craffey A, et al: Calculated risk of chromosomal abnormalities in twin gestations. *Obstet Gynecol* 76:1037, 1990.
125. Brambati B, Tului L, Guerclena S, Alberti E: Ultrasound outcome of first-trimester chorionic villus sampling for genetic investigation in multiple pregnancy. *Obstet Gynecol* 17:209, 2001.
126. McEnerney JK, McEnerney LN: Unfavorable neonatal outcome after intraamniotic injection of methylene blue. *Obstet Gynecol* 35:61, 1983.
127. Van der Pol JC, Wolf H, Boer K, et al: Jejunal atresia related to the use of methylene blue in genetic amniocentesis in twins. *Br J Obstet Gynaecol* 99:141, 1992.
128. Kidd SA, Lancaster PA, Anderson JC, et al: Fetal death after exposure to methylene blue dye during mid-trimester amniocentesis in twin pregnancy. *Prenat Diagn* 16:39, 1996.
129. Bahado-Singh R, Schmitt R, Hobbins JC: New technique for genetic amniocentesis in twins. *Obstet Gynecol* 79:304, 1992.

130. Gilbert WM, Davis SE, Kaplan C, et al: Morbidity associated with prenatal disruption of the dividing membrane in twin gestations. *Obstet Gynecol* 78:623, 1991.
131. Rochon M, Stone J: Invasive procedures in multiple gestations. *Curr Opin Obstet Gynecol* 15:167, 2003.
132. Yaron Y, Bryant-Greenwood PK, Dave N, et al: Multifetal pregnancy reductions of triplets to twins: Comparison with nonreduced triplets and twins. *Am J Obstet Gynecol* 180:1268, 1999.
133. De Cate L, Liebaers I, Foulon W: Outcome of twin gestations after first-trimester chorionic villus sampling. *Obstet Gynecol* 96:714, 2000.
134. Brambati B, Tului L, Guercilena S, Alberti E: Outcome of first-trimester chorionic villus sampling for genetic investigation in multiple pregnancy. *Ultrasound Obstet Gynecol* 17:209, 2001.
135. Antsaklis A, Souka AP, Daskalakis G, et al: Second-trimester amniocentesis vs. chorionic villus sampling for prenatal diagnosis in multiple gestations. *Ultrasound Obstet Gynecol* 20:476, 2002.
136. Evans MI, Goldberg JD, Horenstein J, et al: Selective termination for structural, chromosomal and mendelian anomalies: International experience. *Am J Obstet Gynecol* 181:893, 1999.
137. Eddleman KD, Stone JL, Lynch L, Berkowitz RL: Selective termination of anomalous fetuses in multifetal pregnancies: Two hundred cases at a single center. *Am J Obstet Gynecol* 187:1168, 2002.
138. De Crespigny LC, Robinson HP, Quinn M, et al: Ultrasound-guided fetal blood transfusion for severe rhesus isoimmunization. *Obstet Gynecol* 66:529, 1985.
139. Seeds JW, Bowes WA: Ultrasound-guided fetal intravascular transfusion in severe rhesus isoimmunization. *Am J Obstet Gynecol* 154:1105, 1986.
140. Munne S, Fischer J, Warner A, et al: Preimplantation genetic diagnosis significantly reduces pregnancy loss in infertile couples: A multicenter study. *Fertil Steril* 85:326, 2006.
141. Li M, DeUgarte CM, Surrey M, et al: Fluorescence in situ hybridization reanalysis of day-6 human blastocysts diagnosed with aneuploidy on day 3. *Fertil Steril* 84:1395, 2005.
142. Ray PF, Ao A, Taylor DM, et al: Assessment of the reliability of single blastomere analysis for preimplantation diagnosis of the delta F508 deletion causing cystic fibrosis in clinical practice. *Prenat Diagn* 18:1402, 1998.
143. Baruch S, Adamson GD, Cohen J, et al: Genetic testing of embryos: A critical need for data. *Reprod Biomed Online* 11:667, 2005.
144. Pertl B, Yau SC, Sherlock J, et al: Rapid molecular method for prenatal detection of Down's syndrome. *Lancet* 343:1197, 1994.
145. Pertl B, Kopp S, Kroisel PM, et al: Quantitative fluorescent PCR for the rapid prenatal detection of common aneuploidies and fetal sex. *Am J Obstet Gynecol* 177:899, 1997.
146. Pertl B, Kopp S, Kroisel PM, et al: Rapid detection of chromosome aneuploidies by quantitative fluorescence PCR: First application on 247 chorionic villus samples. *J Med Genet* 36:300, 1999.
147. Oehshorn Y, Bar-Shira A, Jonish A, Yaron Y: Rapid prenatal diagnosis of aneuploidy for chromosomes 21, 18, 13, and X by quantitative fluorescence polymerase chain reaction. *Fetal Diagn Ther* 21:326, 2006.
148. Cirigliano V, Voglino G, Adinolfi M: Non-invasive screening and rapid QF-PCR assay can greatly reduce the need for conventional cytogenetic analyses in prenatal diagnosis. *Reprod Biomed Online* 11:671, 2005.
149. Rickman L, Fiegler H, Carter NP, Bobrow M: Prenatal diagnosis by array-CGH. *Eur J Med Genet* 48:232, 2005.
150. Bianchi DW, Simpson JL, Jackson LG, et al: National Institute of Child Health and Development Fetal Cell Isolation Study. Fetal gender and aneuploidy detection using fetal cells in maternal blood: Analysis of NIFTY I data. *Prenat Diagn* 22:609, 2002.
151. Lo YM, Hjelm NM, Fidler C, et al: Prenatal diagnosis of fetal RhD status by molecular analysis of maternal plasma. *N Engl J Med* 339:1734, 1998.
152. Lo YM, Tein MS, Lau TK, et al: Quantitative analysis of fetal DNA in maternal plasma and serum: implications for noninvasive prenatal diagnosis. *Am J Hum Genet* 62:768, 1998.
153. Bischoff FZ, Sinacori MK, Dang DD, et al: Cell-free fetal DNA and intact fetal cells in maternal blood circulation: Implications for first- and second-trimester noninvasive prenatal diagnosis. *Hum Reprod Update* 8:493, 2002.
154. Camaschella C, Alfarano A, Gottardi E, et al: Prenatal diagnosis of fetal hemoglobin Lepore-Boston disease on maternal peripheral blood. *Blood* 75:2102, 1990.
155. Bianchi DW, Avent ND, Costa JM, van der Schoot CE: Noninvasive prenatal diagnosis of fetal Rhesus D: Ready for Prime(r) Time. *Obstet Gynecol* 106:841, 2005.
156. Van der Schoot CE, Soussan AA, Koclewijn J, et al: Noninvasive antenatal RHD typing. *Transfus Clin Biol* 13:53, 2006.
157. Finning K, Martin P, Daniels G: A clinical service in the UK to predict fetal Rh (Rhesus) D blood group using free fetal DNA in maternal plasma. *Ann N Y Acad Sci* 1022:119, 2004.
158. Lo YM, Lau TK, Zhang J, et al: Increased fetal DNA concentrations in the plasma of pregnant women carrying fetuses with trisomy 21. *Clin Chem* 45:1747, 1999.
159. Jacobs PA, Browne C, Gregson N, Joyce C, White H: Estimates of the frequency of chromosome abnormalities detectable in unselected newborns using moderate levels of banding. *J Med Genet* 29:103, 1992.



## FIRST TRIMESTER SCREENING FOR ANEUPLOIDY

Fergal D. Malone, MD, FACOG, FRCPI

### Fetal Nuchal Translucency

### Nuchal Translucency Screening for Down Syndrome

### Combined First Trimester Testing: Nuchal Translucency with Serum Markers

### Enlarged Nuchal Translucency and Cystic Hygroma in the First Trimester

### Nasal Bone Sonography in the First Trimester

### First Trimester Ductus Venosus Sonography

### First Trimester Tricuspid Regurgitation Evaluation

### Nuchal Translucency Screening in Multiple Gestations

### Implementing Nuchal Translucency-based Screening into General Clinical Practice

#### Nuchal Translucency Quality Control

#### Nuchal Translucency Interpretation

#### Implications for Second Trimester Serum Screening

#### Implications for Second Trimester Ultrasound

#### Availability of Early Prenatal Diagnosis

#### Choosing the Correct Combination of Screening Tests

At present, the ideal time to screen for fetal aneuploidy is during the first trimester of pregnancy. This is a marked change in screening policy due to the significant advances which have been made in antenatal screening for fetal chromosomal abnormalities over the past 20 years. In the past, invasive prenatal diagnosis for Down syndrome with amniocentesis or chorionic villus sampling (CVS) was offered only to women of advanced maternal age (older than 35 years of age at delivery) or those who previously had an affected child. Subsequently, invasive diagnosis was offered to women younger than 35 years of age who had abnormal second trimester multiple-marker serum screening and also to those with abnormal second trimester sonographic signs—so-called soft-markers—of Down syndrome. It should be noted that the most efficient multiple-marker screening test in the second trimester is the “quad” screen, comprising alpha-fetoprotein (AFP), human chorionic gonadotropin (hCG), unconjugated estriol ( $E_3$ ), and inhibin-A (Table 3-1). This approach yields sensitivity for Down syndrome of up to 81%, when sonographic dating is used, for a 5% false-positive rate.<sup>1,2</sup>

However, since the early 1990s, great interest has been directed toward first trimester screening with the use of sonographic and serum screening markers. In a recent survey of perinatologists in the United States, 46% used nuchal translucency sonography and 27% used the serum markers PAPP-A and hCG during the first trimester to screen for Down syndrome (Table 3-2).<sup>3</sup> With the advent of national training programs for nuchal translucency sonography and with the endorsement of many national professional bodies, it is likely that first trimester based screening programs for Down syndrome will become dominant, with only those patients presenting too late for this form of screening being offered second trimester tests.

## FETAL NUCHAL TRANSLUCENCY

The single most powerful marker available today for differentiating Down syndrome from euploid pregnancies is the first trimester sonographic measurement of the fetal

**Table 3-1**

**Pattern of Results Seen With Expanded AFP Screening in Fetal Disorders Used in the Second Trimester**

	AFP	$uE_3$	hCG	Inhibin A
Open NTD	↑↑	No Change	No Change	No Change
Down syndrome	↓↓	↓	↑	↑
Trisomy 18	↓	↓	↓	No Change

AFP, alpha-fetoprotein; hCG, human chorionic gonadotropin; NTD, neural tube defect;  $uE_3$ , unconjugated estriol.

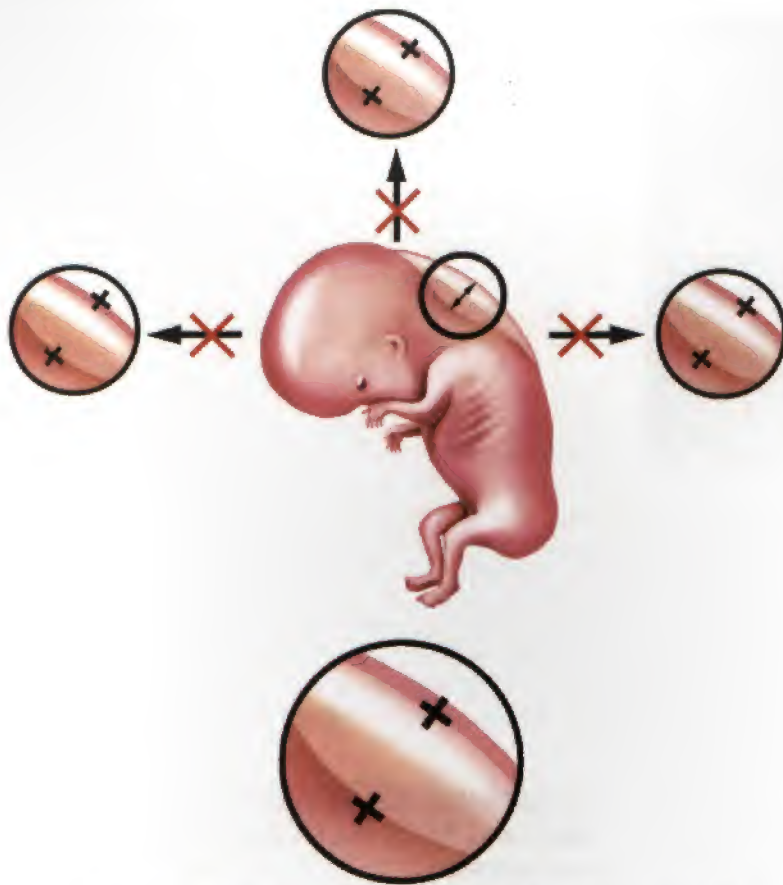
**Table 3-2**

**Nuchal Translucency and Serum Markers Used in First Trimester Screening and their Associations**

Possible Condition	First Trimester Marker		
	NT	PAPP-A	f-βhCG
Trisomy 21	Increased	Low	High
Trisomy 18	Increased	Low	Low
Pregnancy loss <24 weeks	Increased	Very Low	Very Low
Congenital heart defect	Increased	Normal	Normal

NT, nuchal translucency; PAPP-A, pregnancy-associated plasma protein A; f-βhCG, free β human chorionic gonadotropin.

A



## Conventional Measurement

B



**FIGURE 3-1.** A. Conventional measurement for determining the nuchal translucency. Although this illustration demonstrates the recommended placement of the measurement calipers, many investigators use an 'inner to inner' measurement. (Illustration by James A. Cooper, MD, San Diego, CA.) B. Optimizing the technique for first trimester nuchal translucency sonography: Nuchal translucency measurement in a normal fetus at 12 weeks' gestation. Components of a good sonographic screening protocol are evident, including adequate image magnification, mid-sagittal plane, neutral fetal neck position, correct caliper placement. Arrow, amnion.

nuchal translucency space. Nuchal translucency refers to the normal subcutaneous fluid-filled space between the back of the fetal neck and the overlying skin (Fig. 3-1). Normally, this space is small; however, in many fetuses with Down syndrome, this space can be significantly increased (Fig. 3-2). By adhering to a standard ultrasonographic technique, it is

possible to obtain accurate measurements of this area in the vast majority of fetuses between 10 and 14 weeks' gestation (CRL of 36–84 mm). When performing nuchal translucency sonography, it is absolutely essential to ensure optimal technique, which can be attained by focusing on the following criteria<sup>4</sup>:





**FIGURE 3-2.** Increased nuchal translucency measurement of 3.7 mm in a fetus at 12 weeks' gestation with Down syndrome.

- The fetus should be imaged in the midsagittal plane, ideally with the fetal spine down.
- The image should be adequately magnified so that only the fetal head, neck, and upper thorax fill the viewable area.
- The fetal neck should be neutral, with care being taken to avoid measurements in the hyperflexed or hyperextended positions.
- The skin at the fetal back should be clearly differentiated from the underlying amniotic membrane, either by visualizing separate echogenic lines or by noting that the skin line moves with the fetus.
- Measurement calipers should be placed on the inner borders of the echolucent space and should be perpendicular to the long axis of the fetus (see Fig. 3-1).
- Ultrasound and transducer settings should be optimized to ensure clarity of the image and of the borders of the nuchal space in particular. This may require transvaginal sonography in certain situations.

There is a direct correlation between increasing nuchal translucency measurement and risk for Down syndrome, other aneuploidies, major structural malformations, and adverse pregnancy outcome.<sup>1,2,7</sup> Possible causes for the development of this increased fluid-filled space include cardiac failure secondary to structural malformation, abnormalities in the extracellular matrix, and abnormal or delayed development of the lymphatic system.<sup>6,7</sup>

## NUCHAL TRANSLUCENCY SCREENING FOR DOWN SYNDROME

Nuchal translucency sonography is the most powerful marker for general population screening for Down syndrome.<sup>8</sup> The largest study of this form of screening was performed by the Fetal Medicine Foundation based in London.<sup>9</sup> This prospective study of 96,127 unselected patients at 22 centers required nuchal translucency sonography to be performed between 10 and 14 weeks' gestation by specially trained sonographers who used a standardized technique.

The overall Down syndrome detection rate was 77% detection rate, for a 5% false-positive rate.<sup>9</sup> Another large prospective study from the United Kingdom that evaluated the role of nuchal translucency sonography in general population screening was the SURUSS Trial.<sup>2</sup> A total of 39,983 patients had nuchal translucency sonography obtained between 10 and 14 weeks' gestation, and the Down syndrome detection rate was 63%, for a 5% false-positive rate. A large US-based screening program which focused on a more high-risk group of patients (The BUN Trial) revealed a Down syndrome detection rate of 69%, for a 5% false-positive rate, after screening 8216 patients.<sup>10</sup>

The largest prospective trial of all forms of Down syndrome screening yet performed, the FASTER Trial, has also validated the important role of nuchal translucency sonography. This was a multicenter prospective study from 15 centers in the United States in which 36,306 patients from the general population had first trimester nuchal translucency sonography performed.<sup>1</sup> The detection rate for nuchal translucency with maternal age ranged from 70% to 64% at 11 and 13 weeks' gestation respectively, for a 5% false-positive rate.<sup>1</sup> These large studies from varied centers and geographic locations confirm that nuchal translucency sonography must be a key component of first trimester screening programs for fetal Down syndrome.

## COMBINED FIRST TRIMESTER TESTING: NUCHAL TRANSLUCENCY WITH SERUM MARKERS

Together with the clear role of nuchal translucency sonography, research in first trimester screening has consistently shown that pregnancies with fetal Down syndrome are associated with altered levels of certain maternal serum markers, including elevated levels of total hCG and of the free  $\beta$  subunit of hCG (with a median multiple of the median [MoM] of 1.83 in affected cases) and lower levels of pregnancy-associated plasma protein A (with a median MoM of 0.38 in affected cases) (Table 3-2).<sup>11,12</sup> Studies of the combination of free  $\beta$  subunit of hCG, pregnancy-associated plasma protein A, and maternal age uniformly demonstrate a sensitivity for Down syndrome of approximately 60% with a 5% false-positive rate.<sup>12</sup>

These first trimester serum markers are largely independent of nuchal translucency, which has resulted in the development of a combined serum and sonographic screening protocol which would be more effective for screening than either alone. Two large prospective studies have now been published from the United States validating the performance of such combined first trimester screening. The BUN study evaluated 8216 patients and demonstrated a Down syndrome detection rate of 79%, at a 5% false-positive rate, or 64% at a 1% false-positive rate.<sup>10</sup> The FASTER study evaluated 38,033 patients and demonstrated even better Down syndrome detection rates, and showed that performance varied significantly by gestational age.<sup>1</sup> For a 5% false-positive rate, the Down syndrome detection rates using combined serum and sonographic screening were 87%, 85%, and 82% at 11, 12, and 13 weeks' gestation, respectively. For a 1% false-positive rate, the Down syndrome detection rates were 73%, 72%, and 67% at 11, 12, and 13 weeks' gestation respectively.<sup>1</sup>

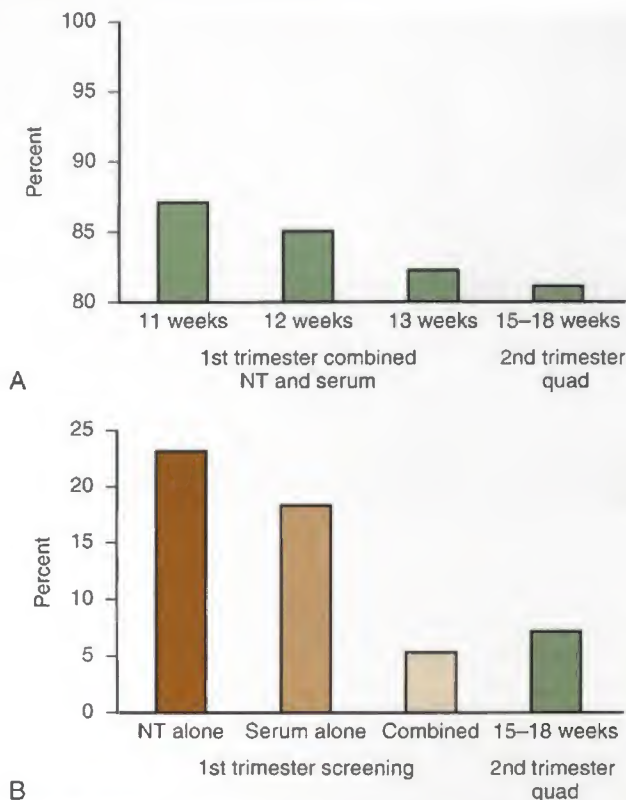


**FIGURE 3-3.** A. Comparison of first- and second trimester screening for Down syndrome: Detection rates of combined first trimester screening at 11, 12, and 13 weeks' gestation, compared with first trimester quad marker serum screening performed at 15 to 18 weeks' gestation (each at 5% false-positive rate). B. Comparison of first- and second trimester screening for Down syndrome: False-positive rates of first trimester nuchal translucency alone, PAPP-A and fβhCG alone, and first trimester combined screening at 12 weeks' gestation, compared with second trimester quad marker serum screening performed at 15 to 18 weeks' gestation (each for 85% detection rate). (Data from Malone FD, Canick JA, Ball RH, et al: A comparison of first-trimester screening, second-trimester screening, and the combination of both for evaluation of risk for Down syndrome. *N Engl J Med* 353:2001, 2005.)

Recently, much debate has occurred regarding the relative performance of these newer first trimester screening programs, compared with the more traditional second trimester serum screening approaches. Previously it has been difficult for clinicians to objectively compare screening programs that occur at different gestational ages because of the differences in aneuploidy prevalence. It is now possible to evaluate objective comparative data upon which the range of screening tests currently available can be directly compared.<sup>1,2</sup> Figure 3-3 summarizes the comparative performance of the various screening options from the FASTER Trial, and demonstrates that first trimester combined screening has very similar performance to second trimester quad marker serum screening.<sup>1</sup> Only when performed at 11 weeks' gestation does first-trimester combined screening have a significantly better performance than second trimester Quad marker serum screening (87% versus 81% Down syndrome detection, respectively, at a 5% false-positive rate). Additionally, the combined first trimester screening test has the lowest false-positive rate, compared with either first trimester component used alone or compared with second trimester serum

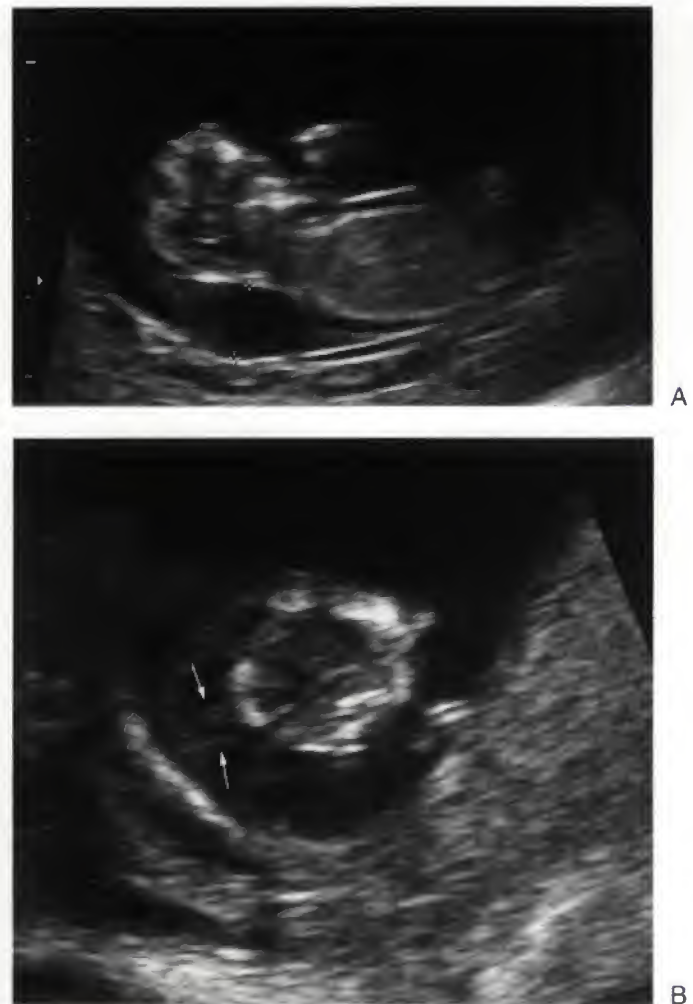


**FIGURE 3-4.** A. Septated cystic hygroma at 12 weeks' gestation: midsagittal sonographic view of a fetus with septated cystic hygroma, demonstrating increased nuchal translucency space (calipers) extending along the entire length of the fetus. B. Septated cystic hygroma at 12 weeks' gestation: transverse view through the fetal neck of the same fetus demonstrating obvious septations (arrows).

screening. It is also important to realize that only the combination of first trimester nuchal translucency sonography with first trimester serum markers comes close to the performance of second trimester quad marker serum screening. Nuchal translucency alone, without being combined with serum markers, has significantly inferior performance characteristics.<sup>1</sup>

### ENLARGED NUCHAL TRANSLUCENCY AND CYSTIC HYGROMA IN THE FIRST TRIMESTER

It is now clear that a subset of fetuses with very large nuchal translucency measurements that have an extremely high risk of fetal aneuploidy or other adverse pregnancy outcomes can be effectively identified in the first trimester. This finding has been described as septated cystic hygroma, and is present when the nuchal translucency space is enlarged extending along the entire length of the fetus, and in which septations are clearly visible (Fig. 3-4).<sup>12</sup> Septated cystic hygroma is



seen in more than one in 300 first trimester pregnancies. In a recent prospective study of routine first trimester sonographic screening, septated cystic hygroma was shown to have a 50% chance of being associated with fetal aneuploidy, with most cases being Down syndrome, as well as cases of Turner syndrome and Trisomy 18.<sup>12</sup> Additionally, among cystic hygroma cases confirmed as being euploid, approximately 50% had a major structural fetal malformation, with most cases including cardiac malformations, as well as other malformations such as skeletal dysplasias. When compared with simple increased nuchal translucency, septated cystic hygroma cases were five times more likely to be aneuploid, 12 times more likely to have cardiac malformations, and six times more likely to result in fetal or neonatal demise.<sup>12</sup>

The practical benefit of being able to counsel patients in the first trimester following the identification of septated cystic hygroma is that there is no need to delay decision making while awaiting serum marker results or using computerized risk calculation algorithms. When faced with a 50% chance of fetal aneuploidy, it is reasonable to offer such patients the immediate option of CVS, and if fetal aneuploidy has been excluded, a detailed fetal anatomic evaluation, including fetal echocardiography, should be performed at 18 to 20 weeks' gestation.<sup>12</sup>

Debate has also occurred regarding the differentiation between septated cystic hygroma and simple enlarged nuchal translucency, with some investigators believing that they are both part of a spectrum of a similar sonographic feature.<sup>13</sup> However, the FASTER Trial, a prospective study of over 38,000 pregnancies, has also now demonstrated that whenever a simple nuchal translucency measurement of 3.0 mm or greater is noted, CVS should be offered immediately because of a minimum risk of aneuploidy of 1 in 6.<sup>14</sup> With such nuchal translucency measurements, there is no role for delaying decision making while awaiting serum marker results, because such additional information does not meaningfully alter the original aneuploidy risk. This finding, therefore, suggests that debating the presence or absence of septations in cases of enlarged nuchal translucency is a moot point, because the risk of aneuploidy either when a nuchal translucency measurement of 3.0 mm or greater is noted, or when a septated cystic hygroma is noted, is sufficiently high to warrant immediate diagnostic testing.<sup>14</sup>

## NASAL BONE SONOGRAPHY IN THE FIRST TRIMESTER

There appears to be a clear association between the absence of the fetal nasal bones on first trimester ultrasound examination and Down syndrome.<sup>15</sup> In a study conducted by Cicero et al,<sup>15</sup> 701 fetuses with increased nuchal translucency were evaluated for the presence or absence of the nose bones during first trimester ultrasonography. The fetal nasal bones could not be visualized in 73% of Down syndrome fetuses (43 of 59) and in only 0.5% of unaffected fetuses (three of 603). The authors also felt that the absence of the fetal nose bone was not related to nuchal translucency thickness and therefore could be combined into a single ultrasound screening modality, with a predicted sensitivity of 85% for a 1% false-positive rate.<sup>15</sup> This study was subsequently expanded to a larger series of 3829 high-risk



**FIGURE 3-5.** First trimester ultrasound examination of a fetus at 13 weeks' gestation, with normal nasal bones. Features of good nasal bone imaging technique are evident, including midsagittal plane, fetal profile facing upward, adequate magnification, and visualization of two parallel lines at the level of the fetal nose, one representing fetal skin (small arrow) and the deeper line representing nasal bones (large arrow).

first trimester pregnancies, in which the detection rate for Down syndrome using absent nasal bones was 67%, for a 2.8% false-positive rate.<sup>16</sup>

Adequate imaging of the fetal nasal bones can be technically challenging in the first trimester, and careful attention to correct technique should, therefore, be paid to ensure consistency in technique. The nasal bones should be visualized on ultrasound along the midsagittal plane with a perfect fetal profile. The fetal spine should be posterior, with slight neck flexion. Two echogenic lines at the fetal nose profile should be visualized; the superficial echogenic line is the nasal skin, and the deeper echogenic line represents the nasal bones. This deeper echogenic line representing the nasal bones should be more echolucent at its distal end (Fig. 3-5). Care should be taken not to perform this evaluation with the ultrasound beam parallel to the plane of the nasal bones, because this might erroneously lead to the conclusion of absent nasal bones.

Although several other studies evaluating the role of first trimester nasal bone sonography as a screening test for fetal Down syndrome have also been published, all were limited by being derived from high-risk patient populations or lacking adequate pregnancy outcome ascertainment.<sup>17</sup> The largest study of first trimester fetal nasal bone sonography published to date, and in which an unselected general patient population has been evaluated, did not confirm a useful role for this form of screening.<sup>17</sup> In a prospective study of 6324 patients having nasal bone sonography by trained and experienced sonographers, adequate views of the fetal profile were obtained in only 76% of cases, and none of the 11 cases of fetal Down syndrome were found to have absent nasal bones.<sup>17</sup> Two further studies of the role of first trimester nasal bone sonography as a screening tool in the general population have also recently been published, and have confirmed these findings that there is only a limited role of this form of screening.<sup>18,19</sup> One study screened 7116 unselected patients from the general population including 12 cases of



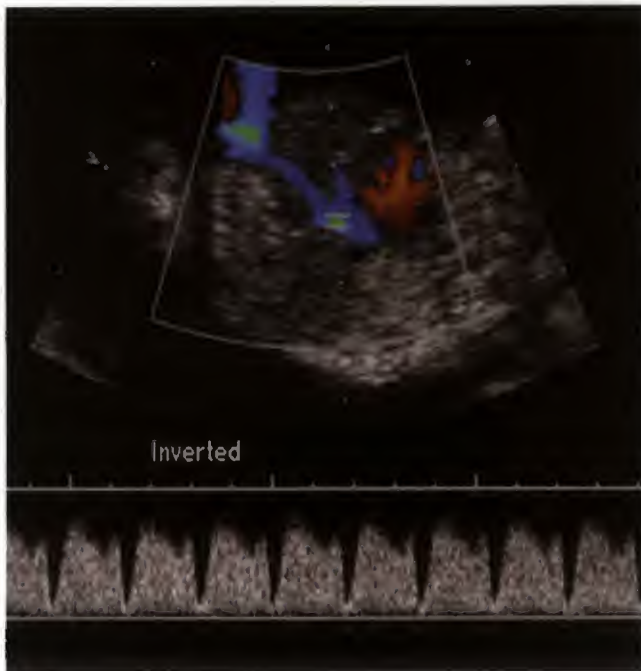


**FIGURE 3-6.** Pulsed-Doppler sonography image of a normal ductus venosus waveform at 12 weeks' gestation. Of note, the ductus venosus can be identified using color flow as a small vessel with turbulent flow. The nadir of flow during the "a" wave remains forward flowing (arrow).

Down syndrome, and screened a further 510 high risk patients including 23 cases of Down syndrome.<sup>18</sup> Absent nasal bones in the first trimester was noted in only 17% of cases in the general population and in 48% of cases in the high-risk population. A further study screened 1800 consecutive patients from the general population, and absent nasal bones was noted in only two of seven (29%) of Down syndrome cases.<sup>19</sup>

Although it is possible that there may be a role for first trimester fetal nasal bone sonography in the hands of select experts as a second-line screening tool in high risk patients, current data would suggest that this form of sonography should not be used as a general population screening tool.

### FIRST TRIMESTER DUCTUS VENOSUS SONOGRAPHY

First trimester Doppler sonographic evaluation of ductus venosus blood flow has been described as an adjunctive test for fetal aneuploidy screening. Forward triphasic pulsatile ductus venosus flow, as illustrated in Figure 3-6, is normal, whereas reversed flow at the time of the atrial contraction has been associated with aneuploidy and fetal cardiac malformations.<sup>20</sup> In a series of early studies date evaluating this association, between 59% and 93% of aneuploid fetuses had abnormal first trimester ductus venosus flow velocities.<sup>8</sup> Abnormal ductus venosus flow velocities were also found in as few as 3% or as many as 21% of normal fetuses. It may, therefore, be possible that fetal ductus venosus flow velocity waveform analysis may be useful to modify a patient's final risk for aneuploidy following completion of the nuchal translucency measurement. This could be used to either improve the detection rate or alternatively to reduce the false-positive rate.



**FIGURE 3-7.** First trimester sonographic evaluation for tricuspid regurgitation in a fetus at 11 weeks' gestation. Note the pulsed-Doppler gate placed across the tricuspid valve, with the angle to the direction of flow close to zero. There is no regurgitation greater than 60 cm/sec.

Although it appears that there is some association between abnormal ductus venosus flow studies and aneuploidy in the first trimester, there are several pitfalls that must be considered. The ductus venosus vessel itself may be as small as 2 mm at 10 to 14 weeks, making it difficult to obtain accurate flow velocity waveforms from such a tiny vessel without contamination of the waveform from neighboring vessels. For example, if the Doppler gate is placed too proximally near the umbilical sinus, the normal continuous venous flow from the umbilical vein may obscure absence of flow during the atrial contraction in the ductus venosus. Alternatively, placement of the Doppler gate too far distally, near the insertion of the ductus venosus into the inferior vena cava, may lead to the erroneous diagnosis of reversal of flow at the atrial contraction, as such reversal of flow is commonly seen in the inferior vena cava. The current consensus appears to be that first trimester ductus venosus Doppler flow studies should be performed only as a secondary screening test in the hands of experienced sonologists at referral centers, either to modify the final risk for aneuploidy or to help predict the prognosis of fetuses with normal chromosomes and an increased nuchal translucency measurement.<sup>21,22</sup>

### FIRST TRIMESTER TRICUSPID REGURGITATION EVALUATION

An association has been suggested between fetal aneuploidy and abnormal tricuspid regurgitation noted during first trimester sonography.<sup>22</sup> To perform this assessment, the fetus should be oriented so that the chest wall is anterior and the fetal heart should be insonated parallel to the ventricular septum. A pulsed-Doppler gate of approximately 3-mm is then placed across the tricuspid valve, with care to ensure that the angle to the direction of flow is as close to zero as possible (Fig. 3-7). Significant tricuspid regurgitation is



considered to be present if a regurgitant jet of at least 60 cm/sec is noted extending to over half of systole.<sup>23</sup>

In a series of 1557 high-risk pregnancies at 11 to 13 weeks' gestation, significant tricuspid regurgitation was noted in only 4% of chromosomally normal fetuses, but was present in 77 of 114 cases (68%) of Down syndrome and 14 of 42 cases (33%) of trisomy 18.<sup>23</sup> These investigators were able to obtain adequate Doppler waveforms of the tricuspid valve in 99% of cases and there was low interobserver variability of measurements.

Although these data are encouraging regarding an association between first trimester tricuspid regurgitation and chromosomal abnormalities, like ductus venosus assessment, it is unclear whether this form of screening will have any role in general population screening. Extrapolation of the results of a screening test from a high-risk population, performed in the hands of experts, to implementation in the general population will likely overstate the true performance of the test. It is likely that first trimester sonography for tricuspid regurgitation may have a role as a second line test, following an initial high-risk nuchal translucency and serum screen. In this setting, it may have a role in reducing the false-positive rate of screening. In one series of 75,821 first trimester pregnancies, addition of tricuspid regurgitation as a second line screening test following nuchal translucency and serum screening resulted in a Down syndrome detection rate of 92% for a false-positive rate of only 2.7%.<sup>22</sup>

## NUCHAL TRANSLUCENCY SCREENING IN MULTIPLE GESTATIONS

The prenatal risk assessment of Down syndrome in multiple gestation pregnancies has been limited before the advent of nuchal translucency-based screening. Maternal serum screening has not been widely used in the setting of multiple gestations because of the potential for discordancy between twins and the impact of different placentas on the various analytes. Nuchal translucency measurements are broadly similar between singleton and twin pregnancies, implying that the Down syndrome detection rates should be similar. The false-positive rate of nuchal translucency screening might be higher in monochorionic twins because some complications unique to monochorionic gestations, such as twin-to-twin transfusion syndrome, might present with increased nuchal translucency measurement.<sup>24</sup>

Options for first trimester screening for Down syndrome therefore include providing either a fetus-specific risk based on nuchal translucency alone, or providing an overall pregnancy risk based on combined serum and sonographic markers. In one series of 448 twin pregnancies, nuchal translucency yielded an 88% detection rate for a 7% false-positive rate.<sup>24</sup> In another series of 206 twin pregnancies screened using nuchal translucency and first trimester serum markers, the Down syndrome detection rate was estimated to be approximately 75% for a 5% false-positive rate.<sup>25</sup> To provide a pregnancy specific risk in twins, a likelihood ratio is calculated for each fetus' nuchal translucency measurement, these two likelihood ratios are then added together, and this is then multiplied by the biochemistry likelihood ratio to provide a final "pseudorisk" calculation.<sup>26</sup> Although additional research on the efficacy of this combined first-trimester screening in multiple gestations is still needed,

nuchal translucency measurement should at least represent an improvement over serum screening in multiple gestations. At present, some centers use nuchal translucency sonography to assist in selecting fetuses for reduction in higher-order multiple gestations.

## IMPLEMENTING NUCHAL TRANSLUCENCY-BASED SCREENING INTO GENERAL CLINICAL PRACTICE

Nuchal translucency sonography has pushed prenatal screening for Down syndrome and other aneuploidies into the first trimester. This has the potential of providing major advantages for patients, such as earlier reassurance when results are normal or safer pregnancy termination if abnormal results are found. However, there are several practical issues that must be resolved before all obstetric providers should consider implementing this form of screening into routine obstetric practice.<sup>27</sup>

### Nuchal Translucency Quality Control

The extent of quality control measures among earlier studies of nuchal translucency screening likely accounts for the large inconsistencies in quoted Down syndrome detection rates.<sup>8</sup> Nuchal translucency ultrasound is extremely operator dependent and will be a poor technique for general population screening if strict guidelines and ongoing quality control systems are not maintained.<sup>28</sup> In one multicenter study in which adequate training and quality control were not addressed, the overall sensitivity for Down syndrome was only 31%.<sup>28</sup> Appropriate training, adherence to a standard technique, and experience are key to its success as a reliable screening tool.

Initial training in nuchal translucency sonography, however, is only one element of the quality control needed to optimize this technique. Systems must also be put in place at each local ultrasound practice to ensure that ongoing quality assurance is maintained. The optimal method of ensuring adequate nuchal translucency quality control at a population level will likely be to track individual sonographers' median nuchal translucency measurements and standard deviations over time. This quality assurance technique has the advantage of being easier to standardize and automate, thereby being more practical for national screening. In the United Kingdom and other countries internationally, the Fetal Medicine Foundation ([www.fetalmedicine.com](http://www.fetalmedicine.com)) has an established system of credentialing of sonologists, together with ongoing audit of measurements. In the United States, the Society for Maternal Fetal Medicine ([www.ntqr.org](http://www.ntqr.org)) has developed a similar system for initial training and interacts with sonologists and laboratory providers to maintain an ongoing nuchal translucency quality review program.

### Nuchal Translucency Interpretation

Mean nuchal translucency measurements increase by approximately 15% to 20% each week from 10 to 14 weeks' gestation.<sup>1,2,29</sup> Therefore, it is inappropriate to use a single millimeter cutoff to define a normal nuchal translucency or a pregnancy that is normal. More appropriate options include using the 95th percentile for a particular gestational age or



multiples of the median (MoMs). Unfortunately, calculation of such cutoff values require a software program to adequately integrate other background data, such as maternal age and maternal serum marker results, into the risk assessment.

Additionally, it is still unclear whether it is valid to use generic population medians to interpret nuchal translucency measurements or whether such medians for risk calculations should be center-specific or sonographer-specific. In the recently completed SURUSS trial from the United Kingdom, the use of sonographer-specific medians resulted in an improvement of 5% in overall Down syndrome detection rates, compared with use of center-specific medians.<sup>2</sup> In another study that addressed the importance of differences in center-specific medians, a Scottish trial of 15 centers evaluating 17,229 patients had individual center nuchal translucency median MoMs ranging from 0.7 to 1.4 MoMs.<sup>30</sup> Ideally, the median MoM should be 1.0. The consequences of such large variability in MoMs between centers on the actual risks quoted to individual patients could be dramatic.

### **Implications for Second Trimester Serum Screening**

Implementing a national nuchal translucency screening program in isolation will likely have a negative impact on current second trimester serum screening programs, because the positive predictive value of second trimester screening might be reduced as much as sixfold after first trimester screening.<sup>27</sup> The number of fetuses with Down syndrome still alive during the second trimester will be significantly reduced because many such fetuses will have already been diagnosed in the first trimester. Sequential screening without appropriate modifications of second trimester serum marker cutoffs will increase the overall false-positive rate, resulting in an increased number of amniocenteses and procedure-related pregnancy losses.<sup>1</sup>

### **Implications for Second Trimester Ultrasound**

Nuchal translucency screening will not obviate the need for second trimester ultrasound for the detection of structural fetal abnormalities. The "genetic sonogram," which evaluates for structural malformations and a range of second trimester soft markers for aneuploidy, such as short femurs, echogenic bowel, echogenic intracardiac foci, and increased nuchal fold, has gained widespread acceptability. A national policy of first trimester screening will likely have a negative impact on the performance of the "genetic sonogram." The positive predictive value of these ultrasonographic soft markers for aneuploidy will decrease because the number of aneuploid fetuses entering the second trimester will be reduced. At present, it is not known what the relevance of these soft markers will be in a population of fetuses that has already undergone nuchal translucency-based screening. If the "genetic sonogram" continues without allowance for the lower prevalence of second trimester aneuploid fetuses, it is likely that more unnecessary amniocenteses will be performed without significant improvement in detection rates. The best way to incorporate the "genetic sonogram" into a

practice in which first trimester screening has already been performed is to rely on likelihood ratios. If a soft marker for Down syndrome is seen at a second trimester ultrasound examination, the appropriate likelihood ratio for that marker should be multiplied by the final Down syndrome risk quoted from first trimester screening, rather than multiplying by the maternal age-related risk.

### **Availability of Early Prenatal Diagnosis**

One of the most compelling arguments in favor of nuchal translucency-based screening for Down syndrome is the shift to earlier diagnosis through CVS at 10 to 13 weeks' gestation. CVS is not as widely available as amniocentesis on a national basis.<sup>3</sup> Early amniocentesis in the first trimester is no longer considered an acceptable alternative to CVS owing to its higher association with fetal loss, fetal clubfoot, and procedure failure.<sup>31</sup> If first trimester screen-positive patients do not have ready access to CVS, they might experience increased anxiety, waiting 3 to 4 weeks for an opportunity to undergo amniocentesis at 15 weeks. Therefore, a policy of first trimester screening for aneuploidy should not be implemented unless first trimester diagnosis with CVS is locally available. If a patient desires the benefit of first trimester screening but CVS is not easily available, then the optimal approach might be to provide the first trimester result at 16 weeks as part of a single integrated screening result in combination with second trimester serum markers.<sup>2,27</sup>

### **Choosing the Correct Combination of Screening Tests**

With the increasing range of Down syndrome screening tests available to obstetric providers today, there is a need for accurate comparative data to evaluate the best combination of tests to implement into practice. The comparative performance of each type of Down syndrome screening has recently been described in the FASTER Trial.<sup>1</sup> These results have shown that the most inefficient test, associated with the highest screen-positive rate, is nuchal translucency sonography performed on its own. First trimester screening seems to derive much of its efficiency by combining nuchal translucency with pregnancy-associated plasma protein A and free  $\beta$  subunit of hCG evaluation. An integrated screen, incorporating nuchal translucency and pregnancy-associated plasma protein A in the first trimester, together with AFP, hCG, unconjugated E<sub>3</sub>, and inhibin-A in the second trimester, seems to be the single most efficient test. In a center without easy access to high-quality nuchal translucency sonography, another reasonable alternative might be a serum-only test, incorporating pregnancy-associated plasma protein A in the first trimester with AFP, hCG, unconjugated E<sub>3</sub>, and inhibin-A in the second trimester, with a single risk being quoted.

It is unlikely that a single screening test will be suitable for all practitioners and their patients. The decision as to which screening test to incorporate into local clinical practice will be based on factors such as gestational age at presentation, availability of high-quality nuchal translucency sonography, and availability of first trimester invasive testing with CVS (Fig. 3–8). Some patients might be most interested in the



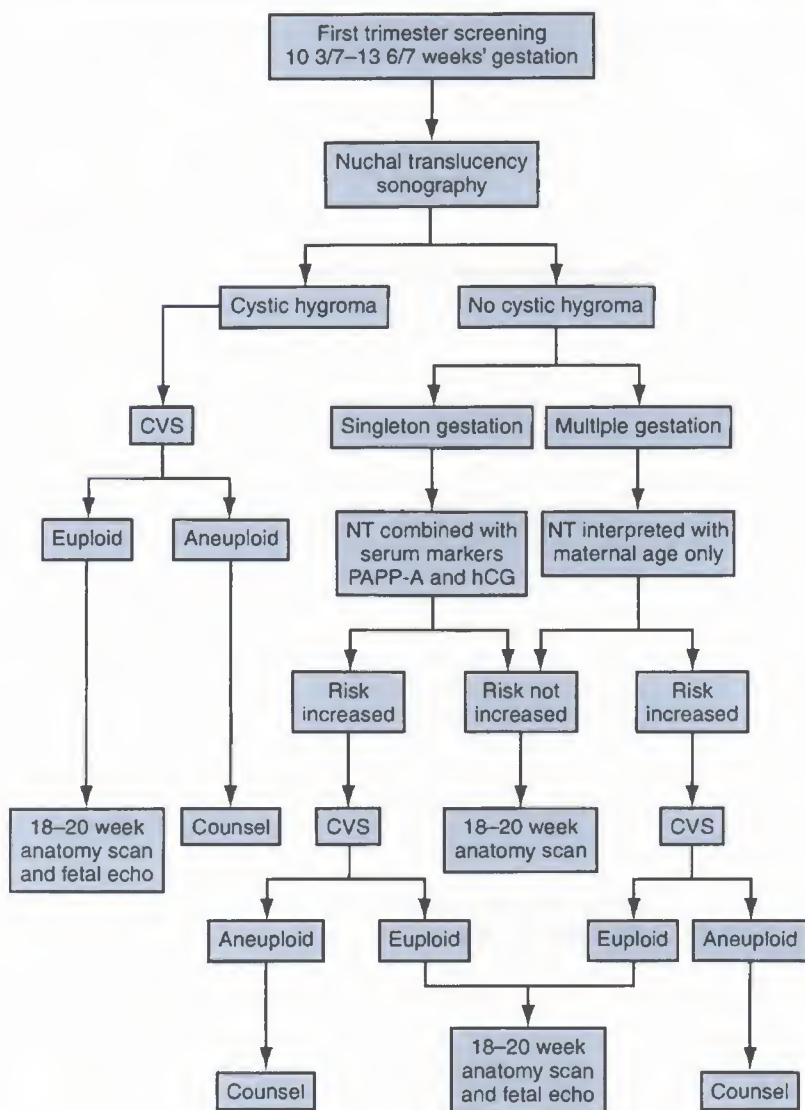


**FIGURE 3–8.** Flow diagram demonstrating screening decision options during the first trimester.

earliest possible screening result; for such patients, combined first trimester nuchal translucency and serum screening might be desired. Other patients might be more interested in the most efficient test, maximizing their detection rate and minimizing the need for amniocentesis; for such patients, a single integrated screen result combining first- and second trimester approaches might be desired. Still other patients might not present for care sufficiently early to take advantage of first trimester screening; for these patients, there should be the option of second trimester serum screening and genetic sonography.

Future directions in Down syndrome screening may also use more sophisticated combinations of tests.<sup>27</sup> Stepwise sequential screening involves providing a risk result after first trimester combined screening. High-risk patients undergo diagnostic testing using CVS, whereas lower risk patients return at 15 weeks' gestation for further screening, such as the second trimester quad serum markers, and have the option of then undergoing amniocentesis. These latter tests however are interpreted using the first trimester marker results to ensure the most accurate risk estimation and to

minimize the overall false-positive rate. Another option may be contingency screening, which involves categorizing patients into three groups after first trimester combined screening. Patients with very high-risk results, such as one in 30 or higher for example, undergo diagnostic testing using CVS, whereas patients with very low-risk results, such as one in 1500 or lower, are reassured and have no further testing. Intermediate patients with risks between these two cutoffs return at 15 weeks' gestation for second trimester quad serum markers. Again, these latter tests however must be interpreted using the first trimester marker results to ensure accuracy of risk estimation and to minimize the overall false-positive rate. Initial models have suggested that such a contingency screening program could yield detection rates as high as 95% for a 5% false-positive rate, but with only 15% of patients needing to return in the second trimester for further tests.<sup>32</sup>

Informed consent regarding this large variety of prenatal screening options for aneuploidy should be an integral part of the screening process itself. Because of the complexity of choices regarding the different screening options, and

because of the range of abnormal outcomes associated with increased nuchal translucency, it will be vital to provide all patients with pretest genetic counseling before embarking on screening.

## References

- Malone FD, Canick JA, Ball RH, et al: A comparison of first-trimester screening, second-trimester screening, and the combination of both for evaluation of risk for down syndrome. *N Engl J Med* 353:2001, 2005.
- Wald NJ, Rodeck C, Hackshaw AK, et al: First- and second-trimester antenatal screening for Down's syndrome: The results of the Serum, Urine and Ultrasound Screening Study (SURUSS). *J Med Screen* 10:56, 2003.
- Egan JF, Kaminsky LM, DeRoche ME, et al: Antenatal Down syndrome screening in the United States in 2001: A survey of maternal-fetal medicine specialists. *Am J Obstet Gynecol* 187:1230, 2002.
- Abuhamad A: Technical aspects of nuchal translucency measurement. *Semin Perinatol* 29:376, 2005.
- Malone FD, Berkowitz RL, Canick JA, D'Alton ME: first-trimester screening for aneuploidy: Research or standard of care? *Am J Obstet Gynecol* 182:490, 2000.
- Nicolaides KH, Heath V, Cicero S: Increased fetal nuchal translucency at 11-14 weeks. *Prenat Diagn* 22:308, 2002.
- Moscato G: Fetal nuchal translucency: A need to understand the physiological basis. *Ultrasound Obstet Gynecol* 5:6, 1995.
- Malone FD, D'Alton ME, for the Society for Maternal Fetal Medicine: first-trimester sonographic screening for Down syndrome. *Obstet Gynecol* 102:1066, 2003.
- Snijders RJ, Noble P, Sebire N, et al: UK multicenter project on assessment of risk of trisomy 21 by maternal age and fetal nuchal-translucency thickness at 10-14 weeks of gestation. *Lancet* 351:343, 1998.
- Wapner R, Thom E, Simpson JL, et al: first-trimester screening for trisomies 21 and 18. *N Engl J Med* 349:1405, 2003.
- Canick JA, Kellner LH: first-trimester serum screening for aneuploidy: Serum biochemical markers. *Semin Perinatol* 23:359, 1999.
- Malone FD, Ball RH, Nyberg DA, et al: first-trimester septated cystic hygroma: Prevalence, Natural history, and pediatric outcome. *Obstet Gynecol* 106:288, 2005.
- Molina FS, Avgidou K, Kagan KO, et al: Cystic hygromas, nuchal edema, and nuchal translucency at 11-14 weeks of gestation. *Obstet Gynecol* 107:678, 2006.
- Comstock CH, Malone FD, Ball RH, et al: Is there a nuchal translucency millimeter measurement above which there is no added benefit from first-trimester serum screening? *Am J Obstet Gynecol* 195:843, 2006.
- Cicero S, Curcio P, Papageorgiou A, et al: Absence of nasal bone in fetuses with trisomy 21 at 11-14 weeks of gestation: An observational study. *Lancet* 358:1665, 2001.
- Cicero S, Longo D, Rembouskos G, et al: Absent nasal bone at 11-14 weeks of gestation and chromosomal defects. *Ultrasound Obstet Gynecol* 22:31, 2003.
- Malone FD, Ball RH, Nyberg DA, et al: first-trimester nasal bone evaluation for aneuploidy in the general population. *Obstet Gynecol* 104:1222, 2004.
- Prifti F, Sairam S, Bhide A, Thilaganathan B: first-trimester nuchal translucency, nasal bones, and trisomy 21 in selected and unselected populations. *Am J Obstet Gynecol* 194:828, 2006.
- Ramos-Corpeas D, Santiago JC, Montoya F: Ultrasonographic evaluation of fetal nasal bone in a low-risk population at 11 - 13 + 6 gestational weeks. *Prenat Diagn* 26:112, 2006.
- Matias A, Gomes C, Flack N, et al: Screening for chromosomal abnormalities at 10-14 weeks: the role of ductus venosus blood flow. *Ultrasound Obstet Gynecol* 12:380, 1998.
- Hecher K: Assessment of ductus venosus flow during the first and early second trimesters: what can we expect? *Ultrasound Obstet Gynecol* 17:285, 2001.
- Nicolaides KH, Spencer K, Avgidou K, et al: Multicenter study of first-trimester screening for trisomy 21 in 75,821 pregnancies: results and estimation of the potential impact of individual risk-oriented two-stage first-trimester screening. *Ultrasound Obstet Gynecol* 25:221, 2005.
- Falcon O, Faiola S, Huggon I, et al: Fetal tricuspid regurgitation at the 11 + 0 to 13 + 6-week scan: association with chromosomal defects and reproducibility of the method. *Ultrasound Obstet Gynecol* 27:609, 2006.
- Sebire NJ, Souka A, Skentou H, et al: Early prediction of severe twin-to-twin transfusion syndrome. *Hum Reprod* 15:2008, 2000.
- Spencer K, Nicolaides KH: Screening for trisomy 21 in twins using first-trimester ultrasound and maternal serum biochemistry in a one stop clinic: a review of three years experience. *Br J Obstet Gynaecol* 110:276, 2003.
- Wald NJ, Rish S, Hackshaw AK: Combining nuchal translucency and serum markers in prenatal screening for Down syndrome in twin pregnancies. *Prenat Diagn* 23:588, 2003.
- Malone FD: Nuchal translucency-based Down syndrome screening: barriers to implementation. *Semin Perinatol* 29:272, 2005.
- Haddow JE, Palomaki GE, Knight GJ, et al: Screening of maternal serum for fetal Down's syndrome in the first trimester. *N Engl J Med* 338:955, 1998.
- Scott F, Boogert A, Sinosich M, et al: Establishment and application of a normal range for nuchal translucency across the first trimester. *Prenat Diagn* 16:629, 1996.
- Crossley JA, Aitken DA, Cameron AD, et al: Combined ultrasound and biochemical screening for Down's syndrome in the first trimester: a Scottish multicenter study. *Br J Obstet Gynaecol* 109:667, 2002.
- Canadian Early and Mid-Trimester Amniocentesis Trial (CEMAT): Randomized trial to assess safety and fetal outcome of early and midtrimester amniocentesis. *Lancet* 351:242, 1998.
- Cuckle H, Benn P, Wright D: Down syndrome screening in the first and/or second trimester: model predicted performance using meta-analysis parameters. *Semin Perinatol* 29:252, 2005.



# THE SECOND TRIMESTER GENETIC SONOGRAM

Lami Yeo, MD and Anthony M. Vintzileos, MD

## Introduction

### Biochemical Serum Marker Screening in the Second Trimester

### Sonographic Features of Fetal Aneuploidy

- Structural Abnormalities
- Nuchal Fold
- Short Long Bones
- Pyelectasis
- Echogenic Intracardiac Focus
- Hyperechoic Bowel
- Choroid Plexus Cysts
- Nasal Bone

- Iliac Wing Angle

- Ear Length

- Extremity Abnormalities

- Single Umbilical Artery

- Other Sonographic Aneuploidy Markers

### Trisomy 21 (Down Syndrome)

### Second Trimester Genetic Sonography

### Trisomy 18 (Edwards Syndrome)

### Trisomy 13 (Patau Syndrome)

### Conclusion

## INTRODUCTION

Unfortunately, aneuploidy occurs in human development. Its frequency varies, depending on the maternal age and also the gestational age of the fetus. With earlier gestational ages and in nonviable gestations, the prevalence of aneuploidy increases. Chromosome abnormalities are the leading cause of pregnancy loss, and at least 95% of chromosomally abnormal conceptions are lost before term. A minimum of 10% to 15% of conceptions are chromosomally abnormal. Aneuploid fetuses account for approximately 6% to 11% of all stillbirths and neonatal deaths.<sup>1</sup> One large study reported that among newborn children, 0.8% had a chromosomal abnormality at birth.<sup>2</sup> It has been common and widespread practice to offer genetic amniocentesis to all women who have increased risks for fetal chromosomal abnormalities, such as advanced maternal age, family history of aneuploidy, or abnormal second trimester serum screening. However, the practice of offering routine invasive testing to all high-risk pregnant women has been challenged, owing to its invasive nature and associated risks such as pregnancy loss.

Over the last several years, it became apparent that many chromosomal abnormalities are associated with fetal structural abnormalities or aneuploidy markers that are capable of being detected during second trimester ultrasonography. This is due to the fact that over the years, there has been an improvement and evolution of high-quality resolution in fetal imaging, such that detailed examination of the fetus is possible. Today, ultrasound provides a very important noninvasive method for the prenatal detection of fetuses with chromosomal abnormalities. In addition, an ultrasound examination provides a tangible and realistic modality because patients can visibly see for

themselves, as compared with relying solely on biochemical screening. Fetuses with trisomies 18 and 13 have many major structural anomalies and, therefore, ultrasound has a high sensitivity in detecting them (up to 83%–100% for trisomy 18)<sup>3,4</sup> and 91% for trisomy 13.<sup>5</sup> However, this may not necessarily apply to Down syndrome cases. Because only 25% of second trimester fetuses with Down syndrome have ultrasonically detectable major congenital anomalies,<sup>6</sup> investigators have been searching for other sonographic markers to increase the sensitivity of detection. This has formed the basis for the emergence and practice of second trimester genetic sonography.

This chapter focuses on second trimester ultrasonography as a means of detecting fetal aneuploidy and specific patterns of malformations associated with the most common autosomal trisomies (Down syndrome, trisomy 18, trisomy 13), and also discusses the significance of individual aneuploidy markers. Because biochemical serum screening in the second trimester is often incorporated into risk calculations with genetic sonography, this also is reviewed.

## BIOCHEMICAL SERUM MARKER SCREENING IN THE SECOND TRIMESTER

Biochemical screening during the second trimester has made a major impact on screening for fetal trisomy 21, although simultaneously, maternal age alone as a screening method has become less important. Screening for Down syndrome in low-risk patients (women <35 years of age) was begun when researchers discovered in the mid-1980s that the mean level of maternal serum alpha-fetoprotein (MSAFP) in Down syndrome pregnancies was 0.7 multiples



of the normal median (MoM).<sup>7-9</sup> Subsequently, it was also realized that in Down syndrome pregnancies, unconjugated estriol levels were lower (0.79 MoM) and human chorionic gonadotropin (hCG) levels were higher (2.04 MoM).<sup>10-13</sup> AFP, unconjugated estriol, and hCG are independent of maternal age and only weakly correlated with each other. Therefore, they can be used in combination to estimate fetal Down syndrome risks. By using the relative risks derived from maternal serum levels of these three analytes, the maternal age-related risk can be modified, and for each individual patient a "triple screen" risk can then be derived.

Triple marker screening has been the preferred screening test for fetal Down syndrome in women younger than 35 years of age, and it is routinely offered in pregnancy over the past several years.<sup>13-16</sup> Multiple marker screening has a significantly higher sensitivity than MSAFP screening alone. In the population of women younger than 35 years of age, the triple marker screen identifies approximately 60% of all Down syndrome pregnancies, for an approximately 5% screen-positive rate. In women 35 years of age and older, it will detect 75% or more of all Down syndrome cases, and also some other aneuploidies.<sup>17</sup> Because maternal age is the basis of the serum screening protocol, both the Down syndrome detection rate and the screen-positive rate increase with maternal age.<sup>18</sup> Different screen-positive cutoffs may be used, depending on the laboratory. For instance, some will use the midtrimester Down syndrome risk of a 35-year-old woman as the screen-positive cutoff (1/270), whereas others select a screen-positive cutoff that results in an acceptable balance between detection rate and screen-positive rate (usually 1/190 or 1/200).

Maternal serum sampling can be done between 15 and 20 weeks of gestation; however, it is most accurate when performed between 16 and 18 weeks. Dating of the pregnancy must be accurate, because incorrect dates will affect the assigned triple-screen risk, and may lead to false-positive or false-negative results. When there is wrong dating (for example, after sonography has been performed), it is essential to either recalculate the results, or have a new blood sample drawn if the original specimen was drawn at less than 15 weeks of gestation. Maternal weight, race, diabetes, and the number of fetuses present are all incorporated into the risk calculation.

Although serum screening is used primarily for the detection of Down syndrome, it may detect other types of fetal aneuploidy, such as trisomy 18. Some other types of aneuploidy that are likely to be missed by serum screening may be lethal (for example, trisomy 13) or sex chromosome abnormalities that have not been found to be associated with profound mental retardation or severe physical or developmental limitations.

Some believe that the free beta subunits of hCG ( $\beta$ -hCG) are superior to the intact hCG molecule, but neither has definitively been proven to be superior. Recently, there has also been the testing and emergence of a new analyte, dimeric inhibin A. This has been the most promising new second trimester analyte and is currently used by many commercial laboratories in combination with the more traditional three analytes. This new four-analyte combination, or "quadruple screen," appears to detect 67% to 76% cases of fetal Down syndrome in women younger than 35 years of age, with a screen-positive rate of 5% or less.<sup>19,20</sup>

For multiple gestations, diagnostic options are somewhat limited. With twins, the risk of Down syndrome should be calculated by considering the maternal age-related risk of Down syndrome and the probability that either or both fetuses could be affected. The midtrimester risk for at least one fetus to have Down syndrome in a twin gestation in women 33 years of age is approximately the same as the risk for a singleton pregnancy in women 35 years of age, therefore justifying discussion regarding invasive testing under these circumstances.<sup>21</sup>

## SONOGRAPHIC FEATURES OF FETAL ANEUPLOIDY

All pregnancies are theoretically at risk for fetal aneuploidy. Additional risk factors include advanced maternal age, abnormal biochemical screening results, history of fetal aneuploidy, known balanced translocation, or other structural rearrangements in one of the parents, and abnormalities visualized on prenatal ultrasound. In aneuploid fetuses, sonography may reveal structural abnormalities, other findings (such as intrauterine growth restriction, polyhydramnios), or aneuploidy markers. "Soft" sonographic markers are variations in normal anatomy that, except for their relationship to aneuploidy (especially trisomy 21), are unlikely to be clinically significant. Compared with structural anomalies, markers are often transient and nonspecific findings which can also occur frequently in euploid fetuses.

Some of the most common sonographic markers seen in the second trimester include nuchal fold thickening, echogenic intracardiac focus, shortened long bones, hyperechoic bowel, renal pyelectasis, choroid plexus cysts (CPCs), clinodactyly, and hypoplastic or absent nasal bone. As a general statement, as the number of identified markers increases, the risk for aneuploidy in the fetus increases as well. Among aneuploid fetuses, although the features may be highly variable from one fetus to the next, certain patterns of anomalies and common features exist (Tables 4-1, 4-2, and 4-3).

Discovering features of fetal aneuploidy on prenatal sonography and detection rates depend on various factors. These include indications for the scan, gestational age, the population examined (high risk versus low risk), quality of imaging, criteria for an abnormal scan, the type of chromosomal abnormality, and experience of the examiner. For instance, although high sensitivities of detection have been reported by experienced examiners in high-risk populations, low sensitivities can be expected from less experienced sonographers in low-risk populations.<sup>22</sup>

## Structural Abnormalities

Structural or major anomalies that may be seen in aneuploid fetuses include central nervous system anomalies, facial abnormalities, cystic hygroma, diaphragmatic hernia, cardiac defects, gastrointestinal abnormalities, genitourinary anomalies, nonimmune hydrops, and extremity abnormalities. Many fetuses with trisomies 18 and 13 have multiple major structural anomalies; however, this may not necessarily apply to Down syndrome cases. Only 25% of second trimester fetuses with Down syndrome have ultrasonographically detectable major congenital anomalies.<sup>6</sup> In two prenatal series



**Table 4-1** Prenatal Sonographic Features of Trisomy 21

	Trisomy 21
Structural abnormalities	Cardiac defects Cystic hygroma Ventriculomegaly/ hydrocephalus Esophageal atresia/ tracheoesophageal fistula Duodenal atresia Omphalocele
Aneuploidy markers	Clinodactyly (hypoplastic middle phalanx of the fifth digit) Echogenic intracardiac focus Hyperechoic bowel (similar echogenicity to iliac bones) Nuchal fold thickening ( $\geq 6$ mm) Pyelectasis (anteroposterior diameter of renal pelvis $\geq 4$ mm) Sandal gap (wide space between first and second toes) Short long bones (femur, humerus, tibia, fibula) Wide iliac angle Two vessel umbilical cord Short ear length Absent or hypoplastic nasal bone
Other findings	Brachycephaly Flat profile Protruding tongue Hydrops Hydrothorax Pericardial effusion Unfused amnion and chorion after 14 weeks

before 20 weeks, structural anomalies were detected by sonography in only 16% to 17% of trisomy 21 fetuses.<sup>23,24</sup>

Infants with Down syndrome have a 50% incidence of cardiac defects, most commonly ventricular septal defects (Fig. 4-1) and common atrioventricular canal defects (Fig. 4-2). Unfortunately, ventricular septal defects can be quite difficult to identify on prenatal sonography and the detection rate may be variable. One group was able to detect heart defects in just over one half of fetuses with Down syndrome.<sup>25</sup> By using nonspecific cardiac findings (such as tricuspid regurgitation, pericardial effusion, and right-left disproportion), DeVore reported abnormal cardiac findings in 76% of fetuses with Down syndrome; however, only 9% showed an atrioventricular septal defect.<sup>26</sup> Cardiac malformations are also found in more than 90% of trisomy 18 and 13 fetuses. In our own recent study of 38 fetuses with trisomy 18, we found that the majority (84%) had major congenital heart disease on ultrasound.<sup>4</sup> Another study also found structural heart defects to be present sonographically in 80% of their cohort of fetuses with trisomy 18.<sup>27</sup>

Identification of cardiac abnormalities on prenatal sonography may increase the risk for fetal aneuploidy. As compared with postnatal studies, a much higher frequency of aneuploidy (22% to 32%) has been found in fetuses with

**Table 4-2** Prenatal Sonographic Features of Trisomy 18

	Trisomy 18
Structural abnormalities	Cardiac defects Cystic hygroma Diaphragmatic hernia Omphalocele Esophageal atresia (with or without tracheoesophageal fistula) Central nervous system Agensis of corpus callosum Ventriculomegaly/ hydrocephalus Large cisterna magna Dandy-Walker malformation Cerebellar dysgenesis Neural tube defect Craniofacial Strawberry-shaped skull Prominent occiput Dolicocephaly Ocular anomalies Micrognathia Cleft lip/palate Small, low-set ears Genitourinary Hydronephrosis Horseshoe kidney Bladder outlet obstruction Duplication abnormalities Genital abnormalities Extremity Limb reduction abnormalities Radial aplasia Clenched hands and/or overlapping digits Clubfeet Rocker-bottom feet Lower extremity/feet abnormalities Contractures/arthrogryposis/ flexion deformities Movement disorders
Aneuploidy markers	Choroid plexus cyst(s) Strawberry-shaped skull Nuchal thickening Single umbilical artery Shortened limbs
Other findings	Intrauterine growth restriction Amniotic fluid abnormalities Umbilical cord cysts Nonimmune hydrops

sonographically detectable cardiac malformations.<sup>28,29</sup> One factor that also contributes to the frequency of aneuploidy is the type of cardiac defect present. For instance, the aneuploidy risk is much higher for hypoplastic heart (Fig. 4-3), atrioventricular canal defects, tetralogy of Fallot, or double-outlet right ventricle as compared with isolated ventricular septal defects or valvular stenosis.<sup>30</sup> In particular, atrioventricular canal defects have a high risk of aneuploidy. In one series of 38 atrioventricular septal defects, the authors found aneuploidy in 58% ( $n = 22$ ): Down syndrome ( $n = 19$ ), trisomy 18 ( $n = 1$ ), trisomy 13 ( $n = 1$ ), and mosaicism ( $n = 1$ ).<sup>31</sup>

**Table 4-3 Prenatal Sonographic Features of Trisomy 13**

Trisomy 13	
Structural abnormalities	Cardiac defects
	Cystic hygroma, nuchal thickening
	Omphalocele
	Central nervous system
	Holoprosencephaly
	Agenesis of corpus callosum
	Ventriculomegaly
	Enlarge cisterna magna
	Abnormal posterior fossa
	Neural tube defects
	Craniofacial
	Microcephaly
	Micrognathia
	Cleft lip and/or palate
	Facial clefts
	Ocular anomalies
	Sloping forehead
	Small ears
	Extremity
	Postaxial polydactyly
	Overlapping digits
	Camptodactyly
	Radial aplasia
	Rocker-bottom feet
	Clubfeet
	Urogenital
	Hydronephrosis
	Cortical cysts
	Horseshoe kidney
	Echogenic kidneys
	Polycystic kidneys
Aneuploidy markers	Echogenic intracardiac focus
	Pyelectasis
Other findings	Single umbilical artery
	Microcephaly
	Intrauterine growth restriction
	Polyhydramnios

*Duodenal atresia* (Fig. 4-4) is usually recognized after 20 to 24 weeks of pregnancy by the documentation of the “double bubble” sign (dilated fluid-filled stomach and proximal duodenum) and evidence of polyhydramnios. This is the leading cause of intestinal obstruction among newborns. Among cases of duodenal atresia detected prenatally, trisomy 21 is present in approximately one third of cases.<sup>30</sup> Therefore, invasive testing for karyotype has been offered when duodenal atresia is prenatally identified (even if this occurs in the third trimester, as it still provides vital information in counseling patients).

*Cystic hygromas* are abnormal cystic masses of lymphatic origin that usually occur in the posterolateral area of the neck (Figs. 4-5 and 4-6). They have a high predisposition to aneuploidy. In fact, aneuploidy is found in more than 60% of fetuses with cystic hygroma. The frequency of aneuploidy varies with the gestational age, and the size and appearance of the hygroma. Large cystic hygromas (typically seen after 14 weeks) tend to have septations (see Fig. 4-5) and carry a high risk of aneuploidy. In the second trimester, about 75% are associated with aneuploidy, and Turner syndrome (45X) accounts for 80% of these.<sup>30</sup> In addition, trisomies 18, 13,

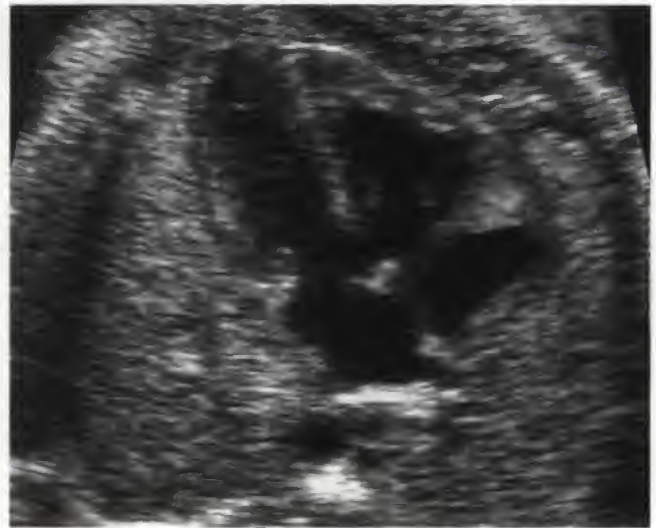


**FIGURE 4-1.** Apical four-chamber view of the fetal heart showing an inlet ventricular septal defect.



**FIGURE 4-2.** Transverse axial view of the fetal chest, showing a complete atrioventricular canal defect of the heart in a Down syndrome fetus. Note the primum atrial septal defect and inlet ventricular septal defect at the crux of the heart, along with a single atrioventricular valve.

and 21 are also found. Because hygromas may occur in fetuses with Down syndrome, they may represent a “severe” form of the spectrum of increased nuchal fold thickening. However, for hygromas seen in the first trimester, the aneuploidy rate is different (lower), and there is a higher proportion of Down syndrome and other chromosomal abnormalities. Therefore, whenever a cervical cystic hygroma is identified on prenatal sonography, invasive testing should be offered.

In a study comparing septated with nonseptated cystic hygromas in the early second trimester, it was found that septated hygromas were more likely (than nonseptated hygromas) to be associated with aneuploidy (72% versus 6%), and other anomalies (52% versus 15%).<sup>32</sup> Isolated cystic





**FIGURE 4-3.** Apical four-chamber view in a third trimester fetus. There is a markedly hypoplastic left heart visualized.

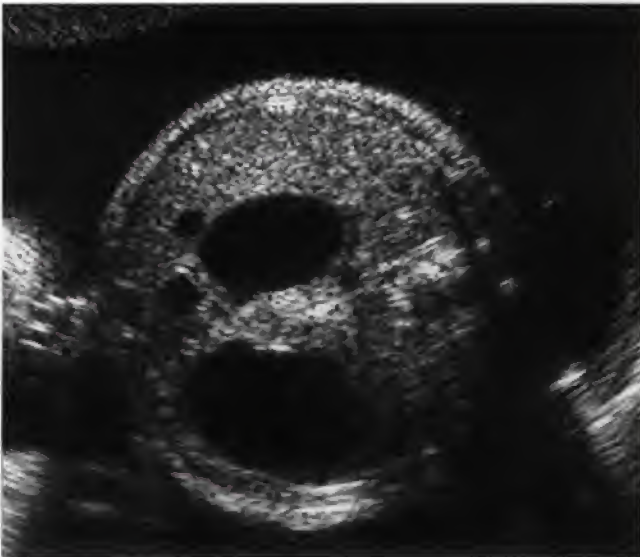


**FIGURE 4-4.** Duodenal atresia in a Down syndrome fetus. A transverse axial scan of the abdomen in the third trimester shows the classic "double-bubble" sign; polyhydramnios was also present.



**FIGURE 4-5.** Turner syndrome fetus with huge, septated cystic hygroma.



**FIGURE 4-6.** Gross image of stillborn fetus showing massive cystic hygroma surrounding the neck.



**FIGURE 4-7.** Transverse axial section of fetal chest, showing evidence of hydrops. Note the bilateral pleural effusions and significant skin edema.

hygromas that occur in an atypical location (noncervical) also do not appear to carry a significant risk of aneuploidy.<sup>30</sup>

In general, *nonimmune hydrops* (Fig. 4-7) can result from a variety of both maternal and fetal causes. It is recognized sonographically by ascites, pericardial effusions, pleural effusions, polyhydramnios, thickened placenta, and skin



**FIGURE 4-8.** Large unilateral pleural effusion (*asterisk*) pushing the heart into the right side of the chest.

edema. Aneuploidy is also a common cause of nonimmune hydrops, accounting for up to 16% of cases.<sup>33</sup> The pathophysiology of hydrops is not clear, but involves congestive heart failure or lymphatic dysplasia. The most common types of karyotype abnormalities that are associated with hydrops include Turner syndrome, trisomies 21, 18, and 13, and triploidy. When we studied the prenatal sonographic features of trisomy 18 fetuses, we found that 13% had evidence of hydrops/pleural effusions.<sup>4</sup> In addition, when nonimmune hydrops is diagnosed before 18 weeks, there is a higher incidence of aneuploidy, as compared with hydrops diagnosed in the latter half of pregnancy.<sup>34</sup> Therefore, when hydrops is diagnosed sonographically and appears to be unexplained, invasive testing should be offered. The combination of generalized hydrops and cystic hygroma, which is referred to as lymphangiectasia, is lethal in prognosis. Lymphangiectasia is associated with aneuploidy in approximately two thirds of cases, especially Turner syndrome. Thus, it should be separated from hydrops without cystic hygroma.

*Hydrothorax* (pleural effusion, chylothorax) has been linked to aneuploidy, especially Turner syndrome, Down syndrome, and trisomy 13. Among 82 cases of isolated fetal pleural effusion (Fig. 4-8) reported in the literature, Down syndrome was present in 4.9%.<sup>33</sup> Therefore, fetal karyotype analysis should be offered whenever hydrothorax is identified on prenatal sonography. It should be noted that *ascites* (Fig. 4-9) may occur in isolation and without other signs of hydrops. This has also been associated with aneuploidy, as reported in an evaluation of 18 fetuses with ascites where 5.6% ( $n = 1$ ) had Down syndrome.<sup>36</sup>

Diaphragmatic hernia (Fig. 4-10) is due to a congenital defect in the fetal diaphragm, with herniation of abdominal viscera into the fetal chest. This abnormality carries an increased risk for chromosomal abnormalities, such as trisomy 18 (most common), trisomy 13, Down syndrome, Turner syndrome, and other chromosomal abnormalities. It appears that the aneuploid frequency has been reported to be from 8% to 34%, most commonly 10% to 20%.<sup>37-39</sup> Therefore, karyotype testing should be offered whenever this defect is identified prenatally.



**FIGURE 4-9.** Transverse axial view of the fetal abdomen, demonstrating ascites and significant skin edema.

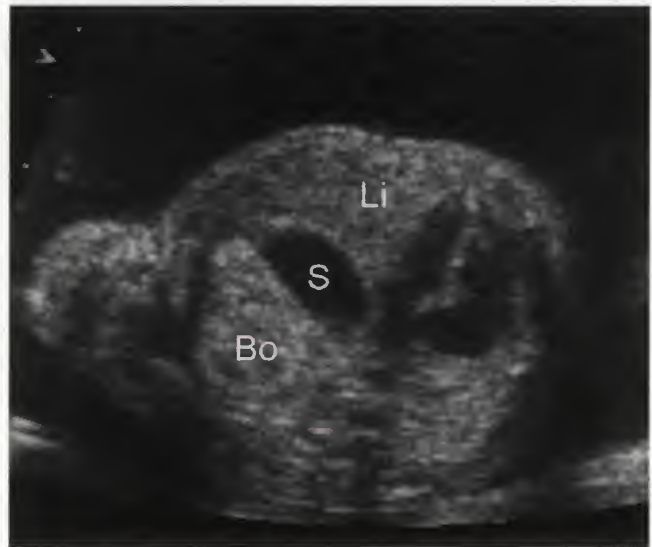


**FIGURE 4-10.** Transverse view through the fetal chest, showing a left-sided diaphragmatic hernia. Note the stomach (*S*), bowel (*Bo*), and liver (*Li*) within the chest cavity, displacing the heart to the right side.

An *omphalocele* (Figs. 4-11 and 4-12) occurs when there is a central abdominal wall defect that results in herniation of intra-abdominal structures into the base of the umbilical cord, which is covered by a membrane. Omphaloceles are associated with other fetal anomalies and aneuploidy in more than one half of the prenatally diagnosed cases. They carry a high risk of aneuploidy, such as trisomies 18 and 13 (most often), Down syndrome, Turner syndrome, and triploidy. Similarly to other fetal malformations, there appears to be a higher frequency of aneuploidy in most prenatal studies (30%–40%) as compared with neonatal studies (with



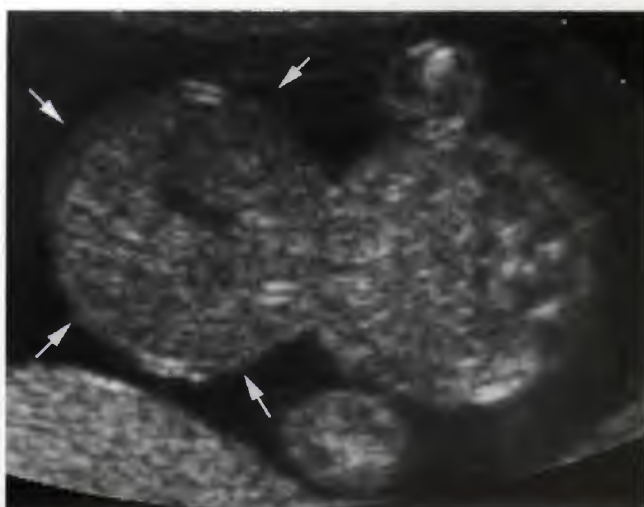


**FIGURE 4-11.** Large liver containing omphalocele (arrows) in a second trimester patient. The omphalocele is larger than the native fetal abdomen.



**FIGURE 4-12.** Second trimester fetus with trisomy 18 with large omphalocele containing both liver (Li) and echogenic bowel. The umbilical cord insertion can be seen by color Doppler on the apex of the herniated sac. Also note the umbilical cord cyst (arrow).

a combined rate of 12%), owing to the presence of more severely anomalous fetuses who die in utero or in the immediate neonatal period.<sup>30</sup> In one study, of 35 cases of omphalocele diagnosed by sonography, 54% had aneuploidy: trisomy 18 ( $n = 17$ ), triploidy ( $n = 1$ ), and Klinefelter syndrome ( $n = 1$ ).<sup>40</sup> In a recent study by our group, we found that of all trisomy 18 fetuses, 18% had an omphalocele identified on prenatal sonography.<sup>4</sup> Patients should be offered invasive testing for karyotype whenever an omphalocele is identified. Omphaloceles with intracorporeal liver (containing bowel only) have a higher aneuploidy risk than those with extracorporeal liver (containing liver) (see Fig. 4-11).<sup>41</sup> One group found an aneuploidy rate of 87% in omphaloceles with intracorporeal liver, versus 9% in extracorporeal liver.<sup>41</sup> When the omphalocele is extracorporeal and no other anomalies are identified, the risk for aneuploidy is low. Chromosomally normal fetuses with omphaloceles and no



**FIGURE 4-13.** Transverse axial scan at midgestation showing ventriculomegaly with a markedly dilated ventricle (arrows).

life-threatening abnormalities may have an excellent outcome after surgery.

Many *central nervous system* abnormalities carry an increased risk for fetal aneuploidy. Cerebral *ventriculomegaly* (Fig. 4-13), which is diagnosed when the atrial diameter of the cranial lateral ventricle reaches 10 mm or more, is a frequent finding. This is often associated with a relative “shrinkage” (inability to fill entirely the width of the lateral ventricle) or “dangling” of the choroid plexus. Ventriculomegaly (even mild) is associated with an increased risk for aneuploidy such as Down syndrome. However, it may also be seen as a normal variant later in the second trimester (after 20 weeks’ gestation) and in male fetuses, in the absence of “dangling” of the choroid plexus.<sup>30</sup> In one study, there were 31 fetuses with isolated borderline ventriculomegaly (10 to 15 mm) and 9.7% ( $n = 3$ ) were found to have aneuploidy (2 Down syndrome, 1 trisomy 13).<sup>42</sup> By reviewing the literature and including their cases, from a total of 234 patients, aneuploidy (mostly Down syndrome) was found in 3.8%. In another large (2743) series of cases, 3.8% were found to be karyotypically abnormal and Down syndrome was present in 2% of all the cases.<sup>23</sup> In chromosomally normal, aneuploid, and Down syndrome fetuses, mild ventriculomegaly was observed in 0.5%, 6.8%, and 5.5%, respectively.<sup>23</sup> Although the odds ratio of mild ventriculomegaly for aneuploidy was 4.4 (95% confidence interval (CI), 1.3 to 93.4), the ventriculomegaly was never isolated in these cases.

*Hydrocephalus* (Fig. 4-14) and *spina bifida* (Fig. 4-15), both together and each alone, have been reported to be associated with various types of karyotypic abnormalities, mainly trisomy 18, 13, and triploidy.<sup>43</sup> In a review of 107 fetuses with central nervous system abnormalities, aneuploidy was found in 3%, 8%, and 33% of fetuses with hydrocephalus, hydrocephalus and spina bifida, and spina bifida alone, respectively.<sup>43</sup> In our study of 38 trisomy 18 fetuses, we found that 19% had neural tube defects, whereas 8% had ventriculomegaly/hydrocephalus.<sup>4</sup> Therefore, if spina bifida is diagnosed prenatally, fetal karyotype testing should be offered.

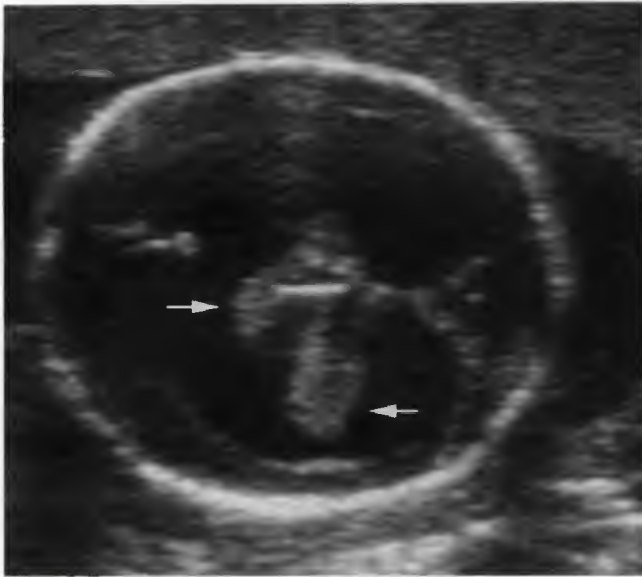


**FIGURE 4-14.** Marked dilation of both lateral ventricles with dangling choroid plexuses (arrows) in a fetus with hydrocephalus.



**FIGURE 4-15.** Three-dimensional sonogram showing the fetal back affected by a neural tube defect (arrow) in the lumbosacral area.

When *cerebellar* abnormalities are detected on prenatal sonography, there is an increased risk for aneuploidy and associated abnormalities.<sup>44</sup> Cerebellar abnormalities include Dandy-Walker malformation (Figs. 4-16 and 4-17), Dandy-Walker variant, and cerebellar hypoplasia with enlargement of the cisterna magna. In both Dandy-Walker malformation and variant, the enlarged fourth ventricle expands through a defect in the cerebellar vermis. With the variant type, there is incomplete vermian agenesis. Trisomy 18 is the most common aneuploidy, but other chromosomal abnormalities may also be observed. It is important to know that subtelomeric rearrangements have been seen related to brain abnormalities, including hypoplastic cerebellum and hydrocephalus<sup>30</sup>; this should be considered when karyotype

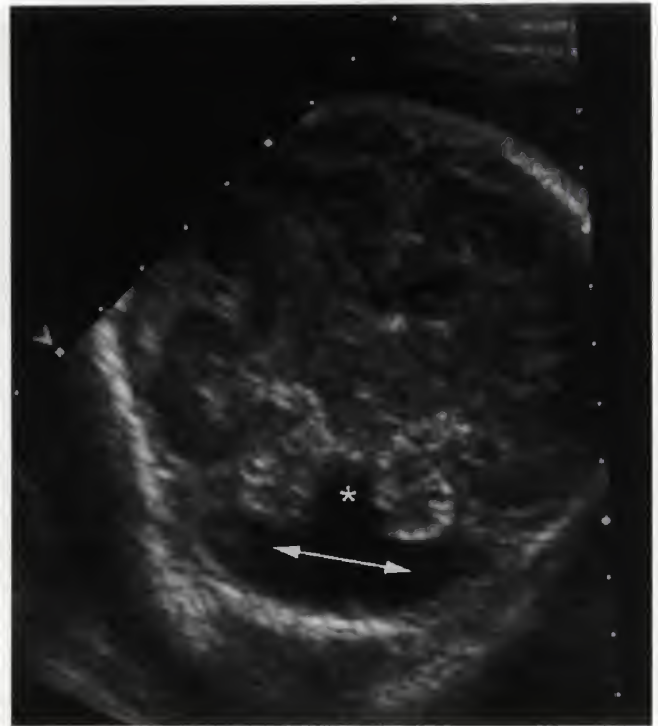


**FIGURE 4-16.** Dandy-Walker malformation in a trisomy 13 fetus. In a transverse axial plane, an enlarged fourth ventricle (arrows) is seen along with a defect in the cerebellar vermis. Note that the cerebellar hemispheres are splayed.

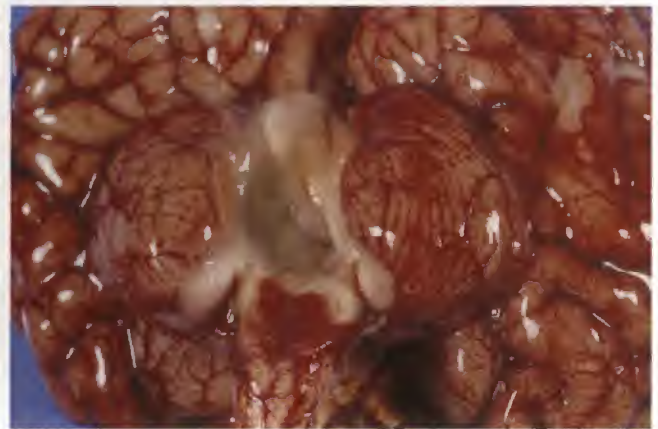


**FIGURE 4-17.** Pathologic specimen of brain shows cerebellar hemispheres bilaterally, but with complete absence of the vermis, consistent with Dandy-Walker malformation.

testing is performed. The Dandy-Walker variant is more strongly associated with aneuploidy (as compared with the malformation type), which is counterintuitive because the variant type is a more subtle anomaly.<sup>45,46</sup> Among those tested, one group found karyotypic anomalies in 53% fetuses with Dandy-Walker variant, as compared with 32% in those with Dandy-Walker malformation.<sup>46</sup>

Although it may be seen in normal fetuses, an enlarged cisterna magna may be indicative of chromosomal abnormalities (especially trisomy 18). This is most commonly visualized in the third trimester, and is less likely in the



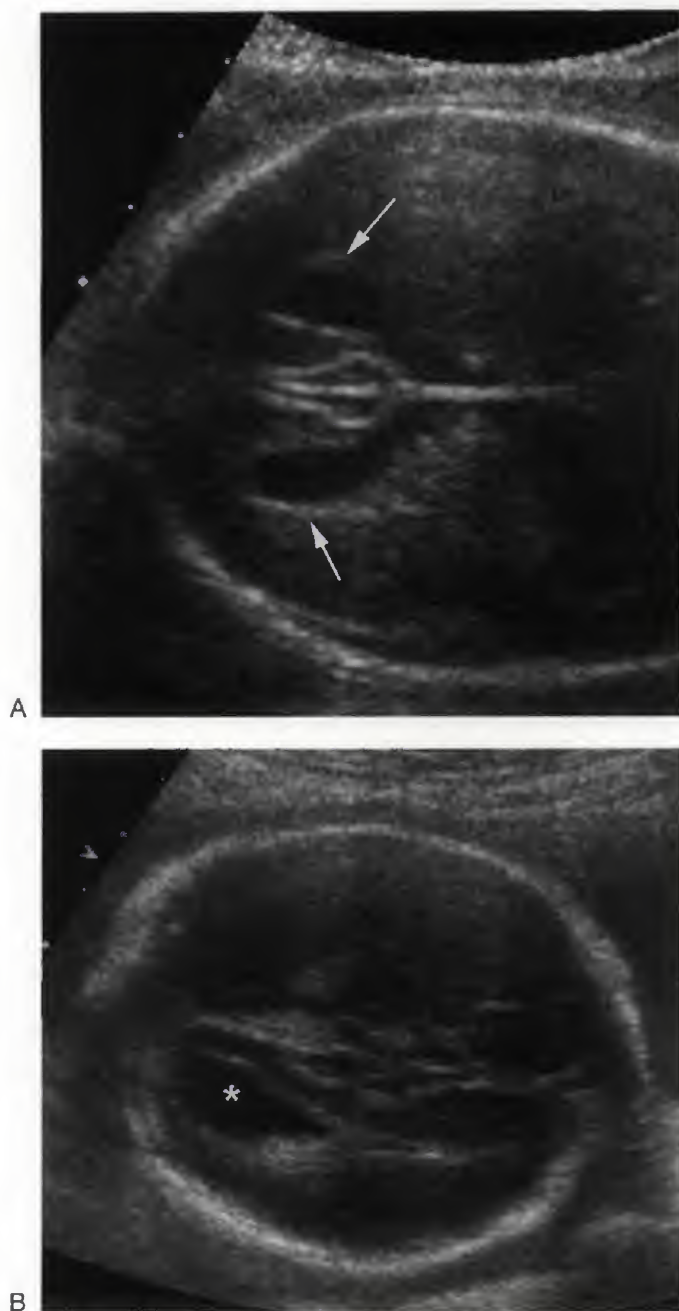


**FIGURE 4-18.** A. Fetus with agenesis of corpus callosum. Widely separated frontal horns (arrows) are seen with absence of the cavum septum pellucidum. B. Transverse axial scan through the lateral ventricle shows the characteristic "teardrop" shape of lateral ventricles or disproportionate enlargement of the occipital horns (colopocephaly) (asterisk), which is indicative of agenesis of corpus callosum.

second trimester.<sup>47,48</sup> One study examined fetuses with vermian agenesis or enlarged cisterna magna, and found that 55% had aneuploidy, most commonly trisomy 18 or trisomy 18 variant.<sup>45</sup> However, it appears that when there is an isolated enlarged cisterna magna (especially after 26 weeks) without other structural anomalies, this is usually associated with a normal karyotype and outcome.<sup>49</sup>

*Agenesis of the corpus callosum* (Fig. 4-18) can be complete or partial. The diagnosis is made by showing absence of the

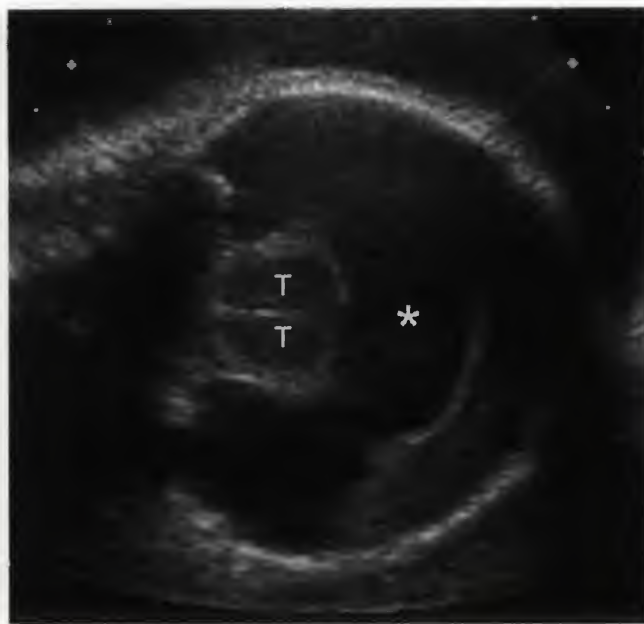


**FIGURE 4-19.** Transaxial view through the head of a trisomy 13 fetus, showing alobar holoprosencephaly. Note the fused thalami (T) surrounded by a single monoventricle (asterisk).

complex formed by the corpus callosum and cavum septum pellucidum, along with various other sonographic findings such as colpocephaly (or disproportionate enlargement of the occipital horns) (see Fig. 4-18). Aneuploidy is found in approximately 20% of cases, and mostly include trisomies 18, 8, and 13.<sup>50</sup> However, a variety of other types of chromosomal abnormalities are also reported. A recent study examined cases of agenesis of the corpus callosum diagnosed prenatally and postnatally.<sup>51</sup> Among the prenatally diagnosed cases, aneuploidy was present in 8%, as compared with 4% in postnatal cases.

*Holoprosencephaly* (Figs. 4-19 and 4-20) is a midline abnormality of the brain, resulting from absent or incomplete division of the prosencephalon (embryonic forebrain), and formation of the midline structures. It is embryologically related to development of the midface, hence, the common association with median facial anomalies (Fig. 4-21) involving the forehead, interorbital structures, nose, premaxilla, and upper lip. There are three major types of holoprosencephaly, depending on the degree of anatomic abnormality: alobar, semilobar, and lobar type. Aneuploidy is present overall in 50% to 60% of fetuses with alobar or semilobar holoprosencephaly. Of the various types of chromosomal abnormalities, trisomy 13 or a variant of trisomy 13 is the most common (found in 50%–75% of those with abnormal karyotype); however, there is a wide variety of other aneuploid types reported. Among fetuses with trisomy 13, holoprosencephaly has been reported in 39%.<sup>5</sup> In the presence of facial or extrafacial abnormalities in addition to holoprosencephaly, the risk for aneuploidy is increased.

*Facial anomalies* are commonly seen in fetuses or neonates with karyotypic abnormalities. Some karyotypically abnormal fetuses or neonates may demonstrate micrognathia (Figs. 4-22 and 4-23), sloping forehead (see Fig. 4-23),



**FIGURE 4-20.** Pathologic specimen of alobar holoprosencephaly in neonate affected with trisomy 13.



**FIGURE 4-21.** Gross pathologic features seen in the face of a neonate with alobar holoprosencephaly. A single eye globe (cyclopia) and a proboscis located above the median eye are present. Also note the clenched hands bilaterally.

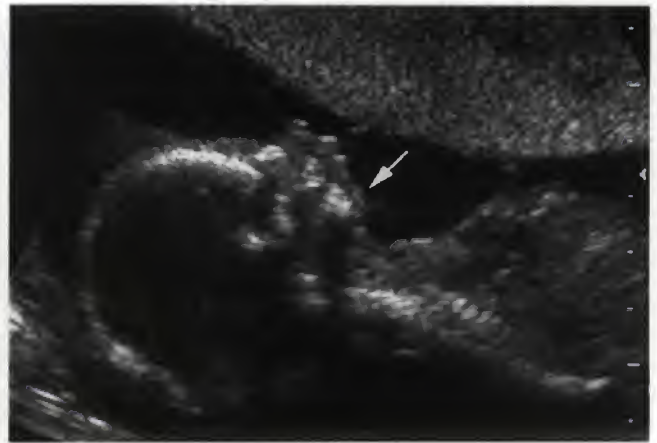


**FIGURE 4-22.** Abnormal facial profile, showing severe micrognathia (arrow).



**FIGURE 4-23.** Gross pathologic features seen in the face of a neonate with trisomy 9. Note the sloping forehead, flat profile, small nose, and micrognathia (arrow).

flattened profile (Fig. 4-24), or retrognathia. In examining the sonographic features of 38 fetuses with trisomy 18, we found that approximately one half (53%) had facial anomalies visualized.<sup>4</sup> Twenty-nine percent had an abnormal profile (excluding micrognathia), 21% had micrognathia, and 18% had hypotelorism.

The presence of *cleft lip/palate* (Figs. 4-25 and 4-26) is associated with aneuploidy (such as trisomies 13 and 18), especially when found together with central nervous system malformations or other abnormalities. A recent study examined fetuses with cleft lip and palate and reported aneuploidy in 0%, 32%, 59%, and 82% in unilateral cleft lip, unilateral cleft lip and palate, bilateral cleft lip and palate, and median cleft lip and palate, respectively.<sup>30</sup> Although some would argue that cleft lip alone has a low risk of aneuploidy and invasive testing is not always necessary, occasionally it is difficult to diagnose cleft palate prenatally and therefore this may represent a false-negative examination for cleft palate. Therefore, amniocentesis should probably be offered to all patients with fetal cleft lip and/or palate diagnosed on ultrasound.





**FIGURE 4-24.** Facial profile of fetus with trisomy 18. The profile is flattened and there is a hypoplastic nasal bone.



**FIGURE 4-25.** Three-dimensional image of the fetal face showing unilateral cleft lip (arrow).

*Ocular anomalies*, such as hypotelorism (Fig. 4-27), hypertelorism, microphthalmia, anophthalmia, and cyclopia (see Fig. 4-21) can be associated with fetal karyotype abnormalities. Most importantly, when they are seen along with other malformations (especially holoprosencephaly), the risk of aneuploidy is particularly increased.

*Genitourinary* abnormalities can be associated with fetal chromosomal abnormalities. The highest frequency of aneuploidy has been reported in those fetuses with urethrovesical obstruction (bladder outlet obstruction), most commonly trisomy 18 or 13.<sup>30</sup> In a cohort of 39 fetuses having obstruction at or distal to the urethrovesical junction,



**FIGURE 4-26.** Three-dimensional image of the fetal face showing bilateral cleft lip.



**FIGURE 4-27.** Marked hypotelorism in a fetus with trisomy 13.

chromosomal abnormalities were reported in 23%.<sup>52</sup> For urinary tract abnormalities occurring more proximally, aneuploidy has been reported with less frequency. For unilateral renal abnormalities including ureteropelvic junction obstruction and multicystic dysplastic kidneys, the risk of aneuploidy is considered to be low.<sup>53</sup> However, amniocentesis for karyotype may still be offered in all cases of multicystic dysplastic kidney (Fig. 4-28) because of the potential for associated chromosomal abnormalities.

In general, although the majority of congenital malformations may increase the risk for fetal aneuploidy, there are still some exceptions. These involve disorders that result from tissue or vascular disruption, such as gastroschisis, tumors, limb-body wall complex, hydranencephaly, and amniotic band syndrome.



**FIGURE 4-28.** Parasagittal scan through the fetal lower abdomen shows large multicystic dysplastic kidney with multiple cysts of varying sizes.



**FIGURE 4-29.** View through the posterior fossa shows normal nuchal fold thickness (0.41 cm) in the second trimester.

## Nuchal Fold

In 80% of newborns with Down syndrome, redundant nuchal skin folds or excess soft tissue in the posterior neck area are present.<sup>54</sup> Nuchal thickening is also present in other chromosomal abnormalities, such as trisomy 18, 13, and Turner syndrome. In some cases, it may even result from cystic hygroma resolution. In 1985, Benacerraf was the first to report thickened soft tissue at the fetal occiput between 15 and 20 weeks of gestation as a sonographic sign for trisomy 21.<sup>55</sup> The authors showed that 33% of fetuses with Down syndrome had a nuchal fold thickening of greater than or equal to 6 mm. By directing a transaxial plane through the fetal head and angled posteriorly to include the cerebellum and occipital bone, the nuchal skin fold thickness can be obtained (Fig. 4-29). Internal anatomic landmarks include

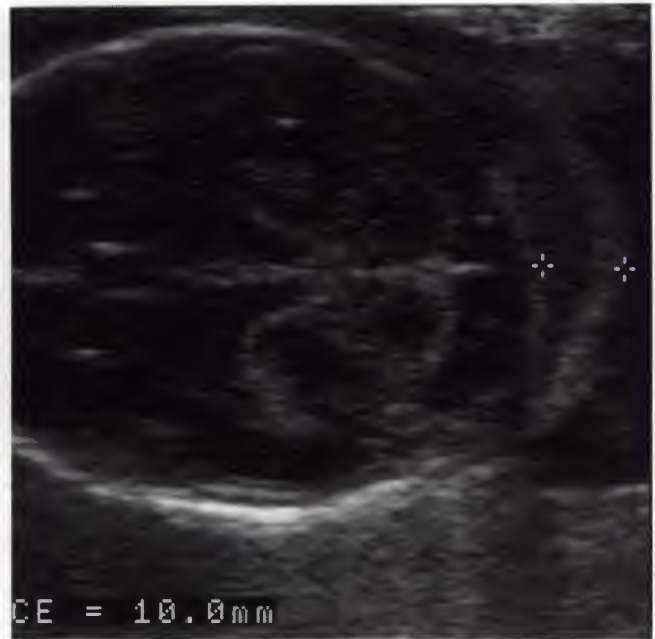


**FIGURE 4-30.** Transaxial plane through the posterior fossa of the fetal head, revealing an increased nuchal skin fold thickness (10 mm) in a 21-week fetus with Down syndrome.

the cavum septum pellucidum, cerebral peduncles, cerebellar hemispheres, and cisterna magna. Measurements are typically performed between 15 and 21 gestational weeks, and are measured by calipers from the outer skull table (or outside the occipital bone) to the outer skin edge. Values of greater than or equal to 5 or 6 mm are considered abnormal or increased (Fig. 4-30). The mean intraobserver and interobserver errors for this measurement are only 0.63 mm and 0.53 mm, respectively, thus making this marker highly reproducible.<sup>56</sup> However, it should be noted that when obtaining the nuchal fold thickness in breech fetuses, fetuses with an extended head on the neck or when increased pressure is placed on the transducer over the fetal head, a false-positive increased thickness may be obtained.

The sensitivity and false-positive rates for nuchal fold thickening (Fig. 4-31) vary with gestational age and the definition of a positive examination. Two large prospective clinical trials have shown the sensitivity of nuchal fold thickness for fetal Down syndrome detection to be 43% and 42%, with positive screening rates of 0.1% and 1.3%, respectively.<sup>56,57</sup> Another group found that by using a cutoff value of greater than or equal to 6 mm, 33% of trisomy 21 fetuses could be detected, with only a 0.1% false-positive rate.<sup>58</sup> They suggested lowering this cutoff to greater than or equal to 5 mm in order to achieve a sensitivity of 77.8% with a 2% false-positive rate. Benacerraf observed that in 303 normal fetal cases, none showed nuchal thickening greater than 5 mm up to 20 weeks' gestation.<sup>57</sup> Therefore, other studies have suggested that using 5 mm is a better cutoff, leading to improved sensitivity with only a slight increase in the false-positive rate.<sup>58,59</sup> At our institution, we use 6 mm or more as the threshold value for abnormal. Multiple other studies have also confirmed the finding that thickened nuchal fold on second trimester sonography is associated



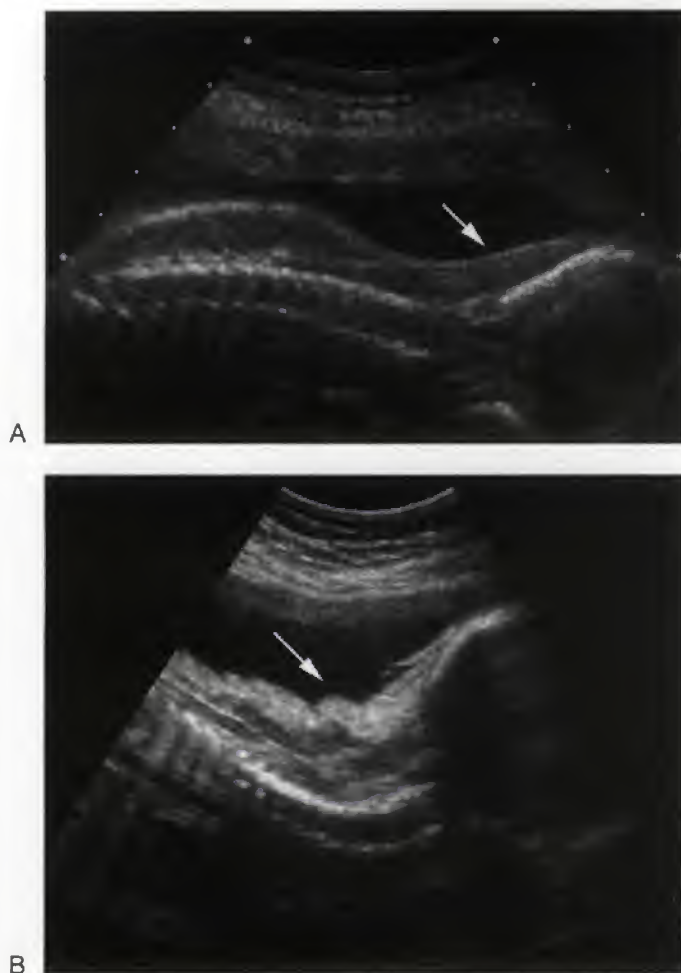


**FIGURE 4-31.** A. Longitudinal image of second trimester fetus with trisomy 21. Increased soft tissue is seen at the back of the head (arrow). Note that the fetal head is in a neutral position with respect to the cervical spine. B. Longitudinal image of a third trimester fetus with known Down syndrome. Note the redundant nuchal skin (arrow). In this case the prominent soft tissue is abnormal. However, extension of the fetal head on the neck, as in this case, may cause normal soft tissue to appear prominent and abnormal.

with a high risk for fetal Down syndrome.<sup>56,60-62</sup> The thickened nuchal fold is one of the most important markers, and the most sensitive and specific single marker for the midtrimester detection of Down syndrome,<sup>55</sup> although absent nasal bone has also recently been shown to have 41% sensitivity and 100% specificity for fetal Down syndrome.<sup>63</sup> Even as an isolated finding, abnormal nuchal fold has been reported to carry a likelihood ratio of at least 11 for Down syndrome.<sup>64,65</sup> Even among women who are not at risk for having a Down syndrome fetus, the thickened nuchal fold is helpful in detecting these affected fetuses.<sup>66</sup> Therefore, nuchal fold as a marker is a powerful tool, even in low-risk patients. Given these results, genetic amniocentesis should be offered when an abnormal nuchal fold measurement is observed, even in a low-risk population.

A very important fact is that although the nuchal thickness may persist throughout the second trimester in some fetuses with trisomy 21, other fetuses will have complete

**Table 4-4**

**Biparietal Diameter/Femur Length Ratio for Detection of Down Syndrome**

Study	Number of Down Syndrome Fetuses	Sensitivity	Positive Screen Rate
Dicke et al <sup>72</sup>	33	18%	4%
Hadlock et al <sup>73</sup>	16	19%	12%
Perella et al <sup>74</sup>	19	26%	23%
Hill et al <sup>75</sup>	22	36%	7%
Brumfield et al <sup>76</sup>	15	40%	2%
Lockwood et al <sup>70</sup>	35	51%	7%
Venacerraf et al <sup>57</sup>	20	70%	5%

resolution.<sup>67</sup> Thus, regression may occur whether or not the fetus has Down syndrome; therefore, once an abnormal nuchal skin measurement is obtained, an amniocentesis should be offered, regardless of whether the nuchal skin thickness resolves.<sup>68</sup>

### Short Long Bones

Because trisomy 21 individuals often have short stature, it is not surprising that the second trimester Down syndrome fetus may have a tendency for short humerus and femur bone lengths. In fact, the somatic and visceral growth profiles of midgestation trisomy 21 fetuses have been described, and it has been shown that the most striking deviations from normal are the short limbs (which are discordant with the head circumference).<sup>69</sup> When measuring long bone lengths, it is important to obtain the measurement with the diaphysis located horizontally in the image, because vertical measurements can falsely "shorten" the length. The most commonly used method for determining short long bone length is to compare the actual with the expected measurement based on biparietal diameter (BPD), rather than using gestational age.

In 1987, it was first shown that a short femur was associated with an increased risk for fetal Down syndrome.<sup>57,70</sup> The femur length can be assessed between 15 and 23 weeks using either a BPD/femur length ratio, or the observed-to-expected femur length ratio.<sup>57,70</sup> By choosing an upper limit of 1.5 standard deviations above the mean in the BPD/femur length ratio, Lockwood found that the sensitivity and false-positive rate was 51% and 7%, respectively, for detecting Down syndrome fetuses (Table 4-4).<sup>70</sup> Benacerraf demonstrated that 68% of trisomy 21 fetuses had ratios of the observed-to-expected femur length of less than 0.91, based on the BPD (Table 4-5).<sup>57</sup> Some investigators have found differences in the diagnostic accuracy of the BPD/femur length ratio, depending upon the gestational age of the fetus.<sup>71</sup> Most specifically, a short femur was most helpful in detecting trisomy 21 between 17 and 19 weeks gestation.

The efficacies of the BPD/femur length ratio and the observed-to-expected femur length ratio for trisomy 21 detection are depicted in Tables 4-4<sup>57,70,72-76</sup> and 4-5.<sup>57,72,75,77-80</sup> As seen, there is a wide range of sensitivities reported, with some studies failing to show a clinically meaningful association between short femur length and Down syndrome. This may be a reflection of the differences

**Table 4-5****Observed to Expected Femur Length Ratio for Detection of Down Syndrome**

Study	Number of Down Syndrome Fetuses	Sensitivity	Positive Screen Rate
Lafollette et al <sup>77</sup>	30	12%	13%
Nyberg et al <sup>78</sup>	49	14%	6%
Dicke et al <sup>72</sup>	33	15%	10%
Benacerraf et al <sup>79</sup>	20	40%	5%
Crist et al <sup>80</sup>	6	50%	6%
Hill et al <sup>75</sup>	22	50%	15%
Benacerraf et al <sup>57</sup>	28	68%	2%

in the populations examined in each of the studies. Because there is variation in fetal femur length with respect to maternal race,<sup>81</sup> it is advisable that in order to optimize sensitivity and specificity, each center should establish its own normal reference data, because mean values and standard deviations may significantly vary from one site to another.

Most data show that trisomy 21 fetuses have slightly shorter femurs (as compared with normal fetuses); however, the reduction in femur length in these fetuses is only minimal and it may not be useful as an isolated marker in screening for Down syndrome. Therefore, as with other sonographic aneuploidy markers, using a combination of markers (versus in isolation) to detect fetal Down syndrome is more useful.

In a 1989 study based on postmortem measurements in trisomy 21 fetuses, it was reported that humeral lengths were shorter than expected.<sup>82</sup> Subsequently, Benacerraf examined the role of humerus length in detecting trisomy 21 fetuses in the second trimester by using the measured-to-expected humerus length ratio of less than 0.90 as a cutoff; 50% of Down syndrome fetuses were identified with a 6.25% false-positive rate.<sup>83</sup> In the same year, our group found that short humerus length had a 54% sensitivity for the ultrasonographic detection of second trimester Down syndrome fetuses (versus 18% for femur length).<sup>84</sup> However, other investigators have found short humeral length to be less useful as a screening marker for trisomy 21 (28% sensitivity and positive screen rate of 9%).<sup>85</sup>

By combining both humerus and femur length assessments, a remarkable reduction in false-positive rates can be achieved.<sup>86</sup> Fetuses with both a short humerus and short femur carry an 11-fold higher risk of having trisomy 21, when compared with the age-based risk.<sup>87</sup> Gender may appear to have a role in influencing long bone lengths. In 1993, one study found that affected male fetuses with Down syndrome had more short femur and humerus measurements than affected female fetuses did, when compared with their normal counterparts.<sup>88</sup> A subsequent study by our group found that affected Down syndrome male fetuses had a greater proportion of short femur and humerus measurements at any given BPD, than did affected female fetuses.<sup>89</sup> However, when another group studied the impact of gender on the sonographic detection of fetal trisomy 21, they did not find statistical significance in the incidences of any of the sonographic markers, including short long bones.<sup>90</sup>

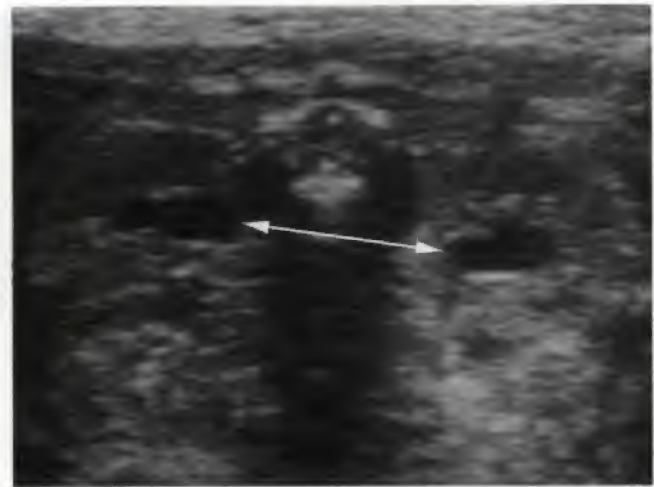


**FIGURE 4-32.** A transverse scan in the second trimester shows bilateral pyelectasis (arrows) in a fetus with Down syndrome.

### Pyelectasis

Renal pyelectasis (or renal pelvic dilation) (Fig. 4-32) is measured in an anteroposterior dimension as the fluid-filled renal pelvis. It should be measured only when the kidneys and spine are positioned directly toward or away from the transducer (versus to the side). Among various centers, the abnormal cutoff varies, but the most common value used is 3 to 4 mm. At our unit, we use a threshold measurement of 4 mm or more in the second trimester. Pyelectasis has been associated with an increased risk for aneuploidy,<sup>91-94</sup> especially for trisomy 21. Its prevalence varies with gestational age, with many cases resolving as the pregnancy advances. However, pyelectasis (especially mild) is a relatively common finding on prenatal sonography and may be seen in 2% to 2.8% of normal fetuses.<sup>92</sup>

In 1990, it was first shown that mild fetal pyelectasis was associated with an increased risk for trisomy 21.<sup>91</sup> By using a cutoff of greater than 4 mm, it was found that 25% of Down syndrome fetuses had pyelectasis.<sup>91</sup> Similarly, one group found that 18.7% of their Down syndrome fetuses had pyelectasis,<sup>56</sup> whereas another showed a 17% incidence of pyelectasis among fetuses with Down syndrome, with a 2% false-positive rate.<sup>92</sup> Among 210 fetuses overall with pyelectasis, 3.3% had Down syndrome.<sup>91</sup> Snijders<sup>95</sup> estimated that mild pyelectasis increased the risk for Down syndrome by 1.6-fold over the baseline risk. Some studies have focused on isolated pyelectasis as a marker for aneuploidy. Of 99 fetuses with isolated pyelectasis, two fetuses had aneuploidy (one of which had Down syndrome).<sup>96</sup> However, in a population of women with advanced maternal age, among the 2.9% of second trimester fetuses with isolated pyelectasis, the authors did not find an increased incidence of aneuploidy.<sup>97</sup>

Overall, although isolated fetal pyelectasis is a sonographic marker that carries a slightly increased risk for trisomy 21, the risk is probably not enough to justify amniocentesis in a low-risk population. However, in a high-risk population, pyelectasis may be used sonographically in combination with other aneuploidy markers, such as nuchal fold, short long bones, and so forth. When present in high-





**FIGURE 4-33.** Apical four-chamber view of the fetal heart, showing an echogenic intracardiac focus (arrow) in the left ventricle. Note the similar brightness to surrounding bone.



**FIGURE 4-34.** Apical four-chamber view of the fetal heart, showing multiple echogenic foci. There are several in the left ventricle, and one focus in the right ventricle.

risk women, even as an isolated marker, the identification of pylectasis may increase the a-priori risk for fetal trisomy 21.

### Echogenic Intracardiac Focus

An echogenic intracardiac focus (EIF) is commonly seen on second trimester sonography, and it is present in 3% to 4% of normal fetuses.<sup>98</sup> It is a discrete, brightly echogenic spot with brightness similar to bone (Fig. 4-33), and appears to be caused by reflection from the papillary muscles and chordae tendinae. Pathologic correlation suggests that EIF correlates with papillary muscle mineralization that may be seen histologically.<sup>99</sup> It may also represent coarse intramyocardial calcifications surrounded by myocardial fibrosis.<sup>100</sup> In low-risk patients, presence of an EIF is not associated with cardiac anomalies.<sup>101-103</sup> The prevalence of EIF appears to be significantly higher among the Asian population, with EIF found three times more often among Asian patients, as compared with whites.<sup>104</sup> Because EIF could be a subjective finding, its detection depends on various factors such as fetal positioning, maternal scanning characteristics, experience of the sonologist, quality and resolution of the ultrasound machine, completeness of the examination, and sonographic technique. Importantly, it is best visualized in an apical four-chamber view, with the apex of the heart pointing either toward or away from the transducer,<sup>105</sup> because it may “disappear” when examining the heart from a subcostal four-chamber view (apex pointing to the side). Although it has been reported that it typically resolves by the third trimester,<sup>103</sup> we have found that with careful sonographic examination, an EIF can still be visualized even in the third trimester.

EIF was considered a normal variant until 1992.<sup>98</sup> In a pathologic study, Roberts was the first to suggest an associ-

ation between mineralization of the papillary muscle and aneuploidy.<sup>106</sup> Microcalcification of the papillary muscle was seen in 2%, 16%, and 39% of normal fetuses, trisomy 21 fetuses, and trisomy 13 fetuses, respectively.<sup>106</sup> Subsequently in 1995, Bromley reported on a series of 1334 second trimester fetuses undergoing amniocentesis, and found that 4.9% had an EIF.<sup>101</sup> Eighteen percent (4/22) of Down syndrome fetuses had an EIF, compared with 4.7% (62/1312) of normal fetuses. They found that in this high-risk population, the sonographic identification of an EIF was associated with a fourfold increase in the risk for trisomy 21.<sup>101</sup> Recently, the same authors found that as an isolated finding, EIF carries a likelihood ratio of 1.4 for fetal trisomy 21.<sup>107</sup> Subsequently, many studies have confirmed an association between Down syndrome and EIF.<sup>108-111</sup> The likelihood ratio of EIF for Down syndrome is estimated to fall in the range of 1.8 to 4.2.<sup>30</sup> However, some investigators have failed to show an association between Down syndrome and EIF.<sup>102,112</sup> An association between EIF and trisomy 13 has also been reported.<sup>5</sup> The authors found EIF in 39% of trisomy 13 fetuses earlier than 20 weeks.

Although an EIF may occur in either or both cardiac ventricles, it is most frequently seen in the left ventricle. One study found EIF in the left ventricle, combined left and right ventricles, and isolated to the right ventricle in 96%, 4.3%, and 0.7% of cases, respectively.<sup>113</sup> It appears that multiple or large EIF (Fig. 4-34) may also further increase the risk for aneuploidy. In other words, when the right ventricle or both ventricles show an echogenic intracardiac focus, the incidence of aneuploidy may be higher than it is for a single, left-sided focus.<sup>109</sup> One group of investigators found that right-sided (Fig. 4-35) and bilateral EIF combined had approximately a twofold greater risk for aneuploidy, as compared with left-sided foci.<sup>109</sup> Among fetuses with an EIF





**FIGURE 4-35.** Echogenic intracardiac focus seen the right ventricle of the heart (arrow).

in the right ventricle, there appeared to be a higher incidence of Down syndrome, as compared with fetuses with EIF isolated to the left ventricle only. Another study found that of 15 fetuses having multiple EIF, 67% ( $n = 10$ ) had abnormal karyotypes, and only two of these had other sonographic abnormalities.<sup>114</sup> Others have also found that EIF involving both cardiac ventricles (see Fig. 4-34) are more often associated with aneuploidy. One group reported that chromosomal abnormalities was more common when EIF involved both ventricles, as compared with either ventricle alone.<sup>111</sup>

In summary, the relationship between an echogenic intracardiac focus and trisomies 21 and 13 has been confirmed in the literature. Therefore, in the high-risk population even when an echogenic intracardiac focus is isolated, this will increase the a priori risk for fetal Down syndrome. However, in low-risk populations when the EIF is isolated and no other sonographic major or minor anomalies are identified, it is considered a "normal variant," and no further evaluation (including fetal karyotyping) is generally recommended.

## Hyperechoic Bowel

As with many other aneuploidy markers, hyperechoic bowel is nonspecific and it can be seen in normal fetuses. Overall, it is not a very frequent finding, as it is found in approximately 0.5% of normal fetuses. Normally in the second trimester, the bowel is homogeneous and has the same echogenicity as the rest of the fetal abdomen, thus appearing nondiscreet and normally unnoticeable. However, in the presence of hyperechoic bowel, one will have a subjective impression of unusually echogenic bowel. Its clinical significance varies with the degree of echogenicity. It has also been shown that the echogenicity of normal bowel increases with transducer frequency, although this effect is uniform (although true hyperechoic bowel tends to be focal).<sup>115</sup> Especially with current ultrasound technology and better sonographic resolution, one should remember that using



**FIGURE 4-36.** Hyperechoic bowel (arrows) in the abdomen (Grade 3) of a Down syndrome fetus. The echogenicity is similar to that of the vertebral bodies.

high-frequency transducers can highlight or exaggerate the echogenicity of fetal bowel, even in the normal fetus. Because the clinical detection of hyperechoic bowel still requires subjective interpretation, some have used a grading system to reduce subjectivity as much as possible.<sup>116</sup> Some will only acknowledge bowel that is markedly echogenic on sonography, whereas others will recognize both moderate and markedly echogenic bowel. A grading system for hyperechoic bowel which has been proposed includes grade 1 (mildly echogenic and typically diffuse), grade 2 (moderately echogenic and typically focal), and grade 3 (very echogenic, similar to that of bone structures).<sup>116</sup> In our unit, we diagnose hyperechoic bowel only if it has sonographic echogenicity similar to the iliac bones.

Hyperechoic bowel is seen with increased frequency in aneuploid fetuses (Fig. 4-36), especially trisomy 21.<sup>24,117-119</sup> In 1990, Nyberg reported an association between chromosomal abnormalities and hyperechoic bowel; of 94 fetuses with Down syndrome, 7% had hyperechoic bowel.<sup>24</sup> Another group examined 50 fetuses with hyperechoic bowel (defined as echogenicity comparable to bone) and found that 16% had aneuploidy, most of whom had Down syndrome.<sup>117</sup> The same group of investigators reported that 12.5% of all second trimester Down syndrome fetuses in their unit had hyperechoic bowel. Hyperechoic bowel appears to increase the risk of trisomy 21 by six- to sevenfold.<sup>64</sup> However, the risk will vary depending on maternal age, presence of other abnormalities, and a variety of other risk factors. The risk of Down syndrome in fetuses with isolated hyperechoic bowel is approximately 1.4% in the general population.<sup>68</sup> Others have reported that isolated hyperechoic bowel would be expected to be associated with a risk of trisomy 21 of approximately 1% to 2% in the general population.<sup>30</sup>

The differential diagnosis of hyperechoic bowel includes congenital infections (such as cytomegalovirus, herpes simplex virus, and parvovirus), meconium ileus (due to cystic fibrosis), and bowel obstruction/atresias/malformations. It may also be associated with prenatal vaginal bleeding and fetal swallowing of blood from intraamniotic hemorrhage.<sup>120</sup> With hyperechoic bowel, there is also an increased risk of



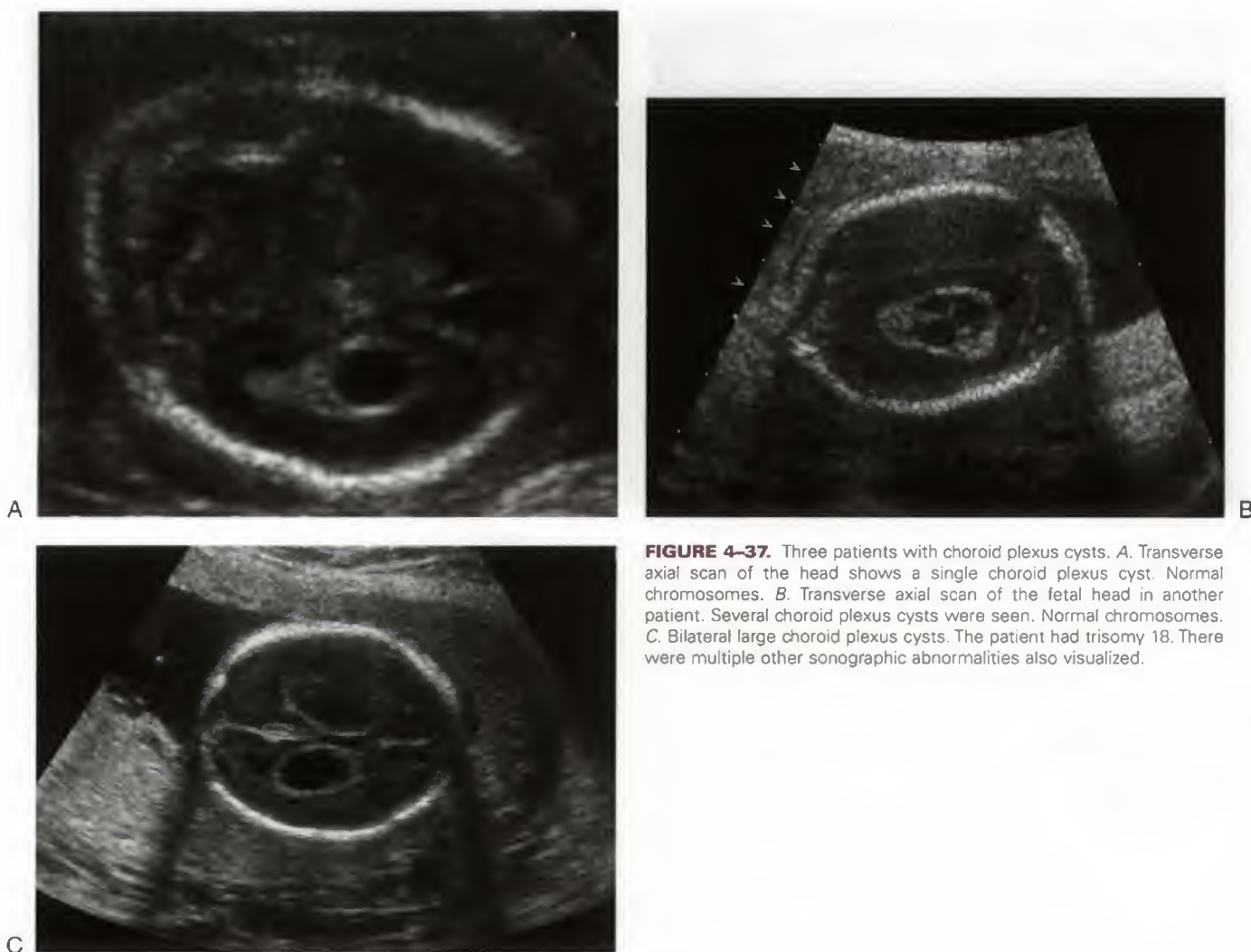


**FIGURE 4-37.** Three patients with choroid plexus cysts. *A.* Transverse axial scan of the head shows a single choroid plexus cyst. Normal chromosomes. *B.* Transverse axial scan of the fetal head in another patient. Several choroid plexus cysts were seen. Normal chromosomes. *C.* Bilateral large choroid plexus cysts. The patient had trisomy 18. There were multiple other sonographic abnormalities also visualized.

poor perinatal outcome, such as fetal demise, intrauterine growth restriction, and placenta-related complications.<sup>120</sup> It has been shown that the risk of both cystic fibrosis and aneuploidy increases with the degree of echogenicity of the fetal bowel.<sup>116,121</sup> From 145 cases of second trimester hyperechoic bowel, one study showed that cystic fibrosis was found in 0%, 2.5%, and 20.8% of fetuses with grades 1, 2, and 3 bowel, respectively.<sup>121</sup> They also found Down syndrome in 0%, 2.5%, and 25% of fetuses with grades 1, 2, and 3 bowel, respectively.

It is important to distinguish hyperechoic bowel from meconium peritonitis, in which the most common and characteristic finding on prenatal sonography is peritoneal calcification. Hyperechoic bowel is also different from hyperechoic meconium seen during the third trimester, which can be normal but is usually confined to the colon.

From a summary of the largest studies of hyperechoic bowel and their outcomes, Nyberg reported that the data indicated an increased risk for fetal or neonatal demise (3%–4%), aneuploidy (about 3%), other anomalies (3%), bowel complication (1%–2%), cystic fibrosis (1%–2%), and congenital infection (1%–2%).<sup>122</sup> Therefore, when hyperechoic bowel is visualized, one should consider maternal

studies for congenital infection, cystic fibrosis carrier status, invasive testing for fetal karyotype, and serial scans throughout the pregnancy to rule out intrauterine growth restriction and bowel malformations/atresias (which may not be evident until the third trimester). In general, the prognosis is favorable once aneuploidy, structural anomalies, infection, cystic fibrosis, and intrauterine growth restriction have been ruled out.

### Choroid Plexus Cysts

The cranial lateral ventricles contain sonolucent cerebrospinal fluid. Within the lateral ventricles lies the brightly echogenic choroid plexus that normally fills the atrium, and may contain cysts (Fig. 4–37). CPCs are a relatively common finding during the second trimester, especially with current improved sonographic technology and resolution. The reported prevalence among normal fetuses is variable and ranges anywhere from 0.3% to 3.6%.<sup>123,124</sup> This variability can be accounted for by various factors, such as indications for referral, completeness of the scan, size criteria for diagnosing cysts, and gestational age. CPCs themselves have no known effect on fetal development and are essentially benign.



In addition, unlike other aneuploidy markers (for example, hyperechoic bowel), there is no known association with other adverse outcomes if the karyotype is normal.

CPCs are seen almost exclusively in fetuses between 16 to 21 weeks of gestational age, and appear to be transient. By the 23rd week of gestation, they are usually undergoing regression and it is uncommon to see them sonographically after 25 to 26 weeks. Cysts may be unilateral or bilateral, single or multiple, and small or large. Commonly, they are multilocular in appearance, and the cysts typically range from between 0.5 cm and 2 cm in size. Occasionally, they may be so large as to fill almost the entire lateral ventricle and expand its walls, giving the false appearance of ventriculomegaly (Fig. 4-37B).

CPCs can be a significant finding because there have been reports in the literature over the years describing the association of CPCs with fetal aneuploidy, specifically with trisomy 18.<sup>125-127</sup> CPCs appear to be present in approximately one third of trisomy 18 fetuses.<sup>126</sup> Because of this association, there is much debate as to whether fetuses having CPCs on ultrasound should undergo karyotyping. It is clearly recommended that when fetuses with CPCs have other sonographic findings, invasive testing should be offered. However, when prenatal sonography by experienced personnel reveals that the CPCs are *isolated*, management should be conservative. However, some investigators believe that fetuses having isolated CPCs and no other anomalies may still carry a risk of aneuploidy high enough to justify amniocentesis. However, the critical component lies in whether an "isolated" CPC is, in fact, truly isolated. This can only be presumed once a detailed fetal survey by experienced examiners has failed to reveal other structural abnormalities/markers. Therefore, it is imperative that all fetuses with CPCs undergo a detailed fetal sonographic anatomic survey by someone who is skilled and experienced in prenatal diagnosis.

Several meta-analyses have been reported in the literature with regard to fetuses with isolated CPCs. One report revealed that 13 of the largest studies had a 0.27% incidence (or 1/374 risk) of trisomy 18 among fetuses with isolated CPCs, thus suggesting that invasive testing is not warranted.<sup>127</sup> Another report found that among 1346 fetuses with isolated CPCs, seven had trisomy 18 and five had Down syndrome.<sup>128</sup> Their study suggested a likelihood ratio of 13.8 (CI 7.7 to 25.0) for trisomy 18, and 1.87 (CI 0.78 to 4.46) for Down syndrome. Table 4-6 contains a summary of reported studies examining the incidence of aneuploidy in fetuses with isolated CPCs. Only one of the large studies (274 fetuses) shows the presence of chromosomal anomalies in cases of isolated CPCs.<sup>129</sup> As seen from the table, of 24 studies, the majority had no cases of aneuploidy, whereas eight studies found an association of isolated CPCs with chromosomal anomalies.

Snijders et al<sup>130</sup> found CPCs in 50% of their fetuses with trisomy 18, and in 1% of chromosomally normal fetuses. However, because the vast majority of affected fetuses showed other sonographic anomalies, the risk (for trisomy 18) of isolated CPCs was only marginally increased, with a likelihood ratio less than 2; however, the presence of just one other abnormality increased the risk 20 times.<sup>130</sup> Recently, we examined the prenatal sonographic features of 38 fetuses with trisomy 18, and found that 50% had CPC identified, but they were always associated with multiple other

Table 4-6

### Summary of Studies of the Incidence of Aneuploidy in Fetuses with Isolated Choroid Plexus Cysts

Study	No. of Cases with Isolated Choroid Plexus Cysts	No. of Chromosomal Anomalies
Achiron et al <sup>145</sup>	29	1
Benacerraf et al <sup>146</sup>	38	0
Chan et al <sup>147</sup>	13	0
Chinn et al <sup>123</sup>	36	0
Chitkara et al <sup>148</sup>	38	0
Clark et al <sup>149</sup>	5	0
DeRoo et al <sup>150</sup>	17	0
Gabrielli et al <sup>151</sup>	61	0
Gray et al <sup>135</sup>	201	0
Gross et al <sup>127</sup>	74	0
Hertzberg et al <sup>152</sup>	31	0
Howard et al <sup>140</sup>	51	1
Kupferminc et al <sup>153</sup>	98	4
Nadel et al <sup>125</sup>	220	0
Nava et al <sup>154</sup>	193	4
Ostlere et al <sup>137</sup>	96	0
Perpignano et al <sup>139</sup>	86	5
Platt et al <sup>141</sup>	67	0
Porto et al <sup>134</sup>	59	2
Shields et al <sup>139</sup>	274	7
Thorpe-Beeston et al <sup>155</sup>	49	0
Twining et al <sup>138</sup>	16	0
Walkinshaw et al <sup>136</sup>	152	4
Zerres et al <sup>156</sup>	14	0

sonographic abnormalities (never isolated).<sup>4</sup> Recently, DeVore also found the prevalence of CPCs in trisomy 18 fetuses to be 53%, and when these cysts were isolated, they were not associated with trisomy 18.<sup>27</sup> In another study by our group, we found that of 98 fetuses with isolated CPCs, none had aneuploidy, whereas of the 13 fetuses with CPCs and major anatomic abnormalities, 100% had trisomy 18.<sup>131</sup> Subsequently, one group of investigators found that all 131 fetuses with isolated CPC had normal karyotypes, and all fetuses with aneuploidy had additional anomalies.<sup>132</sup> In addition, we have shown that from a cost-benefit point of view, invasive testing based on the presence of isolated CPCs is not justified.<sup>133</sup>

Previously, it has also been believed that large cysts (> 1 cm) or bilateral cysts increased the risk for aneuploidy. Some evidence suggests that these larger cysts further increase the risk for trisomy 18 (compared with smaller cysts)<sup>134-138</sup>; however, this should still be regarded within the context of whether other abnormalities are also present or not. Although CPCs always resolve, larger cysts may take longer to undergo this process, lending support to the observation that delayed resolution of CPCs may carry an increased risk for trisomy 18.<sup>30</sup> One must also remember that it has been shown that small, unilateral lesions may be seen in chromosomally abnormal fetuses.<sup>139</sup> Whether CPCs are unilateral or bilateral is probably not significant, although it is probably the case that larger cysts also tend to be bilateral.<sup>30</sup> In our study, of the 19 trisomy 18 fetuses with CPCs, 79% (n = 15) had bilateral cysts; of these, six had a "moth-eaten" appearance of the choroid plexus.<sup>4</sup> On the



other hand, four fetuses had unilateral CPC(s), of whom three had only a single cyst.

Unlike for trisomy 18, a possible relationship between CPC and trisomy 21 is somewhat controversial. Some studies have suggested that CPCs are associated with Down syndrome in the second trimester.<sup>127,134,139-141</sup> However, Bromley showed that the incidence of CPCs in the normal population (1.4%) was the same as the incidence of cysts among fetuses with Down syndrome.<sup>142</sup> Thus, they concluded that the presence of CPCs did not increase a patient's risk for fetal Down syndrome. In a meta-analysis, the authors reported that isolated CPCs were associated with a fetal Down syndrome risk of 1/880, which is the same as that of the general population.<sup>143</sup>

Therefore, in order to increase or decrease one's suspicion of aneuploidy, when CPCs are visualized sonographically, we believe a thorough, detailed examination needs to be performed of the remaining fetal anatomy to rule out other abnormalities. In our experience, if no other anomalies are found (especially when hands are open and ear length is normal), the risk of aneuploidy remains very low (even in a high-risk patient), and invasive testing is not warranted. As described in a recent editorial, it is recommended that when CPC is the only detected sonographic abnormality, it should be emphasized that as an isolated finding in a patient otherwise considered at low risk for fetal aneuploidy, a CPC is not considered clinically significant and does not change the patient from low- to high-risk status.<sup>144</sup> Therefore, although CPCs have been reported to be associated with fetal aneuploidy, if no other major or minor sonographic anomalies are identified in the fetus, and in the absence of other risk factors, this is considered a "normal variant," and no further evaluation is recommended.<sup>144</sup>

Many recommend that if fetal karyotyping is not performed when CPC are identified, follow-up sonograms should be performed to follow the cysts. However, because they always resolve, repeat scans add no value to decision making, with the possible exception of detecting other sonographic anomalies that were previously missed.

## Nasal Bone

In 1866, when Langdon Down first described the features of patients with trisomy 21, he noted that the face was flat and the nose small.<sup>157</sup> This is a common feature of the Down syndrome facies (Fig. 4-38). As a more objective confirmation, absent ossification, hypoplastic or short, and agenesis of the nasal bone have also been described in radiographs of Down syndrome fetuses.<sup>158,159</sup> Keeling et al<sup>158</sup> examined 31 Down syndrome fetuses (12-24 weeks) with radiographs, and found that 61% had hypoplasia or agenesis of the nasal bone. Recently, nasal bone hypoplasia or absence of nasal bone on ultrasonography has been described as a sign of fetal Down syndrome. One of the first ultrasound papers was published in 2001, when Cicero noted that among 59 cases of Down syndrome in the first trimester, 73% had an absent nasal bone with a false-positive rate of only 0.5%.<sup>160</sup> Subsequently, this was followed by a case report series in 2002 that described three second trimester Down syndrome fetuses of high-risk women, in which 66% ( $n = 2$ ) had an absent nasal bone, and the third had a nasal bone length less than 2.5% for gestational age.<sup>161</sup>



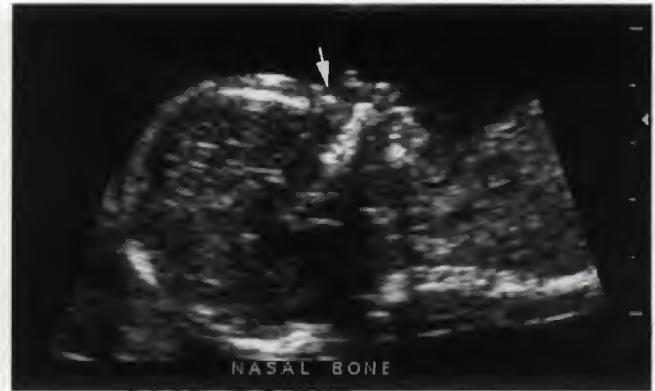
**FIGURE 4-38.** Characteristic Down syndrome facies on three-dimensional imaging, with a small nose and the tongue protruding outwards.

When evaluating the facial profile for the nasal bone, the correct technique and angle of insonation should be used. The profile should be viewed in the midsagittal plane, with care taken to keep the angle of insonation close to 45 degrees or 135 degrees.<sup>161</sup> This technique is recommended in order to avoid artificially causing false nasal bone measurements. With angles less than 45 degrees or greater than 135 degrees, the nasal bone may artificially appear *absent*. On the other hand, as the angle approaches 90 degrees, edges of the bone may become difficult to delineate precisely because of echo scatter, and the measurement may become artificially large. The nasal bone should be visualized as a linear echogenic structure if the correct technique described above is used (Fig. 4-39).

Many studies have examined the sensitivity and false-positive rates in the second trimester, for sonographically absent (Fig. 4-40 and Table 4-7) or hypoplastic/short fetal nasal bone (Fig. 4-41) as a sonographic marker for the detection of Down syndrome. The sensitivities for absent nasal bone have ranged from 28% to 66%, and false-positive rates from 0 to 20%. However, many studies show sensitivities and false-positive rates ranging from 34.6% to 57% and 0% to 3.7%, respectively (see Table 4-7). Importantly, it appears that the sensitivity and false-positive rate of absent nasal bone in detecting Down syndrome approximates that of nuchal fold thickening (40% sensitivity, 0.1% false-positive rate).<sup>172</sup> Recently, through a matched case-control study we examined the usefulness of absent nasal bone by ultrasound in the prenatal detection of second trimester fetuses with Down syndrome.<sup>63</sup> There were 40 fetuses identified with Down syndrome, and in 72.5%



**FIGURE 4-39.** Normal facial profile showing presence of the fetal nasal bone (arrow).



A



B

**FIGURE 4-41.** Hypoplastic nasal bone. A. Facial profile of fetus affected with duplication/deletion aneuploidy. There is a hypoplastic nasal bone (arrow) present. B. Facial profile of another fetus showing a small nasal bone (arrow).



**FIGURE 4-40.** Facial profile of a fetus with trisomy 21, demonstrating an absent nasal bone. Also note the tongue protruding slightly outwards between the lips.

**Table 4-7**

**Summary of Sensitivity and False-positive Rates of Sonographic Absent Fetal Nasal Bone (Second Trimester) in Detecting Down Syndrome**

Author/Year	Down Syndrome (Number of Cases)	Gestational Ages (Weeks)	Sensitivity	FPR	Comments
Sonek 2002 <sup>162</sup>	3	19-22	66%	NA	Third fetus had NB length < 2.5% for gestational age
Bromley 2002 <sup>162</sup>	16	15-20	37%	0.5%	
Cicero 2003 <sup>163</sup>	34	15-22	62%	1.2%	Hypoplastic defined as absent NB or < 2.5 mm
Lee 2003 <sup>164</sup>	20	*21.8±3.0	40-45%	10-20%	3-D sonography
Vintzileos 2003 <sup>63</sup>	40	*19.2±1.5	41%	0%	
Odibo 2004 <sup>165</sup>	18	15-22	28%	2%	
Goncalves 2004 <sup>166</sup>	26	19.6-25.2	34.6%	3.7%	3-D sonography
Zelop 2004 <sup>167</sup>	12	15-22	33%	0%	
Freire-Lizama 2004 <sup>168</sup>	7	15-23	42.8%	0%	28.5% had small NB < 10%
Viora 2005 <sup>169</sup>	18	15-21	55.5%	0.47%	Another 22.2% had hypoplastic NB
Benoit 2005 <sup>170</sup>	14	17-26	57%	NA	
Bergann 2006 <sup>171</sup>	17	18-26	41%	0%	3-D sonography

FPR, false-positive rate; NA, not available; NB, nasal bone; 3-D, three-dimensional.

\*Mean ± standard deviation.



( $n = 29$ ), an adequate facial profile was obtained. Of these 29 fetuses, 12 had an absent nasal bone for a sensitivity of 41%, with a specificity of 100% (or false-positive rate 0%). More importantly, the sensitivity of genetic sonography was increased from 83% to 90% by adding absent nasal bone to the other sonographic aneuploidy markers.<sup>63</sup> Since 2003, we have therefore added this marker to the list of other sonographic aneuploidy markers evaluated during a genetic ultrasound examination. With regard to absent nasal bone, because the specificity is very high (with correspondingly low false-positive rates), it is an ideal marker to add to other more "traditional" markers evaluated during genetic sonography because it does not increase the false-positive rate. Others also have suggested that the association of NBLs to other sonographic markers may further improve sensitivity and reduce the false-positive rate for fetal trisomy 21, allowing the avoidance of unnecessary invasive procedures.<sup>173</sup>

In 2005, we reported that the addition of absent nasal bone as an aneuploidy marker increased the sensitivity of second trimester genetic sonography for Down syndrome from 87% (before including absent nasal bone as a marker) to 92.8%, without increasing the false-positive rate.<sup>174</sup> This significant increase in the detection of trisomy 21 with the addition of absent nasal bone as a marker emphasizes the need to include this marker in the list of aneuploidy markers evaluated during a genetic sonogram. Similarly to our finding, Goncalves found that three of their 26 Down syndrome fetuses had no sonographic markers for this condition at the time of examination.<sup>166</sup> However, among these fetuses, two had absent nasal bone, although one had a normal nasal bone. Bromley et al<sup>162</sup> also found that among their 16 Down syndrome cases, although 13 had other sonographic markers suggesting aneuploidy, three had no other markers. Nevertheless, of these three Down syndrome fetuses that possessed no other sonographic markers, two had absent nasal bone.

We currently use the presence or absence of nasal bone as a sonographic marker for aneuploidy, and we have shown 100% agreement between examiners with respect to presence or absence of nasal bone. However, we believe that if short or hypoplastic nasal bone is going to be used as a marker in detecting Down syndrome, each unit should establish their own sonographic nomograms of NBL in the second trimester which are specific to their respective patient populations. It is only then, that examination of various cutoffs and evaluating their respective efficacies can establish what degree of hypoplastic nasal bone (or NBL) has the most appropriate efficacy for detecting fetal Down syndrome and aneuploidy. This has already been performed by some groups.<sup>175,175</sup> Through normative data of NBLs which have been created, it has been shown that the fetal NBL increases linearly with advancing gestational age.<sup>173,175</sup> There also appears to be some ethnic/racial differences in NBLs. A pilot study examining the fetal nasal bone in the Chinese population found the length to be shorter than that of whites and blacks.<sup>176</sup>

Mean NBLs are shorter and BPD/NBL ratios are greater in fetuses with trisomy 21, as compared with euploid fetuses.<sup>177</sup> In one study examining 16 fetuses with Down syndrome, 37% had no detectable nasal bone, compared with 0.5% of euploid fetuses. An absent nasal bone was found to confer a likelihood ratio of 83 for fetal Down syndrome.<sup>162</sup> In addition,

although absent nasal bone was a powerful marker for trisomy 21, a short nasal bone was also associated with an increased likelihood for trisomy 21 in a high-risk population. By using a BPD/NBL ratio of greater than 10, there was an 81% sensitivity for Down syndrome, with an 11% false-positive rate.<sup>162</sup> Another recent study in 2005 found that of 18 Down syndrome fetuses, 55.5% had an absent nasal bone and an additional 22.2% had hypoplastic nasal bone, with the false-positive rate being only 0.47%.<sup>169</sup> In addition, the BPD/NBL was 10 or greater in 62.5% of fetuses affected by Down syndrome, and in 9.8% of euploid fetuses. They concluded that inclusion of NBL into the second trimester screening protocol could potentially obviate the false-negative cases from other screening tests. Therefore, the measurement of NBL in the second trimester seemed to provide additional benefits beyond the assessment of the presence or absence of the nasal bone.<sup>169</sup>

Recently, three-dimensional (3-D) ultrasonography has been used in the second trimester to allow more accurate visualization of the fetal bony face and the nasal bones.<sup>164,166,170</sup> One group has found that unilateral absence or hypoplasia of the nasal bone is an important observation in Down syndrome fetuses, and that this differentiation may be best demonstrated on 3-D imaging.<sup>170</sup> Although many trisomy 21 fetuses had absent nasal bones concordantly on both two-dimensional (2-D) and subsequent 3-D imaging, there were three fetuses with a discrepancy between the imaging modalities. In these three Down syndrome fetuses, all had absent nasal bones by 2-D imaging, however 3-D sonography showed absence of a unilateral nasal bone in all three, and either hypoplasia ( $n = 2$ ) or normal nasal bone ( $n = 1$ ) on the other side. The authors point out that the finding of unilateral hypoplasia of the nasal bone has not been previously described in studies of 2-D imaging, because the nasal bone is normally viewed in a single parasagittal section.<sup>170</sup> The findings could explain some discrepant findings where there is "absence" of the nasal bone on 2-D imaging, but presence on postmortem x-rays. This new information suggests that when 3-D sonographic equipment is available, suspicious findings of hypoplastic/absent nasal bone should be examined via this modality, and volumes can be stored for later evaluation and rendering.<sup>170</sup> The hope and anticipation is that this may improve the accuracy of sonographic prenatal findings and accordingly, the sensitivity for Down syndrome.

Finally, when absent nasal bone is visualized, this is not necessarily a marker solely for fetal Down syndrome. Lee reported that at least 58 genetic syndromes (including trisomy 18) may be associated with absence of the nasal bone.<sup>164</sup> Another study has found that in 41% of all aneuploid fetuses, the nasal bone was either absent or hypoplastic (see Fig. 4-41).<sup>165</sup>

## Iliac Wing Angle

Children with trisomy 21 have pelvic dysplasia and a wider lateral span of the iliac wing as compared with normal children, thus causing a widened iliac angle. Accordingly, attempts have been made to use this as a possible sonographer marker in the second trimester for fetal Down syndrome. By examining a transverse view of the fetal pelvis, the iliac angle made by the two iliac crests at the pivot point



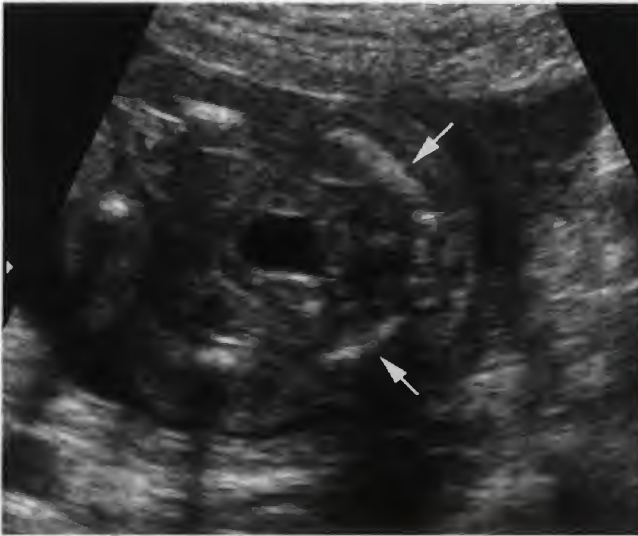


**FIGURE 4-42.** Iliac wing angle on a transverse view through the fetal pelvis, showing a 90-degree angle made by the two iliac crests (arrows) at the sacrum.

of the sacral spine can be measured (Fig. 4-42). One study examined 19 fetuses with trisomy 21, and found that the mean iliac angle was  $80 \pm 19.7$  degrees, as compared with  $63.1 \pm 20.3$  degrees for those with normal karyotypes ( $P = 0.0004$ ).<sup>178</sup> By using an iliac angle of 90 degrees as a cutoff, 36.8% fetuses with Down syndrome were identified, as well as 12.8% of normal fetuses ( $P = 0.003$ ). Other studies have assessed the iliac angle and also found a difference between normal and trisomy 21 fetuses.<sup>179,180</sup> For example, one group found that in their high-risk population, by using a cutoff of greater than or equal to 90 degrees as abnormal, they could detect 90% of Down syndrome fetuses (positive predictive value 33%).<sup>179</sup> Some have also reported using iliac length measurements in screening for trisomy 21.<sup>181</sup> They found that the observed-to-expected iliac length measurement gave a sensitivity of 40% (false-positive rate 2%) for the detection of trisomy 21 fetuses.<sup>181</sup>

However, unlike other aneuploidy markers, which are very reproducible and consistent (such as pyelectasis, single umbilical artery), there is considerable variation in the measurement of the iliac wing angle. The angle may vary, depending on the actual transverse level at which the measurement is taken, and there is also significant intra- and interobserver variability. Several factors affect this measurement, including orientation of spine, axial level, and gestational age.<sup>182</sup> One group found that the iliac angle decreased by 15.7 degrees from the superior to inferior portion of the pelvis, and decreased by as much as 15.6 degrees when the spine is directed to the side.<sup>182</sup> Thus, despite studies toting the utility of this sonographic marker in the second trimester for detecting fetal Down syndrome, if one has a known Down syndrome fetus, depending on which level the angle is measured, the angle can be greater or less than 90 degrees. Therefore, similar to others,<sup>183</sup> because obtaining a standard measurement is difficult and due to variation in the angle measured depending on the various factors described, we have not incorporated this particular

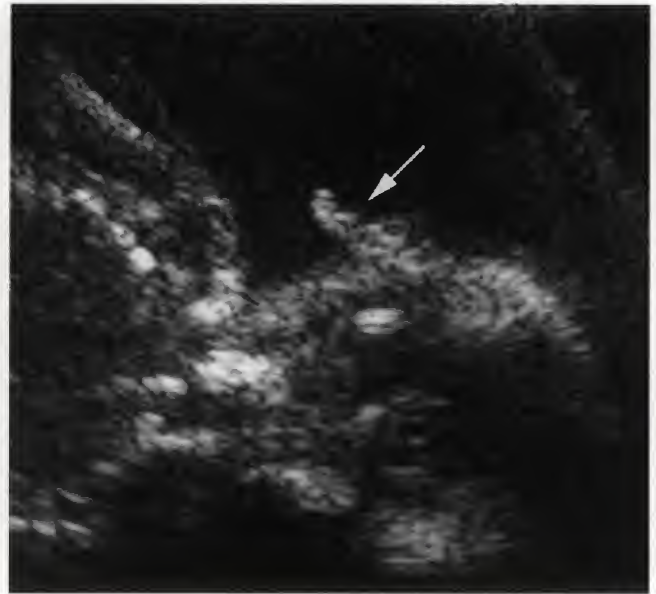


**FIGURE 4-43.** Second trimester fetus with low-set ear (arrow).

marker into our second trimester genetic sonogram. Most experts believe that a widened pelvic angle is not a useful marker, especially when used as part of a screening ultrasound.<sup>184</sup>

## Ear Length

Abnormally small ears have previously been described to be one of the most consistent clinical findings in newborns and infants with aneuploidy, including Down syndrome.<sup>185</sup> As a matter of fact, it has been described by Thelander and Pryor<sup>186</sup> that one of the most striking and consistent growth discrepancies documented in children with Down syndrome is in the development of the external ear. They found that of all the anthropomorphic measurements examined, the longitudinal dimension of the pinna fell the furthest below the expected norm in all age levels studied. In addition, as many as 60% of newborns with Down syndrome and more than 80% to 90% of those with trisomy 18 and 13 have ear anomalies described as a characteristic feature.<sup>187</sup> Low-set ears (Fig. 4-43) with abnormal helix have also been found to be one of the most frequent anomalies (77%) in autopsy cases of trisomy 18.<sup>188</sup>

Therefore, short ear length on prenatal ultrasound has been examined as a potential sonographic marker for the detection of fetal aneuploidy. Several prenatal sonographic studies have noted an association between fetal ear length and aneuploidy. One group found that short ears ( $\geq 1.5$  standard deviations below gestational age average) were associated with fetal chromosomal disorders, with a sensitivity of 73.3%.<sup>189</sup> However, although short ears were always found sonographically in cases with trisomy 18 and 13, it occurred only in about half of the cases with trisomy 21.<sup>189</sup> Lettieri et al<sup>190</sup> prospectively measured second trimester fetal ear lengths and found that most aneuploid fetuses had short ear lengths ( $\leq 10$ th percentile), with a sensitivity of 71%. Another study calculated measured-to-expected ear length ratios and



found that these ratios were significantly lower in fetuses with aneuploidy. They found that a ratio of less than 0.8 had a 75% sensitivity for detecting Down syndrome fetuses and 83.3% sensitivity for detecting trisomy 18.<sup>191</sup> Subsequently, in 1997 another group found the sensitivity of ear length below the 5th percentile for the detection of chromosomal abnormalities to be 80%.<sup>192</sup> Chitkara et al<sup>193</sup> measured sonographic ear lengths in normal fetuses to create a nomogram, and then found that short ear lengths were a useful parameter in predicting fetal aneuploidy.<sup>194</sup> Thirty-two percent (11/34) of fetuses with significant chromosomal abnormalities had short ear lengths, and in six cases, this was the only sonographic finding.<sup>194</sup>

We recently examined the sensitivity of ear length in detecting fetal aneuploidy. First, we established a nomogram for ear length (14–41 weeks) prospectively.<sup>195</sup> Ninety-six fetuses with aneuploidy were identified: trisomy 21 ( $n = 51$ ), trisomy 18 ( $n = 24$ ), trisomy 13 ( $n = 6$ ), Turner syndrome ( $n = 4$ ), and others ( $n = 11$ ). Sixty-three of these aneuploid fetuses had ear lengths less than or equal to 10th percentile for gestational age, for a sensitivity of 66%. We found that of all the Down syndrome fetuses, 41% had an ear length less than or equal to 10th percentile. Twenty-three out of the 24 fetuses with trisomy 18 had ear lengths less than or equal to 10th percentile for gestational age, for a sensitivity of 96%, whereas all six fetuses with trisomy 13 had ear lengths less than or equal to 10th percentile for gestational age, for a sensitivity of 100%.<sup>195</sup> Therefore, short ear length was not as sensitive a marker for trisomy 21 as it was for trisomies 18 (96%) and 13 (100%). Aneuploid ear lengths were also plotted against the nomogram curves for BPD, divided according to the type of aneuploidy. When using ear length against BPD, the sensitivity of all aneuploid fetuses less than or equal to 10th percentile was 43%. When examining the individual aneuploidies, the sensitivities of ear length less than or equal to 10th percentile for BPD for trisomies 21, 18, 13, and other types of aneuploidy were 28%, 87%, 60%, and 27%, respectively. Therefore, we found that the small ears were not related entirely to overall small fetal size, but in almost one half the cases (43%), the fetal ear lengths were disproportionately smaller than their BPDs (especially in trisomy 18 and 13), indicating “true” smaller ears.

In another study, we examined the prenatal detection of fetal trisomy 18 through abnormal sonographic features.<sup>4</sup> Twenty-seven fetuses with trisomy 18 had prenatal ear length measurements available and were defined as short if the ear length was less than 10th percentile for gestational age. We found short ear length to be overall the most sensitive marker for trisomy 18 (96%). It is important to note, however, that this finding was always seen with multiple other abnormalities and never in isolation. Chitkara et al<sup>194</sup> found that from their four cases of trisomy 18, 75% had short ear length, as well as other sonographic abnormalities.

When performing second trimester genetic sonography, we routinely obtain the ear length measurement and incorporate evaluation of fetal ear length as an aneuploidy marker. In addition, when trying to rule out trisomy 18 on prenatal sonography, an attempt should always be made to evaluate the ear length. Although a normal ear length cannot rule out trisomy 18 completely, it should markedly decrease the risk for this condition.



**FIGURE 4-44.** Long-axis view of fetal lower extremity in the second trimester, showing a clubbed foot. Note that the plantar surface of the foot is seen in the same plane as the entire lengths of the tibia and fibula.



**FIGURE 4-45.** Gross pathologic image of neonate demonstrating bilateral clubbed feet.

## Extremity Abnormalities

In addition to being seen frequently in association with spina bifida, *clubfoot* (Figs. 4-44 and 4-45) has been also associated with various types of aneuploidy, including trisomies 18 and 13.<sup>196</sup> In our experience, 32% of trisomy 18 fetuses have clubfeet.<sup>4</sup> In a postmortem study, clubfeet were also present in 23% of trisomy 18 cases.<sup>197</sup> In another study of 26 fetuses with trisomy 18, 38% had evidence of clubfeet on ultrasound.<sup>126</sup> In general, however, most of these aneuploid fetuses will show other sonographic anomalies. Therefore, it is somewhat controversial as to whether an isolated clubfoot justifies invasive testing for karyotype analysis. In one study examining 68 cases of fetuses with apparently isolated clubfoot on ultrasound and having available follow-up, approximately





**FIGURE 4-46.** Gross pathologic image of neonate with trisomy 9, showing a rocker-bottom foot.

6% had aneuploidy (trisomy 21, trisomy 18, 47XXX, 47XXY).<sup>198</sup> However, there were other anomalies some of which were detected only after birth, including mild posterior urethral valves, early renal dysplasia, ventricular septal defects, and hip or other limb abnormalities. Accordingly, the authors recommended that because other subtle associated malformations may not be detected on early second trimester sonography, fetal karyotyping should be offered when isolated clubfoot is visualized on prenatal sonography.<sup>198</sup> On the other hand, in a recent study reviewing 51 cases of isolated clubfoot, other investigators found no additional malformations detected at birth or cases of aneuploidy.<sup>199</sup> Accordingly, the study concluded that provided a thorough fetal sonogram is performed (and is normal), and the patient is considered low risk, an isolated unilateral/bilateral clubfoot does not appear to be an indication for fetal karyotyping.<sup>199</sup>

**Rocker-bottom foot** (Fig. 4-46) occurs when one or both feet appear to have a “rocker-bottom” appearance on sonography (similar to the bottom of a rocking chair), instead of the normal inward arch of the plantar surface of the foot. This finding may be seen in some aneuploidies, such as trisomies 18 and 13. In our series of fetuses with trisomy 18, we found that 29% had evidence of rocker-bottom feet.<sup>4</sup> In a post-mortem study, rocker-bottom feet were present in 10% of trisomy 18 cases.<sup>197</sup> Another group found that of 12 fetuses with trisomy 18, 70% had clubfeet or rocker-bottom feet seen on prenatal sonography.<sup>200</sup>

**Clinodactyly** (or hypoplasia of the middle phalanx of the 5th digit) (Figs. 4-47 and 4-48) is visualized as a curving inward or deviation of the 5th digit of the fetal hand toward the other fingers. It may be seen with Down syndrome, and in a radiographic postmortem study, was seen in about one third of cases.<sup>159</sup> Of infants with trisomy 21, it appears that



**FIGURE 4-47.** Second trimester fetus with Down syndrome showing a hypoplastic middle phalanx of the fifth digit (arrow) and clinodactyly.

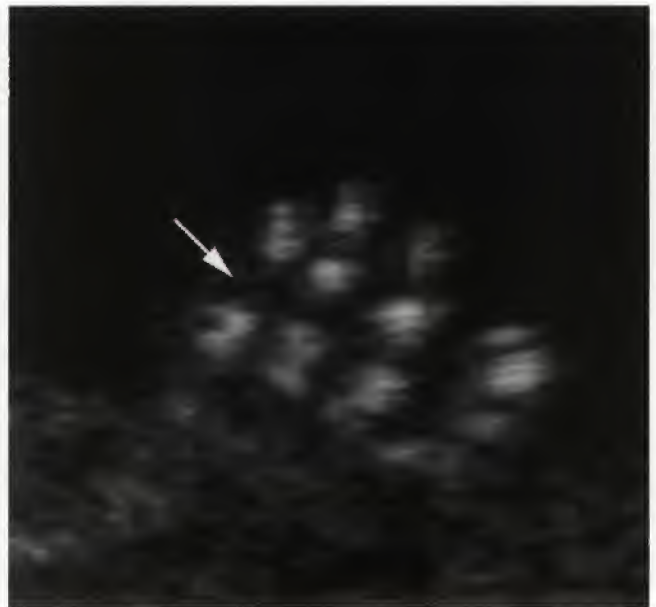


**FIGURE 4-48.** Sonographic view of fetal fingers, showing complete absence of the middle phalanx of the fifth digit (arrow).

60% have this feature.<sup>68</sup> Subsequently, clinodactyly has been examined in both normal and Down syndrome fetuses on second trimester prenatal sonography.<sup>201</sup> By using a ratio (length middle phalanx 5th digit/length middle phalanx 4th digit), some investigators found that the mean ratio for normal and Down syndrome fetuses was 0.85 and 0.59 ( $P = 0.04$ ), respectively. When a cutoff ratio of 0.70 was used, there was a 75% sensitivity for fetal Down syndrome, with an 18% false-positive rate.<sup>201</sup>





**FIGURE 4-49.** Plantar view of the foot in a second trimester fetus with Down syndrome, showing a sandal-gap deformity with wide space between first and second toes (arrow).

Although clinodactyly is often used as an aneuploidy marker for fetal Down syndrome, it should be kept in mind that this is a feature seen in many normal fetuses. In addition, unlike thickened nuchal fold or pyelectasis, the interpretation and impression of clinodactyly is often susceptible to more subjective variability. It can also be a feature that is generally difficult to assess on second trimester sonography and is dependent on fetal positioning. Therefore, whereas evaluation of this marker may be appropriate in the high-risk patient, it should probably not be used in a screening environment, due to its high false-positive rate.

In 1994, the *sandal gap* deformity was described in a fetus with Down syndrome.<sup>202</sup> This occurs when there is separation of the great toe from the second toe (Fig. 4-49), causing a wide space or gap to be visualized on prenatal sonography. Like clinodactyly, sandal gap is also commonly seen among normal fetuses and can therefore be difficult to use in a screening setting. However, in our experience, although many normal fetuses may exhibit this feature, in these cases, it is usually transient, and careful observation will reveal closing of this space during the time of the sonogram. We have noticed that in fetuses with trisomy 21, the sandal gap deformity often remains persistent throughout the observation period, even despite fetal movement. Another point to keep in mind is that the sonographic appearance of the fetal toes may be very similar or even identical to that of the parents (who can show a wide normal variation in appearances), and may therefore be familial and not necessarily indicative of an abnormality or malformation.

Limb reduction malformations (such as *radial aplasia*) (Fig. 4-50) are associated with aneuploidy, especially trisomy 18.<sup>203</sup> In fact, when radial aplasia is identified, trisomy 18 should be in the differential diagnosis.

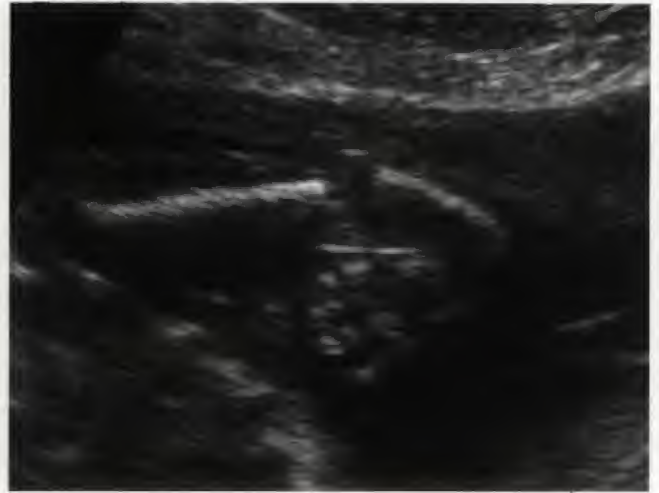


**FIGURE 4-50.** Scan of the arm in a trisomy 18 fetus shows the characteristic appearance of radial aplasia. The hand is turned inwards, and the forearm is shortened. The long humerus bone is also visualized.



**FIGURE 4-51.** Sonogram of fetus with trisomy 18 shows bilateral clenched hands, which persisted throughout the sonographic examination.

*Flexion deformities and movement disorders* are also commonly seen with trisomy 18. In particular, a very characteristic finding of this chromosomal abnormality is fixed flexion of the hands (or *clenched hands*), often having overlapping digits (Figs. 4-51 and 4-52). In fact, some trisomy 18 fetuses even show generalized arthrogryposis or contractures. When examining the prenatal sonographic features of trisomy 18, we found contractures in 18%.<sup>4</sup> We also found bilateral clenched hands and overlapping digits to be highly sensitive (95%) and the second most common sonographic abnormality in fetuses with trisomy 18.<sup>4</sup> Importantly, this feature was seen even at early gestational ages (between 14.6 and 17.6 weeks). This has been documented on fetoscopic observation as early as 14 weeks, suggesting that malpositioning of the fingers in trisomy 18 occurs some time between 12 and



**FIGURE 4-52.** Three-dimensional image of fetus with trisomy 18 shows persistently bilateral clenched hands in front of the face. These hand findings are a characteristic finding of this aneuploidy.

14 weeks of gestation.<sup>204</sup> Another case series has reported overlapping fingers sonographically at 13 weeks.<sup>205</sup> Our sensitivity of 95% is similar to the experience of Shields et al,<sup>206</sup> in which they found the most common sonographic abnormality seen in trisomy 18 fetuses was persistent abnormal positioning of fingers or clenched fist (89%), and to that of Kinoshita et al,<sup>207</sup> who found overlapping fingers and flexion to be the most common external anomaly (84%) on autopsy.<sup>207</sup> Shields et al<sup>206</sup> also state that because the most common sonographic abnormality found in their population of fetuses with trisomy 18 was abnormal positioning of the hands, it is likely that documentation of an open hand, along with use of maternal triple screen, should reduce the number of patients with CPCs who need invasive testing.

Many other studies have also found abnormal hands to be their most common fetal sonographic abnormality in trisomy 18.<sup>126,200,208</sup> In a postmortem study of aneuploid cases, clenched fists were seen in 35% of cases of trisomy 18 at autopsy.<sup>197</sup> Another study of ultrasonographically diagnosed fetal wrist position abnormalities showed 32% to have trisomy 18.<sup>209</sup> We have never sonographically visualized open hands (full extension of all fingers in the same plane as the metacarpals) in fetuses that ultimately prove to have trisomy 18. Our sensitivity of hand abnormalities was not 100%. However, because one fetus was 36 weeks at the time of sonographic examination (the hands were difficult to visualize), and in the other case, the hands were not examined sonographically owing to the patient's request to

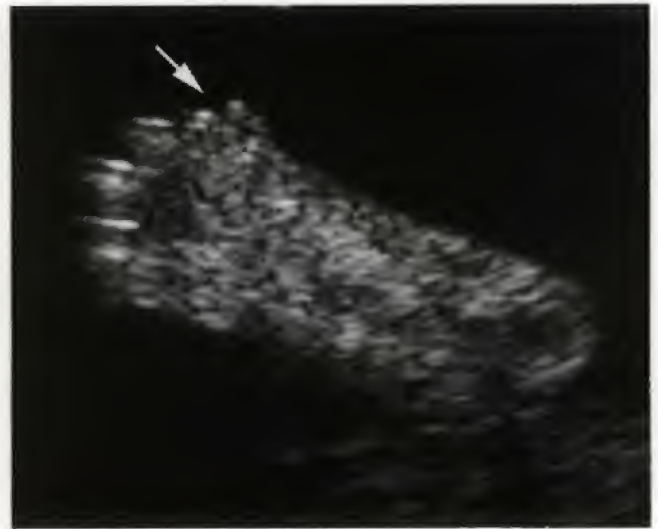


**FIGURE 4-53.** Plantar surface of the foot of a trisomy 18 fetus. Note the very abnormal appearance of the dysplastic toes. The fourth and fifth toes (arrow) are also smaller than the rest.

stop the examination. In both cases, however, delivery and autopsy ultimately showed bilateral clenched hands.

When examining the prenatal sonographic features of trisomy 18, we also found almost two thirds (63%) of our fetuses with trisomy 18 to have lower extremity/feet abnormalities overall.<sup>4</sup> Thirteen percent had evidence of contractures on prenatal sonography, although 16% had an abnormal position/appearance of the toes (Fig. 4-53). In Nyberg's study of 47 fetuses with trisomy 18, he found extremity abnormalities by pathologic examination, sonography, or both, in 93% of fetuses, suggesting that when trisomy 18 is suspected on the basis of other sonographic findings, the hands and feet should be specifically evaluated.<sup>3</sup> Another study found that of 15 fetuses with trisomy 18, the most common sonographic abnormality was abnormal hands or feet (73%).<sup>208</sup>

*Polydactyly* occurs when there is the presence of more than five digits. It is classified as preaxial if the extra digits are located on the radial or tibial side, or postaxial if they are located on the ulnar or fibular side. Most commonly, this extra digit is a simple skin tag (which can be difficult to see sonographically), but bones or a completely duplicated and nonfunctional digit may also be present. Polydactyly is frequently present in fetuses with trisomy 13 (Fig. 4-54).<sup>30</sup>

### Single Umbilical Artery

The normal umbilical cord contains three vessels (two arteries and one vein) that are surrounded by Wharton's jelly. The absence of one of the umbilical arteries (SUA or two-vessel cord) is the most common pathologic condition of the umbilicus in humans and one of the most common malformations in humans, with an incidence of 1% in singleton births, and 4.6% in twin births.<sup>210</sup>

The prenatal diagnosis of SUA (Fig. 4-55) on sonography is not difficult with current, modern sonographic equipment. The basic prenatal screening technique involves an



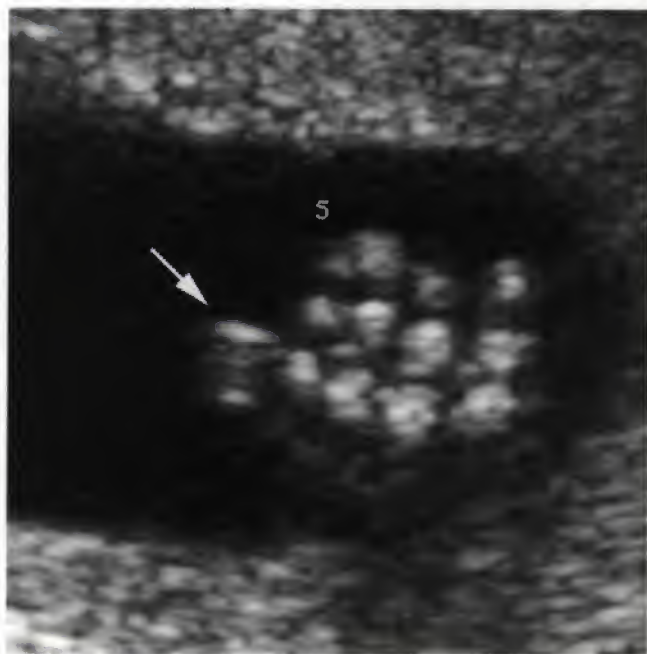


**FIGURE 4-54.** View of the hand of a trisomy 13 fetus, showing postaxial polydactyly (arrow). Both hands were affected similarly.

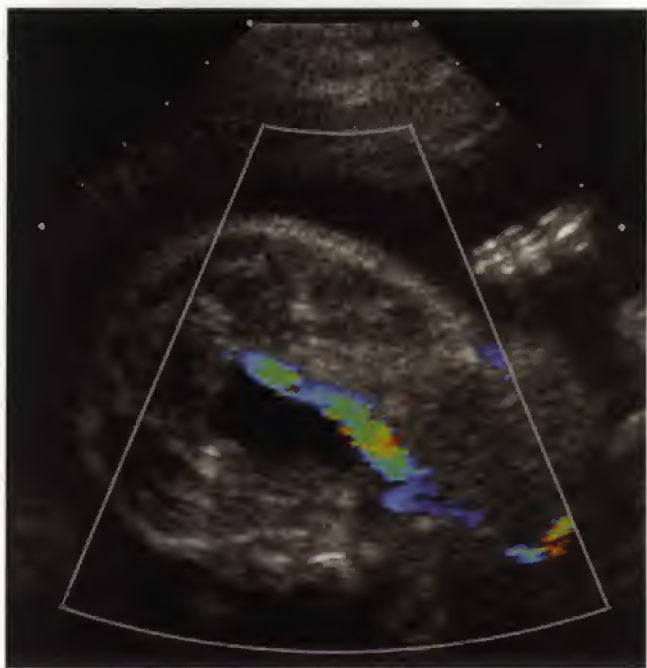
examination of transverse views of a free loop of cord with adequate magnification (see Fig. 4-55). In this view, when there is an SUA, only two vessels are visualized, where the larger vessel is the vein and the smaller vessel is the umbilical artery. Another method that can be used in the prenatal detection of SUA is demonstrating the absent intra-abdominal segment of the missing umbilical artery. This can be detected prenatally by examining the umbilical arteries running alongside and around the fetal bladder in a transverse view of the pelvis (Fig. 4-55B). Examination is greatly enhanced by using color flow Doppler or power Doppler imaging, and appears to be the best screening technique for SUA.

There is a well-known association between SUA and cytogenetic abnormalities. The incidence of cytogenetic abnormalities among fetuses demonstrating SUA has been 17%, with nearly one half of these fetuses having major anomalies.<sup>211,212</sup> Trisomy 18 is the most common aneuploidy associated with SUA.<sup>213</sup> The next most common types of abnormal karyotypes associated with SUA are trisomy 13, Turner syndrome (45X), and triploidy.<sup>213</sup> SUA has an incidence of 11.3% among cytogenetically abnormal pregnancies, and it can be found in 10% to 50% of trisomy 18 fetuses.<sup>214</sup> Of trisomy 13 fetuses, 10% to 50% also have an SUA.<sup>30</sup> In one of our recent studies examining the abnormal sonographic features of trisomy 18, we found that 21% had a single umbilical artery.<sup>4</sup> On the other hand, Down syndrome does not appear to be commonly associated with SUA,<sup>212</sup> although it has been reported. It is important to keep in mind, however, that although SUA has been included as an aneuploidy marker, it is nonspecific and is most commonly seen in normal fetuses.

SUA has also been reported to be associated with an increased risk of congenital anomalies, fetal growth restriction,



A



B

**FIGURE 4-55.** A. Multiple short axis sections through the umbilical cord in a patient with a single umbilical artery. The larger structure in each case is the vein, the smaller, the artery. B. Transverse axial plane of section through the fetal abdomen in a patient with a single umbilical artery. The single umbilical artery is seen adjacent to the urinary bladder.

prematurity, and an increased perinatal mortality rate.<sup>215</sup> The incidence of congenital anomalies has been reported to be 20% in infants with SUA.<sup>211</sup> The risk for congenital anomalies in infants with SUA depends on the ascertainment method (being highest at autopsy), but cases diagnosed sonographically or at term deliveries still have an increased risk of anomalies. The rate of associated fetal anomalies with SUA ranges, in various studies, from 18.4% to more than 47%, with the highest rates of associated malformations reported in pathologic rather than clinical studies.<sup>216</sup>

Neonates with SUA may have anomalies involving a wide variety of organ systems, including central nervous, musculoskeletal, cardiovascular, gastrointestinal, and genitourinary systems.<sup>217</sup> However, no consistent pattern of anomalies has been recognized in association with SUA, and virtually any malformation may be present. SUA also occurs in various genetic syndromes, such as VATER association, Jarcho-Levin syndrome, Meckel-Gruber syndrome, as well as others.<sup>218</sup> Therefore, it is imperative that when a SUA is identified, a targeted and detailed fetal anatomic survey should be performed to rule out concurrent malformations. In addition, given the common association of single umbilical artery with congenital cardiac disease, even in the presence of a normal fetal karyotype, a detailed evaluation of the heart should also be performed in fetuses with SUA.<sup>219</sup>

In a large study of 167 fetuses with SUA, among those cases with postnatal information, 31% had structural abnormalities, often involving multiple organs.<sup>217</sup> The most common organ systems involved were the heart, the gastrointestinal system, and central nervous system, in that order. Importantly, among 85 cases with apparently isolated single umbilical artery at sonography and known fetal outcome, 7% proved to be anomalous at birth, which is considerable.<sup>217</sup> Therefore, although invasive testing in the neonatal period may not be necessary in an uncomplicated infant, a careful and thorough physical examination of the neonate is required to exclude other anomalies.

In fetuses with isolated SUA, there is usually no increased incidence for a chromosome abnormality.<sup>211</sup> However, as with isolated CPCs, this stipulates that a detailed sonogram by experienced personnel should rule out other anomalies. Once the single umbilical artery is believed to be genuinely isolated, in the absence of high-risk factors, invasive prenatal diagnostic procedures for chromosomal analysis may not be routinely indicated, because most fetuses with isolated SUA are karyotypically normal. However, when intrauterine growth restriction or multiple malformations are detected in association with SUA, prenatal karyotyping should be offered. In summary, once SUA is identified sonographically, this should trigger a search for additional abnormalities, but by itself, the finding may not be an indication for chromosome analysis in the low-risk patient. However, patients should be informed that their neonates may be at risk for subtle anomalies which may be found only at the time of birth.

### Other Sonographic Aneuploidy Markers

*Brachycephaly* (anteroposterior shortening) (Fig. 4-56) and frontal lobe shortening can be seen in infants with Down syndrome. Therefore, investigators have tried to evaluate the use of these characteristics in detecting fetuses with trisomy 21.<sup>220,221</sup> In 1998, a report showed that frontal lobe shortening had a sensitivity of 16%, with a false-positive rate of 3%.<sup>221</sup> They suggested that this marker could be used in conjunction with other aneuploidy markers. In examining the frontothalamic distance in 19 fetuses with Down syndrome in the second trimester, another group found that 52% of Down syndrome fetuses had a distance that was less than 10th percentile.<sup>220</sup> By setting the false-positive rate at approximately 5%, the sensitivity of this measurement was 21%.

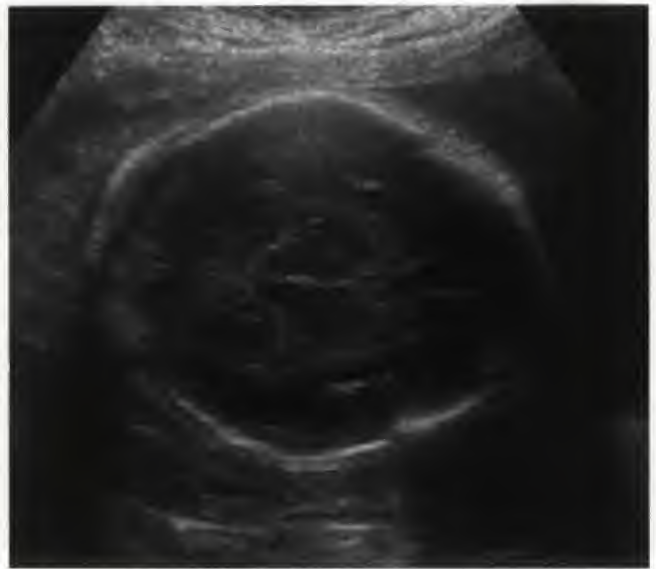


**FIGURE 4-56.** Transaxial image of the fetal head showing brachycephaly in a fetus with trisomy 21.



**FIGURE 4-57.** Transverse view of the head of a second trimester fetus with trisomy 18, showing a strawberry-shaped skull.

In 1992, Nicolaides first described the *strawberry-shaped* skull (Fig. 4-57) seen in fetuses with trisomy 18.<sup>222</sup> They reported this feature in 52% of fetuses with trisomy 18 who, however, had other anomalies seen sonographically, too. Subsequently, another group reported a strawberry-shaped head in 34% of fetuses with trisomy 18.<sup>206</sup> It is believed that although the false-positive rate in normal fetuses is unknown, it is probably about 1%.<sup>223</sup> Once head shape abnormalities are identified, a careful search of the rest of the fetus for abnormal sonographic findings is warranted.



## TRISOMY 21 (DOWN SYNDROME)

Autosomal trisomies are primarily the result of meiotic nondisjunction, which increases with maternal age. The most common autosomal trisomy in live-born infants is Down syndrome, or trisomy 21. The clinical features of Down syndrome were first described by Dr. John Langdon Down in 1866.<sup>157</sup> It was not until almost a century later that the chromosome abnormality was discovered in 1959. Overall, 1 child in 800 is born with Down syndrome.<sup>224</sup> In the United States, it occurs in 1/504 pregnancies during the second trimester,<sup>225</sup> with the prevalence significantly varying with maternal age. The specific risk of trisomy 21 at the time of second trimester amniocentesis varies from 1/274 for women 35 years of age, to 1/10 for women 48 years of age.<sup>226</sup> Many other chromosomal abnormalities are also associated with increasing maternal age, including trisomies 13 and 18. The risk for fetal Down syndrome also changes depending on the gestational age at the time of the examination, due to intrauterine losses of chromosomally abnormal conceptuses. Thus, at birth, the maternal age-specific incidence of Down syndrome is 33% lower than it is at 15 to 20 weeks, and it is 54% lower at birth than it is at 9 to 14 weeks.<sup>226</sup>

The significance of trisomy 21 lies in the fact that it is the single, most common genetic cause of mental retardation. Trisomy 21 is due to the addition of all or a critical portion of chromosome 21, leading to a triplicate or trisomic state. The critical zone for producing the typical phenotypic characteristics of Down syndrome appears to be 21q22.3. Studies examining the parental origins of chromosome 21 in Down syndrome have shown that 95% of cases of trisomy 21 are due to maternal nondisjunction, and only about 5% of cases contain an extra paternal 21. Ninety-five percent of individuals with trisomy 21 have three copies of chromosome 21, whereas the remaining are due to mosaicism or Robertsonian translocation (most involving chromosome 14 or 21). In general, the recurrence risk for Down syndrome is approximately 1%.

The mean survival is approximately 55 years of age, with the early mortality due to the severity of anomalies (especially cardiac). Invariably, mental retardation is present in adults, with mean IQs of 50 to 60.<sup>30</sup> Persons affected with Down syndrome also have increased risks for premature onset of Alzheimer's disease, hearing loss, strabismus, hypothyroidism, leukemia, and premature aging.

Persons with Down syndrome often exhibit characteristic clinical features, such as: short stature, redundant nuchal skin, flat and small nose, small ears, clinodactyly or curving inward of the 5th finger (midphalanx hypoplasia), Simian crease (single palmar crease), brachycephaly, flat occiput, epicanthal folds, protruding tongue, sandal gap (wide space between first and second toes), cardiac defects, ventricular dilation/hydrocephalus, and gastrointestinal abnormalities. Accordingly, with careful examination, it has been shown that many of these dysmorphic features may also be visualized on second trimester sonography (see Fig. 4-38). Therefore, this knowledge has therefore led to the development of the genetic sonogram, which is essentially a noninvasive evaluation tool for Down syndrome.

## SECOND TRIMESTER GENETIC SONOGRAPHY

Over the past years, with the emergence of sophisticated and high-resolution ultrasonography, and a greater proportion of the maternal population achieving pregnancies at an advanced maternal age, the ability to screen for fetal aneuploidy and other fetal abnormalities has achieved monumental importance in the management of obstetric patients. This task can be accomplished through various testing modalities in the second trimester, such as biochemical serum marker screening as previously discussed, detailed ultrasonography, and if indicated, invasive testing. Invasive forms of testing, such as amniocentesis, chorionic villus sampling, and cordocentesis are diagnostic tests that provide almost a 100% diagnostic accuracy of the presence or absence of aneuploidy. Genetic amniocentesis testing has traditionally been offered to patients who are considered to be at high risk for fetal Down syndrome. These are women whose age at the time of delivery is at least 35 years of age have an abnormal serum marker screen, or both. Biochemical screening and ultrasonography, for the purpose of aneuploidy detection, are screening tests associated with a high number of false-positive results. Nevertheless, owing to the potential significant risks of invasive testing such as pregnancy loss, rupture of membranes, bleeding, and infection, many patients choose to undergo screening surveillance initially and then decide upon further, more invasive forms of diagnosis, if necessary.

The first method of screening for fetal Down syndrome was introduced in the early 1970s and was based on maternal age; amniocentesis was offered to women age 35 years of age or more. This is because at 35 years of age, the midtrimester risk for fetal Down syndrome approximates the risk of pregnancy loss due to amniocentesis (1/270). Over the last three decades, there has been a fundamental shift in birth trends observed, with more births occurring in women 35 years of age or older.<sup>225</sup> Women in the group of 35 to 49 years of age made up 4.7% of live births in 1974, as compared with 12.6% in 1997.<sup>225</sup> As a result, the prevalence of fetal Down syndrome during the second trimester has increased from 1/740 in 1974 to 1/504 in 1997. However, although maternal age is strongly correlated with the risk for fetal Down syndrome, most children with Down syndrome are actually born to women younger than 35 years, because most children are born to women in this younger age group.

A wealth of information has been published in the literature regarding the specific use of second trimester genetic ultrasonography for detecting Down syndrome prenatally by examining multiple aneuploidy markers, and it has now gained widespread use. We currently offer second trimester genetic sonography to all (and only) high-risk patients (advanced maternal age at the time of delivery, abnormal second trimester serum screening results, or abnormal first trimester screening results). Many women use the information derived from this sonogram to obtain an adjusted risk for Down syndrome to guide their decision regarding genetic amniocentesis, rather than choosing traditional, invasive testing as a first option. In fact, we have found over the years that genetic sonography has been a patient-driven service. In high-risk patients when the genetic sonogram is normal, the amniocentesis rate is only 3%.<sup>227</sup>



We have also found that the amniocentesis rate increases in direct proportion to the number of abnormal sonographic markers identified, with 100% of patients selecting invasive testing when four or more markers are seen. Since the initiation of our genetic sonography service over a 10-year period, approximately 5000 patients have avoided amniocentesis testing. If the fetal loss rate directly related to amniocentesis is estimated to be between 1/100 and 1/300, then this amounts to between 17 and 50 fetal lives saved, thus attesting to the power of normal genetic sonography.

Maternal age as a screening method may currently identify only 47% of Down syndrome cases, with a false-positive rate that has been increasing in recent years (13%–14%).<sup>225</sup> When advanced maternal age alone is used to screen for Down syndrome, about 140 amniocenteses are needed to discover one trisomy 21 fetus,<sup>6</sup> implying that one normal fetus may be lost for every two fetuses identified with DS. Although combining maternal age and second trimester serum screen identifies approximately 60% to 65% of fetuses with DS,<sup>228</sup> this approach would still require approximately 60 to 70 amniocenteses to detect one fetus with DS.<sup>6</sup> As a result, one normal fetus may be lost as a complication of amniocentesis for every three to four fetuses detected with trisomy 21. Therefore, owing to these reasons, the practice of routinely offering invasive testing to all high-risk pregnant women has been challenged.<sup>228</sup> Genetic sonography reduces the invasive testing rate, and can optimize the selection of candidates for invasive testing in order to decrease procedure-related losses of normal fetuses without significantly decreasing detection rates. Accordingly, the genetic sonogram evolved from a patient's perspective with the purpose of possibly avoiding invasive testing, and many patients use the information derived from genetic ultrasound to guide their decision regarding amniocentesis.

Genetic sonography, which is performed in the second trimester, is a specific targeted examination for fetal aneuploidy, most specifically for trisomy 21, that searches for the presence of fetal structural anomalies, as well as other aneuploidy markers and abnormal fetal biometry.<sup>227</sup> Ideally, it is performed between 18 and 20 weeks of gestation. Because only 25% of Down syndrome fetuses in the second trimester have sonographically detectable major anomalies,<sup>6</sup> the search must involve some of the aforementioned markers in order to increase sensitivity. The sonographic aneuploidy markers that are used may include short long bones, increased nuchal fold thickness (see Figs. 4–30 and 4–31), pyelectasis (see Fig. 4–32), CPCs (see Fig. 4–37), short car length (see Fig. 4–43), wide iliac wing angle (see Fig. 4–42), hyperechoic bowel (see Fig. 4–36), echogenic intracardiac focus (see Figs. 4–33, 4–34, and 4–35), sandal gap toes (see Fig. 4–49), hypoplastic mid-phalanx of 5th digit (see Figs. 4–47 and 4–48), clinodactyly (see Fig. 4–47), and more recently, absent nasal bone (see Figs. 4–40 and 4–41).

Each marker by itself has only a low to moderate sensitivity for Down syndrome. However, there is no question that the risk of fetal trisomy 21 increases with the number of markers present. One should also keep in mind that many of these prenatal sonographic markers, when found in isolation, may not necessarily increase the risk for aneuploidy and can commonly be seen in euploid fetuses. However, when they are found in the context of multiple other sonographic abnormalities or markers, or in high-risk patients, the risk

**Table 4–8**
**Accuracy of Second-trimester Genetic Sonography for the Detection of Down Syndrome**

Author/Year	Sensitivity	False-positive Rate
Benacerraf 1992 <sup>231</sup>	91% (29/32)	13% (77/588)
Nadel 1995 <sup>232</sup>	83% (59/71)	13% (88/694)
DeVore 1995 <sup>233</sup>	87% (13/15)	11% (107/1000)
Nyberg 1995 <sup>234</sup>	50% (9/18)	7% (27/374)
Vintzileos 1996 <sup>235</sup>	93% (13/14)	13% (54/406)
Bahado-Singh 1996 <sup>236</sup>	90% (10/11)	14% (132/962)
Bromley 1997 <sup>237</sup>	83% (44/53)	17% (31/177)
Verdin 1998 <sup>238</sup>	82% (9/12)	10% (44/449)
Nyberg 1998 <sup>239</sup>	68% (97/142)	12% (116/930)
Sohl 1999 <sup>240</sup>	67% (37/50)	17% (448/2639)
Vintzileos 1999 <sup>230</sup>	82% (28/34)	9% (159/1792)
Wax 2000 <sup>241</sup>	71% (5/7)	12% (95/789)
DeVore 2001 <sup>242</sup>	91% (52/57)	13% (260/2000)
<b>TOTAL</b>	<b>77% (363/469)</b>	<b>13% (1507/11,809)</b>

Abnormal test was defined as the presence of  $\geq 1$  abnormal ultrasound markers.

for fetal aneuploidy is increased. A meta-analysis by Smith-Bindman examined more than 50 trials dating back to 1984, and demonstrated that isolated markers (other than increased nuchal fold thickness and structural anomalies) do not have a significant prediction for fetal Down syndrome.<sup>229</sup> However, their sensitivity for multiple (one or more) markers visualized on sonography reached 69%, with a false-positive rate of 8% for detecting Down syndrome. By combining multiple aneuploidy markers, the sensitivity for trisomy 21 can be increased to greater than 80% with false-positive rates of 10% to 15% (by defining as abnormal any ultrasound examination with at least one abnormal marker present).<sup>230,231</sup> The use of multiple sonographic markers improves the sensitivity of sonography for the detection of Down syndrome, but also results in higher false-positive rates. The sensitivity of genetic sonography depends on a variety of factors, such as gestational age, indications for referral, markers examined, experience of the sonologist, and quality of the examination. Benacerraf's group in 1992 first established a sonographic scoring index for fetal aneuploidy by examining multiple markers.<sup>231</sup> Subsequently, many more studies have been published that examine the accuracy of genetic sonography for detecting fetal Down syndrome in high-risk populations (Table 4–8). By defining as abnormal the ultrasound with at least 1 abnormal marker, the overall sensitivity is 77% (50% to 93%) and the false-positive rate is 13% (7% to 17%).

In 1998, a large multicenter collaborative study involving 11 institutions (including our own) examined the sensitivity of sonography in detecting fetal Down syndrome.<sup>243</sup> They found that 85% of Down syndrome fetuses ( $n = 241$ ) had at least one abnormal finding on ultrasound. Recently in 2003, an eight-center study (including our own) evaluated the use of second trimester genetic sonography among high-risk pregnancies, including 176 Down syndrome fetuses.<sup>244</sup> The sensitivity for Down syndrome was 72%, with a range from 64% to 80% at the various centers. Of significance, about



**Table 4-9****Aneuploidy Markers of the Genetic Sonogram at Robert Wood Johnson Medical School****Aneuploidy Marker**

Structural anomalies including cardiac (four-chamber and outflow tracts)
Short femur (observed to expected <10th percentile)
Short humerus (observed to expected <10th percentile)
Pyelectasis (anteroposterior diameter of renal pelvis $\geq 4$ mm)
Nuchal fold thickening ( $\leq 6$ mm)
Echogenic bowel (similar echogenicity to iliac bones)
Choroid plexus cysts ( $> 10$ mm)
Hypoplastic middle phalanx of the fifth digit
Wide space between first and second toes (sandal gap)
Two vessel umbilical cord
Echogenic intracardiac focus, short tibia, short fibula, short ear (since October 1997)
Absent nasal bone (since 2003)

From Yeo L, Vinzileos AM: The use of genetic sonography to reduce the need for amniocentesis in women at high-risk for Down syndrome. *Semin Perinatol* 27:154, 2003.

one half (47%) of Down syndrome fetuses had a thickened nuchal fold of 5 mm or more, making this marker the one with the highest sensitivity.

In 1996, our group was the first to publish data on using second trimester genetic sonography to guide clinical management of women at high risk for fetal Down syndrome.<sup>235</sup> In this study, when one or more abnormal ultrasound markers were present, the sensitivity for trisomy 21 was 93%. Subsequently, once we analyzed our 1999 data, in the presence of a normal genetic ultrasound, we counseled high-risk patients that the likelihood for fetal Down syndrome was reduced by at least 80% from the a priori risk.<sup>227</sup> Over almost a 10-year period (since November 1992) we have evaluated over 5000 fetuses by using genetic sonography; the overwhelming majority (85%) had no markers seen (normal scan), 12% had one abnormal marker present, and 3% had two or more markers present. Eighty-seven percent of fetuses with Down syndrome, 100% of fetuses with trisomy 18, 80% of fetuses with trisomy 13, and 88% of fetuses with other chromosomal abnormalities had abnormal genetic sonograms (one or more abnormal sonographic markers present). When one or more abnormal sonographic markers were present, the sensitivity, specificity, positive and negative predictive values for Down syndrome were 87%, 91%, 11% and 99.8%, respectively. Approximately two thirds of fetuses with trisomy 21 had two or more abnormal sonographic markers seen. Because the greatest sensitivity is provided by using greater than or equal to one markers present, we use this as the abnormal test because the greatest risk reduction for high-risk women will occur in this situation after a normal genetic sonogram.

Currently, at our institution, we target for many specific aneuploidy markers when performing the genetic ultrasound (Table 4-9). These include structural anomalies including cardiac, short femur, short humerus, pyelectasis, nuchal fold thickening, echogenic bowel, CPCs, hypoplastic middle phalanx of the fifth digit, sandal gap, two-vessel

**Table 4-10****Annual Utilization Rates of Genetic Sonography for Detection of Fetal Trisomy 21 (Robert Wood Johnson Medical School)**

Year	Candidates for Prenatal Diagnosis*	Genetic Ultrasound Number (%)	Total Number of Amniocenteses† Number (%)
1993‡	477	2 (0.4%)	475 (99.6%)
1994	495	82 (17%)	423 (85%)
1995	523	251 (48%)	292 (56%)
1996	594	328 (55%)	279 (47%)
1997	793	510 (64%)	315 (40%)
1998	856	662 (77%)	215 (25%)
1999	1285	956 (74%)	405 (31%)
2000	1537	1114 (73%)	468 (30%)
2001	1497	1062 (71%)	488 (32%)
2002	1536	1110 (73%)	493 (32%)

\*Includes advanced maternal age ( $\geq 35$  years of age) with or without abnormal serum biochemistry results, abnormal serum biochemistry results in women  $< 35$  years of age, or family history of chromosome abnormality.

†Includes women who underwent genetic amniocentesis only as their first option and women who underwent amniocentesis after genetic sonography.

‡The genetic sonogram service was available for only 2 months in 1993 (November and December).

From James DK, Stee PJ, Weiner CP, et al: High-Risk Pregnancy: Management Options, 3rd ed. Philadelphia, W.B. Saunders, 2005, Table 8-7.

umbilical cord, echogenic intracardiac focus, short tibia, short fibula, and short ear length. Recently in 2003, we have added absent fetal nasal bone to the list.

Over the years, we have found there is an ever-increasing proportion of high-risk women who prefer to have genetic sonography as the first option rather than amniocentesis (Table 4-10). In 1997, we retrospectively examined the use rates of genetic sonography from 1993 to 1996 and its role in influencing the decision for amniocentesis in women at increased risk for fetal Down syndrome.<sup>245</sup> Over this time period, there was an increasing use trend found, and the most important factors associated with the patient's decision to undergo genetic amniocentesis were (relative risk [RR]; 95% CI): three or more sonographic markers present (RR 189.5; 37.1, 980.0), two sonographic markers present (RR 47.2; 9.8, 267.8), one sonographic marker present (RR 12.7; 5.5, 29.7) and abnormal serum biochemistry (RR 3.0; 1.0, 8.9).<sup>245</sup> Table 4-10 shows the overall increasing use rates of genetic sonography as a first option among high-risk women and the corresponding decreases in the total number of amniocentesis procedures performed since we began offering genetic sonography services in 1993. Since 1998, more than 70% of women chose to undergo genetic sonography as a first option rather than amniocentesis. Accordingly, there has been a decrease in the number of amniocenteses performed. The total amniocentesis rate (sum of amniocentesis as first option plus amniocentesis after genetic sonography) decreased from 99.6% in 1993 to 32% in 2002. This is a 68% reduction rate in the total number of genetic amniocenteses since 1993.

Many other studies have shown that normal second trimester genetic sonography, in effect, reduces the risk for fetal Down syndrome, and therefore reduces the need for



Table 4-11

**Accuracy of Genetic Sonography\* in Detecting Fetal Down Syndrome (According to the Indication for Testing) and Risk for Down Syndrome After Normal Genetic Sonography**

Indication	Sensitivity %	Specificity %	PPV %	NPV %	Risk for Down syndrome after normal genetic sonography	
					Negative LR (CI)	Risk Reduction %
AMA	84	90	7	99.8	0.18 (0.06, 0.54)	82
Abnormal TS	89	86	14	99.7	0.13 (0.04, 0.42)	87
Abnormal TS in less than 35 years of age	90	84	15	99.6	0.12 (0.03, 0.50)	88
Abnormal TS and AMA	86	88	12	99.7	0.16 (0.02, 1.34)	84

\*Presence of > one abnormal sonographic marker considered an abnormal examination result.

AMA, advanced maternal age; CI, confidence interval; LR, likelihood ratio; NPV, negative predictive value; PPV, positive predictive value; TS, triple screen.

From Yeo L, Vintzileos AM: The use of genetic sonography to reduce the need for amniocentesis in women at high-risk for Down syndrome. *Semin Perinatol* 27:156, 2003.

amniocentesis in high-risk patients.<sup>246,248</sup> In 2001, one group studied 1556 high-risk patients (advanced maternal age and/or abnormal triple screen) between 1993 and 1998.<sup>248</sup> They found genetic ultrasound's sensitivity for Down syndrome to be 87% (27/31) with a reduction in the need for amniocentesis by 61%.

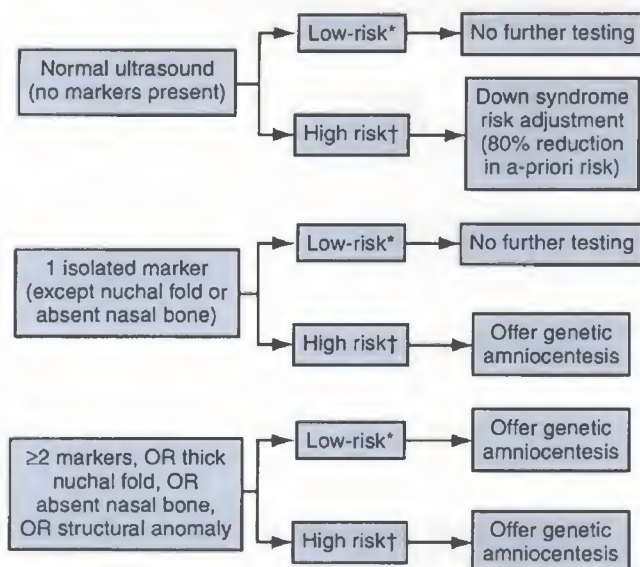
In 1999, we examined whether there were any clinically significant indication-specific variations in the accuracy of genetic sonography for trisomy 21.<sup>249</sup> The indications for genetic ultrasound were grouped into four categories: (1) advanced maternal age (regardless of triple screen results), (2) abnormal triple screen results (regardless of maternal age), (3) abnormal triple screen results in women younger than 35 years of age, and (4) abnormal triple screen results in women older than 35 years of age. We found no significant indication-specific variations to be present.

In looking at updated data with a higher number of patients (Table 4-11), the likelihood of fetal trisomy 21 is reduced by 82% to 88% after a normal genetic ultrasound, depending on the indication for testing.<sup>250</sup> Thus, the degree of risk adjustment after a normal genetic sonogram seems to be independent on the indication for testing, including advanced maternal age, abnormal triple screen, or some combination of the two. We have found that the sensitivity of genetic sonography ranges from 84% among women with advanced maternal age to 90% among women younger than 35 years of age having an abnormal triple screen. Again, there were no significant indication-specific variations in the accuracy of genetic sonography.

Recently, we targeted the value of genetic sonography in the specific population of women with advanced maternal age and normal triple screen.<sup>251</sup> Among 768 patients meeting these criteria, we found the risk for Down syndrome was 0% (0/673) with a normal genetic ultrasound, and the risk was 4.2% (4/95) when the genetic ultrasound was abnormal. There were four fetuses with Down syndrome in this population, and all had abnormal genetic sonography. The maternal triple screen risks in these four Down syndrome fetuses ranged between 1/319 and 1/833. Thus, genetic sonography may indeed increase the detection rate of fetal Down syndrome in women with advanced maternal age and moderate triple screen risks (between 1/275 and 1/1000).

Although second trimester genetic sonography has been advocated for screening the general population, it is our opinion that this should be performed and applied only to the high-risk population, for various reasons. First, considerable expertise is necessary to rule out sonographic fetal malformations (especially subtle cardiac defects) and such expertise is not widely available. Application of genetic sonography to the low-risk population may be inappropriate and even dangerous, due to the high false-positive rates of 12% to 15% in the high-risk population (which is probably higher in low-risk populations). If the presence of any one marker is considered a positive screen in the low-risk patient, the high false-positive rate will lead to considerable anxiety among these patients. In low-risk patients, the a priori risk for fetal Down syndrome may be so low that the presence of only one aneuploidy marker (for example, pyelectasis) does not usually elevate the risk enough to justify amniocentesis. Therefore, it is expected that the positive predictive value, and perhaps even the sensitivity of genetic ultrasound for fetal Down syndrome, may be decreased in the low-risk patient. It is also important to realize that the accuracy of second trimester aneuploidy markers has been mainly studied in high-risk populations and extrapolation of such accuracy to the low-risk patient is not appropriate. In the low-risk population, isolated markers (other than increased nuchal fold thickness, absent nasal bone, or structural anomalies) should not be used as an indication for amniocentesis testing. However, often one may incidentally discover one or more abnormal sonographic markers in the low-risk population. Figure 4-58 reveals the algorithm that we follow at our institution as a clinical practice guideline. It is vital to remember that because the sensitivity of an isolated marker (with the possible exception of increased nuchal fold thickness or absent nasal bone) is so low, clinicians should not recommend amniocentesis in low-risk patients.<sup>252</sup> All sonographic abnormalities involving a major organ/structural anomalies (with a few exceptions), thickened nuchal fold, absent nasal bone, or the presence of two or more aneuploidy markers (or minor structural abnormalities) indicate a high risk for fetal aneuploidy, and invasive testing should be offered, even in the low-risk patient. Certain isolated sonographic fetal abnormalities (for example, gastroschisis) that



SECOND TRIMESTER ULTRASOUND MARKERS  
PRACTICE GUIDELINES

**FIGURE 4-58.** Algorithm for clinical management based on the results of second trimester ultrasound (presence or absence of sonographic markers). Maternal age younger than 35 years of age, serum screen result less than 1/274, or both (*asterisk*). Maternal age 35 years of age and older, serum screen result 1/274 and greater, or both (*dagger*). (Redrawn from Yeo L, Vintzileos AM: The use of genetic sonography to reduce the need for amniocentesis in women at high risk for Down syndrome. *Semin Perinatol* 27:158, 2003.)

are not usually associated with aneuploidy may not require further invasive testing.

In high-risk patients, we use genetic sonography as an adjunct to maternal age and serum screening to adjust the risk for fetal Down syndrome for each individual patient, based on our accuracy. The a priori risk may be based on first trimester combined screening, triple/quadruple screen, or on maternal age (if first or second trimester screen results are not available or were not performed). We then multiply the a priori risk with the negative likelihood ratio, if the examination is normal. For instance, if the risk for fetal Down syndrome by maternal age is 1/274 and the genetic scan is normal, the new adjusted risk for fetal Down syndrome will be 1/274 times 0.20 (or 1/1370) (at least 80% reduction). If only one marker is present (except structural anomaly, thick nuchal fold, or absent nasal bone), we recommend invasive testing only if the patient is high risk. On the other hand, once two or more markers are visualized, we offer invasive testing, regardless of risk status. One should keep in mind and counsel patients that the genetic scan can never reduce their risk of having a Down syndrome fetus to 0%. Either a triple or quadruple screen is acceptable as an a priori risk because most of our findings are based on high-risk patients who underwent serum testing.

We believe that in high-risk patients, a normal ultrasound can reduce considerably the risk of Down syndrome. Hobbins et al<sup>252</sup> supported the position that the most important application of genetic sonography is that when it is normal, it diminishes the possibility of Down syndrome, and consequently, reduces the number of invasive procedures in

Table 4-12

Likelihood Ratios of Isolated Markers in  
Four Large Studies

Marker	Smith-Bindman 2001 <sup>229</sup>	AAURA 2001 <sup>64</sup>	Nyberg 1998 <sup>239</sup>	Bromley 2002 <sup>65</sup>
None	NA	0.4	0.36	0.22
Nuchal fold	17	8.6	11	Infinite
Bright bowel	6.1	5.5	6.7	NA
Short humerus	7.5	2.5	5.1	5.8
Short femur	2.7	2.2	1.5	1.2
EIF	2.8	2	1.8	1.4
Pyelectasis	1.9	1.5	1.5	1.5

EIF, echogenic intracardiac focus; NA, not applicable.

From Benacerraf BR: The role of the second trimester genetic sonogram in screening for fetal Down syndrome. *Semin Perinatol* 29:391, 2005.

high-risk patients. The degree of risk reduction depends on several factors, such as the criteria and number of aneuploidy markers sought, and the sensitivity of the ultrasound. Most recent studies use a negative likelihood ratio ranging somewhere between 0.2 to 0.4 after a normal genetic sonogram, corresponding to a 60% to 80% reduction in risk.

Other centers have used a scoring index system to optimize the clinical management of sonographic markers.<sup>253</sup> The main advantage of this particular method is the ease of use and comprehension. This index is based on the assumption that individual aneuploidy markers are not equally important. In this system, two points are given when structural abnormalities or nuchal thickening is identified, although one point is given for other markers. For those patients having a score of two or more, amniocentesis is then offered. By using a score of two or more, it allowed the authors to detect 81% of fetuses with Down syndrome, with a 4.4% false-positive rate.<sup>231</sup> Subsequently, the scoring index system was modified to incorporate maternal age, by giving one point for age older than or equal to 35 years of age, and two points for age older than or equal to 40 years of age.<sup>254</sup> The authors emphasize that the single most clinically important use of second trimester genetic sonography lies in the risk reduction that is conferred by a normal sonogram (0 score), because it allows the opportunity for many high-risk women to avoid amniocentesis.

Another method which has been used is to integrate the risk of sonographic markers with the a priori risk based on maternal age.<sup>255</sup> This is called age-adjusted ultrasound risk adjustment (AAURA) for fetal Down syndrome and are used for women of all ages. In using this method, sonographic markers are "weighted" by the strength of individual findings, expressed as likelihood ratios. The authors base the individual risk assessment of fetal Down syndrome on maternal age and the presence or absence of each of the ultrasound markers in terms of likelihood ratios. Likelihood ratios of isolated markers have been reported in several studies (Table 4-12). By using likelihood ratios, the post priori risk is then estimated. We do not use these likelihood ratios because in our experience, the overwhelming majority of trisomy 21 fetuses have multiple markers in combination, not in isolation. Therefore, we have been unable to generate stable and reliable positive likelihood ratios of isolated markers. Yet, some investigators are using AAURA, and



report that both the sensitivity of fetal Down syndrome detection and the false-positive rate increase with maternal age. This is believed to be appropriate because older women desire a high sensitivity, and the alternative clinically is amniocentesis for all women age 35 years or older (100% false-positive rate).<sup>30</sup> At the same time, AAURA also minimizes the false-positive rate for younger women (4% false-positive rate) with a satisfactory sensitivity (61.5%).<sup>30</sup> The authors also believe that because sonographic findings are largely independent of both maternal age and biochemical analytes, the risk from biochemical screening (serum markers plus maternal age risk) can be substituted for maternal age risk alone, when known.<sup>30</sup>

It is imperative that every center that performs genetic sonography monitor its sensitivity in detecting fetal Down syndrome in order to provide patients accurate, detailed, and updated counseling regarding their degree of risk reduction when the scan is normal. We continuously monitor our accuracy in detecting fetal Down syndrome in high-risk women. We and other investigators believe that risk adjustment for Down syndrome is institution-specific and that data may not apply to other centers.<sup>256</sup> Some believe also that the use of genetic sonography should be limited to specialized centers.<sup>257</sup>

Another issue to address is whether second trimester genetic sonography is cost effective. We recently analyzed the cost between universal amniocentesis and genetic sonography and found that genetic sonography was cost effective if the sensitivity for detecting Down syndrome was greater than 74%.<sup>258</sup> We also found that genetic sonography resulted in savings to the health care system of 9%, and decreased the loss rate of normal fetuses following amniocentesis by 87%.<sup>258</sup> Genetic sonography is also cost effective in women younger than 35 years of age who are at moderate risk for Down syndrome based on triple screen results, as well as in advanced maternal age patients, who decline amniocentesis after second trimester genetic counseling.<sup>259</sup> Offering genetic sonography to these patients is associated with cost savings for most acceptable genetic ultrasound accuracies. Finally, recent data indicate that combining second trimester genetic sonography with traditional serum markers may significantly improve the diagnostic accuracy of Down syndrome fetuses.<sup>260</sup> Various integrated algorithms combining serum analytes and sonographic markers have been generated (for example, nuchal thickness, humerus length, serum AFP, hCG). However, these algorithms have not been prospectively validated.

## TRISOMY 18 (EDWARDS SYNDROME)

Trisomy 18 (Edwards syndrome, or trisomy E) occurs in approximately 1/8000 births. Trisomy 18 is much more common at conception because 95% of these cases result in spontaneous abortion or stillbirth. Trisomy 18 is the second most common autosomal trisomy and has a uniformly dismal prognosis. Intrauterine demise is common, and it is estimated that of those fetuses alive at 16 weeks, 50% to 90% do not survive to live birth.<sup>261</sup> Survival postnatally is very poor, with the majority dying in early infancy. Those who survive are profoundly mentally and physically retarded, and common problems include failure to thrive, hypotonia, and feeding difficulties.

Pregnancies affected with fetal trisomy 18 have a characteristic pattern on biochemical maternal serum screening in the second trimester. All three serum markers are lower than normal, with median values as follows: AFP, 0.6 MoM; unconjugated estriol, 0.5 MoM; and hCG, 0.3 MoM. The triple marker screen can identify approximately 60% to 75% of fetuses with trisomy 18 when a separate analysis is performed that seeks low levels of all three analytes, with or without consideration of maternal age.<sup>262,263</sup> However, because of the low prevalence of trisomy 18, ultrasound is still recommended following a positive screen for trisomy 18. One study suggested that ultrasound was superior to biochemistry in detecting trisomy 18, although both tests identified affected fetuses missed by the other.<sup>264</sup>

It is well established that those affected with trisomy 18 have many major structural anomalies. In fact, more than 100 different abnormalities involving virtually every organ system has been noted in association with trisomy 18.<sup>265</sup> Neonates with trisomy 18 have many characteristic clinical features, such as cardiac defects, growth restriction, prominent occiput, small mouth, micrognathia, low and pointed ears, mental retardation, clenched hands with overlapping fingers, short sternum, and rocker-bottom feet. Overlapping of fingers most frequently occurs with the index finger overlapping the middle finger, and the 5th finger curving inward. As a result, there is a multitude of sonographic abnormalities/malformations that can be visualized prenatally (see Table 4-2). These include cystic hygroma, cardiac defects, omphalocele, extremity abnormalities, craniofacial defects, spina bifida, diaphragmatic hernia, genitourinary abnormalities, amniotic fluid abnormalities, CPCs, single umbilical artery, umbilical cord cysts and short ear length. An important point is that trisomy 18 fetuses can show an onset of intrauterine growth restriction as early as the second or even first trimester. By the third trimester, almost all are significantly growth restricted; unfortunately, some fetuses with trisomy 18 are delivered by cesarean section before any discovery or knowledge of aneuploidy.<sup>266</sup> Nyberg found that intrauterine growth restriction was present in one half of the fetuses less than 24 weeks gestation, and in 89% of those greater than 24 weeks' gestation.<sup>3</sup> When growth restriction, polyhydramnios, and abnormal hand posturing is visualized, this is highly predictive of trisomy 18 in the third trimester.

Sonography has been shown to have variable but high sensitivity in detecting trisomy 18 (64% to 100%) (Table 4-13), particularly when performing a thorough, anatomic survey. One group found 100% sensitivity of ultrasonography to detect fetuses with trisomy 18; however, this was not restricted to fetal structural anomalies, but also included abnormal measurements.<sup>268</sup> In a sample of 15 fetuses with trisomy 18, Benacerraf et al<sup>268</sup> found that 80% had one or more sonographic abnormalities (range 0-5). Three of the fetuses had no sonographic findings at all; however, these examinations were performed between 16 and 17 weeks. In examining fetuses with trisomy 18 during the early second trimester only, Shields et al<sup>270</sup> found that most, but not all (86%) fetuses had one or more detected abnormalities on ultrasound, with the mean number of abnormalities per fetus being three (range zero to six). In 1993, Nyberg found that when excluding CPCs, 83% (39/47) of fetuses with trisomy 18 had more than one ultrasound abnormalities (range zero to six) identified.<sup>3</sup> DeVore<sup>27</sup> found



**Table 4-13** Sensitivity of Prenatal Sonography in Fetuses with Trisomy 18

Author/Year	Number	Gestational Age in Weeks (Range)*	Sensitivity of U/S in Detecting Trisomy 18	Most Common U/S Abnormality
Bundy 1986 <sup>267</sup>	12	18 (12-40)	75%	IUGR (42%)
Benacerraf 1988 <sup>208</sup>	15	22.7 ± 7.9 (15-35)	80%	Abnormal hands or feet (73%)
Benacerraf 1990 <sup>126</sup>	26	19.4 ± 7.0 (13.5-36)	77%	Abnormal hands (38%) Clubfeet (38%)
Nyberg 1993 <sup>3</sup>	47	14-24 weeks (29 fetuses) >24 weeks (18 fetuses)	83%	IUGR (51%)
Seoud 1994 <sup>268</sup>	12	22.1 ± 5.3	100%†	Flexion hands (70%) Clubfeet or rocker bottom feet (70%)
Salihu 1997 <sup>269</sup>	11	≤24 weeks (7 fetuses) >24 weeks (4 fetuses)	64%	Polyhydramnios (36%)
Shields 1998 <sup>270</sup>	35	17.5 ± 2.0 (14-22)	86%	Abnormal position fingers (89%)
DeVore 2000 <sup>27</sup>	30	17.5 ± 1.5 (14-23)	97%	Structural cardiac defects (80%)
Feuchtbaum 2000 <sup>271</sup>	23	N/A	65%	CPC (43%)
	142	N/A	66%	N/A
Brumfield 2000 <sup>264</sup>	30	14-22	70%	CPC (43%)
Yeo 2003 <sup>4</sup>	38	20.1 (14.6-36.3)	100%	Shortened ear length < 10th percentile (96%)

CPC, choroid plexus cyst; IUGR, intrauterine growth restriction; N/A, not available; U/S, ultrasound.

\*Mean + standard deviation or median given when available

†However, also includes &gt;1 abnormal measurements; not just structural anomalies

that of 30 fetuses with trisomy 18 between 14 to 23 weeks, ultrasound had a very high sensitivity of 97%. The most frequent sonographic abnormality was structural cardiac defects (80%). Others have found a lower sensitivity of ultrasound in detecting trisomy 18.<sup>271</sup> In this study, ultrasound was reportedly normal in 35% of 23 affected fetuses with trisomy 18.

In a recent study, we found that by performing a complete sonographic survey, all trisomy 18 fetuses had four or more sonographic anomalies (one patient had 19 individual fetal anomalies).<sup>4</sup> We found that the sonographic presence of short ear length (96%), bilateral clenched or closed hands or overlapping digits (95%), and central nervous abnormalities (87%) were the most sensitive markers for fetal trisomy 18. We also found that 92% of trisomy 18 fetuses had at least two of four minor sonographic abnormalities (upper extremities/hands, lower extremities/feet, face, ear).<sup>4</sup> This fact emphasizes the importance of thorough prenatal sonographic examination of fetuses, with attention to fine detail in addition to examination of all organ systems after 18 weeks gestation.

For those fetuses at risk for fetal trisomy 18, a complete and detailed prenatal sonogram is indicated. Being aware of the types of malformations that are associated with this aneuploidy is imperative in order to target the sonographic examination appropriately. Similarly to the concept of genetic sonography in screening for fetal Down syndrome, we believe that normal findings from a complete anatomic survey in experienced hands should "decrease" a patient's risk of trisomy 18 (regardless of the presence/absence of CPC or abnormal serum screen results) to an extremely low level sufficient to avoid genetic amniocentesis after appropriate patient counseling.<sup>4</sup> On the other hand, when sono-

graphic findings are visualized that are consistent with trisomy 18, fetal karyotyping should be offered, along with appropriate counseling.

As with trisomy 13, there is little information regarding the recurrence risk for trisomy 18. In general, an empiric risk of approximately 1% is usually given to patients.<sup>272</sup>

## TRISOMY 13 (PATAU SYNDROME)

Trisomy 13 and its congenital abnormalities was first described by Patau in 1960.<sup>265</sup> The birth prevalence is estimated at between 1/5000 and 1/20,000 births.<sup>273</sup> It accounts for approximately 1% of spontaneous first trimester miscarriages and has an extremely poor prognosis. Most children with this chromosomal abnormality die in infancy; the median survival is 2.5 days.<sup>265</sup> Of newborns with trisomy 13, 82% die in the first month and only 5% survive the first 6 months.<sup>263</sup> Survivors have severe mental defects, often have seizures, apnea, feeding difficulties, and failure to thrive. The phenotype is often so characteristic that a diagnosis can be made frequently based on clinical features alone. The features include microcephaly, serious central nervous system abnormalities (such as abnormal posterior fossa, ventriculomegaly, agenesis of corpus callosum), cardiac defects (> 80%), growth restriction, receding forehead, ocular anomalies, cleft lip and palate (60% to 70%), limb deficiencies, rocker-bottom feet or clubfeet, clenched hands with overlapping digits, postaxial polydactyly (75%), omphalocele, and renal abnormalities (such as polycystic kidneys). In particular, alobar holoprosencephaly is a common finding that is often associated with severe midline facial defects, such as midline clefts, microphthalmia, hypotelorism, cyclopia, and absence of the nose.

**Table 4-14** Sensitivity of Prenatal Sonography in Fetuses with Trisomy 13

Author/Year	N	Gestational Age (Weeks)	Sensitivity of U/S in Detecting Trisomy 13	Most Common U/S Abnormalities
Nicolaides 1992 <sup>274</sup>	31	15–39	100%	Abnormal extremities 68% Renal 65% Facial cleft 48% Growth restriction 48% Cardiac 45% Holoprosencephaly 35%
Lehman 199 <sup>55</sup>	33	12–32	91%	Central nervous system 58% Cardiac 48% Facial 48% Growth restriction 48% Holoprosencephaly 39% Renal 33% Extremity 33% Echogenic intracardiac foci 30%
DeVigan 2001 <sup>276</sup>	85	All gestational ages	68.2%	Cardiac 20% Cleft 18% Holoprosencephaly 18% Holoprosencephaly 47% Hypotelorism/cyclopia 40% Abnormal hands/feet 40% Facial cleft 33% Cardiac 33%
Tongsong 2002 <sup>275</sup>	15	16–22	93%	Central nervous system 64% Facial 64% Cardiac 54% Renal 43%
Papp 2006 <sup>277</sup>	28	13–25	89.3%	

U/S, ultrasound.

Because fetuses with trisomy 13 have severe abnormalities, the sensitivity of prenatal sonography for the detection of this aneuploidy is very high (Table 4-14), with most studies reporting sensitivities greater than 90%.<sup>5,274,275</sup> One large study examining data from 11 European countries reported a sensitivity of only 68.2% in 85 cases of trisomy 13.<sup>276</sup> However, the study focused on the detection of major malformations because not all registries recorded soft markers. In addition, the study was performed via routine scanning, and the authors believed that when detailed scanning is undertaken, the performance would be better.<sup>276</sup> In order to achieve a high degree of sensitivity, a detailed and systematic sonographic survey should be performed. Characteristic features of trisomy 13 that can be visualized on prenatal sonography are described in Table 4-3. In one of the largest series of 33 fetuses with trisomy 13, one or more prenatal sonographic findings were found in 91% overall.<sup>5</sup> Some of the most common findings included central nervous system anomalies (58%), cardiac defects (48%), facial anomalies (48%), growth restriction (48%), holoprosencephaly (39%), renal abnormalities (33%) (Fig. 4-59), and extremity abnormalities (33%). Importantly, EIF, which is an aneuploidy marker, were also seen in 30% of cases.

It is important to distinguish trisomy 13 from Meckel-Gruber syndrome, which is an autosomal-recessive disorder that shares some common characteristic features with trisomy 13. This has implications in counseling because this autosomal-recessive disorder, unlike trisomy 13, has a 25% recurrence risk. Meckel-Gruber syndrome is characterized by polycystic kidneys, polydactyly, midline central nervous

**FIGURE 4-59.** Coronal view of the fetal abdomen showing bilateral echogenic kidneys.

system malformations (such as occipital encephalocele, Dandy-Walker malformation), and other features.

There is little information regarding the recurrence risk for trisomy 13. In general, an empiric risk of approximately 1% is usually given to patients.<sup>272</sup>

## CONCLUSION

At present, there is no uniformity in population-based screening for fetal Down syndrome in the United States.



There are many variations, including first trimester screening and/or second trimester serum markers. Regardless of the method used, high sensitivity is important for those women who are high risk, although low false-positive rates are most desirable among low-risk women. Genetic sonography has enabled us to detect fetal aneuploidy, and also diagnose many fetal congenital anomalies in all trimesters of pregnancy. We have come a long way with regard to the potential options that high-risk patients can be given. According to many pregnant women, advanced maternal age alone or abnormal maternal serum screening alone may no longer be indications for invasive testing, and it is clear that for such patients, prenatal sonography is of paramount importance. With the emergence of first trimester screening (both ultrasound and serum), this will also add additional information that in the future may be incorporated into genetic sonography to give individualized risks for Down syndrome to patients. The most appropriate application of genetic sonography pertains to those high-risk women who seek reassurance, and, therefore, risk reduction by a normal genetic sonogram. The power of normal genetic sonography lies in its ability to save fetal lives by avoiding many unnecessary amniocentesis procedures. We have found that although many clinicians may refer patients for genetic sonography, in our experience, it has been over the years mainly a patient-driven service. There are many women who will no longer undergo amniocentesis automatically as a first option, but rather, will choose to use the information from genetic sonography to help guide their decision about invasive testing.

## References

- Alberman ED, Creasy MR: Frequency of chromosomal abnormalities in miscarriages and perinatal deaths. *J Med Genet* 14:313, 1977.
- Nielsen J, Wohler M: Chromosome abnormalities found among 34,910 newborn children: Results from a 13-year incidence study in Arhus, Denmark. *Hum Genet* 87:81, 1991.
- Nyberg DA, Kramer D, Resta RG, et al: Prenatal sonographic findings of trisomy 18: Review of 47 cases. *J Ultrasound Med* 2:103, 1993.
- Yeo L, Guzman ER, Day-Salvatore D, et al: Prenatal detection of fetal trisomy 18 through abnormal sonographic features. *J Ultrasound Med* 22:581, 2003.
- Lehman CD, Nyberg DA, Winter TC, et al: Trisomy 13 syndrome: Prenatal ultrasound findings in a review of 33 cases. *Radiology* 194:217, 1995.
- Vintzileos AM, Egan JF: Adjusting the risk for trisomy 21 on the basis of second-trimester ultrasonography. *Am J Obstet Gynecol* 172:837, 1995.
- Cuckle HS, Wald NJ, Lindenbaum RH: Maternal serum alpha-fetoprotein measurement: A screening test for Down syndrome. *Lancet* 1:926, 1984.
- Cuckle HS, Wald NJ, Thompson SG: Estimating a woman's risk of having a pregnancy associated with Down's syndrome using her age and serum alpha-fetoprotein level. *Br J Obstet Gynaecol* 94:387, 1987.
- New England Regional Genetics Group Prenatal Collaborative Study of Down Syndrome Screening: Combining maternal serum  $\alpha$ -fetoprotein measurements and age to screen for Down syndrome in pregnant women under age 35. *Am J Obstet Gynecol* 160:575, 1989.
- Bogart MH, Pandian MR, Jones OW: Abnormal maternal serum chorionic gonadotropin levels in pregnancies with fetal chromosome abnormalities. *Prenat Diagn* 7:623, 1987.
- Wald NJ, Cuckle HS, Densem JW, et al: Maternal serum unconjugated oestriol as an antenatal screening test for Down's syndrome. *Br J Obstet Gynaecol* 95:334, 1988.
- Wald NJ, Cuckle HS, Densem JW, et al: Maternal serum screening for Down's syndrome in early pregnancy. *BMJ* 297:883, 1988.
- Haddow JE, Palomaki GE, Knight GJ, et al: Prenatal screening for Down's syndrome with use of maternal serum markers. *N Engl J Med* 327:588, 1992.
- Cheng EY, Luthy DA, Zebelman AM, et al: A prospective evaluation of a second-trimester screening test for fetal Down syndrome using maternal serum alpha-fetoprotein, hCG, and unconjugated estriol. *Obstet Gynecol* 81:72, 1993.
- Burton BK, Prins GS, Vorp MS: A prospective trial of prenatal screening for Down syndrome by means of maternal serum  $\alpha$ -fetoprotein, human chorionic gonadotropin, and unconjugated estriol. *Am J Obstet Gynecol* 169:526, 1993.
- Wenstrom KD, Williamson RA, Grant SS, et al: Evaluation of multiple-marker screening for Down syndrome in a statewide population. *Am J Obstet Gynecol* 169:793, 1993.
- American College of Obstetricians and Gynecologists: Prenatal diagnosis of fetal chromosomal abnormalities. 2003 Compendium of Selected Publications 547-557, 2003.
- Haddow JE, Palomaki GE, Knight GJ, et al: Reducing the need for amniocentesis in women 35 years of age or older with serum markers for screening. *N Engl J Med* 330:114, 1994.
- Wald NJ, Densem JW, George L, et al: Prenatal screening for Down's syndrome using inhibin-A as a serum marker. *Prenat Diagn* 16:143, 1996.
- Wenstrom KD, Owen J, Chu DC, et al: Prospective evaluation of free beta-subunit of human chorionic gonadotropin and dimeric inhibin A for aneuploidy detection. *Am J Obstet Gynecol* 181:887, 1999.
- Rodis JF, Egan JF, Crafczy A, et al: Calculated risk of chromosomal abnormalities in twin gestations. *Obstet Gynecol* 76:1037, 1990.
- Stoll C, Dott B, Alembik Y, Roth MP: Evaluation of routine prenatal ultrasound examination in detecting fetal chromosomal abnormalities in a low risk population. *Hum Genet* 91:37, 1993.
- Sohl BD, Scioscia AL, Budorick NE, Moore TR: Utility of minor ultrasonographic markers in the prediction of abnormal fetal karyotype at a prenatal diagnostic center. *Am J Obstet Gynecol* 181:898, 1999.
- Nyberg DA, Resta R, Luthy DA, et al: Prenatal sonographic findings of Down syndrome: review of 94 cases. *Obstet Gynecol* 76:370, 1990.
- Paladini D, Tartagloine A, Agangi A, et al: The association between congenital heart disease and Down syndrome in prenatal life. *Ultrasound Obstet Gynecol* 15:104, 2000.
- DeVore GR: Trisomy 21: 91% detection rate using second-trimester ultrasound markers. *Ultrasound Obstet Gynecol* 16:133, 2000.
- DeVore GR: Second trimester ultrasonography may identify 77 to 97% of fetuses with trisomy 18. *J Ultrasound Med* 19:565, 2000.
- Crawford DC, Chita SK, Allan LD: Prenatal detection of congenital heart disease: factors affecting obstetric management and survival. *Am J Obstet Gynecol* 159:352, 1988.
- Copel JA, Pitu G, Kleinman CS: Congenital heart disease and extracardiac anomalies: associations and indications for fetal echocardiography. *Am J Obstet Gynecol* 154:1121, 1986.
- Nyberg DA, Souter VL: Chromosomal abnormalities. In Nyberg DA, McGahan JP, Pretorius DH, Pitu G (eds): *Diagnostic Imaging of Fetal Anomalies*. Philadelphia, Lippincott Williams & Wilkins, 2003, pp 86-906.
- Delisle MF, Sander GG, Tessier F, Farquharson DF: Outcome of fetuses diagnosed with atrioventricular septal defect. *Obstet Gynecol* 94:763, 1999.
- Bronshtein M, Bar-Hava I, Blumenfeld I, et al: The difference between septated and nonseptated nuchal cystic hygroma in the early second trimester. *Obstet Gynecol* 81:683, 1993.
- Anandakumar C, Biswas A, Wong YC, et al: Management of non-immune hydrops: 8 years' experience. *Ultrasound Obstet Gynecol* 8:196, 1996.
- Iskaros J, Jauniaux E, Rodeck C: Outcome of nonimmune hydrops fetalis diagnosed during the first half of pregnancy. *Obstet Gynecol* 90:321, 1997.
- Hagay Z, Recce A, Roberts A, et al: Isolated fetal pleural effusion: A prenatal management dilemma. *Obstet Gynecol* 81:147, 1993.
- Zelop C, Benacerraf BR: The causes and natural history of fetal ascites. *Prenat Diagn* 14:941, 1994.
- Dillon E, Renwick M, Wright C: Congenital diaphragmatic herniation: Antenatal detection and outcome. *Br J Radiol* 73:360, 2000.



38. Bollmann R, Kalache K, Mau H, et al: Associated malformations and chromosomal defects in congenital diaphragmatic hernia. *Fetal Diagn Ther* 10:52, 1995.
39. Howe DT, Kilby MD, Sirry H, et al: Structural chromosome anomalies in congenital diaphragmatic hernia. *Prenat Diagn* 16:1003, 1996.
40. Gilbert WM, Nicolaides KH: Fetal omphalocele: Associated malformations and chromosomal defects. *Obstet Gynecol* 70:633, 1987.
41. Getachew MM, Goldstein RB, Edge V, et al: Correlation between omphalocele contents and karyotypic abnormalities: Sonographic study in 37 cases. *AJR Am J Roentgenol* 158:133, 1992.
42. Pilu G, Falco P, Gabrielli S, et al: The clinical significance of fetal isolated cerebral borderline ventriculomegaly: Report of 31 cases and review of the literature. *Ultrasound Obstet Gynecol* 14:320, 1999.
43. Nyberg DA, Mack LA, Hirsch J, et al: Fetal hydrocephalus: sonographic detection and clinical significance of associated anomalies. *Radiology* 163:187, 1987.
44. Kolble N, Wisser J, Kurmanavicius J, et al: Dandy-Walker malformation: Prenatal diagnosis and outcome. *Prenat Diagn* 20:318, 2000.
45. Nyberg DA, Mahony BS, Hegge FN, et al: Enlarged cisterna magna and the Dandy-Walker malformation: Factors associated with chromosome abnormalities. *Obstet Gynecol* 77:436, 1991.
46. Chang MC, Russell SA, Callen PW, et al: Sonographic detection of inferior vermian agenesis in Dandy-Walker malformations: prognostic implications. *Radiology* 193:765, 1994.
47. Chen CP, Hung TH, Jan SW, et al: Enlarged cisterna magna in the third trimester as a clue to fetal trisomy 18. *Fetal Diagn Ther* 13:29, 1998.
48. Steiger RM, Porto M, Lagrew DC, et al: Biometry of the fetal cisterna magna: estimates of the ability to detect trisomy 18. *Ultrasound Obstet Gynecol* 5:384, 1995.
49. Haimovici JA, Doubilet PM, Benson CB, et al: Clinical significance of isolated enlargement of the cisterna magna (>10 mm) on prenatal sonography. *J Ultrasound Med* 16:731, 1997.
50. Serur D, Jeret JS, Wisniewski K: Agenesis of the corpus callosum. Clinical, neuroradiological and cytogenetic studies. *Neuropediatr* 19:87, 1986.
51. Goodyear PW, Bannister CM, Russel S, et al: Outcome in prenatally diagnosed fetal agenesis of the corpus callosum. *Fetal Diagn Ther* 16:139, 2001.
52. Nicolaides KH, Snijders RJ, Gosden CM, et al: Ultrasonographically detectable markers of fetal chromosomal abnormalities. *Lancet* 340:704, 1992.
53. Rizzo N, Gabrielli S, Pilu G, et al: Prenatal diagnosis and obstetrical management of multicystic dysplastic kidney disease. *Prenat Diagn* 7:109, 1987.
54. Hall B: Mongolism in newborn infants. *Clin Pediatr* 5:4, 1966.
55. Benacerraf BR, Barss VA, Laboda LA: A sonographic sign for the detection in the second trimester of the fetus with Down's syndrome. *Am J Obstet Gynecol* 151:1078, 1985.
56. Crane JP, Gray DL: Sonographically measured nuchal skinfold thickness as a screening tool for Down syndrome: Results of a prospective clinical trial. *Obstet Gynecol* 77:533, 1991.
57. Benacerraf BR, Gelman R, Frigoletto FD: Sonographic identification of second-trimester fetuses with Down's syndrome. *N Engl J Med* 317:1371, 1987.
58. Borrell A, Costa D, Martinez JM, et al: Early midtrimester fetal nuchal thickness: Effectiveness as a marker of Down syndrome. *Am J Obstet Gynecol* 175:45, 1996.
59. Gray DL, Crane JP: Optimal nuchal skin-fold thresholds based on gestational age for prenatal detection of Down syndrome. *Am J Obstet Gynecol* 171:1282, 1994.
60. Grandjean H, Sarramon MF, AFDPE Study group: Sonographic measurement of nuchal skinfold thickness or detection of Down syndrome in the second-trimester fetus: A multicenter prospective study. *Obstet Gynecol* 85:103, 1995.
61. Watson WJ, Miller RC, Menard K, et al: Ultrasonographic measurement of fetal nuchal skin to screen for chromosomal abnormalities. *Am J Obstet Gynecol* 170:583, 1994.
62. Landwehr Jr JB, Johnson MP, Hume RF, et al: Abnormal nuchal findings on screening ultrasonography: Aneuploidy stratification on the basis of ultrasonographic anomaly and gestational age at detection. *Am J Obstet Gynecol* 175:995, 1996.
63. Vintzileos A, Walters C, Yeo L: Absent nasal bone in the prenatal detection of fetuses with trisomy 21 in a high-risk population. *Obstet Gynecol* 101:905, 2003.
64. Nyberg DA, Souter VL, El-Bastawissi A, et al: Isolated sonographic markers for detection of fetal Down syndrome in the second trimester of pregnancy. *J Ultrasound Med* 10:1053, 2001.
65. Bromley B, Lieberman E, Shipp TD, et al: The genetic sonogram, a method for risk assessment for Down syndrome in the mid trimester. *J Ultrasound Med* 21:1087, 2002.
66. Benacerraf BR, Laboda LA, Frigoletto Jr FD: Thickened nuchal fold in fetuses not at risk for aneuploidy. *Radiology* 184:239, 1992.
67. Bromley B, Benacerraf BR: The resolving nuchal fold in second trimester fetuses: Not necessarily a reassuring finding. *J Ultrasound Med* 14:253, 1995.
68. Benacerraf BR: Ultrasound Evaluation of Chromosomal Abnormalities. In Callen PW (ed): *Ultrasonography in Obstetrics and Gynecology*. Philadelphia: WB Saunders, 2000, pp 38-67.
69. Barr Jr M: Growth profiles of human autosomal trisomies at mid-gestation. *Teratology* 50:395, 1994.
70. Lockwood C, Benacerraf B, Krinsky A, et al: A sonographic screening method for Down syndrome. *Am J Obstet Gynecol* 157:803, 1987.
71. Platt LD, Medearis AL, Carlson DE, et al: Screening for Down syndrome with the femur length/biparietal diameter ratio: A new twist of the data. *Am J Obstet Gynecol* 167:124, 1992.
72. Dicke JM, Gray DL, Songster GS, et al: Fetal biometry as a screening tool for the detection of chromosomally abnormal pregnancies. *Obstet Gynecol* 74:726, 1989.
73. Hadlock FP, Harrist RB, Martinez-Poyer J: Fetal body ratios in second trimester: A useful tool for identifying chromosomal abnormalities. *J Ultrasound Med* 11:81, 1992.
74. Perrella R, Duerinckx AJ, Grant EG, et al: Second-trimester sonographic diagnosis of Down syndrome: Role of femur-length shortening and nuchal fold thickening. *AJR Am J Roentgenol* 151:981, 1988.
75. Hill LM, Guzick D, Belfar HL, et al: The current role of sonography in the detection of Down syndrome. *Obstet Gynecol* 74:620, 1989.
76. Brumfield CG, Hauth JC, Cloud GA, et al: Sonographic measurements and ratios in fetuses with Down syndrome. *Obstet Gynecol* 73:644, 1989.
77. LaFollette L, Filly RA, Anderson R, et al: Fetal femur length to detect trisomy 21: A reappraisal. *J Ultrasound Med* 8:657, 1989.
78. Nyberg DA, Resta RG, Hickok DE, et al: Femur length shortening in the detection of Down syndrome: Is prenatal screening feasible? *Am J Obstet Gynecol* 162:1247, 1990.
79. Benacerraf BR, Chana A, Gelman R, et al: Can sonographers reliably identify anatomy features associated with Down syndrome? *Radiology* 173:377, 1989.
80. Grist TM, Fuller RW, Albiez KL, et al: Femur length in the US prediction of trisomy 21 and other chromosomal abnormalities. *Radiology* 174:837, 1990.
81. Shipp TD, Bromley B, Masciola M, et al: Variation in fetal femur length with respect to maternal race. *J Ultrasound Med* 20:141, 2001.
82. Fitzsimmons J, Droste S, Shepard TH, et al: Long-bone growth in fetuses with Down syndrome. *Am J Obstet Gynecol* 161:1174, 1989.
83. Benacerraf BR, Neuberg D, Frigoletto FD: Humeral shortening in second-trimester fetuses with Down syndrome. *Obstet Gynecol* 77:223, 1991.
84. Rodis JF, Vintzileos AM, Fleming AD, et al: Comparison of humerus length with femur length in fetuses with Down syndrome. *Am J Obstet Gynecol* 165:1051, 1991.
85. Rotmensch S, Luo J, Liberati M, et al: Fetal humeral length to detect Down syndrome. *Am J Obstet Gynecol* 166:1330, 1992.
86. Biagiotti R, Periti E, Cariatì E: Humerus and femur length in fetuses with Down syndrome. *Prenat Diagn* 14:429, 1994.
87. Nyberg DA, Resta RG, Luthy DA, et al: Humerus and femur length shortening in the detection of Down's syndrome. *Am J Obstet Gynecol* 168:534, 1993.
88. Lockwood CJ, Lynch L, Ghidini A, et al: The effect of fetal gender on the prediction of Down syndrome by means of maternal serum alpha-fetoprotein and ultrasonographic parameters. *Am J Obstet Gynecol* 169:1190, 1993.
89. Smulian JC, Vintzileos AM, Ciarleglio L, et al: Gender-specific patterns of second trimester femur and humerus measurements in fetuses with Down's syndrome. *J Matern Fetal Med* 4:225, 1995.
90. Benacerraf BR, Miller WA, Nadel A, et al: Does gender have an impact on the sonographic detection of second-trimester fetuses with Down's syndrome? *Ultrasound Obstet Gynecol* 5:30, 1995.
91. Benacerraf BR, Mandel J, Estroff JA, et al: Fetal pyclectasis: A possible association with Down syndrome. *Obstet Gynecol* 76:58, 1990.



92. Corteville JE, Dicke JM, Crane JP: Fetal pyelectasis and Down syndrome: Is genetic amniocentesis warranted? *Obstet Gynecol* 79:770, 1992.
93. Wilson RD, Lynch S, Lessoway VA: Fetal pyelectasis: Comparison of postnatal renal pathology with unilateral and bilateral pyelectasis. *Prenat Diagn* 17:451, 1997.
94. Wickstrom E, Maizels M, Sabbagha RE, et al: Isolated fetal pyelectasis: Assessment of risk for postnatal uropathy and Down syndrome. *Ultrasound Obstet Gynecol* 8:236, 1996.
95. Snijders RJ, Sebire NJ, Faria M, et al: Fetal mild hydronephrosis and chromosomal defects: Relation to maternal age and gestation. *Fetal Diagn Ther* 10:349, 1995.
96. Wickstrom EA, Thangavelu M, Parilla BV, et al: A prospective study of the association between isolated fetal pyelectasis and chromosomal abnormality. *Obstet Gynecol* 88:379, 1996.
97. Guariglia L, Rosati P: Isolated mild fetal pyelectasis detected by transvaginal sonography in advanced maternal age. *Obstet Gynecol* 92:833, 1998.
98. Levy DW, Mintz MC: The left ventricular echogenic focus: A normal finding. *AJR Am J Roentgenol* 150:85, 1988.
99. Brown DL, Roberts DJ, Miller WA: Left ventricular echogenic focus in the fetal heart: Pathologic correlation. *J Ultrasound Med* 13:613, 1994.
100. Tennstedt C, Chaoui R, Vogel M, et al: Pathologic correlation of sonographic echogenic foci in the fetal heart. *Prenat Diagn* 20:287, 2000.
101. Bromley B, Lieberman E, Laboda L, et al: Echogenic intracardiac focus: a sonographic sign for fetal Down syndrome. *Obstet Gynecol* 86:998, 1995.
102. Achiron R, Lipitz S, Gabbay U, et al: Prenatal ultrasonographic diagnosis of fetal heart echogenic foci: No correlation with Down syndrome. *Obstet Gynecol* 89:945, 1997.
103. Petrikovsky BM, Challenger M, Wyse LJ: Natural history of echogenic foci within ventricles of the fetal heart. *Ultrasound Obstet Gynecol* 5:92, 1995.
104. Shipp TD, Bromley B, Liberman EP, et al: The frequency of the detection of fetal echogenic intracardiac foci with respect to maternal race. *Ultrasound Obstet Gynecol* 15:460, 2000.
105. Ranzini AC, McLean DA, Sharma S, et al: Fetal intracardiac echogenic foci: Visualization depends on the orientation of the 4-chamber view. *J Ultrasound Med* 20:763, 2001.
106. Roberts DJ, Genest D: Cardiac histologic pathology characteristics of trisomies 13 and 21. *Hum Pathol* 23:1130, 1992.
107. Bromley B, Lieberman E, Shipp TD, et al: The Genetic Sonogram: A method of risk assessment for Down syndrome in the midtrimester. *J Ultrasound Med* 21:1087, 2002.
108. Sepulveda W, Cullen S, Nicolaides P, et al: Echogenic foci in the fetal heart: A marker of chromosomal abnormality. *Br J Obstet Gynaecol* 102:490, 1995.
109. Bromley B, Lieberman E, Shipp TD, et al: Significance of an echogenic intracardiac focus in fetuses at high and low risk for aneuploidy. *J Ultrasound Med* 17:127, 1998.
110. Winter TC, Anderson AM, Cheng EY, et al: The echogenic intracardiac focus in second trimester fetuses with trisomy 21: Usefulness as a US marker. *Radiology* 216:450, 2000.
111. Wax JR, Philput C: Fetal intracardiac echogenic foci: does it matter which ventricle? *J Ultrasound Med* 17:141, 1998.
112. How HY, Villafane J, Parihus RR, et al: Small hyperechoic foci of the fetal cardiac ventricle: A benign sonographic finding? *Ultrasound Obstet Gynecol* 4:205, 1994.
113. Bettelheim D, Deutinger J, Bernaschek G: The value of echogenic foci ("golfsballs") in the fetal heart as a marker of chromosomal abnormalities. *Ultrasound Obstet Gynecol* 14:98, 1999.
114. Vibhakar NI, Budorick NE, Scioscia AL, et al: Prevalence of aneuploidy with a cardiac intraventricular echogenic focus in at-risk patient population. *J Ultrasound Med* 18:265, 1999.
115. Vincoff NS, Callen PW, Smith-Bindman R, Goldstein RB: Effect of ultrasound transducer frequency on the appearance of the fetal bowel. *J Ultrasound Med* 18:799, 1999.
116. Nyberg DA, Dubinsky T, Mahony BS, et al: Echogenic fetal bowel: Clinical importance. *Radiology* 188:527, 1993.
117. Bromley B, Doubilet P, Frigoletto FD Jr, et al: Is fetal hyperechoic bowel on second-trimester sonogram an indication for amniocentesis? *Obstet Gynecol* 83:647, 1994.
118. Al-Kouatly HB, Chasen ST, Strelzoff J, et al: The clinical significance of echogenic bowel. *Am J Obstet Gynecol* 185:1035, 2001.
119. Strocker AM, Snijders RJ, Carlson DE, et al: Fetal echogenic bowel: Parameters to be considered in differential diagnosis. *Ultrasound Obstet Gynecol* 16:519, 2000.
120. Sepulveda W, Reid R, Nicolaides P, et al: Second-trimester echogenic bowel and intraamniotic bleeding: Association between fetal bowel echogenicity and amniotic fluid spectrophotometry at 410 nm. *Am J Obstet Gynecol* 174:839, 1996.
121. Slotnick RN, Abuhamad AZ: Prognostic implications of fetal echogenic bowel. *Lancet* 347:85, 1996.
122. Nyberg DA, Neilsen IR: Abdomen and Gastrointestinal Tract. In Nyberg DA, McGahan JP, Pretorius DH, Pilu G (eds): *Diagnostic Imaging of Fetal Anomalies*. Philadelphia: Lippincott Williams & Wilkins, 2003, pp 547-602.
123. Chinn DH, Miller EI, Worthy LM, Towers CV: Sonographically detected fetal choroid plexus cysts: Frequency and association with aneuploidy. *J Ultrasound Med* 10:255, 1991.
124. Ostlere SJ, Irving HC, Lilford RJ: A prospective study of the incidence and significance of fetal choroid plexus cysts. *Prenat Diagn* 9:205, 1989.
125. Nadel AS, Bromley BS, Frigoletto FD, et al: Isolated choroid plexus cysts in the second-trimester fetus: Is amniocentesis really indicated? *Radiology* 185:545, 1992.
126. Benacerraf BR, Harlow B, Frigoletto FD: Are choroid plexus cysts an indication for second-trimester amniocentesis? *Am J Obstet Gynecol* 162:1001, 1990.
127. Gross SJ, Shulman LP, Tolley EA, et al: Isolated fetal choroid plexus cysts and trisomy 18: A review and meta-analysis. *Am J Obstet Gynecol* 172:83, 1995.
128. Yoder PR, Sabbagha RE, Gross SJ, et al: The second-trimester fetus with isolated choroid plexus cysts: a meta-analysis of risk of trisomies 18 and 21. *Obstet Gynecol* 93:869, 1999.
129. Shields LE, Uhrich SB, Easterling TR, et al: Isolated fetal choroid plexus cysts and karyotype analysis: Is it necessary? *J Ultrasound Med* 15:389, 1996.
130. Snijders RJ, Shawa L, Nicolaides KH: Fetal choroid plexus cysts and trisomy 18: assessment of risk based on ultrasound findings and maternal age. *Prenat Diagn* 14:1119, 1994.
131. Yeo L, Guzman ER, Vintzileos AM, et al: Isolated versus nonisolated choroid plexus cysts: Their relationship to aneuploidy and other congenital anomalies. *Am J Obstet Gynecol* 180:558, 1999.
132. Leonardi MR, Wolfe HM, Lanouette JM, et al: The apparently isolated choroid plexus cyst: importance of minor abnormalities in predicting the risk for aneuploidy. *Fetal Diagn Ther* 13:49, 1998.
133. Vintzileos AM, Ananth CV, Fisher AJ, et al: An economic evaluation of prenatal strategies for detection of trisomy 18. *Am J Obstet Gynecol* 179:1220, 1998.
134. Porto M, Murata Y, Warneke LA, et al: Fetal choroid plexus cysts: An independent risk factor for chromosomal anomalies. *J Clin Ultrasound* 21:103, 1993.
135. Gray DL, Winborn RC, Suessen TL, et al: Is genetic amniocentesis warranted when isolated choroid plexus cysts are found? *Prenat Diagn* 16:983, 1996.
136. Walkinshaw S, Pilling D, Spriggs A: Isolated choroid plexus cysts: The need for routine offer of karyotyping. *Prenat Diagn* 14:663, 1994.
137. Ostlere SJ, Irving HC, Lilford RJ: Fetal choroid plexus cysts: A report of 100 cases. *Radiology* 175:753, 1990.
138. Twining P, Zuccollo J, Clewes J, et al: Fetal choroid plexus cysts: A prospective study and review of the literature. *Br J Radiol* 64:98, 1991.
139. Perpignano MC, Cohen HL, Klein VR, et al: Fetal choroid plexus cysts: Beware the smaller cyst. *Radiology* 182:715, 1992.
140. Howard RJ, Tuck SM, Long J, et al: The significance of choroid plexus cysts in fetuses at 18-20 weeks. An indication for amniocentesis? *Prenat Diagn* 12:685, 1992.
141. Platt LD, Carlson DE, Medearis AL, et al: Fetal choroid plexus cysts in the second trimester of pregnancy: A cause for concern. *Am J Obstet Gynecol* 164:1652, 1991.
142. Bromley B, Lieberman R, Benacerraf BR: Choroid plexus cysts: Not associated with Down syndrome. *Ultrasound Obstet Gynecol* 8:232, 1996.
143. Gupta JK, Cave M, Lilford RF, et al: Clinical significance of fetal choroid plexus cysts. *Lancet* 346:724, 1995.
144. Filly RA, Benacerraf BR, Nyberg DA, et al: Choroid plexus cyst and echogenic intracardiac focus in women at low risk for chromosomal anomalies. *J Ultrasound Med* 23:447, 2004.



145. Achiron R, Barkai G, Katznelson B-M, et al: Fetal lateral ventricle choroid plexus cysts: The dilemma of amniocentesis. *Obstet Gynecol* 78:815, 1991.
146. Benacerraf BR, Laboda LA: Cyst of the fetal choroid plexus: A normal variant? *Am J Obstet Gynecol* 160:319, 1989.
147. Chan L, Hixson JL, Laifer SA, et al: A sonographic and karyotypic study of second-trimester fetal choroid plexus cysts. *Obstet Gynecol* 73:703, 1989.
148. Chitkara U, Cogswell C, Norton K, et al: Choroid plexus cysts in the fetus: A benign anatomic variant or pathologic entity? Report of 41 cases and review of the literature. *Obstet Gynecol* 72:185, 1988.
149. Clark SL, DeVore GR, Sabey PL: Prenatal diagnosis of cysts of the fetal choroid plexus. *Obstet Gynecol* 72:585, 1988.
150. DeRoo TR, Harris RD, Sargent SK, et al: Fetal choroid plexus cysts: Prevalence, clinical significance, and sonographic appearance. *AJR Am J Roentgenol* 151:1179, 1988.
151. Gabrielli S, Reece A, Pili G, et al: The clinical significance of prenatally diagnosed choroid plexus cysts. *Am J Obstet Gynecol* 160:1207, 1989.
152. Hertzberg BS, Kay HH, Bowie JD: Fetal choroid plexus lesions: Relationship of antenatal sonographic appearance to clinical outcome. *J Ultrasound Med* 8:77, 1989.
153. Kupferminc MJ, Tamura RK, Sabbagha RE, et al: Isolated choroid plexus cyst(s): An indication for amniocentesis. *Am J Obstet Gynecol* 171:1068, 1994.
154. Nava S, Godmilow L, Recser S, et al: Significance of sonographically detected second-trimester choroid plexus cysts: A series of 211 cases and a review of the literature. *Ultrasound Obstet Gynecol* 4:448, 1994.
155. Thorpe-Berston JG, Gosden M, Nicolaides KH: Choroid plexus cysts and chromosomal defects. *Br J Radiol* 63:783, 1990.
156. Zerres K, Schuler H, Gembruch U, et al: Chromosomal findings in fetuses with prenatally diagnosed cysts of the choroid plexus. *Hum Genet* 89:301, 1992.
157. Down JLH: Observations on an ethnic classification of idiots. *London Hosp Clin Lect Rep* 3:259, 1866.
158. Keeling JW, Hansen BF, Kjaer I: Pattern of malformations in the axial skeleton in human trisomy 21 fetuses. *Am J Med Genet* 68:466, 1997.
159. Stempfle N, Hutten Y, Fredouille C, et al: Skeletal abnormalities in fetuses with Down's syndrome: Radiographic post-mortem study. *Pediatr Radiol* 29:682, 1999.
160. Cicero S, Curcio P, Papageorgiou A, et al: Absence of nasal bone in fetuses with trisomy 21 at 11-14 weeks of gestation: An observational study. *Lancet* 358:1665, 2001.
161. Sonck JD, Nicolaides KH: Prenatal ultrasonographic diagnosis of nasal bone abnormalities in three fetuses with Down syndrome. *Am J Obstet Gynecol* 186:139, 2002.
162. Bromley B, Lieberman E, Shipp TD, et al: Fetal nose bone length: A marker for Down syndrome in the second trimester. *J Ultrasound Med* 21:1387, 2002.
163. Cicero S, Sonck JD, McKenna DS, et al: Nasal bone hypoplasia in trisomy 21 at 15-22 weeks' gestation. *Ultrasound Obstet Gynecol* 21:15, 2003.
164. Lee W, DeVore GR, Comstock CH, et al: Nasal bone evaluation in fetuses with Down syndrome during the second and third trimesters of pregnancy. *J Ultrasound Med* 22:55, 2003.
165. Odibo AO, Sehdev HM, Dunn L, et al: The association between fetal nasal bone hypoplasia and aneuploidy. *Obstet Gynecol* 104:1229, 2004.
166. Goncalves LF, Espinoza J, Lee W, et al: Phenotypic characteristics of absent and hypoplastic nasal bones in fetuses with Down syndrome: description by 3-dimensional ultrasonography and clinical significance. *J Ultrasound Med* 23:1619, 2004.
167. Zelop C, Benn P, Milewski E, et al: Efficacy of absent or shortened nasal bone length for Down syndrome detection in second trimester fetuses. *Am J Obstet Gynecol* 191:545, 2004.
168. Freire-Lizama T, Johnson J: The NOSE (nasal ossification sonographic evaluation) study. *Am J Obstet Gynecol* 191:S144, 2004.
169. Viora E, Errante G, Sciarrone A, et al: Fetal nasal bone and trisomy 21 in the second trimester. *Prenat Diagn* 25:511, 2005.
170. Benoit B, Chaoui R: Three-dimensional ultrasound with maximal mode rendering: A novel technique for the diagnosis of bilateral or unilateral absence or hypoplasia of nasal bones in second-trimester screening for Down syndrome. *Ultrasound Obstet Gynecol* 25:19, 2005.
171. Bergann A, Bamberg C, Eder K, et al: Mid-facial anthropometry in second-trimester fetuses with trisomy 21: A three-dimensional ultrasound study. *Prenat Diagn* 26:158, 2006.
172. Bromley B, Benacerraf BR: The genetic sonogram scoring index. *Semin Perinatol* 27:124, 2003.
173. Bunduki V, Ruano R, Miguelez J, et al: Fetal nasal bone length: Reference range and clinical application in ultrasound screening for trisomy 21. *Ultrasound Obstet Gynecol* 21:156, 2003.
174. Yeo L, Ananth CV, Kontopoulos E, et al: The addition of absent nasal bone increases the sensitivity of second trimester genetic sonography for Down syndrome to 92.8%. *Am J Obstet Gynecol* 191:S25, 2005.
175. Cusick W, Provenzano J, Sullivan CA, et al: Fetal nasal bone length in euploidy and aneuploidy fetuses between 11 and 20 weeks' gestation: A prospective study. *J Ultrasound Med* 23:1327, 2004.
176. Chen M, Lee CP, Leung KY, et al: Pilot study on the midsecond trimester examination of fetal nasal bone in the Chinese population. *Prenat Diagn* 24:87, 2004.
177. Tran LT, Carr DB, Mitumori LM, et al: Second-trimester biparietal diameter/nasal bone length ratio is an independent predictor of trisomy 21. *J Ultrasound Med* 24:805, 2005.
178. Shipp TD, Bromley B, Lieberman E, et al: The second-trimester fetal iliac angle as a sign of Down syndrome. *Ultrasound Obstet Gynecol* 12:15, 1998.
179. Bork MD, Egan JFX, Cusick W, et al: Iliac wing angle as a marker for trisomy 21 in the second trimester. *Obstet Gynecol* 89:734, 1997.
180. Zoppi MA, Ibbas RM, Floris M, et al: Can fetal iliac bone measurement be used as a marker for Down's syndrome screening? *Ultrasound Obstet Gynecol* 12:19, 1998.
181. Abuhamad AZ, Kolm P, Mari G, et al: Ultrasonographic fetal iliac length measurement in the screening for Down syndrome. *Am J Obstet Gynecol* 171:1063, 1994.
182. Kliewer MA, Hertzberg BS, Freed KS, et al: Normal fetal pelvis: Important factors for morphometric characterization with US. *Radiology* 215:453, 2000.
183. Shipp TD, Bromley B, Lieberman E, et al: The iliac angle as a sonographic marker for Down syndrome in second trimester fetuses. *Obstet Gynecol* 89:446, 1997.
184. Grange G, Thoury A, Dupont J, et al: Sonographic measurement of the fetal iliac angle cannot be used alone as a marker for trisomy 21. *Fetal Diagn Ther* 15:41, 2000.
185. Sivan Y, Merlob P, Reisner SH: Assessment of ear length and low set ears in newborn infants. *J Med Genet* 20:213, 1983.
186. Thelander HE, Pryor HB: Abnormal patterns of growth and development in mongolism: An anthropometric study. *Clin Pediatr* 5:493, 1966.
187. Gorlin RJ, Cohen MM, Levin LS: *Syndromes of the Head and Neck*, 3rd ed. Oxford, Oxford University Press, 1990.
188. Kinoshita M, Nakamura Y, Nakano R, et al: Thirty-one autopsy cases of trisomy 18: clinical features and pathological findings. *Pediatr Pathol* 9:445, 1989.
189. Birnholz JC, Farrell EE: Fetal ear length. *Pediatrics* 81:555, 1988.
190. Lettieri L, Rodis JF, Vintzileos AM, et al: Ear length in second-trimester aneuploid fetuses. *Obstet Gynecol* 81:57, 1993.
191. Awwad JT, Azar GB, Karam KS, et al: Ear length: A potential sonographic marker for Down syndrome. *Int J Gynecol Obstet* 44:233, 1994.
192. Shimizu T, Salvador L, Hughes-Benzie R, et al: The role of reduced ear size in the prenatal detection of chromosomal abnormalities. *Prenat Diagn* 17:545, 1997.
193. Chitkara U, Lee L, El-Sayed YY, et al: Ultrasonographic ear length measurement in normal second and third-trimester fetuses. *Am J Obstet Gynecol* 183:230, 2000.
194. Chitkara U, Lee L, Oehlert JW, et al: Fetal ear length measurement: a useful predictor of aneuploidy? *Ultrasound Obstet Gynecol* 19:131, 2002.
195. Yeo L, Guzman ER, Ananth CV, et al: Prenatal detection of fetal aneuploidy by sonographic ear length. *J Ultrasound Med* 22:565, 2003.
196. Benacerraf BR: Antenatal sonographic diagnosis of congenital clubfoot: a possible indication for amniocentesis. *J Clin Ultrasound* 14:703, 1986.
197. Isaksen CV, Eik-Nes SH, Blaas HG, et al: A correlative study of prenatal ultrasound and post-mortem findings in fetuses and infants with an abnormal karyotype. *Ultrasound Obstet Gynecol* 16:37, 2000.



198. Shipp TD, Benacerraf BR: The significance of prenatally identified isolated clubfoot: Is amniocentesis indicated? *Am J Obstet Gynecol* 178:600, 1998.
199. Malone FD, Marino T, Bianchi DW, et al: Isolated clubfoot diagnosed prenatally: is karyotyping indicated? *Obstet Gynecol* 95:437, 2000.
200. Seoud MA, Alley DC, Smith DL, et al: Prenatal sonographic findings in trisomy 13, 18, 21 and 22: A review of 46 cases. *J Reprod Med* 39:781, 1994.
201. Benacerraf BR, Harlow B, Frigoletto Jr FD: Hypoplasia of the middle phalanx of the fifth digit: A feature of the second trimester fetus with Down syndrome. *J Ultrasound Med* 9:389, 1990.
202. Wilkins I: Separation of the great toe in fetuses with Down syndrome. *J Ultrasound Med* 13:229, 1994.
203. Christianson AL, Nelson MM: Four cases of trisomy 18 syndrome with limb reduction malformation. *J Med Genet* 21:293, 1984.
204. Quintero RA, Johnson MP, Mendoza G, et al: Ontogeny of clenched-hand development in trisomy 18 fetuses: a serial transabdominal fetoscopic observation. *Fetal Diagn Ther* 14:68, 1999.
205. Lam YH, Tang MH: Sonographic features of fetal trisomy 18 at 13 and 14 weeks: four case reports. *Ultrasound Obstet Gynecol* 13:366, 1999.
206. Shields LE, Carpenter LA, Smith KM, et al: Ultrasonographic diagnosis of trisomy 18: Is it practical in the early second trimester? *J Ultrasound Med* 17:327, 1998.
207. Kinoshita M, Nakamura Y, Nakano R, et al: Thirty-one autopsy cases of trisomy 18: clinical features and pathological findings. *Pediatr Pathol* 9:445, 1989.
208. Benacerraf BR, Miller WA, Frigoletto FD: Sonographic detection of fetuses with trisomies 13 and 18: accuracy and limitations. *Am J Obstet Gynecol* 158:404, 1988.
209. Paluda SM, Comstock CH, Kirk JS, et al: The significance of ultrasonographically diagnosed fetal wrist position anomalies. *Am J Obstet Gynecol* 174:1834, 1996.
210. Heifetz SA: Single umbilical artery. A statistical analysis of 237 autopsy cases and review of the literature. *Perspect Pediatr Pathol* 8:345, 1984.
211. Nyberg DA, Mahony BS, Luthy D, et al: Single umbilical artery-prenatal detection of concurrent anomalies. *J Ultrasound Med* 10:247, 1991.
212. Byrne J, Blanc WA: Malformations and chromosome anomalies in spontaneously aborted fetuses with single umbilical artery. *Am J Obstet Gynecol* 151:340, 1985.
213. Wu M-H, Chang F-M, Shen M-R, et al: Prenatal sonographic diagnosis of single umbilical artery. *J Clin Ultrasound* 25:425, 1997.
214. Saller DN, Keene CL, Sun C-CJ: the association of single umbilical artery with cytogenetically abnormal pregnancies. *Am J Obstet Gynecol* 163:922, 1990.
215. Parilla BV, Tamura RK, MacGregor SN, et al: The clinical significance of a single umbilical artery as an isolated finding on prenatal ultrasound. *Obstet Gynecol* 85:570, 1995.
216. Lilja M: Infants with single umbilical artery studied in a national registry. General epidemiological characteristics. *Paediatr Perinat Epidemiol* 5:27, 1991.
217. Chow JS, Benson CB, Doubilet PM: Frequency and nature of structural anomalies in fetuses with single umbilical arteries. *J Ultrasound Med* 17:765, 1998.
218. Persutte WH, Hobbins JC: Single umbilical artery: a clinical enigma in modern prenatal diagnosis. *Ultrasound Obstet Gynecol* 6:216, 1995.
219. Abuhamad AZ, Shaffer W, Mari G, et al: Single umbilical artery: Does it matter which artery is missing? *Am J Obstet Gynecol* 173:728, 1995.
220. Bahado-Singh RO, Wyse L, Dorr MA, et al: Fetuses with Down syndrome have disproportionately shortened frontal lobe dimensions on ultrasonographic examination. *Am J Obstet Gynecol* 167:1009, 1992.
221. Winter TC, Reichman JA, Luna JA, et al: Frontal lobe shortening in second-trimester fetuses with trisomy 21: Usefulness as a US marker. *Radiology* 207:215, 1998.
222. Nicolaides KH, Salvesen DR, Snijders RJ, et al: Strawberry-shaped skull in fetal trisomy 18. *Fetal Diagn Ther* 7:132, 1992.
223. Nyberg DA, Mack LA, Hirsch J, Mahony BS: Abnormalities of fetal cranial contour in sonographic detection of spina bifida: evaluation of the "lemon" sign. *Radiology* 167:387, 1988.
224. Hook EB, Porter IH: Population Cytogenetic Studies in Humans. San Diego, Academic Press, 1977.
225. Egan JF, Benn P, Borgida AF, et al: Efficacy of screening for fetal Down syndrome in the United States from 1974 to 1997. *Obstet Gynecol* 96:979, 2000.
226. Snijders RJ, Sundberg K, Holzgreve W, et al: Maternal age and gestation-specific risk for trisomy 21. *Ultrasound Obstet Gynecol* 13:167, 1999.
227. Yeo L, Vintzileos AM: The use of genetic sonography to reduce the need for amniocentesis in women at high-risk for Down syndrome. *Semin Perinatol* 27:152, 2003.
228. Haddow JE, Palomaki GE, Knight GJ, et al: Reducing the need for amniocentesis in women 35 years of age or older with serum markers for screening. *N Engl J Med* 330:114, 1994.
229. Smith-Bindman R, Hosmer W, Feldstein VA, et al: Second-trimester ultrasound to detect fetuses with Down syndrome: A meta-analysis. *JAMA* 285:1044, 2001.
230. Vintzileos AM, Guzman ER, Smulian JC, et al: Indication-specific accuracy of second-trimester genetic ultrasonography for the detection of trisomy 21. *Am J Obstet Gynecol* 181:1045, 1999.
231. Benacerraf BR, Neuberger D, Bromley B, et al: Sonographic scoring index for prenatal detection of chromosomal abnormalities. *J Ultrasound Med* 11:449, 1992.
232. Nadel AS, Bromley B, Frigoletto FD, et al: Can the presumed risk of autosomal trisomy be decreased in fetuses of older women following a normal sonogram? *J Ultrasound Med* 14:297, 1995.
233. DeVore GR, Alf O: The use of color Doppler ultrasound to identify fetuses at increased risk for trisomy 21: an alternative for high-risk patients who decline genetic amniocentesis. *Obstet Gynecol* 85:378, 1995.
234. Nyberg DA, Luthy DA, Cheng EY, et al: Role of prenatal ultrasonography in women with positive screen for Down syndrome on the basis of maternal serum markers. *Am J Obstet Gynecol* 173:1030, 1995.
235. Vintzileos AM, Campbell WA, Rodis JF, et al: The use of second-trimester genetic sonogram in guiding clinical management of patients at increased risk for fetal trisomy 21. *Obstet Gynecol* 87:948, 1996.
236. Bahado-Singh RO, Tan A, Deren O, et al: Risk of Down syndrome and any clinically significant chromosome defect in pregnancies with abnormal triple-screen and normal targeted ultrasonographic results. *Am J Obstet Gynecol* 175:824, 1996.
237. Bromley B, Lieberman E, Benacerraf BR: The incorporation of maternal age into the sonographic scoring index for the detection at 14-20 weeks of fetuses with Down syndrome. *Ultrasound Obstet Gynecol* 10:321, 1997.
238. Verdin SM, Economides DL: The role of ultrasonographic markers for trisomy 21 in women with positive serum biochemistry. *Br J Obstet Gynaecol* 105:63, 1998.
239. Nyberg DA, Luthy DA, Resta RG, et al: Age-adjusted ultrasound risk assessment for fetal Down's syndrome during the second trimester: Description of the method and analysis of 142 cases. *Ultrasound Obstet Gynecol* 12:8, 1998.
240. Sohl BD, Scioscia AL, Budorick NE, et al: Utility of minor ultrasonographic markers in the prediction of abnormal fetal karyotype at a prenatal diagnostic center. *Am J Obstet Gynecol* 181:898, 1999.
241. Wax JR, Guilbert J, Mather J, et al: Efficacy of community-based second trimester genetic ultrasonography in detecting the chromosomally abnormal fetus. *J Ultrasound Med* 19: 689, 2000.
242. Devore GR, Romero R: Combined use of genetic sonography and maternal serum triple-marker screening: An effective method for increasing the detection of trisomy 21 in women younger than 35 years. *J Ultrasound Med* 20:645, 2001.
243. Persutte WH, Hobbins JC, Nyberg DA, et al: Trisomy 21 multicenter collaborative project. *Am J Obstet Gynecol* 178:S22, 1998(abstr).
244. Hobbins JC, Lezotte DC, Persutte WH, et al: An eight center study to evaluate the utility of mid-term genetic ultrasounds among high risk pregnancies. *J Ultrasound Med* 22:33, 2003.
245. Vintzileos AM, Guzman ER, Smulian JC, et al: Choice of second-trimester genetic sonogram for detection of trisomy 21. *Obstet Gynecol* 90:187, 1997.
246. Bahado-Singh RO, Tan A, Deren O, et al: Risk of Down syndrome and any clinically significant chromosome defect in pregnancies with abnormal triple-screen and normal targeted ultrasound results. *Am J Obstet Gynecol* 175:824, 1996.
247. Deren O, Mahoney MJ, Copel JA, et al: Subtle ultrasonographic anomalies: Do they improve the Down syndrome detection rate? *Am J Obstet Gynecol* 178:441, 1998.

248. Pinette MG, Garrett J, Salvo A, et al: Normal midtrimester (17-20 weeks) genetic sonogram decreases amniocentesis rate in a high-risk population. *J Ultrasound Med* 20:639, 2001.
249. Vintzileos AM, Guzman ER, Smulian JC, et al: Indication-specific accuracy of second-trimester genetic ultrasonography for the detection of trisomy 21. *Am J Obstet Gynecol* 181:1045, 1999.
250. Vintzileos AM, Guzman ER, Smulian JC, et al: Down syndrome risk estimation after normal genetic sonography. *Am J Obstet Gynecol* 187:1226, 2002.
251. Vintzileos AM, Guzman ER, Smulian JC, et al: Second-trimester genetic sonography in patients with advanced maternal age and normal triple screen. *Obstet Gynecol* 99:993, 2002.
252. Hobbins JC, Bahado-Singh RO, Lezotte DC: The genetic sonogram in screening for Down syndrome: response to the JAMA study. *J Ultrasound Med* 20:269, 2001.
253. Benacerraf BR, Nadel AS, Bromley B: Identification of second-trimester fetuses with autosomal trisomy by use of a sonographic scoring index. *Radiology* 193:135, 1994.
254. Bromley B, Lieberman E, Benacerraf BR: The incorporation of maternal age into the sonographic scoring index for the detection at 14-20 weeks of fetuses with Down's syndrome. *Ultrasound Obstet Gynecol* 10:321, 1997.
255. Nyberg DA, Souter VL: Use of genetic sonography for adjusting the risk for fetal Down syndrome. *Semin Perinatol* 27:130, 2003.
256. Landwehr JB Jr, Johnson MP, Hume RF, et al: Abnormal nuchal findings on screening ultrasonography: Aneuploidy stratification on the basis of ultrasonographic anomaly and gestational age at detection. *Am J Obstet Gynecol* 175:995, 1996.
257. American College of Obstetricians and Gynecologists: Prenatal diagnosis of fetal chromosomal abnormalities: 2003 Compendium of Selected Publications. Washington, The American College of Obstetricians and Gynecologists, pp 547-557, 2003.
258. Vintzileos AM, Ananth CV, Fisher AJ, et al: An economic evaluation of second-trimester genetic ultrasonography for prenatal detection of Down syndrome. *Am J Obstet Gynecol* 179:1214, 1998.
259. DeVore GR: Is genetic ultrasound cost-effective? *Semin Perinatol* 27:173, 2003.
260. Bahado-Singh R, Cheng CC, Matia P, et al: Combined serum and ultrasound screening for detection of fetal aneuploidy. *Semin Perinatol* 27:145, 2003.
261. Hook EB, Woodbury DF, Albright SG: Rates of trisomy 18 in livebirths, stillbirths, and at amniocentesis. *Birth Defects* XV:81, 1979.
262. Canick JA, Palomaki GE, Osathanondh R: Prenatal screening for trisomy 18 in the second trimester. *Prenat Diagn* 10:546, 1990.
263. Palomaki GE, Haddow JE, Knight CJ, et al: Risk-based prenatal screening for trisomy 18 using alpha-fetoprotein, unconjugated oestriol and human chorionic gonadotropin. *Prenat Diagn* 15:713, 1995.
264. Brumfield CG, Wenstrom KD, Owen J, Davis RO: Ultrasound findings and multiple marker screening in trisomy 18. *Obstet Gynecol* 95:51, 2000.
265. Jones KL: *Smith's Recognizable Patterns of Human Malformation*, 5th ed. Philadelphia, WB Saunders, 1997.
266. Schneider AS, Mennuti MT, Zackai EH: High cesarean section rate in trisomy 18 births: A potential indication for late prenatal diagnosis. *Am J Obstet Gynecol* 140:367, 1981.
267. Bundy AL, Saltzman DH, Poher B, et al: Antenatal sonographic findings in trisomy 18. *J Ultrasound Med* 5:361, 1986.
268. Seoud MA, Alley DC, Smith DL, et al: Prenatal sonographic findings in trisomy 13, 18, 21 and 22: A review of 46 cases. *J Reprod Med* 39:781, 1994.
269. Salihu HM, Boos R, Schmidt W: Antenatally detectable markers for the diagnosis of autosomally trisomic fetuses in at-risk pregnancies. *Am J Perinatol* 14:257, 1997.
270. Shields LE, Carpenter LA, Smith KM, et al: Ultrasonographic diagnosis of trisomy 18: Is it practical in the early second trimester? *J Ultrasound Med* 17:327, 1998.
271. Feuchtbaum LB, Currier RJ, Lorey FW, et al: Prenatal ultrasound findings in affected and unaffected pregnancies that are screen-positive for trisomy 18: The California Experience. *Prenat Diagn* 20:293, 2000.
272. Carey JC: Trisomy 18 and trisomy 13 syndromes. In Cassidy SB, Allanson JE (eds): *Management of genetic syndromes*. New York: Wiley, 2001, pp 419-420.
273. Hill LM: The sonographic detection of trisomies 13, 18, and 21. *Clin Obstet Gynecol* 80:349, 1996.
274. Nicolaides KH, Snijders RJ, Gosden CM, et al: Ultrasonographically detectable markers of fetal chromosomal abnormalities. *Lancet* 340:704, 1992.
275. Tongsong T, Sirichotiyakul S, Wanapirak C, et al: Sonographic features of trisomy 13 at midpregnancy. *Int J Gynecol Obstet* 76:143, 2002.
276. DeVigan C, Baena N, Cariati E, et al: Contribution of ultrasonographic examination to the prenatal detection of chromosomal abnormalities in 19 centres across Europe. *Ann Genet* 44:209, 2001.
277. Papp C, Beke A, Ban Z, et al: Prenatal diagnosis of trisomy 13: Analysis of 28 cases. *J Ultrasound Med* 25:42, 2006.



## FETAL SYNDROMES

Juliana M. Leite, MD, Roberta Granese, MD, Philippe Jeanty, MD, PhD, and Sandra Silva Herbst, MD

**Achondrogenesis**

**Achondroplasia**

**Aicardi Syndrome**

**Alagille Syndrome**

**Amniotic Band Syndrome**

**Apert Syndrome**

**Arnold-Chiari Malformation**

**Arthrogryposis Multiplex Congenita**

**Asphyxiating Thoracic Dysplasia**

**Asplenia-Polysplenia Syndromes**

**Beckwith-Wiedemann Syndrome**

**Campomelic Dysplasia**

**Caudal Regression Syndrome**

**Cerebrohepatorenal Syndrome**

**Charge Association**

**Fetal Alcohol Syndrome, Fetal Alcohol Effects**

**Fetal Cytomegalovirus Infection**

**Fetal Rubella Syndrome**

**Fetal Toxoplasmosis Syndrome**

**Fetal Valproic Acid Exposure Syndrome**

**Fetal Varicella Zoster**

**Fraser Syndrome**

**Fryns Syndrome**

**Goldenhar Syndrome**

**HELLP Syndrome**

**Hereditary Lymphedema I**

**Herpes Simplex Infection**

**Holoprosencephaly**

**Holt-Oram Syndrome**

**Hydrolethrus Syndrome**

**Hypoplastic Left Heart Syndrome**

**Klippel-Feil Syndrome**

**Klippel-Trenaunay-Weber Syndrome**

**Larsen Syndrome**

**Lethal Multiple Pterygium Syndrome**

**Lissencephaly**

**Meckel Syndrome**

**Monosomy X (Turner) Syndrome**

**Noonan Syndrome**

**Osteogenesis Imperfecta**

**Pallister-Killian Syndrome**

**Pena-Shokeir Syndrome**

**Pentalogy of Cantrell**

**Pfeiffer Syndrome**

**Pierre Robin Syndrome**

**Poland Syndrome**

**Prader-Willi Syndrome**

**Prune-Belly Syndrome**

**Roberts Syndrome**

**Septo-Optic Dysplasia**

**Simpson-Golabi-Behmel Syndrome**

**Sirenomelia**

**Smith-Lemli-Opitz Syndrome**

**Thanatophoric Dysplasia**

**Tuberous Sclerosis**

**Twin-to-Twin Transfusion Syndrome**

**VACTERL Association**

**Walker-Warburg Syndrome**

**Wolf-Hirschhorn Syndrome**

Congenital anomalies are typically organized by organ system. This is an excellent organization in that similar disorders are grouped together. However, multisystem syndromes do not fit neatly in the organ category organization.

Usually, the most striking finding or the most unusual finding is the one that leads to the inclusion in one or another group. Yet with the more precise information that one can now acquire, it is time to organize syndromes as a separate subject.

Congenital anomalies, which represent structural abnormalities of the developing embryo or fetus, are often classified into four different types: (1) malformation, (2) deformation, (3) disruption, and (4) dysplasia.

**Malformation.** A morphologic defect of an organ, part of an organ, or larger region of the body that results from an intrinsically abnormal developmental process. The term intrinsic implies that the developmental potential of the primordium or anlage is abnormal from the beginning. Malformations may be single or multiple.

**Deformation.** Deformation refers to an abnormal form, shape, or position of part of the body caused by mechanical forces antenatally, often as a result of intrauterine molding or constraint. The forces that cause deformations may be extrinsic, such as uterine abnormalities, or intrinsic factors, such as oligohydramnios.

**Disruption.** A morphologic defect of an organ, part of an organ, or larger region of the body resulting from the breakdown of previously normal tissue. It is caused by an extrinsic force or internal interference with a developmental process or a vascular insult. Extrinsic factors such as infection, teratogen, or trauma are considered disruptive. Intrauterine vascular accidents are a major cause of disruptions.

**Dysplasia.** An abnormal organization of cells into tissues and its morphologic results. Dysplasia is the process and consequence of abnormal tissue formation. It is casually nonspecific and often affects several organs because of the nature of the underlying cellular disturbances.

When more than one fetal abnormality is identified, several terms are used to describe the causation and pathogenesis.

**Sequence.** A pattern of multiple anomalies that results from a single anomaly or mechanical factor. Also referred to as an anomalad. The resultant secondary problems may be due to a malformation, disruption, or deformation.

**Association.** A nonrandom occurrence in two or more individuals of multiple anomalies not known to be a sequence or syndrome.

**Syndrome.** A pattern of multiple anomalies thought to be pathogenetically related and not known to represent a single sequence.

In the following pages we review several syndromes that should be familiar to sonographers and sonologists either because they are fairly characteristic or common, or because their recognition will affect the management of the pregnancy. The selection of the syndromes included is somewhat artificial, but all can be detected prenatally or will affect the pregnancy. Clearly, this review cannot be exhaustive. The Birth Defect Encyclopedia contained approximately 2000 syndromes, and the Online Mendelian Inheritance in Man (OMIM) recently passed the 10,000-syndrome landmark. Even for physicians dedicated to the subject, this is an unmanageable amount of information to grasp. Rather than attempt to read (let alone memorize) such a large body of knowledge, it is more important to learn how to investigate unusual cases. What are the most noticeable and major of findings? And almost as important, what are the minor or more subtle findings? Once the observations are made, is

there other clinical information of importance? Before rushing to do an amniocentesis, some review of the large database is usually indicated to suggest differential diagnoses and further tests (call the laboratory to see what test tube they want). The London Dysmorphology Database used to be the standard, but OMIM is clearly the easier one to use presently. Even Medline, with the use of Boolean operators (advanced search) is an excellent tool to identify rare conditions. These tools should be readily available.

Another aspect of the prenatal diagnosis of syndrome that must be kept in mind is the progress of molecular genetics. Since the recognition of the disorders of the fibroblast growth receptor factor (FGFR), the classification of the skeletal dysplasias (see Achondroplasia later) has been completely reorganized. These sources should be consulted because it is likely that a genetic or a biochemical test (see Smith-Lemli-Opitz syndrome later) can be made for these disorders that will establish the diagnosis with certainty.

Finally an important aspect of the prenatal diagnosis is the assistance to the parents in making management decisions. This is best done by providing them with contacts with support groups, and here again the Internet has revolutionized the communication between parents formally isolated in small pocket all around the world. A good resource is NORD (National Organization for Rare Disorders), but often a good search with an internet search engine will identify many more sites of interest.

Over the last 5 years, the function of the sonologist has changed significantly from simply identifying some findings to being much more proactive in the making of the differential diagnosis and the establishment of management plans. Often, the sonologist is the first one to identify the disorder, and is the one to establish contacts with the genetics department, dysmorphology specialists, and various cardiologists and surgeons. The ability to provide clear directions to the parents is important, and in this time of turmoil for the family, being the reference point to which they can come back is important. We routinely provide searches and references to our patients and attempt to identify support group so they can get the other parent's information, which is often more realistic than the information provided within the health care system.

## References

- Moore KL, Persaud TVN: The Developing Human: Clinically Oriented Embryology. Philadelphia, WB Saunders, 2002
- Nyhan WL: Structural abnormalities: A systematic approach to diagnosis. Clin Symp 42:2, 1990
- Buyse ML (ed): Birth Defects Encyclopedia. Blackwell Scientific Publication, 1990.
- <http://www.ncbi.nlm.nih.gov/entrez/query.fcgi?db=OMIM&cmd=Limits>
- <http://www.ncbi.nlm.nih.gov/PubMed/>
- <http://www.csmc.edu/genetics/skeldys/nomenclature.html>
- <http://www.rarediseases.org/>



## ACHONDROGENESIS

**Definition.** This group of lethal neonatal chondrodysplasia with short-limb dysplasia contains several entities.

**Synonyms.** Type IA is the Houston-Harris type; type IB is the Parenti-Fraccaro type; and type II is the Langer-Saldino type and is also called chondrogenesis imperfecta, achondrogenesis-hypochondrogenesis type II, and was the type IB achondrogenesis. There are two less common types, III and IV. Types II and IV were isolated by Whiteley and Gorlin on femoral measurement. The validity of these two last types is questioned, with type III probably representing type II and type IV probably representing hypochondrogenesis. These essentially radiologic categories have been modified several times and are being replaced by genetic classification (see later) and thus are mainly of historical interest.

**Prevalence.** Rare, with probably less than 100 cases reported. Birth prevalence is 0.9 to 0.23 per 10,000 births.

**Etiology.** Autosomal recessive (type IB) and dominant (type II).

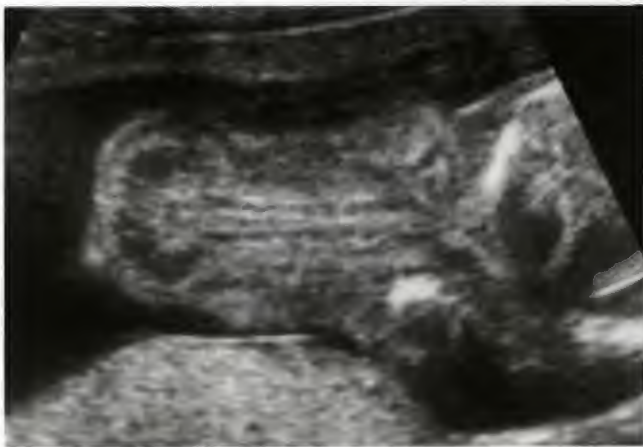


**FIGURE 5-1.** Achondrogenesis. Almost absent mineralization of the spine (note the spinal cord).

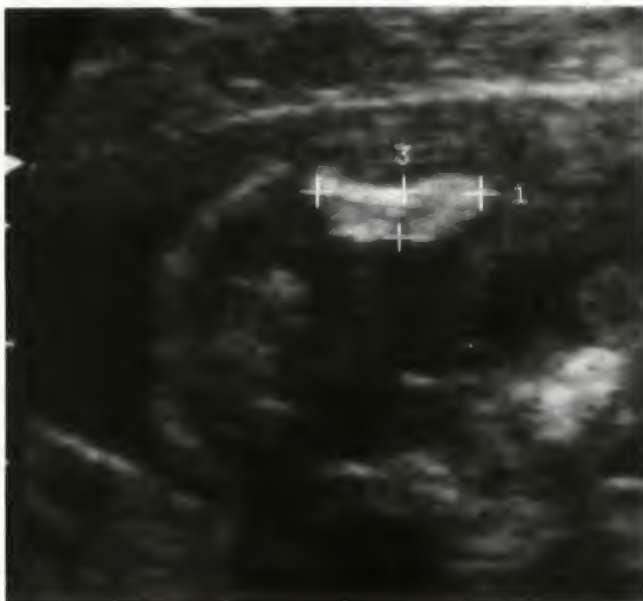


**FIGURE 5-2.** The appearance of transparent bones in which both cortices can be seen.

**Diagnosis.** Type I achondrogenesis is a severe chondrodystrophy characterized radiographically by poor ossification of the spine and pelvic bones, which results in stillbirth or early death. The ultrasound manifestation includes very short limbs and short thin ribs that may have fractures. The short ribs are responsible for the lethal pulmonary hypoplasia and the polyhydramnios from esophageal compression. The abnormal mineralization may or may not be manifested sonographically as bones that are either very echopenic, or in which both cortical can be imaged. Normally, only the proximal cortical side is imaged and the distal side is shadowed by the proximal side. Type II also presents with the same findings but the mineralization deficit is less severe.



**FIGURE 5-3.** Micromelia with the arms not joining in front of the chest.



**FIGURE 5-4.** Achondrogenesis. The appearance of the fetus at 19 weeks.

and the long bones less short. Two cases of large cystic hygromas in association with achondrogenesis have been reported.

**Genetic Anomalies.** Type IA: unknown. Type IB: mutation in the gene for diastrophic dysplasia sulfate transporter gene (DTDST) on the long arm (locus 32-33) of chromosome 5. The diastrophic dysplasia sulfate transporter gene is recessively transmitted and is an allele of the diastrophic dysplasia gene. This is important because the type II (see below) is an autosomal-dominant mutation (and thus involves a new mutation for each case since the disease is lethal) and, therefore, has a much lower likelihood of recurrence than the 25% risk of the type IB. The diagnosis can be made by chorionic villus sampling in at-risk couples. Type II achondrogenesis is the Langer-Saldino type and is caused by new dominant mutation in the type II collagen gene (*COL2A1* gene) on chromosome 12. Therefore, it is more related to hypochondroplasia, spondyloepiphyseal dysplasia, and the Kniest-Stückler syndrome. These may be allelic variants, with hypochondroplasia related to achondrogenesis as hypochondroplasia is related to achondroplasia.

**Differential Diagnosis.** Osteogenesis imperfecta (type II and occasionally type IIc) and hypophosphatasia also

present with demineralization, but the limb shortening is not usually as severe. Abnormal mineralization and shortened trunk length distinguish it from thanatophoric dysplasia in which these are normal.

**Prognosis.** Lethal.

**Management.** Termination of pregnancy can be offered before viability. Standard prenatal care is not altered when continuation of the pregnancy is opted for. Confirmation of diagnosis after birth is important for genetic counseling.

## References

- Knowlton S, Graves C, Tiller GE: Achondrogenesis. *Fetus* 2:7564, 1992.
- Meizner I, Barnhard Y: Achondrogenesis type I diagnosed by transvaginal ultrasonography at 13 weeks' gestation. *Am J Obstet Gynecol* 173:1620, 1995.
- Mahony BS, Filly RA, Cooperberg PL: Antenatal sonographic diagnosis of achondrogenesis. *J Ultrasound Med* 3:333, 1984.
- Wenstrom KD, Williamson RA, Hoover WW, et al: Achondrogenesis type II (Langer-Saldino) in association with jugular lymphatic obstruction sequence. *Prenat Diagn* 9:527, 1989.
- Özeren S, Yüksel A, Tükel T: Prenatal sonographic diagnosis of type I achondrogenesis with a large cystic hygroma. *Ultrasound Obstet Gynecol* 13:75, 1999.

## ACHONDROPLASIA

**Definition.** Rhizomelic micromelia associated with frontal bossing and low nasal bridge.

**Synonyms.** None.

**Prevalence.** Common: 0.5 to 1.5:10,000

**Etiology.** Defective cartilaginous molding of the bone precursor.

**Diagnosis.** This skeletal dysplasia may manifest as homozygous and heterozygous achondroplasia. Patel and Filly have described the methodology for distinguishing the two genetic manifestations of this dysplasia. Their results indicated that those fetuses with femoral lengths that are below the 3rd percentile standard compared with the biparietal diameter (BPD) at 17.0 weeks BPD age and that demonstrate progressive shortening at 20.0 and 23.0 weeks BPD age have homozygous achondroplasia, whereas those fetuses in whom a decrease in femoral length is seen at 17.0 to 23.0 weeks BPD age have heterozygous achondroplasia. In addition, fetuses with heterozygous achondroplasia are expected, and those with homozygous achondroplasia are

not expected, to have a femoral length that exceeds 34 mm at 26.0 weeks BPD age. Fetuses with normal interval growth in femoral length during the second trimester are expected to be unaffected, and an ultrasound scan obtained after 26.0 weeks should help confirm this prediction. The frontal bossing and depressed nasal bridge can also be recognized. Occasionally more subtle anomalies such as the trident hand (an increased interspace between the third and fourth digit) or the lack of widening of the lumbar canal can also be identified.

**Genetic Anomalies.** Achondroplasia is an autosomal-dominant skeletal dysplasia caused by mutation in the

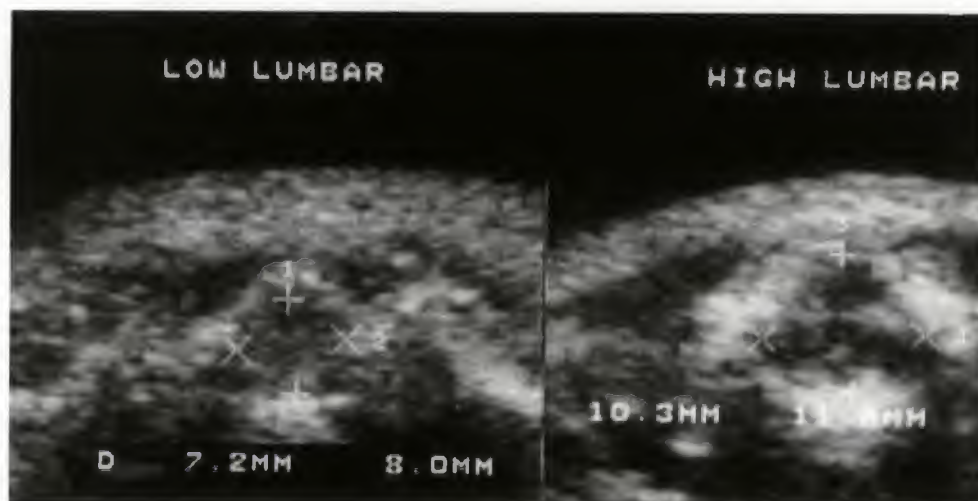


FIGURE 5-5. Short femur in a patient with homozygous achondroplasia.



FIGURE 5-6. Achondroplasia. Frontal bossing.





**FIGURE 5-7.** Achondroplasia. Lack of widening of the spinal canal.

fibroblast growth factor receptor-3 gene, which is located on the short arm of chromosome 4 at the 16.3 locus. Bellus has demonstrated that the anomaly was due to a glycine to arginine substitution at codon 380. These papers are landmarks in our knowledge about skeletal dysplasias. Before these papers, skeletal dysplasias were almost strictly classified by radiologic criteria. These papers marked the beginning of an intense and successful search for gene mapping of skeletal dysplasia, many of which were subsequently recognized to result from alterations of the fibroblast growth factors (I–III).

**Differential Diagnosis.** The differential diagnosis is with multiple conditions, such as

- Thanatophoric dysplasia (narrower chest, platyspondyly, more severe micromelia, no trident hand, more severe polyhydramnios).
- Achondrogenesis (very poor mineralization, with lack of echogenicity of the bones, more severe micromelia, and more severe polyhydramnios).
- Osteogenesis imperfecta type II (poor mineralization (often the proximal aspect of the brain is well seen through the “transparent” skull), variable micromelia, sometimes visible bone angulations from fractures, bell-shaped chest).

- Diastrophic dysplasias in which the micromelia is associated with joint contractures, in particular, abnormal finger and toe positions.

**Prognosis.** Children with achondroplasia have normal intellectual achievements. The major problems are orthopedic (narrow spinal canal and foramen magnum). There is a vibrant support group (The Little People of America) that is very active in resolving the problems of affected individuals.

**Management.** Although termination of pregnancy can be offered before viability, the majority of these children adapt well in society and lead productive lives.

## References

- Patel MD, Filly RA: Homozygous achondroplasia: US distinction between homozygous, heterozygous and unaffected fetuses in the second trimester. *Radiology* 196:541, 1995.
- Moeglin D, Benoit B: Three-dimensional sonographic aspects in the antenatal diagnosis of achondroplasia. *Ultrasound Obstet Gynecol* 18:81, 2001.
- Velinov M, Slaugenhaupt SA, Stoilov I, et al: The gene for achondroplasia maps to the telomeric region of chromosome 4p. *Nat Genet* 6:318, 1994.
- Le Merrer M, Rousseau F, Legeai-Mallet L, et al: A gene for achondroplasia—hypochondroplasia maps to chromosome 4p. *Nat Genet* 6:314, 1994.

## AICARDI SYNDROME

**Definition.** Neurodegenerative disorder was first described in 1965, including cerebral atrophy, intracerebral calcification of the basal ganglia, a chronic cerebrospinal fluid lymphocytosis, and negative serologic investigations for common prenatal infections. It is associated with a developmental arrest, agenesis of the corpus callosum, chorioretinal lacunae, infantile spasm, and physical handicaps.

**Synonyms.** None

**Incidence.** More than 100 cases reported.

**Etiology.** Autosomal-recessive inheritance or possibly an X-linked dominant disorder that occurs de novo in women, and it is lethal in the hemizygous man. It is genetically heterogeneous, with almost 50% of families mapping to the first known locus at 3p21 (AGS1). Another linkage to a

second AGS locus (AGS2) at chromosome 13q14-21 exists, as well as at least one further locus.

### Pathogenesis.

May result from a perturbation of interferon-alpha metabolism.

### Sonographic Findings.

Micro-ophthalmia, choroid plexus cysts, choroid plexus papilloma, Dandy Walker malformation, and dysgenesis of the corpus callosum can be recognized prenatally. Agenesis of the corpus callosum is complete in 72% and partial in 28% of the cases. Infrequently, this syndrome has been associated with cleft lip and palate.

### Implications for Targeted Examinations

- Cerebral anomalies (like calcifications, cerebral cyst, and a high-riding third ventricle characteristic of agenesis of

the corpus callosum) with ultrasound and cerebral magnetic resonance imaging.

- Female fetus.
- Investigate the possibility of parental consanguinity.
- Increase of interferon-alpha level in the fetal blood and cerebrospinal fluid.
- Exclude an infectious etiology.
- Assess the newborn shortly after birth.

**Differential Diagnosis.** Dysgenesis of the corpus callosum.

**Prognosis.** Poor, with most infants dying during the first few years. Those that survive are profoundly mentally retarded later.

**Recurrence Risk.** It is sporadic in nature and affects only female fetuses.

## ALAGILLE SYNDROME

**Definition.** This is a disorder characterized by the association of biliary hypoplasia (manifesting as neonatal cholestasis), pulmonary stenosis, vertebral abnormalities, characteristic facies, ocular and cardiovascular anomalies.

**Synonyms.** Alagille-Watson syndrome, cholestasis with peripheral pulmonary stenosis, arteriohepatic dysplasia, hepatic ductular hypoplasia, jagged I syndrome.

### Etiology.

This is a multisystem autosomal dominant disorder with variable penetrance. The *JAG1* gene on chromosome 20p12.1-p11.23 is currently the only gene known to be implicated in Alagille syndrome.

**Sonographic Findings.** Fetal sonography can reveal facial alterations such as a broad forehead, pointed mandible, and bulbous tip of the nose; cardiac and vascular anomalies such as pulmonary valvular stenosis, peripheral arterial stenosis; skeletal abnormalities such as abnormal vertebrae ("butterfly" vertebrae), a decrease in interpediculate distance in the lumbar spine and in the fingers, varying degrees of foreshortening, and progressive severe intrauterine growth restriction.

**Differential Diagnosis.** Cystic kidney disorders associated with cholestatic liver disease and all the familial intrahepatic

**Management.** Termination of pregnancy can be offered before viability. Standard prenatal care is not altered when continuation of the pregnancy is opted for. Confirmation of diagnosis after birth is important for genetic counseling.

## References

- Ali M, Highet LJ, Lacombe D, et al: A second locus for Aicardi-Goutieres syndrome at chromosome 13q14-21. *J Med Genet* 43:444, 2005.
- Bromley B, Krishnamoorth KS, Benacerraf BR: Aicardi syndrome: prenatal sonographic findings. A report of two cases. *Prenat Diagn* 20:344, 2000
- Le Garrec M, Doret M, Pasquier JC, et al: Prenatal diagnosis of Aicardi-Goutieres syndrome. *Prenat Diagn* 25:28, 2005.
- Neidich JA, Nussbaum RL, Packer RJ, et al: Heterogeneity of clinical severity and molecular lesions in Aicardi syndrome. *J Pediatr* 116:911, 1990.

cholestasis: Zellweger syndrome, cholestasis-lymphedema syndrome, Byler disease, and cholestasis with defective formation of cholic acid. Alpha-1-antitrypsin deficiency may present as neonatal cholestasis with a paucity of intrahepatic bile ducts.

**Associated Anomalies.** It is frequently associated with growth failure, attributed to concurrent congenital anomalies, cholestasis, malabsorption or malnutrition, renal abnormalities, and also unilateral cystic kidney disease with or without renal dysplasia.

**Prognosis.** The vascular anomalies such as basilar artery aneurysms, internal carotid artery anomalies, middle cerebral artery aneurysm, aortic aneurysms and coarctations, internal carotid artery anomaly, and renal artery stenosis are the major cause of morbidity and mortality in the affected children. They account for 34% of the mortality because of the elevated risk of intracranial bleeding. Absent deep tendon reflexes are frequent in the infants as well as elevated



**FIGURE 5-8.** Alagille syndrome. Enlarged main pulmonary artery (arrow). (Courtesy Francis Duchatel, 2002, *thefetus.net*.)



**FIGURE 5-9.** Alagille syndrome. Thickened and stenotic pulmonary valve. (Courtesy Francis Duchatel, 2002, *thefetus.net*.)



transaminases and alkaline phosphatase, posterior embryotoxon in the eye examination, generalized xanthomas, including oral xanthomas, and marked hypodontia. The degree of biliary hypoplasia is variable. Some patients may have severe cholestasis, progress to cirrhosis, and require liver transplantation.

**Management.** This disorder should be suspected in all the infants with cholestasis. It is important to evaluate the newborn also with a renal ultrasound examination.

## References

Albayram F, Stone K, Nagey D, et al: Alagille syndrome: prenatal diagnosis and pregnancy outcome. *Fetal Diagn Ther* 17:182, 2002.

Gauthier F, Hadchouel M: Congenital disorders of the biliary ducts. *Rev Prat* 50:2142, 2000.

Harendza S, Hubner CA, Glaser C, et al: Renal failure and hypertension in Alagille syndrome with a novel JAG1 mutation. *J Nephrol* 18:312, 2005.

Ho NC, Lacbawan F, Francomano CA, et al: Severe hypodontia and oral xanthomas in Alagille syndrome. *Am J Med Genet* 93:250, 2000.

Kamath BM, Spinner NB, Emerick KM, et al: Vascular anomalies in Alagille syndrome: a significant cause of morbidity and mortality. *Circulation* 109:1354, 2004. Epub 2004 Mar 1. Comment in *Circulation* Sep 28;110:e327, 2004; author reply e327.

Lykavieis P, Hadchouel M, Chardot C, et al: Outcome of liver disease in children with Alagille syndrome: a study of 163 patients. *Gut* 49:431, 2001.

Martin SR, Garel L, Alvarez F: Alagille's syndrome associated with cystic renal disease. *Arch Dis Child* 74:232, 1996.

## AMNIOTIC BAND SYNDROME

**Definition.** Amniotic band syndrome is a set of congenital malformations ranging from minor constriction rings and lymphedema of the digits to complex, bizarre multiple congenital anomalies that are attributed to amniotic bands that stick, entangle, and disrupt fetal parts.

**Synonyms.** ADAM complex (amniotic deformities, adhesion, mutilation), amniotic band sequence, amniotic disruption complex, annular grooves, congenital amputation, congenital constricting bands, Streeter's bands, transverse terminal defects of limb, aberrant tissue bands, amniochorionic mesoblastic fibrous strings, amniotic bands.

**Prevalence.** The prevalence is 7.7/10,000 live births, but it can be as high as 178/10,000 for spontaneous abortions. The male-to-female ratio is 1:1.

**Etiology.** Not precisely known. Some theories have been suggested teratogenic, multifactorial, and genetic factors that cause a rupture of the amnion. Teratogenic effect of drugs such as methadone and lysergic acid diethylamide may play an important role in many cases.

**Pathogenesis.** Rupture of the amnion in early pregnancy leads to entrapment of fetal structures by "sticky" mesodermic bands that originate from the chorionic side of the amnion, followed by disruption. It has been suggested that the bands lead to a decreased blood flow in the constricted limb and subsequent natural amputation. This exogenous mechanistic theory does not explain several features of this syndrome, such as why there are reported cases of amniotic band syndrome with histologically normal and intact amniotic lining; why internal abnormalities such as holoprosencephaly,

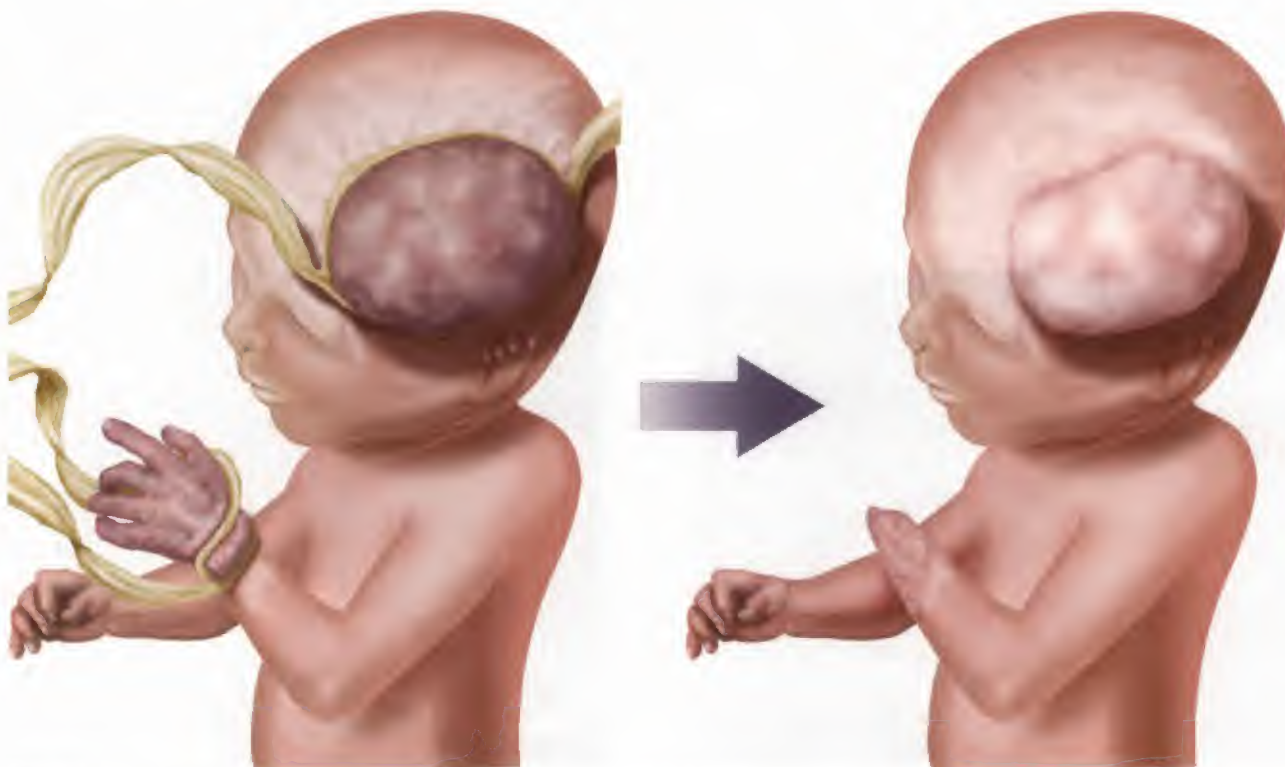


**FIGURE 5-10.** Pathophysiology of amniotic band syndrome. Amniotic band wrapping around the extremity and head resulting in nonembryologic abnormalities such as amputation of the distal limb and a noncentral encephalocele. (Illustration by James A. Cooper, MD, San Diego, CA.)



**FIGURE 5-11.** Amniotic band attached to the fetal head. (Courtesy, Vicente Ruiz, 2005, *thefetus.net*.)

cerebellar dysplasia, heterotopia, cardiac, and renal abnormalities can be seen; and why monozygotic twins are more often affected than dizygotic twins.

**Diagnosis.** The syndrome results in structural anomalies that vary from minor to lethal forms. The most common findings are constriction rings around the digits, arms, and legs; swelling of the extremities distal to the point of constriction; amputation of digits, arms, and legs; asymmetric face; facial clefts; cephalocele; anencephaly; acrania; multiple joint contractures; pterygium; clubfeet, clubhands, and pseudosyndactyly; microphthalmia, uveal coloboma, corneal metaplasia, and unilateral chorioretinal lacunae.

A detailed view of the fetus' face, digits and body with 3-dimensional ultrasound exams, may contribute to the diagnosis.

**Differential Diagnosis.** A uterine synechia or septation can simulate an amniotic band. The amniotic folds can be differentiated because they are not "sticking" to the body.

**Prognosis.** The more severe forms are lethal. Mild manifestations sometimes are found just at birth and do not have impact on survival.

**Recurrence Risk.** No recurrence is expected, except in rare sporadic familial cases, which have been reported in association with epidermolysis bullosa and Ehler-Danlos syndrome.

**Management.** It depends on the extent of the anomalies. Termination of pregnancy can be offered for the severe



**FIGURE 5-12.** Postnatal image showing the amniotic band attached to the skull and the exencephaly. (Courtesy, Vicente Ruiz, 2005, *thefetus.net*.)

forms. Recently, endoscopic release has been reported and may prove beneficial in releasing the constriction band in threatened limb amputation. Endoscopic fetal therapy with lysis of the constriction ring in utero is an option, but intervention is probably not always warranted. Spontaneous lysis of an amniotic band attached to a fetal elbow has been shown.

## References

- Paladini D, Foglia S, Sglavo G, Martinelli P: Congenital constriction band of the upper arm: the role of three-dimensional ultrasound in diagnosis, counseling and multidisciplinary consultation. *Ultrasound Obstet Gynecol* 23:520, 2004.
- Chen CP, Chang TY, Lin YH, et al: Prenatal sonographic diagnosis of acrania associated with amniotic bands. *J Clin Ultrasound* 32:256, 2004.
- Pedersen TK, Thomsen SG: Spontaneous resolution of amniotic bands. *Ultrasound Obstet Gynecol* 18:673, 2001.
- Senúñhes L, Verspyck E, Eurin D, et al: Favourable outcome of a tight constriction band secondary to amniotic band syndrome. *Prenat Diagn* 24:1981, 2004.
- Cincore V, Ninos AP, Pavlik J, et al: Prenatal diagnosis of acrania associated with amniotic band syndrome. *Obstet Gynecol* 102:1176, 2003.
- Sherer DM, Lysikiewicz AJ: Doppler flow velocimetry assisted diagnosis of an intrauterine synechia during pregnancy. *Am J Perinatol* 19:421, 2002.

## APERT SYNDROME

**Definition.** Apert syndrome is a rare developmental deformity characterized by craniofacial and limb malformations accompanied by variable degrees of mental retardation in 50% of the cases. In 1894, Wheaton provided the first description and subsequently, in 1906, Apert summarized the disorder, presenting nine cases.

**Incidence.** The occurrence of Apert syndrome is estimated at 0.0625 to 0.1:10,000 live births. The male-to-female ratio is 1:1.

**Synonyms.** Acrocephalosyndactyly type 1, Apert-Crouzon disease.

**Etiology.** Apert syndrome is an autosomal disorder with dominant inheritance. Most of the cases are sporadic,





**FIGURE 5-13.** Facial abnormality; short and broad head, high cranial vault (acrocephaly), frontal bossing, depressed nasal bridge with prognathism and “mitten hand” deformity (bilateral symmetric syndactyly) of Apert syndrome. (Illustration by James A. Cooper, M.D., San Diego, CA.)

resulting from new mutations. Association with advanced paternal age has been described.

**Sonographic Findings.** Brachycephaly and acrocephaly, high forehead, flat occiput, *craniostylosis* usually involving the coronal sutures, flat face, and hypertelorism. Other ultrasound findings that are present are agenesis of the corpus callosum, mild ventriculomegaly, and fusion of the cervical vertebrae at the level of C5-C6. In the extremities, we can find syndactyly (“mitten hand”) (osseous and cutaneous), usually involving the second, third, and fourth fingers. There is a broad thumb and hallux. Polyhydramnios (caused by the decreased fetal swallowing) and variable degrees of mental retardation have also been found, and their occurrence and intensity seem to correlate with the severity of central nervous system anomalies. The prenatal diagnosis by ultrasound and fetoscopy has been reported in all trimesters of pregnancy. Increased nuchal translucency at the first trimester might be a sonographic marker for the disorder.

**Diagnosis.** The most typical findings in Apert syndrome are craniosynostosis (by synostosis of the coronal sutures), bilateral symmetric syndactyly of the limbs (mitten-like hands and feet), and midfacial hypoplasia. Additional features, which appear with variable frequency, include

- Skeletal anomalies: short and broad head, high cranial vault (acrocephaly), prominent forehead (frontal bossing) hypertelorism and proptosis, depressed nasal bridge with parrot-beaked nose, hypoplastic maxilla, prognathism.
- Cardiac anomalies: pulmonic stenosis, overriding aorta, ventricular septal defects.
- Central nervous system anomalies: hydrocephaly, malformation of the corpus callosum and limbic structures, gyral abnormalities, hypoplasia of the white matter, and heterotopic gray matter.

**Genetic Anomalies.** The most common mutations associated with Apert syndrome are substitution S252W and P253R, which occur in the fibroblast growth factor receptor 2 genes. Genetic molecular studies are recommended for the fetus (by chorionic villus sampling or amniocentesis) and for parents when Apert syndrome is suspected, in particular in those families affected for the first time. The development of molecular techniques for the definitive diagnosis of this



**FIGURE 5-14.** Apert syndrome. Sonogram demonstrating frontal bossing (three-dimensional view). (Courtesy of Luis Izquierdo, 2000, *thefetus.net*.)

condition in prenatal cases was made possible by the finding of the *FGFR2* gene mutations.

**Differential Diagnosis.** Genetic syndromes also characterized by the presence of craniosynostosis such as Crouzon, Pfeiffer, Carpenter, and Saethre-Chotzen may be included in the differential diagnosis. Molecular genetic studies can exclude these disorders.

**Recurrence Risk.** When resulting from a new mutation, the recurrence risk is improbable. If one of the parents carries the disorder, the recurrence risk is 50%.

**Management.** If diagnosed before viability, termination of pregnancy can be offered. After viability, standard obstetric management is not altered. Delivery in a tertiary center is recommended.

## References

- Esser T, Rogalla P, Bamberg C, et al: Application of the three-dimensional maximum mode in prenatal diagnosis of Apert syndrome. *Am J Obstet Gynecol* 193:1743, 2005.
- Ferreira JC, Bernstein PS, Jabs EW, et al: Second-trimester molecular prenatal diagnosis of sporadic Apert syndrome following suspicious ultrasound findings. *Ultrasound Obstet Gynecol* 14:426, 1999.
- Skidmore DL, Pai AP, Toi A, et al: Prenatal diagnosis of Apert syndrome: report of two cases. *Prenat Diagn* 23:1009, 2003.
- Parent P, Le Guern H, Munck MR, et al: Apert syndrome, an antenatal ultrasound detected case. *Genet Counsel* 5:297, 1994.
- Kaufmann K, Baldinger S, Pratt L: Ultrasound detection of Apert syndrome: a case report and literature review. *Am J Perinatol* 14:427, 1997.
- Jones KL: Apert syndrome in Smith's recognizable patterns of human malformation. Philadelphia, WB Saunders Company, 1997, pp 418–419.
- Blank CE: Apert's syndrome (a type of acrocephalosyndactyly). Observations on a British series of thirty-nine cases. *Ann Hum Genet* 24:151, 1960.
- Tunte W, Lenz W: Zur häufigkeit und mutations-rate des Apertsyndroms. *Hum Genet (Berlin)*, 4:101, 1967.
- Erikson JD, Cohen MM Jr: A study of parental age effects on the occurrence of fresh mutations for the Apert syndrome. *Ann Hum Genet* 38:89, 1974.
- Park WJ, Theda C, Maestri NE, et al: Analysis of phenotypic features and FGFR2 mutations in Apert syndrome. *Am J Hum Genet* 57:321, 1995.

## ARNOLD-CHIARI MALFORMATION

**Definition.** The Arnold-Chiari malformation was first identified in 1883 by Cleland. It is characterized by the prolapse of hindbrain structures below the level of the foramen magnum. It can be associated with skeletal abnormalities and neurologic dysfunction. There are three types of Arnold-Chiari malformation (see also Table 5-1):

- Type I: Downward displacement of the cerebellar tonsils beneath the foramen magnum of greater than 4 mm. The fourth ventricle remains in the posterior fossa. This is mainly an incidental computed tomographic discovery.
- Type II: Invariably seen prenatally as a congenital deformity characterized by displacement of cerebellar tonsils, parts of the cerebellum, fourth ventricle, pons, and medulla oblongata through the foramen magnum into the spinal canal. In 95% percent of the cases, it is accompanied by a myelomeningocele and often hydrocephalus.
- Type III: In its most severe form, the condition is associated with large herniation of the posterior fossa contents with myelomeningocele and hydrocephalus.

**Synonym.** The nickname “banana sign” has been applied to the deformity of the cerebellum.

**Incidence.** Commonly associated with spina bifida; rare outside of spina bifida. There is a higher preponderance of Arnold-Chiari type I in female fetuses versus male fetuses (3:2).

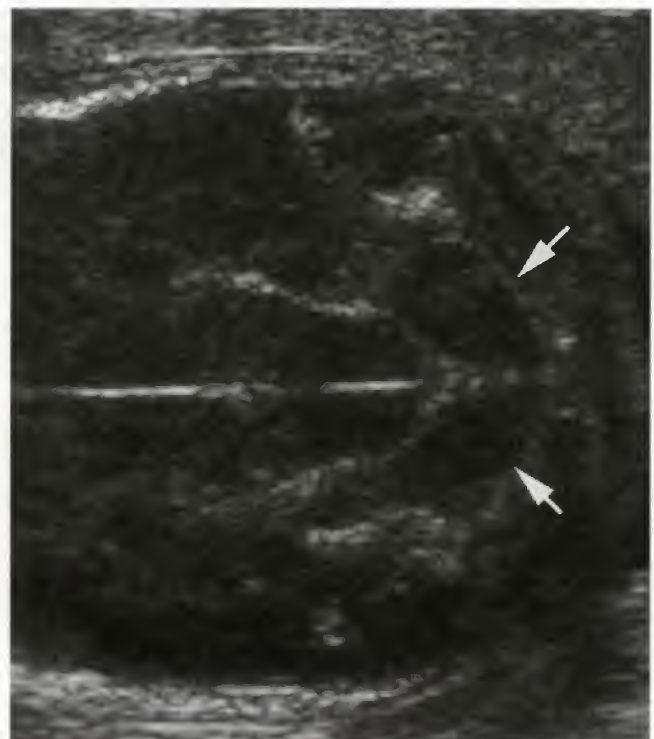


**FIGURE 5-16.** The banana sign: the lobes of the cerebellum have lost their lumpy appearance and the vermian incisures are not as marked as normal (arrows).

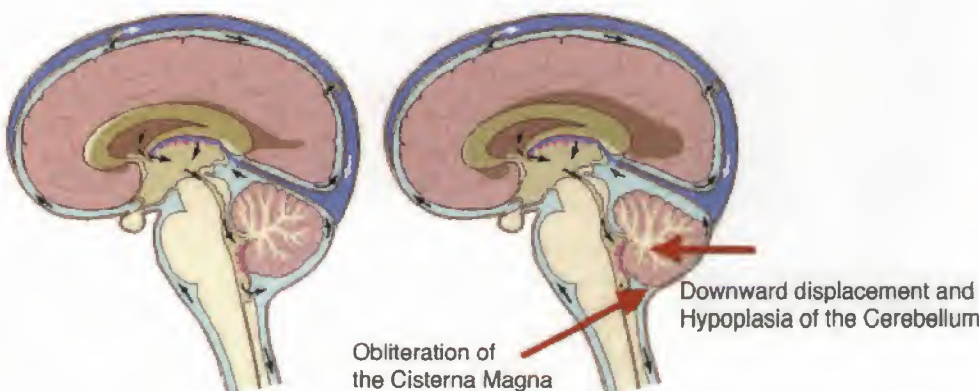


**FIGURE 5-15.** Schematic changes in Arnold-Chiari type II.



**Table 5-1** Intrauterine Visualization of Alterations of Chiari Malformation

Findings	Chiari I	Chiari II	Chiari III
Posterior fossa	Displacement of cerebellar tonsils toward the superior cervical canal	Small posterior fossa with inferior displacement of vermis and superoanterior of cerebellum.	High cervical encephalocele with herniation of content of posterior fossa and/or occipital lobe
Brain	Usually normal	Pointed quadrigeminal plate Dysgenesis of corpus callosum, heterotopia and polymicrogyria	There might be similarity to Chiari II findings
Ventricles	Hydrocephalus (mild to moderate in 20% of cases) Fourth ventricle is small, elongated, and with inferior displacement	Hydrocephalus (90% of cases)	There might be similarity to Chiari II findings
Spinal cord	Hydrosyringomyelia (in 30%–60% of cases)	Myelomeningocele (approximately 100% of cases) Hydrosyringomyelia (in 50%–60% of cases) Diastematomyelia	There might be similarity to Chiari II findings
Associative malformations	Difficult prenatal evaluation Bone anomalies of base of skull	Difficult prenatal evaluation	Posterior bifida spine in topography on C1 and C2

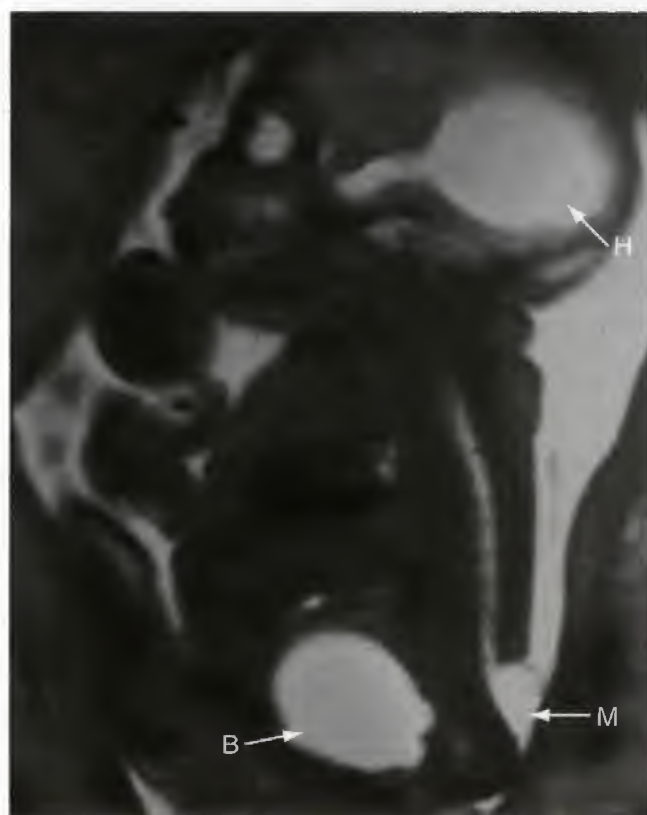


**FIGURE 5-17.** Sagittal T2-weighted (29 weeks) showing marked hydrocephalus (*H*) and a myelomeningocele (*M*). Note the increased volume of the bladder (*B*). (Courtesy of Heron Werner, 2005, *thefetus.net*.)

**Etiology.** Autosomal-recessive inheritance for some forms.

**Pathogenesis.** The abundance of theories regarding the pathogenesis of Chiari malformation reflects the present lack of consensus on the subject. An understanding of the pathogenesis of Chiari malformations must be aimed at examining the pathophysiology at the craniocervical junction. A defect during embryonic development causes underdevelopment of the posterior fossa and blockage of the normal outlets of the fourth ventricle (foramina of Magendie and Luschka), resulting in increased pressure and causing the cerebellar tonsils to descend into the foramen magnum. Accumulated cerebrospinal fluid is then forced caudally through the entrance into the central canal of the spinal cord at the caudal-most portion of the fourth ventricle, because of a pressure gradient.

**Diagnosis.** The displacement of the cerebellum deforms the lateral lobes (which lose their “round shape”) and the vermillion notch to appear more continuous (thus, the banana sign). The diagnosis has been made as early as the first trimester. D’Addario et al have evaluated the angle between the clivus and supra occiput and found it a useful parameter to diagnose Chiari II malformation.

**Genetic Anomalies.** Unknown.

**Differential Diagnosis.** Nonobstructive hydrocephalus, such as

- Dysgenesis of the corpus callosum.
- Aqueductal stenosis.
- Borderline ventriculomegaly.
- Dandy-Walker malformation.
- Porencephaly.
- Schizencephaly.

**Associated Anomalies.** Hydrocephaly from obstruction of the foramina of Magendie, syringomyelia, diastematomyelia.

**Prognosis.** Variable. Poor if other brain abnormalities (migrational abnormalities) are present and if associated with a large or high myelomeningocele.

**Management.** Termination of pregnancy can be offered before viability. For those affected by spina bifida, an experimental intrauterine repair performed between 23 and 30 weeks' gestation has been proposed in a few centers in the United States. Standard prenatal care is not altered when continuation of the pregnancy is chosen. Confirmation of diagnosis after birth is important for genetic counseling.

## ARTHROGRYPOSIS MULTIPLEX CONGENITA

**Definition.** This heterogeneous set of conditions shares limitation of movements and joint ankylosis as main findings.

**Synonyms.** Congenital contractures, fetal akinesia sequence, Pena-Shokeir syndrome.

**Incidence.** 1 to 3:10,000

**Etiology.** Possibly autosomal dominant.

**Pathogenesis.** Arthrogryposis results from decreased in utero motion, either from neural, muscular, connective tissue, infectious origin.

**Diagnosis.** Although the anomalies are obvious when recognized, when the baby is born, the prenatal diagnosis may be challenging when fluid is decreased, and the abnormal limb position appears attributable to the oligohydramnios. Some forms are associated with polyhydramnios and the abnormal limb position (knocked knee), genu recurvatum,



**FIGURE 5-18.** Arthrogryposis multiplex. Fixed flexion deformity of the hips. Also noted is bilateral congenital talipes equino varus. (Courtesy of S. Manohar, MD, 2004, *thefetus.net*.)

## References

- Sicuranza GB, Steinberg P, Figueroa R: Arnold-Chiari malformation in a pregnant woman. *Obstet Gynecol* 102:1191, 2003.
- Cheng JS, Nash JBS, Meyer GA: Chiari type I malformation revisited: Diagnosis and treatment. *Neurologist* 8:357, 2000
- D'Addario V, Pinto V, Del Bianco A, et al: The clivus-supraocciput angle: a useful measurement to evaluate the shape and size of the fetal posterior fossa and to diagnose Chiari II malformation. *Ultrasound Obstet Gynecol* 18:146, 2001.



**FIGURE 5-19.** The postnatal image of a fetus with arthrogryposis multiplex. (Courtesy of S. Manohar, MD, 2004, *thefetus.net*.)

clubfeet, and clubhand) make the diagnosis easy. Polyhydramnios is often a manifestation of decreased swallowing, which may be part of the same pathogenesis as the arthrogryposis itself (muscular or neuronal deficit). An increase in nuchal lucency as well as the characteristic decreased movement can also be seen in the first trimester.

**Genetic Anomalies.** Several anomalies have been linked to the following site 5q35, 9p21-q21, 11p15.5.

**Differential Diagnosis.** Trisomy 18, renal agenesis, and myotonic dystrophy may present with some similar findings.

**Associated Anomalies.** Because of the heterogeneity of the condition, numerous associated anomalies have been described including scoliosis, central nervous system anomalies, and even seizures.

**Prognosis.** The prognosis depends on associated anomalies (respiratory limitations, scoliosis.)

**Management.** Termination of pregnancy can be offered before viability. Standard prenatal care is not altered when continuation the pregnancy is opted for. Confirmation of diagnosis after birth is important for genetic counseling.

## Reference

- Lammens M, Moerman P, Fryns JP, et al: Fetal akinesia sequence caused by nemaline myopathy. *Neuropediatrics* 28:116, 1997.



## ASPHYXIATING THORACIC DYSPLASIA

**Definition.** Autosomal-recessive chondrodysplasia characterized by a small thorax, varying degrees of rhizomelic brachymelia, polydactyly, pelvic abnormalities, and renal anomalies.

**Synonyms.** Jeune syndrome

**Incidence.** Unknown, usually affecting white babies.

**Pathogenesis and Etiology.** Autosomal-recessive disorder.

**Diagnosis.** The most striking ultrasound finding is a very narrow chest with short limbs. The limbs, however, are not as short as those of other lethal conditions such as thanatophoric dysplasia, achondrogenesis, OI type 2, and the short-rib polydactyly syndromes. The increased iliac wing angle, reported in the radiographic literature, has not been reported yet with ultrasound. Pancreatic cysts have been recognized in one case.

**Genetic Anomalies.** The defect is probably located on the short arm of chromosome 12.

**Differential Diagnosis.** Ellis van Creveld syndrome (short arm of chromosome 4) that presents mainly with cardiac anomalies instead of renal anomalies.

**Prognosis.** In spite of the dreadful name, not all newborns are asphyxiated, and with corrective surgery of the chest, some patients have had a fairly normal outcome.

**Management.** Termination of pregnancy can be offered before viability. Standard prenatal care is not altered when



**FIGURE 5-20.** Coronal view of the chest and abdomen of a fetus with asphyxiating thoracic dysplasia. Note the constriction of the chest (arrows). (Courtesy of Adrian Clavelli, 2001, thefetus.net.)

continuation the pregnancy is opted for. Confirmation of diagnosis after birth is important for genetic counseling.

## Reference

Lipson M, Waskey J, Rice J, et al: Prenatal diagnosis of asphyxiating thoracic dystrophy. *Am J Med Genet* 18:273, 1984.

## ASPLENIA-POLYSPLENIA SYNDROMES

**Definition.** This set of syndromes is due to errors of lateralization of the primary field. It results (with simplifi-

cations) in either a fetus with a predominant right-sidedness and an isomeric left side (asplenia: a fetus whose left side is a mirror image of its right side) or left-sidedness and an

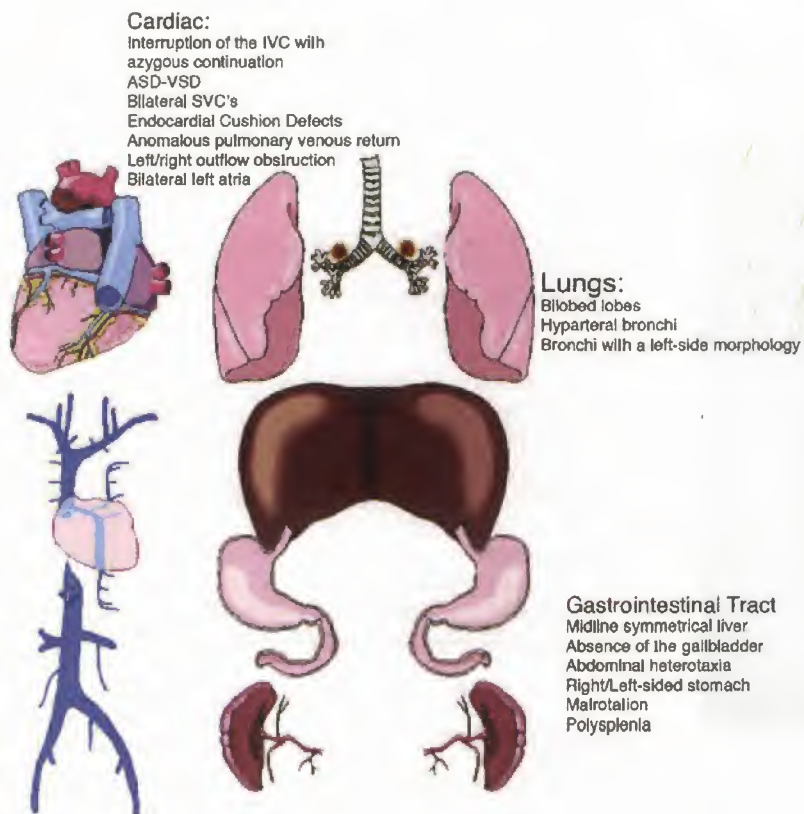


**FIGURE 5-21.** Schematic drawing of the findings in polysplenia. (Courtesy of P. Jeanty, 1999, thefetus.net.)

**Table 5-2** Anomalies Associated With Asplenia-Polysplenia Syndromes

	Asplenia	Polysplenia
<i>Cardiovascular</i>	Bilateral superior vena cava, anomalous pulmonary venous connections, absence of the coronary sinus, endocardial cushion defect, right ventricular outflow tract obstructions, transpositions of the great arteries, isomerism of the atria (both resemble a right atrium), atrial septal defects; the apex of the heart can be in either direction	Anomalous pulmonary venous return, interrupted IVC with (hemi)azygos continuation, atrial and ventricular septal defects, pulmonic stenosis, endocardial cushion defects (less severe than in asplenia)
<i>Spleen</i>	Splenic agenesis or more commonly hypotrophy	Multiple splenules
<i>Lungs</i>	Trilobate lungs with eparterial bronchus	Bilobated lungs with hyparterial bronchus
<i>Liver</i>	Decrease in the normal difference of size between the right and left lobe, independent hepatic vein on the opposite side of the IVC	
<i>Stomach</i>	Right sided or midline	
<i>Bowel</i>	Malrotation (the colon is posterior to the small bowel)	
<i>Complications</i>	Infections	

IVC, inferior vena cava.

isomeric right side (polysplenia: a fetus whose right side is a mirror image of its left side). These fetuses are usually recognized because of the associated cardiac anomalies.

**Synonym.** Ivemark syndrome, heterotaxia, cardiosplenic syndrome.

**Incidence.** The incidence is very low, estimated at 1 in 10,000 to 20,000 live births.

**Etiology.** Autosomal-recessive inheritance with male preponderance in the most of the cases, but there are reports of autosomal-dominant and X-linked inheritance, too. Heterotaxy syndromes could also occur in chromosomal translocation or deletion in sporadic cases.

**Diagnosis.** The diagnosis is usually made by the recognition of the cardiac anomalies, in particular, the presence of atrioventricular septal defect, mesocardia (the axis of the interventricular septum being almost anteroposterior) with an endocardial cushion defect, an intrahepatic segment of the umbilical vein that is also oriented anteroposteriorly, and an odd-looking stomach. The abnormal lobation of the lungs is difficult to recognize, and the only instance when it can be done is when a sliver of pleural fluid is infiltrated between the lobes. Another typical finding is the interruption of the inferior vena cava with azygos continuation. The typical findings include an inferior vena cava that is posterior in the upper abdomen (instead of curving anteriorly to enter the right atrium) and the abrupt decrease in size of the inferior vena cava near the diaphragm. An enlarged azygos arch joining the superior vena cava can also be recognized. The presence of a persistent left superior vena cava is rarely recognized, not because it is a challenging finding, but because it is not sought. Color and pulsed Doppler of the splenic artery has been suggested as an aid in the prenatal diagnosis of the syndrome. Other findings include agenesis of the corpus callosum with pachygyria and hydrocephalus.

**Genetic Anomalies.** Although it was thought that the syndrome resulted from a possible mutation in the gene encoding connexin 43 (CX43), this was not supported by further studies.

**Differential Diagnosis.** The cardiac anomalies (in particular, endocardial cushion defect) without the syndrome and trisomy 18 may be included in the differential diagnosis.

**Associated Anomalies.** Anomalies are listed in Table 5-2.

**Prognosis.** Asplenia tends to be a more severe disease because of the cyanotic heart lesions and the superimposed infections. Although morbidity and mortality in the neonatal period are determined mainly by the cardinal cardiac defects, the visceral anomalies may strongly affect the long-term outcome of these patients.

**Management.** Termination of pregnancy can be offered before viability. Standard prenatal care is not altered when continuation of the pregnancy is chosen. Confirmation of diagnosis after birth is important for genetic counseling. The treatment of the infant is dictated by the cardiac defects.

## References

- Noack F, Sayk F, Ressel A, et al: Ivemark syndrome with agenesis of the corpus callosum: a case report with a review of the literature. *Prenat Diagn* 22:1011, 2002.
- Marton T, Cesko I, Hajdu J, et al: Heterotaxy syndrome, analysis of 13 cases and review of the literature. *Orv Hetil* 143:299, 2002.
- Abuhamad AZ, Robinson JN, Bogdan D, et al: Color Doppler of the splenic artery in the prenatal diagnosis of heterotaxic syndromes. *Am J Perinatol* 16:469, 1999.
- Cesko I, Hajdu J, Marton T, et al: Familial heterotaxy syndrome. Case report and review of the international literature. *Orv Hetil* 139:2775, 1998.
- Berg C, Geipel A, Smrcek J, et al: Prenatal diagnosis of cardiosplenic syndromes: a 10-year experience. *Ultrasound Obstet Gynecol* 22:451, 2003.



## BECKWITH-WIEDEMANN SYNDROME

**Definition.** Beckwith-Wiedemann syndrome is a disorder first described by Beckwith in 1963 and Wiedemann in 1964. It is characterized by the classic triad of macrosomia, omphalocele, and macroglossia.

**Synonym.** Exomphalos-macroglossia-gigantism syndrome.

**Incidence.** The incidence has been estimated to be 0.72:10,000 births, and more than 500 cases are reported in the literature.

**Etiology.** The condition is sporadic in most cases. Beckwith-Wiedemann syndrome has an autosomal-dominant inheritance, with incomplete penetrance and variable expressivity. Rearrangements involving the chromosome



**FIGURE 5-22.** Beckwith-Wiedemann syndrome. The ear-lobe groove (arrow) can be recognized when searched for clinically.



**FIGURE 5-23.** Typical omphalocele (arrow). (Courtesy of Luis Machado, MD, 2000, thefetus.net.)



**FIGURE 5-24.** Coronal plane of section from a fetus at 26 weeks' gestation with subsequently proven Beckwith-Wiedemann syndrome. Bilateral fetal nephromegaly is demonstrated.

11p15 region seem to be the mutation responsible for this disorder.

**Diagnosis.** The detection of macrosomia, omphalocele, and macroglossia associated with normal karyotype makes the diagnosis of Beckwith-Wiedemann syndrome. Other features occurring in variable incidence include nephromegaly, hepatomegaly, small groove earlobe creases, diaphragmatic hernia, hemihypertrophy, exophthalmos, enlargement of the testis, enlarged kidneys, adrenocortical macrocyst, single umbilical artery, and cardiac defects. The most typical findings include macrosomia, polyhydramnios, enlarged placenta, and a distended abdomen. Because most described signs developed after 22 weeks of gestation, a careful follow-up should be carried on until late stages of pregnancy.

**Genetic Anomalies.** Structural anomalies of the chromosome including paternal isodisomy of the 11p15.5 region, isodisomy of 11q, and uniparental disomy may be detected by cytogenetic studies. Thus, aside from a conventional cytogenetic analysis, some authors recommend using polymerase chain reaction of polymorphic loci on 11p15.5, to detect possible maternal deletions or inversions, paternal duplications, and uniparental disomy. These may account for 25% of cases of Beckwith-Wiedemann syndrome.

**Differential Diagnosis.** Down syndrome must be excluded by chromosomal analysis owing to the occurrence of macroglossia in both conditions. Diabetic fetopathy is another cause of macrosomia and, thus, is a differential





**FIGURE 5-25.** Profile of the fetal face in a patient with macroglossia (arrow) and Beckwith-Wiedemann syndrome.

diagnosis. Zellweger syndrome can also combine liver and kidney enlargement, and may be diagnosed prenatally by measuring fatty acid concentration and activity of marker enzymes. Perlman syndrome, a rare entity characterized by hypotonia, facial dysmorphism, gigantism, and visceromegaly including nephromegaly, is another differential diagnosis.

**Complications.** Pancreatic cell hyperplasia may affect 30% to 50% of patients, causing hyperinsulinism and neonatal hypoglycemia on the second or third day of life. Untreated neonatal hypoglycemia is an important complication and may result in further cerebral dysfunction, such as seizures, mild to moderate mental retardation, or neonatal death in more severe cases. Macroglossia can cause variable complications ranging from feeding difficulties to airway obstruction and death. Long-term complications include high risk for abdominal tumors, in particular Wilms tumor (3.7% incidence); hepatoblastoma; neuroblastoma, and adrenal cortical carcinoma. The risk of developing malignant tumors increases when hemihypertrophy is present. Beckwith-Wiedemann syndrome is a favorable biologic marker for survival in children who have intra-abdominal tumors. Benign tumors are associated with this disease.

**Prognosis.** Neonatal mortality rate is approximately 21%, due mainly to congestive heart failure. Among those who survive, the prognosis is in general favorable, depending on the severity of the associated anomalies and long-term complications. Preterm delivery is a complication due to the polyhydramnios and gestational hypertension.

**Management.** When diagnosed before viability, termination can be offered. After viability, sonographic evaluation of fetal growth is suggested. When macrosomia is suspected, cesarean section may be offered owing to the risk of shoulder dystocia. An early diagnosis of Beckwith-Wiedemann syndrome is important for counseling the parents concerning potential risk for developing embryonic tumors, selection of the mode of delivery due to potential adrenal cysts that might bleed during labor, and prevention of neonatal hypoglycemia. Serum alpha-fetoprotein screening, usually in combination with abdominal ultrasound, can lead to early detection of hepatoblastoma. Delivery in a tertiary center is recommended for early abdominal wall defect repair and treatment of the hypoglycemia. Sonographic screening for abdominal tumors is recommended during the first 6 years of life. Aggressive follow-up is warranted in cases of association with hemihypertrophy and nephromegaly with or without evidence of a Wilms tumor precursor.

## References

- Muguerza R, Rodriguez A, Formigo E, et al: Pancreatoblastoma associated with incomplete Beckwith-Wiedemann syndrome: case report and review of the literature. *J Pediatr Surg* 40:1341, 2005.
- Fahmy J, Kaminsky CK, Parisi MT: Perlman syndrome: a case report emphasizing its similarity to and distinction from Beckwith-Wiedemann and prune-belly syndromes. *Pediatr Radiol* 28:179, 1998.
- Wangler MF, Chang AS, Moley KH, et al: Factors associated with preterm delivery in mothers of children with Beckwith-Wiedemann syndrome: a case cohort study from the BWS registry. *Am J Med Genet A* 134:187, 2005.
- Merrot T, Walz J, Anastasescu R, et al: Prenatally detected cystic adrenal mass associated with Beckwith-Wiedemann syndrome. *Fetal Diagn Ther* 19:465, 2004.
- Mulik V, Wellesley D, Sawdy R, et al: Unusual prenatal presentation of Beckwith-Wiedemann syndrome. *Prenat Diagn* 24:501, 2004.
- Rahmah R, Yong JF, Sharifa NA, et al: Bilateral adrenal cysts and ectopic pancreatic tissue in Beckwith-Wiedemann syndrome: is a conservative approach acceptable? *J Pediatr Endocrinol Metab* 17:909, 2004.
- Clericuzio CL, Chen E, McNeil DE, et al: Serum alpha-fetoprotein screening for hepatoblastoma in children with Beckwith-Wiedemann syndrome or isolated hemihyperplasia. *J Pediatr* 143:270, 2003.
- Reish O, Lerer I, Amiel A, et al: Wiedemann-Beckwith syndrome: further prenatal characterization of the condition. *Am J Med Genet* 107:209, 2002.
- Hamada H, Fujiki Y, Obata-Yasuoka M, et al: Prenatal sonographic diagnosis of Beckwith-Wiedemann syndrome in association with a single umbilical artery. *J Clin Ultrasound* 29:535, 2001.
- Borer JC, Kaefer M, Barnewolt CE, et al: Renal findings on radiological followup of patients with Beckwith-Wiedemann syndrome. *J Urol* 161:235, 1999.
- Beckwith JB: Extreme cytomegaly of the adrenal fetal cortex, omphalocele, hyperplasia of kidneys and pancreas, and Leydig-cell hyperplasia. Another syndrome? Presented at annual meeting of western society for pediatric research, Los Angeles, California, November 11, 1963.
- Wiedemann HR: Complex malformation. Familial avec hernie ombilicale et macroglossie—un “syndrome nouveau”? *J Hum Genet* 13:223, 1964.
- Williams DH, Gauthier DW, Maizels M: Prenatal diagnosis of Beckwith-Wiedemann syndrome. *Prenat Diagn* 25:879, 2002.

## CAMPOMELIC DYSPLASIA

**Definition.** Campomelic dysplasia is a congenital disorder characterized by the development of abnormal curvature of the long bones, particularly the lower extremities, such as femur and tibiae. Some authors have classified the disease into two varieties—“long limbed” and “short limbed”—

depending on the type of limbs involved in the pathologic process.

**Synonyms.** Campomelic dysplasia, campomelic syndrome, campomelic dwarfism, congenital bowing of the limbs.

**Prevalence.** The disorder affects 0.02:10,000 live births. Sex reversal occurs in some genotypic male fetuses who lack





**FIGURE 5-26.** Campomelic dysplasia. Bowing of the femur (arrows). Note the gentle curve that differentiates this entity from the more acute angles seen in osteogenesis imperfecta fetuses.

the H-Y antigen. Phenotypic sex ratio is approximately M1:F2.3, karyotypic sex ratio is approximately M2:F1.

**Etiology.** The transmission of campomelic dysplasia is still debated. Autosomal-recessive inheritance is thought to be the most common pattern, although it may also be due to sporadic autosomal-dominant mutation.

**Recurrence Risk.** Depends on the etiology. If transmitted by autosomal-recessive pattern, it has a 25% recurrence risk. When transmitted by autosomal-dominant pattern, it has 50% recurrence risk, but in fact, most are new mutations.

**Diagnosis.** The most characteristic sign of campomelic dysplasia is the marked anterior bowing of the long bones, particularly of the femur and tibia. Severe angulation may mimic fractures. Other sonographic features that are commonly present include growth restriction; bell-shaped narrow chest; 11 pair of ribs; hypoplasia of the midthoracic vertebral bodies, fibula, and scapula; scoliosis; shortness of the limbs; talipes equinovarus; tracheobronchomalacia; flat and small face; high forehead with prominent occiput; low nasal bridge; micrognathia; cleft of the soft palate; hypertelorism; low-set and malformed ears; hydrocephalus; and ambiguous genitalia.

**Genetic Anomaly.** A mutation in SOX9, a sex-determining region of Y (SRY)-related gene, located at 17q24 seems to be associated with the occurrence of both campomelic dysplasia and sex reversal.

**Pathogenesis.** Although many theories have been proposed to explain the development of the anomalies present in this syndrome, (in particular the bowing of the bones), the precise mechanism is not known. Some of the theories are

1. Mechanical stress due to faulty fetal position within the uterus.
2. Primary muscle imbalance and shortening, particularly of the calf muscles causing secondary bending of the tibia.
3. Intrauterine fracture with subsequent healing.
4. Abnormal vascular and cellular elements of perichondrium.
5. Developmental disturbance in the cartilaginous phase of bone formation.

**Associated Anomalies.** Polyhydramnios, and anomalies from the central nervous, cardiac, and renal systems have been described antenatally. After birth, hearing loss may occur.

**Differential Diagnosis.** Osteogenesis imperfecta types I and II, hypophosphatasia, unclassifiable varieties of congenital bowing of the long bones, thanatophoric dysplasia, mesomelic dysplasia (Reinhart variety), Roberts syndrome, and diastrophic dysplasia.

**Prognosis.** Almost all result in neonatal or infant death owing to respiratory complications. Some survivors, including a boy alive at 17 years, have been reported.

**Management.** Before viability, the option of pregnancy termination should be offered. After viability, standard obstetric management is not altered, and respiratory function in the newborn must be supported.

## References

- Khajavi A, Lachman R, Rimo N, et al: Heterogeneity in the campomelic syndromes. Long and short bone varieties. *Radiology* 120:641, 1976.
- Lee FA, Isaacs H, Strauss J: The "campomelic" syndrome. *Am J Dis Child* 124:485, 1972.
- Cordone M, Lituania M, Zampatti C, et al: In utero ultrasonographic features of campomelic dysplasia. *Prenat Diagn* 9:745, 1989.

## CAUDAL REGRESSION SYNDROME

**Definition.** Caudal regression syndrome is a rare congenital defect, characterized by the absence of the sacrum, and defects of variable portions of lumbar spine, associated with anomalies from different systems.

**Synonyms.** Caudal dysplasia sequence, sacral agenesis.

**Prevalence.** 1 to 0.25:10,000 in normal pregnancies and 200 to 250 times higher in diabetic pregnancies.

**Etiology.** Unknown, but associated with maternal diabetes in 16% of the affected.

**Recurrent Risk.** This anomaly is not thought to be hereditary, and the recurrent risk is very small, although it is higher in diabetics.

**Diagnosis.** The sonographic findings are variable, and depend on the extent and severity of the defect. It ranges from complete absence of the sacrum associated with abnor-

malities of the lumbar spine and lower extremities (such as clubfeet and contractions of the knees and hips) to abnormalities of the sacrum, without associated defects. The most typical findings are the absence of a few vertebrae, the shield-like appearance of the fused or approximated iliac wings and the decrease interspace between the femoral heads. Some sonographic planes of section will intersect the fetus at such an angle that no spine is visible, a very striking and probably pathognomonic finding. Decreased movement of the legs is frequently observed. First trimester diagnosis may be difficult to accomplish because of the incomplete ossification of the sacrum at that time. A short crown rump length and abnormal appearance of the yolk sac have been proposed as early sonographic signs of caudal regression syndromes.

**Genetic Anomaly.** Unknown.

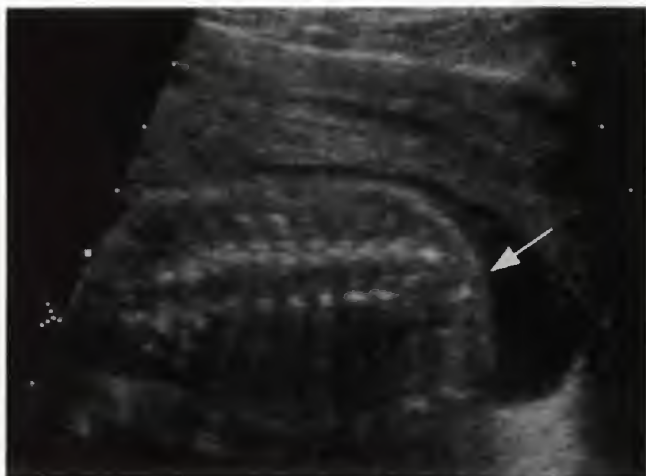


**FIGURE 5-27.** Caudal regression syndrome. Although on superficial examination, this image might pass for normal, note that on the caudal side of the image (on the right, because the ribs can be seen on the left side of the image) the spine terminates (*arrow*) without the usual landmark of the iliac wings and sacrum.



**FIGURE 5-29.** Caudal regression syndrome. The lack of sacrum allows the iliac wings to be approximated, giving them a shield-like appearance (*arrow*).



**FIGURE 5-28.** This same finding is even more striking on the sagittal view of the spine, where the distal end (*arrow*) appears to have been "erased." This is actually the finding that caught the eye of one of my astute sonographers: she was puzzled by the spine "looking too short."



**FIGURE 5-30.** The spinal cord of this fetus is about at 2:00 (compare with the position of the iliac wing on Fig. 5-29). I do not know of any other condition that can provide this same image of a cross-section through a fetal abdomen with no visible spine. All of the other differential diagnoses such as achondrogenesis and the severest forms of osteogenesis imperfecta would not present with the localized anomaly seen here.

**Pathogenesis.** Disruption of the maturation of the caudal portion of the spinal cord complex before 4 weeks' gestation, leading to motricity deficits and neurologic impairment, varying from incontinence of urine and feces to complete neurologic loss.

**Associated Anomalies.** Anomalies of the central nervous, musculoskeletal, genitourinary, cardiac, respiratory, and gastrointestinal systems may be found in association with caudal regression syndrome.

**Differential Diagnosis.** Sirenomelia, which was thought to be the most severe form of caudal regression syndrome (today it is considered a different entity), is the main

differential diagnosis. Fusion of the lower extremities is a typical finding of sirenomelia.

**Prognosis.** Depends on the severity of the spinal defect and associated anomalies, but the vast majority of survivals requires urologic and orthopedic interventions. Severe forms are commonly associated with cardiac, renal, and respiratory problems, which are responsible for early neonatal death.



**Management.** If detected early, pregnancy termination can be offered. Standard prenatal care is not altered if continuation of pregnancy is opted. If born alive, extensive surgery in tertiary center is usually needed to repair the defects.

## CEREBROHEPATORENAL SYNDROME

**Definition.** One of the four syndromes of the “peroxisome biogenesis disorders” or heterogeneous group of human neurodegenerative diseases that results in impairment of many metabolic pathways, especially of the beta-oxidation of very-long-chain fatty acids (VLCFAs), due to deficiency of peroxisomes in liver and kidneys.

**Synonym.** Zellweger syndrome.

**Incidence.** 0.2 to 0.25:10,000. The proportion between male and female fetuses is 1:1. The probable locus is on the long arm of chromosome 7 in the 21-22 regions.

**Etiology.** Autosomal-recessive inheritance with variable expression.

**Pathogenesis.** Peroxisomes are single membrane-bound cell organelles that perform numerous metabolic functions. The inherited peroxisomal disorders appear when these organelles lack one or more of their functions and become impaired. Although multiple organs are affected, the nervous system is affected most.

**Sonographic Findings.** The fetuses demonstrate growth restriction, hypotonicity with decreased movements, and increased nuchal translucency. Abnormal head shape (bulging forehead, wide metopic suture), facial dysmorphism (micrognathia, and buphthalmos), central nervous system (hydrocephalus) periventricular cysts, ventriculomegaly, hepatomegaly with dysgenesis, cardiac anomalies, clinodactyly, and simian creases can also be detected prenatally.

**Differential Diagnosis.** Many aneuploidies may present with similar findings. Down syndrome is commonly misdiagnosed owing to the overlapping of several structural findings.

**Implications for Targeted Examinations.** The initial laboratory diagnosis is suspected by demonstration of elevated very-long-chain fatty acids in plasma and with a detailed

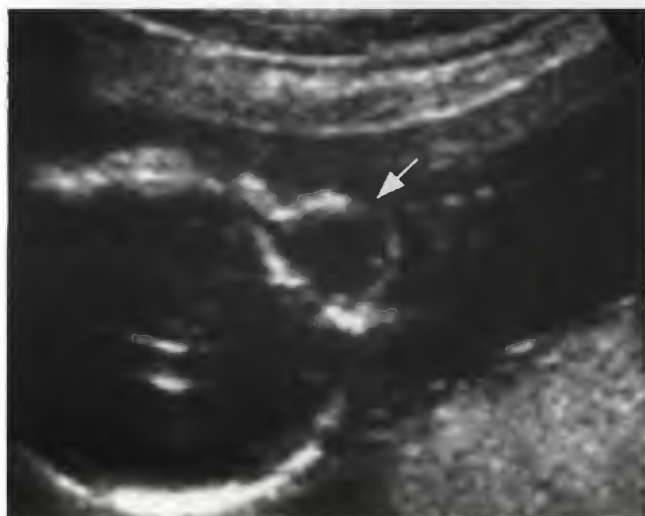


**FIGURE 5-31.** Cerebrohepatorenal syndrome. Buphthalmos. Note the enlarged size of the eye (arrow).

## References

- Jaffe R, Zeituni M, Feigin M: Caudal regression syndrome. *Fetus, Spinal anomalies* 7561:1, 1991.  
Benacerraf BR: Caudal regression syndrome and sirenomelia. In *Ultrasound of Fetal Syndromes*, Churchill Livingstone, New York, 1998, p 250.

correct  
journal?

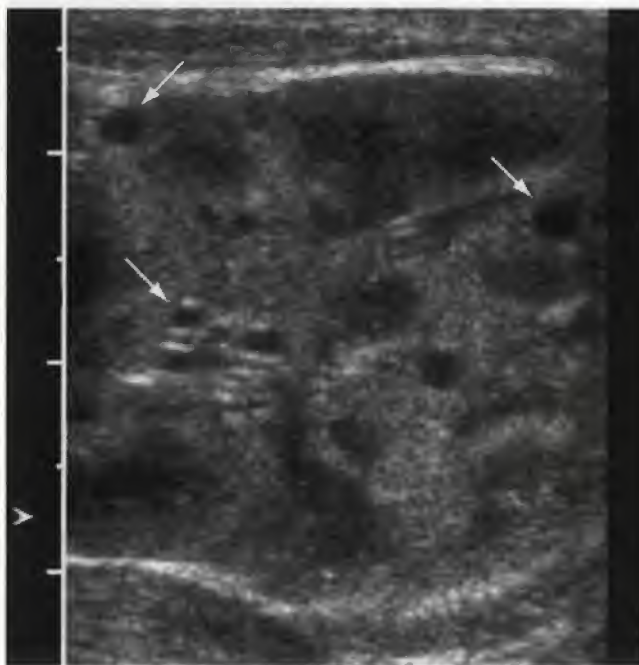


**FIGURE 5-32.** Renal sonogram of a pediatric patient with Zellweger syndrome. Multiple small cysts (arrows) are seen throughout the kidney.

ultrasound scanning. Cultured chorionic villus sampling and amniocentesis with a detection of reduced peroxisomes and abnormal lipid metabolism are essential for a complete classification and to confirm the presumed diagnosis. Some recent studies report also a low estriol level and low concentrations of human chorionic gonadotropin in the maternal serum screening.

**Prognosis.** Most infants with this disorder die within the first year.

**Management.** Termination of pregnancy can be offered before viability. Standard prenatal care is not altered when continuation of the pregnancy is chosen. Confirmation of diagnosis after birth is important for genetic counseling.

## References

- Cuillier F, Cartault F, Lemaire P, et al: Subependymal pseudocysts in the fetal brain revealing Zellweger syndrome. *J Gynecol Obstet Biol Reprod (Paris)* 33:325, 2004.  
Depreter M, Espeel M, Roels F: Human peroxisomal disorders. *Microsc Res Tech* 61:203, 2003.  
Johnson JM, Babul-Hirji R, Chitayat D: First-trimester increased nuchal translucency and fetal hypokinesia associated with Zellweger syndrome. *Ultrasound Obstet Gynecol* 17:344, 2001.  
Lee HF, Mak SC, Wu FW, et al: Zellweger syndrome: report of one case. *Acta Paediatr Taiwan* 42:53, 2001.  
De Graaf IM, Pajkrt E, Keessen M, et al: Enlarged nuchal translucency and low serum protein concentrations as possible markers for Zellweger syndrome. *Ultrasound Obstet Gynecol* 13:268, 1999.  
Steinberg SJ, Elcioglu N, Slade CM, et al: Peroxisomal disorders: clinical and biochemical studies in 15 children and prenatal diagnosis in 7 families. *Am J Med Genet* 85:502, 1999.

## CHARGE ASSOCIATION

**Definition.** Coloboma of the eye, heart defects, atresia of the choanae, retarded mental and growth development, genital anomalies, and ear anomalies with or without deafness (Table 5-3).

**Diagnosis.** Hall (1979) first reported a constellation of nonrandomly associated malformations occurring with choanal atresia. Subsequent authors have validated the CHARGE association and suggested the inclusion of orofacial clefts and esophageal atresia as main features. Tetralogy of Fallot is the most frequent heart defect reported in the CHARGE association. Tellier et al (1998) evaluated 47 CHARGE patients for the frequency of major anomalies, namely, coloboma (79%), heart malformation (85%), choanal atresia (57%), growth and mental retardation (100%), genital anomalies (34%), ear anomalies (91%), and deafness (62%). In addition, they commented on anomalies observed frequently in neonates and infants with the CHARGE syndrome, including minor facial anomalies, neonatal brain stem dysfunction with cranial nerve palsy, and internal ear anomalies such as semicircular canal hypoplasia, which was found in each patient that could be tested. Criteria for poor survival were thought to include male gender, central nervous system and esophageal malformations, and bilateral choanal atresia. A significantly higher mean paternal age at conception, together with concordance in monozygotic twins and the existence of rare familial cases, supported the role of genetic factors such as de novo dominant mutation or subtle submicroscopic chromosome rearrangement.

**Genetics.** A large percentage of children with CHARGE syndrome have a mutation in the *CHD7* gene on chromosome 8. Mutations in this gene can confirm the diagnosis of CHARGE in those cases. Not finding a mutation does NOT rule out the CHARGE syndrome.

**Etiology.** Unclear.

**Recurrence.** Recurrence risk is low. Empiric risk of recurrence is at most 1% to 2%.

**Differential Diagnosis.** 22q11 deletion spectrum/VCF (velocardiofacial) syndrome (sometimes called DiGeorge syndrome) has different facial and ear features; VACTERL association, *PAXα* mutation (coloboma, hearing loss, and renal abnormalities); retinoic embryopathy.

**Prognosis.** Mortality in the first 2 years of life is 20% to 25%. Choanal atresia is a threat to life because young infants cannot establish the habit of mouth breathing.

## References

- The CHARGE Foundation. <http://www.chargesyndrome.org/index.asp>
- Online Mendelian Inheritance in Man (OMIM) <http://www.ncbi.nlm.nih.gov/Omim/searchomim.html>
- Hall BD: Choanal atresia and associated multiple anomalies. *J Pediatr* 95:395, 1979.
- Koletzko B, Majewski F: Congenital anomalies in patients with choanal atresia: CHARGE-association. *Eur J Pediatr* 142:271, 1984.
- Tellier AL, Cormier-Daire V, Abadie V, et al: CHARGE syndrome: report of 47 cases and review. *Am J Med Genet* 76:402, 1998.
- Gorlin RJ: Personal Communication. Minneapolis, MN, 1982.
- Cyran SE, Martínez R, Daniels S, et al: Spectrum of congenital heart disease in CHARGE association. *J Pediatr* 110:576, 1987.

**Table 5-3 Major Characteristics of CHARGE\***

Finding	Includes	Frequency
Coloboma of the eye	Coloboma of the iris, retina, choroids, disc, not including colobomas of the eyelid; microphthalmos (small eyes) or cryptophthalmos (absent eye)	80%–90%
Choanal atresia or stenosis	Unilateral or bilateral: bony or membranous. Unilateral atresia or stenosis may be difficult to diagnose	50%–60%
Cranial nerve dysfunction or anomaly	I–Lack of smell (anosmia) IX/X–Swallowing difficulties VII–Facial palsy–(unilateral or bilateral)	Frequent 70%–90% 40%
Characteristic CHARGE ear	Short, wide ear with little or no lobe, “snipped off” helix, prominent anti-helix that is discontinuous with the tragus, triangular concha, decreased cartilage, often stick out, usually asymmetric Middle ear: ossicular malformations seen on MRI Malformed inner ear (Mondini defect) with deformed cochlea and vestibules seen on MRI	Frequent 80%–90%

MRI, magnetic resonance imaging scan.

\*These are very common in CHARGE and relatively rare in other conditions.

Reproduced with permission from the Charge Syndrome Foundation, <http://www.chargesyndrome.org/index.asp>.

## FETAL ALCOHOL SYNDROME, FETAL ALCOHOL EFFECTS

Alcohol use during pregnancy results in a spectrum of adverse outcomes known as fetal alcohol spectrum disorders. Fetal alcohol syndrome (FAS) is one of these disorders. FAS is characterized by specific facial abnormalities and significant impairments in neurodevelopment and physical growth. Children exposed to alcohol (approximately 45 to

50 g of ethanol per day or equivalent) in utero suffer from growth and mental retardation, physical abnormalities, and immune dysfunction. There is no “threshold,” so some fetuses exhibit signs of fetal alcohol effects at lower exposure. Recommendations for clinicians regarding assessment of thresholds published by the National Institute on Alcohol Abuse and Alcoholism recommend that any woman who reports drinking more than seven drinks per week or more



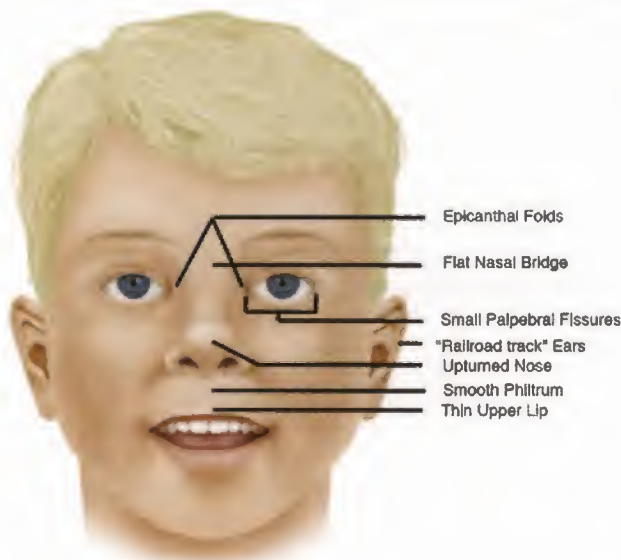


**FIGURE 5-33.** Characteristic facial features in a child with fetal alcohol spectrum disorders. Findings may include a smooth philtrum, thin upper lip, upturned nose, flat nasal bridge and midface, epicanthal folds, small palpebral fissures, and small head circumference. (Reproduced with permission from Darryl Leja, NHGRI, National Institutes of Health; Wattendorf DJ, Muenke M: Fetal alcohol spectrum disorders. *Am Fam Physician* 72:279, 2005.)



**FIGURE 5-34.** Characteristic features of an ear of a child with fetal alcohol spectrum disorders. Note the underdeveloped upper part of the ear parallel to the ear crease below ("railroad track" appearance). (Reproduced with permission from Darryl Leja, NHGRI, National Institutes of Health; Wattendorf DJ, Muenke M: Fetal alcohol spectrum disorders. *Am Fam Physician* 72:279, 2005.)



**FIGURE 5-35.** Characteristic features of a hand of a child with fetal alcohol spectrum disorders. Note the curved fifth finger (clinodactyly) (small arrow) and the upper palmar crease (large arrow) that widens and ends between the second and third fingers ("hockey stick" crease). (Reproduced with permission from Darryl Leja, NHGRI, National Institutes of Health; Wattendorf DJ, Muenke M: Fetal alcohol spectrum disorders. *Am Fam Physician* 72:279, 2005.)

than three drinks on any given day be further assessed for risk of developing alcohol-related problems.

**Synonyms.** None.

**Incidence.** The incidence of FAS ranges from 2 to 30:10,000 live births. This represents the most common form of mental retardation in the United States. In the United States, the prevalence of FAS has been estimated to fall between 0.5 and 2.0 cases per 1000 births. It has been long recognized that the true extent of teratogenic injury from alcohol exposure exceeds the clinically recognized prevalence of FAS, because behavioral and physical teratogenesis may be present in the absence of full expression of the syndrome.

**Etiology.** Direct toxicity of alcohol and its metabolites that cross the placenta and are not detoxified by the fetal liver.

**Diagnosis.** The findings include microcephaly, long round philtrum, small micrognathia, cleft palate, suppression of the Cupid arch, microphthalmia, microcephaly, dysgenesis of the corpus callosum, malformed ears, atrial septal defect, ventricular septal defect, and growth restriction predominantly involving the limbs and occurring early without oligoamnios. This lack of specificity suggests that the FAS facies may be a

common teratogenic expression of exposure to a variety of substances occurring during a defined period of fetal development.

**Differential Diagnosis.** Other conditions that involve growth restriction and microcephaly such as toxoplasmosis, rubella, cytomegalovirus, herpes simplex (TORCH) and chromosomal anomalies.

**Prognosis.** Mental retardation and delay in growth that persists postnatally. Most children with FAS are mildly to moderately retarded, but intellectual ability varies widely. The severity of mental retardation appears related to the severity of growth deficits and dysmorphogenesis, such that the more phenotypically affected individuals have lower IQ scores. Hyperactivity is frequently observed. As adults, mental illness is highly prevalent with FAS, affecting more than 70% in one series in which 60% had alcohol or drug dependence, 44% depression, and 40% psychosis.

## FETAL CYTOMEGALOVIRUS INFECTION

**Definition.** Fetal cytomegalovirus infection is a congenital disorder characterized by hydrops, ascites, ventriculomegaly, and other findings caused by transplacental transmission of cytomegalovirus to the fetus. The double-stranded DNA herpes group virus causes a mild infection or a mononucleosis-type illness in young healthy adults, chronic disease in older adults, and mild to severe congenital infection.

**Synonym.** Congenital cytomegalovirus infection.

**Etiology.** Cytomegalovirus (a double-stranded DNA herpes group virus).

**Incidence.** Congenital cytomegalovirus infection occurs in 0.2% to 2.2% of deliveries. Intrauterine transmission of cytomegalovirus takes place in approximately 40% of infections, and approximately 10% of live-born infants have symptomatic disease at the time of birth and later. Few cases may have isolated findings such as ascites.

**Diagnosis.** Cytomegalovirus infection as well as other congenital infections should be suspected whenever non-immune hydrops is found. Other suggestive findings that may be present are intracranial calcifications and intracranial hemorrhage, microcephaly, brain atrophy, abnormal periventricular echogenicities, intraparenchymal foci, ventriculomegaly, intraventricular adhesions, periventricular pseudocysts, sulcation and gyral abnormal patterns, hypoplastic corpus callosum, cerebellar and cisterna magna abnormalities, signs of striatal artery vasculopathy, splenomegaly, chorioretinitis (an echogenic lining to the vitreous body), occlusion of the foramen ovale (marked by decreased motion of the foramen ovale flap and thickening of the flap), signs of right-sided heart overload from the premature closure, ascites, hyper-echoic bowel, intrauterine growth restriction, and oligohydramnios. Most features are found by ultrasound examinations, at approximately 20 weeks' gestation.

Whenever maternal infection is confirmed, culture and polymerase chain reaction testing of amniotic fluid and cordocentesis is required for serologic studies (search for fetal-specific IgM antibody), although it does not have 100% reliability. Polymerase chain reaction on amniocentesis samples can be made after 21 weeks' pregnancy, after a 7-week interval between diagnosis of maternal infection and antenatal procedure. The diagnosis can also be made by

**Management.** The management of these pregnancies should be aimed at reducing the alcohol consumption; few programs have had much efficacy.

## References

- Bertrand J, Floyd RL, Weber MK, et al: National Task Force on FAS/FAE. Fetal Alcohol Syndrome: Guidelines For Referral and Diagnosis. Atlanta, GA. Centers for Disease Control and Prevention. 2004
- Strömberg K, Mattson SN, Adnams CM, et al: Fetal Alcohol Spectrum Disorders: An International Perspective [Proceedings of Symposia at the 2004 ISBRA Meeting]. *Alcoholism* 29:1121, 2005.
- Jouitteau B, Massias C, Sanyas P: Fetal alcohol syndrome. *J Radiol* 81:1709, 2000.
- Larroque B, Kaminski M: Prenatal alcohol exposure and development at preschool age: main results of a French study. *Alcohol Clin Exp Res* 22:295, 1998.
- Floyd RL, O'Connor MJ, Sokol RJ, et al: Recognition and prevention of fetal alcohol syndrome. *Obstet Gynecol* 106:1059, 2005.
- Chiriboga CA: Fetal drug and ethanol effects. *Learn Neurol* 10:151, 2004.

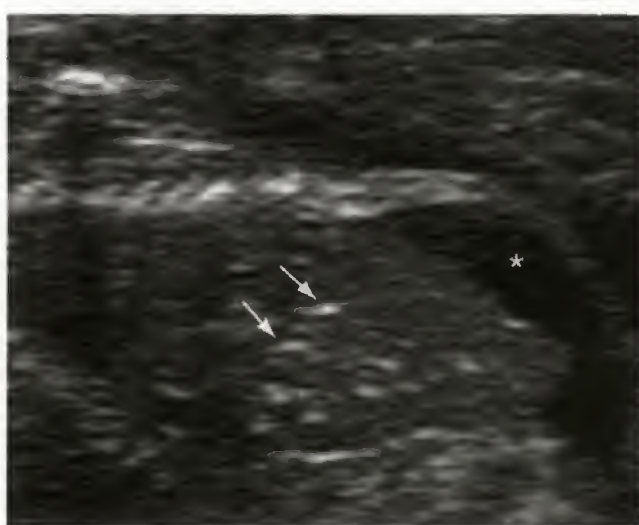


**FIGURE 5-36.** Sonogram of a second trimester fetus with proven cytomegalovirus infection. Hepatic calcifications (arrows) are seen as well as fetal ascites (asterisk).

histologic study of typical inclusion bodies in biopsy or autopsy specimens.

Focal sonographic periventricular increased echogenicity associated with mild ventriculomegaly, without any abnormalities of the cerebral and cerebellar organogenesis or cephalic biometry alteration in the third trimester of pregnancy, should be considered as a marker of encephalitis following cytomegalovirus infection of the fetal brain. Fetal magnetic resonance imaging is a useful adjunct in the evaluation of intrauterine infection with cytomegalovirus.

**Pathogenesis.** The exact mode of transplacental passage is uncertain. The virus replicates in fetal tissues, producing inflammation, tissue necrosis, and organ dysfunction. Cytomegalovirus hepatitis in the neonate can present with an intense inflammatory response involving the portal triads. In these cases, lobular disarray, degeneration of hepatocytes, and cholestasis are also seen. The cause of ascites in congenital cytomegalovirus infection is not certain. Contributing factors may include low serum protein levels due to



hepatic dysfunction and portal obstruction resulting from periportal inflammation.

**Associated Anomalies.** Isolated ascites is an uncommon finding in fetuses with cytomegalovirus infection but may occur. Cardiovascular, gastrointestinal, musculoskeletal, and ocular lesions may be found in association with the classic features. Petechiae, neurosensory hearing loss, and poor intellectual development may also occur after birth.

**Differential Diagnosis.** Because ascites is often the first manifestation of hydrops, the differential diagnosis for fetal ascites is essentially the same as with generalized hydrops, which includes mainly all congenital infections. Conditions that present with intracranial calcifications (such as tuberous sclerosis), hyperechoic bowel (cystic fibrosis and Down syndrome), and hepatomegaly (primary liver disease or extramedullary hematopoiesis) should be considered.

**Prognosis.** In general, neonates with symptomatic cytomegalovirus infection do poorly, with a neonatal mortality rate as high as 30% and a high rate of neurologic handicap in survivors. Cytomegalovirus hepatitis is reversible in survivors, but mental retardation, motor handicaps, and hearing loss are expected long-term sequelae. Late sequelae such as sensorineural hearing loss and neurodevelopmental disorders occur in 10% to 15% of infants lacking symptoms at birth. Pediatric neurologic morbidity is related to the degree of antenatal ventriculomegaly and, when it is greater than 15 mm, it is associated with an increase in abnormal neurologic development.

**Recurrence Risk.** Considering that viral infection confers immunity in the majority, there is just a small theoretical risk of reinfection in another pregnancy.

## FETAL RUBELLA SYNDROME

**Definition.** Fetal rubella syndrome is a congenital disorder resulting from primary maternal infection with the rubella virus. It is characterized mainly by deafness, mental retardation, congenital cataract, heart defects, and other structural anomalies that may be found with variable severity and frequency. During acute rubella in pregnancy, the rate of congenital infection is higher than 90% in the 12 first weeks of pregnancy, approximately 60% in weeks 13 to 17, 25% in weeks 18 to 24, and then increases again during the last month of pregnancy.

**Synonym.** Fetal rubella effects.

**Etiology.** It is caused by a RNA togavirus, which is the only member of the genus Rubivirus. The fetus is infected by transplacental transmission.

**Recurrence Risk.** None.

**Incidence.**

Not precisely known. Administration of rubella vaccine has significantly reduced the incidence of maternal infection, although reinfection after vaccination is possible. The development of fetal infection reaches 50% among those exposed during the first trimester and 20% during the second trimester.

**Diagnosis.** The most frequent sonographic findings are cardiac malformations (in particular, septal defects), eye defects (cataracts, microphthalmia, and retinopathy), microcephaly, hepatomegaly, splenomegaly and growth restriction. Deafness and mental retardation are expected after birth. The confirmation of fetal infection can be made by isolating

**Management.** Termination of pregnancy can be offered before viability. If continuation of the pregnancy is chosen, monthly follow-up with ultrasound is recommended to monitor growth restriction, hydrops, and the other fetal manifestations. Decompression with paracentesis to remove fetal ascites may prevent pulmonary hypoplasia and improve the circulatory system in those cases severely affected.

## References

- Daiminger A, Bader U, Enders G: Pre- and periconceptional primary cytomegalovirus infection: risk of vertical transmission and congenital disease. *Obstet Gynecol Surv* 60:420, 2005.
- Liesnard C, Donner C, Brancart F, et al: Prenatal diagnosis of congenital cytomegalovirus infection: prospective study of 237 pregnancies at risk. *Obstet Gynecol* 95:881, 2000.
- Guibaud L, Attia-Sobol J, Buenerd A, et al: Focal sonographic periventricular pattern associated with mild ventriculomegaly in fetal cytomegalic infection revealing cytomegalic encephalitis in the third trimester of pregnancy. *Prenat Diagn* 24:727, 2004.
- Ortiz JU, Ostermayer E, Fischer T, et al: Severe fetal cytomegalovirus infection associated with cerebellar hemorrhage. *Ultrasound Obstet Gynecol* 23:402, 2004.
- Moinuddin A, McKinstry RC, Martin KA, et al: Intracranial hemorrhage progressing to porencephaly as a result of congenitally acquired cytomegalovirus infection—an illustrative report. *Prenat Diagn* 23:797, 2003.
- Malinge G, Lev D, Zahalka N, et al: Fetal cytomegalovirus infection of the brain: the spectrum of sonographic findings. *AJNR Am J Neuroradiol* 24:28, 2003.
- Graham E, Duhl A, Ural S, et al: The degree of antenatal ventriculomegaly is related to pediatric neurological morbidity. *J Matern Fetal Med* 10:258, 2001.

rubella viral RNA from amniotic fluid samples and applying polymerase chain reaction.

**Associated Anomalies.** Occasionally, the following anomalies can be associated with the classic findings of fetal rubella syndrome: renal disorders, hypospadias, cryptorchidism, meningocele, glaucoma, patent ductus arteriosus, and peripheral pulmonic stenosis.

**Differential Diagnosis.** All of the conditions that can be associated with congenital hepatomegaly and cataracts should be excluded. This includes congenital infections (TORCH), fetal anemia, fetal liver tumor, chondrodysplasia punctata, Neu-Laxova syndrome, Smith-Lemli-Opitz syndrome, and Walker-Warburg syndrome.

**Prognosis.** Intrauterine death may occur. Postnatal impact of the intrauterine infection varies from absence of any defect to all the anomalies mentioned earlier with variable severity. The agent may remain for years in the tissues, causing chronic infection and its complications (such as diabetes mellitus due to chronic viropathy of the pancreas).

**Management.** Termination of pregnancy should be considered every time fetal infection is detected during the first trimester, owing to the severity of the condition in this group. After viability, monthly sonographic monitoring for growth and follow-up of the anomalies is recommended.

**Prevention.** Women found to be susceptible during pregnancy should be offered vaccination postpartum and before discharge from the hospital. Breastfeeding is not a contraindication to receiving the rubella vaccine.



## References

Tang JW, Aarons E, Hesketh LM, et al: Prenatal diagnosis of congenital rubella infection in the second trimester of pregnancy. *Prenat Diagn* 23:509, 2003.

O'Neill JF: The ocular manifestations of congenital infection: a study of the early effect and long-term outcome of maternally transmitted rubella and toxoplasmosis. *Trans Am Ophthalmol Soc* 96:813, 1998.

## FETAL TOXOPLASMOSIS SYNDROME

**Definition.** Toxoplasmosis is caused by infection with the protozoan parasite *Toxoplasma gondii*. Toxoplasmosis is normally asymptomatic in immunocompetent individuals. Acute infections in pregnant women can be transmitted to the fetus and cause severe illness (mental retardation, blindness and epilepsy). The risk of maternal fetal transmission increases with gestational age at the time of exposure, whereas the incidence of severe disease decreases.

**Synonyms.** None.

**Incidence.** An estimated 400 to 4,000 cases of congenital toxoplasmosis occur each year in the United States. Of the 750 deaths attributed to toxoplasmosis each year, 375 (50%) are believed to be caused by eating contaminated meat, making toxoplasmosis the third leading cause of food-borne deaths in this country. The incidence of toxoplasmosis acquisition during pregnancy ranges from 1 to 4 per 10,000. Half of the fetuses escape from the infection, one third has a subclinical infection, and only one tenth has a severe infection.

**Etiology.** Infectious. Women infected with *Toxoplasma* before conception, with rare exceptions, do not transmit the infection to their fetuses. Women infected with *Toxoplasma* after conception can transmit the infection across the placenta to their fetuses. Fetal involvement results from acute infection in the mother; however, those mothers with chronic infection can transmit the disease by reactivation, which is caused by an immunologic dysfunction. The rate of fetal transmission during primary infection is 25%, 54%, and 65%, in the first, second, and third trimesters, respectively.

**Pathogenesis.** The fetus is infected hematogenously through the placenta during parasitemia in the mother.



**FIGURE 5-37.** Severe dilatation of posterior horns of the lateral ventricles in a fetus with toxoplasmosis infection. (Courtesy of Julio Cesar Coub, 2006.)

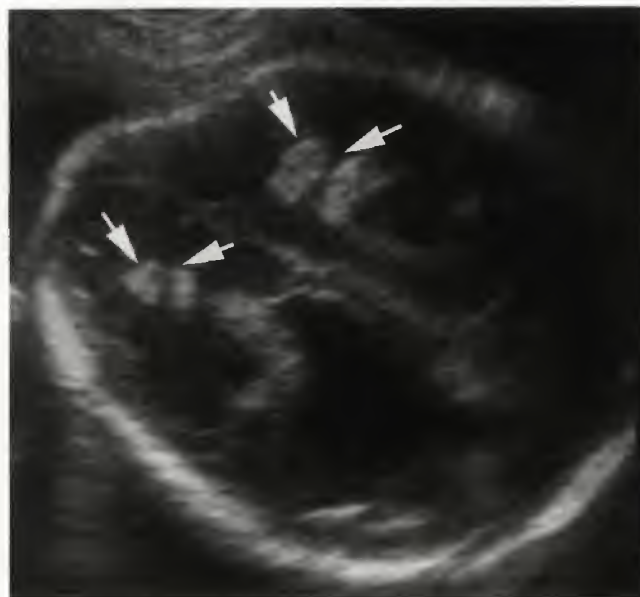


**FIGURE 5-38.** Intracranial calcifications (arrows). (Courtesy of Julio Cesar Coub, 2006.)

Ocular toxoplasmosis causes irreversible damage to the retina in utero. The fetus and infant mount inflammatory responses that may contribute to ocular damage.

**Diagnosis.** The classic triad of signs suggestive of congenital toxoplasmosis includes chorioretinitis, intracranial calcifications, and hydrocephalus. However, most infants infected in utero are born with no obvious signs of toxoplasmosis on routine examination, but many develop learning and visual disabilities later in life. If left untreated, congenital toxoplasmosis can be associated with severe and even fatal disease. Other findings include microcephaly, encephalomyelitis, seizures, mental retardation, ascites, and hepatosplenomegaly. Although the diagnosis used to be made by serologic techniques and cultures, it can now be done with polymerase chain reaction detection of *Toxoplasma gondii* in fetal tissues.

**Differential Diagnosis.** The other TORCH infections.

**Prognosis.** Approximately 75% of congenitally infected newborns are asymptomatic.

**Recurrence Risk.** Typically none.

**Management.** Depending on gestational age and whether the fetus is known to be infected, pregnant women have been treated with the antibiotic spiramycin or with sulfadiazine alone or the combination of pyrimethamine and sulfadiazine. Treatment of acute infection during pregnancy has been associated with an approximately 50% reduction in fetal infection.

**Prevention.** Toxoplasmosis infection can be prevented in large part by cooking meat to a safe temperature, and peeling or thoroughly washing fruits and vegetables before eating; pregnant women should avoid changing cat litter or,



if no one else is available to change the cat litter, use gloves, then wash their hands thoroughly.

## References

Silveira C, Ferreira R, Muccioli C, et al: Toxoplasmosis transmitted to a newborn from the mother infected 20 years earlier. *Am J Ophthalmol* 136:370, 2003.

Roberts F, Mets MB, Ferguson DJ, et al: Histopathological features of ocular toxoplasmosis in the fetus and infant. *Arch Ophthalmol* 119:51, 2001.

Lopez A, Dietz VJ, Wilson M, et al: Preventing congenital toxoplasmosis. *MMWR* 49(RR02):57, 2000.

Vidigal PVT, Santos DVV, Castro FC, et al: Prenatal toxoplasmosis: Diagnosis from amniotic fluid by PCR. *Rev Soc Bras Med Trop* 35:1, 2002.

## FETAL VALPROIC ACID EXPOSURE SYNDROME

**Definition.** Fetal valproic acid exposure syndrome is a syndrome resulting from maternal valproate (anticonvulsant) use during pregnancy and it is characterized by a cluster of minor and major anomalies, including central nervous system dysfunction, spina bifida, developmental delay, intrauterine growth restriction, and cardiac anomalies.

**Synonym.** Depakene exposure.

**Incidence.** Unknown, rare. Any epileptic pregnant mother has two to three times increased risk for congenital anomalies compared with the general population. If the exposure to valproic acid takes place between the 17th and 30th days after fertilization, the incidence of neural tube defects reaches 1% to 2%. In general, the teratogenic risks rise with increasing doses of valproic acid, with a significantly higher malformation risk in doses up to 1000 mg/day.

**Etiology.** Exposure to valproic acid.

**Pathogenesis.** Unknown.

**Diagnosis.** The findings include cardiovascular abnormalities, hypotonia, spina bifida, hypospadias, and limb reductions. The facial appearance can be characterized by an oral cleft, small broad nose, small ears, flat philtrum, a long upper lip with shallow philtrum, and micrognathia/retrognathia. Intrauterine growth restriction, microcephaly, generalized hypertrichosis sparing palms and soles, coarse face, gum hypertrophy, clubfeet and clubhands, musculoskeletal abnormalities, genital abnormalities, and urogenital defects may also be present. Heart defects have also been reported. In 26% of patients with fetal valproic acid exposure syndrome, cardiovascular abnormalities, most frequently ventricular septal defects, aortic or pulmonary stenosis, and persistent ductus arteriosus also occur. Pulmonary hypoplasia is also reported. Epilepsy and mental retardation may develop after birth.

**Genetic Anomalies.** None.

**Associated Anomalies.** Anomalies from different systems have been reported in association with this syndrome, such

as omphalocele, inguinal hernia, duodenal atresia, and scoliosis. Hyperbilirubinemia, hepatotoxicity, transient hyperglycemia, afibrinogenemia, and fetal or neonatal distress may be found.

**Differential Diagnosis.** Other neural tube defects. However, the clinical history in the presence of an association of spina bifida and cardiac anomaly should suggest the diagnosis.

**Prognosis.** Fetuses that present major anomalies have a poor prognosis. Metabolic disturbances may also complicate the neonatal period. These affected children can die in infancy, and the surviving patients can develop mental retardation.

**Recurrence Risk.** If the mother is exposed to valproic acid in a second pregnancy, the teratogenic effect will be the same.

**Management.** When detected in the second trimester, termination of the pregnancy can be offered. If the pregnancy is allowed to continue, no alteration of the management is needed. Many new antiepileptic drugs have been introduced over the past few years, and switching the mother to one of those is recommended. Because of the increased risk of malformations, pregnant women using valproic acid should be informed about the option of prenatal diagnosis by structural ultrasound examination and alpha-fetoprotein analysis of maternal serum.

## References

Stoll C, Audeoud F, Gaugler C, et al: Multiple congenital malformations including generalized hypertrichosis with gum hypertrophy in a child exposed to valproic acid in utero. *Genet Couns* 14:289, 2003.

Kozma C: Valproic acid embryopathy: report of two siblings with further expansion of the phenotypic abnormalities and a review of the literature. *Am J Med Genet* 98:168, 2001.

Janas MS, Arroce M, Hansen SH, et al: Lung hypoplasia—a possible teratogenic effect of valproate. Case report. *APMIS* 106:300, 1998.

Berg K, Open ACC, Nickels PGJ, et al: Complex cardiac defect with hypoplastic right ventricle in a fetus with valproate exposure. *Prenat Diagn* 25:156, 2005.

## FETAL VARICELLA ZOSTER

**Definition.** Fetal varicella zoster is a combination of abnormalities of multiple organs, caused by fetal contamination with maternal chickenpox infection.

**Synonyms.** Congenital varicella syndrome, varicella embryopathy, chickenpox, herpes zoster.

**Incidence.** The incidence of maternal infection with herpes virus varicella is 7:10,000 pregnancies. The risk of fetal involvement among all pregnant women infected with varicella during their gestation varies from 1% to 20%. First trimester varicella infections have been associated with an increased risk of spontaneous abortion. Second trimester

varicella infections have been associated with 2% risk of a congenital syndrome characterized by limb hypoplasia, cutaneous scars, cataracts, microcephaly, and cortical atrophy.

**Etiology.** Herpes virus.

**Recurrence Risk.** Less than 1%.

**Diagnosis.** Maternal infection at any time in pregnancy exposes the fetus to a high risk of transplacental contamination and is indicative of fetal follow-up. The risk of fetal anomalies, however, is higher during the first and second trimesters. Sonographic signs of fetal disease include fetal demise, growth restriction, musculoskeletal abnormalities such as clubfeet and abnormal position of the hands (caused



**FIGURE 5-39.** Varicella zoster infection. The fetal face at autopsy (26 weeks). Note the collapsed cranium, intact skin (very little maceration), disproportionate necrosis of the ocular globes, and flattened midface. (Courtesy of R.R. Lebel, 1992.)

by both necrosis and denervation of the affected tissue), limitation of limb extension due to cicatrices formation, cutaneous scars, limb hypoplasia, chorioretinitis, congenital cataracts, microphthalmia, hydrops, polyhydramnios, hyperechogenic hepatic foci, cerebral anomalies such as ventriculomegaly or atrophy, and microcephaly, disseminated foci of necrosis and microcalcifications, encephalitis, echogenic bowel in the second trimester. The placenta can show a multifocal chronic villitis with multinucleated giant cells. Fetal infection can be demonstrated by detection of varicella-zoster virus DNA by polymerase chain reaction in fetal blood and amniotic fluid or by detection of the specific IgM antibody, in the same fluids.

**Pathogenesis.** Direct damage to fetal tissues by neurotropic virus.

**Associated Anomalies.** Congenital anomalies from multiple organs with variable severity can be associated with varicella embryopathy. Among survivors, development of mental retardation, seizures, and limitation of movements may develop after birth. The virus may cause serious infections, particularly pneumonia, in adult women.

**Differential Diagnosis.** Other viral infections, vascular accidents, amniotic band syndrome.

## FRASER SYNDROME

**Definition.** Fraser syndrome is a rare genetic syndrome with abnormalities of the head, lungs, kidneys, and limbs. It combines acrofacial and urogenital malformations with or without cryptophthalmos.

**Synonym.** Cryptophthalmos-syndactyly syndrome

**Incidence.** 0.043:10,000 live-born infants and 1.1:10,000 stillbirths.

**Prognosis.** The severity of fetal involvement varies from dermatologic lesions to lethal disseminated disease. Limited scarring tends to have an excellent prognosis. Fetal brain disruptions, or severe maternal varicella with development of lethal maternal pneumonia and encephalitis, are indicators of an extremely high risk for fetal demise. The mortality rate varies from 39% to 61%. Early maternal infection (first and early second trimester) has a higher association with fetal anomalies, and third trimester infections have a higher risk for varicella-zoster development at the neonatal period. A life-threatening illness may occur when a newborn is delivered within 5 days of the onset of maternal illness.

**Management.** Termination of pregnancy can be offered before viability. If continuation of the pregnancy is chosen, periodic sonographic evaluation is recommended to search for fetal anomalies, limb contractures, and other signs of fetal compromise. If maternal seroconversion is suspected for the varicella-zoster virus, combining prenatal ultrasound and magnetic resonance imaging may document the extent of tissue damage and assist in the counseling. After a therapeutic abortion, fetal infection can be confirmed by detection of varicella zoster viral DNA in several fetal tissues and placenta, and by histopathologic findings such as miliary calcified necroses in fetal organs.

**Prevention.** Serologic testing and vaccination should be offered to women of childbearing age, and women should be questioned about immunity to varicella preconceptionally. Susceptible pregnancy patients should be counseled to avoid contact with individuals who have chickenpox. If exposure occurs, varicella-zoster immunoglobulin should be administered within 96 hours in an attempt to prevent maternal infection. Also susceptible neonates should receive varicella-zoster immunoglobulin. Acyclovir is active against the varicella-zoster virus, and treatment is indicated in seriously ill adults and neonates.

## References

- Verstraeten H, Vanzielegheem B, Defoort P, et al: Prenatal ultrasound and magnetic resonance imaging in fetal varicella syndrome: correlation with pathology findings. *Prenat Diagn* 23:705, 2003.
- Petignat P, Vial Y, Laurini R, et al: Fetal varicella-herpes zoster syndrome in early pregnancy: ultrasonographic and morphological correlation. *Prenat Diagn* 21:121, 2001.
- Yaron Y, Hassan S, Geva E, et al: Evaluation of fetal echogenic bowel in the second trimester. *Fetal Diagn Ther* 14:176, 1999.
- Hartung J, Enders G, Chaoui R, et al: Prenatal diagnosis of congenital varicella syndrome and detection of Varicella-Zoster virus in the fetus: a case report. *Prenat Diagn* 19:163, 1999.
- Chapman SJ: Varicella in pregnancy. *Semin Perinatol* 22:339, 1998.

**Etiology.** Probably autosomal-recessive transmission because an unusual proportion of infants are born to consanguineous parents.

**Recurrence Risk.** Fraser syndrome has a recurrence risk of 25% among siblings, and therefore, prenatal diagnosis and counseling of the affected families is important.

**Diagnosis.** The diagnosis has been suggested prenatally by the combination of the major and minor characteristics.



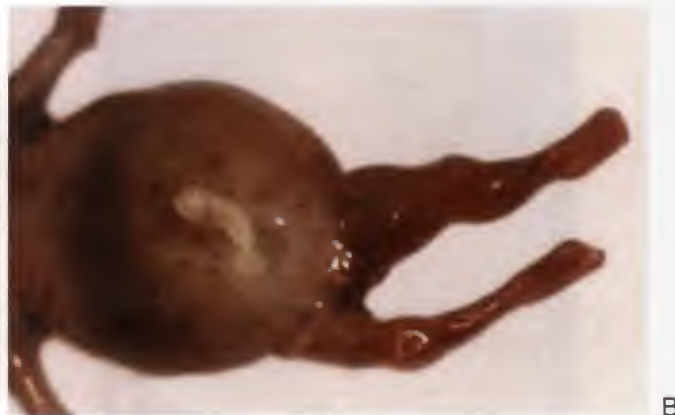


**FIGURE 5-40.** A case of Fraser syndrome diagnosed at 16 weeks' gestation. Megacystis, syndactyly, and oligohydramnios were seen. A. Sonogram demonstrating megacystis (BI) and ascites (asterisk). (B) Neonatal image. Note the distention of the abdominal wall. C. Picture of the postmortem feet showing syndactyly between I, II, and III digits. (A, B, C courtesy of Fabrice Cuillier, 2005, *thefetus.net*.)

Cases are diagnosed on the basis of at least two major criteria and one minor criterion or at least four minor criteria.

The major characteristics are

- Cryptophthalmos.
- Syndactyly.
- Genital anomalies.
- Sibling with Fraser syndrome.

The minor characteristics are

- Alterations of the nose.
- Alterations of the ears.
- Alterations of the larynx.
- Oral clefts (cleft lip and/or palate).
- Umbilical hernia.
- Renal agenesis (unilateral or bilateral).
- Skeletal anomalies.

The prenatal diagnosis of Fraser syndrome can be suspected, but because of the great variety of malformations, the diagnosis will remain doubtful unless a previous child is affected.

**Sonographic Findings.** Hyperechogenic lungs, laryngeal stenosis/atresia, oligohydramnios, ascites, renal agenesis/dysplasia, microphthalmia/hypertelorism, hydrocephalus, syndactyly, ear defects, ambiguous genitalia.

**Pathogenesis.** A defect of apoptosis has been suggested because several of the anomalies result from failure of



**FIGURE 5-41.** Sonogram of another fetus with laryngeal atresia and Fraser syndrome. Bilateral enlarged hyperechogenic lungs and fluid filled bronchi (arrows) are seen. Ascites (asterisk) was present.

programmed cell death (fusion of eyelids, digits, larynx, and vagina).

**Genetic Anomalies.** The Fraser syndrome gene is located to 4q21.

**Associated Anomalies.** Cryptophthalmos, absent or malformed lacrimal ducts, middle and outer ear malformations, high palate, cleavage along the midplane of nares and tongue, hypertelorism, laryngeal stenosis, syndactyly, wide separation of symphysis pubis, displacement of umbilicus and nipples, primitive mesentery of small bowel, maldeveloped kidneys, fusion of labia and enlargement of clitoris, and bicornuate uterus and malformed fallopian tubes.

**Differential Diagnosis.** The differential diagnosis of hyperrechogenic lungs includes congenital diaphragmatic hernia, cystic adenomatoid malformation (type III), sequestered lung, and tracheal or bronchial atresia. The differential diagnosis of the cryptophthalmos includes alobar holoprosencephaly, which should be easy to recognize from the simple hydrocephalus of the Fraser fetuses.

**Prognosis.** Fatal if laryngeal atresia or renal agenesis is present. If cryptophthalmos is the main sign, even surgical

repair will yield very poor vision (20/200 and 20/360) in the rare correctable cases.

**Management.** Depends on the predominant associated anomalies. Termination of the pregnancy can be recommended when renal agenesis or laryngeal atresia is present.

## References

- Okumus N, Onal EE, Turkyilmaz C, et al: Resuscitation failure due to Fraser syndrome in a newborn undiagnosed in the prenatal period. *Resuscitation* 65:221, 2005.
- Lesniewicz R, Sulik M, Midro AT: Microphthalmos and hypertelorism as diagnostic index in ultrasound diagnosis of Fraser syndrome. *Ginekol Pol* 76:147, 2005.
- Berg C, Geipel A, Germer U, et al: Prenatal detection of Fraser syndrome without cryptophthalmos: case report and review of the literature. *Ultrasound Obstet Gynecol* 18:76, 2001.

## FRYNS SYNDROME

**Definition.** Fryns syndrome is a rare congenital disorder characterized by dysmorphic facial features (coarse face with microphthalmia, hypertelorism, facial hair growth, cloudy corneas, broad and flat nasal bridge, cleft lip and palate, microretrognathia, and low-set ears), diaphragmatic hernia, distal limb hypoplasia, and pulmonary hypoplasia. The first description was provided by Fryns in 1979.

**Incidence.** Unknown. Ayme and coworkers reported a prevalence of 0.7:10,000 births in France.

**Etiology.** Autosomal recessive inheritance.

**Recurrence Risk.** 25%.

**Diagnosis.** The phenotypic variability makes the sonographic diagnosis of Fryns syndrome a challenge. The detection of typical facial dysmorphism associated with diaphragmatic hernia (which is a leading sonographic criterion), hypoplastic thorax with widely spaced nipples, hypoplasia or absence of the lobulation of the lungs, distal limb deficiencies with hypoplasia of the terminal phalanges and nails, and postaxial oligodactyly should suggest Fryns syndrome. Development of polyhydramnios late in the second trimester and normal growth or overgrowth of the fetus are also expected. The use of three-dimensional ultrasound may be helpful to precisely define the facial anomalies. Although the frequency of cystic hygroma is not as high as the features mentioned earlier, this defect has been proposed as a sonographic first trimester marker for recurrent cases. Other findings that can be detected are persistent truncus arteriosus, interrupted aortic

arch, left isomerism, complex central nervous system midline malformations, and multiple pterygias. Maternal and amniotic fluid alpha-fetoprotein levels may be elevated, in particular in fetuses that carry open defects.

**Genetic Anomalies.** No specific DNA defect has been identified.

**Differential Diagnosis.** The differential diagnosis includes trisomy 18 (which can be excluded by karyotype), Killian/Teschler-Nicole syndrome (mosaic tetrasomy 12p), Zellweger syndrome (deficiency of peroxisomal enzyme), and Brachman-DeLange syndrome (usually associated with severe growth restriction).

**Associated Anomalies.** Anomalies from skeletal, cardiac, central nervous, gastrointestinal, and genitourinary systems can be associated with Fryns syndrome.

**Prognosis.** The majority of affected infants are stillborn or die in early neonatal period. A few reported infants who survive have severe mental and developmental retardation.

**Management.** When the syndrome is detected before viability, termination of pregnancy can be offered. After viability, standard prenatal care is not altered.

## Reference

- Ramsing M, Gillissen-Kacsbach G, Holzgreve W, et al: Variability in the phenotypic expression of Fryns syndrome: A report of two sibships. *Am J Med Genet* 95:415, 2000.

## GOLDENHAR SYNDROME

**Definition.** Hemifacial microsomia, epibulbar dermoids, preauricular appendages, ear hypoplasia, transverse facial clefts, asymmetry of skull, and spinal anomalies (vertebral segmentation errors).

**Incidence.** This syndrome has an estimated frequency of 1/3000 to 1/5000 newborns, with a minor male-to-female (3/2) predominance.

**Synonyms.** Oculo-auriculo-vertebral spectrum, Goldenhar-Gorlin's syndrome, facio-auriculo-vertebral dysplasia.

**Etiology.** Probably sporadic, with rare cases suggesting an autosomal-recessive or autosomal-dominant inheritance.

**Diagnosis.** The diagnosis is usually made by observing the facial asymmetry (likely to become more common with three-dimensional ultrasound) or a maxillary cleft in association with unilateral microphthalmia. Other findings include anophthalmos, cardiac, or urinary anomalies and lipoma of the corpus callosum.

**Pathogenesis.** Possible fetal hemorrhage in the region of the first and second branchial arches at the time when the blood supply of these arches switches from the stapedia artery to the external carotid artery.

**Genetic Anomalies.** Unknown.

**Associated Anomalies.** Tracheoesophageal fistula, epibulbar dermoids, syringohydromyelia, neurodevelopment





**FIGURE 5-42.** Asymmetry of the face with hypoplasia of the left side and cleft in a fetus with Goldenhar syndrome. (Courtesy of Luc de Catte, 1999, *thefetus.net*.)

delay, occipital meningoencephalocele, tetralogy of Fallot, ventricular septal defects, asplenia syndrome, ventricular

inversion associated with double-outlet right ventricle, pulmonary atresia with ventricular septal defect, double-outlet right ventricle, infradiaphragmatic total anomalous pulmonary venous connection, ectopic and fused kidneys, renal agenesis, vesicoureteral reflux, ureteropelvic junction obstruction, ureteral duplication, multicystic kidney, and single umbilical artery.

**Differential Diagnosis.** Kaufman syndrome (oculo-cerebro-facial syndrome), acrofacial dysostosis, and CHARGE association.

**Prognosis.** Aside from the mental handicaps these patients may have, many complications result from upper airway problems as well as vertebral complications.

**Recurrence Risk.** Probably none unless in an autosomal-dominant/autosomal-recessive inheritance.

**Management.** When the diagnosis is recognized in the early stages of gestation, termination of pregnancy may be offered. In the prenatal period, the management will attempt cosmetic improvements.

## References

- Martinelli P, Maruotti GM, Agangi A, et al: Prenatal diagnosis of hemifacial microsomia and ipsilateral cerebellar hypoplasia in a fetus with oculoauriculovertebral spectrum. *Ultrasound Obstet Gynecol* 24:199, 2004.
- Kita D, Munemoto S, Ueno Y, et al: Goldenhar's syndrome associated with occipital meningoencephalocele-case report. *Neurol Med Chir (Tokyo)* 42:354, 2002.
- Witters I, Schreurs J, Van Wing J, et al: Prenatal diagnosis of facial clefting as part of the oculo-auriculo-vertebral spectrum. *Prenat Diagn* 21:62, 2001.
- De Catte L, Laubach M, Legein J, et al: Early prenatal diagnosis of oculoauriculovertebral dysplasia or the Goldenhar syndrome. *Ultrasound Obstet Gynecol* 8:422, 1996.

## HELLP SYNDROME

**Definition.** HELLP syndrome is an acronym for a severe variant of preeclampsia, characterized by **h**emolysis, **e**levated liver enzymes, and **l**ow platelets. This condition is life threatening for both mother and fetus. Sonographic signs of fetal compromise include intrauterine growth restriction, decreased tonus, decreased movement, and abnormal Doppler of the umbilical and cerebral arteries.

**Incidence.** HELLP syndrome affects 2% to 12% of the patients who develop preeclampsia, and white women seem to be more affected than black women.

**Etiology.** HELLP syndrome is a situation specific of pregnancies complicated by severe preeclampsia.

**Recurrence Risk.** Although the risk of recurrence is not precisely known, every patient affected by HELLP syndrome should be followed in a subsequent pregnancy as a patient at increased risk.

**Diagnosis.** The maternal diagnosis is made by laboratory studies (hemolysis, elevated liver enzymes, and thrombocytopenia—platelets below 100,000, which is the most consistent finding) and clinical signs and symptoms (which includes edema, hypertension, nausea, and abdominal pain due to hepatic hemorrhage and rupture). Although it is agreed that hemolysis, liver dysfunction, and thrombocytopenia must be present to make a diagnosis of HELLP syndrome, there is disagreement over the specific biochemical and

hematologic criteria to be used. The criteria specified by Sibai and Martin are often used. Sibai's criteria include hemolysis as evidenced by an abnormal peripheral smear, lactate dehydrogenase greater than 600 IU/L or total bilirubin greater than 1.2 mg/dl; elevated liver enzymes as evidenced by an aspartate transaminase greater than 70 IU/L and platelets less than 100 000/mm<sup>3</sup>. Martin's criteria include hemolysis as evidenced by a falling hematocrit, lactate dehydrogenase greater than 164 IU/L or a bleeding diathesis; elevated liver enzymes as evidenced an aspartate transaminase greater than 48 IU/L and alanine transaminase greater than 24 IU/L and platelets less than 100 000 mm<sup>3</sup>. The fetal findings include intrauterine growth restriction and reduced amniotic fluid volume, which are fetal responses to the chronic process of decreased placental blood supply, resulting from the maternal hypertension. In a more severe situation, with diminished fetal oxygen reserve, signs of distress may be found, such as decreased tonus, movement, respiratory movement, and abnormal Doppler velocimetry. Fetal demise and neonatal death are not uncommon in severe cases.

**Associated Anomalies.** A very important and dangerous condition that may associates with HELLP syndrome is disseminated intravascular coagulation.

**Differential Diagnosis.** Disorders that can result in liver dysfunction or anemia, such as thrombocytopenic purpura,

thrombotic thrombocytopenic purpura, hemolytic uremic syndrome, gallbladder disease, viral hepatitis, and acute fatty liver of pregnancy.

**Prognosis.** The prognosis is variable, according to the severity of both maternal and fetal status. Maternal morbidity and mortality rates are proportionate to the severity of systemic disease, whereas fetal morbidity and mortality rates are gestational-age dependent in the majority of cases.

**Management.** Patients with HELLP should be considered as having severe preeclampsia. Referral to a tertiary center as well as delivery of term pregnancies is recommended. Cases remote from term of pregnancy should be managed conservatively, with intensive monitoring of both maternal and fetal well-being. Delivery should be accomplished as soon as pulmonary maturity is reached.

## References

- Weinstein L: Syndrome of hemolysis, elevated liver enzymes, and low platelet count: a severe consequence of hypertension in pregnancy. *Am J Obstet Gynecol* 142:159, 1982.
- Sibai BM, Taslimi MM, El-Nazer A, et al: Maternal perinatal outcome associated with the syndrome of hemolysis, elevated liver enzymes, and low platelets in severe preeclampsia-eclampsia. *Am J Obstet Gynecol* 155:501, 1986.
- Goodlin RC: Beware the great imitator—severe preeclampsia. *Contemp Obstet Gynecol* 20:215, 1984.
- Fairlie FM, Sibai BM: Hypertensive diseases in pregnancy. In Reece EA, Hobbs JC, Mahoney MJ, Petrie RH (eds): *Medicine of the Fetus & Mother*. Philadelphia, J.B. Lippincott Company, 1992, pp 925–942.
- Van Dam PA, Renier M, Backelandt M, et al: Disseminated intravascular coagulation and the syndrome of hemolysis, elevated liver enzymes, and low platelets in severe preeclampsia. *Obstet Gynecol* 73:97, 1989.
- Matchaba P, Moodley J: Corticosteroids for HELLP syndrome in pregnancy. *Cochrane Database Syst Rev* (1):CD002076, 2004.
- Sibai BM, Ramadan MK, Usta I, et al: Maternal morbidity and mortality in 442 pregnancies with hemolysis, elevated liver enzymes, and low platelets (HELLP syndrome). *Am J Obstet Gynecol* 169:1000, 1993.
- Martin JN Jr, Blake PG, Perry KG, et al: The natural history of HELLP syndrome: patterns of disease progression and regression. *Am J Obstet Gynecol* 164:1500, 1991.

## HEREDITARY LYMPHEDEMA I

**Definition.** Hereditary lymphedema is a rare disease characterized by a firm edema of the lower extremities that can be generalized to the whole leg or limited to feet or toes. It was first described by Milroy in 1828. In general, it is considered to be a benign disorder with mainly cosmetic importance.

**Synonyms.** Nonne-Milroy lymphedema, early-onset lymphedema, primary congenital lymphedema.

True congenital lymphedema, or hereditary lymphedema type I (OMIM 153100), usually presents either at, or soon after, birth and may be associated with other congenital malformations.

Onset of clinical symptoms in hereditary lymphedema type II (OMIM 153200) usually occurs during or near either puberty or the menopause.

In 1962, a case was reported of congenital chylous ascites in an affected infant, whose father had recurrent swelling of the scrotum beginning at the age of 20 years. In 1964, pleural effusion was observed. In 1965, Esterly described one child with a congenital type, which implies an intrinsic abnormality of the lymph-conducting pathways, or a secondary type, which implies that external factors such as radiotherapy, severe infection, or surgical excision have damaged lymph drainage routes. Most forms of primary lymphedema are thought to be caused by a congenital abnormality of the lymphatic system.

**Incidence.** It is estimated to occur with an incidence of approximately 1 in 6,000 newborn. The male-to-female ratio is 1:2 to 3.

**Etiology.** The disease has autosomal-dominant inheritance with incomplete penetrance (80%–84%), variable expressivity

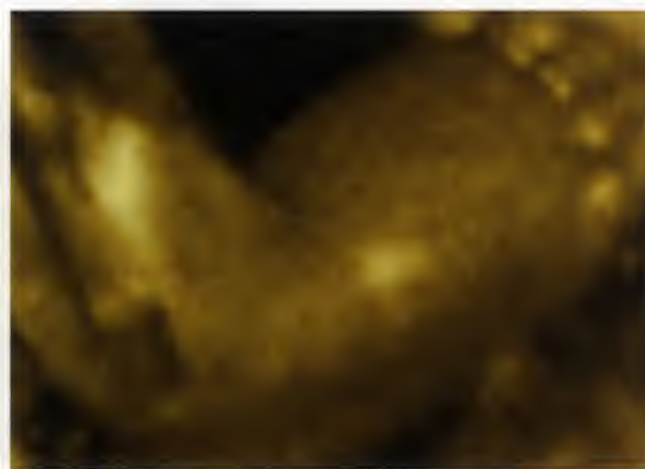


**FIGURE 5-43.** A and B. Two-dimensional and three-dimensional sonograms of a fetus with primary lymphedema demonstrating edema of the lower extremities and feet. (Courtesy of Montse Alegre, 2005, *thefetus.net*.)





**FIGURE 5-44.** Photograph of neonate in Figure 5-43, demonstrating lower extremity edema. (Courtesy of Montse Alegre, 2005, thefetus.net.)

and variable age of onset. These features tend to appear at birth or in infancy.

**Pathogenesis.** All of the anomalies found are due to dysgenesis of lymphatic microvessels. This dysgenesis ranges from mild to severe and even to aplasia of both the lymphatic capillaries and collectors. This condition results from impaired lymph drainage in the presence of normal capillary filtration. It may be either primary in type, which implies an intrinsic abnormality of the lymph-conducting pathways, or secondary in type, which implies that external factors such as radiotherapy, severe infection, or surgical excision have damaged lymph drainage routes. Most forms of primary lymphedema are thought to be caused by a congenital abnormality of the lymphatic system.

**Diagnosis.** This condition is suggested by the finding of isolated edema of the dorsum of feet in the fetus, a normal karyotype, and absence of other significant malformations. The disease has variable expressivity and must be suspected in those fetuses with distal subcutaneous edema of the extremities, most frequently of the lower limbs, but the hands can also be involved. Findings can be present in one extremity or in all of them, and there is no concordance in the time of appearance and degree of involvement of each extremity. Occasionally, persistent or transient pleural effusion and ascites can be found. The rest of the examination is normal. The prenatal diagnosis has been suggested in fetus from 15 weeks of gestation. Chylothorax, ascites, and pericardial effusion have been described in association with the lymphedema.

**Clinical Characteristics.** Lymphedema is present in one or both legs at birth and is painless, nonpitting, with no tendency to ulceration, and no associated varicosities. In the majority of the cases, the lymphedema persists throughout life.

**Genetic Anomalies.** The exact location of the genetic alteration causing the hereditary lymphedema has not been described. However, it has recently been demonstrated that the gene is located to the region 5q34-q35. There is also

evidence that the disorder might be associated with mutations in the FLT4 that encodes the vascular endothelial growth factor receptor-3.

**Differential Diagnosis.** The following dysmorphic syndromes must be considered:

- Turner syndrome.
- Noonan syndrome.
- Lymphedema-distichiasis syndrome (double row of eyelashes).
- Lymphedema and ptosis syndrome.
- Meige lymphedema (hereditary lymphedema type II).
- Congenital recessive type lymphedema.

**Associated Anomalies.** There are reports of associations with distichiasis, hydroceles, atrial septal defect, and characteristic facial changes.

**Prognosis.** Edema, particularly severe below the waist, sometimes complicated with papillomatosis and nail changes. Present in one or both legs, the lymphedema persists throughout life but does not seem to affect longevity. As the patient matures, the overlying skin displays a slightly rosy hue, while the size of the edematous parts remains proportional to the remainder of the body. The morbidity is due to infections. There are few significant complications associated with this disorder. There are case reports of intestinal lymphangiectasia, recurrent septic arthritis, angiosarcoma, and lymphangiosarcoma.

**Management.** If other fetal anomalies are ruled out and fetal karyotype is normal, parental counseling concerning etiology, management, and possible complications is advisable. Several individuals wear compression stockings, which are effective in containing the edema, whereas those who are more severely affected attend hospital for compression pumping to reduce limb size.

## References

- Makhoul IR, Sujov P, Ghanem N, et al: Prenatal diagnosis of Milroy's primary congenital lymphedema. *Prenat Diagn* 22:823, 2002.
- Ferrell RE, Levinson KL, Esmen JH, et al: Hereditary lymphedema: evidence for linkage and genetic heterogeneity. *Hum Mol Genet* 7:2073, 1998.
- Sarda P, Jalaguier J, Montoya F, et al: Hereditary congenital lymphedema with pseudosexual ambiguity. *J Genet Hum* 36:353, 1988.
- Dale RF: Primary lymphoedema when found with distichiasis is of the type defined as bilateral hyperplasia by lymphography. *J Med Genet* 24:170, 1987.
- Fang J, Dagenais SL, Erickson RP, et al: Mutations in FOXC2 (MFH-1), a forkhead family transcription factor, are responsible for the hereditary lymphedema-distichiasis syndrome. *Am J Hum Genet* 67:1382, 2000.
- Herbert FA, Bowen PA: Hereditary late-onset lymphedema with pleural effusion and laryngeal edema. *Arch Intern Med* 143:913, 1983.
- Mucke J, Hoepffner W, Scheersmidt G, et al: Early onset lymphoedema, recessive form—a new form of genetic lymphoedema syndrome. *Eur J Pediatr* 145:195, 1986.
- Evans AL, Brice G, Sotirova V, et al: Mapping of primary congenital lymphedema to the 5q35.3 region. *Am J Hum Genet* 64:547, 1999.
- Irrthum A, Karkkainen MJ, Devriendt K, et al: Congenital hereditary lymphedema caused by a mutation that inactivates VEGFR3 tyrosine kinase. *Am J Hum Genet* 67:295, 2000.
- Karkkainen MJ, Ferrell RE, Lawrence EC, et al: Missense mutations interfere with VEGFR-3 signalling in primary lymphoedema. *Nat Genet* 25:153, 2000.
- Finegold DN, Kimak MA, Lawrence EC, et al: Truncating mutations in FOXC2 cause multiple lymphedema syndromes. *Hum Mol Genet* 10:1185, 2001.



Holberg CJ, Erickson RP, Bernas MJ, et al: Segregation analyses and a genome-wide linkage search confirm genetic heterogeneity and suggest oligogenic inheritance in some Milroy congenital primary lymphedema families. *Am J Med Genet* 98:303, 2001.

Jeltsch M, Kaipainen A, Joukov V, et al: Hyperplasia of lymphatic vessels in VEGF-C transgenic mice. *Science* 276:1423, 1997.

Parsch H, Urbanek A, Wenzel-Hora B: The dermal lymphatics in lymphoedema visualized by indirect lymphography. *Br J Dermatol* 110:431, 1984.

Bollinger A, Isenring G, Franzeck UK, et al: Aplasia of superficial lymphatic capillaries in hereditary and congenital lymphedema (Milroy's disease). *Lymphology* 16:27, 1983.

Pfister G, Saesseli B, Hoffmann U, et al: Diameters of lymphatic capillaries in patients with different forms of primary lymphedema. *Lymphology* 23:140, 1990.

Wheeler ES, Chan V, Wassman R, et al: Familial lymphedema praecox: Meige's disease. *Plast Reconstr Surg* 67:362, 1981.

Mehta SD, Robinson RJ, Bern SA: Pedal manifestations of Milroy's disease. *J Am Podiatr Med Assoc* 86:400, 1996.

Albornoz MA, Myers AR: Recurrent septic arthritis and Milroy's disease. *J Rheumatol* 15:1726, 1988.

Offori TW, Platt CC, Stephens M, et al: Angiosarcoma in congenital hereditary lymphoedema (Milroy's disease)—diagnostic beacons and a review of the literature. *Clin Exp Dermatol* 18:174, 1993.

Brostrom LA, Nilsson U, Kronberg M, et al: Lymphangiosarcoma in chronic hereditary oedema (Milroy's disease). *Ann Chir Gynaecol* 78:320, 1989.

Lev-Sagie A, Hamani Y, Raas-Rothschild A, et al: Prenatal ultrasonographic diagnosis of atypical Nonne-Milroy lymphedema. *Ultrasound Obstet Gynecol* 21:72, 2003.

## HERPES SIMPLEX INFECTION

**Definition.** Prenatal infection by the herpes simplex virus type II, rarely the type I.

**Synonyms.** None.

**Incidence.** Unknown.

**Etiology/Pathogenesis.** Transplacental or transcervical passage of the virus. Almost all neonatal herpes simplex virus infections are the results of a first-episode maternal infection near the time of labor, when the birth occurs before the development of protective maternal antibodies. It is clear that the majority of newborns acquire the virus by contact with infected genital secretions. Because the majority of cases of first episode genital herpes during pregnancy are asymptomatic or unrecognized in 60% to 80% of women, the prevention of neonatal transmission depends on the identification of the herpes simplex virus serologically discordant couple. Herpes simplex type I transforms the HB-I human cell line by association with the human gene for adenylate kinase-1 (on chromosome 9). Women with primary genital herpes simplex infection lesions (symptomatic or asymptomatic) who deliver vaginally have a high risk (33%–50%) of transmitting infection to their neonates. With recurrent disease, the risk of transmission during a vaginal delivery is much lower (<2%–5%).

**Diagnosis.** Growth restriction, microcephaly, hydranencephaly, cerebellar necrosis, chorioretinitis, cataract, and microphthalmia. Hepatosplenomegaly can also be present.

**Genetic Anomalies.** None.

**Associated Anomalies.** Inguinal hernias, aplasia cutis.

**Differential Diagnosis.** Other TORCH infections.

**Recurrence Risk.** Unknown; no siblings have been reported to have been infected.

**Prognosis.** A majority of these babies are born prematurely. Mortality and morbidity rates are high, even though an effective antiviral therapy is now available.

**Management.** Isolation of the virus in amniotic fluid culture does not necessarily mean infection of the fetus. Treatment with acyclovir and vidarabine may be attempted. Studies of acyclovir use among pregnant women suggest that acyclovir treatment orally, near term, reduces the rate of abdominal delivery in women who have frequent recurrences because of a decrease on the incidence of active lesions at delivery. Cesarean delivery is indicated for all women with active genital lesions at the time of the delivery.

**Prevention.** Couples should be educated about the natural history of genital herpes simplex infection. Susceptible pregnant women should avoid sexual contact during the last 6 to 8 weeks of gestation if they partners have active genital infection.

## References

- Nahmias AJ: Neonatal HSV infection Part I: continuing challenges. *Herpes* 11:33, 2004.
- Rouse DJ, Stringer JS: An appraisal of screening for maternal type-specific herpes simplex virus antibodies to prevent neonatal herpes. *Am J Obstet Gynecol* 183:400, 2000.
- Brown ZA: HSV-2 specific serology should be offered routinely to antenatal patients. *Rev Med Virol* 10:141, 2000.

## HOLOPROSENCEPHALY

**Definition.** Holoprosencephaly is a heterogeneous entity of central nervous system anomalies caused by the impaired midline cleavage of the embryonic forebrain. In the most cases, it is associated with midfacial anomalies. Holoprosencephaly is graded according to the severity of the brain's anomaly as alobar, semilobar, and lobar (Table 5–4). In the most severe alobar form, the ventricle is continuous, whereas in the lobar form, an attempt to form occipital horns and abnormal frontal horns is present. Because of a mechanism of reciprocal induction between the brain and the skull, the facial structures are also abnormal. The severity of the facial malformation reflects the severity of the intracranial anomalies.

**Synonyms.** The following are part of the holoprosencephaly complex: arhinencephaly, cebocephaly, ethmocephaly, and cyclopia.

**Incidence.** The incidence is about 6 to 12:10,000 among live-born infants but 40:10,000 in embryos. Half of these are associated with trisomy 13. The sex distribution shows a female predominance.

**Etiology.** Autosomal-dominant, autosomal-recessive, and monogenic inheritance as well as infectious (cytomegalovirus, toxoplasmosis), toxic (hydantoin), and maternal conditions such as gestational diabetes have been reported.

**Pathogenesis.** Failure of sagittal cleavage of the telencephalon that results in the presence of a midline single ventricle with variable degrees of separation. This is probably



due to mutations in the gene for the sonic hedgehog morphogen and genes that encode its downstream intracellular signaling pathway. There is also some evidence for a defect in the cholesterol biosynthesis.

**Diagnosis.** The diagnosis is suggested by numerous findings such as cyclopia, cebocephaly, ethmocephaly, hypotelorism, proboscis; median cleft lip, single ventricular cavity, thalami fusion, absence of median structures, and microcephaly.

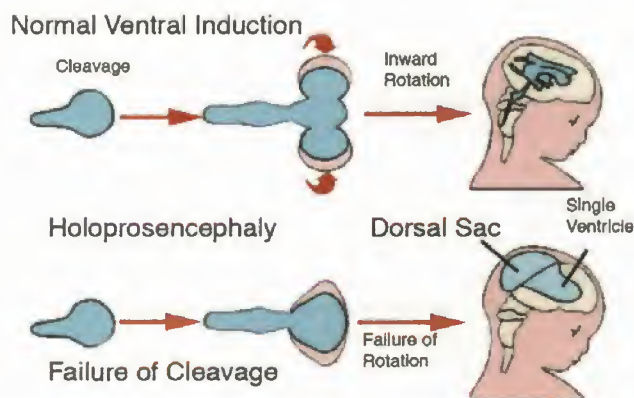


**FIGURE 5-45.** Normal and abnormal brain development leading to holoprosencephaly.



**FIGURE 5-46.** Note the proboscis above the fused eye. (Courtesy of Lenin Montilla, 2004, thefetus.net.)

**Recurrence Risk.** The risk of recurrence depends of the basis for the actual condition, such as chromosome defect or syndrome. Both autosomal-dominant and autosomal-recessive conditions have been described, but incomplete penetrance or an incomplete form or microform can make the interpretations of familial occurrence difficult. The proportion of sporadic cases is estimated to be 68%, with a 6% recurrence rate for sporadic, nonchromosomal forms. In the autosomal-dominant form, the penetrance is estimated as 82% for major types (alobar, semilobar, lobar) and 88% when major and minor types (atypical) were included. Thus, the recurrence risk after an isolated case is 13% for major types and 14% when minor types are included.

**Genetic Anomaly.** Possibly located on the short arm of chromosome 3, the long arm of chromosome 7 or the long arm of chromosome 14.

**Associated Anomalies.** Median cleft lip, proboscis, arhinencephaly, cebocephaly, ethmocephaly, and cyclopia.

**Differential Diagnosis.** The associated aneuploidies (trisomy 13 and 18) should be excluded by karyotype.

**Prognosis.** Depends on the form. The severe forms are usually associated with neonatal death. Some of the mildest form (single front incisor) may have mild to moderate mental retardation and are at risk for pituitary dysfunction.

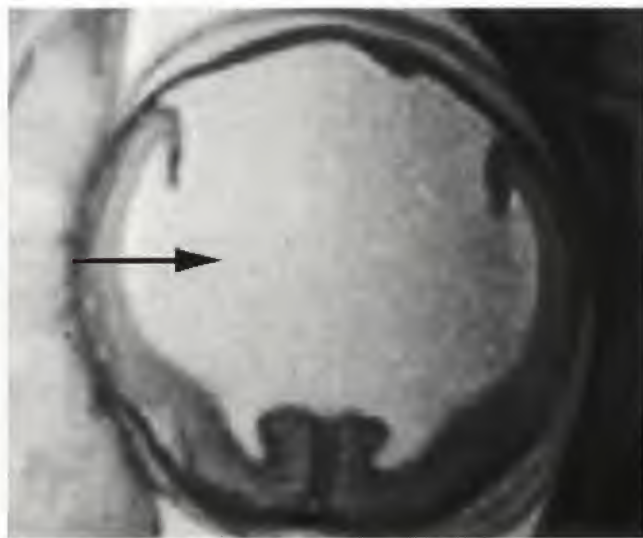


**FIGURE 5-47.** Axial T2 magnetic resonance imaging view of a fetus with alobar holoprosencephaly demonstrating the single common ventricle (arrow). (Courtesy of Heron Werner, 2005, thefetus.net.)

**Table 5-4** Classification of Holoprosencephaly

Findings	Alobar	Semilobar	Lobar
Craniofacial anomaly	Severe	Variable	Mild or absent
Ventricles	Monoventricle	Rudimentary occipital horns	Frontal horns with a rectangular aspect
Septum pellucidum	Absent	Absent	Absent
Falx cerebri	Absent	Partial	Well developed
Interhemispheric fissure	Absent	Partial	Present; some anteroinferior fusion
Thalamus, basal ganglia	Fused	Partially separated	Separated

**Management.** Termination of pregnancy can be offered for the severe cases (semilobar, alobar).

## References

- Blaas HGK, Eriksson AG, Salvesen KA, et al: Brains and faces in holoprosencephaly: pre- and postnatal description of 30 cases. *Ultrasound Obstet Gynecol* 19:24, 2002.
- Odent S, Le Marec B, Munnich A, et al: Segregation analysis in nonsyndromic holoprosencephaly. *Am J Med Genet* 77:139, 1998.
- Parant O, Sarramon MF, Delisle MB, et al: Prenatal diagnosis of holoprosencephaly. A series of twelve cases. *J Gynecol Obstet Biol Reprod (Paris)* 26:687, 1997.
- Ming JE, Roessler E, Muenke M: Human developmental disorders and the Sonic hedgehog pathway. *Mol Med Today* 4:343, 1998.
- Roessler E, Muenke M: Holoprosencephaly: a paradigm for the complex genetics of brain development. *J Inher Metab Dis* 21:481, 1998.
- Lange Y, Steck TL: Four cholesterol-sensing proteins. *Curr Opin Struct Biol* 8:435, 1998.
- Petek E, Kroisel PM, Wagner K: Isolation of a 370 kb YAC fragment spanning a translocation breakpoint at 3p14.1 associated with holoprosencephaly. *Clin Genet* 54:406, 1998.
- Fryns JP: Another holoprosencephaly locus at 7q21.2? *J Med Genet* 35:614, 1998.
- Frints SG, Schrander-Stumpel CT, Schoenmakers EF, et al: Strong variable clinical presentation in 3 patients with 7q terminal deletion. *Genet Couns* 9:5, 1998.
- Vance GH, Nickerson C, Sarnat L, et al: Molecular cytogenetic analysis of patients with holoprosencephaly and structural rearrangements of 7q. *Am J Med Genet* 76:51, 1998.
- Devriendt K, Fryns JP, Chen CP: Holoprosencephaly in deletions of proximal chromosome 14q. *J Med Genet* 35:612, 1998.
- Hall RK, Bankier A, Aldred MJ, et al: Solitary median maxillary central incisor, short stature, choanal atresia/midnasal stenosis (SMMCI) syndrome. *Oral Surg Oral Med Oral Pathol Oral Radiol Endod* 84:651, 1997.

## HOLT-ORAM SYNDROME

**Definition.** The Holt-Oram syndrome consists of congenital heart disease and anomalies of the upper limb (phocomelia (4.5%), radial ray aplasia, triphalangeal thumb, clinodactyly).

**Synonyms.** Heart-hand syndrome. (This syndrome appears genetically distinct from the Heart-hand syndrome types II and III).

**Incidence.** Uncommon.

**Etiology.** Autosomal-dominant inheritance with 100% penetrance and no evidence of reduced fitness. Increasing severity occurs in succeeding generations consistent with anticipation.

**Recurrence Risk.** 50%.

**Diagnosis.** The cardiac lesions include atrial (30%–60%) and ventricular septal defects, patent ductus arteriosus, endocardial cushion defect, hypoplasia of the left ventricle, and conduction disturbances. Seventeen percent have complex cardiac anomalies. The radial ray aplasia varies from a difficult to diagnose triphalangeal thumb to more obvious club hand. The absence of the thumb can also be recognized.



**FIGURE 5-49.** Scan of the left forearm at 24 weeks of gestation. The scan showed the ulna alone. (Courtesy of Fabrice Cullier, 2003, *thefetus.net*.)



**FIGURE 5-48.** Holt-Oram syndrome. Scan of the right forearm made at 22 weeks of gestation. The scan showed a ulna alone with clubbed arm. (Courtesy of Fabrice Cullier, 2003, *thefetus.net*.)





**FIGURE 5-50.** Profile of the left forearm of the fetus at 24 weeks of amenorrhea. The thumb is on the same plane as the fingers and is triphalangeal. (Courtesy of Fabrice Cullier, 2003, *thefetus.net*.)

**Pathogenesis.** Probable cardiomeelic developmental field.

**Genetic Anomaly.** Mutations in two of the T-box genes (TBX5 and TBX3) on chromosome 12q24.1 have been shown to be responsible for the congenital abnormalities associated with Holt-Oram syndrome. TBX5 is only involved in anterior limb development.

**Associated Anomalies.** See definition. A few inconstant anomalies such as renal anomalies have been reported.

**Differential Diagnosis.** The differential diagnosis is usually that of the radial ray aplasia and could include the TAR syndrome, Fanconi anemia, VACTERL association, and the radial ray-choanal atresia.

## HYDROLETHALUS SYNDROME

**Definition.** This syndrome is characterized by multiple developmental defects of fetus such as polydactyly (postaxial in the hands and preaxial in the feet), central nervous system malformations such as hydrocephalus and absent midline structures of the brain, micrognathia, limb anomalies, and several other abnormalities, mostly in the midline structures.

**Synonym.** Salonen-Herva-Norio syndrome.

**Incidence.** Approximately 1 in 20,000. Parents often have some ancestry in an eastern region of Finland, where the syndrome was described for the first time in 1981. Outside of this subgroup, the incidence is very rare.

**Etiology.** Autosomal-recessive lethal malformation syndrome.

**Diagnosis.** The findings of massive hydrocephalus, encephalocele, micrognathia, polydactyly (in particular, a



**FIGURE 5-51.** Profile of the fetus at 24 weeks of amenorrhea. The angulated forearm is seen with the radial ray limb deformation. (Courtesy of Fabrice Cullier, 2003, *thefetus.net*.)

**Prognosis.** Mainly related to the severity of the cardiac and orthopedic handicap.

**Management.** Usually, no alteration of the prenatal care is needed. Great orthopedic progress at pollicization of the index finger to provide opposition have decreased the handicap of some of these children.

## References

- Newbury-Ecob RA, Leanage R, Raeburn JA, et al: Holt-Oram syndrome: a clinical genetic study. *J Med Genet* 33:300, 1996.
- Sletten LJ, Pierpont ME: Variation in severity of cardiac disease in Holt-Oram syndrome. *Am J Med Genet* 65:128, 1996.
- Brons JT, van Geijn HP, Wladimiroff JW, et al: Prenatal ultrasound diagnosis of the Holt-Oram syndrome. *Prenat Diagn* 8:175, 1988.
- Wilson GN: Correlated heart/limb anomalies in Mendelian syndromes provide evidence for a cardiomeelic developmental field. *Am J Med Genet* 76:297, 1998.
- Bonnet D, Terrett J, Pequignot-Viegas E, et al: Gene localisation in 12q12 in Holt-Oram atrio-digital syndrome. *Arch Mal Coeur Vaiss* 88:661, 1995.
- Campbell CE, Casey G, Goodrich K: Genomic structure of TBX2 indicates conservation with distantly related T-box genes. *Mamm Genome* 9:70, 1998.
- Smith J: Brachyury and the T-box genes. *Curr Opin Genet Dev* 7:474, 1997.
- Li QY, Newbury-Ecob RA, Terrett JA, et al: Holt-Oram syndrome is caused by mutations in TBX5, a member of the Brachyury (T) gene family. *Nat Genet* 15:21, 1997.
- Weber M, Wenz W, van Riel A, et al: The Holt-Oram syndrome. Review of the literature and current orthopedic treatment concepts. *Z Orthop Ihre Grenzgeb* 135:368, 1997.

duplicated big toe), syndactyly, cardiac malformation, clubfeet, and polyhydramnios are very suggestive of the diagnosis. Other findings include cleft lip/palate, lung hypoplasia, and endocardial cushion defects. In families in which there has been a previously affected fetus, ultrasound diagnosis can be made in the 11th week of gestation.

**Genetic Anomalies.** It is caused by a missense mutation in a novel gene *HYLS1*.

**Differential Diagnosis.** Other midline malformation syndromes including: Pallister-Hall, Smith-Lemli-Opitz, pseudo-trisomy 13, oro-facial-digital syndrome, some skeletal dysplasias such as the short rib-polydactyly syndromes, and campomelic dysplasia are difficult to distinguish from hydrolethalus. Others include Meckel syndrome, characterized by polydactyly, central nervous system anomalies (cephalocele instead of hydrocephaly), and cystic kidneys;



acrocallosal syndrome, which shows severe mental retardation, agenesis, or hypoplasia of the corpus callosum, polydactyly of fingers and toes, and anencephaly besides other midline defects.

**Prognosis.** Aside from an anecdotal survival of more than a few months, neonatal death is the rule.

**Management.** Termination of pregnancy can be offered before viability. Standard prenatal care is not altered when continuation of the pregnancy is chosen.

## References

- Mee L, Honkala H, Kopra O, et al: Hydroletharus syndrome is caused by a missense mutation in a novel gene HYLS1. *Hum Mol Genet* 14:1475, 2005. Epub Apr 20, 2005.
- Chan BC, Shek TW, Lee CP: First-trimester diagnosis of hydroletharus syndrome in a Chinese family. *Prenat Diagn* 24:587, 2004.
- Shotelersuk V, Punyavoravud V, Phudhichareonrat S, et al: An Asian girl with a 'milder' form of the hydroletharus syndrome. *Clin Dysmorphol* 10:51, 2001.
- Christensen B, Blaas HG, Isaksen CV, et al: Sibs with anencephaly, anophthalmia, clefts, omphalocele, and polydactyly: hydroletharus or acrocallosal syndrome? *Am J Med Genet* 91:231, 2000.
- Visapaa I, Salonen R, Varilo T, et al: Assignment of the locus for hydroletharus syndrome to a highly restricted region on 11q23-25. *Am J Hum Genet* 65:1086, 1999.
- De Ravel TJ, van der Griendt MC, Evan P, et al: Hydroletharus syndrome in a non-Finnish family: confirmation of the entity and early prenatal diagnosis. *Prenat Diagn* 19:279, 1999.
- Norgard M, Yankowitz J, Rhead W, et al: Prenatal ultrasound findings in hydroletharus: continuing difficulties in diagnosis. *Prenat Diagn* 16:173, 1996.

## HYPOPLASTIC LEFT HEART SYNDROME

**Definition.** Hypoplastic left heart syndrome is a congenital cardiac anomaly characterized by the association of a small left ventricle with aortic atresia and mitral hypoplasia or atresia.

**Synonyms.** Aortic atresia.

**Incidence.** Hypoplastic left heart syndrome comprises 10% to 15% of prenatally detected congenital heart diseases, and affects 1.6 per 10,000 live births.

**Etiology.** The etiology of hypoplastic left heart syndrome is not precisely known. Autosomal-recessive, autosomal-dominant, and polygenic inheritance have been suggested. Multifactorial is the more likely form of transmission.

**Recurrence Risk.** The recurrence risk depends on the etiology and varies from 0.5% to 25%, being quoted at around 2% in most of the cases. According to Norwood, the recurrence risk is 4% for those families with one affected child and 25% for those with two or more affected children.

**Diagnosis.** The typical findings seen on four-chamber view include a small, thick-walled and hyperechoic left

ventricle, with weak contractility. Aortic valve atresia, variable degree of hypoplasia of the ascending aorta and poor mitral valve motion are also expected. The presence of an echogenic bundle where the atrioventricular valve should have been is a typical finding of the mitral or tricuspid atresias. In hypoplastic left hearts, the aorta is small or not visible, whereas in hypoplastic right heart the pulmonic artery is hypoplastic or missing. The identification of a small amount of flow (usually only feasible with color Doppler) is important. If the flow is retrograde, the septum is usually intact and the prognosis poor. The presence of antegrade flow signals the presence of a ventricular septal defect.

**Pathogenesis.** Unknown.

**Genetic Anomaly.** A defect at 11q23.3 has been suggested.

**Associated Anomalies.** Aside from the cardiac anomalies (mentioned earlier), extracardiac defects are frequently seen associated with hypoplastic left heart, and the most common are two-vessel cord, craniofacial, gastrointestinal, genitourinary, and central nervous system abnormalities.



**FIGURE 5-52.** Hypoplastic left heart. Four-chamber view. The left ventricle is posterior and to the right of the image. Note how much smaller it is than the right ventricle. There is also a small pericardial effusion in the atrioventricular groove on the right side of the heart.



**FIGURE 5-53.** In the "three-vessel" view the "line-dot-dot" configuration of the pulmonary artery, the ascending aorta and the superior vena cava is incomplete. The hypoplastic ascending aorta is missing between the pulmonary artery and the superior vena cava.



**Differential Diagnosis.** The single ventricles, hypoplastic right ventricles and the severe forms of endocardial cushion defect may all appear similar in the four-chamber view. A careful observation of the position of the atria, atrio-ventricular valves, and great vessels often allows the correct diagnosis.

**Prognosis.** Hypoplastic left heart syndrome is responsible for 25% of cardiac deaths in the first week of life. Almost all of the affected infants die within 6 weeks if they are not treated. Several palliative procedures, including atrial septectomy, banding of the pulmonary artery, and creation of aortopulmonary shunt have been used. Patients undergoing these procedures either died at some time after the operation or have been followed for a very limited period. Thus far, Norwood reconstruction and cardiac transplantation are the most successful techniques, but the success rate is still very limited.

## KLIPPEL-FEIL SYNDROME

**Definition.** Klippel-Feil syndrome first was described by Klippel and Feil in 1975. It is a congenital anomaly characterized by a classic triad including short neck, low posterior hairline, and limited range of motion due to fusion of cervical vertebrae. It now is known that fewer than 50% of patients with congenital defects of the cervical spine have all three signs of this classic triad. Patients with Klippel-Feil syndrome were assigned to one of three types:

- Type I comprises fusion of many cervical and upper thoracic vertebrae into bony blocks.
- Type II has fusion at only one or two vertebrae, and may associate hemivertebrae and fusion of the occipito-atlantoic joint.
- Type III has both cervical fusion and lower thoracic or lumbar fusion.

**Synonyms.** Segmentation syndrome 1.

**Incidence.** It has been estimated that it occurs in approximately 1:40,000 TO 42,000 births, which may be an

**Management.** When the diagnosis is made before viability, the option of pregnancy termination can be offered. After viability, delivery in a tertiary center should be recommended where a cardiovascular team is prepared to undertake surgical care of the infant.

## References

- Alsoufi B, Bennetts J, Verma S, Caldarone CA: New developments in the treatment of hypoplastic left heart syndrome. *Pediatrics* 119:109, 2007.
- Rychik J: Hypoplastic left heart syndrome: from in-utero diagnosis to school age. *Semin Fetal Neonatal Med* 10:553, 2005.
- Tongsong T, Sittiwangkul R, Khunamornpong S, Wanapirak C: Prenatal sonographic features of isolated hypoplastic left heart syndrome. *J Clin Ultrasound* 33:367, 2005.

underestimate because some mild forms may be under-reported. A slight female predominance of approximately 3:2 has been reported.

**Etiopathology.** Anomalies of segmentation of the somites in the 4th to 8th week.

**Diagnosis.** The short neck may be associated with opisthotonos (retroflexion of the head), and the disorganization of the cervical vertebrae is potentially recognizable. It is sometimes associated with ocular malformations, cleft lip and palate and occasional oligodontia in both the primary and permanent dentition, craniofacial asymmetry, maxillary constriction and velopharyngeal insufficiency, persistent trigeminal artery, congenital heart defects and renal (renal agenesis, and genital anomalies. An interesting case of an intramedullary mass thought to be due to this syndrome has also been reported, perhaps due to a maldevelopment of the cervical spine.

**Genetic Anomalies.** Dominant inheritance with reduced penetrance and variable expression of a defective gene on the long arm of chromosome 8 at locus 22.2. Possible role of PAX1 in the pathogenesis of KFS is object of studies. It has



**FIGURE 5-54.** Second trimester sonogram of a fetus with Klippel-Feil syndrome. Persistent retroflexion of the head on the neck should raise suspicion.

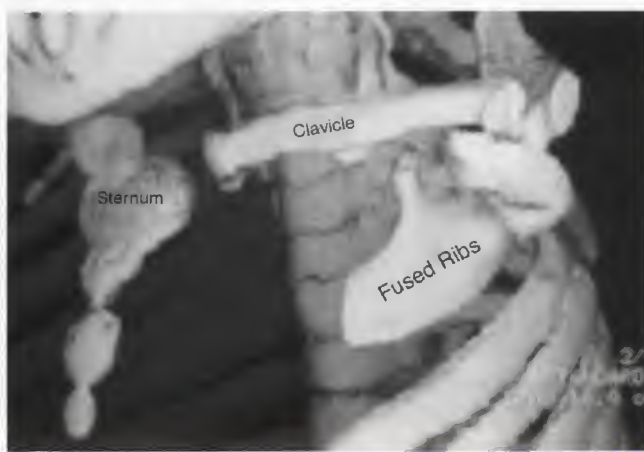


**FIGURE 5-55.** Reformatted computer tomographic scan of a 2-year-old child with Klippel-Feil syndrome. Note the fused ribs. (Courtesy of Ian Suchet, 2002, *thefetus.net*.)



**FIGURE 5-56.** A child with Klippel-Feil syndrome. Note the opisthotonic position, low-set ears, and micrognathia.

been shown that a PAX1 mutant mouse is characterized by vertebral segmentation defects, reminiscent of the human disorder Klippel-Feil syndrome.

**Differential Diagnosis.** Iniencephaly presents with similar opisthotonos but appears more severe (cervical spina

bifida); dyssegmental dysplasia presents with similar vertebral findings but adds short limbs and cephaloceles. It is unclear whether Klippel-Feil syndrome is a discrete entity, or if it is one point on a spectrum of congenital spinal deformities. Only by identifying the link between the genetic etiology and the phenotypic pathological anatomy of the syndrome we'll be able to rationalize the heterogeneity of it.

**Prognosis.** The complications result from the vertebral fusion and include cord compression syndrome, cervical instability, and motility impairment.

**Management.** Termination of pregnancy can be offered before viability. Standard prenatal care is not altered when continuation of the pregnancy is chosen. Confirmation of diagnosis after birth is important for genetic counseling.

## References

- Barbosa V, Maganzini AL, Nieberg LG: Dento-skeletal implications of Klippel-Feil syndrome [a case report]. *N Y State Dent J* 71:48, 2005.
- Erol M, Cakken H, Tan O, et al: Report of a girl with Klippel-Feil syndrome and Poland anomaly. *Genet Couns* 15:469, 2004.
- Dickerman RD, Colle KO, Mitler MA: Intramedullary inflammatory mass dorsal to the Klippel-Feil deformity: error in development or response to an abnormal motion segment? *Spinal Cord* 42:720, 2004.
- Tracy MR, Dormans JP, Kusumi K: Klippel-Feil syndrome: clinical features and current understanding of etiology. *Clin Orthop Relat Res* 424:183, 2004.
- Paksoy Y, Seker M, Kalkan E: Klippel-Feil syndrome associated with persistent urigeminal artery. *Spine* 29:E193, 2004.
- McGaughan JM, Oates A, Donnai D, et al: Mutations in PAX1 may be associated with Klippel-Feil syndrome. *Eur J Hum Genet* 11:468, 2003.
- Klippel M, Feil A: The classic: A case of absence of cervical vertebrae with the thoracic cage rising to the base of the cranium (cervical thoracic cage). *Clin Orthop* 109:3, 1975.
- Tracy MR, Kusumi K: Klippel-Feil syndrome: Clinical features and current understanding of etiology. *Pediatrics* 424:183, 2004.

## KLIPPEL-TRENAUNAY-WEBER SYNDROME

**Definition.** In 1900, Klippel and Trenaunay originally described the entity of limb overgrowth, multiple cutaneous angiomas, and varicose veins, which was confirmed by Parkes-Weber in 1918 and extended by the infrequent finding of arteriovenous fistulae. This syndrome is a rare congenital soft tissue anomaly, with sporadic occurrence, characterized by a triad of multiple hemangiomas, arteriovenous fistulas, and unilateral limb hypertrophy, due to bony and soft tissue overgrowth.

**Synonyms.** Klippel-Trenaunay syndrome; angio-osteohypertrophy syndrome, Parkes-Weber syndrome.

**Incidence.** Rare.

**Etiology.** Happle suggested a predominant inheritance that most satisfactorily explains the findings. Heterozygous individuals for a single gene defect are phenotypically normal. The trait is expressed only when a somatic mutation occurs in the normal allele at an early stage of embryogenesis. The embryo is then a mosaic of homozygous or

heterozygous cell lines for the mutation. This explains the patchy distribution of the defect.

**Pathogenesis.** The exact mechanism causing Klippel-Trenaunay-Weber syndrome is not known. A mesodermal

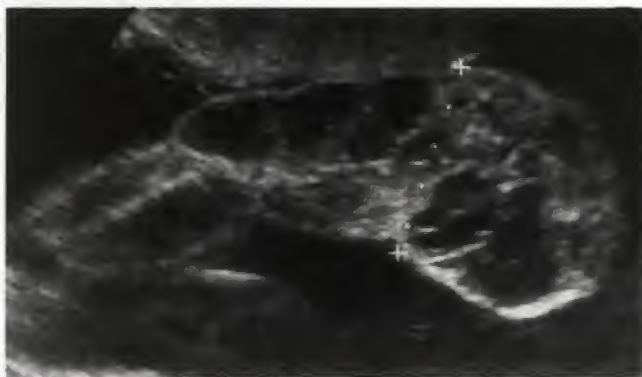


**FIGURE 5-57.** Klippel-Trenaunay-Weber syndrome. Sonogram of the leg of a fetus at 20 weeks' gestation with marked edema. (Courtesy of Carlos Alberto Mejia Escobar, 2000, *thefetus.net*.)



defect affecting angiogenesis and associated with persistence of the embryonic vascular network might explain the vascular anomalies. Others have suggested that a disturbance in the regulation of tissue growth factors is the underlying mechanism.

**Recurrence Risk.** Probably none, although some cases have raised the possibility of autosomal dominance.

**Diagnosis.** May include hydrops fetalis (from high-output cardiac failure) with limbs edema and hypertrophy (more girth than length), ascites, abnormal abdominal hemangiomatous masses, and hepatomegaly. A three-dimensional diagnosis was made recently.

**Genetic Anomaly.** This may be due to a single gene defect on either chromosome 5q or p11.

**Associated Anomalies.** Kasabach-Merritt syndrome of thrombocytopenia due to platelet consumption within the hemangioma, and high-output cardiac failure may complicate the outcome. It is reported also an association with an umbilical cord hemangioma.

**Differential Diagnosis.** Lymphangioma, Proteus syndrome, and fetal thoracic mass (even if color-flow Doppler studies of the mass are negative).

## LARSEN SYNDROME

**Definition.** This syndrome consists of skeletal dysplasia with multiple joint dislocations and short stature and abnormal facial features. There are two forms of the syndrome: a lethal and a nonlethal form. The lethal form is usually fatal due to pulmonary hypoplasia.

**Synonyms.** None.

**Incidence.** It is a rare anomaly with an estimated incidence of 1/100,000 births.

**Etiology.** Both autosomal-dominant and autosomal-recessive patterns of inheritance have been reported.

**Pathogenesis.** Generalized mesenchymal disorder involving connective tissues due to a decreased  $\alpha$ -1/ $\alpha$ -2 chain ratio in type I collagen.

**Diagnosis.** Prenatal diagnosis of Larsen syndrome is difficult and a review of the literature revealed only five previous cases. The abnormal joint with dislocations (hip dislocation, genu recurvatum, clubhands from accessory carpal bones, clubfeet) can be associated with rhizomelic shortening of the upper extremities and with hypoplastic fibula. A coronal cleft in the vertebral body can also be recognized. At the level of the face, a low nasal bridge, frontal bossing, micrognathia, and hypertelorism can be observed. The neurologic defects associated with Larsen syndrome include agenesis of the corpus callosum, hydrocephaly, and hearing defects.

**Associated Anomalies.** Some associated anomalies have also been reported including cleft palate, cervical spine instability, cardiac defects, and pulmonary hypoplasia.

**Genetic Anomalies.** The gene locus is at 3p21.1-p14.1.

**Differential Diagnosis.** It has to be differentiated from the congenital genu recurvatum, arthrogryposis multiplex congenita, Pena-Shokeir phenotype, and cerebro-oculo-facio-skeletal syndrome. In the absence of familial history, these patients are usually identified as having arthrogryposis.

**Prognosis.** When recognized, the tracheomalacia, pulmonary insufficiency, and vertebral instability (cervical kyphosis from marked hypoplasia of one or two vertebral

**Prognosis.** When detected prenatally, the disorder is usually more severe and the prognosis poor when associated with cardiac insufficiency.

**Management.** Termination of pregnancy can be offered in the severe forms; otherwise, no alteration of management is expected. Given the rarity of the disease, there is not enough information available to counsel patients regarding obstetric outcome.

## References

- Yang JI, Kim HS, Ryu HS: Prenatal sonographic diagnosis of Klippel-Trenaunay-Weber syndrome: a case report. *J Reprod Med* 50:291, 2005.
- Rebarber A, Roman AS, Roshan D, et al: Obstetric management of Klippel-Trenaunay syndrome. *Obstet Gynecol* 104:1205, 2004.
- Sahinoglu Z, Uludogan M, Delikara NM: Prenatal sonographic diagnosis of Klippel-Trenaunay-Weber syndrome associated with umbilical cord hemangioma. *Am J Perinatol* 20:1, 2003.
- Heydanus R, Wladimiroff JW, Brandenburg H, et al: Prenatal diagnosis of Klippel-Trenaunay-Weber syndrome: a case report. *Ultrasound Obstet Gynecol* 5:360, 1992.
- Happle R: Mosaicism in human skin. Understanding the patterns and mechanisms. *Arch Dermatol* 129:1460, 1993.



**FIGURE 5-58.** Genu recurvatum in a fetus with Larsen syndrome. (Courtesy Dr. Peter Twining, Nottingham, UK.)

bodies—usually the fourth or fifth cervical vertebra) can be managed to improve the prognosis but probably only for the nonlethal form.

**Management.** Termination of pregnancy can be offered before viability. Standard prenatal care is not altered when continuation of the pregnancy is chosen. Confirmation of diagnosis after birth is important for genetic counseling.

## References

- Shih JC, Peng SS, Hsiao SM, et al: Three-dimensional ultrasound diagnosis of Larsen syndrome with further characterization of neurological sequelae. *Ultrasound Obstet Gynecol* 24:89, 2004.
- Gorincour G, Chotel F, Rudigoz RC, et al: Prenatal diagnosis of congenital genu recurvatum following amniocentesis complicated by leakage. *Ultrasound Obstet Gynecol* 22:643, 2003.



## LETHAL MULTIPLE PTERYGIUM SYNDROME

**Definition.** Massive and early hydrops with cystic hygroma and joint contractions. Pterygium is used to describe webbing of the skin across the joint. The term means "wing-like." Limb pterygia at birth indicate an abnormal developmental process probably occurring in the first trimester and involving reduced mobility of the webbed limb. The severity of the web appears to correlate directly with the degree of hypomobility of the affected joint and with the time in development at which the movement reduction began. This syndrome consists of a constellation of multiple anomalies associated with fetal akinesia sequence and fixation and hypomobility of the joints.

**Incidence.** Unknown but not rare in the first trimester.

**Synonyms.** Lethal contractural syndromes.

**Etiology.** Autosomal-recessive syndrome, with a few cases suggesting an X-linked transmission or a glycogen storage disease type IV.

**Pathogenesis.** The data suggest that the syndrome combines the manifestations of a jugular lymphatic obstruction sequence with those of an early severe fetal akinesia sequence with two possible mechanisms: an abnormally fragile collagen constitution or an early fetal muscular "dystrophy."

**Diagnosis.** In the first trimester, the appearance of a thickened nuchal lucency extending around the whole body and, to a lesser extent, the limbs is characteristic. These fetuses have hydrops and bob along in the fluid when shaken. Occasionally, the diagnosis is not made until later in the pregnancy, at a time when the hypokinesia, the joint contractions, and the multiple pterygia are more visible. Other possible findings are polyhydramnios, craniofacial/ocular anomalies, short forearms of the fetus, pulmonary hypoplasia, diaphragmatic hernia, scoliosis, and fractures.

**Genetic Anomalies.** Unknown.

**Differential Diagnosis.** Some of the severe aneuploidies may also present with hydrops. The arthrogryposes (fetal akinesia sequence), the cerebro-oculo-facio-skeletal syndrome and the Pena-Shokeir syndrome show joint contractions, too, so they should be considered in the differential diagnosis. But the most obvious ultrasound finding in lethal multiple pterygium syndrome is not the contractions but the hydrops. Limited pterygia of the popliteal regions can also be seen in fetuses with caudal regression syndrome. Noonan syndrome also presents with cystic hygroma.



**FIGURE 5-59.** Lethal multiple pterygium syndrome. Photograph of the fetus showing evidence of contracted joints and cystic hygroma.

**Associated Anomalies.** Some vertebral and other bony anomalies may be present.

**Prognosis.** Lethal.

**Management.** Termination of pregnancy can be offered before viability. Standard prenatal care is not altered when continuation of the pregnancy is chosen. Confirmation of diagnosis after birth is important for genetic counseling.

## References

- Cox PM, Bructon LA, Bjelogrić P, et al: Diversity of neuromuscular pathology in lethal multiple pterygium syndrome. *Pediatr Dev Pathol* 6:59, 2003. Epub Nov 7, 2002.
- Sergi C, Poeschl J, Graf M, et al: Restrictive dermopathy: case report, subject review with Kaplan-Meier analysis, and differential diagnosis of the lethal congenital contractural syndromes. *Am J Perinatol* 18:39, 2001.
- Entezami M, Runkel S, Kunze J, et al: Prenatal diagnosis of a lethal multiple pterygium syndrome type II. Case report. *Fetal Diagn Ther* 13:35, 1998.
- Landau D, Mishori-Dery A, Hershkovitz R, et al: A new autosomal recessive congenital contractural syndrome in an Israeli Bedouin kindred. *Am J Med Genet A* 117:37, 2003.

## LISSENCEPHALY

**Definition.** Lissencephaly is a cerebral developmental disorder, with agyria of the brain, which may be accompanied by pachygyria, minimal or no hydrocephalus, a wide cortical mantle, and characteristic dysmorphic features. Miller in 1963 and Dieker in 1969 provided the first descriptions. Lissencephaly is a cerebral developmental disorder with reduced or absent brain gyri, which is caused by disturbed neuronal migration in the neocortex. Two main distinctive types (type I and type II) exist, both with subconditions. Lissencephaly is differentiated in two main groups with subtypes and a third distinctive type:

**LISSENCEPHALY TYPE I.** Characterized by agyria with or without pachygyria, a wide cortical mantle and minimal or no hydrocephalus. Both agyric and pachygyric regions have a four-layer cortex: (1) a molecular layer, (2) an outer cellular layer (true cortex), (3) a cell sparse layer, and (4) a deep cellular layer composed of heterotopic incompletely migrated neurons.

- Miller-Dieker syndrome.
- Norman Roberts syndrome.
- Isolated lissencephaly.

**LISSENCEPHALY TYPE II.** The thickened cortex is disorganized without layering. Vascular bundles and



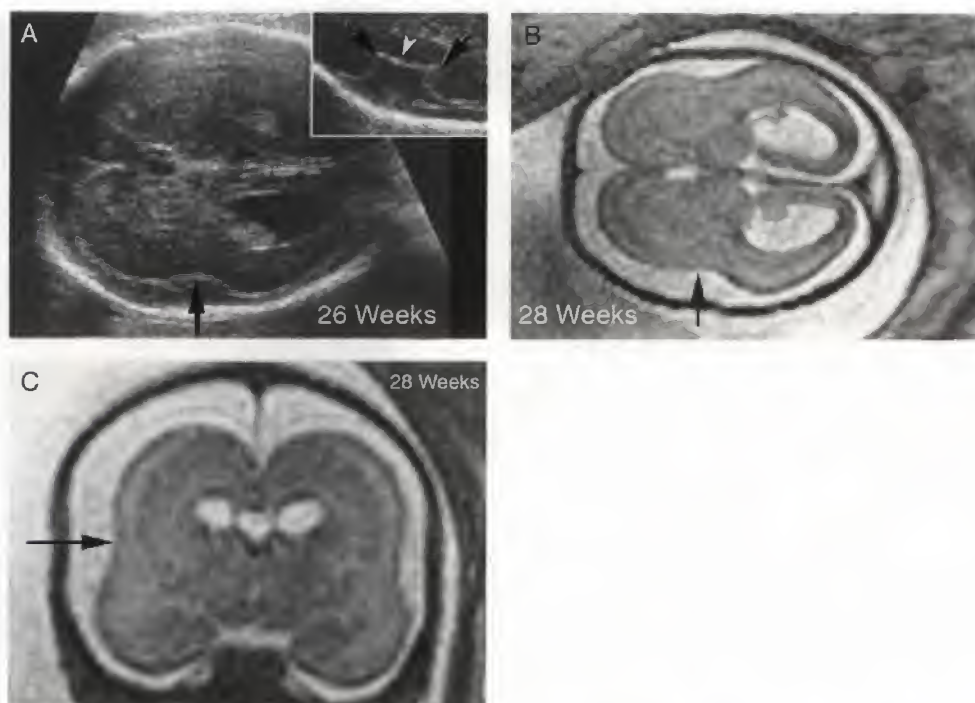


**FIGURE 5-80.** Abnormal Sylvian fissure/insula at 26 weeks. **A.** Axial ultrasound image at 26 weeks in a fetus with lissencephaly associated with Miller-Dieker syndrome shows a shallow, flat Sylvian fissure/insula (arrow) with absence of angularity at the insular margins. Image in the inset shows the expected appearance of the Sylvian fissure/insula in a 26-week normal fetus. Infolding of the operculum should be seen with acute angles (black arrows in inset) at the margins of the insula (white arrowhead in inset) at 24.5 weeks' gestation. **(B)** Axial and **(C)** coronal T2-weighted magnetic resonance images at 28 weeks in the same fetus with Miller-Dieker syndrome showing a shallow Sylvian fissure (arrow). The brain has an hourglass or figure-of-eight appearance on the axial image. Also note the agyria, large subarachnoid space, and mildly dilated occipital horns. (Reproduced with permission from Fong KW, Ghai S, Toi A, et al: Prenatal ultrasound findings of lissencephaly associated with Miller-Dieker syndrome and comparison with pre- and postnatal magnetic resonance imaging. *Ultrasound Obstet Gynecol* 24:716, 2004.)

fibroglial tissue are present in the cortex and subarachnoid space. Lissencephaly type II typically is characterized by hydrocephalus and additional serious central nervous system defects. It is usually part of a syndrome.

- HARD+/-E syndrome.
- COM syndrome.
- Other subtypes.

**NEU-LAXOVA SYNDROME.** Lethal autosomal-recessively inherited disorder consisting of growth restriction, microcephaly, lissencephaly, corpus callosum agenesis, intracranial calcifications, cerebellar hypoplasia, facial dysmorphism, microphthalmia, exophthalmos, cataracts, absent eyelids, hydrops, ichthyosis, contractures of extremities, and syndactyly. A prenatal ultrasound diagnosis was published in 1987, but the sonographic evaluation of central nervous system features was not mentioned.

**Synonyms.** Lissencephaly type I, Miller-Dieker syndrome, chromosome 17p13 syndrome, chromosomal deletion 17p13.

**Prevalence.** Unknown but rare; the male-to-female ratio is 1:2.25.

**Etiology.** Monosomy for the terminal segment of the short arm of chromosome 17, especially band 17p13. It may be discrete.

**Recurrence Risk.** If de novo deletion or translocation occurs, the recurrence risk is low. If the translocation is inherited from one parent (who has a balanced trans-

location), the recurrence risk may be as high as 25%. Affected children will not grow to reproductive age.

**Diagnosis.** Sonographic diagnosis in general is not accomplished earlier than the late second trimester, when the characteristic cerebral anomalies can be noted. The progressive microcephaly and failure of development of both sulci and gyri (which in normal conditions is well defined from 26 to 28 weeks) are suggestive of lissencephaly. The occurrence of polyhydramnios associated with intra-uterine growth restriction is an expected finding for the third trimester. If the condition is severe, polyhydramnios may complicate the diagnosis. Facial dysmorphism is characterized by prominent forehead, short nose, broad and flat nasal bridge, and protuberant upper lip.

**Genetic Anomalies.** Deletion at the 17p13.3 locus.

**Pathogenesis.** Defective neuronal migration with four rather than six layers in the cortex.

**Associated Anomalies.** Duodenal atresia, urinary tract abnormalities, congenital heart defects, cryptorchidism, inguinal hernia, clinodactyly, polydactyly, and ear anomalies may be found.

**Differential Diagnosis.** Isolated lissencephaly sequence, Norman-Roberts syndrome, lissencephaly syndromes type II such as HARD+/-E (Walker-Warburg) syndrome and COM syndrome, and Neu-Laxova syndrome as a third lissencephaly type. All syndromes that may develop microcephaly should be suspected.

**Prognosis.** Usually severe mental retardation affects these patients. Failure to thrive, infantile spasms, and seizures are also expected. The prognosis is poor, and death occurs usually within the first 2 years of life.

**Management.** Karyotyping is recommended to detect the chromosomal defect. Differentiation from lissencephaly type II is important for genetic counseling purposes, considering that type II has an autosomal-recessive pattern of transmission. No causal treatment is available at this time.

## MECKEL SYNDROME

**Definition.** Meckel syndrome is a rare and lethal syndrome characterized by occipital cephalocele, postaxial polydactyly, and dysplastic cystic kidneys. It can be associ-

Usually, the ultrasound diagnosis is made during the third trimester, and termination is not an option. Standard prenatal care is not altered.

## Reference

Ghai S, Fong KW, Toi A, et al: Prenatal US and MR imaging findings of lissencephaly: review of fetal cerebral sulcal development. *Radiographics* 26:389, 2006.



**FIGURE 5-61.** Occipital encephalocele. (Courtesy of Marcos V Sanchez, 2005, *thefetus.net*.)



**FIGURE 5-62.** Meckel's syndrome. Cystic dysplastic kidneys. (Courtesy of Marcos V Sanchez, 2005, *thefetus.net*.)

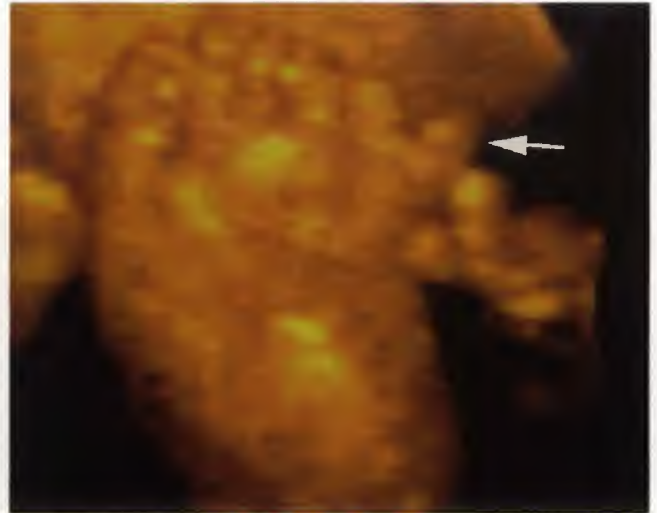


**FIGURE 5-63.** Polydactyly. (Courtesy of Marcos V Sanchez, 2005, *thefetus.net*.)



**FIGURE 5-64.** Photograph of another fetus with Meckel syndrome. Note the small posterior cephalocele, the large abdominal distention due to the bilateral cystic kidneys, and the postaxial polydactyly.



ated with many other conditions, and hepatic fibrosis is one of the most common associations.

**Synonyms.** Dysencephalia splanchnocystica, Meckel syndrome (used in English literature)-this is the preferred appellation and is used by both Medline's Medical Subject Heading and *The Birth Defects Encyclopedia*; Gruber syndrome (used in European literature), Meckel-Gruber syndrome.

**Incidence.** Not precisely known, but authors agree that this is a very rare condition. According to Bergsma, the incidence of Meckel syndrome is 0.2:10,000 live births. Salonen stated that the incidence of Meckel syndrome at birth varies from 0.07 to 0.7:10,000 births. In Finland, the disorder is unusually frequent and reaches 1.1:10,000 births. It is also estimated that this syndrome corresponds to 5% of all neural tube defects.

**Etiology.** Autosomal-recessive inheritance.

**Recurrence Risk.** 25% recurrence risk is involved.

**Genetic Anomalies.** The locus for Meckel syndrome is on chromosome 17, long arm, region 2, bands 1-4. Phenotypic variability and cases that did not have confirmed linkage to 17q suggest that there is some degree of locus heterogeneity.

**Diagnosis.** In 1981, Fraser and Lytwyn suggested that the cystic dysplastic kidneys are a constant anomaly in Meckel syndrome and, therefore, must be present in addition to at least two minor defects to make the diagnosis. This concept is still discussed, and the reported incidence of renal disorder in this syndrome varies from 95% to 100%. Initially, the kidneys develop microscopic cysts that destroy the parenchyma and enlarge the organ up to 10 or 20 times. The syndrome can be confidently detected and diagnosed by sonography at the 11th to 14th gestational week. Unfortunately, the first sonographic finding is often oligohydramnios, which makes the diagnosis more difficult to establish. It is caused by renal dysfunction, and it develops early in the second trimester when the kidneys replace extracellular diffusion as the main source of amniotic fluid. However, some cases of Meckel syndrome have normal amniotic fluid, and thus the presence of normal fluid does not exclude the diagnosis. Sometimes, absence of the bladder can also be recognized. An early sonogram, with normal kidneys, in a family at risk for recurrence, does not exclude Meckel syndrome, and a follow-up at 20 weeks of gestation is recommended.

Occipital cephalocele is present in 60% to 80%. Maternal serum or amniotic fluid-fetoprotein level may be normal, as a membrane may cover the cephalocele. Postaxial polydactyly is present in 55% to 75% of fetuses. Other limb anomalies, such as bowing and shortening, may also be present.

Finding at least two of the three features of the classic triad, in the presence of normal karyotype, makes the diagnosis. There is also a "variant" form of this syndrome that joins the posterior fossa malformation and multicystic kidneys with hepatic fibrosis.

**Differential Diagnosis.** The differential diagnosis will depend on the type of the associated anomalies. Owing to several sonographic similarities between these conditions, trisomy 13 must be excluded by karyotype. Another possible differential diagnosis is autosomal-dominant polycystic kidney disease.

**Associated Anomalies.** The constellation of possible anomalies associated with this syndrome is extensive. In some situations, such a wide phenotypic variation makes the recognition of the disease more difficult.

**Prognosis.** Meckel syndrome is a lethal disorder. Most infants are stillborn or die hours or days after birth. A few sometimes survive a few months with poor quality of life. According to Ramadan, there is one report of a long survivor who died at the age of 28 months. In 1997 Paavola reported another atypical case of a long survivor who died at 18 months of life.

**Management.** A karyotype study should be obtained when Meckel syndrome is suspected in order to exclude chromosomal disorders. If the diagnosis is made before viability, termination can be offered. When the family decides to continue the pregnancy, or if the diagnosis is made after viability, the standard obstetrical management is not altered.

## References

- Nizard J, Bernard JP, Ville Y: Fetal cystic malformations of the posterior fossa in the first trimester of pregnancy. *Fetal Diagn Ther* 20:146, 2005.
- Mittermayer C, Lee A, Brugger PC: Prenatal diagnosis of the Meckel-Gruber syndrome from 11th to 20th gestational week. *Ultraschall Med* 25:275, 2004.

## MONOSOMY X (TURNER) SYNDROME

**Definition.** Chromosomal disorder of female patients, described by Turner in 1938, characterized by the absence of one X sex chromosome (45, XO).

**Synonyms.** Monosomy X, Ullrich-Turner syndrome.

**Incidence.** 2.5 to 5.5:10,000 live-born female infants in the white population. In the Japanese population, it has been estimated to be 7 to 21:10,000 live-born female infants. The incidence in all pregnancies, however, is considered much higher because Turner syndrome accounts for one fourth of the spontaneous abortions caused by chromosomal anomalies.

**Etiology.** The absence of one sex chromosome, in general the paternal chromosome, which occurs sporadically in most cases. Eight to sixteen percent of all cases are

mosaic. Advanced maternal age is not associated with this aneuploidy.

**Pathogenesis.** In general, the cystic hygroma is a large septated cystic mass posterior to the neck, due to a dilatation of the jugular lymphatic sacs. It is caused by a developmental delay in the connection with the venous system, or a primary abnormal dilatation or proliferation of the lymphatic channels interfering with a normal flow between the lymphatic and venous systems.

**Diagnosis.** Cystic hygroma is the most characteristic prenatal feature in this syndrome. Spontaneous remission of the cyst may occur, often resulting in webbing of the neck. Other common findings include lymphedema, in particular of the dorsum of hands and feet, or, in the more severe cases, anasarca, hydrops, short cervical spine, intrauterine growth



**FIGURE 5-65.** Monosomy X. Transverse axial view of the neck demonstrates large septated masses. (Courtesy of P. Jeanty, 1999, *thefetus.net*.)

restriction, short neck, prominent auricles, horseshoe kidney, heart defects (coarctation and bicuspid aortic valve), fetal tachycardia, bone dysplasia, and short stature. Dysgenesis of the ovaries occurs in 90% of cases, causing absent menses and infertility in adult life. Variable degrees of mental and developmental retardation are also frequently seen. Elevated maternal serum  $\beta$  hCG has been reported in association with Turner syndrome.

**Differential Diagnosis.** Head and neck cystic mass, such as cephalocele and meningocele, must be excluded. Often, the angle of junction of the cystic mass with skin can be used in the differential diagnosis. Cystic hygromas that elevate the subcutaneous tissues tend to have a smooth junction angle, whereas cephaloceles that herniate through the skin tend to have an acute angle at their junction. Cystic hygromas may occasionally be present in Robert syndrome, and other autosomal recessive disorders. Chromosomal analysis can exclude these conditions.

**Genetic Anomalies.** Absence or structural abnormalities of one X chromosome, such as deletion of the sex-determining region (XY Yp deletion) or mosaicism (45, X1 46, XX or 45X1 46XY), can also be responsible for this condition.

**Prognosis.** Intrauterine demise occurs in many cases and is generally caused by hydrops, which is the major intra-



**FIGURE 5-66.** The fetus at autopsy. (Courtesy of P. Jeanty, 1999, *thefetus.net*.)

uterine complication. Among survivors, the prognosis depends on the severity of the associated anomalies. Cases of mosaicism tend to have a better prognosis, and in some cases with discrete manifestations, the syndrome remains undiagnosed for years.

**Recurrence Risk.** Considering that Turner syndrome is a sporadic event in the majority of cases, chances of recurrence are extremely low, although not precisely known.

**Management.** A karyotype is recommended when Turner syndrome is suspected. Termination of pregnancy can be offered before viability. After viability, standard prenatal care is not altered.

## References

- Liao AW, Snijders R, Geerts L, et al: Fetal heart rate in chromosomally abnormal fetuses. *Ultrasound Obstet Gynecol* 16:610, 2000.
- Von Kaisenberg CS, Nicolaides KH, Brand-Saberi B: Lymphatic vessel hypoplasia in fetuses with Turner syndrome. *Hum Reprod* 14:823, 1999.

## NOONAN SYNDROME

**Definition.** In 1968, Jacqueline A. Noonan described 19 cases of a syndrome very similar to the disorder described by Turner. Among her patients, 17 had pulmonary stenosis and 2 had patent ductus arteriosus (12 boys and 7 girls). Other anomalies included lymphedema, pterygium coli, deformity of the sternum with precocious closure of sutures resulting in a pectus carinatum superiorly and a pectus excavatum inferiorly, coarctation of the aorta, cryptorchidism, and thrombocytopenia. Aside from this syndrome occurring

in both genders, there is a large phenotypic overlap with Turner syndrome.

**Synonyms.** Turner syndrome with normal XX, pseudo-Turner syndrome, male Turner syndrome, Ullrich syndrome.

**Incidence.** Its prevalence is 4 to 10:10,000 births.

**Etiology.** Autosomal-dominant inheritance with sporadic new mutations.

**Diagnosis.** The initial anomaly most likely to be observed is a posterior nuchal cystic hygroma, which may regress later in the gestation into a nuchal fold redundancy and



pterygium coli. Other fetuses have been suspected because of special facial features (low-set ears, depressed nasal bridge, and large head), congenital heart disease, pleural effusions, renal abnormalities, polyhydramnios, short stature, hydrops and familiar history. Some fetuses have been identified by triple marker screening, too. Congenital heart disease may appear in up to 60% of Noonan syndrome patients. In fact, a cardiac abnormality associated with cervical lymphatic abnormalities may provide the only clues to diagnoses of Noonan syndrome. In the literature, three cases of persistent right umbilical vein with no intrahepatic portion are described associated with Noonan syndrome. In these cases drainage was possible directly into the right atrium, inferior vena cava or inferior vena cava through the iliac vein. Amelioration of early nuchal region findings in a fetus with a normal karyotype and late onset of the more "typical" ultrasonographic changes may limit early prenatal detection. Noonan syndrome is yet diagnosed at birth or during childhood.

**Genetic Anomalies.** X-linked dominant inheritance of either a single mutant gene or a submicroscopic deletion was originally suspected, but now it is recognized that one of the genes for Noonan syndrome is located on chromosome 12 in the 12q24.2-q24.31 region.

**Differential Diagnosis.** Turner syndrome (excluded in boys or otherwise by karyotype) is also unlikely to be

familial, whereas Noonan syndrome has a strong familial predilection; trisomy 21; Escobar syndrome.

**Prognosis.** Fairly normal life expectancy for those without major complications of heart disease. After thoracoamniotic shunting, pleural effusion with hydrops has a 57% survival rate; premature delivery is the leading source of morbidity.

**Management.** Termination of pregnancy can be offered before viability. Standard prenatal care is not altered when continuation of the pregnancy is chosen.

## References

- Joo JG, Beke A, Toth-Pal E, et al: Successful pregnancy in a Noonan syndrome patient after 3 unsuccessful pregnancies from severe fetal hydrops: a case report. *J Reprod Med* 50:373, 2005.
- Piconc O, Benachi A, Mandelbrot L, et al: Thoracoamniotic shunting for fetal pleural effusions with hydrops. *Am J Obstet Gynecol* 191:2047, 2004.
- Bradley E, Kean L, Twining P, et al: Persistent right umbilical vein in a fetus with Noonan's syndrome: a case report. *Ultrasound Obstet Gynecol* 17:76, 2001.
- Achiron R, Heggesh J, Grisaru D, et al: Noonan syndrome: a cryptic condition in early gestation. *Am J Med Genet* 92:159, 2000.
- Nisbet DL, Griffin DR, Chitty LS: Prenatal features of Noonan syndrome. *Prenat Diagn* 19:642, 1999.

## OSTEOGENESIS IMPERFECTA

**Definition.** Heterogeneous group of genetic disorders (classically divided in four types assessed by Sillence: I, II or congenital, III, and IV) characterized by severe bone fragility, leading to abnormal ossification and multiple fractures. The four types are

- *Type I:* does not present prenatal deformities, and the diagnosis is made after birth, when the limb deformities start to develop.
- *Type II:* the most severe form; presents with multiple skeletal malformations, such as bone shortening and angulation due to multiple fractures, demineralization of

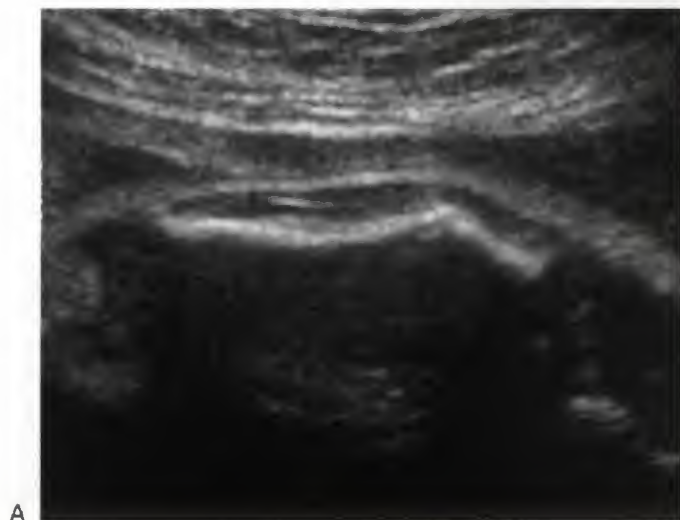


**FIGURE 5-67.** Osteogenesis imperfecta. A and B. Note the fractured femur. (Courtesy of Annette Reuss, 2005, thefetus.net.)

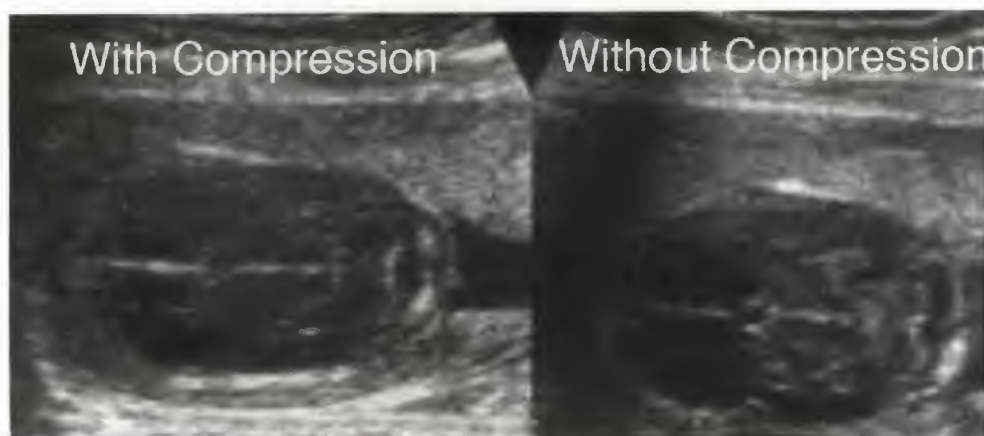


**FIGURE 5-68.** The skull demonstrates markedly decreased echogenicity and is readily compressible even with moderate transducer pressure (*left*).



**FIGURE 5-69.** Frontal x-ray scans of the fetus. Note the poor mineralization and the numerous fractures.

the skull, narrow and bell-shaped chest caused by fractures of the ribs, decreased fetal movement, wrinkling of the surface of the bones due to multiple fractures.

- **Type III:** less severe form than type II, usually presents multiple fractures at birth, with development of progressive bone deformities from neonatal period to adolescence. Detectable as early as second trimester in *type IIIc*.
- **Type IV:** this is the mildest presentation of the disorder, not detectable prenatally. It usually involved premature osteoporosis in the 4th to 5th decades of life.

**Synonyms.** Osteogenesis imperfecta congenital, Van der Hoeve syndrome, Lobstein disease, trias fragilitas osseum, brittle bone disease, and Vrolik disease.

**Incidence.** 0.4:10,000 live births and about half of it (0.19:10,000) represent type II.

**Etiology.** In the majority of the cases of both types I and IV, an autosomal-dominant pattern is involved. Type II is a *de novo* dominant mutation (with a few reports of autosomal recessive pattern), and type III is either autosomal recessive or dominant.

**Recurrence Risk.** Depends on the form of transmission. In general, it ranges from 2% to 5% for type II, if it is not caused by a spontaneous mutation.

**Diagnosis.** The sonographic findings that may be present (in particular in type II) include broad, short, fractured long bones, with a wrinkled appearance caused by callus formation, decreased ossification of the skull, with increased visualization of the intracranial structures, small bell-shaped chest, abnormal skull shape, broad irregular ribs, angulation of the long bones, abnormal face. A typical finding of osteogenesis imperfecta type II is the ability to see both cortices of a bone. Normally, the distal cortex is shadowed by the proximal, but not in the severe demineralization of osteogenesis imperfecta (achondrogenesis and hypophosphatasia may present the same finding). Most of the anomalies can be detected in utero by ultrasound early in the second trimester. A normal ultrasound for a high-risk patient does not exclude the disorder. In general, if the fractures do not occur in utero, the diagnosis is made only after birth.

**Genetic Anomaly.** A disorder in one of the two genes responsible for the type I collagen production (*COL1A1* and *COL1A2*) is the cause of the disease.

**Pathogenesis.** A defect of formation, organization, and chemical composition in type I collagen (which is found in skin, ligaments, tendons, demineralized bone, and dentine) is responsible for decreased mineralization and bone fragility.

**Associated Anomalies.** Kyphoscoliosis, deafness, hypotonia, inguinal hernias, hydrocephalus, hydrops, prenatal grown deficiency.

**Differential Diagnosis.** Hypophosphatasia (infantile form), achondrogenesis, and other short-limbed dwarfisms.



**Prognosis.** Type II osteogenesis imperfecta is uniformly lethal, and the most frequent causes are cerebral hemorrhage and respiratory failure. The other forms develop after birth, progressive deformities of the long bones, and short stature.

**Management.** Owing to the uniformly fatal outcome, termination of pregnancy could be offered at any stage of the gestation when type II is diagnosed. For the other forms, termination could be offered before viability. If continuing the pregnancy is opted for, standard prenatal care should not be altered.

## PALLISTER-KILLIAN SYNDROME

**Definition.** Rare polymalformative complex syndrome characterized by facial dysmorphism, severe mental retardation, and epilepsy.

**Synonyms.** Pallister-Killian syndrome, tetrasomy 12 p, Teschler-Nicola/Killian syndrome.

**Incidence.** Human autosomal tetrasomies are rare. Among them, tetrasomy 12p is undoubtedly the least unusual. It is more common in woman of advanced age.

**Etiology.** Tissue-specific mosaic distribution of an additional isochromosome 12p. The chromosomal abnormality is observed in either a mosaic or a non-mosaic state on selected tissues, such as bone marrow and skin fibroblast. It generally occurs as a mosaic and the pattern intensity varies from one tissue to another. The reference tissue for isochromosome 12p is the skin fibroblast, where the abnormality is most common and clear. All of the cases are sporadic, with only a single preliminary report of recurrence.

**Pathogenesis.** The mechanism of the increased nuchal translucency is unclear. Tetrasomy 12p is not always diagnosed, because the tissues are affected differently. Although it is present in a high percentage of fibroblasts, it is practically absent from the blood. Individuals with Pallister-Killian syndrome are often mosaic of isochromosome 12p, but in some cases, the degree of mosaicism in the chorion villus sample is much lower than that in the fetal tissues subsequently examined. Confined placental mosaicism is a well-recognized phenomenon in a number of chromosomal abnormalities and is said to contribute to their intrauterine survival.

**Diagnosis.** Sonographic findings include facial anomalies as eye defects (hypertelorism), prefrontal edema, flat profile with a small nose and thin lips, but never micrognathia or clefting; fetal hydrops in the first trimester or a thick nuchal fold, pulmonary abnormalities, heart defect, diaphragmatic defects, rhizomelic limb shortening, acral hypoplasia, square hands, syndactyly, polydactyly, urogenital abnormalities, rare acral hypoplasia. Therefore, Palladini thought that the diagnosis of Pallister-Killian syndrome should be considered whenever diaphragmatic hernia and short limbs are detected. In such cases, the detection of the typical profile may contribute to establishing a diagnosis.

**Differential Diagnosis.** It has to be differentiated from Fryns syndrome, chondrodysplasia of Robinow (facial dysmorphism, short limbs and vertebral dysostosis), metabolic disorder (macrosomia, macroglossia), acrocallosal syndrome (preaxial polydactyly along with corpus callosum agenesis), VATER anomaly (with anal imperforation and cardiac malformations).

## References

- Lachman RS, Rappaport V: Fetal imaging in the skeletal dysplasias. *Clin Perinatol* 17:703, 1990.
- Taybi H, Lachman RS: Radiology of syndromes, metabolic disorders, and skeletal dysplasias, 3rd ed. Chicago, Year Book Medical Publishers, 1990, p 761.
- Young ID, Thompson EM, Hall CM, et al: Osteogenesis imperfecta Type IIa: evidence for dominant inheritance. *J Med Genet* 24:386, 1987.



**FIGURE 5-70.** Pallister-Killian syndrome. Postmortem examination demonstrates a flat facial appearance with dysmorphic low-set ears. (Courtesy of Fabrice Cuillier, 2003, thefetus.net.)

**Prognosis.** Phenotypic expression has varied from multiple anomalies resulting in perinatal death to the more characteristic situation of profound mental retardation, coarse facial appearance, pigmentary anomalies, localized alopecia in the temporofrontal area, hypertelorism, and long philtrum. The prognosis is poor. At birth, up-slanting palpebral fissures, a broad nasal bridge, dysmorphic low-set ears, cutaneous edema on the neck and the trunk, and a long philtrum were noted. Tetrasomy 12p is not always diagnosed, because the tissues are differently affected. Although it is present in a high percentage of fibroblasts, it is practically absent from the blood. Less severely affected individuals may present in postnatal life with profound mental retardation, seizures, abnormal skin pigmentation, facial anomalies, and short necks. The psychomotor retardation is extremely severe, and is accompanied by vertebral and joint deformities, with muscular atrophy in older subjects. The blood karyotype is normal. In fibroblast



cultures, the extra chromosome resembles chromosome 20. The appearance of R bands suggests the fusion of two 12p chromosomes.

**Recurrence Risk.** All of the cases of Pallister-Killian syndrome described up to 1997 are sporadic.

**Management.** The diagnosis of Pallister syndrome based on clinical appearance alone is often difficult owing to the broad spectrum of clinical anomalies not specific to this syndrome. When highly suspected on ultrasound examination, prenatal cytogenetic studies are suggested, because survivors are severely mentally retarded. Owing to mosaicism, it is altogether necessary to examine several tissues for the presence of tetrasomy 12p, including circulating lymphocytes in which mosaicism can be low as 1% to 3%, amniocytes, chorionic cells and skin fibroblasts in which mosaicism ranges from 6% to 100%. Fluorescence in situ hybridization is the only accurate way to determine the real distribution of the isochromosome in various tissues. The occurrence of 12p tetrasomy cells decreases with age of the fetus, the mitotic index, and the time the tissues has been in culture.

## PENA-SHOKAIR SYNDROME

**Definition.** Pena-Shokeir syndrome is an inherited disorder characterized by neurogenic arthrogryposis, facial anomalies, pulmonary hypoplasia, and dysmorphic features resulting from fetal akinesia. It was first described by Pena and Shokeir in 1974, and was subsequently included among the phenotypes associated with fetal akinesia deformation sequence.

**Synonyms.** Fetal akinesia/hypokinesia sequence, fetal akinesia deformation sequence, arthrogryposis multiplex congenita with pulmonary hypoplasia.

**Etiology.** Autosomal-recessive inheritance is the most common pattern of transmission. Several descriptions of unusual presentations suggest a heterogenic etiology.

**Recurrence Risk.** The prediction of the recurrence risk is imprecise due to the multifactorial etiology. In most cases, it varies from 0% to 25%.

**Incidence.** Unknown.

**Pathophysiology.** Active fetal movement starts in mid-first trimester and is of major importance for the normal development of the joints and contiguous tissues. Absent or reduced fetal movement leads to stiff joints, pterygia, and abnormal neuromuscular function with decreased fetal swallowing, which causes pulmonary hypoplasia and polyhydramnios.

**Diagnosis.** The combination of abnormal limb position, restrictive fetal movement with reduced or absent response

## References

- Paladini D, Borghese A, Arienzo M, et al: Prospective ultrasound diagnosis of Pallister-Killian syndrome in the second trimester of pregnancy: the importance of the fetal facial profile. *Prenat Diagn* 20:996, 2000.
- Chicca J, Hoffet M, Rousseau O, et al: Pallister-Killian syndrome [(12p)]: First pre-natal diagnosis using cordocentesis in the second trimester confirmed by in situ hybridization. *Clin Genet* 54:294, 1998.
- Langford K, Hodgson S, Sellar M, et al: Pallister-Killian syndrome presenting through nuchal translucency screening for trisomy 21. *Prenat Diagn* 20:670, 2000.
- Gilgenkrantz S, Droulle P, Schweitzer M, et al: Mosaic tetrasomy 12p. *Clin Genet* 28:495, 1985.
- Gadow EC, Lippold S, Serafin E, et al: Prenatal diagnosis and long survival of Fryns' syndrome. *Prenat Diagn* 14:673, 1994.
- Fryns JP: Prenatal diagnosis and long survival of Fryns syndrome. *Prenat Diagn* 15:97, 1995.
- Barthe B, Cohen H, Saada P: Un cas de diagnostic prénatal de syndrome de Fryns. *J Gynecol Obstet Biol Reprod* 24:57, 1995.
- Mathieu M, Piussan C, Thepot F, et al: Collaborative study of mosaic tetrasomy 12p or Pallister-Killian syndrome (ninteen fetuses or children). *Ann Genet* 40:45, 1997.

to acoustic stimulation, growth restriction, polyhydramnios, and pulmonary hypoplasia makes the diagnosis. Low-set malformed ears, hypertelorism, short neck, cleft palate, scalp edema, thoracic deformities, camptodactyly, and micrognathia may also be found. Anomalies less frequently described in association with Pena-Shokeir syndrome include diaphragmatic hernia, gastroschisis, and microcephaly.

**Differential Diagnosis.** Trisomy 18 may present features that overlap with Pena-Shokeir syndrome, in particular craniofacial, limb, and intrathoracic abnormalities. Karyotype analysis makes the differential diagnosis. Nonlethal forms of arthrogryposis present the same set of findings, except for the pulmonary hypoplasia.

**Prognosis.** Pena-Shokeir is a lethal condition. A significant number of the affected fetuses are born prematurely. Of those born at term, 30% are stillborn. Among the survivors, the majority die within a few weeks of life. Pulmonary complication is the main cause of death.

**Management.** Termination of pregnancy can be offered before viability. Standard prenatal care should be changed throughout the pregnancy only for maternal indications.

## Reference

- Paladini D, Tartaglione A, Agangi A, et al: Pena-Shokeir phenotype with variable onset in three consecutive pregnancies. *Ultrasound Obstet Gynecol* 17:163, 2001.

## PENTALOGY OF CANTRELL

**Definition.** This congenital disorder described by Cantrell is characterized by two major defects: ectopia cordis and an abdominal wall defect (most commonly an omphalocele, but gastroschisis can also be present). The other three defects of the pentalogy are disruption of all the interposing structures: the distal sternum, anterior diaphragm, and diaphragmatic pericardium. Variants of the classic form, such as incomplete expressions, have also been reported. It was first described by Cantrell in 1958, and the syndrome occurs sporadically, with variable degrees of expression.

**Synonyms.** Thoracoabdominal ectopia cordis, ectopia cordis; Cantrell-Heller-Ravitch syndrome; pentalogy syndrome; peritoneopericardial diaphragmatic hernia.

**Incidence.** Very rare. Approximately 90 cases have been reported in the literature, and even fewer have had the complete syndrome confirmed.

**Etiology.** Unknown. Sometimes it can be associated with chromosomal abnormalities.

**Diagnosis.** Presence of complete disruption of the anterior chest and abdominal wall, causing the five defects described by Cantrell, is the classic form and may be





**FIGURE 5-71.** Sonogram of an embryo at 10 weeks' gestation with pentalogy of Cantrell. (Courtesy of Fernando Maia, 2005, *thefetus.net*.)



**FIGURE 5-72.** Color Doppler sonogram in the same patient with pentalogy of Cantrell. (Courtesy of Fernando Maia, 2005, *thefetus.net*.)

detected as early as mid-second trimester. The typical finding of cardiac activity outside the chest in association with an omphalocele makes the diagnosis. Karyotype analysis is recommended to exclude chromosomal anomalies. Ascites and pleural effusion may occur due to compression of the contents of both chest and abdomen.

**Genetic Anomalies.** Unknown.

**Pathogenesis.** Developmental failure of a segment of the lateral mesoderm between 14 and 18 days after conception, resulting in failure of ventral wall closure and incomplete external primordial bands fusion.

**Associated Anomalies.** Intracardiac anomalies (i.e., tetralogy of Fallot, ventricular septal defect) are the rule. Others include cranial and facial anomalies, hydrocephalus, anencephaly, chromosomal abnormalities, malrotation of the colon, cystic hygroma, dysplastic kidney, and clubfeet.



**FIGURE 5-73.** Postmortem view of a fetus with pentalogy of Cantrell. (Courtesy of Heron Werner, 2005, *thefetus.net*.)

**Differential Diagnosis.** Isolated thoracic cardiac ectopy, ectopia cordis associated with amniotic band syndrome, body-stalk abnormality, isolated omphalocele, Beckwith-Wiedemann syndrome, chromosomal abnormalities.

**Prognosis.** Survival is rare and depends on the size of the abdominal wall defect, extent of the cardiac defect, and presence of associated anomalies. Rare milder forms may be corrected surgically. Cases presenting a complete extrusion of heart and abdominal contents have an extremely poor prognosis.

**Recurrence Risk.** Unknown. No recurrence has been recorded. One set of monozygotic twins concordant for the syndrome has been reported.

**Management.** Termination of pregnancy can be offered before viability. After viability, periodic ultrasonographic evaluation of the lesions, fetal growth, and delivery in a tertiary center are recommended. After delivery, repair of the omphalocele should not be delayed. Repair of the sternal, diaphragmatic, and pericardial defects can be attempted at the same time. Surgical correction is often difficult secondary to hypoplasia of the thoracic cage and inability to enclose the ectopic heart. Some affected infants have respiratory insufficiency secondary to pulmonary hypoplasia. Recognition and treatment of any intracardiac anomaly is important because congenital heart disease is a source of major morbidity in infants surviving the neonatal period.

## Reference

- Pollio F, Sica C, Pacilio N, et al: Pentalogy of Cantrell: first trimester prenatal diagnosis and association with multicystic dysplastic kidney. *Minerva Ginecol* 55:363, 2003.



## PFEIFFER SYNDROME

**Definition.** The Pfeiffer syndrome is characterized by bilateral coronal craniosynostosis, midface hypoplasia and syndactyly of hands and feet, and congenitally enlarged thumbs. It was originally described in eight persons from three generations by Pfeiffer in 1964. It is divided in three clinical subtypes, with diagnostic and prognostic implications:

- Type I. Classic appearance with craniosynostosis, broad thumbs, syndactyly, and normal intelligence. This form is compatible with life. It has generally good outcome.
- Type II. Cloverleaf skull, ocular proptosis, broad thumbs, variable visceral anomalies, elbow ankylosis, and severe compromise of the central nervous system. Usually results in early death.
- Type III. Craniosynostosis, severe ocular proptosis without cloverleaf skull, elbow ankylosis, and variable visceral anomalies. Affected fetuses have severe neurologic compromise, with poor prognosis and early death.

**Synonyms.** Acrocephalosyndactyly type 5

**Incidence.** Unknown. Since the first description was done, approximately 30 cases have been reported.

**Etiology.** Type I: autosomal-dominant or fresh mutations. Types II and III: sporadic

**Recurrence Risk.** Variable, depending on the etiology. When the transmission has an autosomal-dominant pattern, the recurrence risk is 50%. If caused by fresh mutations, the risk of recurrence is very low.

**Diagnosis.** Sonographic signs of Pfeiffer syndrome include craniofacial anomalies (brachycephaly, acrocephaly, craniosynostosis of the coronal suture, hypertelorism, small nose, and low nasal bridge) and hands and feet anomalies

(partial syndactyly of second and third fingers and second, third, and fourth toes, broad thumb, and big toe).

**Genetic Anomalies.** Pfeiffer syndrome is genetically heterogeneous. Some cases are linked to mutations at the fibroblastic growth factor receptor 1 (*FGFR1*) gene at chromosome 8p11.22-p12. Mutations at the *FGFR2* gene, which map at chromosome 10q25-q26, were also reported. An exclusive paternal origin of a de novo mutation, associated with advanced paternal age, has been described in Pfeiffer syndrome.

**Associated Anomalies.** Choanal atresia, tracheomalacia and bronchomalacia, cloverleaf skull, fused vertebra, Arnold-Chiari malformation, hydrocephalus, and imperforate anus. After birth, seizures and mental retardation may develop.

**Differential Diagnosis.** The main differential diagnosis includes the syndromes that are characterized by craniosynostosis (Apert, Carpenter, Crouzon, kleeblattschädel anomaly, and thanatophoric dysplasia).

**Prognosis.** The prognosis depends on the severity of associated anomalies, mainly on the severity of the central nervous system compromise. Type I has in general a good prognosis. Types II and III are not compatible with life, and death occurs early.

**Management.** Termination of pregnancy can be offered before viability. If continuation of the pregnancy is chosen, periodic sonographic evaluation of the anomalies (central nervous system anomalies in particular) is recommended.

## Reference

Nazarro A, Monica MD, Lonardo F, et al: Prenatal ultrasound diagnosis of a case of Pfeiffer syndrome without cloverleaf skull and review of the literature. *Prenatal Diagn* 24:918, 2004.

## PIERRE ROBIN SYNDROME

**Definition.** The Pierre Robin syndrome is a rare malformation that consists of micrognathia, glossoptosis, and a cleft palate.

**Synonyms.** Cleft palate-micrognathia-glossoptosis, Pierre Robin sequence, Robin anomalad.

**Incidence.** 1:8500 live births.

**Etiology.** Autosomal-recessive inheritance, with a few X-linked cases. Some authors suggested a prenatal and neonatal brain stem dysfunction as a neuroembryological hypothesis to explain the onset of some cases of Pierre Robin sequence.

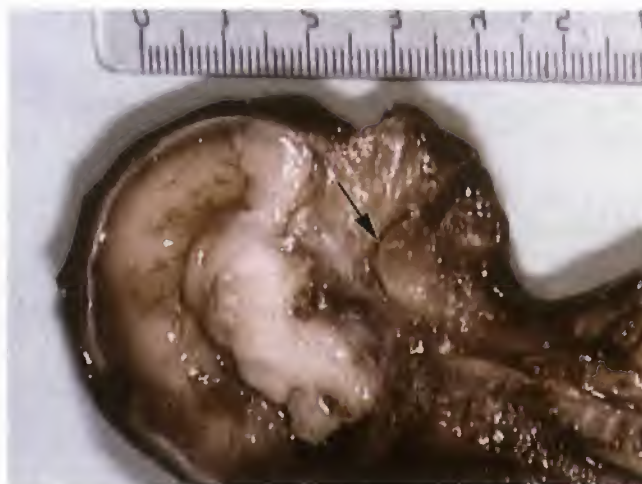


**FIGURE 5-74.** Pierre Robin syndrome. A. Normal autopsy. The tongue (arrow) occupies the anterior part of the mouth and free airway as compared with (B). B. Glossoptosis (arrow) and "no tongue" in the anterior space of the mouth.



**Diagnosis.** The easiest method to establish the diagnosis is to obtain a sagittal section of the face, in which the micrognathia is most visible. Three-dimensional multiplanar imaging increases the likelihood to analyze a true midline sagittal view of the facial profile. Another important clue is often the polyhydramnios resulting from the failure to swallow properly due to the macro-retroglossia. Other findings can be oro-digestive and cardiorespiratory functional disorders.

**Genetic Anomalies.** Unknown (this is a heterogeneous group of conditions).

**Differential Diagnosis.** The agnathia-microstomiasynotia syndrome (otocephaly) resembles a severe form of Pierre Robin syndrome. Other causes of micrognathia include trisomy 13, trisomy 18 and the cerebro-costo-mandibular syndrome characterized by Pierre-Robin anomaly, multiple rib defects and occasional occurrence of intellectual impairment.

**Associated Anomalies.** May be associated with trisomy 18, Stickler syndrome, and other syndromes. Cardiac abnormalities were also commonly detected with an incidence approaching 20%.

## POLAND SYNDROME

**Definition.** Poland syndrome consists of a congenital unilateral absence or hypoplasia of the pectoralis muscle, most frequently involving the sternocostal portion of the pectoralis major muscle, and a variable degree of ipsilateral hand and digit anomalies, including symbrachydactyly. Ipsilateral aplasia of the breast exists in females. Dextrocardia has been reported in several cases.

**Synonyms.** Poland-Moebius syndrome, subclavian artery supply disruption sequence.

**Incidence.** The incidence, reported by different authors, ranges from 1:10,000 to 1:100,000. It is observed more frequently in males than in females; the right side of the body is affected more often than the left.

**Etiology.** The etiology of this syndrome is still discussed. Most of the cases are sporadic, but a familial incidence is described, too. Genetic causes, vascular compromise in the subclavian arteries during early stages of embryogenesis, and teratogenic effects of environmental xenobiotics (cigarette smoking by pregnant women) are different etiologic factors considered.

**Diagnosis.** The chest asymmetry and symbrachydactyly can be recognized, but the long bones are probably too normal to be recognized.

## PRADER-WILLI SYNDROME

**Definition.** Complex, multisystem disorder that affects the central nervous system, with a predilection for the hypothalamus.

**Synonyms.** Prader-Labhart-Willi syndrome.

**Etiology.** It can be considered an autosomal-dominant disorder and is caused by deletion or disruption of a gene or several genes on the paternal chromosomal 15q11-q13 region, or a maternal uniparental disomy (maternal UPD15/mUPD15) of chromosome 15 with normal karyotype (because the genes on the maternal chromosome 15 are virtually

**Prognosis.** Upper airway obstruction, neonatal respiratory distress and feeding problems.

**Management.** Termination of pregnancy can be offered before viability. Standard prenatal care is not altered when continuation of the pregnancy is chosen. Antenatal recognition is important because it allows the pediatrician to provide immediate assistance for the infant. It is a neonatal emergency because the tongue may obstruct the airways and lead to suffocation. Confirmation of diagnosis after birth is important for genetic counseling.

## References

- James PA, Aftimos S: Familial cerebro-costo-mandibular syndrome: a case with unusual prenatal findings and review. *Clin Dysmorphol* 12:63, 2003.
- Lee W, McNie B, Chaiworapongsa T, et al: Three-dimensional ultrasonographic presentation of micrognathia. *J Ultrasound Med* 21:775, 2002.
- Abadie V, Morisseau-Durand MP, Beyler C, et al: Brainstem dysfunction: a possible neuroembryological pathogenesis of isolated Pierre Robin sequence. *Eur J Pediatr* 161:275, 2002.
- Hsieh YY, Chang, CC, Tsai HD, et al: The prenatal diagnosis of Pierre-Robin sequence. *Prenat Diagn* 19:567, 1999.

**Genetic Anomalies.** Not established.

**Differential Diagnosis.** Differential diagnosis in the fetus is limited to those conditions characterized by body asymmetry, such as congenital hemidysplasia with ichthyosiform erythroderma and limb defects (CHILD) syndrome, and to the cluster of anomalies caused by the occurrence of thoracic hemivertebrae, such as chest asymmetry and rib hypoplasia. However, in cases of isolated thoracic hemivertebrae, upper limb malformations are usually absent. The real problem is represented by CHILD syndrome.

**Prognosis.** Aside from the anomalies of the extremity, the prognosis is excellent.

**Management.** Standard prenatal care is not altered. Confirmation of diagnosis after birth is important for genetic counseling.

## References

- Paladino D, D'Armiento MR, Martinelli P: Prenatal ultrasound diagnosis of Poland syndrome. *Obstet Gynecol* 104:1156, 2004.
- Slezak R, Sasiadek M: Poland's syndrome. *Pol Merkuriusz Lek* 9:568, 2000.

inactive through imprinting), or an imprinting center mutation. A small cytogenetic subset of these patients have a so-called small supernumerary marker chromosome (sSMC). The vast majority of fetuses with Prader-Willi syndrome occur sporadically. Deletions account for 70% to 80% of cases; the majority are interstitial deletions, many of which can be visualized by prometaphase banding examination. A minority consist of unbalanced translocations, mostly de novo, which are easily detected by routine chromosome examination. The remainder of cases are the result of maternal uniparental disomy. In most of these latter cases,



cytogenetic examinations yield normal results. However, in a few cases, either balanced translocations, familial or de novo, or supernumerary small marker chromosomes, are observed.

**Diagnosis.** Ultrasound examination may reveal polyhydramnios, decreased fetal movements, malpresentation, characteristic craniofacial features, large biparietal diameter of the fetus, slightly enlarged lateral ventricles, hypoplasia of the corpus callosum, abnormal fetal heart rhythm with prolonged inactive periods and diurnal variation of the incidence of heart rate accelerations, and hypoplastic male external genitalia without intrauterine growth restriction.

**Differential Diagnosis.** Angelman syndrome.

**Prognosis.** The clinical picture manifestation in Prader-Willi syndrome is variable, and depends on the age of the affected child. It is characterized by diminished fetal activity, obesity, muscular hypotonia, mental retardation, short stature, small hands and feet, and hypogonadotropic hypogonadism. The neonate is often profoundly hypotonic, can often present with asphyxia and absence of crying. In addition, there is mild prenatal growth restriction, hyporeflexia, poor feeding due to diminished swallowing and sucking reflexes. Cryptorchidism occurs with hypoplastic penis and scrotum in boys and hypoplastic labiae in girls. Often, the most prominent features such as obesity, mental retardation and behavioral disorders do not become evident until later childhood, which can lead to underdiagnosis or late diagnosis in early childhood. Generally the feeding difficulties improve by the age of 6 months. From 12 to 18 months onward, hyperphagia causes major somatic and psychologic problems. Diminished growth is observed in the majority of infants. Small hands with delicate and tapering fingers and small feet (acromicria) are seen in most infants and adolescents; hand and foot sizes correlate well with length, but not with age, and foot size tends to be smaller than hand size. The face is characterized by a narrow bifrontal diameter, almond-shaped eyes (often in mild upslanted position), strabismus, full cheeks, and diminished mimic activity due to muscular hypotonia. Plethoric obesity becomes the most striking feature. From the age of about 6 years onward, many children present scars from scratching due to itching, and later, almost all show abdominal striae. Depigmentation relative to the familial background is a feature in about three quarters of the patients.

**Recurrence Risk.** Kennerknecht (1992) estimated an overall recurrence risk of 0.4%. However, if two or more siblings are affected, he estimated that the risk to the next sibling would be 50%. This syndrome usually occurs de novo with a very low recurrence risk. However, in rare cases, familial translocations are observed, giving rise to a high recurrence risk.

**Management.** In a karyotypically normal fetus with ambiguous male external genitalia and cerebral anomalies, extensive cytogenetic and molecular biology studies are strongly recommended because of risk of this syndrome. Candidates for prenatal diagnosis of Prader-Willi syndrome are fetuses of pregnancies in which a reduced activity is observed. Because of the long-term implications of this

syndrome, it is important to recognize its features as soon as possible so that early counseling of parents and the affected child is possible and also a prevention of the complications in both pregnancy and labour.

## References

- Prader-Willi syndrome, Online Mendelian Inheritance in Man <http://www.ncbi.nlm.nih.gov/entrez/dispomim.cgi?id=176270> #176270
- Schinkel A: Approaches to the prenatal diagnosis of the Prader-Willi syndrome. (Letter.) *Hum Genet* 74:327, 1986.
- Cassidy SB, Lai L-W, Erickson RP, et al: Trisomy 15 with loss of the paternal 15 as a cause of Prader-Willi syndrome due to maternal disomy. *Am J Hum Genet* 51:701, 1992.
- Purvis-Smith SG, Saville T, Manass S, et al: Uniparental disomy 15 resulting from 'correction' of an initial trisomy 15. (Letter.) *Am J Hum Genet* 50:1348, 1992.
- Hall JG: Genomic imprinting and its clinical implications. (Editorial.) *N Engl J Med* 326:827, 1992.
- Stephenson JBP: Prader-Willi syndrome: neonatal presentation and later development. *Dev Med Child Neurol* 22:792, 1980.
- Chitayat D, Davis EB, McGillivray BC, et al: Perinatal and first year follow-up of patients with Prader-Willi syndrome: normal size of hands and feet. *Clin Genet* 35:161, 1989.
- Butler MG, Meaney FJ: An anthropometric study of 38 individuals with Prader-Labhart-Willi syndrome. *Am J Med Genet* 26: 445, 1987.
- Gunay-Aygun M, Schwartz S, Heeger S, et al: The changing purpose of Prader-Willi syndrome clinical diagnostic criteria and proposed revised criteria. *Pediatrics* 108:e92, 2001. Note: epub.
- Kennerknecht I: Differentiated recurrence risk estimations in the Prader-Willi syndrome. *Clin Genet* 41:303, 1992.
- Haqq AM, Stadler DD, Rosenfeld RG, et al: Circulating ghrelin levels are suppressed by meals and octreotide therapy in children with Prader-Willi syndrome. *J Clin Endocrinol Metab* 88:3573, 2003.
- Carrel AL, Myers SE, Whitman BY, et al: Growth hormone improves body composition, fat utilization, physical strength and agility, and growth in Prader-Willi syndrome: a controlled study. *J Pediatr* 134:215, 1999.
- Delparigi A, Tschop M, Heiman ML, et al: High circulating ghrelin: a potential cause for hyperphagia and obesity in Prader-Willi syndrome. *J Clin Endocrinol Metab* 87:5461, 2002.
- Flori E, Biancalana V, Girard-Lemaire F, et al: Difficulties of genetic counseling and prenatal diagnosis in a consanguineous couple segregating for the same translocation (14;15) (q11;q13) and at risk for Prader-Willi and Angelman syndromes. *Eur J Hum Genet* 12:181, 2004.
- Liehr T, Brude E, Gillessen-Kaesbach G, et al: Prader-Willi syndrome with a karyotype 47,XY,+min(15)(pter->q11.1:) and maternal UPD 15—case report plus review of similar cases. *Eur J Med Genet* 48:175, 2005. Epub Feb 17, 2005.
- L'Hermine AC, Aboura A, Brisset S, et al: Fetal phenotype of Prader-Willi syndrome due to maternal disomy for chromosome 15. *Prenat Diagn* 23:938, 2003.
- Fong BF, De Vries JI: Obstetric aspects of the Prader-Willi syndrome. *Ultrasound Obstet Gynecol* 21:389, 2003.
- Eggermann T, Zerres K, Eggermann K, et al: Uniparental disomy: clinical indications for testing in growth retardation. *Eur J Pediatr* 161:305, 2002. Epub Apr 26, 2002.
- Eiholzer U, Schlumpf M, Nordmann Y, et al: Early manifestations of Prader-Willi syndrome: influence of growth hormone. *J Pediatr Endocrinol Metab* 14:1441, 2001.
- Hiroi H, Kozuma S, Hayashi N, et al: A fetus with Prader-Willi syndrome showing normal diurnal rhythm and abnormal ultradian rhythm on heart rate monitoring. *Fetal Diagn Ther* 15:304, 2000.
- Szpecht-Potocka A: Molecular analysis in Prader-Willi syndrome diagnosis. *Med Wieku Rozwoj* 3:407, 1999.
- Glenn CC, Deng G, Michaelis RC, et al: DNA methylation analysis with respect to prenatal diagnosis of the Angelman and Prader-Willi syndromes and imprinting. *Prenat Diagn* 20:300, 2000.



## PRUNE-BELLY SYNDROME

**Definition.** Prune-belly syndrome is a rare congenital disorder, more common in boys, consisting of deficiency of abdominal wall muscles (absent or hypoplastic), cryptorchidism, and genitourinary malformations.

**Synonym.** Eagle-Barrett syndrome.

**Etiology.** Many theories have been proposed to explain the pathogenesis of this anomaly. The first one proposes that prune-belly syndrome occurs as an abnormal mesodermal development. The developmental arrest of the mesodermal elements would lead to severe abdominal laxity and defective development of the urinary tract. The second theory is that this condition is a result of the urethral obstruction malformation complex. It proposes that pressure atrophy of the abdominal wall muscles occurs when urethral obstruction leads to massive distention of the bladder and ureters. Bladder distention would also interfere with descent of the testes and, thus, be responsible for the bilateral cryptorchidism. The mechanism responsible for the urinary tract dilatation and distention is a flap valve mechanism that results from a hypoplasia of the stromal and epithelial elements of the prostatic urethra. The hypoplasia of these elements leads to an underlying weakness and subsequent sacculation of the prostatic urethra. The last theory is that this is a genetic defect on the basis of the predominance in male fetuses and few familial cases.

**Incidence.** 0.25 to 0.3:10,000 live births, almost exclusively in male fetuses (male-to-female ratio 20:1). The higher incidence of this syndrome in male fetuses has been explained on the basis of the more complex morphogenesis of the male urethra, possibly resulting in obstructive anomalies at several levels.

**Diagnosis.** The diagnosis should be suspected in fetuses with very large abdominal masses. These are, most typically, bladder obstruction caused by urethral valves, urethral agenesis, but also other abdominal masses such as an ovarian cyst. When the etiology is urethral obstruction, oligo-

hydramnios with consequent pulmonary hypoplasia and urinary ascites may result. Usually, the oligohydramnios makes the detection of cryptorchidism impossible. Other findings may be Potter facies, pulmonary hypoplasia, gastric dilatation, short bowel, microileum, microcolon, malrotation of the intestines, imperforate anus, arthrogryposis and club-foot. Additional information can be gained by addition three-dimensional ultrasonography scanning and could be useful for more efficient counseling and therapeutic planning.

**Differential Diagnosis.** Urinary tract anomalies such as megacystis, megaureter, urethral obstruction, and primary vesicourethral reflux are differential diagnoses. Neurogenic bladder and megacystis, microcolon, intestinal hypoperistalsis syndrome may also be considered, although the latter presents with normal amniotic fluid.

**Prognosis.** The prognosis depends on the degree of renal function compromise. Outcome is typically good in cases of prune-belly syndrome with normal amniotic fluid volume. The early urinary obstruction, present in the majority of cases, leads to renal failure, pulmonary hypoplasia, and death in the neonatal period. More than 60% of infants die in the first week of life. Early decompression of severe bladder obstruction improves the prognosis. Fetuses that develop mild urinary tract distention have better prognosis. Mild hydronephrosis and megalourethra may be the only manifestations in these cases.

**Recurrence Risk.** Unknown, but low. A familial occurrence has been seen in some affected patients, suggestive of an X-linked inheritance. A multifactorial, or polygenic, inheritance has also been proposed.

**Management.** Sonographic monitoring of the urinary tract and amniotic fluid volume is required throughout the pregnancy. When early or severe distention of the urinary tract is observed, a vesicoamniotic shunts with vesical decompression and correction of the amniotic fluid levels has been proposed to improve renal and pulmonary function. Anatomic abnormalities that warrant consideration

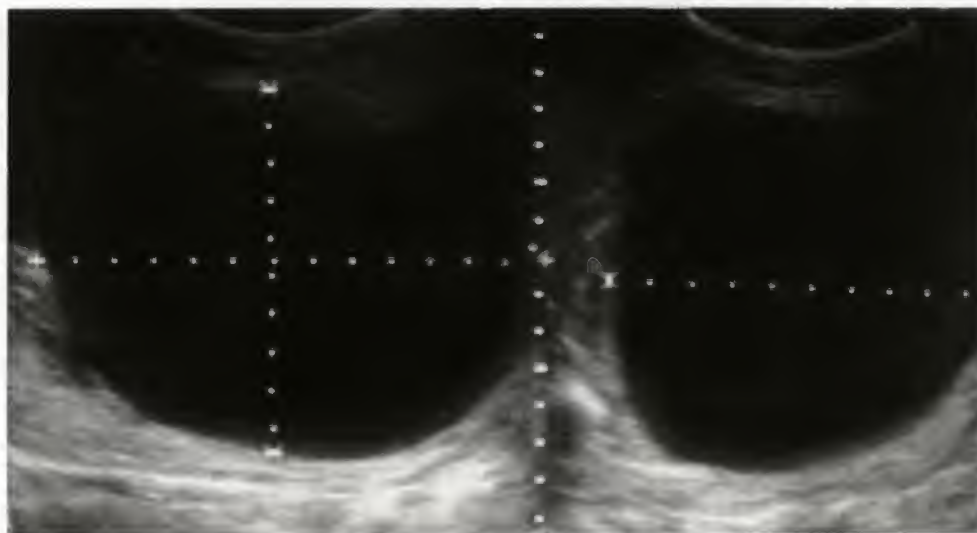
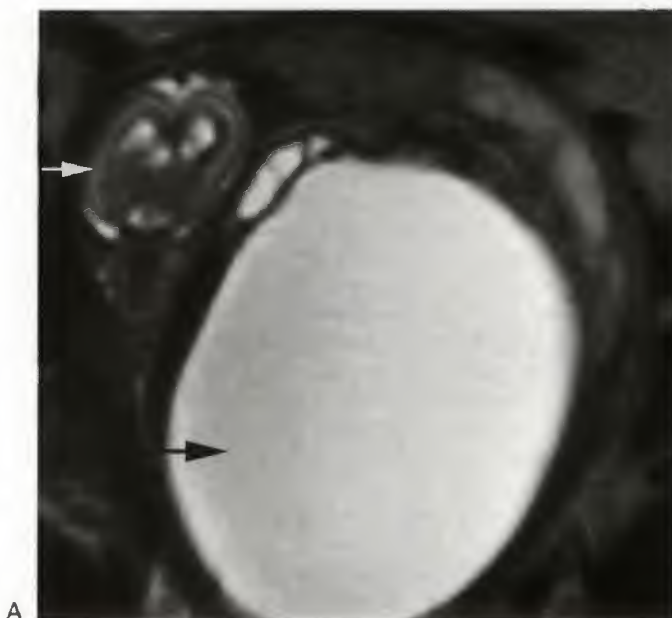
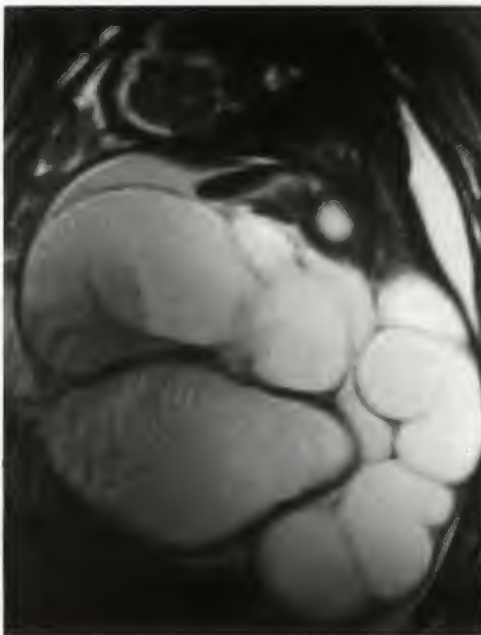


**FIGURE 5-75.** Prune-belly syndrome. Ultrasound demonstrating a markedly dilated urinary bladder (25 weeks). (Courtesy of Heron Werner, 2005, *thefetus.net*.)



A



B

**FIGURE 5-76.** A. Sagittal T2 magnetic resonance imaging scan demonstrating high signal from a markedly dilated urinary bladder (black arrow). Note the size discrepancy of the fetal head (white arrow) at 26 weeks' gestation. B. Coronal T2 magnetic resonance imaging scan demonstrating marked dilatation of the fetal ureter. (A and B courtesy of Heron Werner, 2005, *thefetus.net*.)

of correction are those that interfere with critical fetal organ development. Experimental evidence suggests that fetal urinary tract obstruction, whether intermittent or persistent, can lead to renal dysplasia, which is often irreversible, even



**FIGURE 5-77.** Postmortem neonatal photograph demonstrating a markedly enlarged abdomen with redundant skin. (Courtesy of Heron Werner, 2005, *thefetus.net*.)

if the obstruction is relieved immediately after birth. The percutaneous placement of an indwelling catheter for urinary diversion is one possible therapy. Urinary tract decompression in the early second trimester is desirable to reduce the potential for ongoing damage to the developing kidneys. The benefits of such therapy remain controversial and are yet to be evaluated in a prospective, randomized fashion. As such, urinary diversion should be considered on a case-by-case basis. Additionally, correction of severe oligohydramnios as early as possible should reduce the possibility of pulmonary hypoplasia. Abdominal wall reconstruction for both aesthetics and function is often necessary. Because 75% of individuals with prune-belly syndrome have extra-urinary anomalies, a thorough evaluation, especially cardiac, should be performed.

## References

- Salihu HM, Tchuenguem G, Aliyu MH, et al: Prune belly syndrome and associated malformations. A 13-year experience from a developing country. *West Indian Med J* 52:281, 2003.
- Perez-Brayfield MR, Gatti J, Berkman S, et al: In utero intervention in a patient with prune-belly syndrome and severe urethral hypoplasia. *Urology* 57:1178, 2001.
- Bonilla-Musoles F, Machado LE, Bailao LA, et al: Abdominal wall defects: two- versus three-dimensional ultrasonographic diagnosis. *J Ultrasound Med* 20:379, 2001.
- Leeners B, Sauer I, Schefels J, et al: Prune-belly syndrome: therapeutic options including in utero placement of a vesicoamniotic shunt. *J Clin Ultrasound* 28:500, 2000.
- Leeners B, Sauer I, Funk A: Prune belly syndrome—diagnosis and therapeutic possibilities. *Z Geburtshilfe Neonatol* 203:183, 1999.
- Chen CP, Wang TY, Chuang CY: Sonographic findings in a fetus with megacystis-microcolon-intestinal hypoperistalsis syndrome. *J Clin Ultrasound* 26:217, 1998.
- Hoshino T, Ihara Y, Shirane H, Ota T: Prenatal diagnosis of prune belly syndrome at 12 weeks of pregnancy: case report and review of the literature. *Ultrasound Obstet Gynecol* 12:362, 1998.



## ROBERTS SYNDROME

**Definition.** Roberts syndrome is a rare genetic developmental disorder, characterized by multiple malformations, in particular symmetrical limb abnormality, craniofacial anomalies, and severe mental and growth restriction. It was initially described by Roberts in 1919, and more recently reviewed by Appelt. Herrmann described in 1974, cases of a very similar entity called pseudothalidomide or SC syndrome (SC were the initials of the two families that were originally described). Presently Roberts syndrome and SC phocomelia are considered a single genetic entity, with a wide phenotypic variation.

**Synonyms.** Pseudothalidomide syndrome, tetraamelia syndrome.

**Prevalence.** Unknown.

**Etiology.** This disorder has an autosomal-recessive transmission with marked variability of phenotypic expression. The disease locus was assigned to chromosome 17q21. The unique cytogenetic abnormality, called premature centromere separation, which disrupts the process of chromatid pairing, is responsible for the development of multiple structural anomalies found in Roberts syndrome.

**Recurrence Risk.** The recurrence risk for couples with positive family history is 25%.

**Diagnosis.** The presence of craniofacial anomalies such as midfacial clefts (lip and palate), hypertelorism with prominent eyes and corneal clouding, nose and ear anomalies, prominent premaxilla, micrognathia, midfacial capillary hemangiomas, microcephaly, curly silvery blond hair, symmetric limb abnormality (that range from tetraphocomelia to less serious limb reduction and affect more severely the upper limbs than the lower, and severe mental and growth retardation are very suggestive of Roberts syndrome. Less common findings include oligodactyly, oligohydramnios, heart defects (in particular atrial septal defect and patent ductus arteriosus), diaphragmatic defect, agenesis of the spleen, and adrenal glands, gastrointestinal abnormalities (obstructions), renal anomalies (polycystic or dysplastic kidneys), cryptorchidism, enlarged phallus (compared to rest of the body), hypoplasia of the pelvis, malformed uterus, atresia of the urethra, vagina, and anus.

Sonographic detection of those features is highly indicative of Roberts syndrome. Clinical findings and cytogenetic studies make the diagnosis after birth.

**Genetic Anomaly.** Cytogenic analysis of fetal cells, obtained from chorionic villus sampling in the first trimester, or amniocentesis or cordocentesis during the second and third trimesters, is required to confirm the diagnosis prenatally. The presence of premature centromere separation makes the diagnosis. One negative cytogenetic analysis does not exclude Roberts syndrome. A second analysis using a different type of fetal tissue is required.

**Prognosis.** Most patients born at term with less than 37 cm of birth length and severe facial and limb defects have been stillborn or have died early in childhood. Patients born with more than 37 cm of birth length and less severe defects have better prognosis but the survivors have grown abnormalities and severe mental deficiency. However, survival beyond the infancy is infrequent.

**Management.** When detected before viability, termination of pregnancy can be offered. After viability, standard obstetrical management is not altered. For those families previously affected, chorionic villi sample for cytogenetic studies during the first trimester must be offered.

## References

- Roberts JB: A child with double cleft of lip and palate, protrusion of the intermaxillary portion of the upper jaw and imperfect development of the bones of the four extremities. *Ann Surg* 70:252, 1919.
- Appelt H, Gerken H, Lenz W: Tetraphokomelie mit Lippen-Kiefer-Gaumenspalte und Clitorishypertrophie - Ein Syndrom. *Paediatr Paedol* 2:119, 1966.
- Jones KL, Roberts-SC: Phocomelia in Smith's Recognizable Patterns of Human Malformation. Philadelphia, WB Saunders Company, 1997. pp 298-299.
- German J, Roberts syndrome 1. Cytological evidence for a disturbance in chromatid pairing. *Clin Genet* 16:441, 1979.
- Robins DB, Ladda RL, Thieme GA, et al: Prenatal detection of Roberts-SC Phocomelia syndrome: Report of 2 sibs with characteristic manifestations. *Am J Med Genet* 32:390, 1989.
- Süoui S, Privitera O, Brambati B, et al: First-trimester prenatal diagnosis of Roberts syndrome. *Prenat Diagn* 12:145, 1992.
- Palladini D, Palmieri S, Lecora M, et al: Prenatal ultrasound diagnosis of Roberts syndrome in a family with negative history. *Ultrasound Obstet Gynecol* 7:208, 1996.

## SEPTO-OPTIC DYSPLASIA

**Definition.** Septo-optic dysplasia is a syndrome characterized by anomalies of cerebral midline structures, such as absence of the septum pellucidum, congenital optic nerve dysplasia, and panhypopituitarism, leading to multiple endocrine defects (diabetes insipidus, hypogonadotropic hypogonadism, hypothyroidism, adrenal insufficiency, abnormal thyrotropin releasing hormone test, gonadotropin releasing hormone test, and gonadotropin hormone-releasing hormone). Septo-optic dysplasia may represent a mild form of holoprosencephaly.

**Synonym.** Morsier syndrome

**Incidence.** Unknown but rare.

**Etiopathology.** Although a vascular disruption sequence has been postulated, more recent genetic anomalies seem to explain the findings (see genetic anomalies later). A possible mendelian (autosomal-recessive) inheritance has also been

postulated. Also, illicit drug use may play a causative role in brain development anomalies. In addition, intrauterine exposure to valproic acid has been associated with an increased risk of central nervous system abnormalities, primarily neural tube defects.

### Clinical Findings.

- Central nervous system: seizures, mental retardation, atrophy of the optic nerve, dilatation of the suprasellar cistern, empty sella, cortical atrophy and dystrophic corpus callosum, and anterior cephaloceles have also been described.
- Face: hypotelorism, microphthalmia, visual impairment with nystagmus, unilateral or bilateral disk hypoplasia with double rim appearance (choroidal pigment in the outer margin and pale nerve tissue in the inner), variable visual loss, coloboma, strabismus, astigmatism, bilateral cleft lip and palate, high arched palate and flat nasal bridge.



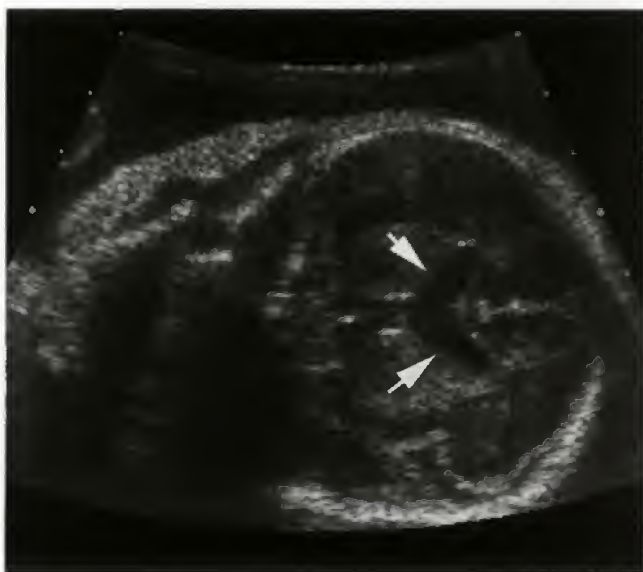


**FIGURE 5-78.** Second trimester sonogram of the fetal head in a patient with septo-optic dysplasia. Absence of the septum pellucidum and communication of the frontal horns of the lateral ventricles (arrows) is seen.

- Endocrine system: low growth rate and short stature. The most common problem is growth hormone deficiency (93%), followed by adrenocorticotrophic hormone deficiency (57%), hypothyroidism (53%), and diabetes, and gonadotropin deficiency. Hypothalamic dysfunction is the basic origin of these endocrine abnormalities. Septo-optic dysplasia is responsible for approximately 4% of all growth hormone deficiencies in children.

**Diagnosis.** Absence of the septum pellucidum is probably the most typical finding. Sometimes, the standard sonographic views of the brain, obtained along the axial planes at midgestation, can fail to identify this absence. It can be explained by the close proximity of the walls of the lateral ventricles, normal in size that could generate an

artifact resembling a normal cavum septum pellucidum. The magnetic resonance demonstration of hypoplastic optic tracts can allow one to make the diagnosis definitively. Hypotelorism, enlarged cerebral ventricles, communicating lateral ventricles, and bilateral cleft lip and palate have also been recognized prenatally.

**Genetic Anomalies.** Mutations of the homeobox gene *HESX1* is suggested as the etiologic cause at least in a subset of patients. An Arg53Cys missense mutation was found in two children within the *HESX1* homeodomain, which destroyed its ability to bind target DNA. Mice that are deficient of the *HESX1* homeobox gene present with neural defects similar to those of septo-optic dysplasia.

**Differential Diagnosis.** Several variants with associated schizencephaly, dysgenesis of the corpus callosum, or microphthalmos, as well as incomplete forms, have been described. Lobar holoprosencephaly may also resemble septo-optic dysplasia.

**Recurrence Risk.** Unknown.

**Prognosis.** The variable degree of mental deficit (from minimal to severe) as well as the presence of multiple endocrine dysfunctions affects the prognosis for each infant. Prevention of hyperthermia (in case of fever), dehydration (fever and diabetes insipidus), and other endocrine dysfunctions should be searched and corrected.

**Management.** Termination of pregnancy can be offered before viability. Standard prenatal care is not altered when continuation of the pregnancy is chosen. Confirmation of diagnosis after birth is important for genetic counseling. Prevention of recurrent hypoglycemic episodes, seizures, and hormonal imbalances may improve the overall prognosis.

## References

- Pilu G, Tani G, Carletti A, et al: Difficult early sonographic diagnosis of absence of the fetal septum pellucidum. *Ultrasound Obstet Gynecol* 25:70, 2005.
- Orrico A, Galli L, Zappella M, et al: Septo-optic dysplasia with digital anomalies associated with maternal multidrug abuse during pregnancy. *Eur J Neurol* 9:679, 2002.
- McMahon CL, Braddock SR: Septo-optic dysplasia as a manifestation of valproic acid embryopathy. *Teratology* 64:83, 2001.

## SIMPSON-GOLABI-BEHMEL SYNDROME

**Definition.** Simpson-Golabi-Behmel syndrome is characterized by a pre- and postnatal overgrowth, a characteristic facial appearance, a high risk for the development of embryonal tumors, and a spectrum of congenital malformations (visceral and skeletal) that overlap those of other overgrowth syndromes.

**Synonyms.** Bulldog syndrome, dysplasia gigantism syndrome, X-linked, Dgsx Golabi-Rosen syndrome, Simpson dysmorphia syndrome, encephalo-tropho-schisis syndrome.

**Etiology.** By Simpson (in 1975) and Behmel (in 1984) who first described this condition.

**Prevalence.** Unknown.

**Etiology.** X-linked syndrome characterized by either deletions or point mutations within the glypican-3 (*GPC3*) gene at Xq26, one member of a multigene family encoding for at least six distinct glycosylphosphatidylinositol-linked cell surface heparan sulfate proteoglycans. Occasionally, these deletions also include the glypican-4 gene (*GPC4*). Not

all individuals with SGBS have demonstrated disruptions of the *GPC3* locus, which raises the possibility that other loci on the X chromosome could be responsible for some cases of this syndrome.

**Diagnosis.** An ultrasound screening can find.

- Characteristic "coarse" face with hypertelorism, a short broad upturned nose, a wide mouth, a straight facial profile with incompetence of the lips, midline groove of tongue, macroglossia, malposition of teeth, submucous cleft, malocclusion, cleft palate, a large maxilla and mandible, a large inferior face height, large anterior cranial base, sometimes also odontogenic keratocysts.
- Macrosomia.
- Skeletal anomalies such as finger hypoplasia, a congenital abnormality of the proximal phalanx, postaxial polydactyly, broad hands, hypoplastic index finger nails.
- Visceral and congenital anomalies such as pulmonar stenosis, heart defects, and severe tachyarrhythmias.



- Diaphragmatic hernia, gastrointestinal malformations, visceromegaly, pyloric stenosis, splenomegaly, large dysplastic kidneys;
- Congenital midline defects such as agenesis of the corpus callosum

Elevated maternal serum alpha-fetoprotein is also present.

**Differential Diagnosis.** Beckwith-Wiedemann syndrome, Sotos' syndrome, Lysosomal diseases, and other syndromes with overgrowth.

**Associated Anomalies.** Wilms tumor, nephroblastomatosis, hepatoblastoma, hepatocellular carcinoma, neuroblastoma, hemangioma.

**Prognosis.** The clinical manifestations of the syndrome are broad, varying from very mild forms in carrier women to infantile lethal forms in affected men. The affected newborns may manifest, besides the findings reported earlier and already revealed by ultrasound, an obstructive sleep apnea syndrome, mental retardation ranging from normal to mildly retarded, tall stature, generalized muscular hypotonia, increased risk for cardiac arrhythmias and for development of embryonal tumors such as neuroblastoma and Wilms' tumor in early childhood. Ambiguous genitalia (micropenis and perineoscrotal hypospadias with cryptorchidism) and supernumerary nipples are also reported. Cardiac defects and conduction disturbances are major components of the syndrome and can be responsible for death in early infancy and perhaps for cardiac arrest in the adult.

**Recurrence Risk.** Unknown.

**Management.** Depends on the predominant associated anomalies. Termination of pregnancy can be offered before viability. If continuation of the pregnancy is chosen, periodic monitoring of fetal growth and evaluation of the structural defects are recommended.

## References

- Yamashita H, Yasuhi I, Ishimaru T, et al: A case of nondiabetic macrosomia with Simpson-Golabi-Behmel syndrome: antenatal sonographic findings. *Fetal Diagn Ther* 10:134, 1995.
- Hughes-Benzie RM, Tolmie JL, McNay M, et al: Simpson-Golabi-Behmel syndrome: disproportionate fetal overgrowth and elevated maternal serum alpha-fetoprotein. *Prenat Diagn* 14:313, 1994.
- Day R, Fryer A: Index finger abnormalities in Simpson-Golabi-Behmel syndrome. *Clin Dysmorphol* 14:35, 2005.
- Paludetti G, Zampino G, Della Marca G, et al: The tongue-base suspension using Repose bone screw system in a child with Simpson-Golabi-Behmel syndrome. Case report. *Int J Pediatr Otorhinolaryngol* 67:1143, 2003.
- Gillan TL, Hughes R, Godbout R, et al: The Simpson-Golabi-Behmel gene, GPC3, is not involved in sporadic Wilms tumorigenesis. *Am J Med Genet A* 122:30, 2003.
- Taniyama T, Kitai N, Iguchi Y, et al: Craniofacial morphology in a patient with Simpson-Golabi-Behmel syndrome. *Cleft Palate Craniofac J* 40:550, 2003.

- Poetke M, Jamil B, Muller U, et al: Diffuse neonatal hemangiomatosis associated with Simpson-Golabi-Behmel syndrome: a case report. *Eur J Pediatr Surg* 12:59, 2002.
- Chiao E, Fisher P, Crisponi L, et al: Overgrowth of a mouse model of the Simpson-Golabi-Behmel syndrome is independent of IGF signaling. *Dev Biol* 243:185, 2002.
- Li M, Shuman C, Fei YL, Cutieongo E, et al: GPC3 mutation analysis in a spectrum of patients with overgrowth expands the phenotype of Simpson-Golabi-Behmel syndrome. *Am J Med Genet* 102:161, 2001.
- DeBaun MR, Ess J, Saunders S: Simpson Golabi Behmel syndrome: progress toward understanding the molecular basis for overgrowth, malformation, and cancer predisposition. *Mol Genet Metab* 72:279, 2001.
- Krimmel M, Reinert S: Multiple odontogenic keratocysts in mental retardation-overgrowth (Simpson-Golabi-Behmel) syndrome. *Br J Oral Maxillofac Surg* 38:221, 2000.
- Veugelaers M, Cat BD, Muyldermans SY, et al: Mutational analysis of the GPC3/GPC4 glypican gene cluster on Xq26 in patients with Simpson-Golabi-Behmel syndrome: identification of loss-of-function mutations in the GPC3 gene. *Hum Mol Genet* 9:1321, 2000.
- Brzustowicz LM, Farrell S, Khan MB, et al: Mapping of a new SGBS locus to chromosome Xp22 in a family with a severe form of Simpson-Golabi-Behmel syndrome. *Am J Hum Genet* 65:779, 1999.
- Lin AE, Neri G, Hughes-Benzie R, et al: Cardiac anomalies in the Simpson-Golabi-Behmel syndrome. *Am J Med Genet* 83:378, 1999.
- Veugelaers M, Vermeesch J, Watanabe K, et al: GPC4, the gene for human K-glypican, flanks GPC3 on xq26: deletion of the GPC3-GPC4 gene cluster in one family with Simpson-Golabi-Behmel syndrome. *Genomics* 53:1, 1998.
- Neri G, Gurrieri F, Zanni G, et al: Clinical and molecular aspects of the Simpson-Golabi-Behmel syndrome. *Am J Med Genet* 79:279, 1998. Comment in *Am J Med Genet* 99:166, 2001.
- Weidle B, Orstavik KH: Simpson-Golabi-Behmel syndrome. A new overgrowth syndrome with increased risk of tumor development. *Tidsskr Nor Lægeforen* 118:1556, 1998.
- Lapunzina P, Badia I, Galoppo C, et al: A patient with Simpson-Golabi-Behmel syndrome and hepatocellular carcinoma. *J Med Genet* 35:153, 1998.
- Verloes A, Massart B, Dehalleux I, et al: Clinical overlap of Beckwith-Wiedemann, Perlman and Simpson-Golabi-Behmel syndromes: a diagnostic pitfall. *Clin Genet* 47:257, 1995.
- Chen E, Johnson JP, Cox VA, et al: Simpson-Golabi-Behmel syndrome: congenital diaphragmatic hernia and radiologic findings in two patients and follow-up of a previously reported case. *Am J Med Genet* 46:574, 1993. Comment in *Am J Med Genet* 87:267, 1999.
- Di Rocco M, Lignana E, Faraci M, et al: The Simpson-Golabi-Behmel syndrome. The stages of a diagnostic procedure. *Minerva Pediatr* 45:163, 1993.
- Gurrieri F, Cappa M, Neri G: Further delineation of the Simpson-Golabi-Behmel (SGB) syndrome. *Am J Med Genet* 44:136, 1992. Comment in *Am J Med Genet* 46:606, 1993.
- Garganta CL, Bodurtha JN: Report of another family with Simpson-Golabi-Behmel syndrome and a review of the literature. *Am J Med Genet* 44:129, 1992.
- Hughes-Benzie RM, Hunter AG, Allanson JE, et al: Simpson-Golabi-Behmel syndrome associated with renal dysplasia and embryonal tumor: localization of the gene to Xqcen-q21. *Am J Med Genet* 43:428, 1992.
- Konig R, Fuchs S, Kern C, et al: Simpson-Golabi-Behmel syndrome with severe cardiac arrhythmias. *Am J Med Genet* 38:244, 1991.
- Neri G, Marini R, Cappa M, et al: Simpson-Golabi-Behmel syndrome: an X-linked encephalo-tropho-schisis syndrome. *Am J Med Genet* 30:287, 1988.

## SIRENOMELIA

**Definition.** A congenital anomaly, caused by a disruptive vascular defect, characterized by fusion of the lower extremities, associated with renal agenesis, absence of the sacrum, rectum, and bladder. It was considered in the past to represent a severe form of caudal regression syndrome.

**Synonyms.** Mermaid syndrome, sirenomelia sequence.

**Etiology.** Although the etiology is unknown, sirenomelia is not believed to be hereditary.

**Recurrence Risk.** Unknown.

**Diagnosis.** The diagnosis of sirenomelia is based on the presence of fusion of the lower extremities associated with other skeletal and lumbar spine deformities, bilateral renal agenesis (which leads to severe oligohydramnios and pulmonary hypoplasia), and heart and abdominal wall





**FIGURE 5-79.** Sirenomelia. The fused extremity and the flipper-like deformity of the foot are characteristic of sirenomelia.

defects. The defect varies from simple cutaneous fusion of the limbs to absence of all long bones but one femur. The defect of the feet is proportional with the defect of the long bones, with a cutaneous defect commonly presenting with a double fused foot with 10 toes, and more severe defects presenting with a more rudimentary foot and ectromelia. Because the legs are fused, the rotation of the legs does not occur and they remain in their fetal position. Thus, the fibulae when present, are between the tibia and the sole of the foot is oriented "ventrally" instead of "dorsally."

**Pathogenesis.** An alteration in early vascular development, leads to a "vitelline arterial steal," in which blood flow is diverted from the caudal region of the embryo to the placenta, resulting in multiple defects of the lower extremities. Many of these fetuses have an aberrant vasculature, with the umbilical arteries connected to the old vitelline arteries (the superior mesenteric arteries).

**Genetic Anomaly.** Unknown.

## SMITH-LEMLI-OPITZ SYNDROME

**Definition.** Smith-Lemli-Opitz syndrome (SLO) is a common autosomal-recessive disorder described in 1964 by Smith et al, characterized by multiple anomalies including typical facial appearance, mental and growth retardation, syndactyly of the second and third toes, genital and other abnormalities of the internal organs. Depending on the severity of the malformations, the prognosis can range from mild intellectual impairment to lethal. The diagnosis was based on clinical features found after birth or in autopsy until 1993, when Irons described the reduced plasma cholesterol levels and elevated levels of cholesterol precursor 7-dehydrocholesterol (7-DHC) in association with SLO. The confirmation of these biochemical findings by many

**Table 5-5** Anomalies Associated With Sirenomelia

Abnormality	Frequency
Abnormal genitalia	Very frequent sign
Agenesis/hypoplasia of kidneys	Very frequent sign
Ambiguous genitalia	Very frequent sign
Bladder anomalies	Very frequent sign
Imperforate anus/anal stenosis	Very frequent sign
Sacroccocyx agenesis	Very frequent sign
Cardiac anomalies	Frequent sign
Radius absent/abnormal	Frequent sign
Spina bifida	Frequent sign
Tracheo-oesophageal fistula	Frequent sign

Reproduced with permission from Orphanet:  
<http://www.orpha.net/consor/cgi-bin/home.php?Lng=GB>.

**Associated Anomalies.** Anomalies are listed in Table 5-5. Cardiac, renal, abdominal wall, chest, and lower spine defects are frequently seen. Single umbilical artery, imperforate anus, and absence of the genitals are commonly found.

**Differential Diagnosis.** Caudal regression syndrome is the main differential diagnosis, and it usually presents with milder deformities compared to sirenomelia and normal amniotic fluid volume. Owing to the bilateral renal agenesis, fetuses affected by sirenomelia frequently have Potter facies. The fusion of the lower extremities, present in sirenomelia, makes the differential diagnosis. Other conditions that should be excluded are Fraser and VATER.

**Prognosis.** This is a lethal condition due to the associated renal agenesis and its complications. Exceptional cases present without renal agenesis and may survive.

**Management.** Termination of pregnancy can be offered before viability. Standard prenatal care is not altered throughout the pregnancy if continuation is opted for.

## References

- Benacerraf BR: Caudal regression syndrome and sirenomelia in ultrasound of fetal syndromes. New York, Churchill Livingstone, 1998, pp 250-254.
- Jones KL: Sirenomelia sequence in Smith's recognizable patterns of human malformation. Philadelphia, WB Saunders Company, 1998, p 634.
- Stevenson RE, Jones KL, Phelan MC, et al: Vascular steal: the pathogenic mechanism producing sirenomelia and associated defects of the viscera and soft tissues. *Pediatrics* 78:451, 1986.
- Orphanet: <http://www.orpha.net/consor/cgi-bin/home.php?Lng=GB>

other researchers proved that cholesterol and its precursors plasma levels could be reliable markers for the prenatal diagnosis. Currently, the cholesterol analysis can be made prenatally using amniotic fluid or, in the first trimester, by chorionic villus sampling. The introduction of biochemical testing for Smith-Lemli-Opitz syndrome has improved the prenatal detection of this syndrome. However, the recognition of ultrasonographic features suggestive of Smith-Lemli-Opitz syndrome is necessary to raise the suspicion, especially in patients who are not aware of their carrier condition and are having their first affected pregnancy. The ultrasonographic examination also evaluates the severity of the anomalies, and thus assists in predicting the outcome. In 1987, Curry proposed the division of the entity



into two classes: type I (the classical syndrome described by Smith) and type II (the most severe cases).

**Synonyms.** Acrodysgenital dwarfism, Lowry-Miller-MacLean syndrome.

**Incidence.** Some authors suggest that Smith-Lemli-Opitz syndrome is the second most common autosomal recessive disorder in North American whites, after cystic fibrosis. The prevalence of this syndrome has been estimated between 0.25:10,000 and 0.5:10,000, but an incidence of 1:10,000 was mentioned in 1997, in a population in Middle Bohemia. Furthermore, with the identification of a metabolic defect, a re-evaluation of these data has been suggested.

**Etiology-Pathogenesis.** Delleire observed in 1966, the autosomal-recessive pattern of transmission. In 1994, Wallace reported a case of balanced translocation in an affected patient and suggested that the gene locus might be at 7q32. Caused by a defect in the cholesterol biosynthesis, Smith-Lemli-Opitz syndrome is the first known genetic syndrome with a metabolic etiology.

**Diagnosis.** The detection of an extremely reduced concentration of cholesterol and abnormal accumulation of 7-dehydrocholesterol in the plasma make the diagnosis in infants and adults. Elevated concentration of 7-dehydrocholesterol at amniotic fluid in the second trimester or at chorionic villus sampling in the first trimester, normally undetectable in both specimens, is a reliable marker for prenatal diagnosis of Smith-Lemli-Opitz syndrome. Cases of Smith-Lemli-Opitz syndrome with normal cholesterol and abnormal 7DHC have been reported and, thus, normal levels of isolated cholesterol do not completely exclude the disorder. Estriol levels in maternal urine late in pregnancy may be reduced, as well as estriol levels in maternal circulation. Half of the fetuses that suffered intrauterine fetal demise with Smith-Lemli-Opitz syndrome were found to have low or undetectable maternal serum estriol levels, raising the speculation that this finding might become a maternal serum screening for this syndrome. The gene for Smith-Lemli-Opitz syndrome has been mapped and mutations have been isolated, but only on experimental basis now.

**Sonographic Findings.** Ultrasonographic findings during prenatal examination may raise the suspicion in patients who do not have familial or past histories of Smith-Lemli-Opitz syndrome and thus, are not aware of their condition of carriers. Ultrasonographic detection of multiple anomalies such as facial anomalies, polydactyly, syndactyly (more common between the second and third toes), single palmar crease, hypospadias and cryptorchidism in the male fetus, ambiguous genitalia, cardiac defects, lung malformations and many others in association with normal karyotype is suggestive of Smith-Lemli-Opitz syndrome. The detection of major anomalies is important to evaluate the severity of the disorder. Detection of increased nuchal translucency, or persisting nuchal edema with nonimmune hydrops are other findings reported in fetuses with Smith-Lemli-Opitz syndrome 8.

**Differential Diagnosis.** The pattern of multisystemic anomalies is characteristic of trisomies 21, 18, and 13, and thus, karyotype is recommended to exclude these disorders. Overlap of Smith-Lemli-Opitz syndrome with disorders such as Meckel syndrome has been reported, due to variability of phenotype in both conditions. The presence of occipital encephalocele as well as dysplastic kidneys favors

**Table 5-6** Associated Anomalies and Peculiarities of Smith-Lemli-Opitz Syndrome

Anatomic Area	Anomaly
Limbs	Syndactyly (of the second and third toes in particular) Postaxial polydactyly Short limbs Clinodactyly Dislocated hips Valgus deformity Radial deviation of the hands Ulnar deviation of the fingers Rocker-bottom feet Abnormal palmar creases Digital whorl dermal ridge pattern
CNS/Head	Microcephaly Trigonocephaly Agenesis of the corpus callosum Seizures Demyelination of cerebral hemispheres, cranial nerves, and peripheral nerves Hydrocephalus Cerebral hypoplasia Cerebellar hypoplasia
Cardiac	Ventricular septal defect Atrial septal defect Atriomegaly Ventriculomegaly
Genitourinary	Hypospadias Cryptorchidism Micropenis Bifidum scrotum Hypoplastic scrotum Microurethra Ambiguous genitalia Prominent clitoral hood Redundant labia minora Hypoplastic labia Rudimentary uterus Ureteropelvic junction obstruction Renal hypoplasia Urethral stenosis Cystic renal dysplasia Male pseudohermaphroditism

CNS, central nervous system.

Meckel syndrome. Genital anomalies and syndactyly support the diagnosis of Smith-Lemli-Opitz syndrome.

**Associated Anomalies.** Although Smith-Lemli-Opitz syndrome more often presents features such as facial, limbs, and genital anomalies associated with growth and mental retardation, the wide phenotype variation is the most important aspect of this disorder. Anomalies from all the systems have been described, and the most common are mentioned in Table 5-6.

## References

- Waterham HR, Wijburg FA, Hennekam RC, et al: Smith-Lemli-Opitz syndrome is caused by mutations in the 7-dehydrocholesterol reductase gene. *Am J Hum Genet* 63:329, 1998.
- Kelley RJ, Hennekam RCM: The Smith Lemli-Opitz syndrome. *J Med Genet* 37:321, 2000.

- Nowaczyk MJM, Wayne JS: The Smith-Lemli-Opitz syndrome: a novel metabolic way of understanding developmental biology, embryogenesis, and dysmorphology. *Clin Genet* 59:375, 2001.
- Tint GS, Salen G, Batta AK, et al: Correlation of severity and outcome with plasma sterol levels in variants of the Smith-Lemli-Opitz syndrome. *J Pediatr* 127:82, 1995.
- Ryan AK, Bartlett K, Clayton P, et al: Smith-Lemli-Opitz syndrome: a variable clinical and biochemical phenotype. *J Med Genet* 35:558, 1998.
- Nowaczyk MJM, Whelan DT, Hill RE: Smith-Lemli-Opitz syndrome: phenotypic extreme with minimal clinical findings. *Am J Med Genet* 78:419, 1998.
- Ryan AK, Bartlett K, Clayton P, et al: Smith-Lemli-Opitz syndrome: A variable clinical and biochemical phenotype. *J Med Genet* 35:558-565, 1998.
- Curry CJ, Carey JC, Holland JS, et al: Smith-Lemli-Opitz syndrome-type II: Multiple congenital anomalies with male pseudo-hermaphroditism and frequent early lethality. *Am J Med Genet* 26:45, 1987.

- Bewley S, Roberts LJ, Mackinson AM, et al: First trimester fetal nuchal translucency: problems with screening the general population 2. *Br J Obstet Gynaecol* 102:386, 1995.
- Chitty LS, Pandya PP: Ultrasound screening for fetal abnormalities in the first trimester. *Prenat Diagn* 17:1269, 1997.
- Hytt JA, Clayton PT, Moscoso G, et al: Increased first trimester nuchal translucency as prenatal manifestation of Smith-Lemli-Opitz syndrome. *Am J Med Genet* 58:374, 1995.
- McGaughan JM, Clayton PT, Mills KA, et al: Prenatal diagnosis of Smith-Lemli-Opitz syndrome. *Am J Med Genet* 56:269, 1995.
- Opitz J: RSH/SLO ('Smith-Lemli-Opitz') syndrome. Historical, genetic and developmental considerations. *Am J Med Genet* 50:344, 1994.
- Pandya P, Kondylis A, Hilbert L, et al: Chromosomal defects and outcome in 1015 fetuses with increased nuchal translucency. *Ultrasound Obstet Gynecol* 5:15, 1995.

## THANATOPHORIC DYSPLASIA

**Definition.** Thanatophoric dysplasia is a lethal congenital form of short-limbed chondrodysplasia, which is divided into two subtypes:

- *Type I* is characterized by extreme rhizomelia, bowed long bones, narrow thorax, a relatively large head, normal trunk length, and absent cloverleaf skull. The spine shows platyspondyly, the cranium has a short base, and frequently, the foramen magnum is decreased in size. The forehead is prominent, and hypertelorism and a saddle nose may be present. The hands and feet are normal, but the fingers are short.
- *Type II* is characterized by short, straight long bones and cloverleaf skull.

**Synonyms.** Thanatophoric dwarfism.

**Incidence.** 0.69:10,000; the male-to-female ratio is 2:1.

**Etiology.** Possibly autosomal-dominant inheritance, but the majority of cases result from new mutations of the fibroblast growth factor receptor 3.

**Recurrence Risk.** A general empiric risk was estimated in 2%.

**Diagnosis.** The sonographic diagnosis can be made in the presence of short-limbed dwarfism, hypoplastic thorax, cloverleaf skull, frontal bossing and simian crease. Femur bowing, narrow thorax, large head size even without ventriculomegaly, and redundant soft tissues are features that become more pronounced with advancing gestation but may not be present in midtrimester. In 70% of cases, thanatophoric dysplasia is associated with polyhydramnios, which may be massive and lead to premature labor. Fetal movements do not seem to be affected by the disease, but a decrease in motion during the third trimester has been reported. Decreased hand flexure is probably responsible for the presence of simian crease. In the absence of cloverleaf



**FIGURE 5-80.** Coronal plane three-dimensional reconstructions show the typical kleeblattschädel or cloverleaf skull of type II thanatophoric dysplasia. (Courtesy of Ana Bircher, 2002, thefetus.net.)



**FIGURE 5-81.** Further three-dimensional surface rendering mode image shows more details. (Courtesy of Ana Bircher, 2002, thefetus.net.)





**FIGURE 5-82.** The upper limbs were short, mostly rhizomelic and maintain a right angle throughout all examinations. (Courtesy of Ana Bircher, 2002, *thefetus.net*.)

skull, the disease should be suspected when severe rhizomelic dwarfism and a narrow thorax are detected. Sonographic measurement of fetal femur length, especially when correlated with biparietal diameter, is a reliable method in the identification of certain forms of short-limbed skeletal dysplasias, as well as thanatophoric dysplasia.

**Pathogenesis.** Characteristic generalized disruption of the growth plate with persistent mesenchyme-like tissue.

**Associated Anomalies.** "Cloverleaf skull" (in type II), horseshoe kidney, hydronephrosis, atrial septal defect, defective tricuspid valve, imperforate anus, and radioulnar synostosis.

**Differential Diagnosis.** Chondroectodermal dysplasia (Ellis-van Creveld syndrome), asphyxiating thoracic dysplasia, short rib–polydactyly syndrome, and homozygous achondroplasia. All short-limbed dwarfism should be considered. If type II is suspected, conditions that have association with craniosynostosis and cloverleaf skull should be excluded (Apert, Crouzon, Pfeiffer, Carpenter, and Kleeblattschadel syndromes).

**Prognosis.** This is a uniformly lethal condition, and in general, affected infants die shortly after birth. The cause of death is respiratory failure due to hypoplastic lungs.

**Management.** The option of pregnancy termination should be offered before viability. Sonographic evaluation of hydrocephalus is recommended, considering that it may cause malpresentation and difficult delivery. If massive hydrocephalus has developed, cephalocentesis or elective cesarean section should be considered to avoid maternal trauma.



**FIGURE 5-83.** Postmortem images of this fetus. (Courtesy of Ana Bircher, 2002, *thefetus.net*.)

## References

- Orioli IM, Castilla EE, Barbosa-Neto JG: The birth prevalence rates for the skeletal dysplasias. *J Med Genet* 23:328, 1986.
- Maroteaux P, Lamy M, Robert JM: Le nanisme thanatophore. *Presse Med* 75:2519, 1967.
- Taybi H, Langman R: *Radiology of Syndromes, Metabolic disorders, and Skeletal Dysplasias*, 3rd ed. Chicago, London, Mosby, 1990.
- Wilcox WR, Tavormina PL, Krakov D, et al: Molecular, radiologic, and histopathologic correlations in thanatophoric dysplasia. *Am J Med Genet* 78:274, 1998.
- Escobar LF, Bixler D, Padilla LM: Quantitation of craniofacial anomalies in utero: fetal alcohol and Crouzon syndromes and thanatophoric dysplasia. *Am J Med Genet* 45:25, 1993.
- Langer LO Jr, Yang SS, Hall JG, et al: Thanatophoric dysplasia and cloverleaf skull. *Am J Med Genet Suppl* 3:167, 1987.
- Brodie SG, Kitoh H, Lachman RS, et al: Platypondylic lethal skeletal dysplasia, San Diego type, is caused by FGFR3 mutations. *Am J Med Genet* 84:476, 1999.
- van der Harten HJ, Brons JT, Dijkstra PF, et al: Some variants of lethal neonatal short-limbed platyspondylic dysplasia: a radiological ultrasonographic, neuropathological and histopathological study of 22 cases. *Clin Dysmorphol* 2:1, 1993.
- Kitoh H, Lachman RS, Brodie SG, et al: Extra pelvic ossification centers in thanatophoric dysplasia and platyspondylic lethal skeletal dysplasia—San Diego type. *Pediatr Radiol* 28:759, 1998.
- <http://www.csmc.edu/genetics/skeldys/default.html>
- Orioli IM, Castilla EE, Barbosa-Neto JG: The birth prevalence rates for the skeletal dysplasias. *J Med Genet* 23:328, 1986.
- Wilcox WR, Tavormina PL, Krakov D, et al: Molecular, radiologic, and histopathologic correlations in thanatophoric dysplasia. *Am J Med Genet* 78:274, 1998.
- Yuce MA, Yardim T, Kurtul M, et al: Prenatal diagnosis of thanatophoric dwarfism in second trimester. A case report. *Clin Exp Obstet Gynecol* 25:149, 1990.
- Chesi M, Brents LA, Eli SA, et al: Activated fibroblast growth factor receptor 3 is an oncogene that contributes to tumor progression in multiple myeloma. *Blood* 97:729, 2001.
- Hertz JM, Junker I, Christensen L, et al: The molecular genetic background of hereditary craniosynostosis and chondrodysplasias. *Ugeskr Laeger* 163:4862, 2001.



Wilkie AO: Fibroblast growth factor receptor mutations and craniosynostosis: three receptors, five syndromes. *Indian J Pediatr* 63:351, 1996.

van Ravenswaaij-Arts CM, Losekoot M: From gene to disease; achondroplasia and other skeletal dysplasias due to an activating mutation in the fibroblast growth factor. *Ned Tijdschr Geneesk* 145:1056, 2001.

Jones KL: *Smith's Recognizable Patterns of Human Malformation*, 5th ed. Philadelphia, London, WB Saunders, 1997.

Yamaguchi K, Honma K: Autopsy case of thanatophoric dysplasia: observations on the serial sections of the brain. *Neuropathology* 21:222, 2001.

Adar R, Monson-Oman E, David P, et al: Differential activation of cysteine-substitution mutants of fibroblast growth factor receptor 3 is determined by cysteine localization. *J Bone Miner Res* 17:860, 2002.

Bellus GA, Spector EB, Speiser PW, et al: Distinct missense mutations of the FGFR3 lys650 codon modulate receptor kinase activation and the severity of the skeletal dysplasia phenotype. *Am J Hum Genet* 67:1411, 2000.

Pediatric database (PEDBASE). Last updated: 11/15/97

Pena SDJ, Goodman HO: The genetics of thanatophoric dwarfism. *Pediatrics* 51:104, 1973.

Nussbaum RL, McInnes RR, Willard HF: *Thompson and Thompson Genetics in Medicine*, 6th ed. Philadelphia, WB Saunders, 2001, p 102.

Benacerraf BMD: *Ultrasound of Fetal Syndromes*. New York, Edinburgh, Churchill Livingstone, 1998.

Chen CP, Chern SR, Shih JC, et al: Prenatal diagnosis and genetic analysis of type I and type II thanatophoric dysplasia. *Prenat Diagn* 21:89, 2001.

Garjian KV, Pretorius DH, Budorick NE, et al: Fetal skeletal dysplasia: three-dimensional US—initial experience. *Radiology* 214:717, 2002.

Budorick NE: The fetal musculoskeletal system. In Callen PW (ed): *Ultrasonography in Obstetric and Gynecology*, 4th ed. Philadelphia, WB Saunders, 2000, pp 343–345.

Romero R, Pilu G, Jeanty P: Prenatal diagnosis of congenital anomalies. Norwalk, CT, Appleton and Lange, 1988, pp 335–339.

Weber M, Johansson R, Cartens C, et al: Thanatophoric dysplasia type II: new entity? *J Pediatr Orthop B* 7:10, 1999.

Winter RM, Knowles SAS, Bieber FR, et al: *The Malformed Fetus and Stillbirth. A diagnostic approach*. Chichester, NY, J Wiley & Son, 1988.

Sawai H, Komori S, Ida A, et al: Prenatal Diagnosis of thanatophoric dysplasia by mutational analysis of the fibroblast growth factor receptor 3 gene and a proposed correction of previously published PCR results. *Prenat Diagn* 19:21, 1999.

Goncalves L, Jeanty P: Fetal biometry of skeletal dysplasias; a multicentric study. *J Ultrasound Med* 13:167, 1996.

Rahemtullah A, Mc Guillivray B, Wilson RD: Suspected skeletal dysplasia: femur length to abdominal circumference ratio can be used in ultrasonographic prediction of fetal outcome. *Am J Obstet Gynecol* 177:864, 1997.

## TUBEROUS SCLEROSIS

**Definition.** This syndrome is associated with facial angiofibroma (often incorrectly called adenoma sebaceum), epilepsy, mental retardation, renal cysts, multiple and bilateral angiofibroma of the kidney, and rhabdomyoma of the heart. Diverse cutaneous manifestations such as hypochromic patches (visible under Wood light) and café-au-lait patches (light brown areas) are also typical of the syndrome. Brain tumors such as ependymoma of the third ventricle and astrocytoma may also be present.

**Synonym.** Bourneville sclerosis and Brissaud.

**Incidence.** 0.3 to 1:10,000. The age of onset is in the first decade of life.



**FIGURE 5-84.** Tuberous sclerosis. Several rhabdomyomas are seen in this four-chamber view of the heart. (Courtesy of Luc Gourand, 2002, *thefetus.net*.)



**FIGURE 5-85.** The typical café-au-lait spot of tuberous sclerosis. (Courtesy of P. Jeanty, 1999, *thefetus.net*)

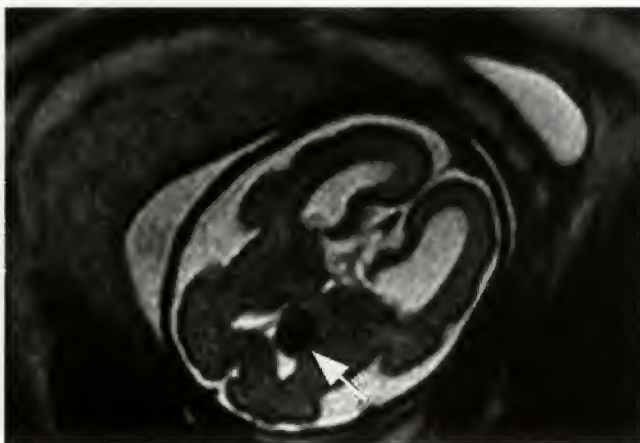


**FIGURE 5-86.** Axial view (T2 weighted) in a fetus of 26 weeks' gestation showing a typical subependymal nodule (arrow). (Courtesy of Heron Werner, 2005, *thefetus.net*.)



**Table 5-7** Main Aspects of Tuberous Sclerosis**Classic triad (<50% of cases):**

Facial lesions,  
Convulsions and  
Mental retardation

**Central Nervous System**

Cortical hamartomas  
Lesion of white substance\*  
Subependymal hamartomas (95%)  
Typical localization: alongside lateral ventricle walls

**Astrocytoma of subependymal giant cells\***

Localization: foramen of Monro  
Obstructive hydrocephaly

**Kidney:**

Cysts  
Angiolioma

**Cardiovascular:**

Rhabdomyoma  
Aneurysm, stenosis, and vascular ectopia

**Liver:**

Leiomyoma  
Adenoma

\*No reports of intrauterine visualization.

**Etiology.** Autosomal-dominant inheritance with a large proportion of fresh mutations (sporadic cases). The expression is highly variable.

**Pathogenesis.** Tubers are the expression of an early disorder of the embryogenesis. The greater the number of tubers, the greater the number of neurologic impairments. They can be found everywhere within the cerebral hemispheres, such as in the subependymal region located in the walls of lateral ventricles and on the surface of the basal ganglia. They may extend into the ventricles in the foramen of Monro area, and they can cause obstruction and hydrocephalus. They may also appear in the cortical gyri and sulcus terminalis. Tuberous sclerosis induces a reduction of the number of neurons, which are substituted by "monster" multinucleated giant neurons. The overgrowth of the fibrillary astrocytes can result in malignant astrocytomas. The sclerosis induces a demyelization, as well as calcium deposition in the glia and the blood vessels, which go through hyaline degeneration.

**Clinical Findings.** Tuberous sclerosis can show a wide variety of signs that involve many organs as a consequence of the multifactorial origin of this genetic disorder (Table 5-7).

**Diagnosis.** The diagnosis is usually suggested by the discovery of cardiac tumors, which resemble small uterine fibroids (round, usually well-delineated homogeneous masses). Between 51% and 86% of cardiac rhabdomyomas are associated with tuberous sclerosis. Occasionally, the finding of a rhabdomyoma during routine second trimester ultrasound examination may lead to the recognition that the

mother is affected. Cardiac rhabdomyomas increase prenatally, may regress in early infancy, remain unchanged during childhood, and regress in adolescence. The rhabdomyomas may cause rhythm disruptions (Wolff-Parkinson-White syndrome, supraventricular tachycardia, paroxysmal arrhythmias) as well as obstructions or regurgitation. Renal angiofibromas have not been recognized prenatally, although this may simply be a matter of time. Some recent unpublished reports have demonstrated that the periventricular subependymal nodules may also be detected.

Two-dimensional Doppler echocardiography is a useful, noninvasive method to diagnose fetal cardiac rhabdomyomas and to monitor their influence on fetal cardiac function. However, it does not help to determine which fetuses affected by rhabdomyomas will develop tuberous sclerosis. Some studies report that 39% of prenatal suspected cardiac rhabdomyomas will be diagnosed at birth as a tuberous sclerosis syndrome. Family history remains the strongest predictor of the syndrome in prenatal counseling, whereas size of the cardiac tumor can not reliably be used. Magnetic resonance imaging can be performed to assess all of the associated malformations.

**Genetic Anomalies.** Tuberous sclerosis C is caused by defects or mutations on two genes, tuberous sclerosis C1 and tuberous sclerosis C2. Only one of the genes needs to be affected for tuberous sclerosis C to be present. The tuberous sclerosis C1 gene, discovered in 1997, is on chromosome 9 and produces a protein called hamartin. The tuberous sclerosis C2 gene, discovered in 1993, is on chromosome 16 and produces a protein called tuberin. These proteins act as tumor suppressors, agents that regulate cell proliferation and differentiation.

**Differential Diagnosis.** The predominant prenatal finding is that of the rhabdomyomas. Other cardiac tumors, such as a fibroma, should also be considered.

**Recurrence Risk.** Low in cases of new mutation; higher in cases of gonadal mosaicism; 50% in cases of parental involvement.

**Prognosis.** When no hydrops results from the presence of the rhabdomyomas, the prognosis depends on the other complications of the disorder. Because of the great variability of expression, an accurate prediction of the status of the child is difficult to infer from the status of the parent. Furthermore, new genetic evidence seems to indicate that the mental prognosis varies with the locus of the defective gene; thus, this may influence the decision about the pregnancy in the future.

**Management.** Termination of the pregnancy may be offered before viability.

## References

- Kivelitz DE, Muhler M, Rake A, et al: MRI of cardiac rhabdomyoma in the fetus. *Eur Radiol* 14:1513, 2004.
- Gamzu R, Achiron R, Hegesh J, et al: Evaluating the risk of tuberous sclerosis in cases with prenatal diagnosis of cardiac rhabdomyoma. *Prenat Diagn* 22:1044, 2002.
- D'Addario V, Pinto V, Di Naro E, et al: Prenatal diagnosis and postnatal outcome of cardiac rhabdomyomas. *J Perinat Med* 30:170, 2002.



## TWIN-TO-TWIN TRANSFUSION SYNDROME

**Definition.** Twin-to-twin transfusion syndrome is a congenital entity unique to monochorionic diamniotic twin pregnancies, characterized by an imbalanced blood exchange between the twins' circulation, which occur through interplacental anastomosis and may cause fetal compromise varying from growth discordance to death of both fetuses. The first description was made by Schatz in late 1800s.

**Synonym.** Stuck twin.

**Etiology.** Vascular anastomosis.

**Recurrence Risk.** Unknown, but very low, considering the small chance to develop a second monochorionic diamniotic twin pregnancy.

**Incidence.** Twin-to-twin transfusion complicates about 15% of monochorionic twin gestations and is responsible for 17% of the perinatal mortality in multiple pregnancies.

**Diagnosis.** Ultrasonographic criteria for the diagnosis of twin-to-twin transfusion syndrome include monochorionic placentation, with visualization of a separating membrane, fetuses of the same sex, mid-pregnancy polyhydramnios-oligohydramnios sequence (polyhydramnios at the recipient's sac and oligohydramnios at the donor's sac), in the absence of other causes of abnormal amniotic fluid volume, and marked growth discordance. Significant weight discordance is considered a difference between the twin's size equal or greater to 20%. Other findings that might be observed include nonvisualization of the donor's bladder with enlarged recipient's bladder, abnormal Doppler systolic/diastolic (S/D) ratio at the umbilical cord, hydrops or evidence of congestive heart failure of either twin (more commonly found at the recipient twin). Milder forms of the disease are more difficult to diagnose owing to the lack of

uniform criteria; however, one should suspect twin-to-twin transfusion syndrome in the presence of amniotic fluid discrepancy between the cavities.

**Pathogenesis.** If embryonic splitting occurs before day 3 after fertilization, two independent fetuses with separate placentas will result. A single placenta with two amniotic cavities occurs if splitting takes place between days 4 and 7. If division of the embryoblast occurs after about 8 days, the twins share a single placenta and amniotic cavity (monochorionic-monoamniotic twins). Division beyond day 12 results in conjoined twins.

When two fetuses share the same placenta, vascular anastomoses develop between their circulations. These anastomoses can be of three types: vein to vein, artery to artery, and artery to vein. Even when there are multiple vascular connections within a single placenta, no transfusion should occur provided the anastomoses are balanced. Placentas from pregnancies with twin-to-twin transfusion syndrome have fewer anastomoses, which are more likely to be solitary and of the deep arteriovenous type than those without twin-to-twin transfusion syndrome. Provided transfusion occurs, the donor or "pump" twin becomes hypovolemic owing to blood loss. Hypoxia develops because of placental insufficiency, which is also responsible for intrauterine growth restriction. Poor renal perfusion leads to oligohydramnios. This latter feature, when severe, is responsible for the classic appearance of the stuck twin: the amniotic sac becomes too small, the amniotic membrane

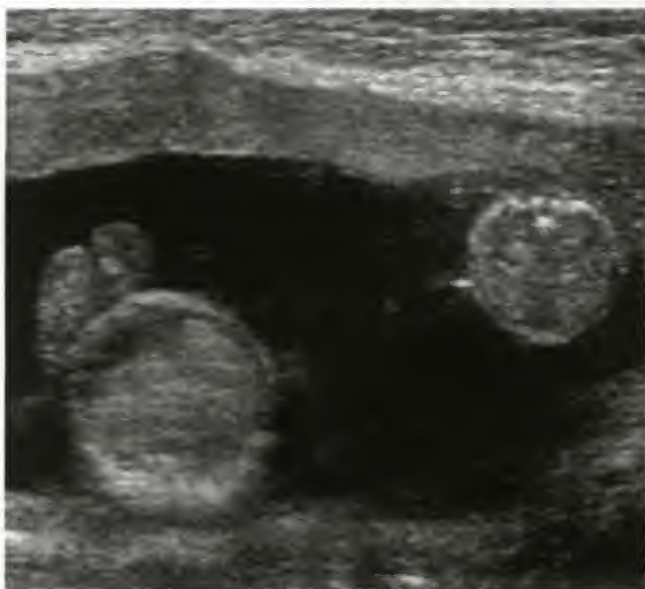


**FIGURE 5-87.** Twin-to-twin transfusion syndrome. The fetuses are visibly discordant in size with the larger fetus on the left (the recipient) demonstrating ascites.



**FIGURE 5-88.** A different case of twin-to-twin transfusion syndrome. The fetus on the maternal right (left side of the image) is held up against the anterior uterus by the dividing membrane (arrows).





**FIGURE 5-89.** Postmortem photograph of twins. The twins are discordant with the larger, recipient twin on the left.

comes in close contact with the body of the “pump” twin, and the fetus appears trapped to the uterine wall. Hypervolemia with increased renal perfusion leads to polyhydramnios in the sac of the recipient twin. Because there is no loss of protein or cellular components from its circulation, colloid osmotic pressure draws water from the maternal compartment across the placenta, establishing a vicious circle of hypervolemia, polyuria, and hyperosmolarity, leading to high-output cardiac failure, hydrops, and polyhydramnios.

In the most severe forms, the diagnosis should not be difficult: a single placenta, massive polyhydramnios in the sac of the recipient twin, a stuck donor twin attached to the uterine wall with poor mobility, and obvious growth discordance. Milder forms of the disease are more difficult to diagnose owing to the lack of uniform criteria. However, one should suspect twin-to-twin transfusion in the presence of amniotic fluid discrepancy between the cavities, regardless of the amount of weight discordance between the twins. An intertwin hemoglobin difference greater than 2.4 g/dl in fetal blood obtained by cordocentesis has been shown to be consistent with stuck twin syndrome.

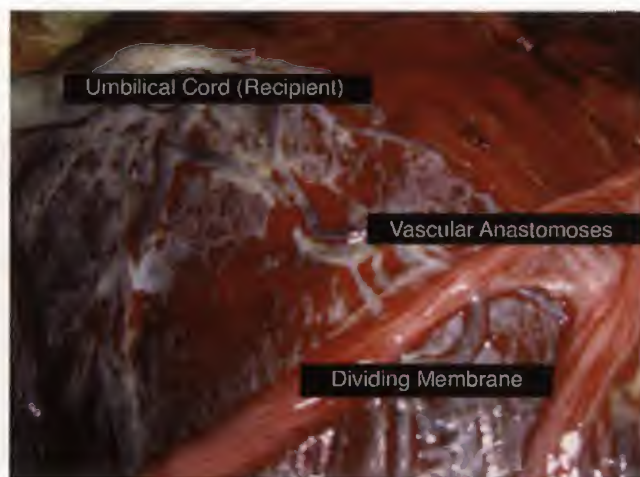


**FIGURE 5-90.** This is another case of twin-to-twin transfusion. Fetal surface of the placenta showing two sacs, a dividing membrane and the vascular anastomoses.

**Associated Anomalies.** The overdistention of the uterus caused by the polyhydramnios can cause preterm labor, amniorrhexis, abruptio placentae, respiratory, and abdominal discomfort. Death of one twin can cause embolic phenomena (twin embolization syndrome) and coagulation problems in the remaining twin, and sequelae such as neurologic, cardiac, and renal diseases are common among survivors.

**Differential Diagnosis.** The differential diagnosis should be mainly concerned with twins of discordant size without transfusion as the underlying pathophysiologic mechanism for the problem. Some authors have proposed a new entity called twin oligohydramnios-polyhydramnios sequence, in which twin-to-twin transfusion is included. Histopathologic studies of the placenta are required to differentiate twin-to-twin transfusion from the other conditions included in twin oligohydramnios-polyhydramnios sequence. Isolated intrauterine growth restriction can be considered if the growth discrepancy is minimal (less than 15%) and the other features of the syndrome are not present. Dichorionic twin pregnancy with fused placentas and growth restriction of one of the fetuses is another condition that can lead to misdiagnosis. This can be excluded if the twins have different sexes or, after birth, by histopathologic analysis of the placenta.

**Prognosis.** When the disease manifests during the second trimester, there is a higher risk of perinatal morbidity and mortality. Intrauterine hypoxia, preterm delivery, and death of one fetus (usually the donor) with subsequent death or hypoxic-ischemic sequelae (see twin embolization syndrome earlier) in the surviving twin are the most common complications to watch for in these pregnancies. The absent end-diastolic flow in the donor's umbilical artery, accompanied by venous pulsation in the recipient's umbilical vein, is usually associated with a poor prognosis. Hydrops or evidence of congestive heart failure of either twin is also associated with ominous prognosis. These signs are found more commonly at the recipient twin.

**Management.** Although efficacy of the therapies available is still controversial, the elevated mortality rate



(which can be as high as 100%) when expectant management is opted for, imposes the necessity of invasive therapy. Treatment includes serial amniocentesis to drain polyhydramnios in the sac of the recipient twin and, more recently, ablation of communicating vessels on the placental surface by neodymium: YAG laser guided by fetoscopy and umbilical cord ligation. Intensive monitoring with weekly nonstress testing, alternating with biophysical profiles, is recommended from the time of diagnosis to delivery.

## VACTERL ASSOCIATION

**Definition.** Initially described in 1973, the vertebral, anal, tracheoesophageal, renal and radial abnormalities (VATER) association represents a defect in mesodermal development at the primitive streak level. More recently, this association has been expanded to include these abnormalities as well as cardiac features and a broader description of limb anomalies (VACTERL). VACTERL is a mnemonically useful acronym for a nonrandom association of malformations including **V** (vertebral anomalies), **A** (anal atresia), **C** (cardiac anomalies), **TE** (tracheoesophageal fistula or esophageal atresia), **R** (renal/urinary anomalies), and **L** (limb defect). Patients are considered to have the VACTERL association when three or more organ systems are involved. The most frequent defects described are tracheoesophageal fistula and anal or vertebral anomalies.

**Synonyms.** VATER sequence, VATER association, VACTERL syndrome.

**Incidence.** Uncommon. Approximately 300 cases have been reported.

**Etiology.** Although VACTERL occurs as a sporadic event in the majority of cases, a high frequency among offspring of diabetic mothers has been observed. Some authors report that prenatal rats exposed to doxorubicin (Adriamycin) demonstrated a similar series of anomalies.

**Recurrence Risk.** Varies from 1% to 50%.

**Pathogenesis.** Defective mesodermal development of unknown origin, possibly a mitochondrial disorder.



**FIGURE 5-91.** VACTERL association. Sonogram of a fetus with anal atresia and a dilated segment of large intestine.

## Reference

Bruner JP, Anderson TL, Rosemond RL: Placental pathophysiology of the twin oligohydramnios-polyhydramnios sequence and the twin-twin transfusion syndrome. *Placenta* 19:81, 1998.

**Diagnosis.** The association of vertebral anomalies (in particular at the lumbosacral level) and renal, heart, and radial defects constitutes the classic manifestation of VACTERL syndrome. It is well known, however that some people who are affected will not present all typical findings. The diagnosis can also be suspected because of polyhydramnios in the presence of a small or absent fetal stomach (the tracheoesophageal fistula), hemivertebrae or scoliosis, or limb (in particular, radius anomalies, club hand, reduction defects, and polydactylies), renal, and cardiac defects. The presence of a supernumerary rib (13 and 14 pairs thoracic, 6 to 7 lumbar) may be recognized, especially with three-dimensional rendering. The ultrasound diagnosis of VACTERL syndrome may be accomplished early in the second trimester, if the fetus is severely affected.

**Genetic Anomalies.** X-linked and autosomal-recessive inheritance.

**Differential Diagnosis.** Nearly half of patients with tracheoesophageal fistula will exhibit other VACTERL malformations. Townes syndrome has many similar features. Because VACTERL syndrome consists of anomalies of multiple systems, chromosomal disorders such as trisomy 18 and trisomy 13 must be excluded by karyotype study. Disorders characterized by the presence of vertebral, renal, and/or radial defects (such as thrombocytopenia absent radius syndrome, Fanconi anemia, Robert's syndrome, Holt-Oram syndrome, Nager syndrome, caudal regression syndrome, sirenomelia, müllerian duct, renal agenesis, upper limb, and rib abnormalities association, ectrodactyly-ectodermal dysplasia syndrome, and Jarcho-Levin syndrome) should be considered.

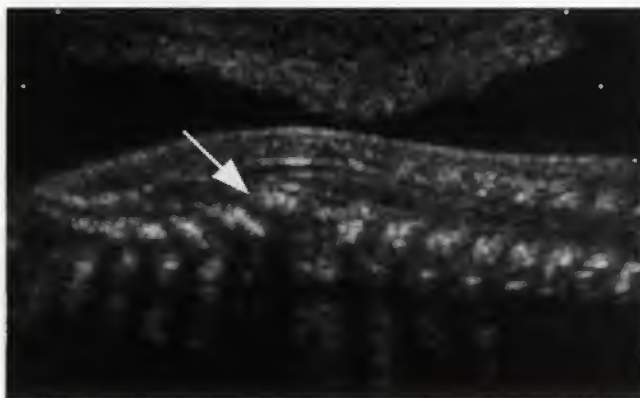


**FIGURE 5-92.** Abnormal vertebrae (arrow) in association with the above-mentioned finding and a radial abnormality (not shown) should arouse suspicion of VACTER association.



**Associated Anomalies.** Numerous. Hydrocephalus is commonly associated.

**Prognosis.** Poor overall but depends on the particular association of anomalies. During the last several decades, the literature has reflected a steady increase in the survival of infants with the VACTERL association. Today most children with the VACTERL association survive.

**Management.** Termination of pregnancy can be offered before viability. Monthly sonographic monitoring of fetal growth and evaluation of the structural defects are recommended. Delivery in a tertiary center is required for prompt surgical repair and rehabilitation. The most common organ system involved is the urinary system with an upper urinary tract anomaly in more than 90% of cases. After birth, patients with the VACTERL association should remain on

antibiotic prophylaxis for urinary tract infection while awaiting the completion of screening. Urologic follow-up is crucial because the majority of patients eventually require genitourinary intervention. Today, surgeons are more apt to correct cardiac and intestinal problems in these cases.

## References

- Kolker AR, Coombs CJ, Meara JG, et al: Patterns of radial dysmorphology with the VACTERL association in the adriamycin-exposed prenatal rat. *Ann Plast Surg* 45:525, 2000.  
 Omim: VACTERL ASSOCIATION WITH HYDROCEPHALUS 276950.  
 Kolon TF, Gray CL, Sutherland RW, et al: Upper urinary tract manifestations of the VACTERL association. *J Urol* 163:1949, 2000.

## WALKER-WARBURG SYNDROME

**Definition.** Walker-Warburg syndrome is a genetic disorder characterized by retinal detachment, cataracts, microphthalmia, and musculoskeletal and central nervous system anomalies (hydrocephalus, lissencephaly type II, cephalocele) associated with mental retardation. It was first reported by Walker in 1942 and reviewed by Warburg in 1971.

**Synonyms.** Lissencephaly type II, HARDE syndrome (hydrocephalus, agyria, retinal dysplasia, and encephalocele), muscle-eye-brain disease, cerebro-oculomuscular syndrome, cerebro-ocular dysplasia-muscular dystrophy, Warburg syndrome, Walker lissencephaly, encephalo-ophthalmic dysplasia, and oculocerebral malformation.

**Incidence.** Unknown.

**Etiology.** Autosomal-recessive inheritance.

**Diagnosis.** Dobyns reviewed 63 cases in 1989 and established the diagnostic criteria, which include lissencephaly type II, cerebellar malformations, retinal malformation (in general, retinal nonattachment), and congenital muscular dystrophy. Indeed, congenital muscular dystrophy is present in 100% of the cases. However, a wide variety of eye and cerebral manifestations have been reported, in addition to the main anomalies including: microphthalmia, buphthalmos, congenital glaucoma, cataract, optic nerve hypoplasia, persistent hyaloid artery, Dandy-Walker malformation, hydrocephalus, cephalocele, microcephaly, and agenesis of the corpus callosum. Based on this wide spectrum of defects, the association of any type of eye with cerebral malformations should raise the suspicion of Walker-Warburg syndrome. The finding of a concentric ring inside the vitreous body (the detached retina) or the presence of lipoma of the corpus callosum is very suggestive of the diagnosis. When prenatal sonographic findings are inconclusive, magnetic resonance imaging, computed tomography, electromyography, and autopsy studies are indicated after birth to provide accurate genetic counseling to the family.

**Genetic Anomalies.** Defect of 9q31.

**Associated Anomalies.** Cleft lip and genital malformations may occasionally be found.

**Differential Diagnosis.** Anomalies associated with lissencephaly such as Miller-Dieker and Neu-Laxova are major differential diagnoses. Other disorders that should be excluded are Meckel syndrome, Fryns syndrome, trisomies



**FIGURE 5-93.** Small cephalocele (arrow) in a fetus with Walker-Warburg syndrome. The previous child of this family was similarly affected.

18 and 13, severe Fukuyama-type congenital muscular dystrophy, and maternal viral infections.

**Recurrence Risk.** The recurrence risk for couples with previously affected children is 25%.

**Prognosis.** Most of the newborns affected by Walker-Warburg syndrome die within the first year of life. Of those few who survive until 5 years of age, the majority have severe mental and developmental retardation.

**Management.** When detected before viability, termination of pregnancy can be offered. After viability, standard prenatal care is not altered.

## References

- Asano Y, Minagawa K, Okuda A, et al: A case of Walker-Warburg syndrome. *Brain Dev* 22:454, 2000.  
 Blin G, Rabbé A, Ansquer Y, et al: First-trimester ultrasound diagnosis in a recurrent case of Walker-Warburg syndrome. *Ultrasound Obstet Gynecol* 26:297, 2005.

## WOLF-HIRSCHHORN SYNDROME

**Definition.** Chromosomal disorder caused by loss of material from the distal aspect of the short arm of chromosome 41.

**Synonyms.** 4p-deletion syndrome, Wolf-Hirschhorn syndrome, Wolf-Hirschhorn chromosome region.

**Incidence.** Approximately 120 cases reported in the world literature, but several times that many are registered in support group.

**Etiology.** Abnormal chromosome breakage during synapsis and recombination. Although it was first thought that the deletion was paternal in origin, it has been found recently that it can be of both maternal and paternal origin. Paternal age is not a causal factor.

**Diagnosis.** The prenatal diagnosis is suggested by the presence of severe intrauterine growth restriction associated

with no Doppler anomaly, normal amniotic fluid, midline defects, and a "downturned mouth."

**Genetic Diagnosis.** Although there may be some difficulty in detecting some small deletions by cytogenetics, the standard cytogenetics (regular-G-banding, high-resolution banding, polymerase chain reaction typing, Southern blot hybridization, and fluorescence in situ hybridization technique) can provide the diagnosis. The gene map locus is 4p16.3.

**Associated Anomalies.** Anomalies are listed in Table 5-8. Differential diagnosis,

- *PITT syndrome*: is very closely related to 4p-. PITT syndrome, or Pitt-Rogers-Danks syndrome (PRDS), is a rare presumed autosomal-recessive syndrome with pre- and postnatal growth retardation, microcephaly, characteristic facial appearance, seizures, unusual palmar creases, and

**Table 5-8** Anomalies Associated with Wolf-Hirschhorn Syndrome

Area	Features
Growth	Severe growth restriction is the rule
Achievements	Psychomotor delay Mental retardation
Central nervous system	Dysgenesis of the corpus callosum Abnormal EEG pattern characterized by generalized or unilateral myoclonic seizures followed by brief atypical absences. Seizure disorders tend to disappear with age
Skull	Microcephaly Dolichocephaly
Face	Scalp defects Greek helmet facial appearance Earlobe anomalies Large rectangular nose continuing to the eyebrows Low-set ears Anterior eye segment anomalies (extropia, blepharoptosis) Coloboma of the eyes Hypertelorism High forehead Downward-slanting palpebral fissures Some ophthalmic features of 4p- syndrome are similar to those of 5p- (cri-du-chat syndrome) Coracoid nose Microretrognathia Facial dysmorphism Cleft lip and palate Down-turned mouth Taurodontism, which is a dental trait characterized by teeth with elongated pulp chambers and apical displacement of the bifurcation and trifurcation of roots. It causes eruption delay and congenitally lost teeth
Heart	Ventricular septal defect Right ventricular hypoplasia
Lungs	Pulmonary isomerism Diaphragmatic hernia
Urinary system	Hypoplastic thorax Renal hypoplasia Polycystic dysplasia Oligomeganephronia (a rare renal hypoplasia characterized by a reduction in the number of reniculi with compensatory hypertrophy of the glomeruli and proximal renal tubules)
Genital	Hypospadias Undescended testes with an irregular distal penis
Spine	Sacral dimples Sacral sinus
Others	Skeletal anomalies

*Continued*



**Table 5-8** Anomalies Associated with Wolf-Hirschhorn Syndrome—Cont'd

Area	Features
	Antibody deficiencies (IgA and IgG2) are mentioned in some cases. The association of antibody defects with 4p- suggests a regulatory gene with the deleted chromosome region that effects the B cell system
	One 8-months-old baby girl developed malignant hyperthermia after cheiloplasty
	Esophageal atresia
	Cystic hygroma
	Large placental chorioangioma
	Hypotrophic placenta, with possible vascular lesions, also without maternal hypertension
Midline fusion defects	Ranging from minor abnormalities such as
	Scalp defect
	Hypertelorism
	Pulmonary isomerism
	Common mesentery
	Hypospadias, that is one of the most prominent and characteristic midline defects in male infants with this syndrome
	Sacral dimple
	to:
	Cleft palate
	Corpus callosum agenesis
	Ventricular septal defect
	Diaphragmatic hernia

EEG, electroencephalography; IgA, immunoglobulin A; IgG2, immunoglobulin G2.

developmental delay. It is also a microdeletion in 4p16.3.

- *Zink finger syndrome*: is considered as a subfamily of 4p-; however signs and symptoms are different.
- *Trisomy 1*: caused by trisomy for some or all regions of chromosome 13, share several features including pre- and postnatal growth retardation, microcephaly, cleft lip and palate, and cardiac anomalies.
- *Other aneuploidies*: Although 4p- is similar to 5p-, 4p- individuals do not have the distinct cry. The ocular features, which distinguish 4p- from other deletions, include normal tearing, some degree of blepharoptosis, and the preponderance of anterior segment signs.

**Prognosis.** Usually lethal; however, four cases have been followed up to 16 years.

**Recurrence Risk.** Unknown.

**Management.** The diagnosis of a growth-restricted fetus with normal amniotic fluid, normal Doppler, and negative infection screen suggest a detailed examination of the fetal brain and heart and a karyotype. Standard cytogenetics cannot always demonstrate a microdeletion; thus, high-resolution banding and molecular analysis should be performed. A three-dimensional ultrasonographic examination is also useful to observe the face of fetuses. An autopsy can reveal delayed bone age.

## References

Sase M, Hasegawa K, Honda R, et al: Ultrasonographic findings of facial dysmorphism in Wolf-Hirschhorn syndrome. *Am J Perinatol* 22:99, 2005.

- Boog G, Le Vaillant C, Collet M, et al: Prenatal sonographic patterns in six cases of Wolf-Hirschhorn (4p-) syndrome. *Fetal Diagn Ther* 19:421, 2004.
- Dietze I, Fritz B, Huhle D, et al: Clinical, cytogenetic and molecular investigation in a fetus with Wolf-Hirschhorn syndrome with paternally derived 4p deletion. Case report and review of the literature. *Fetal Diagn Ther* 19:251, 2004.
- Beaujard MP, Jouannic JM, Bessieres B, et al: Prenatal detection of a de novo terminal inverted duplication 4p in a fetus with the Wolf-Hirschhorn syndrome phenotype. *Prenat Diagn* 25:451, 2005.
- Aslan H, Karaca N, Basaran S, et al: Prenatal diagnosis of Wolf-Hirschhorn syndrome (4p-) in association with congenital hypospadias and foot deformity. *BMC Pregnancy Childbirth* 3:1, 2003.
- Tapper JK, Zhang S, Harirah HM, et al: Prenatal diagnosis of a fetus with unbalanced translocation (4; 13) (p16;q32) with overlapping features of Patau and Wolf-Hirschhorn syndromes. *Fetal Diagn Ther* 17:347, 2002.
- De Keersmaecker B, Albert M, Hillion Y, et al: Prenatal diagnosis of brain abnormalities in Wolf-Hirschhorn (4p-) syndrome. *Prenat Diagn* 22:366, 2002.
- Dufke A, Seidel J, Schoning M, et al: Microdeletion 4p16.3 in three unrelated patients with Wolf-Hirschhorn syndrome. *Cytogenet Cell Genet* 91:81, 2000.
- Petek E, Wagner K, Steiner H, et al: Prenatal diagnosis of partial trisomy 4q26-qter and monosomy for the Wolf-Hirschhorn critical region in a fetus with split hand malformation. *Prenat Diagn* 20:349, 2000.
- Vinals F, Sepulveda W, Selman E: Prenatal detection of congenital hypospadias in the Wolf-Hirschhorn (4p-) syndrome. *Prenat Diagn* 14:1166, 1994.
- Tachdjian G, Fondacci C, Tapia S, et al: The Wolf-Hirschhorn syndrome in fetuses. *Clin Genet* 42:281, 1992.
- Verloes A, Schaaps JP, Herens C, et al: Prenatal diagnosis of cystic hygroma and chorioangioma in the Wolf-Hirschhorn syndrome. *Prenat Diagn* 11:129, 1991.
- Eiben B, Leipoldt M, Schubbe I, et al: Partial deletion of 4p in fetal cells not present in chorionic villi. *Clin Genet* 33:49, 1988.

# ULTRASOUND EVALUATION DURING THE FIRST TRIMESTER OF PREGNANCY

Faye C. Laing, MD, Mary C. Frates, MD, and Carol B. Benson, MD

## Maternal Physiology and Embryo Development

### Development of the Placenta and Fetal Membranes

- Development of the Placenta
- Development of the Uteroplacental Circulation
- Development of the Chorionic "Membrane"
- Development of the Amnion

### Normal Sonographic Anatomy and Landmarks

- Identifying the Gestational Sac
- Blood Flow in Early Pregnancy
- Identifying the Yolk Sac
- Identifying the Embryo and Cardiac Activity
- Identifying Fetal Membranes and the Placenta

### Determining Gestational Age

### First Trimester Complications

- Absent Intrauterine Sac

### Detecting a Sac Without an Embryo or Yolk Sac

### Abnormal Sac Criteria

- Size
- Growth Rate
- Trophoblastic Appearance

## Role of Doppler

### Detecting a Sac With an Embryo

- Cardiac Activity Absent
- Cardiac Activity Present

### Risk Factors for Early Pregnancy Failure

- Gestational Age
- Intrauterine Blood
- Heart Rate

### Small Sac Size—Growth Delay

### Yolk Sac Evaluation

### Amnion Evaluation

### Maternal Factors

### Usefulness of hCG Levels in First Trimester Pregnancy

### Role of Doppler in Predicting Pregnancy Outcome

### Detecting Fetal Anomalies

### Developmental Pitfalls

### Diagnosing Anomalies (Excluding Nuchal Translucency)

### Conclusion

During the first trimester of pregnancy, a unique and dramatic sequence of events occurs, defining the most critical and tenuous period of human development: the remarkable transformation of a single cell into a recognizable human being. The time span for the first trimester is based on menstrual dates; in a patient with a 28-day cycle, it begins 2 weeks before fertilization (on the first day of the last normal menstrual period) and concludes 12 weeks later. In this chapter, gestational age (GA) is used exclusively and is synonymous with menstrual age (MA). This terminology is chosen because menstruation is a visible event that establishes the date of the last normal menstrual period, and because it is consistent with radiologic and obstetric usage. In contrast, embryologic dating begins with conception and is, therefore, 2 weeks later than the first day of the last normal menstrual period. Although embryologic age is scientifically more precise, there is no visible landmark to announce conception, and so, radiologists and obstetricians continue to use MA or GA for pregnancy dating.

Transvaginal sonography is the optimal way to image a patient during the first trimester of pregnancy (Fig. 6-1).

Indications and the need to do this examination are many and include<sup>1</sup>: (1) to identify the location and number of gestational sacs; (2) to assign a GA to the pregnancy; (3) to determine whether an early pregnancy has a normal appearance or whether sonographic indicators are present that predict failure; (4) to evaluate maternal symptoms such as pain or bleeding; (5) to evaluate uterine contents before pregnancy termination; and (6) to guide diagnostic or therapeutic procedures that require visual guidance (that is, chorionic villus sampling, amniocentesis). As ultrasound technology continues to evolve and improve, there is increasing emphasis for early screening of fetal complications. For example, early detection of Down syndrome and other chromosomal abnormalities can now be achieved by measuring the fetal nuchal translucency between 11 and 14 weeks' gestation, and combining this information with maternal age and maternal serum biochemistry levels (pregnancy-associated plasma protein A [PAPP-A], and the free beta subunit of human chorionic gonadotropin).<sup>2,3</sup> Some investigators also suggest that it is possible to examine cardiac and noncardiac fetal anatomy in a low-risk population in the





**FIGURE 6-1.** Sagittal transabdominal scan (A) reveals a normal-appearing retroverted uterus. A transvaginal scan (B) done immediately after the transabdominal study shows the yolk sac within an intrauterine gestational sac.

setting of a routine 11 to 14 week ultrasound scan.<sup>4</sup> Indeed, at this GA, a wide range of congenital anomalies that can affect the central nervous system, heart, ventral wall, urinary tract, and skeleton have been reported.<sup>5</sup> What role three-dimensional (3D) ultrasound will play at this time of development is still unclear, but preliminary work suggests that it can potentially minimize scanning time and provide an excellent way to store scanned data.<sup>6</sup>

To comprehend normal and abnormal sonographic findings in early pregnancy, it is important to understand normal development and to appreciate the rapid and critical sequential changes that are occurring. The first trimester can be divided into preovulation and periovulation, conceptus, embryonic, and fetal phases of development (Table 6-1).<sup>7</sup>

**Table 6-1** Embryology of Early Pregnancy

Period of Development	Weeks	Features
Pre- and periovulation	1-2	Ovarian follicle matures ↑
Ovulation		↑
Corpus luteum Conceptus	3-5	Fertilization ↑
Morula		↑
Blastocyst		↑
Embryonic	6-10	Trilaminar embryo (flat embryo) C-shape embryo ↑
Major organs develop		↑
Yolk sac detaches Fetal	11-12	Fetal growth ↑
		Amniotic and chorionic membranes approach each other (fusion at 17 weeks)

Adapted from Sohaey R, Woodward P, Zweibel WJ: First-trimester ultrasound: The essentials. *Semin Ultrasound CT MR* 17:2, 1996.

The following discussion highlights physiologic, embryologic, and anatomic changes that occur during this time and emphasizes developmental changes as they relate to sonographic images obtained with high-resolution transvaginal transducers. A 28-day cycle is used in this discussion, although a normal cycle may vary in length from 25 to 35 days. For those interested in a more detailed explanation of these events, an excellent source for this material is *The Developing Human: Clinically Oriented Embryology* by Moore and Persaud.<sup>8-18</sup>

## MATERNAL PHYSIOLOGY AND EMBRYO DEVELOPMENT

During the first 2 weeks of pre- and periovulation, cyclic changes occur within both the ovaries and endometrium as a result of the influence of pituitary gonadotropic follicle-stimulating hormone (FSH) and luteinizing hormone (LH) (Fig. 6-2).<sup>17</sup> Initially, under the influence of FSH, a mature ovarian follicle develops. Estrogen elaborated by the follicle causes the functional layer of endometrium to proliferate and become thicker, as the spiral arteries elongate and the uterine glands increase in number and length. As a result of an abrupt surge in LH, ovulation occurs, and an oocyte is extruded, typically on day 14 of the cycle. After ovulation, the follicle collapses and transforms into the glandular corpus luteum, which produces progesterone and a small amount of estrogen. This hormonal activity is responsible for additional histologic changes of the endometrium as it enters the secretory phase, so named because the uterine glands now secrete material rich in glycogen. The glands

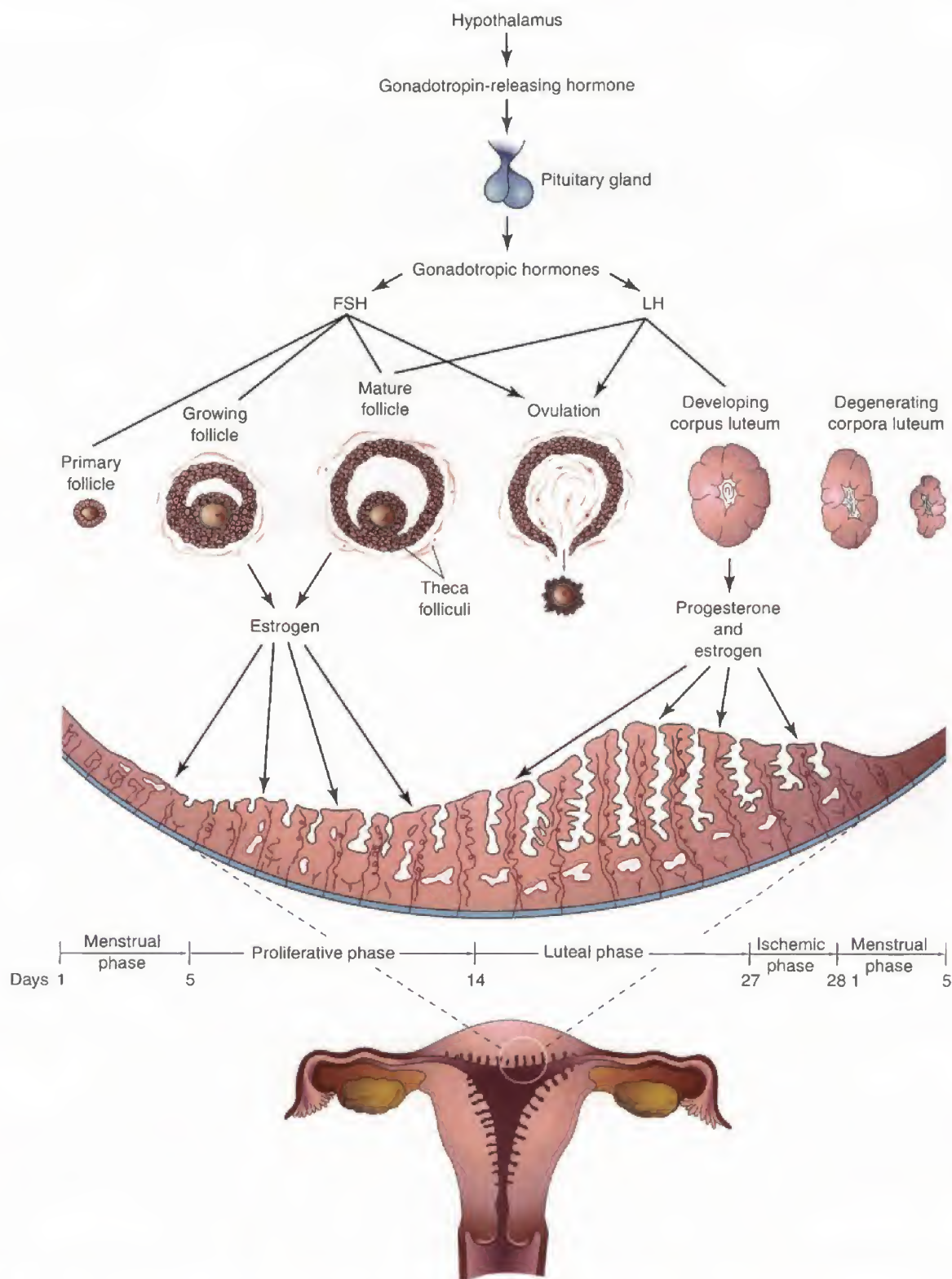


**FIGURE 6-2.** Diagrammatic representation of the relationships between gonadotrophic hormones and changes in the endometrium and ovary during a normal menstrual cycle. Ovarian changes are induced by follicle-stimulating hormone (FSH) and luteinizing hormone (LH). As a result, ovarian hormones are produced (estrogen and progesterone), which promote cyclic changes in the structure and function of the endometrium. (From Moore KL, Persaud TVN: *The Developing Human: Clinically Oriented Embryology*, 7th ed. Philadelphia, WB Saunders, 2003.)



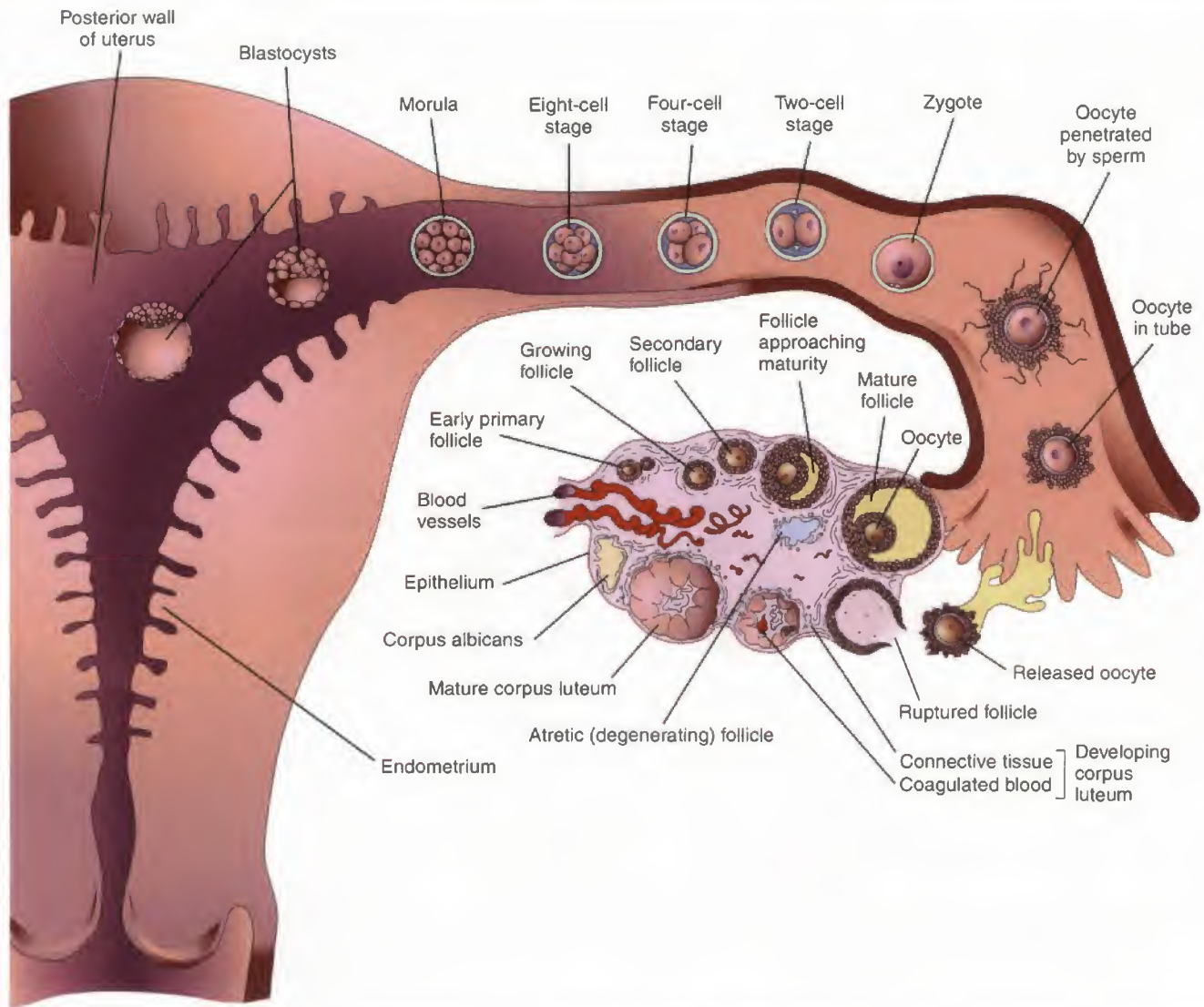


**FIGURE 6-3.** Diagram demonstrating the sequence of ovulation, fertilization, and early development of the embryo. Soon after the morula enters the endometrial cavity, fluid penetrates the cell mass to create the blastocyst. The blastocyst begins to implant into the decidualized endometrium by the end of the 3rd gestational week. (From Moore KL, Persaud TVN: *The Developing Human: Clinically Oriented Embryology*, 7th ed. Philadelphia, WB Saunders, 2003.)

become increasingly wide, tortuous, and saccular, and the uterine spiral arteries become increasingly coiled as they invade the superficial compact layer of endometrium. The endometrium continues to thicken as a result of glandular and vascular growth and increased stromal fluid.

During the 3rd to 5th weeks of the cycle (the conceptus period), fertilization occurs, with subsequent development of the morula, blastocyst, and bilaminar and ultimately trilaminar, or flat, embryo.<sup>7,8,10,16</sup> Fertilization most often occurs within 1 day of ovulation (day 15 of the 28-day cycle), typically in the ampulla, the longest and widest portion of the fallopian tube (Fig. 6-3). At fertilization, fusion of the egg and sperm, each haploid gamete with 23 individual chromosomes, results in a zygote, a diploid cell with 23 pairs, or 46 chromosomes. Over the next 2 days, the cell mass transgresses the tube while dividing repeatedly to form a solid ball of 12 or more cells, called the morula. As the

morula enters the uterine cavity on day 18 or 19 of the cycle, endometrial fluid penetrates the cell mass to create a central cavity. When this occurs, the morula is transformed into a blastocyst, and its tissue is divided into two important layers. The outer cell layer, or trophoblast, ultimately creates the chorionic membranes and the fetal contribution to the placenta. The inner cell layer develops into the embryo, amnion, umbilical cord, and the primary and secondary yolk sacs. By the end of the 3rd week, the blastocyst begins to implant into the decidualized endometrium, a term applied to the functional layer of the thickened and edematous gravid endometrium (Fig. 6-4).

During the 4th week, the blastocyst, measuring only 1 mm in diameter, becomes fully imbedded into endometrial tissue. Not surprisingly, during this process, as trophoblastic tissue invades the endometrium, vaginal bleeding may occur and be confused clinically with an atypical menstrual cycle.

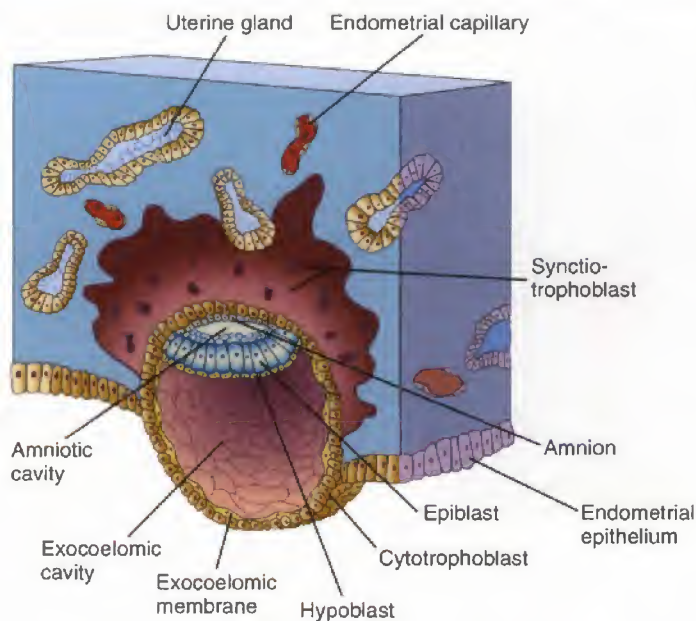


**FIGURE 6-4.** Diagrammatic illustration of blastocyst implanting into the decidualized endometrium. Note the extent of the invading syncytiotrophoblastic tissue, which contributes to the placenta. The amniotic cavity is slitlike at this early stage of development. The exocoelomic cavity becomes the primary yolk sac, and the epiblastic and hypoblastic layers of cells develop into the bilaminar embryonic disk. Despite these ongoing events, sonographic examination cannot yet detect the presence of a pregnancy. (From Moore KL, Persaud TVN: *The Developing Human: Clinically Oriented Embryology*, 7th ed. Philadelphia, WB Saunders, 2003.)

The 4th week is a time of rapid cell proliferation and differentiation, affecting multiple primordial structures. The primary yolk sac shrinks and disappears gradually while the secondary yolk sac forms. The latter structure plays a critical role by providing nutrients for the embryo, serving as the site for initial hematopoiesis, and contributing to the developing gut and reproductive systems.<sup>9</sup> A tiny bilaminar embryo also forms between the secondary yolk sac and developing amnion, and a primitive uteroplacental circulation is established.<sup>8</sup> By the end of this week, the products of conception have attained a diameter of 2 to 3 mm and are at the threshold of detection by state-of-the-art transvaginal ultrasound transducers. In addition, the pregnancy test becomes positive because a measurable quantity of human chorionic gonadotropin (hCG) is produced by trophoblastic tissue.

During the final week of the conceptus stage (5 weeks' GA), normal menstrual flow is absent, and the woman may suspect pregnancy. The products of conception continue to enlarge primarily as a result of expansion of the chorionic cavity, which attains a diameter of 5 mm (Fig. 6-5). This cavity is identified by sonologists as fluid within the "gestational sac." The secondary yolk sac is variably identified by sonographic examination, and the developing bilaminar embryonic disk undergoes the process of gastrulation, which transforms it into a trilaminar disk with three germ layers (endoderm, mesoderm, and ectoderm). Despite these transformations, the embryo remains undetectable by sonography.

Weeks 6 through 10 constitute the embryonic phase, during which time all major internal and external structures begin to form (Table 6-2).<sup>11</sup> Although most organ function remains minimal, the cardiovascular system develops rapidly, and the primordial heart starts to beat at the beginning of the 6th week.<sup>12</sup> The appearance of the embryo changes dramatically as it is transformed from its flat disk-like configuration to a C-shaped structure, and it develops a human-

like appearance (Fig. 6-6). During embryogenesis, crown rump length (CRL) grows rapidly, measuring 30 mm by the end of the 10th week.

The final 2 weeks of the first trimester (11th and 12th weeks GA) begin the fetal period, during which there is continued rapid growth and ongoing organ development.<sup>13</sup> During the initial phase of fetal development, the head is disproportionately large and constitutes one half of the CRL. As body growth subsequently accelerates, relative proportionality becomes apparent.

## DEVELOPMENT OF THE PLACENTA AND FETAL MEMBRANES

### Development of the Placenta

The placenta contains both maternal and fetal tissue. The maternal component is derived from a portion of decidualized endometrium, whereas the fetal component is derived from a portion of chorionic tissue that surrounds the blastocyst.<sup>14</sup>

Endometrium deep to the implanted conceptus, the decidua basalis, forms the maternal component of the placenta. The superficial portion of decidua, which covers the invading conceptus, is the decidua capsularis; the remaining endometrium is the decidua parietalis (also called decidua vera) (Fig. 6-7).

The fetal component of the placenta is derived from trophoblastic tissue, which by 5 weeks' GA develops into chorionic villi that completely encircle the conceptus (see Fig. 6-7A).<sup>15</sup> Initially, these villi are uniform in thickness and are in intimate contact with adjacent decidual tissue. Subsequently, the most superficial two thirds of villi, located immediately beneath the decidua capsularis, degenerate to form the smooth chorion (also called chorion laeve) (see Fig. 6-7B). The remaining villi are in contact with the decidua basalis and are located adjacent to the most deeply



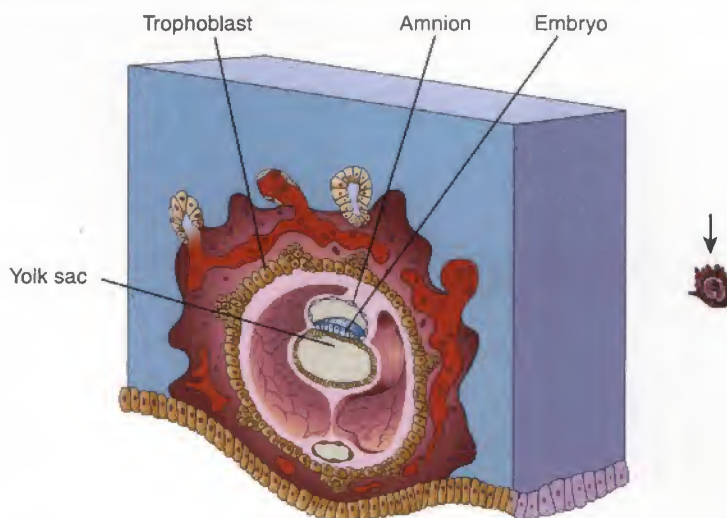


**FIGURE 6-5.** Diagram of the blastocyst at the end of the conceptus stage of development. The gestational sac, which is now visible by sonography, measures approximately 5 mm in diameter and contains the secondary yolk sac lying opposite the amniotic cavity. A developing embryo is interposed between these two fluid-filled cavities. Sonography variably identifies the secondary yolk sac, although the embryo cannot yet be seen. (From Moore KL, Persaud TVN: *The Developing Human: Clinically Oriented Embryology*, 7th ed. Philadelphia, WB Saunders, 2003.)

**Table 6-2** Criteria for Estimating Developmental Stages in Human Embryos

GA (days)	Length (mm)	Main External Characteristics
34–35	1.5–3.0	Flat embryonic disk.
36–37	2.0–3.5	Embryo straight or slightly curved.
38–39	2.5–4.5	Embryo curved owing to head and tail folds.
40–41	3.0–5.0	Upper limb buds appear.
42–44	4.0–6.0	Embryo has C-shaped curve.
45–46	5.0–7.0	Upper limbs are paddle shaped.
47–50	7.0–9.0	Hand plates formed; digital rays present. Lower limbs are paddle shaped.
51–54	8.0–11.0	Foot plates formed.
55–57	11.0–14.0	Digital rays visible in hand plates.
58–60	13.0–17.0	Digital rays clearly visible in foot plates.
61–62	16.0–18.0	Limbs extend ventrally. Trunk elongating and straightening. Midgut herniation prominent.
63–65	18.0–22.0	Upper limbs longer and bent at elbows. Fingers webbed.
66–67	22.0–28.0	Hands and feet approach each other. Fingers are free and longer. Toes webbed. Stubby tail present.
68–69	23.0–28.0	Toes free and longer. Eyelids and external ears more developed.
70	27.0–31.0	Head more rounded and shows human characteristics. External genitalia still have sexless appearance. Distinct bulge still present in umbilical cord, caused by herniation of intestines. Tail has disappeared.

GA, gestational age.

Adapted from Moore KL, Persaud TVN: *Organogenic period: The fourth to eighth weeks*. In Moore KL, Persaud TVN (eds): *The Developing Human: Clinically Oriented Embryology*, 7th ed. Philadelphia, WB Saunders, 2003, pp 78-93.

imbedded portion of the blastocyst. These villi rapidly increase in number, branch profusely, and enlarge as they become the chorion frondosum, the fetal contribution to the definitive placenta.

### Development of the Uteroplacental Circulation

To understand developing uteroplacental circulation, a basic knowledge of the anatomy and physiology of uterine blood flow is helpful. Blood to the uterus is from the paired

uterine arteries, which are branches of the anterior division of the internal iliac artery. As each uterine artery enters the uterus at the uterocervical junction, it ascends along the lateral uterine wall and produces multiple penetrating arcuate branches. When these branches pierce the endometrium, they become the spiral arteries.

With early embryonic development, the spiral arteries located within the decidua basalis become increasingly prominent. Side-by-side maternal and embryonic circulations are established initially as trophoblastic cells form chorionic villi that invade into portions of the decidualized endo-

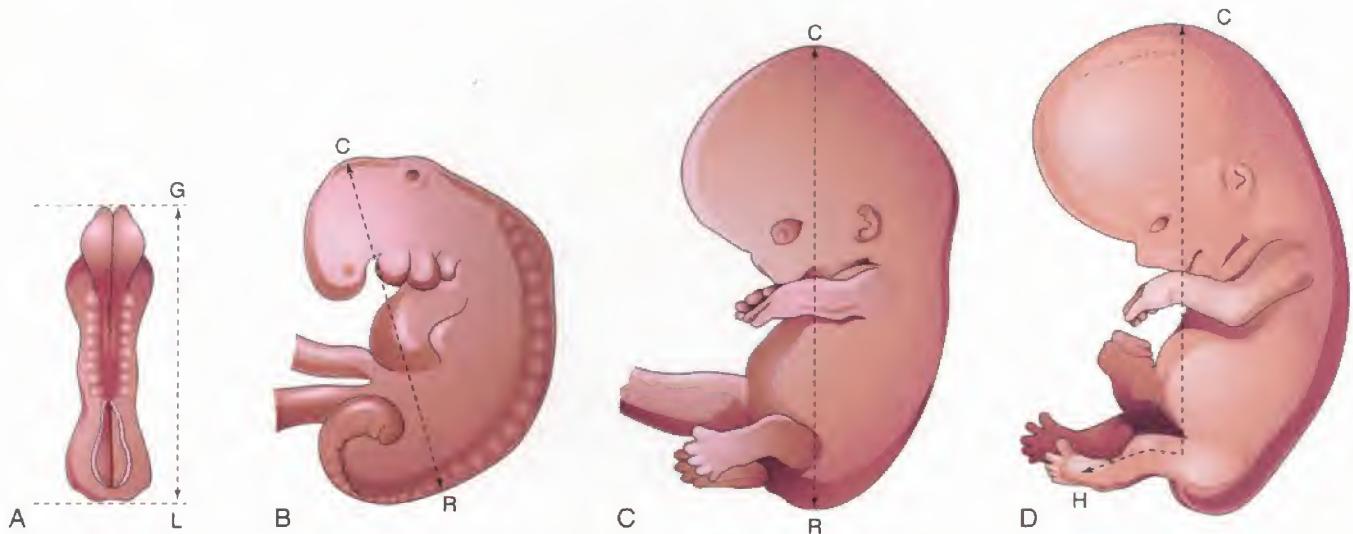


**FIGURE 6-6.** A-D. Sketches during the embryonic phase of development (6 to 10 weeks gestational age) reveal dramatic changes in both the size and shape of the embryo. Initially, the embryo has a flat, disklike configuration (A) without a clearly defined crown or rump. Soon thereafter, it becomes C-shaped (B), and by the end of the embryonic phase of development it has a human-like appearance. (B, C) Methods used to measure crown-rump length and (D) crown-heel length. (From Moore KL, Persaud TVN: *The Developing Human: Clinically Oriented Embryology*, 7th ed. Philadelphia, WB Saunders, 2003.)

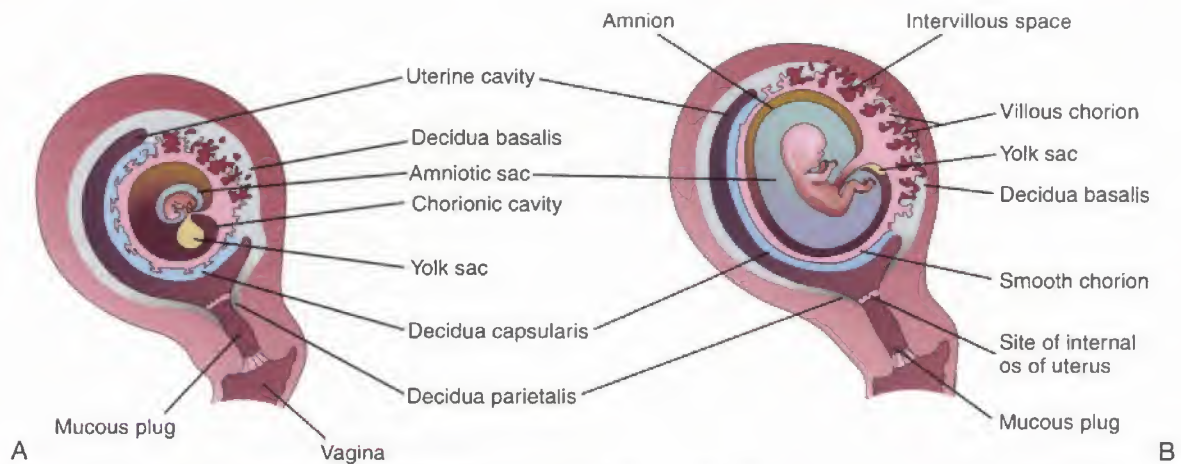


**FIGURE 6-7.** A. At 7 weeks' gestational age, chorionic villi completely surround the gestational sac and are relatively thick where they contact underlying endometrial tissue (decidua basalis). As the sac enlarges, the chorion and overlying decidua (decidua capsularis) protrude into the compressed uterine cavity and come into contact with the decidua parietalis. This anatomic configuration gives rise to the double decidual sac sign. B. The compressed and avascular chorionic tissue becomes smooth and is defined by sonologists as the chorionic "membrane." Because of its fixed anatomic relationship to the developing placenta, in the event of placental bleeding, blood can dissect between the chorionic membrane and overlying decidua, giving rise to a subchorionic hematoma. (From Moore KL, Persaud TVN: *The Developing Human: Clinically Oriented Embryology*, 7th ed. Philadelphia, WB Saunders, 2003.)



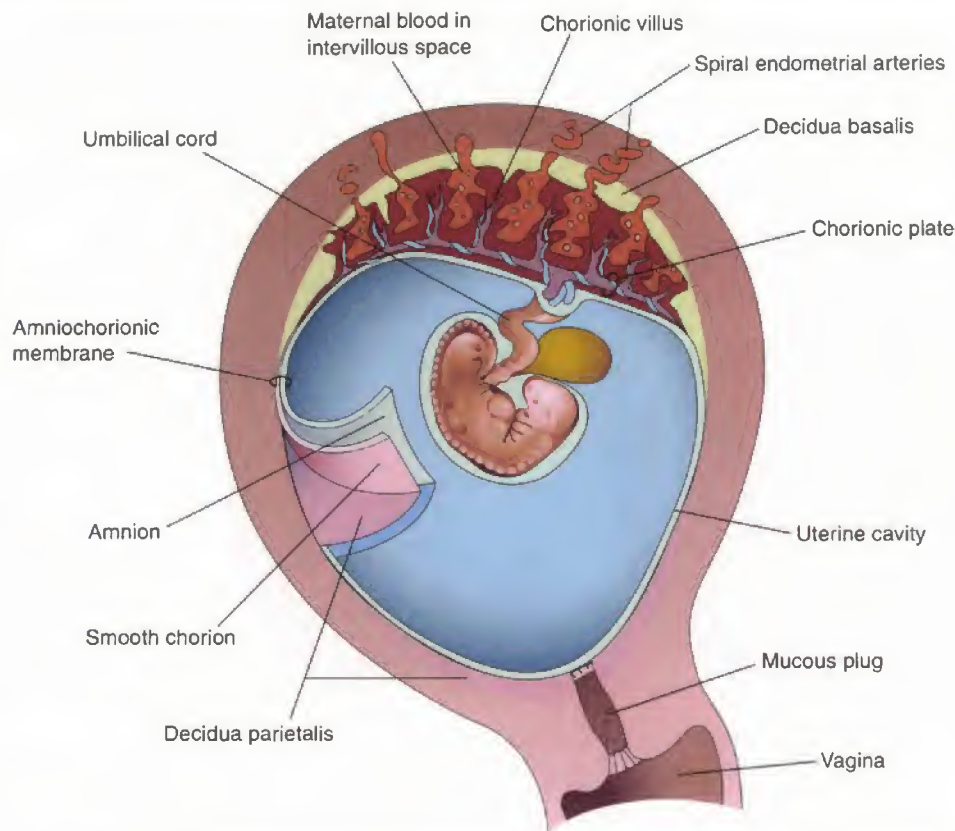


**FIGURE 6-8.** Maternal and embryonic circulations develop side by side as trophoblastic cells form chorionic villi, which invade and erode portions of the decidualized endometrium. The result of this process is development of vascular intervillous spaces that ultimately receive maternal blood from the spiral arteries. This anatomic relationship allows villi containing fetal blood to be surrounded and perfused by maternal blood. (From Moore KL, Persaud TVN: *The Developing Human: Clinically Oriented Embryology*, 7th ed. Philadelphia, WB Saunders, 2003.)

metrium (Fig. 6-8).<sup>14</sup> Before actual maternal-fetal circulation is established, however, the invading trophoblastic cells create plugs within the maternal spiral arteries. The villi simultaneously erode tiny portions of the decidua, which subsequently enlarge to form the intervillous spaces. The intervillous spaces will ultimately receive maternal blood from the spiral arteries, and thus the villi containing fetal blood will be surrounded and perfused by maternal blood by the end of the first trimester.<sup>19</sup> There is some controversy as to how and when in the first trimester the perfusion of villi begins and when actual maternal fetal circulation is initiated. Two hypotheses have been proposed to explain these events.

The first hypothesis is based on studies of first trimester gravid hysterectomy specimens and postulates that until the end of the first trimester there is no communication between maternal and fetal circulations, and intervillous blood flow is absent.<sup>20-28</sup> Early studies suggested that the intervillous spaces are initially filled with clear fluid, possibly filtered maternal plasma.<sup>20</sup> These fluid-filled spaces may create a hypoxic and protective environment for the developing embryo.<sup>29</sup> As the trophoblastic plugs within the spiral arteries dissolve or dislodge by the end of the first trimester, maternal blood begins to circulate into the intervillous spaces. Concurrent with this event is a marked increase in uterine blood flow, which can be documented by sonography.<sup>26</sup>

An alternative hypothesis suggests that transformation of the intervillous space from fluid filled to blood filled occurs gradually throughout the entire first trimester.<sup>30,31</sup> According to this theory, the trophoblastic plugs are incomplete and venous flow is normally present in the intervillous space. The flow is low velocity and has low pulsatility, presumably to prevent the implanting trophoblast from becoming detached from the decidua. This slow flow can be detected by sensitive Doppler techniques by as early as 5.5 gestational weeks.<sup>32-36</sup> Which of these theories best approximates actual physiologic development remains to be determined.

### Development of the Chorionic "Membrane"

The chorion is derived from the superficial two thirds of chorionic villi that, at approximately 10 weeks' GA, become compressed and avascular, and subsequently degenerate into a membrane-like structure (see Fig. 6-7B).<sup>14</sup> Embryologists identify this as the smooth chorion or chorion laeve, whereas ultrasonologists refer to it as the chorionic "membrane." Because the chorionic membrane and chorion frondosum each originate from chorionic villi, these two structures remain in intimate contact throughout gestation. For this reason, the chorionic membrane always extends up to and merges with the edge of the placenta. As is described



later, understanding this anatomic relationship is important for comprehending sonographic findings that accompany placental bleeding.

As the gestational sac grows, it begins to protrude into the compressed uterine cavity (see Fig. 6–7). As a result, the overlying decidua capsularis and smooth chorion come into contact with the decidua parietalis, which is located on the opposite side of the uterine cavity. During the second trimester, the capsularis and parietalis actually fuse and obliterate the uterine cavity. This allows the chorionic membrane to become loosely attached to the decidua parietalis. These anatomic relationships have clinical import because, in the event of placental bleeding, blood can easily dissect into the space between the chorionic membrane and decidua parietalis (see later discussion).<sup>14</sup>

## Development of the Amnion

At 3 to 4 weeks' GA, concurrent with implantation and development of trophoblastic tissue, the amniotic membrane begins to form from cells that originate from the inner blastocyst (see Figs. 6–4, 6–5, and 6–9).<sup>8</sup> This membrane initially surrounds the newly formed amniotic cavity, opposite the newly formed secondary yolk sac, and is attached to the bilaminar embryonic disk, which is contiguous to and lies between the amnion and chorion. As the amnion and its cavity rapidly expand, they surround the growing embryo. The amniotic membrane remains attached to the embryo at the umbilical cord insertion site; as the embryo flexes, its dorsal surface pushes into the amniotic sac. As the umbilical cord elongates, the secondary yolk sac, having completed its functions, is displaced away from the embryo and is readily visible within the shrinking chorionic cavity. Whereas the amniotic cavity continues to expand, the chorionic cavity shrinks and is ultimately obliterated between 12 and 16 weeks.

## NORMAL SONOGRAPHIC ANATOMY AND LANDMARKS

Despite considering the pre- and periovulation period as part of the "first trimester of pregnancy," pregnancy has not yet occurred. However, each month the functional layer of endometrium undergoes anticipatory changes in the event of conception. During menstruation, sonographic images depict the endometrium as a thin central echogenic line because of the opposed endometrial surfaces. Over the next 10 days, before ovulation, the functional layer proliferates, and at sonography a hypoechoic area is perceived surrounding the central linear echo. The total anteroposterior thickness of this multilayered endometrium is approximately 8 mm. Correlation with histologic specimens suggests that this appearance is due to relative homogeneity of endometrial tissue, with the glandular elements remaining straight and orderly.<sup>37,38</sup>

During the conceptus phase of pregnancy (weeks 3 to 5), despite rapid and dramatic changes involving the products of conception, the endometrial appearance is identical to that observed during a nonconceptual cycle. After ovulation, it enters the secretory phase of the cycle, becoming dramatically hyperechogenic, and approaching 14 mm in total thickness. Histologically, the increased echogenicity results not only from new acoustic interfaces that originate

as a result of glandular and vascular tortuosity but also from reflections from glandular secretions, glycogen, and mucus.<sup>37</sup> As the 4th week concludes, despite complete implantation, the blastocyst remains undetectable to even high-resolution vaginal imaging because of its small size (1 mm). During the final week of the conceptus phase, however, just as the patient becomes aware that she may be pregnant, sonography can often identify changes that signal intrauterine implantation.

## Identifying the Gestational Sac

The first definitive sonographic finding to suggest early pregnancy is visualization of the gestational sac. Using vaginal transducers with frequencies of at least 5 MHz, the size threshold for sac detection is 2 to 3 mm, corresponding to between 4 weeks' and 1 day GA and 4 weeks' and 3 days GA (Fig. 6–10).<sup>39–41</sup> At sonography, the earliest appearance of a gestational sac is a small round fluid collection surrounded completely by a hyperechogenic rim of tissue. The central fluid collection is the chorionic cavity, and the surrounding echoes are due to developing chorionic villi and adjacent decidual tissue. As the sac enlarges, the hyperechogenic rim should be at least 2 mm thick, and its echogenicity should exceed the level of myometrial echoes.<sup>42</sup>

To maintain uniformity, gestational sac size should be determined by calculating the mean sac diameter (MSD). This value is obtained by adding the three orthogonal dimensions of the chorionic cavity (excluding the surrounding echogenic rim of tissue) and dividing by 3 (Fig. 6–11).

The position of a normal gestational sac is in the mid- to upper uterus. As the sac implants into the decidualized endometrium, it should be adjacent to the linear central cavity echo complex, without initially displacing or deforming this hyperechogenic anatomic landmark (Fig. 6–12). On the basis of the physiology of sac implantation, Yeh et al,<sup>43</sup> in 1986, described the intradecidual sign. Using this sign with a transabdominal approach, these investigators reported a sensitivity of 92%, specificity of 100%, and accuracy of 93% for diagnosing an early intrauterine pregnancy (IUP). Two subsequent studies, each using a vaginal approach, have been published in an attempt to validate the effectiveness of this sign. The initial report by Laing et al<sup>44</sup> had disappointing results, with a sensitivity of 34% to 66%, specificity of 55% to 73%, and accuracy of 38% to 65%. A subsequent investigation by Chiang et al,<sup>45</sup> had more favorable results, with a sensitivity of 60% to 68%, specificity of 97% to 100%, and accuracy of 67% to 73%. The reason for the disparate results of these two reports is uncertain, but may relate to different criteria used to precisely and confidently identify the thin echogenic line (central uterine stripe) that represents the potential uterine cavity.

Also confounding the problem of identifying an early intrauterine gestational sac with certainty, is that with continued growth, it often changes shape from round to elliptical, and it may develop an irregular contour as a result of adjacent uterine contractions, myomas, implantation bleeds, or a distended maternal urinary bladder. Because even the most favorable reported statistics are not highly sensitive or accurate for documenting the intradecidual sac sign, and because occasionally a pseudogestational sac of an



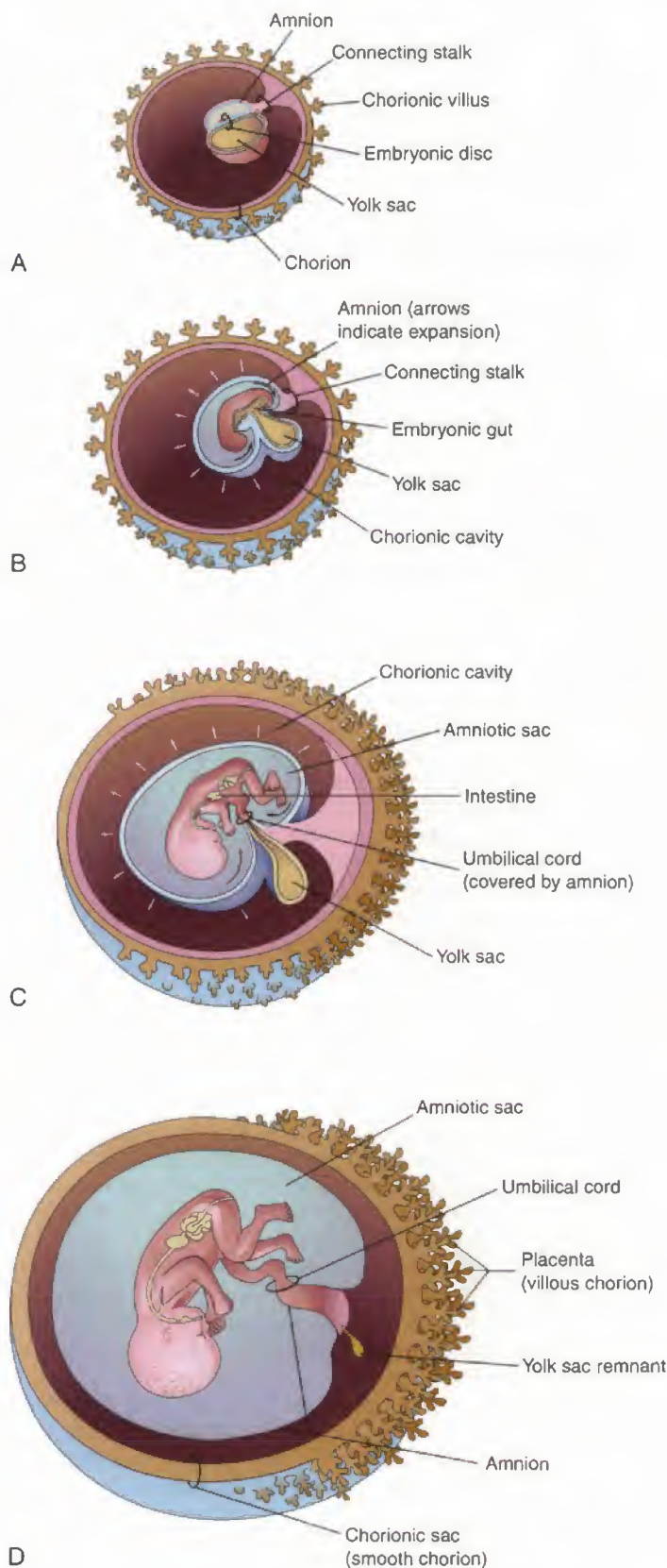


**FIGURE 6-9.** A. At 5 weeks' gestational age, the amniotic membrane surrounds the newly formed amniotic cavity and is opposite the newly formed secondary yolk sac. Interposed between these two cavities is the bilaminar embryonic disc. B. By 6 weeks' gestational age, the rapidly expanding amniotic cavity surrounds the enlarging embryo. Note how the dorsal surface of the embryo pushes into the amniotic sac and how the yolk sac is extruded into the chorionic cavity. At this stage of development, chorionic villi completely encircle the sac. C. At 12 weeks, the amniotic cavity continues to enlarge, whereas the chorionic cavity becomes relatively small but still contains a visible yolk sac. With degeneration of the smooth chorion over the surface of the sac that protrudes into the uterine cavity, the chorionic "membrane" is formed. D. By 22 weeks' gestational age, complete fusion of the amnion and chorionic membranes has occurred, with obliteration of the chorionic cavity. (From Moore KL, Persaud TVN: *The Developing Human: Clinically Oriented Embryology*, 7th ed. Philadelphia, WB Saunders, 2003.)



**FIGURE 6-10.** An early gestational sac, measuring 4 mm in diameter, is visible as a small fluid-filled structure (the chorionic cavity) surrounded by an echogenic rim of tissue (chorionic villi and adjacent decidual tissue) (arrows).

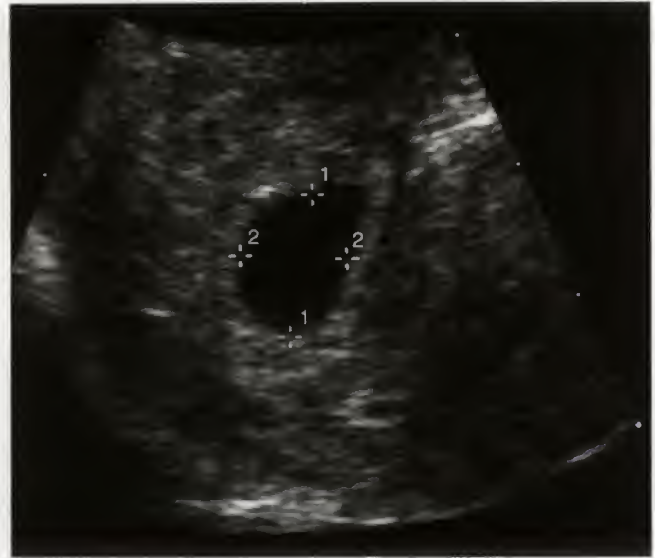


**FIGURE 6-11.** Mean gestational sac diameter is determined by adding the three orthogonal dimensions of the chorionic cavity and dividing by 3. Correct caliper placement is illustrated between calipers one and two. Note that the echogenic choriodecidual reaction is not included in the measurement.

ectopic pregnancy and a gestational sac can have a very similar appearance (Fig. 6-13), the value of this sign appears limited. In cases of very early pregnancy, follow-up sonography should be obtained to document the appearance of the yolk sac or embryo.<sup>44,45</sup>

As the sac enlarges, it gradually impresses and deforms the central cavity echo complex, giving rise to the characteristic sonographic appearance referred to as the double decidual sac sign (see Figs. 6-7 and 6-14).<sup>46,47</sup> This sign, which is universally present when the MSD is 10 mm or greater, consists of two concentric echogenic lines surrounding a portion of the gestational sac. The line closest to the sac represents the combined smooth chorion-decidual capsularis, whereas the adjacent, more peripherally located line represents the decidua parietalis. The uterine cavity is the potential space between these two lines and often contains a trace of fluid. The double decidual sac sign is most effective with transabdominal sonography performed at 5 to 6 weeks' GA because, using this approach, sonographers can confirm the presence of an IUP before a yolk sac is visualized. With the advent of nearly universal transvaginal sonography, the double decidual sac sign has been relegated to a lesser role. The sign may still be useful, however, in patients in whom transvaginal sonography is not possible.

### Blood Flow in Early Pregnancy

The characteristic first trimester main uterine artery waveform obtained at the uterocervical junction consists of high-resistance flow with a prominent diastolic notch, although the notch will occasionally be absent in a normal patient (Fig. 6-15). The diastolic notch typically disappears during the second trimester and in some cases as early as

13 weeks' gestation.<sup>21</sup> Persistence of the diastolic notch into the third trimester correlates with umbilical cord and placental abnormalities.<sup>48</sup>

Doppler signals can also be obtained from the spiral arteries or subchorionic vessels, located at the junction of the myometrium and hyperechogenic choriodecidual tissues. Flow in these vessels is typically pulsatile, with a low-resistance pattern (Fig. 6-16). Deep to the subchorionic vasculature is the intervillous space (Fig. 6-17). In the first trimester, Doppler interrogation at this level reveals a more venouslike flow pattern, which may be difficult to detect (even in a more developed placenta) because of its extremely low velocity.<sup>22</sup>

Over the course of the first trimester, vascular impedance decreases and blood flow velocity increases, and the uteroplacental hemodynamics change from high resistance low volume to the low resistance high velocity state that will continue for the remainder of the pregnancy.<sup>31</sup>

During first trimester sonography, prominent hypoechogenic areas with visible venous flow are occasionally seen around the margins of a gestational sac (Fig. 6-18). These have been termed venous lakes. Unlike true intervillous flow, which is difficult to localize without sensitive Doppler settings, slow flow within these vascular spaces can often be appreciated with gray-scale sonography alone if high-gain settings are used. Because of its extremely low velocity, the flow is difficult to document with color or pulsed Doppler. If no attempt is made to evaluate for the presence of flow, these spaces may be incorrectly considered subchorionic hematomas. Whether these vascular spaces have any significance with regard to pregnancy outcome is uncertain; opinions range from benign to ominous.<sup>49,50</sup> Therefore, when multiple lakes are seen, close sonographic follow-up is probably indicated.





A



B

**FIGURE 6-12.** A. Diagram of the intradecidual sign. The gestational sac (circle) does not displace or deform the central cavity complex (straight black line). The white area represents thickened decidual tissue. (From Laing FC, Brown DL, Price JF, et al: *Intradecidual sign: Is it effective in diagnosis of an early intrauterine pregnancy?* Radiology 204:655, 1997) B. Transvaginal sonogram demonstrates the intradecidual sign. The sac is completely imbedded within the thickened decidual and does not displace or deform the central echo cavity complex (arrows).

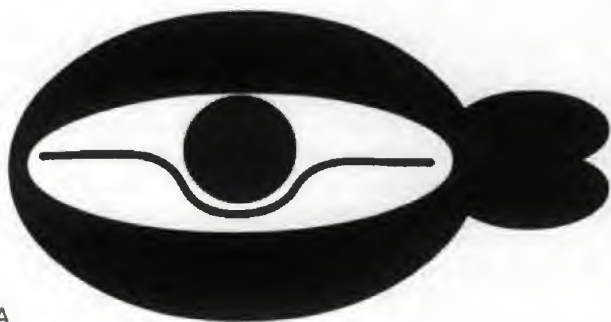


A

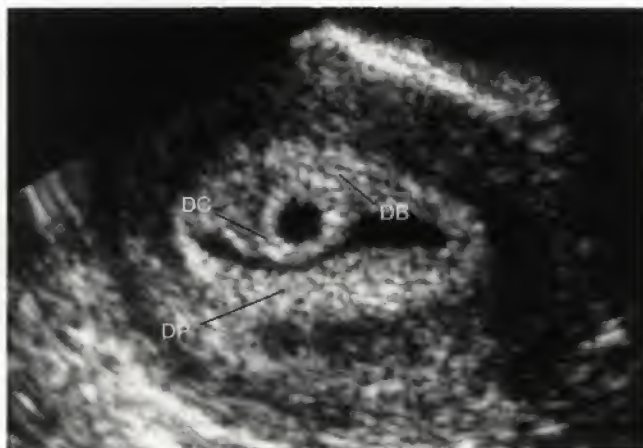


B

**FIGURE 6-13.** Transvaginal sonograms from two patients: one had an intrauterine pregnancy (A) and the other an ectopic pregnancy (B). Similar sonographic findings make it impossible to distinguish the appearance of a gestational sac from a pseudogestational sac.



A



B

**FIGURE 6-14.** A. Diagram of the double decidual sac sign. The gestational sac (circle) protrudes into and displaces the central cavity echo complex (curved line). The white area represents thickened decidual tissue. (From Laing FC, Brown DL, Price JF, et al: *Intradecidual sign: Is it effective in diagnosis of an early intrauterine pregnancy?* Radiology 204:655, 1997) B. Transvaginal sonogram demonstrates the double decidual sac sign. Two concentric lines are due to the echogenic decidual capsularis-smooth chorion (DC) and the peripherally located decidua parietalis (DP). In this patient, the uterine cavity contains a small amount of fluid. The decidua basalis (DB) is slightly more echogenic as a result of developing placental tissue.

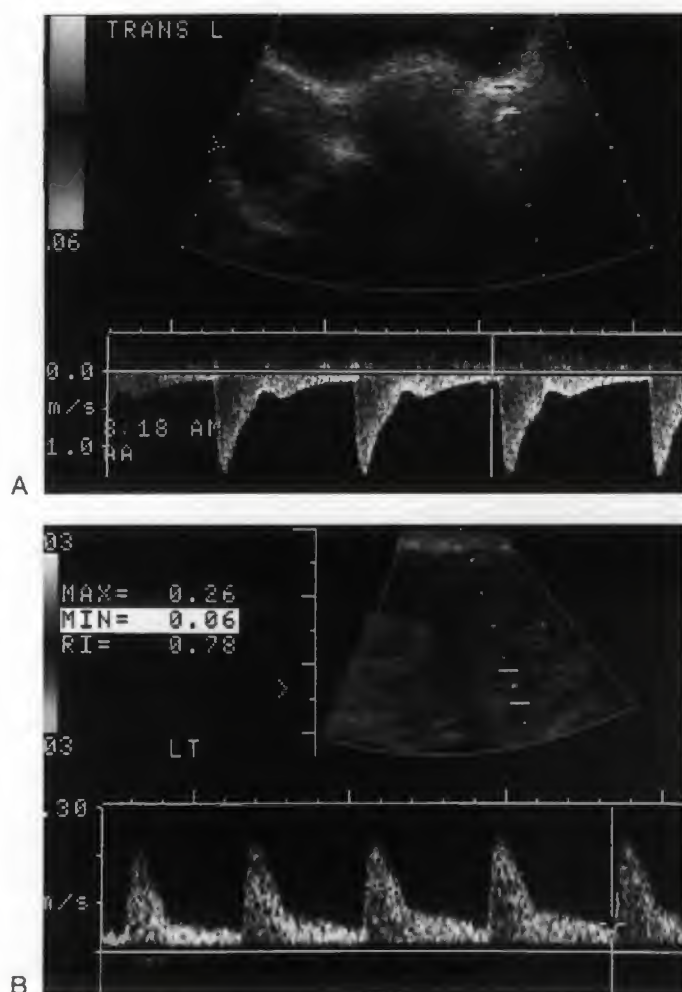


**FIGURE 6-15.** Uterine artery waveforms. A. Tracing of the left uterine artery at 8.4 weeks gestational age shows high systolic velocity and an early diastolic notch. B. In another patient at 6.0 weeks gestational age, the uterine artery tracing lacks a diastolic notch. The outcome was normal.

## Identifying the Yolk Sac

The yolk sac is the first anatomic structure identified within the gestational sac. Embryologically, this is the secondary yolk sac, but because the primary yolk sac cannot be detected by sonography, sonologists refer to this structure simply as the yolk sac. Using a transvaginal approach, it may be visible as early as the beginning of the 5th gestational week (MSD, 5 mm), and it is almost always seen by 5.5 weeks' GA (MSD, 8 mm).<sup>51</sup> Using a transabdominal approach, the yolk sac should be evident by 7 weeks' GA, when the MSD is 20 mm.<sup>52</sup> Because detecting a yolk sac unequivocally confirms that an intrauterine fluid collection represents an early IUP as opposed to a pseudosac associated with an ectopic pregnancy, it is important to optimize scanning parameters to ensure its visualization.<sup>53</sup> Given a choice, the highest possible transducer frequency as well as harmonic imaging should be selected (Fig. 6-19). Detecting the yolk sac is also important for purposes of assigning GA, and to

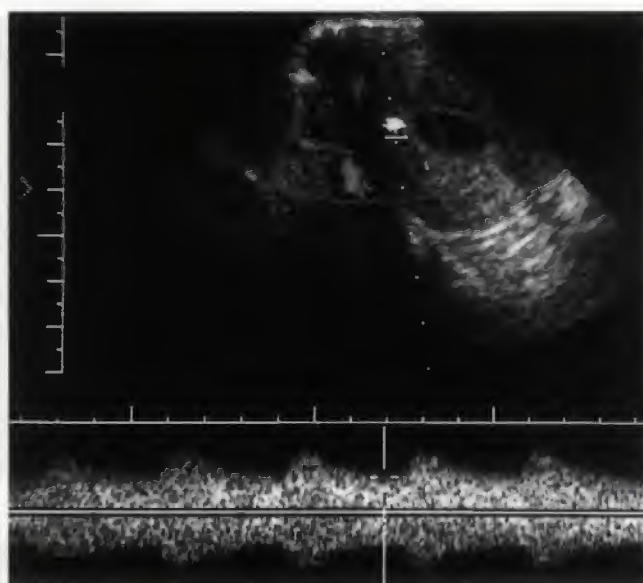


**FIGURE 6-16.** Subchorionic artery Doppler tracing at 7.5 weeks' gestational age is obtained at the junction of the echogenic trophoblast and myometrium and shows a low velocity waveform with prominent diastolic flow.

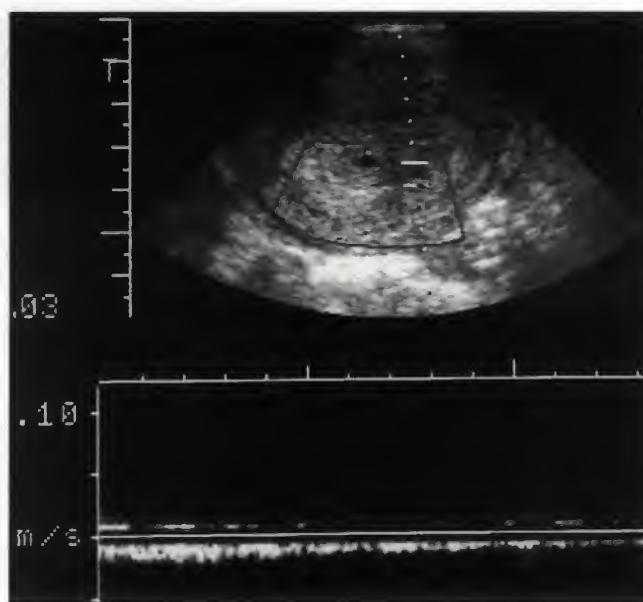


**FIGURE 6-17.** Doppler flow obtained from the intervillous spaces reveals a venouslike waveform with extremely low velocity.

locate the contiguous embryonic disk and early cardiac activity.<sup>51,52,54,55</sup>

The yolk sac is spherical in shape, with a well-defined echogenic periphery and a sonolucent center. Its diameter increases steadily between 5 and 10 weeks' GA to a maximal diameter of 5 to 6 mm<sup>56-58</sup>; this corresponds to a CRL of 30 to 45 mm (Fig. 6-20 and Table 6-3).<sup>58</sup> As the GA advances, the yolk sac separates and ultimately detaches from the



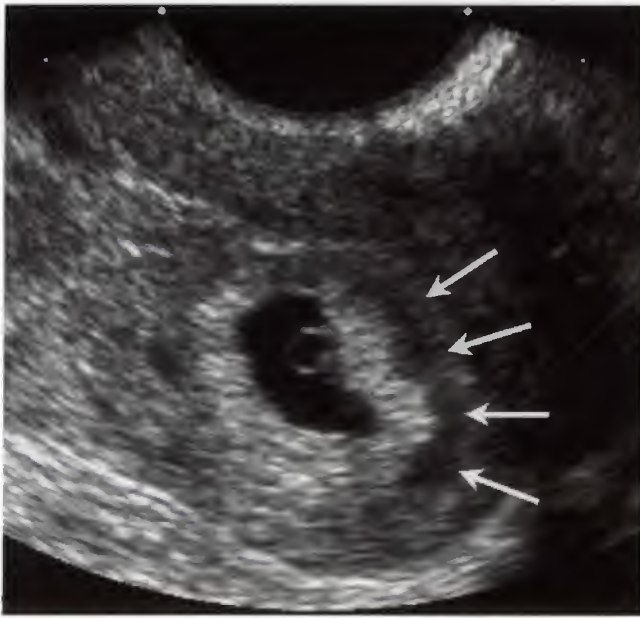


**FIGURE 6-18.** With gray scale imaging, visible flow was obvious within a crescentic area contiguous to the gestational sac (arrows). In this patient, follow-up examination confirmed embryonic demise.

embryo but remains visible within the shrinking chorionic cavity. Subsequently, its diameter decreases,<sup>57,58</sup> and it may occasionally become somewhat irregular in contour.<sup>56</sup> By the end of the first trimester, it is no longer detected by sonography, although, if searched for, it can be found at delivery.<sup>59</sup>

### Identifying the Embryo and Cardiac Activity

Using state-of-the-art vaginal transducers, the embryonic disk is detected initially as a subtle area of focal thickening along the periphery of the yolk sac (Fig. 6-21). Most authorities agree that the threshold for embryo detection is when the disk measures 1 to 2 mm in length. Depending on the investigator, this corresponds to between 5 and 6 weeks' GA<sup>60-63</sup> and a MSD of between 5 and 12 mm.<sup>64-66</sup>

Embryologic investigation suggests that cardiac contractions begin at 36 to 37 days GA.<sup>12</sup> Support for this is found in a series of patients who conceived with assisted reproduction. In these patients, transvaginal sonography detected embryonic cardiac activity at 34 gestational days, with a simultaneous embryonic length of 1.6 mm.<sup>67</sup> Because the human eye is exquisitely sensitive to motion, very early cardiac pulsations can occasionally be appreciated by real-time sonography before the embryo itself is identified. For practical purposes, many sonologists consider the identification of cardiac activity in an embryo with a CRL of less than 5 mm as 6 weeks' GA.<sup>68</sup> Cardiac activity should be detected routinely when the embryo attains a length of 4 to 5 mm.<sup>67,69,70</sup> This corresponds to a GA of 6.0 to 6.5 weeks, at which time the MSD is 13 to 18 mm.<sup>51,65,67,71,72</sup> Using a transabdominal approach, cardiac activity should be evident by 8 weeks' GA, when the MSD is 25 mm.<sup>52</sup>

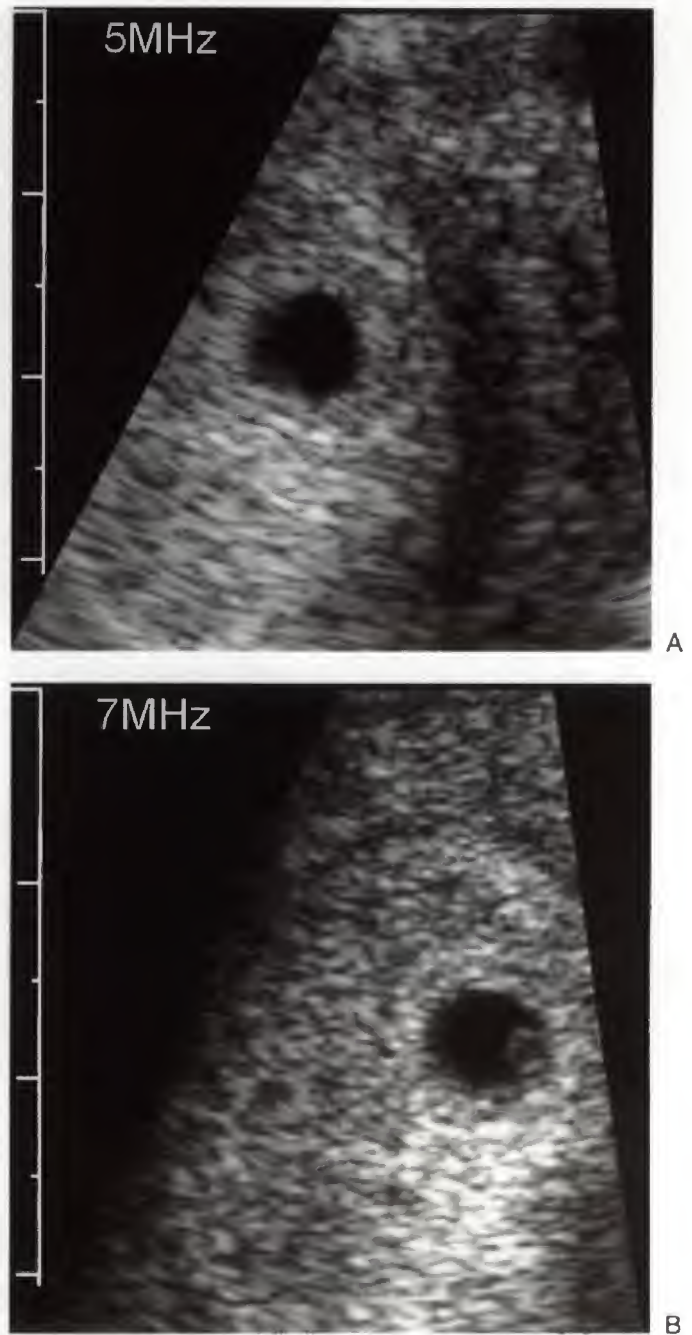


**FIGURE 6-19.** 5.3-week intrauterine gestational sac. A. A transvaginal scan using a 5MHz transducer failed to detect a yolk sac. B. With a 7.5 MHz transducer, a yolk sac is easily seen.

During the first trimester, cardiac rates, which should be recorded using M-mode, vary with GA, but not with the sex of the embryo (Table 6-4 and Fig. 6-22).<sup>72-77</sup> When activity is obtained before 6 weeks, the rate is relatively slow, typically between 100 and 115 beats per minute (BPM) (Fig. 6-23).<sup>72,78-80</sup> Thereafter, it increases rapidly, and by 8 weeks is between 144 and 170 BPM.<sup>72-74</sup> After 9 weeks' GA, the rate plateaus at 137 to 144 BPM.<sup>72</sup> Examining an individual embryo for 15 to 60 minutes reveals almost no

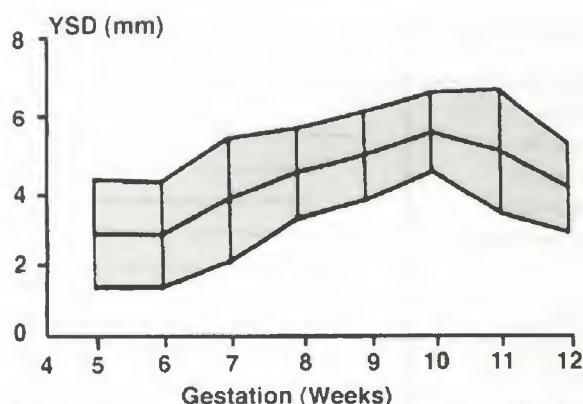


**FIGURE 6-20.** Graph depicting the mean diameter of the yolk sac diameter ( $\pm$  standard deviation) as it relates to the gestational age in weeks. Note the diameter increases steadily to 10 weeks' gestational age and then gradually diminishes. (From Jauniaux E, Jurkovic D, Henriët Y, et al: *Development of the secondary human yolk sac: Correlation of sonographic and anatomic features*. Hum Reprod 6:1160, 1991.)

**Table 6-3**

**Mean Diameter of the Secondary Yolk Sac by Week**

Gestational Age (weeks)	Sonographic Diameter (mm $\pm$ SD)
5	3.01 $\pm$ 0.75
6	2.99 $\pm$ 0.73
7	3.99 $\pm$ 0.86
8	4.72 $\pm$ 0.64
9	5.22 $\pm$ 0.63
10	5.89 $\pm$ 0.56
11	5.35 $\pm$ 0.87
12	4.34 $\pm$ 0.62

Adapted from Jauniaux E, Jurkovic D, Henriët Y, et al: *Development of the secondary human yolk sac: Correlation of sonographic and anatomical features*. Hum Reprod 6:1160, 1991.

variation in cardiac rate<sup>75</sup>; in contrast, comparing embryonic heart rates at different GAs reveals progressively more variation in heart rate with increasing GA.<sup>76</sup>

Sonographic observation throughout the embryonic period (weeks 6 to 10) reveals dramatic transformation of anatomic structures (see Figs. 6-6, 6-24, and 6-25 and Table 6-2). CRL length increases by approximately 1 mm/day.<sup>66,81</sup> During the 6th week of development, with ventral folding of the cranial and caudal ends of the embryo, it changes rapidly from a flat disk into a 3D C-shaped structure.<sup>11</sup> The rapidly developing brain and head become prominent as the rostral neuropore closes, and the caudal neuropore elongates and curves into a tail. Soon thereafter, as the amniotic sac surrounds the developing embryo, the yolk sac, and embryo diverge from one another. Despite the extra-amniotic location of the yolk sac, initially it remains attached to the embryo via the sonographically visible vitelline duct (also called the omphalomesenteric duct) (Fig. 6-26).<sup>82</sup> This structure contains an artery and vein that transport blood elements, nutrients, and primordial sex cells



**FIGURE 6-21.** The embryonic disk is initially seen as a focal thickening along the periphery of the yolk sac (arrow). In this case, its length is approximately 2 mm, corresponding to 6 weeks' gestational age.

**Table 6-4**

**First-Trimester Fetal Heart Rates**

Gestational Age (weeks)	Mean Fetal Heart Rate (beats per minute $\pm$ 1 SD)
5-5.95	101.2 $\pm$ 8.7
6-6.95	124.5 $\pm$ 12.1
7-7.95	128.0 $\pm$ 11.7
8-8.95	144.3 $\pm$ 19.5
9-9.95	138.7 $\pm$ 12.4
10-10.95	136.9 $\pm$ 10.9
11-11.95	139.8 $\pm$ 18.9
12-12.95	137.3 $\pm$ 12.9

Adapted from Hertzberg BS, Mahony BS, Bowie JD: *First trimester fetal cardiac activity: Sonographic documentation of a progressive early rise in heart rate*. J Ultrasound Med 7:573, 1988.

from the yolk sac to the embryo. Between 7 and 8 weeks, limb buds evolve into paddle-shaped upper and lower limbs, with early development of the hands and feet. By the 9th week, the extremities protrude ventrally, the trunk begins to elongate and straighten, and midgut herniation into the umbilical cord is prominent. The 10th week (embryo length, 30 to 35 mm) reveals a distinctly human-appearing embryo, with visible and relatively opposed hands and feet and the tail no longer present (Fig. 6-27). Although a prominent embryologic textbook suggests return of the midgut to the abdomen during the 12th gestational week,<sup>18</sup> sonographic



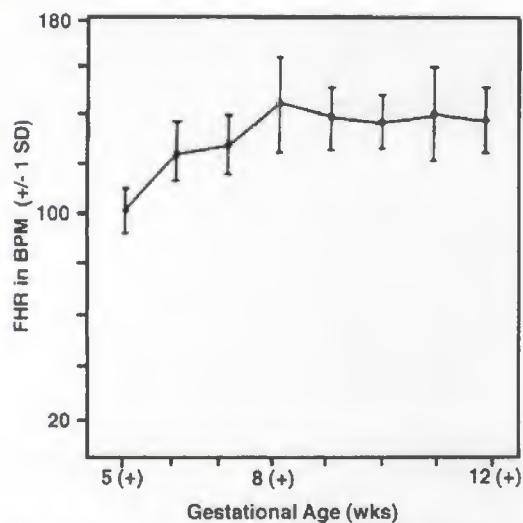


**FIGURE 6-22.** Mean fetal heart rate ( $\pm$  standard deviation) as a function of gestational age. (From Hertzberg BS, Mahony BS, Bowie JD: First trimester fetal cardiac activity: Sonographic documentation of a progressive early rise in heart rate. *J Ultrasound Med* 7:573, 1988.)



**FIGURE 6-23.** Before 6 weeks, the fetal heart rate is relatively slow. In this case, it was determined as 94 beats per minute.

analysis suggests this event is completed by the end of the 11th week.<sup>83-85</sup>

The combination of higher frequency and technologically improved transducers in concert with multiplanar endovaginal 3D image acquisition have heralded a new and exciting method to advance “sonoembryology,” such that it is now possible to visually observe, study, and better understand the rapid growth and dramatic anatomic changes that occur during the first trimester.<sup>86-90</sup> As four-dimensional sonographic technology improves, it has the potential to evaluate early fetal movement and behavior patterns.<sup>91,92</sup> The goal for these types of observations is to improve first

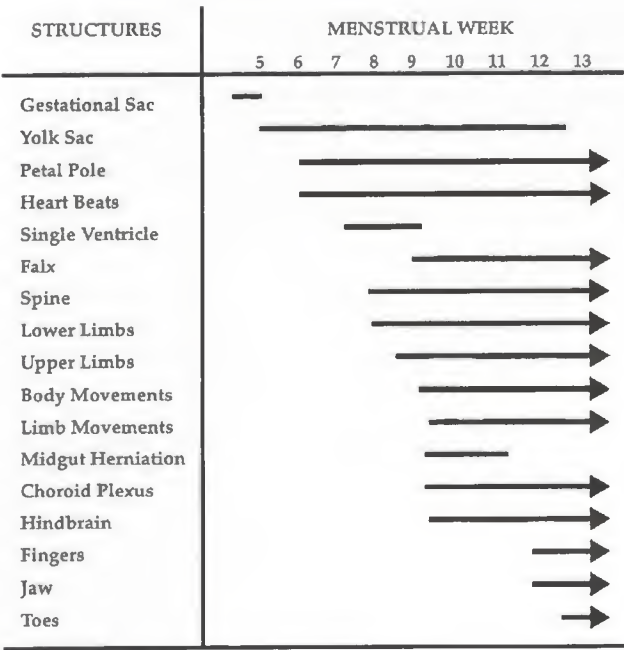


**FIGURE 6-24.** Sequential appearance of embryonic structures and functions during the first-trimester pregnancy. (From Timor-Tritsch IE, Farine D, Rosen MG: A close look at early embryonic development with the high-frequency transvaginal transducer. *Am J Obstet Gynecol* 159:676, 1988.)

trimester assessment of normal anatomic structures, improve evaluation of selected patients at risk for embryologic-fetal malformations, and improve pregnancy dating by basing it on the chronologic and sequential appearance of normal anatomic structures.

### Identifying Fetal Membranes and the Placenta

Recall that, in a normal pregnancy, the first intrasac structure identified by sonography is the yolk sac, visible by 5.5 weeks’ GA. A few days later, the embryonic disk can be detected. Although the amniotic membrane develops concurrently, because it is so thin (0.02 to 0.5 mm),<sup>93</sup> and possibly because it is closely applied to the embryo,<sup>94</sup> it is not normally identified until 6.7 weeks’ at which time the CRL is 7 mm (Fig. 6-28).<sup>95</sup> Rarely, however, it can be seen as a small membranous structure contiguous with the embryo but on the side opposite the yolk sac; the term double bleb sign has been used to describe this anatomic relationship (see Figs. 6-5, 6-9A, and 6-29).<sup>82</sup>

Using vaginal transducers and relatively high-gain settings, the thin amniotic membrane becomes apparent surrounding the embryo, which is now located within the sphere-shaped amniotic cavity or sac. With continued first trimester growth, an interesting linear relationship is apparent with respect to CRL and amniotic sac diameter. Not only do each increase by 1 mm per day but their measurements are equivalent (that is, in a normal pregnancy, a CRL of 12 mm should have an amniotic cavity with a mean diameter of 12 mm).<sup>96</sup>



**FIGURE 6-25.** Two-dimensional sonographic images that depict changes during the first trimester in embryonic size and shape. *A.* At 6.5 weeks' gestational age (GA), it is not possible to differentiate the crown from the rump (embryo is measured between calipers) (compare with Fig. 6-6*A*). *B.* At 8 weeks' GA, the embryo has a C-shaped configuration (compare with Fig. 6-6*B*). The cephalic end becomes prominent and contains an easily visible sonolucent structure: the developing rhombencephalon. The rump may reveal a tail-like appendage. Because of embryonic curvature, length measurement is often a neck-rump length (between calipers) rather than a crown-rump length. *C.* By 10 weeks GA (CRL of 30 mm between calipers), the limbs are becoming visible (*open arrow*), and the gut is herniating into the base of the umbilical cord (*arrow*) (compare with Fig. 6-6*C*). Note that the head is disproportionately large relative to body length. *D.* At the end of the first trimester, the fetus has a human-like appearance (compare with Fig. 6-6*D*). Note the relative proportionality between the head size and overall body length.





**FIGURE 6-26.** As the developing embryo and yolk sac diverge, they remain attached via the vitelline (omphalomesenteric) duct (arrow).

In many cases, only the portion of amnion located perpendicular to the ultrasound beam may be visible (Fig. 6-30). Importantly, in some normal cases, it may not be visible at all, and the inability to visualize the amnion does not predict pregnancy failure (Fig. 6-31). Detection of the amnion and its cavity confirms the presence of an intra-uterine gestational sac. Its size and appearance help determine whether an early pregnancy is progressing normally.

Because the amniotic cavity enlarges more rapidly than the chorionic cavity, the latter structure is obliterated as the amniotic membrane reaches the chorion (see Fig. 6-30). The process of apposition begins in the middle of the first trimester but is often incomplete until 12 to 16 weeks' GA.<sup>59</sup> Once apposed, the amniotic membrane is no longer visible.

In most patients, the chorionic cavity is identified by knowledge of its peripheral anatomic relationship to the amnion. Unless a separate amnion is visible, however, the chorionic cavity cannot be identified with confidence. Occasionally, diffuse low-level echogenic material fills the chorionic cavity, and by virtue of acoustic contrast, this anatomic space is "labeled" (Fig. 6-32).<sup>59,82</sup> The precise nature of these echoes is unknown, but they most likely relate to the relatively thick, proteinaceous material contained within this cavity.<sup>97</sup>

As placental development begins during the 8th gestational week, the hyperechogenic ring surrounding the sac becomes asymmetric, with focal peripheral thickening of the most deeply imbedded portion of the sac. This is due primarily to combined developmental changes occurring within the embryonic and, to a lesser degree, the maternal contributions to the placenta.

## DETERMINING GESTATIONAL AGE

Calculating GA on the basis of menstrual history is often risky. Many women are uncertain of their dates, and even when the menstrual history is known to be correct, individual variations in the time of ovulation can alter the length of a cycle from 25 to 35 days. Despite these variables, experts agree that the most accurate time to date a pregnancy is during the first trimester, when biologic variation is relatively



A



B

**FIGURE 6-27.** A. Three-dimensional image of embryo at 10.4 weeks' gestational age demonstrates proportionally large head, 4 visible extremities, and mild prominence at the base of umbilical cord, consistent with physiologic herniation of the gut into the cord. Comparison with gray scale image of the same embryo (B) shows crown-rump length of 34.8 mm, without discernable anatomic detail.

minimal (Table 6-5).<sup>68,98</sup> Accurate dating is a critical prerequisite for subsequent reliability in fetal growth studies.

The first structure that can be measured for the purpose of calculating GA is the gestational sac. Sac measurements should be obtained if there is no visible yolk sac or embryo. Various methods and formulas have been developed for this

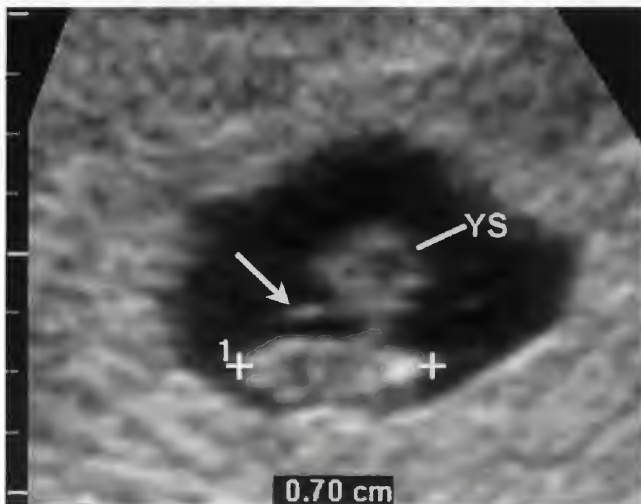


**FIGURE 6-28.** Transvaginal scan of a 6.7-week gestational age embryo (crown rump length of 7 mm) demonstrates a thin echogenic line (arrow) close to the embryo that is due to the amnion. The yolk sac (YS) is visible in the chorionic cavity.



**FIGURE 6-29.** Transvaginal scan of a 5.8-week gestational age embryo (crown rump length, between calipers, measured 2.6 mm) demonstrates the uncommonly observed double bleb sign. Because it is thicker and more echogenic, the outer covering of the yolk sac (YS) is more easily seen than the amniotic membrane (A). In this image, an embryo is difficult to identify, but cardiac activity (118 beats per minute) was recorded.



**FIGURE 6-30.** Because it is so thin, it is not unusual to visualize only the portion of amnion located perpendicular to the ultrasound beam. In this 13.5-week gestational age pregnancy, note that the yolk sac is more visible than the amnion and is located in the relatively small chorionic cavity.



**FIGURE 6-31.** In this normal 8.3-week intrauterine pregnancy, the embryo and yolk sac are clearly seen. Despite relatively high gain settings, the amnion is not visible.

purpose, including sac volumes and mean diameters.<sup>52,64</sup> Because of the ease with which it can be obtained, many authorities use the MSD (see Fig. 6-11). Between 5 and 11 weeks' GA, a simple and convenient method to calculate GA (in days) using sac size is to add 30 to the MSD (in millimeters).<sup>52,99</sup> With this formula, a sac with a mean diameter of 5 mm corresponds to 35 days GA. Whether 3D

ultrasound determination of sac volume will prove superior to conventional methods remains to be shown. Of two published comparative studies, one suggested 3D was superior to conventional two-dimensional volumetry,<sup>100</sup> whereas the other showed equivalent results.<sup>101</sup> Neither study demonstrated prognostic superiority of volumetric measurements with respect to gestational outcome.





**FIGURE 6-32.** Occasionally, in a normal first-trimester pregnancy, the chorionic cavity contains low-level echogenic material. In this example, the amniotic cavity is relatively sonolucent compared with the chorionic cavity.

The next visible landmark that can be used for pregnancy dating is the presence of a yolk sac. A yolk sac without an embryo or cardiac activity, detected by transvaginal scan, corresponds to 5.5 weeks' GA.<sup>68</sup> With normal development, in accordance with the formula noted previously, the MSD should be 8 mm. If cardiac activity is detected but the CRL is too small to measure, the GA is reported as 6 weeks.<sup>68</sup> Between 6 and 12 weeks' GA, determining the CRL measurement is generally considered the most accurate method of dating a pregnancy.<sup>62,63,102-105</sup> When the embryonic disk is detected initially at 6 weeks' GA, it may be too small to actually measure, although cardiac pulsations are frequently visible (see Fig. 6-29). Within days, the length of the linear embryonic disk can be measured, although it is not possible to actually distinguish the crown from the rump (see Figs. 6-6A and 6-25A). As the embryo grows and it assumes a C shape, the cranial end becomes relatively prominent and identifiable (see Figs. 6-6B, 6-25B, and 6-27A). Before 8 weeks' GA, because of rather dramatic flexion of the head, the greatest length along the longest axis is actually a neck-rump measurement.<sup>106</sup> Toward the end of the embryonic phase of development, with gradual extension of the head and regression of the tail, a true crown rump measurement is possible (see Figs. 6-6C and 6-25C).

Robinson,<sup>107</sup> in 1973, initially reported use of the CRL for pregnancy dating. Over the next 2 years, he and Fleming refined their methodology and, in their 1975 landmark article, stated that "a single CRL measure could estimate maturity to within  $\pm 4.7$  days with 95% confidence on the basis of a single measurement."<sup>102</sup> Despite relatively crude equipment, their tables have, quite remarkably, withstood the test of time, although more recent tables (some based on transvaginal studies or pregnancies conceived through assisted reproduction) modified the original numbers to reflect more accurately GA determination in very early pregnancy (Table 6-6).<sup>59,62,63,66,68</sup>

Because normal embryonic growth is almost linear at 1 mm/d,<sup>52,61-63,95</sup> GA in days can also be estimated by adding 42 to the embryonic length (in millimeters). For

**Table 6-5** Guidelines for Dating a Pregnancy During First Trimester

Stage of Development	Gestational Age (weeks)
Gestational sac (no yolk sac, embryo, heartbeat)	5.0
Gestational sac and yolk sac (no embryo, no heartbeat)	5.5
Gestational sac and yolk sac (living embryo, CRL <5 mm) too small to measure	6.0
Embryo/fetus $\geq 5$ mm in length	Age based on CRL (see Table 6-6)

Formulas: mean sac diameter (mm) + 30 = gestation age (days) (between 5 and 11 weeks).

CRL, Crown rump length (mm) + 42 = gestation age (days) (between 6 and 9.5 weeks).

From Benson CB, Doubilet PM: Fetal measurements-normal and abnormal growth. In Rumack CM, Wilson S, Charboneau JW, et al (eds): *Diagnostic Ultrasound*, 3rd ed. St Louis, Elsevier Mosby, 2005, pp 1493-1512.

pregnancies between 43 and 67 days, this determination has a 95% confidence limit of  $\pm 3$  days.<sup>61</sup>

Toward the end of the first trimester, with rapid fetal development and flexion/extension positional changes limiting accurate CRL determination, measurements of the biparietal diameter and femur length become the preferred biometric parameters for calculating GA.<sup>68,108</sup> The primary factor that negatively influences the reliability of first trimester GA determination is measurement error.

## FIRST TRIMESTER COMPLICATIONS

Because of the complex sequence of events that accompany first trimester development, it is not unusual for complications to occur. Approximately 15% of clinically recognized pregnancies are spontaneously miscarried; the loss rate is estimated at two to three times higher with very early and often clinically unrecognized pregnancy.<sup>109,110</sup>

Vaginal spotting or frank bleeding is very common and is experienced by approximately 25% of patients during the first few weeks of pregnancy.<sup>109</sup> Often the bleeding is temporary and self-limited, and is likely due to implantation of the conceptus into the decidualized endometrium. If ultrasound is performed in these patients, the results are usually normal.

In a setting of severe pain, uterine contractions, and a dilated cervix, the pregnancy is doomed to failure. In these cases, ultrasound is not usually indicated but may be used selectively to determine whether retained products of conception are present, which could require curettage.

If the cervix is long and closed in a patient with vaginal bleeding, the diagnosis is *threatened abortion*. This term, applicable in approximately 25% of clinically apparent pregnancies of 20 weeks or less, is used when the patient is clinically considered to have a potentially living embryo. Threatened abortion encompasses a broad range of conditions that are named based on the stage of development

**Table 6-6** Crown Rump Length Measurement Related to Menstrual Age (MA)

		Mean Predicted MA (weeks)				Mean Predicted MA (weeks)	
CRL		Robinson and Fleming <sup>87*</sup>	Hadlock et al <sup>54†</sup>	CRL		Robinson and Fleming <sup>87*</sup>	Hadlock et al <sup>54†</sup>
(cm)	(mm)			(cm)	(mm)		
0.2	2	5.7	5.7	2.9	29	9.9	9.7
0.3	3	5.9	5.9	4.0	40	10.0	9.9
0.4	4	6.1	6.1	3.1	31	10.1	10.0
0.5	5	6.3	6.2	3.2	32	10.2	10.1
0.6	6	6.5	6.4	3.3	33	10.3	10.2
0.7	7	6.7	6.6	3.4	34	10.4	10.3
0.8	8	6.9	6.7	3.5	35	10.5	10.4
0.9	9	7.0	6.9	3.6	36	10.6	10.5
1.0	10	7.2	7.1	3.7	37	10.7	10.6
1.1	11	7.4	7.2	3.8	38	10.8	10.7
1.2	12	7.5	7.4	3.9	39	10.9	10.8
1.3	13	7.7	7.5	4.0	40	11.0	10.9
1.4	14	7.9	7.7	4.1	41	11.1	11.0
1.5	15	8.0	7.9	4.2	42	11.2	11.1
1.6	16	8.2	8.0	4.3	43	11.3	11.2
1.7	17	8.3	8.1	4.4	44	11.4	11.2
1.8	18	8.5	8.3	4.5	45	11.4	11.3
1.9	19	8.6	8.4	4.6	46	11.5	11.4
2.0	20	8.7	8.6	4.7	47	11.6	11.5
2.1	21	8.9	8.7	4.8	48	11.7	11.6
2.2	22	9.0	8.9	4.9	49	11.8	11.7
2.3	23	9.1	9.0	5.0	50	11.9	11.7
2.4	24	9.3	9.1	5.1	51	11.9	11.8
2.5	25	9.4	9.2	5.2	52	12.0	11.9
2.6	26	9.5	9.4	5.3	53	12.1	12.0
2.7	27	9.6	9.5	5.4	54	12.2	12.0
2.8	28	9.7	9.6	5.5	55	12.3	12.1

MA, menstrual age; CRL, crown-rump length.

\*Robinson's data modified by Peter Doubilet, MD. The formula, which is also included in the OBUS computer calculation program, is as follows: MA (in weeks) =  $5.9066 + (2.0943 \times \text{CRL}) - (0.21264 \times \text{CRL}^2) + (0.011206 \times \text{CRL}^3)$  (Courtesy of Peter Doubilet, MD).

†MA =  $1.684969 + (0.315646 \times \text{CRL}) - (0.49306 \times \text{CRL}^2) + (0.004057 \times \text{CRL}^3) - (0.000120456 \times \text{CRL}^4)$ .

From Nyberg DA, Laing FC: Threatened abortion and abnormal first-trimester intrauterine pregnancy. In Nyberg DA, Hill LM, Böhm-Velez M, Mendelson EB (eds): Transvaginal Ultrasound. St. Louis, Mosby-Year book, 1992, p 78.

and the sonographic appearance of the products of conception (Table 6-7).<sup>111</sup> Analysis of these pregnancies suggests that 50% eventually abort; the remaining 50% have a normal outcome.<sup>109</sup> The term *missed abortion*, still common in clinical parlance, does not adequately describe pathophysiologic changes and should be abandoned.<sup>112</sup> Instead, *embryonic demise* should apply when there is clear evidence of a nonliving embryo, and *blighted ovum* should be used to describe an abnormal pregnancy with a gestational sac but no visible embryo. To simplify matters without adversely affecting clinical management, consideration should be given to describing any abnormal intrauterine first trimester pregnancy as one that is *unsuccessful*, or *failed*.

Other entities that can present clinically as threatened abortion are ectopic pregnancy and gestational trophoblastic disease. The findings at ultrasound examination in patients with threatened abortion are often both crucial and pivotal because, in most cases, the sonographic findings not only can determine the precise diagnosis but can also be used to guide therapy. Occasionally, to interpret the ultrasound images correctly, it is also necessary to know the quantitative level of serum hCG (see Usefulness of hCG in First Trimester Pregnancy).

The following section reviews the ultrasound findings in threatened abortion (with the exception of gestational trophoblastic disease and ectopic pregnancy, discussed separately in Chapters 29 and 32). Emphasis is on transvaginal criteria that can be used to differentiate a normal from an abnormal first trimester pregnancy reliably and confidently. As a practical point for discussion, and with regard to the uterus, the sonographic findings are divided into those that reveal an absent intrauterine sac, a sac lacking an embryo, and a sac containing an embryo.

### Absent Intrauterine Sac

If the uterus appears normal on sonographic examination, or if the endometrial echoes appear prominent and no sac is visible, the differential diagnosis includes absence of pregnancy, a very early IUP (normal or abnormal), or an ectopic pregnancy. Assuming a positive pregnancy test, most often the outcome is unfavorable. This is because most patients with threatened abortion present after 6 weeks' GA, when sonographic examination normally reveals intrauterine products of conception.<sup>110</sup>



**Table 6-7 Typical Clinical and Sonographic Findings of Threatened Abortion and Abnormal Intrauterine Pregnancy**

Term	Clinical Signs	Serial hCG Levels	Ultrasound Findings
<b>Normal Outcome</b>			
Threatened abortion	Vaginal bleeding, clots (rarely), closed cervical os	Normal exponential rise	Embryo with cardiac activity  Empty gestational sac (5–6.5 weeks) that subsequently develops with embryo Empty uterus (3–5 weeks)
<b>Abnormal Outcome</b>			
Complete abortion	Complete passage of embryo and gestational tissue	Rapid fall	Empty uterus
Incomplete abortion	Incomplete passage of gestational tissue	Slow fall or plateau	Typical thickened and irregular endometrium or fluid within endometrial cavity
Abortion in progress	Bleeding, often with clots and uterine cramps	Variable; usually plateau	Gestational sac in the process of expulsion
Embryonic (fetal) demise	Lack of uterine growth, absent fetal heart tones when expected	Variable; initial normal rise, then plateau or fall	Discrete embryo lacking cardiac activity
Blighted ovum (anembryonic Pregnancy)	Lack of uterine growth, absent fetal heart tones when expected	Variable; initial normal rise, then plateau or fall	Discrepancy in gestational sac development and embryonic development with little or no embryonic remnant

hCG, human chorionic gonadotropin.

From Nyberg DA, Laing FC: Threatened abortion and abnormal first-trimester intrauterine pregnancy. In Nyberg DA, Hill LM, Böhm-Velez M, et al (eds): Transvaginal Ultrasound. St. Louis, Mosby-Year book, 1992.

When the endometrium is abnormally thick or irregularly echogenic, the differential diagnosis includes intrauterine blood or retained products of conception after an incomplete spontaneous abortion, a decidual reaction associated with an ectopic pregnancy, or decidual changes resulting from an early but not yet visible IUP. Patient history in conjunction with the quantitative level of hCG can often pinpoint the specific cause for the sonographic findings. Failure to detect an intrauterine sac when the hCG level exceeds a specific discriminatory number\* excludes a normal early IUP (see Usefulness of hCG in First Trimester Pregnancy). In the absence of heavy bleeding, the likelihood of an ectopic pregnancy increases.

With heavy vaginal bleeding, retained products of conception or intrauterine blood are likely, although ectopic pregnancy is not completely excluded. Under these circumstances, Doppler evaluation may be useful to detect the presence of retained tissue (Fig. 6-33). When tissue is present, available therapeutic options include surgical intervention (cervical dilatation and curettage), medical management (with a vaginal prostaglandin analog such as misoprostol), or expectant management. Several studies suggest that ultrasound may be useful to predict which patients can be managed expectantly. For example, with detectable blood flow in the presumed intervillous space, Schwärzler et al<sup>113</sup> reported an 80% success rate with spontaneous abortion occurring within 7 days, whereas this happened only 23% of

the time when flow was not detected. Two additional investigations each suggest that expectant management has a better outcome when sonography reveals an incomplete miscarriage (that is, retained products), as opposed to an intact gestational sac (with or without a visible embryo).<sup>114,115</sup>

If the sonographic examination fails to reveal an intrauterine sac and the quantitative hCG level is less than the discriminatory number for sac detection, diagnostic considerations include an early IUP (normal or abnormal) or an ectopic pregnancy. Under these circumstances, the patient's clinical status and her desire to either maintain or terminate the pregnancy should determine whether serial tests (serum hCG or ultrasound or both) should be performed or whether intervention is required. On the basis of clinical considerations, the latter includes laparoscopy, laparotomy, uterine curettage, or administration of methotrexate, or a combination of these.

## DETECTING A SAC WITHOUT AN EMBRYO OR YOLK SAC

When ultrasound examination reveals a sac without an embryo or yolk sac, the diagnosis is limited to one of three entities: (1) a normal early IUP; (2) an abnormal IUP; or (3) a pseudogestational sac in a patient with an ectopic pregnancy.

In theory, an intrauterine sac can be distinguished from a pseudogestational sac because the former is located within the decidua, whereas the latter is within the uterine cavity (see Fig. 6-12).<sup>43</sup> In practice, this distinction is often difficult to make with certainty (see Fig. 6-13). Therefore, a follow-up ultrasound should be obtained to document subsequent appearance of the yolk sac or embryo.<sup>44,45</sup>

\*In this context, a discriminatory number or level refers to the lowest value for which a certain observation should always be detected; in contrast, a threshold number or level refers to the lowest value for which a certain observation can be detected by sonography.



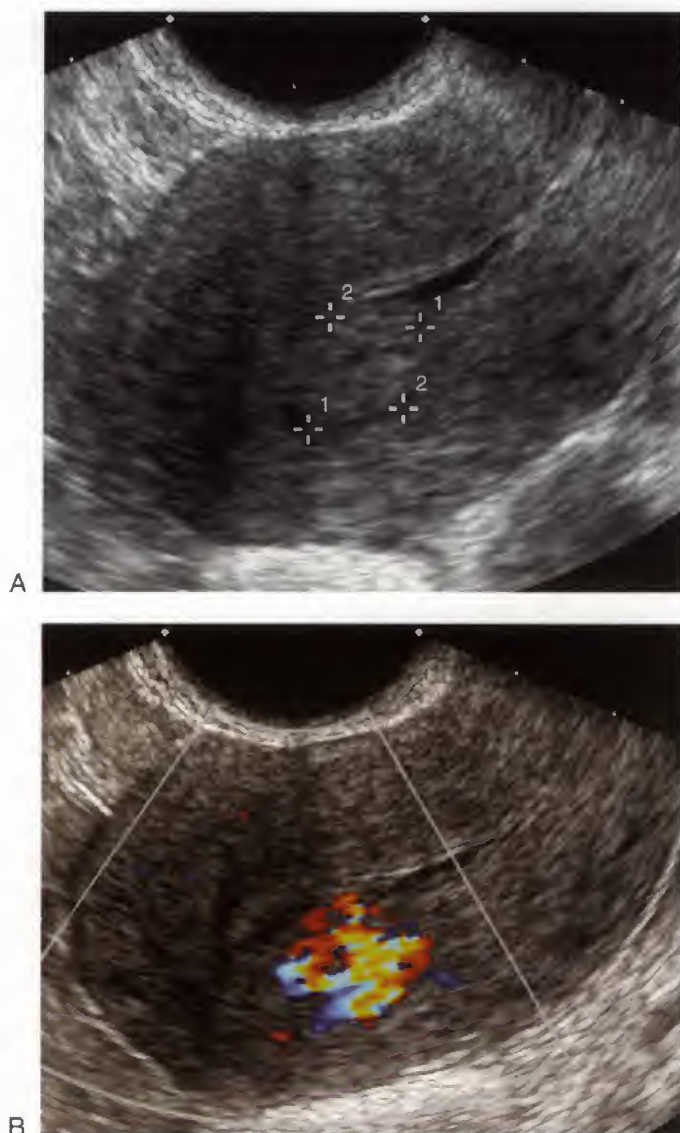


**FIGURE 6-33.** Heavy bleeding occurred in this patient who was reported to be 8.5 weeks pregnant. *A.* Gray scale imaging reveals echogenic material in the endometrial cavity (between calipers). *B.* Color Doppler confirms vascular flow within this material, consistent with retained products of conception. This was surgically confirmed.

## ABNORMAL SAC CRITERIA

### Size

Recall that the threshold for detecting a normal intrauterine sac by transvaginal ultrasound examination is when the sac diameter is only 2 to 3 mm; this corresponds to a GA of slightly more than 4 weeks.<sup>39-41</sup> A sac should be detected consistently by both transabdominal and transvaginal sonography when its mean diameter is 5 mm; this corresponds to a GA of 5 weeks.<sup>52,54</sup>

Specific size criteria can be used to differentiate a normal from an abnormal intrauterine gestational sac. Using a *transabdominal* approach, discriminatory size criteria that suggest an abnormal sac include failure to detect a double

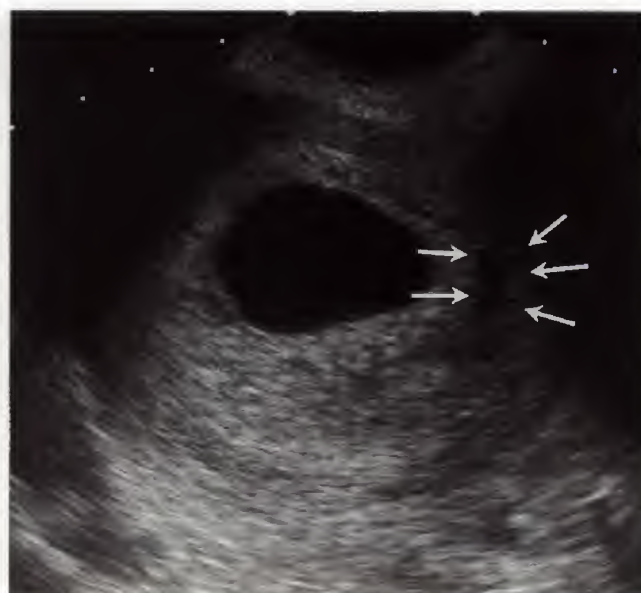


**FIGURE 6-34.** Despite a mean sac diameter of 22 mm, transvaginal sonography failed to reveal either a yolk sac or embryo. This appearance is diagnostic of a failed pregnancy. Note the double decidual sac sign (between arrows), confirming an intrauterine gestational sac and not a pseudogestational sac resulting from an ectopic pregnancy.

decidual sac when the MSD is 10 mm or greater, failure to detect a yolk sac when the MSD is 20 mm or greater, and failure to detect an embryo with cardiac activity when the MSD is 25 mm or greater.<sup>42,47</sup>

Because of superior resolution, a transvaginal approach should be used preferentially to evaluate any intrauterine fluid collection that lacks an embryo. Also, because yolk sac and embryo detection in early pregnancy is critically dependent on transducer frequency, the highest possible transducer frequency should be used to detect these subtle, but critically important anatomic structures (see Fig. 6-19).<sup>53</sup> Generally accepted *transvaginal* discriminatory criteria for determining an abnormal sac include failure to detect a yolk sac when the MSD is 8 mm or greater and failure to detect cardiac activity when the MSD exceeds 16 mm (Fig. 6-34).<sup>51,116</sup>

It is important to understand that these discriminatory criteria should be used as guidelines and that exceptions to these numbers have been reported.<sup>117</sup> If certain findings are not observed at the appropriate time, the results of an ultrasound examination are equivocal, the examination is technically difficult, or the sonographer is inexperienced, caution is warranted. Follow-up ultrasound examination should be obtained in these cases to obviate the risk of terminating a normal IUP.

### Growth Rate

The terms *blighted ovum* and *anembryonic pregnancy* imply that developmental arrest occurred either before formation of the embryo or before it is detectable using currently available equipment. In a series of 3500 consecutive first trimester abortuses, Byrne et al<sup>118</sup> determined that the embryo failed



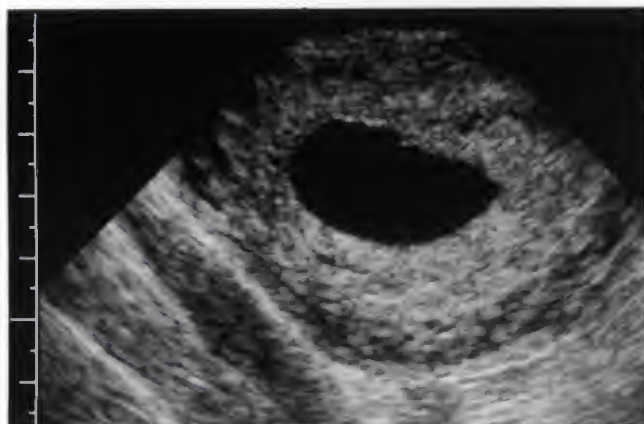


**FIGURE 6-35.** This sac-like structure had a mean diameter of 28 mm, did not contain a yolk sac or embryo, and lacked a double decidual sac sign. The surrounding tissue was abnormally thin and only weakly echogenic. These findings suggest a failed pregnancy, although a pseudogestational sac is not excluded. Doppler may be useful to distinguish between these two entities.

to develop in greater than 60% of cases. Despite an anembryonic state, trophoblastic tissue often continues to function, resulting in continued gestational sac growth, albeit at a diminished rate. Whereas the MSD increases by 1.13 mm/d in a normal gestation, the growth rate of an abnormal sac is only 0.70 mm/d.<sup>52</sup> On the basis of these observations, abnormal sac growth can be diagnosed confidently when the MSD fails to increase by at least 0.6 mm/d.

In possibly abnormal cases and in those with sacs that are less than the discriminatory size for visualizing the yolk sac or cardiac activity, knowledge of normal developmental and sac growth parameters allows sonologists to gauge an appropriate time interval between the initial and follow-up ultrasound examinations. Ideally, the repeat study should aim to identify both the yolk sac and cardiac activity. For example, if the initial MSD is 4 mm, a follow-up study should be done to detect cardiac activity when the sac achieves a diameter of 16 mm. Because normal sac diameter increases by approximately 1 mm/d, an appropriate time interval between the two sonographic examinations is at least 12 days. In contrast, if the initial sonographic examination reveals an MSD of 12 mm (without cardiac activity), the follow-up study should be done approximately 4 days later to determine whether the pregnancy is developing normally.

### Trophoblastic Appearance

Initially described on the basis of transabdominal sonography, an abnormal-appearing choriodecidual or trophoblastic reaction consists of a distorted sac shape; thin (< 2 mm), weakly echogenic, or irregular choriodecidual reaction; and absence of a double decidual sac when the MSD exceeds 10 mm.<sup>42</sup> Often the sac associated with a failing or failed pregnancy has multiple abnormal trophoblastic changes (Fig. 6-35).



**FIGURE 6-36.** This gestational sac has an unusual echogenic convex bulge (arrow). Accurate dating based on in vitro fertilization was 6.0 weeks; a tiny living embryo (not shown) was small for dates, and measured 1.3 mm. Follow up scan 2 weeks later confirmed demise. In very early pregnancies this convex bulge (referred to recently as the “chorionic bump”) should not be mistaken for an embryo without a heartbeat.

Recently, subtle trophoblastic abnormalities have been reported using a vaginal approach. In their investigation of asymptomatic women between 5 and 12 weeks' GA, Bajo et al<sup>19</sup> measured trophoblastic thickness at the embryonic implantation site and noted that in 15% of cases, the difference between the GA (in weeks) and the trophoblastic thickness exceeded 3 mm. This was associated with a 64% miscarriage rate within 7 days of the ultrasound study. A much less common first trimester observation, also associated with a guarded prognosis, consists of an irregular convex bulge that arises from the choriodecidual surface and protrudes into the gestational sac (Fig. 6-36). In a report of 15 patients (prevalence 0.7%) with this so-called chorionic bump, Harris et al<sup>120</sup> reported subsequent miscarriage in 8 (53%) patients. One should be cautious when making this observation, as this protrusion of tissue into the gestational sac may simulate a nonviable embryo adjacent to the developing placenta. The pathophysiology for both of these observations is speculative, but the respective authors suggest early placental insufficiency and a hematoma bulging into the sac. Clearly, the take home message is that “the harder we look, the more we see.”

### ROLE OF DOPPLER

Doppler sonography may also be useful for determining whether an intrauterine sac-like structure that lacks an embryo is a true gestational sac. When a nonspecific-appearing intrauterine fluid collection is identified, Doppler may help differentiate a pseudogestational sac associated with an ectopic pregnancy from an intrauterine gestational sac, either normal or abnormal. Flow around a pseudogestational sac may be either absent or show only a minimal amount of low-velocity flow (< 8 cm/s peak systolic velocity).<sup>121</sup> In contrast, flow around an intrauterine gestational sac typically is high velocity with a low-resistance



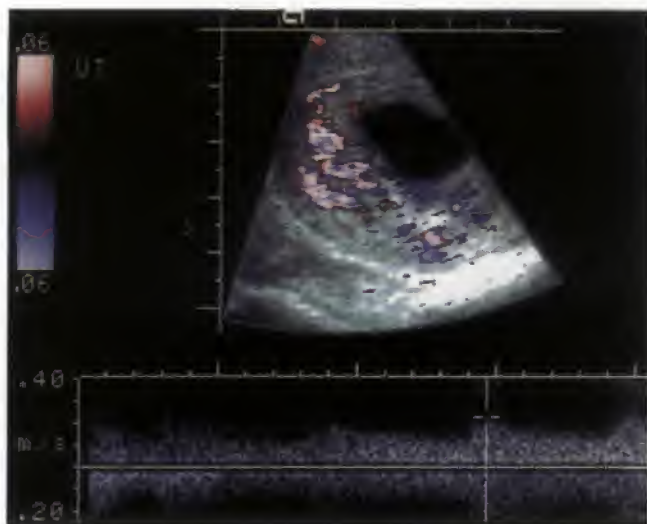


**FIGURE 6-37.** Color Doppler interrogation of an intrauterine fluid collection without a yolk sac or embryo shows extensive myometrial and endometrial blood flow with high peak systolic velocity. Pathology confirmed a failed pregnancy.

pattern (Fig. 6-37). Our personal experience, as well as others, confirms that low-resistance arterial flow may occasionally be detected with pseudogestational sacs.<sup>122</sup> This finding limits the usefulness of Doppler for making this important distinction. Therefore, patients whose initial sonogram demonstrates an intrauterine fluid collection but no adnexal mass or definite IUP should undergo sonographic and clinical follow-up rather than Doppler interrogation. Also, because Doppler sonography delivers more energy than gray-scale ultrasound, its use should be minimized to prevent unnecessary and potentially harmful exposure of an early embryo.<sup>123</sup> Within 1 to 2 weeks, both normal and abnormal IUPs will become more apparent clinically and sonographically. If there is an ectopic pregnancy, follow-up studies will reveal the diagnosis in most patients.

## DETECTING A SAC WITH AN EMBRYO

### Cardiac Activity Absent

When an embryo is visible during a transabdominal ultrasound examination but cardiac activity is absent, the prognosis is usually poor. Occasionally, however, cardiac activity is not detected in a very small embryo because of its size. On the basis of work by Pennell et al,<sup>124</sup> the discriminatory embryonic size for detecting cardiac motion transabdominally has been determined as being 9 mm. In their experience, cardiac activity was absent in 21% of normal pregnancies with a CRL of less than 9 mm.

Not surprisingly, a vaginal approach lowers the discriminatory CRL for detecting cardiac activity. Levi et al<sup>69</sup> suggested a 4-mm CRL cutoff because, in their experience, all normal pregnancies had cardiac activity when embryos achieved this length, whereas cardiac activity was absent in 18% of embryos with a CRL measurement of less than

4 mm. Other investigators used 5 mm as the discriminatory embryonic length for detecting cardiac motion.<sup>70,124</sup> If the length of the embryo is less than the discriminatory value, the patient should be managed expectantly and a repeat ultrasound examination done when the expected CR length exceeds the discriminatory value. Alternatively, or additionally, the level of serum hCG may be useful for determining whether or not a normal IUP is present.

When embryonic length exceeds the discriminatory length and cardiac activity is absent, a nonviable gestation is highly likely. Because this negative observation (failure to perceive a heartbeat) has such important clinical ramifications, caution and certainty are required before reaching this conclusion. To ensure that the measured structure is indeed the embryo, it is useful to note its relationship to the yolk sac. Between 6 and 7 weeks' GA, the embryo and yolk sac are closely applied and contiguous structures (see Fig. 6-21); after 7 weeks' GA, they diverge from one another (see Fig. 6-26). The scan should be performed using the highest transducer frequency available,<sup>53</sup> M-mode and if possible a real-time clip or videotape should be obtained to document absent cardiac activity, and also if possible, a second independent observer should be present to confirm the findings (Fig. 6-38). Interpretive caution must always be exercised whenever a question is raised with regard to either the technical adequacy of the study (maternal or equipment related) or the experience of the examiner. In most cases, embryonic demise is due to a chromosome abnormality that leads to arrested embryonic development.<sup>109,118</sup>

### Cardiac Activity Present

Sonographic detection of cardiac activity not only confirms a living embryo but is also considered a favorable prognostic finding.<sup>69,80,125,126</sup> In general, if cardiac activity is found in an asymptomatic woman examined after 8 weeks' GA, the risk of loss is only 2% to 3%.<sup>127-129</sup> Despite optimism associated with cardiac activity, however, multiple risk factors have been described that increase the possibility of subsequent embryonic-fetal demise.

## RISK FACTORS FOR EARLY PREGNANCY FAILURE

### Gestational Age

An inverse relationship exists between GA and an adverse outcome. When asymptomatic women are examined before 6.5 weeks' GA, the incidence for subsequent demise ranges from 7% to 24%.<sup>66,74,130</sup> This loss rate declines to approximately 2% after 8 weeks.<sup>127-129</sup> Increased early loss most likely reflects a well-recognized high background demise rate as a result of lethal chromosome mutations during this phase of pregnancy.

### Intrauterine Blood

Intrauterine collections of blood are found in many women with first trimester threatened abortion as well as some asymptomatic patients. During early pregnancy, as implantation occurs, the genesis for these collections most likely relates to the erosive effects of the chorion frondosum (the



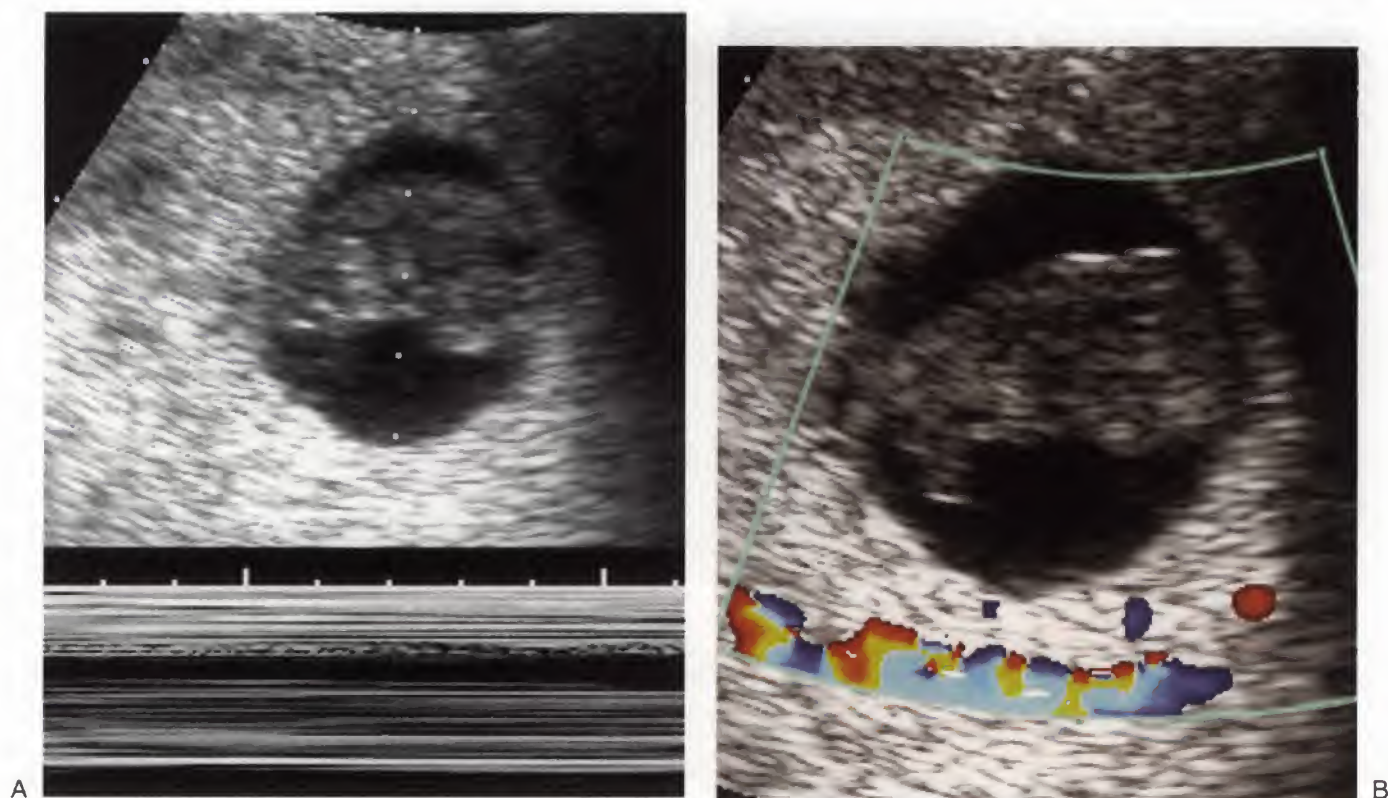


**FIGURE 6-38.** A. Demise of a 9.1-week gestational age embryo can be documented by an M-mode tracing that shows lack of cardiac activity. Color Doppler (B) can also confirm this diagnosis by documenting lack of embryonic blood flow.

fetal contribution to the definitive placenta) as it penetrates into the decidua basalis (the maternal contribution to the definitive placenta). Later it is likely due to venous bleeding associated with separation or abruption of the placental margin or marginal sinus.<sup>131</sup> A range of descriptive words, including intrauterine, perigestational, implantational, or subchorionic, can be used to characterize these maternal hemorrhages. When this occurs, blood dissects along paths of least resistance and ultimately can be located in a variety of positions relative to the developing sac and placenta (Fig. 6-39). As blood tracks away, and becomes remote from the placenta, it often elevates the attached chorionic membrane (smooth chorion), dissecting it and the attached decidua vera. In this manner, it comes to surround the gestational sac. If the collection penetrates into the adjacent endometrial cavity, bleeding becomes clinically apparent. Similar to hematomas throughout the body, the echogenicity of the blood depends on its age and the amount of associated clot (Fig. 6-40). In general, acute hemorrhage is hyperechoic or isoechoic relative to placental tissue. With evolution, liquefaction occurs, and the collection becomes more anolucent but often contains residual low-level echoes.

The literature reveals widely disparate findings regarding pregnancy outcome in women with first trimester vaginal bleeding. Several studies suggested a two- to threefold increased risk of spontaneous abortion,<sup>126,132-135</sup> whereas others reported no increase in miscarriage rate despite a visible intrauterine hematoma.<sup>136,137</sup> One explanation for the varied opinions may relate to the location as opposed to

the size of the hematoma. For example, a small retroplacental hematoma may be associated with a relatively worse prognosis than a larger hematoma situated within the endometrial cavity and away from the placenta.<sup>138</sup> To further confuse this issue, there is also evidence that suggests that first trimester bleeding is associated with an adverse outcome, but this is statistically independent of the presence or absence of a hematoma.<sup>134,139</sup> Other confounding variables either alone or in combination may also play a role in determining pregnancy outcome. These include an increased risk for spontaneous abortion with a progressively larger hematoma, advancing maternal age, earlier GA, bradycardia, smoking, and small sac size.<sup>132,134,135,140</sup> Despite these negative prognostic features, a well-designed study that prospectively evaluated pregnancies between 6 and 13 weeks' GA noted that both symptomatic and asymptomatic women can be assured that their pregnancy has a high likelihood of a favorable outcome if sonography confirms fetal cardiac activity and the scan results are normal.<sup>125</sup> Fortunately, despite vaginal bleeding, the majority of patients with this complication will have a successful pregnancy outcome.

## Heart Rate

When embryonic cardiac activity is first detected between 5 and 6 weeks' GA, the rate is relatively slow (see Figs. 6-22 and 6-23, and Table 6-4). Although mean heart rates of 82 BPM at 5 weeks' GA and 96 BPM at 6 weeks' GA have been reported,<sup>141</sup> most investigators reported a normal



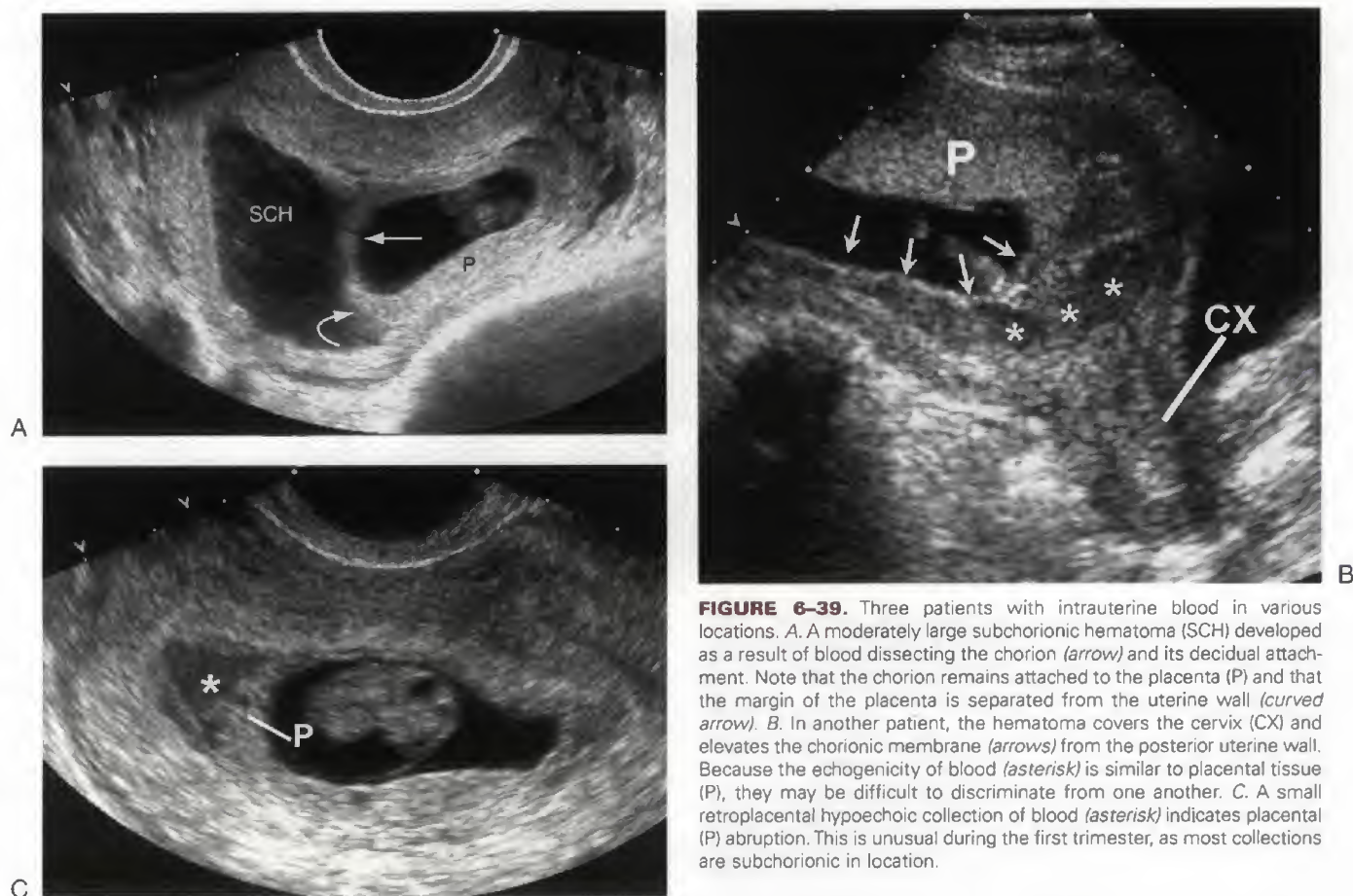


**FIGURE 6-39.** Three patients with intrauterine blood in various locations. *A.* A moderately large subchorionic hematoma (SCH) developed as a result of blood dissecting the chorion (arrow) and its decidual attachment. Note that the chorion remains attached to the placenta (P) and that the margin of the placenta is separated from the uterine wall (curved arrow). *B.* In another patient, the hematoma covers the cervix (CX) and elevates the chorionic membrane (arrows) from the posterior uterine wall. Because the echogenicity of blood (asterisk) is similar to placental tissue (P), they may be difficult to discriminate from one another. *C.* A small retroplacental hypoechoic collection of blood (asterisk) indicates placental (P) abruption. This is unusual during the first trimester, as most collections are subchorionic in location.

range of 100 to 115 BPM between 5 and 6 weeks' GA.<sup>72,78-80</sup> The mean heart rate increases to approximately 140 BPM by 9 weeks' GA.<sup>72</sup> Because of the relatively slow initial heart rate, one report defines bradycardia as less than 100 BPM before 6.2 weeks' GA and less than 120 BPM between 6.3 and 7.0 weeks.<sup>73</sup> Multiple investigations document an adverse outcome with embryonic bradycardia, and this is especially worrisome when vaginal bleeding is also present.<sup>134,135</sup> Close and continued follow up of embryos with early bradycardia (at 6 to 7 weeks' GA) is warranted, because even if the rate normalizes by 8 weeks' GA, there still is a 25% demisc rate by the end of the first trimester (Fig. 6-41).<sup>142</sup> A few case reports document first trimester bradycardia associated with both atrial and ventricular arrhythmias; typically, the outcome is dismal (Fig. 6-42).<sup>143,144</sup> Analysis of first trimester bradycardia also confirms an association with structural and chromosome abnormalities, especially trisomy 18 and triploidy.<sup>145,146</sup> In contrast, other chromosome defects, including trisomy 21, and especially trisomy 13 and Turner syndrome, have an association with first trimester tachycardia (determined at 10-14 weeks' GA).<sup>146</sup> In another investigation, however, that evaluated embryonic heart rates at or before 7 weeks' GA, a rapid early heart rate had a good prognosis, with a high likelihood of a normal outcome.<sup>147</sup>

Nonetheless, because of reported risks associated with cardiac rate abnormalities, consideration should be given

to follow-up ultrasound examinations if the embryonic heart rate is either less than or exceeds the limits of normal for a given GA, or if an irregular rhythm is detected.

### SMALL SAC SIZE-GROWTH DELAY

During the first trimester, the volume of fluid within the gestational sac is not routinely reported because most first trimester sacs contain relatively similar small amounts of fluid. Occasionally, however, the amount of fluid in a first trimester sac is noticeably diminished, resulting in a sac that is small for dates. In two reports evaluating pregnancy outcome in the presence of first trimester oligohydramnios, the incidence of spontaneous abortion was between 80% and 94% despite normal cardiac activity (Fig. 6-43).<sup>148,149</sup> In these studies, oligohydramnios was diagnosed when the difference between the MSD and CRL was less than 5 mm. Even less severe discrepancies, in the range of 5 to 8 mm, are at increased risk for miscarriage, with a reported rate of approximately 25%.<sup>148</sup> This is not surprising when a small sac is present; other adverse prognostic indicators such as embryonic bradycardia, maternal bleeding, and delay in embryonic growth may also be present.<sup>135,138</sup> Although a small sac size is relatively uncommon (observed in 1.9% of fertility patients),<sup>148</sup> this observation can be used to counsel women who present with this finding.



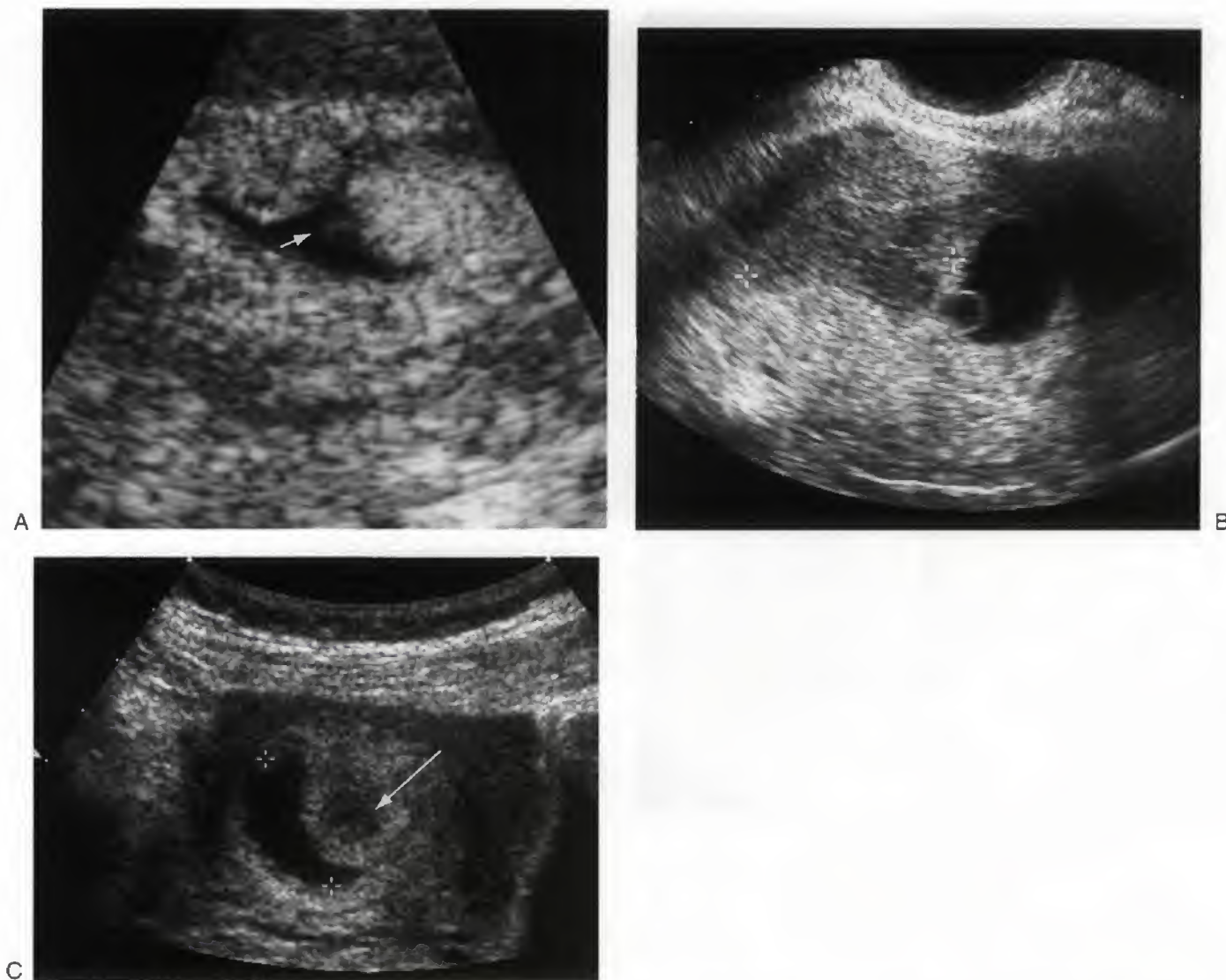


**FIGURE 6-40.** Three patients with intrauterine blood of varying echogenicity. *A.* A large amount of echogenic blood surrounds a very small embryo (arrow). Because the echogenicity of the hematoma is identical to that of placental tissue, they may be very difficult to distinguish from one another. Color Doppler may be helpful to show intraplacental blood flow. *B.* Despite its moderate size, this hematoma (between calipers) is difficult to identify because its echogenicity is similar to adjacent tissue. *C.* On this image, the prominent sonolucent crescent-shaped structure (between calipers) could be misconstrued for a gestational sac. It is, in fact, a subchorionic hematoma, that partially surrounds an adjacent gestational sac (arrow).

Occasionally, a live embryo is seen that is smaller than expected on the basis of accurate dating or prior ultrasound examination. Studies suggest that a smaller-than-expected first trimester CRL measurement reflects early growth restriction that persists throughout pregnancy and is associated with low birthweight, low birthweight percentile, and premature delivery.<sup>150-152</sup> The origin of fetal growth impairment may reflect a defect in early placentation.<sup>153</sup> In these women, first trimester circulating concentration of PAPP-A is decreased; because this trophoblast derived protein is part of a complex system that among other things, controls trophoblastic invasion of the decidua, a paucity of this substance may negatively impact placental development and result in chronic placental dysfunction.

## YOLK SAC EVALUATION

Both the size and appearance of the yolk sac should be considered in early pregnancy, although once cardiac activity is documented, the yolk sac is relegated to secondary status. A normal yolk sac has a maximal diameter of 5 to 6 mm at approximately 10 weeks' GA. Although abnormal yolk sac diameters are generally reported to be associated with subsequent pregnancy failure,<sup>56,57,154,155</sup> one study of 14 cases with yolk sac diameters greater than the 95th percentile for GA reported normal pregnancy outcomes.<sup>156</sup> An interesting observation, recently reported in a group of 18 women with insulin-dependent diabetes, revealed that during their first trimester, the diameter of their yolk sacs

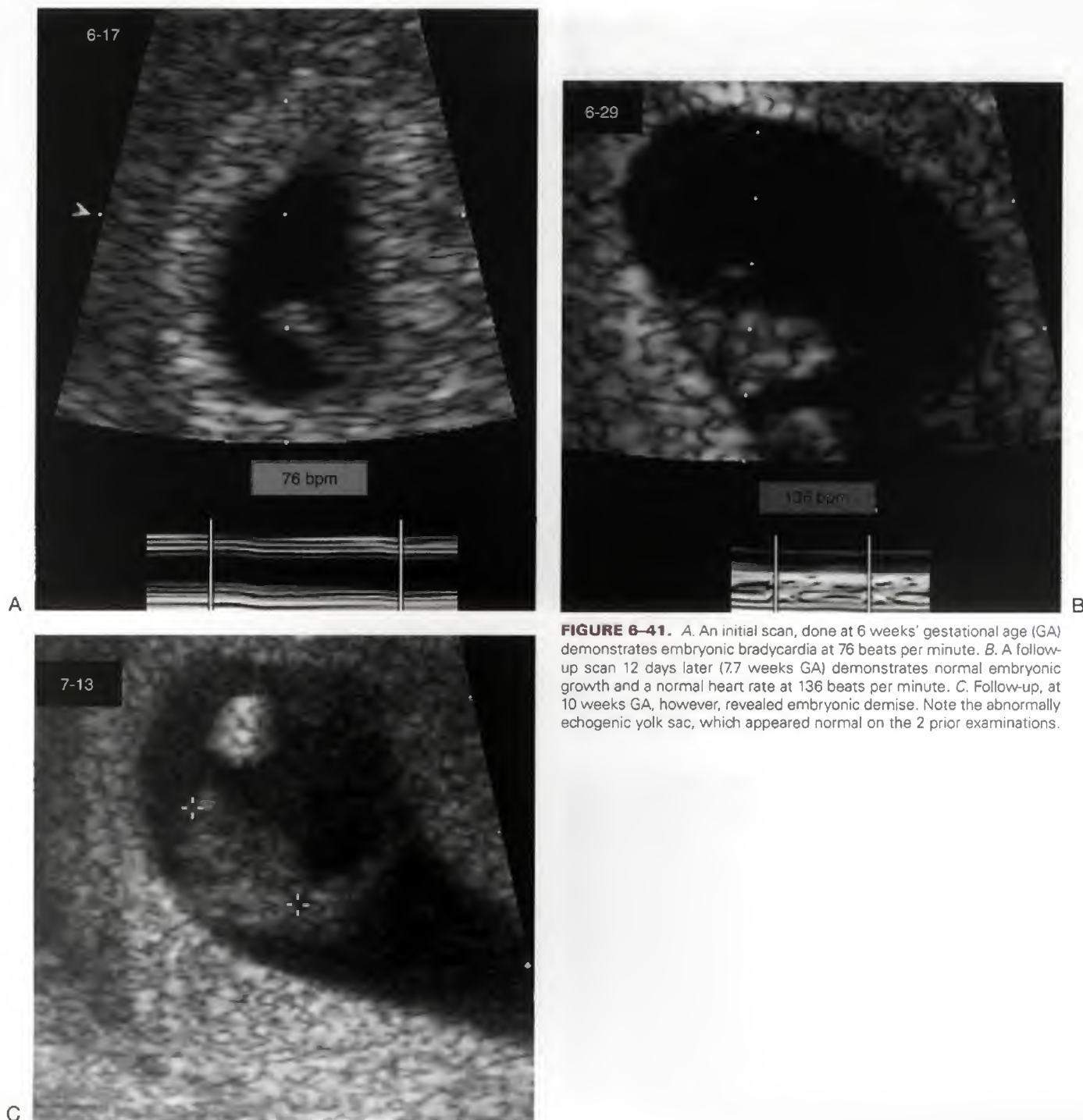


**FIGURE 6-41.** A. An initial scan, done at 6 weeks' gestational age (GA) demonstrates embryonic bradycardia at 76 beats per minute. B. A follow-up scan 12 days later (7.7 weeks GA) demonstrates normal embryonic growth and a normal heart rate at 136 beats per minute. C. Follow-up, at 10 weeks GA, however, revealed embryonic demise. Note the abnormally echogenic yolk sac, which appeared normal on the 2 prior examinations.

was significantly larger when compared with a control group. Unfortunately, the outcome of these pregnancies was not reported, so the diagnostic implication of this observation is unknown.<sup>157</sup>

A practical approach to this issue is to consider any patient with a large yolk sac to be at increased risk for spontaneous abortion. In our experience, follow-up scans reveal that many, but not all, of these patients have subsequent embryonic demise (Fig. 6-44).

An abnormal-appearing yolk sac is also associated with early pregnancy failure.<sup>154</sup> Sporadic case reports suggest that yolk sacs that are abnormally shaped, calcified, echogenic, or double (vitelline duct cyst) are associated with either antecedent or subsequent embryonic demise (Fig. 6-41C).<sup>158,159</sup> Despite an abnormal-appearing yolk sac, whenever cardiac activity is present, follow-up imaging is recommended because, in rare and exceptional cases, the pregnancy may continue to term (Fig. 6-45).



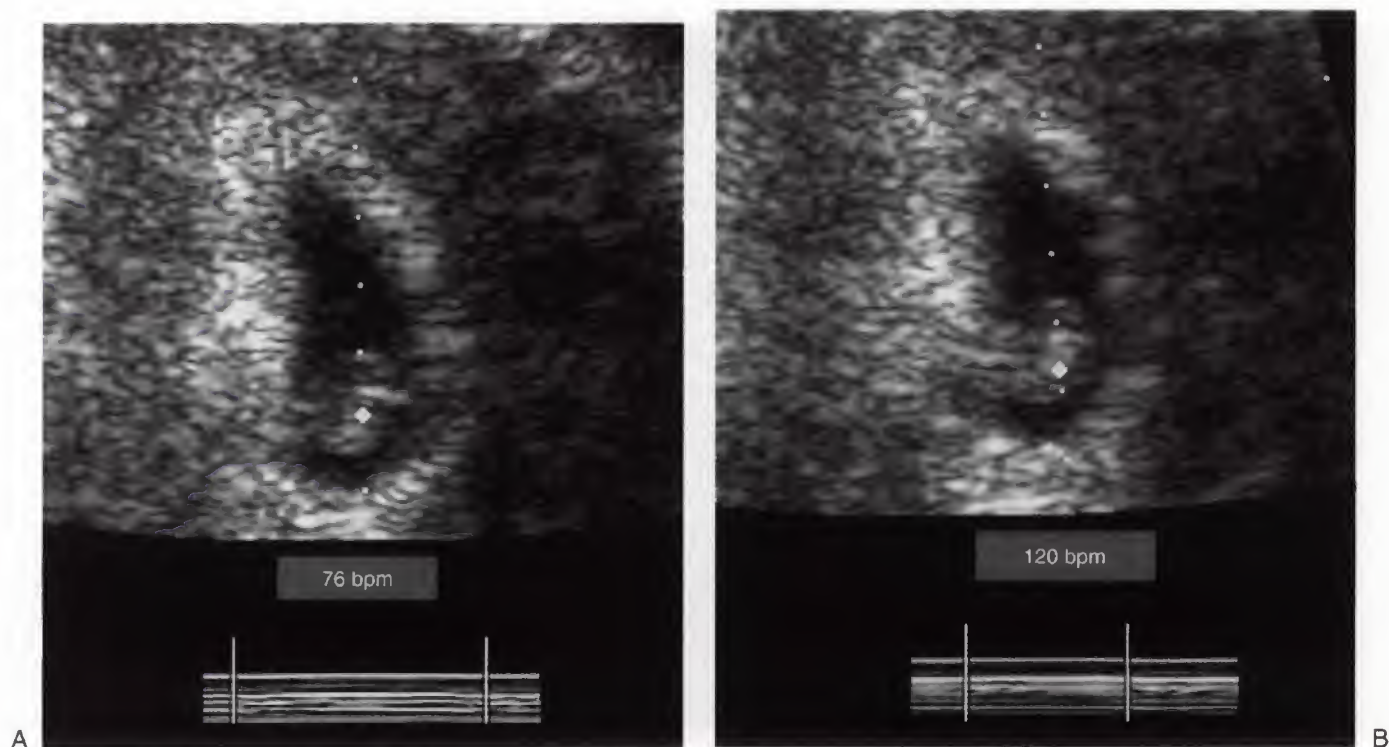


**FIGURE 6-42.** At 7.4 weeks' gestational age, this embryo was noted to have an irregular heart rate, that varied between 76 beats per minute (A), and 120 beats per minute (B). A scan done 2 weeks after this examination revealed demise of the embryo.

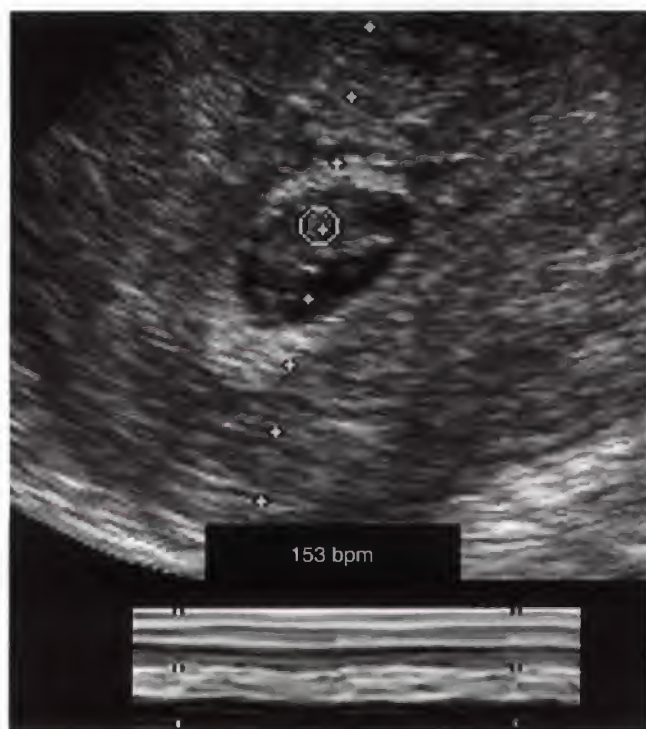


**FIGURE 6-43.** First trimester oligohydramnios is obvious in this sac that contained a living embryo with a normal cardiac rate. Follow-up examination, however, confirmed demise.

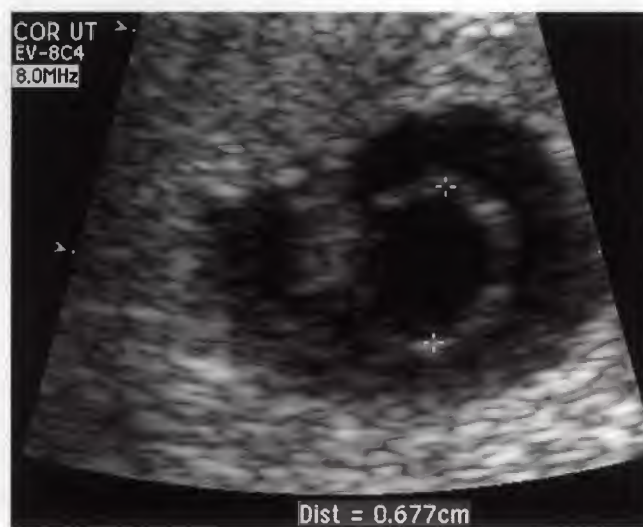


**FIGURE 6-44.** Based on in vitro fertilization, this pregnancy was 7.6 weeks' gestational age. The embryonic length, however, was lagging by more than a week, the heart rate was slow (83 beats per minute), and the yolk sac was large (diameter of 6.7 mm). Follow-up scan confirmed embryonic demise.





**FIGURE 6-45.** This embryo (between calipers), which was 6.5 weeks' gestational age, had an abnormally echogenic yolk sac (arrow). Despite this predictor for a poor outcome, follow-up examination revealed normal growth and development.

## AMNION EVALUATION

Because it is such a thin membrane or perhaps because it initially lies in close proximity to the embryo,<sup>94</sup> the normal amnion may be difficult or impossible to perceive at sonography during the first trimester, and it is not seen normally until the CRL is 7 mm or greater (6.7 weeks' GA) (see Fig. 6-28).<sup>95</sup> In a study of 169 normal and 169 failed pregnancies, the amnion was visible in 34 embryos with a CRL less than 7 mm. In each case, these pregnancies had already failed or subsequently failed.<sup>95</sup> Another investigation that determined amniotic fluid volume in normal first trimester pregnancies could only do so at or after 7 weeks' GA, when the amnion became visible.<sup>160</sup> In 1988, using a transabdominal approach, Yeh et al<sup>82</sup> described the double bleb sign, which was transiently visible between 5 and 7 weeks' GA, and was owing to the contiguously positioned amniotic sac-embryo-yolk sac complex. In our laboratory, despite extensive experience with vaginal sonography during this gestational period, a double bleb appearance is rarely seen in a normal 5- to 7-week GA pregnancy (see Fig. 6-29). When the double bleb appearance is obvious, it is typically associated with impending or frank pregnancy failure. In some cases, it represents two contiguous yolk sacs associated with monozygotic twinning; rarely, it is due to an anomaly such as an umbilical cord cyst (Fig. 6-46).

Abnormal amnion development is suggested when the membrane is easy to see or if its thickness and echogenicity approach that of the yolk sac. Another worrisome finding is an enlarged amniotic cavity relative to the CRL (Fig. 6-47). Recall that in a normal first trimester pregnancy, the mean amniotic sac diameter is approximately equal to the CRL. In Horrow's evaluation of 10 first trimester embryos that subsequently died, each displayed an abnormally large amniotic cavity relative to the size of the embryo and its chorionic cavity (Fig. 6-48).<sup>96</sup> In this report, the difference between the CRL and amniotic cavity diameter was approximately 1 mm in normal pregnancies but almost 9 mm in abnormal pregnancies. As with other adverse prognostic indicators, patients with enlarged or suspicious-

appearing amniotic sacs should be advised to undergo a follow-up ultrasound examination (Fig. 6-49).

Because ultrasound imaging normally detects an embryo before the amnion, a finding that has been reported as highly suggestive of an abnormal pregnancy is visualization of this membrane without detection of an embryo (Fig. 6-50).<sup>161</sup> The majority of cases with an "empty amnion" sign also have an MSD greater than 16 mm, which, in and of itself, is consistent with a failed pregnancy. When this sign is apparent but the sac diameter is less than 16 mm, confirmation of failed pregnancy should be corroborated with the serum hGC level or follow-up ultrasound examination.

If an otherwise empty sac contains an easily visible membrane-like structure, distinction between the abnormal amnion versus a large yolk sac may be difficult or impossible (Fig. 6-51). Nonetheless, abnormal development should be suspected in either case because the presence of a cystic structure larger than 6 mm in diameter without a living embryo is highly suggestive of pregnancy failure.

## MATERNAL FACTORS

Maternal factors that may increase the risk of spontaneous miscarriage include age, smoking, structural uterine abnormalities, and a history of miscarriages.

Maternal age adversely affects outcome. Women older than 34 years are one and one half to five times more likely to miscarry than younger women.<sup>126,129,132,135,140,162</sup> Until age 30, the incidence of miscarriage is approximately 12%; thereafter, the rate increases rapidly, exceeding 50% in women older than 45 years.<sup>162</sup>

Both acquired and congenital structural uterine abnormalities are associated with increased risk of pregnancy loss. In addition to synechiae, acquired structural abnormalities that may affect outcome include fibroids. In women with fibroids, the pregnancy loss rate is almost twice that of women with a normal uterus, and in one study, the loss rate was statistically greater with multiple fibroids, but did not correlate with fibroid size or location.<sup>163</sup> Congenital structural malformations, which are typically of müllerian duct origin, primarily affect the rate of spontaneous abortion as opposed to the rate of conception. Septate uteri consistently have the strongest association with early miscarriage, presumably because of inadequate placental implantation on the poorly vascularized septum.<sup>164</sup> A less common congenital abnormality may be found in women whose mothers were exposed to diethylstilbestrol during pregnancy (daughters of women who took diethylstilbestrol [DES]).<sup>165,166</sup> In these patients, developmental changes may cause cervical incompetence or a hypoplastic, T-shaped configuration of the endometrium, each of which contributes to an abnormally high miscarriage rate.

The prognosis for successful pregnancy in patients with structural uterine abnormalities relates to the specific abnormality and whether it is amenable to surgical correction. In comparison to lethal chromosomal embryonic mutations, these cases are relatively few in number.

The term *recurrent miscarriage* describes the situation of three or more consecutive first trimester spontaneous losses, which affects approximately 1% of couples.<sup>109</sup> Because the cause for this problem is multifactorial, evaluation of these patients requires a broad range of diagnostic tests that



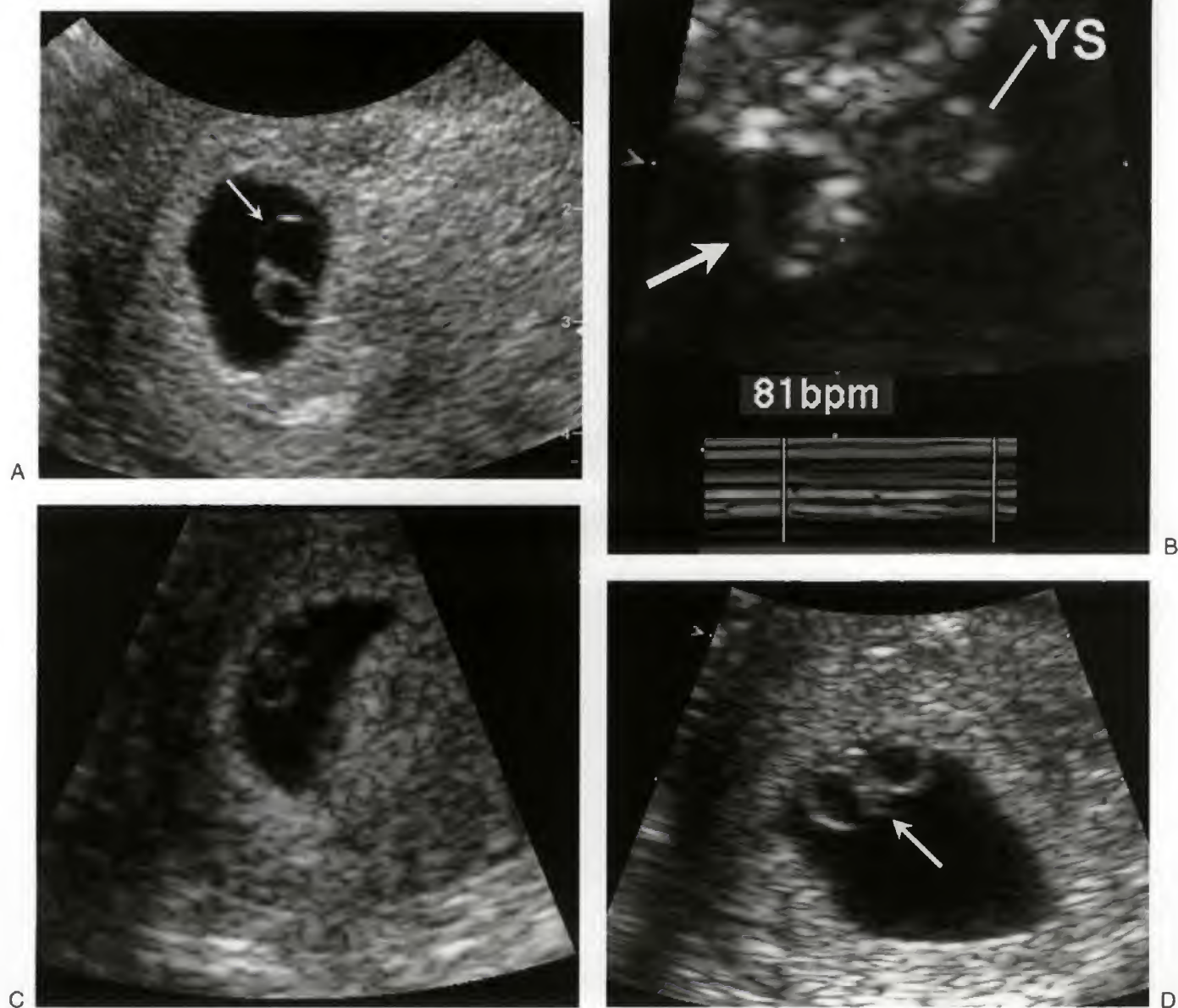


**FIGURE 6-48.** Four different patients, each with what appears to be a prominent double bleb sign. *A.* This is a failed pregnancy, which by accurate dating was 7.8 weeks' gestational age (GA) (arrow points to amnion). *B.* This 7-week GA embryo had bradycardia (81 beats per minute) as well as an abnormally thick amnion (arrow). Follow-up scan confirmed demise. YS, yolk sac. *C.* These two closely opposed round structures represent two yolk sacs associated with monozygotic twinning. *D.* This case, which is virtually identical in appearance to *C*, is due to an umbilical cord cyst adjacent to the yolk sac; a living embryo is between these 2 structures (arrow). The pregnancy subsequently failed at 18 weeks.



**FIGURE 6-47.** In this 6-week intrauterine pregnancy, the diameter of the amniotic cavity (AC) was much too large relative to the embryonic crown-rump length (between calipers). In addition, the amnion (arrow) was too easily seen. Follow-up sonographic examination revealed demise.



**FIGURE 6-49.** In this transabdominal scan, the amnion is too easily seen and slightly irregular, and the amniotic cavity is no longer spherical. Despite these findings, follow-up ultrasound examination revealed a normally developing fetus.

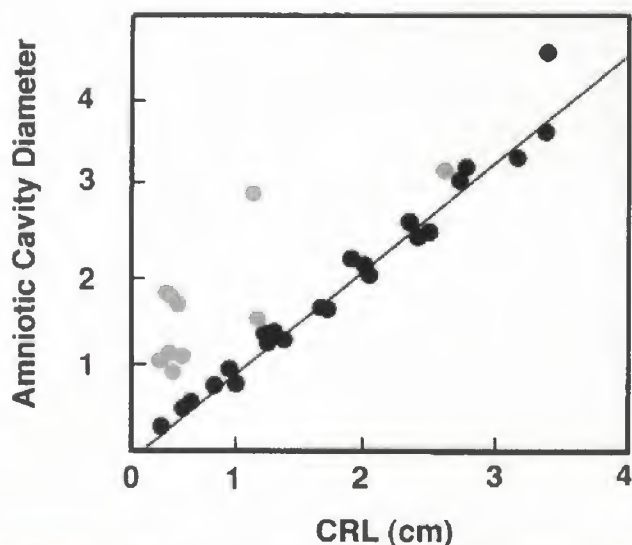


**FIGURE 6-48.** Relationship of the diameter of the amniotic cavity (AC) to the crown-rump length (CRL) in normal (solid circles) and abnormal (gray circles) embryos. As evident from this graph, abnormal pregnancies have a large amniotic cavity diameter. (From Horrow MM: *Enlarged amniotic cavity: A new sonographic sign of early embryonic death*. *AJR Am J Roentgenol* 158:359, 1992.)



**FIGURE 6-50.** This transvaginal scan reveals an easily visible round structure with a mean diameter of 8 mm. The distinction between an abnormal amnion versus a large yolk sac is not always possible, but in this case, a small yolk sac is also present (arrow). Therefore, this appearance is consistent with a failed pregnancy.

evaluate anatomic, hormonal, genetic, and autoimmune factors. Readers interested in the clinical aspects of this topic should consult an up-to-date gynecologic textbook, such as *Danforth's Obstetrics and Gynecology*.<sup>109</sup>

Sonographic findings in patients with recurrent spontaneous abortion depend on when the sonogram is done. Although

approximately three fourths of these patients will have a living embryo demonstrated at some point during the first trimester, follow-up confirms a four to five times greater likelihood of subsequent loss compared with women without a history of recurrent pregnancy loss.<sup>167,168</sup> Because in most cases the pregnancy fails by approximately 8 weeks' GA,



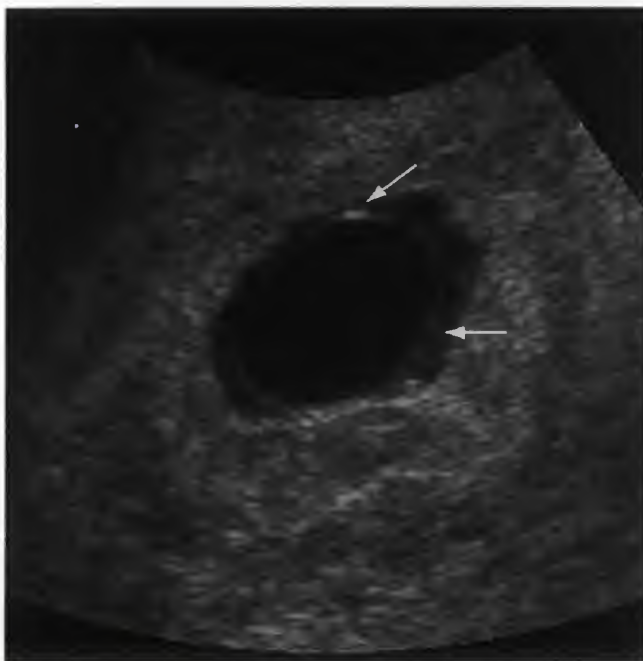


**FIGURE 6-51.** A single, round structure (arrows) with a mean diameter of 9 mm is visible in this gestational sac. It could be either an abnormal amnion or a large yolk sac; in either case, the appearance is abnormal and consistent with a failed pregnancy.

it may be prudent to perform a vaginal sonographic examination at this time (as opposed to earlier) to provide realistic feedback to these patients.<sup>169</sup>

### USEFULNESS OF HCG LEVELS IN FIRST TRIMESTER PREGNANCY

There is no question that high-resolution ultrasound and the quantitative level of serum hCG are complementary and, when used together, optimize the evaluation of patients with threatened abortion. This is particularly true when the initial ultrasound findings are nondiagnostic. Because both gestational sac growth and hCG production relate to trophoblastic function, there is normally an excellent correlation between sac size and hCG level.<sup>170</sup>

If a patient with a threatened abortion has a definitely abnormal gestational sac, a quantitative hCG level is not usually useful. In equivocal cases, or in women at risk for recurrent miscarriage, however, this assay can be extremely helpful for determining whether or not the pregnancy is progressing normally. In most patients with an abnormal IUP, the hCG level is disproportionately low relative to the sac size.<sup>170-173</sup>

Another indication for determining the quantitative hCG level is the presence of a small intrauterine fluid collection that lacks a DDS finding (transabdominal scan) or intra-decidual sign (transvaginal scan). In these cases, the level of hCG may be used to determine whether the intrauterine findings are due to a pseudogestational sac or an early IUP. Most often, ectopic pregnancies are associated with a disproportionately high level of hCG for the size of the fluid collection. Additionally, failure to detect an intrauterine

gestational sac when the hCG value exceeds the discriminatory level places the patient at risk for an ectopic pregnancy.<sup>169,174</sup> Although the discriminatory hCG level for detecting an intrauterine sac varies somewhat from one ultrasound laboratory to another and also depends on the standard against which the hCG is calibrated, it is clear that combining the hCG level with the ultrasound findings significantly improves one's ability to interpret equivocal ultrasound findings and to diagnose ectopic pregnancy.<sup>174,175</sup> Many ultrasound laboratories currently use between 1000 and 2000 mIU/mL (International Reference Preparation) as the hCG level above which an intrauterine gestational sac should normally be visible by transvaginal scanning.<sup>99,176-178</sup>

### ROLE OF DOPPLER IN PREDICTING PREGNANCY OUTCOME

Because energy levels associated with Doppler can be significantly greater than for imaging, and because the greatest potential for risk in ultrasound diagnosis is in fetal Doppler studies,<sup>123</sup> our ultrasound laboratory does not advocate routine use of Doppler in the first trimester. However, using controlled research protocols, several investigations have addressed Doppler applications in early pregnancy. With respect to an IUP (as opposed to ectopic pregnancy), the primary role of Doppler is to determine whether a first trimester pregnancy will have a normal outcome. To do this, attention has been focused on uteroplacental and corpus luteal flow patterns.

Uteroplacental flow can be evaluated by measuring flow velocity or a variety of indexes (systolic-diastolic ratio, resistive index [RI], pulsatility index) that characterize flow patterns within the main uterine artery or subchorionic vessels (spiral arteries). In a normal pregnancy, the indices within these vessels demonstrate a progressive decline from 6 to 12 weeks' gestation.<sup>21,36,179</sup> Histomorphometric anatomic correlation suggests that the basis for this progressive drop in resistance is the establishment of the intervillous circulation.<sup>26</sup> The usefulness of Doppler for predicting pregnancy outcome has not been established; some reports suggest that elevated resistance in the uterine or subchorionic vessels is associated with a high likelihood of spontaneous abortion,<sup>25,49,180</sup> whereas others have found that Doppler analysis of these vessels is not predictive of outcome.<sup>179,181,182</sup>

A second area of investigation is interrogation of corpus luteal blood flow during the first trimester.<sup>183-186</sup> In these studies, conflicting results are also evident; one report suggested a relatively increased corpus luteal RI associated with threatened abortion,<sup>184</sup> whereas another found no significant difference in this measurement compared with that of the control population.<sup>185</sup> Interestingly, both of these studies agreed that the RI was abnormally increased in patients with missed abortion.<sup>184,185</sup> Corpus luteal RIs have also been measured in an effort to predict pregnancy outcome; the results of this investigation show this parameter cannot be used successfully for this purpose.<sup>186</sup>

Although Doppler has not proven useful for predicting a successful first trimester outcome, researchers have confirmed a correlation between first trimester uterine artery resistance and subsequent pregnancy complications. Most authors agree that as early as 11 weeks' GA, elevated uterine artery resistance can identify patients at risk for both intra-

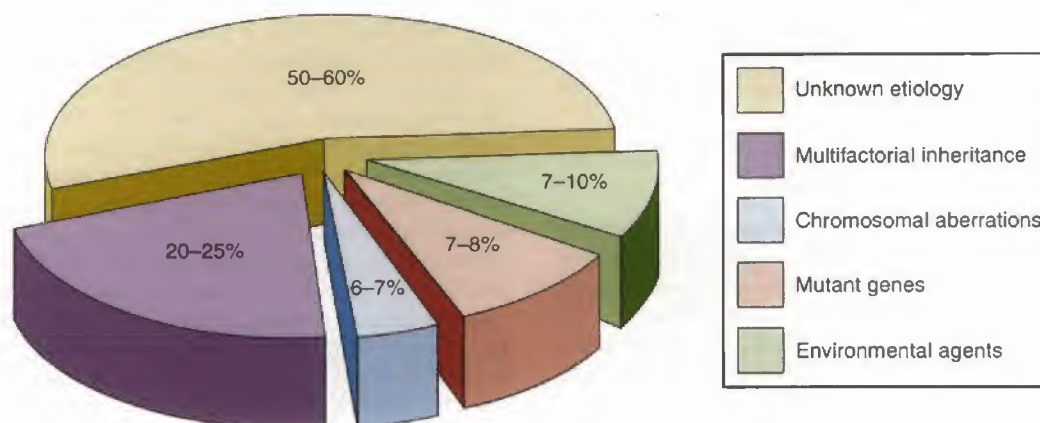


**FIGURE 6-52.** Graphic representation noting the causes of human congenital anomalies. (From Moore KL, Persaud TVN: *The Developing Human: Clinically Oriented Embryology*, 7th ed. Philadelphia, WB Saunders, 2003, pp 158–186.)

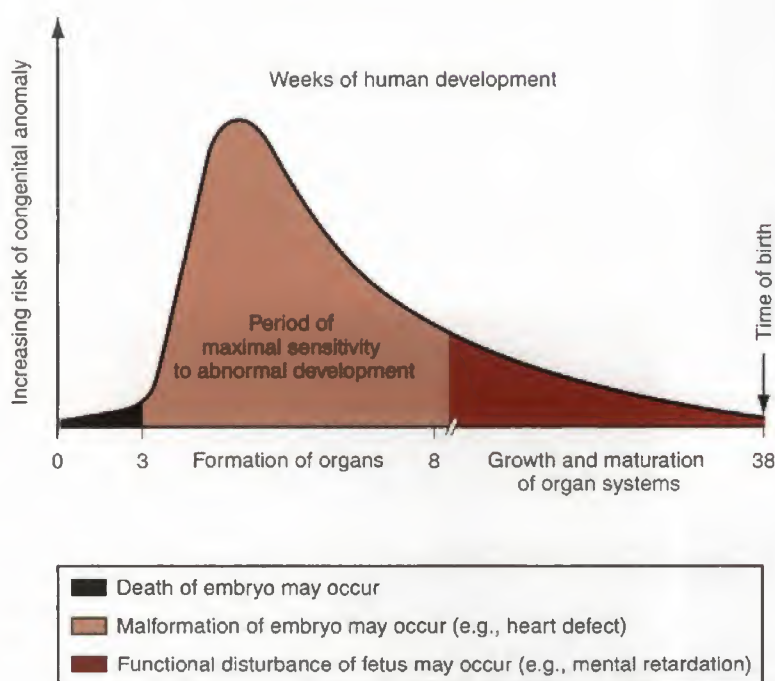


**FIGURE 6-53.** Schematic illustration depicting the risk of developing a congenital anomaly relative to gestational age. (From Moore KL, Persaud TVN: *The Developing Human: Clinically Oriented Embryology*, 7th ed. Philadelphia, WB Saunders, 2003, pp 158–186.)

uterine growth restriction and pregnancy-induced hypertension.<sup>187–189</sup> One explanation for this relationship is inadequate or incomplete trophoblastic invasion of the maternal vessels during the first trimester. Early identification of patients at risk for these complications could allow additional screening and possible intervention.

## DETECTING FETAL ANOMALIES

Congenital fetal malformations can be the result of genetic or chromosomal, environmental, or combined factors. In more than 50% of cases, the origin is unknown; however, when a cause is identified, most are due to chromosomal aberrations (Fig. 6-52). Environmental causes, or teratogens,

are responsible for approximately 10% of anomalies. The timing of exposure of the embryo to a teratogen is critical to pregnancy outcome (Fig. 6-53). Very early exposures (up to 5 weeks' GA) typically have an all-or-none result: the embryo will either die or be unaffected. Exposure during organogenesis (5 to 10 weeks' GA) often affects organ development and results in severe congenital anomalies. Exposure during the fetal phase of development has a variable result.<sup>190</sup>

With continued technologic improvements, imaging of the embryo has progressed far beyond identifying cardiac activity and measuring CRL. Although many congenital anomalies cannot be diagnosed with confidence until the second trimester, gross abnormalities such as large encephaloceles, holoprosencephaly, ventral wall defects, and



conjoined twins can often be detected in the latter part of the first trimester.<sup>4,191,192</sup> Nonetheless, at this early stage of development, anomaly detection remains limited by the small size of the fetus.

## DEVELOPMENTAL PITFALLS

As the embryo develops, several normal anatomic structures undergo developmental changes that can be misinterpreted as abnormal. One potentially confusing cystic space, readily visible in the posterior cranium between 7 and 9 weeks' GA, is the developing rhombencephalon (Fig. 6-54). This structure will ultimately contribute to the fourth ventricle, brain stem,



**FIGURE 6-54.** A well-defined cystic area in the posterior fossa (between calipers) represents the normally developing rhombencephalon in this 8.2-week embryo.

and cerebellum, and it should not be confused with a developing Dandy-Walker malformation or hydrocephalus.

Another potential source of confusion is prominence at the fetal umbilical cord insertion site. Beginning in the 8th week of gestation, physiologic herniation of fetal bowel into the base of the umbilical cord creates a focal mass. This mass can measure up to 7 mm in diameter and typically becomes most prominent at 9 to 10 weeks' GA, concurrent with a 90-degree counterclockwise rotation of the bowel around the base of the superior mesenteric artery (Fig. 6-55). The mass should not measure more than 7 mm, it should resolve by the end of the 11th week GA as the bowel returns to its intra-abdominal location, and it should no longer be seen once the CRL is 45 mm or greater.<sup>83-85</sup>

## DIAGNOSING ANOMALIES (EXCLUDING NUCHAL TRANSLUCENCY)

By 10 weeks' GA, the fetal cranium, brain, neck, trunk, and extremities can be visualized, and gross anomalies can be detected in the first trimester.

*Anencephaly* is characterized by absence of development of the cranium with dystrophic brain tissue in the expected location of the fetal head. When this condition is visible during first trimester sonography, the fetal head has an irregular contour and is not contained by bone. The dystrophic brain tissue may extend beyond the usual location of the head, such as to either side of the face or



**FIGURE 6-55.** A. Ten-week embryo with a rounded mass protruding from the anterior abdominal wall, representing physiologic bowel herniated into the base of the umbilical cord (arrows). With continued normal development, the mass is typically no longer present by 12 weeks' gestational age. B. Three-dimensional image of a 10-week fetus with prominent physiologic bowel at the base of the umbilical cord (arrows).

A



B



**FIGURE 6-56.** Anencephaly. *A.* Twelve-week fetus with absent cranium and dystrophic brain tissue protruding above the face (arrows). The head size is smaller than normal. *B.* Eleven-week fetus (calipers) with anencephaly and dystrophic brain tissue extending anterior to the face (arrows).



**FIGURE 6-57.** Fourteen-week fetus with an occipital defect (between calipers) and encephalocele (arrows) herniated outside the cranium.



**FIGURE 6-58.** Thirteen-week fetus with holoprosencephaly, demonstrating large single ventricle (asterisk) and absence of the falx due to failure of division of the prosencephalon or forebrain.

anterior to the orbits, or the head may appear abnormally small (Fig. 6-56). No calcified cranium will be seen.<sup>193,194</sup>

Large *encephaloceles*, defects in the cranium through which intracranial contents herniate outside the skull, can sometimes be identified (Fig. 6-57). With *holoprosencephaly*, a brain anomaly resulting from failure of cleavage of the prosencephalon into the cerebral hemispheres, the fetal head contains a large central cystic space and the falx and choroid plexus are absent (Fig. 6-58).<sup>195</sup> This devastating anomaly is often seen with trisomy 13 and, therefore, once detected, should prompt counseling for karyotype testing.

The presence of large cystic spaces behind the fetal head, neck, and trunk, like thickening of the nuchal translucency (see Chapter 3), are associated with abnormal chromosomes, particularly trisomies 13, 18, and 21 and Turner syndrome. These fluid collections are called *cystic hygromas* or *lymph-angiectasia*.<sup>196</sup> The cystic spaces may extend down the trunk of the fetus, appearing as a halo around the fetus, or the spaces may be confined to the posterior fetal neck (Fig. 6-59).



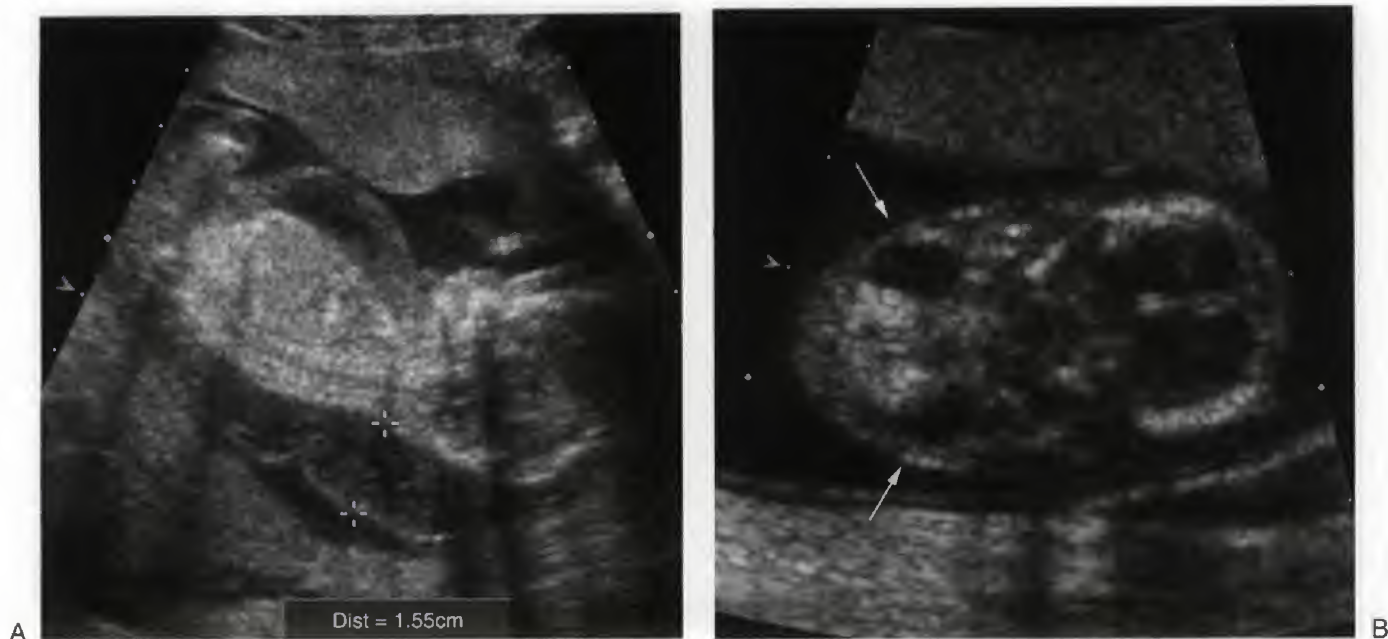


**FIGURE 6-59.** Lymphangiectasia and cystic hygroma. *A.* Fourteen-week fetus encased by marked skin thickening and edema (between calipers) due to diffuse lymphangiectasia. *B.* Coronal image of fetal head and neck of a different fetus demonstrating focal cystic spaces around the neck (arrows) representing a cystic hygroma.

Large ventral wall defects, such as *omphalocele* and *gastroschisis*, can be differentiated from physiologic bowel herniation based on the size of the protruding anterior abdominal wall mass and persistence of the mass beyond 12 weeks' GA. If the size of the mass before 12 weeks' GA is more than 7 mm, a ventral wall defect should be suspected, and follow-up sonography should be performed after 12 weeks' GA to confirm the diagnosis. The protruding mass of an omphalocele typically has a smooth and rounded contour, because the extruded abdominal contents are contained by a peritoneal membrane (Fig. 6-60).<sup>197</sup> The contour of the gastroschisis is typically irregular, because bowel loops protruding through the defect are not contained by a membrane (Fig. 6-61).

*Amniotic band syndrome* is characterized by deformities of the fetus, including ventral wall defects, encephaloceles, and limb amputations. Severe cases of disruption of the fetus can sometimes be diagnosed in the first trimester (Fig. 6-62).<sup>197,198</sup> Normally, by the end of the first trimester, the ventral wall should appear intact and all four extremities should be identified as present.

When monoamniotic twins are present during the early part of the first trimester, it is often difficult to tell whether

they are conjoined or separate but very close together. By the end of the first trimester, however, as the amniotic cavity enlarges, it is usually possible to differentiate true *conjoined twins* from individual monoamniotic twins, and the site of joining may be identified (Fig. 6-63).<sup>199,200</sup>

## CONCLUSION

Transvaginal ultrasound has changed the clinical approach for evaluating patients during the first trimester of pregnancy. In asymptomatic women, it can determine the number of gestational sacs and precisely date the pregnancy. In women who present with threatened abortion, ultrasound is often the first and frequently the only study required to sort out the many differential clinical considerations. In approximately 50% of these patients, the results reveal a normal IUP, and the pregnancy progresses without difficulty. In the remaining patients whose outcomes are abnormal, ultrasound can usually diagnose the specific problem, and expeditious and appropriate therapy can be undertaken. In the few remaining cases, a quantitative hCG determination may be indicated, or serial hCG and ultrasound examinations may be warranted.



**FIGURE 6-80.** Omphaloceles. A. Eleven-week fetus with small rounded mass at the base of the umbilical cord (between calipers) that persisted on follow-up scan after 12 weeks' gestational age. B. Color Doppler sonogram of 12-week fetus with large omphalocele (arrows) demonstrating umbilical vessels traveling through the omphalocele sac. C. Three-dimensional sonogram of same fetus as B demonstrating the rounded omphalocele sac (arrow) anterior to the fetal abdomen.



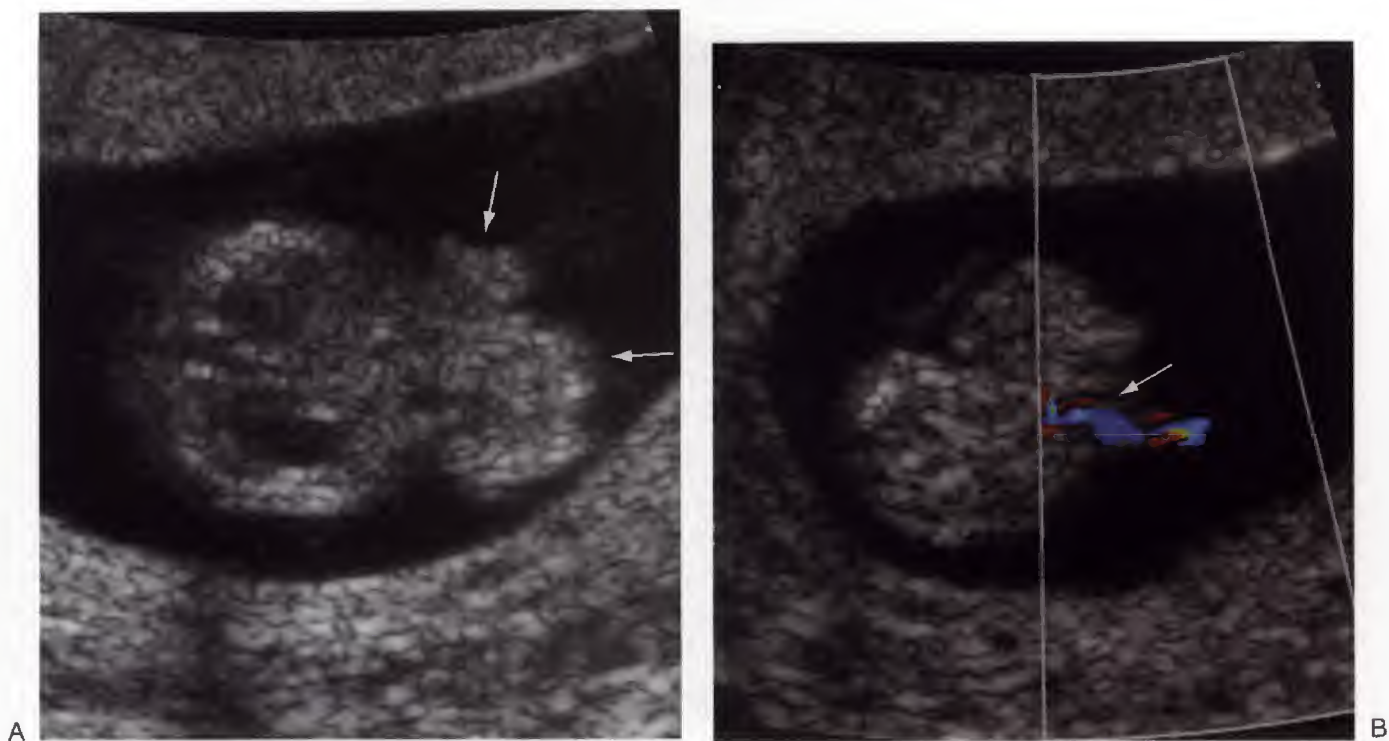


**FIGURE 6-61.** Gastroschisis. *A.* Irregularly shaped mass (arrows) protruding from the anterior abdominal wall of this 14-week fetus, representing bowel loops extruded into the amniotic cavity through the anterior abdominal wall defect. *B.* Color Doppler image demonstrating that the cord insertion (arrow) into the fetal abdomen is intact.



**FIGURE 6-62.** Twelve week fetus (arrows) whose ventral wall is disrupted by amniotic bands and abdominal contents (arrowheads) are protruding outside the body.



**FIGURE 6-63.** Ten-week conjoined twins with two heads (arrows) and fused bodies.

## References

1. Demianczuk NN, Van Den Hof MC, Farquharson D, et al: Diagnostic Imaging Committee of the Executive and Council of the Society of Obstetricians and Gynecologists of Canada. The use of first trimester ultrasound. *J Obstet Gynecol Can* 25:864, 2003.
2. Malone FD, Canick JA, Ball RH, et al: First- and Second-Trimester Evaluation of Risk (FASTER) Research Consortium. First-trimester or second-trimester screening, or both, for Down's syndrome. *N Engl J Med* 353:2001, 2005.
3. Nicolaides KH: First-trimester screening for chromosomal abnormalities. *Semin Perinatol* 29:190, 2005.
4. Fong KW, Toi A, Salem S, et al: Detection of fetal structural abnormalities with US during early pregnancy. *Radiographics* 24:157, 2004.
5. Souka AP, Pilalis A, Kavalakis Y, et al: Assessment of fetal anatomy at the 11-14-week ultrasound examination. *Ultrasound Obstet Gynecol* 24:730, 2004.
6. Michailidis GD, Papageorgiou P, Economides DL: Assessment of fetal anatomy in the first trimester using two- and three-dimensional ultrasound. *Br J Radiol* 75:215, 2002.

7. Sohaey R, Woodward P, Zweibel WJ: First-trimester ultrasound: The essentials. *Semin Ultrasound CT MR* 17:2, 1996.
8. Moore KL, Persaud TVN: Formation of bilaminar embryonic disc and chorionic sac: The second week. In Moore KL, Persaud TVN (eds): *The Developing Human: Clinically Oriented Embryology*, 7th ed. Philadelphia, WB Saunders, 2003, pp 43–57.
9. Moore KL, Persaud TVN: Placenta and fetal membranes. In Moore KL, Persaud TVN (eds): *The Developing Human: Clinically Oriented Embryology*, 7th ed. Philadelphia, WB Saunders, 2003, p 143.
10. Moore KL, Persaud TVN: The beginning of human development: The first week. In Moore KL, Persaud TVN (eds): *The Developing Human: Clinically Oriented Embryology*, 7th ed. Philadelphia, WB Saunders, 2003, pp 31–42.
11. Moore KL, Persaud TVN: Organogenic period: The fourth to eighth weeks. In Moore KL, Persaud TVN (eds): *The Developing Human: Clinically Oriented Embryology*, 7th ed. Philadelphia, WB Saunders, 2003, pp 78–93.
12. Moore KL, Persaud TVN: The cardiovascular system. In Moore KL, Persaud TVN (eds): *The Developing Human: Clinically Oriented Embryology*, 7th ed. Philadelphia, WB Saunders, 2003, pp 330.
13. Moore KL, Persaud TVN: The fetal period: Ninth week to birth. In Moore KL, Persaud TVN (eds): *The Developing Human: Clinically Oriented Embryology*, 7th ed. Philadelphia, WB Saunders, 2003, pp 104–106.
14. Moore KL, Persaud TVN: Placenta and fetal membranes. In Moore KL, Persaud TVN (eds): *The Developing Human: Clinically Oriented Embryology*, 7th ed. Philadelphia, WB Saunders, 2003, pp 120–126.
15. Moore KL, Persaud TVN: Formation of germ layers and early tissue and organ differentiation: The third week. In Moore KL, Persaud TVN (eds): *The Developing Human: Clinically Oriented Embryology*, 7th ed. Philadelphia, WB Saunders, 2003, pp 71–74.
16. Moore KL, Persaud TVN: Formation of germ layers and early tissue and organ differentiation: The third week. In Moore KL, Persaud TVN (eds): *The Developing Human: Clinically Oriented Embryology*, 7th ed. Philadelphia, WB Saunders, 2003, p 60.
17. Moore KL, Persaud TVN: The beginning of human development: The first week. In Moore KL, Persaud TVN (eds): *The Developing Human: Clinically Oriented Embryology*, 7th ed. Philadelphia, WB Saunders, 2003, pp 24–29.
18. Moore KL, Persaud TVN: The digestive system. In Moore KL, Persaud TVN (eds): *The Developing Human: Clinically Oriented Embryology*, 7th ed. Philadelphia, WB Saunders, 2003, p 268.
19. Carbillon L, Challier JC, Alouini S, et al: Uteroplacental circulation development: Doppler assessment and clinical importance. *Placenta* 22:795, 2001.
20. Husin J, Schaaps JP: Echographic and anatomic studies of the maternotrophoblastic border during the first trimester of pregnancy. *Am J Obstet Gynecol* 157:162, 1987.
21. Coppens M, Loquet P, Kollen M, et al: Longitudinal evaluation of uteroplacental and umbilical blood flow changes in normal early pregnancy. *Ultrasound Obstet Gynecol* 7:114, 1996.
22. Jauniaux E: Intervillous circulation in the first trimester: The phantom of the color Doppler obstetric opera. *Ultrasound Obstet Gynecol* 8:73, 1996.
23. Jauniaux E, Jurkovic D, Campbell S: In vivo investigations of the anatomy and the physiology of early human placental circulations. *Ultrasound Obstet Gynecol* 1:435, 1991.
24. Jaffe R, Jauniaux E, Hustin J: Maternal circulation in the first-trimester human placenta: Myth or reality? *Am J Obstet Gynecol* 176:695, 1997.
25. Jaffe R, Woods J: Color Doppler imaging and in vivo assessment of the anatomy and physiology of the early uteroplacental circulation. *Fertil Steril* 60:293, 1993.
26. Jauniaux E, Jurkovic D, Campbell S: Doppler ultrasonographic features of the developing placental circulation: Correlation with anatomic findings. *Am J Obstet Gynecol* 166:585, 1992.
27. Meuris S, Nagy AM, Delogne-Desnoeck J, et al: Temporal relationship between the human chorionic gonadotrophin peak and the establishment of intervillous blood flow in early pregnancy. *Hum Reprod* 10:947, 1995.
28. Schaaps J-P, Tsatsaris V, Goffin F, et al: Shunting the intervillous space: New concepts in human uteroplacental vascularization. *Am J Obstet Gynecol* 192:323, 2005.
29. Umaoka Y, Noda Y, Narimoto K, et al: Effects of oxygen toxicity on early development of mouse embryos. *Mol Reprod Dev* 31:28, 1992.
30. Carbillon L, Ziol M, Challier J-C, et al: Doppler and immunohistochemical evaluation of decidual spiral arteries in early pregnancy. *Gynecol Obstet Invest* 59:24, 2005.
31. Makikallio K, Tekay A, Jouppila P: Uteroplacental hemodynamics during early human pregnancy: A longitudinal study. *Gynecol Obstet Invest* 58:49, 2004.
32. Merce LT, Barco MJ, Bau S: Color Doppler sonographic assessment of placental circulation in the first trimester of normal pregnancy. *J Ultrasound Med* 15:135, 1996.
33. Valentin L, Sladkevicius P, Laurini R, et al: Uteroplacental and luteal circulation in normal first-trimester pregnancies: Doppler ultrasonographic and morphologic study. *Am J Obstet Gynecol* 174:768, 1996.
34. Merce LT, Barco MJ, de la Fuente F: Doppler velocimetry measured in retrochorionic space and uterine arteries during early human pregnancy. *Acta Obstet Gynecol Scand* 68:603, 1989.
35. Simpson NAB, Nimrod C, De Vermette R, et al: Sonographic evaluation of intervillous flow in early pregnancy: Use of echo-enhancement agents. *Ultrasound Obstet Gynecol* 11:204, 1998.
36. Kurjak A, Kupesic S: Doppler Assessment of the intervillous blood flow in normal and abnormal early pregnancy. *Obstet Gynecol* 89:252, 1997.
37. Fleischer AC, Kaleris GC, Machin JE, et al: Sonographic depiction of normal and abnormal endometrium with histopathologic correlation. *J Ultrasound Med* 5:445, 1986.
38. Forrest TS, Elyaderani MK, Muilenburg MI, et al: Cyclic endometrial changes: US assessment with histologic correlation. *Radiology* 167:233, 1988.
39. Timor-Tritsch IE, Farine D, Rosen MG: A close look at early embryonic development with the high-frequency transvaginal transducer. *Am J Obstet Gynecol* 159:676, 1988.
40. Rossavik IK, Torjusen GO, Gibbons WE: Conceptual age and ultrasound measurements of gestational sac and crown-rump length in *in vitro* fertilization pregnancies. *Fertil Steril* 49:1012, 1988.
41. de Crespigny LC, Cooper D, McKenna M: Early detection of intrauterine pregnancy with ultrasound. *J Ultrasound Med* 7:7, 1988.
42. Nyberg DA, Laing FC, Filly RA: Threatened abortion: Sonographic distinction of normal and abnormal gestation sacs. *Radiology* 158:397, 1986.
43. Yeh HC, Goodman JD, Carr L, et al: Intradecidual sign: A US criterion of early intrauterine pregnancy. *Radiology* 161:463, 1986.
44. Laing FC, Brown DL, Price JF, et al: Intradecidual sign: Is it effective in diagnosis of an early intrauterine pregnancy? *Radiology* 204:655, 1997.
45. Chiang G, Levine D, Swire M, et al: The intradecidual sign: Is it reliable for diagnosis of early intrauterine pregnancy? *Am J Roentgenol* 183:7251, 2004.
46. Bradley WG, Fiske CE, Filly RA: The double sac sign of early intrauterine pregnancy: Use in exclusion of ectopic pregnancy. *Radiology* 143:223, 1982.
47. Nyberg DA, Laing FC, Filly RA, et al: Ultrasonographic differentiation of the gestational sac of early intrauterine pregnancy from the pseudogestational sac of ectopic pregnancy. *Radiology* 146:755, 1983.
48. Abuhamad A, Sclater AJ, Carlson EJ, et al: Umbilical artery Doppler waveform notching: Is it a marker for cord and placental abnormalities? *J Ultrasound Med* 21:857, 2002.
49. Jaffe R, Dorgan A, Abramowicz JS: Color Doppler imaging of the uteroplacental circulation in the first trimester: Value in predicting pregnancy failure or complication. *AJR Am J Roentgenol* 164:1255, 1995.
50. Jauniaux E, Zaidi J, Jurkovic D, et al: Comparison of colour Doppler features and pathological findings in complicated early pregnancy. *Hum Reprod* 9:2432, 1994.
51. Levi CS, Lyons EA, Lindsay DJ: Early diagnosis of nonviable pregnancy with transvaginal US. *Radiology* 167:383, 1988.
52. Nyberg DA, Mack LA, Laing FC, et al: Distinguishing normal from abnormal gestational sac growth in early pregnancy. *J Ultrasound Med* 6:23, 1987.
53. Rowling SE, Langer JE, Coleman BG, et al: Sonography during early pregnancy: Dependence of threshold and discriminatory values on transvaginal transducer frequency. *AJR Am J Roentgenol* 172:983, 1999.
54. Cadkin AV, McAlpin J: Detection of fetal cardiac activity between 41 and 43 days of gestation. *J Ultrasound Med* 3:499, 1984.
55. Nyberg DA, Laurence MA, Harvey D, et al: Value of the yolk sac in evaluating early pregnancies. *J Ultrasound Med* 7:129, 1988.



56. Lindsay DJ, Lovett IS, Lyons EA, et al: Yolk sac diameter and shape at transvaginal US: Predictors of pregnancy outcome in the first trimester. *Radiology* 183:115, 1992.
57. Stampone C, Nicotra M, Mutinelli C, et al: Transvaginal sonography of the yolk sac in normal and abnormal pregnancy. *J Clin Ultrasound* 24:3, 1996.
58. Jauniaux E, Jurkovic D, Henriot Y, et al: Development of the secondary human yolk sac: Correlation of sonographic and anatomical features. *Hum Reprod* 6:1160, 1991.
59. Nyberg DA, Hill LM: Normal early intrauterine pregnancy: Sonographic development and hCG correlation. In Nyberg DA, Hill LM, Böhm-Velez M, et al (eds): *Transvaginal Ultrasound*. St. Louis, Mosby-Year Book, 1992, pp 65-84.
60. Yeh HC, Rabinowitz JG: Letter. *J Ultrasound Med* 14:97, 1995.
61. Goldstein SR, Wolfson R: Transvaginal ultrasonographic measurement of early embryonic size as a means of assessing gestational age. *J Ultrasound Med* 13:27, 1994.
62. Daya S: Accuracy of gestational age estimation by means of the fetal crown-rump length measurement. *Am J Obstet Gynecol* 168:903, 1993.
63. Wisser J, Dirschedl P, Krone S: Estimation of gestational age by transvaginal sonographic measurement of the greatest embryonic length in dated human embryos. *Ultrasound Obstet Gynecol* 4:457, 1994.
64. Robinson HP: "Gestational sac" volumes as determined by sonar in the first trimester of pregnancy. *Br J Obstet Gynecol* 82:100, 1975.
65. Robinson HP, Hadlock FP, Shah YP, et al: Combined data comparing menstrual age with average gestational sac size (mean diameter), and crown-rump length. In Nyberg DA, Hill LM, Böhm-Velez M, et al (eds): *Transvaginal Ultrasound*. St. Louis, Mosby-Year Book, 1992, p 335.
66. Hadlock FP, Shah YP, Kanon DJ, Lindsey JV: Fetal crown-rump length: Reevaluation of relation to menstrual age (5-18 weeks) with high-resolution real-time US. *Radiology* 182:501, 1992.
67. Coulam CB, Britten S, Soenksen DM: Early (34-56 days from last menstrual period) ultrasonographic measurements in normal pregnancies. *Hum Reprod* 11:1771, 1996.
68. Benson CB, Doubilet PM: Fetal measurements-normal and abnormal fetal growth. In Rumack CM, Wilson SR, Charboneau JW (eds): *Diagnostic Ultrasound*, 3rd ed. St. Louis, CV Mosby, 2005, pp 1493-1512.
69. Levi CS, Lyons EA, Zheng XH, et al: Transvaginal US: Demonstration of cardiac activity in embryos of less than 5.0 mm in crown-rump length. *Radiology* 176:71, 1990.
70. Brown DL, Emerson DS, Fleker RE, et al: Diagnosis of early embryonic demise by transvaginal sonography. *J Ultrasound Med* 9:631, 1990.
71. Rempen A: Diagnosis of viability in early pregnancy with vaginal sonography. *J Ultrasound Med* 9:711, 1990.
72. Hertzberg BS, Mahony BS, Bowie JD: First trimester fetal cardiac activity: Sonographic documentation of a progressive early rise in heart rate. *J Ultrasound Med* 7:573, 1988.
73. Doubilet PM, Benson CB: Embryonic heart rate in the early first trimester: What rate is normal? *J Ultrasound Med* 14:431, 1995.
74. Stefanou TI, Lolis DE, Sotiriadis AJ, et al: Embryonic heart rate in early pregnancy. *J Clin Ultrasound* 26:33, 1998.
75. Schats R, Jansen CAM, Wladimiroff JW: Embryonic heart activity: Appearance and development in early human pregnancy. *Br J Obstet Gynaecol* 97:989, 1990.
76. Montenegro N, Ramos C, Matias A, et al: Variation of embryonic/fetal heart rate at 6-13 weeks' gestation. *Ultrasound Obstet Gynecol* 11:274, 1998.
77. McKenna DS, Ventolini G, Neiger R, et al: Gender-related differences in fetal heart rate during first trimester. *Fetal Diagn Ther* 21:144, 2006.
78. Achiron R, Tadmor O, Mashiah S: Heart rate as a predictor of first-trimester spontaneous abortion after ultrasound-proven viability. *Obstet Gynecol* 78:330, 1991.
79. Laboda LA, Estroff JA, Benacerraf BR: First trimester bradycardia: A sign of impending fetal loss. *J Ultrasound Med* 8:561, 1989.
80. May DA, Sturtevant NV: Embryonal heart rate as a predictor of pregnancy outcome: A prospective analysis. *J Ultrasound Med* 10:591, 1991.
81. Lasser DM, Peisner DB, Vollebergh J, et al: First-trimester fetal biometry using transvaginal sonography. *Ultrasound Obstet Gynaecol* 3:104, 1993.
82. Yeh HC, Rabinowitz JG: Amniotic sac development: Ultrasound features of early pregnancy-the double bleb sign. *Radiology* 166:97, 1988.
83. Bowerman RA: Sonography of fetal midgut herniation: Normal size criteria and correlation with crown-rump length. *J Ultrasound Med* 12:251, 1993.
84. Timor-Trisch IE, Warren WB, Peisner DB, et al: First-trimester midgut herniation: A high-frequency transvaginal sonographic study. *Am J Obstet Gynecol* 161:831, 1989.
85. Blaas HG, Eik-Nes SH, Kiserud T, et al: Early development of the abdominal wall, stomach and heart from 7 to 12 weeks of gestation: A longitudinal ultrasound study. *Ultrasound Obstet Gynecol* 6:240, 1995.
86. Benoit B, Hafner T, Kurjak A, et al: Three-dimensional sonoembryology. *J Perinat Med* 30:63, 2002.
87. Blaas HG, Taipale P, Torp H, et al: Three-dimensional ultrasound volume calculations of human embryos and young fetuses: A study on the volumetry of compound structures and its reproducibility. *Ultrasound Obstet Gynecol* 27:640, 2006.
88. Yonemoto H, Yoshida K, Kinoshita K, et al: Embryological evaluation of surface features of human embryos and early fetuses by 3-D ultrasound. *J Obstet Gynaecol Res* 28:211, 2002.
89. Acharya G, Morgan H: First-trimester, three-dimensional transvaginal ultrasound volumetry in normal pregnancies and spontaneous miscarriages. *Ultrasound Obstet Gynecol* 19:575, 2002.
90. Hull AD, James G, Salerno CC, et al: Three-dimensional ultrasonography and assessment of the first-trimester fetus. *J Ultrasound Med* 20:287, 2001.
91. Andonotopo W, Medic M, Salihagic-Kadic A, et al: The assessment of fetal behavior in early pregnancy: Comparison between 2D and 4D sonographic scanning. *J Perinat Med* 33:406, 2005.
92. Kurjak A, Carrera J, Medic M, et al: The antenatal development of fetal behavioral patterns assessed by four-dimensional sonography. *J Matern Fetal Neonatal Med* 17:401, 2005.
93. Bourne G: The microscopic anatomy of the human amnion and chorion. *Am J Obstet Gynecol* 79:1070, 1960.
94. Giacomello F: Small sac size as a predictor of poor fetal outcome (letter). *Radiology* 184:578, 1992.
95. Ikegawa A: First-trimester detection of amniotic sac in relation to miscarriage. *J Obstet Gynaecol Res* 23:283, 1997.
96. Horrow MM: Enlarged amniotic cavity: A new sonographic sign of early embryonic death. *Am J Roentgenol* 158:359, 1992.
97. Campbell J, Wathen N, Macintosh M, et al: Biochemical composition of amniotic fluid and extraembryonic coelomic fluid in the first trimester of pregnancy. *Br J Obstet Gynaecol* 99:563, 1992.
98. Kalish RB, Thaler HT, Chasen ST, et al: First- and second-trimester ultrasound assessment of gestational age. *Am J Obstet Gynecol* 191:975, 2004.
99. Nyberg DA, Filly RA, Mahony BS, et al: Early gestation: Correlation of HCG levels and sonographic identification. *AJR Am J Roentgenol* 144:951, 1985.
100. Muller T, Sutterlin M, Pohls U, et al: Transvaginal volumetry of first trimester gestational sac: a comparison of conventional with three-dimensional ultrasound. *J Perinat Med* 28:214, 2000.
101. Acharya G, Morgan H: First-trimester, three-dimensional transvaginal ultrasound volumetry in normal pregnancies and spontaneous miscarriages. *Ultrasound Obstet Gynecol* 19:575, 2002.
102. Robinson HP, Fleming JEE: A critical evaluation of sonar "crown-rump length" measurement. *Br J Obstet Gynaecol* 82:702, 1975.
103. Tunon K, Eik-Nes SH, Grottnum P, et al: Gestational age in pregnancies conceived after in vitro fertilization: A comparison between age assessed from oocyte retrieval, crown-rump length and biparietal diameter. *Ultrasound Obstet Gynecol* 15:41, 2000.
104. Taipale P, Hilesmaa V: Predicting delivery date by ultrasound and last menstrual period in early gestation. *Obstet Gynecol* 97:189, 2001.
105. Salomon LJ, Bernard JP, Duyme M, et al: Revisiting first-trimester fetal biometry. *Ultrasound Obstet Gynecol* 22:63, 2003.
106. Goldstein SR: Embryonic ultrasound measurements: Crown-rump length revisited. *Am J Obstet Gynecol* 165:497, 1991.
107. Robinson HP: Sonar measurement of the fetal crown-rump length as a means of assessing maturity in the first trimester of pregnancy. *Br Med J* 4:28, 1973.
108. Sladkevicius P, Saltvedt S, Almstrom H, et al: Ultrasound dating at 12-14 weeks of gestation. A prospective cross-validation of established dating formulae in in-vitro fertilized pregnancies. *Ultrasound Obstet Gynecol* 26:504, 2005.



109. Branch DW, Scott JR: Early pregnancy loss. In Scott JR, Gibbs RS, Karlan BY, Hanczy AF (eds): *Danforth's Obstetrics and Gynecology*, 9th ed. Philadelphia: Lippincott, Williams & Wilkins, 2003, pp 75-87.
110. Wilcox AJ, Weinberg CR, O'Connor JF, et al: Incidence of early pregnancy loss. *N Engl J Med* 319:189, 1988.
111. Nyberg DA, Laing FC: Threatened abortion and abnormal first-trimester intrauterine pregnancy. In Nyberg DA, Hill LM, Böhm-Velez M, et al (eds): *Transvaginal Ultrasound*. St. Louis, Mosby-Year Book, 1992, pp 85-103.
112. Pridjian G, Moawad AH: Missed abortion: Still appropriate terminology? *Am J Obstet Gynecol* 161:261, 1989.
113. Schwärzler P, Holden D, Nielsen S, et al: The conservative management of first trimester miscarriages and the use of colour Doppler sonography for patient selection. *Human Reproduction* 14:1341, 1999.
114. Sairam S, Khare M, Michailidis G, et al: The role of ultrasound in the expectant management of early pregnancy loss. *Ultrasound Obstet Gynecol* 17:506, 2001.
115. Elson J, Taylor A, Salim R, et al: Expectant management of miscarriage-prediction of outcome using ultrasound and novel biochemical markers. *Hum Reprod* 20:2330, 2005.
116. Schouwink MH, Fong BF, Mol BW, et al: Ultrasonographic criteria for non-viability of first trimester intra-uterine pregnancy. *Early Pregnancy* 4:203, 2000.
117. Rowling SE, Coleman BG, Langer JE, et al: First-trimester US parameters of failed pregnancy. *Radiology* 203:211, 1997.
118. Byrne J, Warburton D, Kline J, et al: Morphology of early fetal deaths and their chromosomal characteristics. *Teratology* 32:297, 1985.
119. Bajo J, Moreno-Calvo FJ, Martínez-Cortés L, et al: Is trophoblastic thickness at the embryonic implantation site a new sign of negative evolution in first trimester pregnancy? *Hum Reprod* 15:1629, 2000.
120. Harris RD, Couto C, Karpovsky C, et al: The chorionic bump: A first-trimester pregnancy sonographic finding associated with a guarded prognosis. *J Ultrasound Med* 25:757, 2006.
121. Dillon EH, Feyock AL, Taylor KJW: Pseudogestational sacs: Doppler US differentiation from normal or abnormal intrauterine pregnancies. *Radiology* 176:359, 1990.
122. Dubinsky TJ, Parvey HR, Maklad N: Endometrial color flow/image directed Doppler imaging: Negative predictive value for excluding ectopic pregnancy. *J Clin Ultrasound* 25:103, 1997.
123. Duck FA: Is it safe to use diagnostic ultrasound during the first trimester? *Ultrasound Obstet Gynecol* 13:385, 1999.
124. Pennell RG, Needleman L, Pajak T, et al: Prospective comparison of vaginal and abdominal sonography in normal early pregnancy. *J Ultrasound Med* 10:63, 1991.
125. Frates MC, Benson CB, Doubilet PM: Pregnancy outcome after a first trimester sonogram demonstrating fetal cardiac activity. *J Ultrasound Med* 12:383, 1993.
126. Siddiqi TS, Caligaris JT, Miodovnik M, et al: The rate of spontaneous abortion after first trimester sonographic demonstration of fetal cardiac activity. *Am J Perinatol* 5:1, 1988.
127. Cashner KA, Christopher CR, Dysert GA: Spontaneous fetal loss after demonstration of a live fetus in the first trimester. *Obstet Gynecol* 70:827, 1987.
128. MacKenzie WE, Holmes DS, Newton JR: Spontaneous abortion rate in ultrasonographically viable pregnancies. *Obstet Gynecol* 71:81, 1988.
129. Pandya PP, Snijders RJM, Psara N, et al: The prevalence of non-viable pregnancy at 10-13 weeks of gestation. *Ultrasound Obstet Gynecol* 7:170, 1996.
130. Howe RS, Isaacson KJ, Albert JL, et al: Embryonic heart rate in human pregnancy. *J Ultrasound Medicine* 10:367, 1991.
131. Nyberg DA, Cyr DR, Mack LA, et al: Sonographic spectrum of placental abruption. *Am J Roentgenol* 148:161, 1987.
132. Bennett GL, Bromley B, Lieberman E, et al: Subchorionic hemorrhage in first-trimester pregnancies: Prediction of pregnancy outcome with sonography. *Radiology* 200:803, 1996.
133. Hill LM, Guzik D, Fries J, et al: Fetal loss rate after ultrasonically documented cardiac activity between 6 and 14 weeks menstrual age. *J Clin Ultrasound* 19:221, 1991.
134. Falco P, Milano V, Pili G, et al: Sonography of pregnancies with first-trimester bleeding and a viable embryo: A study of prognostic indicators by logistic regression analysis. *Ultrasound Obstet Gynecol* 7:165, 1996.
135. Makrydimas G, Sebire NJ, Lolis D, et al: Fetal loss following ultrasound diagnosis of a live fetus at 6-10 weeks of gestation. *Ultrasound Obstet Gynecol* 22:368, 2003.
136. Stabile I, Campbell S, Grudzinskas JC: Threatened miscarriage and intrauterine hematomas: Sonographic and biochemical studies. *J Ultrasound Med* 8:289, 1989.
137. Pedersen JF, Mantoni M: Prevalence and significance of subchorionic hemorrhage in threatened abortion: A sonographic study. *AJR Am J Roentgenol* 154:535, 1990.
138. Nagy S, Bush M, Stone J, et al: Clinical significance of subchorionic and retroplacental hematomas detected in the first trimester of pregnancy. *Obstet Gynecol* 102:94, 2003.
139. Johns J, Hyett J, Jauniaux E: Obstetric outcome after threatened miscarriage with and without a hematoma on ultrasound. *Obstet Gynecol* 102:483, 2003.
140. Benson CB, Doubilet PM, Cooney MJ, et al: Early singleton pregnancy outcome: Effects of maternal age and modes of conception. *Radiology* 203:399, 1997.
141. Merchiers EH, Dhont M, DeSutter PA, et al: Predictive value of early embryonic cardiac activity for pregnancy outcome. *Am J Obstet Gynecol* 165:11, 1991.
142. Doubilet PM, Benson CB: Outcome of first-trimester pregnancies with slow embryonic heart rate at 6-7 weeks gestation and normal heart rate by 8 weeks at US. *Radiology* 236:643, 2005.
143. Vaccaro H, Amor F, Leyton M, et al: Arrhythmia in early pregnancy: A predictor of first-trimester pregnancy loss. *Ultrasound Obstet Gynecol* 12:248, 1998.
144. Wong SF, Chau KT, Ho LC: Fetal bradycardia in the first trimester: An unusual presentation of atrial extrasystoles. *Prenat Diagn* 22:976, 2002.
145. Doubilet PM, Benson CB, Chow JS: Long-term prognosis of pregnancies complicated by slow embryonic heart rates in the early first trimester. *J Ultrasound Med* 18:537, 1999.
146. Liao AW, Snijders R, Geerts L, et al: Fetal heart rate in chromosomally abnormal fetuses. *Ultrasound Obstet Gynecol* 16:610, 2000.
147. Doubilet PM, Benson CB, Chow JS: Outcome of pregnancies with rapid embryonic heart rates in the early first trimester. *Am J Roentgenol* 175:67, 2000.
148. Dickey RP, Olar TT, Taylor SN, et al: Relationship of small gestational sac-crown-rump length differences to abortion and abortus karyotypes. *Obstet Gynecol* 79:554, 1992.
149. Bromley B, Harlow BL, Laboda LA, et al: Small sac size in the first trimester: A predictor of poor fetal outcome. *Radiology* 178:375, 1991.
150. Dickey RP, Gasser RF: Ultrasound evidence for variability in the size and development of normal human embryos before the tenth post-insemination week after assisted reproductive technologies. *Hum Reprod* 8:331, 1993.
151. Smith GCS, Smith MFS, McNay MB, et al: First-trimester growth and the risk of low birth weight. *N Engl J Med* 339:1817, 1998.
152. Kallen K: Increased risk of perinatal/neonatal death in infants who were smaller than expected at ultrasound fetometry in early pregnancy. *Ultrasound Obstet Gynecol* 24:30, 2004.
153. Smith GC: First trimester origins of fetal growth impairment. *Semin Perinatol* 28:41, 2004.
154. Cucuk T, Duru NK, Yenen MC, et al: Yolk sac size and shape as predictors of poor pregnancy outcome. *J Perinat Med* 27:316, 1999.
155. Chama CM, Marupa JY, Obed JY: The value of the secondary yolk sac in predicting pregnancy outcome. *J Obstet Gynaecol* 25:245, 2005.
156. Dugoff L, Persutte WH, Schultz L, et al: Prognostic significance of the large yolk sac [Abstract]. *Am J Obstet Gynecol* 178:S165, 1998.
157. Cosmi E, Piazze JJ, Ruozzi A, et al: Structural-tridimensional study of yolk sac in pregnancies complicated by diabetes. *J Perinat Med* 33:132, 2005.
158. Harris RD, Vincent LM, Askin FB: Yolk sac calcification: A sonographic finding associated with intrauterine embryonic demise in the first trimester. *Radiology* 166:109, 1988.
159. Barzilai M, Lyons EA, Levi CS, et al: Vitelline duct cyst or double yolk sac. *J Ultrasound Med* 8:523, 1989.
160. Weissman A, Iskowitz-Eldor J, Jakobi P: Sonographic measurement of amniotic fluid volume in the first trimester of pregnancy. *J Ultrasound Med* 15:771, 1996.
161. McKenna KM, Feldstein VA, Goldstein RB, et al: The "empty amnion": A sign of early pregnancy failure. *J Ultrasound Med* 14:117, 1995.
162. Gindoff PR, Jewellic R: Reproductive potential in the older woman. *Fertil Steril* 46:989, 1986.
163. Benson CB, Chow JS, Chang-Lee W, et al: Outcome of pregnancies in women with uterine leiomyomas identified by sonography in the first trimester. *J Clin Ultrasound* 29:261, 2001.



164. Cooney MJ, Benson CB, Doubilet PM: Outcomes of pregnancies in women with uterine duplication anomalies. *J Clin Ultrasound* 26:3, 1998.
165. Patton PE: Anatomic uterine defects. *Clin Obstet Gynecol* 37:705, 1994.
166. Daya S: Ultrasonographic evaluation of uterine anomalies. In Jaffe R, Pierson RA, Abramowicz JA (eds): *Imaging in Infertility and Reproductive Endocrinology*. Philadelphia, JB Lippincott, 1994, pp 63-92.
167. van Leeuwen I, Branch DW, Scott JR: First trimester-ultrasonography findings in women with a history of recurrent pregnancy loss. *Am J Obstet Gynecol* 168:111, 1993.
168. Opsahl MS, Pettit DC: First trimester sonographic characteristics of patients with recurrent spontaneous abortion. *J Ultrasound Med* 12:507, 1993.
169. Cunningham DS, Bledsoe LD, Tichenor JR, et al: Ultrasonographic characteristics of first-trimester gestations in recurrent spontaneous aborters. *J Reprod Med* 40:565, 1995.
170. Nyberg DA, Filly RA, Duarte DL, et al: Abnormal pregnancy: Early diagnosis by US and serum chorionic gonadotropin levels. *Radiology* 158:393, 1986.
171. Ong CY, Liao AW, Spencer K, et al: First trimester maternal serum free beta human chorionic gonadotropin and pregnancy associated plasma protein A as predictors of pregnancy complications. *Brit J Obstet Gynecol* 107:1265, 2000.
172. Tong S, Wallace EM, Rombauts L: Association between low day 16 hCG and miscarriage after proven cardiac activity. *Obstet Gynecol* 107:300, 2006.
173. Check JH, Liss JR, Katz Y, et al: Slow rising serial chorionic gonadotropins predict poor pregnancy outcome despite sonographic viability. *Clin Exp Obstet Gynecol* 30:193, 2003.
174. Nyberg DA, Laing FC, Filly RA, et al: Ectopic pregnancy: Diagnosis by sonography correlated with quantitative hCG levels. *J Ultrasound Med* 6:145, 1987.
175. Kadar N, DeVore G, Romero R: Discriminatory hCG zone: Its use in the sonographic evaluation for ectopic pregnancy. *Obstet Gynecol* 58:156, 1981.
176. Caeciatore B, Ylostolo P, Stenman UH, et al: Suspected ectopic pregnancy: Ultrasound findings and hCG levels assessed by immuno-fluorometric assay. *Br J Obstet Gynaecol* 95:497, 1988.
177. Bandi ZL, Schoen I, Waters M: An algorithm for testing and reporting serum choriogonadotropin at clinically significant decision levels with the use of "pregnancy test" reagents. *Clin Chem* 35:545, 1989.
178. Peisner DB, Timor-Tritsch IE: The discriminatory zone of beta-hCG for vaginal probes. *J Clin Ultrasound* 18:280, 1990.
179. Frates MC, Doubilet PM, Brown DL, et al: Role of Doppler ultrasonography in the prediction of pregnancy outcome in women with recurrent spontaneous abortion. *J Ultrasound Med* 15:557, 1996.
180. Leible S, Cumsille F, Walton R, et al: Discordant uterine artery velocity waveforms as a predictor of subsequent miscarriage in early viable pregnancies. *Am J Obstet Gynecol* 179:1587, 1998.
181. Pellizzari P, Pozzan C, Marchiori S, et al: Assessment of uterine artery blood flow in normal first-trimester pregnancies and in those complicated by uterine bleeding. *Ultrasound Obstet Gynecol* 19:366, 2002.
182. Alcázar JL, Ruiz-Perez ML: Uteroplacental circulation in patients with first-trimester threatened abortion. *Fertil Steril* 73:130, 2000.
183. Kurjak A, Crenkovic G, Salihagic A, et al: The assessment of normal early pregnancy by transvaginal color Doppler ultrasonography. *J Clin Ultrasound* 21:3, 1993.
184. Salim A, Zalud I, Farmakides G, et al: Corpus luteum blood flow in normal and abnormal early pregnancy: Evaluation with transvaginal color and pulsed Doppler sonography. *J Ultrasound Med* 13:971, 1994.
185. Alcázar JL, Laparte C, Lopez-Garcia G: Corpus luteum blood flow in abnormal early pregnancy. *J Ultrasound Med* 15:645, 1996.
186. Frates MC, Doubilet PM, Durfee SD, et al: Sonographic and Doppler characteristics of the corpus luteum: Can they predict pregnancy outcome? *J Ultrasound Med* 20:821, 2001.
187. Dugoff L, Lynch AM, Cioffi-Ragan D, et al: First trimester uterine artery Doppler abnormalities predict subsequent intrauterine growth restriction. *Am J Obstet Gynecol* 193:1208, 2005.
188. Perfumo F, Güven M, Ganapathy R, et al: The longitudinal variation in uterine artery blood flow pattern in relation to birth weight. *Obstet Gynecol* 130:764, 2004.
189. Schuchter K, Metzenbauer M, Hafner E, et al: Uterine artery Doppler and placental volume in the first trimester in the prediction of pregnancy complications. *Ultrasound Obstet Gynecol* 18:590, 2001.
190. Moore KL, Persaud TVN: Human birth defects. In Moore KL, Persaud TVN (eds): *The Developing Human: Clinically Oriented Embryology*, 7th ed. Philadelphia, WB Saunders, 2003, pp 157-185.
191. Van Zalen-Sprock RM, Van Vugt JMG, Van Geijn HP: First and early second trimester diagnosis of anomalies of the central nervous system. *J Ultrasound Med* 14:603, 1995.
192. Dugoff L: Ultrasound diagnosis of structural abnormalities in the first trimester. *Prenat Diagn* 22:316, 2002.
193. Chatzipapas IK, Whidow RJ, Economides DL: The 'Mickey Mouse' sign and the diagnosis of anencephaly in early pregnancy. *Ultrasound Obstet Gynecol* 13:196, 1999.
194. Liu IF, Chang CH, Yu CH, et al: Prenatal diagnosis of fetal acrania using three-dimensional ultrasound. *Ultrasound Med Biol* 31:175, 2005.
195. Sepulveda W, Dezerega V, Be C: First-trimester sonographic diagnosis of holoprosencephaly: Value of the "butterfly" sign. *J Ultrasound Med* 23:761, 2004.
196. Malone FD, Ball RH, Nyberg DA, et al: FASTER Trial Research Consortium. First-trimester septated cystic hygroma: Prevalence, natural history, and pediatric outcome. *Obstet Gynecol* 106:288, 2005.
197. Blazer S, Zimmer EZ, Gover A, et al: Fetal omphalocele detected early in pregnancy: associated anomalies and outcomes. *Radiology* 232:191, 2004.
198. Daskalakis G, Sebire NJ, Jurkovic D, et al: Body stalk anomaly at 10-14 weeks of gestation. *Ultrasound Obstet Gynecol* 10:416, 1997.
199. Pajkri E, Jauniaux E: First-trimester diagnosis of conjoined twins. *Prenat Diagn* 25:820, 2005.
200. Vural F, Vural B: First trimester diagnosis of dicephalic parapagus conjoined twins via transvaginal ultrasonography. *J Clin Ultrasound* 33:364, 2005.

# ULTRASOUND EVALUATION OF FETAL BIOMETRY AND NORMAL AND ABNORMAL FETAL GROWTH

Henry L. Galan, MD, Santosh Pandipati, MD, and Roy A. Filly, MD

## Introduction

### Dating a Pregnancy

### First Trimester of Pregnancy (0 to 13 Weeks)

### Second and Third Trimesters of Pregnancy (14 to 42 Weeks)

### Biometry: Following the Rules

Biparietal Diameter

Head Circumference

Abdominal Circumference

Femur Length

### Other Biometric Parameters

### Late Pregnancy

### Calculation of Menstrual Age

## Estimation of Fetal Weight

### Clinical Application of Biometric Parameters

Intrauterine Growth Restriction

*Definition*

*Etiologies*

*Pathophysiology*

*Short- and Long-Term Sequelae*

Assessment of Fetal Status

Doppler Velocimetry

### Accelerated Fetal Growth

### Interval Fetal Growth and Growth Potential

### Conclusions

## INTRODUCTION

Ultrasound has become the essential tool of modern obstetric practice. With advances in technology and computer processing, what was once a mere curiosity has become crucial for the assessment of the placenta, membranes, fluid, and fetal anatomy, as is covered in the other portions of this text. The assignment of pregnancy age is the first task placed before the care provider, and ultrasound is the key modality used for this purpose. Additionally, ultrasound is far superior to the clinical examination for determining adequacy of interval fetal growth. With the development of Doppler technology, one can now assess fetal status to determine pathology earlier than as evidenced by abnormal fetal cardiotocography (CTG). As a result, Doppler ultrasound has become crucial for making management decisions in some high risk settings. The methods for dating a pregnancy, measuring growth, and assessing fetal status using Doppler technology are covered in this chapter.

## DATING A PREGNANCY

Sonography provides an enormous amount of useful information to the practicing obstetrician. Arguably, the

single most useful piece of information that obstetric sonography provides is an accurate determination of menstrual age. It is difficult to imagine a clinical problem encountered during a pregnancy in which an accurate menstrual age is not highly desired before proceeding with an appropriate management plan.

It is important to establish from the outset what is meant by the term *menstrual age* and why it is so important in clinical obstetrics. *Fetal age* actually begins at conception, and an equivalent term is *conceptional age*. However, classically and by current convention, obstetricians date pregnancies in menstrual weeks, beginning from the 1st day of the last normal menstrual period. The appropriate term for this method of dating is *menstrual age*, and this term is used exclusively in this chapter when referring to the duration of a pregnancy.<sup>1</sup> Many obstetricians also use the term *gestational age* (GA). Although GA should be equivalent to *conceptional age*, in clinical obstetric practice GA is used interchangeably with *menstrual age*. The term *conceptional age* should be reserved to describe pregnancies in which the actual date of conception is known; this is uncommon and is usually restricted to patients who have undergone assisted reproduction (e.g., in vitro fertilization, artificial insemination). Even if conceptional age is known, the menstrual age should be calculated from the conceptional age, based on the assumption of midcycle ovulation ( $\text{menstrual age} = \text{conceptional age} + 14 \text{ days}$ ). Once this has been done, the menstrual age is established and should never be changed later in pregnancy. Subsequent fetal measurements then become an index of fetal growth rather than menstrual age.

\*In December, 2005 the ultrasound community lost one of the pioneers in obstetric ultrasound, Dr. Frank P. Hadlock. Since the late 1970s Dr. Hadlock investigated the role of ultrasound in assigning gestational age (GA) and defining abnormal fetal growth patterns. He contributed to this chapter in previous editions. His formulae for weight prediction are still being used today in most ultrasound scanning equipment. He was a superb teacher and friend and will be dearly missed.



**Table 7-1** Methods for Determining Menstrual Age

Clinical or Sonographic Parameter	Variability Estimate ( $\pm 2$ SD)
In vitro fertilization*	$\pm 1$ day
Ovulation induction*	$\pm 3$ days
Artificial insemination*	$\pm 3$ days
Single intercourse record*	$\pm 3$ days
Basal body temperature record*	$\pm 4$ days
First trimester physical examination	$\pm 2$ weeks
Second trimester physical examination	$\pm 4$ weeks
Third trimester physical examination	$\pm 6$ weeks
First trimester sonographic examination (crown rump $\pm 18\%$ of the estimate length)	
Second trimester sonographic examination (head $\pm 18\%$ of the estimate circumference, femur length)	
Third trimester sonographic examination (head $\pm 8\%$ of the estimate circumference, femur length)	

SD, standard deviation.

\*Those are indicators of conceptional age (menstrual age = conceptional age + 14 days)

Adapted from James D. Bowie, M.D., Duke University Medical Center.

Knowledge of menstrual age is important to the obstetrician because it affects clinical management in a number of important ways. First, knowledge of menstrual age is used in early pregnancy for the scheduling of invasive procedures such as chorionic villus sampling and genetic amniocentesis, and in the interpretation of biochemical tests such as expanded maternal serum biomarker screening ("quad-screen") for risk assessment for neural tube defects and chromosomal anomalies (e.g., trisomy 21 and 18) in which the normal range of values changes over time. Second, knowledge of menstrual age allows the obstetrician to anticipate normal spontaneous delivery or to plan elective delivery within the time frame of a term pregnancy (37 to 42 weeks); this also allows the physician to institute measures that will optimize fetal outcome when labor ensues before 37 weeks or fails to ensue after 42 weeks. Third, knowledge of menstrual age is important in evaluating fetal growth because the normal range for the size of any fetal parameter changes with advancing age.<sup>1</sup> Thus, a fetal weight of 2000 g would be normal at 33 weeks but would indicate growth restriction at 36 weeks. When an anomaly is discovered sonographically, the mother's choices are heavily influenced by menstrual age. Virtually all important clinical decisions require knowledge of the menstrual age.

Before the advent of sonography, menstrual age was established by the patient's menstrual history, corroborated, preferably during early pregnancy, by physical examination of uterine size, and confirmed in the postnatal period by physical examination of the neonate.<sup>2,3</sup> All three of these parameters alone or in combination were notoriously inaccurate (Table 7-1), but the menstrual history could be especially misleading for a number of reasons. First, many women may not accurately recall the 1st day of the last normal menstrual period (LMP), particularly if they are not trying to conceive. Also some women commonly misunderstand the question posed and report the last day instead of the 1st day of their last period. Moreover, for those who do remember their LMP, it may be unreliable or misleading

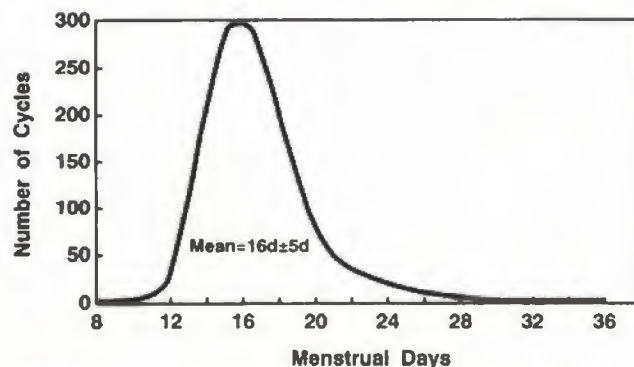


**FIGURE 7-1.** Length of the follicular phase of the menstrual cycle in a large number of patients studied by Matsumoto, Nogami, and Ohkuri.<sup>4</sup> Note that the distribution is skewed to the right, with a higher number of patients ovulating late in the cycle (>day 21) than earlier in the cycle (<day 11). This corresponds to the findings in the study by Waldenström, Axelsson, and Nilsson,<sup>6</sup> in which an early midtrimester ultrasound study agreed with the menstrual history in only about 80% of the cases. In 3%, the age by ultrasound evaluation was greater than expected from the optimal menstrual history (corresponding to early ovulation), and in about 17%, the age by ultrasound evaluation was less than expected from the optimal menstrual history (indicating late ovulation). (Adapted from Matsumoto S, Nogami Y, Ohkuri S: Statistical studies on menstruation: A criticism on the definition of normal menstruation. *Gumma J Med Sci* 11:294, 1962.)

because of oligomenorrhea, abnormal bleeding events, use of hormonal contraceptives, becoming pregnant in the first ovulatory cycle after a recent delivery, or ovulating very early (<day 11) or very late (>day 21) in the menstrual cycle. This latter point may be particularly important, because Matsumoto, Nogami, and Ohkuri<sup>4</sup> reported that early or late ovulation occurs in approximately 20% of the population (Fig. 7-1). Indeed, many pregnancy dating formulae and calculator wheels are based on a 280-day gestation starting from the time of the LMP, which is, in turn, based upon a regular, 28-day menstrual cycle composed of 14 days in the follicular and luteal phases each. It is not surprising, then, that Campbell et al<sup>5</sup> and Waldenström, Axelsson, and Nilsson<sup>6</sup> found that, even in patients with optimal menstrual histories, a single second trimester biparietal diameter (BPD) measurement was more predictive of the estimated date of delivery (EDD) than the date of delivery calculated from the 1st day of the last normal menstrual period. One often hears the statements "This patient has good dates" or "That patient has bad dates." What constitutes "good" as opposed to "bad" dates? Optimal menstrual histories are present when the patient has a certain last normal menstrual period (preferably recorded on a calendar), regular menses, no exposure to hormonal contraceptives, and no unusual bleeding. Thus, it should not be surprising that the most common indications for obstetric sonograms are related to uncertainty regarding the menstrual age.

Sonographic studies designed to evaluate the duration of pregnancy are based on measurements of the fetus, using size as an indirect indicator of menstrual age.<sup>1,7-32</sup> These studies usually relied on cross-sectional evaluation of large numbers of patients with known dates of the beginning of the last normal menstrual period and no compounding variables in the menstrual history to question its validity. Rossavik and Fishburne<sup>33</sup> demonstrated that such populations



are equivalent to populations with known conception dates for studies of this type. Most studies also eliminated patients with multiple gestations and those with a history that might adversely affect fetal growth. In a properly designed cross-sectional analysis of any fetal biometric parameter, measurements are made in a large number of fetuses evenly distributed over the entire range of menstrual ages, with each fetus being measured only once in gestation; the latter point is important in avoiding bias in variability estimates. The data are then analyzed using regression analysis, with menstrual age as the dependent variable, and equations are generated that will predict menstrual age for any given measurement or set of measurements. Most of the published tables that provide predictions of menstrual age from sonographic measurements have been generated in this way.<sup>1</sup>

The value of any given studied biometric parameter (e.g., BPD, head circumference [HC], femur length [FL], ear lobe length, nostril width) is based on ease of obtaining the measurement and the accuracy with which it predicts menstrual age. A measurement that is easily obtained but inaccurate for judging menstrual age is of little value. As well, a measurement that accurately predicts menstrual age but is very difficult to obtain is also usually not valuable. In inexperienced hands, a difficult measurement is often inaccurately obtained, thus nullifying its salutary effect on age prediction. The measurements currently recommended by the American Institute of Ultrasound in Medicine (BPD, HC, abdominal circumference [AC], and FL) are adequate for the purpose of estimating menstrual age; any additional measurement to predict menstrual age must improve current predictors, and thus far none has emerged.

Regardless of the number of sonographic measurements that one uses in predicting menstrual age, it is very important to remember that this is an inference of age from size, and to understand the variability that is associated with any such estimate. The variability, usually the result of measurement error or actual biologic variability in size, is expressed as  $\pm 2$  standard deviations, which should be applicable to 95% of the fetuses in a normal population. One must always keep in mind, however, that 5% of the time estimates will be outside this range. Inspection of the magnitude of the maximum errors observed in the original regression data will give a general idea about the largest mistake one could make prospectively predicting menstrual age in a clinical case setting.

Reporting a menstrual age estimate to one or two decimal places for a given fetal measurement or set of measurements may result in an unreasonable assumption regarding the degree of accuracy by the patient's primary clinician. Importantly, when reporting the menstrual age estimate, it is wise to avoid potential misunderstanding. Cardinal numbers (1, 2, 3, and so on) are used for counting. Ordinal numbers are used to express succession (first, second, third, and so on). Although often used interchangeably, they are not. A fetus in the 20th menstrual week of pregnancy is between the ages of 19 weeks 0 days and 19 weeks 6 days, whereas a fetus that is 20 menstrual weeks is 20 weeks 0 days. The cardinal number is more precise. Sonographic estimates of menstrual age should be reported in cardinal numbers.<sup>34</sup>

As noted earlier, the BPD<sup>5,6</sup> was more predictive of the EDD than the EDD calculated from the 1st day of the last normal menstrual period. Thus, the gold standard that was

used to test the validity of sonographic fetal biometry was less accurate than the sonographic measurement itself. The result is that the breadth of the variation about the mean for any sonographic measurement is in part due to the inaccuracy imposed by using the LMP to construct the axis of the curve defining the sonographic measurement. Understanding variation in measurements is very important. However, in practice, one should always choose the mean measurement for clinical case management. The principal reason to know the variation of a given measurement prediction is to gauge the potential danger to the patient if the mean estimate is very far from reality. During the remainder of this section, clues for gauging the potential for error will be provided.

## FIRST TRIMESTER OF PREGNANCY (0 TO 13 WEEKS)

The earliest unequivocal sign of pregnancy using sonographic evaluation is the demonstration of the "gestational sac."<sup>35-41</sup> Interestingly, the term *gestational sac* is largely an invention of the early sonologists, who used the term to describe the ring-like structure they identified within the womb of women with positive pregnancy tests. The more precise term is *chorionic sac*. It is the developing chorionic villi that generate the bright echogenic ring noted near the endometrial cavity. The fluid contained therein is almost totally chorionic fluid during very early development. With early articulated-arm equipment (static imaging) and transabdominal real-time equipment the gestational sac could not be visualized until approximately 6 menstrual weeks, but with the new high-resolution real-time equipment, particularly those equipped with transvaginal probes, the gestational sac can usually be seen by 5 menstrual weeks. At this early stage in gestation, the average internal diameter of the gestational sac, calculated as the mean of the anteroposterior diameter, the transverse diameter and the longitudinal diameter (the so-called mean sac diameter [MSD]), can provide an estimation of menstrual age in a normally developing pregnancy (Table 7-2). Importantly, the measurement of the MSD is obtained from the interface of the chorionic villi and the chorionic fluid. Therefore, it represents an estimate of the mean internal diameter of the chorionic sac. The wall of the sac is not included.

There is some controversy in the literature regarding the precise age at which sonography can first detect a chorionic (gestational) sac; estimates range from 3 to 5 weeks.<sup>38,42,44</sup> There is less controversy regarding the size of the gestational sac when it is first observed.<sup>44</sup> This is now thought to be approximately 2 to 3 mm MSD. Similarly, most observers agree that the MSD increases about 1 mm per day in early gestation.<sup>36,42,45,46</sup> Controversy returns when one studies age estimates of MSD by various authors.<sup>38,42,43</sup> Embryologic data and recent data gathered by de Crespigny, Cooper, and McKenna<sup>44</sup> leave little doubt that the MSD equals 2 to 3 mm at 4 weeks and 3 to 4 days.<sup>41</sup> It is reasonably safe to assume that a gestational sac reaches 5 mm at 5 weeks.<sup>43</sup> Thus (until an MSD of 25 mm is reached), GA in days can be calculated by adding 30 to the MSD (i.e., MSD at 5 weeks or 35 days = 5 mm).<sup>36,46</sup>

The early embryo cannot be seen at this time, but there are two features that differentiate the gestational sac from



**Table 7-2** Relation Between Mean Sac Diameter, Menstrual Age, and Human Chorionic Gonadotropin Level

Mean Gestational Sac Diameter (mm)	Predicted Age Range (week) = 95% CI*	Predicted hCG (mIU/mL) Range = 95% CI†
2	5.0 (4.5–5.5)	1164 (629–2188)
3	5.1 (4.6–5.6)	1377 (771–2589)
4	5.2 (4.8–5.7)	1629 (863–3036)
5	5.4 (4.9–5.8)	1932 (1026–3636)
6	5.5 (5.0–6.0)	2155 (1226–4256)
7	5.6 (5.1–6.1)	2704 (1465–4990)
9	5.9 (5.4–6.3)	3785 (2085–6870)
10	6.0 (5.5–6.5)	4470 (2400–9075)
11	6.1 (5.6–6.6)	5297 (2952–9058)
12	6.2 (5.8–6.7)	6267 (3502–11,218)
13	6.4 (5.9–6.8)	7415 (4145–13,267)
14	6.5 (6.0–7.0)	8773 (4894–15,726)
15	6.6 (6.2–7.1)	10,379 (5767–18,682)
16	6.7 (6.3–7.2)	12,270 (6776–22,235)
17	6.9 (6.4–7.3)	14,528 (7964–26,501)
18	7.0 (6.5–7.5)	17,188 (9343–31,621)
19	7.1 (6.6–7.6)	20,337 (10,951–37,761)
20	7.3 (6.8–7.7)	24,060 (12,820–45,130)
21	7.4 (6.9–7.8)	28,464 (15,020–53,970)
22	7.5 (7.0–8.0)	33,675 (17,560–64,570)
23	7.6 (7.2–8.1)	39,843 (20,573–77,164)
24	7.8 (7.3–8.2)	47,138 (24,067–93,325)

\*Predicted age from mean sac diameter is from Daya S, Wood S, Ward S, et al: Early pregnancy assessment with transvaginal ultrasound scanning. Can Med Assoc J 144:441, 1991. Reprinted with permission from the Canadian Medical Association.

†Predicted hCG from mean sac diameter is from Nyberg DA, Filly RA, Filho DLD, et al: Abnormal pregnancy; Early diagnosis by US and serum chorionic gonadotropin levels. Radiology 158:393, 1986. (The hCG was calibrated against the Second International Standard.)  
CI, confidence interval; hCG, human chorionic gonadotropin.

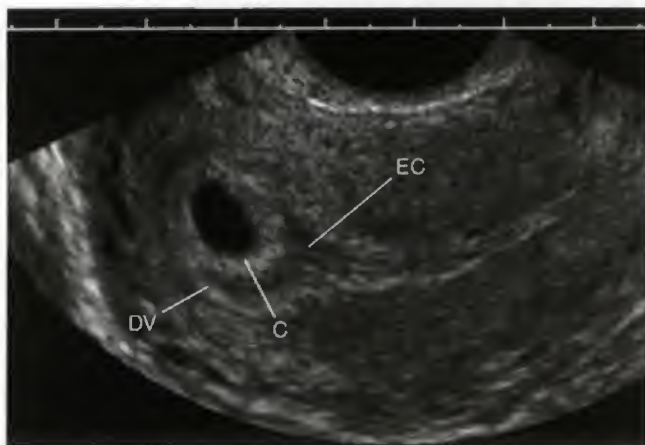


**FIGURE 7-2.** The double decidual sac sign is a misnomer. This sonographic feature typical of early gestations simply should be called the double sac sign because of the origin of only one of the decidia. The origin of the inner of the double rings (the endometrial cavity [EC]) is less echogenic than the deeper layer (closer to the myometrium). It is the less echogenic superficial layer of the decidua vera (DV) that provides the "separation" between the more echogenic chorionic villi (C) and deeper decidua vera rings.

the pseudogestational sac of an ectopic gestation. One is the double sac sign, which is created by visualization of the deep layer of the decidua parietalis and the early villi separated by the less echogenic layer and more superficial layer of decidua parietalis (Fig. 7-2).<sup>18,50</sup> Also of value is the intradecidual sign, wherein the developing sac, imbedded in the decidua,

deviates the endometrial cavity reflection (Fig. 7-3).<sup>49</sup> Visualization of an embryo or embryonic structure is a more reliable sign than either of the features just mentioned. The earliest embryonic structure detectable by sonography is the yolk sac. This can be seen using high-resolution vaginal probes during the 5th menstrual week (MSDs usually range from 6 to 12 mm when a yolk sac is seen in the absence of a concomitant embryo) (Fig. 7-4).

The MSD becomes progressively less reliable for predicting menstrual age as the first trimester of pregnancy advances. Once the embryo can be visualized, the measurement of choice for estimation of menstrual age becomes the crown rump length (CRL). The developing embryo can be consistently detected with transvaginal transducers when the CRL reaches 5 mm and can be detected when it is as small as 2 mm. If the embryo can be visualized and measured, then MSD is no longer used to predict age. The embryo achieves a CRL of 5 mm when the MSD equals approximately 14 mm. MSDs of 14 mm or less are very precise for predicting menstrual age in normal pregnancies. The accuracy of MSD measurements only deteriorates after this time. As a general principle, embryonic or fetal measurements are more precise than measurements of the gestational sac. In addition, the earlier the measurement, the more accurate it will be. Therefore, MSD measurements between 2 and 14 mm (i.e., before the embryo can be seen) are highly reliable because they represent the earliest possible sonographic measurement.

By the 6th menstrual week, one can usually identify the early embryo and usually cardiac activity, as well, in normally developing pregnancies (Fig. 7-5A). However, better visual-

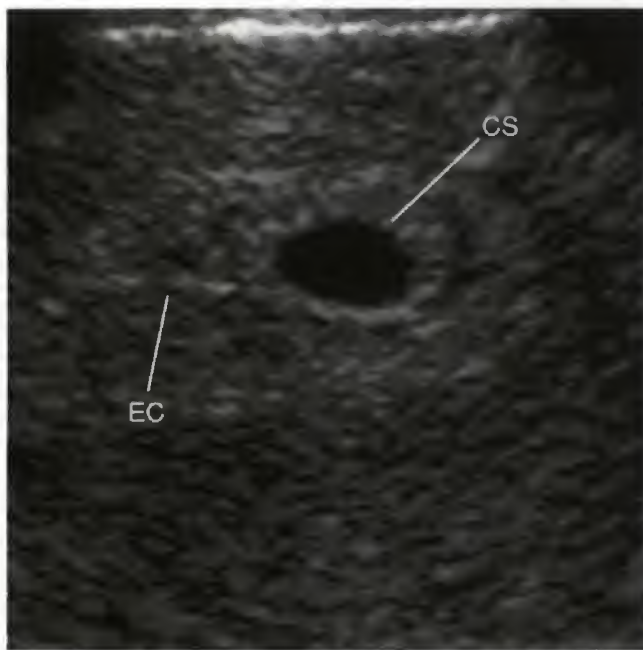


**FIGURE 7-3.** Transvaginal sonogram demonstrating the "intradecidual sign." Note that the chorionic sac (CS) displaces the endometrial cavity (EC), indicating that the chorionic sac actually resides within the decidual vera and not within the endometrial cavity.

ization of the early embryo can be made between 7 and 13 menstrual weeks (see Fig. 7-5B). Warren et al<sup>41</sup> demonstrated the developmental landmarks of the embryo during this time frame (Fig. 7-6). Although these anatomic features can provide clues to the age of the fetus, better estimates of menstrual age can be made by measurement of the CRL.<sup>23,29,31,39,51-60</sup> Strictly speaking, investigators and clinical sonologists do not truly measure the CRL when determining the length of first trimester embryos and fetuses.<sup>61</sup> The early embryo/fetus is curved (see Fig. 7-5B). The conventional measurement that is obtained is the maximal straight-line length of the fetus (see Fig. 7-5B).<sup>61</sup> The true CRL is depicted in Figure 7-5C. An additional measurement that can be considered is the maximum axial length of the fetus depicted in Figure 7-5D. However, despite the minor inaccuracy of nomenclature, the maximal straight-line length as measured by virtually all practicing sonologists will be referred to in this chapter as the CRL. When using the CRL to predict menstrual age, one should use the average CRL measurement from three satisfactory images. Modern instruments compute the menstrual age from this measurement. Alternatively, one may refer to published tables for estimation of menstrual age (Table 7-3).

In general, there has been extreme uniformity in the CRL data from various centers dating back to the original studies of Robinson<sup>51</sup> and Robinson and Fleming,<sup>52</sup> and it

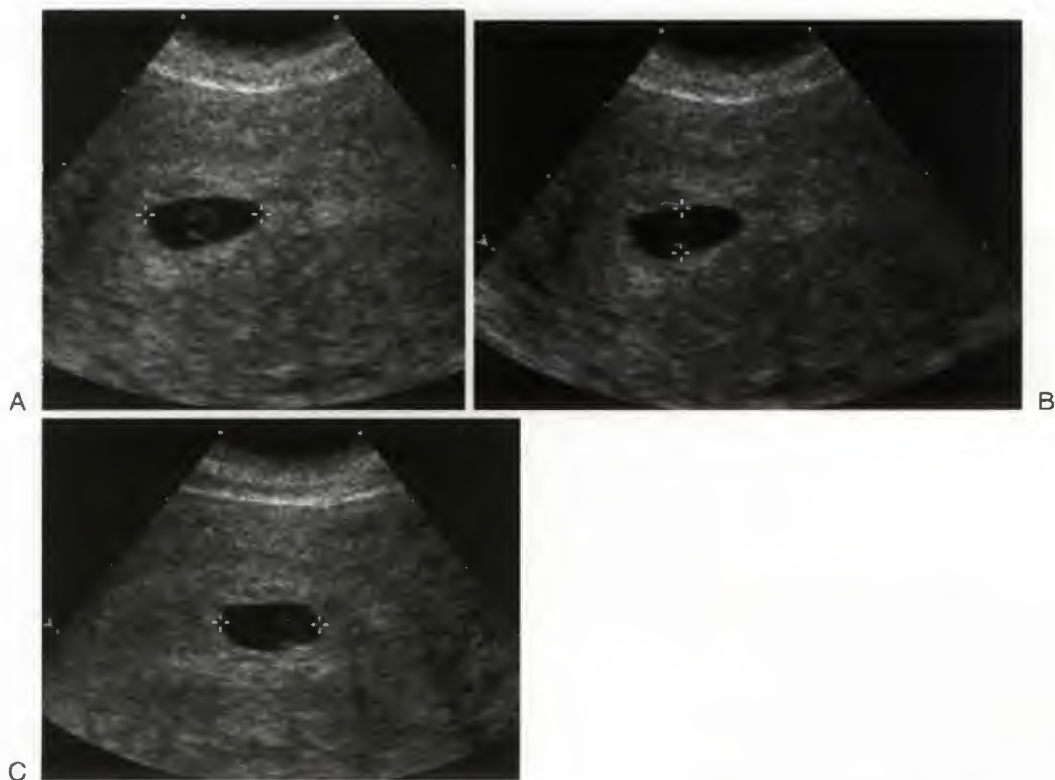


**FIGURE 7-4.** This high-resolution transvaginal real-time image demonstrates a yolk sac before the embryo is visible. Thus, a crown rump length cannot be measured at this stage of embryonic development. A-C. Instead, a mean diameter of the chorionic sac is determined, the "mean sac diameter." Three measurements—length (A), depth (B), and width (C) are obtained, summed, and then divided by three. The length and depth are measured on the same longitudinally oriented image, whereas the width is measured on a transversely oriented image. Note as well that the measurements are obtained from the interface of the chorionic fluid with the rim of chorionic villi; the "wall" is not included.



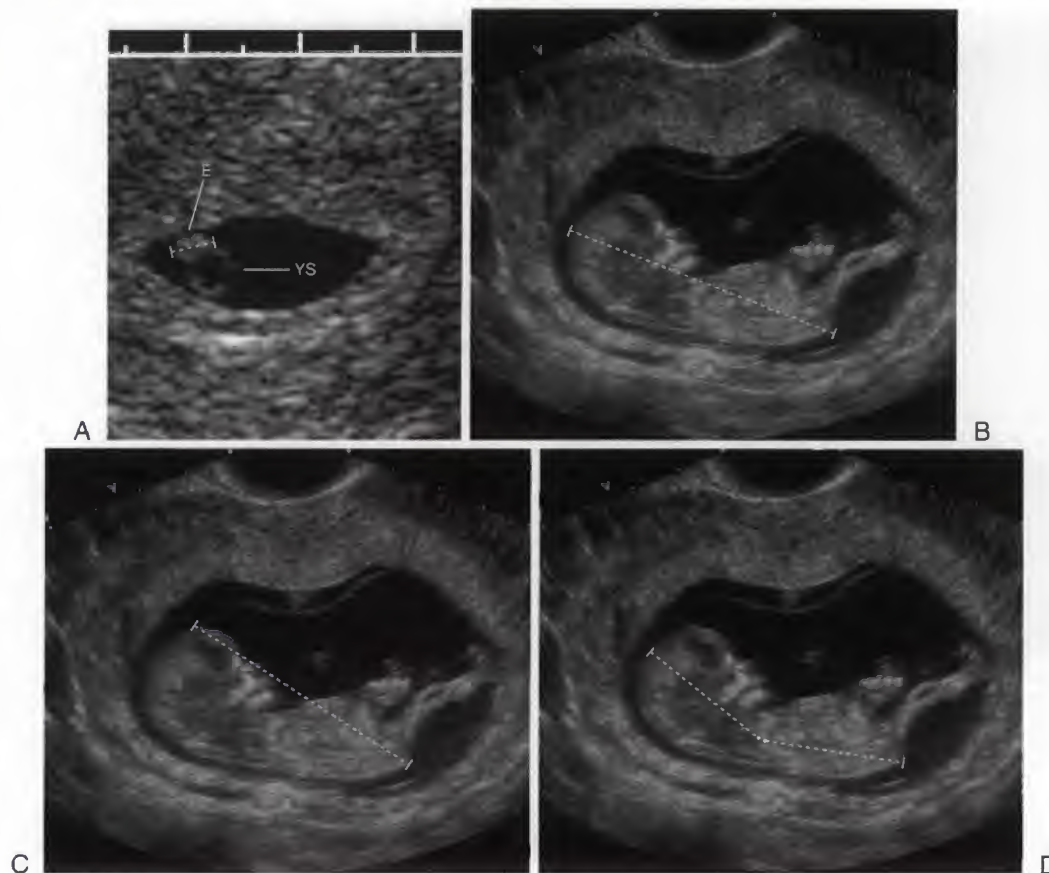


**FIGURE 7-5.** A. This high resolution transvaginal real-time image demonstrates the early embryo (E), which measures approximately 3 mm in this case, corresponding to a menstrual age of approximately 6 weeks  $\pm$  8% (3 days). The yolk sac (YS) is identified immediately adjacent to the embryo because there is no yolk stalk at this stage of embryonic development. B. This high-resolution transvaginal real-time image demonstrates the typical measurement of the crown rump length. This measurement is the maximum straightline length and not a true crown rump length. C. Cursor position to measure the true crown rump length. D. Method of measuring the maximal axial length.

has been demonstrated that measurements made with static image equipment, transabdominal real-time equipment, and transvaginal real-time equipment demonstrate no significant differences. Additionally, Silva et al<sup>59</sup> evaluated patients with known dates of conception using high-resolution transvaginal probes, and their data correspond closely with those of the early investigators. The only difficulty with the older studies is that they do not provide data before 7 weeks. This posed a problem when estimating the menstrual age of embryos detected earlier than 7 weeks. In a comprehensive study of CRL, Hadlock et al<sup>23</sup> developed measurement tables establishing menstrual age for CRL as small as 2 mm and extended the range of CRL, data up to measurements as large as 12 cm (see Table 7-3). The majority of the early studies on CRL demonstrated that the accuracy of the method in predicting menstrual age was 3 to 5 days ( $\pm$  2 standard deviations [SD]).<sup>51-53</sup>

In a study by MacGregor et al,<sup>56</sup> however, the accuracy of the technique was demonstrated to decrease as pregnancy advanced into the late first trimester. Hadlock et al<sup>23</sup> concurred that accuracy decreases as the first trimester of pregnancy nears its end. Because MacGregor's study population had known dates of conception, this increase in variability with advancing pregnancy was believed to

represent early biologic variability in embryonic or fetal size. In an effort to simplify the reporting of variability estimates, Hadlock et al evaluated variability as a percentage of the predicted age and demonstrated that the variability is relatively uniform at 8% for CRL measurements between 2 mm and 12 cm. Thus, for a CRL menstrual age prediction of 8 weeks, the 95% confidence interval is 8 weeks  $\pm$  8% = 8 weeks  $\pm$  0.64 week. Similarly, for a CRL age estimation of 15 weeks, the variability would be 15 weeks  $\pm$  8% = 15 weeks  $\pm$  1.2 weeks. The optimal time for prediction of menstrual age from CRL measurements is between 6 and 9 weeks.

Benson and Doubilet<sup>8</sup> recommended the following rules of thumb for visual estimates of early first trimester menstrual age. If a chorionic (gestational) sac with no yolk sac or embryo is seen, estimate the age at 5 menstrual weeks. If a chorionic (gestational) sac with a yolk sac but no embryo is seen, estimate the age at 5.5 menstrual weeks. If a chorionic (gestational) sac with a tiny embryo (<5 mm) adjacent to the yolk sac is seen, estimate the age at 6 menstrual weeks. Although these are simple visual estimates, their accuracy is uncanny.

Other measurements of the fetus can also be made in the first trimester of pregnancy. For example, Bovicelli et al<sup>54</sup> in 1981 evaluated the fetal BPD in comparison with the first

PERCENT OF EMBRYONIC STRUCTURES  
PRESENT OR ABSENT

☐ STRUCTURE PRESENT

☒ STRUCTURE ABSENT

WEEKS OF GESTATION	4	5	6	7	8	9	10	11	12
GESTATIONAL SAC ONLY	100								
YOLK SAC	0	91	100						
FETAL POLE WITH HEART MOTION	0	0	86	100					
SINGLE VENTRICLE	0	0	6	82	70	25	0	0	0
FALX	0	0	0	0	30	75	100	100	100
MIDGUT HERNIATION	0	0	0	0	100	100	100	50	0
TOTAL CASES	6	11	15	17	10	13	15	11	6

**FIGURE 7-6.** Sequential appearance of morphologic features as the chorionic sac, yolk sac, embryo, and fetus develop in the first trimester of pregnancy. Although used by the authors, "fetal pole" is an inexact term. Embryo and fetus are preferred terms. Note that the chorionic (gestational) sac is identified in all normal pregnancies beginning at 5 menstrual weeks. The yolk sac is seen in all normal pregnancies from 6 menstrual weeks onward, and the embryo is seen in all normal pregnancies from 7 menstrual weeks onward. Although of some interest scientifically, the appearance times of the cerebral "ventricle" (vesicle), falx, and midgut herniation are not of value in precise pregnancy dating. (From Warren WB, Timor-Tritsch I, Peisner DB, et al: Dating the early pregnancy by sequential appearance of embryonic structures. *Am J Obstet Gynecol* 161:747, 1989.)

**Table 7-3** Predicted Menstrual Age (MA)\* from Crown Rump Length (CRL)<sup>†</sup> Measurements<sup>‡</sup>

CRL	MA	CRL	MA	CRL	MA	CRL	MA	CRL	MA	CRL	MA
0.2	3.7	2.2	8.9	4.2	11.1	6.2	12.6	8.2	14.2	10.2	16.1
0.3	5.9	2.3	9.0	4.3	11.2	6.3	12.7	8.3	14.2	10.3	16.2
0.4	6.1	2.4	9.1	4.4	11.2	6.4	12.8	8.4	14.3	10.4	16.3
0.5	6.2	2.5	9.2	4.5	11.3	6.5	12.8	8.5	14.4	10.5	16.4
0.6	6.4	2.6	9.4	4.6	11.4	6.6	12.9	8.6	14.5	10.6	16.5
0.7	6.6	2.7	9.5	4.7	11.5	6.7	13.0	8.7	14.6	10.7	16.6
0.8	6.7	2.8	9.6	4.8	11.6	6.8	13.1	8.8	14.7	10.8	16.7
0.9	6.9	2.9	9.7	4.9	11.7	6.9	13.1	8.9	14.8	10.9	16.8
1.0	7.2	3.0	9.9	5.0	11.7	7.0	13.2	9.0	14.9	11.0	16.9
1.1	7.2	3.1	10.0	5.1	11.8	7.1	13.3	9.1	15.0	11.1	17.0
1.2	7.4	3.2	10.1	5.2	11.9	7.2	13.4	9.2	15.1	11.2	17.1
1.3	7.5	3.3	10.2	5.3	12.0	7.3	13.4	9.3	15.2	11.3	17.2
1.4	7.7	3.4	10.3	5.4	12.0	7.4	13.5	9.4	15.3	11.4	17.3
1.5	7.9	3.5	10.4	5.5	12.1	7.5	13.6	9.5	15.3	11.5	17.4
1.6	8.0	3.6	10.5	5.6	12.2	7.6	13.7	9.6	15.4	11.6	17.5
1.7	8.1	3.7	10.6	5.7	12.3	7.7	13.8	9.7	15.5	11.7	17.6
1.8	8.3	3.8	10.7	5.8	12.3	7.8	13.8	9.8	15.6	11.8	17.7
1.9	8.4	3.9	10.8	5.9	12.4	7.9	13.9	9.9	15.7	11.9	17.8
2.0	8.6	4.0	10.9	6.0	12.5	8.0	14.0	10.0	15.9	12.0	17.9
2.1	8.7	4.1	11.0	6.1	12.6	8.1	14.1	10.1	16.0	12.1	18.0

\*Measured in weeks.

<sup>†</sup>Measured in centimeters.

<sup>‡</sup>The 95% confidence interval is  $\pm 8\%$  of the predicted age.

From Hadlock FP, Shah YP, Kanon DJ, et al: Fetal crown-rump length: Reevaluation of relation to menstrual age (5–18 weeks) with high resolution real-time US. *Radiology* 182:501, 1992.



trimester CRL for predicting menstrual age between 7 and 13 weeks, and in 1982 Selbing<sup>39</sup> reported a similar study. Both groups demonstrated that the first trimester BPD is an accurate predictor of menstrual age but is not more accurate than the CRL and adds little, if anything, to the age estimate based on the CRL. Reece et al<sup>31</sup> demonstrated similar results using early fetal "abdominal" (torso) circumference in the first trimester of pregnancy. Most recently, Sladkevicius et al<sup>62</sup> compared 21 different CRL-based dating formulae to three different BPD-based dating formulae obtained at 12 to 14 weeks GA by abdominal ultrasound in 167 singleton pregnancies conceived following in vitro fertilization, and thus had definitively known pregnancy ages. Their findings showed that five of the CRL formulae generated very accurate pregnancy ages, and although the BPD formulae were also quite accurate, they had smaller random measurement errors than the CRL formulae. This led the authors to conclude that the BPD is a superior measurement than the CRL at 12 to 14 weeks for dating purposes. No measurements of the AC, HC, or FL were performed in this study, and thus, comments cannot be made about them in comparison to the CRL. In practice, the use of high-resolution vaginal probes allows very acceptable images of the head, abdomen, and femur for measurements of HC, BPD, AC, and FL from 10 weeks on. However, because these additional measurements are not necessarily more accurate than the CRL length in predicting age from 10 to 13 weeks and their use in conjunction with the CRL does not further improve age estimation, it is difficult to justify their use. Moreover, they are technically more difficult to obtain than the CRL measurement, and at least thus far their routine use is not warranted in the first trimester. The transition between first and second trimesters (13 to 14 weeks) is the appropriate time to make the transition from CRL to BPD, HC, AC, and FL.

In summary, the accuracy of first trimester fetal measurements in predicting menstrual age is well documented; there is very little biologic size variability during this time. This is in contrast to the third trimester of pregnancy, in which individual genetic expressions in fetal size can result in a very heterogeneous population. It is also well established that once menstrual age has been determined or corroborated by very early MSD (2 to 14 mm) or embryonic or fetal CRL in the first trimester of pregnancy, the menstrual age of the pregnancy is established and should *never* be changed based on biometric measurements made later in pregnancy.

Indeed, the same can be said of sonographic estimation of age at any time. An earlier measurement supersedes a later measurement, and sonographic estimates of age before 20 weeks gestation are highly reliable for pregnancy dating. In nearly all cases, sonographic estimates of age before 20 weeks gestation (except those with assisted conception and those maintaining basal body temperature charts) represent the most accurate scientific information establishing the menstrual age.

An important issue is the timing of the sonogram when the dates are uncertain. It has already been stated that the earlier the measurement is obtained, the more accurate is the estimate because biologic variability increases throughout gestation. Unfortunately, an age estimate at 7 menstrual weeks will be extremely accurate but provides little other useful information about the fetus, placenta, amniotic fluid volume, and cervix. An alternative is to wait until the second trimester

is under way before performing the sonogram to establish dates (15 to 18 weeks). Because dates are in question, the uterine size estimate is important in planning the timing of the early second trimester examination. If this second option is elected, dating accuracy will suffer. However, the accuracy at 15 to 18 weeks is still excellent and adequate for all clinical purposes. The value of waiting is that a large amount of additional information about the health of the pregnancy is obtained. Of course, there is also the possibility of obtaining both first trimester and second trimester sonograms, but this is associated with a significant increase in cost. The greatest accuracy per medical dollar spent is achieved in the first trimester. The greatest value per medical dollar spent is achieved in the early second trimester. If the dates of a pregnancy are clinically truly uncertain, the earliest possible ultrasound is advised to ensure the highest accuracy in assigning GA. This information may ultimately prove to be essential for the long-term management of the pregnancy, and therefore worth the additional expenditure up front.

## SECOND AND THIRD TRIMESTERS OF PREGNANCY (14 TO 42 WEEKS)

In the second trimester of pregnancy, the fetus has grown sufficiently in size so that remarkable anatomic detail can be visualized (see Chapter 9). Many structures can be identified and measured during this time,<sup>22,23,33,63,64</sup> but the basic fetal measurements used to estimate age are the BPD, HC, AC, and FL.<sup>1</sup> With training and practice, these measurements can be obtained with a high degree of consistency and accuracy. One must always remember, however, that the images and measurements must be made with great care in every case, and one must be certain to duplicate the technique of the investigator whose data one is using. Using measurements from poor images or images that depict fetal anomalies should be avoided.

Modern instrumentation computes the age estimate virtually in real time on the viewing screen because the cursors are fit to the structure being measured. The examiner should avoid the temptation to "massage" the endpoints of the measurement because the age computation on the viewing screen is smaller or larger than their preconceived notion of what the biometry should be. Instead, it is crucial to learn the rules for obtaining each measurement and to adhere to them rigorously; only then can the results be interpreted in a rational way.

## BIOMETRY: FOLLOWING THE RULES

Crucial decisions may be made on the basis of fetal biometric measurements. Therefore, each clinical specialist must be well schooled in the proper techniques of obtaining these measurements. It is not necessary to repeat every erroneously taken measurement because correcting the measurement probably will not influence the interpretation of the case if the error is small. However, it is important that the interpreter can recognize the error and has a sense of both the magnitude and the direction of the error. For example, suppose that a BPD was erroneously measured in a fetus of 21 weeks menstrual age, known by early embryonic CRL. The erroneous measurement is 4.7 cm and



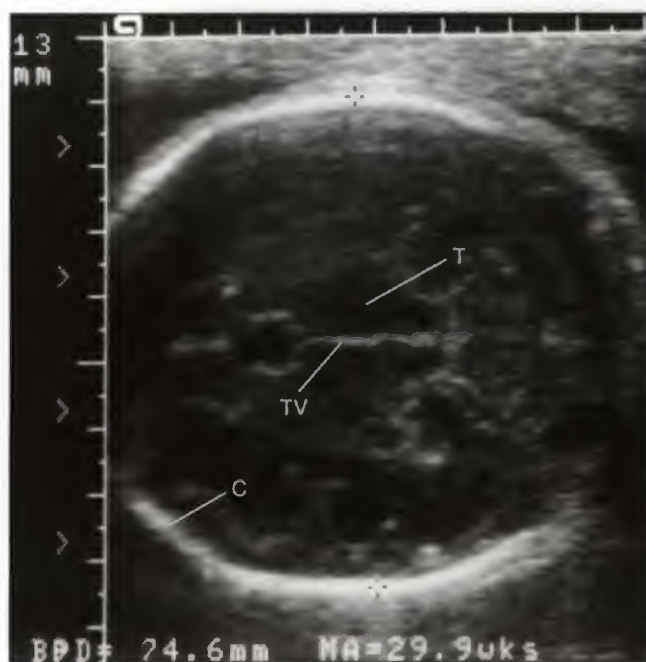


**FIGURE 7-7.** An accurate biparietal diameter can be obtained through any plane of section that intersects the third ventricle (TV) and thalami (T). The margins of the calvaria (C) must be symmetric. The first criterion ensures that the plane of section is taken at the proper craniocaudal plane. The second criterion ensures that the transducer is oriented perpendicular to the central axis of the head. Note the measurement is 74.6 mm.

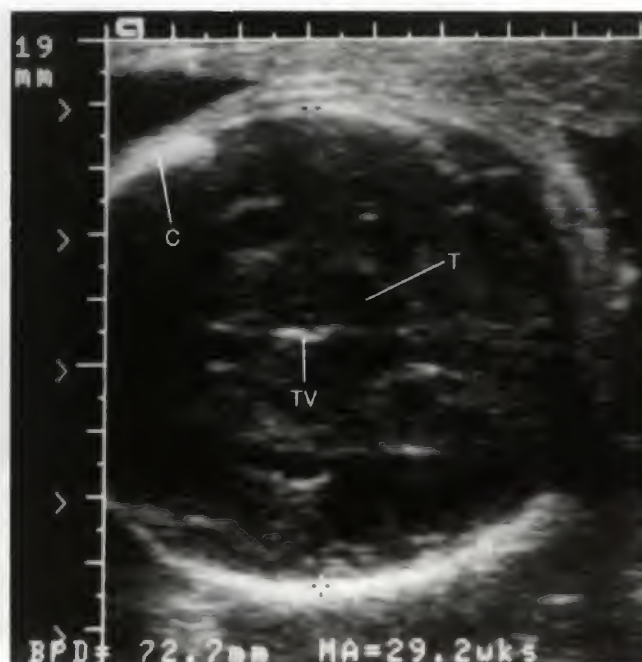


**FIGURE 7-8.** Image of same fetus as in Figure 7-7 taken minutes apart. This biparietal diameter measurement meets the criterion of being taken through the third ventricle (TV) and thalami (T) but does not meet the criterion of demonstrating symmetric calvaria (C). The BPD measured from this plane (72.7 mm) is 2 mm smaller than the properly measured BPD of 74.6 mm (see Fig. 7-7). This degree of error is probably not clinically significant.

the predicted age by BPD is, therefore, 20.2 weeks. Analysis of the error leads one to recognize that the BPD was slightly undermeasured. One can recognize that a BPD predicting 20.2 weeks is within the normal range. Correcting the error would push the measurement toward the known menstrual age. Clearly, there is no reason to spend the time correcting the error. Note that this comment is only applicable for the occasional slight error in measurement and is not appropriate to systematic or large-scale errors that should be rectified expeditiously.

Potential errors in biometric measurements are numerous and can be engendered by equipment misregistration, aberrations of transducers, and type of transducer to name a few. It is important to ensure through the equipment manufacturer that the instrument is properly adjusted to make accurate linear measurements in every direction on the viewing screen, that biometric tables are accurately entered in the machine computation package, and finally, that subsequent computations are accurate. Although one does not have direct control over these adjustments, the wise sonologist never assumes that instrumentation is always accurate in this arena. *Aside from optimizing the image, one can only control two aspects of biometric measurement. One can choose the plane of section, and one can choose the endpoints of measurement* (Figs. 7-7 to 7-12).

The BPD can be appropriately measured through any plane of section that traverses the third ventricle and thalami (see Fig. 7-7).<sup>65</sup> Early in the history of BPD measurement, the BPD was defined as the widest distance between the parietal eminences. The “widest” BPD is not always obtained

though a plane of section that traverses the third ventricle and thalami. Occasionally, the “widest” BPD is obtained in a more cephalad location.<sup>65</sup> However, rather than dutifully searching for the widest diameter, it is now convention to measure all fetuses at the same anatomic plane in all centers across the country. The advantages of every practitioner obtaining the BPD in the same way are obvious. Searching for the widest BPD is likely to engender errors because there will be a tendency to accept an erroneous measurement wherein the error overestimates the measurement.

Any plane of section through a 360-degree arc that passes through the thalami and third ventricle is acceptable for measuring the BPD. This means that an accurate measurement can be obtained through an infinite number of planes (the significance of this point is made clear later). The rules for measuring the BPD are as follows. First, the correct plane of section is through the third ventricle and thalami, as noted. Second, the calvaria are smooth and symmetric bilaterally. Third, the cursors are consistently positioned in one of the three following ways: outer edge of near calvarial wall to inner edge of far calvarial wall, inner edge of near calvarial wall to outer edge of far calvarial wall, or middle of near calvarial wall to middle of far calvarial wall. Measuring from the outer edge of the near calvarial wall to the outer edge of the far calvarial wall is inappropriate. The first two criteria define the precise plane of section. Because there are two criteria that must be met to obtain a proper plane of section, the BPD measurement should be considered as a “two-dimensional” measurement. The third criterion describes the proper endpoints of measurement. Because the



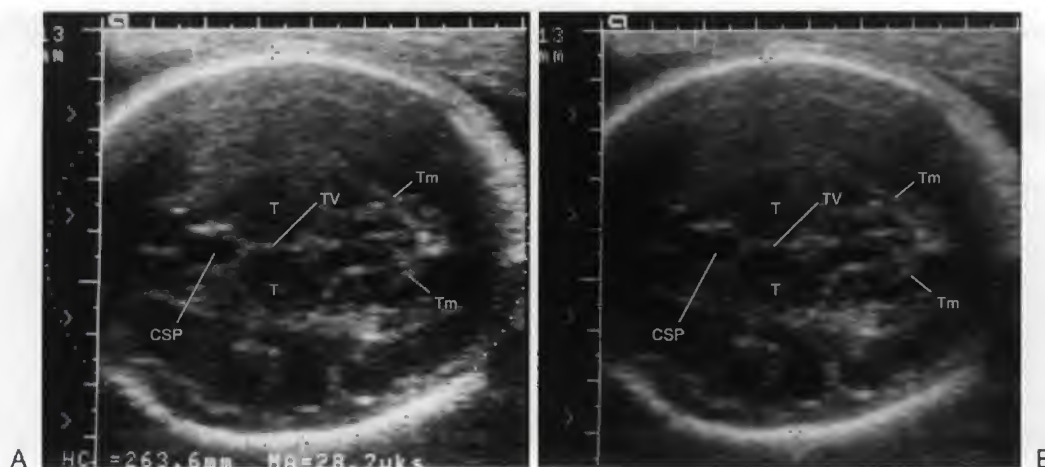


**FIGURE 7-9.** Image of same fetus as in Figure 7-7 taken minutes apart. As with Figure 7-7, this plane of section fulfills the two criteria for measuring a biparietal diameter (BPD) (T, thalamic nucleus; TV, third ventricle). A. However, it also fulfills the third criterion necessary to measure a head circumference; the plane is properly oriented to the skull base. Demonstrating the cavum septi pellucidum (CSP) anteriorly and the tentorial hiatus posteriorly (Tm, tentorium) documents proper orientation of the plane of section to the skull base. Because this plane of section accurately meets all criteria for an HC measurement and because the ellipse is carefully fit to the calvarial margins, one may correctly assume that 263.6 mm is highly accurate. B. Note that the BPD measurement is 74.2 mm, only a 0.4-mm difference from that of Figure 7-7, demonstrating that any plane through the thalami and third ventricle with symmetric calvaria accurately measures the BPD.

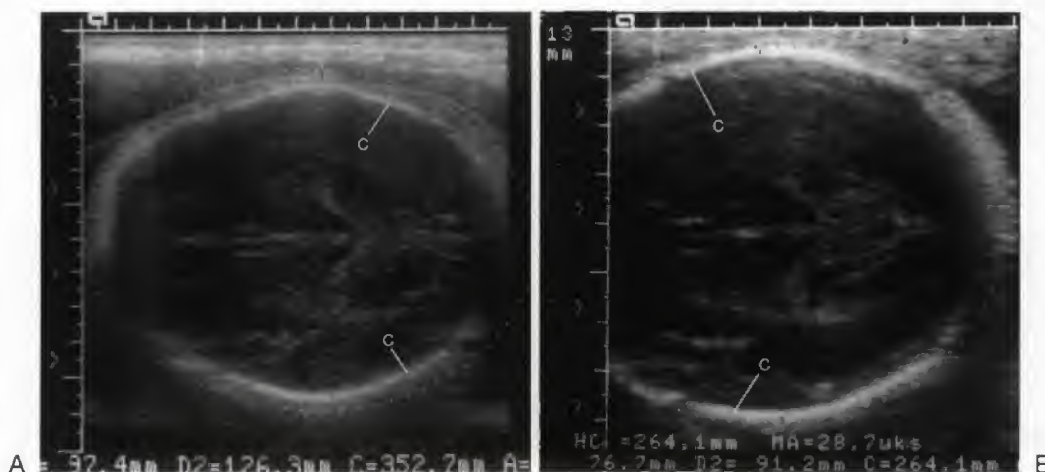


**FIGURE 7-10.** Image of same fetus as in Figure 7-7 taken minutes apart. A. One reason for the development of the long linear transducer was to encompass the entire fetal calvaria in late pregnancy to measure both the biparietal and an occipitofrontal diameters necessary to compute a head circumference. Later, as measurement technology advanced, this requirement was also deemed necessary so that the computer-generated ellipse could be seen to "fit" the calvarial margin throughout. An error, however, was made during this measurement. The sonographer fit the ellipse to the scalp margin rather than the calvarial margin (C). B. With shorter linear transducers, the ellipse approximated a portion of the calvarial margin. This does not create a significant error. There is no need to purchase a long linear transducer solely for the purpose of demonstrating the entire perimeter of a third trimester fetal head.

calvaria are brightly echogenic and symmetric and the thalami are symmetric about the third ventricle, the BPD is a measurement that can be obtained with great consistency and accuracy. The symmetry makes it easy to see that the correct plane of section has been obtained. Common errors in BPD are illustrated in Figures 7-8 and 7-124.

Recall that the BPD can be obtained through an infinite number of planes. However, in the strictest sense, the HC is best obtained through a single plane of section. Thus, the HC is a more difficult measurement to obtain consistently correctly. The correct plane of section parallels the base of the skull. Therefore, the plane is more cephalad anteriorly

than it is posteriorly. Whereas when obtaining a properly measured BPD the transducer must be correctly oriented in two planes, the HC requires that the transducer be properly oriented in three planes. Because there are three criteria that must be met to obtain a proper plane of section, the HC measurement should be considered as a three-dimensional measurement. To measure the BPD the transducer must be (1) perpendicular to the parietal bones and (2) positioned at the correct cephalocaudal position to intersect the third ventricle and thalami. To measure the HC, the two criteria for the BPD must be fulfilled, and the transducer plane must be properly oriented to the skull base. Because the skull base

is very irregularly shaped, it is not used to orient the plane of the HC. Instead brain anatomy landmarks are used.

The rules for measuring the HC are as follows. The correct plane of section is through the third ventricle and thalami in the central portion of the brain (as with the BPD),

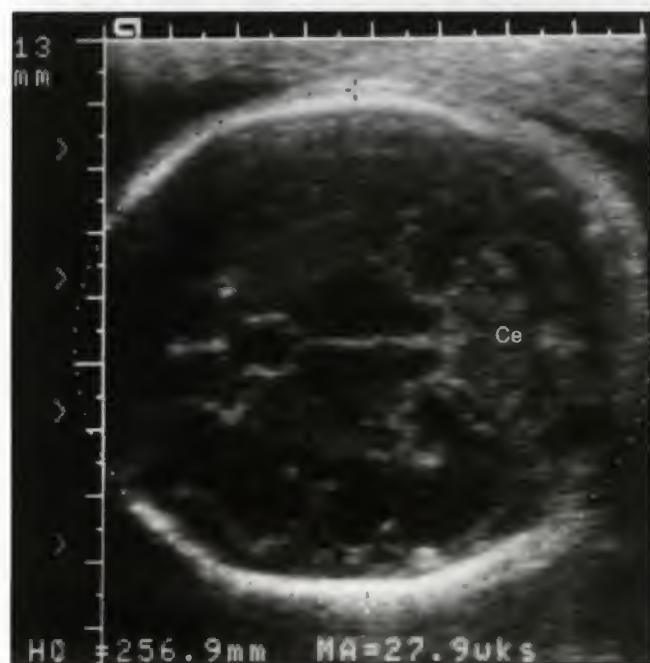


**FIGURE 7-11.** This is the same image as Figure 7-7 now used to measure the head circumference (HC). The plane of section meets all necessary criteria for biparietal diameter measurement but is not properly oriented to the skull base for HC measurement. Note that the cerebellum (Ce) rather than the tentorial hiatus is demonstrated posteriorly. The HC measured from this plane of section is 256.9 mm compared with 263.6 mm measured from the proper plane (compare with Fig. 7-9A).

but the cavum septi pellucidi must be visible in the anterior portion of the brain and the tentorial hiatus must be visible in the posterior portion of the brain. Some refer to this anatomy as an "arrow." The cavum septi pellucidi and frontal horns are the "feathers." The third ventricle and sylvian aqueduct are the "shaft." The ambient and quadrigeminal cisterns and the tentorial hiatus are the "arrowhead." The calvaria must be smooth and symmetric bilaterally. After the proper plane of section is obtained, the cursors are positioned at the outer edge of the near calvarial wall and the outer edge of the far calvarial wall. Most modern equipment then will allow a computer-generated ellipse to be fit to the calvarial margins (see Fig. 7-9A). The entire perimeter of the calvaria need not be demonstrated to accurately measure the HC.<sup>66</sup> The ellipse adequately estimates the head perimeter even when it is not entirely imaged (see Fig. 7-10).

Note several features. First, a properly measured BPD can be obtained on the same image as a properly oriented HC measurement (see Fig. 7-9B). The reverse is not necessarily true (see Figs. 7-11 and 7-12). Second, the proper position of the cursors to measure the HC is inappropriate for BPD measurements (compare Fig. 7-9A and B). Thus, if the BPD is measured first on the image, the cursors must then be moved before the computer-generated ellipse is fit to the calvarial margins for HC determination. Finally, it is important to be certain that the ellipse is fit to the calvaria and not the skin of the scalp (see Fig. 7-10A). Again, an analysis of an observed error should give the interpreter a sense of both the direction and magnitude of the error. If, for example, the sonographer fit the ellipse to the skin of the scalp and not to the calvaria, the error will increase the HC measurement (i.e., the "direction" of the error), and in a late, large fetus the error will be great (i.e., the "magnitude" of the error). In a young fetus the magnitude of the error will be small.

The FL measurement is technically the easiest of the common biometric measurements. This is due to the

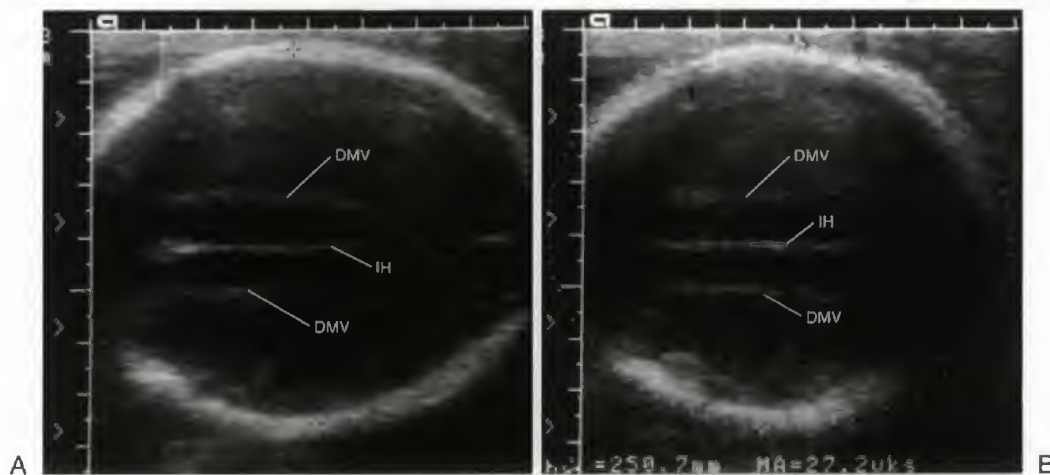


**FIGURE 7-12.** Image of same fetus as in Figure 7-7 taken minutes apart. A. This biparietal diameter (BPD) measurement fulfills the criterion of symmetric calvaria but was not obtained through the thalami and third ventricles. It was obtained too near the vertex. The three "lines" seen in this image have been commonly displayed in the ultrasound literature. The central line is the interhemispheric fissure (IH). The lateral lines are composite reflections from the deep medullary veins (DMV) draining the periventricular white matter. Therefore, this plane is obtained cephalad to the lateral ventricular bodies, BPD measurement in this plane underestimates age. Compare this measurement of 71.9 mm with that obtained in the correct plane as illustrated in Figure 7-7 (74.6 mm). B. The head circumference (HC) measured in this plane also underestimates age. Compare the measurement of 250.7 mm with the correctly measured HC of 263.6 mm obtained in this fetus (compare with Fig. 7-9A).



essentially one-dimensional nature of the measurement. The transducer need only be aligned to the long axis of the bone to obtain a proper plane of section. No other transducer adjustment is necessary. However, that does not mean that errors in measurement or observational errors are rare.<sup>10,67,68</sup> Quite the contrary is true.

The first feature to understand about the FL measurement is that one does not actually measure the entire femur. Only the ossified portions of the diaphysis and metaphysis are measured (Fig. 7-13).<sup>10</sup> The cartilaginous ends of the femur are excluded. The ossified portion of the femur is more visible sonographically than the nonossified ends. Nonetheless, the cartilaginous ends of the femur are readily demonstrated (Fig. 7-14). Although the cartilaginous ends are excluded, they are the keys to accuracy and consistency in femoral length measurements. To obtain the measurement accurately, the transducer must be aligned to the long axis of the diaphysis. How does one know that the transducer is properly aligned? One method is to accept the longest femoral length as the most accurate measurement. This assumes that the only potential error is to undermeasure the bone because the transducer is improperly aligned to the bone. This is a false assumption.



**FIGURE 7-13.** Radiograph of the femur from a term neonatal autopsy specimen. Sonographic measurements of the "femur" include only the ossified portion of the diaphysis (D) and metaphysis (M). The cartilaginous femoral head (FH), greater trochanter (GT), and distal epiphysis (DE) are not included in the measurement. When it ossifies, the distal femoral epiphyseal (DFE) secondary ossification center is also not included in the measurement.

Proper alignment of the transducer to the long axis of the femur is ensured by demonstrating that both the femoral head or the greater trochanter and the femoral condyle are simultaneously in the plane of section (Fig. 7-15).<sup>10</sup> If these two structures are seen, the plane is unambiguously through

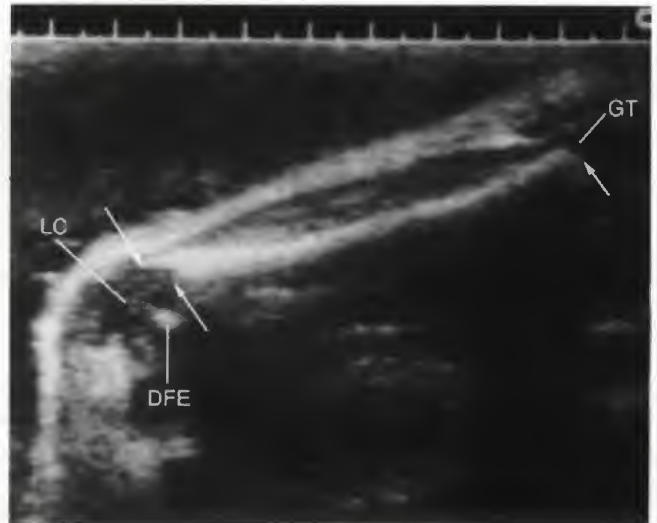


**FIGURE 7-15.** This sonogram demonstrates the femur of a middle third trimester fetus. This is an ideal image from which to measure the femur. Because the greater trochanter (GT) and lateral condyle (LC) of the distal epiphysis are seen, one may be confident that the proper plane through the long axis of the femoral diaphysis has been obtained. The only remaining task is to position the endpoints of measurement properly (i.e., the electronic cursors). The proximal cursor is easily placed at the junction of bone and cartilage (*short arrow*). However, a choice must be made distally. Should the "point" (*long arrow*) along the lateral margin be included? Compare with Figure 7-13. No such ossified "point" exists. This structure, only seen sonographically, should not be included in the measurement and introduces a significant overestimate of femur size if included. The only way to choose properly the correct endpoint for placing the distal measurement cursor is to demonstrate clearly the junction of the distal epiphysis with the metaphysis (*short arrow*). As well, this image clearly depicts the ossification center (DFE) of the distal epiphysis.

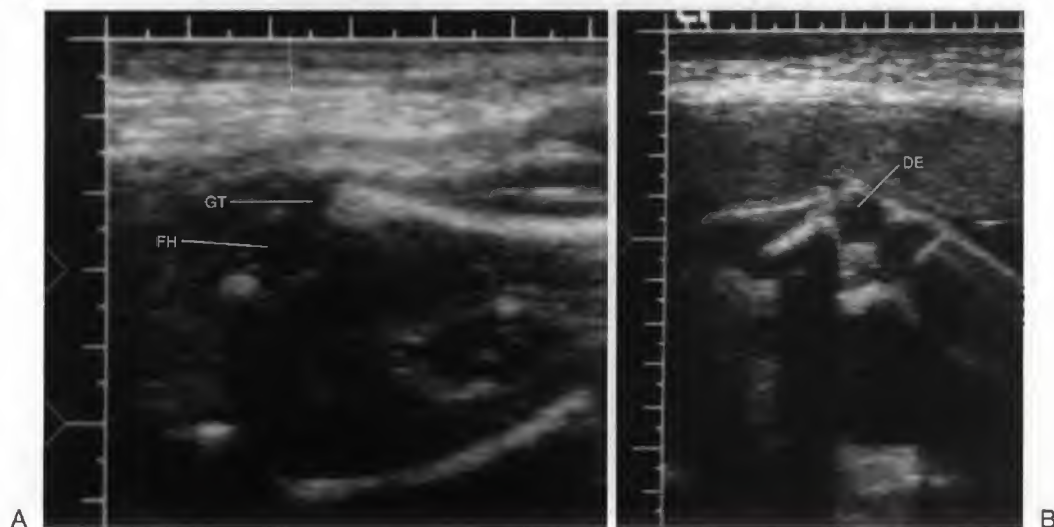


**FIGURE 7-14.** A. Sonogram of the proximal fetal femur. Compare with Figure 7-13. The cartilaginous greater trochanter (GT) and femoral head (FH) are not included in the femoral measurement but are clearly seen. B. Sonogram of the distal femur (compare with Fig. 7-13). The cartilaginous distal epiphysis (DE) is also clearly seen but is not included in the femoral measurement. Although not included in the measurements, the cartilaginous ends of the femur are the keys to obtaining highly accurate and reproducible femoral measurements. See text.

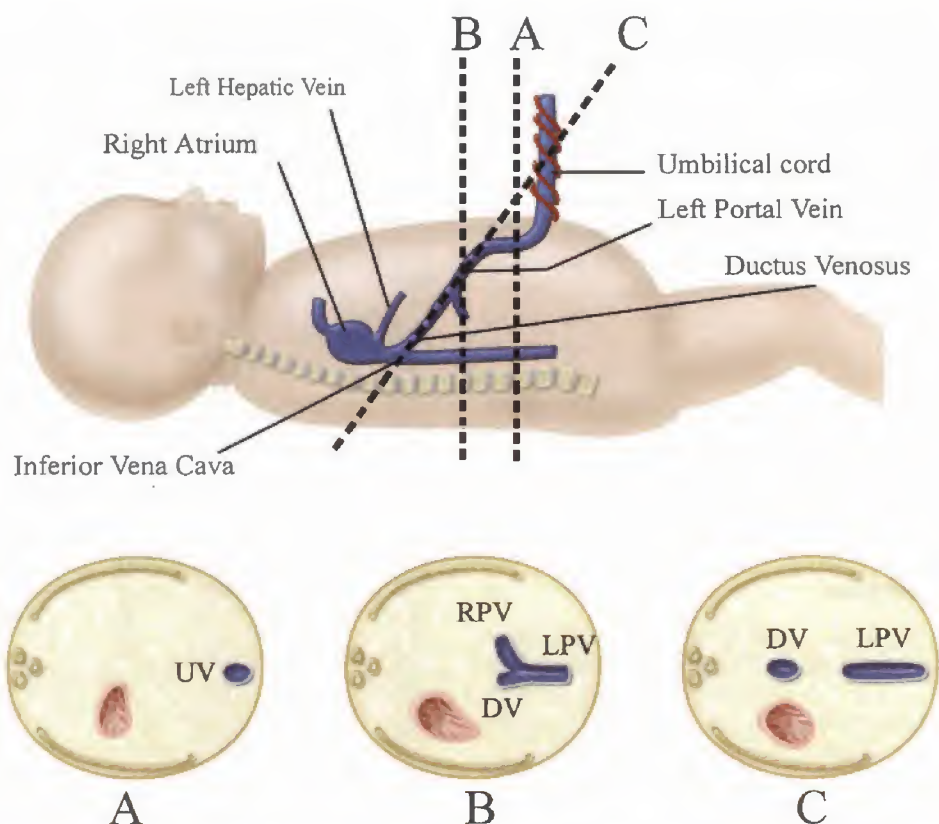


**FIGURE 7-16.** Umbilical venous circulation through the fetal liver. A. Plane of section depicting the umbilical vein (UV) in short axis (correlate with Fig. 7-17A). This plane is too caudal for abdominal circumference measurement. B. Plane of section through the junction of the left (LPV) and right (RPV) portal veins (correlate with Fig. 7-17B). This is the correct level for AC measurement (DV, ductus venosus). C. Plane of section aligned along the course of the LPV (correlate with Fig. 7-17C). Note that this plane is too inclined in a craniocaudal axis. (Illustration by James A. Cooper, MD, San Diego, CA.)

the femoral long axis. Thus, once can be confident that the proper plane of section to obtain an accurate measurement has been chosen. The only remaining task is to position the electronic cursors properly at the correct endpoints of measurement. Again, it is the cartilaginous ends that direct precise placement of the measurement cursors. The cursors are positioned at the junction of the bone with the cartilage (see Fig. 7-15). It is important not simply to choose the end of the brightest reflection as the endpoint of measurement because of an entity that has been called the “distal femoral point.” The distal femoral point is not part of the bony metaphysis.<sup>10</sup> Including it significantly overmeasures the femur. Therefore, the rules for measurement of the femur are as follows. First, align the transducer to the femur and freeze the plane that shows both the cartilaginous femoral head and distal condyle. Then place the measurement cursors at the junction of the cartilage and bone, being careful to avoid the distal femoral point.

Finally, the AC is the most difficult of the four measurements that are ordinarily obtained. As with the HC, the AC is a three-dimensional measurement. Unfortunately, the abdominal anatomy is not symmetric like the brain anatomy. Further, there is no bright calvarial margin to check the perpendicularity of the planar axis and to provide easily seen endpoints of measurement.

The AC is measured in a location that estimates liver size. The liver is the largest organ in the fetal torso, and its size reflects aberrations of growth, both growth restriction and macrosomia. Therefore, one does not measure the circumference at the fetal “waist” (umbilicus) as one would in an adult. The fetal AC is measured at the position where the transverse-diameter of the liver is the greatest. This can be determined sonographically as the position where the right and left portal veins are continuous with one another (Fig. 7-16).<sup>69</sup> Some refer to this anatomic confluence of the intrahepatic portal veins as “the hockey stick.”

Therefore, the rules of measurement of the fetal AC are as follows. The correct cephalocaudal plane is the position where the right and left portal veins are continuous with one another. Second, the appearance of the lower ribs is symmetric. Finally, the shortest length of the umbilical segment of the left portal vein is depicted. If a long segment is seen, then the transducer is erroneously angled inferiorly instead of perpendicular to the midline (see Fig. 7-16C).<sup>69</sup> After this plane of section is frozen on the screen, the ellipse is fit to the skin edge. Note that this is distinctly different from the HC, where one specifically does not fit the ellipse to the skin edge but rather to the calvarial edge. Importantly, the skin margin may abut other soft tissue structures like the placenta or myometrium and be relatively inconspicuous.



Remember that the rib margin is easily seen, and one may mistakenly fit the ellipse margin to the rib instead of the skin. This will significantly undermeasure the AC. Although this error will have relatively little effect on the estimate of menstrual age, it will have a much greater effect on the weight estimate.

There will be many times when the landmarks for fetal AC measurement are less than optimally documented. In this circumstance, the reader should rely on the following rule: "round" covers a multitude of sins. This rule implies that, when the desired anatomic landmarks are difficult to demonstrate, the circumference estimate, wherein the transverse and anteroposterior diameters of the abdomen are equal or nearly so, is likely to be the more accurate compared with estimates wherein the diameters are disparate. In compliance with this concept, excessive pressure with the transducer should be avoided because it distorts the shape of the abdomen.

### Biparietal Diameter

The BPD has received the greatest amount of attention in the literature as a means of establishing menstrual age.<sup>12,22,23,28,33,63,64,70</sup> The measurement technique and pitfalls were described earlier. The menstrual age can be determined by using a standard reference table (Table 7-4). However, modern instruments immediately compute an age as the measurement is being obtained.

All reports on the BPD have demonstrated it to be an accurate predictor of menstrual age before 20 weeks. For example, Hadlock, Harrist, and Martinez-Poyer<sup>22</sup> demonstrated the variability to be  $\pm 1$  week (2 SD) in a population of 1771 patients with optional menstrual histories seen between 14 and 20 weeks (Table 7-5). Persson and Weldner<sup>64</sup> and Rossavik and Fishburne<sup>33</sup> reported similar results in patients with known dates of conception, as did Crespigny and Speirs<sup>70</sup> in a large series of patients whose dates were confirmed by CRL in the first trimester of pregnancy. In addition, Campbell et al<sup>5</sup> and Waldenström, Axelsson, and Nilsson,<sup>6</sup> in independent studies, demonstrated that a BPD obtained between 14 and 20 menstrual weeks is a better predictor of the estimated date of confinement than an optimal menstrual history. Virtually all studies demonstrated a progressive increase in variability from 20 weeks to term, but the degree to which the variability increases in the late third trimester of pregnancy has been a subject of some disagreement in the literature.<sup>12,28,70,71</sup> Most early authors concluded that the variability during this time frame is approximately  $\pm 3\frac{1}{2}$  weeks (2 SD), but Kurtz et al<sup>28</sup> reported the variability to be  $\pm 2$  weeks during this time. This difference most likely is a statistical phenomenon, because the mathematical evaluation by Kurtz et al was performed on mean values from a number of different centers and does not directly include any of the raw data from the more than 25,000 patients who form the basis of their report. The variability they reported, then, represents the confidence interval of the mean and should not be comparable to the standard deviation reported by others.<sup>12</sup> In studies of patients with optimal menstrual histories, the variability of late third trimester BPD age predictions has been consistently demonstrated to be approximately  $\pm 3\frac{1}{2}$  weeks. This has been confirmed in a large series of patients

**Table 7-4**

#### Predicted Menstrual Age for Biparietal Diameter (BPD) Measurements

BPD (cm)	Menstrual Age (week)	BPD (cm)	Menstrual Age (week)
2.6	13.9	6.2	25.3
2.7	14.2	6.3	25.7
2.8	14.5	6.4	26.1
2.9	14.7	6.5	26.4
3.0	15.0	6.6	26.8
3.1	15.3	6.7	27.2
3.2	15.6	6.8	27.6
3.3	15.9	6.9	28.0
3.4	16.2	7.0	28.3
3.5	16.5	7.1	28.7
3.6	16.8	7.2	29.1
3.7	17.1	7.3	29.5
3.8	17.4	7.4	29.9
3.9	17.7	7.5	30.4
4.0	18.0	7.6	30.8
4.1	18.3	7.7	31.2
4.2	18.6	7.8	31.6
4.3	18.9	7.9	32.0
4.4	19.2	8.0	32.5
4.5	19.5	8.1	32.9
4.6	19.9	8.2	33.3
4.7	20.2	8.3	33.8
4.8	20.5	8.4	34.2
4.9	20.8	8.5	34.7
5.0	21.2	8.6	35.1
5.1	21.5	8.7	35.6
5.2	21.8	8.8	36.1
5.3	22.2	8.9	36.5
5.4	22.5	9.0	37.0
5.5	22.8	9.1	37.5
5.6	23.2	9.2	38.0
5.7	23.5	9.3	38.5
5.8	23.9	9.4	38.9
5.9	24.2	9.5	39.4
6.0	24.6	9.6	39.9
6.1	25.0	9.7	40.5
Variability Estimates ( $\pm 2$ SD) (week)			
12-18		$\pm 1.2$	
18-24		$\pm 1.7$	
24-30		$\pm 2.2$	
30-36		$\pm 3.1$	
36-42		$\pm 3.2$	

SD, standard deviation.

From Hadlock FP, Deter RL, Harrist RB, et al: Fetal biparietal diameter: A critical reevaluation of the relation to menstrual age by means of real-time ultrasound. *J Ultrasound Med* 1:97, 1982; Hadlock FP, Deter LR, Harrist RB, et al: Estimating fetal age: Computer-assisted analysis of multiple fetal growth parameters. *Radiology* 152:497, 1984.

in Australia in whom the menstrual ages were confirmed in early pregnancy by CRL.<sup>70</sup> Both of the later studies, however, eliminated patients with head shape abnormalities, multiple gestation, or diseases likely to adversely affect fetal growth. The large variability associated with third trimester use of the BPD has been confirmed in a study by Benson and Doubilet<sup>7</sup> of patients whose menstrual histories had been established early in pregnancy by CRL; in this study, however, no attempt was made to eliminate multiple

**Table 7-5** Variability ( $\pm 2$  SD) in Predicting Menstrual Age From Sonographic Measurements (14 to 20 Weeks)

Parameter	Hadlock, Harrist, and Martinez-Poyer <sup>22</sup>	Rossavik and Fishburne <sup>33</sup>	Persson and Weldner <sup>64</sup>	Benson and Doubilet <sup>7</sup>
Biparietal diameter	0.94	1.02	0.92	1.40
Head circumference	0.84	0.92	ND	1.20
Abdominal circumference	1.04	1.12	ND	2.10
Femur length	0.96	ND	0.98	1.40
Biparietal diameter, femur length	0.80	ND	0.78	ND
Head circumference, femur length	0.76	ND	ND	ND

ND, no date; SD, standard deviation.

**Table 7-6** Variability ( $\pm 2$  SD) in Predicting Menstrual Age in the Second Half of Pregnancy

Parameter	20-26 Weeks	26-32 Weeks	32-42 Weeks
Biparietal diameter	2.1	3.8	4.1
Corrected biparietal diameter	1.9	3.3	3.8
Head circumference	1.9	3.4	3.8
Abdominal circumference	3.7	3.0	4.5
Femur length	2.5	3.1	3.5

SD, standard deviation.

Adapted from Benson CB, Doubilet PM: Sonographic prediction of gestational age: Accuracy of second and third trimester fetal measurements. *AJR Am J Roentgenol* 157:1275, 1991.

gestations or patients with potential growth disturbances. These authors found that the variability in predicting menstrual age using BPD reached a peak of approximately 4.1 weeks (2 SD) in the late third trimester of pregnancy (Table 7-6).

In certain circumstances (e.g., ruptured membranes, breech presentations, multiple gestations), shape changes in the fetal head may lead to even greater errors than those mentioned here. If one suspects that the shape of the calvarium is other than typical, one should measure the cephalic index of the head to assess head shape (see Fig. 7-5). The cephalic index is calculated from the BPD and the fronto-occipital diameter (FOD) measured from the outer edge of the calvaria to the outer edge of the calvaria:

$$\text{Cephalic index} = \frac{\text{BPD}}{\text{FOD}} \times 100$$

Technically, manufacturers usually compute a cephalic index from the HC ellipse long and short axes. Because the short axis of the HC ellipse is not truly a BPD, a slight and clinically insignificant error is introduced into cephalic indexes computed in this way. In the first in utero study on this subject, Hadlock et al<sup>11</sup> evaluated 316 patients between 14 and 40 menstrual weeks and demonstrated that the cephalic index was essentially age independent over time, with a mean value of 78.3 and an SD of 4.4. They concluded that a cephalic index greater than 1 SD above or below the mean (<74, >83) may be associated with a significant

alteration in the BPD measurement expected for a given menstrual age and that the HC can be used effectively as an alternative means of establishing age in such cases. Gray et al<sup>72</sup> found minimal changes in the mean value of age.

Doubilet and Greenes<sup>9</sup> recommended an alternative approach to potential head shape variations by routinely calculating a shape-corrected BPD based on an idealized cephalic index of 78:

$$\text{Shape-corrected BPD} = \left( \frac{\text{BPD} \times \text{FOD}}{1.265} \right)$$

As expected, when this shape correction is performed, the BPD is equivalent to the HC in accuracy of menstrual age prediction because it has been rendered shape independent.<sup>7,9</sup>

## Head Circumference

The neonatal HC is an important measurement of neonatal head growth and has gained importance as an in utero ultrasound measurement because it is independent of head shape. The measurement is made as described earlier (see Fig. 7-9A). If an ultrasonic system does not have the computer-generated ellipse ability, reliable estimates of HC also can be calculated using the shortest and longest axes of the fetal head measured outer to outer (the same measurements used to calculate the cephalic index). Although ideally one should use the formula for the circumference of an ellipse for this calculation, adequate estimates of the HC can be made using the formula  $(D1 + D2) \times 1.57$ . When the cephalic index indicates extreme dolicocephaly (value <70), the HC should not be calculated by this formula. The computer-generated ellipse should be used. The menstrual age can then be determined using a standard reference table (Table 7-7), although modern instruments compute the menstrual age from the HC as the measurement is being obtained.

Several authors demonstrated that HC is one of the most reliable individual parameters for estimation of menstrual age.<sup>14,73</sup> This is due to its shape independence and the fact that it represents a balance between ease of measurement (and, therefore, measurement accuracy) and predictive validity for age. For example, in 1982, Law and MacRae<sup>73</sup> demonstrated in a series of 594 patients that the HC was superior to the BPD as a predictor of menstrual age. This has been a consistent finding in studies by Hadlock et al.<sup>18,21,22</sup> Hill et al<sup>27</sup> and Benson and Doubilet<sup>7</sup> also reported similar conclusions



**Table 7-7****Predicted Menstrual Age for Head Circumference Measurements (8.5–36.0 cm)**

Head Circumference (cm)	Menstrual Age (week)	Head Circumference (cm)	Menstrual Age (week)
8.5	13.7	22.5	24.4
9.0	14.0	23.0	24.9
9.5	14.3	23.5	25.4
10.0	14.6	24.0	25.9
10.5	15.0	24.5	26.4
11.0	15.3	25.0	26.9
11.5	15.6	25.5	27.5
12.0	15.9	26.0	28.0
12.5	16.3	26.5	28.6
13.0	16.6	27.0	29.2
13.5	17.0	27.5	29.8
14.0	17.3	28.0	30.3
14.5	17.7	28.5	31.8
15.0	18.1	29.0	31.6
15.5	18.4	29.5	32.2
16.0	18.8	30.0	32.8
16.5	19.2	30.5	33.5
17.0	19.6	31.0	34.2
17.5	20.0	31.5	34.9
18.0	20.4	32.0	35.5
18.5	20.8	32.5	36.3
19.0	21.2	33.0	37.0
19.5	21.6	33.5	37.7
20.0	22.1	34.0	38.5
20.5	22.5	34.5	39.2
21.0	23.0	35.0	40.0
21.5	23.4	35.5	40.8
22.0	23.9	36.0	41.6
Variability Estimates ( $\pm 2$ SD) (week)			
12–18		$\pm 1.3$	
18–24		$\pm 1.6$	
24–30		$\pm 2.2$	
30–36		$\pm 2.7$	
34–42		$\pm 3.4$	

SD, standard deviation.

From Hadlock FP, Deter RL, Harrist RB, Park SK: Fetal head circumference: Relation to menstrual age. *AJR Am J Roentgenol* 138:649, 1982. Copyright 1982, American Roentgen Ray Society.

in independent studies. As with the other individual parameters, however, the variability in age prediction from HC increases with advancing menstrual age (see Table 7-7). For example, Hadlock, Harrist, and Martinez-Poyer<sup>22</sup> and Rossavik and Fishburne<sup>33</sup> demonstrated that this parameter can predict menstrual age to within  $\pm 1$  week (2 SD) before 20 weeks' gestation. Benson and Doubilet<sup>7</sup> demonstrated that the variability in predicting age from HC increases progressively throughout pregnancy, reaching a peak of approximately  $\pm 3.8$  weeks (2 SD) in the late third trimester (see Tables 7-5 and 7-6).

### Abdominal Circumference

The measurement of the fetal AC is made as described previously (Figs. 7-16 and 7-17). If the sonographic instrument is not equipped with a computer-generated ellipse measure-

ment capability, the circumference can be calculated using the transverse and anteroposterior diameters of the abdomen (measured from skin edge to skin edge) and the formula  $(D1 + D2) \times 1.57$ . The menstrual age can then be determined using a standard reference table (Table 7-8). However, as noted earlier, modern instruments immediately compute an age as the measurement is being obtained.

Of the four basic ultrasound measurements, the AC has generally had the largest reported variability.<sup>7,18,21,27</sup> This is partly attributable to the fact that AC is more acutely affected by growth disturbances than the other basic parameters (see Tables 7-5 and 7-6). The observed variability is probably due more to measurement error than biologic variability (Fig. 7-18). Most authors have gone to extremes to exclude patients with growth disturbances from their study populations. Furthermore, of the four recommended measurements, AC measurements are the most difficult to obtain. The greatest differences in accuracy between AC and the other parameters in the study by Benson and Doubilet<sup>7</sup> were observed in the second trimester of pregnancy, a point at which growth variations would be expected to be minimal (see Table 7-6).

In early pregnancy and in normally growing fetuses, the AC is only slightly less accurate on average than the other basic measurements if one strictly adheres to the rules of measurement. Similar results have been reported by Hill et al,<sup>27</sup> who demonstrated that the variability in predicting menstrual age (14 to 43 weeks) from AC in 265 normal weight fetuses was slightly less than that associated with the BPD. As with all other parameters, however, the variability in predicting menstrual age based on AC increases as pregnancy advances. For example, in a retrospective study of patients with menstrual dates corroborated by early CRL, Benson and Doubilet<sup>7</sup> reported variability of  $4\frac{1}{2}$  weeks (2 SD) in the late third trimester of pregnancy (see Table 7-6).

### Femur Length

Because of its size, visibility, and ease of measurement the femur is generally preferred over the other long bones as a means of predicting menstrual age. The FL measurement was described in detail earlier (see Figs. 7-13 to 7-15). Although virtually all of the early work in femur biometry was done on white populations, it has been demonstrated that these measurements are not altered in any appreciable way in other races.<sup>21,30</sup> Obviously, in any fetus suspected of having an osteochondral dysplasia, the FL should be excluded from calculation of menstrual age. Estimates of menstrual age can be obtained from standard reference tables (Table 7-9). However, as noted earlier, modern instruments immediately compute an age while the measurement is being obtained.

Most studies suggest that the FL is an accurate predictor of menstrual age in the early second trimester (2 SD =  $\pm 1$  week), but again variability increases as pregnancy advances. Furthermore, reported variability throughout the remainder of pregnancy from several laboratories has been inconsistent (see Tables 7-5 and 7-6).<sup>13,16,74,75</sup> For example, Jeanty et al<sup>74</sup> reported a uniform variability for the FL age estimate of  $\pm 2.1$  weeks throughout the second and third trimesters of pregnancy, suggesting that the FL is just as accurate in predicting age at 40 weeks as it is at 14 weeks.

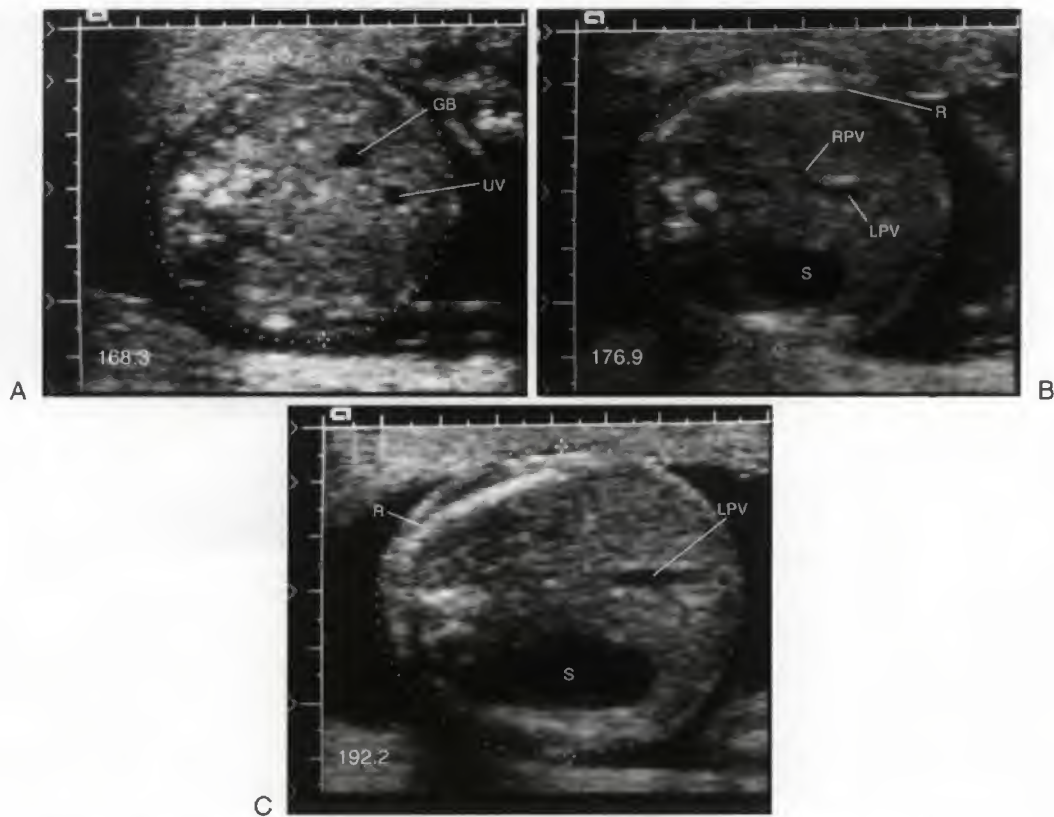


**FIGURE 7-17.** Abdominal circumference (AC) measurements correlated with Figure 7-16. Each measurement was obtained in the same fetus within minutes of one another. *A.* The abdominal circumference depicted here is obtained at the wrong craniocaudal plane. It is obtained in too caudal a position. This can be determined by two observations. First, the plane cuts through the short axis of the umbilical vein (UV) (correlate with Fig. 7-16A). Second, no ribs are visible laterally. Compare with the correct plane of section in *B* (GB, gallbladder). *B.* This is a properly oriented and measured AC. Note that it measures 176.9 mm. The ribs (R) are symmetric, and the junction of the right (RPV) and left (LPV) portal veins is seen. By contrast, the circumference measured in Figure 7-17A is only 168.3 mm. Note that the body of the fetal stomach (S) is nearly always visible in a well-performed AC measurement. In *A*, the gallbladder, a more caudal structure, is visible rather than the stomach. *C.* In this plane of section, a long length of the left portal vein (LPV) is seen rather than the junction of the right and left portals, as noted in Figures 7-16B and 7-17B. This indicates that the plane of section is inclined relative to the body axes. If the reader compares Figure 17B and C, one will note that in the latter the abdominal section is more elliptically shaped than in the former. The circumference is increased by this error (192.2 mm compared with 176.9 mm). It is because this latter error is very common that the rule “round covers a multitude of errors” applies.

Hadlock et al<sup>25</sup> believed that this is a statistical phenomenon resulting from the use of the wrong test of the variability estimate. Furthermore, although Hill et al<sup>27</sup> found FL to be the most accurate of all the individual parameters in predicting menstrual age, Ott<sup>76</sup> found it to be the least accurate. Hadlock et al<sup>18</sup> and Benson and Doubilet<sup>7</sup> found the FL to be roughly equivalent in accuracy to the other parameters in estimating menstrual age, reaching a peak variability of approximately  $\pm 3.5$  weeks in the late third trimester of pregnancy.

It is important to emphasize, as stated earlier, that variability of fetal head and femur measurements (BPD/HC/FL) is small early in gestation. Many tables list variability of these measurements as a grouped range, for example, 12 to 18 weeks =  $\pm 1.3$  weeks. Although the variability of slightly greater than one week is often acceptable and normal in most of the second trimester, one should be suspicious when this is found, early in the second trimester, for example, 12 to 14 weeks. A BPD, HC or FL 1 week less than the other measurements may be an early sign of microcephaly in the

case of a slightly smaller fetal head or trisomy 21 or a short limbed bony dysplasia in the case of a slightly smaller femur.

## OTHER BIOMETRIC PARAMETERS

A number of other fetal structures can be imaged and measured with current high-resolution real-time ultrasound equipment. These measurements may rarely play a role when either the transverse axial image necessary for measurement of the BPD and HC or the proper plane for femur measurement is not obtainable. For example, when the head is in a direct occiput posterior position, the orbits are easily imaged, and several authors have published normal data for both the binocular distance and the interorbital and intraorbital diameters (see Appendix A-24).<sup>77,78</sup> When the fetus is in a direct occiput anterior position, the posterior fossa is closer to the transducer, and the cerebellum can be seen to advantage. Hill et al<sup>26</sup> published normal data for the transverse diameter of the cerebellum (transverse cerebellar diameter), and some authors believe that it is preferable to other head



**Table 7-8** Predicted Menstrual Age for Abdominal Circumference Measurements

Abdominal Circumference (cm)	Menstrual Age (week)	Abdominal Circumference (cm)	Menstrual Age (week)
10.0	15.6	23.5	27.7
10.5	16.1	24.0	28.2
11.0	16.5	24.5	28.7
11.5	16.9	25.0	29.2
12.0	17.3	25.5	29.7
12.5	17.8	26.0	30.1
13.0	18.2	26.5	30.6
13.5	18.6	27.0	31.1
14.0	19.1	27.5	31.6
14.5	19.5	28.0	32.1
15.0	20.0	28.5	32.6
15.5	20.4	29.0	33.1
16.0	20.8	29.5	33.6
16.5	21.3	30.0	34.1
17.0	21.7	30.5	34.6
17.5	22.2	31.0	35.1
18.0	22.6	31.5	35.6
18.5	23.1	32.0	36.1
19.0	23.6	32.5	36.6
19.5	24.0	33.0	37.1
20.0	24.5	33.5	37.6
20.5	24.9	34.0	38.1
21.0	25.4	34.5	38.7
21.5	25.9	35.0	39.2
22.0	26.3	35.5	39.7
22.5	26.8	36.0	40.2
23.0	27.3		
Variability Estimates ( $\pm 2$ SD) (week)			
	12-18	$\pm 1.0$	
	24-30	$\pm 2.2$	
	30-36	$\pm 3.0$	
	36-42	$\pm 2.5$	

SD, standard deviation.

From Hadlock FP, Deter RL, Harrist RB, Park SK: Fetal abdominal circumference as a predictor of menstrual age. *AJR Am J Roentgenol* 139:367, 1982. Copyright 1982, American Roentgen Ray Society.

measurements for age prediction in cases in which fetal growth may be altered (Table 7-10).<sup>79</sup> Other notable measurements that may be used as substitute variables for predicting menstrual age include virtually all of the long bones of the arms and legs (see Appendices A-17 and A-18). In addition, normal data have been published for use of the fetal foot length (the growth of which appears to be spared in cases of intrauterine growth restriction) and fetal clavicle length measurements as predictors of menstrual age. The variability associated with age predictions based on these additional biometric parameters is outlined in Table 7-11. These measurements might be useful in certain circumstances, but in general, the basic fetal measurements previously mentioned serve as adequate indicators of menstrual age in most cases.

## LATE PREGNANCY

Occasionally, an obstetrician is first confronted with a pregnant woman who is uncertain of her dates and has

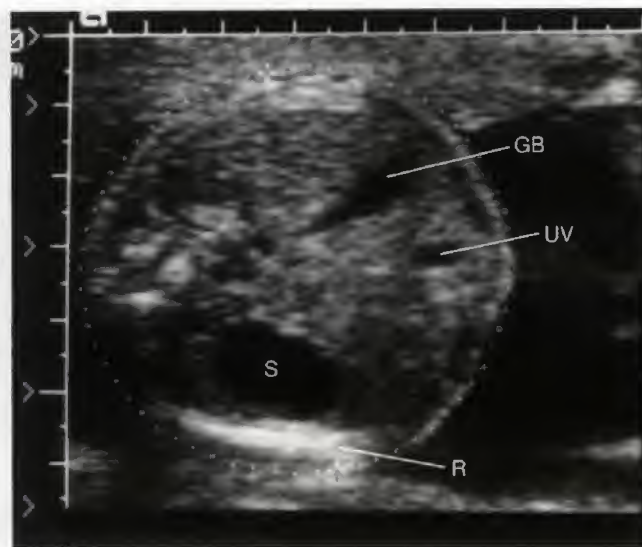


**FIGURE 7-18.** In this plane of section, the acoustic beam enters the abdomen at a more caudal site and exits at a more cranial site. This is evident by two observations. First, no rib is seen on the "up" side of the abdomen and a length of rib (R) is seen on the "down" side. As well, the gallbladder (GB) is seen on the "up" side, whereas the body and fundus of the stomach (S) are seen on the "down" side (UV, umbilical vein). Note that the error introduced by this off-axis plane is less than that introduced by the off-axis plane depicted in Figure 7-17C. Importantly, recognizing the anatomic signals of error depicted in Figures 7-17A and C and 7-18 give the examiner both knowledge of the direction and magnitude of the error and suggest the change in transducer alignment needed to correct the error.

already reached the third trimester. Although the accuracy of first trimester ultrasound for predicting GA is  $\pm 3$  to 5 days, and  $\pm 7$  days for 12 to 18 weeks' GA,<sup>80</sup> biometric data are unreliable in the third trimester. This situation becomes clinically relevant when a determination for delivery may become necessary. Owing to the relatively slow maturation of the fetal pulmonary system in relation to all other organ systems, the risk of neonatal respiratory distress syndrome is non-negligibly high, even at near-term GA. This risk is essentially gone once a fetus has reliably achieved 39 weeks' menstrual age. Indeed, the American College of Obstetricians and Gynecologists (ACOG) stipulates strict criteria to ensure pulmonary maturity for the elective delivery of a fetus before 39 0/7 weeks' GA.<sup>81</sup> If one of these criteria is successfully met, the obstetrician can reliably assume pulmonary maturity. These criteria include

- Fetal heart tones that have been documented for 20 weeks by non-electronic fetoscope or for 30 weeks by Doppler.
- The passage of 36 weeks since a serum or urine human chorionic gonadotropin pregnancy test was found to be positive by a reliable laboratory.
- Ultrasound measurement of a crown-rump length at 6 to 11 weeks' GA that supports a current GA equal to or greater than 39 weeks.
- Ultrasound measurement at 12 to 20 weeks of gestation that supports a clinically determined GA of 39 weeks or greater.

While there is no foolproof means of determining menstrual age in the circumstance of uncertain LMP and no early

**Table 7-9****Predicted Menstrual Age for Femur Lengths (1.0–7.9 cm)**

Femur Length (cm)	Age (Week)	Femur Length (cm)	Age (Week)
1.0	12.8	4.5	24.5
1.1	13.1	4.6	24.9
1.2	13.4	4.7	25.3
1.3	13.6	4.8	25.7
1.4	13.9	4.9	26.1
1.5	14.2	5.0	26.5
1.6	14.5	5.1	27.0
1.7	14.8	5.2	27.4
1.8	15.1	5.3	27.8
1.9	15.4	5.4	28.2
2.0	15.7	5.5	28.7
2.1	16.0	5.6	29.1
2.2	16.3	5.7	29.6
2.3	16.6	5.8	30.0
2.4	16.9	5.9	30.5
2.5	17.2	6.0	30.9
2.6	17.6	6.1	31.4
2.7	17.9	6.2	31.9
2.8	18.2	6.3	32.3
2.9	18.6	6.4	32.8
3.0	18.9	6.5	33.3
3.1	19.2	6.6	33.8
3.2	19.6	6.7	34.2
3.3	19.9	6.8	34.7
3.4	20.3	6.9	35.2
3.5	20.7	7.2	36.7
3.6	21.8	7.3	37.2
3.9	22.1	7.4	37.7
4.0	22.5	7.5	38.3
4.1	22.9	7.6	38.8
4.2	23.3	7.7	39.3
4.3	23.7	7.8	39.8
4.4	24.1	7.9	40.4
Variability Estimates ( $\pm 2$ SD) (week)			
12–18		$\pm 1.0$	
18–24		$\pm 1.8$	
24–30		$\pm 2.0$	
30–36		$\pm 2.4$	
36–42		$\pm 3.2$	

SD, standard deviation.

From Hadlock FP, Deter RL, Harrist RB, Park SK: Fetal femur length as a predictor of menstrual age: Sonographically measured. *AJR Am J Roentgenol* 138:875, 1982. Copyright 1982, American Roentgen Ray Society.

ultrasound measurements, the fetal skeleton can provide some clues as to the duration of the pregnancy. Long bone ossification begins at the primary ossification center in the diaphysis starting at the end of the embryonic period. The secondary ossification centers appear later, with those of the heel and knee preceding all others. The bone growth occurring at these centers is referred to as the epiphysis.<sup>82</sup> The distal femoral epiphysis, which is not included in the measurement of the femoral shaft, is not seen before 28 weeks' GA, but it is observed in 94% of fetuses at 34 weeks GA, and in an even greater proportion of older fetuses (see Figs. 7-15 and 7-19).<sup>82,83</sup> These ossification centers appear earlier, on average, in female fetuses (Fig. 7-20).<sup>84</sup> The size of the distal femoral ossification center also cor-

**Table 7-10****Predicted Menstrual Ages for Transverse Cerebellar Diameters of 14 to 56 mm**

Cerebellum (mm)	Menstrual Age (Week)	Cerebellum (mm)	Menstrual Age (Week)
14	15.2	35	29.4
15	15.8	36	30.0
16	16.5	37	30.6
17	17.2	38	31.2
18	17.9	39	31.8
19	18.6	40	32.3
20	19.3	41	32.8
21	20.0	42	33.4
22	20.7	43	33.9
23	21.4	44	34.4
24	22.1	45	34.8
25	22.8	46	35.3
26	23.5	47	35.7
27	24.2	48	36.1
28	24.9	49	36.5
29	25.5	50	36.8
30	26.2	51	37.2
31	26.9	52	37.5
32	27.5	54	38.0
33	28.1	55	38.3
34	28.8	56	38.5
Variability Estimates ( $\pm 2$ SD) (week)			
12–18		$\pm 1.0$	
18–24		$\pm 1.8$	
24–30		$\pm 2.0$	
30–36		$\pm 2.4$	
36–42		$\pm 3.2$	

SD, standard deviation.

From Hill LM, Guzik D, Fries J, et al: Transverse cerebellar diameter in estimating gestational age in the large-for-gestational age fetus. *Obstet Gynecol* 75:983, 1990. Reprinted with permission from the American College of Obstetricians and Gynecologists.

**Table 7-11****Variability ( $\pm 2$  SD) Estimates for Secondary Biometric Parameters**

Parameter	12–18 Weeks	18–24 Weeks	24–30 Weeks	30–36 Weeks	36–42 Weeks
Binocular distance <sup>77</sup>	1.8	2.4	3.0	4.0	4.0
Cerebellar diameter <sup>20</sup>	1.0	1.8	2.0	2.4	3.2
Clavicle length <sup>63</sup>	6.5	6.5	6.5	6.5	6.5
Radius length <sup>25</sup>	1.8	2.2	2.9	3.5	4.1
Ulna length <sup>73</sup>	3.6	3.6	3.6	3.6	3.6
Tibia length <sup>73</sup>	3.5	3.5	3.5	3.5	3.5
Foot length <sup>54</sup>	1.2	1.7	2.2	2.6	3.1

SD, standard deviation.

relates with late GA (Fig. 7-21).<sup>85</sup> The proximal tibial epiphysis is not seen before 34 weeks' GA but does occur in 35% of 35-week-old fetuses, 80% of 37 week fetuses, and 100% of fetuses at or beyond 39 weeks GA.<sup>82</sup> Thus, visualization of the distal femoral and proximal tibial epiphyseal ossification centers is helpful for confirming biometric data predicting menstrual age in late pregnancy (see Fig. 7-19).<sup>84,85</sup>



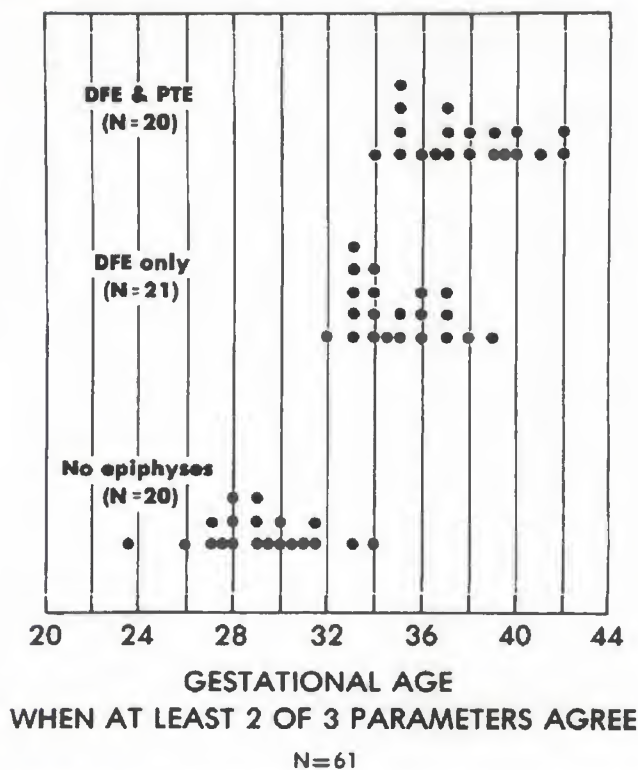


**FIGURE 7-19.** Appearance time of the distal femoral (DFE) and proximal tibial (PTE) epiphyseal ossification centers in a mixed group of 61 fetuses that were well dated. (From Chinn DH, Bolding DB, Callen PW, et al: *Ultrasonographic identification of fetal lower extremity epiphyseal ossification centers. Radiology 147:815, 1983.*)

The appearance time of the epiphyseal ossification centers is insufficiently accurate to use as a sole arbiter of menstrual age in late pregnancy but can serve more as a confirmatory observation that the biometric data are accurate. For example if one encounters a fetus whose biometric measurements suggest a menstrual age of 36 weeks but in whom neither an ossified distal femoral or proximal tibial epiphyseal ossification center is visible, the possibility that the calculated menstrual age is erroneous is high. Potentially, such a fetus is macrosomic.

Additional GA markers exist. These include the transverse cerebellar diameter and foot length (the growth of both are spared in fetal growth restriction (see earlier as well as Tables 7-10 and 7-11), placental grading, small intestinal peristalsis, colonic echogenicity, and the presence or absence of colonic haustra.<sup>82</sup> Placental grading is based on echogenicity attributed to increasing calcium and fibrous deposition with advancing age.<sup>82,86</sup> On a grading system of 1 to 3, with 3 representing the most advanced or matured placenta, the distribution at term is 45% for grade 1, 55% for grade 2, and 5% to 10% for grade 3.<sup>87</sup> Although it is unusual to find a grade 1 placenta at or beyond 42 weeks' GA, grade 2 occurs 55% of the time, and grade 3, 45% of the time. Correlation between placental grading and pulmonic maturity is highly controversial, and various disorders have been shown to affect the sonographic appearance of the placenta (e.g., "premature" maturation with maternal chronic hypertension, and "delayed" maturation with diabetes mellitus and

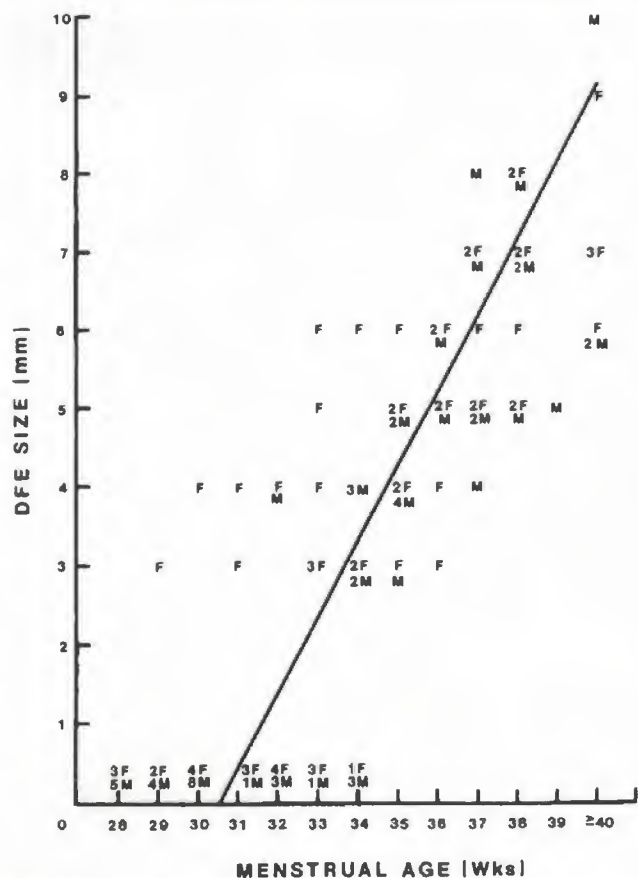


**FIGURE 7-20.** Variation in the distal femoral epiphyseal ossification centers (DFE) appearance time and size in male and female fetuses. (From Mahony SB, Callen PW, Filly RA: *The distal femoral epiphyseal ossification center in the assessment of third trimester menstrual age: Sonographic identification and measurement. Radiology 155:201, 1985.*)

isoimmunization).<sup>82,88</sup> Placental grading should *not* be used to determine fetal lung maturity.

With advancing GA, small-intestinal peristalsis "matures," developing into more vigorous and longer duration peristaltic waves. Just as with placental maturation, a grading system has been described for small intestinal peristalsis<sup>82</sup>:

- Grade 0: Small intestinal peristalsis is absent.
- Grade 1: Few sporadic waves of small intestinal peristalsis in up to 3 discrete areas, present for durations of less than 3 seconds.
- Grade 2: Moderate waves of small intestinal peristalsis in more than 3 discrete areas, present for durations longer than 3 seconds.
- Grade 3: Active waves of small intestinal peristalsis that are seen throughout the observation interval.

Intestinal peristalsis can be seen as early as 18 weeks' GA. Grade 1 peristalsis can be observed in 88% of fetuses before 29 weeks' gestation, and grade 3 peristalsis in 80% of fetuses between 37 and 38 weeks' GA.<sup>89</sup>

Colonic echogenicity is another sonographic marker that has been described. With advancing GA, there is an increase in luminal meconium content and a reduction in water leading to progressively increased echogenicity. When com-

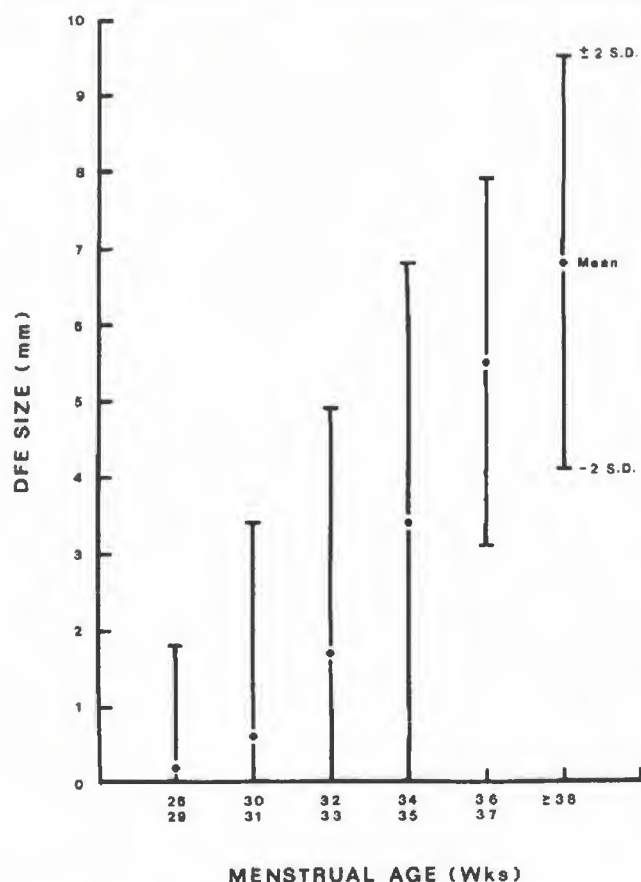


**FIGURE 7-21.** Mean diameter of the distal femoral epiphyseal ossification centers (DFE) with increasing age of late third trimester fetuses. (From Mahony SB, Callen PW, Filly RA: The distal femoral epiphyseal ossification center in the assessment of third trimester menstrual age: Sonographic identification and measurement. *Radiology* 155:201, 1985.)

pared with the appearance of other intra-abdominal structures, this echogenicity can also be graded<sup>82</sup>:

- Grade 0: The abdomen is uniform in appearance, and the colon is not identified.
- Grade 1: The colonic contents have an echo-free appearance. This is essentially identical to that of the bladder and the stomach; the colonic haustra can be identified.
- Grade 2: Intermediate. The colon appears more echodense than the bladder but less than the liver.
- Grade 3: The colonic contents have an echogenicity essentially equal to that of the liver

Grade 0 colonic echogenicity is present in 82% of fetuses less than 29 weeks' GA, but grade 3 is seen in 85% of fetuses older than 39 weeks' GA.<sup>89</sup> Finally, colonic haustra can be observed using ultrasound starting at 30 weeks' GA, and thus, can serve as an independent marker of a GA of at least 30 weeks.

Clearly, there is a point in pregnancy after which reliance on biometric parameters to date the pregnancy is invalid and serious errors can be made. After this point, it is no longer possible to "know" the menstrual age of the pregnancy. The use of secondary markers as described earlier can only provide a rough estimate of GA that is far too

imprecise to assign an exact date. Thus, the only information that can be reliably obtained from third trimester sonograms is the fetal weight and, by a follow-up study, whether interval growth is normal. Experts disagree regarding the point in pregnancy when sonographic estimates of age become too unreliable to use. However, all agree that the accuracy begins to deteriorate rapidly after the 20th week. The exact cutoff is debatable but lies somewhere in the range of 24 to 28 menstrual weeks.

## CALCULATION OF MENSTRUAL AGE

The literature is replete with articles that focus on predicting menstrual age using ultrasound measurements of the fetus.<sup>5,32</sup> A common theme among these articles is that the variability in predicting menstrual age increases as pregnancy advances for all fetal parameters (see Tables 7-5 and 7-6). The increase in variability is undoubtedly for the most part due to actual differences in fetal size, because it has been demonstrated consistently in populations with optimal menstrual histories, with known dates of conception, and in whom age was established early in pregnancy by use of the CRL measurement. For example, Hadlock, Harrist, and Martinez-Poyer<sup>22</sup> studied 1771 patients with excellent menstrual histories and demonstrated that any of the individual parameters can provide accurate estimates of menstrual age (2 SD =  $\pm 1$  week) between 14 and 20 weeks. Persson and Weldner<sup>64</sup> and Rossavik and Fishburne<sup>33</sup> demonstrated similar results in patients with known dates of conception (see Table 7-5). In a large study of patients whose dates were confirmed by the gold standard of early CRL dating, Benson and Doubilet<sup>7</sup> demonstrated that age estimates from individual parameters reach a maximum variability of approximately  $\pm 4$  weeks in the late third trimester of pregnancy (see Table 7-6). Thus, one should try to establish menstrual age as early in pregnancy as possible.

Which measurements should one use to predict age in a given case? Hadlock et al<sup>18</sup> suggested that one should avoid the tendency to place excessive emphasis arbitrarily on any one measurement because, in a given case, any measurement could provide the best estimate of age. With this idea in mind, they postulated that multiple fetal measurements should be used in combination to provide a composite age estimate. The use of multiple measurements is especially important when one considers several points. (1) If one is using only one parameter and makes an imaging or measurement error, the magnitude of the error in age prediction could be significantly greater than the reported variability for that parameter. (2) It is not uncommon for normal fetuses to have measurements that are above or below the expected mean value at a given age and these differences are not always in the same direction. For example, a fetus may have a 75 percentile head size and a 25 percentile abdominal size. (3) The process of plane selection of the fetal head, abdomen, and femur allows a detailed look at important anatomic structure and, therefore, facilitates detection of abnormalities in these areas, including hydrocephalus, encephalocele, bowel obstruction, ascites, renal abnormalities, and dwarfism.

The initial approach of Hadlock et al<sup>18</sup> was to use a simple averaging technique in which the estimates of age are added and divided by the number of estimates made. For example,



consider the following measurements obtained in the early second trimester:

BPD	3.3 cm = 15.9 weeks
HC	12.4 cm = 16.2 weeks
AC	10.0 cm = 15.6 weeks
FL	2.2 cm = 16.3 weeks
Composite age	16.0 weeks $\pm$ 1 week

However, these authors subsequently developed regression equations for use in predicting age from any single measurement or combination of measurements,<sup>18</sup> and these equations have been validated prospectively.<sup>21</sup> These regression equations have become routine in usage in clinical practice. However, if an ultrasonic system is not equipped with an appropriate computation software package, the simple averaging technique gives approximately equivalent results.

The development of this multiple parameter dating approach raises two questions immediately. The first is how many measurements of the fetus must one make to obtain the best estimate of menstrual age? Hadlock et al<sup>18</sup> examined this issue over the entire 14- to 42-week age range and demonstrated that the use of the four basic measurements results in the greatest accuracy (lack of systematic bias), greatest precision (lowest range of variability), and smallest maximum observed errors. Although some authors questioned the validity of the method,<sup>71</sup> Hill et al<sup>27</sup> validated the models in an independent study. Moreover, Hill et al demonstrated that the addition of a fifth parameter (radius length) does not add to the accuracy of the method. From a purely statistical point of view, both Hadlock et al<sup>16</sup> and Hill et al<sup>27</sup> were unable to demonstrate significant improvement beyond the two-parameter model based on HC and FL. Persson and Weldner<sup>64</sup> reported similar results in a large study between 14 and 20 weeks (see Table 7-5). Although the variability of the two-parameter (HC, FL) model increases as pregnancy advances, it is relatively constant at 8% when expressed as a percentage of the estimate. For example, if the composite age estimate based on these two parameters is 20 weeks, then the variability associated with that estimate is 20 weeks  $\pm$  1.6 weeks. In the late third trimester, a composite age estimate of 40 weeks would have a corresponding variability of 40 weeks  $\pm$  3.2 weeks. Because the four-parameter method results in the lowest variability estimates, it is most commonly used in clinical practice.

The second important question that comes to mind using the multiple-parameter dating technique is how disparate the individual measurements can be and still be acceptable for incorporation into the composite age estimate. For example, if measurement of the fetal head (BPD or HC) gave an age estimate of 20 weeks and measurement of the FL gave an age estimate of 14 weeks, one would know empirically that the two cannot be averaged to provide a composite age. The fetus is almost certainly abnormal. To deal with this issue one can rely on fetal body ratio data as delineated in Tables 7-12 and 7-13. For example, if the BPD is to be used in the age estimate, one should first examine the cephalic index. If it indicates an abnormal head shape, the BPD should either be eliminated in favor of the HC or corrected for head shape.<sup>9,11,72</sup> One can then measure the relationship between FL and HC. If this is normal, then both measurements can be used for the prediction of age.<sup>20</sup> If the FL:HC ratio is high, the head measurement should be deleted

**Table 7-12** Normal Body Ratio Data (14–21 Weeks)

Menstrual Week	Cephalic Index (SD = 3.7) <sup>71</sup>	Femur/BPD $\times$ 100 (SD = 4.0) <sup>24</sup>	Femur/HC $\times$ 100 (SD = 1.0) <sup>24</sup>	Femur/AC $\times$ 100 (SD = 1.3) <sup>24</sup>
14	81.5	58.0	15.0	19.0
15	81.0	59.0	15.7	19.3
16	80.5	61.0	16.4	19.8
17	80.1	63.0	16.9	20.3
18	79.7	65.0	17.5	21.8
19	79.4	67.0	18.1	21.0
20	79.1	69.0	18.4	21.3
21	78.8	70.0	18.6	21.5

BPD, biparietal diameter; HC, head circumference; AC, abdominal circumference.

**Table 7-13** Normal Fetal Body Ratios (22–40 Weeks)

Menstrual Week	Cephalic Index (SD = 4.4) <sup>11</sup>	Femur/BPD $\times$ 100 (SD = 5.0) <sup>85</sup>	Femur/HC $\times$ 100 (SD = 1.1) <sup>20</sup>	Femur/AC $\times$ 100 (SD = 1.3) <sup>17</sup>
22	78.3	77.4	18.6	21.6
23	78.3	77.6	18.8	21.7
24	78.3	77.8	19.0	21.7
25	78.3	78.0	19.2	21.8
26	78.3	78.2	19.4	21.8
27	78.3	78.4	19.6	21.9
28	78.3	78.6	19.8	21.9
29	78.3	78.8	20.0	21.9
30	78.3	79.0	20.3	22.0
31	78.3	79.2	20.5	22.0
32	78.3	79.4	20.7	22.1
33	78.3	79.6	20.9	22.1
34	78.3	79.8	21.1	22.2
35	78.3	80.0	21.4	22.2
36	78.3	80.2	21.6	22.2
37	78.3	80.4	21.8	22.3
38	78.3	80.6	22.0	22.3
39	78.3	80.8	22.2	22.3
40	78.3	81.0	22.4	22.4

BPD, biparietal diameter; HC, head circumference; AC, abdominal circumference.

because of possible microcephaly; if this ratio is low, the FL age estimate should be deleted because of possible dwarfism.<sup>20</sup> These decisions are based on the assumption of normal anatomy of the head and long bones.

If AC is to be included in the age estimate, one must examine the relationship between FL and AC (FL/AC  $\times$  100). If this ratio is low, one should avoid using the AC because of possible macrosomia; and if it is high, one should avoid using the AC because of possible intrauterine growth restriction.<sup>17</sup> Because the AC may be affected by abnormal fetal growth, one can make a strong case for eliminating it from the age estimation procedure altogether, particularly in the third trimester of pregnancy.<sup>7</sup> This case is even stronger in view of the inability to demonstrate a statistically significant improvement in the age estimation procedure by adding additional parameters to the combination of HC and FL.<sup>18,22</sup>



The limiting factor in menstrual age estimates from fetal biometry is likely due to the genetic variation in actual fetal size as pregnancy advances and, to a lesser extent, the measurement errors associated with their use. Thus, it is unlikely that additional biometric parameters will add to the accuracy of the dating procedure using ultrasound evaluation. It is possible, and ever likely, that certain nonbiometric observations may prove helpful in narrowing the variability associated with ultrasound age estimates.<sup>1</sup> These observations include the degree of placental maturation,<sup>96</sup> amniotic fluid volume,<sup>97</sup> and maturation of the fetal bowel pattern (as explained above).<sup>96,98</sup> The presence of a grade 3 placenta, low amniotic fluid volume (in the absence of ruptured membranes, fetal renal disease, or growth restriction), and a mature fetal bowel pattern would make one favor the higher end of the age estimate based on fetal biometry. For example, in the presence of the above-mentioned ancillary findings, if the biometric age estimate based on FL and head size was 34 weeks  $\pm$  2.7 weeks, one would favor the high end of the estimate (36.7 weeks). These ancillary findings are useful and can be further supported by looking for epiphyseal ossification centers to correlate with late estimates of menstrual age.<sup>85</sup> Thus, in the case just described, the presence of the distal femoral and proximal tibial epiphyseal ossification centers would again favor the higher end of the age estimate, that is, 36.7 weeks (see earlier for more information on fetal maturation markers). Additional parameters for measurement, such as the fetal clavicle and foot, have also been looked at for estimation of age, and the latter appears to be immune to the effects of growth restriction.<sup>99-101</sup>

The menstrual age based on the LMP dates should never be changed late in pregnancy based solely on ultrasound measurements. Great caution is mandatory when menstrual age based on the LMP differs from sonographic biometry late in pregnancy. All available clinical information must be carefully scrutinized before dates are "changed" in late pregnancy. Whenever this course of action is chosen, the potential for serious error must be forefront in the minds of the managing clinicians. More obvious, if dates have been established early in pregnancy by sonographic biometry, changing the dates based on later sonographic biometry is a formula for disaster.

## ESTIMATION OF FETAL WEIGHT

Once biometric parameters have been measured, an estimate of fetal weight can be made. A number of techniques exist to perform this function. Formulas and nomograms for the estimation of fetal weight using combinations of BPD, HC, AC, and FL have been developed. Among the common fetal weight formulas are Shepard's and Hadlock's (see Appendix B).<sup>90-92</sup> These formulas have been validated, and, for example, the Shepard formula predicts fetal weight within 10% of the actual weight in 85% of cases.<sup>90</sup> The Hadlock formula improves upon this by the incorporation of three fetal parameters, reducing the random error by 15% to 25% less than with models utilizing two parameters.<sup>82</sup> Most modern ultrasound equipment comes with computer packages that will automatically calculate an estimated fetal weight (EFW) based on one of these formulas. If such a function is not available, one can refer to 2  $\times$  2 nomogram tables that use two biometric parameters to provide an

estimate of fetal weight (e.g., BPD and AC, or AC and FL; see Appendix B-5).

One can compare the estimated fetal weight with established cross-sectional population-based growth curves. Lubchenco et al<sup>93</sup> in 1963 first described such a growth curve based on live-born birthweights of neonates born to white and Hispanic women in Denver, Colorado (5000 feet above sea level) from 24 to 42 weeks' GA. Brenner et al followed this up with a growth curve based upon white and black infants delivered in Cleveland and aborted fetuses from North Carolina.<sup>91</sup> Differences exist among these population-based growth curves due to the inherent variation in populations studied based on numerous factors, including altitude, ethnicity, socioeconomic status, and time period. In an effort to overcome these limitations, Alexander et al<sup>95</sup> described 1991 United States national birthweight data from over three million live births from 20 to 44 weeks' GA. Nevertheless, all of these growth curves are based on birthweight, and not *fetal* weight. Because they are composite curves based on the endpoint of fetal growth at each successive GA, they are not true representations of the actual rate of fetal growth. Indeed, neonates born at earlier GAs are more likely to be born owing to other complications of pregnancy that may, in turn, result in inclusion of an abnormally high number of infants with intrauterine growth restriction (IUGR) at these time points, thereby possibly misrepresenting fetal weight at extremes of GA. This becomes quite relevant for clinical circumstances when one has a heightened suspicion for the potential development of growth restriction (see section on IUGR later). Despite these limitations, use of these growth curves has become commonplace because there currently does not exist a more superior method of determining fetal weight growth percentile (see later on individualized growth curves).

## CLINICAL APPLICATION OF BIOMETRIC PARAMETERS

### Intrauterine Growth Restriction

#### Definition

In any given population, there is a normal distribution of fetal size at each GA. Inherently, a fraction of fetuses will be small and large. Although fetuses at the extremes of size may be within the spectrum of normal and achieving their growth potential (see the section on individualized growth curves, later), it is more likely that the majority of these fetuses are growing abnormally, either underachieving or overachieving their potential. The terms small for gestational age (SGA) and IUGR have been confusingly used interchangeably. In 1967, Battaglia and Lubchenco<sup>102</sup> defined SGA as birthweight being below the 10th percentile for GA. Whereas IUGR has been defined using a number of different criteria, including that for SGA, it is now generally a term reserved for the clinical circumstance of a fetus that is underachieving its growth potential. This is the way IUGR will be used in this chapter, while SGA will be a term reserved for constitutionally small fetuses that are meeting their growth potential as best as can be clinically determined.

A number of criteria have been used to capture a fetal population most at risk for abnormal growth. Among those



used to ascribe IUGR, the most common is a EFW less than the 10th percentile for GA. Alternative criteria include an EFW less than the 3rd, 5th, and 15th percentiles, as well as less than 2 standard deviations (SD) below the mean. The AC has also been used as a defining biometric parameter, because it is believed that among all fetal measures, pathologic growth affects hepatic size, and thus the AC first. An AC less than the 10th percentile, the 2.5th percentile, and 2 SDs below the mean for GA have all been used as defining criteria. Overly strict criteria may have very high positive predictive values, but may miss a sizable number of fetuses that also have pathologic growth. More specifically, although the 10th percentile will have a higher false-positive rate, it may detect the fetus genetically set to be at the 50th percentile but is pathologically small at the 9th percentile. As Dr. John Hobbins of the University of Colorado Health Sciences Center puts it rather eloquently: "The fetus genetically programmed to be in the 90th percentile who is born in the 20th percentile may be in more trouble than a baby born to a jockey and a gymnast who is in the 8th percentile." For the purpose of screening out a high-risk population, obstetric practitioners most commonly use a definition of less than the 10th percentile, and this will be the definition used in this chapter.

### **Etiologies**

There are a number of causes of IUGR. A traditional method of distinguishing the etiologies of IUGR is symmetric versus asymmetric growth, in which the former is a situation when all biometric measurements are symmetrically lagging and the latter is when they are lagging asymmetrically (e.g., the BPD lags less than the AC that is expected for the GA at hand). Symmetric growth lag has been shown to occur from genetic disorders (e.g., trisomy 18), fetal infections (e.g., rubella and cytomegalovirus), congenital malformations, and a variety of syndromes (e.g., Cornelia de Lange).<sup>103</sup> Asymmetric growth lag tends to occur in situations of relative nutritional and oxygen deprivation. The basis of this distinction based upon patterns of symmetry comes from the thought that global insults to the fetus lead to a total restriction in fetal growth, whereas nutritional and oxygen deficiencies lead to an asymmetric growth pattern with preferential preservation of vital structures first such as the brain (thus, a head-to-body disproportion, or an AC lag relative to head parameters). This is of course prone to inaccuracy, because a late gestation fetus that has been exposed to a chronically nutritionally deficient or hypoxic environment through a major portion of pregnancy can also show growth lag of all fetal parts to a similar extent and, hence, may appear to be symmetrically restricted. Some forms of growth restriction may fall into either symmetric or asymmetric categories and, hence, do not easily lend themselves to classification. An example of this occurs in monochorionic twin gestations that are at risk for developing twin-twin transfusion syndrome, in which one twin (the donor) pumps a portion of its blood to the other twin (the recipient) through anomalous placental vascular anastomoses. The donor twin often develops significant anemia, growth restriction, and severe oligohydramnios, whereas the recipient twin becomes plethoric, congested, and edematous. The recipient twin is at profound risk for developing cardiac failure and subsequent hydrops

fetalis (please refer to other portions of this text for further information on this condition).

Pathologic growth that is the end result of inadequate nutrient and oxygen delivery to the fetus through the uteroplacental unit is attributed to uteroplacental insufficiency (UPI). Owing to the broad range of causes of IUGR, and because the major cause of IUGR is UPI, the remainder of this section will focus on IUGR of UPI etiology. It is important to remember that UPI is a terminal condition with a multifactorial etiology. A number of conditions can lead to UPI, and growth restriction as a result. These can be divided into placental and maternal disorders. Examples of placental causes include placental abruption of a chronic nature, placenta previa, mosaicism (e.g., localized placental trisomy 16), marginal or velamentous cord insertion, and primary placental disorders. Maternal etiologies can include behavioral states, such as smoking and cocaine abuse, and any chronic medical condition that affects systemic oxygenation or vasculature, and therefore also afflicts uteroplacental circulation and oxygen delivery: chronic lung disease (chronic obstructive pulmonary disease, emphysema), pre-existing diabetes mellitus, chronic hypertension, collagen vascular disorders (e.g., systemic lupus erythematosus), acquired thrombophilias (e.g., antiphospholipid antibody syndrome [APAS]), and inherited thrombophilias (e.g., Factor V Leiden or prothrombin 20210A mutation). The end result of all of these conditions is poor placentation, with a resultant reduction in placental blood flow or chronic hypoxemia.

### **Pathophysiology**

The development of an adequate interface between the maternal and fetal circulations at the level of the placenta is vital to proper fetal growth, because a poor interface does not allow for adequate nutrient and oxygen delivery, nor for adequate removal of fetal metabolic wastes. As explained earlier, factors that affect any component of this interface can alter placental development, and thus fetal growth, in a detrimental fashion.

Placental development is an ongoing process throughout gestation, with key developments occurring in each trimester. The first trimester is marked by placental attachment, angiogenesis, cellular transport mechanisms for glucose, amino acids, and fatty acids, and the onset of fetal cardiac activity to facilitate distribution and disposal of various substances between the maternal-fetal circulations.<sup>103</sup> A number of maternal adaptations start in the first trimester, including postprandial hyperglycemia, intravascular volume expansion, and relative refractoriness to vasoactive substances. The second trimester is characterized by trophoblastic invasion into the uterine spiral arteries and vascular remodeling, resulting in the development of a low-resistance circuit, a massive increase in total villous surface area vastly improving capacity for maternal-fetal exchange, and a significant increase in fetal cardiac output. A resultant exponential increase in placental size is matched by an exponential fetal growth spurt. Finally, in the third trimester, the fetus prepares for an eventual extrauterine existence; longitudinal growth, along with establishment of fetal stores, especially body fat, is key to this goal.

IUGR is primarily the result of disturbances in placental vascular development.<sup>103</sup> In early pregnancy, miscarriage



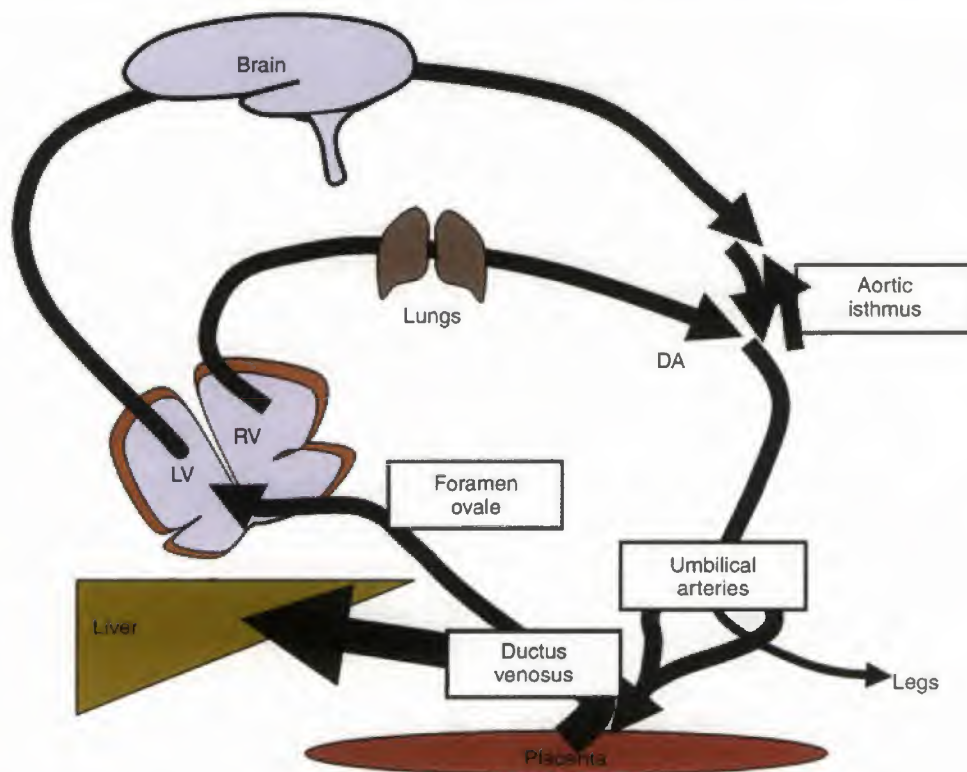


**FIGURE 7-22.** Fetoplacental blood flow. Note the presence of the ductus venosus, foramen ovale, and ductus arteriosus (DA) that are unique to the fetal circulation. LV, left ventricle; RV, right ventricle. (From Gabbe SG, Niebyl JR, Simpson JL: *Obstetrics: Normal and Problem Pregnancies*, 5th ed. Philadelphia, Churchill Livingstone, 2007.)

may result from inhibited angiogenesis and poor placental adherence. Later in gestation, inadequate trophoblastic invasion into the maternal spiral and radial arteries leads to the failure of establishment of a low-resistance circuit that is key to further fetal growth. As discussed earlier, a number of causes of IUGR exist. These conditions can affect the placenta directly, such as maternal placental floor infarcts and fetal villous obliteration, or may inhibit the maternal and fetal placental vascular flow, as in vaso-occlusive conditions (e.g., APAS). Stillbirth can occur in situations in which the insult is severe and early in onset, with inability for compensatory mechanisms to overcome the challenge. In cases in which compensation can initially occur and fetal survival is possible, one may yet encounter failure of adequate interval fetal growth in the second and third trimesters. In mild cases, only a relative reduction in fetal stores may be noticed at birth (i.e., a reduction in body fat and a reduction in the AC due to decreased hepatic glycogen stores), but in more severe cases, chronic hypoxia and metabolic acidosis may result, with possible profound implications for neonatal and later life.

The fetal response to UPI can be categorized into early and late cardiovascular adaptations that are relevant to sonographic assessment of fetal status (see later). Early adaptation is characterized by changes in blood flow to favor nutrient and oxygen distribution to essential organs, especially the brain (Fig. 7-22). Umbilical venous volume is reduced in early stages of UPI (persistent reduction in umbilical venous volume can lead to a diminished fetal blood volume, and hence reduced fetal renal perfusion; oligohydramnios can be

the end result).<sup>104</sup> This leads to greater diversion of the relatively nutrient- and oxygen-rich umbilical venous blood through the ductus venosus away from the liver and to the fetal heart; through the foramen ovale, this blood then enters the left side of the heart, and from there, moves on to the coronary and cerebral circulations.<sup>105,106</sup> Facilitating this shunting is an elevation in right ventricular afterload owing to the high resistance of the pulmonary vasculature as well as the rising placental resistance seen in UPI; a reduction in left ventricular afterload occurs as well owing to a drop in cerebral vascular resistance.<sup>107-111</sup> Thus, there is a relative increase in left ventricular cardiac output compared with the right.<sup>112,113</sup> Late changes occur with progressive UPI and increasing placental resistance with development of oligohydramnios. Cardiac output declines owing to the rising afterload, resulting in reduced forward flow. As a result, the ability to handle preload is also significantly diminished, leading to an elevated central venous pressure and inhibition in forward venous flow.<sup>114-118</sup> The final stage is global myocardial dysfunction and dilatation.<sup>119</sup> At this juncture, fetal acidosis is an ominous clinical finding. Holosystolic tricuspid insufficiency and spontaneous fetal heart rate decelerations herald impending death.<sup>119</sup>

### Short- and Long-Term Sequelae

As one might expect, fetuses with IUGR face a number of immediate challenges as neonates. When combined with prematurity, risks include increased mortality, necrotizing enterocolitis, and respiratory distress syndrome.<sup>120</sup> When



delivered at term, these neonates still face significant complications, including increased risk for mortality, transient tachypnea of the newborn, hypothermia (temperature  $<36^{\circ}\text{C}$ ), hypoglycemia, polycythemia, hyperviscosity, hyperbilirubinemia, and impaired immune function.<sup>121–128</sup> Although a significant number of moderately growth restricted fetuses go on to catch up in growth based on height and weight by 18 years of age, those fetuses that are below the 3rd percentile for birthweight have greater difficulty in doing so, and tend to have lower weight and shorter stature than their appropriate for GA (AGA) counterparts throughout childhood and adolescence.<sup>129,130</sup> It is clear that growth-restricted, prematurely born infants are at increased risk for neurodevelopmental abnormalities and cognitive impairment.<sup>131,132</sup> Term IUGR infants are also at risk for learning difficulties, behavioral problems, and worse school performance than term AGA children.<sup>130,131,133</sup>

Interestingly, it has been hypothesized that growth-restricted infants may be prone to developing adult disorders. Known as the fetal origins of adult disease, or the Barker hypothesis, the supposition is that a poor in utero environment leads to fetal maladaptive changes that persist into infancy, childhood, and adulthood. Although useful for survival in a relatively hostile intrauterine environment, these changes, predominantly vascular in nature, become detrimental in the long term. Conditions that have been attributed to IUGR include hypertension, stroke, diabetes mellitus, atherosclerosis/hypercholesterolemia, and obesity.<sup>134–137</sup> Although highly intriguing, definitive causality has not yet been established between IUGR and these conditions.

## Assessment of Fetal Status

Fetal status fundamentally refers to the state of fetal oxygenation and acid-base equilibrium. A clinical circumstance of UPI jeopardizes oxygen and nutrient delivery to the fetus, necessitating an adaptive response, as explained in part earlier. Fetal compromise occurs when there is failure of such a response, or when these adaptive mechanisms are overcome with ongoing and worsening UPI. With timely intervention, a fetus can be saved from injury and even death. The often difficult challenge that confronts the obstetrician is the necessity to balance the risks of injury and intrauterine fetal demise with prolongation of pregnancy in the setting of IUGR against those associated with potential iatrogenic prematurity. Thus, evaluating fetal status is crucial to proper management of the IUGR fetus.

Once a fetus is identified to be at-risk by an ultrasound-derived weight estimate below the 10th percentile for GA, and it is clear that UPI is the primary pathologic culprit, the obstetrician should initiate fetal surveillance. Traditional methods have included nonstress testing (a particular form of cardiotocography, called CTG), amniotic fluid measurement, and biophysical profiling. It is now clear that abnormalities in findings using these modalities are relatively late in occurrence, with fetal acidosis often being already present by the time of evaluation (see below, and Fig. 7–23A and B).<sup>103</sup> Placental insufficiency can be detected noninvasively with ultrasound imaging, and with the relatively recent development of Doppler ultrasound, even fetal acid-base status can be inferred. Once acidosis sets in, intrauterine demise may soon follow. Thus, a method to identify a preacidotic state in

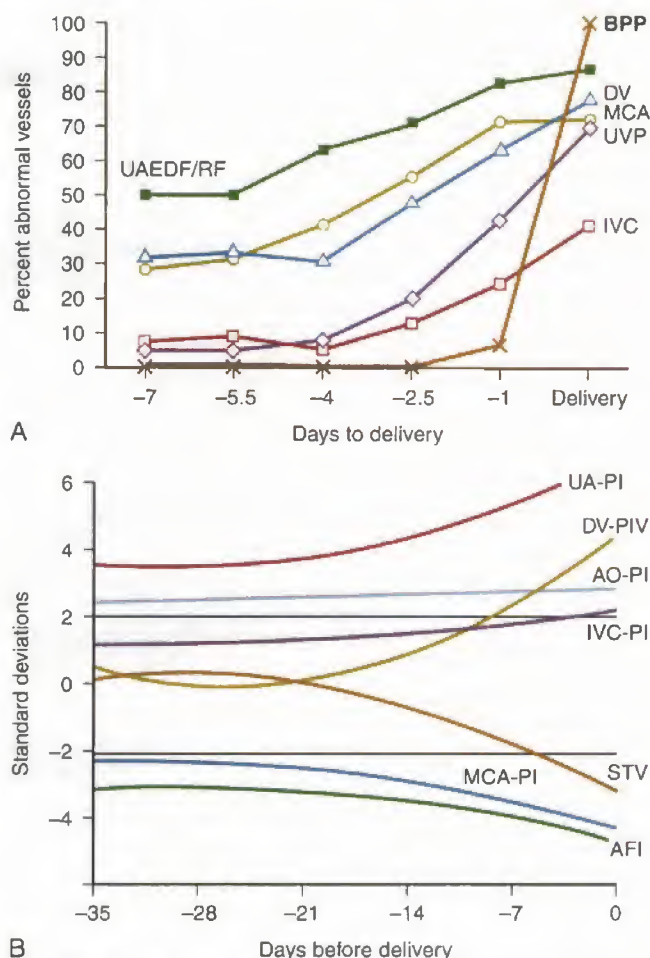


**FIGURE 7-23.** A. Timing of fetal responses to placental insufficiency. BPP, biophysical profile; DV, ductus venosus; IVC, inferior vena cava; MCA, middle cerebral artery; UAEDF/RF, umbilical artery end diastolic flow/reverse flow; UVP, umbilical venous pulsations. Note that numerous Doppler abnormalities occur before the onset of an abnormal BPP. B. Timing of fetal responses to placental insufficiency. Note that the timing of the loss of short-term variability on CTG correlates quite well with the onset of abnormal ductus venosus Doppler velocimetry. Thus, this is a direct link between a biophysical abnormality and abnormal ultrasound findings. Note also that worsening AFI (and therefore, development of, or worsening of, oligohydramnios) is a relatively late occurrence. AFI, amniotic fluid index; AO, aorta; DV, ductus venosus; IVC, inferior vena cava; MCA, middle cerebral artery; PI, pulsatility index; STV, short-term variability; UA, umbilical artery. (From Gabbe SG, Niebyl JR, Simpson JL: *Obstetrics: Normal and Problem Pregnancies*, 5th ed. Philadelphia, Churchill Livingstone, 2007)

an IUGR fetus becomes essential to have if one is to intervene in a timely fashion. The development of Doppler ultrasound has provided just such a tool.

## Doppler Velocimetry

Doppler ultrasound is based on the principle of the Doppler effect, so named for Johann Christian Doppler, who identified this occurrence in 1842. Simply put, when energy is reflected from a moving boundary, the frequency of the reflected energy varies in relation to the velocity of the moving boundary. In sonographic terms, the Doppler phenomenon depends upon the ability of an ultrasound beam to be



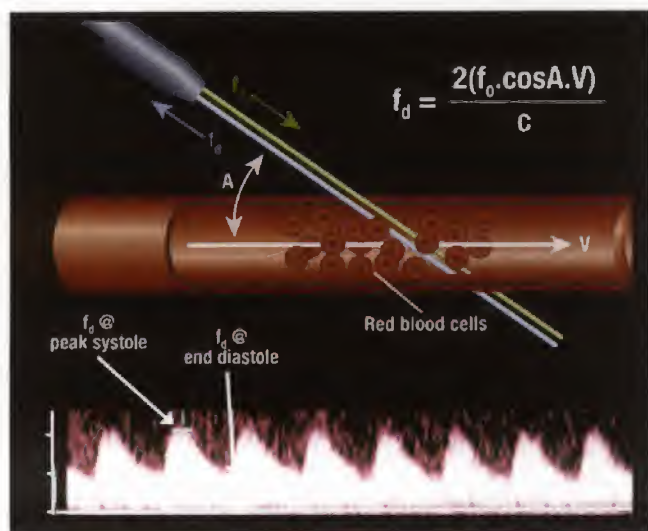


**FIGURE 7-24.** Doppler effect. The Doppler phenomenon depends upon the ability of an ultrasound beam to be changed in frequency when encountering a moving object, and in this circumstance, red blood cells. (From Abuhamad A: Does Doppler U/S improve outcomes in growth-restricted fetuses? *Contemporary Ob/Gyn* 48:56, 2003.)



**FIGURE 7-25.** Umbilical artery Doppler waveform, shown as velocity (V) versus time (t). S, systolic; D diastolic. Note that there is forward (positive) flow throughout the entire duration of the fetal cardiac cycle.

changed in frequency when encountering a moving object, and in this circumstance, red blood cells (Fig. 7-24) (see Chapter 22).

With interrogation of a blood vessel of interest, such as an umbilical artery, a characteristic waveform is generated (Fig. 7-25). In fact, as gestation advances and placental resistance declines in normal pregnancies, the umbilical artery Doppler waveform changes, reflecting a relatively greater and greater diastolic forward flow (Fig. 7-26). As one might surmise, in the setting of progressive UPI and elevated placental resistance, diastolic forward flow in the umbilical artery declines. Various Doppler indices exist to measure such placental resistance, and include S/D ratio, pulsatility index, and resistive index (Table 7-14). These measures are independent of the angle of insonation, because the generated waveform will reproduce both systolic and diastolic flows proportionately (Fig. 7-27A). Nonetheless, insonation of the vessel of interest as close to zero degrees as possible will yield a waveform with the most pronounced systolic and diastolic flows (Fig. 7-27B).

As explained earlier, UPI is associated with progressive worsening of placental resistance. This results in alterations in the maternal blood flow to the uteroplacental circuit, as well as fetal cardiovascular adaptive responses that can be

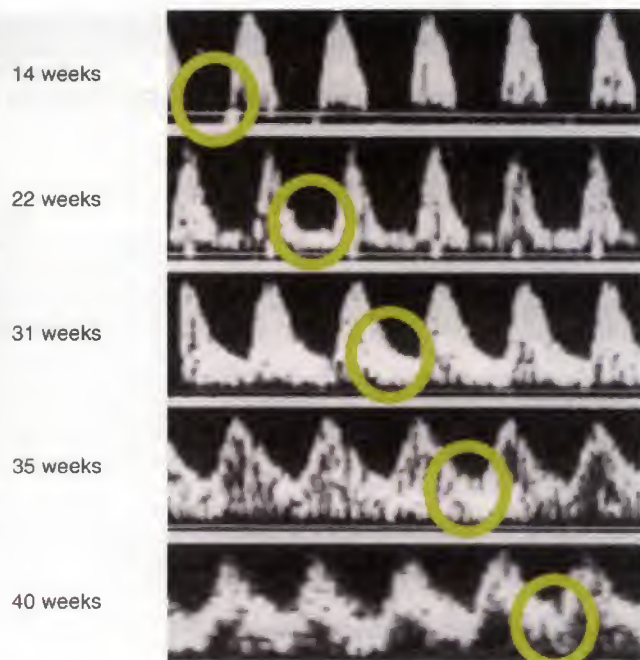


**FIGURE 7-26.** Normal umbilical artery Doppler waveform with advancing gestational age. Note the relative increase in diastolic forward flow with later gestational ages (and hence, a smaller S/D ratio with advancing age) as highlighted by the yellow circles. It is normal to have absent end-diastolic flow in the first and very early second trimesters.

detected by Doppler ultrasound of relevant vessels. Doppler interrogation of the fetal arterial system provides an indirect assessment of placental resistance, whereas the fetal venous system provides an assessment of the fetal cardiac function. By evaluating both fetal arterial and venous circulations, as well as the maternal uterine arteries, one can gauge the progression of UPI and IUGR well in advance of the development of oligohydramnios and fetal heart rate abnormalities.<sup>103</sup> Maternal evaluation can identify patients at risk for developing IUGR, pre-eclampsia, and placental abruption, whereas fetal evaluation can identify situations at risk for hypoxemia and acidosis based on the severity of Doppler findings.<sup>138,139</sup>

The earliest stages of placental pathology can be detected by the presence of diastolic notching in the maternal uterine arteries at 12 to 14 weeks' gestation, and when this persists beyond 24 weeks, it is highly reflective of abnormal placental resistance (Fig. 7-28A and B).<sup>140-142</sup> This has been associated with adverse pregnancy outcomes such as IUGR, placental abruption, and pre-eclampsia.<sup>143-145</sup> It has been observed by us that in circumstances of a lateralized placenta, a diastolic notch may appear only on the side ipsilateral to the placenta. On the fetal side, reduced umbilical artery end-diastolic velocity (EDV) can be seen when as little as 30% of the villous vessels are abnormal; with 70% abnormality, there can be complete absence (AEDV) or even reversal of umbilical artery end-diastolic velocity (REDV; Fig. 7-29).<sup>146,147</sup> Thus, with progressive worsening of UPI, the umbilical artery S/D ratio will become increasingly larger until it can no longer be calculated when there is AEDV. As previously mentioned, in early stages of UPI, fetal adaptive



**Table 7-14** Umbilical Artery Doppler Indices of Resistance

Gestational Age (Weeks)	Umbilical Artery Doppler (Resistive Index and Systolic: Diastolic Ratio)					
	Percentiles					
	5th		50th		95th	
	Resistive Index	Systolic: Diastolic Ratio	Resistive Index	Systolic: Diastolic Ratio	Resistive Index	Systolic: Diastolic Ratio
16	0.70	3.39	0.80	5.12	0.90	10.5
17	0.69	3.27	0.79	4.86	0.89	9.46
18	0.68	3.16	0.78	4.63	0.88	8.61
19	0.67	3.06	0.77	4.41	0.87	7.90
20	0.67	2.97	0.76	4.22	0.86	7.30
21	0.65	2.88	0.75	4.04	0.85	6.78
22	0.64	2.79	0.74	3.88	0.84	6.33
23	0.63	2.71	0.73	3.73	0.83	5.94
24	0.62	2.64	0.72	3.59	0.82	5.59
25	0.61	2.57	0.71	3.46	0.81	5.28
26	0.60	2.50	0.70	3.34	0.80	5.01
27	0.59	2.44	0.69	3.22	0.79	4.76
28	0.58	2.38	0.68	3.12	0.78	4.53
29	0.57	2.32	0.67	3.02	0.77	4.33
30	0.56	2.26	0.67	2.93	0.76	4.14
31	0.55	2.21	0.65	2.84	0.75	3.97
32	0.54	2.16	0.64	2.76	0.74	3.81
33	0.53	2.11	0.63	2.68	0.73	3.67
34	0.52	2.07	0.62	2.61	0.72	3.53
35	0.51	2.03	0.61	2.54	0.71	3.40
36	0.50	1.98	0.60	2.47	0.70	3.29
37	0.49	1.94	0.59	2.41	0.69	3.18
38	0.47	1.90	0.57	2.35	0.67	3.08
39	0.46	1.87	0.56	2.30	0.67	2.98
40	0.45	1.83	0.55	2.24	0.65	2.89
41	0.44	1.80	0.54	2.19	0.64	2.81
42	0.43	1.76	0.53	2.14	0.63	2.73

Note: Resistive index =  $0.97199 - 0.01045 \times \text{gestational age}$  ( $SD = 0.06078$ ); systolic: diastolic ratio =  $11(1 - \text{resistive index})$ .

Adapted from Kofinas AD, Espeland MA, Penry M, et al: Uteroplacental Doppler flow velocity waveforms in normal pregnancy: a statistical exercise and the development of appropriate reference values. *Am J Perinatol* 9:94, 1992.

mechanisms lead to increased left ventricular output and decreased cerebral resistance. Cerebral arteries such as the middle cerebral artery (MCA) of the circle of Willis are part of a high impedance vascular bed with low end-diastolic flow velocities (Fig. 7-30). The MCA is a representative vessel that can be easily interrogated with Doppler ultrasound. In UPI, the MCA EDV is increased, and thus the MCA is characterized by a lower S/D ratio than normal (Fig. 7-31A to C).<sup>148</sup> This finding is often referred to as "brain-sparing."<sup>103</sup> These early changes in fetal blood flow, with elevated umbilical artery S/D ratio and a reduced MCA S/D ratio, are seen in fetuses that are at risk for developing hypoxemia but are typically not associated with acidosis.<sup>149-151</sup>

As discussed earlier, in the situation of late fetal adaptation with advanced UPI, fetal cardiac function begins to fail and venous return begins to diminish. In this circumstance, Doppler assessment of the fetal venous circulation becomes necessary. Umbilical venous and portal circulations have waveforms that are steady and without pulsations. In contrast, central venous or precordial venous structures (ductus venosus, hepatic veins and the inferior vena cava [IVC]) have flow velocity waveforms that reflect central venous pressure changes characterized by triphasic wave-

forms (S, D, and *a* waves). The central venous waveforms are thus typically composed of systolic and diastolic peaks (S and D waves) that occur upon ventricular contraction and passive diastolic filling (Fig. 7-32).<sup>103</sup> A trough that occurs following the D wave, the *a* wave, is generated when there is a sudden increase in right atrial pressure due to the atrial contraction in late diastole and, as a result, an inhibition to venous return (see Fig. 7-32).<sup>103</sup> With severe right ventricular dysfunction, this atrial contraction can generate reverse flow along the venous system through the IVC, ductus venosus, and even into the umbilical vein in the most extreme circumstances in which the circulation is normally steady and without pulsations (Fig. 7-33A to C).<sup>103</sup> Venous back flow during atrial contraction (and hence a reversal in the *a* wave on Doppler interrogation) in the IVC and ductus venosus is most reflective of fetal metabolic acidemia as confirmed by percutaneous umbilical cord blood sampling (PUBS; see Fig. 7-33B).<sup>152,153</sup> These findings precede the holosystolic tricuspid insufficiency and ominous spontaneous fetal heart rate decelerations that portend impending death as described earlier.

The clinical utility of Doppler ultrasound should be obvious. The scientific literature shows that this sonographic

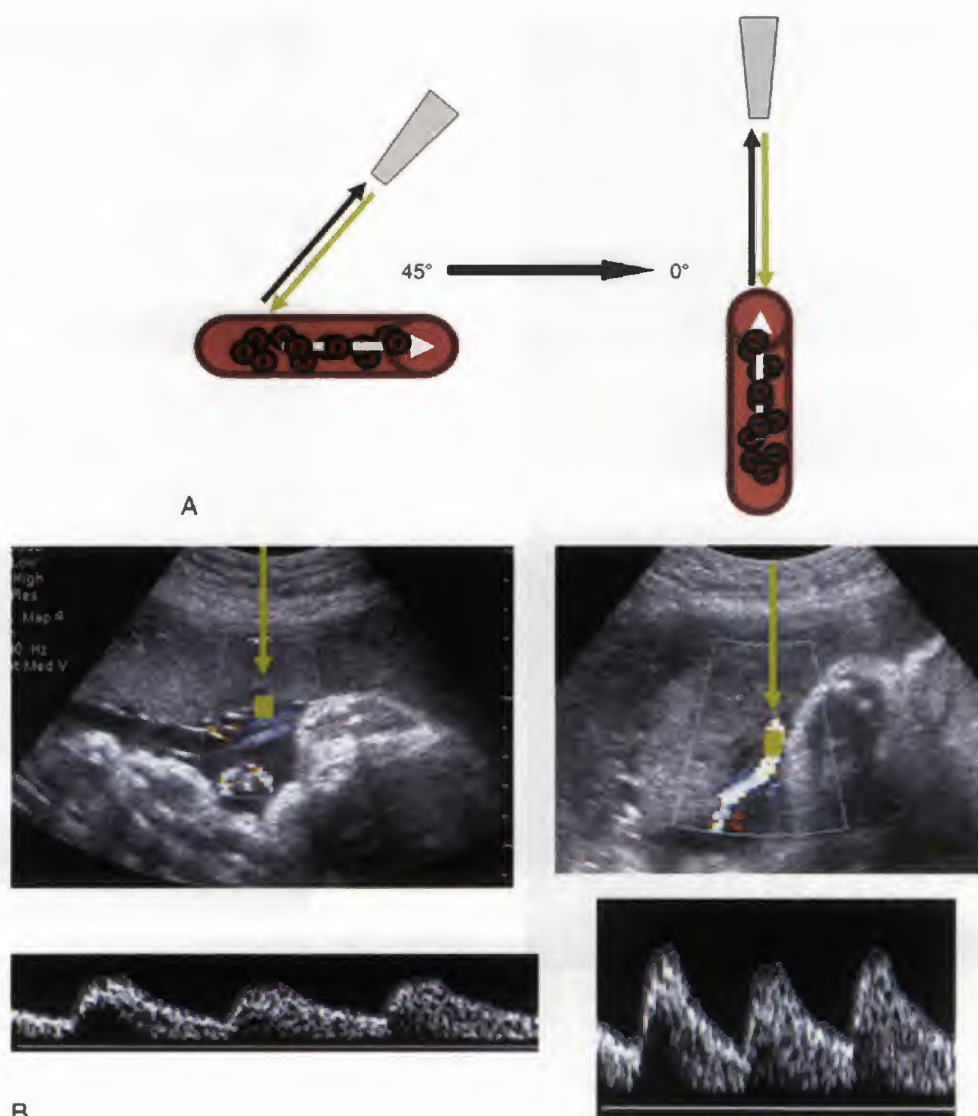


**FIGURE 7-27.** A. Angle of insonation in Doppler ultrasound. The frequency shift is directly proportional to the speed with which the RBCs are moving within a particular vessel and it is also dependent on the cosine of the angle the ultrasound beam makes with the blood vessel (as shown in the equation with Fig. 7-24). Ideally one should obtain an angle as close as possible to 0 degrees. (Courtesy John Hobbins, MD, University of Colorado Health Sciences Center, Denver, CO.) B. Angle of insonation in Doppler ultrasound. Note the difference in waveforms generated depending upon the insonation angle. On the image on the right the beam is parallel to the vessel and on the image on the left the beam is almost perpendicular to the vessel.

modality, when appropriately used, reduces not only mortality, but also morbidity. The finding of AEDV or REDV marks a pregnancy that is at an 80-fold increased risk for perinatal mortality, and when intervention is appropriately timed, a roughly 40% reduction in mortality can be achieved.<sup>154–157</sup> With the addition of venous Doppler assessment, the very preterm severely growth-restricted fetus can be better managed. Indeed, in 50% to 70% of cases, venous Doppler abnormalities occur before abnormal findings on fetal heart rate monitoring or biophysical profile (see Fig. 7-23A and B).<sup>158</sup> In circumstances in which there is a normal umbilical artery waveform and normal CTG testing, no fetuses have been shown to have hypoxemia/acidemia.<sup>159</sup> When there is abnormality in the umbilical artery waveform, and CTG remains normal, only 5% of fetuses have hypoxemia/acidemia. Finally, when there is

abnormality in both the umbilical artery Doppler velocimetry and CTG testing, 60% of fetuses can be found to have hypoxemia/acidemia by PUBS. Thus, the ideal time to deliver the IUGR fetus is before one sees abnormalities in the fetal heart rate tracing and only in the umbilical and venous circulations. A suggested algorithm for the management of the fetus with IUGR is shown in Figure 7-34.

## ACCELERATED FETAL GROWTH

Accelerated fetal growth is generally referred to as macrosomia or large for GA (LGA). Although they are not mutually exclusive of one another, macrosomia and LGA are defined differently. LGA was originally defined by neonatologists as a way of defining newborns who had birthweights that were greater than 90th percentile for a given GA. Obstetricians



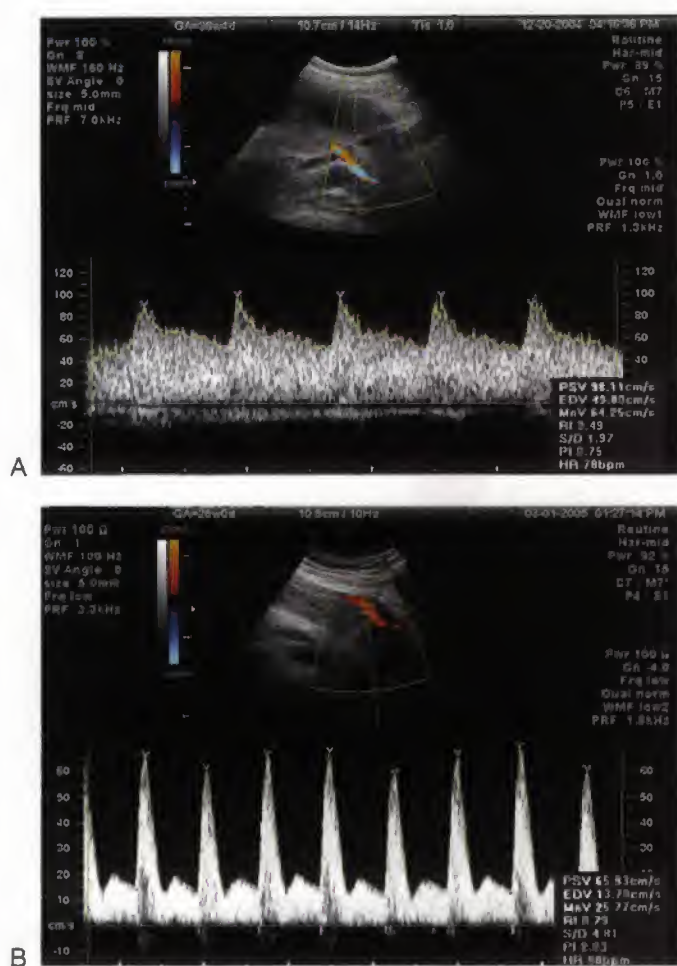


**FIGURE 7-28.** A. Normal uterine artery waveform. Note the lush flow during both maternal systole and diastole, and thus the low S/D ratio ( $< 2$ ). B. Abnormal uterine artery waveform. Note the diastolic notch and the relative reduction in diastolic flow (and thus, an abnormally elevated S/D ratio). (A and B Courtesy Wayne Persutte, PhD, RDMS, Platte River Perinatal Clinic, University of Colorado Health Sciences Center, Denver, CO.)

and perinatologists subsequently moved the use of LGA back in time into the prenatal period to describe the fetus who had an EFW greater than 90th percentile for GA. In contrast, macrosomia, refers to fetal growth as depicted by EFW that has surpassed a specific weight (either 4000 g or 4500 g) regardless of the GA. Many obstetricians define macrosomia as an EFW greater than 4000 g because this identifies a group at greater risk for maternal and fetal injury than fetuses weighing less than 4000 g. Although the ACOG supports either definition, they also cite the particularly sharply increased incidence of maternal and fetal injury with fetal weights greater than 4500 g.<sup>160</sup> From a clinical viewpoint, the important issue is that a clinician be consistent with the definition used personally in practice. The associated factors or causes of LGA or macrosomia include maternal obesity, pregestational and gestational diabetes, erythroblastosis fetalis and other causes of hydrops fetalis, prior macrosomic infant, and postdates pregnancy ( $> 42$  weeks). There are also nonchromosomal genetic syndromes (e.g., Beckwith-Weidemann syndrome) that make up a very small percentage of macrosomic infants that are seen clinically.

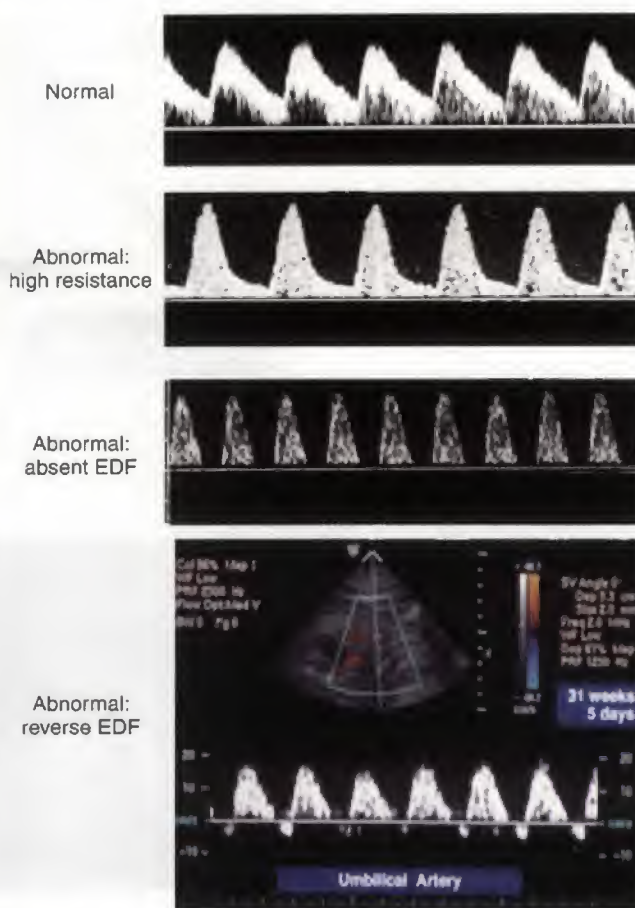


**FIGURE 7-29.** Appearance of umbilical artery waveform with progression of worsening uteroplacental insufficiency. This increase seen across gestation in diastolic flow is a result of the processes of branching angiogenesis at the end of the first trimester and beginning of the second, and nonbranching angiogenesis that starts at the end of the second trimester.

It is important to attempt to define the cause of a given LGA fetus antenatally, especially if the cause is gestational diabetes because intervention with either hypoglycemic agents or insulin can affect outcomes. However, the primary clinical concern with macrosomia is the risk of adverse events surrounding delivery, and this is particularly important clinically given that macrosomia complicates approximately 10% of all live births.<sup>161</sup> Ten percent is a sizable number when one considers that there are nearly 4 million births per year in the United States alone. Table 7-15 shows recent birthweight percentiles from 3.8 million deliveries occurring in 1991. Maternal adverse events include increased risks of postpartum hemorrhage, sphincter and rectal lacerations, and a twofold increased risk of cesarean delivery.<sup>159-163</sup> Although maternal injury is important, fetal injury associated with shoulder dystocia accounts for a significant percentage of obstetric litigation. Fetal trauma may result in brachial plexus injury (C5 and C6 injury—Erb-Duchenne palsy), clavicular fracture, humeral fracture, hypoxic-ischemic encephalopathy, and death.<sup>164</sup> Because cesarean section can obviate the adverse events associated with macrosomia,



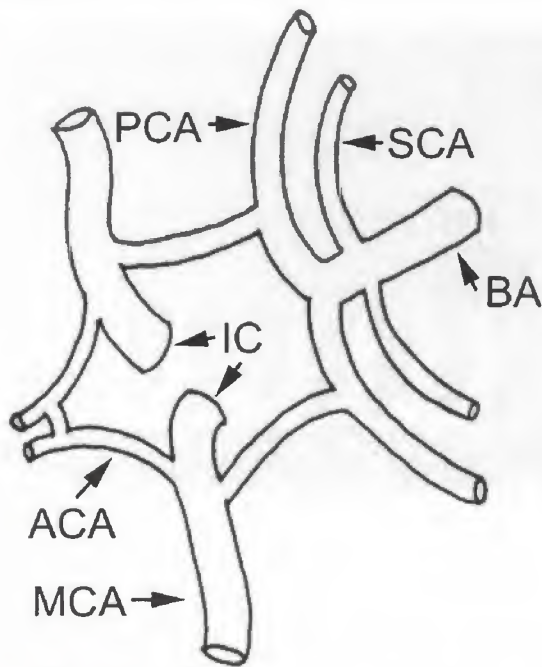


**FIGURE 7-30.** Circle of Willis. The Circle of Willis is supplied by the internal carotid and the vertebral arteries. It is made up by communicating vessels between the posterior, middle and anterior cerebral arteries. The middle cerebral artery (MCA) carries 80% of cerebral blood flow. Of the cerebral vessels, the MCA is the most accessible to ultrasound. ACA, anterior cerebral artery; BA, basilar artery; IC, internal carotid artery; PCA, posterior cerebral artery; SCA, superior cerebellar artery. (From Veille JC, Hanson R, Tatum K, et al: Longitudinal quantitation of MCA blood flow in normal human fetuses. *AJOG* 169:1393, 1993.)

concerted efforts have been made to predict macrosomia antenatally in hopes of identifying at-risk pregnancies.

Available tools for diagnosing macrosomia antenatally include assessment of maternal risk factors, clinical examination of uterine size (fundal height), and ultrasound. However, prenatal diagnosis of macrosomia is often difficult even with the use of ultrasound given that 40% of these fetuses have no identifiable risk factors at birth.<sup>165</sup> The EFW is obtained from an equation that contains several fetal variables obtained from two-dimensional measurements with the AC, in general, being most heavily weighted in the formulas. Published studies to date have not been able to demonstrate the superiority of ultrasound based fetal weights over that of clinical estimates. One study comparing fetal weights derived by ultrasound, Leopold maneuvers, and maternal perception found no statistical differences between the three groups. Curiously, the maternal perception of fetal weight was closer to the actual weights than the other two methods.<sup>167-169</sup> Although a variety of fetal biometric parameters, indices, and ratios have been reported in an attempt to identify the macrosomic fetus, the best endpoint to use for the diagnosis of fetal macrosomia is the EFW, for which the accuracy is at best marginal. In nondiabetic patients, ultrasound measurements used to diagnose macrosomia carry a sensitivity up to 50%, a specificity of 99%, a positive predictive value of up to 44%, and a negative predictive value of 60% to 99%.<sup>170-175</sup> In spite of more than 45 published formulas for EFW, accurate diagnosis of macrosomia requires waiting until birth and

weighing the newborn. Benacerraf et al have shown that even when birthweight is greater than 4500 g, only half of these fetuses fell within 10% of the EFW by ultrasound. Furthermore, EFWs need to exceed 4800 g in order for 50% of the fetuses to reach the 4500 g macrosomic cutoff, or greater than 4700 g for 50% to be above 4000 g.<sup>170,176,177</sup>

Increased amniotic fluid volume can be seen in the large for GA and macrosomic fetus. The prevalence of polyhydramnios is higher in pregnancies of nondiabetic mothers with a LGA fetus than with a non-LGA fetus.<sup>178</sup> When the EFW is above the 90th percentile, LGA can be diagnosed with greater confidence in the presence of polyhydramnios.

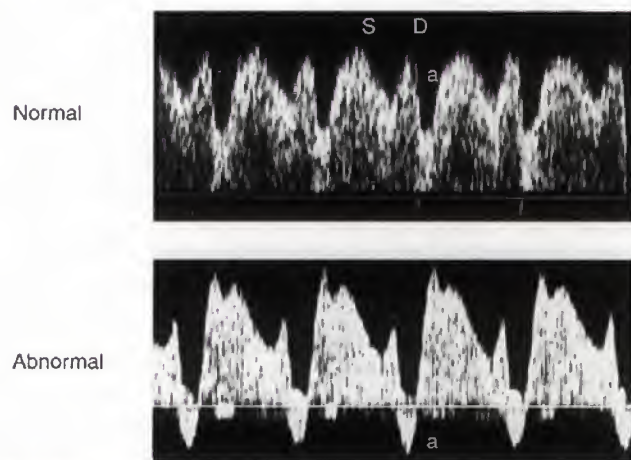
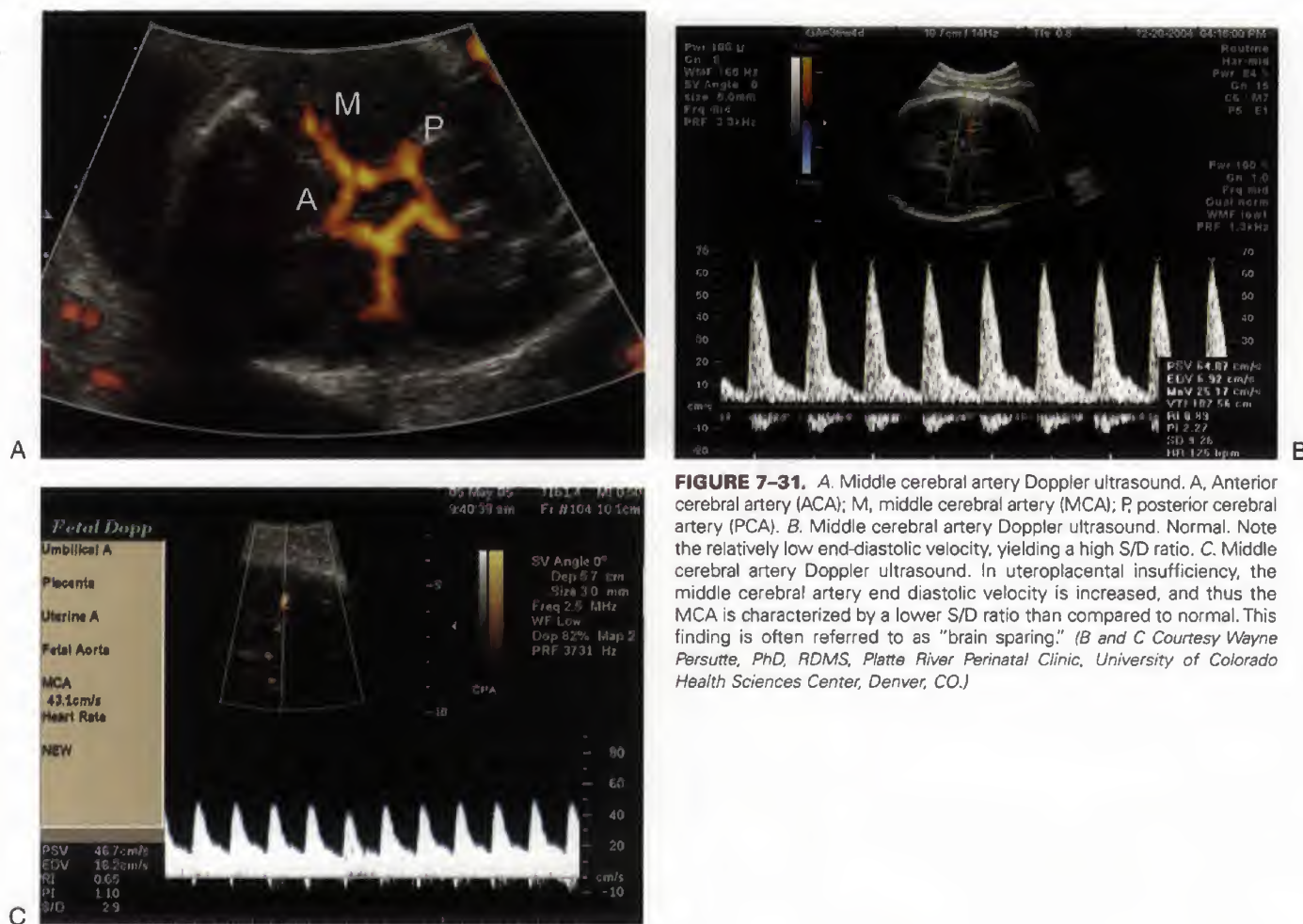
Although the incidence of shoulder dystocia in the general population has been reported to be up to 2.8%, the rate increases up to 9% in pregnancies complicated by gestational or preexisting diabetes.<sup>179</sup> The excess glycogen deposition that occurs in the diabetic pregnancy results in an overall larger torso with development of body to head disproportion. This leads to a larger than average shoulder girth with an increased risk for shoulder dystocia. The risk of shoulder dystocia is further increased when there is a macrosomic fetus in the diabetic patient. The rate of shoulder dystocia increases up to 23% with an EFW greater than 4000 g and up to 50% with an EFW greater than 4500 g. This has led obstetricians to perform elective cesarean sections for such patients to avoid shoulder dystocia. However, the risk of shoulder dystocia remains elevated in diabetic patients whose fetus may still be below 4000 g. This has lead individuals to investigate the utility of formulas using ultrasound parameters in predicting shoulder dystocia.<sup>180-182</sup> In the study by Cohen et al., 415 diabetic patients with an EFW between 3800 and 4200 g resulted in the occurrence of 31 shoulder dystocias. Using the formula of abdominal diameter (calculated as AC divided by 3.14) minus the BPD, if the value obtained was greater than 2.6, then there was a 30% shoulder dystocia rate and if the value was less than 2.6, then there was a 0% rate of shoulder dystocia. As such, the negative predictive value appears most useful. However, it must be kept in mind that the overall number of patients in this study and in others trying to predict shoulder dystocia, remain small.

In summary, birthweight assessment remains the only accurate way to diagnose the macrosomic infant. It is unfortunate that ultrasound remains unreliable for the prenatal detection of macrosomia. However, there may be some promise with the use of formulas such as that by Cohen et al.<sup>180</sup> for predicting shoulder dystocia in the diabetic patient. With the advent of three-dimensional ultrasound, perhaps volumetric measures will provide greater diagnostic accuracy for the prenatal diagnosis of macrosomia.

## INTERVAL FETAL GROWTH AND GROWTH POTENTIAL

Once fetal age has been firmly established, the determination of fetal growth becomes necessary in the high-risk pregnancy. As discussed earlier, various conditions and disorders predispose the fetus to poor or accelerated fetal growth. These conditions may be pre-existing in the mother (e.g., chronic hypertension, collagen vascular diseases, and APAS) or may be gestational (e.g., gestational diabetes, multiple pregnancy, and velamentous cord insertion), thereby marking





such a pregnancy as being "high risk." In these circumstances, interval growth assessment becomes a necessary part of fetal surveillance. Inherent in determining interval growth is the necessity for at least two temporally spaced measurements of biometric parameters. Given that growth is continuous rather than sporadic, and that the identification of growth is limited by the technical capability of the ultrasound equipment used, the recommended interval between ultrasound evaluations of fetal growth is three weeks, because shorter intervals increase the likelihood of a false-positive diagnosis of abnormal growth.<sup>183,184</sup>

Traditional methods of determining abnormal growth involve sequential measurements of interval growth and comparison of these biometric parameters to GA based population tables as described above (see Tables 7-4 and 7-7 to 7-9). One can also use these biometric parameters to estimate a fetal weight, and use this in comparison with population-based fetal weight for any particular GA (see earlier, and Table 7-15). Growth curve standards derived from cross-sectional data depend upon the assumption that the sample studied is composed of a single group of normally

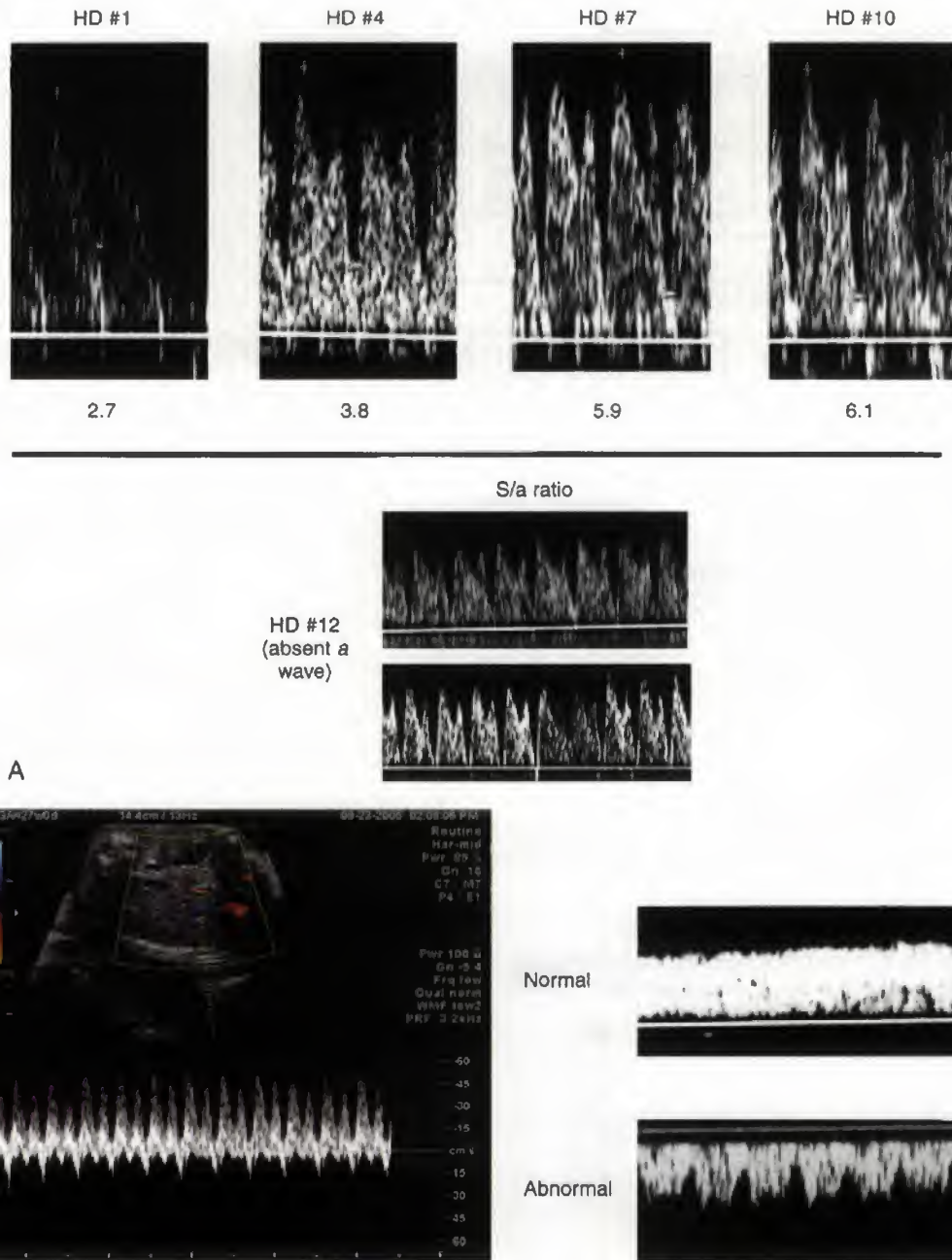


**FIGURE 7-33.** A. Progressive changes in the ductus venosus waveform with worsening uteroplacental insufficiency. Venous back flow during atrial contraction (and hence a reversal in the a wave on Doppler interrogation) in the IVC and ductus venosus is most reflective of fetal metabolic acidemia. Note the progression of diminishment of the a wave with each successive Doppler assessment. HD, hospital day. B. Abnormal ductus venosus waveform. Note the reversal in the a wave. (Courtesy Wayne Persutte, PhD, RDMS, Platte River Perinatal Clinic, University of Colorado Health Sciences Center, Denver, CO.) C. Normal and abnormal umbilical vein waveforms. With severe right ventricular dysfunction that occurs in progressive and severe UPI, the atrial contraction can generate reverse flow along the venous system through the IVC, ductus venosus, and even into the umbilical vein in the most extreme circumstances where the circulation is normally steady and without pulsations.



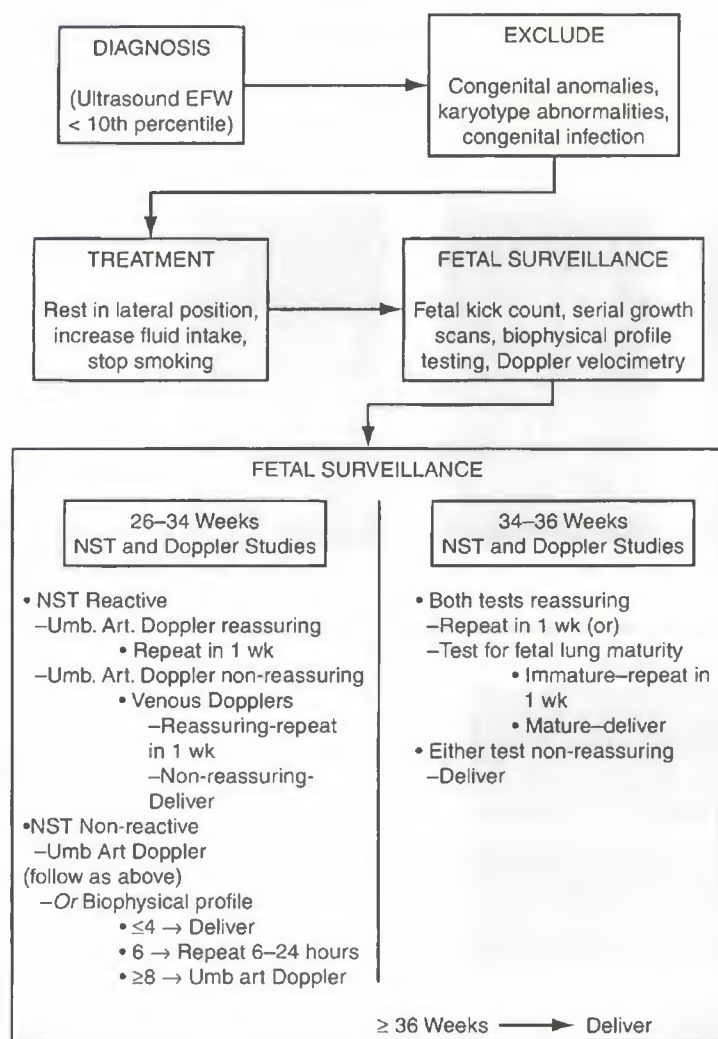


**FIGURE 7-34.** Suggested algorithm for the management of IUGR.

**Table 7-15** Birthweight Percentiles at Term in 1991

GA	50th	Birthweight (g) 90th	95th
37	3117	3755	3956
38	3263	3867	4027
39	3400	3980	4107
40	3495	4060	4185
41	3527	4094	4217
42	3522	4098	4213

GA, gestational age.

Modified from Alexander GR, Himes JH, Kaufmann RB, et al: A United States national reference for fetal growth. *Obstet Gynecol* 87:163, 1996.

growing fetuses having similar growth trajectories that show only random variation, and that the group is applicable to the clinical situation at hand. Using traditional cross-sectional methods, one assumes that a fetus initially measuring at the 15th percentile, that on remeasurement several weeks later, drops below the 10th percentile is a fetus at significant risk as opposed to one that remains at the 15th percentile, and

hence, is on its individual growth curve (Fig. 7-35). But what is one to do with the fetus that is determined to be anatomically and genetically normal but upon initial measurement is below the 10th percentile, for example, at the 8th percentile, and remains at the 8th percentile at several subsequent measurements performed at appropriate time intervals (Fig. 7-36)? If both parents are “small,” then one may assume that such a fetus is also constitutionally small, and the fact that the fetus maintains its growth percentile is reassuring. However, if the parents are both average or “large” in size, then even though such a fetus maintains its growth percentile, one may still have heightened concern for IUGR, and should initiate Doppler velocimetry assessment. One other circumstance to consider is the scenario in which, during fetal growth surveillance of a high risk pregnancy, one detects a fetus that is falling off its growth curve (i.e., crossing centiles) but remains above the 10th percentile at all times (e.g., goes from 50th percentile to 25th to the 15th percentile). Such a situation should also raise the level of concern, and such a fetus should heighten the frequency of surveillance, including the initiation of amniotic fluid assessment, regular CTG, and if appropriate, biophysical profiling. Doppler velocimetry has not been adequately

## NORMAL RANGE OF FETAL WEIGHT

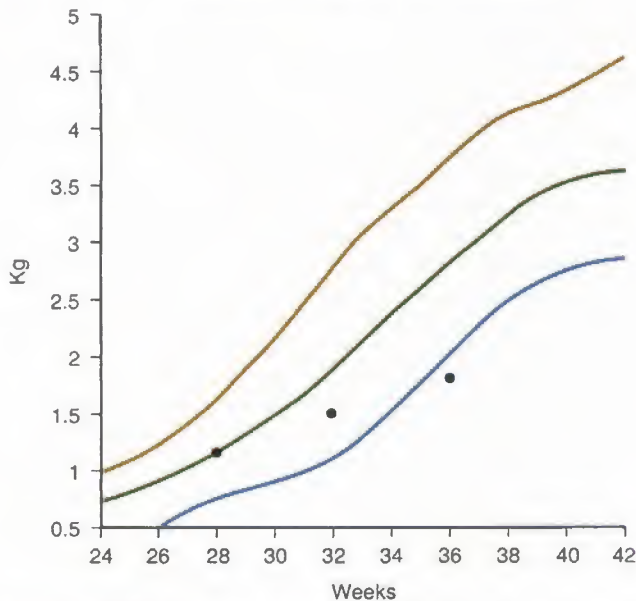


**FIGURE 7-35.** Fetal growth curve showing abnormal interval growth with crossing of centiles. Green line represents the mean, purple means 90th percentile, and blue means 10th percentile.

## NORMAL RANGE OF FETAL WEIGHT

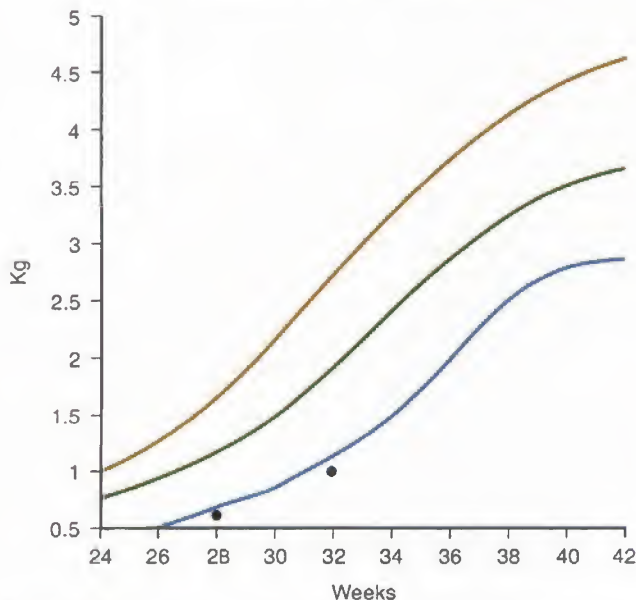


**FIGURE 7-36.** Fetal growth curve showing a constitutionally small fetus. The fetal weight at each gestational age is maintaining its own growth curve despite being less than the 10th percentile. Green line represents the mean, purple 90th percentile, and blue 10th percentile.

validated in fetuses that measure above the 10th percentile, and so may be used only with significant caution. In essence, a very small proportion of fetuses that measure above the 10th percentile for GA, and a sizable proportion of fetuses that measure below the 10th percentile, are truly pathologically growth-restricted (as a corollary, a similar case can

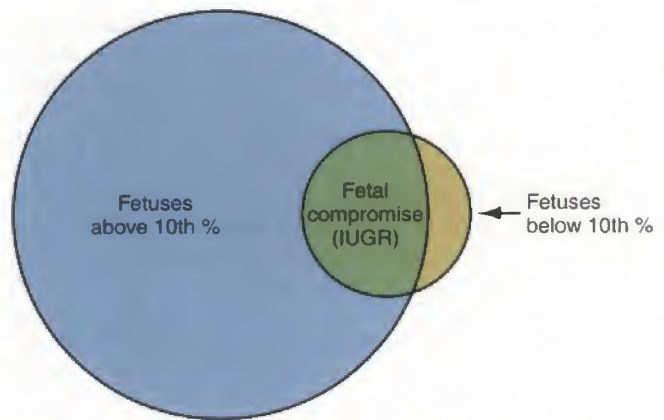


**FIGURE 7-37.** A very small proportion of fetuses that measure above the 10th percentile for gestational age, and a sizable proportion of fetuses that measure below the 10th percentile, are truly pathologically growth restricted (corresponding to the area demarcated "fetal compromise").

be made at the other end of the spectrum, when one is concerned with the large fetus). Figure 7-37 illustrates this graphically. Thus, the traditional method of identifying the potentially growth-restricted fetus may miss abnormally growing fetuses that are above the 10th percentile, and may falsely heighten concern regarding normally growing fetuses that happen to be below the 10th percentile.

Because of this limitation of population-based reference ranges to assess fetal growth, individualized growth models have been proposed by several investigators.<sup>185-187</sup> By defining a growth curve specific to a particular fetus, the obvious limitations of population-based growth charts can be eliminated. Two different methods have been described to generate individualized growth curves (IGCs). The first was developed by Rossavik, and is based on the premise that in a normal fetus, normal growth before 28 weeks' GA predicts the subsequent normal growth pattern for that particular fetus; thus, each individual fetus acts as its own control. Two scans are obtained between 14 and 27 weeks' GA, separated by an interval of at least 5 weeks, and are sufficient to generate an IGC for that particular fetus. Growth curves can be generated for each ultrasound parameter (e.g., HC, AC, FL) and for EFW.<sup>186,188-192</sup> A third and later scan is then necessary to determine whether the fetus is following its particular IGC. An extension of this method employing three-dimensional ultrasound has been proposed using fractional thigh volume measurements.<sup>193</sup> The premise of this technique is that human newborns have 15% body fat, which accounts for 46% of variance in birthweight. A significant correlation exists between fetal/neonatal limb volume and birthweight, so three-dimensional ultrasound scans of fractional thigh volume at at least two time points before 28 weeks' GA can be used to establish an individualized growth curve for a particular fetus. The Rossavik method has even been described for fetuses that are a part of a twin gestation.<sup>193</sup> The Rossavik method is limited by its dependency upon normal second trimester growth, and is useful in circumstances when a growth abnormality, if it is to occur, does so in the third trimester.

Because this approach is cumbersome in clinical practice by requiring three sets of scans, other models have been



developed that account for variables that contribute to the majority of the variance to newborn size. These include fetal gender, maternal weight at the first antenatal visit, height, ethnic group, and parity.<sup>187,194</sup> Gardosi et al describe the generation of customized antenatal longitudinal growth charts based on these parameters.<sup>187</sup> The estimated size of a fetus can thus be projected at term and estimated for any specific time point in gestation. Deviation from this projected growth pattern can be identified by serial sonographic biometric measurements. In a retrospective study of 4179 pregnancies, with adjusted centiles, 28% of babies conventionally designated SGA (<10th percentile) and 22% of those designated LGA (>90th percentile) were within normal limits for the pregnancy.<sup>187</sup> Conversely, 24% and 26% of babies identified as small or large, respectively, with adjusted centiles were missed by conventional unadjusted centile assessment. Using these customized charts, babies designated as SGA had higher perinatal morbidity and mortality than normally grown babies and than those defined as SGA by traditional cross-sectional, population-based curves.<sup>195,196</sup>

Although theoretically sound, the widespread use of individualized growth curves has not yet occurred, in part due to inadequate large-scale prospective evidence for improved perinatal outcomes and favorable cost-benefit ratios. Undoubtedly, such data will be forthcoming in the not-too-distant future. A number of questions remain with regard to IGCs. These questions will need to be thoroughly addressed before widespread adoption and replacement of traditional methods can become possible:

1. Should all fetuses undergo individualized or customized growth curve development?
2. How much of a deviation from an individualized growth curve is important for any given fetus?
3. When should Doppler ultrasound surveillance be initiated?
4. What of multiple gestations, especially those prone to non-UPI causes of IUGR, for example, monochorionic gestations?
5. Do there need to be gender- or ethnicity-specific modifications to the Rossavik formula for development of a more clinically relevant individualized growth curve (i.e., is there a need to integrate the Gardosi and Rossavik models)?

## CONCLUSIONS

1. Biometric estimates of age infer age from size and are, therefore, less accurate as pregnancy progresses because of biologic variability in fetal size and associated measurement errors. This increase in variability is relatively constant at 8% when expressed as a percentage of the estimate.
2. If age is known unequivocally by conceptional data, the age is established (menstrual age = conceptional age + 14 days) and should usually not be changed based on ultrasound measurements.
3. If a patient's menstrual dates are in question or not known, the patient should be seen for biometric dating early in pregnancy. The highest accuracy is obtained in the first trimester by CRL (2 SD = 8% of the estimate). However, little is lost in dating accuracy if one waits

until the uterine size suggests 18 weeks and a large amount of ancillary information is gained. For example, if a CRL obtained at 6 to 9 weeks' GA yields an EDD that is greater than 5 days off of that generated by conceptional dating (i.e., use of LMP), then one should defer assignment of the EDD and GA to the ultrasound. Subsequent ultrasound measurements become an index of growth rather than of age.

4. Beyond the first trimester of pregnancy, age estimates should be based on the multiple parameter technique, preferably before 20 weeks. The optimal combination of parameters is based on HC and FL. For example, in circumstances in which first trimester ultrasound dating is unavailable, and if biometric parameters that are measured before 20 weeks' GA yield an EDD that is greater than 7 days off of that generated by conceptional dating, then one should defer assignment of the EDD and GA to the ultrasound. Subsequent ultrasound measurements become an index of growth rather than of age.
5. There is a point in pregnancy after which sole reliance on biometric parameters to date the pregnancy is invalid. After that point, the only information that can be reliably obtained from sonograms is the fetal weight and, by a follow-up study, whether the interval growth is normal. In this setting, the appearance time of the epiphyseal ossification centers (as well as other discussed maturation markers) can be used as an internal check on the accuracy of the biometric estimate of menstrual age.
6. SGA and IUGR have been confusingly used interchangeably. Although IUGR has been defined using a number of different criteria, including that for SGA, it is now generally a term reserved for the clinical circumstance of a fetus that is underachieving its growth potential. A number of criteria have been used to capture a fetal population most at risk for abnormal growth. Among those used to ascribe IUGR, the most common is an EFW less than the 10th percentile for GA.
7. The fetal response to UPI insufficiency can be categorized into early and late cardiovascular adaptations that are relevant to sonographic assessment of fetal status. Early adaptation is characterized by changes in blood flow to favor nutrient and oxygen distribution to essential organs, especially the brain. Late changes occur with progressive UPI and increasing placental resistance with development of oligohydramnios. The final stage is global myocardial dysfunction and dilatation. At this juncture, fetal acidosis is an ominous clinical finding. Holosystolic tricuspid insufficiency and spontaneous fetal heart rate decelerations herald impending death.
8. Once a fetus is identified to be at-risk by an ultrasound-derived weight estimate below the 10th percentile for GA, and it is clear that UPI is the primary pathologic culprit, fetal surveillance should be initiated. Traditional methods have included non-stress testing, amniotic fluid measurement, and biophysical profiling. It is now clear that abnormalities in findings using these modalities are relatively late in occurrence, with fetal acidosis often being already present by the time of evaluation. Placental insufficiency can be detected noninvasively with Doppler ultrasound, allowing one to identify a preacidotic state in an IUGR fetus. This is essential to preventing adverse



fetal outcomes because once acidosis sets in, permanent fetal injury and intrauterine demise may soon follow.

9. Doppler interrogation of the fetal arterial system provides an indirect assessment of placental resistance, whereas the fetal venous system provides an assessment of the fetal cardiac function. By evaluating both fetal arterial and venous circulations, as well as the maternal uterine arteries, one can gauge the progression of UPI and IUGR well in advance of the development of oligohydramnios and fetal heart rate abnormalities.
10. The earliest stages of placental pathology can be detected by the presence of diastolic notching in the maternal uterine arteries at 12 to 14 weeks' gestation, and when this persists beyond 24 weeks, it is highly reflective of abnormal placental resistance. With progressive worsening of UPI, the umbilical artery S/D ratio will become increasingly larger until it can no longer be calculated when there is AEDV. Reduced umbilical artery EDV can be seen when as little as 30% of the villous vessels are abnormal; with 70% abnormality, there can be complete absence or even reversal of umbilical artery EDV.
11. In early stages of UPI, fetal adaptive mechanisms lead to increased left ventricular output and decreased cerebral resistance. In UPI, the MCA EDV is increased, and thus, the MCA is characterized by a lower S/D ratio than normal. This finding is often referred to as "brain sparing." These early changes in fetal blood flow, with elevated umbilical artery S/D ratio and a reduced MCA S/D ratio are seen in fetuses that are at risk for developing hypoxemia, but are typically not associated with acidosis.
12. When there is abnormality in the umbilical artery waveform, and CTG remains normal, only 5% of fetuses have hypoxemia/acidemia. When there is abnormality in both the umbilical artery Doppler velocimetry and CTG testing, 60% of fetuses can be found to have hypoxemia/acidemia by PUBS. Thus, the ideal time to deliver the IUGR fetus is before one sees abnormalities in the fetal heart rate tracing and only in the umbilical and venous circulations.
13. The scientific literature shows that Doppler ultrasound reduces not only mortality, but also morbidity in the setting of IUGR. The finding of AEDV or REDV marks a pregnancy that is at an 80-fold increased risk for perinatal mortality, and when intervention is appropriately timed, a roughly 40% reduction in mortality can be achieved. With the addition of venous Doppler assessment, the very preterm severely growth-restricted fetus can be better managed before permanent fetal injury or death occurs.
14. Macrosomia and LGA are defined differently. LGA describes the fetus that has an EFW greater than 90th percentile for GA. In contrast, macrosomia, refers to fetal growth as depicted by EFW that has surpassed a specific weight regardless of the GA. The ACOG supports either 4000 or 4500 g as the criterion for macrosomia, and the organization cites the particularly sharply increased incidence of maternal and fetal injury with fetal weights greater than 4500 g.
15. The primary clinical concern with macrosomia is the risk of adverse events surrounding delivery. This is particularly important clinically given that macrosomia complicates approximately 10% of all live births. Maternal adverse events include increased risks of postpartum hemorrhage, sphincter and rectal lacerations, and a 2-fold increased risk of cesarean delivery. Fetal trauma associated with shoulder dystocia may result in brachial plexus injury (C5 and C6 injury - Erb-Duchenne Palsy), clavicular fracture, humeral fracture, hypoxic-ischemic encephalopathy and death.
16. Inherent in determining interval growth is the necessity for at least two temporally spaced measurements of biometric parameters. Given that growth is continuous rather than sporadic, and that the identification of growth is limited by the technical capability of the ultrasound equipment used, the recommended interval between ultrasound evaluations of fetal growth is 3 weeks, because shorter intervals increase the likelihood of a false-positive diagnosis of abnormal growth.

## References

1. Hadlock FP: Sonographic estimation of fetal age and weight. *Radiol Clin North Am* 28:39, 1990.
2. Beazley JM, Underhill RA: Fallacy of the fundal height. *BMJ* 4:404, 1970.
3. Alexander GR, de Caunes F, Hulsey TC, et al: Validity of postnatal assessments of gestational age: A comparison of the method of Ballard et al. and early ultrasonography. *Am J Obstet Gynecol* 167:891, 1992.
4. Matsumoto S, Nogami Y, Ohkuri S: Statistical studies on menstruation. A criticism on the definition of normal menstruation. *J Med Sci* 11:294, 1962.
5. Campbell S, Warsof SL, Little D, Cooper DJ: Routine ultrasound screening for the prediction of gestational age. *Obstet Gynecol* 65:613, 1985.
6. Waldenström U, Axelsson U, Nilsson S: A comparison of the ability of a sonographically measured biparietal diameter and the last menstrual period to predict the spontaneous onset of labor. *Obstet Gynecol* 76:33, 1990.
7. Benson CB, Doubilet PM: Sonographic prediction of gestational age: Accuracy of second- and third-trimester fetal measurements. *AJR Am J Roentgenol* 157:1275, 1991.
8. Benson CB, Doubilet PM: Fetal measurements: Normal and abnormal fetal growth. In Rumack CM, Wilson SR, Charboneau JW (eds): *Obstetric and Fetal Sonography*, 2nd ed. St. Louis, MO, Mosby-Year Book, 1998.
9. Doubilet PM, Greenes RA: Improved prediction of gestational age from fetal head measurements. *AJR Am J Roentgenol* 142:797, 1984.
10. Goldstein RB, Filly RA, Simpson G: Pitfalls in femur length measurements. *J Ultrasound Med* 6:203, 1987.
11. Hadlock FP, Deter RL, Carpenter RL, et al: The effect of head shape on the accuracy of BPD in estimating fetal gestational age. *AJR Am J Roentgenol* 137:83, 1981.
12. Hadlock FP, Deter RL, Harrist RB, et al: Fetal biparietal diameter: Rational choice of plane of section for sonographic measurement. *AJR Am J Roentgenol* 138:871, 1982.
13. Hadlock FP, Harrist RB, Deter RL, et al: Fetal femur length as a predictor of menstrual age: Sonographically measured. *AJR Am J Roentgenol* 138:875, 1982.
14. Hadlock FP, Deter RL, Harrist RB, et al: Fetal head circumference: Relation to menstrual age. *AJR Am J Roentgenol* 138:649, 1982.
15. Hadlock FP, Deter RL, Harrist RB, et al: Fetal abdominal circumference as a predictor of menstrual age. *AJR Am J Roentgenol* 139:367, 1982.
16. Hadlock FP, Harrist RB, Deter RL, et al: A prospective evaluation of fetal femur length as a predictor of gestational age. *J Ultrasound Med* 2:111, 1983.
17. Hadlock FP, Deter RL, Harrist RB, et al: A date-independent predictor of intrauterine growth retardation: Femur length/abdominal circumference ratio. *AJR Am J Roentgenol* 141:979, 1983.



18. Hadlock FP, Deter RL, Harrist RB, et al: Estimating fetal age: Computer-assisted analysis of multiple fetal growth parameters. *Radiology* 152:497, 1984.
19. Hadlock FP, Deter RL, Roecker E, et al: Relation of fetal femur length to neonatal crown-heel length. *J Ultrasound Med* 3:1, 1984.
20. Hadlock FP, Harrist RB, Shah Y, et al: The femur length/head circumference relation in obstetric sonography. *J Ultrasound Med* 3:439, 1984.
21. Hadlock FP, Harrist RB, Shah YP, et al: Estimating fetal age using multiple parameters: A prospective evaluation in a racially mixed population. *Am J Obstet Gynecol* 156:955, 1987.
22. Hadlock FP, Harrist RB, Martinez-Poyer J: How accurate is second trimester fetal dating? *J Ultrasound Med* 10:557, 1992.
23. Hadlock FP, Shah YP, Karon DJ, et al: Fetal crown-rump length: Reevaluation of relation to menstrual age (5-18 weeks) with high-resolution real-time US. *Radiology* 182:501, 1992.
24. Hadlock FP, Harrist RB, Martinez-Poyer J: Fetal body ratios in second trimester: A useful tool for identifying chromosomal abnormalities? *J Ultrasound Med* 11:81, 1992.
25. Hill LM, Guzick D, Thomas ML, et al: Fetal radius length: A critical evaluation of race as a factor in gestational age assessment. *Am J Obstet Gynecol* 161:193, 1989.
26. Hill LM, Guzick D, Rivello D, et al: The transverse cerebellar diameter cannot be used to assess gestational age in the small for gestational age fetus. *Obstet Gynecol* 75:329, 1990.
27. Hill LM, Guzick D, Hixson J, et al: Composite assessment of gestational age: A comparison of institutionally derived and published regression equations. *Am J Obstet Gynecol* 167:551, 1992.
28. Kurtz AB, Wapner RJ, Kurtz RJ, et al: Analysis of biparietal diameter as an accurate indicator of gestational age. *J Clin Ultrasound* 8:319, 1980.
29. Pedersen JF: Fetal crown-rump length measurement by ultrasound in normal pregnancy. *Br J Obstet Gynaecol* 89:926, 1982.
30. Ruvalo KA, Filly RA, Callen PW: Evaluation of fetal femur length for prediction of gestation age in a racially mixed obstetric population. *J Ultrasound Med* 6:417, 1987.
31. Reece EA, Scioscia AL, Green J, et al: Embryonic trunk circumference: A new biometric parameter for estimation of gestational age. *Am J Obstet Gynecol* 156:713, 1987.
32. Rose BL, Lamb FJ: Multiple simultaneous predictors of gestational age. An application of Bayes' theorem. *Am J Perinatol* 5:44, 1988.
33. Rossavik IK, Fishburne JI: Conceptional age, menstrual age, and ultrasound age: A second-trimester comparison of pregnancies of known conception date with pregnancies dated from the last menstrual period. *Obstet Gynecol* 73:243, 1989.
34. Amersi S, Grimes DA: The case against using ordinal numbers for gestational age. *Obstet Gynecol* 91:623, 1998.
35. Bernaschek G, Rendlstorfer R, Csaicsib P: Vaginal sonography versus serum human chorionic gonadotropin in early detection of pregnancy. *Am J Obstet Gynecol* 158:608, 1988.
36. Nyberg DA, Filly RA, Filho DL, et al: Abnormal pregnancy: Early diagnosis by US and serum chorionic gonadotropin levels. *Radiology* 158:393, 1986.
37. Daya S, Woods S, Ward S, et al: Early pregnancy assessment with transvaginal ultrasound scanning. *Can Med Assoc J* 144:441, 1991.
38. Yeh HC, Rabinowitz JG: Amniotic sac development: Ultrasound features of early pregnancy—the double bleb sign. *Radiology* 167:97, 1988.
39. Selbing A: Gestational age and ultrasonic measurement of gestational sac, crown-rump length and biparietal diameter during first 15 weeks of pregnancy. *Acta Obstet Gynecol Scand* 61:233, 1982.
40. Goldstein I, Zimmer EA, Tamir A, et al: Evaluation of normal gestational sac growth: Appearance of embryonic heartbeat and embryo body movements using the transvaginal technique. *Obstet Gynecol* 77:885, 1991.
41. Warren WB, Timor-Tritsch I, Peisner DB, et al: Dating the early pregnancy by sequential appearance of embryonic structures. *Am J Obstet Gynecol* 161:747, 1989.
42. Hellman LM, Kobayashi M, Fillisti L, et al: Growth and development of the human fetus prior to the twentieth week of gestation. *Am J Obstet Gynecol* 103:789, 1969.
43. Nyberg DA, Filly RA, Mahony BS, et al: Early gestation: Correlation of HCG levels and sonographic identification. *AJR Am J Roentgenol* 144:951, 1985.
44. de Crespigny LC, Cooper D, McKenna M: Early detection of intrauterine pregnancy with ultrasound. *J Ultrasound Med* 7:7, 1988.
45. Batzer IR, Weiner S, Corson SL, et al: Landmarks during the first forty-two days of gestation demonstrated by the beta-subunit of human chorionic gonadotropin and ultrasound. *Am J Obstet Gynecol* 146:973, 1983.
46. Sauerbrei E, Cooperberg PL, Poland BJ: Ultrasound demonstration of the normal fetal yolk sac. *J Clin Ultrasound* 8:217, 1980.
47. Moore K: *The Beginning of Development: The First Week*, 3rd ed. Philadelphia, WB Saunders, 1982.
48. Nyberg DA, Laing FC, Filly RA, et al: Ultrasonographic differentiation of the gestational sac of early intrauterine pregnancy from the pseudogestational sac of ectopic pregnancy. *Radiology* 146:755, 1983.
49. Yeh HC, Goodman JD, Carr L, et al: Intradecidual sign: A US criterion of early intrauterine pregnancy. *Radiology* 161:463, 1986.
50. Cadkin AV, McAlpin J: The decidual-chorionic sac: A reliable sonographic indicator of intrauterine pregnancy prior to detection of a fetal pole. *J Ultrasound Med* 3:539, 1984.
51. Robinson HP: Sonar measurement of fetal crown-rump length as means of assessing maturity in first trimester of pregnancy. *BMJ* 4:281, 1973.
52. Robinson HP, Fleming JE: A critical evaluation of sonar "crown-rump length" measurements. *Br J Obstet Gynaecol* 82:702, 1975.
53. Drumm JE, Clinch J, MacKenzie G: The ultrasonic measurement of fetal crown-rump length as a method of assessing gestational age. *Br Obstet Gynaecol* 83:417, 1976.
54. Bovicelli L, Orsini LF, Rizzo N, et al: Estimation of gestational age during the first trimester by real-time measurement of fetal crown-rump length and biparietal diameter. *J Clin Ultrasound* 9:71, 1981.
55. Nelson LH: Comparison of methods for determining crown-rump measurement by real-time ultrasound. *J Clin Ultrasound* 9:67, 1981.
56. MacGregor SN, Tamura RK, Sabbagha RE, et al: Underestimation of gestational age by conventional crown-rump length dating curves. *Obstet Gynecol* 70:344, 1987.
57. Vollebbergh JH, Jongsma HW, van Dongen PW: The accuracy of ultrasonic measurement of fetal crown-rump length. *Eur J Obstet Gynecol Reprod Biol* 30:253, 1989.
58. Koornstra G, Wattel E, Exalto N: Crown-rump length measurements revisited. *Eur J Obstet Gynecol* 35:131, 1990.
59. Silva PD, Mahairas G, Schaper AM, et al: Early crown-rump length. A good predictor of gestational age. *J Reprod Med* 35:641, 1990.
60. Evans J: Fetal crown-rump length values in the first trimester based upon ovulation timing using the luteinizing hormone surge. *Br J Obstet Gynaecol* 98:48, 1991.
61. Deter RL, Buster JE, Casson PR, et al: Individual growth patterns in the first trimester: Evidence for difference in embryonic fetal growth rates. *Ultrasound Obstet Gynecol* 13:90, 1999.
62. Sladkevicius P, Saltvedt S, Almstrom H, et al: Ultrasound dating at 12-14 weeks of gestation: a prospective cross-validation of established dating formulae in *in-vitro* fertilized pregnancies. *Ultrasound Obstet Gynecol* 26:504, 2006.
63. Kopta MM, May RR, Crane JP: A comparison of the reliability the estimated date of confinement predicted by crown-rump length and biparietal diameter. *Am J Obstet Gynecol* 145:562, 1983.
64. Persson PH, Weldner BM: Reliability of ultrasound fetometry estimating gestational age in the second trimester. *Acta Obstet Gynecol Scand* 65:481, 1986.
65. Shepard M, Filly RA: A standardized plane for biparietal diameter measurement. *J Ultrasound Med* 1:145, 1982.
66. Simpson GF, Filly RA: Comparison of fetal head circumference measurements using standard and long linear array transducer. *J Diagn Med Sonogr* 4:2, 1988.
67. Mahony BS, Filly RA: High-resolution sonographic assessment of the fetal extremities. *J Ultrasound Med* 3:489, 1984.
68. Abrams SL, Filly RA: Curvature of the fetal femur: A normal sonographic finding. *Radiology* 156:490, 1985.
69. Chinn DH, Filly RA, Callen PW: Ultrasonic evaluation of fetal umbilical and hepatic vascular anatomy. *Radiology* 144:153, 1982.
70. de Crespigny LC, Speirs AL: A new look at biparietal diameter Aust N Z J Obstet Gynaecol 29:26, 1989.
71. Kurtz AB, Needleman L: *Ultrasound Assessment of Fetal Age*, 2nd ed. Philadelphia, WB Saunders, 1988.
72. Gray DL, Songster GS, Parvin CA, et al: Cephalic index: A gestational age-dependent biometric parameter. *Obstet Gynecol* 74:600, 1989.
73. Law RG, MacRae KD: Head circumference as an index of fetal age. *J Ultrasound Med* 1:281, 1982.



74. Jeanty P, Rodesch F, Delbeke D, et al: Estimation of gestational age from measurements of fetal long bones. *J Ultrasound Med* 3:75, 1984.
75. Warda AH, Deter RL, Rossavik IK, et al: Fetal femur length: A critical reevaluation of the relationship to menstrual age. *Obstet Gynecol* 67:69, 1985.
76. Ott WJ: Accurate gestational dating. *Obstet Gynecol* 67:311, 1985.
77. Mayden KL, Tortora M, Berkowitz RL, et al: Orbital diameters. A new parameter for prenatal diagnosis and dating. *Am J Obstet Gynecol* 144:289, 1982.
78. Jeanty P, Canuraine F, Cousaert E, et al: The binocular distance. A new way to estimate fetal age. *J Ultrasound Med* 3:241, 1984.
79. Vinkesteyn AS, Mulder PG, Wladimiroff JW: Fetal transverse cerebellar diameter measurements in normal and reduced fetal growth. *Ultrasound Obstet Gynecol* 15:47, 2000.
80. Reece EA, Gabrielli S, Degennaro N, et al: Dating through pregnancy: a measure of growing up. *Obstet Gynecol Surv* 44:544, 1989.
81. ACOG Educational Bulletin #230. Assessment of fetal lung maturity. November 1996.
82. Reece EA, Goldstein I, Hobbins JC: Fundamentals of Obstetric and Gynecologic Ultrasound. Stamford, CT, Appleton and Lange, 1994.
83. Goldstein I, Lockwood C, Balanger K et al: Ultrasonographic assessment of gestational age with the distal femoral and proximal tibial ossification centers in the third trimester. *Am J Obstet Gynecol* 158:127, 1988.
84. Chinn DH, Bolding DB, Callen PW, et al: Ultrasonographic identification of fetal lower extremity epiphyseal ossification centers. *Radiology* 147:815, 1983.
85. Mahony B, Callen P, Filly RA: The distal femoral epiphyseal ossification centers in the assessment of third trimester menstrual age: Sonographic identification and measurement. *Radiology* 155:201, 1984.
86. Grannum PA, Berkowitz RL, Hobbins JC: The ultrasonic changes in the maturing placenta and their relation to fetal pulmonary maturity. *Am J Obstet Gynecol* 133:915, 1979.
87. Grannum PA, Hobbins JC: The placenta. *Radiol Clin North Am* 20:353, 1982.
88. Kazzi GM, Gross TL, Rosen MG, et al: The relationship of placental grade, fetal lung maturity, and neonatal outcome in normal and complicated pregnancies. *Am J Obstet Gynecol* 148:54, 1984.
89. Goldstein I, Lockwood C, Hobbins JC: Ultrasound assessment of fetal intestinal development in the evaluation of gestational age. *Obstet Gynecol* 70:682, 1987.
90. Shepard MJ, Richards VA, Berkowitz RL, et al: An evaluation of two equations for predicting fetal weight by ultrasound. *Am J Obstet Gynecol* 142:47, 1982.
91. Hadlock FP, Harrist RB, Fearnycough TC, et al: Use of femur length/abdominal circumference ratio in detecting the macrosomic fetus. *Radiology* 154:503, 1985.
92. Hadlock FP, Harrist RB, Sharman RS, et al: Estimation of fetal weight with the use of head, body, and femur measurements—a prospective study. *Am J Obstet Gynecol* 151:333, 1985.
93. Lubchenco LO, Hansman C, Dressler M, et al: Intrauterine growth as estimated from live born birth-weight data at 24 to 42 weeks of gestation. *Pediatrics* 37:403, 1967.
94. Brenner WE, Edelman DA, Hendricks CH: A standard of fetal growth for the United States of America. *Am J Obstet Gynecol* 126:555, 1976.
95. Alexander GR, Himes JH, Kaufmann RB, et al: A United States national reference for fetal growth. *Obstet Gynecol* 87:163, 1996.
96. Perrucha RA, Platt LD: Relationship of placental grade to gestational age. *Am J Obstet Gynecol* 144:733, 1982.
97. Rutherford SE, Phelan JP, Smith CV, et al: The four-quadrant assessment of amniotic fluid volume: An adjunct to antepartum fetal heart rate testing. *Obstet Gynecol* 70:353, 1987.
98. Zilianti M, Fernandez S: Correlation of ultrasonic images of fetal intestine with gestational age and fetal maturity. *Obstet Gynecol* 62:569, 1982.
99. Yarkoni S, Schmidt W, Jeanty P, et al: Clavicular measurement: A new biometric parameter for fetal evaluation. *J Ultrasound Med* 4:467, 1985.
100. Mercer BM, Sklar S, Shariatmadar A, et al: Fetal foot length as a predictor of gestational age. *Am J Obstet Gynecol* 156:350, 1987.
101. Hohler CW, Quetel TA: Comparison of ultrasound femur length and biparietal diameter in late pregnancy. *Am J Obstet Gynecol* 141:759, 1981.
102. Battaglia FC, Lubchenco LO: A practical classification of newborn infants by weight and gestational age. *J Pediatr* 71:159, 1967.
103. Baschat AA: Pathophysiology of fetal growth restriction: Implications for diagnosis and surveillance. *Obstet Gynecol Surv* 59(8):617, 2004.
104. Rigano S, Bozzo M, Ferrazzi E, et al: Early and persistent reduction in umbilical vein blood flow in the growth-restricted fetus: a longitudinal study. *Am J Obstet Gynecol* 185:834, 2001.
105. Bellotti M, Pennati G, De Gasperi C, et al: Simultaneous measurements of umbilical venous, fetal hepatic, and ductus venosus blood flow in growth-restricted human fetuses. *Am J Obstet Gynecol* 190:1347, 2004.
106. Kiserud T: The ductus venosus. *Semin Perinatol* 25:11, 2001.
107. Rizzo G, Capponi A, Chaoui R, et al: Blood flow velocity waveforms from peripheral pulmonary arteries in normally grown and growth-retarded fetuses. *Ultrasound Obstet Gynecol* 8:87, 1996.
108. Griffin D, Bilardo K, Masini L, et al: Doppler blood flow waveforms in the descending thoracic aorta of the human fetus. *Br J Obstet Gynaecol* 91:997, 1984.
109. Akalin-Sel T, Nicolaides KH, Peacock J, et al: Doppler dynamics and their complex interrelation with fetal oxygen pressure, carbon dioxide pressure, and pH in growth-retarded fetuses. *Obstet Gynecol* 84:439, 1994.
110. Wladimiroff JW, Tonge HM, Stewart PA: Doppler ultrasound assessment of cerebral blood flow in the human fetus. *Br J Obstet Gynaecol* 93:471, 1986.
111. Arbeille P, Maulik D, Fignon A, et al: Assessment of the fetal PO<sub>2</sub> changes by cerebral and umbilical Doppler on lamb fetuses during acute hypoxia. *Ultrasound Med Biol* 21:861, 1995.
112. Reed KL, Anderson CF, Shenker L: Changes in intracardiac Doppler flow velocities in fetuses with absent umbilical artery diastolic flow. *Am J Obstet Gynecol* 157:774, 1987.
113. Al Ghazali W, Chita SK, Chapman MG, et al: Evidence of redistribution of cardiac output in asymmetrical growth retardation. *Br J Obstet Gynaecol* 96:697, 1987.
114. Makikallio K, Jouppila P, Rasanen J: Retrograde net blood flow in the aortic isthmus in relation to human fetal arterial and venous circulations. *Ultrasound Obstet Gynecol* 19:147, 2002.
115. Rizzo G, Arduini D: Fetal cardiac function in intrauterine growth retardation. *Am J Obstet Gynecol* 165:876, 1991.
116. Rizzo G, Capponi A, Rinaldo D, et al: Ventricular ejection force in growth-retarded fetuses. *Ultrasound Obstet Gynecol* 5:247, 1995.
117. Gudmundsson S, Tulzer G, Huhta JC, et al: Venous Doppler in the fetus with absent end-diastolic flow in the umbilical artery. *Ultrasound Obstet Gynecol* 7:262, 1996.
118. Hecher K, Campbell S, Doyle P, et al: Assessment of fetal compromise by Doppler ultrasound investigation of the fetal circulation. Arterial, intracardiac, and venous blood flow velocity studies. *Circulation* 91:129, 1995.
119. Rizzo G, Capponi A, Pietropolli A, et al: Fetal cardiac and extracardiac flows preceding intrauterine death. *Ultrasound Obstet Gynecol* 4:139, 1994.
120. Bernstein IM, Horbar JD, Badger GJ, et al: Morbidity and mortality among very-low-birth-weight neonates with intrauterine growth restriction. The Vermont Oxford Network. *Am J Obstet Gynecol* 182:198, 2000.
121. Doctor BA, O'riordan MA, Kirchner HL, et al: Perinatal correlates and neonatal outcomes of small for gestational age infants born at term gestation. *Am J Obstet Gynecol* 185:652, 2001.
122. Kramer MS, Olivier M, McLean FH, et al: Impact of intrauterine growth retardation and body proportionality on fetal and neonatal outcome. *Pediatrics* 86:707, 1990.
123. Hakanson DO, Oh W: Hyperviscosity in the small-for-gestational age infant. *Biol Neonate* 37:109, 1980.
124. Ferguson AC: Prolonged impairment of cellular immunity in children with intrauterine growth retardation. *J Pediatr* 93:52, 1978.
125. Williams RL, Creasy RK, Cunningham GC, et al: Fetal growth and perinatal viability in California. *Obstet Gynecol* 59:624, 1982.
126. Wennergren M, Wennergren G, Vilbergsson G: Obstetric characteristics and neonatal performance in a four-year small for gestational age population. *Obstet Gynecol* 72:615, 1988.
127. Piper JM, Xenakis EM, McFarland M: Do growth-retarded premature infants have different rates of perinatal morbidity and mortality than appropriately grown premature infants? *Obstet Gynecol* 87:169, 1996.



128. Kok JH, den Ouden AL, Verloove-Vanhorick SP, et al: Outcome of very preterm small for gestational age infants: the first nine years of life. *Br J Obstet Gynaecol* 105:162, 1998.
129. Karlberg J, Albertsson-Wikland K: Growth in full-term small-for-gestational-age infants: from birth to final height. *Pediatr Res* 38:733, 1995.
130. Paz I, Seidman DS, Danon YL, et al: Are children born small for gestational age at increased risk of short stature? *Am J Dis Child* 147:337, 1993.
131. Yanney M, Marlow M: Paediatric consequences of fetal growth restriction. *Semin Neonatol* 9:411, 2004.
132. McCarton, CM, Wallace, IF, Divon, M, et al: Cognitive and neurologic development of the premature, small for gestational age infant through age 6: comparison by birth weight and gestational age. *Pediatrics* 98:1167, 1996.
133. O'Keeffe, MJ, O'Callaghan, M, Williams, GM, et al: Learning, cognitive, and attentional problems in adolescents born small for gestational age. *Pediatrics* 112:301, 2003.
134. Barker, DJP: Early growth and cardiovascular disease. *Arch Dis Child* 80:305, 1999.
135. Barker, DJP: Fetal origins of coronary heart disease. *BMJ* 311:171, 1995.
136. Barker, DJ, Osmond, C, Simmonds, SJ, et al: The relation of small head circumference and thinness at birth to death from cardiovascular disease in adult life. *BMJ* 306:422, 1993.
137. Sallout B, Walker M: The fetal origin of adult diseases. *J Obstet Gynaecol* 23:555, 2003.
138. Weiner CP: The relationship between the umbilical artery systolic/diastolic ratio and umbilical blood gas measurements in specimens obtained by cordocentesis. *Am J Obstet Gynecol* 162:1198, 1990.
139. Bilardo CM, Nicolaides KH, Campbell S: Doppler measurements of fetal and uteroplacental circulations: relationship with umbilical venous blood gases measured at cordocentesis. *Am J Obstet Gynecol* 162:115, 1990.
140. Meekins JW, Pijnenborg R, Hanssens M, et al: A study of placental bed spiral arteries and trophoblast invasion in normal and severe pre-eclamptic pregnancies. *Br J Obstet Gynaecol* 101:679, 1994.
141. Harrington K, Carpenter RG, Goldfrad C, et al: Transvaginal Doppler ultrasound of the uteroplacental circulation in the early prediction of pre-eclampsia and intrauterine growth retardation. *Br J Obstet Gynaecol* 104:674, 1997.
142. Bower S, Bozzo M, Ferrazzi E, et al: Early and persistent reduction in umbilical vein blood flow in the growth-restricted fetus: a longitudinal study. *Am J Obstet Gynecol* 185:834, 2001.
143. Griffin D, Cohen-Overbeek T, Campbell S: Fetal and utero-placental blood flow. *Clin Obstet Gynaecol* 10:565, 1983.
144. Bower S, Bewley S, Campbell S: Improved prediction of preeclampsia by two-stage screening of uterine arteries using the early diastolic notch and color Doppler imaging. *Obstet Gynecol* 82:78, 1993.
145. Papageorgiou AT, Yu CK, Bindra R, et al: Fetal Medicine Foundation Second Trimester Screening Group: Multicenter screening for pre-eclampsia and fetal growth restriction by transvaginal uterine artery Doppler at 23 weeks of gestation. *Ultrasound Obstet Gynecol* 18:441, 2001.
146. Giles WB, Trudinger BJ, Baird PJ: Fetal umbilical artery flow velocity waveforms and placental resistance: pathological correlation. *Br J Obstet Gynaecol* 92:31, 1985.
147. Morrow RJ, Adamson SL, Bull SB, et al: Effect of placental embolization on the umbilical artery velocity waveform in fetal sheep. *Am J Obstet Gynecol* 161:1055, 1989.
148. Wladimiroff JW, Tonge HM, Stewart PA: Doppler ultrasound assessment of cerebral blood flow in the human fetus. *Br J Obstet Gynaecol* 93:471, 1986.
149. Akalin-Sel T, Nicolaides KH, Peacock J, et al: Doppler dynamics and their complex interrelation with fetal oxygen pressure, carbon dioxide pressure, and pH in growth-retarded fetuses. *Obstet Gynecol* 84:439, 1994.
150. Arceille P, Maulik D, Fignon A, et al: Assessment of the fetal PO<sub>2</sub> changes by cerebral and umbilical Doppler on lamb fetuses during acute hypoxia. *Ultrasound Med Biol* 21:861, 1995.
151. Baschat AA: Integrated fetal testing in growth restriction: combining multivessel Doppler and biophysical parameters. *Ultrasound Obstet Gynecol* 21:1, 2003.
152. Hecher K, Snijders R, Campbell S, et al: Fetal venous, intracardiac, and arterial blood flow measurements in intrauterine growth retardation: relationship with fetal blood gases. *Am J Obstet Gynecol* 173:10, 1995.
153. Rizzo G, Capponi A, Arduini D, et al: The value of fetal arterial, cardiac and venous flows in predicting pH and blood gases measured in umbilical blood at cordocentesis in growth retarded fetuses. *Br J Obstet Gynaecol* 102:963, 1995.
154. Thornton JG, Lilford RJ: Do we need randomized trials of antenatal tests of fetal well being? *Br J Obstet Gynaecol* 100:197, 1993.
155. Alfrevic Z, Neilson JP: Doppler ultrasonography in high-risk pregnancies: systematic review with meta-analysis. *Am J Obstet Gynecol* 172:1379, 1995.
156. Divon MY: Umbilical artery Doppler velocimetry: clinical utility in high-risk pregnancies. *Am J Obstet Gynecol* 174:10, 1996.
157. Giles W, Bisits A: Clinical use of Doppler ultrasound in pregnancy: information from six randomised trials. *Fetal Diagn Ther* 8:247, 1993.
158. Romero R, Kalache KD, Kadar N: Timing the delivery of the pre-term severely growth-restricted fetus: venous Doppler, cardiotocography on the biophysical profile? Opinion in *Ultrasound Obstet Gynecol* 19:118, 2002.
159. Ferrazzi E, Bulfamante G, Mezzopane R, et al: Uterine Doppler velocimetry and placental hypoxic-ischemic lesion in pregnancies with fetal intrauterine growth restriction. *Placenta* 20:389, 1999.
160. Fetal Macrosomia. American College of Obstetricians and Gynecologists Practice Bulletin. Clinical management Guidelines for Obstetrician-Gynecologists. Number 22, November 2000.
161. Ventura SJ, Martin JA, Curtin SC, et al: Births: final data for 1998. *Natl Vital Stat Rep* 48:1, 2000.
162. Gherman RB, Goodwin TM, Souter I, et al: The McRoberts' maneuver for the alleviation of shoulder dystocia: how successful is it? *Am J Obstet Gynecol* 176:656, 1997.
163. Bérard J, Dufour P, Vinatier D, et al: Fetal macrosomia : risk factors and outcome. A study of the outcome concerning 100 cases >4500g. *Eur J Obstet Gynecol Reprod Biol* 77:51, 1998.
164. Shoulder Dystocia. American College of Obstetricians and Gynecologists Practice Bulletin. Clinical management Guidelines for Obstetrician-Gynecologists. Number 40, November 2002.
165. Boyd ME, Usher RH, McLean FH: Fetal macrosomia prediction, risks, proposed management. *Obstet Gynecol* 61:715, 1983.
166. Chauhan SP, Cowan BD, Magann EF, et al: Intrapartum detection of a macrosomic fetus: clinical versus 8 sonographic models. *Aust N Z J Obstet Gynaecol* 35:267, 1995.
167. Johnstone FD, Prescott RJ, Steel JM, et al: Clinical and ultrasound prediction of macrosomia in diabetic pregnancy. *Br J Obstet Gynaecol* 103:747, 1996.
168. Chauhan SP, Hendrix NW, Magann EF, et al: Limitations of clinical and sonographic estimates of birth weight: experience with 1034 parturients. *Obstet Gynecol* 91:72, 1998.
169. Chauhan SP, Sullivan CA, Lutton TD, et al: Parous patients' estimate of birth weight in postterm pregnancy. *J Perinatol* 15:192, 1995.
170. Smith GC, Smith MF, McNay MB, et al: The relation between fetal abdominal circumference and birth weight: findings in 3512 pregnancies. *Br J Obstet Gynaecol* 104:181, 1997.
171. O'Reilly-Green CP, Divon MY: Receiver operating characteristic curves of sonographic estimated fetal weight for prediction of macrosomia in prolonged pregnancies. *Ultrasound Obstet Gynecol* 9:403, 1997.
172. Tamura RK, Sabbagha RE, Depp R: Diabetic macrosomia: accuracy of third trimester. *Ultrasound Obstet Gynecol* 67:828, 1986.
173. Chervenak JL, Divson MY, Hirsch J, et al: macrosomia in the post-date pregnancy: is routine ultrasonographic screening indicated? *Am J Obstet Gynecol* 161:753, 1989.
174. Pollack RN, Hauer-Pollack G, Divon MY: Macrosomia in postdates pregnancies: the accuracy of routine ultrasonographic screening. *Am J Obstet Gynecol* 167:7, 1992.
175. Sandmire HF: Whither ultrasonic prediction of fetal macrosomia? *Obstet Gynecol* 82:860, 1993.
176. Benacerraf BR, Gelman R, Frigoletto FD Jr: Sonographically estimated fetal weights: accuracy and limitation. *Am J Obstet Gynecol* 159:1118, 1988.
177. McLaren RA, Puckett JL, Chauhan SP: Estimators of birth weight in pregnant women requiring insulin: a comparison of seven sonographic models. *Obstet Gynecol* 85:565, 1995.
178. Benson CB, Coughlin BF, Doubilet PM: Amniotic fluid volume in large-for-gestational-age fetuses of nondiabetic mothers. *J Ultrasound Med* 10:149, 1991.

179. Uvena-Celebrezze J, Catalano PM: The infant of the woman with gestational diabetes mellitus. *Clin Obstet Gynecol* 43:127, 2000.
180. Cohen B, Penning S, Major C, et al: Sonographic prediction of shoulder dystocia in infants of diabetic mothers. *Obstet Gynecol* 88:10, 1996.
181. Elliott JP, Garite TJ, Freeman RK, et al: Ultrasonic prediction of fetal macrosomia in diabetic patients. *Obstet Gynecol* 60:159, 1982.
182. Winn HN, Holcomb W, Shumway JB, et al: The neonatal bisacromial diameter: a prenatal sonographic evaluation. *J Perinat Med* 25:484, 1997.
183. Mongelli M, Sverker EK, Tambyrajia R: Screening for fetal growth restriction: a mathematical model of the effect of time interval and ultrasound error. *Obstet Gynecol* 92:908, 1998.
184. Bobrow CS, Soothill P: Fetal growth velocity: a cautionary tale. *Lancet* 353:1460, 1999.
185. Eik-Nes SH, Grottnum P, Persson PH, Marsal K: Prediction of fetal growth by ultrasound biometry. I. Methodology. *Acta Obstet Gynecol Scand* 61:53, 1982.
186. Rossavik IK, Deter RL: Mathematical modeling of fetal growth: I. Basic principles. *J Clin Ultrasound* 12:529, 1984.
187. Gardosi J, Chang A, Kalyan B, et al: Customised antenatal growth charts. *Lancet* 339:283, 1992.
188. Deter RL, Rossavik IR, Harrist RB, et al: Mathematical modeling of fetal growth: Development of individual growth curve standards. *Obstet Gynecol* 68:151, 1986.
189. Simon NV, Deter RL, Shearer DM, et al: Prediction of normal fetal growth by the Rossavik growth model using two scans before 27 weeks, menstrual age. *J Clin Ultrasound* 17:237, 1989.
190. Deter RL, Rossavik IR, Harrist RB: Development of individualized growth curve standanrds for estimated fetal weight: I. Weight estimation procedure. *J Clin Ultrasound* 16:215, 1988.
191. Deter RL, Rossavik IR, Carpenter RJ: Development of individualized growth curve standanrds for estimated fetal weight: II. Weight prediction during the third trimester and at birth. *J Clin Ultrasound* 17:83, 1989.
192. Lee W, Deter RL, McNie B, et al: Individualized growth curve assessment of fetal soft tissue using fractional thigh volume. *Ultrasound Obstet Gynecol* 24:767, 2004.
193. Deter RL, Bishong X, Milner LL: Prenatal prediction of neonatal growth status in twins using individualized growth assessment. *J Clin Ultrasound* 24:53, 1996.
194. Gardosi J, Mul T, Mongelli M, et al: Analysis of birthweight and gestational age in antepartum stillbirths. *Br J Obstet Gynaecol* 105:524, 1998.
195. Clausson B, Gardosi J, Francis A, et al: Perinatal outcome in SGA births defined by customized versus population based birthweight standards. *Br J Obstet Gynaecol* 108:830, 2001.
196. de Jong CL, Gardosi J, Dekker GA, et al: Application of a customised birthweight standard in the assessment of perinatal outcome in a high risk population. *Br J Obstet Gynaecol* 105:531, 1998.



# ULTRASOUND EVALUATION OF MULTIPLE PREGNANCIES

James F. X. Egan, MD and Adam F. Borgida, MD

## Introduction

## Etiology of Twins

## Diagnosis of Twins

## "Vanishing" Twins

## Perinatal Loss in Twin Gestations

## Placentation

Chorionicity and Amnionicity

First Trimester

Second and Third Trimesters

Membrane Insertion, "Twin Peak" Sign

Membrane Thickness

Membrane Layers

Multiple Sonographic Markers to Determine

Chorionicity/Amnionicity

Monoamniotic Twins

## Conjoined Twins

## "Stuck" Twin

## Twin-to-Twin Transfusion Syndrome

## Acardiac Twins

## Aneuploidy Screening in Twin Gestations

## Invasive Testing in Twin Gestations

## Cervical Length and Spontaneous Preterm Birth

## Multifetal Pregnancy Reduction

## Twins Discordant for Anomalies

## Method Used for Selective Reduction of the Anomalous Fetus

## Twin Growth

Intrapartum Use of Ultrasound in Twin Gestations

## Conclusion

## INTRODUCTION

Ultrasound has revolutionized the care of women carrying twins. It begins with the diagnosis of twins and continues through the determination of chorionicity, cervical length measurement in predicting preterm delivery of twins, ultrasound screening for structural abnormalities and aneuploidy, management of complications unique to twins, and the intrapartum role of ultrasound in vaginal twin deliveries.<sup>1-3</sup> The problems found in twins are also seen in the increasing number of higher order multiples born in the United States and throughout the world.

Upon learning of a twin gestation, most parents are struck with joy and awe. The obstetrician and sonographic practitioner, however, are faced with numerous problems including prematurity, decreased survival, impaired growth, increased structural abnormalities, and aneuploidy.<sup>1-6</sup> Approximately 14% to 25% of twins are growth restricted and 25% require admission to neonatal intensive care units.<sup>7,8</sup> The risk of cerebral palsy is four times greater for twins than singletons, and 17 times greater for triplets than singletons.<sup>9,10</sup> The fetal death rate for twins of 15.5/1000 live births is almost four times higher than that of singletons, which is 4.3/1000 live births.<sup>11</sup> The likelihood of not surviving the first year of life is 7-fold greater for twins than for singletons.<sup>12,13</sup> Twin-specific problems include twin-to-twin

transfusion syndrome (TTTS), monochorionic-monoamniotic twin placentation and variations of conjoined twins. Management decisions for one twin must consider the impact on the co-twin.<sup>14,15</sup> Maternal complications such as preeclampsia and diabetes are two to three times more common in twin gestations than in singletons.<sup>16,17</sup> Despite these risks, twins generally result in a successful pregnancy for both the parents and health care providers.

Twin gestations accounted for 3.2% of all live births in the United States in 2003.<sup>4</sup> Multiple gestations have increased 1.33-fold in the United States over the past decade from 75,858 of 3,612,258 live births (1/48) in 1980 to 128,665 of 4,089,950 live births (1/31) in 2003. When considered as the proportion of pregnancies rather than live births (Fig. 8-1), twins comprised 1/94 pregnancies in 1980 and 1/62 in 2003. Figure 8-2 tracks the changes in the number of twin, triplet, and quadruplet live births in the United States from 1990 to 2003. All three categories of multiples increased from 1990 to 1998. From 1998 to 2003, however, the number of quadruplets declined, triplets leveled off, and the rate of increase in twins has slowed. Most multiple pregnancies are twins. They comprised 96.9% of all multiples in 1990, but this percentage decreased steadily to 95.7% in 2000 before increasing to 96% in 2001.

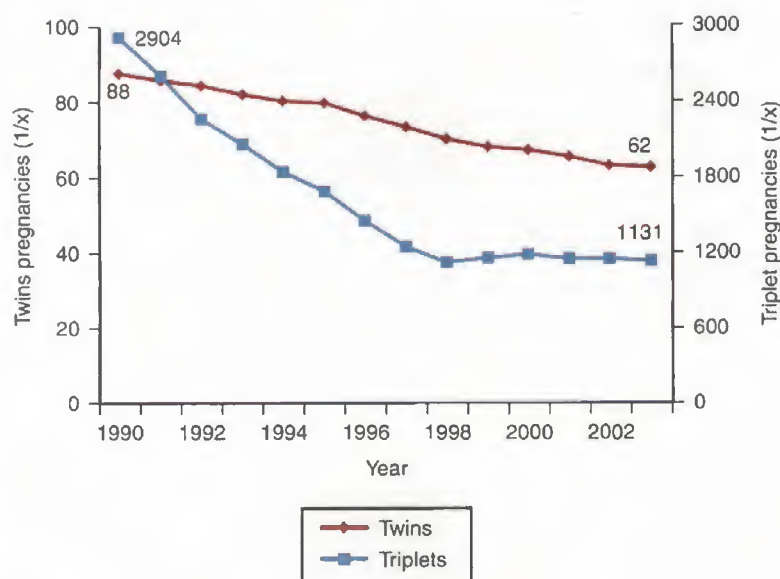


**FIGURE 8-1.** Twin and triplet pregnancies (expressed as 1/x) in the United States from 1990 to 2003. (From *Nativity Data Set: National Center for Health Statistics: Centers for Disease Control and Prevention, Atlanta CD-ROM 1997–2002: Series 21 11,12,14,15*; and Yinon Y, Yagel S, Tepperberg-Dikawa M, et al: Prenatal diagnosis and outcome of congenital cytomegalovirus infection in twin pregnancies. *Br J Obstet Gynaecol* 113:295, 2006.)

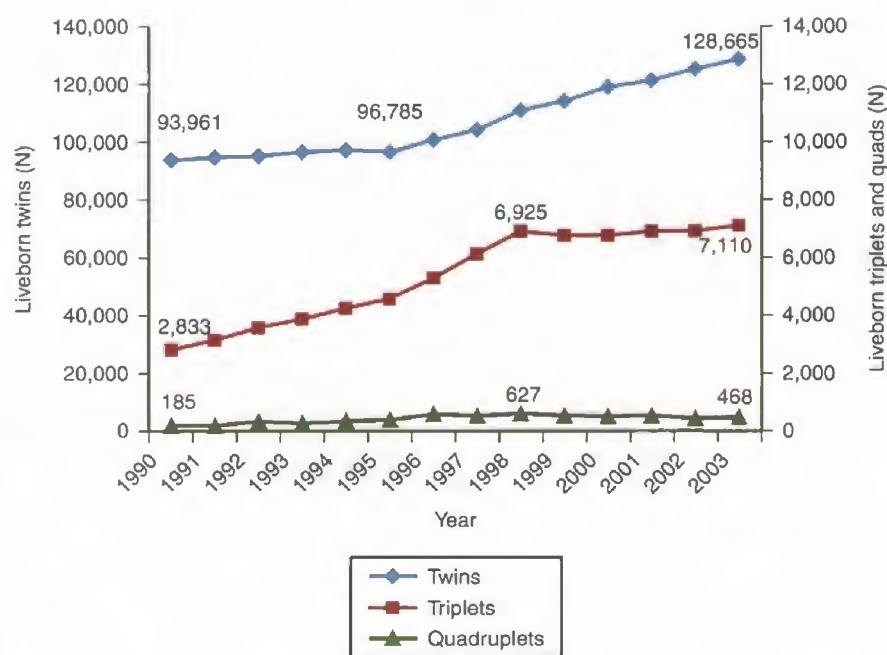


**FIGURE 8-2.** The number of twin, triplet, and quadruplet live births in the United States from 1990 to 2003.

## ETIOLOGY OF TWINS

Twin embryology differs from that of singletons in that there are two embryos with one or two placentas. Twins are either monozygotic or dizygotic depending on the number of eggs fertilized at conception (Fig. 8-3).<sup>2</sup> Monozygotic twins, often called “identical” by nonmedical personnel, result from one egg being fertilized by one sperm that divides into two embryos within two to 14 days after fertilization. These twins have the same genetic makeup and are contemporaneous “clones” of one another. The rate of monozygotic twinning is constant throughout the world at approximately 1/250 pregnancies.<sup>2</sup> The timing of cleavage in monozygotic twinning determines the type of placentation and the like-

lihood of complications. Figure 8-4 is based on the classic report by Benirschke and Kim.<sup>2</sup> It depicts the first 17 days after ovulation in a monozygotic twin gestation and demonstrates three types of placentation: dichorionic-diamniotic (about 1/3, occurring on day 0–3), monochorionic-diamniotic (about 2/3, occurring on day 4–8), and monochorionic-monoamniotic (< 1%, occurring on day 9–12) that may result from this type of twinning (Table 8-1). Although the incidence of monozygotic twinning has been relatively constant throughout the world in spontaneous twin gestations (Table 8-2), it may be increased by assisted reproductive technologies, particularly those methods that alter the zona pellucida around the time of fertilization, or where there is



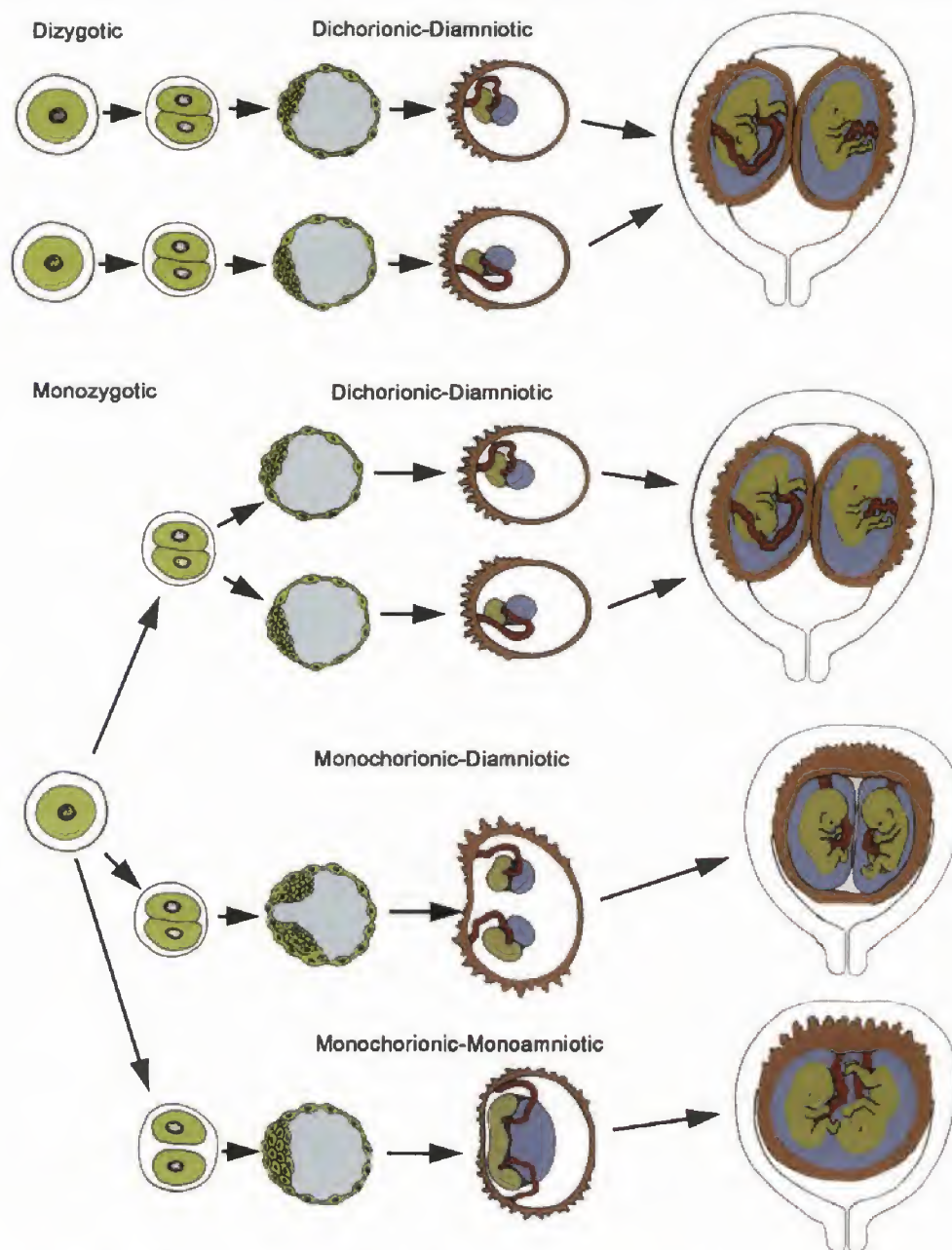


**FIGURE 8-3.** Diagram of the development and placentation of dizygotic and monozygotic twins. The degree to which monozygotic twins share placentas, chorions, and amnions depends on the stage of development at which splitting occurs. (Modified from Larsen WJ: *Human Embryology*, 2nd ed. New York, Churchill Livingstone, 1997.)

delayed blastocyst implantation.<sup>18,19</sup> Dizygotic twinning varies by race, geographic area, maternal age, and the availability of assisted reproductive technologies.<sup>20,21</sup> In the 1980s, the highest rate of dizygotic twinning was seen in an area of Nigeria, where it was 49/1000 live births. The lowest rate was found in Japan at 1.3/1000 live births (see Table 8-2).<sup>22</sup> This increased rate in Nigerian women is due to a higher baseline level of follicle-stimulating hormone.<sup>20</sup> The maternal age peak for spontaneous multiples is 37 years of age.<sup>21</sup>

With the greater access to assisted reproductive technologies, the geographic differences in dizygotic twinning have

blurred in developed countries. To assess the impact of assisted reproductive technologies on multiple births, Bardis et al<sup>23</sup> reported on a survey of all deliveries for 1 week of 2003 in the United Kingdom. Of the 6913 deliveries, there were 100 twins (1.4%) and one triplet gestation (0.01%). Assisted reproductive technology was used to achieve 1.9% of all pregnancies delivered. The multiple pregnancy rate in the assisted reproductive technology group was 13.5% compared with 1.2% in spontaneous conceptions. Because of the greater morbidity and mortality seen with multiple gestations, fertility clinics have reduced the number of embryos trans-

## MONOZYGOTIC TWINNING

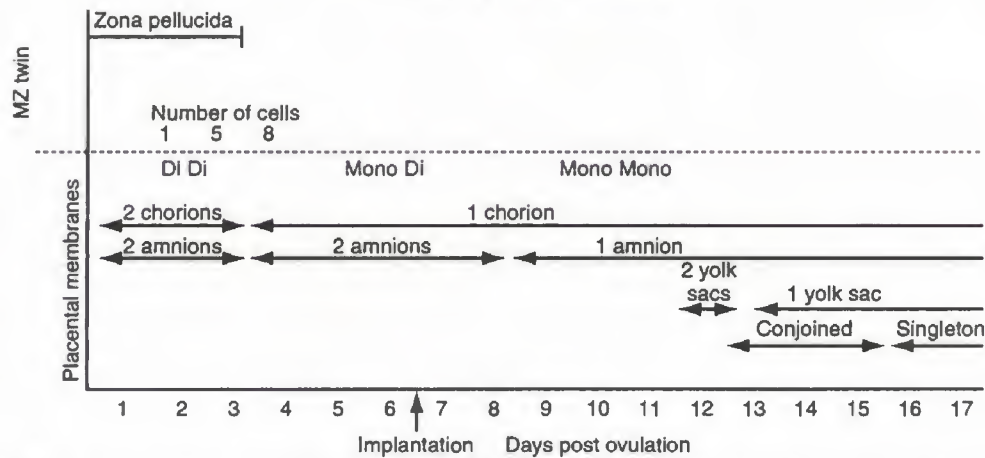


**FIGURE 8-4.** The timing of monozygotic twinning demonstrating the impact of the day cleavage occurs on placentation and complications, that is, monochorionic monoamniotic placenta or conjoined twins. (From Benirschke K: *Multiple pregnancy (First of two parts)*. *N Engl J Med* 288:1276, 1973.)

**Table 8-1** Types of Monozygotic Twins Related to Time of Division After Ovum Fertilization

Chorion	Amnion	Time to Division (Days)	Frequency
Dichorionic	Diamniotic	0-3	25%
Monochorionic	Diamniotic	4-8	75%
Monochorionic	Monoamniotic	9-12	~1%
Monochorionic	Monoamniotic (conjoined twins)	13-15	Rare

**Table 8-2** Geographic Twinning Rates per 1000 Births

Geographic Area	Monozygotic	Dizygotic
Nigeria	5.0	49.0
United States		
Black	4.7	11.1
White	4.2	7.1
England and Wales	3.5	8.8
Japan	3.0	1.3

Adapted from MacGillivray I: Epidemiology of twin pregnancy. *Semin Perinatol* 10:4, 1986.

ferred for each cycle. This has decreased the rate of increase in the number of high order multiples. Figures 8-1 and 8-2 show a flattening of the curve for triplets in the United States from 1998 to 2003.<sup>4</sup> Despite the lower number of embryos transferred in each cycle, the likelihood of a successful pregnancy has not decreased. Single embryo transfer is becoming more generally accepted. Crintini et al<sup>24</sup> reported on 107 infertility patients, of whom 41 had single embryo transfers and 66 had two blastocysts transferred. There was no difference in the implantation rate in 238 cycles in which one or two embryos were transferred (76% versus 66%, respectively) or in the pregnancy rate (76% versus 79%). Twinning rates, however, (3% versus 62%, respectively) differed dramatically.

Dizygotic twins, often called "fraternal" by nonmedical personnel, result from the fertilization of two eggs by two sperm (see Figs. 8-3 and 8-5). The genetic makeup of these twins differs from one another. Dizygotic twinning varies by race, advancing maternal age, geography, season, ethnic origin, and increasing parity.<sup>21,25</sup> The most dramatic increases have been seen with the use of assisted reproductive technologies.<sup>19</sup> With very rare exceptions, dizygotic twins always have a dichorionic-diamniotic placenta, but monozygotic twins may have either a dichorionic-diamniotic or monochorionic-diamniotic placenta depending on the

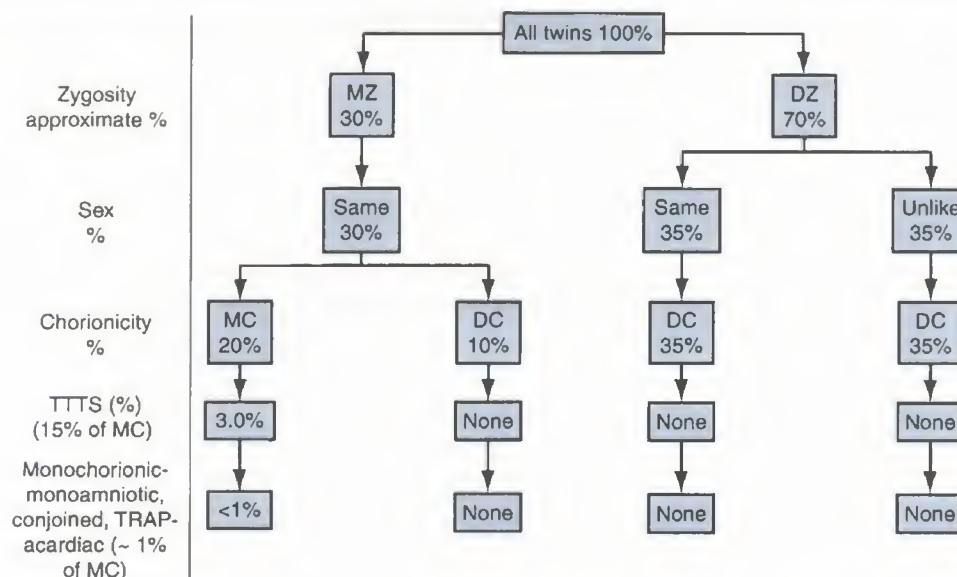
timing of the twinning event (see Fig. 8-4).<sup>26</sup> The type of placentation is the most important predictor of the pregnancy-related complications in twin gestations. Chorionicity, not zygosity, determines the likelihood of many twin-related complications.<sup>27,28</sup> A primary goal when performing an ultrasound in a patient with a multiple pregnancy, is to determine chorionicity.

## DIAGNOSIS OF TWINS

Ultrasound is crucial for the diagnosis of twins. Before the availability of prenatal ultrasound, up to 50% of twin gestations were first discovered at the time of delivery. A clinical suspicion of multiple gestation should be raised when a patient has a larger than expected uterine size, if a patient's pregnancy associated symptoms, for example, hyperemesis gravidarum, seem excessive, or if she became pregnant using assisted reproductive technologies.<sup>29,30</sup>

Every obstetric ultrasound should begin with a complete imaging sweep of the uterus. We always start in the suprapubic area and scan cephalad in a transverse axial plane until we reach the top of the uterine fundus. This sweep images the entire contents of the uterus and allows the sonographer to count the number of embryos or fetuses, determine their presentation and lie and document the situs,





MZ monozygous, DZ dizygous, MC monochorionic, DC dichorionic, TTTS twin to twin transfusion syndrome, TRAP twin reversed arterial perfusion.

**FIGURE 8-5.** Approximate distribution of monozygous and dizygous twinning with chorionicity and complications of monozygous twins as a percent of all twins. This represents the approximate distribution of twin gestations in the United States by zygosity and chorionicity. Both monochorionic and dichorionic twin gestations are at greater risk for maternal and fetal/neonatal complications (such as preeclampsia, diabetes, structural fetal abnormalities, aneuploidy, growth restriction) when compared with singleton gestations. Complications found only in monochorionic twin gestations include twin-to-twin transfusion (TTTS), monochorionic-monoamniotic twins, twin reversed arterial perfusion (TRAP) acardiac twins, conjoined twins, and fetus in fetu.

or left and right sides, of each fetus. This should be routinely done on every obstetric ultrasound so that multiple pregnancies and situs abnormalities are not missed.

Important sonographic details to note in the first trimester include the number of gestational sacs, the location of the placenta or placentas, the presence and characteristics of the dividing membrane or membranes, amniotic fluid status, the number of yolk sacs and the fetal heart rates.<sup>3,5,31</sup> This information helps to determine chorionicity, which is essential for the provider when counseling patients regarding potential complications.<sup>32</sup>

## “VANISHING” TWINS

In 1986, Landy et al<sup>33</sup> reported on 1000 first trimester pregnancies with an incidence of twinning of just over 3%. They found approximately 20% of these twin gestations resulted in singleton live births, with or without vaginal bleeding. They called this the “vanishing twin” phenomenon. In a prospective series of 68 twin pregnancies diagnosed with two fetal heartbeats, dichorionic and monochorionic twins diagnosed earlier than 8 weeks were significantly more likely to result in a singleton pregnancy than those diagnosed after 8 weeks.<sup>34</sup> Dichorionic twins were more likely to result in one or two viable newborns when compared with similarly aged monochorionic-diamniotic twins (Fig. 8-6).

The prognosis for singletons resulting from a vanishing twin depends on the number of sacs seen initially and the timing of the loss of the co-twin. Dickey et al<sup>35</sup> found that 15% of singleton in vitro fertilization (IVF) births began as a higher order gestation. Schieve et al<sup>36</sup> noted that the greater

the number of fetal hearts seen on an early twin ultrasound examination the greater the subsequent risk of low birth weight for both singletons (such as “vanishing twins”) and twins. Pinborg et al<sup>37</sup> reported that of all IVF singletons born, 10.4% resulted from a twin gestation early in pregnancy. In their 624 IVF singletons, who were survivors of a vanishing co-twin identified by sonography in week 8, there was a higher incidence of preterm delivery and infant mortality when compared with 5237 singletons. These complications, however, were gestational age dependent. When they stratified the neonatal outcomes by the time of vanishing as early (< 8 weeks), intermediate (> 8 and < 22 weeks), and late (> 22 weeks), delivery at less than 32 weeks was 1.9%, 5.3%, and 21.4% respectively, and a neonatal intensive care unit stay of greater than 28 days was 8.7%, 15.7%, and 43.8% for early, intermediate, and late losses of a co-twin respectively. Neurodevelopmental disorders were also higher with a loss at a later gestational age with 3.3% early, 8.0% intermediate and 9.7% in the late “vanishing” group. In general, if a twin “vanished” at less than 8 weeks, the pregnancy outcomes were comparable with singletons from early singleton gestations. This highlights the importance of careful and repeated ultrasound examinations in the early stages of pregnancy to correctly diagnose and follow twins. We discuss the “appearing twin” later in this chapter.

## PERINATAL LOSS IN TWIN GESTATIONS

Perinatal losses are greater in twin gestations than in singletons. Infant mortality rates in 1999 were more than five times higher at 32.9/1000 for live-born twins compared

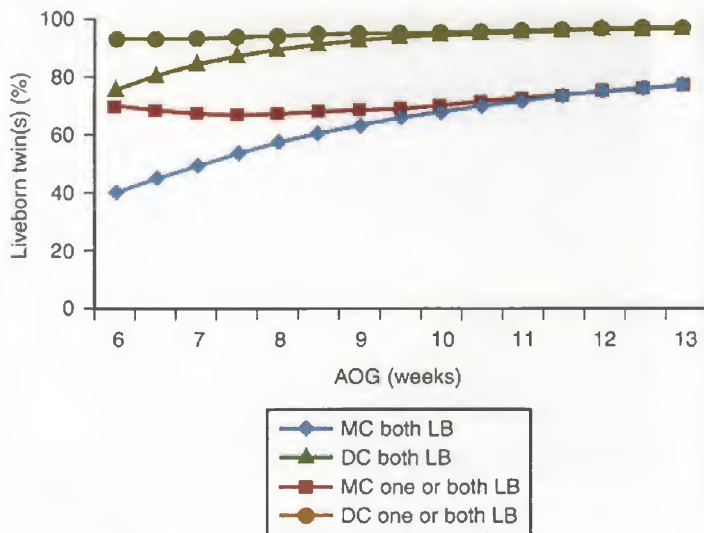


**FIGURE 8-6.** The probability of delivering live-born twins, by chorionicity, when two fetal heartbeats were seen on a normal first trimester ultrasound.

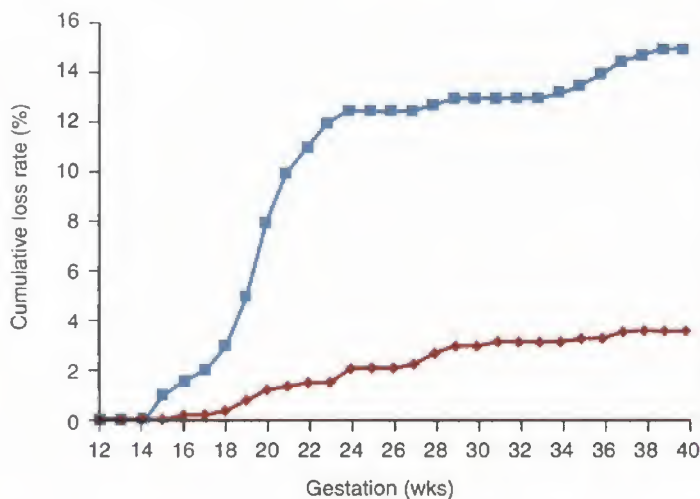


**FIGURE 8-7.** Cumulative loss rate by chorionicity from 12 weeks to term in twin gestations.

with 6.2/1000 for live-born singletons in the United States.<sup>1</sup> Survival in twins depends on chorionicity, which determines the level of risk for anomalies, growth problems, and prematurity.<sup>32</sup> Sebire et al<sup>32</sup> reported that cumulative loss rate from 12 weeks to term was approximately 3% for dichorionic and almost 15% for monochorionic twins (Fig. 8-7). The excess losses for monochorionic twins relate to TTTS, prematurity, congenital abnormalities and monoamniotic-monochorionic placentation. Because these losses are more likely to occur between 16 and 22 weeks (see Fig. 8-7), we suggest that ultrasound examinations be performed every 1 to 2 weeks during that time period for known monochorionic-diamniotic twin gestations to screen for TTTS and, if necessary, to develop a management plan. Figure 8-8 shows an ultrasound of a 21-week twin gestation with a fetal demise of one twin. The head circumference and abdominal circumference of the twin with the demise are

much smaller than those of the living twin. Figure 8-9 is a photograph of a fetus papyraceus, or mummified remains of the lost twin found in the folds of the membranes of the placenta after delivery of the surviving twin at 38 weeks.

Although monochorionic twins are at greater risk of complications than dichorionic twins, they represent only 20% of all twins (see Fig. 8-5). Most perinatal losses in twins are due to problems with prematurity, anomalies, or growth. Figure 8-10 compares the gestational age at delivery of the 121,346 twin versus 3,902,691 singleton live-born infants in the United States in 2002.<sup>4</sup> At 28, 32, and 35 weeks' gestation, 0.8%, 2%, and 6.3% of singletons had delivered compared with 5.8%, 15.5%, and 41.9% of twins. This demonstrates a 6.7- to 8-fold higher risk of a preterm delivery at every week from 22 to 35 weeks for twins. Maternal and fetal complications including preeclampsia, gestational diabetes, and cerebral palsy are also increased.<sup>11</sup> Cerebral



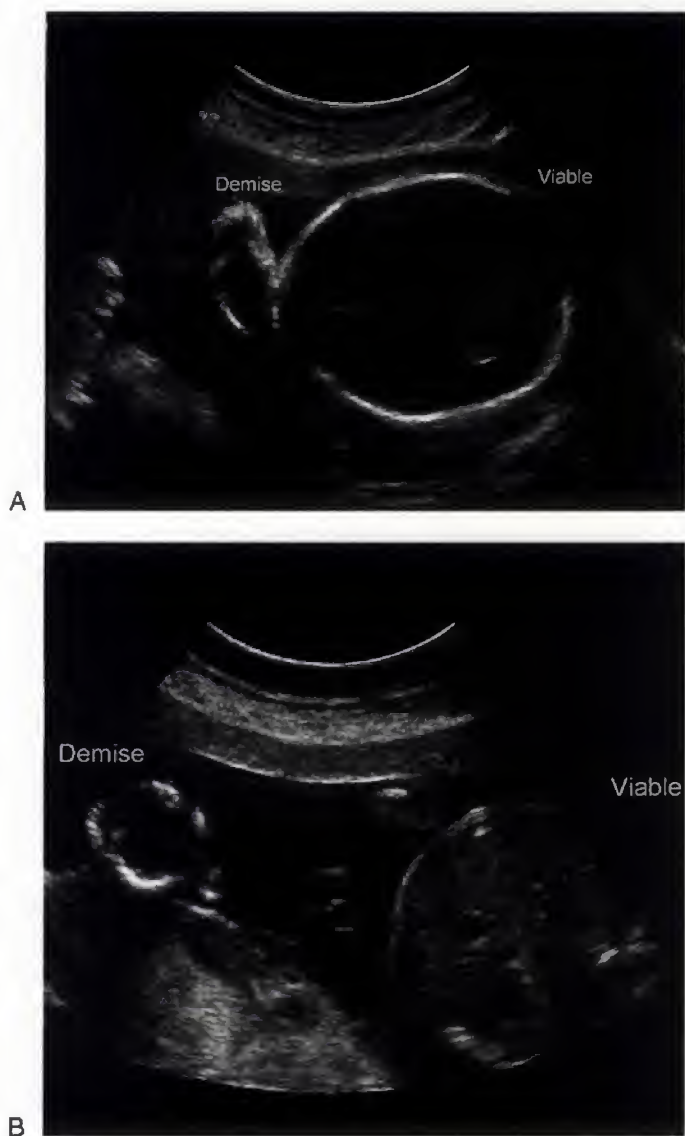


**FIGURE 8-8.** Fetal demise of one twin with a surviving co-twin at 21 weeks' gestation. *A.* The collapsed cranium of the twin with the fetal demise compared with the surviving twin's cranium. *B.* The abdominal circumference of the fetal demise is compared with that of the surviving twin.

palsy rates increase with higher order multiples. They are 2.3/1000 in singleton live births, 12.6/1000 in twins, and 44.8/1000 in triplet gestations.<sup>38</sup>

## PLACENTATION

### Chorionicity and Amnionicity

One of the most important, and sometimes overlooked roles a sonographic practitioner plays in the management of twins is the identification of chorionicity. This is generally a straightforward diagnosis for the sonographer/sonologist in the late first and early second trimester. Ultrasound is very useful in determining placentation, especially chorionicity and amnionicity, and these are very important in predicting



**FIGURE 8-9.** Fetus papyraceus resulting from a midtrimester fetal demise of a co-twin. This fetus was noted on inspection of the placenta and membranes following a term delivery of the surviving twin. (Pathology image courtesy of Melinda Sanders, MD, and Erika Walz, PA, University of Connecticut Health Center, Farmington, CT.)

twin pregnancy complications.<sup>3,5,32</sup> Although ultrasound can almost always determine chorionicity, it only determines zygosity in a subset of twins (see Fig. 8-5).

### First Trimester

First trimester evaluation is in the best time to determine chorionicity and amnionicity in multiple gestations. The diagnosis becomes more difficult as pregnancy progresses. First trimester diagnosis is based on the number of gestational sacs, amnions, and yolk sacs (Table 8-3 and Fig. 8-11). Transvaginal sonography is often used in the first trimester because these structures may be difficult to visualize transabdominally. Sonographers do almost as well as perinatologists in determining chorionicity. Weisz et al<sup>39</sup> compared the accuracy of sonographers and perinatologists in determining chorionicity in 172 twin cases before 14 weeks. The overall rate of agreement on the diagnosis of chorionicity was 90.1%. With dichorionic twins, they agreed on 118 of 119 (99.2%), whereas in monochorionic-diamniotic twins, there was agreement in 94.5%. Sonographers diagnosed 10 monochorionic-monoamniotic twins that were later diagnosed as monochorionic-diamniotic. This is a difficult diagnosis, however, that is often overcalled by both perinatologists and sonographers on the first or second scan. Because of this, we sometimes bring a woman back for two or three scans before diagnosing monochorionic-monoamniotic twins. Monteagudo<sup>40</sup> showed the use of first trimester vaginal sonography in correctly determining chorionicity and amnionicity in 43 twin pregnancies. The number of gestational sacs correlates with amnionicity; however, as discussed later, underestimation is possible.

Another diagnostic pitfall in the first trimester is the "appearing" twin. Doubilet and Benson<sup>41</sup> have reported their experience with transvaginal ultrasound at 5.0 to 5.9 weeks' gestation and concluded that 30/220 (13.6%) twin pregnancies were diagnosed as singletons on initial evaluation. Monochorionic twins were more likely to be

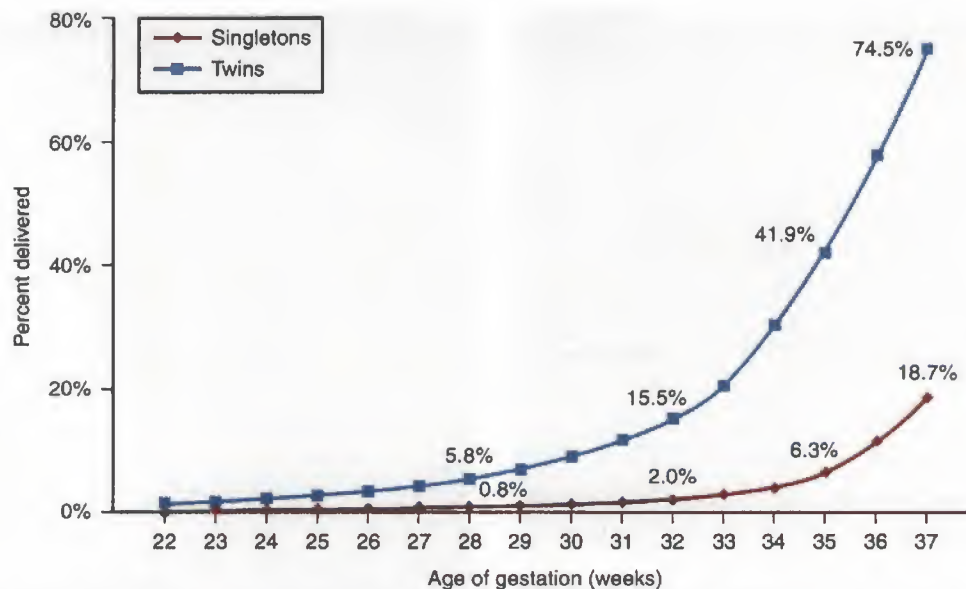


**FIGURE 8-10.** The distribution of twin versus singleton live births delivered from 22 to 37 weeks in the United States in 2002. (From *Nativity Data Set: National Center for Health Statistics: Centers for Disease Control and Prevention, Atlanta CD-ROM 1997–2002; Series 21 11, 12, 14, 15.*)

**Table 8-3**

**Sonographic Determination of Chorionicity and Amnionicity in First Trimester Twin Gestations**

Placantation	Gestational Sacs	Yolk Sacs	Embryos/ Sac	Amniotic Cavities
DC, DA	2	2	1	2
MC, DA	1*	2	2*	2
MC, MA	1*	1 or partially divided*	2*	1

\*Amnionicity cannot be determined by this finding.

DC, dichorionic; DA, diamniotic; MC, monochorionic; MA, monoamniotic.

“appearing” twins. Of those initially diagnosed as singletons, 24/213 (11.3%) were dichorionic twin gestations, whereas 6/7 (85.7%) were monochorionic gestations. They reported that the pregnancy outcomes for the “appearing” twin gestations were comparable with other twin gestations.

The timing of the visualization of membranes and yolk sac depends on chorionicity and gestational age (see Fig. 8-4). Bromley and Benacerraf<sup>42</sup> retrospectively reviewed the sonographic images of monochorionic twin pregnancies scanned between 6 and 9.5 weeks. This study included 20 diamniotic and two monoamniotic pregnancies. In diamniotic pregnancies less than 8 weeks, only yolk sacs and no dividing membranes were visualized. Two yolk sacs were noted in all but one case on scanning at a later gestational age (Fig. 8-12). In the monoamniotic cases, a single yolk sac was noted at 9 weeks with a single amnion around both embryos. A similar study correlating yolk sacs with amnionicity was performed by Shen et al<sup>43</sup> in 20 monochorionic-diamniotic pregnancies under 11 weeks' gestation. In 85% (17/20) of monochorionic-diamniotic pregnancies, two yolk sacs were noted. In three, only one yolk sac was noted. To summarize, seeing two yolk

sacs is confirmation of diamniotic twins; however, a single yolk sac requires further confirmation before the diagnosis of monoamniotic twins should be made. The only criteria diagnostic of monochorionic-monoamniotic twins is the finding of a single amniotic cavity (see Table 8-3).

## Second and Third Trimesters

The steps in determining placentation in the second and third trimesters include documentation of gender, placental masses, and characterization of the dividing membrane(s). If differing genders or two distinct placentas are noted, then dichorionic placentation has occurred.<sup>2</sup> If the same gender is present and there is one placenta, the type of placentation may be dichorionic-diamniotic, monochorionic-diamniotic, monochorionic-monoamniotic, or monochorionic with conjoined twins.<sup>44</sup> The intertwin dividing membrane ultrasound characteristics must then be evaluated to determine placentation.<sup>45,46</sup>

## Membrane Insertion, “Twin-Peak” Sign

Perhaps the most useful ultrasonographic marker for determining chorionicity is the appearance of the membrane at its insertion onto the chorionic plate or fetal surface of the placenta. Finberg<sup>46</sup> first reported the ultrasonographic appearance of the dividing membrane as it inserts onto the chorionic plate of the placenta. When the groove between the membranes at the insertion into the placenta appears thick, it is called the lambda or “twin-peak” sign, and a fused dichorionic-diamniotic placentation is likely (Figs. 8-13 and 8-14). If the insertion clearly joins the chorionic plate of the placenta as a thin, wispy membrane, it is called “T” sign, and a monochorionic-diamniotic placentation is likely (Fig. 8-15). Wood et al<sup>47</sup> reported the diagnostic utility of the twin-peak or lambda sign to determine chorionicity in a prospective series, with chorionicity confirmed by pathology





**FIGURE 8-11.** The first trimester is the best time to evaluate the chorionicity and amnionicity of twin gestations. *A.* Sonogram in a 10-week monochorionic-diamniotic gestation. A thin dividing membrane (arrow) from the two apposed amniotic sacs is seen. *B.* Sonogram from a 7-week dichorionic-diamniotic gestation. Both amnions (arrows) surrounding the developing embryos are well seen in this diamniotic twin pregnancy. Dichorionicity is confirmed by the thick intertwin membrane.

postdelivery. The twin-peak sign correctly predicted 34/36 dichorionic pregnancies, whereas its absence correctly predicted seven of eight monochorionic pregnancies. This yielded an overall positive-predictive value of 97%. Sepulveda et al<sup>48</sup> studied the impact of advancing gestational age on the twin-peak sign, comparing its sonographic presence at a 10- to 14-week scan with that at 16 and 20 weeks. Of the 101 twin pregnancies with a twin-peak sign at 10 to 14 weeks, 98 still had it at the 16-week scan. At the 20-week scan, however, only 87/101 pregnancies had the twin-peak sign. Therefore, advancing gestational age negatively affects the diagnosis of the twin-peak sign. Sepulveda also used a variation of the twin-peak sign to



**FIGURE 8-12.** Sonogram from a 6.5-week dichorionic-diamniotic twin pregnancy. Although the amniotic membranes are not well seen, both yolk sacs (arrows) in this diamniotic pregnancy are well seen.

assess chorionicity retrospectively and prospectively in triplet pregnancies. He called the junction of the three interfetal membranes the “epsilon zone” (Fig. 8-16).<sup>49</sup> In 19/20 triplet pregnancies prospectively studied, chorionicity was correctly diagnosed in the first trimester. There were 16 trichorionic pregnancies and four dichorionic pregnancies in this study.

The correct diagnosis of chorionicity and amnionicity in twin pregnancies is often straightforward early in gestation, when the division between the two gestational sacs are thick in dichorionic gestations (see Fig. 8-11*B*). If one is attempting to determine the chorionicity of twins in the second or third trimester and the diagnosis is equivocal, an attempt should be made to obtain and evaluate, early, first trimester scans if they were done previously, when the diagnosis can be more certain.

### Membrane Thickness

A thicker dividing membrane is more likely to be seen in a dichorionic-diamniotic placenta. (see Figs. 8-13, 8-14, and 8-15). In a retrospective study of twin pregnancies, Hertzberg et al<sup>50</sup> determined that a thick dividing membrane (greater than 1 mm) indicated dichorionic-diamniotic twins in 38 of 42 cases. Townsend, Simpson, and Filly retrospectively reviewed 75 twin pregnancies to determine chorionicity based on membrane thickness. They found that a thick membrane predicted dichorionic-diamniotic placentation 83% of the time and was seen 89% of the time at the first sonogram.<sup>51</sup> A thin membrane predicted 83% of monochorionic placentations but was seen only 54% of the time. A similar study from Winn et al<sup>52</sup> used a membrane thickness of 2 mm or more as a cutoff. This accurately predicted monochorionic and dichorionic twins 82% and 95% of the time. Stagiannis et al<sup>53</sup> studied the reproducibility of membrane thickness to predict chorionicity. In their study, 27

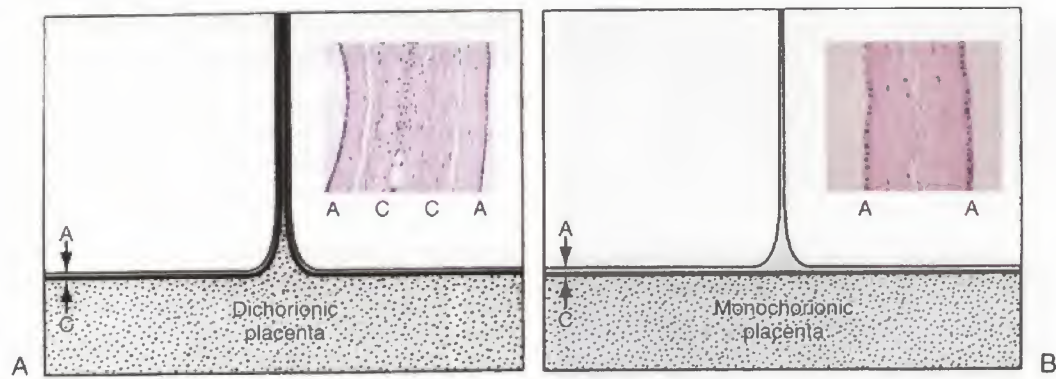


**FIGURE 8-13.** “Twin-peak” sign with placental pathology of fetal membranes. **A.** Diagram of the “twin-peak” sign in dichorionic twin gestations. The chorion (C) and amnion (A) of each twin reflect away from the fused placenta to form the intertwin membrane. A potential space exists between the membranes, which are filled with the amniotic and chorionic mesoderm as seen in the pathology images of dichorionic membranes (*see inset*). **B.** In monozygotic-diamniotic twins the intertwin membrane is composed of only two amnions. A single chorion does not allow the chorionic mesoderm to access the potential space between the diamniotic membranes as seen in the pathology sample of monozygotic fetal membranes (*see inset*). (Pathology image courtesy of Melinda Sanders, MD, and Erika Walz, PA, University of Connecticut Health Center, Farmington, CT; from Finberg HJ: The “twin peak” sign: Reliable evidence of dichorionic twinning. *J Ultrasound Med* 11:571, 1992.)

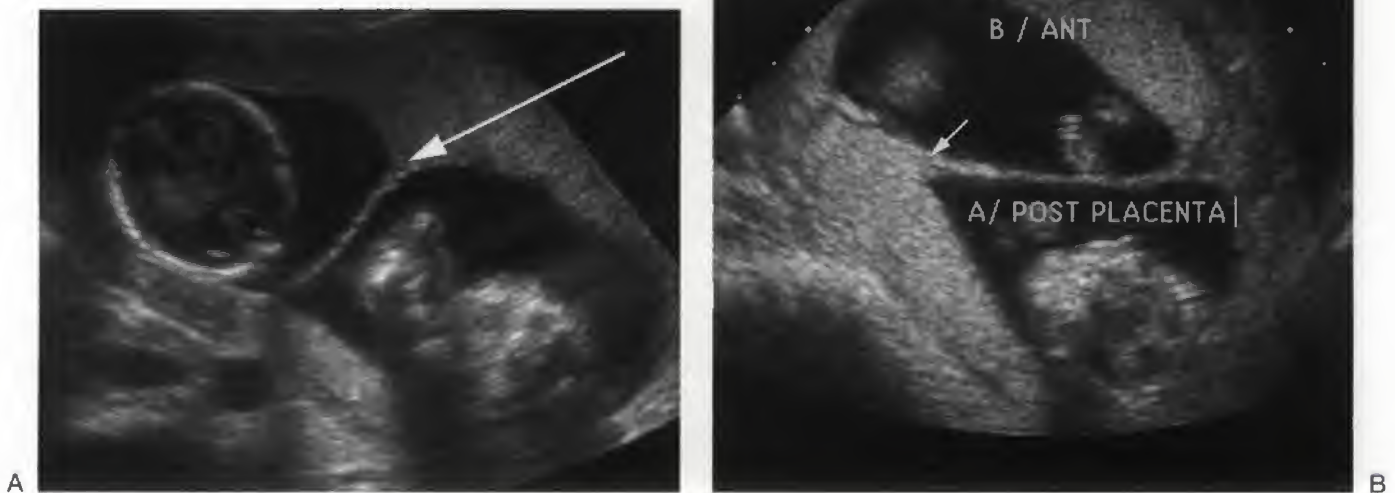


**FIGURE 8-14.** **A.** The lambda, or “twin-peak” sign is demonstrated by the thicker placental membranes which widen (*arrow*) as they touch down on the chorionic plate indicating a fused dichorionic-diamniotic placenta. **B.** In cases where the placentas are on opposite sides and clearly separate, as in this case, observation of the twin-peak sign is not necessary to make the diagnosis of dichorionicity. One can still see the insinuation of the chorion (placental tissue) (*arrow*) into the dividing membrane.

twin pregnancies were scanned by two observers blinded to chorionicity on 52 occasions at five areas of the membranes. Membrane thickness measurements closest to the placenta were the most reproducible, but significant variation in membrane thickness does occur, particularly in the second and third trimesters.

### Membrane Layers

D’Alton et al<sup>45</sup> prospectively studied 69 consecutive twin pregnancies to assess chorionicity by counting the number of layers in the dividing membrane visualized by ultrasound. If two layers were seen, a monozygotic pregnancy was diagnosed. If more than two were seen, a dichorionic pregnancy





**FIGURE 8-15.** T-sign as a thin wispy placental membrane joins the chorionic plate (arrow), indicating a monochorionic, diamniotic placenta.



**FIGURE 8-16.** Trichorionic triplets imaged in the first trimester. Three separate gestational sacs meeting at the junction of the three interfetal membranes (the "epsilon zone" is identified).

was predicted. Confirmation was obtained after delivery by histopathology (see Fig. 8-13). Ultrasound counting of the membrane layers correctly predicted chorionicity in 68/69 twin pregnancies. There was 100% accuracy in predicting the 51 dichorionic pregnancies and 94.4% accuracy in predicting the 18 monochorionic pregnancies. Vayssiere et al<sup>54</sup> performed a similar prospective study counting membrane layers and correctly predicted chorionicity in 60/63 twin pregnancies.

## Multiple Sonographic Markers to Determine Chorionicity/Amnionicity

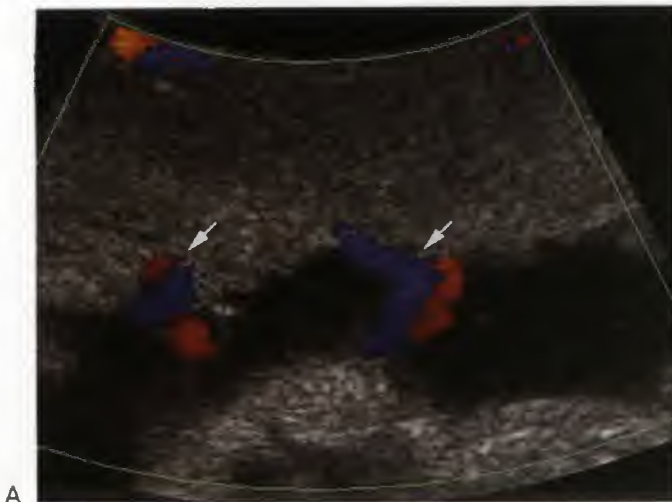
No single sonographic marker of chorionicity is completely reliable. The use of multiple markers enhances the accuracy of predicting chorionicity. Scardo et al<sup>55</sup> prospectively studied the accuracy of multiple sonographic markers to predict chorionicity and amnionicity in 100 consecutive twin pregnancies with postdelivery confirmation. They assessed placental number, fetal gender, membrane thickness, and presence of the twin-peak sign (see Figs. 8-14 and 8-15). They performed an average of 3.6 ultrasound examinations, starting at a mean gestational age of 22.6 weeks. Use of the composite sonographic markers had at least a 91% sensitivity and specificity for correctly determining chorionicity. The timing of these examinations was relatively late in gestation. With the greater acceptance of first trimester ultrasound, the accuracy of determining chorionicity should improve. Carroll et al<sup>56</sup> performed a similar study to predict chorionicity at 10 to 14 weeks' gestation using the number of placental sites, presence of a twin-peak sign, and intertwin membrane thickness. This study included 150 pregnancies with postnatal confirmation of chorionicity and included 116 dichorionic and 34 monochorionic pregnancies. Prenatal ultrasound correctly predicted chorionicity in 139/150 pregnancies (93.3%). The most accurate predictors of dichorionic placentation were the twin-peak sign or separate placentas with a sensitivity and specificity of 97.4% and 100%, respectively.

## Monoamniotic Twins

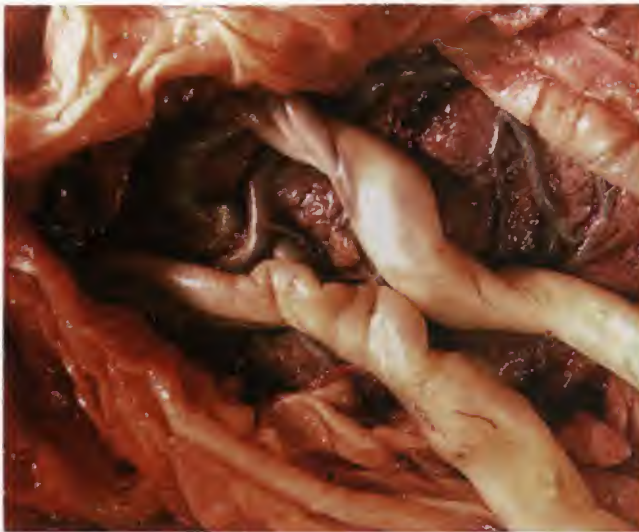
When the dividing membrane is not seen early in the ultrasound evaluation of a twin pregnancy, the diagnosis of monochorionic-monoamniotic twins should be considered. This occurs in approximately 1% of all monochorionic twins (see Figs. 8-3, 8-4, and 8-5). We require several examinations to search for the dividing membrane before making this diagnosis, because the membrane may not initially be apparent by ultrasound. Distinguishing monochorionic-monoamniotic twins from a "stuck" twin in an oligohydramniotic sac can be difficult. Normal amniotic fluid volume and two free-floating twins with no visualized membrane separating them should clinch the diagnosis of monochorionic-monoamniotic twins. Visualization of two cord insertions into the chorionic plate of the placenta in very close proximity to one another is also suggestive of monochorionic-monoamniotic twins (Fig. 8-17).

Color and two-dimensional ultrasound readily show the umbilical cord entanglement that leads to the strikingly increased mortality for monochorionic-monoamniotic twins (Fig. 8-18).<sup>2,57-59</sup> Nyberg et al<sup>60</sup> first reported ultrasound evidence of cord entanglement as a sign of monochorionic-monoamniotic twins. Townsend and Filly confirmed this finding in five sets of nonconjoined, monochorionic-monoamniotic twin pregnancies (Fig. 8-19).<sup>61</sup> Subsequent studies have supported this finding, which is characteristic of monochorionic-monoamniotic twin pregnancies. Overton et al<sup>62</sup> reported using color flow and pulsed wave Doppler to insonate a common cord mass to confirm monochorionic-monoamniotic twins in the first trimester (Fig. 8-20). First trimester vaginal sonography using color Doppler has also





A



B

**FIGURE 8-17.** A. Cord insertions are seen in close proximity to one another in a monoamniotic-placenta by using color-flow Doppler. B. Placenta showing both umbilical cords close to one another with no intervening membranes. (Pathology image courtesy of Melinda Sanders, MD, and Erika Walz, PA, University of Connecticut Health Center, Farmington, CT.)

demonstrated cord entanglement.<sup>63</sup> Sonography may also be useful in the antenatal management of monoamniotic-monoamniotic twins. Belfort et al<sup>64</sup> reported extremely high blood flow velocities associated with umbilical vein compression by the entangled cords when following three monoamniotic-monoamniotic twin pregnancies (Fig. 8-21). Abuhamad et al<sup>65</sup> followed two monoamniotic-monoamniotic twin pregnancies with longitudinal Doppler flow velocities of the umbilical artery. Notching of the umbilical artery waveform was associated with increased narrowing of the umbilical vessels secondary to cord entanglement. Doppler interrogation of the aggregate cord mass may also demonstrate arterial flow, at differing heart rates in both fetuses, which is called a “galloping” Doppler pattern (Fig. 8-22). As with all multiple gestations, a velamentous insertion of the umbilical cord (that is, where the cord inserts into the mem-



**FIGURE 8-18.** Color-flow Doppler interrogation of adjacent abdominal cord insertions and tangled cords in monoamniotic-monoamniotic twins.



**FIGURE 8-19.** A two-vessel umbilical cord wrapped around a three-vessel umbilical cord in monoamniotic-monoamniotic twins.

branes rather than the chorionic plate) is more common in monoamniotic-monoamniotic placentas (Fig. 8-23).

Several different protocols have been proposed for the management of monoamniotic-monoamniotic twins. Because of the rarity of this condition, there are no randomized clinical trials. Rodis et al<sup>57</sup> showed that with daily antenatal surveillance after viability, the double survival rate for monoamniotic-monoamniotic twins was greater than 90%. They suggest serial sonograms, steroids to enhance fetal lung maturity, and daily nonstress tests starting at 24 to 26 weeks. They also recommended delivery by cesarean birth after documentation of fetal lung maturity at 33 to 34 weeks. Carr et al<sup>58</sup> reported that fetal mortality does not increase in monoamniotic twins after 30 weeks' gestation. A literature review by Roque et al<sup>59</sup> summarizing the outcomes of 133 monoamniotic-monoamniotic twin pregnancies, however,





A



B

**FIGURE 8-20.** A. Tangled cords in monoamniotic twins. A color flow Doppler sonogram shows flow in entangled umbilical cords conferring monochorionicity. B. Gross pathology of the entangled umbilical cords. (Courtesy of Sjurk Westra, MD, UCLA School of Medicine, Los Angeles, CA.)

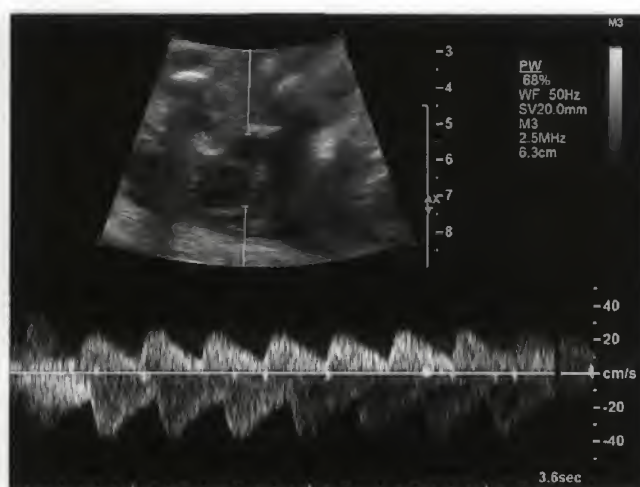


**FIGURE 8-22.** Doppler flow of entangled cords showing bidirectional arterial flow at different heart rates that has been called "galloping" fetal heart rates.

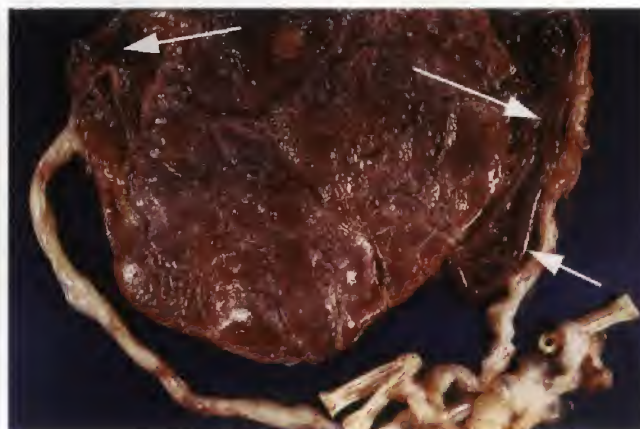


**FIGURE 8-23.** Velamentous cord insertions (arrows) on both placentas of a monochorionic-monoamniotic twin pregnancy. (Courtesy of Melinda Sanders, MD, and Erika Walz, PA, University of Connecticut Health Center, Farmington, CT.)

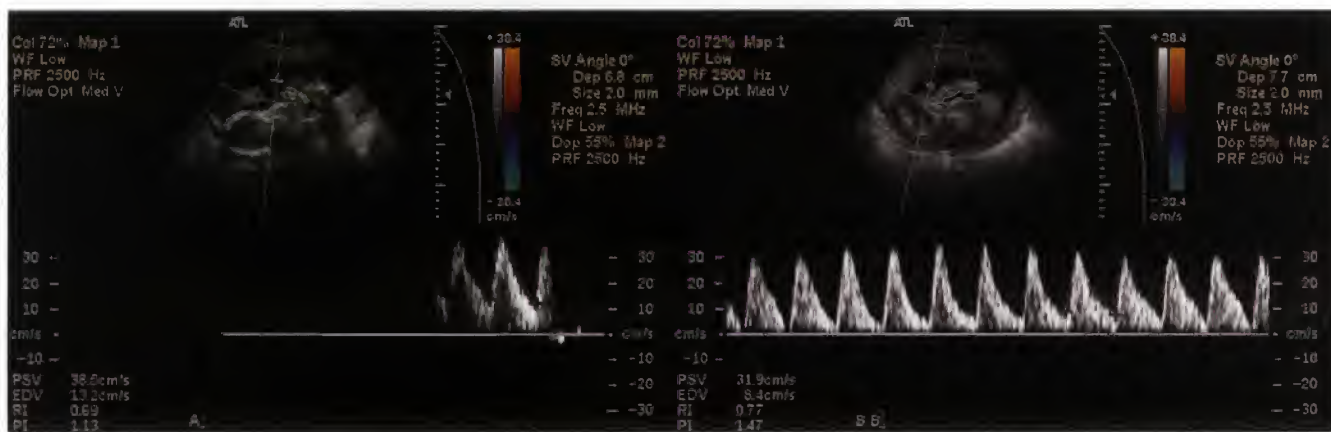


**FIGURE 8-21.** Pulse wave Doppler of the umbilical arteries in a monochorionic-monoamniotic twin pregnancy. Twin A shows normal diastolic flow, whereas twin B has diminished diastolic flow suggesting increased pressures downstream due to cord compression.

reported a significant increase in perinatal loss after 32 weeks' gestation and recommended elective delivery at 32 weeks. An 11-center retrospective report on 96 monochorionic-monoamniotic twin pregnancies showed that intense inpatient fetal surveillance was superior to less intense outpatient fetal surveillance.<sup>66</sup> There was a 14.8% risk of intrauterine fetal loss in the 44 pregnancies managed as outpatients, although there were no fetal losses in the group admitted for monitoring. The protocols differed in the two arms of the study, however, and the results are therefore not comparable. The outpatient management consisted of electronic fetal monitoring one to three times per week compared with 1 hour, two to three times daily for the inpatient group. Thus, it is unclear if daily outpatient testing would accomplish similar results to those provided by the inpatient protocol. All studies on monochorionic-monoamniotic twins agree that they present the caregiver with a very high-risk clinical problem and require intense fetal surveillance beginning at viability and ending in a premature, often planned cesarean birth.

## CONJOINED TWINS

The rare phenomenon of conjoined twins occurs in a monochorionic monoamniotic twin when the embryo divides at 13 to 15 days from conception (see Figs. 8-3, 8-4, and 8-5). The two fetal poles may be attached at varying sites (Table 8-4). The location of the shared sites provides the basis for the nomenclature describing conjoined twins. The most common conjoined twins are the omphalopagus or thoracopagus twins, which are joined at the abdomen or chest respectively (Fig. 8-24).<sup>67</sup>

Ultrasound features of conjoined twins include visualizing the twins in the same relative positions in all views, direct opposition of the twins from each other, and extreme extension of the fetal spine.<sup>68</sup> Inseparable skin contours must

be persistent and at the same anatomic level to avoid a false diagnosis. An early ultrasound finding suggestive of conjoined twins is a bifid appearing fetal pole (Fig. 8-25).<sup>69</sup> Several pitfalls in the diagnosis have been described. Diamniotic twins in close proximity with a dividing membrane that is difficult to visualize may lead to a false-positive diagnosis. If the conjoined twins are very anomalous, a singleton fetus may be falsely diagnosed.<sup>70</sup> Finally, a discordant presentation (breech, vertex) may occur if the connection site is pliable.<sup>71,72</sup>

Numerous variations in the types of conjoined twins may occur, and the prognosis for survival is generally very poor.<sup>72</sup>

**Table 8-4** Types of Conjoined Twins

Inferior conjunction: lower body in single or twins joined by some lower portion of body
Diprosopus: two faces with one head and body
Dicephalus: two heads with one body
Ischiopagus: joined by inferior sacrum and coccyx
Pygopagus: joined by posterolateral sacrum and coccyx
Superior conjunction: upper body is single or twins joined by some upper portion of body
Dipygus: single head, thorax, abdomen with two pelvis and four legs
Syncephalus: facial fusion with or without thoracic fusion
Craniopagus: joined at the head
Middle conjunction: fusion of midportion of the body, separate above and below
Thoracopagus: thoracic fusion
Omphalopagus (xiphopagus): joined from umbilicus to xiphoid cartilage
Thoraco-omphalopagus: thoracic and abdominal fusion
Rachipagus: vertebral fusion above sacrum

Adapted from Guttmacher AF, Nichols BC: Teratology of conjoined twins. Birth Defects 3:3, 1967.

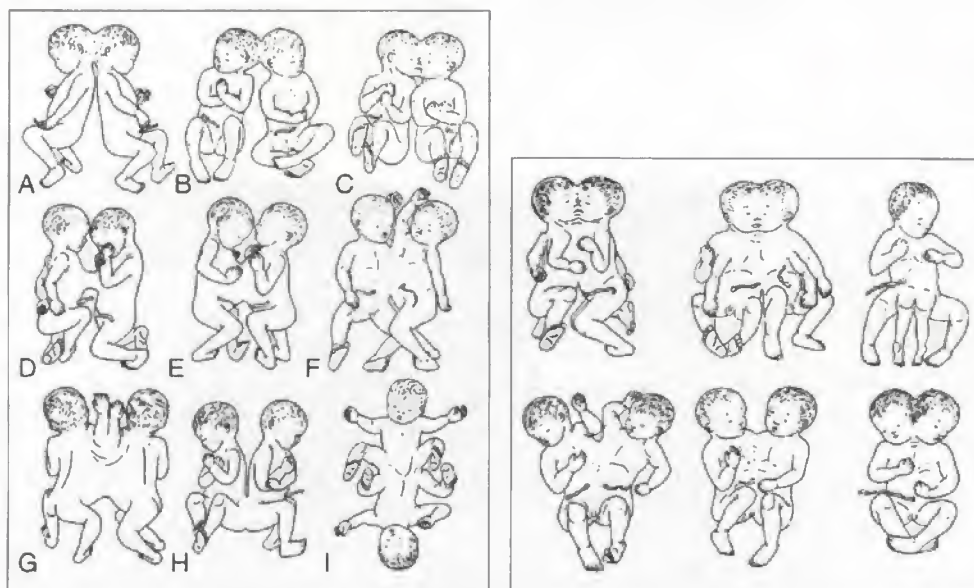


**FIGURE 8-24.** Different types of conjoined twins. Left, Cases of limited fusions in which heads and limbs are separate and retain their identity. A to C, craniopagus; D to G, thoracopagus; H and I, pygopagus. Right, Cases of more extensive fusion. (From Patten BM: Human Embryology, 3rd ed New York, McGraw Hill, 1968.)



When conjoined twins are diagnosed, there should be a systematic approach to define which major organs are present in each fetus, which are shared, and what vascular communications are present.<sup>72</sup> Detailed scanning or fetal magnetic resonance imaging at 20 weeks or more provides a reliable picture of structural anomalies and of shared viscera. Fetal echocardiography is especially informative with thoracopagus conjoined twins (Fig. 8-26).<sup>73</sup> Spitz et al<sup>74</sup> reviewed the ultrasound diagnosis and prognosis of conjoined twins. Sharing of the cardiac and liver structures is not uncommon, and fetuses with a shared heart have a particularly bad prognosis.<sup>74</sup> The previously mentioned steps help determine

the prognosis for postnatal separation. A review of the experience at the Children's Hospital of Philadelphia, described 14 sets of conjoined twins.<sup>75</sup> Ten of the 14 were thoracoomphalopagus (Fig. 8-27). Associated anomalies included cardiac malformations in 11 of 14, congenital diaphragmatic hernia in four of 14 and abdominal wall defects in two of 14. Only 5/28 individual newborns survived after separation highlighting the grave prognosis.

The first trimester diagnosis of conjoined twins has also been described (see Fig. 8-25). In a review of the literature, Pajkrt and Jauniaux<sup>76</sup> reported that monochorionic-monoamniotic twins may be misdiagnosed as conjoined twins owing to limited fetal movement. They also reported that in pregnancies that continued after the diagnosis of conjoined twins, approximately one half died in utero and another 44% died during the neonatal period.

### "STUCK" TWIN

An ominous ultrasound finding is the "stuck" twin. In this setting, one twin has normal or increased amniotic fluid and the other has severe oligohydramnios that makes that amniotic



**FIGURE 8-25.** Dicephalus-conjoined twins seen on an 11-week ultrasound. Two fetal heads (*arrows*) and a single thorax and abdomen are seen.



**FIGURE 8-27.** Newborn conjoined thoraco-omphalopagus twins.



**FIGURE 8-26.** Thoracopagus twins showing shared great vessels (*arrow*) using grayscale and color Doppler imaging.



**FIGURE 8-28.** Thin membrane (arrow) reflecting between the head and the back of the thorax in the oligohydramniotic sac of the "stuck" twin.

sac adhere to the sidewall of the uterus and confines the fetus to that area of the uterus. There are several causes of a stuck twin including bilateral, renal agenesis or other renal anomalies in the affected twin, severe growth restriction with oligohydramnios, or TTTS.<sup>77</sup> To diagnose a stuck twin, the sonographer/sonologist must perform a careful evaluation, looking for a dividing membrane. The fluid around the unaffected twin may be normal, but it is increased if TTTS is the cause.<sup>78</sup> The most informative areas around the fetus to find the dividing membrane are near the fetal neck, chin, or limbs. This is where a thin membrane may be seen bridging the gaps between fetal small parts (Fig. 8-28). The pregnant mother can be shifted from side to side to assure that the stuck twin does not move in the amniotic cavity. The diagnosis of a stuck twin is made when there is normal fluid or polyhydramnios around one twin, severe oligohydramnios around the stuck twin, and an adherent membrane is seen encasing this fetus and restricting fetal movement in the uterine cavity (Fig. 8-29). In some cases, the membranes around the stuck twin may form a "sling" (Fig. 8-30). The cause of the stuck twin must then be determined. A careful evaluation may reveal fetal anomalies to explain the oligohydramnios such as bilateral renal agenesis or multicystic dysplastic kidneys. These may be difficult to diagnose with the oligohydramnios but would be suggested by normal, rather than increased, amniotic fluid around the unaffected twin. Diagnostic amniocentesis improves the prenatal diagnosis of fetal anomalies and may help to diagnose ruptured membranes in cases of oligohydramnios.<sup>79,80</sup> The amniocentesis of fluid around a stuck twin also improves the ability of the sonographer to perform a more informative anatomic survey. The instilled fluid can be aspirated for karyotype and infection studies.

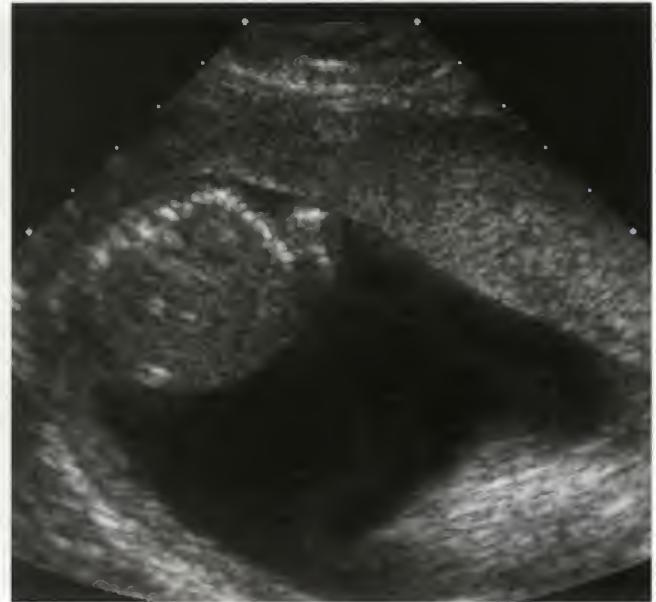


**FIGURE 8-29.** "Stuck" twin. Note the position of the fetus stuck against the right anterior wall of the uterus. The fetal position persisted despite maternal position change. The membrane is not visible in this image.

## TWIN-TO-TWIN TRANSFUSION SYNDROME

If the evaluation of the stuck twin has some, or all of the following features, the diagnosis of TTTS must be considered:

Monochorionic placentation

Same sex fetuses

Oligohydramnios (see Fig. 8-29) around one twin and polyhydramnios around the other

Velamentous cord insertion (see Fig. 8-23)

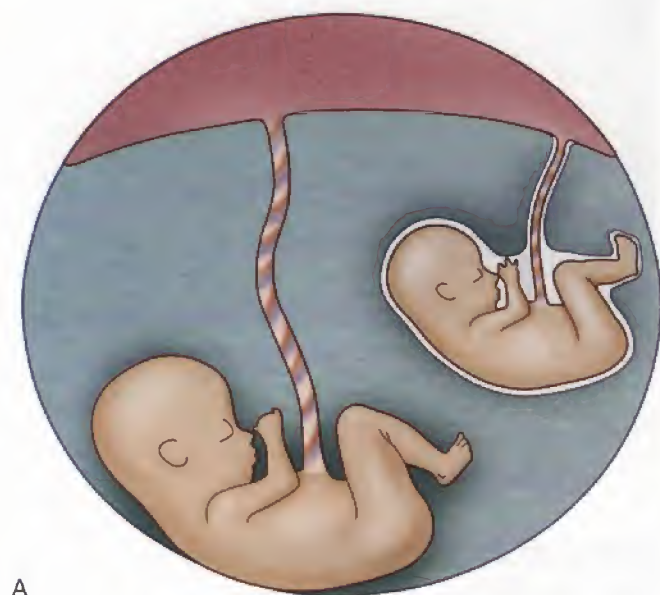
An enlarged bladder in the recipient twin, who has polyhydramnios (Fig. 8-31)

No bladder seen in the donor twin

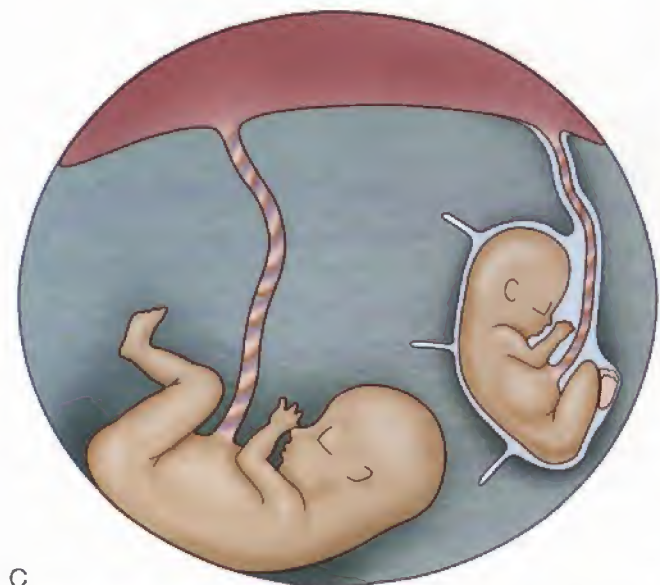
Size discrepancy with the recipient twin significantly larger than the donor

Ultrasound is extremely helpful in establishing the diagnosis and improving the survival of infants with TTTS. There are numerous theories about the pathophysiology of TTTS including abnormal placentation, unbalanced vascular communications, and velamentous cord insertion. Vascular communications are found in up to 98% of monochorionic placentas. Therefore, unidirectional or unbalanced blood flow is necessary to explain the changes noted in TTTS.<sup>77</sup> These anastomoses may be arterial to venous (AVA) (Figs. 8-32 and 8-33), arterial to arterial (AAA), and venous to venous. AVA anastomoses are commonly present in monochorionic placentas. In fact, the majority of monochorionic-diamniotic placentas have AVA connections, often greater than one and often bidirectional. The presence of such a connection does not necessarily result in TTTS. Fichera et al<sup>81</sup> evaluated the use of Doppler ultrasound to detect AAA in monochorionic-diamniotic twin pregnancies.





A



C



B



D

**FIGURE 8-30.** Twin-to-twin transfusion syndrome (TTTS) with a "sling" around the "stuck" twin. When there is little to no amniotic fluid in the amniotic sac of the donor "stuck" twin, the membrane appears as a sling around the fetus. In the absence of amniotic fluid in this sac, the fluid surrounding this twin may wrongly be assumed to be in its sac, when in fact it is the fluid in the adjacent recipient twin's sac with polyhydramnios. A. A pregnancy with TTTS in which the fetus on the right is enshrouded by its membrane in an oligohydramniotic sac. B. In this case of TTTS, the donor twin is in an anhydramniotic sac. The apposed membranes appear as a single membrane (arrow). The surrounding amniotic fluid (asterisks) is in the other twin's amniotic sac. C. A pregnancy with TTTS in which the fetus on the right is enshrouded by its membrane in an oligohydramniotic sac. Redundant amnion is seen projecting from the fetus and at times presents a confusing appearance. D. Scan of a donor fetus with severe oligohydramnios and redundant amnion (arrow) seen projecting into the amniotic fluid of the other fetus. (A and C courtesy of Vickie A. Feldstein, MD, University of California School of Medicine, San Francisco, CA.)

They are important because they appear to function as a compensatory mechanism for the other vascular imbalances. Superficial chorionic vessels between the cord insertions were identified by color, and the vessels were interrogated with pulsed wave Doppler.<sup>82</sup> AAA were documented by the presence of bidirectional arterial flow in these vessels (see Fig. 8-33E). The presence of AAA was associated with a lower likelihood of TTTS. If TTTS did develop, it was generally not severe.<sup>82</sup> Several studies have identified early ultrasound findings in monochorionic-diamniotic pregnancies that may predict TTTS, such as an increased nuchal translucency or alterations of flow in the fetal ductus venosus (Fig. 8-34).<sup>82,83</sup> The in utero transfusion often leads to anemia in the donor and polycythemia in the recipient twin, which may be reflected in the placenta after delivery (Fig. 8-35).

Quintero et al<sup>84</sup> defined severe TTTS as the presence of polyhydramnios (maximum vertical pocket of amniotic fluid of  $> 8$  cm) and oligohydramnios (maximum vertical pocket of amniotic fluid of  $< 2$  cm). He proposed a staging system

using visualization of the bladder in the donor twin, the presence or absence of hydrops in either twin, pulsed Doppler studies of the middle cerebral artery, umbilical artery and umbilical vein, and the demise of one or both twins (Fig. 8-36). In stage I, the bladder of the donor twin was still visible, whereas in stage II, the bladder was not visualized but the Doppler studies were normal. By stage III, there were Doppler abnormalities; in stage IV, hydrops was present; and in stage V, there was a demise of one or both twins (Table 8-5). Taylor et al<sup>85</sup> found that although this staging system was not useful for prediction of fetal outcome on initial evaluation, an increase in stage carried with it a higher risk of earlier perinatal loss. Thus, staging may be more useful in monitoring disease progression. Untreated TTTS that develops earlier than 26 weeks has a perinatal mortality rate of 90%.<sup>86</sup>

A systematic approach should be used in the management of TTTS. We suggest documenting the maximum fluid pocket around the recipient twin, visualization of the fetal bladders, establishing growth curves for each, evaluating the cervical length, and performing pulsed wave Doppler of the umbilical arteries of each fetus. If the amniotic fluid volume becomes excessive around the recipient, the cervical length is becoming shorter, or Doppler interrogation reveals absent or reverse end-diastolic velocity, intervention should be considered (see Fig. 8-36). Hydrops in either the donor or recipient fetus can occur and therapy at this point should be directed at optimizing the outcome for the nonhydropic fetus.

There are several treatment protocols for TTTS, although evidence is mounting that the preferred therapy for severe TTTS is laser photocoagulation of the communicating vessels. Therapies include serial amnioreductions of the polyhydramnios around the recipient twin, needle hole septostomy of the intervening twin membrane, laser ablation of the communicating placental vessels, and cord ligation of one twin, usually the anomalous or hydropic fetus. Pregnancy termination may be considered in cases with very early onset and severe findings. The risks and



**FIGURE 8-31.** Enlarged fetal bladder (arrow) noted in a recipient twin in twin-to-twin transfusion syndrome.

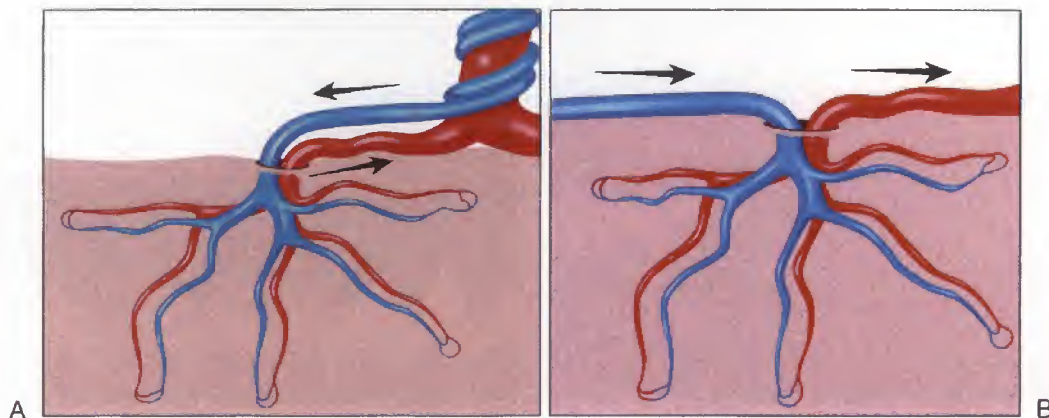


**FIGURE 8-32.** Illustrations of (A) normal-paired branch vessels from the umbilical cord and (B) arteriovenous anastomosis in monochorionic twin placenta. A, Normal paired branches of the umbilical artery (blue) and umbilical vein (red) are seen coursing together on the fetal surface of the placenta. Blood flows from the umbilical cord toward the placenta by way of the umbilical artery and returns by way of the umbilical vein. B, Unpaired vessels course on the fetal surface of the placenta. A branch of the donor umbilical artery (blue) meets a branch of the recipient umbilical vein (red) where they enter and exit the placental cotyledon by way of a common foramen. Note that the arteriovenous communication occurs deep within the placenta. (Courtesy of Vickie Feldstein, MD, University of California, San Francisco, School of Medicine, San Francisco, CA.)



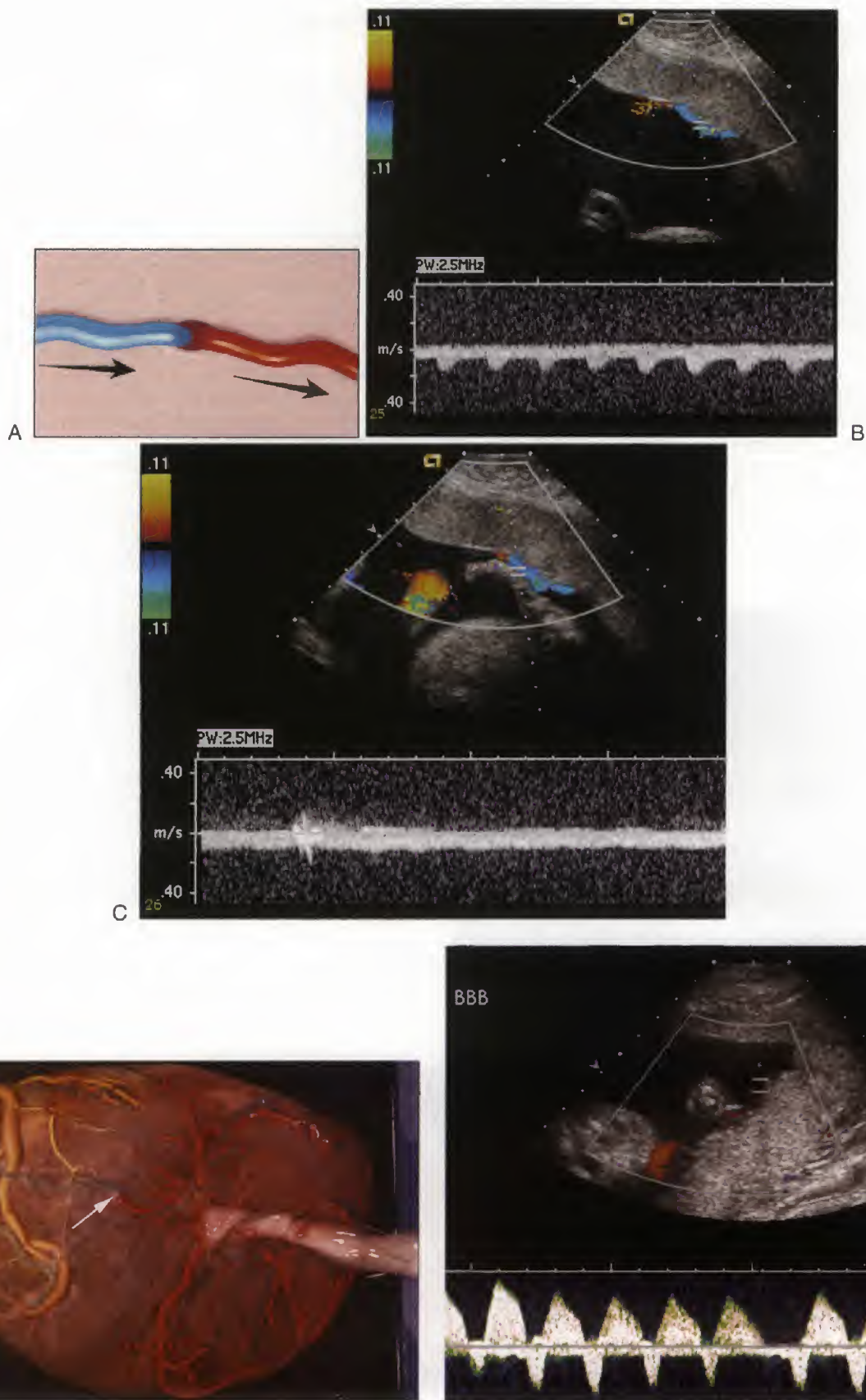


**FIGURE 8-33.** Color and pulsed Doppler of the surface-communicating vessels in monozygotic twins. **A.** Arteriovenous anastomosis in a monozygotic placenta. Overview from the fetal surface of the placenta shows feeding branch of umbilical artery from donor (blue) and draining branch of umbilical vein of recipient (red) entering the placenta via a common foramen. **B, C.** Color Doppler ultrasound study demonstrates an unpaired vascular structure on the placental surface. Spectral Doppler waveforms reveal a feeding arterial branch (**B**) and draining venous branch (**C**), with flow directed from the donor toward the recipient. (Courtesy of Vickie Feldstein, MD, University of California, San Francisco, School of Medicine, San Francisco, CA.) **D.** Placental pathology injection study showing an A-V anastomosis (arrow) with donor-feeding arterial branch blue and recipient-draining venous branch red. (Courtesy of Geoffrey Machin, MD, Permanente Medical Group, Oakland, CA.) **E.** Pulsed-wave color Doppler insonation of placental surface vessel showing the characteristic periodic bidirectional interference pattern of an arterioarterial anastomosis.

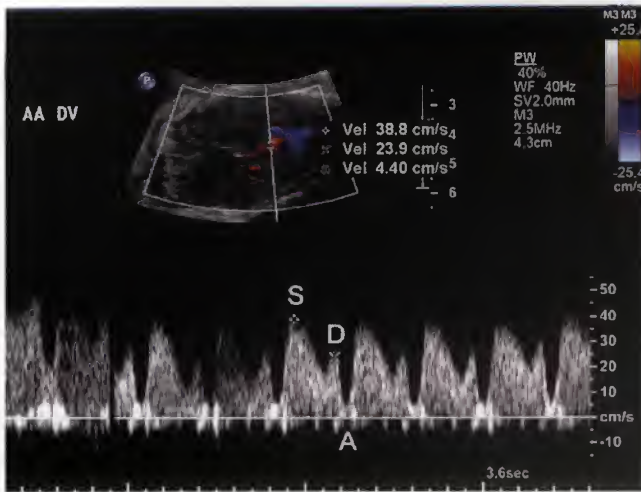


**FIGURE 8-34.** Twin A with reduced flow in the ductus venosus during atrial contractions at 23 weeks in a fetus with twin-to-twin transfusion syndrome.



**FIGURE 8-35.** Placenta in a case of twin-to-twin transfusion syndrome. The donor's placental disc is paler, suggesting fetal anemia, whereas the recipient's placental disc is darker, suggesting polycythemia. The donor's hematocrit was 22% and the recipient's was 54%. (Courtesy of Melinda Sanders, MD, and Erika Walz, PA, University of Connecticut Health Center, Farmington, CT.)

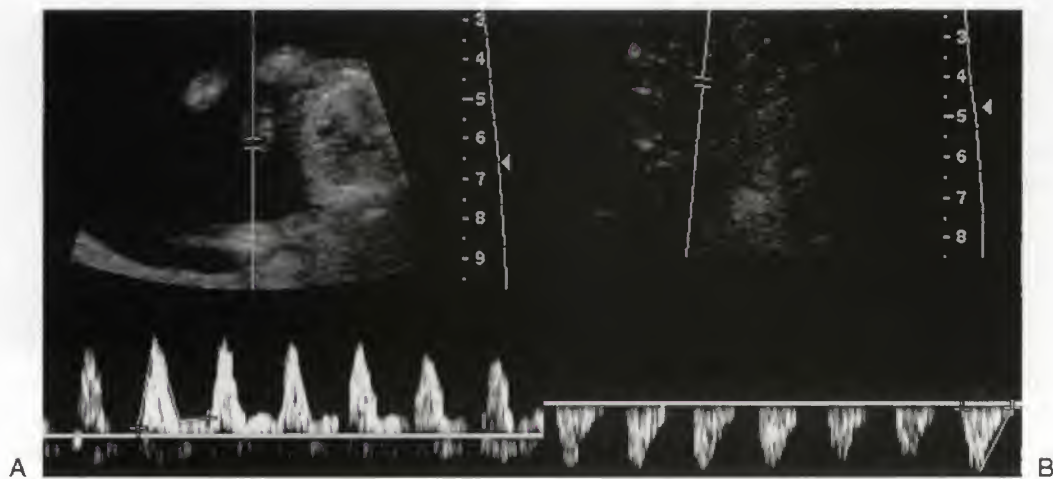


**FIGURE 8-36.** Pulsed wave Doppler in a twin-to-twin transfusion syndrome case with abnormal umbilical artery flow. Note the absent end-diastolic flow for twin B.

**Table 8-5** Staging of Twin-to-Twin Transfusion Syndrome<sup>64</sup>

Stage	Amniotic Fluid	Fetal Bladder	MCA Doppler, Umbilical Artery or Vein	Hydrops	Fetal Demise
I	Donor-oligohydramnios Recipient-polyhydramnios	Normal	Normal	No	No
II	As above	Donor bladder not seen	Normal	No	No
III	As above	As above	Abnormal	No	No
IV	As above	As above	Abnormal	Yes, either twin	No
V	As above	As above	Abnormal	Yes, either twin	Yes, either twin



benefits of each therapy should be carefully discussed. In cases with hydrops of one fetus, cord ligation may be performed after consideration of the impact on the surviving co-twin. As the blood pressure of the dying fetus collapses, the vascular communications between the twins allow blood from the surviving twin to move down the pressure gradient to the dying twin. In this setting, a double fetal death or neurologic impairment of the survivor may occur.<sup>85,87</sup> Sacrificing the hydropic fetus by cord ligation should prevent hypoperfusion of the surviving twin. When one twin has a coexisting major anomaly, cord ligation has been performed.<sup>88</sup>

Therapeutic amniocentesis can be rapidly performed for TTTS as a primary treatment or as a temporizing measure before transfer to a center for laser photocoagulation. Two practical methods have been described. The wall suction method described by Elliott et al<sup>89,90</sup> and the vacuum bottle method described by Dolinger et al.<sup>91</sup> Both adequately remove the excessive amniotic fluid from the recipient twin's sac. We use an 18- or 20-gauge spinal needle and place the needle in the cavity away from the fundus of the uterus. By avoiding the fundus, the needle is less likely to pull out of the amniotic cavity as the uterine fundus shrinks from the decreasing in amniotic fluid volume. Removal of large quantities of amniotic fluid can be achieved safely.<sup>90</sup> A recommended endpoint is a maximum amniotic fluid depth around the recipient twin of 5 to 6 cm. Frequent assessment of fluid, fetal growth, and Doppler flow can be used to guide the timing of repeat procedures.

In some cases, only one therapeutic amniocentesis resolves the oligohydramnios-polyhydramnios seen in TTTS. This finding led to the hypothesis that an amnioseptostomy may be used as a treatment for TTTS.<sup>92</sup> By creating several needle holes in the dividing membrane, one allows free flow of fluid between the sacs, and equilibration of amniotic fluid in the two sacs may be achieved. A randomized trial of 73 pregnancies complicated by TTTS comparing amnioreduction with amniotic membrane septostomy has been performed.<sup>93</sup> The trial was stopped early when an interim analysis found no difference in the primary outcome of at least one twin surviving. In the amnioreduction group, at least one twin survived in 78% of cases compared with 80% in the septostomy group. The only potential advantage was that a single procedure was needed in 68% of the patients treated by septostomy compared with 46% of patients treated by amnioreduction. Concern exists, however, that septostomy may create monoamniotic twins with the potential for cord entanglement.<sup>94</sup> The dividing membrane may also rupture spontaneously leading to monoamniotic twins.<sup>95,96</sup>

Laser surgery to separate the placental vascular communications between monochorionic twins in TTTS has been described.<sup>97</sup> Few centers exist for this technically challenging procedure. The vessels are sometimes difficult to visualize owing to placental location or previous amniocenteses, and preterm labor and rupture of membranes are known complications of the procedure (Fig. 8-37). A randomized trial of pregnancies with severe TTTS diagnosed before 26 weeks' gestation compared laser therapy with serial amnioreduction.<sup>98</sup> The trial was ended prematurely when laser separation study arm showed significantly better survival of at least one twin at 28 days and 6 months of newborn life compared with pregnancies treated by amnioreduction. A more important finding was that more infants were free of

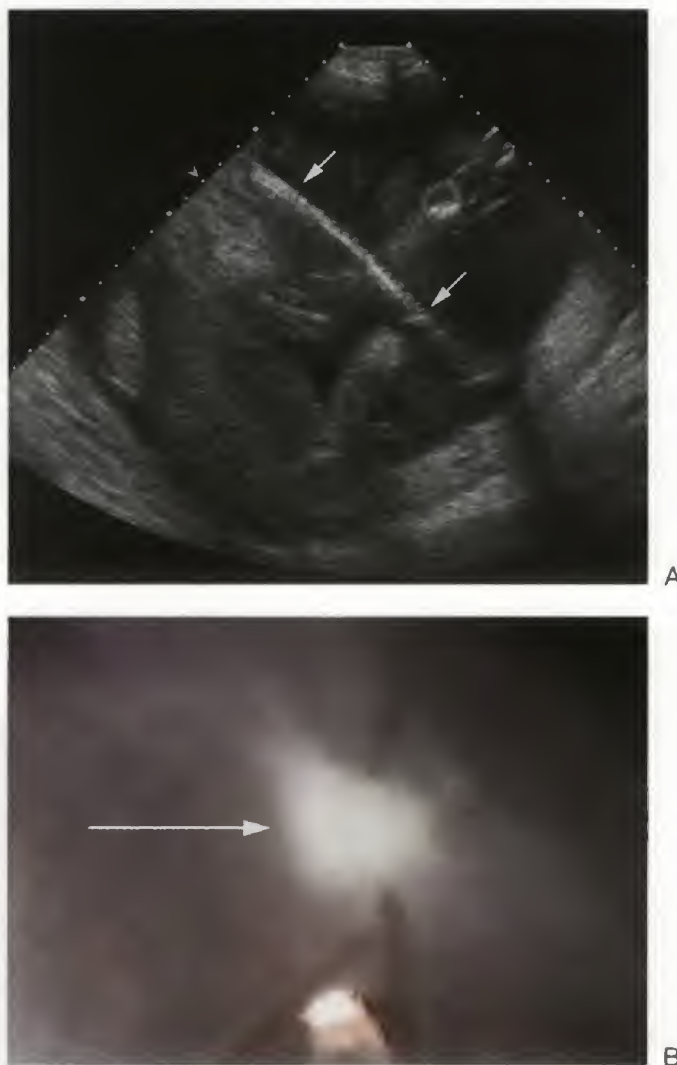


**FIGURE 8-37.** A. Sonogram demonstrating laparoscope with laser (arrows) near an arteriovenous connection on the placental surface. B. Laser cautery of communicating placental vessels (arrow) using fetoscopy. (Courtesy of Julian E. De Lia, MD, St. Joseph Regional Medical Center, Milwaukee, WI.)

neurologic complications at 6 months of age in the laser treated group (52%) than in the amnioreduction group (31%). The interventional trials of TTTS highlight the fact that pregnancies complicated by severe TTTS are at very high risk for obstetric complications including the loss of one or both twins and have the potential for impaired neurologic outcomes in surviving twins despite current treatments.

## ACARDIAC TWINS

An unusual and rare form of monochorionic twins is the acardiac twin. This may represent an extreme form of TTTS. One theory on the pathogenesis of acardiac twins was proposed by Driggers et al.<sup>99</sup> They described the ultrasound and postmortem evaluation of monochorionic twins with an early TTTS. The recipient twin had a severely hypoplastic heart and hydrops. They theorized that the



**FIGURE 8-38.** Acardiac twin with absence of formed cranium. Diffuse anasarca is seen with a focal cystic hygroma (arrow).

early TTTS led to cardiac dysfunction in the recipient twin followed by the twin reverse arterial perfusion (TRAP) of the recipient twin. This perfusion occurs through AAA on the placental surface carrying deoxygenated blood from the umbilical arterial circulation of the donor to the very abnormal recipient twin. The “rescue” of a dying fetus and evolution to an acardiac twin is called the TRAP sequence.<sup>100</sup> This perfusion with deoxygenated blood has been suggested as the mechanism leading to the typical ultrasound findings in acardiac twins. The recipient fetus is oxygenated through reverse flow in its umbilical arteries, which primarily nourish the structures in the lower trunk of the fetus. This preferential circulation to the caudal aspects of the recipient leads to the typical anatomic findings of an absent or vestigial head and heart. Early ultrasound detection of the TRAP sequence may be difficult. The acardiac twin may be mistaken for a fetal demise because no cardiac activity is present. Repeat studies document the acardiac twin. Early findings may also include cystic hygroma or increased long bone length, because the lower extremities of the acardiac twin are often preferentially perfused (Fig. 8-38). The acardiac twin typically has some recognizable fetal features such as limbs or bones, but there is no cardiac activity and major anomalies are the rule. Careful ultrasound examination of the placental surface of the acardiac twin can identify vascular connections to the donor twin through AAA.<sup>101</sup> This leads to flow into the acardiac twin through its umbilical cord (Fig. 8-39).

Doppler ultrasound of the communicating vessels, the size of the recipient twin relative to the acardiac twin, and cardiac dysfunction/hydrops of the donor twin predict the outcome for the donor twin and help direct treatment during pregnancy.<sup>102</sup> In 10 pregnancies, poor outcomes were

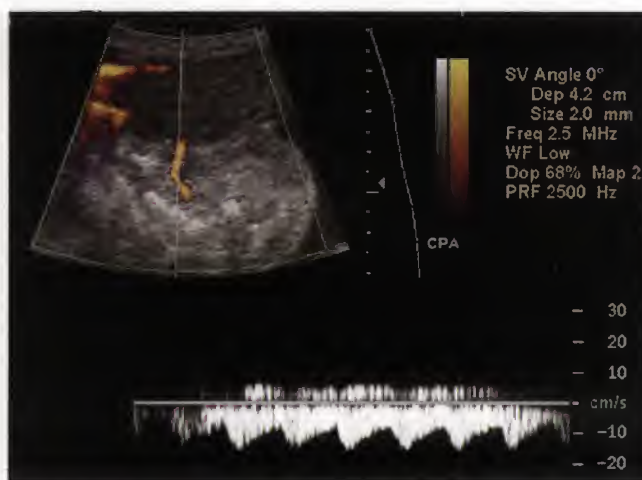


**FIGURE 8-39.** Color and pulsed Doppler imaging of an acardiac twin showing pulsatile flow from the donor twin.



**FIGURE 8-40.** Acardiac twin demonstrating the amorphous, vestigial structures cephalad and caudad as the distance from the umbilical cord arterial circulation increases. (Pathology images courtesy of Melinda Sanders, MD, and Erika Walz, PA, University of Connecticut Health Center, Farmington, CT.)

associated with a rapid growth of the acardiac twin or when the pulsatility index of the perfusing vessel was less than that of the donor twin.<sup>103</sup> Another study compared resistive indices and showed that a large difference ( $> 0.20$ ) in the index between the donor and recipient twin was associated with improved outcomes.<sup>102</sup> The decision to proceed to an ablative procedure requires serial ultrasonographic evaluations. Moore et al<sup>104</sup> reported the outcomes of 49 acardiac twin pregnancies. They found a significant correlation between the weight ratios of the twins. If the size of the acardiac twin exceeded 70% of donor twin's estimated fetal weight, there was a significant increase in preterm birth, polyhydramnios, and heart failure of the pump twin (Fig. 8-40). The weight of the acardiac twin can be estimated in grams by the formula:  $(1.2 \times \text{longest length}^2) - (1.7 \times \text{longest length})$ .<sup>104</sup> Therefore, a relatively large weight of the acardiac twin may



be an indication for prenatal treatment. Other indications for therapy include polyhydramnios, cardiac dysfunction, and hydrops of the pump twin.

Tan and Sepulveda reviewed the literature for pregnancy outcomes after prenatal interruption of the vascular connections to the acardiac twin.<sup>105,106</sup> Of the 71 cases treated by invasive procedures, 40 were treated by cord occlusion and 31 by intrafetal (acardiac twin) ablation of communicating vessels. The overall donor twin survival rate was 76%, with a median gestational age at delivery of 36 weeks. Intrafetal ablation of the umbilical vessels was superior to cord occlusion. It had an 87% success rate compared with 65% for cord occlusion and a mean gestational age at delivery of 37 weeks compared with 32 weeks for cord occlusion. The methods of intrafetal ablation of the communicating vessels included alcohol, monopolar diathermy, interstitial laser, and radiofrequency. Radiofrequency ablation appears to be the most efficacious. If the acardiac mass remains small compared with the donor fetus, complications are less likely.

## ANEUPLOIDY SCREENING IN TWIN GESTATIONS

Advancing maternal age is a known risk factor for autosomal trisomies, the most common of which is Down syndrome. The average age of a woman delivering twins in the United States has increased from 27.8 years of age in 1991 to 29.3 in 2001.<sup>107,108</sup> The average age for all mothers in the United States in 2001 was 27.4 years of age. The percent of all mothers 35 years of age or older giving birth has increased from 8.9% in 1990 to 13.7% in 2002. Of all women delivering multiple gestations, the percentage of women 35 years of age or older has increased from 11.4% in 1990 to 21% in 2001.<sup>4</sup> Thus, mothers of twins are older and have an a priori increased risk for Down syndrome. Advances in reproductive technology have also played a major role in the increase in multiple gestations in the United States. Women using assisted reproductive technology are more likely to be older and in their later reproductive years.

The risk of Down syndrome in a twin pregnancy is greater than the age-specific risk in a singleton gestation. The precise difference, however, is difficult to determine. Rodis et al<sup>109</sup> calculated a theoretical maternal age-specific risk for Down syndrome in twin pregnancies. They assumed that the probability of Down syndrome was independent among the twins and that survivals were comparable with singletons. They stated that a risk of one, or the other, or both twins being affected was approximately 80% higher than the singleton maternal age-specific risk. This risk approximated the singleton risk of a woman 2 or 3 years older. Lee et al<sup>110</sup> used a similar model but corrected for maternal race and zygosity. They concluded that the twin risk per pregnancy approached that of the singleton risk for a mother 3 or 4 years older. For example, a woman 32 years of age carrying twins would be quoted a Down syndrome risk for that pregnancy equal to that of a woman 35 or 36 years of age with a singleton pregnancy.

These theoretical estimates did not correspond to data on live-born twins. Wald et al<sup>111</sup> found a lower risk of Down syndrome in twins than the Rodis or Meyers studies postulated. In a meta-analysis of four cohort studies of 64

Down syndrome twins, the live birth prevalence of Down syndrome in twin pregnancies was only 18% higher than singletons. They concluded that the risk for a twin pregnancy resulting in a live-born with Down syndrome does not differ significantly from that of a singleton gestation. Doyle et al<sup>112</sup> in a study of 106 twin live births with Down syndrome found an even greater disparity from the theoretical estimates. He found that the prevalence was only 3% higher than singletons. This discrepancy between the estimated and the observed live-born twins may be explained by a higher intrauterine lethality for Down syndrome affected twins. Therefore, the prevalence of Down syndrome may be higher in the first and second trimester than at birth.<sup>3</sup>

Antenatal screening for Down syndrome in a twin gestation uses the same principles and methods generally applied to singletons, that is, maternal age, serum screening, and ultrasound. These modalities are employed to better estimate the specific risk of Down syndrome for that pregnancy. An antenatal diagnosis may be made by either chorionic villous sampling or amniocentesis. Both the screening and the diagnosis are complicated by the fact that the fetuses may be discordant for abnormal ultrasound findings and for aneuploidy, and that an invasive test, or fetal intervention, places both fetuses at risk.

Using live-birth data to assess Down syndrome risk in the second trimester requires a correction for fetal losses in both affected and unaffected pregnancies. With twin gestations, two corrections are necessary. The first is for the natural losses seen in the second and third trimesters for unaffected and Down syndrome fetuses, and the second is for the differential in twin losses based on chorionicity. Unaffected singletons have a loss rate of 1.46% from the midtrimester to term,<sup>113</sup> whereas 15.7% of singleton Down syndrome fetuses are lost from 16 weeks to term. Estimates of loss for Down syndrome twins from the second trimester to term are not available. Using birth certificate data and observed-to-expected Down syndrome ratios, we estimated the live-born Down syndrome incidence in 1990 and the yearly incidence from 1995 to 2000.<sup>107</sup> There was a 1.8-fold increase in the contribution of multiples to Down syndrome live births from 2.6% in 1990 to 4.6% by the year 2000 (Table 8-6).<sup>3</sup>

This increase in Down syndrome fetuses in multiple gestations reinforces the need for Down syndrome screening. We have reviewed the lack of consensus on the age-related Down syndrome risks for twins. Maternal serum tests also use different norms (approximately twice the value used in singletons if the analyte is higher in Down syndrome pregnancies, or one half if the analyte is lower in Down syndrome) that factor in the contribution of both fetuses. Because fetuses can be discordant for aneuploidy, the individual contribution of each fetus to the serum analytes is not known. Therefore, the serum screen results are averaged for the pregnancy. Testing for Down syndrome in the first trimester uses serum screening with pregnancy associated plasma protein A (PAPP-A) and the free beta subunit of human chorionic gonadotropin (hCG). Spencer et al<sup>114</sup> found that the normal PAPP-A in twins was 1.86 multiple of the median (MoM) greater than in singletons and the free beta was 2.099 MoM. Ultrasound screening requires that both fetuses are imaged and implies that structural markers or anomalies in twins carry with them similar implications for Down syndrome (likelihood ratios) and other aneuploidies.



**Table 8-6** Contribution of Multiple Gestations to Down Syndrome Livebirth Prevalence<sup>3</sup>

Year	Total Live Births	Total Down Syndrome*	Down Syndrome from Multiple Gestations	% Down Syndrome from Multiple Gestations
1990	4,158,212	5900	152	2.6%
1995	3,899,589	6292	174	2.8%
1996	3,891,494	6498	231	3.6%
1997	3,880,894	6629	271	4.1%
1998	3,945,192	6850	294	4.3%
1999	3,963,465	6955	315	4.5%
2000	4,063,823	7264	334	4.6%

\*Assuming no antenatal intervention.

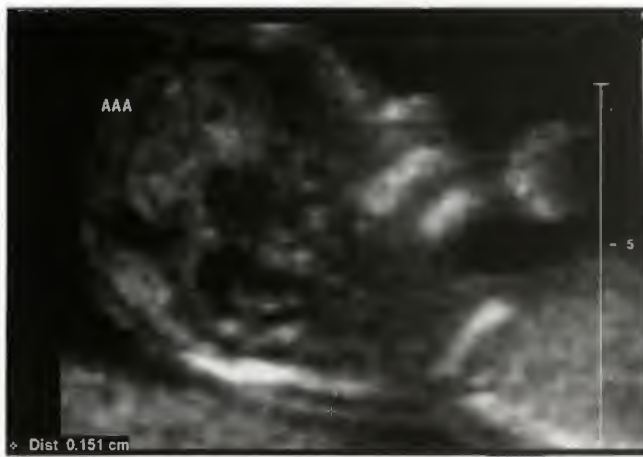


**FIGURE 8-41.** Nuchal translucency in a twin gestation generally differs even in monozygotic-diamniotic twins.

First trimester ultrasound is performed to assess nuchal translucency (Fig. 8-41). Normative measures of nuchal translucency in unaffected and fetuses with Down syndrome are approximately the same in both singletons and twins. Maymon et al<sup>115</sup> reported agreement of the mean nuchal translucency in singletons (1.5 mm/0.5) and in twins (1.5 mm/0.17). When evaluated using the mean MoM standard deviation (SD), the nuchal translucency MoM for singletons was 0.9 (0.5), whereas in twins, it was 0.9 (0.4). There was no statistically significant difference in either the actual values or the MoMs for nuchal translucency.

Spencer<sup>114</sup> developed a theoretical first trimester twin Down syndrome detection model using a fixed 5% false-positive rate. Nuchal translucency and maternal age detected 75.2% of both discordant (that is, one twin positive and one twin negative) and concordant Down syndrome twins. Using free beta hCG, PAPP-A, and maternal age, there was a 51.5% detection rate if the twins were discordant for Down syndrome and 55.4% detection rate if they both had Down syndrome. When age, the serum screen, and ultrasound were combined in the first trimester (that is, nuchal translucency, free beta hCG, PAPP-A, and maternal age), there was a 79.7% detection rate in twins discordant for Down syndrome and an 81.3% detection rate if both had Down syndrome.

Although first trimester screening is becoming more popular, most Down syndrome screening in the United States is still done in the second trimester. A survey of maternal fetal medicine specialists in the United States in 2001 revealed that of the time they spent on antenatal diagnosis, 87.3% was devoted to second trimester screening and 12.7% to first trimester screening.<sup>116</sup> Second trimester screening also uses maternal age, the serum screen, and ultrasound, or some combination of the three. The second trimester serum screen values for twins are also approximately twice (or one half) the level of singleton norms. Wald et al<sup>117</sup> reported that the mean MoMs for twins were 2.23 for the maternal serum alpha-fetoprotein, 1.65 for estriol, 2.01 for hCG, and 1.99 for inhibin-A. Neveaux et al<sup>118</sup> estimated the second trimester serum screen values for Down syndrome twins depend on whether one or both of the fetuses are affected. If one twin was affected, the maternal serum alpha-fetoprotein was 1.89 MoMs, whereas if both were affected, it was 1.62 MoMs. The estriol was 1.47 MoM if one twin was affected and 1.22 MoM if both were affected, whereas the hCG was 3.26 MoM if one was affected and 4.51 MoM when both were affected. Maymon et al<sup>115</sup> estimated the false-positive rates for second trimester serum screening and determined the amniocentesis rates in twins versus singletons. The false-positive rate for the triple test in twins was higher at 15% compared with 6% in singletons, and the amniocentesis rate was 18.3% in twins and 7.5% in singletons. The differences in both the false-positive and amniocentesis rates were statistically significant. A summary of the efficacy of antenatal Down syndrome screening in twins can be seen on Table 8-7.

**Table 8-7**

### The Efficacy of Antenatal Down Syndrome Screening in Twins

Test	Sens. (%)	FPR (%)	LR
Maternal age $\geq 35$ : U.S. 2000	50.2	13.4	3.7
First Trimester:			
Maternal age, hCG, PAPP-A <sup>114</sup>	52	5	10.4
First Trimester:			
Maternal age, hCG, PAPP-A, NT <sup>114</sup>	80.3	5	16.0
Second Trimester:			
Maternal age, triple screen <sup>115</sup>	53	5	10.6

FPR, false positive rate; hCG, human chorionic gonadotropin; LR, likelihood ratio; NT, nuchal translucency; PAPP-A, pregnancy associated plasma protein A; Sens., sensitivity.



**Table 8-8**

**The Estimated Down Syndrome Detection Rate in Twins by Chorionicity at a 5% False-Positive Rate Using Maternal Age, Ultrasound, and the Serum Screen<sup>119</sup>**

Twin Pregnancy	Nuchal Translucency (mm) (%)	Combined test (%) <sup>*</sup>	Integrated test (%) <sup>**</sup>
Monochorionic	73	84	93
Dichorionic	68	70	78
All twins	69	72	80
Singletons	73	85	95

<sup>\*</sup>NT, free beta-hCG. PAPP-A at 10-13 weeks with maternal age

<sup>\*\*</sup>NT, PAPP-A at 10 to 13 weeks and AFP, estriol, and free beta-hCG, and inhibin A at 14 to 22 weeks with maternal age.

AFP, alpha fetoprotein; hCG, human chorionic gonadotropin; NT, nuchal translucency; PAPP-A, pregnancy associated plasma protein A

Both first and second trimester serum and ultrasound test results may be combined in the integrated test in singletons and twins. This includes nuchal translucency, PAPP-A, and free beta hCG or hCG in the first trimester and the quad screen in the second trimester. Wald estimated the Down syndrome detection rate in twins by chorionicity at a 5% FPR<sup>119</sup> (Table 8-8).

A survey of maternal fetal medicine specialists in the United States in 2001 found that 97.6% of them used the serum screen for antenatal diagnosis and 91.5% used ultrasound.<sup>116</sup> Those using ultrasound focused on anomalies (83.4%), biometry (77.9%), and the genetic sonogram (77.9%). Of the second trimester markers identified, those most commonly used were major anomalies, cardiac abnormalities, nuchal fold thickness, short femur or humerus, echogenic bowel, ventriculomegaly, and pyelectasis. Those used less than 50% of the time were echogenic intracardiac focus, choroid plexus cyst, two-vessel umbilical cord, clinodactyly, sandal gap deformity, and a wide pelvic angle. When these markers were identified, the Down syndrome risk was modified using likelihood ratios, or the ratio of the incidence of the marker in the exposed (that is, Down syndrome fetuses) over its incidence in the unexposed (that is, unaffected fetuses). This risk modification can be performed when these markers are isolated or when they are found in combination. Using maternal age and the genetic sonogram in singleton pregnancies, the sensitivities for Down syndrome range from 80.5% to 91.2% and the false-positive rates range from 4% to 14%. The extension of this methodology to twin gestations, although intuitively attractive, has not been critically evaluated.

## INVASIVE TESTING IN TWIN GESTATIONS

Invasive testing using either chorionic villous sampling or amniocentesis carries a slightly greater risk than that found in singletons. Ghidini et al<sup>120</sup> reported on 101 twin pregnancies in which an amniocentesis was performed and 108 twins with no amniocentesis. The miscarriage rate for the twin gestations who had the amniocentesis was 3.5% and it was 3.2% without the amniocentesis, demonstrating a slightly higher miscarriage rate in the group with the

amniocentesis. Several other studies quote higher loss rates than singletons; however, most losses are not related to the procedure.<sup>121</sup>

## CERVICAL LENGTH AND SPONTANEOUS PRETERM BIRTH

Twin gestations are at increased risk for preterm delivery (see Fig. 8-10). The mean age at delivery for live-born twins in the United States has decreased from 35.8 weeks' gestation in 1991 to 35.4 weeks' gestation in 2001.<sup>4</sup> Despite the increase in dizygotic twinning from assisted reproductive technologies, and therefore, in dichorionic gestations, the percent of twins delivering at less than 37 weeks has increased from 65% in 1991 to 74.5% in 2001.<sup>1</sup> Cervical length is a predictor of term and preterm delivery in twins. A normal cervical length usually results in a near-term delivery. Imseis et al<sup>122</sup> found that a cervical length of greater than 35 mm between 24 and 26 weeks' gestation indicated a low risk of delivery at less than 34 weeks' gestation in twins. A cervical length of greater than 35 mm had a 49% sensitivity, 94% specificity and 97% positive predictive value for a delivery greater than 34 weeks' gestation. Several studies suggest that a short cervical length at 20 to 28 weeks of gestation places a twin gestation at significant risk of a preterm delivery. Souka et al<sup>123</sup> found that a cervical length measurement of less than 25 mm at 23 weeks' gestation was strongly correlated with a spontaneous preterm delivery. Goldenberg et al<sup>124</sup> compared cervical length with other predictors of twin preterm delivery. Using a cervical length of less than 25 mm at 24 weeks' gestation, they found that it was a better predictor of preterm delivery at less than 32, 35, and 37 weeks' gestation than the presence of bacterial vaginosis, a positive fetal fibronectin, and other risk factors. In the 147 sets of twins, a cervical length of less than 25 mm at 24 weeks was associated with a delivery at less than 32 weeks' gestation in 26.9%. If the cervical length was less than 25 mm at 28 weeks however, only 13.2% delivered at less than 32 weeks' gestation. Guzman et al<sup>125</sup> used a slightly different cervical length cutoff and a different gestational age time frame but arrived at similar conclusions. If the cervical length was less than 2.0 mm between 15 and 24 weeks' gestation, there was a 50% delivery rate at less than 32 weeks' gestation. If the cervical length between 25 and 28 weeks was less than 2.0 mm, the rate of delivery at less than 32 weeks gestation was 16.1%. Table 8-9 summarizes the efficacy of a 23-week cervical length ultrasound to predict a spontaneous preterm delivery in twin gestations. As with almost every complication of twins chorionicity influences the rate of preterm deliveries for a given cervical length. Monochorionic-diamniotic twins have a preterm delivery rate of 9.1% at less than 28 weeks compared with 1.5% for dichorionic-diamniotic twins. Therefore, chorionicity alters the efficacy of cervical length as a screening tool to predict preterm delivery.<sup>126</sup> In general, a short cervix in a monochorionic-diamniotic twin is of more concern than a short cervix in a dichorionic-diamniotic twin.

Newman et al<sup>127</sup> investigated the impact of cervical cerclage on the obstetric outcome of twin gestations with a shortened cervical length in a nonrandomized prospective study. They followed 147 consecutive twin mothers who



**Table 8-9** Efficacy of Cervical Length at 23 Weeks to Predict Spontaneous Preterm Delivery in Twin Gestations

	N	CL ≤ 20 mm (%)	CL ≤ 25 mm (%)	CL ≤ 30 mm (%)	Del. < 32 wks. (%)	Del. < 35 wks. (%)	Sens. (%)	False pos. rate (%)	False neg. rate (%)
Goldenberg et al <sup>124</sup>	147		17.7		8.8		53.8	14.2	5.0
			17.7			32.0	29.8	12.0	27.3
Yang et al <sup>160</sup>	65		9.2		9.2		50.0	5.1	5.1
			9.2			23.1	53.3	8.0	11.5
Vayssiere et al <sup>161</sup>	242			12.8	5.4		46.2	10.9	3.3
	225			12.9		14.7	27.3	10.4	12.2
Guzman et al <sup>125</sup>	131	17.6			9.2		41.7	15.1	6.5
	129	18.0				17.2*	36.4	14.2	13.3
Sperling et al <sup>126</sup>	383		7.6		6.0		30.4	6.1	4.5
			7.6			18.5	19.7	14.1	16.1

\* ≤ 34 weeks.

CL, cervical length; Del., delivery; wks., weeks; Sens., sensitivity; pos., positive; neg., negative.

underwent transvaginal ultrasonographic cervical length measurement between 18 and 26 weeks' gestation. As expected, the risk of preterm delivery increased with decreasing cervical length. Those with cervical lengths less than 25 mm were offered a cervical cerclage. Twenty-one of 128 twin gestations underwent cerclage, for a cervical length of less than 25 mm. When the twin pregnancies were stratified into cervical length quartiles, midtrimester cerclage did not alter the risks of preterm delivery when compared with restricted maternal activity.

## MULTIFETAL PREGNANCY REDUCTION

Owing to the increased risk of prematurity and the concomitant long-term risks of neonatal morbidity associated with higher order multiple gestations, multifetal pregnancy reduction has evolved as a modality to decrease the number of fetuses in the index pregnancy. The early experience reported 85 first trimester reductions in which all but five were reduced from triplets or higher to twins.<sup>128</sup> Reductions were performed with transabdominal injection of intracardiac potassium chloride on dichorionic-diamniotic pregnancies because vascular anastomoses in monochorionic placentas would place the co-twin at risk. The mean gestational age at delivery was 35.7 weeks, but eight pregnancies lost all of the fetuses. A transvaginal approach for the potassium chloride delivery has also been tried.<sup>129</sup> A single center's series of 290 consecutive cases of multifetal pregnancy reduction compared the transabdominal with the transvaginal route. They found a higher total pregnancy loss rate for those performed transvaginally (16.7%) compared with those done transabdominally (2.7%).<sup>130</sup>

Other factors affect the loss rate in multifetal pregnancy reduction. There is a learning curve for the procedure. The pregnancy loss rates for multifetal pregnancy reductions are inversely proportional to the operator's experience.<sup>131</sup> Loss rates also vary by the number of fetuses at the start and at the conclusion of the procedure. In a report of a multicenter experience with 3513 completed reductions, the pregnancy loss rates were 15.4% for a starting number of six fetuses or more, 11.4% for a starting number of five fetuses, 7.3% for a starting number of four fetuses, and 4.5% for a starting number of three fetuses. Loss rates with a final number of

fetuses of three, two, or one were 18.4%, 6.0%, and 6.7%, respectively. In a single-center experience on 1000 consecutive multifetal pregnancy reductions, the overall complete pregnancy loss rate was 5.9%.<sup>132</sup> The loss rate was lowest with a starting number of two fetuses (2.5%) and remained stable for reductions with starting numbers of three, four, or five fetuses but increased thereafter to 12.9% for six or more fetuses. Loss rates also increased as the finishing numbers increased. The rate of prematurity also rose with a higher finishing number. A final number of one, two, or three had a loss rate of 3.5% to 5.5% to 16.7% respectively. The mean gestational age at delivery for final singletons was 37.9 weeks; for twins, 35.3 weeks, and for triplets, 33.5 weeks. Note that these gestational ages are very similar to unreduced pregnancies with a similar number of fetuses. A comparison of reduced twins from triplets to nonreduced twins and triplets also confirmed that pregnancy losses and prematurity can be diminished with multifetal pregnancy reduction.<sup>133</sup> Given the potential impact for pregnancy loss and prematurity associated with a twin gestation, some practitioners now offer the reduction of twins to a singleton gestation.<sup>134</sup> Chorionic villous sampling has been used to guide multifetal pregnancy reduction.<sup>134-136</sup>

## TWINS DISCORDANT FOR ANOMALIES

The finding of an anomalous fetus in a twin gestation is not uncommon.<sup>14</sup> The background risk for major anomalies in all singleton pregnancies is 2% to 3%, and this is doubled for twins. There is a 3-fold increase in anomalies in monozygotic twins that may be related to the underlying cause of monozygotic twinning.<sup>137</sup> Structural cardiac abnormalities in monozygotic twins without TTTS are four times more common than the background risk.<sup>138</sup> The management of one anomalous fetus with a normal co-twin is problematic. The options for addressing this dichotomy depend on the severity of the anomaly, the gestational age at diagnosis, the health of the co-twin and the potential for the anomalous fetus to affect the long-term success of the pregnancy.

When an abnormality is found in one twin, selective reduction of that twin is possible. Evans et al<sup>139</sup> reported on selective reduction in 345 twin pregnancies. The total pregnancy loss at less than 24 weeks was 7% and after 24 weeks



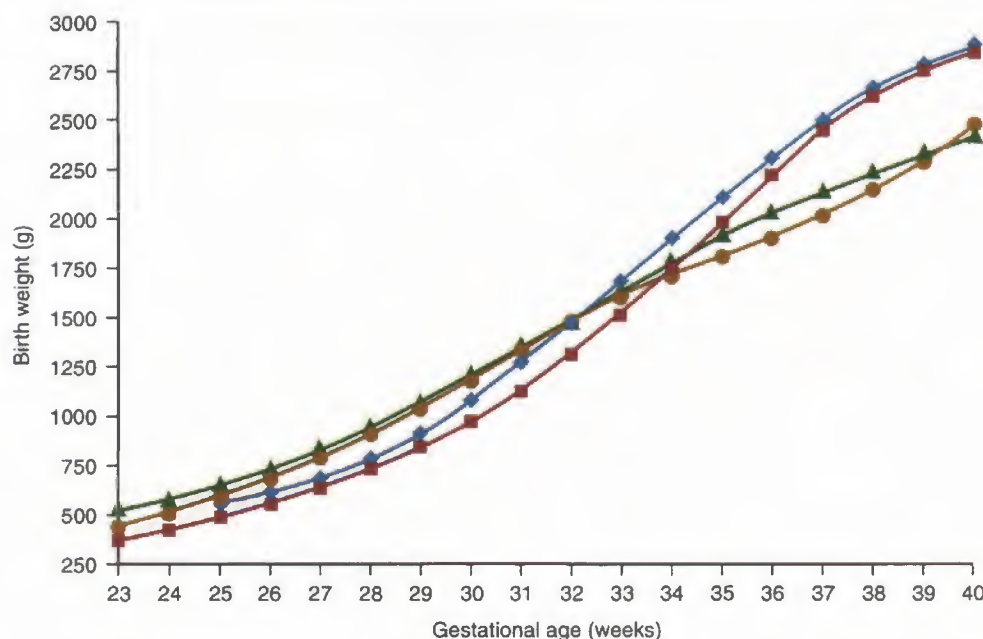


**FIGURE 8-42.** Growth curves for twin gestations by chorionicity. Tenth-percentile growth curves of published nomograms of singletons reported by Brenner WE, Edelman DA, Hendricks CH (squares) and Zhang and Bowes (diamonds) and of monochorionic twins (closed circles) and dichorionic twins (open circles) reported by Ananth CV, et al. (Modified from Ananth CV, Vintzileos AM, Shen-Schwartz S, et al: Standards of birthweight in twin gestations stratified by placental chorionicity. *Obstet Gynecol* 91:91, 1998. Reprinted with permission from the American College of Obstetricians and Gynecologists.)

was 0.9%. Of the twins delivering after 24 weeks, 12.4% delivered between 25 to 32 weeks and 79.8% delivered at greater than 32 weeks. For triplets, the loss rate was 12.8% before 24 weeks and for quadruplets it was 14.3% before 24 weeks.<sup>140</sup>

## METHOD USED FOR SELECTIVE REDUCTION OF THE ANOMALOUS FETUS

Selective termination in a dichorionic twin pregnancy uses transabdominal injection of potassium chloride into the fetal heart. Generally the needle is inserted into the left side of the fetal heart and remains in situ for several minutes to document fetal asystole. Rescanning is usually performed to confirm the fetal demise. Evans published the earliest experience in a multicenter study of 183 cases of selective fetocide.<sup>141</sup> The fetal loss rate before 24 weeks was 8.3% with potassium chloride, and 41.7% with air embolization. A subsequent report of 402 cases using only potassium chloride injection found a 7.5% fetal loss rate before 24 weeks' gestation.<sup>139</sup>

## TWIN GROWTH

An important and easily obtained measure of fetal well-being in a multiple gestation is fetal growth. Growth discrepancy is calculated by subtracting the estimated fetal weight of the smaller fetus from the larger fetus and dividing by the weight of the larger fetus. Discordant birthweight is a diagnosis made on serial ultrasound examinations that can predict adverse pregnancy outcomes, especially for the smaller fetus.<sup>142-144</sup> However, even in very discordant twins,

the size of the smaller fetus may frequently be appropriate for gestational age.<sup>144</sup> Yinon et al<sup>145</sup> has shown that in a small-for-gestational-age discordant twin, there is a much higher risk for adverse outcome than in an appropriate-for-gestational age discordant twin. Prospectively, therefore, pregnancy management should not be based on discordance alone. Additionally, there is controversy over the degree of discordance that can accurately be predicted by a single ultrasound examination.<sup>146,147</sup> Serial biometry is a more accurate method to predict problematic discordant fetal growth.<sup>148,149</sup> Twin growth is similar to that of singletons until 30 to 32 weeks' gestation and varies by chorionicity as seen in Figure 8-42.<sup>150,151</sup> After 32 weeks, the placental reserve may limit fetal growth, leading to an asymmetric growth pattern (that is, lag in the abdominal circumference) seen in the third trimester. This asymmetric pattern typical of intrauterine growth restriction predicts the increased potential for adverse pregnancy outcomes.<sup>152,153</sup>

Because twins are at greater risk for growth abnormalities, they are followed more frequently than singleton gestations. The minimum time between ultrasound examinations to determine that the weight difference, that is, from that found on the previous scan, is meaningful is two weeks.<sup>154</sup> Serial ultrasound examinations are usually performed in twin gestations at monthly intervals for normally growing twins and at 2-week intervals when growth abnormalities are documented or suspected. Monochorionic twins are at greater risk of growth disturbances, especially from 16 to 22 weeks and are followed at 1- to 2-week intervals during this time frame to screen for TTTS (see Fig. 8-7).<sup>32</sup>

First trimester discordance in size can also be useful for predicting potential adverse outcomes. Kalish showed that a crown rump length (CRL) discordance greater than 10% among 159 twins between 11 and 14 weeks was associated

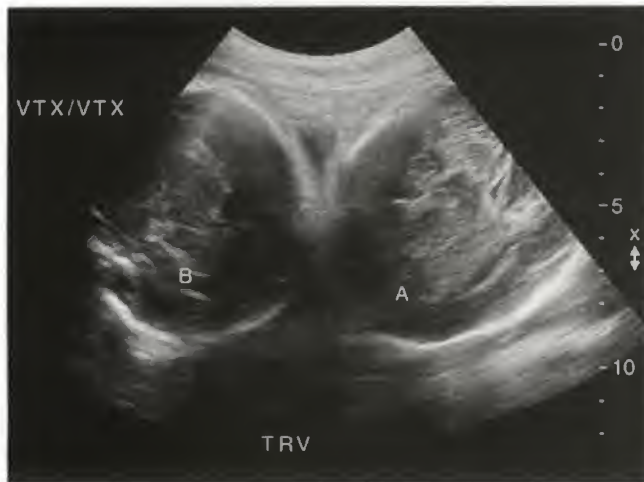


**FIGURE 8-43.** Vertex-vertex presentations in a twin gestation.

with nearly a 10-fold increased risk for fetal structural or chromosomal anomalies.<sup>155</sup> The same group showed that in 130 twin pregnancies, a greater than 3-day difference in CRL between 11 and 14 weeks predicted nearly a 6-fold increased risk for birthweight discordance greater than 20%.<sup>156</sup> Salomon et al<sup>157</sup> also found that when a CRL discrepancy was more than the 95th percentile, there was an increased risk of fetal aneuploidy.<sup>157</sup> Unlike almost everything else in twins, this was not influenced by chorionicity.

### Intrapartum Use of Ultrasound in Twin Gestations

Multiple gestations pose numerous problems in the delivery room.<sup>158,159</sup> There is a higher incidence of prematurity, abnormal fetal lie, abnormal placentation, cord accidents, and retained placentas. Because of this, we believe that ultrasound is an essential component in the intrapartum management of twins. Estimation of fetal weight, fetal lie, and presentation are best accomplished by ultrasound in twin pregnancies (Fig. 8-43). If the presenting fetus is in a transverse lie, ultrasound aids in the decision regarding the uterine incision. A transverse fetal lie with the fetal back down is generally delivered through a vertical uterine incision. If the fetal lie and estimated weights support a decision for a vaginal birth, ultrasound is very helpful in visualizing the position of the second twin during the second stage.<sup>159</sup> Ultrasound can ensure that no cord or fetal small parts are presenting. If the operator decides to perform a version of the second fetus, the ultrasound is often useful during the procedure. Even when a breech extraction is planned, ultrasound assists the clinician to correctly identify the fetal ankles aiding in the delivery process.

### CONCLUSION

Multiple gestations pose interesting and exciting challenges to parents, obstetricians, and sonographers. We have reviewed the role of ultrasound in the diagnosis of twins, the determination of chorionicity, the management of complications unique to twins, the value of cervical length screening

to predict prematurity, the use of ultrasound in screening for aneuploidy in multiples, and the intrapartum role of ultrasound in twin gestations. Ultrasound is a valuable tool for the obstetrician and sonographer to improve the diagnosis of twins and higher order multiples to guide the care and management of complications relating to multiple gestations.

### References

1. Russell RB, Petrini JR, Damus K, et al: The changing epidemiology of multiple births in the United States. *Obstet Gynecol* 101:129, 2003.
2. Benirschke K: Multiple pregnancy (First of two parts). *N Engl J Med* 288:1276, 1973.
3. Egan JF, Borgida AF: Multiple gestations: The importance of ultrasound. *Obstet Gynecol Clin North Am* 31:141, 2004.
4. Natality Data Set: National Center for Health Statistics: Centers for Disease Control and Prevention, Atlanta CD-ROM 1997-2002; Series 21 11,12,14,15.
5. Sperling L, Tabor A: Twin pregnancy: the role of ultrasound in management. *Acta Obstet Gynecol Scand* 80:287, 2001.
6. Modena AB, Berghella V: Antepartum management of multifetal pregnancies. *Clin Perinatol* 32:443, 2005.
7. Mauldin J, Newman RB: Neurologic morbidity associated with multiple gestation. *Female Patient* 23:27, 1998.
8. Etner SL, Christiansen CL, Callahan TL, Hall JE: How low birth weight and gestational age contribute to increased inpatient costs for multiple births. *Inquiry* 98:325, 1997.
9. Elliott JP, Radin TG: Quadruplet pregnancy: Contemporary management and outcome. *Obstet Gynecol* 80:421, 1992.
10. Grether JK, Nelson KB, Cummins SK: Twinning and cerebral palsy: Experience in four northern California counties, births 1983 through 1985. *Pediatrics* 92:854, 1993.
11. ACOG Practice Bulletin #56: Multiple gestation: Complicated twin, triplet, and high-order multifetal pregnancy. *Obstet Gynecol* 104:869, 2004.
12. Luke B, Minogue J: The contribution of gestational age and birth weight to perinatal viability in singletons versus twins. *J Matern Fetal Med* 3:263, 1994.
13. Kiely JL, Kleinman JC, Kiely M: Triplets and higher-order multiple births: Time trends and infant mortality. *Am J Dis Child* 146:862, 1992.
14. Rustico MA, Baicrù MG, Covicello D, et al: Managing twins discordant for fetal anomaly. *Prenat Diagn* 25:766, 2005.
15. Malone FD, D'Alton ME: Management of multiple gestations complicated by a single anomalous fetus. *Curr Opin Obstet Gynecol* 9:213, 1997.
16. Roach VJ, Lau TK, Wilson D, et al: The incidence of gestational diabetes in multiple pregnancy. *Aust N Z J Obstet Gynaecol* 38:56, 1998.
17. Sibai BM, Hauth J, Caritis S, et al: Hypertensive disorders in twin versus singleton gestations. National Institute of Child Health and Human Development Network of Maternal-Fetal Medicine Units. *Am J Obstet Gynecol* 182:938, 2000.
18. Wenstrom KD, Syrop CH, Hammit DG, et al: Increased risk of monozygotic twinning associated with assisted reproduction. *Fertil Steril* 60:510, 1993.
19. Blickstein I: Monozygoticity in perspective. *Ultrasound Obstet Gynecol* 27:235, 2006.
20. Nylander PP: The factors that influence twinning rates. *Acta Genet Med Gemellol (Roma)* 30:189, 1981.
21. Campbell DM, Campbell AJ, MacGillivray I: Maternal characteristics of women having twin pregnancies. *J Biosoc Sci* 6:463, 1974.
22. MacGillivray I: Epidemiology of twin pregnancy. *Semin Perinatol* 10:4, 1986.
23. Bardis N, Maruthini D, Balen AH: Modes of conception and multiple pregnancy: a national survey of babies born during one week in 2003 in the United Kingdom. *Fertil Steril* 84:1727, 2005.
24. Criniti A, Thyer A, Chow G, et al: Elective single blastocyst transfer reduces twin rates without compromising pregnancy rates. *Fertil Steril* 84:1613, 2005.
25. Hall JG: Twinning. *Lancet* 362:735, 2003.
26. Souter VL, Kapur RP, Nyholt DR, et al: A report of dizygous monozygotic twins. *N Engl J Med* 349:154, 2003.



27. Dube J, Dodds L, Aronson BA: Does chorionicity or zygosity predict adverse perinatal outcomes in twins? *Am J Obstet Gynecol* 186:579, 2002.
28. Carroll SG, Tyfield L, Reeve L, et al: Is zygosity or chorionicity the main determinant of fetal outcome in twin pregnancies? *Am J Obstet Gynecol* 193:757, 2005.
29. Egan JF, Vinzilos AM, Turner G, Fleming A, et al: Correlation of uterine fundal height with ultrasonic measurements in twin gestations. *J Matern Fetal Med* 3:18, 1994.
30. Sebire NJ, Souka A, Skentou H, et al: First trimester diagnosis of monoamniotic twin pregnancies. *Ultrasound Obstet Gynecol* 16:223, 2000.
31. Mahony BS, Filly RA, Callen PW: Amnionity and chorionicity in twin pregnancies: Prediction using ultrasound. *Radiology* 155:205, 1985.
32. Sebire NJ, Snijders RJ, Hughes K, et al: The hidden mortality of monochorionic twin pregnancies. *Br J Obstet Gynaecol* 104:1203, 1997.
33. Landy HJ, Weiner S, Corson SL, et al: The "vanishing twin": Ultrasonographic assessment of fetal disappearance in the first trimester. *Am J Obstet Gynecol* 155:14, 1986.
34. Benson CB, Doubilet PM, Laks MP: Outcome of twin gestations following sonographic demonstration of two heart beats in the first trimester. *Ultrasound Obstet Gynecol* 3:343, 1993.
35. Dickey RP, Taylor SN, Lu PY, et al: Spontaneous reduction of multiple pregnancy: incidence and effect on outcome. *Am J Obstet Gynecol* 186:77, 2002.
36. Schieve LA, Meikle SF, Ferre C, et al: Low and very low birth weight in infants conceived with use of assisted reproductive technology. *N Engl J Med* 346:731, 2002.
37. Pinborg A, Lidegaard O, La Cour Freiesleben N, et al: Consequences of vanishing twins in IVF/ICSI pregnancies. *Hum Reprod* 20:2821, 2005.
38. Pharoah PO, Cooke T: Cerebral palsy and multiple births. *Arch Dis Child Fetal Neonatal Ed* 75:F174, 1996.
39. Weisz B, Pandya P, Dave R, et al: Scanning for chorionicity: comparison between sonographers and perinatologists. *Prenat Diagn* 25:835, 2005.
40. Monteagudo A: Sonographic assessment of chorionicity and amnionity in twin pregnancies: How, when and why? *Croat Med J* 39:191, 1998.
41. Doubilet PM, Benson CB: "Appearing twin": Undercounting of multiple gestations on early first trimester sonograms. *J Ultrasound Med* 17:199, 1998.
42. Bromley B, Benacerraf B: Using the number of yolk sacs to determine amnionity in early first trimester monochorionic twins. *J Ultrasound Med* 14:415, 1995.
43. Shen O SA, Belleer U, Rabinowitz R: Number of yolk sacs does not predict amnionity in early first-trimester monochorionic multiple gestations. *Ultrasound Obstet Gynecol* 27:53, 2006.
44. Sepulveda W: Chorionicity determination in twin pregnancies: Double trouble. *Ultrasound Obstet Gynecol* 10:79, 1997.
45. D'Alton ME, Dudley DK: The ultrasonographic prediction of chorionicity in twin gestation. *Am J Obstet Gynecol* 160:557, 1989.
46. Finberg HJ: The "twin peak" sign: Reliable evidence of dichorionic twinning. *J Ultrasound Med* 11:571, 1992.
47. Wood SL, St Onge R, Connors G, et al: Evaluation of the twin peak or lambda sign in determining chorionicity in multiple pregnancy. *Obstet Gynecol* 88:6, 1996.
48. Sepulveda W, Sebire NJ, Hughes K, et al: The lambda sign at 10-14 weeks of gestation as a predictor of chorionicity in twin pregnancies. *Ultrasound Obstet Gynecol* 7:421, 1996.
49. Sepulveda W, Sebire NJ, Odibo A, et al: Prenatal determination of chorionicity in triplet pregnancy by ultrasonographic examination of the ipsilateral zone. *Obstet Gynecol* 88:855, 1996.
50. Hertzberg BS, Kurtz AB, Choi HY, et al: Significance of membrane thickness in the sonographic evaluation of twin gestations. *AJR Am J Roentgenol* 148:151, 1987.
51. Townsend RR, Simpson GF, Filly RA: Membrane thickness in ultrasound prediction of chorionicity of twin gestations. *J Ultrasound Med* 7:327, 1988.
52. Winn HN, Gabrielli S, Reece EA, et al: Ultrasonographic criteria for the prenatal diagnosis of placental chorionicity in twin gestations. *Am J Obstet Gynecol* 161:1540, 1989.
53. Stagiannis KD, Sepulveda W, Southwell D, et al: Ultrasonographic measurement of the dividing membrane in twin pregnancy during the second and third trimesters: A reproducibility study. *Am J Obstet Gynecol* 173:1546, 1995.
54. Vayssiere CF, Heim N, Camus EP, et al: Determination of chorionicity in twin gestations by high-frequency abdominal ultrasonography: Counting the layers of the dividing membrane. *Am J Obstet Gynecol* 175:1529, 1996.
55. Scardo JA, Ellings JM, Newman RB: Prospective determination of chorionicity, amnionity, and zygosity in twin gestations. *Am J Obstet Gynecol* 173:1376, 1995.
56. Carroll SG, Soothill PW, Abdel-Fattah SA, et al: Prediction of chorionicity in twin pregnancies at 10-14 weeks of gestation. *Br J Obstet Gynaecol* 109:182, 2002.
57. Rodis JF, McIlveen PF, Egan JF, et al: Monoamniotic twins: Improved perinatal survival with accurate prenatal diagnosis and antenatal fetal surveillance. *Am J Obstet Gynecol* 177:1046, 1997.
58. Carr SR, Aronson MP, Coustan DR: Survival rates of monoamniotic twins do not decrease after 30 weeks' gestation. *Am J Obstet Gynecol* 163:719, 1990.
59. Roque H, Gillen-Goldstein J, Funai E, et al: Perinatal outcomes in monoamniotic gestations. *J Matern Fetal Neonatal Med* 13:414, 2003.
60. Nyberg DA, Filly RA, Golbus MS, et al: Entangled umbilical cords: A sign of monoamniotic twins. *J Ultrasound Med* 3:29, 1984.
61. Townsend RR, Filly RA: Sonography of nonconjoined monoamniotic twin pregnancies. *J Ultrasound Med* 7:665, 1988.
62. Overton TG, Denbow ML, Duncan KR, et al: First-trimester cord entanglement in monoamniotic twins. *Ultrasound Obstet Gynecol* 13:140, 1999.
63. Sherer DM, Sokolovski M, Haratz-Rubinstein N: Diagnosis of umbilical cord entanglement of monoamniotic twins by first-trimester color Doppler imaging. *J Ultrasound Med* 21:1307, 2002.
64. Belfort MA, Moise KJ, Jr, Kirshon B, et al: The use of color flow Doppler ultrasonography to diagnose umbilical cord entanglement in monoamniotic twin gestations. *Am J Obstet Gynecol* 168:601, 1993.
65. Abuhamad AZ, Mari G, Copel JA, et al: Umbilical artery flow velocity waveforms in monoamniotic twins with cord entanglement. *Obstet Gynecol* 86:674, 1995.
66. Heyborne KD, Porreco RP, Garite TJ, et al: Improved perinatal survival of monoamniotic twins with intensive inpatient monitoring. *Am J Obstet Gynecol* 192:96, 2005.
67. Edmonds LD, Layde PM: Conjoined twins in the united states, 1970-1977. *Teratology* 25:301, 1982.
68. Koontz WL, Herbert WN, Seeds JW, et al: Ultrasonography in the antepartum diagnosis of conjoined twins: A report of two cases. *J Reprod Med* 28:627, 1983.
69. Maggio M, Callan NA, Hamod KA, et al: The first-trimester ultrasonographic diagnosis of conjoined twins. *Am J Obstet Gynecol* 152:833, 1985.
70. Weingast GR, Johnson ML, Pretorius DH, et al: Difficulty in sonographic diagnosis of cephalothoracopagus. *J Ultrasound Med* 3:421, 1984.
71. Harper RG, Kenigsberg K, Sia CG, et al: Xiphopagus conjoined twins: A 300-year review of the obstetric, morphopathologic, neonatal, and surgical parameters. *Am J Obstet Gynecol* 137:617, 1980.
72. Barth RA, Filly RA, Goldberg JD, et al: Conjoined twins: Prenatal diagnosis and assessment of associated malformations. *Radiology* 177:201, 1990.
73. Tongsong T, Khunamornpong S, Piyamongkol W, et al: Prenatal sonographic delineation of the complex cardiac anatomy of thoracopagus twins. *Ultrasound Obstet Gynecol* 25:189, 2005.
74. Spitz L: Conjoined twins. *Prenat Diagn* 25:814, 2005.
75. MacKenzie TC, Crombleholme TM, Johnson MP, et al: The natural history of prenatally diagnosed conjoined twins. *J Pediatr Surg* 37:303, 2002.
76. Pajkrt E, Jauniaux E: First-trimester diagnosis of conjoined twins. *Prenat Diagn* 25:820, 2005.
77. Galea P, Jain V, Fisk NM: Insights into the pathophysiology of twin-twin transfusion syndrome. *Prenat Diagn* 25:777, 2005.
78. Maymon R, Mendelovic S, Schachter M, et al: Diagnosis of conjoined twins before 16 weeks' gestation: The 4-year experience of one medical center. *Prenat Diagn* 25:839, 2005.
79. Pryde PG, Hallak M, Lauria MR, et al: Severe oligohydramnios with intact membranes: An indication for diagnostic amniocentesis. *Fetal Diagn Ther* 15:46, 2000.
80. Fisk NM, Ronderos-Dumit D, Soliani A, et al: Diagnostic and therapeutic transabdominal amniocentesis in oligohydramnios. *Obstet Gynecol* 78:270, 1991.



81. Fichera A, Mor E, Soregaroli M, Frusca T: Antenatal detection of arterio-arterial anastomoses by Doppler placental assessment in monochorionic twin pregnancies. *Fetal Diagn Ther* 20:519, 2005.
82. Matias A, Ramalho C, Montenegro N: Search for hemodynamic compromise at 11–14 weeks in monochorionic twin pregnancy: Is abnormal flow in the ductus venosus predictive of twin-twin transfusion syndrome? *J Matern Fetal Neonatal Med* 18:79, 2005.
83. Matias A, Montenegro N, Arcias JC: Anticipating twin-twin transfusion syndrome in monochorionic twin pregnancy: Is there a role for nuchal translucency and ductus venosus blood flow evaluation at 11–14 weeks? *Twin Res* 3:65, 2000.
84. Quintero RA, Morales WJ, Allen MH, et al: Staging of twin-twin transfusion syndrome. *J Perinatol* 19:550, 1999.
85. Taylor MJ, Govender L, Jolly M, et al: Validation of the Quintero staging system for twin-twin transfusion syndrome. *Obstet Gynecol* 100:1257, 2002.
86. Haverkamp F, Lex C, Hanisch C, et al: Neurodevelopmental risks in twin-to-twin transfusion syndrome: preliminary findings. *Eur J Paediatr Neurol* 5:21, 2001.
87. Robyr R, Quarello E, Ville Y: Management of fetofetal transfusion syndrome. *Prenat Diagn* 25:786, 2005.
88. Quintero RA, Romero R, Reich H, et al: In utero percutaneous umbilical cord ligation in the management of complicated monochorionic multiple gestations. *Ultrasound Obstet Gynecol* 8:16, 1996.
89. Elliott JP, Sawyer AT, Radin TG, et al: Large-volume therapeutic amniocentesis in the treatment of hydramnios. *Obstet Gynecol* 84:1025, 1994.
90. Elliott JP, Urig MA, Clewell WH: Aggressive therapeutic amniocentesis for treatment of twin-twin transfusion syndrome. *Obstet Gynecol* 77:537, 1991.
91. Dolinger MB, Donnenfeld AE: Therapeutic amniocentesis using a vacuum bottle aspiration system. *Obstet Gynecol* 91:143, 1998.
92. Saade GR, Belfort MA, Berry DL, et al: Amniotic septostomy for the treatment of twin oligohydramnios-polyhydramnios sequence. *Fetal Diagn Ther* 13:86, 1998.
93. Moise Jr KJ, Dorman K, Lamvu G, et al: A randomized trial of amnioreduction versus septostomy in the treatment of twin-twin transfusion syndrome. *Am J Obstet Gynecol* 193:701, 2005.
94. Feldman DM, Odibo A, Campbell WA, et al: Iatrogenic mono-amniotic twins as a complication of therapeutic amniocentesis. *Obstet Gynecol* 91:815, 1998.
95. Sherer DM, Bitton C, Stimpf R, et al: Cord entanglement of monochorionic diamniotic twins following spontaneous antepartum septostomy sonographically simulating a true knot of the umbilical cord. *Ultrasound Obstet Gynecol* 26:676, 2005.
96. Nasrallah FK, Faden YA: Antepartum rupture of the intertwin-dividing membrane in monochorionic diamniotic twins: A case report and review of the literature. *Prenat Diagn* 25:856, 2005.
97. De Lia J, Emery MC, Sheafar SA, et al: Twin transfusion syndrome: Successful in utero treatment with digoxin. *Int J Gynaecol Obstet* 23:197, 1985.
98. Senat MV, Deprest J, Boulvain M, et al: Endoscopic laser surgery versus serial amnioreduction for severe twin-to-twin transfusion syndrome. *N Engl J Med* 351:136, 2004.
99. Driggers RW, Blakemore KJ, Bird C, et al: Pathogenesis of acardiac twinning: Clues from an almost acardiac twin. *Fetal Diagn Ther* 17:185, 2002.
100. Van Allen MI, Smith DW, Shepard TH: Twin reversed arterial perfusion (TRAP) sequence: A study of 14 twin pregnancies with acardius. *Semin Perinatol* 7:285, 1983.
101. Benson CB, Bieber FR, Genest DR, et al: Doppler demonstration of reversed umbilical blood flow in an acardiac twin. *J Clin Ultrasound* 17:291, 1989.
102. Dashe JS, Fernandez CO, Twickler DM: Utility of Doppler velocimetry in predicting outcome in twin reversed-arterial perfusion sequence. *Am J Obstet Gynecol* 185:135, 2001.
103. Brassard M, Fouron JC, Leduc L, et al: Prognostic markers in twin pregnancies with an acardiac fetus. *Obstet Gynecol* 94:409, 1999.
104. Moore TR, Gale S, Benirschke K: Perinatal outcome of forty-nine pregnancies complicated by acardiac twinning. *Am J Obstet Gynecol* 163:907, 1990.
105. Tan TY, Sepulveda W: Acardiac twin: A systematic review of minimally invasive treatment modalities. *Ultrasound Obstet Gynecol* 22:409, 2003.
106. Wong AE, Sepulveda W: Acardiac anomaly: Current issues in prenatal assessment and treatment. *Prenat Diagn* 25:796, 2005.
107. Egan JF, Benn PA, Zelop CM, et al: Down syndrome births in the United States from 1989 to 2001. *Am J Obstet Gynecol* 191:1044, 2004.
108. Yinon Y, Yagel S, Tepperberg-Dikawa M, et al: Prenatal diagnosis and outcome of congenital cytomegalovirus infection in twin pregnancies. *Br J Obstet Gynaecol* 113:295, 2006.
109. Rodis JF, Vintzileos AM, Campbell WA, et al: Intrauterine fetal growth in discordant twin gestations. *J Ultrasound Med* 9:443, 1990.
110. Lee DH, Cottrell JR, Sanders RC, et al: OEIS complex (omphalocele-exstrophy-imperforate anus-spinal defects) in monozygotic twins. *Am J Med Genet* 84:29, 1999.
111. Wald NJ, Cuckle HS: Recent advances in screening for neural tube defects and Down's syndrome. *Fetal diagnosis of genetic defects*. Baillieres Clin Obstetrics Gynecol 1:649, 1987.
112. Doyle LW, Cauchi M, De Crespigny LC, et al: Fetal intravascular transfusion for severe erythroblastosis: Effects on haematology and survival. *Aust N Z J Obstet Gynaecol* 26:192, 1986.
113. Egan JF, Benn P, Borgida AF, et al: Efficacy of screening for fetal Down syndrome in the United States from 1974 to 1997. *Obstet Gynecol* 96:979, 2000.
114. Spencer K: Screening for trisomy 21 in twin pregnancies in the first trimester: Does chorionicity impact on maternal serum free beta-hCG or PAPP-A levels? *Prenat Diagn* 21:715, 2001.
115. Maymon R, Dreazen E, Rozinsky S, et al: Comparison of nuchal translucency measurement and second-trimester triple serum screening in twin versus singleton pregnancies. *Prenat Diagn* 19:727, 1999.
116. Egan JF, Kaminsky LM, Deroche ME, et al: Antenatal Down syndrome screening in the United States in 2001: A survey of maternal-fetal medicine specialists. *Am J Obstet Gynecol* 187:1230, 2002.
117. Wald NJ, Kennard A, Hackshaw A, et al: Antenatal screening for Down's syndrome. *J Med Screen* 4:181, 1997.
118. Nevoux LM, Palomaki GE, Knight GJ, et al: Multiple marker screening for Down syndrome in twin pregnancies. *Prenat Diagn* 16:29, 1996.
119. Wald NJ, Rish S, Hackshaw AK: Combining nuchal translucency and serum markers in prenatal screening for Down syndrome in twin pregnancies. *Prenat Diagn* 23:588, 2003.
120. Ghidini A, Lynch L, Hicks C, et al: The risk of second-trimester amniocentesis in twin gestations: a case-control study. *Am J Obstet Gynecol* 169:1013, 1993.
121. Appelman Z, Furman B: Invasive genetic diagnosis in multiple pregnancies. *Obstet Gynecol Clin North Am* 32:97, 2005.
122. Imseis HM, Albert TA, Iams JD: Identifying twin gestations at low risk for preterm birth with a transvaginal ultrasonographic cervical measurement at 24 to 26 weeks' gestation. *Am J Obstet Gynecol* 177:1149, 1997.
123. Souka AP, Heath V, Flint S, et al: Cervical length at 23 weeks in twins in predicting spontaneous preterm delivery. *Obstet Gynecol* 94:450, 1999.
124. Goldenberg RL, Iams JD, Miodovnik M, et al: The preterm prediction study: Risk factors in twin gestations. National Institute of Child Health and Human Development Maternal-Fetal Medicine Units Network. *Am J Obstet Gynecol* 175:1047, 1996.
125. Guzman ER, Walters C, O'Reilly-Green C, et al: Use of cervical ultrasonography in prediction of spontaneous preterm birth in twin gestations. *Am J Obstet Gynecol* 183:1103, 2000.
126. Sperling L, Kil C, Larsen LU, et al: How to identify twins at low risk of spontaneous preterm delivery. *Ultrasound Obstet Gynecol* 26:138, 2005.
127. Newman RB, Krombach RS, Myers MC, et al: Effect of cerclage on obstetrical outcome in twin gestations with a shortened cervical length. *Am J Obstet Gynecol* 186:634, 2002.
128. Lynch L, Berkowitz RL, Chikara U, et al: First-trimester transabdominal multifetal pregnancy reduction: A report of 85 cases. *Obstet Gynecol* 75:735, 1990.
129. Timor-Tritsch IE, Peisner DB, Monteagudo A, et al: Multifetal pregnancy reduction by transvaginal puncture: evaluation of the technique used in 134 cases. *Am J Obstet Gynecol* 168:799, 1993.
130. Timor-Tritsch IE, Bashiri A, Monteagudo A, et al: Two hundred ninety consecutive cases of multifetal pregnancy reduction: Comparison of the transabdominal versus the transvaginal approach. *Am J Obstet Gynecol* 191:2085, 2004.
131. Evans MI, Berkowitz RL, Wapner RJ, et al: Improvement in outcomes of multifetal pregnancy reduction with increased experience. *Am J Obstet Gynecol* 184:972, 2001.



132. Stone J, Eddleman K, Lynch L, et al: A single center experience with 1000 consecutive cases of multifetal pregnancy reduction. *Am J Obstet Gynecol* 187:1163, 2002.
133. Yaron Y, Bryant-Greenwood PK, Dave N, et al: Multifetal pregnancy reductions of triplets to twins: Comparison with nonreduced triplets and twins. *Am J Obstet Gynecol* 180:1268, 1999.
134. Evans MI, Kaufman MI, Urban AJ, et al: Fetal reduction from twins to a singleton: A reasonable consideration? *Obstet Gynecol* 104:102, 2004.
135. Brambati B, Tului L, Camurri L, et al: First-trimester fetal reduction to a singleton infant or twins: Outcome in relation to the final number and karyotyping before reduction by transabdominal chorionic villus sampling. *Am J Obstet Gynecol* 191:2035, 2004.
136. Eddleman KA, Stone JL, Lynch L, et al: Chorionic villus sampling before multifetal pregnancy reduction. *Am J Obstet Gynecol* 183:1078, 2000.
137. Nicolaides K, Sebire N, Snijder MJ: The 11–14 Week Scan. New York: Parthenon, 1999.
138. Karatza AA, Wolfenden JL, Taylor MJ, et al: Influence of twin-twin transfusion syndrome on fetal cardiovascular structure and function: Prospective case-control study of 136 monochorionic twin pregnancies. *Heart* 88:271, 2002.
139. Evans MI, Goldberg JD, Horenstein J, et al: Selective termination for structural, chromosomal, and mendelian anomalies: International experience. *Am J Obstet Gynecol* 181:893, 1999.
140. Evans MI, Britt DW: Fetal reduction. *Semin Perinatol* 29:321, 2005.
141. Evans MI, May M, Drugan A, et al: Selective termination: Clinical experience and residual risks. *Am J Obstet Gynecol* 162:1568, 1990.
142. Blickstein I, Friedman A, Caspi B, et al: Ultrasonic prediction of growth discordancy by intertwin difference in abdominal circumference. *Int J Gynaecol Obstet* 29:121, 1989.
143. Babson SG, Phillips DS: Growth and development of twins dissimilar in size at birth. *N Engl J Med* 289:937, 1973.
144. Blickstein I, Keith LG: Neonatal mortality rates among growth-discordant twins, classified according to the birth weight of the smaller twin. *Am J Obstet Gynecol* 190:170, 2004.
145. Yinon Y, Mazkereth R, Rosentzweig N, et al: Growth restriction as a determinant of outcome in preterm discordant twins. *Obstet Gynecol* 105:80, 2005.
146. Caravello JW, Chauhan SP, Morrison JC, et al: Sonographic examination does not predict twin growth discordance accurately. *Obstet Gynecol* 89:529, 1997.
147. Chauhan SP, Shields D, Parker D, et al: Detecting fetal growth restriction or discordant growth in twin gestations stratified by placental chorionicity. *J Reprod Med* 49:279, 2004.
148. Senoo M, Okamura K, Murotsuki J, et al: Growth pattern of twins of different chorionicity evaluated by sonographic biometry. *Obstet Gynecol* 95:656, 2000.
149. Ong S, Lim MN, Fitzmaurice A, et al: The creation of twin centile curves for size. *Br J Obstet Gynaecol* 109:753, 2002.
150. Ananth CV, Demissie K, Hanley ML: Birth weight discordancy and adverse perinatal outcomes among twin gestations in the United States: The effect of placental abruption. *Am J Obstet Gynecol* 188:954, 2003.
151. Ananth CV, Vintzileos AM, Shen-Schwarz S, et al: Standards of birth weight in twin gestations stratified by placental chorionicity. *Obstet Gynecol* 91:917, 1998.
152. Blickstein I, Goldman RD, Mazkereth R: Adaptive growth restriction as a pattern of birth weight discordance in twin gestations. *Obstet Gynecol* 96:986, 2000.
153. Dashe JS, McIntire DD, Lucas MJ, et al: Effects of symmetric and asymmetric fetal growth on pregnancy outcomes. *Obstet Gynecol* 96:321, 2000.
154. Ayres A, Johnson TR: Management of multiple pregnancy: Prenatal care-part I. *Obstet Gynecol Surv* 60:527, 2005.
155. Kalish RB, Chasen ST, Gupta M, et al: First trimester prediction of growth discordance in twin gestations. *Am J Obstet Gynecol* 189:706, 2003.
156. Kalish RB, Gupta M, Perni SC, et al: Clinical significance of first trimester crown-rump length disparity in dichorionic twin gestations. *Am J Obstet Gynecol* 191:1437, 2004.
157. Salomon LJ, Cavicchioni O, Bernard JP, et al: Growth discrepancy in twins in the first trimester of pregnancy. *Ultrasound Obstet Gynecol* 26:512, 2005.
158. Ramsey PS, Repke JT: Intrapartum management of multifetal pregnancies. *Semin Perinatol* 27:54, 2003.
159. Ayres A, Johnson TR: Management of multiple pregnancy: Labor and delivery. *Obstet Gynecol Surv* 60:550, 2005.
160. Yang JH, Kuhlman K, Daly S, et al: Prediction of preterm birth by second trimester cervical sonography in twin pregnancies. *Ultrasound Obstet Gynecol* 15:288, 2000.
161. Vayssières C, Favre R, Audibert F, et al: Cervical length and funneling at 22 and 27 weeks to predict spontaneous birth before 32 weeks in twin pregnancies: A French prospective multicenter study. *Am J Obstet Gynecol* 187:1596, 2002.

# ULTRASOUND EVALUATION OF NORMAL FETAL ANATOMY

Roy A. Filly, MD and Vickie A. Feldstein, MD

## Superficial Anatomy of the Fetus

### Musculoskeletal System

### Cardiovascular System

### Gastrointestinal System

## Respiratory System

### Genitourinary System

### Central Nervous System

Our understanding of normal fetal anatomy as seen on sonograms continues to be an area of considerable growth. Instrumentation has improved steadily, yielding both improved and more consistent image quality. Among the most significant advancements for fetal imaging has been the ability to choose the depth of the zone of best focus of the ultrasonic beam and to select frequency without changing transducers. With these capabilities, the area of anatomy being observed can be consistently inspected with the focused portion of the beam at an optimum frequency, both highly significant advantages. More recently, three-dimensional sonographic imaging has expanded our ability to evaluate the fetus in a near-infinite number of tomographic planes as well as with surface-rendered viewing.

Furthermore, sonologists have gradually improved their understanding of the anatomy portrayed on in utero sonograms. Unquestionably, clearer images have led the way to our improved understanding, but other factors have been involved. Not the least of these has been the surge in ultrasonic imaging of premature neonates.<sup>1,2</sup> These tiny neonates are the equivalent of second trimester fetuses as early, at times, as 24 weeks. Visualization of their brain<sup>1,2</sup> (Fig. 9-1) and abdominal (Fig. 9-2) anatomy in the more ideal ex utero environment, which permits the use of higher frequency transducers, a greater selection of planes of section, and comparison with other imaging modalities, has done much to improve our understanding of fetal anatomy. This information can be, to a large extent, extrapolated to younger fetuses. Also, magnetic resonance imaging continues to be a growth area in fetal imaging. Our ability to compare sonographic anatomy of the fetus with that portrayed on magnetic resonance imaging further enhances our understanding of fetal sonographic anatomy.<sup>3-7</sup>

The ability of sonography to detect intrafetal structures depends on a balance between spatial resolution and contrast.<sup>8</sup> This balance, however, strongly favors contrast as the more important aspect of perception. For example, a large white dot on a white wall is difficult or impossible to see because no contrast differential exists even though the eye can spatially resolve easily a tiny black dot (high contrast)

on the same wall. Structures possessing high levels of subject contrast can be consistently detected at a smaller size (often equating to an earlier age) than those displaying poor contrast. Although sonographic contrast agents are available for imaging in adults and children, current agents do not cross the placenta in sufficient concentration to affect fetal organs.<sup>9</sup> Therefore, sonologists possess no agents to alter contrast of fetal organs and thus are totally dependent on subject contrast (inherent contrast) for visualization of internal fetal morphologic details. Clearly, spatial resolution is also a critical feature in defining morphology but has not been the limiting factor in demonstrating fetal anatomy. Fortunately, sophisticated modern sonographic imaging systems have the ability to choose varying contrast settings, which enhance inherent tissue differences.

Another technology that has improved fetal imaging, particularly for earlier gestations, is the intracavitary (transvaginal) transducer.<sup>10-12</sup> Certain aspects of fetal, indeed embryonic, anatomy can be seen with amazing detail (Fig. 9-3). Although this methodology is crucial to modern imaging, we intend to concentrate our discussion on anatomy visualized by transabdominal transducers in fetuses beyond the 14th week. When examining later pregnancies, in the context of fetal anatomic imaging, we use transvaginal transducers predominantly to visualize the presenting part when transabdominal transducers fail to adequately image this region of the fetus's anatomy (i.e., distal sacrum in a fetus in breech presentation).

Other parameters, important in fetal imaging, also cannot be controlled. Sonography is a tomographic technique. Appropriate positioning for obtaining the best tomographic plane is always desirable. However, we are unable to control fetal position to attain this end. We also cannot control maternal body habitus or the amount of amniotic fluid, both of which may dramatically alter our ability to discern fetal anatomy. Despite these problems, a large number of fetal structures are consistently visible sonographically.

High-resolution, real-time scanners with their flexible approach to imaging are mandatory for modern fetal sonography.<sup>13-15</sup> In the following sections, various aspects of fetal



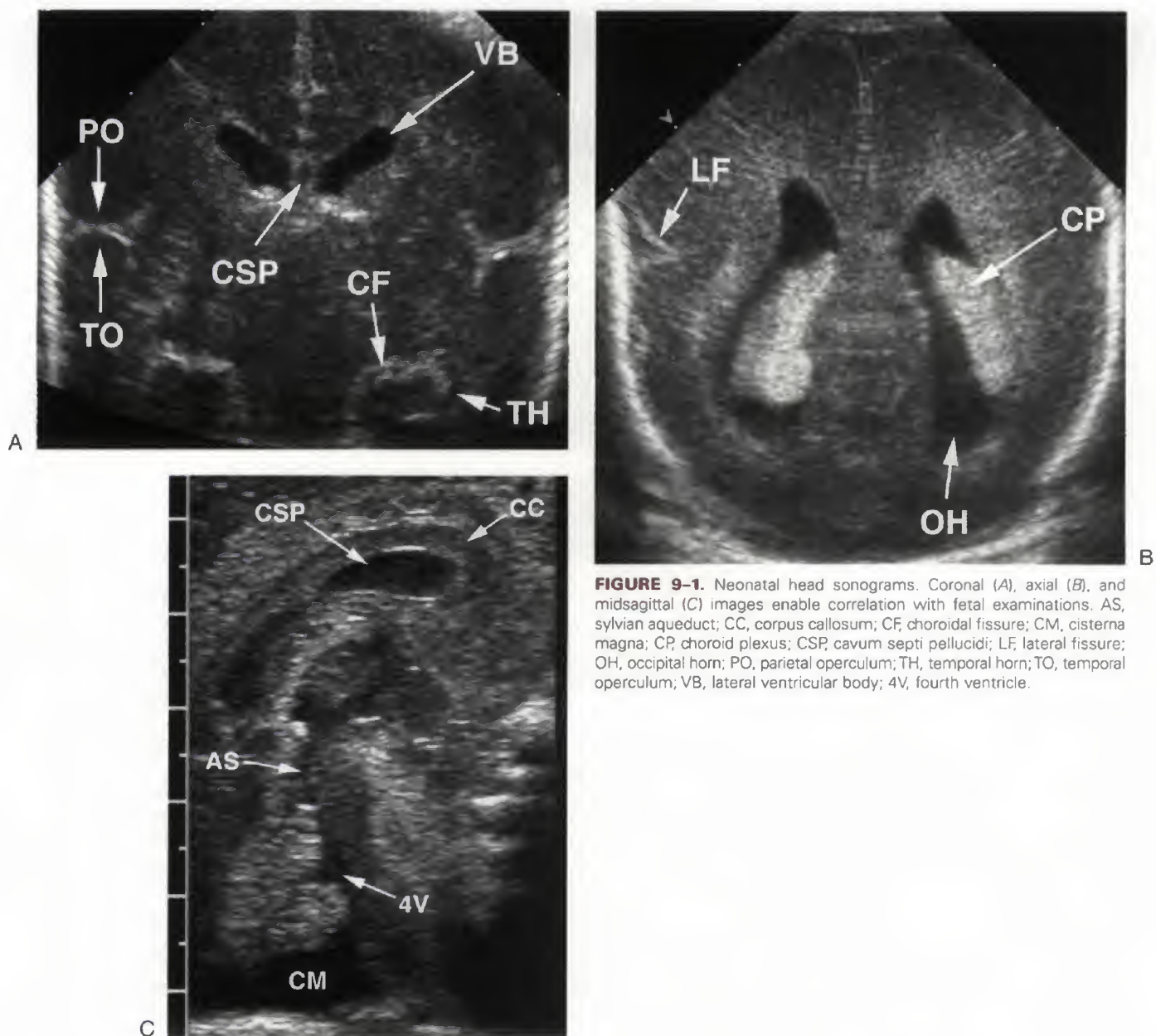


**FIGURE 9-1.** Neonatal head sonograms. Coronal (A), axial (B), and midsagittal (C) images enable correlation with fetal examinations. AS, sylvian aqueduct; CC, corpus callosum; CF, choroidal fissure; CM, cisterna magna; CP, choroid plexus; CSP, cavum septi pellucidum; LF, lateral fissure; OH, occipital horn; PO, parietal operculum; TH, temporal horn; TO, temporal operculum; VB, lateral ventricular body; 4V, fourth ventricle.

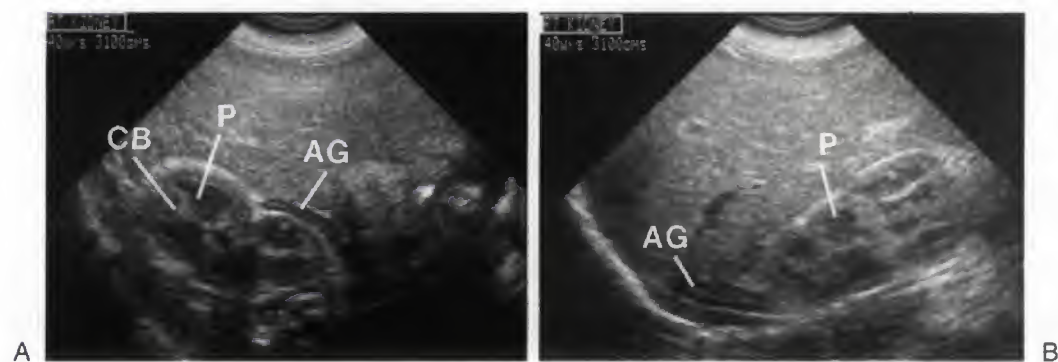


**FIGURE 9-2.** Neonatal abdominal sonograms. A. Transverse axial image. B. Parasagittal image. AG, adrenal gland, both cortex (thicker and darker) and medulla (thinner and brighter); CB, Bertin column; P, medullary pyramid of the kidney.



**FIGURE 9-3.** Transvaginal sonogram of a 17-mm embryo. This mid-sagittal view demonstrates the large early fourth ventricle formed by the folding of the rhombencephalon (R). A, amnion.

anatomy are detailed as seen on such instrumentation. An estimate is made of the ability of ultrasound instrumentation to consistently demonstrate the anatomic part under consideration as well as an attempt to estimate when the fetus has attained sufficient size such that the anatomic structure is large enough to be detected. It is important to recall that size and visualization may be relative at any given stage of development. For example, in a small fetus with a well-distended urinary bladder, identification of the bladder is relatively easy. Alternatively, identification of the bladder will be difficult in a term fetus that has recently voided. The urine, in this instance, provides the "contrast" that ordinarily makes the urinary bladder an easy structure to perceive. If this contrast agent drains away, the size of the fetus (and thus its bladder) will not rescue one from the loss of contrast. Important also is the concept that the human eye sees best in the "relative" rather than the "absolute" sense of size. Thus, in a young fetus, the cerebral ventricle is much more readily seen than in an older fetus because the relative size of the ventricle compared with overall brain size is larger early (even though the absolute size is larger later).

If the sonographer begins with a specific intent to image a particular fetal part, it is frequently possible to succeed.<sup>8,16</sup> To accomplish this end, the sonographer must (1) assess the precise fetal position; (2) consider whether the anatomic part of interest is best visualized in planes perpendicular to the fetal long axis or parallel to the fetal long axis; and (3) adjust acoustic imaging parameters, particularly time-gain compensation, and transducer angulation to visualize the area to best advantage. Obviously, such rules are the same throughout all of sonography. The challenge of imaging intrafetal structures is to apply these rules when fetal position is

changing such that the current scanning plane is no longer applicable for the part one wishes to visualize.

The flexibility offered by real-time sonographic systems enables one to survey the fetus quickly to determine precise position. Second, the sonographic tomograms, which are rapidly generated (virtually "real-time" imaging), enable one to view a large volume of the fetus with closely spaced sections. Such a rapid look at many contiguous tomograms eliminates one of the basic flaws of tomographic imaging of a moving target. Finally, fetal movements are viewed directly, which enables one to quickly reorient the transducer to the optimal plane of section to image the structure of interest. As digital image storage and viewing continues to expand, cine clip technology has greatly improved the capture and viewing of many fetal parts, especially those that are in motion, such as the heart. Currently, three-dimensional imaging systems have reached a clinically relevant stage of development.<sup>17-19</sup> These instruments depend on "volume imaging." That is, a volume of tissue (the fetus) is insonated and the data are gathered in the processing computer. From this "volume," three-dimensional images are generated. Of perhaps greater importance in the future, individual planes of section in virtually any orientation can be computed. When and if it becomes possible to generate equivalent planar images to those obtained with a hand-held transducer, the current method of "fluoroscopic" sonography, the entire nature of sonography will change. The technical challenges of sonography will be greatly reduced (Fig. 9-4). Three-dimensional imaging of fetal anatomy will be covered in a separate chapter.

Fetal parts of interest to the sonologist fall into three major categories of subject contrast that subsequently determine the relative ease with which the structure is sonographically visible: (1) structures that generate high-amplitude reflections (e.g., ossified bones, submucosa of fetal bowel); (2) structures that generate no internal echoes (e.g., fluid-containing viscera); and (3) those that generate midrange gray echoes (e.g., the parenchymal organs such as the lungs, brain, spleen, liver, kidneys, muscles). The categories are listed from most visible to least visible. Within the last category, one may anticipate seeing a spectrum of gray shades that will enable distinction between several parenchymal organs and intraorgan components. For example, the medullary portions of the fetal renal parenchyma generate lower amplitude internal echoes than do the surrounding cortical tissues and Bertin septa, thus enabling recognition of this separate component of renal tissue (Fig. 9-5).<sup>20</sup>

A feature of critical importance for organ imaging is the fetal position. Clearly, a prone fetus is in an optimal position for imaging the kidneys, ordinarily difficult to perceive, but in a poor position to demonstrate the urinary bladder, which is usually easy to image. Determination of fetal position should be accomplished in all obstetric sonographic examinations from the second trimester onward. The fetal position should be determined as precisely as possible before an interpretation of fetal anatomy is begun, because the position of a structure will often influence our interpretation. The general fetal orientation is first assessed (i.e., longitudinal, oblique, or transverse). Once this is determined, the presentation (i.e., cephalic, breech) and location of the fetal spine are noted. If, for example, the fetal spine is on the maternal left side and the fetus is in a cephalic presentation,



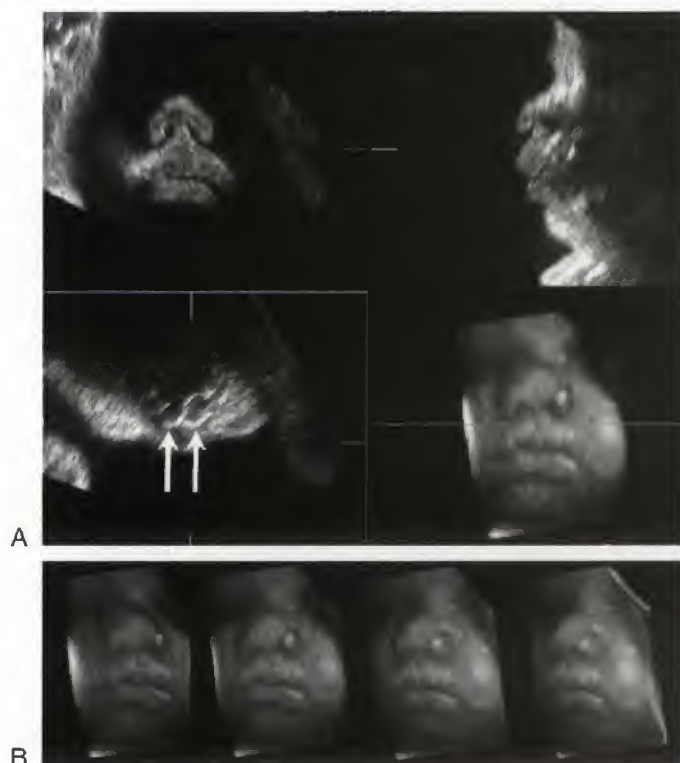


**FIGURE 9-4.** Normal face in a 35-menstrual-week fetus. *A.* Multiplanar and volume-rendered images of the fetal face are displayed. Upper left, a coronal view through the nose and lips is seen. Upper right, a sagittal or profile view of the face is seen. Lower left, an axial plane through the anterior alveolar ridge of the primary palate is shown. Lower right, a volume-rendered image of the face using surface and light techniques is shown. A line is visible crossing the upper lip of the fetus, which identifies the level of the axial plane in the lower left box. Note two tooth buds in the anterior alveolar ridge (arrows). *B.* Images from multiple rotations of the fetal face are shown. Generally, a volume is rotated with a knob on the work panel to provide the impression of three-dimensionality. (From Pretorius DH, Nelson TR: *Three-dimensional ultrasound in gynecology and obstetrics*. *Ultrasound Q* 14:218, 1998.)

one can judge that the fetus is lying on its left side (Fig. 9-6). Conversely, if the fetus is breech, then it must be lying on its right side. The reverse is the case for breech and cephalic fetuses when the fetal spine lies on the maternal right side. In the transverse or oblique fetal positions, the same rules apply but with a different orientation.

Such an analysis of fetal position is vital for proper interpretation of abdominal and thoracic situs and for identification of abnormal fetal structures. For instance, a rounded, fluid-filled structure in the left posterior portion of the upper fetal abdomen may be assumed to represent the fundus of the fetal stomach. However, a structure of identical appearance but located on the right side of the upper fetal abdomen must be interpreted as a pathologic lesion or an abnormality of situs.

It is important to recall that pathologic structures are frequently more visible than their normal counterparts (e.g., dilated small bowel loops are easier to detect than normal small bowel loops). However, it is even more important to keep in mind that the most difficult pathologic observation is to recognize the absence of a structure that ordinarily

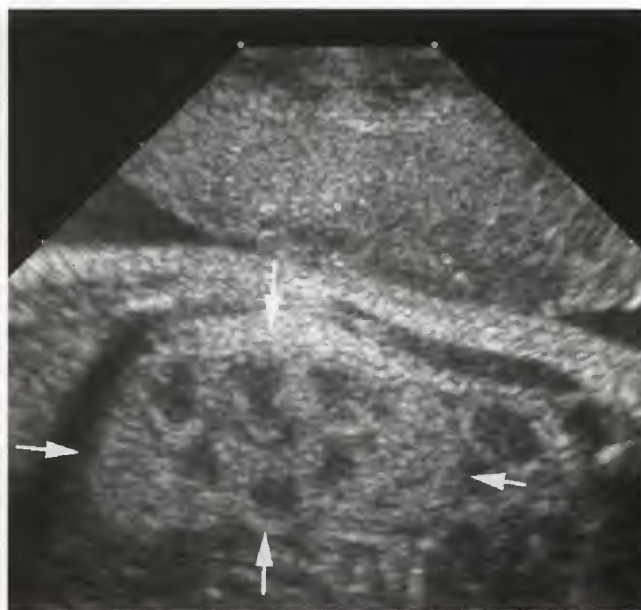


**FIGURE 9-5.** Sonogram of a fetal kidney in longitudinal axis (arrows). The medullary pyramids (darker, triangle-shaped areas) are distinguished from surrounding cortical tissues and septa of Bertin.

could be visualized (e.g., a missing portion of an extremity or the inability to see the stomach when esophageal atresia without tracheoesophageal fistula is present).

## SUPERFICIAL ANATOMY OF THE FETUS

Routine sonography for obstetric indications rarely requires a survey of superficial fetal structures. However, when an anomaly is suspected, a careful look at superficial features of the fetus becomes important or even mandatory. Superficial anatomy considered in this section includes the face, ears, hair, and external genitalia. Importantly, technologic advancements in three-dimensional renderings of fetal sonograms have had a dramatic impact on visualization of superficial fetal anatomy.<sup>21-23</sup> Please refer to Chapter 24 for details.

The fetal face can be viewed with considerable clarity with two-dimensional sonography. Expectant mothers are often surprised to see their fetus so clearly (Figs. 9-7 to 9-9). The brow, cheeks, eyelids (and occasionally even eyelashes), nose, lips, and chin can be seen with consistency. The nose and lips are the more important to image in detail (to exclude clefting). The alae, column, and nares can be clearly depicted (Figs. 9-10 and 9-11). The upper lip is more important diagnostically than the lower lip and fortunately easier to see. Visualization is usually good enough to identify the philtrum. The cheeks are prominent, as expected, and the subcutaneous tissues of the cheek, because of the presence of a large fat pad, are brightly echogenic (Fig. 9-12). The profile is also readily demonstrated (see Fig. 9-9) and provides useful information about the brow (e.g., frontal bossing), chin (e.g., hypognathia), and nose (e.g., midface hypoplasia and the Down syndrome).

The ears can be visualized quite well and their progressive maturation noted.<sup>24</sup> The external auditory canal, helix (and

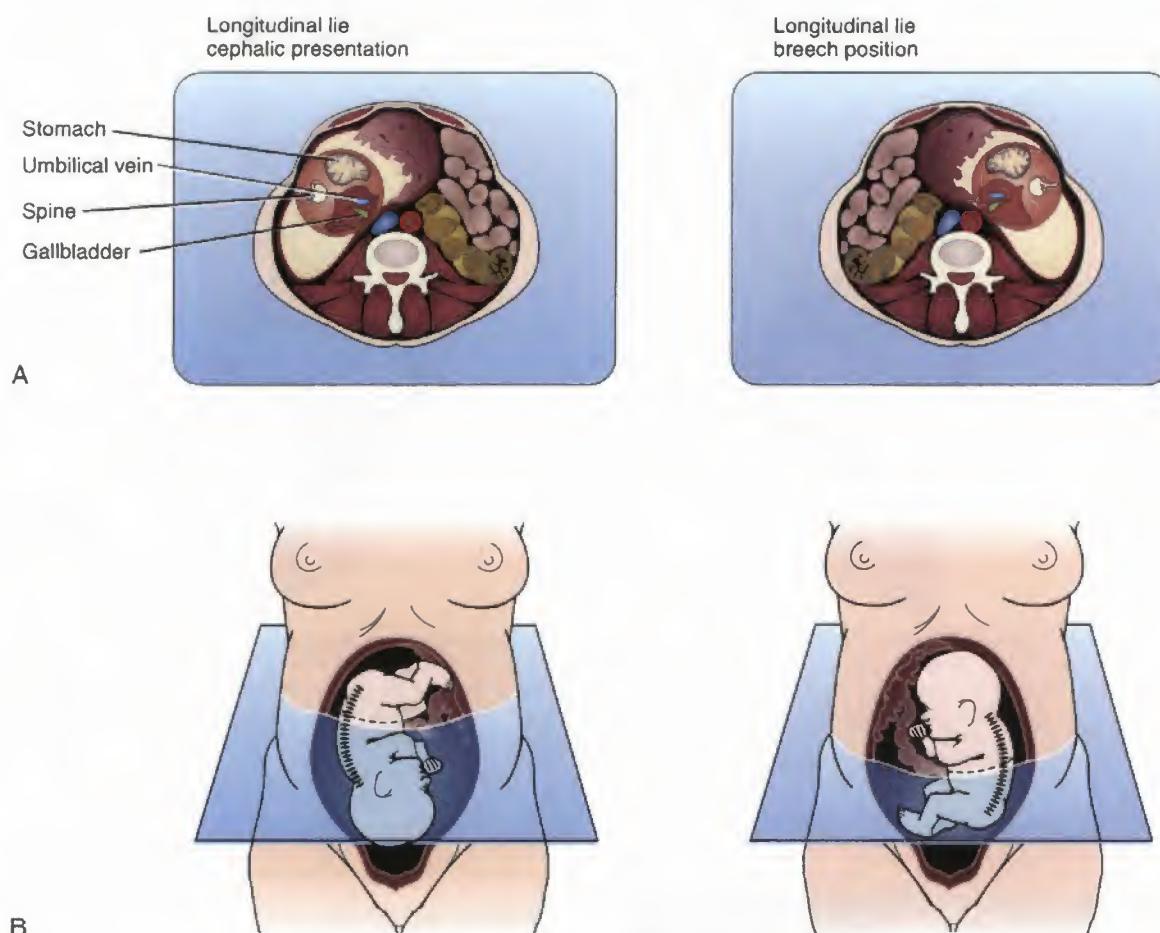


**FIGURE 9-6.** Knowledge of the plane of section across the maternal abdomen (longitudinal or transverse) as well as the position of the fetal spine and left-sided (stomach) and right-sided (gallbladder) structures can be used to determine fetal lie and presenting part. **A.** This transverse scan of the gravid uterus demonstrates the fetal spine on the maternal right with the fetus lying with its right side down (stomach anterior, gallbladder posterior). Because these images are viewed looking up from the patient's feet, the fetus must be in a longitudinal lie and in cephalic presentation. **B.** When the gravid uterus is scanned transversely and the fetal spine is on the maternal left, with the right side down, the fetus is in a longitudinal lie and in breech presentation. *Continued*



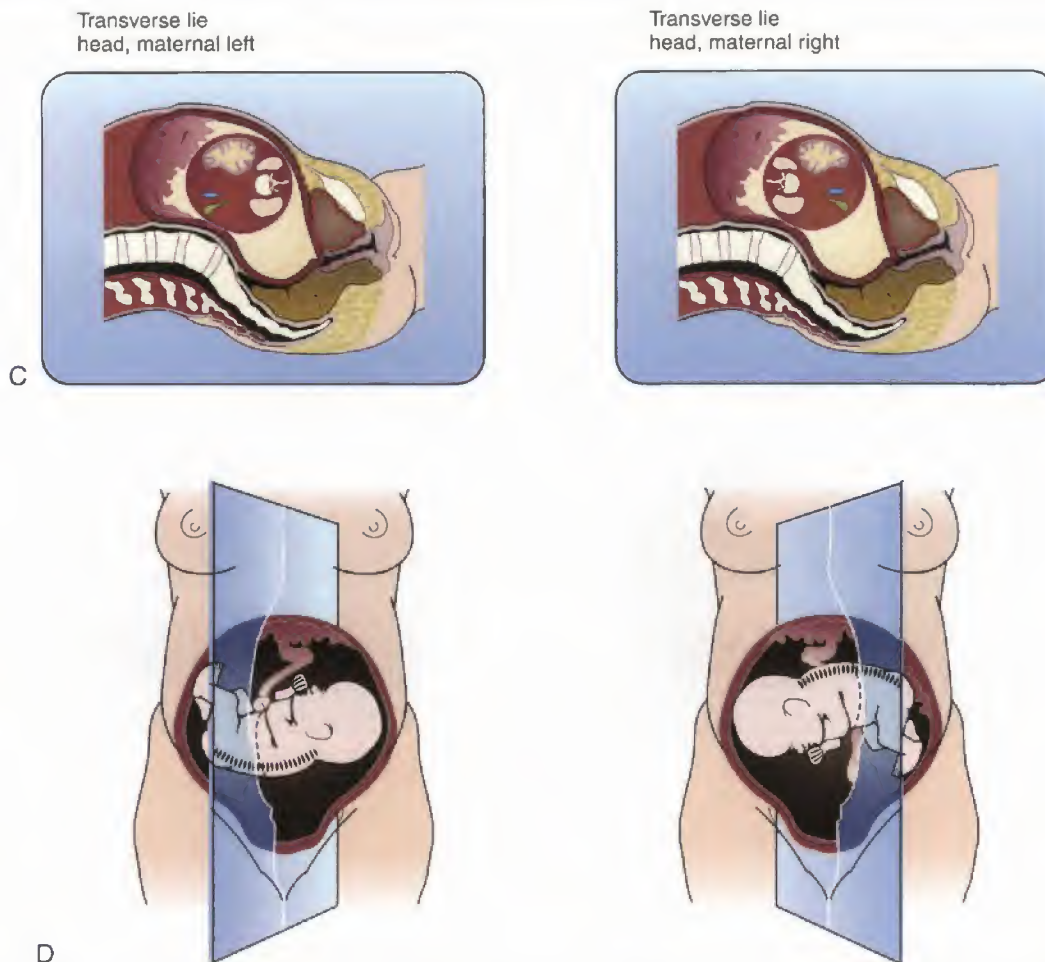


**FIGURE 9-6 cont'd.** C. When a longitudinal plane of section demonstrates the fetal body to be transected transversely and the fetal spine is nearest the lower uterine segment, with the fetal right side down, the fetus is in a transverse lie with the fetal head on the maternal left. D. When a longitudinal plane of section demonstrates the fetal body to be transected transversely and the fetal spine is nearest the uterine fundus with the fetal right side down, the fetus is in a transverse lie with the fetal head on the maternal right. Although real-time scanning of the gravid uterus quickly allows the observer to determine fetal lie and presentation, this maneuver of identifying specific right- and left-sided structures within the fetal body forces one to determine fetal position accurately and identify normal and pathologic fetal anatomy.

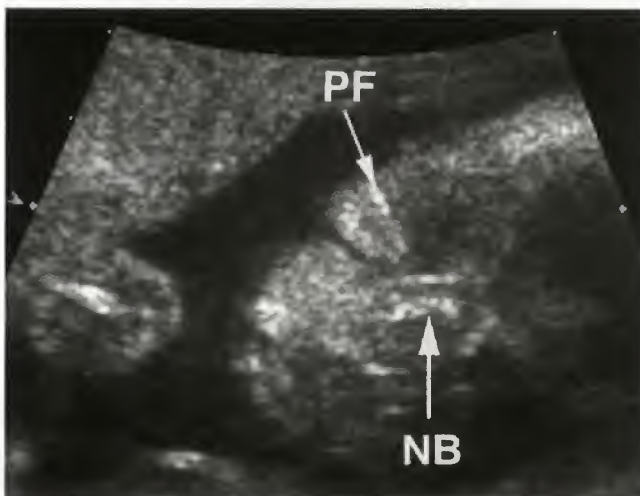


**FIGURE 9-7.** Coronal section of the fetal face that demonstrates the palpebral fissures (PF) particularly well. NB, nasal bone.

antihelix in older fetuses), lobule, and tragus can be depicted (Fig. 9-13), but the relative position of the ear (e.g., as in low-set ears) is difficult to judge—a task more readily accomplished with three-dimensional imaging. The ear may be protuberant and can be mistaken for an abnormality, especially an encephalocele.<sup>25</sup>

Scalp hair is readily perceived in late fetuses (that have some). The bright linear echoes protruding from or paralleling the scalp and neck are quite conspicuous. Indeed, the only benefit of recognizing hair is not to be misled into mistaking long hair for a pathologic process, namely, an encephalocele or cystic hygroma, because longer hair, wet and matted by the amniotic fluid, may trap some of the fluid between it and the skin of the occiput or neck, creating the false impression of a cystic mass in this location (Fig. 9-14).

The external genitalia can be appreciated from early second trimester onward. Gender can be quite accurately assigned.<sup>26-28</sup> Ordinarily, this is not of clinical consequence. However, in certain circumstances, gender should always be

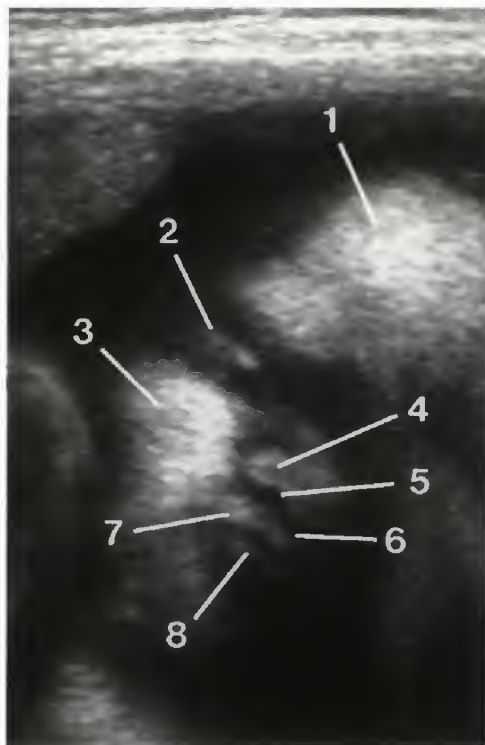
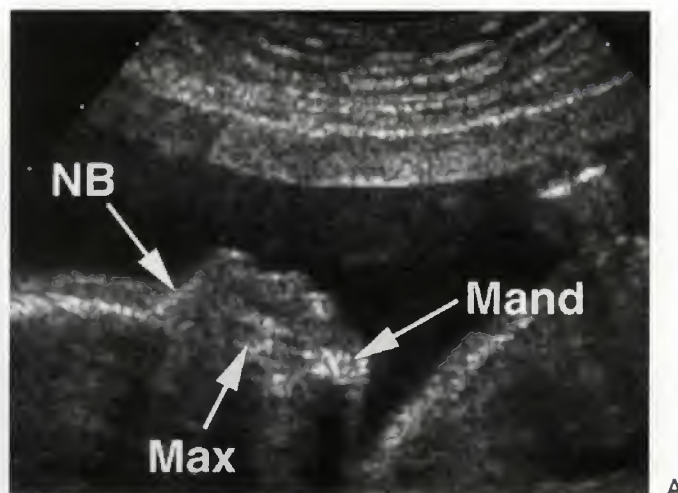
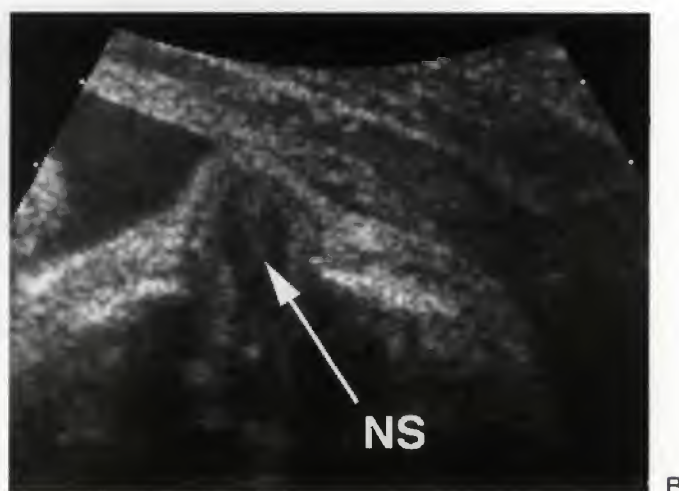


**FIGURE 9-8.** Sonogram of the fetal face. Even though this image is a tomogram with relatively little depth, facial features are seen well. Amniotic fluid surrounding the face provides the "contrast" for visualization. 1, brow; 2, eyelid; 3, cheek; 4, ala of nose; 5, nostril; 6, philtrum; 7, upper lip; 8, lower lip.



A



B

**FIGURE 9-9.** A. Midsagittal view of the fetal face ("profile" view). B. Axial sonogram through the nose. Note that the cartilaginous nasal septum (NS) is well seen. NB, nasal bone; Mand, mandible; Max, maxilla.

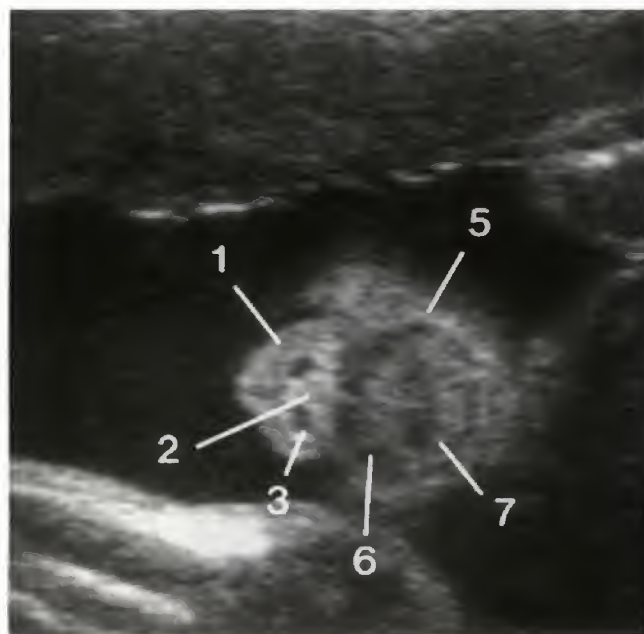


**FIGURE 9-10.** "Coronal" sonogram of the nose and mouth. Nasal structure is particularly well seen. 1, ala; 2, column; 3, nostril. The mouth displays less detail, although consistent and characteristic layering of echoes is seen. These layers are (presumably) the subcutaneous fat (5) and muscular tissue (6), the orbicularis oris muscle, and (7) the mucosal tissue.

determined. These include all living twins in which a single placental site is seen or when monozygotic twinning, other than for reasons of placentation, would be considered detrimental to pregnancy outcome.<sup>29</sup> All fetuses with suspected lower urinary tract obstruction should have gender determined because the differential diagnosis is different in boys and girls. Certain other circumstances would require gender determination if karyotyping were refused or impractical to perform. These include, but are not limited to, risk for X-linked disorders or when the Turner syndrome is suspected because of a dysmorphic feature (e.g., cystic hygroma).

Female gender should be assigned only by identification of the major and minor labia (Fig. 9-15). Assigning female gender because of an inability to see a penis will result in many diagnostic errors. Male genitalia are readily seen (Fig. 9-16). The penis and scrotum are most obvious. Testes may be seen in the scrotal sac, sometimes as early as the beginning of the third trimester (the testes are intraabdominal during most of gestation, but are often visualized in the presence of ascites). Details of the penis, including the glans,



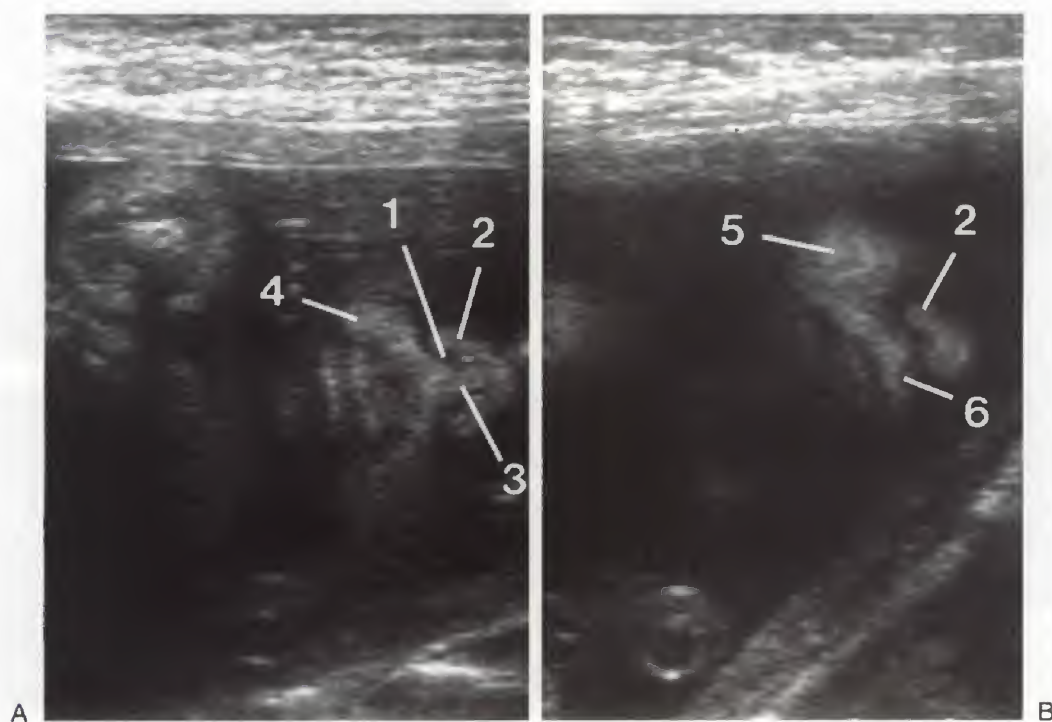


**FIGURE 9-11.** A. True coronal image of the nose and upper lip. 1, nostril; 2, ala; 3, column; 4, upper lip. B. Inclined coronal image demonstrates a slightly different perspective. 5, cheek; 6, philtrum.

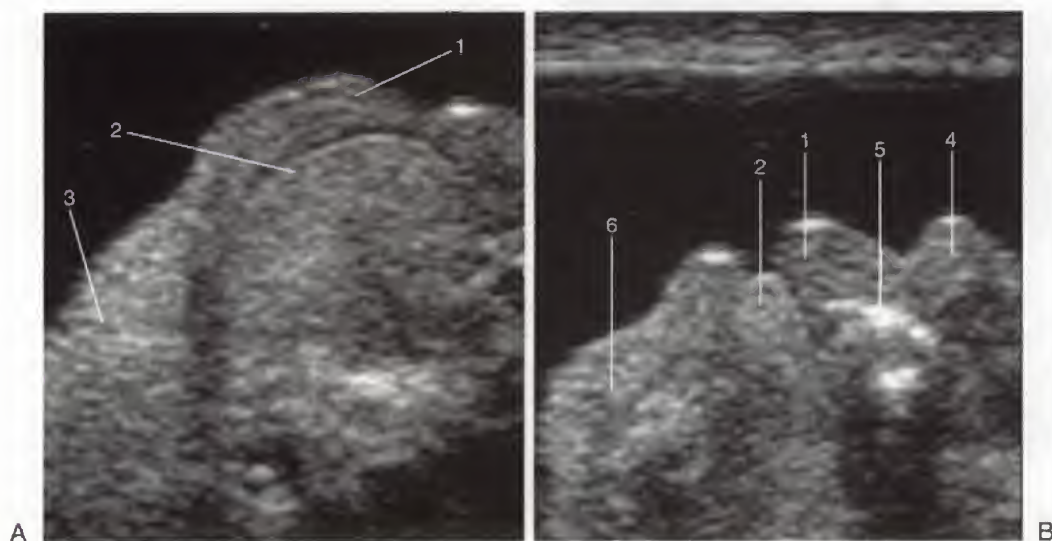


**FIGURE 9-12.** A. Axial section of the fetal face demonstrating the tongue. 1, lip; 2, tongue; 3, fat pad of cheek. B. Midsagittal section of the fetal face demonstrating the tongue. 4, nose; 5, maxilla; 6, chin.

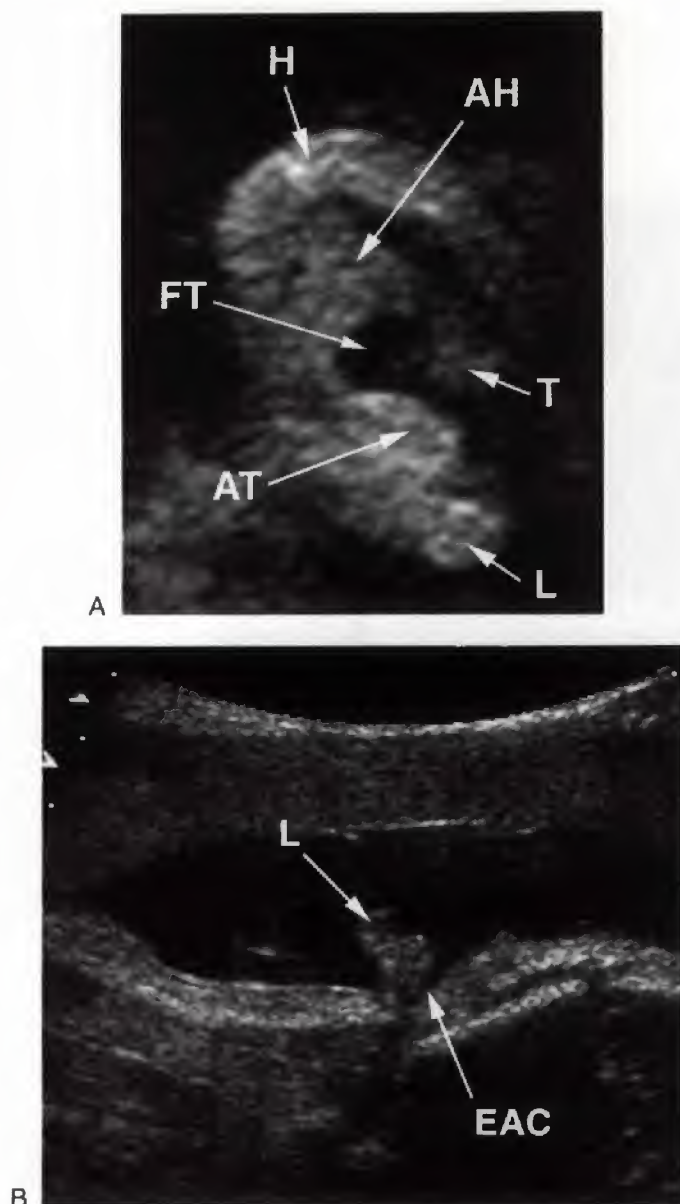


**FIGURE 9-13.** Parasagittal (A) and coronal (B) sonograms of the fetal ear. AH, antihelix; AT, antitragus; EAC, external auditory canal; FT, fossa triangularis; H, helix; L, lobule; T, tragus.

urethra, and corpora cavernosa, may be appreciated (Fig. 9-17). Even the foreskin is visible in some cases.

## MUSCULOSKELETAL SYSTEM

Real-time ultrasonography provides the most appropriate format for imaging fetal bones. The resolution and flexibility offered by such systems enable one to survey the fetal skeleton rapidly. Of all structures within the fetus, the ossified portions of the skeleton possess the highest level of subject contrast and thus are seen earlier and more consistently than any other organ system.<sup>13,30-33</sup> Indeed, sonography surpasses all other imaging modalities in fetal

skeletal imaging. Although radiographs of abortuses demonstrate bony morphology more advantageously than would a sonogram,<sup>34,35</sup> the reverse is true of fetuses in the womb, where overlying maternal soft tissues and bones, fetal movement, and inappropriate fetal position defeat radiographic techniques in visualization of the early fetal skeleton. With volume imaging (three-dimensional sonography) special processing can give a more global view of fetal skeletal structures than can be achieved with two-dimensional sonography.<sup>36-38</sup> This enhances the image and diagnostic process for assessment of both normalcy and pathology.

Fetal position is extremely important. The posterior elements of the fetal spine may be clearly imaged with the fetus in a prone or decubitus position but are difficult to image when the fetus is supine.<sup>39</sup> Similarly, the extremities are imaged to excellent advantage when floating freely in the amniotic fluid. The same extremity tucked under the fetus will be quite difficult to image.

Despite these potential problems, fetal skeletal structures remain the earliest and most readily recognized fetal anatomic structures. Indeed, the earliest structures seen with consistency are the ossification centers of the maxilla, mandible, and clavicle, the first bones of the human body to ossify.<sup>13</sup> The calvaria can be imaged from the late first trimester onward. The same is true of the long bones of the upper and lower extremity (Fig. 9-18). Visibility of bony detail rapidly increases, and by 15 to 16 menstrual weeks (sometimes earlier), even phalanges can be visualized. Bones of only 2 to 3 mm in size can be consistently imaged by sonography, provided that no unusual impediments to the scanning procedure exist (Fig. 9-19). Many specific bony structures can be depicted. Bones in both the appendicular and axial skeleton are well imaged.

It is important to clarify that sonography has the capacity to visualize not only the ossified portions of the fetal skeleton but also the cartilaginous portions.<sup>13</sup> Cartilaginous ends of the long bones may be seen by the early second trimester. Indeed, bones entirely in cartilage can be seen sonographically (Fig. 9-20). It is equally important to recognize that the full thickness of the ossified diaphysis of long bones is not seen sonographically.<sup>40</sup> This is due to acoustic shadowing. The cartilaginous ends of long bones help us to recognize this aberration. By matching up the width of the epiphysis, the full thickness of which can be seen, with the apparent "width" of the bony diaphysis, it is clear that these are unequal (Figs. 9-21 and 9-22). This observation helps to correct some perceptual errors that can lead to erroneous diagnoses. For example, the inability to see the full thickness of the femoral diaphysis creates the impression that the fetal femur farther from the transducer is bowed (Fig. 9-23).<sup>40</sup> This error is caused by visualization of only the medial cortex of the femoral diaphysis (which is normally curved) (Fig. 9-24). However, the inability to "visually correct" this normal curvature by simultaneous observation of the "straight" lateral cortex causes the perceptual error.

The majority of the bones of the appendicular skeleton can be seen in early to middle second trimester, although phalanges may be difficult to perceive in some instances. It is a general rule of appendicular skeletal imaging that the more proximal a bone, the more readily it is identified. This rule in one sense is untrue of the hands and feet, in which the metacarpals and metatarsals are seen more readily and



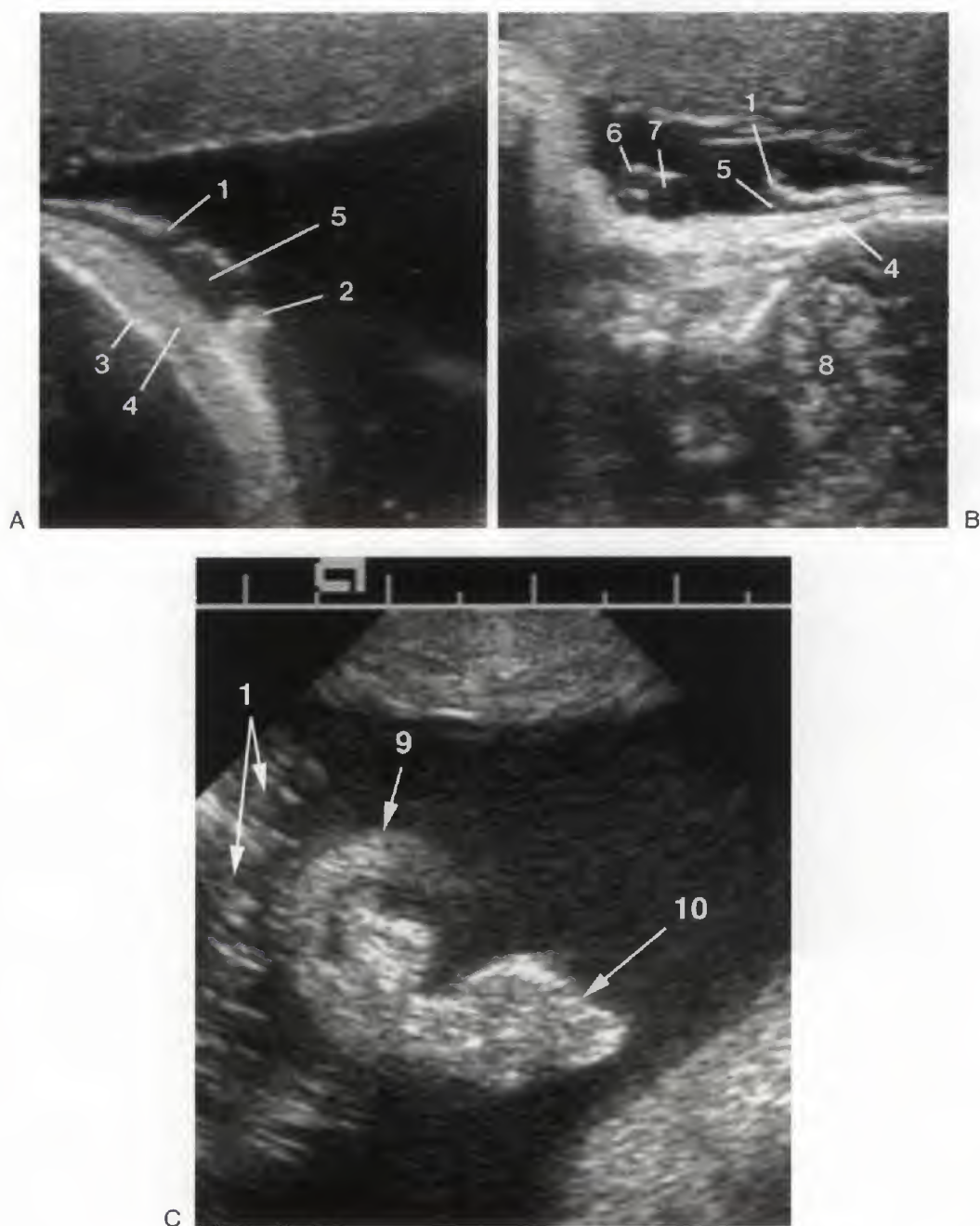


**FIGURE 9-14.** A. Hair (1) may be mistaken for the outer membrane of a cystic mass in an older fetus. 2, Portion of ear; 3, occipital bone; 4, subcutaneous tissues and muscles in the occipital region; 5, "trapped" amniotic fluid. B. Scan at 90 degrees to A. This image clarifies that the fetus is normal. 6, umbilical artery; 7, umbilical vein; 8, cerebellum. C. Parasagittal plain through a different fetus demonstrates hair (1) above the ear. 9, helix; 10, lobule.

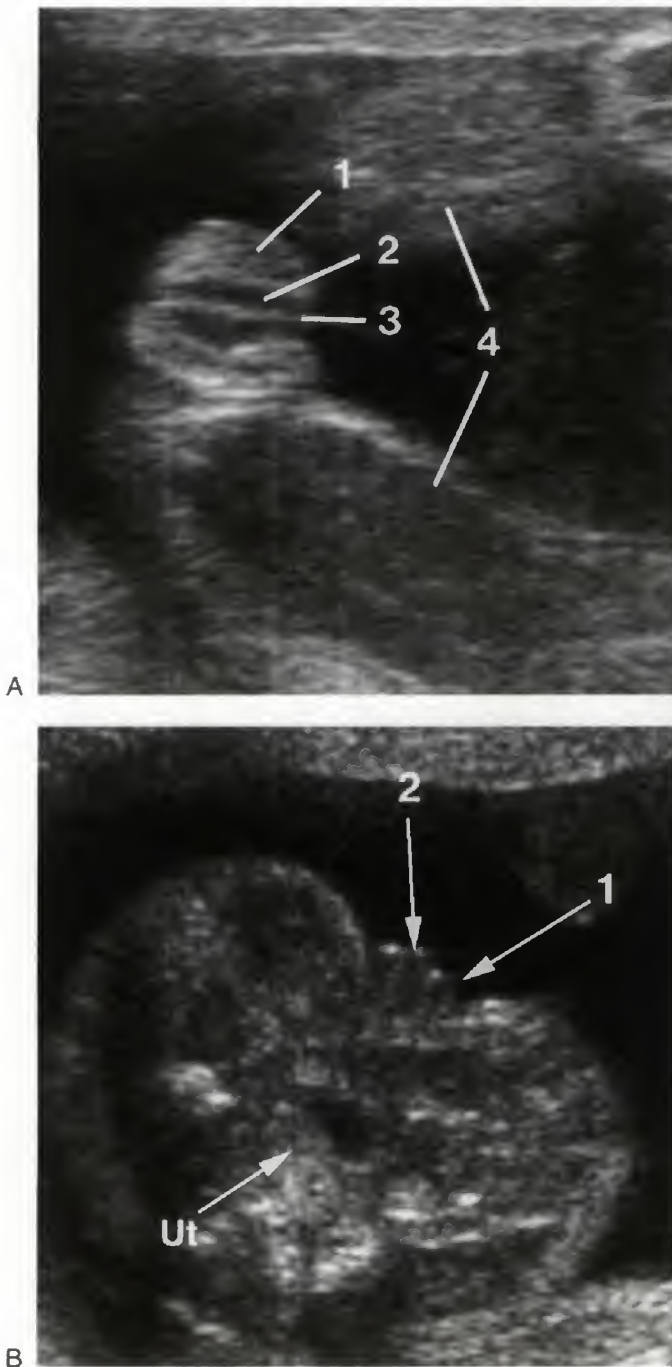


**FIGURE 9-15.** Coronal (A) and axial (B). External (and "internal") female genitalia. Of interest, the uterus (Ut) can be seen to asymmetrically indent the bladder of female fetuses (*Ants Toi, MD - personal communication*). 1, major labium; 2, minor labium; 3, vaginal cleft; 4, thighs.

earlier than either the carpal or tarsal bones (see Figs. 9-19 and 9-25). This is because the metacarpals and metatarsals are well ossified at 4 months, whereas the carpals and tarsals (except for the tarsal calcaneus and talus) remain cartilaginous throughout pregnancy. The tarsal calcaneus and talus ossify between the 5th and 6th months, whereas the remaining tarsals and carpals do not ossify until after birth (Figs. 9-26 and 9-27).

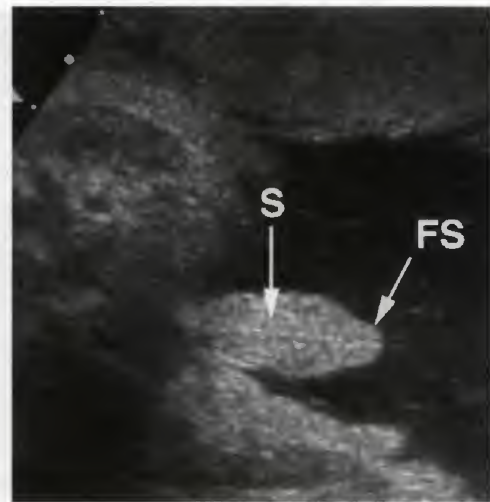


**FIGURE 9-16.** Nonerect fetal penis seen sonographically. FS, foreskin; S, shaft.

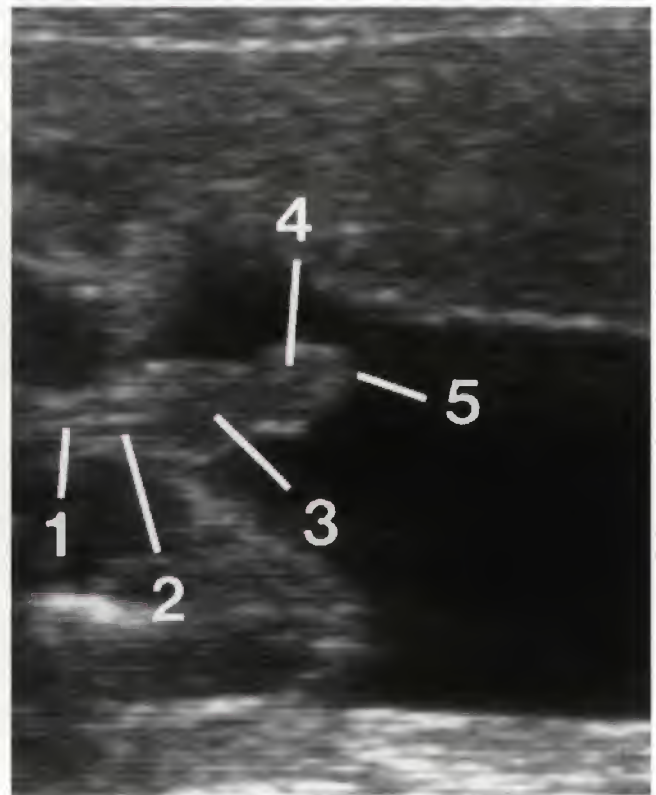


**FIGURE 9-17.** Details in an erect fetal penis. 1, urethra; 2, corpus cavernosum; 3, shaft; 4, glans; 5, foreskin.

The scapula (Figs. 9-28 and 9-29), clavicle (Fig. 9-30), humerus (see Figs. 9-28 and 9-31), radius (Fig. 9-32), ulna (see Figs. 9-31 and 9-32), metacarpals (see Figs. 9-19 and 9-32), and phalanges (see Figs. 9-19 and 9-33) can be imaged in most cases. Interestingly, the clavicle may be difficult to see, presumably because of the flexed position of the fetal neck, which draws the calvaria into a position that obscures the clavicle. Nonetheless, if one desires to see the clavicle,





**FIGURE 9-18.** Sonogram of a 10½-week-old embryo demonstrates the tiny (approximately 1 mm) primary ossification center of the femur (arrow). (From Mahony BS, Filly RA: High-resolution sonographic assessment of the fetal extremities. *J Ultrasound Med* 3:489, 1984.)

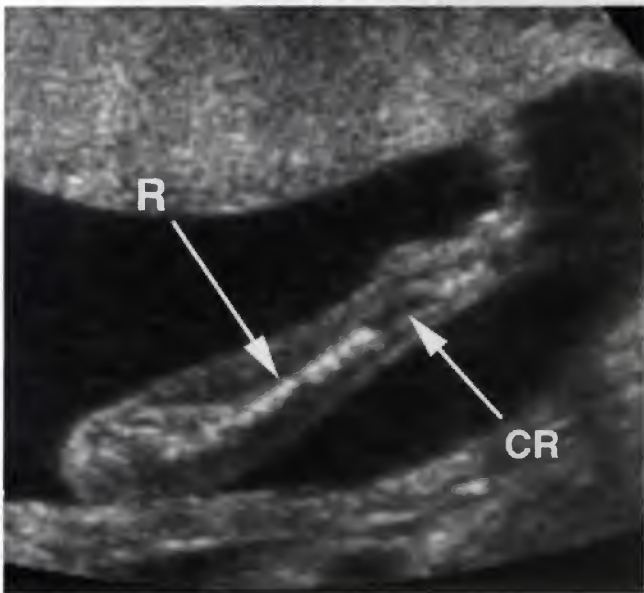
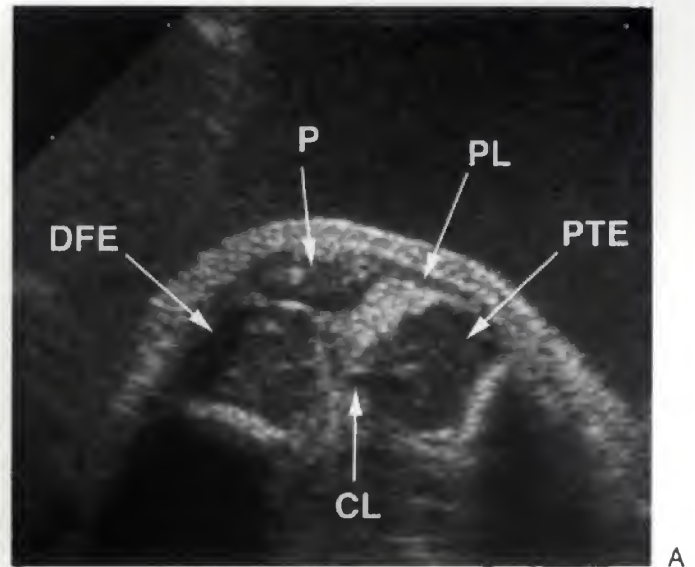
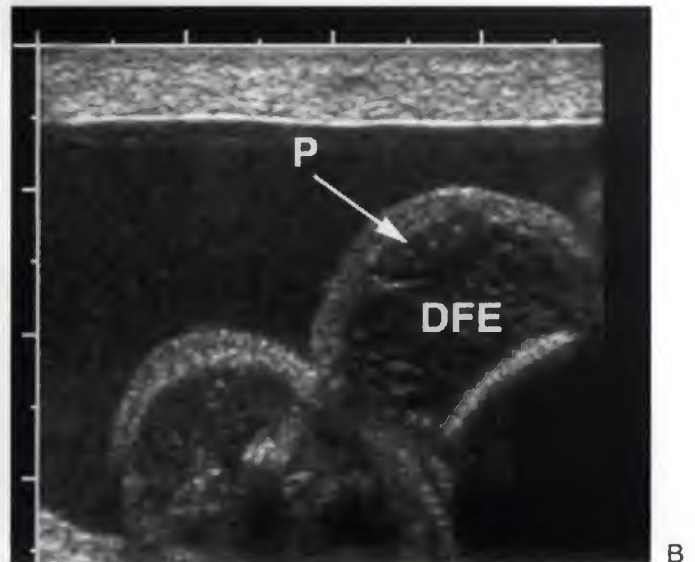


**FIGURE 9-19.** Sonogram of a 20-week fetal forearm and wrist. CR, cartilaginous carpal bones; R, radial diaphysis (distal radial epiphysis is also cartilaginous).

this can nearly always be accomplished. Indeed, measurements exist for normal clavicular length at various gestational ages.<sup>41</sup> Similarly, the femur (Figs. 9-34 to 9-37), tibia (Figs. 9-38 and 9-39), fibula (see Fig. 9-38), metatarsals (see Figs. 9-25 and 9-26), and phalanges (see Fig. 9-25) of the lower extremity can be appreciated well sonographically.



A



B

**FIGURE 9-20.** A. Midsagittal sonogram of the fetal knee. B. Axial sonogram (similar to the knee radiograph called the "sunrise view"). CL, posterior cruciate ligament; DFE, distal femoral epiphysis; P, patella (a bone that is entirely cartilaginous); PL, patellar ligament; PTE, proximal tibial epiphysis. Note the echogenic synovium located between the patella, patella ligament and the epiphyses.

The figures demonstrating the hip joint, femur, and knee (see Figs. 9-34 to 9-38) may be reviewed to appreciate the remarkably detailed anatomy that can be achieved with high-resolution sonography.

The simplest way to identify the types of long bones of the extremity viewed on the sonogram is to obtain planes of section that traverse the short axis of the limb. Sonograms obtained in such a plane through the forearm and calf will demonstrate two bones. In the lower leg, the more lateral bone is the fibula, and the medial bone is the tibia (see Fig. 9-38). This method works as well in the forearm but is less precise because pronation may cause the radius and ulna to "cross." In the normal fetus, the tibia and fibula and

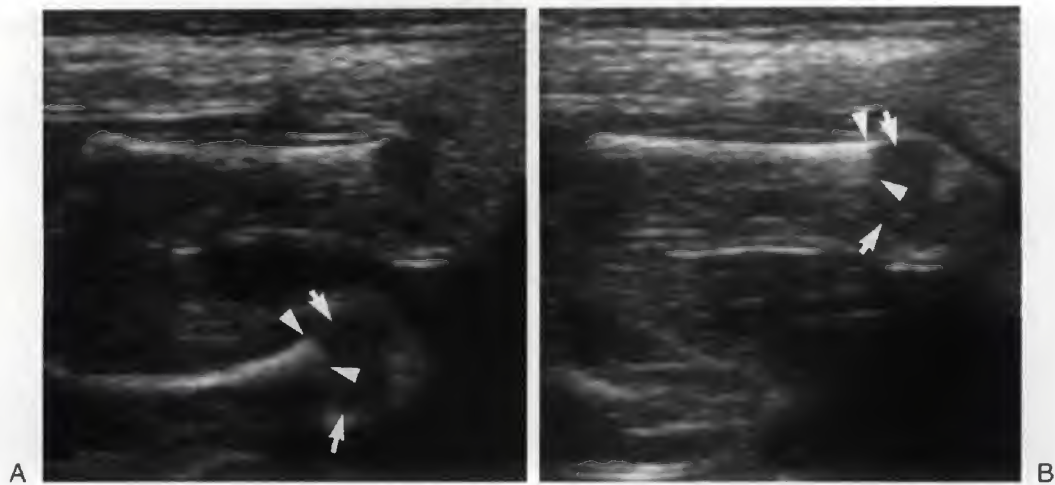


**FIGURE 9-21.** A. Sonogram best demonstrating the femur farther from the transducer. Arrows mark the edges of the distal epiphysis. Arrowheads mark the apparent “edges” of the distal femoral diaphysis. The more medial edge of the diaphysis matches the edge of the medial condyle, but the lateral edges of “diaphysis” and lateral condyle are widely disparate. B. The same exercise can be performed on the nearer femur. Again, arrows mark the edges of the distal epiphysis and arrowheads mark the “edges” of the femoral diaphysis. Shadowing by the bone but not the cartilage causes this deceptive appearance.



**FIGURE 9-22.** Sector sonogram of the distal femur taken such that the lines of sight from the transducer intersect the inferior end of the femoral metaphysis at the epiphyseal plate (1). By this maneuver, the full thickness of the distal ossified femur is seen sonographically (compare with Fig. 9-21). Now, the thickness of the epiphysis (arrows) and ossified femoral shaft match perfectly. 2, patella; 3, secondary ossification center of the distal femoral epiphysis.

radius and ulna end at the same level distally (see Fig. 9-32). Proximally, of course, the ulna is longer than the radius (see Fig. 9-31) and the tibia is longer than the fibula. This allows both ready differentiation of the tibia and fibula in the lower extremity and of the radius from the ulna in the upper extremity. That both paired long bones of the upper and

lower extremity end at the same level distally is important in assessing possible limb reduction abnormalities.

The hand can be assessed more critically than the foot.<sup>42-44</sup> With patience, one can usually discern all four fingers and the thumb. The hand is frequently clenched in a fist-like fashion, which can complicate the counting of fingers. However, even under this circumstance, one can frequently make the necessary observations. The toes, although smaller than the fingers, can be seen relatively well with modern equipment (see Figs. 9-25 and 9-27). If difficulty arises, it is usually the functionally less important fourth and fifth toes that are not seen.

It is possible in the late third trimester fetus to identify the distal femoral (see Figs. 9-22 and 9-40) and proximal tibial (see Fig. 9-40) epiphyseal ossification centers.<sup>45,46</sup> Ossification of these epiphyses, as seen on radiographs, is known to be an indicator of fetal maturity. Identification of the epiphyseal ossification centers about the knee provides a different type of parameter that sonologists can use in the assessment of gestational age in the third trimester of pregnancy. In general, visualization of a distal femoral epiphyseal ossification center indicates a gestational age of at least 33 weeks (Figs. 9-41 to 9-43). Similarly, the same data suggest that demonstration of the proximal tibial epiphysis indicates a gestational age of at least 35 weeks. These ossification centers appear earlier, on average, in female fetuses (see Fig. 9-42).<sup>46</sup> The size of the distal femoral ossification center correlates with late gestational age (see Fig. 9-43).<sup>46</sup> The proximal humeral epiphyseal ossification center is usually the last to ossify of the secondary ossification centers.

As stated earlier, many bones of the fetal appendicular skeleton are entirely cartilaginous. Some of these still can be imaged sonographically. Indeed, the patella can be seen rather commonly (see Figs. 9-20 and 9-22). This bone does not begin to ossify until after birth. All of the carpal and most of the tarsal bones are entirely cartilaginous (see Figs. 9-19, 9-25, 9-26, and 9-32). The carpal bones cannot be seen discretely. Rather, they are perceived as a conglom-



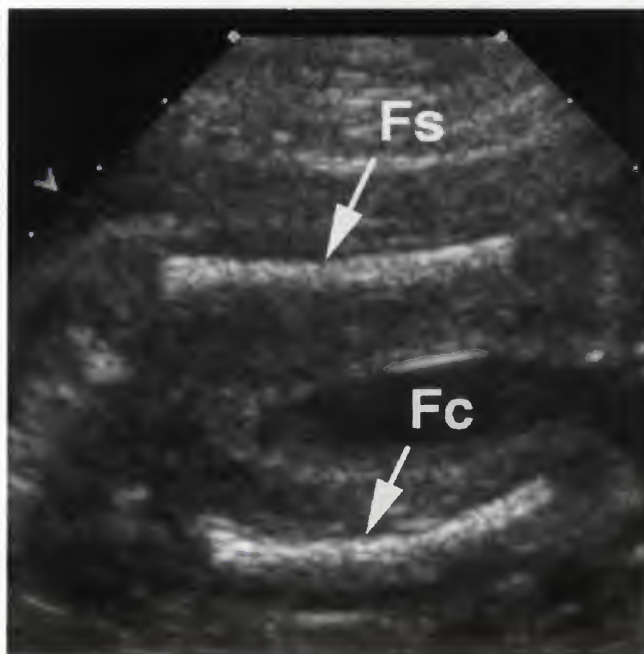


**FIGURE 9-23.** The diaphysis of the femur nearer to the transducer appears straight (Fs). The full thickness of the diaphysis is not seen. The diaphysis of the femur farther from the transducer appears curved (Fc). Compare with Figure 9-24. This is a normal shape of the medial aspect of the bone. However, the straight lateral cortex seen in the radiograph but not the sonogram visually compensates the curvature because the full thickness of bone is not perceived.



**FIGURE 9-24.** Radiograph of a midtrimester fetal femur. Note that our eye compensates for the curvature of the medial diaphyseal cortex (curved arrows) by noting the straight lateral diaphyseal cortex (straight arrows). Compare with Figure 9-23.

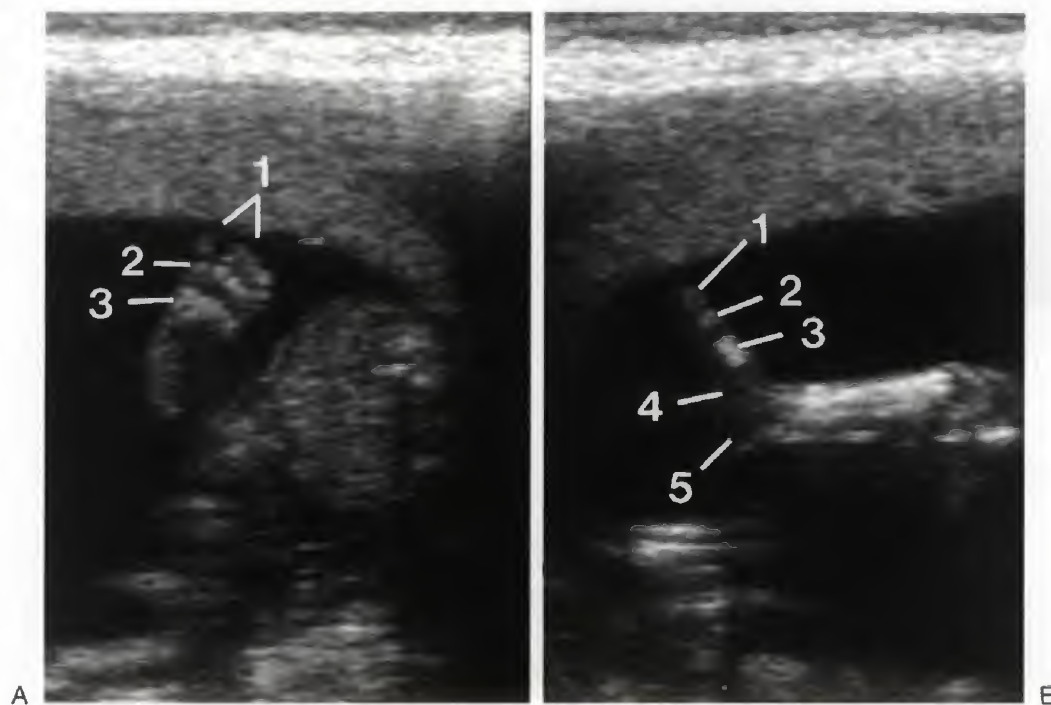


**FIGURE 9-25.** Fetal foot at 16 weeks' gestation in transverse axial (A) and parasagittal (B) planes. 1, toes; 2, proximal phalangeal ossification centers; 3, metatarsal ossification centers; 4, tarsal cuboid in cartilage; 5, tarsal calcaneus in cartilage.

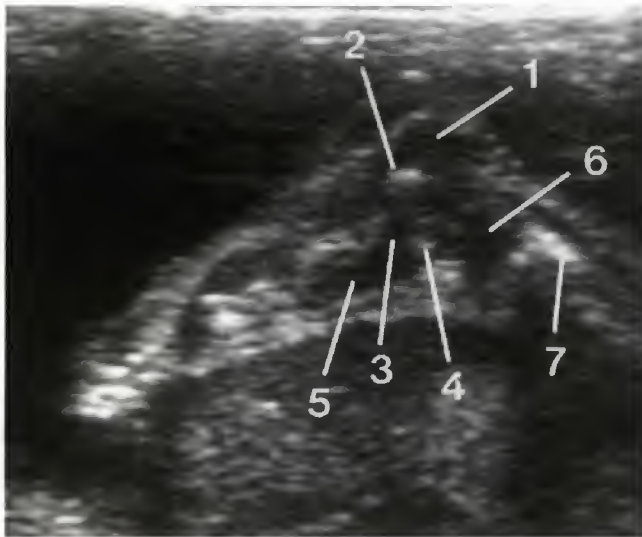


**FIGURE 9-26.** Midsagittal sonogram of the fetal foot in late second trimester. 1, cartilaginous calcaneus; 2, primary ossification center of calcaneus; 3, cartilaginous talus; 4, primary ossification center of talus; 5, tarsal navicular in cartilage; 6, distal tibial epiphysis; 7, distal tibial diaphysis.

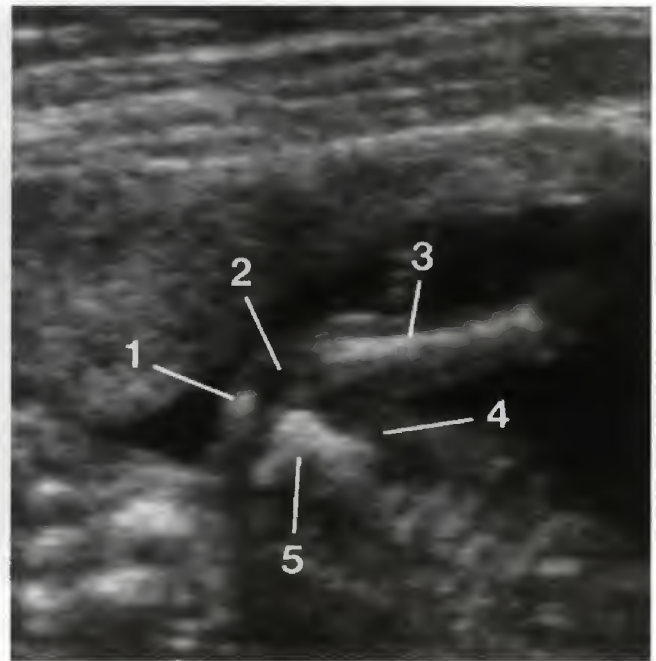


**FIGURE 9-28.** Coronal sonogram of the shoulder and upper arm. 1, distal clavicle; 2, cartilaginous humeral head; 3, ossified humeral diaphysis; 4, latissimus dorsi muscle; 5, scapula.

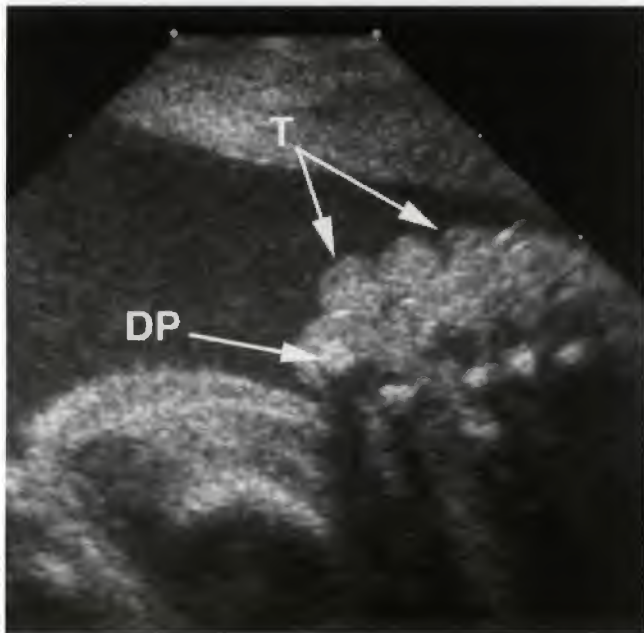


**FIGURE 9-27.** Axial sonogram of the fetal toes (T) demonstrating the soft tissues. Little bony structure is seen although the distal phalanx (DP) of the great toe is visible.

erate hypoechoic band spanning the gap from the distal radius and ulna to the proximal metacarpal ossification centers (see Fig. 9-32). Of course, this gap also includes the cartilaginous epiphyses of the long bones as well. Conversely, some of the tarsal bones can be discretely identified from time to time (see Figs. 9-25 and 9-26). These include, most

notably, the early tarsal calcaneus and talus (before 24 weeks) and the tarsal navicular and cuboid throughout gestation.

Visualization of the cartilaginous ends of the long bones assists in their measurement in two ways. The measurement of fetal long bones is confined to the ossified portion. A potential error is to foreshorten the bone by failing to obtain the plane of section through the true long axis of the bone. To avoid underestimating length, this shortcoming is often compensated for by assuming the “longest” measurement obtained in several attempts to be the most accurate, an assumption that can lead to serious overestimates, as is discussed shortly. However, if both cartilaginous ends of the desired bone to be measured are seen, this guarantees that the plane of section has passed through the longest axis of the bone (Fig. 9-44). The only remaining task to minimize error is to accurately position measurement cursors at the ends of the bone.

Another common misconception in measurement of the femur is that no other tissue in proximity to the bony termination will yield an echo of equal brightness to the bone. Thus, one should always place measurement cursors from the edge of the distal brightest reflection to the edge of the proximal brightest reflection. This long-standing belief is unfortunately erroneous, especially in older fetuses, although younger fetuses are not exempt from this potentially significant error in femur length estimation.<sup>47</sup> Figure 9-45 demonstrates that a nonosseous, but nonetheless equally bright, reflection is returned from tissues distal to the epiphyseal plate but in immediate contiguity with the distal femoral metaphysis. This is called the distal femoral point for lack of a more precise anatomic term.<sup>47</sup> That this point is not part of the ossified femur can be determined by noting its relationship to the cartilaginous lateral condyle. The



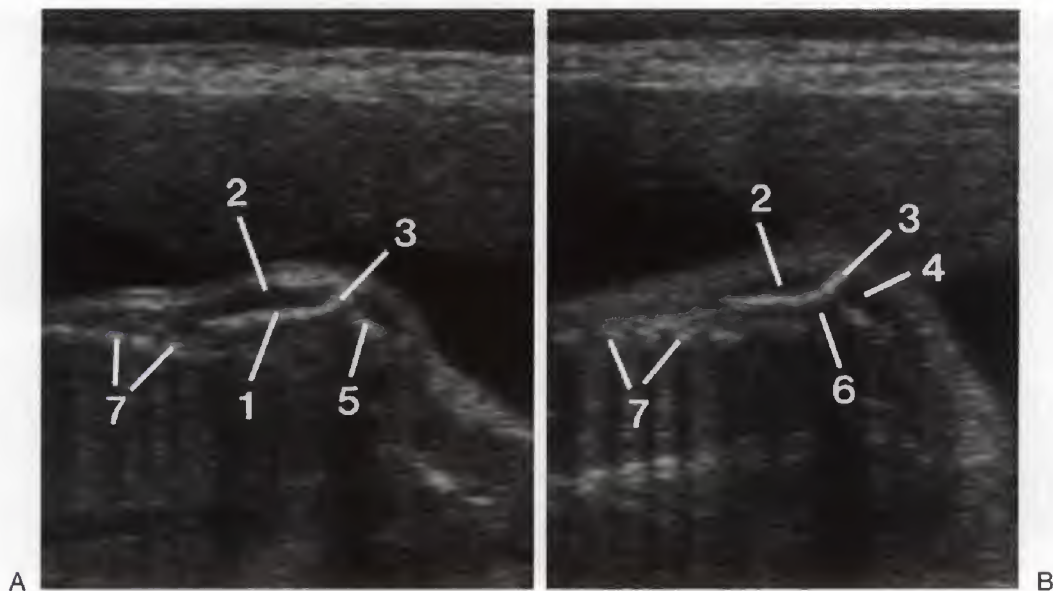


**FIGURE 9-29.** A and B. Parasagittal sonograms of the scapula. 1, infraspinous fossa; 2, infraspinatus muscle; 3, scapular spine; 4, supraspinatus muscle; 5, supraspinous fossa; 6, subscapularis muscle; 7, ribs in short axis.

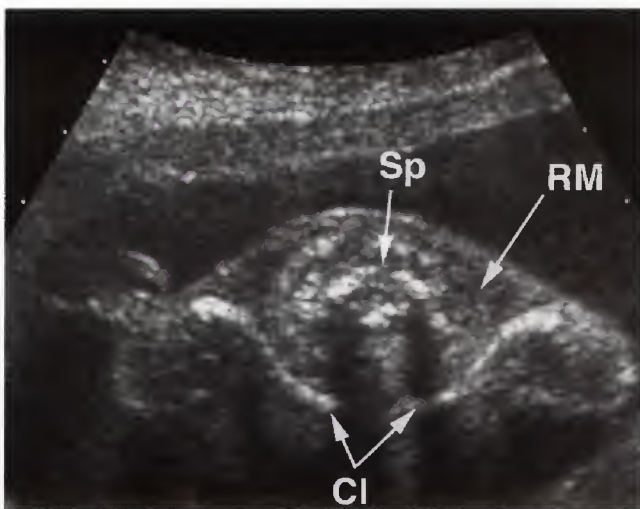


**FIGURE 9-30.** Axial sonogram of the clavicles (CI). Sp, spine; RM, rhomboid muscle.

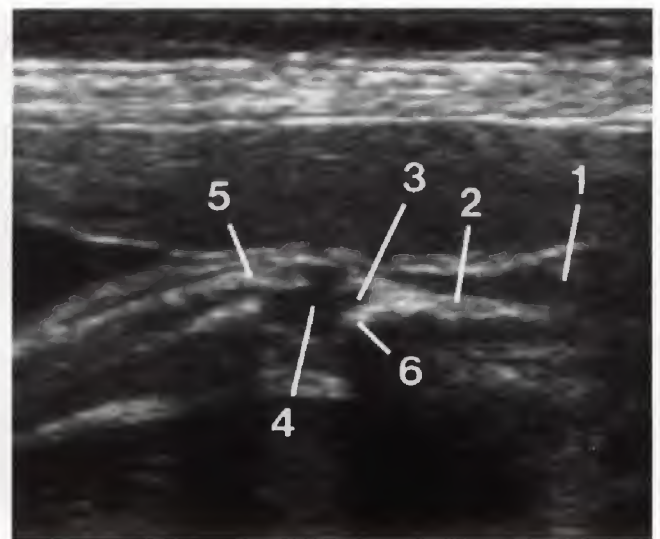


**FIGURE 9-31.** Fetal elbow, hand pronated, coronal sonogram. 1, triceps muscle; 2, ossified humeral diaphysis; 3, cartilaginous olecranon fossa; 4, conglomerate cartilages about the elbow joint; 5, proximal ulnar diaphysis; 6, medial humeral epicondyle.

femoral metaphysis ends at the beginning of the distal femoral epiphysis and does not overlap the edge of the epiphysis. Compare the radiograph of the fetal femur in Figure 9-24 with the sonogram of the fetal femur in Figure 9-45. No such *ossified* femoral point exists.

Sonography, from time to time, demonstrates rather extraordinary features of the musculoskeletal system of the extremities. At present, no known diagnostic usefulness for this information has been established, nor is it possible to demonstrate such structures with the consistency necessary to use their visualization in diagnostic pursuits. However, several of these remarkable features are demonstrated in Figures 9-46 to 9-48.

Many bones or components of bones of the axial skeleton are also routinely visualized. In the skull region, one can perceive a number of bones individually or as a conglomerate. The greater wings of the sphenoid and petrous ridge are easily identified and define the anterior, middle, and posterior cranial fossae (Fig. 9-49). The orbits can be visualized without difficulty unless the more anteriorly positioned orbit severely shadows the more posteriorly positioned orbit (Fig. 9-50). Standards have been established for fetal interorbital distances to evaluate hypotelorism and

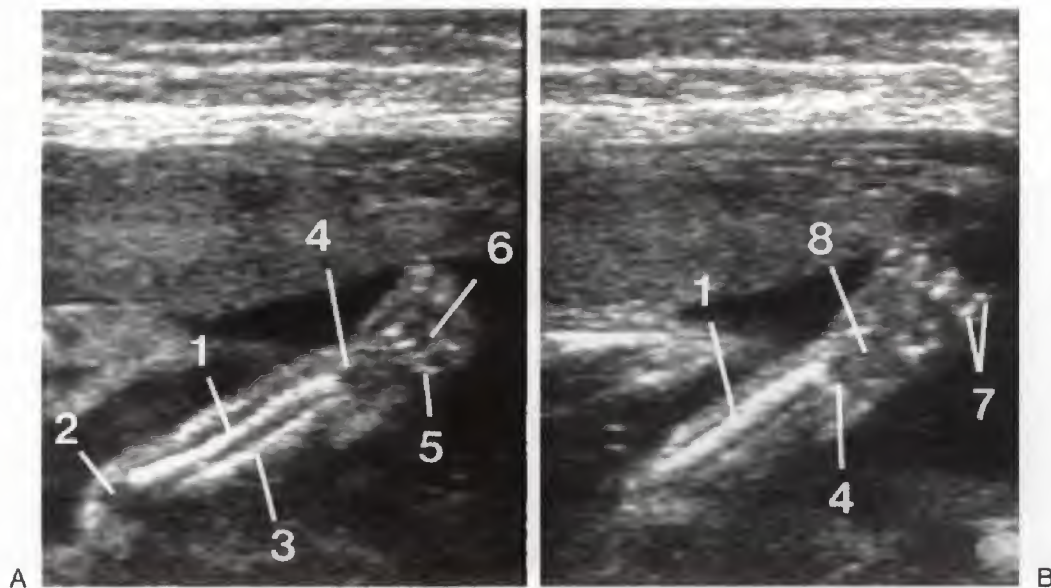


**FIGURE 9-32.** *A* and *B*. Coronal sonograms of the forearm and wrist. 1, ulnar diaphysis; 2, olecranon in cartilage; 3, radial diaphysis; 4, distal ulnar epiphysis; 5, metacarpal diaphysis; 6, distal metacarpal epiphysis; 7, phalangeal ossification centers; 8, carpal arch seen as a conglomerate cartilage.

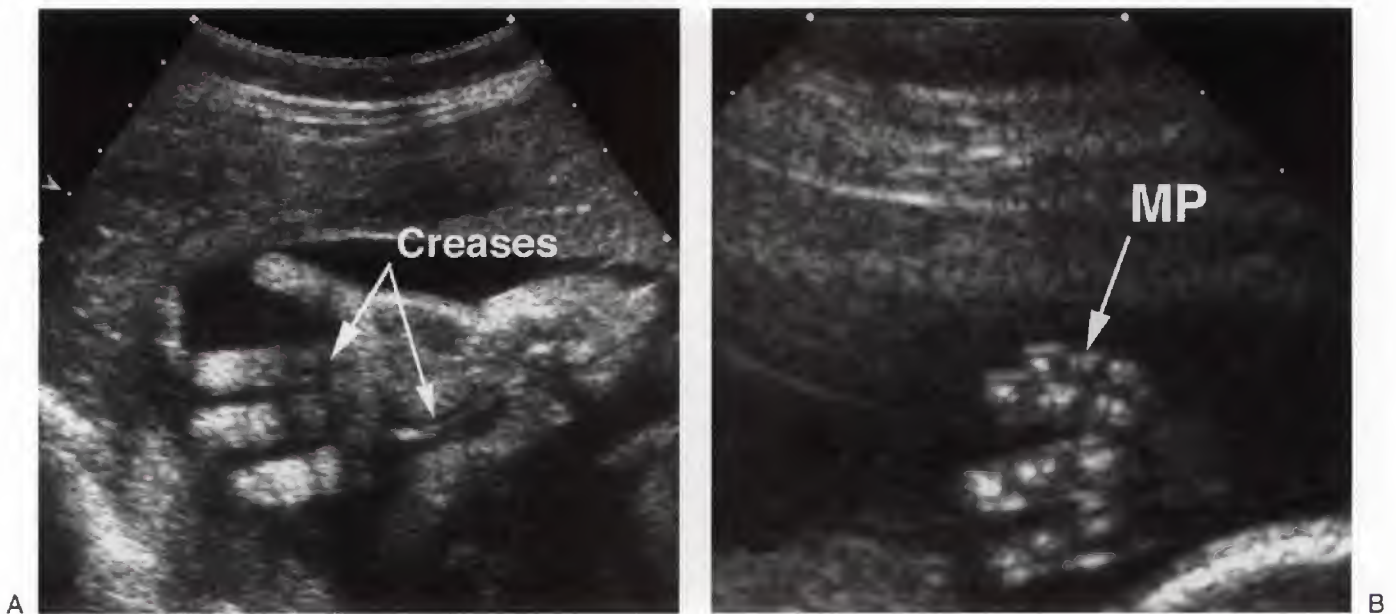


**FIGURE 9-33.** *A*. Coronal sonogram of the fetal hand demonstrating the soft tissues of the fingers and palm. Creases at the interphalangeal joints and palmar creases are seen. *B*. Coronal sonogram of the hand demonstrating some of the bony detail of the developing phalanges. MP, middle phalanx.



hypertelorism.<sup>48</sup> In older fetuses, surprising detail of the intraorbital contents can be appreciated, including the wall of the globe, lens, retrobulbar fat, optic nerve, and rectus muscles (Fig. 9-51). Portions of the maxilla and nearly the entire mandible can be identified, as can the bony nasal ridge (see Fig. 9-50). Similarly, the frontal, parietal, and squama of the temporal and occipital bones, the bones making up the calvaria, can be seen clearly. The cartilaginous

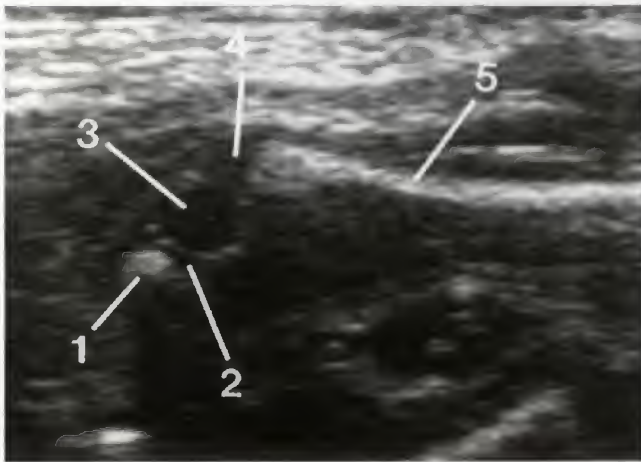


**FIGURE 9-34.** Coronal image of the fetal hip. 1, ischial ossification center; 2, cartilaginous acetabulum; 3, femoral head in cartilage; 4, greater trochanter in cartilage; 5, femoral diaphysis. Note the echogenic synovium between the cartilaginous acetabulum and the femoral head. Refer to Figure 9-20A.

zones of articulation of these bones, the coronal, sagittal, and lambdoid sutures, are commonly visible (Fig. 9-52). The fontanels may be seen as well (Fig. 9-53). These anatomic features are particularly well seen in three-dimensional reconstructions of the calvaria, as demonstrated in Chapter 24. Sutures and fontanels are the windows for brain imaging (Fig. 9-54). Although many individuals who perform sonography do not realize that they are employing sutures and fontanels to image the fetal brain, they visually ascertain that, as they move the transducer, “fuzzy” brain images suddenly become clearer. The reason, of course, is that as they move the transducer the beam inevitably passes through a suture or fontanel, enabling even the unsophisticated imager to take advantage of these gaps between the calvarial plates.

The ribs, spine, and pelvis are easily imaged and serve as excellent anatomic landmarks. In the pelvis, the iliac ossification centers are easily observed from early second trimester onward (ossified at 2.5 to 3 fetal months). Ischial ossification (see Fig. 9-34) is present at 4 months, but pubic ossification is not present until 6 months.

The spine is an extremely important structure in fetal diagnosis.<sup>39,49-51</sup> With the advent of maternal serum alpha-fetoprotein screening, as well as the concurrent development of sophisticated high-resolution ultrasound imaging technology, the potential exists to diagnose nearly all lesions of spina bifida before the 20th week of pregnancy.<sup>52</sup> These changes in obstetric care mandate that the morphology of the fetal spine be well understood by sonologists. The sequence of development of ossification centers in the fetal vertebral column has been extensively studied in the past with radiologic and histologic methods.<sup>34,35</sup> Each vertebra usually has three primary ossification centers, one for the

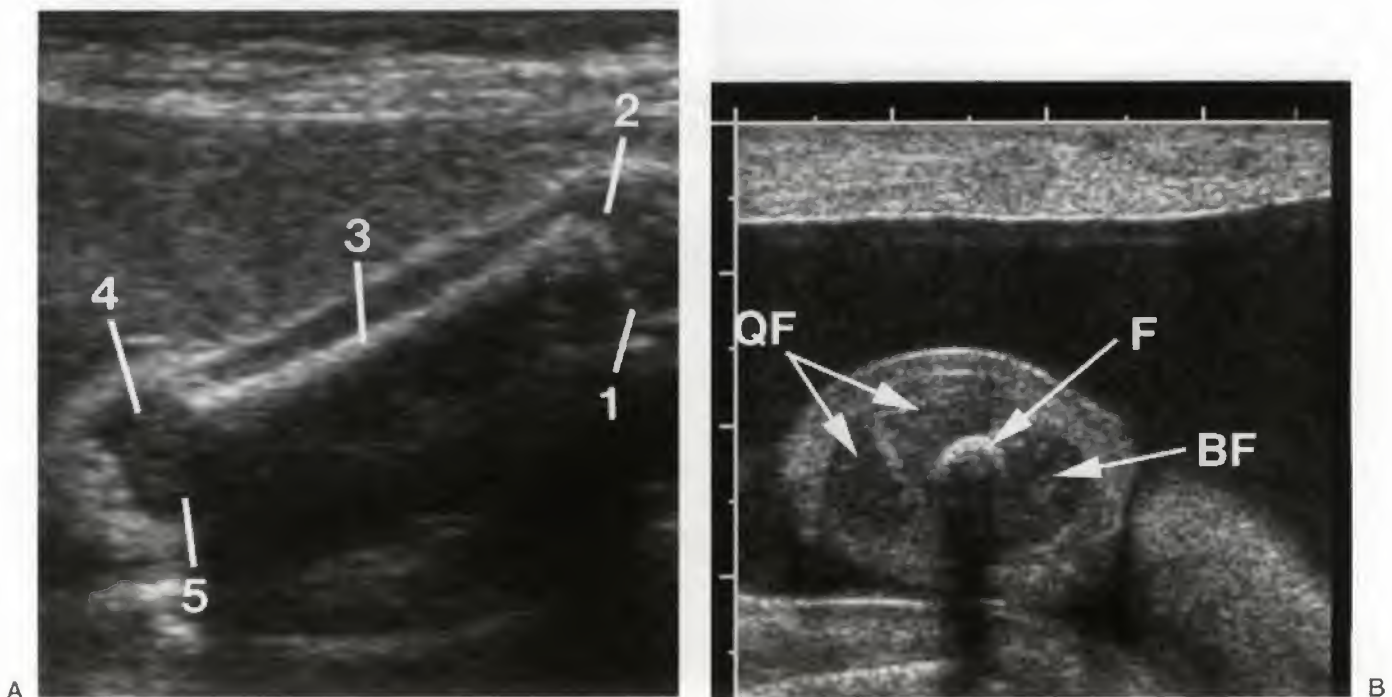


**FIGURE 9-35.** A and B. Longitudinal (A) and transverse axial (B) sonograms of the fetal thigh. 1, posterior hip joint capsule; 2, greater trochanter; 3, femoral diaphysis; 4, lateral condyle; 5, medial condyle; QF, quadriceps femoris muscle; BF, biceps femoris muscle; F, femoral diaphysis.

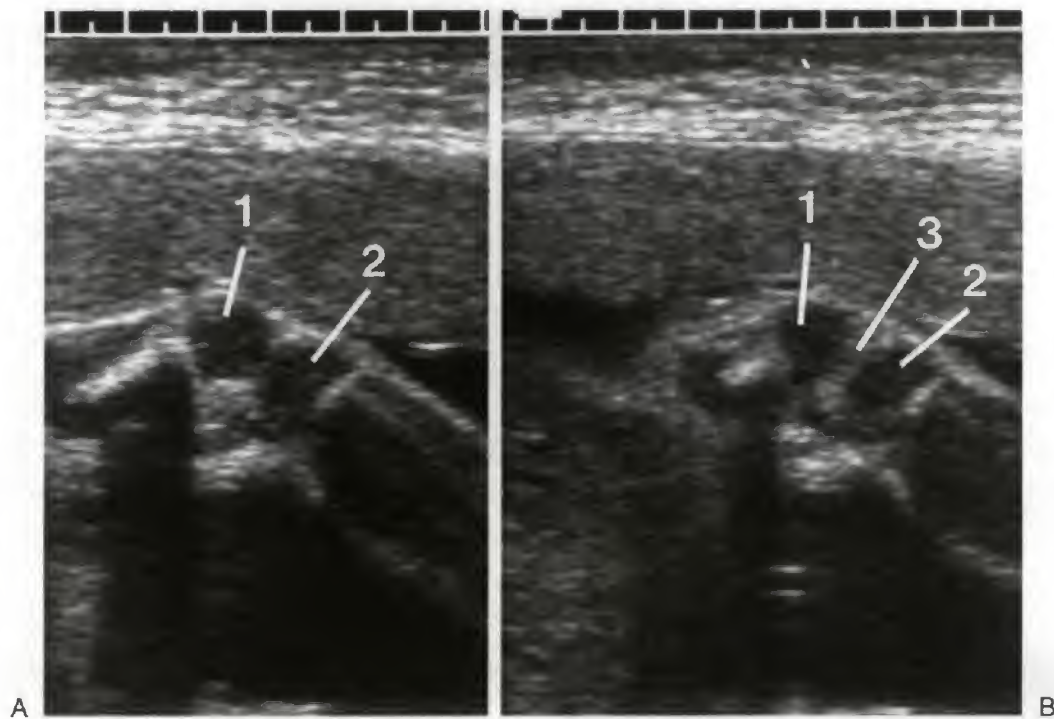


**FIGURE 9-36.** A. Parasagittal sonogram of the fetal knee. The femoral condyle (1) articulates with the tibial plateau (proximal tibial epiphysis). B. Midsagittal sonogram of the fetal knee. Note the gap (3) between the distal femoral epiphysis (1) and the proximal tibial epiphysis (2). This is due to the intercondylar notch (see Fig. 9-37).

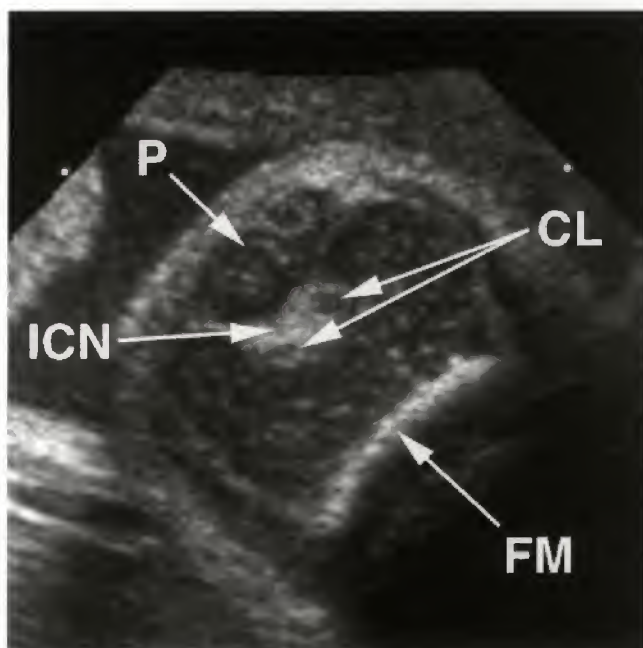


**FIGURE 9-37.** Axial sonogram of the knee in flexion. CL, cruciate ligaments; FM, femoral metaphysis; ICN, intercondylar notch [note the brightly echogenic synovium within the joint]; P, patella.

body (centrum) and one on each side of the posterior neural arch. The centra are ossified first in the lower thoracic and upper lumbar regions, followed by progressive ossification in both the cephalic and caudal directions. By contrast, and in general, the ossification centers for the posterior neural arch appear in a more standard cephalocaudal direction. The posterior neural arch first begins to ossify (sonographically recognizable high-amplitude reflections) at the base of the transverse process (Fig. 9-55). Ossification proceeds from this center to progressively include the laminae and pedicles. The progression of ossification of the laminae is more important for the diagnosis of neural tube defects because spina bifida is the most consistently demonstrable dysmorphic lesion in open spinal defects. This abnormality is recognized sonographically by an abnormal outward flaring of the posterior neural arch ossification centers.

Varying degrees of maturation of spinal ossification are present at differing levels of the spine when we are most frequently called on to assess normalcy of the fetal spine.<sup>39</sup> Although there are some exceptions as noted previously, ossification in the neural arch first appears at the base of the transverse process. Early posterior neural arch ossification then progresses anteriorly into the pedicles, also contributing a portion of the vertebral body, and posteriorly into the laminae. Additionally, craniocaudal extension into



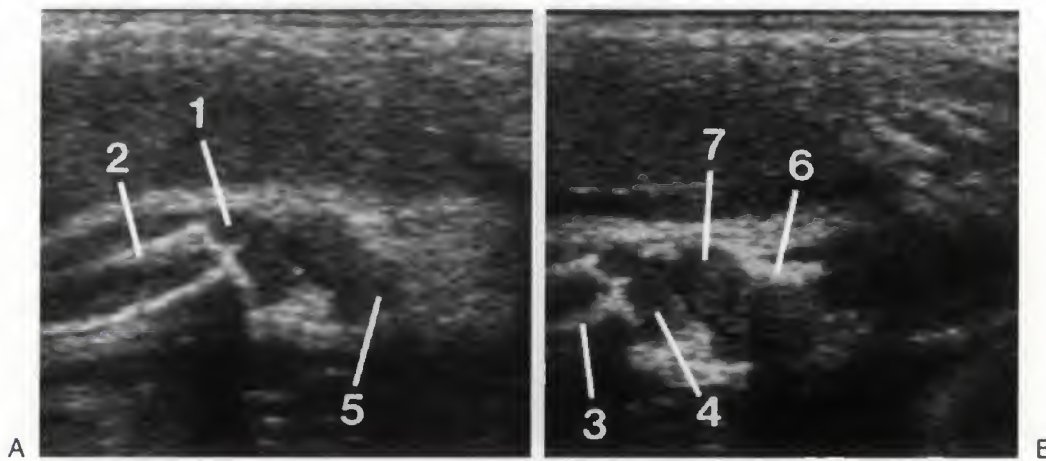


**FIGURE 9-38.** A and B. Coronal sonograms of the knee (off axis). 1, proximal fibular epiphysis; 2, fibular diaphysis; 3, tibial diaphysis; 4, proximal tibial epiphysis; 5, patella; 6, femoral metaphysis; 7, lateral femoral condyle.

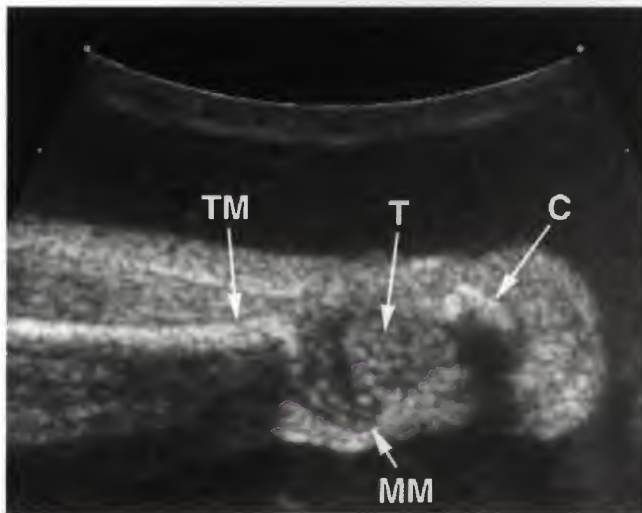


**FIGURE 9-39.** Axial sonogram of the distal tibia and a portion of the ankle joint. C, calcaneus; TM, tibial metaphysis; MM, medial malleolus; T, talus (a bone that is entirely cartilaginous).

the articular processes and lateral extension into the transverse processes occur. Because the critical observation in the diagnosis of open spinal neural tube defects is the demonstration of spina bifida (seen as an outward flaring of the posterior arch ossification centers), the ideal situation to confirm normalcy is to observe the antithesis of this pathologic state (e.g., inward angulation of the laminae). This indeed is the case when visible ossification is present in the normal laminae (Fig. 9-56). Unfortunately, there is insufficient ossification of the laminae to perceive inward angulation of the posterior neural arch ossification centers in the lower spine to confirm normalcy of the fetal spine during the crucial stage of gestation when this sonographic diagnosis must be made (18 to 22 menstrual weeks) (see Fig. 9-55).<sup>49,52</sup> This is particularly important when considering the most

common location of such lesions (e.g., lumbar and sacral regions).<sup>49</sup> Easily identifiable ossification of the laminae is visible in the cervical region in all fetuses by 18 to 19 menstrual weeks, whereas thoracic ossification of the laminae is only partially visible during the 18- to 19-menstrual-week period.<sup>39</sup> There is no ossification of the laminae in the lumbar or sacral regions of fetuses examined before 19 menstrual weeks (see Fig. 9-55). The thoracic vertebrae consistently demonstrate partial ossification of the laminae in the range of 20 to 22 weeks; the lumbar region does not demonstrate a similar degree of ossification until 22 to 24 weeks (Fig. 9-57). The sacral spine reveals no evidence of ossification in the laminae before 22 weeks. Only after 25 weeks is there consistently recognizable ossification of the arch in the sacral region (Fig. 9-58). Fetal position (either prone or decubitus) does not appear to affect appreciably the ability to discern the degree of neural arch ossification, although the prone position usually results in the clearest images (Fig. 9-59). If the fetus is supine, a critical examination of the posterior neural arch cannot be carried out (Fig. 9-60).<sup>39</sup>

The spine may be seen in both longitudinal and transverse axial planes. Although both planes are important, the transverse axial plane demonstrates the anatomy to best advantage. On longitudinal planes of section, the posterior elements are seen as "parallel" bands of echoes. In fact, they are not precisely parallel because they flare in the upper cervical region and converge in the sacrum. In addition, careful scanning usually discloses a slight widening of the lumbar area. It is important not to mistake this slight lumbar widening as a pathologic event. Because the fetal spine is normally kyphotic, usually one cannot visualize the entire spine in a single longitudinal coronal plane. For this reason, transverse axial planes of section are necessary to be certain that the entire spine has been imaged on a segment-by-segment basis. Caution must be exercised as well to ensure that the spine has been examined in its entirety on transverse planes. At the cephalic end, no problem arises because one encounters the calvaria. However, the caudal end is more difficult. One can successfully use the ischial ossification

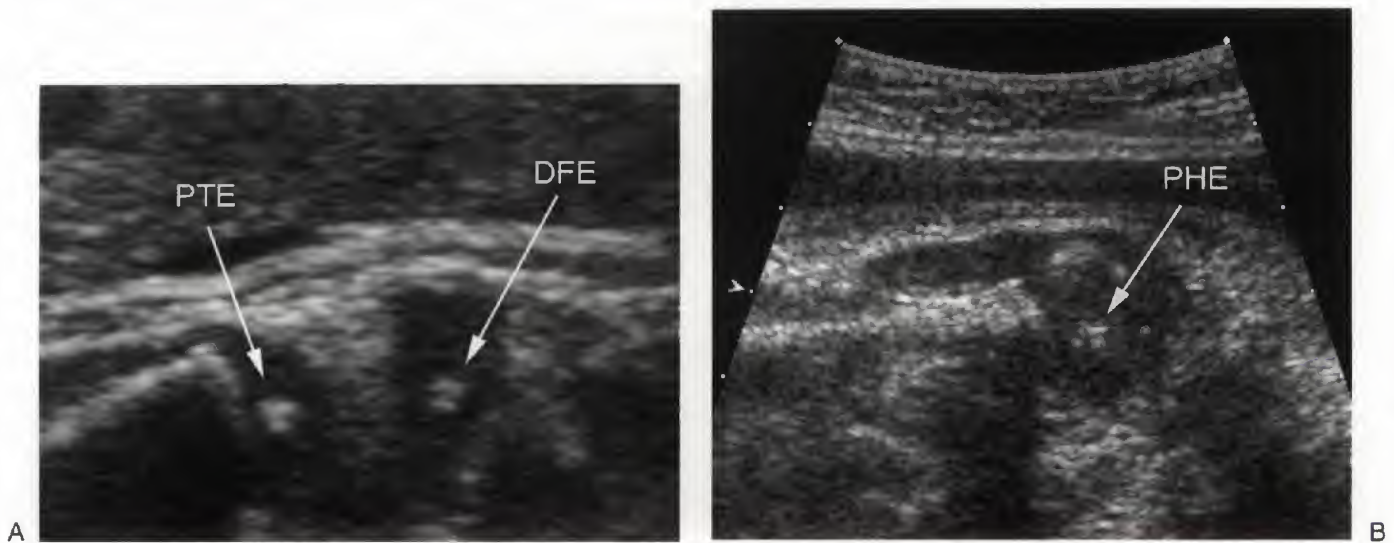


**FIGURE 9-40.** A. Coronal sonogram of the distal thigh in a term fetus. DFE, ossification center of distal femoral epiphysis; PTE, ossification center of proximal tibial epiphysis. Note the large and similar sizes of the ossification centers, a virtually certain sign of a near-term fetus. B. Coronal sonogram through the proximal humerus shows an early secondary ossification center in the humeral head, another finding indicating a later gestation. PHE, ossification center of proximal humeral epiphysis.

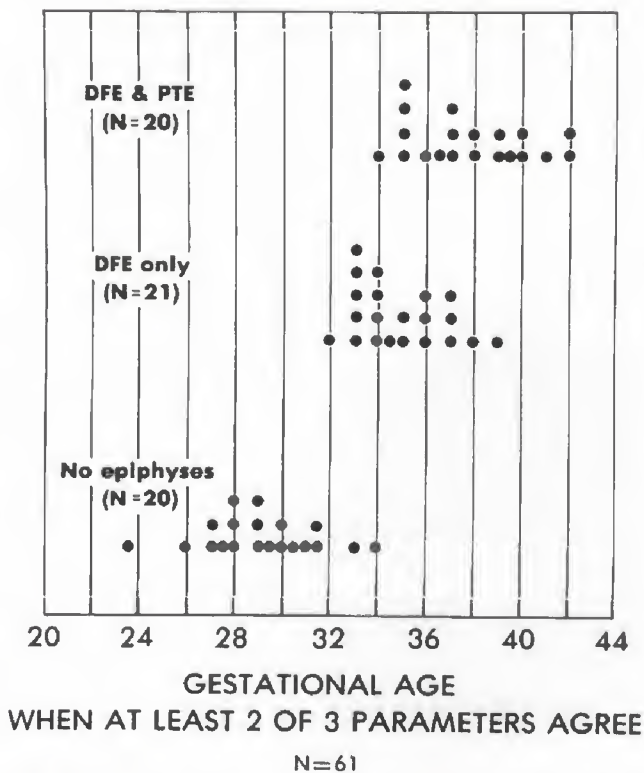


**FIGURE 9-41.** Appearance time of the distal femoral epiphysis (DFE) and proximal tibial epiphysis (PTE) in a mixed group of 61 fetuses when two of the following three dating parameters agreed: last menstrual period, early sonogram, and Dubowitz scores. (From Chinn DH, Bolding DB, Callen PW, et al: Ultrasonographic identification of fetal lower extremity epiphyseal ossification centers. *Radiology* 147:815, 1983.)

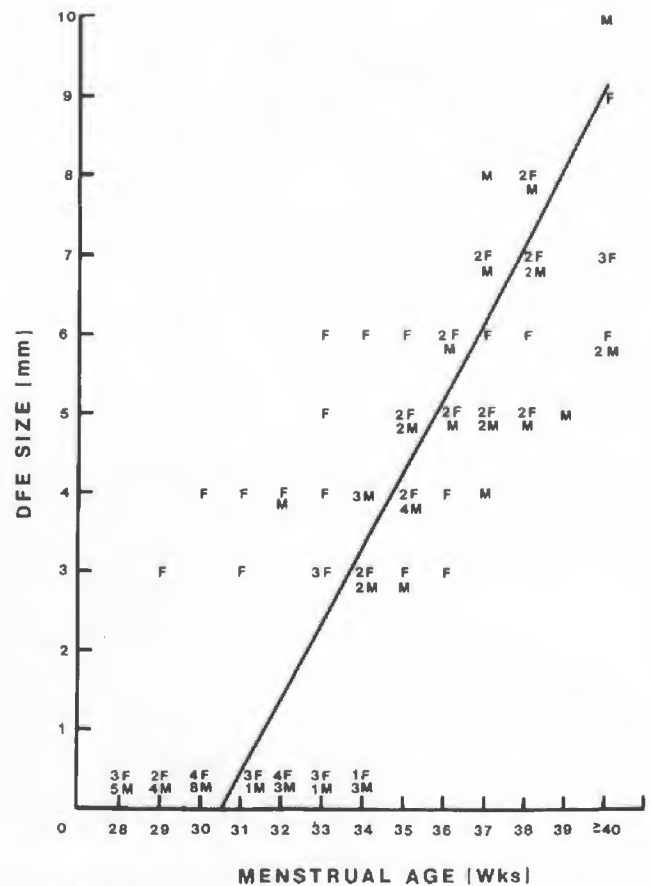


**FIGURE 9-42.** Variation in the distal femoral epiphysis (DFE) appearance time and size in male and female fetuses. (From Mahony SB, Callen PW, Filly RA: The distal femoral epiphyseal ossification center in the assessment of third trimester menstrual age: Sonographic identification and measurement. *Radiology* 155:201, 1985.)



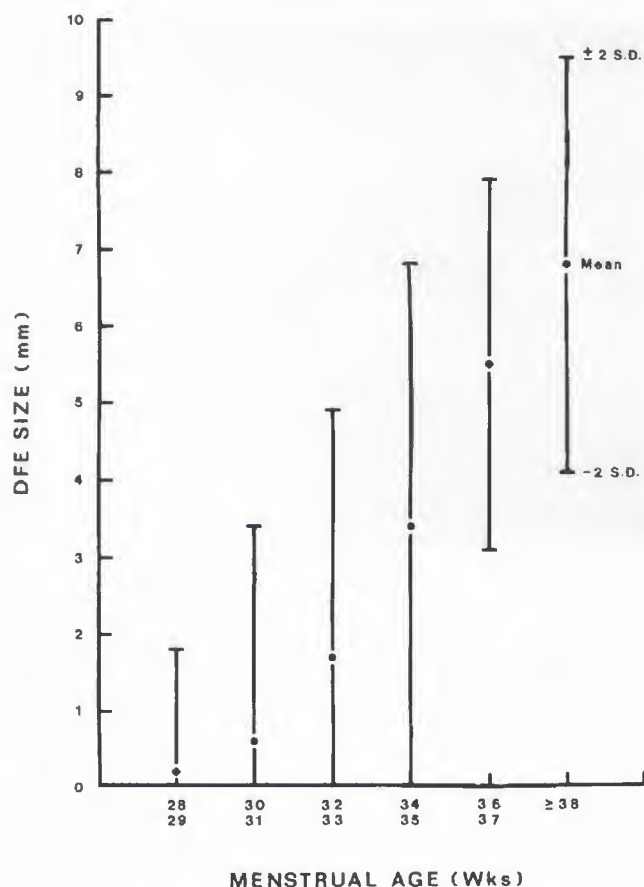


**FIGURE 9-43.** Mean diameter of the distal femoral epiphysis (DFE) with increasing age. (From Mahony SB, Callen PW, Filly RA: *The distal femoral epiphyseal ossification center in the assessment of third trimester menstrual age: Sonographic identification and measurement. Radiology 155:201, 1985.*)

centers as landmarks to ensure that the caudal end of the spine has been reached (Fig. 9-61). In older fetuses, both spinal and spinal canal anatomy can often be quite dramatically depicted (Fig. 9-62).

Cartilaginous structure in the axial skeleton is less conspicuous than in the appendicular skeleton but nonetheless is visible in virtually all fetuses. The sutures of the calvarial vault already have been noted. The cartilaginous neurocentral synchondrosis of the spine (the junction of the

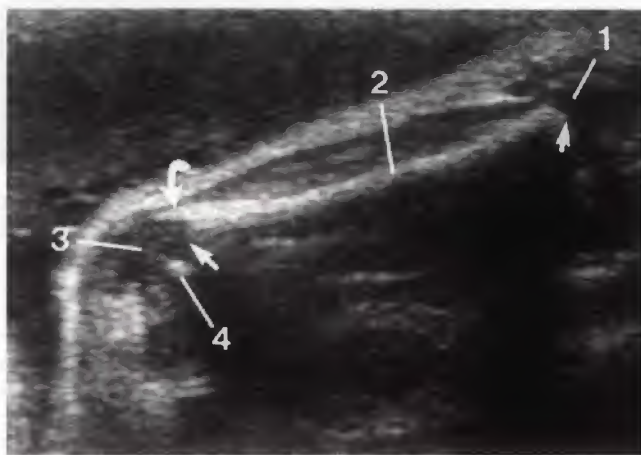


**FIGURE 9-45.** View of the fetal femur, third trimester. A bright reflector (curved arrow) is seen in continuity with the lateral femoral metaphysis. This structure is not part of the ossified femur. Endpoints of femur measurement are marked by straight arrows. 1, greater trochanter; 2, femoral diaphysis; 3, lateral condyle; 4, ossification center of the distal epiphysis.

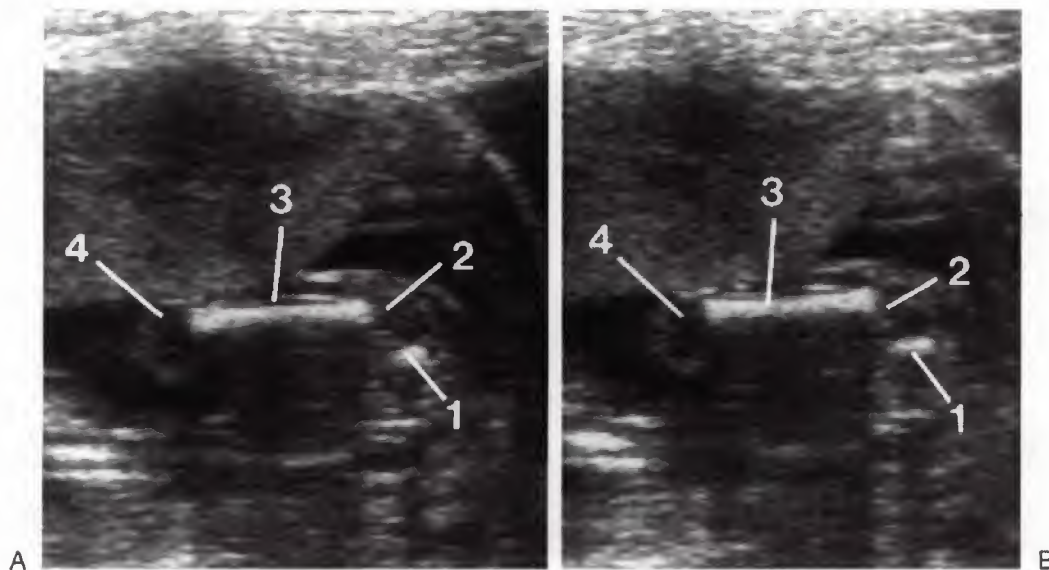


**FIGURE 9-44.** A and B. Two views of the femur for measurement. Visualization of the proximal (2) and distal (4) cartilaginous bone ensures that the plane of section is through the long axis of the diaphysis (3). Only proper positioning of the cursors remains to ensure an accurate measurement. 1, ischial ossification center.

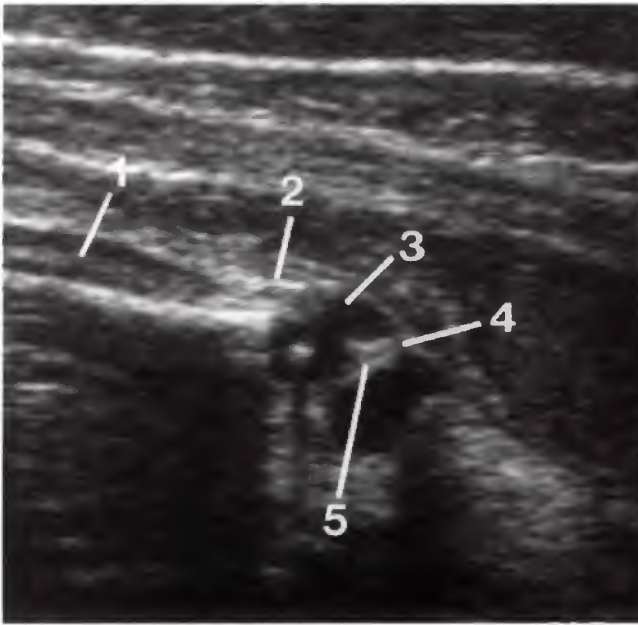


**FIGURE 9-46.** Midsagittal sonogram of the extended knee. In addition to structures pointed out in earlier figures, note the quadriceps muscle (1), the quadriceps tendon (2), the patella (3), the patellar ligament (4), and synovium (5) contained by the knee joint.

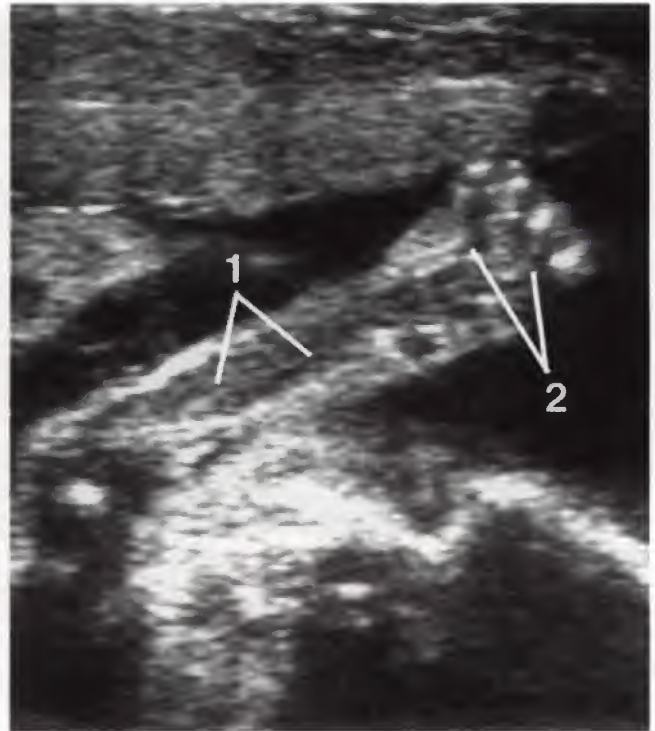


**FIGURE 9-48.** Coronal sonogram through the dorsal soft tissues of the forearm and hand. 1, extensor muscle group; 2, extensor tendons.

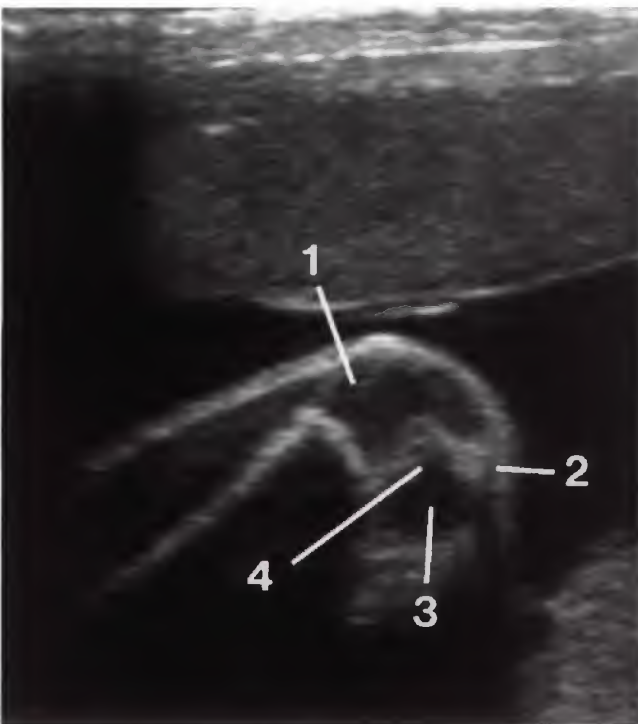


**FIGURE 9-47.** Midsagittal sonogram of the fetal knee in flexion. 1, distal femoral epiphysis; 2, patellar ligament; 3, proximal tibial epiphysis. These three structures marginate the knee joint. Within the knee joint is a large quantity of highly echogenic tissue, presumably synovium. Clearly outlined by the bright "synovium" is the cruciate ligament (4).

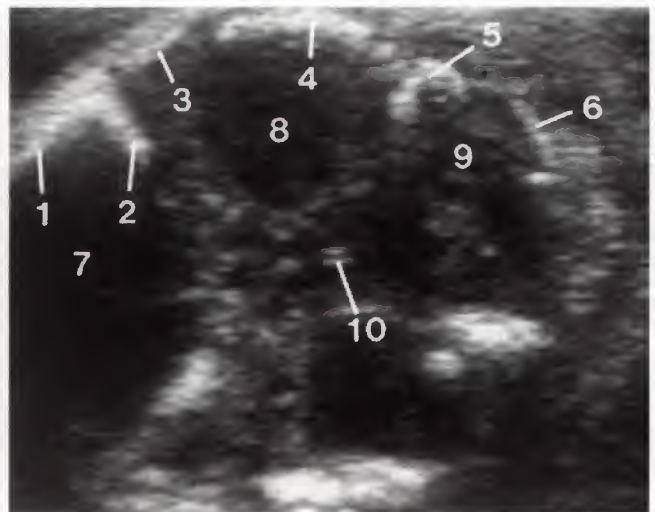


**FIGURE 9-49.** Transverse axial sonogram near the skull base. 1, frontal bone; 2, greater wing of sphenoid bone; 3, parietal bone; 4, temporal bone; 5, petrous ridge; 6, occipital bone; 7, anterior cranial fossa; 8, middle cranial fossa; 9, posterior cranial fossa; 10, basilar artery.



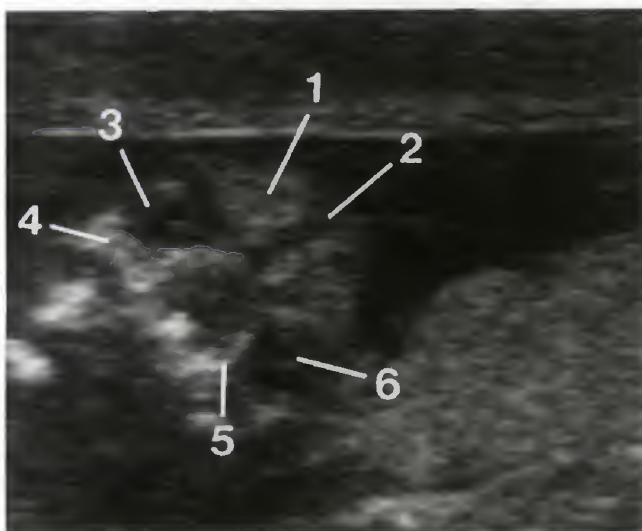


**FIGURE 9-50.** Fetal orbits, early second trimester. 1, frontal bone; 2, metopic suture; 3, orbit; 4, maxilla; 5, nasal bone; 6, lens.

centrum and the posterior ossification centers) is visible in all fetuses from the end of the first trimester onward (see Figs. 9-55 to 9-59).<sup>39</sup> Similarly, the gaps between the vertebral body ossification centers are a composite of the nonossified margin of the adjoining vertebral bodies plus the intervertebral disk (see Fig. 9-60). The margin of cartilage in the vertebral body is best appreciated posteriorly, lying between the ossification center and the dura of the spinal canal (see Fig. 9-62C and D). As well, the spinous processes of the posterior neural arch are occasionally seen; these structures again are entirely composed of cartilage in fetal life (see Fig. 9-62C).

One feature that cannot be well judged on sonograms is the degree of ossification of the bones. Thus, increased ossification, as in osteopetrosis, is completely unrecognized on sonograms. Similarly, diminished ossification is poorly judged. Only in the most extremely osteopenic bone can one appreciate diminished ossification on sonograms. Examples are the nearly nonossified calvaria in fetuses with osteogenesis imperfecta lethalis or recessive hypophosphatasia,<sup>53-55</sup> or the spine in fetuses with achondrogenesis.<sup>56</sup>

Little space is devoted to the fetal muscular system, even though many muscles and muscle groups may be seen quite well (see Figs. 9-28 and 9-29). In general, normal muscles are quite hypoechoic, at times so much so that they simulate fluid collections. This is most notable of the abdominal wall musculature, which may simulate ascites (pseudoascites) (Fig. 9-63).<sup>37</sup> At present, high-resolution sonographic equipment decreases the propensity to “overcall” ascites caused by this artifactual situation because the layers of the abdominal wall can be seen quite clearly.<sup>58</sup>

The abdominal wall muscles, the internal and external oblique and the transversus abdominis, are, at times, so clearly visible that the individual layers can be detected (Fig. 9-64). More commonly seen as a single layer of muscles, this tissue is easily recognized as lying within the abdominal wall by noting its position between the subcutaneous fat and the peritoneal fat. The latter is traced from the

paranephric fat as it curves onto the flank. Furthermore, the abdominal wall muscles “meet” the ends of the lower thoracic ribs, whereas ascites would pass “between” the ribs and the abdominal viscera.<sup>58</sup>

## CARDIOVASCULAR SYSTEM

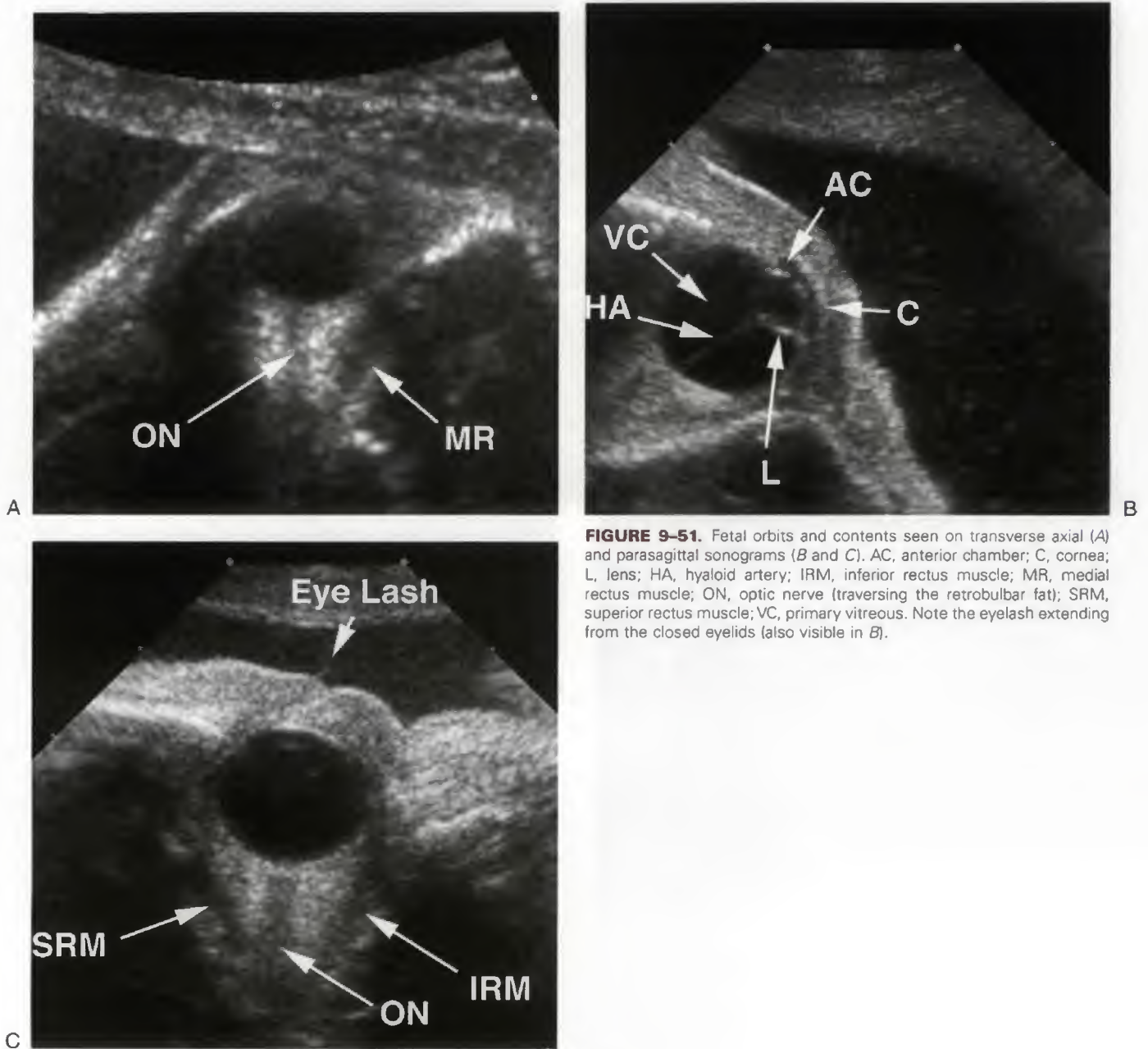
The anatomy of the heart and great vessels is discussed in detail in Chapter 14. In this chapter, the focus is on those fetal vessels visible within the uterus and fetal corpus that are not covered elsewhere. Indeed, a surprisingly large number of individual fetal blood vessels can be seen. Color Doppler sonography has greatly added to our ability to consistently demonstrate fetal vessels.

The fetal circulation begins in the placenta. In virtually all second and third trimester fetuses, one can detect the surface (fetal) vessels of the placenta, and with color Doppler sonography, one can even appreciate that these vessels penetrate the placental substance. The surface vessels coalesce at the cord “insertion.” The identification of the cord insertion has become important because of the advent of percutaneous umbilical (fetal) blood sampling for diagnosis and management (see Chapter 17).<sup>59</sup> The cord “insertion” is often easily seen, but if not, it is worthwhile to search for large placental surface vessels and trace these to the cord and to use color Doppler sonography.

The normal umbilical cord is composed of two arteries and a vein (Fig. 9-65). The cord is virtually always coiled and sometimes extremely so. This leads to a variety of appearances of the cord when viewed with tomographic sections as generated by sonography (Fig. 9-66). Indeed, the “simple” task of counting cord vessels can be made quite frustrating by the coils. To obtain the correct count of cord vessels consistently, one must rely on a true transverse axial section of the cord vessels. Longitudinal or oblique views can be misleading.

These vessels enter the fetus, by definition, at the umbilicus and there immediately diverge.<sup>60</sup> The umbilical vein proceeds cephalically (Fig. 9-67); the umbilical arteries egress from a caudal direction. The umbilical arteries proceed along the margin of the urinary bladder from their origin at the iliac arteries in their course toward the umbilicus (Fig. 9-68). As they course along the bladder margin, they should not be mistaken for dilated ureters, a distinction easily made by interrogating them with color Doppler sonography. Regardless of the degree of bladder distention, normal umbilical arteries *always* flank the bladder wall. Thus, this relationship can be employed both to detect the umbilical arteries or the urinary bladder, particularly when pathology has altered the expected appearance of the bladder. Although not representing certain evidence of a three-vessel cord, the identification of two umbilical arteries flanking the bladder lumen represents excellent evidence for a three-vessel cord and, employing color Doppler sonography, constitutes the easiest method of “confirming” a three-vessel cord.

The umbilical vein joins the fetal portal circulation. The fetal portal circulation is seen with a high degree of consistency on sonograms. Obviously, the larger the fetus, the more readily one will see the smaller elements of this system. Importantly, many of the illustrations seen in the literature incorrectly interpret the fetal umbilical and portal venous anatomy. Confusion has led not only to improper





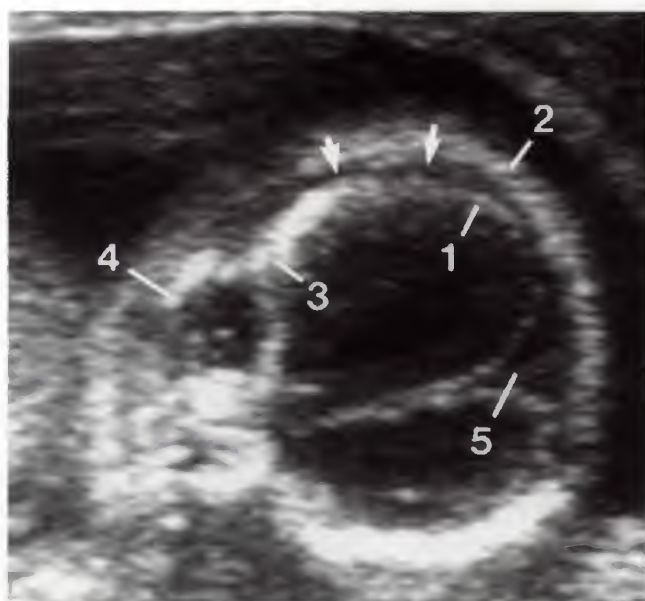


**FIGURE 9-52.** Oblique view demonstrating the coronal suture (arrows). 1, frontal bone; 2, parietal bone; 3, greater wing of sphenoid bone; 4, maxilla; 5, interhemispheric fissure with brain edges showing brightly reflective covering of pia-arachnoid.

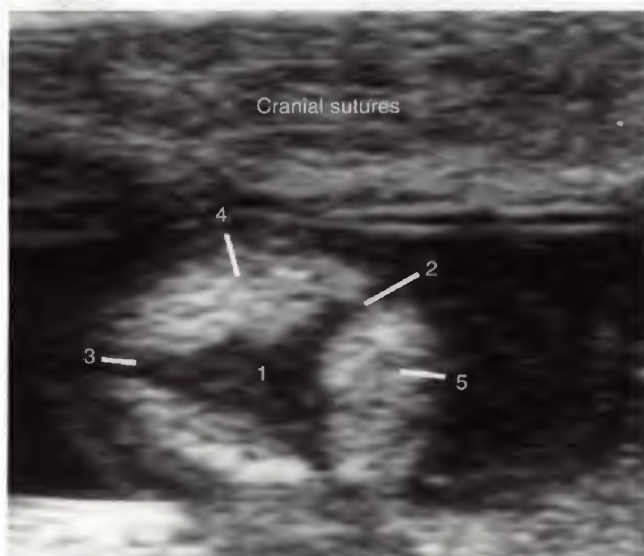


**FIGURE 9-53.** Transverse axial sonogram of the posterior fontanel (1). 2, lambdoid suture; 3, sagittal suture; 4, parietal bone; 5, occipital bone.

nomenclature but also to use of inappropriate landmarks for obtaining important fetal measurements. With a clear understanding of fetal portal vein anatomy, one can avoid these pitfalls and better appreciate fetal and adult segmental hepatic anatomy.

The dynamics of fetal circulation determine the details of fetal hepatic portal venous and segmental anatomy.<sup>61</sup> Because there are no blood-diverting branches of the umbilical vein, the volume of placental blood entering the left portal venous

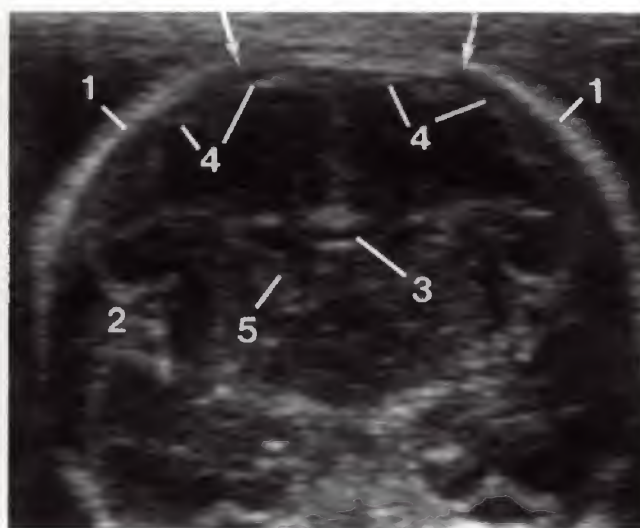


**FIGURE 9-54.** The sonographic beam was directed through the anterior fontanel (arrows) in a midtrimester fetus enabling recognition of striking detail in the fetal brain because of the "bone-free window." 1, parietal bone; 2, lateral fissure; 3, corpus callosum; 4, brain edges over the most cephalic portions of the parietal lobes; 5, head of caudate nucleus.

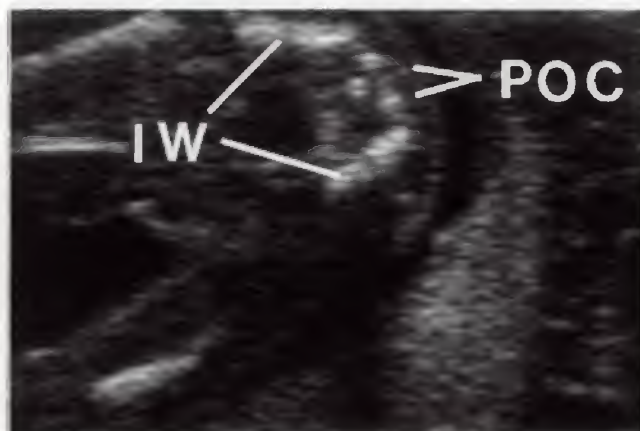


**FIGURE 9-55.** Early ossification centers in the sacral spine. Anteriorly is the centrum, and posteriorly (POC) the ossifications of the posterior arch appear near the base of the transverse processes. IW, iliac wings. (From Filly RA, Simpson GF, Linkowski G: Fetal spine morphology and maturation during the second trimester: Sonographic evaluation. *J Ultrasound Med* 6:631, 1987)

system equals that in the umbilical vein. Thus, the umbilical vein and the portion (umbilical segment) of the left portal vein that it joins have the same diameter (see Fig. 9-67). Therefore, the left portal vein of the fetus is larger than the right, the reverse of the situation seen in the child and adult. From this point, blood may reach the right atrium through several avenues. A common misconception of the fetal circulation is that the bulk of umbilical venous blood bypasses the liver capillary bed through a large patent ductus

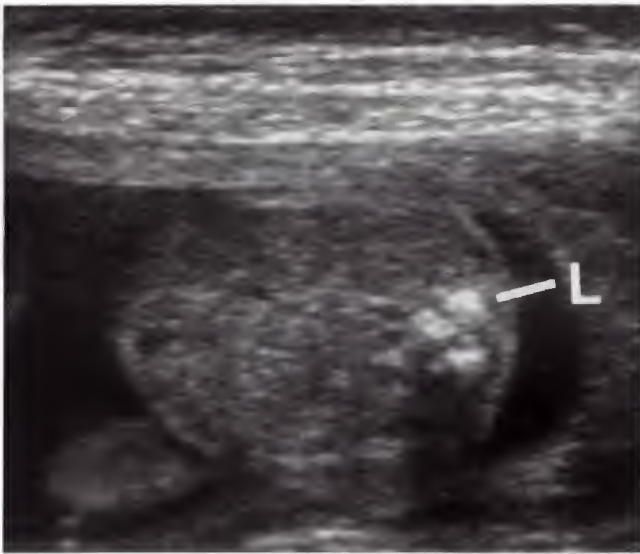


**FIGURE 9-56.** Lumbar vertebra, transverse axial sonogram. The laminae (L) demonstrate early ossification causing the appearance of "inward angulation" of the posterior arch. (From Filly RA, Simpson GF, Linkowski G: *Fetal spine morphology and maturation during the second trimester: Sonographic evaluation.* *J Ultrasound Med* 6:631, 1987)

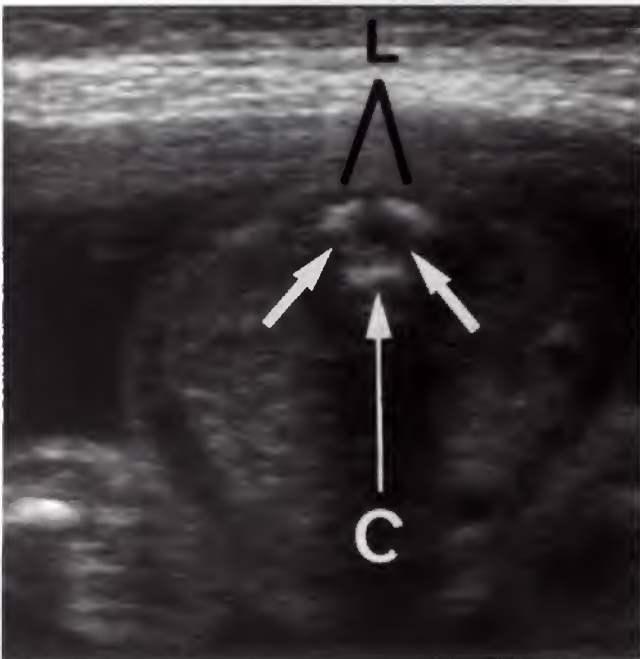


**FIGURE 9-57.** Lumbar spine, transverse axial sonogram, 23 weeks. Well-defined ossification of the laminae (L). C, centrum; arrows, neurocentral synchondroses. (From Filly RA, Simpson GF, Linkowski G: *Fetal spine morphology and maturation during the second trimester: Sonographic evaluation.* *J Ultrasound Med* 6:631, 1987)

venous. However, in utero, the ductus venosus averages only one seventh the diameter of the umbilical vein<sup>62</sup> and even may be closed (see Fig. 9-67).<sup>63</sup> It should be remembered, however, that the peripheral resistance of the hepatic vascular bed is not present in the ductus venosus, enabling this smaller caliber vessel to carry a larger quantity of blood

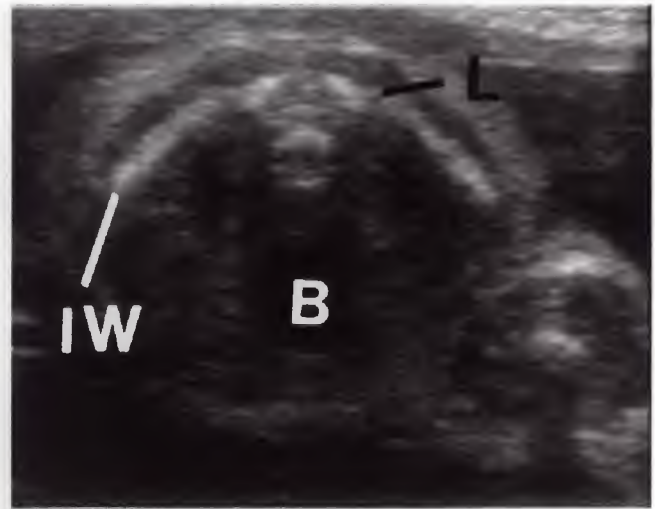


**FIGURE 9-58.** Sacral spine, transverse axial sonogram, 26 weeks. B, bladder; IW, iliac wing; L, laminae. (From Filly RA, Simpson GF, Linkowski G: *Fetal spine morphology and maturation during the second trimester: Sonographic evaluation.* *J Ultrasound Med* 6:631, 1987)

than might be expected. Nonetheless, a significant portion of umbilical venous blood, which carries the highest concentration of nutrients and oxygen in the fetus, actually circulates through the left lobe of the fetal liver through branches supplying the medial and lateral segments before entering the systemic venous system through the left and middle hepatic veins (Fig. 9-69). Although the right lobe of the liver receives a small amount of umbilical venous blood from the left portal vein, the bulk of blood entering the right portal vein is derived from the main portal vein, which, in the fetus, contains low concentrations of both nutrients and oxygen.<sup>63</sup> The unequal distribution of nutrients to the fetal liver partially accounts for the relatively large size of the left lobe of the fetal liver. After closure of the umbilical vein at birth, the nutrient supply to the entire liver equalizes and the relative size of the left lobe decreases.

In the fetus, the umbilical vein courses cephalically in the free margin of the falciform ligament (see Fig. 9-67). As noted earlier, it joins the umbilical portion of the left portal vein near the caudal margin of the left intersegmental fissure of the liver.<sup>64</sup> After birth, the umbilical vein thromboses, collapses, and ultimately becomes the ligamentum teres hepatis, a classic marker of left intersegmental fissure (indeed, for a very long time this structure was considered the line of division of the left and right hepatic lobes). The precise line of division between the umbilical vein and the umbilical segment of the left portal vein is the point at which the most anterior of the medial and lateral segmental branches to the left hepatic lobe egress the left portal vein (the branches to segments 3 and 4). Remember, the umbilical vein has no blood diverting branches. Therefore, those two hepatic intraparenchymal vessels had to originate from the umbilical segment of the left portal vein.

The umbilical portion of the left portal vein has a predominantly posterior course but also courses superiorly in the left intersegmental fissure (see Fig. 9-67). As noted



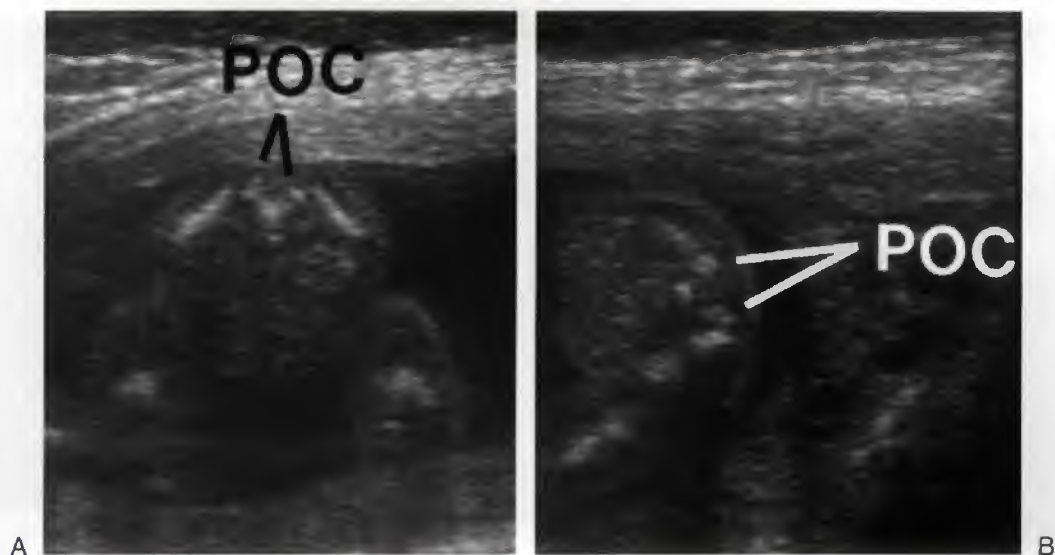


**FIGURE 9-59.** Transverse axial sonograms, sacral spine, same fetus in prone (A) and decubitus (B) positions. The posterior arch (POC) anatomy is seen well in either position. (From Filly RA, Simpson GF, Linkowski G: *Fetal spine morphology and maturation during the second trimester: Sonographic evaluation.* *J Ultrasound Med* 6:631, 1987.)

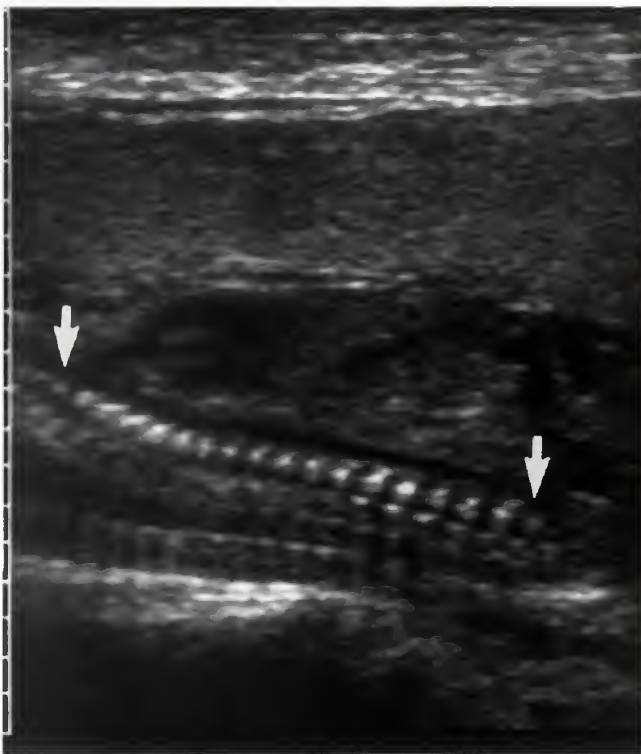


**FIGURE 9-60.** Supine fetus, second trimester. The vertebral bodies, lying between the arrows, are clearly seen but the posterior arch cannot be well appreciated. Note that the vertebral body ossification centers smoothly align along their anterior surfaces.

earlier, its branches supply the medial and lateral segments of the left lobe of the liver.<sup>65</sup> The left portal vein then courses abruptly to the right, exits the left intersegmental fissure, and forms the transverse portion (pars transversa) of the left portal vein (see Figs. 9-69 and 9-70). The pars transversa joins imperceptibly with the right portal vein at the main

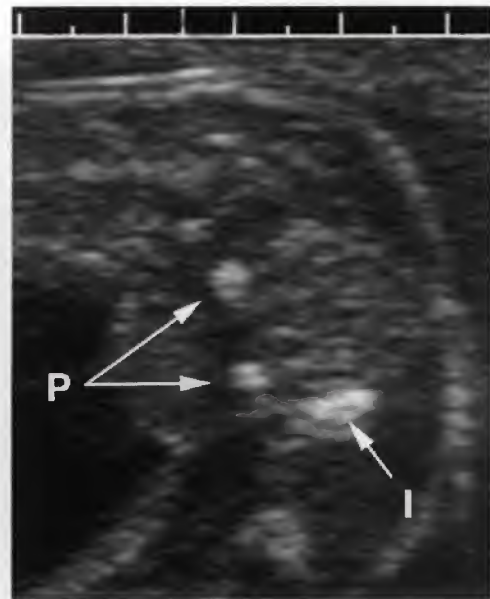


**FIGURE 9-61.** Axial sonogram of the pelvis demonstrating the early ossification centers of the pubis (P). Also seen is an ischial ossification (I).

lobar fissure. The ductus venosus originates from the pars transversa (but occasionally more rightward).<sup>66</sup> The ductus continues posteriorly but assumes a more cephalad course than the umbilical portion of the left portal vein (see Fig. 9-70). It continues as an unbranched structure to join the left or, less commonly, the middle hepatic vein (this distinction is somewhat artificial as the left hepatic vein, the middle hepatic vein and the ductus venosus most commonly form a confluence before entering the inferior vena cava). In this position, the ductus venosus lies in the superior extension of the gastrohepatic ligament, which separates the developing

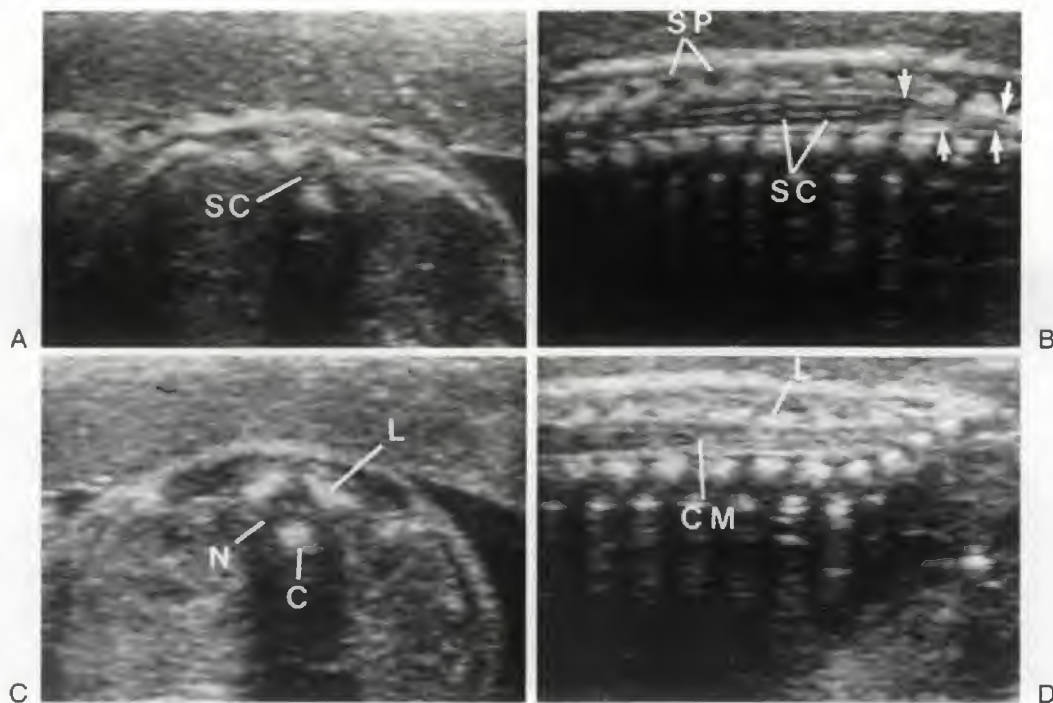


**FIGURE 9-62.** A and B. Lumbar spine of 27-week fetus, axial sections. C, centrum; L, laminae; N, neurocentral synchondrosis; SC, spinal cord. C and D. Longitudinal scans of the thoracolumbar (C) and lumbosacral (D) spine. CM, conus medullaris; arrows, dura; L, laminae; SC, spinal cord [note bright linear echo from central canal]; SP, spinous process [in cartilage]. (From Filly RA, Simpson GF, Linkowski G: *Fetal spine morphology and maturation during the second trimester: Sonographic evaluation*. *J Ultrasound Med* 6:631, 1987.)

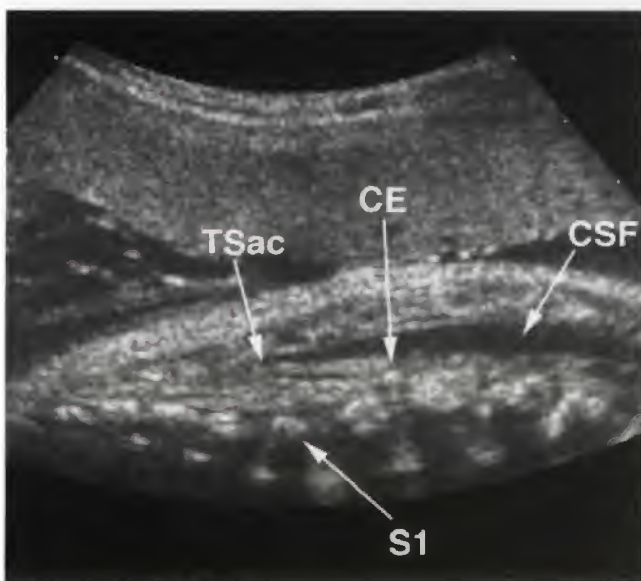


**FIGURE 9-63.** Midsagittal sonogram of the fetal spine demonstrating the termination of the thecal sac (TSac). The S1 vertebral body is marked. Overlying the echogenic cauda equina (CE) (echogenic due to the leptomeninges that cover the nerve roots) is lucent cerebrospinal fluid (CSF).

caudate lobe posteriorly from the medial and lateral segments of the left hepatic lobe anteriorly (the gastrohepatic ligament, the dominant ligament of the lesser omentum, also separates the greater and lesser peritoneal cavities). After birth, the ductus venosus closes and becomes the fibrous ligamentum venosum.<sup>64</sup>

Sonograms of the upper portion of the fetal abdomen clearly demonstrate the anatomy just described (see Figs. 9-67 to 9-70). Because the umbilical vein courses cephalically, transversely oriented planes of section intersect this vessel's short axis (see Fig. 9-64). Slight cephalad movement of the transducer demonstrates a position at which this venous structure abruptly courses posteriorly (see Figs. 9-69 and 9-70). This posteriorly coursing vein represents the umbilical portion of the left portal vein rather than the cephalic portion of the umbilical vein, as it is commonly mislabeled in the literature. That this vessel is indeed the left portal vein is easily observed as branches to the medial and lateral segments of the left lobe are noted to arise from this vein (see Figs. 9-69 and 9-70). When the umbilical portion of the left portal vein is seen throughout its entire course, one can be certain that some angulation has been introduced into the scan plane because this venous structure courses not only posterior but slightly cephalad (see Fig. 9-67). A variety of branches of the umbilical segment of the left portal vein are



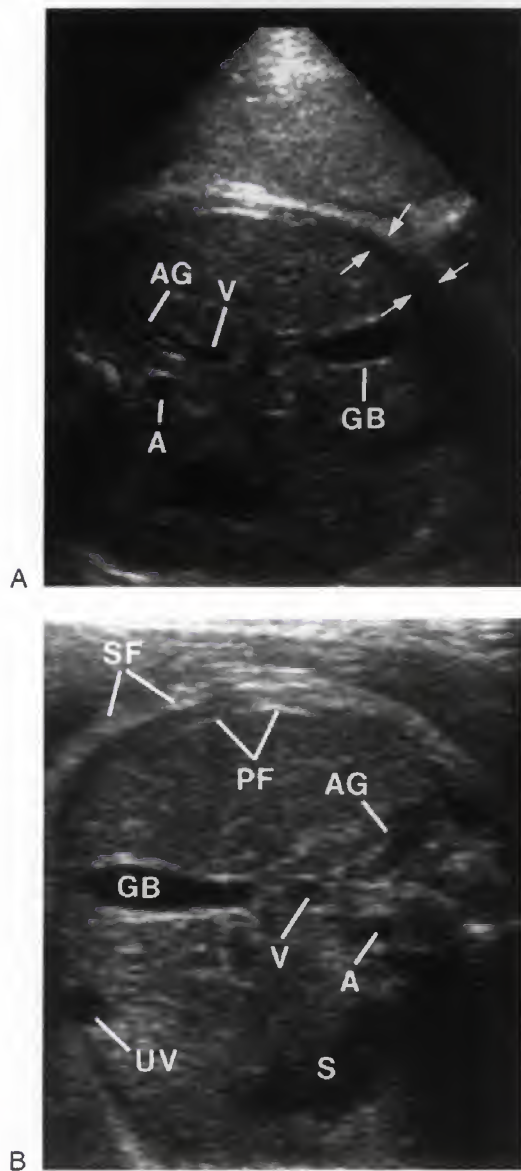


**FIGURE 9-64.** *A* and *B*. Transverse axial sonograms, fetal abdomen. *A*. Hypoechoic abdominal wall musculature (arrows) may erroneously give the impression that ascites is present. *A*, aorta; *AG*, adrenal gland; *V*, vena cava; *GB*, gallbladder. *B*. Abdominal wall musculature lies between the subcutaneous fat (*SF*) and the properitoneal fat (*PF*). Individual layers can be appreciated. *S*, stomach; *UV*, umbilical vein.

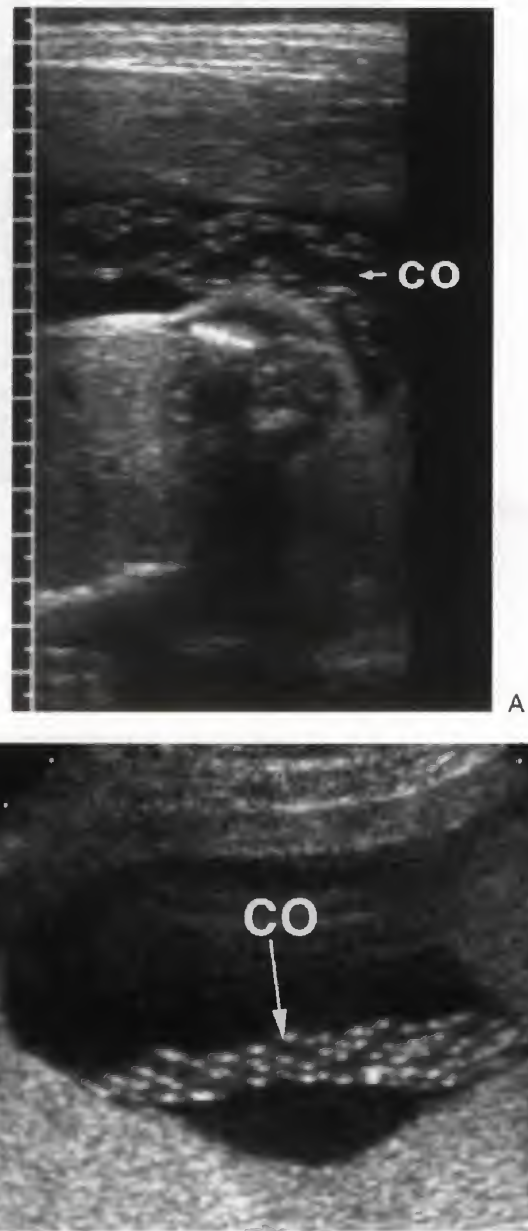


**FIGURE 9-65.** *A*. Longitudinal sonogram of a three-vessel umbilical cord (*CO*) with a typical amount of coiling. *B*. Longitudinal sonogram of a three-vessel umbilical cord (*CO*) with a greater than usual amount of coiling (controversy exists as to whether this is a variant or an abnormal circumstance).

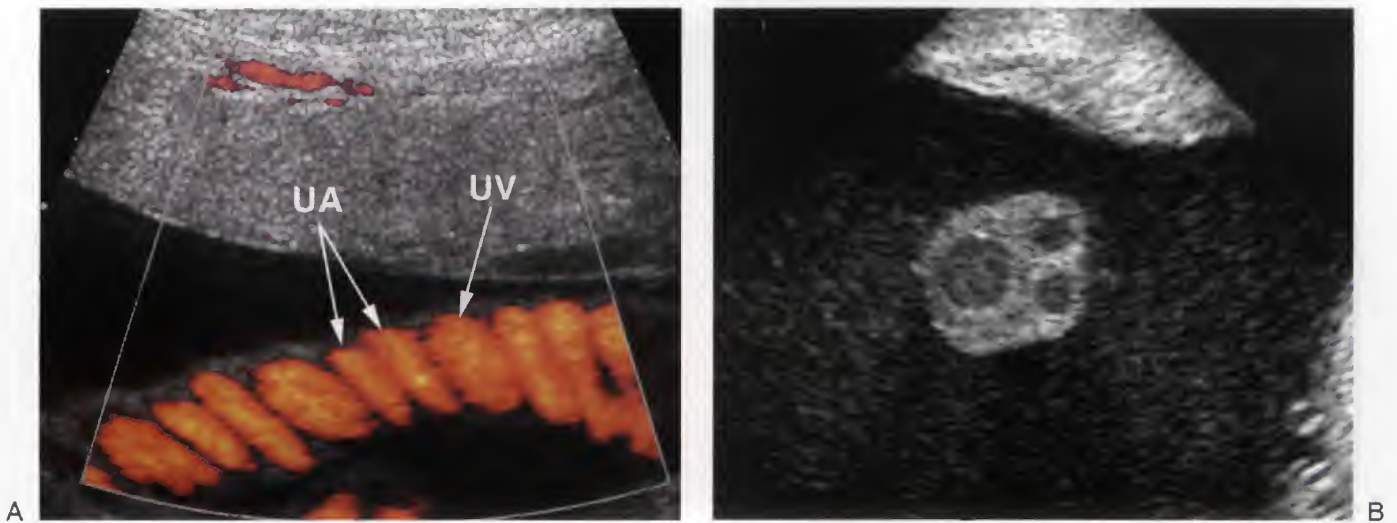


**FIGURE 9-66.** A. Longitudinal nondirectional color Doppler sonogram of the umbilical cord. The umbilical vein (UV) is interlaced by the two umbilical arteries (UA). B. Transverse axial sonogram of the umbilical cord.

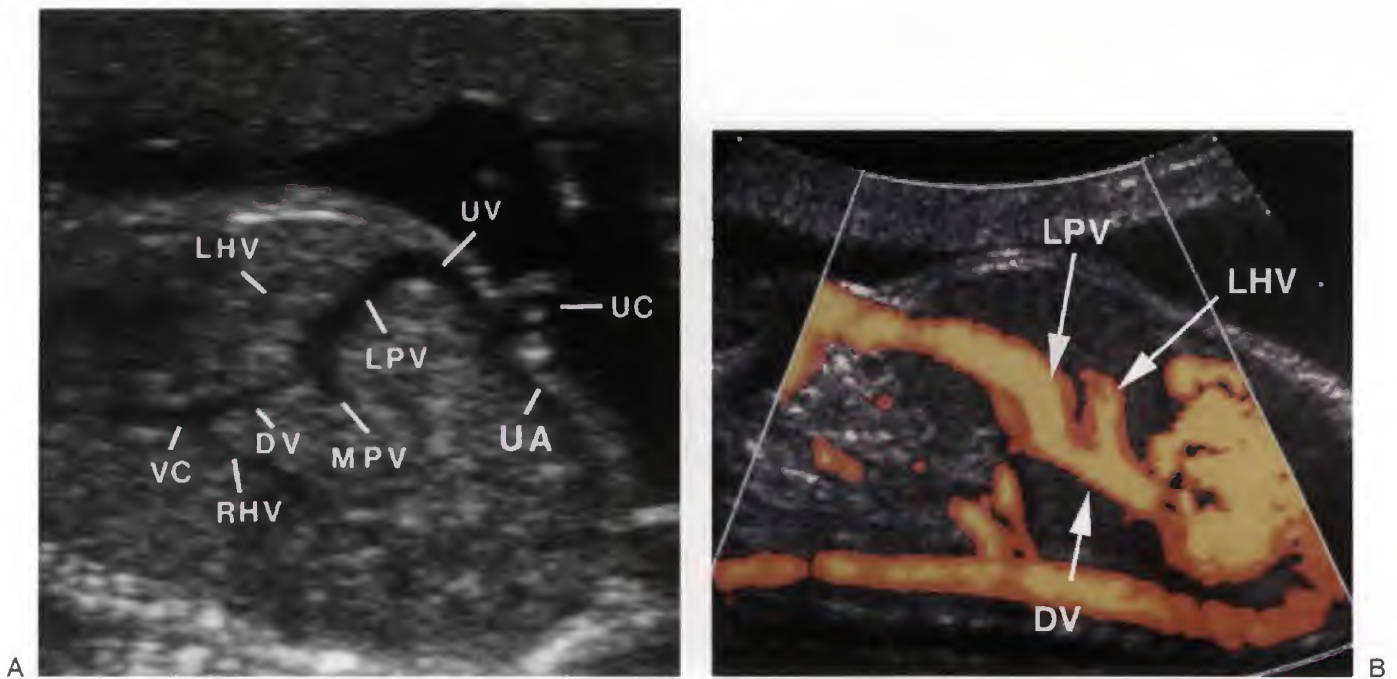


**FIGURE 9-67.** A and B. Midsagittal sonograms of the umbilical circulation in gray scale (A) and nondirectional color Doppler (B). DV, ductus venosus; LHV, left hepatic vein; LPV, umbilical segment of left portal vein; MPV, main portal vein; RHV, right hepatic vein; UA, umbilical artery; UC, umbilical cord; UV, umbilical vein; VC, inferior vena cava.





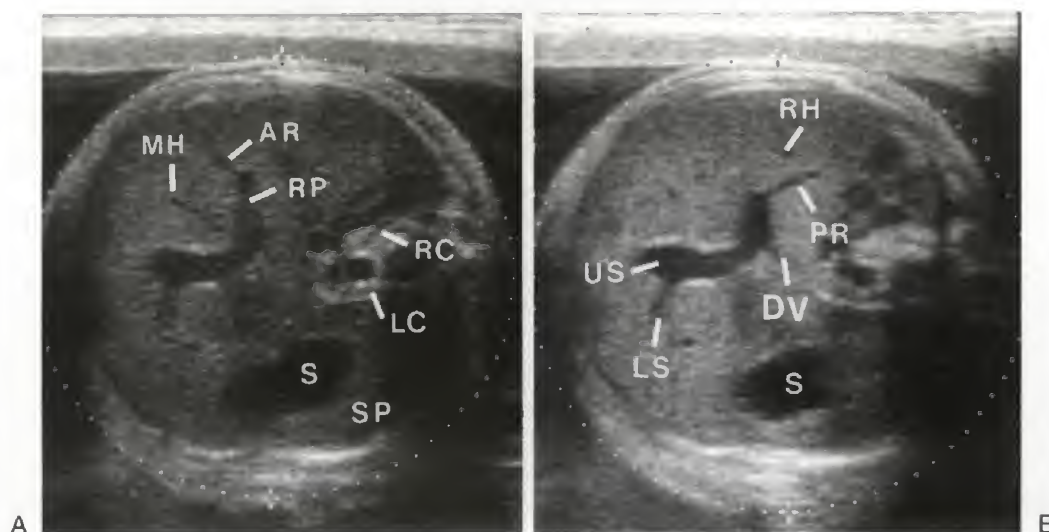


**FIGURE 9-70.** A and B. Transverse axial sonograms of fetal liver. DV, ductus venosus (alternatively, this may represent a partial section through the main portal vein—see Fig. 9-69B); AR, anterior division of right portal vein; LS, lateral segmental branch; MH, middle hepatic vein; PR, posterior division of right portal vein; RC and LC, right and left diaphragmatic crura; RH, right hepatic vein; RP, right portal vein; S, stomach SP spleen; US, umbilical segment of left portal vein.

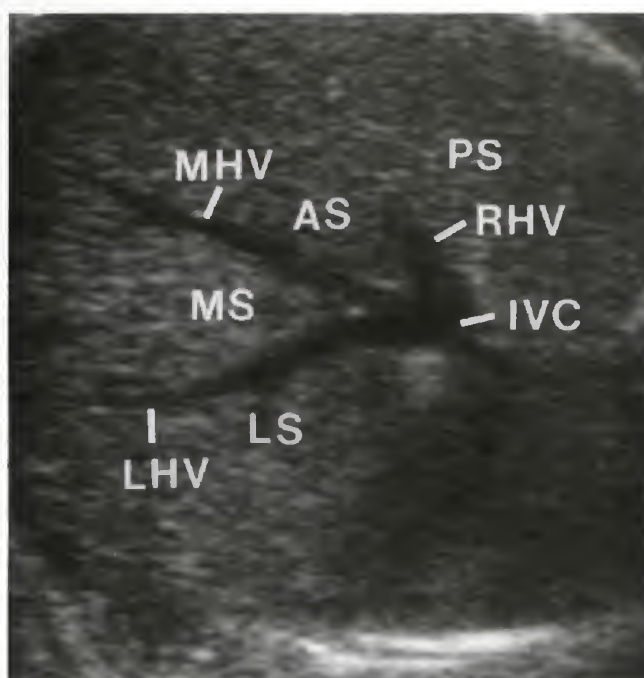


**FIGURE 9-71.** Sonogram through the long axis of the proximal fetal hepatic veins. IVC, inferior vena cava; LHV, left hepatic vein; MHV, middle hepatic vein; RHV, right hepatic vein. These veins divide the liver into lobes and segments. AS and PS, anterior and posterior segments of the right hepatic lobe; MS and LS, medial and lateral segments of the left hepatic lobe.

all pregnancies should include a four-chamber heart view (Fig. 9-73). Outlet views of the cardiac ventricles are recommended in the most recent guidelines.<sup>68</sup> Useful information about the position and size of the great vessels can be quickly gleaned from a transverse axial view of the upper medi-

astinum by simply moving the transducer cephalically from the four-chamber heart view. This section traverses the superior vena cava, the ascending and descending thoracic aorta, the pulmonary artery, and the ductus arteriosus (coursing from the pulmonary artery to the descending thoracic aorta) (Fig. 9-74).

The vessels arising from the transverse aorta are frequently visible and include the brachiocephalic, left common carotid, and left subclavian arteries (Fig. 9-75A). The common carotid arteries and jugular veins are also commonly seen in the neck of older fetuses. The brachial artery and vein are less frequently seen adjacent to the humerus but again can be found using color Doppler sonography.

Intracranial arterial structures are easily perceived using color Doppler sonography (Fig. 9-76). These include the vessels of the circle of Willis seen in the basilar cisterns surrounding the inferior portion of the third ventricle. Also, the middle cerebral artery can be identified coursing in the sylvian cistern, the posterior cerebral artery in the ambient cistern, the anterior cerebral arteries in the interhemispheric cistern (near the genu of the corpus callosum), and the basilar artery in the interpeduncular cistern. Also commonly seen is the pericallosal artery after the formation of the corpus callosum commences and proceeds to its body.

The abdominal aorta and inferior vena cava are easily identified, as are the common iliac arteries and veins (see Fig. 9-75B and C). Other branches of the abdominal aorta can be consistently visualized using color Doppler sonography. These include the celiac axis, the superior mesenteric artery, and the renal arteries. Similarly, the renal veins can be consistently seen.

In the leg, the superficial femoral artery and vein (Fig. 9-77) may be visualized in older fetuses. When the knee is extended, it is not difficult to trace these vessels to the level of the popliteal artery and vein, a virtually impossible task when the knee is flexed.



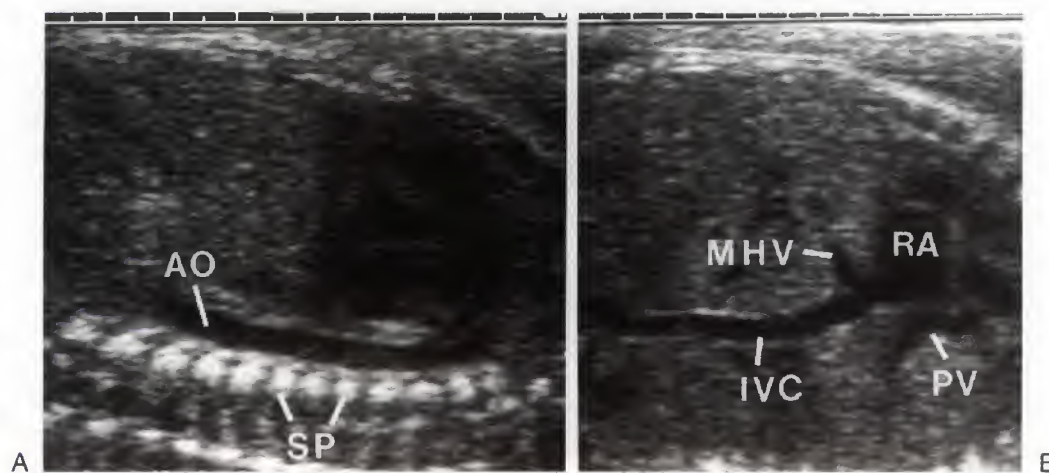


**FIGURE 9-72.** A. Longitudinal view of the aorta (AO). SP, spine. B. Longitudinal view of the inferior vena cava (IVC). MHV, middle hepatic vein; PV, pulmonary vein; RA, right atrium.

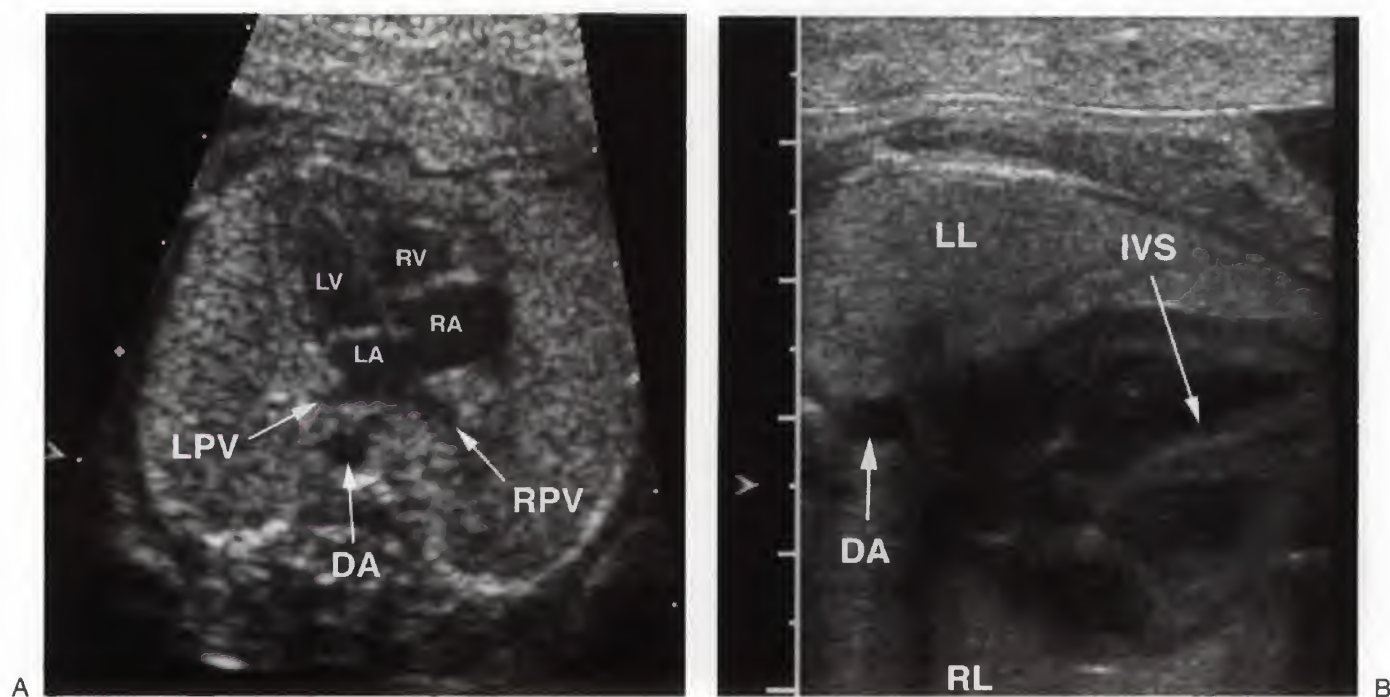


**FIGURE 9-73.** A and B. Transverse axial sonograms through the fetal thorax, the "four-chamber view." In A, the fetus is supine. In B, the fetus is in right decubitus position. DA, descending thoracic aorta; IVS, interventricular septum; LA, left atrium; LL, left lung; LPV, left pulmonary vein; LV, left ventricle; RA, right atrium; RL, right lung; RPV, right pulmonary vein; RV, right ventricle.

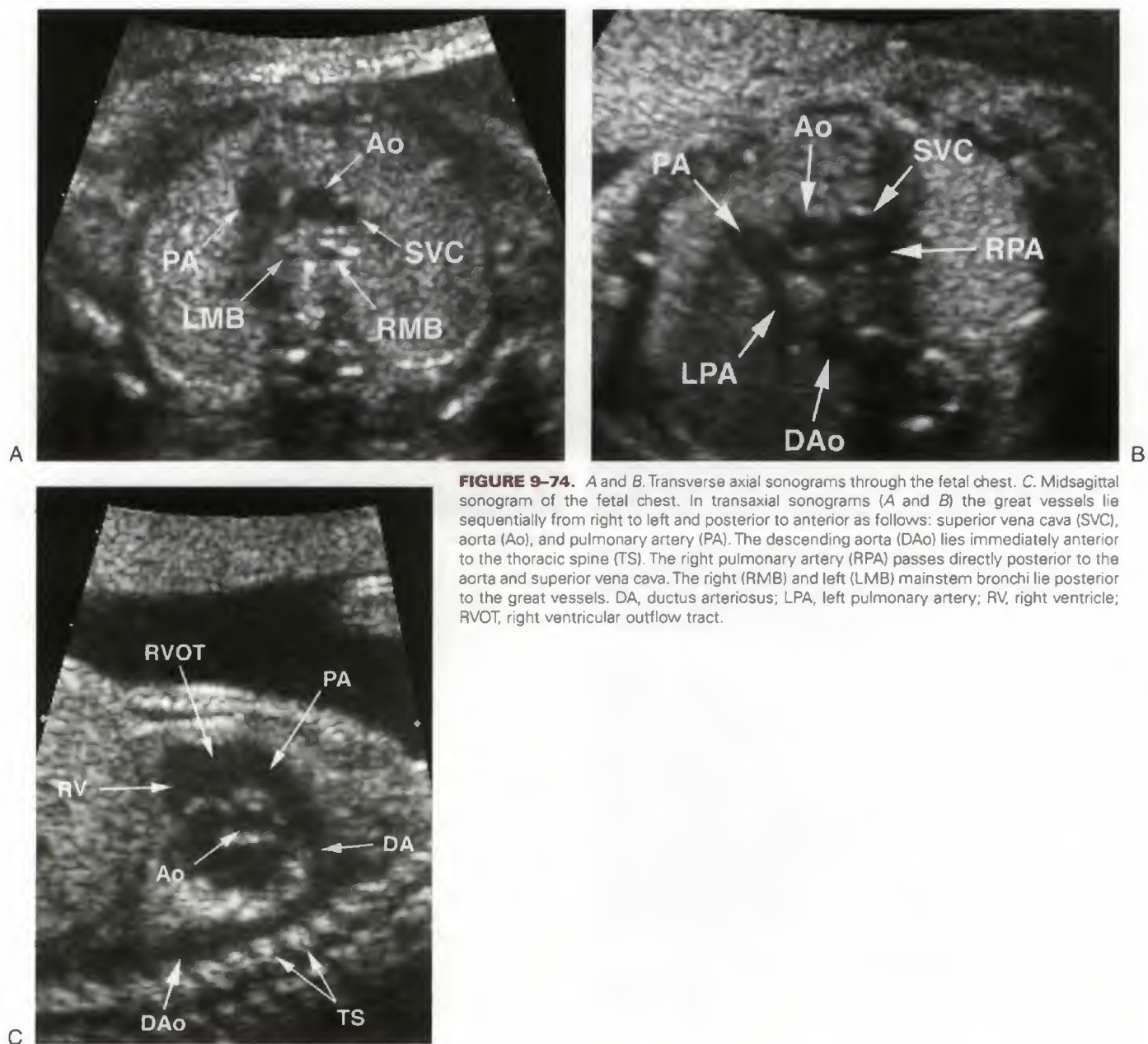


**FIGURE 9-74.** A and B. Transverse axial sonograms through the fetal chest. C. Midsagittal sonogram of the fetal chest. In transaxial sonograms (A and B) the great vessels lie sequentially from right to left and posterior to anterior as follows: superior vena cava (SVC), aorta (Ao), and pulmonary artery (PA). The descending aorta (DAo) lies immediately anterior to the thoracic spine (TS). The right pulmonary artery (RPA) passes directly posterior to the aorta and superior vena cava. The right (RMB) and left (LMB) mainstem bronchi lie posterior to the great vessels. DA, ductus arteriosus; LPA, left pulmonary artery; RV, right ventricle; RVOT, right ventricular outflow tract.



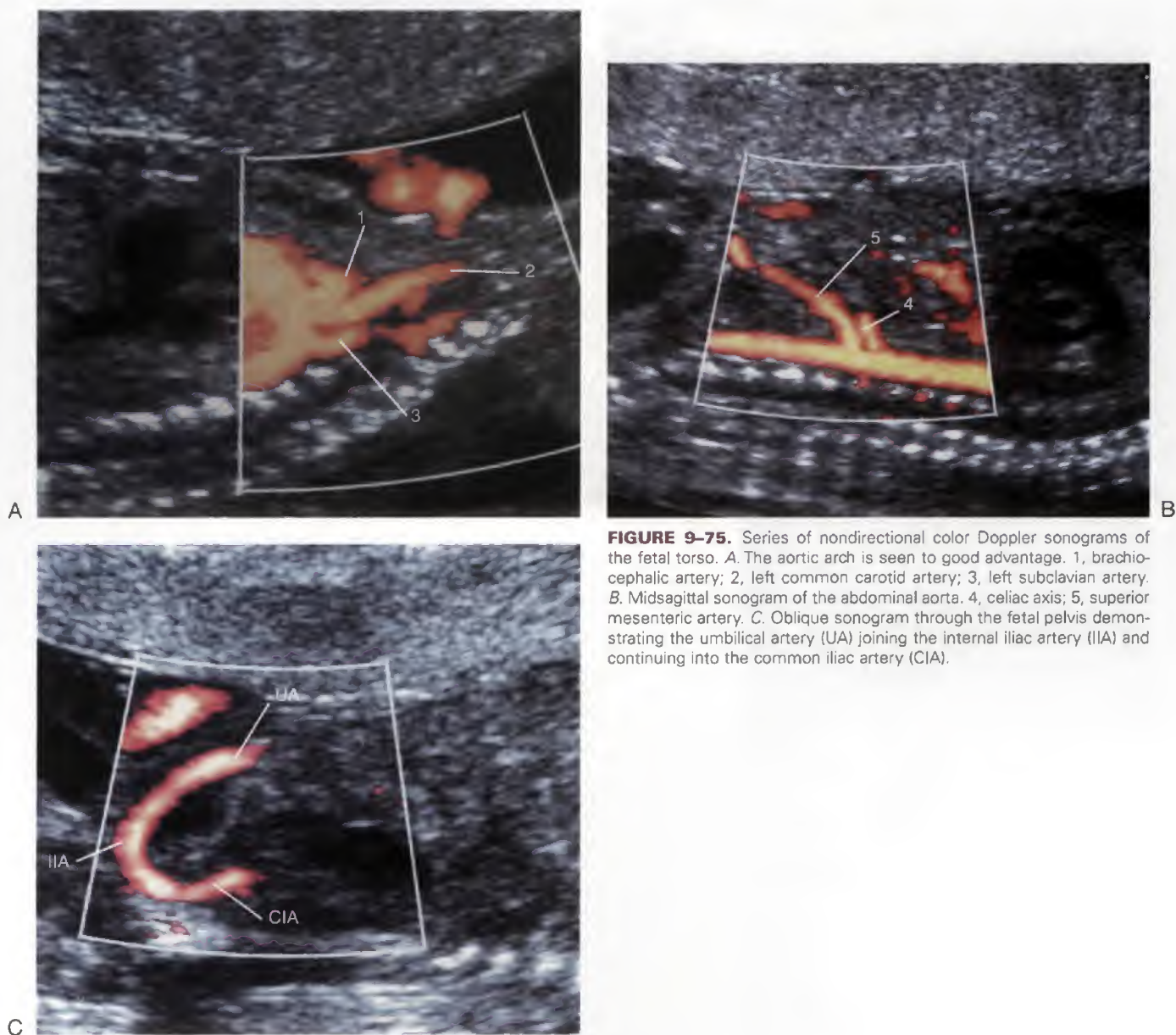


**FIGURE 9-75.** Series of nondirectional color Doppler sonograms of the fetal torso. *A.* The aortic arch is seen to good advantage. 1, brachiocephalic artery; 2, left common carotid artery; 3, left subclavian artery. *B.* Midsagittal sonogram of the abdominal aorta. 4, celiac axis; 5, superior mesenteric artery. *C.* Oblique sonogram through the fetal pelvis demonstrating the umbilical artery (UA) joining the internal iliac artery (IIA) and continuing into the common iliac artery (CIA).

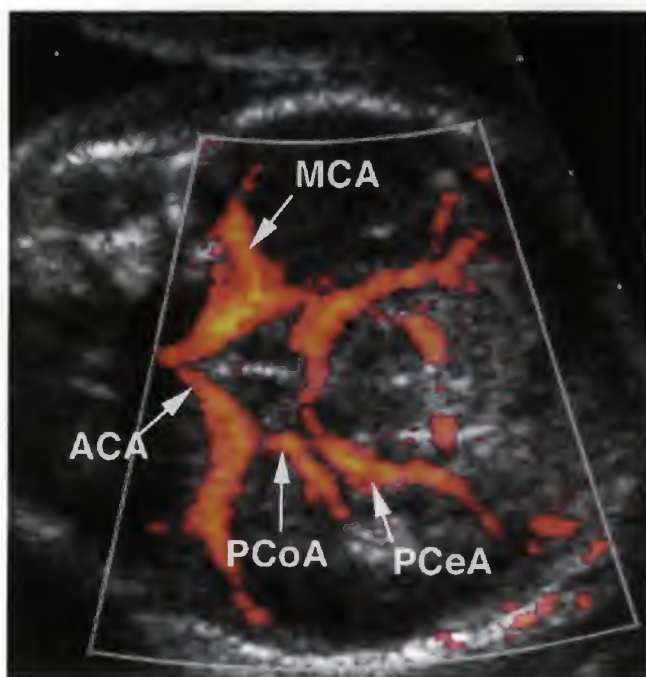


**FIGURE 9-76.** The circle of Willis is well seen on this non-directional color Doppler image. ACA, anterior cerebral artery; MCA, middle cerebral artery; PCeA, posterior cerebral artery; PCoA, posterior communicating artery.

## GASTROINTESTINAL SYSTEM

Many components of the gastrointestinal system can be seen sonographically, some as early as the end of the first trimester.<sup>69</sup> The largest parenchymal organ of the system and of the torso, the liver, is seen consistently from the second trimester onward, although its margins are often indistinct in the earlier phases of pregnancy. Conversely, the other major parenchymal organ of the gastrointestinal system, the pancreas, is much less commonly seen, even in third trimester fetuses. For lack of a better section in which to include it, the spleen is considered with the gastrointestinal tract. This organ is also visible consistently in the second trimester, but, like the liver, its margins are frequently indistinct. Conversely, those portions of the fetal gastrointestinal system that consistently contain fluid, the stomach (see Figs. 9-64, 9-69, and 9-70) and gallbladder (see Figs. 9-63 and 9-64), are among the earliest and most consistently seen of fetal structures.

The components within and about the oral cavity are seen relatively well on sonography.<sup>70</sup> The lips and cheeks have been described in the section on superficial anatomy (see Figs. 9-10 and 9-11). Also consistently seen is the tongue (Fig. 9-78). The tongue is seen to best advantage during swallowing movements. The gingival ridge with tooth buds is seen commonly in fetuses of 20 weeks or more (see Fig. 9-784). The hard palate is difficult to define consistently but with practice can be detected. For this reason, cleft palate is more difficult to detect than cleft lip. Clefting of the soft palate is difficult to diagnosis sonographically because the soft palate cannot be recognized discretely. The

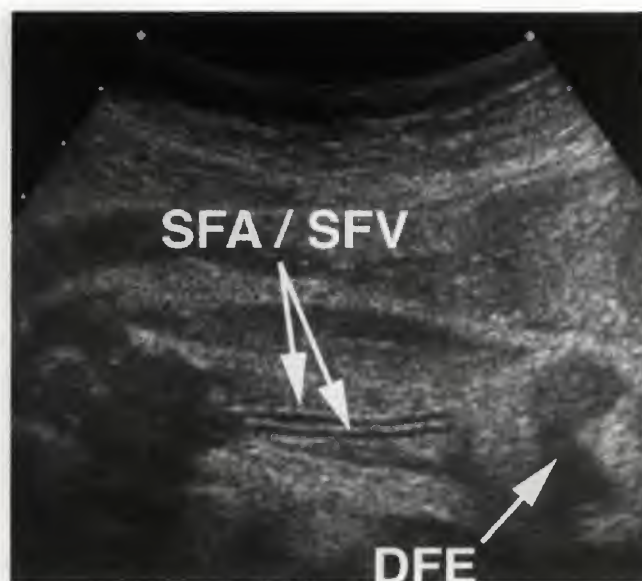


**FIGURE 9-77.** Superficial femoral artery and vein (SFA/SFV) seen side by side in the mid and distal thigh. DFE, distal femoral epiphysis.

oropharynx and laryngeal pharynx frequently contain fluid and thus are seen relatively often when sought (see Figs. 9-78 and 9-79). Transverse axial scans through the upper neck are quite successful for visualization of the pharynx, but longitudinal coronal images, more difficult to obtain, display the anatomy to greater advantage. In longitudinal coronal planes, the continuity of the pharyngeal zones can be appreciated as well as the larynx protruding into the pharynx (see Fig. 9-79). The piriform sinuses, valleculae, and glottis may be appreciated.

The mid- and distal esophagus may be seen surprisingly often when sought (Fig. 9-80).<sup>70</sup> The proximal esophagus is extraordinarily difficult, if not impossible, to visualize in the normal fetus. The mid- and distal esophagus may be seen, although inconsistently, in both longitudinal coronal and transverse axial images. The key to identification of this structure is the descending thoracic aorta, a structure easily seen. The mid- and distal portions of the esophagus lie immediately anterior to the descending thoracic aorta. The aorta is first visualized in a longitudinal coronal plane. The transducer is then slowly moved anteriorly. As the aorta disappears from view, the esophagus comes into view but is much more difficult to recognize. It is seen as five parallel linear echoes. The hyperechoic serosa and lumen and the hypoechoic muscular wall (Fig. 9-81) create these. Conceptually, one could apply a similar strategy to visualization of the upper third of the esophagus. In this instance, one would image the trachea (see the following section) in a longitudinal coronal plane and then slowly move the transducer posteriorly. As the trachea disappears, the esophagus should again come into view. Unfortunately, this concept, although anatomically correct, is practically unsuccessful.

The stomach and gallbladder are the only portions of the subdiaphragmatic fetal gastrointestinal system that consistently contain fluid (see Figs. 9-63, 9-64, 9-69, and 9-70).<sup>69,71,72</sup>



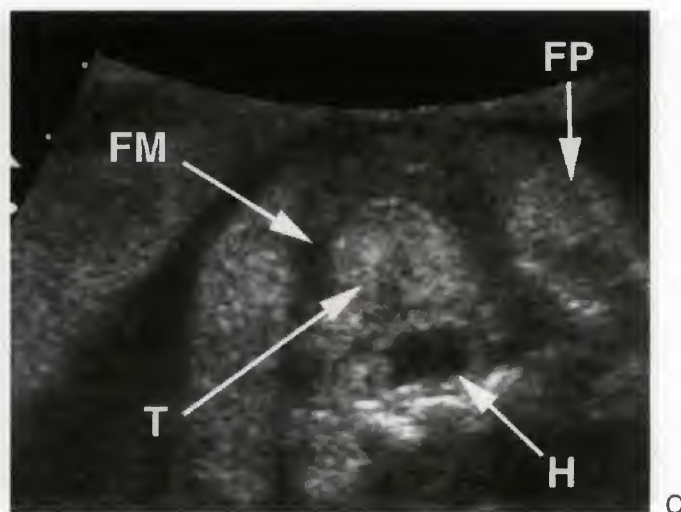
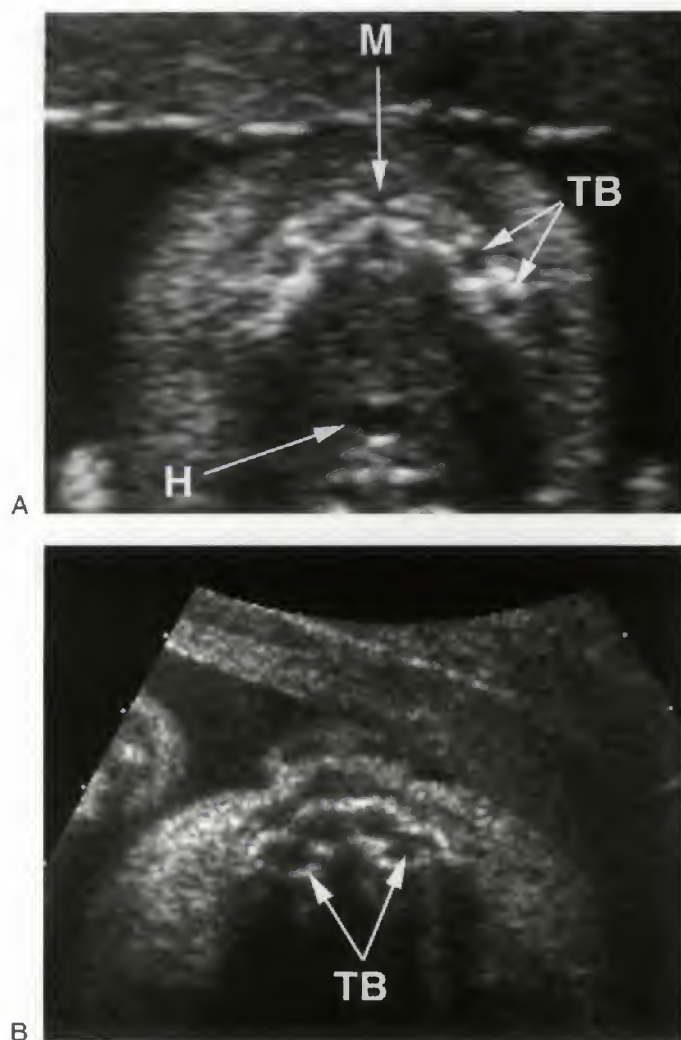


**FIGURE 9-78.** Transverse axial sonograms of the (A), mandible; (B) maxilla, and (C) tongue. FM, facial musculature; FP, cheek fat pads (Bichat); H, hypopharynx; M, mandibular mentum; TB, tooth buds; T, tongue.

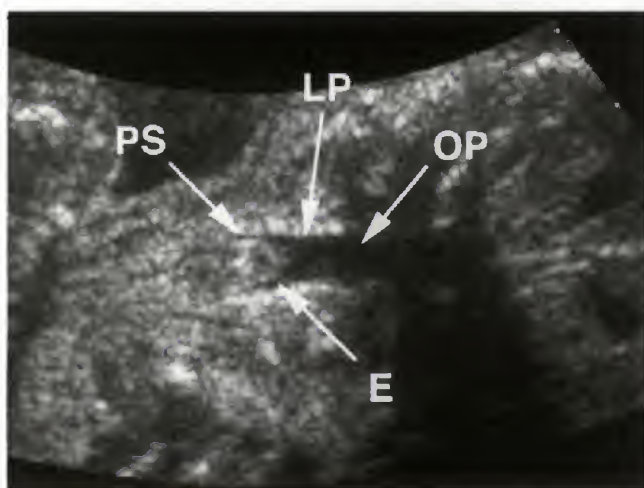


**FIGURE 9-79.** Coronal sonogram of the fetal hypopharynx. The fluid-filled oropharynx (OP) and laryngopharynx (LP) are well seen. Fluid slightly distends the piriform sinuses (PS). E, epiglottis.

Thus, any fluid-containing small bowel should be viewed with suspicion, although in late fetuses one not infrequently sees very small amounts of normal succus entericus in the small bowel lumen, usually made more obvious by accompanying peristalsis. Fluid contained within the normal fetal stomach is almost entirely imbibed. The fetus begins to swallow amniotic fluid at approximately 16 weeks.<sup>71,72</sup> The volume that the fetus swallows increases dramatically throughout pregnancy and reaches 400 to 500 mL by term. There is a relative proportionality between the volume of urine produced and the amount of amniotic fluid imbibed by the fetus. In the absence of a patent esophagus, the stomach will be empty (invisible) except in two circumstances. First, and most common, is the concomitant presence of a tracheoesophageal fistula, enabling the fetus to “breathe” fluid into the esophagus and thence to the stomach.<sup>73</sup> More likely, the gastric fluid comes from the fluid produced by the lung that then drains through the fistula into the stomach rather than by “breathing” fluid into the trachea and thence through the fistula. This pathologic

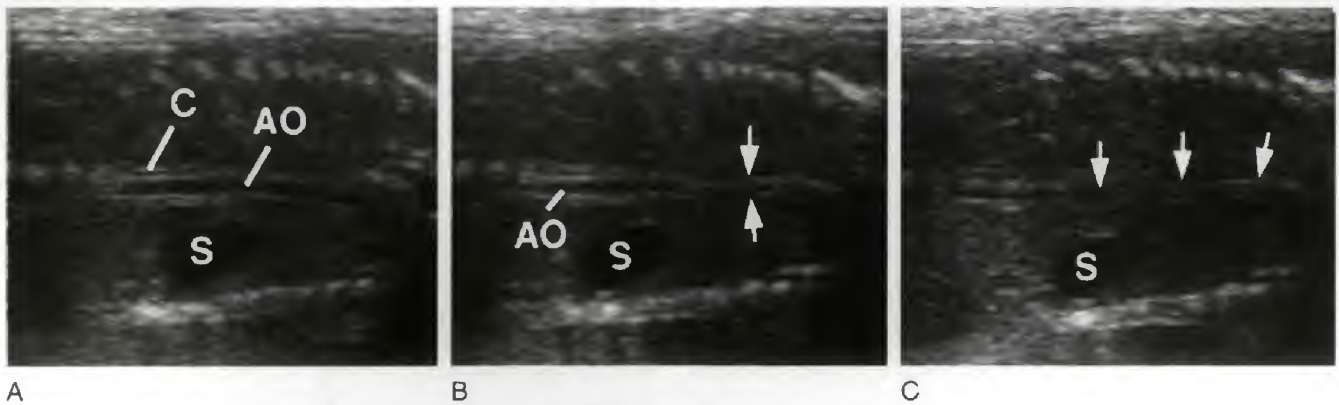


**FIGURE 9-80.** A-C. Coronal sonograms depicting demonstration of the mid and distal esophagus. First (A), the descending aorta (AO) is localized. C, diaphragmatic crura; S, stomach. As the transducer is moved anteriorly (B and C), the esophagus (arrows) comes into view.

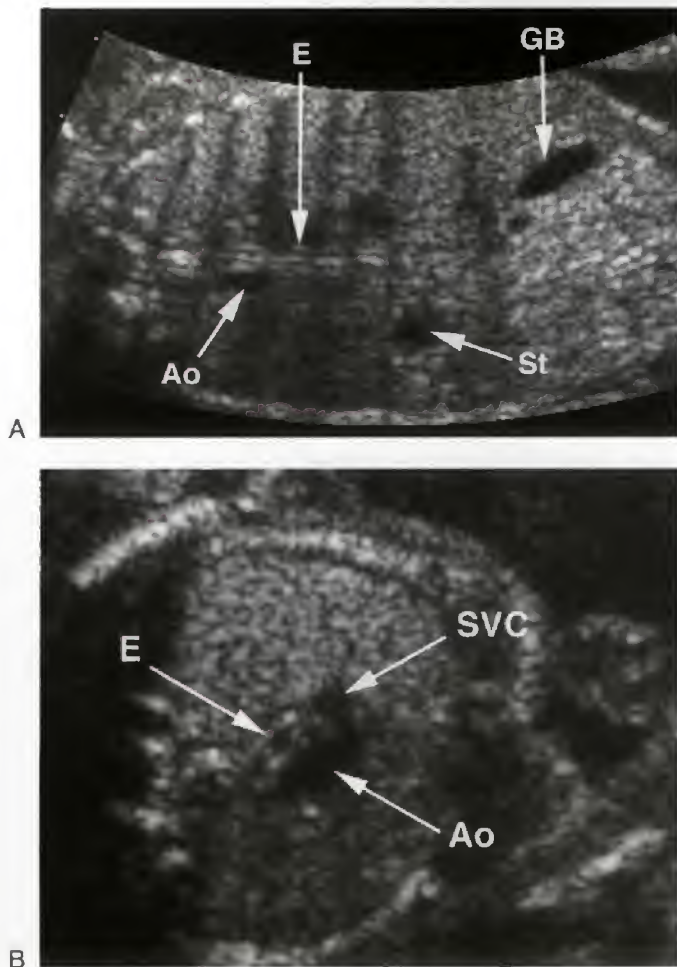


**FIGURE 9-81.** Coronal (A) and transverse axial (B) sonograms demonstrating the esophagus (E). The serosa and lumen appear hyper-echoic, and the muscular wall is hypoechoic. St, stomach; GB, gallbladder, Ao, aorta, SVC, superior vena cava. Distally, the esophagus lies anterior to the descending aorta (compare with Fig. 9-80). Proximally, it lies posterior to the transverse aorta (B) and medial to the ascending aorta (A).

event is commonly associated with polyhydramnios in late pregnancy but not always before 24 weeks. Second, the association of esophageal atresia without tracheoesophageal fistula but with a second proximal gastrointestinal tract atresia or obstruction will allow secretions from the stomach to accumulate within the gastric lumen.

The stomach varies considerably in size depending, presumably, on how much amniotic fluid has been recently imbibed by the fetus.<sup>71,72</sup> A prominent stomach never should be taken as sole evidence of obstruction. When the stomach is well distended, its various parts (i.e., the fundus, body, and antrum) can be identified (Fig. 9-82). The fundus is most posterior, whereas the antrum is most anterior. The incisura angularis can be noted when the stomach is well distended. The incisura angularis is a notch of variable depth that is usually found along the lesser curvature between the body and antrum of the stomach.<sup>74</sup>

Small bowel becomes progressively more visible through the second and third trimesters. Meconium begins accumulating in the small bowel during early and middle second trimester. This may impart the appearance of a “conglomerate” zone of increased echogenicity in the mid- and lower abdomen of the fetus. This should not be mistaken either for an abnormal mass (pseudomass of bowel)<sup>75-77</sup> or of a bowel abnormality. With passage of time, and somewhat dependent on ease of imaging, discrete small bowel loops become visible (Fig. 9-83). With modern equipment, the bowel wall is seen to good advantage. The submucosa and serosa display greater echogenicity than the muscular layers, the thinner muscularis mucosa and thicker muscularis propria. Later in pregnancy, deposition of fat in the mesentery probably accentuates the separation of individual bowel loops and increases echogenicity in the region of the abdomen where the small bowel resides.

Importantly, “increased echogenicity” of the bowel has been implicated as a harbinger of several serious abnormalities of the fetus.<sup>78,79</sup> Therefore, it is important to discriminate increased echogenicity of the bowel content (potentially indicating a problem) from echogenicity caused



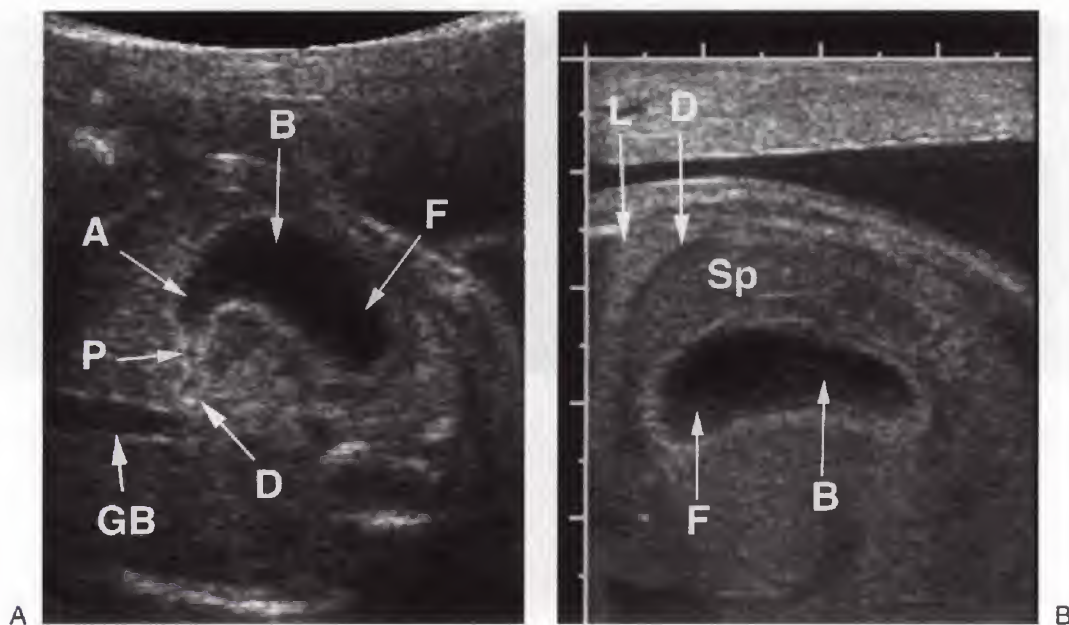


**FIGURE 9-82.** A. Coronal image of the stomach demonstrating all portions of the stomach including the fundus (F), body (B), antrum (A), and pylorus (P). The duodenal bulb (D) (not containing fluid) lies adjacent to the gallbladder (GB). B. Axial sonogram of the fetal stomach showing the fundus (F) and body (B). A portion of the left lung (L) and spleen (Sp) are included. D, diaphragm.

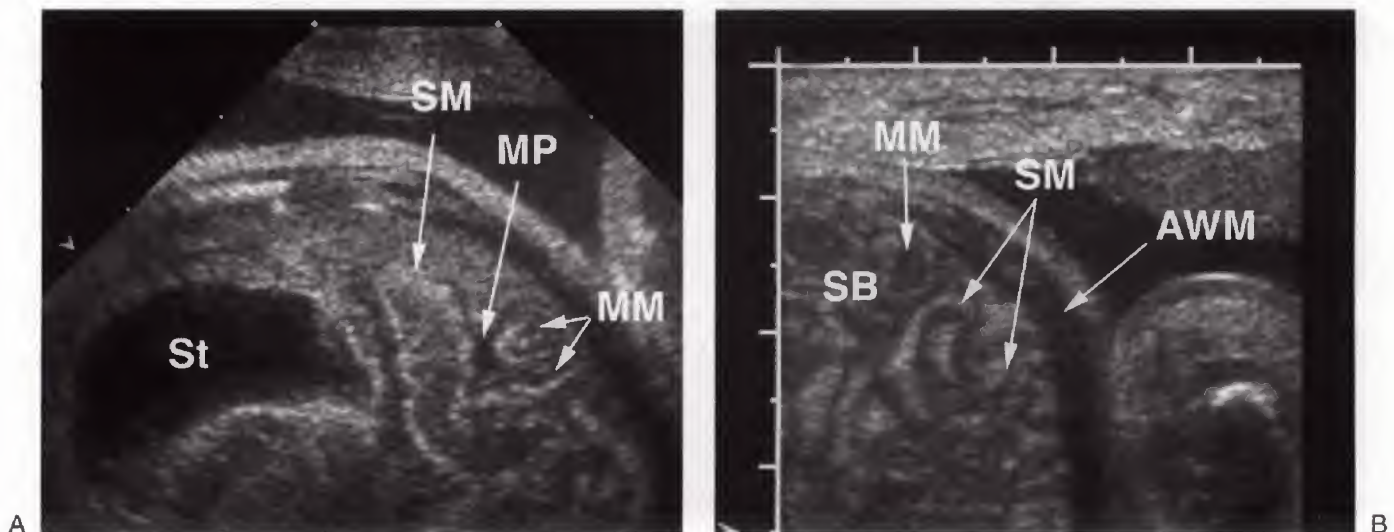


**FIGURE 9-83.** A and B. Discrete small bowel (SB) loops are clearly visible on images through the fetal abdomen. The morphology of the bowel wall is well shown. The dominant feature of the small bowel wall is the submucosa (SM) which demonstrates bright echoes (not to be mistaken for "echogenic bowel"). The muscularis propria (MP) which demonstrates darker gray echoes lies "outside" of the submucosa and the muscularis mucosa (MM, also dark) lies "inside" of the submucosa. Note that the anterior abdominal wall musculature (AWM), like all musculature, demonstrates darker gray echoes. If one looks closely, one can appreciate the more echogenic small bowel mucosa "sandwiched" between the layers of muscularis mucosa. St, stomach.

by normal bowel structure, but perceived in conglomerate to represent "increased bowel echogenicity" (unlikely to indicate a problem). Examining to see if the echogenicity is due to well-visualized submucosa or mesenteric fat will avoid these issues. Generally, high-frequency transducers demonstrate the submucosa of the small bowel to much

greater advantage, thus giving the examiner the impression that the bowel is "echogenic".<sup>80</sup> When transducers with frequencies greater than 5 MHz are being employed, the probability that fetal bowel wall structure has resulted in an impression of "increased echogenicity" is great. Confirmation with lower frequency transducers should be done. By late

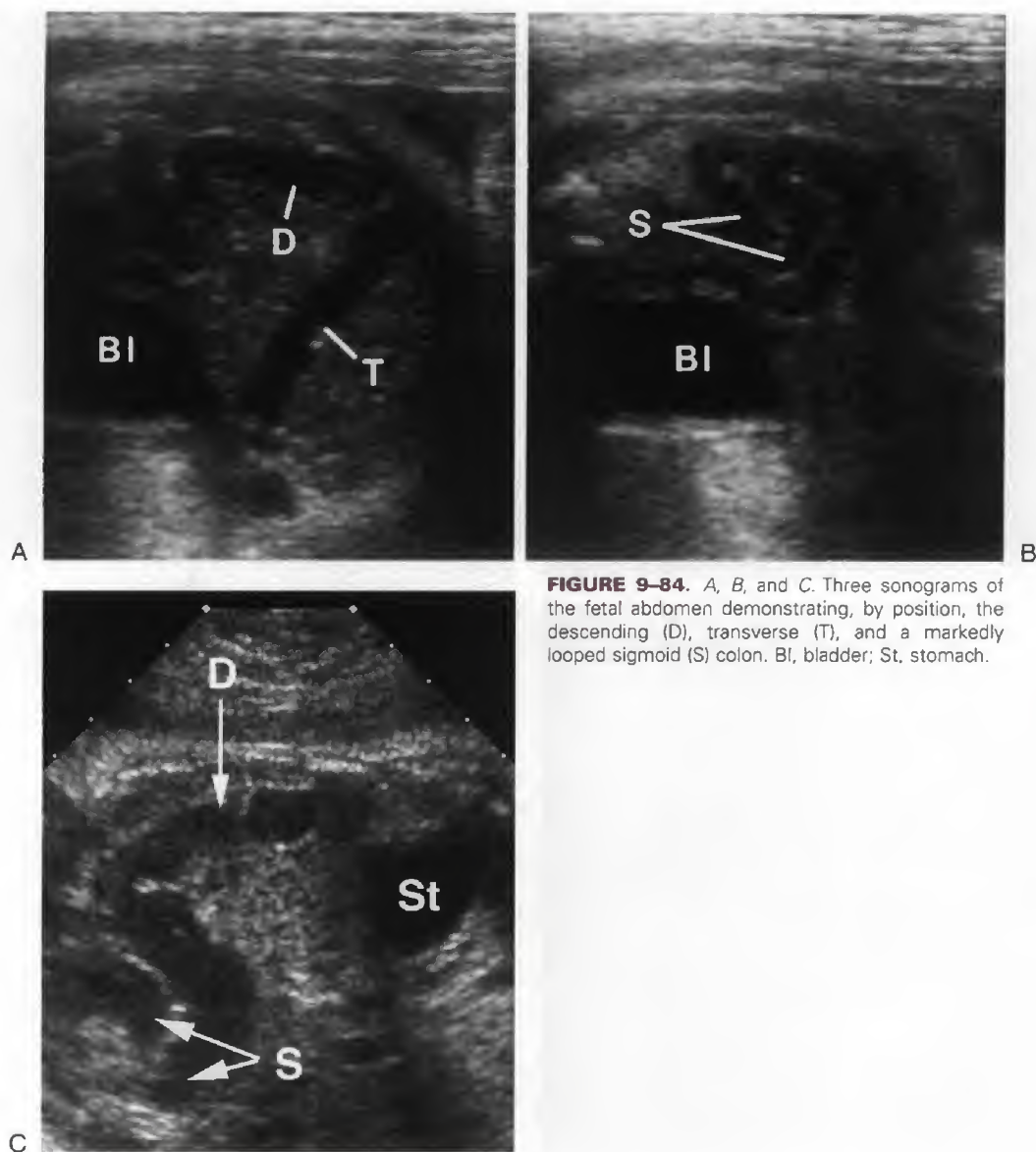


**FIGURE 9-84.** A, B, and C. Three sonograms of the fetal abdomen demonstrating, by position, the descending (D), transverse (T), and a markedly looped sigmoid (S) colon. Bl, bladder; St, stomach.

pregnancy, almost regardless of equipment quality, discrete small bowel containing small amounts of fluid (succus entericus) can be visualized in nearly all fetuses.<sup>81</sup>

The colon tends to become visible near the beginning of the third trimester and, again, is seen progressively better with increasing gestational age.<sup>81,82</sup> The colon tends to be relatively hypoechoic (Figs. 9-84 and 9-85). As such, colon should not be mistaken for dilated small bowel. It is the characteristic course of the colon that most readily permits distinction from pathologically dilated small bowel. The ascending colon courses along the right flank (see Fig. 9-84A) in relation to the right kidney. As it approaches the liver, it bends leftward, in the hepatic flexure (see Fig. 9-84A). The transverse colon courses along the free edge of the liver (see Figs. 9-84A and 9-85A) and passes inferior to the stomach. At the splenic flexure, the colon turns posteriorly and again comes into intimate relationship with the kidney; of course, in this instance it is the left

kidney. Frequently, when imaging the kidneys, the colon is detected. Indeed, when a kidney is absent, the colon occupies the renal fossa and should not be misinterpreted as a normal or abnormal kidney. Finally, the sigmoid colon arcs over the urinary bladder to join the rectum (see Figs. 9-84B and 9-85B). Occasionally, haustral markings can be noted in the colon wall. A redundant sigmoid colon (see Fig. 9-85B) should not be mistaken for dilated small bowel.

The liver, as noted earlier, is proportionately larger in the fetus than in the child or adult.<sup>83</sup> Similarly, in the early second trimester, the liver constitutes 10% of the total fetal weight but only 5% of the total weight at term. The fetal liver, in addition, has a substantially larger left lobe. Indeed, the fetal liver spans the entire width of the abdomen throughout pregnancy, the left lobe always contacting the left abdominal wall. This would be unusual but possible in an adult.



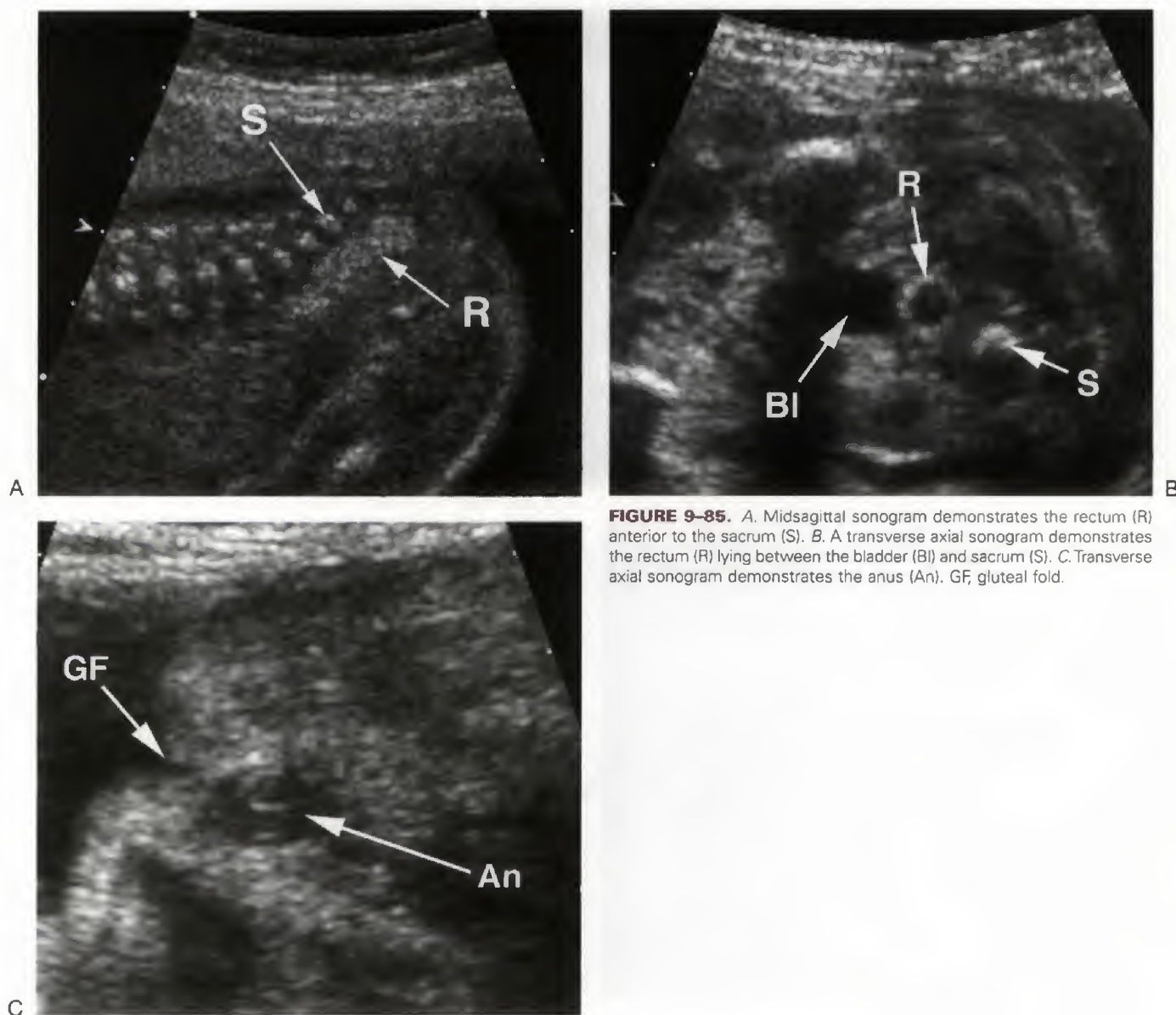


**FIGURE 9-85.** A. Midsagittal sonogram demonstrates the rectum (R) anterior to the sacrum (S). B. A transverse axial sonogram demonstrates the rectum (R) lying between the bladder (Bl) and sacrum (S). C. Transverse axial sonogram demonstrates the anus (An). GF, gluteal fold.

The two major segments of each hepatic lobe can be seen in older fetuses (see Fig. 9-71) and to some extent even in early second trimester fetuses.<sup>61,64</sup> The lateral segment of the left lobe extends to the left of the umbilical segment of the left portal vein (see Figs. 9-9 and 9-70). The medial segment of the left lobe is the tissue lying between the gallbladder (or middle hepatic vein more superiorly) and the umbilical segment of the left portal vein or the intersegmental fissure more caudally (Fig. 9-86). The right lobe is all of the hepatic tissue lying to the right of the gallbladder, middle hepatic vein, and inferior vena cava (see Figs. 9-64 and 9-70). These latter three structures all reside in the main lobar fissure. The left portal vein and left hepatic vein mark the left intersegmental fissure. Finally, the right intersegmental fissure is marked by the right hepatic vein cephalically and its anterior branch inferiorly.

As noted earlier, the pancreas is difficult to perceive at any gestational age. The pancreatic tissue lies posterior to the stomach, an area that can be visualized consistently in the fetus. However, discrete perception of the pancreas requires demonstration of the splenic vein and origin of the superior mesenteric artery in a transverse axial plane of section (Fig. 9-87). The pancreas then is the band of tissue between these vessels and the posterior gastric wall. Occasionally, the pancreas is slightly greater in echogenicity than the peripancreatic tissues and organs, making visualization easier.

The spleen is not truly a gastrointestinal organ (see Figs. 9-70 and 9-82B). The spleen is bounded by the diaphragm superiorly, the lower ribs laterally, the stomach medially, and the diaphragm and kidney posteriorly. It is only the inferior margin that is difficult to delimit. In the

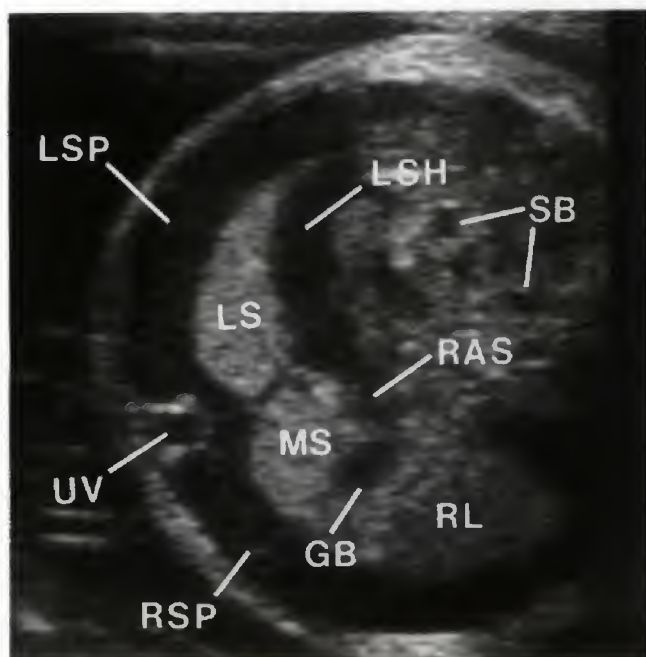


**FIGURE 9-86.** Transverse axial sonogram of the fetal abdomen after an intraperitoneal transfusion for Rh isoimmunization enables recognition of many peritoneal spaces, including the right (RSP) and left (LSP) subphrenic spaces and the right anterior (RAS) and left subhepatic (LSH) spaces. Segmental anatomy of the fetal liver is also well seen, including the medial (MS) and lateral (LS) segments of the left hepatic lobe. GB, gallbladder; RL, right hepatic lobe; SB, small bowel; UV, umbilical vein.

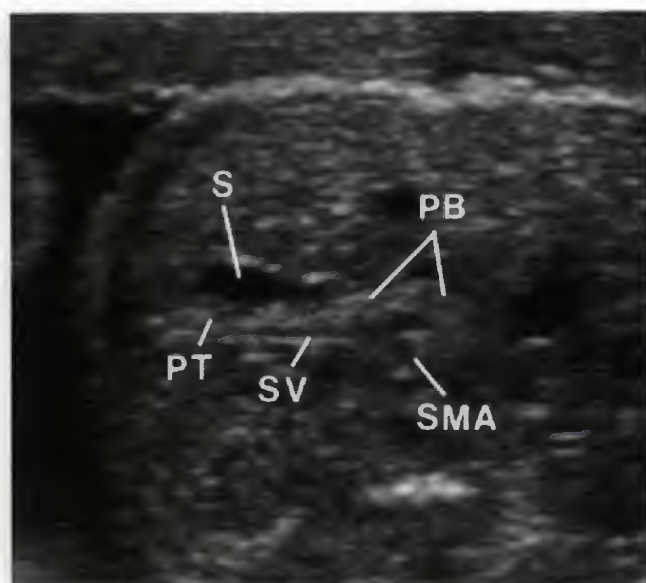
fetus, the spleen echogenicity is similar to that of the liver. In the adult, the liver is slightly less echogenic than the spleen.<sup>84-87</sup> The spleen grows progressively through fetal life, and nomograms of splenic size are available in the literature.<sup>84</sup>

## RESPIRATORY SYSTEM

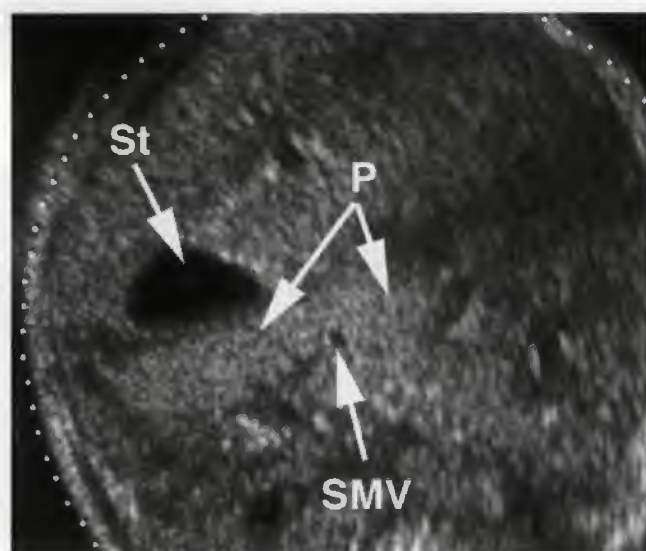
The upper respiratory tract system is seen partially. The nose has been previously illustrated (see Figs. 9-10 and 9-11). The nasal cavity, septum, and palate can be detected with practice. As noted earlier, portions of the pharynx and hypopharynx are commonly visible because of the presence of fluid.<sup>70</sup> The piriform sinuses are seen when fluid filled (see Fig. 9-79). When relatively large amounts of fluid are present in the pharynx of an older fetus, the epiglottis may be seen protruding into the fluid (Fig. 9-88). The epiglottis is particularly visible during swallowing.

The larynx is virtually always visible when the hypopharynx is fluid filled (see Figs. 9-79 and 9-88). Details of laryngeal anatomy are not particularly evident, but the larynx itself is easily recognized as a superior constriction of the tracheal fluid column protruding into the hypopharynx and flanked by the piriform sinuses. If the head is markedly flexed, the overlying mandible frequently defeats efforts to visualize the larynx and hypopharynx.

The trachea is a relatively easy structure to visualize (Figs. 9-88 to 9-90).<sup>70</sup> Again, this is predominantly because it is consistently fluid filled. The lungs produce fluid that is



A



B

**FIGURE 9-87.** A and B. The fetal pancreas is not commonly seen discretely but is well depicted in these examples. When sought, it can often be detected. Those who perform abdominal sonograms in adults and children will recognize the familiar landmarks. In example B the pancreas (P) is enlarged (Beckwith-Wiedemann syndrome). The pancreas lies between the splenic vein (SV) and the posterior stomach wall (S). PB, pancreatic body; PT, pancreatic tail; SMA, superior mesenteric artery; SMV, superior mesenteric vein.

not only expelled into the trachea. Additionally, the trachea, along much of its length, is flanked by the conspicuous pulsations of the common carotid arteries. The trachea usually can be traced to its distal end, passing posterior to the aortic arch (see Fig. 9-89A), but the carina and bronchi are quite difficult to perceive. Because mainstem bronchi are usually invisible, smaller ramifications of the bronchi are, for all intents and purposes, universally invisible at this time in the development of fetal sonography.

The right and left pulmonary arteries and pulmonary veins (Figs. 9-91 and 9-92) are visible in a large percentage of second and third trimester fetuses. However, one



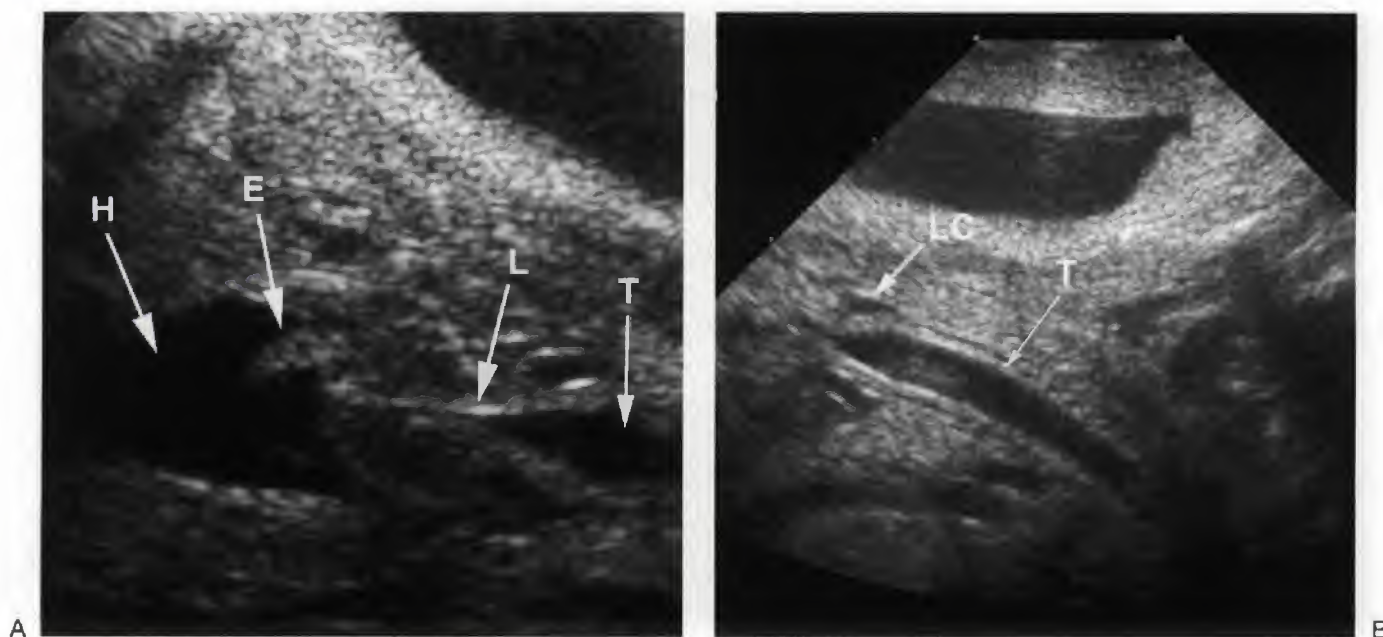


**FIGURE 9-88.** A and B. Coronal sections through the hypopharynx (H), epiglottis (E), larynx (L), and trachea (T). LC, laryngeal cartilage.

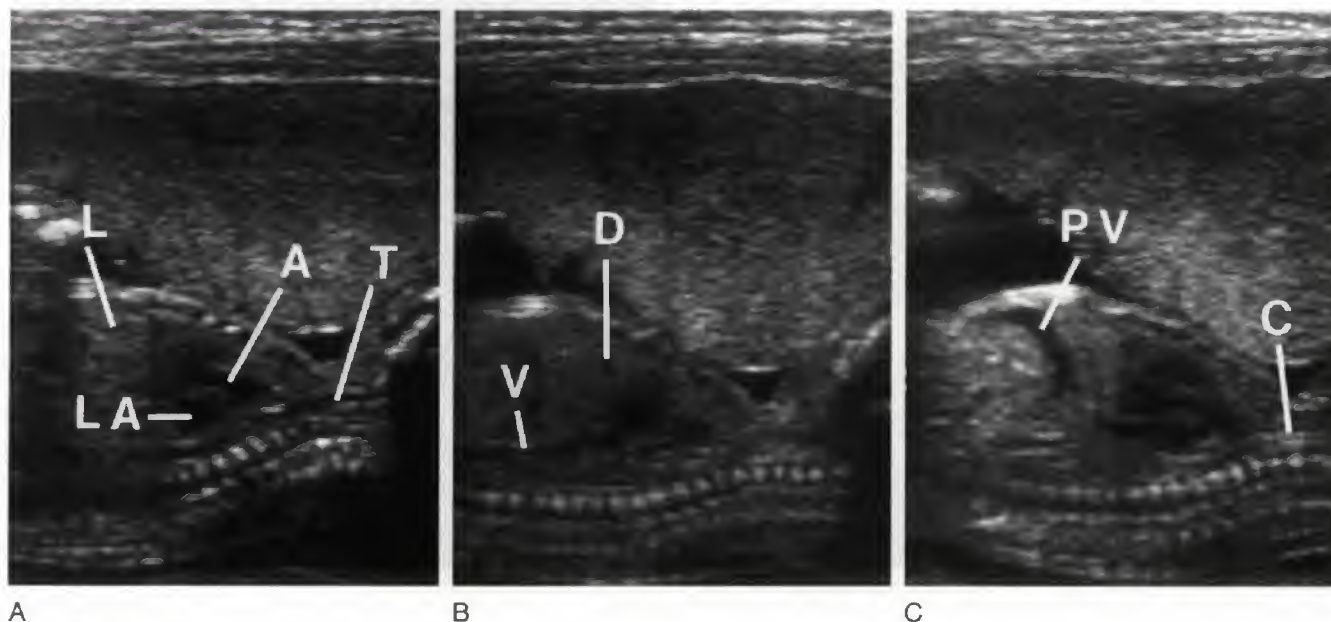


**FIGURE 9-89.** Relationships of mediastinal and neck structures. Three midsagittal (A) or parasagittal (B and C) sonograms demonstrate the trachea (T) down to the level of the aortic arch (A). The cervical esophagus (C) lies posterior to the trachea in the neck (note again the muscular and mucosal layering). D, diaphragm; L, liver; LA, left atrium; PV, left portal vein; V, inferior vena cava.

generally pursues visualization of these major vessels during examination of the heart rather than the lungs. Details of the pulmonary arterial and venous anatomy are found in Chapter 14.

The lung (at least lung tissue) can be seen from late first trimester onward. Early in pregnancy, definition of the lung is drawn more from the structures that surround it. These

heart (and to a lesser extent other mediastinal structures) medially. Inferiorly, the early lung blends imperceptibly with the liver. These two organs are equal in echogenicity throughout some of the second trimester. As pregnancy progresses, the lung becomes more echogenic than the liver (Fig. 9-93). The reason for this is unknown. It was speculated that this difference may signal pulmonary

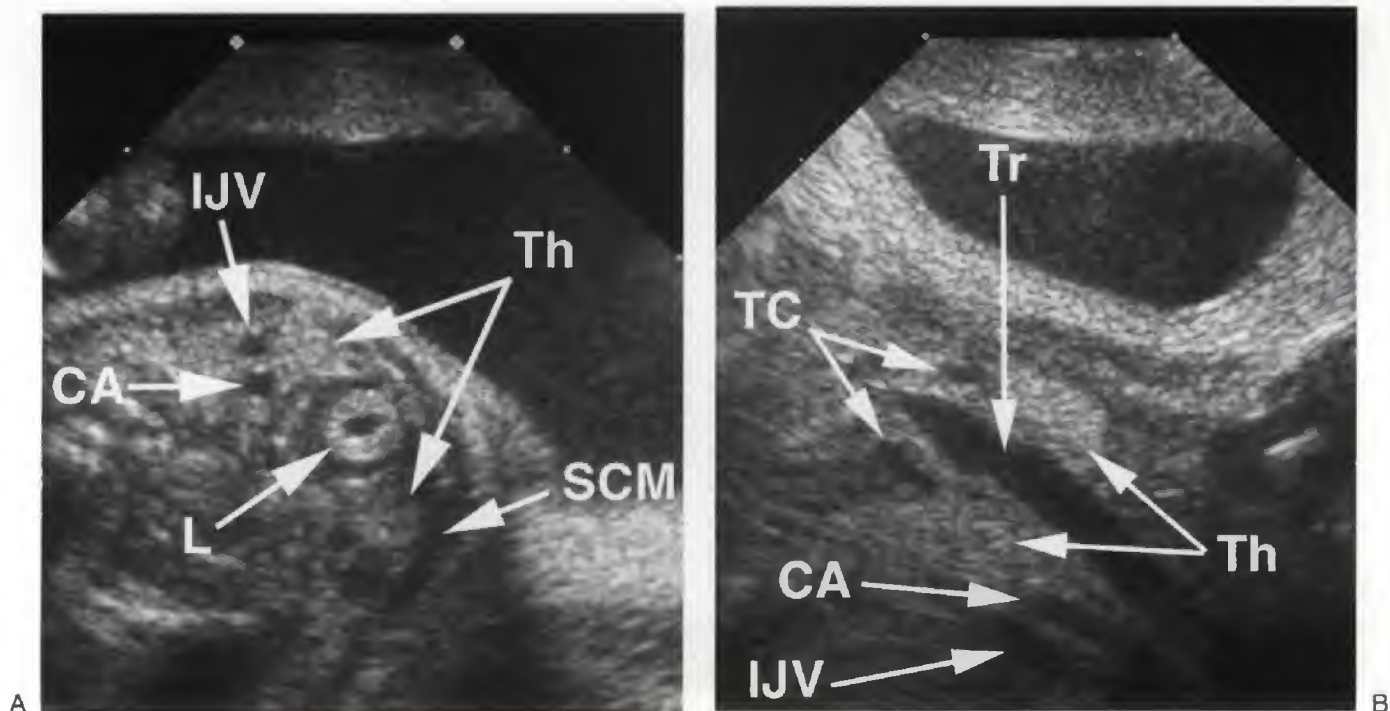


**FIGURE 9-90.** Transverse axial (A) and longitudinal (B) sonograms of the fetal neck. CA, carotid artery; IJV, internal jugular veins; L, larynx; SCM, sternocleidomastoid muscle; TC, thyroid cartilages; Th, thyroid lobes; Tr, trachea.

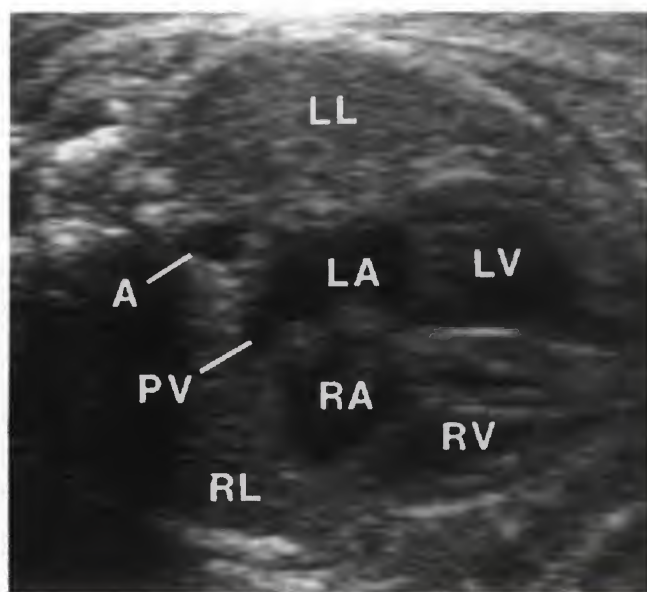


**FIGURE 9-91.** Transverse axial sonogram of the fetal thorax. A, descending aorta; LA, left atrium; LL, left lung; LV, left ventricle; PV, pulmonary vein; RA, right atrium; RL, right lung; RV, right ventricle.



**FIGURE 9-92.** Axial section through the fetal thorax. LL, left lung; RL, right lung; arrows, pulmonary veins.

of greater echogenicity than the liver can be seen earlier in pregnancy than lung maturity can possibly develop.<sup>88,89</sup> Furthermore, the muscular portion of the diaphragm becomes progressively more visible with fetal growth and the hypertrophy of the diaphragmatic muscle that occurs as the fetus “breathes” against atelectatic, fluid-filled lungs

(Fig. 9-94). These markers of the inferior extent of the lung improve pulmonary tissue visibility with advancing gestational age. Discrete pulmonary lobes are not visible in the normal fetus, but when a pleural effusion is present, insinuation of fluid into the major fissures (and the minor fissure on the right) marks lobar boundaries.



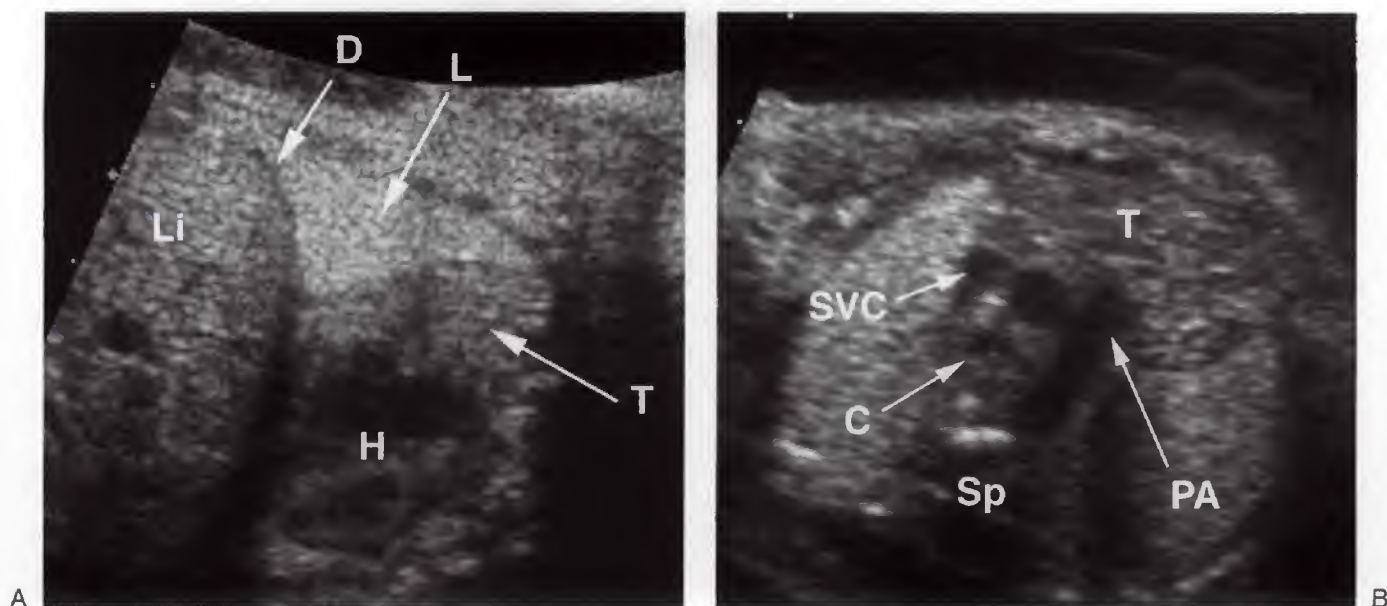


**FIGURE 9-93.** Coronal sonogram (A) through the fetal chest. Echogenicity differences between lung (L) and liver (Li) and lung and thymus (T) are easily seen in this older fetus. B. Axial sonogram through the fetal chest. Again, the echogenicity differences between the lung and thymus (T) are easily seen. C, carina; D, diaphragm; H, heart; PA, pulmonary artery; Sp, spine; SVC, superior vena cava.



**FIGURE 9-94.** The muscular diaphragm (D) is relatively hypoechoic. L, liver.

## GENITOURINARY SYSTEM

Although the extreme variability of fetal positioning and the lack of subject contrast between kidney and the surrounding tissues do not permit consistent identification of both fetal kidneys, normal fetal kidneys are commonly identified in their paraspinous location as early as 15 menstrual weeks. Visualization typically becomes consistent by the 20th week.<sup>90</sup>

In longitudinal section, fetal kidneys appear as bilateral elliptic structures, and in transverse section, they have a circular appearance adjacent to the lumbar spinal ossification centers bilaterally (Fig. 9-95). Later in pregnancy, hyperechogenic retroperitoneal fat, which surrounds the kidneys, assists in their sonographic visualization (see Figs. 9-95 and 9-96). The fetal renal pyramids can frequently be discriminated from the surrounding cortex and columns of Bertin in most fetuses and are arranged in an anterior and posterior row (see Fig. 9-95A) in a configuration corresponding to the calices that contact the apices of the pyramids (the papillae).<sup>20</sup> The echotexture of the normal fetal renal cortex, which usually approximates or may even be slightly greater than that of the surrounding tissues, highlights the relatively echopenic pyramids. The characteristic position of the pyramids avoids any potential confusion with renal parenchymal cysts. Confusion with dilated calices is avoided by noting the interspaced columns of Bertin and the lack of communication with dilated infundibula and pelvis. Within the renal sinus of fetuses, there is generally a paucity, or more commonly a frank absence, of fat. Intrarenal collecting structures, the pelvis and infundibula, are commonly seen in fetuses because they frequently contain fluid,<sup>91,92</sup> a topic that is addressed in Chapter 16.

The fetal kidneys grow throughout gestation. Standards for renal length, width, thickness, volume, and circumference have been established as a function of menstrual age and correspond with measurements of renal size obtained on stillborn fetuses postnatally.<sup>93-95</sup> Throughout pregnancy, the ratio of kidney circumference to abdominal circumference remains relatively constant at 0.27 to 0.30. Such measurements are more efficient for detecting enlarged kidneys than small kidneys. Diminution in renal size is more difficult to detect because the exact renal border, especially of small

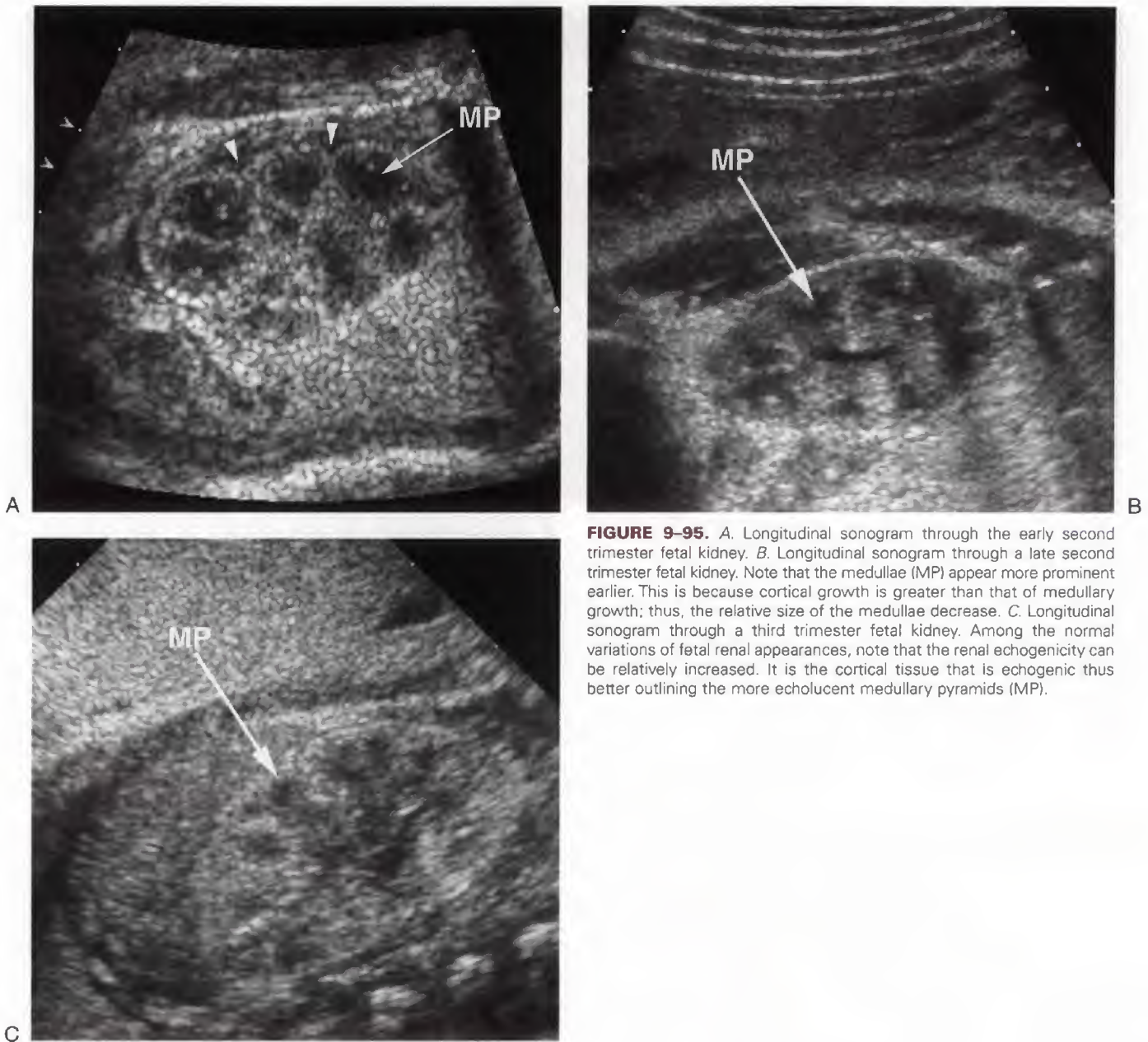


**FIGURE 9-95.** A. Longitudinal sonogram through the early second trimester fetal kidney. B. Longitudinal sonogram through a late second trimester fetal kidney. Note that the medullae (MP) appear more prominent earlier. This is because cortical growth is greater than that of medullary growth; thus, the relative size of the medullae decrease. C. Longitudinal sonogram through a third trimester fetal kidney. Among the normal variations of fetal renal appearances, note that the renal echogenicity can be relatively increased. It is the cortical tissue that is echogenic thus better outlining the more echolucent medullary pyramids (MP).

kidneys, may be partially obscured, because the plane of section may not be through the longest renal axis, and because of the wide standard deviation in renal size.<sup>93-95</sup>

The normal fetal ureter is, for all intents and purposes, not identifiable in fetuses. Uncommonly, one may see a normal ureter, but visualization of a fetal ureter should always suggest pathologic dilatation. However, as early as 15 menstrual weeks, the normal fetal urinary bladder can be identified (see Fig. 9-68). Only a few cubic centimeters of bladder urine would be needed to allow ready visualization in a young fetus. Because the fetus normally fills and empties the urinary bladder every 30 to 45 minutes, the bladder will frequently be seen to increase in size and to empty during the course of a sonographic examination.<sup>96-98</sup> Similarly, fetuses in whom the urinary bladder is not visualized can be

examined at intervals for bladder filling. If the bladder cannot be seen in the presence of oligohydramnios, sequential imaging to test for bladder filling is mandatory.

At 32 weeks of gestation, the maximum fetal bladder volume measures 10 mL. By term, the normal fetal bladder volume quadruples. Similarly, fetal urine production, as calculated by determination of change in bladder volume with time, increases from 9.6 mL/h at 30 weeks to 27.3 mL/h at 40 weeks' menstrual age.<sup>96,97</sup> Of course, term fetuses void; thus, the bladder may be empty.<sup>98</sup> Filling and emptying of the fetal urinary bladder confirms that the fetus produces urine but does not indicate the "quality" of urine produced. The normal fetal urinary bladder, the wall of which is very thin and virtually invisible when the bladder is well distended, occupies a midline position within the fetal pelvis (Fig. 9-97).



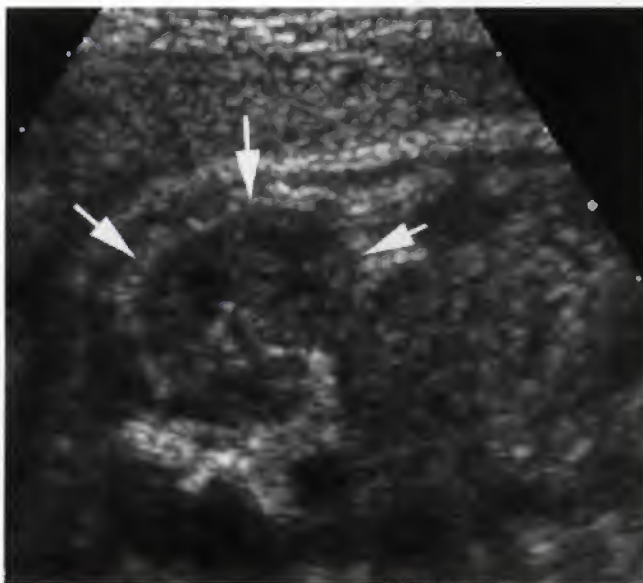


**FIGURE 9-96.** Transverse axial sonogram of a fetal kidney margined by perirenal fat (arrows). The brightly echogenic perirenal fat helps to sonographically outline the less echogenic renal parenchyma.

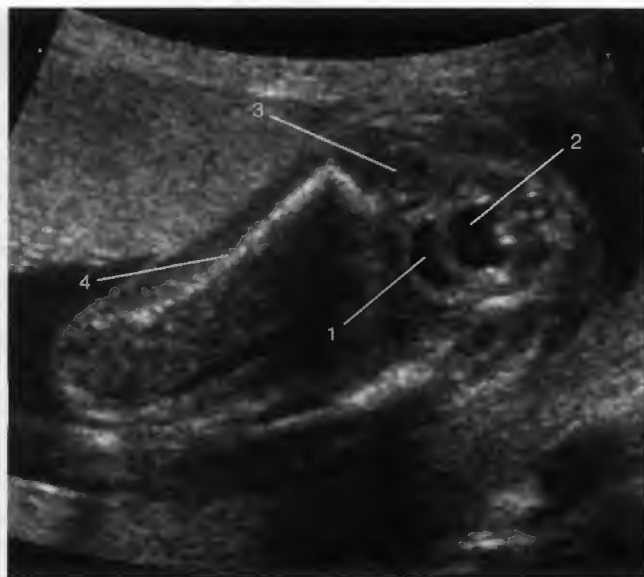
Changes in volume of the urinary bladder with time differentiate it from cystic pathologic pelvic structures. Recall that the umbilical arteries always flank the urinary bladder regardless of the degree of bladder distention. This anatomic relationship is extremely useful for identification of a persistently empty urinary bladder or the confirmation of a massively overdistended bladder.

The normal fetal urethra may be identified, from time to time, as an hyperechogenic line extending the length of an erect penis (see Fig. 9-17). In female and in male fetuses examined when the penis is flaccid, the normal urethra is difficult or impossible to identify. The uterus and ovaries cannot be visualized in normal female fetuses. The testes can be visualized in male fetuses only after they have descended into the scrotum. The prostate cannot be visualized. The external genitalia were discussed previously in the *Superficial Anatomy of the Fetus* section.

The fetal adrenal gland, although not part of the genitourinary system, is seen quite routinely when searching for the kidneys (see Figs. 9-96 and 9-98).<sup>99,100</sup> Indeed, even in the presence of agenesis of one or both kidneys, the adrenal glands can be appreciated in their expected paraspinous locations. The fetal adrenal glands may often be imaged after 30 menstrual weeks. The adrenal glands have a specific size, shape, and echogenicity. The echo pattern is so characteristic that the cortex and medulla can be appreciated separately (see Figs. 9-63, 9-64, and 9-98). In the fetus, both adrenal glands cap the upper renal poles (in the adult the left adrenal gland most often lies anterior to the upper pole).<sup>100</sup> The right adrenal is seen more consistently. Its upper portion lies immediately posterior to the proximal inferior vena cava (see Fig. 9-98).

## CENTRAL NERVOUS SYSTEM

The fetal brain was one of the first areas of investigational interest in the diagnosis of fetal anomalies.<sup>101</sup> This was a



A



B

**FIGURE 9-97.** A. Transverse axial sonogram through the fetal pelvis. 1, urinary bladder; 2, rectum; 3, femoral head; 4, femoral diaphysis. B. Oblique axial sonogram through the fetal pelvis with nondirectional color Doppler. The umbilical arteries (UA) mark the lateral margins of the bladder (BL).

result of two factors: (1) the fetal head was imaged routinely to obtain a biparietal diameter for the determination of gestational age; and (2) central nervous system anomalies are among the most common birth defects. At first, only gross morphologic aberrations such as anencephaly or advanced hydrocephalus were discovered prenatally. Because instrumentation has improved to the present day, many malformations of the brain can be diagnosed with accuracy even before 20 weeks of development.<sup>102-107</sup>

The path to the diagnosis of anomalous development, as always, begins with a firm grasp of normal developmental anatomy. Initially, many errors were made when interpreting normal fetal intracranial anatomy as seen by sonography.<sup>108-110</sup> This was due to the unusual circumstance that “fluid” and

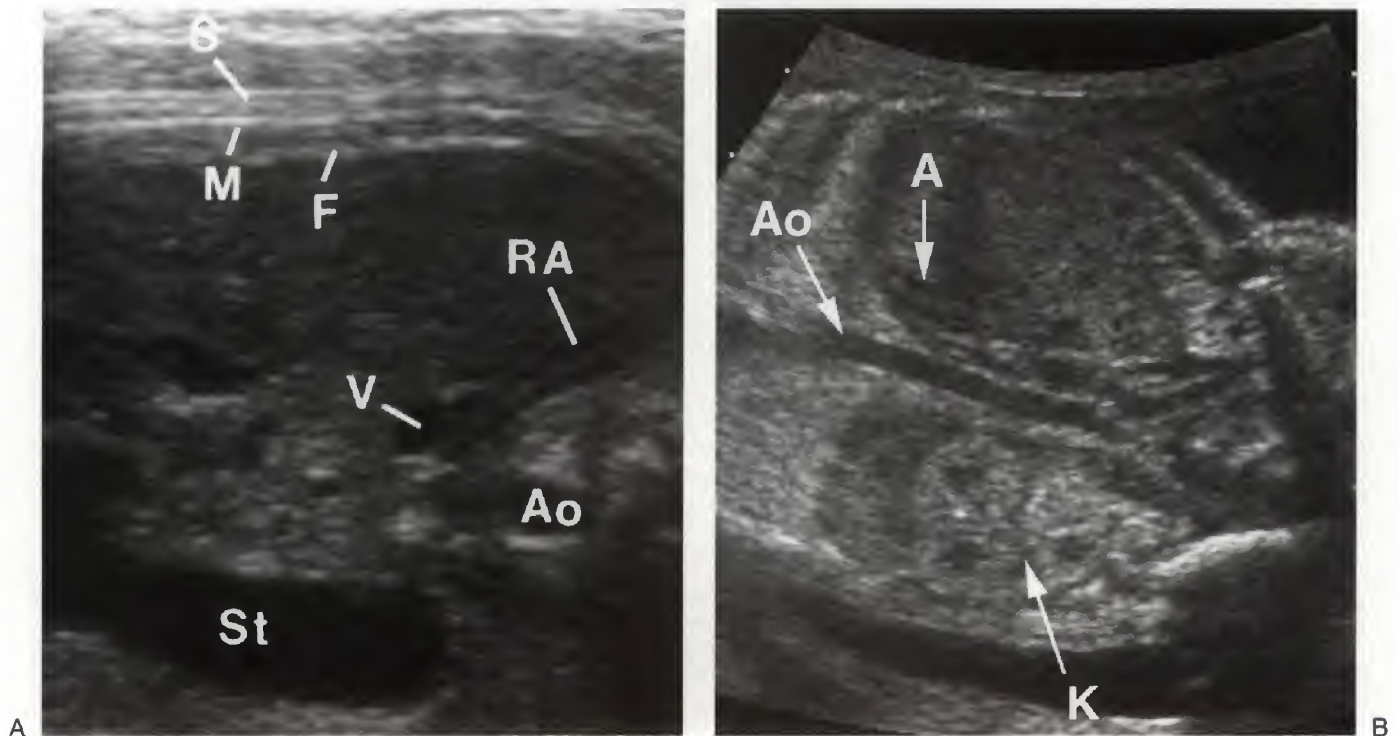


**FIGURE 9-98.** A. Transverse axial sonogram of the right adrenal gland (RA), although much anatomy can be seen on this image of the upper fetal abdomen. Note both limbs of the right adrenal gland immediately posterior to the inferior vena cava (V) and a portion of the left adrenal gland (unlabeled) to the left of the aorta (Ao). The abdominal wall, including the subcutaneous fat (S), muscle layers (M), and properitoneal fat (F), is well seen. St, stomach. B. Coronal sonogram of the adrenal (A) demonstrating its typical triangular "hat" appearance. K, opposite kidney.

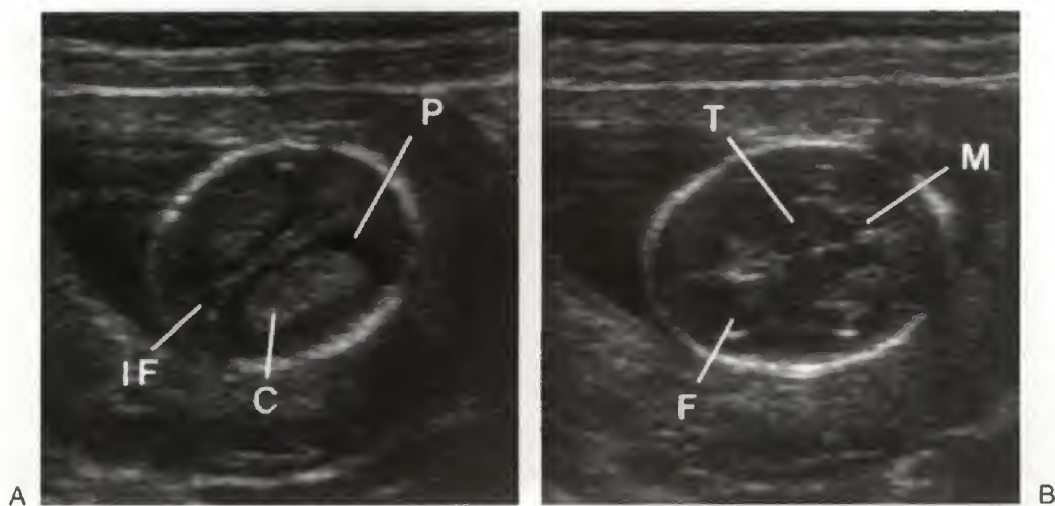


**FIGURE 9-99.** A. Transverse axial scan at the level of the lateral ventricular atria in a 14-week-old fetus. The brain parenchyma (P) is very lucent. C, choroid plexus; IF, interhemispheric fissure. B. Slightly caudal scan demonstrates well-developed thalami (T) and midbrain (M). The frontal horns (F) are large and filled with cerebrospinal fluid.



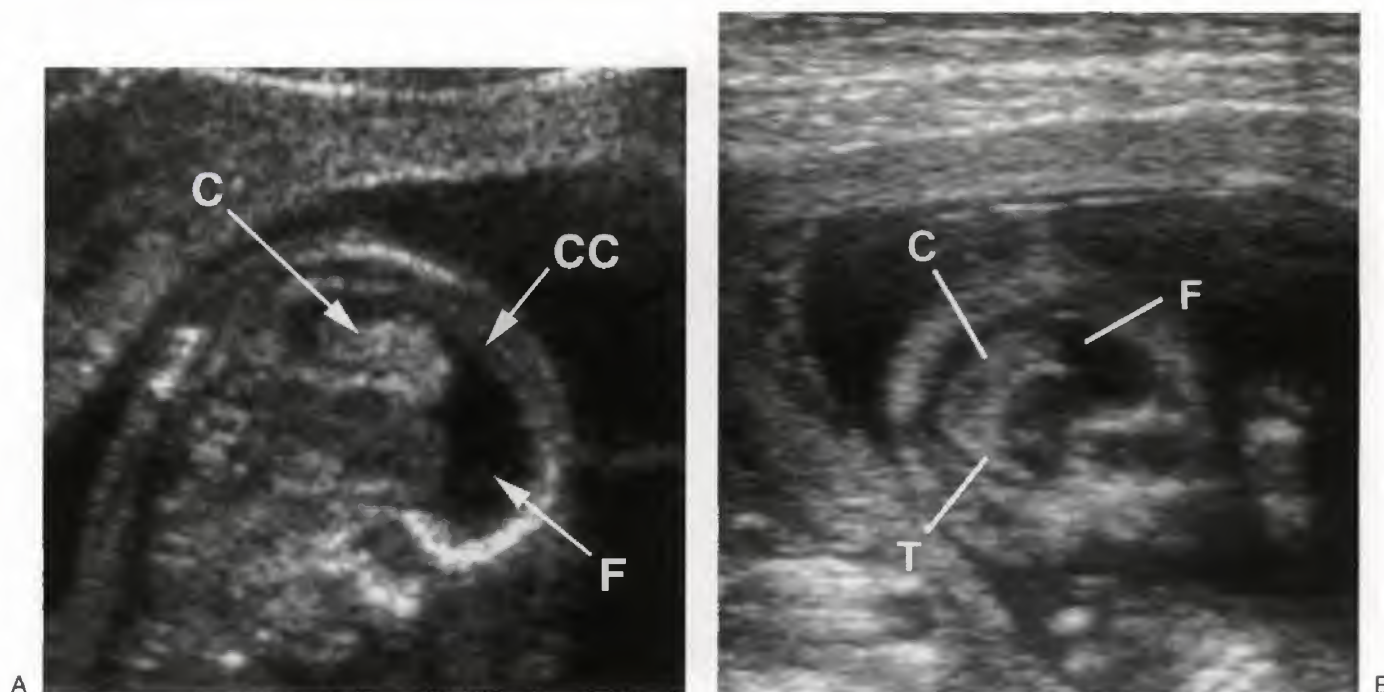


**FIGURE 9-100.** A and B. Parasagittal sonograms in late first trimester demonstrate that, even this early in development, choroid plexus (C) fills the posterior and inferior portions of the ventricle. Specular reflectors demarcate the frontal horn (F) that is devoid of choroid plexus and thus seen as a “fluid-containing” portion of the ventricular system. The early temporal horn is seen (T). Note absence of an occipital horn. Choroid (C) fills the body, atrium, and early temporal horn. Note as well how remarkably thin the cerebral cortical (CC) tissue is.

“solid” areas of the brain did not behave in an anticipated manner. It was initially expected that the sonographic appearance of the lateral ventricles would be dominated by cerebrospinal fluid, which would render them echolucent. Instead, their appearance was dominated by highly echogenic choroid plexus (Figs. 9-99 to 9-102).<sup>111,112</sup> Conversely, the bulk of neural tissue, the telencephalon, diencephalon, and mesencephalon, is quite echopenic compared with other solid tissues in the human body (see Fig. 9-99).<sup>111,113</sup> The more recent entrant into the area of diagnostic sonography can well imagine the potential for misinterpretation among early researchers when the largest fluid-containing areas of the brain yielded the greatest amplitude echoes, whereas the solid tissue yielded the lowest. To further complicate matters, dramatic changes occur as brain development progresses, resulting in ever-changing positions of certain “landmarks.” These changes had never been observed *in vivo*, and post-mortem examination of the brain can be at variance with its appearance during life.

A series of key observations led to the clear delineation of normal developmental neuroanatomy as viewed sonographically. These observations included recognition of the fetal third ventricle, the brightly echogenic choroid plexus,<sup>111</sup> and pulsating vasculature in several cisterns.<sup>113</sup> The first two identified the supratentorial ventricular system. The last enabled identification of the sylvian cistern (middle cerebral artery pulsation), interpeduncular cistern (basilar artery pulsation), and ambient cisterns (posterior cerebral artery pulsations) (see Fig. 9-76). The landmarks established by these observations provided a framework for subsequent identification of other specific neural structures.

Later in the course of the development of sonography, the neonatal brain came under study (see Figs. 9-1 and 9-103).<sup>1,2,112</sup> Interestingly, this resulted in much greater understanding of the appearance of the *fetal* brain because examination of “newborn children” now begins commonly as early as 25 to 26 weeks of development in the preterm infant (essentially a second trimester fetus) (see Fig. 9-1). Investigators then began to apply neuroanatomy as learned from the neonatal brain, which was imaged with great clarity through the anterior fontanel, to the developing fetal brain. The following analysis of fetal intracranial anatomy is presented on the basis of these observations.

The fetal head can be clearly discriminated from the fetal torso when an embryo reaches a crown rump length of 10 to 15 mm. By the 10th to 11th weeks after the last normal menstrual period (see Fig. 9-3), one can already begin to appreciate anatomy inside the developing fetal head. At this point, the intracranial tissue components consist almost entirely of the thalamus and corpus striatum, which yield the symmetric appearance of the brain as these structures narrow the developing third ventricle into a midline specular reflector.

By the end of the first trimester, the thalamus, third ventricle, midbrain, brain stem, and cerebellar hemispheres have achieved an appearance that will remain largely unchanged, other than progressive enlargement, throughout the remaining period of sonographic observation of the fetus (see Fig. 9-99). Therefore, the vast majority of the changes that are observed—and they are substantial—relate to the growth and development of the telencephalon. As mentioned earlier, by the end of the first and beginning of the second

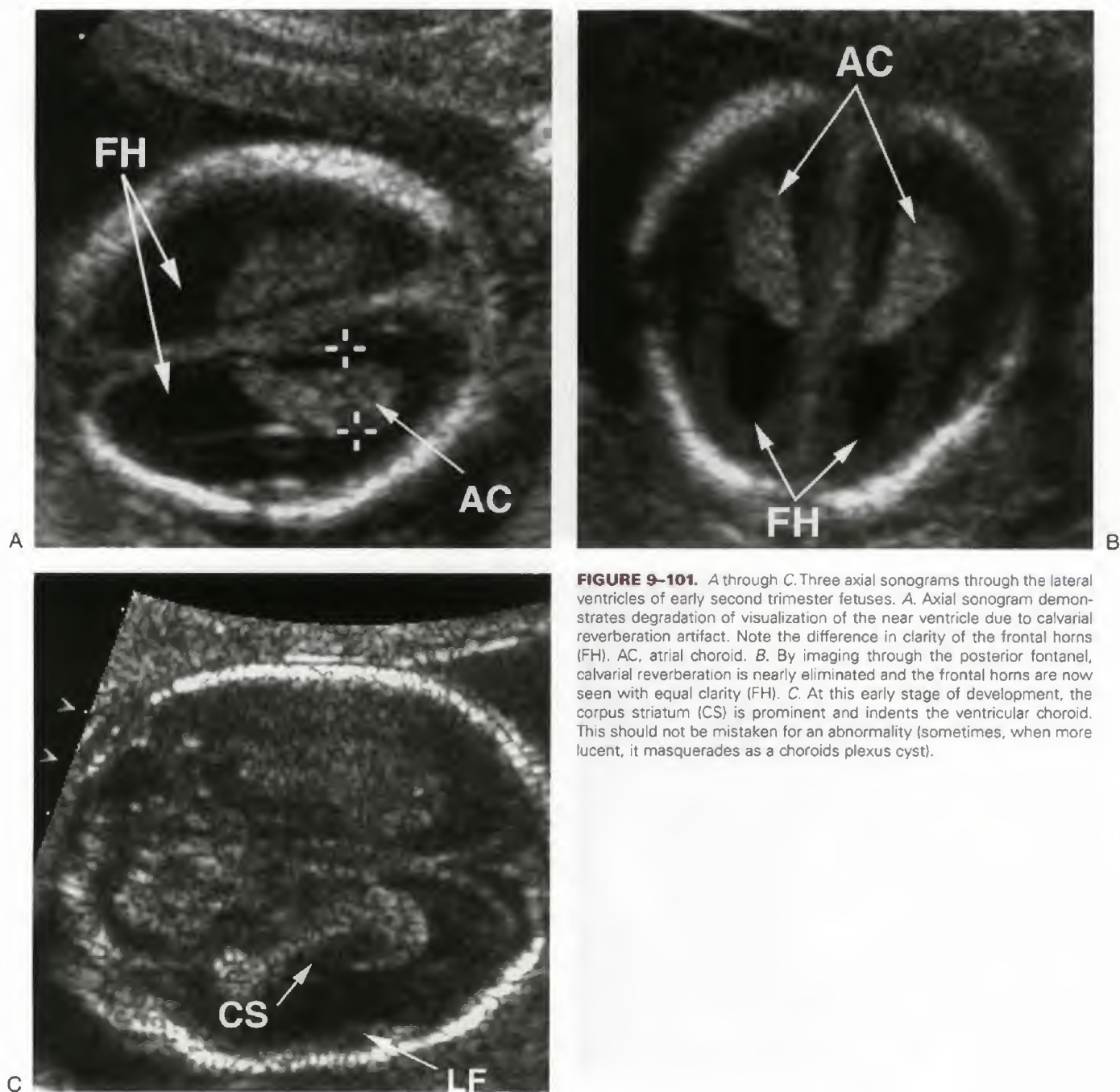


**FIGURE 9-101.** A through C. Three axial sonograms through the lateral ventricles of early second trimester fetuses. A. Axial sonogram demonstrates degradation of visualization of the near ventricle due to calvarial reverberation artifact. Note the difference in clarity of the frontal horns (FH). AC, atrial choroid. B. By imaging through the posterior fontanel, calvarial reverberation is nearly eliminated and the frontal horns are now seen with equal clarity (FH). C. At this early stage of development, the corpus striatum (CS) is prominent and indents the ventricular choroid. This should not be mistaken for an abnormality (sometimes, when more lucent, it masquerades as a choroids plexus cyst).



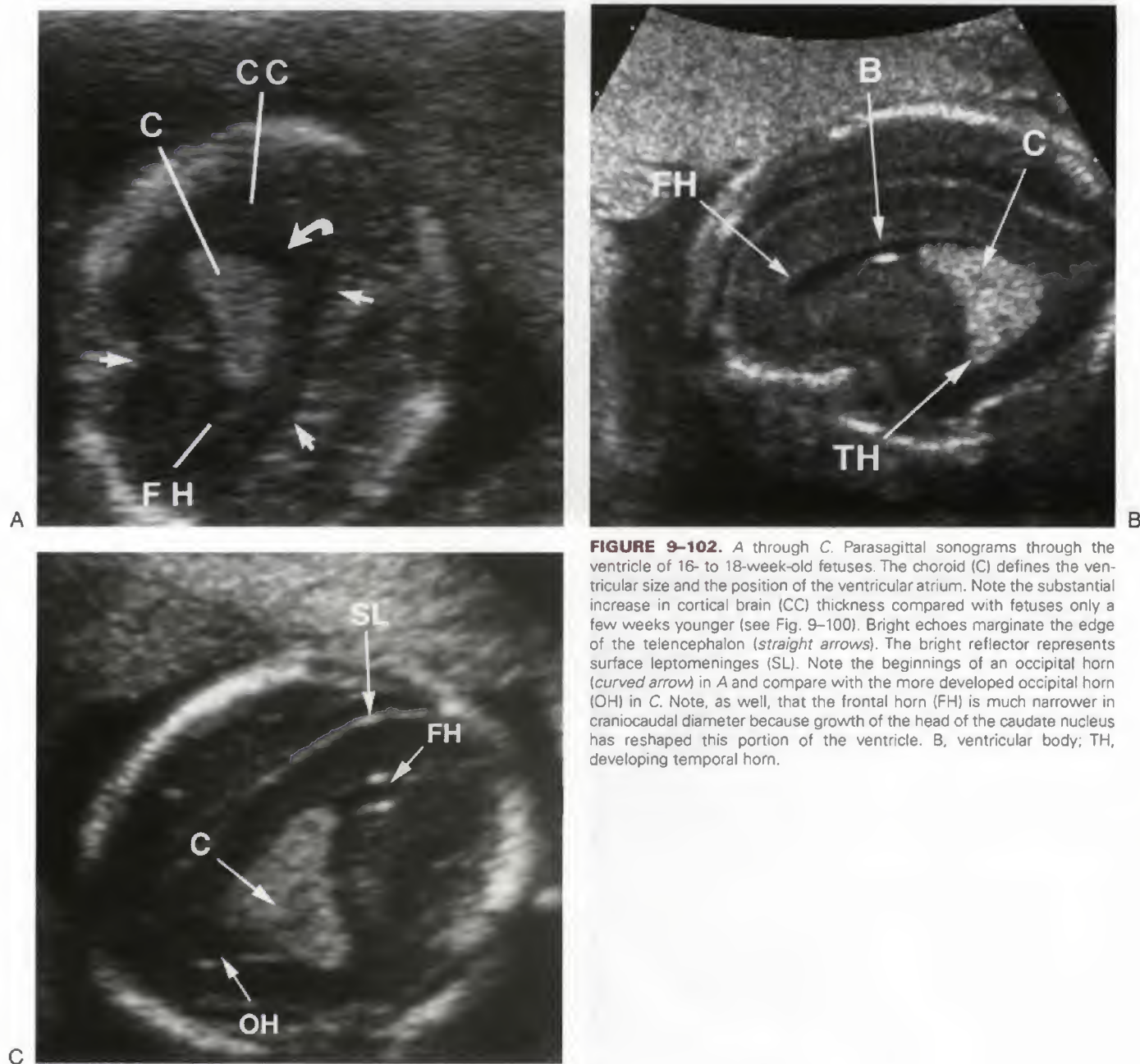


**FIGURE 9-102.** A through C. Parasagittal sonograms through the ventricle of 16- to 18-week-old fetuses. The choroid (C) defines the ventricular size and the position of the ventricular atrium. Note the substantial increase in cortical brain (CC) thickness compared with fetuses only a few weeks younger (see Fig. 9-100). Bright echoes marginate the edge of the telencephalon (*straight arrows*). The bright reflector represents surface leptomeninges (SL). Note the beginnings of an occipital horn (*curved arrow*) in A and compare with the more developed occipital horn (OH) in C. Note, as well, that the frontal horn (FH) is much narrower in craniocaudal diameter because growth of the head of the caudate nucleus has reshaped this portion of the ventricle. B, ventricular body; TH, developing temporal horn.

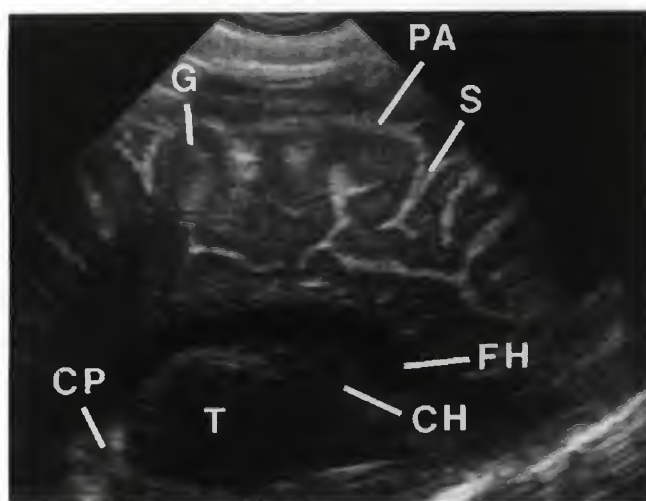


**FIGURE 9-103.** Parasagittal sonogram of the brain of a 6-month-old child. Gyri (G) are well developed. Pia-arachnoid (PA) tissues cover the surface of the brain and make the sulci (S) highly conspicuous. Careful inspection of gyri shows that cortical "gray matter" is less echogenic than the "white matter" (this is almost certainly not a difference due to gray and white matter distinction but to the vessels coursing through the central gyrus). CH, caudate head; CP, choroid plexus; FH, frontal horn; T, thalamus.

trimesters, the lateral ventricles (see Figs. 9-99 and 9-100) dominate the sonographic appearance of the telencephalon. The brightly echogenic choroid plexus dominates these in turn. By 12 to 13 weeks, the lateral ventricles can be clearly seen, appear ovoid, and are largely filled with choroid plexus. Only the frontal horns are devoid of choroid plexus as they are throughout life (see Figs. 9-99B, 9-100, and 9-101). At this stage of development, only the rudiment of a temporal horn (see Fig. 9-100B) and an occipital horn has yet to develop. The frontal horn, body of the ventricle, and atrium of the ventricle are large and easily detected. The choroid is the easiest structure to recognize because of its size and high-amplitude echogenicity. Conversely, the mantle of developing cerebral cortex surrounding the lateral ventricle is more difficult to delineate because of its low-amplitude echogenicity (Fig. 9-99A), but a demarcation between the lateral ventricle and the cerebral mantle can be appreciated from specular reflections arising from the walls of the lateral ventricle (see Figs. 9-99B and 9-100B). These, of course, are seen where the acoustic beam intersects the ventricular wall perpendicularly. By 16 to 18 weeks the mantle of developing cortical tissue has thickened appreciably (compare Figs. 9-100 and 9-102). As the occipital lobe has increased in volume, an occipital horn of the lateral ventricle has gradually appeared (see Figs. 9-100 through 9-102).

The relative echogenicity of structures, which will be viewed throughout the remainder of gestation, is largely established at this time. Two types of tissue are brightly echogenic and, therefore, most easily seen during the examination of the fetal brain. These tissues are the choroid plexus, as noted earlier, and the brain coverings: the dura (pachymeninx) and pia-arachnoid (leptomeninges). Interestingly, the choroid develops from the vascular pia. The leptomeninges demarcate the edges of the brain with a brightly reflective

margin of echoes (see Figs. 9-102 through 9-104). Peripheral to this brightly echogenic margin are the subarachnoid spaces that contain cerebrospinal fluid (Figs. 9-103 through 9-105). A feature that confounds the inexperienced sonologist is the relative lack of change in echogenicity between the peripheral (i.e., cortical brain) tissue and the cerebrospinal fluid space as seen across the brightly reflecting marginal echo from the pia-arachnoid (indeed, the cerebrospinal fluid-containing space may be more echogenic) (see Figs. 9-104 and 9-105). This perceptual problem originates from the anticipation that the subarachnoid spaces should be anechoic, whereas the brain parenchyma should be brightly echogenic. This reasonable assumption is untrue in many instances. Recall that these spaces have both cerebrospinal fluid and pia-arachnoid tissue within them. It is the relative amount of these two components that determines the sonographic appearance of the subarachnoid spaces. Small subarachnoid cisterns (such as the basal and perimesencephalic cisterns) have an appearance dominated by pia-arachnoid and thus are seen as brightly echogenic spaces (Fig. 9-106). This is not to say that these cisterns are devoid of cerebrospinal fluid, but the fluid does not significantly influence their sonographic appearance. Conversely, larger subarachnoid spaces, such as those over the convexities of the hemispheres (see Fig. 9-103 and 9-104) and the cisterna magna (Fig. 9-107), have an appearance dominated by cerebrospinal fluid. Thus, they behave, in the sonographic sense, as one would anticipate for a fluid-containing cavity. Intermediate-sized subarachnoid spaces will have both anechoic zones from visible cerebrospinal fluid and brightly echogenic zones from visible pia-arachnoid tissues (see Figs. 9-104 through 9-106). The bright margination provided by the leptomeninges enable one to visualize, for example, the midbrain quite elegantly (see Fig. 9-106). Without these margin echoes, our perception of the midbrain would be greatly hindered.

As noted earlier, brightly reflecting structures dominate the appearance of the fetal brain as seen by the sonologist. The choroid plexus and brain coverings (pia-arachnoid and dura) are the two major components within the developing calvaria that produce bright reflections. The important dural structures from the perspective of sonographic fetal brain anatomy are the falx cerebri and the tentorium (see Figs. 9-104 through 9-108). Occasionally, neural structure generates high-amplitude reflections. This is particularly true of the basal ganglia, especially the lenticular nuclei (see Fig. 9-107). The cerebellar vermis and the surface tissues of the cerebellar hemispheres also appear very bright (Figs. 9-109 and 9-110), but this appearance is again secondary to leptomeninges. The cerebellar folia "drag" meninges below the "surface" of the hemisphere, making the surface tissues appear bright (Fig. 9-109B). The cerebellar vermis has the greatest number of folia and intertwined meninges. Thus, it often appears strikingly hyperechogenic (Fig. 9-110B).

Also important as high-amplitude echoing structures are specular reflections from the walls of the ventricular system (see Figs. 9-99B, 9-100B, 9-101A and 9-102C). Such reflections occur when the ultrasonic beam strikes the smooth ventricular wall perpendicularly or nearly so. Thus, one would assume that points and lines of brightness so produced might vary from moment to moment depending on the direction in which the transducer was pointed. This,



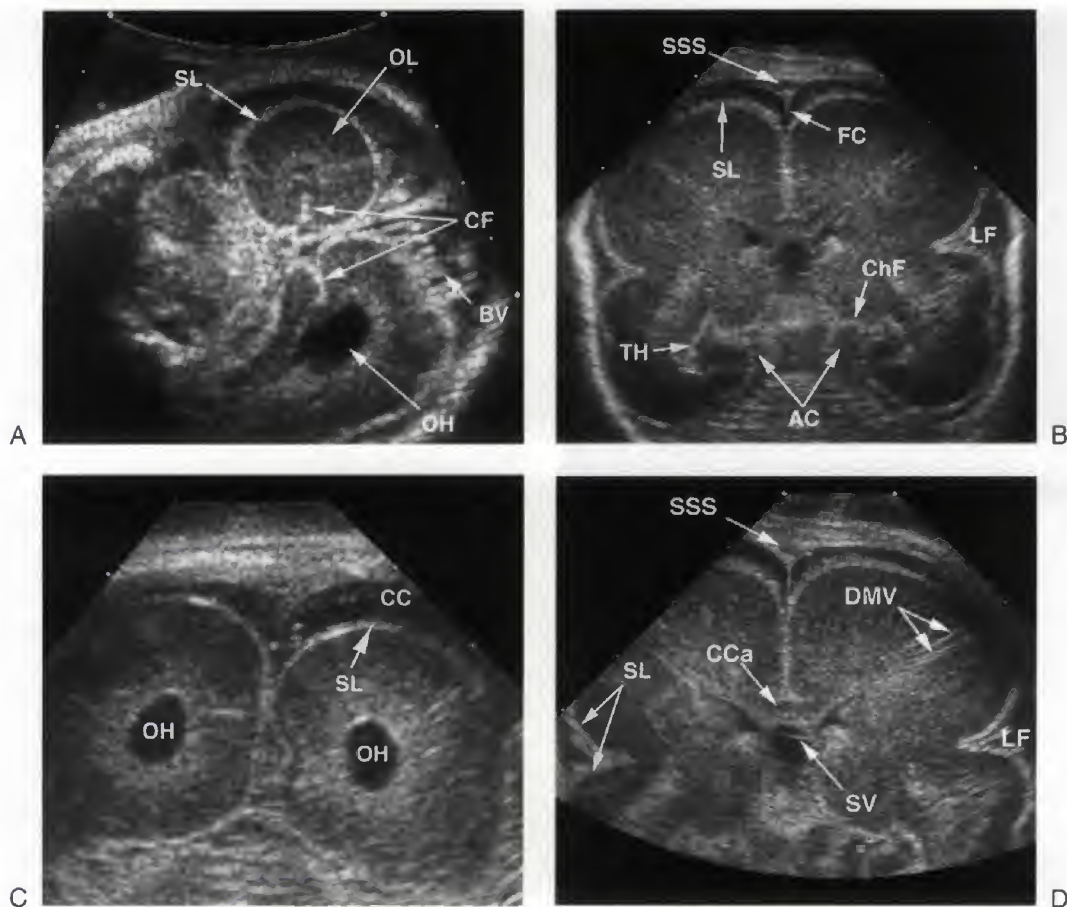


**FIGURE 9-104.** A through D. Sequence of sonogram obtained through fontanels and sutures. This technique enables one to see symmetrical brain anatomy. The surface leptomeninges (SL) are crucial to discriminating of the edge of the brain tissue and the adjacent cisterns. BV, bridging veins; CC, convexity cistern; CCa, corpus callosum; CF, calcarine fissure; ChF, choroidal fissure; DMV, deep medullary veins; FC, falx cerebri; LF, lateral fissure; OH, occipital horn; OL, occipital lobe; SSS, superior sagittal sinus; SV, septal vein; TH, temporal horn.

however, is not the case for two reasons. First, fetal brain images are predominantly produced in transverse axial planes (appropriate for both biparietal diameter and head circumference measurements) (see Figs. 9-99B and 9-101A) and less commonly coronal or parasagittal (see Fig. 9-102C) planes. In these planes, the beam tends to intersect the ventricular system perpendicularly at the same interfaces. Second, the curvature of the bony calvaria limits the number of axial, coronal, and parasagittal planes that can be achieved as a result of significant beam divergence when the beam intersects curved portions of calvaria. Thus, the specular reflections from the ventricular walls tend to be seen in stable locations and can be used as important and reproducible anatomic landmarks.

Additionally, within the substance of the brain, most notably in the region of the cerebral white matter tracks, other bright reflections are noted (see Figs. 9-104 to 9-106, and 9-111). Earlier, these reflectors were mistaken for the lateral ventricular walls, with which they are contiguous (see Figs. 9-105 and 9-108).<sup>110,113,114</sup> The origins of these reflections are blood vessels draining the deeper white matter regions (see Figs. 9-104D, 9-105, 9-108, and 9-111).<sup>115</sup> Interestingly, pia accompanies these vessels as they course through the brain substance. Therefore, again it is the

leptomeninges that account for bright echoes in the fetal brain. Thus, the brightly echoing structures of the fetal brain, including the surface echoes, cisterns, draining veins of the deep white matter, and choroid plexus, are all tied to the pia mater. As Dr. James Bowie observed one day regarding the *grand unifying theory of bright echoes in the brain*, "it's all pia" (personal communication, 1991).

The sonographic "skeleton" of the developing fetal brain originates from the brightly reflective structures just considered. Using these structures as the framework, numerous discrete neural tissue areas are discernible sonographically (see Figs. 9-106, 9-107 and 9-112).<sup>1,2</sup> As the brain develops, multiple areas of the telencephalon, diencephalon, midbrain, pons, and cerebellum become anatomically identifiable. These are recognized by variations in the echogenicity of specific nuclei and tracts that pass through these zones (see Figs. 9-105, 9-107, 9-109B, 9-110, 9-111A, and 9-112). Several brain nuclei, as well as some other areas of neural tissue, demonstrate a moderate increase in echo amplitude compared with surrounding brain elements (see Figs. 9-105, 9-107, 9-112 and 9-113). These nuclei demonstrate lower amplitude signals than choroid or leptomeninges. Among these structures are the caudate and lenticular nuclei, separated by the internal capsule. Less commonly, the

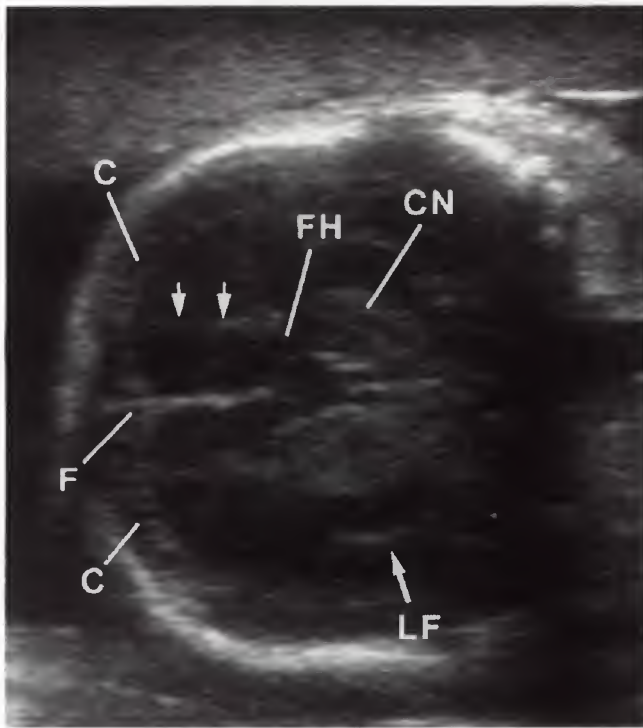


**FIGURE 9-105.** Coronal section through the heads of the caudate nuclei (CN). The frontal horn (FH), which is not well seen, drapes over the caudate. Extending between the ventricular margin and the edge of the brain are linear echogenic structures previously mistaken for ventricles (arrows). Also seen are bridging strands of pia-arachnoid through the cistern (C) over the convexities (probably bridging veins covered with pia-arachnoid). F, falx; LF, lateral fissure.

claustrum, margined by the extreme and external capsules, is visible. Similarly, the substantia nigra (Fig. 9-106B) in the midbrain and dentate nuclei of the cerebellum (Fig. 9-107A, not labeled) are discernible. Also the pars ventralis (belly) of the pons is seen as a zone of moderate echogenicity as opposed to the pars dorsalis (tegmentum), which returns low-amplitude echoes (Fig. 9-114).<sup>1</sup>

It is important for sonologists to be familiar with the appearance of the lateral ventricles as they change throughout growth and development of the fetal brain. By 18 to 20 weeks, easily recognizable occipital horns and temporal horns are visible (see Fig. 9-102). The lateral ventricles have achieved their adult components. From this point onward, the lateral ventricles change in shape and proportion as influenced by neural tissues growing adjacent to their walls. For example, the growth of the caudate nucleus markedly reshapes the frontal horn of the lateral ventricles (see Fig. 9-102).<sup>116</sup> However, throughout the period of observation of fetal lateral ventricles (from 13 to 40 weeks), the size of the atria remains largely unchanged. The transverse diameter of the ventricular atrium at the level of the glomus of the choroid plexus shows an average dimension of approximately 7 mm and an upper limit of 10 mm throughout the second and third trimesters.<sup>117</sup> This is the most convenient area to recognize fetal ventricular enlargement, as is discussed in detail in the section on ventriculomegaly in Chapter 10.<sup>111,112,117</sup> It is important to note that the frontal (anterior) and occipital (posterior) horns of the lateral ventricles do not possess choroid plexus (see Figs. 9-100 through 9-102). Between 24 weeks and term, the telencephalon undergoes little structural change other

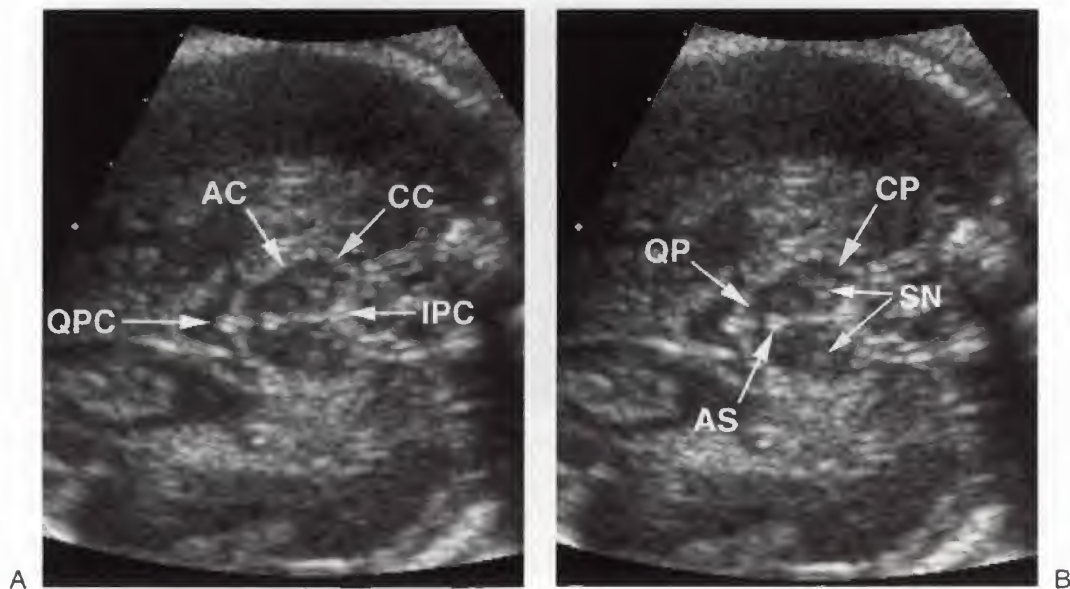


**FIGURE 9-106.** A and B. Sonogram demonstrating the midbrain. The midbrain is seen well because of the sharp outline provided by the brightly echogenic perimesencephalic cisterns (the leptomeninges provide the bright line of demarcation). AC, ambient cistern; CC, crural cistern; IPC, interpeduncular cistern; QPC, quadrigeminal plate cistern. These marginate the cerebral peduncles (CP) and the quadrigeminal plate (QP). AS, aqueduct of Sylvius; SN, substantia nigra.



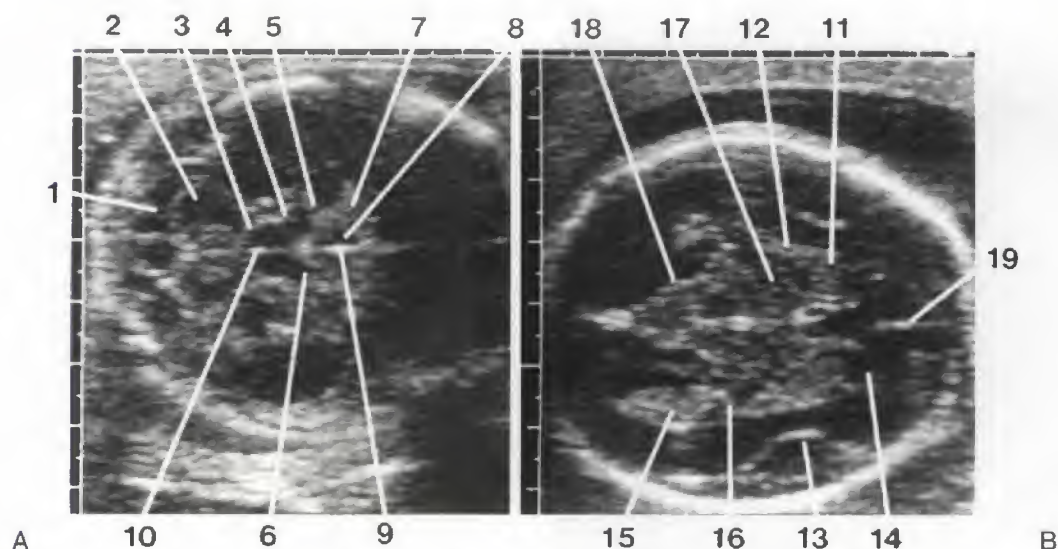


**FIGURE 9-107.** A and B. Transverse axial sonograms demonstrating many discrete neural structures. Note the varying echogenicities of the cisterns. Large cisterns (1, cistern magna) have an appearance dominated by cerebrospinal fluid. Small cisterns (7, basal cisterns) are dominated by pia-arachnoid. 2, cerebellar hemisphere; 3, quadrigeminal cistern; 4, ambient cistern; 5, crural cistern; 6, interpeduncular cistern (note walls of basilar artery centrally in this cistern); 8, hypothalamus; 9, inferior recess of third ventricle; 10, sylvian aqueduct; 11, head of caudate; 12, lentiform nuclei; 13, lateral fissure; 14, frontal horn; 15, atrial choroid; 16, posterior limb of internal capsule; 17, thalamus; 18, tentorial hiatus; 19, falx cerebri.

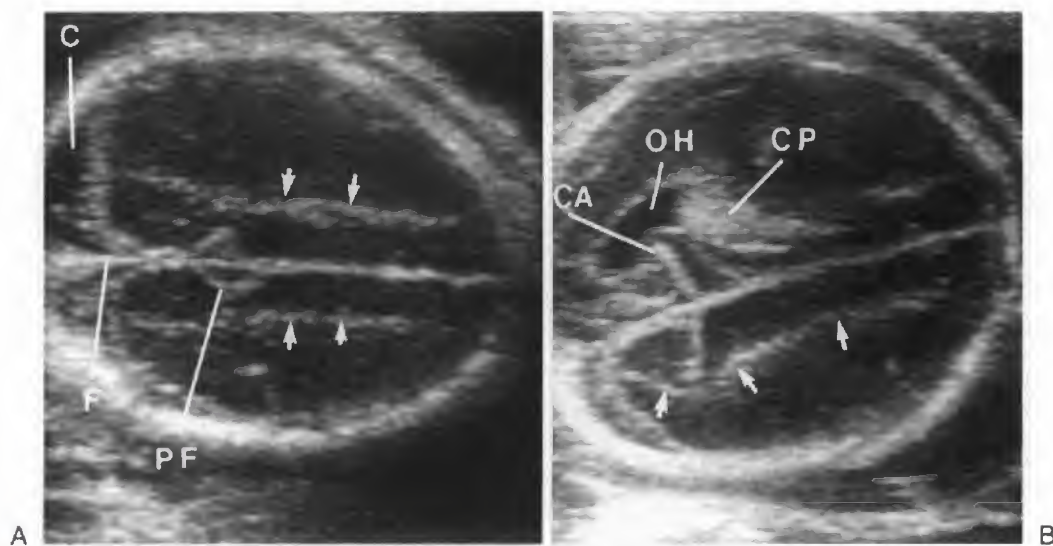


**FIGURE 9-108.** A. Transverse axial sonogram near the vertex. Bright linear echoes (arrows) often mistaken for lateral ventricles are clearly seen. Note that these echoes extend to the brain edge. C, convexity cistern with cerebrospinal and hair-like bridging veins covered by brightly echogenic pia-arachnoid; F, falx; PF, parieto-occipital fissure. B. Off-axis scan through both the lateral ventricle and the linear echo (arrow) seen in A. The occipital horn (OH) is now well seen. Note again that the linear echo extends to the brain edge, whereas the occipital horn is entirely margined by brain tissue. CA, calcar avis; CP, choroid.

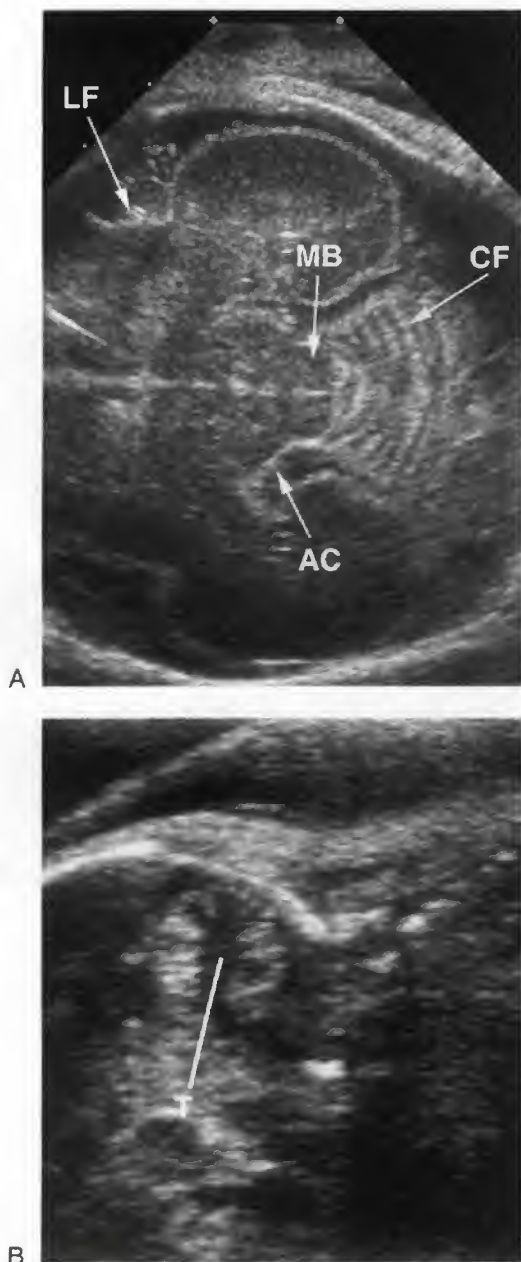


**FIGURE 9-109.** A. Posterior fossa view (transverse axial) demonstrating cerebellar folia (CF). AC, ambient cistern; LF, lateral fissure; MB, midbrain. B. Parasagittal sonogram of the posterior fossa. Cerebellar white matter tracts (T) are well seen. The bright margin of the cerebellum is "artificial" in that it is due to reflections from leptomeninges drawn into the cerebellum by folia formation (gray matter is hypoechoic).

than increased cortical growth and the consequent increase in convolutions (and thus sulcal markings), which can be recognized adjacent to the convexities (Figs. 9-115A and 9-116A).<sup>118</sup> The increase in brain volume causes the lateral ventricles, which are growing more slowly, to become progressively less conspicuous.

As opposed to sulci, which are narrow and develop later as gyri form, fissures are broader, present earlier in development, and can be seen before 20 weeks.<sup>119</sup> Of the two that

are commonly seen, the parieto-occipital fissure, an indentation medially adjacent to the interhemispheric cistern, is smaller (see Figs. 9-108A, 9-111B and 9-115A). The lateral fissure (insula and sylvian fossa/fissure) is a deep groove in the lateral margin of the developing telencephalon.<sup>117,120,121</sup> The groove is seen as a smooth depression as early as 14 weeks (Fig. 9-101C).<sup>119</sup> Subsequently, its appearance gradually changes as the fronto-parietal and temporal opercula develop (see Figs. 9-105, 9-107, 9-109, 9-112, and 9-116).<sup>119</sup> This important fissure results in frequent confusion because it causes a portion of the brain surface to be invaginated deeply into the hemisphere (see Figs. 9-105, 9-107, 9-109, and 9-112). The pia-arachnoid on the surface of the insula, the tissue at the base of the lateral fissure, generates a curvilinear reflection that appears to lie within the brain substance rather than at its "edge." This echo is often mistaken for a specular reflection from the lateral wall of the lateral ventricle, an error leading to misdiagnoses of hydrocephalus. With progressive growth of the temporal and parietal lobes, this fissure progressively closes, burying the previously exposed insular cortex behind the developing temporal and parietal opercula (see Figs. 9-116 and 9-117). By term (38 to 42 weeks), the lateral fissure closes and ultimately becomes the sylvian cistern complex.

Other fissures and sulci become visible at predictable times during fetal brain development. This developmental sequence, or the failure thereof, enables one to diagnose or exclude certain brain malformations associated with migrational abnormalities. Among these are either the absence of formation of fissures and sulci (lissencephalic anomalies) or the appearance of fissures and sulci in aberrant locations (dysplastic brain).<sup>119,122</sup> The calcarine fissure (sulcus) (Fig. 9-104A) is associated with the parieto-occipital fissure. The calcarine fissure angles caudally from the mid portion of the parieto-occipital fissure, creating a prominent fold in the medial occipital lobe (the two fissures form a "Y" lying on its side). The calcarine fissure's greatest importance is that, as it grows, it indents the medial aspect of the occipital horn, thereby actually changing the shape of the ventricle at the junction of the atrium and occipital horn (the other piece of developing brain that greatly reshapes ventricular configuration is the caudate nucleus). The folded tissue is called the "calcar avis" (translated meaning the "bird's heel," which it somewhat resembles [at least to the anatomist who described it—I would have called it the "bird's beak"]) (see Figs. 9-108B and 9-116B). The calcarine fissure is easily seen on coronal sections of the posterior brain (see Fig. 9-104A). In the coronal plane, one would think that it is the parieto-occipital fissure except that the coronal plane favors visualization of the calcarine fissure, whereas the axial plane favors visualization of the parieto-occipital fissure (see Fig. 9-115B). The calcarine fissure (sulcus) becomes visible by the 24th week.<sup>119</sup> The cingulate sulcus, the sulcus that parallels the superior surface of the corpus callosum (see Fig. 9-114), also becomes visible at approximately the same time as the calcarine sulcus.<sup>119</sup> The cingulate sulcus is important in that it does not form when there is complete agenesis of the corpus callosum. Thus, the formation of the corpus callosum is the "causative" element determining sulcation of the medial frontoparietal cortex. Because the cingulate sulcus is the first of the medial sulci to develop, its presence is helpful in excluding complete callosal agenesis.



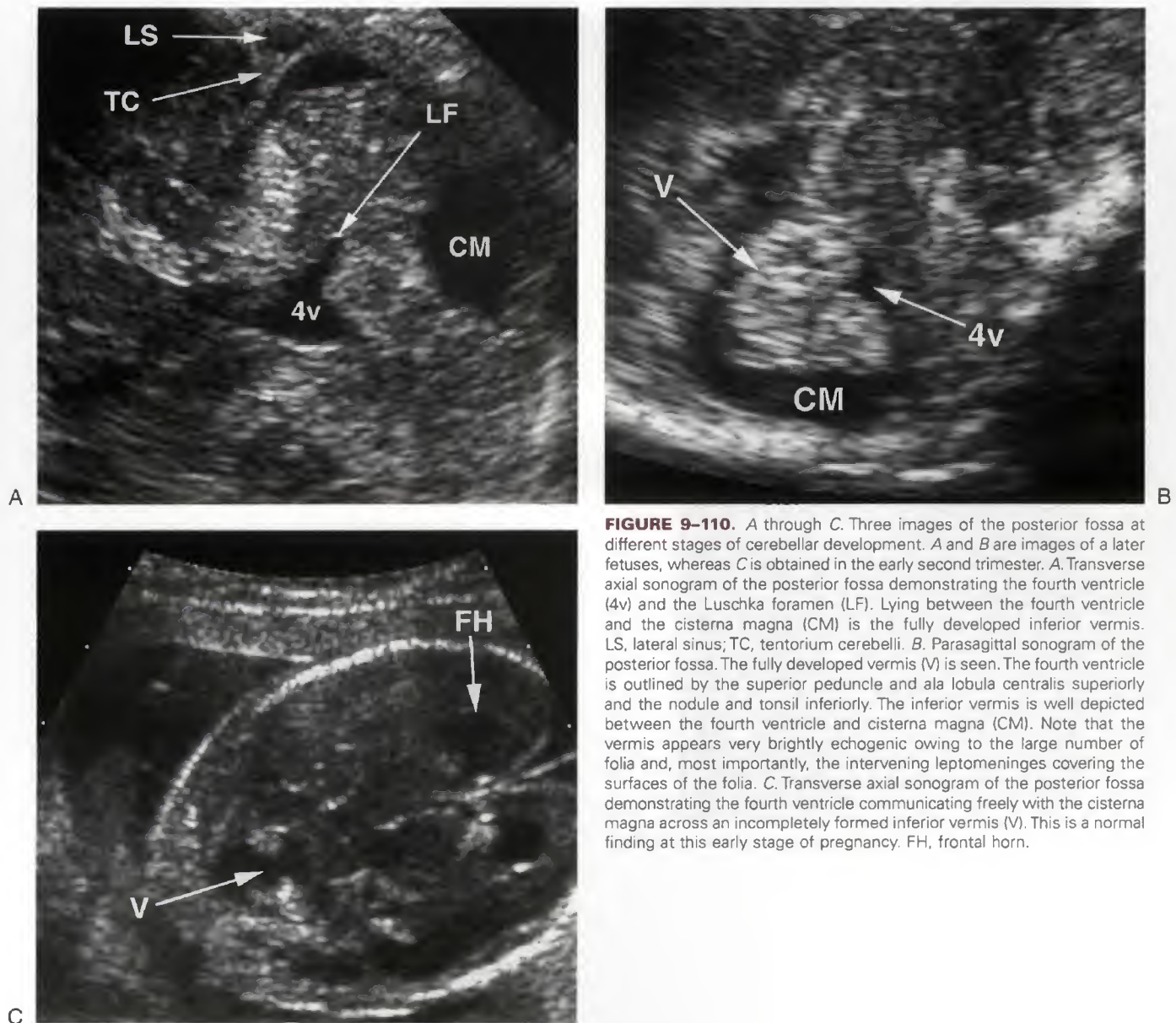


**FIGURE 9-110.** A through C. Three images of the posterior fossa at different stages of cerebellar development. *A* and *B* are images of a later fetus, whereas *C* is obtained in the early second trimester. *A*. Transverse axial sonogram of the posterior fossa demonstrating the fourth ventricle (4v) and the Luschka foramen (LF). Lying between the fourth ventricle and the cisterna magna (CM) is the fully developed inferior vermis. LS, lateral sinus; TC, tentorium cerebelli. *B*. Parasagittal sonogram of the posterior fossa. The fully developed vermis (V) is seen. The fourth ventricle is outlined by the superior peduncle and ala lobula centralis superiorly and the nodule and tonsil inferiorly. The inferior vermis is well depicted between the fourth ventricle and cisterna magna (CM). Note that the vermis appears very brightly echogenic owing to the large number of folia and, most importantly, the intervening leptomeninges covering the surfaces of the folia. *C*. Transverse axial sonogram of the posterior fossa demonstrating the fourth ventricle communicating freely with the cisterna magna across an incompletely formed inferior vermis (V). This is a normal finding at this early stage of pregnancy. FH, frontal horn.

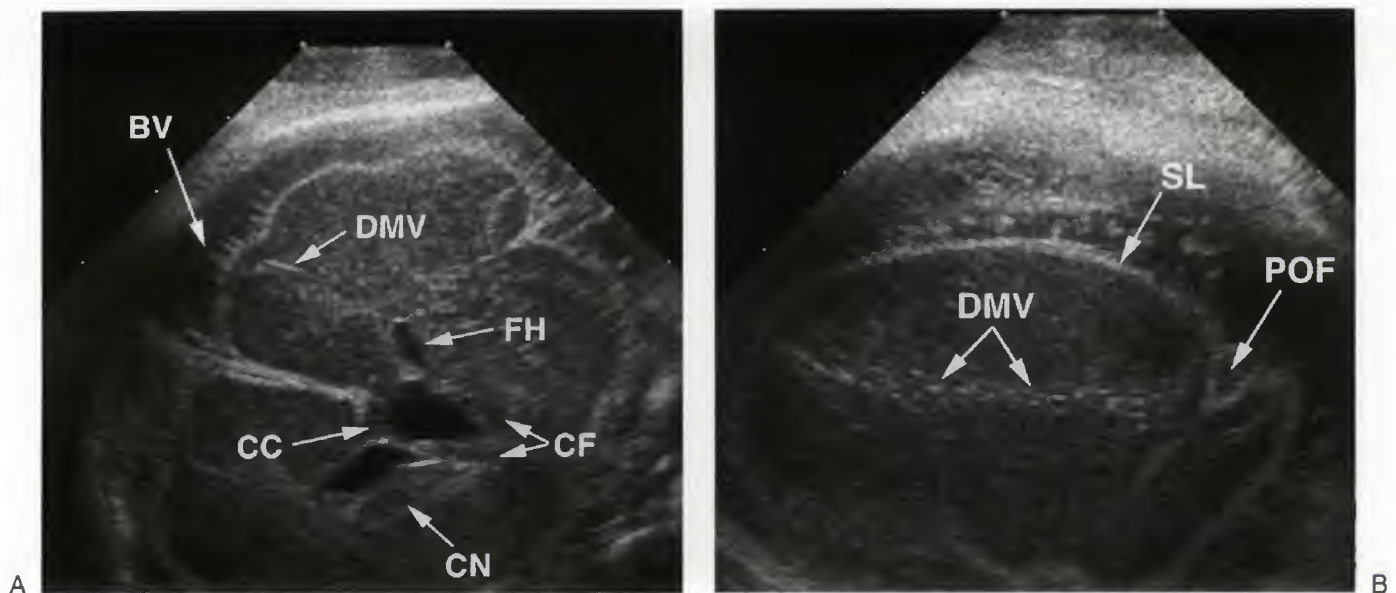


**FIGURE 9-111.** A. Coronal plane. B. Parasagittal plane. The deep medullary veins (DMV) and the bridging veins (BV) are invested with pia mater and thus are brightly reflective. Brightly reflective surface leptomeninges (SL) demarcate the brain surface and help to discreetly detect fissures and sulci such as the parieto-occipital fissure (POF). CC, corpus callosum; CF, columns of the fornix; CN, caudate nucleus; FH, frontal horn.

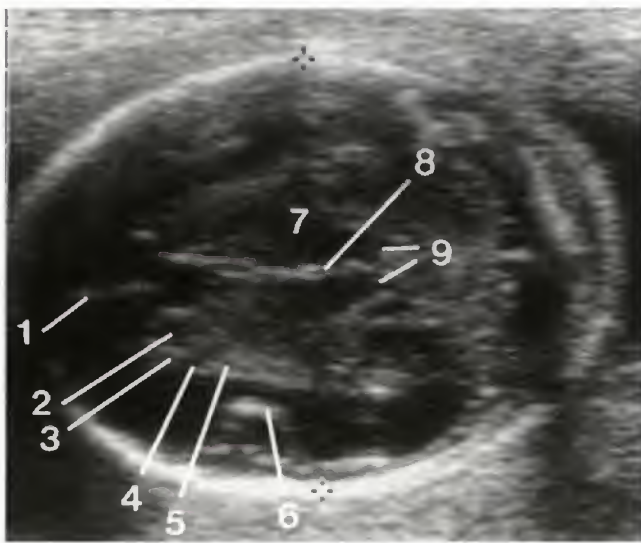


**FIGURE 9-112.** Transverse axial sonogram. 1, falx; 2, frontal horn; 3, caudate head; 4, anterior limb of internal capsule; 5, lentiform nuclei; 6, lateral sulcus; 7, thalamus; 8, third ventricle; 9, quadrigeminal bodies.

Finally, the sulci over the convexities gradually become increasingly visible from the beginning of the third trimester onward.<sup>119</sup> Among other recognizable sulci are sulci on the inferior frontal lobe that help define the gyrus rectus (see Figs. 9-116 and 9-117).

A structure of great importance in fetal neuroanatomy is the corpus callosum (Fig. 9-118). The corpus callosum begins its development between the 10th and 11th weeks of

gestation. It has achieved its adult configuration by the end of the 17th week. The development starts at the genu and proceeds posteriorly to the splenium. However, the rostrum (the most anterior part of the corpus callosum) forms last. The rostrum is not usually seen on prenatal sonograms. Sonographic imaging of the corpus callosum for the detection of abnormal formation should not be attempted in earnest until after 17 weeks (see Fig. 9-118D). The best views of the corpus callosum are obtained in the midsagittal plane (see Figs. 9-114B and 9-118B). However information about the corpus callosum can be obtained in other planes of section. The body and genu can be seen in coronal and axial planes (see Figs. 9-111A, 9-113A, and 9-118A). Unfortunately, when partial agenesis (dysgenesis) of the corpus callosum is present, it is typically the splenium and distal body that are missing. Importantly, the splenium can be imaged in axial planes of section, although with some difficulty, because the plane of section must approach from the occipital region (see Fig. 9-118C). Occipital ossification and the smaller posterior fontanel make this approach difficult at times. An extremely helpful structure, both in terms of visualization of the corpus callosum and for excluding complete agenesis of the corpus callosum, is the cavum septi pellucidi/cavum vergae complex (see Fig. 9-113). The cavum septi pellucidi is the median cleft between the two laminae of the septum pellucidum. Sometimes called the fifth ventricle, it is not. It is not lined by ependyma. The cavum vergae (described by the Italian anatomist, Verga) is the posterior extension of the cavum septi pellucidi (see Fig. 9-113C). The actual line of division is the fornix, but as the fornix is not visible in a midsagittal plane, I use the Monroe foramen to demarcate the end of one cavum and the beginning of the other (see Fig. 9-113C). The corpus callosum is the roof of the cavae, and the roof of the third ventricle is the floor of the cava. Fortunately, we



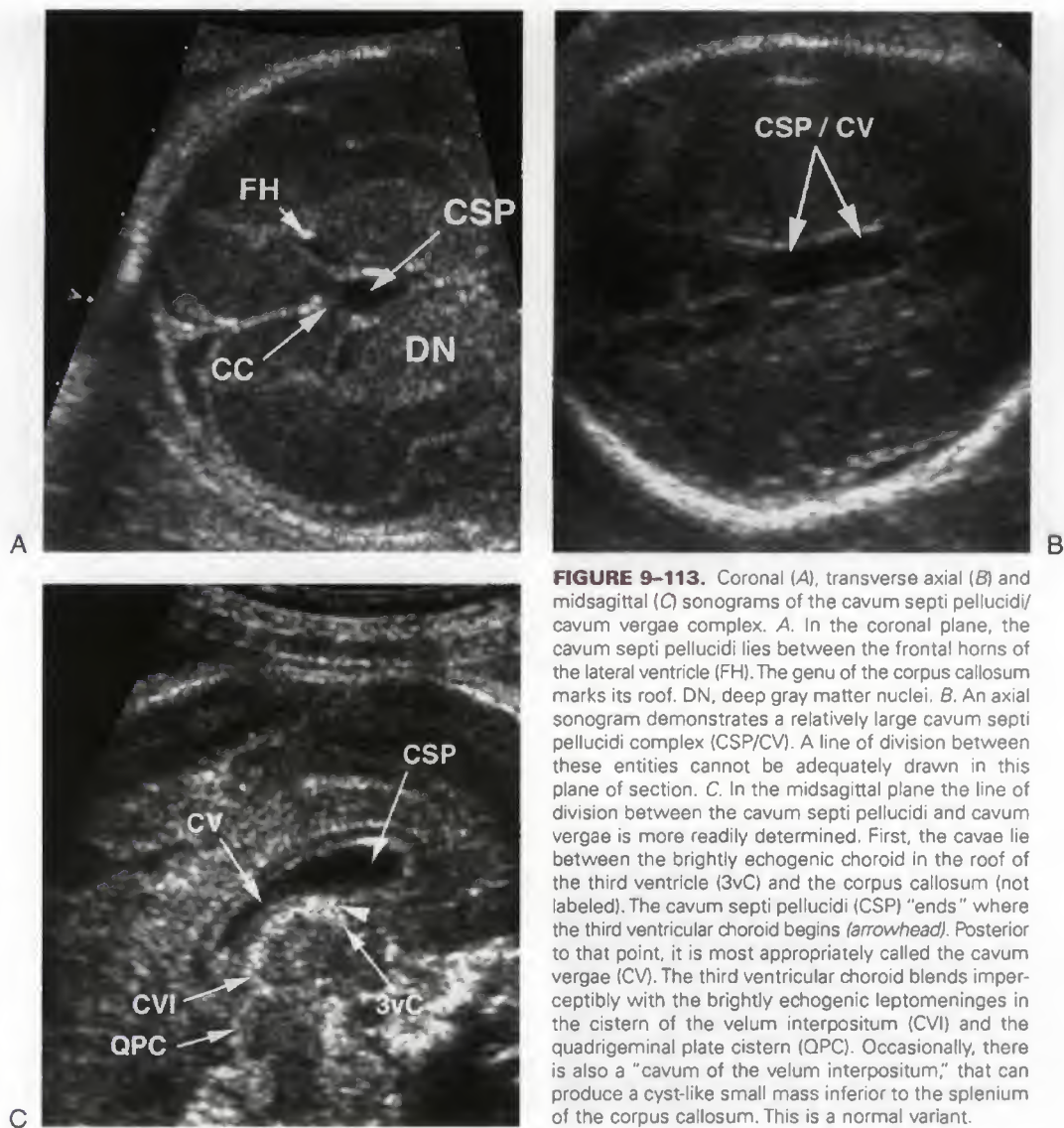


**FIGURE 9-113.** Coronal (A), transverse axial (B) and midsagittal (C) sonograms of the cavum septi pellucidi/cavum vergae complex. A. In the coronal plane, the cavum septi pellucidi lies between the frontal horns of the lateral ventricle (FH). The genu of the corpus callosum marks its roof. DN, deep gray matter nuclei. B. An axial sonogram demonstrates a relatively large cavum septi pellucidi complex (CSP/CV). A line of division between these entities cannot be adequately drawn in this plane of section. C. In the midsagittal plane the line of division between the cavum septi pellucidi and cavum vergae is more readily determined. First, the cavae lie between the brightly echogenic choroid in the roof of the third ventricle (3vC) and the corpus callosum (not labeled). The cavum septi pellucidi (CSP) "ends" where the third ventricular choroid begins (arrowhead). Posterior to that point, it is most appropriately called the cavum vergae (CV). The third ventricular choroid blends imperceptibly with the brightly echogenic leptomeninges in the cistern of the velum interpositum (CVI) and the quadrigeminal plate cistern (QPC). Occasionally, there is also a "cavum of the velum interpositum," that can produce a cyst-like small mass inferior to the splenium of the corpus callosum. This is a normal variant.

have an excellent marker of the roof of the third ventricle. This is because the third ventricular choroid recurves along the roof (see Figs. 9-113C and 9-118B). The most anterior extent of the third ventricular choroids (see Fig. 9-113C) marks the position of the Monroe foramen and thus is a very reasonable dividing line between the cavum septi pellucidi and the cavum vergae. In axial planes of section, a reasonable line of division cannot be drawn (see Fig. 9-113B). A final aspect of callosal development is that formation of the cingulate gyrus (and thus the cingulate sulcus) is dependent on the formation of the corpus callosum (see Fig. 9-114).

The cerebellar vermis, like the corpus callosum, is also a late structure to develop (see Fig. 9-110). Indeed, of the major parts of the fetal brain to develop, the cerebellar vermis is last in line. The cerebellum is well imaged throughout the second and third trimesters (except near term when occipital ossification is sufficiently great to thwart passage of the acoustic beam) (see Figs. 9-109, 9-110, 9-114, and

9-118B). Like the corpus callosum, the cerebellar vermis develops from "front to back." Thus, the inferior portion of the vermis does not complete its formation until relatively late (in the range of the 18th gestational week). Sonographically, one detects the inferior vermis lying between the fourth ventricle and the cisterna magna (see Figs. 9-110A, 9-110B, and 9-114A). In midsagittal planes, the fourth ventricle is outlined by the superior peduncle and ala lobula centralis superiorly and the nodule and tonsil inferiorly. The inferior vermis is well depicted between the fourth ventricle and cisterna magna. Note that the vermis appears very brightly echogenic owing to its large number of folia (see Fig. 9-110B) and, most importantly, the intervening leptomeninges covering the surfaces of the folia. By contrast, in a 16- to 17-week-old fetus, a transverse axial sonogram of the posterior fossa typically demonstrates the fourth ventricle communicating freely with the cisterna magna across an incompletely formed inferior vermis (see Fig. 9-110C). This

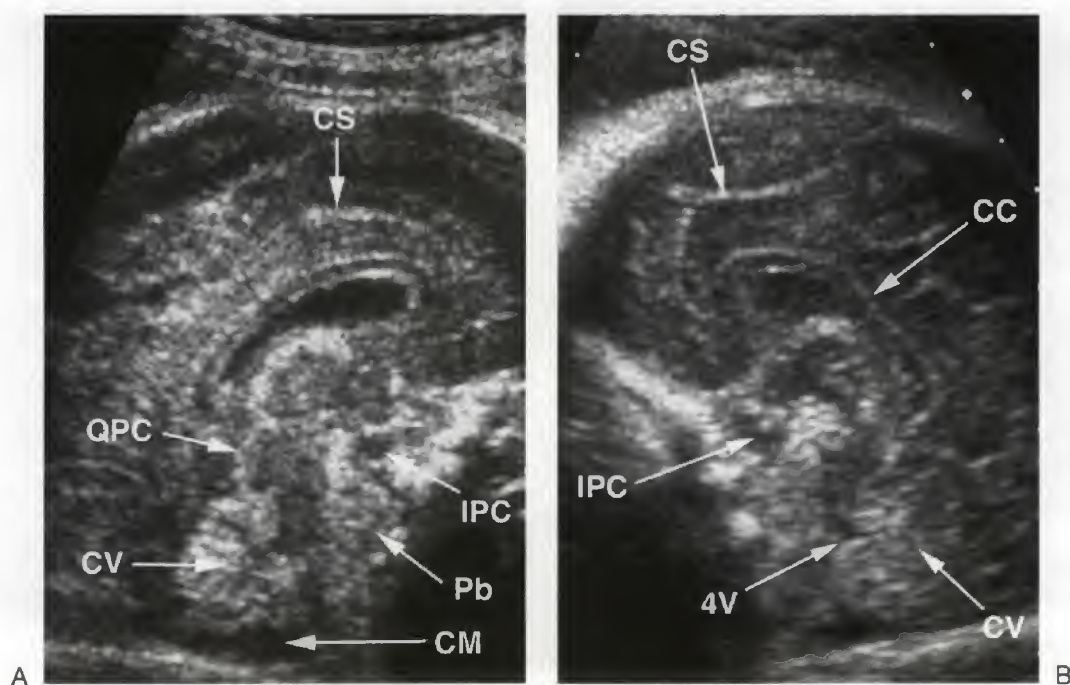


**FIGURE 9-114.** Midsagittal sonograms of a younger (*A*) and older (*B*) fetus. The cingulate sulcus (CS) is readily seen. The cingulate gyrus (not labeled) lies between the cingulate sulcus and the corpus callosum (CC). In the older fetus, more visible sulci along the medial frontal and parietal lobes are visible (*B*). 4v, fourth ventricle; CM cisterna magna; CV, cerebellar vermis; IPC, interpeduncular cistern; Pb, belly of pons; QPC, quadrigeminal plate cistern.

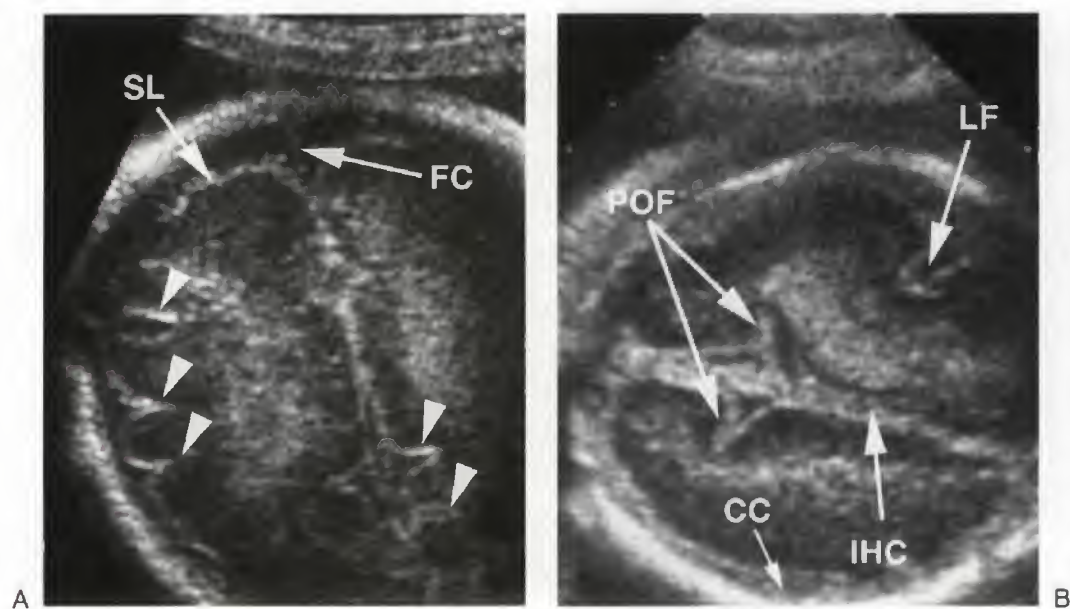


**FIGURE 9-115.** *A*. Younger fetus. *B*. Older fetus. Sonograms concentrating on the brain surface. In the younger fetus, the brain surface is relatively smooth, although some of the major developing fissures are visible. POF, parieto-occipital fissure; LF, lateral fissure. In the older fetus, numerous sulci and gyri are visible (arrowheads). CC, convexity cistern; FC, falx cerebri; IHC, interhemispheric cistern.



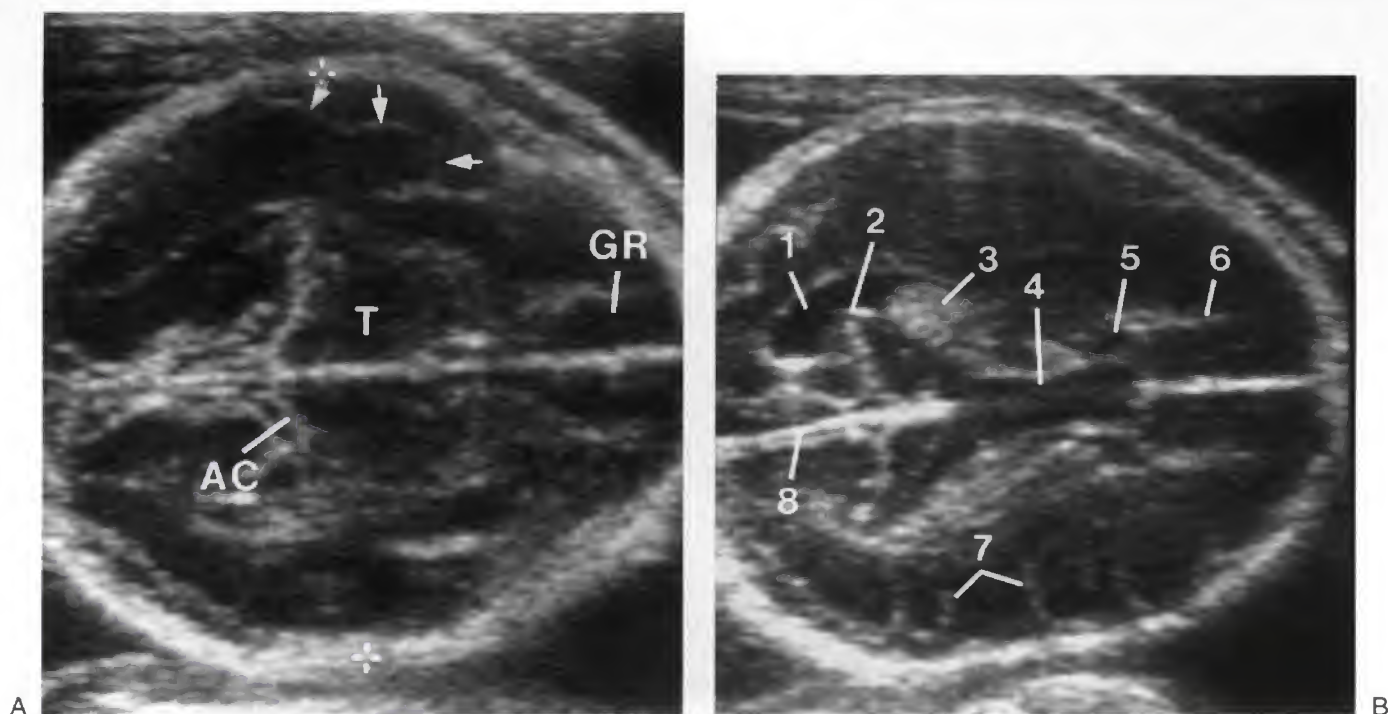


**FIGURE 9-116.** A and B. Transverse axial sonograms of a fetus with little calcification of the calvaria (recessive osteogenesis imperfecta). A. Note the lack of near calvarial reverberation artifact enabling visualization of the near temporal lobe with greater clarity than the far temporal lobe (*short arrows*). AC, ambient cistern; GR, gyrus rectus; T, thalamus. B. Note the clarity with which the near ventricle is visualized. 1, occipital horn; 2, calcar avis; 3, atrial choroid; 4, corpus callosum [it is very unusual to see so much of the corpus callosum in an axial plane]; 5, frontal horn; 6, veins in the deep white matter; 7, sulci; 8, falx cerebri.

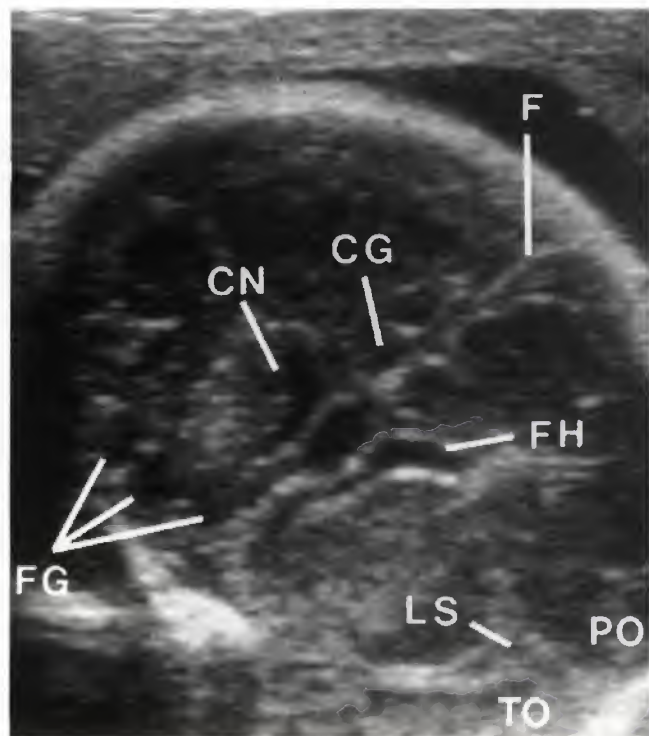


**FIGURE 9-117.** Coronal sonogram, anteriorly. CG, cingulate gyrus; CN, caudate nucleus; F, falx; FG, frontal gyri; FH, frontal horn; LS, lateral sulcus; PO, parietal operculum; TO, temporal operculum.

is a normal finding at this early stage of pregnancy. The cerebellar hemispheres are outlined by the fluid in the cisterna magna (see Fig. 9-110). The fourth ventricle can be depicted throughout the second and third trimesters unless technical imaging problems confound its visualization (indeed, the “fourth ventricle” is even seen in the first trimester [see Fig. 9-3]).

One of the difficulties in mastering the sonographic anatomy of intracranial structures is the usual inability to see both hemispheres of the brain symmetrically.<sup>123</sup> The hemisphere nearest to the transducer is virtually always “clouded” over by reverberation artifacts generated as the acoustic beam passes through the near calvarial wall. Calvarial ossification appears to be at the root of this artifact because the artifact is markedly reduced in fetuses with recessive osteogenesis imperfecta or other bone dysplasias wherein calvarial ossification is nearly absent (see Fig. 9-116). Unfortunately, essentially all other fetuses possess calvarial ossification. The following rule should always be applied: The sonologist must assume that the intracranial anatomy of the fetus is symmetric, whether normal or abnormal, unless images document an asymmetry. Visualization of the near hemisphere requires that we use bone-free windows in the near calvaria. The “windows” are the anterolateral and posterolateral fontanels in axial approach or the anterior and posterior fontanels in coronal imaging. Because the anterolateral and posterolateral fontanels are nearer to the base of the brain than to the vertex, using the anterolateral

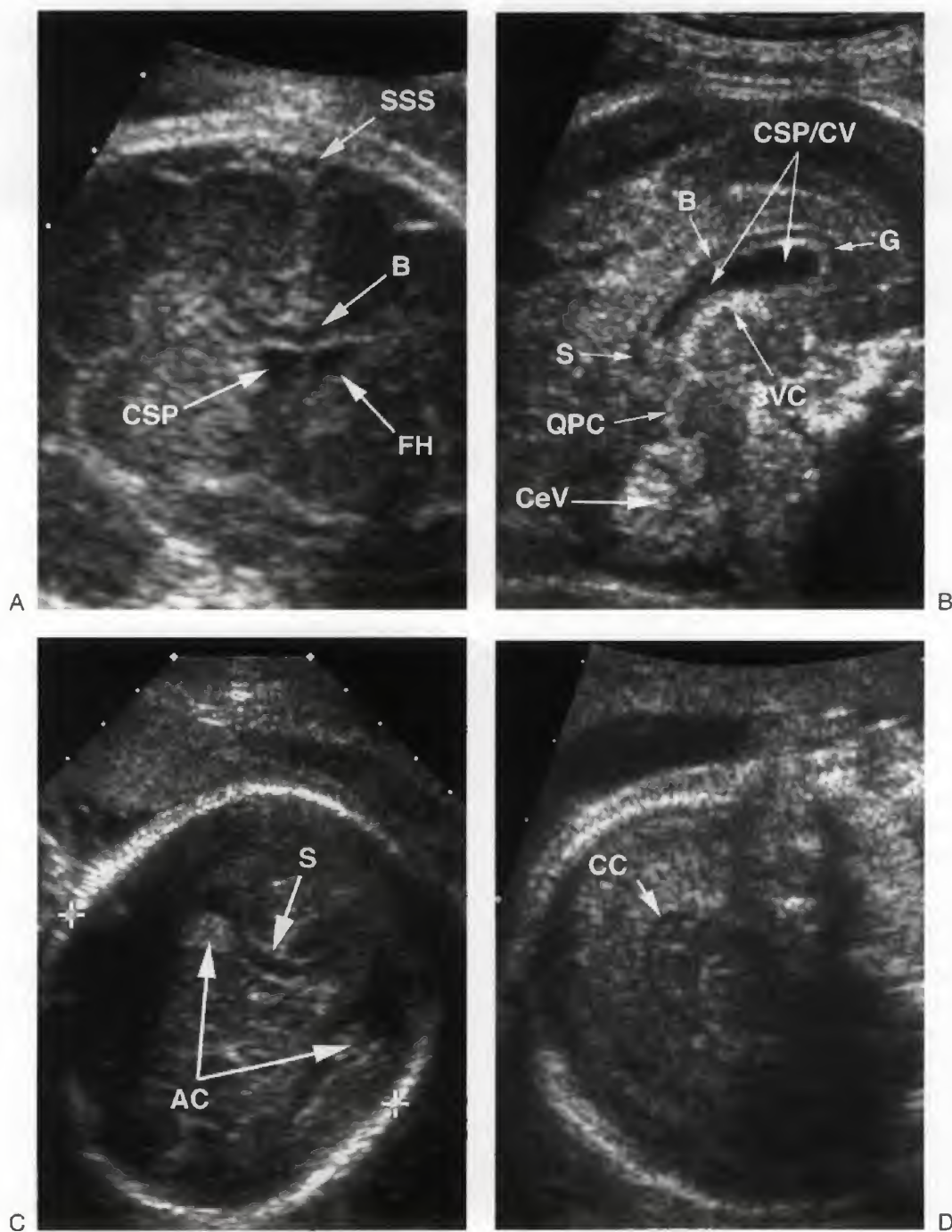


**FIGURE 9-118.** A. Coronal section through the body (B) of the corpus callosum. B. Midsagittal sonograms show the corpus callosum to best advantage. B, body; G, genu; S, splenium. C. Axial view "aimed" at the occiput demonstrates the splenium (S), the most crucial portion of the corpus callosum to demonstrate. In an "occiput up" fetus, a midsagittal sonogram of the corpus callosum would be nearly impossible to obtain. D. Nineteen-week-old fetus with corpus callosum well demonstrated. 3VC, choroid plexus in the roof of the third ventricle; AC, atrial choroids; CeV, vermis of the cerebellum; CSP, cavum septi pellucidum; CV, cavum vergae; FH, frontal horn; QPC, quadrigeminal plate cistern; SSS, superior sagittal sinus.



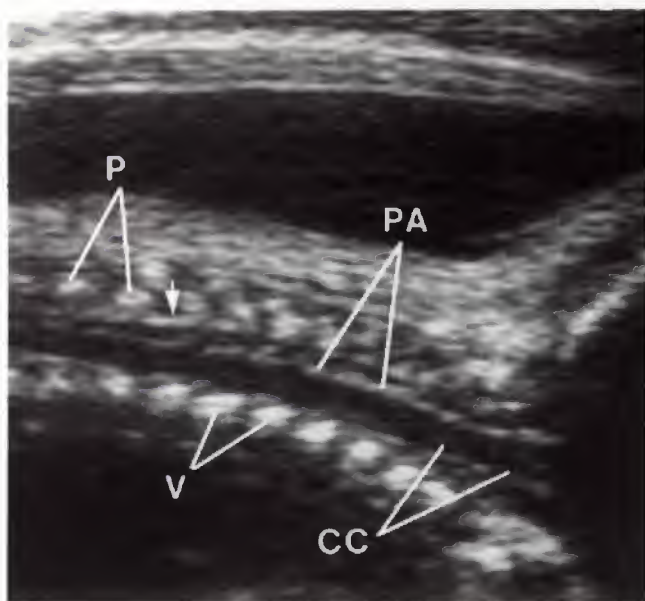


**FIGURE 9-119.** Longitudinal sonogram at the craniocervical junction demonstrating the cervical cord (CC). P, posterior arch ossification centers; PA, pia-arachnoid; V, vertebral body ossification centers; arrow, dura.

and posterolateral fontanel results in images of the near hemisphere that are off axis to the axial plane (at least in most images). Therefore, caution must be exercised in the interpretation of the off axis planes, particularly when judging the size of the near ventricular atrium.

As noted earlier, the fetal spine is seen well from 15 to 16 weeks onward. However, we often delay evaluation for suspected myelomeningocele until 18 to 20 weeks of gestation. This is due to significant and favorable maturational changes in the spine that occur during this period. The posterior ossification centers begin at the base of the transverse processes (see Figs. 9-55 to 9-60). As ossification progresses, the laminae become visible (see Figs. 9-56 to 9-58 and 9-62). The inward angulation of the normal laminae is the opposite of the outward splaying of the laminae seen in spina bifida, an optimal situation for detecting this anomaly. Spina bifida, of course, is the bony anomaly seen in all myelomeningoceles. The spinal cord neural tissue, like that of most brain tissue, is echogenic (see Fig. 9-62). The conus medullaris (see Fig. 9-62D) and the craniocervical junction (Fig. 9-119) can be seen, albeit inconsistently, in nearly all fetuses by 18 to 20 menstrual weeks. The tissues surrounding the cord (leptomeninges) are brightly echogenic, as are those that surround the brain, and the dura is usually also seen discretely as a linear bright reflector (see Fig. 9-62C and D, and 9-63). In fetuses with myelomeningoceles, determination of the most cephalic spinal level of the lesion is an important factor in prognosis. This level can be determined by counting up from the last ossified vertebral segment (assumed to be S-4 in the second trimester and S-5 in the third trimester) (Fig. 9-120).

## References

1. Yousefzadeh DK, Naidich TP: US anatomy of the posterior fossa in children: correlation with brain sections. *Radiology* 156:353, 1985.

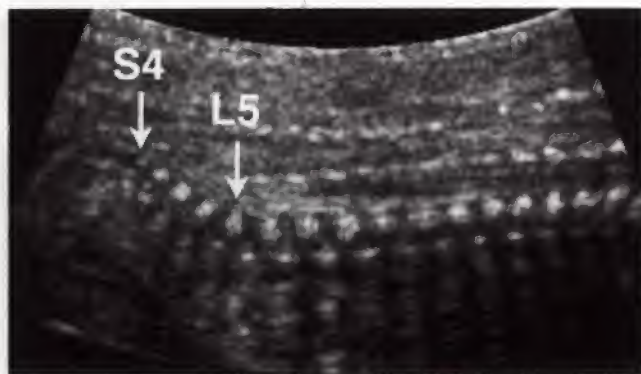


**FIGURE 9-120.** Sagittal plane of section of the spine in a 21-week-old fetus. The spinal level can be determined by counting up from the last ossified vertebral segment (assumed to be S-4 in the second trimester and S-5 in the third trimester). In this case, the S-4 ossification center and L5 spinal segment are seen.

2. Naidich TP, Gusnard DA, Yousefzadeh DK: Sonography of the internal capsule and basal ganglia in infants: 1. Coronal sections. *AJNR Am J Neuroradiol* 6:909, 1985.
3. Amin RS, Nikolaidis P, Kawashima A, et al: Normal anatomy of the fetus at MR imaging. *Radiographics* 19 Spec No:S201, 1999.
4. Coakley FV, Glenn OA, Qayyum A, et al: Fetal MRI: a developing technique for the developing patient. *AJR Am J Roentgenol* 182:243, 2004.
5. Glenn OA: Fetal central nervous system MR imaging. *Neuroimaging Clin N Am* 16:1, 2006.
6. Levine D, Smith AS, McKenzie C: Tips and tricks of fetal MR imaging. *Radiol Clin North Am* 41:729, 2003.
7. Trop I, Levine D: Normal fetal anatomy as visualized with fast magnetic resonance imaging. *Top Magn Reson Imaging* 12:3, 2001.
8. Filly RA, Callen PW: Ultrasonographic evaluation of normal fetal anatomy. In Sanders RC, James AE (eds): *The Principles and Practice of Ultrasonography in Obstetrics and Gynecology*, 2nd ed. New York, Appleton Century Crofts, 1980.
9. Simpson DH, Burns PN, Averkiou MA: Techniques for perfusion imaging with microbubble contrast agents. *IEEE Trans Ultrason Ferroelectr Freq Control* 48:1483, 2001.
10. Monteagudo A, Timor-Tritsch IE: First trimester anatomy scan: pushing the limits. What can we see now? *Curr Opin Obstet Gynecol* 15:131, 2003.
11. Souka AP, Nicolaides KH: Diagnosis of fetal abnormalities at the 10-14-week scan. *Ultrasound Obstet Gynecol* 10:429, 1997.
12. Timor-Tritsch IE: Transvaginal sonographic evaluation of fetal anatomy at 14 to 16 weeks. Why is this technique not attractive in the United States? *J Ultrasound Med* 20:705, 2001.
13. Mahony BS, Filly RA: High-resolution sonographic assessment of the fetal extremities. *J Ultrasound Med* 3:489, 1984.
14. Cooperberg PL, Chow T, Kite V, et al: Biparietal diameter: a comparison of real time and conventional B scan techniques. *J Clin Ultrasound* 4:421, 1976.
15. Docker MF, Setuatre RS: Comparison between linear array real time ultrasonic scanning and conventional compound scanning in the measurement of the fetal biparietal diameter. *Br J Obstet Gynaecol* 84:924, 1977.
16. Filly RA: Sonographic anatomy of the normal fetus. In Harrison MR, Golbus MS, Filly RA (eds): *The Unborn Patient: Prenatal Diagnosis and Treatment*, 2nd ed. Philadelphia, WB Saunders, 1991.
17. Benaceraf BR, Shipp TD, Bromley B: Three-dimensional US of the fetus: volume imaging. *Radiology* 238:988, 2006.
18. Dyson RL, Pretorius DH, Budorick NE, et al: Three-dimensional ultrasound in the evaluation of fetal anomalies. *Ultrasound Obstet Gynecol* 16:321, 2000.
19. Goncalves LF, Lee W, Espinoza J, et al: Three- and 4-dimensional ultrasound in obstetric practice: does it help? *J Ultrasound Med* 24:1599, 2005.



20. Bowic JD, Rosenberg ER, Andreotti RF, et al: The changing sonographic appearance of fetal kidneys during pregnancy. *J Ultrasound Med* 2:505, 1983.
21. Hata T, Yonehara T, Aoki S, et al: Three-dimensional sonographic visualization of the fetal face. *AJR Am J Roentgenol* 170:481, 1998.
22. Rotten D, Levailant JM: Two- and three-dimensional sonographic assessment of the fetal face. 2. Analysis of cleft lip, alveolus and palate. *Ultrasound Obstet Gynecol* 24:402, 2004.
23. Rotten D, Levailant JM: Two- and three-dimensional sonographic assessment of the fetal face. 1. A systematic analysis of the normal face. *Ultrasound Obstet Gynecol* 23:224, 2004.
24. Birnholz JC: The fetal external ear. *Radiology* 147:819, 1983.
25. Fink IJ, Chinn DH, Callen PW: A potential pitfall in the ultrasonographic diagnosis of fetal encephalocele. *J Ultrasound Med* 2:313, 1983.
26. Elejalde BR, de Elejalde MM, Heitman T: Visualization of the fetal genitalia by ultrasonography: a review of the literature and analysis of its accuracy and ethical implications. *J Ultrasound Med* 4:633, 1985.
27. Birnholz JC: Determination of fetal sex. *N Engl J Med* 309:942, 1983.
28. Natsuyama E: Sonographic determination of fetal sex from twelve weeks of gestation. *Am J Obstet Gynecol* 149:748, 1984.
29. Mahony BS, Filly RA, Callen PW: Amnionity and chorionity in twin pregnancies: prediction using ultrasound. *Radiology* 155:205, 1985.
30. Filly RA, Golbus MS: Ultrasonography of the normal and pathologic fetal skeleton. *Radiol Clin North Am* 20:311, 1982.
31. Filly RA, Golbus MS, Carey JC, et al: Short-limbed dwarfism: ultrasonographic diagnosis by mensuration of fetal femoral length. *Radiology* 138:653, 1981.
32. O'Brien GD, Queenan JT, Campbell S: Assessment of gestational age in the second trimester by real-time ultrasound measurement of the femur length. *Am J Obstet Gynecol* 139:540, 1981.
33. Jeanty P, Kirkpatrick C, Dramaix-Wilmet M, et al: Ultrasonic evaluation of fetal limb growth. *Radiology* 140:165, 1981.
34. Meyer DB, O'Rahilly R: Roentgenographic investigation of the human skeleton during early fetal life. *Am J Roentgenol Radium Ther Nucl Med* 76:455, 1956.
35. Bagnall KM, Harris PF, Jones PR: A radiographic study of the human fetal spine. 2. The sequence of development of ossification centres in the vertebral column. *J Anat* 124:791, 1977.
36. Garjian KV, Pretorius DH, Budorick NE, et al: Fetal skeletal dysplasia: three-dimensional US—initial experience. *Radiology* 214:717, 2000.
37. Riccabona M, Johnson D, Pretorius DH, et al: Three dimensional ultrasound: display modalities in the fetal spine and thorax. *Eur J Radiol* 22:141, 1996.
38. Yanagihara T, Hata T: Three-dimensional sonographic visualization of fetal skeleton in the second trimester of pregnancy. *Gynecol Obstet Invest* 49:12, 2000.
39. Filly RA, Simpson GF, Linkowski G: Fetal spine morphology and maturation during the second trimester. Sonographic evaluation. *J Ultrasound Med* 6:631, 1987.
40. Abrams SL, Filly RA: Curvature of the fetal femur: a normal sonographic finding. *Radiology* 156:490, 1985.
41. Yarkoni S, Schmidt W, Jeanty P, et al: Clavicular measurement: a new biometric parameter for fetal evaluation. *J Ultrasound Med* 4:467, 1985.
42. Jeanty P, Romero R, d'Alton M, et al: In utero sonographic detection of hand and foot deformities. *J Ultrasound Med* 4:595, 1985.
43. Benacerraf BR, Frigoletto FD: Prenatal ultrasound diagnosis of clubfoot. *Radiology* 155:211, 1985.
44. Hashimoto BE, Filly RA, Callen PW: Sonographic diagnosis of clubfoot in utero. *J Ultrasound Med* 5:81, 1986.
45. Chinn DH, Bolding DB, Callen PW, et al: Ultrasonographic identification of fetal lower extremity epiphyseal ossification centers. *Radiology* 147:815, 1983.
46. Mahony BS, Callen PW, Filly RA: The distal femoral epiphyseal ossification center in the assessment of third-trimester menstrual age: sonographic identification and measurement. *Radiology* 155:201, 1985.
47. Goldstein RB, Filly RA, Simpson G: Pitfalls in femur length measurements. *J Ultrasound Med* 6:203, 1987.
48. Jeanty P, Cantraine F, Coussaert E, et al: The binocular distance: a new way to estimate fetal age. *J Ultrasound Med* 3:241, 1984.
49. Dennis MA, Drose JA, Pretorius DH, et al: Normal fetal sacrum simulating spina bifida: "pseudodysraphism." *Radiology* 155:751, 1985.
50. Abrams SL, Filly RA: Congenital vertebral malformations: prenatal diagnosis using ultrasonography. *Radiology* 155:762, 1985.
51. Birnholz JC: Fetal lumbar spine: measuring axial growth with US. *Radiology* 158:805, 1986.
52. Hashimoto BE, Mahony BS, Filly RA, et al: Sonography, a complementary examination to alpha-fetoprotein testing for fetal neural tube defects. *J Ultrasound Med* 4:307, 1985.
53. Brown BS: The prenatal ultrasonographic diagnosis of osteogenesis imperfecta lethalis. *J Can Assoc Radiol* 35:63, 1984.
54. Kousseff BG, Mulivor RA: Prenatal diagnosis of hypophosphatasia. *Obstet Gynecol* 57:9S, 1981.
55. Merz E, Goldhofer W: Sonographic diagnosis of lethal osteogenesis imperfecta in the second trimester: case report and review. *J Clin Ultrasound* 14:380, 1986.
56. Mahony BS, Filly RA, Cooperberg PL: Antenatal sonographic diagnosis of achondrogenesis. *J Ultrasound Med* 3:333, 1984.
57. Rosenthal SJ, Filly RA, Callen PW, et al: Fetal pseudoascites. *Radiology* 131:195, 1979.
58. Hashimoto BE, Filly RA, Callen PW: Fetal pseudoascites: further anatomic observations. *J Ultrasound Med* 5:151, 1986.
59. Dallos F: Fetal blood sampling under ultrasound guidance. In Harrison MR, Golbus MS, Filly RA (eds): *The Unborn Patient: Prenatal Diagnosis and Treatment*, 2nd ed. Philadelphia: WB Saunders, 1991.
60. Moore KL: The placenta and fetal membranes. In Moore KL (ed): *The Developing Human: Clinically Oriented Embryology*, 4th ed. Philadelphia: WB Saunders, 1988.
61. Chinn DH, Filly RA, Callen PW: Ultrasonic evaluation of fetal umbilical and hepatic vascular anatomy. *Radiology* 144:153, 1982.
62. Barron DH: The changes in the fetal circulation at birth. *Physiol Rev* 24:277, 1944.
63. Emery JL: Functional asymmetry of the liver. *Ann N Y Acad Sci* 111:37, 1963.
64. Marks WM, Filly RA, Callen PW: Ultrasonic anatomy of the liver: a review with new applications. *J Clin Ultrasound* 7:137, 1979.
65. Gupta SC, Gupta CD, Arora AK: Intrahepatic branching patterns of portal vein. A study by corrosion cast. *Gastroenterology* 72:621, 1977.
66. Rosen MS, Reich SB: Umbilical venous catheterization in the newborn: identification of correct positioning. *Radiology* 95:335, 1970.
67. Hattan RA, Rees GK, Johnson ML: Normal fetal anatomy. *Radiol Clin North Am* 20:271, 1982.
68. AIUM Practice Guideline for the performance of an antepartum obstetric ultrasound examination. *J Ultrasound Med* 22:1116, 2003.
69. Goldstein RB, Callen PW: Ultrasound evaluation of the fetal thorax and abdomen. In Callen PW (ed): *Ultrasonography in Obstetrics and Gynecology*, 2nd ed. Philadelphia, WB Saunders, 1988.
70. Cooper C, Mahony BS, Bowic JD, et al: Ultrasound evaluation of the normal fetal upper airway and esophagus. *J Ultrasound Med* 4:343, 1985.
71. Pritchard JA: Fetal swallowing and amniotic fluid volume. *Obstet Gynecol* 28:606, 1966.
72. Abramovich DR: Fetal factors influencing the volume and composition of liquor amnii. *J Obstet Gynaecol Br Commonw* 77:865, 1970.
73. Pretorius DH, Meier PR, Johnson ML: Diagnosis of esophageal atresia in utero. *J Ultrasound Med* 2:475, 1983.
74. Gross BH, Filly RA: Potential for a normal fetal stomach to simulate the sonographic "double bubble" sign. *J Can Assoc Radiol* 33:39, 1982.
75. Grand RJ, Watkins JB, Torti FM: Development of the human gastrointestinal tract. A review. *Gastroenterology* 70:790, 1976.
76. Manco LG, Nunan FA Jr, Sohnen H, et al: Fetal small bowel simulating an abdominal mass at sonography. *J Clin Ultrasound* 14:404, 1986.
77. Fakhry J, Reiser M, Shapiro LR, et al: Increased echogenicity in the lower fetal abdomen: a common normal variant in the second trimester. *J Ultrasound Med* 5:489, 1986.
78. Al-Kouatly HB, Chasen ST, Streltsoff J, et al: The clinical significance of fetal echogenic bowel. *Am J Obstet Gynecol* 185:1035, 2001.
79. Kesrouani AK, Guibourdenche J, Muller F, et al: Etiology and outcome of fetal echogenic bowel. Ten years of experience. *Fetal Diagn Ther* 18:240, 2003.
80. Vincoff NS, Callen PW, Smith-Bindman R, et al: Effect of ultrasound transducer frequency on the appearance of the fetal bowel. *J Ultrasound Med* 18:799; quiz 805, 1999.
81. Zilianti M, Fernandez S: Correlation of ultrasonic images of fetal intestine with gestational age and fetal maturity. *Obstet Gynecol* 62:569, 1983.



82. Nyberg DA, Mack LA, Patten RM, et al: Fetal bowel. Normal sonographic findings. *J Ultrasound Med* 6:3, 1987.
83. Crelin ES: *Functional Anatomy of the Newborn*. New Haven, CT, Yale University Press, 1973.
84. Schmidt W, Yarkoni S, Jeanty P, et al: Sonographic measurements of the fetal spleen: clinical implications. *J Ultrasound Med* 4:667, 1985.
85. Potter EL: *Pathology of the Fetus and Infant*. Chicago, Year Book Medical, 1961.
86. Gruenewald P, Hoang Ngoc M: Evaluation of body and organ weights in perinatal pathology. I. Normal standards derived from autopsies. *Am J Clin Pathol* 34:247, 1960.
87. Mittlestaedt CA: Ultrasound of the spleen. *Semin Ultrasound* 2:233, 1981.
88. Fried AM, Loh FK, Umer MA, et al: Echogenicity of fetal lung: relation to fetal age and maturity. *AJR Am J Roentgenol* 145:591, 1985.
89. Cayea PD, Grant DC, Doubilet PM, et al: Prediction of fetal lung maturity: inaccuracy of study using conventional ultrasound instruments. *Radiology* 155:473, 1985.
90. Lawson TL, Foley WD, Berland LL, et al: Ultrasonic evaluation of fetal kidneys. *Radiology* 138:153, 1981.
91. Hoddick WK, Filly RA, Mahony BS, et al: Minimal fetal renal pyelectasis. *J Ultrasound Med* 4:85, 1985.
92. Arger PH, Coleman BG, Mintz MC, et al: Routine fetal genitourinary tract screening. *Radiology* 156:485, 1985.
93. Grannum P, Bracken M, Silverman R, et al: Assessment of fetal kidney size in normal gestation by comparison of ratio of kidney circumference to abdominal circumference. *Am J Obstet Gynecol* 136:249, 1980.
94. Jeanty P, Dramaix-Wilmet M, Elkhazen N, et al: Measurements of fetal kidney growth on ultrasound. *Radiology* 144:159, 1982.
95. Bertagnoli L, Lalatta F, Gallicchio R, et al: Quantitative characterization of the growth of the fetal kidney. *J Clin Ultrasound* 11:349, 1983.
96. Wladimiroff JW, Campbell S: Fetal urine-production rates in normal and complicated pregnancy. *Lancet* 1:151, 1974.
97. Campbell S, Wladimiroff JW, Dewhurst CJ: The antenatal measurement of fetal urine production. *J Obstet Gynaecol Br Commonw* 80:680, 1973.
98. Chamberlain PF, Manning FA, Morrison I, et al: Circadian rhythm in bladder volumes in the term human fetus. *Obstet Gynecol* 64:657, 1984.
99. Rosenberg ER, Bowie JD, Andreotti RF, et al: Sonographic evaluation of fetal adrenal glands. *AJR Am J Roentgenol* 139:1145, 1982.
100. Co CS, Filly RA: Normal fetal adrenal gland location. *J Ultrasound Med* 5:117, 1986.
101. Goldberg BB, Isard HJ, Gershon-Cohen J, et al: Ultrasonic fetal cephalometry. *Radiology* 87:328, 1966.
102. Hidalgo H, Bowie J, Rosenberg ER, et al: Review. In utero sonographic diagnosis of fetal cerebral anomalies. *AJR Am J Roentgenol* 139:143, 1982.
103. Fiske CE, Filly RA: Ultrasound evaluation of the normal and abnormal fetal neural axis. *Radiol Clin North Am* 20:285, 1982.
104. Pasto ME, Kurtz AB: The prenatal examination of the fetal cranium, spine, and central nervous system. *Semin Ultrasound CT MR* 5:170, 1984.
105. Filly RA: Ultrasonography. In Harrison MR, Golbus MS, Filly RA (eds): *The Unborn Patient: Prenatal Diagnosis and Treatment*, 1st ed. Orlando, FL, Grune & Stratton, 1984, pp 33-123.
106. Carrasco CR, Stierman ED, Harnsberger HR, et al: An algorithm for prenatal ultrasound diagnosis of congenital CNS abnormalities. *J Ultrasound Med* 4:163, 1985.
107. Edwards MSD, Filly RA: Diagnosis and management of fetal disorders of the central nervous system. In Hoffman HJ, Epstein F (eds): *Disorders of the Developing Nervous System: Diagnosis and Treatment*. Boston, Blackwell Scientific Publications, 1986, pp 55-73.
108. Young GB: The "arrow" pattern. A new "anatomical" fetal biparietal diameter. *Radiology* 137:445, 1980.
109. Jeanty P, Chervenak FA, Romero R, et al: The sylvian fissure: a commonly mislabeled cranial landmark. *J Ultrasound Med* 3:15, 1984.
110. Denkhau H, Winsberg F: Ultrasonic measurement of the fetal ventricular system. *Radiology* 131:781, 1979.
111. Chinn DH, Callen PW, Filly RA: The lateral cerebral ventricle in early second trimester. *Radiology* 148:529, 1983.
112. Fiske CE, Filly RA, Callen PW: The normal choroid plexus: ultrasonographic appearance of the neonatal head. *Radiology* 141:467, 1981.
113. Johnson ML, Dunne MG, Mack LA, Rashbaum CL: Evaluation of fetal intracranial anatomy by static and real-time ultrasound. *J Clin Ultrasound* 8:311, 1980.
114. Jeanty P, Dramaix-Wilmet M, Delbeke D, et al: Ultrasonic evaluation of fetal ventricular growth. *Neuroradiology* 21:127, 1981.
115. Hertzberg BS, Burger PC, Bowie JD, et al: Sonographic characteristics of small cerebral blood vessels. An in vivo and postmortem study. *J Ultrasound Med* 9:697, 1990.
116. Day WR: Casts of foetal lateral ventricles. *Brain* 82:109, 1959.
117. Siedler DE, Filly RA: Relative growth of the higher fetal brain structures. *J Ultrasound Med* 6:573, 1987.
118. Worthen NJ, Gilbertson V, Lau C: Cortical sulcal development seen on sonography: relationship to gestational parameters. *J Ultrasound Med* 5:153, 1986.
119. Toi A, Lister WS, Fong KW: How early are fetal cerebral sulci visible at prenatal ultrasound and what is the normal pattern of early fetal sulcal development? *Ultrasound Obstet Gynecol* 24:706, 2004.
120. Pilu G, De Palma L, Romero R, et al: The fetal subarachnoid cisterns: an ultrasound study with report of a case of congenital communicating hydrocephalus. *J Ultrasound Med* 5:365, 1986.
121. Laing FC, Stamler CE, Jeffrey RB: Ultrasonography of the fetal subarachnoid space. *J Ultrasound Med* 2:29, 1983.
122. Fong KW, Ghai S, Toi A, et al: Prenatal ultrasound findings of lissencephaly associated with Miller-Dieker syndrome and comparison with pre- and postnatal magnetic resonance imaging. *Ultrasound Obstet Gynecol* 24:716, 2004.
123. Reuter KL, D'Orsi CJ, Raptopoulos VD, et al: Sonographic pseudosymmetry of the prenatal cerebral hemispheres. *J Ultrasound Med* 1:91, 1982.

# ULTRASOUND EVALUATION OF THE FETAL NEURAL AXIS

Gianluigi Pilu, MD

## Normal Sonographic Anatomy of the Fetal Central Nervous System

### Magnetic Resonance Imaging of the Fetal Brain

#### Ventriculomegaly

#### Neural Tube Defects

Anencephaly

Spina Bifida

Cephalocele

#### Midline Anomalies

Agenesis of the Corpus Callosum

Dandy-Walker Malformation

#### Destructive Cerebral Lesions

#### Disorders of Nerve Cell Proliferation

Intracranial Tumors

#### Anomalies of Neuronal Migration

#### Vascular Abnormalities

#### Intracranial Cysts

#### Conclusions

Central nervous system (CNS) malformations are some of the most common of all congenital abnormalities. Neural tube defects are the CNS malformations most frequently encountered at birth and amount to approximately 1 to 2 cases per 1000 births. The incidence of intracranial abnormalities with an intact neural tube is uncertain because it is likely that most of these escape detection at birth and only become manifest in later life. Long-term follow-up studies suggest that the incidence may be as high as one in 100 births.<sup>1</sup>

Ultrasound has been used for nearly 30 years as the main modality to help diagnose fetal CNS anomalies. In recent years, fetal magnetic resonance imaging (MRI) has emerged as a promising new technique that may add, in selected cases, important information,<sup>2,3</sup> although the real advantage over ultrasound remains debated.<sup>4,5</sup> In this chapter, the investigation of the fetal brain and the identification of CNS anomalies are reviewed.

## NORMAL SONOGRAPHIC ANATOMY OF THE FETAL CENTRAL NERVOUS SYSTEM

The fetal cerebrum undergoes major developmental changes throughout the entire gestation. High resolution transvaginal probes have allowed detailed investigation of the human embryo in vivo in the very first part of pregnancy (Figs. 10-1 and 10-2). Starting from 7 weeks' gestation, the primary cerebral vesicles can be identified as fluid-filled areas with transvaginal sonography. From 11 weeks' gestation, the brightly echogenic choroid plexuses filling the large lateral ventricles are the most prominent intracranial structures (see Fig. 10-1). In the second trimester, a detailed sonographic examination of the already well-developed cerebral structures, allowing the detection of most anomalies, is feasible. How-

ever, the results of an obstetric sonogram greatly depend upon the level of expertise of the sonographer and the time dedicated to the scan. In evaluating the fetal brain, a distinction must be made between a basic examination (frequently referred to as a level one, routine, or standard scan) and a fetal neurosonogram (or level two examination). The basic scan is fundamentally a screening examination for low-risk patients, and there is a general consensus that it is conveniently carried out by two transverse axial views of the head, demonstrating the lateral ventricles, basal ganglia, cavum septum pellucidum, and posterior fossa (Fig. 10-3).<sup>6</sup> Measurement of the biparietal diameter, head circumference and internal diameter of the atrium is recommended. Some advocate also measurement of the transverse cerebellar diameter and/or cisterna magna depth.<sup>7</sup>

A fetal neurosonogram is a diagnostic examination, usually performed in a patient at increased risk of fetal anomalies and may include coronal and sagittal views of the head that are more difficult to obtain but that have the advantage of delineating more clearly, subtle details of intracranial anatomy, particularly by using a vaginal probe in fetuses in cephalic presentation (Fig. 10-4). Three-dimensional ultrasound is a useful adjunct to the bidimensional examination in that it allows visualization of scanning planes difficult or impossible to obtain directly (Fig. 10-5).<sup>8</sup>

The examination of the fetal spine requires expertise and meticulous scanning, and the results are heavily dependent on the fetal position. Sonography demonstrates the ossification centers of the vertebrae (one inside the body, one at the junction of the lamina and pedicle on each side) that appear brightly echogenic. Three types of scanning planes can be used to evaluate the integrity of the spine. In *transverse planes*, the vertebrae have different anatomic configurations dependent upon the spinal level imaged (Fig. 10-6). Fetal



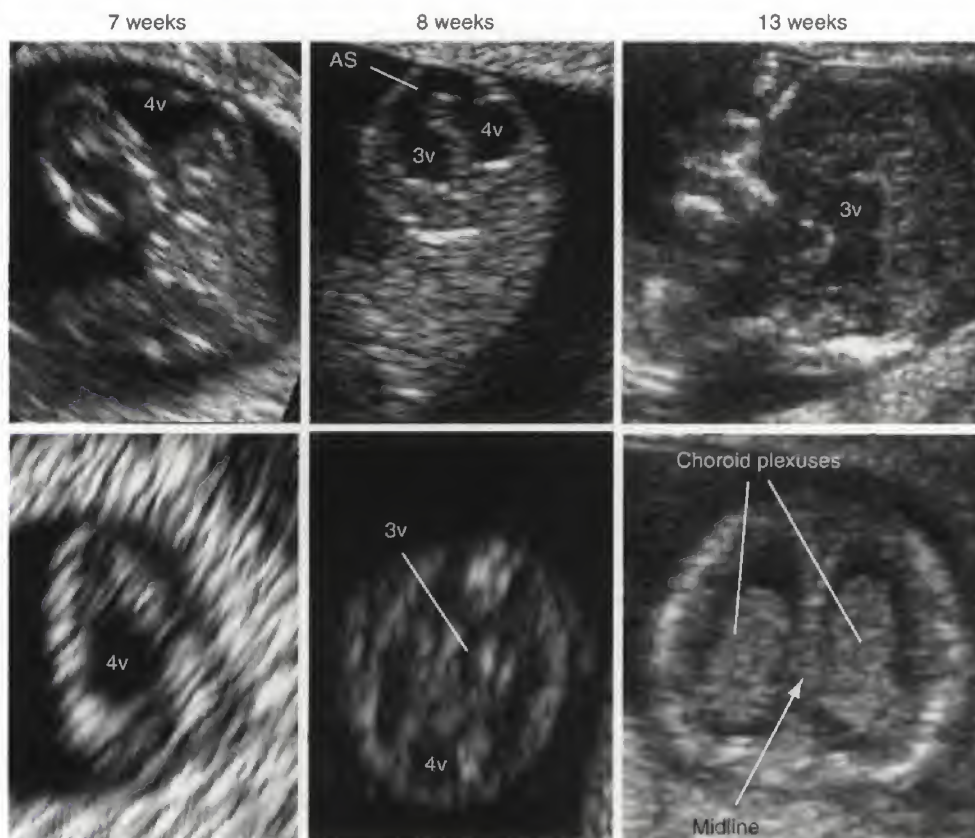


**FIGURE 10-1.** Sonography of the embryonic and early fetal brain as demonstrated by sagittal sections (*upper row*) and axial sections (*lower row*). At 7 weeks' gestation (transvaginal scan), the rhombencephalic vesicle, that will give rise to the fourth ventricle (4v) is usually the only demonstrable structure: at 8 weeks (transvaginal scan) the remaining two primary vesicles of the brain can be demonstrated: the mesencephalic vesicle, which will give rise to the aqueduct of Sylvius (AS), and the prosencephalic vesicle, which will develop into the third ventricle; at 13 weeks, the intracranial anatomy is dominated by the prominent choroid plexuses of the lateral ventricles. The midline can also be clearly visualized at this time in gestation.

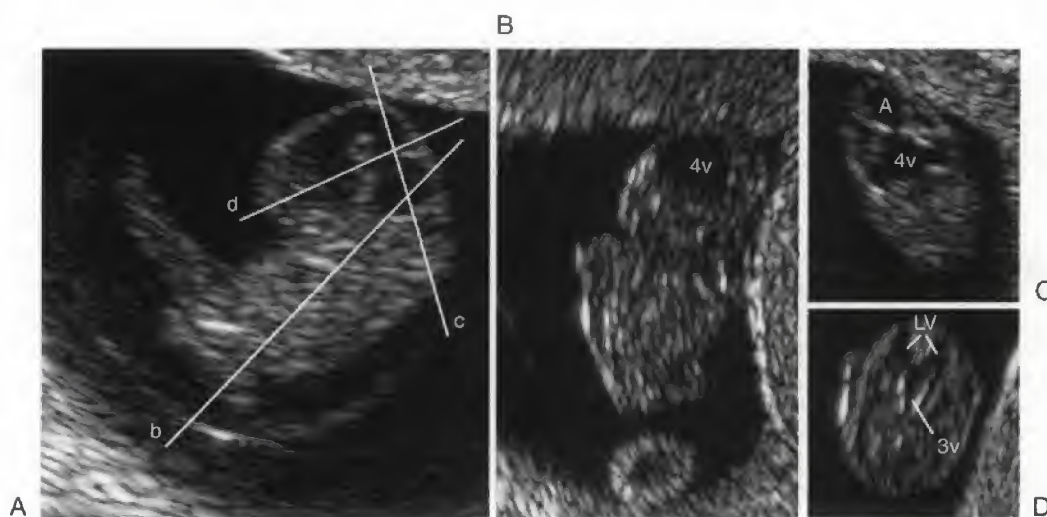


**FIGURE 10-2.** Multiplanar sonography of the primary cerebral vesicles at 8 weeks + 4 days' gestation with a 10 MHz transvaginal transducer. The rhombencephalic vesicle (4v), the mesencephalic vesicle (A), the prosencephalic vesicle (3v), and the tiny cavities of the telencephalic vesicles (LV) can be readily appreciated. The labeled lines on figure (A) represent the planes of section shown on the other images (B), (C), and (D).

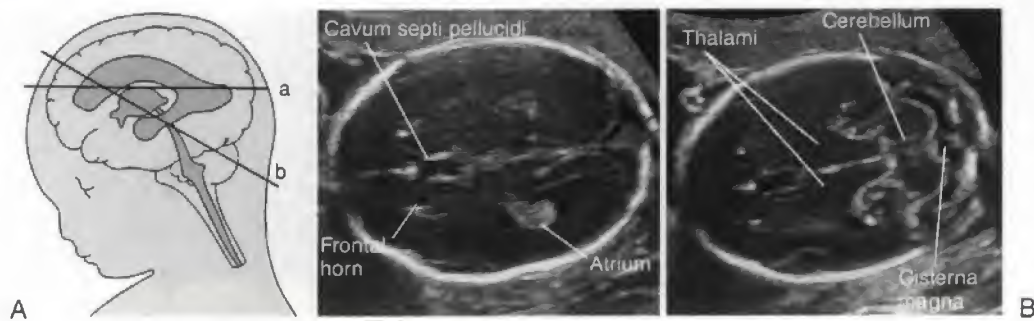


**FIGURE 10-3.** The transventricular (A) and transcerebellar (B) views in a normal midtrimester fetus. The cavum septum pellucidum, atrium of the lateral ventricle, and the cisterna magna are all well seen.

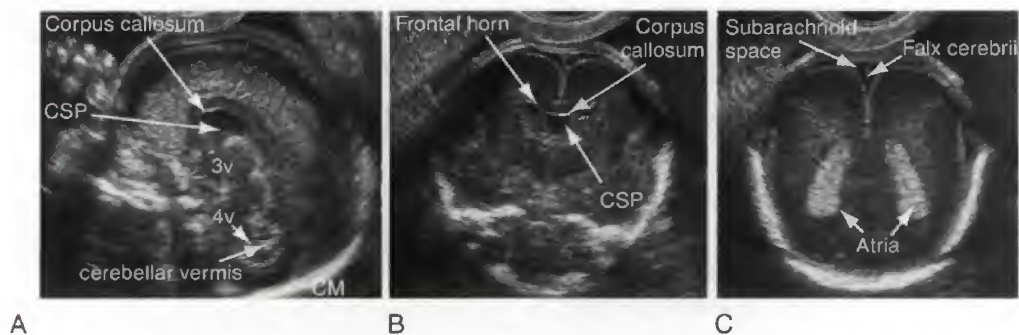


**FIGURE 10-4.** Sagittal (A) and coronal sections (B, C) of a normal midtrimester fetus. CSP, cavum septi pellucidum; 3v, third ventricle; 4v, fourth ventricle.

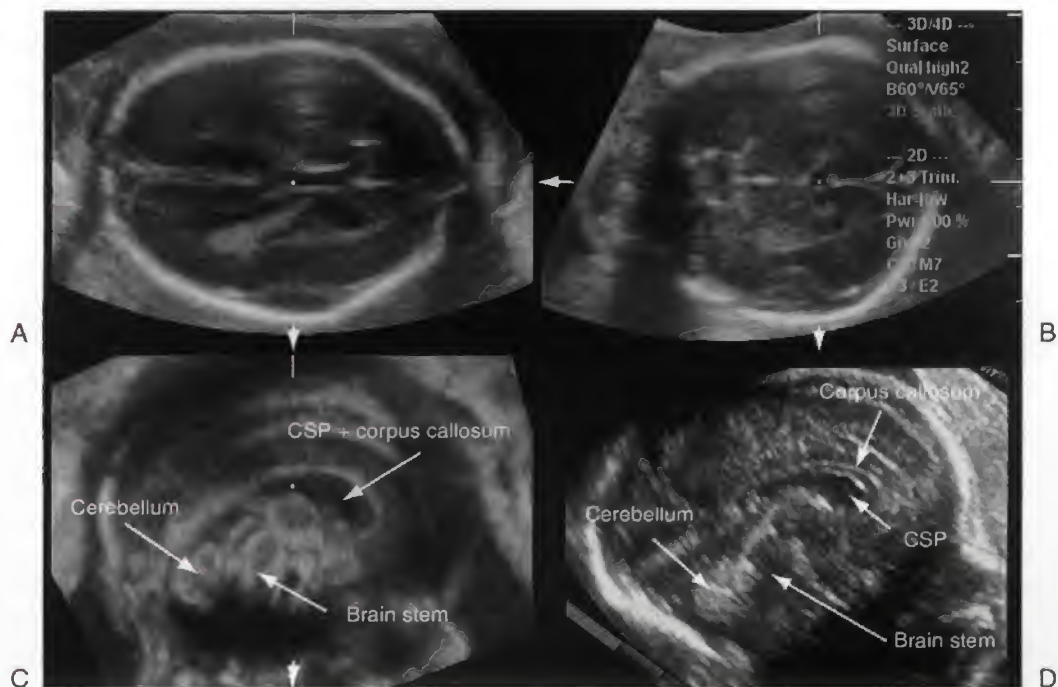


**FIGURE 10-5.** Multiplanar imaging of the fetal brain using three-dimensional sonography. The data volume has been obtained with the probe aligned along the axial plane (A). Two orthogonal sections have been reconstructed demonstrating simultaneously the coronal (B) and midsagittal planes (C). There is an excellent correlation between the midsagittal plane reconstructed from the ultrasound volume and (D) the corresponding plane obtained with standard two-dimensional ultrasound. CSP, cavum septum pellucidum.



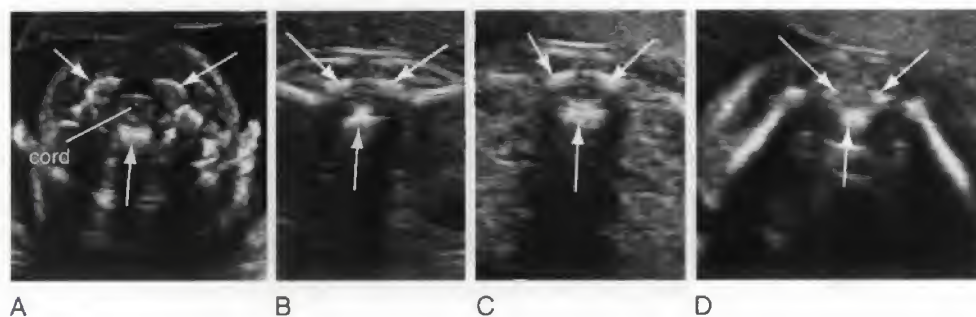


**FIGURE 10-6.** Transverse views of the fetal spine in the cervical (A), thoracic (B), lumbar (C), and sacral area (D) vertebral bodies and lamina/pedicles (arrows).

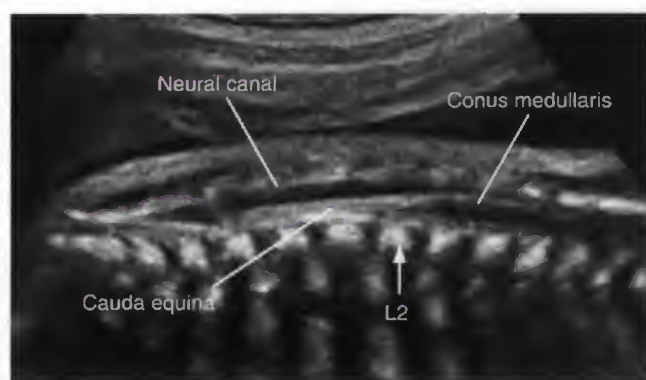


**FIGURE 10-7.** Sagittal view of the fetal spine.

thoracic and lumbar vertebrae have a triangular shape, with the ossification centers surrounding the neural canal. The first cervical vertebrae are quadrangular in shape, and the sacral vertebrae are flat. Examination of the spine is a dynamic process. While using the axial approach, the ultrasound transducer is swept along the entire length of the spine. In *sagittal planes* the ossification centers of the vertebral body and posterior arches form two parallel lines that converge in the sacrum. When the fetus is prone, a true sagittal section can also be obtained, directing the ultrasound beam across the unossified spinous process. This allows visualization of the neural tube and of the spinal cord within it. In the second and third trimester of gestation, the conus medullaris is usually found at the level of L2–L3 (Fig. 10-7).<sup>9</sup> In *coronal planes*, one, two, or three parallel lines are visualized, depending on the orientation of the sound beam (Fig. 10-8).

Integrity of the neural canal is inferred by the regular disposition of the ossification centers of the spine and the presence of soft tissue covering the spine. If a true sagittal section can be obtained, visualizing the conus medullaris in its normal location further strengthens the diagnosis of normalcy.

In the basic examination, a longitudinal view of the spine should always be demonstrated. However, detailed evaluation is complex, and usually requires an expert, or level 2, scan.<sup>10</sup>

## MAGNETIC RESONANCE IMAGING OF THE FETAL BRAIN

MRI has been used in obstetric patients for diagnosis of fetal cerebral anomalies. The MRI procedure is not believed to be hazardous to the fetus, and new equipment allows fast scanning at a reasonable level of resolution. In general, the anatomy is well depicted in fetuses older than 20 weeks' gestation. Compared with ultrasound, MRI has a lower spatial resolution but is particularly valuable because of greater contrast resolution (Fig. 10-9). It has been found to be particularly valuable in the assessment of migrational disorders, intracranial hemorrhage (ICH), and complex cerebral anomalies. Furthermore, it is not influenced by fetal position, skull calcification, and oligohydramnios. There is a controversy in the current literature whether MRI provides additional diagnostic information to the sonographic examination when the sonogram is performed by an expert.<sup>4,5</sup> Nevertheless, the use of MRI in obstetric patients is becoming widespread.<sup>2</sup> It should be stressed, however, that often with current technology, this technique gives the best results only after fetal viability, when termination of pregnancy is no longer possible in most countries.

## VENTRICULOMEGALY

Enlargement of the lateral cerebral ventricles (Fig. 10-10) can be regarded as a nonspecific marker of abnormal brain development and is encountered with many different cerebral anomalies. Therefore, evaluation of the integrity of the cerebral lateral ventricles is of particular importance while screening for fetal cerebral anomalies. Although many different approaches to the evaluation of the integrity of lateral ventricles have been proposed, measurement of the internal width of the atrium of the lateral ventricle at the level of the glomus of the choroid plexus is currently favored.<sup>11</sup> Under normal conditions, the measurement is less than 10 mm, whereas a value of more than 15 mm indicates *severe ventriculomegaly* and is often associated with an intracranial malformation at birth. The outcome of these fetuses is variable and depends largely on the underlying etiology of the ventricular dilatation. The available studies suggest that fetuses with isolated severe ventriculomegaly have an increased risk of perinatal death and a probability of severe neurologic sequelae in the range of 50% of survivors.<sup>12</sup> An

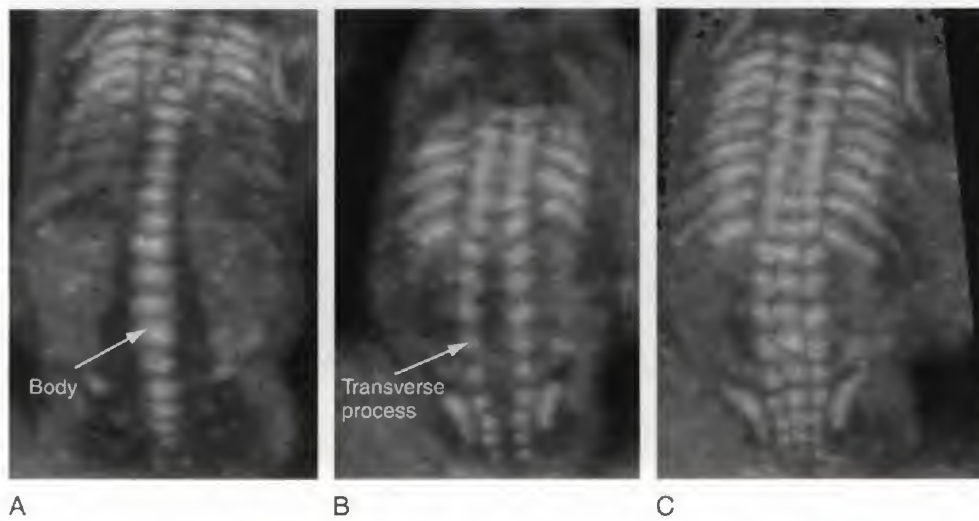


**FIGURE 10-8.** Three-dimensional coronal views of the fetal spine obtained reslicing an ultrasound volume. Depending on the orientation and thickness of the ultrasound beam, (A) the bodies of the vertebrae, (B) the transverse processes, or (C) both can be demonstrated.

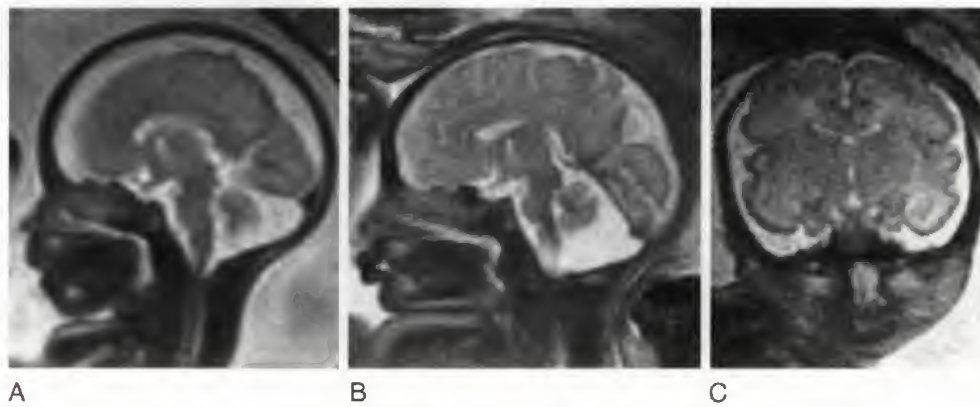


**FIGURE 10-9.** Magnetic resonance image of the fetal brain in the second (A) and third trimester (B,C).

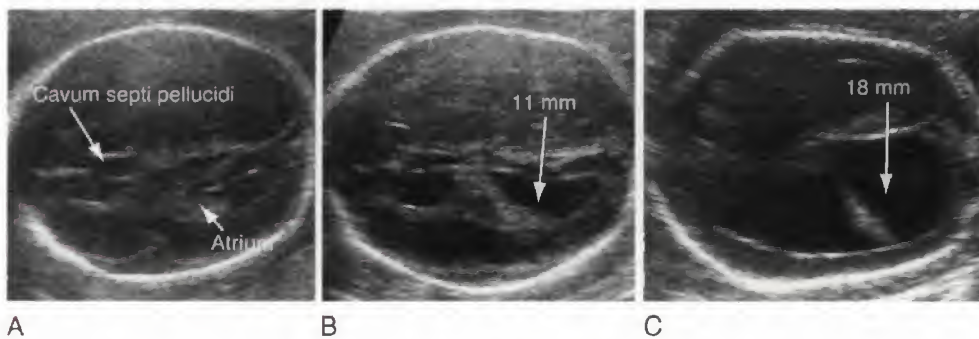


**FIGURE 10-10.** Normal transventricular scan (A) demonstrating an atrium of lateral ventricle of normal size, (B) mild ventriculomegaly, and (C) severe ventriculomegaly.



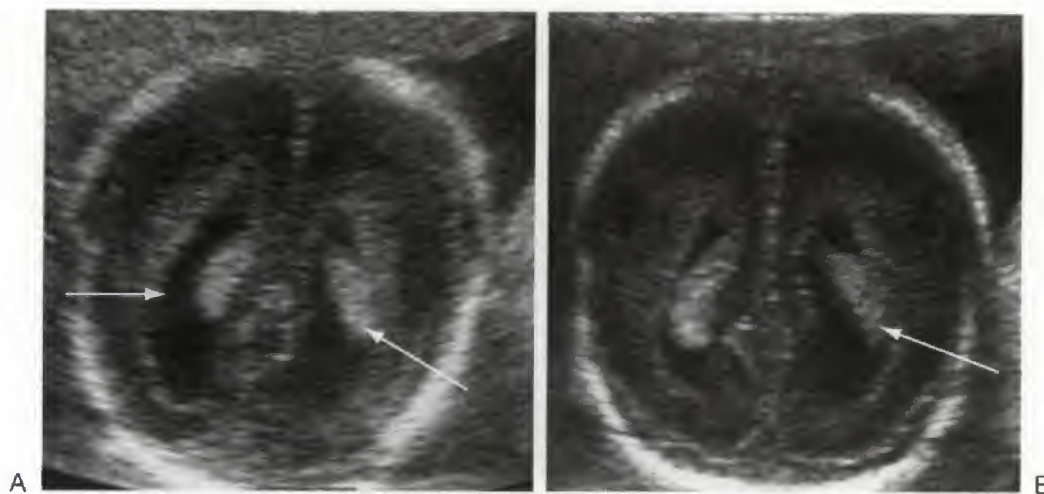


**FIGURE 10-11.** Bilateral (A) and unilateral (B) mild ventriculomegaly.

intermediate value of the atrial width, 10 to 15 mm, is commonly referred to as *mild ventriculomegaly*. It is associated with an increased probability of cerebral and extracerebral malformations, aneuploidies, and infections and, therefore, these patients should be carefully evaluated in a referral center. Fetuses with *isolated* mild ventriculomegaly usually have a good outcome, and in most instances, the ventricles stabilize or return to normal size throughout gestation. However, these fetuses run an increased risk of neurologic compromise and, in some cases, develop severe cerebral anomalies, including hydrocephalus, white matter injury, and cortical plate abnormalities, in the last part of the gestation or after birth.<sup>13</sup> The risk is particularly increased when the atrial width is greater than 12 mm, when the dilatation affects both lateral ventricles and in female fetuses (Fig. 10-11).<sup>13</sup> It has been suggested that the term mild ventriculomegaly should be limited only to cases with atrial measurements of 10 to 12 mm, whereas values of 12.1 to 15 mm should be referred to as *moderate* ventriculomegaly, because they tend to have in general a worse outcome.<sup>14</sup>

Congenital hydrocephalus has genetic implications. It should be stressed that the experience thus far indicates that antenatal ultrasound is unreliable for predicting the recurrence of isolated ventriculomegaly, and particularly of the X-linked variety, because in many cases, enlargement of the lateral ventricles develops only late in gestation or after birth. DNA analysis for the X-linked variety is now available and should be considered, although the exact sensitivity remains uncertain.<sup>15-17</sup>

When the diagnosis of severe ventriculomegaly is made before viability, many parents would probably request termination of pregnancy. In continuing pregnancies, no modifications of standard obstetric management are required. A cesarean section is recommended only in those cases with associated macrocrania. Cephalocentesis to reduce cranial size is associated with significant morbidity and is indicated only in cases with a presumption of a severe prognosis.<sup>18</sup>

**Table 10-1**

**Incidence of Neural Tube Defects in Various Geographic Areas**

	Spina Bifida Incidence per 1000 Births	Anencephaly Incidence per 1000 Births
South Wales	4.1	3.5
Southampton	3.2	1.9
Birmingham, UK	2.8	2.0
Charleston		
White	1.5	1.2
Black	0.6	0.2
Alexandria	.0	3.6
Japan	0.3	0.6

Modified from Brocklehurst G. In Vinken PJ, Bruyn GW (eds): Handbook of Clinical Neurology vol 32. Amsterdam, Elsevier/North Holland Biomedical Press, 1978, pp 519-578.

## NEURAL TUBE DEFECTS

The average incidence of neural tube defects, is 1 to 2 in 1000 births, with a peak of 7 in 1000 in South Wales (Table 10-1).<sup>1</sup> The multifactorial etiology of these anomalies is well established (Tables 10-2 and 10-3).

### Anencephaly

*Anencephaly* is characterized by the absence of the cranial vault and telencephalon. Necrotic remnants of the brain stem and rhombencephalic structures are covered by a vascular membrane. Associated malformations are common and include spina bifida, cleft lip/palate, clubfoot, and omphalocele. Polyhydramnios is frequently found. The diagnosis is easy in the second and third trimester, and relies on the demonstration of the absence of the cranial vault

**Table 10-2 Recognized Causes of Neural Tube Defects**

Multifactorial inheritance
Anencephaly, meningomyelocele, meningocele, and encephalocele
Single mutant genes
Meckel syndrome, autosomal recessive (phenotype includes occipital encephalocele and rarely anencephaly)
Median-cleft face syndrome, possibly autosomal dominant (phenotype includes anterior encephalocele)
Robert syndrome, autosomal-recessive inheritance (phenotype includes anterior encephalocele)
Syndrome of anterior sacral meningomyelocele and anal stenosis—ominant, either autosomal or X-linked
Jarcho-Levin syndrome, autosomal-recessive inheritance (phenotype includes meningomyelocele)
HARDE syndrome autosomal-recessive inheritance (phenotype includes encephalocele)
Chromosome abnormalities
13 trisomy
18 trisomy
Triploidy
Other abnormalities, such as unbalanced translocation and ring chromosome
Probably hereditary, but mode of transmission not established
Syndrome of occipital encephalocele, myopia, and retinal dysplasia
Anterior encephalocele among Bantus and Thais
Teratogens
Valproic acid (phenotype includes spina bifida)
Aminopterin/amethopterin (phenotype includes anencephaly and encephalocele)
Thalidomide (phenotype includes, rarely, anencephaly and meningomyelocele)
Maternal predisposing factors
Diabetes mellitus (anencephaly more frequent than spina bifida)
Specific phenotypes, but without known cause
Syndrome of craniofacial and limb defects secondary to aberrant tissue bands (phenotype includes multiple encephaloceles)
Cloacal exstrophy (phenotype includes myelocystocele)
Sacroccygeal teratoma (phenotype includes meningomyelocele)

Modified from Main DM, Mennuti MT: Neural tube defects: Issues in prenatal diagnosis and counseling. *Obstet Gynecol* 67; 1, 1986.

(Fig. 10-12). Anencephaly is considered to be the final stage of acrania, as a consequence of disruption of abnormal brain tissue unprotected by the calvarium.<sup>19</sup> Although the term acrania is often used in conjunction with anencephaly, the term implies absence of the entire skull, including the skull base, which is not true in anencephaly.<sup>20,21</sup> The skull base is present in anencephaly and the calvarium is absent (acalvaria). Although the fetal head can be positively

**Table 10-3 Estimated Incidence of Neural Tube Defects (NTD) Based on Specific Risk Factors in the United States**

Population	Incidence per 1000 Live Births
Mother as reference	
General incidence	1.4-1.6
Women undergoing amniocentesis for Advanced maternal age	1.5-3.0
Women with diabetes mellitus	20
Women on valproic acid in first trimester	10-20
Fetus as reference	
One sibling with NTD	15-30
Two siblings with NTD*	57
Parent with NTD	11
Half sibling with NTD	8
First cousin (mother's sister's child)	10
Other first cousins	3
Sibling with severe scoliosis secondary to multiple vertebral defects	15-30
Sibling with occult spina dysraphism	15-30
Sibling with sacroccygeal teratoma or hamartoma	~15-30

\*Risk is higher in British studies. Risk increases further for three or more siblings or combinations of other close relatives.

Modified from Main DM, Mennuti MT: Neural tube defects: Issues in prenatal diagnosis and counseling. *Obstet Gynecol* 67:1, 1986.

identified by vaginal sonography as early as the 7th week of gestation, the diagnosis may be difficult in the first trimester. Absent calvarial mineralization before 10 to 12 weeks' gestation makes the differentiation of normal and abnormal brain difficult. Therefore, a cephalic pole, albeit overtly abnormal, is usually present in early gestation, and may be difficult to identify and differentiate from the normal brain before 11 weeks' gestation (see Fig. 10-12).<sup>22</sup>

## Spina Bifida

The term *spina bifida* refers to incomplete closure of the bony elements of the spine (lamina and spinous processes) posteriorly.<sup>23-25</sup> Spina bifida is commonly subdivided into open and closed forms.<sup>26</sup> Open spina bifida is predominant at birth and is a full-thickness defect of the skin, underlying soft tissues and vertebral arches exposing the neural canal. The defect may be covered by a thin meningeal membrane, an extension of dura and arachnoid *without neural tissue* through the posterior spina bifida (meningocele). In the presence of neural tissue inside the sac, the lesion is defined as a myelomeningocele, a term often used to indicate all cases of spina bifida aperta. The defect may vary considerably in size. The lumbar, thoracolumbar, or sacrolumbar areas are most frequently affected. Leakage of cerebrospinal fluid through the defect causes an increased concentration of alpha-fetoprotein (AFP) in the amniotic fluid and maternal serum.<sup>10</sup> Closed spina bifida is characterized by a vertebral schisis covered by skin. The skin is usually pigmented,



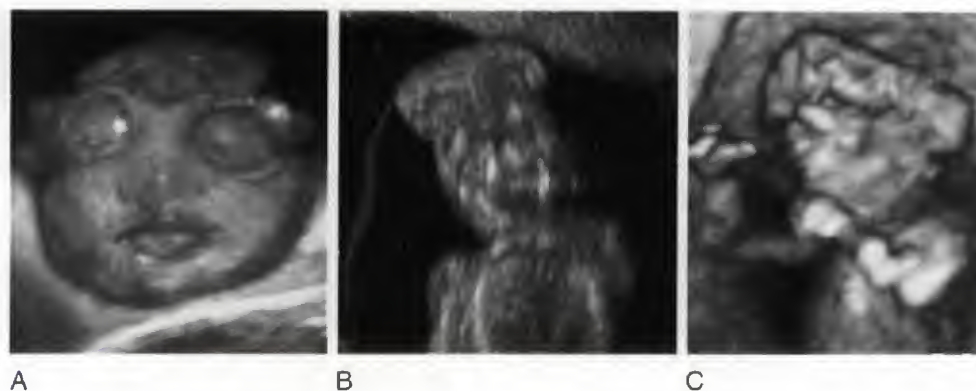


**FIGURE 10-12.** Anencephaly in the third (A) and second trimester (B,C). (A. Courtesy of Renato Ximenes, Sao Paulo, Brazil.)

dimpled, or composed of areas with hypertrichosis. A subcutaneous mass, a meningocele or lipoma, may be present. Maternal serum and amniotic fluid AFP are usually within normal limits.<sup>27</sup>

Developmentally, there is a localized failure of closure of the neural folds (neural tube) in patients with myelomeningoceles. As a result, the neural tube remains open and the neural folds remain in continuity with the cutaneous ectoderm at the skin surface.<sup>23</sup> The spinal cord, which is open at the skin surface, is referred to as the *neural placode*.<sup>23</sup> Failure of separation of the neural placode and cutaneous ectoderm prevents the tissue destined to form the pedicles and lamina to migrate properly relative to the neural ectoderm.<sup>23</sup> As a result, the pedicles and lamina are everted, facing posterolaterally instead of posteromedially, and the spinal canal undergoes fusiform enlargement in the area of the spina bifida (Fig. 10-13).<sup>23</sup>

Open spina bifida can be identified sonographically by demonstrating the defect of the neural tube that is constantly associated with separation of the posterior processes of the vertebrae, absence of posterior soft tissues, and (frequently) with the cyst formed by the myelomeningocele (see Fig. 10-13). Prenatal recognition has been reported as early as the first trimester.<sup>28</sup> However, in everyday practice, the diagnosis remains difficult even at midgestation and always requires meticulous scanning. The experience of the operator, the quality of the equipment and the amount of time dedicated to the scan continue to represent critical factors. The accuracy of referral centers is close to 100%.<sup>10</sup> The sensitivity of routine nontargeted examinations at midgestation is extremely variable in different studies, and it is probably about 40% when ultrasound is the only method and about 80% when ultrasound is used in conjunction with maternal serum AFP screening.<sup>29-32</sup> Examination of the fetal head can assist the sonologist, because open spina bifida is consistently associated with easily recognizable cranial abnormalities.<sup>33,34</sup> Leakage of cerebrospinal fluid leads to displacement of the cerebellar vermis, fourth ventricle, and medulla oblongata through the foramen magnum inside the upper cervical canal (Chiari type II or Arnold-Chiari malformation). Sonographically, this results in small head measurement at midgestation, obliteration of the cisterna magna, small size and abnormal shape of the cerebellum that is impacted deep into the posterior fossa (banana sign),

and frontal concavity (lemon sign) (Fig. 10-14). The observation of a normal appearance of the cerebellum and a normal cisterna magna virtually excludes a myelomeningocele. Hydrocephalus of variable degree is present in virtually all cases of spina bifida aperta at birth but in less than 70% of cases in the midtrimester.<sup>33,34</sup> It should be noted that other intracranial abnormalities are often seen in association with a myelomeningocele and Chiari II malformation (Table 10-4).<sup>23</sup> In particular, abnormalities of the corpus callosum are seen in 70% to 90% of affected patients.<sup>23</sup> These abnormalities consist of hypoplasia or absence of the splenium and rostrum of the corpus callosum.<sup>23</sup>

Closed spina bifida is associated with normal intracranial anatomy and normal AFP, and therefore, is often difficult to diagnose, with the possible exception of cases associated with large subcutaneous lesions, such as meningoceles or, more frequently, lipomas (Fig. 10-15).<sup>27</sup>

Although anencephaly is invariably fatal, the outcome for infants with open spina bifida is dictated by the site and extension of the lesion. The mortality rate remains high in the long term and many of the survivors suffer from significant disabilities such as lower limb paralysis or dysfunction and incontinence.<sup>35</sup> Sagittal views are most useful in assessing the severity and location of the lesion. The top or the most cephalic extent of the bone malformation in spina bifida is often referred to as "the level of the lesion." This level can be determined by counting up from the last ossified vertebral segment (assumed to be S-4 in the second trimester and S-5 in the third trimester). If it is technically difficult to assess the lower spine, one can assume that the last rib indicates T-12 and the top of the iliac wing indicates L-5 to S-1 (see Fig. 10-13B).<sup>36</sup> Recently, attempts have been made at intrauterine repair of spina bifida and it has been suggested that these operations may reduce the morbidity of the affected infants. Although preliminary evidence suggests an improvement in the posterior fossa abnormality, the final analysis of improvement in outcome will have to await large multicenter studies. It has been suggested that elective caesarean section may be beneficial to the infants in reducing the rate of neurologic complications and particularly the level of motor paralysis.<sup>37</sup> However, these results remain a matter of debate.<sup>37-39</sup>

The outcome of closed spina bifida is difficult to predict in utero. These infants usually do not develop Arnold-Chiari

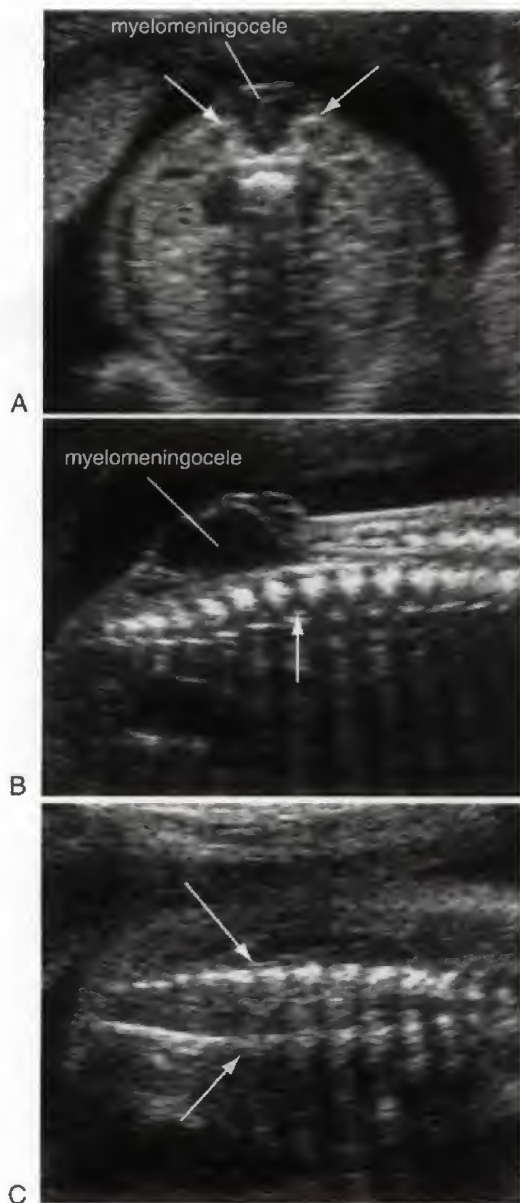


**FIGURE 10-13.** Myelomeningocele in a midtrimester fetus. *A.* The posterior elements of the spine (*arrows*) are splayed outward. The myelomeningocele is flat in this plane of section. *B.* Although the defect in the spine cannot be recognized in this view, the fluid-filled myelomeningocele is well seen. The last ossified spinal segment in this second trimester fetus is S4, and thus, counting upward, the top of the lesion is at the L2-L3 level (*arrow*). *C.* Coronal plane of section demonstrating fusiform enlargement of the spinal canal (*arrows*) in the area of the spina bifida.

malformation and hydrocephalus. However, particularly those with subcutaneous masses may suffer from neurologic sequelae of variable entity.<sup>40</sup>

### Cephalocele

The term *cephalocele* indicates a protrusion of intracranial contents through a bony defect of the skull. In most cases, the lesion arises from the midline. They are the most

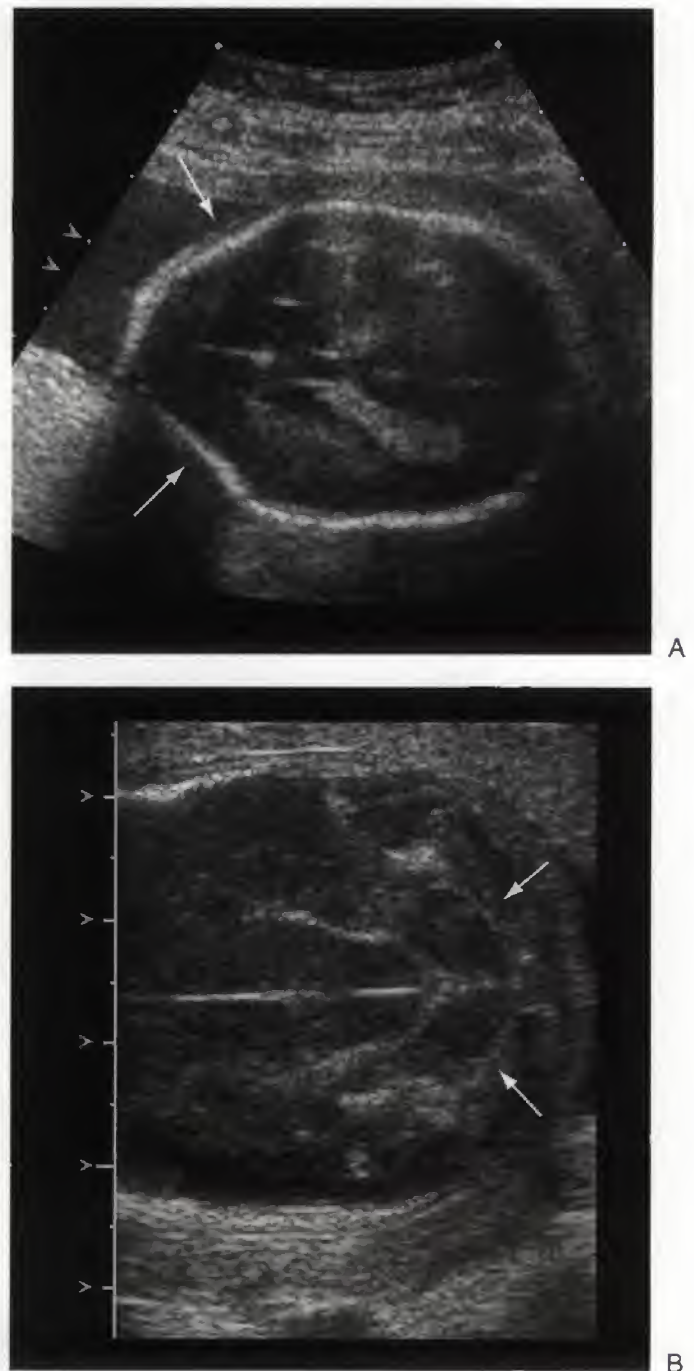


**FIGURE 10-14.** The cranial signs associated with open spina bifida. *A.* The lemon sign from the frontal concavity (*arrows*). *B.* The banana sign of the compressed cerebellar hemispheres (*arrows*).

common in the occipital area in the white populations in Europe and North America, accounting for approximately 80% of cephaloceles in that group.<sup>41</sup> In southeast Asia, the most common location for cephaloceles is the fronto-ethmoidal region.<sup>41-43</sup> Parietal cephaloceles are the least common and often associated with significant underlying brain abnormalities.<sup>41,43</sup> Encephaloceles are characterized by the presence of brain tissue inside the lesion. When only meninges protrude, the term cranial meningocele should be



used. Cephaloceles often cause impaired cerebrospinal fluid circulation and hydrocephalus. Massive encephaloceles may be associated with microcephaly. Cephaloceles are frequently associated with other anomalies or are part of a syndrome (Table 10-5).

Fetal cephaloceles should be suspected when a paracranial mass is seen on sonography (Fig. 10-16). The diagnosis of encephalocele is easy, because the presence of brain tissue inside the sac is striking on ultrasound.<sup>44,45</sup> Differentiation of a cranial meningocele from soft tissue edema or a cystic hygroma of the neck may be difficult. Demonstration of the bony defect in the skull would allow a proper diagnosis but cranial meningoceles are often associated with extremely small (few millimeters) defects that are not amenable to antenatal sonographic recognition. Indirect clues can assist the diagnosis. Cranial cephaloceles are very often associated with ventriculomegaly. The major differential diagnostic consideration is that of cystic hygromas. Cystic

hygromas arise from the region of the neck, have multiple internal septations and a thick wall, and are often associated with generalized soft tissue edema and hydrops.

The pediatric literature suggests that the outcome of cephaloceles is mainly related to the presence or absence of brain tissue inside the lesion. However, the largest available antenatal series reports a dismal prognosis for both varieties.<sup>44,45</sup>

**Table 10-4**

### Frequency of Brain and Spine Anomalies in Patients With Chiari II Malformations

Anomaly	Frequency
Myelomeningocele	Always
Hydrocephalus	Almost always
Dysplastic tentorium	Almost always
Small posterior fossa	Almost always
Luckenschädel	Almost always
Caudal Displacement of brainstem	Usually
Cervicomedullary kink	Usually
Upward Cerebellar Herniation	Usually
Large massa intermedia	Usually
Elongated cranial nerves	Usually
Tectal beak	Usually
Callosal hypogenesis	Usually
Syringohydromyelia	~50%
Malformations of cortical development	Occasionally
Aqueductal stenosis	Occasionally

From Barkovich AJ: Congenital malformations of the brain and skull. In Barkovich AJ (ed), *Pediatric Neuroimaging*, 4th ed. Philadelphia, Lippincott Williams & Wilkins, 2005.

**Table 10-5** Conditions Associated with Cephaloceles

Amniotic band syndrome (sporadic)
Multiple cephaloceles, predominantly anterior
Amputations of digits or limbs
Bizzare oral clefts Chemke syndrome (AR)
Hydrocephaly
Agrya
Cerebellar dysgenesis cryptophthalmos syndrome (AR)
Forehead skin covers one or both eyes
Ear abnormalities
Soft tissue syndactyly dyssegmental dysplasia (AR)
Short limb dysplasia
Metaphyseal widening
Small thorax
Micrognathia
Frontonasal dysplasia (sporadic, some cases are familial)
Frontal cephalocele
Ocular hypertelorism meckel syndrome (AR)
Polycystic kidneys
Polydactyly
Microphthalmia
Orofacial clefting
Ambiguous genitalia von Voss syndrome (?)
Agenesis of the corpus callosum
Phocomelia
Urogenital anomalies
Thrombocytopenia Warfarin syndrome
Nasal hypoplasia
Bone stippling
Limb shortening
Hydrocephaly

Modified from Cohen MM Jr, Lemire RJ: Syndromes with cephaloceles. *Teratology* 25:161, 1982.

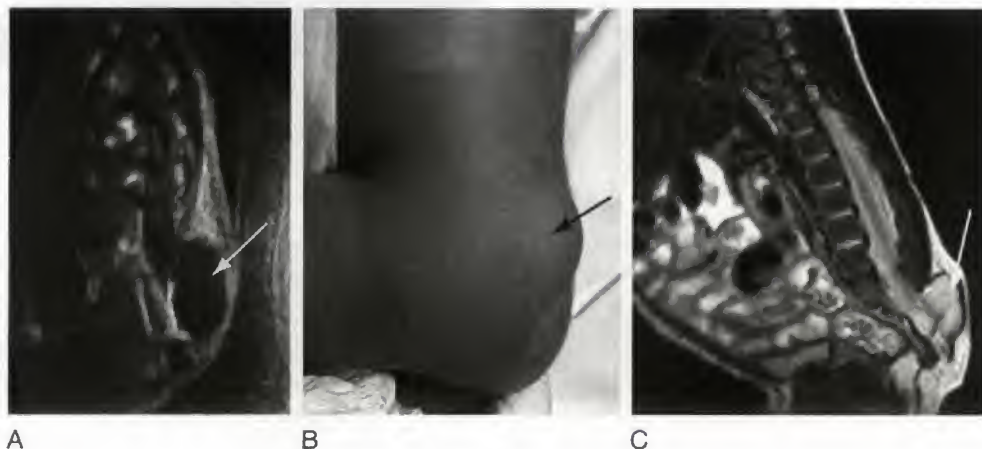


**FIGURE 10-15.** Closed spina bifida with lipoma. (A) Prenatal sonogram, (B) postnatal appearance, and (C) magnetic resonance imaging of the spine.

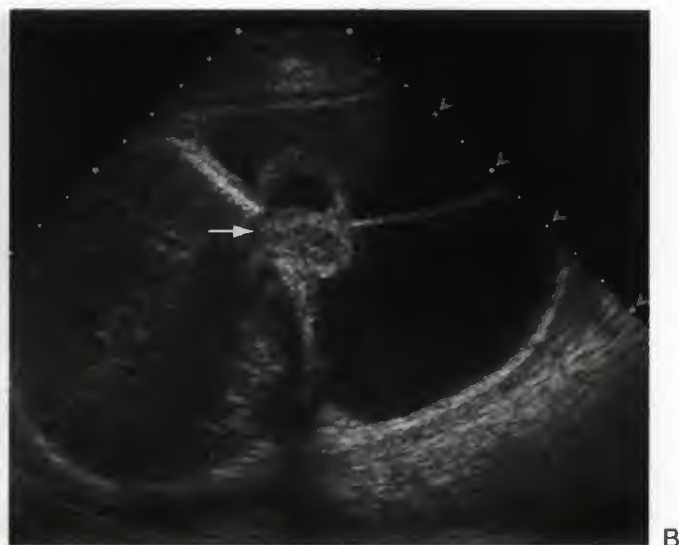
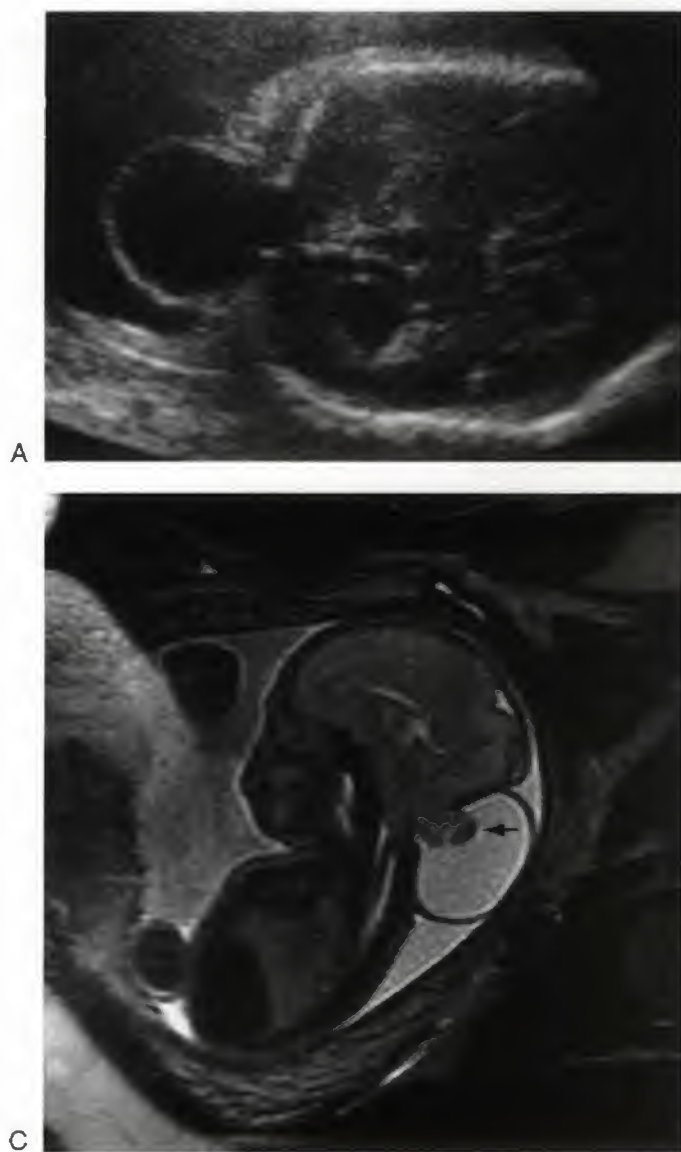


**FIGURE 10-16.** Fetal cephaloceles. A. Cranial meningocele. B. Encephalocele with small amount of brain seen herniating through the defect (arrow) in the calvarium. C. MRI from the same patient demonstrating the cystic and brain components (arrow) of the encephalocele. MRI, magnetic resonance imaging scan.

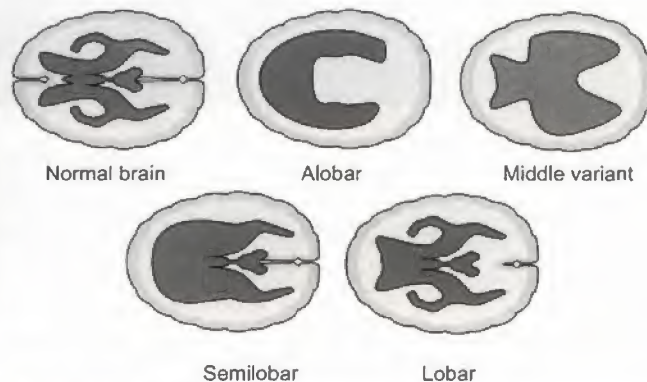


**FIGURE 10-17.** Schematic representation of a normal brain compared with different varieties of holoprosencephaly.

## MIDLINE ANOMALIES

Midline cerebral anomalies include a group of brain defects that encompass a wide spectrum of severity and are typically associated with craniofacial malformations.

The *holoprosencephalies* are complex abnormalities of the forebrain that share in common an incomplete separation of the cerebral hemispheres and formation of diencephalic structures.<sup>46</sup> The most widely accepted classification of these disorders (Fig. 10-17) recognizes four major varieties: the alobar, semilobar, and lobar types, plus the more recently described middle interhemispheric variant. In the *alobar* variety, the most pronounced one, the interhemispheric fissure, falx cerebri, and corpus callosum are totally absent; there is a single primitive ventricle (holoventricle); the thalami are fused in the midline; and there is absence of the third ventricle, neurohypophysis, and olfactory bulbs and tracts. In *semilobar* holoprosencephaly, the two cerebral hemispheres are partially separated posteriorly but there is still a single

ventricular cavity. In both the alobar and semilobar forms, the roof of the ventricular cavity, the *tela choroidea*, normally enfolded within the brain, may balloon out between the cerebral convexity and the skull to form a cyst of variable size, called the *dorsal sac*. Alobar and semilobar holoprosencephaly are often associated with microcephaly, less frequently with macrocephaly, which is invariably due to a dorsal cyst and/or internal obstructive hydrocephalus. In the lobar variety, the interhemispheric fissure is well developed posteriorly and anteriorly, but there is still a variable degree of fusion of the cingulate gyrus and of the lateral ventricles, and absence of the septum pellucidum. In the middle interhemispheric variant of holoprosencephaly, fusion occurs mostly at the level of the bodies of lateral ventricles, whereas



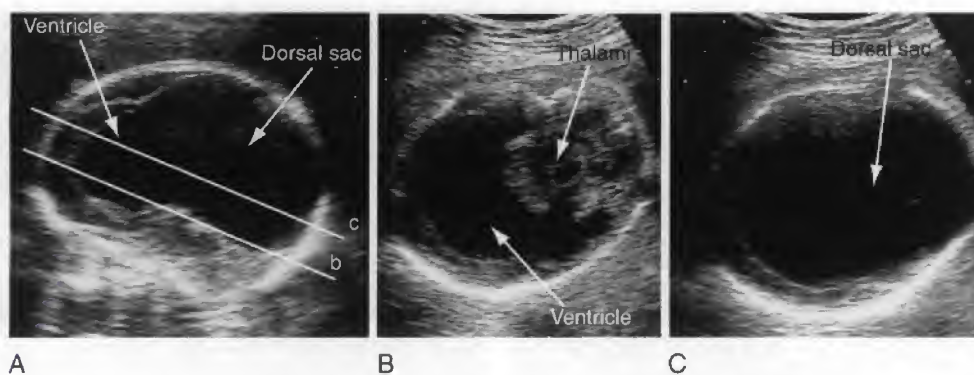


**FIGURE 10-18.** Multiplanar sonography of alobar holoprosencephaly in the midtrimester. *A.* Median plane demonstrating the single ventricular cavity, which has a rim of cortex anteriorly and amply communicates posteriorly with a dorsal sac. *B.* Axial scan at the level of the thalami, demonstrating the crescent shaped single ventricle and the absence of the midline in the anterior cortex. *C.* In a slightly craniad axial plane than the previous one, the communication between the ventricular cavity and the dorsal sac is demonstrated.

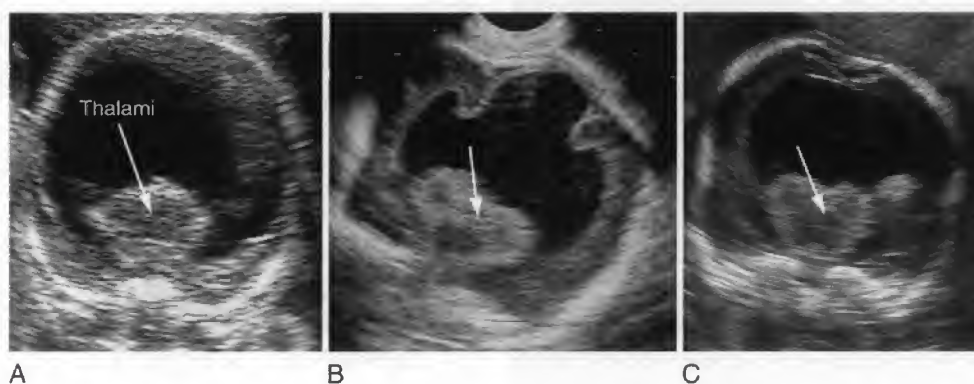


**FIGURE 10-19.** Different varieties of alobar holoprosencephaly (*A*) pancake type: only a thin rim of cortex is present, and the ventricular cavity continues anteriorly and posteriorly with a large dorsal sac; (*B*) cup variety: the cortex is partially enfolded over the ventricular cavity with a better delineation of the transition between the ventricle and the dorsal sac; (*C*) ball variety: the cortex is completely enfolded over the ventricular cavity, and there is no dorsal sac. All varieties share in common a very similar bulb-like appearance of the thalami (arrows).

the frontal horns and posterior horns are relatively well developed.<sup>47</sup> In patients with semilobar holoprosencephaly the splenium of the corpus callosum is present without the genu or body of the corpus callosum.<sup>41,48,49</sup> As Barkovich states:

Holoprosencephaly is the only brain anomaly described in which the posterior corpus callosum forms in the absence of anterior callosal formation.<sup>41 (p 367)</sup>

Alobar and semilobar holoprosencephaly are typically and almost constantly associated with facial anomalies that can be regarded as the consequence of hypoplasia of the midfacial structures. The malformations span between cyclopia and severe hypotelorism with median cleft lip/palate. The nose may be absent, replaced by a proboscis, or extremely flattened.<sup>46</sup> Conversely, facial anomalies are rarely encountered in the lobar form and middle interhemispheric variant.

Holoprosencephaly at birth is exceedingly rare. This anomaly has a high intrauterine fatality rate and is not infrequently encountered in prenatal studies. The etiology is heterogeneous. In most cases, the anomaly is isolated and

sporadic. In other cases, chromosomal abnormalities have been found (trisomy 13 and polyploidy) and anatomic abnormalities are found.

Prenatal diagnosis of alobar holoprosencephaly depends on the demonstration of a single rudimentary cerebral ventricle, that may protrude posteriorly through the incompletely enfolded cortex to form a dorsal sac (Fig. 10-18). According to the degree of enfoldment of the cortex over the ventricular cavity and the presence or absence of a dorsal sac, three varieties of alobar holoprosencephaly are commonly distinguished: the pancake, the cup, and the ball type (Fig. 10-19). Additional findings include the presence of typical facial anomalies. Similar findings are expected with the semilobar type. The middle interhemispheric variant of alobar holoprosencephaly is featured by relatively well-formed frontal horns that are fused in the midline without the intervening septum pellucidum and communicate posteriorly with a single rudimentary cavity (Fig. 10-20). Recognition of the lobar variety has also been reported, although the differentiation from other cerebral anomalies such as the simple agenesis of the septum pellucidum is always difficult. Although this condition may be suspected in

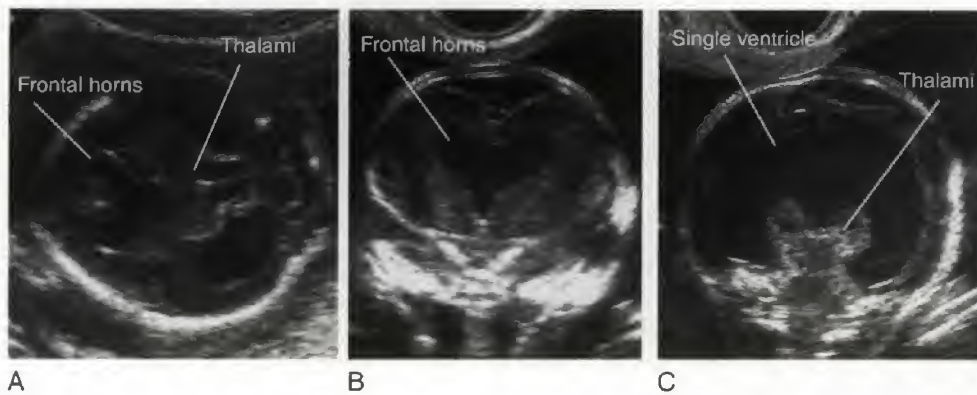


**FIGURE 10-20.** Middle interhemispheric variant of holoprosencephaly in the axial (A), anterior coronal (B), and midcoronal plane (C). The frontal horns are well developed and there is a partial formation of the interhemispheric fissure. However the midcoronal plane reveals a common ventricular cavity with hypoplastic undivided thalami.

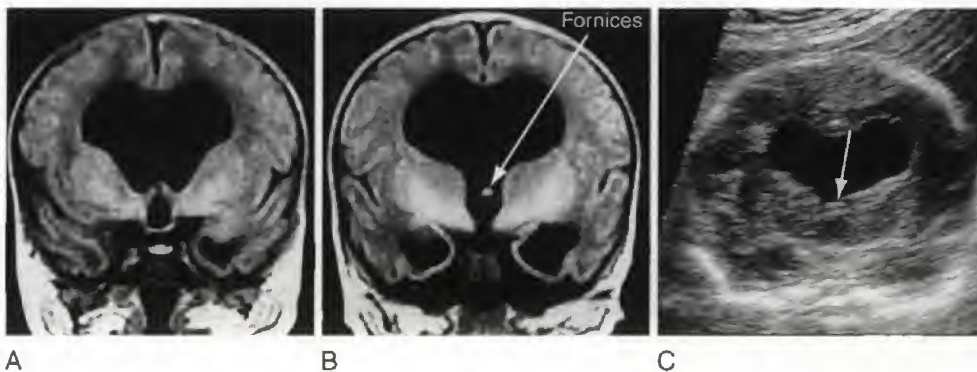


**FIGURE 10-21.** Lobar holoprosencephaly. (A, B) Postnatal magnetic resonance image; (C) prenatal ultrasound study. The frontal horns are fused centrally, as well as the fornices (arrow), which form a thick fascicle running in the floor of the cavity.



**FIGURE 10-22.** A. Color Doppler demonstration of anterior cerebral artery (ACA) branching in a normal fetus and giving rise to the pericallosal artery. B. Lobar holoprosencephaly: the interhemispheric fissure is shallow and the arteries branching from the anterior cerebral artery run on the surface of the brain (serpent crawling). C. In agenesis of the corpus callosum, the arteries ascend vertically without forming a loop. 3v, third ventricle.

axial scans, mainly because of the concomitance of absence of the septum pellucidum and ventriculomegaly, the coronal scan is more informative in that it demonstrates the flat squared roof of the frontal horns as well as the ample inferior communication with the inferior third ventricle. The presence of the fused fornices, which appear as a linear structure running within the third ventricle from the anterior to the posterior commissure, is a frequent and very specific finding with this condition (Fig. 10-21).<sup>50,51</sup> As in

lobar holoprosencephaly, the interhemispheric fissure is shallow anteriorly owing to the fusion of the frontal lobes and the branches of the anterior cerebral artery run along the surface of the brain giving rise on color Doppler imaging to a typical sign that has been referred to as the serpent crawling under the skull (Fig. 10-22).<sup>52</sup>

The invariably poor prognosis for infants affected by alobar and semilobar holoprosencephaly is well established. Thus far, cases diagnosed in utero with lobar holopros-



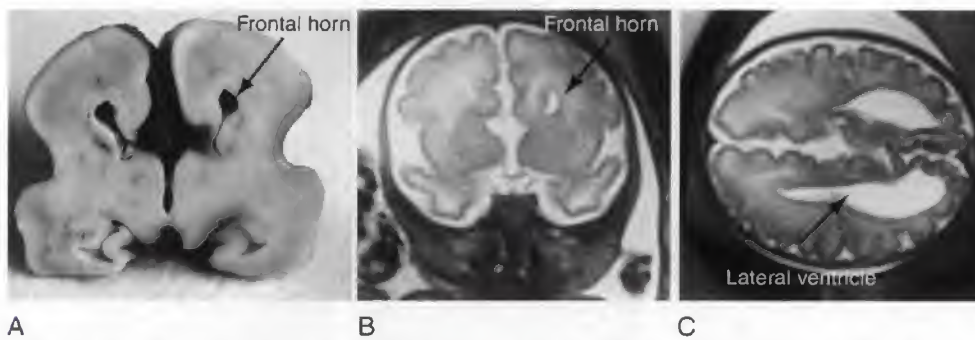


**FIGURE 10-23.** Complete agenesis of the corpus callosum: (A) pathology in a midtrimester fetus; (B, C) magnetic resonance at 32 weeks. Apart from the absence of the corpus callosum, a number of abnormal findings can be appreciated including the increased separation of the hemispheres, the comma-shaped frontal horns, and the teardrop shape of the lateral ventricles in the axial plane, referred to as colpocephaly.

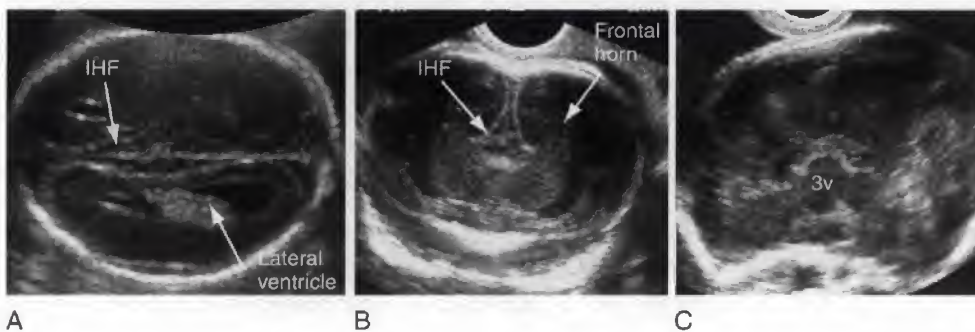


**FIGURE 10-24.** Sonography of fetal agenesis of the corpus callosum. A. In the axial plane, the interhemispheric fissure (IHF) appears wider than usual without evidence of the cavum septi pellucidum. B. In the coronal and (C) sagittal plane, no corpus callosum or cavum septi pellucidum can be seen above the third ventricle (3v).

encephaly have also had extremely poor neurologic development.<sup>50,52</sup>

## Agenesis of the Corpus Callosum

*Agenesis of the corpus callosum* (ACC) is an anomaly of uncertain prevalence and clinical significance. Estimates of 0.3% to 0.7% in the general population and 2% to 3% in the developmentally disabled are usually quoted.<sup>53,54</sup> The etiology is heterogeneous. Genetic factors are probably predominant. The high frequency of associated malformations and chromosomal aberrations suggest that ACC is often a part of a widespread developmental disturbance.

ACC may be either complete or partial. In the latter case, also referred to as dysgenesis of the corpus callosum, the caudal portion (splenium and body) is missing to varying degrees.

The diagnosis of ACC is possible from midgestation onward<sup>55</sup> but is a challenge even for expert sonologists.<sup>56</sup> The anatomic elements useful for the diagnosis are summarized in Figure 10-23. With complete ACC, there is no septum pellucidum, the two hemispheres tend to be more separated than usual in the central part of the brain, and

there are typical modifications in the morphology of the lateral ventricle. In the coronal section, the frontal horns are separated more than usual and have a comma-like shape, whereas in the transverse axial plane, the lateral ventricles have a teardrop-like shape that is due to the combination of the posterior enlargement of the atria and occipital horn with frontal horns that have a normal size but are more separated than usual. This finding is referred to as colpocephaly. The third ventricle may be rostrally displaced. In routine examinations, an increased atrial width with a typical teardrop configuration of the lateral ventricles and failure to visualize the cavum septum pellucidum should alert the physician to the possibility of fetal ACC. Once a suspicion has been formulated, a direct diagnosis is possible by demonstrating the absence of the corpus callosum on coronal and sagittal scans (Fig. 10-24). These views are at times difficult to obtain, in particular in fetuses in vertex presentation. However, vaginal sonography is of great advantage in such cases. Abnormal branching of the anterior cerebral artery can also be demonstrated with the use of color Doppler ultrasound (see Fig. 10-22).

Diagnosis of partial ACC has also been reported, but the sonographic findings are even more elusive than with the



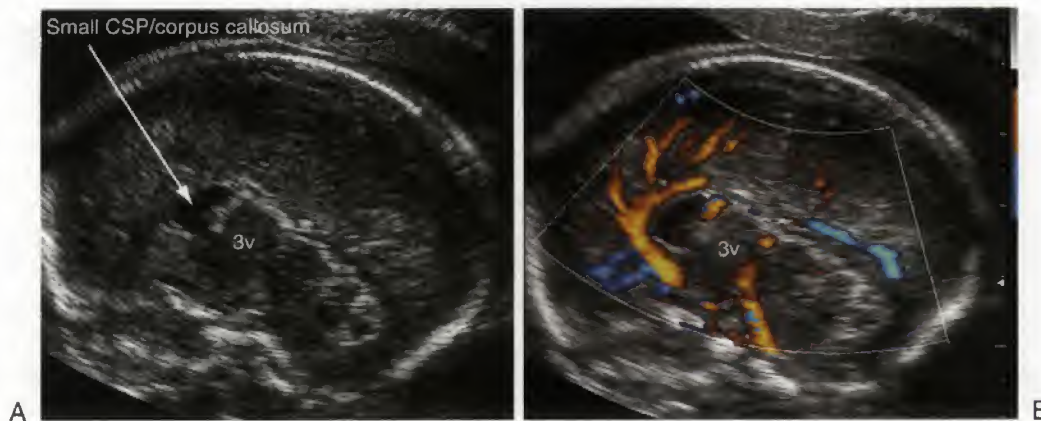


**FIGURE 10-25.** Partial agenesis of the corpus callosum. *A.* In this fetus at 21 weeks' gestation, the corpus callosum/cavum septi pellucidi complex is much smaller than normal; in fact it does not entirely cover the third ventricle, but only reaches about midway. *B.* The corpus callosum appears thin and barely discernible with gray scale imaging and can be positively identified only when highlighted by the course of the pericallosal artery.

complete form (Fig. 10-25).<sup>55,57</sup> The cavum septi pellucidi is usually present, and the axial sections may be completely unremarkable. Identification of partial ACC requires a median section demonstrating that the posterior portion of the corpus callosum is absent. This results in the corpus callosum forming an incomplete arch over the area of the third ventricle. The incomplete corpus callosum tends also to be thinner and on top forms an angle that is more open posteriorly than usual.

Midline interhemispheric cysts may be seen in association with ACC. Barkovich et al<sup>41</sup> divide ACC with interhemispheric cysts into two major groups: Type 1, in which the interhemispheric cyst is a diverticulum of the ventricular system and thus communicates with the ventricles and type 2, in which multiple cysts are present that do not communicate with the ventricles. Type 2 ACC with interhemispheric cyst is often associated with subcortical heterotopia. Of note, as with all types of cysts, the cysts associated with callosal agenesis may not develop or become apparent on imaging until late in gestation.<sup>41,58,59</sup> These cysts can be associated with macrocephaly or frank hydrocephalus at birth.<sup>41,58,59</sup>

ACC, be it complete or partial, is frequently a part of syndromes or multiple malformations (Table 10-6). The most common mentioned is Aicardi syndrome, an X-linked dominant disorder consisting of infantile spasms, callosal agenesis or hypogenesis, chorioretinopathy, severe global developmental delay, and medically refractory epilepsy.<sup>41,60,61</sup> Imaging may demonstrate: callosal agenesis or hypogenesis, heterotopias, cortical dysplasia, posterior fossa cysts, cerebellar hypoplasia, choroid plexus papillomas, and microphthalmia. When ACC is an isolated finding it is associated with a normal to borderline intellectual development in most cases.<sup>55,62</sup> However, long-term studies indicate a progressive decrease in intellectual capacity throughout the years, and most infants tend to have significant difficulties in school.<sup>63</sup> ACC has also been linked to psychosis.<sup>64</sup>

*Absence of the septum pellucidum* is the rule with holoprosencephaly and ACC. It may also occur with other intracranial anomalies, such as deMorsier syndrome, or septo-optic dysplasia, cortical abnormalities, and schizencephaly, and it may also be present as an isolated finding (Fig. 10-26).<sup>47,65-67</sup>

The differential diagnosis is frequently difficult. However, pediatric data suggest that the prognosis is usually severe, with more than 90% of cases demonstrating mental retardation or severe neurologic abnormalities when associated with other anomalies and 66% demonstrating motor defects or mental delay when isolated.<sup>67</sup>

## Dandy-Walker Malformation

The term *Dandy-Walker syndrome or malformation* was originally described in 1914 by Dandy and Blackfan in which a rare malformation of the posterior fossa consisting of marked cystic dilatation of the fourth ventricle with anterior and superior displacement of a vermis with complete or partial agenesis was seen.<sup>68</sup> Three additional cases and a review of the literature were reported by Taggart and Walker in 1942.<sup>69</sup> In an additional report and review of the malformation in 1954, Benda labeled this abnormality as the Dandy-Walker malformation.<sup>70</sup> Since the original description, a number of other abnormalities of the posterior fossa with similarities to the Dandy-Walker malformation have been described including the Dandy-Walker variant (partial agenesis of the vermis without a large dilated cystic fourth ventricle), megacisterna magna and Blake's pouch cyst. Some investigators have suggested that all of these entities be grouped and referred to as the Dandy-Walker complex.<sup>49</sup> The difficulty in using one term to describe these entities is that the prognosis for each can be different. Strictly described, the Dandy-Walker malformation should be used to describe (1) marked cystic dilatation of the fourth ventricle, which may fill much of the posterior fossa; (2) hypogenesis or agenesis of the cerebellar vermis; and (3) superior displacement of the tentorium and lateral sinuses. The cisterna magna is compressed and reduced to a virtual space between the dilated fourth ventricle and the dura mater.<sup>71</sup> The cerebellar hemispheres are often anterolaterally displaced. Hydrocephalus, although frequently seen in cases of Dandy-Walker malformation, is not necessary for the diagnosis.

Sonographically, the median plane is the most important one for the diagnosis. The cystic fourth ventricle extends superiorly, displacing the cerebellar vermis (which is frequently



**Table 10-6****Syndromes Featuring Agenesis of the Corpus Callosum***Frequent in:*

Acrocallosal syndrome (AR)  
 Aicardi syndrome (X-linked dominant)  
 Andermann syndrome (AR)  
 Cerebro-oculo-facio-skeletal (COFS) syndrome (AR)  
 Fryns syndrome (AR)  
 Marden-Walker syndrome (AR)  
 Meckel Gruber syndrome (AR)  
 Microphthalmia-linear skin defects syndrome (X-linked dominant)

Miller Diexer syndrome (lissencephaly syndrome)

Neu-Laxova syndrome (AR)

Septo-Optic dysplasia sequence

Walker-Warburg syndrome (X-linked dominant)

Zellweger syndrome (AR)

*Occasionally in:*

Apert syndrome (AR)

Baller-Gerold syndrome (AR)

Calloso-genital dysplasia syndrome (AR)

Coffin-Siris syndrome (?AR)

Congenital microgastria-limb reduction complex (unknown)

Crouzon syndrome (AD)

Duplication 4p syndrome

Fetal alcohol syndrome

Fetal warfarin syndrome

FG syndrome (X-linked recessive)

Fronto-nasal dysplasia sequence (sporadic/AD)

Gorlin syndrome (AD)

Greig cephalopolysyndactyly syndrome (AD)

Hydrolethrus syndrome (AR, X-linked dominant)

Lens dysplasia (X-linked recessive)

Marshall-Smith syndrome (unknown)

Oculo-auriculo-vertebral spectrum (unknown)

Oculo-cerebro-cutaneous syndrome (Delleman syndrome) (unknown)

Opitz syndrome (AD, X-linked recessive)

Oral-facio-digital syndrome type 1 (X-linked dominant)

Peters' Plus syndrome (AR)

Radial aplasia-thrombocytopenia syndrome (AR)

Rubinstein-Taybi syndrome (Sporadic)

Shapiro syndrome (X-linked recessive)

Simpson-Golabi-Behmel syndrome (X-linked recessive)

Trisomy 8 syndrome

Trisomy 13 syndrome

Trisomy 18 syndrome

X-linked hydrocephalus spectrum (X-linked recessive)

XO syndrome

XXXXY syndrome (hypoplastic)

Yunis-Varon syndrome

Metabolic disorders

AR, autosomal recessive; AD, autosomal dominant.

Modified from Blum A, Andre M, Droulle P, et al: Prenatal echographic diagnosis of corpus callosum agenesis. The Norway experience 1982-1989. Genet Counsel 1:115, 1990 and Jones KL: Recognizable Patterns of Human malformations. Philadelphia, WB Saunders, 1997.

hypoplastic) and elevates the *tentorium cerebelli* and the *torcular Herophili* above its normal position (Fig. 10-27). Dandy-Walker malformation is frequently associated with other neural defects, mostly with other midline anomalies, such as ACC and holoprosencephaly. Other deformities include encephaloceles, polycystic kidneys, cardiovascular defects, and facial

clefting. Table 10-7 lists the most frequent associations. Even if isolated, it has been generally considered to have a poor prognosis. However, recent experience with MRI in infants suggests that those cases in which the vermis appears hypoplastic have a subnormal intelligence in 85% of cases versus only 15% of those in which the vermis appears to be intact.<sup>72,73</sup> In a study by Boddaert et al, the cerebellar vermis was considered normal with MRI if it was possible to document three main anatomic landmarks in the median plane: the fastigium point that corresponds to the posterior apex of the fourth ventricle and the two main fissures.<sup>72</sup> A similar approach has also been suggested for antenatal studies. Both MRI and multiplanar, possibly, transvaginal ultrasound can be used. However, it is expected that the small size of the vermis and the difficulty in obtaining an exact median plane will, at times, represent major limiting factors, particularly in early gestation.

Dandy-Walker malformation is exceedingly rare, with an estimated incidence of about 1:30,000 births, and is found in 4% to 12% of all cases of infantile hydrocephalus. However, minor variations of this condition are frequently encountered, attested by an increasing number of reports, both in the prenatal and pediatric literature. The term *Dandy-Walker complex* (or *continuum*) is used to indicate the spectrum of abnormal findings that share in common an enlargement of the posterior fossa (fourth ventricle or cisterna magna) and the impression of a V-shaped cleft in the cerebellar vermis in the axial plane (Fig. 10-28).<sup>72,74,75</sup> When other anomalies are excluded, however, careful evaluation of the posterior fossa anatomy may help determine the specific abnormality and prognosis (Fig. 10-29).

Enlargement of the cisterna magna, referred to as a *megacisterna magna*, was a diagnosis introduced by Gonsette et al<sup>76,77</sup> to describe a series of adult patients with markedly enlarged posterior fossa cisterns due to cerebellar atrophy. Since the original description, the term has been "loosely applied" to describe an enlarged retrocerebellar space (cisterna magna) and a normal and intact vermis and normal cerebellar hemispheres.<sup>77</sup> In prenatal sonograms, if the cisterna magna depth is greater than 10 mm and the cerebellar vermis appears intact and in its normal position, the condition is usually referred to as *megacisterna magna*. Although this is a risk factor for associated malformations including aneuploidies (trisomy 18 in particular),<sup>78,79</sup> most isolated cases are of no consequence.<sup>8,40,74,80</sup> If there is the impression of a V-shaped cleft in the cerebellum in the axial plane and the median plane reveals a vermis that is intact with a cyst in the posterior fossa the diagnosis is most likely a *Blake's pouch cyst*, and the prognosis is usually good.<sup>40,81</sup> A *Blake's pouch cyst* represents herniation of the inferior aspect of the fourth ventricle through the foramen of Magendie into the vallecule and retroversian cistern.<sup>40</sup>

In 1976 Harwood-Nash introduced the term *Dandy-Walker variant* to describe "an outpouching of an ependymal lined cyst from the fourth ventricle" associated with dysplasia of the vermis.<sup>77,82</sup> A hypoplastic superiorly rotated vermis is the landmark of *vermian hypoplasia* previously referred to as Dandy-Walker variant, a condition that is frequently associated with other intracranial anomalies and carries a very high risk of abnormal neurodevelopment.<sup>72-74</sup> Distinction between an intact and an hypoplastic vermis is far from simple. From approximately midgestation, under normal



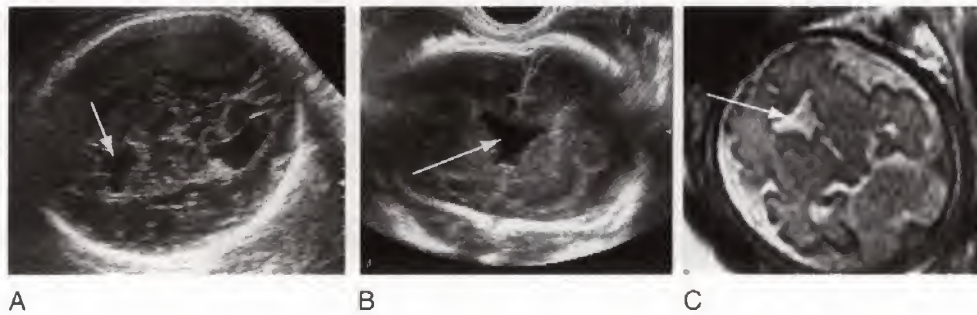


**FIGURE 10-26.** Absence of the septum pellucidum (arrow) in axial and coronal (A, B) sonograms and (C) intrauterine magnetic resonance imaging.

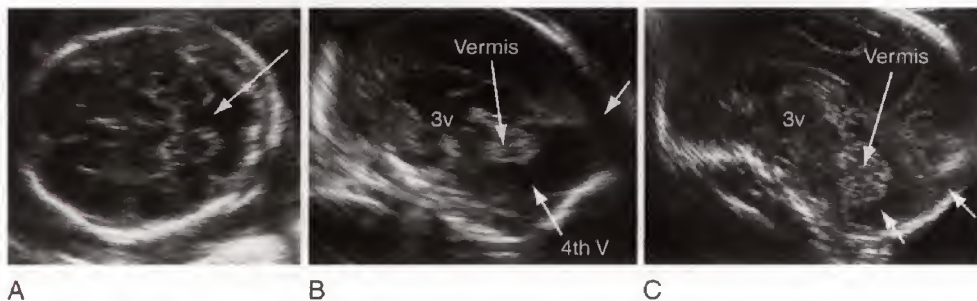


**FIGURE 10-27.** Dandy-Walker malformation. In the axial plane (A) a large fourth ventricle with a V-shaped defect in the cerebellum is seen (arrow); (B) in the sagittal plane, the cisterna magna appears large (in fact, the cystic fourth ventricle) (arrow) and the cerebellar vermis is displaced superiorly and rotated. Comparing this image with the normal appearance of this section (C), it can also be observed that the cerebellar vermis is small and shapeless, and that the fourth ventricle expands superiorly, from which a superior dislocation of the tentorium and torcular herophili can be inferred (arrows). 3v, third ventricle.

conditions, it is usually possible with either sonography or MRI to demonstrate the fastigium of the fourth ventricle and the two main fissures in the median plane.<sup>72-74</sup> With hypoplasia of the vermis, these landmarks cannot be identified. Nomograms of the normal size of the vermis throughout gestation are also available (Table 10-8).<sup>83</sup>

In our own experience, isolated megacisterna magna and Blake's pouch cyst represent the bulk of the posterior fossa anomalies that are diagnosed antenatally.<sup>8</sup> Although the data thus far are limited and the neurologic risk cannot be predicted precisely, it would seem that in the majority of these cases, the prognosis is good. It should be noted that there are some authors who believe that both conditions (megacisterna magna and Dandy-Walker variant) may represent a Blake's pouch cyst.<sup>77</sup>

The greatest diagnostic challenge is probably represented by *Joubert syndrome*, an anomaly with autosomal-recessive transmission that is featured by absence or hypoplasia of the vermis, which is not rotated. In a pregnancy at specific risk, the condition can be suspected when a communication is seen between the fourth ventricle and a cisterna magna of normal size in the transverse plane (Fig. 10-30).<sup>84</sup> In the absence of the vermis, the two hemispheres impinge on the midline, and therefore, the median plane is of little use. However, at times, it may demonstrate a fourth ventricle of slightly irregular shape.<sup>84</sup> In the absence of a positive familial history, however, this finding has a very low predictive value and most cases we have seen were found to be normal at birth.

Caution is warranted while making the diagnosis of a minor variety of the Dandy-Walker continuum, the Dandy-Walker variant, or inferior vermian agenesis. Development of the cerebellar vermis is incomplete before 20 weeks' gestation, and thus a defect and abnormality of the vermis may be suspected if imaged too early.<sup>85</sup> Even in cases diagnosed after 20 weeks, there is evidence that isolated inferior vermian hypoplasia is overdiagnosed prenatally, even with the use of MRI. Thus, postnatal confirmation is warranted.<sup>86</sup> In a study correlating the Dandy-Walker malformation complex and postmortem pathology, Phillips et al<sup>87</sup> found that two sonographic variables in the transverse axial plane correlated well with the pathologic diagnosis: the severity of the vermian defect and the shape of the gap between the hemispheres in transverse cerebellar images. A trapezoidal gap, with a broad dorsal base and relatively straight sides, corresponded to hypoplasia of aplasia of the vermis at autopsy (see Fig. 10-27A). However, a keyhole-shaped gap with convex sides was not associated with macroscopic or microscopic cerebellar pathology<sup>87</sup> (Fig. 10-28C).

In general, meticulous scanning with a multiplanar approach is recommended in cases with a suspicion of a posterior fossa anomaly. The poor correlation that has been demonstrated in several studies between antenatal diagnosis and autopsy findings is probably related to the use of only axial planes, which can be extremely misleading. In the axial plane, entities that are clinically different, such as Dandy-Walker malformation, vermian hypoplasia, and Blake's pouch cyst may be difficult to distinguish from one



**Table 10-7****Abnormalities Associated With Dandy-Walker Malformation****Malformations**

Holoprosencephaly  
 Agenesis of the corpus callosum  
 Neural tube defects  
 Cleft lip  
 Congenital heart disease  
 Cornelia de Lange syndrome  
 Goldenhar syndrome  
 Kidney abnormalities  
 Facial hemangiomas  
 Klippel-Feil syndrome  
 Polysyndactyly

**Mendelian**

Warburg (AR)  
 Aase-Smith (AD)  
 Ruvalcaba syndrome (AD/X-linked)  
 Coffin-Siris (AR)  
 Oro-facio-digital syndrome type II (AR)  
 Meckel Gruber syndrome (AR)  
 Aicardi syndrome (X-linked dominant)  
 Ellis van Creveld (AR)  
 Fraser cryptophthalmus (AR)

**Chromosomal**

45,X  
 6p-  
 9q+  
 dup 5p  
 dup 8p  
 dup 8q  
 trisomy 9  
 triploidy  
 dup 17q

**Environmental**

Rubella  
 Coumadin  
 Alcohol  
 Cytomegalovirus  
 Diabetes  
 Isotretinoin

AR, autosomal recessive; AD, autosomal dominant.

Adapted from Murray JC, Johnson JA, Bird TD: Dandy-Walker malformation: etiologic heterogeneity and empiric recurrence risk. Clin Genet 28:272, 1985.

another. Because the diagnosis of midline anomalies depends on section planes of the fetal head that are sometimes difficult to obtain, we have found that three-dimensional ultrasound is frequently of considerable help. Multiplanar slicing of a volume obtained from axial scans usually provide images of diagnostic quality.<sup>8</sup>

**DESTRUCTIVE CEREBRAL LESIONS**

Many congenital anomalies of the brain are not the consequence of an embryogenetic malformative process but are due to a destructive process. The pathophysiology is frequently unclear and the condition remains idiopathic. However, a link with obstetric complications of different nature is frequently found.

Intracranial hemorrhage (ICH) is usually found at the level of the lateral ventricles, although it can occur in other anatomic locations. It is a frequent complication in premature infants, although rarely, it may occur antenatally, as a consequence of coagulopathy or trauma, or other yet unexplained factors. The sonographic appearance of an ICH is extremely variable depending on the severity and the time since it occurred (Fig. 10-31).<sup>88</sup> When imaging the fetal head in an axial plane of section, the imaging plane needs to be symmetric without any angulation. The normal choroid plexus on one side may simulate a germinal matrix hemorrhage when the imaging plane is asymmetric. Blood that accumulates into the ventricles appears initially as a hyperechogenic collection. With time, the blood clot retracts and demonstrates an anechoic core, and is frequently associated with ventricular dilatation (grade 3 hemorrhage). Large hemorrhagic collections may be complicated by infarcts and destruction of the surrounding white matter. (grade 4 hemorrhage). The prognosis in these cases is severe. In a review of the literature, perinatal death occurred in about 50% of cases and 50% of survivors had neurologic compromise at long-term follow-up. There was a correlation between the outcome and the grade of the hemorrhage. The prognosis was more favorable with grade 1 and 2 hemorrhages (hemorrhage limited to the germinal matrix or lateral ventricles without ventriculomegaly), that at times may even resolve in utero, and was usually severe with grade 3 and 4 lesions (intraventricular hemorrhage associated with severe ventriculomegaly and white matter destruction respectively).<sup>88</sup>

Congenital *porencephaly* is defined as the presence of cystic cavities within the brain matter (Fig. 10-32). The cavities

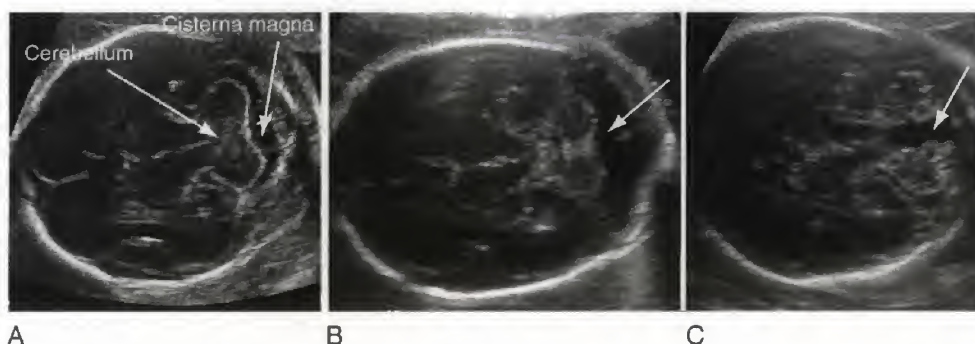


**FIGURE 10-28.** A. The normal transcerebellar scan compared with variations of the Dandy-Walker. B. Enlarged cisterna magna and normal-appearing vermis (arrow). C. A cerebellar cleft (arrow) suggesting a vermian defect.

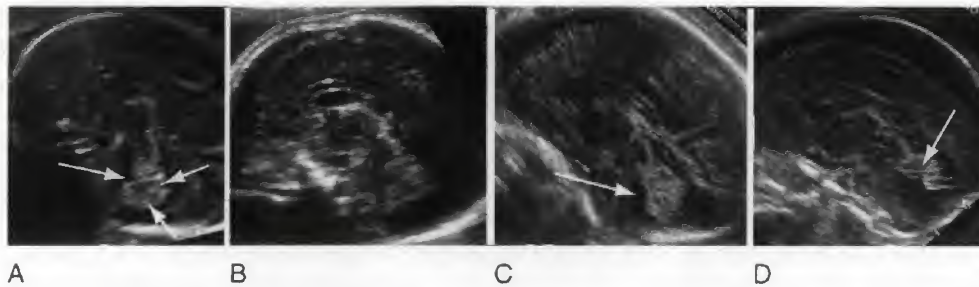


**FIGURE 10-29.** A. The normal midsagittal view demonstrating the main landmarks of the cerebellar vermis (fastigium of fourth ventricle and the two main fissures) (arrows) is compared with variations of the Dandy-Walker continuum: (B) enlargement of the cisterna magna with an intact vermis (megacisterna magna); (C) upward rotation (arrow) of a seemingly intact vermis (Blake's pouch cyst); and (D) upward rotation of an hypoplastic vermis (arrow) (vermian hypoplasia).

**Table 10-8** Normal Values (Mean + Standard Deviation) of the Cerebellar Vermis

Gestational Age (weeks)	Anteroposterior Diameter (mm)	Superoinferior Diameter (mm)	Circumference (mm)	Area (cm <sup>2</sup> )
21-22	10.6±1.4	11.1±1.1	43.8±3.3	0.9±0.2
23-24	12.9±1.1	12.3±1.4	47.5±5.5	12±0.2
25-26	13.5±2.1	13.6±0.9	50.9±4.4	1.4±0.2
27-28	16.3±2.7	16.0±1.6	58.9±6.8	2.0±0.5
29-30	17.5±2.2	17.7±2.1	64.7±6.5	2.3±0.4
31-32	19.0±1.9	19.2±1.1	70.7±6.9	2.8±0.4
33-34	19.2±1.9	21.2±2.3	72.7±8.3	3.0±0.8
35-36	21.4±1.5	19.8±1.0	77.6±5.1	3.4±0.3
37-38	22.1±3.8	23.0±4.6	80.7±9.9	3.9±1.4
39-40	25.7±2.3	25.0±2.6	86.7±7.0	4.9±0.7

Reproduced with permission from Malinger G, Ginath S, Lerman-Sagie T, et al: The fetal cerebellar vermis: normal development as shown by transvaginal ultrasound. *Prenat Diagn* 21:687, 2001.

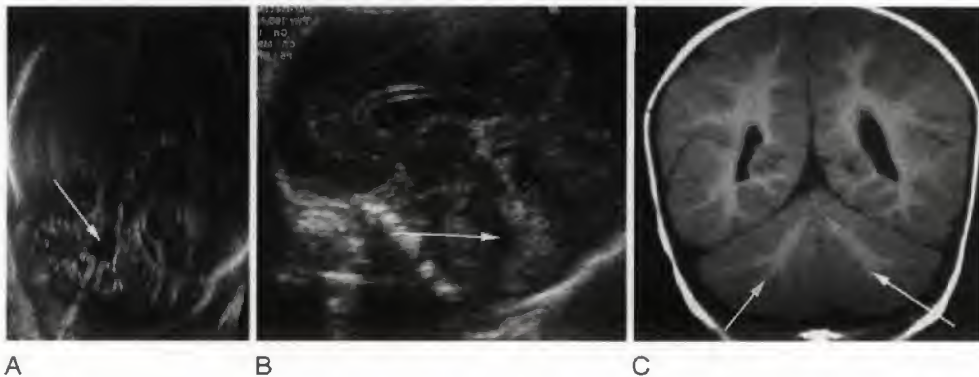


**FIGURE 10-30.** Joubert syndrome. The sonographic findings are limited to the presence of a communication between the fourth ventricle (arrow) and the cisterna magna (A) and an abnormal shape of the fourth ventricle (arrow) (B). C. Postnatally, magnetic resonance imaging demonstrates the absence of the cerebellar vermis between the cerebellar hemispheres (arrows). (Courtesy Philippe Jeanty, Nashville, TN.)

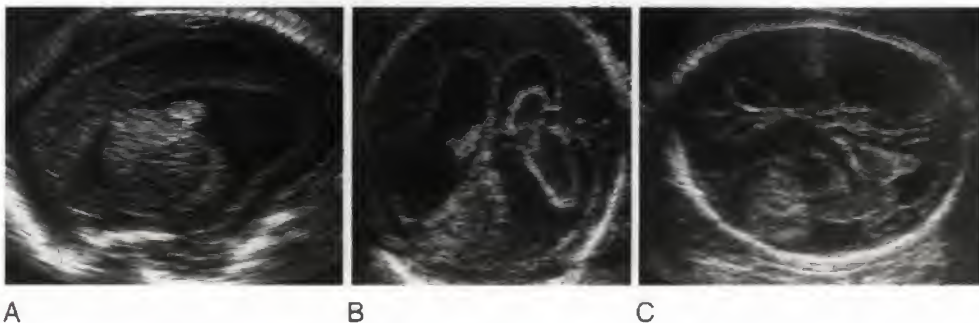


**FIGURE 10-31.** Types of intracranial hemorrhage: (A) soon after the hemorrhage, the blood is intensely echogenic; this is grade II hemorrhage; (B) an old hemorrhage; the coronal scan demonstrates a typical blood clot and ventricular enlargement (grade 3 hemorrhage); (C) hemorrhage associated with destruction of the cortex (grade 4 hemorrhage).



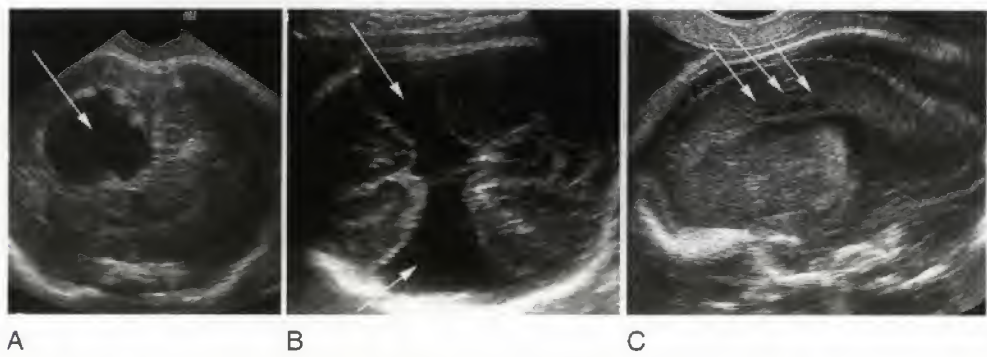


**FIGURE 10-32.** Destructive lesions of the fetal brain: A. Porencephalic cyst (arrow). B. Schizencephaly (arrows). C. Periventricular leukomalacia (arrows).

usually communicate with the ventricular system, the subarachnoid space, or both.<sup>89</sup> Loss of cerebral tissue may derive from a morphogenetic disorder (true porencephaly or *schizencephaly*). More frequently, it is the consequence of an intrauterine disruption (pseudoporencephaly or encephaloclastic porencephaly). The developmental form is typically bilateral and symmetric, and is frequently associated with microcephaly. In *pseudoporencephaly* a unilateral lesion is usually found. In both cases, there is a wide variability in the size of the lesion.<sup>89</sup> Cerebrospinal fluid turnover is often impaired and hydrocephalus is present. *Hydranencephaly* can be regarded as an extreme form of pseudoporencephaly. Most of the cerebral hemispheres are replaced by fluid. The brain stem and rhombencephalic structures are usually spared. The head may be small, of normal size, or extremely enlarged. The etiology is heterogeneous. Congenital infections including toxoplasmosis and cytomegalovirus (CMV), and intrauterine narrowing or occlusion of the internal carotid arteries have been reported. Accurate antenatal diagnosis of both schizencephaly and porencephaly has been reported. However, it should be stressed that porencephaly is a disruption that usually occurs only in the third trimester.

The outcome of infants with a congenital destructive process of the brain is dictated by the size and location of the lesion. Extensive porencephaly, particularly if associated with hydrocephalus or microcephaly, and hydranencephaly have a uniformly poor outcome.<sup>89</sup>

*Periventricular leukomalacia* is a degenerative disorder of the white matter that is most frequently encountered in premature infants and is frequently associated with a poor prognosis. The cystic variety of this condition has been described recently in the fetus. The diagnosis is made by demonstrating multiple small cysts close to the upper corner of the lateral ventricles (see Fig. 10-32C).<sup>90</sup>

*Intrauterine infection* in general is one of the major causes of congenital brain lesions, and CMV in particular is one of the leading causes of brain damage in children. Fetuses with CMV infection affecting the brain may present with a wide range of intracranial abnormalities. The most frequent findings in our experience include echogenic bowel and abnormal intracranial anatomy. The cerebral findings are pleomorphic and include periventricular and intraparenchymal echogenicity, ventriculomegaly, cerebellar hypoplasia, microcephaly and cortical abnormalities.<sup>91</sup>

Although the experience thus far is scanty, it would seem that ultrasound plays a limited role in the prenatal diagnosis

Table 10-9		Diagnosis of Fetal Microcephaly (Biparietal Diameter (mm) SD Below the Mean)				
Week	Mean	-1	-2	-3	-4	-5
20	48	45	42	40	37	34
21	51	48	46	43	40	37
22	54	52	49	46	43	41
23	57	55	52	49	46	44
24	61	58	55	52	49	47
25	64	61	58	55	53	50
26	67	64	61	58	56	53
27	69	67	64	61	58	56
28	72	70	67	64	61	59
29	75	72	69	67	64	61
30	78	75	72	69	67	64
31	80	77	74	72	69	66
32	82	79	77	74	71	68
33	84	81	79	76	73	70
34	86	83	80	78	75	72
35	87	85	82	79	76	74
36	89	86	83	80	78	75
37	90	87	84	82	79	76
38	91	88	85	83	80	77
39	92	89	86	83	81	78
40	92	89	87	84	81	78
41	93	90	87	85	82	79
42	93	91	88	85	82	80

From Chervenak FA, Jeanty P, Cantraine F, et al: The diagnosis of microcephaly. *Am J Obstet Gynecol* 149:512, 1984.

of CMV infection. In our experience, while examining a pregnant patient with recent infection, the positive predictive value of abnormal sonographic findings in the prediction of symptomatic neonatal infection is in the range of 80%, but the sensitivity is only 20%.

### DISORDERS OF NERVE CELL PROLIFERATION

The association between decreased head size and reduction of both brain mass and total cell number in *microcephalic infants* is well established. However, the threshold of abnormality is uncertain. Some authors suggest employing a head circumference below 2 standard deviations (SDs) from the mean as diagnostic criterion. Others prefer to consider head circumference below 3 SDs as abnormal (Table 10-9). The



incidence of microcephaly obviously varies in different surveys, depending on the definition used to identify the lesion.

Microcephaly should not be considered as a single clinical entity but rather as a symptom of many etiologic disturbances, including both environmental and genetic factors (Table 10-10). Microcephaly is featured by a typical disproportion in size between the skull and the face. The forehead is sloping. The brain is small, with the cerebral hemispheres affected to a greater extent than the diencephalic and rhomboencephalic structures. Abnormal convoluted patterns, including macrogyria, microgyria, and agyria, are frequently found. The ventricles may be enlarged. Microcephaly is frequently found in cases of porencephaly, lissencephaly, and holoprosencephaly.

Many difficulties arise in attempting to identify fetal microcephaly. The utility of head measurements alone may be hampered by incorrect dating or intrauterine growth restriction. Furthermore, the natural history of fetal microcephaly is largely unknown. A progressive development of the lesion interfering with early recognition has been described. A comparison of biometric parameters such as the head circumference–abdominal circumference ratio and the femur length–biparietal diameter ratio has been suggested. Nevertheless, both false-positive and false-negative diagnoses occur frequently.<sup>92</sup> It is clear that the predictive value of ultrasound biometry has significant limitations. A qualitative evaluation of the intracranial structures is a very useful adjunct to biometry because many cases of microcephaly are associated with morphologic derangement, particularly with ventriculomegaly, schizencephaly, and disorders of ventral induction. Demonstration of a sloping forehead also increases the index of suspicion (Fig. 10-33).<sup>93</sup>

The final outcome of microcephaly is uncertain. Infants with a small head have a significantly increased risk of neurologic compromise, and there is a correlation with the size of the head. When the head circumference is extremely small (e.g., 4 SDs or more below the mean) and there are associated abnormalities, the prognosis tends to be severe.

*Megalencephaly*, that is, an abnormally large brain, is usually found in individuals of normal and even superior intelligence, but it may be associated with mental retardation and neurologic impairment.<sup>94</sup> Megalencephaly is also a part of congenital anomalies and syndromes such as Beckwith-Wiedemann syndrome, achondroplasia, neurofibromatosis, and tuberous sclerosis (Table 10-11). Obstetric and pediatric sonographers are frequently challenged by the problem of megalencephaly, a condition that should be suspected in the presence of abnormally large head measurements without evidence of hydrocephalus or intracranial masses. In such cases, examination of the parents may be of help, because asymptomatic megalencephaly is frequently familial.

## Intracranial Tumors

Fetal *intracranial tumors* are rare. The incidence has been estimated at 0.34 per million live births. There are several classifications of congenital brain tumors (Table 10-12). In a review of 48 cases diagnosed antenatally,<sup>95</sup> teratomas accounted for 62% of cases. Neuroepithelial tumors were present in 15%, lipomas in 10%, and craniopharyngiomas in 6%. The origin of tumors diagnosed in utero is frequently difficult to ascertain, given the large dimensions of the mass.

**Table 10-10** Classification of Microcephaly

- I. Microcephaly with associated malformations
  - A. Genetic
    1. Chromosomal aberrations
      - Down syndrome
      - Trisomy 13 syndrome
      - Trisomy 18 syndrome
      - Trisomy 22 syndrome
      - 4p- syndrome
      - Cat cry (5p-) syndrome
      - 18p- syndrome
      - 18q- syndrome
    2. Single gene defects
      - Bloom syndrome (AR)
      - Borjeson-Forssman-Lehmann syndrome (XLR)
      - Cockayne syndrome (AR)
      - DeSanctis-Cacchione syndrome (AR)
      - Dubowitz syndrome (AR)
      - Fanconi pancytopenia (AR)
      - Focal dermal hypoplasia (XLD)
      - Incontinentia pigmenti (XLD)
      - Lissencephaly syndrome (AR)
      - Meckel-Gruber syndrome (AR)
      - Menkes syndrome (XLR)
      - Roberts syndrome (AR)
      - Seckel bird-headed dwarfism (AR)
      - Smith-Lemli-Opitz syndrome (AR)
  - B. Environmental
    1. Prenatal infections
      - Rubella syndrome
      - Cytomegalovirus disease
      - Herpesvirus hominis
      - Toxoplasmosis
    2. Prenatal exposure to drugs or chemicals
      - Fetal alcohol syndrome
      - Fetal hydantoin syndrome
      - Aminopterin syndrome
    3. Maternal phenylketonuria
  - C. Unknown etiology
    1. Recognized syndromes
      - Coffin-Sins syndrome
      - DeLange syndrome
      - Johanson-Blizzard syndrome
      - Langer-Giedion syndrome
      - Rubenstein-Taybi syndrome
      - Williams syndrome
    2. Undefined combinations
- II. Microcephaly without associated malformations
  - A. Genetic
    1. Primary microcephaly (AR)
    2. Paine syndrome (XLR)
    3. Alpers disease (AR)
    4. Inborn errors of metabolism
      - Disorders of folic acid metabolism (AR)
      - Hyperlysinemia (AR)
      - Methylmalonic acidemia (AR)
      - Phenylketonuria (AR)
  - B. Environmental
    1. Prenatal exposure to radiation
    2. Fetal malnutrition
    3. Perinatal trauma or hypoxia
    4. Postnatal infections
  - C. Unknown etiology; happy puppet syndrome

AD, autosomal dominant; AR, autosomal recessive; XLR, X-linked recessive. Adapted from Ross ME, Frias JL: In Vinken PJ, Bruyn GW (eds): *Handbook of Clinical Neurology*, vol 30. Amsterdam, Elsevier 'North Holland Biomedical Press, 1997, pp 507-524.



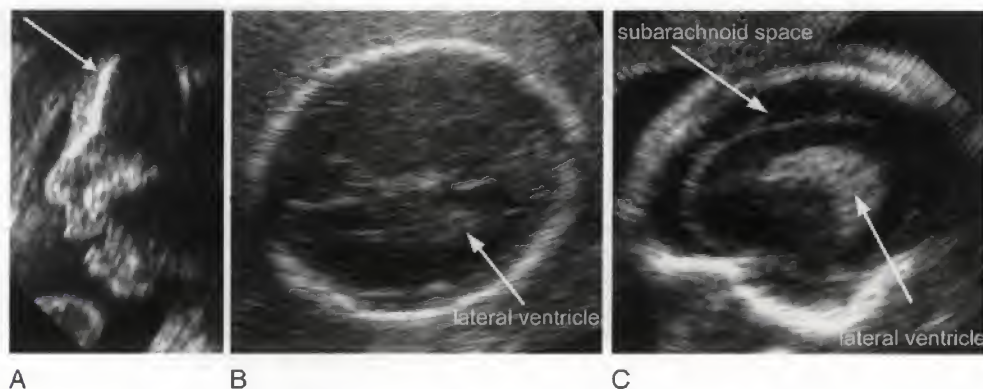


**FIGURE 10-33.** Sonography of fetal microcephaly at 22 weeks. *A.* A profile view reveals sloping of the forehead (arrow). *B.* A transabdominal scan reveals suboptimal resolution of intracranial details; there is the impression of enlargement of the subarachnoid space, and the occipital horn is not visualized. *C.* Vaginal sonography reveals a large layer of subarachnoid space surrounding a shrinking brain; the shape of the lateral ventricle is immature, with no developed occipital horn.

**Table 10-11**

**Syndromes and Malformations  
Associated with Megalencephaly**

Benign familial megalencephaly (autosomal dominant)  
 Unilateral megalencephaly (sporadic)  
 Megalencephaly with neurologic compromise, familial  
 (X-linked recessive?)  
 Achondroplasia (autosomal dominant)  
 Thanatophoric dysplasia (sporadic, autosomal recessive)  
 Beckwith-Wiedemann syndrome (sporadic, autosomal  
 dominant)  
 Lipomatosis, angiomatosis, macrocephaly (Bannayan-Zonana  
 syndrome) (autosomal dominant)  
 Neurofibromatosis (autosomal dominant)  
 Fragile X syndrome (X-linked recessive)

However, most of the lesions are supratentorial, in contrast to the more frequent infratentorial location of brain tumors occurring in older children.

Fetal intracranial tumors are frequently associated with macrocephaly, ventricular enlargement, intracranial calcifications, and hemorrhage. Ventriculomegaly is most frequently the cause of obstruction to cerebrospinal fluid circulation. However, overproduction of fluid may occur with teratomas and choroid plexus papillomas. Polyhydramnios is present in 40% of cases. In most cases, the mechanism is probably related to failure of swallowing, whether this is neurologically induced or is the consequence of mechanical obstruction to the pharynx. Hydrops has also been reported, most frequently as a consequence of arteriovenous shunting within the large tumoral mass, causing high-output cardiac failure. Facial dysmorphism is frequent with large tumors. There is well-established association between interhemispheric lipomas and ACC. There is no established association between fetal and neonatal tumors and chromosomal aberrations.

A brain tumor is suspected when mass-occupying lesions, cystic areas, or solid areas are seen within the fetal head (Fig. 10-34). Ultrasound does not allow a specific diagnosis of the histologic variety. Fetal teratomas, astrocytomas and

**Table 10-12**

**Classification of Congenital Intracranial  
Tumors**

Embryonic tumors  
 Teratoma  
 Epidermoid  
 Dermoid  
 Germinal tumors  
 Germinoma  
 Embryonal carcinoma  
 Choriocarcinoma  
 Endodermal sinus tumor  
 Teratoma  
 Neuroblastic tumors  
 Medulloblastoma  
 Neuroblastoma  
 Retinoblastoma  
 Tumors related to embryonal remnant tissues  
 Craniopharyngioma  
 Chordoma  
 Tumors of ependymal origin  
 Ependymoma  
 Subependymal mixed glioma  
 Choroid plexus papilloma  
 Glioblastoma multiforme  
 Malignant astrocytoma  
 Tumors associated with genetic diseases  
 Tuberous sclerosis (Bourneville's disease)  
 Neurofibromatosis (Von Recklinghausen's disease)  
 Systemic angiomas of the central nervous system and  
 eye (Von Hippel-Lindau's disease)  
 Colloid cyst of the third ventricle  
 Heterotopia and hamartoma  
 Lipoma  
 Vascular tumors: hemangioblastoma

Adapted from Mori K: *Neuroradiology and Neurosurgery*. New York, Thieme-Stratton, 1985; Wilson CB, Moossy J, Boldrey E, et al: *Pathology of intracranial tumors*. In Newton TH, Potts DC (eds): *Radiology of the Skull and Brain*. Anatomy and Pathology. St. Louis, CV Mosby, 1977.

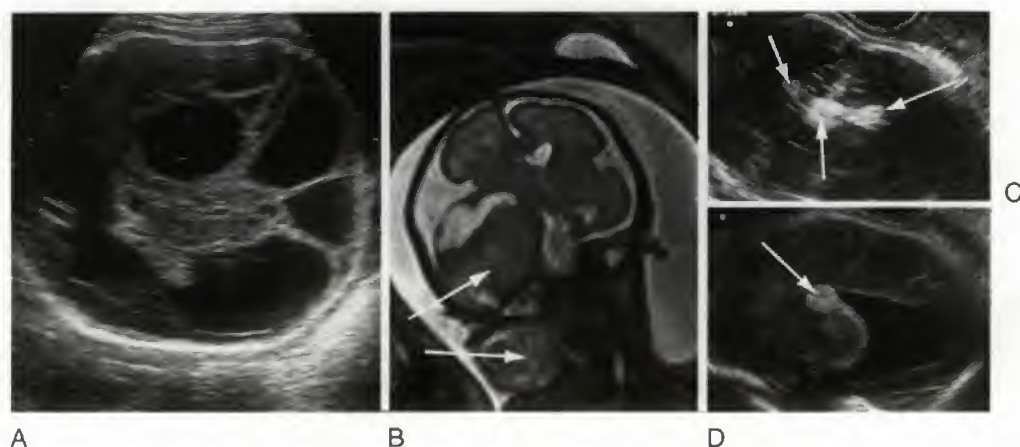


**FIGURE 10-34.** Fetal intracranial tumors: A and B. Intracranial teratoma (arrows). C and D. Multiple lipomas (arrows) in a fetus with associated agenesis of the corpus callosum.

craniopharyngiomas have a similar appearance, that is, a complex mass distorting the brain architecture, possibly associated with macrocephaly, ventriculomegaly and intracranial calcifications. Intracranial lipomas are well-defined hyperechogenic areas, usually located in the midline, in the position normally occupied by the corpus callosum, and within the bodies of lateral ventricles. Eventually, choroid plexus papillomas appear as large choroid plexuses, most frequently in association with ventriculomegaly and subarachnoid space enlargement.<sup>95</sup>

The natural history of fetal brain tumors is uncertain. However, the available data suggest that even very severe lesions may develop rapidly in late gestation. In fact, several cases have been reported in which midtrimester sonograms were unremarkable. Teratomas may be associated with increased maternal serum and amniotic fluid AFP.

The differential diagnosis of brain tumors include other space-occupying intracranial lesions. At times, it may be particularly challenging to distinguish between a tumor and a fresh intraparenchymal hemorrhage. Cerebral hemorrhage usually lacks the mass effect that is found with tumors. In these cases, serial sonograms (in 2 to 3 weeks) most severe ICHs are expected to result in cavitation, ventriculomegaly, and blood clot formation) or antenatal MRI will usually solve the problem.

The prognosis of congenital tumors is poor. In a review of 48 cases, the overall mortality rate was 77%.<sup>95</sup> No clear data are available with regard to the degree of neurologic impairment in survivors, but this is expected to be high as well. The histologic type of the tumor is certainly a major factor. In a postnatal series, the 1-year survival rate of teratomas was only 7%, compared with rates of 44% in patients with astrocytomas and 50% in patients with choroid plexus papillomas. There are many limitations to the antenatal diagnosis of the specific types of tumor. However, large complex masses distorting intracranial anatomy (usually teratomas, astrocytomas, or craniopharyngiomas) were found to have an overall survival rate of only 14%. On the other hand, intracranial lipomas, with a specific ultrasound appearance, were associated with a survival rate of 100% and no developmental handicap.<sup>95</sup>

## ANOMALIES OF NEURONAL MIGRATION

The neuronal cells that form the gray matter originate internally to the brain, on the surface of the lateral ventricles, and only later migrate along radially aligned glial cells to the surface of the brain. The migration occurs in different waves that last for several weeks. Most of the process takes place between 8 weeks' and 16 weeks' gestation but continues up to 25 weeks. Once the neuronal cells have reached their destination on the surface of the brain, they undergo a process of maturation and differentiation, grow axons and dendrites, and develop synapses with other neurons, giving rise to a well-ordered, six-layer cortex. Migration abnormalities are characterized by the incomplete formation of the cortical layers, with abnormal locations of neurons that have failed to reach their final destination. In general, the cortex is thickened by a large, disorganized layer of neurons. Conversely, the white matter underneath the cortex is thinned by failure of production of axons by the disorganized neuronal cells. Macroscopically, the main finding is an alteration in the convolutional pattern of the brain, which may be associated with modifications in brain mass and size of the ventricles.

Failure of neuron migration includes a broad spectrum of anomalies: absence to severe reduction of convolutions (*lissencephaly*), increased number of small convolutions (*polymicrogyria*), *unilateral megalencephaly*, *schizencephaly*, and *gray matter heterotopias*. The migrational process may be arrested by environmental factors (ischemia, teratogens), but a genetic predisposition is clearly present at least for some anomalies.

Postnatally, the technique of choice for the diagnosis of this condition is MRI, which allows a clear discrimination between white and gray matter. However, sonographic detection of typical macroscopic abnormalities of brain anatomy (clefts in the cortex, gyral anomalies, and so on) has led us to suspect and even diagnose these conditions antenatally, although usually only in late gestation (Fig. 10-35).<sup>96</sup> In the past, it was assumed that abnormalities of sulcal development such as *lissencephaly*, could not be diagnosed until 27 to 28 weeks.<sup>97</sup> A recent study by Toi et al<sup>98</sup> documented the appearance time of the parieto-occipital fissure, calcarine fissure, cingulate, and some convexity sulci. In their



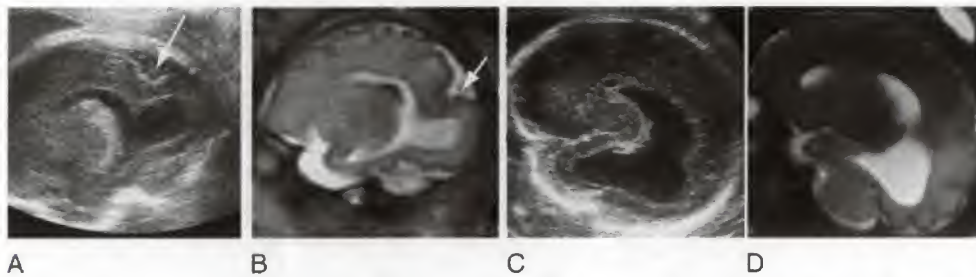


**FIGURE 10-35.** Fetal cortical abnormalities demonstrated by sonography and magnetic resonance imaging. *A* and *B*. Abnormal convolution associated with unusual shape of the cortex (arrows) and underlying lateral ventricle. *C* and *D*. This fetus at 34 weeks' gestation has a very smooth brain and an unusual echogenicity of the cortex.

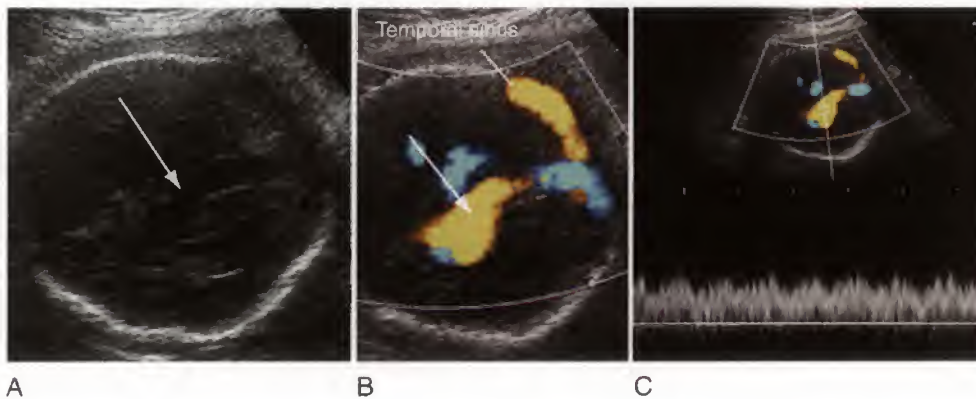


**FIGURE 10-36.** Complex arteriovenous malformation with dilatation of the vein of Galen in a third trimester fetus. *A*. Axial view of the head demonstrating increased echogenicity of the cortex with poor delineation of anatomic details and a fluid-filled midline tortuous lesion (arrow) in the posterior third of the brain, at the level of the vein of Galen cistern. *B*. Color Doppler demonstrates blood flow within the fluid-filled lesion and typically dilated venous sinuses. *C*. Spectral Doppler demonstrating high velocity pulsatile venous blood flow in the enlarged vein of Galen.

study, they noted the youngest age at which a specific sulcus was first visible in any fetus and also the age after which the sulcus was visible in all fetuses. Sulci could be seen by transabdominal ultrasound as early as 18.5 weeks. Medial hemispheric sulci and the insula were visible earlier and more confidently than convexity sulci. The earliest gestational ages at which specific sulci could be seen in any fetus were as follows: parieto-occipital fissure, 18.5 weeks; calcarine sulcus, 18.5 weeks; cingulate sulcus, 23.2 weeks; and convexity sulci, 23.2 weeks. In their series, the gestational ages at which these sulci were always visible were: parieto-occipital fissure, greater than 20.5 weeks; calcarine sulcus, greater than 21.9 weeks; cingulate sulcus, greater than 24.3 weeks; and convexity sulci, greater than 27.9 weeks. Failure of sulcation beyond these stated gestational ages may allow one to suspect lissencephaly.

## VASCULAR ABNORMALITIES

Vascular anomalies of the fetal brain are rare, and only a handful of cases have been described thus far. The majority of reports concentrate upon the vein of Galen vascular malformations. More recently, thrombosis of the dural sinuses has been described.

The term aneurysm of the vein of Galen indicates a spectrum of arteriovenous malformations, ranging from a

single large aneurysmal dilatation of the vein of Galen to multiple communications between the vein and the carotid and vertebrobasilar systems.<sup>99</sup> Three types are described: (1) arteriovenous fistula, (2) arteriovenous malformation with ectasia of the vein of Galen, and (3) varix of the vein of Galen. The arteriovenous fistula is frequently manifest in the fetal or neonatal period with high-output heart failure due to cardiac overload. Both the ectasia and the varix tend to present later in life with bleeding episodes and are not associated with cardiac failure. Arteriovenous fistulae associated with a varix are not part of the definition when they are located elsewhere in the brain.

Prenatally, the typical finding is an elongated anechoic area at the level of the cistern of the vein of Galen, with color and pulsed Doppler evidence of turbulent venous and blood arterial flow (Fig. 10-36).<sup>100</sup> The cerebral architecture may be intact, or it may be distorted because of the concomitance of ventriculomegaly, porencephaly, and brain edema, which is inferred by increased echogenicity of the cortex. The dural sinuses and neck vessels are frequently enlarged, and signs of cardiac overload may be present, including cardiomegaly, hepatosplenomegaly, soft tissue edema, polyhydramnios and hydrops. Color Doppler may help in identifying the origin of the vessels feeding the lesion, an observation that may have practical implications for assessing the prognosis. MRI has also been used in these cases.



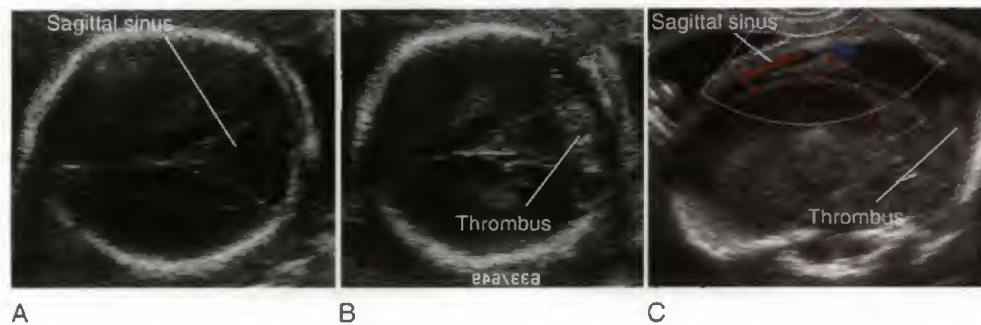


**FIGURE 10-37.** Congenital thrombosis of the dural sinuses. *A.* A large fluid collection is seen posteriorly to the brain (*long arrow*), corresponding to the dilated superior sagittal sinus. *B.* Within the greatly enlarged sinus, a thrombus is seen as an echogenic mass. *C.* Color Doppler ultrasound demonstrates stop of blood flow (*arrow*) within the enlarged portion of the superior sagittal sinus.

Although vein of Galen aneurysms may become symptomatic in the elderly, they are more frequently seen in the neonatal period. The common clinical features in the neonate are cardiomegaly with congestive heart failure and increased intracranial pressure with hydrocephaly or cranial bruit. Focal neurologic deficit, seizure, and hemorrhages are less common findings. The available experience with prenatal diagnosis suggests a mortality rate in the range of 50%, and normal development in about 50% of survivors.<sup>89,100,101</sup> The outcome was strongly dependent on the antenatal evidence of other intracranial abnormalities (hydrocephalus, brain edema, porencephaly) and hydrops. When any of these abnormalities was found, the prognosis was always poor. In general, cases with a normal postnatal development had isolated vascular lesions, without cerebral or cardiovascular compromise in utero and were treated after birth with angiographic embolization.<sup>101</sup>

*Dural sinus thrombosis* is a well-known entity in the neonatal period that has been documented in utero as well. The etiology includes trauma; systemic conditions such as sepsis, meningitis, and dehydration; and hypercoagulopathy caused by polycythemia or deficiency of physiologic anticoagulants (antithrombin, protein C or protein S, factor V Leiden mutation). Prematurity and perinatal asphyxia are considered predisposing factors. A possible role of maternal pre-eclampsia has also been suggested. However, in up to 40% of cases, the condition is idiopathic.<sup>102</sup>

In the cases thus far diagnosed in utero, ultrasound revealed a dilated superior sagittal sinus containing a thrombus. Color Doppler has documented the interruption of blood flow at the level of the dilated sinuses (Fig. 10-37).<sup>102</sup> MRI and MRI angiography are the techniques of choice for the diagnosis after birth and have been used antenatally as well.

The clinical presentation of thrombosis of the dural sinuses in newborn infants is variable. Symptoms include seizures, unexplained irritability, macrocephaly, or a bulging fontanel. Postnatal studies reveal that in general thrombosis of the cerebral venous circulation is an important and under-recognized cause of seizures in term infants. The natural history is variable. In the absence of perinatal asphyxia, normal neurodevelopmental outcome is likely and the risk of seizure recurrence is low. A poor outcome should be expected especially in preterm neonates, and in cases of secondary cerebral sinus thrombosis. Associated imaging

signs such as infarction or ventricular hemorrhage are correlated with poor prognosis. Sequelae may also depend on the location of the thrombus. In a recent study, all patients with permanent neurologic disability had thrombosis of the deep veins with an associated deep cerebral infarction; in contrast, all patients with thrombosis without infarction or with superficial cortical venous infarction had uniformly a good outcome.<sup>103</sup>

## INTRACRANIAL CYSTS

Intracranial arachnoid cysts are accumulations of clear cerebrospinal-like fluid between the dura and the brain substance. The histologic diagnosis is not always available, and the term is frequently used to indicate any intracranial cyst located in the subarachnoid space.

Arachnoid cysts have been found anywhere in the central nervous system including the spinal canal. The most frequent locations are the surface of the cerebral hemispheres in the sites of the major fissures (sylvian, rolandic, and inter-hemispheric), the region of sella turcica, the anterior fossa, and the middle fossa. Less frequently, they are seen in the posterior fossa. Most of the cases diagnosed antenatally involve supratentorial cysts, in the midline, sylvian fissure, and ambient cistern. Arachnoid cysts may be primary (congenital) or secondary (acquired). Congenital types are believed to be formed by maldevelopment of the leptomeninges and do not freely communicate with the subarachnoid space. Acquired types are formed as the result of hemorrhage, trauma, and infection, and often communicate with the subarachnoid space. Arachnoid cysts have the potential to grow as the result of either some communication with the subarachnoid space from a ball-valve mechanism or cerebrospinal fluid production by a choroid plexus-like tissue contained within the cyst wall. Large arachnoid cysts can cause obstructive ventriculomegaly by compressing the foramen of Monro or the aqueduct posteriorly, or by blocking the basal cisterns. Hydrocephalus and macrocephaly are the most common presentations in the neonatal period. Arachnoid cysts have been reported very rarely in association with other anomalies. The list includes trisomy 18, tetralogy of Fallot, sacroccygeal tumor, and neurofibromatosis.

Ultrasound examination of arachnoid cysts demonstrates a well-defined anechoic lesion with adjacent mass effect,



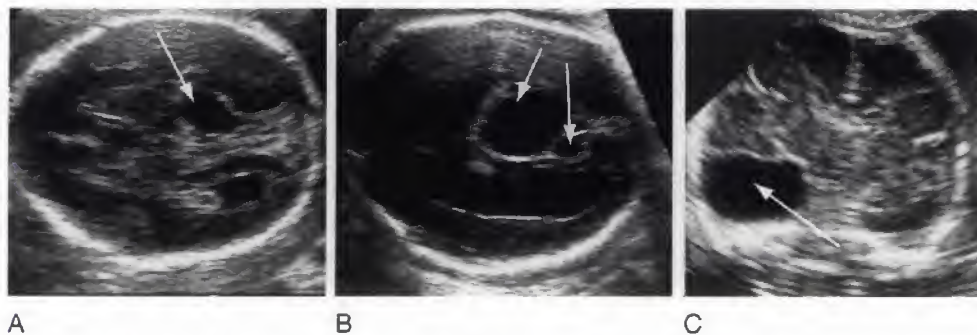


**FIGURE 10-38.** Sonograms of fetuses with arachnoid cysts. A. A small cyst (arrow) in the ambient cistern. B. A midline bilocular cyst (arrows). C. A very large cyst (arrow) arising from the sylvian fissure.

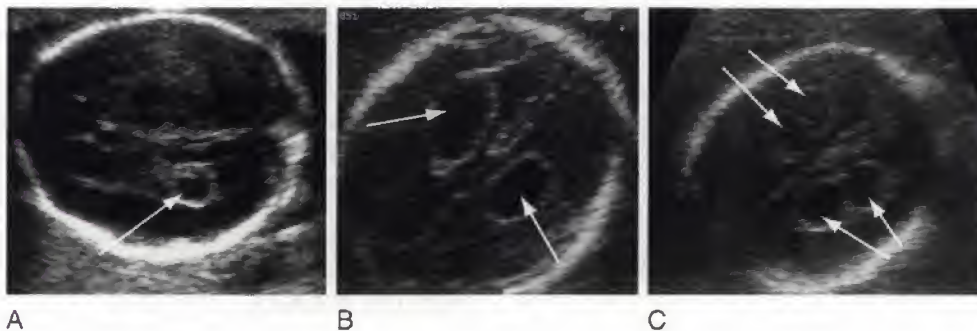


**FIGURE 10-39.** Choroid plexus cyst (arrow). A. Single and small (arrow). B. Large bilateral (arrows). C. Multiple (arrows).

occasionally associated with hydrocephalus (Fig. 10-38). The overall majority of arachnoid cysts diagnosed in utero thus far have been recognized only in the third trimester. In a few cases, unremarkable sonograms had been obtained in the midtrimester. Therefore, it is likely that most of these lesions develop only in late gestation. Differentiating fetal arachnoid cysts from other intracranial fluid collections may be difficult at times. However, in the largest available series, multiplanar brain imaging and vaginal sonography of vertex fetuses were found to be extremely effective.<sup>89</sup> Porencephalic cysts are located inside the brain substance, whereas arachnoid cysts lie between the skull and brain surface. Furthermore, the majority of congenital porencephalic cysts communicate with the lateral ventricles. In schizencephaly, the fluid-filled collection connects the lateral ventricles to the subarachnoid space.

A posterior fossa arachnoid cyst is distinguished from the Dandy-Walker complex by demonstrating the integrity of the cerebellar vermis. Another useful clue is the demonstration that arachnoid cysts tend to be laterally positioned and result in an asymmetric posterior fossa.

In many cases, arachnoid cysts are asymptomatic, but they may cause epilepsy, mild motor or sensory abnormalities, or hydrocephalus. Hydrocephalus and macrocephaly are the most common presentations in the neonatal period.

Neurosurgical series in general suggest a good prognosis, with absence of symptoms in more than 70% of cases. The location of the cyst has influence on the final outcome. In one series, temporal cysts were found to have the best outcome, with more than 90% of patients recovering completely

or with only slight deficits, and there were no deaths. The other locations were associated with a significantly poorer outcomes. In particular, posterior fossa arachnoid cysts had the worst outcomes.<sup>104,105</sup>

Gliopendymal cysts are thought to derive from displaced neuroectodermal tissue and have the same ultrasound appearance of arachnoid cysts.<sup>106</sup> Differentiation between these two entities is usually possible only on the basis of histologic examination. However, the diagnosis of a gliopendymal cyst should be favored when the cyst is in the midline and is associated with ACC (see earlier). The distinction may not be clinically relevant, because it is uncertain whether the prognostic implications are different.

*Choroid plexus cysts* appear as round sonolucent areas in the substance of the choroid plexus of the lateral ventricles (Fig. 10-39). They have been described with increasing frequency over the last decade. Surveys of low-risk pregnant patients indicate that the frequency of this finding in the midtrimester is in the range of 1%. However, the real incidence is probably dependent on the resolution of the ultrasound equipment, the attention of the operator, and the definition of the choroid plexus cyst that is employed. Although on average, the incidence in most studies is in the range of 1%, figures as high as 3.6% have been reported.<sup>107,108</sup>

Choroid plexus cysts may be unilateral or bilateral, and occasionally are multiple. They are typically found at the level of the atrium of lateral ventricles, less frequently within the bodies. When examined with high-resolution ultrasound equipment, the choroid plexus of the lateral ventricle often appears slightly heterogeneous. To be called a choroid plexus



cyst, the lesion should measure at least 2 mm in diameter. Large cysts up to 14 mm may be seen, and usually contain internal septations.

The diagnosis of a choroid plexus cyst is readily made in the majority of cases by noting the typical location within the atria of lateral ventricles, with a normal appearance of the surrounding fetal brain. The only problem that can be encountered at times is differentiating a large choroid plexus cyst slightly distending the cavity of a ventricle from primary ventriculomegaly. In such cases, the most important clue is the demonstration that choroid plexus cysts have a thick echogenic wall and tend to have internal septations. In dubious cases, a follow-up scan may be useful as most choroid plexus cysts usually rapidly decrease in size and may even disappear with advancing gestation. A localized intraventricular bleed may result in a blood clot resembling an abnormality of the choroid plexus. However, the clot is less regular than a choroid plexus cysts and the surrounding ventricle is usually enlarged.

However, fetal choroid plexus cysts are benign findings that are at times associated with an increased likelihood of trisomy 18. The available data do not indicate an association with other chromosomal aberrations, including trisomy 21.<sup>109,110</sup> In 80% to 90% of fetuses with trisomy 18, anatomic deformities are detected by ultrasound.<sup>79</sup> On the basis of these data, a prudent approach is to perform a thorough sonographic examination of the fetus when a choroid plexus cyst is identified. This examination should include evaluation of the hands and feet, and a thorough examination of the fetal heart. If an additional ultrasound abnormality is identified, chromosomal analysis should be offered to the patient. There is debate as to how the patient with an isolated choroid plexus cyst should be counseled. Some investigators believe that when the cyst is isolated and a thorough ultrasound evaluation reveals no other abnormalities that the cyst may be considered a normal variant.<sup>111</sup> Snijders and co-workers<sup>110</sup> have reported that in the presence of a choroid plexus cyst, the risk of trisomy 18 is increased 1.5 times over the baseline. Additional reassurance can be obtained by correlating ultrasound findings with serum biochemical markers.

From time to time, suggestions have been made that the risk of aneuploidy is related to the size of the cyst, whether it is unilateral or bilateral, and whether it is persistent or disappears. From the available literature, no evidence supports any of these suggestions. Small cysts, unilateral cysts, and transient cysts have been documented in association with aneuploidies.

Isolated choroid plexus cysts do not modify standard obstetric management. Because no deleterious effect on the fetus has been thus far reported with this finding, there is no need in our opinion for follow-up scans. A handful of very large cysts of the choroid plexuses causing intracranial hypertension have been described in the neurosurgical literature, but these cysts represent probably a separate clinical entity.<sup>112</sup>

## CONCLUSIONS

Modern ultrasound equipment yields a unique potential for the evaluation of the normal and abnormal fetal central nervous system. A large number of congenital anomalies can be consistently recognized. Transvaginal sonography is

extending antenatal diagnosis to very early gestation MRI can be used to improve the accuracy of the diagnosis in selected cases.

Nevertheless, there are many limits to the prenatal diagnosis of CNS anomalies. Some studies of low-risk patients undergoing basic examinations have reported sensitivities in excess of 80%.<sup>31,113</sup> However, these results probably far overestimate the diagnostic potential of the technique. These surveys had invariably very short follow-up and almost only included open neural tube defects, whose recognition was probably facilitated by systematic screening with maternal serum AFP. Pitfalls of prenatal ultrasound are well documented and occur for a number of reasons. One of the most important limitations is related to continuing brain development in the second half of gestation and into the neonatal period that limits the detection of anomalies such as microcephaly and cortical malformations. Furthermore, some cerebral lesions are not due to faulty embryologic development but represent the consequence of acquired prenatal, perinatal, and postnatal insults. Even in expert hands, some types of anomalies may be difficult or impossible to diagnose in utero, in a proportion that is yet impossible to determine with precision.<sup>114</sup>

On the other hand, when an anomaly is identified, counseling the parents and deciding a sensible obstetric management is frequently difficult. Some cerebral anomalies have outcomes that can be predicted with reasonable precision. This is certainly the case with catastrophic lesions such as anencephaly and severe holoprosencephaly, as well as with anomalies that are invariably detected at birth, such as spina bifida. However, there is a large number of conditions that can be accurately identified in utero and yet have an unclear natural history. ACC, mild ventriculomegaly, and minor variations of the Dandy-Walker continuum are remarkable examples with this regard.

## References

1. Myrianthopoulos NC: Epidemiology of central nervous system malformations. In Vinken PJ, Bruyn GW (eds): *Handbook of Clinical Neurology*. Amsterdam, Elsevier, 1977, pp 139-171.
2. Griffiths PD, Paley MN, Widjaja E, et al: In utero magnetic resonance imaging for brain and spinal abnormalities in fetuses. *BMJ* 331:562, 2005.
3. Levine D, Barnes PD, Robertson RR, et al: Fast MR imaging of fetal central nervous system abnormalities. *Radiology* 229:51, 2003.
4. Malinge G, Lev D, Lerman-Sagie T: Is fetal magnetic resonance imaging superior to neurosonography for detection of brain anomalies? *Ultrasound Obstet Gynecol* 20:317, 2002.
5. Malinge G, Ben-Sira L, Lev D, et al: Fetal brain imaging: a comparison between magnetic resonance imaging and dedicated neurosonography. *Ultrasound Obstet Gynecol* 23:333, 2004.
6. Filly RA, Cardoza JD, Goldstein RB, Barkovich AJ: Detection of fetal central nervous system anomalies: a practical level of effort for a routine sonogram. *Radiology* 172:403, 1989.
7. Serhatiluglu S, Kocakoc E, Kiris A, et al: Sonographic measurement of the fetal cerebellum, cisterna magna, and cavum septum pellucidum in normal fetuses in the second and third trimesters of pregnancy. *J Clin Ultrasound* 31:194, 2003.
8. Pili G, Segata M, Ghi T, et al: Diagnosis of midline anomalies of the fetal brain with the three-dimensional median view. *Ultrasound Obstet Gynecol* 27:522, 2006.
9. Robbin ML, Filly RA, Goldstein RB: The normal location of the fetal conus medullaris. *J Ultrasound Med* 13:541, 1994.
10. Filly RA, Callen PW, Goldstein RB: Alpha-fetoprotein screening programs: what every obstetric sonologist should know. *Radiology* 188:1, 1993.



11. Cardoza JD, Goldstein RB, Filly RA: Exclusion of fetal ventriculomegaly with a single measurement: the width of the lateral ventricular atrium. *Radiology* 169:711, 1988.
12. Gupta JK, Bryce FC, Lilford RJ: Management of apparently isolated fetal ventriculomegaly. *Obstet Gynecol Surv* 49:716, 1994.
13. Pilu G, Falco P, Gabrielli S, et al: The clinical significance of fetal isolated cerebral borderline ventriculomegaly: report of 31 cases and review of the literature. *Ultrasound Obstet Gynecol* 14:320, 1999.
14. Gaglioti P, Danelon D, Bontempo S, et al: Fetal cerebral ventriculomegaly: outcome in 176 cases. *Ultrasound Obstet Gynecol* 25:372, 2005.
15. Lyonnet S, Pelet A, Royer G, et al: The gene for X-linked hydrocephalus maps to Xq28, distal to DXS52. *Genomics* 14:508, 1992.
16. Serville F, Benit P, Saugier P, et al: Prenatal exclusion of X-linked hydrocephalus-stenosis of the aqueduct of Sylvius sequence using closely linked DNA markers. *Prenat Diagn* 13:4359, 1993.
17. Rogers JG, Danks DM: Prenatal diagnosis of sex-linked hydrocephalus. *Prenat Diagn* 3:269, 1983.
18. Chervenak FA, McCullough LB: Ethical analysis of the intrapartum management of pregnancy complicated by fetal hydrocephalus with macrocephaly. *Obstet Gynecol* 68:720, 1986.
19. Bronshtein M, Ornoy A: Acrania: anencephaly resulting from secondary degeneration of a closed neural tube: two cases in the same family. *J Clin Ultrasound* 19:230, 1991.
20. Casellas M, Ferrer M, Rovira M, et al: Prenatal diagnosis of exencephaly. *Prenat Diagn* 13:417, 1993.
21. Weissman A, Diukman R, Auslander R: Fetal acrania: five new cases and review of the literature. *J Clin Ultrasound* 25:511, 1997.
22. Johnson SP, Sebire NJ, Snijders RJ, et al: Ultrasound screening for anencephaly at 10-14 weeks of gestation. *Ultrasound Obstet Gynecol* 9:14, 1997.
23. Barkovich AJ: Congenital anomalies of the spine. In Barkovich AJ (ed): *Pediatric Neuroimaging*, 4th ed. Philadelphia, Lippincott, Williams & Wilkins, 2005.
24. French BN: The embryology of spinal dysraphism. *Clin Neurosurg* 30:295, 1983.
25. Schut L, Pizzi FJ, Bruce DA: Occult spinal dysraphism. In McLaurin RL (ed): *Myelomeningocele*. New York, Grune & Stratton, 1977, pp 349-368.
26. Tortori-Donati P, Rossi A, Cama A: Spinal dysraphism: a review of neuroradiological features with embryological correlations and proposal for a new classification. *Neuroradiology* 42:471, 2000.
27. Ghi T, Pilu G, Falco P, et al: Prenatal diagnosis of open and closed spina bifida. *Ultrasound Obstet Gynecol* 28:899, 2006.
28. Blaas HG, Eik-Nes SH, Isaksen CV: The detection of spina bifida before 10 gestational weeks using two- and three-dimensional ultrasound. *Ultrasound Obstet Gynecol* 16:25, 2000.
29. Boyd PA, Wellesley DG, De Walle HE, et al: Evaluation of the prenatal diagnosis of neural tube defects by fetal ultrasonographic examination in different centres across Europe. *J Med Screen* 7:169, 2000.
30. Grandjean H, Larroque D, Levi S: The performance of routine ultrasonographic screening of pregnancies in the Eurofetus Study. *Am J Obstet Gynecol* 181:446, 1999.
31. Ewigman BG, Crane JP, Frigoletto FD, et al: Effect of prenatal ultrasound screening on perinatal outcome. RADIUS Study Group. *N Engl J Med* 329:821, 1993.
32. Garne E, Loane M, Dolk H, et al: Prenatal diagnosis of severe structural congenital malformations in Europe. *Ultrasound Obstet Gynecol* 25:6, 2005.
33. Nicolaides KH, Campbell S, Gabbe SG, et al: Ultrasound screening for spina bifida: cranial and cerebellar signs. *Lancet* 2:72, 1986.
34. Pilu G, Romero R, Reece EA, et al: Subnormal cerebellum in fetuses with spina bifida. *Am J Obstet Gynecol* 158:1052, 1988.
35. Bruner JP, Tulipan N: Tell the truth about spina bifida. *Ultrasound Obstet Gynecol* 24:595, 2004.
36. Kollias SS, Ball WS Jr, Prenger EC: Cystic malformations of the posterior fossa: differential diagnosis clarified through embryologic analysis. *Radiographics* 13:1211, 1993.
37. Luthy DA, Wardinsky T, Shurtleff DB, et al: Cesarean section before the onset of labor and subsequent motor function in infants with meningomyelocele diagnosed antenatally. *N Engl J Med* 324:662, 1991.
38. Shurtleff DB, Luthy DA, Nyberg DA, et al: Meningomyelocele: management in utero and post natum. *Ciba Found Symp* 181:270; discussion 280, 1994.
39. Shurtleff DB, Luthy DA, Nyberg DA, et al: The outcome of fetal myelomeningocele brought to term. *Eur J Pediatr Surg* 4(Suppl 1):25, 1994.
40. Tortori-Donati P, Fondelli MP, Rossi A, et al: Cystic malformations of the posterior cranial fossa originating from a defect of the posterior membranous area. Mega cisterna magna and persisting Blake's pouch: two separate entities. *Childs Nerv Syst* 12:303, 1996.
41. Barkovich JA: Congenital malformations of the brain and skull. In Barkovich JA (ed): *Pediatric Neuroimaging*, 4th ed. Philadelphia, Lippincott Williams & Wilkins, 2005.
42. Diebler C, Dulac O: Cephaloceles: clinical and neuroradiological appearance. Associated cerebral malformations. *Neuroradiology* 25:199, 1983.
43. Naidich TP, Altman NR, Brannan BH, et al: Cephaloceles and related malformations. *AJNR Am J Neuroradiol* 13:655, 1992.
44. Budorick NE, Pretorius DH, McGahan JP, et al: Cephalocele detection in utero: sonographic and clinical features. *Ultrasound Obstet Gynecol* 5:77, 1995.
45. Goldstein RB, LaPidos AS, Filly RA: Fetal cephaloceles: diagnosis with US. *Radiology* 180:803, 1991.
46. Blaas HG, Eriksson AG, Salvesen KA, et al: Brains and faces in holoprosencephaly: pre- and postnatal description of 30 cases. *Ultrasound Obstet Gynecol* 19:24, 2002.
47. Malinger G, Lev D, Kidron D, et al: Differential diagnosis in fetuses with absent septum pellucidum. *Ultrasound Obstet Gynecol* 25:42, 2005.
48. Barkovich AJ: Apparent atypical callosal dysgenesis: analysis of MR findings in six cases and their relationship to holoprosencephaly. *AJNR Am J Neuroradiol* 11:333, 1990.
49. Barkovich AJ, Norman D: Anomalies of the corpus callosum: correlation with further anomalies of the brain. *AJR Am J Roentgenol* 151:171, 1988.
50. Pilu G, Sandri F, Perolo A, et al: Prenatal diagnosis of lobar holoprosencephaly. *Ultrasound Obstet Gynecol* 2:88, 1992.
51. Pilu G, Ambrosetto P, Sandri F, et al: Intraventricular fused fornices: a specific sign of fetal lobar holoprosencephaly. *Ultrasound Obstet Gynecol* 4:65, 1994.
52. Bernard JP, Drummond CL, Zaarour P, et al: A new clue to the prenatal diagnosis of lobar holoprosencephaly: the abnormal pathway of the anterior cerebral artery crawling under the skull. *Ultrasound Obstet Gynecol* 19:605, 2002.
53. Han JS, Benson JE, Kaufman B, et al: MR imaging of pediatric cerebral abnormalities. *J Comput Assist Tomogr* 9:103, 1985.
54. Jeret JS, Serur D, Wisniewski K, et al: Frequency of agenesis of the corpus callosum in the developmentally disabled population as determined by computerized tomography. *Pediatr Neurol* 12:101, 1985.
55. Pilu G, Sandri F, Perolo A, et al: Sonography of fetal agenesis of the corpus callosum: a survey of 35 cases. *Ultrasound Obstet Gynecol* 3:318, 1993.
56. Bennett GL, Bromley B, Benacerraf BR: Agenesis of the corpus callosum: prenatal detection usually is not possible before 22 weeks of gestation. *Radiology* 199:447, 1996.
57. Volpe P, Paladini D, Resta M, et al: Characteristics, associations and outcome of partial agenesis of the corpus callosum in the fetus. *Ultrasound Obstet Gynecol* 27:509, 2006.
58. Pierre-Kahn A, Hanlo P, Sonigo P, et al: The contribution of prenatal diagnosis to the understanding of malformative intracranial cysts: state of the art. *Childs Nerv Syst* 16:619, 2000.
59. Smith AS, Levine D: Appearance of an interhemispheric cyst associated with agenesis of the corpus callosum. *AJNR Am J Neuroradiol* 25:1037, 2004.
60. Aicardi G, Lefebvre J, Lerrieux-Koechlin A: A new syndrome: spasm in flexion, callosal agenesis, ocular abnormalities. *Electroencephalogr Clin Neurophysiol* 19:609, 1965.
61. Rosser TL, Acosta MT, Packer RJ: Aicardi syndrome: spectrum of disease and long-term prognosis in 77 females. *Pediatr Neurol* 27:343, 2002.
62. Gupta JK, Lilford RJ: Assessment and management of fetal agenesis of the corpus callosum. *Prenat Diagn* 15:301, 1995.
63. Moutard ML, Kieffer V, Feingold J, et al: Agenesis of corpus callosum: prenatal diagnosis and prognosis. *Childs Nerv Syst* 19:471, 2003.
64. Lewis SW, Reveley MA, David AS, et al: Agenesis of the corpus callosum and schizophrenia: a case report. *Psychol Med* 18:341, 1988.
65. Lepinard C, Coutant R, Boussin F, et al: Prenatal diagnosis of absence of the septum pellucidum associated with septo-optic dysplasia. *Ultrasound Obstet Gynecol* 25:73, 2005.



66. Pilu G, Tani G, Carletti A, et al: Difficult early sonographic diagnosis of absence of the fetal septum pellucidum. *Ultrasound Obstet Gynecol* 25:70, 2005.
67. Belhocine O, Andre C, Kalifa G, et al: Does asymptomatic septal agenesis exist? A review of 34 cases. *Pediatr Radiol* 35:410, 2005.
68. Dandy WE, Blackfan KD: Internal hydrocephalus: an experimental, clinical, and pathological study. *Am J Dis Child* 8:406, 1914.
69. Taggart Jr, JK, Walker AE: Congenital atresia of the foramina of Luschka and Magendie. *Arch Neurol Psychiatr* 48:5628, 1942.
70. Benda CE: The Dandy-Walker syndrome or the so-called atresia of the foramen Magendie. *J Neuropathol Exp Neurol* 13:14, 1954.
71. Calabro F, Arcuri T, Jinkins JR: Blake's pouch cyst: an entity within the Dandy-Walker continuum. *Neuroradiology* 42:290, 2000.
72. Boddart N, Klein O, Ferguson N, et al: Intellectual prognosis of the Dandy-Walker malformation in children: the importance of vermian lobulation. *Neuroradiology* 45:320, 2003.
73. Klein O, Pierre-Kahn A, Boddart N, et al: Dandy-Walker malformation: prenatal diagnosis and prognosis. *Childs Nerv Syst* 19:484, 2003.
74. Adamsbaum C, Moutard ML, Andre C, et al: MRI of the fetal posterior fossa. *Pediatr Radiol* 35:124, 2005.
75. Guibaud L, des Portes V: Plea for an anatomical approach to abnormalities of the posterior fossa in prenatal diagnosis. *Ultrasound Obstet Gynecol* 27:477, 2006.
76. Gonsette R, Potvliege R, Andre-Balissaux G, et al: [Mega-cisterna magna: clinical, radiologic and anatomopathologic study]. *Acta Neurol Psychiatr Belg* 68:559, 1968.
77. Nelson MD Jr, Maher K, Gilles FH: A different approach to cysts of the posterior fossa. *Pediatr Radiol* 34:720, 2004.
78. Nyberg DA, Mahony BS, Hegge FN, et al: Enlarged cisterna magna and the Dandy-Walker malformation: factors associated with chromosome abnormalities. *Obstet Gynecol* 77:436, 1991.
79. Nyberg DA, Kramer D, Resta RG, et al: Prenatal sonographic findings of trisomy 18: review of 47 cases. *J Ultrasound Med* 12:103, 1993.
80. Adam R, Greenberg JO: The mega cisterna magna. *J Neurosurg* 48:190, 1978.
81. Zalc Y, Gilboa Y, Gabis L, et al: Rotation of the vermis as a cause of enlarged cisterna magna on prenatal imaging. *Ultrasound Obstet Gynecol* 27:490, 2006.
82. Harwood-Nash DC: *Neuroradiology in Infants and Children*. Mosby, St. Louis, 1976.
83. Malinge G, Ginath S, Lerman-Sagie T, et al: The fetal cerebellar vermis: normal development as shown by transvaginal ultrasound. *Prenat Diagn* 21:687, 2001.
84. Doherty D, Glass IA, Siebert JR, et al: Prenatal diagnosis in pregnancies at risk for Joubert syndrome by ultrasound and MRI. *Prenat Diagn* 25:4427, 2005.
85. Bromley B, Nadel AS, Pauker S, et al: Closure of the cerebellar vermis: evaluation with second trimester US. *Radiology* 193:761, 1994.
86. Limperopoulos C, Robertson RL, Estroff JA, et al: Diagnosis of inferior vermian hypoplasia by fetal magnetic resonance imaging: potential pitfalls and neurodevelopmental outcome. *Am J Obstet Gynecol* 194:1070, 2006.
87. Phillips JJ, Mahony BS, Siebert JR, et al: Dandy-Walker malformation complex: Correlation between ultrasonographic diagnosis and postmortem neuropathology. *Obstet Gynecol* 107:685, 2006.
88. Ghi T, Simonazzi G, Perolo A, et al: Outcome of antenatally diagnosed intracranial hemorrhage: case series and review of the literature. *Ultrasound Obstet Gynecol* 22:121, 2003.
89. Pilu G, Falco P, Perolo A, et al: Differential diagnosis and outcome of fetal intracranial hypoechoic lesions: report of 21 cases. *Ultrasound Obstet Gynecol* 9:229, 1997.
90. Ghi T, Brondelli L, Simonazzi G, et al: Sonographic demonstration of brain injury in fetuses with severe red blood cell alloimmunization undergoing intrauterine transfusions. *Ultrasound Obstet Gynecol* 23:428, 2004.
91. Malinge G, Lev D, Zahalka N, et al: Fetal cytomegalovirus infection of the brain: the spectrum of sonographic findings. *AJNR Am J Neuroradiol* 24:28, 2003.
92. Bromley B, Benacerraf BR: Difficulties in the prenatal diagnosis of microcephaly. *J Ultrasound Med* 14:303, 1995.
93. Pilu G, Falco P, Milano V, et al: Prenatal diagnosis of microcephaly assisted by vaginal sonography and power Doppler. *Ultrasound Obstet Gynecol* 11:357, 1998.
94. DeMyer W: Megalencephaly: types, clinical syndromes, and management. *Pediatr Neurol* 2:321, 1986.
95. Schlembach D, Bornemann A, Rupprecht T, et al: Fetal intracranial tumors detected by ultrasound: a report of two cases and review of the literature. *Ultrasound Obstet Gynecol* 14:407, 1999.
96. Malinge G, Lev D, Lerman-Sagie T: Abnormal sulcation as an early sign for migration disorders. *Ultrasound Obstet Gynecol* 24:704, 2004.
97. Fong KW, Ghai S, Toi A, et al: Prenatal ultrasound findings of lissencephaly associated with Miller-Dieker syndrome and comparison with pre- and postnatal magnetic resonance imaging. *Ultrasound Obstet Gynecol* 24:716, 2004.
98. Toi A, Lister WS, Fong KW: How early are fetal cerebral sulci visible at prenatal ultrasound and what is the normal pattern of early fetal sulcal development? *Ultrasound Obstet Gynecol* 24:706, 2004.
99. Johnston IH, Whittle IR, Besser M, et al: Vein of Galen malformation: diagnosis and management. *Neurosurgery* 20:747, 1987.
100. Sepulveda W, Platt CC, Fisk NM: Prenatal diagnosis of cerebral arteriovenous malformation using color Doppler ultrasonography: case report and review of the literature. *Ultrasound Obstet Gynecol* 6:282, 1995.
101. Rodesch G, Hui F, Alvarez H, et al: Prognosis of antenatally diagnosed vein of Galen aneurysmal malformations. *Childs Nerv Syst* 10:79, 1994.
102. Visentin A, Falco P, Pilu G, et al: Prenatal diagnosis of thrombosis of the dural sinuses with real-time and color Doppler ultrasound. *Ultrasound Obstet Gynecol* 17:322, 2001.
103. Medlock MD, Olivero WC, Hanigan WC, et al: Children with cerebral venous thrombosis diagnosed with magnetic resonance imaging and magnetic resonance angiography. *Neurosurgery* 31:870, discussion 876, 1992.
104. Marinov M, Undjian S, Wetzka P: An evaluation of the surgical treatment of intracranial arachnoid cysts in children. *Childs Nerv Syst* 5:177, 1989.
105. Richard KE, Dahl K, Sanker P: Long-term follow-up of children and juveniles with arachnoid cysts. *Childs Nerv Syst* 5:184, 1989.
106. Hassan J, Sepulveda W, Teixeira J, et al: Gliopendymal and arachnoid cysts: unusual causes of early ventriculomegaly in utero. *Prenat Diagn* 16:729, 1996.
107. Chinn DH, Miller EI, Worthy LM, et al: Sonographically detected fetal choroid plexus cysts. Frequency and association with aneuploidy. *J Ultrasound Med* 10:255, 1991.
108. Gupta JK, Cave M, Lilford RJ, et al: Clinical significance of fetal choroid plexus cysts. *Lancet* 346:724, 1995.
109. Bromley B, Lieberman R, Benacerraf BR: Choroid plexus cysts: not associated with Down syndrome. *Ultrasound Obstet Gynecol* 8:232, 1996.
110. Snijders RJ, Shawa L, Nicolaides KH: Fetal choroid plexus cysts and trisomy 18: assessment of risk based on ultrasound findings and maternal age. *Prenat Diagn* 14:1119, 1994.
111. Coco C, Jeanty P: Karyotyping of fetuses with isolated choroid plexus cysts is not justified in an unselected population. *J Ultrasound Med* 23:899, 2004.
112. Neblett CR, Robertson JW: Symptomatic cysts of the telencephalic choroid plexus. *J Neurol Neurosurg Psychiatry* 34:324, 1971.
113. Crane JP, LeFevre ML, Winborn RC, et al: A randomized trial of prenatal ultrasonographic screening: impact on the detection, management, and outcome of anomalous fetuses. The RADIUS Study Group. *Am J Obstet Gynecol* 171:392, 1994.
114. Malinge G, Lerman-Sagie T, Waternberg N, et al: A normal second-trimester ultrasound does not exclude intracranial structural pathology. *Ultrasound Obstet Gynecol* 20:51, 2002.



# ULTRASOUND EVALUATION OF THE FETAL FACE AND NECK

Gianluigi Pilu, MD, Maria Segata, MD, and Antonella Perolo, MD

## Craniofacial Anomalies

Normal Sonographic Anatomy of the Fetal Face  
 Typical Facial Clefts  
 Atypical Facial Clefts  
 Orbital and Ocular Defects  
 Micrognathia, Retrognathia, and Macroglossia  
 Tumors of the Face  
 Facial Dysmorphism

## Craniosynostosis

### Anomalies of the Neck

Nuchal Cystic Hygroma  
 Other Neck Masses

### Conclusions

## CRANIOFACIAL ANOMALIES

Craniofacial anomalies include a wide spectrum of malformations. Accurate sonographic diagnosis is possible from early gestation onward and has been described in many publications.<sup>1-5</sup> However, a meticulous scanning technique is required that may be difficult to apply in all examinations. Part of the problem is the reconstruction from tomographic planes of the complex tridimensional anatomy of the face. Furthermore, the face is frequently difficult or impossible to access owing to the position of the fetus. Most national guidelines for the standard examination of fetal anatomy include only a few views of the fetal face, mostly demonstration of orbits and eyes, but do not consider feasible an examination of nose, lips, and chin. The accuracy of referral centers in the investigation of high-risk patients is universally reported to be very high.<sup>2-6</sup> Conversely, the sensitivity of standard examinations in a low-risk group of patients is extremely variable, but tends to be low, in the range of 20% to 40%, with a general tendency to recognize facial malformations associated with other anomalies and to miss the isolated ones.<sup>7-10</sup>

Craniofacial malformations may be clinically relevant when seen in isolation, and they may also be associated with other congenital anomalies or be a part of a syndrome. Evaluation of the face is indeed an important part of the clinical genetic examination that is performed postnatally. Therefore, any time a fetal anomaly is identified, the diagnostic workup should include a detailed examination of the fetal face. Apart from obvious malformations, such examinations may also identify subtle dysmorphism that may be crucial for a definitive diagnosis.

## Normal Sonographic Anatomy of the Fetal Face

With two-dimensional (2D) ultrasound, a combination of planes must be used to assess facial anomalies (Fig. 11-1).<sup>1,3,4,6</sup> The following discussion applies mostly to the midtrimester fetus. However, many details of facial anatomy can be identified as early as 11 weeks, particularly by using transvaginal sonography. In the third trimester of gestation, the examination frequently fails because of intrauterine crowding and unfavorable fetal position. Necessary prerequisites of sonography of the fetal face are that it is accessible and there is a pocket of amniotic fluid in front of it, particularly for three-dimensional scanning.

The midsagittal plane is one of the most useful images in that it allows visualization of the profile, which is also one of the most easily recognizable sonographic images of the fetus for the parents. The forehead, nose, and jaw are readily appreciated in this view, which is important to assess the integrity of these structures as well (Table 11-1).

Although the fetal profile is an extremely important view, axial or coronal planes must be obtained to assess the integrity of eyes and lips. A transverse axial scan slightly caudal to the one commonly used for the determination of the biparietal diameter easily reveals orbits and eyes (Table 11-2). The lens and extraocular structures such as muscles, retro-orbital fat, and optic nerve may be visualized. Movements of the eyes are frequently seen during fetal life. It should be remembered that they are usually not synchronous and conjugated. Nomograms for binocular distance, interocular distance, and ocular diameter are available (Table 11-3). By moving the transducer caudally, the superior lip and palate can be visualized. Further caudal movements display the tongue inside the oral cavity and the mandible.

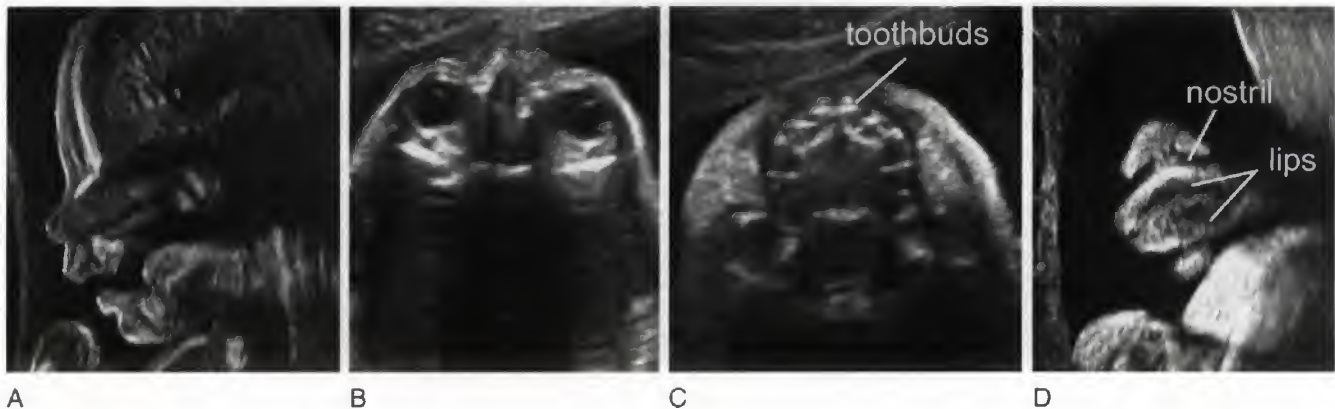


**FIGURE 11-1.** Sagittal (A), axial (B, C), and coronal (D) views of the fetal head demonstrating the relevant details of facial anatomy.

**Table 11-1** Normal Appearance of Fetal Facial Features on Ultrasound in the Midsagittal Section Plane

Structure	Normal Appearance
Forehead	Almost linear immediately above the articulation between the nasal bones and the frontal bone, followed by a smooth backwards bend. This view allows measurement of the thickness of the frontal skin (at the level of the middle of the frontal bend).
Nasal bones	Oblique along a frontocaudal direction. This view allows measurement of the length of the nasal bones and of the superior facial angle (angle between the vertical section of the frontal bone and the nasal bones).
Nasal soft tissues	The columella is oblique or horizontal but should not be vertical.
Upper lip	The philtrum is linear, and should present no bulging. This view allows measurement of the length of the philtrum.
Secondary palate	Thick echoic line, beginning at the alveolar level, and extending horizontally backward. Its middle is marked by a notch, present on both the superior and inferior edges, and corresponds to the transverse palatal suture. <sup>32</sup> The notch is mostly visible on the superior edge.
Oral cavity	The tongue is slightly oblique upward (10–15°). Its tip lies immediately behind the alveolar ridge.
Inferior lip	Rests edge to edge with the upper lip. Both lips are arranged along the same axis; there should be no anteroposterior shift between them.
Chin	At the level of the vertical line traced on the prefrontal skin (esthetic vertical line of the face).

From Rotten D, Levailant JM: Two- and three-dimensional sonographic assessment of the fetal face. 1. A systematic analysis of the normal face. *Ultrasound Obstet Gynecol* 23:224, 2004.

**Table 11-2** Normal Appearance of Fetal Facial Features on Ultrasound in the Axial Section Planes

Structure	Normal Appearance
Orbits	The interorbital axis is perpendicular to the strict sagittal axis. This view allows measurement of the inner and outer interorbital lengths.
Nasal septum, malar	The nasal septum is perpendicular to the axial plane. The two malar arches are symmetric with regard arches to the nasal septum
Upper lip, maxilla	There is no lack of continuity of the upper lip. The maxilla appears as a regular, U-shaped echoic alveolus, secondary plate bend. The alveolus and tooth buds appear as hypoechoic spots regularly layered along the alveolar ridge. There is no shift between adjacent alveoli. The hard palate appears as an echoic structure, with a complex shape. The anterior part is semicircular and lies immediately posterior to the alveolar ridge. The posterior part presents as a rectangle-shaped figure, with a notch on its distal side. This view allows measurement of the size of the maxilla.
Oral cavity	The tongue occupies the totality of the oral cavity, and is glued to the alveolar ridge. Posteriorly, the tongue ends at the oropharynx level. This view allows measurement of the width and length of the tongue.
Mandible	Appears as a regular V-shaped echoic image. Both hemimandibles are almost rectilinear. The symphysis menti is clearly visible. The alveoli appear as regularly layered phypoechoic spots. This view allows measurement of the size of the mandible (for example, mandible width and computation of mandible width/maxilla width ratio).

From Rotten D, Levailant JM: Two- and three-dimensional sonographic assessment of the fetal face. 1. A systematic analysis of the normal face. *Ultrasound Obstet Gynecol* 23:224, 2004.



**Table 11-3** Growth of the Ocular Parameters

Age (Weeks)	Binocular Distance (mm)			Interocular Distance (mm)			Ocular Diameter (mm)		
	5th	50th	95th	5th	50th	95th	5th	50th	95th
11	5	13	20	—	—	—	—	—	—
12	8	15	23	4	9	13	1	3	6
13	10	18	25	5	9	14	2	4	7
14	13	20	28	5	10	14	3	5	8
15	15	22	30	6	10	14	4	6	9
16	17	25	32	6	10	15	5	7	9
17	19	27	34	6	11	15	5	8	10
18	22	29	37	7	11	16	6	9	11
19	24	31	39	7	12	16	7	9	12
20	26	33	41	8	12	17	8	10	13
21	28	35	43	8	13	17	8	11	13
22	30	37	44	9	13	18	9	12	14
23	31	39	46	9	14	18	10	12	15
24	33	41	48	10	14	19	10	13	15
25	35	42	50	10	15	19	11	13	16
26	36	44	51	11	15	20	12	14	16
27	38	45	53	11	16	20	12	14	17
28	39	47	54	12	16	21	13	15	17
29	41	48	56	12	17	21	13	15	18
30	42	50	57	13	17	22	14	16	18
31	43	51	58	13	18	22	14	16	19
32	45	52	60	14	18	23	14	16	19
33	46	53	61	14	19	23	15	17	19
34	47	54	62	15	19	24	15	17	20
35	48	55	63	15	20	24	15	18	20
36	49	56	64	16	20	25	16	18	20
37	50	57	65	16	21	25	16	18	21
38	50	58	65	17	21	26	16	18	21
39	51	59	66	17	22	26	16	19	21
40	52	59	67	18	22	26	16	19	21

From Romero R, Pilu G, Jeanty P, et al: Prenatal Diagnosis of Congenital Anomalies. Norwalk, CT, Appleton & Lange, 1988, p 83.

Coronal planes provide similar information to the axial ones (Table 11-4). However, a section tangential to the anterior face and demonstrating the tip of the nose, nostrils, and upper lip is probably the most useful one in assessing the integrity of the upper lip. The nostrils typically appear as two small anechoic areas. In this scanning plane, demonstrating that the hyperechogenic upper lip separates the anechoic nostrils from the oral rim virtually excludes the presence of cleft lip (CL).

The principles of three-dimensional (3D) ultrasound are described in detail elsewhere in this text (see Chapter 24). Diagnosis of craniofacial anomalies is one of the most important areas of application of this technique in obstetric sonography. The advantages over standard 2D ultrasound include the visualization of scanning planes that are physically impossible or very difficult to obtain; the demonstration of the surface of the face; and the possibility to have panoramic views of the entire face (Fig. 11-2). The limitations of the technique are the same as that for 2D sonograms. If the fetal face is not accessible or there is not a pocket of amniotic fluid separating the face from the surrounding structures, a 3D view will be of little help. However, in expert hands, a satisfying examination is possible in

**Table 11-4**

### Normal Appearance of the Fetal Facial Features on Ultrasound in the Coronal Section Planes

Structure	Normal Appearance
Nose-mouth view	The nostrils are symmetric. The columella is visualized as an intact line.
Alveolus, nasal septum	The alveolar ridge is regular and appears as an echoic band where tooth buds appear as hypoechoic holes. The nasal septum is perpendicular to the alveolar ridge lining.
Hard palate	Bow-shaped, with a symmetric bend. On each side, it is in continuity with the malar bone.
Retropalatal region	The vomer bone appears as a medial echoic spot isolated in an empty space, with no visible supporting structure acquisition

From Rotten D, Levailant JM: Two- and three-dimensional sonographic assessment of the fetal face. 1. A systematic analysis of the normal face. *Ultrasound Obstet Gynecol* 23:224, 2004.



**FIGURE 11-2.** Three-dimensional ultrasound: multiplanar analysis demonstrating simultaneously sagittal (A), axial (B), and coronal views (C) of the fetal face.



**FIGURE 11-3.** Three-dimensional ultrasound: surface rendering of the fetal face at 11 weeks (A), 19 weeks (B), and 37 weeks (C).

the majority of cases in the second to early third trimester. The relative value of 2D over 3D ultrasound has been debated.<sup>6,11</sup> In expert hands, 2D ultrasound is extremely precise in the identification and categorization of craniofacial malformations and we have not found any significant diagnostic advantage from the use of 3D.<sup>6</sup> It has been suggested that 3D ultrasound of fetal craniofacial anomalies has other potential benefits, such as offering the parents a realistic and understandable image of the fetal anomaly, and allowing better communication with the specialists involved in the management of the infant. Most of the experience with 3D ultrasound has been derived from referral centers. The impact of this technique in standard examinations has yet to be assessed. In general, 3D ultrasound is complex and probably beyond the scope of a basic evaluation of fetal anatomy in low-risk pregnancies. However, it is possible that four-dimensional ultrasound, which allows a rapid and accurate

visualization of the external surface of the fetus, could prove useful for assessment of facial anatomy in such settings.

Once an ultrasound volume has been acquired, it can be studied with a variety of approaches. Thus far, three modes have been reported to be useful in the diagnosis of craniofacial anomalies. The multiplanar mode consists in the simultaneous demonstration of three orthogonal planes whose direction is chosen by the operator. Typically, the volume is obtained from the profile view of the fetus, which is displayed on the upper left corner of the screen, while the two perpendicular planes are demonstrated in the upper right and lower quadrants (see Fig. 11-2). The advantage is that it may be difficult at times to obtain the exact plane in a moving fetus. The surface mode allows one to visualize the external surface of the fetal face when it is surrounded by fluid (Fig. 11-3). Eventually, the maximum or transparent mode allows one to demonstrate the brightest echoes



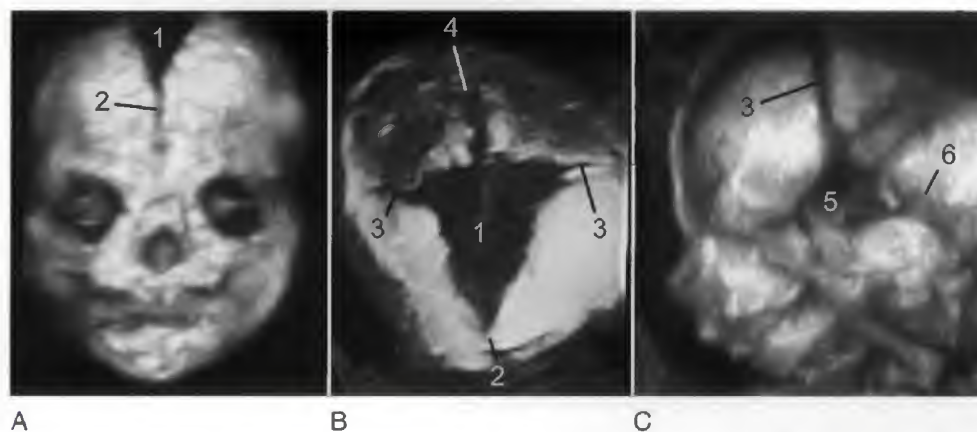


**FIGURE 11-4.** Three-dimensional ultrasound: the skeleton of the face and skull is clearly demonstrated with the maximum or transparent mode. The different sutures and fontanel are depicted in the coronal (A), superior (B), and lateral view (C) of the skull: 1. bregmatic fontanel; 2. frontal or metopic suture; 3. coronal suture; 4. parietal suture; 5. sphenoid fontanel; 6. mastoid suture.

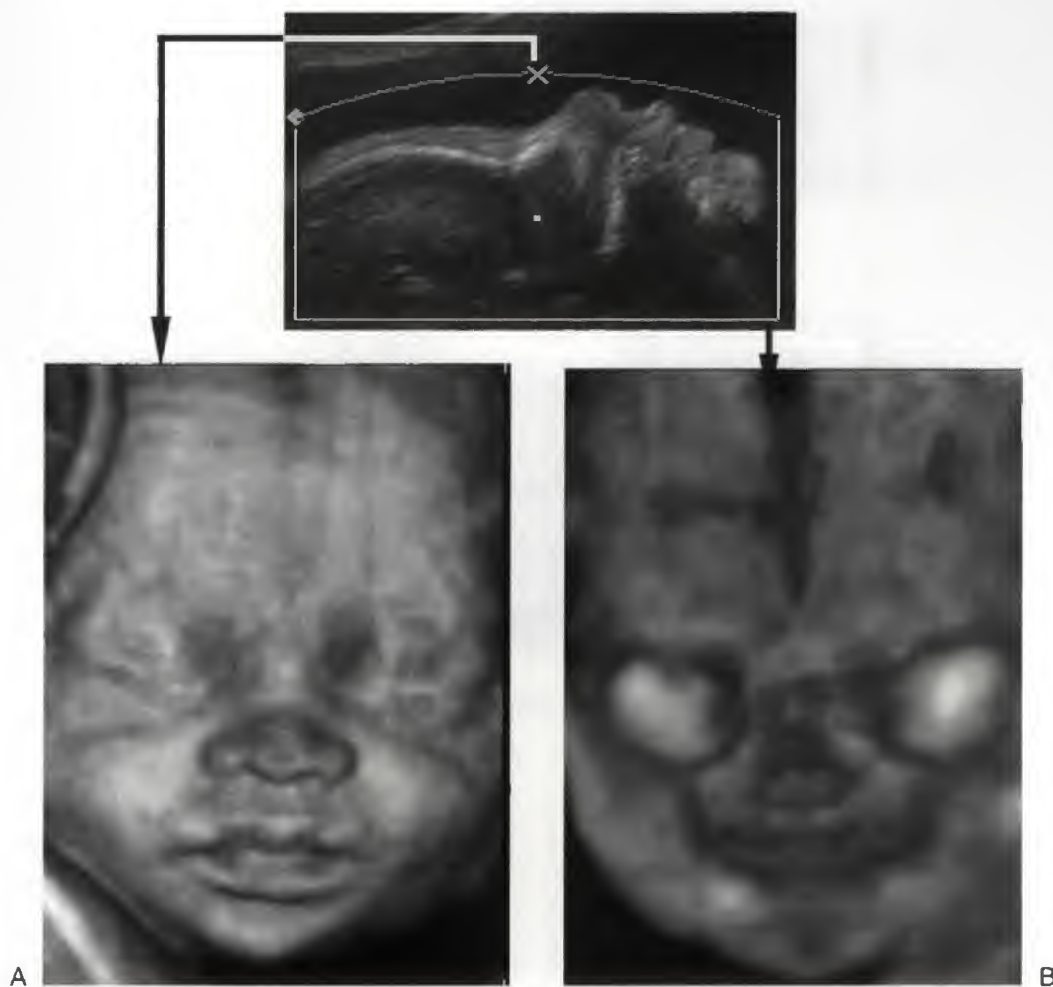


**FIGURE 11-5.** Three-dimensional ultrasound: anterior (A) and reverse view (B) of the fetal face. The same ultrasound volume is used, and only the point of view is changed. The reverse view provides an image of the anterior palate and nasal fossa.

within the volume and it can be used to visualize the skull (Fig. 11-4).

One limitation of 2D ultrasound is the difficulty in visualizing clearly the posterior portion of the palate, owing to shadowing artifacts arising from the anterior palate. 3D sonography often overcomes this difficulty. One approach

is the so-called reverse view of the face, that is, once the volume has been acquired, the face is viewed in surface mode from the back instead from the front (Fig. 11-5).<sup>11,12</sup> Another approach consists in insonating the face at an angle that demonstrates the palate (Figs. 11-6 and 11-7).<sup>13</sup>





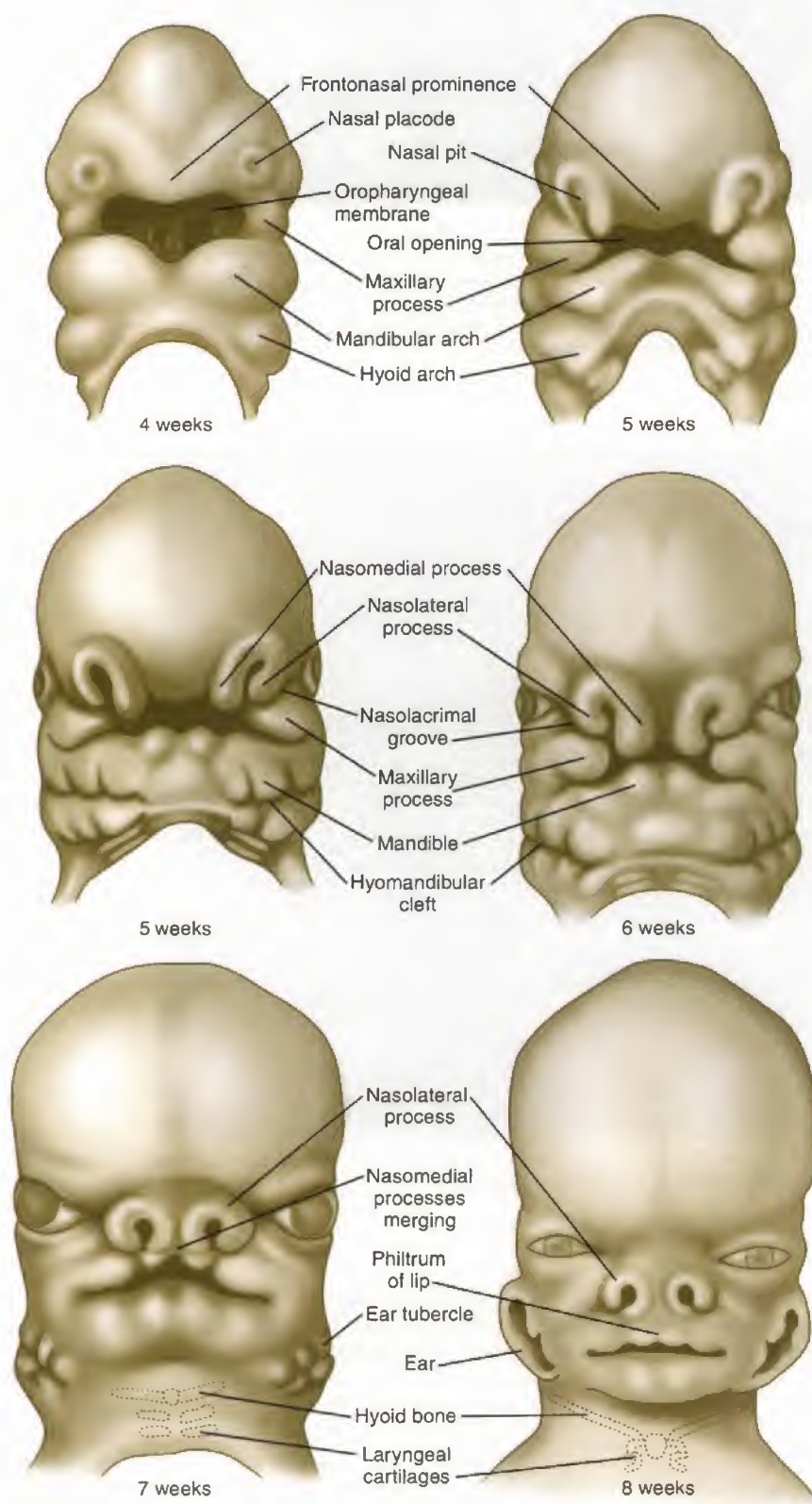


**FIGURE 11-8.** Frontal views of the heads of human embryos from 4 to 8 weeks of age. (From Carlson BM [ed]: *Human Embryology and Developmental Biology*, 3rd ed. Philadelphia, Mosby/Elsevier, 2004, p 322.)

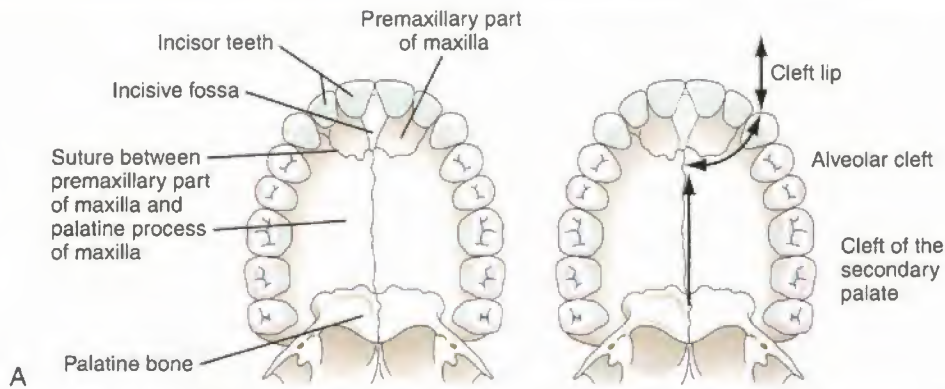


**FIGURE 11-9.** A. Drawing of the human palate in the axial plane highlights the anatomy of the premaxillary part of the maxilla and the lateral palatine processes of the secondary palate. Their points of fusion are indicated by the black lines between them. The four incisor teeth arise from the premaxillary portion of the primary palate, and the remaining teeth, from the canines posteriorly, arise from the lateral palatine processes of the secondary palate. (Adapted and reprinted from Moore KL: *The Developing Human: Clinically Oriented Embryology*, 6th ed. Philadelphia, WB Saunders, 1998, p 245.) B. Schematic representation of the various cleft constituents of the palate. (From Rotten D, Levailant JM: Two and three-dimensional sonographic assessment of the fetal face. 2. Analysis of cleft lip, alveolus and palate. *Ultrasound Obstet Gynecol* 24:402, 2004.)

prominence, maxillary prominence, and mandibular prominence) are separated by grooves that eventually undergo fusion and obliteration. The palate originates from the fusion of three palatine processes. The median palatal process originates from the medial nasal prominences, and the two lateral ones originate from the maxillary processes. The palatine processes fuse also with the nasal septum, which divides the nasal cavities. The palate is commonly divided in three parts: the anterior or primary palate, the posterior or secondary palate, and the soft palate (Fig. 11-9). Typical facial clefts derive presumably from failure of fusion of the different bony structures and overlying soft tissues, with persistence of the embryologic grooves (Fig. 11-10).

CL-CP and isolated CP are two different anomalies. With exceedingly rare exceptions, recurrences are type specific. If the index case has CL-CP, there is no increased risk for isolated CP, and vice versa. Roughly, of all cases with typical facial clefts, 25% have CL, 50% have CL-CP, and 25% have CP.

In the vast majority of cases, typical facial clefts have a multifactorial etiology. The empiric risks of recurrence for these cases are reported in Table 11-5. In some cases, however, facial clefts are a part of well-established genetic and nongenetic syndromes. The claimed risk associated with intake of diazepam and steroidal agents has not been confirmed in carefully controlled studies. Chromosomal abnormalities are rare in postnatal series but rather frequent in the prenatal ones.<sup>2,6,17,18</sup> The discrepancy may be due to a high rate of intrauterine selection of aneuploid fetuses, as well as to the inclusion of an excess of atypical clefts.

Facial clefts encompass a broad spectrum of severity. The typical CL appears as a linear defect extending from one side of the lip into the nostril (Table 11-6). CL-CP may extend through the alveolar ridge and hard palate, reaching the floor of the nasal cavity or even the floor of the orbit (Table 11-7). CP may include defects of the hard palate, the soft palate, or both or the submucosal tissue (see Table 11-8 and Fig. 11-10).

Associated anomalies are found in 50% of patients with isolated CP and in only 13% of those with CL-CP. An

incidence of 60% has been found in embryos and fetuses with facial clefting. In the majority of patients, the associated anomalies do not conform to an established syndrome. In cases of either isolated CL or CP, the most frequent anomaly is clubfoot, whereas in cases of CL-CP, it is polydactyly. Of particular importance is the association with congenital heart disease. No specific pattern could be identified. Specific associations with well-described syndromes are shown in Table 11-9.

The sonographic diagnosis of CL in the fetus depends on demonstration of a groove extending from one of the nostrils inside the lip and possibly the alveolar ridge. With standard 2D ultrasound, facial clefts can be recognized and categorized by a combination of coronal and axial scans. In our experience, CL is best visualized in an anterior coronal plane, demonstrating a linear defect extending from one nostril to the oral rim, usually associated with distortion of both upper lip and nose (Fig. 11-11). Extension of the defect into the palate is better demonstrated in an axial scan of the maxilla (Fig. 11-12). By angling the transducer, it is usually possible to evaluate the degree of extension of the defect, that is to identify whether the lesion is limited to the most anterior part of the palate or the alveolar ridge, or it continues into the posterior palate (see Fig. 11-12). Indirect sonographic findings can also be noted that correlate with the type of defect. In all typical clefts with bilateral CL-CP, the axial and sagittal views demonstrate a protrusion of the central portion of the palate and lip that is commonly referred to as the premaxillary pseudomass (Fig. 11-13). With bilateral CL-CP there is a major distortion of facial anatomy, and the pseudomass is a more obvious and reliable finding than the visualization of the clefts itself.<sup>19</sup> Conversely, with unilateral CL-CP or bilateral CL, the profile view is always unremarkable. The diagnosis of CL-CP, mostly of the bilateral type, has been described even in early gestation, at 11 to 14 weeks, predominantly because of the demonstration of a premaxillary pseudomass.

If a satisfying ultrasound volume can be acquired, the diagnosis of cleft lip is easy. The transparent mode can be used to demonstrate whether the palate is involved or not



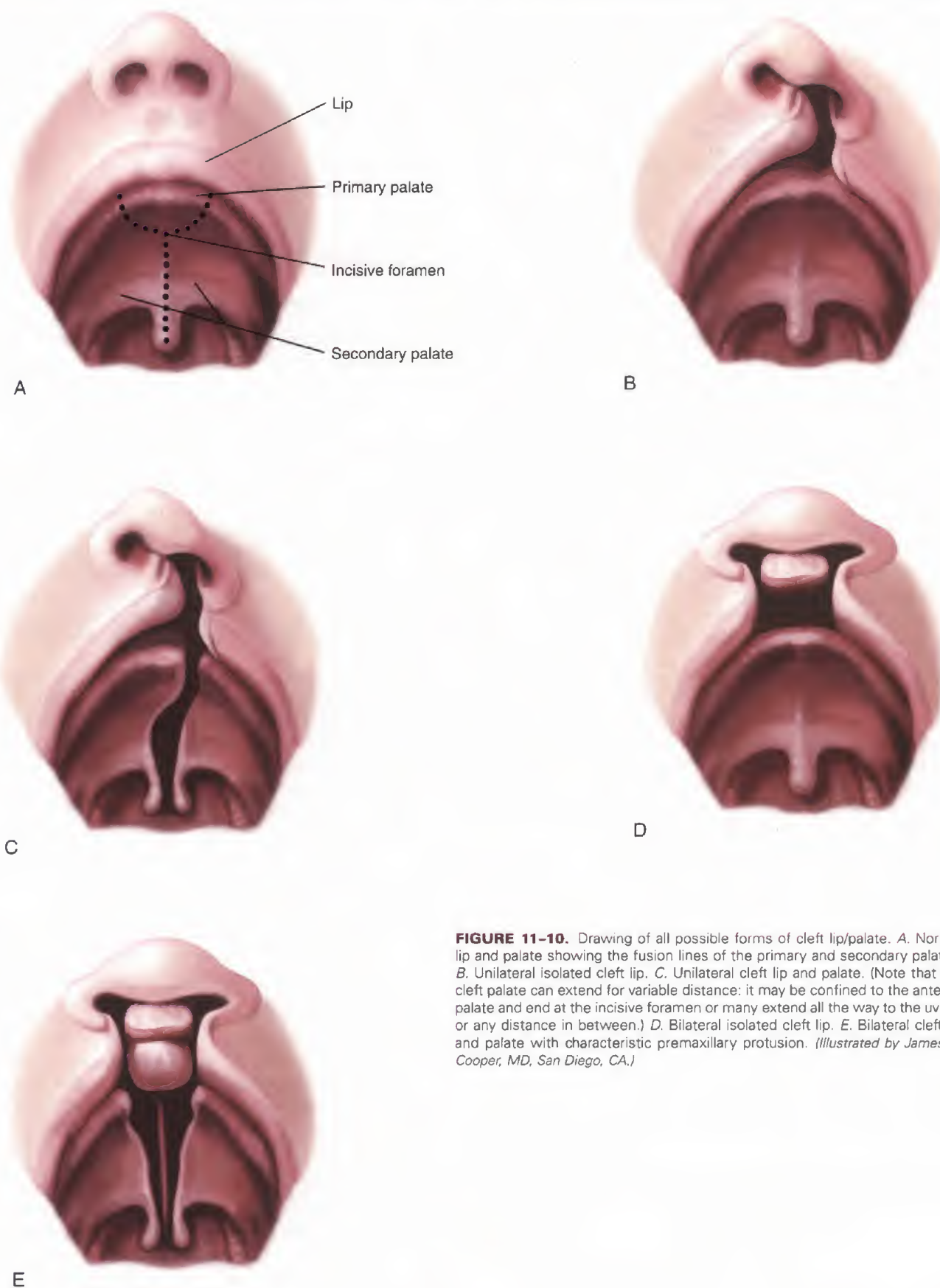


**FIGURE 11-10.** Drawing of all possible forms of cleft lip/palate. A. Normal lip and palate showing the fusion lines of the primary and secondary palates. B. Unilateral isolated cleft lip. C. Unilateral cleft lip and palate. (Note that the cleft palate can extend for variable distance: it may be confined to the anterior palate and end at the incisive foramen or many extend all the way to the uvula, or any distance in between.) D. Bilateral isolated cleft lip. E. Bilateral cleft lip and palate with characteristic premaxillary protusion. (Illustrated by James A. Cooper, MD, San Diego, CA.)

**Table 11-5****Risk of Recurrent Cleft Lip/Cleft Palate in Subsequent Offspring**

Variable	Cleft Lip/Palate (%)
Unaffected parent	
No affected offspring	0.1
No affected offspring plus 1 affected first cousin	0.4
One affected offspring	4.0
Two affected offspring	9.0
One affected offspring plus one affected relative	4.0
Affected parents	
One parent plus no affected offspring	4.0
One parent plus one affected offspring	10-17
Two parents plus one affected offspring	60.0

(Fig. 11-14). If the palate is insonated at an angle, the degree of internal extension of the cleft can be appreciated (Fig. 11-15). Magnetic resonance imaging may also be used in selected cases, as it is effective for evaluating the involvement of the palate (Fig. 11-16) and may also allow the diagnosis of CP, which is difficult if not impossible with ultrasound.

The prognosis of facial clefts depends primarily on the presence and type of associated anomalies. Mild clefts, such as lineal indentations of the lips or submucosal cleft of the soft palate, may not require surgical correction. Larger defects cause cosmetic, swallowing, and respiratory problems. Recent advances in surgical technique have produced good cosmetic and functional results. Cases that are associated with a defect in the posterior palate represent the greatest challenge for surgical correction, as the soft palate is involved in the process of swallowing and vocalizing. Furthermore, auditory tubal disorders may lead in time to acoustic problems and deafness.

**Table 11-6****Sonographic Characteristics of Unilateral or Bilateral Cleft Lip**

Section Plane	Unilateral Cleft	Bilateral Cleft
Sagittal and parasagittal	The midsagittal view is usually normal. The parasagittal views show the cleft of the upper lip as a defect between two thickened zones, with visible asymmetry between both sides of the defect. The narinal bridge is always complete, but there is a flattened narinal bend.	The normal image of the lip is replaced by the protruding premaxillary prolabium. The prolabium is stuck to the nose, which is consequently flattened. The columella cannot be analyzed.
Axial	The loss of continuity of the labial arc is clearly apparent. The nostrils are asymmetric and distorted, but the nasal aisles are always present, constituting a bridge over the cleft.	On each side, the protruding premaxillary prolabium is separated from the remaining upper lip extremities by the clefts. Both nostrils are flattened but complete.
Coronal	The loss of lip continuity is clearly apparent.	The defects in lip continuity are clearly apparent.

From Rotten D, Levailant JM: Two- and three-dimensional sonographic assessment of the fetal face. 2. Analysis of cleft lip, alveolus and palate. *Ultrasound Obstet Gynecol* 24:402, 2004

**Table 11-7****Sonographic Characteristics of Unilateral or Bilateral Cleft Alveolus**

Section Plane	Unilateral Cleft	Bilateral Cleft
Axial	The alveolar defect ranges from a simple slant to a cleft involving the alveolus and pre-maxilla. Clefts involving the alveolus present as a defect in alveolar continuity: - a simple irregularity in the alveolar lining signals an alveolar slant; - a defect in alveolar regularity with anteroposterior shift between the two hemimaxillae signals a cleft involving the alveolus and pre-maxilla.	The pre-maxilla is protruded together with the prolabium. The premaxillary mass is analyzed (size, soft tissue and bone content). The external parts of both alveoli are symmetrical.
Coronal	There is a defect in alveolar continuity, with missing buds.	There is a median defect in alveolar continuity. This contrasts with an intact hard palate.

From Rotten D, Levailant JM: Two- and three-dimensional sonographic assessment of the fetal face. 2. Analysis of cleft lip, alveolus and palate. *Ultrasound Obstet Gynecol* 24:402, 2004.



**Table 11-8** Sonographic Characteristics of Unilateral or Bilateral Secondary Palate Cleft

Section Plane	Secondary Palate Cleft With a Unilateral CLA	Secondary Palate Cleft With a Bilateral CLA
Midsagittal and parasagittal	The successive views show a defect in hard palate continuity. This defect is asymmetric. It is not strictly median, but lateralized, usually towards the same side as the CLA cleft.	An hyperechoic midline image is present in the midsagittal view. Care must be taken: although a median line is present it is not the palate, but the vomer bone. On each side of the sagittal view, the parasagittal views show the hard palate defects
Axial	When looking for the palate caudally to the alveolus (remember that the alveoli are separated by a defect and a shift), one does not find it. The only apparent image is that of an oblique vomer bone (10–5°)	The anteroposterior hyperechoic line corresponding to the vomer bone is present Anteriorly, it extends onto the premaxillary prolabium On each side of this median structure, the cleft is readily apparent.
Coronal	Medially, the palatal arch is interrupted by a defect. Actually, this defect is not symmetric, but lateralized on the same side as the CLA cleft. Thus, the two half arches are not symmetrical. The wider half is on the non-pathologic side. The vomer bone is deflected toward the half arch situated on the pathologic side, and rests on it.	The hard palate cannot be imaged. The vomer appears as a suspended midline line, with no supportive structure to rest on. The palatal arch is reduced to two small lateral structures.

From Rotten D, Levailant JM: Two- and three-dimensional sonographic assessment of the fetal face. 2. Analysis of cleft lip, alveolus and palate. *Ultrasound Obstet Gynecol* 24:402, 2004

## Atypical Facial Clefts

Approximately 3% of clefts occur in portions of the face different from the line joining the nostrils to the posterior palate. The prevalence is much higher in prenatal studies due to both the high intrauterine fatality rate that is associated with some of these conditions and probably the higher detection rate due to the frequency of associated malformations.

The atypical cleft that has been reported most frequently in prenatal diagnosis series is the median cleft or Tessier cleft number 0. This is a quadrangular defect in the central portion of the upper lip and palate, usually associated with a flattened nose. It accounts for less than 1% all cases of cleft lip. It is considered to represent the consequence of underdevelopment of the frontonasal prominence, which normally joins the two maxillary prominences. Development of the midface is induced by the prechordal mesenchyme, which is also responsible for the differentiation of the midline structures of the brain. This explains the frequent association of median clefts with alobar or semilobar holoprosencephaly.<sup>20,21</sup> The typical combination of findings in these cases include hypotelorism, flat nose, and median CL (Fig. 11-17).

Median CL may also occur in association with hypertelorism (increased orbital distance), a combination that is pathognomonic of the "median cleft face syndrome" or "frontonasal dysplasia."<sup>22</sup> The pathogenesis is much different in these cases. The premaxilla is present, as well as the nose that is usually bifid, and the brain is normal in most cases. The diagnosis relies on the demonstration of a wide central defect involving both the upper lip and the palate in axial or coronal scans.

The prognosis of a median cleft depends entirely on the association with other anomalies. Median cleft face syndrome is usually associated with normal intelligence. Radical cosmetic surgery may be required. Alobar and semilobar holoprosencephaly associated with median clefts and hypotelorism both have a extremely poor prognosis. Severe holoprosencephaly is also associated with other craniofacial anomalies due to underdevelopment of the midface that include a combination of hypotelorism/cyclopia, absence of a nose, and presence of a proboscis (Fig. 11-18).<sup>20,21</sup>

Bilateral CL-CP is usually associated with anterior displacement of the premaxilla. In a minority of cases, it may occur without protrusion and a flat facial profile.<sup>2</sup> This is a different and more extreme anomaly than typical CL-CP, which is probably pathophysiologically connected to median CL, and usually associated with multiple anomalies and chromosomal aberrations, trisomy 18 in particular (Fig. 11-19).

The most common atypical cleft found at birth is the lateral one (or Tessier number 7), which has an estimated incidence of one in 3000 to 5600 live births and may be either unilateral (more frequently on the left side) or bilateral.<sup>23,24</sup> It is probably due to defective development of the branchial arches and is characterized by a variable degree of widening of the oral commissure (macrostomia) associated with hypoplasia of the lateral skeleton of the face (maxilla, zygomatic bone, ascending branch of the mandible) and external ear. A handful of cases have been diagnosed antenatally. Sonographic findings include unusual deepening of the corners of the mouth and asymmetry between the two sides of the face. 3D ultrasound is particularly valuable for recognizing lateral clefts (Fig. 11-20). The

**Table 11-9****Most Frequent Syndromes Associated With Facial Clefts****Chromosomal aberrations**

- Deletion 4p (Wolf-Hirschhorn syndrome)
- Trisomy 10
- Trisomy 13
- Trisomy 18
- Trisomy 22
- Trisomy 9

**Malformations and sequences**

- Amniotic bands
- Arthrogryposis
- Camptomelic dysplasia
- Caudal regression syndrome/syrenomelia
- CHARGE association
- Diastrophic dysplasia
- Ectrodactyly, ectodermal dysplasia, clefting
- Holoprosencephaly
- Hydrolethrus
- Majewski (short rib-polydactyly syndrome, type II)
- Median cleft face (frontonasal dysplasia)

**Syndromes**

- Crouzon
- Femoral hypoplasia, unusual facies
- Fryns
- Goldenhar
- Gorlin
- Klippel-Feil
- Larsen
- Marfan
- Meckel-Gruber
- Multiple pterygiums
- MURCS association
- Nager
- Neu-Laxova
- Oral-facial-digital (Mohr)
- Pena Shokeir
- Pierre Robin
- Roberts
- Shprintzen
- Smith-Lemli-Opitz
- Treacher Collins
- Van der Woude
- Alker-Warburg

central portion of the face, nose, lips and alveolar ridge are well visualized with a standard 2D scan. However, the lateral part of the fetal face is not equally accessible. A panoramic view of the entire face in surface mode is certainly the best approach for this diagnosis.<sup>24</sup> Atypical facial clefts probably can also occur also with a disruptive mechanisms, as it is attested by cases of amniotic band syndrome.<sup>2</sup>

Lateral clefts of the face are usually isolated malformations. Surgical correction is possible but is extremely challenging owing to the association with underlying skeletal abnormalities involving the mandible. Ear abnormalities are also frequent.



**FIGURE 11-11.** Anterior coronal plane of the fetal face demonstrating unilateral cleft lip.

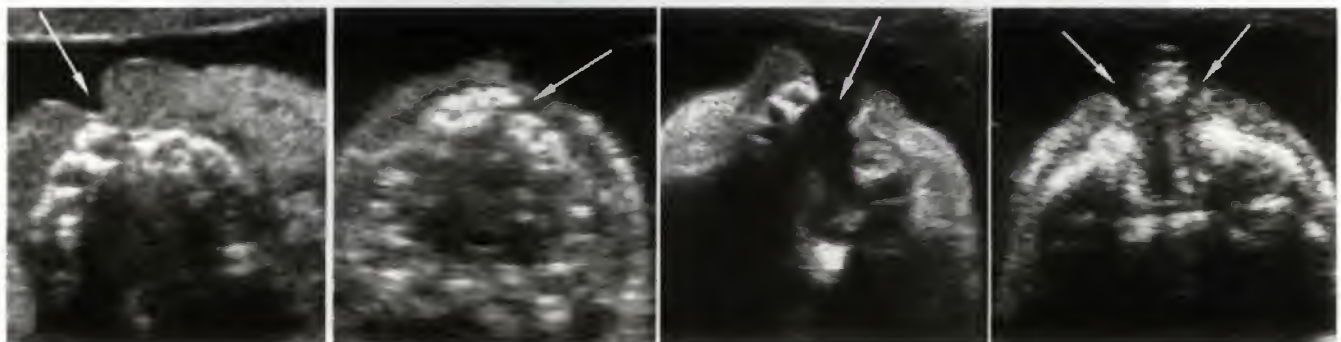


**FIGURE 11-12.** Axial planes of the maxilla in fetuses with facial clefts: *A.* Isolated cleft lip (arrow): the alveolar ridge is intact albeit irregular in shape as it frequently happens in these cases. *B.* Unilateral cleft lip and palate: the defect only extends to the alveolar ridge (arrow); note that one toothbud is missing but that the secondary palate does look intact; this defect is frequently referred to as cleft alveolus. *C.* Unilateral cleft lip and palate; the defect is seen extending to the secondary palate (arrow). *D.* Bilateral cleft lip and palate (arrows); the anterior protrusion of the central portion of the maxilla (or premaxilla) indicates that the defect extends posteriorly to the secondary palate.



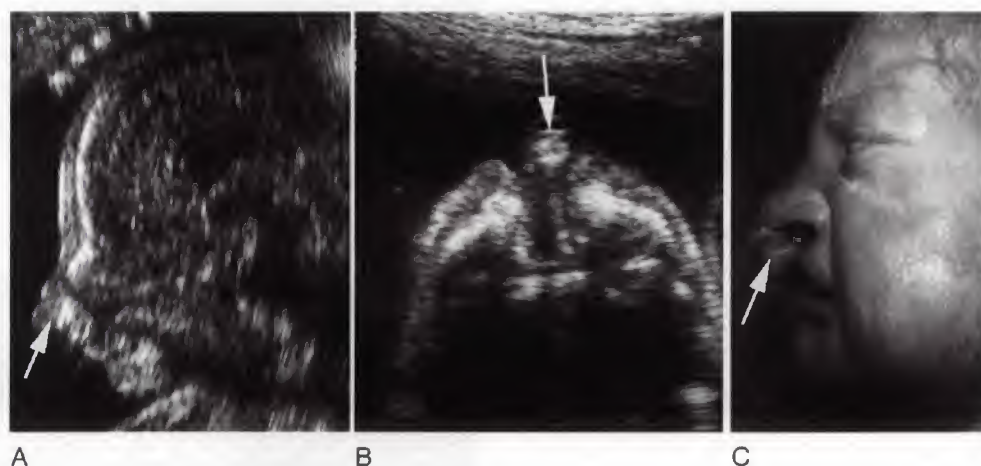


**FIGURE 11-13.** Protrusion of the premaxilla (arrows) in a fetus with bilateral cleft lip and palate: (A) sagittal view; (B) axial view; (C) postnatal image for comparison.

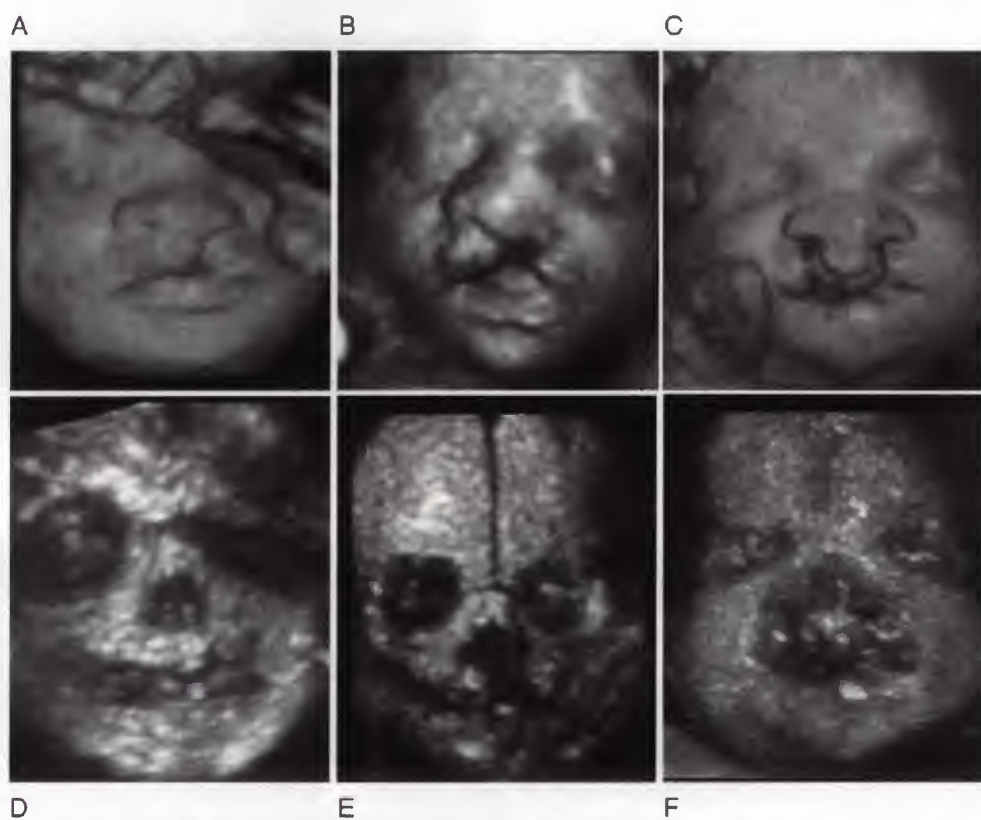


**FIGURE 11-14.** Three-dimensional ultrasound of cleft lip in surface mode (A, B, C) and maximum mode (D, E, F). A. Unilateral cleft lip. B, E. Unilateral cleft lip and palate. C, F. Bilateral cleft lip and palate.

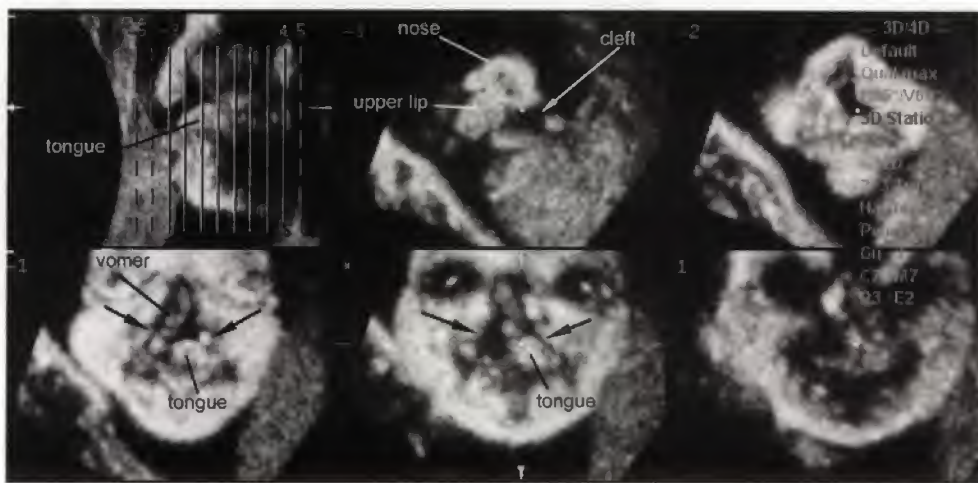


**FIGURE 11-15.** Three-dimensional ultrasound of unilateral cleft lip and palate: TUI (multiple slices) of a volume obtained with angled insonation of the fetal palate. A comparison between the reference sagittal view and the coronal slices allows one to identify the defect extending into the secondary palate (arrows).

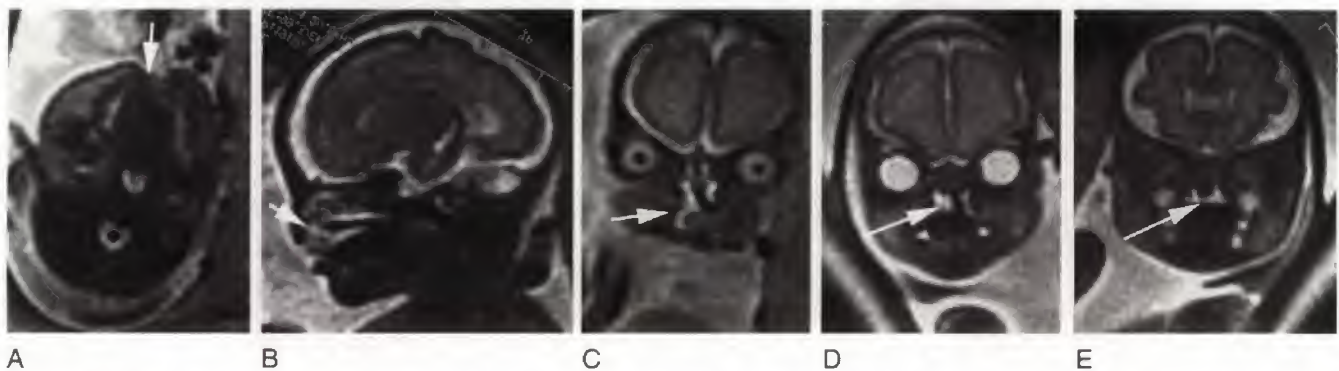


**FIGURE 11-16.** Magnetic resonance imaging of a third trimester fetus with unilateral cleft lip and palate (arrow) in the axial (A), sagittal (B), and coronal planes (C, D, E). Extension of the defect to the entire secondary palate is well demonstrated.

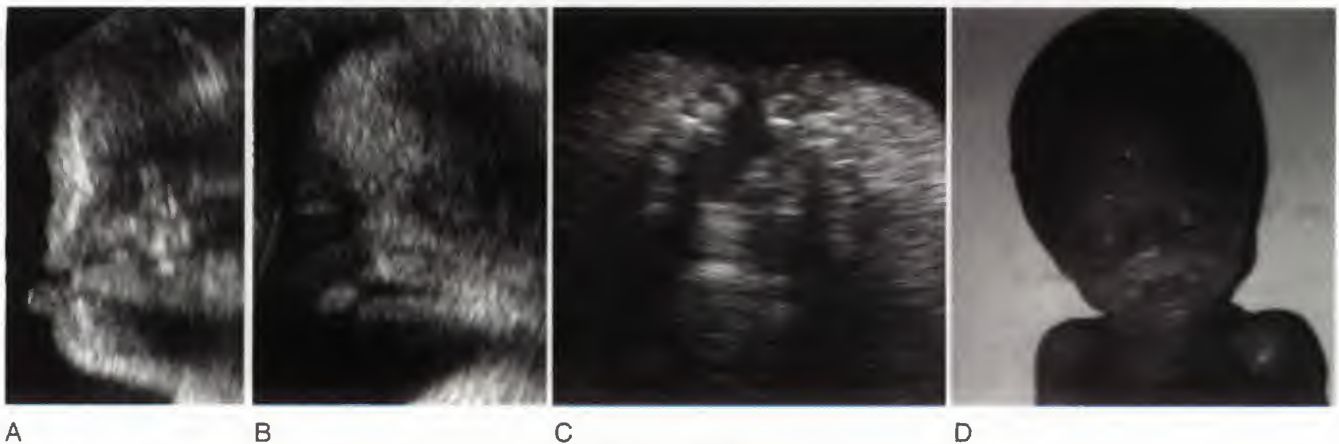


**FIGURE 11-17.** Median cleft lip and flattened nose in a fetus with alobar holoprosencephaly seen in (A) sagittal, (B) coronal, (C) axial planes of section and (D) postnatally.



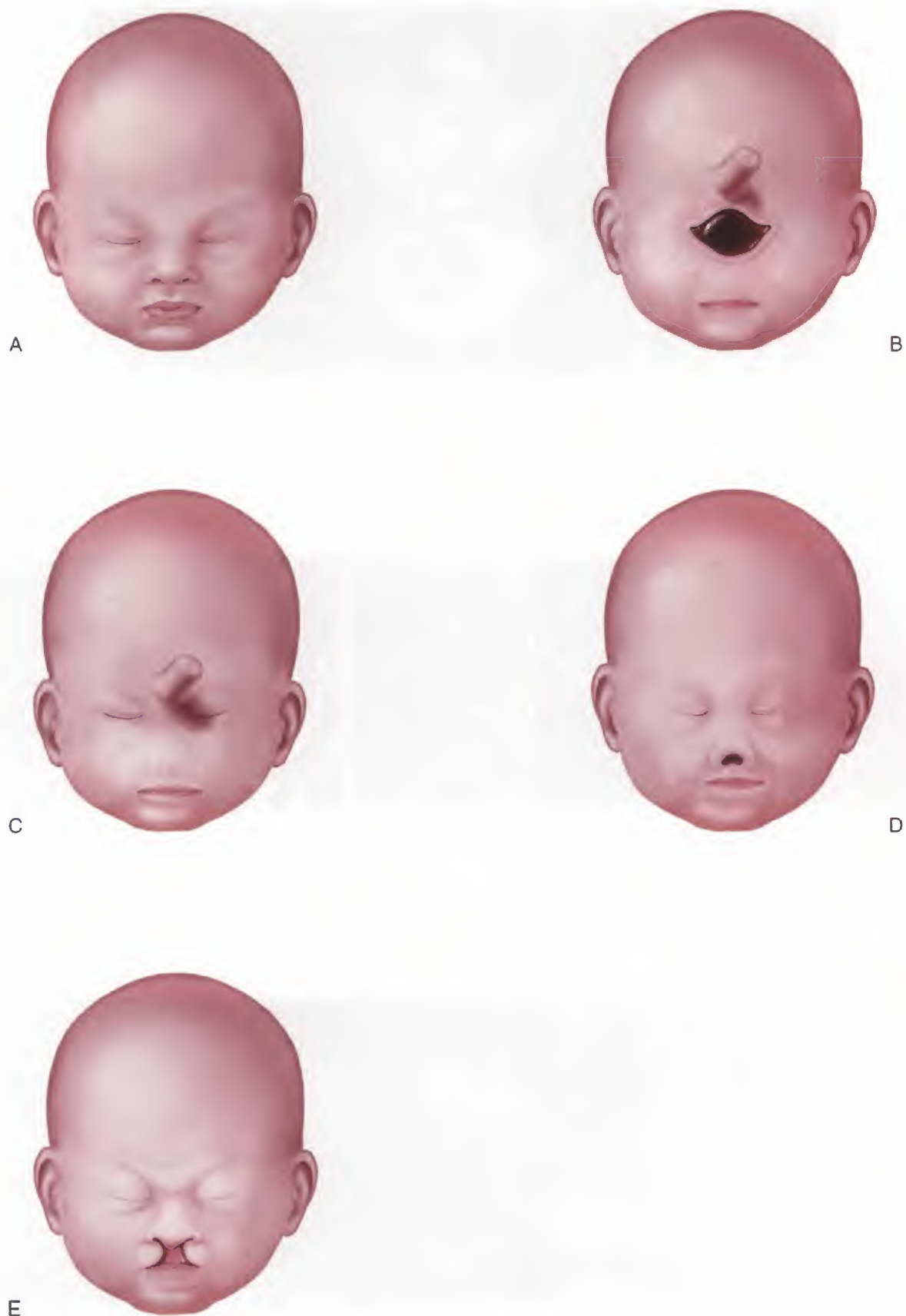


**FIGURE 11-18.** Facial abnormalities associated with holoprosencephaly compared with the normal face. A. Normal face. B. Cyclopia. C. Ethmocephaly. D. Cebocephaly. E. Midline cleft. (Modified from Coates TL, McGahan JP: *The fetal face*. In McGahan JP, Porto A (eds): *Diagnostic Obstetrical Ultrasound*. Philadelphia, JB Lippincott, 1994, p. 212. Illustration by James A. Cooper, MD, San Diego, CA.)

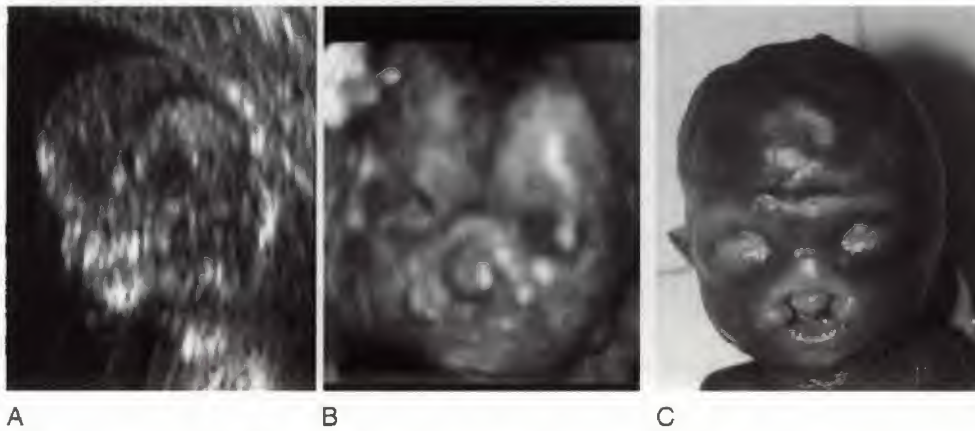


**FIGURE 11-19.** Bilateral cleft lip and palate with flat face: (A) profile view at 12 weeks; (B) surface mode at 14 weeks; (C) postnatal image.

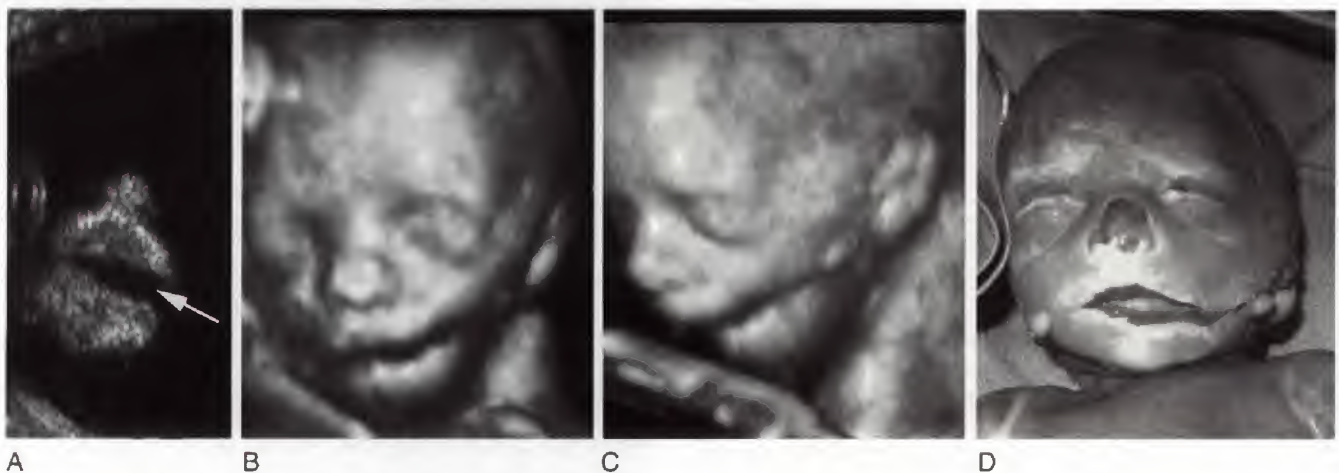


**FIGURE 11-20.** Lateral cleft of the fetal face: (A) anterior coronal scan demonstrating the lips and nose; an asymmetry in the shape of the mouth is noted (arrow); (B, C) three-dimensional ultrasound: surface mode demonstrates a lateral cleft associated with a typically sunken cheek and a skin tag; (D) postnatal image.

## Orbital and Ocular Defects

In early development, the eyes are placed laterally in the primitive face in a fashion similar to that of lower animals with panoramic vision. As gestation progresses, they migrate toward the midline, creating favorable conditions for the development of stereoscopic vision. Hypertelorism is an increased interorbital distance, and this can be either an isolated finding or associated with many clinical syndromes or malformations. Mild hypertelorism is a common variant. However, there is a high likelihood of mental retardation when either associated anomalies or an extreme degree of hypertelorism is found. The most common anomalies with hypertelorism are the median cleft face syndrome; craniosynostoses such as Apert, Crouzon, and Pfeiffer syndromes; agenesis of the corpus callosum; and anterior encephaloceles. Hypertelorism per se results only in cosmetic problems and possible impairment of stereoscopic binocular vision. For severe cases, a number of operative procedures, such as

canthoplasty, orbitoplasty, surgical positioning of the eyebrows, and rhinoplasty, have been proposed.

Hypotelorism (decreased interorbital distance) is almost always found in association with other severe anomalies, almost invariably with holoprosencephaly. The prognosis, which depends on the associated anomalies, is usually very poor.<sup>2,3,20,21</sup>

Microphthalmia is defined as a decreased size of the eyeball, and anophthalmia refers to the absence of the eye; however, the term anophthalmia should be reserved for the pathologist, who must demonstrate not only absence of the eye but also of optic nerves, chiasma, and tracts. Microphthalmia/anophthalmia, which is either unilateral or bilateral, is usually associated with many genetic syndromes. Prenatal diagnosis of microphthalmia is based on the demonstration of decreased ocular diameters (Fig. 11-21) and careful examination of the intraorbital anatomy is indicated to identify lens, pupil, and optic nerve.<sup>25</sup> Congenital microphthalmia is frequently associated with visual disorders and



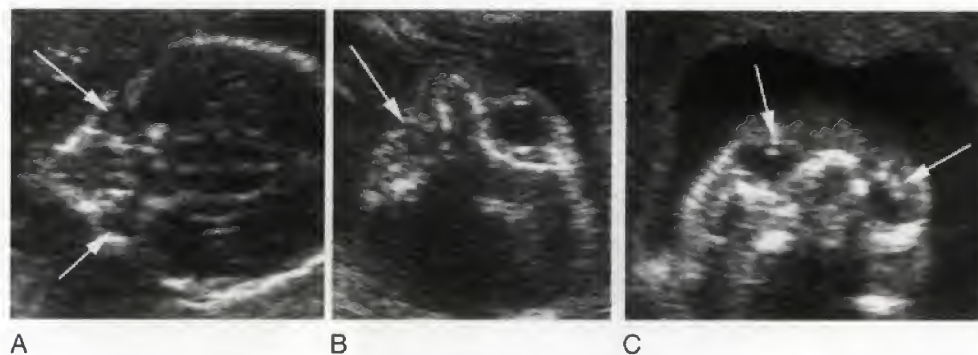


**FIGURE 11-21.** Ocular anomalies: (A, B) bilateral and unilateral microphthalmia (arrows); (C) cataract (arrows).

with other anomalies. Goldenhar syndrome (found in about 1 per 5000 births) is associated with hypoplasia of one half of the face (hemifacial microsomia) that often includes unilateral anophthalmia, and ear, dental, and facial abnormalities (Fig. 11-21).<sup>26</sup> It has been reported that at least in some cases, microphthalmia may develop throughout gestation and early prenatal diagnosis may be impossible.<sup>25</sup>

A cataract is a clouding of the lens in the eye that affects vision. Most cataracts are related to aging. Cataracts are very common in older people. Rarely, this is found at birth, and in these cases the disease is usually bilateral. Sonographically, cataract is associated with an echogenic lens<sup>25</sup> (see Fig. 11-21). In the majority of cases, cataracts are a part of multiple anomalies and syndromes, or are associated with congenital infections. Congenital cataract can be treated by removal of the lens. The prognosis however depends largely on the associated anomalies.

Congenital obstruction of the nasolacrimal duct results in cystic dilatation of the proximal part of the duct. Dacrocystocele has been identified prenatally as an anechoic mass medial and slightly inferior to the eye<sup>27</sup> (Fig. 11-22). Although the differential diagnosis includes an anterior encephalocele, hemangioma, and a dermoid cyst, the sonographic appearance is typical. Postnatally, dacrocystoceles resolve spontaneously in about 90% of cases within the first 6 months of life.

### Micrognathia, Retrognathia, and Macroglossia

The mandible forms the floor of the oral cavity and contains the tongue. If the mandible is severely hypoplastic (micrognathia) or posteriorly displaced (retrognathia), a typical malformative sequence occurs: the tongue is displaced superiorly and posteriorly, leading to both abnormal closure of the palatine process, which results in either a cleft palate or a high arched palate, and glossoptosis that may cause suffocation at birth. This sequence is frequently referred to as the Robin anomalad. It may be a sporadic isolated finding (in about 40% of cases), or it may be associated with other anomalies or with recognized genetic and nongenetic syndromes including Treacher Collins, Robin and Robert syndromes, chromosomal abnormalities (mainly trisomy 18 and triploidy), and teratogen exposure. Otocephaly is a rare, lethal, sporadic abnormality characterized by severe hypo-

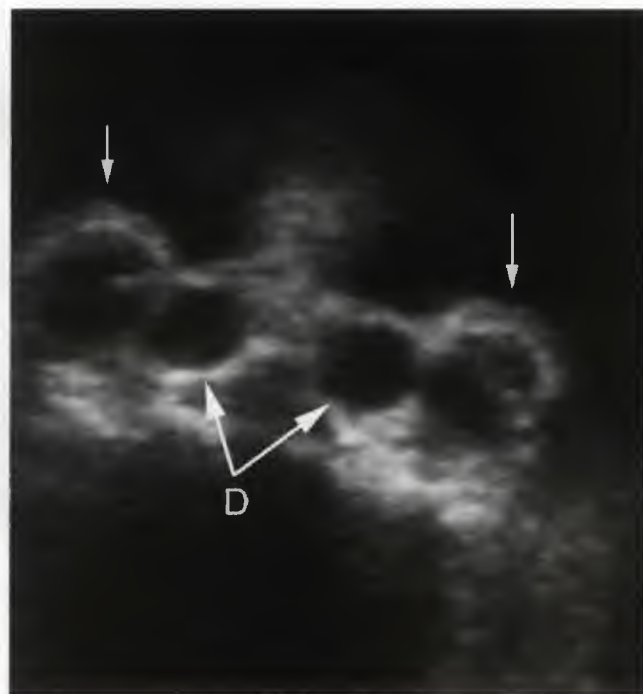


**FIGURE 11-22.** Bilateral dacrocystoceles (D) in a second trimester fetus. Orbits are indicated by arrows.

plasia of the mandible (agnathia) and severe midline defects, including holoprosencephaly, anterior encephalocele, cyclopia, aglossia, microstomia, and midfacial location of the ears (so-called ear-head).

Micrognathia/retrognathia encompass a wide spectrum of severity, and probably most mild cases can not be recognized in utero. Conversely, severe forms can be identified since early gestation<sup>28</sup> and different approaches have been suggested from time to time. Probably, the simplest one is the profile view to demonstrate that the midportion of the mandible is not aligned with the maxilla (Fig. 11-23).<sup>3,29</sup> In this view, the upper lip is usually very prominent and the chin is receding. However, this is a subjective observation and, at times, is associated with many uncertainties. The index of suspicion increases when the tongue appears to be displaced posteriorly and superiorly.<sup>30</sup> Measurement of the

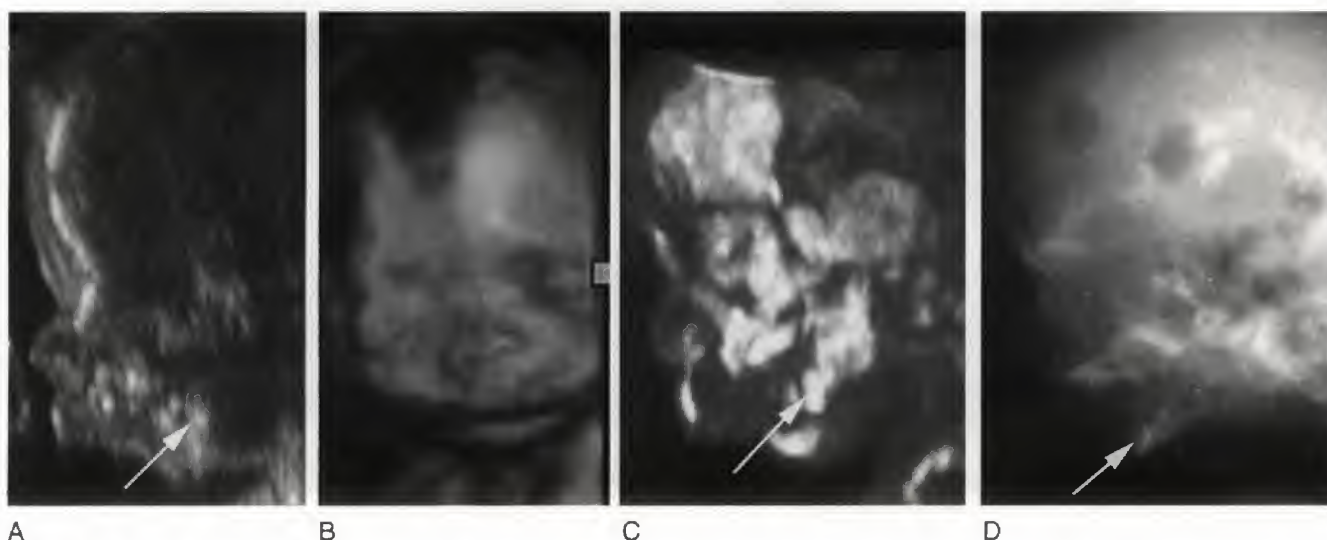


**FIGURE 11-23.** Severe micrognathia (arrows) in a fetus with dysmorphic facies and multiple anomalies: (A) sagittal view of the fetal face demonstrating protruding upper lip and small chin; (B) three-dimensional ultrasound, surface mode, demonstrating abnormal face with small chin and hypertelorism; (C) three-dimensional ultrasound, maximum mode demonstrating the small mandible; (D) postnatal radiograph.

mandible has also been proposed.<sup>5,31,32</sup> Distinguishing micrognathia from retrognathia is not simple, and the two conditions frequently coexist.<sup>5</sup> Intrauterine development of micrognathia, limiting early prenatal diagnosis, has been suggested as contributing to the difficulty of diagnosis.<sup>29</sup> With 3D ultrasound in transparent mode, the entire mandible can be visualized and this may increase diagnostic precision<sup>33</sup> (see Fig. 11-23).

Severe micrognathia can be a neonatal emergency due to airway obstruction by the tongue in the small oral cavity. If prenatal diagnosis is made, a pediatrician should be present in the delivery room and be prepared to intubate the infant.<sup>29,34</sup> However, the prognosis depends mostly on the presence of associated anomalies.<sup>34,35</sup> Probably, only the most severe cases and those with associated malformations are detected in utero, and this may explain the poor outcome of most neonatal series.

The fetal tongue can be identified as early as 14 weeks' gestation.<sup>36</sup> Malformations of the tongue include microglossia and macroglossia.<sup>36</sup> Macroglossia is defined as a resting tongue that protrudes beyond the teeth or alveolar ridge.<sup>36,37</sup> Sonography has demonstrated macroglossia in patients with trisomy 21 and Beckwith-Weidemann syndrome (Fig. 11-24). However, macroglossia may also be seen in patients with hypothyroidism, storage diseases, and other genetic syndromes.<sup>36,38</sup>

## Tumors of the Face

Epignathus is a very rare teratoma arising from the oral cavity or pharynx. Most cases of epignathus arise from the sphenoid bone. Some arise from the hard and soft palate, the pharynx, the tongue, and jaw. From their sites of origin, the tumors grow into the oral or nasal cavity or intracranially. The tumors, which are usually benign, consist of tissues derived from any of the three germinal layers; most of them contain adipose tissue, cartilage, bone, and nervous



**FIGURE 11-24.** Beckwith-Weidemann in a second trimester fetus. A protruding tongue is well seen (arrow) in the profile view.

tissue. Prenatal diagnosis is suggested by the demonstration of a solid tumor arising from the oral cavity (Fig. 11-25); calcifications and cystic components may also be present.<sup>39,40</sup> A careful examination of the brain is important because the tumor may grow intracranially. The outlook depends on the size of the lesion and the involvement of vital structures. Lesions detected antenatally have been very large. Polyhydramnios has been associated with poor prognosis. The major cause of neonatal death is asphyxia due to airway obstruction. Surgical resection and normal postoperative course are possible.



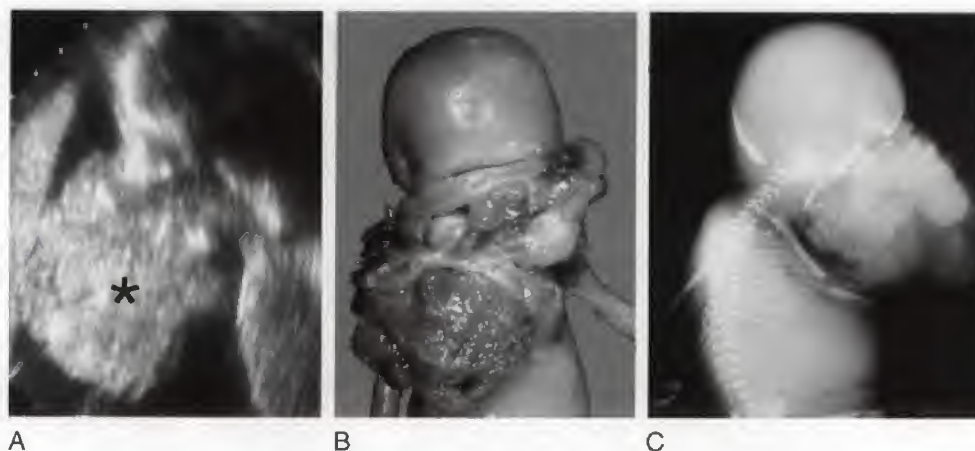


**FIGURE 11-25.** Epignathus. A. Antenatal sonogram demonstrating a large mass (asterisk). B, C. Postnatal images in a similar case. (B, C. courtesy of Frank Chervenak, MD, New York, NY and [www.thefetus.net](http://www.thefetus.net)).

Myoblastoma is a very rare benign tumor, which usually arises from the oral cavity. The tumor occurs in females exclusively, and it may be the consequence of excessive production of estrogens by the fetal ovaries under human chorionic gonadotropin stimulation. The ultrasound features are those of a large solid mass protruding from the fetal mouth. Vascular connections between the tumor and the floor of the oral cavity may be demonstrated using color Doppler ultrasound. Polyhydramnios (due to pharyngeal compression) is common.

Intracranial teratomas may grow outside the skull and protrude from the orbits (Fig. 11-26).

## Facial Dysmorphism

Modern high-resolution ultrasound allows detailed evaluation of the fetal face, and an expert sonologist can perform on a living fetus in early gestation an anatomic examination that in many ways is similar to the clinical evaluation that can be performed on a live infant. Facial dysmorphism is now amenable to antenatal detection, and 3D sonography is certainly valuable in these settings (Fig. 11-27). The detection of even subtle facial findings has been useful to diagnose or corroborate the diagnosis of syndromes in pregnancies at increased risk.<sup>6,26,29,32,33,41-51</sup> However, some caution is necessary because facial features may demonstrate extreme variations in normal individuals.

Among the facial dysmorphisms that can be reliably identified, Binder syndrome or maxillonasal dysplasia is characterized by the association of an extremely small and flat nose, a convex upper lip, and malocclusion. Antenatally, the profile view is particularly striking, with an extremely small and flat nose that does not form an angle with the forehead<sup>42,43</sup> (Fig. 11-28). This condition does not seem to affect neurologic development, and surgical treatment is available.<sup>52</sup> However, an association with chondrodysplasia punctata has been described.



**FIGURE 11-26.** Orbital teratoma. Large cystic and solid mass (arrow) projecting beyond the orbit.

## CRANIOSYNOSTOSIS

Premature ossification and closure of the cranial sutures results in the abnormal shape and size of the skull. In severe cases, this condition can also cause compression on cranial nerves and increased pressure on the growing brain. The final result depends upon the sutures that are involved and the time the closure takes place. Craniosynostosis (or cranio-stenosis) occurs in about 1 of 2500 births. In most cases, only one suture is affected and the condition is isolated and

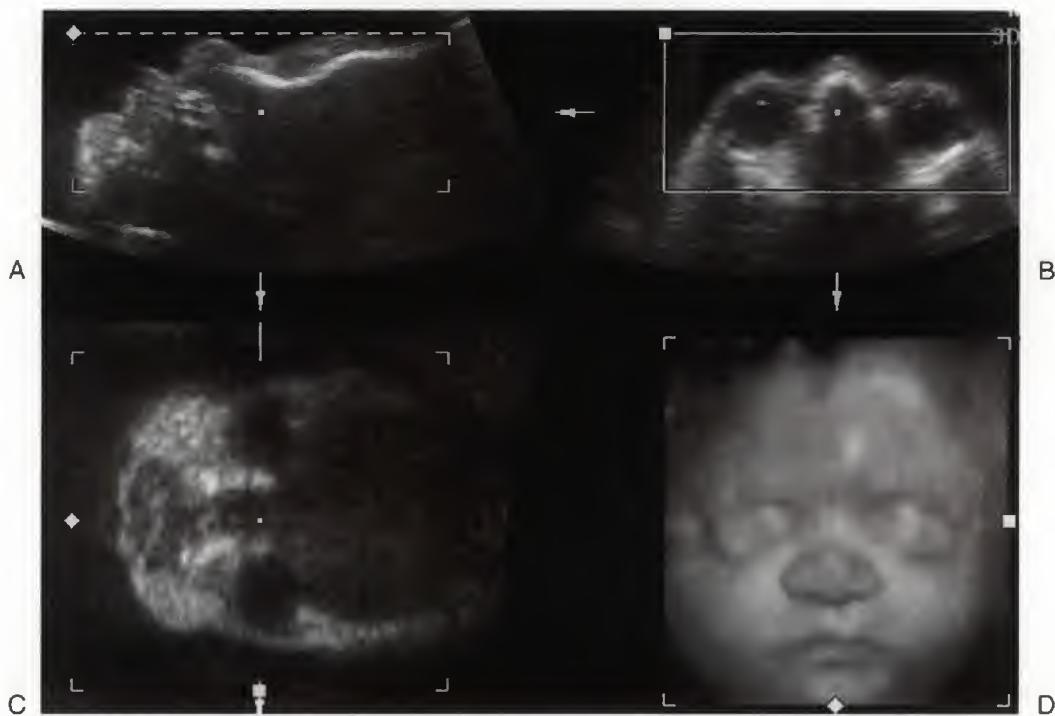


**FIGURE 11-27.** This fetus had increased nuchal translucency in the late first trimester, and a thick nuchal fold and polyhydramnios in the second trimester. Although the bidimensional examination of the fetal face (*A, B, C*) is negative, the surface mode (*D*) reveals unusual facies with antimongoloid slanting of the eyelids. Noonan syndrome was diagnosed after birth.

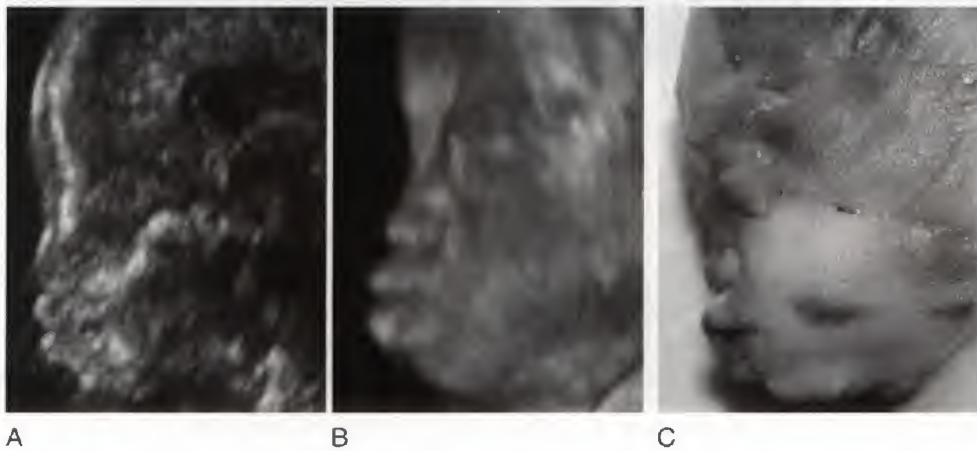


**FIGURE 11-28.** Binder syndrome: (*A*) sagittal view of the face; (*B*) fetal profile in three-dimensional surface mode ultrasound; (*C*) postnatal image. Note the small and flat nose with absence of any angle between forehead and nose.

sporadic. However, in a minority of cases, closure of multiple sutures is possible and associated anomalies are present. Craniosynostosis is a part of many genetic syndromes. The genetic defect underlying some of these has been identified. Most frequently this is a mutation in the genes encoding the fibroblast growth factor receptors 1, 2, and 3.

The most frequent craniosynostosis is due to closure of the sagittal suture, which is responsible for about half of the cases, resulting in an elongated head (scaphocephaly). The second most frequent type is due to closure of the coronal suture that results in a very flat, recessed forehead (brachycephaly).

Crouzon and Apert syndromes are the most common of the craniosynostosis syndromes. The main findings include premature closure of the coronal suture, hypoplasia of the midface, exophthalmos, and polydactyly/syndactyly of the hands and feet. Crouzon syndrome occurs in approximately 1 in 25,000 births. It may be transmitted as an autosomal-dominant genetic condition or appear as a fresh mutation. The appearance of an infant with Crouzon syndrome can vary in severity from a mild presentation with subtle midface characteristics to severe forms with multiple cranial sutures fused and marked midface and ocular problems. The incidence of Apert syndrome is approximately 1 in 100,000.





**FIGURE 11-29.** Craniosynostosis syndromes: (A) Apert syndrome; (B) Pfeiffer syndrome, lethal variety (cloverleaf skull); (C) trigonocephaly.

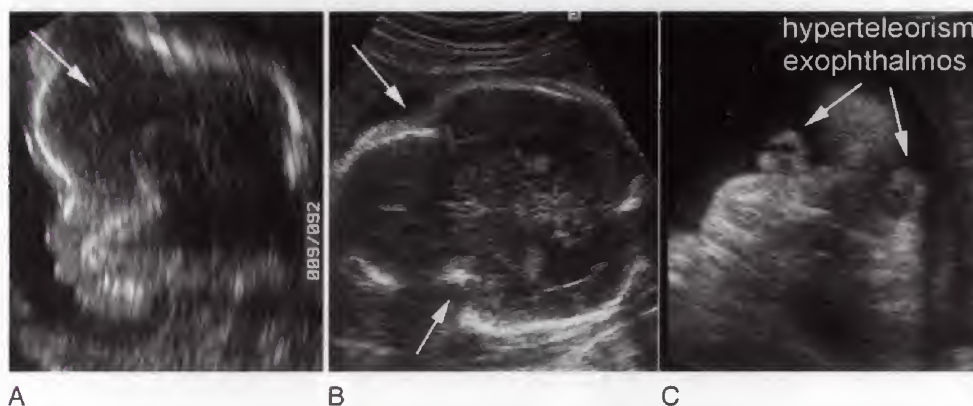


**FIGURE 11-30.** Antenatal sonogram from the case demonstrated in Figure 11-25B: (A, B) sagittal and axial sonograms demonstrating the cloverleaf skull (arrows); (C) exophthalmos and hypertelorism.

births and most cases are fresh mutations. The general features of a child with Apert syndrome are similar to those in a child with Crouzon syndrome (Fig. 11-29). However, there is not as much variability between cases and the degree of presentation is more severe. Other types of craniosynostosis syndromes that have been diagnosed in utero include Pfeiffer syndrome, which is characterized by closure of all sutures with cloverleaf skull, and trigonocephaly, which is due to closure of the metopic suture that results in a triangular forehead (see Fig. 11-29). Type II thanatophoric dysplasia is also associated with craniosynostosis.

The experience with prenatal diagnosis of craniosynostosis is limited and consists mostly of case reports and small series of severe types.<sup>6,45,46,48,53-60</sup> Most likely, the majority of cases are missed antenatally. We are aware of many infants that were diagnosed after birth with craniosynostosis and had completely unremarkable prenatal sonograms. Dolicocephaly due to compression is a frequent finding during fetal life, and we expect that differentiation from the most frequent type of craniosynostosis, closure of the sagittal suture, would be impossible in most cases. Even severe forms may be associated only with subtle findings, particularly in early gestation. Craniosynostosis should be suspected in the presence of an

abnormal skull shape<sup>54</sup> (Fig. 11-30). Failure to visualize the sutures, which are normally seen as linear interruptions of the echogenic calvarium, increase the index of suspicion.<sup>54</sup> Recently, reports on 3D ultrasound suggest that this technique may be valuable in the diagnosis of craniosynostosis.<sup>6,53,55</sup> Apart from the demonstration of panoramic views of the cranium using the standard surface mode (Fig. 11-31), the transparent or maximum mode allows one to better visualize the sutures, which is particularly useful for demonstrating the abnormal compensatory opening of the patent sutures that occurs when there is craniosynostosis. With premature closure of the coronal sutures, for example, there is a typical enlargement of the metopic one<sup>56,61</sup> (Fig. 11-32).

## ANOMALIES OF THE NECK

Current ultrasound equipment allows the visualization of the main anatomic structures of the neck: upper airways and esophagus, vessels, and spine. A detailed investigation of the cervical structures is usually possible as early as the 18th week of gestation. However, flexion of the head and an unfavorable position of the fetus can make the examination difficult. Views of the fetal neck at 25 weeks of gestation are

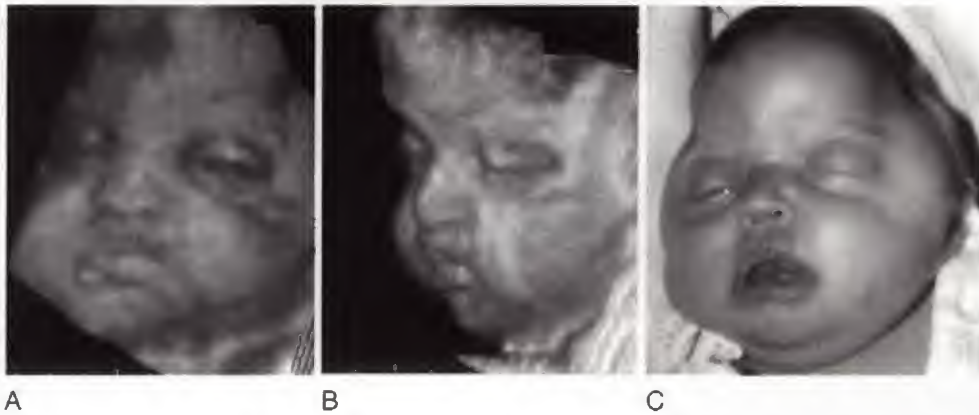


**FIGURE 11-31.** Pfeiffer syndrome, lethal variety: (A, B) three-dimensional surface mode (C) compared with a postnatal image.

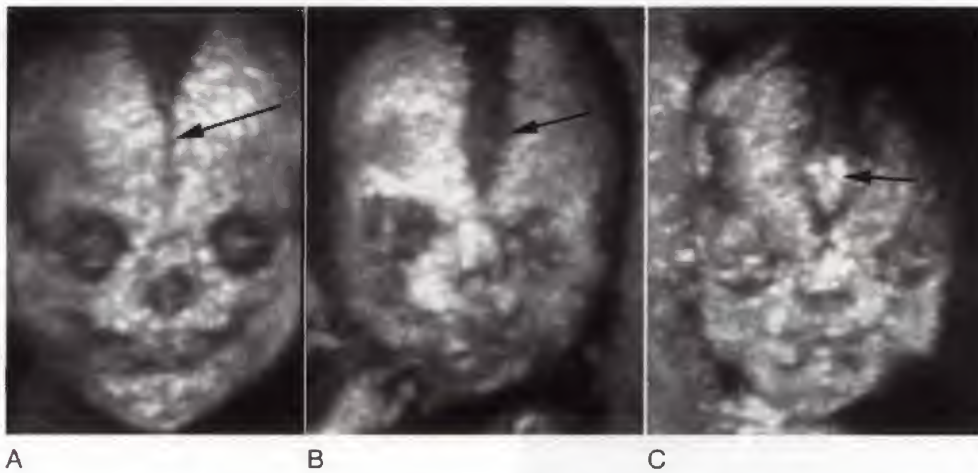


**FIGURE 11-32.** The metopic suture (arrow) in a normal fetus (A) and in two fetuses with cranosynostosis and multiple anomalies (B, C). Note the presence of a wormian bone in (C).

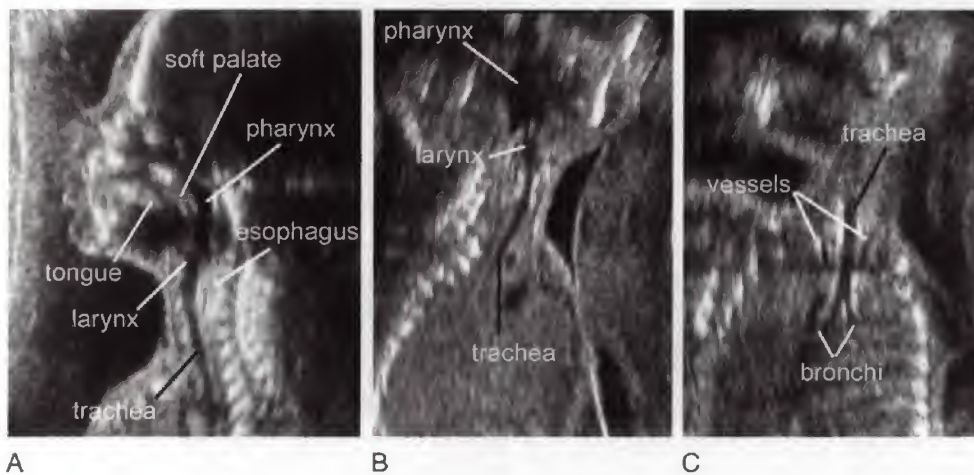


**FIGURE 11-33.** The fetal neck structures at 25 weeks' gestation.

provided in Figure 11-33. Most anatomic components of this area are demonstrated in these sonograms. The tongue is seen filling the oral cavity. Shadowing from the facial bones obscures the hard palate, but its position can be inferred by the curvature of the tongue and by the soft palate. Real-time examination greatly enhances the under-

standing of these structures, because movement of both the tongue and the soft palate is frequently seen. Behind the soft palate and below a high-level echo complex presumably arising from the sphenoid, the fluid-filled pharyngeal cavity is seen and can be followed until it bifurcates into the larynx and hypopharynx. With high-resolution ultrasound, the



esophagus may be seen, as a multilayered structure. The serosa and the mucosa appear as echogenic lines, interposed within the hypoechogenic muscular walls. With slight angulation of the transducer, the main neck vessels, the common carotid artery, and the jugular veins are demonstrated, and the identification is facilitated by the use of color Doppler. At closer inspection, minute details, such as the vocal cords, may be appreciated. On real-time ultrasound examination, it is frequently possible to demonstrate the contractions of the vestibulum of the larynx.

## Nuchal Cystic Hygroma

The term hygroma means moist tumor. Cystic hygromas are anomalies of the lymphatic system characterized by single or multiple cysts within the soft tissues. In the fetus, they usually occur in the nuchal region, much less frequently in the axillary region or anterior neck region. Nuchal cystic hygroma is associated in the majority of cases with generalized lymphatic obstruction, and the term lymphatic obstruction sequence has been proposed. In the embryo, the lymphatic system drains into the jugular lymphatic sac. A communication between this primitive structure and the jugular vein is formed at 40 days of gestation (conceptional age). Failure of development of this communication results

in lymphatic stasis. Dilatation of the jugular lymphatic sac leads to the formation of cystic structures in the cervical region. If a connection between the lymphatic and the venous system does not occur at this point, a progressive peripheral lymphedema and nonimmune hydrops will develop, leading to early intrauterine death<sup>62</sup> (Fig. 11-34). If the connection is formed, the sequence is interrupted, and the fluid collections are resorbed. The redundant skin will give rise to webbed neck (pterygium colli), which is a typical manifestation of many genetic and nongenetic conditions. Uplifting and anterior rotation of the ears and an abnormal hair pattern are other consequences of overdilatation of the jugular lymphatic sac. Distention of the tributary lymphatics may result in peripheral lymphedema, which, in turn, may give rise to redundancy of the skin of the face and puffy hands and feet, with deep-set narrow nails. It has also been suggested that transitory ascites may result in laxity of the anterior abdominal wall and prune-belly syndrome.<sup>62</sup>

Sonographically, overdilatation of the jugular lymphatic sacs that are located in both sides of the neck results in the formation of a cystic structure that is usually partitioned by a thick fibrous band corresponding to the nuchal ligament. Within the cystic structure, thinner septa are seen and probably represent fibrous structures of the neck or deposits of fibrin, giving to the lesion a typical honeycomb appearance (Fig. 11-35). Most cases seen in the second trimester have decreased amounts of amniotic fluid, and a few have either normal fluid or polyhydramnios. The size of the lesions may vary greatly from small collections of fluid to enormous cysts that may be larger than the fetus. In cases of generalized hydrops, pleural effusions, ascites, and severe skin edema are present.

There is a correlation between increased nuchal translucency and cystic hygroma. Cystic hygroma can be regarded as the most severe end of the spectrum of increased nuchal translucency. Typically, when nuchal translucency is in excess of 4 mm, septa are seen within it. The prevalence of nuchal cystic hygroma depends upon gestational age. Nuchal cystic hygromas have a high rate of intrauterine selection, and they are exceedingly rare at birth. Conversely, they are found in 1:250 fetuses at 11 to 14 weeks.<sup>63</sup>

Nuchal cystic hygromas are frequently found in association with chromosomal aberrations and, consequently, with a wide variety of anatomic defects. In the first trimester, autosomal trisomies and trisomy 21 in particular are more

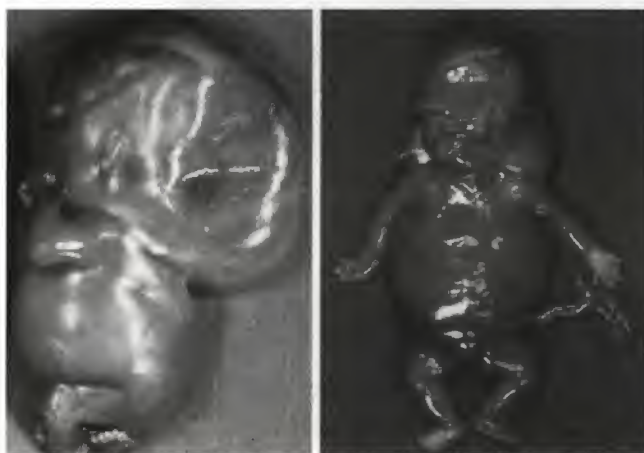


**FIGURE 11-34.** Cystic nuchal hygroma with lymphatic obstruction sequence.

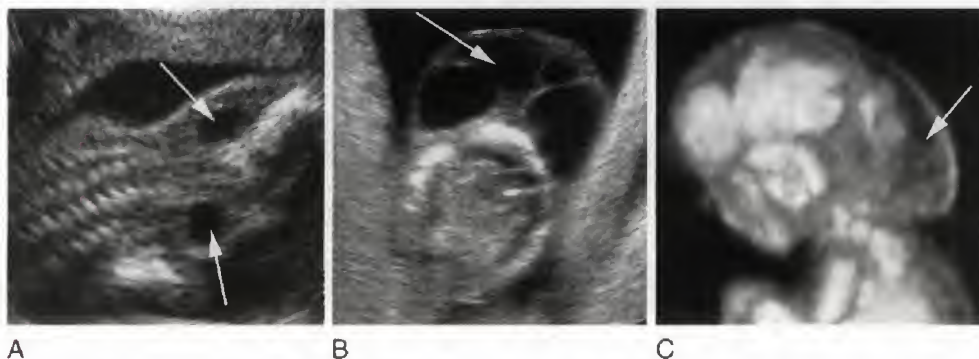


**FIGURE 11-35.** Nuchal cystic hygroma: (A) small hygroma in a second trimester fetus: two separate fluid accumulations are seen on each side of the neck (arrows); (B) large cystic hygroma (arrow) in a fetus at 14 weeks' gestation; (C) three-dimensional ultrasound in surface mode in a fetus with a cystic hygroma (arrow).

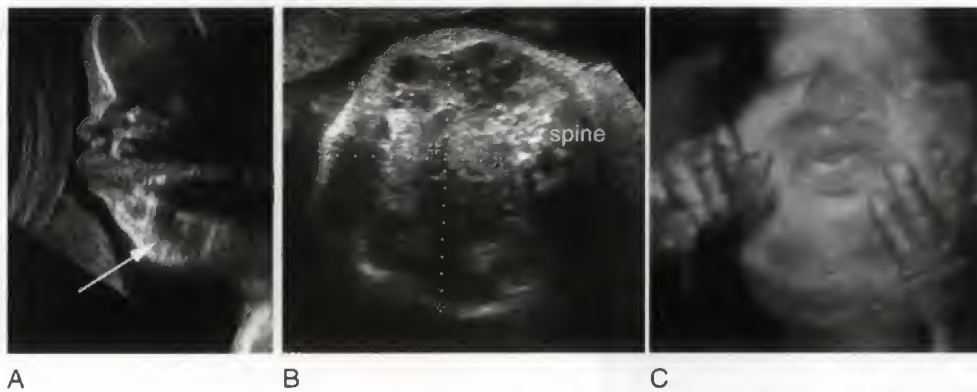


**FIGURE 11-36.** Although the antenatal diagnosis was cervical teratoma, this fetus was found at birth to have a cavernous lymphangioma infiltrating the neck tissues. A, B. Two-dimensional sonograms demonstrating the large neck mass. C. Surface rendered 3D sonogram demonstrating the mass.

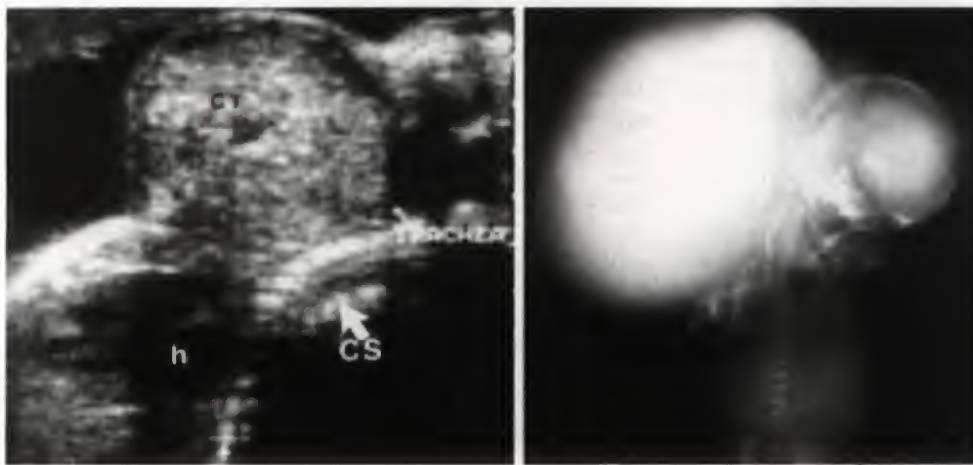


**FIGURE 11-37.** Large cervical teratoma.

frequent.<sup>63</sup> In the midtrimester, Turner syndrome is predominant.<sup>62</sup> Nuchal cystic hygroma with normal karyotype can be inherited as an autosomal recessive trait.<sup>64</sup> Webbed necks or redundant skin are found in genetic and nongenetic syndromes, such as Noonan syndrome, familial pterygium colli, and fetal alcohol syndrome.

The prognosis depends upon the gestational age and the association with hydrops or other anomalies. Of cases diagnosed at 11 to 14 weeks' gestation, only 17% will have an intact survival. The mortality rate of cases seen at mid-gestation is close to 100%.<sup>63</sup>

### Other Neck Masses

Lymphangiomas and hemangiomas have overlapping histopathologic and sonographic findings, and are the most frequent neck tumors in infancy. Associated anomalies and hydrops are rarely seen, and very frequently the lesion is only diagnosed in late gestation. Sonographically, they appear as a complex mass of variable dimensions, usually infiltrating the surrounding tissues (Fig. 11-36).<sup>65,66</sup> The prognosis is usually severe. These tumors can cause polyhydramnios and dystocia, as well as airway obstruction or swallowing difficulties after birth.<sup>67</sup> Surgical resection is

usually required but is associated with many complications (facial nerve palsy, mandibular maldevelopment, malocclusion, abnormal tooth eruption, and speech difficulties). Infiltration of the surrounding tissues frequently requires multiple operations.

Cervical teratomas are rare tumors that vary in size and generally consist of a mixture of cystic and solid components, frequently with internal calcifications<sup>68,69</sup> (Fig. 11-37). Obstruction of the airways and esophagus leads frequently to polyhydramnios and acute respiratory failure in the newborn period. With large masses, the prognosis is poor with a high risk of perinatal death. In infants, surviving surgical correction is difficult because these tumors tend to be large, and extensive neck dissection and multiple additional procedures are necessary to achieve complete resection of the tumor with acceptable functional and cosmetic results.<sup>69</sup>

Fetal goiter (enlargement of the thyroid gland) can be associated with hyperthyroidism, hypothyroidism or an euthyroid state. Congenital hypothyroidism occurs in about 1 in 4000 live births. However most hypothyroid infants have primary thyroid dysgenesis (absent or hypoplastic thyroid gland), secondary (pituitary) or tertiary (hypothalamic) hypothyroidism, which are associated with a normal or





**FIGURE 11-38.** Fetal goiter (arrow) that was found to be associated with hypothyroidism as a consequence of excessive maternal propylthiouracil assumption.

small thyroid gland. Only a minority have thyroid dysmorphogenesis or hypothyroidism secondary to intrauterine exposure to antithyroid medications, which are associated with goiter in the newborn period. The two drugs primarily responsible for the latter are iodide preparations and propylthiouracil. Iodide preparations are administered as expectorant medications, and radiopaque dyes are used in amniography. Maternal ingestion of as little as 12 mg/day may result in congenital hypothyroidism. About 1% of mothers exposed to propylthiouracil have hypothyroid infants.

Ultrasound diagnosis of goiter is based on the demonstration of a solid, anteriorly located symmetric mass, which may result in hyperextension of the fetal head<sup>70-73</sup> (Fig. 11-38). Polyhydramnios is common due to mechanical obstruction of the esophagus. The prognosis depends on the basic cause of the goiter. Fetal blood sampling can aid in determining fetal thyroid status, especially in women suffering from Graves' disease in which either transplacental transfer of drugs or thyroid-stimulating antibodies may result in fetal goiter.<sup>70,71</sup> Maternal therapy usually corrects fetal hyperthyroidism. Direct fetal therapy in cases of fetal hypothyroidism can be undertaken by amniocentesis, and this can result in resolution of the fetal goiter.<sup>70,71</sup>

The differential diagnosis of neck masses is frequently difficult. The ultrasound findings of anterior hygroma/hemangioma and cervical teratoma overlap.<sup>67</sup> In general, cervical teratomas are mostly solid, may contain calcifications, and are well demarcated from surrounding tissues. Conversely, hygromas/hemangiomas tend to have significant

fluid components and to infiltrate the tissues of the neck and face. Goiter has always a solid appearance, is well demarcated from the surrounding tissues, is relatively small compared with the previous lesions, and when it is large, it is bilobed.

In general, any mass growing in the anterior neck region of the fetus particularly if large and associated with polyhydramnios may be associated with a potentially lethal airway obstruction at birth. In these cases, delivery of the fetus in a tertiary care center is always recommended. An ex utero intrapartum treatment (EXIT) procedure may also be considered. This process involves a cesarean section in which only the head of the fetus is delivered at first to allow pediatricians to ensure airway access by either intubation or tracheotomy while the fetus is still attached to the umbilical cord and placenta.<sup>74-76</sup>

## CONCLUSIONS

Facial clefts are frequent malformations. However, evaluation of the fetal face is difficult with standard sonographic techniques and these anomalies are frequently missed. Other facial anomalies, such as micrognathia, ocular anomalies, and craniosynostosis are rare, and even in expert hands, they may be difficult to recognize. Nuchal cystic hygroma is one of the most frequent anomalies diagnosed antenatally. Large masses occurring in the anterior neck be associated with respiratory insufficiency and require individualized treatment in tertiary care centers.

## References

1. Benacerraf BR, Frigoletto FD Jr, Bieber FR: The fetal face: ultrasound examination. *Radiology* 153:495, 1984.
2. Nyberg DA, Sickler GK, Hegge FN, et al: Fetal cleft lip with and without cleft palate: US classification and correlation with outcome. *Radiology* 195:677, 1995.
3. Pilu G, Reece EA, Romero R, et al: Prenatal diagnosis of craniofacial malformations with ultrasonography. *Am J Obstet Gynecol* 155:45, 1986.
4. Rotten D, Levailant JM: Two- and three-dimensional sonographic assessment of the fetal face. 2. Analysis of cleft lip, alveolus and palate. *Ultrasound Obstet Gynecol* 24:402, 2004.
5. Rotten D, Levailant JM, Martinez H, et al: The fetal mandible: a 2D and 3D sonographic approach to the diagnosis of retrognathia and micrognathia. *Ultrasound Obstet Gynecol* 19:122, 2002.
6. Ghi T, Perolo A, Banzi C, et al: Two-dimensional ultrasound is accurate in the diagnosis of fetal craniofacial malformation. *Ultrasound Obstet Gynecol* 19:543, 2002.
7. Jones MC: Prenatal diagnosis of cleft lip and palate: detection rates, accuracy of ultrasonography, associated anomalies, and strategies for counseling. *Cleft Palate Craniofac J* 39:169, 2002.
8. Stoll C, Dott B, Alembik Y, Roth M: Evaluation of prenatal diagnosis of cleft lip/palate by foetal ultrasonographic examination. *Ann Genet* 43:11, 2000.
9. Sohan K, Freer M, Mercer N, et al: Prenatal detection of facial clefts. *Fetal Diagn Ther* 16:196, 2001.
10. Wayne C, Cook K, Sairam S, et al: Sensitivity and accuracy of routine antenatal ultrasound screening for isolated facial clefts. *Br J Radiol* 75:584, 2002.
11. Campbell S, Lees C, Moscoso G, et al: Ultrasound antenatal diagnosis of cleft palate by a new technique: the 3D "reverse face" view. *Ultrasound Obstet Gynecol* 25:12, 2005.
12. Campbell S, Lees CC: The three-dimensional reverse face (3D RF) view for the diagnosis of cleft palate. *Ultrasound Obstet Gynecol* 22:552, 2003.
13. Pilu G, Segata M: A novel technique to visualize the normal and cleft fetal secondary palate: angled insonation and three-dimensional ultrasound. *Ultrasound Obstet Gynecol* 29:159, 2007.



14. Ghi T, Tani G, Savelli L, et al: Prenatal imaging of facial clefts by magnetic resonance imaging with emphasis on the posterior palate. *Prenat Diagn* 23:970, 2003.
15. Kazan-Tannus JF, Levine D, McKenzie C, et al: Real-time magnetic resonance imaging aids prenatal diagnosis of isolated cleft palate. *J Ultrasound Med* 24:1533, 2005.
16. Bellis TH, Wohlgenuth B: The incidence of cleft lip and palate deformities in the south-east of Scotland (1971-1990). *Br J Orthod* 26:121, 1999.
17. Berge SJ, Plath H, Van de Vondel PT, et al: Fetal cleft lip and palate: sonographic diagnosis, chromosomal abnormalities, associated anomalies and postnatal outcome in 70 fetuses. *Ultrasound Obstet Gynecol* 18:422, 2001.
18. Nicolaides KH, Salvesen DR, Snijders RJ, et al: Fetal facial defects: associated malformations and chromosomal abnormalities. *Fetal Diagn Ther* 8:1, 1993.
19. Nyberg DA, Hegge FN, Kramer D, et al: Premaxillary protrusion: a sonographic clue to bilateral cleft lip and palate. *J Ultrasound Med* 12:331, 1993.
20. Pihu G, Romero R, Rizzo N, et al: Criteria for the prenatal diagnosis of holoprosencephaly. *Am J Perinatol* 4:41, 1987.
21. Blaas HG, Eriksson AG, Salvesen KA, et al: Brains and faces in holoprosencephaly: pre- and postnatal description of 30 cases. *Ultrasound Obstet Gynecol* 19:24, 2002.
22. Martinelli P, Russo R, Agangi A, et al: Prenatal ultrasound diagnosis of frontonasal dysplasia. *Prenat Diagn* 22:375, 2002.
23. Presti F, Celentano C, Marczazzo L, et al: Ultrasound prenatal diagnosis of a lateral facial cleft (Tessier number 7). *Ultrasound Obstet Gynecol* 23:606, 2004.
24. Pihu G, Visentin A, Ambrosini G, et al: Three-dimensional sonography of unilateral Tessier number 7 cleft in a mid-trimester fetus. *Ultrasound Obstet Gynecol* 26:98, 2005.
25. Bronshtein M, Zimmer E, Gershoni-Baruch R, et al: First- and second-trimester diagnosis of fetal ocular defects and associated anomalies: report of eight cases. *Obstet Gynecol* 77:443, 1991.
26. Volpe P, Gentile M: Three-dimensional diagnosis of Goldenhar syndrome. *Ultrasound Obstet Gynecol* 24:798, 2004.
27. Battaglia C, Artini PG, D'Ambrogio G, et al: Prenatal ultrasonographic evidence of transient dacryocystoceles. *J Ultrasound Med* 13:897, 1994.
28. Hsieh YY, Chang CC, Tsai HD, et al: The prenatal diagnosis of Pierre-Robin sequence. *Prenat Diagn* 19:567, 1999.
29. Pihu G, Romero R, Reece EA, et al: The prenatal diagnosis of Robin anomaly. *Am J Obstet Gynecol* 154:630, 1986.
30. Bronshtein M, Blazer S, Zalel Y, et al: Ultrasonographic diagnosis of glossoposis in fetuses with Pierre Robin sequence in early and mid pregnancy. *Am J Obstet Gynecol* 193:1561, 2005.
31. Paladini D, Morra T, Teodoro A, et al: Objective diagnosis of micrognathia in the fetus: the jaw index. *Obstet Gynecol* 93:382, 1999.
32. Paladini D, Tartaglione A, Lamberti A, et al: Prenatal ultrasound diagnosis of Nager syndrome. *Ultrasound Obstet Gynecol* 21:195, 2003.
33. Lee W, McNie B, Chaiworapongsa T, et al: Three-dimensional ultrasonographic presentation of micrognathia. *J Ultrasound Med* 21:775, 2002.
34. van den Elzen AP, Semmekrot BA, Bongers EM, et al: Diagnosis and treatment of the Pierre Robin sequence: results of a retrospective clinical study and review of the literature. *Eur J Pediatr* 160:47, 2001.
35. Vetraino IM, Lee W, Bronsteen RA, et al: Clinical outcome of fetuses with sonographic diagnosis of isolated micrognathia. *Obstet Gynecol* 102:801, 2003.
36. Achiron R, Ben Arie A, Gabbay U, et al: Development of the fetal tongue between 14 and 26 weeks of gestation: in utero ultrasonographic measurements. *Ultrasound Obstet Gynecol* 9:39, 1997.
37. Weiss LS, White JA: Macroglossia: a review. *J La State Med Soc* 142:13, 1990.
38. Emmanouil-Nikoloussi EN, Kerameos-Foroglou C: Developmental malformations of human tongue and associated syndromes (review). *Bull Group Int Rech Sci Stomatol Odontol* 35:5, 1992.
39. Chervenak FA, Tortora M, Moya FR, et al: Antenatal sonographic diagnosis of epignathus. *J Ultrasound Med* 3:235, 1984.
40. Gull I, Wolman I, Har-Toov J, et al: Antenatal sonographic diagnosis of epignathus at 15 weeks of pregnancy. *Ultrasound Obstet Gynecol* 13:271, 1999.
41. Cohen J, Ghezzi F, Goncalves L, et al: Prenatal sonographic diagnosis of Treacher Collins syndrome: a case and review of the literature. *Am J Perinatol* 12:416, 1995.
42. Cook K, Prefumo F, Presti F, et al: The prenatal diagnosis of Binder syndrome before 24 weeks of gestation: case report. *Ultrasound Obstet Gynecol* 16:578, 2000.
43. Cuillier F, Cartault F, Lemaire P, et al: Maxillo-nasal dysplasia (Binder syndrome): antenatal discovery and implications. *Fetal Diagn Ther* 20:301, 2005.
44. Drolshagen LF, Durmon G, Berumen M, et al: Prenatal ultrasonographic appearance of "Cornelia de Lange" syndrome. *J Clin Ultrasound* 20:470, 1992.
45. Hansen WF, Rijhsinghani A, Grant S, et al: Prenatal diagnosis of Apert syndrome. *Fetal Diagn Ther* 19:127, 2004.
46. Leo MV, Suslak L, Ganesh VL, et al: Crouzon syndrome: prenatal ultrasound diagnosis by binocular diameters. *Obstet Gynecol* 78:906, 1991.
47. Levaillant JM, Gerard-Blanluet M, Holder-Espinasse M, et al: Prenatal phenotypic overlap of Costello syndrome and severe Noonan syndrome by tri-dimensional ultrasonography. *Prenat Diagn* 26:340, 2006.
48. Menashe Y, Ben Baruch G, Rabinovitch O, et al: Exophthalmus—prenatal ultrasonic features for diagnosis of Crouzon syndrome. *Prenat Diagn* 9:805, 1989.
49. Paladini D, D'Armiento M, Ardovino I, et al: Prenatal diagnosis of the cerebro-oculo-facio-skeletal (COFS) syndrome. *Ultrasound Obstet Gynecol* 16:91, 2000.
50. Roy S, Sinsky A, Williams B, et al: Congenital epulis: prenatal imaging with MRI and ultrasound. *Pediatr Radiol* 33:800, 2003.
51. Urban M, Hartung J: Ultrasonographic and clinical appearance of a 22-week-old fetus with Brachmann-de Lange syndrome. *Am J Med Genet* 102:73, 2001.
52. Munro IR, Sinclair WJ, Rudd NL: Maxillonasal dysplasia (Binder's syndrome). *Plast Reconstr Surg* 63:657, 1979.
53. Benacerraf BR, Spiro R, Mitchell AG: Using three-dimensional ultrasound to detect craniosynostosis in a fetus with Pfeiffer syndrome. *Ultrasound Obstet Gynecol* 16:391, 2000.
54. Delahaye S, Bernard JP, Renier D, et al: Prenatal ultrasound diagnosis of fetal craniosynostosis. *Ultrasound Obstet Gynecol* 21:347, 2003.
55. Esser T, Rogalla P, Bamberg C, et al: Application of the three-dimensional maximum mode in prenatal diagnosis of Apert syndrome. *Am J Obstet Gynecol* 193:1743, 2005.
56. Faro C, Chaoui R, Wegrzyn P, et al: Metopic suture in fetuses with Apert syndrome at 22-27 weeks of gestation. *Ultrasound Obstet Gynecol* 27:28, 2006.
57. Gollin YG, Abuhamad AZ, Inati MN, et al: Sonographic appearance of craniofacial dysostosis (Crouzon syndrome) in the second trimester. *J Ultrasound Med* 12:625, 1993.
58. Hill LM, Grzybek PC: Sonographic findings with Pfeiffer syndrome. *Prenat Diagn* 14:47, 1994.
59. Hill LM, Thomas ML, Peterson CS: The ultrasonic detection of Apert syndrome. *J Ultrasound Med* 6:601, 1987.
60. Martinelli P, Paladini D, D'Armiento M, et al: Prenatal diagnosis of cloverleaf skull in the subtype 2 Pfeiffer syndrome. *Clin Dysmorphol* 6:89, 1997.
61. Faro C, Benoit B, Wegrzyn P, et al: Three-dimensional sonographic description of the fetal frontal bones and metopic suture. *Ultrasound Obstet Gynecol* 26:618, 2005.
62. Chervenak FA, Isaacson G, Blakemore KJ, et al: Fetal cystic hygroma. Cause and natural history. *N Engl J Med* 309:822, 1983.
63. Malone FD, Ball RH, Nyberg DA, et al: First-trimester septated cystic hygroma: prevalence, natural history, and pediatric outcome. *Obstet Gynecol* 106:288, 2005.
64. Dallapiccola B, Zelante L, Perla G, et al: Prenatal diagnosis of recurrence of cystic hygroma with normal chromosomes. *Prenat Diagn* 4:383, 1984.
65. Paladini D, Vassallo M, Sglavo G, et al: Cavernous lymphangioma of the face and neck: prenatal diagnosis by three-dimensional ultrasound. *Ultrasound Obstet Gynecol* 26:300, 2005.
66. Viora E, Grassi Pirrone P, Comoglio F, et al: Ultrasonographic detection of fetal cranio-facial hemangioma: case report and review of the literature. *Ultrasound Obstet Gynecol* 15:431, 2000.
67. Yoshida S, Kikuchi A, Naito S, et al: Giant hemangioma of the fetal neck, mimicking a teratoma. *J Obstet Gynaecol Res* 32:47, 2006.
68. Treعت JC, Claramunt V, Larraz J, et al: Prenatal ultrasound diagnosis of fetal teratoma of the neck. *J Clin Ultrasound* 12:509, 1984.
69. Kerner B, Flaum E, Mathews H, et al: Cervical teratoma: prenatal diagnosis and long-term follow-up. *Prenat Diagn* 18:51, 1998.



70. Abuhamad AZ, Fisher DA, Warsof SL, et al: Antenatal diagnosis and treatment of fetal goitrous hypothyroidism: case report and review of the literature. *Ultrasound Obstet Gynecol* 6:368, 1995.
71. Agrawal P, Ogilvy-Stuart A, Lees C: Intrauterine diagnosis and management of congenital goitrous hypothyroidism. *Ultrasound Obstet Gynecol* 19:501, 2002.
72. Matsumoto T, Miyakoshi K, Kasai K, et al: Fetal goitrous hypothyroidism followed by neonatal transient hyperthyroidism. A case report. *Fetal Diagn Ther* 18:459, 2003.
73. Perrotin F, Sembely-Taveau C, Haddad G, et al: Prenatal diagnosis and early in utero management of fetal dysmorphogenetic goiter. *Eur J Obstet Gynecol Reprod Biol* 94:309, 2001.
74. Harrison MR, Adzick NS, Flake AW, et al: Correction of congenital diaphragmatic hernia in utero VIII: Response of the hypoplastic lung to tracheal occlusion. *J Pediatr Surg* 31:1339, 1996.
75. Hirose S, Farmer DL, Lee H, et al: The ex utero intrapartum treatment procedure: Looking back at the EXIT. *J Pediatr Surg* 39:375; discussion 375, 2004.
76. Larsen ME, Larsen JW, Hamersley SL, et al: Successful management of fetal cervical teratoma using the EXIT procedure. *J Matern Fetal Med* 8:295, 1999.

# THE FETAL MUSCULOSKELETAL SYSTEM

Luís F. Gonçalves, MD, Juan Pedro Kusanovic, MD, Francesca Gotsch MD, Jimmy Espinoza, MD, and Roberto Romero MD

## Development of the Fetal Skeleton

Skeletogenesis (Genetics and Embryology)  
Endochondral Ossification  
Intramembranous Ossification

## Skeletal Dysplasias

Birth Prevalence and Contribution to Perinatal Mortality  
Classification of Skeletal Dysplasias  
*International Nosology and Classification of Constitutional Disorders of Bone*  
*Molecular-Pathogenetic Classification of Skeletal Dysplasias*  
Lethal Skeletal Dysplasias  
Terminology Frequently Used to Describe Bone Dysplasias  
Biometry of the Fetal Skeleton in the Diagnosis of Bone Dysplasias  
Clinical Presentation  
Diagnostic Imaging and the Prenatal Diagnosis of Skeletal Dysplasias  
Approach to the Diagnosis of Skeletal Dysplasias  
*Evaluation of the Long Bones*  
*Prediction of Pulmonary Hypoplasia*  
*Evaluation of Hands and Feet*  
*Evaluation of the Fetal Cranium*  
*Evaluation of the Fetal Face*  
*Evaluation of the Fetal Spine*  
*Evaluation of the Internal Organs*  
*Newborn Evaluation*  
Increased Nuchal Translucency and Skeletal Dysplasia

## Osteochondrodysplasias

Achondroplasia, Thanatophoric Dysplasia, and Hypochondroplasia  
*Achondroplasia*  
*Thanatophoric Dysplasia*  
*Hypochondroplasia*  
Fibrochondrogenesis, Atelosteogenesis  
*Fibrochondrogenesis*  
*Atelosteogenesis*  
Achondrogenesis  
Osteogenesis Imperfecta and Hypophosphatasia  
*Osteogenesis Imperfecta*  
*Hypophosphatasia*  
Diastrophic Dysplasia  
Kniest-Like Disorders  
*Kniest Syndrome*  
Dyssegmental Dysplasia  
Campomelic Dysplasia

Skeletal Dysplasias Characterized by a Hypoplastic Thorax

*Asphyxiating Thoracic Dysplasia (Jeune Syndrome)*  
*Short Rib-Polydactyly Syndromes*  
*Chondroectodermal Dysplasia*

Skeletal Dysplasias With Predominant Membranous Bone Involvement

*Cleidocranial Dysplasia*  
*Yunis-Varon Syndrome*

Limb Deficiency or Congenital Amputations

Syndromes With Absent Limbs and Facial Anomalies

*Aglossia-Adactylia Syndrome*  
*Moebius Syndrome*

Limb Reduction Defects Associated With Other Anomalies

*Congenital Hemidysplasia With Ichthyosiform Erythroderma and Limb Defects*  
*Fibula Aplasia Complex Brachydactyly (Du Pan Syndrome)*  
*Splenogonadal Fusion Syndrome*  
*Adams-Oliver Syndrome*  
*Phocomelia*  
*Roberts Syndrome and SC Phocomelia Syndrome*  
*Grebe Syndrome*  
*Thrombocytopenia With Absent Radius Syndrome*  
*Congenital Short Femur (Proximal Femoral Focal Deficiency)*

## Split Hand and Foot Deformities

## Ectrodactyly Ectodermal Dysplasia-Cleft Lip/Palate Syndrome

## Clubhands

Radial Clubhand  
Radial Clubhand and Hematologic Disorders  
*Fanconi Anemia*  
*Thrombocytopenia With Absent Radius Syndrome*  
*Aase Syndrome*  
*Holt-Oram Syndrome*  
Radial Clubhand and Scoliosis  
*VATER Association*  
*Goldenhar Syndrome*  
*Klippel-Feil syndrome*  
Other Conditions Associated With Radial Clubhand  
*Ulnar Clubhand*  
Polydactyly  
Arthrogryposis

## Clubfoot



## DEVELOPMENT OF THE FETAL SKELETON

The skeleton is composed of two tissues (bone and cartilage), three cell types (osteoblasts, osteoclasts, and chondrocytes), and more than 200 skeletal elements spread throughout the body.<sup>1,2</sup> Skeletal tissues derive from three embryonic cell lineages: (1) cranial neural crest cells, which originate the craniofacial skeleton, including the calvarium, midface, mandible and teeth; (2) paraxial mesoderm cells or somites, which are the embryologic precursors of the axial skeleton; and (3) the lateral plate mesoderm, which is responsible for limb formation.<sup>1,3-6</sup> Embryologically, limb buds begin to develop during the 4th week of embryonic life (6th menstrual week) as clusters of mesenchymal cells covered by a layer of ectoderm.<sup>1-3</sup> Mesenchymal models of bone (anlagen) form around the 5th week of embryonic life (7th menstrual week) (Fig. 12-1).<sup>3</sup> Development of the upper limbs antecedes that of the lower limbs in bud appearance, differentiation, and establishment of final relative limb size. Limbs develop in a proximodistal sequence, with the anlagen of the humerus and femur forming first, followed by the radius and the ulna, the tibia and the fibula, the metacarpal and the metatarsal bones, and, finally, the phalanges.<sup>1,2,7</sup>

### Skeletogenesis (Genetics and Embryology)

Skeletogenesis involves four steps: patterning, organogenesis, growth, and homeostasis.<sup>6</sup> Patterning is the process by which the final size, shape, number and arrangement of bones are determined.<sup>2,6</sup> This process takes place long before skeletogenesis, and three signaling regions have been identified: (1)

an apical ectodermal ridge; (2) an area consisting of ectoderm covering the sides of the bud; and (3) a zone of polarizing activity.<sup>3</sup> The apical ectodermal ridge consists of densely packed ectodermal cells located at the tip of the limb bud, which express several fibroblast growth factors (FGFs) that initiate and control limb outgrowth.<sup>5,8,9</sup> The ectoderm covering the sides of the bud regulates dorsoventral patterning.<sup>5</sup> The zone of polarizing activity is located on the posterior limb bud margin. It is responsible for antero-posterior patterning and, thus, the formation of digits.<sup>9,10</sup> Besides FGFs, several other genes are involved in the control of limb patterning, including Sonic hedgehog (Shh), GLI-Kruppel family member GLI3 (Gli3), sal-like 1 (Sall1), Hoxd13, Hoxa13, bone morphogenetic/cartilage-derived morphogenetic protein (CDMP), growth differentiation factors (GDFs), noggin (Nog), t-box family 4 and 5 (Tbx-4 and Tbx-5), Wnt7-a, radical fringe (Rfng), engrailed (en), and LIM homeobox transcription factor 1 beta (Lmx1b).<sup>1</sup>

Bone and cartilage are formed during the organogenesis period, which consists of three phases: condensation, cell differentiation, and histogenesis. Condensation is pivotal in skeletal development, because the templates for the future bones (anlagen) are defined at this stage.<sup>4</sup> Condensation initiation, boundary set, proliferation, adhesion, and growth are regulated by complex interactions between extracellular matrix molecules, cell surface receptors, cell adhesion molecules (e.g., fibronectin, tenascin, Noggin, syndecan, and N-CAM), homeobox genes (e.g., Hoxa-2, Hoxa-13, Hoxd-11, and Hoxd-11-13), transcription factors (e.g. runt related transcription factor 2 [RUNX2], winged-helix transcription factor [CFKH-1], mesenchyme forkhead 1 [MFH-1], paired box transcription factors 1 and 9 [PAX-1, PAX-9], periaxin 1 and 2 [PRX-1 and PRX-2], scleraxis, and mammalian

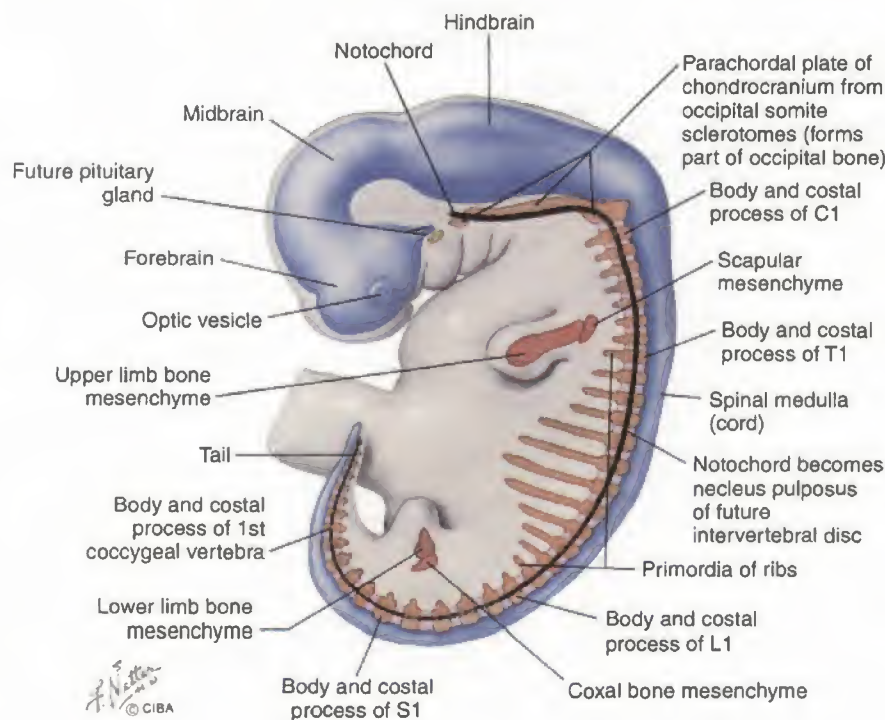


**FIGURE 12-1.** Diagram of the mesenchymal precartilage primordia of the axial and appendicular skeletons at 5 weeks' embryologic age (7 weeks' menstrual age). These develop further and eventually ossify to form skeletal structures as designated. Several central nervous system structures are also designated. (Illustration by Netter FH; from Crelin ES: *Development of the musculoskeletal system*. CIBA Clin Symp 33:6, 1981. Used with permission from CIBA-GEIGY Corporation, Summit, N.J.)



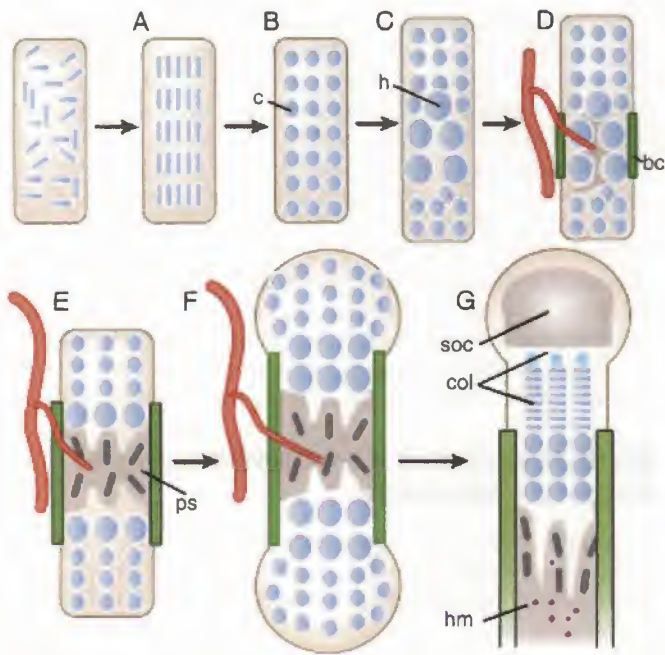


**FIGURE 12-2.** Endochondral bone formation. **A.** Mesenchymal cells condense. **B.** Cells of condensations become chondrocytes (c). **C.** Chondrocytes at the center of condensation stop proliferating and become hypertrophic (h). **D.** Perichondrial cells adjacent to hypertrophic chondrocytes become osteoblasts, forming bone collar (bc). Hypertrophic chondrocytes direct the formation of mineralized matrix, attract blood vessels, and undergo apoptosis. **E.** Osteoblasts of primary spongiosa accompany vascular invasion, forming the primary spongiosa (ps). **F.** Chondrocytes continue to proliferate, lengthening the bone. Osteoblasts of primary spongiosa are precursors of eventual trabecular bone; osteoblasts of bone collar become cortical bone. **G.** At the end of the bone, the secondary ossification center (soc) forms through cycles of chondrocyte hypertrophy, vascular invasion, and osteoblast activity. The growth plate below the secondary center of ossification forms orderly columns of proliferating chondrocytes (col). Hematopoietic marrow (hm) expands in marrow space along with stromal cells. (From Kronenberg HM: *Developmental regulation of the growth plate*. *Nature* 423:332, 2003.)

SRY box 9 [SOX-9]), and growth factors (e.g. bone morphogenetic proteins, fibroblast growth factor-2 [FGF-2], transforming growth factor  $\beta$ ).<sup>11</sup>

Cell differentiation and histogenesis (osteogenesis) initiate during the 7th week of embryonic development (9th menstrual week), with bones developing by either endochondral or membranous ossification.<sup>6</sup>

## Endochondral Ossification

The axial and appendicular skeletons are formed by endochondral ossification (Fig. 12-2). Cartilaginous models of the future bones differentiate within mesenchymal condensations during the 6th week of development (8th menstrual week), with primary ossification centers developing in the middle of the anlagen between the 7th and 12th week of development (9th to 14th menstrual weeks).<sup>3</sup> SOX9 plays an important role in chondrogenesis and, indeed, mutations in this gene cause campomelic dysplasia, a severe skeletal disorder characterized by congenital bowing and angulation of the long bones (especially of the tibia), hypoplastic scapulae, sex reversal in male fetuses, and a high lethality rate due to respiratory distress.<sup>1</sup> Another gene involved in chondro-

genesis is procollagen type II alpha 1 (COL2A1), which encodes collagen type II.<sup>1,12</sup>

Within primary ossification centers, hypertrophic cartilage matrix is degraded, chondrocytes undergo apoptosis, osteoblasts replace the disappearing cartilage with trabecular bone, and bone marrow is formed.<sup>1</sup> Simultaneously, osteoblasts in the perichondrium begin to deposit a collar of compact bone matrix along the diaphysis.<sup>1,12</sup> Osteoblast differentiation is controlled by RUNX2<sup>13</sup> and Osterix,<sup>14</sup> whereas proliferation is controlled by the low-density lipoprotein receptor-related protein 5 (LPR5) signaling pathway.<sup>2</sup> Eventually, cartilage in the center of the anlagen degrades, mineralizes, and is removed by osteoclasts.<sup>3,4</sup> Vascular ingrowth is stimulated by vascular endothelial growth factor, with the influx of osteoprogenitor cells occurring at the same time that the bone matrix is deposited along the periosteum of the mid-shaft.<sup>3,4,15</sup> Some of these invading cells differentiate into hematopoietic stem cells, whereas others differentiate into osteoclasts or osteoblasts.<sup>6</sup>

Secondary ossification centers begin to appear at the extremities of bones (epiphysis) later in pregnancy.<sup>3</sup> The portion of cartilage trapped between the expanding primary and secondary ossification centers is known as the growth plate or physis.<sup>3</sup> This structure is responsible for the longitudinal growth of long bones until definitive fusion between epiphyses and diaphyses occurs at the end of puberty.<sup>3,4,12</sup> Longitudinal growth is coordinated by Indian hedgehog (Ihh), a stimulator of chondrocyte proliferation at the growth plate.<sup>1</sup> Bone mass, shape, and strength are maintained throughout development and adult life by balancing bone destruction and formation. Homeostasis is the process that controls the continuing remodeling of bones.<sup>6</sup>

It is important to realize that when a long bone is imaged by ultrasound, only the diaphyses are measured, because the epiphyses usually are not clearly visualized. With favorable conditions, good images of the epiphysis can be obtained, especially when high frequency transducers are used (Fig. 12-3). Secondary ossification centers may often be visualized by ultrasound in the third trimester. The distal femoral ossification center may be seen at approximately 32 to 33 weeks of gestation, the proximal tibial epiphyseal center at 34 to 35 weeks, and the proximal humeral epiphyseal ossification center at 37 to 38 weeks of gestation (Fig. 12-4A and B). When all three centers are identified, it is likely that the fetus is at least 37 weeks. These ossification centers may be seen slightly earlier in female fetuses than in male fetuses. The timeline for the radiographic and histologic appearance of primary and secondary ossification centers is illustrated in Figure 12-4C.

The axial skeleton (e.g., vertebrae and the dorsal part of the ribs) originates from the somites. Formation of new somites and detachment of these structures from the paraxial mesoderm occur in the craniocaudal direction in a highly organized fashion.<sup>5</sup> A molecular clock produced by oscillations of cycling genes (e.g. c-hairy-1, lunatic fringe [l-fng], and naked cuticle 1 [nkd1]) stimulates Notch receptor signaling waves that sweep through the paraxial mesoderm.<sup>16-19</sup> Spatial coordination is provided by a decreasing gradient of FGF8 from the posterior to the anterior pole of the embryo.<sup>5,18,20</sup> Differential expression of delta-like (Dll) proteins determines the size and polarity of the somites,<sup>5</sup> which mature as they move rostrally and differentiate into



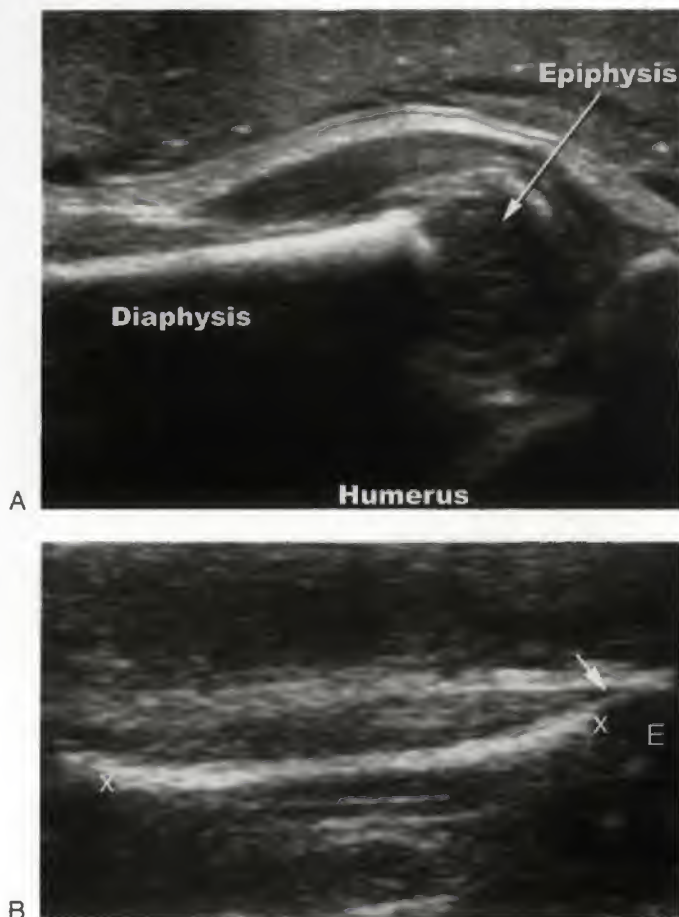


**FIGURE 12-3.** A. Proximal humeral epiphysis imaged with a high-frequency linear transducer (10 MHz) in a fetus at 29 weeks' gestation. B. Measurement of the femur in a third trimester patient. The femur should be measured along the ossified bone (between the Xs). The specular reflection from the surface of the femoral epiphysis (arrow) should not be measured.

dermatomyotomes and sclerotomes.<sup>5,18</sup> Dermatomyotomes give rise to the appendicular and axial musculatures, as well as the dorsal epithelium. The sclerotome is the precursor of the axial skeleton, and its formation is initiated and controlled by Sonic hedgehog.<sup>5,21,22</sup>

### Intramembranous Ossification

The craniofacial skeleton and clavicles develop by intramembranous ossification.<sup>1</sup> This process differs from endochondral ossification by the direct differentiation of mesenchymal cells into osteoblasts, which produce a bone matrix rich in type I collagen.<sup>1-3,12,15</sup> Bone remodeling is accomplished by the continuous and concerted action of osteoblasts (cells that produce bone matrix) and osteoclasts (cells that remove bone).

### SKELETAL DYSPLASIAS

Abnormal development, growth, or maintenance of cartilage and bone tissues result in skeletal dysplasias. Skeletal dysplasias are a heterogeneous group of disorders affecting

the development of chondro-osseous tissues and resulting in abnormalities in the size and shape of various segments of the skeleton. Despite recent advances in imaging and molecular genetics,<sup>23-25</sup> accurate prenatal diagnosis of skeletal dysplasias remains a clinical challenge.<sup>26</sup> Although 253 osteochondrodysplasias and 45 genetically determined dysostoses have been included in the most recent revision of the International Nosology and Classification of Constitutional Disorders of Bone<sup>27</sup> (and more will probably be identified as distinct entities), the number that can be recognized with the use of sonography in the antepartum period is considerably smaller. In subsequent sections of this chapter, we review the birth prevalence, classification, and molecular genetics of skeletal dysplasias that are identifiable at birth.

### Birth Prevalence and Contribution to Perinatal Mortality

In a large multicenter study conducted in Italy, the birth prevalence of skeletal dysplasias recognizable in the neonatal period, excluding limb amputations, was estimated as 2.4/10,000 births.<sup>28</sup> Twenty-three percent of the affected

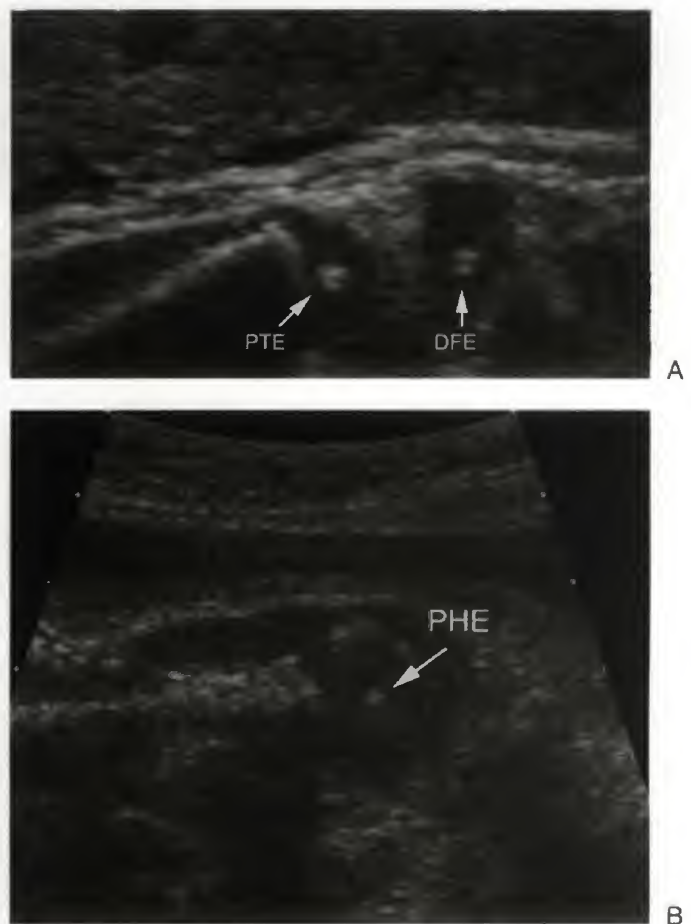


**FIGURE 12-4.** A. Sonogram of the lower extremity at the knee in a fetus at 35 weeks' gestation. Increased echogenicity from the secondary ossification centers of distal femoral (DFE) and proximal tibial (PTE) epiphyses are seen. B. Sonogram of the proximal humerus in a fetus at 38 weeks' gestation. Ossification of the proximal humeral epiphyseal ossification center (PHE) is well seen.

*Continued*

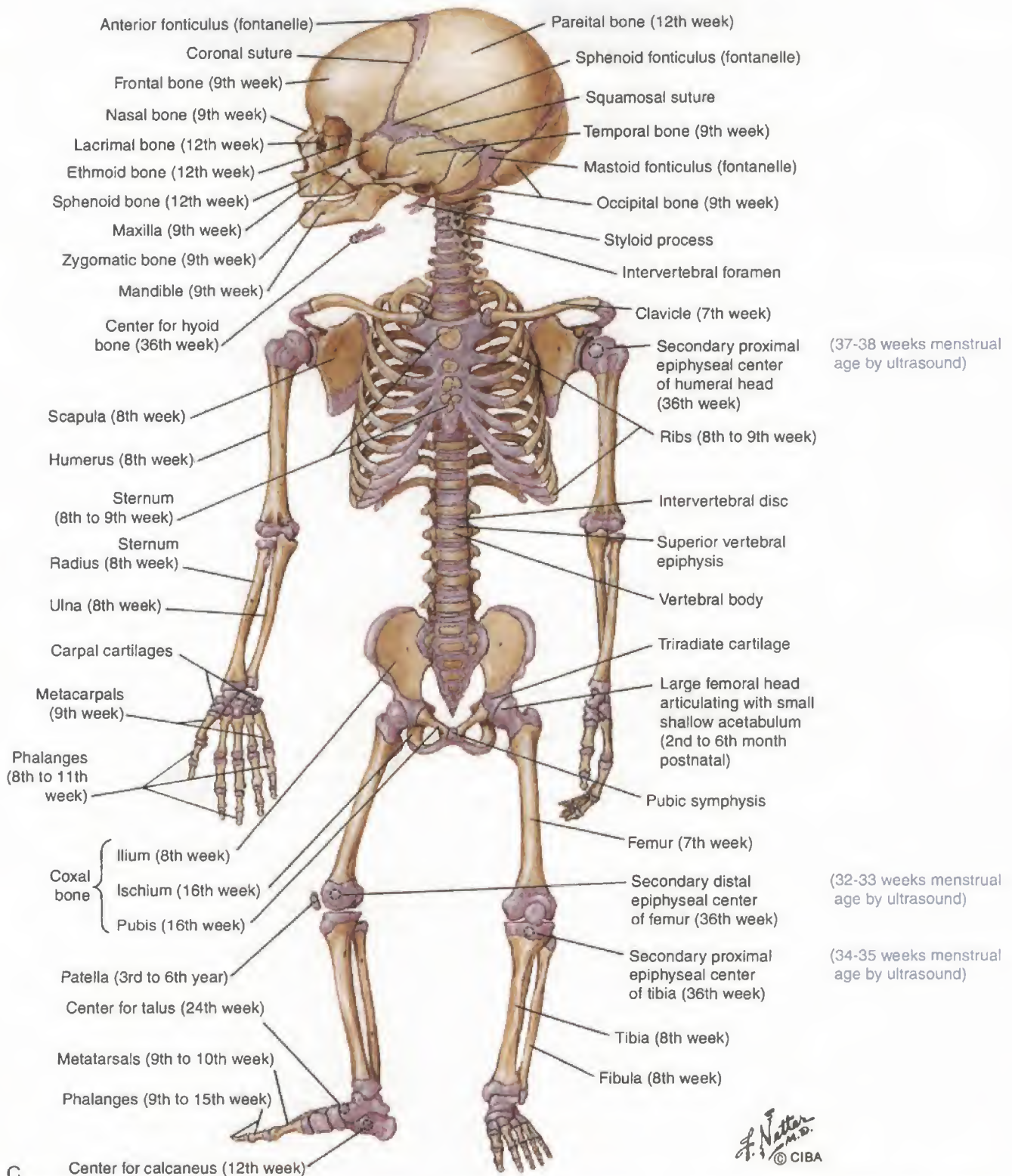


**FIGURE 12-4 cont'd. C.** Diagram of the skeleton of a full-term newborn. The times that the ossification centers appear are designated in embryologic weeks (add 2 weeks for menstrual age). These times are somewhat different than those using ultrasound because ultrasound is more sensitive for detection of ossification than radiographic methods. All refer to the primary ossification centers unless otherwise designated. Only at birth are the lower extremities the same lengths as the upper extremities; subsequently, the lower extremities grow to become longer than the upper extremities. (C by Netter FH; from Crelin ES: *Development of the musculoskeletal system* CIBA Clin Symp 33:13, 1981. Used with permission from CIBA-GEIGY Corporation, Summit, NJ.)



**Table 12-1****Birth Prevalence of Skeletal Dysplasias  
(per 10,000 total births)**

	Birth Prevalence (per 10,000)	Frequency Among Perinatal Deaths
Thanatophoric dysplasia	0.69	1:246
Achondroplasia	0.37	—
Achondrogenesis	0.23	1:639
Osteogenesis imperfecta type II	0.18	1:799
Osteogenesis imperfecta (other types)	0.18	—
Asphyxiating thoracic dysplasia	0.14	1:3,196
Chondrodysplasia punctata	0.09	—
Campomelic dysplasia	0.05	1:3,196
Chondroectodermal dysplasia	0.05	1:3,196
Larsen's syndrome	0.05	—
Mesomelic dysplasia (Larger's type)	0.05	—
Others	0.46	1:800

From Camera G, Mastroiacovo P: Birth prevalence of skeletal dysplasias in the Italian multicentric monitoring system for birth defects. In Papadatos CJ, Bartsocas CS (eds): *Skeletal Dysplasias*. New York, Alan R. Liss, 1982, p 441.

infants were stillborn, whereas 32% died during the first week of life. The overall frequency of skeletal dysplasias among perinatal deaths was 9.1 per 1000. This study also reported on the birth prevalence of the different skeletal dysplasias and their relative frequency among perinatal deaths (Table 12-1). The four most common skeletal dysplasias were thanatophoric dysplasia, achondroplasia, osteogenesis imperfecta (OI), and achondrogenesis. Thanatophoric dysplasia and achondrogenesis accounted for 62% of all lethal skeletal dysplasias, and the most common nonlethal skeletal dysplasia was achondroplasia.<sup>28</sup> In another large series performed in western Scotland, the prevalence of skeletal dysplasias at birth was 1.1 per 10,000 births. The most frequent conditions were thanatophoric dysplasia (1/42,000), OI (1/56,000), chondrodysplasia punctata (1/84,000), campomelic syndrome (1/112,000), and achondrogenesis (1/112,000).<sup>29</sup> Rasmussen et al<sup>30</sup> reported a prevalence of 2.14/10,000 deliveries in a longitudinal study, which included elective pregnancy termination, stillborn infants at more than 20 weeks of gestation, and live-born infants diagnosed by the 5th day of life. The rate of lethal cases in this latter study was 0.95/10,000 deliveries.<sup>30</sup> Other studies reporting on the prevalence of skeletal dysplasias are summarized in Table 12-2.<sup>28-39</sup> Of interest, the study reporting the highest prevalence of skeletal dysplasias at birth (9.5/10,000 births) was conducted in a population with a high rate of consanguineous unions.<sup>39</sup>

## Classification of Skeletal Dysplasias

### International Nosology and Classification of Constitutional Disorders of Bone

Over the past 30 years, the classification of skeletal dysplasias has evolved from one based on clinical/

**Table 12-2****Overall Birth Prevalence of  
Osteochondrodysplasias – Summary of  
12 Studies**

Reference	Rate per 10,000	Comment
Gustavson and Jorulf <sup>31</sup>	4.7	In newborns
Camera and Mastroiacovo <sup>28</sup>	2.4	In neonates
Connor et al. <sup>29</sup>	1.1	Lethal skeletal dysplasias in neonates
Weldner et al. <sup>32</sup>	7.5	
Orioli et al. <sup>33</sup>	2.3	First 3 days of life
Stoll et al. <sup>34</sup>	3.2	First 8 days of life
Andersen and Hauge <sup>35</sup>	7.6	Diagnosed in all ages
Andersen <sup>36</sup>	1.5	Lethal chondrodysplasias only
Kallen et al. <sup>37</sup>	1.6	No details about age
Rasmussen et al. <sup>30</sup>		
All cases	2.1	In first 5 days of life
Lethal chondrodysplasias	0.95	
Gordienko et al. <sup>38</sup>	3.1	
Al Gazali et al. <sup>39</sup>	9.5	Newborns and stillbirths > 500 gr; Prevalence of consanguinity: 72%

radiologic/pathologic descriptions to one that also includes the underlying molecular abnormality for those conditions for which the defect is known.<sup>40</sup>

The first uniform classification, proposed in 1977, was called International Nomenclature for Skeletal Dysplasias. The classification was based purely on descriptive findings of either clinical or radiologic nature.<sup>41</sup> Since its initial publication, the classification has undergone three revisions. In 1992,<sup>42-44</sup> it was reoriented based on radiologic diagnosis and morphologic criteria, and similar conditions were grouped into families, depending on the presumed pathogenetic similarities. Five years later, the classification was reorganized to take into account information regarding genes or protein defects underlying the families of disorders.<sup>45,46</sup> Thus, those disorders for which a genetic defect was well documented were regrouped into distinct families based on specific mutations. These included, for example, the "achondroplasia group" of disorders with mutations in the fibroblast growth factor receptor 3 gene, the "diastrophic dysplasia group" of disorders with mutations in the diastrophic dysplasia sulfate transporter gene, the type II collagenopathies with mutations in the type II collagen gene, and the type XI collagenopathies with mutations in the cartilage oligomeric protein gene. Several new groups were added, including the lethal skeletal dysplasias group, the fragmented bones group, and the miscellaneous neonatal severe dysplasia group. The classification was last revised during the 5th Meeting of the International Skeletal Dysplasia Society, which took place in Oxford, England in



2001; it is now called the International Nosology and Classification of Constitutional Disorders of Bones (2001).<sup>27</sup> Although this classification remains a combination of morphologic and molecular groupings of disorders, genetically determined dysostoses were added to skeletal dysplasias (or osteochondrodysplasias), because these two groups overlap in clinical practice. Dysostoses are skeletal malformations that occur during the first 8 weeks of embryonic life and for which the phenotype is static, that is, the phenotype does not evolve throughout life.<sup>27</sup> In contrast, skeletal dysplasias, which often present after the embryonic period, are characterized by a more general involvement of the skeleton, and the phenotype continues to evolve throughout life.<sup>27</sup> Genetically determined dysostoses have been divided into three groups: those with predominant cranial and facial involvement (e.g., Crouzon syndrome), those with predominant axial involvement (e.g., spondylocostal dysostoses), and those with predominant involvement of the extremities (e.g., Fanconi syndrome). The full version of the International Nosology and Classification of Constitutional Disorders of Bones<sup>27</sup> can be downloaded from the International Skeletal Dysplasia Society website (<http://www.isds.ch/ISDSframes.html>).

### **Molecular-Pathogenetic Classification of Skeletal Dysplasias**

As acknowledged earlier, at least in part, by the above-mentioned nosology classification, evolving knowledge regarding the molecular basis of skeletal dysplasias indicates that a spectrum of phenotypes share a similar genetic basis.<sup>24,25,47–51</sup> For example, disorders that originate during patterning are generally caused by Hox or Pax genes.<sup>6</sup> In contrast, growth defects are frequently caused by mutations in genes that encode for extracellular matrix products or for regulatory signal peptides.<sup>6</sup> Therefore, a parallel molecular classification based on the structure and function of implicated genes and proteins has been developed to help further understand the pathogenesis of individual disorders. The Molecular-Pathogenetic Classification of Genetic Disorders of the Skeleton is presented in Table 12-3,<sup>24</sup> and complements the International Nosology and Classification of Constitutional Disorders of Bone.<sup>27</sup> Skeletal disorders with a well-documented genetic and biochemical basis have been assigned to one of seven groups: (1) defects in extracellular structural proteins; (2) defects in metabolic pathways (including enzymes, ion channels and transporters); (3) defects in folding and degradation of macromolecules; (4) defects in hormones and signal transduction mechanisms; (5) defects in nuclear proteins and transcription factors; (6) defects in oncogenes and tumor suppressor genes; and (7) defects in RNA and DNA processing and metabolism.

The reader is reminded that only approximately one third of bone dysplasias have had their molecular basis elucidated, and that new genes involved in skeletal dysplasias are continually being discovered.<sup>25</sup> We review the mutations associated with specific skeletal dysplasias in subsequent sections of this chapter.

### **Lethal Skeletal Dysplasias**

Of special interest to perinatologists are the group of lethal osteochondrodysplasias, which were classified by Spranger

and Maroteaux<sup>52</sup> into 11 subgroups based on radioanatomic manifestations (Table 12-4). The purpose of this classification was to facilitate differential diagnosis, and the groups do not necessarily constitute pathogenetic families.

### **Terminology Frequently Used to Describe Bone Dysplasias**

Shortening of the extremities can involve the entire limb (micromelia), the proximal segment (rhizomelia), the intermediate segment (mesomelia), or the distal segment (acromelia) (Fig. 12-5). The diagnosis of rhizomelia or mesomelia requires comparing the dimensions of the bones of the legs and forearm with those of the thighs and arms. Figures 12-6 and 12-7 display the relationships between the humerus and ulna, as well as the femur and tibia, which can be used for the objective assessment of rhizomelia and mesomelia. Table 12-5 presents a list of skeletal dysplasias characterized by rhizomelia, mesomelia, and micromelia.

Several skeletal dysplasias feature alterations of the hands and feet. The term polydactyly refers to the presence of more than five digits. It is classified as postaxial if the extra digits are on the ulnar or fibular side, and preaxial if they are located on the radial or tibial side. Syndactyly refers to soft tissue or bony fusion of adjacent digits. Clinodactyly consists of deviation of a finger (or fingers).

The most common spinal abnormality seen in skeletal dysplasias is platyspondyly, which consists of the flattening of the vertebrae (Fig. 12-8).<sup>53–59</sup> Kyphosis and scoliosis can also be identified in utero (Figs. 12-9 and 12-10).<sup>60–64</sup> Prenatal diagnosis of hemivertebra (Fig. 12-11)<sup>60,65,66</sup> and coronal clefting of vertebral bodies have been made.<sup>63,67</sup>

### **Biometry of the Fetal Skeleton in the Diagnosis of Bone Dysplasias**

Long bone biometry has been used extensively for the prediction of gestational age. Nomograms for this purpose make use of the long bone as the independent variable and the estimated fetal age as the dependent variable. However, the type of nomogram required to assess the normality of bone dimensions uses gestational age as the independent variable and long bone length as the dependent variable. For the proper use of these nomograms, the clinician must know the accurate gestational age of the fetus. Therefore, patients at risk for skeletal dysplasias are advised to seek prenatal care at an early gestational age in order to assess all clinical estimators of gestational age. Tables 12-6 and 12-7 present nomograms for the measurement of limb biometry for the upper and lower extremities, respectively. Comparisons between limb dimensions and the head circumference can be used for patients presenting with uncertain gestational age (Figs. 12-12 and 12-13). Although some investigators have employed the biparietal diameter for this purpose, the head circumference has the advantage of being shape independent. A limitation of this approach is that it assumes that the cranium is not involved in the dysplastic process, and this may not be the case in some skeletal dysplasias.

The nomograms and figures in this chapter provide the mean, the 5th, and the 95th percentiles of limb biometric parameters. The reader should be aware that 5% of the general population would fall outside these boundaries.



**Table 12-3** Molecular-Pathogenetic Classification of Genetic Disorders of the Skeleton

Gene or Protein	Inheritance	Clinical Phenotype	References
Group 1: Defects in extracellular structural proteins			
<i>COL1A1</i> , <i>COL1A2</i> (collagen 1 $\alpha 1$ , $\alpha 2$ chains)	AD	Family: Osteogenesis imperfecta	Byers, 1990 <sup>1044</sup> ; Prockop et al, 1994 <sup>1045</sup>
<i>COL2A1</i> (collagen 2 $\alpha 1$ chain)	AD	Family: achondrogenesis 2, hypochondrogenesis, congenital spondyloepiphyseal dysplasia (SEDC), Kniest, Stickler arthro-ophthalmopathy, familial osteoarthritis, other variants	Spranger et al, 1994 <sup>1046</sup>
<i>COL9A1</i> , <i>COL9A2</i> , <i>COL9A3</i> (collagen 9 $\alpha 1$ , $\alpha 2$ , $\alpha 3$ chains)	AD	Multiple epiphyseal dysplasia (MED; two or more variants)	Lohiniva et al, 2000 <sup>1047</sup> ; Sipayde et al, 2000 <sup>1048</sup>
<i>COL10A1</i> (collagen 10 $\times 1$ chain)	AD	Metaphyseal dysplasia Schmid	Wallis et al, 1996 <sup>1049</sup>
<i>COL11A1</i> , <i>COL11A2</i> (collagen 11 $\alpha 1$ , $\alpha 2$ chains)	AR, AD	Oto-spondylo-megaepiphyseal dysplasia (OSMED); Stickler (variant), Marshall syndrome	Melkonimi et al, 2000 <sup>1050</sup> ; Spranger, 1998 <sup>1051</sup>
COMP (cartilage oligomeric matrix protein)	AD	Pseudoachondroplasia, multiple epiphyseal dysplasia (MED, one form)	Briggs et al, 1998 <sup>1052</sup>
MATN3 (matrilin-3)	AD	Multiple epiphyseal dysplasia (MED; one variant)	Chapman et al, 2001 <sup>1053</sup>
Perlecan	AR	Schwartz-Jampel type 1; Dyssegmental dysplasia	Arikawa-Hirasawa et al, 2001 <sup>508</sup>
Group 2: Defects in metabolic pathways (including enzymes, ion channels, and transporters)			
TNSALP (tissue nonspecific alkaline phosphatase)	AR, AD	Hypophosphatasia (several forms)	Mornet et al, 1998 <sup>465</sup>
ANKH (pyrophosphate transporter)	AD	Craniometaphyseal dysplasia	Nurnberg et al, 2001 <sup>1054</sup> ; Reichenberger et al, 2001 <sup>1055</sup>
DTDST/SLC26A2 (diastrophic dysplasia sulfate transporter)	AR	Family: achondrogenesis 1B, atelosteogenesis 2, diastrophic dysplasia, recessive multiple epiphyseal dysplasia (rMED)	Rossi and Superti-Furga, 2001 <sup>470</sup> ; Superti-Furga et al, 1996 <sup>580</sup> ; Superti-Furga et al, 1996 <sup>1056</sup>
PAPSS2 (phosphoadenosine-phosphosulfate-synthase 2)	AR	Spondylo-epi-metaphyseal dysplasia Pakistani type	ul Haque et al, 1998 <sup>1057</sup>
TCIRG1 (osteoblast proton pump subunit)	AR	Severe infantile osteopetrosis	Fratini et al, 2000 <sup>1058</sup>
CIC-7 (chloride channel 7)	AR	Severe osteopetrosis	Kornak et al, 2001 <sup>1059</sup>
Carboanhydrase II	AR	Osteopetrosis with intracranial calcifications and renal tubular acidosis	Venta et al, 1991 <sup>1061</sup>
Vitamin K-epoxide reductase complex	AR	Chondrodysplasia punctata with vitamin K-dependent coagulation defects	Oldenburg et al, 2000 <sup>1061</sup> ; Pauli, 1988 <sup>1062</sup> ; Pauli et al, 1987 <sup>1063</sup>
MGP (matrix Gla protein)	AR	Keutel syndrome (pulmonary stenosis, brachytelephalangism, cartilage calcifications and short stature)	Munroe et al, 1999 <sup>1064</sup>
ARSE (arylsulfatase E)	XLR	X-linked chondrodysplasia punctata (CDPX1)	Franco et al, 1995 <sup>1065</sup>
3- $\beta$ -hydroxysteroid-dehydrogenase	XLD	CHILD syndrome	Konig et al, 2000 <sup>774</sup>
3- $\beta$ -hydroxysteroid $\Delta(8)\Delta(7)$ isomerase	XLD	X-linked chondrodysplasia punctata, Conradi-Hünemann type (CDPX2); CHILD syndrome	Braverman et al, 1999 <sup>1066</sup> ; Grange et al, 2000 <sup>1067</sup>
PEX7 (peroxisomal receptor/importer)	AR	Rhizomelic chondrodysplasia punctata 1	Motley et al, 1997 <sup>1068</sup>
DHAPAT (Di-hydroxy-acetophosphate-acyltransferase, peroxisomal enzyme)	AR	Rhizomelic chondrodysplasia punctata 2	Ofman et al, 1998 <sup>1069</sup>
Alkyl-di-hydroxy-diacetophosphate synthase (AGPS; peroxisomal enzyme)	AR	Rhizomelic chondrodysplasia punctata 3	de Vet et al, 1998 <sup>1070</sup>

Continued

**Table 12-3** Molecular-Pathogenetic Classification of Genetic Disorders of the Skeleton—Cont'd

Gene or Protein	Inheritance	Clinical Phenotype	References
Group 3: Defects in folding and degradation of macromolecules			
Sedlin (endoplasmic reticulum protein with unknown function)	XR	X-linked spondyloepiphyseal dysplasia (SED-XL)	Gedeon et al, 1999 <sup>1071</sup>
Cathepsin K (lysosomal proteinase)	AR	Pycnodysostosis	Hou et al, 1999 <sup>1072</sup>
Lysosomal acid hydrolases and transporters (sulfatase, glycosidase, translocase, etc.)	AR, XLR	Lysosomal storage diseases: mucopolysaccharidoses, oligosaccharidoses, glycoproteinoses (several forms)	Leroy and Wiesmann, 1993 <sup>1073</sup>
Targeting system of lysosomal enzymes (GlcNAc-1-phosphotransferase)	AR	Mucopolipidosis II (I-cell disease), mucopolipidosis III	Leroy and Wiesmann, 1993 <sup>1073</sup>
Matrix metalloproteinase 2 (MMP2)	AR	Torg type osteolysis (nodulosis arthropathy and osteolysis syndrome)	Martignetti et al, 2001 <sup>1074</sup>
Group 4: Defects in hormones and signal transduction mechanisms			
25- $\alpha$ -hydroxycholecalciferol-1-hydroxylase	AR	Vitamin D-dependent rickets type 1 (VDDR1)	Kitanaka et al, 1998 <sup>1075</sup>
1, 25- $\alpha$ -dihydroxy-vitamin D3 receptor	AR	Vitamin D-resistant rickets with end-organ unresponsiveness to vitamin D3 (VDDR2)	Hughes et al, 1988 <sup>1076</sup>
CASR (calcium "sensor"/receptor)	AD	Neonatal severe hyperparathyroidism with bone disease (if affected fetus in unaffected mother); familial hypocalciuric hypercalcemia	Bai et al, 1997 <sup>1077</sup>
PTH/PTHrP receptor	AD (activating mutations)	Metaphyseal dysplasia Jansen	Schipani et al, 1996 <sup>1078</sup>
	AR (inactivating mutation)	Lethal dysplasia (Blomstrand)	Zhang et al, 1998 <sup>1079</sup>
Stimulatory Gs alpha protein of adenylate cyclase (GNAS1)	AD	Pseudohypoparathyroidism (Albright hereditary osteodystrophy and several variants) with constitutional haploinsufficiency mutations; McCune-Albright syndrome with somatic mosaicism for activating mutations	Patten et al, 1990 <sup>1080</sup>
PEX proteinase	XL	Hypophosphatemic rickets, X-linked semidominant type (impaired cleavage of FGF23)	The HYP Consortium, 1995 <sup>1081</sup> ; Sabbagh et al, 2000 <sup>1082</sup>
Fibroblast growth factor 23 (FGF23)	AD	Hypophosphatemic rickets, autosomal dominant type (resistant of PEX cleavage)	The ADHR Consortium, 2000 <sup>1083</sup>
Fibroblast growth factor receptor 1 (FGFR1)	AD	Craniosynostosis syndromes (Pfeiffer, other variants)	Wilkie, 1997 <sup>1084</sup>
FGFR2	AD	Craniosynostosis syndromes (Apert, Crouzon, Pfeiffer; several variants)	Wilkie, 1997 <sup>1084</sup>
FGFR3	AD	Thanatophoric dysplasia, achondroplasia, hypochondroplasia, SADDAN; craniosynostosis syndromes (Crouzon with acanthosis nigricans, Muenke nonsyndromic craniosynostosis)	Passos-Bueno et al, 1999 <sup>270</sup> ; Wilkie, 1997 <sup>1084</sup>
Orphan receptor tyrosine kinase (ROR-2)	AR	Robinow syndrome	Afzal et al, 2000 <sup>1085</sup> ; Van Bokhoven et al, 2000 <sup>1086</sup>
Receptor activator of nuclear factor $\kappa$ B; RANK (TNFRSF11A)	AD	Brachydactyly type B	Oldridge et al, 2000 <sup>1087</sup>
Transforming growth factor $\beta$ 1 (TGF $\beta$ 1)	AD	Familial expansile osteolysis	Hughes et al, 2000 <sup>1088</sup>
Cartilage-derived morphogenetic protein 1 (CDMP1)	AD	Diaphyseal dysplasia (Camurati-Engelmann)	Janssens et al, 2000 <sup>1089</sup>
Noggin ("growth factor," TGF antagonist)	AD	Acromesomelic dysplasia Grebe/Hunter-Thompson	Thomas et al, 1997 <sup>828</sup> ; Thomas et al, 1996 <sup>1090</sup>
	AD	Brachydactyly type C	Polinkovsky et al, 1997 <sup>1091</sup>
	AD	Multiple synostosis syndrome; synphalangism and hypoaacusis syndrome	Gong et al, 1999 <sup>1092</sup>

Continued



**Table 12-3** Molecular-Pathogenetic Classification of Genetic Disorders of the Skeleton—Cont'd

Gene or Protein	Inheritance	Clinical Phenotype	References
<i>delta-like 3</i> , intercellular signaling (DLL3)	AR	Spondylocostal dysostosis (one form)	Bulman et al, 2000 <sup>1093</sup>
Indian hedgehog signal molecule (IHH)	AD	Brachydactyly A1	Gao et al, 2001 <sup>1094</sup>
C7orf2 (orphan receptor)	AR	Acheiropodia	Ianakiiev et al, 2001 <sup>1095</sup>
Sclerostin; cystine knot secreted protein (SOST)	AR	Sclerosteosis, van Buchem disease	Balemans et al, 2001 <sup>1096</sup>
LDL receptor-related protein 5 (LRP5)	AR	Osteoporosis-pseudoglioma syndrome	Gong et al, 2001 <sup>1097</sup>
Growth regulator/growth factor (WISP3)	AR	Progressive pseudorheumatoid dysplasia	Hurvitz et al, 1999 <sup>1098</sup>
Group 5: Defects in nuclear proteins and transcription factors			
SOX9 (HMG-type DNA binding protein/transcription factor)	AD	Campomelic dysplasia	Wegner et al, 1994 <sup>1099</sup>
GII3 (zinc finger gene)	AD	Greig cephalopolysyndactyly, polydactyly type A and others, Pallister-Hall syndrome	Kalff-Suske et al, 1999 <sup>1100</sup> ; Radhakrishna et al, 1999 <sup>1101</sup>
TRPS1 (zinc finger gene)	AD	Tricho-rhino-phalangeal syndrome (types 1-3)	Momeni et al, 2000 <sup>1102</sup>
EVC (leucine-zipper gene)	AR	Chondroectodermal dysplasia (Ellis-van Creveld)	Ruiz-Perez et al, 2000 <sup>703</sup>
TWIST (helix-loop-helix transcription factor)	AD	Craniosynostosis Saethre-Chotzen	el Chouzzi et al, 1997 <sup>1103</sup>
P63 (p53 related transcription factor)	AD	EEC syndrome, Hay-Wells syndrome, limby-mammary syndrome, split hand-split foot malformation (some forms)	Celli et al, 1999 <sup>859</sup> ; McGrath et al, 2001 <sup>1104</sup> ; van Bokhoven et al, 2001 <sup>1105</sup>
CBFA-1 (core binding factor A1; runt-type transcription factor)	AD	Cleidocranial dysplasia	Mundlos et al, 1997 <sup>715</sup>
LXM1B (LIM homeodomain protein)	AD	Nail-patella syndrome	Dreyer et al, 1998 <sup>1106</sup>
DLX3 (distal-less 3 homeobox gene)	AD	Trichodontoosseous syndrome	Price et al, 1998 <sup>1107</sup>
HOXD13 (homeobox gene)	AD	Synpolydactyly	Akarsu et al, 1996 <sup>1108</sup>
MSX2 (homeobox gene)	AD (gain of function) AD (loss of function)	Craniosynostosis, Boston type Parietal foramina	Jabs et al, 1993 <sup>1109</sup> Wilkie et al, 2000 <sup>1110</sup>
ALX4 (homeobox gene)	AD	Parietal foramina (cranium bifidum)	Mavrogiannis et al, 2001 <sup>1111</sup>
SHOX (short stature-homeobox)	Pseudo-autosomal	Léri-Weill dyschondrosteosis, idiopathic short stature?	Shears et al, 1998 <sup>1112</sup>
TBX3 (T-box 3, transcription factor)	AD	Ulnar-mammary syndrome	Bamshad et al, 1997 <sup>1114</sup>
TBX5 (T-box 5, transcription factor)	AD	Holt-Oram syndrome	Li et al, 1997 <sup>939</sup>
EIF2AK3 (transcription initiation factor kinase)	AR	Wolcott-Rallison syndrome (neonatal diabetes mellitus and spondyloepiphyseal dysplasia)	Delepine et al, 2000 <sup>1114</sup>
NEMO (NFκB essential modulator; kinase activity)	XL	Osteopetrosis, lymphedema, ectodermal dysplasia and immunodeficiency (OLEDAID)	Doffinger et al, 2001 <sup>1115</sup> ; Smahi et al, 2000 <sup>1116</sup>
Group 6: Defects in oncogenes and tumor suppressor genes			
EXT1, EXT2 (exostosin-1, exostosin-2; heparan-sulfate polymerases)	AD	Multiple exostoses syndrome types 1, type 2	Cheung et al, 2001 <sup>1117</sup> ; Duncan et al, 2001 <sup>1118</sup> ; Lind et al, 1998 <sup>1119</sup>
SH3BP2 ( <i>c-Abi</i> binding protein)	AD	Cherubism	Ueki et al, 2001 <sup>1120</sup>
Group 7: Defects in RNA and DNA processing and metabolism			
RNAse MRP-RNA component	AR	Cartilage-hair-hypoplasia	Ridanpaa et al, 2001 <sup>1121</sup> ; Bonafé et al, 2002 <sup>1122</sup>
Adenosine deaminase (ADA)	AR	Severe combined immunodeficiency (SCID) with (facultative) metaphyseal changes	Hirschhorn 1995 <sup>1123</sup>

AD, autosomal dominant; AR, autosomal recessive; XLD, X-linked dominant; XLR, X-linked recessive.

From Superti-Furga A, Bonafé L, Rimoin DL: Molecular-pathogenetic classification of genetic disorders of the skeleton. *Am J Med Genet* 106:282, 2001.

**Table 12-4** Nosology of Lethal Osteochondrodysplasias

<b>1. Hypophosphatasia and morphologically similar disorders</b>		<b>7. Lethal metatropic dysplasia and similar disorders</b>	
1.01	Hypophosphatasia	7.01	Lethal metatropic dysplasia (hyperchondrogenesis)
1.02	Probable hypophosphatasia	7.02	Isolated case
1.03	Lethal metaphyseal dysplasia	7.03	Isolated case
<b>2. Chondrodysplasia punctata and similar disorders</b>		7.04	Fibrochondrogenesis
2.01	Rhizomelic chondrodysplasia punctata	7.05	Schneckenbecken dysplasia
2.02	Lethal chondrodysplasia punctata, X-linked dominant	7.06	Isolated case
2.03	Greenberg dysplasia	7.07	Isolated case
2.04	Dappled diaphysis dysplasia	7.08	Isolated case
<b>3. Achondrogenesis and similar disorders</b>		<b>8. Kniest-like disorders</b>	
3.01	Achondrogenesis I-A (Houston Harris)	8.01	Dyssegmental dysplasia, Silverman type
3.02	Achondrogenesis I-B (Fraccaro)	8.02	Dyssegmental dysplasia, Rolland-Desbuquois
3.03	New lethal osteochondrodysplasia	8.03	Lethal Kniest disease
3.04	Achondrogenesis II (Langer-Saldino)	8.04	Chondrodysplasia resembling Kniest dysplasia
3.05	Hypochondrogenesis	8.05	Isolated case
<b>4. Thanatophoric dysplasia and similar disorders</b>		8.06	Blomstrand chondrodysplasia
4.01	Thanatophoric dysplasia, type 1	<b>9. Lethal osteochondrodysplasias with pronounced diaphyseal abnormalities</b>	
4.02	Thanatophoric dysplasia, type 2	9.01	Campomelic syndrome
4.03	Homozygous achondroplasia	9.02	Stuve-Wiedemann syndrome
4.04	Lethal achondrodysplasia	9.03	Boomerang dysplasia
4.05	Glasgow variant	9.04	Atelosteogenesis
<b>5. Platypondylic lethal chondrodysplasias</b>		9.05	Disorder resembling atelosteogenesis
5.01	Platypondylic chondrodysplasia, Torrance type	9.06	De la Chapelle dysplasia
5.02	Platypondylic chondrodysplasia, San Diego type	9.07	McAlister dysplasia
5.03	Platypondylic chondrodysplasia, Luton type	9.08	Pseudodystrophic dysplasia
5.04	Platypondylic chondrodysplasia, Shiraz type	<b>10. Osteogenesis imperfecta and similar disorders</b>	
5.05	Opsismodysplasia	10.01	Osteogenesis imperfecta II-A
5.06	Sixth form of platyspondylic chondrodysplasia	10.02	Osteogenesis imperfecta II-B
5.07	Seventh form of platyspondylic chondrodysplasia	10.03	Osteogenesis imperfecta II-C
<b>6. Short rib polydactyly syndromes</b>		10.04	Isolated case
6.01	Short rib polydactyly syndrome, type I (Saldino-Noonan)	10.05	Astley-Kendall dysplasia
6.02	Short rib polydactyly syndrome, type II (Verma-Naumoff)	<b>11. Lethal disorders with gracile bones</b>	
6.03	Short rib polydactyly syndrome, type III (Le Marec)	11.01	Fetal hypokinesia phenotype
6.04	Short rib polydactyly syndrome, type IV (Yang)	11.02	Lethal osteochondrodysplasia with gracile bones
6.05	Short rib polydactyly syndrome, type V	11.03	Lethal osteochondrodysplasia with intrauterine over-tubulation
6.06	Short rib polydactyly syndrome, type VI (Majewski)		
6.07	Short-rib-polydactyly syndrome, type VII (Beemer)		

From Spranger J, Maroteaux P: The lethal osteochondrodysplasias. *Adv Hum Genet* 19:1, 1990.

Ideally, a more stringent criterion, such as the 1st percentile of limb growth for gestational age, should be used for diagnosis. Unfortunately, none of the currently available nomograms have been based on a sufficient number of patients to provide an accurate discrimination between the 5th and the 1st percentiles. However, most skeletal dysplasias diagnosed in utero or at birth are associated with dramatic long bone shortening, and under these circumstances, the precise boundary used (1st or 5th percentile) is not critical. An exception to this is achondroplasia, in which limb biometry is mildly affected until the third trimester, when abnormal growth can be detected by examining the slope of growth of the femur length.<sup>68</sup> In a study including 127 cases of 17 skeletal dysplasias, Gonçalves and Jeanty<sup>69</sup> concluded, with the use of discriminant analysis, that the degree of shortening of the femur length can be used as the initial step in distinguishing among the five most common disorders: thanatophoric dysplasia, OI type II, achondrogenesis, achondroplasia, and hypochondroplasia. Gabrielli et al.<sup>70</sup> evaluated the possibility of an early diagnosis of skeletal dysplasias in high-risk patients. A total of 149 consecutive,

uncomplicated singleton pregnancies at 9 to 13 weeks after amenorrhea were scanned by transvaginal ultrasound. Eight additional patients with previous pregnancies affected with skeletal dysplasias were evaluated with serial examinations every 2 weeks from 10 to 11 weeks of gestation onward. Significant correlations between femur length and both crown rump length and biparietal diameter were found. Of the five cases with skeletal dysplasias, two (one with recurrent OI, the other with recurrent achondrogenesis) were diagnosed in the first trimester. The results of this study suggest that an early evaluation of the fetus and the correlation of femur length with crown rump length and of femur length with biparietal diameter might be helpful in the early diagnosis of severe skeletal dysplasias. In less severe cases, however, biometric evaluation appeared to be of limited value. Nomograms for long bone measurements according to crown rump length in a large population of normal fetuses examined between 11 and 14 weeks of gestation have been recently published and their role in the early assessment of pregnancies at risk for skeletal dysplasias remains to be determined.<sup>71</sup>



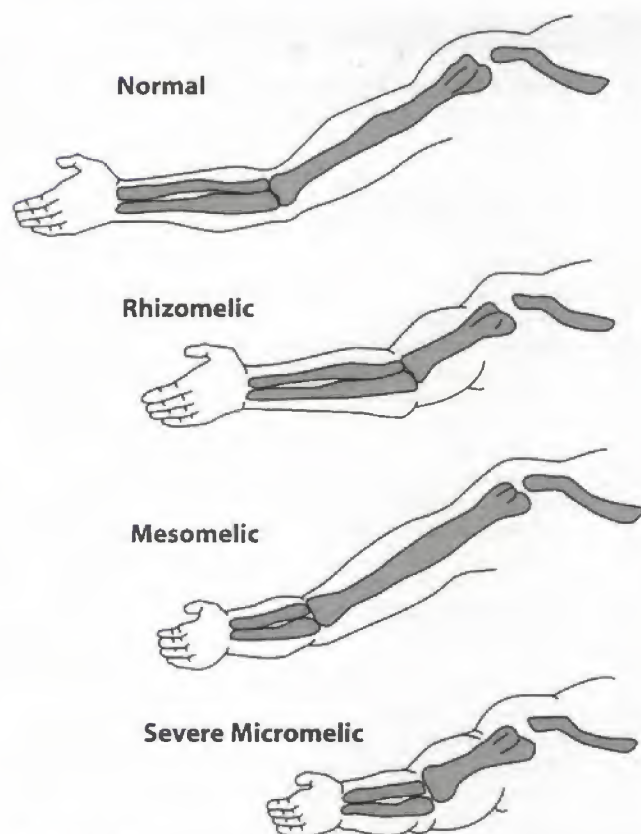


**FIGURE 12-5.** Varieties of short limb dysplasia according to the segment involved.

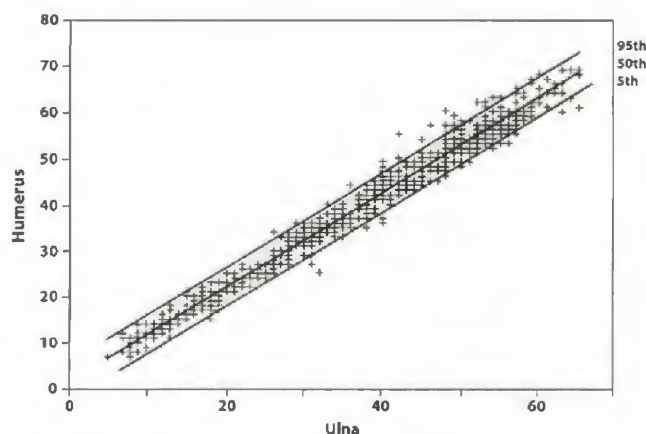


**FIGURE 12-6.** Relationship between the lengths of the ulna and the humerus.

## Clinical Presentation

The challenge of antenatal diagnosis of skeletal dysplasias generally presents itself in one of two ways: (1) a patient who has delivered an infant with a skeletal dysplasia and desires antenatal assessment in a subsequent pregnancy; or (2) the incidental finding of a shortened, bowed, or anomalous extremity during a routine sonographic examination. In

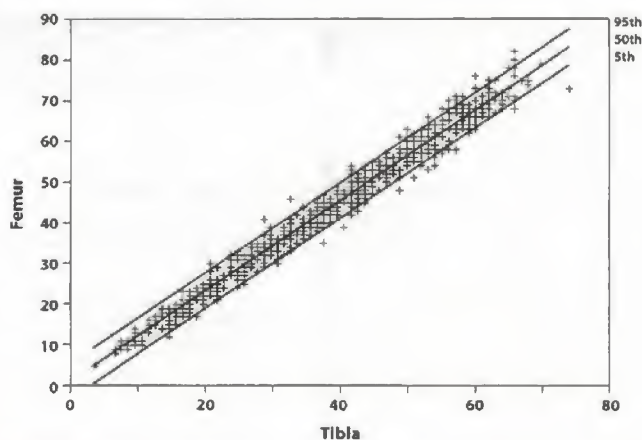


**FIGURE 12-7.** Relationship between the lengths of the tibia and femur.

**Table 12-5**

### Skeletal Dysplasias Characterized by Rhizomelia, Mesomelia, and Micromelia

#### *Rhizomelia*

- Thanatophoric dysplasia
- Atelosteogenesis
- Chondrodysplasia punctata (rhizomelic type)
- Congenital short femur
- Achondroplasia
- Hypochondroplasia

#### *Mesomelia*

- Mesomelic dysplasia (Langer, Reinhardt, and Robinow types)
- Ellis-van Creveld syndrome (chondroectodermal dysplasia)

#### *Acromesomelia*

- Ellis-van Creveld syndrome (chondroectodermal dysplasia)

#### *Micromelia*

- Achondrogenesis
- Atelosteogenesis
- Short-rib-polydactyly syndrome
- Diastrophic dysplasia
- Fibrochondrogenesis
- Osteogenesis imperfecta (type II)
- Kniest dysplasia
- Dyssegmental dysplasia
- Roberts syndrome

patients at risk, the examination is easier when the particular phenotype is known. The inability to obtain reliable information about skeletal mineralization and the involvement of other systems (e.g., skin) with sonography is a limiting factor in the establishment of an accurate diagnosis after the identification of an incidental finding. Another limitation is the paucity of information about the in utero natural history of these disorders.

Despite these difficulties and limitations, good medical reasons justify attempting an accurate prenatal diagnosis of skeletal dysplasias. A number of these disorders are uniformly lethal (see Table 12-4), whereas others are associ-



A



B

**FIGURE 12-8.** A. Longitudinal scan of the spine in a fetus with thanatophoric dysplasia and platyspondyly. The intervertebral discs (*white arrows*) are greater in height than the vertebra (*black arrows*), which are flat. B. Lateral spine x-ray from a fetus with platyspondyly and thanatophoric dysplasia. Note the markedly flattened vertebrae.

ated with mental retardation.<sup>72</sup> In addition, there is a group of disorders associated with thrombocytopenia for which vaginal delivery may expose the infants to the risk of intracranial hemorrhage. Accurate diagnosis of skeletal dysplasias is therefore important for prenatal counseling.



**FIGURE 12-9.** Coronal scan of the fetal spine by two-dimensional ultrasound showing scoliosis.



**FIGURE 12-10.** Three-dimensional rendered images of the fetal spine showing scoliosis.

### Diagnostic Imaging and the Prenatal Diagnosis of Skeletal Dysplasias

Despite the increasing availability of molecular testing, a comprehensive molecular diagnostic search for all skeletal dysplasias is not possible at this time. Indeed, as mentioned in a previous section of this chapter, only about one third of skeletal dysplasias have had their molecular basis defined.<sup>25</sup> Therefore, the role of diagnostic imaging in the prenatal investigation of skeletal dysplasias are (1) to narrow the

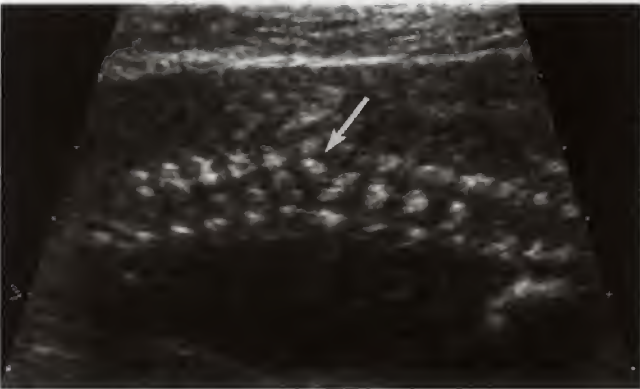


differential diagnosis of skeletal dysplasias so that appropriate confirmatory molecular tests can be selected, (2) to predict lethality; and (3) to identify the fetus with a skeletal dysplasia early enough in pregnancy so that the diagnostic workup can be completed before the limit of fetal viability.<sup>73-77</sup>

Ultrasound is the primary imaging modality used for the initial diagnostic evaluation of an affected fetus, and several studies have explored the role of ultrasound in the detection

of skeletal dysplasias.<sup>53,68,78-88</sup> The first was a prospective analysis of a high-risk population (15 women, 16 cases) carrying a genetic risk for skeletal dysplasias conducted by Kurtz et al.<sup>68</sup> Based on second trimester findings, five abnormal fetuses among 16 fetuses at risk were correctly diagnosed. Weldner et al.<sup>32</sup> screened 12,453 patients in the second and third trimesters, and estimated the prevalence of skeletal dysplasias detectable by prenatal ultrasound as 7.5/10,000. Sharony et al.<sup>84</sup> studied fetuses and stillbirths referred from other centers for suspected skeletal dysplasia. Most of the cases were sporadic, and the most common final diagnoses were OI (16%) and thanatophoric dysplasia (14%). Table 12-8 summarizes the diagnostic accuracy of two-dimensional ultrasound (2DUS) for prenatal diagnosis of skeletal dysplasias.<sup>26,38,88-91</sup>

Several investigators have proposed that three-dimensional ultrasonography (3DUS) may improve the diagnostic accuracy for prenatal diagnosis of skeletal dysplasia.<sup>92-104</sup> The rationale for this expectation is that the availability of rendering algorithms to reconstruct the fetal skeleton may allow the observation of phenotypic features not detectable by 2DUS. For example, Garjian et al.<sup>95</sup> and Krakow et al.<sup>102</sup> reported on the diagnosis of additional facial<sup>95,102</sup> and scapular anomalies,<sup>95</sup> as well as abnormal calcification patterns<sup>102</sup> in fetuses with skeletal dysplasias. Moeglin and Benoit,<sup>98</sup> on the other hand, used the multiplanar visualization method to demonstrate the pointed appearance of the

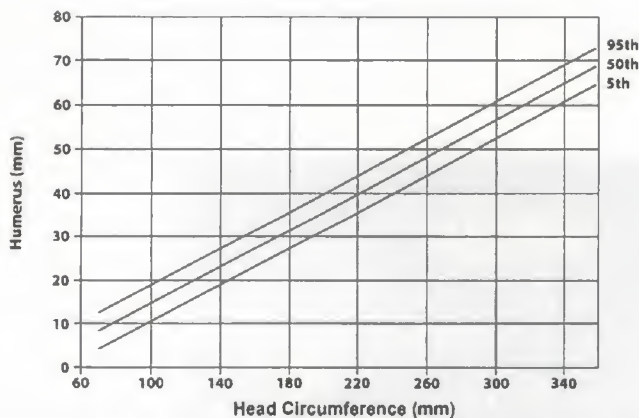
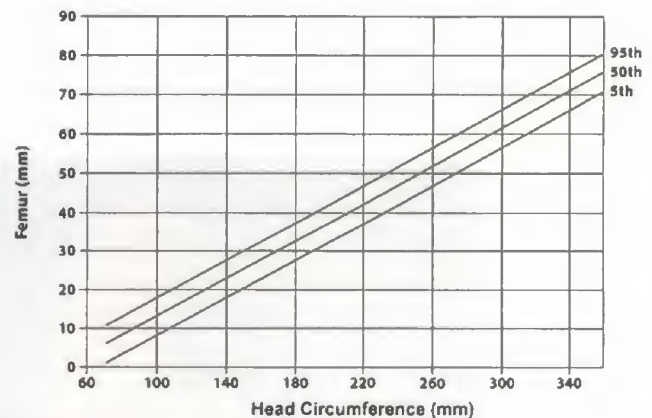


**FIGURE 12-11.** Coronal scan of the fetal spine showing lateral hemivertebra (arrow) in the thoracic segment.

Table 12-6 Normal Values for the Leg (millimeters)									
Week	Tibia Percentile			Fibula Percentile			Femur Percentile		
	5th	50th	95th	5th	50th	95th	5th	50th	95th
12	—	7	—	—	6	—	4	8	13
13	—	10	—	—	9	—	6	11	16
14	7	12	17	6	12	19	9	14	18
15	9	15	20	9	15	21	12	17	21
16	12	17	22	13	18	23	15	20	24
17	15	20	25	13	21	28	18	23	27
18	17	22	27	15	23	31	21	25	30
19	20	25	30	19	26	33	24	28	33
20	22	27	33	21	28	36	26	31	36
21	25	30	35	24	31	37	29	34	38
22	27	32	38	27	33	39	32	36	41
23	30	35	40	28	35	42	35	39	44
24	32	37	41	29	37	45	37	42	46
25	34	40	45	34	40	45	40	44	49
26	37	42	47	36	42	47	42	47	51
27	39	44	49	37	44	50	45	49	54
28	41	46	51	38	45	53	47	52	56
29	43	48	53	41	47	54	50	54	59
30	45	50	55	43	49	56	52	56	61
31	47	52	57	42	51	59	54	59	63
32	48	54	59	42	52	63	56	61	65
33	50	55	60	46	54	62	58	63	67
34	52	57	62	46	55	65	60	65	69
35	53	58	64	51	57	62	62	67	71
36	55	60	65	54	58	63	64	68	73
37	56	61	67	54	59	65	65	70	74
38	58	63	68	56	61	65	67	71	76
39	59	64	69	56	62	67	68	73	77
40	61	66	71	59	63	67	70	74	79

**Table 12-7** Normal Values for the Arm (millimeters)

Week	Humerus Percentile			Ulna Percentile			Radius Percentile		
	5th	50th	95th	5th	50th	95th	5th	50th	95th
12	—	9	—	—	7	—	—	7	—
13	6	11	16	5	10	15	6	10	14
14	9	14	19	8	13	18	8	13	17
15	12	17	22	11	16	21	11	15	20
16	15	20	25	13	18	23	13	18	22
17	18	22	27	16	21	26	14	20	26
18	20	25	30	19	24	29	15	22	29
19	23	28	33	21	26	31	20	24	29
20	25	30	35	24	29	34	22	27	32
21	28	33	38	26	31	36	24	29	33
22	30	35	40	28	33	38	27	31	34
23	33	38	42	31	36	41	26	32	39
24	35	40	45	33	38	43	26	34	42
25	37	42	47	35	40	45	31	36	41
26	39	44	49	37	42	47	32	37	43
27	41	46	51	39	44	49	33	39	45
28	43	48	53	41	46	51	33	40	48
29	45	50	55	43	48	53	36	42	47
30	47	51	56	44	49	54	36	43	49
31	48	53	58	46	51	56	38	44	50
32	50	55	60	48	53	58	37	45	53
33	51	56	61	49	54	59	41	46	51
34	53	58	63	51	56	61	40	47	53
35	54	59	64	52	57	62	41	48	54
36	56	61	65	53	58	63	39	48	57
37	57	62	67	55	60	65	45	49	53
38	59	63	68	56	61	66	45	49	54
39	60	65	70	57	62	67	45	50	54
40	61	66	71	58	63	68	46	50	55

**FIGURE 12-12.** Relationship between the head circumference and the length of the humerus.**FIGURE 12-13.** Relationship between the head circumference and the length of the femur.

upper femoral diaphysis in achondroplasia. Three-dimensional reconstruction of the fetal bones is best performed using the maximum intensity projection mode, a rendering algorithm that prioritizes the display of voxels with the highest gray levels contained within a region of interest selected by the user<sup>95,98</sup> (Fig. 12-14). If the fetus is

examined early enough in the pregnancy, the entire skeleton can be included within the region of interest, and therefore, panoramic visualization can be achieved.<sup>95</sup> However, the diagnosis may still be missed, because the phenotypic characteristics of some skeletal dysplasias do not manifest until later in pregnancy. Case reports and small series of skeletal



dysplasias have been published describing phenotypic characteristics or skeletal features for which 3DUS may provide additional information (Table 12-9).<sup>93,95-98,100-103,105</sup>

Three-dimensional helical computerized tomography (3DHCT) has recently been proposed as an adjunctive imaging modality for the prenatal diagnosis of skeletal dysplasias (Fig. 12-15).<sup>106</sup> Like 3DUS, postprocessing techniques such as maximum intensity projection, surface rendering, and volume rendering can be used for three-dimensional reconstruction.<sup>107-109</sup> Long bone measurements obtained by postmortem helical CT studies have been compared with those obtained within 24 hours of delivery by ultrasound, and a significant correlation between the two methods was observed.<sup>110</sup> Excellent panoramic images of the fetal skeleton can be obtained by 3DHCT without superimposition of the maternal skeleton (which occurs with radiography). Ruano et al<sup>106</sup> compared the phenotypic characteristics of three skeletal dysplasias [achondroplasia ( $n=3$ ), OI ( $n=2$ ), and chondrodysplasia punctata ( $n=1$ )] visualized by prenatal 3DHCT, 3DUS, and 2DUS. Deformation of the fetal pelvis and an increase in the intervertebral space of the lumbar vertebrae were diagnosed more often using 3DHCT than 2DUS and 3DUS. In

contrast, some phenotypic characteristics of fetuses with skeletal dysplasias were demonstrated only by ultrasound: phalangeal hypoplasia, point-calcified epiphysis (both by 2DUS and 3DUS), and facial dysmorphism (by 3DUS only). Although the overall count of correct phenotypic characteristics detected prenatally favored 3DHCT over 3DUS (94.3% [33/35] versus 77.1% [27/35],  $p=0.03$ , McNemar's test for correlated samples), the diagnostic performance of 3DHCT was not superior to that of 3DUS, because the correct prenatal diagnosis was established by both modalities in all cases. Provided that the two diagnostic methods have comparable diagnostic accuracy, 3DUS has two important advantages over 3DHCT, namely the lack of radiation exposure and wider availability in the clinical setting. It is also noteworthy that the overall experience with 3DUS for the diagnosis of skeletal dysplasias is still limited.<sup>92-105,111-116</sup> Nevertheless, even in this study, 3DUS performed better than 2DUS, both in the identification of phenotypic characteristics (77.1% [27/35] versus 51.4% [18/35],  $p=0.004$ , McNemar's test for correlated samples) and in establishing an accurate diagnosis.

## Approach to the Diagnosis of Skeletal Dysplasias

A proposed systematic approach to the prenatal diagnosis of skeletal dysplasias is summarized in Table 12-10 and described in greater detail in the following section.

### Evaluation of the Long Bones

**Measurements.** All long bones should be measured in all extremities. Comparisons with other segments should be performed to establish whether the limb shortening is predominantly rhizomelic, mesomelic, or acromelic, or whether it involves all segments (see Figs. 12-5, 12-6, 12-7, and 12-14). A detailed examination of each bone is necessary

**Table 12-8**

**Accuracy of Prenatal Ultrasound for Diagnosis of Skeletal Dysplasias**

Author	Year	Number of Cases	Correct Diagnosis (%)
Gordienko et al <sup>38</sup>	1996	26	73 (9)
Gaffney et al <sup>88</sup>	1998	35	31 (11)
Tretter et al <sup>90</sup>	1998	27	48 (13)
Herish et al <sup>91</sup>	1998	23	48 (11)
Doray et al <sup>89</sup>	2000	47	60 (28)
Parilla et al <sup>26</sup>	2003	31	65 (20)



**FIGURE 12-14.** Comparison between the surface rendering mode (A) and the maximum intensity projection mode (B), for the visualization of the fetal leg of a fetus with mesomelic shortening of the long bones. With the surface rendering mode, the external surface of the leg is visualized. By switching the rendering algorithm to maximum intensity projection, only the voxels with the highest intensity are displayed, with clear depiction of the mesomelic shortening of the long bones (the tibia and fibula are proportionately shorter than the femur).

**Table 12-9** Additional Phenotypic Findings and Improved Visualization in Cases of Skeletal Dysplasias by Prenatal 3DUS as Compared to 2DUS in Published Reports

Skeletal Dysplasia	Phenotypic Characteristics Identified Better by 3DUS than 2DUS
Platyospondylic lethal chondrodysplasia <sup>93</sup> Campomelic dysplasia <sup>95,109,116</sup>	Enhanced visualization of femoral and tibial bowing; Better characterization of the facial soft tissues with surface rendering Micrognathia; Flat face; Hypoplastic scapulae; Bifid foot; Fan-like position of the toes
Thanatophoric dysplasia <sup>95-97,102</sup>	Improved characterization of frontal bossing and depressed nasal bridge; Demonstration of redundant skin folds; Low-set dysmorphic ears
Achondroplasia <sup>98,102</sup>	Improved characterization of frontal bossing and depressed nasal bridge; Superior evaluation of the epiphyses and metaphyses of the long bones, with demonstration of a vertical metaphyseal slope; Caudal narrowing of the interpedicular distance; Clear visualization of trident hand; Better visualization of disproportion between limb segments
Chondrodysplasia punctata, rhizomelic form <sup>102</sup>	Improved characterization of the Binder facies (depressed nasal bridge, mid-face hypoplasia, small nose with upturned alae); Identification of laryngeal stippling
Achondrogenesis <sup>102</sup>	Panoramic demonstration of short neck and severe shortening of all segments of the limbs
Jarcho-Levin syndrome <sup>101</sup> Spondylocostal dysostosis <sup>111</sup> Larsen syndrome <sup>105</sup> Cleidocranial dysplasia <sup>115</sup>	Vertebral defects with absence of ribs and transverse process Fan-like rib cage with rib fusion Genu recurvatum, midface hypoplasia, low set ears Widened cranial sutures, poor mineralization of the occipital bones, pseudoarthrosis of the clavicle
Apert syndrome <sup>113,114</sup>	Coronal craniosynostosis

2DUS, two-dimensional ultrasound; 3DUS, three-dimensional ultrasound.

Phenotypic characteristics of osteogenesis imperfecta,<sup>95</sup> short rib–polydactyly syndrome,<sup>100</sup> and Apert's syndrome<sup>102</sup> have also been described using 3DUS, although no additional findings to 2DUS were observed.

to exclude the absence or hypoplasia of individual bones (fibula, tibia, ulna, radius, clavicles, and scapulae).<sup>85,117-120</sup>

**Degree of Mineralization.** An attempt should be made to characterize the degree of mineralization. This can be assessed by examining the acoustic shadow behind the bone and the echogenicity of the bone itself. Signs of demineralization include the visualization of an unusually prominent falx and the absence or decreased echogenicity of the spine. It should be stressed that there are limitations for the sonographic evaluation of mineralization of long bones and that other structures, such as the skull, may be better suited for this assessment (Fig. 12-16).

**Degree of Long Bone Curvature.** At present, there is no objective means of assessing long bone curvature, and experience is the only tool assisting the operator in discerning the boundary between normality and abnormality. Campomelia (excessive bowing, Fig. 12-17) is characteristic of certain disorders (e.g., campomelic dysplasia).

**Metaphyseal Flaring.** Metaphyseal flaring denotes widening at the level of the metaphyseal growth plate. It can be observed in many conditions, including achondroplasia, hypochondroplasia, hypochondrogenesis, asphyxiating thoracic dysplasia, chondrodysplasia punctata, diastrophic dysplasia, hypophosphatasia, Kniest dysplasia, kyphomelic dysplasia, metatropic dysplasia, and OI.<sup>121</sup>

**Fractures.** The possibility of fractures should be considered, because they can be present in some conditions

(e.g., OI, Fig. 12-18). The fractures may be extremely subtle, or may lead to angulation and separation of the segments of the affected bone (Fig. 12-19).

### Prediction of Pulmonary Hypoplasia

Several skeletal dysplasias are associated with a hypoplastic thorax. This is extremely important because chest restriction leads to pulmonary hypoplasia, a frequent cause of death in these conditions (see Table 12-4). When a severe skeletal dysplasia is diagnosed, the presence of marked thoracic involvement and pulmonary hypoplasia will allow the clinician to counsel the parents regarding prognosis despite the fact that the specific type of dysplasia may not be known. A number of ultrasonographic parameters have been investigated for the prediction of pulmonary hypoplasia. These include measurements of the thorax and lungs, ratios between thoracic measurements and other biometric parameters, Doppler velocimetry of the pulmonary arteries, Doppler evaluation of tracheal fluid flow, and more recently, three-dimensional volumetric measurements of the fetal lungs by either ultrasound or magnetic resonance imaging (MRI).

**Evaluation of Thoracic and Lung Dimensions by Two-Dimensional Ultrasound.** Thoracic and lung biometry have been extensively studied to identify fetuses at high risk for pulmonary hypoplasia.<sup>122-133</sup> Table 12-11 lists skeletal



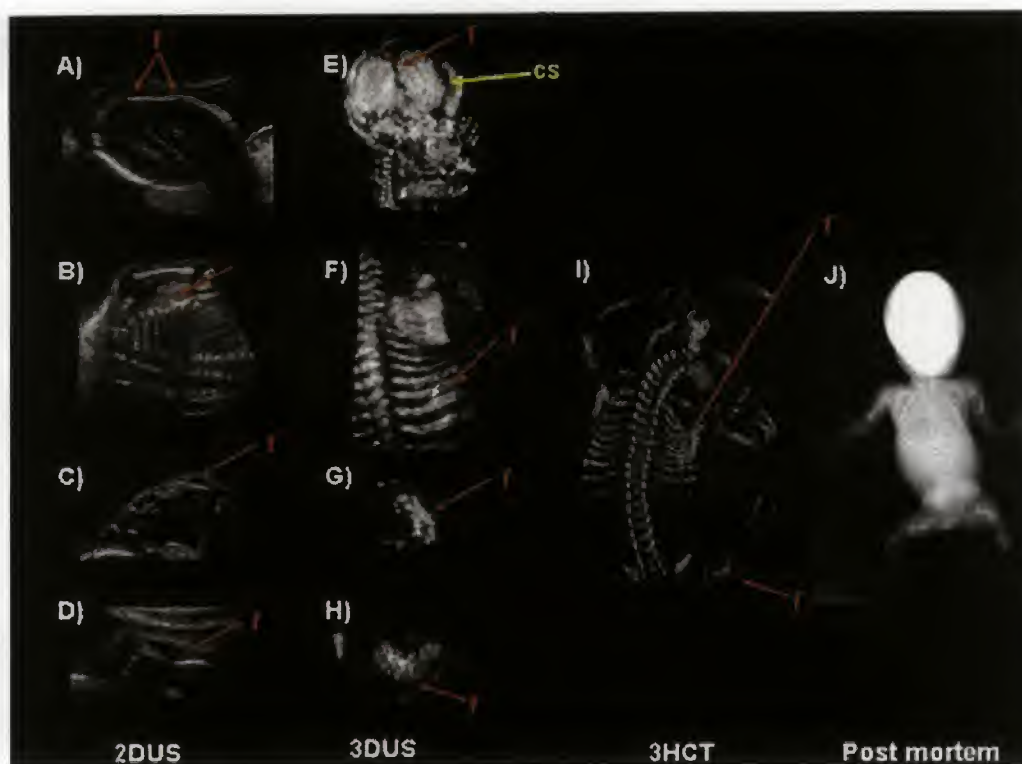


**FIGURE 12-15.** Comparison of phenotypic features of osteogenesis imperfecta by three-dimensional helical computer tomography (3DHCT), three-dimensional ultrasound (3DUS), two-dimensional ultrasound (2DUS), and postmortem radiographs. Prenatal diagnosis of osteogenesis imperfecta at 33 weeks of gestation by 2D-US, 3D-US, and 3-HCT. *A.* 2DUS: transverse section of fetal head with a skull fracture (f) deformed due to the transducer pressure. *B.* 2DUS: coronal section of fetal thorax showing irregular ribs (arrow). *C.* 2DUS: sagittal section of the right arm showing a short and bowed arm (f). *D.* 2DUS: sagittal section of fetal femur with a fracture (f). *E.* 3DUS: three-dimensional rendered bone mode image showing lateral view of fetal skull with a fracture (f) that could be differentiated from a normal coronal suture (CS) by the location and the deforming aspect depending on the transducer pressure; this was confirmed at postmortem examination. *F.* 3DUS: rendered bone mode demonstrating posterior view of fetal thorax showing fractured and irregular ribs (f). *G.* 3DUS: rendered bone mode image showing short and bowing radius and cubitus (f). *H.* 3DUS: rendered bone mode image showing a fractured femur (f). *I.* 3DHCT: posterior view of entire fetus confirming fractures of ribs and femur (f) as well as decreased mineralization of the skull. *J.* Postmortem radiologic examination, confirming shortening, bowing and fracture of long bones. (From Ruano R, Molho M, Roume J, et al: Prenatal diagnosis of fetal skeletal dysplasias by combining two-dimensional and three-dimensional ultrasound and intrauterine three-dimensional helical computer tomography. *Ultrasound Obstet Gynecol* 24:134, 2004.)

dysplasias associated with altered thoracic dimensions, whereas Figures 12-20 and 12-21 illustrate features associated with a hypoplastic thorax.

Methods used to measure the bony thorax, chest, lungs, and heart by 2DUS are illustrated in Figure 12-22. Thoracic dimensions in fetuses with known gestational age can be evaluated by the nomograms reproduced in Tables 12-12 and 12-13. When gestational age is uncertain, age-independent ratios, such as the thoracic-to-abdominal circumference ratio (normal value: 0.77 to 1.01) and the thoracic-to-head circumference ratio (normal value: 0.56 to 1.04) can be used.<sup>123</sup>

A summary of the diagnostic accuracy of biometric parameters for the diagnosis of pulmonary hypoplasia is presented in Table 12-14.<sup>124-130,133-139</sup> Of particular interest are the measurements of the right lung diameter or the ratio between right lung diameter/bony thoracic circumference proposed by Merz et al.<sup>131</sup> In a study of 32 fetuses with a postnatal diagnosis of pulmonary hypoplasia (skeletal dysplasias [ $n = 7$ ], renal agenesis [ $n = 11$ ], diaphragmatic hernia [ $n = 7$ ], and hydrothorax [ $n = 2$ ]), all had a right lung diameter below the 5th percentile for age, regardless of the primary disorder.<sup>136</sup> In a subsequent study of 19 fetuses with

congenital diaphragmatic hernia, Bahlmann et al<sup>137</sup> demonstrated that the ratio of right lung diameter/bony thoracic circumference detected all fetuses with pulmonary hypoplasia with 100% sensitivity and 100% specificity.

**Short Femur Length and Prediction of Lethality in Skeletal Dysplasias.** Rahemtullah et al<sup>140</sup> studied 18 cases of skeletal dysplasias, and all lethal cases were associated with a femur length/abdominal circumference ratio of 0.16. Although the test detected lethal cases with 100% sensitivity, two cases of achondroplasia were erroneously identified as lethal with this method. A less pragmatic approach has been proposed by Hersh et al,<sup>91</sup> who were able to predict lethality in 23 out of 25 cases of skeletal dysplasias with a femur length below the first percentile for age, after combining this information with other sonographic findings (i.e., bell-shaped thorax, decreased bone echogenicity, or both).

**Lung Volumetry by Three-Dimensional Ultrasound**  
Fetal lung volumetry by 3DUS has been performed using two techniques: multiplanar<sup>141-146</sup> (Fig. 12-23) and VOCAL (Virtual Organ Computer-Aided AnaLysis, GE Medical Systems, Milwaukee, Wisconsin) (Fig. 12-24).<sup>147-154</sup> Nomograms for lung volumetry by 3DUS have been proposed by several investigators.<sup>141-143,149,152,153,155,156</sup>

**Table 12–10**
**Steps for Examination of the Fetus With a Suspected Skeletal Dysplasia by Two-Dimensional and Three-Dimensional Ultrasound**

1. Measure all long bones
2. Compare with other segments and classify the limb shortening as:
  - a. Rhizomelia
  - b. Mesomelia
  - c. Acromelia
  - d. Severe micromelia
3. Qualitative assessment of long bones:
  - a. Demineralization
  - b. Fractures
  - c. Bowing
  - d. Metaphyseal flaring
  - e. Absence of bones
4. Measure chest dimensions to determine risk of pulmonary hypoplasia
5. Evaluation of hands and feet
  - a. Digits (polydactyly/syndactyly)
  - b. Positional deformities
6. Evaluation of the cranium
  - a. Macrocrania
  - b. Frontal bossing
  - c. Cloverleaf skull
  - d. Hypertelorism/Hypotelorism
7. Facial clefts
8. Examination of the spine
  - a. Platyspondyly
  - b. Demineralization
  - c. Hemi vertebrae
  - d. Coronal clefts
  - e. Vertebral disorganization
9. Evaluation of internal organs, including echocardiography
10. Fetal motion
11. Amniotic fluid volume



**FIGURE 12-16.** Demineralization of the skull in a case of osteogenesis imperfecta. The lateral ventricle and choroid plexus in the near field are well seen due to lack of normal mineralization of the calvarium. Normally reverberation artifact from the calvarium would obscure these structures.



A



B

**FIGURE 12-17.** Bowing of the lower extremity (arrows) in a case of (A) thanatophoric dysplasia and (B) campomelic dysplasia.

Kalache et al.<sup>147</sup> demonstrated that both the 3D multiplanar and 3D VOCAL modes can be used to measure pulmonary volumes in fetuses, an observation that was subsequently confirmed by Moeglin et al.<sup>152</sup> A potential advantage of the VOCAL technique is the possibility of obtaining fine contours of the lungs, which may be particularly valuable when the outline of the organ in question is irregular, such as in cases of congenital diaphragmatic hernia. In contrast, lung volume measurements obtained by the 3D multiplanar technique are faster, taking usually less than 5 minutes to perform.<sup>152</sup> Volumes are best estimated when datasets are acquired using a transverse view of the fetal thorax.<sup>143,153</sup> Ruano et al.<sup>154</sup> compared volumetric measurements of the fetal lungs obtained using the VOCAL method and the actual volume at autopsy in eight cases of congenital diaphragmatic hernia and 25 controls without pulmonary malformations. The mean relative error of 3DUS to estimate the actual lung volume was -7.19% (range: -42.70% to +18.11%) in cases of congenital diaphragmatic



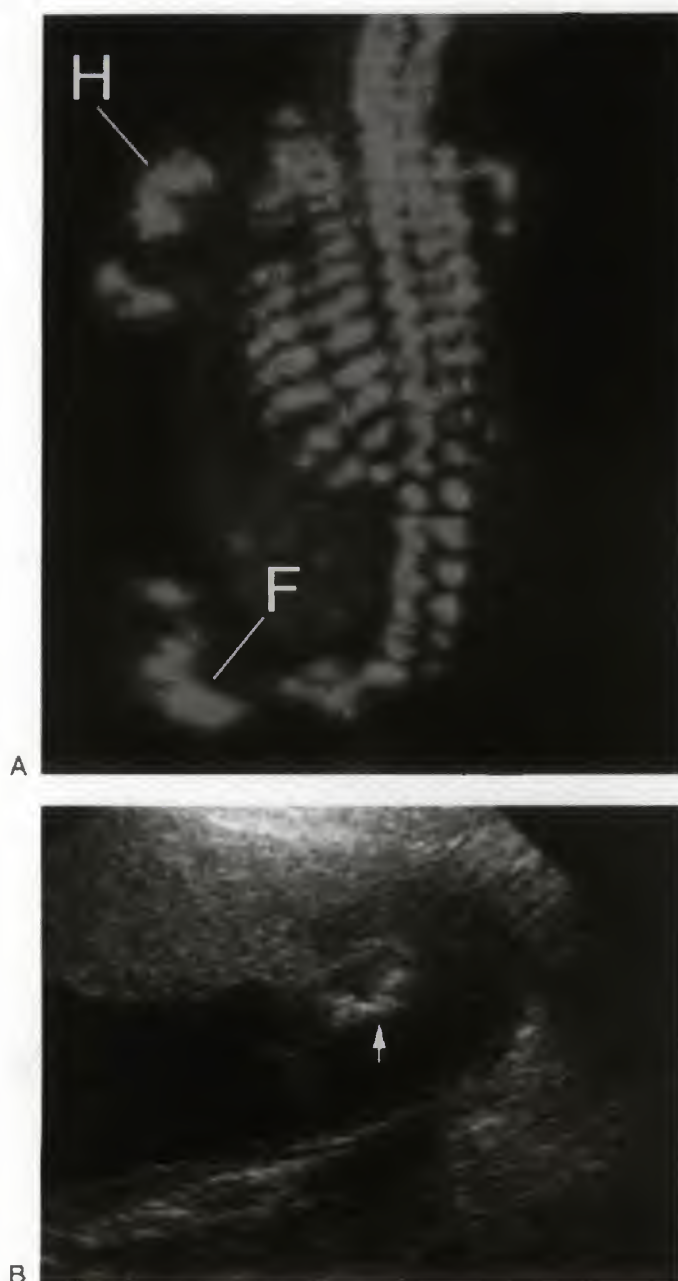


**FIGURE 12-18.** A. Three-dimensional ultrasonography in a case of osteogenesis imperfecta type II. The volume dataset was rendered using the maximum intensity (skeletal) mode. Multiple fractures in the ribs are present. Note the severe bowing and shortening of the left femur (F) and humerus (H). (B) Sonogram of a fetus with osteogenesis imperfecta type II. The femur is markedly shortened (arrow) with multiple fractures.



**FIGURE 12-19.** In utero fracture in a case of osteogenesis imperfecta. The arrows indicate the hypoechoic fracture line.

**Table 12-11**

**Skeletal Dysplasias Associated With Altered Thoracic Dimensions**

**Long, narrow thorax**

- Asphyxiating thoracic dysplasia (Jeune)
- Chondroectodermal dysplasia (Ellis-van Creveld)
- Metatropic dysplasia
- Fibrochondrogenesis
- Atelosteogenesis
- Camptomelic dysplasia
- Jarcho-Levin syndrome
- Achondrogenesis
- Osteogenesis imperfecta congenital
- Hypophosphatasia
- Dyssegmental dysplasia
- Cleidocranial dysplasia

**Short thorax**

- Osteogenesis imperfecta (type II)
- Kniest's dysplasia (metatropic dysplasia type II)
- Pena-Shokeir syndrome

**Hypoplastic thorax**

- Short rib-polydactyly syndrome (type I, type II)
- Thanatophoric dysplasia
- Cerebrocostomandibular syndrome
- Cleidocranial dysplasia syndrome
- Homozygous achondroplasia
- Melnik-Needles syndrome (osteodysplasty)
- Fibrochondrogenesis
- Otopalatodigital syndrome type II

hernia and -0.72% (range: -30.25% to +19.22%) in normal fetuses.

We have recently compared the diagnostic efficiency of lung volume measurements by 3DUS with that of biometric parameters measured by 2DUS in the identification of lethal pulmonary hypoplasia in 41 fetuses with musculoskeletal disorders (see Table 12-14). Lethal pulmonary hypoplasia was diagnosed in 34.1% of cases (14/41). Ninety-three

percent (13/14) of the fetuses with pulmonary hypoplasia had lung volumes below the 5th percentile for gestational age; however, because the number of false-positive diagnoses was too high (48.1% [13/27]), the test is unlikely to be clinically useful. The parameters with the highest diagnostic efficiency to predict lethal pulmonary hypoplasia in this population were (1) the right lung diameter (sensitivity 71.4% [10/14], specificity 92.6% [25/27], positive-predictive value



**FIGURE 12-20.** Longitudinal section of a fetus with thanatophoric dysplasia. Note the significant disproportion between the chest and abdomen.



**FIGURE 12-21.** Extremely short ribs in a fetus with short rib-polydactyly syndrome.

83.3% [10/12], negative predictive value 86.2% [25/29], and diagnostic efficiency 85.4% [35/41]); (2) thoracic circumference/abdominal circumference ratio (sensitivity 85.7% [12/14], specificity 85.2% [23/27], positive-predictive value 75.0% [12/16], negative predictive value 92.0% [23/25], and diagnostic efficiency 85.4% [35/41]); and (3) the femur length/abdominal circumference ratio (sensitivity 85.7% [12/14], specificity 85.2% [23/27], positive-predictive value 75.0% [12/16], negative predictive value 92.0% [23/25], and diagnostic efficiency 85.4% [35/41]).

**Evaluation of Lung Volume or Signal Intensity by Magnetic Resonance Imaging.** Parameters proposed to evaluate lung volume by MRI include the relative lung volume (ratio of observed over expected lung volume), lung volume over estimated fetal weight ratio (LV/EFW), and the lung over spinal fluid signal intensity ratio (L/SF).<sup>157-164</sup>

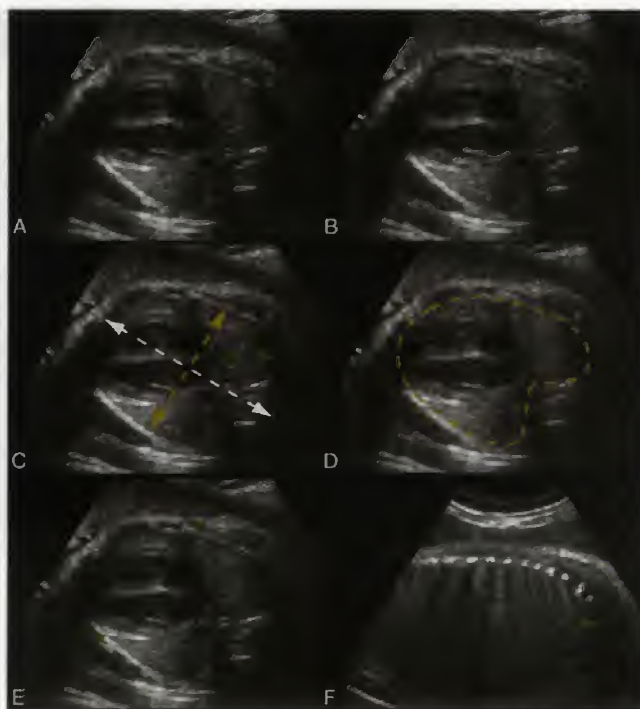


**FIGURE 12-22.** A to F Illustration of the various methods to measure thoracic, lung, and heart dimensions.

Rypens et al<sup>157</sup> determined normal lung volume biometry across gestational age in 336 fetuses with normal lungs. Normal fetal lung volume increased with gestational age. There was, however, a constant ratio between the volume of the left and right lung volumes, with right lung volume accounting for 56% of the total fetal lung volume. MRI volumes corresponded to 90% of the volumes measured by pathologic examination.

Williams et al<sup>160</sup> calculated relative lung volume in a group of 91 fetuses with sonographically normal lungs and compared the measurements to 28 fetuses at risk for pulmonary hypoplasia. The mean relative lung volume was significantly smaller in the group of fetuses at risk for pulmonary hypoplasia ( $34\% \pm 15\%$  versus  $102\% \pm 17\%$ ,  $p < 0.001$ ). Tanigaki et al<sup>161</sup> compared the diagnostic performance of LV/EFW determined by MRI to three ultrasonographic parameters commonly used to assess the risk of pulmonary hypoplasia at birth. In a population of 17 fetuses at risk for pulmonary hypoplasia, a FLV/EFW below the 5th percentile for age was the most accurate diagnostic parameter.

Signal intensity ratios to predict lung hypoplasia have also been evaluated.<sup>162-164</sup> Kuwashima et al<sup>162</sup> proposed that the lungs of fetuses with pulmonary hypoplasia would have low intensity signals, as opposed to fetuses with normal lung development. Osada et al<sup>163</sup> compared LV/EFW between 58 normal fetuses and 29 fetuses at risk for pulmonary hypoplasia. In addition to LV/EFW, the authors also evaluated lung signal intensities expressed as a proportion of the spinal fluid signal intensity lung/spinal fluid (L/SF). Although diagnostic indices were not reported in this study, ROC analysis showed that simultaneous



**Table 12-12** Fetal Thoracic Circumference Measurements (Centimeters)

Gestational Age (wk)	No.	Predictive Percentiles								
		2.5	5	10	25	50	75	90	95	97.5
16	6	5.9	6.4	7.0	8.0	9.1	10.3	11.3	11.9	12.4
17	22	6.8	7.3	7.9	8.9	10.0	11.2	12.2	12.8	13.3
18	31	7.7	8.2	8.8	9.8	11.0	12.1	13.1	13.7	14.2
19	21	8.6	9.1	9.7	10.7	11.9	13.0	14.0	14.6	15.1
20	20	9.5	10.0	10.6	11.7	12.8	13.9	15.0	15.5	16.0
21	30	10.4	11.0	11.6	12.6	13.7	14.8	15.8	16.4	16.9
22	18	11.3	11.9	12.5	13.5	14.6	15.7	16.7	17.3	17.8
23	21	12.2	12.8	13.4	14.4	15.5	16.6	17.6	18.2	18.8
24	27	13.2	13.7	14.3	15.3	16.4	17.5	18.5	19.1	19.7
25	20	14.1	14.6	15.2	16.2	17.3	18.4	19.4	20.0	20.6
26	25	15.0	15.5	16.1	17.1	18.2	19.3	20.3	21.0	21.5
27	24	15.9	16.4	17.0	18.0	19.1	20.2	21.3	21.9	22.4
28	24	16.8	17.3	17.9	18.9	20.0	21.2	22.2	22.8	23.3
29	24	17.7	18.2	18.8	19.8	21.0	22.1	23.1	23.7	24.2
30	27	18.6	19.1	19.7	20.7	21.9	23.0	24.0	24.6	25.1
31	24	19.5	20.0	20.6	21.6	22.8	23.9	24.9	25.5	26.0
32	28	20.4	20.9	21.5	22.6	23.7	24.8	25.8	26.4	26.9
33	27	21.3	21.8	22.5	23.5	24.6	25.7	26.7	27.3	27.8
34	25	22.2	22.8	23.4	24.4	25.5	26.6	27.6	28.2	28.7
35	20	23.1	23.7	24.3	25.3	26.4	27.5	28.5	29.1	29.6
36	23	24.0	24.6	25.2	26.2	27.3	28.4	29.4	30.0	30.6
37	22	24.9	25.5	26.1	27.1	28.2	29.3	30.3	30.9	31.5
38	21	25.9	26.4	27.0	28.0	29.1	30.2	31.2	31.9	32.4
39	7	26.8	27.3	27.9	28.9	30.0	31.1	32.2	32.8	33.3
40	6	27.7	28.2	28.8	29.8	30.9	32.1	33.1	33.7	34.2

From Chitkara U, Rosenberg J, Chervenak FA, et al: Prenatal sonographic assessment of the fetal thorax: normal values. *Am J Obstet Gynecol* 156:1069, 1987.

**Table 12-13** Fetal Thoracic Length Measurements (Centimeters)

Gestational Age (wk)	No.	Predictive Percentiles								
		2.5	5	10	25	50	75	90	95	97.5
16	6	0.9	1.1	1.3	1.6	2.0	2.4	2.8	3.1	3.2
17	22	1.1	1.3	1.5	1.8	2.2	2.6	3.0	3.2	3.4
18	31	1.3	1.4	1.7	2.0	2.4	2.8	3.2	3.4	3.6
19	21	1.4	1.6	1.8	2.2	2.7	3.0	3.4	3.6	3.8
20	20	1.6	1.8	2.0	2.4	2.8	3.2	3.6	3.8	4.0
21	30	1.8	2.0	2.2	2.6	3.0	3.4	3.7	4.0	4.1
22	18	2.0	2.2	2.4	2.8	3.2	3.6	3.9	4.1	4.3
23	21	2.2	2.4	2.6	3.0	3.4	3.8	4.1	4.3	4.5
24	27	2.4	2.6	2.8	3.1	3.5	3.9	4.3	4.5	4.7
25	20	2.6	2.8	3.0	3.3	3.7	4.1	4.5	4.7	4.9
26	25	2.8	2.9	3.2	3.5	3.9	4.3	4.7	4.9	5.1
27	24	2.9	3.1	3.3	3.7	4.1	4.5	4.9	5.1	5.3
28	24	3.1	3.3	3.5	3.9	4.3	4.7	5.0	5.4	5.4
29	24	3.3	3.5	3.7	4.1	4.5	4.9	5.2	5.5	5.6
30	27	3.5	3.7	3.9	4.3	4.7	5.1	5.4	5.6	5.8
31	24	3.7	3.9	4.1	4.5	4.9	5.3	5.6	5.8	6.0
32	28	3.9	4.1	4.3	4.6	5.0	5.4	5.8	6.0	6.2
33	27	4.1	4.3	4.5	4.8	5.2	5.6	6.0	6.2	6.4
34	25	4.2	4.4	4.7	5.0	5.4	5.8	6.2	6.4	6.6
35	20	4.4	4.6	4.8	5.2	5.6	6.0	6.4	6.6	6.8
36	23	4.6	4.8	5.0	5.4	5.8	6.2	6.5	6.8	7.0
37	22	4.8	5.0	5.2	5.6	6.0	6.4	6.7	7.0	7.1
38	21	5.0	5.2	5.4	5.8	6.2	6.5	6.9	7.1	7.3
39	7	5.2	5.4	5.6	6.0	6.4	6.7	7.1	7.3	7.5
40	6	5.4	5.6	5.8	6.1	6.5	6.9	7.3	7.5	7.7

From Chitkara U, Rosenberg J, Chervenak FA, et al: Prenatal sonographic assessment of the fetal thorax: normal values. *Am J Obstet Gynecol* 156:1069, 1987.

**Table 12-14** Biometric Parameters Proposed by Different Authors for the Evaluation of Lung Hypoplasia

Author, Year <sup>‡</sup>	Parameter	Fetuses at risk	Prevalence (%)	Sensitivity (%)	Specificity (%)	Accuracy (%)	Population
Nimrod et al, 1986 <sup>124</sup>	TC	45	38	88	96	93	PROM; oligohydramnios; pleural effusion; other conditions affecting lung growth
Fong et al, 1988 <sup>126</sup>	TC	18	60	60	88	72	Prolonged PROM; oligohydramnios; fetal malformations associated with lung hypoplasia
Songster et al, 1989 <sup>127</sup>	FL/TC	26	42	80	92	88	PROM; urinary tract anomalies; fetal skeletal dysplasias; IUGR; TTTS
Vintzileos et al, 1989 <sup>128</sup>	TC	13	69	33	57	46	Severe oligohydramnios > 5 weeks' duration
	TA			33	71	54	
	TA-HA			50	71	62	
	(TC × 100)/AC			33	86	62	
	CA/HA			67	86	77	
Roberts and Mitchell, 1990 <sup>134</sup>	(TA-HA) × 100/CA	20	60	83	86	85	PROM < 25 weeks of gestation > 7 days' duration
	LL			92	100	95	
	TC			67	100	80	
	TC/AC			75	100	88	
	TC/CA			80	90	87	
Ohlsson et al, 1992 <sup>135</sup>	TC/FL	58	28	80	97	91	PROM < 30 weeks and 19 cases of congenital anomalies
	LA	19	79	100	75	95	
	TC/FL			55	97	90	
Maeda et al, 1993 <sup>130</sup>	LA						Non immune hydrops; polycystic kidneys; PROM; diaphragmatic hernia; immune hydrops; trisomy 18
Yoshimura et al, 1996 <sup>133</sup>	TC	21 <sup>†</sup>		100	83	90	Case-control study: 21 patients at risk for pulmonary hypoplasia (renal anomalies associated with pulmonary hypoplasia; thanatophoric dysplasia; prolonged PROM < 26 weeks of gestation); 30 PROM patients with normal lung function
	TA			100	87	92	
	TC/AC			90	90	90	
	LA			81	100	93	
	TA-HA	16 <sup>†</sup>	†	100	87	91	
	TA/HA			69	100	89	
	TA-HA/TA			69	97	87	
	LA/TA			31	100	76	
Merz et al, 1999 <sup>136</sup>	LD	32	*	100			Skeletal dysplasias (n=7); renal agenesis (n=11); diaphragmatic hernia (n=7); hydrothorax (n=2)
	TTD			53	*	*	
	TSD			47			
	TC			47			
Bahlmann et al, 1999 <sup>137</sup>	TC	17	82	14	100	29	Diaphragmatic hernia
	LD			100	100	100	
	LD/TC			100	100	100	
Heling et al, 2001 <sup>138</sup>	TTD	29	55	44	50	46	Bilateral renal agenesis; bilateral multicystic kidneys; chronic PROM < 25 weeks of gestational age; hydrothorax prolonged oligohydramnios due to PROM or congenital renal disease
	APTD			57	42	52	
	LL			29	66	42	
Laudy et al, 2002 <sup>139</sup>	TC	40	43	94	38	61	
	CC/TC			76	50	61	
	TC/AC			69	71	70	
	LD			71	93	82	
	TC/AC			86	85	85	
	FL/AC			86	85	85	
	TC			71	89	83	
Gonçalves et al, 2006	LA/TA	41	34	57	89	78	Fetuses with musculoskeletal disorders
	HV/TLV			64	89	78	
	LD/TC			29	96	73	
	TLV			93	52	66	
	TA-HA/TA			50	59	56	
	RCP/AC			85	36	54	

AC, abdominal circumference; APTD, anteroposterior thoracic diameter; CC, cardiac circumference; FL, femur length; HA, heart area; HV, heart volume; IUGR, intrauterine growth restriction; LA, lung area; LD, lung diameter; LL, lung length; PROM, premature rupture of the membranes; RCP, rib cage perimeter; TA, thoracic area; TC, thoracic circumference; TLV, total lung volume; TTD, transverse thoracic diameter; TTTS, twin-to-twin transfusion syndrome.

\*All fetuses had pulmonary hypoplasia

<sup>†</sup>Case-control study; all fetuses in the column "Fetuses at risk" had pulmonary hypoplasia; 30 gestational age-matched control fetuses were studied.

<sup>‡</sup>Only papers for which data to calculate at least the sensitivity were included.



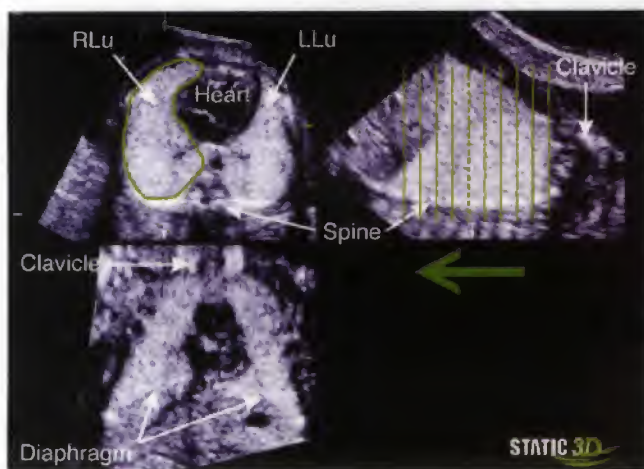


**FIGURE 12-23.** Three-dimensional fetal lung measurements using the multiplanar technique. Illustration of the image sequences (green vertical lines) used to obtain transverse views of the lung. The right lung (RLu) is outlined. Fetal lung volume is obtained by scrolling through the transverse plane (green arrow). LLu, left lung. (From Kalache KD, Espinoza J, Chaiworapongsa T, et al: Three-dimensional ultrasound fetal lung volume measurement: a systematic study comparing the multiplanar method with the rotational (VOCAL) technique. *Ultrasound Obstet Gynecol* 21:111, 2003.)

measurement of fetal lung volume and signal intensity by MRI had an area under the curve of 0.990 to predict lung hypoplasia, compared with 0.930 and 0.955 for lung volume or L/SF ratio alone. Keller et al<sup>164</sup> evaluated signal intensities of lung/liver, lung/amniotic fluid, lung/muscle, liver/fluid, and liver/muscle for the prediction of lung hypoplasia. In contrast to the study of Osada et al,<sup>163</sup> these signal intensity ratios did not differ significantly from those in the normal population.

**Doppler Assessment of Tracheal Fluid Flow.** Kalache et al<sup>165</sup> have proposed that the volume of lung fluid displaced in the trachea could be useful for the analysis of fetal lung function. The investigators tested this hypothesis in a case-control study that included six cases of congenital diaphragmatic hernia diagnosed prenatally and a control group of five healthy fetuses matched for gestational age to each case. Parameters analyzed included (1) the length of the inspiratory phase; (2) the length of the expiratory phase; (3) the peak velocities during inspiration and expiration; and (4) the volume estimation of the displaced fluid in the trachea during breathing (calculated as volume = velocity time integral [VTI]  $\times \pi \times [d \times 0.5]^2$ ). The estimated breathing-related tracheal volume flow in uncomplicated pregnancies increased with gestational age (from  $0.21 \pm 0.10$  ml/breath at 26 weeks to  $1.37 \pm 0.48$  ml/breath at 36 weeks of gestation), and was significantly lower in fetuses with diaphragmatic hernia who died of pulmonary hypoplasia. Tracheal volume flow in survivors was comparable to controls.

**Doppler Velocimetry of the Pulmonary Arteries.** Underdevelopment and structural changes of the pulmonary vascular bed in cases of pulmonary hypoplasia may result in increased pulmonary vascular resistance and reduced pulmonary arterial compliance.<sup>166</sup> Therefore, several investigators have attempted to use Doppler measurements of the pulmonary arteries and of its branches in an attempt to



**FIGURE 12-24.** Three-dimensional model of the right lung volume obtained using VOCAL. Note the indentation of the fetal heart (asterisk). The frontal view is shown on the left and the lateral view on the right. (From Kalache KD, Espinoza J, Chaiworapongsa T, et al: Three-dimensional ultrasound fetal lung volume measurement: a systematic study comparing the multiplanar method with the rotational (VOCAL) technique. *Ultrasound Obstet Gynecol* 21:111, 2003.)

identify fetuses at risk for pulmonary hypoplasia.<sup>139,167-171</sup> Mitchell et al<sup>167</sup> evaluated the resistance index of the peripheral pulmonary arteries for the prediction of pulmonary hypoplasia in 10 fetuses with bilateral multicystic dysplastic kidneys. The resistance index of the peripheral pulmonary arteries was above the 95th percentile for gestational age in 80% of the cases with pulmonary hypoplasia.

Subsequent studies have yielded contradictory results. Achiron et al<sup>168</sup> found that the pulsatility index of the peripheral pulmonary arteries were within normal limits in four fetuses with proven pulmonary hypoplasia, suggesting that the PI of the lung circulation would be a poor test to predict lung hypoplasia. Chaoui et al<sup>169</sup> reported that only six of nine fetuses with lung hypoplasia had an elevated pulsatility index in the main branches of the left and right pulmonary arteries. Similarly, Laudy et al<sup>139</sup> studied 40 fetuses at risk for pulmonary hypoplasia and found that Doppler velocimetry indices of the proximal and middle pulmonary branches were not better than chest biometry to predict pulmonary hypoplasia.

In contrast, Yoshimura et al<sup>170</sup> reported low peak systolic velocities in four out of five fetuses, and increased pulsatility index in five out of five fetuses with confirmed pulmonary hypoplasia (thanatophoric dysplasia [ $n = 2$ ], nonimmune hydrops [ $n = 2$ ] and bilateral renal agenesis [ $n = 1$ ]). Rizzo et al,<sup>171</sup> in a population of 20 fetuses with prolonged preterm premature rupture of the membranes, found that an elevated pulsatility index in a peripheral pulmonary artery observed 2 weeks after membrane rupture detected the subsequent development of pulmonary hypoplasia with a sensitivity of 62.5%, specificity of 94.6%, positive predictive value of 83.3%, and negative predictive value of 78.5%. Finally, Fuke et al<sup>172</sup> proposed the use of acceleration time/ejection time at the main branches of the pulmonary arteries to identify fetuses at risk for pulmonary hypoplasia. The normal ratio is  $0.17 \pm 0.04$  for the right and  $0.15 \pm 0.04$  for the left pulmonary arteries, and this ratio does not change with gestational age. The test correctly identified five of six fetuses with pulmonary hypoplasia among the 17 fetuses at risk. All 11 normal fetuses had a normal acceleration time/ejection time of the pulmonary arteries.





**FIGURE 12-25.** Three-dimensional rendered volume using the maximum intensity (skeletal) mode showing postaxial polydactyly (arrow).

### Evaluation of Hands and Feet

Hands and feet should be examined to exclude polydactyly (Fig. 12-25), brachydactyly, and extreme postural deformities such as those seen in diastrophic dysplasia. Table 12-15 shows a nomogram of the fetal foot size throughout gestation. Table 12-16 displays disorders associated with hand and foot deformities. Disproportion between hands and feet and the other parts of the extremity may also be a sign of a skeletal dysplasia. Figure 12-26 illustrates the relationship between femur and foot length. The femur length/foot length ratio is nearly constant from 14 to 40 weeks of gestation, with a mean value of  $0.99 \pm 0.06$  (standard deviation). A ratio below 0.87 is considered abnormal.<sup>173</sup> Although fetuses with skeletal dysplasias have been reported to have abnormally low ratios, more experience is required to establish the diagnostic value of this method.<sup>174</sup> It is expected that a small proportion of normal fetuses may have an abnormal ratio. As in the case of other limb biometric parameters, large deviations from the lower limit of normal are likely to be significant.

### Evaluation of the Fetal Cranium

Several skeletal dysplasias are associated with defects of membranous ossification and, therefore, affect skull bones. Examination of the skull bones may reveal poor ossification (see Fig. 12-16), frontal bossing (Fig. 12-27), or cloverleaf deformity (Fig. 12-28). Table 12-17 presents abnormalities of the skull and face in the different skeletal dysplasias.

### Evaluation of the Fetal Face

Sonographic examination of facial features is of major importance in the assessment and diagnosis of fetuses with skeletal dysplasias, because many of these disorders are

**Table 12-15**

**Nomogram of Fetal Foot Size Throughout Gestation (Centimeters)**

Gestational Age (weeks)	N	Percentile				
		5th	10th	50th	90th	95th
15	18	1.4	1.5	1.8	2.2	2.3
16	446	1.6	1.7	2.1	2.5	2.6
17	375	1.9	2.0	2.4	2.8	2.9
18	613	2.2	2.3	2.7	3.1	3.2
19	1160	2.5	2.6	3.0	3.3	3.4
20	929	2.8	2.9	3.2	3.6	3.7
21	552	3.1	3.2	3.5	3.9	4.0
22	360	3.4	3.5	3.9	4.2	4.3
23	222	3.7	3.8	4.2	4.6	4.7
24	177	4.0	4.1	4.5	4.9	5.0
25	125	4.3	4.4	4.8	5.1	5.2
26	123	4.6	4.7	5.1	5.4	5.5
27	108	4.8	4.9	5.3	5.7	5.8
28	74	5.1	5.2	5.6	5.9	6.0
29	66	5.3	5.4	5.8	6.2	6.3
30	65	5.6	5.7	6.1	6.4	6.5
31	62	5.8	5.9	6.3	6.7	6.8
32	65	6.0	6.1	6.5	6.9	7.0
33	39	6.3	6.4	6.8	7.1	7.2
34	37	6.5	6.6	7.0	7.4	7.5
35	24	6.8	6.9	7.3	7.6	7.7
36	15	7.0	7.1	7.5	7.9	8.0
37	17	7.3	7.4	7.7	8.1	8.2

From Meirowitz NB, Ananth CV, Smulian JC, et al: Foot length in fetuses with abnormal growth. *J Ultrasound Med* 19:201, 2000.

**Table 12-16**

**Skeletal Dysplasias Associated with Polydactyly and Syndactyly**

Postaxial polydactyly
Chondroectodermal dysplasia
Short rib–polydactyly syndrome (type I, type II)
Asphyxiating thoracic dysplasia
Otopalatodigital syndrome
Mesomelic dysplasia, Werner type (associated with absence of thumbs)
Preaxial polydactyly
Chondroectodermal dysplasia
Short rib–polydactyly syndrome type II
Carpenter's syndrome
Syndactyly
Poland syndrome
Acrocephalosyndactylies (Carpenter syndrome, Apert syndrome)
Otopalatodigital syndrome type II
Mesomelic dysplasia, Werner type
TAR syndrome
Jarcho-Levin syndrome
Brachydactyly
Mesomelic dysplasia, Robinow type
Otopalatodigital syndrome
Hitchhiker thumbs
Diastrophic dysplasia
Clubfoot deformity
Diastrophic dysplasia
Osteogenesis imperfecta
Kniest dysplasia
Spondyloepiphyseal dysplasia

TAR, thrombocytopenia–radial aplasia.



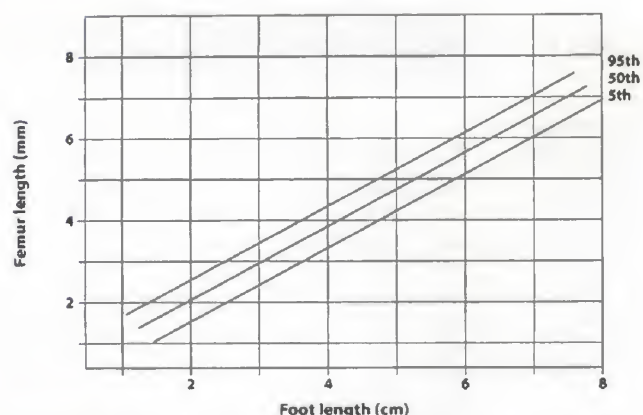


**FIGURE 12-26.** Relationship between femur and foot length.



**FIGURE 12-27.** Frontal bossing in a sagittal scan in a fetus with achondroplasia.

associated with typical abnormalities.<sup>175</sup> Sonographic evaluation of the fetal face is easily performed in a high percentage of patients from 16 to 20 weeks of gestation onward. The single most reliable view in detecting facial abnormalities is the sagittal view, because it permits determination of mid-face hypoplasia, which occurs in several skeletal dysplasias, such as thanatophoric dysplasia, achondroplasia, campomelic dysplasia, OI type I, and spondyloepiphyseal dysplasia congenita.<sup>81,176</sup>

In median clefting, the central portion of the upper lip is absent, and on the midline sagittal view, no upper lip will be demonstrated. In bilateral cleft lip, the midline view will have variable appearance, depending on the amount of residual premaxillary tissue present in the midline. In unilateral cleft lip, the midline sagittal scan may be relatively normal but the parasagittal view will reveal the cleft. Clefts should subsequently be confirmed by imaging the lips in the coronal plane.

Cleft palate occurs in 66% of patients with cleft lip. Isolated cleft palate is more difficult to diagnose with ultrasound because of shadowing of facial bones. 3DUS has been



**FIGURE 12-28.** Cloverleaf skull in a patient with thanatophoric dysplasia.

shown to be superior to 2DUS for the prenatal diagnosis of cleft lip and palate.<sup>177-179</sup> Potential advantages of 3DUS over 2DUS include (1) a true coronal view of the lips can be displayed, even when the original scanning plane was obtained from a different orientation; (2) 3D standardized multiplanar imaging makes it easier to successfully demonstrate the maxillary tooth-bearing alveolar ridge in suspected cases; and (3) the maxillary tooth-bearing alveolar ridge can be more accurately localized by multiplanar technique because this region can be easily mistaken for the mandibular ridge.<sup>180,181</sup> Rendered views of the cleft lip/palate have been described as being particularly useful for patient counseling.<sup>180,182,183</sup> A novel technique for visualization of the fetal palate, called the 3D reverse face view, has recently been proposed for the antenatal characterization of facial clefting, in particular clefting of the hard palate.<sup>184</sup> This technique consists of rotating the volume dataset 180 degrees around the vertical axis in order to examine the secondary palate. Campbell et al<sup>185</sup> reported preliminary results of this technique in eight cases of suspected orofacial clefting. A cleft in the soft palate was missed in only one case.

Micrognathia is also frequently observed in cases of skeletal dysplasia (Table 12-18).<sup>186-188</sup> In an attempt to provide an objective tool to diagnose micrognathia prenatally, Palladini et al<sup>189</sup> proposed the jaw index, which is computed as the ratio between the anteroposterior mandibular diameter and the biparietal diameter. In a population of 198 malformed fetuses, 11 of which had micrognathia at necropsy or at birth, a jaw index below 23 correctly identified all cases of micrognathia with a false-positive rate of 2%. Rotten et al<sup>190</sup> proposed two parameters to differentiate between retrognathia and micrognathia: the inferior facial

**Table 12-17****Skeletal Dysplasias Associated With Skull and Face Deformities****Large head**

Achondroplasia  
 Achondrogenesis  
 Thanatophoric dysplasia  
 Osteogenesis imperfecta  
 Cleidocranial dysplasia  
 Hypophosphatasia  
 Campomelic dysplasia  
 Short-rib polydactyly syndrome, type III  
 Robinow mesomelic dysplasia  
 Otopalatodigital syndrome

**Cloverleaf skull**

Thanatophoric dysplasia  
 Campomelic dysplasia

**Other craniosynostosis**

Apert syndrome  
 Carpenter's syndrome

**Congenital cataracts**

Condrosynostosis punctata

**Cleft palate**

Asphyxiating thoracic dysplasia  
 Kniest dysplasia  
 Dystrophic dysplasia  
 Spondyloepiphyseal dysplasia  
 Campomelic dysplasia  
 Jarcho-Levin syndrome  
 Ellis-van Creveld syndrome  
 Short rib-polydactyly syndrome, type II  
 Metatropic dysplasia  
 Otopalatodigital syndrome, type II  
 Dyssegmental dysplasia  
 Robert syndrome

**Short upper lip**

Chondroectodermal dysplasia

**Micrognathia**

Campomelic dysplasia  
 Dystrophic dysplasia  
 Weissenbacher-Zweymüller syndrome  
 Otopalatodigital syndrome  
 Pena-Shokeir syndrome  
 Thrombocytopenia-radial aplasia (TAR) syndrome  
 Langer syndrome

**Table 12-18****Skeletal Dysplasias Associated With Micrognathia**

Campomelic dysplasia  
 Diastrophic dysplasia  
 Otopalatodigital syndrome  
 Achondrogenesis  
 Mesomelic dysplasia  
 Pena-Shokeir syndrome  
 Treacher-Collins syndrome  
 Nager acrofacial dysostosis  
 Oromandibular limb hypogenesis  
 Goldenhar syndrome  
 Atelosteogenesis  
 Hydrothelium syndrome



**FIGURE 12-29.** Inferior facial angle. The inferior facial angle is defined as the angle between two lines traced on a sagittal profile view of the fetal face: (1) a reference line, orthogonal to the vertical part of the forehead, at the level of the synostosis of the nasal bones; and (2) the profile line, joining the tip of the mentum to the anterior border of the more protruding lip.

angle (Fig. 12-29), and the mandible width (MD/MX) ratio (Fig. 12-30). The inferior facial angle is used to diagnose retrognathia. It is defined as the angle between two lines traced on a sagittal profile view of the fetal face: (1) a reference line, orthogonal to the vertical part of the forehead, at the level of the synostosis of the nasal bones; and (2) the profile line, joining the tip of the mentum to the anterior border of the more protruding lip. In a population of fetuses at high risk for facial anomalies, an inferior facial angle less than 50 degrees identified retrognathia with a sensitivity of 100% and a specificity of 98.9%. The MD/MX ratio is computed using transverse sections of the mandible and maxilla, with the actual measurements performed 10 mm posteriorly to the anterior osseous border. An MD/MX ratio less than 0.785 between 18 and 28 weeks of gestation correctly identified micrognathia in three cases of Treacher Collins syndrome.

Intraorbital and interorbital diameters should also be measured, because hypertelorism may occur in cases of skeletal dysplasia (Table 12-19).

### Evaluation of the Fetal Spine

Sonographic assessment of the fetal spine is another component of the examination of fetuses with suspected skeletal dysplasias. The following parameters should be assessed:

**Vertebral Bodies.** Fetal vertebral bodies are composed of three ossification centers representing the vertebral body and two laminae.<sup>191-194</sup> Abnormalities of the ossification centers of the fetal vertebral body may result in bony defects, such as hemivertebrae (see Fig. 12-11), butterfly vertebrae, or block vertebrae causing congenital scoliosis (see Figs. 12-9 and 12-10). A study of the associated anomalies



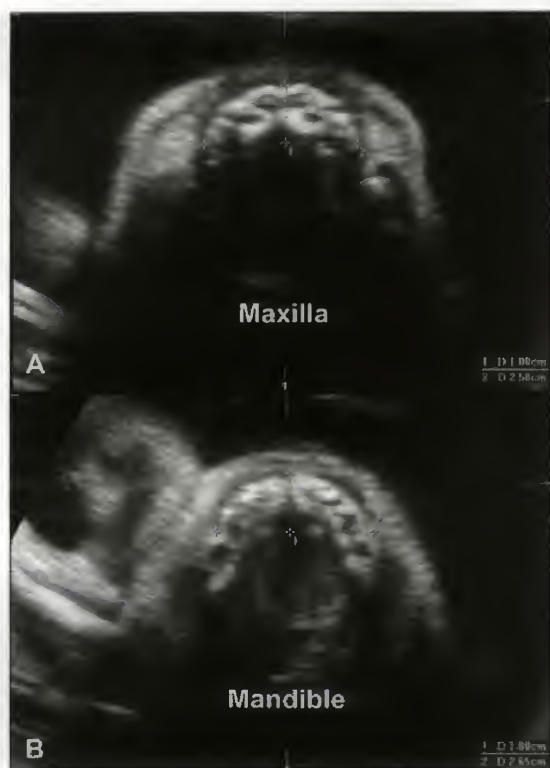


**FIGURE 12-30.** Mandible/maxilla (MD/MX) ratio. The MD/MX ratio is calculated using transverse sections of the mandible (B) and maxilla (A), with measurements performed 10 mm posteriorly to the anterior osseous border.

in 27 cases of prenatally detected hemivertebrae noted that, although 11 fetuses had no other abnormal findings, 16 had additional associated anomalies.<sup>191</sup> These included cardiac, gastrointestinal, renal, facial, extremity, and cranial anomalies. Seven fetuses had bilateral renal agenesis (Potter sequence). Only five of the fetuses with additional anomalies survived. Usually these anomalies are not a risk factor for aneuploidy. Rib defects are often associated with thoracic vertebral body anomalies.

Platyspondyly may be diagnosed with current high-resolution sonography (see Fig. 12-8).<sup>195</sup> Objective evaluation may be performed by computing a ratio between measurements of the vertebral interspace to vertebral body height.<sup>53</sup>

Clefting of the vertebrae may be complete or incomplete, or coronal or sagittal.<sup>63</sup> Coronal vertebral clefts are a result of missed fusion between the anterior and posterior primary ossification centers beyond 16 weeks of gestation, and can be observed by sonography in utero.<sup>196,197</sup> Sagittal clefts in the vertebral bodies are believed to represent localized splitting of the notochord due to adhesions between ectoderm and endoderm during the embryonic period. The role of vertebral clefting in the diagnosis of skeletal dysplasias was assessed by searching the database at the International Skeletal Dysplasia Registry in a study conducted by Westvik and Lachman.<sup>197</sup> Coronal and sagittal clefts were present in 40 different conditions. Coronal clefts were more common than sagittal clefts and were mainly located in the thoracolumbar region. Clefts were most frequently observed in

**Table 12-19**

### Skeletal Dysplasias Associated With Hypertelorism

Otopalatodigital syndrome  
 Arthrogryposis multiplex congenital  
 Larsen syndrome  
 Roberts syndrome  
 Cleidocranial dysplasia  
 Achondroplasia  
 Camptomelic dysplasia  
 Coffin syndrome  
 Klippel-Feil syndrome  
 Apert's syndrome  
 Sprengel deformity  
 Mesomelic dysplasia  
 Holt-Oram syndrome

atelosteogenesis (88%), followed by chondrodysplasia punctata (79%), dyssegmental dysplasia (73%), Kniest dysplasia (63%), and short rib-polydactyly syndrome (SRPS) (53%).<sup>197</sup> The authors concluded that vertebral clefts are of major diagnostic value in these groups of skeletal dysplasias.

**Spinal Curvature.** The most common osseous anomaly causing scoliosis is unilateral unsegmented bar with contralateral hemivertebrae.<sup>191,198-201</sup> Spinal dysraphism may occur with congenital scoliosis, and this possibility should be examined carefully. An apparent etiologic relationship exists between neural tube defects and other vertebral anomalies. Siblings of infants with congenital scoliosis have a 4% risk of neural tube defects.<sup>202</sup> This increased risk is present in siblings of children with a single hemivertebrae, as well as multiple vertebral anomalies (with or without neural arch defects). The differential diagnosis of fetal scoliosis includes neural tube defects, large abdominal wall defects, amniotic band syndrome, caudal regression, and hemivertebrae. Nonossification of the lumbar vertebral bodies has been detected in achondrogenesis and other diseases.<sup>203-205</sup>

### Evaluation of the Internal Organs

A detailed examination of the cardiovascular, genitourinary, gastrointestinal, and central nervous system (CNS) organs should be performed in all fetuses with skeletal anomalies. Some syndromes present with specific abnormalities of the internal organs, thus helping in the differential diagnoses of these entities. For example, congenital heart disease is a prominent feature of Ellis-van Creveld syndrome<sup>206</sup> and Holt-Oram syndrome.<sup>207</sup>

### Newborn Evaluation

Even when all efforts have been made to establish an accurate prenatal diagnosis, a careful study of the newborn is always required.<sup>87</sup> The evaluation should include a detailed physical examination performed by a geneticist or an individual with experience in the field of skeletal dysplasias and radiographs of the skeleton. The radiographs should include anterior, posterior, lateral, and Towne views of the skull, as well as anteroposterior views of the spine, extremities, and scapula,<sup>208</sup> with separate films of hands and



feet. Examination of the skeletal radiographs will permit precise diagnoses in a large proportion of cases, because the classification of skeletal dysplasias is largely based on radiographic findings. In lethal skeletal dysplasias, histologic examination of the chondro-osseous tissue should be performed, because this information may help the physician reach a specific diagnosis. Chromosomal studies should be included, because there is a specific group of constitutional bone disorders associated with cytogenetic abnormalities. Biochemical studies are helpful in some cases (e.g., hypophosphatasia). DNA restriction and enzymatic activity assays should be considered if the phenotype suggests a metabolic disorder (e.g., mucopolysaccharidosis). Molecular diagnosis can be performed for disorders in which a specific genetic mutation has been identified, and it is recommended that DNA be saved in all cases.<sup>24,25,209</sup>

### Increased Nuchal Translucency and Skeletal Dysplasia

In chromosomally normal pregnancies, nuchal translucency (NT) thickness is associated with an increased risk of major anomalies,<sup>210-213</sup> including skeletal dysplasias.<sup>101,213-217</sup> For example, in the multicenter screening project for trisomy 21 using the combination of maternal age and NT, 100,000 pregnancies were included, and an association between nuchal translucency and a wide range of skeletal dysplasias was found among these patients.<sup>210</sup> In addition, several case reports and small series have also suggested that in chromosomally normal fetuses an association may exist between increased NT thickness and skeletal anomalies. Table 12-20 summarizes these data.

## OSTEOCHONDRODYSPLASIAS

A growing number of skeletal dysplasias have been recognized in utero, and a complete account of each disorder is

beyond the scope of this chapter. The following discussion presents only a few of the most common disorders relevant to prenatal diagnosis.

### Achondroplasia, Thanatophoric Dysplasia, and Hypochondroplasia

Achondroplasia, thanatophoric dysplasia, and hypochondroplasia are discussed in the same section, because these disorders are caused by different mutations in the fibroblast growth factor receptor-3 (*FGFR3*) gene.<sup>218-225</sup> Mutations in *FGFR3* are gain-of-function mutations that produce a constitutively active protein capable of initiating intracellular signal pathways in the absence of ligand binding.<sup>226,227</sup> This activation leads to premature maturation of the bone.<sup>227</sup> The critical clinical difference between thanatophoric dysplasia and achondroplasia/hypochondroplasia is severe shortening of the ribs in thanatophoric dysplasia, resulting in restricted lung volumes, respiratory insufficiency, and death within hours or days.<sup>228</sup>

#### Achondroplasia

The most common nonlethal skeletal dysplasia is achondroplasia, an autosomal-dominant condition with complete penetrance and an estimated prevalence ranging from 1:10,000 to 1:50,000 births.<sup>229-231</sup> It is clinically characterized by rhizomelic shortening of the limbs and mild limb bowing, exaggerated lumbar lordosis, and an enlarged head.<sup>232</sup> The bones of the hands and feet are short (brachydactyly). The head is large (macrocephaly), with frontal bossing, midface hypoplasia, a flattened nasal bridge, and a broad mandible. The problems in the prenatal diagnosis of this condition have been discussed in detail by Kurtz and colleagues.<sup>233</sup> Moreover, Modaff et al<sup>234</sup> provided data about the frequency of prenatal misdiagnosis of achondroplasia and illustrated the difficulty of making this diagnosis.

**Table 12-20** Skeletal Dysplasias Associated With Increased Thickness of Nuchal Translucency

Skeletal Dysplasia	Author (Year)
Achondrogenesis	Hewitt, 1993 <sup>1125</sup> , Soothill and Kyle, 1997 <sup>1126</sup> , Fisk et al, 1991 <sup>377</sup>
Achondroplasia	Fukada et al, 1997 <sup>1127</sup> , Hernadi and Torocsik, 1997 <sup>1128</sup>
Asphyxiating thoracic dysplasia	Ben Ami et al, 1997 <sup>584</sup> ; Hsieh et al, 1999 <sup>1129</sup>
Blomstrand osteochondrodysplasia	den Hollander et al, 1997 <sup>1130</sup>
Campomelic acampomelic dysplasia	Michel-Calemard et al, 2004 <sup>216</sup>
Campomelic dysplasia	Hafner et al, 1998 <sup>1131</sup>
Cleidocranial dysplasia	Hiippala et al, 2001 <sup>1132</sup>
Chondroectodermal dysplasia (Ellis-van Creveld)	Venkat-Raman et al, 2005 <sup>673</sup>
Ectrodactyly ectodermal dysplasia	Leung, MacLachlan, and Sepulveda, 1995 <sup>1133</sup>
Fanconi anemia	Terçanlı et al, 2001 <sup>890</sup>
Fetal akinesia deformation sequence	Souka et al, 1998 <sup>213</sup> ; Hyett et al, 1997 <sup>1134</sup>
	Madazli et al, 2002 <sup>1038</sup> ; Makrydimas et al, 2004 <sup>1040</sup>
	Souka et al, 2002 <sup>215</sup>
Hypophosphatasia	Eliyahu, 1997 <sup>1135</sup> ; Souka 1998 <sup>213</sup>
Jarcho-Levin syndrome	Makrydimas et al, 2001 <sup>214</sup>
Osteogenesis imperfecta II	Hill and Leary, 1998 <sup>622</sup>
Short rib-polydactyly syndrome	Hewitt, 1993 <sup>1125</sup>
Sirenomelia	Souka, 1998 <sup>213</sup> ; Hyett et al, 1995 <sup>1136</sup> ; Maymon Ogle, and Chitty, 1999 <sup>1137</sup> ;
Smith Lemli Opitz syndrome	Sharp et al, 1997 <sup>1138</sup> ; Hobbins et al, 1994 <sup>1139</sup>
Thanatophoric dysplasia	Souka, 1998 <sup>213</sup> ; Ferreira et al, 2004 <sup>1140</sup>
Thrombocytopenia-radial aplasia	Witters et al, 2005 <sup>217</sup>
VACTERL association	Souka, 1998 <sup>213</sup>





**FIGURE 12-31.** A. Illustration demonstrating separation between the third and fourth digit. B. Photograph of a child with achondroplasia and trident hand. C. In utero sonogram of a fetus with achondroplasia and trident hand with separation between the third and fourth digits (arrow). (Illustrations courtesy of Philippe Jeanty, MD, Nashville, TN.)

They retrospectively collected data from 37 consecutive referrals of infants with achondroplasia in whom ultrasound was performed prenatally. Nine of the 37 (24%) infants had a positive family history of achondroplasia; all nine were correctly diagnosed prenatally. Of the 28 infants with no family history of achondroplasia, 16 (57%) were recognized to have abnormalities on ultrasound, although none were diagnosed with certainty. Five received an appropriate diagnosis of "most likely" achondroplasia and four others were given a nonspecific (but appropriate) diagnosis of some skeletal dysplasia, not otherwise specified. In seven instances (25%), an incorrect diagnosis of a lethal or very severe disorder was assigned.

The major difficulty in the antenatal diagnosis is that the long bone growth in this disease is not recognized in most cases until the third trimester of pregnancy.<sup>69,233</sup> However, prenatal diagnosis of achondroplasia is possible and has been reported.<sup>235-238</sup> For example, the trident hand (an increased interspace between the third and fourth digit) is a specific finding for achondroplasia<sup>239,240</sup> (Fig. 12-31). A distinct difference in the femoral length growth curves of homozygous, heterozygous, and unaffected children of achondroplastic parents was described by Patel et al<sup>241</sup> Fetuses with homozygous achondroplasia demonstrated early shortening of the femurs less than 3rd percentile at 14.0 to 16.5 weeks, biparietal diameter age (mean 15.6 weeks), whereas the fetuses



with heterozygous achondroplasia were affected later in pregnancy with femoral shortening less than 3rd percentile at 18.2 to 26.2 weeks biparietal diameter age (mean 21.5 weeks).<sup>241</sup> Recently, Tonni et al<sup>231</sup> reported the association of first trimester increased nuchal translucency in a fetus with achondroplasia, and Karadimas et al<sup>242</sup> reported a fetus with achondroplasia and multiple craniosynostoses.

More than 99% of the individuals with achondroplasia have one of two mutations in the *FGFR3* gene, which is located on the short arm of chromosome 4 at the 16.3 locus.<sup>243-245</sup> The most common mutation is a guanine-to-adenine (G-to-A) transition at nucleotide 1138 in the amino acid 380. About 1% of affected individuals have a guanine-to-cytosine (G-to-C) transversion at the same nucleotide.<sup>218,246</sup> A point mutation is called transition when a pyrimidine replaces a pyrimidine or a purine replaces a purine, and transversion when a pyrimidine replaces a purine or vice versa.<sup>209</sup> The G380R mutation has been shown to result in constitutive activation of the *FGFR3* gene, which inhibits the chondrocyte proliferation and differentiation, and is responsible for the shortness of the long bones. Prenatal diagnosis in pregnancies in which one or both parents have achondroplasia is possible by molecular diagnosis, using chorionic villus sampling (CVS) or amniocentesis.<sup>238,247,248</sup> Molecular analysis can also identify mutations in fetuses suspected to have achondroplasia based on ultrasound findings, making prenatal diagnosis more effective.

Heterozygous achondroplasia is compatible with a normal life and intellectual development. However, cervicomedullary junction abnormalities, which may lead to compression, put the infant with achondroplasia at risk for lethal sequelae.<sup>249</sup> Cervicomedullary decompressive surgery can be life saving by decreasing neurologic complications associated with damage of the spinal cord, and may eliminate the profound central apnea that can cause sudden death.<sup>250</sup> In the homozygous state (which occurs in 25% of the offspring of two parents with achondroplasia), the disease is usually lethal during the first 2 years of life.<sup>229</sup> However, a case of survival for 37 months has been reported.<sup>251</sup> The radiologic characteristics of homozygous achondroplasia lie between those of thanatophoric dysplasia and heterozygous achondroplasia.

Administration of growth hormone (GH) has been proposed for the treatment of achondroplasia.<sup>252</sup> With the aim of determining the effectiveness of GH treatment on the short stature of individuals with achondroplasia, Tanaka et al<sup>253</sup> conducted a long-term treatment study in 42 children (16 boys and 26 girls, aged 3 to 14 years) with achondroplasia. After evaluation of the hypothalamic-pituitary function and point mutation analysis, children were treated with GH for over 2 years. Post-treatment growth velocity and body proportion parameters were determined. The annual height gain during GH therapy was significantly greater than that before therapy ( $3.9 \pm 1.0$  cm/year before treatment vs  $6.5 \pm 1.8$  cm/year for the first year, and  $4.6 \pm 1.6$  cm/year for the second year of treatment) and body disproportion was not aggravated.<sup>253</sup> However, individual variability in response to GH treatment was observed.<sup>254</sup> Other innovative therapeutic approaches have been considered, including down-regulation of the tyrosine kinase activity of the *FGFR3* by selective chemical inhibitors,<sup>230</sup> blocking antibodies to interfere with the binding of FGF ligands to *FGFR3*,<sup>230</sup> and targeted overexpression of C-type natriuretic peptide.<sup>255</sup>

**SADDAN (Severe Achondroplasia With Developmental Delay and Acanthosis Nigricans)** Tavormina et al<sup>256</sup> identified a *FGFR3* missense mutation in four unrelated individuals with skeletal dysplasias approaching the severity observed in thanatophoric dysplasia type I. Three of the four individuals developed extensive areas of acanthosis nigricans beginning in early childhood, suffered from severe neurologic impairments, and survived past infancy without prolonged life support measures. The *FGFR3* mutation (A1949T:Lys650Met) occurs at the nucleotide adjacent to the thanatophoric dysplasia type II mutation (A1948G:Lys650Glu) and results in a different amino acid substitution. The authors of the study referred to the phenotype caused by the Lys650Met mutation as "severe achondroplasia with developmental delay and acanthosis nigricans" (SADDAN) because it differs significantly from the phenotypes of other known *FGFR3* mutations. SADDAN is also associated with unusual bone deformities, such as femoral bowing with reverse (i.e., posterior apex) tibial and fibular bowing, and so-called ram's horn bowing of the clavicle. This condition has not been associated with cloverleaf skull or craniosynostosis.<sup>257</sup>

### Thanatophoric Dysplasia

Thanatophoric dysplasia is the most common lethal skeletal dysplasia.<sup>28</sup> It is characterized by severe rhizomelia, normal trunk length with narrow thorax, and a large head with prominent forehead. It occurs in 0.24 to 0.69 of 10,000 births.<sup>29,30,220,258</sup> Two subtypes (I and II) have been identified, which are phenotypically differentiated by the skull shape and femur morphology. Type I typically presents with bowed "telephone receiver" femurs<sup>259</sup> (Fig. 12-32) and no cloverleaf skull, whereas the type II phenotype is characterized by a severe cloverleaf skull (see Fig. 12-28) and short, straight long bones.<sup>43,260</sup> Mild cloverleaf skull has been described in patients with the type I subtype.<sup>259,261,262</sup> Cloverleaf skull may result from premature closure of the coronal and lambdoid sutures, defective development of the cranial base with secondary synostosis, or a primary developmental disorder of the brain with secondary deformation of the skull. The differential diagnosis between the two types depends on the radiographic findings and histology. Both types of thanatophoric dysplasia are inherited in an autosomal-dominant manner. The majority of cases of thanatophoric dysplasia (all type I and most cases of type II) are sporadic. Some familial cases of type II have been reported.<sup>263-268</sup>

Distinct mutations in the *FGFR3* gene cause each one of the two types of thanatophoric dysplasia.<sup>229,263,266,269</sup> Three common mutations (R248C, Y373C, and S249C) are found in approximately 90% of the patients with thanatophoric dysplasia type I.<sup>226,270,271</sup> One mutation, K650E, is found in almost all cases of thanatophoric dysplasia type II.<sup>272-274</sup> Camera et al<sup>275</sup> reported an individual with the common thanatophoric dysplasia type I mutation and the clinical phenotype of achondroplasia. Although mosaicism was considered as a possible explanation for the milder phenotype, no trace of mosaicism was found in buccal mucosal cells or blood.

Prenatal sonographic findings depend on the specific type of thanatophoric dysplasia.<sup>196</sup> The association between cloverleaf skull and micromelia is specific to thanatophoric



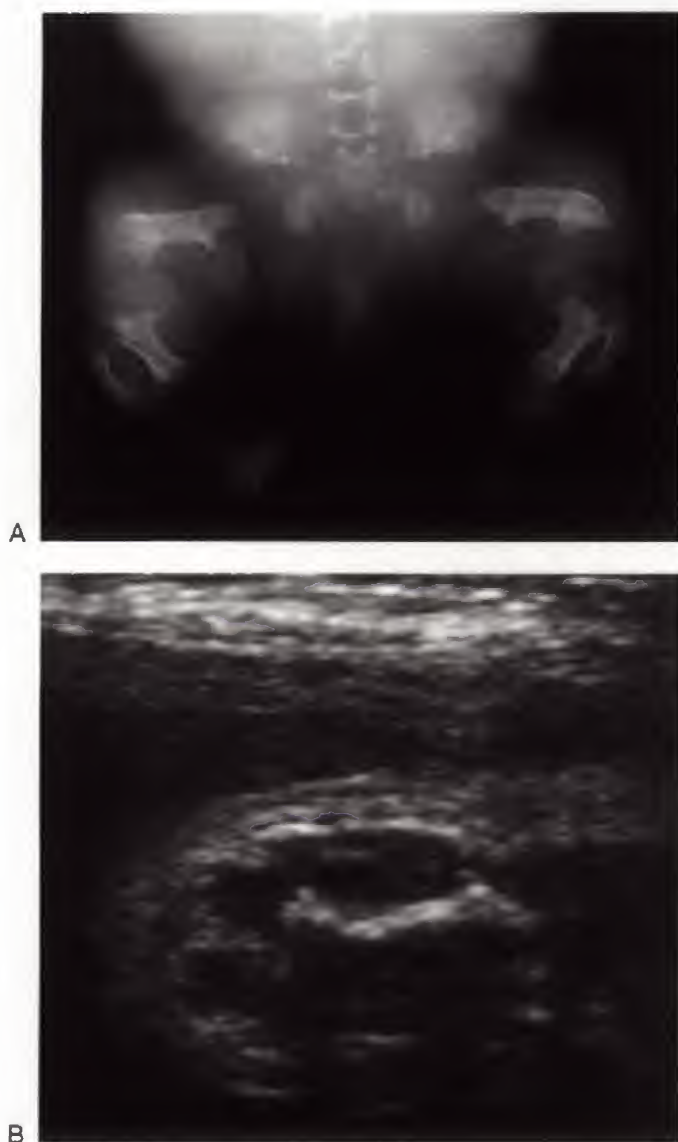


**FIGURE 12-32.** A. Radiograph of a patient with thanatophoric dysplasia. Marked limb shortening and characteristic bowed "telephone receiver" femurs are demonstrated. B. Sonogram of a fetus with thanatophoric dysplasia with marked femoral shortening and bowing.

dysplasia. Although campomelic syndrome may be also associated with cloverleaf skull, micromelia is not a feature of that condition. Ventriculomegaly, macrocranium, and polyhydramnios are frequently seen. Cerebellar hypoplasia is observed in approximately 37% of the cases in postnatal series.<sup>228</sup> There is a relatively large calvarium with a prominent forehead (Fig. 12-33), a saddle nose, and hypertelorism. Additional findings include short ribs, platyspondyly (see Fig. 12-8), and short and broad tubular bones in the hands and feet.

Thanatophoric dysplasia is associated with a specific pattern of brain malformations, characterized by megalencephaly (100%), hippocampal dysplasia (100%), rudimentary dentate gyrus (100%), polymicrogyria (97%), enlarged temporal lobes (93%), abnormal deep transverse sulci across



**FIGURE 12-33.** Prominent forehead (frontal bossing) in a fetus with thanatophoric dysplasia.

the inferomedial temporal lobe (88%), subependymal neuronal heterotopia (81%), and subarachnoid neuroglial heterotopia (79%).<sup>228</sup> This pattern of brain anomalies has been extensively described in the neuropathology literature and has been observed with similar frequency in thanatophoric dysplasia types I and II.<sup>228</sup> Research conducted in mouse models for thanatophoric dysplasia suggests that the cortical malformations observed in thanatophoric dysplasia result from compound disturbances in cortical patterning, proliferation, and apoptosis. The result is gyral pattern abnormalities, regional dysplasia, and altered surface area (especially temporal lobe hyperplasia and premature sulcation).<sup>228,276,277</sup> Macroscopic gyral abnormalities and enlargement of the temporal lobe probably occur in all cases of thanatophoric dysplasia, are thought to be specific for the disease, and are already present at mid gestation by the time that obstetric ultrasonography is performed.<sup>228,278</sup>

The differential diagnoses of thanatophoric dysplasia include SRPS, homozygous achondroplasia (in which both parents are typically affected), and asphyxiating thoracic dysplasia (differentiated by slight shortening of the long bones and normal vertebrae). On a review of the radiologic findings of several cases of thanatophoric dysplasia, Horton and colleagues<sup>279</sup> were able to discern a group of distinct entities characterized by severe platyspondyly. These disorders include the Torrance, San Diego, Lutton, and Shiraz types of platyspondylic lethal osteochondrodysplasias. Differential diagnosis among these entities is based on histologic and radiologic characteristics. Individuals with platyspondylic lethal skeletal dysplasia-San Diego type have *FGFR3* mutations that have been previously reported in association with thanatophoric dysplasia type I.<sup>280</sup>

Thanatophoric dysplasia is a uniformly lethal disorder, although survival for several months has been reported in isolated cases.<sup>268,279,281-284</sup> Prenatal sonographic diagnosis has been documented,<sup>97,204,285-302</sup> including a case in a triplet pregnancy.<sup>192</sup> Prenatal diagnosis by CVS or amniocentesis is available.<sup>96,303-305</sup>



## Hypochondroplasia

Hypochondroplasia is an autosomal-dominant disorder that resembles achondroplasia,<sup>306</sup> although the clinical symptoms and radiologic features in the hypochondroplasia are generally milder than those seen in the achondroplasia. Hypochondroplasia can result from a mutation in the *FGFR3* gene,<sup>307,308</sup> even though genetic heterogeneity has been suspected.<sup>309</sup> The incidence and prevalence of this disorder have not been determined, at least in part because of lack of agreement on a definitive set of diagnostic criteria, which makes it difficult to review data from the many studies reported in the literature. Most cases occur sporadically as a result of a new mutation.<sup>310</sup>

Two *FGFR3* mutations (C1620A and C1620G) result in a lysine for asparagine substitution at codon 540 (N540K) and have been shown to cause hypochondroplasia.<sup>219,311</sup> Several other *FGFR3* mutations have been proposed to cause a small number of cases of hypochondroplasia. In addition, the *IGF-1* gene has been proposed to be linked to hypochondroplasia in a subset of cases, although no pathogenetic mutations have been identified.<sup>309</sup>

The differential diagnosis between this condition and achondroplasia is based on the sparing of the head and the lack of tibial bowing in hypochondroplasia.<sup>306,312-316</sup> However, it is noteworthy that medial temporal lobe dysgenesis, similar to that observed in patients with thanatophoric dysplasia, has been recently described in three patients with a C1620A mutation in the *FGFR3* gene.<sup>317,318</sup> Although this condition is generally first detected during childhood, prenatal diagnosis has been reported in fetuses at risk.<sup>236,313</sup> Deviation of the fetal growth curve for femur length from the normal values and a normal growth curve for biparietal diameter has been suggested as a potential ultrasonographic marker for the prenatal diagnosis of hypochondroplasia.<sup>319</sup> DNA-based diagnosis through CVS or amniocentesis may be possible. It has been recommended that molecular analysis should include both the achondroplasia and hypochondroplasia mutations.<sup>320</sup>

## Fibrochondrogenesis, Atelosteogenesis

Fibrochondrogenesis and atelosteogenesis have a clinical presentation similar to that of thanatophoric dysplasia. The differential diagnosis between these disorders in utero is difficult. Fibrochondrogenesis and atelosteogenesis are extremely rare, and only a few cases of each have been reported.<sup>63,321-328</sup>

### Fibrochondrogenesis

Fibrochondrogenesis is a very rare lethal chondrodysplasia, with only 15 cases reported until now.<sup>329</sup> The first case was described in 1978 by Lazzaroni-Fossati et al.<sup>330</sup> This disorder is inherited in an autosomal-recessive fashion and characterized by micromelia with significant metaphyseal flaring, normal head size, flat face, flattened nasal bridge with anteverted nostrils, prominent eyes, undermineralized skull, platyspondyly, clefting of the vertebral bodies, and a narrow and bell-shaped thorax.<sup>329,331-333</sup> Metaphyseal flaring is not a feature of thanatophoric dysplasia.<sup>321,330,334,335</sup> This condition has been described in four consanguineous families.<sup>322,330,333,336</sup> Other conditions to be considered in the

differential diagnosis include metatropic dysplasia and Kniest dysplasia. Histologic examination is characterized by chondrocytes with fibroblastic appearance and poor endochondral ossification.<sup>323,333</sup> Prenatal diagnosis of fibrochondrogenesis by ultrasound has been reported as early as 17 weeks of gestation.<sup>321-323</sup> The recurrence risk for fibrochondrogenesis is 25%, which emphasizes the importance of genetic counseling.<sup>323</sup> At present, the molecular defect involved in fibrochondrogenesis is not known.<sup>337</sup>

### Atelosteogenesis

Atelosteogenesis includes a heterogeneous group of disorders with overlapping phenotypic features. It is a lethal chondrodysplasia characterized by severe micromelia (with hypoplasia of the distal segments of the humerus and femur), bowing of long bones, flat nasal bridge, cleft palate, micrognathia, narrow chest with short ribs, coronal and sagittal vertebral clefts,<sup>63</sup> and dislocation at the level of the elbow and knee. Clubfoot deformities may also be present.<sup>338</sup> Three subtypes of atelosteogenesis have been described based on radiologic and pathologic findings.<sup>339-342</sup> Silience et al<sup>342</sup> retrospectively collected data from 17 referrals of fetuses and newborns with atelosteogenesis during a 20-year period. Clinically, all cases had marked limb shortening. Micrognathia, a flattened nasal bridge, and cleft palate were more common in atelosteogenesis type II, as was pulmonary hypoplasia. Talipes was present in 80% of the cases of atelosteogenesis type I. Radiographic findings of atelosteogenesis type I (five cases) showed distal hypoplasia of the femur; the humerus was absent or segment shaped; the radius, ulna, and tibia were bowed; there was absence of the fibula; and all cases had coronal clefts in the lumbar vertebra. In atelosteogenesis type II (11 cases), the femora were shortened with expanded club-like ends and not distally tapered, and the humeri presented with distal hypoplasia and pointing. The forearm was shorter due to distal hypoplasia of the ulnae and proximal hypoplasia of the radii. In the lower limbs, the tibiae were short and bowed, and the fibulae had proximal or distal hypoplasia and pointing. The sacrum was horizontal. All cases had an S-shaped cervical spine. Only one case of atelosteogenesis type III was reported, with distal tapering of the femur and humerus, absence of ossification of the fibula, and an S-shaped cervical spine.<sup>342</sup>

Atelosteogenesis types I and III are sporadic and caused by missense mutations in the gene encoding filamin B, a protein that has a role in vertebral segmentation, joint formation, and endochondral ossification.<sup>343</sup> Atelosteogenesis type II is inherited with an autosomal-recessive pattern, and it is caused by a mutation in the diastrophic dysplasia sulfate transporter (DTDST) gene (*SLC26A2*).<sup>344-347</sup> It overlaps phenotypically and genetically with diastrophic dysplasia and achondrogenesis type IB.<sup>342,348,349</sup>

Differential diagnoses include diastrophic dysplasia and de la Chapelle dysplasia.<sup>350,351</sup> Three cases of a lethal dysplasia termed boomerang dysplasia (so-called boomerang-like tibia) may actually represent the same disorder as atelosteogenesis type I.<sup>352</sup>

### Achondrogenesis

Achondrogenesis, also known as anosteogenesis, is a lethal chondrodysplasia characterized by extreme micromelia, a



short trunk, and macrocrania. The birth prevalence ranges from 0.09 to 0.23 in 10,000 births.<sup>29,30,84,88,90</sup> Traditionally, this disorder has been classified into two types: the more severe form, which is type I achondrogenesis (Parenti-Fraccaro), and type II achondrogenesis (Langer-Saldino), the less severe form. In 1998, type I was subdivided into two types: type IA (Houston-Harris) and type IB (Fraccaro).<sup>353,354</sup> And although hypochondrogenesis had been considered a separate disorder from achondrogenesis, evidence now suggests that hypochondrogenesis and achondrogenesis type II are phenotypic variants of the same disorder.<sup>355-357</sup> Indeed, clinically and radiologically, achondrogenesis type II, hypochondrogenesis, and neonatal spondyloepiphyseal dysplasia congenita form a continuous spectrum of disease.<sup>358</sup> The fundamental biochemical disorder seems to be allelic mutations of the gene coding for type II procollagen.<sup>359</sup> Whitley and Gorlin proposed a different classification dividing achondrogenesis into four types,<sup>359</sup> but their proposal has not gained widespread acceptance.

Type IA achondrogenesis (Houston-Harris) is characterized by micromelia, lack of ossification of vertebral bodies but ossification of the pedicles in the cervical, and an upper thoracic region, and short ribs with multiple fractures. The calvarium is demineralized. Type IB (Fraccaro), which is a recessively inherited chondrodysplasia, is caused by a mutation in the *DTDS* gene<sup>360-362</sup> and is similar to type IA. The calvarium, however, is ossified, and fractured ribs cannot be seen. Although vertebral bodies are minimally ossified or not at all, the pedicles show some degree of ossification. Type II achondrogenesis is characterized by micromelia, a lack of mineralization of all or many of the vertebral bodies, sacrum, and ischium, an enlarged calvarium with normal ossification, variable shortening of the ribs, and an absence of fractures (Fig. 12-34).<sup>363</sup> Table 12-21 illustrates the characteristics of the different types of achondrogenesis.<sup>364,365</sup>

Prenatal diagnosis should be suspected on the basis of micromelia, lack of vertebral ossification, and a large head with various degrees of ossification of the calvarium.<sup>203,363-376</sup> Polyhydramnios and hydrops have been associated with achondrogenesis. However, sonographic examinations of affected fetuses do not demonstrate fluid accumulation in body cavities. The hydropic appearance of these fetuses and neonates is probably attributable to redundancy of soft tissue mass over a limited skeletal frame. An association between cystic hygromas and achondrogenesis has been reported in a fetus with normal chromosomal constitution.<sup>363,365,377</sup>

Achondrogenesis types IA and IB are inherited in an autosomal-recessive pattern, whereas most cases of achondrogenesis type II and hypochondrogenesis have been sporadic (new autosomal-dominant mutations). Some severe cases of type II achondrogenesis follow an autosomal-recessive pattern.<sup>378</sup>

The primary defect in achondrogenesis type IA is unknown. The only gene known to be associated with achondrogenesis type IB is *SLC26A2* (*DTDS*), which encodes a sulfate transporter protein.<sup>379</sup> Because the basic defect in achondrogenesis type IB has been identified, diagnosis by molecular study is possible. The distinction between achondrogenesis type IB (which has a recurrence risk of 25%), and the more frequent autosomal dominant achondrogenesis type II, which has a lower recurrence risk, is important for genetic counseling. A couple at risk of

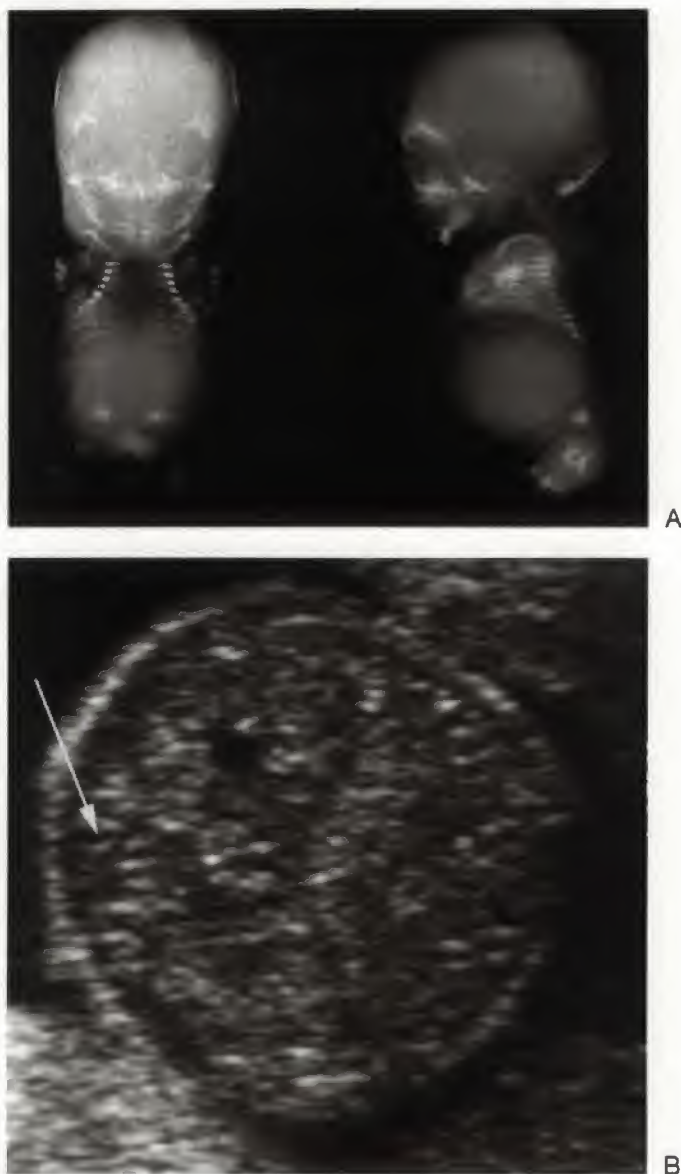


**FIGURE 12-34.** A. Frontal and lateral views in a case of achondrogenesis type II. There is no mineralization of the spine and ischial bones. The thorax is bell shaped, with short and straight ribs and no fractures. Long bones are short, with metaphyseal flaring and cupping. B. Transverse axial sonogram in a fetus with achondrogenesis. The lack of ossification of the spine (arrow) makes determination of anterior and posterior aspects of the fetus difficult in this view.

having a child with achondrogenesis type IB may take advantage of the possibility of molecular prenatal diagnosis by CVS or amniocentesis.<sup>344,348,360</sup> Achondrogenesis type II/hypochondrogenesis results from mutations in the *COL2A1* gene.<sup>380</sup> Prenatal diagnosis by molecular analysis of the *COL2A1* gene is available.

### Osteogenesis Imperfecta and Hypophosphatasia

OI and hypophosphatasia are discussed together because they are characterized by skeletal demineralization.



**Table 12-21 Radiologic Differences Between Achondrogenesis Type I (A-B), Type II, and Hypochondrogenesis**

	Type IA (Houston-Harris)	Type IB (Fraccaro)	Type II (Langer-Saldino)	Hypochondrogenesis
Skull	Membranous calvarium	All parts of ossified skull well seen	Normal ossification	Normal ossification
Long bones	Extremely shortened with metaphyseal cupping and spurs Rectangular bones	Arms and legs shorter than with type IA with minimal ossification; abundant metaphyseal spiking or spurring on lower leg bones Square or stellate bones	Short and bowed with metaphyseal flaring and cupping Mushroom stem bones	Less bowed and shortened with irregular or smooth metaphyses
Spine	Vertebral bodies unossified, with partly ossified pedicles	Vertebral bodies minimally or not ossified, pedicles ossified	Variable pattern of ossified or unossified vertebral bodies and pedicles	Thoracic and upper lumbar vertebral bodies ossified but still platyspondylic Cervical and lower lumbar bodies unossified
Pelvis	Poorly formed and ossified, with crenated iliac bones Ischial bones poorly ossified, pubic bones unossified	Iliac bones same aspect as in type IA Ischial and pubic bones unossified	Halberd-like iliac bones with unossified ischial and pubic bones	Near normally developed iliac bones with partial ossification of ischial bones and unossified pubic bones
Thorax	Short and barrel-shaped Short ribs with cupped metaphyses and multiple fractures	Same as in type IA with unfractured ribs	Short and barrel or bell shaped with short unfractured ribs	Near normal but shallow cage with short unfractured ribs

From Spranger J: Pattern recognition in bone dysplasias. In Papadatos CJ, Bartsocas CS (eds): Endocrine Genetics and Genetics of Growth. New York, Alan R. Liss, 1985, p 315.

### Osteogenesis Imperfecta

The term OI was introduced over a century ago to describe a newborn with extremely brittle bones (see Figs. 12-16, 12-18, and 12-19). At present, the term refers to a heterogeneous group of disorders caused, in most cases, by mutations in one or two structural genes for type I procollagen.<sup>381-387</sup> Extraskelatal malformations are variably associated with the disorder and include blue sclera, dentinogenesis imperfecta, hyperlaxity of ligaments and skin, hearing impairment, and presence of wormian bones on skull radiographs.<sup>387</sup> Advanced paternal age is considered a risk factor for OI.<sup>388</sup> The prevalence of OI is 0.18 per 10,000 births.<sup>29,30</sup>

The most popular classification is that proposed by Sillence and colleagues.<sup>389</sup> A modification of this classification has been recently put forward by Rauch and Glorieux,<sup>387</sup> and includes three additional types (V, VI, and VII [Table 12-22]). Clinically, the most relevant characteristic of OI is bone fragility, with severity increasing in the following order: (1) type I; (2) types IV, V, VI and VII; (3) type III; and (4) type II.<sup>387</sup>

In type I (autosomal dominant), there are no prenatal deformities. After birth, patients suffer from bone fragility, blue sclera (all ages), and hearing loss. There is osteoporosis, a normal calvarium, and no dentinogenesis imperfecta. Fractures may range from none to multiple, especially vertebral fractures that can lead to mild scoliosis.<sup>387</sup> Mutations resulting in OI type I cause premature termination codons that lead to decreased production of type I procollagen.<sup>384</sup>

Type II is an autosomal-dominant condition.<sup>390</sup> It is also known as the perinatal variety and is uniformly lethal. Other features are almost no ossification of the skull; beaded ribs; shortened, crumpled long bones; and multiple fractures in utero (see Fig. 12-18). The thorax is short but not narrow. Type II is subclassified into three subtypes (IIA, IIB, and IIC) according to radiologic criteria: subtype A has short, broad, crumpled long bones, angulation of tibias, and continuously beaded ribs; subtype B has short, broad, crumpled femurs, angulation of tibias but normal ribs or ribs with incomplete beading; and subtype C has long, thin, inadequately modeled long bones with multiple fractures and thin beaded ribs.<sup>391</sup>

Type III (autosomal recessive and rare) is a nonlethal variety characterized by blue sclera and multiple fractures present at birth. The sclera becomes white with time. The membranous skull is severely deossified, and the long bones are mildly shortened but with marked angulations. Type IIB and type III OI are difficult to distinguish and may represent different degrees of severity of the same disorder.<sup>392</sup>

In type IV (autosomal dominant), the long bones and sclera are normal. There is mild to moderate osseous fragility, and 25% of the newborns have fractures. There is significant heterogeneity in the expression of the disease, even within the same family.<sup>393</sup> From this heterogeneous group, Rauch and Glorieux have recently identified three separate clinical entities based on distinct clinical and bone histological features. These disorders have been classified as OI types V, VI, and VII (see Table 12-22).<sup>387,393-396</sup> Type V



**Table 12-22** Expanded Sillence Classification of Osteogenesis Imperfecta

Type	Clinical Severity	Typical Features	Typically Associated Mutations
I	Mild non-deforming osteogenesis imperfecta	Normal height or mild short stature; blue sclera; no dentinogenesis imperfecta	Premature stop codon in <i>COL1A1</i>
II	Perinatal lethal	Multiple rib and long bone fractures at birth; pronounced deformities; broad long bones; low density of skull bones on radiographs; dark sclera	Glycine substitutions in <i>COL1A1</i> or <i>COL1A2</i>
III	Severely deforming	Very short; triangular face; severe scoliosis; grayish sclera; dentinogenesis imperfecta	Glycine substitutions in <i>COL1A1</i> or <i>COL1A2</i>
IV	Moderately deforming	Moderately short; mild to moderate scoliosis; grayish or white sclera; dentinogenesis imperfecta	Glycine substitutions in <i>COL1A1</i> or <i>COL1A2</i>
V	Moderately deforming	Mild to moderate short stature; dislocation of radial head; mineralized interosseous membrane; hyperplastic callus; white sclera; no dentinogenesis imperfecta	Unknown
VI	Moderately to severely deforming	Moderately short; scoliosis; accumulation of osteoid in bone tissue, fish scale pattern of bone lamellation; white sclera; no dentinogenesis imperfecta	Unknown
VII	Moderately deforming	Mild short stature; short humeri and femora; coxa vara; white sclera; no dentinogenesis imperfecta	Unknown

From Rauch F, Glorieux PF: Osteogenesis imperfecta. *Lancet* 363:1377, 2004.

is characterized by moderate to severe bone fragility, calcification of the interosseous membrane at the forearm that severely limits movements of the hand, and predisposition to develop hyperplastic calluses. The characterization of type VI is based on bone histology showing an increased amount of osteoid and an abnormal pattern of lamellation. OI type VII is a recessive disorder with bone fragility, rhizomelia, and coxa vara. This type has been described only in a community of Native Americans in northern Quebec.<sup>387</sup>

OI type I is caused by a premature stop codon in *COL1A1*.<sup>382</sup> Types II, III and IV typically result from mutations that lead to substitutions for glycine within the triple helical domain of the pro- $\alpha$  chain, disrupting the normal folding of the molecule and initiating the production of abnormal collagen.<sup>397,398</sup> Approximately 90% of the patients with a clinical diagnosis of OI have a mutation in either the *COL1A1* or *COL1A2* gene, resulting in abnormal molecular constitution of procollagen type I.<sup>387,398-401</sup> Gene mutations associated with types V, VI, and VII have not been identified.<sup>387</sup>

The natural history of OI in utero is variable. Prenatal diagnosis of OI type II has been reported numerous times,<sup>95,402-423</sup> even as early as 12 weeks of gestation by either 2DUS or 3DUS.<sup>424-427</sup> It is important to note, however, that in some cases, fractures and limb shortening may not be observed until the second or even the third trimesters.<sup>428-430</sup> A typical sonographic finding associated with OI type II is the improved visualization of intracranial structures. Prenatal diagnosis of OI types I, III, and IV have also been reported using either ultrasound, biochemistry or molecular techniques.<sup>431-435</sup> The differential diagnosis should consider other skeletal disorders such as hypophosphatasia, achondrogenesis, and campomelic dysplasia.

### Hypophosphatasia

Hypophosphatasia is a rare autosomal-recessive inherited disorder with an estimated incidence of 1:100,000.<sup>436</sup> It is characterized by demineralization of bones and low alkaline phosphatase (ALP) in serum and other tissues.<sup>437</sup> The severity of the disease is inversely related to serum levels of ALP activity.<sup>438</sup> ALP acts on pyrophosphate and other phosphate esters, leading to the accumulation of inorganic phosphates that are critical for the formation of bone crystals. Bone fragility is thought to be the result of deficient generation of bone crystals.<sup>439</sup>

Hypophosphatasia is a condition that has been subdivided into six clinical types according to the age of onset: (1) perinatal (lethal), (2) infantile, (3) childhood, (4) adult, (5) odontohypophosphatasia, and (6) pseudohypophosphatasia.<sup>440</sup> The perinatal form is associated with stillbirth or early neonatal death due to either intracranial hemorrhage or respiratory insufficiency secondary to poorly developed ribs and reduced thoracic cavity volume.<sup>441,442</sup> The infantile variant may cause craniosynostosis and nephrocalcinosis from hypercalcemia and hypercalciuria during the first year of life, and is often fatal. Premature loss of deciduous teeth and rickets are the cardinal clinical features of childhood hypophosphatasia. In the adult form, recurrent metatarsal stress fractures and pseudofractures in long bones can be the hallmark. Odontohypophosphatasia refers to especially mildly affected individuals who have dental, but no skeletal, manifestations. The teeth are predisposed to cavities and may be lost prematurely. Pseudohypophosphatasia is an extremely rare variant characterized by typical clinical, radiologic, and biochemical findings of infantile hypophosphatasia with the exception that the total serum ALP concentrations are normal or increased.<sup>440</sup> The perinatal



and infantile varieties have an autosomal recessive pattern of inheritance, whereas the childhood, adult, and odontohypophosphatasia forms can be transmitted as either an autosomal-dominant or autosomal-recessive trait.<sup>443</sup>

Fetuses with congenital hypophosphatasia have generalized demineralization of the skeleton, with shortening and bowing of tubular bones. Multiple fractures are present. The generalized and marked demineralization of the cranial vault results in deformation of the skull after external compression. This sonographic sign is also present in some cases of OI type II and achondrogenesis type IA. Prenatal diagnosis of this condition has been reported with ultrasound<sup>444-454</sup> and by assaying ALP in tissue obtained by CVS<sup>437,455,456</sup> or amniotic fluid culture. ALP measurement in amniotic fluid is not a reliable means of making a diagnosis of hypophosphatasia because most of the ALP in amniotic fluid is of intestinal origin.<sup>457,458</sup> The involved enzymes in hypophosphatasia are bone and liver ALPs, and these isoenzymes contribute only 16% of the total amniotic fluid enzymatic activity.<sup>459</sup> Therefore, although prenatal diagnosis by DNA analysis is possible,<sup>460</sup> this requires sequencing the entire gene, which increases the complexity of the process.

Hypophosphatasia has been shown to be caused by mutations in the ALP liver (*ALPL*) gene, also called the tissue non-specific alkaline phosphatase (*TNSALP*) gene, located on chromosome 1 p36.1-p34.<sup>461,462</sup> A large spectrum of mutations is observed in the white population.<sup>463,464</sup> At present, 178 mutations have been reported and a list is maintained in a recently updated database (<http://www.sesep.uvsq.fr/Data base.html>) and about 80% of all mutations are missense.<sup>438</sup> Missense mutations in the gene lead to variable residual enzymatic activity and the extremely high phenotypic heterogeneity observed in hypophosphatasia.<sup>221,465</sup>

## Diastrophic Dysplasia

Diastrophic dysplasia is an autosomal-recessive disease with low frequency in most populations, but the condition is highly prevalent in Finland, with a carrier frequency of 1% to 2%.<sup>466</sup> It is characterized by micromelia, clubfoot, hand deformities, multiple joint flexion contractures, and scoliosis.<sup>467</sup> The diagnosis may be difficult at birth because of phenotypic variability, and milder cases are often diagnosed at a later age.<sup>468</sup> The clinical features include rhizomelic-type micromelia, joint contractures, hand deformities with an abducted position of the thumbs (so-called hitchhiker thumb [Figs. 12-35 and 12-36]), spine disorders (e.g., scoliosis, kyphosis, spina bifida occulta, spinal stenosis, lumbar lordosis) and severe talipes equinovarus. The head is normal, but micrognathia and cleft palate may be associated with this disease. Diastrophic dysplasia is a generalized disorder of cartilage leading to destruction of the cartilage matrix, formation of fibrous scar tissue and subsequent ossification. The latter process is responsible for the contractures. Mutations in the *DTDST* gene (*SLC26A2*), located on chromosome 5q32-q33.1,<sup>469,470</sup> are associated with reduced sulfate transport in chondrocytes, resulting in undersulfation of proteoglycans, leading to abnormal cartilage formation.<sup>470-473</sup> Five common *SLC26A2* mutations (R279W, IVS1+2T->C, DELV340, R178X, and C653S) account for approximately 65% of disease alleles.<sup>470</sup> Sequence



**FIGURE 12-35.** Three-dimensional rendered volume of a fetus with diastrophic dysplasia showing a hitchhiker thumb.



**FIGURE 12-36.** Hitchhiker thumb in diastrophic dysplasia.

analysis of the coding region can detect mutations in greater than 90% of alleles in individuals with typical clinical, radiologic, and histologic features.<sup>470</sup>

Prenatal diagnosis of diastrophic dysplasia has been made in patients at risk,<sup>62,64,468,474-477</sup> based on severe shortening and bowing of all long bones. Sepulveda et al<sup>478</sup> reported



clearer visualization of the limbs and face deformities by 3DUS. Prenatal diagnosis in at-risk pregnancies in which the familial mutations have been identified can be accomplished by DNA analysis of fetal cells obtained by CVS or amniocentesis.<sup>479</sup> Biochemical studies of fibroblasts and/or chondrocytes are available and may be useful for cases in which molecular genetic tests fail to identify *SLC26A2* mutations.<sup>480</sup> This disorder has a wide spectrum, and some cases may not be diagnosable in utero.

Diastrophic dysplasia is not universally lethal. Intelligence and sexual development are unaffected. However, joint contractures and painful osteoarthritis are associated with severe physical handicaps that require corrective orthopedic surgery.<sup>466</sup> There is an increased mortality rate in the neonatal period and infancy due to upper airway obstruction secondary to tracheobronchomalacia and medullary compression caused by severe cervical kyphosis.<sup>466,481</sup>

Differential diagnoses include arthrogryposis multiplex congenita, atelosteogenesis type II, and pseudodiastrophic dysplasia. Pseudodiastrophic dysplasia has a similar presentation as diastrophic dysplasia<sup>482</sup> and is inherited in an autosomal recessive pattern.<sup>30</sup> Histologic examination is required for differential diagnosis, since the distinctive morphologic abnormalities of the growth plate noted in diastrophic dysplasia have not been observed in pseudodiastrophic dysplasia. Cetta et al<sup>483</sup> demonstrated that a patient with pseudodiastrophic dysplasia had no defect in the *DTDST* gene and that both sulfate uptake by skin fibroblasts as well as sulfation of proteoglycans were normal.

## Kniest-Like Disorders

The term Kniest-like disorders is used in reference to a group of conditions that share histologic and radiologic characteristics with Kniest syndrome but differ in terms of clinical presentation and inheritance.<sup>484</sup>

### Kniest Syndrome

In 1952, Dr. Wilhelm Kniest<sup>485</sup> published the case of a 3.5-year-old girl with "skeletal changes showing a certain relationship to classical chondrodystrophy but differing in many of its manifestations." His publication clarified the phenotypic differences between this condition and other forms of chondrodystrophies. Kniest syndrome is one of the type II collagenopathies, which are disorders that not only impair fetal growth, but are also characterized by ocular and otolaryngological abnormalities.<sup>486–489</sup> The pattern of inheritance is autosomal dominant,<sup>265</sup> and these diseases are caused by usually de novo mutations in the *COL2A1* gene.<sup>487,489,490</sup> Other type II collagenopathies include spondyloepiphyseal dysplasia and Stickler dysplasia type I.<sup>491</sup>

Phenotypic features of Kniest syndrome include rhizomelic shortening of the long bones with widened metaphyses and prominent joints. Spinal involvement is common and characterized by platyspondyly and coronal clefts. The thorax is broad and short. Other manifestations, which may be detected during prenatal life, include micrognathia and cleft palate.<sup>492</sup> However, Kniest syndrome may be difficult to recognize during the second trimester because long bone biometry does not become remarkably abnormal until the third trimester of pregnancy.<sup>492</sup> The prognosis varies widely,

ranging from long-term survival with short stature, kyphoscoliosis, and craniofacial anomalies, to lethality in the neonatal period secondary, to tracheomalacia and respiratory distress.<sup>493</sup> Other long-term disabilities include feeding difficulties, hearing impairment, and blindness.<sup>492</sup>

## Dyssegmental Dysplasia

Dyssegmental dysplasia is a disorder characterized by anarchic ossification of the vertebral bodies (anyspondyly), metaphyseal flaring, and severe bowing of the long bones.<sup>494,495</sup> Two distinct types have been recognized: the mild Rolland-Desbuquois and the lethal Silverman-Handmaker.<sup>494,497–499</sup> Encephaloceles are frequently present in the Silverman-Handmaker type,<sup>496</sup> and prenatal diagnosis has been established in patients at risk.<sup>497,500–502</sup> The Silverman-Handmaker type is caused by a functional null mutation in the gene encoding Perlecan (*HSPG2*).<sup>503</sup> The Rolland-Desbuquois type has milder radiographic features resembling Kniest dysplasia and, although long-term survival is possible, a substantial proportion of affected individuals die during the first year of life.<sup>263,493</sup> Decreased levels of matrix metalloproteinase-2 and the tissue inhibitor of metalloproteinase-1 have been reported in cases of the Rolland-Desbuquois type of dyssegmental dysplasia.<sup>504</sup> The inheritance of both conditions is autosomal recessive.<sup>264,495</sup> Other disorders associated with vertebral disorganization include Jarcho-Levin syndrome and mesomelic dysplasia.

## Campomelic Dysplasia

Campomelic dysplasia is a rare lethal disorder first described by Maroteaux in 1971.<sup>506</sup> The prevalence varies between 0.05 and 1.6/10,000.<sup>506,507</sup> The disorder is characterized by bowing of the long bones of the lower extremities, an enlarged and elongated skull with a peculiarly small face, hypoplastic scapulae, and several associated anomalies such as micrognathia, cleft palate, talipes equinovarus, congenital dislocation of the hip, macrocephaly, hydrocephalus, hydronephrosis, and congenital heart defects.<sup>390</sup> The most important and significant features are bowing of the femur and tibia; other tubular bones are normal in length (see Fig. 12–17B). The thorax is narrow, can be bell shaped, and 11 pairs of ribs are usually present. Cervical vertebrae are hypoplastic and poorly ossified.<sup>508</sup> In the largest clinical and genetic study conducted to date, which included 36 patients with CMD, Mansour et al<sup>506</sup> concluded that campomelic dysplasia is a sporadic autosomal-dominant condition.

There are two short-bone varieties of campomelic dysplasia, representing distinct syndromes: (1) the normocephalic form, known as kyphomelic dysplasia, and (2) the craniostenotic type, which appears to be identical to Antley-Bixler syndrome. Antenatal diagnosis of campomelic dysplasia has been reported several times,<sup>90,116,196,509–516</sup> and the differential diagnoses include OI, thanatophoric dysplasia, and hypophosphatasia.

A unique aspect of campomelic dysplasia is that 75% of affected infants with a male karyotype present with sex reversal syndrome and have female or ambiguous genitalia.<sup>517,518</sup> The histology of the gonads varies from gonads with testicular differentiation to dysgenetic gonads with primary follicles. Indeed, mutations in the *SOX-9* gene,



**Table 12-23 Disorders With Thoracic Dysplasia and Polydactyly**

	Asphyxiating Thoracic Dysplasia (Jeune)	Chondroectodermal Dysplasia (Ellis-van Creveld)	Short-Rib Polydactyly Syndrome Type I (Saldino-Noonan)	Short-Rib Polydactyly Syndrome Type II (Majewski)	Short Rib Syndrome Type III (Naumoff)	Short Rib Syndrome Type IV (Beamer-Langer)
Relative prevalence	Common	Uncommon	Common	Extremely rare	Rare	Rare
Clinical features						
Thoracic constriction	++	+	+++	+++	+++	+++
Polydactyly	+	++	++	++	++	++
Limb shortening	+	+	+++	+	++	++
Congenital heart disease	-	++	++	++	-	-
Other abnormalities	Renal disease	Ectodermal dysplasia	Genitourinary and gastrointestinal anomalies	Cleft lip and palate	Renal abnormality	Cleft lip and palate and genitourinary and gastrointestinal anomalies
Radiographic features						
Tubular bone shortening	+	+	+++	++	+++	++
Distinctive features in femora	-	-	Pointed ends	-	Marginal spurs	-
Short, horizontal ribs	++	++	+++	+++	+++	+++
Vertical shortening of ilia and flat acetabula	++	++	++	-	++	-
Defective ossification of vertebral bodies	-	-	++	-	+	++
Shortening of skull base	-	-	-	-	+	-

+, not common; +++, most common; -, absent

Reproduced with permission from Cremim BJ: Bone Dysplasias of Infancy. A Radiological Atlas. Berlin: Springer-Verlag; 1978.

which is also a fundamental testis-differentiation gene common to all vertebrates,<sup>519</sup> have been reported in several patients with this disorder.<sup>517,518,520-523</sup> These mutations interfere with DNA binding by *SOX-9* or truncate the C-terminal transactivation domain and thereby impede the ability of *SOX-9* to activate target genes during organ development.<sup>522</sup> Chromosomal translocations involving 17q have also been observed in several affected individuals.<sup>524-529</sup>

Campomelic dysplasia is frequently lethal in infancy, although some cases of survivors have been reported.<sup>509,530-534</sup> The cause of death is respiratory distress due to tracheomalacia.

### Skeletal Dysplasias Characterized by a Hypoplastic Thorax

The dysplastic process involves the ribs and other bones of the rib cage in many skeletal dysplasias. A reduction in thoracic dimensions leads to restriction of lung growth and, consequently, pulmonary hypoplasia. Lung hypoplasia is the main cause of death in lethal skeletal dysplasias. There are specific groups of dysplasias in which thoracic hypoplasia is a cardinal feature. These include asphyxiating thoracic

dysplasia, Ellis-van Creveld syndrome, SRPS, and campomelic syndrome. Table 12-23 illustrates the criteria for the differential diagnoses of the first three of these conditions. Other disorders presenting with altered thoracic dimensions are thanatophoric dysplasia, atelosteogenesis, fibrochondrogenesis, achondrogenesis, and Jarcho-Levin syndrome (Fig. 12-37).<sup>535</sup>

#### Asphyxiating Thoracic Dysplasia (Jeune Syndrome)

Asphyxiating thoracic dysplasia, or Jeune syndrome,<sup>536</sup> is a rare autosomal-recessive condition, with an estimated prevalence of 0.14/10,000 births.<sup>537-539</sup> Asphyxiating thoracic dysplasia is characterized by a combination of a small thorax, varying degrees of brachymelia, polydactyly, pelvic abnormalities, and renal involvement.<sup>540</sup> Phenotypic expression is wide and includes lethal,<sup>541</sup> mild,<sup>538,542</sup> and latent<sup>539</sup> forms. In severe cases, thoracic narrowing is responsible for pulmonary hypoplasia, respiratory failure, and early infancy death.<sup>543</sup> Conversely, the presence and the degree of renal involvement<sup>544-556</sup> constitute the main prognostic factor in the milder forms.<sup>542,553,557</sup> Individuals





**FIGURE 12-37.** Jarcho-Levin syndrome. There is dramatic spinal shortening with disorganization of the vertebral bodies, a characteristic chest deformity (crab-like appearance with posterior fusion and anterior flaring of the ribs), and unaffected long bones.

surviving childhood are likely to have a clinical course complicated by respiratory distress, recurrent pulmonary infections,<sup>544</sup> hepatic,<sup>547,554,556-563</sup> and pancreatic involvement.<sup>564,565</sup> Ocular/retinal manifestations have been sporadically described in association with Jeune syndrome.<sup>547,566-568</sup>

**Skeletal Findings.** The thorax is described as narrow and bell shaped, and the ribs are short, broad and horizontally oriented.<sup>545,569</sup> Brachymelia, if present, is predominantly of the rhizomelic type.<sup>566,570,571</sup> Long bones may be bowed<sup>569,571</sup> and have visible proximal ossification centers at birth in two thirds of the cases.<sup>571</sup> Postaxial polydactyly is not a constant finding, with both the upper and lower limbs variably affected.<sup>557,569,570,572,573</sup> Pelvic findings include small-squared iliac wings, a trident pelvis (shortened ilia with a downward hook of the greater sciatic notches), and horizontal acetabular roofs with spur-shaped projections.<sup>540,570,571,573</sup> A handlebar-like conformation of clavicles has been reported.<sup>540,571</sup> Cleft lip and palate can also occur.

**Renal Findings.** The degree of renal involvement is the main prognostic factor for individuals surviving the neonatal period.<sup>542,545,547,552,557</sup> Renal failure can occur during childhood<sup>545,547,551,553</sup> and may require renal transplantation.<sup>544,546,549</sup> Cystic or scleroatrophic changes, partly indistinguishable from those associated with juvenile

nephronophthisis, are the two characteristic histologic patterns of renal involvement.<sup>545,548,552</sup> Cystinuria has also been described in patients with Jeune syndrome.<sup>550,575</sup>

**Hepatic Findings.** Liver involvement ranges from subclinical to biliary cirrhosis and progressive portal hypertension<sup>558,560,576</sup> requiring transplantation during childhood.<sup>558</sup> Intralobular bile ducts loss, portal tract periphery bile duct proliferation and fibrosis are the most frequent histologic findings.<sup>547,554,558</sup> Because liver involvement at early stages can be subclinical and manifest as early as in the neonatal period,<sup>561,563</sup> early diagnostic work-up and close follow-up of hepatic function has been proposed.<sup>560</sup>

**Other Findings.** Ophthalmologic evaluation of long-term survivors has revealed a wide spectrum of retinal anomalies. Pigmentation, dystrophy, degeneration, and aplasia have been reported among long-term survivors.<sup>547,567,568,577</sup> Visual loss and night blindness have been sporadically reported as the initial manifestation of mild forms of the Jeune syndrome.<sup>568</sup> Other associated anomalies include Dandy Walker malformation,<sup>561,578</sup> agenesis of the corpus callosum,<sup>561</sup> situs inversus,<sup>579</sup> neuroectodermal tumor in the soft tissue of the chest wall,<sup>549</sup> Hirschsprung disease,<sup>580</sup> and asplenia.<sup>579</sup>

**Prenatal Diagnosis.** Prenatal sonographic diagnosis of Jeune syndrome<sup>540,557,569-572,574,581-586</sup> has been reported several times in the literature. A positive familial history contributes to second trimester recognition of recurrent forms,<sup>569-571,581</sup> whereas diagnosis in low-risk pregnancies is more challenging and has been reported in the third trimester.<sup>540</sup>

Although the locus for asphyxiating thoracic dystrophy maps to chromosome 15q13, mutation analysis of two candidate genes (*GREMLIN* and *FORMIN*) did not reveal pathogenic mutations.<sup>587</sup> Thus, molecular diagnosis for this condition is not available clinically at the time of this writing.<sup>588</sup>

**Surgical Management for Respiratory Distress.** Lateral thoracic expansion, a surgical procedure that attempts to enlarge the thoracic cage by separating ribs from their periosteum and plating them together with titanium struts, has been performed in a handful of patients with asphyxiating thoracic dysplasia, resulting in improvement in respiratory function and/or eliminating the need for external ventilators.<sup>589-592</sup>

### Short Rib-Polydactyly Syndromes

SRPSs are an heterogeneous group of disorders inherited as an autosomal-recessive trait.<sup>45,593</sup> Traditionally, four major types of short rib-polydactyly syndromes have been described: type I (Saldino-Noonan),<sup>594</sup> type II (Majewski),<sup>595</sup> type III (Verma-Naumoff),<sup>596</sup> and type IV (Beemer-Langer).<sup>597</sup> These conditions are classified within the family short rib dysplasia with or without polydactyly group, which also includes asphyxiating thoracic dysplasia (Jeune syndrome) and chondroectodermal dysplasia (Ellis-van Creveld dysplasia).<sup>27</sup> Because SRPSs I through IV are lethal in the newborn period because of the severe pulmonary hypoplasia and associated anomalies and, conversely, Ellis-van Creveld and Jeune syndromes are not uniformly lethal,<sup>598</sup> accurate prenatal diagnosis is important in order to provide adequate counseling.





**FIGURE 12-38.** Short rib-polydactyly syndrome. There is severe shortening of all long bones, very short and horizontal ribs, and postaxial polydactyly in all four extremities. Note the angulation of the bones in the forearm.

SRPSs I through IV are characterized by short limbs/micromelic dwarfism, constricted thorax, usually polydactyly, and multiple anomalies of major organs (Fig. 12-38).<sup>599-603</sup> Spranger and Maroteaux have indicated that the absence of polydactyly does not exclude the diagnosis of this entity.<sup>52,604-606</sup> In fact, although polydactyly is a constant feature in SRPS type II (Majewski) and is commonly found in types I and III (Saldino-Noonan and Verma-Naumoff),<sup>607</sup> patients with SRPS type IV (Beemer) seldom have polydactyly.<sup>597,608,609</sup>

**Differential Diagnosis.** SRPSs have been identified prenatally by 2DUS<sup>579,604,605,610-629</sup> and 3DUS,<sup>100,630</sup> as well as by fetoscopy.<sup>631</sup> Table 12-23 illustrates the differential diagnosis and features of the disorders characterized by polydactyly and a narrow thorax. Differential diagnosis is often a challenging task, especially before birth, because a high degree of overlap exists in clinical and radiologic features. Indeed, there is debate as to whether the various forms of SRPSs are related to different genes, to different mutations on the same gene, or due to variability of expression of the same mutant gene.<sup>602,603,632-637</sup>

**Molecular Diagnosis.** The molecular basis of the SRPSs has not been elucidated. Urioste<sup>638</sup> recognized a balanced pericentric inversion of chromosome 4 in a proband with clinical and radiologic manifestations of SRPS and proposed that the disorder could be due to disruption of a gene in the 4p16 region (the same region where the gene for



**FIGURE 12-39.** Postaxial polydactyly in a fetus with Ellis-van Creveld syndrome.

Ellis-van Creveld syndrome maps). However, this association has been subsequently excluded both in a family with SRPS III,<sup>639</sup> as well as in 10 unrelated cases of SRPS III by sequence analysis.<sup>640</sup>

### Chondroectodermal Dysplasia

Chondroectodermal dysplasia, also known as Ellis-van Creveld syndrome, is a rare autosomal-recessive condition with an estimated birth prevalence of 1/60,000 in the general population and 5/1,000 among the Amish community of Lancaster County, Pennsylvania.<sup>641-643</sup> Ellis-van Creveld syndrome is defined by the tetrad of chondrodysplasia, ectodermal dysplasia, polydactyly, and congenital heart disease.<sup>644</sup> The combination and severity of each of these features is extremely variable, and as a consequence, the clinical course and prognosis range from death in the neonatal period because of cardiopulmonary complications<sup>645-647</sup> to long-term survival.<sup>648</sup>

**Skeletal Findings.** In Ellis-van Creveld syndrome, the long bones most commonly present mesomelic<sup>206,649-653</sup> or acromesomelic shortening.<sup>644,650,654-660</sup> The presence and severity of rib cage dysplasia is an important factor in determining prognosis. A narrow thorax with short and horizontal ribs is frequently associated with pulmonary hypoplasia, early respiratory failure, and recurrent pulmonary infections.<sup>645-647,650,661,662</sup>

Postaxial polydactyly (Figs. 12-39 and 12-40) can involve the hands and feet in several combinations: only hands bilaterally,<sup>206,600,644,649-651,653,655,659,662-666</sup> both hands and both feet,<sup>646-650,652,657,667-673</sup> or both hands and one foot.<sup>654,671,674,675</sup> Clinodactyly<sup>644,648,666</sup> and syndactyly<sup>646,650,659,662,663,673,676-680</sup> have also been reported. Bowing of the long bones,<sup>600,644,650,654,655,658,659,673</sup> genu valgus,<sup>643,644,648,652,656,664,669-671,676,677</sup> and pelvic radiologic anomalies (including broad, squared and vertically short ilia, trident configuration of the acetabula, spur-like projections at the acetabular roof)<sup>643,646,649,653,662,663,666,672,673,679</sup> are additional phenotypic features. The vertebrae and skull have a normal appearance.<sup>649,672</sup>



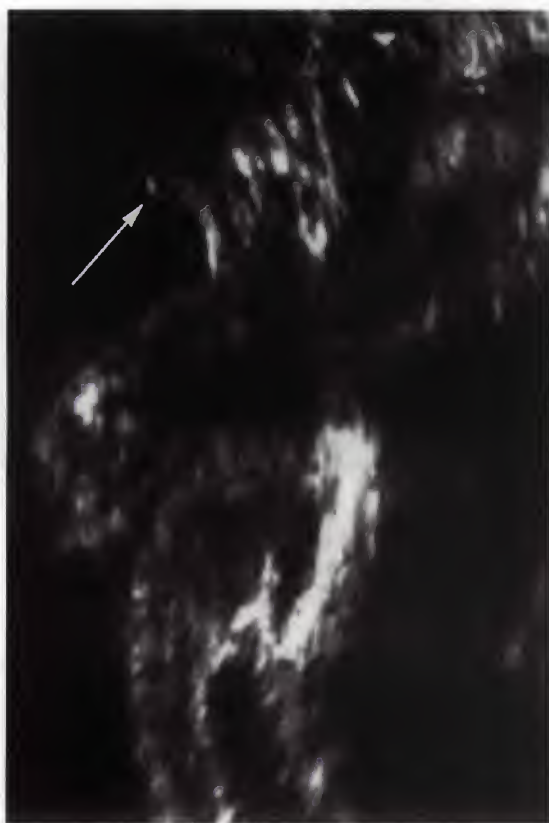


**FIGURE 12-40.** Sonographic image of the hand shown in Figure 12-39. Note the abnormal angulation of the extra digit on the ulnar side of the forearm (arrow).

**Cardiac Defects.** Congenital heart disease occurs in up to 60% of affected individuals,<sup>680,681</sup> and its presence and severity are strongly correlated to mortality rate.<sup>649</sup> The most common cardiac anomalies are those characterized by defects of the endocardial cushion closure, such as atrial septal defects,<sup>206,647,649,651,661,664,667,671,673,674,677</sup> ventricular septal defects,<sup>653,659,662</sup> atrioventricular septal defects,<sup>684</sup> atrioventricular canal,<sup>643,660,669,671,679,683</sup> and single atrium.<sup>646,649,652,657,660,663,665,667,678,684-687</sup> Mitral clefts,<sup>648,657,660</sup> complex cardiac malformations,<sup>660,663,679</sup> and complete situs inversus<sup>656</sup> have also been reported in Ellis-van Creveld syndrome.

**Ectodermal Dysplasia.** Clinical manifestations of ectodermal dysplasia are present in 70% of cases.<sup>669</sup> The most frequent are dystrophic changes of the fingernails, thin and sparse hair, and oral and dental abnormalities.<sup>644,649,661</sup> Short upper lip, multiple and hyperplastic frenula, and fusion of the upper lip to the gingival margin are common in patients with Ellis-van Creveld syndrome.<sup>657,670,676</sup> Dental anomalies include dysmorphic cone-shaped and microdontic teeth, taurodontism, delay in eruption or anodontia,<sup>206,644,649,650,653-656,666,670,671,677,678,683,686,687</sup> natal, and neonatal teeth.<sup>645,663,665,676,690,691</sup> Sporadic cases of micrognathia<sup>672,678,688,690</sup> and mandibular malocclusion<sup>690</sup> have been reported. This variety of oral manifestations requires multidisciplinary dental treatment, with special attention to the high incidence of cardiac defects in these patients<sup>676</sup>

**Other Manifestations.** CNS anomalies can occasionally occur in association with Ellis-van Creveld syndrome, including ventriculomegaly,<sup>663</sup> Arnold Chiari malformation,<sup>662</sup> Dandy Walker anomaly,<sup>643</sup> and spina bifida occulta.<sup>656</sup> The kidneys are rarely involved, although there are sporadic reports of renal agenesis, congenital megaureter,<sup>678</sup> renal medullary dysplasia,<sup>691</sup> and nephronophthisis.<sup>671</sup> An association between Ellis-van Creveld syndrome and bile duct dysplasia requiring liver transplantation has been reported.<sup>655,691</sup> Thymic hypoplasia,<sup>684</sup> Hodgkin's disease, nodular sclerosing at young age,<sup>692</sup> and retinal dystrophy<sup>668</sup> are other less common associations.

**Prenatal Diagnosis.** Prenatal diagnosis by ultrasound has been reported during second<sup>648,649,653,669,677,681,695-700</sup> and third trimesters,<sup>600,646,647,651,662,667,675,679,693-698</sup> as well as in the first trimester.<sup>651</sup> Fetoscopy has been performed in selected cases.<sup>667,693,695</sup>

**Differential Diagnosis.** Differentiating between Ellis-van Creveld and Jeune syndrome can be challenging<sup>699</sup> because there is a great degree of overlap in the phenotypic features of these two conditions.<sup>671,700</sup> McKusick-Kaufman syndrome shares with Ellis-van Creveld postaxial polydactyly and heart defects,<sup>701</sup> but differentiating characteristics include absence of chondrodysplasia and ectodermodyplasia, as well as the presence of hydrometrocolpos.<sup>702</sup> Weyers acrofacial dysostosis, an autosomal-dominant condition, shares with Ellis-van Creveld the mild short stature, postaxial polydactyly, dental and nail dystrophy. On the other hand, thoracic dysplasia and congenital heart disease are not typical features in Weyers acrofacial dysostosis. Linkage and haplotype analysis raised the possibility that Weyers acrofacial dysostosis is the heterozygous expression of a mutation that, in the homozygous form, causes Ellis-van Creveld syndrome.<sup>703,704</sup>

**Genetics and Molecular Diagnosis.** Mutations on two nonhomologous genes named *EVC1*<sup>703,705</sup> and *EVC2*,<sup>706,707</sup> both mapping to the short arm of chromosome 4 (4p16) in a head-to-head configuration, are candidates for Ellis-van Creveld syndrome. However, it has been recently reported that mutations in either the *EVC1* or *EVC2* gene are not uniformly found in all subjects with a phenotypic diagnosis of Ellis-van Creveld syndrome.<sup>708</sup> Typing of microsatellite markers flanking the *EVC* locus has been reported for first trimester diagnosis of Ellis-van Creveld syndrome in a family with a previously affected child.<sup>675</sup> There is debate about the possibility of partial manifestations in heterozygous carriers.<sup>648,666,674,686,703</sup>

## Skeletal Dysplasias With Predominant Membranous Bone Involvement

A group of skeletal dysplasias is characterized by disruption in the process of intramembranous bone ossification. These include cleidocranial dysplasia, Yunis-Varom syndrome, and isolated parietal foramina. Among these disorders, cleidocranial dysplasia is the one that has been more often diagnosed prenatally.

### Cleidocranial Dysplasia

Cleidocranial dysplasia is an autosomal-dominant condition characterized by clavicular aplasia or hypoplasia,



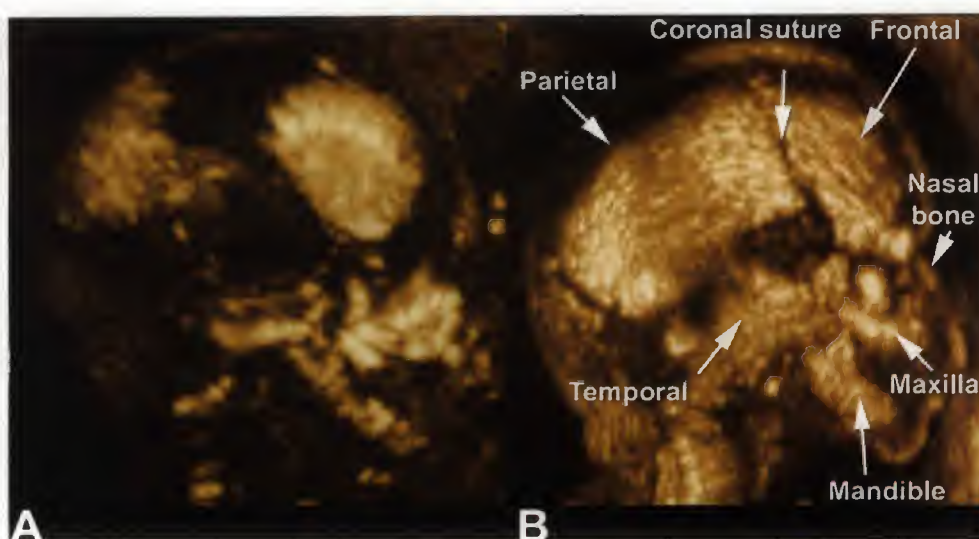


**FIGURE 12-41.** A. Three-dimensional rendering of the fetal skull at 18 3/7 weeks of gestation using the maximum intensity projection mode demonstrates widening of the coronal suture, absence of the squamous portion of the temporal bone, and absence of the nasal bones in a fetus with cleidocranial dysplasia. B. Labeled three-dimensional image of a normal fetal skull at 18 3/7 weeks (control). (From Soto E, Richani K, Goncalves LF, et al: *Three-dimensional ultrasound in the prenatal diagnosis of cleidocranial dysplasia associated with B-cell immunodeficiency*. *Ultrasound Obstet Gynecol* 27:574, 2006.)

brachycephaly, midface hypoplasia, patent or delayed closure of fontanels (Fig. 12-41), delayed eruption of permanent teeth, and relatively short stature.<sup>709-712</sup> The incidence of cleidocranial dysplasia is estimated to be 0.5/100,000 live births.<sup>713</sup> Cleidocranial dysplasia is caused by mutations in the human osteoblast-specific transcription factor gene (*RUNX2*),<sup>714-717</sup> formerly known as *CBFA1* (core-binding factor  $\alpha$ -1),<sup>718</sup> located in chromosome 6p21.<sup>719-721</sup> The *RUNX2* gene is essential for osteoblast differentiation and, thus, affects both membranous and endochondral bone formation.<sup>722,723</sup> *RUNX2* induces and regulates the expression of genes involved in bone matrix formation and remodeling by modification of chromatin or interaction with co-regulatory proteins.<sup>724,725</sup>

Prenatal diagnosis of cleidocranial dysplasia by ultrasound has been reported as early as 14 weeks of gestation.<sup>726</sup> The most common finding is the detection of unilateral and bilateral hypoplastic and hypomineralized clavicles, although pseudoarthrosis (fracture) of the clavicle (Fig. 12-42) has also been reported.<sup>115</sup> Other features include hypomineralization/poor ossification of the cranial bones and/or pelvis, large fontanels with wide sutures, obvious corpus callosum, brachycephaly, fronto-parietal-occipital bossing, low nasal bridge, and long bones below the fifth percentile.<sup>727-733</sup> Molecular prenatal diagnosis for *RUNX2* mutations can be accomplished by analysis of fetal tissue, or obtained by CVS or amniocentesis.<sup>734</sup>

The differential diagnosis includes disorders characterized by poor mineralization of the calvarium, such as hypophosphatasia, as well as disorders that have fracture/pseudoarthrosis of the clavicle as one of the characteristic phenotypic features (e.g., congenital pseudoarthrosis of the clavicle and Yunis-Varon syndrome). Congenital pseudoarthrosis defines a spontaneous fracture that progresses to nonunion and is associated with abnormal movement at the site. The mechanisms proposed for this clavicular defect include an

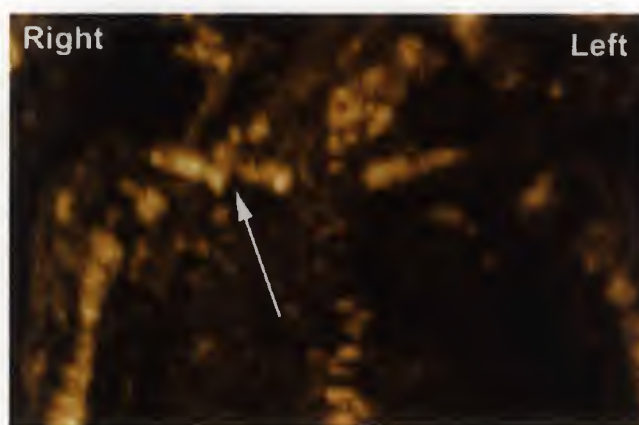


**FIGURE 12-42.** Three-dimensional rendering of the fetal shoulders using the maximum intensity projection mode in a fetus with cleidocranial dysplasia. The arrow points to a site of pseudoarthrosis (fracture) of the clavicle. (From Soto E, Richani K, Goncalves LF, et al: *Three-dimensional ultrasound in the prenatal diagnosis of cleidocranial dysplasia associated with B-cell immunodeficiency*. *Ultrasound Obstet Gynecol* 27:574, 2006.)

abnormal elevation of the first rib and right subclavian artery<sup>735,736</sup> or a failure of fusion of the two ossification centers (congenital pseudoarthrosis).<sup>735</sup> Yunis-Varon syndrome is described in the next section.

### Yunis-Varon Syndrome

Yunis-Varon syndrome is an autosomal-recessive disorder that shares characteristics with cleidocranial dysplasia but, in addition, includes micrognathia, bilateral absence of the thumbs and distal phalanges of the fingers, as well as hypoplasia of the great toes.<sup>737</sup> This condition has not been diagnosed prenatally.



**Table 12-24** Congenital Amputations

Absent limbs only
Single absent limb
Multiple absent limbs
Absent limbs with rings
Congenital ring constriction syndrome
Absent limbs and face anomaly
Aglossia-adactylia syndromes
Möebius syndrome
Absent limbs with other anomalies
Ichthyosiform skin (CHILD syndrome)
Fibula agenesis-complex brachydactyly (du Pan's syndrome)
Splenogonadal fusion
Skull and scalp defects (Adams-Oliver syndrome)
Phocomelia
Thalidomide syndrome
Thrombocytopenia with absent radii syndrome
Robert's pseudothalidomide-SC syndrome
Grebe syndrome
Proximal femoral focal deficiency
Femoral hypoplasia-unusual facies syndrome
Femur-fibula-ulna complex
Femur-tibia-radius complex
Split hand/split foot (SH/SF) syndromes
Only SH/SF
SH/SF and absent long bones
Ectrodactyly, ectodermal dysplasia, cleft lip and palate syndrome
Others
Split foot and triphalangeal thumb, autosomal dominant
Split foot, or split hand and central polydactyly (see central polydactyly)
SH/SF and congenital nystagmus (Karsch-Neugebauer syndrome)
SH/SF and renal malformations (Acrorenal syndrome)
Split foot and mandibulofacial dysostosis (Fontaine syndrome), autosomal dominant

Reproduced with permission from Goldberg MD: *The Dysmorphic Child: An Orthopedic Perspective*. New York, Raven Press, 1987.

## Limb Deficiency or Congenital Amputations

On occasion, the only identifiable anomaly is the absence of an extremity (limb deficiency) or a segment of an extremity (congenital amputation) (Table 12-24).<sup>738</sup> These disorders differ from osteochondrodysplasias, and the terms usually used to refer to limb reduction abnormalities include<sup>739</sup>:

- Amelia: absence of a limb or limbs
- Hemimelia: absence of a longitudinal segment of a limb (e.g. radial aplasia, radial hypoplasia)
- Phocomelia: hypoplasia of the limbs, with hands and feet attached to the shoulder and hips
- Acheira: absence of the hands
- Apodia: absence of a foot or feet
- Acheiropodia: absence of hands and feet.

The overall incidence of congenital limb reduction deformities ranges from 0.49 to 3.5 per 10,000 births (Table 12-25).<sup>740,741</sup> It has been estimated that approximately 50% of these limb reduction defects are simple transverse reduction deficiencies

**Table 12-25**

Prevalence of Different Types of Limb Reduction Malformations in Hungary, 1975-1977

Type	Total	Population Prevalence (per 1000 Births)
Terminal transverse	79	0.14
Radial	13	0.09
Ulnar	41	0.11
Split hand and/or foot	20	0.04
Ring constriction	62	0.49
Total	274	0.49

From Bod M, Czeizel A, Lenz W: Incidence at birth of different types of limb reduction abnormalities in Hungary 1975-1977. *Hum Genet* 65:27, 1983.



**FIGURE 12-43.** Sonogram of a fetus with radial aplasia. The hand deviates toward the side of the absent bone (radius).

of one forearm or hand without associated anomalies.<sup>740,741</sup> The remainder consist of multiple reduction deficiencies, with an approximate 23% incidence of additional anomalies of the internal organs or craniofacial structures.<sup>738</sup>

Limb deficiencies can present alone or as part of a specific syndrome. An isolated limb deficiency of the upper extremity (e.g., distal segment of an arm) is generally an isolated anomaly. The hand often deviates in the direction of the absent bone (Fig. 12-43). In contrast, congenital amputation of the leg generally occurs within the context of a syndrome, as do bilateral amputations or reduction of all limbs.<sup>742</sup>

Isolated amputation of an extremity can be due to amniotic band syndrome, exposure to a teratogen, or a vascular accident. In most cases, the anomaly is sporadic, and the risk of recurrence is negligible. Sonographic findings related to these conditions have been reviewed in depth by Bromley and Benacerraf.<sup>743</sup>



In the largest study conducted to date, which included a population of 709,030 births from 20 malformation registries in 12 European countries, the overall prenatal detection rate for limb reduction defects was 35.6% (89/250), with a higher detection rate observed among cases with associated malformations (49.1% [55/112]). The frequency of chromosomal anomalies in the presence of associated malformations was 14.3% (16/112), with eight cases of trisomy 18, two cases of trisomy 21, and one case each of triple X, Klinefelter syndrome, deletion 7q, + isochromosome 12p, deletion 3q and unbalanced translocation t(5;14)(p13;q13). Among fetuses with a normal karyotype and associated anomalies, 33.9% (38/112) had syndromic disorders or associations, including amniotic bands, VATER association, Poland syndrome, Hanhart syndrome, Brachmann-De Lange syndrome, thrombocytopenia-radial aplasia (TAR) syndrome, limb bodywall complex, caudal regression syndrome, Fanconi anaemia, ulnar mammary syndrome, Holt-Oram syndrome, Roberts syndrome, femur-fibula-ulna syndrome, Aarskog syndrome, Adams-Oliver syndrome, Oto-facio-digital type 2 syndrome, Robinow syndrome, Carey-Fineman-Ziter syndrome, and twin-reversed arterial perfusion sequence.

The following section reviews syndromes in which a limb amputation or deficiency is associated with other anomalies. We follow the classification proposed by Goldberg (see Table 12-24).<sup>738</sup>

## Syndromes With Absent Limbs and Facial Anomalies

### ***Aglossia-Adactylia Syndrome***

Aglossia-adactylia syndrome consists of transverse amputations of the limbs and malformations of the mouth, including micrognathia, vestigial tongue (hypoglossia), dental abnormalities, and ankylosis of the tongue to the hard palate, the floor of the mouth, or the lips (glossopalatine ankylosis). The spectrum of anomalies of the extremities is variable, ranging from absent digits to severe deficiencies of all four extremities. Intelligence is generally normal. The condition is sporadic and has been attributed to a vascular accident.<sup>744,745</sup> It includes the Moebius sequence, Hanhart syndrome, glossopalatine ankylosis syndrome, limb deficiency-splenogonadal fusion syndrome, and Charlie M syndrome.<sup>746-751</sup> There is confusion in the classification of these patients because of the associated anomalies and the frequency of overlapping features. Although some authors have considered Hanhart syndrome and glossopalatine ankylosis syndrome as distinct entities, differential diagnosis is extremely difficult.<sup>752</sup>

### ***Moebius Sequence***

The Moebius sequence consists of a number of facial anomalies attributed to paralysis of the sixth and seventh cranial nerves.<sup>753</sup> Limited jaw mobility and micrognathia are present.<sup>754,755</sup> Ptosis is also a common feature. The Moebius sequence is generally sporadic, but autosomal-dominant, autosomal-recessive, and X-linked recessive forms have been described.<sup>756-758</sup> A large study conducted in Brazil documented the association between exposure to misoprostol during early pregnancy and vascular disruption defects,

including Moebius sequence and transverse limb reduction defects.<sup>759</sup> The associated limb reduction anomalies (25% of cases) are generally present in the upper extremities and range from transverse deficiencies to absent digits. Mental retardation occurs in 10% of the cases.<sup>756</sup> The Moebius, Poland, and Klippel-Feil syndromes have been considered subclavian artery supply disruption sequences, based on the hypothesis that interruption of the early embryonic blood supply to the subclavian artery, vertebral artery, and their branches may lead to these conditions.<sup>757,760-766</sup>

## Limb Reduction Defects Associated With Other Anomalies

### ***Congenital Hemidysplasia With Ichthyosiform Erythroderma and Limb Defects***

Congenital hemidysplasia with ichthyosiform erythroderma and limb defects (CHILD syndrome) is a defect characterized by strict demarcation of the lesions to one side of the midline.<sup>767-769</sup> The presence of unilateral defects of long bones is an important feature of the syndrome.<sup>770</sup> Limb deficiencies may vary from hypoplasia of phalanges or metacarpals to complete absence of an extremity. The calvarium, scapulae, or ribs may also be involved. Zellweger syndrome, chondrodysplasia punctata, and warfarin embryopathy may present with similar findings. Visceral anomalies include congenital heart disease,<sup>770,771</sup> unilateral hydronephrosis, hydroureter, and unilateral absence of the kidney, fallopian tube, ovaries, adrenal gland, and thyroid. CHILD syndrome predominantly affects females (by a ratio of 19:1)<sup>772,773</sup> and is caused by mutations in the NSDHL gene (NAD[P]H steroid dehydrogenase-like protein), located at Xq28 and encoding a  $\beta$ -hydroxysteroid dehydrogenase involved in the cholesterol biosynthetic pathway.<sup>774-776</sup>

### ***Fibula Aplasia Complex Brachydactyly (Du Pan Syndrome)***

Fibula aplasia complex brachydactyly (Du Pan syndrome) is an extremely rare condition characterized by bilateral agenesis of the fibula with abnormalities of the metacarpals and proximal phalanges. Limb reduction defects can involve the lower extremities.<sup>777</sup> An autosomal-recessive pattern of inheritance has been suggested.<sup>778</sup> Faiyaz-Ul-Haque et al<sup>779</sup> have examined genomic DNA from a family with Du Pan syndrome for mutations in the *CDMP1* gene. Affected individuals were homozygous for a missense mutation, *T1322C*, in the coding region of the *CDMP1* gene. Homozygous *CDMP1* mutations also cause Hunter-Thompson and Grebe syndromes.<sup>780</sup>

### ***Splenogonadal Fusion Syndrome***

Splenogonadal fusion syndrome is characterized by limb reduction defects and splenogonadal fusion.<sup>781,782</sup> Most reported cases have occurred in boys.<sup>783</sup> Typically, there is a mass in the scrotum, and an ectopic spleen is identified during surgery.<sup>784</sup> There is a continuous type in which the normally located spleen is connected to the gonad by bands or cords of splenic tissue.<sup>785</sup> A review of 14 reported cases indicates that there is some overlap between this syndrome



and the aglossia-adactylia syndrome or Hanhart syndrome.<sup>786</sup>

### **Adams-Oliver Syndrome**

Adams-Oliver syndrome is a group of disorders characterized by the association of limb reduction defects and scalp anomalies (aplasia cutis and deficiency of bony calvarium).<sup>787</sup> Sporadic and familial cases have been reported.<sup>788</sup> Other organ systems may be involved, and there are reports of associated cardiovascular, brain, pulmonary and renal anomalies.<sup>789-795</sup> Becker et al<sup>796</sup> reported prenatal diagnosis by ultrasound of two cases of Adams-Oliver syndrome in the same family, the first at 13 weeks and the second at 23 weeks of gestation. Both cases showed limb reduction defects and, in the second case, the scalp defect was diagnosed as an echo-free space between the scalp and bone.

### **Phocomelia**

In phocomelia, the extremities resemble those of a seal. Typically, the hands and feet are present, but the intervening arms and legs are absent. Hands and feet may be normal or abnormal. Three syndromes must be considered in the differential diagnosis of phocomelia: Roberts syndrome, some varieties of the TAR syndrome, and Grebe syndrome. Phocomelia also can be caused by exposure to thalidomide.<sup>797</sup> Prenatal diagnosis of phocomelia has been reported by 3DUS.<sup>798</sup>

### **Roberts Syndrome and SC Phocomelia Syndrome**

Roberts syndrome is an autosomal-recessive disorder characterized by the association of tetraphocomelia and craniofacial dysmorphism, including macrocephaly, hypertelorism, shallow orbits, facial clefting defects, and hypoplastic nasal alae.<sup>799-802</sup> The upper extremities are generally more severely affected than the lower extremities. Polyhydramnios has been noted, and other anomalies associated with the syndrome include horseshoe kidney, ventriculomegaly, cephalocele, and spina bifida.<sup>803</sup> Roberts syndrome is caused by mutations in the *ESCO2* gene (establishment of cohesion 1 homolog 2).<sup>804</sup>

SC phocomelia syndrome is an allelic disorder caused by mutations in the *ESCO2* gene<sup>802</sup> with a similar, but milder phenotype than Roberts syndrome. SC phocomelia (named after the first descriptions in two families with surnames beginning with S and C, respectively)<sup>805</sup> is characterized by (1) nearly symmetric reductive malformations of the limbs, resembling phocomelia; (2) flexion contractures of various joints; (3) minor anomalies, including capillary hemangioma of the face, forehead and ears, hypoplastic cartilages of the ears and nose, micrognathia, scanty silvery-blond hair, and cloudy corneas; (4) growth restriction; and (5) mental retardation.<sup>264</sup> Mental retardation may be mild and survival into adulthood is common.<sup>802</sup>

Differentiation between the two conditions is based on phenotypic characteristics only, as the phenotype cannot be predicted by the genotype. Prenatal diagnosis for both conditions has been reported.<sup>26,803,806-817</sup>

### **Grebe Syndrome**

Grebe syndrome (Grebe-Quelle-Salgado chondrodystrophy) is an autosomal-recessive nonlethal acromesomelic skeletal disorder. It was first described in two girls by Grebe,<sup>818</sup> and subsequently in 47 Brazilian individuals by Quelle-Salgado.<sup>819</sup> The prevalence at birth has been estimated as 5:1,000,000.<sup>820</sup> Affected individuals have normal head, neck, and trunk skeleton, relatively normal humeri and femora, short and deformed radii, ulnae, tibiae, and fibulae, and severe abnormalities of hands and feet. Polydactyly is frequent. Digits are very small and have been variously described bulbous,<sup>821</sup> bud-like,<sup>822</sup> mere knobs,<sup>823</sup> globular appendages,<sup>824</sup> or stubby toe-like fingers.<sup>825</sup> The proximal and middle phalanges of the fingers and toes are invariably absent, while the distal phalanges are present.<sup>824</sup> Radiographic documentation has provided information on subtle clinical characteristics for obligate heterozygotes: polydactyly, brachydactyly, hallux valgus, and metatarsus adductus.<sup>824-827</sup> The disease is caused by a missense mutation in the gene encoding cartilage-derived morphogenetic protein-1 (CDMP-1).<sup>828</sup> Survivors have normal intelligence and develop normal secondary sexual characteristics. Prenatal diagnosis of Grebe syndrome has been made based on the phenotypic features of the disease (acromesomelic dysplasia and dysmorphic distal appendages with normal craniofacial and axial skeletal development),<sup>821,829,830</sup> as well as by the identification of mutations in the CDMP-1 gene.<sup>830</sup>

### **Thrombocytopenia With Absent Radius Syndrome**

TAR syndrome is discussed in detail in the section on radial clubhand deformities.

### **Congenital Short Femur (Proximal Femoral Focal Deficiency)**

Proximal femoral focal deficiency, or congenital short femur, refers to a group of disorders encompassing a wide range of congenital developmental anomalies of the femur. The disorder has been classified into five groups: type I, simple hypoplasia of the femur; type II, short femur with angulated shaft; type III, short femur with coxa vara (most common); type IV, absent or defective proximal femur; and type V, absent or rudimentary femur.<sup>831,832</sup> (Fig. 12-44). One or both femora can be affected, although the right femur is more frequently involved. Anomalies of the upper limbs can also be present and do not exclude the diagnosis.<sup>29</sup> Proximal femoral focal deficiency syndrome may be associated with umbilical or inguinal hernias. If both femora are affected, it is important to examine the face carefully, because the disorder may be bilateral femoral hypoplasia and unusual facies syndrome,<sup>833,834</sup> which consists of bilateral femoral hypoplasia and facial anomalies, including short nose with broad tip, long philtrum, micrognathia, and cleft palate. Long bone abnormalities can extend to other segments of the lower extremities (absent fibula) and to the upper extremities. Femoral focal deficiency syndrome is considered a sporadic condition, but a familial form has been described. Except in bilateral proximal focal deficiency, the diagnosis is usually suspected when there is unilateral short femur, in the absence of other anomalies.<sup>834-838</sup>





**FIGURE 12-44.** Second trimester sonogram in a fetus with proximal femoral focal deficiency. The right femur (arrow) is significantly shorter than the left.

If the defect is unilateral, it may correspond to the femur-fibula-ulnar or femur-tibia-radius complex. These two syndromes have different implications for genetic counseling: the former is nonfamilial, whereas the second has a strong genetic component.<sup>839</sup>

## SPLIT HAND AND FOOT DEFORMITIES

The term split-hand-and-foot syndrome is used to refer to a group of disorders characterized by splitting of the hand and foot into two parts. Other terms include lobster-claw deformity, ectrodactyly, and aborted fingers.<sup>774,840</sup> The conditions are classified into typical and atypical varieties.<sup>841</sup> The typical form consists of absence of both the finger and the metacarpal bone, resulting in a deep V-shaped central defect that clearly divides the hand into an ulnar and a radial part. It occurs in 1 per 90,000 live births and has a familial tendency (usually inherited in an autosomal dominant fashion).<sup>842</sup> The atypical variety is characterized by a much wider cleft formed by a defect of the metacarpals and the middle fingers. As a consequence, the cleft is U shaped and wide, with only thumb and small finger remaining. The atypical variety occurs in 1 per 150,000 live births.<sup>843</sup>

Although a complex system for the classification of these disorders, based on the distribution of remaining fingers, has been proposed,<sup>844</sup> it is not helpful in differential diagnosis and syndrome classification. Split-hand-and-foot deformities can occur as isolated anomalies or as part of a more complex syndrome. The syndromic types are more frequently encountered.

The split-hand-and-foot and absent-long-bones syndromes include two conditions in which there is split hand and aplasia of the tibia or split foot with aplasia of the ulna. However, skeletal anomalies are not limited to these bones; the clavicle, femur, and fibula can also be affected. The pattern of inheritance of these disorders has not been clearly

determined. Autosomal-dominant, recessive, and X-linked recessive patterns have been proposed.<sup>845</sup>

## ECTRODACTYLY ECTODERMAL DYSPLASIA-CLEFT LIP/PALATE SYNDROME

Ectrodactyly ectodermal dysplasia-cleft lip/palate syndrome is an autosomal-dominant condition characterized by the triad of ectrodactyly, ectodermal dysplasia, and facial clefting.<sup>846</sup> Ectrodactyly generally involves the four extremities, with more severe deformities of the hands.<sup>847,848</sup> The spectrum of ectodermal defects is wide and includes hypopigmentation, dry skin, sparse hair, and dental defects.<sup>849-852</sup> Tear duct anomalies and decreased lacrimal secretions lead to chronic keratoconjunctivitis and severe loss of visual acuity.<sup>853,854</sup> Cleft lip is generally bilateral. Obstructive uropathy often occurs in this condition.<sup>855</sup> Intelligence is generally normal.<sup>858</sup> Mutations in the *P63* gene account for most cases of ectodermal dysplasia-cleft lip/palate syndrome.<sup>846,857</sup>

A different group of syndromes involves associations of the split-hand-and-foot deformity with other anomalies. These entities include split foot and triphalangeal thumb, split foot and hand and central polydactyly, Karsch-Neugebauer syndrome (split hand and foot with congenital nystagmus), and mandibulofacial dysostosis (Fontaine syndrome).<sup>858</sup>

## CLUBHANDS

Clubhand deformities are classified into two main categories: radial and ulnar. Radial clubhand includes a wide spectrum of disorders that encompass absent thumb, thumb hypoplasia, thin first metacarpal, and absent radius (Table 12-26). Ulnar clubhand is much less frequent than radial clubhand and ranges from mild deviations of the hand on the ulnar side of the forearm to complete absence of the ulna. Although radial clubhand is frequently syndromic, ulnar clubhand is usually an isolated anomaly.<sup>859-862</sup> Table 12-27 displays conditions that present with ulnar ray defects.

Whenever a clubhand is identified, it is important to conduct a thorough examination of the fetus and newborn to delineate associated anomalies that may suggest a syndrome. Fetal blood-sampling procedures and fetal echocardiography are recommended. A complete blood cell count, including platelets, is important to establish the diagnosis of Fanconi pancytopenia, TAR syndrome, and Aase syndrome. A fetal karyotype is indicated because several chromosomal abnormalities (e.g., trisomy 18, trisomy 21, and other structural aberrations) have been reported in association with clubhand deformities. Congenital heart disease is an important feature of the Holt-Oram syndrome, the Lewis upper limb-cardiovascular syndrome, and some cases of TAR syndrome.

### Radial Clubhand

The term isolated radial clubhand indicates that the clubhand is not part of a recognized syndrome.<sup>862,863</sup> However, this does not exclude that other anomalies may be



**Table 12-26** Radial Ray Defects: A Differential Diagnosis of Congenital Deficiency of the Radius and Radial Ray

- I. Isolated: nonsyndromatic
- II. Syndromes with blood dyscrasias
  - A. Fanconi anemia
  - B. Thrombocytopenia with absent radii syndrome
  - C. Aase syndrome: congenital anemia, nonopposable triphalangeal thumb, scaphoid and distal radius hypoplasia, radioulnar synostosis, short stature with narrow shoulders, autosomal recessive (see Diamond-Blackfan syndrome for a similar, perhaps identical, syndrome)
- III. Syndromes with congenital heart disease
  - A. Holt-Oram syndrome
  - B. Lewis upper limb–cardiovascular syndrome: more extensive arm malformations and more complex heart anomalies than with Holt-Oram but probably not a separate syndrome, autosomal dominant
- IV. Syndromes with craniofacial abnormalities
  - A. Nager acrofacial dysostosis
  - B. Radial clubhand and cleft lip and/or cleft palate: sporadic
  - C. Juberg-Hayward syndrome: cleft lip and palate, hypoplastic thumbs, short radius, radial head subluxation, autosomal recessive
  - D. Baller-Gerold syndrome: craniosynostosis, bilateral radial clubhand, absent/hypoplastic thumb, autosomal recessive
  - E. Rothmund-Thomson syndrome: prematurely aged skin changes, juvenile cataract, sparse gray hair, absent thumbs, radial clubhands, occasional knee dysplasia (see Progeria syndromes)
  - F. Duane-radial dysplasia syndrome: abnormal ocular movements: inability to abduct and eyeball retraction with adduction, radius and radial ray hypoplasia, vertebral anomalies, renal malformation, autosomal dominant (see Klippel-Feil variants)
  - G. The IVIC syndrome (Instituto Venezolano de Investigaciones Cientificas): radial ray deficiency, hypoplastic or absent thumbs and radial clubhands, impaired hearing, abnormal movements of extraocular muscles with strabismus, autosomal dominant
  - H. LARD syndrome (lacrimo-auriculo-radial-dental; Levy-Hollister): absent lacrimal structures, protuberant ears, thumb and radial hypoplasia, abnormal teeth, autosomal dominant
  - I. Radial defects with ear anomalies and cranial nerve 7 dysfunction
  - J. Radial hypoplasia, triphalangeal thumb, hypospadias, diastema or maxillary central incisors, autosomal dominant
- V. Syndromes with congenital scoliosis
  - A. VATER association
  - B. Goldenhar syndrome (oculoauriculovertebral dysplasia)
  - C. Klippel-Feil syndrome
- VI. Radial aplasia and chromosome aberrations
- VII. Syndromes with mental retardation
  - A. Seckel's syndrome (bird-headed dwarfism): microcephaly, beaklike protrusion of nose, mental retardation, absent/hypoplastic thumbs, bilateral dislocated hips
- VIII. Thalidomide embryopathy (of historical interest, but some 60% had radial clubhand)

Reproduced with permission from Goldberg MD: The Dysmorphic Child: An Orthopedic Perspective. New York, Raven Press, 1987.

present (e.g., scoliosis and congenital heart disease). Isolated nonsyndromic radial clubhand is generally a sporadic disorder.<sup>859-862</sup> A detailed list of conditions associated with radial clubhands is presented in Table 12-26.

## Radial Clubhand and Hematologic Disorders

Radial clubhand may be part of the three syndromes characterized by hematologic abnormalities: Fanconi pancytopenia, TAR syndrome, and Aase syndrome.

### Fanconi Anemia

Fanconi anemia (pancytopenia) is an autosomal-recessive disease characterized by the association of bone marrow failure (anemia, leukopenia, and thrombocytopenia)<sup>864</sup> and skeletal anomalies, including radial clubhand with absent thumbs, radial hypoplasia, and a high frequency of chromosomal instability (demonstrated in amniotic fluid cells or fetal lymphocytes as a high frequency of chromosomal

breakage after incubation with diepoxy-butane).<sup>865-868</sup> Approximately 25% of affected individuals do not have limb reduction anomalies. Associated findings include microcephaly, congenital dislocation of the hips, scoliosis, as well as cardiac, pulmonary, and gastrointestinal anomalies.<sup>869-871</sup> Intrauterine growth restriction is common. Up to 25% of the patients will show some degree of mental deficiency. It is assumed that the basic defect is related to the inability to repair DNA damage, in particular that of so-called DNA cross-links. At present, at least 11 complementation groups (A, B, C D1/BRCA2, D2, E, F, G, I, J, and L)<sup>872</sup> and eight associated genes have been identified: *FANCA*, *FANCC*, *FANCD2*, *FANCE*, *FANCF*, *FANCG/XRCC9*, *FANCL* and *FANCD1 (BRCA2)*.<sup>873-880</sup> About 200 mutations have been described, and among these, mutations in the gene for complementation group FA-A (*FANCA*) account for approximately 65% of the cases.<sup>872</sup> Prenatal diagnosis has been reported many times.<sup>837,881-891</sup> Molecular genetic testing is currently available for mutation analysis of the common Ashkenazi Jewish *FANCC* mutation and sequence analysis for *FANCA*, *FANCC*, *FANCF*, and *FANCG*.<sup>892</sup> For those cases



**Table 12-27** Ulnar Ray Defects: A Differential Diagnosis of Congenital Deficiency of the Ulna and Ulnar Ray

- I. Isolated: nonsyndromatic absent ulna
- II. Ulna hypoplasia and skeletal deficiency elsewhere
  - A. Ulna aplasia with lobster claw deformity of hand and/or foot, autosomal dominant
  - B. Femur-fibula-ulna complex
- III. Syndromes with ulna deficiency
  - A. Cornelia de Lange's syndrome
  - B. Miller syndrome (postaxial acrofacial dysostosis): absent ulna and ulnar rays and absent fourth and fifth toes; Treacher-Collins mandibulofacial hypoplasia, autosomal recessive; distinguish from Nagai preaxial acrofacial dysostosis
  - C. Pallister ulnar-mammary syndrome: hypoplasia of ulna and ulnar rays; hypoplasia of the breast and absence of apocrine sweat glands, autosomal dominant
  - D. Pillay syndrome (ophthalmomandibulomelic dysplasia): absent distal third of ulna, absent olecranon, hypoplastic trochlea and proximal radius, fusion of interphalangeal joints in ulnar fingers, knee dysplasia; corneal opacities, fusion of temporomandibular joint, autosomal dominant
  - E. Weyers' oligodactyly syndrome: deficiency of ulna and ulnar rays, antecubital webbing, short sternum, malformed kidney and spleen, cleft lip and palate, sporadic
  - F. Schnitzel's syndrome: absent/hypoplastic fourth, fifth metacarpals and phalanges, hypogenitalism, anal atresia, autosomal dominant
  - G. Mesomelic dwarfism, Reinhardt-Pfeiffer type (ulno-fibula dysplasia): a generalized bone dysplasia but with a disproportionate hypoplasia of the ulna and fibula, autosomal dominant
  - H. Mesomelic dwarfism, Langer's type: a generalized bone dysplasia, but with aplasia of the distal ulna and proximal fibula and hypoplasia of the mandible

Reproduced with permission from Goldberg MD: *The Dysmorphic Child: An Orthopedic Perspective*. New York, Raven Press, 1987.

in which the affected gene and parental mutations are not known (e.g., in case of radial ray abnormalities identified by ultrasound but negative family history), chromosome breakage studies after exposure to DNA cross-linking agents,<sup>885-887</sup> or single-cell parameter flow cytometry of amniotic fluid cell cultures, or bivariate flow cytometry of umbilical cord cell cultures<sup>893</sup> have been used for prenatal diagnosis. The rationale for the use flow cytometry to test for Fanconi anemia is the hypersensitivity Fanconi anemia cells to alkylating agents leading to elevated G2-phase cell fractions in positive cases.<sup>893</sup>

### **Thrombocytopenia With Absent Radius Syndrome**

TAR syndrome is an autosomal recessive disorder characterized by thrombocytopenia (platelet count of less than 100,000/mm<sup>3</sup>) and bilateral absence of the radius.<sup>895-898</sup> Thumbs and metacarpals are always present. The ulna and humerus may be absent, and clubfoot deformities may occur. Congenital heart disease is present in 33% of the cases (e.g., tetralogy of Fallot and septal defects). Delivery by cesarean section is recommended, because these fetuses are at risk for intracranial hemorrhage.<sup>899,900</sup> TAR has been successfully diagnosed in utero many times.<sup>899-914</sup>

### **Aase Syndrome**

Aase syndrome is an autosomal-recessive condition characterized by congenital hypoplastic anemia and a radial clubhand with bilateral triphalangeal thumb and a hypoplastic distal radius.<sup>915-918</sup> Cardiac defects (ventricular septal defects and coarctation of the aorta) may be present.<sup>919</sup> Triphalangeal thumbs are a feature of several

bone dysostoses and malformation syndromes. They may also occur in random association with other defects, and as isolated, often familial, anomalies.<sup>920</sup> The differential diagnosis of this condition includes Holt-Oram syndrome, Diamond-Blackfan syndrome,<sup>921,922</sup> chromosomal abnormalities, and fetal hydantoin syndrome.

### **Holt-Oram Syndrome**

Holt-Oram syndrome is an autosomal-dominant disorder characterized by congenital heart disease (mainly atrial septal defects, secundum type, and ventricular septal defects),<sup>207,921,923-926</sup> aplasia or hypoplasia of the radius, and triphalangeal or absent thumbs.<sup>927,928</sup> Limb defects are often asymmetric, with the left side being more affected than the right side. There is no correlation between the severity of the limb defects and cardiac anomalies.<sup>929,930</sup> Indeed, some individuals have only a skeletal anomaly.<sup>932</sup> Other findings include hypertelorism, chest wall, and vertebral anomalies.<sup>931-934</sup> This condition has been diagnosed prenatally by 2DUS and 3DUS.<sup>931,935-939</sup> Holt-Oram syndrome is caused by mutations in the *TBX5* gene,<sup>939,940</sup> and pre-implantation diagnosis of this condition has been reported.<sup>941</sup> The upper limb-cardiovascular syndrome described by Lewis and colleagues is probably not a separate entity from Holt-Oram syndrome.<sup>942</sup>

### **Radial Clubhand and Scoliosis**

Radial clubhand may also be associated with congenital scoliosis. The three syndromes that should be considered part of the differential diagnosis include VATER association, some cases of the Goldenhar syndrome, and the Klippel-Feil syndrome.<sup>943</sup>



### VATER Association

VATER association is the result of a defective mesodermal development during embryogenesis before the 35th day of gestation.<sup>944-947</sup> The typical findings are vertebral segmentation defects (70%), anal atresia (80%), tracheoesophageal fistula (70%), esophageal atresia, and radial and renal defects (65% and 53%, respectively).<sup>948,949</sup> Other anomalies include a single umbilical artery (35%) and congenital heart disease, occurring in nearly 50% of the patients.<sup>950-955</sup> VATER association occurs sporadically, although recurrence within a sibship has been reported.<sup>953</sup> Prenatal diagnosis by sonography has been reported.<sup>66,955-965</sup>

### Goldenhar Syndrome

Goldenhar syndrome is characterized by hemifacial microsomia, vertebral anomalies, and radial defects.<sup>966-970</sup> Alterations in the morphogenesis of the first and second brachial arches result in hypoplasia of the malar, maxillary, or mandibular region; microtia; and ocular and oropharyngeal anomalies.<sup>970-975</sup> Prenatal diagnosis has been reported.<sup>972,977-979</sup>

### Klippel-Feil Syndrome

Klippel-Feil syndrome is characterized by fusion of any two the cervical vertebrae, resulting in short neck, low posterior hair line, and restricted mobility of the upper spine. Several associated anomalies may be present, including spina bifida, cleft palate, rib abnormalities, lung disorders, congenital heart disease, and limb anomalies.<sup>980</sup> Klippel-Feil syndrome has not been diagnosed prenatally.

### Other Conditions Associated With Radial Clubhand

Radial clubhand has also been reported in association with several chromosomal anomalies, including trisomies 18 and 21, deletion of the long arm of 13, and ring formation of chromosome 4.<sup>868,981,982</sup>

Some disorders present with craniofacial abnormalities and radial clubhand deformities. These conditions are sporadic and have common features that make a prenatal differential diagnosis difficult. The most common craniofacial anomaly is cleft lip and palate. Uuspaa's study of 3225 cases with orofacial cleft showed a 2.8% association with upper extremity deformities.<sup>983</sup>

### Ulnar Clubhand

Ulnar clubhand usually occurs as an isolated, nonsyndromic anomaly. Syndromes that may have ulnar clubhand as part of their phenotype (e.g., Poland syndrome) are described in Table 12-27.<sup>984</sup>

### Polydactyly

Polydactyly is the presence of an additional digit (see Fig. 12-25).<sup>985,986</sup> The extra digit may range from a fleshy nubbin to a complete digit with controlled flexion and extension (see Figs. 12-39 and 12-40). Polydactyly can be



**FIGURE 12-45.** Femoral hypoplasia—unusual facies syndrome. Note the absence of the left femur and only a tiny portion of ossified bone on the right side. There is partial fusion of the tibia and fibula. Of interest is the presence of preaxial polydactyly (arrows) in both feet.

classified as postaxial (the most common form), preaxial, and central (see Table 12-16). Postaxial polydactyly occurs on the ulnar side of the hand and fibular side of the foot.<sup>987-989</sup> Preaxial polydactyly is present on the radial side of the hand and the tibial side of the foot (Fig. 12-45).<sup>990</sup> Central polydactyly consists of an extra digit that is usually hidden between the long and the ring finger.<sup>991-994</sup>

Evidence from mouse models suggests that many types of polydactyly involve the hedgehog pathway, either directly or indirectly. Specifically, mutations in the downstream effector of Shh, *GLI3*, give rise to several polydactyly phenotypes, the mildest of which are postaxial polydactyly type I and preaxial polydactyly type IV (or Creig cephalopolysyndactyly).<sup>5</sup> Postaxial polydactyly type I is about 10 times more frequent in blacks than in whites, and is characterized by an extra digit that is well developed and articulates with the fifth digit or an extra metacarpal/metatarsal.<sup>264</sup> Creig cephalopolysyndactyly is characterized by pre- or postaxial polysyndactyly of variable degrees, frontal bossing, and hypertelorism.<sup>5</sup> The most severe malformations are found in Pallister-Hall syndrome, which is characterized by hypothalamic hamartomas, craniofacial anomalies, polysyndactyly, and anal defects.<sup>994</sup>

Although the majority of cases of polydactyly are isolated and inherited as an autosomal-dominant trait, polydactyly is



**Table 12-28** Disorders of the Developing Motor System on All Levels, Leading to Immobilization

Disorders of the developing neuromuscular system
Loss of anterior horn cells
Radicular disease with collagen proliferation
Peripheral neuropathy with neurofibromatosis
Congenital myasthenia
Neonatal myasthenia (maternal myasthenia gravis)
Amyoplasia congenital
Congenital muscular dystrophy
Central core disease
Congenital myotonic dystrophy
Glycogen accumulation myopathy
Disorders of developing connective tissue or connective tissue disease
Muscular and articular connective tissue dystrophy
Articular defects by mesenchymal dysplasia
Increased collagen synthesis
Disorders of developing medulla or medullar disease
Congenital spinal epidural hemorrhage
Congenital duplication of the spinal canal
Disorders of brain development (e.g., porencephaly or brain disease)
Congenital encephalopathy

a phenotypic trait in 119 disorders (97 syndromic and 22 nonsyndromic), 39 of which are caused by mutations in known genes and 16 are mapped to a locus in the genome.<sup>995</sup> Central polydactyly is often bilateral and may be associated with other hand and foot malformations.<sup>991-993</sup> Preaxial polydactyly, however, especially when a triphalangeal thumb is present, is more likely to be part of a syndrome.

## Arthrogryposis

The term arthrogryposis multiplex congenita (AMC) refers to multiple joint contractures present at birth in an intact skeleton.<sup>996-999</sup> The condition is present in 3 per 10,000 live births.<sup>999,1000</sup>

Normal fetal movement between 7 and 8 weeks of gestation onward is important for the development of the joints; limitation of the fetal joint motion leads to the development of contractures and AMC.<sup>1001,1002</sup> This has been confirmed in animal models,<sup>1003</sup> including chick and rat embryos injected with tubocurarin and botulism toxins,<sup>1004,1005</sup> viral myopathy induced by coxsackie A viruses,<sup>1006</sup> and cross-section of the spinal cord.<sup>1007</sup> Therefore, AMC is a syndrome, not a specific disorder. The incidence of the different underlying causes of AMC is variable in the literature. Neurologic, muscular, connective tissue, skeletal abnormalities, and intrauterine crowding can lead to impaired fetal motion and AMC.<sup>1001,1002</sup> Table 12-28 shows a list of motor disorders that can lead to AMC. In a series of 74 children, Banker<sup>1009</sup> found that the most common causes of AMC were neurogenic disorders, followed by myopathic disorders. Similarly, in an autopsy series of 75 fetuses and newborns, Swinyard<sup>1009</sup> reported CNS disorders as a cause of AMC in 75% of the cases, followed by muscular disorders in 10% to 15%. In contrast, Quinn et al<sup>1010</sup> reported that only 5 of 21 cases of lethal AMC were of neurogenic etiology, whereas 11 were myogenic and 5 were of uncertain pathology.

The etiology of AMC may derive from hereditary conditions,<sup>1012-1018</sup> infectious agents, drugs, toxins and fetal alcohol syndrome.<sup>1003,1004,1021</sup> Maternal hyperthermia has also been associated with AMC.<sup>1020</sup> Maternal antibodies specific for a fetal acetylcholine receptor have been reported to cause fetal AMC without evidence of maternal myasthenia gravis.<sup>1021,1023</sup> In addition, plasma from human mothers of fetuses with AMC, when injected into pregnant mice, causes deformities in the offspring.<sup>1023</sup> The pattern of inheritance depends on the specific cause of AMC.<sup>1024</sup> In a series of 350 cases, Hall<sup>1025</sup> found that 46% of them corresponded to a syndrome with no recurrence risk, 23% corresponded to disorders inherited with a Mendelian pattern (autosomal dominant, autosomal recessive, or X-linked), 20% were unknown conditions, 6% were associated with environmental disorders, 3% were chromosomal, and 2% were multifactorial in origin.

The recurrence risk varies depending on the underlying cause. Hall and Reed<sup>1020</sup> found that in 20% of 350 patients, no diagnosis was made. They concluded that, in this situation, the risk for recurrence would be 4.7% if only the limbs were affected, 7% if the CNS was involved, and 1.4% if the limbs and another area were involved.

In most cases of AMC, deformities are usually symmetric and involve the four limbs (Fig. 12-46). Anomalies of the lower extremities only, or bimelic involvement, can also occur. The severity of the deformities increases distally in the involved limb, with the hands and feet typically being the most affected.

Cardinal findings on prenatal ultrasonography include absence of fetal movement on real-time examination and severe flexion deformities.<sup>1026-1041</sup> Four-dimensional ultrasonography may help to better characterize the phenotype prenatally.<sup>1043</sup> Zelop and Benacerraf<sup>1033</sup> evaluated the clinical significance and outcome of postural deformities and contractures of the upper extremities detected prenatally. Among 52 fetuses with sonographically detected abnormalities





**FIGURE 12-46.** Arthrogryposis multiplex congenita. There is flexion of the upper limbs with hyperextension of the lower limbs.

of the upper extremities, 26 (59%) had aneuploidies, mostly trisomy 18 (88% [23/26]). Fetuses with a normal karyotype presented with a variety of syndromic conditions, including three cases of arthrogryposis multiplex congenita, and one case each of Pierre-Robin sequence, Freeman-Sheldon, and Whistler syndrome requiring gastroscopy-tube placement, and bilateral syndactyly requiring multiple corrective surgical procedures. The survival rate was 5% (8/52), and only one of the survivors was phenotypically normal after birth.

Many congenital anomalies are associated with AMC. The most frequent are cleft palate, Klippel-Feil syndrome, meningocele, and congenital heart disease. Ten percent of patients with AMC have associated anomalies of the CNS.<sup>997</sup>

The prognosis of AMC depends on the specific cause. Although some cases are uniformly lethal, others are associated with mild to moderate handicap. In a retrospective study of 828 cases of AMC, Fahy and Hall<sup>1043</sup> found that polyhydramnios is a poor prognostic sign.

## CLUBFOOT

Clubfoot (talipes equinovarus) is a congenital malformation of the bones of the ankle and foot resulting in the adduction of the forefoot, inversion of the heel, and plantar flexion of the forefoot and ankle.<sup>1141</sup> There is subluxation of the



**FIGURE 12-47.** Sonogram of the lower extremity in a fetus with unilateral clubfoot. Normally, when the tibia and fibula are seen, only a portion of the foot is seen in the same plane. The abnormal medial deviation of the foot results in all structures being seen en face.

talo-calcaneo-navicular joint. As a result of this malformation, the dorsal aspect of the foot is often rotated medially, which assumes a clublike appearance.<sup>1142</sup> The sonographic diagnosis is made when the metatarsals and phalanges of the foot are seen in the same plane as the tibia and fibula<sup>1142,1144</sup> (Fig. 12-47).

The severity of the clubfoot deformity varies from a postural deformity often requiring no treatment; an isolated clubfoot deformity, needing casting and possible surgery, often with a favorable outcome; or a complex clubfoot abnormality associated with other chromosomal, neuromuscular, or structural abnormalities. Clubfoot may also result from restriction of movement in utero as in severe oligohydramnios.<sup>1142</sup> The prevalence is often stated as one per 1000 live births, with a 2:1 male-to-female predisposition.<sup>1145</sup> Several series have demonstrated that an initially diagnosed isolated clubfoot abnormality was noted to be complex and associated with other abnormalities either later in pregnancy or in the neonatal period.<sup>1142,1146</sup> False-positive diagnoses are more prevalent when unilateral clubfoot is suspected than when bilateral clubfoot was suspected or diagnosed.<sup>1142</sup> The association of an isolated clubfoot abnormality with aneuploidy is controversial. Shipp and Benacerraf found that 5.9% of 87 fetuses with isolated clubfoot had an abnormal karyotype and concluded that amniocentesis is indicated after that diagnosis.<sup>1149</sup> Other investigators came to the opposite conclusion.<sup>1142,1143,1148</sup> In the series by Malone et al,<sup>1141</sup> there were no cases of aneuploidy on karyotype when the clubfoot was isolated.



## References

- Olsen BR, Reginato AM, Wang W: Bone development. *Ann Rev Cell Dev Biol* 16:191, 2000.
- Karsenty G: The complexities of skeletal biology. *Nature* 423:316, 2003.
- Moore KL, Persaud TVN: The skeletal system. In Moore KL, Persaud TVN (eds): *The Developing Human—Clinically Oriented Embryology*. Philadelphia, WB Saunders, 1998, p 384–402.
- Savarirayan R, Rimoin DL: Skeletal dysplasias. *Adv Pediatr* 51:209, 2004.
- Kornak U, Mundlos S: Genetic disorders of the skeleton: a developmental approach. *Am J Hum Genet* 73:447, 2003.
- Mundlos S: Skeletal morphogenesis. *Methods Mol Biol* 136:61, 2000.
- Summerbell D, Lewis JH, Wolpert L: Positional information in chick limb morphogenesis. *Nature* 244:492, 1973.
- Brand-Saberi B, Krenn V, Christ B: The control of directed myogenic cell migration in the avian limb bud. *Anat Embryol (Berl)* 180:555, 1989.
- Koussoulakos S: Vertebrate limb development: from Harrison GGOs limb disk transplantations to targeted disruption of *Hox* genes. *Anat Embryol (Berl)* 209:93, 2004.
- MacCabe JA, MacCabe AB, Abbott UK, et al: Limb development in diplopodia: a polydactylous mutation in the chicken. *J Exp Zool* 191:383, 1975.
- Hall BK, Miyake T: All for one and one for all: condensations and the initiation of skeletal development. *Bioessays* 22:138, 2000.
- Kronenberg HM: Developmental regulation of the growth plate. *Nature* 423:332, 2003.
- Ducy P: Cbfa1: a molecular switch in osteoblast biology. *Dev Dyn* 219:461, 2000.
- Nakashima K, Zhou X, Kunkel G, et al: The novel zinc finger-containing transcription factor osterix is required for osteoblast differentiation and bone formation. *Cell* 108:17, 2002.
- Zelzer E, Olsen BR: The genetic basis for skeletal diseases. *Nature* 423:343, 2003.
- Conlon RA, Reaume AG, Rossant J: Notch1 is required for the coordinate segmentation of somites. *Development* 121:1533, 1995.
- Palmeirim I, Henrique D, Ish-Horowicz D, et al: Avian hairy gene expression identifies a molecular clock linked to vertebrate segmentation and somitogenesis. *Cell* 91:639, 1997.
- Baker RE, Schnell S, Maini PK: A clock and wavefront mechanism for somite formation. *Dev Biol* 293:16, 2006.
- Ishikawa A, Kitajima S, Takahashi Y, et al: Mouse *Nkd1*, a Wnt antagonist, exhibits oscillatory gene expression in the PSM under the control of Notch signaling. *Mechanisms of Development* 121:1443, 2004.
- Dubrulle J, McGrew MJ, Pourquie O: FGF signaling controls somite boundary position and regulates segmentation clock control of spatiotemporal *HOX* gene activation. *Cell* 106:219, 2001.
- Fan CM, Tessier-Lavigne M: Patterning of mammalian somites by surface ectoderm and notochord: evidence for sclerotome induction by a hedgehog homolog. *Cell* 79:1175, 1994.
- Johnson RL, Laufer E, Riddle RD, et al: Ectopic expression of Sonic hedgehog alters dorsal-ventral patterning of somites. *Cell* 79:1165, 1994.
- Maymon E, Romero R, Ghezzi F, et al: Fetal skeletal anomalies. In Fleischer A, Manning F, Jeanty P, et al (eds): *Sonography in Obstetrics and Gynecology: Principles and Practice*. New York, McGraw-Hill, 2001, p 445–506.
- Superti-Furga A, Bonafé L, Rimoin DL: Molecular-pathogenetic classification of genetic disorders of the skeleton. *Am J Med Genet* 106:282, 2001.
- Superti-Furga A: Growing bone knowledge. *Clin Genet* 66:399, 2004.
- Parilla BV, Leeth EA, Kambich MP, et al: Antenatal detection of skeletal dysplasias. *J Ultrasound Med* 22:255, 2003.
- Hall CM: International nosology and classification of constitutional disorders of bone (2001). *Am J Med Genet* 113:65, 2002.
- Camera G, Mastroiacovo P: Birth prevalence of skeletal dysplasias in the Italian multicentric monitoring system for birth defects. In Papadatos CJ, Bartsocas CS (eds): *Skeletal Dysplasias*. New York, Alan R. Liss, 1982, p 441.
- Connor JM, Connor RA, Sweet EM, et al: Lethal neonatal chondrodysplasias in the West of Scotland 1970–1983 with a description of a thanatophoric, dysplasia-like, autosomal recessive disorder, Glasgow variant. *Am J Med Genet* 22:243, 1985.
- Rasmussen SA, Bieber FR, Benacerraf BR, et al: Epidemiology of osteochondrodysplasias: changing trends due to advances in prenatal diagnosis. *Am J Med Genet* 61:49, 1996.
- Gustavson KH, Jorulf H: Different types of osteochondrodysplasia in a consecutive series of newborns. *Helv Paediatr Acta* 30:307, 1975.
- Weldner BM, Persson PH, Ivarsson SA: Prenatal diagnosis of dwarfism by ultrasound screening. *Arch Dis Child* 60:1070, 1985.
- Orioli IM, Castilla EE, Barbosa-Neto JG: The birth prevalence rates for the skeletal dysplasias. *J Med Genet* 23:328, 1986.
- Stoll C, Dott B, Roth MP, Alembik Y: Birth prevalence rates of skeletal dysplasias. *Clin Genet* 35:88, 1989.
- Andersen PE, Jr., Hauge M: Congenital generalised bone dysplasias: a clinical, radiological, and epidemiological survey. *J Med Genet* 26:37, 1989.
- Andersen PE Jr: Prevalence of lethal osteochondrodysplasias in Denmark. *Am J Med Genet* 32:484, 1989.
- Kallen B, Knudsen LB, Mutchinick O, et al: Monitoring dominant germ cell mutations using skeletal dysplasias registered in malformation registries: an international feasibility study. *Int J Epidemiol* 22:107, 1993.
- Gordienko IY, Grechanina EY, Sopko NI, et al: Prenatal diagnosis of osteochondrodysplasias in high risk pregnancy. *Am J Med Genet* 63:90, 1996.
- Al Gazali LI, Bakir M, Hamid Z, et al: Birth prevalence and pattern of osteochondrodysplasias in an inbred high risk population. *Birth Defects Res Part A Clin Mol Teratol* 67:125, 2003.
- Savarirayan R, Rimoin DL: The skeletal dysplasias. *Best Pract Res Clin Endocrinol Metab* 16:547, 2002.
- International nomenclature of constitutional diseases of bone. Revision—May, 1977. *J Pediatr* 93:614, 1978.
- International Nomenclature of Constitutional Diseases of Bone—revision, May, 1983. *Australas Radiol* 30:163, 1986.
- Spranger J: International classification of osteochondrodysplasias. The International Working Group on Constitutional Diseases of Bone. *Eur J Pediatr* 151:407, 1992.
- Lachman RS, Tiller GE, Graham JM Jr, et al: Collagen, genes and the skeletal dysplasias on the edge of a new era: a review and update. *Eur J Radiol* 14:1, 1992.
- Lachman RS: International nomenclature and classification of the osteochondrodysplasias (1997). *Pediatr Radiol* 28:737, 1998.
- Lachman RS: Introduction and overview. *Pediatr Radiol* 28:735, 1998.
- Erlacher A, Filvaroff EH, Gitelman SE, et al: Toward a molecular understanding of skeletal development. *Cell* 80:371, 1995.
- Gilbert-Barnes E, Opitz JM: Abnormal bone development: histopathology of skeletal dysplasias. *Birth Defects Orig Artic Ser* 30:103, 1996.
- Horton WA: Progress in human chondrodysplasias: molecular genetics. *Ann N Y Acad Sci* 785:150, 1996.
- Horton WA: Molecular genetic basis of the human chondrodysplasias. *Endocrinol Metab Clin North Am* 25:683, 1996.
- Reardon W: Skeletal dysplasias detectable by DNA analysis. *Prenat Diagn* 16:1221, 1996.
- Spranger J, Maroteaux P: The lethal osteochondrodysplasias. *Adv Hum Genet* 19:1, 1990.
- Rouse GA, Filly RA, Toomey F, Grube GL: Short-limb skeletal dysplasias: evaluation of the fetal spine with sonography and radiography. *Radiology* 174:177, 1990.
- Brodie SG, Lachman RS, Jewell AF, et al: Lethal osteosclerotic osteochondrodysplasia with platyspondyly, metaphyseal widening, and intracellular inclusions in sibs. *Am J Med Genet* 80:423, 1998.
- Chen CP, Chern SR, Shih SL, et al: Kyphomelic dysplasia in two sib fetuses. *J Med Genet* 35:65, 1998.
- Chitayat D, Gruber H, Mullen BJ, et al: Hydrops-ectopic calcification-moth-eaten skeletal dysplasia (Greenberg dysplasia): prenatal diagnosis and further delineation of a rare genetic disorder. *Am J Med Genet* 47:272, 1993.
- Seller MJ, Berry AC, Maxwell D, et al: A new lethal chondrodysplasia with platyspondyly, long bone angulation and mixed bone density. *Clin Dysmorphol* 5:213, 1996.
- Trajkovski Z, Vrcakovski M, Saveski J, et al: Greenberg dysplasia (hydrops-ectopic calcification-moth-eaten skeletal dysplasia): prenatal ultrasound diagnosis and review of literature. *Am J Med Genet* 111:415, 2002.



59. Wilcox WR, Lucas BC, Loebel B, et al: Pacman dysplasia: report of two affected sibs. *Am J Med Genet* 77:272, 1998.
60. Benacerraf BR, Greene MF, Barss VA: Prenatal sonographic diagnosis of congenital hemivertebra. *J Ultrasound Med* 5:257, 1986.
61. Song TB, Kim YH, Oh ST, et al: Prenatal ultrasonographic diagnosis of congenital kyphosis due to anterior segmentation failure. *Asia Oceania J Obstet Gynaecol* 20:31, 1994.
62. Gembruch U, Niesen M, Kehrberg H, et al: Diastrophic dysplasia: a specific prenatal diagnosis by ultrasound. *Prenat Diagn* 8:539, 1988.
63. Nores JA, Rotmensch S, Romero R, et al: Atelosteogenesis type II: sonographic and radiological correlation. *Prenat Diagn* 12:741, 1992.
64. Tongsong T, Wanapirak C, Sirichotiyakul S, et al: Prenatal sonographic diagnosis of diastrophic dwarfism. *J Clin Ultrasound* 30:103, 2002.
65. Ryu JK, Cho JY, Choi JS: Prenatal sonographic diagnosis of focal musculoskeletal anomalies. *Korean J Radiol* 4:243, 2003.
66. Weisz B, Achiron R, Schindler A, et al: Prenatal sonographic diagnosis of hemivertebra. *J Ultrasound Med* 23:853, 2004.
67. Herzberg AJ, Effmann EL, Bradford WD: Variant of atelosteogenesis? Report of a 20-week fetus. *Am J Med Genet* 29:883, 1988.
68. Kurtz AB, Wapner RJ: Ultrasonographic diagnosis of second-trimester skeletal dysplasias: a prospective analysis in a high-risk population. *J Ultrasound Med* 2:99, 1983.
69. Goncalves L, Jeanty P: Fetal biometry of skeletal dysplasias: a multicentric study. *J Ultrasound Med* 13:977, 1994.
70. Gabrielli S, Falco P, Pilu G, et al: Can transvaginal fetal biometry be considered a useful tool for early detection of skeletal dysplasias in high-risk patients? *Ultrasound Obstet Gynecol* 13:107, 1999.
71. De Biasio P, Prefumo F, Lantieri PB, et al: Reference values for fetal limb biometry at 10-14 weeks of gestation. *Ultrasound Obstet Gynecol* 19:588, 2002.
72. Coffin GS, Siris E, Wegienka LC: Mental retardation with osteocartilaginous anomalies. *Am J Dis Child* 112:205, 1966.
73. Baker ER, Goldberg MJ: Diagnosis and management of skeletal dysplasias. *Semin Perinatol* 18:283, 1994.
74. Azouz EM, Teebi AS, Eyedoux P, et al: Bone dysplasias: an introduction. *Can Assoc Radiol J* 49:105, 1998.
75. Vanhoenacker FM, Van Hul W, Gielen J, et al: Congenital skeletal abnormalities: an introduction to the radiological semiology. *Eur J Radiol* 40:168, 2001.
76. Unger S: A genetic approach to the diagnosis of skeletal dysplasia. *Clin Orthop* 401:32, 2002.
77. Goncalves LF, Espinoza J, Mazor M, et al: Newer imaging modalities in the prenatal diagnosis of skeletal dysplasias. *Ultrasound Obstet Gynecol* 24:115, 2004.
78. Pretorius DH, Rumack CM, Manco-Johnson ML, et al: Specific skeletal dysplasias in utero: sonographic diagnosis. *Radiology* 159:237, 1986.
79. Donnemfeld AE, Mennuti MT: Second trimester diagnosis of fetal skeletal dysplasias. *Obstet Gynecol Surv* 42:199, 1987.
80. McGuire J, Manning F, Lange I, et al: Antenatal diagnosis of skeletal dysplasia using ultrasound. *Birth Defects Orig Artic Ser* 23:367, 1987.
81. Escobar LF, Bixler D, Weaver DD, et al: Bone dysplasias: the prenatal diagnostic challenge. *Am J Med Genet* 36:488, 1990.
82. Kurtz AB, Needleman L, Wapner RJ, et al: Usefulness of a short femur in the in utero detection of skeletal dysplasias. *Radiology* 177:197, 1990.
83. Spirt BA, Oliphant M, Gottlieb RH, et al: Prenatal sonographic evaluation of short-limbed dwarfism: an algorithmic approach. *Radiographics* 10:217, 1990.
84. Sharony R, Browne C, Lachman RS, et al: Prenatal diagnosis of the skeletal dysplasias. *Am J Obstet Gynecol* 169:668, 1993.
85. Bowerman RA: Anomalies of the fetal skeleton: sonographic findings. *AJR Am J Roentgenol* 164:973, 1995.
86. MacDonald MR, Welsh MP: Perinatal approach to skeletal dysplasia. *Nebr Med J* 80:334, 1995.
87. Carvalho L, Soares M, Feijoo MJ, et al: A collaborative approach to the diagnosis of a lethal short limb skeletal dysplasia. *Genet Couns* 8:139, 1997.
88. Gaffney G, Manning N, Boyd PA, et al: Prenatal sonographic diagnosis of skeletal dysplasias—a report of the diagnostic and prognostic accuracy in 35 cases. *Prenat Diagn* 18:357, 1998.
89. Doray B, Favre R, Viville B, et al: Prenatal sonographic diagnosis of skeletal dysplasias. A report of 47 cases. *Ann Genet* 43:163, 2000.
90. Tretter AE, Saunders RC, Meyers CM, et al: Antenatal diagnosis of lethal skeletal dysplasias. *Am J Med Genet* 75:518, 1998.
91. Hersh JH, Angle B, Pietrantonio M, et al: Predictive value of fetal ultrasonography in the diagnosis of a lethal skeletal dysplasia. *South Med J* 91:1137, 1998.
92. Merz E, Bahlmann F, Weber G, et al: Three-dimensional ultrasonography in prenatal diagnosis. *J Perinat Med* 23:213, 1995.
93. Steiner H, Spitzer D, Weiss-Wichert PH, et al: Three-dimensional ultrasound in prenatal diagnosis of skeletal dysplasia. *Prenat Diagn* 15:373, 1995.
94. Ploekinger-Ulm B, Ulm MR, Lee A, et al: Antenatal depiction of fetal digits with three-dimensional ultrasonography. *Am J Obstet Gynecol* 175:571, 1996.
95. Garjian KV, Pretorius DH, Budorick NE, et al: Fetal skeletal dysplasia: three-dimensional US—initial experience. *Radiology* 214:717, 2000.
96. Chen CP, Chern SR, Shih JC, et al: Prenatal diagnosis and genetic analysis of type I and type II thanatophoric dysplasia. *Prenat Diagn* 21:89, 2001.
97. Machado LE, Bonilla-Musoles F, Raga F, et al: Thanatophoric dysplasia: ultrasound diagnosis. *Ultrasound Q* 17:235, 2001.
98. Moeglin D, Benoit B: Three-dimensional sonographic aspects in the antenatal diagnosis of achondroplasia. *Ultrasound Obstet Gynecol* 18:81, 2001.
99. Kos M, Hafner T, Funduk-Kurjak B, et al: Limb deformities and three-dimensional ultrasound. *J Perinat Med* 30:40, 2002.
100. Viora E, Sciarone A, Bastonero S, et al: Three-dimensional ultrasound evaluation of short-rib polydactyly syndrome type II in the second trimester: a case report. *Ultrasound Obstet Gynecol* 19:88, 2002.
101. Clementschitsch G, Hasenohrl G, Steiner H, et al: [Early Diagnosis of a Fetal Skeletal Dysplasia Associated with Increased Nuchal Translucency with 2D and 3D Ultrasound]. *Ultraschall Med* 24:349, 2003.
102. Krakow D, Williams J III, Poehl M, et al: Use of three-dimensional ultrasound imaging in the diagnosis of prenatal-onset skeletal dysplasias. *Ultrasound Obstet Gynecol* 21:467, 2003.
103. Seow KM, Huang LW, Lin YH, et al: Prenatal three-dimensional ultrasound diagnosis of a campomelic dysplasia. *Arch Gynecol Obstet* 269:142, 2004.
104. Benoit B: The value of three-dimensional ultrasonography in the screening of the fetal skeleton. *Childs Nerv Syst* 19:403, 2003.
105. Shih JC, Peng SS, Hsiao SM, et al: Three-dimensional ultrasound diagnosis of Larsen syndrome with further characterization of neurological sequelae. *Ultrasound Obstet Gynecol* 24:89, 2004.
106. Ruano R, Molho M, Roume J, et al: Prenatal diagnosis of fetal skeletal dysplasias by combining two-dimensional and three-dimensional ultrasound and intrauterine three-dimensional helical computer tomography. *Ultrasound Obstet Gynecol* 24:134, 2004.
107. Wilting JE: Technical aspects of spiral-CT. *Medica Mundi* 43:34, 1989.
108. Brink JA: Technical aspects of helical (spiral) CT. *Radiol Clin North Am* 33:825, 1995.
109. Heiken JP, Brink JA, Vannier MW: Spiral (helical) CT. *Radiology* 189:647, 1993.
110. Brailon PM, Buenerd A, Lapillonne A, et al: Skeletal and total body volumes of human fetuses: assessment of reference data by spiral CT. *Pediatr Radiol* 32:354, 2002.
111. Wong GY, Wong SF, Chan WP, Ng WF: Three-dimensional ultrasound findings of spondylocostal dysostosis in the second trimester of pregnancy. *Ultrasound Obstet Gynecol* 27:580, 2006.
112. Blaumeiser B, Loquet P, Wuyts W, et al: Prenatal diagnosis of Pfeiffer syndrome type II. *Prenat Diagn* 24:644, 2004.
113. Esser T, Rogalla P, Bamberg C, et al: Application of the three-dimensional maximum mode in prenatal diagnosis of Apert syndrome. *Am J Obstet Gynecol* 193:1743, 2005.
114. Faro C, Chaoui R, Wegrzyn P, et al: Metopic suture in fetuses with Apert syndrome at 22-27 weeks of gestation. *Ultrasound Obstet Gynecol* 27:28, 2006.
115. Soto E, Richani K, Goncalves LF, et al: Three-dimensional ultrasound in the prenatal diagnosis of cleidocranial dysplasia associated with B-cell immunodeficiency. *Ultrasound Obstet Gynecol* 27:574, 2006.
116. Promsonthi P, Wattanasrichaigoon D: Prenatal diagnosis of campomelic dysplasia with three-dimensional ultrasound. *Ultrasound Obstet Gynecol* 27:583, 2006.



117. Pashayan H, Fraser FC, McIntyre JM, et al: Bilateral aplasia of the tibia, polydactyly and absent thumb in father and daughter. *J Bone Joint Surg Br* 53:495, 1971.
118. Luthy DA, Hall JG, Graham CB: Prenatal diagnosis of thrombocytopenia with absent radii. *Clin Genet* 15:495, 1979.
119. Filkins K, Russo J, Bilinski I, et al: Prenatal diagnosis of thrombocytopenia absent radius syndrome using ultrasound and fetoscopy. *Prenat Diagn* 4:139, 1984.
120. Graham M: Congenital short femur: prenatal sonographic diagnosis. *J Ultrasound Med* 4:361, 1985.
121. Hall CM, Washbrook J: REAMS: Radiological Electronic Atlas of Skeletal Malformation Syndromes. (1.0). 2000. London, Oxford Press Electronic Publishing.
122. DeVore GR, Horenstein J, Platt LD: Fetal echocardiography. VI. Assessment of cardiothoracic disproportion—a new technique for the diagnosis of thoracic hypoplasia. *Am J Obstet Gynecol* 155:1066, 1986.
123. Chitkara U, Rosenberg J, Chervenak FA, et al: Prenatal sonographic assessment of the fetal thorax: normal values. *Am J Obstet Gynecol* 156:1069, 1987.
124. Nimrod C, Davies D, Iwanicki S, et al: Ultrasound prediction of pulmonary hypoplasia. *Obstet Gynecol* 68:495, 1986.
125. Johnson A, Callan NA, Bhutani VK, et al: Ultrasonic ratio of fetal thoracic to abdominal circumference: an association with fetal pulmonary hypoplasia. *Am J Obstet Gynecol* 157:764, 1987.
126. Fong K, Ohlsson A, Zalev A: Fetal thoracic circumference: a prospective cross-sectional study with real-time ultrasound. *Am J Obstet Gynecol* 158:1154, 1988.
127. Songster GS, Gray DL, Crane JP: Prenatal prediction of lethal pulmonary hypoplasia using ultrasonic fetal chest circumference. *Obstet Gynecol* 73:261, 1989.
128. Vintzileos AM, Campbell WA, Rodis JF, et al: Comparison of six different ultrasonographic methods for predicting lethal fetal pulmonary hypoplasia. *Am J Obstet Gynecol* 161:606, 1989.
129. D'Alton M, Mercer B, Riddick E, et al: Serial thoracic versus abdominal circumference ratios for the prediction of pulmonary hypoplasia in premature rupture of the membranes remote from term. *Am J Obstet Gynecol* 166:658, 1992.
130. Maeda H, Nagata H, Tsukimori K, et al: Prenatal evaluation and obstetrical management of fetuses at risk of developing lung hypoplasia. *J Perinat Med* 21:355, 1993.
131. Merz E, Wellek S, Bahlmann F, Weber G: [Normal ultrasound curves of the fetal osseous thorax and fetal lung]. *Geburtshilfe Frauenheilkd* 55:77, 1995.
132. Abuhamad AZ, Sédoule-Murphy SJ, Kolm P, et al: Prenatal ultrasonographic fetal rib length measurement: correlation with gestational age. *Ultrasound Obstet Gynecol* 7:193, 1996.
133. Yoshimura S, Masuzaki H, Gotoh H, et al: Ultrasonographic prediction of lethal pulmonary hypoplasia: comparison of eight different ultrasonographic parameters. *Am J Obstet Gynecol* 175:477, 1996.
134. Roberts AB, Mitchell JM: Direct ultrasonographic measurement of fetal lung length in normal pregnancies and pregnancies complicated by prolonged rupture of membranes. *Am J Obstet Gynecol* 163:1560, 1990.
135. Ohlsson A, Fong K, Rose T, et al: Prenatal ultrasonic prediction of autopsy-proven pulmonary hypoplasia. *Am J Perinatol* 9:334, 1992.
136. Merz E, Miric-Tesanic D, Bahlmann F, et al: Prenatal sonographic chest and lung measurements for predicting severe pulmonary hypoplasia. *Prenat Diagn* 19:614, 1999.
137. Bahlmann F, Merz E, Hallermann C, et al: Congenital diaphragmatic hernia: ultrasonic measurement of fetal lungs to predict pulmonary hypoplasia. *Ultrasound Obstet Gynecol* 14:162, 1999.
138. Heling KS, Tennstedt C, Chaoui R, et al: Reliability of prenatal sonographic lung biometry in the diagnosis of pulmonary hypoplasia. *Prenat Diagn* 21:649, 2001.
139. Laudy JA, Tibboel D, Robben SG, et al: Prenatal prediction of pulmonary hypoplasia: clinical, biometric, and Doppler velocity correlates. *Pediatrics* 109:250, 2002.
140. Rahemtullah A, McGillivray B, Wilson RD: Suspected skeletal dysplasias: femur length to abdominal circumference ratio can be used in ultrasonographic prediction of fetal outcome. *Am J Obstet Gynecol* 177:864, 1997.
141. Lee A, Kratochwil A, Stumpfen I, et al: Fetal lung volume determination by three-dimensional ultrasonography. *Am J Obstet Gynecol* 175:588, 1996.
142. Laudy JA, Janssen MM, Struyk PC, et al: Three-dimensional ultrasonography of normal fetal lung volume: a preliminary study. *Ultrasound Obstet Gynecol* 11:13, 1998.
143. Pohls UG, Rempen A: Fetal lung volumetry by three-dimensional ultrasound. *Ultrasound Obstet Gynecol* 11:6, 1998.
144. Bahmaic A, Hughes SW, Clark T, et al: Serial fetal lung volume measurement using three-dimensional ultrasound. *Ultrasound Obstet Gynecol* 16:154, 2000.
145. Osada H, Iitsuka Y, Masuda K, et al: Application of lung volume measurement by three-dimensional ultrasonography for clinical assessment of fetal lung development. *J Ultrasound Med* 21:841, 2002.
146. Gerards FA, Engels MA, Twisk JW, et al: Normal fetal lung volume measured with three-dimensional ultrasound. *Ultrasound Obstet Gynecol* 27:134, 2006.
147. Kalache KD, Espinoza J, Chaiworapongsa T, et al: Three-dimensional ultrasound fetal lung volume measurement: a systematic study comparing the multiplanar method with the rotational (VOCAL) technique. *Ultrasound Obstet Gynecol* 21:111, 2003.
148. Kalache KD, Espinoza J, Chaiworapongsa T, et al: Three-dimensional reconstructed fetal lung using VOCAL. *Ultrasound Obstet Gynecol* 21:205, 2003.
149. Ruano R, Benachi A, Joubin L, et al: Three-dimensional ultrasonographic assessment of fetal lung volume as prognostic factor in isolated congenital diaphragmatic hernia. *BJOG* 111:423, 2004.
150. Ruano R, Joubin L, Sonigo P, et al: Fetal lung volume estimated by 3-dimensional ultrasonography and magnetic resonance imaging in cases with isolated congenital diaphragmatic hernia. *J Ultrasound Med* 23:353, 2004.
151. Ruano R, Benachi A, Martinovic J, et al: Can three-dimensional ultrasound be used for the assessment of the fetal lung volume in cases of congenital diaphragmatic hernia? *Fetal Diagn Ther* 19:87, 2004.
152. Moeglin D, Talmant C, Duyme M, et al: Fetal lung volumetry using two- and three-dimensional ultrasound. *Ultrasound Obstet Gynecol* 25:119, 2005.
153. Peralta CF, Cavoretto P, Csapo B, et al: Lung and heart volumes by three-dimensional ultrasound in normal fetuses at 12-32 weeks' gestation. *Ultrasound Obstet Gynecol* 27:128, 2006.
154. Ruano R, Martinovic J, Dommergues M, et al: Accuracy of fetal lung volume assessed by three-dimensional sonography. *Ultrasound Obstet Gynecol* 26:725, 2005.
155. Chang CH, Yu CH, Chang FM, et al: Volumetric assessment of normal fetal lungs using three-dimensional ultrasound. *Ultrasound Med Biol* 29:935, 2003.
156. Sabogal JC, Becker E, Bega G, et al: Reproducibility of fetal lung volume measurements with 3-dimensional ultrasonography. *J Ultrasound Med* 23:347, 2004.
157. Rypens F, Metens T, Rocourt N, et al: Fetal lung volume: estimation at MR imaging—initial results. *Radiology* 219:236, 2001.
158. Coakley FV, Lopoo JB, Lu Y, et al: Normal and hypoplastic fetal lungs: volumetric assessment with prenatal single-shot rapid acquisition with relaxation enhancement MR imaging. *Radiology* 216:107, 2000.
159. Paek BW, Coakley FV, Lu Y, et al: Congenital diaphragmatic hernia: prenatal evaluation with MR lung volumetry—preliminary experience. *Radiology* 220:63, 2001.
160. Williams G, Coakley FV, Qayyum A, et al: Fetal relative lung volume: quantification by using prenatal MR imaging lung volumetry. *Radiology* 233:457, 2004.
161. Tanigaki S, Miyakoshi K, Tanaka M, et al: Pulmonary hypoplasia: prediction with use of ratio of MR imaging-measured fetal lung volume to US-estimated fetal body weight. *Radiology* 232:767, 2004.
162. Kuwashima S, Nishimura G, Iimura F, et al: Low-intensity fetal lungs on MRI may suggest the diagnosis of pulmonary hypoplasia. *Pediatr Radiol* 31:669, 2001.
163. Osada H, Kaku K, Masuda K, et al: Quantitative and qualitative evaluations of fetal lung with MR imaging. *Radiology* 231:887, 2004.
164. Keller TM, Rake A, Michel SC, et al: MR assessment of fetal lung development using lung volumes and signal intensities. *Eur Radiol* 14:984, 2004.
165. Kalache KD, Chaoui R, Hartung J, et al: Doppler assessment of tracheal fluid flow during fetal breathing movements in cases of congenital diaphragmatic hernia. *Ultrasound Obstet Gynecol* 12:27, 1998.



166. Laudy JA, Wladimiroff JW: The fetal lung. 2: Pulmonary hypoplasia. *Ultrasound Obstet Gynecol* 16:482, 2000.
167. Mitchell JM, Roberts AB, Lee A: Doppler waveforms from the pulmonary arterial system in normal fetuses and those with pulmonary hypoplasia. *Ultrasound Obstet Gynecol* 11:167, 1998.
168. Achiron R, Heggesh J, Mashiah S, et al: Peripheral right pulmonary artery blood flow velocimetry: Doppler sonographic study of normal and abnormal fetuses. *J Ultrasound Med* 17:687, 1998.
169. Chaoui R, Kalache K, Tennstedt C, et al: Pulmonary arterial Doppler velocimetry in fetuses with lung hypoplasia. *Eur J Obstet Gynecol Reprod Biol* 84:179, 1999.
170. Yoshimura S, Masuzaki H, Miura K, et al: Diagnosis of fetal pulmonary hypoplasia by measurement of blood flow velocity waveforms of pulmonary arteries with Doppler ultrasonography. *Am J Obstet Gynecol* 180:441, 1999.
171. Rizzo G, Capponi A, Angelini E, et al: Blood flow velocity waveforms from fetal peripheral pulmonary arteries in pregnancies with preterm premature rupture of the membranes: relationship with pulmonary hypoplasia. *Ultrasound Obstet Gynecol* 15:98, 2000.
172. Fuke S, Kanzaki T, Mu J, et al: Antenatal prediction of pulmonary hypoplasia by acceleration time/ejection time ratio of fetal pulmonary arteries by Doppler blood flow velocimetry. *Am J Obstet Gynecol* 188:228, 2003.
173. Campbell J, Henderson A, Campbell S: The fetal femur/foot length ratio: a new parameter to assess dysplastic limb reduction. *Obstet Gynecol* 72:181, 1988.
174. Hershey DW: The fetal femur/foot length ratio: a new parameter to assess dysplastic limb reduction. *Obstet Gynecol* 73:682, 1989.
175. Turner GM, Twining P: The facial profile in the diagnosis of fetal abnormalities. *Clin Radiol* 47:389, 1993.
176. Escobar LF, Bixler D, Padilla LM, et al: Fetal craniofacial morphometrics: in utero evaluation at 16 weeks' gestation. *Obstet Gynecol* 72:674, 1988.
177. Chen ML, Chang CH, Yu CH, et al: Prenatal diagnosis of cleft palate by three-dimensional ultrasound. *Ultrasound Med Biol* 27:1017, 2001.
178. Chmait R, Pretorius D, Jones M, et al: Prenatal evaluation of facial clefts with two-dimensional and adjunctive three-dimensional ultrasonography: a prospective trial. *Am J Obstet Gynecol* 187:946, 2002.
179. Mittermayer C, Blaicher W, Brugger PC, et al: Foetal facial clefts: prenatal evaluation of lip and primary palate by 2D and 3D ultrasound. *Ultraschall Med* 25:120, 2004.
180. Johnson DD, Pretorius DH, Budorick NE, et al: Fetal lip and primary palate: three-dimensional versus two-dimensional US. *Radiology* 217:236, 2000.
181. Lee W, Kirk JS, Shaheen KW, et al: Fetal cleft lip and palate detection by three-dimensional ultrasonography. *Ultrasound Obstet Gynecol* 16:314, 2000.
182. Pretorius DH, Nelson TR: Fetal face visualization using three-dimensional ultrasonography. *J Ultrasound Med* 14:349, 1995.
183. Mittermayer C, Lee A: Three-dimensional ultrasonographic imaging of cleft lip: the winners are the parents. *Ultrasound Obstet Gynecol* 21:628, 2003.
184. Campbell S, Lees CC: The three-dimensional reverse face (3D RF) view for the diagnosis of cleft palate. *Ultrasound Obstet Gynecol* 22:552, 2003.
185. Campbell S, Lees C, Moscoso G, et al: Ultrasound antenatal diagnosis of cleft palate by a new technique: the 3D "reverse face" view. *Ultrasound Obstet Gynecol* 25:12, 2005.
186. Prows CA, Bender PL: Beyond Pierre Robin sequence. *Neonatal Netw* 18:13, 1999.
187. Pilu G, Reece EA, Romero R, et al: Prenatal diagnosis of craniofacial malformations with ultrasonography. *Am J Obstet Gynecol* 155:45, 1986.
188. Bromley B, Benacerraf BR: Fetal micrognathia: associated anomalies and outcome. *J Ultrasound Med* 13:529, 1994.
189. Paladini D, Morra T, Teodoro A, et al: Objective diagnosis of micrognathia in the fetus: the jaw index. *Obstet Gynecol* 93:382, 1999.
190. Rotten D, Levallant JM, Martinez H, et al: The fetal mandible: a 2D and 3D sonographic approach to the diagnosis of retrognathia and micrognathia. *Ultrasound Obstet Gynecol* 19:122, 2002.
191. Abrams SL, Filly RA: Congenital vertebral malformations: prenatal diagnosis using ultrasonography. *Radiology* 155:762, 1985.
192. Zelof CM, Pretorius DH, Benacerraf BR: Fetal hemivertebrae: associated anomalies, significance, and outcome. *Obstet Gynecol* 81:412, 1993.
193. Achiron R, Lipitz S, Grisaru D, et al: Second-trimester ultrasonographic diagnosis of segmental vertebral abnormalities associated with neurological deficit: a possible new variant of occult spinal dysraphism. *Prenat Diagn* 16:760, 1996.
194. Kozlowski K, Bieganski T, Gardner J, et al: Osteochondrodysplasies with marked platyspondyly and distinctive peripheral anomalies. *Pediatr Radiol* 29:1, 1999.
195. Wells TR, Landing BH, Bostwick FH: Studies of vertebral coronal cleft in rhizomelic chondrodysplasia punctata. *Pediatr Pathol* 12:593, 1992.
196. Lachman RS: Fetal imaging in the skeletal dysplasias: overview and experience. *Pediatr Radiol* 24:413, 1994.
197. Westvik J, Lachman RS: Coronal and sagittal clefts in skeletal dysplasias. *Pediatr Radiol* 28:764, 1998.
198. McMaster MJ: Occult intraspinal anomalies and congenital scoliosis. *J Bone Joint Surg Am* 66:588, 1984.
199. McMaster MJ, David CV: Hemivertebra as a cause of scoliosis. A study of 104 patients. *J Bone Joint Surg Br* 68:588, 1986.
200. McMaster MJ: Congenital scoliosis caused by a unilateral failure of vertebral segmentation with contralateral hemivertebrae. *Spine* 23:998, 1998.
201. McMaster MJ, Singh H: Natural history of congenital kyphosis and kyphoscoliosis. A study of one hundred and twelve patients. *J Bone Joint Surg Am* 81:1367, 1999.
202. Connor JM, Connor AN, Connor RA, et al: Genetic aspects of early childhood scoliosis. *Am J Med Genet* 27:419, 1987.
203. Johnson VP, Yiu-Chiu VS, Wierda DR, et al: Midtrimester prenatal diagnosis of achondrogenesis. *J Ultrasound Med* 3:223, 1984.
204. Mahony BS, Filly RA, Callen PW, et al: Thanatophoric dwarfism with the cloverleaf skull: a specific antenatal sonographic diagnosis. *J Ultrasound Med* 4:151, 1985.
205. Sorge G, Ruggieri M, Lachman RS: Spondyloperipheral dysplasia. *Am J Med Genet* 59:139, 1995.
206. Katsouras CS, Thomadakis C, Michalis LK: Cardiac Ellis-van Creveld syndrome. *Int J Cardiol* 87:315, 2003.
207. Bossert T, Walther T, Gummert J, et al: Cardiac malformations associated with the Holt-Oram syndrome—report on a family and review of the literature. *Thorac Cardiovasc Surg* 50:312, 2002.
208. Mortier GR, Rimoin DL, Lachman RS: The scapula as a window to the diagnosis of skeletal dysplasias. *Pediatr Radiol* 27:447, 1997.
209. Francomano CA: The genetic basis of dwarfism. *N Engl J Med* 332:58, 1995.
210. Nicolaides KH, Azar G, Byrne D, et al: Fetal nuchal translucency: ultrasound screening for chromosomal defects in first trimester of pregnancy. *BMJ* 304:867, 1992.
211. Pandya PP, Kondylis A, Hilbert L, et al: Chromosomal defects and outcome in 1015 fetuses with increased nuchal translucency. *Ultrasound Obstet Gynecol* 5:15, 1995.
212. Brady AF, Pandya PP, Yuksel B, et al: Outcome of chromosomally normal livebirths with increased fetal nuchal translucency at 10-14 weeks' gestation. *J Med Genet* 35:222, 1998.
213. Souka AP, Snijders RJ, Novakov A, et al: Defects and syndromes in chromosomally normal fetuses with increased nuchal translucency thickness at 10-14 weeks of gestation. *Ultrasound Obstet Gynecol* 11:391, 1998.
214. Makrydimas G, Souka A, Skentou H, et al: Osteogenesis imperfecta and other skeletal dysplasias presenting with increased nuchal translucency in the first trimester. *Am J Med Genet* 98:117, 2001.
215. Souka AP, Raymond FL, Mornet E, et al: Hypophosphatasia associated with increased nuchal translucency: a report of two affected pregnancies. *Ultrasound Obstet Gynecol* 20:294, 2002.
216. Michel-Calemard L, Lesca G, Morel Y, et al: Campomelic acampomelic dysplasia presenting with increased nuchal translucency in the first trimester. *Prenat Diagn* 24:519, 2004.
217. Witters I, Claerhout P, Fryns JP: Increased nuchal translucency thickness in thrombocytopenia-absent-radius syndrome. *Ultrasound Obstet Gynecol* 26:581, 2005.
218. Shiang R, Thompson LM, Zhu YZ, et al: Mutations in the transmembrane domain of FGFR3 cause the most common genetic form of dwarfism, achondroplasia. *Cell* 78:335, 1994.
219. Bellus GA, McIntosh I, Smith EA, et al: A recurrent mutation in the tyrosine kinase domain of fibroblast growth factor receptor 3 causes hypochondroplasia. *Nat Genet* 10:357, 1995.
220. Wilcox WR, Tavormina PL, Krakow D, et al: Molecular, radiologic, and histopathologic correlations in thanatophoric dysplasia. *Am J Med Genet* 78:274, 1998.



221. Ozono K: Recent advances in molecular analysis of skeletal dysplasia. *Acta Paediatr Jpn* 39:491, 1997.
222. Climent C, Lorda-Sanchez I, Urioste M, et al: [Achondroplasia: molecular study of 28 patients]. *Med Clin (Barc)* 110:492, 1998.
223. Cohen MM Jr: Achondroplasia, hypochondroplasia and thanatophoric dysplasia: clinically related skeletal dysplasias that are also related at the molecular level. *Int J Oral Maxillofac Surg* 27:451, 1998.
224. Wilkin DJ, Szabo JK, Cameron R, et al: Mutations in fibroblast growth-factor receptor 3 in sporadic cases of achondroplasia occur exclusively on the paternally derived chromosome. *Am J Hum Genet* 63:711, 1998.
225. Lemyre E, Azouz EM, Teebi AS, et al: Bone dysplasia series. Achondroplasia, hypochondroplasia and thanatophoric dysplasia: review and update. *Can Assoc Radiol J* 50:185, 1999.
226. Rousseau F, el Ghouzzi V, Delezoide AL, et al: Missense FGFR3 mutations create cysteine residues in thanatophoric dwarfism type I (TD1). *Hum Mol Genet* 5:509, 1996.
227. Cohen MM Jr: Some chondrodysplasias with short limbs: molecular perspectives. *Am J Med Genet* 112:304, 2002.
228. Hevner RF: The cerebral cortex malformation in thanatophoric dysplasia: neuropathology and pathogenesis. *Acta Neuropathol (Berl)* 110:208, 2005.
229. Vajo Z, Francomano CA, Wilkin DJ: The molecular and genetic basis of fibroblast growth factor receptor 3 disorders: the achondroplasia family of skeletal dysplasias, Muenke craniosynostosis, and Crouzon syndrome with acanthosis nigricans. *Endocr Rev* 21:23, 2000.
230. Aviczer D, Golembo M, Yayon A: Fibroblast growth factor receptor-3 as a therapeutic target for Achondroplasia—genetic short limbed dwarfism. *Curr Drug Targets* 4:353, 2003.
231. Tonni G, Ventura A, De Felice C: First trimester increased nuchal translucency associated with fetal achondroplasia. *Am J Perinatol* 22:145, 2005.
232. Ramaswami U, Rumsby G, Hindmarsh PC, et al: Genotype and phenotype in hypochondroplasia. *J Pediatr* 133:99, 1998.
233. Kurtz AB, Filly RA, Wapner RJ, et al: In utero analysis of heterozygous achondroplasia: variable time of onset as detected by femur length measurements. *J Ultrasound Med* 5:137, 1986.
234. Modaff P, Horton VK, Pauli RM: Errors in the prenatal diagnosis of children with achondroplasia. *Prenat Diagn* 16:525, 1996.
235. Elejalde BR, de Elejalde MM, Hamilton PR, et al: Prenatal diagnosis in two pregnancies of an achondroplastic woman. *Am J Med Genet* 15:437, 1983.
236. Huggins MJ, Mernagh JR, Steele L, et al: Prenatal sonographic diagnosis of hypochondroplasia in a high-risk fetus. *Am J Med Genet* 87:226, 1999.
237. Chitayat D, Fernandez B, Gardner A, et al: Compound heterozygosity for the achondroplasia-hypochondroplasia FGFR3 mutations: prenatal diagnosis and postnatal outcome. *Am J Med Genet* 84:401, 1999.
238. Mesoraca A, Pilu G, Perolo A, et al: Ultrasound and molecular mid-trimester prenatal diagnosis of de novo achondroplasia. *Prenat Diagn* 16:764, 1996.
239. Guzman ER, Day-Salvatore D, Westover T, et al: Prenatal ultrasonographic demonstration of the trident hand in heterozygous achondroplasia. *J Ultrasound Med* 13:63, 1994.
240. Cordone M, Lituanica M, Bocchino G, et al: Ultrasonographic features in a case of heterozygous achondroplasia at 25 weeks' gestation. *Prenat Diagn* 13:395, 1993.
241. Patel MD, Filly RA: Homozygous achondroplasia: US distinction between homozygous, heterozygous, and unaffected fetuses in the second trimester. *Radiology* 196:541, 1995.
242. Karadimas C, Trouvas D, Haritatos G, et al: Prenatal diagnosis of achondroplasia presenting with multiple-suture synostosis: a novel association. *Prenat Diagn* 26:258, 2006.
243. Francomano CA, Orúz de Luna RI, Hefferon TW, et al: Localization of the achondroplasia gene to the distal 2.5 Mb of human chromosome 4p. *Hum Mol Genet* 3:787, 1994.
244. Le Merrer M, Rousseau F, Legeai-Mallet L, et al: A gene for achondroplasia-hypochondroplasia maps to chromosome 4p. *Nat Genet* 6:318, 1994.
245. Velinov M, Slangenaupt SA, Stoilov I, et al: The gene for achondroplasia maps to the telomeric region of chromosome 4p. *Nat Genet* 6:314, 1994.
246. Rousseau F, Bonaventure J, Legeai-Mallet L, et al: Mutations in the gene encoding fibroblast growth factor receptor-3 in achondroplasia. *Nature* 371:252, 1994.
247. James PA, Shaw J, du Sart D, et al: Molecular diagnosis in a pregnancy at risk for both spondyloepiphyseal dysplasia congenita and achondroplasia. *Prenat Diagn* 23:861, 2003.
248. Schrijver I, Lay MJ, Zehnder JL: Rapid combined genotyping assay for four achondroplasia and hypochondroplasia mutations by real-time PCR with multiple detection probes. *Genet Test* 8:185, 2004.
249. Lachman RS: Neurologic abnormalities in the skeletal dysplasias: a clinical and radiological perspective. *Am J Med Genet* 69:33, 1997.
250. Ho NC, Guarnieri M, Brant LJ, et al: Living with achondroplasia: quality of life evaluation following cervico-medullary decompression. *Am J Med Genet A* 131:163, 2004.
251. Pauli RM, Conroy MM, Langer LO Jr, et al: Homozygous achondroplasia with survival beyond infancy. *Am J Med Genet* 16:459, 1983.
252. Seino Y, Moriwake T, Tanaka H, et al: Molecular defects in achondroplasia and the effects of growth hormone treatment. *Acta Paediatr Suppl* 88:118, 1999.
253. Tanaka H, Kubo T, Yamate T, et al: Effect of growth hormone therapy in children with achondroplasia: growth pattern, hypothalamic-pituitary function, and genotype. *Eur J Endocrinol* 138:275, 1998.
254. Weber G, Prinster C, Meneghel M, et al: Human growth hormone treatment in prepubertal children with achondroplasia. *Am J Med Genet* 61:396, 1996.
255. Yasoda A, Komatsu Y, Chusho H, et al: Overexpression of CNP in chondrocytes rescues achondroplasia through a MAPK-dependent pathway. *Nat Med* 10:80, 2004.
256. Tavormina PL, Bellus GA, Webster MK, et al: A novel skeletal dysplasia with developmental delay and acanthosis nigricans is caused by a Lys650Met mutation in the fibroblast growth factor receptor 3 gene. *Am J Hum Genet* 64:722, 1999.
257. Bellus GA, Bamshad MJ, Przylepa KA, et al: Severe achondroplasia with developmental delay and acanthosis nigricans (SADDAN): phenotypic analysis of a new skeletal dysplasia caused by a Lys650Met mutation in fibroblast growth factor receptor 3. *Am J Med Genet* 85:53, 1999.
258. Spranger J: [International nomenclature of constitutional bone diseases (the Paris nomenclature)]. *Fortschr Geb Rontgenstr Nuklearmed* 115:283, 1971.
259. Brodie SG, Kitch H, Lipson M, et al: Thanatophoric dysplasia type I with syndactyly. *Am J Med Genet* 80:260, 1998.
260. Weber M, Johannisson R, Carstens C, et al: Thanatophoric dysplasia type II: new entity? *J Pediatr Orthop B* 7:10, 1998.
261. Iannaccone G, Gerlini G: The so-called "Cloverleaf Skull Syndrome." A report of three cases with a discussion of its relationships with thanatophoric dwarfism and the craniosynostoses. *Pediatr Radiol* 2:175, 1974.
262. Jasnosz KM, MacPherson TA: Perinatal pathology casebook. Thanatophoric dysplasia with cloverleaf skull. *J Perinatol* 13:162, 1993.
263. Yang SS, Heidelberger KP, Brough AJ, et al: Lethal short-limbed chondrodysplasia in early infancy. In Rosenberg HS, Bocklandt RP (eds): *Perspectives in Pediatric Pathology*. Chicago, Year Book Medical Publishers, 1976, p 1.
264. Online Mendelian Inheritance in Man, OMIM (TM). McKusick-Nathans Institute for Genetic Medicine, Johns Hopkins University (Baltimore, MD) and National Center for Biotechnology Information, National Library of Medicine (Bethesda, MD), 2000 World Wide Web URL: <http://www.ncbi.nlm.nih.gov/omim/>. 2006.
265. McKusick VA, Francomano CA, Antonarakis SE: *Mendelian Inheritance in Man: Catalogs of Autosomal Dominant, Autosomal Recessive, and X-Linked Phenotypes*. Baltimore, Johns Hopkins University Press, 1990.
266. Tavormina PL, Shiang R, Thompson LM, et al: Thanatophoric dysplasia (types I and II) caused by distinct mutations in fibroblast growth factor receptor 3. *Nat Genet* 9:321, 1995.
267. Partington MW, Gonzales-Crussi F, Khakee SG, et al: Cloverleaf skull and thanatophoric dwarfism. Report of four cases, two in the same sibship. *Arch Dis Child* 46:656, 1971.
268. Schild RL, Hunt GH, Moore J, et al: Antenatal sonographic diagnosis of thanatophoric dysplasia: a report of three cases and a review of the literature with special emphasis on the differential diagnosis. *Ultrasound Obstet Gynecol* 8:62, 1996.
269. d'Avis PY, Robertson SC, Meyer AN, et al: Constitutive activation of fibroblast growth factor receptor 3 by mutations responsible for



- the lethal skeletal dysplasia thanatophoric dysplasia type I. *Cell Growth Differ* 9:71, 1998.
270. Passos-Bueno MR, Wilcox WR, et al: Clinical spectrum of fibroblast growth factor receptor mutations. *Hum Mutat* 14:115, 1999.
  271. Li D, Liao C, Ma X: Prenatal diagnosis and molecular analysis of type I thanatophoric dysplasia. *Int J Gynaecol Obstet* 91:268, 2005.
  272. Rousseau F, Saugier P, Le Merrer M, et al: Stop codon FGFR3 mutations in thanatophoric dwarfism type I. *Nat Genet* 10:11, 1995.
  273. Gorlin RJ: Fibroblast growth factors, their receptors and receptor disorders. *J Craniomaxillofac Surg* 25:69, 1997.
  274. Bellus GA, Spector EB, Speiser PW, et al: Distinct missense mutations of the FGFR3 lys650 codon modulate receptor kinase activation and the severity of the skeletal dysplasia phenotype. *Am J Hum Genet* 67:1411, 2000.
  275. Camera G, Baldi M, Strisciunglio G, et al: Occurrence of thanatophoric dysplasia type I (R248C) and hypochondroplasia (N540K) mutations in two patients with achondroplasia phenotype. *Am J Med Genet* 104:277, 2001.
  276. Iwata T, Chen L, Li C, et al: A neonatal lethal mutation in FGFR3 uncouples proliferation and differentiation of growth plate chondrocytes in embryos. *Hum Mol Genet* 9:1603, 2000.
  277. Inglis-Broadgate SL, Thomson RE, Pellicano F, et al: FGFR3 regulates brain size by controlling progenitor cell proliferation and apoptosis during embryonic development. *Dev Biol* 279:73, 2005.
  278. Knisely AS, Ambler MW: Temporal-lobe abnormalities in thanatophoric dysplasia. *Pediatr Neurosci* 14:169, 1988.
  279. Horton WA, Rimoin DL, Hollister DW, et al: Further heterogeneity within lethal neonatal short-limbed dwarfism: the platyspondylic types. *J Pediatr* 94:736, 1979.
  280. Brodie SG, Kitoh H, Laehman RS, et al: Platyspondylic lethal skeletal dysplasia, San Diego type, is caused by FGFR3 mutations. *Am J Med Genet* 84:476, 1999.
  281. Moir DH, Kozlowski K: Long survival in thanatophoric dwarfism. *Pediatr Radiol* 5:123, 1976.
  282. Stensvold K, Ek J, Hovland AR: An infant with thanatophoric dwarfism surviving 169 days. *Clin Genet* 29:157, 1986.
  283. Baker KM, Olson DS, Harding CO, et al: Long-term survival in typical thanatophoric dysplasia type I. *Am J Med Genet* 70:427, 1997.
  284. Dominguez R, Talmachoff P: Diagnostic imaging update in skeletal dysplasias. *Clin Imaging* 17:222, 1993.
  285. Fink IJ, Filly RA, Callen PW, et al: Sonographic diagnosis of thanatophoric dwarfism in utero. *J Ultrasound Med* 1:337, 1982.
  286. Chervenak FA, Blakemore KJ, Isaacson G, et al: Antenatal sonographic findings of thanatophoric dysplasia with cloverleaf skull. *Am J Obstet Gynecol* 146:984, 1983.
  287. Beetham FG, Reeves JS: Early ultrasound diagnosis of thanatophoric dwarfism. *J Clin Ultrasound* 12:43, 1984.
  288. Burrows PE, Stannard MW, Pearrow J, et al: Early antenatal sonographic recognition of thanatophoric dysplasia with cloverleaf skull deformity. *AJR Am J Roentgenol* 143:841, 1984.
  289. Elejalde BR, de Elejalde MM: Thanatophoric dysplasia: fetal manifestations and prenatal diagnosis. *Am J Med Genet* 22:669, 1985.
  290. Weiner CP, Williamson RA, Bonsib SM: Sonographic diagnosis of cloverleaf skull and thanatophoric dysplasia in the second trimester. *J Clin Ultrasound* 14:463, 1986.
  291. Meizner I, Levy A, Carmi R, et al: Early prenatal ultrasonic diagnosis of thanatophoric dwarfism. *Isr J Med Sci* 26:287, 1990.
  292. Kassanos D, Botsis D, Katassos T, et al: Prenatal sonographic diagnosis of thanatophoric dwarfism. *Int J Gynaecol Obstet* 34:373, 1991.
  293. Corsello G, Maresi E, Rossi C, et al: Thanatophoric dysplasia in monozygotic twins discordant for cloverleaf skull: prenatal diagnosis, clinical and pathological findings. *Am J Med Genet* 42:122, 1992.
  294. Gerihauser H, Schuster C, Immervoll H, et al: [Prenatal diagnosis of thanatophoric dwarfism]. *Ultraschall Med* 13:41, 1992.
  295. Camera G, Dodero D, Camandona F, et al: [Prenatal diagnosis of thanatophoric dysplasia at 21st week of pregnancy]. *Pathologica* 85:215, 1993.
  296. Marin-Ruiz R, Alarcon HC, Montiel RW, et al: [Thanatophoric dysplasia. Its prenatal ultrasonic diagnosis. A case report]. *Ginecol Obstet Mex* 61:344, 1993.
  297. van der Harten HJ, Brons JT, Dijkstra PF, et al: Some variants of lethal neonatal short-limbed platyspondylic dysplasia: a radiological ultrasonographic, neuropathological and histopathological study of 22 cases. *Clin Dysmorphol* 2:1, 1993.
  298. Szatmary FP, Szabo L, Toth T, et al: [Prenatal diagnosis of thanatophoric dysplasia]. *Orv Hetil* 136:75, 1995.
  299. Todros T, Sciarrone A, Voglino G, et al: [Prenatal diagnosis of thanatophoric dysplasia at the 20th week of pregnancy using ultrasonography]. *Pathologica* 87:723, 1995.
  300. Yuce MA, Yardim T, Kurtul M, et al: Prenatal diagnosis of thanatophoric dwarfism in second trimester. A case report. *Clin Exp Obstet Gynecol* 25:149, 1998.
  301. Sun CC, Grumbach K, DeCosta DT, et al: Correlation of prenatal ultrasound diagnosis and pathologic findings in fetal anomalies. *Pediatr Dev Pathol* 2:131, 1999.
  302. Sahinoglu Z, Uludogan M, Gurbuz A, et al: Prenatal diagnosis of thanatophoric dysplasia in the second trimester: ultrasonography and other diagnostic modalities. *Arch Gynecol Obstet* 269:57, 2003.
  303. Sawai H, Komori S, Ida A, et al: Prenatal diagnosis of thanatophoric dysplasia by mutational analysis of the fibroblast growth factor receptor 3 gene and a proposed correction of previously published PCR results. *Prenat Diagn* 19:21, 1999.
  304. De Biasio P, Prefumo F, Baffico M, et al: Sonographic and molecular diagnosis of thanatophoric dysplasia type I at 18 weeks of gestation. *Prenat Diagn* 20:835, 2000.
  305. Chen CP, Chern SR, Chang TY, et al: Second trimester molecular diagnosis of a stop codon FGFR3 mutation in a type I thanatophoric dysplasia fetus following abnormal ultrasound findings. *Prenat Diagn* 22:736, 2002.
  306. Hall BD, Spranger J: Hypochondroplasia: clinical and radiological aspects in 39 cases. *Radiology* 133:95, 1979.
  307. Cohn DH: Mutations affecting multiple functional domains of FGFR3 cause different skeletal dysplasias: a personal retrospective in honor of John Wasmuth. *Ann N Y Acad Sci* 785:160, 1996.
  308. Matsui Y, Yasui N, Kimura T, et al: Genotype phenotype correlation in achondroplasia and hypochondroplasia. *J Bone Joint Surg Br* 80:1052, 1998.
  309. Mullis PE, Patel MS, Brickell PM, et al: Growth characteristics and response to growth hormone therapy in patients with hypochondroplasia: genetic linkage of the insulin-like growth factor I gene at chromosome 12q23 to the disease in a subgroup of these patients. *Clin Endocrinol (Oxf)* 34:265, 1991.
  310. Bailey AJ, Sims TJ, Stancescu V, et al: Abnormal collagen cross-linking in the cartilage of a diastrophic dysplasia patient. *Br J Rheumatol* 34:512, 1995.
  311. Prinos P, Costa T, Sommer A, et al: A common FGFR3 gene mutation in hypochondroplasia. *Hum Mol Genet* 4:2097, 1995.
  312. Scott GJ Jr: Achondroplastic and hypochondroplastic dwarfism. *Clin Orthop* 114:18, 1976.
  313. Stoll C, Manini P, Bloch J, Roth MP: Prenatal diagnosis of hypochondroplasia. *Prenat Diagn* 5:423, 1985.
  314. Stoilov I, Kilpatrick MW, Tsiouras P, et al: Possible genetic heterogeneity in hypochondroplasia. *J Med Genet* 32:492, 1995.
  315. Angle B, Hersh JH, Christensen KM: Molecularly proven hypochondroplasia with cloverleaf skull deformity: a novel association. *Clin Genet* 54:417, 1998.
  316. Prinster C, Carrera P, Del Maschio M, et al: Comparison of clinical-radiological and molecular findings in hypochondroplasia. *Am J Med Genet* 75:109, 1998.
  317. Grosso S, Farnetani MA, Berardi R, et al: Medial temporal lobe dysgenesis in Muenke syndrome and hypochondroplasia. *Am J Med Genet A* 120:88, 2003.
  318. Kannu P, Hayes IM, Mandelstam S, et al: Medial temporal lobe dysgenesis in hypochondroplasia. *Am J Med Genet A* 138:389, 2005.
  319. Kataoka S, Sawai H, Yamada H, et al: Radiographic and genetic diagnosis of sporadic hypochondroplasia early in the neonatal period. *Prenat Diagn* 24:45, 2004.
  320. Karadimas C, Sifakis S, Valsamopoulos P, et al: Prenatal diagnosis of hypochondroplasia: report of two cases. *Am J Med Genet A* 140:998, 2006.
  321. Hunt NC, Vujanic GM: Fibrochondrogenesis in a 17-week fetus: a case expanding the phenotype. *Am J Med Genet* 75:326, 1998.
  322. Megarbane A, Haddad S, Berjaoui L: Prenatal ultrasonography: clinical and radiological findings in a boy with fibrochondrogenesis. *Am J Perinatol* 15:403, 1998.
  323. Randrianaiivo H, Haddad G, Roman H, et al: Fetal fibrochondrogenesis at 26 weeks' gestation. *Prenat Diagn* 22:806, 2002.
  324. Chervenak FA, Isaacson G, Rosenberg JC, et al: Antenatal diagnosis of frontal cephalocele in a fetus with atelosteogenesis. *J Ultrasound Med* 5:111, 1986.



325. Bejjani BA, Oberg KC, Wilkins I, et al: Prenatal ultrasonographic description and postnatal pathological findings in atelosteogenesis type I. *Am J Med Genet* 79:392, 1998.
326. Schultz C, Langer LO, Laxova R, et al: Atelosteogenesis type III: long term survival, prenatal diagnosis, and evidence for dominant transmission. *Am J Med Genet* 83:28, 1999.
327. Ueno K, Tanaka M, Miyakoshi K, et al: Prenatal diagnosis of atelosteogenesis type I at 21 weeks' gestation. *Prenat Diagn* 22:1071, 2002.
328. Wessels MW, den Hollander NS, de Krijger RR, et al: Prenatal diagnosis of boomerang dysplasia. *Am J Med Genet A* 122:148, 2003.
329. Kulkarni ML, Matadh PS, Praveen Prabhu SP, et al: Fibrochondrogenesis. *Indian J Pediatr* 72:355, 2005.
330. Lazzaroni-Fossati F, Stanescu V, Stanescu R, et al: [Fibrochondrogenesis]. *Arch Fr Pediatr* 35:1096, 1978.
331. Eteson DJ, Adomian GE, Ornoy A, et al: Fibrochondrogenesis: radiologic and histologic studies. *Am J Med Genet* 19:277, 1984.
332. Al Gazali LI, Bakalnova D, Bakir M, et al: Fibrochondrogenesis: clinical and radiological features. *Clin Dysmorphol* 6:157, 1997.
333. Leeners B, Funk A, Cotarello CL, et al: Two sibs with fibrochondrogenesis. *Am J Med Genet* 127A:318, 2004.
334. Whitley CB, Langer LO Jr, Ophoven J, et al: Fibrochondrogenesis: lethal, autosomal recessive chondrodysplasia with distinctive cartilage histopathology. *Am J Med Genet* 19:265, 1984.
335. Martinez-Frias ML, Garcia A, Cuevas J, et al: A new case of fibrochondrogenesis from Spain. *J Med Genet* 33:429, 1996.
336. Al Gazali LI, Bakir M, Dawodu A, Haas D: Recurrence of fibrochondrogenesis in a consanguineous family. *Clin Dysmorphol* 8:59, 1999.
337. Hall CM, Elcioglu NH: Metatropic dysplasia lethal variants. *Pediatr Radiol* 34:66, 2004.
338. Maroteaux P, Spranger J, Stanescu V, et al: Atelosteogenesis. *Am J Med Genet* 13:15, 1982.
339. Sillence DO, Lachman RS, Jenkins T, et al: Spondylumerofemoral hypoplasia (giant cell chondrodysplasia): a neonatally lethal short-limbed skeletal dysplasia. *Am J Med Genet* 13:7, 1982.
340. Yang SS, Roskamp J, Liu CT, et al: Two lethal chondrodysplasias with giant chondrocytes. *Am J Med Genet* 15:615, 1983.
341. McAlister WH, Crane JP, Bucy RP, et al: A new neonatal short limbed dwarfism. *Skeletal Radiol* 13:271, 1985.
342. Sillence D, Worthington S, Dixon J, et al: Atelosteogenesis syndromes: a review, with comments on their pathogenesis. *Pediatr Radiol* 27:388, 1997.
343. Krakow D, Robertson SP, King LM, et al: Mutations in the gene encoding filamin B disrupt vertebral segmentation, joint formation and skeletogenesis. *Nat Genet* 36:405, 2004.
344. Hastbacka J, Superti-Furga A, Wilcox WR, et al: Atelosteogenesis type II is caused by mutations in the diastrophic dysplasia sulfate-transporter gene (DTDST): evidence for a phenotypic series involving three chondrodysplasias. *Am J Hum Genet* 58:255, 1996.
345. Sillence DO, Kozlowski K, Rogers JG, et al: Atelosteogenesis: evidence for heterogeneity. *Pediatr Radiol* 17:112, 1987.
346. Stern HJ, Graham JM Jr, Lachman RS, et al: Atelosteogenesis type III: a distinct skeletal dysplasia with features overlapping atelosteogenesis and oto-palato-digital syndrome type II. *Am J Med Genet* 36:183, 1990.
347. Superti-Furga A, Neumann L, Riebel T, et al: Recessively inherited multiple epiphyseal dysplasia with normal stature, club foot, and double layered patella caused by a DTDST mutation. *J Med Genet* 36:621, 1999.
348. Rossi A, van der Harten HJ, Beemer FA, et al: Phenotypic and genotypic overlap between atelosteogenesis type 2 and diastrophic dysplasia. *Hum Genet* 98:657, 1996.
349. Newbury-Ecob R: Atelosteogenesis type 2. *J Med Genet* 35:49, 1998.
350. De la CA, Maroteaux P, Havu N, et al: [A rare lethal bone dysplasia with recessive autosomic transmission]. *Arch Fr Pediatr* 29:759, 1972.
351. Whitley CB, Burke BA, Granroth G, et al: de la Chapelle dysplasia. *Am J Med Genet* 25:29, 1986.
352. Kozlowski K, Sillence D, Cortis-Jones R, et al: Boomerang dysplasia. *Br J Radiol* 58:369, 1985.
353. Borochowitz Z, Ornoy A, Lachman R, et al: Achondrogenesis II-hypochondrogenesis: variability versus heterogeneity. *Am J Med Genet* 24:273, 1986.
354. Borochowitz Z, Lachman R, Adomian GE, et al: Achondrogenesis type I: delineation of further heterogeneity and identification of two distinct subgroups. *J Pediatr* 112:23, 1988.
355. Spranger J: Pattern recognition in bone dysplasias. In Papadatos CJ, Bartsocas CS (eds): *Endocrine Genetics and Genetics of Growth*. New York, Alan R. Liss, 1985, p 315.
356. Godfrey M, Keene DR, Blank E, et al: Type II achondrogenesis-hypochondrogenesis: morphologic and immunohistopathologic studies. *Am J Hum Genet* 43:894, 1988.
357. van der Harten HJ, Brons JT, Dijkstra PF, et al: Achondrogenesis-hypochondrogenesis: the spectrum of chondrogenesis imperfecta. A radiological, ultrasonographic, and histopathologic study of 23 cases. *Pediatr Pathol* 8:571, 1988.
358. Murray LW, Bautista J, James PL, et al: Type II collagen defects in the chondrodysplasias. I. Spondyloepiphyseal dysplasias. *Am J Hum Genet* 45:5, 1989.
359. Whitley CB, Gorlin RJ: Achondrogenesis: new nosology with evidence of genetic heterogeneity. *Radiology* 148:693, 1983.
360. Superti-Furga A: Achondrogenesis type 1B. *J Med Genet* 33:957, 1996.
361. Cai G, Nakayama M, Hiraki Y, et al: Mutational analysis of the DTDST gene in a fetus with achondrogenesis type 1B. *Am J Med Genet* 78:58, 1998.
362. Wenstrom KD, Williamson RA, Hoover WW, et al: Achondrogenesis type II (Langer-Saldino) in association with jugular lymphatic obstruction sequence. *Prenat Diagn* 9:527, 1989.
363. Won HS, Yoo HK, Lee PR, et al: A case of achondrogenesis type II associated with huge cystic hygroma: prenatal diagnosis by ultrasonography. *Ultrasound Obstet Gynecol* 14:288, 1999.
364. Ozeren S, Yuksel A, Tukul T: Prenatal sonographic diagnosis of type I achondrogenesis with a large cystic hygroma. *Ultrasound Obstet Gynecol* 13:75, 1999.
365. Golbus MS, Hall BD, Filly RA, et al: Prenatal diagnosis of achondrogenesis. *J Pediatr* 91:464, 1977.
366. Anteby SO, Aviad I, Weinstein D: Prenatal diagnosis of achondrogenesis. *Radiol Clin (Basel)* 46:109, 1977.
367. Smith WL, Breitweiser TD, Dinno N: In utero diagnosis of achondrogenesis, type I. *Clin Genet* 19:51, 1981.
368. Mahony BS, Filly RA, Cooperberg PL: Antenatal sonographic diagnosis of achondrogenesis. *J Ultrasound Med* 3:333, 1984.
369. Benacerraf B, Osathanondh R, Bieber FR: Achondrogenesis type I: ultrasound diagnosis in utero. *J Clin Ultrasound* 12:357, 1984.
370. Glenn LW, Teng SS: In utero sonographic diagnosis of achondrogenesis. *J Clin Ultrasound* 13:195, 1985.
371. Schramm T, Nerlich A: [Sonographic diagnosis of a case of type 1 achondrogenesis in the 2d trimester]. *Geburtshilfe Frauenheilkd* 49:917, 1989.
372. Balakumar K: Antenatal diagnosis of Parenti-Fraccaro type achondrogenesis. *Indian Pediatr* 27:496, 1990.
373. Jeelson UC, Prabhu S, Nambiar D: Prenatal diagnosis of achondrogenesis. *Indian Pediatr* 27:190, 1990.
374. Mandjee D, Clement F, Belin M, et al: [Achondrogenesis. Ultrasonic diagnosis and clinical and anatomopathologic comparison]. *Rev Fr Gynecol Obstet* 86:391, 1991.
375. Boudier E, Zurlinden B, Cour A, et al: [Antenatal diagnosis of achondrogenesis. Two successive cases in the same family]. *J Gynecol Obstet Biol Reprod (Paris)* 20:623, 1991.
376. Tongsong T, Srisomboon J, Sudasna J: Prenatal diagnosis of Langer-Saldino achondrogenesis. *J Clin Ultrasound* 23:56, 1995.
377. Fisk NM, Vaughan J, Smidt M, et al: Transvaginal ultrasound recognition of nuchal edema in the first-trimester diagnosis of achondrogenesis. *J Clin Ultrasound* 19:586, 1991.
378. Chen H, Liu CT, Yang SS: Achondrogenesis: a review with special consideration of achondrogenesis type II (Langer-Saldino). *Am J Med Genet* 10:379, 1981.
379. Superti-Furga A, Hastbacka J, Wilcox WR, et al: Achondrogenesis type IB is caused by mutations in the diastrophic dysplasia sulphate transporter gene. *Nat Genet* 12:100, 1996.
380. Vissing H, D'Alessio M, Lee B, et al: Glycine to serine substitution in the triple helical domain of pro-alpha 1 (II) collagen results in a lethal perinatal form of short-limbed dwarfism. *J Biol Chem* 264:18265, 1989.
381. Kuivaniemi H, Tromp G, Prockop DJ: Mutations in collagen genes: causes of rare and some common diseases in humans. *FASEB J* 5:2052, 1991.



382. Willing MC, Pruchno CJ, Atkinson M, et al: Osteogenesis imperfecta type I is commonly due to a COL1A1 null allele of type I collagen. *Am J Hum Genet* 51:508, 1992.
383. Willing MC, Deschenes SP, Slayton RL, et al: Premature chain termination is a unifying mechanism for COL1A1 null alleles in osteogenesis imperfecta type I cell strains. *Am J Hum Genet* 59:799, 1996.
384. Wang Q, Orrison BM, Marini JC: Two additional cases of osteogenesis imperfecta with substitutions for glycine in the alpha 2(I) collagen chain. A regional model relating mutation location with phenotype. *J Biol Chem* 268:25162, 1993.
385. Dyne KM, Valli M, Forlino A, et al: Deficient expression of the small proteoglycan decorin in a case of severe/lethal osteogenesis imperfecta. *Am J Med Genet* 63:161, 1996.
386. Byers PH, Steiner RD: Osteogenesis imperfecta. *Annu Rev Med* 43:269, 1992.
387. Rauch F, Glorieux PF: Osteogenesis imperfecta. *Lancet* 363:1377, 2004.
388. Orioli IM, Castilla EE, Scarano G, et al: Effect of paternal age in achondroplasia, thanatophoric dysplasia, and osteogenesis imperfecta. *Am J Med Genet* 59:209, 1995.
389. Sillence DO, Senn A, Danks DM: Genetic heterogeneity in osteogenesis imperfecta. *J Med Genet* 16:101, 1979.
390. Young ID, Thompson EM, Hall CM, et al: Osteogenesis imperfecta type IIA: evidence for dominant inheritance. *J Med Genet* 24:386, 1987.
391. Sillence DO, Barlow KK, Garber AP, et al: Osteogenesis imperfecta type II delineation of the phenotype with reference to genetic heterogeneity. *Am J Med Genet* 17:407, 1984.
392. Sillence DO, Barlow KK, Cole WG, et al: Osteogenesis imperfecta type III. Delineation of the phenotype with reference to genetic heterogeneity. *Am J Med Genet* 23:821, 1986.
393. Andersen PE Jr, Hauge M: Osteogenesis imperfecta: a genetic, radiological, and epidemiological study. *Clin Genet* 36:250, 1989.
394. Glorieux FH, Rauch F, Plotkin H, et al: Type V osteogenesis imperfecta: A new form of brittle bone disease. *Journal of Bone and Mineral Research* 15:1650, 2000.
395. Glorieux FH, Ward LM, Rauch F, et al: Osteogenesis imperfecta type VI: A form of brittle bone disease with a mineralization defect. *J Bone Miner Res* 17:30, 2002.
396. Ward LM, Rauch F, Travers R, et al: Osteogenesis imperfecta type VII: an autosomal recessive form of brittle bone disease. *Bone* 31:12, 2002.
397. Byers PH, Starman BJ, Cohn DH, et al: A novel mutation causes a perinatal lethal form of osteogenesis imperfecta. An insertion in one alpha 1(I) collagen allele (COL1A1). *J Biol Chem* 263:7855, 1988.
398. Wenstrup RJ, Cohn DH, Cohen T, et al: Arginine for glycine substitution in the triple-helical domain of the products of one alpha 2(I) collagen allele (COL1A2) produces the osteogenesis imperfecta type IV phenotype. *J Biol Chem* 263:7734, 1988.
399. Barsh GS, Byers PH: Reduced secretion of structurally abnormal type I procollagen in a form of osteogenesis imperfecta. *Proc Natl Acad Sci U S A* 78:5142, 1981.
400. Barsh GS, Roush CL, Bonadio J, et al: Intron-mediated recombination may cause a deletion in an alpha 1 type I collagen chain in a lethal form of osteogenesis imperfecta. *Proc Natl Acad Sci U S A* 82:2870, 1985.
401. Chu ML, Gargiulo V, Williams CJ, et al: Multixon deletion in an osteogenesis imperfecta variant with increased type III collagen mRNA. *J Biol Chem* 260:691, 1985.
402. Chervenak FA, Romero R, Berkowitz RL, et al: Antenatal sonographic findings of osteogenesis imperfecta. *Am J Obstet Gynecol* 143:228, 1982.
403. Milsom I, Mattsson LA, Dahlen-Nilsson I: Antenatal diagnosis of osteogenesis imperfecta by real time ultrasound: two case reports. *Br J Radiol* 55:310, 1982.
404. Elejalde BR, de Elejalde MM: Prenatal diagnosis of perinatally lethal osteogenesis imperfecta. *Am J Med Genet* 14:353, 1983.
405. Griffin ER III, Webster JC, Almaro VP: Ultrasonic and radiological features of osteogenesis imperfecta congenita: case report. *Mil Med* 148:157, 1983.
406. Patel ZM, Shah HL, Madon PF, Ambani LM: Prenatal diagnosis of lethal osteogenesis imperfecta (OI) by ultrasonography. *Prenat Diagn* 3:261, 1983.
407. Stephens JD, Filly RA, Callen PW, et al: Prenatal diagnosis of osteogenesis imperfecta type II by real-time ultrasound. *Hum Genet* 64:191, 1983.
408. Woo JS, Ghosh A, Liang ST, et al: Ultrasonic evaluation of osteogenesis imperfecta congenita in utero. *J Clin Ultrasound* 11:42, 1983.
409. Aylsworth AS, Seeds JW, Guilford WB, et al: Prenatal diagnosis of a severe deforming type of osteogenesis imperfecta. *Am J Med Genet* 19:707, 1984.
410. Brown BS: The prenatal ultrasonographic diagnosis of osteogenesis imperfecta lethalis. *J Can Assoc Radiol* 35:63, 1984.
411. Ghosh A, Woo JS, Wan CW, et al: Simple ultrasonic diagnosis of osteogenesis imperfecta type II in early second trimester. *Prenat Diagn* 4:235, 1984.
412. Bradley FJ, Essex T: Osteogenesis imperfecta: report of 2 cases. *J Am Osteopath Assoc* 85:462, 1985.
413. Carpenter MW, Abuelo D, Neave C: Midtrimester diagnosis of severe deforming osteogenesis imperfecta with autosomal dominant inheritance. *Am J Perinatol* 3:80, 1986.
414. Merz E, Goldhofer W: Sonographic diagnosis of lethal osteogenesis imperfecta in the second trimester: case report and review. *J Clin Ultrasound* 14:380, 1986.
415. Brons JT, van der Harten HJ, Wladimiroff JW, et al: Prenatal ultrasonographic diagnosis of osteogenesis imperfecta. *Am J Obstet Gynecol* 159:176, 1988.
416. Munoz C, Filly RA, Golbus MS: Osteogenesis imperfecta type II: prenatal sonographic diagnosis. *Radiology* 174:181, 1990.
417. Pfutzenreuter N, Panzer F, Bastert G: Prenatal diagnosis of osteogenesis imperfecta congenita; a case report. *Eur J Obstet Gynecol Reprod Biol* 34:189, 1990.
418. Constantine G, McCormack J, McHugo J, et al: Prenatal diagnosis of severe osteogenesis imperfecta. *Prenat Diagn* 11:103, 1991.
419. Morin LR, Herlicoviez M, Loisel JC, et al: Prenatal diagnosis of lethal osteogenesis imperfecta in twin pregnancy. *Clin Genet* 39:467, 1991.
420. D'Ottavio G, Tamaro LF, Mandruzzato G: Early prenatal ultrasonographic diagnosis of osteogenesis imperfecta: a case report. *Am J Obstet Gynecol* 169:384, 1993.
421. Berge LN, Marton V, Tranebjærg L, et al: Prenatal diagnosis of osteogenesis imperfecta. *Acta Obstet Gynecol Scand* 74:321, 1995.
422. Chen FP, Chang LC: Prenatal diagnosis of osteogenesis imperfecta congenita by ultrasonography. *J Formos Med Assoc* 95:386, 1996.
423. Tongsong T, Wanapirak C, Sirianguk S: Prenatal diagnosis of osteogenesis imperfecta type II. *Int J Gynaecol Obstet* 61:33, 1998.
424. DiMaio MS, Barth R, Koprivnikar KE, et al: First-trimester prenatal diagnosis of osteogenesis imperfecta type II by DNA analysis and sonography. *Prenat Diagn* 13:589, 1993.
425. Buisson O, Senat MV, Laurenceau N, et al: [Update on prenatal diagnosis of osteogenesis imperfecta type II: an index case report diagnosed by ultrasonography in the first trimester]. *J Gynecol Obstet Biol Reprod (Paris)* 31:672, 2002.
426. McEwing RL, Alton K, Johnson J, et al: First-trimester diagnosis of osteogenesis imperfecta type II by three-dimensional sonography. *J Ultrasound Med* 22:311, 2003.
427. Ruano R, Picone O, Benachi A, et al: First-trimester diagnosis of osteogenesis imperfecta associated with encephalocele by conventional and three-dimensional ultrasound. *Prenat Diagn* 23:539, 2003.
428. Bishop NJ: Osteogenesis imperfecta calls for caution. *Nat Med* 5:466, 1999.
429. Bischoff H, Freitag P, Jundt G, et al: Type I osteogenesis imperfecta: diagnostic difficulties. *Clin Rheumatol* 18:48, 1999.
430. Bulas DI, Stern HJ, Rosenbaum KN, et al: Variable prenatal appearance of osteogenesis imperfecta. *J Ultrasound Med* 13:419, 1994.
431. Robinson LP, Worthen NJ, Lachman RS, et al: Prenatal diagnosis of osteogenesis imperfecta type III. *Prenat Diagn* 7:7, 1987.
432. Thompson EM: Non-invasive prenatal diagnosis of osteogenesis imperfecta. *Am J Med Genet* 45:201, 1993.
433. Pepin M, Atkinson M, Starman BJ, et al: Strategies and outcomes of prenatal diagnosis for osteogenesis imperfecta: a review of biochemical and molecular studies completed in 129 pregnancies. *Prenat Diagn* 17:559, 1997.
434. Nuytink L, Sayli BS, Karen W, et al: Prenatal diagnosis of osteogenesis imperfecta type I by COL1A1 null-allele testing. *Prenat Diagn* 19:873, 1999.



435. Ries L, Frydman M, Barkai G, et al: Prenatal diagnosis of a novel COL1A1 mutation in osteogenesis imperfecta type I carried through full term pregnancy. *Prenat Diagn* 20:876, 2000.
436. Mornet E, Simon-Bouy B: [Genetics of hypophosphatasia]. *Arch Pediatr*;11:444, 2004.
437. Mornet E, Muller F, Ngo S, et al: Correlation of alkaline phosphatase (ALP) determination and analysis of the tissue non-specific ALP gene in prenatal diagnosis of severe hypophosphatasia. *Prenat Diagn* 19:755, 1999.
438. Komaru K, Ishida Y, Amaya Y, et al: Novel aggregate formation of a frame-shift mutant protein of tissue-nonspecific alkaline phosphatase is ascribed to three cysteine residues in the C-terminal extension. Retarded secretion and proteasomal degradation. *FEBS J* 272:1704, 2005.
439. Vandevijver N, Die-Smulders CE, Offermans JP, et al: Lethal hypophosphatasia, spur type: case report and fetopathological study. *Genet Couns* 9:205, 1998.
440. Whyte MP: Hypophosphatasia and the role of alkaline phosphatase in skeletal mineralization. *Endocr Rev* 15:439, 1994.
441. Terada S, Suzuki N, Ueno H, et al: A congenital lethal form of hypophosphatasia: histologic and ultrastructural study. *Acta Obstet Gynecol Scand* 75:502, 1996.
442. Sergi C, Mornet E, Troeger J, et al: Perinatal hypophosphatasia: radiology, pathology and molecular biology studies in a family harboring a splicing mutation (648+1A) and a novel missense mutation (N400S) in the tissue-nonspecific alkaline phosphatase (TNSALP) gene. *Am J Med Genet* 103:235, 2001.
443. Sawai H, Kanazawa N, Tsukahara Y, et al: Severe perinatal hypophosphatasia due to homozygous deletion of T at nucleotide 1559 in the tissue nonspecific alkaline phosphatase gene. *Prenat Diagn* 23:743, 2003.
444. Wladimiroff JW, Niermeijer MF, van der Harten JJ, et al: Early prenatal diagnosis of congenital hypophosphatasia: case report. *Prenat Diagn* 5:47, 1985.
445. Warren RC, McKenzie CF, Rodeck CH, et al: First trimester diagnosis of hypophosphatasia with a monoclonal antibody to the liver/bone/kidney isoenzyme of alkaline phosphatase. *Lancet* 2:856, 1985.
446. Yagel S, Milwidsky A, Ornoy A, et al: Imaging case of the month. Hypophosphatasia. *Am J Perinatol* 2:261, 1985.
447. DeLange M, Rouse GA: Prenatal diagnosis of hypophosphatasia. *J Ultrasound Med* 9:115, 1990.
448. Hall C: Pre-natal diagnosis of lethal dwarfism using ultrasound. *Radiogr Today* 57:22, 1991.
449. Kleinman G, Uri M, Hull S, et al: Perinatal ultrasound casebook. Antenatal findings in congenital hypophosphatasia. *J Perinatol* 11:282, 1991.
450. Tongsong T, Sirichotiyakul S, Siriengkul S: Prenatal diagnosis of congenital hypophosphatasia. *J Clin Ultrasound* 23:52, 1995.
451. Moore CA, Curry CJ, Henthorn PS, et al: Mild autosomal dominant hypophosphatasia: in utero presentation in two families. *Am J Med Genet* 86:410, 1999.
452. Pauli RM, Modaff P, Sipes SL, et al: Mild hypophosphatasia mimicking severe osteogenesis imperfecta in utero: bent but not broken. *Am J Med Genet* 86:434, 1999.
453. Gortzak-Uzan L, Sheiner E, Gohar J: Prenatal diagnosis of congenital hypophosphatasia in a consanguineous Bedouin couple. A case report. *J Reprod Med* 45:588, 2000.
454. Tongsong T, Pongsatha S: Early prenatal sonographic diagnosis of congenital hypophosphatasia. *Ultrasound Obstet Gynecol* 15:252, 2000.
455. Sato S, Matsuo N: Genetic analysis of hypophosphatasia. *Acta Paediatr Jpn* 39:528, 1997.
456. Brock DJ, Barron L: First-trimester prenatal diagnosis of hypophosphatasia: experience with 16 cases. *Prenat Diagn* 11:387, 1991.
457. Rudd NL, Miskin M, Hoar DI, et al: Prenatal diagnosis of hypophosphatasia. *N Engl J Med* 295:146, 1976.
458. Rattenbury JM, Blau K, Sandler M, et al: Letter: Prenatal diagnosis of hypophosphatasia. *Lancet* 1:306, 1976.
459. Orimo H, Nakajima E, Hayashi Z, et al: First-trimester prenatal molecular diagnosis of infantile hypophosphatasia in a Japanese family. *Prenat Diagn* 16:559, 1996.
460. Henthorn PS, Whyte MP: Infantile hypophosphatasia: successful prenatal assessment by testing for tissue-non-specific alkaline phosphatase isoenzyme gene mutations. *Prenat Diagn* 15:1001, 1995.
461. Weiss MJ, Cole DE, Ray K, et al: A missense mutation in the human liver/bone/kidney alkaline phosphatase gene causing a lethal form of hypophosphatasia. *Proc Natl Acad Sci U S A* 85:7666, 1988.
462. Smith M, Weiss MJ, Griffin CA, et al: Regional assignment of the gene for human liver/bone/kidney alkaline phosphatase to chromosome 1p36.1-p34. *Genomics* 2:139, 1988.
463. Mornet E, Taillandier A, Peyramaure S, et al: Identification of fifteen novel mutations in the tissue-nonspecific alkaline phosphatase (TNSALP) gene in European patients with severe hypophosphatasia. *Eur J Hum Genet* 6:308, 1998.
464. Spentchian M, Merrien Y, Herasse M, et al: Severe hypophosphatasia: characterization of fifteen novel mutations in the ALPL gene. *Hum Mutat* 22:105, 2003.
465. Zurutuza L, Muller F, Gibrat JF, et al: Correlations of genotype and phenotype in hypophosphatasia. *Hum Mol Genet* 8:1039, 1999.
466. Hastbacka J, de la Chapelle A, Mahtani MM, et al: The diastrophic dysplasia gene encodes a novel sulfate transporter: positional cloning by fine-structure linkage disequilibrium mapping. *Cell* 78:1073, 1994.
467. Horton WA, Rimoin DL, Lachman RS, et al: The phenotypic variability of diastrophic dysplasia. *J Pediatr* 93:609, 1978.
468. Kaitila I, Ammala P, Karjalainen O, et al: Early prenatal detection of diastrophic dysplasia. *Prenat Diagn* 3:237, 1983.
469. Hastbacka J, Kaitila I, Sistonen P, et al: Diastrophic dysplasia gene maps to the distal long arm of chromosome 5. *Proc Natl Acad Sci U S A* 87:8056, 1990.
470. Rossi A, Superti-Furga A: Mutations in the diastrophic dysplasia sulfate transporter (DTDST) gene (SLC26A2): 22 novel mutations, mutation review, associated skeletal phenotypes, and diagnostic relevance. *Hum Mutat* 17:159, 2001.
471. Superti-Furga A, Hastbacka J, Rossi A, et al: A family of chondrodysplasias caused by mutations in the diastrophic dysplasia sulfate transporter gene and associated with impaired sulfation of proteoglycans. *Ann N Y Acad Sci* 785:195, 1996.
472. Karniski LP: Mutations in the diastrophic dysplasia sulfate transporter (DTDST) gene: correlation between sulfate transport activity and chondrodysplasia phenotype. *Hum Mol Genet* 10:1485, 2001.
473. Megarbane A, Farkh I, Haddad-Zebani S: How many phenotypes in the DTDST family chondrodysplasias? *Clin Genet* 62:189, 2002.
474. Gollop TR, Eigier A: Prenatal ultrasound diagnosis of diastrophic dysplasia at 16 weeks. *Am J Med Genet* 27:321, 1987.
475. Jung C, Sohn C, Sergi CL: Case report: prenatal diagnosis of diastrophic dysplasia by ultrasound at 21 weeks of gestation in a mother with massive obesity. *Prenat Diagn* 18:378, 1998.
476. Wax JR, Carpenter M, Smith W, et al: Second-trimester sonographic diagnosis of diastrophic dysplasia: report of 2 index cases. *J Ultrasound Med* 22:805, 2003.
477. Severi FM, Bocchi C, Sanseverino F, et al: Prenatal ultrasonographic diagnosis of diastrophic dysplasia at 13 weeks of gestation. *J Matern Fetal Neonatal Med* 13:282, 2003.
478. Sepulveda W, Sepulveda-Swatson E, Sanchez J: Diastrophic dysplasia: prenatal three-dimensional ultrasound findings. *Ultrasound Obstet Gynecol* 23:312, 2004.
479. Hastbacka J, Salonen R, Laurila P, et al: Prenatal diagnosis of diastrophic dysplasia with polymorphic DNA markers. *J Med Genet* 30:265, 1993.
480. Bonafe L, Superti-Furga A: Diastrophic dysplasia. *GeneReviews at GeneTests: Medical Genetics Information Resource (database online)*. 2004. Copyright, University of Washington, Seattle. 1997-2005. Available at <http://www.genetests.org>. Accessed 2-18-2005.
481. Remes V, Helenius I, Peltonen J, et al: Lung function in diastrophic dysplasia. *Pediatr Pulmonol* 33:277, 2002.
482. Eteson DJ, Beluffi G, Burgio GR, et al: Pseudodiastrophic dysplasia: a distinct newborn skeletal dysplasia. *J Pediatr* 109:635, 1986.
483. Cetta G, Rossi A, Burgio GR, et al: Diastrophic dysplasia sulfate transporter (DTDST) gene is not involved in pseudodiastrophic dysplasia. *Am J Med Genet* 73:493, 1997.
484. Hooshang T, Ralph SL: *Radiology of Syndromes, Metabolic Disorders, and Skeletal Dysplasias*. Chicago, Year Book Medical Publishers, 1983.
485. Kniest W: Zur Abgrenzung der Dysostosis enchondralis von der Chondrodystrophie. *Z Kinderheilk* 70:633, 1952.
486. Siggers CD, Rimoin DL, Dorst JP, et al: The Kniest syndrome. *Birth Defects Orig Artic Ser* 10:193, 1974.
487. Winterpacht A, Hilbert M, Schwarze U, et al: Kniest and Stickler dysplasia phenotypes caused by collagen type II gene (COL2A1) defect. *Nat Genet* 3:323, 1993.



488. Fernandes RJ, Wilkin DJ, Weis MA, et al: Incorporation of structurally defective type II collagen into cartilage matrix in kniest chondrodysplasia. *Arch Biochem Biophys* 355:282, 1998.
489. Weis MA, Wilkin DJ, Kim HJ, et al: Structurally abnormal type II collagen in a severe form of Kniest dysplasia caused by an exon 24 skipping mutation. *J Biol Chem* 273:4761, 1998.
490. Wilkin DJ, Bogaert R, Lachman RS, et al: A single amino acid substitution (G103D) in the type II collagen triple helix produces Kniest dysplasia. *Hum Mol Genet* 3:1999, 1994.
491. Nishimura G, Haga N, Kitoh H, et al: The phenotypic spectrum of COL2A1 mutations. *Hum Mutat* 26:36, 2005.
492. Chen H: *Atlas of Genetic Diagnosis and Counselling*. Totowa, NJ: Humana Press, 2006.
493. Chen H, Yang SS, Gonzalez E: Kniest dysplasia: neonatal death with necropsy. *Am J Med Genet* 6:171, 1980.
494. Handmaker SD, Campbell JA, Robinson LD, et al: Dyssegmental dwarfism: a new syndrome of lethal dwarfism. *Birth Defects Orig Artic Ser* 13:79, 1977.
495. Aleck KA, Grix A, Clericuzio C, et al: Dyssegmental dysplasias: clinical, radiographic, and morphologic evidence of heterogeneity. *Am J Med Genet* 27:295, 1987.
496. Fasanelli S, Kozlowski K, Reiter S, et al: Dyssegmental dysplasia (report of two cases with a review of the literature). *Skeletal Radiol* 14:173, 1985.
497. Andersen PE, Jr., Hauge M, Bang J: Dyssegmental dysplasia in siblings: prenatal ultrasonic diagnosis. *Skeletal Radiol* 17:29, 1988.
498. Prabhu VG, Kozma C, Leftridge CA, et al: Dyssegmental dysplasia Silverman-Handmaker type in a consanguineous Druze Lebanese family: long term survival and documentation of the natural history. *Am J Med Genet* 75:164, 1998.
499. Stoll C, Langer B, Gasser B, et al: Sporadic case of dyssegmental dysplasia with antenatal presentation. *Genet Couns* 9:125, 1998.
500. Kim HJ, Costales F, Bouzouki M, et al: Prenatal diagnosis of dyssegmental dwarfism. *Prenat Diagn* 6:143, 1986.
501. Hsieh YY, Chang CC, Tsai HD, et al: Prenatal diagnosis of dyssegmental dysplasia. A case report. *J Reprod Med* 44:303, 1999.
502. Izquierdo LA, Kushnir O, Aase J, et al: Antenatal ultrasonic diagnosis of dyssegmental dysplasia: a case report. *Prenat Diagn* 10:587, 1990.
503. Arikawa-Hirasawa E, Wilcox WR, Le AH, et al: Dyssegmental dysplasia, Silverman-Handmaker type, is caused by functional null mutations of the perlecan gene. *Nat Genet* 27:431, 2001.
504. Uchida K, Ueno H, Takizawa N, Okada Y: Reduced levels of MMP-2 and TIMP-1 in dyssegmental dysplasia. *J Bone Miner Res* 18:381, 2003.
505. Maroteaux P, Spranger J, Opitz JM, et al: [The campomelic syndrome]. *Presse Med* 79:1157, 1971.
506. Mansour S, Hall CM, Pembrey ME, et al: A clinical and genetic study of campomelic dysplasia. *J Med Genet* 32:415, 1995.
507. Normann EK, Pedersen JC, Stiris G, van der Hagen CB: Campomelic dysplasia—an underdiagnosed condition? *Eur J Pediatr* 152:331, 1993.
508. Houston CS, Opitz JM, Spranger JW, et al: The campomelic syndrome: review, report of 17 cases, and follow-up on the currently 17-year-old boy first reported by Maroteaux et al in 1971. *Am J Med Genet* 15:3, 1983.
509. Fryns JP, van den Berghe K, van Assche A, van den Berghe H: Prenatal diagnosis of campomelic dwarfism. *Clin Genet* 19:199, 1981.
510. Redon JY, Le Grevellec JY, Marie F, et al: [Prenatal diagnosis of campomelic dysplasia]. *J Gynecol Obstet Biol Reprod (Paris)* 13:437, 1984.
511. Slater CP, Ross J, Nelson MM, et al: The campomelic syndrome—prenatal ultrasound investigations. A case report. *S Afr Med J* 67:863, 1985.
512. Winter R, Rosenkranz W, Hofmann H, et al: Prenatal diagnosis of campomelic dysplasia by ultrasonography. *Prenat Diagn* 5:1, 1985.
513. Cordone M, Lituania M, Zampatti C, et al: In utero ultrasonographic features of campomelic dysplasia. *Prenat Diagn* 9:745, 1989.
514. Tennstedt C, Bartho S, Bollmann R, et al: [Osteochondrodysplasias. Prenatal diagnosis and pathological-anatomic findings]. *Zentralbl Pathol* 139:71, 1993.
515. Sanders RC, Greyson-Fleg RT, Hogge WA, et al: Osteogenesis imperfecta and campomelic dysplasia: difficulties in prenatal diagnosis. *J Ultrasound Med* 13:691, 1994.
516. Tongsong T, Wanapirak C, Pongsatha S: Prenatal diagnosis of campomelic dysplasia. *Ultrasound Obstet Gynecol* 15:428, 2000.
517. Foster JW, Dominguez-Steglich MA, Guioli S, et al: Campomelic dysplasia and autosomal sex reversal caused by mutations in an SRY-related gene. *Nature* 372:525, 1994.
518. Wunderle VM, Critcher R, Hastie N, et al: Deletion of long-range regulatory elements upstream of SOX9 causes campomelic dysplasia. *Proc Natl Acad Sci U S A* 95:10649, 1998.
519. Kanai Y, Hiramatsu R, Matoba S, et al: From SRY to SOX9: Mammalian Testis Differentiation. *J Biochem (Tokyo)* 138:13, 2005.
520. Goji K, Nishijima E, Tsugawa C, et al: Novel missense mutation in the HMG box of SOX9 gene in a Japanese XY male resulted in campomelic dysplasia and severe defect in masculinization. *Hum Mutat Suppl* 1:S114, 1998.
521. Hageman RM, Cameron EJ, Sinclair AH: Mutation analysis of the SOX9 gene in a patient with campomelic dysplasia. *Hum Mutat (Suppl 1)*:S112, 1998.
522. McDowall S, Argentaro A, Ranganathan S, et al: Functional and structural studies of wild type SOX9 and mutations causing campomelic dysplasia. *J Biol Chem* 274:24023, 1999.
523. Pop R, Zaragoza MV, Gaudette M, et al: A homozygous nonsense mutation in SOX9 in the dominant disorder campomelic dysplasia: a case of mitotic gene conversion. *Hum Genet* 117:43, 2005.
524. Maraia R, Saal HM, Wanga D: A chromosome 17q de novo paracentric inversion in a patient with campomelic dysplasia; case report and etiologic hypothesis. *Clin Genet* 39:401, 1991.
525. Young ID, Zuccollo JM, Maltby EL, et al: Campomelic dysplasia associated with a de novo 2q:17q reciprocal translocation. *J Med Genet* 29:251, 1992.
526. Tommerup N, Schempp W, Meinecke P, et al: Assignment of an autosomal sex reversal locus (SRA1) and campomelic dysplasia (CMPD1) to 17q24.3-q25.1. *Nat Genet* 4:170, 1993.
527. Ninomiya S, Narahara K, Tsuji K, et al: Acampomelic campomelic syndrome and sex reversal associated with de novo t(12;17) translocation. *Am J Med Genet* 56:31, 1995.
528. Savarirayan R, Bankier A: Acampomelic campomelic dysplasia with de novo 5q:17q reciprocal translocation and severe phenotype. *J Med Genet* 35:597, 1998.
529. Pfeifer D, Kist R, Dewar K, et al: Campomelic dysplasia translocation breakpoints are scattered over 1 Mb proximal to SOX9: evidence for an extended control region. *Am J Hum Genet* 65:111, 1999.
530. Beluffi G, Fraccaro M: Genetical and clinical aspects of campomelic dysplasia. *Prog Clin Biol Res* 104:53, 1982.
531. Ray S, Bowen JR: Orthopaedic problems associated with survival in campomelic dysplasia. *Clin Orthop* 185:77, 1984.
532. Cooke CT, Mulcahy MT, Cullity GJ, et al: Campomelic dysplasia with sex reversal: morphological and cytogenetic studies of a case. *Pathology* 17:526, 1985.
533. Offiah AC, Mansour S, McDowall S, et al: Surviving campomelic dysplasia has the radiological features of the previously reported ischio-pubic-patella syndrome. *J Med Genet* 39:e50, 2002.
534. Mansour S, Offiah AC, McDowall S, et al: The phenotype of survivors of campomelic dysplasia. *J Med Genet* 39:597, 2002.
535. Romero R, Ghidini A, Eswara MS, et al: Prenatal findings in a case of spondylocostal dysplasia type I (Jarcho-Levin syndrome). *Obstet Gynecol* 71:988, 1988.
536. Jeune M, Carron R: Dystrophic thoracique asphyxiante caractere familial. *Arch Fr Pediatr* 12:276, 1955.
537. Mastrup LP, Host A: [The Jeune syndrome, asphyxiating thoracic dysplasia. A review and description of 2 siblings]. *Ugeskr Laeger* 147:1676, 1985.
538. Capilupi B, Olappi G, Cornaglia AM, et al: [Asphyxiating thoracic dysplasia or Jeune's syndrome. Description of 2 mild familial cases]. *Pediatr Med Chir* 18:529, 1996.
539. Kozlowski K, Masel J: Asphyxiating thoracic dystrophy without respiratory disease: report of two cases of the latent form. *Pediatr Radiol* 5:30, 1976.
540. Chen CP, Lin SP, Liu FF, et al: Prenatal diagnosis of asphyxiating thoracic dysplasia (Jeune syndrome). *Am J Perinatol* 13:495, 1996.
541. Poggiani C, Gasparoni MC, Mangili G, et al: Asphyxiating thoracic dysplasia in a lethal form: radiological and sonographic findings. *Minerva Pediatr* 52:63, 2000.
542. Giorgi PL, Gabrielli O, Bonifazi V, et al: Mild form of Jeune syndrome in two sisters. *Am J Med Genet* 35:280, 1990.
543. Reiterer F, Muller WD, Wendler H: [Variance in the clinical picture and course of asphyxiating thoracic dysplasia (Jeune syndrome)]. *Klin Padiatr* 198:340, 1986.



544. Banerjee D, Desai A, Burke GW, et al: Retransplantation in a patient with type 2 Jeune's syndrome. *Am J Kidney Dis* 39:E9, 2002.
545. Ozcay F, Derbent M, Demirhan B, et al: A family with Jeune syndrome. *Pediatr Nephrol* 16:623, 2001.
546. Amirou M, Bourdat-Michel G, Pinel N, et al: Successful renal transplantation in Jeune syndrome type 2. *Pediatr Nephrol* 12:293, 1998.
547. Novakovic I, Kostic M, Popovic-Rolovic M, et al: [Jeune's syndrome (3 case reports)]. *Srp Arh Celok Lek* 124(Suppl 1):244, 1996.
548. Bernstein J: Glomerulocystic kidney disease—nosological considerations. *Pediatr Nephrol* 7:464, 1993.
549. Redmond J, III, Richter MP, Stein HD, et al: Primitive neuroectodermal tumor of the chest wall in a patient with Jeune's syndrome and renal transplant. *Am J Kidney Dis* 21:449, 1993.
550. Clayton-Smith J: Jeune syndrome and cystinuria. *Am J Med Genet* 41:531, 1991.
551. Ring E, Zobel G, Ratschek M, et al: Retrospective diagnosis of Jeune's syndrome in two patients with chronic renal failure. *Child Nephrol Urol* 10:88, 1990.
552. Donaldson MD, Warner AA, Trompeter RS, et al: Familial juvenile nephronophthisis, Jeune's syndrome, and associated disorders. *Arch Dis Child* 60:426, 1985.
553. Shah KJ: Renal lesion in Jeune's syndrome. *Br J Radiol* 53:432, 1980.
554. Edelson PJ, Spackman TJ, Belliveau RE, et al: A renal lesion in asphyxiating thoracic dysplasia. *Birth Defects Orig Artic Ser* 10:51, 1974.
555. Caraballo A, Lopez BA, Martin GJ, et al: [Thoracic asphyxiating dystrophy and renal disease (author's transl)]. *An Esp Pediatr* 10:88, 1977.
556. Herdman RC, Langer LO: The thoracic asphyxiating dystrophy and renal disease. *Am J Dis Child* 116:192, 1968.
557. Tongsong T, Chanprapaph P, Thongpadungroj T: Prenatal sonographic findings associated with asphyxiating thoracic dystrophy (Jeune syndrome). *J Ultrasound Med* 18:573, 1999.
558. Yerian LM, Brady L, Hart J: Hepatic manifestations of Jeune syndrome (asphyxiating thoracic dystrophy). *Semin Liver Dis* 23:195, 2003.
559. Esmer C, Alvarez-Mendoza A, Lieberman E, et al: Liver fibrocystic disease and polydactyly: proposal of a new syndrome. *Am J Med Genet* 101:12, 2001.
560. Labrune P, Fabre M, Trioche P, et al: Jeune syndrome and liver disease: report of three cases treated with ursodeoxycholic acid. *Am J Med Genet* 87:324, 1999.
561. Trabelsi M, Hammou-Jeddi A, Kammoun A, et al: [Asphyxiating thoracic dysplasia associated with hepatic ductal hypoplasia, agenesis of the corpus callosum and Dandy-Walker syndrome]. *Pediatric* 45:35, 1990.
562. Landing BH, Wells TR, Lipsey AJ, et al: Morphometric studies of cystic and tubulointerstitial kidney diseases with hepatic fibrosis in children. *Pediatr Pathol* 10:959, 1990.
563. Whitley CB, Schwarzenberg SJ, Burke BA, et al: Direct hyperbilirubinemia and hepatic fibrosis: a new presentation of Jeune syndrome (asphyxiating thoracic dystrophy). *Am J Med Genet Suppl* 3:211, 1987.
564. Georgiou-Theodoropoulos M, Agapitos M, Theodoropoulos P, et al: Jeune syndrome associated with pancreatic fibrosis. *Pediatr Pathol* 8:541, 1988.
565. Hopper MS, Boulton JE, Watson AR: Polyhydramnios associated with congenital pancreatic cysts and asphyxiating thoracic dysplasia. A case report. *S Afr Med J* 56:32, 1979.
566. Casteels I, Demandt E, Legius E: Visual loss as the presenting sign of Jeune syndrome. *Eur J Paediatr Neurol* 4:243, 2000.
567. Wilson DJ, Weleber RG, Beals RK: Retinal dystrophy in Jeune's syndrome. *Arch Ophthalmol* 105:651, 1987.
568. Phillips CI, Stokoe NL, Bartholomew RS: Asphyxiating thoracic dystrophy (Jeune's disease) with retinal aplasia: a sibship of two. *J Pediatr Ophthalmol Strabismus* 16:279, 1979.
569. Elejalde BR, de Elejalde MM, Pansch D: Prenatal diagnosis of Jeune syndrome. *Am J Med Genet* 21:433, 1985.
570. Schinzel A, Savoldelli G, Briner J, et al: Prenatal sonographic diagnosis of Jeune syndrome. *Radiology* 154:777, 1985.
571. den Hollander NS, Robben SG, Hoozeboom AJ, et al: Early prenatal sonographic diagnosis and follow-up of Jeune syndrome. *Ultrasound Obstet Gynecol* 18:378, 2001.
572. Lipson M, Waskey J, Rice J, et al: Prenatal diagnosis of asphyxiating thoracic dysplasia. *Am J Med Genet* 18:273, 1984.
573. Tahernia AC, Stamps P: "Jeune syndrome" (asphyxiating thoracic dystrophy). Report of a case, a review of the literature, and an editor's commentary. *Clin Pediatr (Phila)* 16:903, 1977.
574. Chen SH, Chung MT, Chang FM: Early prenatal diagnosis of Jeune syndrome in a low-risk pregnancy. *Prenat Diagn* 23:606, 2003.
575. Rinaldi S, Dionisi-Vici C, Goffredo B, et al: Jeune syndrome associated with cystinuria: report of two sisters. *Am J Med Genet* 37:301, 1990.
576. Hudgins L, Rosengren S, Treem W, et al: Early cirrhosis in survivors with Jeune thoracic dystrophy. *J Pediatr* 120:754, 1992.
577. Bard LA, Bard PA, Owens GW, et al: Retinal involvement in thoracic-pelvic-phalangeal dystrophy. *Arch Ophthalmol* 96:278, 1978.
578. Silengo M, Gianino P, Longo P, et al: Dandy-Walker complex in a child with Jeune's asphyxiating thoracic dystrophy. *Pediatr Radiol* 30:430, 2000.
579. Majewski E, Ozturk B, Gillesen-Kaesbach G: Jeune syndrome with tongue lobulation and preaxial polydactyly, and Jeune syndrome with situs inversus and asplenia: compound heterozygosity Jeune-Mohr and Jeune-Ivemark? *Am J Med Genet* 63:74, 1996.
580. Aurora P, Wallis CE: Jeune syndrome (asphyxiating thoracic dystrophy) associated with Hirschsprung disease. *Clin Dysmorphol* 8:259, 1999.
581. Panero Lopez AL, Puyol Bul PJ, Belaustegui CA, et al: [Asphyxiating thoracic dysplasia in 2 dizygotic twins]. *An Esp Pediatr* 26:453, 1987.
582. Skiptunas SM, Weiner S: Early prenatal diagnosis of asphyxiating thoracic dysplasia (Jeune's syndrome). Value of fetal thoracic measurement. *J Ultrasound Med* 6:41, 1987.
583. Kapoor R, Saha MM, Gupta NC: Antenatal diagnosis of asphyxiating thoracic dysplasia. *Indian Pediatr* 26:495, 1989.
584. Ardura FJ, Alvarez GC, Rodriguez FM, et al: [Asphyxiating thoracic dysplasia associated with proximal myopathy and arachnoid cyst]. *An Esp Pediatr* 33:592, 1990.
585. Ben Ami M, Perlitz Y, Haddad S, et al: Increased nuchal translucency is associated with asphyxiating thoracic dysplasia. *Ultrasound Obstet Gynecol* 10:297, 1997.
586. Das BB, Nagaraj A, Fayemi A, et al: Fetal thoracic measurements in prenatal diagnosis of Jeune syndrome. *Indian J Pediatr* 69:101, 2002.
587. Morgan NV, Bacchelli C, Gissen P, et al: A locus for asphyxiating thoracic dystrophy, ATD, maps to chromosome 15q13. *J Med Genet* 40:431, 2003.
588. GeneTests: Medical Genetics Information Resource (database online). Copyright, University of Washington Seattle. 1993-2005. Updated weekly. Available at <http://www.genetests.org>. 2005. Accessed 2-20-2005.
589. Davis JT, Ruberg RL, Leppink DM, et al: Lateral thoracic expansion for Jeune's asphyxiating dystrophy: a new approach. *Ann Thorac Surg* 60:694, 1995.
590. Davis JT, Heistein JB, Castile RG, et al: Lateral thoracic expansion for Jeune's syndrome: midterm results. *Ann Thorac Surg* 72:872, 2001.
591. Mutabagani K, Humphrey R, Helstein J, et al: The lateral thoracic expansion for Jeunes asphyxiating dystrophy: experience at a single institution. *Saudi Med J* 24:S33, 2003.
592. Davis JT, Long FR, Adler BH, et al: Lateral thoracic expansion for Jeune syndrome: evidence of rib healing and new bone formation. *Ann Thorac Surg* 77:445, 2004.
593. Grote W, Weisner D, Janig U, et al: Prenatal diagnosis of a short-rib-polydactyly syndrome type Saldino-Noonan at 17 weeks' gestation. *Eur J Pediatr* 140:63, 1983.
594. Saldino RM, Noonan CD: Severe thoracic dystrophy with striking micromelia, abnormal osseous development, including the spine, and multiple visceral anomalies. *Am J Roentgenol Radium Ther Nucl Med* 114:257, 1972.
595. Majewski F, Pfeiffer RA, Lenz W, et al: [Polysyndactyly, short limbs, and genital malformations—a new syndrome?] *Z Kinderheilkd* 111:118, 1971.
596. Naumoff P, Young LW, Mazer J, et al: Short rib-polydactyly syndrome type 3. *Radiology* 122:443, 1977.
597. Beemer FA, Langer LO Jr, Klep-de Pater JM, et al: A new short rib syndrome: report of two cases. *Am J Med Genet* 14:115, 1983.
598. Silience D, Kozlowski K, Bar-Ziv J, et al: Perinatally lethal short rib-polydactyly syndromes. Variability in known syndromes. *Pediatr Radiol* 17:474, 1987.



599. Wladimiroff JW, Niermeijer MF, Laar J, et al: Prenatal diagnosis of skeletal dysplasia by real-time ultrasound. *Obstet Gynecol* 63:360, 1984.
600. Muller LM, Cremin BJ: Ultrasonic demonstration of fetal skeletal dysplasia. Case reports. *S Afr Med J* 67:222, 1985.
601. Lavanya R, Pratap K: Short rib polydactyly syndrome—a rare skeletal dysplasia. *Int J Gynaecol Obstet* 50:291, 1995.
602. Sarafoglou K, Funai EF, Fefferman N, et al: Short rib-polydactyly syndrome: more evidence of a continuous spectrum. *Clin Genet* 56:145, 1999.
603. Elcioglu NH, Hall CM: Diagnostic dilemmas in the short rib-polydactyly syndrome group. *Am J Med Genet* 111:392, 2002.
604. Scarano G, Della MM, Capece G, et al: A case of short-rib syndrome without polydactyly in a stillborn: a new type? *Birth Defects Orig Artic Ser* 30:95, 1996.
605. Wu MH, Kuo PL, Lin SJ: Prenatal diagnosis of recurrence of short rib-polydactyly syndrome. *Am J Med Genet* 55:279, 1995.
606. Shindel B, Wise S: Recurrent short rib-polydactyly syndrome with unusual associations. *J Clin Ultrasound* 27:143-46, 1999.
607. Yang SS, Roth JA, Langer LO Jr: Short rib syndrome Beemer-Langer type with polydactyly: a multiple congenital anomalies syndrome. *Am J Med Genet* 39:243, 1991.
608. Passarge E: Familial occurrence of a short rib syndrome with hydrops fetalis but without polydactyly. *Am J Med Genet* 14:403, 1983.
609. Winter RM: A lethal short rib syndrome without polydactyly. *J Med Genet* 25:349, 1988.
610. Thomson GS, Reynolds CP, Cruickshank J: Antenatal detection of recurrence of Majewski dwarf (short rib-polydactyly syndrome type II Majewski). *Clin Radiol* 33:509, 1982.
611. Gembruch U, Hansmann M, Fodisch HJ: Early prenatal diagnosis of short rib-polydactyly (SRP) syndrome type I (Majewski) by ultrasound in a case at risk. *Prenat Diagn* 5:357, 1985.
612. Meizner I, Bar-Ziv J: Prenatal ultrasonic diagnosis of short-rib polydactyly syndrome (SRPS) type III: a case report and a proposed approach to the diagnosis of SRPS and related conditions. *J Clin Ultrasound* 13:284, 1985.
613. Steffelaar JW, Lankhorst PF, Reuss A, et al: [Prenatal diagnosis in a primigravida of the short rib-polydactyly syndrome using echography]. *Ned Tijdschr Geneesk* 132:405, 1988.
614. Meizner I, Bar-Ziv J: Prenatal ultrasonic diagnosis of short rib polydactyly syndrome, type I. A case report. *J Reprod Med* 34:668, 1989.
615. de Sierra TM, Ashmead G, Bilenker R: Prenatal diagnosis of short rib (polydactyly) syndrome with situs inversus. *Am J Med Genet* 44:555, 1992.
616. Benacerraf BR: Prenatal sonographic diagnosis of short rib-polydactyly syndrome type II, Majewski type. *J Ultrasound Med* 12:552, 1993.
617. Cideciyan D, Rodriguez MM, Haun RL, et al: New findings in short rib syndrome. *Am J Med Genet* 46:255, 1993.
618. Prudlo J, Stoltenburg-Diederich G, Jimenez E, et al: Central nervous system alterations in a case of short-rib polydactyly syndrome, Majewski type. *Dev Med Child Neurol* 35:158, 1993.
619. Meizner I, Barnhard Y: Short-rib polydactyly syndrome (SRPS) type III diagnosed during routine prenatal ultrasonographic screening. A case report. *Prenat Diagn* 15:665, 1995.
620. Montemarano H, Bulas DI, Chandra R, Tift C: Prenatal diagnosis of glomerulocystic kidney disease in short-rib polydactyly syndrome type II, Majewski type. *Pediatr Radiol* 25:469, 1995.
621. Fujisawa K: [Saldino-Noonan syndrome (short rib polydactyly syndrome type I)]. *Ryokibetsu Shokogun Shirizu* 15:297, 1996.
622. Dugoff L, Coffin CT, Hobbins JC: Sonographic measurement of the fetal rib cage perimeter to thoracic circumference ratio: application to prenatal diagnosis of skeletal dysplasias. *Ultrasound Obstet Gynecol* 10:269, 1997.
623. Hill LM, Leary J: Transvaginal sonographic diagnosis of short-rib polydactyly dysplasia at 13 weeks' gestation. *Prenat Diagn* 18:1198, 1998.
624. den Hollander NS, van der Harten HJ, Laudy JA, et al: Early transvaginal ultrasonographic diagnosis of Beemer-Langer dysplasia: a report of two cases. *Ultrasound Obstet Gynecol* 11:298, 1998.
625. Golombeck K, Jacobs VR, von Kaisenberg C, et al: Short rib-polydactyly syndrome type III: comparison of ultrasound, radiology, and pathology findings. *Fetal Diagn Ther* 16:133, 2001.
626. Sirichotiyakul S, Tongsong T, Wanapirak C, et al: Prenatal sonographic diagnosis of Majewski syndrome. *J Clin Ultrasound* 30:303, 2002.
627. Naki MM, Gur D, Zemheri E, et al: Short rib-polydactyly syndrome. *Arch Gynecol Obstet* 272:173, 2005.
628. Sridhar S, Kishore R, Thomas N, et al: Short rib polydactyly syndrome-Type I. *Indian J Pediatr* 71:359, 2004.
629. Kumru P, Aka N, Kose G, et al: Short rib polydactyly syndrome type 3 with absence of fibulae (Verma-Naumoff syndrome). *Fetal Diagn Ther* 20:410, 2005.
630. Chen CP, Shih JC, Tzen CY, et al: Recurrent short-rib polydactyly syndrome: prenatal three-dimensional ultrasound findings and associations with congenital high airway obstruction and pyelectasia. *Prenat Diagn* 25:417, 2005.
631. Toftager-Larsen K, Benzie RJ: Fetoscopy in prenatal diagnosis of the Majewski and the Saldino-Noonan types of the short rib-polydactyly syndromes. *Clin Genet* 26:56, 1984.
632. Hentze S, Sergi C, Troeger J, et al: Short-rib-polydactyly syndrome type Verma-Naumoff-Le Marec in a fetus with histological hallmarks of type Saldino-Noonan but lacking internal organ abnormalities. *Am J Med Genet* 80:281, 1998.
633. Ho NC, Francomano CA, van Allen M: Jeune asphyxiating thoracic dystrophy and short-rib polydactyly type III (Verma-Naumoff) are variants of the same disorder. *Am J Med Genet* 90:310, 2000.
634. Franceschini P, Guala A, Vardeu MP, et al: Short rib-dysplasia group (with/without polydactyly): report of a patient suggesting the existence of a continuous spectrum. *Am J Med Genet* 59:359, 1995.
635. Martínez-Frías ML, Bermejo E, Urioste M, et al: Lethal short rib-polydactyly syndromes: further evidence for their overlapping in a continuous spectrum. *J Med Genet* 30:937, 1993.
636. Bernstein R, Isdale J, Pinto M, et al: Short rib-polydactyly syndrome: a single or heterogeneous entity? A re-evaluation prompted by four new cases. *J Med Genet* 22:46, 1985.
637. Silience DO: Non-Majewski short rib-polydactyly syndrome. *Am J Med Genet* 7:223, 1980.
638. Urioste M, Martínez-Frías ML, Bermejo E, et al: Short rib-polydactyly syndrome and pericentric inversion of chromosome 4. *Am J Med Genet* 49:94, 1994.
639. Krakow D, Salazar D, Wilcox WR, et al: Exclusion of the Ellis-van Creveld region on chromosome 4p16 in some families with asphyxiating thoracic dystrophy and short-rib polydactyly syndromes. *Eur J Hum Genet* 8:645, 2000.
640. Takamine Y, Lachman RS, Field FM, et al: Occipital projections in the skeletal dysplasias. *Pediatr Radiol* 34:530, 2004.
641. McKusick VA, Egeland JA, Eldridge R, et al: Dwarfism in the amish. The Ellis-Van Creveld syndrome. *Bull Johns Hopkins Hosp* 115:306, 1964.
642. McKusick VA: Genetic studies in American inbred populations with particular reference to the Old Order Amish. *Isr J Med Sci* 9:1276, 1973.
643. Zangwill KM, Boal DK, Ladda RL: Dandy-Walker malformation in Ellis-van Creveld syndrome. *Am J Med Genet* 31:123, 1988.
644. Arya L, Mendiratta V, Sharma RC, et al: Ellis-van Creveld Syndrome: a report of two cases. *Pediatr Dermatol* 18:485, 2001.
645. Guillozet N, Mbode J: Chondroectodermal dysplasia in an African child: a case report. *J Natl Med Assoc* 72:597, 1980.
646. Horigome H, Hamada H, Sohda S, et al: Prenatal ultrasonic diagnosis of a case of Ellis-van Creveld syndrome with a single atrium. *Pediatr Radiol* 27:942, 1997.
647. Tongsong T, Chanprapaph P: Prenatal sonographic diagnosis of Ellis-van Creveld syndrome. *J Clin Ultrasound* 28:38, 2000.
648. Da Silva EO, Janovitz D, de Albuquerque SC: Ellis-Van Creveld syndrome: report of 15 cases in an inbred kindred. *J Med Genet* 17:349, 1980.
649. Al Kheniaiz S, Al Sannaa N, Teebi AS: What syndrome is this? Chondroectodermal dysplasia—the Ellis-van Creveld syndrome. *Pediatr Dermatol* 18:68, 2001.
650. Caffey J: [Chondroectodermal dysplasia (Ellis-Van Creveld disease).] *Am J Roentgenol Radium Ther Nucl Med* 68:875, 1952.
651. Dugoff L, Thieme G, Hobbins JC: First trimester prenatal diagnosis of chondroectodermal dysplasia (Ellis-van Creveld syndrome) with ultrasound. *Ultrasound Obstet Gynecol* 17:86, 2001.
652. Durairaj M, Rao VD, Devarajan LV, et al: Ellis-van Creveld syndrome (chondro ectodermal dysplasia) associated with single atrium. *Indian Pediatr* 12:703, 1975.



653. Feingold M: Ellis-van Creveld syndrome. *Clin Pediatr (Phila)* 5:431, 1966.
654. Behar A, Rachmilewitz E: Ellis-Van Creveld syndrome. Report of one case associated with abiotrophy of elastic tissue in the cardiovascular system. *Arch Intern Med* 113:606, 1964.
655. Black D, Reutter J, Johnson M, et al: Liver transplantation in Ellis-van Creveld syndrome: a case report. *Pediatr Transplant* 6:255, 2002.
656. Donlan MA, Murphy JJ, Brakel CA: Ellis-van Creveld syndrome associated with complete situs inversus. *Clin Pediatr (Phila)* 8:366, 1969.
657. Hattab FN, Yassin OM, Sasa IS: Oral manifestations of Ellis-van Creveld syndrome: report of two siblings with unusual dental anomalies. *J Clin Pediatr Dent* 22:159, 1998.
658. Kushnick T, Paya K, Mamunes P: Chondroectodermal dysplasia: Ellis-van Creveld syndrome. *Am J Dis Child* 103:77, 1962.
659. Lal H, Manchanda SS, Thaman OP: Chondroectodermal dysplasia (Ellis-Van Creveld syndrome): (a case report). *Indian J Pediatr* 32:10, 1965.
660. Lynch JI, Perry LW, Takakuwa T, et al: Congenital heart disease and chondroectodermal dysplasia. Report of two cases, one in a Negro. *Am J Dis Child* 115:80, 1968.
661. George E, DeSilva S, Lieber E, et al: Ellis van Creveld syndrome (chondroectodermal dysplasia, MIM 22550) in three siblings from a non-consanguineous mating. *J Perinat Med* 28:425, 2000.
662. Sergi C, Voigtlander T, Zoubaa S, et al: Ellis-van Creveld syndrome: a generalized dysplasia of enchondral ossification. *Pediatr Radiol* 31:289, 2001.
663. Blackburn MG, Belliveau RE: Ellis-van Creveld syndrome. A report of previously undescribed anomalies in two siblings. *Am J Dis Child* 122:267, 1971.
664. Gauri LA, Panwar RB, Misra SN: Ellis-van Creveld syndrome. *J Indian Med Assoc* 85:307, 1987.
665. Sajeev CG, Roy TN, Venugopal K: Images in cardiology: Common atrium in a child with Ellis-Van Creveld syndrome. *Heart* 88:142, 2002.
666. Spranger S, Tariverdian G: Symptomatic heterozygosity in the Ellis-van Creveld syndrome? *Clin Genet* 47:217, 1995.
667. Bui TH, Marsk L, Eklof O, et al: Prenatal diagnosis of chondroectodermal dysplasia with fetoscopy. *Prenat Diagn* 4:155, 1984.
668. Calver D, Keast-Butler J, Taylor D: The extra digit. A pointer to the eye? *Trans Ophthalmol Soc U K* 101:35, 1981.
669. Goor D, Rotem Y, Friedman A, et al: Ellis-van Creveld syndrome in identical twins. *Br Heart J* 27:797, 1965.
670. Hunter ML, Roberts GJ: Oral and dental anomalies in Ellis van Creveld syndrome (chondroectodermal dysplasia): report of a case. *Int J Paediatr Dent* 8:153, 1998.
671. Moudgil A, Bagga A, Kamil ES, et al: Nephronophthisis associated with Ellis-van Creveld syndrome. *Pediatr Nephrol* 12:20, 1998.
672. Qureshi F, Jacques SM, Evans MI, et al: Skeletal histopathology in fetuses with chondroectodermal dysplasia (Ellis-van Creveld syndrome). *Am J Med Genet* 45:471, 1993.
673. Venkat-Raman N, Sebire NJ, et al: Increased first-trimester fetal nuchal translucency thickness in association with chondroectodermal dysplasia (Ellis-Van Creveld syndrome). *Ultrasound Obstet Gynecol* 25:412, 2005.
674. Goldblatt J, Minutillo C, Pemberton PJ, et al: Ellis-van Creveld syndrome in a Western Australian aboriginal community. Postaxial polydactyly as a heterozygous manifestation? *Med J Aust* 157:271, 1992.
675. Torrente I, Mangino M, De Luca A, et al: First-trimester prenatal diagnosis of Ellis-van Creveld syndrome using linked microsatellite markers. *Prenat Diagn* 18:504, 1998.
676. Cahuana A, Palma C, Gonzales W, et al: Oral manifestations in Ellis-van Creveld syndrome: report of five cases. *Pediatr Dent* 26:277, 2004.
677. Prabhu SR, Daftary DK, Dholakia HM: Chondroectodermal dysplasia (Ellis-van Creveld syndrome): report of two cases. *J Oral Surg* 36:631, 1978.
678. Rosemberg S, Carneiro PC, Zerbini MC, et al: Brief clinical report: chondroectodermal dysplasia (Ellis-van Creveld) with anomalies of CNS and urinary tract. *Am J Med Genet* 15:291, 1983.
679. Guschmann M, Horn D, Gasiorek-Wiens A, et al: Ellis-van Creveld syndrome: examination at 15 weeks' gestation. *Prenat Diagn* 19:879, 1999.
680. Santos JM, Pipa J, Antunes L, et al: [The Ellis-Van Creveld syndrome. Apropos 2 clinical cases]. *Rev Port Cardiol* 13:45, 58, 1994.
681. Moore TC: Chondroectodermal dysplasia (Ellis-Van Creveld syndrome) with bronchial malformation and neonatal tension lobar emphysema. *J Thorac Cardiovasc Surg* 46:1, 1963.
682. Levin SE, Dansky R, Milner S, et al: Atrioventricular septal defect and type A postaxial polydactyly without other major associated anomalies: a specific association. *Pediatr Cardiol* 16:242, 1995.
683. Goor D, Rotem Y, Strnberg M, Neufeld HN: Persistent common atrioventricular canal in the Ellis-Van Creveld syndrome. A case report. *Acta Cardiol* 22:368, 1967.
684. Akar H, Konuralp C, Baysal K, et al: Ellis-van Creveld syndrome associated with thymic hypoplasia. *Asian Cardiovasc Thorac Ann* 10:336, 2002.
685. Digilio MC, Marino B, Giannotti A, et al: Single atrium, atrioventricular canal/postaxial hexodactyly indicating Ellis-van Creveld syndrome. *Hum Genet* 96:251, 1995.
686. Fryns JP: Postaxial polydactyly as heterozygote manifestation in Ellis-van Creveld syndrome? *Am J Med Genet* 39:500, 1991.
687. Giknis FL: Single atrium and the Ellis-van Creveld syndrome. *J Pediatr* 62:558, 1963.
688. Serotkin A, Stamberg J, Waber L: Duplication 17q mosaicism: an infant with features of Ellis-van Creveld syndrome. *J Med Genet* 25:258, 1988.
689. Leung AK: Natal teeth. *Am J Dis Child* 140:249, 1986.
690. Pratesi C, Carattoli MT: [The Ellis-Van Creveld syndrome. (Description of a case with associated micrognathia)]. *Riv Clin Pediatr* 77:57, 1966.
691. Bohm N, Fukuda M, Staudt R, et al: Chondroectodermal dysplasia (Ellis-van Creveld syndrome) with dysplasia of renal medulla and bile ducts. *Histopathology* 2:267, 1978.
692. Datta V, Chaturvedi P: Ellis-Van Creveld syndrome associated with nodular sclerosing Hodgkin's disease and nephrotic syndrome. *Indian J Pediatr* 67:929, 2000.
693. Isajiw G: Prenatal diagnosis with fetoscopy. *N Engl J Med* 297:949, 1977.
694. Hobbins JC, Mahoney MJ: Fetoscopy in continuing pregnancies. *Am J Obstet Gynecol* 129:440, 1977.
695. Mahoney MJ, Hobbins JC: Prenatal diagnosis of chondroectodermal dysplasia (Ellis-van Creveld syndrome) with fetoscopy and ultrasound. *N Engl J Med* 297:258, 1977.
696. Zimmer EZ, Weinraub Z, Rajman A, et al: Antenatal diagnosis of a fetus with an extremely narrow thorax and short limb dwarfism. *J Clin Ultrasound* 12:112, 1984.
697. Berardi JC, Moulis M, Laloux V, et al: [Ellis-van Creveld syndrome. Contribution of echography to prenatal diagnosis. Apropos of a case]. *J Gynecol Obstet Biol Reprod (Paris)* 14:43, 1985.
698. Frikiche A, Verloes A, Stassen M, et al: [Ellis-Van Creveld syndrome. Apropos of a case diagnosed in utero]. *Rev Med Liege* 44:68, 1989.
699. Kozlowski K, Szmigiel C, Barylak A, et al: Difficulties in differentiation between chondroectodermal dysplasia (Ellis-van Creveld syndrome) and asphyxiating thoracic dystrophy. *Australas Radiol* 16:401, 1972.
700. Brueton LA, Dillon MJ, Winter RM: Ellis-van creveld syndrome, Jeune syndrome, and renal-hepatic-pancreatic dysplasia: separate entities or disease spectrum? *J Med Genet* 27:252, 1990.
701. Digilio MC, Marino B, Giannotti A, et al: Atrioventricular canal defect and postaxial polydactyly indicating phenotypic overlap of Ellis-van Creveld and Kaufman-McKusick syndromes. *Pediatr Cardiol* 18:74, 1997.
702. Castel Y, Toudie L, Alix D, et al: [Postaxial polydactyly in a female neonate associated with hydrocolpos due to vaginal atresia and with a congenital cardiopathy: the McKusick-Kaufman syndrome]. *J Genet Hum* 30:329, 1982.
703. Ruiz-Perez VL, Ide SE, Strom TM, et al: Mutations in a new gene in Ellis-van Creveld syndrome and Weyers acrodermal dysostosis. *Nat Genet* 24:283, 2000.
704. Howard TD, Gutmacher AE, McKinnon W, et al: Autosomal dominant postaxial polydactyly, nail dysrophy, and dental abnormalities map to chromosome 4p16, in the region containing the Ellis-van Creveld syndrome locus. *Am J Hum Genet* 61:1405, 1997.
705. Polymeropoulos MH, Ide SE, Wright M, et al: The gene for the Ellis-van Creveld syndrome is located on chromosome 4p16. *Genomics* 35:1, 1996.



706. Galdzicka M, Patnala S, Hirshman MG, et al: A new gene, EVC2, is mutated in Ellis-van Creveld syndrome. *Mol Genet Metab* 77:291, 2002.
707. Ruiz-Perez VL, Tompson SW, Blair HJ, et al: Mutations in two nonhomologous genes in a head-to-head configuration cause Ellis-van Creveld syndrome. *Am J Hum Genet* 72:728, 2003.
708. Takamine Y, Krejci P, Mekikian PB, et al: Mutations in the EVC1 gene are not a common finding in the Ellis-van Creveld and short rib-polydactyly type III syndromes. *Am J Med Genet A* 130:96, 2004.
709. Cooper SC, Flaitz CM, Johnston DA, et al: A natural history of cleidocranial dysplasia. *Am J Med Genet* 104:1, 2001.
710. Jarvis JL, Keats TE: Cleidocranial dysostosis. A review of 40 new cases. *Am J Roentgenol Radium Ther Nucl Med* 121:5, 1974.
711. Mundlos S: Cleidocranial dysplasia: clinical and molecular genetics. *J Med Genet* 36:177, 1999.
712. Zhou G, Chen Y, Zhou L, et al: CBFA1 mutation analysis and functional correlation with phenotypic variability in cleidocranial dysplasia. *Hum Mol Genet* 8:2311, 1999.
713. Lachman RS: Skeletal dysplasias. In Taybi H, Lachman R (eds): *Radiology of Syndromes, Metabolic Disorders, and Skeletal Dysplasias*. St. Louis, Mosby, 1996, pp 745-951.
714. Lee B, Thirunavukkarasu K, Zhou L, et al: Missense mutations abolishing DNA binding of the osteoblast-specific transcription factor OSF2/CBFA1 in cleidocranial dysplasia. *Nat Genet* 16:307, 1997.
715. Mundlos S, Otto F, Mundlos C, et al: Mutations involving the transcription factor CBFA1 cause cleidocranial dysplasia. *Cell* 89:773, 1997.
716. Quack I, Vonderstrass B, Stock M, et al: Mutation analysis of core binding factor A1 in patients with cleidocranial dysplasia. *Am J Hum Genet* 65:1268, 1999.
717. Otto F, Kanegane H, Mundlos S: Mutations in the RUNX2 gene in patients with cleidocranial dysplasia. *Hum Mutat* 19:209, 2002.
718. Otto F, Thornell AP, Crompton T, et al: Cbfa1, a candidate gene for cleidocranial dysplasia syndrome, is essential for osteoblast differentiation and bone development. *Cell* 89:765, 1997.
719. Feldman GJ, Robin NH, Bruceton LA, et al: A gene for cleidocranial dysplasia maps to the short arm of chromosome 6. *Am J Hum Genet* 56:938, 1995.
720. Mundlos S, Mulliken JB, Abramson DL, et al: Genetic mapping of cleidocranial dysplasia and evidence of a microdeletion in one family. *Hum Mol Genet* 4:71, 1995.
721. Gelb BD, Cooper E, Shevell M, et al: Genetic mapping of the cleidocranial dysplasia (CCD) locus on chromosome band 6p21 to include a microdeletion. *Am J Med Genet* 58:200, 1995.
722. Otto F, Thornell AP, Crompton T, et al: Cbfa1, a candidate gene for cleidocranial dysplasia syndrome, is essential for osteoblast differentiation and bone development. *Cell* 89:765, 1997.
723. Komori T, Yagi H, Nomura S, et al: Targeted disruption of Cbfa1 results in a complete lack of bone formation owing to maturational arrest of osteoblasts. *Cell* 89:755, 1997.
724. Lian JB, Stein JL, Stein GS, et al: Runx2/Cbfa1 functions: diverse regulation of gene transcription by chromatin remodeling and co-regulatory protein interactions. *Connect Tissue Res* 44(Suppl 1):141, 2003.
725. Lian JB, Stein GS: Runx2/Cbfa1: a multifunctional regulator of bone formation. *Curr Pharm Des* 9:2677, 2003.
726. Stewart PA, Wallerstein R, Moran E, et al: Early prenatal ultrasound diagnosis of cleidocranial dysplasia. *Ultrasound Obstet Gynecol* 15:154, 2000.
727. Hassan J, Sepulveda W, Teixeira J, et al: Prenatal sonographic diagnosis of cleidocranial dysostosis. *Prenat Diagn* 17:770, 1997.
728. Paladini D, Lamberti A, Agangi A, et al: Cleidocranial dysostosis. Prenatal ultrasound diagnosis of a late onset form. *Ultrasound Obstet Gynecol* 16:100, 2000.
729. Chen CP, Hung HY, Chang TY, et al: Second-trimester nasal bone hypoplasia/aplasia associated with cleidocranial dysplasia. *Prenat Diagn* 24:399, 2004.
730. Stewart PA, Wallerstein R, Moran E, et al: Early prenatal ultrasound diagnosis of cleidocranial dysplasia. *Ultrasound Obstet Gynecol* 15:154, 2000.
731. Winer N, Le Caignec C, Quere MP, et al: Prenatal diagnosis of a cleidocranial dysplasia-like phenotype associated with a de novo balanced t(2q;6q)(q36;q16) translocation. *Ultrasound Obstet Gynecol* 22:648, 2003.
732. Hamner LH III, Fabbri EL, Browne PC: Prenatal diagnosis of cleidocranial dysostosis. *Obstet Gynecol* 83:856, 1994.
733. Zheng Q, Sebald E, Zhou G, et al: Dysregulation of chondrogenesis in human cleidocranial dysplasia. *Am J Hum Genet* 77:305, 2005.
734. Cavalli P, Santorelli FM, Bontardelli M, et al: Prenatal exclusion of cleidocranial dysplasia. *Prenat Diagn* 23:945, 2003.
735. Alldred AJ: Congenital pseudarthrosis of the clavicle. *J Bone Joint Surg Br* 45-B:312, 1963.
736. Lloyd-Roberts GC, Apley AG, Owen R: Reflections upon the aetiology of congenital pseudarthrosis of the clavicle. With a note on cranio-cleido dysostosis. *J Bone Joint Surg Br* 57:24, 1975.
737. Yunis E, Varon H: Cleidocranial dysostosis, severe micrognathism, bilateral absence of thumbs and first metatarsal bone, and distal aphalangia: a new genetic syndrome. *Am J Dis Child* 134:649, 1980.
738. Goldberg MJ: *The Dysmorphic Child: An Orthopedic Perspective*. New York, Raven Press, 1987.
739. Romero R, Pilu G, Jeanty P, et al: Skeletal dysplasias. In Romero R, Pilu G, Jeanty P (eds): *Prenatal Diagnosis of Congenital Anomalies*. Norwalk, CT, Appleton & Lange, 1987, pp 311-402.
740. Bod M, Czeizel A, Lenz W: Incidence at birth of different types of limb reduction abnormalities in Hungary 1975-1977. *Hum Genet* 65:27, 1983.
741. Stoll C, Wiesel A, Queisser-Luft A, et al: Evaluation of the prenatal diagnosis of limb reduction deficiencies. EUROSCAN Study Group. *Prenat Diagn* 20:811, 2000.
742. Zhu J, Miao L, Xu C, et al: [Analysis of 822 infants with limb reduction defect in China]. *Hua Xi Yi Ke Da Xue Xue Bao* 27:400, 1996.
743. Bromley B, Benacerraf B: Abnormalities of the hands and feet in the fetus: sonographic findings. *AJR Am J Roentgenol* 165:1239, 1995.
744. Lecannellier J, Vischer D: [The aglossia-adactylia syndrome]. *Helv Paediatr Acta* 31:77, 1976.
745. Tuncbilek E, Yalcin C, Atas M: Aglossia-adactylia syndrome (special emphasis on the inheritance pattern). *Clin Genet* 11:421, 1977.
746. Marti-Herrero M, Cabrera-Lopez JC, Toledo L, et al: [Moebius syndrome. Three different forms of presentation]. *Rev Neurol* 27:975, 1998.
747. Cuvelier B, Cousin J, Pauli A, et al: [Aglossia-adactylia syndrome: two new cases (author's transl)]. *Ann Pediatr (Paris)* 28:433, 1981.
748. Canete ER, Gil RR, Alvarez MR, et al: [Hanhart syndrome (aglossia-adactylia syndrome). Report of 2 cases]. *An Esp Pediatr* 33:465, 1990.
749. Deffez JP, Rostand B, Allain P, et al: [An unusual aglossia-adactylia syndrome (author's transl)]. *Rev Stomatol Chir Maxillofac* 82:241, 1981.
750. Grippaudo FR, Kennedy DC: Oromandibular-limb hypogenesis syndromes: a case of aglossia with an intraoral band. *Br J Plast Surg* 51:480, 1998.
751. Robinow M, Marsh JL, Edgerton MT, et al: Discordance in monozygotic twins for aglossia-adactylia, and possible clues to the pathogenesis of the syndrome. *Birth Defects Orig Artic Ser* 14:223, 1978.
752. Lammens M, Moerman P, Fryns JP, et al: Neuropathological findings in Moebius syndrome. *Clin Genet* 54:136, 1998.
753. d'Orey C, Melo MJ, Costa A, et al: [Moebius syndrome in newborn infants]. *Arch Pediatr* 4:897, 1997.
754. Baraitser M: Genetics of Mobius syndrome. *J Med Genet* 14:415, 1977.
755. Bonanni P, Guerrini R: Segmental facial myoclonus in moebius syndrome. *Mov Disord* 14:1021, 1999.
756. Abramson DL, Cohen MM Jr, Mulliken JB: Mobius syndrome: classification and grading system. *Plast Reconstr Surg* 102:961, 1998.
757. Matsui A, Nakagawa M, Okuno M: Association of atrial septal defect with Poland-Moebius syndrome: vascular disruption can be a common etiologic factor. A case report. *Angiology* 48:269, 1997.
758. Jorrel H, Roussey M, Le Marec B: MCA/MR syndrome with oligodactyly and Mobius anomaly in first cousins: new syndrome or familial facial-limb disruption sequence? *Am J Med Genet* 34:506, 1989.
759. Vargas FR, Schuler-Faccini L, Brunoni D, et al: Prenatal exposure to misoprostol and vascular disruption defects: a case-control study. *Am J Med Genet* 95:302, 2000.
760. Bavinck JN, Weaver DD: Subclavian artery supply disruption sequence: hypothesis of a vascular etiology for Poland, Klippel-Feil, and Mobius anomalies. *Am J Med Genet* 23:903, 1986.



761. Brill CB, Peyster RG, Keller MS, et al: Isolation of the right subclavian artery with subclavian steal in a child with Klippel-Feil anomaly: an example of the subclavian artery supply disruption sequence. *Am J Med Genet* 26:933, 1987.
762. Farina D, Gatto G, Leonessa L, et al: Poland syndrome: a case with a combination of syndromes. *Panminerva Med* 41:259, 1999.
763. Larrandaburu M, Schuler L, Ehlers JA, et al: The occurrence of Poland and Poland-Moebius syndromes in the same family: further evidence of their genetic component. *Clin Dysmorphol* 8:93, 1999.
764. Lipson AH, Gillerot Y, Tannenberg AE, et al: Two cases of maternal antenatal splenic rupture and hypotension associated with Moebius syndrome and cerebral palsy in offspring. Further evidence for a utero placental vascular aetiology for the Moebius syndrome and some cases of cerebral palsy. *Eur J Pediatr* 155:800, 1996.
765. St Charles S, DiMario FJ Jr, Grunnet ML: Mobius sequence: further in vivo support for the subclavian artery supply disruption sequence. *Am J Med Genet* 47:289, 1993.
766. Marques-Dias MJ, Gonzalez CH, Rosemberg S: Mobius sequence in children exposed in utero to misoprostol: neuropathological study of three cases. *Birth Defects Res A Clin Mol Teratol* 67:1002, 2003.
767. Happle R, Koch H, Lenz W: The CHILD syndrome. Congenital hemidysplasia with ichthyosiform erythroderma and limb defects. *Eur J Pediatr* 134:27, 1980.
768. Hebert AA, Esterly NB, Holbrook KA, et al: The CHILD syndrome. Histologic and ultrastructural studies. *Arch Dermatol* 123:503, 1987.
769. Hashimoto K, Topper S, Sharata H, et al: CHILD syndrome: analysis of abnormal keratinization and ultrastructure. *Pediatr Dermatol* 12:116, 1995.
770. Hoeger PH, Adwani SS, Whitehead BF, et al: Ichthyosiform erythroderma and cardiomyopathy: report of two cases and review of the literature. *Br J Dermatol* 139:1055, 1998.
771. Happle R, Effendy I, Megahed M, et al: CHILD syndrome in a boy. *Am J Med Genet* 62:192, 1996.
772. Happle R, Mittag H, Kuster W: The CHILD nevus: a distinct skin disorder. *Dermatology* 191:210, 1995.
773. Holmes LB, Redline RW, Brown DL, et al: Absence/hypoplasia of tibia, polydactyly, retrocerebellar arachnoid cyst, and other anomalies: an autosomal recessive disorder. *J Med Genet* 32:896, 1995.
774. König A, Happle R, Bornholdt D, et al: Mutations in the NSDHL gene, encoding a 3beta-hydroxysteroid dehydrogenase, cause CHILD syndrome. *Am J Med Genet* 90:339, 2000.
775. Bittar M, Happle R: CHILD syndrome avant la lettre. *J Am Acad Dermatol* 50:S34, 2004.
776. Hummel M, Cunningham D, Mullett CJ, et al: Left-sided CHILD syndrome caused by a nonsense mutation in the NSDHL gene. *Am J Med Genet A* 122:246, 2003.
777. Lipson AH: Amelia of the arms and femur/fibula deficiency with splenogonadal fusion in a child born to a consanguineous couple. *Am J Med Genet* 55:265, 1995.
778. Ahmad M, Abbas H, Wahab A, et al: Fibular hypoplasia and complex brachydactyly (Du Pan syndrome) in an inbred Pakistani kindred. *Am J Med Genet* 36:292, 1990.
779. Faiyaz-Ul-Haque M, Ahmad W, Zaidi SH, et al: Mutation in the cartilage-derived morphogenetic protein-1 (CDMP1) gene in a kindred affected with fibular hypoplasia and complex brachydactyly (DuPan syndrome). *Clin Genet* 61:454, 2002.
780. Savarirayan R, White SM, Goodman FR, et al: Broad phenotypic spectrum caused by an identical heterozygous CDMP-1 mutation in three unrelated families. *Am J Med Genet A* 117:136, 2003.
781. Voshenrich R, Bartkowski R, Fischer U, et al: [Splenogonadal fusion]. *Rofo* 155:191, 1991.
782. Bonneau D, Roume J, Gonzalez M, et al: Splenogonadal fusion limb defect syndrome: report of five new cases and review. *Am J Med Genet* 86:347, 1999.
783. Pauli RM, Greenlaw A: Limb deficiency and splenogonadal fusion. *Am J Med Genet* 13:81, 1982.
784. Bearss RW: Splenic-gonadal fusion. *Urology* 16:277, 1980.
785. Moore PJ, Hawkins EP, Galliani CA, et al: Splenogonadal fusion with limb deficiency and micrognathia. *South Med J* 90:1152, 1997.
786. Bonafede RP, Beighton P: Autosomal dominant inheritance of scalp defects with ectrodactyly. *Am J Med Genet* 3:35, 1979.
787. Fryns JP, Legius E, Demareel P, et al: Congenital scalp defect, distal limb reduction anomalies, right spastic hemiplegia and hypoplasia of the left arteria cerebri media. Further evidence that interruption of early embryonic blood supply may result in Adams-Oliver (plus) syndrome. *Clin Genet* 50:505, 1996.
788. Verdyck P, Holder-Espinasse M, Hul WV, et al: Clinical and molecular analysis of nine families with Adams-Oliver syndrome. *Eur J Hum Genet* 11:457, 2003.
789. Ishikiriya S, Kaou B, Udagawa A, et al: Congenital heart defect in a Japanese girl with Adams-Oliver syndrome: one of the most important complications. *Am J Med Genet* 43:900, 1992.
790. Bamforth JS, Kaurah P, Byrne J, et al: Adams Oliver syndrome: a family with extreme variability in clinical expression. *Am J Med Genet* 49:393, 1994.
791. Zapata HH, Sletten LJ, Pierpont ME: Congenital cardiac malformations in Adams-Oliver syndrome. *Clin Genet* 47:80, 1995.
792. Lin AE, Westgate MN, van der Velde ME, et al: Adams-Oliver syndrome associated with cardiovascular malformations. *Clin Dysmorphol* 7:235, 1998.
793. Savarirayan R, Thompson EM, Abbott KJ, et al: Cerebral cortical dysplasia and digital constriction rings in Adams-Oliver syndrome. *Am J Med Genet* 86:15, 1999.
794. Swartz EN, Sanatani S, Sandor GG, et al: Vascular abnormalities in Adams-Oliver syndrome: cause or effect? *Am J Med Genet* 82:49, 1999.
795. Amor DJ, Leventer RJ, Hayllar S, et al: Polymicrogyria associated with scalp and limb defects: variant of Adams-Oliver syndrome. *Am J Med Genet* 93:328, 2000.
796. Becker R, Kunze J, Horn D, et al: Autosomal recessive type of Adams-Oliver syndrome: prenatal diagnosis. *Ultrasound Obstet Gynecol* 20:506, 2002.
797. Newman CG: The thalidomide syndrome: risks of exposure and spectrum of malformations. *Clin Perinatol* 13:555, 1986.
798. Lee A, Kratochwil A, Deuvinger J, et al: Three-dimensional ultrasound in diagnosing phocomelia. *Ultrasound Obstet Gynecol* 5:238, 1995.
799. Waldenmaier C, Aldenhoff P, Klemm T: The Roberts' syndrome. *Hum Genet* 40:345, 1978.
800. Sinha AK, Verma RS, Mani VJ: Clinical heterogeneity of skeletal dysplasia in Roberts syndrome: a review. *Hum Hered* 44:121, 1994.
801. de Ravel TJ, Seftel MD, Wright CA: Tetra-amelia and splenogonadal fusion in Roberts syndrome. *Am J Med Genet* 68:185, 1997.
802. Schule B, Oviedo A, Johnston K, et al: Inactivating mutations in ESCO2 cause SC phocomelia and Roberts syndrome: no phenotype-genotype correlation. *Am J Hum Genet* 77:1117, 2005.
803. Benzacken B, Savary JB, Manouvrier S, et al: Prenatal diagnosis of Roberts syndrome: two new cases. *Prenat Diagn* 16:125, 1996.
804. Vega H, Waisfisz Q, Gordillo M, et al: Roberts syndrome is caused by mutations in ESCO2, a human homolog of yeast ECO1 that is essential for the establishment of sister chromatid cohesion. *Nat Genet* 37:468, 2005.
805. Herrmann J, Feingold M, Tuffli G, et al: A familial dysmorphic genetic syndrome of limb deformities, characteristic facial appearance and associated anomalies: the "pseudothalidomide" or "SC-syndrome." *Birth Defects Orig Artic Ser* V:81, 1969.
806. Grundy HO, Burlbaw J, Walton S, et al: Roberts syndrome: antenatal ultrasound—a case report. *J Perinat Med* 16:71, 1988.
807. Robins DB, Ladda RL, Thieme GA, et al: Prenatal detection of Roberts-SC phocomelia syndrome: report of 2 sibs with characteristic manifestations. *Am J Med Genet* 32:390, 1989.
808. Tomkins DJ: Premature centromere separation and the prenatal diagnosis of Roberts syndrome. *Prenat Diagn* 9:450, 1989.
809. Sherer DM, Shah YG, Kliensky N, et al: Prenatal sonographic features and management of a fetus with Roberts-SC phocomelia syndrome (pseudothalidomide syndrome) and pulmonary hypoplasia. *Am J Perinatol* 8:259, 1991.
810. Hirschhorn K, Kaffe S: Prenatal diagnosis of Roberts syndrome. *Prenat Diagn* 12:976, 1992.
811. Stiovi S, Privitera O, Brambati B, et al: First-trimester prenatal diagnosis of Roberts syndrome. *Prenat Diagn* 12:145, 1992.
812. Gruber A, Rabinerson D, Kaplan B, et al: Prenatal diagnosis of Roberts syndrome. *Prenat Diagn* 14:511, 1994.
813. Sharma AK, Jain A, Phadke SR, et al: Prenatal diagnosis of Roberts syndrome. *Indian Pediatr* 31:1261, 1994.
814. Otano L, Matayoshi T, Gadow EC: Roberts syndrome: first-trimester prenatal diagnosis. *Prenat Diagn* 16:770, 1996.
815. Paladini D, Palmieri S, Lecora M, et al: Prenatal ultrasound diagnosis of Roberts syndrome in a family with negative history. *Ultrasound Obstet Gynecol* 7:208, 1996.



816. Concolino D, Sperli D, Cinti R, et al: A mild form of Roberts/SC phocomelia syndrome with asymmetrical reduction of the upper limbs. *Clin Genet* 49:274, 1996.
817. Dalal AB, Phadke SR: Twin pregnancy with Roberts syndrome in one fetus and trisomy 18 in the other. *J Clin Ultrasound* 34:146, 2006.
818. Grebe H: Die Achondrogenesis: ein einfach rezessives Erbmerkmal. *Folia Hered Path* 2:23, 1952.
819. Quelce-Salgado A: A new type of dwarfism with various bone aplasias and hypoplasias of the extremities. *Acta Genet Stat Med* 14:63, 1964.
820. Kumar D: Grebe syndrome. In Buyse ML (ed): *Birth Defects Encyclopedia*. Cambridge, Blackwell Science, 1990, pp 813-814.
821. Kulkarni ML, Kulkarni BM, Nasser PU: Antenatal diagnosis of Grebe syndrome in a twin pregnancy by ultrasound. *Indian Pediatr* 32:1007, 1995.
822. Rittler M, Higa S: Grebe syndrome: a second case with extremely severe manifestations. *J Med Genet* 34:1038, 1997.
823. Garcia-castro JM, Perez-Comas A: Nonlethal achondrogenesis (Grebe-Quelce-Salgado type) in two Puerto Rican sibships. *J Pediatr* 87:948, 1975.
824. Costa T, Ramsby G, Cassia F, et al: Grebe syndrome: clinical and radiographic findings in affected individuals and heterozygous carriers. *Am J Med Genet* 75:523, 1998.
825. Kumar D, Curtis D, Blank CE: Grebe chondrodysplasia and brachydactyly in a family. *Clin Genet* 25:68, 1984.
826. Beighton P: Heterozygous manifestations in the heritable disorders of the skeleton. *Pediatr Radiol* 27:397, 1997.
827. Curtis D: Heterozygote expression in Grebe chondrodysplasia. *Clin Genet* 29:455, 1986.
828. Thomas JT, Kilpatrick MW, Lin K, et al: Disruption of human limb morphogenesis by a dominant negative mutation in CDMP1. *Nat Genet* 17:58, 1997.
829. Munoz Rojas MV, Goncalves LF: Grebe-Quelce-Salgado chondrodysplasia: prenatal diagnosis of two new cases in unrelated families in Southern Brazil. *Am J Med Genet* 113:193, 2002.
830. Cordero DR, Goldberg Y, Basel D, et al: Prenatal sonographic diagnosis of Grebe syndrome. *J Ultrasound Med* 25:115, 2006.
831. Hamanishi C: Congenital short femur. Clinical, genetic and epidemiological comparison of the naturally occurring condition with that caused by thalidomide. *J Bone Joint Surg Br* 62:307, 1980.
832. Daend DL, Smith DW, Scott CI, et al: Femoral hypoplasia—unusual facies syndrome. *J Pediatr* 86:107, 1975.
833. Sanpera I Jr, Fixsen JA, Sparks LT, et al: Knee in congenital short femur. *J Pediatr Orthop B* 4:159, 1995.
834. Makino Y, Inoue T, Shiota K, et al: A case of congenital familial short femur diagnosed prenatally. *Fetal Diagn Ther* 13:206, 1998.
835. Hadi HA, Wade AL: Prenatal diagnosis of unilateral proximal femoral focal deficiency in diabetic pregnancy: a case report. *Am J Perinatol* 10:285, 1993.
836. Kalaycioglu A, Aynaci O: Proximal focal femoral deficiency, contralateral hip dysplasia in association with contralateral ulnar hypoplasia and cleft hand: a case report and review of literatures of PFFD and/or FFU. *Okajimas Folia Anat Jpn* 78:83, 2001.
837. Filly AL, Robnett-Filly B, Filly RA: Syndromes with focal femoral deficiency: strengths and weaknesses of prenatal sonography. *J Ultrasound Med* 23:1511, 2004.
838. Goncalves LF, De Luca GR, Vitorello DA, et al: Prenatal diagnosis of bilateral proximal femoral hypoplasia. *Ultrasound Obstet Gynecol* 8:127, 1996.
839. Sen Gupta DK, Gupta SK: Familial bilateral proximal femoral focal deficiency. Report of a kindred. *J Bone Joint Surg Am* 66:1470, 1984.
840. Frey M, Williams J: What is your diagnosis? Radiographic diagnosis—ectrodactyly. *J Am Vet Med Assoc* 206:619, 1995.
841. Miura T, Suzuki M: Clinical differences between typical and atypical cleft hand. *J Hand Surg [Br]* 9:311, 1984.
842. Glicenstein J, Guero S, Haddad R: [Median clefts of the hand. Classification and therapeutic indications apropos of 29 cases]. *Ann Chir Main Memb Super* 14:253, 1995.
843. Tada K, Yonenobu K, Swanson AB: Congenital central ray deficiency in the hand—a survey of 59 cases and subclassification. *J Hand Surg [Am]* 6:434, 1981.
844. van den BH, Dequeker J, Fryns JP, et al: Familial occurrence of severe ulnar aplasia and lobster claw feet: a new syndrome. *Hum Genet* 42:109, 1978.
845. Verma IC, Joseph R, Bhargava S, et al: Split-hand and split-foot deformity inherited as an autosomal recessive trait. *Clin Genet* 9:8, 1976.
846. Brunner HG, Hamel BCJ, Van Bokhoven H: The p63 gene in EEC and other syndromes. *J Med Genet* 39:377, 2002.
847. Roelfsema NM, Cobben JM: The EEC syndrome: a literature study. *Clin Dysmorphol* 5:115, 1996.
848. Rudiger RA, Haase W, Passarge E: Association of ectrodactyly, ectodermal dysplasia, and cleft lip-palate. *Am J Dis Child* 120:160, 1970.
849. Miller CI, Hashimoto K, Shwayder T, et al: What syndrome is this? Ectrodactyly, ectodermal dysplasia, and cleft palate (EEC) syndrome. *Pediatr Dermatol* 14:239, 1997.
850. Kasmann B, Ruprecht KW: Ocular manifestations in a father and son with EEC syndrome. *Graefes Arch Clin Exp Ophthalmol* 235:512, 1997.
851. Buss PW, Hughes HE, Clarke A: Twenty-four cases of the EEC syndrome: clinical presentation and management. *J Med Genet* 32:716, 1995.
852. Kronic AL, Vesic SA, Goldner B, et al: Ectrodactyly, soft-tissue syndactyly, and nodulocystic acne: coincidence or association? *Pediatr Dermatol* 14:31, 1997.
853. Gershoni-Baruch R, Goldscher D, Hochberg Z: Ectrodactyly-ectodermal dysplasia-clefting syndrome and hypothalamo-pituitary insufficiency. *Am J Med Genet* 68:168, 1997.
854. Maas SM, de Jong TP, Buss P, et al: EEC syndrome and genitourinary anomalies: an update. *Am J Med Genet* 63:472, 1996.
855. Leiter E, Lipson J: Genitourinary tract anomalies in lobster claw syndrome. *J Urol* 115:339, 1976.
856. Penchaszadeh VB, de Negrotti TC: Ectrodactyly-ectodermal dysplasia-clefting (EEC) syndrome: dominant inheritance and variable expression. *J Med Genet* 13:281, 1976.
857. Celli J, Duijf P, Hamel BC, et al: Heterozygous germline mutations in the p53 homolog p63 are the cause of EEC syndrome. *Cell* 99:143, 1999.
858. Halal F, Homys M, Perreault G: Acro-renal-ocular syndrome: autosomal dominant thumb hypoplasia, renal ectopia, and eye defect. *Am J Med Genet* 17:753, 1984.
859. Blauth W, Sonnichsen S: [Congenital clubhand]. *Orthopade* 15:160, 1986.
860. Bujdosó G, Lenz W: Monodactylous splithand-splitfoot. A malformation occurring in three distinct genetic types. *Eur J Pediatr* 133:207, 1980.
861. Goldberg MJ, Meyn M: The radial clubhand. *Orthop Clin North Am* 7:341, 1976.
862. Wood VE: Congenital thumb deformities. *Clin Orthop* 195:7, 1985.
863. Chan KM, Lamb DW: Triphalangeal thumb and five-fingered hand. *Hand* 15:329, 1983.
864. Carroll RE, Louis DS: Anomalies associated with radial dysplasia. *J Pediatr* 84:409, 1974.
865. Alter BP: Bone marrow failure syndromes. *Clin Lab Med* 19:113-33, 1999.
866. Glanz A, Fraser FC: Spectrum of anomalies in Fanconi anaemia. *J Med Genet* 19:412, 1982.
867. Grill F, Freilinger W, Strobl W: [Treatment of a radial club hand]. *Z Orthop Ihre Grenzgeb* 134:324, 1996.
868. Rotman MB, Manske PR: Radial clubhand and contralateral duplicated thumb. *J Hand Surg [Am]* 19:361, 1994.
869. Bueno LO, Bueno MI, Jimenez VA, et al: [A girl with pancytopenia, short stature and minor skeletal abnormalities]. *An Esp Pediatr* 46:409, 1997.
870. Nilsson LR: Chronic pancytopenia with multiple congenital abnormalities (Fanconi's anaemia). *Acta Paediatr* 49:518, 1960.
871. Prindull G, Stubbe P, Kratzer W: Fanconi's anemia. I. Case histories, clinical and laboratory findings in six affected siblings. *Z Kinderheilkd* 120:37, 1975.
872. Levran O, Diotti R, Pujara K, et al: Spectrum of sequence variations in the FANCA gene: an International Fanconi Anemia Registry (IFAR) study. *Hum Mutat* 25:142, 2005.
873. Strathdee CA, Duncan AM, Buchwald M: Evidence for at least four Fanconi anaemia genes including FAOC on chromosome 9. *Nat Genet* 1:196, 1992.
874. Lo TF Jr, Rooimans MA, Bosnoyan-Collins L, et al: Expression cloning of a cDNA for the major Fanconi anaemia gene, FAA. *Nat Genet* 14:320, 1996.



875. Ianzano L, D'Apolito M, Centra M, et al: The genomic organization of the Fanconi anemia group A (FAA) gene. *Genomics* 41:309, 1997.
876. Digweed M: [Molecular basis of Fanconi's anemia]. *Klin Padiatr* 211:192, 1999.
877. de Winter JP, Rooimans MA, van der Weel L, et al: The Fanconi anaemia gene FANCF encodes a novel protein with homology to ROM. *Nat Genet* 24:15, 2000.
878. Timmers C, Taniguchi T, Hejna J, et al: Positional cloning of a novel Fanconi anemia gene, FANCD2. *Mol Cell* 7:241, 2001.
879. Howlett NG, Taniguchi T, Olson S, et al: Biallelic inactivation of BRCA2 in Fanconi anemia. *Science* 297:606, 2002.
880. Meetei AR, de Winter JP, Medhurst AL, et al: A novel ubiquitin ligase is deficient in Fanconi anemia. *Nat Genet* 35:165, 2003.
881. Auerbach AD, Warburton D, Bloom AD, et al: Preliminary communication: prenatal detection of the Fanconi anemia gene by cytogenetic methods. *Am J Hum Genet* 31:77, 1979.
882. Auerbach AD, Adler B, Chaganti RS: Prenatal and postnatal diagnosis and carrier detection of Fanconi anemia by a cytogenetic method. *Pediatrics* 67:128, 1981.
883. Voss R, Kohn G, Shaham M, et al: Prenatal diagnosis of Fanconi anemia. *Clin Genet* 20:185, 1981.
884. Marx MP, Dawson B, Hcyns AD: Prenatal diagnosis of Fanconi's anemia. *S Afr Med J* 62:348, 1982.
885. Shipley J, Rodeck CH, Garrett C, et al: Mitomycin C induced chromosome damage in fetal blood cultures and prenatal diagnosis of Fanconi's anemia. *Prenat Diagn* 4:217, 1984.
886. Auerbach AD, Sagi M, Adler B: Fanconi anemia: prenatal diagnosis in 30 fetuses at risk. *Pediatrics* 76:794, 1985.
887. Dallapiccola B, Doria Lamba CL, Ferranti G, et al: Monitoring of pregnancies at risk for Fanconi's anemia by chorionic villi sampling. *Acta Haematol* 73:157, 1985.
888. Murr-Orlando M, Llerena JC Jr, Birjandi F, et al: FACC gene mutations and early prenatal diagnosis of Fanconi's anaemia. *Lancet* 342:686, 1993.
889. Kwee ML, Lo TF Jr, Arwert F, et al: Early prenatal diagnosis of Fanconi anaemia in a twin pregnancy, using DNA analysis. *Prenat Diagn* 16:345, 1996.
890. Tercanli S, Miny P, Siebert MS, et al: Fanconi anemia associated with increased nuchal translucency detected by first-trimester ultrasound. *Ultrasound Obstet Gynecol* 17:160, 2001.
891. Merrill A, Rosenblum-Vos L, Driscoll DA, et al: Prenatal diagnosis of Fanconi anemia (Group C) subsequent to abnormal sonographic findings. *Prenat Diagn* 25:20, 2005.
892. Shimamura A, Moreau L, D'Andrea A: Fanconi anemia. Copyright, University of Washington Seattle. 1993-2005. Updated weekly. *GeneTests: Medical Genetics Information Resource* (database online). 2004. Accessed 2-20-2005.
893. Bechtold A, Friedl R, Kalb R, et al: Prenatal exclusion/confirmation of Fanconi anemia via flow cytometry: a pilot study. *Fetal Diagn Ther* 21:118, 2006.
894. Hall JG, Levin J, Kuhn JP, et al: Thrombocytopenia with absent radius (TAR). *Medicine (Baltimore)* 48:411, 1969.
895. de Alarcon PA, Graeve JA, Levine RF, et al: Thrombocytopenia and absent radii syndrome: defective megakaryocytopoiesis-thrombocytopoiesis. *Am J Pediatr Hematol Oncol* 13:77, 1991.
896. Ballmaier M, Schulze H, Strauss G, et al: Thrombopoietin in patients with congenital thrombocytopenia and absent radii: elevated serum levels, normal receptor expression, but defective reactivity to thrombopoietin. *Blood* 90:612, 1997.
897. Sekine I, Hagiwara T, Miyazaki H, et al: Thrombocytopenia with absent radii syndrome: studies on serum thrombopoietin levels and megakaryopoiesis in vitro. *J Pediatr Hematol Oncol* 20:74, 1998.
898. Miceli S, Jure MA, de Saab OA, et al: A clinical and bacteriological study of children suffering from haemolytic uraemic syndrome in Tucuman, Argentina. *Jpn J Infect Dis* 52:33, 1999.
899. de Vries LS, Connell J, Bydder GM, et al: Recurrent intracranial haemorrhages in utero in an infant with alloimmune thrombocytopenia. Case report. *Br J Obstet Gynaecol* 95:299, 1988.
900. Shelton SD, Paulyson K, Kay HH: Prenatal diagnosis of thrombocytopenia absent radius (TAR) syndrome and vaginal delivery. *Prenat Diagn* 19:54, 1999.
901. Luthy DA, Mack L, Hirsch J, et al: Prenatal ultrasound diagnosis of thrombocytopenia with absent radii. *Am J Obstet Gynecol* 141:350, 1981.
902. Daffos F, Forestier F, Kaplan C, et al: Prenatal diagnosis and management of bleeding disorders with fetal blood sampling. *Am J Obstet Gynecol* 158:939, 1988.
903. Hedberg VA, Lipton JM: Thrombocytopenia with absent radii. A review of 100 cases. *Am J Pediatr Hematol Oncol* 10:51, 1988.
904. Donnenfeld AE, Wiseman B, Lavi E, et al: Prenatal diagnosis of thrombocytopenia absent radius syndrome by ultrasound and cordocentesis. *Prenat Diagn* 10:29, 1990.
905. Fromm B, Niethard FU, Marquardt E: Thrombocytopenia and absent radius (TAR) syndrome. *Int Orthop* 15:95, 1991.
906. Deloos J, Moerman P, van den Berghe K, et al: Tetrachomelia and bilateral femorotibial synostosis. A severe variant of the thrombocytopenia-absent radii (TAR) syndrome? *Genet Couns* 3:91, 1992.
907. Labrune P, Pons JC, Khalil M, et al: Antenatal thrombocytopenia in three patients with TAR (thrombocytopenia with absent radii) syndrome. *Prenat Diagn* 13:463, 1993.
908. Donnenfeld AE: Prenatal diagnosis of thrombocytopenia in TAR syndrome. *Prenat Diagn* 14:73, 1994.
909. Weinblatt M, Petrikovsky B, Bialer M, et al: Prenatal evaluation and in utero platelet transfusion for thrombocytopenia absent radii syndrome. *Prenat Diagn* 14:892, 1994.
910. Boute O, Depret-Mosser S, Vinatier D, et al: Prenatal diagnosis of thrombocytopenia-absent radius syndrome. *Fetal Diagn Ther* 11:224, 1996.
911. Ergur A, Yergok YZ, Ertekin A, et al: Prenatal diagnosis of an uncommon syndrome: thrombocytopenia absent radius (TAR). *Zentralbl Gynakol* 120:75, 1998.
912. Urban M, Opitz C, Bommer C, et al: Bilaterally cleft lip, limb defects, and haematological manifestations: Roberts syndrome versus TAR syndrome. *Am J Med Genet* 79:155, 1998.
913. Tongsong T, Sirichotiyakul S, Chanprapaph P: Prenatal diagnosis of thrombocytopenia-absent-radius (TAR) syndrome. *Ultrasound Obstet Gynecol* 15:256, 2000.
914. Bellver J, Lara C, Perez-Aytes A, et al: First-trimester diagnosis of thrombocytopenia-absent radius (TAR) syndrome in a triplet pregnancy. *Prenat Diagn* 25:332, 2005.
915. Muis N, Beemer FA, van Dijken P, et al: The Aase syndrome. Case report and review of the literature. *Eur J Pediatr* 145:153, 1986.
916. D'Avanzo M, Pistoia V, Tolone C, et al: Aase-Smith syndrome: report of a new case. *Br J Haematol* 70:125, 1988.
917. Hing AV, Dowton SB: Aase syndrome: novel radiographic features. *Am J Med Genet* 45:413, 1993.
918. Yetgin S, Balci S, Irken G, et al: Aase-Smith syndrome: report of a new case with unusual features. *Turk J Pediatr* 36:239, 1994.
919. Pfeiffer RA, Ambros E: [The Aase syndrome: hereditary autosomal recessive congenital erythropoiesis insufficiency and triphalangeal thumbs]. *Monatsschr Kinderheilkd* 131:235, 1983.
920. Dror Y, Durie P, Marcon P, et al: Duplication of distal thumb phalanx in Shwachman-Diamond syndrome. *Am J Med Genet* 78:67, 1998.
921. Schneider MD, Schwartz RJ: Heart or hand? Unmasking the basis for specific Holt-Oram phenotypes. *Proc Natl Acad Sci U S A* 96:2577, 1999.
922. McLennan AC, Chitty LS, Rissik J, et al: Prenatal diagnosis of Blackfan-Diamond syndrome: case report and review of the literature. *Prenat Diagn* 16:349, 1996.
923. Bennhagen RG, Menahem S: Holt-Oram syndrome and multiple ventricular septal defects: an association suggesting a possible genetic marker? *Cardiol Young* 8:128, 1998.
924. Bohm M: Holt-Oram syndrome. *Circulation* 98:2636, 1998.
925. James MA, McCarroll HR Jr, Manske PR: Characteristics of patients with hypoplastic thumbs. *J Hand Surg [Am]* 21:104, 1996.
926. Wilson GN: Correlated heart/limb anomalies in Mendelian syndromes provide evidence for a cardiomeic developmental field. *Am J Med Genet* 76:297, 1998.
927. Brockhoff CJ, Kober H, Tsilimangas N, et al: Holt-Oram syndrome. *Circulation* 99:1395, 1999.
928. Cachat F, Rapatsalaky A, Sekarski N, et al: [Three different types of atrial septal defects in the same family]. *Arch Mal Coeur Vaiss* 92:667, 1999.
929. Elbaum R, Royer M, Godart S: Radial club hand and Holt-Oram syndrome. *Acta Chir Belg* 95:229, 1995.
930. Sletten LJ, Pierpont ME: Variation in severity of cardiac disease in Holt-Oram syndrome. *Am J Med Genet* 65:128, 1996.
931. Brons JT, van Geijn HP, Wladimiroff JW, et al: Prenatal ultrasound diagnosis of the Holt-Oram syndrome. *Prenat Diagn* 8:175, 1988.



932. Matsuoka R: [Holt-Oram syndrome]. *Ryokibetsu Shokogun Shirizu* 267, 1996.
933. Newbury-Ecob RA, Leanage R, Raeburn JA, Young ID: Holt-Oram syndrome: a clinical genetic study. *J Med Genet* 33:300, 1996.
934. Zhang KZ, Sun QB, Cheng TO: Holt-Oram syndrome in China: a collective review of 18 cases. *Am Heart J* 111:572, 1986.
935. Muller LM, De Jong G, Van Heerden KM: The antenatal ultrasonographic detection of the Holt-Oram syndrome. *S Afr Med J* 68:313, 1985.
936. Tongsong T, Chanprapaph P: Prenatal sonographic diagnosis of Holt-Oram syndrome. *J Clin Ultrasound* 28:98, 2000.
937. Lehner R, Goharkhay N, Tringler B, et al: Pedigree analysis and descriptive investigation of three classic phenotypes associated with Holt-Oram syndrome. *J Reprod Med* 48:153, 2003.
938. Sepulveda W, Enriquez G, Martinez JL, et al: Holt-Oram syndrome: contribution of prenatal 3-dimensional sonography in an index case. *J Ultrasound Med* 23:983, 2004.
939. Li QY, Newbury-Ecob RA, Terrett JA, et al: Holt-Oram syndrome is caused by mutations in *TBX5*, a member of the Brachyury (T) gene family. *Nat Genet* 15:21, 1997.
940. Basson CT, Huang T, Lin RC, et al: Different *TBX5* interactions in heart and limb defined by Holt-Oram syndrome mutations. *Proc Natl Acad Sci U S A* 96:2919, 1999.
941. He J, McDermott DA, Song Y, et al: Preimplantation genetic diagnosis of human congenital heart malformation and Holt-Oram syndrome. *Am J Med Genet A* 126:93, 2004.
942. Lewis KB, Bruce RA, Baum D, et al: The upper limb-cardiovascular syndrome. An autosomal dominant genetic effect on embryogenesis. *JAMA* 193:1080, 1965.
943. Chemke J, Nisani R, Fischel RE: Absent ulna in the Klippel-Feil syndrome: an unusual associated malformation. *Clin Genet* 17:167, 1980.
944. Masuno M: [VATER association (VACTERL association)]. *Ryokibetsu Shokogun Shirizu* 15:309, 1996.
945. Medina-Escobedo G, Rida-Sanz C: [The VATER association]. *Boi Med Hosp Infant Mex* 49:231, 1992.
946. Temtamy SA, Miller JD: Extending the scope of the VATER association: definition of the VATER syndrome. *J Pediatr* 85:345, 1974.
947. Quillin SP, Gilula LA: Imaging rounds #111. VATER association. *Orthop Rev* 21:85, 88, 89, 1992.
948. Corsello G, Maresi E, Corrao AM, et al: VATER/VACTERL association: clinical variability and expanding phenotype including laryngeal stenosis. *Am J Med Genet* 44:813, 1992.
949. Quan L, Smith DW: The VATER association. Vertebral defects, Anal atresia, T-E fistula with esophageal atresia, Radial and Renal dysplasia: a spectrum of associated defects. *J Pediatr* 82:104, 1973.
950. Botto LD, Khoury MJ, Mastroiacovo P, et al: The spectrum of congenital anomalies of the VATER association: an international study. *Am J Med Genet* 71:8, 1997.
951. Unuvar E, Oguz F, Sahin K, et al: Coexistence of VATER association and recurrent urolithiasis: a case report. *Pediatr Nephrol* 12:141, 1998.
952. Werner W, Beintker M, Schubert J, et al: [The VATER syndrome from the urologic viewpoint]. *Urologe A* 37:203, 1998.
953. Auchterlonie IA, White MP: Recurrence of the VATER association within a sibship. *Clin Genet* 21:122, 1982.
954. Ozbey H, Ozbey N: Association of ambiguous genitalia with VATER anomalies. *Pediatr Surg Int* 12:230, 1997.
955. Tongsong T, Wanpirak C, Piyamongkol W, et al: Prenatal sonographic diagnosis of VATER association. *J Clin Ultrasound* 27:378, 1999.
956. Claiborne AK, Blocker SH, Martin CM, et al: Prenatal and postnatal sonographic delineation of gastrointestinal abnormalities in a case of the VATER syndrome. *J Ultrasound Med* 5:45, 1986.
957. Harris RD, Nyberg DA, Mack LA, et al: Anorectal atresia: prenatal sonographic diagnosis. *AJR Am J Roentgenol* 149:395, 1987.
958. McGahan JP, Leebe JM, Lindfors KK: Prenatal sonographic diagnosis of VATER association. *J Clin Ultrasound* 16:588, 1988.
959. Froster UG, Wallner SJ, Reusche E, et al: VACTERL with hydrocephalus and branchial arch defects: prenatal, clinical, and autopsy findings in two brothers. *Am J Med Genet* 62:169, 1996.
960. Miller OF, Kolon TF: Prenatal diagnosis of VACTERL association. *J Urol* 166:2389, 2001.
961. Tercanli S, Troeger C, Fahnstich H, et al: [Prenatal diagnosis and management in VACTERL association]. *Z Geburtshilfe Neonatol* 205:65, 2001.
962. Tongsong T, Chanprapaph P, Khunamornpong S: Prenatal diagnosis of VACTERL association: a case report. *J Med Assoc Thai* 84:143, 2001.
963. Krapp M, Geipel A, Germer U, et al: First-trimester sonographic diagnosis of distal urethral atresia with megalourethra in VACTERL association. *Prenat Diagn* 22:422, 2002.
964. Ardiat E, Houfflin-Debarge V, Besson R, et al: Prenatal diagnosis of congenital megalourethra associated with VACTERL sequence in twin pregnancy: favorable postnatal outcome. *Ultrasound Obstet Gynecol* 21:619, 2003.
965. Chen CP, Shih JC, Chang JH, et al: Prenatal diagnosis of right pulmonary agenesis associated with VACTERL sequence. *Prenat Diagn* 23:515, 2003.
966. Rollnick BR, Kaye CI, Nagatoshi K, et al: Oculoauriculovertebral dysplasia and variants: phenotypic characteristics of 294 patients. *Am J Med Genet* 26:361, 1987.
967. Lal P, Agrawal P, Krishna A: Goldenhar syndrome. *Indian Pediatr* 34:837, 1997.
968. Manfre L, Genuardi P, Tortorici M, et al: Absence of the common crus in Goldenhar syndrome. *AJNR Am J Neuroradiol* 18:773, 1997.
969. Altamar-Rios J: [Goldenhar's syndrome: a case report]. *An Otorrinolaringol Ibero Am* 25:491, 1998.
970. Ferraris S, Silengo M, Ponzzone A, et al: Goldenhar anomaly in one of triplets derived from in vitro fertilization. *Am J Med Genet* 84:167, 1999.
971. Tamas DE, Mahony BS, Bowie JD, et al: Prenatal sonographic diagnosis of hemifacial microsomia (Goldenhar-Gorlin syndrome). *J Ultrasound Med* 5:461, 1986.
972. Matsuo K: [Oculoauriculovertebral syndrome (Goldenhar syndrome)]. *Ryokibetsu Shokogun Shirizu* 15:287, 1996.
973. Tekkok IH: Syringomyelia as a complication of Goldenhar syndrome. *Childs Nerv Syst* 12:291, 1996.
974. Araneta MR, Moore CA, Olney RS, et al: Goldenhar syndrome among infants born in military hospitals to Gulf War veterans. *Teratology* 56:244, 1997.
975. Luchtenberg M, Blotiu A, Lindemann G, et al: [Anomalies of the efferent lacrimal ducts in Goldenhar syndrome]. *Klin Monatsbl Augenheilkd* 213:aA8, 1998.
976. Jeanty P, Zaleski W, Fleischer AC: Prenatal sonographic diagnosis of lipoma of the corpus callosum in a fetus with Goldenhar syndrome. *Am J Perinatol* 8:89, 1991.
977. De Catte L, Laubach M, Legein J, et al: Early prenatal diagnosis of oculoauriculovertebral dysplasia or the Goldenhar syndrome. *Ultrasound Obstet Gynecol* 8:422, 1996.
978. Kita D, Munemoto S, Ueno Y, et al: Goldenhar's syndrome associated with occipital meningoencephalocele—case report. *Neurol Med Chir (Tokyo)* 42:354, 2002.
979. Martinelli P, Maruotti GM, Agangi A, et al: Prenatal diagnosis of hemifacial microsomia and ipsilateral cerebellar hypoplasia in a fetus with oculoauriculovertebral spectrum. *Ultrasound Obstet Gynecol* 24:199, 2004.
980. Thompson GH: The neck. In Behrman GH, Kliegman RM, Jenson HB (eds): *Behrman: Nelson Textbook of Pediatrics*. Philadelphia, WB Saunders, 2004, pp 2288–2290.
981. Gausewitz SH, Meals RA, Setoguchi Y: Severe limb deficiency in Poland's syndrome. *Clin Orthop* 185:9, 1984.
982. Swanson AB, Tada K, Yonenobu K: Ulnar ray deficiency: its various manifestations. *J Hand Surg [Am]* 9:658, 1984.
983. Uuspaa V: Upper extremity deformities associated with the orofacial clefts. *Scand J Plast Reconstr Surg* 12:157, 1978.
984. David TJ: Preaxial polydactyly and the Poland complex. *Am J Med Genet* 13:333, 1982.
985. de la Torre J, Simpson RL: Complete digital duplication: a case report and review of ulnar polydactyly. *Ann Plast Surg* 40:76, 1998.
986. Graham TJ, Ress AM: Finger polydactyly. *Hand Clin* 14:49, 1998.
987. De Smet L: Ulnar dimelia. *Acta Orthop Belg* 65:382, 1999.
988. Kaplan BS, Bellah RD: Postaxial polydactyly, ulnar ray dysgenesis, and renal cystic dysplasia in sibs. *Am J Med Genet* 87:426, 1999.
989. Bader B, Grill F, Lamprecht E: [Polydactyly of the foot]. *Orthopade* 28:125, 1999.
990. Kleanthous JK, Kleanthous EM, Hahn PJ Jr: Polydactyly of the foot. Overview with case presentations. *J Am Podiatr Med Assoc* 88:493, 1998.
991. Goodman RM, Sternberg M, Shem-Tov Y, et al: Acrocephalo-polysyndactyly type IV: a new genetic syndrome in 3 sibs. *Clin Genet* 15:209, 1979.



992. Lowry RB: Editorial comment: variability in the Smith-Lemli-Opitz syndrome: overlap with the Meckel syndrome. *Am J Med Genet* 14:429, 1983.
993. Khaldi F, Bennaceur B, Hammou A, et al: An autosomal recessive disorder with retardation of growth, mental deficiency, ptosis, pectus excavatum and camptodactyly. *Pediatr Radiol* 18:432, 1988.
994. Kang S, Graham JM Jr, Olney AH, et al: GLI3 frameshift mutations cause autosomal dominant Pallister-Hall syndrome. *Nat Genet* 15:266, 1997.
995. Biesecker LG: Polydactyly: how many disorders and how many genes? *Am J Med Genet* 112:279, 2002.
996. Porter HJ: Lethal arthrogryposis multiplex congenita (fetal akinesia deformation sequence, FADS). *Pediatr Pathol Lab Med* 15:617, 1995.
997. Gordon N: Arthrogryposis multiplex congenita. *Brain Dev* 20:507, 1998.
998. Seringe R: [Congenital equinovarus clubfoot]. *Acta Orthop Belg* 65:127, 1999.
999. Thompson GH, Bilencer RM: Comprehensive management of arthrogryposis multiplex congenita. *Clin Orthop* 194:6, 1985.
1000. Burglen L, Amiel J, Viollot L, et al: Survival motor neuron gene deletion in the arthrogryposis multiplex congenita-spinal muscular atrophy association. *J Clin Invest* 98:1130, 1996.
1001. Swinyard CA, Bleck EE: The etiology of arthrogryposis (multiple congenital contracture). *Clin Orthop* 194:15, 1985.
1002. Hall JG: Arthrogryposis multiplex congenita: etiology, genetics, classification, diagnostic approach, and general aspects. *J Pediatr Orthop B* 6:159, 1997.
1003. Jacobson L, Polizzi A, Vincent A: An animal model of maternal antibody-mediated arthrogryposis multiplex congenita (AMC). *Ann N Y Acad Sci* 841:565, 1998.
1004. Drachman DB, Coulombre AJ: Experimental clubfoot and arthrogryposis multiplex congenita. *Lancet* 2:523, 1962.
1005. Moessinger AC: Fetal akinesia deformation sequence: an animal model. *Pediatrics* 72:857, 1983.
1006. Drachman DB, Weiner LP, Price DL, et al: Experimental arthrogryposis caused by viral myopathy. *Arch Neurol* 33:362, 1976.
1007. Drachman DA, Sokoloff L: The role of movement in embryonic joint development. *Development* 14:401, 1966.
1008. Banker BQ: Neuropathologic aspects of arthrogryposis multiplex congenita. *Clin Orthop* 194:30, 1985.
1009. Swinyard CA: Concepts of multiple congenital contractures (arthrogryposis) in man and animals. *Teratology* 25:247, 1982.
1010. Quinn CM, Wigglesworth JS, Heckmatt J: Lethal arthrogryposis multiplex congenita: a pathological study of 21 cases. *Histopathology* 19:155, 1991.
1011. Hall JG: Genetic aspects of arthrogryposis. *Clin Orthop* 194:44, 1985.
1012. Herva R, Leisti J, Kirkinen P, et al: A lethal autosomal recessive syndrome of multiple congenital contractures. *Am J Med Genet* 20:431, 1985.
1013. Lerman-Sagie T, Levi Y, Kidron D, et al: Syndrome of osteopetrosis and muscular degeneration associated with cerebro-oculo-facio-skeletal changes. *Am J Med Genet* 28:42, 1987.
1014. Illum N, Reske-Nielsen E, Skovby F, et al: Lethal autosomal recessive arthrogryposis multiplex congenita with whistling face and calcifications of the nervous system. *Neuropediatrics* 19:186, 1988.
1015. Hennekam RC, Barth PG, Van Lookeren CW, et al: A family with severe X-linked arthrogryposis. *Eur J Pediatr* 150:656, 1991.
1016. Krakowiak PA, O'Quinn JR, Bohnsack JF, et al: A variant of Freeman-Sheldon syndrome maps to 11p15.5-pter. *Am J Hum Genet* 60:426, 1997.
1017. Shohat M, Lotan R, Magal N, et al: A gene for arthrogryposis multiplex congenita neuropathic type is linked to D5S394 on chromosome 5qter. *Am J Hum Genet* 61:1139, 1997.
1018. Zori RT, Gardner JL, Zhang J, et al: Newly described form of X-linked arthrogryposis maps to the long arm of the human X chromosome. *Am J Med Genet* 78:450, 1998.
1019. Hall JG, Reed SD: Teratogens associated with congenital contractures in humans and in animals. *Teratology* 25:173, 1982.
1020. Smith DW, Clarren SK, Harvey MA: Hyperthermia as a possible teratogenic agent. *J Pediatr* 92:878, 1978.
1021. Vincent A, Newland C, Brueton L, et al: Arthrogryposis multiplex congenita with maternal autoantibodies specific for a fetal antigen. *Lancet* 346:24, 1995.
1022. Riemersma S, Vincent A, Beeson D, et al: Association of arthrogryposis multiplex congenita with maternal antibodies inhibiting fetal acetylcholine receptor function. *J Clin Invest* 98:2358, 1996.
1023. Jacobson L, Polizzi A, Morris-Kay G, et al: Plasma from human mothers of fetuses with severe arthrogryposis multiplex congenita causes deformities in mice. *J Clin Invest* 103:1031, 1999.
1024. Rivera MR, Avila CA, Kofman-Alfaro S: Distal arthrogryposis type IIB: probable autosomal recessive inheritance. *Clin Genet* 56:95, 1999.
1025. Hall JG: An approach to research on congenital contractures. *Birth Defects Orig Artic Ser* 20:8, 1984.
1026. Goldberg JD, Chervenak FA, Lipman RA, et al: Antenatal sonographic diagnosis of arthrogryposis multiplex congenita. *Prenat Diagn* 6:45, 1986.
1027. Gorczyca DP, McGahan JP, Lindfors KK, et al: Arthrogryposis multiplex congenita: prenatal ultrasonographic diagnosis. *J Clin Ultrasound* 17:40, 1989.
1028. Kirkinen P, Herva R, Leisti J: Early prenatal diagnosis of a lethal syndrome of multiple congenital contractures. *Prenat Diagn* 7:189, 1987.
1029. Miskin M, Rothberg R, Rudd NL, et al: Arthrogryposis multiplex congenita—prenatal assessment with diagnostic ultrasound and fetoscopy. *J Pediatr* 95:463, 1979.
1030. Socol ML, Sabbagha RE, Elias S, et al: Prenatal diagnosis of congenital muscular dystrophy producing arthrogryposis. *N Engl J Med* 313:1230, 1985.
1031. Ajayi RA, Keen CE, Knott PD: Ultrasound diagnosis of the Pena-Shokeir phenotype at 14 weeks of pregnancy. *Prenat Diagn* 15:762, 1995.
1032. Sepulveda W, Stagiannis KD, Cox PM, et al: Prenatal findings in generalized amyoplasia. *Prenat Diagn* 15:660, 1995.
1033. Zelop C, Benacerraf B: Sonographic diagnosis of fetal upper extremity dysmorphism: significance and outcome. *Ultrasound Obstet Gynecol* 8:391, 1996.
1034. Dudkiewicz I, Achiron R, Ganel A: Prenatal diagnosis of distal arthrogryposis type 1. *Skeletal Radiol* 28:233, 1999.
1035. Scott H, Hunter A, Bedard B: Non-lethal arthrogryposis multiplex congenita presenting with cystic hygroma at 13 weeks gestational age. *Prenat Diagn* 19:966, 1999.
1036. Tongsong T, Chanprapaph P, Khunamornpong S: Prenatal ultrasound of regional akinesia with Pena-Shokeir phenotype. *Prenat Diagn* 20:422, 2000.
1037. Paladini D, Tartaglione A, Agangi A, et al: Pena-Shokeir phenotype with variable onset in three consecutive pregnancies. *Ultrasound Obstet Gynecol* 17:163, 2001.
1038. Madazli R, Tuysuz B, Aksoy F, et al: Prenatal diagnosis of arthrogryposis multiplex congenita with increased nuchal translucency but without any underlying fetal neurogenic or myogenic pathology. *Fetal Diagn Ther* 17:29, 2002.
1039. Witters I, Moerman P, Fryns JP: Fetal akinesia deformation sequence: a study of 30 consecutive in utero diagnoses. *Am J Med Genet* 113:23, 2002.
1040. Makrydimas G, Sotiriadis A, Papapanagiotou G, et al: Fetal akinesia deformation sequence presenting with increased nuchal translucency in the first trimester of pregnancy. *Fetal Diagn Ther* 19:332, 2004.
1041. Lam YH, Tang MH: Sonographic diagnosis of limb reduction defects in a fetus with haemoglobin Bart's disease at 12 weeks of gestation. *Prenat Diagn* 19:983, 1999.
1042. Ruano R, Dumez Y, Dommergues M: Three-dimensional ultrasonographic appearance of the fetal akinesia deformation sequence. *J Ultrasound Med* 22:593, 2003.
1043. Fahy MJ, Hall JG: A retrospective study of pregnancy complications among 828 cases of arthrogryposis. *Genet Couns* 1:3, 1990.
1044. Byers PH: Brittle bones—fragile molecules: disorders of collagen gene structure and expression. *Trends Genet* 6:293, 1990.
1045. Prockop DJ, Kuivaniemi H, Tromp G: Molecular basis of osteogenesis imperfecta and related disorders of bone. *Clin Plast Surg* 21:407, 1994.
1046. Spranger J, Winterpacht A, Zabel B: The type II collagenopathies: a spectrum of chondrodysplasias. *Eur J Pediatr* 153:56, 1994.
1047. Lohiniva J, Paasilta P, Seppanen U, et al: Splicing mutations in the COL3 domain of collagen IX cause multiple epiphyseal dysplasia. *Am J Med Genet* 90:216, 2000.
1048. Spayde EC, Joshi AP, Wilcox WR, et al: Exon skipping mutation in the COL9A2 gene in a family with multiple epiphyseal dysplasia. *Matrix Biol* 19:121, 2000.



1049. Wallis GA, Rash B, Sykes B, et al: Mutations within the gene encoding the alpha 1 (X) chain of type X collagen (COL10A1) cause metaphyseal chondrodysplasia type Schmid but not several other forms of metaphyseal chondrodysplasia. *J Med Genet* 33:450, 1996.
1050. Melkonimi M, Brunner HG, Manouvrier S, et al: Autosomal recessive disorder otospondyloomegaepiphyseal dysplasia is associated with loss-of-function mutations in the COL11A2 gene. *Am J Hum Genet* 66:368, 2000.
1051. Spranger J: The type XI collagenopathies. *Pediatr Radiol* 28:745, 1998.
1052. Briggs MD, Morier GR, Cole WG, et al: Diverse mutations in the gene for cartilage oligomeric matrix protein in the pseudoachondroplasia-multiple epiphyseal dysplasia disease spectrum. *Am J Hum Genet* 62:311, 1998.
1053. Chapman KL, Morier GR, Chapman K, et al: Mutations in the region encoding the von Willebrand factor A domain of matrilin-3 are associated with multiple epiphyseal dysplasia. *Nat Genet* 28:393, 2001.
1054. Nurnberg P, Thiele H, Chandler D, et al: Heterozygous mutations in ANKH, the human ortholog of the mouse progressive ankylosis gene, result in craniometaphyseal dysplasia. *Nat Genet* 28:37, 2001.
1055. Reichenberger E, Tiziani V, Watanabe S, et al: Autosomal dominant craniometaphyseal dysplasia is caused by mutations in the transmembrane protein ANK. *Am J Hum Genet* 68:1321, 2001.
1056. Superti-Furga A, Rossi A, Steinmann B, et al: A chondrodysplasia family produced by mutations in the diastrophic dysplasia sulfate transporter gene: genotype/phenotype correlations. *Am J Med Genet* 63:144, 1996.
1057. ul Haque MF, King LM, Krakow D, et al: Mutations in orthologous genes in human spondyloepimetaphyseal dysplasia and the brachymorphic mouse. *Nat Genet* 20:157, 1998.
1058. Fratini A, Orchard PJ, Sobacchi C, et al: Defects in TCIRG1 subunit of the vacuolar proton pump are responsible for a subset of human autosomal recessive osteopetrosis. *Nat Genet* 25:343, 2000.
1059. Kornak U, Kasper D, Bosl MR, et al: Loss of the CIC-7 chloride channel leads to osteopetrosis in mice and man. *Cell* 104:205, 2001.
1060. Venta PJ, Wely RJ, Johnson TM, et al: Carbonic anhydrase II deficiency syndrome in a Belgian family is caused by a point mutation at an invariant histidine residue (107 His→Tyr): complete structure of the normal human CA II gene. *Am J Hum Genet* 49:1082, 1991.
1061. Oldenburg J, von Brederlow B, Fregin A, et al: Congenital deficiency of vitamin K dependent coagulation factors in two families presents as a genetic defect of the vitamin K-epoxide-reductase-complex. *Thromb Haemost* 84:937, 2000.
1062. Pauli RM: Mechanism of bone and cartilage maldevelopment in the warfarin embryopathy. *Pathol Immunopathol Res* 7:107, 1988.
1063. Pauli RM, Lian JB, Mosher DF, et al: Association of congenital deficiency of multiple vitamin K-dependent coagulation factors and the phenotype of the warfarin embryopathy: clues to the mechanism of teratogenicity of coumarin derivatives. *Am J Hum Genet* 41:566, 1987.
1064. Munro PB, Olgunturk RO, Fryns JP, et al: Mutations in the gene encoding the human matrix Gla protein cause Keutel syndrome. *Nat Genet* 21:142, 1999.
1065. Franco B, Meroni G, Parenti G, et al: A cluster of sulfatase genes on Xp22.3: mutations in chondrodysplasia punctata (CDPX) and implications for warfarin embryopathy. *Cell* 81:15, 1995.
1066. Braverman N, Lin P, Moebius FF, et al: Mutations in the gene encoding 3 beta-hydroxysteroid-delta 8, delta 7-isomerase cause X-linked dominant Conradi-Hunermann syndrome. *Nat Genet* 22:291, 1999.
1067. Grange DK, Kratz LE, Braverman NE, et al: CHLD syndrome caused by deficiency of 3beta-hydroxysteroid-delta8, delta7-isomerase. *Am J Med Genet* 90:328, 2000.
1068. Motley AM, Hettema EH, Hogenhout EM, et al: Rhizomelic chondrodysplasia punctata is a peroxisomal protein targeting disease caused by a non-functional PTS2 receptor. *Nat Genet* 15:377, 1997.
1069. Ofman R, Hettema EH, Hogenhout EM, et al: Acyl-CoA: dihydroxyacetonephosphate acyltransferase: cloning of the human cDNA and resolution of the molecular basis in rhizomelic chondrodysplasia punctata type 2. *Hum Mol Genet* 7:847, 1998.
1070. de Vet EC, Ijlst L, Oostheim W, et al: Alkyl-dihydroxyacetonephosphate synthase. Fate in peroxisome biogenesis disorders and identification of the point mutation underlying a single enzyme deficiency. *J Biol Chem* 273:10296, 1998.
1071. Gedeon AK, Colley A, Jamieson R, et al: Identification of the gene (SEDL) causing X-linked spondyloepiphyseal dysplasia tarda. *Nat Genet* 22:400, 1999.
1072. Hou WS, Bromme D, Zhao Y, et al: Characterization of novel cathepsin K mutations in the pro and mature polypeptide regions causing pycnodysostosis. *J Clin Invest* 103:731, 1999.
1073. Leroy JG, Wiesmann U: Disorders of lysosomal enzymes. In Royce PM, Steinmann B (eds): *Connective Tissue and its Heritable Disorders*. New York, Wiley-Liss, 1993, pp 613-640.
1074. Martignetti JA, Aqeel AA, Sewairi WA, et al: Mutation of the matrix metalloproteinase 2 gene (MMP2) causes a multicentric osteolysis and arthritis syndrome. *Nat Genet* 28:261, 2001.
1075. Kitanaka S, Takeyama K, Murayama A, et al: Inactivating mutations in the 25-hydroxyvitamin D<sub>3</sub> 1alpha-hydroxylase gene in patients with pseudovitamin D-deficiency rickets. *N Engl J Med* 338:653, 1998.
1076. Hughes MR, Malloy PJ, Kieback DG, et al: Point mutations in the human vitamin D receptor gene associated with hypocalcemic rickets. *Science* 242:1702, 1988.
1077. Bai M, Pearce SH, Kifor O, et al: In vivo and in vitro characterization of neonatal hyperparathyroidism resulting from a de novo, heterozygous mutation in the Ca<sup>2+</sup>-sensing receptor gene: normal maternal calcium homeostasis as a cause of secondary hyperparathyroidism in familial benign hypocalciuric hypercalcemia. *J Clin Invest* 99:88, 1997.
1078. Schipani E, Langman CB, Parfitt AM, et al: Constitutively activated receptors for parathyroid hormone and parathyroid hormone-related peptide in Jansen's metaphyseal chondrodysplasia. *N Engl J Med* 335:708, 1996.
1079. Zhang P, Jobert AS, Couvineau A, et al: A homozygous inactivating mutation in the parathyroid hormone/parathyroid hormone-related peptide receptor causing Blomstrand chondrodysplasia. *J Clin Endocrinol Metab* 83:3365, 1998.
1080. Patten JL, Johns DR, Valle D, et al: Mutation in the gene encoding the stimulatory G protein of adenylate cyclase in Albright's hereditary osteodystrophy. *N Engl J Med* 322:1412, 1990.
1081. The HYP Consortium: A gene (PEX) with homologies to endopeptidases is mutated in patients with X-linked hypophosphatemic rickets. *Nat Genet* 11:130, 1995.
1082. Sabbagh Y, Jones AO, Tenenhouse HS: PHEXdb, a locus-specific database for mutations causing X-linked hypophosphatemia. *Hum Mutat* 16:1, 2000.
1083. The ADHR Consortium: Autosomal dominant hypophosphataemic rickets is associated with mutations in FGF23. *Nat Genet* 26:345, 2000.
1084. Wilkie AO: Craniosynostosis: genes and mechanisms. *Hum Mol Genet* 6:1647, 1997.
1085. Afzal AR, Rajab A, Fenske CD, et al: Recessive Robinow syndrome, allelic to dominant brachydactyly type B, is caused by mutation of ROR2. *Nat Genet* 25:419, 2000.
1086. Van Bokhoven H, Celli J, Kayserili H, et al: Mutation of the gene encoding the ROR2 tyrosine kinase causes autosomal recessive Robinow syndrome. *Nat Genet* 25:423, 2000.
1087. Oldridge M, Fortuna AM, Maringa M, et al: Dominant mutations in ROR2, encoding an orphan receptor tyrosine kinase, cause brachydactyly type B. *Nat Genet* 24:275, 2000.
1088. Hughes AE, Ralston SH, Marken J, et al: Mutations in TNFRSF11A, affecting the signal peptide of RANK, cause familial expansile osteolysis. *Nat Genet* 24:45, 2000.
1089. Janssens K, Gershoni-Baruch R, Guanabens N, et al: Mutations in the gene encoding the latency-associated peptide of TGF-beta 1 cause Camurati-Engelmann disease. *Nat Genet* 26:273, 2000.
1090. Thomas JT, Lin K, Nandedkar M, et al: A human chondrodysplasia due to a mutation in a TGF-beta superfamily member. *Nat Genet* 12:315, 1996.
1091. Polinkovsky A, Robin NH, Thomas JT, et al: Mutations in CDMP1 cause autosomal dominant brachydactyly type C. *Nat Genet* 17:18, 1997.
1092. Gong Y, Krakow D, Marcelino J, et al: Heterozygous mutations in the gene encoding noggin affect human joint morphogenesis. *Nat Genet* 21:302, 1999.
1093. Bulman MP, Kusumi K, Frayling TM, et al: Mutations in the human distal homologue, DLL3, cause axial skeletal defects in spondylocostal dysostosis. *Nat Genet* 24:438, 2000.
1094. Gao B, Guo J, She C, et al: Mutations in *IIH*, encoding Indian hedgehog, cause brachydactyly type A-1. *Nat Genet* 28:386, 2001.



1095. Ianakiev P, van Baren MJ, Daly MJ, et al: Acheiropodia is caused by a genomic deletion in C7orf2, the human orthologue of the Lmbr1 gene. *Am J Hum Genet* 68:38, 2001.
1096. Balemans W, Ebeling M, Patel N, et al: Increased bone density in sclerosteosis is due to the deficiency of a novel secreted protein (SOST). *Hum Mol Genet* 10:537, 2001.
1097. Gong Y, Slee R, Group O-PC: Human bone mass accrual is affected by mutations in the low density lipoprotein receptor-related protein 5 gene [Abstract]. *Am J Hum Genet* 69:S189, 2001.
1098. Hurvitz JR, Suwairi WM, Van Hul W, et al: Mutations in the CCN gene family member WISP3 cause progressive pseudorheumatoid dysplasia. *Nat Genet* 23:94, 1999.
1099. Wagner T, Wirth J, Meyer J, et al: Autosomal sex reversal and campomelic dysplasia are caused by mutations in and around the SRY-related gene SOX9. *Cell* 79:1111, 1994.
1100. Kalfi-Suske M, Wild A, Topp J, et al: Point mutations throughout the GLI3 gene cause Greig cephalopolysyndactyly syndrome. *Hum Mol Genet* 8:1769, 1999.
1101. Radhakrishna U, Bornholdt D, Scott HS, et al: The phenotypic spectrum of GLI3 morphopathies includes autosomal dominant preaxial polydactyly type-IV and postaxial polydactyly type-A/B; No phenotype prediction from the position of GLI3 mutations. *Am J Hum Genet* 65:645, 1999.
1102. Momeni P, Glockner G, Schmidt O, et al: Mutations in a new gene, encoding a zinc-finger protein, cause tricho-rhino-phalangeal syndrome type I. *Nat Genet* 24:71, 2000.
1103. el Ghouzi V, Le Merrer M, Perrin-Schmitt F, et al: Mutations of the TWIST gene in the Saethre-Chotzen syndrome. *Nat Genet* 15:42, 1997.
1104. McGrath JA, Duijf PH, Doetsch V, et al: Hay-Wells syndrome is caused by heterozygous missense mutations in the SAM domain of p63. *Hum Mol Genet* 10:221, 2001.
1105. Van Bokhoven H, Hamel BC, Bamshad M, et al: p63 Gene mutations in EEC syndrome, limb-mammary syndrome, and isolated split hand-split foot malformation suggest a genotype-phenotype correlation. *Am J Hum Genet* 69:481, 2001.
1106. Dreyer SD, Zhou G, Baldini A, et al: Mutations in LMX1B cause abnormal skeletal patterning and renal dysplasia in nail patella syndrome. *Nat Genet* 19:47, 1998.
1107. Price JA, Bowden DW, Wright JT, et al: Identification of a mutation in DLX3 associated with tricho-dento-osseous (TDO) syndrome. *Hum Mol Genet* 7:563, 1998.
1108. Akarsu AN, Stoilov I, Yilmaz E, et al: Genomic structure of HOXD13 gene: a nine polyalanine duplication causes synpolydactyly in two unrelated families. *Hum Mol Genet* 5:945, 1996.
1109. Jabs EW, Muller U, Li X, et al: A mutation in the homeodomain of the human MSX2 gene in a family affected with autosomal dominant craniosynostosis. *Cell* 75:443, 1993.
1110. Wilkie AO, Tang Z, Elanko N, et al: Functional haploinsufficiency of the human homeobox gene MSX2 causes defects in skull ossification. *Nat Genet* 24:387, 2000.
1111. Mavrogiannis LA, Antonopoulou I, Baxova A, et al: Haploinsufficiency of the human homeobox gene ALX4 causes skull ossification defects. *Nat Genet* 27:17, 2001.
1112. Shears DJ, Vassal HJ, Goodman FR, et al: Mutation and deletion of the pseudoautosomal gene SHOX cause Leri-Weill dyschondrosteosis. *Nat Genet* 19:70, 1998.
1113. Bamshad M, Lin RC, Law DJ, et al: Mutations in human TBX3 alter limb, apocrine and genital development in ulnar-mammary syndrome. *Nat Genet* 16:311, 1997.
1114. Delepine M, Nicolino M, Barrett T, et al: EIF2AK3, encoding translation initiation factor 2-alpha kinase 3, is mutated in patients with Wolcott-Rallison syndrome. *Nat Genet* 25:406, 2000.
1115. Doffinger R, Smahi A, Bessia C, et al: X-linked anhidrotic ectodermal dysplasia with immunodeficiency is caused by impaired NF-kappaB signaling. *Nat Genet* 27:277, 2001.
1116. Smahi A, Courtois G, Vabres P, et al: Genomic rearrangement in NEMO impairs NF-kappaB activation and is a cause of incontinentia pigmenti. The International Incontinentia Pigmenti (IP) Consortium. *Nature* 405:466, 2000.
1117. Cheung PK, McCormick C, Crawford BE, et al: Etiological point mutations in the hereditary multiple exostoses gene EXT1: a functional analysis of heparan sulfate polymerase activity. *Am J Hum Genet* 69:55, 2001.
1118. Duncan G, McCormick C, Tufaro F: The link between heparan sulfate and hereditary bone disease: finding a function for the EXT family of putative tumor suppressor proteins. *J Clin Invest* 108:511, 2001.
1119. Lind T, Tufaro F, McCormick C, et al: The putative tumor suppressors EXT1 and EXT2 are glycosyltransferases required for the biosynthesis of heparan sulfate. *J Biol Chem* 273:26265, 1998.
1120. Ueki Y, Tiziani V, Santanna C, et al: Mutations in the gene encoding c-Abl-binding protein SH3BP2 cause cherubism. *Nat Genet* 28:125, 2001.
1121. Ridanpaa M, van Eenennaam H, Pelin K, et al: Mutations in the RNA component of RNase MRP cause a pleiotropic human disease, cartilage-hair hypoplasia. *Cell* 104:195, 2001.
1122. Bonafe L, Schmitt K, Eich G, et al: RMRP gene sequence analysis confirms a cartilage-hair hypoplasia variant with only skeletal manifestations and reveals a high density of single-nucleotide polymorphisms. *Clin Genet* 61:146, 2002.
1123. Hirschhorn R: Adenosine deaminase deficiency: molecular basis and recent developments. *Clin Immunol Immunopathol* 76:S219, 1995.
1124. Meirowitz NB, Ananth CV, Smulian JC, et al: Foot length in fetuses with abnormal growth. *J Ultrasound Med* 19:201, 2000.
1125. Hewitt B: Nuchal translucency in the first trimester. *Aust N Z J Obstet Gynaecol* 33:389, 1993.
1126. Soothill P, Kyle P: Fetal nuchal translucency test for Down's syndrome. *Lancet* 350:1629, 1997.
1127. Fukada Y, Yasumizu T, Takizawa M, et al: The prognosis of fetuses with transient nuchal translucency in the first and early second trimester. *Acta Obstet Gynecol Scand* 76:913, 1997.
1128. Hernadi L, Torocsik M: Screening for fetal anomalies in the 12th week of pregnancy by transvaginal sonography in an unselected population. *Prenat Diagn* 17:753, 1997.
1129. Hsieh YY, Hsu TY, Lee CC, et al: Prenatal diagnosis of thoracopelvic dysplasia. A case report. *J Reprod Med* 44:737, 1999.
1130. den Hollander NS, van der Harten HJ, Vermeij-Keers C, et al: First-trimester diagnosis of Blomstrand lethal osteochondrodysplasia. *Am J Med Genet* 73:345, 1997.
1131. Hafner E, Schuchter K, Liebhart E, et al: Results of routine fetal nuchal translucency measurement at weeks 10-13 in 4233 unselected pregnant women. *Prenat Diagn* 18:29, 1998.
1132. Hiipala A, Eronen M, Taipale P, et al: Fetal nuchal translucency and normal chromosomes: a long-term follow-up study. *Ultrasound Obstet Gynecol* 18:18, 2001.
1133. Leung KY, MacLachlan NA, Sepulveda W: Prenatal diagnosis of ectrodactyly: the 'lobster claw' anomaly. *Ultrasound Obstet Gynecol* 6:443, 1995.
1134. Hyett J, Noble P, Sebire NJ, et al: Lethal congenital arthrogryposis presents with increased nuchal translucency at 10-14 weeks of gestation. *Ultrasound Obstet Gynecol* 9:310, 1997.
1135. Eliyahu S, Weiner E, Lahav D, et al: Early sonographic diagnosis of Jarcho-Levin syndrome: a prospective screening program in one family. *Ultrasound Obstet Gynecol* 9:314, 1997.
1136. Hyett JA, Clayton PT, Moscoso G, et al: Increased first trimester nuchal translucency as a prenatal manifestation of Smith-Lemli-Opitz syndrome. *Am J Med Genet* 58:374, 1995.
1137. Maymon R, Ogle RF, Chitty LS: Smith-Lemli-Opitz syndrome presenting with persisting nuchal oedema and non-immune hydrops. *Prenat Diagn* 19:105, 1999.
1138. Sharp P, Haan E, Fletcher JM, et al: First-trimester diagnosis of Smith-Lemli-Opitz syndrome. *Prenat Diagn* 17:355, 1997.
1139. Hobbins JC, Jones OW, Gottesfeld S, et al: Transvaginal ultrasonography and transabdominal embryoscopy in the first-trimester diagnosis of Smith-Lemli-Opitz syndrome, type II. *Am J Obstet Gynecol* 171:546, 1994.
1140. Ferreira A, Matias A, Brandao O, et al: Nuchal translucency and ductus venosus blood flow as early sonographic markers of thanatophoric dysplasia. A case report. *Fetal Diagn Ther* 19:241, 2004.
1141. Malone FD, Marino T, Bianchi DW, et al: Isolated clubfoot diagnosed prenatally: is karyotyping indicated? *Obstet Gynecol* 95:437, 2000.
1142. Mammen L, Benson CB: Outcome of fetuses with clubfeet diagnosed by prenatal sonography. *J Ultrasound Med* 23:479, 2003.
1143. Hashimoto BE, Filly RA, Callen PW: Sonographic diagnosis of clubfoot in utero. *J Ultrasound Med* 5:81, 1986.
1144. Bar-On E, Mashiach R, Inbar O, et al: Prenatal ultrasound diagnosis of clubfoot: Outcome and recommendations for counseling and follow-up. *J Bone Joint Surg* 87-B:990, 2004.
1145. Yamamoto H: A clinical, genetic and epidemiologic study of congenital clubfoot. *Jpn J Hum Genetics* 24:37, 1979.



1146. Rijhsinghani A, Yankowitz J, Kanis AB, et al: Antenatal sonographic diagnosis of clubfoot with particular attention to the implications of isolated clubfoot. *Ultrasound Obstet Gynecol* 12:103, 1998.
1147. Shipp TD, Benacerraf BR: The significance of prenatally identified isolated clubfoot: is amniocentesis indicated? *Am J Obstet Gynecol* 178:600, 1998.
1148. Woodrow N, Tran T, Umstad M, et al: Mid-trimester ultrasound diagnosis of isolated talipes equinovarus: accuracy and outcome for infants. *Aust N Z J Obstet Gynaecol* 38:301, 1998.

# ULTRASOUND EVALUATION OF THE FETAL THORAX

Juriy W. Wladimiroff, MD, PhD, Titia E. Cohen-Overbeek, MD, and Jacqueline A. M. Laudy, MD, PhD

## The Fetal Lung

### Normal Lung Development

### Lung Hypoplasia

### Congenital Cystic Adenomatoid Malformation

### Bronchopulmonary Sequestration

### Congenital High Airway Obstruction (Laryngeal Atresia)

## Other Lung Abnormalities

### The Fetal Diaphragm

#### Normal Development

### Congenital Diaphragmatic Hernia

### Congenital Hydrothorax

In this chapter, normal and abnormal development of fetal intrathoracic organs are discussed, with emphasis on the lungs and diaphragm. Each intrathoracic abnormality may not only have an impact on its own organ functioning but may also have an effect on neighboring organ systems such as diaphragmatic hernia resulting in lung hypoplasia. Diagnostic ultrasound and lately ultrafast magnetic resonance imaging (MRI) play a major role in the detection of fetal intrathoracic pathology. When additional imaging is required, the role of MRI and three-dimensional (3D) ultrasound in the elucidation of intrathoracic normal anatomy and pathologic conditions are discussed.

## THE FETAL LUNG

The prenatal diagnosis of fetal abnormalities originating from the lung is dependent upon the sonographic appearance of intrathoracic space-occupying lesions.<sup>1</sup> The normal lung is of moderate echogenicity, which may vary in echogenicity from hypoechoic to isoechoic to hyperechoic when compared with the adjacent liver (Fig. 13-1).<sup>2</sup> Fetal lung lesions must be distinguished from extrapulmonic masses, such as a diaphragmatic hernia, in which intrathoracic stomach, intestine, and liver are present. Whereas fetal congenital cystic adenomatoid malformation (CCAM) is characterized by either a cystic or a solid hyperechoic mass, bronchopulmonary sequestration (BPS) appears as a well-defined uniformly hyperechoic solid mass mostly situated in the left basal lung.<sup>3</sup> Based on the concept that each unit of embryonic lung includes a bronchial bud supplied by a systemic capillary plexus derived from the primitive aorta and containing a small branch of the pulmonary artery, Achiron et al<sup>4</sup> attempted to group lung lesions according to (1) presence/absence of lung; (2) normal/abnormal lung; and (3) normal/abnormal vascular supply. This system would group congenital lung lesions into one of five groups of dysplasias. Although the concept is intriguing, it may also introduce confusion into an already complex topic.<sup>5</sup> This chapter adheres to the more conventional systems of classification.

## NORMAL LUNG DEVELOPMENT

Human lung development is divided into five stages: embryonic, pseudoglandular, canalicular, saccular, and alveolar (Fig. 13-2). The transition between stages occurs gradually, and there is considerable overlap from one stage to the next, and also between areas within the lung and between various gestational ages and individuals.<sup>6</sup>

During the embryonic stage, the lung arises as a diverticulum from the caudal end of the laryngotracheal groove of the foregut at the end of the fourth week. During the next few weeks, this diverticulum grows gradually caudally to form the primitive trachea. The end of the diverticulum divides into two sacs, the lung buds. By the end of the sixth week, all bronchopulmonary segments have been formed. During the pseudoglandular stage, conducting airways are formed by repeated dichotomous branching resulting in a tree of narrow, thick, epithelial-lined tubules. By the 16th week of gestation, the tracheobronchial tree has been formed. During the canalicular stage (16-28 weeks), the basic structure of the gas-exchanging portion of the lung is formed and vascularized. At the beginning of the saccular stage (28-36 weeks) airways terminate in large smooth-walled cylindrical structures and are subdivided by ridges called crests. The crests protrude into saccules. The end result of the saccular stage is a rapid increase in the gas exchange of the lung and rapid thinning of the interstitium. The alveolar stage (36 weeks-term) is characterized by further thinning of the blood-gas barrier, increase of surfactant production, and progressive branching of the respiratory airways.

Prenatal growth and development of the pulmonary blood vessels is closely linked to that of the bronchial tree. The sixth bronchial arches appear at about 5 weeks and develop into the main pulmonary arterial trunk with right and left branches during the next few weeks of the pseudoglandular period. By 7 weeks of gestation, the adult pattern of vessels connecting heart and lungs is established. The normal cardiac and pulmonary arterial and venous blood flow connections are illustrated in Figure 13-3. The pulmonary arteries and veins can be seen using color Doppler flow imaging (Fig. 13-4).



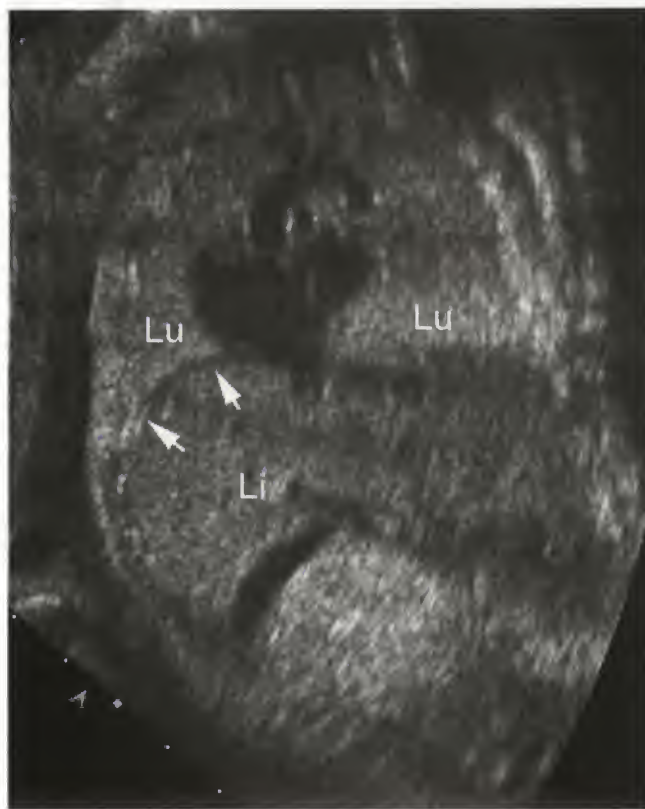


**FIGURE 13-1.** Slightly angled coronal sonographic plane of section in a late second trimester pregnancy demonstrating normal lungs (Lu) slightly more echogenic than the liver (Li). The hypoechoic muscular diaphragm (arrows) is seen on one side.

The in utero pulmonary vascular circuit is a high-resistance, high-pressure, low-flow system.<sup>7</sup> In the fetus, normal gas exchange is placental in origin and pulmonary blood flow is low, merely supplying nutritional requirements for lung growth and some metabolic functions.<sup>8</sup> In human fetuses, the total cardiac output supplying the lungs increases from 13% at 20 weeks to 25% at 30 weeks and remains constant during the remainder of pregnancy.<sup>9</sup> This implies that pulmonary blood flow increases and pulmonary vascular resistance decreases with advancing gestation.

Fetal lung development incorporates a combination of two processes: lung growth and lung maturation, which are related, but appear to be separately controlled. A normal amount of amniotic fluid is important for fetal lung growth.<sup>10</sup> Fetal intrapulmonary fluid is formed by active transport across pulmonary epithelium into the tracheobronchial lumen, where it establishes positive pressure within the developing lung. Lung-liquid volume and intratracheal pressure are maintained within very precise ranges by the larynx, which through unknown mechanisms regulates the efflux of lung liquid volume from the trachea to the amniotic space.<sup>10</sup> Lung liquid contributes up to one third of amniotic fluid volume. Fetal breathing movements in humans can be recorded by ultrasonography from about 10 weeks of gestation. These respiratory movements produce significant changes in intrathoracic pressure, which may influence lung development.<sup>11</sup>

## LUNG HYPOPLASIA

Pulmonary hypoplasia is defined as the incomplete or defective development of the lung resulting in overall reduced size due to reduced numbers or size of acini.<sup>12</sup> With the incidence of lung hypoplasia being 1.1 per 1000 live births and a mortality rate of more than 50%, fetal lung hypoplasia poses a major diagnostic challenge.<sup>13</sup> It is seen in greater than 10% of neonatal autopsies and occurs in association with other malformations, most commonly congenital diaphragmatic hernia, severe skeletal dysplasias and severe renal abnormalities.<sup>12,14</sup> Early evaluation of the adequacy of fetal lung volumes used the subjective appearance of the bony thorax, measurements of the fetal thoracic circumference (TC) (Table 13-1), and the relationship of the thoracic circumference to the abdominal circumference (AC) (the thoracic circumference/abdominal circumference ratio) (Fig. 13-5).<sup>15,16</sup> These measurements, of course, were only indirect assessments of fetal lung volume. Actual fetal lung size was initially estimated from two-dimensional (2D) ultrasound images. Measurements included lung area, lung circumference, and lung length/diameter.<sup>17-21</sup> Lung length has been established in a plane through the long axis of the thorax from the superior end of the sternum to the level of the diaphragm or the inferior surface of the heart<sup>16</sup> or from the apex to the base of the lung.<sup>19</sup> Others studied the ratio of lung area to head circumference (LHR),<sup>22</sup> lung length to thoracic circumference<sup>23</sup> and lung length multiplied by the width to head circumference,<sup>24</sup> particularly in cases of congenital diaphragmatic hernia (Fig. 13-6). From the data thus far, it appears that none of those biometric parameters is reliable enough to predict pulmonary hypoplasia with certainty. The introduction of 3D ultrasonography would allow for the assessment and correction of surface irregularities.<sup>25</sup> The more conventional 3D sonographic approach involves scrolling through one plane of the multiplanar display while delineating the lungs in a different plane. Alternatively, the VOCAL technique (Virtual Organ Computer-Aided Analysis, General Electric medical systems) allows volume calculations around a fixed axis through a number of sequential steps.<sup>26</sup> Whereas in an in vitro setting, rotational measurement of volume proved to be superior to the conventional technique,<sup>25</sup> in vivo study of fetal lung

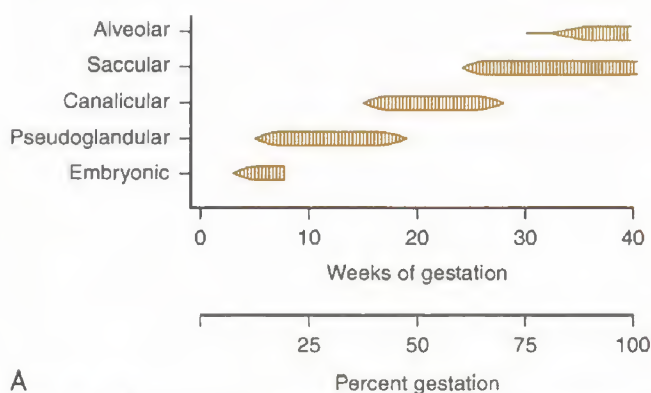


**FIGURE 13-2.** A. The five stages of normal fetal lung development. (From Pringle KC: *Human fetal lung development and related animal models*. Clin Obstet Gynecol 3:502, 1986.) Continued

## STAGES OF LUNG DEVELOPMENT

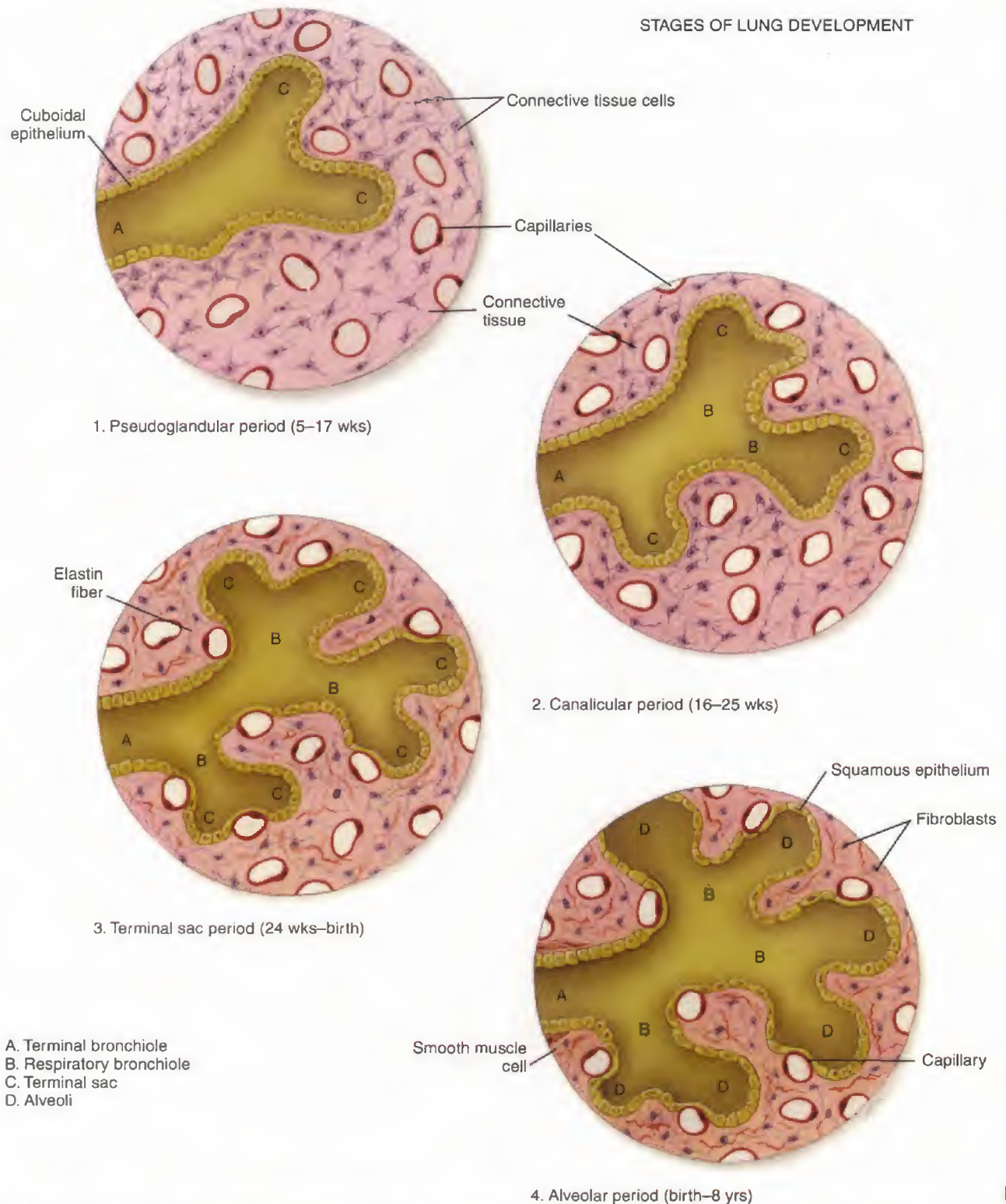


**FIGURE 13–2 cont'd.** B. Histologic sections illustrating progressive stages of lung development. 1. Pseudoglandular period (about 8 weeks). 2. Late canalicular period (about 24 weeks). 3. Early terminal sac period (about 26 weeks). 4. Newborn infant. Early alveolar period. Note that the alveolo-capillary membrane is thin and that some of the capillaries have begun to bulge into the primordial alveoli. (From Moore KL, Persaud TVN, Shiota K [eds]: *Color Atlas of Clinical Embryology*, 2nd ed. Philadelphia, WB Saunders Company, 2000.)

Continued



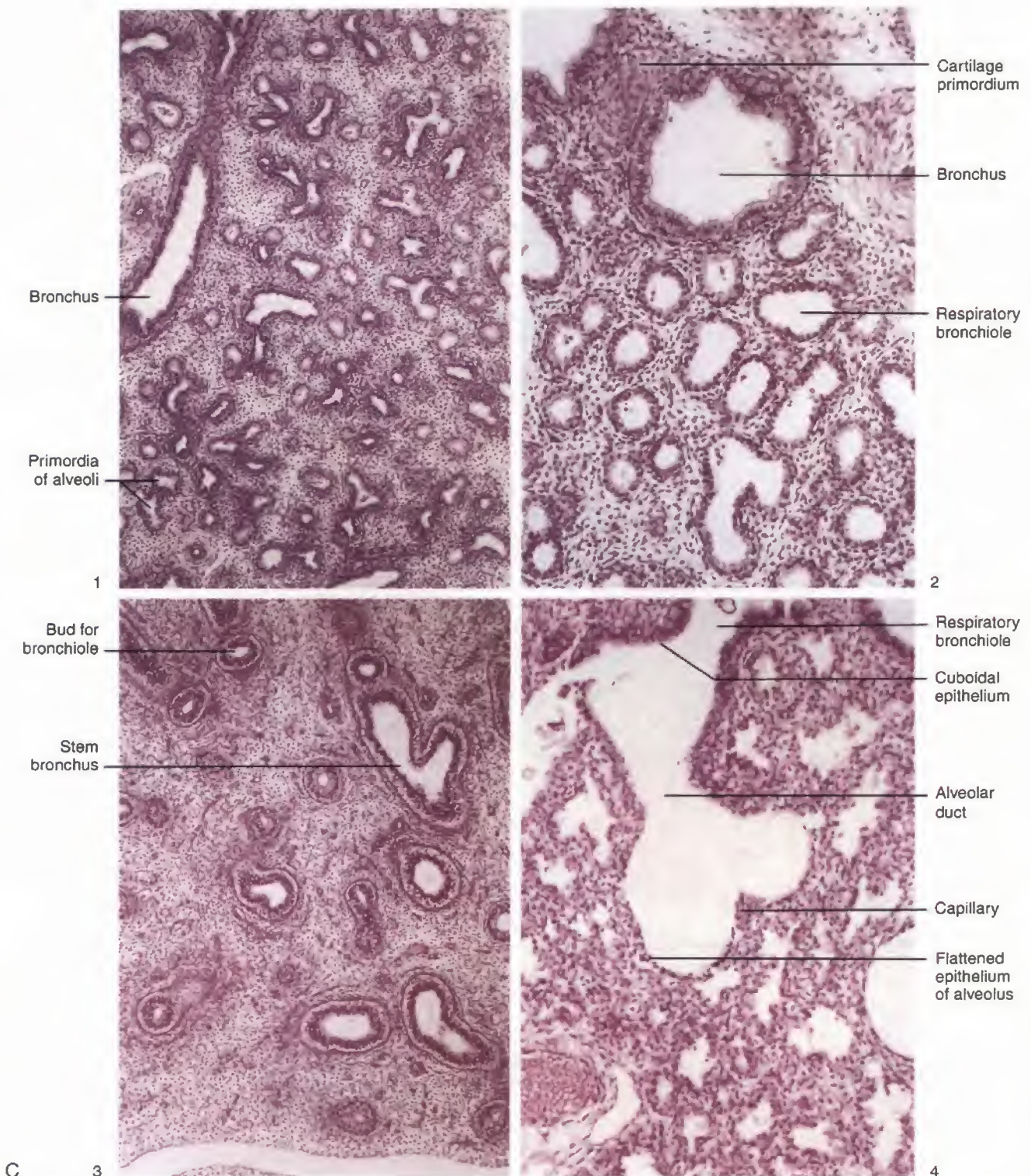


**FIGURE 13-2 cont'd.** C. Photomicrographs of sections of developing human lungs. 1. Pseudoglandular period, 8 weeks. Note the glandular appearance of the lung at this stage. 2. Canalicular period, 16 weeks. The lumina of the bronchi and terminal bronchioles are enlarging. 3. Canalicular period, 18 weeks. Note that many blood vessels are developing in the mesenchyme surrounding the sections of bronchi and terminal bronchioles. 4. Terminal sac period, 24 weeks. Observe the thin-walled terminal sacs (primitive alveoli) that have developed at the ends of the respiratory bronchioles. Also observe that the number of blood vessels has increased and that some of them are closely associated with the terminal sacs or primordial alveoli. (From Moore KL, Persaud TVN, Shiota K [eds]: *Color Atlas of Clinical Embryology*, 2nd ed. Philadelphia, WB Saunders Company, 2000.)



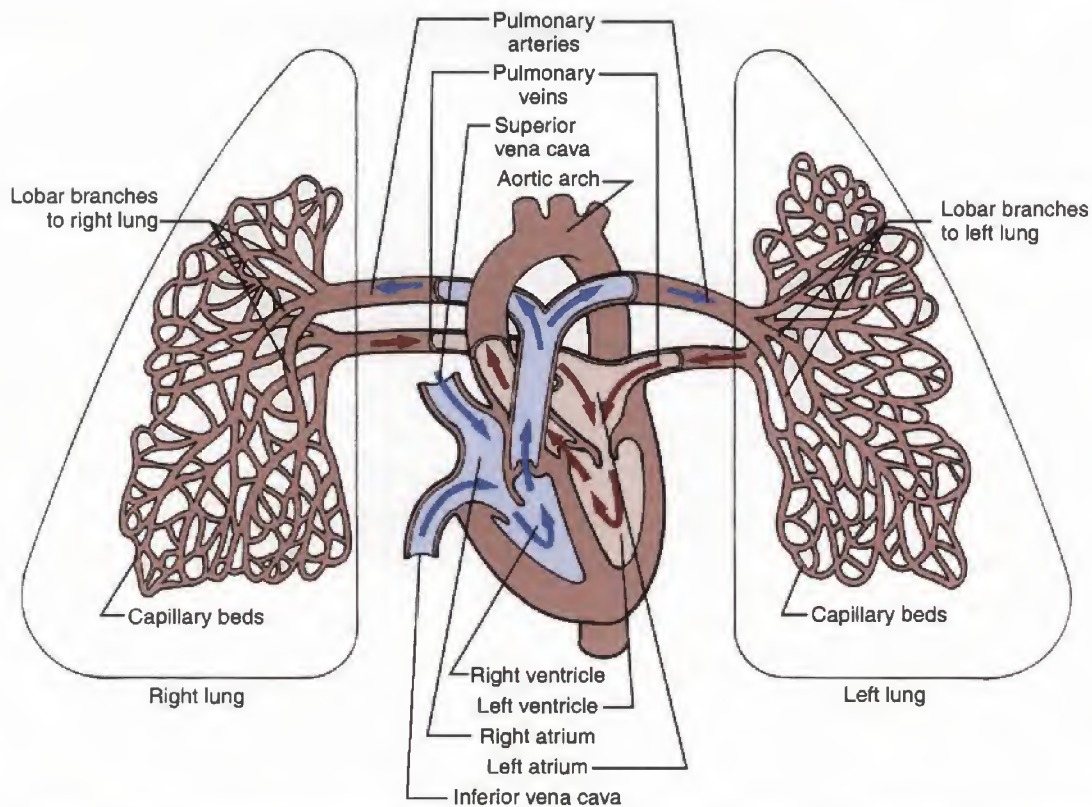


**FIGURE 13-3.** The pulmonary circulation. The right and left pulmonary veins and arteries and the branching capillaries are illustrated. (From Brashers VL: *Structure and function of the pulmonary system*. In McCance KL, Huether SE [eds]: *Pathophysiology: The Biologic Basis for Disease in Adults and Children*. St. Louis, Elsevier, Mosby, 2006.)



**FIGURE 13-4.** Color Doppler image of a transverse cross-section of normal fetal lungs at 27 weeks of gestation demonstrating the pulmonary artery (red) and vein (blue).

volume demonstrated that the rotational method with VOCAL was less reproducible than the common multiplanar technique.<sup>26</sup> On the other hand, Moeglin et al<sup>27</sup> found no statistically significant difference between lung volume values obtained using the two 3D sonographic ultrasound modes. Not only different 3D ultrasound techniques but also different methods for measuring fetal lung volume have been reported. For the most part in earlier work, fetal lung volume was obtained by subtracting fetal heart volume from thoracic volume.<sup>28</sup> The disadvantage of this approach is the inclusion of mediastinal structures (thymus, trachea, esophagus, and great vessels) in the measurement of lung volume. Accuracy may be improved by direct determination of fetal lung volume, including separate measurement of the left and right lungs.<sup>29,30</sup>

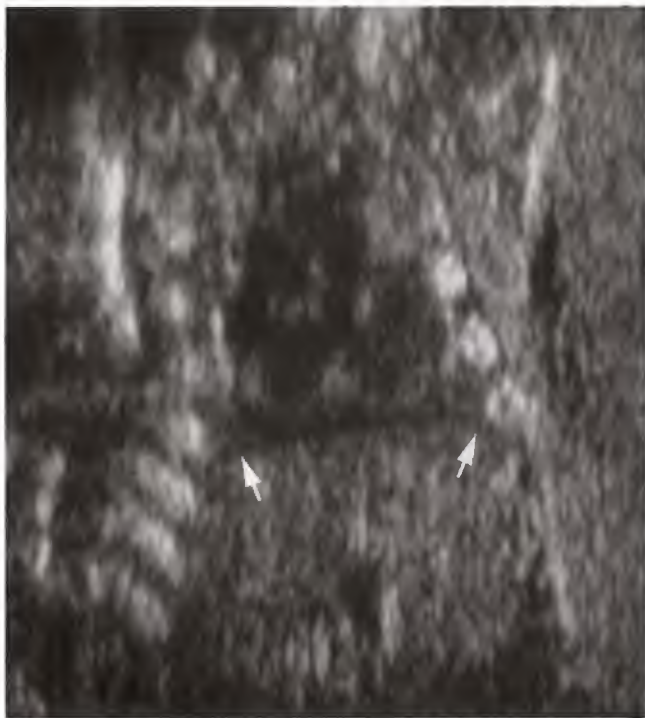
Most reports on direct lung volume measurement by 3D ultrasonography provide a definition of the upper and lower border, such as the level of the clavicle, and the dome of the diaphragm. This was the case in the study by Gerards<sup>29</sup> and was further highlighted by Peralta et al,<sup>31</sup> who also emphasize the importance of defining the medial border of the lungs and distinction from the heart and mediastinal organs as well as the lateral border of the lungs and distinction from the thoracic cage.



**Table 13-1** Fetal Thoracic Circumference Measurements\*

Gestational Age (wk)	No.	Predictive Percentiles								
		2.5	5	10	25	50	75	90	95	97.5
16	6	5.9	6.4	7.0	8.0	9.1	10.3	11.3	11.9	12.4
17	22	6.8	7.3	7.9	8.9	10.0	11.2	12.2	12.8	13.3
18	31	7.7	8.2	8.8	9.8	11.0	12.1	13.1	13.7	14.2
19	21	8.6	9.1	9.7	10.7	11.9	13.0	14.0	14.6	15.1
20	20	9.5	10.0	10.6	11.7	12.8	13.9	15.0	15.5	16.0
21	30	10.4	11.0	11.6	12.6	13.7	14.8	15.8	16.4	16.9
22	18	11.3	11.9	12.5	13.5	14.6	15.7	16.7	17.3	17.8
23	21	12.2	12.8	13.4	14.4	15.5	16.6	17.6	18.2	18.8
24	27	13.2	13.7	14.3	15.3	16.4	17.5	18.5	19.1	19.7
25	20	14.1	14.6	15.2	16.2	17.3	18.4	19.4	20.0	20.6
26	25	15.0	15.5	16.1	17.1	18.2	19.3	20.3	21.0	21.5
27	24	15.9	16.4	17.0	18.0	19.1	20.2	21.3	21.9	22.4
28	24	16.8	17.3	17.9	18.9	20.0	21.2	22.2	22.8	23.3
29	24	17.7	18.2	18.8	19.8	21.0	22.1	23.1	23.7	24.2
30	27	18.6	19.1	19.7	20.7	21.9	23.0	24.0	24.6	25.1
31	24	19.5	20.0	20.6	21.6	22.8	23.9	24.9	25.5	26.0
32	28	20.4	20.9	21.5	22.6	23.7	24.8	25.8	26.4	26.9
33	27	21.3	21.8	22.5	23.5	24.6	25.7	26.7	27.3	27.8
34	25	22.2	22.8	23.4	24.4	25.5	26.6	27.6	28.2	28.7
35	20	23.1	23.7	24.3	25.3	26.4	27.5	28.5	29.1	29.6
36	23	24.0	24.6	25.2	26.2	27.3	28.4	29.4	30.0	30.6
37	22	24.9	25.5	26.1	27.1	28.2	29.3	30.3	30.9	31.5
38	21	25.9	26.4	27.0	28.0	29.1	30.2	31.2	31.9	32.4
39	7	26.8	27.3	27.9	28.9	30.0	31.1	32.2	32.8	33.3
40	6	27.7	28.2	28.8	29.8	30.9	32.1	33.1	33.7	34.2

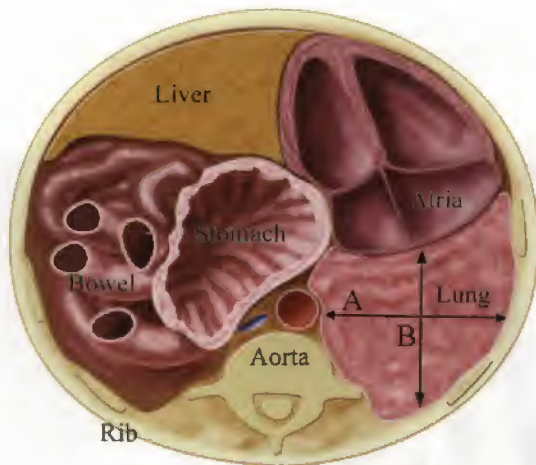
\*Measurements in centimeters.

From Chitkara U, Rosenberg J, Clivernek FA, et al: Prenatal sonographic assessment of the fetal thorax: Normal values. *Am J Obstet Gynecol* 156:1069, 1987.**FIGURE 13-5.** Coronal plane of section in a fetus with a severe skeletal dysplasia. Owing to marked shortening of the ribs and bony thorax, the lungs are markedly hypoplastic. The heart occupies much of the thorax (diaphragm, arrows).

In the past 6 to 7 years, there have been a number of interesting reports using MRI to image the lungs.<sup>32-34</sup> The development of the single-shot rapid-acquisition with relaxation enhancement sequence, a rapid spin-echo-based T2-weighted sequence, has been a major step forward in fetal MRI.<sup>32</sup> On MRI, the lungs are well depicted on T2-weighted images (Fig. 13-7).<sup>33,34</sup> Fast-spin echo T2-weighted MR images of the fetal thorax provide a well-defined contrast between the fetal parenchyma and surrounding structures, which include the trachea, esophagus, diaphragm, and thoracic wall structures.<sup>35</sup> Moreover, the MR signal intensity of the fetal lung is a good indicator of fetal lung maturation.<sup>36</sup> MRI has been shown to be helpful in determining ipsilateral lung volume in cases of congenital diaphragmatic hernia (Fig. 13-8).<sup>36</sup>

The question arises whether there is a preference for 3D ultrasonography or MRI for the determination of fetal lung volume development. 3D ultrasonography has the advantage of cost-effectiveness, ease and speed of use, and patient acceptability.<sup>30</sup> On the other hand, optimal 3D ultrasound resolution may not always be possible owing to fetal position, oligohydramnios, maternal obesity, fetal cardiac activity, and fetal (breathing) movements. The accurate delineation of the contour of the lung may be hampered because of reduced differentiation between fetal lung and liver.

The next question is whether these techniques will suffice in detecting lethal pulmonary hypoplasia. We know that prolonged and severe oligohydramnios, particularly during the canalicular phase of lung development, may cause a

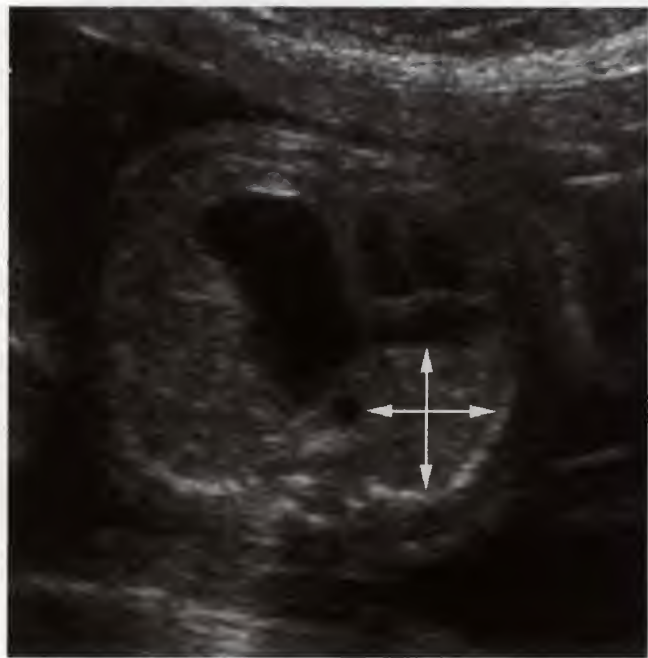


$$\frac{\text{LHR} = A \times B \text{ (mm)}}{\text{HC (mm)}}$$



A

Head Circumference



B

**FIGURE 13-6.** A. Diagrammatic illustration of the method for measuring the lung to head ratio (LHR) in a fetus with congenital diaphragmatic hernia. The measurement of the right lung (in the typical left congenital diaphragmatic hernia) uses a transverse axial plane of section of the fetal thorax at the level of the four-chamber view of the fetal heart. The plane of section should be symmetric so that a single rib is seen on each side. A measurement in millimeters (mm) is made from the thoracic aorta to the lateral inner chest wall (A). Another measurement, also in mm, is made in a plane perpendicular to the first measurement from the outer wall of the atrium to the inner aspect of the posterior chest wall (B). These two measurements are multiplied by one another and divided by the measurement of the head circumference also in mm. (From Roy A. Filly, MD, San Francisco, CA. Illustration by James A. Cooper, MD, San Diego, CA.) B. Transverse axial sonogram of a fetus with a left congenital diaphragmatic hernia. The two diameters (arrows) used in measuring the remaining area of the right lung are shown.



delay or even an arrest in pulmonary vascular development, resulting in reduced lung volume and raised pulmonary vascular resistance.<sup>37</sup> Doppler velocimetry of the fetal arterial lung circulation has shown that peak systolic velocity (PSV) in the proximal pulmonary artery flow velocity waveform is reduced in lethal lung hypoplasia (Fig. 13-9).<sup>38</sup>

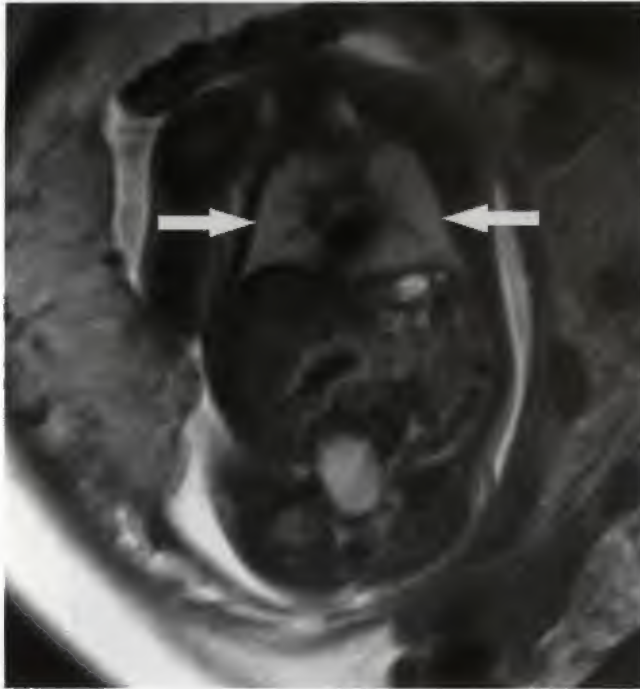


**FIGURE 13-7.** MRI obtained in 29-year-old pregnant woman at 30 weeks' gestation in whom detailed prenatal ultrasound depicted a normal fetal chest and fetal abdomen; MRI was performed because placenta accreta was suspected. Coronal single-shot rapid acquisition with relaxation enhancement (T2-weighted MR image 8/90, 4-mm section) of the fetal chest and fetal abdomen shows lungs (arrows) with high signal intensity. Use of this sequence facilitated easy identification of the lungs and planimetry. (From Williams G, Coakley FV, Qayyum A, et al: *Fetal relative lung volume: Quantification by using prenatal MR imaging lung volumetry*. *Radiology* 233:457, 2004.)

Nevertheless, as a single test it turned out not to be reliable enough for clinical application. A combination of clinical (onset, duration, degree of oligohydramnios), biometric (thoracic to abdominal ratio) and Doppler (PSV in proximal lung artery) parameters demonstrated a PPV of 100%, an overall accuracy of 93%, and a sensitivity of 71%.<sup>39</sup> Again, the clinical significance of this combined test is limited as a result of the restrictions in obtaining the necessary components of it and the low sensitivity of the combination. In another study, a raised pulsatility index (PI) in the arterial lung circulation was found in a substantial number of fetuses

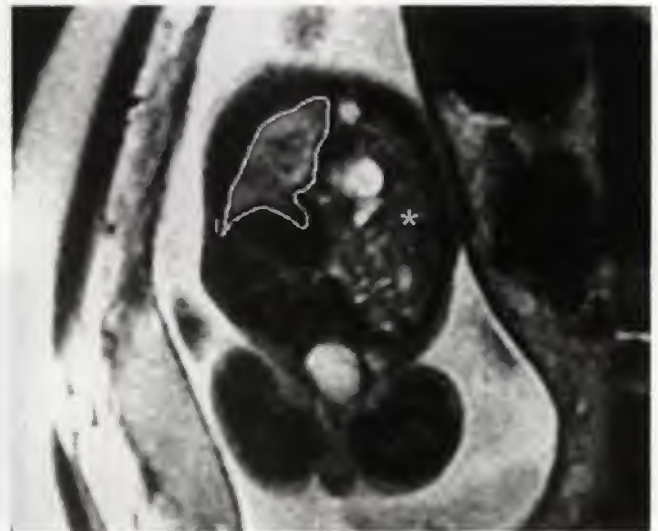


**FIGURE 13-8.** Twenty-six-year-old woman at 24 weeks' gestation. Detailed prenatal ultrasound demonstrated a left CDH. A coronal single-shot RARE T2-weighted (TR/TE = 4/90 msec) 4 mm section of the fetal chest illustrates the technique of lung planimetry. The lung edge has been traced to calculate the lung volume for the section. The right lung cross-sectional area is being measured. The left lung is not visible, and the left hemithorax contains herniated bowel and stomach (asterisk). (From Coakley FV, Lopoo JB, Lu Y, et al: *Normal and hypoplastic fetal lungs: Volumetric assessment with prenatal single-shot rapid acquisition with relaxation enhancement MR imaging*. *Radiology* 216:107, 2000.)

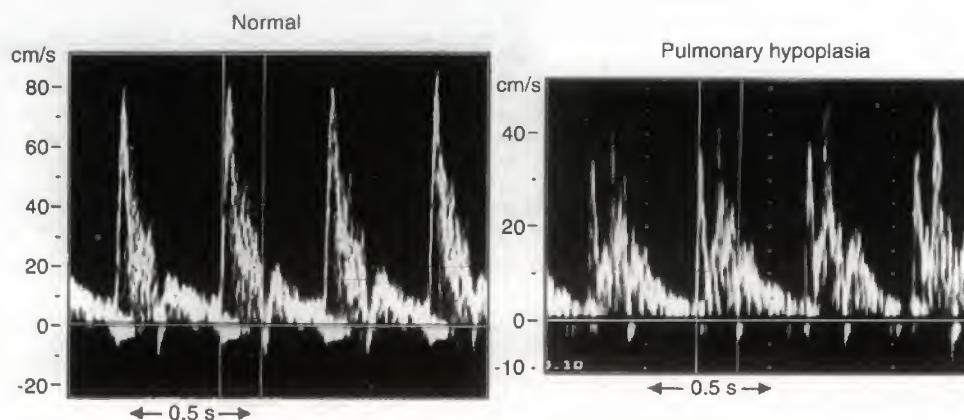


**FIGURE 13-9.** Fetal proximal pulmonary artery flow velocity waveform during normal lung development (left) and in lung hypoplasia (right) at 34 weeks of gestation. Note the reduced velocity and two-pronged nature of the latter waveform. (From Laudy JA, Gaillard JLJ, van der Anker JN, et al: *Doppler ultrasound imaging: A new technique to detect lung hypoplasia before birth? A case report*. *Ultrasound Obstet Gynecol* 7:189, 1996.)



that had developed lung hypoplasia.<sup>40</sup> Of interest is the nonreactivity of the flow pattern in the proximal pulmonary artery during exposure to maternal breathing, by mask, of 60% oxygenated air.<sup>41</sup> This test, with a PPV of 79%, a sensitivity of 92%, and a specificity of 82%, seems quite promising. A different approach was taken by Fuke et al,<sup>42</sup> who found the acceleration time/ejection time ratio in the fetal-pulmonary arterial flow velocity waveform to be reduced in the presence of lung hypoplasia. Whether 3D ultrasound, MRI, and Doppler ultrasound will ultimately produce a test that is clinically applicable and reliable, is as yet unclear.

## CONGENITAL CYSTIC ADENOMATOID MALFORMATION

CCAM of the lung is a benign hamartomatous or dysplastic tumor characterized by overgrowth of terminal bronchioles with a reduction in number of alveoli.<sup>43</sup> These malformations are rare, with an incidence of 1 in 5000 live births.<sup>44</sup> CCAM develops during the pseudoglandular period (7–16 weeks), that is characterized by expansion of the conducting airways and peripheral lung tubules that branch and form buds resulting in acinar tubules. Vascularization of peripheral lung mesenchyme as well as closure of the pleural and peritoneal cavity takes place.<sup>45</sup> The cystic components of CCAM are lined by respiratory epithelium. There is usually communication with the normal tracheobronchial tree and vascularization from the pulmonary artery.<sup>46</sup> A possible gene interaction (*HOX B-5*; *FGF-7*; *PDGFB* gene) with CCAM has been suggested.<sup>47–49</sup> CCAM is usually unilateral and lobar. In the late 1970s, Stocker et al<sup>12</sup> classified the more common types of CCAM into three categories: type 1, in which there is a large or predominant cyst (3 to 10 cm in diameter), compressing the normal parenchyma; type 2, composed of multiple cysts (0.5 to 2.0 cm in diameter) evenly distributed and blending with the adjacent normal parenchyma; and type 3, the small cystic or solid type. More recently, two additional subtypes of CCAM have been added to the classification; type 0, also known as acinar dysplasia, or agenesis with tissue that consists of bronchus-like structures and type IV consisting of a large peripheral cyst of the distal acinus lined predominantly with alveolar type cells. With this classification, Stocker<sup>12</sup> proposed that the designation of CCAM be changed to congenital pulmonary airway malformation (CPAM), owing to the fact that only three of the five types were cystic and only one type (type 3) adenomatoid. Adzick<sup>50</sup> proposed a prenatal classification of CCAM, based on ultrasound. In this classification, CCAM was either macrocystic or microcystic. Macrocystic lesions contain single or multiple cysts that are 5 mm or more in diameter and, therefore, are discernable on ultrasound; the prognosis is often more favorable (Fig. 13–10). Microcystic lesions appear as a solid hyperechogenic mass based on numerous acoustic interfaces (Fig. 13–11). Depending on the size of these lesions, esophageal compression may occur, resulting in reduced fetal swallowing and subsequent polyhydramnios. On prenatal MRI, microcystic lesions present as hyperintense and homogeneous T2-weighted images compared with normal lungs.<sup>51</sup> Macrocysts can be demonstrated on MRI.<sup>52</sup> Changes in thoracic position of other lung lobes, mediastinum, and cardiac structures must be identified.<sup>53</sup> Power Doppler sonog-

raphy allows evaluation of the vascular supply of these lesions.<sup>46</sup> The natural history of CCAM is unpredictable in that it may grow or regress. The latter occurs in about 15% of cases and may be due to decompression into the tracheobronchial tree, outgrowth of blood supply or torsion around the vascular pedicle with infarction.<sup>54,55</sup> On the other hand, development of fetal hydrops must be considered as a sign of impending fetal death (Fig. 13–12).

Quantification of CCAM can be achieved through measuring tumor volume and dividing this volume by head

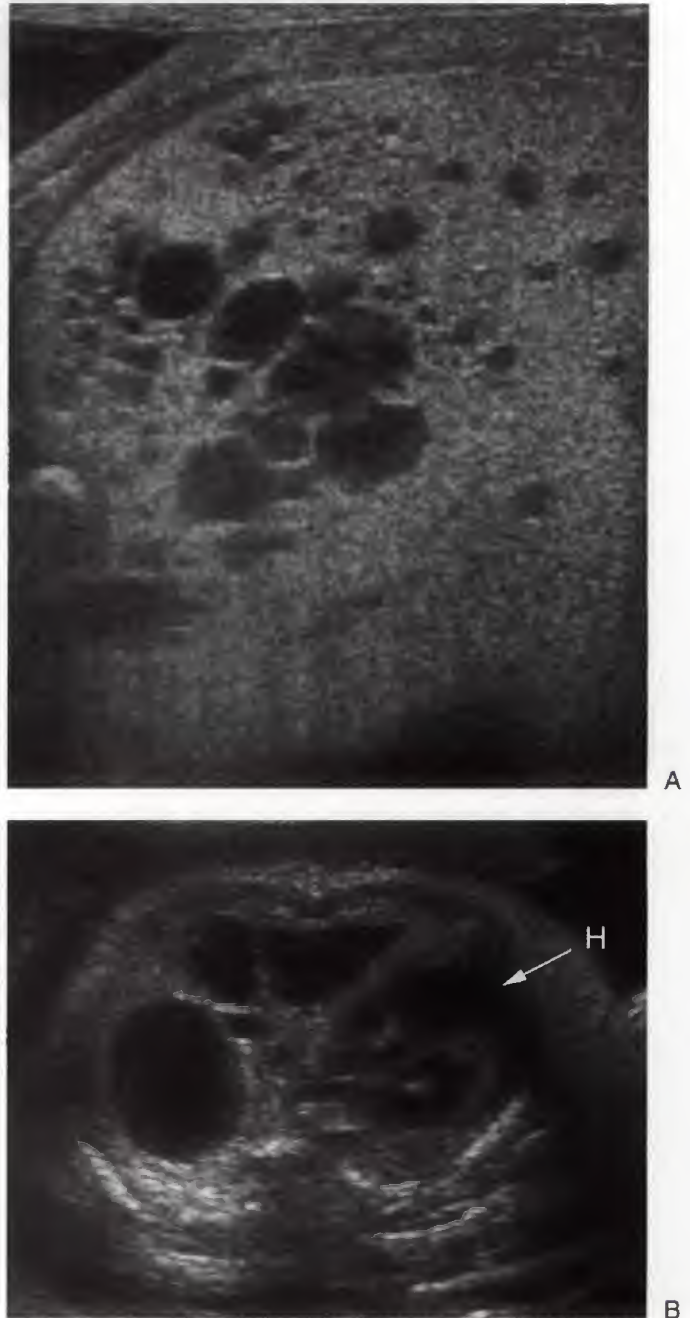


**FIGURE 13–10.** Macrocystic CCAM. A. Macrocystic CCAM with small to moderate sized cysts. Surrounding hyperechogenic tissue characteristic of microcystic CCAM is also seen. B. Macrocystic CCAM with three large cysts adjacent to the heart (H).



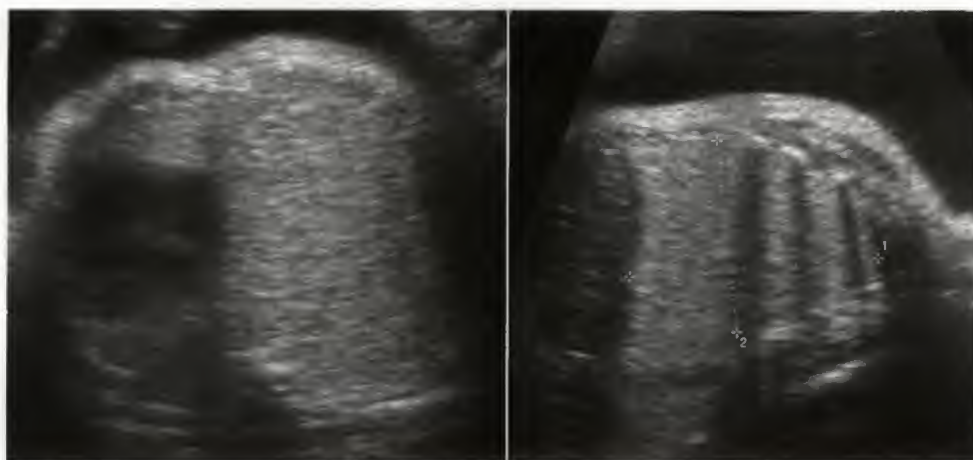


**FIGURE 13-11.** Microcystic adenomatoid malformation of the fetal lungs at 30 weeks of gestation on a transverse (*left*) and longitudinal (*right*) cross-section.



**FIGURE 13-12.** Microcystic adenomatoid malformation of the lung with fetal hydrops (ascites, *arrows*).

circumference to standardize for gestational age.<sup>56</sup> Most cases of prenatally diagnosed CCAM have a good outcome.<sup>57,58</sup> In cases of a large macrocystic CCAM that causes displacement of surrounding thoracic organs, prenatal treatment can be considered by means of cyst aspiration or thoraco-amniotic shunting.<sup>43,59</sup> The latter will be more effective and prevent fluid accumulation. These procedures should be considered before 32 to 33 weeks of gestation, and delivery should be contemplated beyond this gestational age. Microcystic CCAM is not amenable to shunting, but in the presence of fetal hydrops has been treated by means of open fetal surgery providing there were no other abnormalities or abnormal karyotype.<sup>50</sup> Recently, it has been noted that prenatal steroids may help in the resolution of hydrops fetalis in fetuses with CCAM. The prognosis of the various forms of CCAM are often dictated more by the mass effect on adjacent structures (heart, great vessels) rather than the specific type. It should be noted that histological changes of

CCAM and BPS (see later in this chapter) can occur within the same lesion (sometimes referred to as a hybrid lesion). When CCAM is found within a BPS, it is most often histological Type 2.<sup>60</sup>

CCAM should be differentiated from other lung lesions such as (1) congenital lobar emphysema characterised by lobar over-inflation without destruction of the alveolar septae<sup>61</sup> and (2) bronchopulmonary sequestration.

## BRONCHOPULMONARY SEQUESTRATION

BPS represents masses of nonfunctioning lung tissue that do not have a connection to the normal tracheobronchial tree and are supplied by an anomalous systemic artery and usually situated in the lower lobes.<sup>50</sup> Bronchopulmonary sequestrations are rare and are encountered in approximately 1.1% to 1.8% of all pulmonary resections.<sup>62</sup> They are categorized as intralobar and extralobar. In both instances, arterial blood supply is from the systemic circulation (aortic branch) and venous drainage is either by means of the pulmonary veins (intralobar) or by means of the systemic veins (extralobar).<sup>46</sup> Intralobar BPS accounts for 75% of all pulmonary sequestrations.<sup>63</sup> The intralobar variety consists of an abnormal segment of lung tissue that shares the visceral pleural covering of the normal lung. Intralobar BPS has only rarely been reported prenatally. Extralobar BPS consists of a discrete accessory lobe of the lung with its own pleural covering.<sup>63</sup>

They are typically found in the thorax and on the left side (65% to 90%) of cases.<sup>62,64-66</sup> Extralobar BPS may also be found in the mediastinum or pericardium.<sup>62</sup> Approximately 10% to 15% of extralobar sequestrations are found within or below the diaphragm.<sup>64,67</sup> The arterial supply is systemic from an anomalous artery arising from the thoracic or abdominal aorta.<sup>63</sup> The venous drainage is usually systemic through the azygous, hemiazygous veins, or the superior vena cava.<sup>62,63</sup> Extralobar sequestration occurs more frequently in males than females with a 4:1 ratio. Extralobar bronchopulmonary sequestration is associated with other fetal anomalies in approximately two thirds of cases, notably congenital diaphragmatic hernia, and foregut abnor-



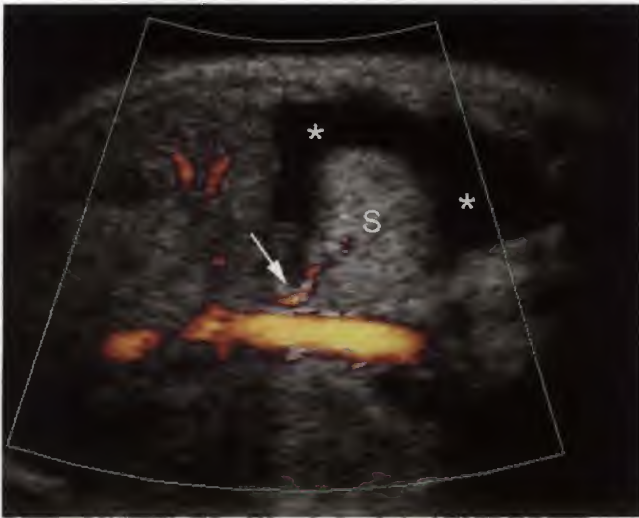


**FIGURE 13-13.** Fetal bronchopulmonary sequestration (S) with supplying vessel (arrow) at 34 weeks' gestation. Pleural effusion (asterisk).

malities.<sup>64,68</sup> The prognosis of BPS generally is good; pleural effusions and subsequently fetal hydrops may develop in a small percentage of affected fetuses.

On ultrasound examination BPS appears as a well-defined, solid, and triangular mass,<sup>53</sup> although cystic areas may be seen. Therefore, it is not surprising that BPS may mimic CCAM and vice versa. A diagnosis of BPS becomes more likely in the presence of a systemic vascular supply as established by 2D color or 2D power Doppler and/or unilateral pleural effusion (Fig. 13-13). As in CCAM, MRI has demonstrated to be helpful in the diagnosis of BPS. On T2-weighted images, there is a wedge-shaped area of very high and homogeneous signal intensity (Fig. 13-14).<sup>69</sup> In contrast to CCAM, a considerable number (approximately 68%) of BPS lesions regress dramatically before birth.<sup>50</sup> Obstetric management consists of careful monitoring in the majority of cases. Early delivery may be contemplated after 32 to 33 weeks of gestation. In earlier stages, intervention by means of thoracocentesis or thoracoamniotic shunting can be considered in the presence of associated pleural effusions and fetal hydrops. Subdiaphragmatic extralobar bronchopulmonary sequestrations may simulate adrenal or renal masses, from which they should be distinguished (Fig. 13-15).

### CONGENITAL HIGH AIRWAY OBSTRUCTION (LARYNGEAL ATRESIA)

Congenital high airway obstruction syndrome (CHAOS) was defined by Hedrick et al<sup>70</sup> in 1994 as upper airway obstruction that is diagnosed in utero by ultrasound, with concomitant findings of large hyperechogenic lungs, flattened or inverted diaphragms, dilated airways distal to the obstruction, and fetal ascites or hydrops (Fig. 13-16).<sup>70,71</sup>

Complete or near-complete obstruction of the upper airway in utero results in obstructed flow of fetal lung fluid and elevated intratracheal pressure, distension of the tracheobronchial tree, and lung expansion leading to tracheobronchomalacia, respiratory distress syndrome, and

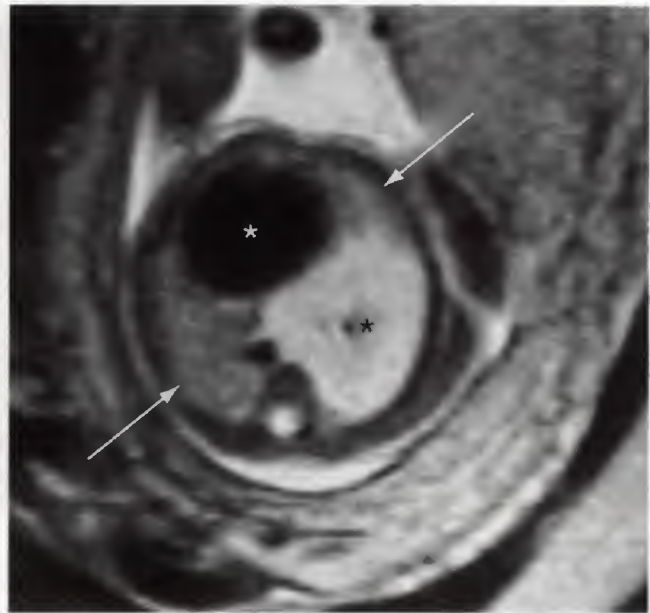


**FIGURE 13-14.** Prenatal magnetic resonance imaging (MRI) appearances of typical extralobar sequestration in fetus at 22 weeks' gestation. Axial T2-weighted single-shot rapid acquisition with relaxation enhancement (RARE) MRI (TR/effective TE, infinite/100) of fetal chest. Sequestration (black asterisk) is visible as large left-sided triangular mass of increased signal intensity, relative to displaced and compressed normal lungs (arrows). Lungs and heart (white asterisk) are displaced to right. (From Dhingra R, Coakley FV, Albanese CT, et al: Prenatal sonography and MR imaging of pulmonary sequestration. *Am J Roentgenol* 180:433, 2003.)

capillary leak of unknown mechanism.<sup>72</sup> The markedly enlarged lungs cause cardiac and caval compression and in utero heart failure as manifested by ascites, hydrops, and placentomegaly. The cause of CHAOS varies and is most commonly caused by laryngeal atresia, subglottic stenosis, or a laryngeal web.<sup>72</sup>

Since 1989, when the first prenatal diagnosis was reported, upper airway obstruction has been reported with increasing frequency.<sup>73,74</sup> It can be an isolated finding or can be present as part of Fraser syndrome, which includes tracheal or laryngeal atresia, renal agenesis, microphthalmia, cryptophthalmos and polydactyly, or syndactyly. The detection of this syndrome is important because it has autosomal-recessive inheritance.<sup>66,74,75</sup>

The sonographic findings include bilateral and uniform hyperechogenicity of the fetal lungs, as well as ascites.<sup>74</sup> The hyperechogenicity is caused by the overdistention of the alveoli by lung fluid, whereas ascites is the result of the compression of the right atrium and great veins by hyperplastic lungs. It has been proposed that the overdistention of the air spaces with lung liquid promotes alveolar proliferation by redistribution of cells.<sup>76</sup> Although polyhydramnios represents a common additional finding, it is thought to be a late event during the natural history of the upper respiratory atresia.<sup>74,77</sup>

Figure 13-17 summarizes the pathophysiologic mechanisms, as well as the ultrasonographic findings of upper respiratory atresia sequence.<sup>74</sup> The differential diagnosis includes bilateral CCAM, type 3.



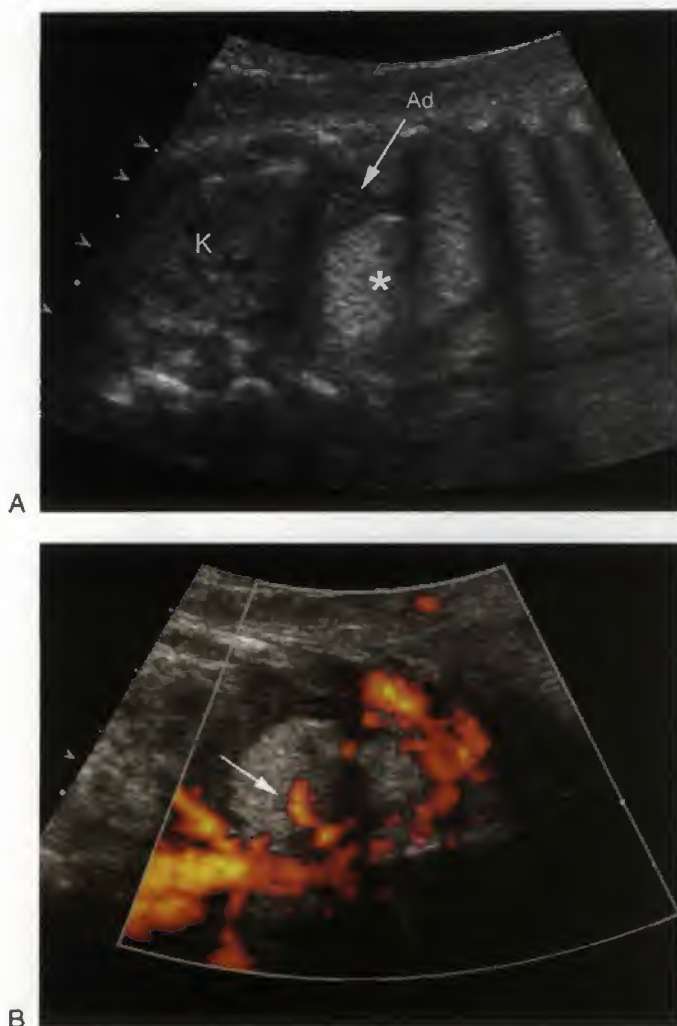


**FIGURE 13-15.** Subdiaphragmatic extralobar bronchopulmonary sequestration. *A.* Longitudinal plane of section in fetus with a subdiaphragmatic mass (asterisk). This lesion is clearly separate from the adjacent adrenal gland (Ad) and the kidney (K) and proved to be a subdiaphragmatic extralobar bronchopulmonary sequestration. *B.* Color Doppler image from the same patient demonstrating the systemic arterial blood supply (arrow) to this lesion from the aorta.

## OTHER LUNG ABNORMALITIES

Other lung lesions include congenital lobar inflation (congenital lobar emphysema), bronchogenic cysts, and neurenteric cysts. Congenital lobar emphysema is characterized by progressive hyperexpansion of the lung parenchyma in a segment or lobe of the lung owing to obstruction of the supplying bronchus.<sup>78,79</sup> The right middle and upper lobes are most commonly affected.<sup>80</sup> Prenatally, congenital lobar emphysema has been described as a uniformly echogenic lesion with associated mass effect. A prenatal diagnosis has, however, been rare, probably owing to the fact that cellular and fluid composition of the affected lobe is very similar to normal lung upon ultrasound examination.<sup>80</sup>

Bronchogenic cysts (Fig. 13-18) develop from abnormal budding of the ventricular diverticulum of the foregut



**FIGURE 13-16.** Coronal sonogram in a fetus with laryngeal atresia. Bilaterally enlarged hyperechogenic lungs are seen. Dilated fluid filled bronchi (arrows) and ascites (asterisks) are seen as well. Li, liver.

resulting in focal cystic duplication of the tracheobronchial tree.<sup>80</sup> They may present as single or, less commonly, as multiple lesions.<sup>81</sup> The dimensions of bronchogenic cysts vary from a few millimeters to greater than 5 cm.<sup>81</sup> The walls of the cysts contain fibrous tissue and small amounts of cartilage, and the content of the cysts may be watery or viscid.

Neurenteric cysts are posterior enteric remnants that result from incomplete separation of the notochord from the foregut in the third to fourth weeks of embryogenesis.<sup>82-84</sup> The presumed cause of the incomplete separation is a persistent communication or adhesion between the ectoderm of the spinal cord and the endoderm of the foregut before neural tube closure. Approximately 90% of neurenteric cysts occur in the right posterior mediastinum, superior to the carina, and about 50% are associated with vertebral abnormalities such as scoliosis, hemivertebra, and butterfly vertebrae.<sup>82,84,85</sup> These cysts may be unilocular, however, they often have an internal septation (Fig. 13-19). Mediastinal neurenteric cysts may displace and compress adjacent lungs, airways, the heart and great vessels, and those with coexistent intraspinal lesions may have signs and symptoms of central nervous system (CNS) abnormalities. The outcome depends mostly on the extent of displacement and functional impairment of the adjacent organs, and on the associated CNS defects. These cysts may cause pulmonary hypoplasia and severe postnatal respiratory distress requiring prolonged ventilatory support.<sup>85,86</sup> The cyst size does not seem to be directly related to prognosis. The differential diagnosis for a large cyst within the thorax is predominantly a CCAM of the lung. Other possibilities include bronchopulmonary sequestration, bronchogenic cyst, congenital diaphragmatic hernia, and teratoma.<sup>87</sup> The association with vertebral abnormalities makes the diagnosis of a neurenteric cyst almost certain.

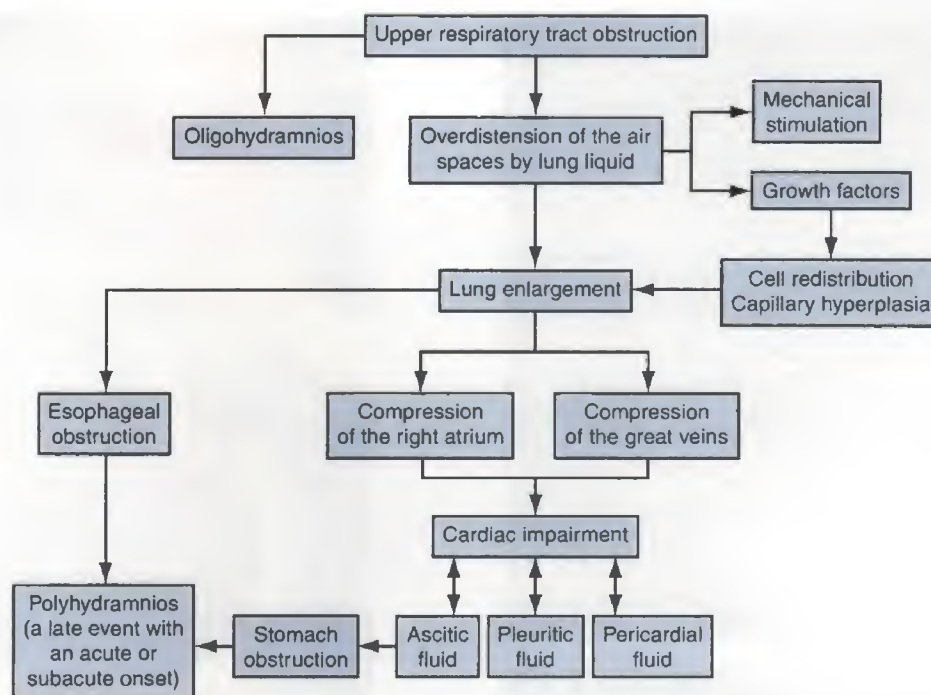


**FIGURE 13-17.** The pathophysiological mechanisms, as well as the ultrasonographic findings of upper respiratory atresia sequence. (From Kassanos D, Christodoulou CN, Agapitos E, et al: Prenatal ultrasonographic detection of the tracheal atresia sequence. *Ultrasound Obstet Gynecol* 10:133, 1997.)

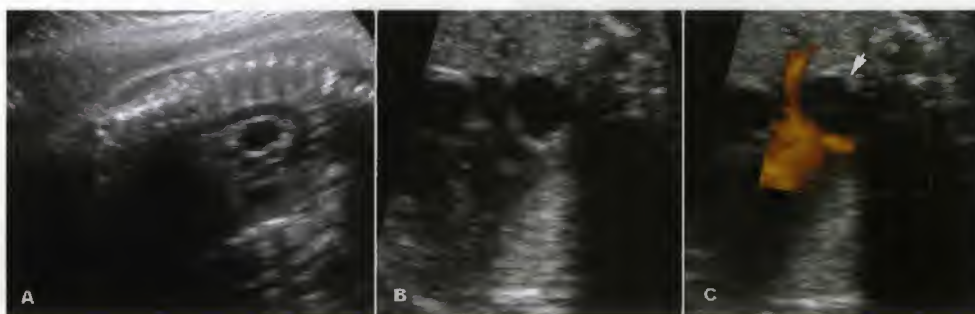


**FIGURE 13-18.** Bronchogenic cyst (arrow) in a longitudinal (A) and transverse (B) cross-section and in a transverse cross-section with color flow (C) at 28 weeks of gestation.

## THE FETAL DIAPHRAGM

### Normal Development

The diaphragm can be described as a dome-shaped musculo-tendinous septum between the thoracic and abdominal cavity consisting of a central aponeurotic segment and a peripheral muscular part. The embryologic development ends around the 8th week of conception. The development consists of the fusion of four different components, that is, ventrally from the septum transversum (mesoderm), which fuses with the pleuroperitoneal membranes, with the dorsal foregut mesentery, and laterally with muscular components of the thoracic wall. The normal diaphragm allows the

passage of organs, vessels, and nerves from the thoracic into the abdominal cavity. The normal diaphragm can be observed directly as a smooth hypoechoic line between the lungs and the liver or spleen.

### CONGENITAL DIAPHRAGMATIC HERNIA

Congenital diaphragmatic hernia occurs in approximately 1 of 2200 live births and is associated with a high degree of morbidity and mortality.<sup>88</sup> Congenital diaphragmatic hernia is characterized by protrusion of abdominal viscera into the thoracic cavity through a diaphragmatic defect (Fig. 13-20). Consequently, lung development may be impaired and may



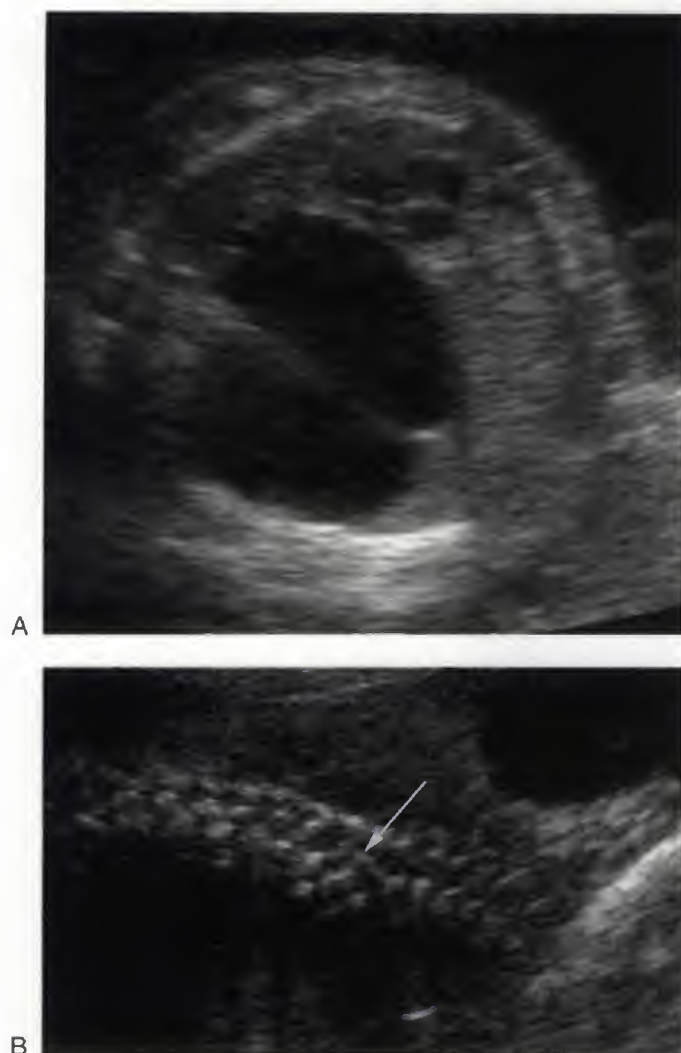


**FIGURE 13-19.** A. Transverse axial sonogram in a 28-week-gestation fetus with a neurenteric cyst. A septated cyst is seen in the right hemithorax. B. Abnormal thoracic vertebrae (arrow) are seen at the same site as the cyst.

even result in pulmonary hypoplasia. It is hypothesized that the cause of diaphragmatic hernia is a result of a primary diaphragmatic defect with secondary migration of abdominal organs into the thoracic cavity or a delayed fusion of the four diaphragmatic components. Almost all hernias occur through the posterolaterally located Bochdalek foramina, which characteristically involves the left side (75%). Foramen of Morgagni hernias occur in the anteromedial retrosternal part of the diaphragm as a result of maldevelopment of the septum transversum. In more than one half of the cases of congenital diaphragmatic hernia, associated structural or chromosomal abnormalities have been found.<sup>89</sup> Polyhydramnios, which is thought to result from gastrointestinal obstruction, is common and is frequently the indication for initial ultrasound examination.<sup>90</sup> The differential diagnosis of fetal diaphragmatic hernia includes cystic adenomatoid malformation of the lung, bronchogenic cysts, and bronchopulmonary sequestration. Congenital heart disease constitutes the majority of associated anomalies. The incidence of an

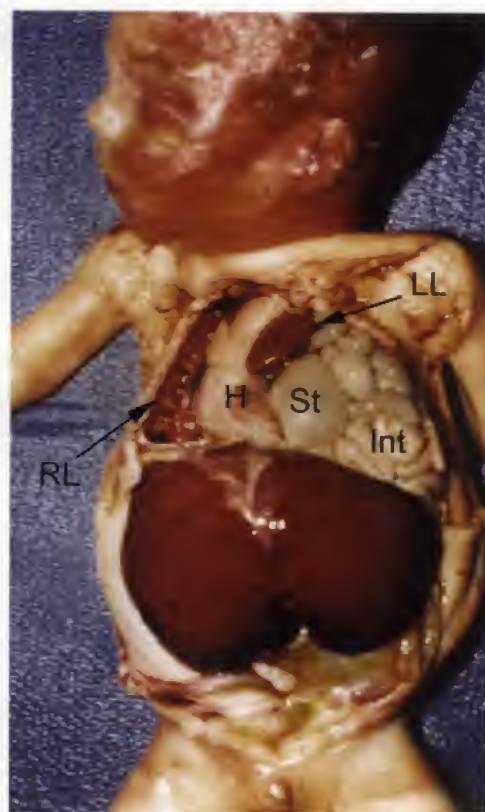


**FIGURE 13-20.** Postmortem photograph of a fetus with a left-sided congenital diaphragmatic hernia. The left lung (LL) is compressed by the large volume of herniated viscera, including the stomach (St) and intestine (Int). Note the compression of the right lung (RL) as well. In this fetus, the liver was not herniated into the chest. H, heart.

abnormal karyotype is approximately 10% but may rise to 20% when only fetuses with multiple anomalies were included. Polyhydramnios occurs in about 75%.<sup>91</sup> A systematic review of 35 studies reporting data for congenital diaphragmatic hernia between 1985 and 1998 showed a median overall mortality rate of 58% for infants diagnosed in utero, 48% if born alive, and 33% postoperatively.<sup>92</sup> The most significant cause of mortality in infants with congenital diaphragmatic hernia is not pulmonary hypertension but iatrogenic injury to their hypoplastic lungs.<sup>93</sup>

The most typical sonographic features of a left congenital diaphragmatic hernia are absence of the fluid-filled stomach in its normal position in the abdomen, displacement of the heart across the mediastinum to the right side, bowel and liver in the left chest, inability to identify the left lung, and presence of the fluid filled stomach adjacent to the heart (Fig. 13-21). Most frequently, the left lobe of the liver herniates, to varying degrees, into the left hemithorax. The position of the stomach is often a clue to the degree of liver herniation. A more anteriorly positioned stomach often means there is little liver herniation, whereas a posteriorly positioned liver often means a large degree of liver herniation. The liver herniation can best be appreciated on coronal planes of section. The position of the portal vein and left hepatic veins make identification of the left lobe of the



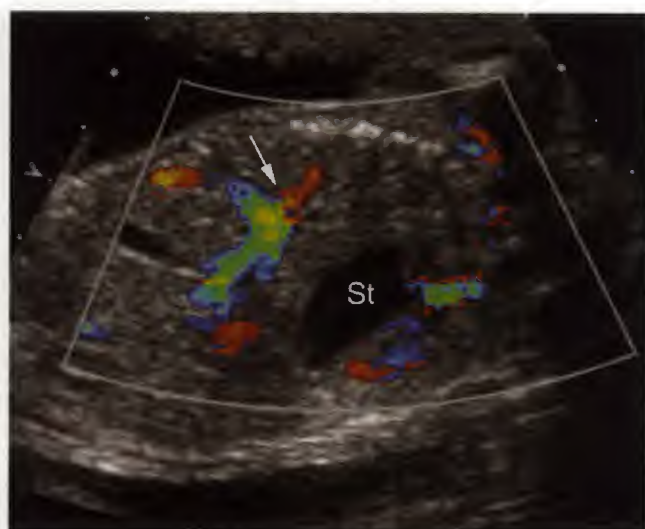


**FIGURE 13-21.** Transverse axial sonogram in a fetus with a left congenital diaphragmatic hernia. The heart (H) is displaced to the right. The left lung was not visible, however, the compressed right lung (RL) was seen. Herniated liver (Li) is seen as a triangle of soft tissue anterior to the stomach (St) and adjacent to the heart. Bo, bowel.

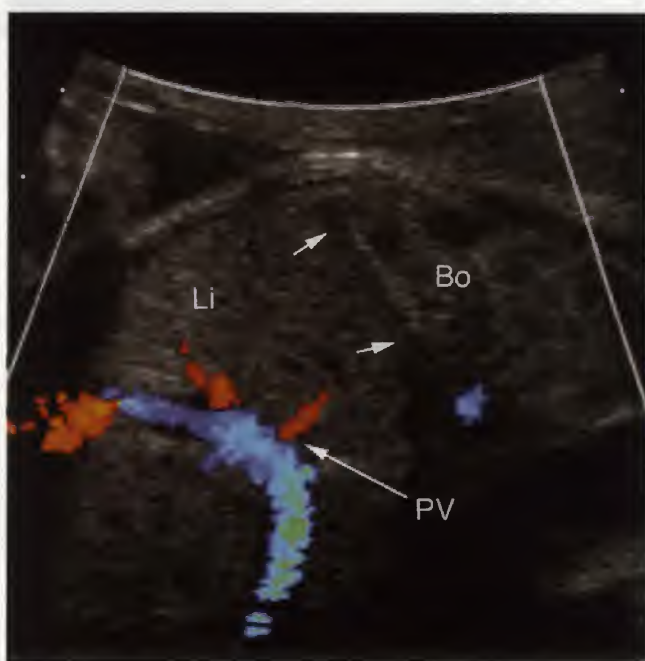
liver more certain (Fig. 13-22). It should be remembered that a diaphragmatic hernia does not imply complete absence of the diaphragm. As such, a ridge of remaining left diaphragm may be seen on various planes of section (Fig. 13-23). Right-sided diaphragmatic hernias are less common and may be more difficult to diagnose. The echogenicity of the herniated liver may simulate the echogenicity of the normal lung. Observation of the fetal gallbladder or portal vessels will allow one to make the correct diagnosis.

Various biometric parameters have been proposed for the prediction of fetal outcome in the presence of diaphragmatic hernia such as fetal pulmonary artery size,<sup>65</sup> fetal lung diameter,<sup>22</sup> and lung diameter/thoracic circumference ratio.<sup>23</sup> Currently, the most widely used method for the antenatal prediction of outcome is the LHR ratio (see Fig. 13-6).<sup>22,94</sup> Recently, a significant association between LHR and lung volume was established, validating the use of LHR in the assessment of fetal lung growth.<sup>95</sup> In another study, however, the percentage of liver that herniated into the chest, and not fetal lung size, correlated with outcome in fetuses with congenital diaphragmatic.<sup>96</sup> A correlation has been found between lung volume as determined by MRI and ultrasound determined LHR in fetuses with isolated left congenital diaphragmatic hernia following adjustment for gestational age and birth weight.<sup>36</sup> MRI has been demonstrated to be more sensitive than ultrasound for detecting thoracic herniation (Fig. 13-24).<sup>97</sup> MRI appears to be most helpful in evaluation of right diaphragmatic hernia because it usually contains liver and bowel.<sup>52</sup> Until recently, the only options available to couples with a fetus diagnosed with congenital diaphragmatic hernia was termination of pregnancy or to await outcome at the time of delivery.

An alternative approach was open surgery with the risk of premature labor and premature rupture of the membranes.<sup>98</sup> Lately, a novel approach of minimal access fetal surgery



A



B

**FIGURE 13-22.** A. Left congenital diaphragmatic hernia with herniation of stomach (St) bowel and liver into the left hemithorax. Identification of the portal vein (arrow) extending into the thorax confirms that part of the liver has herniated. B. Left congenital diaphragmatic hernia in which only intestine (Bo) and stomach have herniated into the left chest. The normal position of the portal vein (arrow) below the diaphragm (arrows) confirms the absence of liver (Li) herniation.

is being explored. Using a fetoscope, videoscopic tracheal intubation is carried out. The current strategy is the placement of an intratracheal detachable balloon to facilitate tracheal occlusion with the objective to induce lung growth. The balloon can be removed in later gestation using a similar technique or by ultrasound guided puncture.<sup>71,95</sup>

## CONGENITAL HYDROTHORAX

Congenital fetal hydrothorax or pleural effusions may be associated with generalized edema and ascites or may occur





**FIGURE 13-23.** Left congenital diaphragmatic hernia with liver (Li) herniation into the left hemithorax. The liver can be seen extending superiorly above the ridge of remaining diaphragm (arrows). St, stomach.



**FIGURE 13-24.** Left congenital diaphragmatic hernia at 26 weeks' gestation, with partial upward herniation of liver into left hemithorax ("liver-up" congenital diaphragmatic hernia). Coronal T1-weighted spoiled gradient-echo magnetic resonance imaging scan (TR/TE, 140/4.2; flip angle, 700) shows upward herniation of left hepatic lobe (arrow). (From Leung JWW, Coakley FV, Hricak H, et al: Prenatal MRI of congenital diaphragmatic hernia. *AJR Am J Roentgenol* 174:1607, 2000.)



**FIGURE 13-25.** Longitudinal cross-section of bilateral fetal hydrothorax at 36 weeks of gestation. Note the clear contour of the left and right fetal lung.

in isolation (Fig. 13-25). In both instances, fetal lung compression, and when prolonged, lung hypoplasia may develop, leading to severe respiratory problems in the neonatal period. The incidence of congenital fetal hydrothorax is estimated at approximately 1 in 15,000 pregnancies. Fluid accumulation can be unilateral or bilateral. Chylothorax is the most common cause of congenital hydrothorax. A mortality rate of more than 50% has been reported.<sup>99</sup> Lesions associated with pleural effusions include CCAM, BPS, congenital diaphragmatic hernia, congenital heart disease, cystic hygroma, and infection. Depending on the degree of fluid accumulation, mediastinal compression occurs with reduced fetal swallowing, resulting in polyhydramnios and risk of premature labor. Insertion of a thoracoamniotic shunt seems the most promising approach.<sup>100,101</sup> It does not only aim at reversing fetal hydrothorax but may prevent development of lung hypoplasia and polyhydramnios. Shunting may also assist in differentiation between hydrops due to primary accumulation of pleural effusions and other causes of hydrothorax, notably infections. In the latter instance, drainage will not resolve the hydrops.<sup>102</sup>

## References

- Hubbard AM, Crombleholme TM: Anomalies and malformations affecting the fetal/neonatal chest. *Semin Roentgenol* 33:117, 1998.
- Fried AM, Loh FK, Umer MA, et al: Echogenicity of fetal lung: Relation to fetal age and maturity. *AJR Am J Roentgenol* 145:591, 1985.
- Dhingsa R, Coakley FV, Albanese CT, et al: Prenatal sonography and MR imaging of pulmonary sequestration. *AJR Am J Roentgenol* 180:433, 2003.
- Achiron R, Hegesh J, Yagel S: Fetal lung lesions: A spectrum of disease. New classification based on pathogenesis, two-dimensional and color Doppler ultrasound. *Ultrasound Obstet Gynecol* 24:107, 2004.
- Sebire NJ: Fetal lung lesions: A new classification of fetal lung dysplasia. *Ultrasound Obstet Gynecol* 24:590, 2004.
- Pringle KC: Human fetal lung development and related animal models. *Clin Obstet Gynecol* 29:502, 1986.



7. Emmerson DS, Cartier MS: The fetal pulmonary circulation. In Copel JA, Reed KL, eds. *Doppler Ultrasound in Obstetrics and Gynecology*. New York, Raven Press Ltd, 1995, p 307.
8. Heymann MA: Control of the pulmonary circulation in the fetus and during the transitional period to air breathing. *Eur J Obstet Gynecol Reprod Biol* 84:127, 1999.
9. Rasanen J, Wood DC, Weiner S, et al: Role of the pulmonary circulation in the distribution of human fetal cardiac output during the second half of pregnancy. *Circulation* 94:1068, 1996.
10. Greenough A: Pulmonary Hypoplasia. In Chervenak FA, Isaacson GC, Campbell S, eds. *Ultrasound in Obstetrics and Gynecology*. Little, Brown and Company, Boston, 1993, pp 903.
11. Harding R, Hooper SB, Dickson KA: A mechanism leading to reduced lung expansion and lung hypoplasia in fetal sheep during oligohydramnios. *Am J Obstet Gynecol* 163:1904, 1990.
12. Stocker JT: The respiratory tract. In Stocker JT, Dehner LP, eds. *Pediatric Pathology*, 2nd ed. Philadelphia, Lippincott, Williams and Wilkins, 2001.
13. Moessinger AC, Santiago A, Paneth NS, et al: Time-trends in necropsy prevalence and birth prevalence of lung hypoplasia. *Paediatr Perinat Epidemiol* 3:421, 1989.
14. Page DV, Stocker JT: Anomalies associated with pulmonary hypoplasia. *Am Rev Respir Dis* 125:216, 1982.
15. Callan NA, Colmorgen GH, Weiner S: Lung hypoplasia and prolonged preterm ruptured membranes: A case report with implications for possible prenatal ultrasonic diagnosis. *Am J Obstet Gynecol* 151:756, 1985.
16. Chitkara U, Rosenberg J, Chervenak FA, et al: Prenatal sonographic assessment of the fetal thorax: Normal values. *Am J Obstet Gynecol* 156:1069, 1987.
17. Heling KS, Tennstedt C, Chaoui R, et al: Reliability of prenatal sonographic lung biometry in the diagnosis of pulmonary hypoplasia. *Prenat Diagn* 21:649, 2001.
18. Ishikawa S, Kamata S, Usui N, et al: Ultrasonographic prediction of clinical pulmonary hypoplasia: Measurement of the chest/trunk-length ratio in fetuses. *Pediatr Surg Int* 19:172, 2003.
19. Lipshutz GS, Albanese CT, Feldstein VA, et al: Prospective analysis of lung-to-head ratio predicts survival for patients with prenatally diagnosed congenital diaphragmatic hernia. *J Pediatr Surg* 32:1634, 1997.
20. Roberts AB, Mitchell JM: Direct ultrasonographic measurement of fetal lung length in normal pregnancies and pregnancies complicated by prolonged rupture of membranes. *Am J Obstet Gynecol* 163:1560, 1990.
21. Stone P, Grant S, Sadler L, et al: The use of ultrasound measurement of fetal lung length to predict neonatal respiratory outcome after prolonged premature rupture of the membranes. *Fetal Diagn Ther* 20:152, 2005.
22. Laudy JA, Van Gucht M, Van Dooren MF, et al: Congenital diaphragmatic hernia: An evaluation of the prognostic value of the lung-to-head ratio and other prenatal parameters. *Prenat Diagn* 23:634, 2003.
23. Bahlmann F, Merz E, Hallermann C, et al: Congenital diaphragmatic hernia: Ultrasonic measurement of fetal lungs to predict pulmonary hypoplasia. *Ultrasound Obstet Gynecol* 14:162, 1999.
24. Keller RL, Glidden DV, Paek BW, et al: The lung-to-head ratio and fetoscopic temporary tracheal occlusion: prediction of survival in severe left congenital diaphragmatic hernia. *Ultrasound Obstet Gynecol* 21:244, 2003.
25. Raine-Fenning NJ, Clewes JS, Kendall NR, et al: The interobserver reliability and validity of volume calculation from three-dimensional ultrasound datasets in the in vitro setting. *Ultrasound Obstet Gynecol* 21:283, 2003.
26. Kalache KD, Espinoza J, Chaiworapongsa T, et al: Three-dimensional ultrasound fetal lung volume measurement: a systematic study comparing the multiplanar method with the rotational (VOCAL) technique. *Ultrasound Obstet Gynecol* 21:111, 2003.
27. Moeglin D, Talmant C, Duyme M, et al: Fetal lung volumetry using two- and three-dimensional ultrasound. *Ultrasound Obstet Gynecol* 25:119, 2005.
28. Laudy JA, Janssen MM, Struyk PC, et al: Three-dimensional ultrasonography of normal fetal lung volume: A preliminary study. *Ultrasound Obstet Gynecol* 11:13, 1998.
29. Gerards FA, Engels MA, Twisk JW, et al: Normal fetal lung volume measured with three-dimensional ultrasound. *Ultrasound Obstet Gynecol* 27:134, 2006.
30. Ruano R, Martinovic J, Dommergues M, et al: Accuracy of fetal lung volume assessed by three-dimensional sonography. *Ultrasound Obstet Gynecol* 26:725, 2005.
31. Peralta CF, Cavoretto P, Csapo B, et al: Lung and heart volumes by three-dimensional ultrasound in normal fetuses at 12-32 weeks' gestation. *Ultrasound Obstet Gynecol* 27:128, 2006.
32. Levine D, Barnes PD, Sher S, et al: Fetal fast MR imaging: reproducibility, technical quality, and conspicuity of anatomy. *Radiology* 206:549, 1998.
33. Osada H, Kaku K, Masuda K, et al: Quantitative and qualitative evaluations of fetal lung with MR imaging. *Radiology* 231:887, 2004.
34. Sabogal JC, Becker E, Bega G, et al: Reproducibility of fetal lung volume measurements with 3-dimensional ultrasonography. *J Ultrasound Med* 23:347, 2004.
35. Rypens F, Metens T, Rocourt N, et al: Fetal lung volume: Estimation at MR imaging-initial results. *Radiology* 219:236, 2001.
36. Paek BW, Coakley FV, Lu Y, et al: Congenital diaphragmatic hernia: Prenatal evaluation with MR lung volumetry—Preliminary experience. *Radiology* 220:63, 2001.
37. Gorinour G, Bouvenot J, Mourot MG, et al: Prenatal prognosis of congenital diaphragmatic hernia using magnetic resonance imaging measurement of fetal lung volume. *Ultrasound Obstet Gynecol* 26:738, 2005.
38. Laudy JA, Gaillard JL, van Anker JN, et al: Doppler ultrasound imaging: a new technique to detect lung hypoplasia before birth? *Ultrasound Obstet Gynecol* 7:189, 1996.
39. Laudy JA, Tibboel D, Robben SG, et al: Prenatal prediction of pulmonary hypoplasia: Clinical, biometric, and Doppler velocity correlates. *Pediatrics* 109:250, 2002.
40. Rizzo G, Capponi A, Angelini E, et al: Blood flow velocity waveforms from fetal peripheral pulmonary arteries in pregnancies with preterm premature rupture of the membranes: Relationship with pulmonary hypoplasia. *Ultrasound Obstet Gynecol* 15:98, 2000.
41. Broth RE, Wood DC, Rasanen J, et al: Prenatal prediction of lethal pulmonary hypoplasia: The hyperoxygenation test for pulmonary artery reactivity. *Am J Obstet Gynecol* 187:940, 2002.
42. Fuke S, Kanzaki T, Mu J, et al: Antenatal prediction of pulmonary hypoplasia by acceleration time/ejection time ratio of fetal pulmonary arteries by Doppler blood flow velocimetry. *Am J Obstet Gynecol* 188:228, 2003.
43. Wilson RD, Hedrick HL, Liechty KW, et al: Cystic adenomatoid malformation of the lung: Review of genetics, prenatal diagnosis, and in utero treatment. *Am J Med Genet* 140:151, 2006.
44. Stocker JT, Madewell JE, Drake RM: Congenital cystic adenomatoid malformation of the lung. Classification and morphologic spectrum. *Hum Pathol* 8:155, 1977.
45. Whitsett JA, Wert SE, Trapnell BC: Genetic disorders influencing lung formation and function at birth. *Hum Mol Genet* 13:207, 2004.
46. Johnson AM, Hubbard AM: Congenital anomalies of the fetal/neonatal chest. *Semin Roentgenol* 39:197, 2004.
47. Liechty KW, Crombleholme TM, Quinn TM, et al: Elevated platelet-derived growth factor-B in congenital cystic adenomatoid malformations requiring fetal resection. *J Pediatr Surg* 34:805, 1999.
48. Simonet WS, DeRose ML, Bucay N, et al: Pulmonary malformation in transgenic mice expressing human keratinocyte growth factor in the lung. *Proc Natl Acad Sci U S A* 92:12461, 1995.
49. Volpe MV, Pham L, Lessin M, et al: Expression of Hoxb-5 during human lung development and in congenital lung malformations. *Birth Defects Res A Clin Mol Teratol* 67:550, 2003.
50. Adzick NS: Management of fetal lung lesions. *Clin Perinatol* 30:481, 2003.
51. Levine D, Barnewolt CE, Mehta TS, et al: Fetal thoracic abnormalities: MR imaging. *Radiology* 228:379, 2003.
52. Hubbard AM: Prenatal magnetic resonance imaging for fetal abnormalities. In Milunsky A, ed. *Genetic Disorders of the Fetus*. London, Johns Hopkins University Press, 2004, pp 944.
53. Goldstein RB: Ultrasound evaluation of the fetal thorax. In Callen PW, ed. *Ultrasonography in Obstetrics and Gynecology*, 4th ed. Philadelphia, WB Saunders, 2000, pp 426-455.
54. Adzick NS, Harrison MR: Management of the fetus with a cystic adenomatoid malformation. *World J Surg* 17:342, 1993.
55. Miller JA, Corteville JE, Langer JC: Congenital cystic adenomatoid malformation in the fetus: Natural history and predictors of outcome. *J Pediatr Surg* 31:805, 1996.
56. Crombleholme TM, Coleman B, Hedrick H, et al: Cystic adenomatoid malformation volume ratio predicts outcome in prenatally diagnosed



- cystic adenomatoid malformation of the lung. *J Pediatr Surg* 37:331, 2002.
57. Duncombe GJ, Dickinson JE, Kikiros CS: Prenatal diagnosis and management of congenital cystic adenomatoid malformation of the lung. *Am J Obstet Gynecol* 187:950, 2002.
58. Illanes S, Hunter A, Evans M, et al: Prenatal diagnosis of echogenic lung: Evolution and outcome. *Ultrasound Obstet Gynecol* 26:145, 2005.
59. Davenport M, Warne SA, Cacciaguerra S, et al: Current outcome of antenally diagnosed cystic lung disease. *J Pediatr Surg* 39:549, 2004.
60. Zangwill BC, Stocker JT: Congenital cystic adenomatoid malformation within an extralobar pulmonary sequestration. *Pediatr Pathol* 13:309, 1993.
61. Gilbert-Barness E, Debich-Spicer D: Respiratory system. In Gilbert-Barness E, Debich-Spicer D, eds. *Embryo and Fetal Pathology*. Cambridge, Cambridge University Press, 2004, pp 470-489.
62. Rosado-de-Christenson ML, Frazier AA, Stocker JT, et al: From the archives of the AFIP. Extralobar sequestration: Radiologic-pathologic correlation. *Radiographics* 13:425, 1993.
63. Frazier AA, Rosado de Christenson ML, Stocker JT, et al: Intralobar sequestration: Radiologic-pathologic correlation. *Radiographics* 17:725, 1997.
64. Stocker JT: Sequestrations of the lung. *Semin Diagn Pathol* 3:106, 1986.
65. Case records of the Massachusetts General Hospital. Weekly clinicopathological exercises. Case 14-1991. A 17-year-old boy with a left posterior intrathoracic mass. *N Engl J Med* 324:980, 1991.
66. Fraser RG, Pare JAP, Pare PD, et al, eds. *Diagnosis of Diseases of the Chest*, 3rd ed. Philadelphia, WB Saunders Company, 1991.
67. Lager DJ, Kuper KA, Haake GK: Subdiaphragmatic extralobar pulmonary sequestration. *Arch Pathol Lab Med* 115:536, 1991.
68. Gerle RD, Jaretzki A 3rd, Ashley CA, et al: Congenital bronchopulmonary-foregut malformation. Pulmonary sequestration communicating with the gastrointestinal tract. *N Engl J Med* 278:1413, 1968.
69. Hubbard AM, Adzick NS, Crombleholme TM, et al: Congenital chest lesions: Diagnosis and characterization with prenatal MR imaging. *Radiology* 212:43, 1999.
70. Hedrick MH, Ferro MM, Filly RA, et al: Congenital high airway obstruction syndrome (CHAOS): A potential for perinatal intervention. *J Pediatr Surg* 29:271, 1994.
71. Hartnick CJ, Rutter M, Lang F, et al: Congenital high airway obstruction syndrome and airway reconstruction: An evolving paradigm. *Arch Otolaryngol Head Neck Surg* 128:567, 2002.
72. Lim FY, Crombleholme TM, Hedrick HL, et al: Congenital high airway obstruction syndrome: natural history and management. *J Pediatr Surg* 38:940, 2003.
73. Arizawa M, Imai S, Suehara N, et al: Prenatal diagnosis of laryngeal atresia. *Nippon Sanka Fujinka Gakkai Zasshi* 41:907, 1989.
74. Kassanos D, Christodoulou CN, Agapitos E, et al: Prenatal ultrasonographic detection of the tracheal atresia sequence. *Ultrasound Obstet Gynecol* 10:133, 1997.
75. Fraser GR: Our genetical 'load': A review of some aspects of genetical variation. *Ann Hum Genet* 25:387, 1962.
76. Keeling JW: *Fetal Pathology*. London, Churchill Livingstone, 1994.
77. Silver MM, Thurston WA, Patrick JE: Perinatal pulmonary hyperplasia due to laryngeal atresia. *Hum Pathol* 19:110, 1988.
78. Barnes NA, Pilling DW: Bronchopulmonary foregut malformations: Embryology, radiology and quandary. *Eur Radiol* 13:2659, 2003.
79. Kravitz RM: Congenital malformations of the lung. *Pediatr Clin North Am* 41:453, 1994.
80. Winters WD, Effmann EL: Congenital masses of the lung: Prenatal and postnatal imaging evaluation. *J Thorac Imaging* 16:196, 2001.
81. Bagolan P, Bilancioni E, Nahom A, et al: Prenatal diagnosis of a bronchogenic cyst in an unusual site. *Ultrasound Obstet Gynecol* 15:66, 2000.
82. Uludag S, Madazli R, Erdogan E, et al: A case of prenatally diagnosed fetal neurenteric cyst. *Ultrasound Obstet Gynecol* 18:277, 2001.
83. Reed JC, Sobonya RE: Morphologic analysis of foregut cysts in the thorax. *Am J Roentgenol Radium Ther Nucl Med* 120:851, 1974.
84. Strollo DC, Rosado-de-Christenson ML, Jett JR: Primary mediastinal tumors: Part II. Tumors of the middle and posterior mediastinum. *Chest* 112:1344, 1997.
85. Ryckman FC, Rosenkrantz JG: Thoracic surgical problems in infancy and childhood. *Surg Clin North Am* 65:1423, 1985.
86. Adzick NS, Harrison MR, Crombleholme TM, et al: Fetal lung lesions: Management and outcome. *Am J Obstet Gynecol* 179:884, 1998.
87. Wilkinson CC, Albanese CT, Jennings RW, et al: Fetal neurenteric cyst causing hydrops: Case report and review of the literature. *Prenat Diagn* 19:118, 1999.
88. Graham G, Devine PC: Antenatal diagnosis of congenital diaphragmatic hernia. *Semin Perinatol* 29:69, 2005.
89. Puri P, Gorman F: Lethal nonpulmonary anomalies associated with congenital diaphragmatic hernia: implications for early intrauterine surgery. *J Pediatr Surg* 19:29, 1984.
90. Harrison MR, Langer JC, Adzick NS, et al: Correction of congenital diaphragmatic hernia in utero, V. Initial clinical experience. *J Pediatr Surg* 25:47, 1990.
91. Manni M, Heydanus R, Den Hollander NS, et al: Prenatal diagnosis of congenital diaphragmatic hernia: A retrospective analysis of 28 cases. *Prenat Diagn* 14:187, 1994.
92. Beresford MW, Shaw NJ: Outcome of congenital diaphragmatic hernia. *Pediatr Pulmonol* 30:249, 2000.
93. Langham MR, Jr, Kays DW, Beierle EA, et al: Twenty years of progress in congenital diaphragmatic hernia at the University of Florida. *Am Surg* 69:45, 2003.
94. Heling KS, Wauer RR, Hammer H, et al: Reliability of the lung-to-head ratio in predicting outcome and neonatal ventilation parameters in fetuses with congenital diaphragmatic hernia. *Ultrasound Obstet Gynecol* 25:112, 2005.
95. Jani J, Peralta CF, Van Schoubroeck D, et al: Relationship between lung-to-head ratio and lung volume in normal fetuses and fetuses with diaphragmatic hernia. *Ultrasound Obstet Gynecol* 27:545, 2006.
96. Walsh DS, Hubbard AM, Olutoye OO, et al: Assessment of fetal lung volumes and liver herniation with magnetic resonance imaging in congenital diaphragmatic hernia. *Am J Obstet Gynecol* 183:1067, 2000.
97. Hubbard AM, Crombleholme TM, Adzick NS, et al: Prenatal MRI evaluation of congenital diaphragmatic hernia. *Am J Perinatol* 16:407, 1999.
98. Kitano Y, Flake AW, Crombleholme TM, et al: Open fetal surgery for life-threatening fetal malformations. *Semin Perinatol* 23:448, 1999.
99. Longaker MT, Laberge JM, Dansereau J, et al: Primary fetal hydrothorax: Natural history and management. *J Pediatr Surg* 24:573, 1989.
100. Blott M, Nicolaides KH, Greenough A: Pleuroamniotic shunting for decompression of fetal pleural effusions. *Obstet Gynecol* 71:798, 1988.
101. Rodeck CH, Fisk NM, Fraser DI, et al: Long-term in utero drainage of fetal hydrothorax. *N Engl J Med* 319:1135, 1988.
102. Ville YG, Nicolaides K, Campbell S: Prenatal diagnosis of fetal malformations by ultrasound. In Milunsky A, ed. *Genetic Disorders and the Fetus*. London, Johns Hopkins University Press, 2004, pp 836-900.

# ULTRASOUND EVALUATION OF THE FETAL HEART

Shi-Joon Yoo, MD, FRCPC and Edgar Jaeggi, MD

## Introduction

### Congenital Heart Diseases

Sonographic Technique, Basic Standard Views, and Anatomy

Imaging Technique and Normal Anatomy

Clues to the Abnormalities

*Transverse View of the Upper Abdomen*

*Four-Chamber View*

*Ventricular Disproportion*

*Atrial, AV, and Ventricular Septal Defects*

*Three-Vessel View*

*Left and Right Ventricular Outflow Tract Views*

*Transposition of the Great Arteries*

*Single and Double Outlet Ventricle*

*Basal Short-Axis View*

*Aortic and Ductal Arch Views*

Prenatal and Postnatal Treatment Options and Outcomes of

Congenital Heart Diseases

### Cardiac Tumors

### Cardiac Rhythm

Normal Fetal Cardiac Rhythm

Sonographic Techniques for Cardiac Rhythm Assessment

*M Mode Echocardiography*

*Pulsed Wave Doppler*

*Other Noninvasive Methods*

Abnormal Cardiac Rhythms

*Irregular Cardiac Rhythm*

*Bradycardia*

*Tachycardia*

*Examination for Pregnant Women with Anti-Ro/SSA and Anti-La/SSB Antibodies*

### Cardiac Function

Physiology of the Fetal Cardiovascular System

### Cardiac Cycle

Techniques for Cardiac Functional Assessment

*Shortening Fraction*

*Cardiac Output*

*Diastolic Function*

*Myocardial Performance Index*

Abnormal Cardiac Function

## INTRODUCTION

Prenatal ultrasound for detection of fetal anomalies has become a routine part of the pregnancy management in most advanced countries. Fetal cardiac examination is an indispensable part of the prenatal ultrasound because of the following well-recognized reasons. First, congenital heart diseases (CHDs) are common congenital anomalies. The incidence of moderate to severe forms of CHD is about 6/1000 live births.<sup>1</sup> The incidence increases to 75/1000 live births if all mild lesions, such as bicuspid aortic valve and tiny muscular ventricular septal defects are included. The prenatal incidence of CHD is much higher with a tendency for an excess of complex lesions. Second, CHD is frequently associated with other noncardiac anomalies and chromosomal abnormalities.<sup>2-4</sup> Extracardiac anomalies are found in 8% to 42% of patients with CHD. The incidence of chromosomal abnormalities ranges from 5% to 13% in live births with CHD<sup>2,3,5</sup> and 15% to 50% in prenatal series.<sup>6-8</sup> More than 50% of fetuses with abnormal chromosomes have cardiac anomalies. Nonchromosomal syndromes and associations comprise 1% to 5% of patients with CHD.<sup>3</sup> Therefore, the presence of a congenital cardiac defect is an indication for chromosomal study and detailed ultrasound assessment of the extracardiac structures. Third, CHD is associated

with significant neonatal and childhood morbidity and mortality. Approximately one quarter of all infant deaths are due to congenital malformations and one third of these deaths are related to CHD.<sup>9,10</sup> CHD is the leading cause of neonatal and childhood deaths, not only because of the complexity of the malformations but also due to its high incidence. Prenatal diagnosis of significant CHD has a positive impact on the postnatal management with reduced surgical delays, shorter intensive care unit stays, and avoidance of severe hemodynamic compromise. Some cardiac lesions, such as complete transposition of the great arteries, require delivery at a tertiary care center for urgent postnatal management. A few congenital cardiac abnormalities, such as atrial flutter, bradycardia with atrioventricular block, critical aortic stenosis, and critical pulmonary stenosis, require in utero medication or intervention.<sup>11-14</sup> Fourth, despite efforts to improve prenatal anomaly detection by introducing structured educational programs with basic ultrasound recommendations, cardiac anomalies continue to be overlooked and a huge variation in detection rates persists between geographic areas and centers.<sup>15-17</sup>

Fetal cardiac examination is performed either as a part of screening fetal sonography for a low-risk population or as a



**Table 14-1** High-risk Groups for Congenital Heart Disease

Fetal Risk Factors	Maternal Risk Factors	Familial Risk Factors
Chromosomal abnormality	Maternal disease	Family history of congenital heart disease
Extracardiac anomaly	Congenital heart disease	Siblings
Omphalocele	Diabetes	Parents
Esophageal atresia	Collagen vascular disease	Family history of syndromes associated with congenital heart disease
Duodenal atresia	Anti-Ra/Lo antibody positive	Tuberous sclerosis
Diaphragmatic hernia	Phenylketonuria	Noonan syndrome
VACTERL association	Exposure to drugs, teratogens, or infections	Holt-Oram syndrome
Increased nuchal translucency	Alcohol	Chromosome 22q11 deletion
Nuchal fold thickening	Anticonvulsants	
Nonimmune hydrops	Lithium	
Polyhydramnios	Retinoic acid	
Oligohydramnios	Rubella, Coxsackie,	
Fetal cardiac dysrhythmia	Cytomegalovirus	
	Parvovirus B19	

VACTERL, Vertebral, Anal, Cardiac, TracheoEsophageal, Renal and Radial, and Limb abnormalities.

complete diagnostic test for groups at high risk for CHD (Table 14-1). The majority of the babies with CHD are born to parents with no identifiable risk factors. Therefore, the rate of detection of CHD depends largely on the sensitivity of the prenatal screening ultrasound. The earlier trials for fetal cardiac screening relied on a four-chamber view alone.<sup>18,19</sup> However, this approach has proved inadequate for detection of abnormalities of visceral and atrial situs, the ventricular outflow tracts, and great arteries.<sup>20,21</sup> Therefore, the screening examination should be extended to include the views for situs determination as well as the views for assessment of the ventricular outflow tracts and great arteries.<sup>22-24</sup> Because the extended examination is rather extensive and complex, a well-standardized protocol should be set in order to reduce the examination time, while maintaining a high degree of diagnostic accuracy.

Fetal cardiac examination should be performed when adequate images can be obtained for diagnosis in the majority of routine patients. The ideal timing is a compromise between examining sufficiently late not to miss late-developing lesions, and yet offering the diagnosis as early as possible for patients to have additional testing, including chromosomal study and to consider the options, if any, applicable to their particular diagnosis.<sup>25</sup> The fetal heart can be visualized transvaginally as early as 9 weeks of gestation and abdominally by 11 weeks.<sup>26</sup> Fetal echocardiography, using both transvaginal and transabdominal approaches, at or before 16 weeks of gestation on fetuses at risk of CHD, allowed distinction between a normal and abnormal cardiac appearance in the majority of cases.<sup>27,28</sup> However, the earlier scan is technically more difficult and less accurate than the second trimester scan, whereas some forms of cardiac malformations do not become evident in the early period of pregnancy. As a result, some of the late-developing lesions may go undetected during early evaluation.<sup>25,29,30</sup> Therefore, fetal cardiac examination is usually performed at 18 to 22 weeks of gestation in the countries where the legal limit of termination of pregnancy is 24 weeks. The earlier scan is justifiably applicable for patients at increased risk of congenital anomalies.<sup>25,26</sup>

Fetal cardiac examination requires a high-resolution ultrasound system with color and power Doppler, pulsed

and continuous wave spectral Doppler and M-mode capabilities. The transducer is chosen according to the gestational age, the size of the mother, and the amount of amniotic fluid. Usually a 5- to 7.5-MHz convex or sector transducer is adequate for the 15- to 30-week scans. A 3-MHz transducer can be required for an obese mother or when there is polyhydramnios. A 3-MHz transducer may also be required after the late second trimester. In general, it is preferable to use a transducer with the highest possible frequency. It is essential to record the real-time images on a digital storage system.

The major part of the screening fetal cardiac examination is real-time grey-scale imaging of the cardiac and major vascular structures with color Doppler interrogation of the ventricular inlets and outflow tracts, and great arteries. Identification and assessment of the vascular anatomy can be further facilitated by power Doppler technique.

Three-dimensional ultrasound has become available for fetal imaging. Its applications to fetal facial and musculoskeletal abnormalities have been well established. It has also been proven very useful for fetal cardiac examination (Fig. 14-1).<sup>31-33</sup> Following the acquisition of the volume dataset, the images are reconstructed offline in any desired planes. The image reconstruction enables the examiner to evaluate series of two-dimensional images in multiple views, evaluate intracardiac anatomy at different depth planes, and recreate casts of blood flow of the chambers and great vessels. This new technology not only enhances the ability of the examiner to identify normal and complex fetal heart anatomy but also facilitates routine image data acquisition by inexperienced personnel. Recent technology allows real-time three-dimensional or four-dimensional ultrasound for instantaneous acquisition of the volume data of the whole heart.

This chapter is divided into four parts according to the pathology and purposes of examinations: Part I, Congenital Heart Diseases; Part II, Cardiac Tumors; Part III, Cardiac Rhythm; Part IV, Cardiac Function.

Each part discusses the sonographic techniques, basic standard views and essential anatomy, the clues to the abnormalities, and the prenatal and postnatal treatment options and outcomes.



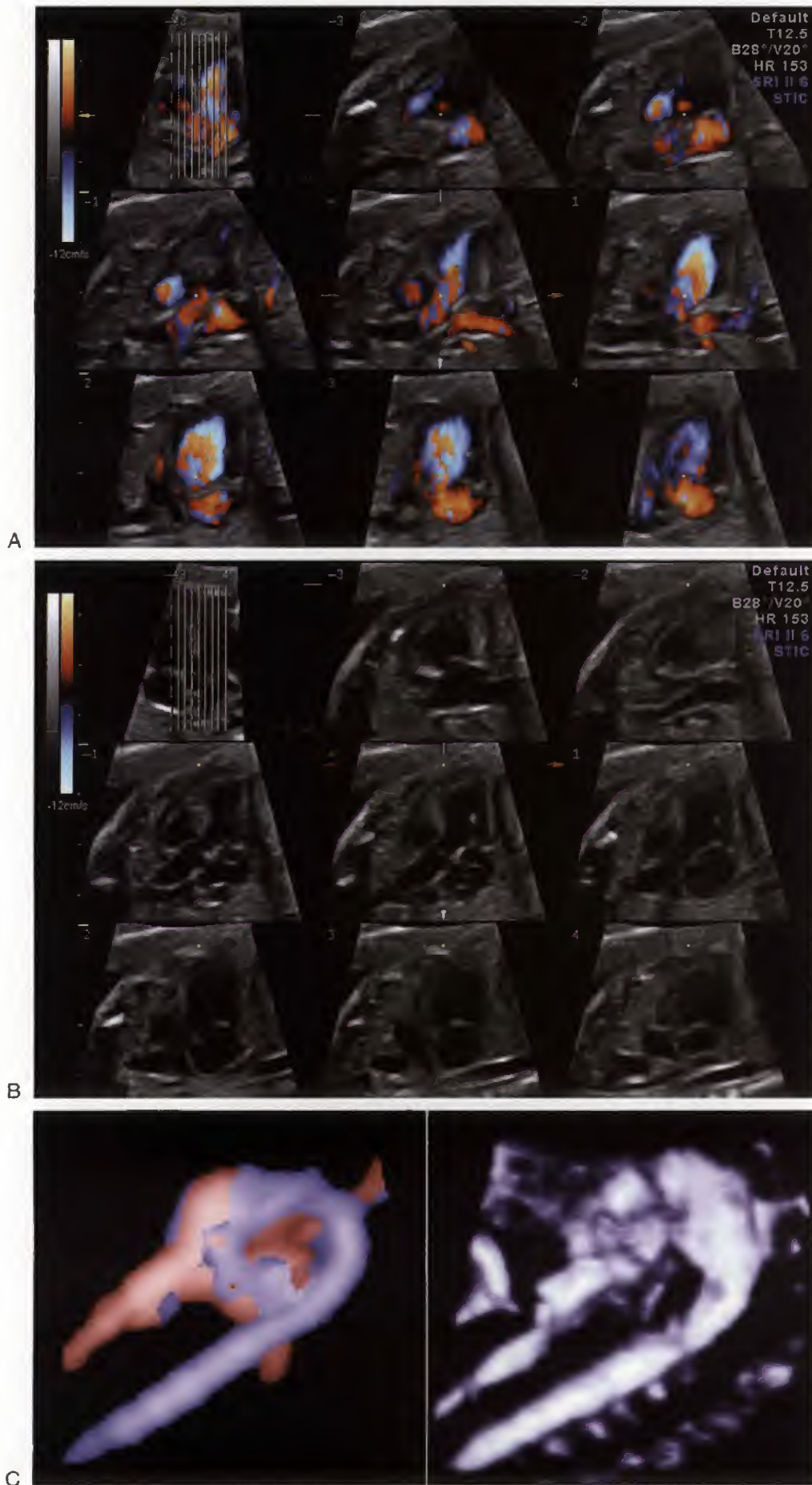


**FIGURE 14-1.** Three-dimensional echocardiograms obtained by spatiotemporal image correlation technique. *A.* Color Doppler spatiotemporal image correlation images. The left upper image is a five-chamber view showing the line cursors for oblique sagittal reformation. The oblique sagittal images are parallel slices that are orthogonal to the plane of the left upper image. *B.* Gray-scale images. Color signal is deleted from the images shown in *A.* *C.* Three-dimensional volume-rendered images from color and power Doppler data.



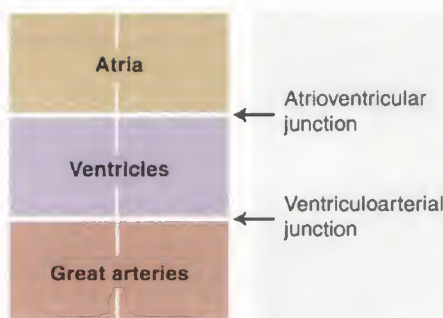


FIGURE 14-2. Basic cardiac segments and junctions.

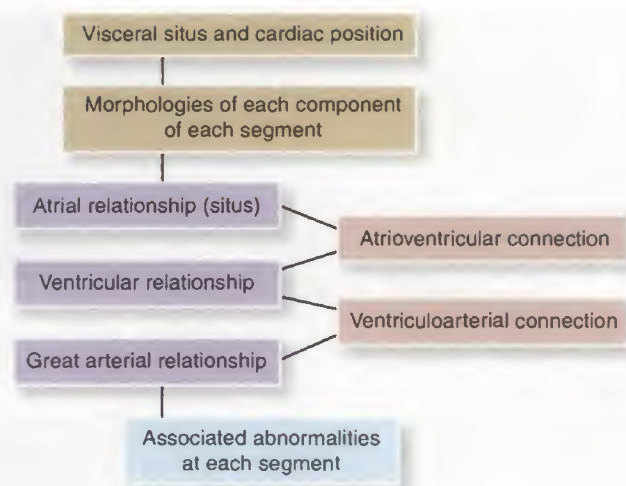


FIGURE 14-3. Steps of sequential segmental approach to congenital heart disease.

## CONGENITAL HEART DISEASES

### Sonographic Technique, Basic Standard Views, and Anatomy

For structural evaluation, the heart is assessed in a step-by-step fashion using sequential segmental analysis.<sup>34,35</sup> In this approach, the heart is considered to consist of three segments: the *atria*, the *ventricles*, and the *great arteries*, and two connectors: the *atrioventricular (AV) junction* and the *ventriculoarterial junction* (Fig. 14-2). The key steps of the sequential segmental approach include (Fig. 14-3)

1. Determination of the visceral situs and position of the heart.
2. Identification of the morphologies of each component of each segment.
3. Assessment of the spatial relationships between the components of each segment.
  - a. Atrial relationship or situs
  - b. Ventricular relationship
  - c. Great arterial relationship
4. Determination of the connections between the segments at the AV and ventriculoarterial junctions.
  - a. AV connection
  - b. Ventriculoarterial connection
5. Evaluation of the associated malformation at each cardiac segment.

Sequential segmental approach can be achieved by continuous sweeping of the sonographic probe from the upper abdomen to the superior mediastinum in the orthogonal planes to the fetal body axis and along the long- and short-axis planes of the heart. In making a journey through the fetal heart and great vessels, the following landmark views should be obtained as the standard views for the complete anatomical assessment (Fig. 14-4)

1. Transverse view of the upper abdomen.
2. Four-chamber view.
3. Three-vessel view.
4. Left ventricular outflow tract view.
5. Right ventricular outflow tract view.
6. Basal short-axis view.
7. Aortic arch view.

### Imaging Technique and Normal Anatomy

Fetal cardiac examination should begin with determination of the position and orientation of the fetus relative to the long axis of the mother and identification of the right and left sides of the fetus. This step can be quickly performed by sweeping the transducer in the transverse and longitudinal planes of the maternal body. It is essential not to determine the right and left sides of the fetus according to the position of the stomach because it can be on the wrong side. For the beginners, a doll can be positioned on the maternal abdomen to facilitate this step.

Once the right and left sides of the fetus are defined, the transverse view of the upper abdomen is obtained for the determination of the visceral situs, which is the first step of sequential segmental analysis (see Fig. 14-4).<sup>34</sup> It is strongly advised not to start the cardiac examination with the heart. The transverse view of the upper abdomen is the view that is used for the measurement of the abdominal circumference. In this view, the larger lobe of the liver and gallbladder are on the right, and the stomach on the left (Fig. 14-5). The cross-section of the abdominal aorta is at the left anterior corner of the spine, whereas the cross-section of the inferior vena cava is on the right. The inferior vena cava is an anterior structure compared with the aorta because it courses forward as it connects to the right atrium. In a well-taken image, a sickle-shaped spleen can be seen behind the stomach.

The transducer is then moved, along the long axis of the fetal body, toward the fetal head to obtain a four-chamber view (see Fig. 14-4).<sup>18,19</sup> Because the transducer is swept from the upper abdomen to the four-chamber plane, it is important to follow the inferior vena cava connecting to the right atrium. In the four-chamber view, the heart occupies approximately one third of the thoracic area and the cardiac axis is directed  $45 \pm 20$  degrees leftward from the coronal or sagittal plane (Fig. 14-6).<sup>36,37</sup> In the first and second trimesters, the cardiac chambers seen in the four-chamber view are symmetric in size. The right atrium and ventricle become slightly larger than the left atrium and ventricle

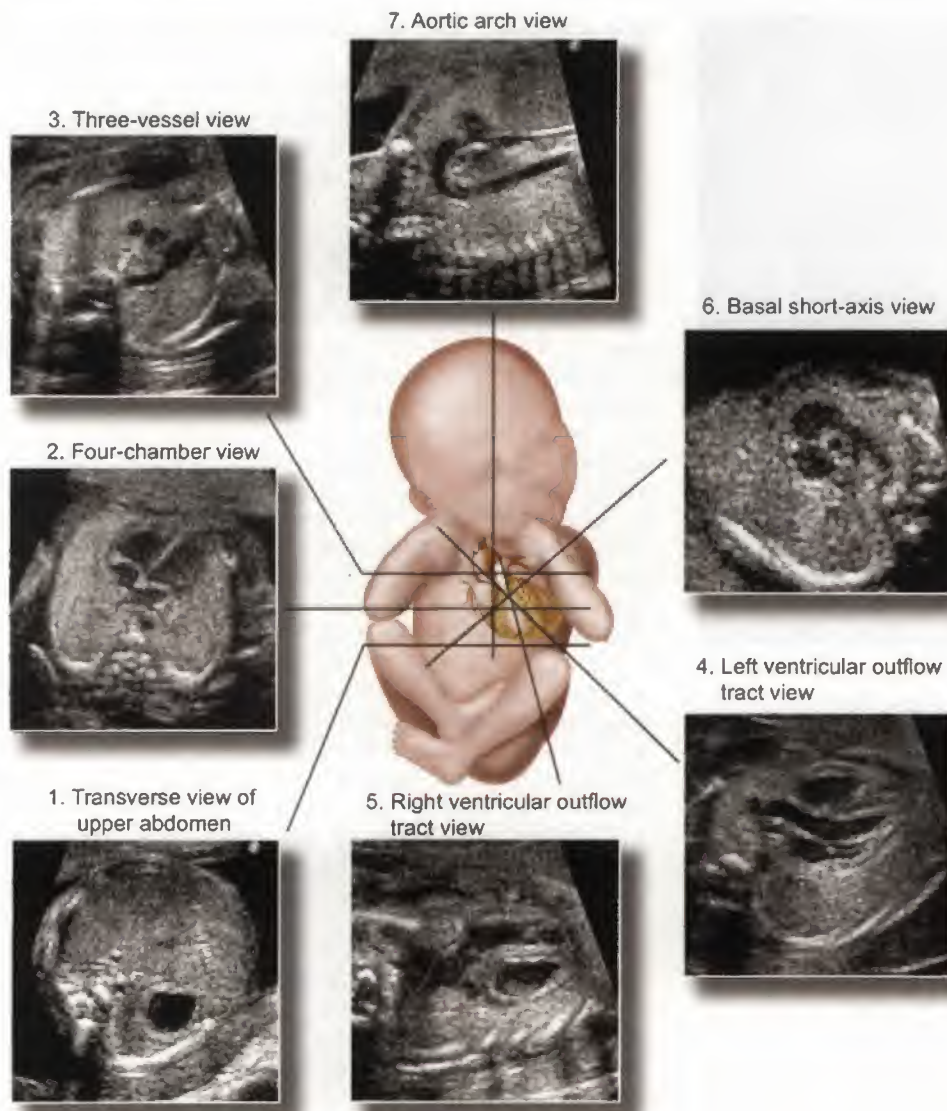


**FIGURE 14-4.** Basic sonographic views for fetal cardiac examination. (Illustration by Shi-Joon Yoo, MD, and James A. Cooper, MD.)

in the third trimester.<sup>38,39</sup> The septum between the four chambers of the heart consists of three parts: atrial, AV, and ventricular (see Fig. 14-6B, C). The AV septum is present between the right atrium and left ventricle because the tricuspid valve has a more apical attachment to the septum than the mitral valve.<sup>40</sup> The central part of the atrial septum is the thin and mobile primum septum (see Fig. 14-6C). In the normal fetus, this part of the septum bulges toward the left atrium as the blood flows from the right atrium into the left atrium through the foramen ovale. The pulmonary veins are identifiable in the four-chamber view. Color and power Doppler techniques are helpful in identifying the pulmonary veins (see Fig. 14-6E). When color Doppler is used for identification of the pulmonary veins, the velocity setting should be set at less than 30 cm/second. Usually, the pulmonary veins that are seen in the four-chamber view are the lower veins, which course slightly forward as they connect to the left atrium. The upper pulmonary veins are more superior and anterior as compared with the lower veins and,

therefore, are not shown in the regular four-chamber view. The lowest section through the four chambers shows the coronary sinus as a small tubular structure between the left ventricle and the orifice of the inferior vena cava (see Fig. 14-6F).<sup>41</sup> In the apical part of the right ventricle, a muscle bundle called 'the moderator band' crosses the cavity. It may be seen as a muscle bundle extending from the septum to the parietal wall (see Fig. 14-6B), but is more often seen as a muscle mass obliterating the apical part of the cavity (see Fig. 14-6A and C). The septal attachment of the AV valves and the presence of the moderator band are the two most important morphologic criteria for ventricular identification. On the other hand, differences in trabeculation pattern between the right and left ventricles are hardly recognizable on the fetal ultrasound examination. The function of the tricuspid and mitral valves should be assessed using color Doppler with a velocity set at 60 to 80 cm/second (see Fig. 14-6G). Trivial tricuspid regurgitation is not uncommon and is usually transient (see Fig. 14-6H).<sup>42,43</sup>



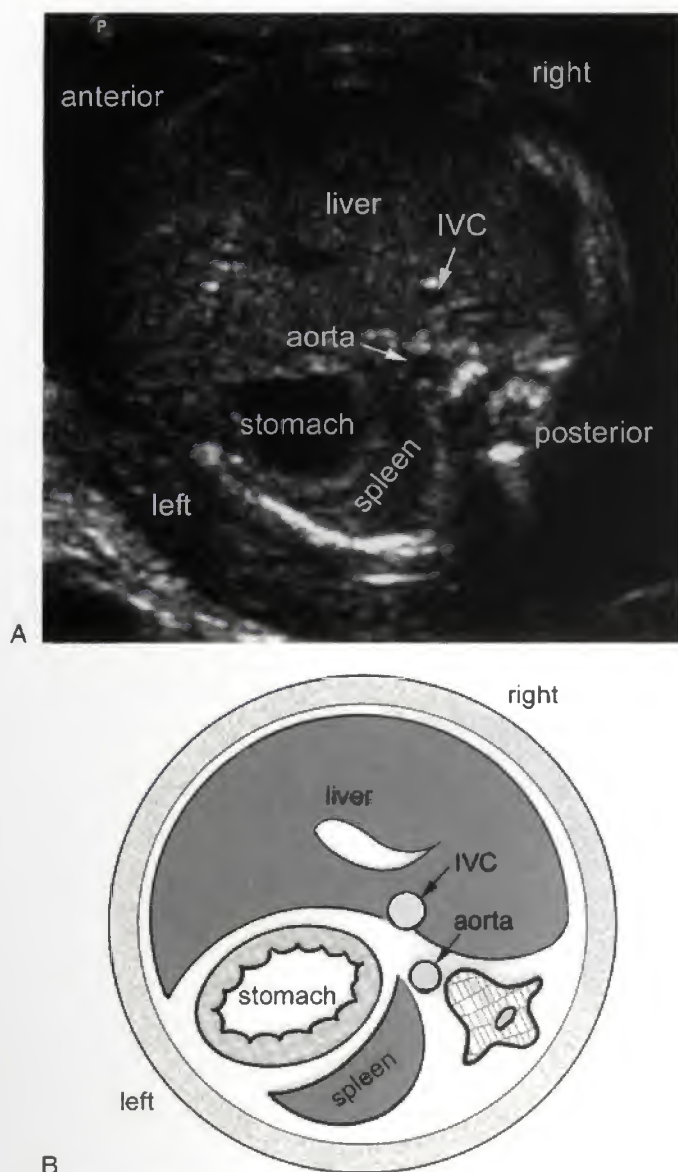


**FIGURE 14-5.** Transverse view of the upper abdomen (A) and corresponding diagram (B). The larger lobe of the liver is on the right, and the stomach on the left. The descending aorta (ao) is at the left anterior aspect of the spine. The inferior vena cava (IVC) is on the right side of the midline. Note that the inferior vena cava is located anteriorly at some distance from the spine as it courses forward to connect to the right atrium above this level.

A recent study using three-dimensional color Doppler technique showed mild-to-moderate tricuspid regurgitation in 83% of fetuses in the early second trimester.<sup>43</sup> However, substantial tricuspid regurgitation in the first trimester is frequently a marker of cardiac malformations or chromosomal defects in the absence of structural heart disease.<sup>44-46</sup> The cross-section of the descending aorta is seen behind the heart at the left anterior aspect of the vertebral body. The cross-section of the esophagus can occasionally be seen as an echolucent structure adjacent to the aorta when the fetus swallows amniotic fluid. In contrast to the vascular structures, the esophagus barely demonstrates signal using color or

power Doppler, and disappears and reappears in a few seconds or minutes.

From the four-chamber plane, the transducer is moved upward along the long axis of the fetal body. The four-chamber view changes into a 'five-chamber view' in which the aortic valve is seen to arise from the left ventricular outflow tract in the center of the four chambers (see Fig. 14-6I). Further upward movement of the transducer creates a three-vessel view in which the oblique section of the main pulmonary artery and cross-sections of the ascending aorta and superior vena cava (SVC) are seen (see Figs. 14-4 and 14-7).<sup>47,48</sup> The three vessels are arranged in a straight line from the left anterior to the right posterior aspect of the mediastinum with a decreasing order of the size. In the adjacent planes shown by slight downward or upward movement or angulation of the transducer, the right and left pulmonary arteries, and the ductal and aortic arches are visualized. In fact, there are three arches in the upper mediastinum; the ductal, aortic, and azygos venous arches (see Fig. 14-7C, F, and G). In addition, the trachea and the major bronchi are identifiable because they contain fluid in fetal life (see Fig. 14-7B, D, and G). Therefore, the position of the aortic arch relative to the trachea can be well defined. Normally, the aortic arch is a sausage-like structure coursing obliquely from right anterior to left posterior on the left side of the trachea. To emphasize the presence of the trachea in the three-vessel view, the term three vessels and trachea view has been suggested.<sup>49,50</sup> The aortic and ductal arches make a V-shaped confluence at the descending aorta (see Fig. 14-7C and F). In the V-view, the ductal arch is slightly bigger than the aortic arch. After it arises from the main pulmonary artery, the right pulmonary artery takes a long horizontal course in front of the tracheal bifurcation before it reaches the right lung hilum (see Fig. 14-7). On the contrary, the left pulmonary artery courses obliquely backward and leftward to reach the left lung hilum. Also seen in the transverse view of the upper mediastinum at the level of the aortic arch is the innominate vein coursing horizontally in front of the ascending aorta. The identification of the various vascular structures in the upper mediastinum can be facilitated with color and power Doppler interrogation. However, the vessel sizes should not be measured by color or power Doppler as the vessels look significantly bigger because of the blooming effect. Anterior to the three vessels, the thymus is seen as an area of different echogenicity as compared with the lungs (see Fig. 14-7G).<sup>51-53</sup> Its echogenicity is similar to or slightly more than that of the adjacent lungs in the early second trimester and it becomes less echogenic in later pregnancy. It typically contains spindle-shaped echogenic spots that make its differentiation from the lungs possible. Its transverse diameter in millimeters is slightly smaller than the gestational age in weeks in the second trimester and becomes slightly larger as the pregnancy approaches the term.<sup>54</sup>

The ventricular outflow tract views need special maneuvers (Fig. 14-8).<sup>23,55</sup> The transducer is moved back to a four-chamber plane. Then the transducer is moved around the fetal thorax until the sonographic beam is positioned perpendicular to the ventricular septum. This procedure aligns the ventricular septum horizontally in the image. In this particular position, the left ventricular outflow tract view can be obtained simply by rotating the transducer 20 to

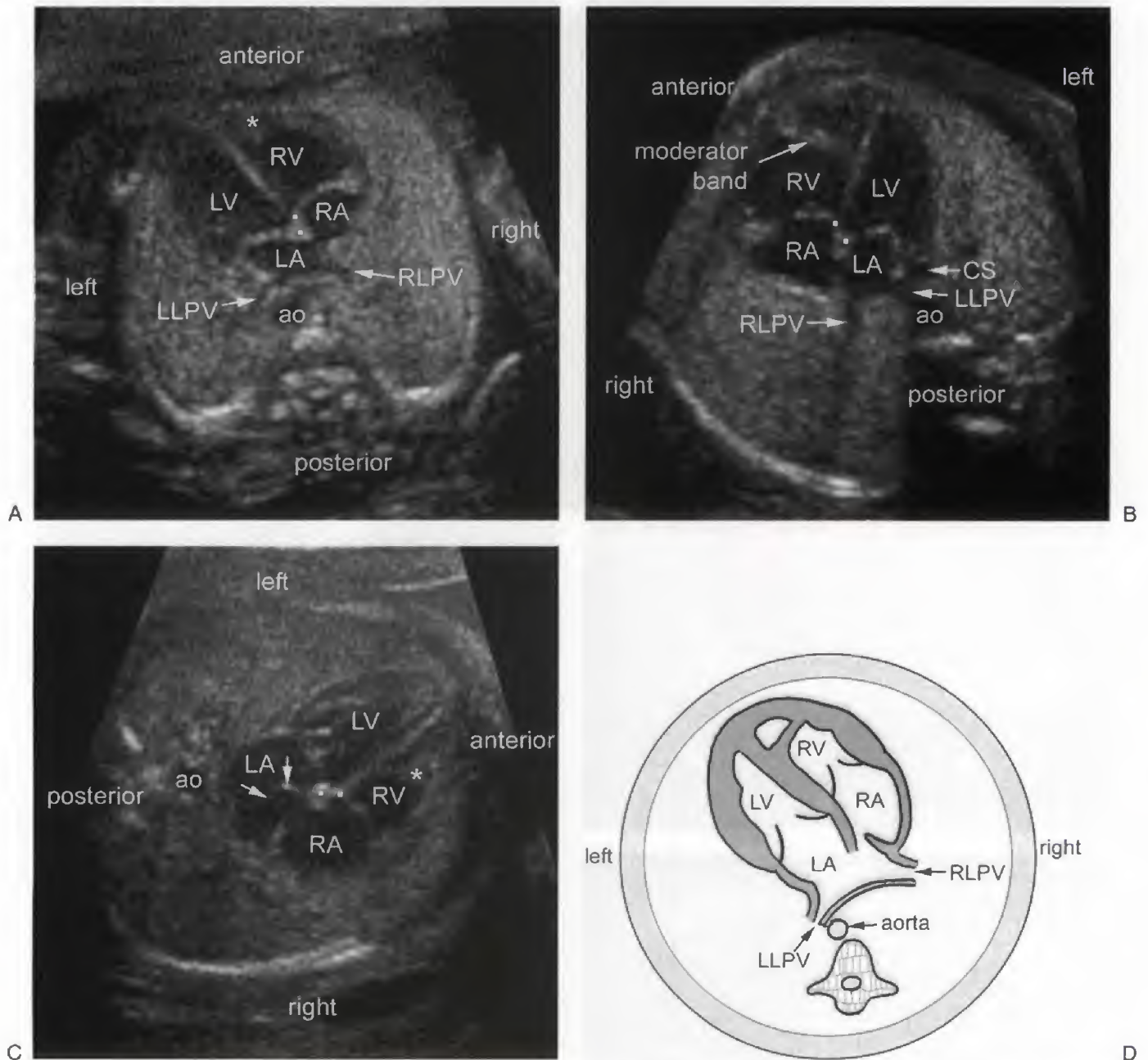
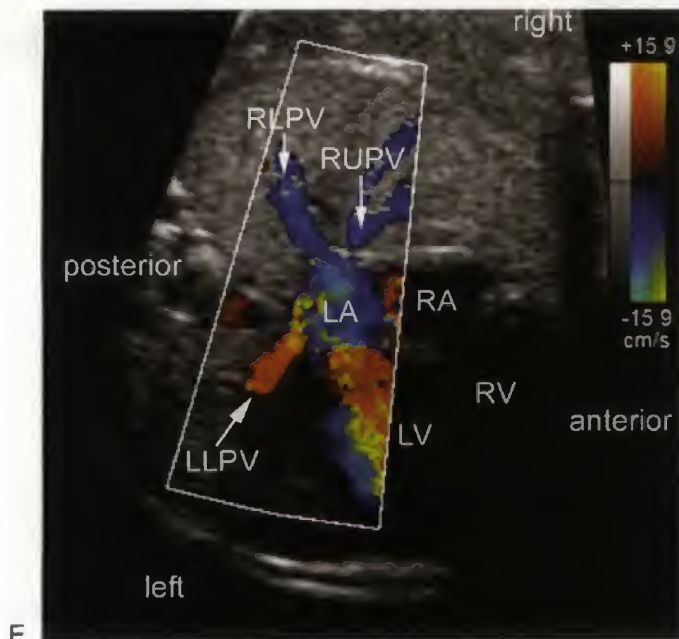


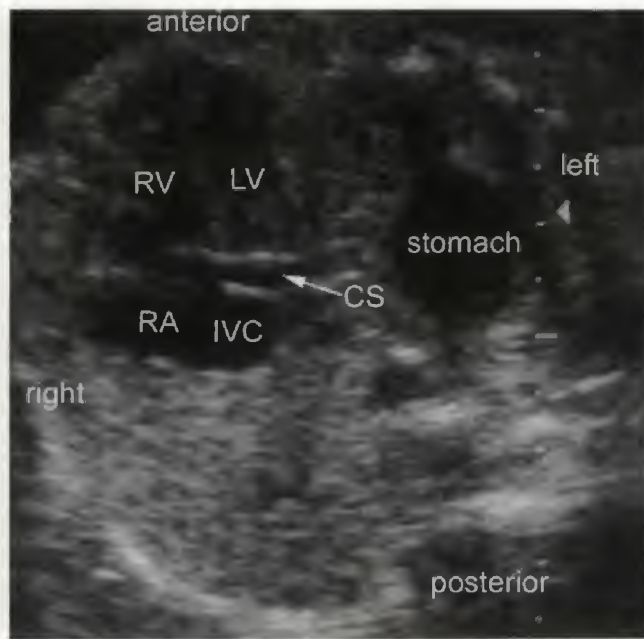
**FIGURE 14-6.** Four-chamber and five-chamber views (A–D). Three different four-chamber views and diagram (D). The right- and left-sided chambers are symmetric in size. The atrioventricular valves have offset attachments (dots in A–C) to the septum with the tricuspid valve having more apical attachment than the mitral valve. The apex of the right ventricle (RV) is obliterated in A and C by the moderator band (*asterisk*). The moderator band can also be seen as a distinct muscle bundle as shown in B. Right and left lower pulmonary veins (RLPV and LLPV) course obliquely forward as they connect to the left atrium (LA). The central part of the atrial septum is the septum primum (*arrows* in C). It is thin and mobile, and bulges into the left atrium. The descending aorta (ao) is seen at the left anterior corner of the spine.

*Continued*

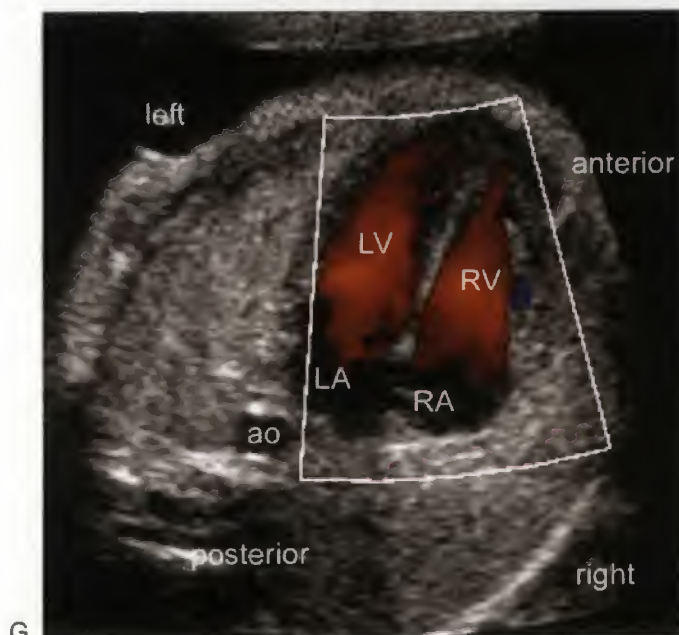




E



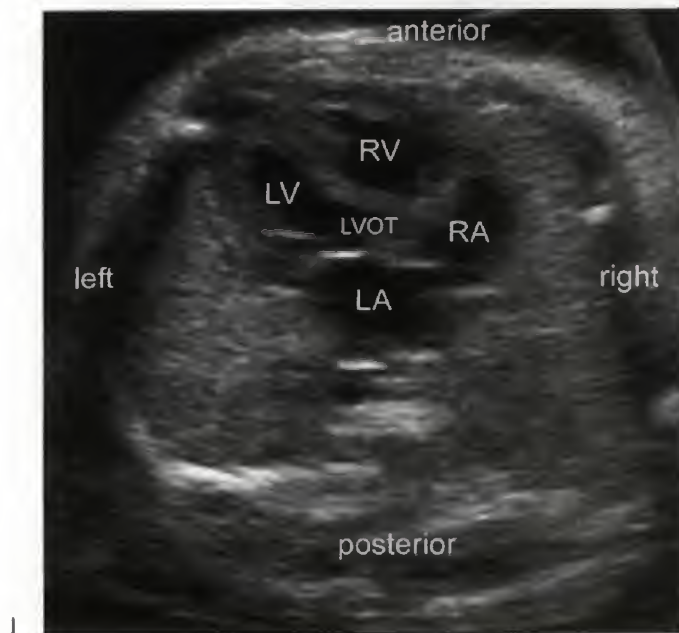
F



G



H



I

**FIGURE 14-8 cont'd.** E. Color Doppler image in four-chamber plane showing both lower pulmonary veins and the right upper pulmonary vein (RUPV). Both lower pulmonary veins course obliquely forward, whereas the right upper pulmonary vein courses obliquely backward as it connects to the left atrium. F. A lower section below the four-chamber view. The coronary sinus (CS) is seen as a tubular structure between the left ventricle (LV) and the inferior vena caval orifice (IVC). Note that its proximal part of the coronary sinus can be seen as a small round circle at the left atrioventricular junction in a regular four-chamber view as shown in B. G. Color Doppler image shows flow through the atrioventricular valves. H. Color Doppler image and Doppler spectrum show trivial tricuspid regurgitation (TR). E and A are the early and late diastolic peaks of the tricuspid inflow, respectively. I. Five-chamber view. A section slightly cranial to the regular four-chamber shows the left ventricular outflow tract (LVOT). RA, right atrium.

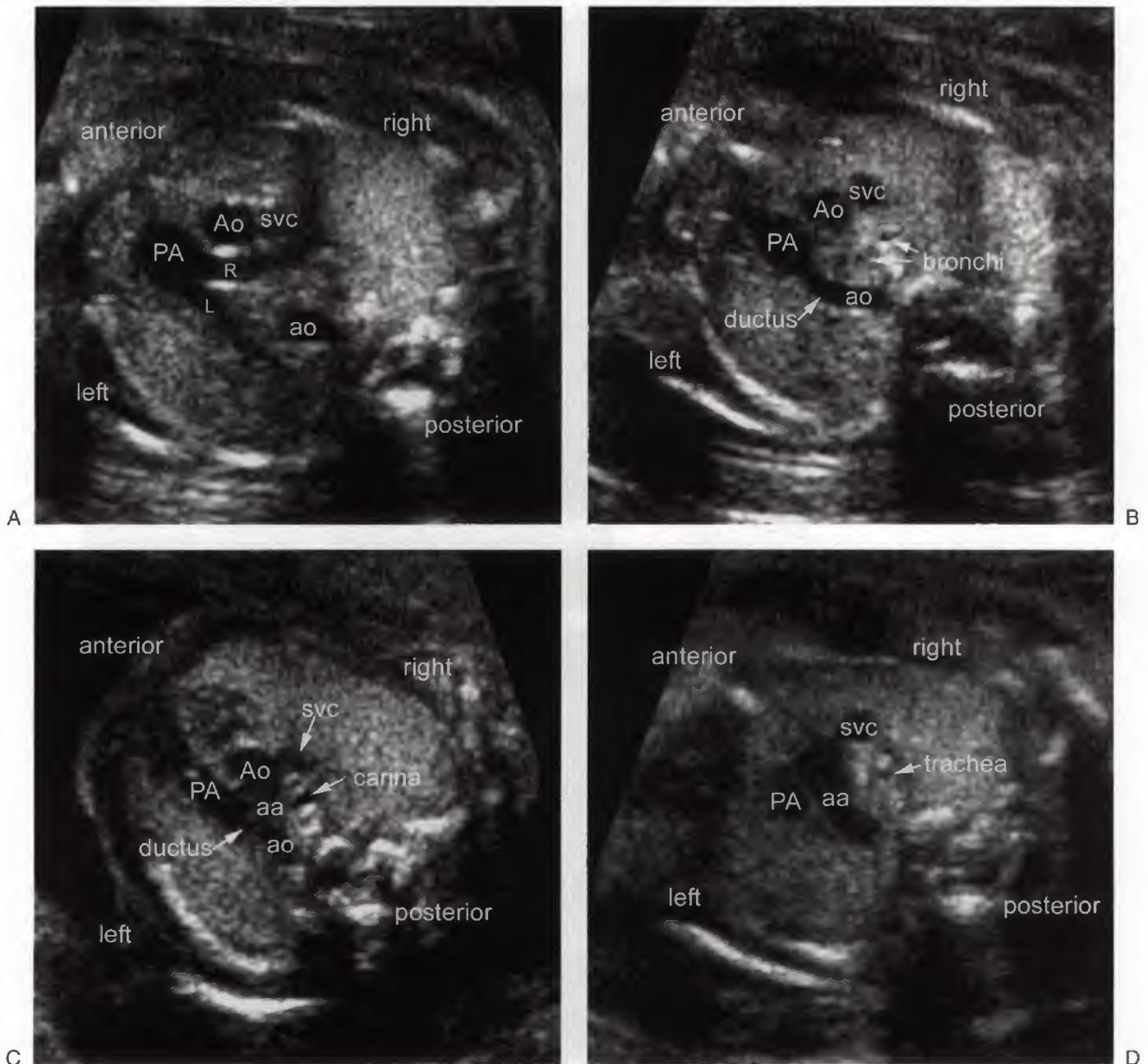


**FIGURE 14-7.** Three-vessel view and its vicinity. A–E. Serial transverse views of the upper mediastinum and a diagram (E) showing the anatomy of the three-vessel view. In its most basal cut (A), the main pulmonary artery (PA) branches into the right (R) and left (L) pulmonary arteries. Above this level (B), where the main pulmonary artery continues to the descending aorta (ao) through the ductus arteriosus, the following three vessels: the main pulmonary artery, the ascending aorta (Ao) and superior vena cava (svc) are aligned in a straight line from the left anterior aspect to the right posterior aspect of the thorax. The three vessels are sized in a decreasing order with the main pulmonary artery being the largest and the superior vena cava the smallest. The right and left bronchi, filled with fluid, are seen in the middle mediastinum. Immediately above this level (C), the aortic arch (aa) and ductus arteriosus form a V-shaped confluence at the descending aorta on the left side of the carina of the trachea. In the most cranial level of the three vessels (D), the sausage-shaped aortic arch is seen on the left side of the trachea.

*Continued*



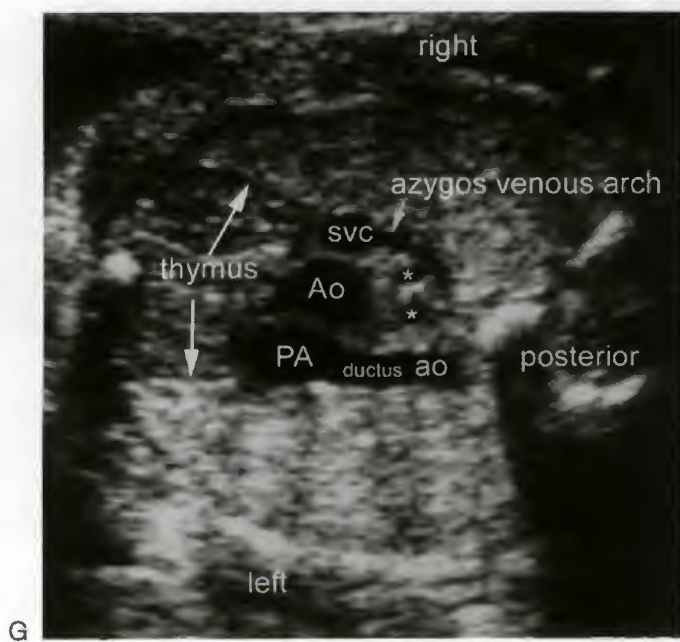
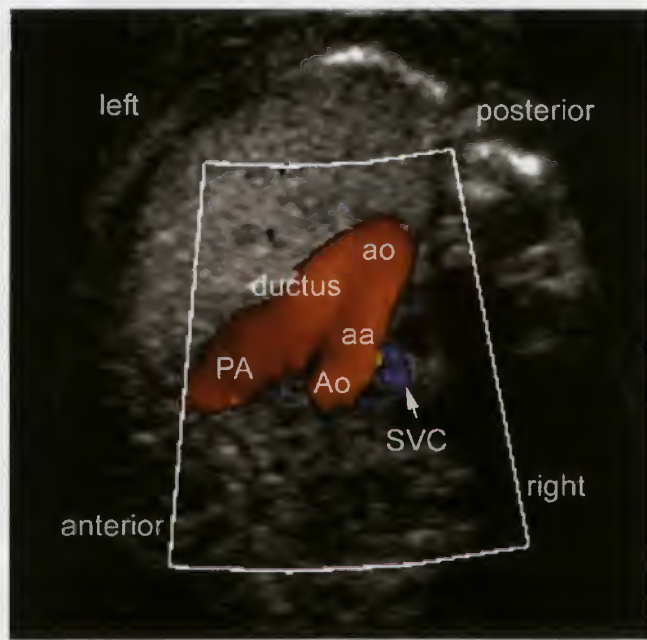
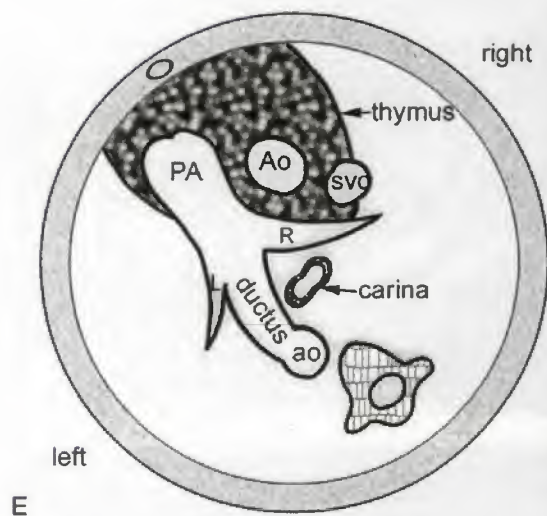


**FIGURE 14-7 cont'd.** *F.* Color Doppler image in three-vessel plane shows a V-shaped confluence of the aortic arch and ductus arteriosus at the descending aorta. *G.* Three-vessel view taken from the right side of the fetus shows the thymus demarcated by thin echogenic lines. The echogenicity of the thymus is slightly different from the adjacent lungs. The thymus contains spindle-shaped echogenic spots. Note the azygos venous arch on the right side. Asterisks are right and left main bronchi.



**FIGURE 14-8.** Left and right ventricular outflow tract views. A. Composite diagram showing how the ventricular outflow tract views are obtained in a fetus in supine cephalic presentation. The scan starts from any transducer position for a four-chamber view (panel a). In step I, the transducer is moved around the fetal chest until the ventricular septum is seen horizontally in the four-chamber view (panel b). In step II, the transducer is rotated 20 to 30 degrees (clockwise in this example with a fetus laying in supine cephalic presentation) towards the cardiac apex until the left ventricular outflow tract view (panel c) is shown. In step III, the transducer is moved upward towards the fetal head until the right ventricular outflow tract view (panel d) is shown. (Modified with permission from Yoo SJ, Lee YH, Kim ES, et al: *Tetralogy of Fallot in the fetus: Findings at targeted sonography. Ultrasound Obstet Gynecol* 14:29, 1999.) B–D. Left ventricular outflow tract views and diagram. Both the inlet and outlet of the left ventricle (LV) are seen. The anterior leaflet of the mitral valve is the anterior border of the left ventricular inlet in diastole, and the posterior border of the left ventricular outlet during systole. The aortic and mitral valves are in direct contact (asterisk). The left ventricular outflow tract courses upward and slightly forward. *Continued*



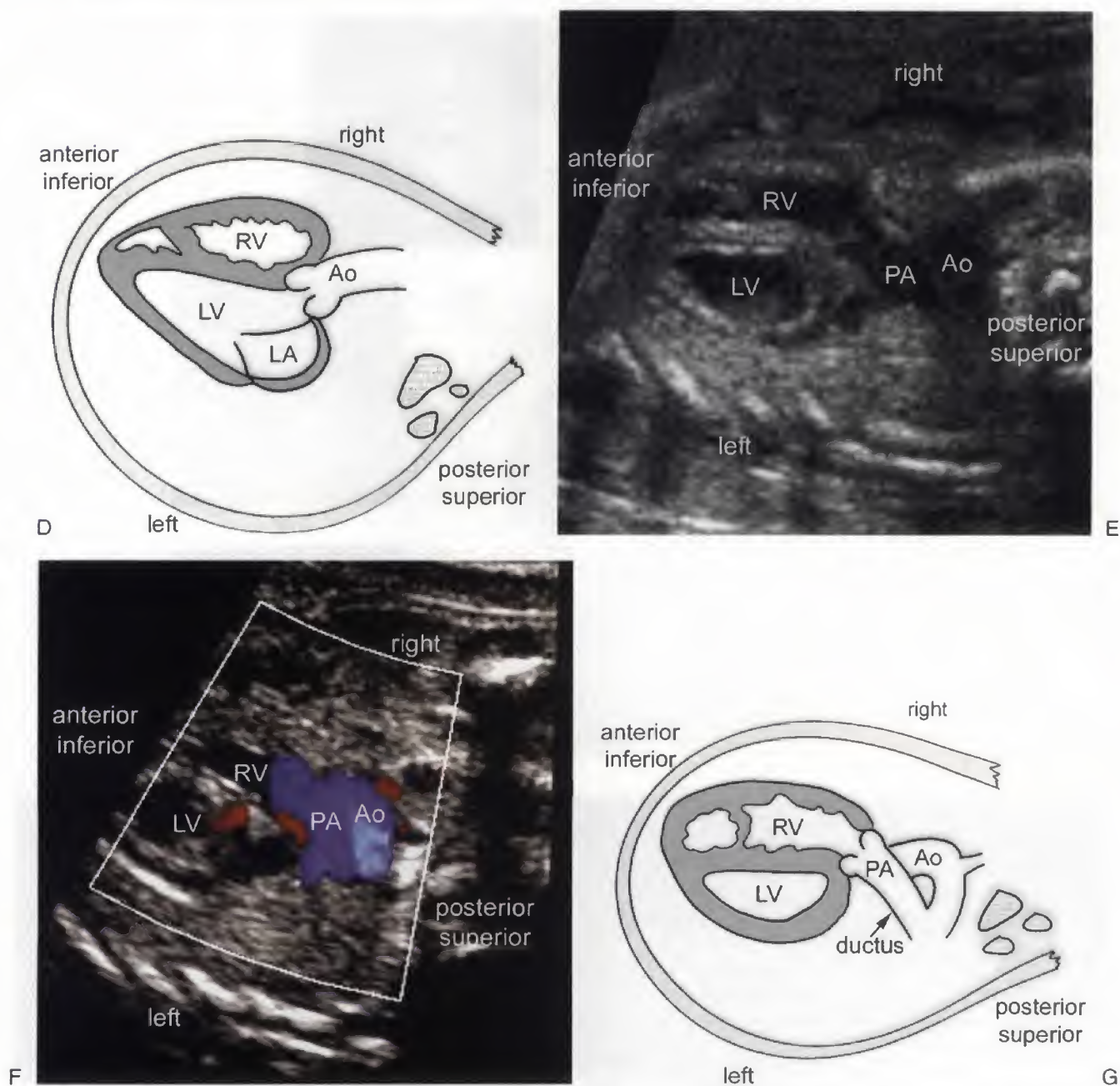


**FIGURE 14-8 cont'd.** E–G. Right ventricular outflow tract views and diagram. The right ventricular (RV) outflow tract leads to the main pulmonary artery (PA) upward and backward. Note the crossing nature of the ventricular outflow tracts to the arterial trunks by comparing the left and right ventricular outflow tract views. Ao, ascending aorta; ao, descending aorta; LA, left atrium; RA, right atrium.

30 degrees clockwise or counterclockwise toward the cardiac apex. By sliding the transducer upward toward the fetal head from this plane, the right ventricular outflow tract view can be obtained. By moving the transducer slightly up and down along the fetal thorax, the crossing nature of the ventricular outflow tracts can be clearly appreciated. Occasionally, the ventricular septum is hard to place perpendicular to the sonographic beam. In this situation, the transducer is positioned to the apex of the heart and then angled cranially toward the fetal head so that the sonographic beam is aligned parallel with the long axis of the

heart. This latter maneuver, however, is more difficult than the former. The left ventricular outflow tract view demonstrates not only the left ventricular outflow tract but also the left ventricular inlet, with the anterior leaflet of the mitral valve demarcating the two (see Fig. 14-8B to D). The aortic valve is in direct contact with the mitral valve, and therefore, the left ventricular outflow tract is not completely muscular. This is in contrast to the right ventricle, in which there is discontinuity between the pulmonary and tricuspid valves because of the presence of an intervening muscular crest that is called crista supraventricularis or ventriculoinfundibular



fold. Therefore, the right ventricular outflow tract is a completely muscular tunnel. The ventricular septum seen in the left ventricular outflow tract view is the more anterior part of the ventricular septum as compared with the septum seen in the four-chamber view. The part of the ventricular septum that abuts the aortic valve is the membranous septum, which is most commonly involved in ventricular septal defects. Commonly, this area of the septum normally appears defective because the septum has a curved configuration and the septum below the aortic valve is the thin membranous part, which makes the diagnosis of a small ventricular septal defect in this region very difficult. In the right ventricular outflow tract view, the right ventricular outflow tract leads to the main pulmonary artery upward and backward (see Fig. 14-8E to G). This is in contrast with the left ventricular outflow tract that courses upward and forward. In the left and right ventricular outflow tract views, the blood flow across the aortic and pulmonary valves should be assessed by using color Doppler with a velocity set at 80 to 100 cm/sec (see Fig. 14-8C and F).

The basal short-axis view is rather difficult to obtain. This view is an oblique view through the right lobe of the liver and the left shoulder (see Figs. 14-4 and 14-9). When an oblique section through these two structures is obtained, the transducer is angled up and down until the cross-sectioned aortic valve is encircled by the right atrium, right ventricle, main pulmonary artery, and right pulmonary artery. This view clearly shows the discontinuity between the tricuspid and pulmonary valves due to the crista supraventricularis or ventriculoinfundibular fold separating the two valves (*asterisks* in Fig. 14-9A). This view is best for assessing patency of the right ventricular outflow tract. As seen in the left ventricular outflow tract view, the part of the septum abutting the tricuspid valve is the membranous septum and, therefore, may appear defective. After the main pulmonary artery bifurcates into the right and left pulmonary arteries, the right pulmonary artery courses rightward along the posterior wall of the aortic valve, whereas the left pulmonary artery continues to the descending aorta through the ductus arteriosus. A different but equivalent anatomy can be seen in right anterior oblique long axis view of the right ventricle (see Fig. 14-9D). This view visualizes the three components of the right ventricle, namely the inlet, trabecular, and outlet parts. The three vessels are also visualized in their oblique or longitudinal sections.

The aortic arch view can be obtained from a three-vessel view. The transducer is moved around the fetal thorax until the sonographic beam is aligned with the cross-sections of the ascending and descending aorta (Fig. 14-10).<sup>55,56</sup> The cross-sections of the ascending and descending aorta are then seen vertically in the three-vessel view. In this position, the transducer is rotated 90 degrees in either clockwise or counterclockwise direction and the aortic arch is shown as a candy cane configuration. The ductal arch view can be obtained in a similar manner. The transducer is moved around the fetal thorax until the oblique section of the main pulmonary artery and the cross-section of the ascending aorta are aligned vertically in the three-vessel view. Then, the transducer is rotated 90 degrees in either direction and a hockey stick view of the ductal arch is produced. In the aortic arch view, the ascending aorta arises from the center of the heart between the right and left atria and, therefore,

is some distance from the anterior chest wall. The aortic arch view shows the right innominate, left carotid, and left subclavian arteries arising from the greater curvature side of the arch. On the other hand, the ductal arch arises far anteriorly, immediately behind the anterior chest wall, as its proximal part is the main pulmonary artery. It takes a rather long course backward as it connects to the descending aorta through the ductus arteriosus. In contrast to the aortic arch, the ductal arch does not give rise to any branch to the head and neck. When the fetus is in either right or left lateral decubitus position, the candy cane and hockey stick views are not possible to obtain. Both arches are then assessed in transverse views (see Fig. 14-7B to F). In the later pregnancy, the ductus arteriosus may become tortuous and a faulty diagnosis of the aneurysm of the ductus arteriosus can be entertained (see Fig. 14-10F).

Normal measurement data for cardiac and major vascular dimensions are listed in the appendix.

## Clues to the Abnormalities

Table 14-2 lists the key anatomic structures that should be investigated and the clues to the presence of CHD at each screening view.

## Transverse View of the Upper Abdomen

The transverse view of the upper abdomen provides the main information regarding whether the visceral situs is normal or abnormal, and if it is abnormal, the pattern of situs most likely present. This is important because situs abnormalities are harbingers of CHD (Tables 14-3 and 14-4).<sup>34,57-60</sup>

The term visceral situs refers to the pattern of arrangement of the body organs relative to the midline or sagittal plane. There are three types of visceral situs: namely, *situs solitus*, *situs inversus*, and *heterotaxy* (Fig. 14-11).<sup>58,61</sup> The visceral situs can usually be determined by observing the location of the liver, stomach, abdominal aorta, and inferior vena cava as seen in the transverse view of the upper abdomen.

In *situs solitus*, the larger lobe of the liver and gall bladder are seen on the right and the stomach on the left (see Fig. 14-5). The spleen can be identified along the posterolateral wall of the stomach as a sickle-shaped structure. The abdominal aorta is located posteriorly at the left anterior aspect of the spine. The inferior vena cava is located more anteriorly on the right as it connects to the right-sided right atrium. In *situs inversus*, these right-left relationships are inverted (Fig. 14-12A). *Situs inversus* may escape detection if the right and left sides of the fetal body are not defined in the beginning of the fetal echocardiographic examination.

*Heterotaxy* (Greek, *heteros* [other than] + *taxis* [arrangement]) indicates an arrangement of the organs that is different from the orderly arrangement of either *situs solitus* or *situs inversus* (see Fig. 14-12B and C).<sup>61</sup> *Heterotaxy* has often been called *situs ambiguus*, which means uncertain situs. However, 'situs ambiguus' is not an appropriate term, because the organ arrangement in *heterotaxy* is not uncertain but rather complex or hard to define.<sup>34</sup> Abdominal *heterotaxy* is characterized by jumbled-up arrangement of the nonpaired organs. *Heterotaxy* is almost always associated with asplenia or polysplenia.<sup>57,58,62-68</sup> *Heterotaxy* with



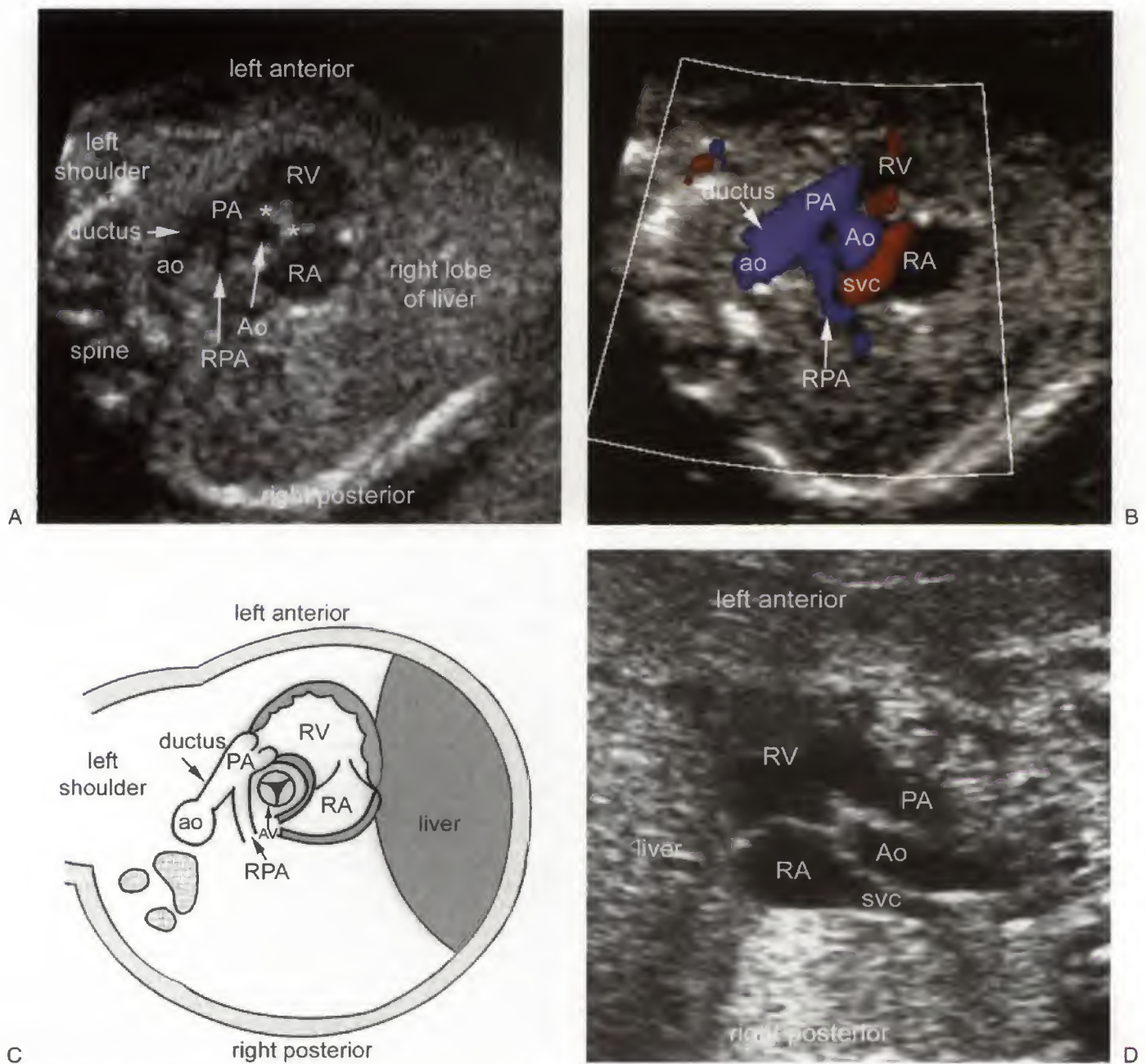


**FIGURE 14-9.** Basal short-axis view and an alternative view. A–C. Basal-short axis views and diagram. The cross-section of the aortic valve (AV) or the ascending aortic root (Ao) is encircled by the right atrium (RA), right ventricle (RV), main pulmonary artery (PA) and right pulmonary artery (RPA). Note the discontinuity between the tricuspid and pulmonary valve annuli (*asterisks*). The right ventricular outflow tract is widely open. The main pulmonary artery connects to the descending aorta (ao) through the ductus arteriosus. (D) Right anterior oblique view of the right ventricle. This view is equivalent to the x-ray angiographic right anterior oblique view. The three components of the right ventricle, the inlet, apical trabecular, and outlet parts are well shown. The three vessels—the main pulmonary artery, the ascending aorta, and the superior vena cava (SVC)—are aligned as they are typically seen in the three-vessel view.

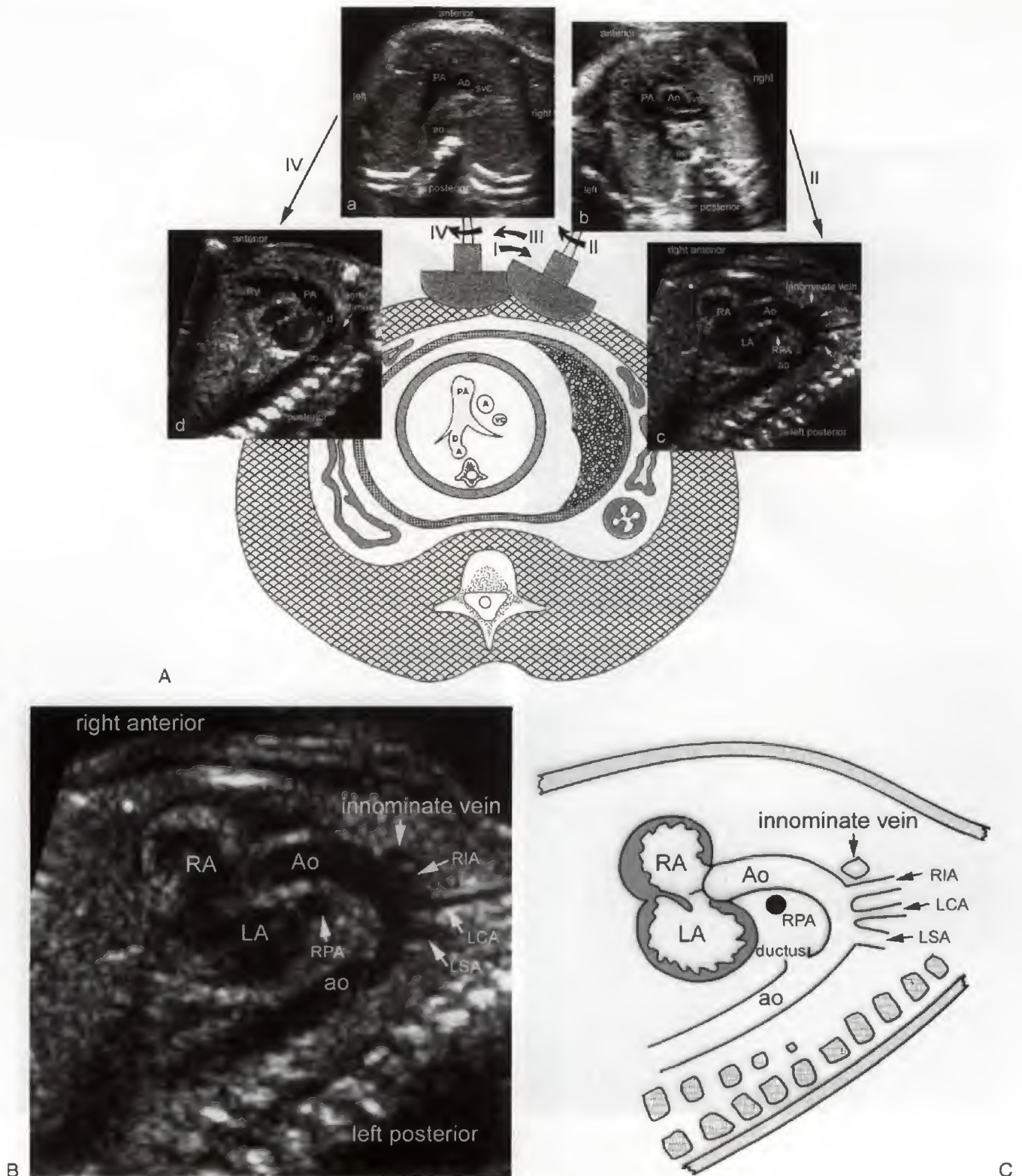


**FIGURE 14-10.** Aortic and ductal arch views. **A.** Composite diagram showing how the aortic and ductal arch views are obtained in a fetus in supine cephalic presentation. The scan starts from any transducer position for a three-vessel view (*panel a*). In step I, the transducer is moved around the fetal chest until the ascending aorta (Ao) and descending aorta (ao) are aligned vertically in the three-vessel view (*panel b*). In step II, the transducer is rotated 90 degrees either clockwise or counterclockwise until the aortic arch is seen as a candy cane-like structure (*panel c*). In step III, the transducer is moved back to a three-vessel view and moved around the fetal chest until the main pulmonary artery (PA) and the descending aorta (ao) are vertically aligned (*panel a*). In step IV, the transducer is rotated 90 degrees either clockwise or counterclockwise until the ductal arch is seen as a hockey stick-like structure (*panel d*). (Modified with permission from Yoo SJ, Lee YH, Kim ES, et al: *Tetralogy of Fallot in the fetus: Findings at targeted sonography. Ultrasound Obstet Gynecol* 14:29, 1999.) **B and C.** Aortic arch views and diagram. The aortic arch arises from the space between the right (RA) and left (LA) atria, and therefore, its origin is some distance away from the anterior chest wall. The aortic arch gives rise to the right innominate or brachiocephalic (RIA), left common carotid (LCA), and left subclavian (LSA) arteries. The cross-section of the innominate vein is seen in front of the right innominate artery. The cross-section of the right pulmonary artery (RPA) is seen immediately behind the ascending aorta. *Continued*



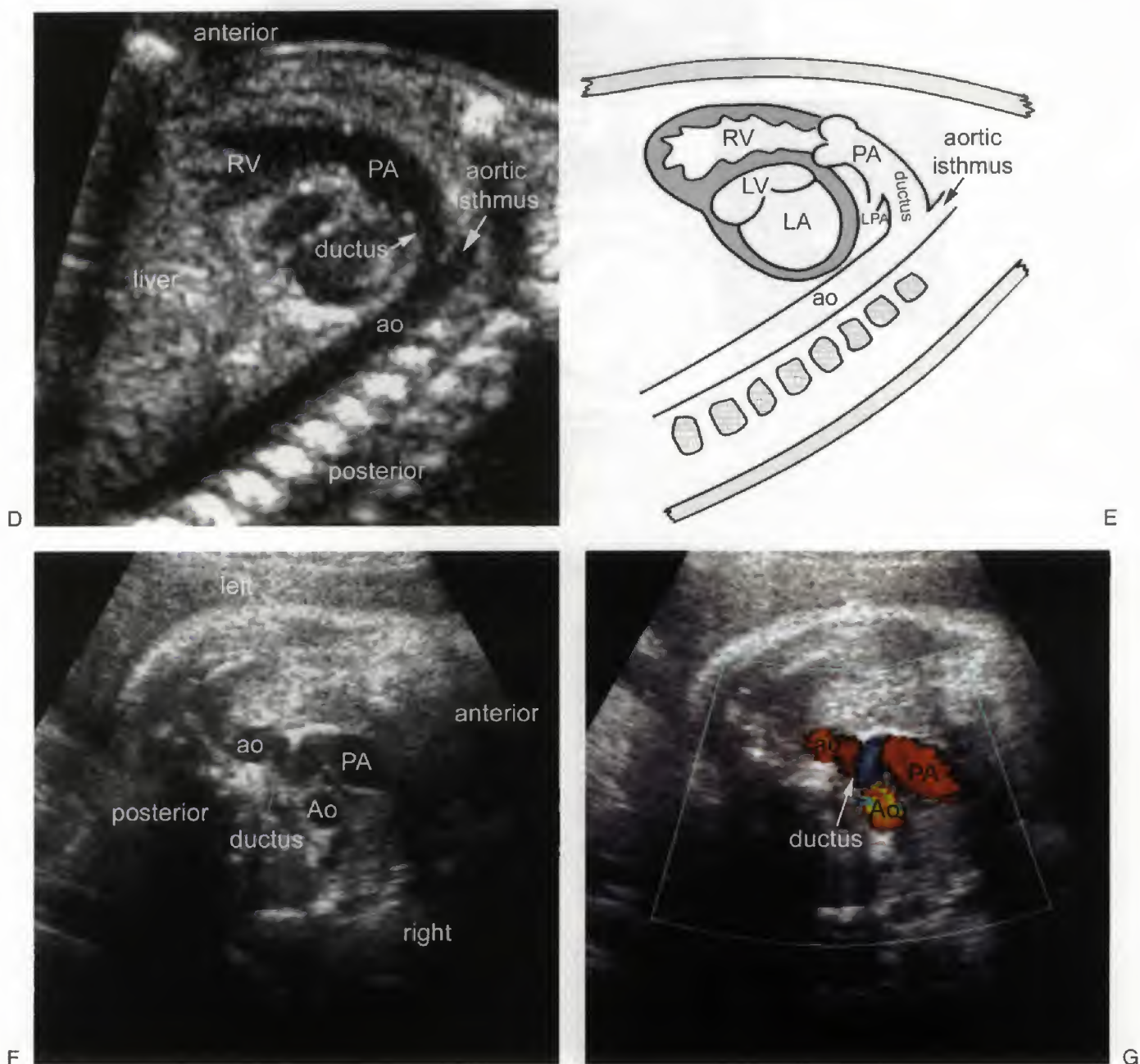


**FIGURE 14-10 cont'd.** *D* and *E*. Ductal arch views and diagram. The ductus arteriosus connects the main pulmonary artery to the descending aorta, thus forming a hockey stick-shaped arch. As its proximal part is the main pulmonary artery, its origin is immediately behind the anterior chest wall. In contrast to the aortic arch, it does not give rise to any head and neck branches. *F* and *G*. Tortuous ductus arteriosus in a fetus at 35 weeks of gestation. The ductus arteriosus tends to become tortuous in later pregnancy. It can be mistaken for an aneurysm of the ductus arteriosus. Color Doppler image (*G*) shows a U-loop of the ductus arteriosus with blue and red signals. LPA, left pulmonary artery.

**Table 14-2** Clues to the Abnormality at Each Sonographic View

Sonographic View	Structures to Investigate	Clues to Abnormalities
Transverse view of upper abdomen	Larger lobe of the liver Stomach Abdominal aorta Inferior vena cava	Abnormal position of the stomach and liver Absent or multiple spleens Aorta and inferior vena cava on the same side of the spine Interruption of the inferior vena cava
Four-chamber view	Position, size and axis of the heart Size symmetry of cardiac chambers and great vessels Pulmonary veins Atrioventricular valve attachment and function Moderator band Septal integrity	Cardiac malposition Displaced heart Abnormal cardiac axis Abnormal atrioventricular connections; discordant connection, univentricular connection Cardiomegaly Asymmetric chamber and valve size Atrial, ventricular or atrioventricular septal defect Apical displacement of the septal leaflet of the tricuspid valve Abnormal pulmonary venous connections
Three-vessel view	Vessel number, alignment and size Position and size of aortic and ductal arches Trachea and bronchi Branch pulmonary arteries	Dilatation of the aorta, pulmonary trunk or superior vena cava Discrepancy in great arterial size Abnormal vessel alignment Abnormal vessel arrangement Aortapulmonary window Only two vessels Additional vessel Right descending aorta Abnormal origin or course of a pulmonary artery Ductal constriction or aneurysm Small or absent thymus
Left and right ventricular outflow tract views	Crossing nature of outflow tracts to arterial trunks Patency of outflow tracts and semilunar valves Septal integrity	Abnormal ventriculoarterial connections: transposition, double outlet right or left ventricle; and single arterial trunk Ventricular septal defect Overriding aorta or pulmonary trunk Abnormal dimension of the outflow tracts and/or arterial valves
Basal short-axis view	Crista supraventricularis Sub pulmonary outflow tract Size of aortic valve and left ventricular outflow tract	Ventricular septal defect in the outlet septum Right ventricular outflow tract narrowing Small size of the aortic valve
Aortic and ductal arch views	Position, contour and size of aortic and ductal arches Patency of the aortic arch Aortic arch branches	Ascending aorta smaller than descending aorta Focal or diffuse narrowing of the aortic arch Interruption of the aortic arch Right aortic arch Double aortic arch Ductal constriction or aneurysm Vessel behind the trachea

**Table 14-3** Incidence of Congenital Heart Disease in Various Forms of Cardiac Malposition<sup>1, 57-60</sup>

Visceral Situs and Heart Position	Incidence of Heart Defects
Situs solitus with levocardia (normal heart position)	<1%
Situs solitus with dextrocardia	>90%
Situs inversus with dextrocardia	10%–50%
Situs inversus with levocardia	>95%
Heterotaxy with right isomerism	~100%
Heterotaxy with left isomerism	Majority

asplenia is characterized by a symmetric liver extending from one side of the abdomen to the other with the stomach on either side (see Fig. 14-12B). In most cases of asplenia, the inferior vena cava and abdominal aorta are juxtaposed on the same side of the spine, with the former being located in front of the latter.<sup>62,64,67,69,70</sup> Heterotaxy with polysplenia also shows an abnormally disposed liver with the stomach on either side (see Fig. 14-12C). In most cases of heterotaxy with polysplenia, the liver has an asymmetric contour with one side being larger than the other. In 75% to 90% of cases of polysplenia, the inferior vena cava shows interruption of its suprarenal-infrahepatic segment and connects instead to the azygos or hemiazygos vein to drain into the SVC.<sup>63-65,69,70</sup> Interruption of the inferior vena cava is suspected when two, rather than one, vessels are seen in front of the spine in



**Table 14-4****Abnormal Findings at Transverse View of the Upper Abdomen**

Abnormal Finding	Significance
Stomach on the right side	The body situs is abnormal
Mirror-image arrangement of the liver, stomach, inferior vena cava, and abdominal aorta	The situs is inverted.
Transverse liver	Either right isomerism or left isomerism. Left isomerism tends to show some asymmetry of the hepatic configuration.
Piggy-backed abdominal aorta behind the inferior vena cava on the same side of the spine (so-called juxtaposition)	Highly suggestive of right isomerism. The dilated azygos vein receiving the interrupted inferior vena cava can occasionally be seen on the same side of the spine but the aorta is the anterior vessel.
Interruption of the inferior vena cava	Occurs in 75%–90% of left isomerism and rarely in other types of body situs.
Multiple spleens or lobulated single spleen	Means polysplenia and occurs in left isomerism with few exceptions.
No identifiable spleen	Can be due to technical limitation but is typically seen in right isomerism with few exceptions.

the transverse view of the upper abdomen and thorax (Figs. 14-12C and 14-13). The two vessels are usually of a similar size and aligned side by side or obliquely, with the azygos or hemiazygos vein located more posteriorly. This relationship can also be appreciated in the coronal plane. The splenic status can be assessed by scrutinizing the posterolateral aspect of the stomach. In asplenia, the hepatic tissue extends posteriorly along the greater curvature of the stomach. In polysplenia, a few small splenic masses can be identified along the greater curvature of the stomach (see Fig. 14-12C). In the thorax, heterotaxy is characterized by symmetry in the lung lobation, the bronchial and pulmonary arterial branching, and the shape of the atrial appendages. Most cases of heterotaxy and asplenia have both sides resembling the normal right side (right isomerism or bilateral right-sidedness), whereas most with heterotaxy and polysplenia have both sides resembling the normal left side (left isomerism or bilateral left sidedness). Investigation of the symmetry of these paired organs is a difficult task in the fetus, although it is not impossible, whereas symmetric arrangement per se is of little functional significance.<sup>34,71</sup> It is very important, however, to thoroughly investigate the systemic and pulmonary venous drainage when the fetus shows abnormal visceral arrangement. CHD is exceedingly common in the presence of heterotaxy. Asplenia with right isomerism is almost always associated with severe CHD. Although left isomerism with polysplenia is also commonly associated with CHD, it is occasionally seen sporadically

and incidentally among patients receiving medical attention for purposes other than treatment for cardiac disease. Table 14-5 lists the CHDs and extracardiac defects that are commonly associated with the two forms of heterotaxy.

### Four-Chamber View

The four-chamber view is an excellent screening view for detection of CHDs in the fetus. A four-chamber screening is able to detect 50% to 60% of cardiac malformations.<sup>20,21</sup> It provides information about the position of the heart in the thorax, the overall heart size, the size of the individual chambers, the pulmonary venous connections to the atrial segment, the morphologic characteristics of the ventricles, the type of AV connection, and the integrity of the atrial, AV and ventricular septa (see Table 14-2).

The position of the heart is defined as levocardia, dextrocardia, or mesocardia according to where the main cardiac mass is located (Table 14-6 and Fig. 14-14). These terms are used only when the abnormal cardiac position is related primarily to the abnormality of the situs or the heart. When the heart is abnormally positioned secondary to the pulmonary, pleural, or diaphragmatic pathology, it is better to describe the side to which the heart is displaced. It is also preferable not to use the terms dextroversion, levoverion, dextroposition, and dextrorotation because they are defined differently among users and, therefore, confusing. Cardiac malposition is defined as any heart position other than levocardia in situs solitus.<sup>57,58,61</sup> This definition of cardiac malposition refers not only to cardiac position but also to the appropriateness of the cardiac position in relation to the body situs. Therefore, levocardia in situs inversus is also an example of cardiac malposition. CHD is very common when there is cardiac malposition (see Table 14-3).

The displacement of the heart from extracardiac causes is often due to a mass effect from a primary lesion (see Table 14-6).<sup>59,60,72</sup> These causes include diaphragmatic hernia or eventration, echogenic or cystic lung lesions such as cystic adenomatoid malformation, pulmonary sequestration, and bronchial atresia, lung tumor, and unilateral pleural effusion. The displacement of the heart can also be due to decreased volume of one lung, as in scimitar syndrome, unilateral absence of a branch pulmonary artery, and primary hypoplasia of a lung (see Fig. 14-14D).<sup>73</sup>

As discussed earlier, the cardiac axis is approximately 45 degrees away from the sagittal and coronal planes.<sup>36,37</sup> An abnormal base-apex axis of the heart is a clue to the diagnosis of a congenital malformation. The cardiac axis is directed more leftward in tetralogy of Fallot (see Fig. 14-14A) and truncus arteriosus, and when there is right chamber dilatation as in Ebstein anomaly, coarctation of aorta and hypoplastic left heart syndrome.<sup>36,37,55</sup> On the contrary, the cardiac axis tends to be directed more forward or even to the right in congenitally corrected transposition of the great arteries or double inlet left ventricle with discordant ventriculoarterial connection (see Fig. 14-14C).<sup>60,74-78</sup>

The AV connection and interventricular relationship are best defined in a four-chamber view.<sup>34</sup> To demonstrate this view, the ventricles should be identified according to their morphologic features. The septal attachment of the AV valves and the presence of the moderator band are the two most important morphologic criteria for ventricular identifi-

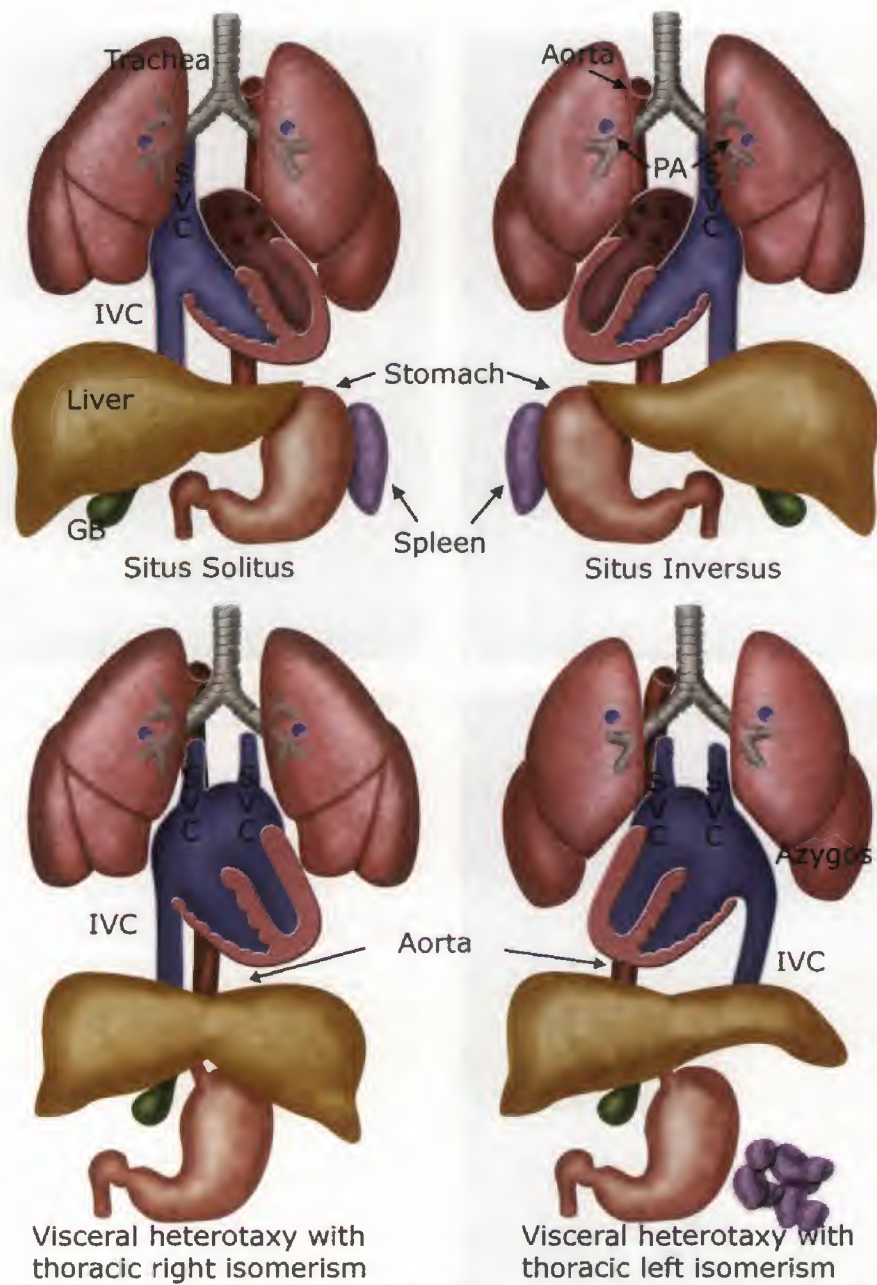


**FIGURE 14-11.** Types of visceral situs. GB, gallbladder; IVC, inferior vena cava; PA, branch pulmonary artery; SVC, superior vena cava. (Illustration by Shi-Joon Yoo, MD, and James A. Cooper, MD.)



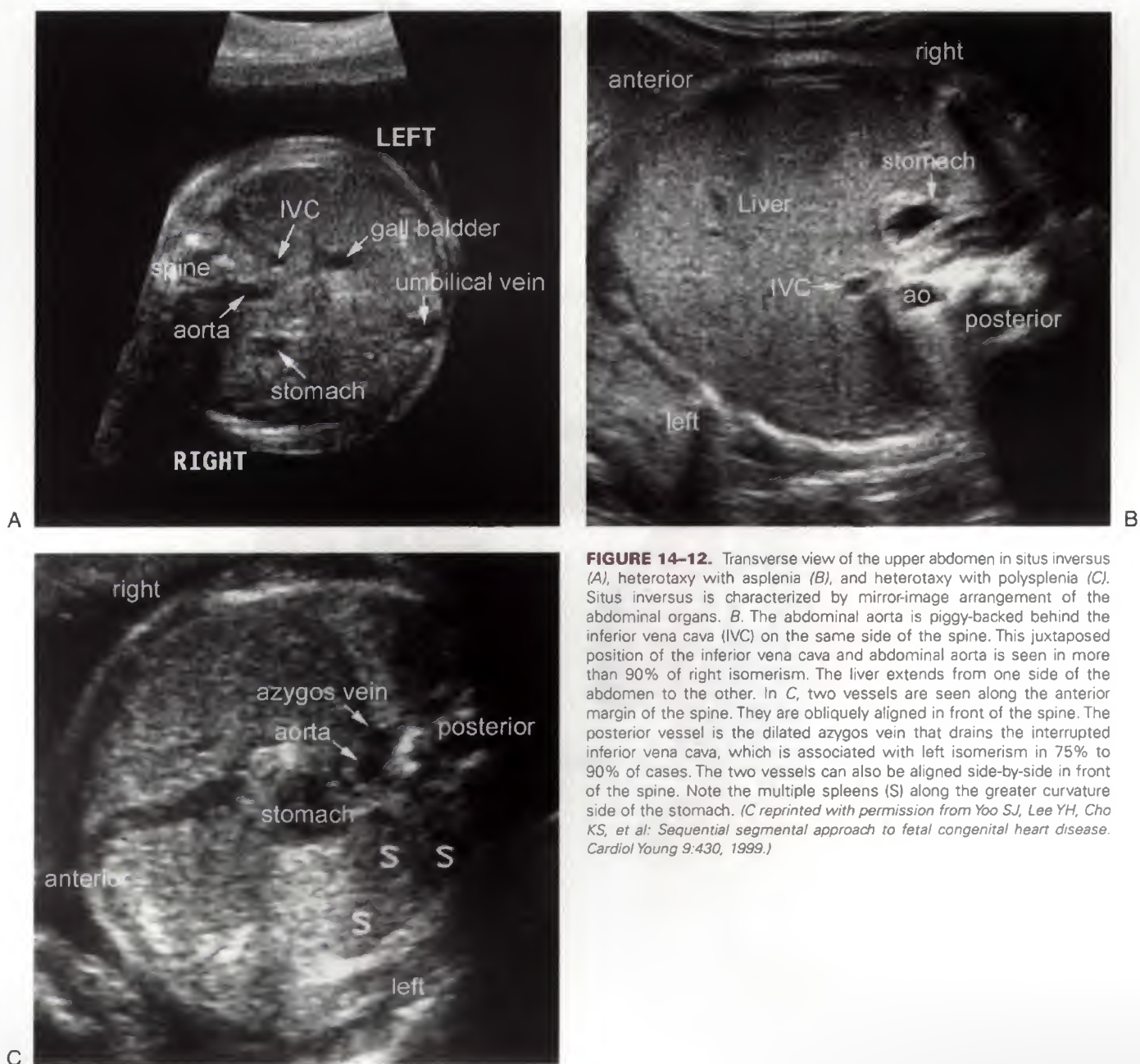


**FIGURE 14-12.** Transverse view of the upper abdomen in situs inversus (A), heterotaxy with asplenia (B), and heterotaxy with polysplenia (C). Situs inversus is characterized by mirror-image arrangement of the abdominal organs. B. The abdominal aorta is piggy-backed behind the inferior vena cava (IVC) on the same side of the spine. This juxtaposed position of the inferior vena cava and abdominal aorta is seen in more than 90% of right isomerism. The liver extends from one side of the abdomen to the other. In C, two vessels are seen along the anterior margin of the spine. They are obliquely aligned in front of the spine. The posterior vessel is the dilated azygos vein that drains the interrupted inferior vena cava, which is associated with left isomerism in 75% to 90% of cases. The two vessels can also be aligned side-by-side in front of the spine. Note the multiple spleens (S) along the greater curvature side of the stomach. (C reprinted with permission from Yoo SJ, Lee YH, Cho KS, et al: Sequential segmental approach to fetal congenital heart disease. *Cardiol Young* 9:430, 1999.)

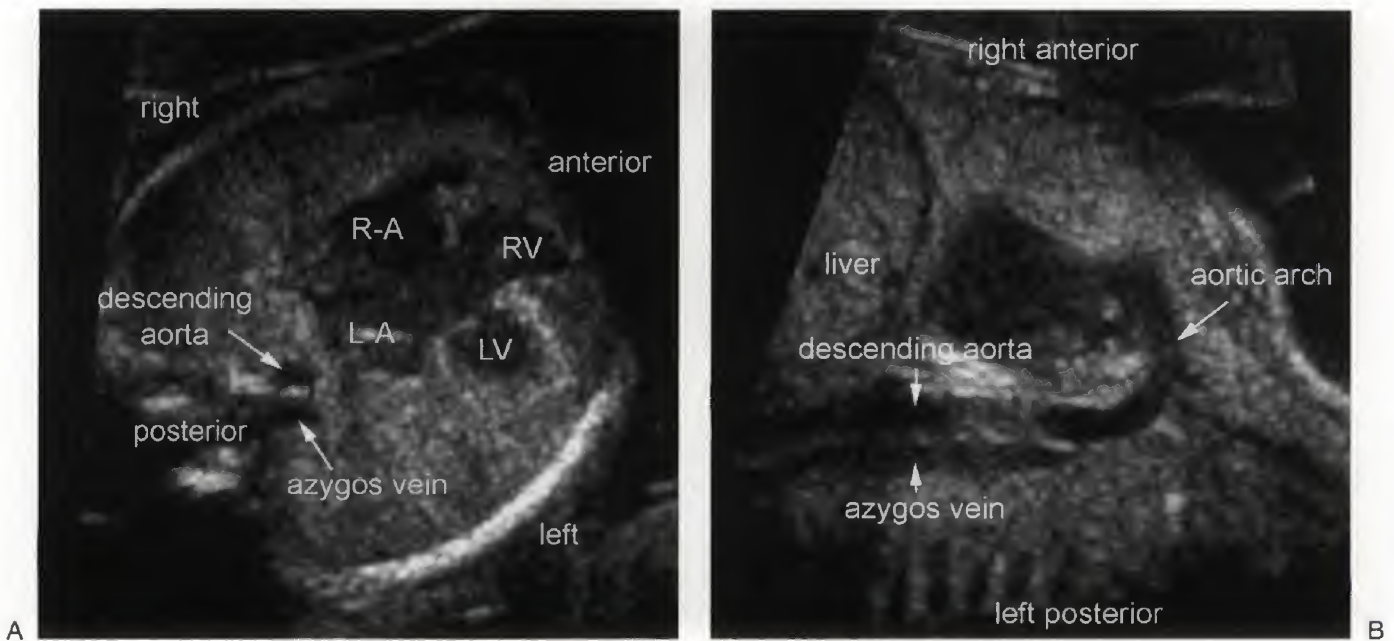


**FIGURE 14-13.** Left isomerism with interruption of the inferior vena cava. Two parallel large vessels are seen in front of the spine in both four-chamber (A) and oblique coronal (B) views. This is the characteristic feature of interrupted inferior vena cava with azygos or hemiazygos venous connection. L-A, left-sided atrium; LV, left ventricle; R-A, right-sided atrium; RV, right ventricle.

**Table 14-5** Common Cardiac and Extracardiac Defects in Right and Left Isomerisms<sup>57, 58, 62-66</sup>

	Right Isomerism	Left Isomerism
<b>Cardiac defects</b>		
Bilateral superior venae cavae	45%	45%
Absence of coronary sinus	~100%	~60%
Interruption of the inferior vena cava	<2.5%	75%–90%
Juxtaposition of the aorta and inferior vena cava	>90%	Uncommon
Extracardiac type of total anomalous pulmonary venous connection	50%, with obstruction in 50%	Rare
Atrioventricular septal defect	90%	50%
Atrioventricular connection	Univentricular in 70%	Biventricular in ~75%
Ventriculoarterial connection	Concordant only in 4%	Concordant in ~70%
Pulmonary atresia or stenosis	80%	30%
Left-sided obstructive lesion	<5%	~30%
Heart block/bradycardia	Rare	Common
<b>Extracardiac defects</b>		
Intestinal malrotation	Virtually all	Virtually all
Common extracardiac defects	Partial thoracic stomach (hiatal hernia) in ~25%	Biliary atresia and/or small or absent gallbladder in 20%, Urinary anomalies in 17%

cation (see Fig. 14-6). Once the morphologies of the ventricles are identified, the spatial relationship between the ventricles is defined. The ventricular relationship with the right ventricle on the right and the left ventricle on the left is called the d-loop ventricular relationship because it is the consequence of d-looping of the straight heart tube during embryogenesis (see Fig. 14-14A). The opposite relationship with the right ventricle on the left and the left ventricle on the right is called 'l-loop' ventricular relationship

(Fig. 14-14C). The pattern by which the atria are connected to the underlying ventricle or ventricles can be divided into biventricular and univentricular connections (Fig. 14-15).

Biventricular AV connections (see Fig. 14-15A) are either concordant or discordant when there is situs solitus or situs inversus. Discordant AV connection is almost always associated with discordant ventriculoarterial connection (Fig. 14-16). In this situation, the physiologic consequence of the discordant connection at the AV junction is cancelled



**Table 14-6** Abnormal Position of the Heart

Category	Significance
Dextrocardia or mesocardia (without lung, pleural or bony pathology)	Means that there is a congenital heart disease except for few exceptions.
Rightward displacement of the heart due to right lung hypoplasia	Differential diagnoses include scimitar syndrome, agenesis of the right pulmonary artery and primary right lung hypoplasia.
Leftward displacement of the heart due to left lung hypoplasia	Differential diagnosis includes agenesis of the left pulmonary artery and left lung hypoplasia.
Anterior displacement of the heart	Bilateral diaphragmatic hernia

out by another discordant connection at the ventriculo-arterial junction and, therefore, is rightfully called congenitally corrected transposition of the great arteries. When there is right or left isomerism, the AV connections are neither concordant nor discordant. Traditionally, these have been described as ambiguous connections. The AV connections in right or left isomerism, nonetheless, are not ambiguous. Instead, they need proper description.<sup>34</sup> Thus, they may be precisely described as right or left isomeric atria with biventricular connection to the ventricles exhibiting either a d-loop or l-loop ventricular relationship.

Univentricular AV connections (see Fig. 14-15*B*) are either in a form of double inlet connection or with absence of one AV connection, resulting in both atria connecting exclusively or mostly to one ventricle. Double inlet can lead to the main chamber of right or left ventricular morphology or to a solitary and indeterminate ventricle. Double inlet left ventricle is the most common type of double inlet in which the small right ventricle is usually located at the left upper aspect of the ventricular mass and there is discordant ventriculoarterial connection in the majority of cases (Fig. 14-17). Absent AV connections are seen involving more commonly the right AV junction than the left. The absent right AV connection is the key pathologic feature of tricuspid atresia (Fig. 14-18). The absent connection means that the atrium and the ventricle are apposed to each other but separated by the atrial and ventricular walls that are invaginated to the center of the heart.

### Ventricular Disproportion

When there is univentricular connection, it is often difficult to precisely distinguish the morphologically right from the morphologically left ventricle by fetal ultrasound. In this setting, the morphology of the ventricles can be defined just by observing where the rudimentary chamber is located.<sup>34</sup> The presence of the rudimentary ventricular chamber at the anterior and superior aspect of the main ventricular chamber indicates that the main ventricular chamber is the morphologically left ventricle (see Figs. 14-17 and 14-18). On the contrary, the presence of the rudimentary ventricular chamber at the posterior and inferior corner of the main

chamber indicates that the main ventricular chamber is the morphologically right ventricle (Fig. 14-19).

In the setting of normal situs solitus and normal AV and ventriculoarterial connections, the four-chamber view frequently shows asymmetry in the cardiac chambers.<sup>38,39,79</sup> Commonly, the asymmetry is due to dilated right atrium and right ventricle. Dilatation of the right atrium and ventricle means that there is increased blood flow volume through or valvar regurgitation on the right side of the heart, although it can also be due to right-sided heart failure (Table 14-7).

The most common causes of ventricular disproportion with right-sided dominance are the right-sided lesions. Significant tricuspid regurgitation is most often due to Ebstein malformation in which the septal and posterior leaflets of the tricuspid valve have their attachments downward into the right ventricle and are hypoplastic and dysplastic (Fig. 14-20).<sup>80</sup> As the displaced leaflets fail to align properly with the anterior leaflet, tricuspid regurgitation ensues during ventricular systole. Dilatation of the right atrium and right ventricle varies according to the severity of regurgitation. Uncommonly, the edges of the displaced septal and posterior leaflets are fused to the edge of the anterior leaflet, resulting in tricuspid stenosis with little regurgitation. In this stenotic form of Ebstein malformation, the right ventricle is not significantly dilated, whereas the right atrium is dilated. Tricuspid regurgitation can also be due to dysplastic valve leaflet without displaced attachments. Severe tricuspid regurgitation may be associated with progressive development of pulmonary stenosis or atresia and right-sided heart failure with hydrops fetalis.<sup>80-82</sup> A markedly dilated right atrium and right ventricle can be associated with atrial flutter. Severe cardiomegaly of any cause is complicated by significant lung hypoplasia that may further complicate the intrauterine and postnatal courses. A small pulmonary artery size in the presence of right atrial dilatation is suggestive of restricted flow through the pulmonary valve. This is typically seen with tricuspid regurgitation with or without pulmonary stenosis or atresia (Fig. 14-21).<sup>80</sup> In the majority of cases with pulmonary atresia or critical stenosis with intact ventricular septum, the right atrium is markedly dilated due to tricuspid regurgitation, whereas the right ventricle is markedly hypertrophied and its cavity shows a variable degree of hypoplasia.<sup>83</sup> Less commonly, pulmonary atresia is associated with a dilated right ventricle. This latter category has a much poorer prognosis, and the pulmonary atresia or severe stenosis is secondary to the tricuspid pathology. The sole source of blood supply to the pulmonary arteries in pulmonary atresia with intact ventricular septum is the ductus arteriosus. On color Doppler interrogation, one may recognize the forward flow in the right ventricle and retrograde flow in the main pulmonary artery kissing at the atretic pulmonary valve (see Fig. 14-21*C*). A small main pulmonary artery may not be obvious at fetal ultrasound.<sup>47</sup> Pulmonary atresia with a hypertrophied hypoplastic right ventricle is commonly associated with coronary arterial abnormalities that include dilatation with fistulous communication with the right ventricle, ostial stenosis and interruption of coronary arterial luminal patency.<sup>84</sup> Communications between the coronary arteries and hypoplastic hypertensive right ventricle can be demonstrated with color Doppler interrogation.<sup>85</sup>

Trivial tricuspid regurgitation is not uncommon but it is rarely significant when it is seen in the 18- to 20-week scan

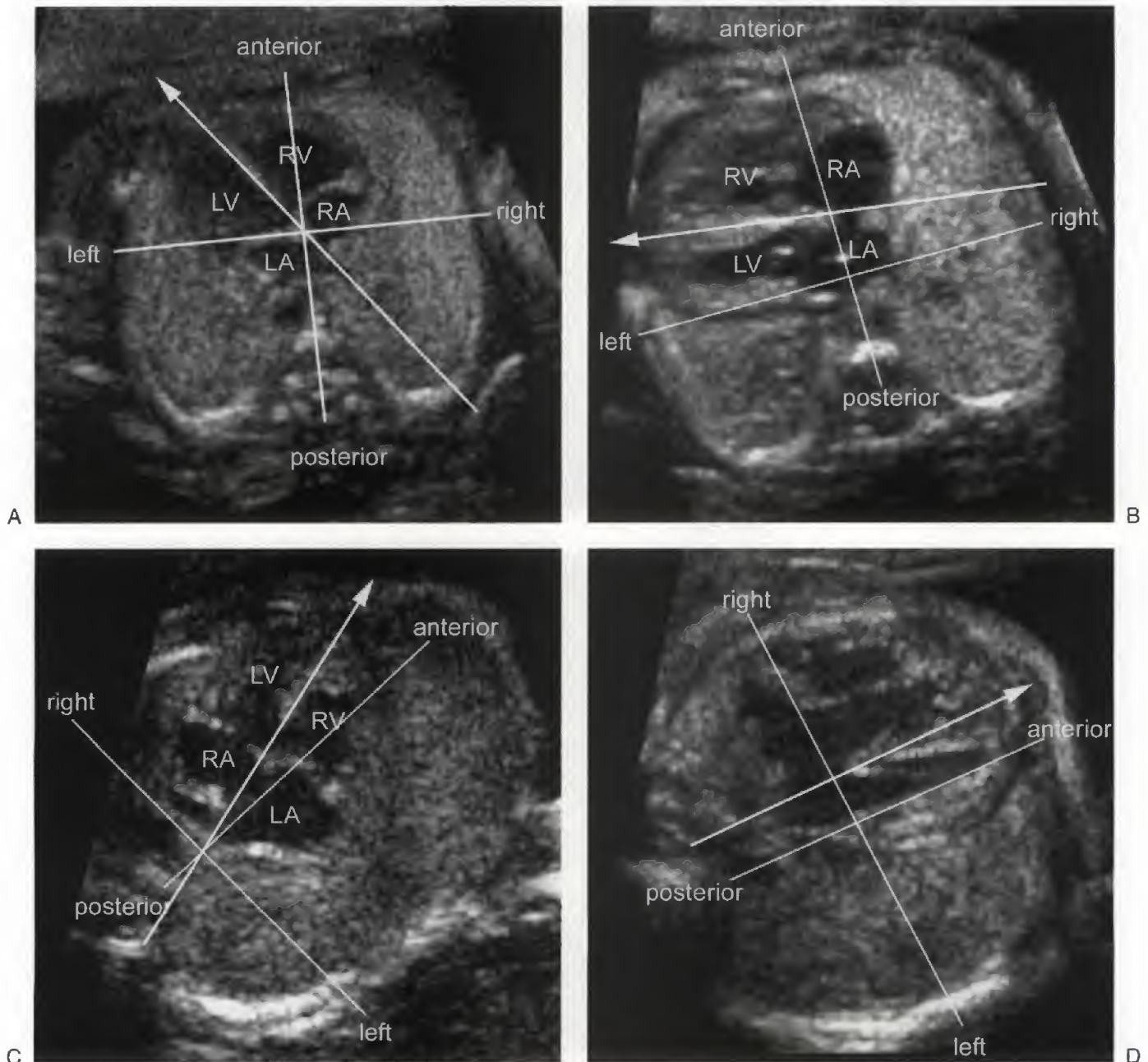


**FIGURE 14-14.** Normal and abnormal positions of the heart. *A.* Levocardia in a normal fetus. Approximately two thirds of the cardiac mass is located in the left thorax. The cardiac axis (*arrow*) is approximately 45 degrees off the coronal or sagittal plane and points in the left anterior direction. *B.* Levocardia with leftward rotation of the cardiac axis in a fetus with tetralogy of Fallot. The cardiac axis (*arrow*) lies in a coronal plane and is directed toward the left lateral chest wall. *C.* Dextrocardia in a fetus with corrected transposition of the great arteries. The major part of the cardiac mass is located in the right thorax. The cardiac axis (*arrow*) points in the right anterior direction. *D.* Rightward displacement of the heart due to right lung hypoplasia in a fetus with scimitar syndrome. The heart is located in the right thorax while its axis (*arrow*) pointing directly forward. When the heart is abnormally positioned secondary to extracardiac pathology, it is simply described as displaced. LA, left atrium; LV, left ventricle; RA, right atrium; RV, right ventricle.



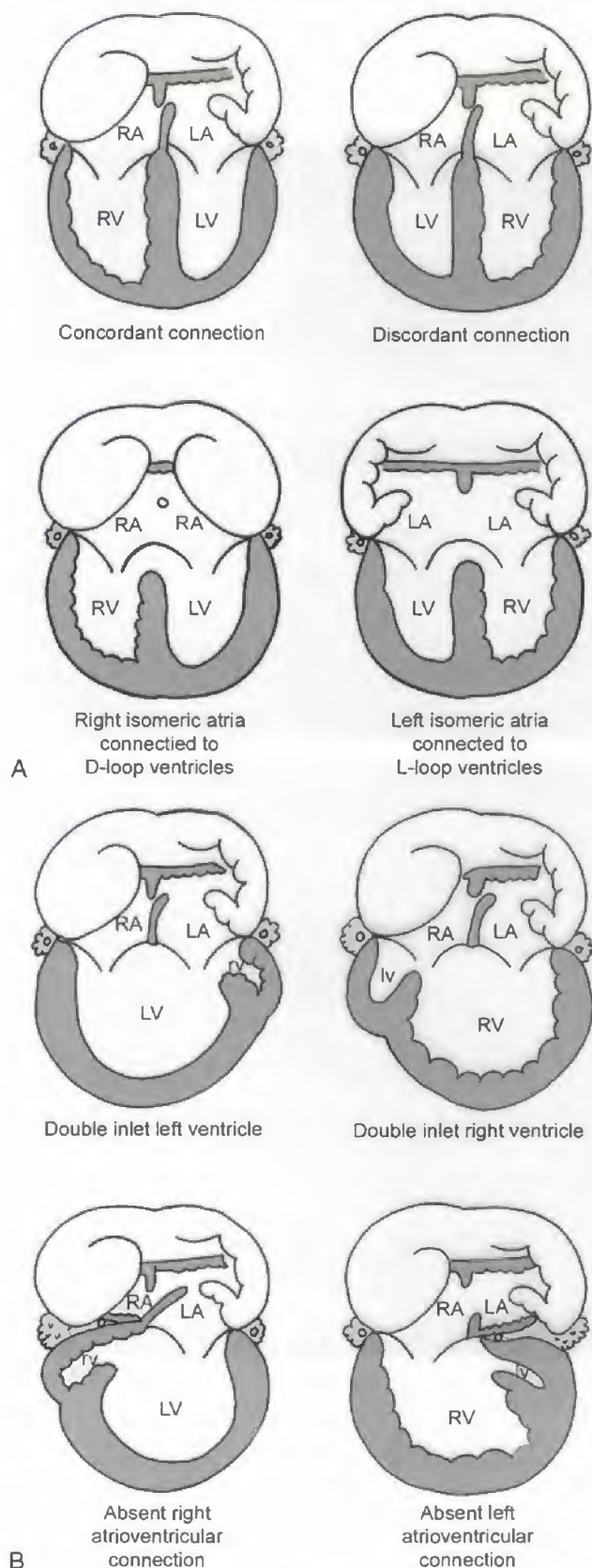


**FIGURE 14-15.** Biventricular (A) and univentricular atrioventricular connections (B). LA, left atrium; LV (lv), left ventricle; RA, right atrium; RV (rv), right ventricle.

and usually disappears in the later pregnancy or after birth (see Fig. 14-6H).<sup>42,43</sup> However, tricuspid regurgitation in the first trimester is often associated with chromosomal abnormalities, especially when it is seen with abnormal nuchal translucency.<sup>44-46</sup>

Less common causes of ventricular disproportion with right-sided dominance are the left-sided obstructive lesions and anomalous pulmonary venous connections. Obstructive lesions of the left side of the heart, including various forms of mitral valve stenosis and left ventricular outflow tract obstruction, result in reduced flow into the left ventricle and, therefore, cause right-sided dominance with reduced right-to-left shunt or overt left-to-right shunt through the patent foramen ovale (Figs. 14-22 and 14-23). It has also been suggested that significant dilatation of the coronary sinus can contribute to left ventricular inflow obstruction.<sup>86-88</sup> The diagnosis of left-sided obstructive lesions can be made by morphologic assessment and measurement of the mitral valve, aortic valve, and aortic arch, as well as color and spectral Doppler interrogation (see Figs. 14-22 and 14-23). Generalized smallness of the left side of the heart with various combinations of obstructive lesions is designated Shone syndrome. The more severe form of underdevelopment of the left-sided structures is the hypoplastic left heart syndrome, in which the degree of left ventricular hypoplasia precludes any form of biventricular repair (see Fig. 14-23).

Anomalous pulmonary venous connection is also a rare cause of ventricular and great arterial disproportion with right-sided dominance.<sup>89-91</sup> The disproportion is typically seen in total anomalous pulmonary venous connection (Fig. 14-24). In the presence of a large atrial septal defect or with infradiaphragmatic drainage, right-sided heart dilatation may not occur until late in pregnancy. Partial anomalous pulmonary venous return is unlikely to cause any significant disproportion of the chambers (Fig. 14-25). The diagnosis of anomalous pulmonary venous drainage can only be reliably excluded by direct examination of the routes of pulmonary venous drainage to the left atrium using color and power Doppler mapping (see Fig. 14-6E). It is important to know that the confluent pulmonary vein in anomalous pulmonary venous connection is very close to the posterior wall of the left atrium and, therefore, could be mistakenly considered to connect normally to the left atrium. Isolated dilatation of the SVC can be a clue to the diagnosis of anomalous drainage to the systemic vein.<sup>92</sup>

Dilatation of the right ventricle in an otherwise normally structured heart without significant tricuspid regurgitation is described as ventricular discrepancy with right-sided dominance (Figs. 14-26 and 14-27). Earlier studies emphasized that right-sided dominance is highly predictive of coarctation or other forms of aortic arch obstruction.<sup>93,94</sup> However, right-sided dominance is not a consistent fetal sonographic finding of coarctation, occurring in only 60% of infants with coarctation.<sup>94</sup> Furthermore, right-sided dominance does not distinguish between fetuses with coarctation and those without.<sup>95,96</sup> Therefore, it is important to assess the size and configuration of the aortic arch when there is right-sided dominance. As a rule of thumb, right-sided dominance should be considered more significant when the ascending aorta is smaller than the SVC or descending aorta or when the aortic arch is significantly smaller than

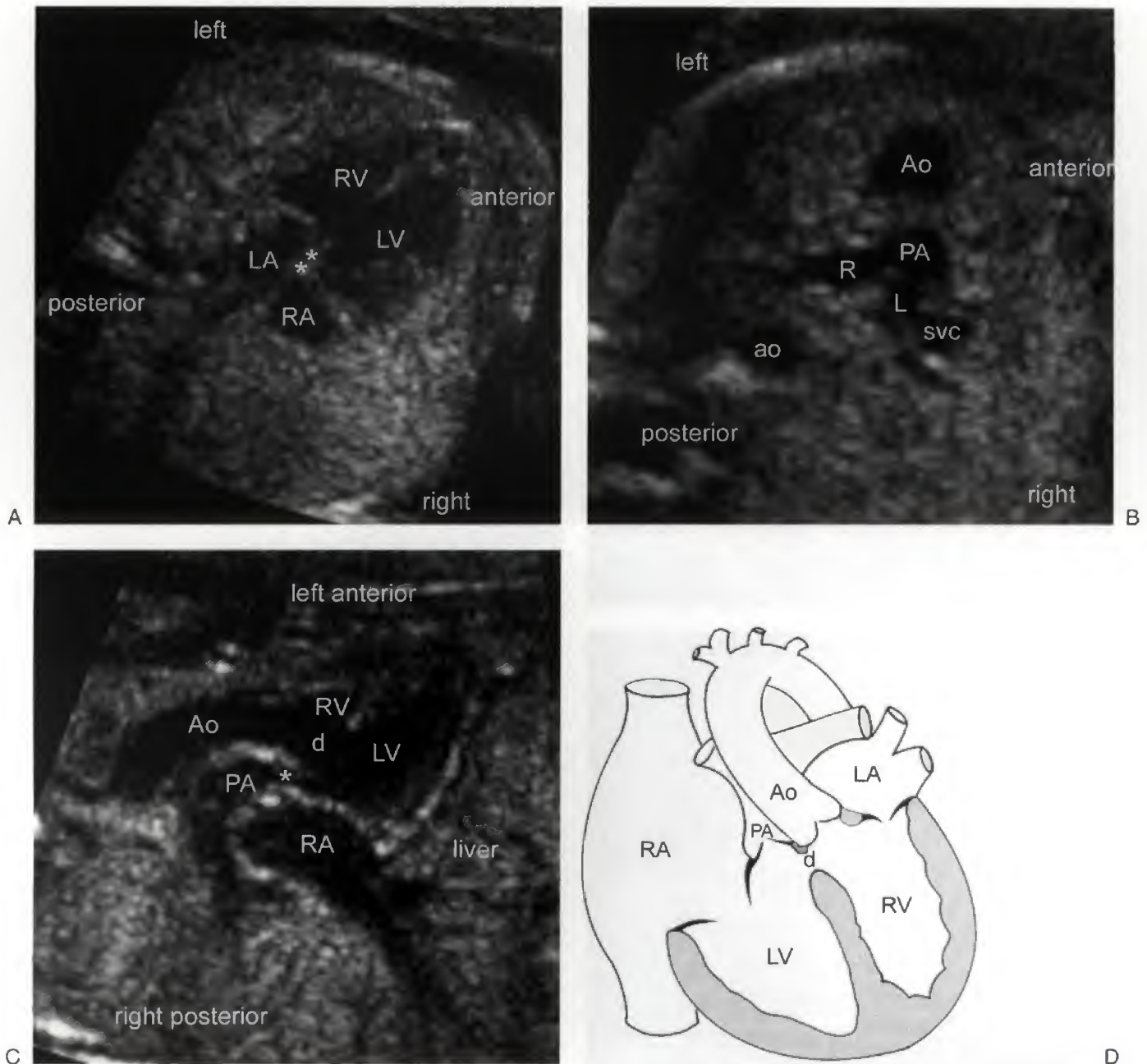


**FIGURE 14-16.** Discordant atrioventricular and ventriculoarterial connections (congenitally corrected transposition of the great arteries). **A.** Four-chamber view shows levocardia and l-loop ventricular relationship with the morphologically right ventricle (RV) on the left and the morphologically left ventricle (LV) on the right. Note the more apical attachment of the left-sided atrioventricular valve to the septum (asterisks). **B.** Three-vessel view shows grossly abnormal great artery relationship with the ascending aorta (Ao) on the left anterior aspect of the main pulmonary artery (PA). This position is most commonly seen in and highly suggestive of corrected transposition of the great arteries in situs solitus. **C.** Right anterior oblique view shows superoinferior relationship of the parts of the ventricles and discordant ventriculoarterial connection. The subpulmonary outflow tract (asterisk) shows narrowing. **D.** Diagrammatic representation of the case. Ao, descending aorta; d, ventricular septal defect; L, left pulmonary artery; LA, left atrium; R, right pulmonary artery; RA, right atrium; SVC, superior vena cava.



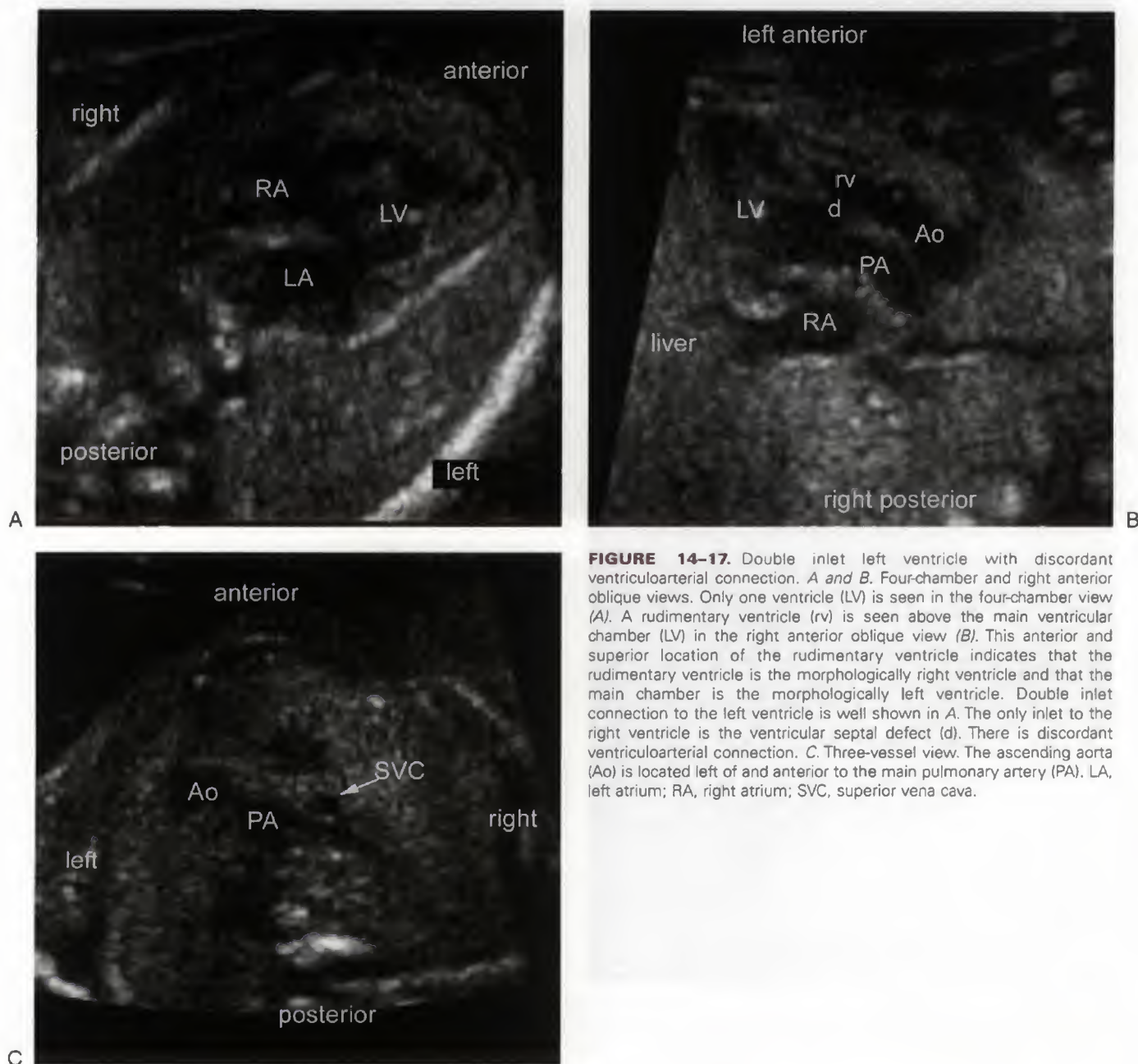


**FIGURE 14-17.** Double inlet left ventricle with discordant ventriculoarterial connection. *A and B.* Four-chamber and right anterior oblique views. Only one ventricle (LV) is seen in the four-chamber view (*A*). A rudimentary ventricle (rv) is seen above the main ventricular chamber (LV) in the right anterior oblique view (*B*). This anterior and superior location of the rudimentary ventricle indicates that the rudimentary ventricle is the morphologically right ventricle and that the main chamber is the morphologically left ventricle. Double inlet connection to the left ventricle is well shown in *A*. The only inlet to the right ventricle is the ventricular septal defect (d). There is discordant ventriculoarterial connection. *C.* Three-vessel view. The ascending aorta (Ao) is located left of and anterior to the main pulmonary artery (PA). LA, left atrium; RA, right atrium; SVC, superior vena cava.

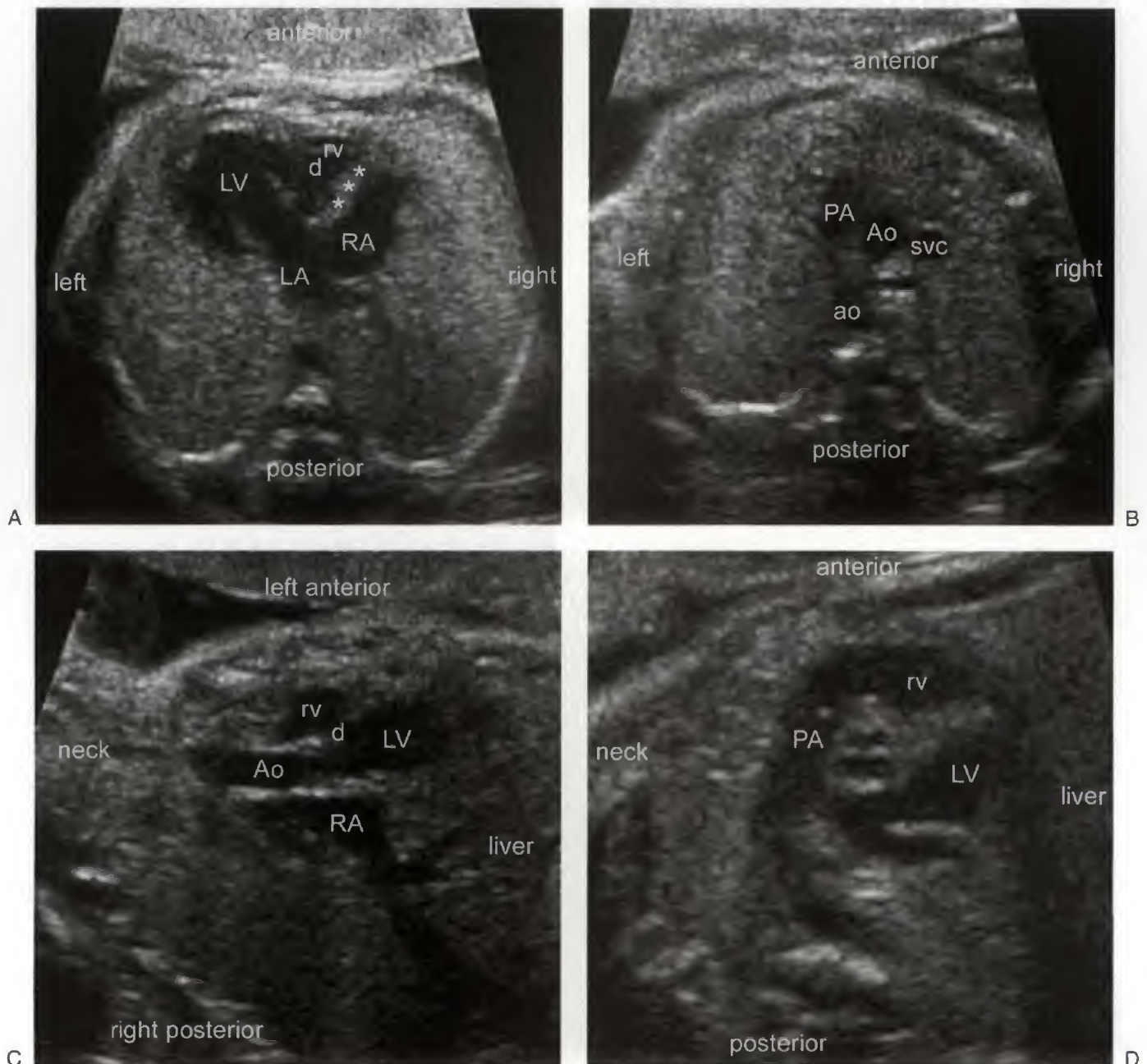


**FIGURE 14-18.** Tricuspid atresia with normally related and connected great arteries. *A.* Four-chamber view shows that the muscular floor (*asterisks*) separates the right atrium (RA) from the underlying small right ventricle (rv). There is an unrestrictive ventricular septal defect (d) between the large left ventricle (LV) and the small right ventricle. *B.* Three-vessel view shows a normal relationship and size of the three vessels. *C.* Oblique sagittal view through the right ventricle shows the pulmonary artery (PA) arising from the right ventricle. *D.* Oblique sagittal view through the left ventricular outflow tract shows the aorta (Ao) arising from the left ventricle. ao, descending aorta; LA, left atrium; SVC, superior vena cava.





**FIGURE 14-19.** Univentricular connection to the morphologically right ventricle. Sagittal view shows the small rudimentary chamber (lv) at the posterior inferior aspect of the main chamber (RV). The rudimentary chamber can be regarded as the morphologically left ventricle because of its posterior and inferior location. Ao, ascending aorta. (Reprinted with permission from Yoo SJ, Lee YH, Cho KS, et al: Sequential segmental approach to fetal congenital heart disease. *Cardiol Young* 9:430, 1999.)

**Table 14-7**

**Causes of Right-sided Dominance in the Four-Chamber View in the Presence of Normal Segmental Connections**

**With An Identifiable Cardiac Defect**

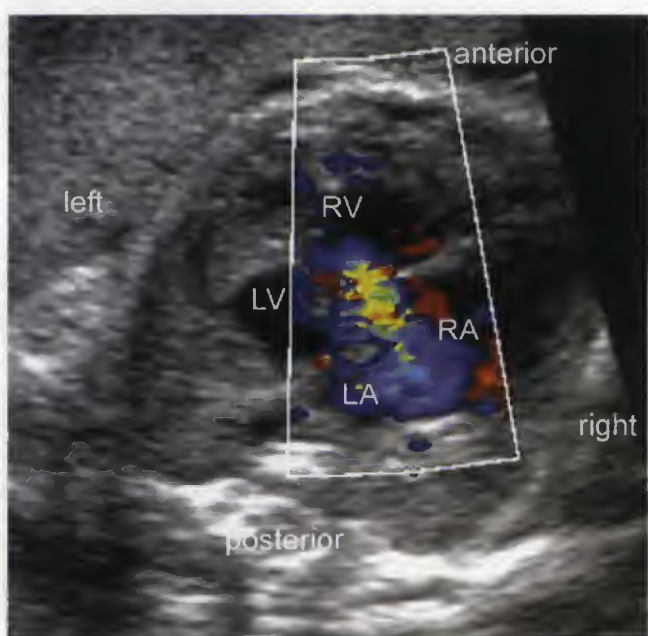
Tricuspid regurgitation  
Ebstein malformation  
Dysplastic tricuspid valve  
Unguarded tricuspid valve  
Pulmonary atresia with intact ventricular septum  
Left-sided obstructive lesion  
Mitral stenosis: supravalvar, valvar and subvalvar  
Critical aortic stenosis  
Hypoplastic left heart syndrome  
Coarctation of the aorta  
Anomalous pulmonary venous connection

**Without An Identifiable Cardiac Defect**

Coarctation of aorta  
Constriction of ductus arteriosus  
Extracardiac arteriovenous malformation  
Vein of Galen aneurysm  
Hepatic arteriovenous malformation  
Intrauterine growth restriction  
Idiopathic



**A**

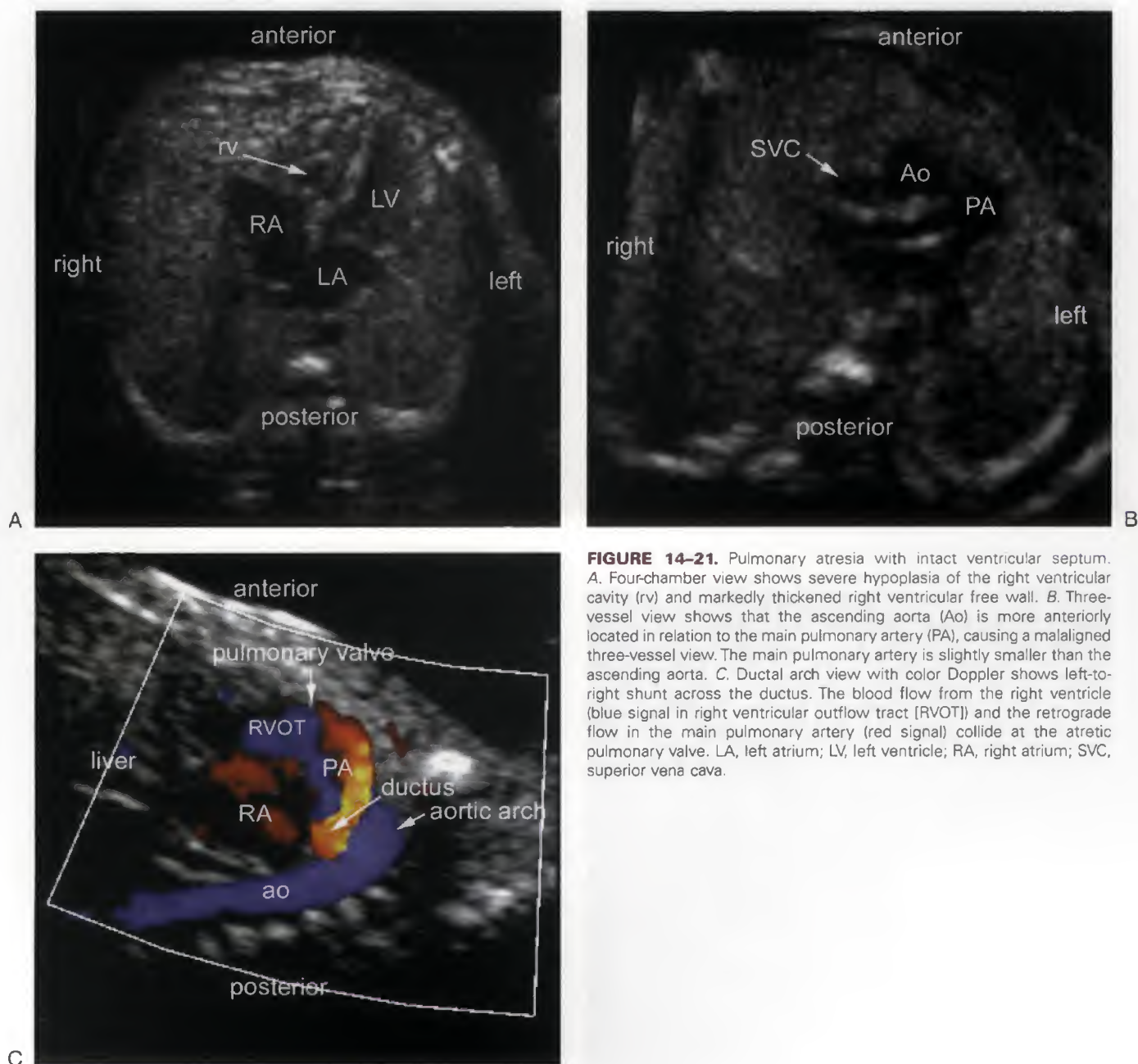


**B**

**FIGURE 14-20.** Ebstein's malformation. A. Four-chamber view shows a big heart with dilatation of the right atrium (RA) and right ventricle (RV). Note the displaced attachment of the septal leaflet of the tricuspid valve (upper asterisk). The anterior leaflet of the mitral valve has a normal insertion to the septum (lower asterisk). The anterior leaflet of the tricuspid valve is large, whereas the septal leaflet is small. B. Color Doppler image in the same view as A shows moderate tricuspid regurgitation. LA, left atrium; LV, left ventricle.

the ductal arch in the three-vessel view (see Figs. 14-26C and 14-27B). Reversed flow in the aortic arch is an important supportive sign of the obstructive lesion of the aortic arch.<sup>97</sup> Right-sided dominance is less predictive of the coarctation of aorta in later pregnancy because the right ventricle is normally bigger than the left ventricle as the pregnancy approaches the term.<sup>38,39,96</sup> In fact, actual coarctation of the

aorta with a posterior shelf or waist lesion is uncommon in the fetus (see Fig. 14-27C). It is speculated that the aorta develops real narrowing with posterior shelf when the ductus arteriosus closes after birth in most isolated coarctations. Obvious coarctation of the aorta is usually a manifestation of a more complex form of aortic arch obstruction associated with other significant heart disease.





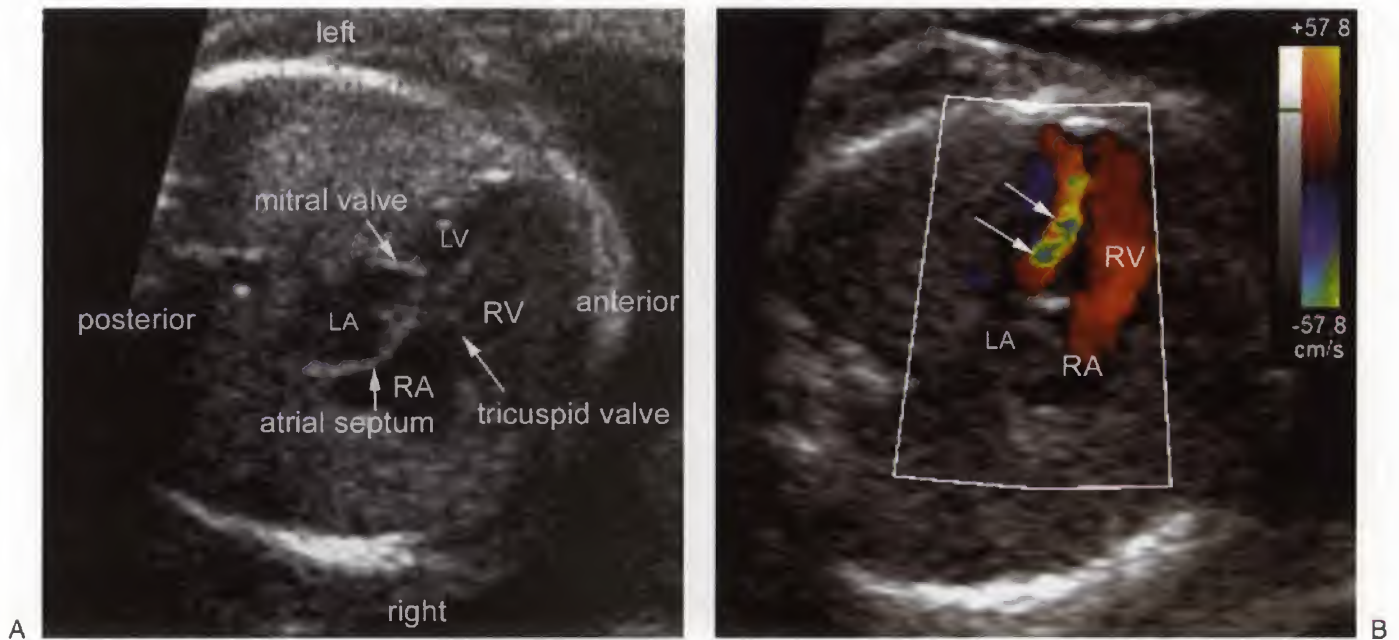


**FIGURE 14-22.** Mitral stenosis. *A.* Four-chamber view shows that the left ventricle (LV) is smaller than the right ventricle (RV). The mitral valve leaflets are thickened. Note that the atrial septum is bowed toward the right atrium (RA). *B.* Color Doppler image in four-chamber view shows flow acceleration (arrows) through the mitral valve. LA, left atrium.

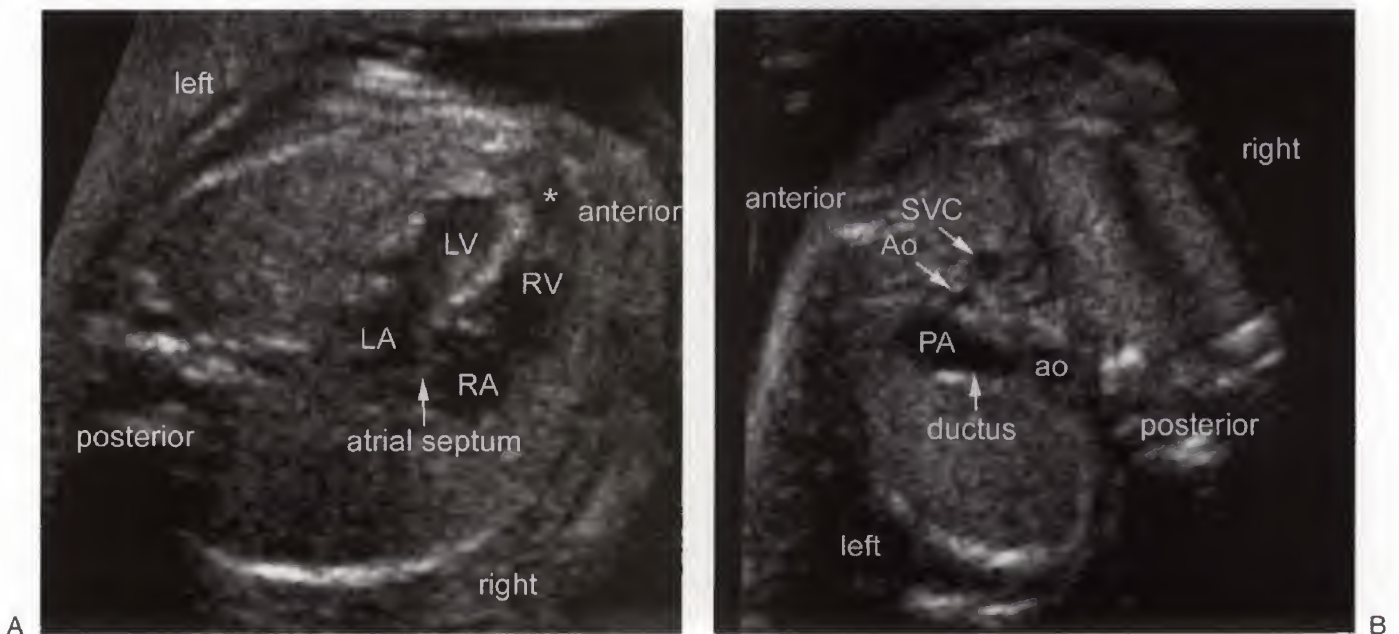


**FIGURE 14-23.** Hypoplastic left-sided heart syndrome. *A.* Four-chamber view shows that the left ventricle (LV) is very small. The cardiac apex (asterisk) is formed by the right ventricle (RV). The flap valve of the fossa ovalis is bowed toward the right atrium (RA) due to reversed shunt across the foramen ovale. Hyperechogenic endocardial surface of the left ventricle suggests endocardial fibroelastosis. *B and C.* Continued

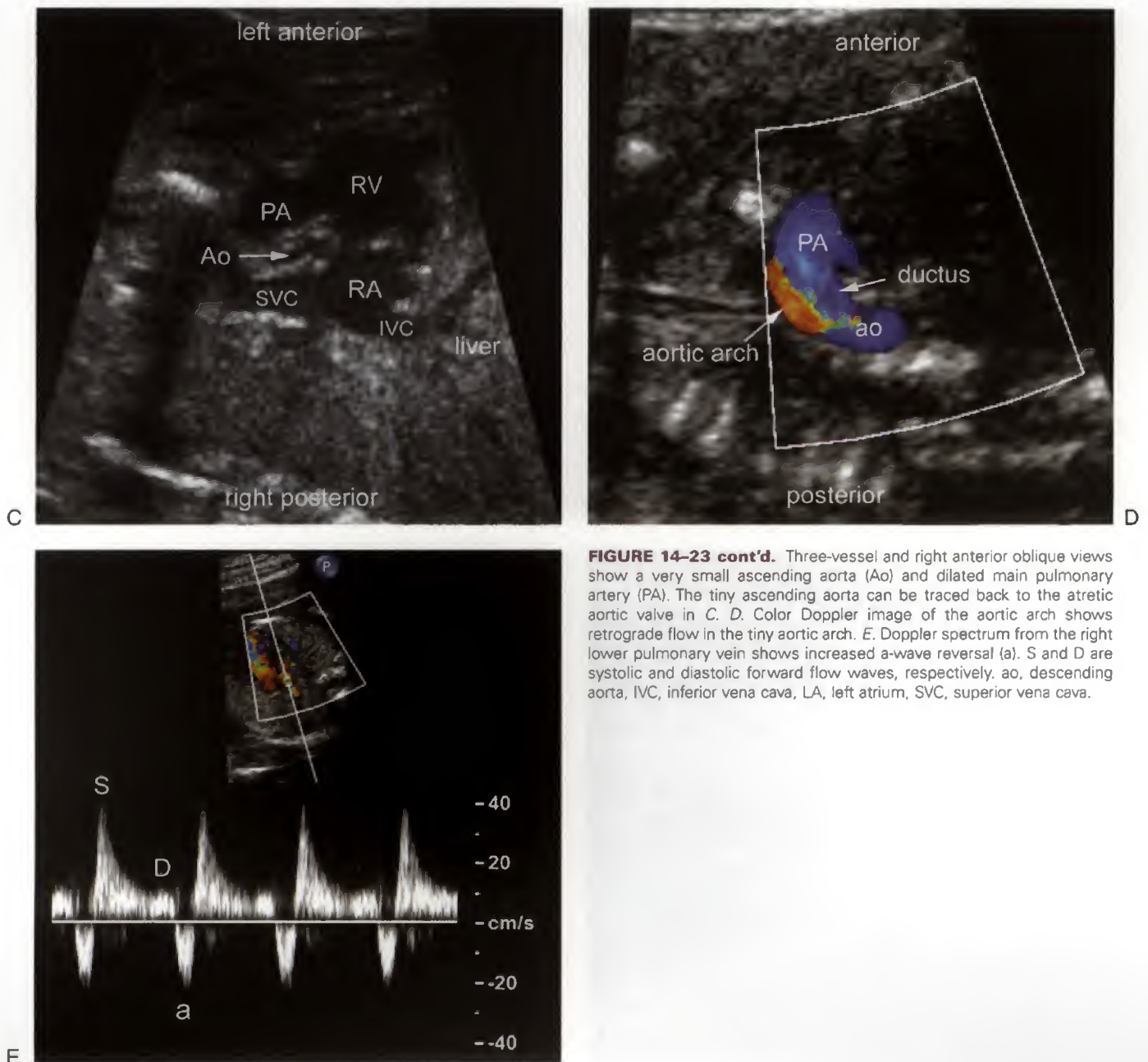


**FIGURE 14-23 cont'd.** Three-vessel and right anterior oblique views show a very small ascending aorta (Ao) and dilated main pulmonary artery (PA). The tiny ascending aorta can be traced back to the atretic aortic valve in *C*. *D*. Color Doppler image of the aortic arch shows retrograde flow in the tiny aortic arch. *E*. Doppler spectrum from the right lower pulmonary vein shows increased a-wave reversal (a). S and D are systolic and diastolic forward flow waves, respectively. ao, descending aorta, IVC, inferior vena cava, LA, left atrium, SVC, superior vena cava.



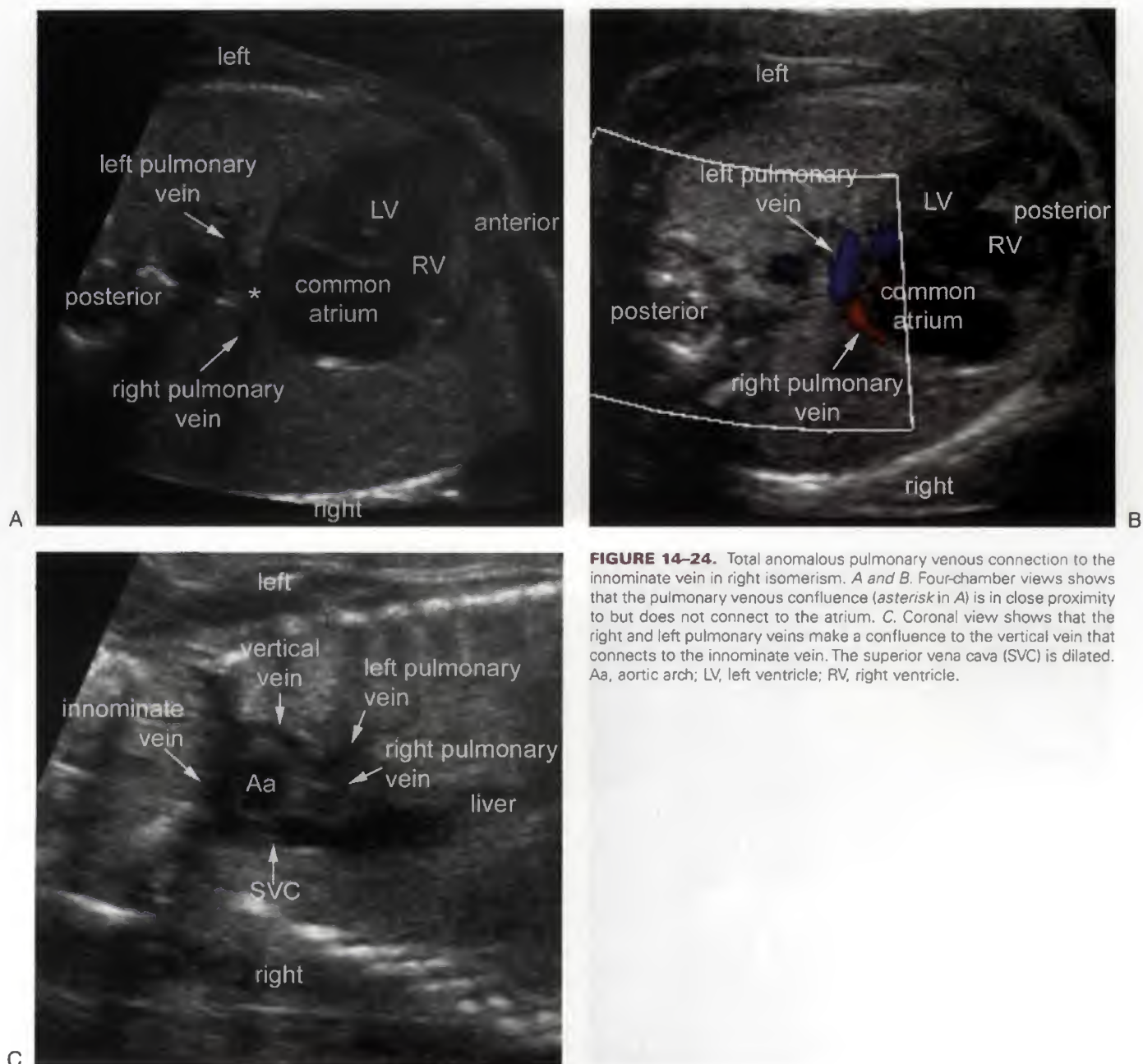


**FIGURE 14-24.** Total anomalous pulmonary venous connection to the innominate vein in right isomerism. *A and B.* Four-chamber views shows that the pulmonary venous confluence (asterisk in *A*) is in close proximity to but does not connect to the atrium. *C.* Coronal view shows that the right and left pulmonary veins make a confluence to the vertical vein that connects to the innominate vein. The superior vena cava (SVC) is dilated. Aa, aortic arch; LV, left ventricle; RV, right ventricle.

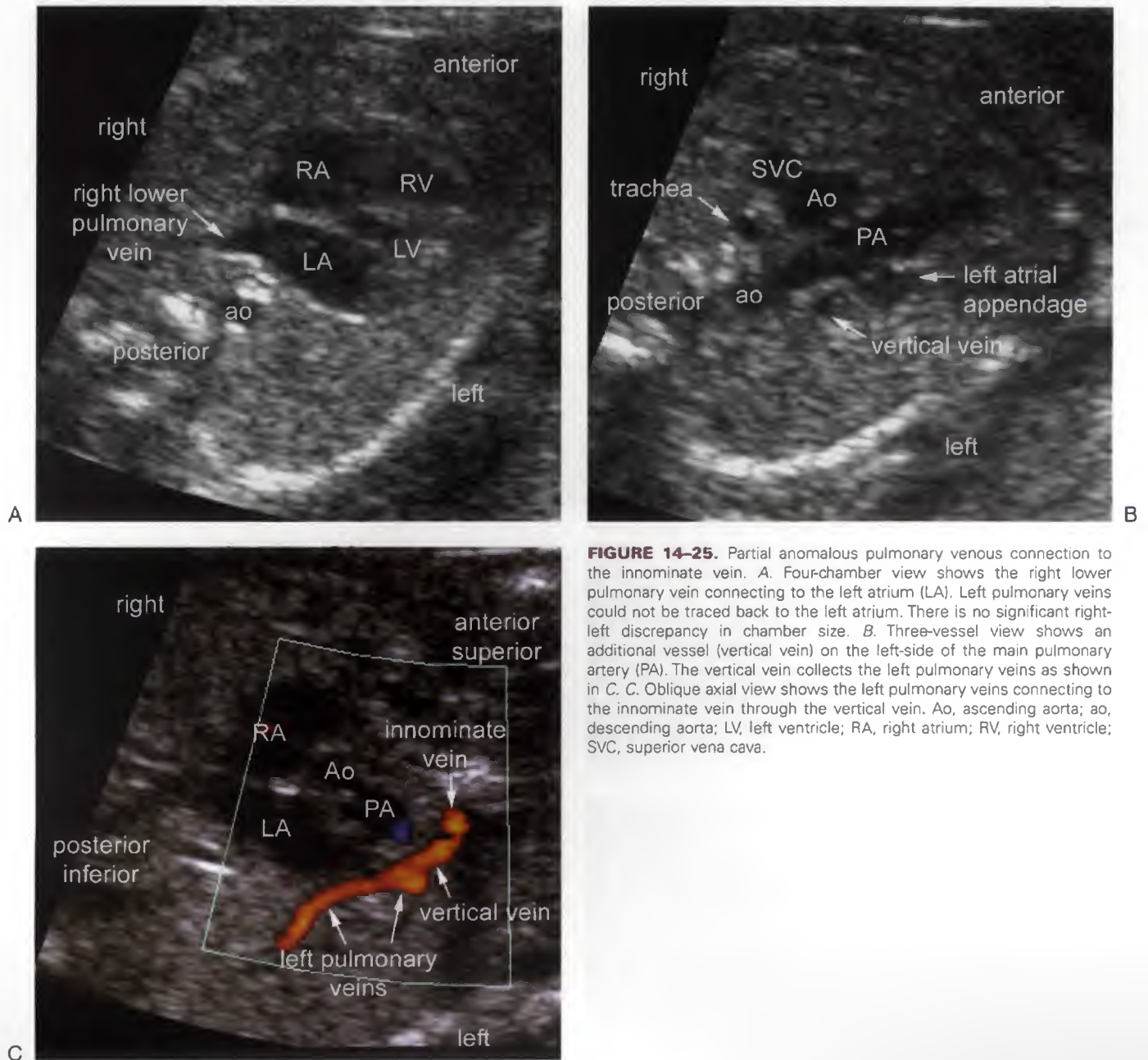


**FIGURE 14-25.** Partial anomalous pulmonary venous connection to the innominate vein. **A.** Four-chamber view shows the right lower pulmonary vein connecting to the left atrium (LA). Left pulmonary veins could not be traced back to the left atrium. There is no significant right-left discrepancy in chamber size. **B.** Three-vessel view shows an additional vessel (vertical vein) on the left-side of the main pulmonary artery (PA). The vertical vein collects the left pulmonary veins as shown in **C.** **C.** Oblique axial view shows the left pulmonary veins connecting to the innominate vein through the vertical vein. Ao, ascending aorta; ao, descending aorta; LV, left ventricle; RA, right atrium; RV, right ventricle; SVC, superior vena cava.



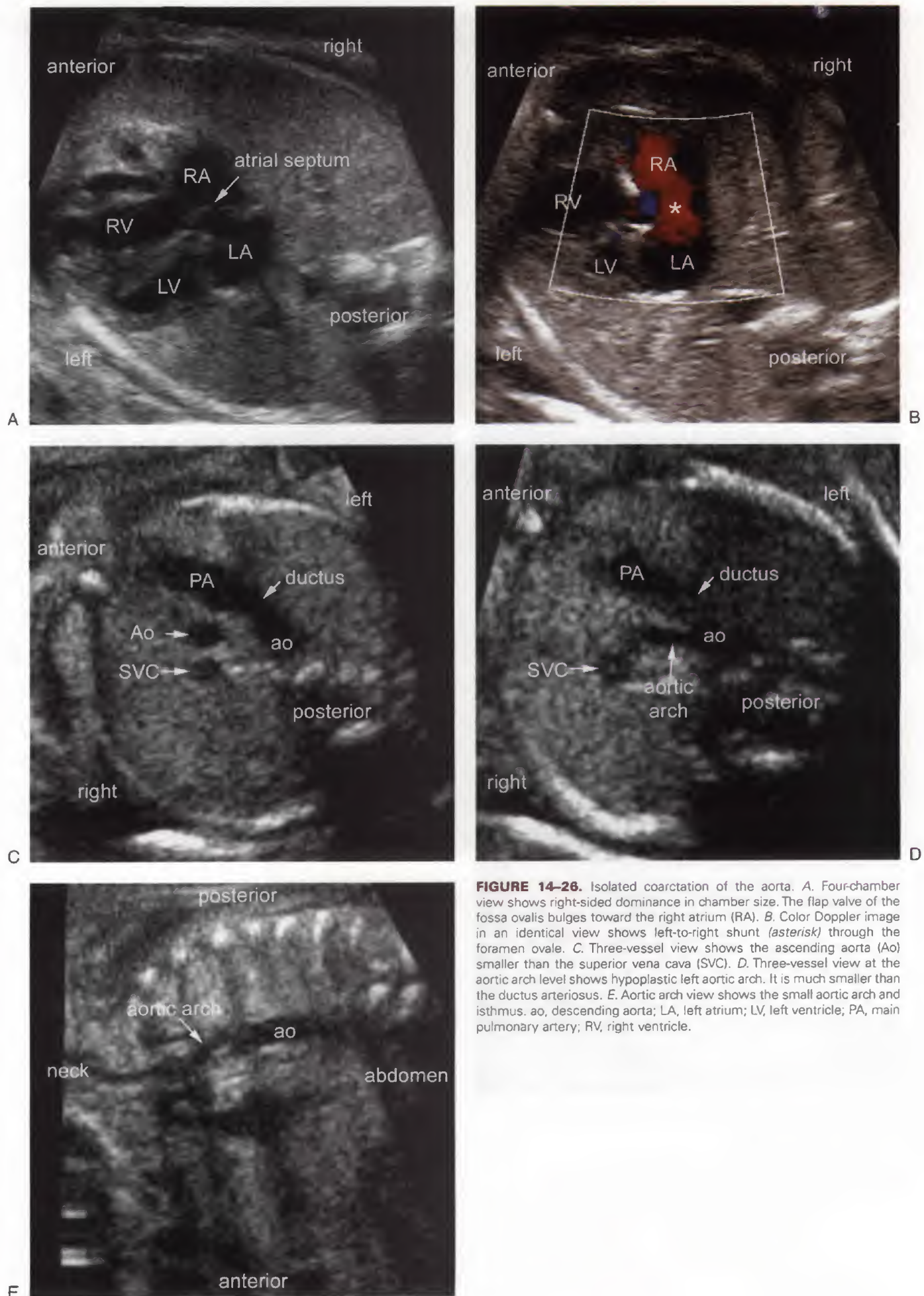


**FIGURE 14-28.** Isolated coarctation of the aorta. **A.** Four-chamber view shows right-sided dominance in chamber size. The flap valve of the fossa ovalis bulges toward the right atrium (RA). **B.** Color Doppler image in an identical view shows left-to-right shunt (*asterisk*) through the foramen ovale. **C.** Three-vessel view shows the ascending aorta (Ao) smaller than the superior vena cava (SVC). **D.** Three-vessel view at the aortic arch level shows hypoplastic left aortic arch. It is much smaller than the ductus arteriosus. **E.** Aortic arch view shows the small aortic arch and isthmus. ao, descending aorta; LA, left atrium; LV, left ventricle; PA, main pulmonary artery; RV, right ventricle.



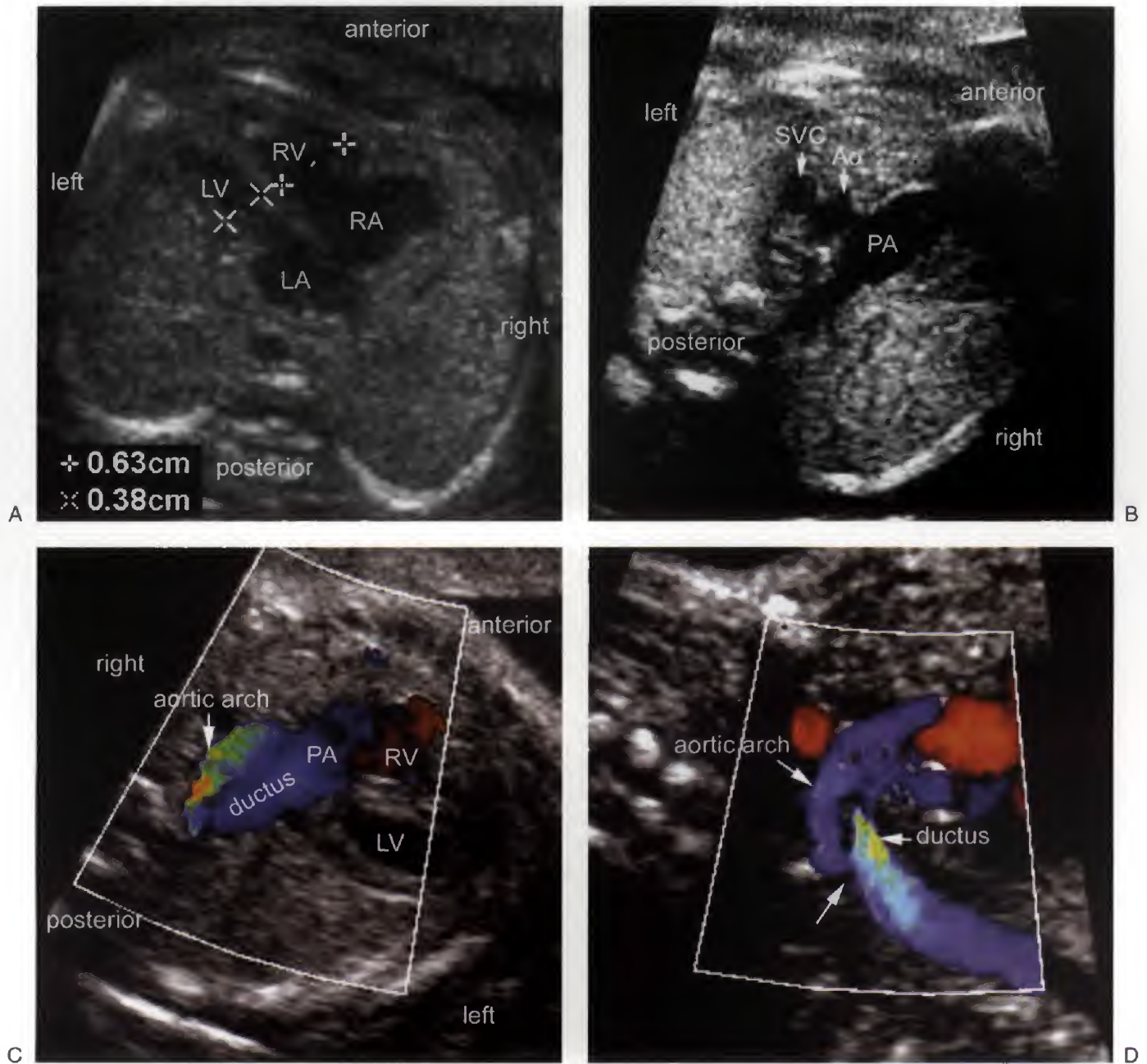


**FIGURE 14-27.** Isolated coarctation of the aorta with posterior shelf. A. Four-chamber view shows the right-sided dominance in chamber size. B. Three-vessel view shows the large main pulmonary artery (PA) and small ascending aorta (Ao). C. Oblique axial view through the aortic and ductal arches shows the aortic arch to be much narrower than the ductus arteriosus. There is flow acceleration in the aortic arch. D. Aortic arch view shows diffuse narrowing of the aortic arch. There is an indentation (arrow) in the posterior wall of the aorta where the ductus arteriosus makes a confluence with the aortic arch. This is not a common finding of isolated coarctation in fetus. LA, left atrium; LV, left ventricle; RA, right atrium; RV, right ventricle; SVC, superior vena cava.

Ductal constriction is also associated with right-sided dominance (Fig. 14-28).<sup>98-100</sup> Ductal constriction is classically seen with maternal administration of cyclo-oxygenase inhibitors such as indomethacin but are also seen without use of a triggering agent. When it is associated with cyclo-oxygenase inhibitor therapy, ductal constriction is reversible. Because delayed diagnosis of ductal constriction can lead to right heart failure with hydrops, intrauterine death and persistent pulmonary hypertension in newborns, its early

recognition is important. Ductal constriction is characterized by acute cardiomegaly with tricuspid regurgitation, right atrial and ventricular dilatation, and right ventricular hypertrophy and dyskinesia. Because of high right ventricular diastolic pressure, the tricuspid valve barely opens in diastole. The diagnosis is made by documenting flow acceleration through the narrow ductus arteriosus (see Fig. 14-28C). It has been suggested that the tortuous ductus arteriosus in later pregnancy also contributes to restricted



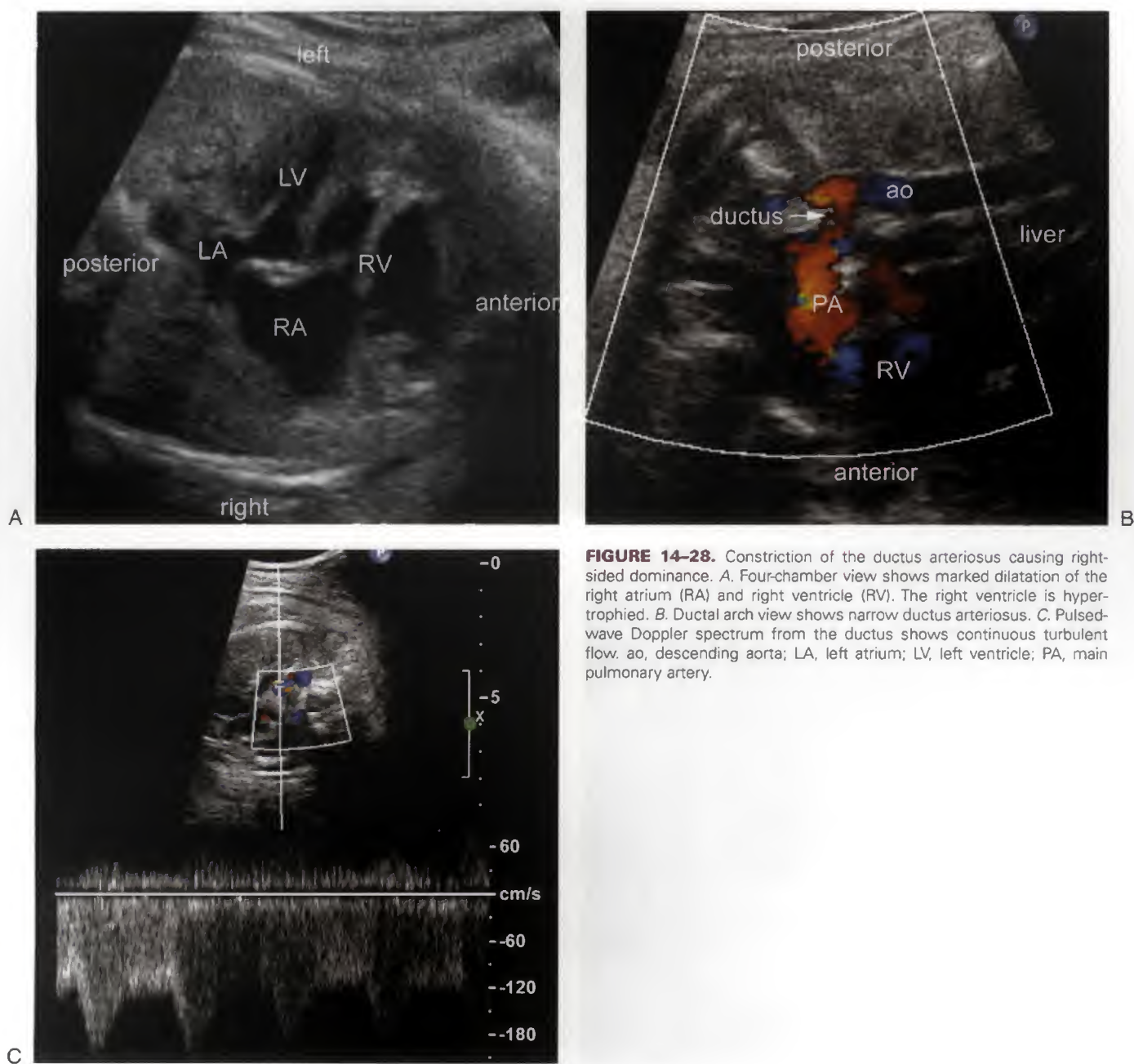


**FIGURE 14-28.** Constriction of the ductus arteriosus causing right-sided dominance. *A.* Four-chamber view shows marked dilatation of the right atrium (RA) and right ventricle (RV). The right ventricle is hypertrophied. *B.* Ductal arch view shows narrow ductus arteriosus. *C.* Pulsed-wave Doppler spectrum from the ductus shows continuous turbulent flow. ao, descending aorta; LA, left atrium; LV, left ventricle; PA, main pulmonary artery.

ductal flow, which needs yet to be proven based on a larger population study.<sup>101</sup> One should be aware that the ductus arteriosus can be small, without physiologic constriction, when there is reduced blood flow from the right ventricle into the pulmonary artery as in tetralogy of Fallot and that the ductus arteriosus is absent in tetralogy of Fallot with absent pulmonary valve syndrome and pulmonary atresia with major aortopulmonary collateral arteries (MAPCA).<sup>55,100</sup>

Extracardiac arteriovenous malformations with hyperdynamic circulation, such as a vein of Galen malformation and hepatic arteriovenous malformation, may also cause dilated right atrium and right ventricle. In fact, coarctation of the aorta is seen in approximately 40% of patients with a vein of Galen malformation (Fig. 14-29).<sup>102</sup> It is considered

to be due to diminished blood flow through the aortic isthmus because of diversion of the blood flow into the vein of Galen malformation.

It is very important to know that right-sided dominance is also seen in some fetuses with intrauterine growth restriction as well as in those with tricuspid regurgitation or anomalous pulmonary venous connections.<sup>91</sup> In fact, mild to even moderate degree of right-sided dominance is not uncommon in the absence of a cardiovascular defect.

Doppler interrogation of flow through the patent foramen ovale is helpful in the differential diagnosis of the causes of dilatation of the right atrium and right ventricle. When there is left-to-right shunt through the patent foramen ovale, especially when the flap valve of the fossa ovalis

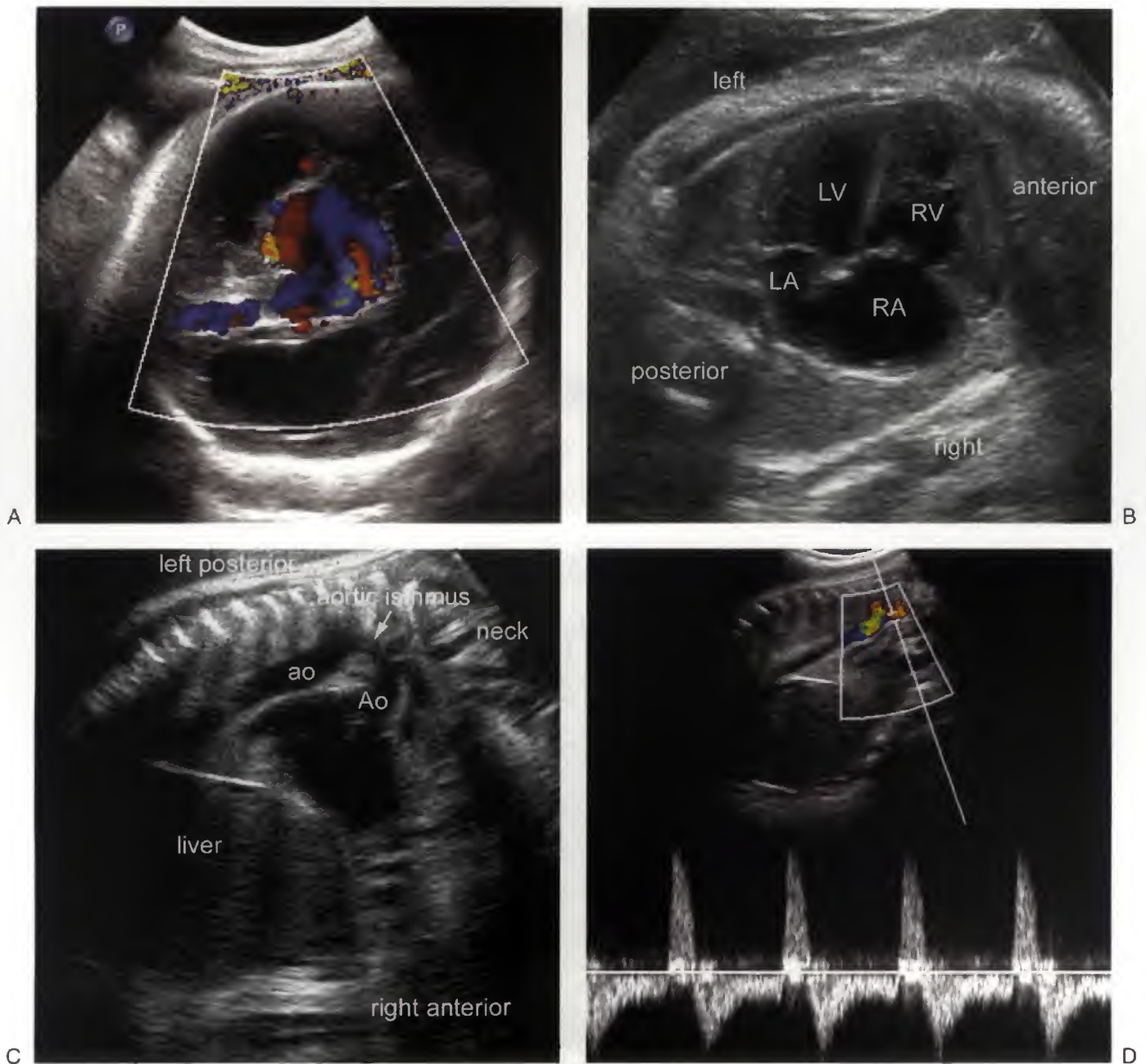


**FIGURE 14-29.** Vein of Galen malformation with coarctation of aorta. *A.* Transverse view of the brain shows an aneurysmally dilated vein of Galen and hydrocephalus. *B.* Four-chamber view shows cardiomegaly with right atrial (RA) and right ventricular (RV) dilatation. The right ventricle is also hypertrophied. *C.* Aortic arch view shows narrow aortic isthmus. *D.* Spectral Doppler tracing of the aortic isthmus shows systolic forward and diastolic retrograde flow. Ao, ascending aorta; ao, descending aorta; LA, left atrium; LV, left ventricle.

bulges into the right atrium, it is highly suggestive of a left-sided obstructive lesion that may have already developed or will develop later (see Figs. 14-22*A*, 14-23*A* and 14-26*A*).<sup>96</sup> When a severe left-side obstructive lesion is associated with a restrictive patent foramen ovale, pulmonary venous blood flow shows increased reversed flow with atrial contraction (see Fig. 14-23*F*).<sup>103-105</sup> When there is right-to-left shunt through the patent foramen ovale, it is more likely a primary right-sided lesion such as tricuspid valve pathology with

or without right ventricular outflow tract obstruction, or anomalous pulmonary venous connection, or intrauterine growth retardation.

Left-sided dominance is much less common and usually seen with right ventricular hypoplasia, with or without right ventricular outflow tract obstruction. It can also be seen with tricuspid valve pathology causing reduction of the blood flow into the right ventricle, such as a straddling tricuspid valve. In the majority of cases of pulmonary atresia with



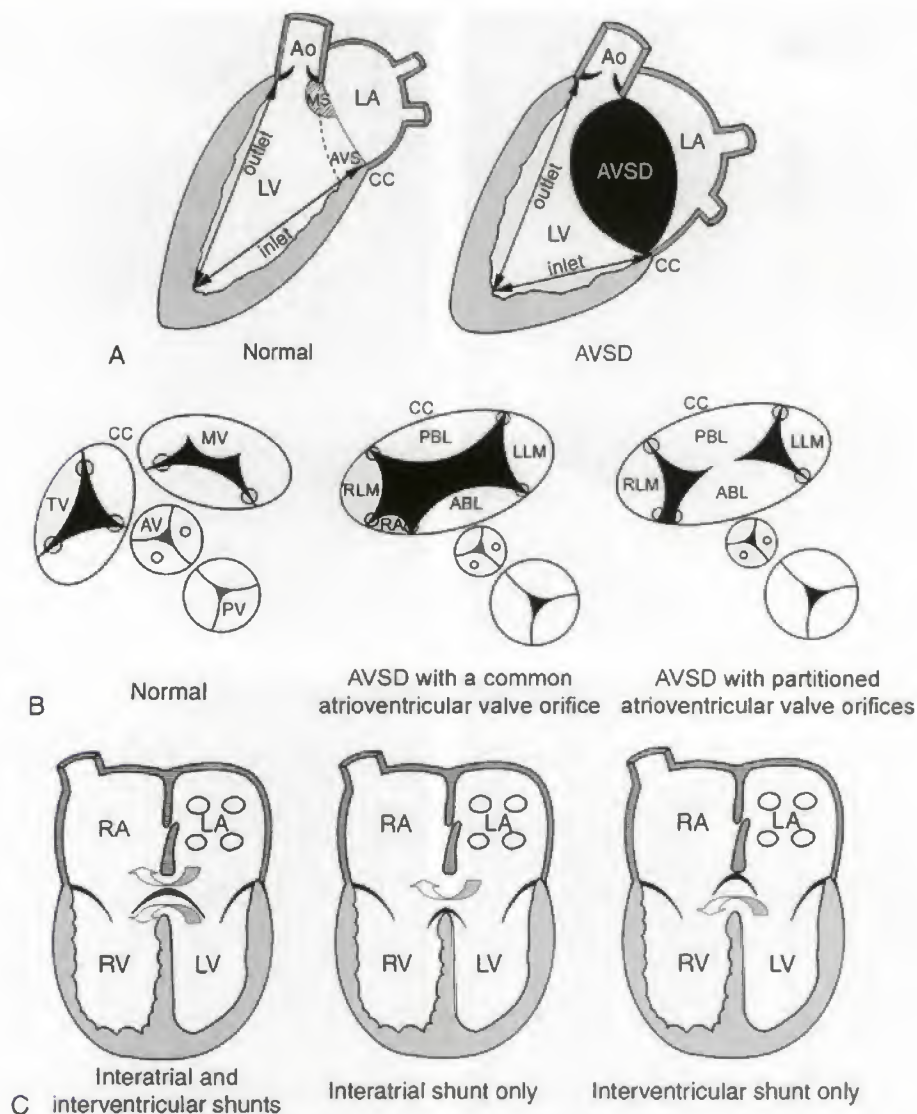


**FIGURE 14-30.** Diagrams showing characteristic features of atrioventricular septal defect (AVSD). **A.** Left ventricle seen from the left side showing inlet-outlet disproportion and increased distance between the aorta (Ao) and crux cordis (CC) in AVSD. **B.** Atrioventricular valves seen from above. Note the wedged position of the aortic valve (AV) between the tricuspid (TV) and mitral (MV) valves in the normal heart. The aortic valve has an unwedged position in AVSD with an increased distance between the aortic valve and crux cordis because of a common atrioventricular annulus. The five leaflets of AVSD are the anterior and posterior bridging leaflets (ABL and PBL), the left and right lateral mural leaflets (LLM and RLM), and the right anterior leaflet (RA). **C.** Level of shunts. The level of shunt across the AVSD is determined by the relationship of the bridging leaflets to the septal margins of the defect. AVS, atrioventricular septum; LA, left atrium; LV, left ventricle; MS, membranous septum; PV, pulmonary valve; RA, right atrium; RV, right ventricle.

intact ventricular septum, the right atrium is dilated but the right ventricle shows severe myocardial hypertrophy with hypoplastic cavity (see Fig. 14-21A).

### **Atrial, AV, and Ventricular Septal Defects**

Atrial, AV, and ventricular septal defects can be seen in the four-chamber view. The so-called secundum atrial septal defect or fossa ovalis defect that involves the flap valve of the fossa ovalis cannot be diagnosed, unless it is very large because the flap valve of the fossa ovalis is a delicate membranous structure that shows floppy movement with flow across the patent foramen ovale. A defect involving the most posterior and superior part of the atrial septum is a superior sinus venosus defect and is almost always associated with

anomalous connection of the right upper pulmonary vein to the SVC. The defect involving the most posterior and inferior part of the atrial septum is an inferior sinus venosus defect and is associated with the inferior vena cava draining partially or totally into the left atrium. Both types of sinus venosus defects are rare.

The AV septal defect is characterized by a large septal defect in the center of the heart at the AV junction (Fig. 14-30). The AV septal defect is more than a simple septal defect. It is also characterized by a common AV annulus with abnormal arrangement of the valve leaflets, an unwedged position of the aortic valve, and a short dimension of the ventricular inlet with inlet-outlet disproportion of the left ventricle (see Fig. 14-30A). The AV valve consists of five leaflets: anterior and posterior bridging

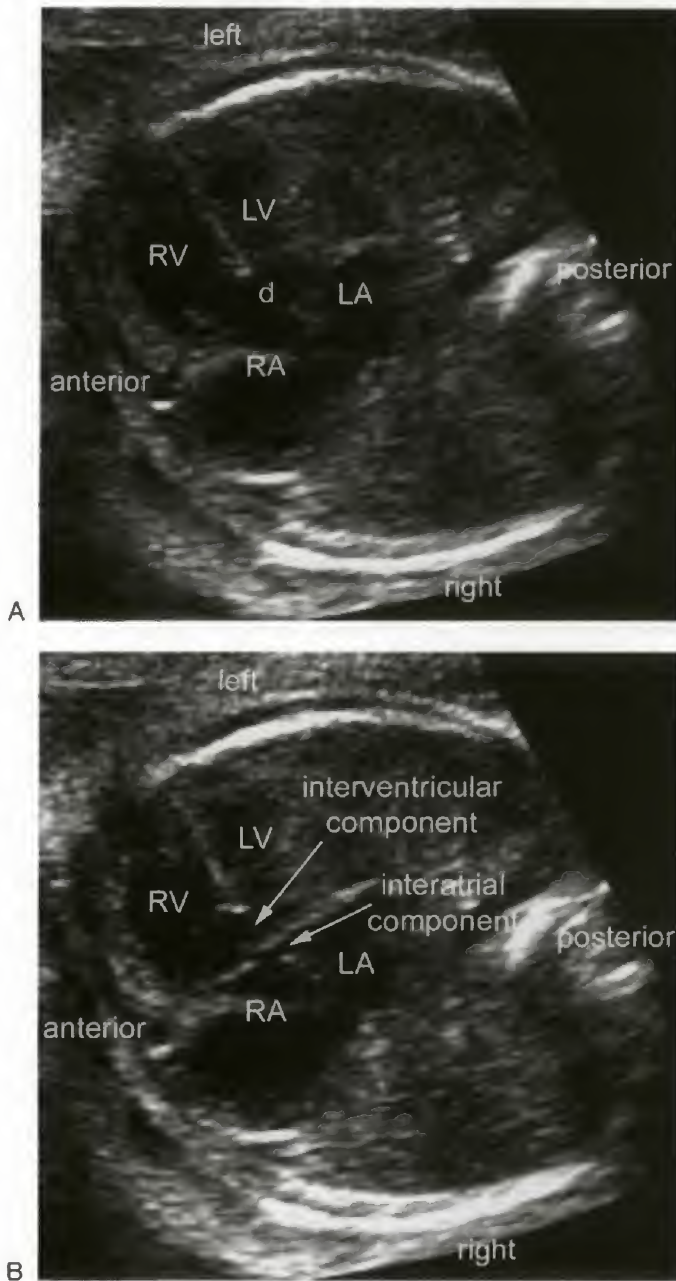


**FIGURE 14-31.** Atrioventricular septal defect with both interatrial and interventricular shunts. *A.* A diastolic frame shows an atrioventricular septal defect (d). *B.* A systolic frame shows that the defect is divided into interatrial and interventricular components by the bridging leaflets. Note the shortened length of the ventricular inlet, which is only slightly longer than the atrial length. LA, left atrium; LV, left ventricle; RA, right atrium; RV, right ventricle.

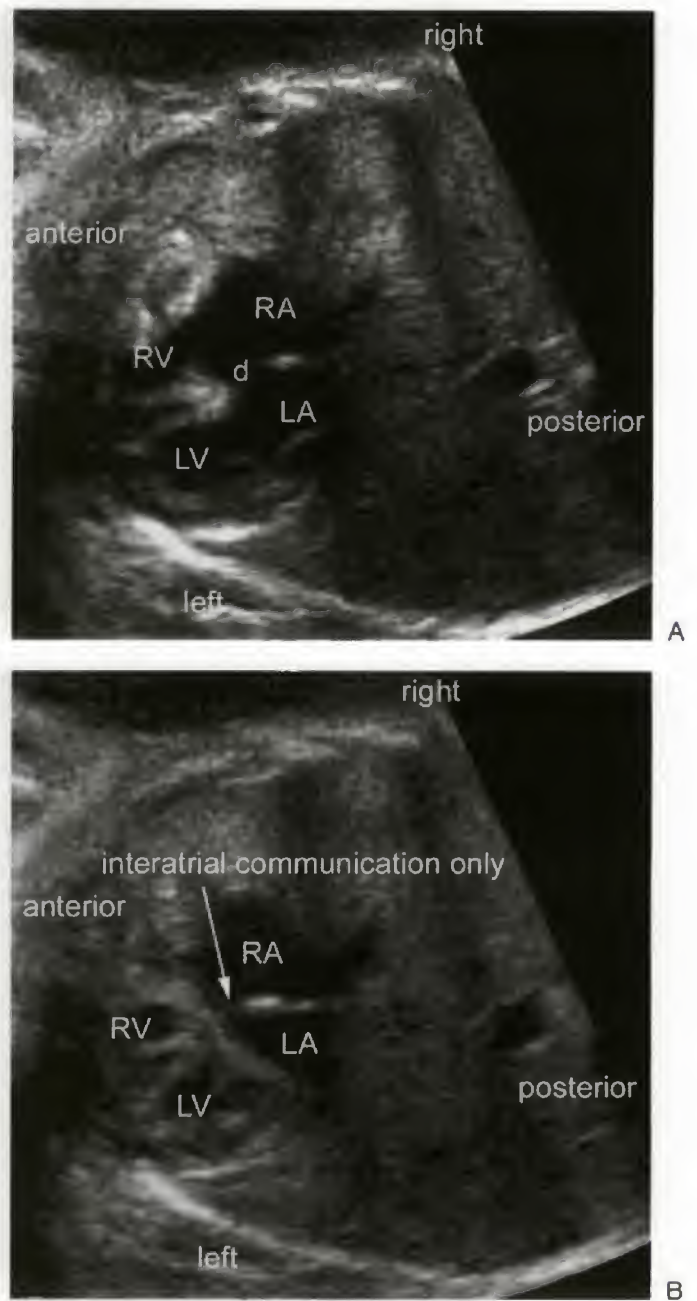


**FIGURE 14-32.** Atrioventricular septal defect with interatrial shunt only (primum atrial septal defect). *A.* A diastolic frame shows an atrioventricular septal defect (d). *B.* A systolic frame shows that the bridging leaflets are attached to the ventricular septal crest making the defect exclusively interatrial. Note that the length of the ventricle is almost equal to the length of the atrium, suggesting shortened ventricular inlet. LA, left atrium; LV, left ventricle; RA, right atrium; RV, right ventricle.

leaflets, right and left lateral mural leaflets, and a right anterior leaflet between the right lateral mural and anterior bridging leaflets (see Fig. 14-30*B*). The right anterior leaflet can be vestigial. The valve orifice can be a common orifice for the right and left chambers. There can be partitioned right and left orifices when the anterior and posterior bridging leaflets are fused through a tongue of tissue. AV septal defects show different levels of shunts according to the relationship of the AV valve leaflets to the septum (see Fig. 14-30*C*). When the anterior and posterior bridging

leaflets do not attach to either the atrial or ventricular septal crest, there are two levels of shunting, interatrial and interventricular (Fig. 14-31). Less commonly, the bridging leaflets are attached to the ventricular septal crest, rendering the defect an exclusively interatrial communication (Fig. 14-32). This latter variant is also called primum atrial septal defect. Very rarely, the leaflets attach to the atrial septal crest, rendering the defect an exclusively interventricular communication. It is usually not difficult to make the diagnosis



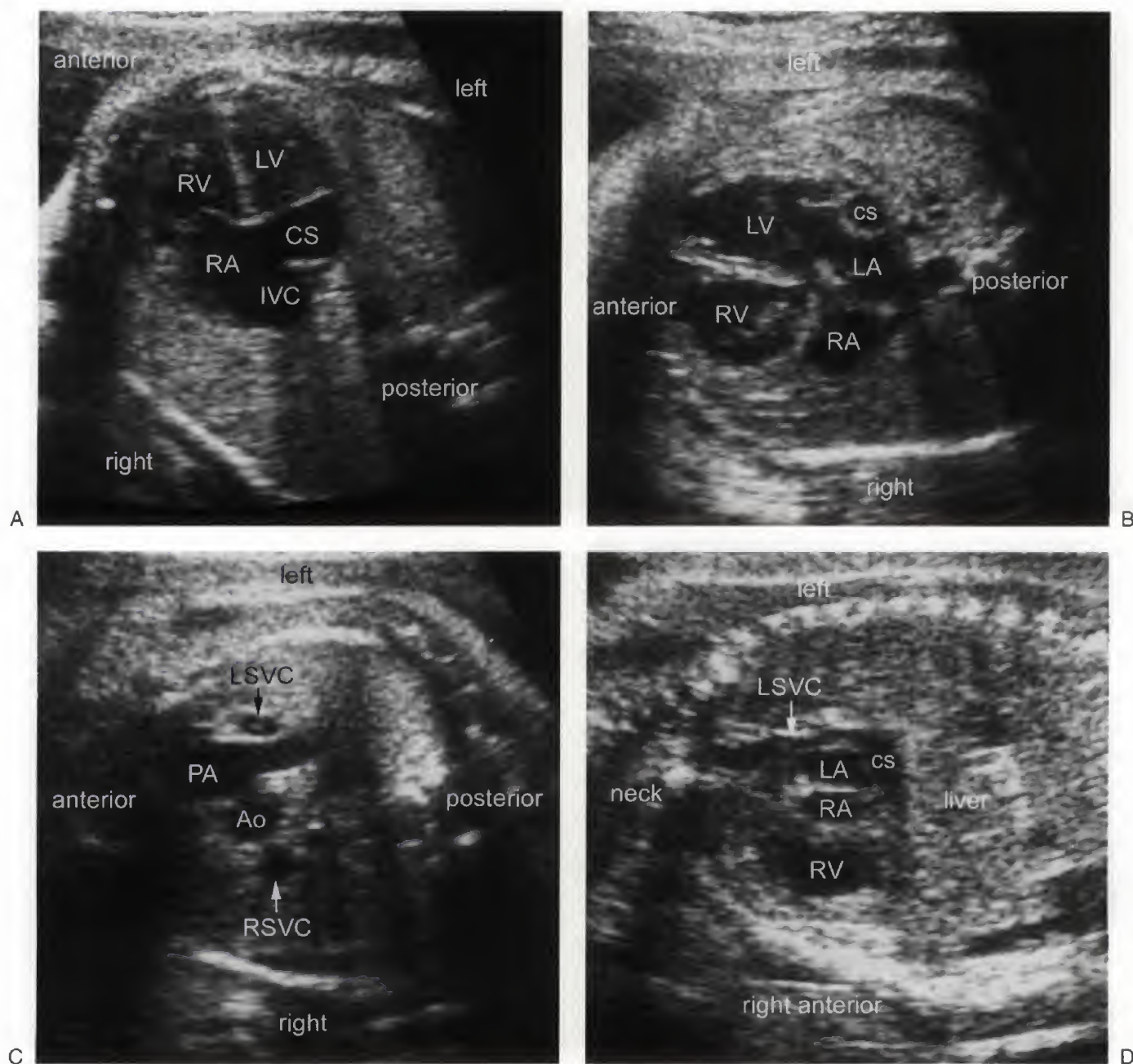


**FIGURE 14-33.** Bilateral superior venae cavae. *A.* Axial view through the lower part of the four chambers shows the dilated coronary sinus (CS). Both the coronary sinus and inferior vena cava (IVC) open to the right atrium (RA). The dilated coronary sinus opening can be mistaken for an atrioventricular septal defect. *B.* True four-chamber view shows that the lower part of the atrial septum is intact. The dilated coronary sinus is seen at the left atrioventricular junction above the mitral valve annulus. *C.* Three-vessel view shows four vessels. The additional vessel is the left superior vena cava (LSVC) on the opposite side of the right superior vena cava (RSVC). A similar finding is also seen in partial or total anomalous pulmonary venous connection to the innominate vein. *D.* Oblique coronal view shows the dilated left superior vena cava and coronary sinus forming a J-shaped channel along the left atrium (LA). Ao, ascending aorta; LA, left atrium; LV, left ventricle; PA, main pulmonary artery; RV, right ventricle.

of AV septal defect by using a four-chamber view. The defect is seen as a large defect with the bridging leaflets free floating across the defect or attached to the ventricular septal crest (see Figs. 14-31 and 14-32). Also seen in AV septal defects is the shortening of the inlet. This feature can be appreciated by calculating the atrial-to-ventricular length ratio in the four-chamber view.<sup>106,107</sup> In the normal heart, the atrial length is approximately half of the ventricular

length. In AV septal defects, the atrial length is more than two thirds of the ventricular length, with the ratio approaching almost 1:1 in many cases. This appearance will be helpful when the sonographic window is poor and does not allow proper visualization or when the defect needs to be differentiated from an inlet ventricular septal defect. The AV septal defect can be mimicked by a dilated coronary sinus in association with persistent left SVC (Fig. 14-33).<sup>108</sup>

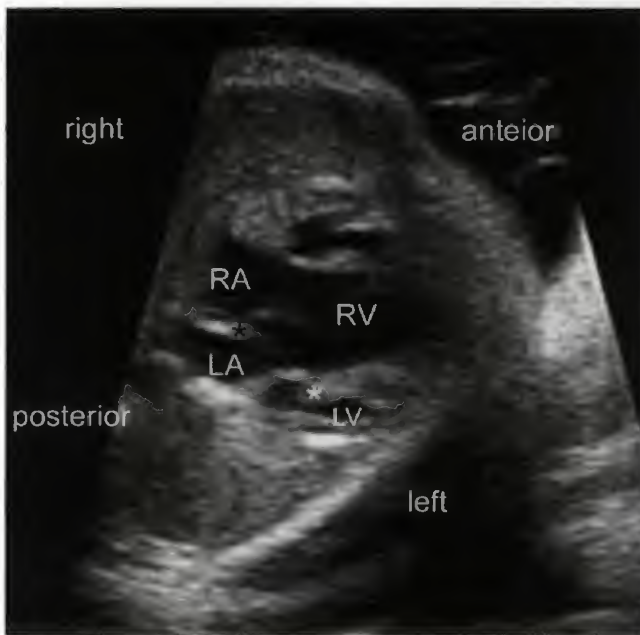


**FIGURE 14-34.** Atrioventricular septal defect with severe hypoplasia of the left ventricle. The ventricular septum is not aligned with the atrial septum. The ventricular septal crest and lower tip of the defective atrial septum are marked by asterisks. The left ventricle (LV) is very hypoplastic. The ventricular septum can be mistaken for a papillary muscle. LA, left atrium; RA, right atrium; RV, right ventricle.



**FIGURE 14-35.** Common atrium with a strand of remnant atrial septum in right isomerism. There is a large complete form of atrioventricular septal defect with a common atrial cavity. Only a thin strand of remnant atrial septum traverses the common atrial cavity. The strand is seen as a dot (arrow) in the center of the common atrium. This finding is highly suggestive of right isomerism. LV, left ventricle; RV, right ventricle.

According to the size of the ventricles, AV septal defects are classified into balanced, right-dominant, and left-dominant types (Fig. 14-34). The AV septal defect is often associated with obstruction of the left ventricular outflow tract and aortic arch. Left ventricular outflow tract narrowing can be due to the anterior bridging leaflet itself, abnormal accessory tissue from the AV valve, fibrous ridge, or prominent muscle bundle between the aortic and AV valves. However, it should be emphasized that the left ventricular outflow tract should be assessed during systolic phase. In diastole, the left ventricular outflow tract characteristically appears narrowed with the appearance of a goose-neck because the anterior bridging leaflet is displaced forward and downward. This goose-neck deformity of the left ventricular outflow tract should not be mistaken for an obstructive lesion. Most importantly, the AV septal defect is associated with a chromosomal abnormality in approximately 50% of cases.<sup>109,110</sup> Interestingly, uncomplicated AV septal defects are more commonly associated with chromosomal abnormalities. AV septal defect is particularly common in visceral heterotaxy. It is seen in 90% of right isomerism and 50% of left isomerism (see Table 14-5). The type of AV septal defect is often characteristic of its association with right isomerism: the atria are a common chamber with only a strand of remnant atrial septal tissue in the center. The remnant atrial septal tissue is seen as a central dot in the common atrium in the four-chamber view (Fig. 14-35).

Inlet ventricular septal defects are not common. They are either perimembranous defects extending toward the ventricular inlet along the annulus of the septal leaflet of the tricuspid valve or muscular defects. The perimem-

branous inlet defect is bordered superiorly by the tricuspid and mitral valves, which appear to be continuous. Therefore, it is often difficult to differentiate it from the AV septal defect in the four-chamber view, in which situation the calculation of the atrial-to-ventricular length ratio can be helpful.<sup>106,107</sup> The most important difference is the lower part of the atrial septum, which is intact in ventricular septal defect. It is interesting that both AV septal defects and perimembranous inlet ventricular septal defects are commonly associated with trisomy 21.<sup>111</sup>

Pericardial fluid is also best seen in four-chamber view. The normal pericardial space contains a small amount of fluid that is seen as an echolucent stripe along the outer margin of the heart.<sup>112</sup> The fluid in the pericardial space moves toward the apex in systole and toward the base in diastole. This movement of the pericardial fluid can be appreciated with color Doppler. As the flowing fluid is seen as a linear structure in two-dimensional images, it can be mistaken for a coronary vessel. A pathologic amount of pericardial effusion may arise from or be associated with a variety of conditions including structural heart disease, impaired cardiac function, trisomy 21 and other chromosomal abnormalities, and infectious processes.<sup>113,114</sup> A gross amount of pericardial effusion in an otherwise normal heart is an indication for fetal karyotyping.<sup>114</sup>

### Three-Vessel View

The three-vessel view provides important clues to the diagnosis of almost all lesions involving the ventricular outflow tracts and great vessels (see Fig. 14-10).<sup>47-50</sup> The abnormalities



**Table 14–8** Abnormal Findings at Three-Vessel View<sup>47</sup>

Abnormal Findings		Congenital Heart Diseases
Abnormal vessel size	Small ascending aorta and large main pulmonary artery	Coarctation of the aorta Interruption of the aortic arch Hypoplastic left heart syndrome Critical aortic stenosis
	Small main pulmonary artery and large ascending aorta	Tetralogy of Fallot Pulmonary atresia with ventricular septal defect Pulmonary atresia or critical stenosis with intact ventricular septal defect
	Dilated main pulmonary artery	Ebstein malformation Pulmonary valve stenosis Pulmonary regurgitation
	Dilated ascending aorta	Aortic valve stenosis Aortic regurgitation Marfan syndrome
	Dilated superior vena cava	Interruption of the inferior vena cava Supracardiac cardiac type of total or partial anomalous pulmonary venous connection Right-side heart failure Vein of Galen aneurysm
Abnormal vessel alignment	Anterior displacement of ascending aorta with small main pulmonary artery	Tetralogy of Fallot Double-outlet right ventricle with subpulmonary stenosis
	Posterior displacement of small ascending aorta	Hypoplastic left heart syndrome Interruption of the aortic arch
	Side-by-side relationship with same arterial size	Double-outlet right ventricle Some complete transposition of the great arteries
	Side-by-side relationship with ascending aorta	Double-outlet right ventricle with subaortic stenosis Complete transposition with subaortic stenosis
Abnormal vessel arrangement	Right anterior ascending aorta (triangular arrangement)	Complete transposition of the great arteries Some double-outlet right ventricle
	Left anterior ascending aorta	Corrected transposition of the great arteries Double-inlet left ventricle with transposition
	Left-sided superior vena cava	Absence of right superior vena cava
Abnormal vessel number	One artery	Truncus arteriosus Pulmonary atresia with ventricular septal defect and absent or hypoplastic main pulmonary artery
	Four vessels	Bilateral superior venae cavae Partial anomalous pulmonary venous connection

that can be seen in the three-vessel view include abnormal vessel size, alignment, arrangement, and number (Table 14–8).

The size of the great arterial trunks can easily be compared in the three-vessel view. Usually, the size of the vessel reflects the amount of blood flow passing through it. Therefore, there is a reciprocal relationship in size between the ascending aorta and the main pulmonary artery. A small ascending aorta and large pulmonary artery suggest diversion of the blood flow into the main pulmonary artery.<sup>47–50</sup> When the ascending aorta is smaller than either the SVC or the descending aorta, it can safely be considered small (see Figs. 14–23B, 14–26C, 14–26D, 14–27B). In the presence of concordant AV and ventriculoarterial connections, preferential flow into the main pulmonary artery occurs when an obstructive lesion or lesions exist in the left side of the heart, as discussed in the previous section. These lesions are associated with variable degree of hypoplasia of

the left heart or the aortic arch, or both. Preferential flow to the right side of the heart also occurs with anomalous pulmonary venous connection, although it is not a constant finding.<sup>89–91</sup> Without preferential flow to it, a large main pulmonary artery can be due to poststenotic dilatation when there is pulmonary valve stenosis.<sup>47,48</sup>

A small main pulmonary artery and a large ascending aorta suggest diversion of the blood flow into the ascending aorta. In the presence of normally related cardiac chambers and great arteries, preferential flow into the ascending aorta occurs most commonly with tricuspid valve regurgitation and/or obstructive right heart lesions such as tricuspid or pulmonary stenosis.

The main pulmonary artery is characteristically small in tetralogy of Fallot (Fig. 14–36).<sup>47,48,55</sup> Morphologically, tetralogy of Fallot is characterized by leftward anterior and superior deviation of the outlet or infundibular septum

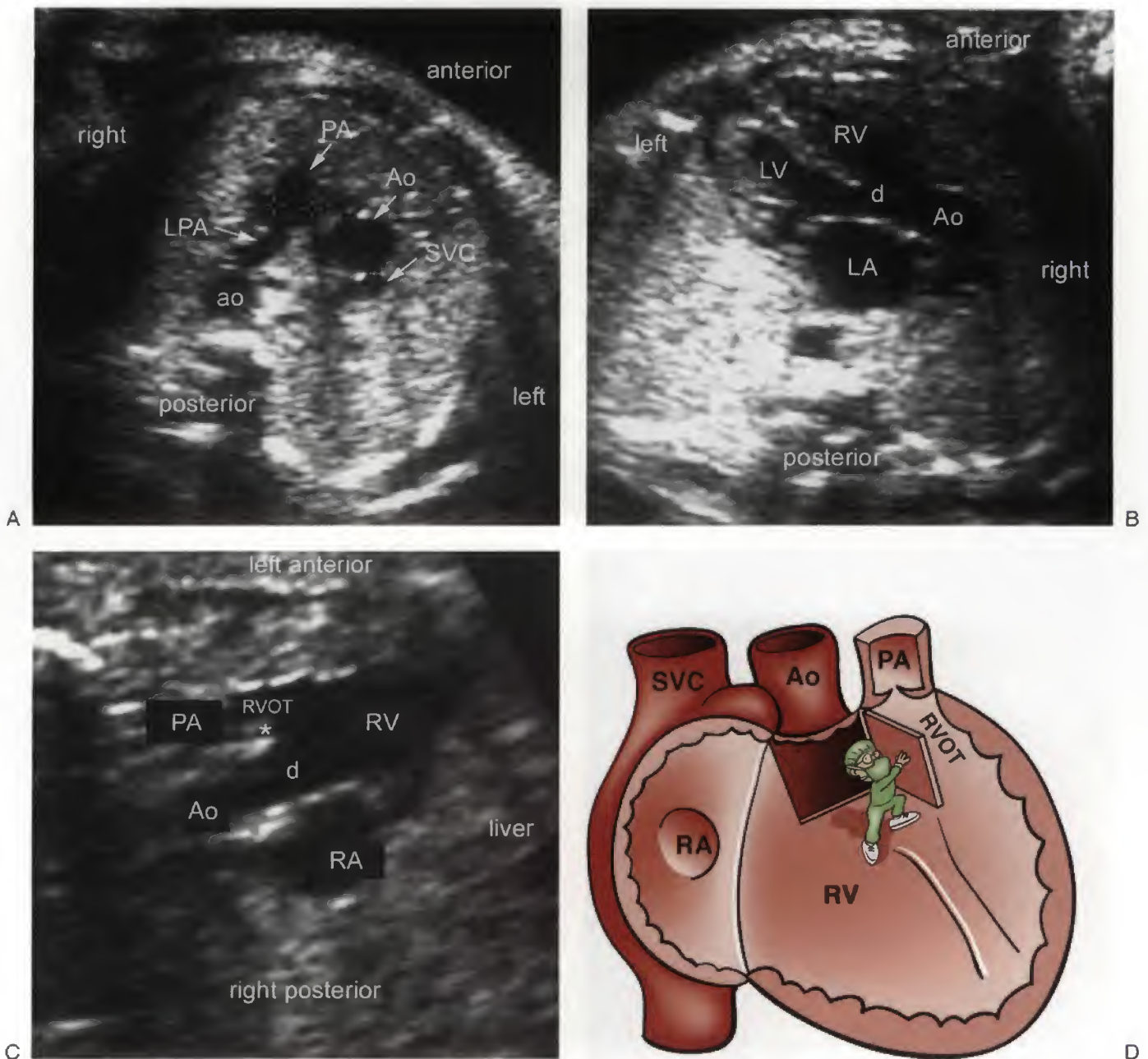


**FIGURE 14-36.** Tetralogy of Fallot. A. Three-vessel view shows malalignment of the three vessels with anterior displacement of the large ascending aorta (Ao) and mild posterior displacement of the small main pulmonary artery (PA). B. Left ventricular outflow tract view shows a large perimembranous ventricular septal defect (d). The aorta overrides the ventricular septum. C. Right anterior oblique view of the right ventricle (RV) shows narrowing of the right ventricular outflow tract (RVOT) due to leftward anterior deviation of the outlet septum (asterisk). The ventricular septal defect is seen posterior to the deviated outlet septum. D. Cartoon showing pathogenetic mechanism of tetralogy of Fallot. The essential feature of tetralogy is leftward, anterior and superior deviation of the outlet septum causing right ventricular outflow tract narrowing and malalignment type of ventricular septal defect. ao, descending aorta; LA, left atrium; LV, left ventricle; RA, right atrium; RV, right ventricle; SVC, superior vena cava. (A reprinted with permission from Yoo SJ, Lee YH, Kim ES, et al: Tetralogy of Fallot in the fetus: Findings at targeted sonography. *Ultrasound Obstet Gynecol* 14:29, 1999.)

relative to the rest of the ventricular septum, causing a large malalignment type of ventricular septal defect, and subpulmonary and pulmonary stenosis (see Fig. 14-36C). The main pulmonary artery is invariably small and the ascending aorta dilated, which tends to be more obvious with advancing gestation.<sup>115,116</sup> The only exception to this rule is when tetralogy is associated with absent pulmonary valve syndrome, which will be discussed later in this section. As

the ventricular septal defect in tetralogy involves the outlet part of the septum, it is not seen in the four-chamber view (see Fig. 14-14B) unless the defect extends to the inlet part of the septum or tetralogy is associated with an AV septal defect. As discussed earlier, the four-chamber view may show leftward deviation of the cardiac axis (see Fig. 14-14B).

Without preferential flow into it, a large ascending aorta can be due to poststenotic dilatation when there is aortic



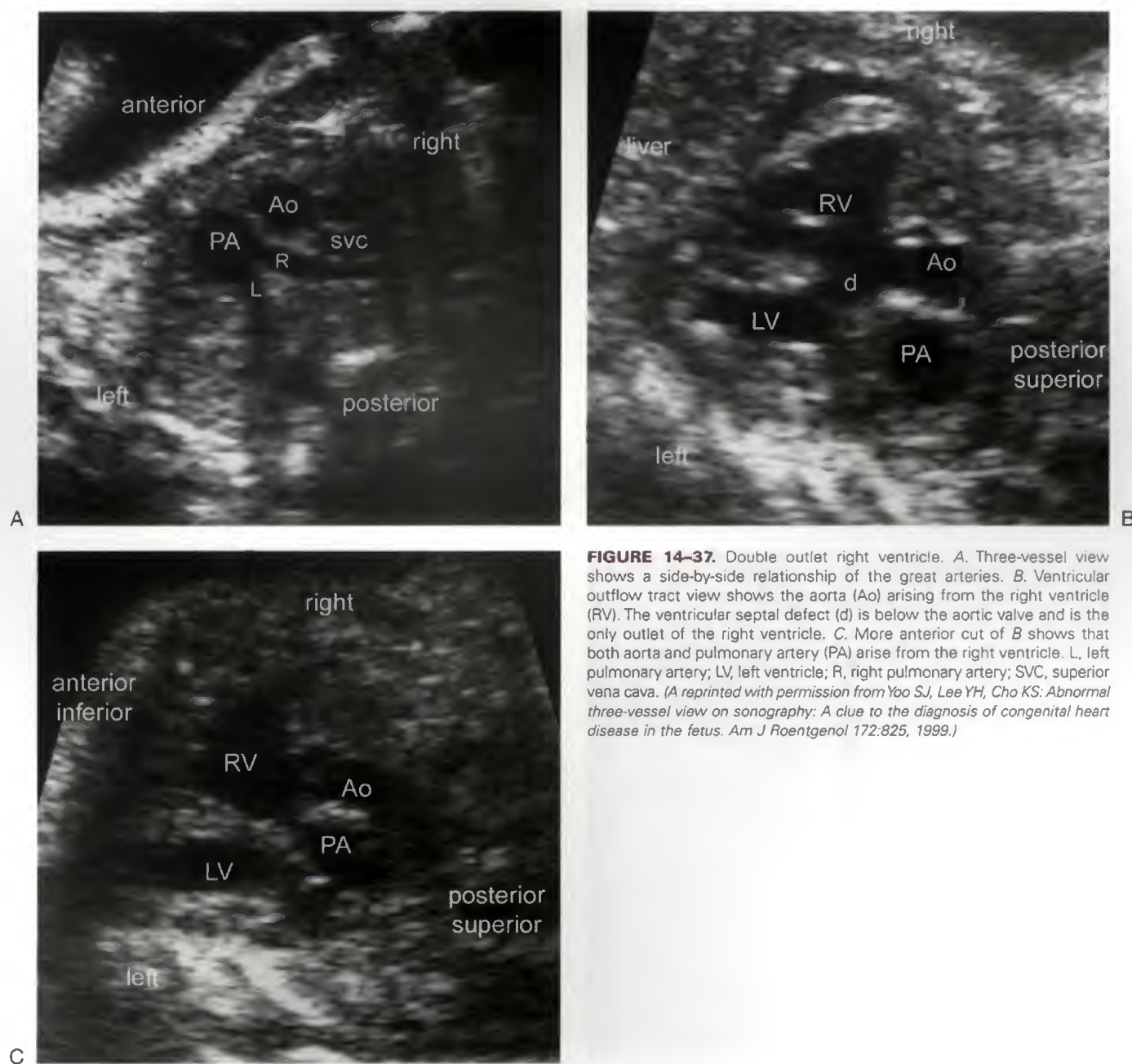


**FIGURE 14-37.** Double outlet right ventricle. *A.* Three-vessel view shows a side-by-side relationship of the great arteries. *B.* Ventricular outflow tract view shows the aorta (Ao) arising from the right ventricle (RV). The ventricular septal defect (d) is below the aortic valve and is the only outlet of the right ventricle. *C.* More anterior cut of *B* shows that both aorta and pulmonary artery (PA) arise from the right ventricle. L, left pulmonary artery; LV, left ventricle; R, right pulmonary artery; SVC, superior vena cava. (A reprinted with permission from Yoo SJ, Lee YH, Cho KS: Abnormal three-vessel view on sonography: A clue to the diagnosis of congenital heart disease in the fetus. *Am J Roentgenol* 172:825, 1999.)

valve stenosis.<sup>47</sup> Marfan syndrome is a possible cause for an unexplained dilatation of the aorta.<sup>117</sup>

Dilatation of the SVC is seen in interruption of the inferior vena cava with azygos or hemiazygos venous continuation, arteriovenous malformations such as vein of Galen aneurysm, and right-sided heart failure.<sup>102</sup> It is also dilated when there is anomalous pulmonary venous drainage into the innominate vein or directly into the SVC.<sup>92</sup>

Abnormal vessel alignment refers to the three vessels not aligning in a straight line in spite of their left-right order being preserved. Most commonly, abnormal alignment is caused by anterior displacement of the ascending aorta with or without posterior displacement of the main pulmonary artery. This form of abnormal alignment is seen in most cases

of tetralogy of Fallot in which the dilated ascending aorta is displaced anteriorly and to the right, and the smaller main pulmonary artery is displaced posteriorly (see Fig. 14-36).<sup>47,48,55</sup> It is also seen in double outlet right ventricle in which the great arteries are often located side by side (Fig. 14-37). Occasional cases of complete transposition of the great arteries may also show a similar arterial relationship.

Less commonly, abnormal alignment is caused by posterior displacement of the ascending aorta (see Fig. 14-23*B*). This form of abnormal alignment suggests severe obstructive lesions of the left side of the heart, such as hypoplastic left heart syndrome and interruption of the aortic arch.

Abnormal vessel arrangement refers to a gross distortion of the left-right order of the three vessels. The most common

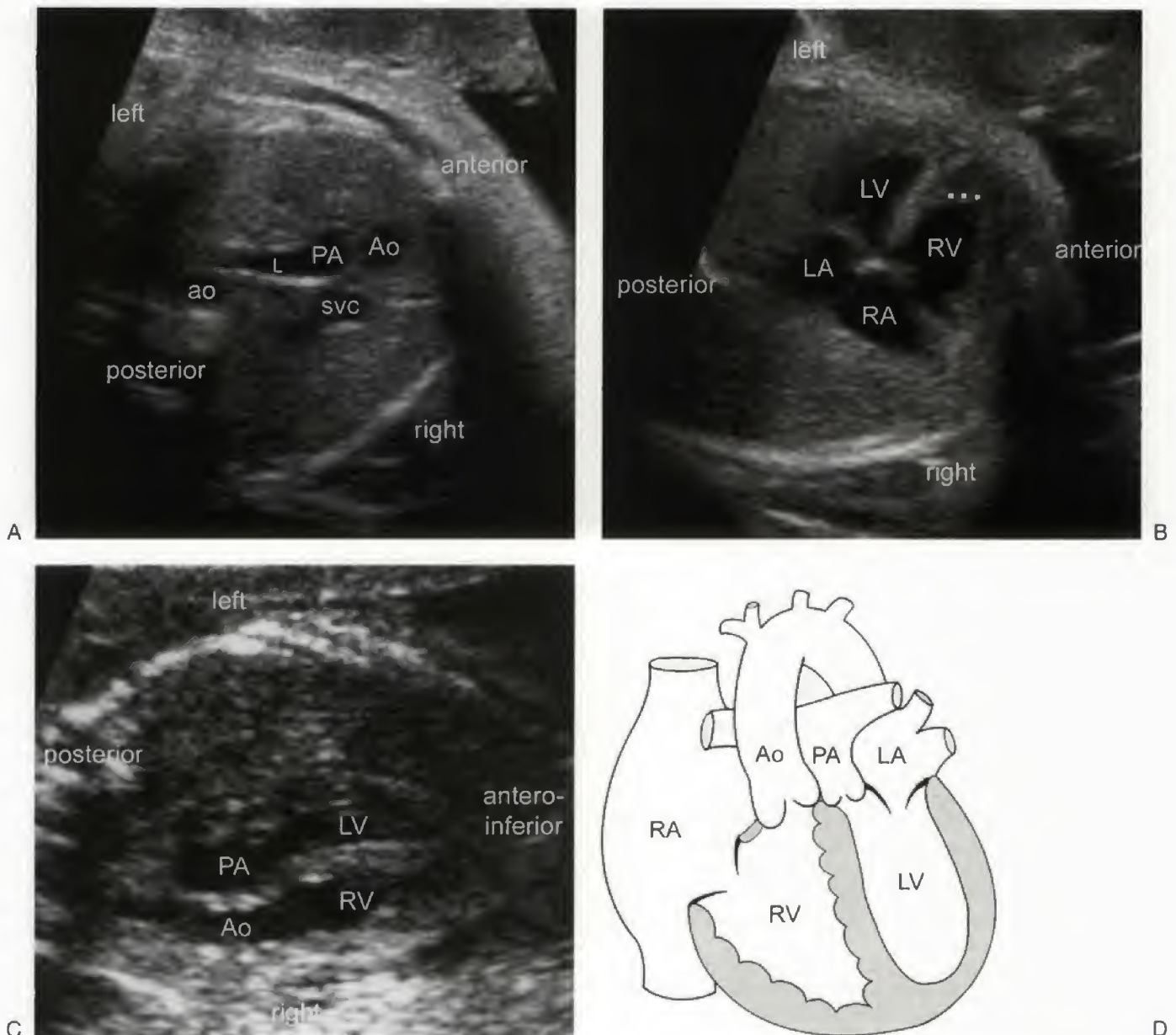


**FIGURE 14-38.** Complete transposition of the great arteries. *A.* Three-vessel view shows triangular arrangement of the three vessels. The aorta (Ao) is located right and anterior to the main pulmonary artery (PA). *B.* Four-chamber view shows normal cardiac anatomy. The apex of the right ventricle (RV) is obliterated by the moderator band (asterisks). *C.* Ventricular outflow tract view shows discordant ventriculoarterial connection with parallel courses. *D.* Diagram shows the anatomy of complete transposition of the great arteries. ao, descending aorta; L, left pulmonary artery; LA, left atrium; LV, left ventricle; PA, main pulmonary artery; RA, right atrium; RV, right ventricle; SVC, superior vena cava. (C reprinted with permission from Yoo SJ, Lee YH, Cho KS, et al: Sequential segmental approach to fetal congenital heart disease. *Cardiol Young* 9:430, 1999.)

abnormal arrangement is a triangular arrangement (Fig. 14-38).<sup>34,47,48</sup> The ascending aorta is located right anterior or directly anterior to the main pulmonary artery. This arrangement is seen in most cases of complete transposition of the great arteries and in some cases of double outlet right ventricle. Complete transposition is characterized by discordant ventriculoarterial connections in the presence of concordant AV connections. As a consequence, the systemic and pulmonary circulations have parallel circuits, which do not permit survival after birth if there is no mixing channel between the two circuits. In the majority of cases

with complete transposition, the ascending aorta is located right anteriorly to the main pulmonary artery, showing a triangular arrangement of the three vessels (see Fig. 14-38). However, there are significant variations in the great arterial relationship in complete transposition.

A less common form of abnormal arrangement is a reversed position of the great arterial trunks; that is, the ascending aorta being located to the left of and anterior to the main pulmonary artery (see Figs. 14-16B and 14-17C).<sup>34,47,48</sup> This is typically seen in congenitally corrected transposition of the great arteries (see Fig. 14-16B).



As discussed earlier in this chapter, corrected transposition refers to a condition in which both AV and ventriculoarterial connections are discordant. A reversed great arterial position is also seen in double inlet left ventricle with discordant ventriculoarterial connection (see Fig. 14–17C). In all of these conditions, a significant discrepancy in size of the main pulmonary artery and ascending aorta suggests an obstructive lesion of the outflow that leads to the smaller of the two. Very rarely, the right SVC is not present and the systemic venous return from the upper body to the right atrium occurs through the left SVC by way of the coronary sinus.<sup>118</sup>

Presence of only two vessels in the three-vessel view is rare but suggests that one arterial trunk is missing or severely hypoplastic or that only one arterial trunk is present.<sup>47,48,55</sup> It is most commonly seen in tetralogy of Fallot with pulmonary atresia (in other words, pulmonary atresia with ventricular septal defect) when the main pulmonary artery is not formed or severely hypoplastic. Only two vessels are typically seen in truncus arteriosus in which a single arterial trunk arises from the heart and gives rise to the ascending aorta, pulmonary arteries and coronary arteries (Fig. 14–39). At its most proximal plane of section, the common truncus is seen as a large arterial root. Immediately above this basal view through the truncal base, the pulmonary arteries arise from the posterior or right posterior wall of the truncus. The differentiation between common truncus and pulmonary atresia is clinically important. In pulmonary atresia, survival of the newborn depends on a patent ductus arteriosus or MAPCA as the sole vascular connection securing pulmonary artery perfusion (Fig. 14–40).<sup>55,120</sup>

Four vessels in the three-vessel view are most commonly seen with bilateral superior venae cavae (see Fig. 14–33).<sup>47,48,121</sup> The persistent left SVC is located at the left posterior aspect of the main pulmonary artery. Four vessels are also seen in partial or total anomalous pulmonary venous connection to the innominate vein in which the vertical vein connecting the anomalous vein to the innominate vein is an additional vessel (see Fig. 14–25).<sup>122</sup>

An abnormal communication between the two arterial trunks characterizes the aortopulmonary window. The defect can involve the proximal or distal part or the entire length of the main pulmonary artery. The distal and total types can be associated with abnormal origin of the right pulmonary artery from the ascending aorta, and are frequently associated with interruption of the aortic arch. The diagnosis can be suspected when the three-vessel view shows a defect between the ascending aorta and main pulmonary artery in the presence of normal aortic and pulmonary valves in the ventricular outflow tract views.<sup>123,124</sup>

A branch pulmonary artery can be absent or hypoplastic (Table 14–9). Unilateral absence of a branch pulmonary artery is characterized by agenesis of the proximal branch pulmonary artery with its distal part connected to the ipsilateral ductus arteriosus. The absent branch pulmonary artery is almost always on the opposite side of the aortic arch. After birth, the affected lung loses its major blood supply as the ductus arteriosus closes. The branch pulmonary arteries are small when there is severe obstruction of pulmonary outflow tract, as in tetralogy of Fallot with severe pulmonary stenosis or atresia. When tetralogy of Fallot with pulmonary atresia (that is, pulmonary atresia with

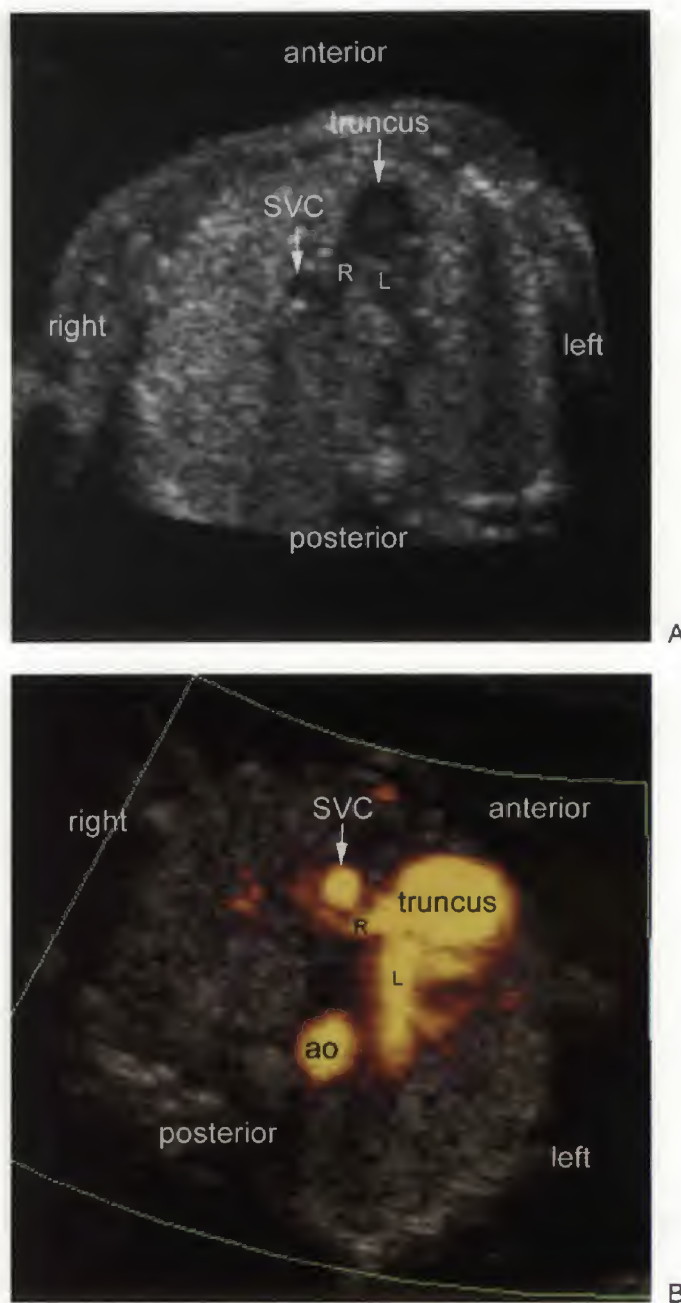


**FIGURE 14–39.** A and B. Truncus arteriosus. Three-vessel view shows only two vessels. The truncus gives rise to the right (R) and left (L) pulmonary arteries. SVC, superior vena cava.

ventricular septal defect) is associated with MAPCA, the branch pulmonary arteries can be hypoplastic or absent. Lung hypoplasia is associated with hypoplasia of the branch pulmonary artery. Hypoplasia of the right lung and right pulmonary artery is typically seen in scimitar syndrome. When a large part of a lung is supplied by an aberrant systemic artery, as in pulmonary sequestration, the ipsilateral branch pulmonary artery may be hypoplastic. Congenital diaphragmatic hernia is associated with variable degree of branch pulmonary artery hypoplasia. The antenatal branch pulmonary artery size correlates with lung weight and there-



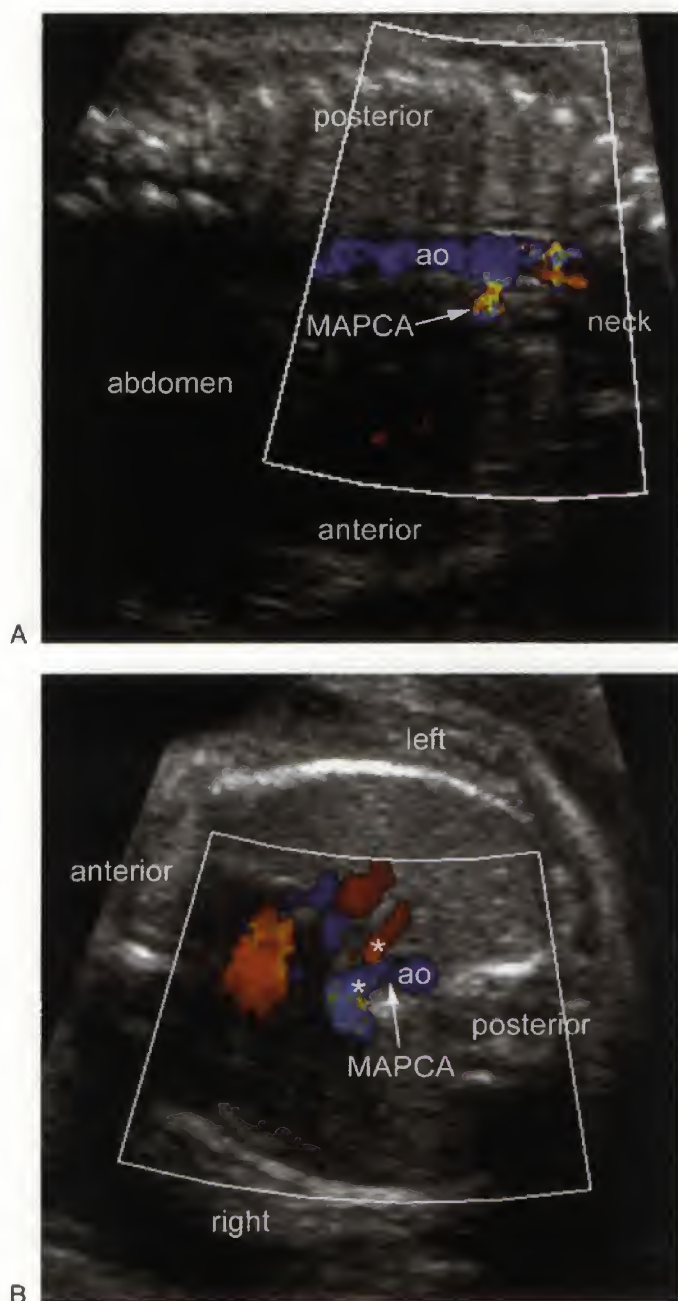


**FIGURE 14-40.** Major aortopulmonary collateral artery in tetralogy of Fallot with pulmonary atresia. *A*. Sagittal view shows a major aortopulmonary collateral artery (MAPCA) arising from the anterior wall of the descending aorta (ao). *B*. Axial view shows the collateral artery bifurcating into branches (asterisks) to both lungs.

fore with postnatal outcome.<sup>124</sup> The draining pulmonary veins of the lung having a small or absent pulmonary artery is small unless there is an alternative source of blood supply.<sup>73</sup>

The left pulmonary artery can have a very distal origin from the main pulmonary artery and course leftward through the space between the trachea and esophagus, a condition called pulmonary artery sling. This condition is commonly associated with abnormal branching of the airway and severe stenosis of the distal trachea. A branch

**Table 14-9** Abnormalities of Branch Pulmonary Arteries

Categories	Significances
Absence	Unilateral absence of right or left pulmonary artery Unilateral or bilateral in pulmonary atresia with ventricular septal defect and major aortopulmonary collateral arteries
Hypoplasia	Bilateral Congenital heart disease with severe pulmonary outflow tract obstruction Diaphragmatic hernia Hypoplastic bony thorax Unilateral Scimitar syndrome Lung hypoplasia Pulmonary sequestration
Dilatation	Constricted ductus arteriosus Absent pulmonary valve syndrome
Abnormal course	Left pulmonary artery sling
Abnormal origin	Anomalous origin of a branch pulmonary artery from the ascending aorta Proximal origin Distal origin

pulmonary artery can have an abnormal origin from the proximal or distal ascending aorta (Fig. 14-41). This diagnosis can be facilitated by color or power Doppler interrogation.<sup>125</sup>

As discussed elsewhere in this chapter, dilated branch pulmonary arteries are seen with a constricted ductus arteriosus (see Table 14-9).<sup>98-100</sup> As the ductus arteriosus closes in the fetus, blood from the right side of the heart is totally directed through the high-resistance, fluid-filled lungs, resulting in dilatation of the branch pulmonary arteries and increased right ventricular afterload with right-sided heart dilatation and tricuspid regurgitation. Color and spectral Doppler interrogation of the constricting ductus shows turbulent flow with high velocity. A peak systolic velocity of greater than 1.5 m/second with increased diastolic flow velocity is suggestive of ductal constriction.

The branch pulmonary arteries are aneurysmally dilated when tetralogy of Fallot is associated with absent pulmonary valve syndrome (Fig. 14-42).<sup>55,126-128</sup> This condition is usually associated with congenital absence of ductus arteriosus, suggesting that the pathogenetic mechanism of the dilatation of the branch pulmonary arteries is similar to that seen with premature closure of the ductus arteriosus. The ductus arteriosus can be aneurysmally dilated in later pregnancy (Fig. 14-43).<sup>129-131</sup>

Ductus arteriosus aneurysms may be observed in patients with connective tissue abnormalities such as Marfan, Ehlers-Danlos, and Larsen syndromes. Spontaneous rupture, erosion, thromboembolism, infection, and compression of adjacent structures are some of the reported complications, although most regress spontaneously.<sup>117,131</sup> The ductus arteriosus aneurysm is best seen in the three-vessel view.<sup>130</sup> It should be differentiated from the normal tortuous course



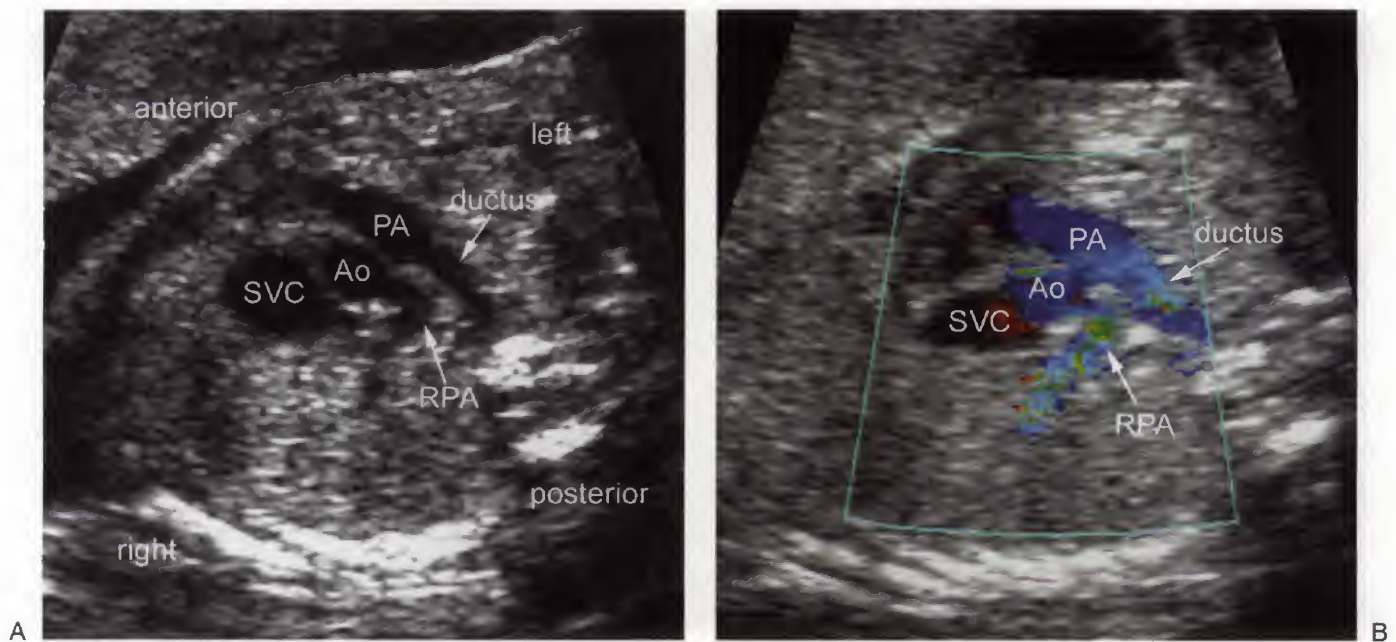


**FIGURE 14-41.** A, B. Origin of the right pulmonary artery from the aorta. Three-vessel views show anomalous origin of the right pulmonary artery (RPA) from the posterior wall of the ascending aorta (Ao). PA, main pulmonary artery; SVC, superior vena cava. (Reprinted with permission from Jung MJ, Yoo SJ: Prenatal diagnosis of anomalous origin of the right pulmonary artery from the ascending aorta. *Cardiol Young* 12:186, 2002.)

of the ductus in late pregnancy (see Fig. 14-10F). Severely tortuous ductus, however, can be associated with physiologic ductal constriction with right-sided chamber enlargement.<sup>101</sup>

When there is a normal left aortic arch, the descending aorta is located at the left anterior aspect of the vertebral body. A right-sided descending aorta is strongly suggestive of a positional abnormality of the aortic arch, most commonly a right aortic arch and less commonly a double aortic arch (Figs. 14-44 and 14-45).<sup>133,134</sup> In double aortic arch, the descending aorta seen in the three-vessel view can be on either side or even in the midline. Very rarely, the aortic arch is left sided relative to the trachea but crosses the midline behind the esophagus to descend on the right side. This rare condition is called circumflex retro-esophageal aortic arch. This condition also occurs with a right aortic arch having a left-sided descending aorta. Any vessel seen behind the trachea in the three-vessel or its adjacent view is an additional sign for an aortic arch anomaly (see Figs. 14-44 and 14-45).<sup>133,134</sup> A retroesophageal vessel can be either an aberrant branch arising from the descending aorta or a part of the double or retroesophageal aortic arch. As mentioned earlier, the left pulmonary artery in pulmonary artery sling courses through the space between the distal trachea and esophagus.

Various syndromes related to chromosome 22q11 deletion are often associated with tetralogy of Fallot, truncus arteriosus, interruption of the aortic arch and aortic arch anomalies.<sup>134,135</sup> Chromosome 22q11 deletion is usually associated with thymic hypoplasia or aplasia. Therefore, when a cardiac defect that has a high incidence of association with chromosome 22q11 deletion is found, the status of the thymus can be evaluated by using a three-vessel view.<sup>52,53</sup> As mentioned, the transverse diameter of the thymus in millimeters is slightly smaller than the gestational

age in weeks in the second trimester and becomes slightly larger as the pregnancy approaches term.<sup>54</sup>

### Left and Right Ventricular Outflow Tract Views

Abnormalities of the ventricular outflow tracts are not only common but also relatively serious and complex. Ventricular outflow tract abnormalities can be categorized into two groups: those occurring as an isolated or complex lesion in the presence of normal ventriculoarterial connection, and those occurring as a complex malformation with abnormal ventriculoarterial connection.

The ventricular septal defect visualized in ventricular outflow tract views is most commonly a perimembranous defect with outlet extension (Fig. 14-46). These defects are seen below the aortic valve in the left ventricular outflow tract view. It is not unusual for the aortic valve to have a mildly overriding position relative to the ventricular septal crest in this view because the defect involves the curved part of the ventricular septum. One may imagine how a simple defect can be seen to override the ventricular septum by mentally removing the part of the septum below the aortic valve seen in a normal left ventricular outflow tract view. On the other hand, this part of the septum may be seen as falsely defective because of the partial volume effect of the oblique cut of the curved septum and the thinness of the membranous septum. Because shunting across a ventricular septal defect in an otherwise normal heart is minimal and for a brief period in the systolic phase, it is difficult to perceive the shunt flow by color Doppler interrogation.<sup>135</sup> Obviously, three-dimensional ultrasound is of significant help.<sup>136</sup> The ventricular septal defects of so-called malalignment type are more readily discernable. The malalignment involves the

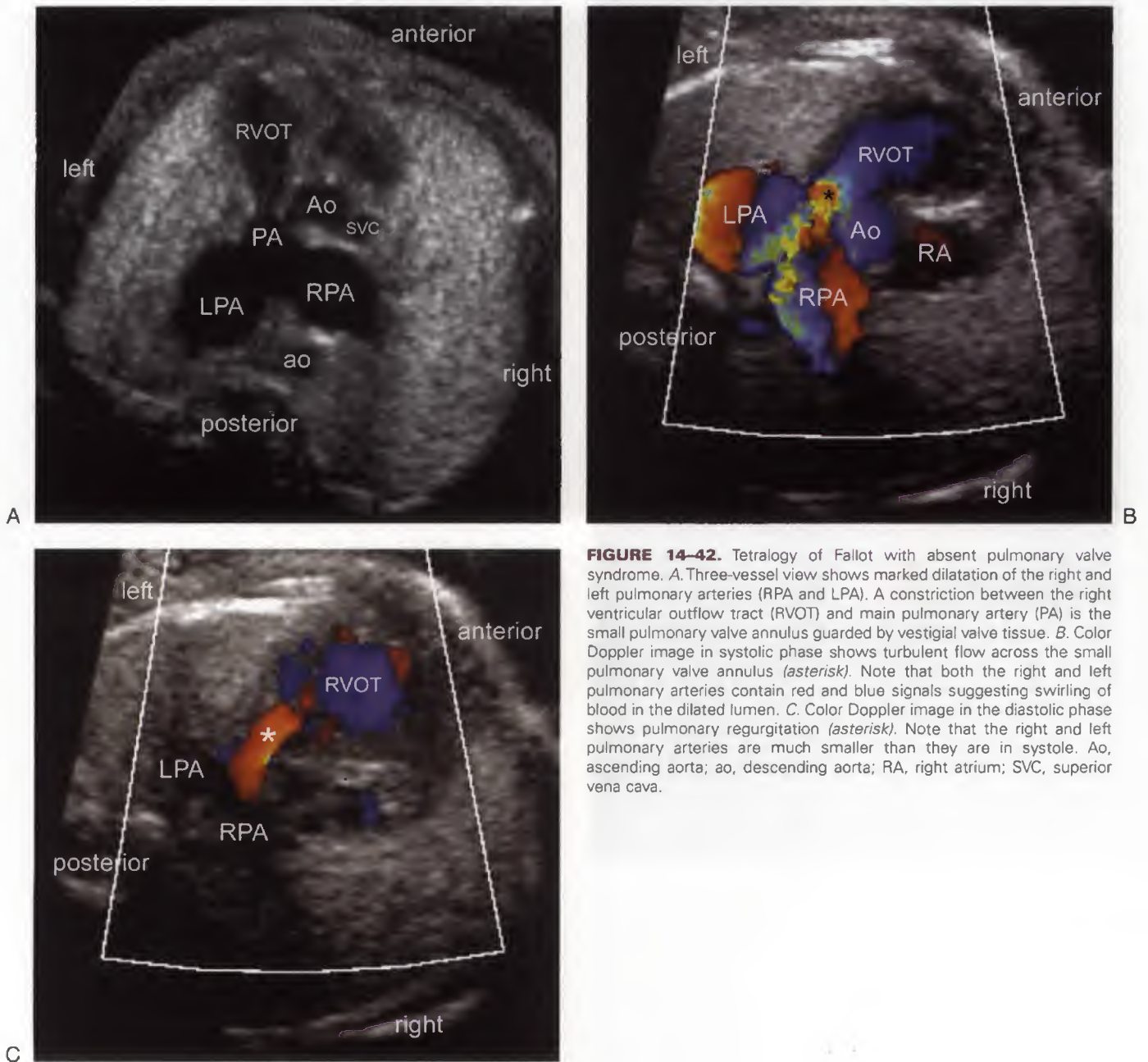


**FIGURE 14-42.** Tetralogy of Fallot with absent pulmonary valve syndrome. **A.** Three-vessel view shows marked dilatation of the right and left pulmonary arteries (RPA and LPA). A constriction between the right ventricular outflow tract (RVOT) and main pulmonary artery (PA) is the small pulmonary valve annulus guarded by vestigial valve tissue. **B.** Color Doppler image in systolic phase shows turbulent flow across the small pulmonary valve annulus (*asterisk*). Note that both the right and left pulmonary arteries contain red and blue signals suggesting swirling of blood in the dilated lumen. **C.** Color Doppler image in the diastolic phase shows pulmonary regurgitation (*asterisk*). Note that the right and left pulmonary arteries are much smaller than they are in systole. Ao, ascending aorta; ao, descending aorta; RA, right atrium; SVC, superior vena cava.



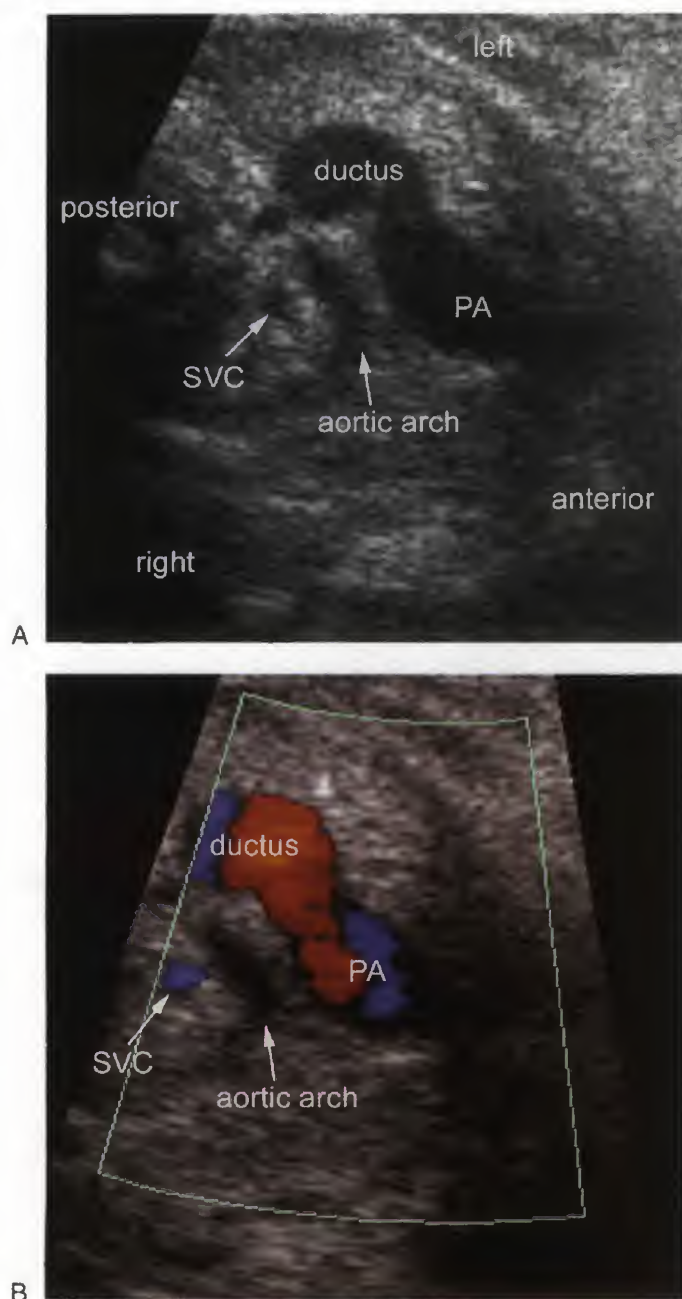


**FIGURE 14-43.** Aneurysm of the ductus arteriosus in a fetus at 34 weeks of gestation. *A*, Three-vessel view shows that the ductus arteriosus is markedly dilated at its aortic end. *B*, Color Doppler image in the same plane as *A* shows swirling blood flow within the dilated part of the ductus arteriosus. This condition should be differentiated from a normal tortuous ductus arteriosus seen in late gestation as shown in Fig. 14-10 *F* and *G*. PA, main pulmonary artery; SVC, superior vena cava.

outlet septum below the semilunar valves and is either forward or backward. The forward or anterior malalignment of the outlet septum encroaches on the right ventricular outflow tract and is typically seen in tetralogy of Fallot (see Fig. 14-36). It is often better appreciated in a short-axis or right anterior oblique view than in ventricular outflow tract views. The backward or posterior malalignment of the outlet septum encroaches on the left ventricular outflow tract and can be easily appreciated in a left ventricular outflow tract

view. The malaligned outlet septum is seen as a teardrop hanging from the aortic valve. When there is significant malalignment, interventricular shunt flow is readily visible with color Doppler. Significant posterior malalignment is associated with various forms of aortic arch obstruction including coarctation, tubular hypoplasia, or interruption. The doubly committed defects involving the most cranial part of the ventricular septum below the pulmonary valve may escape detection in this view.

The obstructive lesions of the left ventricular outflow tract include fibrous ridge, fibromuscular tunnel, accessory tissue arising from the mitral valve, and aortic valvar stenosis, all of which are difficult to identify during a fetal cardiac examination. Left ventricular outflow tract obstruction is often associated with the presence of muscle tissue between the aortic and mitral valves causing discontinuity between the two valves. This muscular crest is called the left ventriculoinfundibular fold. Turbulent flow with increased velocity during color and spectral Doppler examination supports the evidence for outflow tract obstruction. The obstructive lesion of the right ventricular outflow tract is characteristically seen in tetralogy of Fallot and best seen in a short-axis or right anterior oblique long axis view (see Fig. 14-36*C*). An aberrant muscle bundle can cross the right ventricular outflow tract causing progressive obstruction. Pulmonary valve stenosis is seldom evident in the second trimester scan, whereas it is not uncommon postnatally, suggesting that it is an evolving lesion.

The ventricular outflow tract views are the key planes for the assessment of the ventriculoarterial connections. The ventriculoarterial connections are classified as concordant, discordant, double outlet, and single outlet (Fig. 14-47). In defining the ventriculoarterial connections, a great artery is considered to be connected to a ventricle when more than half of its valve area is committed to that ventricle. Abnormal ventriculoarterial connections are characterized by loss of the normal crossing nature of the routes from the ventricular outflow tracts to the great arterial trunks.

### **Transposition of the Great Arteries**

Discordant ventriculoarterial connection is found when the connection between the ventricles and great arterial trunks is reversed, that is, the right ventricle is connected to the aorta and the left ventricle to the pulmonary artery (see Fig. 14-47). Discordant ventriculoarterial connection is commonly called transposition of the great arteries when it is associated with either concordant or discordant AV connection. Discordant ventriculoarterial connection in the presence of concordant AV connection is the essential feature of complete transposition of the great arteries (see Fig. 14-38). Discordant ventriculoarterial connection in the presence of discordant AV connection is the essential feature of congenitally corrected transposition (see Fig. 14-16). In the classic forms of both complete and corrected transposition, the aorta is supported by a completely muscular infundibulum, whereas the pulmonary artery is not. In most cases of transposition, the ventricular outflow tracts are parallel to each other with the right ventricular outflow tract leading to the aorta positioned anterior to the left ventricular outflow tract leading to the pulmonary artery (see Figs. 14-16*C* and 14-38*C*). As discussed in the prior section

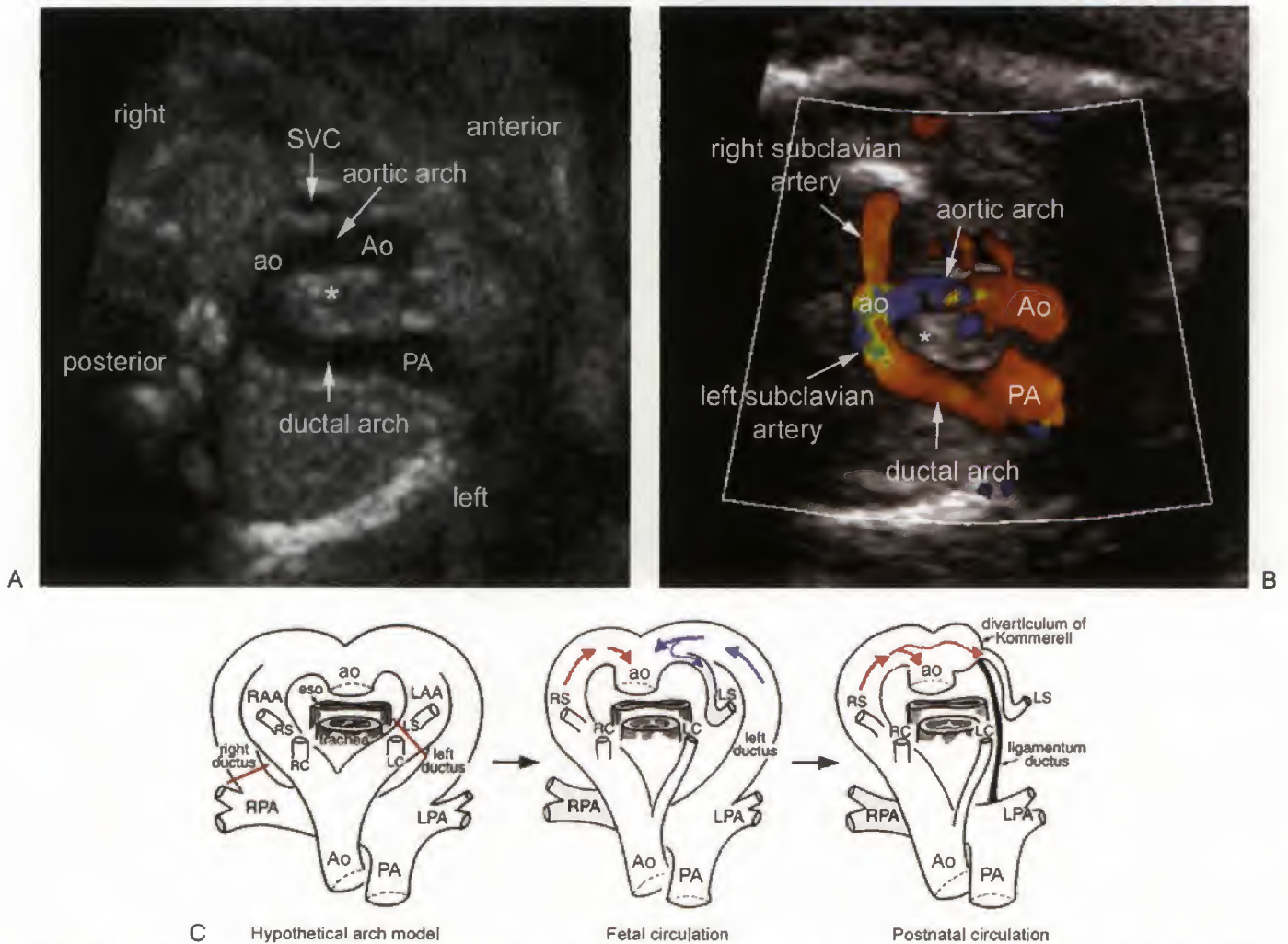


**FIGURE 14-44.** Right aortic arch with aberrant left subclavian artery. *A* and *B*. Three-vessel views show U-shaped vascular loop around the trachea (asterisk). The aortic arch is on the right side of the trachea, with the ductal arch on the left side. The proximal segment of the left subclavian artery connects the aortic and ductal arches, and the blood flow through this segment is reversed. After birth this segment persists as the aortic diverticulum of Kommerell. Note the wide gap between the ascending aorta (Ao) and main pulmonary artery (PA). *C*. Diagrams showing hypothetical morphogenesis. ao, descending aorta; eso, esophagus; LAA, left aortic arch; LC, left common carotid artery; LPA, left pulmonary artery; LS, left subclavian artery; RAA, right aortic arch; RC, right common carotid artery; RPA, right pulmonary artery; RS, right subclavian artery. SVC, superior vena cava. (C reprinted with permission from Yoo SJ, Min JY, Lee YH, et al: *Fetal sonographic diagnosis of aortic arch anomalies*. *Ultrasound Obstet Gynecol* 22:535, 2003.)



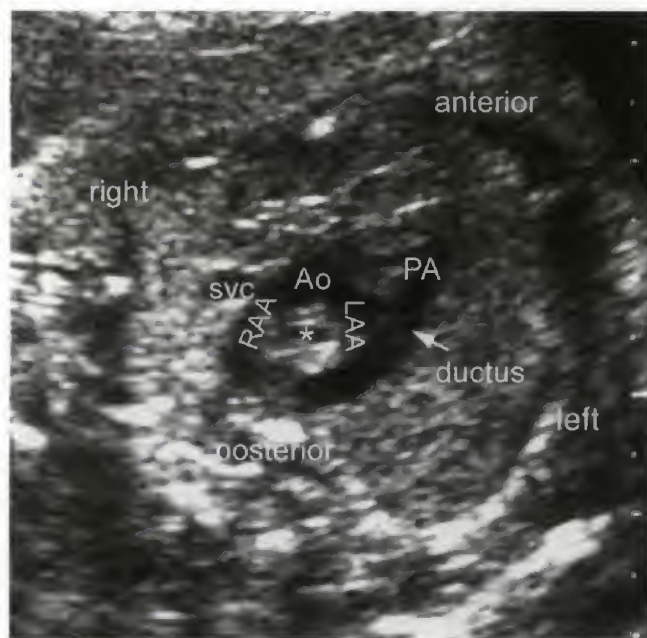


**FIGURE 14-45.** Double aortic arch. Three-vessel view shows that the right and left aortic arches (RAA and LAA) form a complete circle around the trachea (asterisk). The ductus arteriosus is patent on the left side. The aortic arches together with the main pulmonary artery (PA) and ductus arteriosus form a figure of 6 or 9 configuration. Ao, ascending aorta; SVC, superior vena cava. (Reprinted with permission from Yoo SJ, Min JY, Lee YH, et al: *Fetal sonographic diagnosis of aortic arch anomalies*. *Ultrasound Obstet Gynecol* 22:535, 2003.)

about the three-vessel view, the majority of cases with complete transposition have the aorta right anterior to the pulmonary artery (see Fig. 14-38A), whereas the majority of the cases with corrected transposition have the aorta left anterior to the pulmonary artery (see Fig. 14-16B).<sup>34,47,48</sup> A ventricular septal defect is found in approximately 40% of complete transpositions and in 60% to 70% of corrected transpositions. In both, left ventricular outflow tract obstruction is common. The obstruction can be due to posterior malalignment of the outlet septum relative to the rest of the septum, fibrous ridge, fibromuscular tunnel, accessory tissue from the mitral valve, or pulmonary valve stenosis. Right ventricular outflow tract obstruction is less common in both complete and corrected transposition. Size discrepancy of the great arterial trunks in the three-vessel view is a telltale sign of ventricular outflow tract obstruction. Corrected transposition is frequently associated with regurgitation of the left-sided tricuspid valve, either due to valve dysplasia or Ebstein malformation (Fig. 14-48).<sup>74-78</sup> Also possible in corrected transposition is delayed or blocked AV conduction with arrhythmia, as will be discussed later.

### Single and Double Outlet Ventricle

Double outlet can be from the right or left ventricle. Double-outlet right or left ventricle is a type of ventriculoarterial connection in which both great arteries arise exclusively or predominantly from the morphologically right or left ventricle. It is very important to understand that the term double-outlet ventricle is used only to describe how the great arteries arise from or connect to the underlying

ventricles. Therefore, tetralogy of Fallot with more than 50% override of the aortic valve over the ventricular septum has theoretically a double-outlet right ventricular connection. As with discordant ventriculoarterial connection, double-outlet ventricle can occur with any type of atrial situs and any type of AV connection. Double-outlet ventricle is associated with a ventricular septal defect in almost all cases. The ventricular septal defect is the sole outlet of the left ventricle when there is double-outlet right ventricle and the sole outlet of the right ventricle when there is double-outlet left ventricle. The location of the ventricular septal defect relative to the great arterial trunk dictates the hemodynamic consequence of double-outlet ventricle (Fig. 14-49), although the presence or absence of the aortic or pulmonary outflow tract obstruction is also an important contributing factor. Therefore, the ventricular septal defects in double-outlet ventricle are classified as subaortic, subpulmonary, doubly committed, and noncommitted. When double-outlet right ventricle is associated with a subaortic ventricular septal defect, the physiology is that of an isolated ventricular septal defect. When double-outlet right ventricle is associated with a subpulmonary defect, the physiology is that of complete transposition with a ventricular septal defect. When the defect is doubly committed or noncommitted, the physiology depends on the intracardiac streaming of the blood flow. The diagnosis of double outlet and the proximity of the great arterial trunks to the ventricular septal defect should be assessed by using the ventricular outflow tract views (see Fig. 14-37). Of note, the ventriculoarterial connection should be analyzed by a full sweep through the ventricular outflow tracts because appearance in a single view can be misleading. The great arteries tend to have a side-by-side, parallel relationship, with the aorta on the right side, when there is situs solitus and concordant AV connection (see Fig. 14-37C). In the majority of cases with double-outlet right ventricle, both great arteries are supported by a completely muscular infundibulum. Double-outlet right ventricle with subaortic ventricular septal defect is often associated with subpulmonary obstruction, whereas double-outlet right ventricle with subpulmonary defect is often associated with subaortic obstruction or an obstructive lesion of the aortic arch. Double-outlet left ventricle is extremely rare and shows wide morphological variation.

Single-outlet from the heart can be through a single arterial trunk or truncus arteriosus. Single arterial trunk is present when one arterial trunk is missing. It can be a form of pulmonary atresia when the main pulmonary arterial trunk is not formed or is atretic and the aorta is the sole outlet of the ventricle. On the other hand, aortic atresia is not associated with single arterial trunk because the ascending aorta is patent to the level of the aortic valve and gives rise to the coronary arteries. Truncus arteriosus or common arterial trunk is a condition in which one arterial trunk arises from the base of the ventricles by way of a single arterial valve to give rise to the systemic, coronary, and one or both pulmonary arteries (see Fig. 14-39). In almost all cases, there is a large ventricular septal defect immediately underneath the common arterial valve or truncal valve. The common arterial valve usually overrides the ventricular septum, but may have exclusive commitment to either the right or left ventricle. The truncal valve is often stenotic or regurgitant.<sup>119</sup> The ventricular septal defect and the origin of

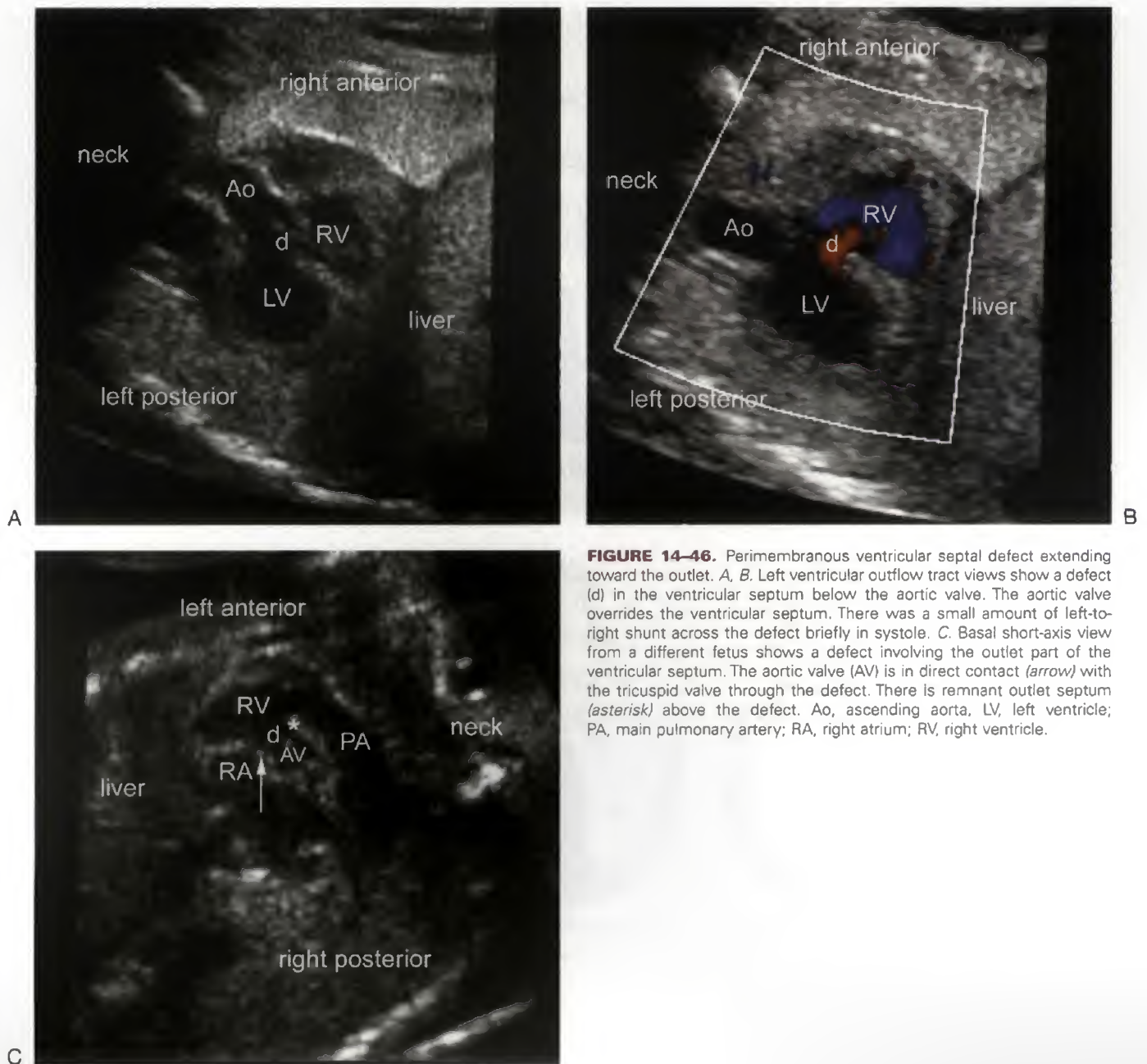


**FIGURE 14-46.** Perimembranous ventricular septal defect extending toward the outlet. *A, B.* Left ventricular outflow tract views show a defect (*d*) in the ventricular septum below the aortic valve. The aortic valve overrides the ventricular septum. There was a small amount of left-to-right shunt across the defect briefly in systole. *C.* Basal short-axis view from a different fetus shows a defect involving the outlet part of the ventricular septum. The aortic valve (*AV*) is in direct contact (*arrow*) with the tricuspid valve through the defect. There is remnant outlet septum (*asterisk*) above the defect. *Ao*, ascending aorta; *LV*, left ventricle; *PA*, main pulmonary artery; *RA*, right atrium; *RV*, right ventricle.



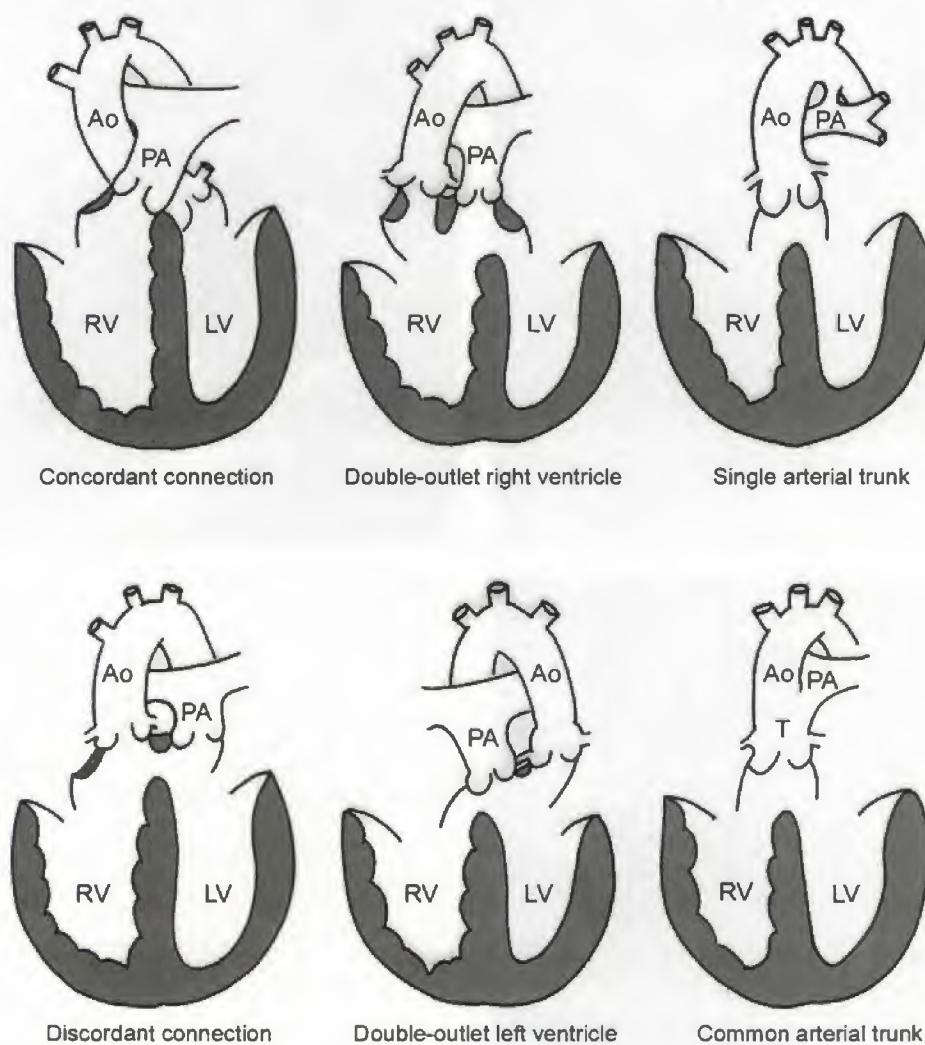


**FIGURE 14-47.** Types of ventriculoarterial connections. Ao, ascending aorta; LV, left ventricle; PA, main pulmonary artery; RV, right ventricle; T, truncus.

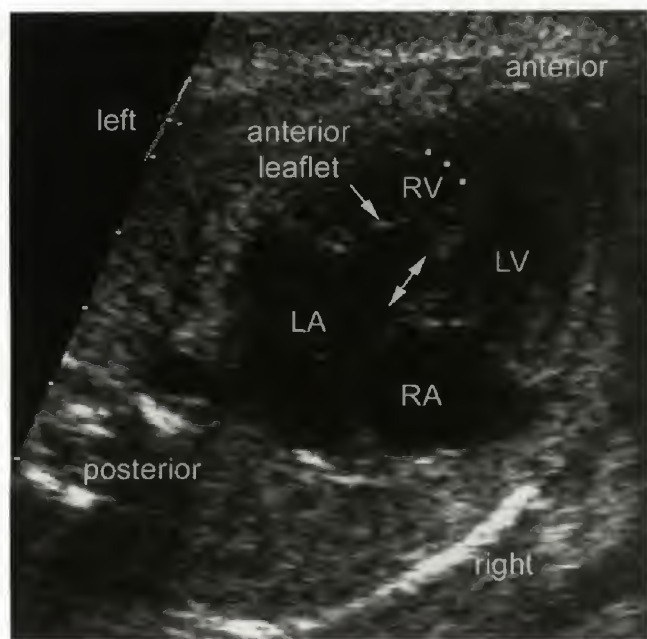


**FIGURE 14-48.** Corrected transposition of the great arteries with Ebstein malformation of the left-sided tricuspid valve. A moderator band (dots) is seen in the apical part of the left-sided right ventricle (RV). There is discordant atrioventricular connection. Septal attachment of the left-sided tricuspid valve is apically displaced. The anterior leaflet of the tricuspid valve is adherent to the septal leaflet, causing tricuspid stenosis. LA, left atrium; LV, left ventricle; RA, right atrium.

the common arterial trunk are best seen in the left ventricular outflow tract view, a finding that is very similar to that of tetralogy of Fallot. Only two vessels are seen in three-vessel view, but this finding is not specific for truncus and is also seen when the main pulmonary artery is not formed or is very small, as in tetralogy of Fallot with pulmonary atresia (in other words, pulmonary atresia with ventricular septal defect).<sup>47,48</sup> To make the diagnosis of truncus arteriosus, one should visualize the origins of the pulmonary arteries from the proximal ascending aorta.<sup>137,138</sup> Truncus arteriosus is occasionally associated with interruption of the aortic arch.

### Basal Short-Axis View

The basal short-axis view is of particular value in the definitive diagnosis of tetralogy of Fallot (see Fig. 14-35C). The essence of tetralogy is the leftward, anterior, and superior deviation of the outlet septum, causing subpulmonary outflow tract narrowing and an outlet-type of ventricular septal defect. This single most important feature of tetralogy is best appreciated in the basal short-axis view or right anterior oblique view of the right ventricle. In addition, the enlarged aortic root can easily be contrasted to the diminutive pulmonary valve. The aberrant muscle bundle in the right ventricle can also be detected but the significance of its presence is often questionable.

Because this view visualizes the outlet septum extending from the tricuspid to the pulmonary valve, the ventricular septal defect involving this area can be identified and its type determined.<sup>55</sup> However, the intact membranous septum

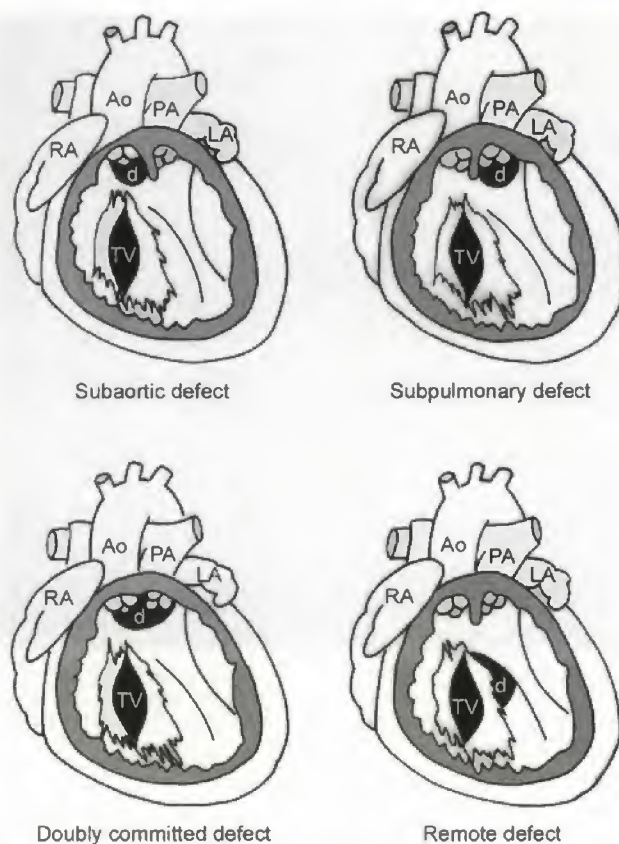


**FIGURE 14-49.** Types of ventricular septal defect in double outlet right ventricle. Ao, ascending aorta; d, ventricular septal defect; LA, left atrium; PA, main pulmonary artery; RA, right atrium; TV, tricuspid valve.

around the tricuspid valve insertion can be mistaken for a defect.

### Aortic and Ductal Arch Views

The aortic arch view is useful in the diagnosis of an obstructive lesion of the aortic arch. As a rule-of-thumb, an obstructive lesion should be suspected when the ascending aorta is smaller than the descending aorta, which can also be appreciated in the three-vessel view (see Figs. 14-26 and 14-27). Discrete coarctation can be seen as a sharp indentation of the posterior wall of the descending aorta on the opposite side of the ductal confluence (see Fig. 14-27). Importantly, discrete coarctation is usually seen in association with an intracardiac left-sided obstructive lesion during fetal life. Isolated coarctation rarely shows overt indentation of the posterior wall of the descending aorta in fetal life. Posterior indentation or shelf lesion is considered to develop when the ductus closes after birth. As has been discussed earlier, fetuses having right-sided dominance of the ventricular and great arterial size are at risk of postnatal development of isolated coarctation.<sup>93-96</sup> Obstructive lesions of the aortic arch can also be suspected from the so-called V- or Y-confluence view of the arches. When the aortic arch is significantly smaller than the ductal arch, tubular hypoplasia of the aortic arch must be suspected (see Fig. 14-26D). When there is interruption, the aorta courses straight to its last branch without forming an arch or an arc (Fig. 14-50).



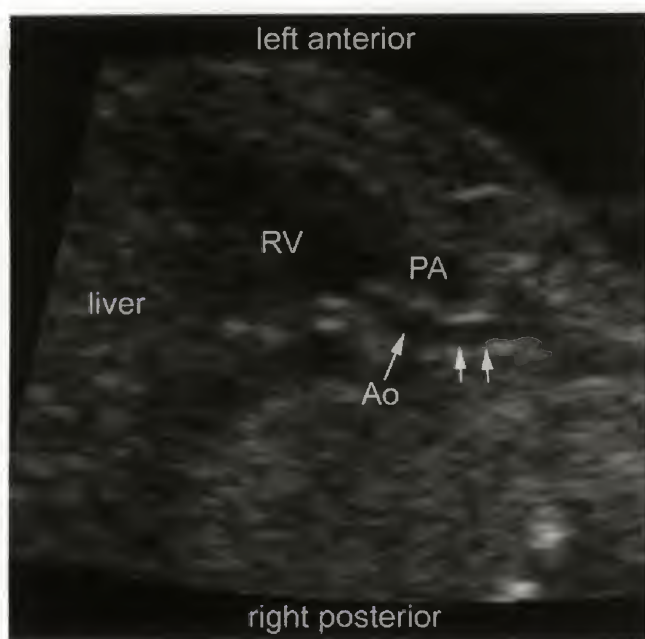


**FIGURE 14-50.** Interrupted aortic arch. Oblique sagittal view shows the left common carotid artery (arrows), in this case, as the direct continuation of the ascending aorta (Ao). PA, main pulmonary artery; RV, right ventricle.

The positional abnormalities of the aortic arch can better be appreciated in the three-vessel view.

### Prenatal and Postnatal Treatment Options and Outcomes of Congenital Heart Diseases

Indeed, fetal cardiac anomalies are recognizable by contemporary ultrasound imaging and often represent a more severe spectrum of cardiovascular disease than those seen after birth. A pediatric cardiologist should be involved in parental counseling as a key figure in detailed lesion diagnosis and in counseling parents about the prognosis of the lesion. Reported outcome data of specific cardiac lesions are useful in providing crude information about the overall prognosis. However, because the pathology spectrum of many defects is far from being uniform, counseling on prognosis and management should be adapted to the individual patient. The task of the fetal cardiologist is to help parents find the best solution for the family.

A timely and precise prenatal diagnosis allows appropriate counseling of the parents, and prenatal and postnatal management planning. It provides the opportunity for detailed ultrasound assessment of extracardiac malformations and chromosomal studies. Prenatal diagnosis enables stratification of cases into those that need in utero intervention, those that need delivery at a tertiary care center for an urgent postnatal management, and those that do not require urgent postnatal treatment. A timely diagnosis of a severe cardiac defect with poor prenatal and postnatal outcome also enables the parents to opt for termination of the pregnancy.

The course of an individual malformation in fetal life is often different from what would be expected postnatally. For instance, there is an increased incidence of spontaneous

**Table 14-10**

#### Ductus-Dependent Congenital Heart Disease

Ductus-Dependent Pulmonary Circulation	Ductus-Dependent Systemic Circulation
Pulmonary atresia or critical pulmonary stenosis with intact ventricular septum	Critical aortic stenosis
Tetralogy of Fallot with severe pulmonary stenosis or atresia	Hypoplastic left heart syndrome
Other forms of complex defect with severe pulmonary stenosis or atresia	Severe coarctation of aorta
Complete transposition of the great arteries	Interruption of the aortic arch
	Complete transposition of the great arteries

intrauterine demise in any fetus with chromosomal anomalies.<sup>6,7</sup> Fetal loss is also common in cardiac anomalies that are associated with severe AV or semilunar valve regurgitation,<sup>128,139</sup> in unbalanced AV septal defects with complete AV block,<sup>140</sup> and congestive heart failure.

In utero treatment includes drug therapy for fetal arrhythmias with heart failure, which is discussed in Part III of this chapter, and balloon dilatation of severe aortic or pulmonary valvar stenosis.<sup>11-14</sup> For most structural cardiac anomalies, however, antenatal treatment is neither warranted nor available.

The decision to transfer to a tertiary care center for planned delivery and immediate postnatal management depends on whether the systemic or pulmonary circulation will largely depend on the persistent patency of the ductus arteriosus after birth. Defects requiring persistent postnatal patency of the ductus arteriosus are called ductus-dependant CHDs (Table 14-10).<sup>97,141</sup> They include severe obstructive lesions of either the right or left side of the heart and lesions that require mixing of the systemic and pulmonary circulation through the ductus for survival. Because transition of the circulation and closure of vital fetal shunts occur at the same time as in healthy newborns, babies with ductus-dependant circulation are often asymptomatic and may escape detection immediately after delivery. They become increasingly and rather rapidly cyanotic, tachypneic, and hypotensive as the ductus arteriosus progressively constricts between 1 and 2 days of age. Not surprisingly, there is reduced morbidity and mortality associated with the fetal diagnosis of ductus-dependent cardiac lesions and in utero transfer to centers providing optimal neonatal care.<sup>142-144</sup>

Neonatal treatment includes the immediate intravenous administration of prostaglandin E1 to maintain the patency of the ductus arteriosus until surgery. Often, interventional catheter procedures are required to improve blood flow mixing through the atrial septum (balloon atrioseptostomy in complete transposition of the great arteries) or to improve blood flow through obstructed valves (balloon dilatation of severe semilunar valve stenosis or atresia). A few specific congenital heart lesions that are not obviously ductus dependent but affect the lungs or airway may also require urgent postnatal care. These include Ebstein disease and tetralogy of Fallot with absent pulmonary valve.<sup>128,139</sup>

Postnatal treatment options include surgical treatment, catheter intervention, medical follow-up for potential



**Table 14-11** Functionally Single Ventricle

Hearts With Univentricular Atrioventricular Connection	Hearts With Biventricular Atrioventricular Connection, One Ventricle Being Too Small
Tricuspid atresia	Pulmonary atresia with intact ventricular septum
Mitral atresia	Hypoplastic left heart syndrome
Double inlet right ventricle	Severe form of critical aortic stenosis
Double inlet left ventricle	Unbalanced form of atrioventricular septal defect
Double inlet indeterminate ventricle	Double outlet right ventricle with an underdeveloped ventricle
Severe form of unbalanced atrioventricular connection	Severe straddling of tricuspid or mitral valve

spontaneous resolution, and compassionate care. When treatment is required, surgical management is the ultimate option in the majority of cases. In a few conditions such as aortic valve stenosis, pulmonary valve stenosis, and peripheral pulmonary artery stenosis, balloon dilatation by catheter intervention is the primary choice. In addition, many of the patent ductus arteriosi, secundum atrial septal defects, and ventricular septal defects can be closed by placing a device through an interventional procedure.

There are two distinct pathways of surgical treatment for CHD: biventricular and univentricular repairs, depending mostly on the size of the ventricles and the anatomy of the AV valves. Biventricular repair is an ideal option for any CHD. However, there are cases in which one ventricle is not large enough to support either the systemic or pulmonary circulation after a biventricular repair. Rarely, one ventricle is entirely absent. Such cases include hypoplastic left heart syndrome, unbalanced forms of AV septal defect, tricuspid atresia, and double inlet ventricles, and are collectively termed as functionally single ventricles or univentricular hearts (Table 14-11). The goal of the univentricular repair is to use the functionally single ventricle as the chamber to support the systemic circulation whereas the pulmonary circulation is maintained by the pressure gradient between the systemic and pulmonary venous systems without the aid of ventricular systole.

Biventricular repair is a single-stage operation in most cases, although some complicated defects require staged operations. The timing of surgery depends on whether the systemic or pulmonary circulation is ductus dependent. Most ductus-dependant lesions require surgical repair within a few days of life. Most nonductus-dependent defects are repaired between the ages of 3 months and a few years, according to the hemodynamic impact of the defect on the cardiac function and pulmonary vasculature. Univentricular repair usually consists of three staged operations. The first stage consists of either a systemic-to-pulmonary arterial shunt for cases with pulmonary stenosis or atresia and pulmonary arterial hypoplasia, or pulmonary arterial banding for those with no significant pulmonary stenosis. Systemic-to-pulmonary arterial shunt operation is usually performed in the first few days of life, whereas pulmonary artery banding is performed in a few weeks depending on the patient's

condition. Cases with mild pulmonary stenosis and good pulmonary arterial growth do not require a first stage operation. The second-stage operation is the bidirectional cavopulmonary connection (bidirectional Glenn) in which the SVC or caeve are connected, end-to-side, to the pulmonary artery on the same side. This operation is usually performed at the age of 6 to 9 months, although it can be performed earlier or later. The third stage operation is the modified Fontan operation in which the inferior vena cava is connected to the pulmonary artery by using an intra-cardiac tunnel or extracardiac conduit. It is also called the total cavopulmonary connection. This procedure is usually performed 12 to 24 months following the bidirectional cavopulmonary connection. Each stage of univentricular repair is associated with significant mortality and morbidity, which varies according to the underlying pathology. Prognosis tends to be better when the main ventricular chamber is the morphologically left ventricle rather than the morphologically right ventricle. The postoperative prognosis of major CHDs is summarized in Table 14-12.<sup>145</sup> However, this information should be used cautiously because the outcome is often influenced by other associated factors including institutional policies and standards. More detailed information is beyond the scope of this chapter.

## CARDIAC TUMORS

Primary cardiac tumors are uncommon in the fetus and neonate.<sup>146</sup> However, cardiac tumors are seen more frequently in fetuses than in neonates, occurring in 0.1% to 0.2% of fetal echocardiographic series.<sup>147,148</sup> This is due to the widespread use of ultrasound as a screening tool for all pregnancies. The majority of the fetal cardiac tumors are rhabdomyomas, with an incidence ranging from 50% to greater than 90%.<sup>147-150</sup> Other less common fetal cardiac tumors include fibroma, teratoma, hemangioma, lipoma, and myxoma.

*Rhabdomyomas* are hamartomatous proliferative lesions that are associated with tuberous sclerosis in 50% to 80% of cases.<sup>147-152</sup> More than 50% of cases with tuberous sclerosis have cardiac rhabdomyomas. Rhabdomyomas are characteristically multiple in nature. On fetal ultrasound, they are seen as homogeneously hyperechogenic, round masses (Fig. 14-51). Not uncommonly, a large predominant mass is seen with tiny satellite tumors. Small tumors may be associated with subtle changes in myocardial echogenicity without showing obvious masses. Even a single detectable tumor in the fetus does not exclude a rhabdomyoma. Although multiplicity of the tumor is sufficient to establish the diagnosis of rhabdomyomas, multifocal localized nodular hypertrophy of the myocardium is a rare cause of multiple masses on ultrasound.<sup>153</sup> Tumors tend to appear in early second trimester, increase in size until the early third trimester, and then regress during later pregnancy and in the first few years of life. Because brain tubers are difficult to detect sonographically, magnetic resonance imaging has been used.<sup>154</sup>

*Fibroma* is second in frequency following rhabdomyoma.<sup>147-150,155</sup> The ventricular septal myocardium is the most common site, followed by right and left ventricular free wall. Usually, fibromas are solitary, homogeneously echogenic mass but there may be associated areas of cystic degeneration.



**Table 14-12 Risk Categories and Mortality Rates of Surgical Procedures**

Risk Category (Mortality Rate)	Diseases or Procedures
1 (0.4%)	Secundum ASD, PAPVC, PDA > 30d, COA > 30d
2 (3.8%)	VSD, Primum ASD, Common atrium, ASD and VSD, LV-RA shunt, TAPVC > 30d, Coronary artery fistula, AP window, Pulmonary stenosis, TOF, Pulmonary artery stenosis, Pulmonary valve replacement, Aortic stenosis > 30d, Subaortic stenosis, COA ≤ 30d, Vascular rings, Bidirectional cavopulmonary anastomosis
3 (8.5%)	Complete AVSD, TOF with pulmonary atresia, DORV, Complete TGA (arterial switch operation), Cor triatriatum, COA with VSD, Mitral valvotomy, mitral valve replacement, Left ventricular outflow tract patch, Aortic valve replacement, Ross procedure, Tricuspid valvotomy, valvuloplasty or valve replacement, Ebstein anomaly > 30d, Reimplantation of anomalous pulmonary artery, Systemic-to-pulmonary artery shunt, RV-pulmonary artery conduit, Fontan procedure
4 (19.4%)	AS ≤ 30d, Konno procedure for complex LV outflow tract obstruction, Interrupted or hypoplastic aortic arch, Complete TGA with VSD (arterial switch with VSD closure), Complete TGA with VSD and subpulmonary stenosis (Rastelli), Corrected TGA (double switch operation), Truncus arteriosus, Unifocalization for TOF with pulmonary atresia, TAPVC ≤ 30d,
5 (NA)	Ebstein anomaly ≤ 30d, Truncus arteriosus with interrupted aortic arch
6 (47.7%)	Hypoplastic left heart syndrome (stage 1 Norwood operation), Damus-Kaye-Stansel operation

ASD, atrial septal defect; AVSD, atrioventricular septal defect; COA, coarctation of the aorta; DORV, double outlet right ventricle; LV, left ventricle; PAPVC, partial anomalous pulmonary venous connection; PDA, patent ductus arteriosus; RA, right atrium; TAPVC, total anomalous pulmonary venous connection; TGA, transposition of the great arteries; TOF, Tetralogy of Fallot. Modified from Jenkins, KJ, Gauvreau K, Newberger JW, et al: Consensus-based method for risk adjustment for surgery for congenital heart disease. *J Thorac Cardiovascul Surg* 123:110, 2002.

Fibromas may cause either inflow or outflow obstruction of the right or left or both ventricles, depending on their location and size. Fibromas arising from the ventricular septum may cause heart block and arrhythmias. Occasionally, cardiac fibromas are observed with extracardiac malformations or syndromes that include nevoid basal cell carcinoma (Gorlin) syndrome, cleft lip and palate, and Beckwith-Wiedemann syndrome. Spontaneous regression of fibroma is rare.

*Teratoma* is a rare tumor originating mainly from the pericardium and, less commonly, from the atrial or ventricular myocardium.<sup>147-150,156,157</sup> Typically, intrapericardial teratomas are attached to the great arterial roots. The tumor is characterized by a mass of heterogeneous echogenicity with solid and cystic components. It is associated with pericardial effusion that contains echogenic debris in the majority of cases. The pericardial effusion is often massive, causing life-threatening tamponade that requires in

utero pericardiocentesis or fetal surgery. Similar to teratomas in other locations, the mass may contain calcifications or bones. However, one should be aware that calcification of the myocardium can result from dystrophic deposition of calcium in the areas of myocardial ischemia, necrosis, bleeding, fibrosis, or infection.<sup>158</sup> Calcific myocardial deposits are also reported in chromosomal abnormalities. Calcification of the tension apparatus of the mitral or tricuspid valve is not uncommon and known as an echogenic focus. The relationship between echogenic ventricular focus and chromosomal abnormalities is discussed elsewhere in this textbook.

*Hemangioma* is also a rare tumor originating from any location in the heart or pericardium, with the right atrium being the most common location (Fig. 14-52).<sup>147-150,159</sup> Similar to teratoma, pericardial effusion is commonly associated and may need in utero pericardiocentesis. Cardiac hemangiomas may be associated with multiple hemangiomas

in the skin and elsewhere. Other forms of vascular tumors including lymphangiomas are also reported in the literature. Generally, vascular tumors are associated with a favorable outcome. Hemangiomas tend to regress spontaneously, having the best prognosis of all cardiac tumors.<sup>147-150</sup>

The prognosis during fetal and postnatal life depends mainly on the location and size of the tumor or tumors.<sup>147-150</sup>

Poor prognostic factors include intracardiac flow obstruction, altered valve function with regurgitation, arrhythmias, large pericardial effusion, and fetal hydrops. Rarely, compression or involvement of the coronary artery by the tumor may result in fatal outcome. Postnatal prognosis also depends on spontaneous regression or growth of the tumor and associated malformations or syndromes. Surgical results are best for hemangiomas, followed by teratomas. Complete excision is often difficult in large fibromas and cardiac transplantation may be required.

## CARDIAC RHYTHM

### Normal Fetal Cardiac Rhythm

The cardiac conduction system is composed of highly specialized muscle tissue that is able to generate the cardiac impulse, transport it across the fibrous ring of the AV junction, and deliver it throughout the ventricles. After originating within the sinus node, the electrical impulse proceeds by way of atrial tissue to the AV node, the His-Purkinje system, and the ventricular myocardium. The electrical impulse is physiologically delayed within the compact AV node, which functions as a filter against the propagation of abnormally fast atrial rates or very premature atrial beats to the ventricles. The normal fetal cardiac rhythm is regular with a 1:1 AV relationship. The sequential mode of AV depolarization results in rhythmic contraction and relaxation of atrial and ventricular myocardium, allowing coordinated filling and emptying of the heart. The heart rate increases rapidly in early gestation until it reaches the peak rate of  $175 \pm 20$  beats per minute at approximately 8 weeks.<sup>160,161</sup> Then, the heart rate gradually decreases to  $140 \pm 20$  beats per minute at

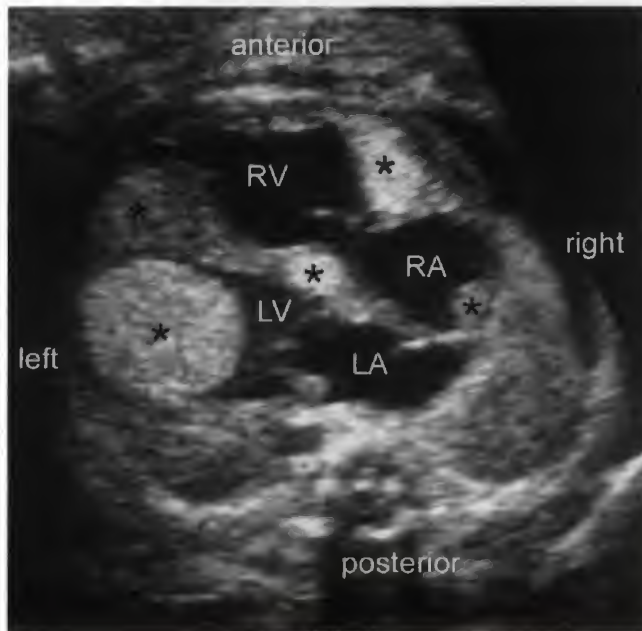


**FIGURE 14-51.** Rhabdomyomas. Four-chamber view shows multiple tumors (asterisks) involving both ventricles, interventricular septum and right atrium (RA). LA, left atrium; LV, left ventricle; RV, right ventricle.

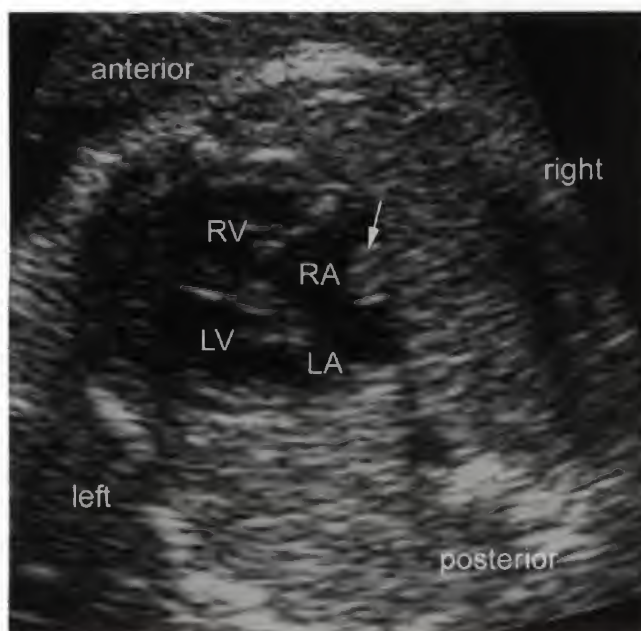


**FIGURE 14-52.** Hemangioma. A. Four-chamber view at 32 weeks shows a round protruding mass (arrow) arising from the posterior wall of the right atrium (RA). B. Four-chamber view at 35 weeks shows growth of the mass and development of an echolucent cystic area. The removed mass showed histological features of hemangioma with central hemorrhage. LA, left atrium; LV, left ventricle; RV, right ventricle.



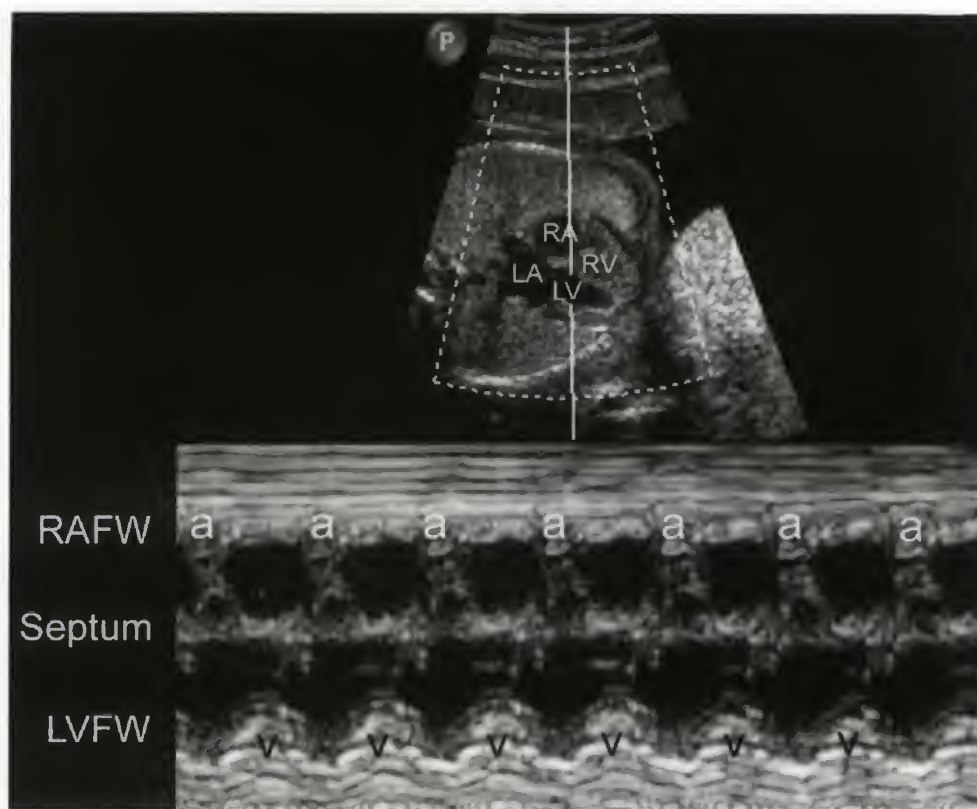


**FIGURE 14-53.** Normal M-mode tracing for cardiac rhythm assessment using four-chamber view. The M-mode beam is directed through the atrial and ventricular walls to demonstrate atrial and ventricular systolic wall motions simultaneously. Atrial contractions (a's) are followed by ventricular contractions (V's). LA, left atrium; LV, left ventricle; LVFW, left ventricular free wall; RA, right atrium; RAFW, right atrial free wall; RV, right ventricle.

20 weeks and  $130 \pm 20$  beats per minute toward term, as a result of increasing parasympathetic influence on the electrical conduction system after the first trimester.<sup>162,163</sup>

### Sonographic Techniques for Cardiac Rhythm Assessment

As in extrauterine life, the classification of fetal rhythm and conduction anomalies relies primarily on the chronology of atrial and ventricular electrophysiologic events. However, the assessment of the fetal cardiac rhythm is more challenging because a conventional real-time electrocardiogram cannot be obtained. M mode and pulsed wave Doppler echocardiography have been used as surrogates because they enable the study of atrial and ventricular electrical events indirectly by their respective mechanical consequences.<sup>164,165</sup>

#### M Mode Echocardiography

Guided by real-time two-dimensional echocardiography, the M mode ultrasound beam is aligned simultaneously through the atrial and ventricular walls to record the sequence of their systolic wall motions. The preferred M mode beam direction is through the atrial and ventricular walls immediately above and below the AV junction because these parts show the most pronounced lateral excursion during a cardiac cycle (Fig. 14-53). A limitation of M mode tracings is that the onset and maximal timing of the atrial and ventricular systolic events are not well-defined and,

therefore, the precise measurement of the time interval between atrial and ventricular contractions (AV time-interval) is not possible.

#### Pulsed Wave Doppler

In comparison with M mode, Doppler flow waves that represent atrial and ventricular systolic events are more clearly delineated. By placing the Doppler cursor across the SVC and the ascending aorta, it is possible to record the flow velocity patterns from both vessels simultaneously (SVC/Aorta Doppler) (Fig. 14-54, *upper panel*). The beginning of the retrograde flow in the SVC reflects the onset of atrial systole, whereas the beginning of the aortic forward flow marks the beginning of ventricular systole. Alternatively, the blood flow through the mitral valve and left ventricular outflow tract can be sampled simultaneously by placing the cursor on the anterior leaflet of the mitral valve in the left ventricular outflow tract view (inflow/outflow Doppler) (see Fig. 14-54, *lower panel*). This technique makes use of the fact that the anterior leaflet is the anterior border of the left ventricular inlet in diastole and the posterior border of the outlet in systole. The beginning of the A-wave of the mitral valve flow is the onset of atrial systole, whereas the beginning of the flow through the left ventricular outflow tract marks the beginning of ventricular systole.

For simple determination of the fetal cardiac rhythm and rate, pulsed Doppler assessment of umbilical artery flow pattern is a convenient and rapid ultrasound method. M

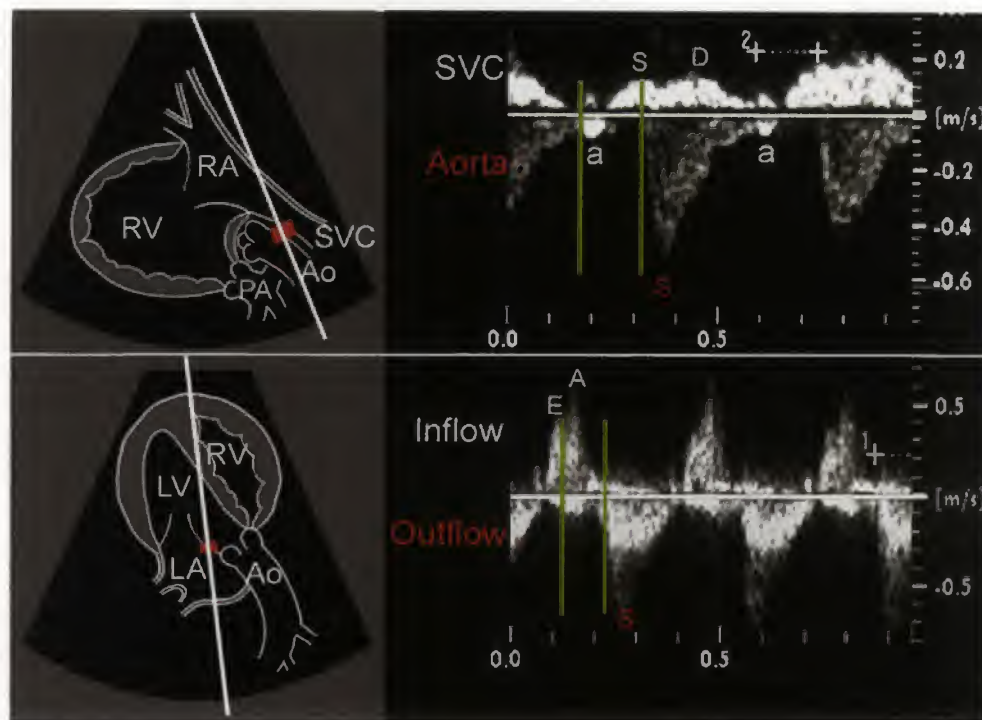


**FIGURE 14-54.** Pulsed Doppler flow curves showing normal atrioventricular relationship of cardiac rhythm. *Upper panel,* Simultaneous Doppler tracing from the superior vena cava (SVC) and ascending aorta (Ao). The superior vena caval flow curve consists of systolic (S) and diastolic (D) forward waves followed by small atrial reversed wave (a). The aortic flow curve consists of a single forward peak (S in red). The atrioventricular time interval is the time lapse between the onsets of the vena caval a-wave and aortic S-wave (between green lines). *Lower panel,* Simultaneous Doppler tracings from the left ventricular inflow and outflow tracts. The inflow flow curve consists of an E wave during early diastolic filling and A wave during atrial contraction. The outflow flow curve shows a single forward wave (S) in systole. The atrioventricular time interval is the time lapse between the onsets of the A and S waves (between green lines). LA, left atrium; LV, left ventricle; PA, main pulmonary artery; RA, right atrium; RV, right ventricle.

mode and spectral Doppler can be used to evaluate all types of fetal arrhythmia. Both pulsed Doppler methods are equally useful to evaluate the integrity of AV conduction during normal cardiac rhythm. Reference values of mechanical AV time intervals vary among different imaging modalities and gradually prolong as a result of increasing gestational age. Normal AV time-interval values are  $190 \pm 36$  ms by M mode,  $120 \pm 11$  ms by inflow/outflow Doppler, and  $111 \pm 17$  ms by SVC/aorta Doppler.<sup>165</sup>

### Other Noninvasive Methods

Transabdominal fetal electrocardiography (ECG) and magnetocardiography have recently become commercially available.<sup>166,167</sup> Fetal ECG is based on signal averaging of electrocardiographic complexes and does not allow beat-to-beat analysis. As a consequence, ECG is not helpful in the diagnosis of fetal rhythm and conduction abnormalities with irregular heart rates. Fetal magnetocardiogram provides better signal quality than ECG because of more favorable transmission properties of magnetic signals. Both magnetocardiograms and electrocardiograms may provide useful information on cardiac time intervals such as the QRS and QT duration. Assessment of myocardial movement by using tissue Doppler technique is an emerging tool for fetal cardiac rhythm disturbances and ventricular function (Fig. 14-55).<sup>168</sup>

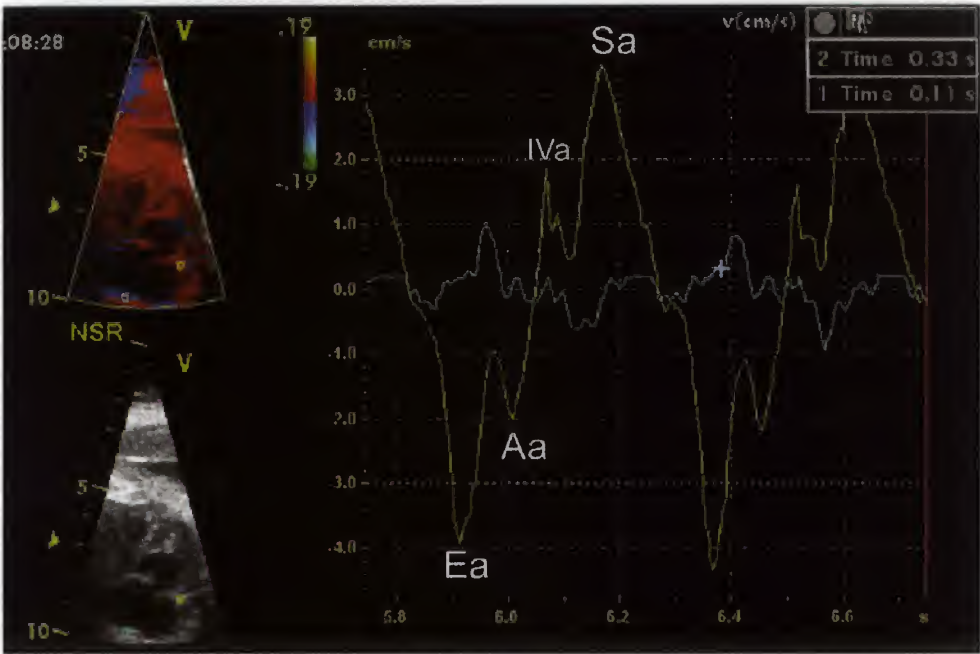
## Abnormal Cardiac Rhythms

Fetal rhythm abnormalities affect at least 2% of pregnancies and are a common reason for referral to fetal cardiologists.<sup>169-171</sup> They may present (1) as an irregularity of the cardiac rhythm, (2) an abnormally slow or fast heart rate, or (3) a combination of abnormal rate and rhythm. Intermittent or sustained irregularity of the cardiac rhythm is usually caused by premature extracontractions and is by far the most common fetal rhythm abnormality (Table 14-13). Less common but potentially life threatening are intermittent or sustained episodes of excessively fast (tachycardia,  $> 180$  beats per minute) or slow (bradycardia,  $< 100$  beats per minute) heart rates. Sustained bradycardia is typically the result of complete AV block, sinus bradycardia, or atrial bigeminy. Supraventricular tachycardia, atrial flutter, and sinus tachycardia are the main causes of fetal tachycardia. Appropriate management depends on accurate diagnosis. Ultrasound is essential to determine the arrhythmia mechanism and the impact on cardiac function, to detect associated cardiac defects or tumors, and to survey the fetal heart rate and well-being for example, during antiarrhythmic treatment.

### Irregular Cardiac Rhythm

Irregularity of the fetal cardiac rhythm with normal or near-normal average heart rates is most often related to premature beats that are generated by ectopic pacemaker





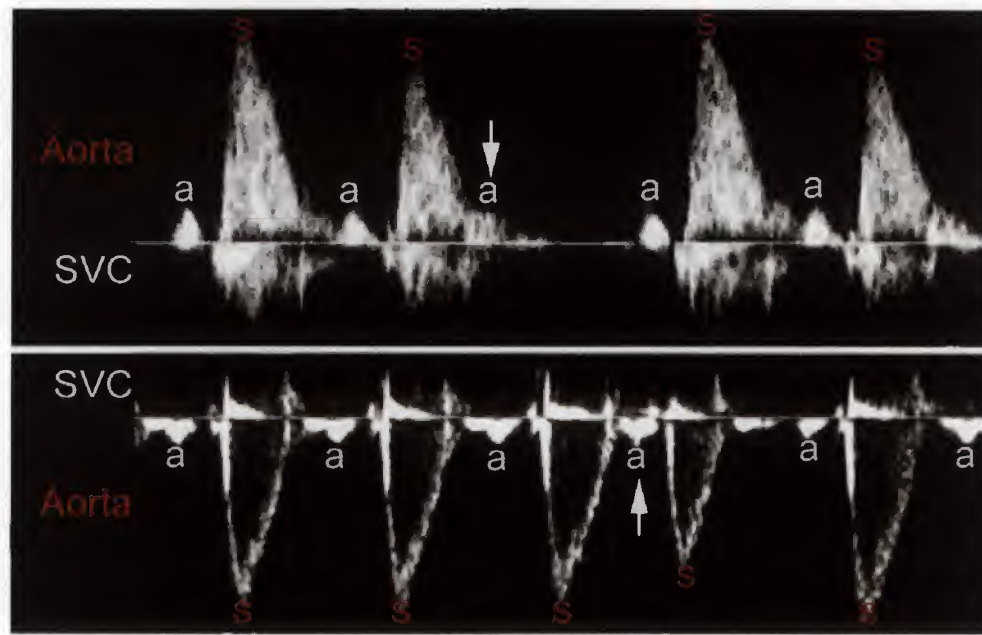
**FIGURE 14-55.** Sequential analysis of atrial (green) and ventricular (yellow) longitudinal wall motion by tissue Doppler. The typical Doppler curve (yellow) obtained from the base of the ventricles during sinus rhythm is composed of four waves. Two diastolic waves are produced by longitudinal tissue motion away from the apex, during early diastolic filling (Ea) and during atrial contraction (Aa). This is followed by two systolic waves towards the apex: the isovolumetric contraction (IVa) and the Sa wave. Atrioventricular time interval is the time lapse between the onsets of Aa and IVa waves.

Table 14-13      Fetal Arrhythmias: Mechanisms, Frequency, and Treatment Recommendations for Obstetricians <sup>169-171</sup>			
Arrhythmias	Frequency	Management Recommendation	Prognosis
Minor arrhythmias	90%		
Premature atrial contractions	Very common	Weekly monitoring of heart rate	Typically resolves SVT in 1%
Premature ventricular contractions	Rare	Weekly monitoring of heart rate	Usually resolves VT rare
Brief sinus tachy/bradycardia	Common	None	Excellent
Major arrhythmias	10%		
Complete atrioventricular block	35%	Urgent referral to tertiary care center	Irreversible Isolated: survival > 90% With LAI: survival < 10%
Supraventricular tachycardia	40%	Urgent referral to tertiary care center	Often resolves after birth No hydrops: survival > 96% Hydrops: survival 65-75%
Atrial flutter	10%-15%	Urgent referral to tertiary care center	Resolves after birth Survival > 90%
Ventricular tachycardia	Rare	Urgent referral to tertiary care center	Variable

LAI, left isomerism; SVT, supraventricular tachycardia; VT, ventricular tachycardia.

tissue usually located in the atria and rarely in the ventricles. The incidence of premature beats is not established in the healthy fetus, but ectopic atrial beats are quite common findings in healthy premature and term babies. *Premature atrial contractions (PACs)* can be observed at any gestational age but are most common in the last trimester in otherwise uneventful pregnancies.<sup>169</sup> PACs may be conducted to the ventricles or blocked within the AV node depending on the

degree of prematurity of the atrial event and thus present either as an extra beat or a missed beat on auscultation or ultrasound examination (Fig. 14-56). PACs are usually transient and benign findings. In the presence of an accessory AV conduction pathway, however, they may occasionally trigger reentrant supraventricular tachycardia. PACs have also been associated with structural heart disease (up to 2%), intracardiac tumors and redundancy of the



**FIGURE 14-56.** Premature atrial contractions. Simultaneous Doppler tracing of the superior vena cava (SVC) and ascending aorta showing isolated blocked (upper panel) and conducted (lower panel) premature atrial contractions (arrows). A, atrial contraction; S, ventricular contraction.

membrane of the foramen ovale. Multiple blocked PACs such as in atrial bigeminy may lower the fetal heart rate below 100 beats per minute and need to be differentiated from more serious causes of bradycardia. *Premature ventricular contractions (PVCs)* are rarely diagnosed antenatally. In general, they are equally well tolerated and benign but may occasionally be associated with intrinsic myocardial disease. The vast majority of fetuses with atrial and ventricular premature beats do not need any prenatal and postnatal treatment, and delivery should not be expedited based on these findings alone. However, because of the potential risk of progression to fetal tachyarrhythmias (see later), it appears prudent to monitor fetuses with frequent premature beats on a weekly or biweekly basis by auscultation or Doppler until the arrhythmia resolves.

### Bradycardia

Brief episodes of sinus bradycardia of less than 1- to 2-minutes' duration are frequent and benign findings during the first and second trimester and do not require any treatment. Transient sinus bradycardia is not uncommon during fetal ultrasound examination when the fetal head is compressed by the probe. A more sustained decrease in average fetal heart rate may be observed during sinus bradycardia and atrial bigeminy with blocked premature atrial beats, whereas the bradycardia is always permanent in complete AV block. Because the ventricular rate is often regular and comparable among these rhythm anomalies, ultrasound imaging is essential for their diagnostic differentiation.

During *sinus bradycardia*, M mode and Doppler echocardiography reveal a regular atrial rate below 100 beats per minute with a normal 1:1 AV activation sequence. Sustained sinus bradycardia may be caused by a number of serious conditions including fetal hypoxia and acidosis, long QT

syndrome, and congenital sinus node dysfunction.<sup>172</sup> Runs of ventricular tachycardia and 2:1 AV block are additional findings suggesting fetal long QT syndrome, which carries a guarded prognosis. Careful examination and, in the absence of a fetal magnetocardiogram, postnatal ECG are recommended in these children and their family members because early detection and treatment of long QT patients may be life-saving.

Sustained *atrial bigeminy* and trigeminy with blocked premature beats may lower the average heart rate of the fetus to 60 to 100 beats per minute and be confused with second- or third-degree AV block. Blocked premature beats and AV block are characterized by a higher atrial than ventricular rate. In AV block, however, the time intervals between consecutive atrial impulses hardly vary, whereas every second event occurs prematurely in atrial bigeminy (Fig. 14-57). This differentiation is important because bradycardia secondary to blocked premature beats resolves spontaneously without treatment, whereas complete AV block is an irreversible and potentially life-threatening disorder.

*AV block* refers to a delay of electrical conduction within the AV node, the bundle of His, or the bundle branches. First-degree AV block is characterized by a prolonged electrical AV conduction time but all impulses are conducted. Because 1:1 AV conduction is maintained, it is not possible to diagnose first-degree AV block without measurement of the AV time intervals. Second-degree AV block refers to a failure to conduct some, but not all atrial impulses to the ventricles. In 2:1 AV block every second atrial beat is conducted to the ventricles. In third degree or complete AV block (CAVB), the electrical AV communication is completely interrupted and atria and ventricles beat independently at their intrinsic rates. Typically, the ventricular rate in CAVB is between 40 and 80 beats per minute.<sup>140</sup> CAVB affects about 1 in 15,000 live-born babies



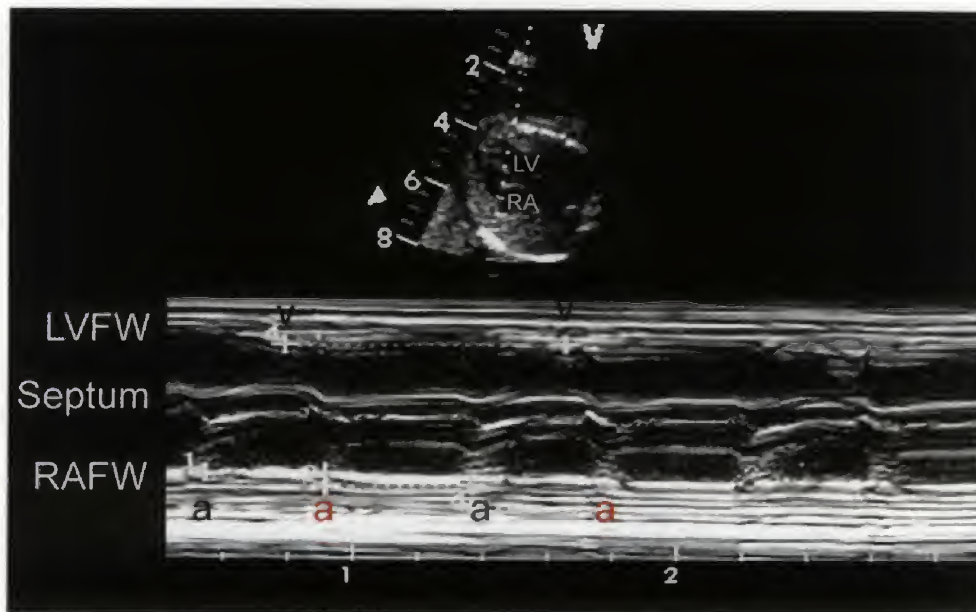


**FIGURE 14-57.** Atrial bigeminy. M-mode tracing through the atrial and ventricular walls shows that every second atrial beat (a's in red) occurs prematurely and is not conducted to the ventricle, resulting in ventricular bradycardia (V-V rate: 67 beats per minute). A, atrial contraction; LVFW, left ventricular free wall; RAFW, right atrial free wall; V, ventricular contraction.

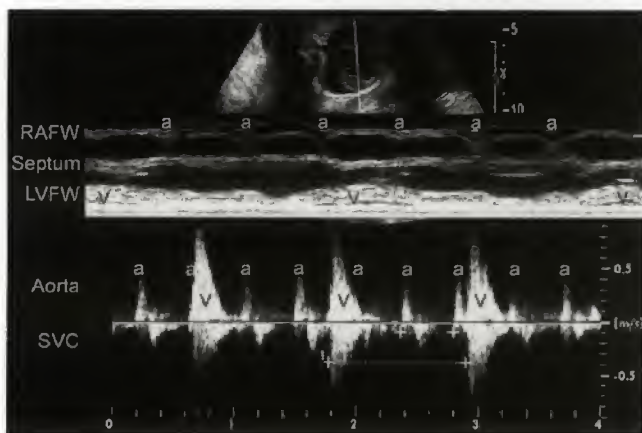


**FIGURE 14-58.** Atrioventricular block. M-mode tracing of the atrial and ventricular walls (upper panel) and simultaneous Doppler tracing of the superior vena cava (SVC) and ascending aorta (lower panel) showing complete atrioventricular dissociation related to complete atrioventricular block. The atrial rate (a-a) is 140 beats per minute and the ventricular rate (V-V) is 54 beats per minute. LVFW, left ventricular free wall; RAFW, right atrial free wall.

but is definitely more frequent in utero, accounting for 30% to 40% of the major fetal arrhythmias. In approximately half of the cases, heart block is associated with structural cardiac lesions, most importantly left isomerism and congenitally corrected transposition (Fig. 14-58). The outcome of fetal CAVB with left isomerism is extremely poor.<sup>140,173</sup> As an isolated disorder, CAVB is mainly associated with the transplacental passage of maternal autoantibodies to 48-kDa SSB/La, 52-kDa and/or 60-kDa SSA/Ro ribonucleoproteins.<sup>174-176</sup> These antibodies are typically found in mothers with systemic lupus erythematosus or

Sjogren syndrome, but may be demonstrated in 1% to 2% of pregnant women with no clinical evidence of autoimmune disease.<sup>174</sup> The anti-Ro/La antibodies progressively enter the fetal circulation in the second trimester and may elicit an immune-mediated tissue injury resulting in progressive destruction of the AV node, myocardial inflammation, endocardial fibroelastosis, and dilated cardiomyopathy in the susceptible offspring.<sup>175-177</sup> CAVB emerging after 20 weeks' gestation affects 1% to 2% of the cohort of antibody-positive mothers, whereas other cardiac manifestations are less common.<sup>174,178</sup> The recurrence risk of immune-mediated CAVB in subsequent pregnancies is 8% to 18%.<sup>175</sup> There is a significant risk of demise, particularly in CAVB with fetal hydrops, poor ventricular function, heart rate of 55 beats or less per minute, and/or premature delivery.<sup>173,176,177,179</sup> Numerous, often controversial, preventive and therapeutic approaches have been used to improve pregnancy outcome.<sup>11</sup> Theoretically, all pregnant women with anti-Ro/La antibodies, who are, therefore, at risk of delivering a child with CAVB, may be considered for preventive treatment. Indeed, this approach has been chosen for a small number of pregnancies that were treated with maternal plasma exchange, and administration of maternal immunoglobulin, steroid, or azathioprine.<sup>180,181</sup> Considering the low fetal risk of less than 2% of developing CAVB, it is difficult to advocate preventive treatment for the entire cohort of mainly unaffected fetuses and mothers. The rationale to treat a fetus with CAVB is not to reverse the block to a normal rhythm because the complete block is an irreversible disease. The treatment is primarily to mitigate or prevent concomitant myocardial inflammation and to augment fetal heart rate. Fluorinated steroids (dexamethasone, betamethasone) are only minimally metabolized by the placenta and become useful when anti-inflammatory fetal treatment is desired. Maternal

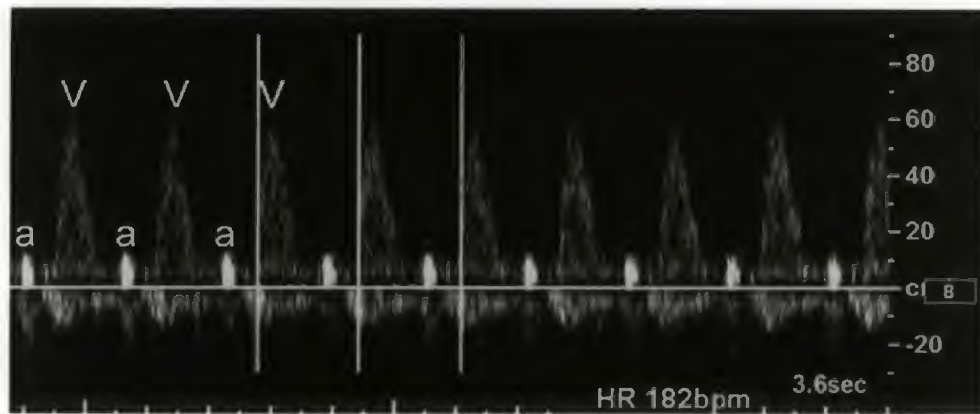


**FIGURE 14-59.** Tachycardia with 1:1 atrioventricular relationship. Simultaneous Doppler tracing of the superior vena cava and ascending aorta showing fetal tachycardia of 182 beats per minute with normal 1:1 atrioventricular relationship and atrioventricular time intervals. This form of tachycardia may be caused by sinus tachycardia, permanent junctional reciprocating tachycardia (PJRT), and atrial ectopic tachycardia (AET). A, atrial contraction; V, ventricular contraction.

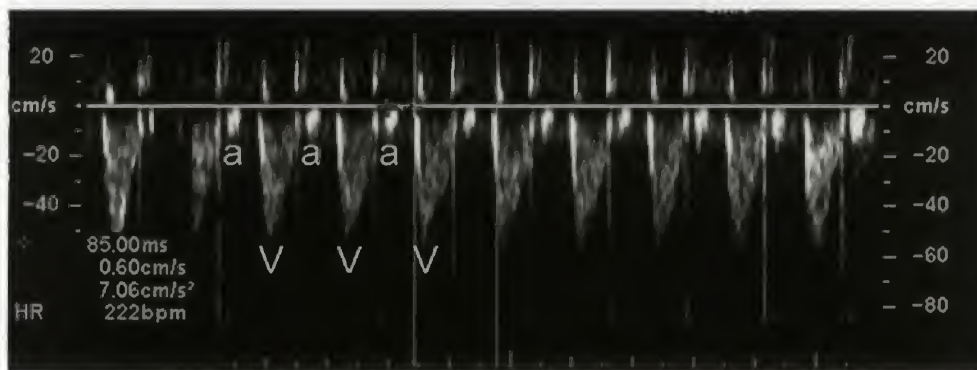


**FIGURE 14-60.** Supraventricular tachycardia. Simultaneous Doppler tracing of the superior vena cava and ascending aorta showing a fetal tachycardia of 222 beats per minute with an 1:1 atrioventricular relationship. The ventricular contraction (V) is closely followed by the atrial contraction (a) suggesting re-entrant SVT as the underlying arrhythmia mechanism.

dexamethasone administration has been shown to improve AV block, hydrops, and myocardial dysfunction.<sup>182</sup> Beta-stimulation may be used to increase the fetal heart rate and myocardial contractility.<sup>11,183</sup> Indeed, recent data suggest that the introduction of transplacental glucocorticoid and  $\beta$ -mimetic fetal therapy has a beneficial effect on outcome but without improving the AV block.<sup>11</sup> Most cases require permanent pacing for class I American Heart Association/American College of Cardiology indications during the first year of life.<sup>84,175</sup>

### Tachycardia

Disorders that lead to an intermittent or sustained increase in heart rate more than 180 beats per minute account for about two third of major fetal arrhythmias. According to the origin of the fast rhythm, tachycardias are classified into sinus tachycardia, supraventricular tachycardia, and ventricular tachycardia.<sup>160,185-189</sup> Echocardiography is again the diagnostic cornerstone in establishing the arrhythmia mechanism and the hemodynamic consequences. The different mechanisms may be distinguished by analysis of the atrial and ventricular chronological relationship and by documentation of the AV and ventriculoatrial (VA) time-

intervals. All forms of tachyarrhythmias may be asymptomatic but, at the other end of the spectrum, may lead to congestive heart failure, dilated cardiomyopathy, neurologic lesions, and even death. Fetal hydrops has been associated with a mortality risk of up to 35%.<sup>186</sup>

*Sinus tachycardia* is characterized by atrial rates of 180 to 200 beats per minute, normal 1:1 AV conduction and some variability of the fetal heart rate (Fig. 14-59). A variety of fetal and maternal conditions may be responsible for sustained sinus tachycardia including fetal distress, anemia, infections, maternal  $\beta$ -stimulation and fetal thyrotoxicosis secondary to thyroid-stimulating maternal autoantibodies. The importance of sinus tachycardia is recognizing and treating the underlying cause.

*Supraventricular tachycardia (SVT)* encompasses tachycardias with three different mechanisms that includes (1) AV reentrant tachycardia (AVRT) related to a fast retrograde conducting accessory pathway; (2) permanent junctional reciprocating tachycardia (PJRT) related to a slow retrograde conducting pathway; and (3) atrial ectopic tachycardia (AET) due to enhanced atrial focal automaticity. They may be differentiated based on their arrhythmia pattern and the AV and VA relationship. AVRT is by far the most common mechanism of fetal SVT 159 (Fig. 14-60). The onset and



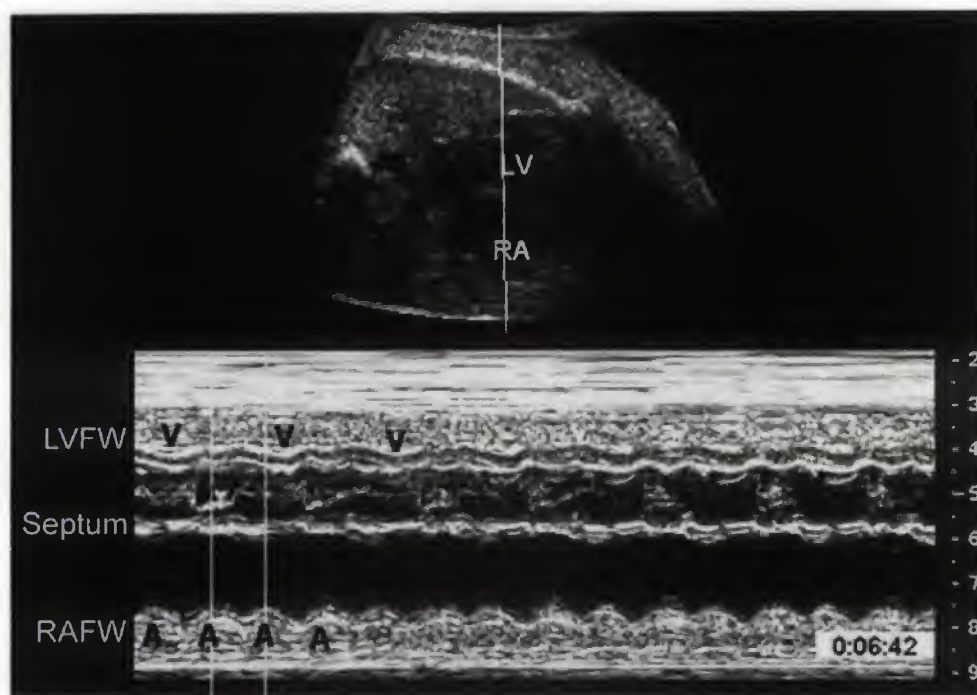


**FIGURE 14-61.** Atrial flutter. M-mode tracing through the left ventricle (LV) and right atrium (RA) shows a fast atrial (A) rate (420 beats per minute) that is twice the ventricular (V) rate (210 beats per minute). The underlying arrhythmia is atrial flutter with 2:1 atrioventricular conduction. LVFW, left ventricular free wall; RAFW, right atrial free wall.

termination of reentrant SVT is sudden. Heart rates range between 180 and 300 beats per minute, and the arrhythmia pattern may be intermittent or incessant.

*Atrial flutter* is the result of an atrial electrical reentrant circuit and is mainly observed in the third trimester.<sup>187,188</sup> Atrial rates range between 300 and 550 beats per minute, which is sufficiently fast that only every second or third atrial beat is conducted to the ventricles through the AV node. As a consequence, ventricular response rates are usually between 150 and 250 beats per minute (Fig. 14-61).

*Ventricular tachycardia* is extremely rare in the fetus. Intermittent runs of ventricular rates between 170 and 400 beats per minute exceed the atrial rate, and there is complete dissociation between atrial and ventricular events. Nevertheless, if the AV node is able to conduct retrograde to the atrium, a 1:1 AV relationship is possible and ventricular tachycardia becomes difficult to differentiate from reentrant SVT. Long QT syndrome should be suspected when there is bradycardia during sinus rhythm, intermittent or permanent complete heart block, or both.<sup>189</sup>

Following the diagnosis of any major arrhythmia, imminent referral to a fetal tertiary care center with expertise in the surveillance and treatment of the mother and fetus is advised. In theory, three management options are available for fetal SVT and atrial flutter: (1) observation, (2) antiarrhythmic drug therapy, and (3) expedited delivery. Close pregnancy monitoring only is a valid option if the fetus presents with intermittent, brief runs of tachycardia in the absence of hemodynamic impairment. Prolonged or permanent episodes of tachycardia may significantly affect the fetal cardiovascular function and rapid and permanent conversion to sinus rhythm to prevent or resolve heart

failure is a primary goal. If a fetus presents with a major tachyarrhythmia after 35 weeks of gestation, expedited delivery followed by postnatal conversion is an option. At an earlier gestational age, the risks associated with premature delivery probably outweigh the potential hazards of fetal-maternal pharmacologic treatment. There is considerable experience in the transmaternal treatment of fetal tachyarrhythmias with a number of antiarrhythmic agents, including digoxin,<sup>164,186,190</sup> procainamide (class Ia),<sup>191</sup> flecainide (class Ic),<sup>186</sup> sotalol and amiodarone (class III).<sup>164,190,192</sup> Direct fetal administration of adenosine, digoxin, and/or amiodarone, for example, into the umbilical vein, has been successfully used for the acute treatment of incessant, poorly tolerated SVT.<sup>193,194</sup> Any antiarrhythmic treatment other than digoxin should be initiated in-hospital while monitoring the fetal and maternal cardiac rhythm. Permanent pharmacologic suppression of fetal tachyarrhythmia is achievable in most cases. Once the arrhythmia is under control, the successful antiarrhythmic treatment should be maintained until delivery with weekly controls of the fetal cardiac rhythm. Most newborns with fetal SVT require antiarrhythmic drug treatment for at least 6 to 12 months after birth. By contrast, once sinus rhythm has been established after birth, recurrence of atrial flutter is uncommon and no long-term drug treatment is usually required.

### **Examination for Pregnant Women With Anti-Ro/SSA and Anti-La/SSB Antibodies**

About 1% to 2% of all pregnant women have anti-Ro/SSA and/or anti-La/SSB autoantibodies, most without any



antibody-related symptoms.<sup>174</sup> These antibodies increasingly enter the fetal circulation in midgestation and may induce a progressive destruction of the AV node in about 1% to 2% of anti-Ro/La antibody-positive pregnancies. As a result of this insult, the electrical AV conduction progressively prolongs to complete heart block after 20 weeks' gestation. Complete AV block may be preventable if the disease can be recognized and treated at an early stage of AV nodal damage, which is clinically characterized by a short-lived appearance of first or second degree AV block.<sup>195</sup> Doppler ultrasound allows simple and reproducible measurement of the mechanical AV time-intervals and thus represents a suitable tool in serially monitoring of the fetuses at risk of immune-mediated heart block. Normal AV time-intervals by SVC/aorta and inflow/outflow Doppler are in general below 140 ms independent of the fetal age. Transplacental fetal steroid treatment to prevent the progression to irreversible complete fetal AV block should be considered if there is significant lengthening of the AV time-intervals compatible with first or higher degree AV block in an anti-Ro/La antibody positive pregnancy between 20 and 24 weeks' gestation.

## CARDIAC FUNCTION

### Physiology of the Fetal Cardiovascular System

There are profound differences in the cardiovascular system before and after birth. The most important is that the placenta rather than the lungs is the major source of oxygenation in the fetus. The oxygenated blood from the placenta returns to the fetus through the umbilical venous system (Fig. 14-62). About 20% to 30% of the umbilical venous blood then bypasses the liver through a narrow, trumpet-shaped vessel, called the ductus venosus.<sup>196</sup> The narrowing of the ductus venosus transforms the continuous, low-velocity umbilical venous blood flow into a pulsatile high-velocity jet, reaching peak velocities up to 75 cm/sec. The flow acceleration gives the oxygenated blood enough momentum to preferentially stream across the foramen ovale into the left side of the heart, which supplies the upper extremities, the brain, and the coronary arteries; only a small proportion passes across the aortic isthmus into the descending aorta. In contrast, poorly oxygenated blood returning to the heart from the superior and inferior venae cavae is mainly directed into the right ventricle and then ejected into the pulmonary arterial trunk. A small proportion passes through the pulmonary circulation, but the majority is directed through the ductus arteriosus to the descending aorta, from which the blood flow is distributed to the abdominal organs, to tissues of the lower trunk and extremities, as well as to the placenta. Thus, in the fetal circulation both ventricles simultaneously eject blood into the systemic circulation. The combined ventricular output is about 450 ml/min/kg of fetal body weight, of which the right heart contributes 20% to 30% more than the left side.<sup>197</sup> Other major differences of fetal circulation as compared with postnatal circulation include a faster heart rate at 120 to 150 beats per minute, lower arterial blood pressure and peripheral resistance, and lower myocardial compliance and contractility. The latter is explained by an

increased constraint owing to fluid filled lungs, a higher proportion of non-contractile elements, and rigid type 1 collagen in the fetal myocardium, and a delay in calcium ion removal by the immature sarcoplasmic reticulum.<sup>198,199</sup> Maturation changes such as an increase in myocardial adrenergic receptor density, a switch to more mature contractile protein isoforms, and better calcium ion handling result in a steady improvement of the myocardial function with advancing gestation.

## CARDIAC CYCLE

Knowledge of fetal cardiac physiology is essential to understanding cardiovascular ultrasound findings. The cardiac cycle consists of five phases (Fig. 14-63). Three repetitive cardiac events are responsible for the antegrade delivery of blood during each cardiac cycle: ventricular contraction in systole, then active ventricular relaxation, and atrial contraction in diastole. With the onset of ventricular contraction, the AV valves close and the intraventricular pressure rises without ventricular shortening until it exceeds the pressure in the great arteries. Because the ventricular volumes do not change in this initial period of ventricular contraction, this period is called the isovolumetric contraction (IC) period. With further ventricular contraction, the ventricular pressure exceeds the pressures in the great arteries, the semilunar valves open, and the blood is ejected from the ventricles into the great arteries. Ventricular contraction during ejection of the stroke volume causes rapid descent of the AV valvar fibrous ring, allowing increased forward flow through the venae cavae, which is called an S-wave on Doppler tracing. As the ventricular pressure falls below the pressures of the great arteries, the semilunar valves close. The ventricular pressure then decreases with ventricular relaxation until the atrial pressures exceed the ventricular pressures. Because the ventricular volumes do not change in this initial period of active ventricular relaxation, the period is called isovolumetric relaxation (IR) period. With further relaxation, the ventricular pressures drop below the atrial pressures, and the AV valves open. This allows rapid inflow of blood into both ventricles during early diastole (E-wave), a fall in atrial pressures, and an increase in systemic venous forward flow (D-wave). As the pressure gradient across the AV valves diminishes, the atrial contraction contributes to ventricular filling in late diastole (A-wave). The rapid rise in atrial pressure during atrial systole is transmitted into the venous system, and results in reversed flow (a-wave) in the hepatic veins and venae cavae, and decreased antegrade flow in the ductus venosus and pulmonary veins.

### Techniques for Cardiac Functional Assessment

Echocardiography is an excellent tool to indirectly assess fetal cardiac function and blood flow. A brief but global assessment of the fetal cardiac function should be incorporated in a basic ultrasound examination. This should include an eyeball assessment of the ventricular contractility (Do both ventricles become noticeably smaller in systole?), as well as Doppler assessment of ventricular inflow and ductus venosus flow. More detailed assessment of the



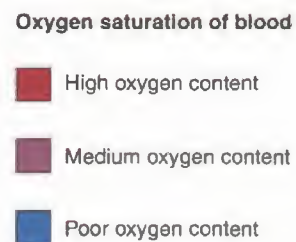


**FIGURE 14-62.** The fetal circulation. The colors indicate the oxygen saturation of the blood, and the arrows show the course of the blood from the placenta to the heart. Observe that three shunts permit most of the blood to bypass the liver and lungs: ductus venosus, foramen ovale, and ductus arteriosus. The poorly oxygenated blood returns to the placenta for oxygen and nutrients through the umbilical arteries. (From Moore K, Persaud TVN: *Before We Are Born: Essentials of Embryology and Birth Defects*, 6th ed. Philadelphia, WB Saunders, 2003.)

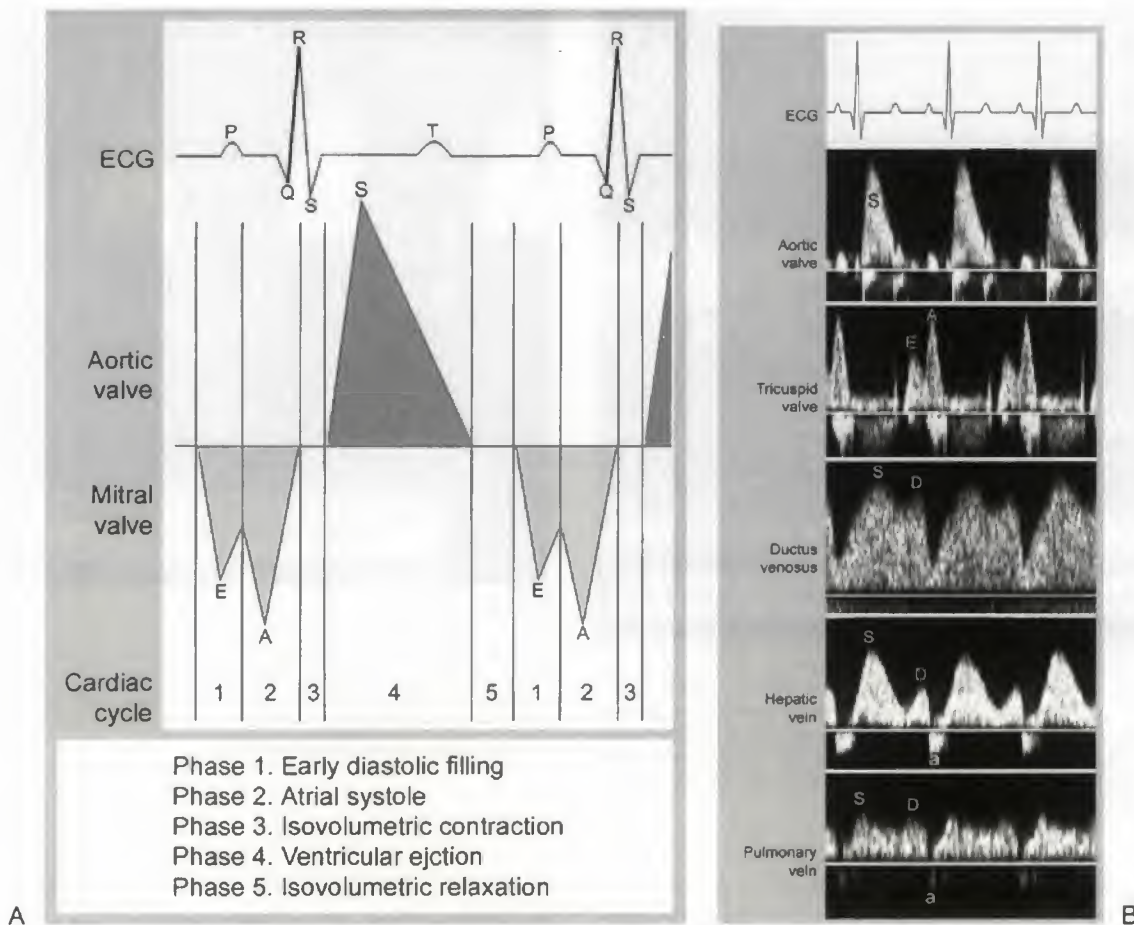


**FIGURE 14-63.** Correlation of cardiac phases (A) and Doppler tracings of normal venous, intracardiac and arterial blood flow (B). Electrical depolarization of the atria (P) and ventricles (QRS) precedes atrial (A) and ventricular (S) contractions, respectively. The largest proportion of ventricular filling occurs with atrial contraction in late diastole (A-wave in Phase 2). The rapid rise in atrial pressure is transmitted into the venous system (a-wave). With the onset of the ventricular contraction, atrioventricular valves close and the ventricular pressure rises without change in ventricular volume (isovolumetric contraction in Phase 3). When the ventricular pressure exceeds the pressure in the great arteries, the semilunar valves open, marking the onset of ventricular systole (arterial S-wave in Phase 4). Ventricular shortening during ejection of the stroke volume causes a rapid descent of the atrioventricular valve ring, allowing increased venous forward flow towards the atria (venous S-waves). When the ventricular pressure falls below the diastolic pressure in the great arteries, the semilunar valves close, marking the beginning of isovolumetric relaxation (Phase 5). When the ventricular pressure drops below the atrial pressure at the end of isovolumetric relaxation, the atrioventricular valves open. This is followed by a rapid inflow of blood into both ventricles during early diastole (E-wave in Phase 1), a fall in atrial pressure and an increase in systemic venous forward flow (D-wave).

cardiac and hemodynamic state is required in certain fetal (e.g., hydrops, growth restriction) and maternal (e.g., diabetes, multiple pregnancies) conditions.

### Shortening Fraction

M mode ultrasound from a four-chamber view or, alternatively, a left ventricular short axis view is the simplest way to quantify changes in chamber and wall dimensions during the cardiac cycle.<sup>200</sup> To accomplish this, the real-time-directed M mode cursor is placed perpendicular to the interventricular septal wall at the level of the chordae tendinae of the AV valves, and the M mode tracing is recorded (Fig. 14-64). This allows the examiner to measure the end-systolic (ESD) and end-diastolic (EDD) diameters as the respective maximal and minimal inward excursions of the ventricular wall. Shortening Fraction (SF) is then calculated using the equation:  $SF = [(EDD - ESD) \times 100] / EDD$ . SF of

both right and left ventricles is 28% to 40%. An abnormal shortening fraction is usually indicative of myocardial compromise or significant increase in ventricular workload.

### Cardiac Output

Measurement of the cardiac output (CO) is useful in conditions that may lead to high output failure, such as agenesis of the ductus venosus, vascular tumors, and acardiac twins.<sup>201,202</sup> The cardiac output is quantified by using the equation:  $CO = A \times \text{Velocity time integral} \times HR$ , where A is the cross-sectional area ( $A = 2 \pi r^2$ ) of the valve, Velocity time integral is the area under the curve of the wave form, and HR is the heart rate. Pulsed Doppler signals should be obtained as parallel as possible to the blood flow direction, placing the sample volume immediately distal to the tips of the interrogated valve leaflet. The left CO can be estimated with reasonable accuracy at the mitral or aortic



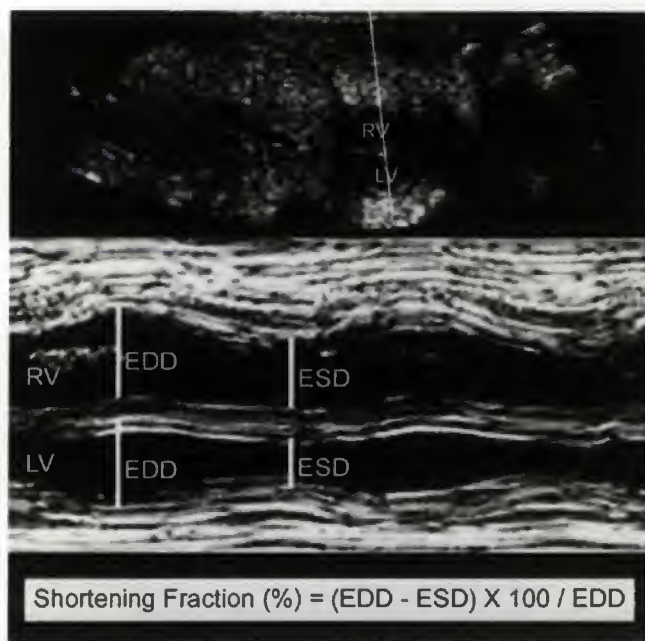


**FIGURE 14-64.** M-mode tracing of ventricular dimensions and myocardial thickness. After obtaining a short axis view of the fetal heart, the M-mode cursor is positioned through the two ventricles, aligned perpendicular to the ventricular septum. The resulting M-mode tracing allows the measurement of end-diastolic (EDD) and end-systolic (ESD) ventricular dimensions for calculation of the shortening fraction. LV, left ventricle; RV, right ventricle.

valve and the right CO, at the tricuspid or pulmonary valve.<sup>203,204</sup> The normal weight-corrected combined fetal CO is about 450 ml/min/kg, of which the right heart contributes 20% to 30% more than the left heart.<sup>197</sup>

### Diastolic Function

Useful information on ventricular filling characteristics is indirectly obtained by ventricular inflow characteristics; the duration of the left ventricular IR time; and the systemic and pulmonary venous Doppler flow patterns.<sup>205,206</sup> *Ventricular filling* is examined by positioning the Doppler gate immediately distal to the respective AV valve. After about 10 weeks' gestation, the characteristic inflow waveform has a biphasic flow pattern representing early diastolic filling during ventricular relaxation (E-wave) and late diastolic filling during atrial contraction (A-wave), respectively (see Fig. 14-63). Peak A-wave velocity exceeds the peak E-wave velocity because ventricular filling of the fetus relies mainly on atrial contraction. Presumably due to improved ventricular relaxation, peak E-wave velocity increases in a linear fashion with advancing gestation, whereas there is little or no change in peak A.<sup>206</sup> As a result, the average E/A ratios increase from approximately 0.6 at 20 weeks' gestation to 0.75 to 0.9 close to term.<sup>207</sup> As diastolic inflow velocity profile relates primarily to changing pressure gradients between the atria and ventricles, it is influenced by numerous variables including intrinsic myocardial and valvar properties, loading conditions and heart rate. *Left ventricular IR time* (Fig. 14-65) can be determined from the interval between aortic valve closure and the onset of

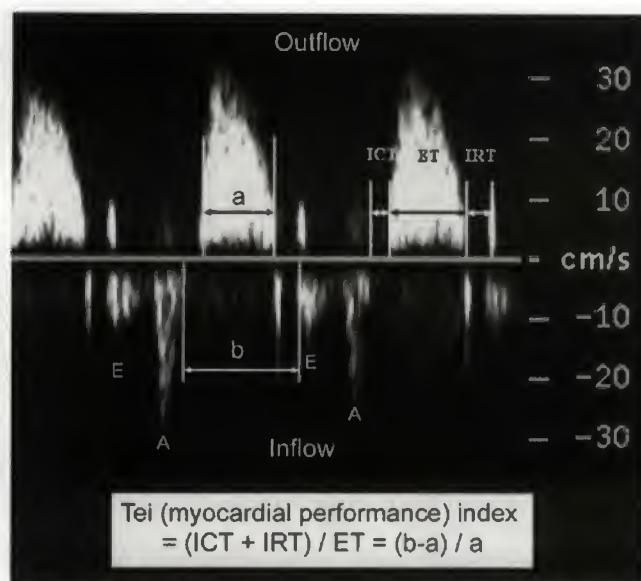


**FIGURE 14-65.** Simultaneous Doppler tracing of the left ventricular inflow and outflow, and calculation of Tei index or myocardial performance index (MPI). The left ventricular isovolumetric contraction time (ICT) is the time interval between the mitral valve closure and the aortic valve opening. The left ventricular isovolumetric relaxation time (IRT) is the time interval between aortic valve closure and the onset of mitral inflow. ET stands for ventricular ejection time.

transmitral flow by pulsed Doppler. To allow precise measurement of this short time interval, tracings should be recorded at a sweep speed of greater than 200 mm/sec. The normal IR time is less than 60 ms.<sup>208,209</sup> Prolonged relaxation time correlates with abnormal early diastolic filling. Pulsed Doppler examination of the inferior vena cava or hepatic vein, ductus venosus, and umbilical vessels is increasingly incorporated into the routine assessment of the fetus. The ultrasound beam for Doppler tracing should be aligned parallel to the blood flow direction for the assessment of velocity measurement, whereas the flow velocity ratios such as systolic/diastolic ratio, resistance index, and pulsatility index do not require parallel alignment of the ultrasound beam. The flow velocity of the inferior vena cava is primarily influenced by right atrial and ventricular pressure, whereas those of the ductus venosus and pulmonary veins more closely represent the left side of the heart. Venous flow waveforms are typically characterized by a biphasic forward flow during systole (S-wave) and early diastole (D-wave) and a short trough (a-wave) during atrial systole (see Fig. 14-63B). The degree of a-wave flow reversal varies considerably between individual veins. In the ductus venosus, blood flow remains antegrade also during atrial contraction, unlike in the venae cavae and hepatic veins. In the inferior vena cava, the ratio of peak reverse flow to peak systolic flow (preload index) is constant throughout gestation and lies between 0 and 0.37.<sup>209</sup> The ratio of the duration of reverse flow during atrial contraction to systolic forward flow declines under normal conditions from around 25% to 5% between 12 weeks and term.<sup>210</sup> With abnormal diastolic filling of the heart, the venous D-wave diminishes or disappears altogether,



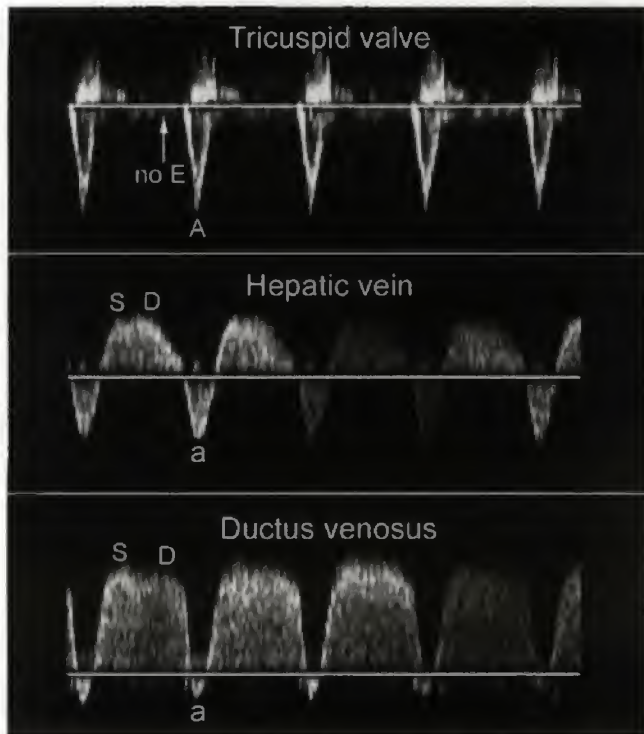


**FIGURE 14-66.** Abnormal diastolic function. Tricuspid inflow is abnormally short and occurs only in late diastole (A-wave). In addition there is increased reversal of blood flow during atrial contraction (a) in the hepatic vein and ductus venosus secondary to increase in end-diastolic ventricular pressure. S, systolic flow; D, early diastolic flow.

whereas the a-wave flow reversal secondary to atrial contraction increases. Abnormal early and late diastolic systemic venous flow may be observed in various conditions such as congestive heart failure and obstructive right-sided heart lesions. Transmission of venous pulsations into the portal and umbilical venous circulation correlates with increasing degrees of cardiac compromise. The end-stage finding of abnormal venous Doppler is atrial pulsations in the umbilical cord usually in association with fetal hydrops (Fig. 14-66).

### Myocardial Performance Index

The Tei index or myocardial performance index is a Doppler index of combined systolic and diastolic function.<sup>208,211-213</sup> The index is calculated by the sum of isovolumetric contraction and isovolumetric relaxation time-intervals divided by ejection time of the ventricle (see Fig. 14-65). Reference data for the mid- and late-gestational right and left-ventricular Tei indices differ between studies, ranging between  $0.35 \pm 0.05$  and  $0.53 \pm 0.13$ .<sup>208,211,213</sup> It has been used to assess the fetal cardiac status in normal and abnormal pregnancy conditions, including diabetes, twin-to-twin syndrome, fetal growth restriction, and congestive heart failure (see Fig. 14-66).

### Abnormal Cardiac Function

Abnormal fetal cardiac function is usually associated with disorders of the heart muscles or abnormal ventricular

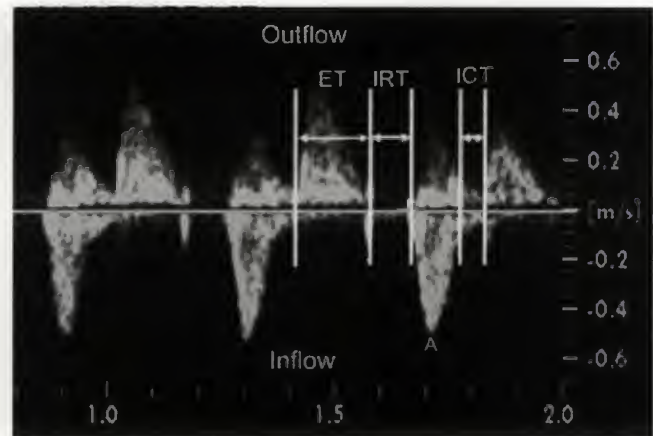


**FIGURE 14-67.** Diastolic dysfunction in cardiomyopathy. Simultaneous Doppler tracing of the left ventricular inflow and outflow shows prolonged isovolumetric relaxation (IRT; 88 ms) and increased myocardial performance index (MPI = 1). ET, ejection time; ICT, isovolumetric contraction time.

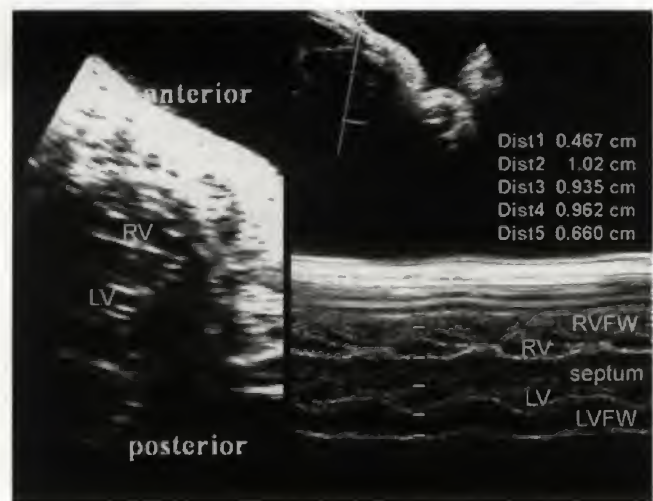


**FIGURE 14-68.** Severe global myocardial hypertrophy. Mid-ventricular short axis view and M-mode tracing shows marked myocardial hypertrophy. LV, left ventricle, LVFW, left ventricular free wall, RV, right ventricle, RVFW, right ventricular free wall.

loading conditions. Numerous reversible and irreversible conditions may influence the fetal myocardial performance including genetic disorders, viral infections, maternal autoimmune diseases, twin-to-twin transfusion syndrome (TTTS), arrhythmias, high output states, and placental failure.

*Cardiomyopathies* are not rare in fetus. The distinction between hypertrophic and dilated forms of cardiomyopathy may help in understanding and perhaps treating the underlying cause. Regardless of the cause, both may present with severe systolic and diastolic dysfunction, fetal hydrops, and even intrauterine demise. (Fig. 14-67)

*Hypertrophic cardiomyopathy (HCM)* is diagnosed when the ventricular wall thickness measures more than 2 standard deviations above the mean for gestational age (Fig. 14-68).<sup>214</sup> Increased wall stiffness may lead to poor diastolic filling of the heart and diminish the cardiac output. Intrinsic causes



include Noonan syndrome, familial HCM,  $\alpha$ -thalassemia, and other rare disorders.<sup>215</sup> Maternal diabetes is the most common extrinsic cause. Insufficient maternal blood glucose control causes fetal hyperglycemia, which stimulates the fetal pancreatic insulin production and secretion. Hyperinsulinemia and hyperglycemia in turn causes generalized fetal macrosomia and organomegaly. HCM with disproportionate septal hypertrophy occurs in 30% of infants of diabetic mothers<sup>216</sup> and these morphologic changes are already detectable by echocardiography in mid gestation.<sup>217</sup> The septal hypertrophy seen in the setting of well-controlled maternal diabetes progresses from midtrimester to term without affecting cardiac filling and ejection and, moreover, spontaneously resolves during infancy.<sup>217,218</sup> Contrary to the usually good prognosis of myocardial hypertrophy, severe HCM that is clinically indistinguishable from familial forms may occasionally be observed in association with maternal diabetes. Disproportionate ventricular septal hypertrophy may also cause obstruction of the left ventricular outflow. Thus, a careful examination of the fetal cardiac four-chamber and outflow tract views should be included in ultrasound assessment of diabetic pregnancies. TTTS complicates 10% to 15% of monochorionic multiple pregnancies.<sup>219</sup> Placental vascular anastomoses provide the basis for intertwin transfusion, resulting in unbalanced volume loading of the donor and recipient twins. The donor presents with chronic hypovolemia and oligohydramnios. Conversely, the recipient fetus is volume-overloaded with polyuria and polyhydramnios, and ventricular hypertrophy and hydrops may develop. Right ventricular outflow obstruction related to right ventricular muscle hypertrophy occurs in about 10% and may regress after successful intrauterine laser treatment or after birth.<sup>220</sup>

*Dilated cardiomyopathy (DCM)* presents with dilated, poorly contracting ventricles, AV regurgitation and often hydrops fetalis. DCM can be divided into two categories: myocardial damage due to inflammation and ischemia, and high output failure. Treatable high output failure may ensue when the cardiac output is massively increased for example, because of severe anemia, massive arteriovenous shunting, agenesis of ductus venosus, TTTS, or an acardiac twin. DCM may also be related to infection (parvovirus, cytomegalovirus, coxsackie B virus, adenovirus, toxoplasmosis), inflammation (maternal anti-Ro/La antibodies), and hereditary conditions (familial DCM).

A third form, *restrictive cardiomyopathy*, is unusual and mainly associated with endocardial fibroelastosis. Fibrosis of the endomyocardium should be suspected if the endocardium shows areas of persistently increased echogenicity on echocardiography. Endocardial fibroelastosis is commonly associated with maternal anti-Ro/La autoantibodies. Impaired diastolic filling decreases cardiac output of the affected fetus although the systolic function appears normal.

## Acknowledgments

We are very grateful to Drs. Alessandra Bernasconi and Alexanadra Jevremovic who informed us of the list of good cases, reviewed our draft manuscript so meticulously, and made valuable comments and corrections. We thank Ms. Jennifer Russell for reference management, Mrs. Eul Kyung Kim for making diagrams, and Ms. Harpal K. Gahunia for proofreading of the final manuscript.

## References

- Hoffman JI, Kaplan S: The incidence of congenital heart disease. *J Am Coll Cardiol* 39:1890, 2002.
- Kramer HH, Majewski F, Trampisch HJ, et al: Malformation patterns in children with congenital heart disease. *Am J Dis Child* 141:789, 1987.
- Grech V, Gatt M: Syndromes and malformations associated with congenital heart disease in a population-based study. *Int J Cardiol* 68:151, 1999.
- Eskedal L, Hagemo P, Eskild A, et al: A population-based study of extra-cardiac anomalies in children with congenital cardiac malformations. *Cardiol Young* 14:600, 2004.
- Ferencz C, Neill CA, Boughman JA, et al: Congenital cardiovascular malformations associated with chromosome abnormalities: an epidemiologic study. *J Pediatr* 114:79, 1989.
- Allan LD, Sharland GK, Chita SK, et al: Chromosomal anomalies in fetal congenital heart disease. *Ultrasound Obstet Gynecol* 1:8, 1991.
- Paladini D, Calabro R, Palmieri S, et al: Prenatal diagnosis of congenital heart disease and fetal karyotyping. *Obstet Gynecol* 81:679, 1993.
- Moore JW, Binder GA, Berry R: Prenatal diagnosis of aneuploidy and deletion 22q11.2 in fetuses with ultrasound detection of cardiac defects. *Am J Obstet Gynecol* 191:2068, 2004.
- Gillum RF: Epidemiology of congenital heart disease in the United States. *Am Heart J* 127:919, 1994.
- Boneva RS, Botto LD, Moore CA, et al: Mortality associated with congenital heart defects in the United States: trends and racial disparities, 1979-1997. *Circulation* 103:2376, 2001.
- Jaeggi ET, Fouron JC, Silverman ED, et al: Transplacental fetal treatment improves the outcome of prenatally diagnosed complete atrioventricular block without structural heart disease. *Circulation* 110:1542, 2004.
- Tworzetzky W, Wilkins-Haug L, Jennings RW, et al: Balloon dilation of severe aortic stenosis in the fetus: potential for prevention of hypoplastic left heart syndrome: candidate selection, technique, and results of successful intervention. *Circulation* 110:2125, 2004.
- Makikallio K, McElhinney DB, Levine JC, et al: Fetal aortic valve stenosis and the evolution of hypoplastic left heart syndrome: patient selection for fetal intervention. *Circulation* 113:1401, 2006.
- Galindo A, Gutierrez-Larraya F, Velasco JM, et al: Pulmonary balloon valvuloplasty in a fetus with critical pulmonary stenosis/atresia with intact ventricular septum and heart failure. *Fetal Diagn Ther* 21:100, 2006.
- Montana E, Khoury MJ, Cragan JD, et al: Trends and outcomes after prenatal diagnosis of congenital cardiac malformations by fetal echocardiography in a well defined birth population, Atlanta, Georgia, 1990-1994. *J Am Coll Cardiol* 28:1805, 1996.
- Jaeggi ET, Sholler GF, Jones OD, et al: Comparative analysis of pattern, management and outcome of pre- versus postnatally diagnosed major congenital heart disease: a population-based study. *Ultrasound Obstet Gynecol* 17:380, 2001.
- Garne E, Stoll C, Clementi M: Euroscan group evaluation of prenatal diagnosis of congenital heart diseases by ultrasound: Experience from 20 European registries. *Ultrasound Obstet Gynecol* 17:386, 2001.
- Allan LD, Crawford DC, Chita SK, et al: Prenatal screening for congenital heart disease. *Br Med J (Clin Res Ed)* 292:1717, 1986.
- Copel JA, Pilu G, Green J, et al: Fetal echocardiographic screening for congenital heart disease: The importance of the four-chamber view. *Am J Obstet Gynecol* 157:648, 1987.
- Bromley B, Estroff JA, Sanders SP, et al: Fetal echocardiography: Accuracy and limitations in a population at high and low risk for heart defects. *Am J Obstet Gynecol* 166:1473, 1992.
- Sharland GK, Allan LD: Screening for congenital heart disease prenatally: Results of a 2 1/2-year study in the South East Thames Region. *Br J Obstet Gynaecol* 99:220, 1992.
- Achiron R, Glaser J, Gelernter I, et al: Extended fetal echocardiographic examination for detecting cardiac malformations in low risk pregnancies. *BMJ* 304:671, 1992.
- DeVore GR: The aortic and pulmonary outflow tract screening examination in the human fetus. *J Ultrasound Med* 11:345, 1992.
- Yagel S, Cohen SM, Achiron R: Examination of the fetal heart by five short-axis views: A proposed screening method for comprehensive cardiac evaluation. *Ultrasound Obstet Gynecol* 17:367, 2001.
- Allan LD: Cardiac anatomy screening: What is the best time for screening in pregnancy? *Curr Opin Obstet Gynecol* 15:143, 2003.



26. Souka AP, Pilalis A, Kavalakis I, et al: Screening for major structural abnormalities at the 11- to 14-week ultrasound scan. *Am J Obstet Gynecol* 194:393, 2006.
27. Comas GC, Calindo A, Martinez JM, et al: Early prenatal diagnosis of major cardiac anomalies in a high-risk population. *Prenat Diagn* 22:585, 2002.
28. Carvalho JS, Moscoso G, Tekay A, et al: Clinical impact of first and early second trimester fetal echocardiography on high risk pregnancies. *Heart* 90:921, 2004.
29. Guariglia L, Rosati P: Transvaginal sonographic detection of embryonic-fetal abnormalities in early pregnancy. *Obstet Gynecol* 96:328, 2000.
30. Smrcek JM, Berg C, Geipel A, et al: Detection rate of early fetal echocardiography and in utero development of congenital heart defects. *J Ultrasound Med* 25:187, 2006.
31. Chaoui R, Hoffmann J, Heling KS: Three-dimensional (3D) and 4D color Doppler fetal echocardiography using spatio-temporal image correlation (STIC). *Ultrasound Obstet Gynecol* 23:535, 2004.
32. Devore GR: Three-dimensional and four-dimensional fetal echocardiography: A new frontier. *Curr Opin Pediatr* 17:592, 2005.
33. Paladini D, Vassallo M, Sglavo G, et al: The role of spatio-temporal image correlation (STIC) with tomographic ultrasound imaging (TUI) in the sequential analysis of fetal congenital heart disease. *Ultrasound Obstet Gynecol* 27:555, 2006.
34. Yoo SJ, Lee YH, Cho KS, et al: Sequential segmental approach to fetal congenital heart disease. *Cardiol Young* 9:430, 1999.
35. Carvalho JS, Ho SY, Shinebourne EA: Sequential segmental analysis in complex fetal cardiac abnormalities: A logical approach to diagnosis. *Ultrasound Obstet Gynecol* 26:105, 2005.
36. Smith RS, Comstock CH, Kirk JS, et al: Ultrasonographic left cardiac axis deviation: A marker for fetal anomalies. *Obstet Gynecol* 85:187, 1995.
37. Shipp TD, Bromley B, Hornberger LK, et al: Levorotation of the fetal cardiac axis: A clue for the presence of congenital heart disease. *Obstet Gynecol* 85:97, 1995.
38. Tan J, Silverman NH, Hoffman JL, et al: Cardiac dimensions determined by cross-sectional echocardiography in the normal human fetus from 18 weeks to term. *Am J Cardiol* 70:1459, 1992.
39. Shapiro I, Degani S, Leibovitz Z, et al: Fetal cardiac measurements derived by transvaginal and transabdominal cross-sectional echocardiography from 14 weeks of gestation to term. *Ultrasound Obstet Gynecol* 12:404, 1998.
40. Vetrano IM, Huang R, Comstock CH: The normal offset of the tricuspid septal leaflet in the fetus. *J Ultrasound Med* 21:1099, 2002.
41. Rein AJ, Nir A, Nadjari M: The coronary sinus in the fetus. *Ultrasound Obstet Gynecol* 15:468, 2000.
42. Smrcek JM, Gembruch U: Longitudinal observations in normally grown fetuses with tricuspid valve regurgitation: Report of 22 cases. *Prenat Diagn* 19:197, 1999.
43. Messing B, Porat S, Imbar T, et al: Mild tricuspid regurgitation: A benign fetal finding at various stages of pregnancy. *Ultrasound Obstet Gynecol* 26:606, 2005.
44. Huggon IC, DeFigueiredo DB, Allan LD: Tricuspid regurgitation in the diagnosis of chromosomal anomalies in the fetus at 11-14 weeks of gestation. *Heart* 89:1071, 2003.
45. Faiola S, Tsoi E, Huggon IC, et al: Likelihood ratio for trisomy 21 in fetuses with tricuspid regurgitation at the 11 to 13 + 6-week scan. *Ultrasound Obstet Gynecol* 26:22, 2005.
46. Falcon O, Faiola S, Huggon I, et al: Fetal tricuspid regurgitation at the 11 + 0 to 13 + 6-week scan: association with chromosomal defects and reproducibility of the method. *Ultrasound Obstet Gynecol* 27:609, 2006.
47. Yoo SJ, Lee YH, Kim ES, et al: Three-vessel view of the fetal upper mediastinum: An easy means of detecting abnormalities of the ventricular outflow tracts and great arteries during obstetric screening. *Ultrasound Obstet Gynecol* 9:173, 1997.
48. Yoo SJ, Lee YH, Cho KS: Abnormal three-vessel view on sonography: A clue to the diagnosis of congenital heart disease in the fetus. *Am J Roentgenol* 172:825, 1999.
49. Yagel S, Arbel R, Anteby EY, et al: The three vessels and trachea view (3VT) in fetal cardiac scanning. *Ultrasound Obstet Gynecol* 20:340, 2002.
50. Vinals F, Heredia F, Giuliano A: The role of the three vessels and trachea view (3VT) in the diagnosis of congenital heart defects. *Ultrasound Obstet Gynecol* 22:358, 2003.
51. Zalel Y, Gamzu R, Mashiach S, et al: The development of the fetal thymus: An in utero sonographic evaluation. *Prenat Diagn* 22:114, 2002.
52. Chaoui R, Kalache KD, Heling KS, et al: Absent or hypoplastic thymus on ultrasound: a marker for deletion 22q11.2 in fetal cardiac defects. *Ultrasound Obstet Gynecol* 20:546, 2002.
53. Barrea C, Yoo SJ, Chitayat D, et al: Assessment of the thymus at echocardiography in fetuses at risk for 22q11.2 deletion. *Prenat Diagn* 23:9, 2003.
54. Cho JY, Min JY, Yoo SJ, et al: Normal thymus diameter at fetal ultrasound. *Ultrasound Obstet Gynecol* 29:634, 2007.
55. Yoo SJ, Lee YH, Kim ES, et al: Tetralogy of Fallot in the fetus: Findings at targeted sonography. *Ultrasound Obstet Gynecol* 14:29, 1999.
56. Yoo SJ, Min JY, Lee YH, et al: Fetal sonographic diagnosis of aortic arch anomalies. *Ultrasound Obstet Gynecol* 22:535, 2003.
57. Moller JH: Malposition of the heart. In Moller JH, Neal WA (eds): *Fetal, Neonatal and Infant Cardiac Disease*. Norwalk, Appleton & Lange, 1990, pp 755.
58. Hagler DJ, O'Leary PW: Cardiac malpositions and abnormalities of atrial and visceral situs. In Emmanouilides GC, Allen HD, Riemenschneider TA, et al (eds): *Moss and Adams' Heart disease in infants, children, and adolescents including the fetus and young adult*. Baltimore, Williams & Wilkins, 1991, pp 1307.
59. Walmsley R, Hishitani T, Sandor GG, et al: Diagnosis and outcome of dextrocardia diagnosed in the fetus. *Am J Cardiol* 94:141, 2004.
60. Bernasconi A, Azancot A, Simpson JM, et al: Fetal dextrocardia: Diagnosis and outcome in two tertiary centres. *Heart* 91:1590, 2005.
61. Stanger P, Rudolph AM, Edwards JE: Cardiac malpositions: An overview based on study of sixty-five necropsy specimens. *Circulation* 56:159, 1977.
62. Phoon CK, Neill CA: Asplenia syndrome: Insight into embryology through an analysis of cardiac and extracardiac anomalies. *Am J Cardiol* 73:581, 1994.
63. Phoon CK, Villegas MD, Ursell PC, et al: Left atrial isomerism detected in fetal life. *Am J Cardiol* 77:1083, 1996.
64. Berg C, Geipel A, Smrcek J, et al: Prenatal diagnosis of cardiopulmonary syndromes: A 10-year experience. *Ultrasound Obstet Gynecol* 22:451, 2003.
65. Berg C, Geipel A, Kamil D, et al: The syndrome of left isomerism: Sonographic findings and outcome in prenatally diagnosed cases. *J Ultrasound Med* 24:921, 2005.
66. Freedom RM, Jaeggi ET, Lim JS, et al: Hearts with isomerism of the right atrial appendages—One of the worst forms of disease in 2005. *Cardiol Young* 15:554, 2005.
67. Lim JS, McCrindle BW, Smallhorn JF, et al: Clinical features, management, and outcome of children with fetal and postnatal diagnoses of isomerism syndromes. *Circulation* 112:2454, 2005.
68. Taketazu M, Loughheed J, Yoo SJ, et al: Spectrum of cardiovascular disease, accuracy of diagnosis, and outcome in fetal heterotaxy syndrome. *Am J Cardiol* 97:720, 2006.
69. Atkinson DE, Drant S: Diagnosis of heterotaxy syndrome by fetal echocardiography. *Am J Cardiol* 82:1147, 1998.
70. Lin JH, Chang CI, Wang JK, et al: Intrauterine diagnosis of heterotaxy syndrome. *Am Heart J* 143:1002, 2002.
71. Berg C, Geipel A, Kohl T, et al: Fetal echocardiographic evaluation of atrial morphology and the prediction of laterality in cases of heterotaxy syndromes. *Ultrasound Obstet Gynecol* 26:538, 2005.
72. Allan LD, Lockhart S: Intrathoracic cardiac position in the fetus. *Ultrasound Obstet Gynecol* 3:93, 1993.
73. Abdullah MM, Lacro RV, Smallhorn J, et al: Fetal cardiac dextro-position in the absence of an intrathoracic mass: Sign of significant right lung hypoplasia. *J Ultrasound Med* 19:669, 2000.
74. McEwing RL, Chaoui R: Congenitally corrected transposition of the great arteries: Clues for prenatal diagnosis. *Ultrasound Obstet Gynecol* 23:68, 2004.
75. Chiappa E, Micheletti A, Sciarone A, et al: The prenatal diagnosis of, and short-term outcome for, patients with congenitally corrected transposition. *Cardiol Young* 14:265, 2004.
76. Bader R, Perrin D, Yoo SJ: Congenitally corrected transposition of the great arteries with Ebstein malformation and hypoplasia of the aortic arch in a fetus. *Fetal Pediatr Pathol* 23:257, 2004.
77. Sharland G, Tingay R, Jones A, et al: Atrioventricular and ventriculo-arterial discordance (congenitally corrected transposition of the great arteries): Echocardiographic features, associations, and outcome in 34 fetuses. *Heart* 91:1453, 2005.



78. Paladini D, Volpe P, Marasini M, et al: Diagnosis, characterization and outcome of congenitally corrected transposition of the great arteries in the fetus: a multicenter series of 30 cases. *Ultrasound Obstet Gynecol* 27:281, 2006.
79. Hornung TS, Heads A, Hunter AS: Right ventricular dilatation in the fetus: A study of associated features and outcome. *Pediatr Cardiol* 22:215, 2001.
80. Lang D, Oberhoffer R, Cook A, et al: Pathologic spectrum of malformations of the tricuspid valve in prenatal and neonatal life. *J Am Coll Cardiol* 17:1161, 1991.
81. Hornberger LK, Sahn DJ, Kleinman CS, et al: Tricuspid valve disease with significant tricuspid insufficiency in the fetus: Diagnosis and outcome. *J Am Coll Cardiol* 17:167, 1991.
82. Song TB, Lee JY, Kim YH, et al: Prenatal diagnosis of severe tricuspid insufficiency in Ebstein's anomaly with pulmonary atresia and intact ventricular septum: A case report. *J Obstet Gynaecol Res* 26:223, 2000.
83. Todros T, Paladini D, Chiappa E, et al: Pulmonary stenosis and atresia with intact ventricular septum during prenatal life. *Ultrasound Obstet Gynecol* 21:228, 2003.
84. Sandor GG, Cook AC, Sharland GK, et al: Coronary arterial abnormalities in pulmonary atresia with intact ventricular septum diagnosed during fetal life. *Cardiol Young* 12:436, 2002.
85. Baschat AA, Love JC, Stewart PA, et al: Prenatal diagnosis of ventriculocoronary fistula. *Ultrasound Obstet Gynecol* 18:39, 2001.
86. Cochrane AD, Marath A, Mee RB: Can a dilated coronary sinus produce left ventricular inflow obstruction? An unrecognized entity. *Ann Thorac Surg* 58:1114, 1994.
87. Jouannic JM, Picone O, Martinovic J, et al: Diminutive fetal left ventricle at mid-gestation associated with persistent left superior vena cava and coronary sinus dilatation. *Ultrasound Obstet Gynecol* 22:527, 2003.
88. Dibardino DJ, Fraser CD Jr, Dickerson HA, et al: Left ventricular inflow obstruction associated with persistent left superior vena cava and dilated coronary sinus. *J Thorac Cardiovasc Surg* 127:959, 2004.
89. Allan LD, Sharland GK: The echocardiographic diagnosis of totally anomalous pulmonary venous connection in the fetus. *Heart* 85:433, 2001.
90. Valsangiacomo ER, Hornberger LK, Barrea C, et al: Partial and total anomalous pulmonary venous connection in the fetus: Two-dimensional and Doppler echocardiographic findings. *Ultrasound Obstet Gynecol* 22:257, 2003.
91. Wessels MW, Frohn-Mulder IME, Cromme-Dijkhuis AH, et al: In utero diagnosis of intra-diaphragmatic total anomalous pulmonary venous return. *Ultrasound Obstet Gynecol* 8:206, 1996.
92. Respondek-Liberska M, Janiak K, Moll J, et al: Prenatal diagnosis of partial anomalous pulmonary venous connection by detection of dilatation of superior vena cava in hypoplastic left heart: A case report. *Fetal Diagn Ther* 17:298, 2002.
93. Benacerraf BR, Saltzman DH, Sanders SP: Sonographic sign suggesting the prenatal diagnosis of coarctation of the aorta. *J Ultrasound Med* 8:65, 1989.
94. Brown DL, Durfee SM, Hornberger LK: Ventricular discrepancy as a sonographic sign of coarctation of the fetal aorta: How reliable is it? *J Ultrasound Med* 16:95, 1997.
95. Hornberger LK, Sahn DJ, Kleinman CS, et al: Antenatal diagnosis of coarctation of the aorta: A multicenter experience. *J Am Coll Cardiol* 23:417, 1994.
96. Sharland GK, Chan KY, Allan LD: Coarctation of the aorta: Difficulties in prenatal diagnosis. *Br Heart J* 71:70, 1994.
97. Berning RA, Silverman NH, Villegas M, et al: Reversed shunting across the ductus arteriosus or atrial septum in utero heralds severe congenital heart disease. *J Am Coll Cardiol* 27:481, 1996.
98. Luchese S, Manica JL, Zielinsky P: Intrauterine ductus arteriosus constriction: Analysis of a historic cohort of 20 cases. *Arq Bras Cardiol* 81:405, 2003.
99. Auer M, Brezinka C, Eller P, et al: Prenatal diagnosis of intrauterine premature closure of the ductus arteriosus following maternal diclofenac application. *Ultrasound Obstet Gynecol* 23:513, 2004.
100. Trevett TN Jr, Cotton J: Idiopathic constriction of the fetal ductus arteriosus. *Ultrasound Obstet Gynecol* 23:517, 2004.
101. Mielke G, Peukert U, Krapp M, et al: Fetal and transient neonatal right heart dilatation with severe tricuspid valve insufficiency in association with abnormally S-shaped kinking of the ductus arteriosus. *Ultrasound Obstet Gynecol* 5:338, 1995.
102. McElhinney DB, Halbach VV, Silverman NH, et al: Congenital cardiac anomalies with vein of Galen malformations in infants. *Arch Dis Child* 78:548, 1998.
103. Crowe DA, Allan LD: Patterns of pulmonary venous flow in the fetus with disease of the left heart. *Cardiol Young* 11:369, 2001.
104. Taketazu M, Barrea C, Smallhorn JF, et al: Intrauterine pulmonary venous flow and restrictive foramen ovale in fetal hypoplastic left heart syndrome. *J Am Coll Cardiol* 43:1902, 2004.
105. Michelfelder E, Gomez C, Border W, et al: Predictive value of fetal pulmonary venous flow patterns in identifying the need for atrial septoplasty in the newborn with hypoplastic left ventricle. *Circulation* 112:2974, 2005.
106. Machlitt A, Heling KS, Chaoui R: Increased cardiac atrial-to-ventricular length ratio in the fetal four-chamber view: A new marker for atrioventricular septal defects. *Ultrasound Obstet Gynecol* 24:618, 2004.
107. Yoo SJ: What does an increased atrial-to-ventricular length ratio mean in fetuses with atrioventricular septal defect? *Ultrasound Obstet Gynecol* 24:597, 2004.
108. Park JK, Taylor DK, Skeels M, et al: Dilated coronary sinus in the fetus: Misinterpretation as an atrioventricular canal defect. *Ultrasound Obstet Gynecol* 10:126, 1997.
109. Huggon IC, Cook AC, Smeeton NC, et al: Atrioventricular septal defects diagnosed in fetal life: Associated cardiac and extra-cardiac abnormalities and outcome. *J Am Coll Cardiol* 36:593, 2000.
110. Fesslova V, Villa L, Nava S, et al: Spectrum and outcome of atrioventricular septal defect in fetal life. *Cardiol Young* 12:18, 2002.
111. Paladini D, Palmieri S, Lamberti A, et al: Characterization and natural history of ventricular septal defects in the fetus. *Ultrasound Obstet Gynecol* 16:118, 2000.
112. Yoo SJ, Min JU, Lee YH: Normal pericardial fluid in the fetus: Color and spectral Doppler analysis. *Ultrasound Obstet Gynecol* 18:248, 2001.
113. Slesnick TC, Ayres NA, Altman CA, et al: Characteristics and outcomes of fetuses with pericardial effusions. *Am J Cardiol* 96:599, 2005.
114. Sharland G, Lockhart S: Isolated pericardial effusion: An indication for fetal karyotyping? *Ultrasound Obstet Gynecol* 6:29, 1995.
115. Hornberger LK, Sanders SP, Sahn DJ, et al: In utero pulmonary artery and aortic growth and potential for progression of pulmonary outflow tract obstruction in tetralogy of Fallot. *J Am Coll Cardiol* 25:739, 1995.
116. Pepas LP, Savis A, Jones A, et al: An echocardiographic study of tetralogy of Fallot in the fetus and infant. *Cardiol Young* 13:240, 2003.
117. Koenigsberg M, Factor S, Cho S, et al: Fetal Marfan syndrome: Prenatal ultrasound diagnosis with pathological confirmation of skeletal and aortic lesions. *Prenat Diagn* 1:241, 1981.
118. Pasquini L, Belmar C, Seale A, et al: Prenatal diagnosis of absent right and persistent left superior vena cava. *Prenat Diagn* 26:700, 2006.
119. Volpe P, Paladini D, Marasini M, et al: Common arterial trunk in the fetus: Characteristics, associations, and outcome in a multicentre series of 23 cases. *Heart* 89:1437, 2003.
120. Miyashita S, Chiba Y: Prenatal demonstration of major aortopulmonary collateral arteries with tetralogy of Fallot and pulmonary atresia. *Fetal Diagn Ther* 19:100, 2004.
121. Machevin-Surugue E, David N, Verspyck E, et al: Dilated coronary sinus in prenatal echocardiography: identification, associations and outcome. *Prenat Diagn* 22:898, 2002.
122. Patel CR, Lane JR, Spector ML, et al: Totally anomalous pulmonary venous connection and complex congenital heart disease: Prenatal echocardiographic diagnosis and prognosis. *J Ultrasound Med* 24:1191, 2005.
123. Valsangiacomo ER, Smallhorn JF: Images in cardiovascular medicine: Prenatal diagnosis of aortopulmonary window by fetal echocardiography. *Circulation* 105:E192, 2002.
124. Sokol J, Bohn D, Larco RV, et al: Fetal pulmonary artery diameters and their association with lung hypoplasia and postnatal outcome in congenital diaphragmatic hernia. *Am J Obstet Gynecol* 186:1085, 2002.
125. Jung MJ, Yoo SJ: Prenatal diagnosis of anomalous origin of the right pulmonary artery from the ascending aorta. *Cardiol Young* 12:186, 2002.
126. Yeager SB, Van Der Velde ME, Waters BL, et al: Prenatal role of the ductus arteriosus in absent pulmonary valve syndrome. *Echocardiography* 19:489, 2002.



127. Moon-Grady AJ, Tacy TA, Brook MM, et al: Value of clinical and echocardiographic features in predicting outcome in the fetus, infant, and child with tetralogy of Fallot with absent pulmonary valve complex. *Am J Cardiol* 89:1280, 2002.
128. Volpe P, Paladini D, Marasini M, et al: Characteristics, associations and outcome of absent pulmonary valve syndrome in the fetus. *Ultrasound Obstet Gynecol* 24:623, 2004.
129. Dyamenahalli U, Smallhorn JF, Geva T, et al: Isolated ductus arteriosus aneurysm in the fetus and infant: A multi-institutional experience. *J Am Coll Cardiol* 36:262, 2000.
130. Jackson CM, Sandor GG, Lim K, et al: Diagnosis of fetal ductus arteriosus aneurysm: importance of the three-vessel view. *Ultrasound Obstet Gynecol* 26:57, 2005.
131. Tseng JJ, Jan SL: Fetal echocardiographic diagnosis of isolated ductus arteriosus aneurysm: A longitudinal study from 32 weeks of gestation to term. *Ultrasound Obstet Gynecol* 26:50, 2005.
132. Achiron R, Rotstein Z, Heggesh J, et al: Anomalies of the fetal aortic arch: A novel sonographic approach to in-utero diagnosis. *Ultrasound Obstet Gynecol* 20:553, 2002.
133. Yoo SJ, Min JY, Lee YH, et al: Fetal sonographic diagnosis of aortic arch anomalies. *Ultrasound Obstet Gynecol* 22:535, 2003.
134. Wilson DI, Goodship JA, Burn J, et al: Deletion within chromosome 22q11 in familial congenital heart disease. *Lancet* 340:573, 1992.
135. Lethor JP, Marcon F, de Moor M, et al: Physiology of ventricular septal defect shunt flow in the fetus examined by color Doppler M-mode. *Circulation* 101:E93, 2000.
136. Yagel S, Valsky DV, Messing B: Detailed assessment of fetal ventricular septal defect with 4D color Doppler ultrasound using spatio-temporal image correlation technology. *Ultrasound Obstet Gynecol* 25:97, 2005.
137. Tometzi AJ, Suda K, Kohl T, et al: Accuracy of prenatal echocardiographic diagnosis and prognosis of fetuses with conotruncal anomalies. *J Am Coll Cardiol* 33:1696, 1999.
138. Tongsong T, Sirichotiyakul S, Sukpan K, et al: Prenatal features of a truncus arteriosus with pulmonary atresia and pulmonary circulation derived from the ductus arteriosus. *J Ultrasound Med* 23:1221, 2004.
139. McElhinney DB, Salvin JW, Colan SD, et al: Improving outcomes in fetuses and neonates with congenital displacement (Ebstein's malformation) or dysplasia of the tricuspid valve. *Am J Cardiol* 96:582, 2005.
140. Jaeggi ET, Hornberger LK, Smallhorn JF, et al: Prenatal diagnosis of complete atrio-ventricular block associated with structural heart disease since 1990: Combined experience of two tertiary care centers and review of the literature. *Ultrasound Obstet Gynecol* 26:16, 2005.
141. Mielke G, Steil E, Kendziorra H, et al: Ductus arteriosus-dependent pulmonary circulation secondary to cardiac malformations in fetal life. *Ultrasound Obstet Gynecol* 9:25, 1997.
142. Soongswang J, Adatia I, Newman C, et al: Mortality in potential arterial switch candidates with transposition of the great arteries. *J Am Coll Cardiol* 32:753, 1998.
143. Tworetzky W, McElhinney DB, Reddy VM, et al: Improved surgical outcome after fetal diagnosis of hypoplastic left heart syndrome. *Circulation* 103:1269, 2001.
144. Bonnet D, Coltri A, Butera G, et al: Detection of transposition of the great arteries in fetuses reduces neonatal morbidity and mortality. *Circulation* 99:916-918, 1999.
145. Jenkins KJ, Gauvreau K, Newberger JW, et al: Consensus-based method for risk adjustment for surgery for congenital heart disease. *J Thorac Cardiovasc Surg* 123:110, 2002.
146. Isaacs H Jr: Fetal and neonatal cardiac tumors. *Pediatr Cardiol* 25:252, 2004.
147. Groves AM, Fagg NL, Cook AC, et al: Cardiac tumours in intra-uterine life. *Arch Dis Child* 67:1189, 1992.
148. Holley DG, Martin GR, Brenner JL, et al: Diagnosis and management of fetal cardiac tumors: a multicenter experience and review of published reports. *J Am Coll Cardiol* 26:516, 1995.
149. Geipel A, Krapp M, Germer U, et al: Perinatal diagnosis of cardiac tumors. *Ultrasound Obstet Gynecol* 17:17, 2001.
150. Zhou QC, Fan P, Peng QH, et al: Prenatal echocardiographic differential diagnosis of fetal cardiac tumors. *Ultrasound Obstet Gynecol* 23:165, 2004.
151. D'Addario V, Pinto V, Di Naro E, et al: Prenatal diagnosis and postnatal outcome of cardiac rhabdomyomas. *J Perinat Med* 30:170, 2002.
152. Tworetzky W, McElhinney DB, Margossian R, et al: Association between cardiac tumors and tuberous sclerosis in the fetus and neonate. *Am J Cardiol* 92:487, 2003.
153. Tehrani M, Vettriano IM, Chang CH: Localized nodular hypertrophy mimicking rhabdomyoma in the fetal heart: Prenatal sonographic and pathology findings. *Pediatr Dev Pathol* 7:192, 2004.
154. Sonigo P, Elmaleh A, Fermont L, et al: Prenatal MRI diagnosis of fetal cerebral tuberous sclerosis. *Pediatr Radiol* 26:1, 1996.
155. Kim TH, Kim YM, Han MY, et al: Perinatal sonographic diagnosis of cardiac fibroma with MR imaging correlation. *AJR Am J Roentgenol* 178:727, 2002.
156. Tollens M, Grab D, Lang D, et al: Pericardial teratoma: Prenatal diagnosis and course. *Fetal Diagn Ther* 18:432, 2003.
157. Ramirez JA, Mon CR, Perez EO, et al: Fetal intrapericardial teratoma. *Ultrasound Obstet Gynecol* 23:416-418, 2004.
158. Simchen MJ, Toi A, Silver M, et al: Fetal cardiac calcifications: Report of four prenatally diagnosed cases and review of the literature. *Ultrasound Obstet Gynecol* 27:325, 2006.
159. Tongsong T, Sirichotiyakul S, Sittiwangkul R, et al: Prenatal sonographic diagnosis of cardiac hemangioma with postnatal spontaneous regression. *Ultrasound Obstet Gynecol* 24:207, 2004.
160. Tannirandorn Y, Manotaya S, Uerpaiojkit B, et al: Reference intervals for first trimester embryonic/fetal heart rate in a Thai population. *J Obstet Gynaecol Res* 26:367, 2000.
161. Hanprasertpong T, Phupong V: First trimester embryonic/fetal heart rate in normal pregnant women. *Arch Gynecol Obstet* 274:257, 2006.
162. Friedman WF, Pool PE, Jacobowitz D, et al: Sympathetic innervation of the developing rabbit heart: Biochemical and histochemical comparisons of fetal, neonatal, and adult myocardium. *Circ Res* 23:25, 1968.
163. Wheeler T, Murrills A: Patterns of fetal heart rate during normal pregnancy. *Br J Obstet Gynaecol* 85:18, 1978.
164. Jaeggi E, Fouron JC, Fournier A, et al: Ventriculo-atrial time interval measured on M-mode echocardiography: A determining element in the diagnosis, treatment and prognosis of fetal supraventricular tachycardia. *Heart* 79:582, 1998.
165. Fouron JC, Proulx F, Miro J, et al: Doppler and M-mode ultrasonography to time fetal atrial and ventricular contractions. *Obstet Gynecol* 96:732, 2000.
166. Taylor MJ, Smith MJ, Thomas M, et al: Non-invasive fetal electrocardiography in singleton and multiple pregnancies. *Brit J Obstet Gynecol* 110:668, 2003.
167. Menendez T, Achenbach S, Beinder E, et al: Usefulness of magnetocardiography for the investigation of fetal arrhythmias. *Am J Cardiol* 88:334, 2001.
168. Nii M, Shimizu M, Roman KS, et al: Doppler tissue imaging in the assessment of atrioventricular conduction time: Validation of a novel technique and comparison with electrophysiologic and pulsed wave Doppler-derived equivalents in an animal model. *J Am Soc Echocardiogr* 19:314, 2006.
169. Kleinman CS, Nehgme RA: Cardiac arrhythmias in the human fetus. *Pediatr Cardiol* 25:234, 2004.
170. Krapp M, Kohl T, Simpson JM, et al: Review of diagnosis, treatment, and outcome of fetal atrial flutter compared with supraventricular tachycardia. *Heart* 89:913, 2003.
171. Jaeggi ET, Nii M: Fetal brady- and tachyarrhythmias: New and accepted diagnostic and treatment methods. *Semin Fetal Neonatal Med* 10:504, 2005.
172. Hofbeck M, Ulmer H, Beinder E, et al: Prenatal findings in patients with prolonged QT interval in the neonatal period. *Heart* 77:198, 1997.
173. Schmidt KG, Ulmer HE, Silverman NH, et al: Perinatal outcome of fetal complete atrioventricular block: a multicenter experience. *J Am Coll Cardiol* 17:1360, 1991.
174. Gladman G, Silverman ED, Yuk-Law, et al: Fetal echocardiographic screening of pregnancies of mothers with anti-Ro and/or anti-La antibodies. *Am J Perinatol* 19:73, 2002.
175. Buyon JP, Hiebert R, Copel J, et al: Autoimmune-associated congenital heart block: Demographics, mortality, morbidity and recurrence rates obtained from the national lupus registry. *J Am Coll Cardiol* 31:1658, 1998.
176. Moak JP, Barron KS, Hougen TJ, et al: Congenital heart block: development of late-onset cardiomyopathy, a previously underappreciated sequela. *J Am Coll Cardiol* 37:238, 2001.
177. Jaeggi ET, Hamilton RM, Silverman ED, et al: Outcome of children with fetal, neonatal or childhood diagnosis of isolated complete heart block: A single institution's experience of 30 years. *J Am Coll Cardiol* 39:130, 2002.



178. Brucato A, Frassi M, Franceschini F, et al: Risk of congenital complete heart block in newborns of mothers with anti-Ro/SSA antibodies detected by counterimmuno-electrophoresis: A prospective study of 100 women. *Arthritis Rheum* 44:1832, 2001.
179. Groves AMM, Allan LD, Rosenthal E: Outcome of isolated congenital complete heart block diagnosed in utero. *Heart* 75:190, 1996.
180. Kaaja R, Julkunen H, Ammala P, et al: Congenital heart block: Successful prophylactic treatment with intravenous gamma globulin and corticosteroid therapy. *Am J Obstet Gynecol* 165:1333, 1991.
181. van der Leij JN, Visser GH, Bink-Boelkens MT, et al: Successful outcome of pregnancy after treatment of maternal anti-Ro (SS-A) antibodies with immunosuppressive therapy and plasmapheresis. *Prenat Diagn* 14:1003, 1994.
182. Saleeb S, Copel J, Friedman D, et al: Comparison of treatment with fluorinated glucocorticoids to the natural history of autoantibody associated congenital heart block. *Arthritis Rheum* 42:2335, 1999.
183. Eronen M, Heikkilä P, Teramo K: Congenital complete heart block in the fetus: Hemodynamic features, antenatal treatment, and outcome in six cases. *Pediatr Cardiol* 22:385, 2001.
184. ACC/AHA guidelines for implantation of cardiac pacemakers and antiarrhythmic devices: A report of the American College of Cardiology/American Heart Association Task Force on practice guidelines (Committee on Pacemaker Implantation). *J Am Coll Cardiol* 31:1175, 1998.
185. Van Engelen AD, Weijtens O, Brenner JI, et al: Management, outcome and follow-up of fetal tachycardia. *J Am Coll Cardiol* 24:1371, 1994.
186. Simpson JM, Sharland GK: Fetal tachycardias: Management and outcome of 127 consecutive cases. *Heart* 79:576, 1998.
187. Jaeggi E, Fouron JC, Drblík S: Atrial flutter in the fetal period: Diagnosis, clinical features, treatment and outcome. A review. *J Pediatr* 132:335, 1998.
188. Lisowski LA, Verheijen PM, Benatar AA, et al: Atrial flutter in the perinatal age group: Diagnosis, management and outcome. *J Am Coll Cardiol* 35:771, 2000.
189. Hofbeck M, Ulmer H, Beinder E, et al: Prenatal findings in patients with prolonged QT interval in the neonatal period. *Heart* 77:198, 1997.
190. Fouron JC, Fournier A, Proulx F, et al: Management of fetal tachyarrhythmia based on superior vena cava/aorta Doppler flow recordings. *Heart* 89:1211, 2003.
191. Friedman JK, Walsh EP, Saul JP: Response of fetal tachycardia to transplacental procainamide. *Cardiol Young* 6:235, 1996.
192. Strasburger JF, Cuneo BF, Michon MM, et al: Amiodarone therapy for drug-refractory fetal tachycardia. *Circulation* 109:375, 2004.
193. Hansmann M, Gembruch U, Bald R, et al: Fetal tachyarrhythmias: Transplacental and direct treatment of the fetus—a report of sixty cases. *Ultrasound Obstet Gynecol* 1:162, 1991.
194. Kohl T, Tercanli S, Kececioğlu D, et al: Direct fetal administration of adenosine for the termination of incessant supraventricular tachycardia. *Obstet Gynecol* 85:873, 1995.
195. Raboisson MJ, Fouron JC, Sonesson SE, et al: Fetal Doppler echocardiographic diagnosis and successful steroid therapy of Luciani-Wenckebach phenomenon and endocardial fibroelastosis related to maternal anti-Ro and anti-La antibodies. *J Am Soc Echocardiogr* 18:375, 2005.
196. Kiserud T, Rasmussen S, Skulstad S: Blood flow and the degree of shunting through the ductus venosus in the human fetus. *Am J Obstet Gynecol* 182:147, 2000.
197. Arduini D, Rizzo G, Romanini C: Fetal cardiac output measurements in normal and pathologic states. In Copel JA, Reed KL (eds): *Doppler Ultrasound in Obstetrics and Gynecology*. New York, Raven Press, 1995, p 271.
198. Fisher DJ, Tate CA, Phillips S: The role of dicarboxylic anion transport in the slower Ca<sup>2+</sup> uptake in fetal cardiac sarcoplasmic reticulum. *Pediatr Res* 32:664, 1992.
199. Marjjanowski MMH, van der Loos CM, Mohrschladt MF, et al: The neonatal heart has a relatively high content of total collagen and type I collagen, a condition that may explain the less compliant state. *J Am Coll Cardiol* 23:1204, 1994.
200. DeVore GR, Siassi B, Platt LD: Fetal echocardiography. IV. M-mode assessment of ventricular size and contractility during the second and third trimesters of pregnancy in the normal fetus. *Am J Obstet Gynecol* 150:981, 1984.
201. Silverman NH: Fetal heart failure. In Copel JA, Reed KL (eds): *Doppler Ultrasound in Obstetrics and Gynecology*. New York, Raven Press, 1995, pp 231.
202. Jaeggi ET, Fouron JC, Hornberger LK, et al: Agenesis of the ductus venosus that is associated with extrahepatic umbilical vein drainage: Prenatal features and clinical outcome. *Am J Obstet Gynecol* 187:1031, 2002.
203. Kenny JF, Plappert T, Doubilet P, et al: Changes in intracardiac blood flow velocities and right and left ventricular stroke volumes with gestational age in the normal human fetus: A prospective Doppler echocardiographic study. *Circulation* 74:1208, 1986.
204. De Smedt MC, Visser GH, Meijboom EJ: Fetal cardiac output estimated by Doppler echocardiography during mid- and late gestation. *Am J Cardiol* 60:338, 1987.
205. Tulzer G, Khowsathit P, Gudmundsson S, et al: Diastolic function of the fetal heart during second and third trimester: A prospective longitudinal Doppler-echocardiographic study. *Eur J Pediatr* 153:151, 1994.
206. Harada K, Rice MJ, Shiota T, et al: Gestational age- and growth-related alterations in fetal right and left ventricular diastolic filling patterns. *Am J Cardiol* 79:173, 1997.
207. Rizzo G, Arduini D: Fetal cardiac function in intrauterine growth retardation. *Am J Obstet Gynecol* 165:876, 1991.
208. Friedman D, Kim M, Glickstein JS: Fetal cardiac function assessed by Doppler myocardial performance index (Tei Index). *Ultrasound Obstet Gynecol* 21:33, 2003.
209. Kanzaki T, Chiba Y: Evaluation of the preload condition of the fetus by inferior vena caval blood flow pattern. *Fetal Diagn Ther* 5:168, 1990.
210. Huisman TW, Stewart PA, Wladimiroff JW: Flow velocity waveforms in the fetal inferior vena cava during the second half of normal pregnancy. *Ultrasound Med Biol* 17:679, 1991.
211. Eidem BW, Edwards JM, Cetta F: Quantitative assessment of fetal ventricular function: Establishing normal values of the myocardial performance index in the fetus. *Echocardiography* 18:9, 2001.
212. Tsutsumi T, Ishii M, Eto G, et al: Serial evaluation for myocardial performance in fetuses and neonates using a new Doppler index. *Pediatr Int* 41:722-727, 1999.
213. Falkensammer CB, Paul J, Huhta JC: Fetal congestive heart failure: Correlation of Tei-index and Cardiovascular-score. *J Perinat Med* 29:390, 2001.
214. Tan J, Silverman NH, Hoffman JI, et al: Cardiac dimensions determined by cross-sectional echocardiography in the normal human fetus from 18 weeks to term. *Am J Cardiol* 70:1459, 1992.
215. Pedra SR, Smallhorn JF, Ryan G, et al: Fetal cardiomyopathies: pathogenic mechanisms, hemodynamic findings, and clinical outcome. *Circulation* 106:585, 2002.
216. Tyrala EE: The infant of the diabetic mother. *Obstet Gynecol Clin North Am* 23:221, 1996.
217. Macklon NS, Hop WCJ, Wladimiroff JW: Fetal cardiac function and septal thickness in diabetic pregnancy: A controlled observational and reproducibility study. *Br J Obstet Gynaecol* 105:661, 1998.
218. Jaeggi ET, Fouron JC, Proulx F: Fetal cardiac performance in uncomplicated and well-controlled maternal type 1 diabetes. *Ultrasound Obstet Gynecol* 17:311, 2001.
219. Sebire NJ, Snijders RJ, Hughes K, et al: The hidden mortality of monochorionic twin pregnancies. *Br J Obstet Gynaecol* 104:1203, 1997.
220. Loughheed J, Sinclair BG, Fung Kee Fung K, et al: Acquired right ventricular outflow tract obstruction in the recipient twin in twin-twin transfusion syndrome. *J Am Coll Cardiol* 38:1533, 2001.

# THE GASTROINTESTINAL TRACT AND ABDOMINAL WALL

Moshe Bronshtein, MD, Shrager Blazer, MD, and Etan Z. Zimmer, MD

## Embryology

### Esophagus

Esophageal Atresia

#### *Incidence*

#### *Associated Anomalies*

#### *Prenatal Diagnosis*

#### *Timing of Diagnosis*

Esophageal and Duodenal Atresia or

Pyloric Atresia

Enteric Duplication Cysts

Laryngotracheoesophageal Cleft

Split Notochord Syndrome and Neurenteric Cysts

### Stomach

Gastric Size

Gastric Emptying Cycles

Nonvisualization of the Stomach

Congenital Microgastria

Location of the Stomach

Pyloric Atresia and Epidermolysis Bullosa

Prenatal Diagnosis

Intraluminal Gastric Masses

Gastric Duplication

### Duodenum

Duodenal Obstruction

#### *Statistics*

#### *Prenatal Diagnosis*

#### *Transient Double Bubble Sign*

#### *Midabdominal Cystic*

#### *Mass—Differential Diagnosis*

### Jejunum and Ileum

Idiopathic Transient Early Intestinal Fluid Dilatation

Jejunioileal Atresia

Prenatal Diagnosis

Meconium Ileus

### Bowel Perforation

Meconium Peritonitis

Prenatal Diagnosis

Meconium Cyst/Pseudocyst

Meckel Diverticulum

Prenatal Diagnosis

Small Intestine Duplication

Congenital Intestinal Pseudo-Obstruction

Congenital Chloride Diarrhea

### Colon

#### Fetal Defecation

Hirschsprung Disease

Prenatal Diagnosis

#### Anal Atresia

Prenatal Diagnosis

#### Hyperchogenic Bowel

Sonographic Definition

Summary

Volvulus

Intrauterine Intussusception

Malrotation

Cloacal Dysgenesis Sequence

Suspected Pathology of the Gastrointestinal Tract: A Practical

Approach (The 12 Commandments)

### Liver

Hepatic Circulation

Hepatic Volume

Hepatomegaly

Simple Transient Idiopathic Cysts in Early Pregnancy

Polycystic Liver Disease

Hepatic Mesenchymal Hamartoma

#### Hepatic Masses

Hepatic Hemangioma

Hepatoblastoma

Liver Calcifications

Gallbladder

Gallbladder—Anatomic Variants

Shape

Location

#### *Persistent Right Umbilical Vein*

Nonvisualized Gallbladder

Nonvisualized Gallbladder as an Isolated Finding

Late-Onset Disappearance of Gallbladder

Fetal Gallstones (Sludge in Gallbladder)

Extrahepatic Biliary Atresia

Prenatal Diagnosis

Choledochal Cyst

Prenatal Diagnosis

### Spleen

Splenomegaly

Splenic Cyst

### Pancreas

Annular Pancreas

Pancreatic Cyst

Pancreatoblastoma

#### Idiopathic Intra-Abdominal Cysts

#### Abdominal Wall

Physiological Midgut Herniation

Omphalocele (Exomphalos)

#### *Associated Anomalies*

#### *Prognosis*

Prenatal Diagnosis

Isolated Omphalocele—The Authors' Experience

Omphalocele and Beckwith-Wiedemann Syndrome

Gastroschisis

Incidence and Etiology

Associated Anomalies

Mode of Delivery

Prognosis

Prenatal Diagnosis

#### Midline Disruption Sequence

#### Cloacal Exstrophy Sequence

Vesicoallantoic Cyst/Patent Urachus



**A**ntenatal malformations of the gastrointestinal tract are being recognized with increasing frequency. This is due in part to improved technologic advances in sonographic imaging as well as a better understanding of the sonographic manifestations of gastrointestinal disease. As is discussed later in this chapter, often the initial sonographic clue to a gastrointestinal tract malformation is an indirect sonographic sign rather than observation of the abnormality itself; that is, polyhydramnios in cases of jejunal atresia and absence of a fluid-filled stomach in cases of esophageal atresia.

## EMBRYOLOGY

The gastrointestinal tract begins its development early in the 3rd and 4th weeks. Longitudinal and lateral folding of the embryo results in incorporation of the dorsal part of the yolk sac.<sup>1</sup> Thus, the endoderm germ cell layer is incorporated into the embryo and forms the primordial (primitive) gut tube (Fig. 15-1).<sup>1</sup> This primitive gut is closed at the cranial end by the oropharyngeal membrane and at its caudal end by the cloacal membrane.<sup>2</sup> The endoderm of the primitive gut gives rise to most of the epithelium and glands of the digestive tract. The epithelium at the cranial and caudal ends of the tract are derived from the ectoderm of the stomodeum (primitive mouth) and proctodeum (anal pit), respectively. The muscular, connective tissue and other layers of the wall of the digestive tract are derived from the splanchnic mesenchyme surrounding the primitive gut.<sup>2</sup> In the anterior part of the embryo, the incorporation of the endoderm into the head fold results in the formation of the foregut, whereas in the posterior part of the embryo the hindgut forms.<sup>2</sup> The foregut is divided into a cranial and a caudal portion. The cranial portion develops in the head

and neck as the pharynx. In the middle region, the midgut forms, and initially this is in direct continuity with the yolk sac. In addition to the primitive gut tube, the endoderm layer also gives rise to the parenchyma of the two large glandular organs associated with the gastrointestinal duct, the liver and pancreas.<sup>1</sup>

## ESOPHAGUS

The esophagus runs from the pharynx to the stomach. It is usually collapsed and is visualized as two to four echogenic lines, representing the anterior and posterior esophageal walls. Occasionally, the esophagus may be filled with fluid and consequently depicted as a tiny tube.<sup>3,4</sup>

Because of its nonlinearity, the esophagus is impossible to depict in its entirety and the cervical, thoracic, and abdominal portions are usually imaged separately. If at all feasible, the cervical section of the esophagus is best imaged in a sagittal plane; the thoracic section is best visualized behind and parallel to the trachea, and the distal abdominal section deviates from the spine and becomes visible upon its entrance into the stomach (Figs. 15-2 and 15-3).

Depiction of the esophagus (using transvaginal transducers) is easier in early pregnancy (12–16 weeks) than in late pregnancy, and as a general rule is best conducted in the late pregnancy with a high-resolution linear transducer.

Malinger et al<sup>4</sup> were able to see three different patterns of esophageal motility between 19 and 25 weeks. The most frequent pattern was a simultaneous, synchronized opening of the esophageal lumen from the oropharynx to the lower esophageal sphincter, lasting 3 seconds on average, without any peristaltic waves. The second pattern consisted of a segmental opening of the esophageal lumen in conjunction

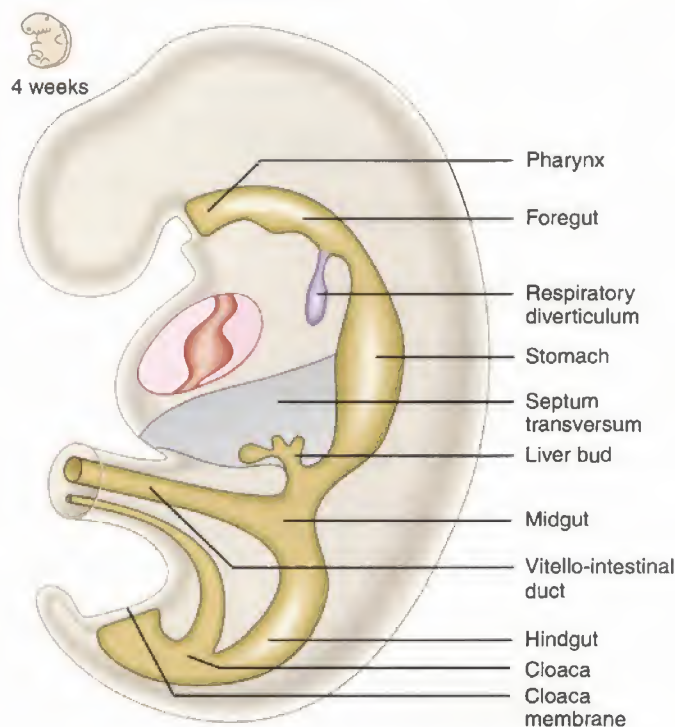


**FIGURE 15-1.** The gut tube in a 4-week embryo. (From Mitchell B, Sharma R: *Embryology: An Illustrated Colour Text*. Edinburgh, Elsevier/Churchill Livingstone, 2005, p. 39)

with peristaltic activity advancing from the pharynx through the mediastinum and into the stomach. The third pattern of motility was imaged in only one of 52 fetuses, in which the authors could see the passage of particulate contents as they moved upwards from the stomach into the pharynx.

## Esophageal Atresia

### Incidence

Esophageal atresia (EA) occurs with a prevalence between 1:5500 and 1:6000 births. More than 90% have an associated tracheoesophageal fistula (TEF).<sup>5-7</sup> The main five types of this anomaly are presented in Figure 15-4. In the most common form (type A, 82%) the upper esophagus ends in a

blind pouch and the TEF is connected to the distal esophagus.

### Associated Anomalies

Up to 64% of infants have associated anomalies,<sup>5-7</sup> most often with VATER/VACTER (vertebral, anorectal, trachea, esophagus, cardiac, renal, and limb) association. Aneuploidy is also common and ranges between 5% to 10% in different series. The risk of Down syndrome is 30 times higher than expected in the general population.<sup>5,8,9</sup>

The outcome of fetuses and infants with esophageal atresia is still unfavorable. Sparey et al<sup>6</sup> reported a perinatal mortality of 21%, primarily as a result of associated anomalies. Long-term morbidity, mainly related to dysphagia, was present in 25% of infants older than 24 months old.

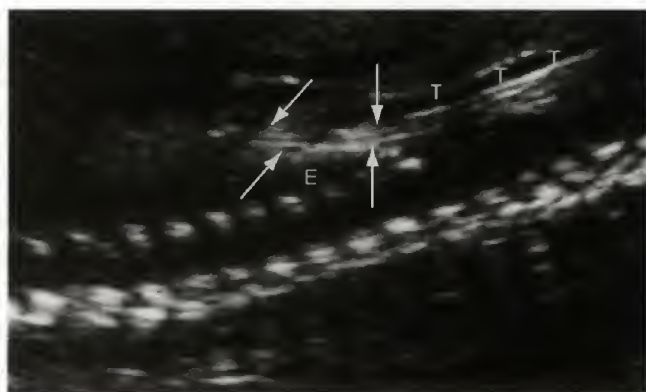


**FIGURE 15-2.** Thoracic esophagus. The esophagus (E) is marked by arrows. The lumen of the trachea is marked by the T letters.

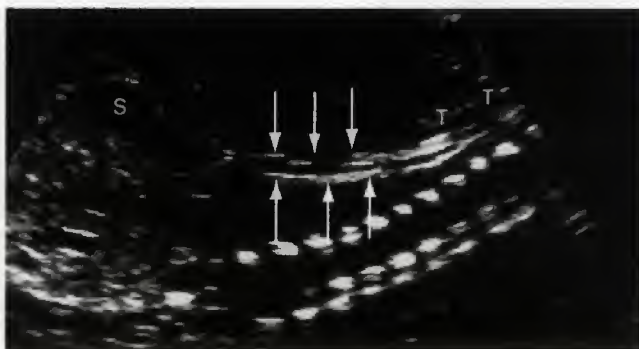


**FIGURE 15-3.** The distal esophagus (arrows) and its entrance into the stomach (S). The trachea is marked by the T letters.

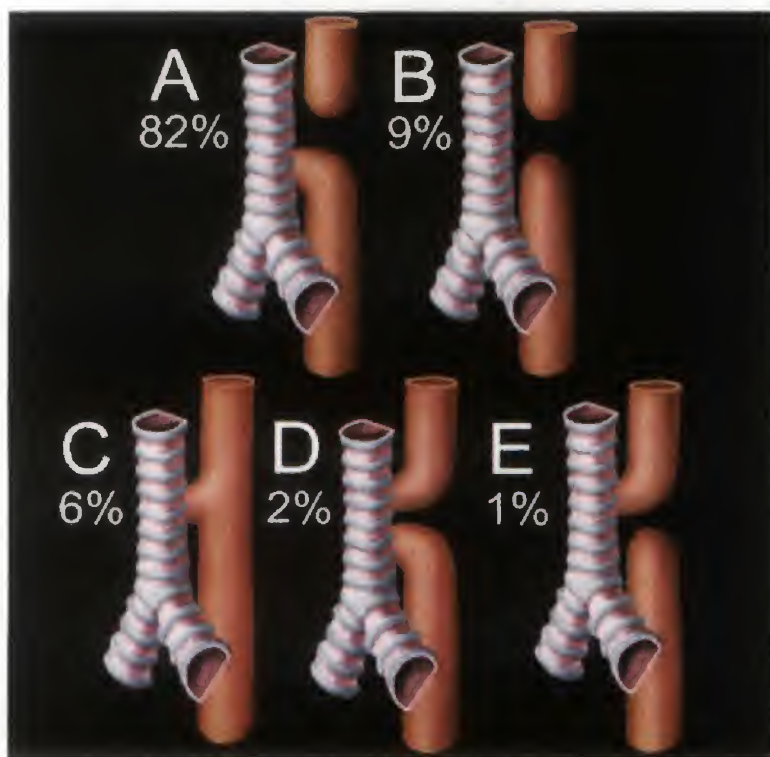


**FIGURE 15-4.** Graphic illustration of the main five types of esophageal atresia with and without tracheoesophageal fistula. (From Donnelly LF, Jones BV, O'Hara SM, et al [eds]: *Diagnostic Imaging, Pediatrics*, 1st ed. Salt Lake City, Amirsys Inc., 2005, p. 44.)





**FIGURE 15-5.** The pouch sign: *Left*, The pouch (arrow) is depicted on a sagittal section of the neck. *Right*, After a short time period, the pouch disappeared. (Courtesy of B. Vijayaraghavan: [www.thefetus.net](http://www.thefetus.net).)

### Prenatal Diagnosis

The main sonographic markers of esophageal atresia are<sup>10-15</sup>:

1. A small or absent stomach.
2. Polyhydramnios.
3. Pouch sign of the esophageal blind end.

Because of the obstructed esophagus, less fluid is swallowed by the fetus and instead of arriving in the stomach it accumulates in the amniotic cavity. However, because a small or absent stomach and/or polyhydramnios may also be present in other anomalies, these sonographic features may only be regarded as indirect, inexplicit markers of esophageal atresia.

Stringer et al<sup>11</sup> noted that the predictive value for EA varies between 39% for a small stomach with polyhydramnios to 56% whenever polyhydramnios is present in the absence of the stomach. Isolated polyhydramnios occurs in 1:50 pregnancies in the general population. Considering the known incidence of esophageal atresia, it is estimated that isolated polyhydramnios will be the only marker of esophageal atresia in about 1% of cases. It is our experience that the presence of severe polyhydramnios and a nonvisualized stomach over a prolonged time period with no upper gastrointestinal tract obstructive anomaly (for example, pressure from a goiter, et cetera) increases significantly the likelihood of EA.

In the last decade, several case reports have focused on the problematic detectability of the pouch sign, which represents the dilated blind end of the esophagus (Fig. 15-5).<sup>10,12-17</sup> Its detection is not a simple task, because it fills and empties periodically, probably in correspondence with fetal swallowing. Furthermore, depending on the nature of the anomaly, the pouch may be located in the cervical region or mediastinum. Schulman et al<sup>14</sup> noted that a detailed ultrasound examination may last up to 20 or 30 minutes because repeated scans of suspected regions are required.

They suggest the following sonographic views:

1. Coronal, through the fetal neck and chest, to visualize the upper airway; hypopharynx, larynx, and trachea.
2. Sagittal section of the fetus.
3. Two axial views: One at the level of the thyroid gland, and one at the level of the three great vessels and trachea.

The pouch sign has not been examined in large series, and, therefore, it is not yet possible to accurately define its sensitivity in detecting EA. Schulman et al<sup>14</sup> found a pouch sign in all of their nine fetuses with EA whereas Langer et al<sup>13</sup> detected the esophageal pouch in only one of six fetuses with EA. Of note, all current reports on the detection of the pouch sign are in fetuses in the second half of pregnancy.

A single umbilical artery is also a possible marker of esophageal atresia. Torfs et al<sup>5</sup> noted that all types of esophageal atresia were significantly associated with a single umbilical artery. In our series of 450 fetuses with a single umbilical artery in early pregnancy there were three cases of esophageal atresia.

Because of the insufficient predictive value of ultrasound in the detection of esophageal atresia, several investigators examined the benefit of performing a magnetic resonance imaging (MRI) examination. MRI was found to increase the accuracy of diagnosis; however, the current data provided are mainly from case reports and large series are not yet available.<sup>13,18,19</sup> Overall, the sensitivity of detecting EA/TEF is low; about 60% to 70% of cases are not detected in utero, mainly because polyhydramnios and small or nonvisualized stomachs are not apparent.

### Timing of Diagnosis

There are currently no reports on the detection of a nonvisualized stomach with polyhydramnios in fetuses with esophageal atresia before 18 weeks' gestation. The authors have seen three fetuses with esophageal atresia in which a normal-looking stomach and a normal amount of amniotic fluid were observed at 14 to 16 weeks' gestation. Polyhydramnios and nonvisualization of the stomach were noted only on a repeat scan at 20 weeks' gestation.

Therefore, it is possible that in many cases of esophageal atresia there is a tracheoesophageal fistula in early pregnancy. These fistulae probably start to narrow as pregnancy continues. If complete obliteration occurs, a small or nonvisualized stomach is expected. Occasionally the fistulous canal between the trachea and the distal portion of the esophagus is replaced by a ligamentous cord.<sup>20</sup> However, if the fistula does not obliterate completely, the stomach may be imaged.

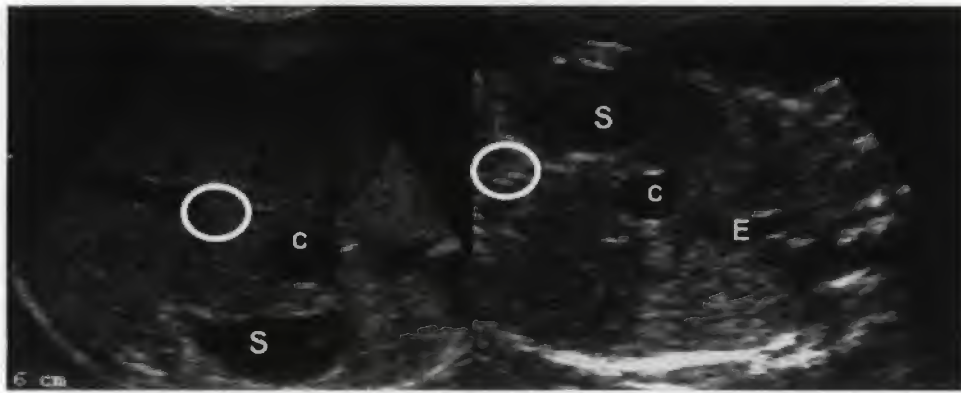


**FIGURE 15-6.** Esophageal duplication cyst. *Left*, A transverse section, the stomach (S) and a cyst (c) in the posterior mediastinum. *Right*, A parasagittal section the cyst is located superiorly to the stomach (S) and the esophagus (E) is depicted. Caution: This is not the bubble of the duodenal atresia, which is expected to be located in the midabdomen and inferior to the stomach (white circle).

### Esophageal and Duodenal Atresia or Pyloric Atresia

Esophageal atresia may occur in combination with other atresias in the gastrointestinal tract.<sup>21-23</sup>

The association of esophageal and duodenal atresia without a tracheoesophageal fistula creates a closed loop of bowel involving the distal esophagus, stomach, and duodenum. Ultrasound will reveal a huge C-shaped fluid collection in the fetal abdomen, which may extend into the chest, or a cystic mass in the chest with dilation of stomach and first portion of the duodenum. The differential diagnosis in such cases includes diaphragmatic hernia, gastrointestinal obstruction, duplication cysts of the gastrointestinal tract, or a cystic anomaly of the lung.

### Enteric Duplication Cysts

Enteric duplication cysts are rare congenital anomalies that may arise anywhere in the gastrointestinal tract. About one half of cases are in the midgut, one third in the foregut (esophagus stomach and proximal part of duodenum), and 13% occur in the colon. The duplication cysts form in parallel with the normal lumen of the gastrointestinal tract when two channels instead of one lumen develop between 6 and 8 weeks of fetal life. The walls of these cysts are composed of muscular and mucosal epithelium. Approximately one third of infants with enteric duplications have associated anomalies such as the split notochord syndrome, gastrointestinal malformations, and duplication of bladder, urethra, internal, and external genitalia. Children may suffer from various medical disorders such as peptic ulceration of the ectopic gastric tissue, hemoptysis in cases of fistula into a bronchus, infection of mediastinal cysts, and gastrointestinal obstructions. It is important to note that malignant transformations have been reported in some duplication cysts. Resection of duplication cysts is regarded as a standard of care because of the high incidence of associated disorders as well as the possibility of malignancy.<sup>24-28</sup>

Esophageal duplication cysts account for about 10% of all mediastinal masses in children, with the majority occurring in the mid- to distal esophagus (Fig. 15-6). Their incidence

is about 1:8200 births, with a 2:1 male sex predominance.<sup>26</sup> Most esophageal duplications have a cystic form, whereas a tubular form is apparent in only 5% to 10% of cases.<sup>24</sup> The cystic form is sonographically imaged as a cyst or single viscous loop. The tubular form may represent as a hyper-echogenic mass adjacent to the normal gastrointestinal lumen (Fig. 15-7).

### Laryngotracheoesophageal Cleft

A laryngotracheoesophageal cleft (LTEC) is an abnormality in the formation of the tracheoesophageal septum or a failure of the septum to reach the appropriate level. Several classifications of this anomaly have been suggested.<sup>29-32</sup>

Associated anomalies are common; mainly gastrointestinal, cardiac, pulmonary, and genitourinary. LTEC also appears in three specific syndromes: Opitz-Frias, Pallister-Hall, and VACTER. Samuel et al,<sup>29</sup> who reported seven fetuses with LTEC, noted that all of them had a lung abnormality and esophageal atresia with a tracheoesophageal fistulae. Agastria was seen in four cases and microgastria in three cases. Infants suffer from repeated episodes of aspiration, chemical pneumonia, feeding problems, and a very high mortality rate.<sup>29-32</sup>

The prenatal sonographic diagnosis should be suggested in cases of polyhydramnios, agastria or microgastria, and cystic anomalies in the lung.<sup>29,30</sup> Because of the high incidence of associated anomalies, a detailed evaluation of all fetal organs is mandatory.

### Split Notochord Syndrome and Neurenteric Cysts

Split notochord syndrome is a rare anomaly in which a cleft of the vertebral column is associated with gastrointestinal and central nervous system anomalies. Neurenteric cysts may also be present.<sup>33-35</sup> Almog et al<sup>34</sup> reported on a fetus who had a stomach abnormally located in the right posterior mediastinum, with severe scoliosis and vertebral distortion. Agangi et al<sup>35</sup> reported on a fetus in which a cystic mass involving the lower part of the sacrum and an oblongated





**FIGURE 15-7.** Gastric duplication: *Left*, An hyperechogenic mass (M), which appears solid, is seen compressing the stomach (s) posteriorly; *Right*, Magnetic resonance scan clarifies that the mass (m) is actually a viscus behind the stomach (s). (From Levine D: *State of the art: Obstetric MR imaging. Radiology* 211:609, 1999.)



**FIGURE 15-8.** Split notochord syndrome. *Left*, A cystic mass observed on a transverse section of the chest. *Right*, In a lower transverse section a split vertebra (V) is connected to the cystic mass (arrow).

perineal structure closely resembling an intestinal loop were observed. The postnatal diagnosis was a protruding colon segment, imperforate anus, and lipomyelomeningocele. Sonographers should therefore be aware that prenatal findings of vertebral anomalies associated with intra-thoracic or intra-abdominal cystic masses may be suggestive of split notochord syndrome (Fig. 15-8). In many cases it is possible to image peristaltic movements inside the cystic mass. These peristaltic movements may be of help in the differential diagnosis of other cystic anomalies in the chest (bronchogenic cyst, cystic adenomatoid malformation, pulmonary sequestration) and in the abdomen (choledochal, omental, mesenteric, and ovarian cysts).

## STOMACH

The fetal stomach first appears as a cystic structure in the upper left abdomen. It can be imaged in approximately 30% of fetuses at 8 weeks' gestation and should be observed in all fetuses at 11 weeks' gestation (Figs. 15-9 and 15-10).<sup>36</sup>

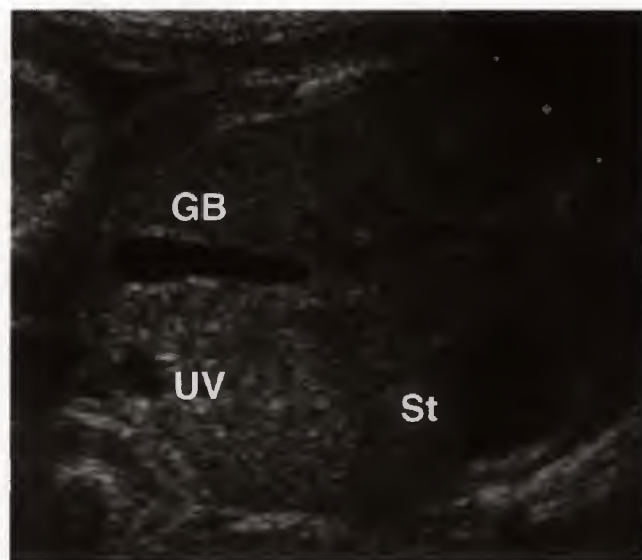


**FIGURE 15-9.** A normal transverse/diagonal section of the fetal abdomen. GB, gallbladder; St, stomach; UV, umbilical vein.

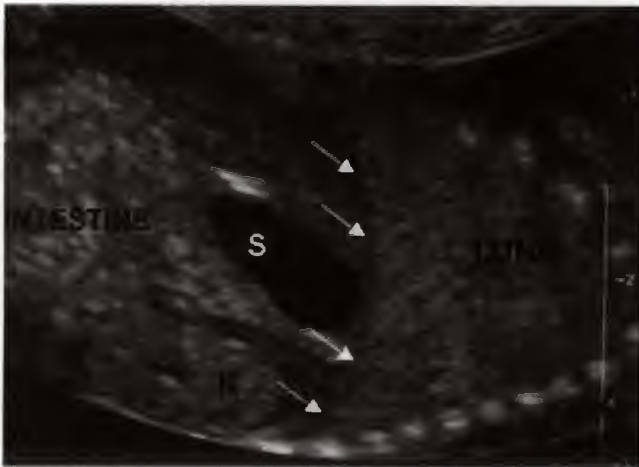


**FIGURE 15-10.** Normal parasagittal section of chest and abdomen. S, stomach; K, kidney. The demarcation line of the diaphragm is marked by arrows.

## Gastric Size

The dimensions of the stomach are defined as the largest area including the pyloric site on transverse or oblique scanning planes. The transverse section at the center of the gastric corpus is used for transverse and anteroposterior measurements. The gastric volume is calculated as a prolate ellipsoid. Several investigators have found a correlation among gastric area, gastric volume, and gestational age.<sup>37-39</sup> However, the size of the stomach is influenced by the amount of amniotic fluid swallowed by the fetus, the amount of gastric secretions, and the rate of pyloric passage of gastric content. It seems, also, that gastric compliance normally varies between fetuses. Although in some fetuses a large stomach is always apparent, in others a small stomach is always depicted. Therefore, fluctuations in gastric size are expected and should be regarded as a physiologic phenomenon. Zimmer et al<sup>40</sup> performed serial measurements of the stomach 20 minutes apart in 146 fetuses between 14 and 41 weeks' gestation. The mean percentage change between each of the paired measurements was 16.6% to 43.1% for the different stomach dimensions.

In addition to the normal physiologic changes in the gastric size, sonographers should be aware that the stomach is an asymmetric organ and standardization of landmarks for its measurements is not always simple. Pathology in gastric size including nonvisualization should therefore be suggested only after several repeated scans. It should be remembered that a small amount of fluid in the stomach does not exclude the diagnosis of esophageal atresia. Either normal gastric secretions or aspiration and flow through a patent tracheoesophageal fistula may result in a small amount of gastric fluid.

## Gastric Emptying Cycles

Cyclic changes in gastric size have been noted starting at 12 weeks' gestation. Sase et al<sup>41,42</sup> performed continuous recordings of the stomach for 1 to 2 hours and sampled the gastric area ratio (gastric area divided by the area of the fetal abdominal transverse section) every minute. They found

that the gastric emptying cycles last 30 to 100 minutes before 24 weeks' gestation, about 40 minutes at 32 to 35 weeks' gestation and more than 80 minutes at term. The gastric volume near term is approximately 10 mL and the volume decrease with gastric emptying is about 60%. It was therefore estimated that gastric emptying accounts for a daily absorption of about 250 mL of swallowed amniotic fluid. Because the fetus swallows nearly 500 mL of amniotic fluid, it is suggested that the extra amount of fluid passes passively through the pylorus independent of the gastric emptying cycles.

## Nonvisualization of the Stomach

Nonvisualization of the fetal stomach has been reported in 0.07% to 0.4% of pregnancies. The fetal outcome was abnormal in 48% to 100% of these cases.<sup>43,44</sup>

Many of the fetuses had associated anomalies. The main disorders that should be suggested are

1. Mechanical obstruction of the esophagus.
  - a. Esophageal atresia.
  - b. Tumors of the pharynx, esophagus, or mediastinum.
  - c. Goiter.
  - d. Diaphragmatic hernia.
  - e. Intrathoracic masses such as large cystic adenomatoid malformations and tracheal atresia.
2. Anatomic disorders of the swallowing system, such as severe cleft palate.
3. Neurogenic disorders of the swallowing system.

The amount of amniotic fluid may be increased, decreased, or normal in cases of a nonvisualized stomach. Polyhydramnios is attributed to a decrease in the amount of amniotic fluid swallowed by the fetus. Oligohydramnios probably occurs in cases of a sick fetus with decreased production of amniotic fluid. In the authors' experience, *transient* nonvisualization of the stomach is not associated with an adverse outcome.

## Congenital Microgastria

Congenital microgastria is an extremely rare anomaly that is believed to be a result of impairment of normal foregut development. Associated anomalies have been reported in many of these children, asplenia, Opitz syndrome, and laryngotracheoesophageal cleft being the most common anomalies.<sup>45-47</sup>

The sonographic diagnosis relies on the depiction of a very small stomach on repeated scans. The main differential diagnosis is a small stomach secondary to esophageal atresia. Of note, in congenital microgastria the amniotic fluid volume may be normal,<sup>45</sup> whereas in esophageal atresia, polyhydramnios is a common finding. Postnatal surgical interventions such as gastric augmentation may be necessary in some cases because these children may be reluctant to feed normally and may suffer from malnutrition, growth restriction, and respiratory tract infections.<sup>46,47</sup> However, in some cases, increased spitting up for several months is the only finding in infants who are otherwise healthy. The authors have seen two such cases; in one of the cases the mother reported that she also had increased spitting up during infancy. Therefore, it is important to tell parents that fetal microgastria may in some cases have a favorable outcome.





**FIGURE 15-11.** A markedly dilated stomach at week 15.

**Enlarged Stomach With Normal Amount of Amniotic Fluid.** This is usually a normal anatomic variant with no adverse clinical outcome (Fig. 15-11).

**Enlarged Stomach With Polyhydramnios.** This anomaly is usually a result of a gastric outlet obstruction, that is, atresia of the pylorus, duodenum, or ileum and jejunum. Rarely, a very dilated C-shaped stomach may be observed in cases of both outlet (pylorus or duodenum) obstruction and inlet obstruction (esophageal atresia). In such cases reflux of fluid from the stomach into the esophagus is not possible.

### Location of the Stomach

An abnormal location of the stomach is an important marker of other possible anomalies (Fig. 15-12):

1. Displacement in various directions
  - a. Diaphragmatic hernia
  - b. Subdiaphragmatic pulmonary sequestration
  - c. Adrenal masses
2. Complete situs inversus. Subjects with this anomaly may also suffer from the Kartagener syndrome.
3. Dextrogastrica or left-sided stomach with dextrocardia. These findings are common in the heterotaxy syndrome or polysplenia/asplenia syndrome.
4. Hypoplastic lung

### Pyloric Atresia and Epidermolysis Bullosa

The incidence of pyloric atresia is approximately 1:100,000 live births. A familial occurrence has been reported and an autosomal, recessive transmission has been suggested. Associated anomalies have been reported in 30% to 44% of these fetuses.<sup>48-51</sup> The association with epidermolysis bullosa



**FIGURE 15-12.** Abnormal location of the stomach. Fetus with a left diaphragmatic hernia. The fluid-filled stomach is not seen in its normal location within the fetal abdomen. The stomach (St) is located within the thorax adjacent to the fetal heart (H). Lu, lung.

requires special attention. Epidermolysis bullosa is an inherited autosomal-recessive disease characterized by increased skin fragility, resulting in blisters and erosions after minor trauma. Mutations in 10 structural genes expressed in the cutaneous basement membrane zone have been reported. The association of epidermolysis bullosa and pyloric stenosis is highly lethal.

### Prenatal Diagnosis

1. Dilated stomach and polyhydramnios.
2. Esophageal dilatation due to gastroesophageal reflux (Fig. 15-13).<sup>52</sup>
3. Markers of skin denudation or blistering in Epidermolysis Bullosa.
  - a. Snowflake appearance of amniotic fluid.<sup>53</sup>
  - b. External deformities and skin strikingly adhered to various organs.<sup>48</sup>
4. High levels of maternal serum alphafetoprotein and acetylcholinesterase in epidermolysis bullosa.
5. DNA analysis and skin biopsy in epidermolysis bullosa.<sup>48,54</sup>

### Intraluminal Gastric Masses

Echogenic masses or debris are sometimes depicted within the fetal stomach (Fig. 15-14). Previously, this finding was mainly reported in fetuses after amniocentesis. It was suggested that these masses are the result of blood and cytogenetic material swallowed by the fetus.<sup>55,56</sup> Improvement of ultrasound resolution has made it possible to see such masses in many cases in which no amniocentesis was performed. Therefore, it seems that this is a normal finding and any

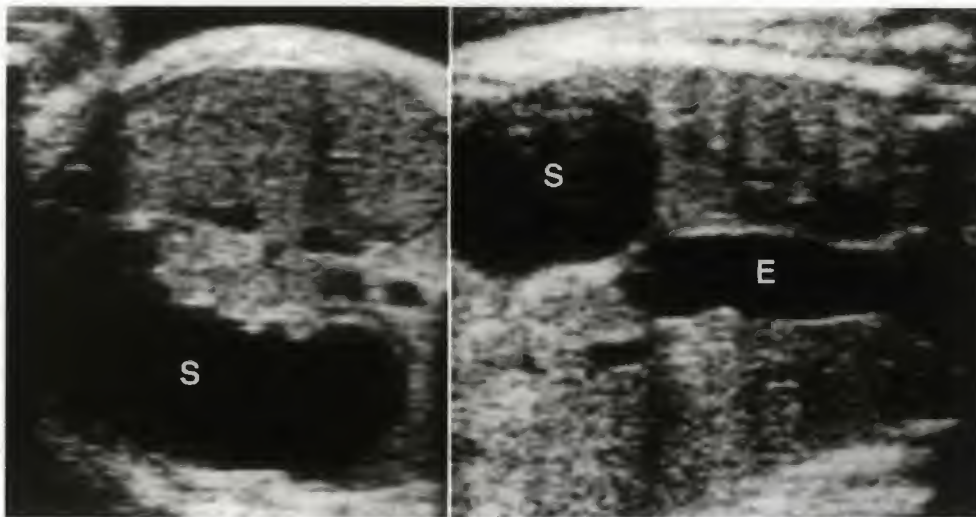


**FIGURE 15-13.** Pyloric atresia. *Left*, A large stomach (S) on a transverse section. *Right*, In a sagittal section the severely dilated esophagus (E) is observed. (Courtesy of V. Suma: [www.thefetus.net](http://www.thefetus.net).)

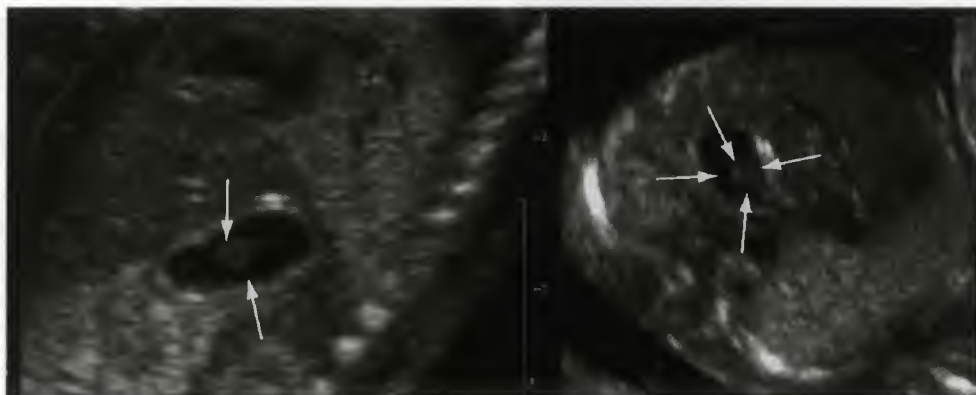


**FIGURE 15-14.** Intragastric echoes (arrows). *Left*, sagittal section; *Right*, transverse section.

debris or sludge (skin cells, or defecated meconium, for instance) swallowed by the fetus may produce such an ultrasound image.

### Gastric Duplication

Gastric duplication accounts for 8% of alimentary tract duplications. They may be either cystic or tubular, and usually appear along the greater curvature of the stomach. The female-to-male ratio is 2:1. In about one half of cases there are associated anomalies. Most common are duplications in other parts of the alimentary tract as well as vertebral anomalies.<sup>57-59</sup>

## DUODENUM

The duodenum can be imaged on a transverse view of the fetal abdomen slightly caudal to the region of the pylorus. It is divided into four parts, with the head of the pancreas located inside the loop (Fig. 15-15). Usually two close echogenic lines are depicted representing the collapsed

duodenum. Levine et al<sup>60</sup> studied 123 low-risk pregnancies at 16 to 39 weeks' gestation and found a collapsed duodenum in all these cases. They therefore concluded that any distention of the duodenum raises the possibility of a pathologic disorder.

Using transvaginal scanning in early pregnancy, it is our experience that a short transient fluid-filled, almost cystic, dilatation of a part or the whole duodenum may be observed in normal fetuses likely representing a peristaltic wave (Fig. 15-16).

### Duodenal Obstruction

Congenital duodenal obstruction has a reported incidence of 1:5000 to 10,000 live births and is the most common cause of fetal small bowel obstruction. The cause of duodenal atresia and stenosis is unknown. Failure of recanalization of the duodenal lumen, or intrauterine vascular ischemia during embryonic life are the most favored theories. The incidence of the anomaly is approximately equal in male and female fetuses and there is no racial predilection.<sup>61,62</sup>



There are several mechanical factors that may also cause an obstruction of the duodenum.

1. Annular pancreas
2. Intestinal malrotation or volvulus
3. Superior mesenteric artery syndrome<sup>63</sup>

### Statistics

Nearly 70% of fetuses with duodenal obstruction have other structural anomalies, mainly anomalies of the gastrointestinal system and heart. Duodenal obstruction is also part of 23

different syndromes (OMIM, Online Mendelian Inheritance in Man).<sup>64</sup> One half of the children are born prematurely, and in 75% of cases, polyhydramnios is apparent.

Duodenal atresia is a classic marker of Down syndrome. The reported incidence of Down syndrome in these fetuses is 24% to 35%, with an overall risk ratio of 300.<sup>65-69</sup> It is the authors' experience that in early pregnancy, most fetuses with Down syndrome have other associated anomalies, mainly increased nuchal edema. Therefore, in cases of normal biochemical markers and absence of nuchal edema, the risk of Down syndrome in fetuses with isolated duodenal atresia is significantly decreased to a risk ratio of nearly 30.

The outcome of patients with duodenal obstruction relies on the success rate of surgical procedures and severity of associated anomalies. A long-term follow-up over 30 years revealed a mortality rate of 9% and 12% of patients suffering from late complications.<sup>70</sup>

### Prenatal Diagnosis

The prenatal sonographic diagnosis of duodenal obstruction has been reported in 87% of cases.<sup>71</sup> It mainly relies on the depiction of the double bubble sign.<sup>22,23,71-74</sup> Polyhydramnios may also be observed in about 40% of cases mainly in the second half of pregnancy. In the double bubble sign, the dilated stomach and the first portion of the duodenum appear side by side across the midline of the upper fetal abdomen (Fig. 15-17). The double bubble sign has been observed as early as 12 weeks' gestation,<sup>22,72</sup> however, in many cases, this sonographic sign has been observed only in the second half of pregnancy. The main reason for the late appearance of the double bubble sign is probably related to the hydrostatic pressure needed to dilate the duodenum and the degree of obstruction. In most cases, duodenal atresia occurs below the ampulla of Vater. In order to dilate the first portion of the duodenum above the ampulla of Vater, a large amount of swallowed amniotic fluid is needed in addition to a forward and backward obstruction which prevents the outflow into the intestine and backflow from the stomach to the esophagus. Another possible reason is that earlier in pregnancy, mild dilation of the duodenum is less than the resolution of the transabdominal scanning approach.

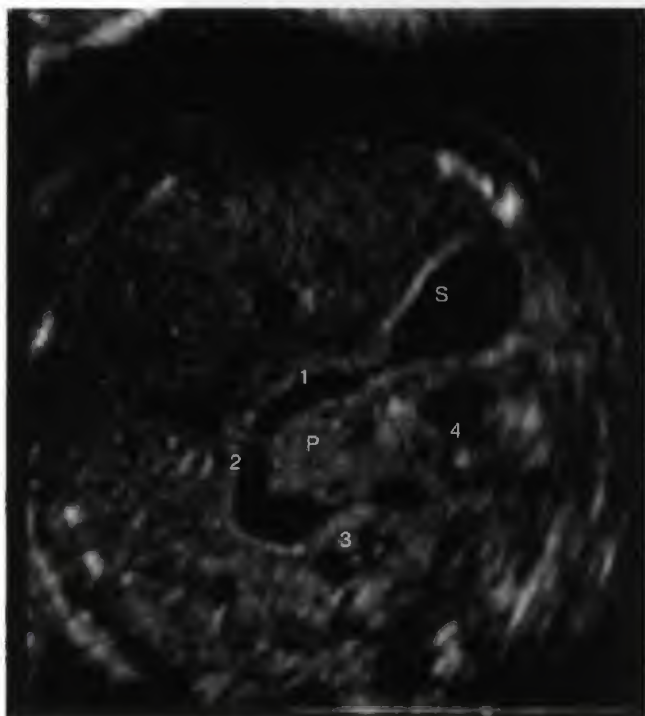


**FIGURE 15-15.** Duodenal distention in a case of jejunal atresia. All parts of the duodenum (1, 2, 3, 4) are distended and encircle the pancreas (P). S, stomach.

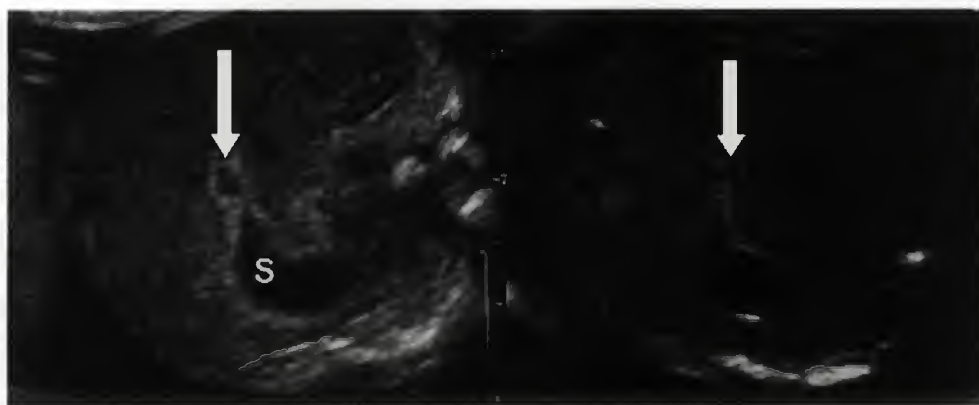


**FIGURE 15-16.** Duodenal peristalsis in early pregnancy. *Left*, A dilated segment of the duodenum (arrow) in continuity with the stomach (S). *Right*, After a few seconds the peristaltic wave disappeared.

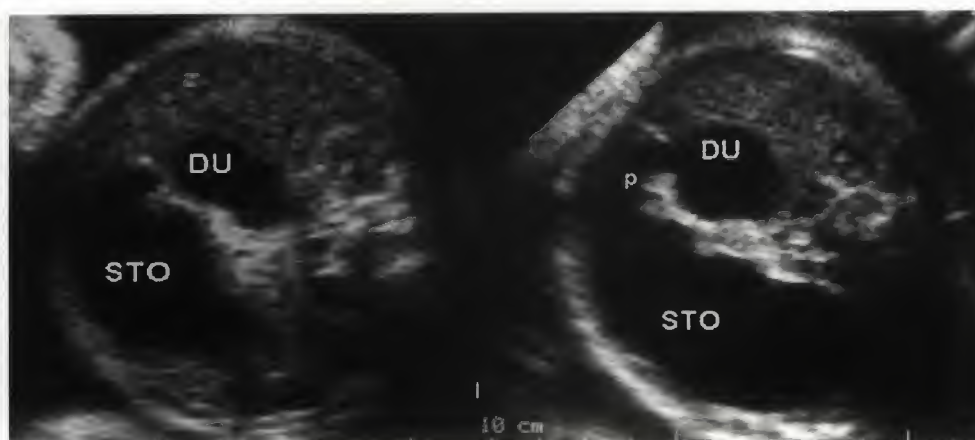


**FIGURE 15-17.** The double bubble sign in duodenal atresia. *Left*, The dilated stomach (STO) and duodenum (DU). *Right*, During a peristaltic wave, the communication through the pylorus (p) is observed.

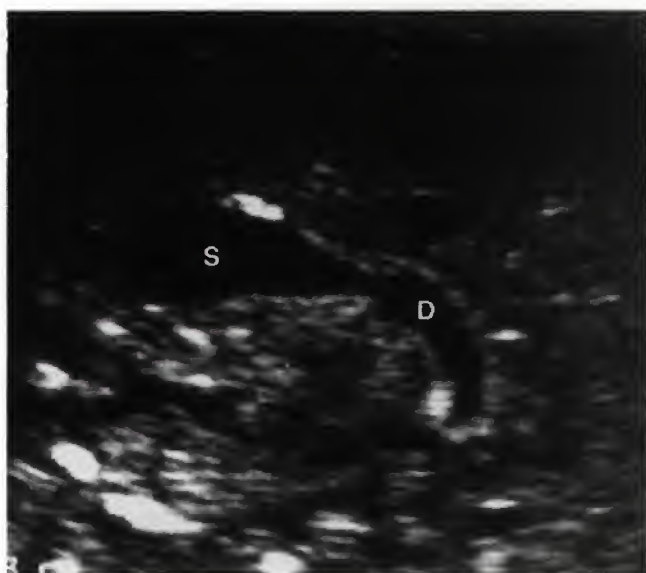


**FIGURE 15-18.** Transient dilation of the first part of the duodenum (D). S, stomach.

### **Transient Double Bubble Sign**

Sonographic pitfalls in the diagnosis of duodenal obstruction are possible. Zimmer and Bronstein<sup>73</sup> reported on three fetuses at 15 weeks' gestation in which a double bubble sign was observed but disappeared on repeated scans after 10 to 15 minutes. All of these fetuses had a normal karyotype and were healthy at delivery. Since this publication, the authors have seen seven more cases of a transient double bubble sign in early pregnancy (Fig. 15-18). In one of these cases, trisomy 21 was detected and in another case the double bubble sign appeared again at 23 weeks' gestation and the fetus was found to have duodenal obstruction. In another case, the dilation of the duodenum remained until week 19 and then disappeared. The newborn was found to be healthy. Therefore, it seems that a transient double bubble sign in early pregnancy is not always an innocent finding and follow-up of these fetuses is mandatory.

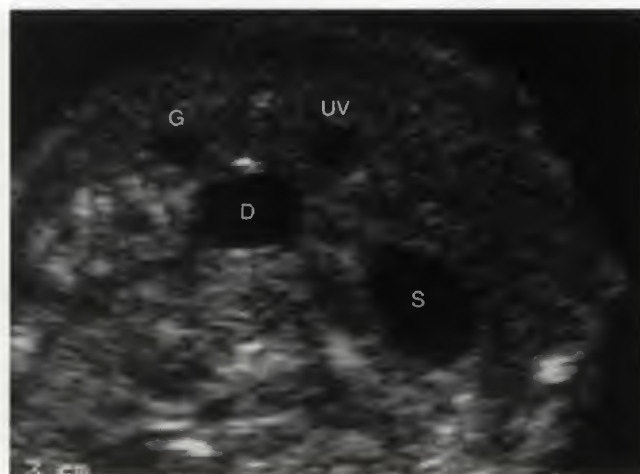


**FIGURE 15-19.** Duodenal duplication cyst. The cystic structure (D) near the stomach (S) was believed to be a dilated duodenum. The correct diagnosis was found in the newborn. G, gallbladder, UV, umbilical vein.

A double bubble sign may also appear in other anomalies of the duodenum and stomach. Malon et al<sup>75</sup> noted a double bubble sign in a case of duodenal duplication. We also had a fetus with this finding (Fig. 15-19). Yoshizato et al<sup>76</sup> found a double bubble sign in a case of pyloric stenosis and a dilated gastric antrum (Box 15-1).

### **Midabdominal Cystic Mass—Differential Diagnosis**

The most common disorders to be suggested in cases of an ultrasonic finding of a cystic mass at the midabdominal level are listed in Box 15-2.

In order to facilitate a proper diagnosis the following examinations are suggested:

1. Location of the cystic mass. A cystic finding above the level of the pylorus and posterior to it excludes the possibility of a duodenal anomaly.



**BOX 15-1 Duodenal Dilatation: Etiology**

1. Duodenal atresia or stenosis
2. Annular pancreas
3. Transient idiopathic dilation<sup>73</sup>
4. Superior mesenteric artery syndrome<sup>63</sup>
5. Segmental dilatation of duodenum<sup>77</sup>

**BOX 15-2 Midabdominal Cystic Mass: Differential Diagnosis**

1. Choledochal cyst
2. Extrahepatic biliary atresia
3. Hepatic cyst
4. Peritoneal/omental cyst
5. Bronchogenic cyst
6. Neurenteric cyst
7. Cystic hygroma
8. Pyloric atresia
9. Pancreatic cyst
10. Intestinal duplication cyst especially those of the duodenum<sup>78,79</sup>

2. Amniotic fluid level of digestive enzymes. A normal level of digestive enzymes excludes the possibility of extrahepatic biliary atresia. It usually also excludes a duodenal obstruction. A very low level or absence of enzymes is a marker of extrahepatic biliary atresia, whereas an increase in the level of digestive enzymes is expected in obstructions below the ampulla of Vater.
3. Search for associated structural anomalies. An anomaly of the vertebrae may be suggestive of a neurenteric cyst, whereas an anomaly of the diaphragm may serve as a clue to a bronchogenic cyst.
4. Amniotic fluid volume. An increase in amniotic fluid volume is common in obstruction of the gastrointestinal tract, whereas a normal amount of amniotic fluid decreases the probability of such an anomaly.

**JEJUNUM AND ILEUM**

The jejunum is located in the upper left side of the abdomen, and the ileum is located in the lower right side (Fig. 15-20). In early pregnancy, high-resolution ultrasonography portrays the small intestine as a sac of transparent “worms inside which small pieces of cotton wool move about.” The latter’s density/crowdedness and size differ between fetuses, and quite often within the fetus itself as well.

Up to 17 weeks’ gestation, peristalsis is obvious and full intestinal contents are seen (Fig. 15-21). After 18 weeks, peristaltic movements slow down and a gradual decrease in the intestinal content takes place, which makes the content appear as fluid or mucous. The intestine then remains nearly empty until close to term (Fig. 15-22). Of note, the sonographic features of the intestine rely highly on the resolution of the ultrasound machine used, transducer frequency, and the woman’s body habitus. The intestinal loops of a fetus in an obese woman, for instance, will be hardly depicted in a basic ultrasound scanner, presenting



**FIGURE 15-20.** The anatomic intra-abdominal location of jejunum and ileum.



**FIGURE 15-21.** Normal image of small intestine until week 17. It looks like transparent worms inside which small pieces of cotton wool move about.

only an image of “nonhomogenous clouds,” whereas a high-resolution scanner will increase the loops’ echogenicity.

**Idiopathic Transient Early Intestinal Fluid Dilatation**

Transient slight to moderate intestinal dilatation without intra-abdominal meconium or ascites is not rare in early pregnancy.<sup>80</sup> It occurs in about 1:400 fetuses at 14 to 17 weeks’ gestation and usually disappears at 18 to 22 weeks’ gestation. Maternal elevated temperature has been reported within 3 weeks of fetal findings in many of these cases. The authors

had more than 80 fetuses with this sonographic finding who had a favorable outcome (Fig. 15-23). Despite this reassuring data, it is suggested to search for possible cystic fibrosis, TORCH infection, and chromosomal anomalies. In addition, a sonographic follow-up until complete disappearance of intestinal dilatation is indicated.

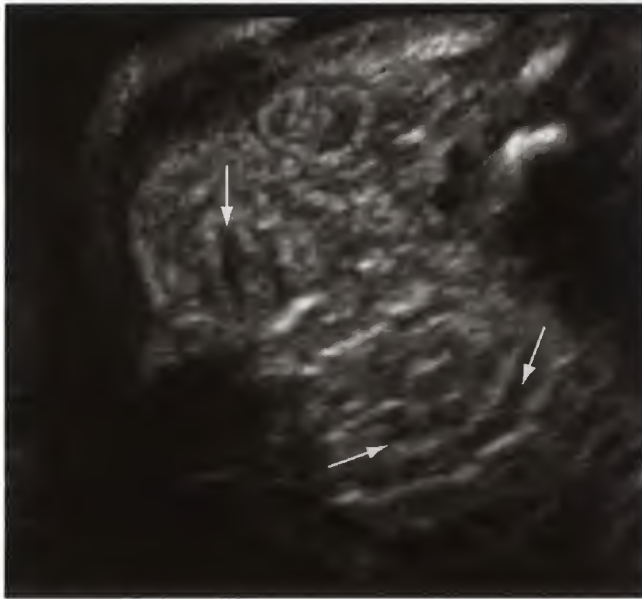


**FIGURE 15-22.** Normal image of small intestine between weeks 20 and 22. The lumen of the intestine contains a small amount of mucous (arrows).

## Jejunioileal Atresia

The jejunioileal atresia rate is 1.3 to 2.9 per 10,000 live births. An association with multiple pregnancies, the black race, vaginal bleeding during pregnancy and low birth weight has been noted.<sup>83,64,83-85</sup> A hereditary form of intestinal atresia has also been observed.<sup>86,87</sup> Chromosomal anomalies occur in less than 1% of cases. This is in contrast with duodenal atresia, in which chromosomal anomalies are very common.

An ischemic insult to the developing midgut during fetal development has been widely accepted as the underlying cause of jejunioileal atresia.<sup>86</sup> The presence of volvulus or intussusception has also been noted in many of these fetuses.<sup>87</sup> It is still unclear, however, whether these anomalies are the result or the cause of the intestinal atresia.

Jejunioileal atresias are classified as follows (Fig. 15-24):

**Type I.** This is a mucosal defect resulting in obstruction. The muscular wall is normal with an intact mesentery.

**Type II.** A fibrous cord connects two atretic bowel ends. The mesentery is intact.

**Type IIIa.** The two blind ends of the bowel are separated by a V-shaped defect in the mesentery.

**Type IIIb.** This type is also called "apple peel" or "Christmas tree" atresia. Two blind, completely separated ends of the bowel coiled around a mesenteric vessel.

**Type IV.** Multiple obstruction of any combination of types I to III.

Traditionally, jejunal and ileal atresia have been grouped together as intestinal atresia. However, there are data indicating that jejunal and ileal atresias may be considered as separate diseases. First, jejunal atresia is twice as common

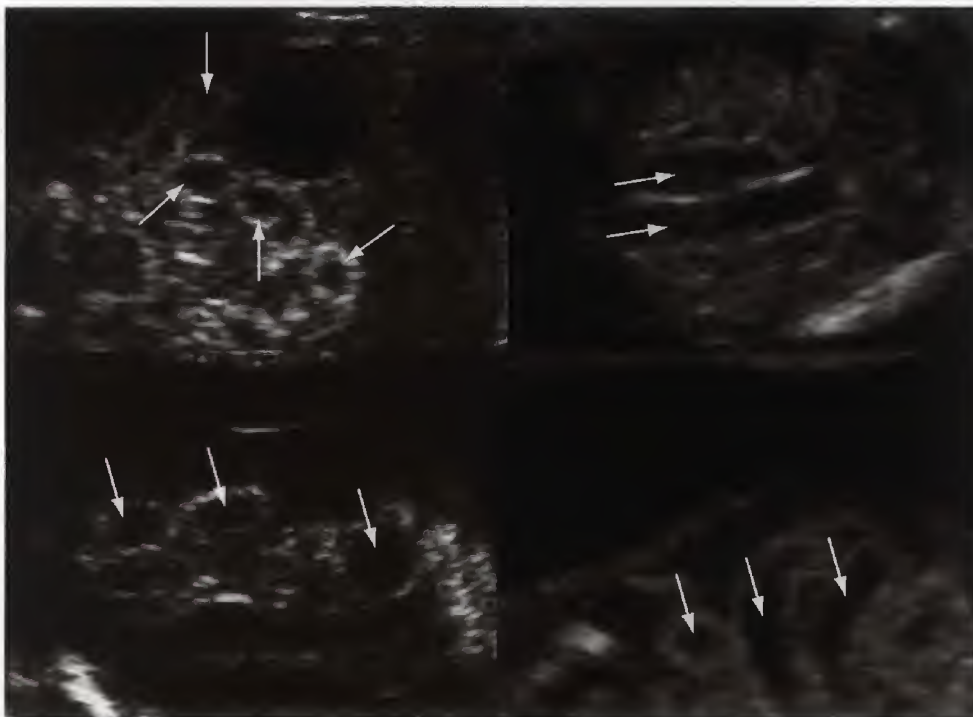


**FIGURE 15-23.** Idiopathic transient dilatation of small bowel (arrows) in four different fetuses between weeks 14 and 16.



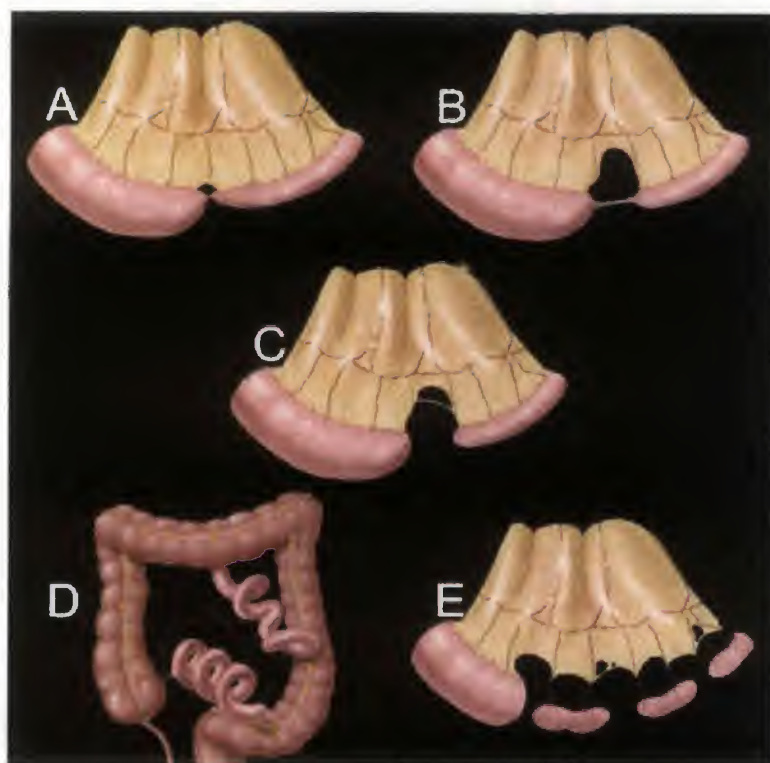


**FIGURE 15-24.** Graphic presentation of jejunoileal atresia: type 1 (A); type 2 (B); type 3a (C); type 3b (D); and type 4 (E). (From Donnelly LF, Jones BV, O'Hare SM, et al [eds]: *Diagnostic Imaging, Pediatrics*. 1st ed. Salt Lake City, Amirsys Inc., 2005, p. 18.)



**FIGURE 15-25.** Jejunol atresia. *Left*, Fetal stomach. *Middle*, Perigastric, very dilated bowel loops. *Right*, Autopsy demonstrating the abnormal loops. (Courtesy of F. Cuillier; [www.thefetus.net](http://www.thefetus.net).)

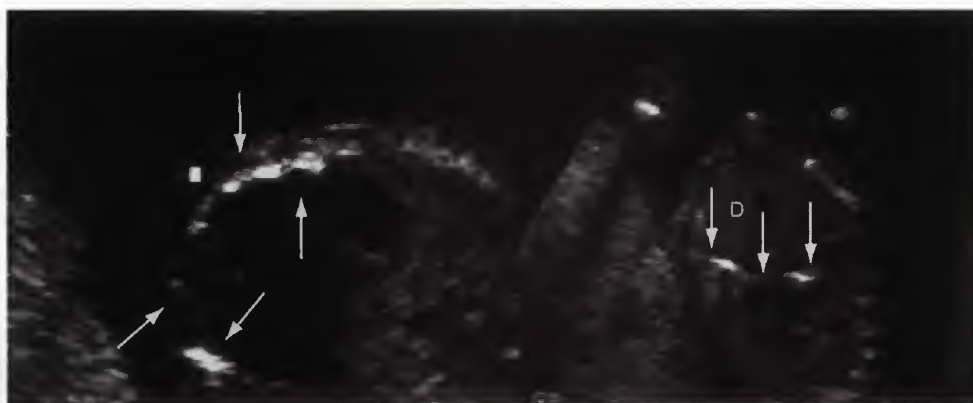
as ileal atresia. Second, Heij et al<sup>88</sup> and Sweeney et al<sup>89</sup> found that many cases of jejunal atresia were multiple atresias as opposed to an ileal atresia that had a single atresia in the vast majority of cases. Sweeney et al<sup>89</sup> noted an associated anomaly in only 1 of 45 patients with ileal atresia as opposed to 16 of 38 patients with jejunal atresia who had associated anomalies (cystic fibrosis, malrotation, congenital heart disease, Down syndrome, anorectal and vertebral anomalies, neural tube defect, and microcephaly). Third, antenatal perforation occurred rather frequently in ileal atresia but was significantly less common in jejunal atresia.<sup>88</sup>

### Prenatal Diagnosis

Sonographic features of intestinal atresia have been observed in 51% to 86% of fetuses in different series. The most common sonographic markers are hyperechogenic bowel, enlarged stomach, dilated bowel, intraperitoneal echogenic material, and polyhydramnios.<sup>90-93</sup> However, it is of importance to note that there are differences between jejunal and ileal atresia. The jejunum has a higher compliance and therefore marked dilatation of the intestinal loops, enlarged stomach, and polyhydramnios are common (Fig. 15-25). In contrast, the compliance of the ileum is much lower and

**Table 15-1** Sonographic Comparison Between Jejunal and Ileal Atresia in the Second Half of Pregnancy

	Intestinal Loops	Stomach	Peritoneal Calcification	Ascites	Associated Anomalies	Polyhydramnios
Jejunum	Marked dilation of loops, most of them on the left abdominal side. Enlargement of duodenum is common.	Large	Frequent	Very rare	Frequent	Frequent
Ileum	Usually only minor dilation of a few loops.	Normal	Frequent	Frequent	Rare	Rare

**FIGURE 15-26.** First clue of jejunal obstruction at week 15. An hyperechogenic rim is observed (arrows). Left, Transverse section. Right, Sagittal section. D, diaphragm.

most of the fluid passing in the intestine has already been absorbed. Therefore, perforation is more common, but dilation of the loops, changes in configuration of stomach and polyhydramnios are less common or even not observed.

Sonographers should be aware that in many cases of jejunoileal atresia the sonographic findings are noted only in the third trimester of pregnancy. In contrast, normal dilatation of intestinal loops in early pregnancy may actually occur during peristaltic movements. Repeated scans for several minutes are advocated in such cases to exclude the possibility of a false-positive diagnosis of intestinal obstruction (Table 15-1).

The following case presents the development of jejunal obstruction in early pregnancy; at 15 weeks' gestation, peritoneal calcifications were observed (Fig. 15-26). Amniocentesis for digestive enzymes revealed very high levels of liver enzymes suggesting an obstruction in the upper gastrointestinal tract. At 19 weeks' gestation ultrasound depicted marked dilation of the whole duodenum (but not of the jejunum) with a normal stomach and amniotic fluid volume (Fig. 15-27). The pregnancy was terminated and the post mortem examination revealed an apple peel atresia (Fig. 15-28). It seems therefore that in early pregnancy, dilation of the duodenum may precede the dilatation of the obstructed jejunum.

## Meconium Ileus

Meconium ileus describes a condition in which a meconium plug obstructs the small intestine. Cystic fibrosis is the leading cause of meconium ileus. Although virtually all

**FIGURE 15-27.** Jejunal obstruction at week 19. The four dilated parts of the duodenum (1, 2, 3, and 4). The echogenic deposits are marked by arrows. S, stomach.

patients with meconium ileus will be shown to have cystic fibrosis, only approximately 15% to 20% of infants with cystic fibrosis present with intestinal obstruction related to meconium ileus.<sup>94,95</sup> Other possible but less frequent reasons for meconium ileus are cytomegalovirus and syphilis.<sup>96,97</sup>



Occasionally, no cause is determined and the disorder is regarded as idiopathic.

The main prenatal sonographic marker is hyperechogenic bowel with dilated loops containing meconium. Less specific markers are intraperitoneal echogenic material, ascites, dilated bowel loops, and meconium pseudocysts.<sup>94,95,98</sup> In cases of cystic fibrosis, nonvisualization of the gallbladder may also be noted.<sup>95</sup> These sonographic findings may also present in cases of bowel perforation and an accurate differential diagnosis is therefore not always possible. A search for cystic fibrosis, TORCH, digestive enzymes, and fetal karyotype is therefore indicated.

## BOWEL PERFORATION

### Meconium Peritonitis

The incidence of intrauterine bowel perforation is 3.3 in 100,000 births.<sup>95,98</sup> The underlying cause of perforation is unknown in the vast majority of cases. Possible causes are stenosis, atresia, volvulus, intussusception, cystic fibrosis,<sup>95</sup>

and infections such as parvovirus B19, cytomegalovirus and hepatitis.<sup>99-101</sup>

Traditionally, the term meconium peritonitis is used because it is believed that the leakage of meconium into the fetal abdomen leads to an aseptic chemical inflammation. In our experience in early pregnancy (52,000 examinations between weeks 14–16), the incidence of meconium spillage into the peritoneal cavity is 1:1000, and 20% of these occurrences are associated with gross structural anomalies.

### Prenatal Diagnosis

The main sonographic markers reported in the literature are intraperitoneal calcifications, hyperechogenic dilated bowel loops, ascites, and polyhydramnios.<sup>98,102-105</sup> It is our experience that the calcified meconium may present in several forms: as a continuous curvilinear form on the entire border of the peritoneum (“Sock-like” appearance) (Figs. 15–29 and 15–30); in a scattered form (Fig. 15–31); and as an isolated focus. The most frequent location of the focus is in the left upper abdominal quadrant behind the stomach (Fig. 15–32).

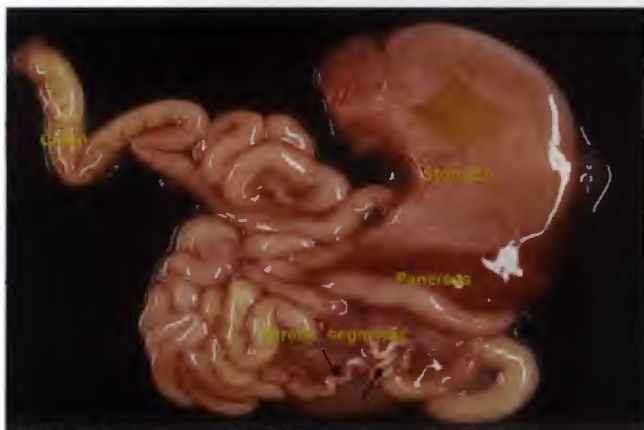


**FIGURE 15-28.** Autopsy week 19. The atretic segments of the jejunum are marked by arrows. (Courtesy of Dr. Dvora Kidron.)



**FIGURE 15-30.** Subdiaphragmatic calcifications (arrows) at week 15. The newborn had a normal outcome.

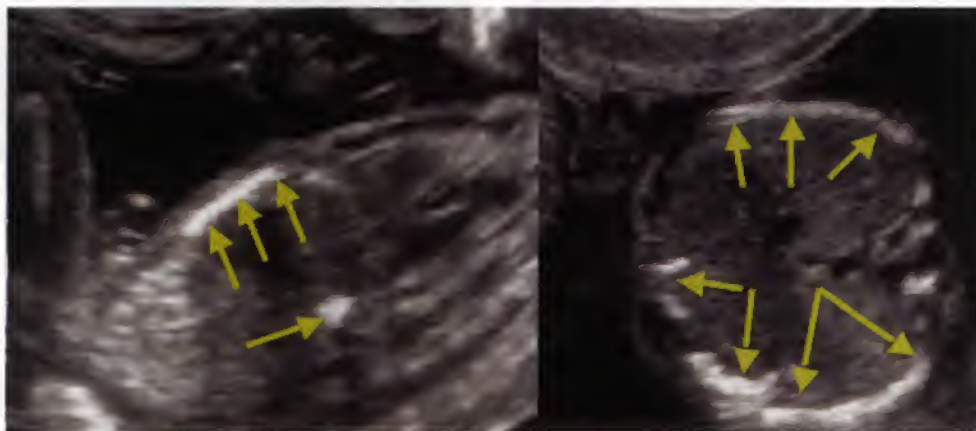


**FIGURE 15-29.** Hyperechogenic rim (arrows) at week 15. Left, Sagittal section. Right, Transverse section. The newborn had a normal outcome.

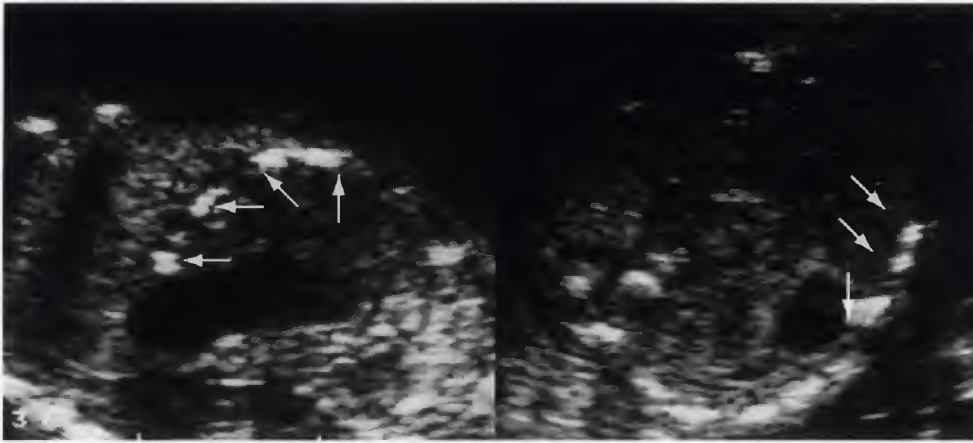


**FIGURE 15-31.** Scattered calcifications (arrows) at week 16. Left, Sagittal section. Right, Transverse section. The newborn had a normal outcome.

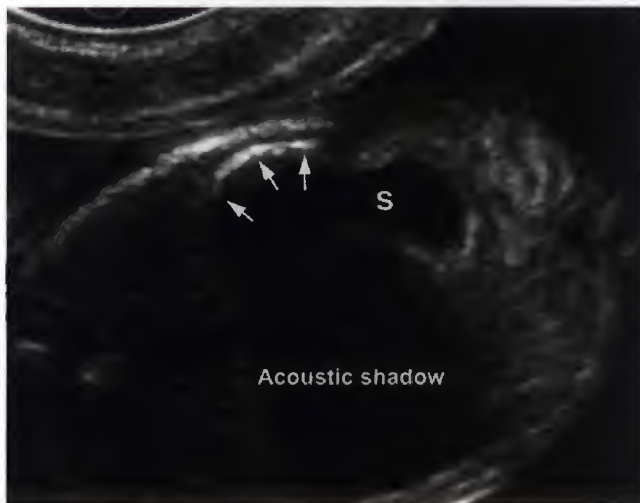


**FIGURE 15-32.** Perigastric calcification (arrows) projecting an acoustic shadow. S, stomach.

### Meconium Cyst/Pseudocyst

Another sonographic appearance of bowel perforation is a meconium cyst or pseudocyst. It usually appears in early pregnancy as a cyst encircled by an hyperechogenic rim or bright spots with acoustic shadows behind them (Fig. 15-33). In some cases the cyst resolves later in pregnancy and the sonographic image resembles hyperechogenic bowel.

We recommend dividing cases of bowel perforation into two groups:

**Primary or Idiopathic Perforation of Bowel Without Intestinal Obstruction.** Primary or idiopathic perforation of bowel represents 96% of cases of bowel perforation. All of them appear in the first and early second trimester. The only sonographic finding is intraperitoneal calcifications. There is no evidence of ascites, polyhydramnios, or dilation of bowel loops. Intrauterine spontaneous sealing of the perforation occurs in most cases, and there are no clinical nor histologic findings of peritonitis in the fetus. The infants outcome is favorable and the only clue to an intrauterine episode of

bowel perforation is the postnatal radiographic finding of intra-abdominal calcifications.

**Secondary Perforation of Bowel.** Secondary perforation of bowel is a result of intestinal obstruction due to intestinal atresia, volvulus, cystic fibrosis, and so forth. It is uncommon and usually appears only in late pregnancy. The main sonographic findings are ascites, polyhydramnios, dilatation of bowel loops, and intraperitoneal calcifications.

Removal of debris and reduction of the intra-abdominal pressure may improve the mesenteric vascular supply for healing of the ruptured intestinal hole. It may also reduce lung compression and prevent pulmonary hypoplasia.<sup>106</sup> Postnatal surgery is mandatory in infants with clinical manifestation of bowel perforations or obstruction. The survival rate in most series is high (Box 15-3).<sup>98,102-105</sup>

### Meckel Diverticulum

Meckel diverticulum (Fig. 15-34) is apparent in 2% of the population and is regarded as the most common congenital anomaly of the gastrointestinal tract.<sup>107,108</sup> The diverticulum that protrudes from the distal part of the ileum is a remnant of the embryonic yolk sac, which may also be referred to as the omphalomesenteric duct or vitelline duct. It usually contains all layers of the intestine but heterotopic tissue may also be present. Recently, Park et al<sup>109</sup> reviewed the records of 1476 patients in whom a Meckel diverticulum was found during surgery. Only 16% of cases were symptomatic. The most common clinical presentation in adults was bleeding and obstruction in children. Among the symptomatic patients, the male-to-female ratio was approximately 3:1. Being a common anomaly, it is of interest that only few cases have been detected in utero. It can therefore be suggested that the vast majority of these diverticulae are asymptomatic in the fetus and their sonographic features are similar to those of normal intestine.

### Prenatal Diagnosis

Meckel diverticulum may be visualized only in cases of obstruction or intussusception. Even in these cases, the sonographic appearance is not characteristic and presents as



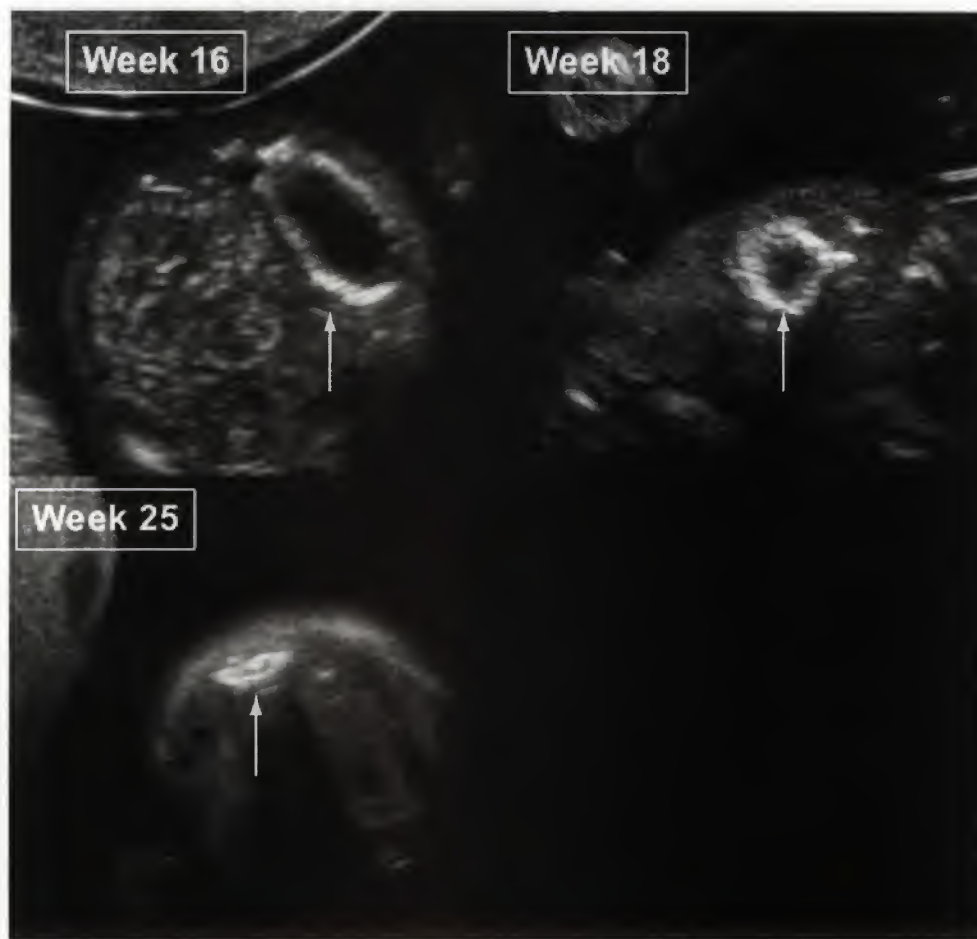


**FIGURE 15-33.** Shrinkage of a meconium cyst (arrow) throughout gestation.

#### **BOX 15-3 Suggested Workup in Fetuses with Intra-abdominal Calcifications**

1. Detailed scanning of all fetal organs including echocardiography
2. Search for cystic fibrosis
3. Search for infections, mainly TORCH
4. Fetal karyotype
5. Evaluation of digestive enzymes level in the amniotic fluid.

an intra-abdominal cyst or dilated bowel with various types of echogenicity and content, with or without peristalsis (Figs. 15-35 and 15-36).<sup>110,111</sup>

### **Small Intestine Duplication**

Duplications may occur along the entire length of the gastrointestinal tract but are most common in the small intestine, in particular the terminal ileum, which represents more than 70% of the small intestinal duplications. They usually lie on the mesenteric side of the bowel, and their size can be only a few millimeters or as long as the whole

intestine. The most common clinical findings in neonates and infants are vomiting, abdominal distention, volvulus, and intussusception.<sup>27,112</sup>

The prenatal differential diagnosis is not always easy and includes other intra-abdominal cystic anomalies.<sup>28,113,114</sup> The following factors may expedite a more definitive diagnosis of a duplication cyst:

1. Depiction of peristalsis in the cyst wall is highly suggestive of an intestinal origin
2. Early appearance (in the first and early second trimester)
3. Single loop dilatation

### **Congenital Intestinal Pseudo-Obstruction**

Congenital intestinal pseudo-obstruction (CIPO) is a rare condition with an incidence of less than 1:100,000. It is characterized by recurrent episodes of intestinal paralytic obstruction with no causative mechanical factor. Visceral neuropathy or myopathy has been detected in many but not all cases. Associated urologic disorders are very common, mainly megacystis and in utero hydronephrosis. Parents should be informed that despite progress in treatment, the reported incidence of mortality is up to 25%.<sup>115-117</sup>

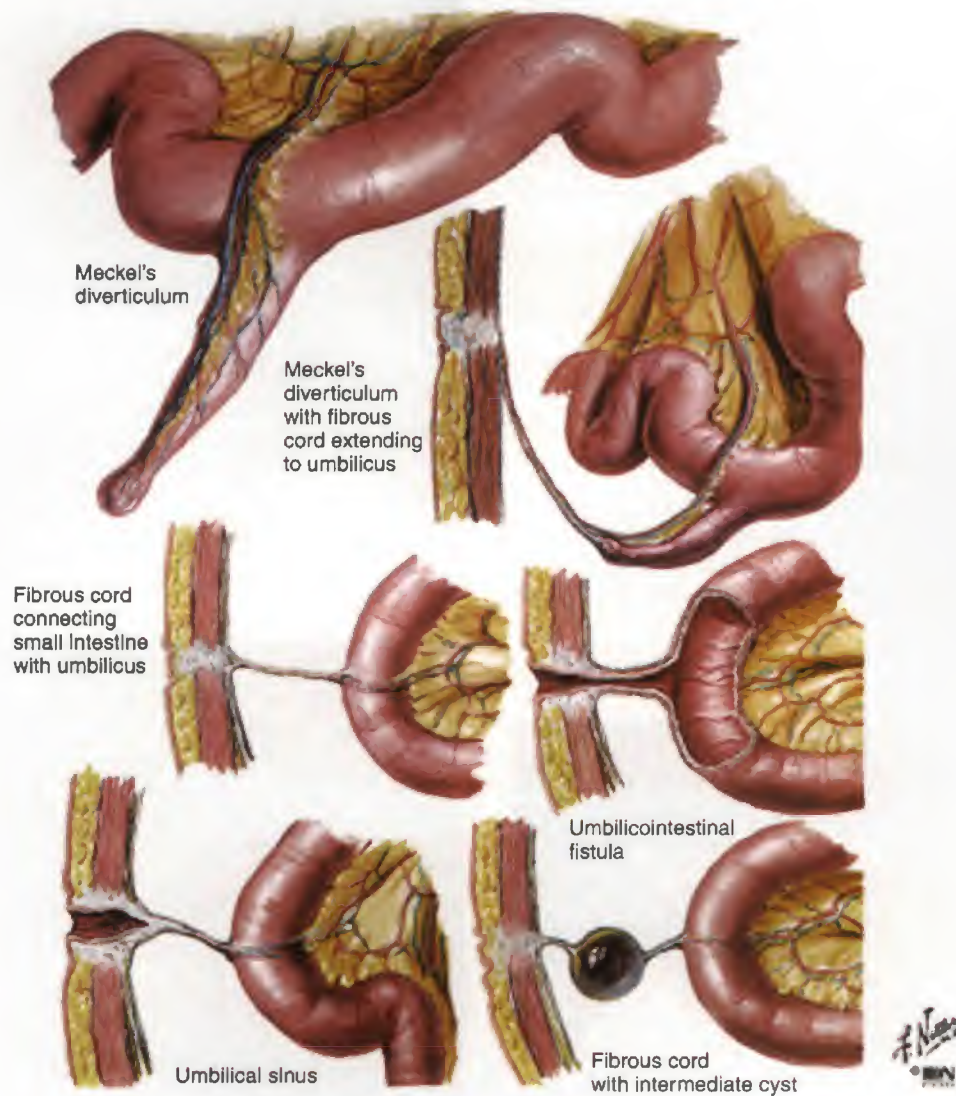


**FIGURE 15-34.** Meckel diverticulum: various morphologic forms. (From netterimages.com, with permission.)

The characteristic findings on prenatal ultrasound are moderately dilated intestinal fluid-filled loops with reduced or absent peristalsis (Fig. 15-37). Polyhydramnios and megacystis may be observed in many of the cases.<sup>115</sup> Of note, there are no ascites or meconium in the peritoneum, which is of help in the differential diagnosis from jejunoileal atresia. Other differential diagnoses to be considered are Hirschsprung disease and congenital chloride diarrhea.

### **Congenital Chloride Diarrhea**

Congenital chloride diarrhea is an autosomal-recessive disorder of chloride transport in the distal ileum and colon. It is characterized by life-long watery diarrhea of prenatal onset with high fecal chloride concentration. The anomaly is very rare. However, a high incidence of 1:3200 to 13,000

was reported in Kuwait and Finland.<sup>118,119</sup> On ultrasound, polyhydramnios and slight-to-moderate distension of intestinal loops with peristalsis are observed (Fig. 15-38).

The differential diagnosis from CIPO relies on the presence of peristalsis as opposed to reduced or absent peristalsis in CIPO. The disorder should also be differentiated from jejunoileal atresia, in which intestinal loops distention is much more obvious and ascites and intraperitoneal meconium are apparent in many cases (Table 15-2).<sup>120</sup>

### **COLON**

It is difficult to sonographically differentiate between the small intestine and colon in the first half of pregnancy. The diagnosis is mainly based on the peripheral location of the colon. Later in pregnancy, the haustral folds may be



imaged. The rectosigmoid may be depicted by transvaginal ultrasound in the first trimester as an echogenic structure below the urinary bladder. Later its lumen becomes visible. Nomograms of the diameters of the descending colon and the rectum in the second half of pregnancy are currently available (Figs. 15-39, 15-40, and 15-41).<sup>120</sup> Normally, there is some sludgy content in the colon (Figs. 15-42 and 15-43), whereas the detection of increased fluid in the colon raises the possibility of a pathologic process.

Presently, there are very few and controversial reports on fetal colonic peristalsis. Although no colonic peristalsis was detected in a number of published studies,<sup>122,123</sup> according to our experience, high resolution ultrasound is capable of revealing active peristalsis of the rectosigmoid as early as at 22 and 23 weeks of gestation.

## FETAL DEFECATION

Passage of meconium in utero is a frequent finding in the last weeks of pregnancy. Its incidence increases with advancing gestational age. A widely accepted concept suggests that fetuses do not normally defecate, and that the presence of



**FIGURE 15-37.** Intestinal pseudo-obstruction at week 31. (Courtesy Dr. Ori Shen.)

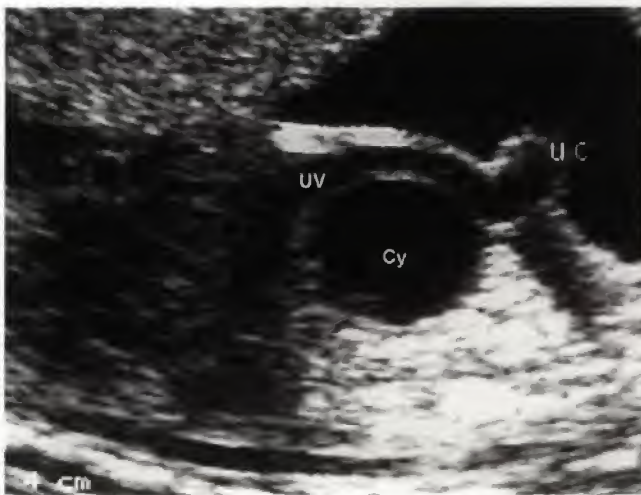


**FIGURE 15-35.** Meckel diverticulum at week 16. The cyst (cy) is encircled by the umbilical vein (uv). Umbilical cord (uc).

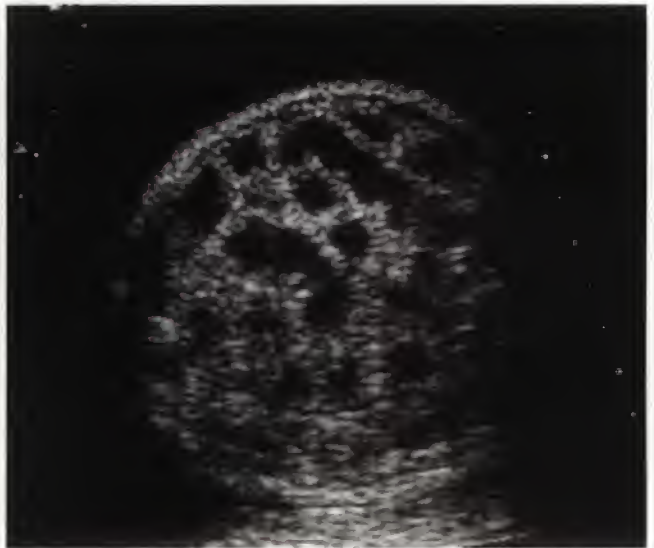


**FIGURE 15-38.** Chloride diarrhea at week 32. (From Husu S, Nelson N, Selbing A: Prenatal bowel dilatation: Congenital chloride diarrhoea. *Arch Dis Child Fetal Neonatal* Ed 85:F65, 2001.)

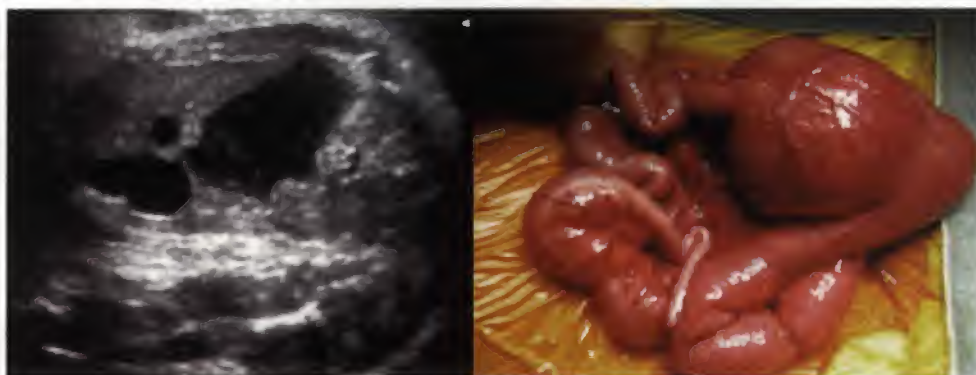


**FIGURE 15-36.** Meckel diverticulum at week 32. Left, A large cystic structure containing sludge. Right, Operative finding. (Reproduced with permission of F. Jacquemard, [www.thefetus.net](http://www.thefetus.net).)

**Table 15-2****The Comparison Between Congenital Intestinal Pseudo-Obstruction (CIPO) and Congenital Chloride Diarrhea (CCD)**

CIPO			
Prognosis	Peristalsis	Sonographic Findings	Incidence
Mortality: 25% Prematurity: 14% Urinary anomalies: 10%	Absent	Moderate fluid filled enlargement of the entire ileum and jejunum; polyhydramnions; No ascites or meconial spillage.	CIPO Incidence: Rare
CCD			
Prognosis	Peristalsis	Sonographic Findings	Incidence
Mortality: 6% Prematurity: Very common Urinary anomalies: No	Good peristalsis	Moderate fluid filled enlargement of the entire ileum and jejunum; polyhydramnions; No ascites or meconium spillage.	CCD Incidence: Rare—Except in Finland and Kuwait

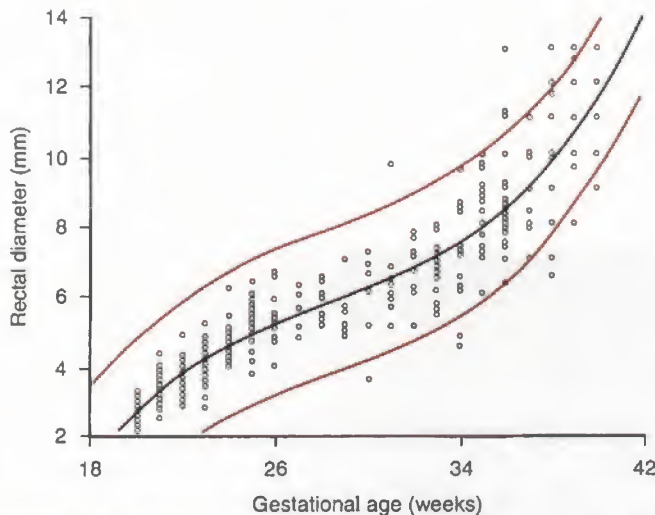


**FIGURE 15-39.** Regression analysis of rectal diameter and gestational week using a cubic model. The 95% confidence interval is shown. (From Zalel Y, Perlitz Y, Gamzu R, et al: In-utero development of the fetal colon and rectum: Sonographic evaluation. *Ultrasound Obstet Gynecol* 21:161, 2003.)

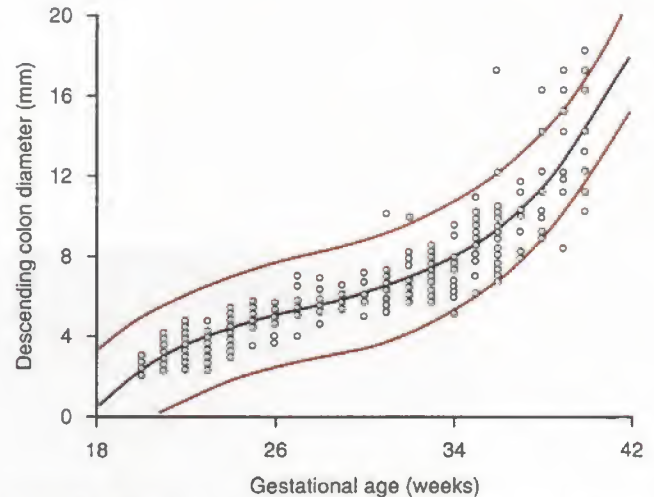


**FIGURE 15-40.** Regression analysis of descending colon diameter and gestational week using a cubic model. The 95% confidence interval is shown. (From Zalel Y, Perlitz Y, Gamzu R, et al: In-utero development of the fetal colon and rectum: Sonographic evaluation. *Ultrasound Obstet Gynecol* 21:161, 2003.)

meconium-stained amniotic fluid implies fetal hypoxia.<sup>124</sup> However, there are some publications indicating that fetal defecation is a physiologic event. Animal models have demonstrated defecation to be independent of fetal distress.<sup>125,126</sup> Ramon et al<sup>127</sup> observed fetal defecation throughout pregnancy in humans. They defined fetal defecation as the expulsion of rectal content through the anus into the amniotic fluid. The diameter and area of the anus were measured sonographically at times of maximum anal aperture in 240 fetuses between 15 and 41 weeks of gestation. One or more defecations were noted in all fetuses. The frequency of defecation was highest between weeks 28 and 34 of gestation. The expulsion of meconium has also been observed using color Doppler imaging (Fig. 15-44), and three- and four-dimensional ultrasonography.<sup>128</sup>

**Authors' opinion:** We agree that fetal defecation is a physiologic process that occurs throughout pregnancy. The main issues strengthening this belief are related to the

following facts: In all early pregnancies, we see a variable amount of echogenic sludge in the amniotic fluid, using high frequency vaginal transducers (Fig. 15-45); the features and echogenicity of this sludge are similar to those of the meconium inside the fetal intestine; the echogenic debris which is sometimes detected in the fetal stomach also has an appearance similar to meconium (see Fig. 15-14). It is therefore possible that the fetus that is known to swallow its amniotic fluid also swallows its own meconium. In very rare occasions, it is possible to visualize the defecation process in the young fetus (Fig. 15-46). There is a correlation between the levels of intestinal and liver enzymes and normal or abnormal fetal defecation process in early and midpregnancy.<sup>129</sup>

### Hirschsprung Disease

Hirschsprung disease is caused by an abnormal innervation of the bowel beginning in the internal anal sphincter and



Week of gestation	Number	Descending colon diameter (mm)		Rectal diameter (mm)	
		Mean	95% CI	Mean	95% CI
19–20	10	3.52	0.79–6.26	3.64	1.45–5.82
21	16	3.59	0.86–6.32	3.79	1.61–5.97
22	28	3.69	0.96–6.41	3.95	1.78–6.13
23	29	3.82	1.09–6.54	4.14	1.97–6.31
24	29	3.98	1.26–6.7	4.34	2.17–6.52
25	29	4.18	1.46–6.9	4.57	2.40–6.74
26	13	4.43	1.70–7.15	4.82	2.64–6.99
27	7	4.71	1.99–7.43	5.08	2.91–7.26
28	7	5.04	2.32–7.76	5.38	3.20–7.55
29	7	5.42	2.69–8.14	5.69	3.52–7.87
30	8	5.84	3.12–8.57	6.04	3.86–8.21
31	10	6.32	3.60–9.05	6.41	4.23–8.58
32	11	6.86	4.13–9.58	6.80	4.63–8.98
33	17	7.45	4.72–10.17	7.23	5.05–9.40
34	14	8.10	5.37–10.82	7.68	5.51–9.85
35	29	8.81	6.09–11.53	8.17	5.99–10.34
36	32	9.59	6.87–12.31	8.68	6.51–10.85
37	18	10.44	7.71–13.16	9.23	7.06–11.40
38	26	11.35	8.63–14.08	9.81	7.64–11.98
39	17	12.34	9.61–15.07	10.43	8.25–12.61
40	22	13.40	10.66–16.15	11.08	8.89–13.26

**FIGURE 15–41.** Descending colon and rectal diameters according to gestational age. (From Zalel Y, Perlitz Y, Gamzu R, et al: *In-utero development of the fetal colon and rectum: Sonographic evaluation. Ultrasound Obstet Gynecol* 21:161, 2003.)



**FIGURE 15–44.** A. Ultrasound image at 33 weeks showing the anus (A) of the fetus and the left and right glutei (LG, RG) in an inferior view before the defecation. AES, anal external sphincter. B. Image of similar projection of the anus during defecation. The defecation flow is shown by color Doppler. (From Ramon y Cajal CL, Ocampo Martínez R: *Picture of the month: In-utero defecation. Ultrasound Obstet Gynecol* 19:531, 2002.)

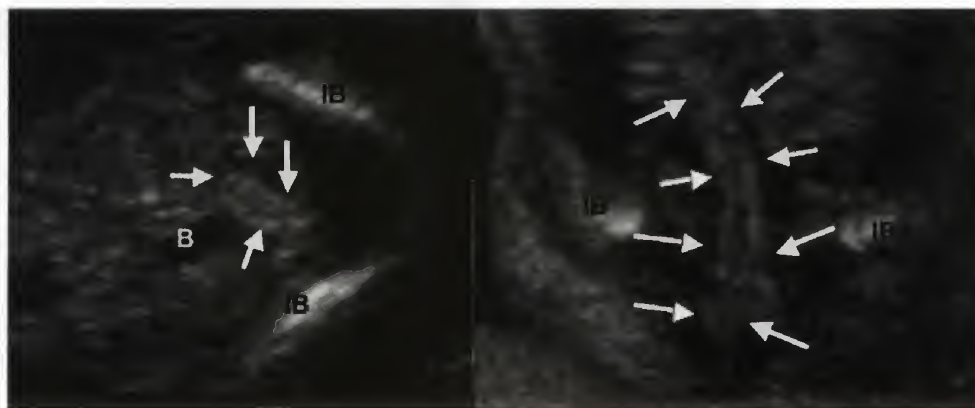


**FIGURE 15–42.** The rectosigmoid in a coronal section at week 15 in two fetuses (arrows). IB, iliac bone. On the left the bladder (B) is also depicted.

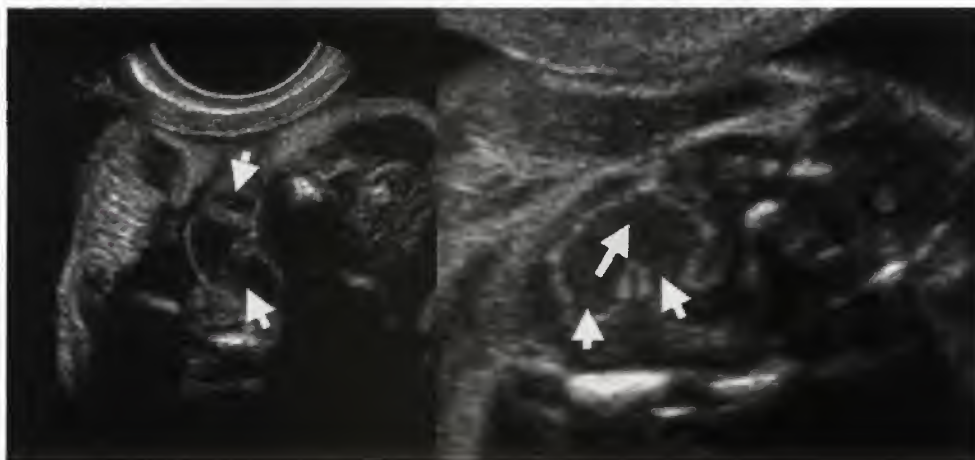


**FIGURE 15–43.** The rectosigmoid in a coronal section at week 23 in two fetuses. The content's sludge-like appearance is marked by arrows.



**FIGURE 15-45.** Intra-amniotic floating echogenic debris at week 15.

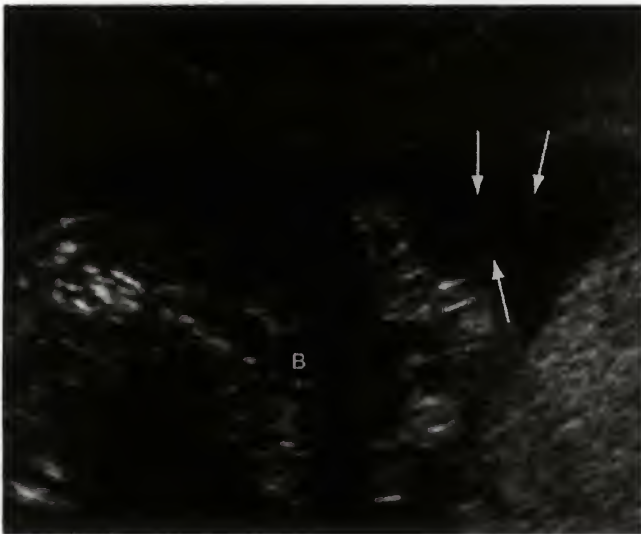


**FIGURE 15-46.** Fetal defecation at week 16. The defecated echogenic debris is marked by arrows. B, bladder. (Courtesy of Dr. Israel Shapiro.)

extending proximally to involve a variable length of gut. It is the most common origin of intestinal obstruction in neonates with an incidence of 1:5000 live births. Male fetuses are affected more often than female fetuses (4:1). Associated anomalies are observed in 11% to 22% of cases, and trisomy 21 is detected in 3% to 10% of affected infants. Genetic factors appear to play a role in the disease with a familial history in about 5% of cases. The mortality rate of this pathology is 16% to 17%.<sup>130,131</sup>

### Prenatal Diagnosis

Only few reports on the prenatal sonographic diagnosis of the disease have been published.<sup>132,133</sup> The main sonographic markers of this disorder are nonspecific, namely, bowel distention and polyhydramnios (Fig. 15-47). The correct diagnosis is usually made only in the first weeks of neonatal life.

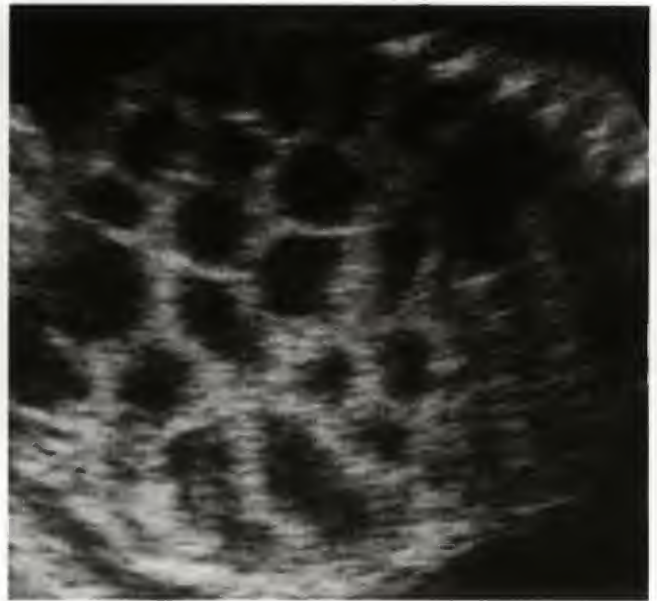


**FIGURE 15-47.** Hirschsprung disease, third trimester. Multiple dilated loops. (Reproduced with permission from L.F. Goncalves, [www.thefetus.net](http://www.thefetus.net).)

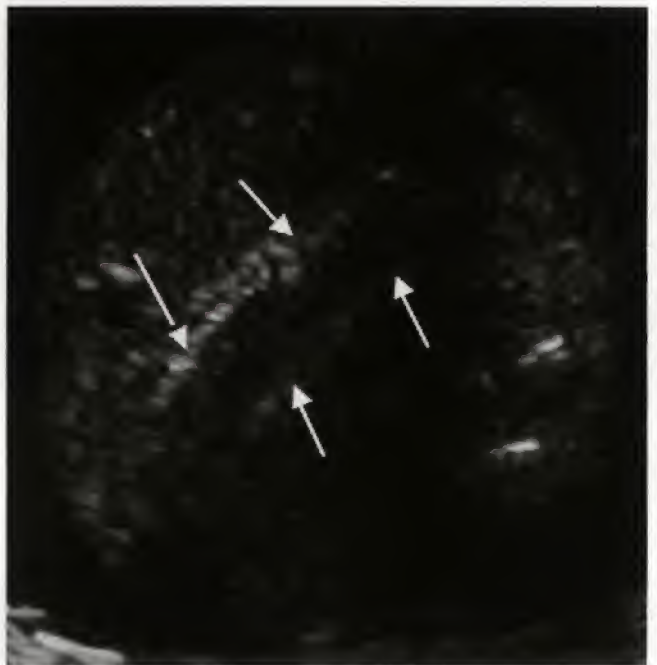


**FIGURE 15-48.** Hirschsprung disease at week 16. The dilated descending colon is marked by arrows.

We have observed two cases in which dilated hyperechogenic bowel was detected at 15 weeks' of gestation (Fig. 15-48); along with other sonographic structural anomalies. Amniocentesis revealed trisomy 21 in both cases, and an aganglionic colon was found on post-mortem examination after termination of pregnancy. Thus, the echogenic intestine depicted in some fetuses with Down syndrome may actually represent Hirschsprung disease.



## ANAL ATRESIA

Anal atresia is the most frequent congenital anal anomaly, with an incidence of about 4:10,000 births. It may be subdivided into a high, low, and intermediate atresia according to the termination of the anal canal relatively to the levator ani muscle.<sup>134–136</sup> Anal atresia has been described in more than 50 syndromes and malformative disorders, the most common being VATER and VACTER associations.<sup>64,134–136</sup>

Out of 1425 cases of anal atresia observed in the EUROCAT survey,<sup>135</sup> 36% were isolated and 64% were accompanied with other malformations. High atresia was present in 10% of cases, whereas low atresia was present in 90% of cases. Forrester and Merz,<sup>136</sup> evaluating the data of 124 cases, found chromosomal anomalies in 8.1% and a family history in 2.4%. Stoll et al<sup>134</sup> reported that the recurrence risk for first degree relatives of probands was 3.7%, with the prevalence rate of nonanal atresia malformations being more than twice as high as that in controls.

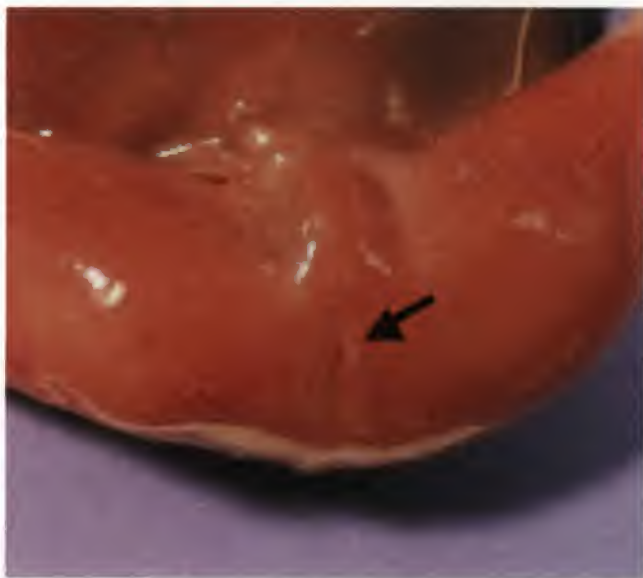


**FIGURE 15-49.** Autopsy at week 17. The arrow points toward the anal membrane. (Courtesy Dr. Lisa L. Maroun.)

## Prenatal Diagnosis

Because anal atresia may be present in cases of VATER/VACTER association, the demonstration of anomalies mainly in the vertebrae, heart, kidney, limbs, and esophagus should alert the sonographer to the possibility of anal atresia (Fig. 15-49). Currently, the prenatal detection rate of anal atresia is still low. Stoll et al<sup>91</sup> reported a detection rate of only 8.2%.<sup>7,63</sup> Most publications are actually case reports, and some of them are observations made in early pregnancy.

The main sonographic markers of anal atresia include<sup>137–143</sup> dilated fetal intestinal loops with fluid inside the lumen (Fig. 15-50); a U- or V-shaped segment of distal bowel in the lower abdomen or pelvis, separated from the bladder with mild ascites; and intraluminal colonic calcifications, which probably represent enterolithiasis. The enterolithiasis is most likely the result of solidification and condensation of the stacked meconium (see Figs. 15-50 and 15-51).

The authors<sup>144</sup> have observed a fetus in which dilation of the bowel was noticed at 15 weeks of gestation. Although no intestinal anomaly could be detected on monthly follow-up scans, anal atresia was found in the newborn after delivery. Taipale et al<sup>143</sup> reported a fetus with an imperforate anus in which dilated bowel was first detected at 12 weeks of

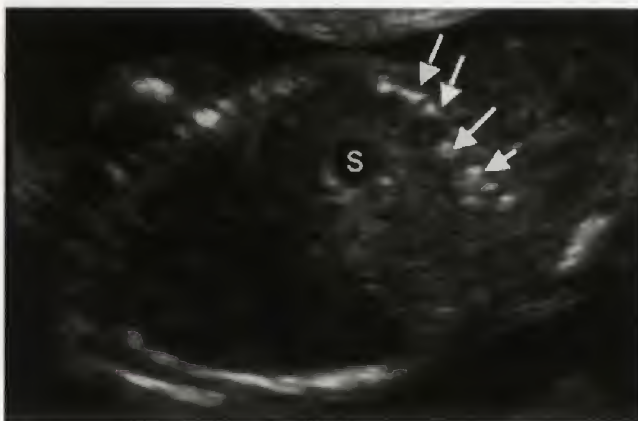


**FIGURE 15-51.** Anal atresia at week 16. The enterolithiasis in the dilated descending colon is marked by arrows. S, stomach.



**FIGURE 15-50.** Anal atresia at week 15. Two sagittal sections of the same fetus. The dilated, fluid-filled rectosigmoid and descending colon is marked by white arrows. In the right figure, the enterolithiasis is marked by a black arrow.

gestation and then again in the third trimester. However, in the second trimester, the intestine appeared to be of normal size. It seems, therefore, that dilatation of the bowel in early pregnancy is a possible marker for anal atresia and the anomaly may be overlooked if only a midpregnancy ultrasound examination is performed. We believe that in the future, the studies of digestive enzymes in the amniotic fluid will be included in the work-up of fetuses with an intestinal dilation at early stages of pregnancy, as this examination has proved to be most helpful in the diagnosis of anal atresia.<sup>129</sup>

## HYPERCHOGENIC BOWEL

### Sonographic Definition

The echogenicity of the intestine approaches that of surrounding bone (Fig. 15-52).

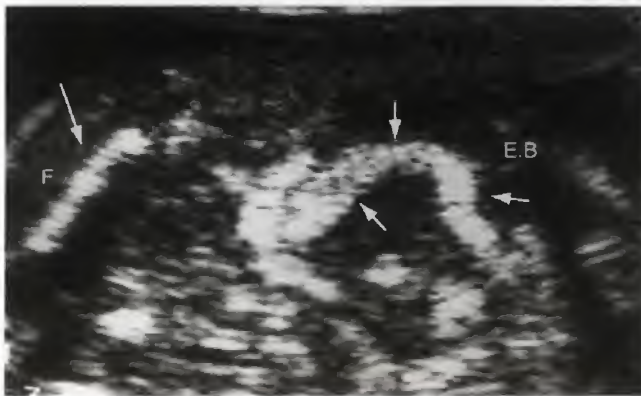


**FIGURE 15-52.** Hyperechogenic bowel (EB). The echogenicity of the bowel (*thin arrows*) is similar to that of the femur (F and *bold arrow*).

Prevalence is 0.2% to 1.8% in second trimester fetuses. The lack of a reliable objective method to evaluate bowel echogenicity leaves the diagnosis of this anomaly entirely in the hands of the subjective interpretation of the observer. The original description of increased bowel echogenicity used relatively low frequency transducers without newer harmonic imaging signal processing. Thus, one's own subjective assessment of bowel echogenicity and the artificial enhancement of transducer frequency, gain, and image processing may have an apparent impact on the interpreted echogenicity level of the bowel (Fig. 15-53).<sup>145-149</sup> It is therefore critical that the diagnosis of hyperechogenic bowel is made only by experienced and highly skilled sonographers who use ultrasound machines with which they are familiar (Tables 15-3 and 15-4).

### Summary

The diagnosis of hyperechogenic bowel should be made by experienced sonographers who are quite familiar with their ultrasound machines. In cases of hyperechogenic bowel, a search for structural anomalies, chromosomal disorders, infections, and cystic fibrosis should be performed. If these disorders are excluded and the maternal alpha-fetoprotein is normal, parents can be counselled that there is a very high probability of a favorable fetal outcome.

### Volvulus

Volvulus is a condition in which bowel loops twist around the mesenteric artery or its branches. The ischemic necrosis may lead to intestinal atresia. It is, however, also possible that intestinal atresia develops first and is complicated by volvulus because of increased peristalsis in the dilated intestine proximal to the site of atresia. The incidence of fetal volvulus is difficult to determine because most data comes from case

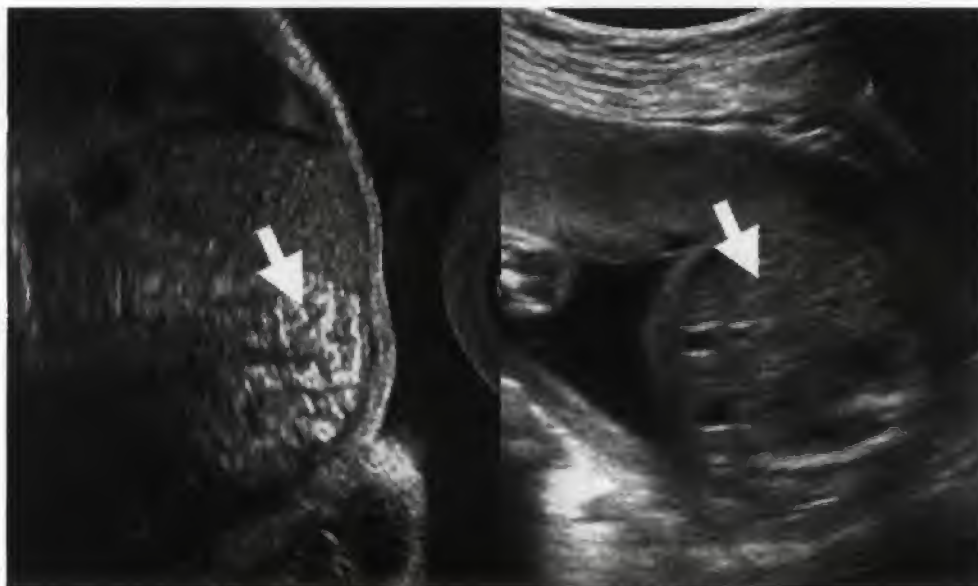


**FIGURE 15-53.** The impact of ultrasound frequency on bowel echogenicity. *Left*, Echogenic bowel (*arrow*) depicted by high frequency transvaginal ultrasound. *Right*, Transabdominal scanning with lower frequency of the same fetus did not show bowel increased echogenicity.



reports. Of note however is the study of Komuro et al,<sup>87</sup> who found a volvulus in 14 of 48 newborns with jejunal atresia.

The characteristic sonographic marker of volvulus in fetuses and children is the whirlpool sign. The twisted bowel loop and its accompanying mesentery and mesenteric vessels exhibit a whirlpool-like configuration (Fig. 15-54).<sup>162-165</sup> Color

Doppler imaging may facilitate the diagnosis by visualizing the twisted mesenteric vessels.<sup>162,163</sup> Sonographers should be aware that the whirlpool sign is not depicted in all cases of fetal volvulus. In some instances the sonographic appearance is nonspecific, in which dilated loops of bowel, ascites, intra-abdominal cystic mass, and polyhydramnios are seen.<sup>166,167</sup>

**Table 15-3**

**Physical Causes for Increased Echogenicity of the Bowel**

1. Swallowed blood and/or meconium. Both of these matters will make the intestine seem hyperechogenic once they reach it. Prospective studies have shown that amniocentesis, chorionic villus sampling, and umbilical cord puncture during intrauterine transfusions are associated with an increase in bowel echogenicity up to 4 weeks following the procedure.<sup>150,151</sup>
2. Thick meconium (constipation). Transient constipation is probably the most common reason for hyperechogenic bowel in normal fetuses. It is also a significant marker of cystic fibrosis.
3. Fluid inside or outside the intestine or in the intestinal wall. The echogenicity in such cases is the result of the different acoustic impedance of the adjacent media (that is, intestinal tissue versus fluid). The main clinical disorders are infection, obstruction with or without perforation, Hirschsprung disease, and intestinal ischemia.
4. Meconium between bowel loops. On ultrasound, meconium outside the intestine is more echogenic than meconium inside the intestinal lumen, and usually occurs in cases of bowel perforation. The latter may be present in cases of obstruction or cystic fibrosis, although in many cases the reason for it is unknown.

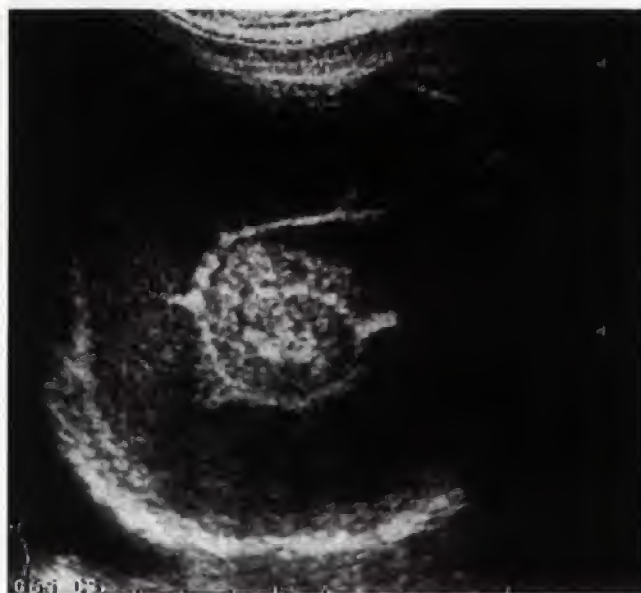


**FIGURE 15-54.** Volvulus: Dilated bowel loop showing a whirlpool-like configuration, at week 34. (From Has R, Gunay S: 'Whirlpool' sign in the prenatal diagnosis of intestinal volvulus. *Ultrasound Obstet Gynecol* 20:307, 2002.)

**Table 15-4**

**Clinical Causes of Hyperechogenic Bowel**

1. Transient, benign and idiopathic. We believe that the underlying cause of hyperechogenic bowel is transient constipation in the fetus with no clinical implications.
2. Chromosomal disorders. Chromosomal anomalies, especially trisomy 21, have been observed in fetus with an hyperechogenic bowel.<sup>152-157</sup> It has been suggested that in aneuploid fetuses bowel motility is decreased, leading to increased water absorption from meconium and constipation. Actually, Hirschsprung disease is common in trisomy 21. The hyperechogenic bowel appears with other structural anomalies in many aneuploid fetuses. However, an isolated finding of hyperechogenic bowel is also associated with an increased risk of chromosomal anomalies.<sup>154,156</sup>
3. Cystic fibrosis. The abnormal pancreatic enzymatic secretion and the thick viscous meconium may cause meconium ileus and even perforation. Cystic fibrosis has been reported in 0% to 13% of fetuses with hyperechogenic bowel.<sup>152-155,157</sup> The differences between studies probably reflect the considerable ethnic variation of this disease. In the white population, the incidence is 1:2500 to 5000, whereas in Asian Americans, it is 1:35,000.<sup>158</sup> The risk of cystic fibrosis is much higher if the parents are carriers of the disease, although the absence of familial history does not preclude the possibility that the fetus is an index case.
4. Infection. Cytomegalovirus is the most common infection leading to paralytic ileus and perforation. However, hyperechogenic bowel has been reported in association with many other infections such as toxoplasma, rubella, varicella, and herpes simplex.<sup>155,157</sup> Of note, despite these data there are recent large studies in which only very few or no infections at all were found in fetuses with hyperechogenic bowel.<sup>153,155</sup>
5. Intrauterine growth restriction. Restriction of blood supply and bowel ischemia in these fetuses is probably the reason of the hyperechogenic appearance of the bowel.<sup>153,154,157,159</sup> Doppler studies in intrauterine growth restriction fetuses with hyperechogenic bowel revealed a significant decrease in the pulsatility index in the superior mesenteric artery and celiac trunk.<sup>160</sup>
6. Intrauterine fetal demise. Intrauterine fetal demise was reported in up to 5.8% of fetuses with an hyperechogenic bowel.<sup>159</sup> The echogenicity of the bowel is probably a result of hypoperfusion and bowel ischemia.
7. Thalassaemia. Fetuses affected by homozygous alpha-thalassaemia-1 are severely anemic and hypoxic. Hyperechogenic bowel has been observed in up to 31% of these cases.<sup>161</sup> Therefore, it is recommended to examine high-risk populations with fetal hyperechogenic bowel for thalassaemia.



## Intrauterine Intussusception

Intrauterine intussusception is regarded as an uncommon clinical finding, accounting for only few cases of neonatal intestinal obstruction (Shimotake). Therefore, of interest is the report of Komuro et al<sup>87</sup> who found intussusception in 12/48 cases of neonatal jejunoileal atresia. The prenatal sonographic findings are usually nonspecific, namely ascites, dilated bowel loops, and features of meconium peritonitis.<sup>169-170</sup> Shimotake et al<sup>169</sup> reported on a fetus in whom, in addition to the above-mentioned sonographic findings, they also detected a "target-like" appearance suggestive of intrauterine intussusception in the abdomen.

## Malrotation

Malrotation of the intestine occurs as a result of failure of normal intestinal rotation and fixation, which usually is completed by the 12th week of gestation (Fig. 15-55). The reported incidence of the anomaly is as high as 2.86 per 10,000 live births and fetal deaths, and about 90% of symptomatic cases are discovered by the first year of life.<sup>171</sup> The incidence of associated anomalies is very high reaching 94% in a large series.<sup>171</sup> The most common anomalies are in the gastrointestinal tract mainly volvulus, diaphragmatic hernia, abdominal wall defects, heterotaxia syndrome, and situs inversus.<sup>171-176</sup> The prenatal sonographic diagnosis has been reported in few cases, relying on nonspecific markers such as dilation of bowel loops (Fig. 15-56), ascites, intra-abdominal cysts, situs inversus, and displacement of the fetal stomach.<sup>174,177-179</sup>

## Cloacal Dysgenesis Sequence

Cloacal dysgenesis sequence is a very rare anomaly defined as absence of anal, genital, and urinary orifices associated with smooth perineum. More than 80% of fetuses also have other major anomalies, mainly absent or dysplastic kidneys, hydronephrosis, megacystis, and pulmonary hypoplasia. Ultrasound may reveal a dilated fluid-filled colon with enterolithiasis, cystic structures in the pelvis, abnormalities of the genitalia and urinary tract, and oligohydramnios (Fig. 15-57).<sup>180-182</sup>

## Suspected Pathology of the Gastrointestinal Tract: A Practical Approach (The 12 Commandments)

1. Intestinal dilatation. The most common associated problems are
  - a. Cystic fibrosis. In 75% of cases with this disease the fetal gallbladder will not be seen, and there is a low level of digestive enzymes.
  - b. Intrauterine infections—mainly TORCH
  - c. Structural anomalies. Detailed scanning of all fetal organs is mandatory. Special attention should be paid to the heart, genitalia, urinary tract, and umbilical cord.
  - d. Chromosomal anomalies.
2. Intestinal content
  - a. It should be remembered that in a dilated and obstructed intestine there is usually a problem with fluid absorption. Therefore, the presence of solid intestinal contents (excluding cases of cystic fibrosis) decreases significantly the probability of pathology.
- b. The presence of enterolithiasis in a fluid-filled segment of the colon is suggestive of anal atresia or a fistula between the urinary system and colon.
3. Ascites
  - a. Ascites is the most significant marker of bowel perforation, especially if an increase in its amount is noted with progress of pregnancy. The ascites in such cases might be a solitary finding or present with bowel dilation and peritoneal calcifications.
  - b. Ascites may not present in perforation of the upper gastrointestinal tract, especially in early pregnancy.
4. The length and width of dilated bowel loops
  - a. An isolated dilation of a single loop, especially if depicted in early pregnancy, raises the possibility of a duplication cyst, particularly if debris is present within the cyst.
  - b. The more proximal the obstruction, the larger the diameter of the dilated loops. The largest dilations will be noted in those loops located on the left side of the fetus (the jejunum).<sup>29,31-33</sup>
  - c. In cases of both proximal and distal obstruction of the stomach, a huge C-shape fluid filled stomach will appear.
  - d. After exclusion of cystic fibrosis, the presence of solid content in dilated loops (especially of the colon) usually has a good prognosis. In contrast, fluid-filled dilated loops are a marker of a pathologic process.
5. Anatomy and physiology
  - a. The presence of clear fluid in the colon and rectosigmoid (albeit a transient event) raises the possibility of anal atresia.
  - b. Dilation of the transverse colon in the second half of pregnancy is usually a normal physiologic finding as long as the small intestine seems normal.
  - c. Depiction of a distended duodenum around the pancreas is a marker of an obstruction.
  - d. It is currently impossible to know with certainty whether only one intestinal obstruction takes place, and unfeasible to pinpoint the precise location of the obstruction, and the length of the atretic intestine.
6. Peristalsis
  - a. Today no standardized method exists that quantitatively assesses peristaltic movements, and activity is assessed subjectively.
  - b. The presence or absence of peristalsis is a possible sonographic marker in many differential diagnoses. It serves as a definitive diagnostic finding only in cases of CIPO and congenital chloride diarrhea.
7. Intraperitoneal calcifications
  - a. In cases of an isolated finding of intraperitoneal calcification, a search for chromosomal anomalies, cystic fibrosis, infections, and digestive enzymes should be performed. Should all these tests prove normal, the probability of pathology in the newborn is very low.
8. Amniotic fluid volume
  - a. There might not be an increase in amniotic fluid volume in cases of gastrointestinal obstruction.



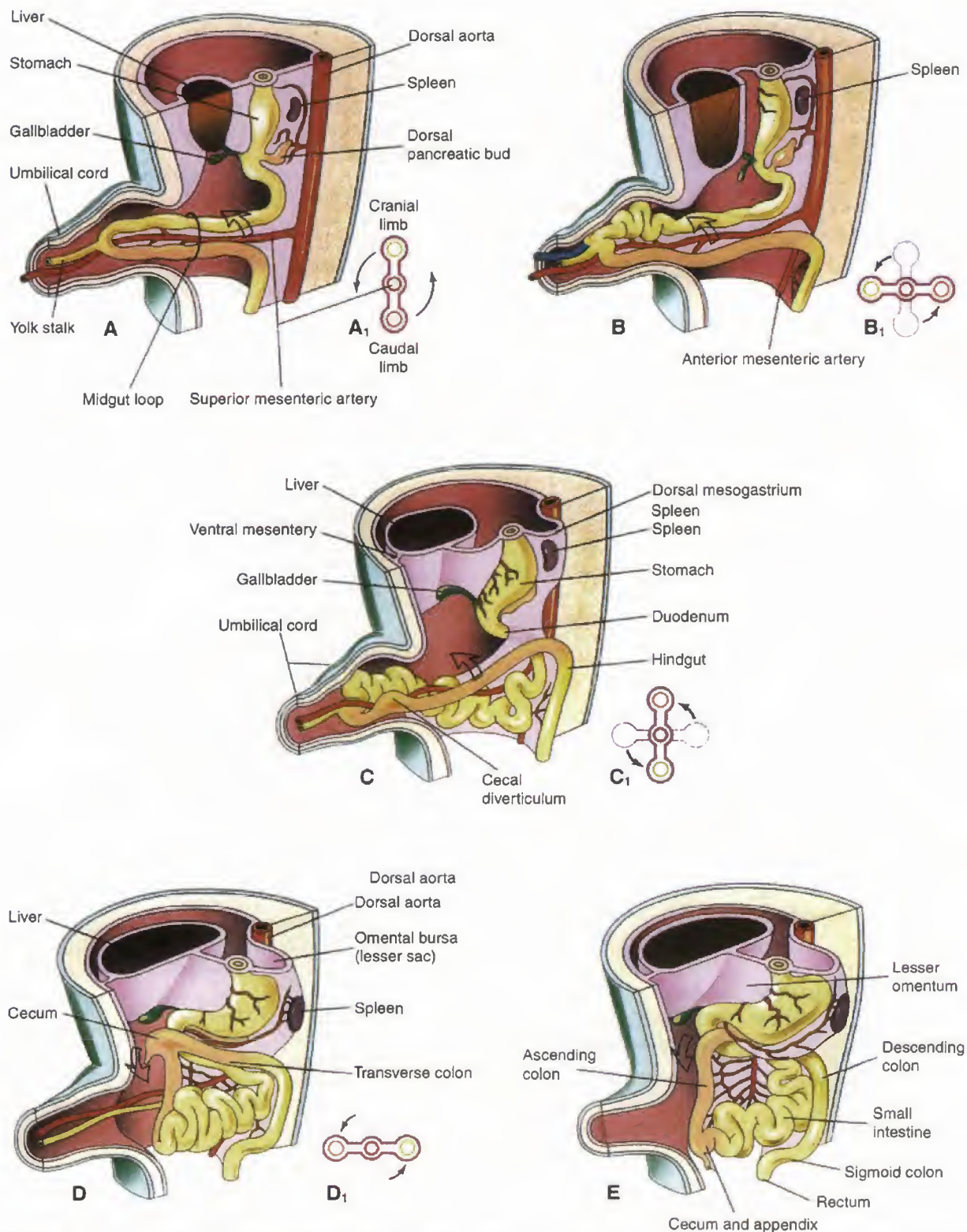


**FIGURE 15-55.** Process of physiologic herniation and reduction. At the beginning of the 8th menstrual week, a loop of midgut herniates into the proximal umbilical cord (A). The relationship to the superior mesenteric artery (SMA) to the bowel is illustrated in A1. At a later stage (B), the midgut begins to rotate 90 degrees counterclockwise (B1). At about the 12th menstrual week, the midgut returns to the abdomen (C and D), and at the same time progressive counterclockwise rotation occurs until the midgut has undergone a total of 270-degree rotation (C1 and D1). The final position of the cecum in the right lower quadrant is achieved later in the fetal period (E). (From Moore KL, Persaud TVN: *The Developing Human: Clinically Oriented Embryology*. Philadelphia, WB Saunders, 1998.)

- b. If there is an increase in amniotic fluid volume, it usually starts in the second half of pregnancy.
- c. Upper gastrointestinal obstruction (esophagus, stomach, duodenum, and jejunum) are quite often associated with polyhydramnios. In contrast, polyhydramnios is much less common in low gastrointestinal obstructions (ileum, colon, rectum, and anus).
- d. Polyhydramnios is common in congenital systemic diseases of the bowel (CIPO and congenital chloride diarrhea).
- e. The presence of "snowflakes" in the fluid is suggestive of epidermolysis bullosa in cases of pyloric atresia.
- 9. Digestive enzymes in the amniotic fluid
  - a. Digestive enzymes of the intestine and liver can be examined at 18 to 22 weeks' gestation.
  - b. A very low level of enzymes is suggestive of biliary atresia or cystic fibrosis.
  - c. A very high level of enzymes is suggestive of an obstruction of the duodenum or jejunum below the ampula of Vater, and fetal vomiting.

- d. A normal level of enzymes reduces significantly the probability of biliary atresia or intestinal obstruction.

#### 10. MRI

There are at present no convincing studies that MRI is better than ultrasound in the detection of gastrointestinal obstruction. We believe that in the future, MRI will be of value in the differential diagnosis between tubular duplications of the gastrointestinal tract, and other intra-abdominal echogenic findings. It will probably also be of help in the diagnosis of intra-hepatic solid tumors and bleeding.

#### 11. Ultrasound machines

Sonographers are advised to make habitual use of the machines they have grown accustomed to, as transducer frequency and gain and image processing can artificially enhance the apparent level of echogenicity of the bowel, leading to misinterpretation of sonographic findings.

#### 12. Parents consultation

We are still in the process of becoming familiarized with the various anomalies of the digestive system. Because a large portion of them bear resemblance to each other and share the same sonographic markers, making precise diagnoses is sometimes unfeasible, and parents should be informed of all possible differential diagnoses including normal outcome.



**FIGURE 15-56.** Malrotation at week 28. An amorphous mass (AM) and dilated colon.

## LIVER

The liver is an asymmetric structure. Its upper border is at the diaphragm. In a midclavicular parasagittal section of the right chest and abdomen the upper third is occupied by the lung, the middle third is occupied by the liver and the lower third is occupied by the intestine. In a midclavicular parasagittal section of the left chest and abdomen the upper third is occupied by the lung, about a quarter is occupied by the liver, and the remaining is occupied by the stomach and intestine. Sonographic differentiation between the fetal right and left lobes is not possible. An increase in the ultrasound attenuation coefficient of the liver as a function of gestational age has been observed. It has been suggested that this change is related to the increase in glycogen storage in the fetal liver.<sup>183,184</sup>



**FIGURE 15-57.** Cloacal dysgenesis. *Left*, A cystic conglomerate is seen in the pelvis. *Middle and Right*, Abnormal genitalia. (Reproduced with permission from F. Cuillier, [www.thefetus.net](http://www.thefetus.net).)



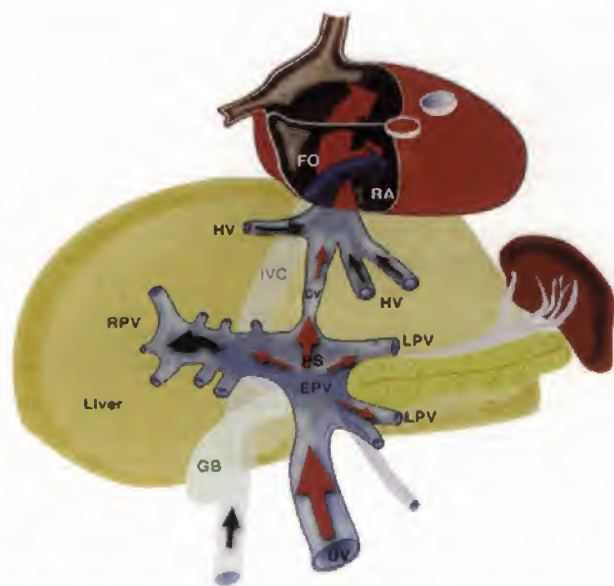


**FIGURE 15-58.** Schematic representation of the fetal umbilical, portal and hepatic venous circulations. The arrows indicate the direction of blood flow and the color, the degree of oxygen content (red, high; purple, medium; blue, low). The arrows indicate the direction of blood flow. DV, ductus venosus; EPV, extrahepatic portal vein; FO, foramen ovale; GB, gallbladder; HV, hepatic veins; IVC, inferior vena cava; LPV, left portal vein; PS, portal sinus; RA, right atrium; RPV, right portal vein; UV, umbilical vein. (From Mavrides E, Moscoso G, Carvacho JS, et al: *The anatomy of the umbilical, portal and hepatic venous systems in the human fetus at 14–19 weeks of gestation. Ultrasound Obstet Gynecol* 18:598, 2001.)

## Hepatic Circulation

A schematic representation of the venous circulation is presented in Figure 15-58. There is an oblique insertion of the umbilical vein into the liver. Inside the liver there is a trifurcation—right and left portal veins, and the ductus venosus, which continues to the inferior vena cava (Fig. 15-59).

## Hepatic Volume

The fetal hepatic volume may be estimated through measurements of hepatic length, circumference, and area using two- and three-dimensional ultrasound. Several studies have shown a high correlation among the liver volume, gestational age, and fetal weight in normal fetuses, whereas in small-for-gestational-age fetuses, the liver volume is decreased.<sup>185–188</sup> Of note, because of the asymmetric configuration of the liver, accurate measurements of the liver dimensions is not a simple task in daily practice, and many sonographers assess the liver's size subjectively.

## Hepatomegaly

Hepatomegaly, or hepatosplenomegaly, may be present in severe isoimmunization, congestive heart failure, infections, macrosomia, neoplasms, metabolic disorders such as Gaucher disease,<sup>188</sup> pyruvate kinase deficiency,<sup>190</sup> syphilis,<sup>191</sup> and overgrowth disorders like Beckwith-Wiedemann syndrome. Hepatosplenomegaly with and without hydrops is a possible marker of Down syndrome. Several studies have shown that

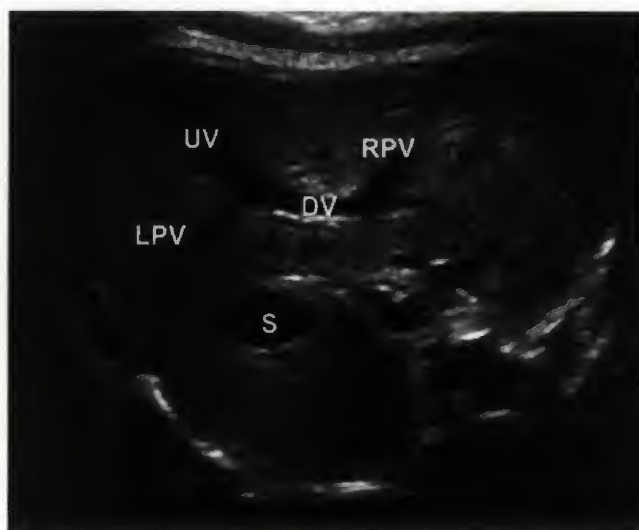


**FIGURE 15-59.** Hepatic venous circulation in a transverse/diagonal section. DV, ductus venosus; LPV, left portal vein; RPV, right portal vein; S, stomach; UV, umbilical vein.

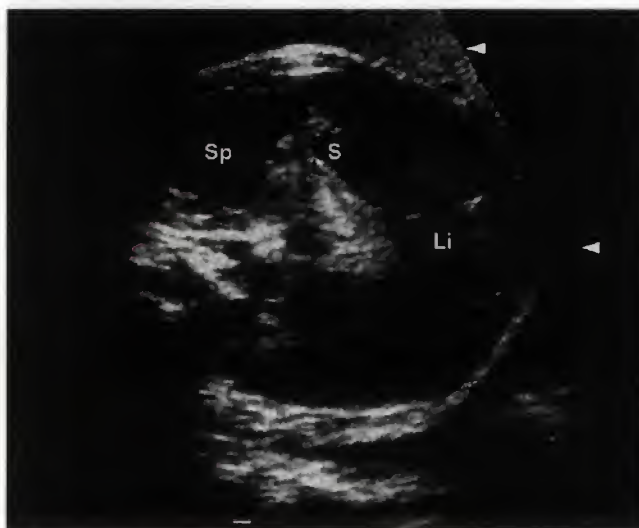


**FIGURE 15-60.** Hepatosplenomegaly in transient myeloploiesis and trisomy 21. Li, liver; Sp, spleen; S, stomach. (From Hamada H, Yamada N, Watanabe H, et al: *Hypoechoic hepatomegaly associated with transient abnormal myeloploiesis provides clues to trisomy 21 in the third-trimester fetus. Ultrasound Obstet Gynecol* 17:442, 2001.)

fetuses with trisomy 21 may have a transient myeloproliferative disorder in the second half of pregnancy (Fig. 15-60).<sup>192–197</sup> The increased liver in these cases may have normal, hypoechogenic, or hyperechogenic appearance. Fetal blood sampling will reveal leukocytosis with predominance of immature blast forms (Box 15-4).

## Simple Transient Idiopathic Cysts in Early Pregnancy

In early pregnancy (14–16 weeks gestation), the authors have noted simple cysts in 1 in 2500 fetuses. These cysts are of various sizes ranging from very small ones to cysts of

10 mm. They may be located in different parts of the liver and disappear in the second half of pregnancy (Fig. 15-61). After labor the infant's liver functions tests are normal. Very rarely such cysts may also first present in the third trimester of pregnancy after a normal scan in the second trimester (Fig. 15-62).<sup>198</sup>

### Polycystic Liver Disease

There are several forms of polycystic liver disease. One of them is the Caroli disease, which is a rare autosomal recessive disorder, characterized by cystic dilatation of the intrahepatic bile ducts. Associated polycystic kidney disease is common. The main clinical manifestations are recurrent cholangitis, jaundice, cirrhosis, cholangiocarcinoma, and

renal impairment. The prenatal diagnosis has been reported in very few cases, presenting as a cluster of cystic lesions in the liver (Fig. 15-63).<sup>199-202</sup> Polycystic kidneys may also be observed.

### Hepatic Mesenchymal Hamartoma

Hepatic mesenchymal hamartoma is a rare benign tumor, usually presenting as a rapidly growing mass in the first two

#### BOX 15-4 Hepatic Cysts-Classification

##### A. Isolated Cyst (Location Everywhere, But Usually in the Periphery)

1. Simple transient idiopathic cysts
2. Lymphangioma

##### B. Polycystic Liver

1. Several forms with and without polycystic kidneys

##### C. Multiple Septated Cysts (Mesenchymal Hamartoma)

##### D. Hilar Cysts (Location in the Hilus of the Liver)

1. Choledochal cysts
2. Extrahepatic biliary atresia



**FIGURE 15-62.** A hepatic cyst that first appeared in the third trimester gradually disappeared after birth.

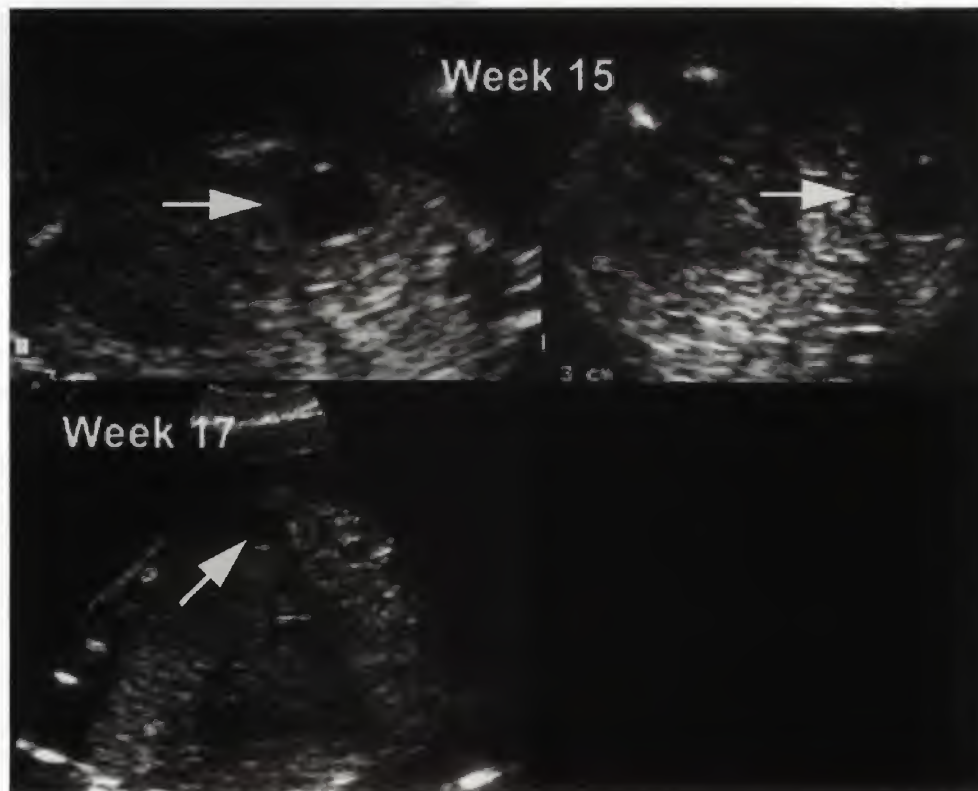


**FIGURE 15-61.** Simple transient idiopathic hepatic cysts (arrows) in three fetuses.





**FIGURE 15-63.** Caroli disease. A multicystic liver at week 30 (left) and in the newborn (right). (From Yuksel A, Has R, Isikoglu M, et al: Prenatal diagnosis of Caroli's disease. *Ultrasound Obstet Gynecol* 19:525, 2002.)

years of life. Because of its fast growth rate, it may cause hydrops, cardiac failure, and even fetal demise in utero. The sonographic appearance is of several cysts separated by thick septa. However, it may also present as a solid or mixed (solid and cystic) mass.<sup>203-207</sup> Absence of atrioventricular malformations is of help in the differential diagnosis from large hemangiomas.

Nonimmune hydrops might be a sequela of mesenchymal hamartoma. An association between hepatic mesenchymal hamartoma and cystic changes in the placenta due to mesenchymal stem villous hyperplasia has been reported by several investigators.<sup>204,207</sup> The underlying etiology of this association is not yet well understood. Resection of the tumor is the treatment of choice in cases of a large mass. In utero drainage of the cysts may be considered in premature fetuses, but its value is questionable because of the rapid reaccumulation of fluid in these cysts.<sup>204</sup>

## HEPATIC MASSES

### Hepatic Hemangioma

Hepatic hemangiomas are the most common benign tumors of the liver in the fetus and neonate. Synonyms used to describe this condition include hepatic arteriovenous malformation or hemangioendothelioma. They usually regress after an initial rapid growth, with complete involution by 12 to 18 months. Although benign, they can be life-threatening due to high output cardiac failure with and without hydrops, hemolytic anemia, severe thrombocytopenia, and disseminated intravascular coagulopathy (Kasabach-Merritt sequence).<sup>208-212</sup> Corticosteroids are the treatment of choice in infancy, as they cause vasoconstriction of the rapidly proliferating endothelial cells that line the vascular channels. Morris et al<sup>208</sup> have shown that maternal corticosteroid therapy was of value also in pregnancy, leading to a progressive decrease in the fetal hepatic mass.

The prenatal sonographic findings may vary depending on the tumor size (Fig. 15-64). Large tumors have a hypoechogenic appearance and atrioventricular malformations are noted. The feeding artery may show high velocity and low impedance blood flow, whereas the draining vein has an

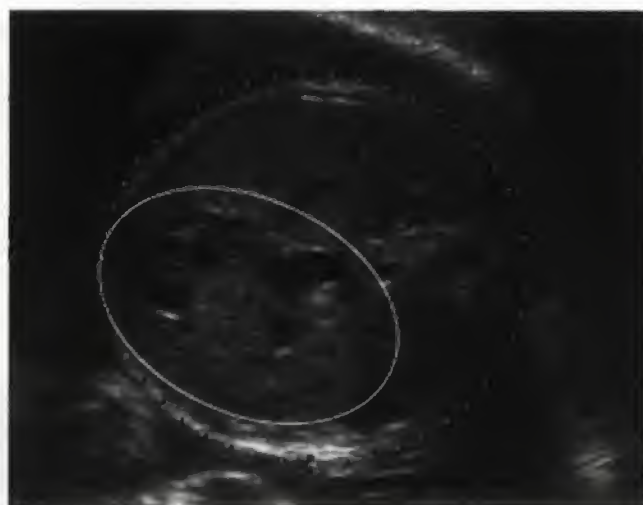


**FIGURE 15-64.** Hemangioendothelioma presenting as a conglomerate of cystic and solid elements (white circle). (Reproduced with permission from G. Ochoa, [www.thefetus.net](http://www.thefetus.net).)

antegrade blood flow pattern with low pulsatility.<sup>208-210</sup> Small tumors have a hyperechogenic appearance with no sonographic evidence of supplying or draining blood vessels.<sup>210,212</sup> It is possible that these small masses actually present intra-uterine involution of the hemangioma. Because of possible fetal complications, cord blood sampling is advocated and infusion of blood products should be considered in premature fetuses with an obvious hematologic disorder.

### Hepatoblastoma

Hepatoblastoma is the most common hepatic malignancy in young children. However, its incidence is very rare at approximately one per one million children younger than 15 years of age. The sonographic appearance is of a lobulated mass with an internal structure resembling spokes of a wheel<sup>213</sup> or a solid mass.<sup>214</sup>

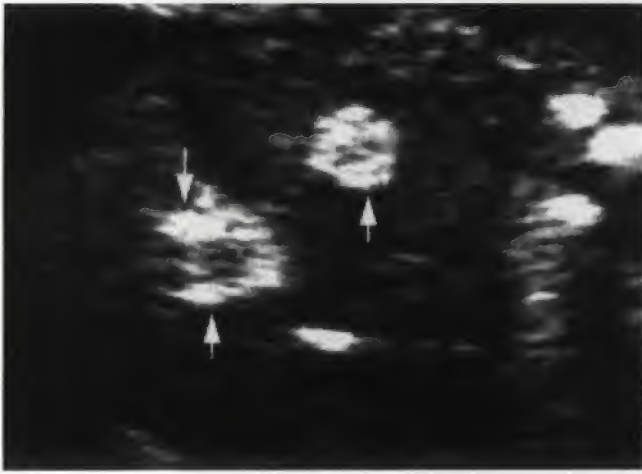


**FIGURE 15-65.** Liver calcifications (arrows) at week 18. The calcifications disappeared at week 32, and the outcome was favorable.

## Liver Calcifications

The reported incidence of fetal liver calcifications is 1:1000 to 1:1750. In many cases, this is a transient idiopathic phenomenon without any consequences. In few cases an underlying pathology is detected, mainly infections (primarily cytomegalovirus), vascular pathologies such as hematoma, thromboemboli of hepatic and portal veins, tumors of the liver, and different chromosomal anomalies.<sup>215-218</sup>

Fetuses may have one, two, or more calcified foci (Fig. 15-65), or even diffuse calcification of the liver as well as peritoneal and intestinal calcifications. The incidence of associated anomalies varies in the different series. Bronshtein and Blazer<sup>215</sup> found associated anomalies in 21% of cases, whereas Simchen et al<sup>218</sup> found associated anomalies in 65% of fetuses. The presence of an isolated sonographic finding of calcification does not exclude the possibility of an infection or aneuploidy. It is therefore suggested to perform a detailed sonographic examination in these fetuses and consider a search for chromosomal anomalies and viral infections.

## Gallbladder

Initially, the gallbladder is a solid mass at 4 weeks of embryonic life, and a definitive lumen develops by recanalization of the epithelium at the 7th week. Bile is formed by the liver at approximately 12 weeks' of gestation, entering the gallbladder and the intestinal system. When this fails to occur, the gallbladder remains atretic and does not develop. On ultrasound, the gallbladder appears at 7 to 14 weeks of gestation, as a teardrop of fluid with variable dimensions, and later gets a shape of a small club. It can be detected in 70% of fetuses at 13 weeks of gestation, and in 99% of cases at 15 weeks of gestation. In the second and third trimesters, the gallbladder is imaged as a small oval or rectangular cyst-like structure located to the right of the intrahepatic umbilical vein, at the lower border of the liver, close to the intestinal loops.

## Gallbladder-Anatomic Variants

Different anatomic variants of the gallbladder can be observed, and no clinical implication has been noted in these different forms, as far as they are a solitary finding in the fetus.

### Shape

The most common variants include duplication of gallbladder, huge gallbladder, L-shaped gallbladder, and transient septum (Fig. 15-66).

### Location

#### **Persistent Right Umbilical Vein**

The gallbladder may be located to the left of the umbilical vein in cases of a persistent right umbilical vein (Fig. 15-67). Early in embryonic development there are two umbilical veins. The right umbilical vein atrophies and the left umbilical vein persists. Persistent right umbilical vein may result from failure of the right umbilical vein to regress resulting in a right umbilical vein that persists and coexists with the left umbilical vein. The right umbilical vein may replace the left umbilical vein, or the right umbilical vein may persist and bypass the liver draining aberrantly into the inferior vena cava or the right atrium. Sonographically, the umbilical vein drains into the right portal vein rather than the left portal vein, the intrahepatic umbilical vein is located lateral and not medial to the gallbladder and the portal vein (often described 'hockey stick') configuration curves toward the stomach rather than parallel or away from it to the right. According to the literature, as well as our experience with 98 fetuses, the frequency of this location is 2 to 4 in 1000 pregnancies. There is a low probability of additional structural anomalies; however, when this is a solitary finding it is regarded as a benign anatomical variant with a favorable outcome.<sup>219-223</sup> Other anatomic variants appear under the umbilical vein or floating and surrounded by the intestinal loops.

## Nonvisualized Gallbladder

According to the authors' experience with more than 52,000 scans between 14 and 16 weeks' gestation, nonvisualization of the gallbladder is noted in 1:560 pregnancies. A nonvisualized gallbladder was defined as the inability to depict it on two targeted ultrasound examinations within a 1-week period. In about 25% of fetuses with a nonvisualized gallbladder, other structural and chromosomal anomalies are also observed. The main structural anomalies are Potter syndrome, abnormal kidneys, hydrops, diaphragmatic hernia, and mesomelia. The major chromosomal anomalies include triploidy (in 30% of cases), trisomy 9, 18, 20, and sex chromosome disorders.<sup>224</sup>

### **Nonvisualized Gallbladder as an Isolated Finding**

The following disorders may be present:

1. Gallbladder agenesis. The incidence is about 13 to 65 in 100,000 in general population, including 1% of nonvisualized gallbladder (NVG) cases. Agenesis is an



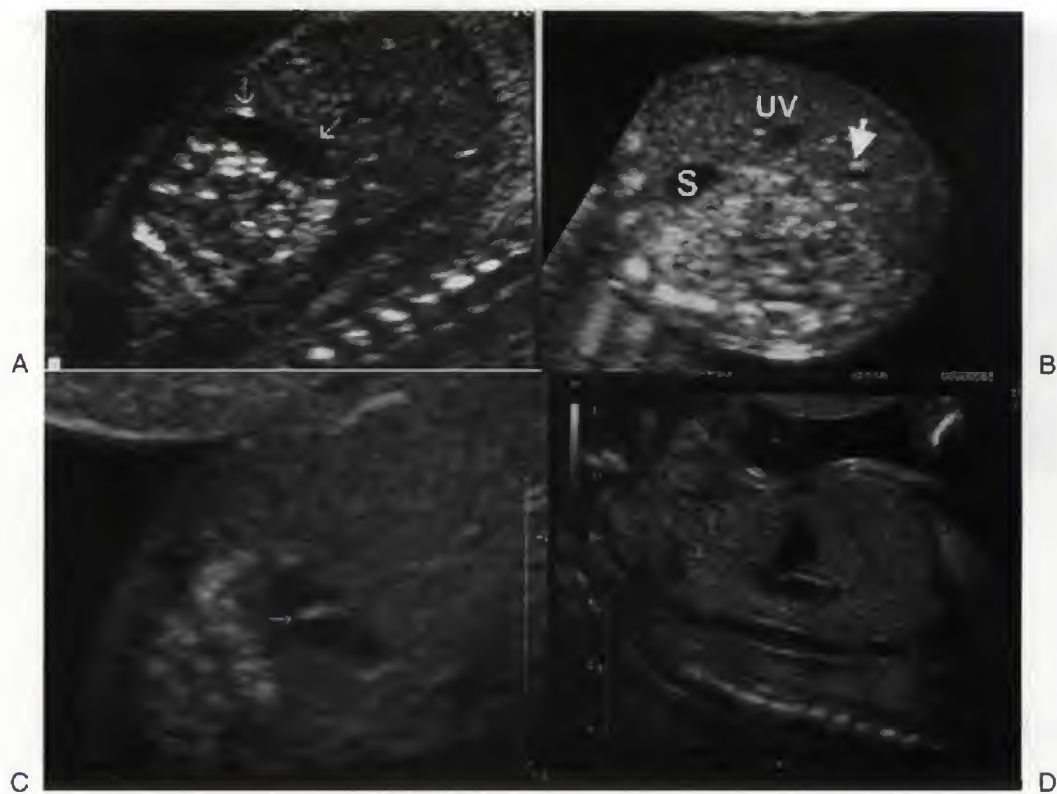


**FIGURE 15-66.** Normal variability in size and shape of the gallbladder. *A.* A huge gallbladder (*arrows*) at week 15. *B.* A small gallbladder (*arrow*) at week 15. Stomach (*s*) and the umbilical vein (*UV*) are depicted. *C.* A septated gallbladder week 15. *D.* An L-shaped gallbladder at week 24.

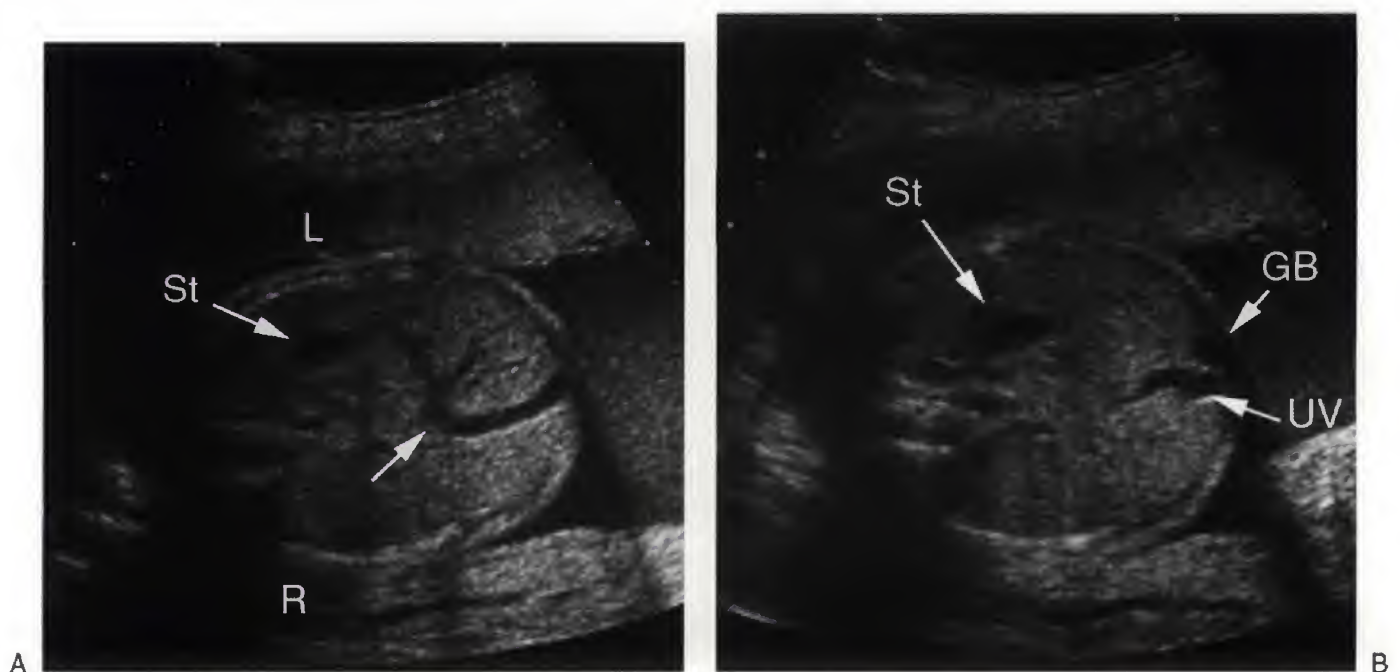


**FIGURE 15-67.** Persistent right umbilical vein. *A.* Transverse axial scan demonstrating the portal vein (*arrows*) curving toward rather than away from the stomach (*St*). L, left; R, right. *B.* Transverse scan demonstrating the umbilical vein (*UV*) to the right of the gallbladder (*GB*). Stomach (*St*).



**FIGURE 15-68.** Gallstones. *Left*, The sludge and stones (arrows) at week 35. *Right*, The normal empty gallbladder in the same newborn.

anatomic variant that usually has no clinical sequelae. Because of the familial tendency of this anomaly, ultrasound examination of the parents may be suggested in case of suspicion of such anomaly in the fetus.<sup>225</sup>

2. Cystic fibrosis. Less than 1% of fetuses with NVG will have cystic fibrosis, whereas the gallbladder is not detected in 75% of fetuses with cystic fibrosis. Cystic fibrosis is also associated with a low level of intestinal and liver enzymes in the amniotic fluid. This phenomenon might be of help in the prenatal diagnosis of the disease.<sup>95</sup>
3. Extrahepatic biliary atresia. This rare anomaly is discussed later in the chapter.

In summary, in all cases of NVG a search for chromosomal anomalies, cystic fibrosis, and digestive enzymes should be performed.

### Late-Onset Disappearance of Gallbladder

The authors observed four cases in which a gallbladder was depicted at 14 and 16 weeks' gestation but could not be seen later in pregnancy. In all these cases postnatal ultrasound revealed a normal gallbladder, and the infants had no medical disorders.

### Fetal Gallstones (Sludge in Gallbladder)

There are several case reports of fetuses with sludge in the gallbladder appearing as a pear-shaped hyperechoic structure. Usually, the gallbladder sludge mimics intrahepatic calcifications or hyperechoic bowel. In most cases, this sonographic feature has been described in the second and third trimesters, and disappeared in the first postnatal month (Fig. 15-68).<sup>226-228</sup> Brown et al<sup>226</sup> reported on the presence of gallstones until the age of 4.5 years, with all of them being asymptomatic.

### Extrahepatic Biliary Atresia

The prevalence of biliary atresia is 0.73 to 0.85 in 10,000 live births.<sup>229,230</sup> Biliary atresia is the leading cause of extrahepatic obstructive jaundice in the newborn and is the single

most frequent indication for liver transplantation in childhood.<sup>229</sup> It may be either isolated or associated with other malformations, mainly polysplenia, cardiac defects, and intra-abdominal anomalies. There are several variants of biliary atresia ranging from complete atresia to atresia of the choledochal duct. The French classification based on the anatomical pattern of the extrahepatic biliary tract remnants is most helpful for sonographers (Fig. 15-69).<sup>231,232</sup>

### Prenatal Diagnosis

There are few case reports on the detection of fetal biliary atresia.<sup>233-237</sup> The diagnosis is mainly based on nonvisualization of the gallbladder, depiction of a cystic structure in the hepatic region or specifically in the hilum, and detection of low levels of liver enzymes in the amniotic fluid. The differentiation from a choledochal cyst is important.

Using the above-mentioned classification, the following work-up is proposed:

**Types 1 and 3.** The gallbladder exists in these cases. Hence, the diagnosis will be overlooked in the general low-risk population. In patients with a family history of biliary atresia it is suggested to evaluate amniotic fluid liver enzymes even when the fetal gallbladder is depicted.

**Type 2.** These cases may be identified by the presence of a cyst in the liver hilum, or nonvisualization of the gallbladder. A cyst in the liver hilum may also represent a choledochal cyst. Matsubara et al<sup>238</sup> and Casaccia et al<sup>239</sup> noted that the size of the choledochal cyst increased steadily as gestational age advanced, whereas the size of the cyst in congenital biliary atresia remained unchanged throughout pregnancy. However, these are only case reports, and patients should therefore be informed about the risk of biliary atresia in every case of a cyst in the liver hilum. We suggest examining liver enzymes in such pregnancies.

**Type 4.** In such cases, there is nonvisualization of the gallbladder. Evaluation of liver enzymes is recommended.

### Choledochal Cyst

The incidence of choledochal cysts in Western countries is 1 per 100,000 live births. In Eastern countries such as Japan the incidence of this disorder is much higher. The female-to-male ratio is 3 to 4:1, and familial occurrences are scarce.



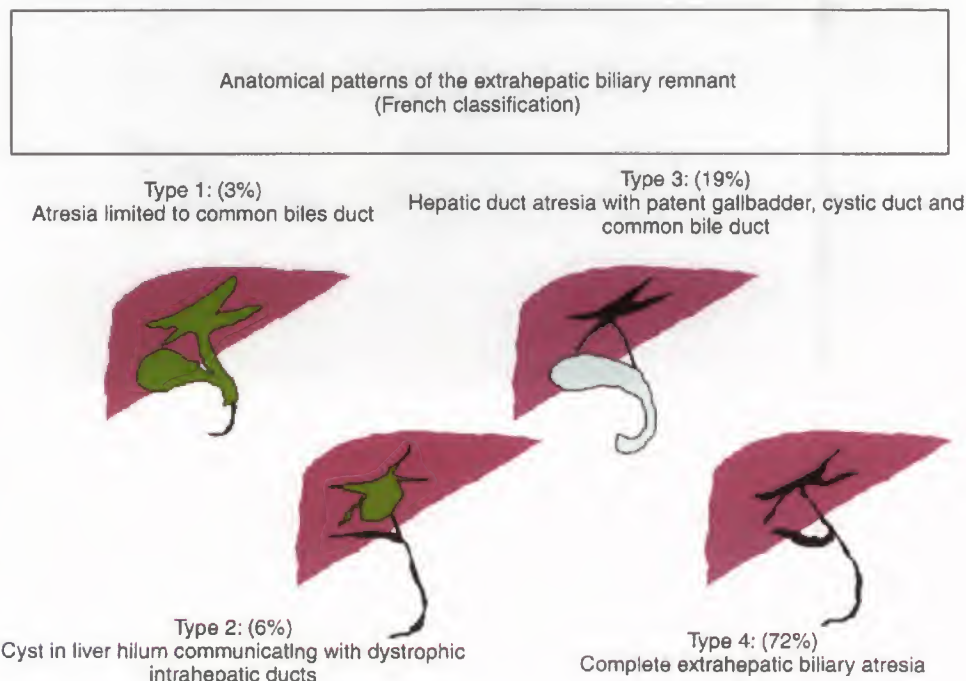


**FIGURE 15-69.** Anatomic patterns of the extrahepatic biliary remnant (French classification). (Courtesy of Dr. Christophe Chardot.)

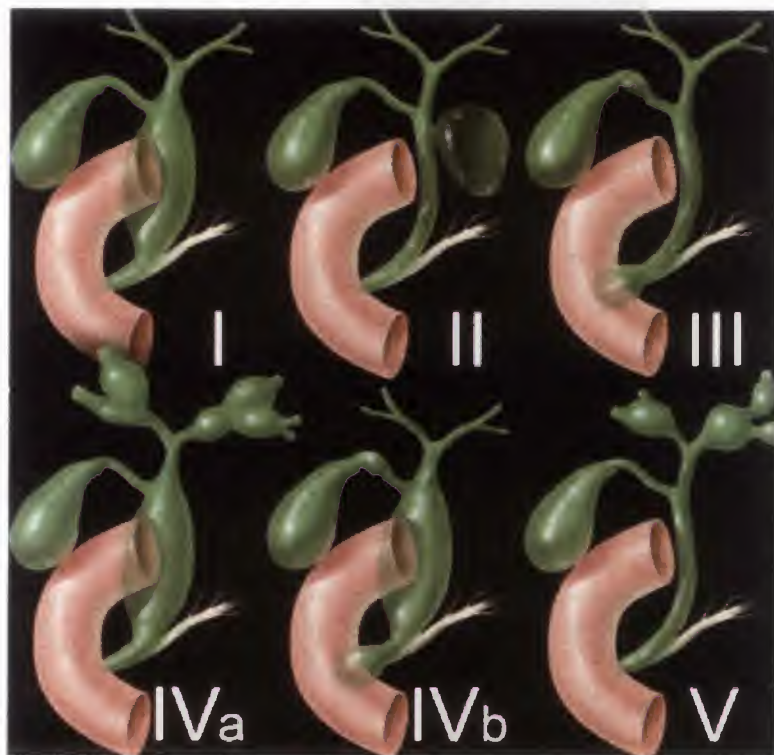


**FIGURE 15-70.** Graphic shows various types of choledochal malformation. Note the anomalous pancreaticobiliary junction; pancreatic duct insert into common bile duct proximal to the sphincter of Oddi. (From Donnelly LF, Jones BV, O'Hara SM, et al [eds]: *Diagnostic Imaging: Pediatrics*, 1st ed. Salt Lake City, Amirsys Inc., 2005, p. 96.)

The cause of these cysts is still unclear. The two leading theories suggest<sup>240</sup>

1. Pancreaticobiliary maljunction allowing pancreatic secretions to reflux into the biliary duct system.

There are five types of cystic anomalies of the choledochus (Todani classification) (Fig. 15-70).<sup>240</sup>

Excision of this cyst in infancy is advocated in order to prevent complications such as cholangitis and liver fibrosis. Of note, internal drainage procedures without cyst excision



**FIGURE 15-71.** Choledochal cyst: The elongated gallbladder (GB) and the round cyst (cyst) in the hepatic hilus resembles the exclamation mark. UV, umbilical vein.

avorable prognosis reported in the literature, we observed a fetus in which the choledochal cyst disappeared during pregnancy. In another case, the choledochal cyst diagnosed in utero, is currently asymptomatic and decreasing in size in the child.

### Prenatal Diagnosis

The presence of a cystic structure in the hepatic hilus should always alert the physician to a possibility of a choledochal cyst.<sup>238,239</sup> The authors noted that such cysts visualized in the same plane with the gallbladder provide an image of an exclamation mark (Fig. 15-71). The main differential diagnosis includes external biliary atresia and an isolated hepatic hilar cyst.

### SPLEEN

Several investigators presented nomograms of the spleen showing a relationship between its size and gestational age.<sup>242,243</sup> However, the spleen and liver have a similar echogenicity, and it is therefore difficult to precisely separate between these two organs while performing an ultrasound examination. The authors therefore believe that a reliable measurement of the normal spleen is not always accurate.

### Splenomegaly

Because of the above-mentioned limitation, the sonographic diagnosis of splenomegaly mainly relies on the following three findings<sup>244</sup>:

1. The stomach is displaced anteriorly and to the midline by the enlarged spleen.
2. The spleen is very close to the anterior abdominal wall (Fig. 15-72).

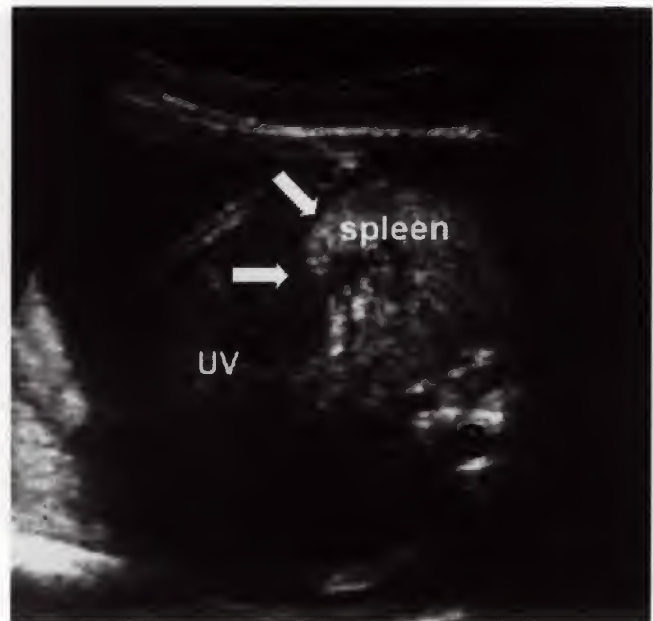


**FIGURE 15-72.** Enlarged hyperechogenic spleen (arrows) in a case of cytomegalovirus infection. S, spine; UV, umbilical vein. (Courtesy of Dr. Ron Auslander.)

3. Color Doppler imaging depicts multiple ramifications of the splenic artery and vein.

Splenomegaly may present in various fetal disorders, the most common of which are

1. Rh isoimmunization and other forms of fetal anemia.<sup>245,246</sup>
2. Infectious disorders such as cytomegalovirus.<sup>244</sup>
3. Metabolic disorders such as Gaucher disease, and pyruvate kinase deficiency.<sup>189,190</sup>
4. Transient myeloproliferative disorder, which sometimes appears in fetuses with Down syndrome.<sup>192-197</sup>
5. Overgrowth disorders such as Beckwith-Wiedemann syndrome.

### Splenic Cyst

Congenital splenic cysts are rare, of unknown origin, and usually present as an isolated finding. Spontaneous postnatal regression of these cysts has been described in many cases.<sup>247-249</sup> Large cysts (larger than 40 mm) call for special attention because of possible acute complications such as rupture, hemorrhage, and infection during childhood. Surgery or aspiration of cysts and sclerosis are therefore the recommended treatment in large cysts.<sup>249</sup> The sonographic differential diagnosis in the fetus includes cystic lesions in the upper left abdomen, mainly in the adrenal, kidney, mesentery, and gastrointestinal duplication cysts.

### PANCREAS

It is very difficult to sonographically differentiate between a normal pancreas, intestinal loops, and retroperitoneal texture. Occasionally, the pancreas can be depicted in the space



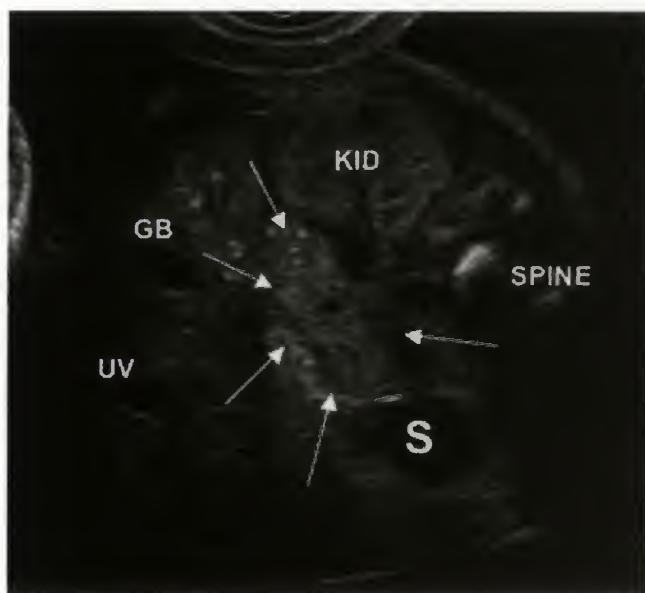


**FIGURE 15-73.** Pancreas. The normal pancreas is marked by arrows. S, stomach; GB, gallbladder; KID, kidney; UV, umbilical vein.

between the stomach, gallbladder, umbilical vein, and kidney. This image is best attained in a transverse axial plane of section at the level of the kidney (Fig. 15-73). Hata et al<sup>250</sup> were able to depict the pancreas in 80% of cases at 20 and 23 weeks' gestation, whereas at 36 and 39 weeks' gestation they could image the pancreas only in 38.4% of cases.

### Annular Pancreas

The annular pancreas arises from persistence of the dorsal pancreatic bud, creating a constricting ring around the duodenum. The anomaly is rare and accounts for only 1% of neonatal intestinal obstruction. However, associated anomalies occur in 10% to 20% of these cases, mainly duodenal obstruction, intestinal malrotation, and Down syndrome.<sup>251</sup>

An annular pancreas should therefore be suspected whenever the double bubble sign of duodenal obstruction is observed. There are a few reports of sonographic imaging of the annular pancreas, as an echogenic structure around the duodenum, immediately under the dilated segment.<sup>251,252</sup>

In the authors' experience depiction of an annular pancreas is difficult, and in most cases of duodenal obstruction, only a double bubble sign is depicted.

### Pancreatic Cyst

Congenital pancreatic cysts are rare and there is a female predominance. They arise from a developmental anomaly of the pancreatic ductal system. The cysts are either solitary or multiple and may even be so numerous to transform the pancreas into a cystic mass. The cysts are usually asymptomatic but may cause abdominal distension and pressure on adjacent viscera in the postnatal period. Excision of the cyst or internal drainage by cystoenterostomy is the treatment of choice in complicated cases.<sup>253,254</sup> Associated anomalies

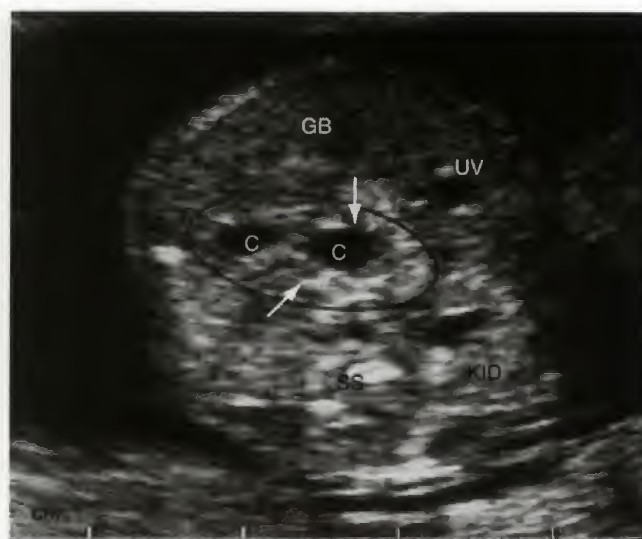


**FIGURE 15-74.** Polycystic pancreas at week 16 (Jeune syndrome). Two cysts (C) inside the demarcated pancreas. GB, gallbladder; KID, kidney; SS, spine; UV, umbilical vein.

have been observed in many of these fetuses. The most common are<sup>253-257</sup>

1. Polycystic disease of pancreas and kidney.
2. von Hippel-Lindau disease.
3. Asphyxiating thoracic dysplasia, short-limb dwarfism. (Jeune syndrome [Fig. 15-74]).
4. Hemihypertrophy.
5. Beckwith-Wiedemann syndrome.

The prenatal diagnosis of a pancreatic cyst should be suggested in cases of a sonographic findings of a cyst in the upper abdomen in the space between the stomach, gallbladder, umbilical vein, and kidney.<sup>253,255-257</sup>

### Pancreatoblastoma

Pancreatoblastoma is a rare tumor. The treatment of choice in childhood is chemotherapy and complete resection.<sup>258,259</sup> The association with Beckwith-Wiedemann syndrome was observed in some cases.<sup>260,261</sup> There are only very few reports on the antenatal findings in pancreatoblastoma. Cacciari<sup>262</sup> observed an amorphous structure with some features resembling a kidney (Fig. 15-75), whereas Pelizzo et al<sup>260</sup> found an isolated intra-abdominal cyst.

### Idiopathic Intra-Abdominal Cysts

A unique type of fetal cystic mass of unknown origin has been observed by the authors in the first and early second trimesters of pregnancy. These cysts are usually located laterally, and may have an hyperechogenic rim. They may occupy up to 60% of the abdominal diameter (Fig. 15-76). A connection between these cysts and abdominal organs could not be identified. A gradual reduction in their size is noted with advancing gestation, and in some cases, the cyst disappears completely, whereas in other cases, a small

hyperechogenic mass remains with features resembling hyperechogenic bowel. It is therefore possible that some of these cysts may actually be meconium cysts. Fetal outcome in all these cases has been favorable. Because of the unknown origin of these cysts, fetuses should be followed by repeated scans to exclude other cystic pathologies. There is a high probability that the cysts will disappear and the fetus will be healthy.

## ABDOMINAL WALL

### Physiological Midgut Herniation

During normal embryonic life, a rapid elongation of the gut and its mesentery as well as simultaneous marked growth and expansion of the liver occurs. The abdominal cavity becomes too small to contain all the intestinal loops, and they enter the extra-embryonic coelom in the umbilical cord

(Figs. 15–55 and 15–77). This process of physiologic midgut herniation takes place during the 6th week of development. During the 10th week, the intestine returns into the abdominal cavity; this process referred to as reduction of the midgut hernia. Timor-Tritsch et al<sup>263</sup> observed such normal herniation in 64% of fetuses at 8 weeks, in 100% during weeks 9 and 10, and in 25% of cases at 11 weeks of gestation. None of the fetuses studied at 12 weeks had a midgut herniation.

### Omphalocele (Exomphalos)

An omphalocele is a defect in the ventral abdominal wall whereby the herniated intra-abdominal content is covered by a membrane consisting of peritoneum and amnion. The small bowel is the most common herniated viscera (Fig. 15–78). Less common are the liver, spleen, stomach, and large bowel. Although bowel is the most common herniated viscera, in moderate to large omphaloceles liver is



**FIGURE 15-75.** Pancreatoblastoma at week 35. An amorphous pancreas is marked by arrows. Sp, spine. (Reproduced with permission from A. Cacciara, [www.thefetus.net](http://www.thefetus.net).)



**FIGURE 15-77.** Physiologic midgut herniation (arrow) at week 10.



**FIGURE 15-76.** Idiopathic intra-abdominal cyst at week 16. Left, transverse; Right, sagittal. S, stomach; K, kidney.





**FIGURE 15-78.** Omphalocele. *Left*, Ultrasound at week 15 showing the intestinal content inside the umbilical cord (arrows). *Right*, The neonate.

invariably present. The prevalence of omphalocele varies considerably in the literature, ranging between 0.74 and 3.9 per 10,000 births.<sup>264-267</sup>

### **Associated Anomalies**

Associated anomalies are observed in 67% to 88% of fetuses. Cardiac defects are present in 50% of cases, gastrointestinal anomalies in 40%, and chromosomal anomalies (mainly, trisomy 13, 18, and 21, and sex chromosome abnormalities) in 30% to 40% of cases.<sup>265,267-273</sup> An association has been observed between the content of the omphalocele and chromosomal defects. Karyotype abnormalities are more common in omphaloceles containing only bowel, and are much less frequent in omphaloceles with liver herniation only.<sup>274-276</sup> Currently, omphalocele is listed in 58 different syndromes.<sup>64</sup>

### **Prognosis**

The prognosis is related to the presence of associated structural and chromosomal anomalies. In a recent evaluation of 90 fetuses mainly with nonisolated omphalocele, the overall prognosis was generally poor.<sup>271</sup> However, review of the literature published between 1985 and 2003<sup>277</sup> revealed that most children with an isolated omphalocele fully participate in normal activities and education without reduction in their quality of life.

### **Prenatal Diagnosis**

The sonographic diagnosis of omphalocele is based on the presence of an abdominal wall defect with herniation of intestinal loops and liver (Fig. 15-79) as well as other abdominal organs into the omphalocele's sac. The umbilical cord is seen at the apex of the sac. It is the authors' experience that in most cases, it is possible to detect an edematous and cystic Wharton jelly around the trapped intestine. The cause and significance of these cysts are not clear (Fig. 15-80).



**FIGURE 15-79.** Omphalocele at week 13. The liver (L) inside the omphalocele sac (arrows).

### **Isolated Omphalocele—The Authors' Experience**

In case of an omphalocele detected at 14 and 16 weeks' gestation, a meticulous detailed targeted sonographic survey of all fetal organs (including echocardiography) is performed. It is our experience that an isolated omphalocele is not associated with chromosomal anomalies. However, because the question of chromosomal anomalies in an isolated omphalocele has not been addressed in large series, we still offer fetal karyotyping in all cases of omphalocele detection.

We have also noticed that on occasion a small isolated omphalocele detected in early pregnancy (14–16 weeks) may

disappear later in pregnancy and the newborns are healthy at birth (Fig. 15-81). Usually these omphaloceles contain only one or few intestinal loops.<sup>269</sup> The reason for a permanent or transient disappearance of an omphalocele is not yet clear, and very few reports on this phenomenon have been published.<sup>278,279</sup> If no associated anomalies are detected and the karyotype is normal, there is still a need to perform follow-up scans in pregnancy in order to detect possible markers of the Beckwith-Wiedemann syndrome.

### Omphalocele and Beckwith-Wiedemann Syndrome

Beckwith-Wiedemann syndrome has been reported in 10% to 22% of fetuses with isolated omphalocele.<sup>271,272</sup> It should be emphasized that it is yet not clear at which gestational age the classic signs of Beckwith-Wiedemann syndrome, namely, macroglossia, organomegaly, cystic and enlarged pancreas and abnormal kidneys, are apparent on ultrasound

examination (Fig. 15-82). There are even reports of late manifestation of the characteristic findings of this syndrome after delivery.<sup>280</sup> A careful ultrasound follow-up throughout gestation is therefore advocated in order to provide parents and caregivers with the maximum information for the ideal management of the pregnancy. Furthermore, it is worthwhile to follow up fetuses with omphalocele after birth (ultrasound of kidneys and adrenals) in order to exclude the possibility of Wilms' tumor and adrenal tumors, which may develop in the Beckwith-Wiedemann syndrome (Box 15-5).

### Gastroschisis

Gastroschisis is a paraumbilical defect of the abdominal wall, that is almost always right sided, resulting in evisceration of the abdominal content into the amniotic cavity (Fig. 15-84). As opposed to omphalocele, the herniated content in gastroschisis is not covered by membranes. The term "gastroschisis minor" denotes a small defect in which only omentum protrudes through the abdominal wall.

### Incidence and Etiology

The incidence of gastroschisis varies significantly between different geographic areas. For example, its rate is 4.4 per 10,000 births in southwest of England,<sup>281</sup> 3.01 per 10,000 births in Hawaii,<sup>282</sup> and 0.47 per 10,000 births in Japan.<sup>265</sup> A remarkable increase in the incidence of the anomaly was observed over the two last decades in many countries. The underlying reason for this increase is not yet elucidated. Several causative factors, including exposure to drugs, chemicals and smoking, have been suggested but they remain unsubstantiated.<sup>265</sup> Of interest, many studies have shown that gastroschisis is associated with a lower overall maternal age than omphalocele.<sup>264,265,267,270,283</sup>

### Associated Anomalies

The incidence of associated structural and chromosomal anomalies is lower than that in omphalocele. Chromosomal aberrations have been detected in 0% to 3%.<sup>265,267,270,272,273</sup> The reported incidence of structural anomalies ranges between 5% in England and Wales,<sup>281</sup> 18.8% in Japan<sup>12</sup> and 51% in France.<sup>267</sup> The most common disorder is intestinal

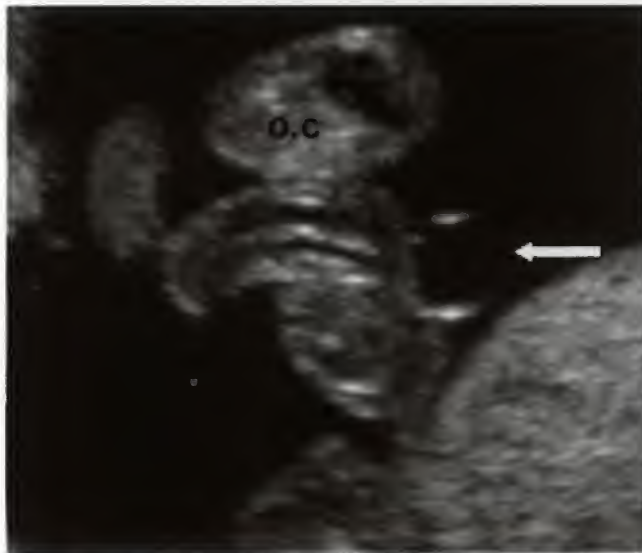


**FIGURE 15-80.** Omphalocele (oc) and Wharton jelly cyst (arrow) at week 16.



**FIGURE 15-81.** Transient omphalocele. Left, Omphalocele at week 15 (arrows). Right, Normal umbilical cord in the same fetus at week 20 (wide arrow).



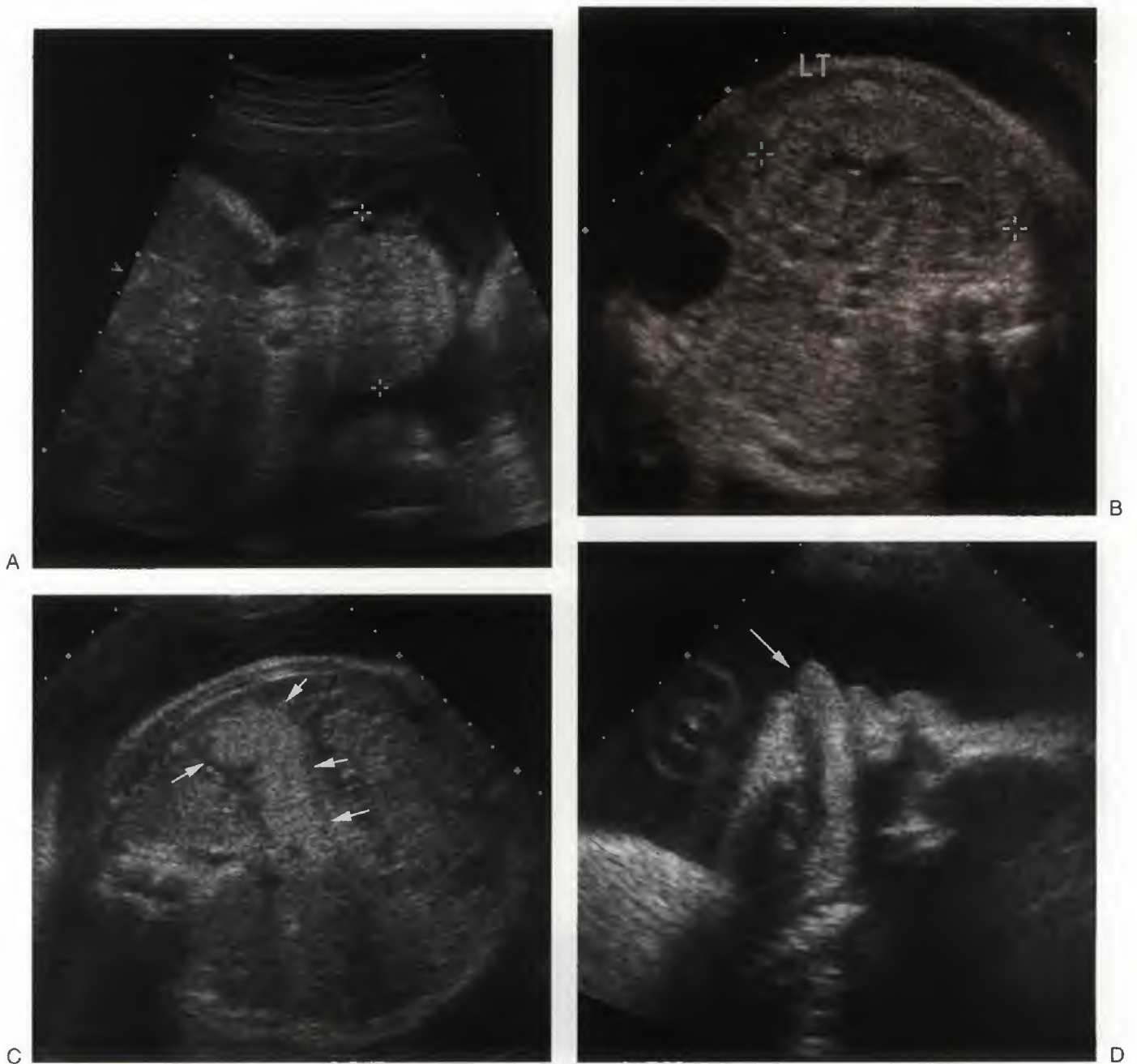


**FIGURE 15-82.** Omphalocele with Beckwith-Wiedemann syndrome. *A.* An omphalocele with predominant liver herniation is seen. *B.* An enlarged fetal kidney is identified. *C.* Markedly enlarged pancreas (*arrows*). *D.* Macroglossia with a protruding tongue (*arrow*).

atresia (10%–20%), which in some cases also causes intussusception and volvulus.<sup>267,277,283–285</sup> It has been suggested that the main reasons for the intestinal damage are exposure to the amniotic fluid and constriction at the abdominal wall defect resulting in ischemia.<sup>285</sup>

## Mode of Delivery

There is currently a trend to deliver these fetuses by a cesarean section assuming that more damage may be caused to the herniated intestine during vaginal delivery. However, studies addressing this issue failed to show a difference in

fetal morbidity or mortality between vaginal and abdominal deliveries.<sup>285–289</sup>

## Prognosis

The survival rate is approximately 92% in fetuses with no other major anomalies.<sup>272,277,288,290,291</sup> Long-term outcomes are mainly related to the gastrointestinal condition. Approximately 10% of patients will have hypoperistalsis syndrome.<sup>277</sup> Other problems, including severe neurologic and developmental disorders, have also been reported in some cases.<sup>272</sup>

## Prenatal Diagnosis

The characteristic sonographic finding is that of cauliflower-like intestinal loops floating freely in the amniotic fluid (Fig. 15–85). The diagnosis can be made in the first trimester.<sup>292</sup> Unlike cases of omphalocele, there is no membranous sac and the umbilical cord is usually normally inserted left of the abdominal wall defect. Evisceration of the liver or other abdominal organs is rare. Marked dilatation and thickening of herniated bowel may be a sign of intestinal damage; however, the accuracy of ultrasound in determining abnormal bowel in this condition has been disappointing. In the third trimester, the normal fluid-filled herniated colon should not be mistaken for abnormally dilated bowel.

### BOX 15–5 Differential Diagnosis of Omphalocele

1. Gastroschisis is discussed later in the chapter.
2. Midline disruption sequence is discussed later in the chapter.
3. Physiological midgut herniation. Physiological midgut herniation may be large; Therefore, it may not be possible to differentiate it from an omphalocele containing solely intestinal loops in the first trimester. Only omphaloceles containing liver may definitely be diagnosed in the first trimester.
4. Umbilical cord. Cyst, edema, lymphangioma, or calcified Wharton jelly (Fig. 15–83).
5. Umbilical hernia

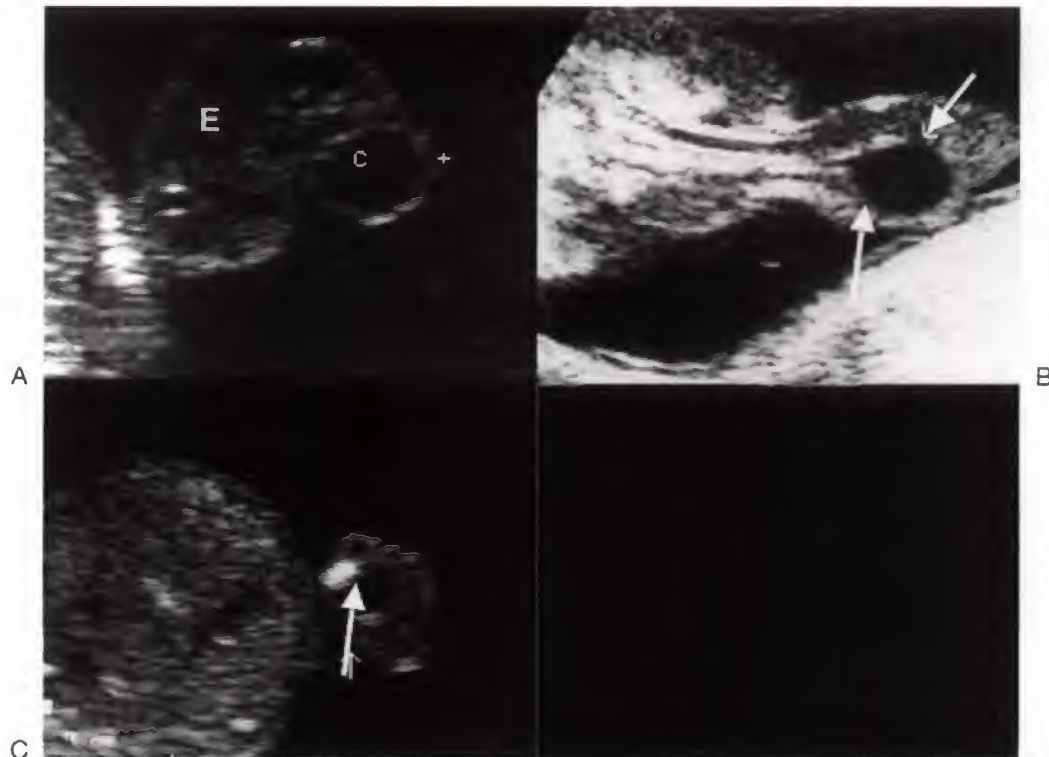


**FIGURE 15–83.** Differential diagnosis of omphalocele. A. An edematous cord (E) with a cyst (c). B. A medium size umbilical cyst (arrows). C. A small umbilical cyst and calcified focus (arrow).



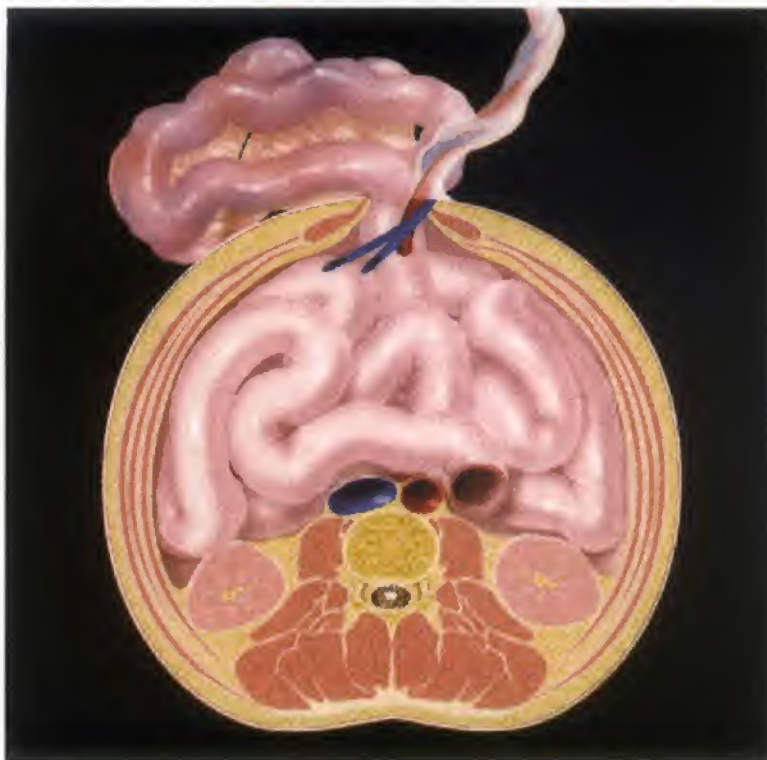


**FIGURE 15–84.** A. Graphic presentation of an abdominal wall defect with herniation of small bowel. The defect is to the right and adjacent to the normally inserted umbilical cord. (From Donnelly LF, Jones BV, O'Hara SM, et al [eds]: *Diagnostic Imaging: Pediatrics*, 1st ed. Salt Lake City, Amirsys Inc., 2005, p. 66.) B. Newborn with gastroschisis. Herniated bowel is seen to the right of the umbilical cord. In this case the bowel is thickened and matted. (From Clark DA, *Atlas of Neonatology: A companion to Avery's Diseases of the Newborn*. Philadelphia, WB Saunders Co., 2000.)





**FIGURE 15-85.** Gastroschisis. A, and B. Two different sections of the same fetus at week 15. The extra-abdominal intestine is marked by bold arrows. Umbilical cord (thin arrows on A). C. Gastroschisis (arrows) in another fetus at week 13.

Additional differential diagnoses include

1. Midline disruption sequence.
2. Cloacal extrophy or bladder extrophy.
3. Cystic or edematous umbilical cord.

## MIDLINE DISRUPTION SEQUENCE

During the 4th week of gestation, the embryo begins to undergo a process of folding that converts it from a flat germ disc into a three-dimensional structure. The cephalic, lateral, and caudal edges are brought together along the ventral midline, and the endodermal, mesodermal and ectodermal layers fuse to the corresponding layer on the opposite side. The fusion process of the amnion also starts at this stage and the amniotic sac encircles the fetus (Fig. 15-86). A defect in these embryologic processes results in fetal anomalies. The extent of malformation depends on the time of insult and size of damaged embryonic zone. As to the abdominal wall, if the damaged embryonic zone is large an evisceration of many abdominal organs is expected. In case of an improper closing of the amnion, part of the eviscerated organs will be located outside the amniotic sac (Fig. 15-87).<sup>293</sup> In addition to the abdominal wall, malformations observed in other structures may involve the limbs, lower urinary system, cloaca, and external genitalia.

Many syndromes and variations of abdominal wall defects have been described. The spectrum of midline disruption

syndromes is wide and includes many anomalies. A careful review of the literature reveals that there is significant overlapping between these syndromes and that the differences are often hardly distinguishable. Furthermore, the terminology is not always clear and many synonyms are used to denote such syndromes.<sup>293-302</sup> The authors therefore assume that the different anomalies reported are actually variable forms of a large spectrum of midline disruption. Midline disruption anomalies are rare, and hence, it is difficult to determine their incidence. Among 52,000 pregnancies examined by the authors, there were seven fetuses with a midline disruption sequence. The earliest diagnosis was made at 8 weeks of gestation (Box 15-6).

## CLOACAL EXSTROPY SEQUENCE

The best known variant of this anomaly is the OEIS complex characterized by omphalocele, extrophy of bladder, imperforate anus, and spinal anomalies. The main sonographic findings of cloacal extrophy are nonvisualization of the bladder, anterior abdominal wall defect, or a cystic mass protruding from the anterior abdominal wall, omphalocele, skeletal anomalies, and abnormal genitalia (Fig. 15-88).<sup>303,304</sup>

## Vesicoallantoic Cyst/Patent Urachus

When a cystic structure is seen adjacent to the lower anterior abdominal wall, the diagnosis of omphalocele is often



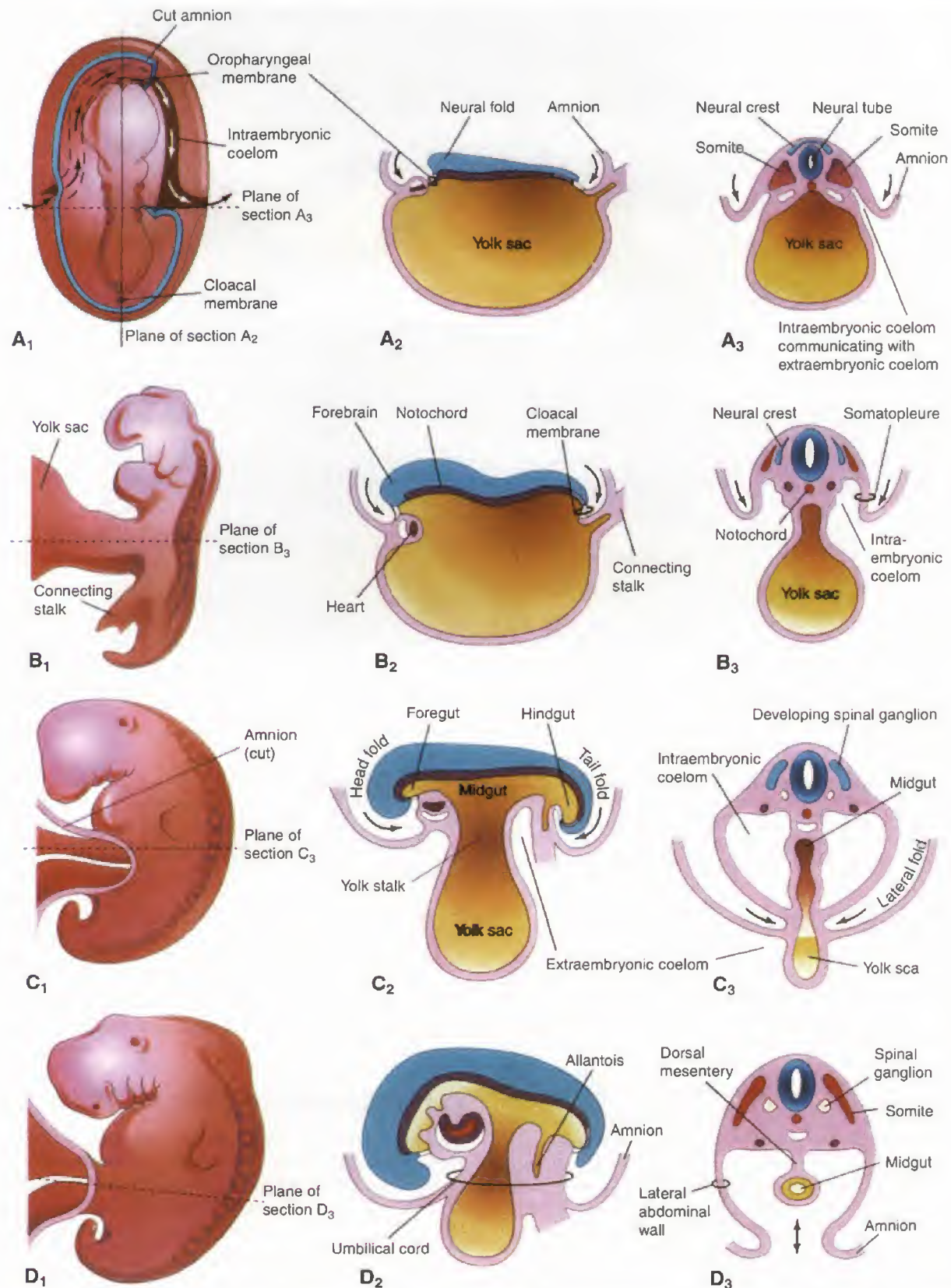


**FIGURE 15-86.** Illustration of serial embryonic development during the 4th week of development (6th menstrual week). A1-A3 is the beginning of the 4th week, B1-B3 at 22 days, C1-C3 at 26 days, D1-D3 at 28 days. B1, C1, and D1 are lateral views at the plane of section designated in A1, A2 to D2 are sagittal views, and A3 to D3 are transverse views at planes designated at A1 to D1. (From Moore KL, Persaud TVN: *The Developing Human: Clinically Oriented Embryology*. Philadelphia, WB Saunders, 1998.)

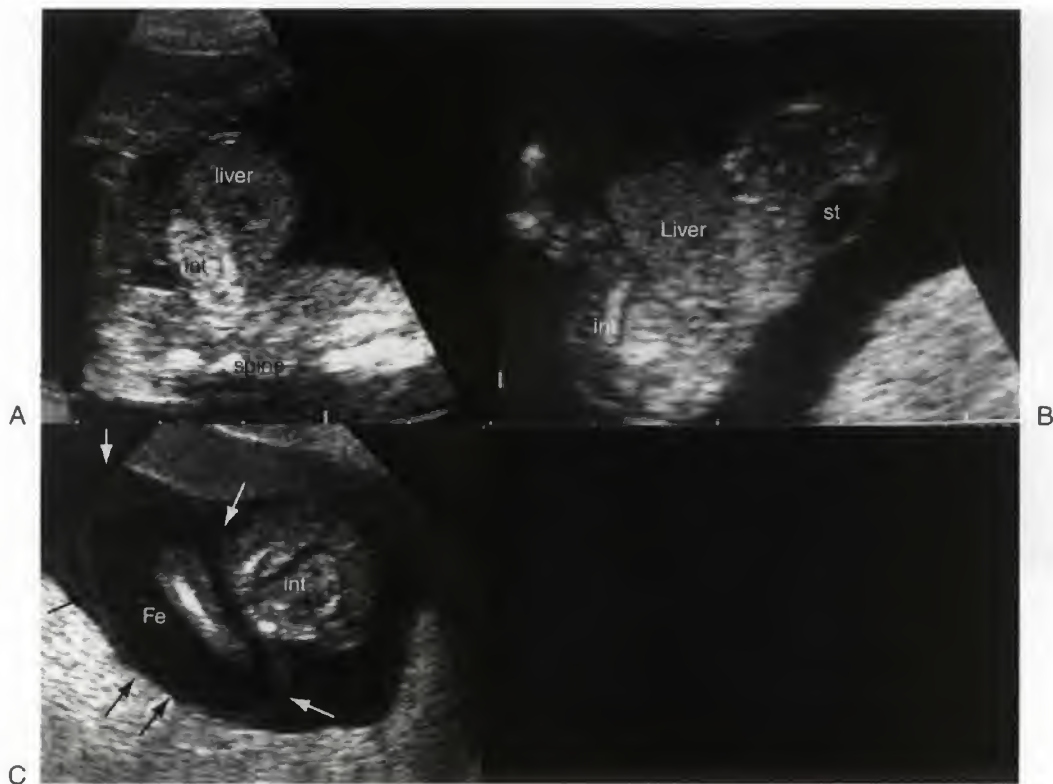


**FIGURE 15-87.** Midline disruption sequence. Three fetuses with different expression of the anomaly. *A.* A mild form, only part of the liver and intestine (int) are herniated. *B.* A severe form, the whole liver, stomach (st) and intestine (int) are herniated. *C.* The most severe form, the intra-abdominal content (int) lies outside the amniotic sac (arrows). The amniotic sac contained only the skeleton. Fe, femur.

#### BOX 15-6 Terminology and Synonyms Used for Anomalies of the Midline Disruption Sequence

Pentalogy of Cantrell  
 Thoracoabdominal eventration  
 Thoracoabdominal syndrome  
 Limb body-wall complex  
 Limb body-wall deficiency syndrome

Body wall defects with limb-reduction anomalies  
 Body stalk anomaly  
 Fissure of the abdominal wall with eventration of the abdominal organs  
 Dysplasia umbilicofetalis



**FIGURE 15-88.** Cloacal exstrophy. *Left,* The herniated cloaca with a urinary bladder. *Right,* The newborn. (Reproduced with permission from R. Jaffe, [www.thefetus.net](http://www.thefetus.net).)





**FIGURE 15-89.** Vesico-allantoic cyst/patent urachus. A cyst (Cy) adjacent to the anterior abdominal wall is seen in continuity (asterisk) with the fetal urinary bladder (Bl).

suspected. When the cyst is seen to connect to the fetal urinary bladder (located normally within the fetal pelvis), the diagnosis of a vesico-allantoic cyst/patent urachus should be entertained (Fig. 15-89).

The allantois is an embryonic structure that develops as a diverticulum from the yolk sac. The allantois becomes incorporated into the embryo, connecting the ventral aspect of the urogenital sinus to the external portion of the umbilicus.<sup>305</sup> The urachus is an embryologic remnant of the allantois. The lumen of the allantois eventually becomes obliterated and the urachus closes to form the median umbilical ligament.<sup>306</sup>

A patent urachus is rare, with an incidence of 1% to 2.5% per 100,000.<sup>307</sup> As mentioned previously, whereas an omphalocele is often first suspected when a cystic mass is seen, the presence of a fluid-filled mass in direct communication with the fetal urinary bladder, as well as the absence of bowel contents, allows one to discriminate between the two. This is important because the prognosis is far different with few associated abnormalities when a patent urachus is seen.<sup>306</sup>

## References

- Embryology: An Illustrated Colour Text. Philadelphia, Elsevier Limited, 2005.
- The Developing Human: Clinically Oriented Embryology, 6th ed. Philadelphia, WB Saunders, 1998.
- Avni EF, Rypens F, Milaire J, et al: Fetal esophagus: Normal sonographic appearance. *J Ultrasound Med* 13:175, 1994.
- Malinge G, Levine A, Rotmens S, et al: The fetal esophagus: Anatomical and physiological ultrasonographic characterization using a high-resolution linear transducer. *Ultrasound Obstet Gynecol* 24:500, 2004.
- Torfs CP, Curry CJ, Bateson TF, et al: Population-based study of urachoesophageal fistula and esophageal atresia. *Teratology* 52:220, 1995.
- Sparey C, Jawaheer G, Barrett AM, et al: Esophageal atresia in the Northern Region Congenital Anomaly Survey, 1985-1997: Prenatal diagnosis and outcome. *Am J Obstet Gynecol* 182:427, 2000.
- Forrester MB, Merz RD: Epidemiology of oesophageal atresia and tracheo-oesophageal fistula in Hawaii, 1986-2000. *Public Health* 119:483, 2005.
- Kallen B, Mastroiacovo P, Robert E, et al: Major congenital malformations in Down syndrome. *Am J Med Genet* 65:160, 1996.
- Bianca S, Bianca M, Ettore G, et al: Oesophageal atresia and Down syndrome. *Downs Syndr Res Pract* 8:29, 2002.
- Satoh S, Takashima T, Takeuchi H, et al: Antenatal sonographic detection of the proximal esophageal segment: specific evidence for congenital esophageal atresia. *J Clin Ultrasound* 23:419, 1995.
- Stringer MD, McKenna KM, Goldstein RB, et al: Prenatal diagnosis of esophageal atresia. *J Pediatr Surg* 30:1258, 1995.
- Kalache KD, Wauer R, Mau H, et al: Prognostic significance of the pouch sign in fetuses with prenatally diagnosed esophageal atresia. *Am J Obstet Gynecol* 182:978, 2000.
- Langer JC, Hussain H, Khan A, et al: Prenatal diagnosis of esophageal atresia using sonography and magnetic resonance imaging. *J Pediatr Surg* 36:804, 2001.
- Shulman A, Mazkereth R, Zalel Y, et al: Prenatal identification of esophageal atresia: The role of ultrasonography for evaluation of functional anatomy. *Prenat Diagn* 22:669, 2002.
- Centini G, Rosignoli L, Kenanidis A, et al: Prenatal diagnosis of esophageal atresia with the pouch sign. *Ultrasound Obstet Gynecol* 21:494, 2003.
- Has R, Gunay S: Upper neck pouch sign in prenatal diagnosis of esophageal atresia. *Arch Gynecol Obstet* 270:56, 2004.
- Yagel S, Sonigo P, Rousseau V, et al: Esophageal atresia diagnosed with three-dimensional ultrasonography. *Ultrasound Obstet Gynecol* 26:307, 2005.
- Levine D, Barnewolt CE, Mehta TS, et al: Fetal thoracic abnormalities: MR imaging. *Radiology* 228:379, 2003.
- Matsuoka S, Takeuchi K, Yamanaka Y, et al: Comparison of magnetic resonance imaging and ultrasonography in the prenatal diagnosis of congenital thoracic abnormalities. *Fetal Diagn Ther* 18:447, 2003.
- Langman J, Sadler TW: Langman's Medical Embryology, 6th ed. Baltimore, Williams & Wilkins, 1990.
- Pameijer CR, Hubbard AM, Coleman B, et al: Combined pure esophageal atresia, duodenal atresia, biliary atresia, and pancreatic ductal atresia: Prenatal diagnostic features and review of the literature. *J Pediatr Surg* 35:745, 2000.
- Dundas KC, Walker J, Laing IA: Oesophageal and duodenal atresia suspected at the 12 week booking scan. *BJOG* 108:225, 2001.
- Marquette GP, Skoll MA, Yong SL, et al: First-trimester imaging of combined esophageal and duodenal atresia without a tracheoesophageal fistula. *J Ultrasound Med* 23:1232, 2004.
- Cheyne N, Rat P, Couailler JF, et al: Tubular duplication of the esophagus. Contribution of magnetic resonance imaging in anatomical analysis before surgery. *Surg Radiol Anat* 22:289, 2000.
- Carachi R, Azmy A: Foregut duplications. *Pediatr Surg Int* 18:371, 2002.
- Wootton-Gorges SL, Eckel GM, Poulos ND, et al: Duplication of the cervical esophagus: A case report and review of the literature. *Pediatr Radiol* 32:533, 2002.
- Puligandla PS, Nguyen LT, St-Vil D, et al: Gastrointestinal duplications. *J Pediatr Surg* 38:740, 2003.
- Gul A, Tekoglu G, Aslan H, et al: Prenatal sonographic features of esophageal and ileal duplications at 18 weeks of gestation. *Prenat Diagn* 24:969, 2004.
- Samuel M, Burge DM, Griffiths DM: Prenatal diagnosis of laryngotracheoesophageal clefts. *Fetal Diagn Ther* 12:260, 1997.
- Noonily MJ, Farmer DL, Flake AV: The association of complete laryngotracheoesophageal cleft with left lung agenesis: Pathophysiological clues provided by an experiment of nature. *J Pediatr Surg* 33:1546, 1998.
- Carr MM, Clarke KD, Webber E, et al: Congenital laryngotracheoesophageal cleft. *J Otolaryngol* 28:112, 1999.
- Kawaguchi AL, Donahoe PK, Ryan DP: Management and long-term follow-up of patients with types III and IV laryngotracheoesophageal clefts. *J Pediatr Surg* 40:158, 2005.
- Perera GB, Milne M: Neurenteric cyst: Antenatal diagnosis by ultrasound. *Australas Radiol* 41:300, 1997.
- Almog B, Leibovitch L, Achiron R: Split notochord syndrome—Prenatal ultrasonographic diagnosis. *Prenat Diagn* 21:1159, 2001.



35. Agangi A, Paladini D, Bagolan P, et al: Split notochord syndrome variant: Prenatal findings and neonatal management. *Prenat Diagn* 25:23, 2005.
36. Blaas HG, Eik-Nes SH, Kiserud T, et al: Early development of the abdominal wall, stomach and heart from 7 to 12 weeks of gestation: A longitudinal ultrasound study. *Ultrasound Obstet Gynecol* 6:240, 1995.
37. Sase M, Asada H, Okuda M, et al: Fetal gastric size in normal and abnormal pregnancies. *Ultrasound Obstet Gynecol* 19:467, 2002.
38. Ben-Haroush A, Yogev Y, Peled Y, et al: Correlation between fetal gastric size and amniotic fluid volume. *J Clin Ultrasound* 33:119, 2005.
39. Kepkep K, Tuncay YA, Goynumer G, et al: Nomogram of the fetal gastric size development in normal pregnancy. *J Perinat Med* 33:336, 2005.
40. Zimmer EZ, Chao CR, Abramovich G, et al: Fetal stomach measurements: Not reproducible by the same observer. *J Ultrasound Med* 11:663, 1992.
41. Sase M, Miwa I, Sumie M, et al: Ontogeny of gastric emptying patterns in the human fetus. *J Matern Fetal Neonatal Med* 17:213, 2005.
42. Sase M, Miwa I, Sumie M, et al: Gastric emptying cycles in the human fetus. *Am J Obstet Gynecol* 193:1000, 2005.
43. McKenna KM, Goldstein RB, Stringer MD: Small or absent fetal stomach: Prognostic significance. *Radiology* 197:729, 1995.
44. Brumfield CG, Davis RO, Owen J, et al: Pregnancy outcomes following sonographic nonvisualization of the fetal stomach. *Obstet Gynecol* 91:905-, 1998.
45. Hill LM: Congenital microgastria: absence of the fetal stomach and normal third trimester amniotic fluid volume. *J Ultrasound Med* 13:894, 1994.
46. Kroes EJ, Festen C: Congenital microgastria: A case report and review of literature. *Pediatr Surg Int* 13:416, 1998.
47. Menon P, Rao KL, Cutinha HP, et al: Gastric augmentation in isolated congenital microgastria. *J Pediatr Surg* 38:E4, 2003.
48. Lepinard C, Descamps P, Meneguzzi G, et al: Prenatal diagnosis of pyloric atresia-junctional epidermolysis bullosa syndrome in a fetus not known to be at risk. *Prenat Diagn* 20:70, 2000.
49. Okoye BO, Parikh DH, Buick RG, et al: Pyloric atresia: Five new cases, a new association, and a review of the literature with guidelines. *J Pediatr Surg* 35:1242, 2000.
50. Ilce Z, Erdogan E, Kara C, et al: Pyloric atresia: 15-year review from a single institution. *J Pediatr Surg* 38:1581, 2003.
51. Nakamura H, Sawamura D, Goto M, et al: Epidermolysis bullosa simplex associated with pyloric atresia is a novel clinical subtype caused by mutations in the plectin gene (PLEC1). *J Mol Diagn* 7:28, 2005.
52. Rizzo G, Capponi A, Arduini D, et al: Prenatal diagnosis of gastroesophageal reflux by color and pulsed Doppler ultrasonography in a case of congenital pyloric atresia. *Ultrasound Obstet Gynecol* 6:290, 1995.
53. Meizner I, Carmi R: The snowflake sign. A sonographic marker for prenatal detection of fetal skin denudation. *J Ultrasound Med* 9:607, 1990.
54. De Jenlis Sicot B, Druelle P, Kacet N, et al: Prenatal findings in epidermolysis bullosa with pyloric atresia in a family not known to be at risk. *Ultrasound Obstet Gynecol* 25:607, 2005.
55. Fakhry J, Shapiro LR, Schechter A, et al: Fetal gastric pseudomasses. *J Ultrasound Med* 6:177, 1987.
56. Daly-Jones E, Sepulveda W, Hollingsworth J, et al: Fetal intraluminal gastric masses after second trimester amniocentesis. *J Ultrasound Med* 13:963, 1994.
57. Richards DS, Langham MR, Anderson CD: The prenatal sonographic appearance of enteric duplication cysts. *Ultrasound Obstet Gynecol* 7:17, 1996.
58. Ozmen MN, Onderoglu L, Ciftci AO, et al: Prenatal diagnosis of gastric duplication cyst. *J Ultrasound Med* 16:219, 1997.
59. Rodriguez CR, Eire PF, Lopez GA, et al: Asymptomatic gastric duplication in a child: Report of a new case and review of the literature. *Pediatr Surg Int* 21:421, 2005.
60. Levine D, Goldstein RB, Cadrin C: Distention of the fetal duodenum: Abnormal finding? *J Ultrasound Med* 17:213, 1998.
61. Dalla Vecchia LK, Grosfeld JL, West KW, et al: Intestinal atresia and stenosis: A 25-year experience with 277 cases. *Arch Surg* 133:490, 1998.
62. Forrester MB, Merz RD: Population-based study of small intestinal atresia and stenosis, Hawaii, 1986-2000. *Public Health* 118:434, 2004.
63. Caspi B, Deutsch H, Grunshpan M, et al: Prenatal manifestation of superior mesenteric artery syndrome. *Prenat Diagn* 23:932, 2003.
64. <http://www3.ncbi.nlm.nih.gov/entrez/omim>
65. Kallen B, Mastroiacovo P, Robert E: Major congenital malformations in Down syndrome. *Am J Med Genet* 65:160, 1996.
66. Stoll C, Alembik Y, Dott B, et al: Study of Down syndrome in 238,942 consecutive births. *Ann Genet* 41:44, 1998.
67. Torfs CP, Christianson RE: Anomalies in Down syndrome individuals in a large population-based registry. *Am J Med Genet* 77:431, 1998.
68. Kava MP, Tullu MS, Muranjan MN, et al: Down syndrome: Clinical profile from India. *Arch Med Res* 35:31, 2004.
69. Singh MV, Richards C, Bowen JC: Does Down syndrome affect the outcome of congenital duodenal obstruction? *Pediatr Surg Int* 20:586, 2004.
70. Escobar MA, Ladd AP, Grosfeld JL, et al: Duodenal atresia and stenosis: Long-term follow-up over 30 years. *J Pediatr Surg* 39:867, 2004.
71. Lawrence MJ, Ford WD, Furness ME, et al: Congenital duodenal obstruction: Early antenatal ultrasound diagnosis. *Pediatr Surg Int* 16:342, 2000.
72. Tsukerman GL, Krapiva GA, Kirillova IA: First-trimester diagnosis of duodenal stenosis associated with oesophageal atresia. *Prenat Diagn* 13:371, 1993.
73. Zimmer EZ, Bronshtein M: Early diagnosis of duodenal atresia and possible sonographic pitfalls. *Prenat Diagn* 16:564, 1996.
74. Traubici J: The double bubble sign. *Radiology* 220:463, 2001.
75. Malone FD, Crombleholme TM, Nores JA, et al: Pitfalls of the 'double bubble' sign: A case of congenital duodenal duplication. *Fetal Diagn Ther* 12:298, 1997.
76. Yoshizato T, Satoh S, Taguchi T, et al: Intermittent 'double bubble' sign in a case of congenital pyloric atresia. *Fetal Diagn Ther* 17:334, 2002.
77. Cuming T, Asif M, Babu R, et al: Congenital segmental dilatation of the duodenum-Differential diagnosis for an antenatally-diagnosed intra-abdominal cyst. *Eur J Pediatr Surg* 11:133, 2001.
78. Yamataka A, Pringle KC: A case with duodenal duplication cyst: Prenatal diagnosis and surgical management. *Fetal Diagn Ther* 13:39, 1998.
79. Borgnon J, Durand C, Gourlaouen D, et al: Antenatal detection of a communicating duodenal duplication. *Eur J Pediatr Surg* 13:130, 2003.
80. Grignon A, Dubois J, Ouellet MC, et al: Echogenic dilated bowel loops before 21 weeks' gestation: A new entity. *AJR Am J Roentgenol* 168:833, 1997.
81. Cragan JD, Martin ML, Moore CA, et al: Descriptive epidemiology of small intestinal atresia, Atlanta, Georgia. *Teratology* 48:441, 1993.
82. Harris J, Kallen B, Robert E: Descriptive epidemiology of alimentary tract atresia. *Teratology* 52:15, 1995.
83. Martinez-Frias ML, Castilla EE, Bermejo E, et al: Isolated small intestinal atresias in Latin America and Spain: Epidemiological analysis. *Am J Med Genet* 93:355, 2000.
84. Seashore JH, Collins FS, Markowitz RI, et al: Familial apple peel jejunal atresia: Surgical, genetic, and radiographic aspects. *Pediatrics* 80:540, 1987.
85. Bilodeau A, Prasil P, Cloutier R, et al: Hereditary multiple intestinal atresia: Thirty years later. *J Pediatr Surg* 39:726, 2004.
86. Werler MM, Sheehan JE, Mitchell AA: Association of vasoconstrictive exposures with risks of gastroschisis and small intestinal atresia. *Epidemiology* 14:349, 2003.
87. Komuro H, Hori T, Amagai T, et al: The etiologic role of intrauterine volvulus and intussusception in jejunoileal atresia. *J Pediatr Surg* 39:1812, 2004.
88. Heij HA, Moorman-Voestermans CG, Vos A: Atresia of jejunum and ileum: Is it the same disease? *J Pediatr Surg* 25:635, 1990.
89. Sweeney B, Surana R, Puri P: Jejunoileal atresia and associated malformations: Correlation with the timing of in utero insult. *J Pediatr Surg* 36:774, 2001.
90. Weissman A, Goldstein I: Prenatal sonographic diagnosis and clinical management of small bowel obstruction. *Am J Perinatol* 10:215, 1993.
91. Sioll C, Alembik Y, Dott B, et al: Evaluation of prenatal diagnosis of congenital gastro-intestinal atresias. *Eur J Epidemiol* 12:611, 1996.
92. Font GE, Solari M: Prenatal diagnosis of bowel obstruction initially manifested as isolated hyperechoic bowel. *J Ultrasound Med* 17:721, 1998.



93. Wax JR, Hamilton T, Cartin A, et al: Congenital jejunal and ileal atresia: Natural prenatal sonographic history and association with neonatal outcome. *J Ultrasound Med* 25:337, 2006.
94. Irish MS, Ragi JM, Karamanoukian H, et al: Prenatal diagnosis of the fetus with cystic fibrosis and meconium ileus. *Pediatr Surg Int* 12:434, 1997.
95. Muller F, Simon-Bouy B, Girodon E, et al: Predicting the risk of cystic fibrosis with abnormal ultrasound signs of fetal bowel: results of a French molecular collaborative study based on 641 prospective cases. *Am J Med Genet* 110:109, 2002.
96. Siplovich I, Davies MR, Kaschula RO, et al: Intestinal obstruction in the newborn with congenital syphilis. *J Pediatr Surg* 23:810, 1988.
97. Dechelotte PJ, Mulliez NM, Bouvier RJ, et al: Pseudo-meconium ileus due to cytomegalovirus infection: A report of three cases. *Pediatr Pathol* 12:73, 1992.
98. Eckoldt F, Heling KS, Woderich R, et al: Meconium peritonitis and pseudo-cyst formation: prenatal diagnosis and post-natal course. *Prenat Diagn* 23:904, 2003.
99. Zerbini M, Gentilomi GA, Gallinella G, et al: Intra-uterine parvovirus B19 infection and meconium peritonitis. *Prenat Diagn* 18:599, 1998.
100. McDuffie RS Jr, Bader T: Fetal meconium peritonitis after maternal hepatitis A. *Am J Obstet Gynecol* 180:1031, 1999.
101. Su VH, Wang PH, Yuan CC, et al: Fetal meconium peritonitis in the infant of a woman with fulminant hepatitis B. A case report. *J Reprod Med* 47:952, 2002.
102. Dirkes K, Crombleholme TM, Craigo SD, et al: The natural history of meconium peritonitis diagnosed in utero. *J Pediatr Surg* 30:979, 1995.
103. Kamata S, Nose K, Ishikawa S, et al: Meconium peritonitis in utero. *Pediatr Surg Int* 16:377, 2000.
104. Shyu MK, Shih JC, Lee CN, et al: Correlation of prenatal ultrasound and postnatal outcome in meconium peritonitis. *Fetal Diagn Ther* 18:255, 2003.
105. Chan KL, Tang MH, Tse HY, et al: Meconium peritonitis: Prenatal diagnosis, postnatal management and outcome. *Prenat Diagn* 25:676, 2005.
106. Shyu MK, Chen CD, Hsieh FJ, et al: Intrauterine intervention in a case of recurrent meconium peritonitis. *Prenat Diagn* 14:993, 1994.
107. Albu I, Munteanu V, Florescu P, et al: The ileal diverticulum. Morpho-clinical and epidemiological study. *Rom J Morphol Embryol* 39:37, 1993.
108. Matsagas MI, Fatouros M, Koulouras B, et al: Incidence, complications, and management of Meckel's diverticulum. *Arch Surg* 130:143, 1995.
109. Park JJ, Wolff BG, Tollefson MK, et al: Meckel diverticulum: The Mayo Clinic experience with 1476 patients (1950-2002). *Ann Surg* 241:529, 2005.
110. Aultman CJ, Samples TL: In utero appearance of a giant Meckel's diverticulum. *Pediatr Radiol* 26:398, 1996.
111. Rushford MP, Stys SJ, Latchaw LA, et al: Prenatal sonographic detection of meckel diverticulum in utero with postnatal radiologic and surgical confirmation. *J Ultrasound Med* 23:319, 2004.
112. Schalamon J, Schleef J, Hollwarth ME: Experience with gastrointestinal duplications in childhood. *Langenbecks Arch Surg* 385:402, 2000.
113. Chen M, Lam YH, Lin CL, et al: Sonographic features of ileal duplication cyst at 12 weeks. *Prenat Diagn* 22:1067, 2002.
114. Foley PT, Sithasanan N, McEwing R, et al: Enteric duplications presenting as antenatally detected abdominal cysts: Is delayed resection appropriate? *J Pediatr Surg* 38:1810, 2003.
115. Faure C, Goulet O, Ategbo S, et al: Chronic intestinal pseudoobstruction syndrome: Clinical analysis, outcome, and prognosis in 105 children. French-Speaking Group of Pediatric Gastroenterology. *Dig Dis Sci* 44:953, 1999.
116. Lapointe SP, Rivet C, Goulet O, et al: Urological manifestations associated with chronic intestinal pseudo-obstructions in children. *J Urol* 168:1768, 2002.
117. Mousa H, Hyman PE, Cocjin J, et al: Long-term outcome of congenital intestinal pseudoobstruction. *Dig Dis Sci* 47:2298, 2002.
118. Holmberg C: Congenital chloride diarrhoea. *Clin Gastroenterol* 15:583, 1986.
119. Badawi MH, Zaki M, Ismail EA, et al: Congenital chloride diarrhoea in Kuwait: A clinical reappraisal. *J Trop Pediatr* 44:296, 1998.
120. Lundkvist K, Ewald U, Lindgren PG: Congenital chloride diarrhoea: A prenatal differential diagnosis of small bowel atresia. *Acta Paediatr* 85:295, 1996.
121. Zalel Y, Perlitz Y, Gamzu R, et al: In-utero development of the fetal colon and rectum: Sonographic evaluation. *Ultrasound Obstet Gynecol* 21:161, 2003.
122. Nyberg DA, Mack LA, Patten RM, et al: Fetal bowel. Normal sonographic findings. *J Ultrasound Med* 6:3, 1987.
123. Parulekar SG: Sonography of normal fetal bowel. *J Ultrasound Med* 10:211, 1991.
124. Kimble RM, Trudinger B, Cass D: Fetal defaecation: Is it a normal physiological process? *J Paediatr Child Health* 35:116, 1999.
125. Ciftci AO, Tanyel FC, Ercan MT, et al: In utero defecation by the normal fetus: A radionuclide study in the rabbit. *J Pediatr Surg* 31:1409, 1996.
126. Ciftci AO, Tanyel FC, Karnak I, et al: In-utero defecation: Fact or fiction? *Eur J Pediatr Surg* 9:376, 1999.
127. Ramon y Cajal CL, Martinez RO: Defecation in utero: A physiologic fetal function. *Am J Obstet Gynecol* 188:153, 2003.
128. Ramon Y Cajal CL, Martinez RO: Prenatal observation of fetal defecation using four-dimensional ultrasonography. *Ultrasound Obstet Gynecol* 26:794, 2005.
129. Bourdelat D, Muller F, Droulle P, et al: Anatomical and sonographical studies on the development of fecal continence and sphincter development in human fetuses. *Eur J Pediatr Surg* 11:124, 2001.
130. Russell MB, Russell CA, Niebuhr E: An epidemiological study of Hirschsprung's disease and additional anomalies. *Acta Paediatr* 83:68, 1994.
131. Ryan ET, Ecker JL, Christakis NA, et al: Hirschsprung's disease: associated abnormalities and demography. *J Pediatr Surg* 27:76, 1992.
132. Eliyahu S, Yanai N, Blondheim O, et al: Sonographic presentation of Hirschsprung's disease. A case of an entirely aganglionic colon and ileum. *Prenat Diagn* 14:1170, 1994.
133. Suzuki S: Megacolon in a fetus during the first trimester. *Prenat Diagn* 21:422, 2001.
134. Stoll C, Alembik Y, Roth MP, et al: Risk factors in congenital anal atresias. *Ann Genet* 40:197, 1997.
135. Cuschieri A, EUROCAT Working Group: Descriptive epidemiology of isolated anal anomalies: A survey of 4.6 million births in Europe. *Am J Med Genet* 103:207, 2001.
136. Forrester MB, Merz RD: Descriptive epidemiology of anal atresia in Hawaii, 1986-1999. *Teratology* 66 Suppl 1:S12, 2002.
137. Harris RD, Nyberg DA, Mack LA, et al: Anorectal atresia: Prenatal sonographic diagnosis. *AJR Am J Roentgenol* 149:395, 1987.
138. Anderson S, Savader B, Barnes J, et al: Enterolithiasis with imperforate anus. Report of two cases with sonographic demonstration and occurrence in a female. *Pediatr Radiol* 18:130, 1988.
139. Grant T, Newman M, Gould R, et al: Intraluminal colonic calcifications associated with anorectal atresia. Prenatal sonographic detection. *J Ultrasound Med* 9:411, 1990.
140. Mandell JJ, Lillehei CW, Greene M, et al: The prenatal diagnosis of imperforate anus with rectourinary fistula: Dilated fetal colon with enterolithiasis. *J Pediatr Surg* 27:82, 1992.
141. Tongsong T, Chanpraph P: Prenatal diagnosis of isolated anorectal atresia with colonic perforation. *J Obstet Gynaecol Res* 27:241, 2001.
142. Lam YH, Shek T, Tang MH: Sonographic features of anal atresia at 12 weeks. *Ultrasound Obstet Gynecol* 19:523, 2002.
143. Taipale P, Rovamo L, Hilesmaa V: First-trimester diagnosis of imperforate anus. *Ultrasound Obstet Gynecol* 25: 187, 2005.
144. Bronshtein M, Zimmer EZ: Early sonographic detection of fetal intestinal obstruction and possible diagnostic pitfalls. *Prenat Diagn* 16:203, 1996.
145. Blickstein I, Smith-Levin M, Gurewitsch E, et al: Computed sonography: Requiem to echogenicity assessment? *Gynecol Obstet Invest* 44:244, 1997.
146. Smith-Levin M, Blickstein I, Albrecht-Shach AA, et al: Quantitative assessment of gray-level perception: Observers' accuracy is dependent on density differences. *Ultrasound Obstet Gynecol* 10:346, 1997.
147. Khandelwal M, Silva J, Chan L, et al: Three-dimensional ultrasonographic technology to assess and compare echodensity of fetal bowel, bone, and liver in the second trimester of pregnancy. *J Ultrasound Med* 18:691, 1999.
148. Vincoff NS, Callen PW, Smith-Bindman R, et al: Effect of ultrasound transducer frequency on the appearance of the fetal bowel. *J Ultrasound Med* 18:799, 1999.
149. Harrison KL, Martinez D, Mason G: The subjective assessment of echogenic fetal bowel. *Ultrasound Obstet Gynecol* 16:524, 2000.



150. Lee HJ, Cho JY: Quantitative assessment of fetal bowel echogenicity: Comparison of harmonic, compound, and fundamental sonographic images. *J Clin Ultrasound* 31:302, 2003.
151. Petrikovsky B, Smith-Levin M, Holsten N: Intra-amniotic bleeding and fetal echogenic bowel. *Obstet Gynecol* 93:684, 1999.
152. Berlin BM, Norton ME, Sugarman EA, et al: Cystic fibrosis and chromosome abnormalities associated with echogenic fetal bowel. *Obstet Gynecol* 94:135, 1999.
153. Ghose J, Mason GC, Martinez D, et al: Hyperechogenic fetal bowel: A prospective analysis of sixty consecutive cases. *BJOG* 107:426-429, 2000.
154. Strocker AM, Snijders RJ, Carlson DE, et al: Fetal echogenic bowel: Parameters to be considered in differential diagnosis. *Ultrasound Obstet Gynecol* 16:519, 2000.
155. Al-Kouatly HB, Chasen ST, Streltsoff J, et al: The clinical significance of fetal echogenic bowel. *Am J Obstet Gynecol* 185:1035, 2001.
156. Nyberg DA, Souter VL, El-Bastawissi A, et al: Isolated sonographic markers for detection of fetal Down syndrome in the second trimester of pregnancy. *J Ultrasound Med* 20:1053, 2001.
157. Simon-Bouy B, Satre V, Ferec C, et al: Hyperechogenic fetal bowel: A large French collaborative study of 682 cases. *Am J Med Genet A* 121:209, 2003.
158. Palomaki GE, FitzSimmons SC, Haddow JE: Clinical sensitivity of prenatal screening for cystic fibrosis via CFTR carrier testing in a United States panethnic population. *Genet Med* 6:405, 2004.
159. Al-Kouatly HB, Chasen ST, Karam AK, et al: Factors associated with fetal demise in fetal echogenic bowel. *Am J Obstet Gynecol* 185:1039, 2001.
160. Achiron R, Mazkereth R, Orvieto R, et al: Echogenic bowel in intrauterine growth restriction fetuses: Does this jeopardize the gut? *Obstet Gynecol* 100:120, 2002.
161. Lam YH, Tang MH, Lee CP, et al: Echogenic bowel in fetuses with homozygous alpha-thalassemia-1 in the first and second trimesters. *Ultrasound Obstet Gynecol* 14:180, 1999.
162. Shimanuki Y, Aihara T, Takano H, et al: Clockwise whirlpool sign at color Doppler US: An objective and definite sign of midgut volvulus. *Radiology* 199:261, 1996.
163. Yoo SJ, Park KW, Cho SY, et al: Definitive diagnosis of intestinal volvulus in utero. *Ultrasound Obstet Gynecol* 13:200, 1999.
164. Has R, Gunay S: 'Whirlpool' sign in the prenatal diagnosis of intestinal volvulus. *Ultrasound Obstet Gynecol* 20:307, 2002.
165. Patino MO, Munden MM: Utility of the sonographic whirlpool sign in diagnosing midgut volvulus in patients with atypical clinical presentations. *J Ultrasound Med* 23:397, 2004.
166. Miyakoshi K, Ishimoto H, Tanigaki S, et al: Prenatal diagnosis of midgut volvulus by sonography and magnetic resonance imaging. *Am J Perinatol* 18:447, 2001.
167. Jequier S, Hanquinet S, Bugmann P, et al: Antenatal small-bowel volvulus without malrotation: Ultrasound demonstration and discussion of pathogenesis. *Pediatr Radiol* 33:263, 2003.
168. Wang NL, Yeh ML, Chang PY, et al: Prenatal and neonatal intussusception. *Pediatr Surg Int* 13:232, 1998.
169. Shimotake T, Go S, Tsuda T, et al: Ultrasonographic detection of intrauterine intussusception resulting in ileal atresia complicated by meconium peritonitis. *Pediatr Surg Int* 16:43, 2000.
170. Yang JL, Kim HS, Chang KH, et al: Intrauterine intussusception presenting as fetal ascites at prenatal ultrasonography. *Am J Perinatol* 21:241, 2004.
171. Forrester MB, Merz RD: Epidemiology of intestinal malrotation, Hawaii, 1986-99. *Paediatr Perinat Epidemiol* 17:195, 2003.
172. Rescorla FJ, Shedd FJ, Grosfeld JL, et al: Anomalies of intestinal rotation in childhood: Analysis of 447 cases. *Surgery* 108:710, 1990.
173. Chang J, Brueckner M, Touloukian RJ: Intestinal rotation and fixation abnormalities in heterotaxia: Early detection and management. *J Pediatr Surg* 28:1281, 1993.
174. Chikhlard A, De Lagausie P, Garel C, et al: Situs inversus and bowel malrotation: Contribution of prenatal diagnosis and laparoscopy. *J Pediatr Surg* 35:1217, 2000.
175. Chao HC, Kong MS, Chen JY, et al: Sonographic features related to volvulus in neonatal intestinal malrotation. *J Ultrasound Med* 19:371, 2000.
176. Choi M, Borenstein SH, Hornberger L, et al: Heterotaxia syndrome: The role of screening for intestinal rotation abnormalities. *Arch Dis Child* 90:813, 2005.
177. Littlewood Teele R, Pease PW, et al: Malrotation in newborns following antenatal diagnosis of intra-abdominal cyst. *Pediatr Radiol* 28:717, 1998.
178. DeRusso PA, Benson J, Lau H: Intestinal malrotation and omental cyst presenting as fetal ascites. *J Pediatr Gastroenterol Nutr* 36:283, 2003.
179. Cassart M, Massez A, Lingier P, et al: Sonographic prenatal diagnosis of malpositioned stomach as a feature of uncomplicated intestinal malrotation. *Pediatr Radiol* 36:358, 2006.
180. Liang X, Ioffe OB, Sun CC: Cloacal dysgenesis sequence: Observations in four patients including three fetuses of second trimester gestation. *Pediatr Dev Pathol* 1:281, 1998.
181. Qureshi F, Jacques SM, Yaron Y, et al: Prenatal diagnosis of cloacal dysgenesis sequence: Differential diagnosis from other forms of fetal obstructive uropathy. *Fetal Diagn Ther* 13:69, 1998.
182. Sahinoglu Z, Mulayim B, Ozden S, et al: The prenatal diagnosis of cloacal dysgenesis sequence in six cases: Can the termination of pregnancy always be the first choice? *Prenat Diagn* 24:10, 2004.
183. Carson PL, Meyer CR, Chiang EH, et al: Ultrasound attenuation coefficient in the fetal liver as a function of gestational age. *Ultrasound Med Biol* 16:399, 1990.
184. Carson PL, Chiang EH, Rubin JM, et al: Pre- to postnatal reduction in ultrasound attenuation coefficient of the liver. *Invest Radiol* 26:8, 1991.
185. Laudy JA, Janssen MM, Struyk PC, et al: Fetal liver volume measurement by three-dimensional ultrasonography: A preliminary study. *Ultrasound Obstet Gynecol* 12:93, 1998.
186. Boito SM, Laudy JA, Struijk PC, et al: Three-dimensional US assessment of hepatic volume, head circumference, and abdominal circumference in healthy and growth-restricted fetuses. *Radiology* 223:661, 2002.
187. Kuno A, Hayashi Y, Akiyama M, et al: Three-dimensional sonographic measurement of liver volume in the small-for-gestational-age fetus. *J Ultrasound Med* 21:361, 2002.
188. Chang CH, Yu CH, Chang FM, et al: The assessment of normal fetal liver volume by three-dimensional ultrasound. *Ultrasound Med Biol* 29:1123, 2003.
189. Rowlands S, Murray H: Prenatal ultrasound findings in a fetus diagnosed with Gaucher's disease (type 2) at birth. *Prenat Diagn* 17:765, 1997.
190. Ghidini A, Sirtori M, Romero R, et al: Hepatosplenomegaly as the only prenatal finding in a fetus with pyruvate kinase deficiency anemia. *Am J Perinatol* 8:44, 1991.
191. Hollier LM, Harstad TW, Sanchez RJ, et al: Fetal syphilis: Clinical and laboratory characteristics. *Obstet Gynecol* 97:947, 2001.
192. Macones GA, Johnson A, Tilley D, et al: Fetal hepatosplenomegaly associated with transient myeloproliferative disorder in trisomy 21. *Fetal Diagn Ther* 10:131, 1995.
193. Baschat AA, Wagner T, Malisius R, et al: Prenatal diagnosis of a transient myeloproliferative disorder in trisomy 21. *Prenat Diagn* 18:731, 1998.
194. Hartung J, Chaoui R, Wauer R, et al: Fetal hepatosplenomegaly: An isolated sonographic sign of trisomy 21 in a case of myeloproliferative disorder. *Ultrasound Obstet Gynecol* 11:453, 1998.
195. Hamada H, Yamada N, Watanabe H, et al: Hypochoic hepatomegaly associated with transient abnormal myelopoiesis provides clues to trisomy 21 in the third-trimester fetus. *Ultrasound Obstet Gynecol* 17:442, 2001.
196. Smrcok JM, Baschat AA, Germer U, et al: Fetal hydrops and hepatosplenomegaly in the second half of pregnancy: a sign of myeloproliferative disorder in fetuses with trisomy 21. *Ultrasound Obstet Gynecol* 17:403, 2001.
197. Ogawa M, Hosoya N, Sato A, et al: Is the degree of fetal hepatosplenomegaly with transient abnormal myelopoiesis closely related to the postnatal severity of hematological abnormalities in Down syndrome? *Ultrasound Obstet Gynecol* 24:83, 2004.
198. Macken MB, Wright JR Jr, Lau H, et al: Prenatal sonographic detection of congenital hepatic cyst in third trimester after normal second-trimester sonographic examination. *J Clin Ultrasound* 28:307, 2000.
199. Hussman KL, Friedwald JP, Gollub MJ, et al: Caroli's disease associated with infantile polycystic kidney disease. Prenatal sonographic appearance. *J Ultrasound Med* 10:235, 1991.
200. Brau I, Laberge JM, Khalife S, et al: Regression of antenatally diagnosed localized Caroli's disease. *J Pediatr Surg* 35:1390, 2000.



201. Yuksel A, Has R, Isikoglu M, et al: Prenatal diagnosis of Caroli's disease. *Ultrasound Obstet Gynecol* 19:525, 2002.
202. Sgro M, Rossetti S, Barozzino T, et al: Caroli's disease: Prenatal diagnosis, postnatal outcome and genetic analysis. *Ultrasound Obstet Gynecol* 23:73, 2004.
203. Mittermayer C, Bertschheim D, Horcher E, et al: Prenatal sonographic detection of a giant multiseptate hepatic cyst in the third trimester. *Ultrasound Obstet Gynecol* 20:97, 2002.
204. Tsao K, Hirose S, Sydorak R, et al: Fetal therapy for giant hepatic cysts. *J Pediatr Surg* 37:E31, 2002.
205. Kamata S, Nose K, Sawai T, et al: Fetal mesenchymal hamartoma of the liver: Report of a case. *J Pediatr Surg* 38:639, 2003.
206. Ramirez-Garrido F, Lopez Gonzalez-Garrido Jde D, Ruiz-Lopez MJ, et al: Prenatal and post-natal imaging of an hepatic mesenchymal hamartoma. *Eur J Pediatr* 162:57, 2003.
207. Laberge JM, Patenaude Y, Desilets V, et al: Large hepatic mesenchymal hamartoma leading to mid-trimester fetal demise. *Fetal Diagn Ther* 20:141, 2005.
208. Morris J, Abbott J, Burrows P, et al: Antenatal diagnosis of fetal hepatic hemangioma treated with maternal corticosteroids. *Obstet Gynecol* 94:813, 1999.
209. Meirowitz NB, Guzman ER, Underberg-Davis SJ, et al: Hepatic hemangioendothelioma: prenatal sonographic findings and evolution of the lesion. *J Clin Ultrasound* 28:258, 2000.
210. Gembruch U, Baschat AA, Gloeckner-Hoffmann K, et al: Prenatal diagnosis and management of fetuses with liver hemangiomas. *Ultrasound Obstet Gynecol* 19:454, 2002.
211. Pott Bartsch EM, Pack BW, Yoshizawa J, et al: Giant fetal hepatic hemangioma. Case report and literature review. *Fetal Diagn Ther* 18:59, 2003.
212. Chou SY, Chiang HK, Chow PK, et al: Fetal hepatic hemangioma diagnosed prenatally with ultrasonography. *Acta Obstet Gynecol Scand* 84:301, 2005.
213. Shih JC, Tsao PN, Huang SF, et al: Antenatal diagnosis of congenital hepatoblastoma in utero. *Ultrasound Obstet Gynecol* 16:94, 2000.
214. Aviram R, Cohen JJ, Komreich L, et al: Prenatal imaging of fetal hepatoblastoma. *J Matern Fetal Neonatal Med* 17:157, 2005.
215. Bronshtein M, Blazer S: Prenatal diagnosis of liver calcifications. *Obstet Gynecol* 86:739, 1995.
216. Stein B, Bromley B, Michlewicz H, et al: Fetal liver calcifications: Sonographic appearance and postnatal outcome. *Radiology* 197:489, 1995.
217. Koopman E, Wladimiroff JW: Fetal intrahepatic hyperechogenic foci: Prenatal ultrasound diagnosis and outcome. *Prenat Diagn* 18:339, 1998.
218. Simchen MJ, Toi A, Bona M, et al: Fetal hepatic calcifications: Prenatal diagnosis and outcome. *Am J Obstet Gynecol* 187:1617, 2002.
219. Hill LM, Mills A, Peterson C, Boyles D: Persistent right umbilical vein: Sonographic detection and subsequent neonatal outcome. *Obstet Gynecol* 84:923, 1994.
220. Kirsch CF, Feldstein VA, Goldstein RB, et al: Persistent intrahepatic right umbilical vein: A prenatal sonographic series without significant anomalies. *J Ultrasound Med* 15:371, 1996.
221. Shen O, Tadmor OP, Yagel S: Prenatal diagnosis of persistent right umbilical vein. *Ultrasound Obstet Gynecol* 8:31, 1996.
222. Blazer S, Zimmer EZ, Bronshtein M: Persistent intrahepatic right umbilical vein in the fetus: a benign anatomic variant. *Obstet Gynecol* 95:433, 2000.
223. Wolman I, Gull I, Fait G, et al: Persistent right umbilical vein: Incidence and significance. *Ultrasound Obstet Gynecol* 19:562, 2002.
224. Blazer S, Zimmer EZ, Bronshtein M: Nonvisualization of the fetal gallbladder in early pregnancy: Comparison with clinical outcome. *Radiology* 224:379, 2002.
225. Kabiri H, Domingo OH, Tzamas CD: Agnecsis of the gallbladder. *Curr Surg* 63:104, 2006.
226. Brown DL, Teale RL, Doubilet PM, et al: Echogenic material in the fetal gallbladder: Sonographic and clinical observations. *Radiology* 182:73, 1992.
227. Petrikovsky B, Klein V, Holsten N: Sludge in fetal gallbladder: Natural history and neonatal outcome. *Br J Radiol* 69:1017, 1996.
228. Munjuluri N, Elgharaby N, Acolet D, et al: Fetal gallstones. *Fetal Diagn Ther* 20:241, 2005.
229. Yoon PW, Bresce JS, Olney RS, et al: Epidemiology of biliary atresia: A population-based study. *Pediatrics* 99:376, 1997.
230. Caton AR, Druschel CM, McNutt LA: The epidemiology of extrahepatic biliary atresia in New York State, 1983-98. *Paediatr Perinat Epidemiol* 18:97, 2004.
231. Gauthier F, Luciani JL, Chardot C, et al: Determinants of life span after Kasai operation at the era of liver transplantation. *Tohoku J Exp Med* 181:97, 1997.
232. Chardot C, Carton M, Spire-Bendelac N, et al: Prognosis of biliary atresia in the era of liver transplantation: French national study from 1986 to 1996. *Hepatology* 30:606, 1999.
233. Iwai N, Deguchi E, Sasaki Y, et al: Antenatal diagnosis of biliary atresia (noncorrectable cyst type): A case report. *Eur J Pediatr Surg* 9:340, 1999.
234. Ben-Ami M, Perlitz Y, Shalev S, et al: Prenatal diagnosis of extrahepatic biliary duct atresia. *Prenat Diagn* 22:583, 2002.
235. Burc L, Vuillard E, Guibourdenche J, et al: Prenatal diagnosis and follow up of biliary atresia. *BJOG* 108:1108, 2001.
236. Hasegawa T, Sasaki T, Kimura T, et al: Prenatal ultrasonographic appearance of type IIId (uncorrectable type with cystic dilatation) biliary atresia. *Pediatr Surg Int* 18:425, 2002.
237. Fujishiro J, Iwanaka T, Arai M, et al: Disappearing cyst of the hepatic hilum in uncorrectable biliary atresia. *Pediatr Surg Int* 21:116, 2005.
238. Matsubara H, Oya N, Suzuki Y, et al: Is it possible to differentiate between choledochal cyst and congenital biliary atresia (type I cyst) by antenatal ultrasonography? *Fetal Diagn Ther* 12:306, 1997.
239. Casaccia C, Bilancioni E, Nahom A, et al: Cystic anomalies of biliary tree in the fetus: Is it possible to make a more specific prenatal diagnosis? *J Pediatr Surg* 37:1191, 2002.
240. Clifton MS, Goldstein RB, Slavotinek A, et al: Prenatal Diagnosis of Familial Type I Choledochal Cyst. *Pediatrics* 117:e596, 2006.
241. Todani T, Watanabe Y, Narusue M, et al: Congenital bile duct cysts: Classification, operative procedures, and review of thirty-seven cases including cancer arising from choledochal cyst. *Am J Surg* 134:263, 1977.
242. Hata T, Deter RL: A review of fetal organ measurements obtained with ultrasound: Normal growth. *J Clin Ultrasound* 20:155, 1992.
243. Aoki S, Hata T, Kitao M: Ultrasonographic assessment of fetal and neonatal spleen. *Am J Perinatol* 9:361, 1992.
244. Chaoui R, Zidan-Marin T, Wisser J: Marked splenomegaly in fetal cytomegalovirus infection: Detection supported by three-dimensional power Doppler ultrasound. *Ultrasound Obstet Gynecol* 20:299, 2002.
245. Oepkes D, Meerman RH, Vandenbussche FP, et al: Ultrasonographic fetal spleen measurements in red blood cell-alloimmunized pregnancies. *Am J Obstet Gynecol* 169:121, 1993.
246. Bahado-Singh R, Oz U, Mari G, et al: Fetal splenic size in anemia due to Rh-alloimmunization. *Obstet Gynecol* 92:828, 1998.
247. Garel C, Hassan M: Focal and neonatal splenic cyst-like lesions. US follow-up of seven cases. *Pediatr Radiol* 25:360, 1995.
248. Lopes MA, Ruano R, Bunduki V, et al: Prenatal diagnosis and follow up of congenital splenic cyst: a case report. *Ultrasound Obstet Gynecol* 17:439, 2001.
249. Saada J, Parant O, Kessler S, et al: Prenatal diagnosis and outcome of congenital splenic cyst: Report of two cases. *Prenat Diagn* 26:9, 2006.
250. Hata K, Hata T, Kitao M: Ultrasonographic identification and measurement of the human fetal pancreas in utero. *Int J Gynaecol Obstet* 26:61, 1988.
251. Weiss H, Sherer DM, Manning FA: Ultrasonography of fetal annular pancreas. *Obstet Gynecol* 94:852, 1999.
252. Pachi A, Maggi E, Giancotti A, et al: Ultrasound diagnosis of fetal annular pancreas. *J Perinat Med* 17:361, 1989.
253. Kebapci M, Aslan O, Kaya T, et al: Prenatal diagnosis of giant congenital pancreatic cyst of a neonate. *AJR Am J Roentgenol* 175:1408, 2000.
254. Boulanger SC, Borowitz DS, Fisher JF, et al: Congenital pancreatic cysts in children. *J Pediatr Surg* 38:1080, 2003.
255. Bronstein M, Reichler A, Borochoy Z, et al: Early prenatal diagnosis of polycystic pancreas with narrow thorax and short limb dwarfism. *Am J Med Genet* 49:6, 1994.
256. Fremont B, Poulain P, Odent S, et al: Prenatal detection of a congenital pancreatic cyst and Beckwith-Wiedemann syndrome. *Prenat Diagn* 17:276, 1997.
257. Sepulveda W, Carstens E, Sanchez J, et al: Prenatal diagnosis of congenital pancreatic cyst: Case report and review of the literature. *J Ultrasound Med* 19:349, 2000.



258. Klimstra DS, Wenig BM, Adair CF, et al: Pancreatoblastoma. A clinicopathologic study and review of the literature. *Am J Surg Pathol* 19:1371, 1995.
259. Defachelles AS, Martin De Lassalle E, Boutard P, et al: Pancreatoblastoma in childhood: clinical course and therapeutic management of seven patients. *Med Pediatr Oncol* 37:47, 2001.
260. Pelizzo G, Conoscenti G, Kalache KD, et al: Antenatal manifestation of congenital pancreatoblastoma in a fetus with Beckwith-Wiedemann syndrome. *Prenat Diagn* 23:292, 2003.
261. Muguerza R, Rodriguez A, Formigo E, et al: Pancreatoblastoma associated with incomplete Beckwith-Wiedemann syndrome: Case report and review of the literature. *J Pediatr Surg* 40:1341, 2005.
262. Cacciari A, Gabrielli S, Ferrari M, et al: Pancreatoblastoma. <http://www.thefetus.net/>
263. Timor-Tritsch IE, Warren WB, Peisner DB, et al: First-trimester midgut herniation: A high-frequency transvaginal sonographic study. *Am J Obstet Gynecol* 161:831, 1989.
264. Byron-Scott R, Haan E, Chan A, et al: A population-based study of abdominal wall defects in South Australia and Western Australia. *Paediatr Perinat Epidemiol* 12:136, 1998.
265. Suita S, Okamatsu T, Yamamoto T, et al: Changing profile of abdominal wall defects in Japan: results of a national survey. *J Pediatr Surg* 35:66, 2000.
266. Barisic I, Clementi M, Hausler M, et al: Evaluation of prenatal ultrasound diagnosis of fetal abdominal wall defects by 19 European registries. *Ultrasound Obstet Gynecol* 18:309, 2001.
267. Stoll C, Alembik Y, Dott B, et al: Risk factors in congenital abdominal wall defects (omphalocele and gastroschisis): a study in a series of 265,858 consecutive births. *Ann Genet* 44:201, 2001.
268. Gibbin C, Touch S, Broth RE, et al: Abdominal wall defects and congenital heart disease. *Ultrasound Obstet Gynecol* 21:334, 2003.
269. Blazer S, Zimmer EZ, Gover A, et al: Fetal omphalocele detected early in pregnancy: associated anomalies and outcomes. *Radiology* 232:191, 2004.
270. Hwang PJ, Kousseff BG: Omphalocele and gastroschisis: An 18-year review study. *Genet Med* 6:232, 2004.
271. Brantberg A, Blaas HG, Haugen SE, et al: Characteristics and outcome of 90 cases of fetal omphalocele. *Ultrasound Obstet Gynecol* 26:527, 2005.
272. Boyd PA, Bhattacharjee A, Gould S, et al: Outcome of prenatally diagnosed anterior abdominal wall defects. *Arch Dis Child Fetal Neonatal Ed* 78:F209, 1998.
273. Garne E, Loane M, Dolk H, et al: Prenatal diagnosis of severe structural congenital malformations in Europe. *Ultrasound Obstet Gynecol* 25:6, 2005.
274. Nyberg DA, Fitzsimmons J, Mack LA, et al: Chromosomal abnormalities in fetuses with omphalocele. Significance of omphalocele contents. *J Ultrasound Med* 8:299, 1989.
275. Getachew MM, Goldstein RB, Edge V, et al: Correlation between omphalocele contents and karyotypic abnormalities: sonographic study in 37 cases. *AJR Am J Roentgenol* 158:133, 1992.
276. St-Vil D, Shaw KS, Lallier M, et al: Chromosomal anomalies in newborns with omphalocele. *J Pediatr Surg* 31:831, 1996.
277. Wilson RD, Johnson MP: Congenital abdominal wall defects: An update. *Fetal Diagn Ther* 19:385, 2004.
278. Bromley B, Benacerraf BR: Transient omphalocele. *J Ultrasound Med* 12:688, 1993.
279. Achiron R, Soriano D, Lipitz S, et al: Fetal midgut herniation into the umbilical cord: Improved definition of ventral abdominal anomaly with the use of transvaginal sonography. *Ultrasound Obstet Gynecol* 6:256, 1995.
280. Chitayat D, Rothchild A, Ling E, et al: Apparent postnatal onset of some manifestations of the Wiedemann-Beckwith syndrome. *Am J Med Genet* 36:434, 1990.
281. Penman DG, Fisher RM, Noblett HR, et al: Increase in incidence of gastroschisis in the south west of England in 1995. *Br J Obstet Gynaecol* 105:328, 1998.
282. Forrester MB, Merz RD: Epidemiology of abdominal wall defects, Hawaii, 1986-1997. *Teratology* 60:117, 1999.
283. Tan KH, Kilby MD, Whittle MJ, et al: Congenital anterior abdominal wall defects in England and Wales 1987-93: retrospective analysis of OPCS data. *BMJ* 313:903, 1996.
284. Saxena AK, Hulskamp G, Schleef J, et al: Gastroschisis: A 15-year, single-center experience. *Pediatr Surg Int* 18:420, 2002.
285. Langer JC: Abdominal wall defects. *World J Surg* 27:117, 2003.
286. Snyder CL: Outcome analysis for gastroschisis. *J Pediatr Surg* 34:1253, 1999.
287. Salvesen KA: Fetal abdominal wall defects—easy to diagnose—and then what? *Ultrasound Obstet Gynecol* 18:301, 2001.
288. Strauss RA, Balu R, Kuller JA, et al: Gastroschisis: The effect of labor and ruptured membranes on neonatal outcome. *Am J Obstet Gynecol* 189:1672, 2003.
289. Snyder CL, St Peter SD: Trends in mode of delivery for gastroschisis infants. *Am J Perinatol* 22:391, 2005.
290. Driver CP, Bruce J, Bianchi A, et al: The contemporary outcome of gastroschisis. *J Pediatr Surg* 35:1719, 2000.
291. Durfee SM, Downard CD, Benson CB, et al: Postnatal outcome of fetuses with the prenatal diagnosis of gastroschisis. *J Ultrasound Med* 21:269, 2002.
292. Guzman ER: Early prenatal diagnosis of gastroschisis with transvaginal ultrasonography. *Am J Obstet Gynecol* 162:1253, 1990.
293. Vermeij-Keers C, Hartwig NG, van der Werff JF: Embryonic development of the ventral body wall and its congenital malformations. *Semin Pediatr Surg* 5:82, 1996.
294. Zimmer EZ, Bronshtein M: Early sonographic diagnosis of fetal midline disruption syndromes. *Prenat Diagn* 16:65, 1996.
295. Hsieh YY, Lee CC, Chang CC, et al: Prenatal sonographic diagnosis of Cantrell's pentalogy with cystic hygroma in the first trimester. *J Clin Ultrasound* 26:409, 1998.
296. Becker R, Runkel S, Entezami M: Prenatal diagnosis of body stalk anomaly at 9 weeks of gestation. Case report. *Fetal Diagn Ther* 15:301, 2000.
297. Colpaert C, Bogers J, Hertveldt K, et al: Limb-body wall complex: 4 new cases illustrating the importance of examining placenta and umbilical cord. *Pathol Res Pract* 196:783, 2000.
298. Paul C, Zosmer N, Jurkovic D, Nicolaides K: A case of body stalk anomaly at 10 weeks of gestation. *Ultrasound Obstet Gynecol* 17:157, 2001.
299. Luchr B, Lipsett J, Quinlivan JA: Limb-body wall complex: A case series. *J Matern Fetal Neonatal Med* 12:132-137, 2002.
300. Daskalakis G, Pilalis A, Papadopoulos D, et al: Body stalk anomaly diagnosed in the 2nd trimester. *Fetal Diagn Ther* 18:342, 2003.
301. Smrcek JM, Germier U, Krokowski M, et al: Prenatal ultrasound diagnosis and management of body stalk anomaly: analysis of nine singleton and two multiple pregnancies. *Ultrasound Obstet Gynecol* 21:322, 2003.
302. Wu JL, Fang KH, Yeh GP, et al: Using color Doppler sonography to identify the perivesical umbilical arteries: a useful method in the prenatal diagnosis of omphalocele-exstrophy-imperforate anus-spinal defects complex. *J Ultrasound Med* 23:1211, 2004.
303. Austin PF, Homsy YL, Gearhart JP, et al: The prenatal diagnosis of cloacal exstrophy. *J Urol* 160:1179, 1998.
304. Kaya H, Oral B, Dittrich R, et al: Prenatal diagnosis of cloacal exstrophy before rupture of the cloacal membrane. *Arch Gynecol Obstet* 263:142, 2000.
305. Donnfeld AE, Mennuti MT, Templeton JM, et al: Prenatal sonographic diagnosis of a vesico-allantoic abdominal wall defect. *J Ultrasound* 8:43, 1989.
306. Tolaymat LL, Maher JE, Kleinman GE, et al: Persistent patent urachus with allantois: a case report. *Ultrasound Obstet Gynecol* 10:366, 1997.
307. Nix JT, Menville JG, Albert M, et al: Congenital patent urachus. *J Urol* 79:264, 1957.



## THE FETAL GENITOURINARY TRACT

Fred E. Avni, MD, PhD, Brigitte Maugey-Laulom, MD, Marie Cassart, MD, PhD, Danielle Eurin, MD, Anne Massez, MD, and Michelle Hall, MD

### Embryology

Bladder and Urethra

The Normal Urinary Tract

*Bladder*

*Kidneys*

*Evidence of a Normally Functioning Urinary Tract*

The Abnormal Urinary Tract

*Abnormal Renal Number*

*Renal Duplication*

*Abnormal Kidney Location*

*Abnormal Kidney Size*

*Urinary Tract Dilatation*

*Hyperechoic Kidneys*

*Cystic Renal Diseases*

### Sonographic Patterns/Ultrasound and Pathologic Correlations

Diseases With Known Genetic Transmission

*Autosomal-Recessive Polycystic Kidney Disease*

*Autosomal-Dominant Polycystic Kidney Disease*

*Glomerulocystic Kidneys*

*Medullary Cystic Dysplasia*

*Unclassified Cystic Diseases*

Diseases Without Genetic Transmission

*Multicystic Dysplastic Kidney*

*Obstructive Dysplasia*

*Simple Renal Cyst*

*Renal Tumors*

*Acquired Renal Pathologies*

Other Congenital Renal Disorders

*Congenital Nephrotic Syndrome*

*Bladder, Urethra, and Urachus*

### Fetal Genital Tract

Normal Genitalia

Ambiguous Genitalia

Male Genital Anomalies

*Hypospadias/Epispadias*

*Scrotum*

Female Genital Anomalies

*Ovarian Cysts*

*Hydrocolpos—Vaginal Malformations*

### Fetal Adrenals

Normal Adrenals

Adrenogenital Syndrome

Adrenal Masses

## EMBRYOLOGY

Structurally and functionally, the urogenital system can be divided into two entirely different components—the urinary system and the genital system. Both of these develop from a common mesodermal ridge of tissue, the intermediate mesoderm, along the posterior wall of the abdominal cavity. Initially, the excretory ducts of both systems enter a common cavity, the cloaca.<sup>1</sup>

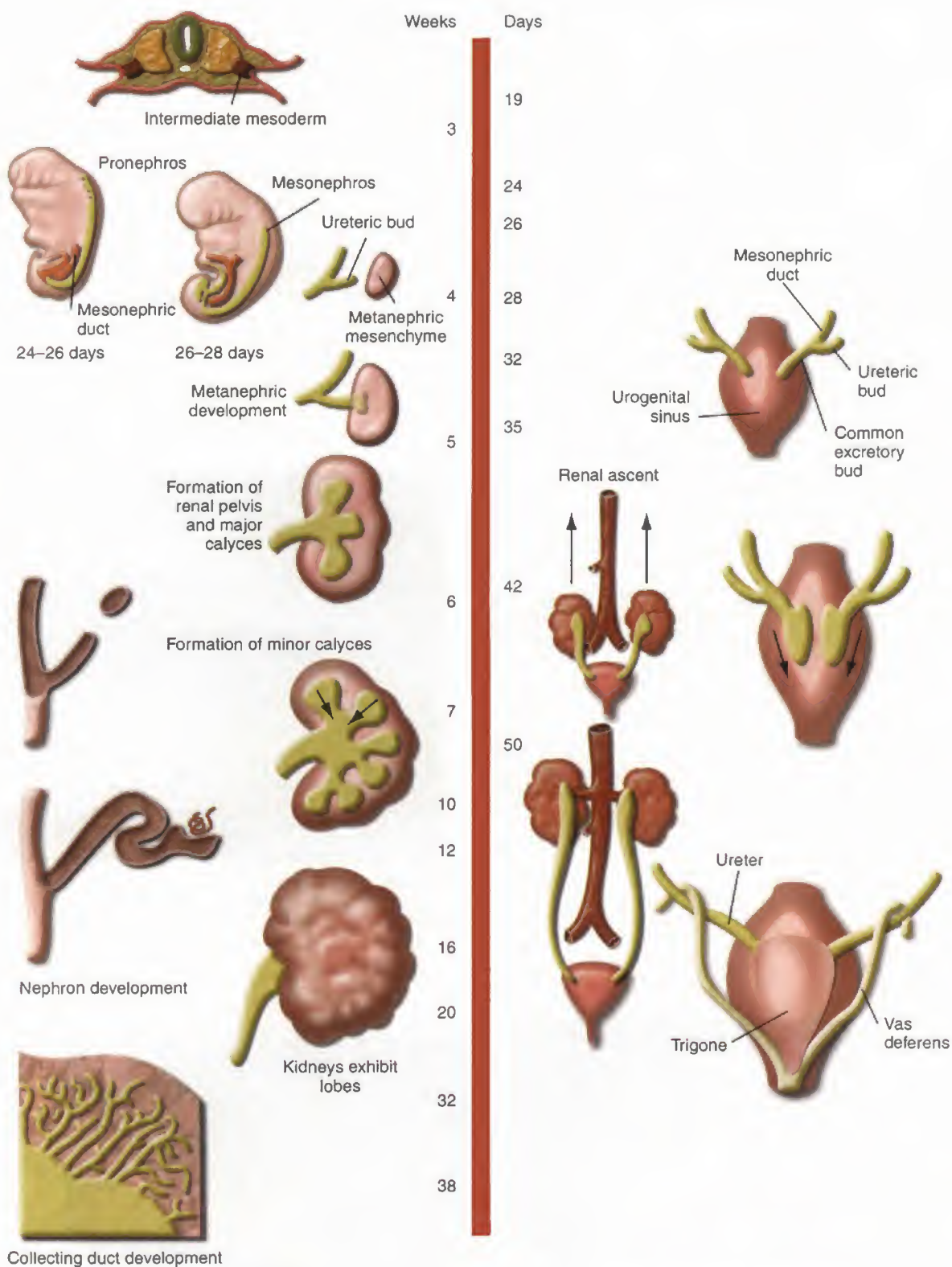
Human embryos develop three sets of excretory organs or kidney systems during intrauterine life.<sup>1,3</sup> The embryonic kidneys, which are formed in a cranial to caudal sequence, in order of appearance are the pronephros, the mesonephros, and the metanephros. The pronephros, analogous to the kidneys in primitive fishes and the mesonephros, which are well developed and analogous to the kidneys of amphibians, both regress in utero. The third set of kidneys, the metanephroi, become the permanent kidneys (Fig. 16-1).<sup>2,3</sup>

The pronephros is seen in the 3rd week of development and completely degenerates by the start of the 5th week. The second kidney, the mesonephros, also regresses by the 4th month; however, it serves as an excretory organ for the

embryo while the definitive kidney begins its development. Certain elements of the mesonephros are retained in the mature urogenital system as part of the reproductive tract.<sup>3</sup>

The metanephros, or definitive kidney, forms in the sacral region as a pair of new structures called the metanephric diverticulum or ureteric bud. It emanates from the distal portion of the mesonephric duct and comes in contact with and penetrates the metanephric mesenchymal blastema (metanephric mesoderm) at approximately the 28th day.<sup>2,3</sup>

The ureteric bud and metanephric mesoderm exert reciprocal inductive effects toward each other, and the proper differentiation of these structures depends on these inductive signals. The metanephric mesoderm induces the ureteric bud to branch, and in turn, the ureteric bud induces the metanephric mesoderm to condense and undergo mesenchymal-epithelial conversion. The nephron, which consists of the glomerulus, proximal tubule, loop of Henle, and distal tubule, is thought to derive from the metanephric mesoderm, whereas the collecting system, consisting of collecting ducts, calyces, pelvis, and ureter, is formed from the ureteric bud (see Fig. 16-1).<sup>3</sup>



A

Kidney development

Ureter and bladder development

B

**FIGURE 16-1.** The timeline of urogenital system development in the kidney (A) and ureter and bladder (B). (Modified from Park JM: *Normal and anomalous development of the urogenital system*. In Walsh PC: *Campbell's Urology*, 8th ed. Philadelphia, WB Saunders, 2002, p 1737. Copyright © 2002 Saunders, An Imprint of Elsevier; and Larsen WJ: *Human Embryology*. New York, Churchill Livingstone, 1997.) (Illustration by James A. Cooper, MD, San Diego, CA.)



The division of the ureteric bud results in the eventual pelvicalyceal patterns and their corresponding renal lobules. The first few divisions of the ureteric bud give rise to the renal pelvis, major and minor calyces, and collecting tubules. Thereafter, the first generations of collecting ducts are formed. When the ureteric bud first invades the metanephric mesoderm, its expanded end forms an ampulla that will eventually give rise to the renal pelvis. By the 6th week, the ureteric bud has bifurcated at least four times, yielding 16 branches. These branches then coalesce to form two to four major calyces extending from the renal pelvis. By the 7th week, the next four generations of branches also fuse, forming the minor calyces. By the 32nd week, approximately 11 additional generations of bifurcation have resulted in approximately 1 to 3 million branches, which will become the collecting duct tubules. In humans, although renal maturation continues to take place postnatally, nephrogenesis is completed before birth.<sup>3</sup>

### Bladder and Urethra

During the 4th to 7th weeks of development, the cloaca is divided by the urorectal septum into the urogenital sinus anteriorly and the anal canal posteriorly. The urogenital sinus is divided into three parts, of which the upper and largest part is the urinary bladder. Initially the bladder is continuous with the allantois, but when the lumen of the allantois is obliterated, a thick fibrous cord, the urachus, remains and connects the apex of the bladder with the umbilicus. The next part is a somewhat narrow canal, the pelvic part of the urogenital sinus, which in the male embryo, gives rise to the prostatic and membranous parts of the urethra and the entire urethra in female embryos. The caudal urogenital sinus forms the phallic urethra in the male embryo and the distal vaginal vestibule in the female embryo.<sup>1,2</sup>

## The Normal Urinary Tract

### Bladder

Urine is first produced by the kidneys during the 9th week of embryonic life. At this stage, the urine in the bladder can be visualized as a fluid-filled structure within the fetal pelvis (Fig. 16-2).

During the second and third trimester, the bladder will empty and refill continuously every 25 to 30 minutes. This cycle can be monitored during the sonographic examination. The position of the fetal bladder can virtually always be identified, because it lies between the umbilical arteries within the fetal pelvis. These arteries are readily seen with the use of color Doppler imaging. At the end of the pregnancy, this cycle decreases, especially in female fetuses possibly due to hormonal influence on the fetal bladder neck. This may induce a pseudomegabladder (see later) (Figs. 16-3 and 16-4).<sup>4,5</sup>



**FIGURE 16-2.** Fetal bladder in the first trimester at 12 weeks' gestational age. Sagittal scan of the fetus. The bladder is seen as a small cystic structure (arrow) in the fetal pelvis.

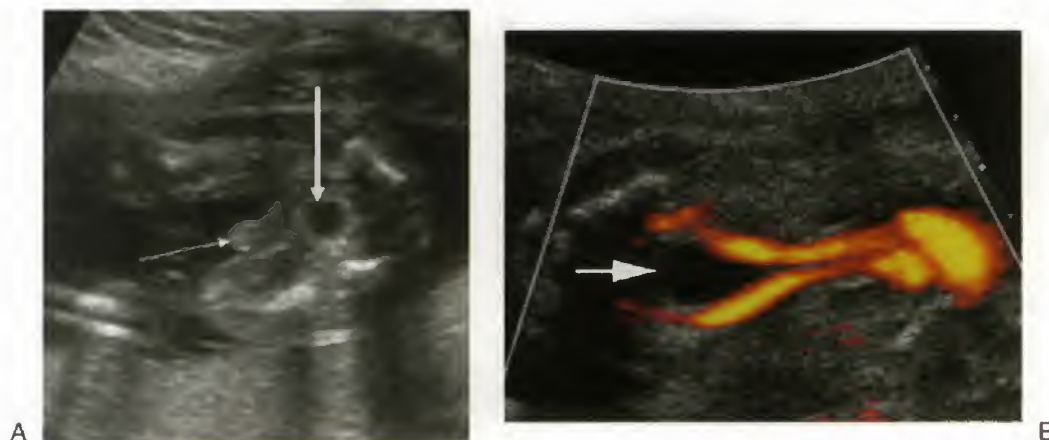


**FIGURE 16-3.** Fetal bladder in the second trimester (male fetus). A. Transverse scan through the fetal pelvis demonstrating the bladder (thick arrow) and the fetal sex (thin arrow). B. Color Doppler of the umbilical arteries at both sides of the bladder (arrow).

## Kidneys

With the use of transvaginal probes, fetal anatomic structures can be visualized earlier than with transabdominal ultrasound (US). Therefore, the fetal kidneys can be demonstrated at approximately 11 weeks transvaginally and at 12 weeks using transabdominal probes. During the first trimester, the kidneys appear as hyperechoic oval structures at both sides of the spine (their hyperechogenicity can be compared to that of the liver or spleen) (Fig. 16-5). This echogenicity will progressively decrease, and during the third trimester, the cortical echogenicity will always be less than that of the liver or spleen. Simultaneous to the decreased echogenicity, corticomedullary (CMD) differentiation will appear at approximately 14 to 15 weeks. This should always be demonstrated in fetuses older than 18 weeks. Prominent pyramids should not be misinterpreted as calyceal dilatation (Fig. 16-6). The fetal kidneys' growth can be evaluated throughout pregnancy by measuring renal length and comparing it to normal charts. (As a simple rule, renal growth is 1.1 mm/gestational week.) During the second and

third trimesters, the kidneys are easily identified by imaging the dorsolumbar spine and scanning on either side in parasagittal and transverse axial sections. Urine distending the renal pelvis may help in their identification. Under normal conditions, the fetal ureters are not visible.<sup>4-6</sup>

## Evidence of a Normally Functioning Urinary Tract

In addition to the visualization of the bladder and normal kidneys, the assessment of the urinary tract (UT) should include an evaluation of the amniotic fluid volume. After 14 weeks, two thirds of the normal amniotic fluid is produced by fetal urination and one third from pulmonary fluid. A normal volume of amniotic fluid is mandatory for proper development of the fetal lung. A normal sized thorax can be confirmed by measuring thoracic diameters or thoracic circumference.<sup>7</sup>

## The Abnormal Urinary Tract

The overall prevalence of renal tract anomalies is estimated at 5/1000 births. The percentage is likely higher when considering transient anomalies. Anomalies involving the UT are numerous and variable. They can be isolated or



**FIGURE 16-4.** Sagittal scan through the fetal abdomen. Fetal bladder (arrow) in the third trimester.

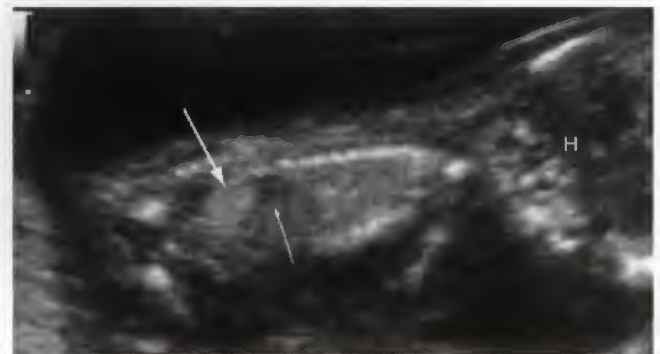


**FIGURE 16-5.** Fetal kidney, first trimester. Parasagittal scan of a first trimester fetus. The kidney appears as a hyperechoic small oval mass (thick arrow). The adrenal above it is hypoechoic (thin arrow). H, fetal head.



**FIGURE 16-6.** Second and third trimester kidneys. A. Second trimester. Sagittal scan through a kidney (K) that appears hyperechoic but with corticomedullary differentiation. Ch, chest. B. Third trimester. The kidney is limited by the crosses. Corticomedullary differentiation is clearly visible.



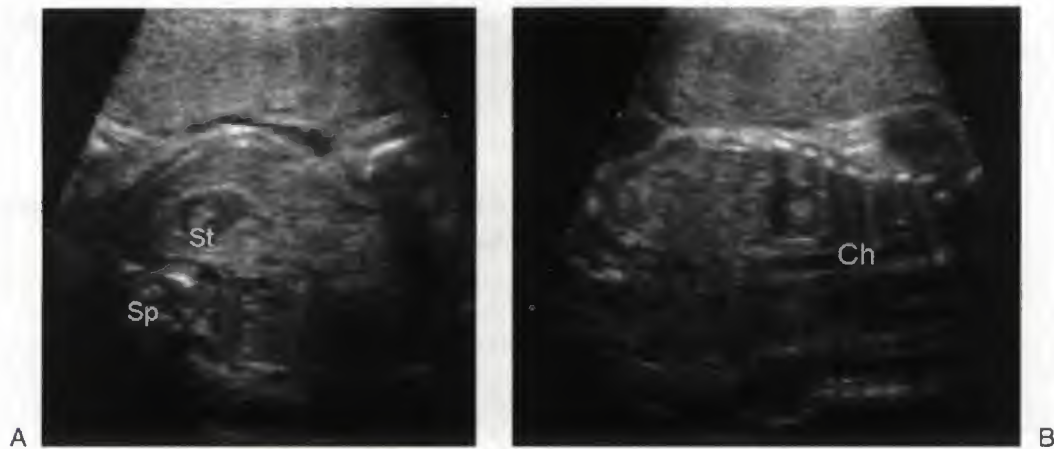


**FIGURE 16-7.** Bilateral renal agenesis, third trimester. A. Transverse scan of the fetal abdomen. Marked oligohydramnios. No renal structure is visible. Sp, spine; St, stomach. B. Sagittal scan of the fetal trunk of the same patient. No renal structure is visible. Ch, chest.

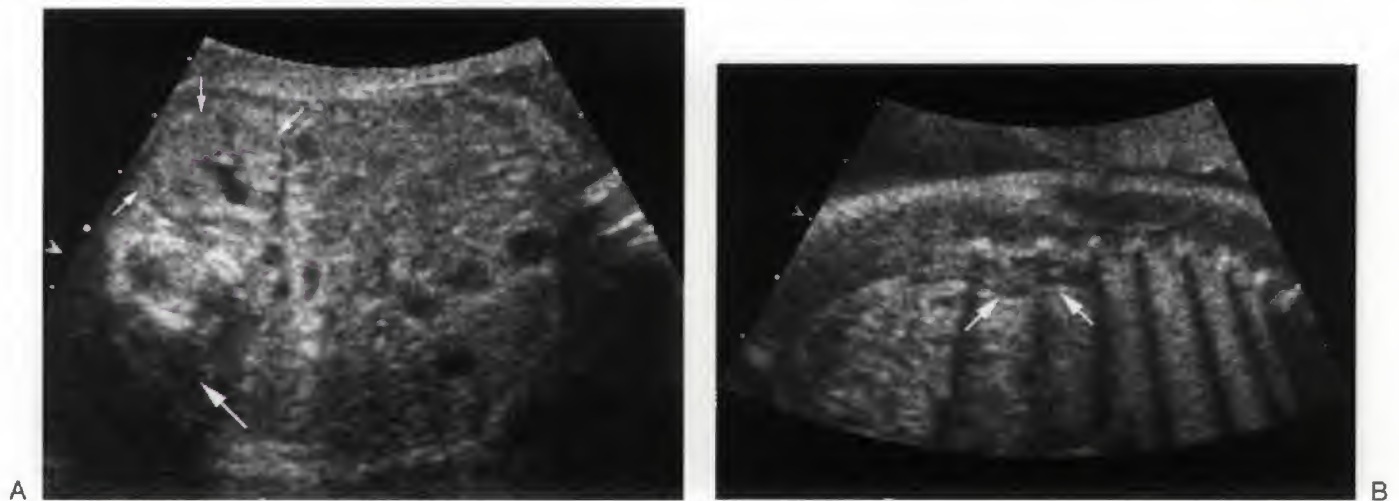


**FIGURE 16-8.** A. Transverse axial scan in a fetus with unilateral renal agenesis. The kidney is not seen in the renal fossa (large arrow). Normal contralateral kidney (small arrows). B. Sagittal scan in the same patient. The adrenal gland (arrows) on the same side as the absent kidney, is now elongated in what has been described as "the lying down adrenal sign."

appear in association with another organ system's anomalies. Therefore, the sonographic examination should be as meticulous as possible in order to visualize possible associated features. These additional findings will determine the prognosis.<sup>8-14</sup>

### Abnormal Renal Number

Bilateral renal agenesis is incompatible with extrauterine life. This condition, at times referred to as Potter's syndrome, results in pulmonary hypoplasia and musculoskeletal abnormalities. The diagnosis is based initially on anhydramnios after 15 weeks and on the nonvisualization of normal renal structures (Fig. 16-7). The bladder is empty (very rarely, a small fluid-filled structure can be observed in the fetal pelvis. It might correspond to retrograde filling of the bladder). Whenever there is a question as to whether the kidneys are present, fetal magnetic resonance imaging (MRI) may help

with the diagnosis. Enlarged, globular adrenals should not be misinterpreted as dysplastic kidneys.<sup>15-18</sup>

Unilateral agenesis occurs in 1/500 pregnancies. At the time of sonography, a normal kidney will not be identified in either lumbar area. When no other complication or malformation is present, the prognosis for postnatal life is excellent (Fig. 16-8). The ipsilateral adrenal gland is usually present, and appears globular and should not be mistaken for the kidney. Without the adjacent kidney, the adrenal gland may be elongated in appearance in what has been called "the lying down adrenal sign" (see Fig. 16-8B). In case of left renal agenesis, the left colonic flexure occupies the empty lumbar fossa and should not be confused with a cystic kidney or a dilated ureter. Whenever one or both lumbar fossas are empty, the kidneys should be searched for in an ectopic location (see later) (noteworthy, renal agenesis can theoretically result from the in utero regression of multicystic renal dysplasia).<sup>19-21</sup>

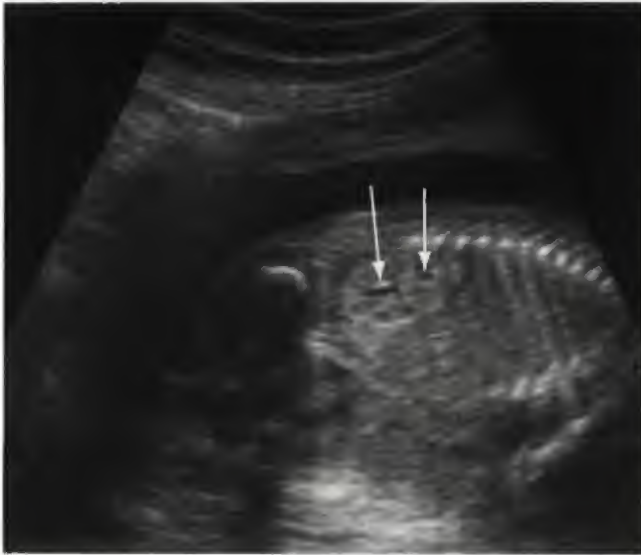


**FIGURE 16-9.** Uncomplicated renal duplication (second trimester). Parasagittal scan through one kidney. Some urine distends the two separated collecting systems (arrows).



**FIGURE 16-10.** Ectopic pelvic kidney, third trimester. Oblique view of the fetal abdomen. The pelvic kidney (K) lies above the bladder (B). Ab, fetal abdomen.

### Renal Duplication

When no complication occurs, renal duplication is a benign condition and should be considered a normal variant (Fig. 16-9). If complicated, it should be included in the differential diagnosis of UT dilatation (see later).

### Abnormal Kidney Location

There are various ectopic locations possible for the kidney. The ectopic kidney is recognizable thanks to its characteristic CMD. An ectopic kidney is usually smaller and may be malrotated. Complications such as dilatation or dysplasia

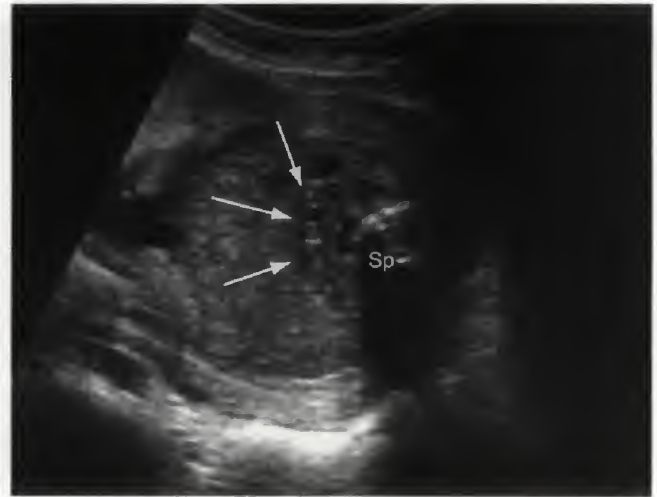


**FIGURE 16-11.** Horseshoe kidney, third trimester. Transverse scan through the middle fetal abdomen. The two kidneys fuse on the midline (arrows). Sp, spine.

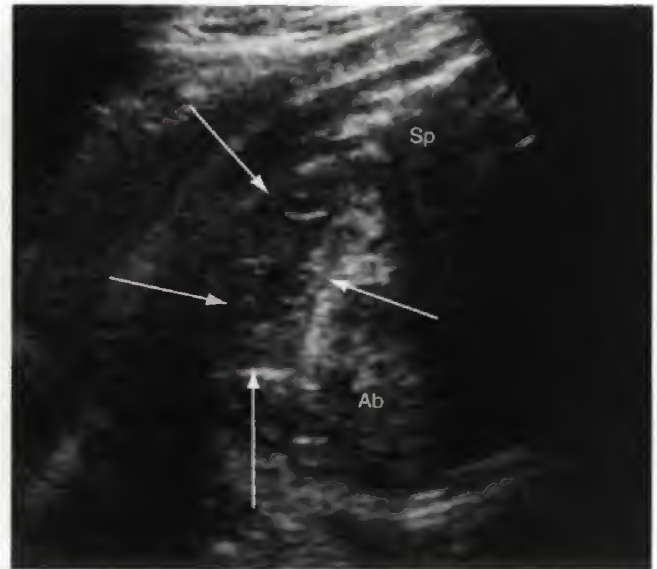


**FIGURE 16-12.** Crossed fused ectopia, third trimester. Transverse oblique view of the fetal abdomen (Ab) demonstrating the two fused kidneys (limited by the arrows). Sp, spine.

do occur. One or both kidneys can be ectopic. The pelvic location is the commonest location for ectopic kidneys to appear (Fig. 16-10). Other ectopic locations include horseshoe, crossed fused ectopia (both kidneys lie on the same side), and intrathoracic ectopia. In horseshoe kidneys, a bridge of renal tissue can be visualized in front of the spine (Fig. 16-11). Crossed ectopia should be differentiated from duplex kidneys. In crossed (fused) ectopia, there is an angulation between the two kidneys, whereas in duplication, the two renal moieties lie in the same continuous plane (Fig. 16-12).<sup>22,23</sup>



### Abnormal Kidney Size

The kidneys must be systematically measured whenever their echogenicity is abnormal or whenever the amniotic fluid volume is reduced.

*Small kidneys* (below -2 standard deviations [SDs]) are usually seen when hypoplasia or dysplasia (or both) resulting from an embryologic maldevelopment, secondary to reflux (reflux nephropathy), obstruction, or to an ischemic phenomenon is present. Small kidneys may also result from so-called tubular dysgenesis associated with the maternal ingestion of angiotensin II antagonists. The prognosis of small kidneys depends on the remaining renal function. Cases with oligohydramnios have the poorest prognosis.<sup>24,25</sup>

Dysplastic renal parenchyma appears hyperechoic and is often associated with parenchymal cysts. Dysplastic and ischemic kidneys are part of the differential diagnosis of hyperechoic kidneys (see later). The differential diagnosis of *enlarged kidneys* (above +2 SDs) includes renal dilatation, cystic kidneys, syndromes with organomegaly (i.e., Beckwith-Wiedemann syndrome) and renal tumors (see later).

### Urinary Tract Dilatation

Dilatation of the renal pelvis is a common finding on obstetric US. Its frequency is evaluated at approximately 1% to 4% of all pregnancies. Yet, all dilatations do not have the same clinical relevance; furthermore, their antenatal and postnatal evolution is variable. This has led to abundant and somewhat controversial literature about the best work-up and follow-up after birth.<sup>13,26,27</sup>

**Definition.** Various criteria are used in order to objectively evaluate renal dilatation. In our experience, the best criterion is the measurement of the anteroposterior diameter of the renal pelvis on a transverse scan of the fetal abdomen (Fig. 16-13). Using this measurement, several threshold values have been applied in order to be able to predict the postnatal outcome, especially in cases with moderate dilatation (less than 15 mm). Many authors agree that the upper limit should be 4 mm during the second and 7 mm during the third trimester of the pregnancy (see Figs. 16-13 to 16-15). These limits are set in order to detect not only

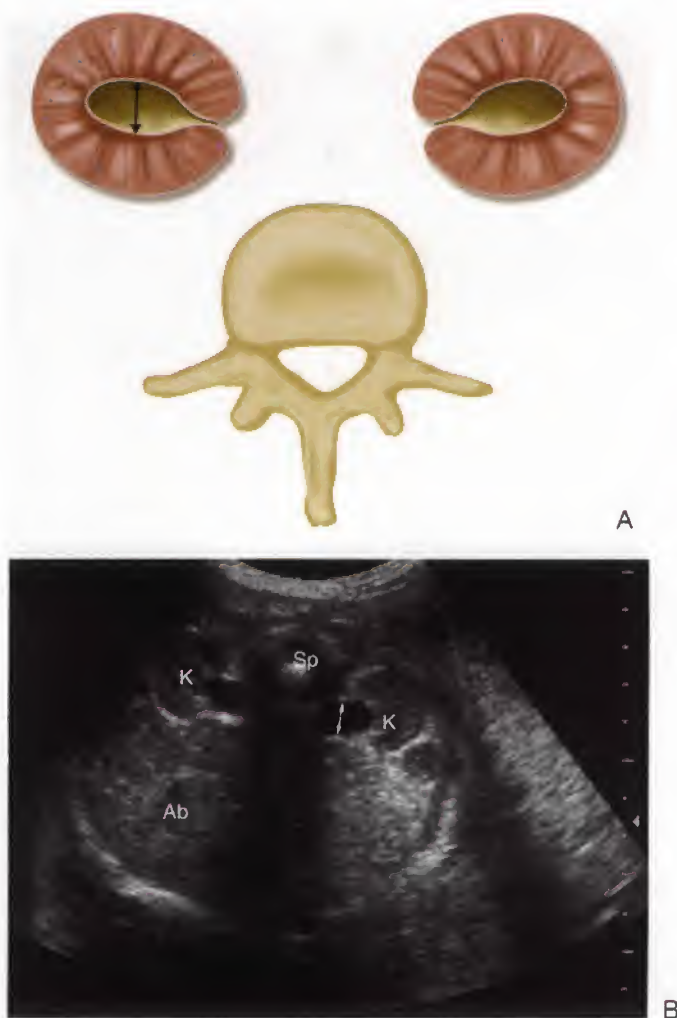


**FIGURE 16-13.** Bilateral mild dilatation. (A) Illustration demonstrating the method for measuring the degree of dilatation. A transverse axial plane of section of the fetal abdomen is obtained and an anteroposterior measurement of the renal pelvis is obtained. (Illustration by James A. Cooper, MD, San Diego, CA.) (B) Transverse sonographic scan through both kidneys (K) demonstrating a mildly distended renal pelvis and the method of measuring the renal pelvis (arrows). Ab, fetal abdomen; Sp, spine.

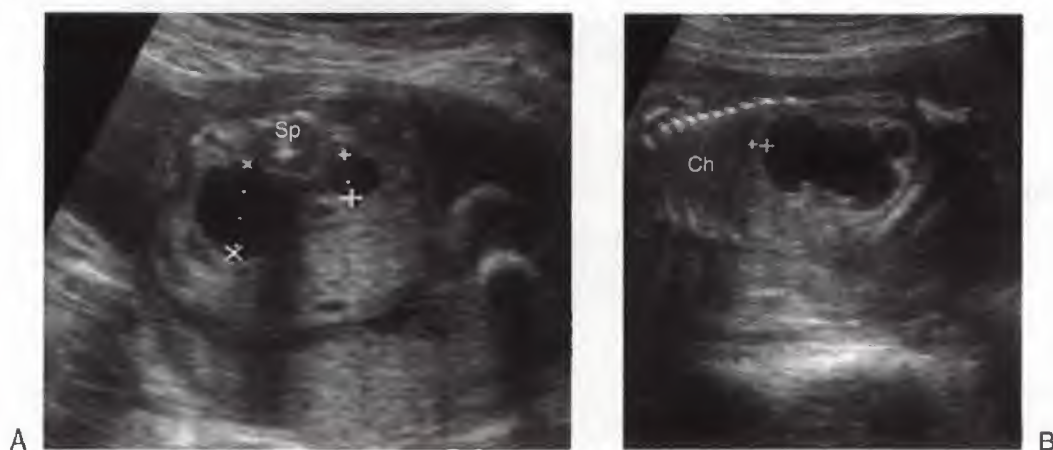


**FIGURE 16-14.** Bilateral asymmetric dilatation (case of ureteropelvic obstruction), third trimester. A. Transverse scan through fetal abdomen. Marked left (20 mm between calipers) and moderate right (10 mm) dilatation. Sp, spine. B. Sagittal scan through the left kidney. Marked pyelocalyceal dilatation. The renal cortex is thinned (2 mm) and hyperechoic suggesting dysplasia. Ch, fetal chest.

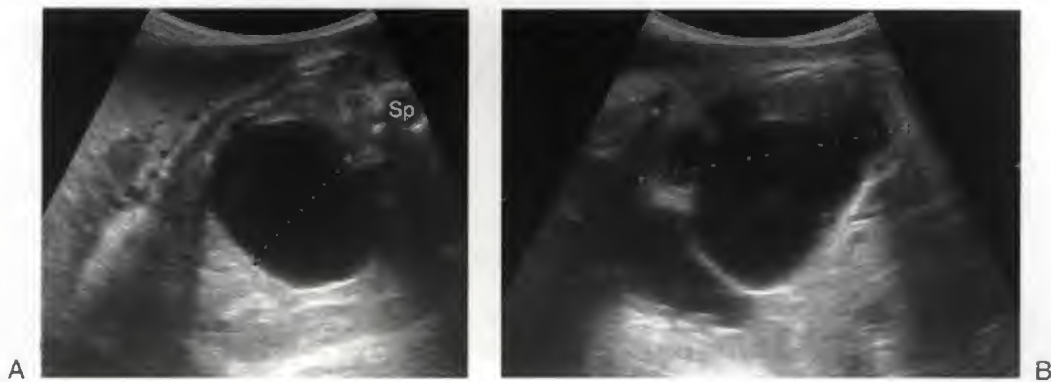


**FIGURE 16-15.** Massive right renal dilatation. Case of ureteropelvic obstruction. *A.* Transverse scan through the fetal abdomen demonstrating marked dilatation of the renal pelvis (36 mm between calipers). Sp, fetal spine. *B.* Sagittal scan through the dilated kidney measuring 72 mm between the calipers.

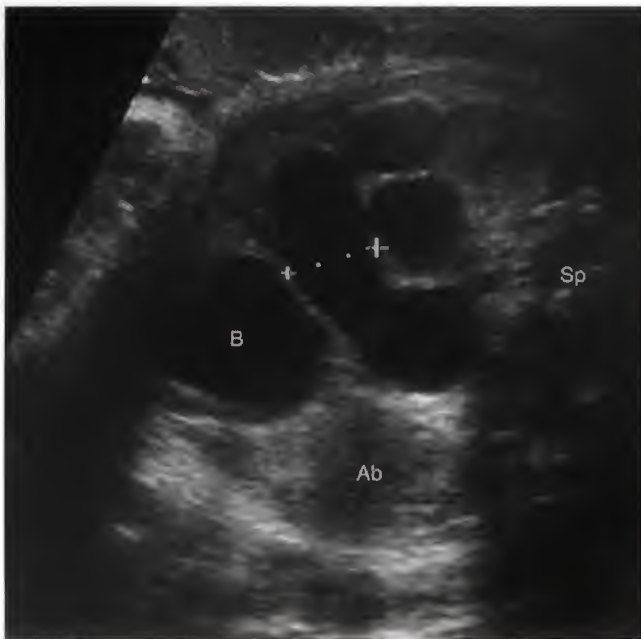


**FIGURE 16-16.** Ureteral dilatation (case of ureteropelvic obstruction). Transverse scan of the fetal abdomen demonstrating the dilated tortuous ureter (12 mm between the calipers). Ab, abdomen; B, bladder; Sp, spine.

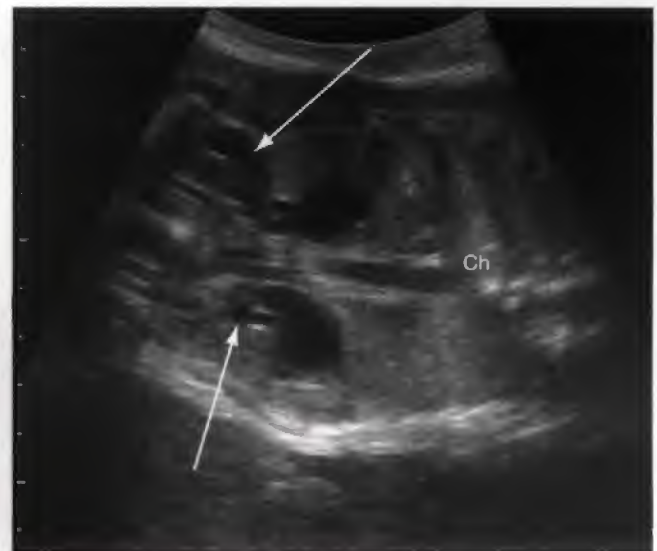


**FIGURE 16-17.** Ureteral dilatation (case of vesicoureteric reflux). Coronal view of the fetal trunk showing bilateral pelvic and ureteral dilatation (arrows). Ch, chest.

patients that will need corrective surgery (in case of obstructive dilatation) but also the majority of fetuses and neonates presenting with vesicoureteric reflux. These patients are at risk for developing complications and eventually worsening renal function.<sup>27-35</sup>

Pyelectasis refers to a visible renal pelvis below the significant threshold. During the second trimester, there are reports of this feature as a minor sign of chromosomal anomaly.<sup>32</sup> Other sonographic evidence of an abnormality of the UT includes the visibility of the fetal ureter during pregnancy (Figs. 16-16 and 16-17) and the demonstration of an enlarged bladder (more than 3 cm length during the second and 5 cm during the third trimester) (Fig. 16-18).<sup>34,36</sup>

**Findings During Obstetric Ultrasound.** Abnormalities resulting in dilatation of the UT can be found at any time

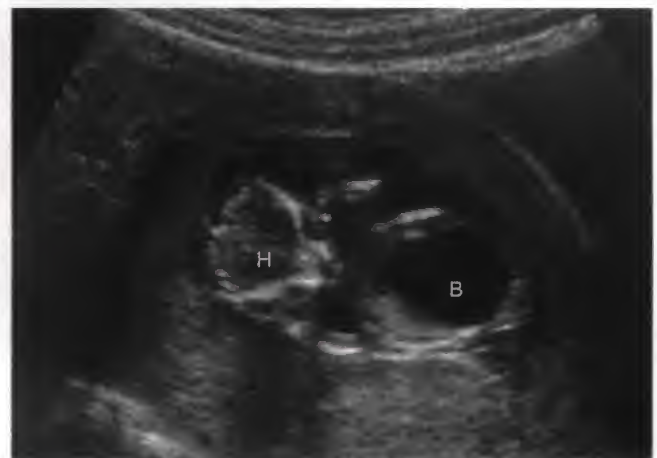


**FIGURE 16-18.** Megacystis, early second trimester (case of urethral atresia). Frontal view through the fetal head and abdomen. The abdomen is filled by the distended urinary bladder (B). H, fetal head.



during pregnancy. The degree of dilatation may increase or decrease during each trimester. Therefore, in order to screen all potentially abnormal cases, some authors advocate performing one sonographic examination during each trimester.<sup>33</sup> This is controversial, because most abnormalities, particularly mild UT dilatation, do not change significantly during pregnancy and, therefore, are unlikely to alter pregnancy and fetal management.

**Table 16–1 Causes of Urinary Tract Dilatation**

UPJ obstruction
Nonobstructive dilatation
UVJ obstruction
VUR
Duplication
Megacalycoses
Infundibular stenosis
Bladder outlet obstruction
So-called megacystis-megaureter association
Megacystis microcolon-hypospadias syndrome

UPJ, ureteropelvic obstruction; UVJ, ureterovesical junction obstruction; VUR, vesicoureteric reflux.

Once dilatation of the collecting system has been detected in utero, the subsequent evaluation should answer three major questions: the origin of the dilatation, the coexistence of associated anomalies, and finally, the prognosis of the malformation. The most common cause for UT dilatation is ureteropelvic obstruction (UPJ). Other causes include ureterovesical junction obstruction (UVJ), vesicoureteric reflux (VUR), complicated duplex kidneys, and bladder outlet obstruction (BOO) (Table 16–1).

In cases of UPJ obstruction, the renal pelvis is dilated. As mentioned earlier, the threshold measurement on a transverse scan of the kidney is 7 mm for mild dilatation, between 7 and 15 mm for moderate dilatation, and more than 15 mm for marked dilatation. The more dilated the system, the more likely there is to be a decrease in renal function after birth. Furthermore, thinned, hyperechogenic renal cortices with cysts often correspond to obstructive dysplasia and impaired function (Fig. 16–19). Yet, unfortunately, there is often no direct correlation between the renal appearance and postnatal function (see Figs. 16–14 and 16–15).<sup>34–38</sup>

Noteworthy, obstruction may lead to leakage (rupture of a renal calyx or even bladder), and to urinary extravasation either as a perirenal urinoma or as ascites. The functional significance of the leakage is not straightforward. In some

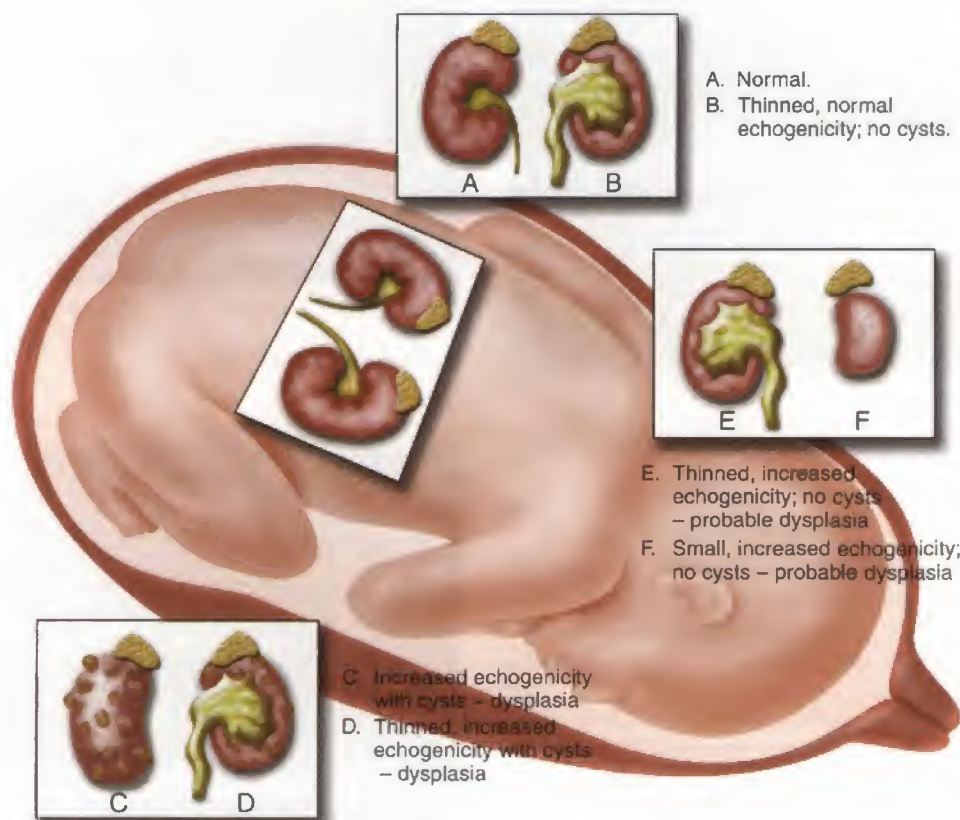


**FIGURE 16–19.** Urinary tract obstruction produces a varied response from the kidneys. A. The kidney may remain normal in distal obstruction, without reflux. B. Pelvocaliectasis may attenuate the parenchymal thickness. C. The kidney may suffer cystic dysplasia (parenchymal cysts), become fibrotic (increased echogenicity), and cease to function (lack of pelvocaliectasis). D. Alternatively, it may undergo cystic dysplasia with parenchymal cysts and increased echogenicity but continue to have pelvocaliectasis and a thinned parenchyma. If no cysts are visible but the parenchyma is of greatly increased echogenicity, either with (E) or without (F) pelvocaliectasis, dysplasia is probably, but not invariably present. (Illustration by James A. Cooper, M., San Diego, CA.)

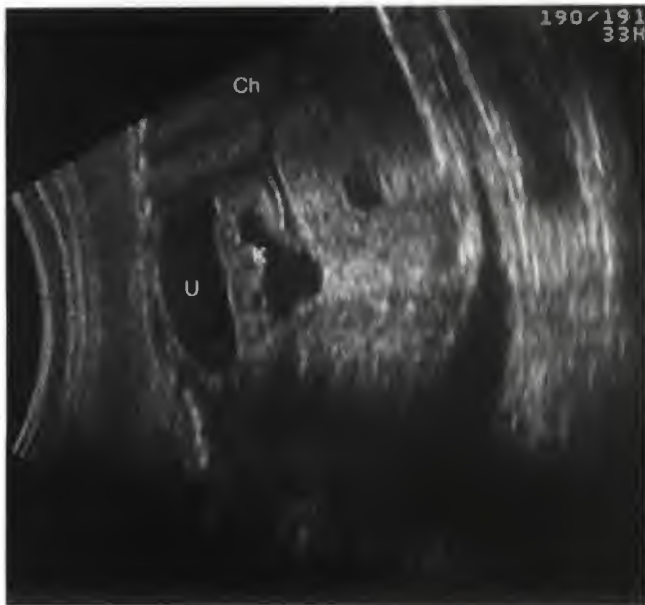


**FIGURE 16-20.** Perirenal urinoma (secondary to a ureteropelvic obstruction), end second trimester. Rotated coronal scan demonstrating the dilated kidney (K) and perirenal urinoma (U). Ch, chest.

instances, it may protect the renal parenchyma, whereas in others renal growth is impaired (Fig. 16-20).<sup>24,39,40</sup>

The main differential diagnosis of UPJ obstruction is *nonobstructive dilatation* (which is a postnatal diagnosis), multicystic dysplastic kidney (MDK) (part of cystic renal diseases, see below) and UVJ obstruction. Rarer differential diagnoses of UPJ obstruction are megacalycoses due to medullary hypoplasia (the calyces are more dilated than the renal pelvis) and infundibular stenosis (no medullary hypoplasia, but still calyceal dilatation).

The diagnosis of UVJ obstruction is based on the demonstration of a dilated ureter. Peristaltic waves modify the caliber of the ureter (see Fig. 16-16).<sup>12-14,36</sup> The dilatation may increase in utero, but it usually decreases after birth. In most instances, it is not possible to differentiate between dilatation secondary to UVJ obstruction from that secondary to high-grade vesicoureteric reflux (see Fig. 16-17). A hint for a differential diagnosis is the variability of the diameter of the renal pelvis during one single examination. This would favor VUR.

*Renal duplication* is usually easy to demonstrate once dilatation has developed. Various complications may occur at the level of renal duplications; for instance, obstruction at the upper or lower moiety or MDK at the upper or lower moiety. Both can be associated with distal insertion of the ureter ending either as an ureterocele or into an ectopic extravascular insertion. The ureterocele is seen as a septum within the bladder. It may prolapse into the urethra and result in acute in utero obstruction. The parenchyma related to obstruction may be thinned and dysplastic. The ectopic extravascular insertion may be difficult to diagnose in utero (Figs. 16-21 and 16-22).<sup>41-44</sup>

Finally, the level of UT obstruction can be located below the bladder. The most frequent cause in male fetuses is posterior urethral valves (PUVs). The condition may or not

induce dilatation of the upper UT. The dilatation can be unilateral or bilateral, and may be related to obstruction or to VUR.<sup>45,46</sup> The degree of associated dysplasia is also variable. There seems to be a correlation between cortical echogenicity and the degree of obstructive dysplasia (Figs. 16-19 and 16-23).<sup>37</sup>

In cases of obstruction, the bladder “reacts” in different ways: it can enlarge, its wall can thicken, or the bladder may rupture and urinary ascites appears; other protective decompressive mechanisms may develop through VUR, urinomas, extravasation, or recanalization of the urachus (Fig. 16-24).<sup>39</sup>

Bladder enlargement due to obstruction secondary to PUV must be differentiated from other causes of BOO and from other causes of large bladder without obstruction (Table 16-2). Urethral atresia may result in megacystis detected during the first trimester and oligohydramnios (see Fig. 16-18); the condition often has a poor prognosis. A dilated penile urethra may be seen. Megacystis-megaureter association is related to massive VUR (Fig. 16-25). In such a case, the amniotic fluid volume is normal. Megacystis-microcolon-hypoperistalsis syndrome is a rare condition occurring in female fetuses with a poor postnatal prognosis (see later).<sup>46-49</sup>

**Prognosis and In Utero Treatment.** Whenever a renal anomaly (mainly dilatation) is detected, a complete survey of the fetal anatomy should be performed in order to detect associated malformations that would indicate the need for chromosomal analysis or the possibility of polymalformative syndromes; both worsen the prognosis.<sup>10,50,51</sup>

In cases of dilatation, the prognosis will depend upon the type and extent of anomalies. Features of poor prognosis include early diagnosis, bilateral marked dilatation, persistently obstructed bladder, oligohydramnios, and secondary lung hypoplasia. Bilateral renal dilatation and BOO have an increased risk of associated chromosomal anomalies, and therefore, in such cases, an evaluation of fetal chromosomes may be warranted. The finding of associated hyperechogenic and cystic renal parenchyma is frequently but only partially informative (positive predictive value [PPV] = 59%, negative predictive value [NPV] = 56%) about renal function. Conversely, normal cortical echogenicity does not exclude dysplasia.

The role of measuring urinary electrolytes in the fetal urine obtained through transabdominal puncture is controversial. There are discrepancies in the predictive values of urine biochemistry owing to small sample size, variations in cutoff values, gestational age, and sampling frequency. Fetuses with renal damage show decreased urinary concentrating especially of sodium and calcium without clear convincing confirmation. Measurements of B<sub>2</sub>-immunoglobulin on C cystatin in the fetal urines allow a better accuracy (Table 16-3). The outcome of vesicoamniotic shunting is also controversial. Although technically relatively easy, the long-term results have not been convincing.<sup>52-56</sup>

**Management of Fetal Renal Pelvic Dilatation After Birth.** It is of utmost importance that any information relevant for the proper postnatal management is correctly transmitted to the postnatal team that will be in charge of the newborn. A variety of findings may be seen in the neonate after birth that suggest an abnormality of the UT (Table 16-4). After birth, some conditions require an





**FIGURE 16-21.** Renal duplication - Obstructed upper pole and ectopic ureterocele (third trimester). A. Illustration demonstrating duplication of the collecting system. Typically the upper pole moiety is obstructed and the lower pole moiety often demonstrates reflux. The ureter from the upper pole moiety inserts more medial and caudal into the bladder than the ureter from the lower pole. This is referred to as the Meyer-Wiegert rule. Dilatation of the submucosal portion of the ureter results in a ureterocele. (Illustration by James A. Cooper, M.D., San Diego, CA.) B. Sagittal scan through the left kidney demonstrating the dilated upper pole (UP) and normal lower pole (LP). C. Sagittal scan through the bladder (B) displaying the ureterocele (arrow).

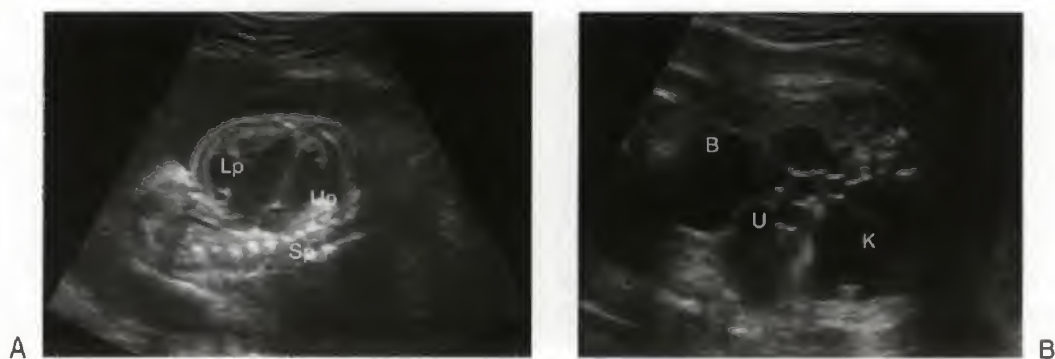


**FIGURE 16-22.** Complicated duplex system, third trimester. A. Sagittal scan of the left kidney. Both the upper (Up) and lower pole (Lp) are dilated. Sp, fetal spine. B. Transverse scan of the fetal abdomen demonstrating the dilated kidney (K), the dilated ureters (U; they should not be confused with dilated intestinal tract), and the urinary bladder (B).



**FIGURE 16-23.** Posterior urethral valves and obstructive dysplasia. A. Coronal scan demonstrates a distended bladder (BI), dilated ureters (U) and a dilated posterior urethra (PU). B. Bilateral hydronephrosis and hyperechogenic kidneys suggesting dysplasia. C. A sonogram slightly later of one of the kidneys confirms obstructive cystic dysplasia (arrows).

immediate confirmation and therapeutic maneuvers. For instance, obstructive PUVs or prolapsed ectopic ureterocele into the urethra leading to oligoanuria necessitate immediate treatment. In case of such suspicions, US and a voiding cystourethrogram (VCUG) should be performed immediately after birth in order to confirm the anomaly.<sup>57</sup>

In all other cases, the work-up should be planned without emergency. There is controversy regarding the respective role of US and VCUG in the postnatal work-up. Some authors advocate the systematic use of a VCUG in every case of antenatal detection of UT dilatation; for others, only patients with persistent dilatation should undergo a VCUG.<sup>58,59</sup> Whatever the choice, all patients are put under prophylactic antibiotic therapy until a final diagnosis and a final therapeutic decision is made.

Practically, we have applied an algorithm based on US examinations (Fig. 16-26). An US including the kidneys, bladder, and ureters should be performed during the first week of life in order to verify the UT abnormality. The sonographic analysis should be as detailed as possible, and any significant anomaly should lead one to perform a VCUG. If the examination is negative, a repeat sonographic examination should be performed at the age of 1 month. Again, if any abnormality is found, a VCUG should be

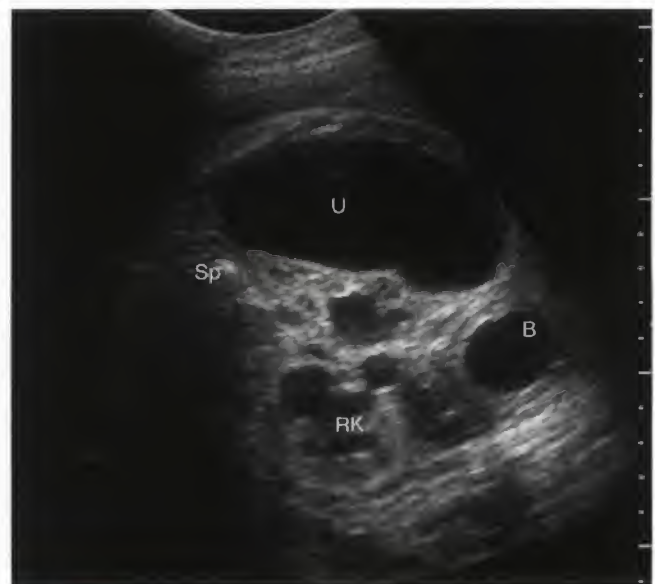


**FIGURE 16-24.** Posterior urethral valves and urinoma, third trimester. Transverse scan of the fetal abdomen. The bladder (B) is small and its wall thickened. At the level of the left kidney, a large urinoma (U) has developed. The right kidney (RK) is just moderately dilated. Sp, spine.



performed, but if no anomaly is demonstrated, no further evaluation is needed. At this stage, any prophylactic antibiotic therapy should be stopped.<sup>60</sup>

The role of VCUG is clearly to detect vesicoureteric reflux that will render long-term follow-up and persistent prophylaxis necessary. This attitude is intended to reduce unnecessary complications that are associated with high grades of VUR. It will also demonstrate anomalies of the urethra and potentially abnormal ureteral endings. Follow-up studies include US (every 6 months for a period of 2 years) in order to verify renal growth, VCUG every year to monitor the reflux, and MAG3 isotopic studies in order to verify renal function.<sup>61-63</sup>

If no reflux is present, complementary imaging is necessary in order to determine the origin of the dilatation. Renal function is assessed through isotopic studies; the morphology of complex or complicated UT malformations are best evaluated by MRI. The technique is particularly helpful for the assessment of the severely dilated UT and complicated duplex systems with dilatation of the upper and lower pole moieties. Also, the technique is able to provide information on the functional status of the kidney. It will help the surgeon in optimizing treatment.<sup>64</sup> After this evaluation and if a conservative attitude is elected, a sonographic

**Table 16-2** Causes of Large Bladder

Urethral atresia (prune-belly syndrome)  
Megalourethra  
Posterior urethral valves  
Anterior urethral valves  
Prolapse of ureterocele  
Megacystis megaureter (vesicoureteric reflux)  
Megacystis microcolon hypoperistalsis syndrome  
"Normal variant" in female fetuses

**Table 16-3**

**Fetal Urinary Biochemistry—Good Prognosis**

Analyte	Value
Sodium*	< 100 mg/dl
Chloride*	< 90 mg/dl
Osmolality*	< 200 mg/dl
Calcium†	< 8 mg/dl
β <sub>2</sub> -Microglobulin‡	< 4.0 mg/L
Total Protein§	< 20 mg/dl
Cystatin C¶	< 1 mg/L

\*Glick PL, Harisson MR, Golbus MS, et al: Management of the fetus with congenital hydronephrosis. II. Prognostic criteria and selection for treatment. *J Pediatr Surg* 20:376, 1985.

†Nicolaidis KH, Cheng HH, Snijders RJM, et al: Fetal urine biochemistry in the assessment of obstructive uropathy. *Am J Obstet Gynecol* 166:932, 1992.

‡Mandelbrot L, Dumez Y, Muller F, et al: Prenatal prediction of renal function in fetal obstructive uropathies. *J Perinat Med* 19:283, 1991.

§Johnson MP, Bukowski TP, Kihier K, et al: Fetal urine albumin/globulin ratio in the in utero evaluation of obstructive uropathies [Abstract]. *Am J Hum Genet* 51:259, 1992.

¶Muller F, Bernard M-A, Benkirane A, et al: Fetal urine cystatin C as a predictor of postnatal renal function in bilateral uropathies. *Clinical Chemistry* 45:2292, 1999.

**Table 16-4**

**Characteristics Suggesting an Abnormality of the Urinary Tract on Neonatal Ultrasound**

Pelvic dilatation greater than 7 mm  
Calyceal dilatation  
Parenchymal thinning  
Lack of cortico-medullary differentiation  
Small kidney  
Thickening of the pelvic wall  
Thickening of the ureteral wall  
Ureteral dilatation above 3 mm  
Enlarged bladder

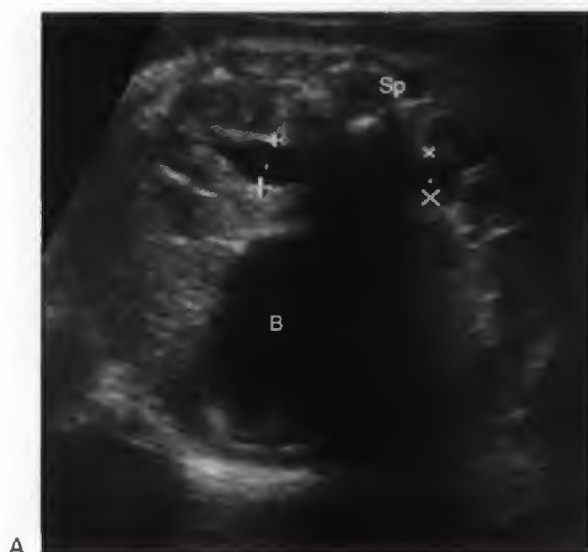


**FIGURE 16-25.** Megacystis megaureter association, third trimester. Transverse scan (A and B) of the fetal abdomen showing variation in the dilatation of the renal pelvis at two different moments during the same examination. The bladder (B) is markedly enlarged. At birth there was bilateral grade V reflux. Sp, spine.

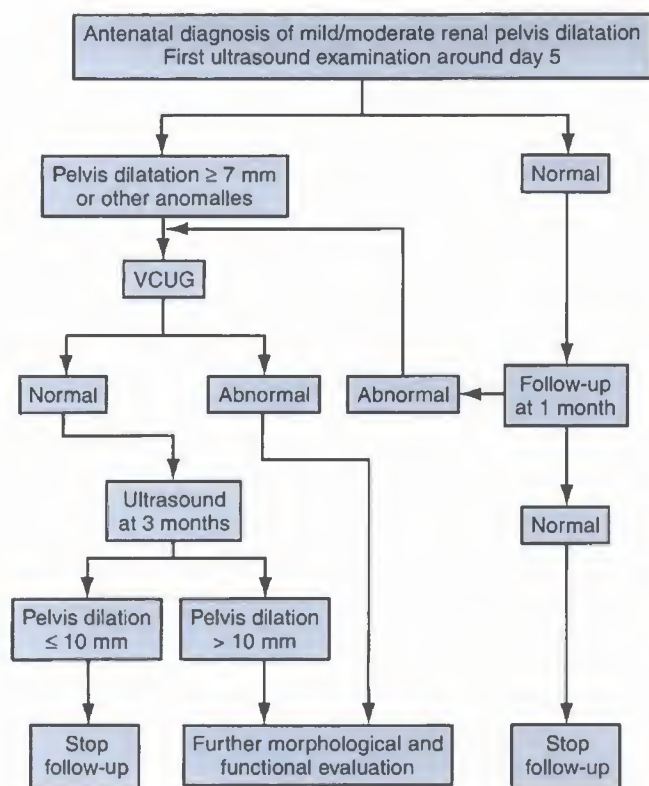


**FIGURE 16-26.** Postnatal imaging strategy in infants with mild to moderate fetal renal pelvic dilatation.

follow-up is advised in order to follow renal growth and dilatation. It has been shown that a large proportion of UT dilatation resolves spontaneously.<sup>63</sup>

The length of follow-up must be adapted to the type of anomaly. If the dilatation of the renal pelvis measures less than 10 mm, a baseline US can be performed at 3 months; if no further dilatation occurs, the follow-up can be stopped because worsening rarely occurs. For dilatation greater than 10 mm or for ureteral dilatation, a longer follow-up is needed. During the period of follow-up (2 to 3 years), it is also important to exclude worsening of the renal function that would suggest the need for alternative treatment.<sup>65-67</sup> Using this algorithm, very few abnormal cases escape the work up and the risk of complications is very low. Some centers use the grading system of the Society of Fetal Urology, although its value in management and prognosis is uncertain (Fig. 16-27).

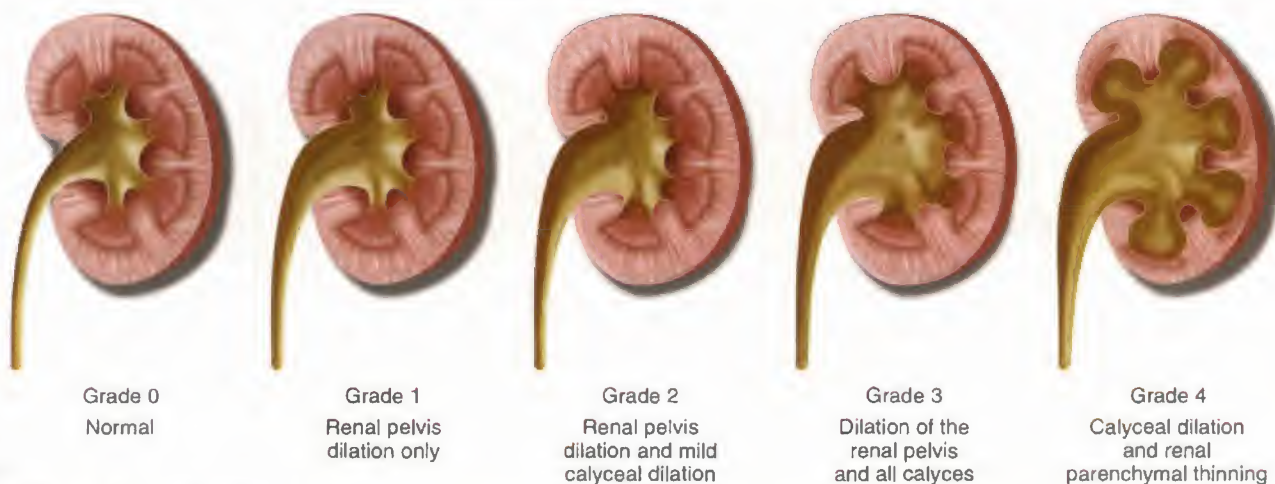
### **Hyperechoic Kidneys**

Hyperechogenicity of the fetal kidney is defined by comparison with the adjacent liver or spleen. This is difficult to assess in the first and second trimester because the kidney is "physiologically" hyperechoic (or isoechoic at the end of the second trimester) relative to the liver. It is easier to characterize after 28 weeks when the renal cortex should always be hypoechoic compared to the liver and spleen.

Hyperechogenicity of *both fetal kidneys* can result from various diseases (Table 16-5).

SOCIETY OF FETAL UROLOGY GRADING SYSTEM OF CONGENITAL HYDRONEPHROSIS		
Grade	Central renal complex	Renal parenchymal thickness
0	Intact	Normal
I	Mild splitting of pelvis (dilation)	Normal
II	Moderate splitting of pelvis and calyces, but complex, confined within renal border	Normal
III	Marked splitting, pelvis dilated outside renal borders and calyces dilated	Normal
IV	Further pelvicalyceal dilation	Thinned

A



B

**FIGURE 16-27.** A. Description. B. Illustration demonstrating the ultrasound grading system of hydronephrosis from the Society of Fetal Urology. (Illustration by James A. Cooper, MD, San Diego, CA.)



**Table 16-5** Causes of Bilateral Hyperechoic Kidneys<sup>(7, 65-69, 76, 103-112)</sup>

	Corticomedullary Differentiation	Isolated Malformation	Polymalformative
Obstructive dysplasia	—	++	—
Hereditary cystic diseases			
ADPKD	+ or —	+++	(+)
ARPKD	— or reversed	+++	
GCD	—	+	+++
MCD	+		+++
Syndromes with other abnormalities			
Overgrowth syndromes			++
Beckwith-Wiedemann	+		
Perlman	+		
Zellweger	+		++
Ivemark	+ or —		++
Diabetes and renal cysts	+ or —		++
Bardet-Biedl	+ or —		
Meckel-Gruber	+ or —		++
Nonhereditary fetal diseases			
Renal vein thrombosis	+ or —	++	
Infection	+	++	+
Intoxication	+	++	
Metabolic diseases (undescribed)	+ or reversed	++	
Maternal diseases	+	++	
Chromosomal anomalies	+ or —		+++
Congenital nephrotic syndromes	+ or —	++	
Nephrostomatosis	+ or —	++	
Normal variant	+	++	

ADPKD, autosomal-dominant polycystic kidney disease; ARPKD, autosomal-recessive polycystic kidney disease; GCD, glomerulocystic disease; MCD, medullary cystic disease.

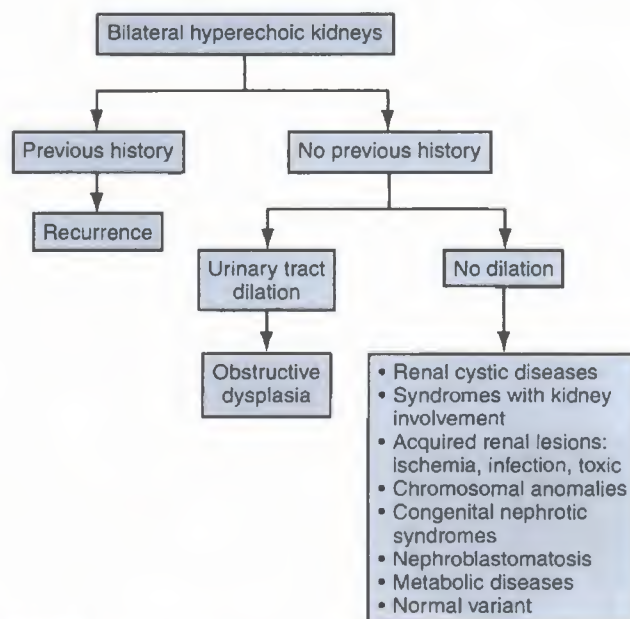
The main etiologies are obstructive dysplasia and cystic renal disease (see later). There are many other causes that include syndromes, acquired fetal renal diseases (renal vein thrombosis [RVT], infections, toxic agents), maternofetal disease, and congenital nephrotic syndromes. However, hyperechoic kidneys may also be seen as a normal variant. Therefore, the work-up of hyperechoic kidneys should include a detailed sonographic evaluation of the kidneys and UT; a detailed analysis of the family history and of the natural course of the disease (see Table 16-5 and Fig. 16-28).<sup>10,68-72</sup>

The prognosis is defined by the suspected diagnosis, the associated malformations, and chromosomal anomalies. Again, oligohydramnios is associated with a poor prognosis.

*Hyperechogenicity of one kidney:* unilateral hyperechogenicity can be seen with unilateral multicystic dysplasia, unilateral obstructive dysplasia, a renal tumor, or unilateral RVT (see later) (Fig. 16-29).

### Cystic Renal Diseases

**Classification of Renal Cystic Diseases.** Typically, renal cystic diseases are separated into diseases with or without hereditary transmission (Table 16-6). Parenchymal dysplasia is the most frequent cause of noninherited renal cysts. Autosomal-dominant polycystic kidney disease (ADPKD) is the most frequent cause of inherited cystic disease. Yet, with recent developments in genetics, this separation has become less clear. For instance, there are some rare cases of MDKs with familial transmission (the so-called “renal adysplasia”).<sup>73</sup>

**FIGURE 16-28.** Etiologies of bilateral hyperechoic kidneys.

The group with clearly identifiable genetic transmission includes autosomal-recessive polycystic kidney disease (ARPKD) and ADPKD, medullary cystic disease (MCD), and certain cases of glomerulocystic diseases. The latter can be encountered as an isolated finding or, more often, as part



**FIGURE 16-29.** Unilateral hyperechoic kidney, case of (cystic) dysplasia, second trimester. Sagittal scan through the right kidney. The renal parenchyma is hyperechoic and contains a cyst in the upper pole (arrow). The lower pole is dilated (case of multicystic dysplastic kidney in the upper pole of a duplex system). Ch, chest.

of a syndrome in which inheritance may or may not be known (see later). Among the polymalformative syndromes, renal cystic disease can be the main and essential finding or just an accessory anomaly.<sup>10,74-77</sup>

**Sonographic Evaluation.** The sonographic evaluation has to be as detailed as possible because some features are essential for the differential diagnosis. The kidneys have to be measured and compared with studies establishing “size versus gestational age” nomograms.<sup>6</sup> The overall echogenicity must be appreciated by comparing the parenchymal echogenicity with that of the liver or spleen (especially in the third trimester). Noteworthy, evaluating hyperechogenicity is somewhat subjective and is also dependent on the equipment used and maternal obesity. The presence or absence of CMD is an important differentiating criterion. Normal CMD, that is, hypolucent medullae relative to cortex is present in the second trimester. Finally the detection of renal cysts, their size, and their location are useful in the differential diagnosis (see Table 16-5).

## SONOGRAPHIC PATTERNS/ ULTRASOUND AND PATHOLOGIC CORRELATIONS

### Diseases With Known Genetic Transmission

#### Autosomal-Recessive Polycystic Kidney Disease

ARPKD has an incidence of 1 in 20,000 live births and often causes fetal and neonatal death. Renal failure and

**Table 16-6**

### Classification of Cystic Diseases of the Kidney in the Fetus

#### Genetic diseases

- Autosomal-recessive polycystic kidney disease
- Autosomal-dominant polycystic kidney disease
- Glomerulocystic kidney disease
- Medullary cystic dysplasia associated with syndromes

#### Nongenetic diseases

##### Renal dysplasia

- Multicystic dysplastic kidney disease\*
- Obstructive cystic dysplasia

##### Nongenetic nondysplastic cysts

- Simple cyst
- Multilocular cyst
- Medullary sponge kidney\*

\*Some cases described with genetic transmission.

hepatic fibrosis develop in many babies who survive the perinatal period. Mutations in the *PKHD1* gene are usually demonstrated in this disease.<sup>77</sup> Yet, because some infants do survive the neonatal period with few or little symptoms, additional genes are probably involved.

The disease is characterized by marked elongation of the collecting tubules that expand into multiple small cysts. The cystic dilatation of the tubules is variable and predominates in the medulla. The outer cortex is spared because it contains no tubules. There is associated biliary dysgenesis. Hepatic fibrosis has been described on pathologic examination of affected fetuses.<sup>78</sup>

The sonographic presentation varies according to the severity of involvement. The most typical presentation is that of markedly enlarged hyperechoic kidneys (+4 → +15 SD), without CMD (Fig. 16-30A and B). This appearance can be observed in the second trimester. The patterns may evolve, and the size of the kidneys may continuously increase during the third trimester. Other findings include oligohydramnios and lung hypoplasia, and therefore, the prognosis is usually poor. There are no other malformations associated with ARPKD. The list of differential diagnoses includes glomerulocystic disease and Bardet-Biedl syndrome (BBS) (see later).<sup>79,80</sup> In these two diseases, the parenchyma is more homogenous than in ARPKD. When the kidneys are not as enlarged (+2 → +6 SD), the diagnosis may be more difficult to ascertain. A hypoechoic outer cortical rim that is usually present in the recessive type may help in suggesting the diagnosis (see Fig. 16-30C). Cysts (greater than 3 mm) may be already apparent in the fetus in the third trimester; they may appear unilateral, and their number varies. This finding occurs in one third of diagnosed fetal cases but is not specific.<sup>81</sup>

Another presentation of ARPKD can be reversed CMD with large (+2 → +4 SD) kidneys (Fig. 16-31). This finding is probably related to increased number of interfaces within the medullae, and to inspissated material within the dilated tubules. It is an important observation because there are very few other causes of reversed CMD. These patients have a better prognosis when the amniotic fluid volume is preserved. The differential diagnosis includes metabolic



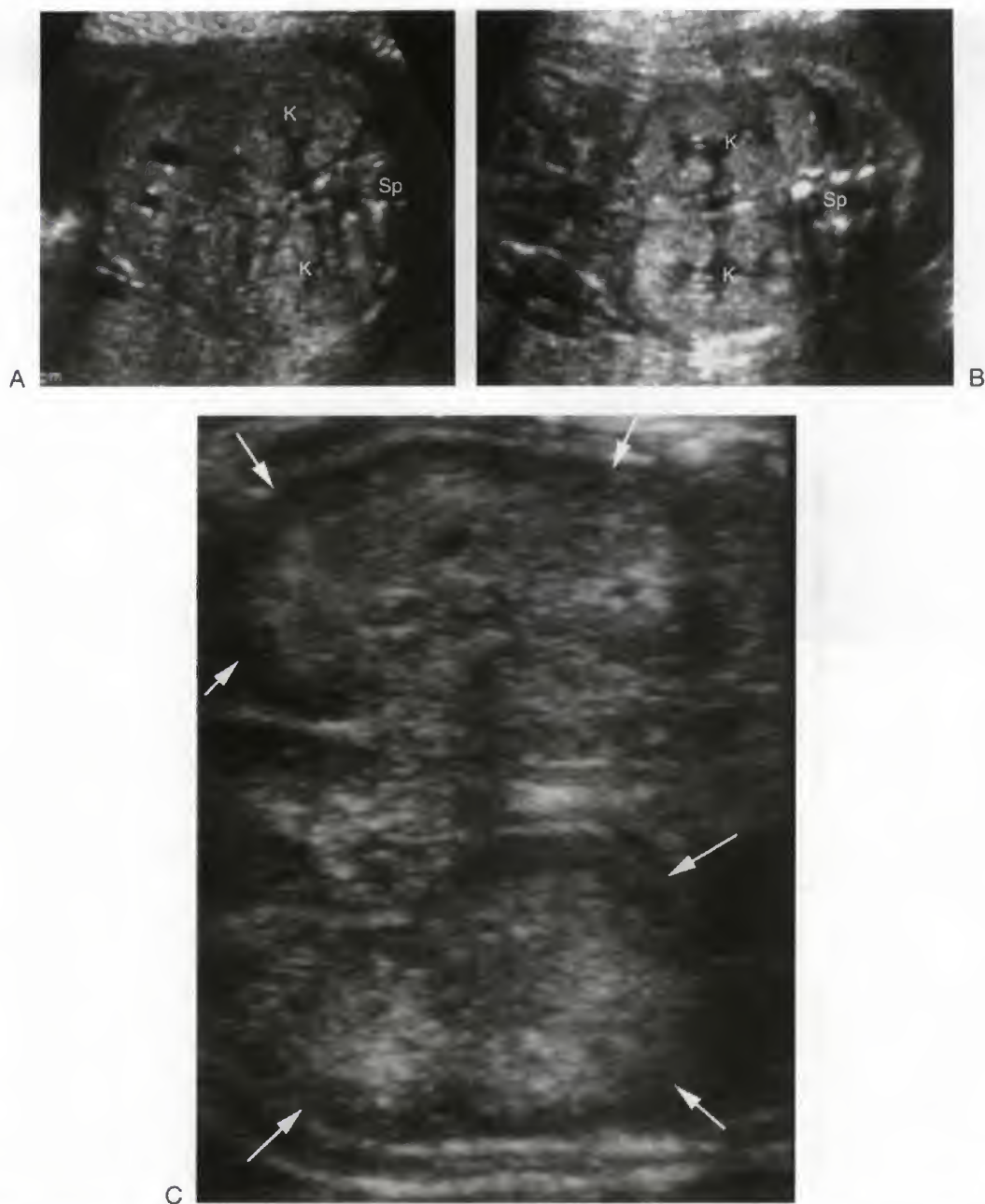


**FIGURE 16-30.** Autosomal-recessive polycystic kidney. A. Second trimester transverse scan of the kidneys (K) that appear large (+3 SD), hyperechoic, and without corticomedullary differentiation. Sp, spine. B. Second trimester, sagittal scan of the kidneys (K). Sp, spine. C. Third trimester transverse scan through the kidneys. They are still large and hyperechoic, but the peripheral cortex is somewhat hypoechoic (arrows) (cortical rim sign).

disorders and intrauterine growth restriction. The liver abnormalities, for example, hepatic fibrosis, are not demonstrated in utero.<sup>78,82-88</sup>

### **Autosomal-Dominant Polycystic Kidney Disease**

ADPKD is the most common form of polycystic kidneys disease in humans and occurs in 1 in 800 live births. ADPKD is an inherited condition that includes at least three phenotypically indistinguishable but genetically distinct

entities caused by mutations in three genes—*PKD1*, *PKD2*, and *PKD3*. The *PKD1* gene is located on chromosome arm 16p in 90% of patients and is related to spontaneous mutation in 10%. ADPKD is transmitted as an autosomal-dominant trait, with almost 100% penetrance if patients live long enough. Because of the variable expressivity and spontaneous mutation, a family history is not found in nearly one half of patients. Defective polycystins appear to contribute to cyst formation by affecting epithelial cell maturation, resulting in the development of cysts of varying sizes in the cortex and medulla.<sup>77</sup> There is likely one or more other

genes involved because some obvious cases have neither of these mutations.

The disease is characterized by the presence of multiple cysts that develop on the wall of collecting tubules and nephrons. The cysts are scattered within the cortex and medulla. These cysts enlarge progressively and are typically identified in early adulthood. Cysts may also develop in the liver, spleen and pancreas in adults.<sup>89</sup>

In the fetus, a pattern highly suggestive of the disease has been recently described by Brun et al<sup>90</sup> and was encountered in more than 80% of affected patients in the third trimester. They found moderately enlarged kidneys (1-2 SD above the

mean) which have hyperechoic cortices and relatively hypoechoic medullae (Fig. 16-32). For the authors, the hyperechoic cortex is probably related to the presence of multiple microcysts that predominate at this stage in the cortex. In most cases, the amniotic fluid volume was normal.<sup>90</sup> Although the exact sensitivity of the pattern is unknown, its demonstration should prompt a familial inquiry including sonography of the parents and grandparents because 50% of cases with the dominant form are discovered following the sonographic detection. However, it is estimated that an unknown percentage of cases of ADPKD are the result of a new mutation. A list of differential diagnoses exists for this pattern and should be considered (Table 16-7 and Fig. 16-33). For some patients, only long-term follow-up will establish the final diagnosis.

As mentioned earlier, in ADPKD, cysts develop only later in adulthood, yet, exceptionally, cysts may be encountered in utero.<sup>90,91</sup> Several other sonographic patterns may be



**FIGURE 16-31.** Autosomal-recessive polycystic kidney disease, third trimester. Sagittal scan. Enlarged hyperechoic kidney (K) with hyperechoic medulla (reversed corticomedullary differentiation). L, liver.

**Table 16-7**

**Differential Diagnoses for Moderately Enlarged Hyperechoic Kidneys With Persisting Corticomedullary Differentiation (+1 → +2 SD)**

- Autosomal-dominant polycystic kidney disease
- Ischemic disease (twin-twin transfusion disease)
- Cytomegalovirus infection
- Deficient maternal neuropeptidase
- Metabolic disease
- Nephrotic syndrome
- Transitory (?)

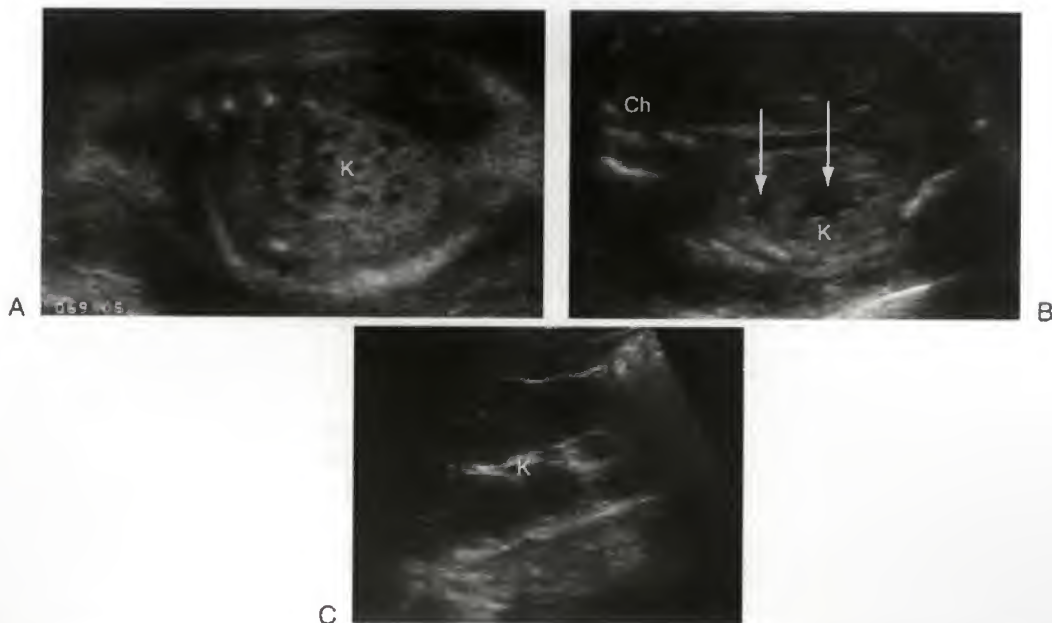


**FIGURE 16-32.** Autosomal-dominant polycystic kidney disease (ADPKD, associated with an uropathy), third trimester. A. Sagittal scan through the right kidney (K). The renal cortex is hyperechoic compared to the liver. The corticomedullary differentiation is preserved. B. Sagittal scan through the left kidney (K). The findings are similar, but there is a duplex system associated with mild upper and lower pole dilatation (arrows). Ch, chest. C. Maternal right kidney (K), sagittal scan. Typical cystic involvement confirming ADPKD.





**FIGURE 16-33.** Simpson-Golabi syndrome revealed as hyperechoic kidneys with parenchymal cysts, Third trimester. Sagittal scan through the kidney that appears moderately enlarged with corticomedullary differentiation. One cyst is visible (arrow).

encountered and suggest ADPKD. First, the kidneys may have a normal appearance in utero; the percentage of cases with a completely normal pattern is unknown. In a few patients affected by autosomal-dominant polycystic kidneys, the kidneys may be diffusely hyperechoic and markedly enlarged (+4 → +8 SD) without CMD. Cysts may develop in utero or after birth in the subcapsular area. This pattern corresponds to the “glomerulocystic variant” of the disease (Fig. 16-34).<sup>80,92-94</sup> The prognosis is still good unless oligo-hydramnios develops. In such case, hypertension and renal failure may develop rapidly after birth.

Interestingly, other UT malformations may be present in association with ADPKD. These include unilateral MDK, UPJ obstruction, duplex systems, and even congenital metabolic diseases.<sup>90</sup>

After birth, as mentioned earlier, the cysts progressively develop; cystic renal involvement may be asymmetric in the infant and child, whereas in some cases, there is a reduction in renal size following birth.<sup>89-91,95-97</sup>

### Glomerulocystic Kidneys

On histopathology, glomerulocystic kidneys (GLC) are defined as kidneys that contain cysts that correspond to distended Bowman spaces. Five to 10 percent of the spaces must be affected in order to establish such a diagnosis. Glomerular cysts are not specific to a simple disorder. They can be present with other types of renal cystic diseases, both inherited and sporadic, in certain syndromes, and in dysplastic kidneys (Table 16-8).

On sonographic examination, the classic GLCs appear enlarged (+4 → +8 SD), hyperechoic, and without CMD (Fig. 16-35). The most suggestive feature is when subcapsular cortical cysts are present (see Figs. 16-34 and 16-35). They can develop in utero or after birth. When present, the diagnosis is straightforward. This finding may help to characterize various syndromes in association with GLC

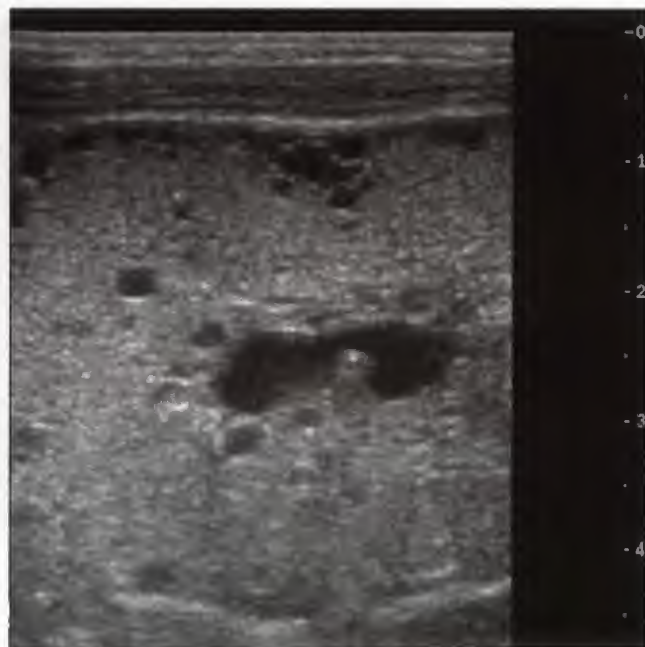


**FIGURE 16-34.** Autosomal-dominant polycystic kidney disease (ADPKD), glomerulocystic form in a neonate. Sagittal scan through the enlarged kidney, which appears hyperechoic with multiple tiny cysts, mostly peripheral. The father was affected by ADPKD.

**Table 16-8** Glomerulocystic Kidneys

Glomerulocystic kidney disease
Autosomal-dominant polycystic kidney disease in young infants
Dominant glomerulocystic kidney disease in older patients
Sporadic nonsyndromal glomerulocystic kidney disease
Familial hypoplastic glomerulocystic disease
Glomerulocystic kidneys in heritable malformative syndromes
Tuberous sclerosis
Orofaciodigital syndrome type 1
Trisomy 13
Short rib polydactyly syndromes
Jeune syndrome (asphyxiating thoracic dystrophy)
Zellweger syndrome
Familial nephronophthisis
Glomerular cysts in dysplastic kidneys
Diffuse cystic dysplasia
Renal-hepatic-pancreatic dysplasia (Ivemark II)

when other malformations coexist. The prognosis will be based on associated findings and on the volume of amniotic fluid. The cysts may develop after birth only.<sup>80,92-94,98</sup>

### Medullary Cystic Dysplasia

MCD, in which cysts involve mainly the medullary tubules, is a feature of many syndromes. It may be associated with glomerulocystic changes as well (see Table 16-8). Tubulointerstitial fibrosis may develop progressively. The renal findings seen in MCD are the renal histologic changes

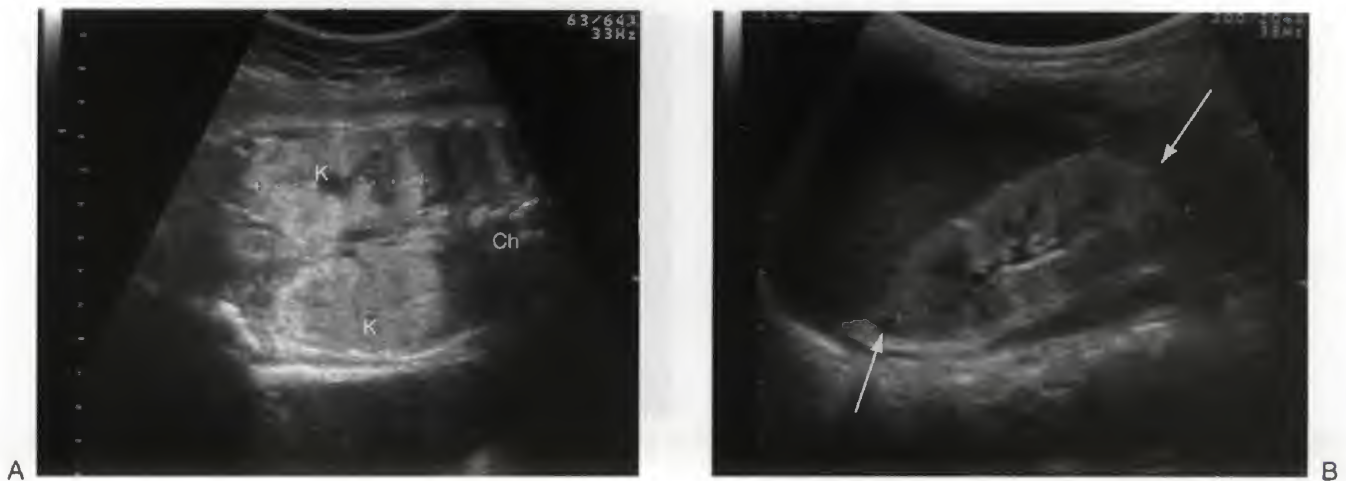


**FIGURE 16-35.** Glomerulocystic kidney in a “diabetes and renal cyst syndrome.” *A.* In utero, third trimester. Front view through both kidneys (K), which appear enlarged and hyperechoic without corticomedullary differentiation. Ch, chest. *B.* At birth, sagittal scan through the right kidney. Small peripheral cysts have now appeared (arrows).

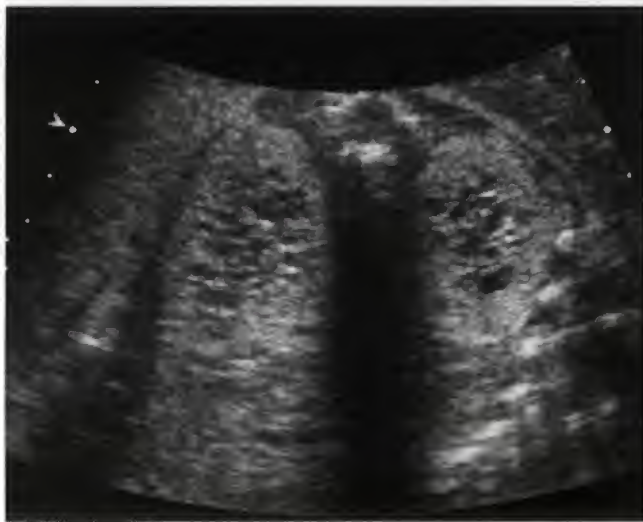


**FIGURE 16-36.** Medullary cystic dysplasia, case of Meckel-Gruber syndrome. Transverse scan of the fetal abdomen. Both kidneys display an abnormal pattern: diffusely cystic changes involving the entire kidney. (An occipital encephalocele was also present, which is not shown.)



**FIGURE 16-37.** Bardet-Biedl syndrome, third trimester. Transverse scan of the fetal abdomen. Both kidneys (K) are enlarged without corticomedullary differentiation. (Polydactyly, which is not shown, was also present.) Sp, spine.

typically encountered in the Meckel-Gruber syndrome. The medullary cystic changes develop very early in the pregnancy and are obvious as early as the end of the first trimester. The demonstration of anomalies of the central nervous system and of the extremities (polydactyly) render the diagnosis even more certain. On sonography, the kidneys are enlarged, a pseudo-cortico-medullary differentiation is present already at the end of the first trimester and the medulla is very prominent. This pattern as demonstrated at this early stage is very typical<sup>99</sup> (Fig. 16-36).

Cystic dysplasia is also common in BBS. The renal lesions are not concentrated in the medullary areas but are more diffuse. The sonographic pattern is that of diffuse hyper-

echoic, slightly or markedly enlarged kidneys. Cysts may be present in utero or develop after birth. Polydactyly is a classic associated finding in utero. The other abnormalities of BBS develop later in childhood (Fig. 16-37).<sup>79,99-102</sup>

### Unclassified Cystic Diseases

Macrocysts may be encountered in cases of tuberous sclerosis. The cysts have specific histopathologic features that include eosinophilic epithelium. Other evidence of the disease, such as cardiac rhabdomyomas and intracerebral lesions, may be present in utero. Several other syndromes include microcysts or macrocysts (e.g., Ivemark syndrome) (Fig. 16-38).<sup>103,104</sup>



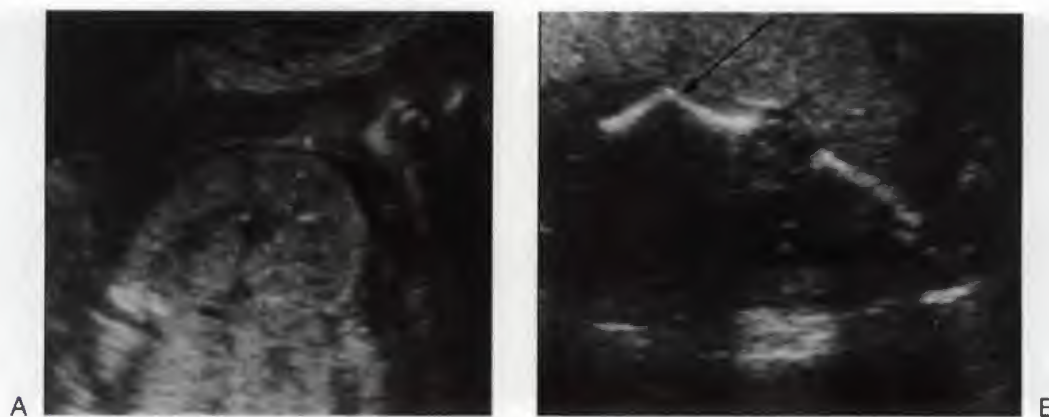


**FIGURE 16-38.** Ivermark II syndrome, second trimester. *A.* Sagittal scan through the hyperechoic kidney, corticomedullary differentiation. *B.* Associated limb deformity: an angulated femur is visible (arrow).

## Diseases Without Genetic Transmission

### Multicystic Dysplastic Kidney

Among the group without hereditary transmission, MDK is one of the most common diseases (although as mentioned earlier, there is known to be an inheritable subgroup<sup>73</sup>). The sonographic findings in patients with MDK are usually straightforward: unilateral involvement with noncommunicating cysts of variable size, variable amount of hyperechoic stroma, no normal cortex or medulla, irregular renal contours, and no identifiable collecting system (Figs. 16-39 and 16-40). The cysts can be large, presenting as a large fetal abdominal mass, or on the contrary, microcystic. MDK may also develop in the upper part of a duplex system (see Fig. 16-29) or be located in an ectopic position (Fig. 16-41). The size of the cysts may decrease in utero or after birth (see Fig. 16-40). Therefore, the entire MDK may “disappear” and give the appearance of renal agenesis. Unilateral involvement carries a good prognosis, although there may be an anomaly affecting the contralateral kidney (i.e., UPJ obstruction). The condition can be



**FIGURE 16-39.** Multicystic dysplastic kidney (MDK), third trimester. Transverse scan of the fetal abdomen. The MDK is limited by the calipers (47.9 mm). Sp, spine.

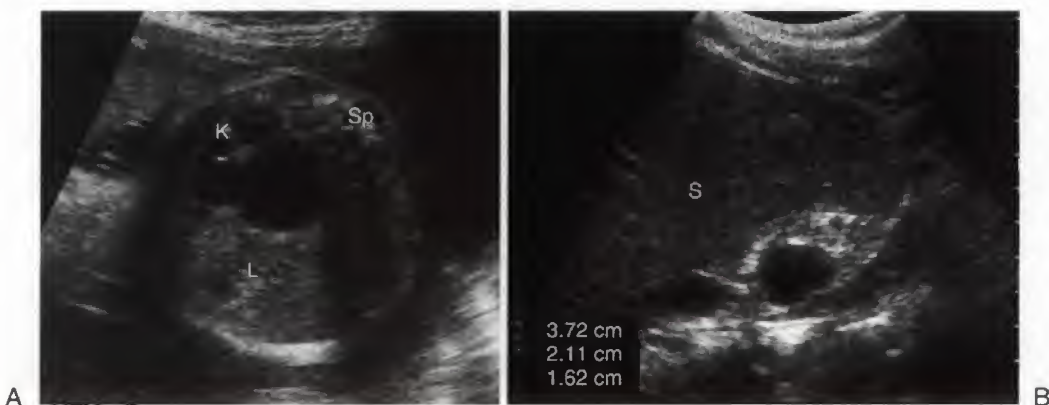


**FIGURE 16-40.** Multicystic dysplastic kidney (MDK), spontaneous involution. *A.* In utero transverse scan of the fetal abdomen. Typical MDK of the left kidney (K). L, liver, Sp, spine. *B.* At age 1 year, sagittal scan of the left flank. The size of the cysts have decreased and only two remained. S, spleen.

associated with other system's malformations (Fig. 16-42). When MDK is an isolated finding, there is no increased risk of chromosomal anomaly. Cases with bilateral involvement (1 out of 15 cases) are associated with severe oligohydramnios and pulmonary hypoplasia; they carry a poor prognosis (Fig. 16-43).<sup>21,105-107</sup>



**FIGURE 16-41.** Multicystic dysplastic kidney (MDK) of an ectopic pelvic kidney (second trimester). Frontal view of the fetal abdomen. The hyperechoic MDK is visible (arrows) in the pelvis, to the right of the aorta and iliac artery.

### Obstructive Dysplasia

Obstructive renal dysplasia is the other most common cause for nonhereditary fetal renal cystic disease and hyperechoic kidneys. In such cases, there is a dilatation of the upper and lower UT associated with hyperechogenicity of the renal parenchyma and ultimately cysts of variable sizes within the renal cortex. The renal function is usually impaired (Figs. 16-19 and 16-44).<sup>73,104,108</sup>

### Simple Renal Cyst

Simple renal cysts are uncommon in the fetus. They may disappear "spontaneously."<sup>109,110</sup> The discovery of a cyst necessitates simple US follow-up in order to exclude the development of a more diffuse distribution and other cystic diseases (Fig. 16-45).

**The Work-Up of Fetal Cystic Disease.** The basis for the work-up must rely on the following:

- The sonographic patterns at presentation and on follow-up (see Tables 16-5, 16-7, and 16-9 to 16-12; and Fig. 16-28).
- Associated malformations.<sup>10,104</sup>
- Family history.

The discovery of abnormal kidneys on obstetrical US in cases of a positive familial history signifies the likelihood of recurrence of the disease. In the absence of family history, the diagnosis will be based on the sonographic patterns at presentation and associated malformations. Complementary

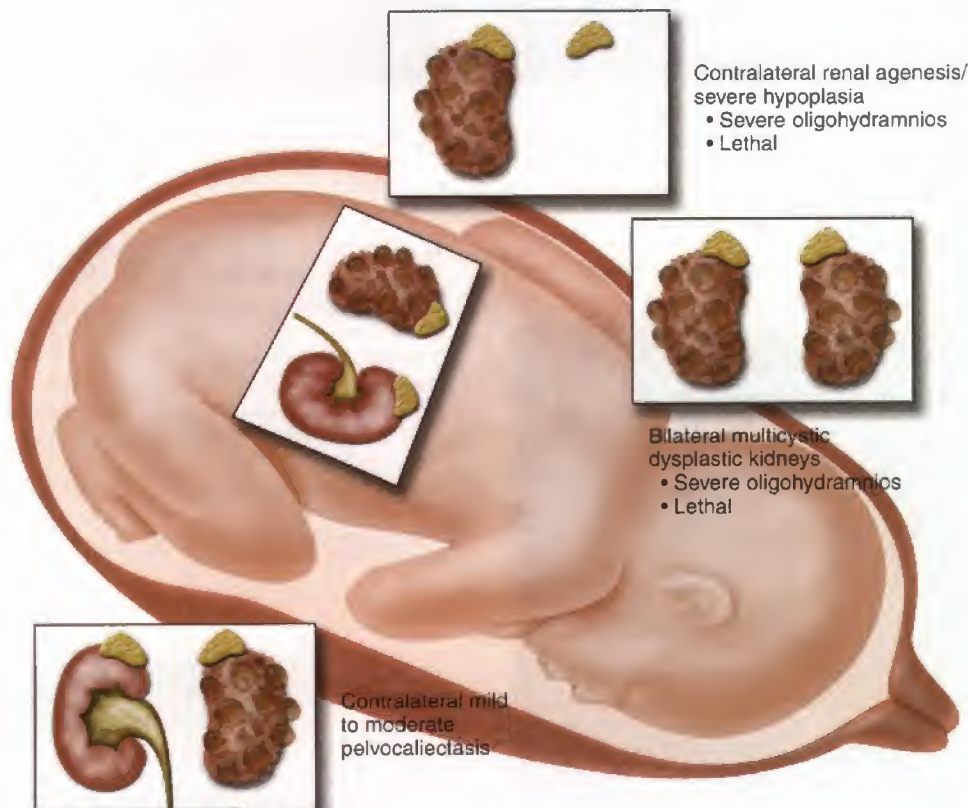


**FIGURE 16-42.** The multicystic dysplastic kidney is essentially nonfunctional. Attention must be focused on the contralateral kidney, because it is the only potentially functional kidney. (Illustration by James A. Cooper, MD, San Diego, CA.)



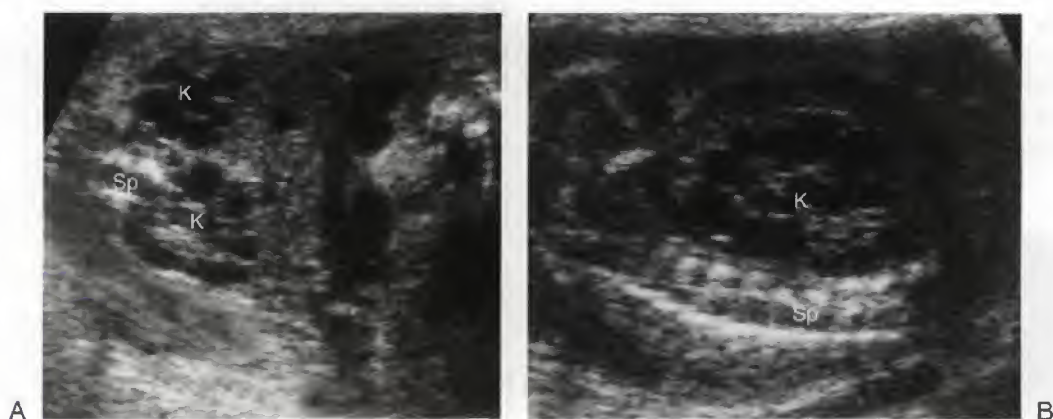


**FIGURE 16-43.** Bilateral multicystic dysplastic kidney (MDK), second trimester. A. Transverse scan of both kidneys showing the bilateral MDK. Anhydramnios is associated. K, kidneys. B. Sagittal scan through the kidney (K). Sp, spine.

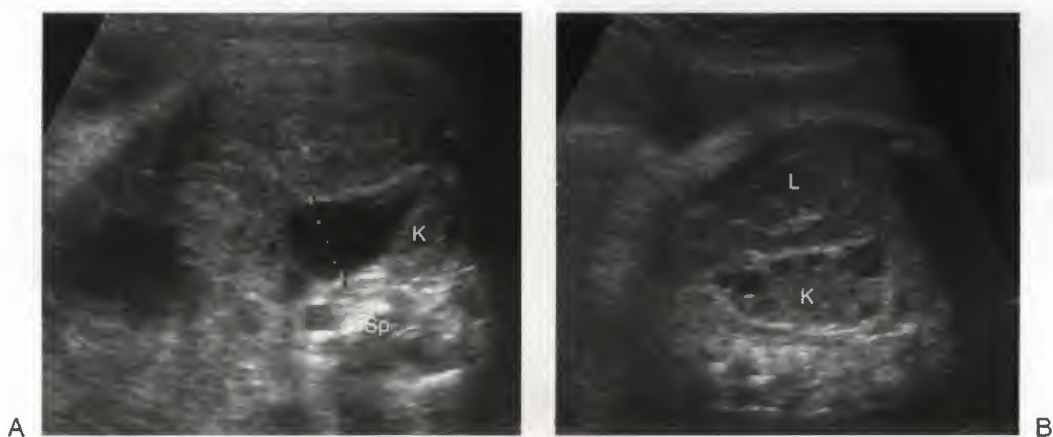


**FIGURE 16-44.** Obstructive dysplasia, third trimester. A. Transverse scan through the right kidney (K) demonstrating renal pelvis dilatation (25 mm). Sp, spine. B. Sagittal scan through the external part of the right kidney (K): multiple parenchymal cysts are visible as evidence of dysplasia. L, liver.

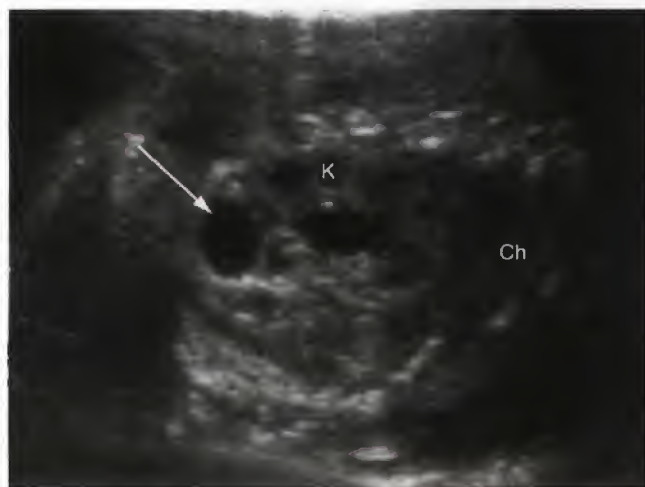


**FIGURE 16-45.** Solitary renal cyst, third trimester. Sagittal scan through the left kidney (K). A cyst is visible (arrows) at its lower pole. The renal pelvis is slightly dilated. Ch, chest

**Table 16-9** Sonographic Patterns at Presentation

- Unilateral single cyst (see Table 16-10);
- Unilateral multiple cysts (see Table 16-11);
- Bilateral cysts (see Table 16-12);
- Hyperechoic kidneys (Tables 16-5 and 16-7, Fig. 16-28):
  - With cortico-medullary differentiation (CMD)
  - Without CMD
  - Reversed CMD
  - With medullary cyst
  - With cortical cyst
  - With subcortical cysts

**Table 16-10** Unilateral Single Cyst (The Rest of the Kidney is Normal)

- Simple renal cyst
- Unilateral Dominant cystic disease
- Cystic tumor
- Non renal cyst
- Urinoma

**Table 16-11** Unilateral Multiple Cysts

MDKD  
 Unilateral obstructive dysplasia  
 Unilateral dominant cystic disease

MDKD, multicystic dysplastic kidney disease.

**Table 16-12** Bilateral Multiple Cysts

Bilateral MDKD (oligohydramnios)  
 Bilateral obstructive dysplasia (urinary tract dilatation)  
 ADPKD  
 ARPKD  
 Subcortical cysts (glomerulocystic kidneys)  
 Syndromes with cystic dysplasia  
 Meckel-Gruber medullary cysts  
 Tuberous sclerosis (macrocyts)  
 Ivemark II  
 Bardet-Biedl syndrome (cortical cysts)

ADPKD, autosomal-dominant polycystic kidney disease; ARPKD, autosomal-recessive polycystic kidney disease; MDKD, multicystic dysplastic kidney disease.

examination such as MRI should be performed as required by the sonographic findings. Subsequently, once the most common or the most typical diagnoses are considered, other diagnoses should also be considered whenever the maternal history reveals specific symptoms (e.g., diabetes, some metabolic diseases).<sup>111-117</sup>

### Renal Tumors

More than half of all congenital abdominal masses found in the neonate originate in the kidney. In the fetus, the most common renal tumor is the mesoblastic nephroma (Fig. 16-46). It appears as a solid tumor that is sometimes difficult to delineate from the adjacent renal parenchyma. The tumor can appear partially cystic. In utero, polyhydramnios is typically associated and hypertension develops after birth. Cases of fetal renal Wilms' tumor have been reported as solid or partially cystic tumors. The prognosis is good. Bilateral involvement suggests nephroblastomatosis, which is a condition with multiple benign nodular lesions.

Patients with Beckwith-Wiedemann syndrome, congenital aniridia, and Perlman and Drash syndromes are at risk of developing renal tumors. The main differential diagnosis of a cystic renal tumor includes MDK.<sup>113,114,117-120</sup> Solid masses adjacent to the kidney, such as neuroblastoma and subdiaphragmatic pulmonary sequestration, should be differentiated from true renal masses.

### Acquired Renal Pathologies

Renal anomalies can occur during pregnancy because of a maternal disease or because of ischemic damage (or both). For instance, maternal diabetes and twin pregnancy increases the risk for RVT in the fetus. Sonographically, at

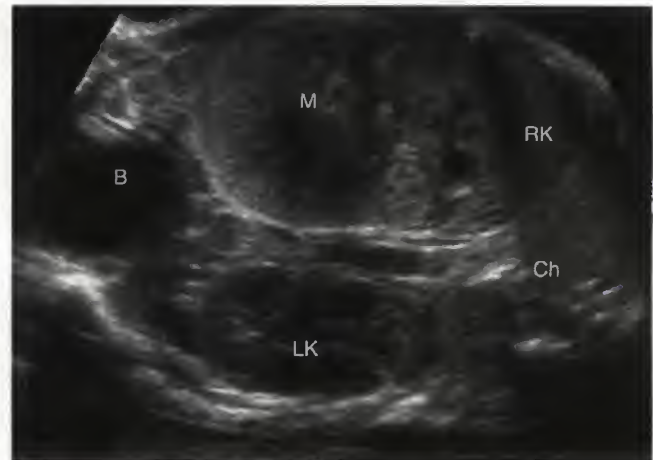


**FIGURE 16-46.** Mesoblastic nephroma, third trimester. Sagittal scan of the fetal trunk. A large round solid mass (M) has developed in the lower pole of the right kidney (RK). B, bladder; Ch, chest; LK, left kidney.

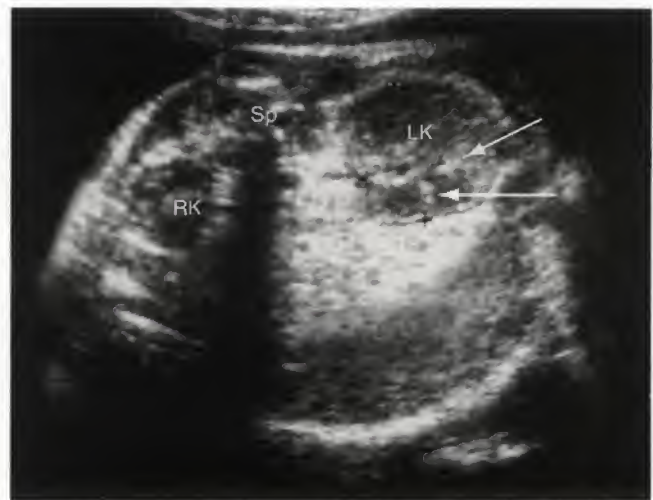


**FIGURE 16-47.** Subacute renal vein thrombosis, third trimester. Transverse scan of both kidneys. The left kidney (LK) is larger and more globular than the right one (RK). Some hyperechoic stripes are visible (arrows). Sp, spine. (Courtesy of P Sonigo MD, Paris, France.)

the acute stage of the thrombosis, the volume of the affected kidney and its echogenicity increase. In some cases, Doppler analysis may confirm the thrombosis. Rapidly, collateral vessels develop and the renal vascularization becomes almost normal. Some vascular calcifications in the interlobar areas may remain as sequelae (Fig. 16-47). A thrombus within the inferior vena cava and adrenal hemorrhage may be associated findings.<sup>119</sup> Maternal deficit in neuropeptidase may induce an acute transient glomerulonephritis in the fetus that results in increased volume and echogenicity. Transient renal failure may occur at birth (Fig. 16-48).<sup>122</sup> Maternofetal infection may involve the kidneys and present with increased echogenicity as demonstrated in some cases with cytomegalovirus.



## Other Congenital Renal Disorders

### Congenital Nephrotic Syndrome

Congenital nephrotic syndrome may rarely affect the fetus. The kidneys appear diffusely hyperechoic usually without CMD. The placenta is thick, and polyhydramnios is present. The proteinemia can be detected in the amniotic fluid. A particular association is the Drash syndrome that includes pseudohermaphroditism and a particular nephrotic syndrome (mesangial sclerosis). Patients affected by the syndrome carry an increased risk for Wilms' tumor (Fig. 16-49).<sup>12,123-126</sup>

### Bladder, Urethra, and Urachus

As mentioned earlier, the bladder is the first structure of the UT to be seen in the fetal pelvis at approximately 9 to 10 weeks that indicates urine is being produced. Its demonstration is an important part of the obstetric US assessment of normal fetal development. Anomalies of the UT can be suspected whenever the bladder is enlarged (more than 3 cm length in the second trimester, more than 6 cm in the third trimester of the pregnancy) or not visible during an entire examination.

Whenever an *enlarged bladder (megacystis)* is demonstrated, BOO should be suspected first. During the first and early second trimester, it could result from urethral atresia and prune-belly syndrome. The kidneys may appear hyperechoic owing to obstructive dysplasia. The prognosis is poor (see Figs. 16-18 and 16-23).<sup>127,128</sup> In the second and third trimester in the male fetus, megacystis almost always results from PUV. The bladder wall may be thickened, and the upper UT may or may not be dilated with hyperechoic renal parenchyma corresponding to obstructive dysplasia. The condition can also be associated with perirenal urinoma due to extravasation.

The differential diagnosis of an enlarged bladder should include marked vesicoureteric reflux and megacystis-microcolon-hypopertalsis syndrome (see Table 16-2). The latter occurs virtually always in female fetuses. The short colon is difficult to assess by US and is easier to demonstrate by fetal MR imaging.<sup>18</sup> Finally, one should not forget to

consider a pseudoenlarged bladder in the third trimester female fetus.<sup>46,127-129</sup>

When the *bladder is not visible*, the amount of amniotic fluid helps to differentiate cases secondary to lack of urine production from bladder malformation. In case of oligohydramnios or anhydramnios, absent or nonfunctioning kidneys should be suspected (bilateral renal agenesis, bilateral MDKs). When the amount of amniotic fluid is just slightly reduced, intrauterine growth restriction and



**FIGURE 16-49.** Congenital nephrotic syndrome, third trimester. Frontal view of both kidneys (K), which appear enlarged and hyperechoic, with poor corticomedullary differentiation. Oligohydramnios was associated. Ch, chest.

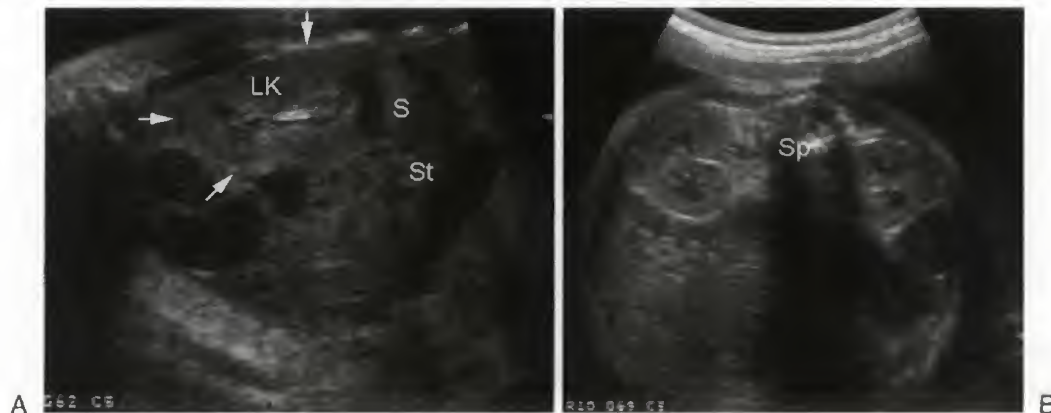


**FIGURE 16-48.** Acute glomerulonephritis secondary to maternal deficit in neuropeptidase. Third trimester scan. A, Sagittal scan of the left kidney (LK) with a thick hyperechoic cortex (arrows). S, spleen; St, stomach. B, Transverse scan through both kidneys that display the same thick hyperechoic appearance. Sp, spine.

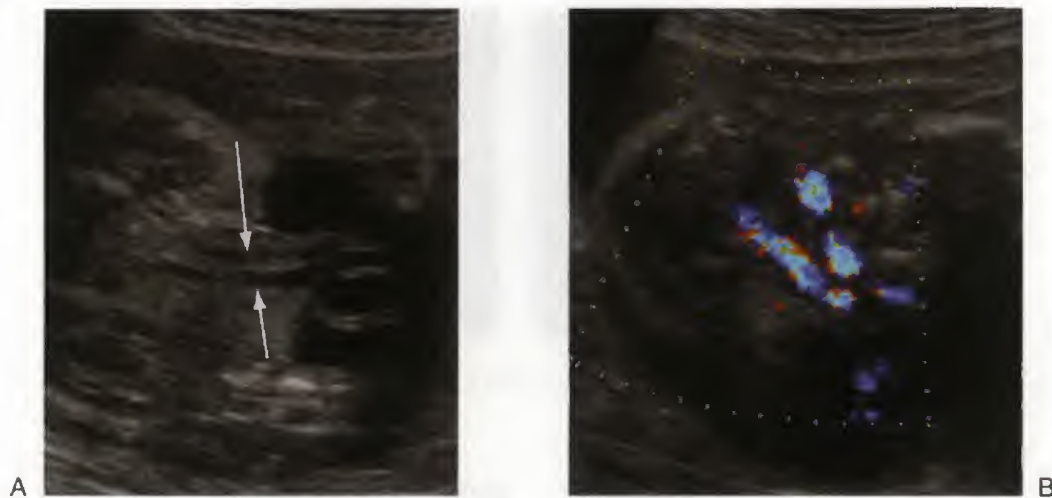


**FIGURE 16-50.** Bladder exstrophy, late second trimester. A. Transverse scan through the fetal pelvis. The bladder structure is recognized between the two umbilical arteries (arrows). B. Color Doppler confirms the absence of bladder structure.

maternofetal infection should be considered.<sup>130</sup> **One should never assume that the explanation for oligohydramnios or anhydramnios is due to rupture of the membranes until one has demonstrated a functioning UT by identification of the urinary bladder and/or the kidneys.**

If the amount of amniotic fluid is normal, a bladder malformation should be considered. In case of bladder exstrophy, no bladder is seen between the umbilical arteries (Fig. 16-50). Instead, a soft tissue mass is seen just below the umbilicus corresponding to the open bladder (mucosa). In the male fetus, the penis is shortened and widened, and the gender ambiguous. The condition has to be differentiated from the omphalocele-exstrophy-imperforate anus (OEIS) complex, in which an omphalocele is present as well.<sup>130-134</sup> An abnormal bladder may also be observed in cases of cloacal malformation sequence (persistence of the urogenital sinus). In this condition, there is a single opening draining the bladder, the vagina, and eventually the colon. It may be difficult to differentiate between these different structures by US alone (Fig. 16-51).<sup>18,133,134</sup>

In the male fetus, the main malformation involving the urethra is PUV (see earlier). This condition results in BOO at variable degrees. On US, the distended posterior urethra can sometimes be clearly demonstrated (see Fig. 16-23). The prognosis is also variable depending on the degree of obstruction and renal dysplasia. Anterior valves are very rarely demonstrated in utero. The main differential diagnosis is megalourethra (Fig. 16-52), in which is a deficient spongy tissue around the urethra, which is dilated to a variable extent.<sup>135,136</sup>

Under normal conditions, the urachus is not seen in utero because this canal becomes fibrotic after the first trimester. Anomalies related to a (partially) patent urachus include patent distended urachus in association with a BOO or an urachal cyst that should always be included in the differential diagnosis of midabdominal cysts.<sup>49,137,138</sup>

Another finding related to the embryo-fetal development of the allantoic-urachal complex is the discovery of a cyst

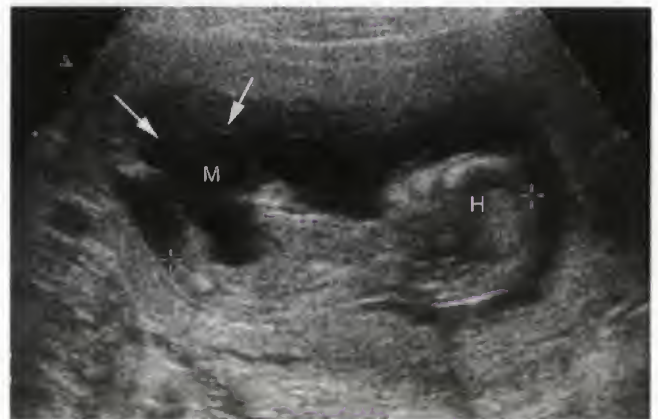


**FIGURE 16-51.** Persistence of urogenital sinus, end of first trimester. Sagittal scan of the fetus. At the level of the fetal pelvis, a cystic polylobulated mass (M) replaces the normal anatomy. No bladder is seen. H, head.

(allantoic cyst) connected to the bladder but developed within the umbilical cord. These cysts resolve or rupture spontaneously at birth; in some cases, the urachus has to be repaired surgically after birth (Fig. 16-53).

## FETAL GENITAL TRACT

### Normal Genitalia

The determination of fetal sex is possible during the obstetric sonographic examination. The improvement of high-resolution US and the use of transvaginal probes allow detailed visualization of the fetal genital anatomy often at the end of the first trimester.

Up to 11 weeks, the external genitalia are identical in both sexes. After 14 weeks, when a rapid growth of the penis occurs, the differences between both are evident. On the sagittal scan, the penis points upward, whereas the clitoris



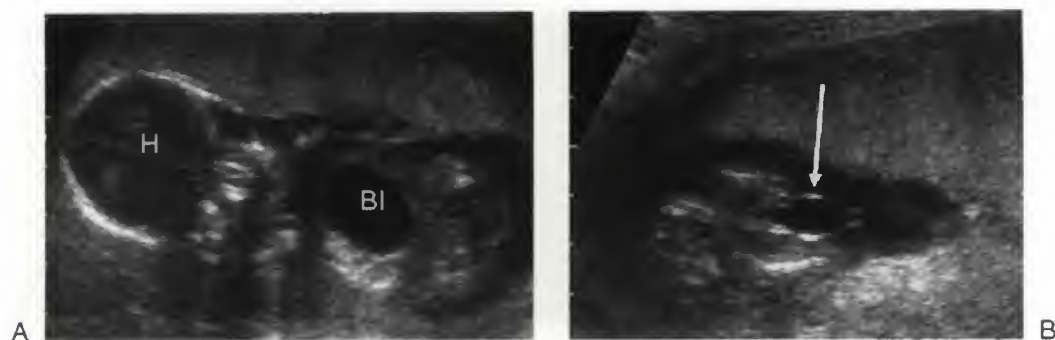


**FIGURE 16-52.** Megabladder and megalourethra, second trimester. A. Coronal view of the fetus. The bladder (Bl) occupies most of the fetal abdomen (urinary tract was bilaterally dilated as well). H, fetal head. B. Transverse axial view through the penis showing the dilated urethra (arrow) without spongy tissue around it.

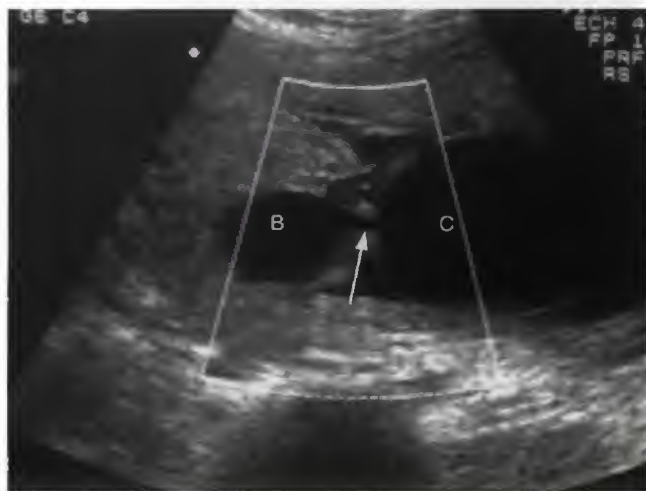


**FIGURE 16-53.** Allantoic cyst, third trimester. A large cyst (C) located within the umbilical cord connects with the bladder (B) through a small channel (arrow). No other malformation is visible.

points downward (Fig. 16-54). During the second trimester, the difference between both sexes becomes even more obvious because the labia or the scrotum and penis are more clearly visible.

The testes can be identified within the scrotum after 26 weeks (Fig. 16-55), and minor degrees of hydrocele is a normal finding. During the third trimester, the labia major and minor can be visualized. Under normal circumstances, the ovaries are usually not identified. On the contrary, during the (late) second and third trimester, the normal uterus can be visualized owing to its physiologic hypertrophy secondary to hormonal influence. The uterus appears as a round or oval mass within the fetal pelvis interposed between the rectum and fetal urinary bladder (Fig. 16-56). The normal endometrium appears hyperechoic.

The determination of the sex is important not only for the parents but also in the presence of specific familial diseases (i.e., hemophilia) or in case of various morphologic anomalies (ovarian cysts, BOO, and so on).<sup>139-142</sup>

## Ambiguous Genitalia

Ambiguous genitalia is characterized by a difficulty to assign the fetal gender during the US examination in the second or



**FIGURE 16-54.** Male sex, first trimester. Sagittal sign. Sagittal scan of the fetus. The penis points upward (arrow).

third trimester. The examiner is unable to differentiate between a short penis and a hypertrophied clitoris. Furthermore, a bifid scrotum can be misinterpreted as the labia major (Fig. 16-57). The condition can be isolated or part of various syndromes; therefore, and as usual, the sonogram examination should be as detailed as possible and chromosomal analysis should be obtained. Two classic associations should be underscored. Ambiguous genitalia can be part of a cloacal malformation in which there is a common opening of the bladder, vagina, and rectum. On the other hand, ambiguous genitalia can be associated and the clue to the diagnosis of an adrenogenital syndrome (AGS). In the female fetus affected by AGS, the clitoris is hypertrophied; the demonstration of enlarged wrinkled adrenals (see later) are typical for this diagnosis. A genitourethral fistula may exist as well but is difficult to demonstrate. In boys with AGS, the disease may develop unrecognized unless the adrenals hypertrophy.<sup>143-148</sup>

## Male Genital Anomalies

### Hypospadias/Epispadias

Hypospadias is a frequent malformation of the penis that appears shorter and broadened. During micturition, the jet

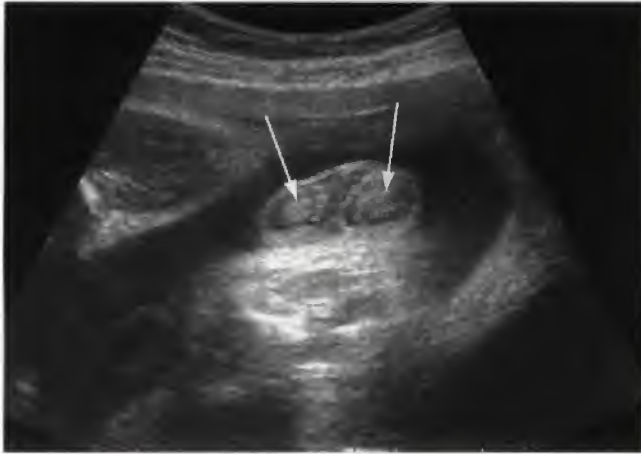


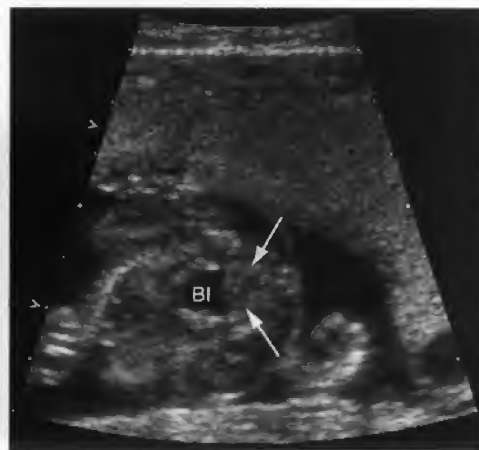
**FIGURE 16-55.** Normal scrotum, third trimester. The two testes are clearly identified (*arrows*).



**FIGURE 16-57.** Ambiguous genitalia, third trimester. Scan through the scrotum. The two hemiscrotum are separated by a penis that is too short (*arrow*) (split scrotum sign).



A



B

**FIGURE 16-56.** Normal female sex. A. Scan through the major and minor labia (*arrows*). B. Transverse scan through the pelvis of a female fetus. Note how the uterus (*arrows*) is interposed between the rectum and bladder (BI) and indents the bladder. In a male fetus no soft tissue will be seen between the rectum and bladder.





**FIGURE 16-58.** Hypospadias, third trimester. Scan through the distal end of the penis (arrow), which appears somewhat shortened and broadened.

**Table 16-13**

**Differential Diagnosis of Peritoneal (Partially) Cystic Masses in the Female Fetus**

Ovarian cyst  
Duplication cyst  
Urachal cyst (midline)  
Hydrocolpos (midline)  
Lymphangioma (cystic)  
Mesenteric cyst  
Teratoma (cystic)  
Meconium pseudocyst

is directed downward. It is usually an isolated finding but can be associated with numerous syndromes (Fig. 16-58). Epispadias is one end of a spectrum, and bladder exstrophy is at the other extreme. The urethral opening lies on the dorsal part of the penis. It is a difficult sonographic diagnosis.<sup>148,149</sup>

### Scrotum

As mentioned earlier, the testes can be visualized within the scrotum at approximately 26 weeks. An isolated undescended testis is not an abnormal finding in utero. A small amount of peritesticular fluid can also be considered as a normal variant. If the fluid collection is hyperechogenic, meconium peritonitis should be suspected. Scrotal intestinal hernia can also be observed in utero. It is important to note that the testis may undergo torsion in utero or in the neonatal period. At the acute stage, the testis is large and hypoechoic. At the chronic stage, the testis appears small and sometimes calcified.<sup>150-153</sup>

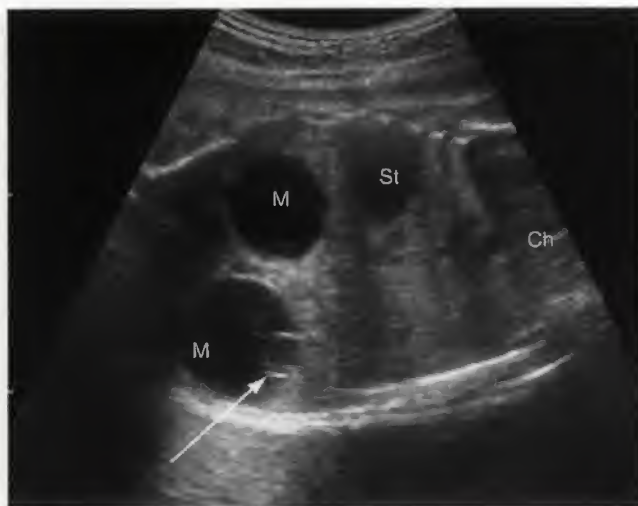


**FIGURE 16-59.** Bilateral ovarian cysts, third trimester. Frontal view of the fetal trunk demonstrating two cystic masses (M). In one of them, a smaller cyst is visible (daughter cyst sign) (arrow). Ch, chest; St, stomach.

## Female Genital Anomalies

### Ovarian Cysts

The ovarian cyst is the commonest cause of cystic mass in the female fetus. Such cysts result from maternofetal hormonal influence and are equivalent to follicles. These cysts may be small or large (> 8 cm), unilateral or bilateral (rare), unique or multiple (rare). They are usually completely cystic; the presence of small cyst within the cyst is a useful diagnostic sign (so-called daughter cyst sign). Torsion and bleeding may occur in utero and result in various types of echogenicities within the cyst (completely echogenic, fluid/fluid level, septa, and so on). The differential diagnosis includes other causes of cystic or semicystic masses (Table 16-13 and Figs. 16-59 to 16-61). Spontaneous involution occurs in utero or after birth, but the cyst may also rupture. Treatment is controversial because some authors favor in utero puncture, whereas some favor postnatal surgery and others a conservative attitude. If a conservative attitude is elected, a close clinical and US follow-up with a monthly follow-up for 6 months should be considered.<sup>155-162</sup> It is important to note that bilateral ovarian cysts may be a symptom of hypothyroidism or associated with maternal diabetes.

### Hydrocolpos—Vaginal Malformations

Vaginal malformations and atresia lead to hydrocolpos, which is visualized as a midline cystic mass (Fig. 16-62). A clue to the diagnosis is the demonstration of the uterine cervix at the superior aspect of the cystic mass. The condition can be part of a cloacal malformation, associated with renal agenesis/MDK or part of syndromes (i.e., Drash, BBS, and so on) (Fig. 16-63).<sup>163-166</sup>

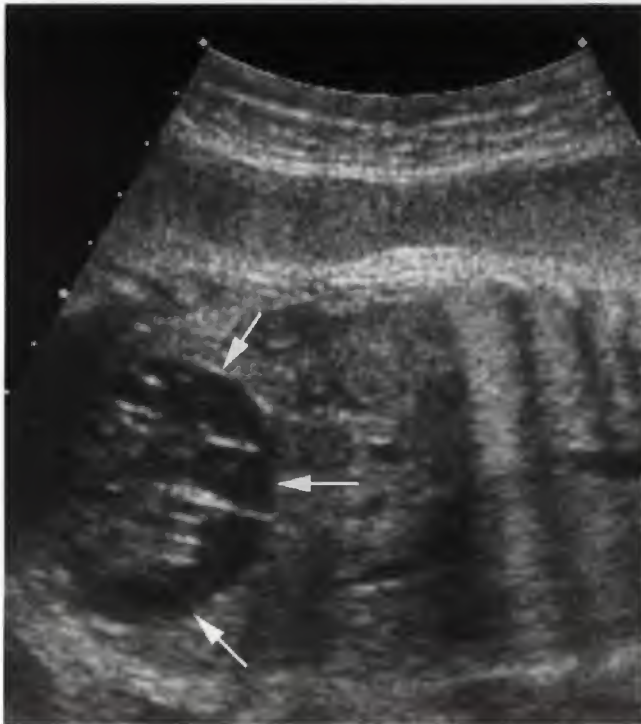


**FIGURE 16-80.** Large ovarian cyst, third trimester. Very large cystic mass is seen within the pelvis and lower abdomen (*arrows*). Fibrinous strands are seen within the cyst characteristic of hemorrhage.



**FIGURE 16-62.** Hydrocolpos, third trimester. Echogenic mass (M) above the bladder (B) corresponding to a hydrocolpos filled with mucous.



**FIGURE 16-81.** Choledochal cyst, third trimester. Cystic mass (M) in the right flank connected to biliary ducts (*arrows*) and corresponding to a choledochal cyst. Sp, spine.

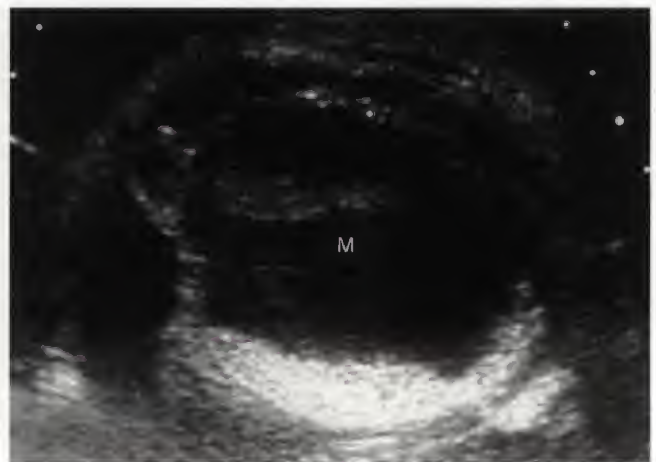


**FIGURE 16-63.** Cloacal malformation, third trimester. Transverse scan through the fetal pelvis. One single (cystic) cavity (M) is visible draining the bladder and vagina. It contains an echogenic material (mucous?).



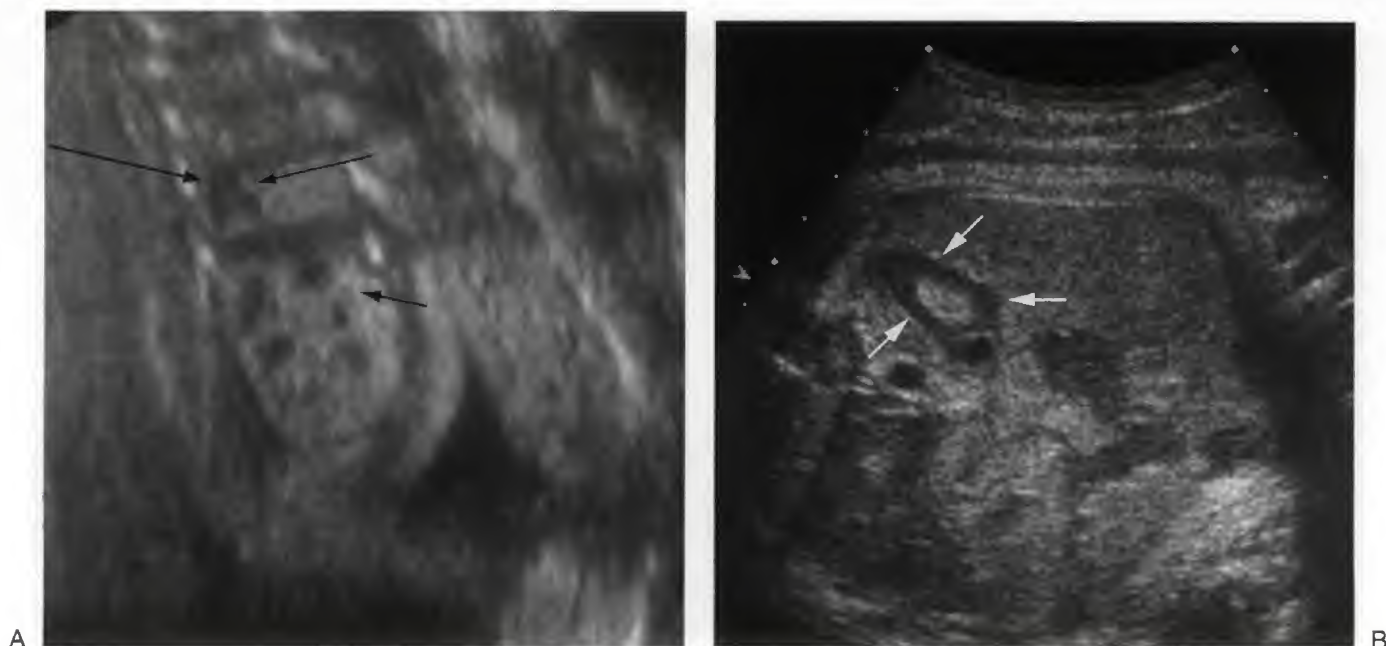


**FIGURE 16-64.** Normal adrenals. A. Second trimester. Coronal view. The triangle-shaped adrenal is visible (*arrows*) above the kidney (*short arrow*). B. Third trimester. Transverse scan. The right adrenal is visible (*arrows*) with a cortico (hypoechoic)-medullary (hyperechoic) differentiation.

## FETAL ADRENALS

### Normal Adrenals

The fetal adrenals are easily demonstrated, especially using transvaginal probes at the end of the first trimester (see Fig. 16-5). They appear as pyramid-shaped hyperechoic structures at the superior aspect of the hyperechoic kidneys. At that stage, their size is approximately half that of the kidney. Progressively, during the second trimester, CMD “appears” (hyperechoic cortex, hyperechoic medulla). The shape is that of an inverted “V” on the superior aspect of the kidney. The size of the gland increases but relatively less than the kidney. During the third trimester, the appearance of the fetal adrenals is very similar to that of the neonatal adrenals (Y-shaped, hypoechoic cortex, hyperechoic medulla) (Fig. 16-64).

In cases of renal agenesis, the adrenal is usually present and more globular or may be elongated (the lying down adrenal sign) (see Fig. 16-8). It should not be misinterpreted as a dysplastic kidney.<sup>167,168</sup>

### Adrenogenital Syndrome

In case of AGS, the adrenals may enlarge as early as the second trimester. They may display the so-called cerebriform wrinkled pattern (Fig. 16-65). The condition is associated with ambiguous genitalia in the female fetus (see earlier). Several authors have proposed using maternal corticotherapy, once the condition has been ascertained, in order to reduce the virilization of the female fetus.<sup>167,169,170</sup>

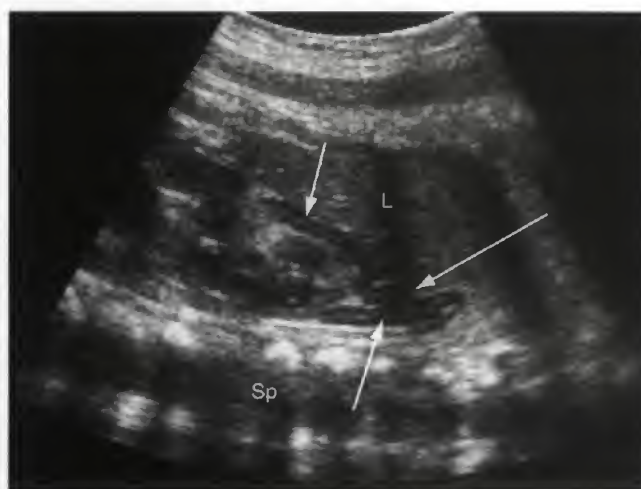


**FIGURE 16-65.** Adrenogenital syndrome, third trimester. Sagittal scan through the right flank demonstrating the hypertrophied adrenal (*arrows*). L, liver; Sp, spine.

### Adrenal Masses

Whenever a mass is detected in the suprarenal area, a neuroblastoma should be suspected first regardless of the pattern of the mass. Neuroblastoma may present as a cystic, a solid or more complex appearance. Color Doppler imaging may demonstrate increasing vascularization of the hyperechoic regions of the mass. The prognosis of antenatal

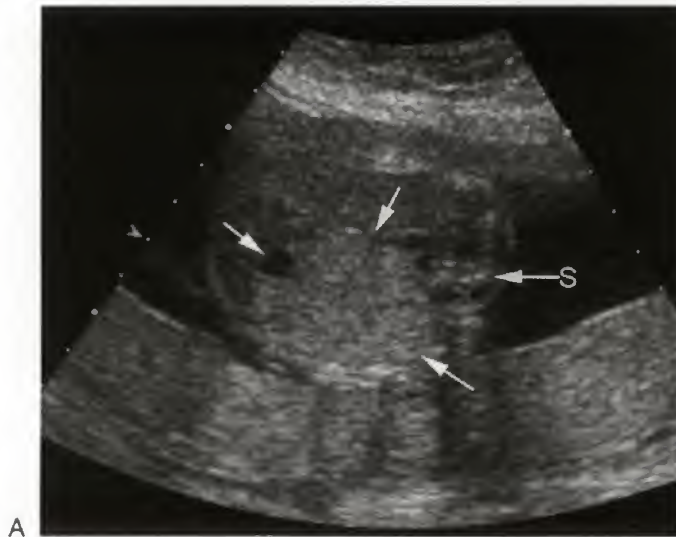


**FIGURE 16-66.** Neuroblastoma. A. Transverse axial scan of the fetal abdomen in a second trimester fetus. A large paraspinal solid mass (arrows) with a single cystic component is seen. This was a neuroblastoma at birth. S, spine. B. Partially cystic mass (between calipers) corresponding to the neuroblastoma. Sp, spine.



**FIGURE 16-67.** Adrenal cyst, third trimester. Transverse scan of the fetal abdomen. A small cyst (arrow) is visible within the adrenal. Sp, spine.

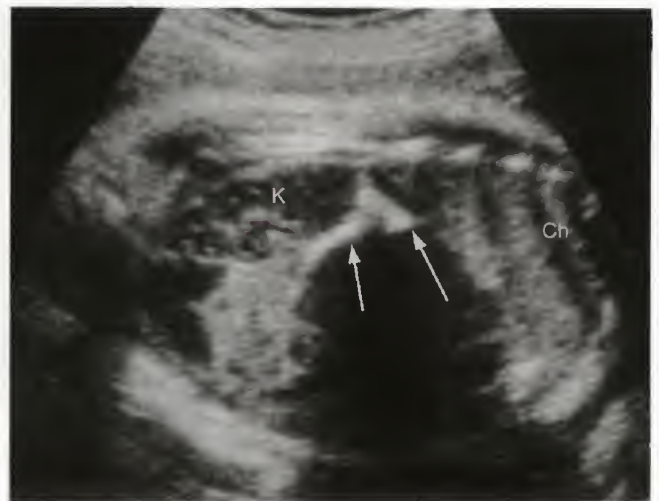


**FIGURE 16-68.** Wolman syndrome, third trimester. Sagittal scan through the fetal trunk. The adrenal appears completely calcified (arrows). Ch, chest; K, kidney. (Courtesy of F Didier MD, Nancy, France.)

neuroblastoma is excellent even when hepatic metastases are present. Furthermore, some cases of spontaneous involution have been reported (Fig. 16-66). The differential diagnosis should include adrenal hemorrhage, associated or not with RVT, and adrenal cysts (Fig. 16-67). Bilateral calcifications are unusual and may suggest Wolman syndrome (Fig. 16-68). Isolated, uncomplicated small cysts may be observed at the level of the adrenals (see Fig. 16-67). Their size is usually small and they disappear spontaneously. Large cysts develop in association with the Beckwith-Wiedemann syndrome. These cysts may bleed, and their appearance becomes more complex. Extra-adrenal causes, such as subdiaphragmatic pulmonary sequestration, should also be included in the differential diagnosis (Table 16-14).<sup>171-185</sup>

**Table 16-14** Differential Diagnosis of an Adrenal Mass

Neuroblastoma
Adrenal hemorrhage
Adrenal carcinoma
Adrenal cyst
Adrenal cyst with B-W syndrome
MDK of a duplex kidney
Splenic or hepatic cyst
Choledochal cyst
Infradiaphragmatic sequestration
Peridiaphragmatic B-P malformation

B-W, Beckwith-Wiedemann; MDK, multicystic dysplastic kidney.



## References

- Sadler TW (ed): Langman's Medical Embryology, 9th ed. Philadelphia, Lippincott, Williams and Wilkins, 2004.
- Moore KL, Persaud TVN: The Developing Human; Clinically Oriented Embryology, 6th ed. Philadelphia, WB Saunders Company, 1998, pp 305-318.
- Park JM: Normal and Anomalous Development of the Urogenital System. In Walsh PC (ed): Campbell's Urology, 8th ed. Philadelphia, WB Saunders Company, 2002.
- Rosati P, Guaniglia L: Transvaginal assessment of fetal urinary tract in early pregnancy. *Ultrasound Obstet Gynecol* 7:95, 1996.
- Chamberlain PF, Manning FD, Morrison I, et al: Circadian reflux in bladder volume in the term human fetus. *Obstet Gynecol* 64:657, 1984.
- Cohen ML, Cooper J, Eisenberg P, et al: Normal length of fetal kidneys. *AJR Am J Roentgenol* 157:545, 1991.
- Thomas IF, Smith DW: Oligohydramnios: cause of the non-renal features of Potter's syndrome including pulmonary hypoplasia. *J Pediatr* 84:811, 1974.
- Dillon E, Ryall A: A 10 year audit of antenatal US detection of renal disease. *Br J Radiol* 71:497, 1998.
- Richmond S, Atkins J: A population-based study of the prenatal diagnosis of congenital malformations over 16 years. *BJOG* 112:1349, 2005.
- Wellesley D, Howe DT: Fetal renal anomalies and genetic syndromes. *Prenat Diagn* 21:992, 2001.
- Wiesel A, Queisser-Luft A, Clementi M, et al: Prenatal detection of congenital renal malformations by fetal US examination: an analysis of 709,030 births in 12 European countries. *Eur J Med Genet* 48:131, 2005.
- Zhou Q, Cardoza JD, Barth R: Prenatal ultrasound of congenital renal malformations. *AJR Am J Roentgenol* 173:1371, 1999.
- Gunn TR, Dennot MD, Mora J, et al: Antenatal diagnosis of urinary tract abnormalities after 28 weeks gestation. *Am J Obstet Gynecol* 172:479, 1995.
- Gloor JM, Ogburn PL, Robert MD, et al: Urinary tract anomalies detected by prenatal US examination at Mayo Clinic. *Mayo Clin Proc* 70:526, 1995.
- Bronshtein M, Amito A, Achiron R, et al: The early prenatal diagnosis of renal agenesis. *Prenat Diagn* 14:291, 1994.
- Latini JM, Curtis MR, Cendron M, et al: Prenatal failure to visualize kidneys: a spectrum of disease. *Urology* 52:306, 1998.
- Hoffman CK, Filly RA, Callen PW: The lying down sign: a US indicator of renal agenesis or ectopia. *J Ultrasound Med* 11:533, 1992.
- Cassart M, Massez A, Metens T, et al: Complementary role of fetal MR imaging after US in assessing unilateral urinary tract anomalies. *AJR Am J Roentgenol* 182:689, 2004.
- Sherer DM, Thompson HO, Armstrong B, et al: Prenatal US diagnosis of unilateral renal agenesis. *J Clin Ultrasound* 18:648, 1990.
- Mandell J, Browly B, Peter CA, Benaceraff BR: Prenatal findings associated with unilateral non-functioning or absent kidney. *J Urol* 152:176, 1994.
- Mesrobian H, Rushton HG, Bulas D: Unilateral renal agenesis may result from in utero regression of multicystic renal dysplasia. *J Urol* 150:793, 1993.
- Jeanty P, Romero R, Kepple D, et al: Prenatal diagnoses in unilateral empty renal fossa. *J Ultrasound Med* 9:651, 1990.
- Meizner I, Bernhard Y: Bilateral fetal pelvic kidneys. *J Ultrasound Med* 14:487, 1995.
- Avni EF, Thoua Y, Van Gansbeke D, et al: The development of hypodysplastic kidney. *Radiology* 164:123, 1985.
- Oliveira EA, Diniz JS, Cabral ACV, et al: Prognostic factors in fetal hydronephrosis: a multivariate analysis. *Pediatr Nephrol* 13:859, 1999.
- Ismaili K, Avni EF, Piepsz A, et al: Current management of infants with renal pelvis dilation: a survey by French-speaking pediatric nephrologists and urologists. *Pediatr Nephrol* 19:966, 2004.
- Ismaili K, Hall M, Donner C, et al: Results of systematic screening for minor degrees of fetal renal pelvis dilatation in an unselected population. *Am J Obstet Gynecol* 188:242, 2003.
- Stocks A, Richards D, Freutzen B, et al: Correlation of prenatal renal pelvic anteroposterior diameter with outcome in infancy. *J Urol* 155:1060, 1996.
- Elder J: Commentary: importance of antenatal diagnosis of vesico-ureteral reflux. *J Urol* 148:1750, 1992.
- John U, Kähler C, Schulz SV, et al: The impact of renal pelvic diameter on postnatal outcome. *Prenat Diagn* 24:591, 2004.
- Mouriquand PDE, Troisfontaines E, Wiloos DT: Antenatal and perinatal uronephrology: current questions and dilemmas. *Pediatr Nephrol* 13:938, 1999.
- Dremsek PA, Gindi K, Voigt P, et al: Renal pyelectasis in fetuses and neonates. *AJR Am J Roentgenol* 168:1017, 1997.
- Economou G, Egginton JA, Brookfield SK: The importance of late pregnancy scans for renal tract abnormalities. *Prenat Diagn* 14:177, 1994.
- Anderson N, Claudice-Engle T, Allau R, et al: Detection of obstruction uropathy in the fetus. *AJR Am J Roentgenol* 164:719, 1995.
- Stocks A, Richards D, Freutzen B, et al: Correlation of prenatal renal pelvic antero-posterior diameter with postnatal outcome. *J Urol* 155:1050, 1996.
- Maizels M, Reisman ME, Slom LS: Grading nephroureteral dilatation detected in the first year of life: correlation with obstruction. *J Urol* 148:609, 1992.
- Kaefer M, Peters CA, Petik AB, et al: Increased renal echogenicity: a US sign for differentiating between obstructive and nonobstructive etiologies of in utero bladder distension. *J Urol* 158:1026, 1997.
- Chudleigh T: Mild pyelectasis. *Prenat Diagn* 21:916, 2001.
- Kaefer M, Keating MA, Adams MC, et al: PUV, pressure pop-offs and bladder function. *J Urol* 154:708, 1995.
- Callen PW, Bolding D, Filly RA, et al: US evaluation of fetal paranephric pseudocysts. *J Ultrasound Med* 2:309, 1983.
- Jee LD, Rickwood AMK, Williams ML, et al: Experience with duplex system anomalies detected by prenatal US. *J Urol* 49:808, 1993.
- Vergani P, Centi P, Locatelli A, et al: Accuracy of prenatal US diagnosis of duplex renal system. *J Ultrasound Med* 18:463, 1999.
- Abu Lamad AZ, Horton GE, Horton SH, et al: Renal duplications anomalies in the fetus. *Ultrasound Obstet Gynecol* 7:174, 1996.
- Austin PF, Cain MP, Casale AJ, et al: Prenatal outlet obstruction secondary to ureteroceles. *Urology* 52:1132, 1998.
- Montemarano H, Bulas DI, Rushton G, et al: Bladder distension and pyelectasis in the male fetus. *J Ultrasound Med* 17:743, 1998.
- Dinneen MD, Dhillon DK, Ward HC, Duffy PA, et al: Antenatal diagnosis of PUV. *J Urol* 72:364, 1993.
- Carlsson SA, Hokegard KA, Mattson LA: Megacystis microcolon hypoperistalsis syndrome. *Acta Obstet Scand* 71:645, 1992.
- Mandell J, Lebowitz RL, Peters CA, et al: Prenatal diagnosis of megacystis megaureter association. *J Urol* 148:1487, 1992.
- Persutte WH, Lenke RR, Kropp KA, et al: Antenatal diagnosis of patent urachus. *J Ultrasound Med* 7:399, 1988.
- Carpenter MW, Corrado F, Sung J: Lethal fetal renal anomalies and obstetric outcome. *Eur J Obstet Gynecol Reprod Med* 89:149, 2000.
- Stachler M, Downer C, Van Regemorter N, et al: Should determination of fetal karyotype be systematic for all malformations detected by obstetrical US. *Prenat Diagn* 25:567, 2005.
- Spitzer A: The current approach to the assessment of fetal renal function: fact or fiction. *Pediatr Nephrol* 10:230, 1996.
- Brussières L, Laborde K, Souberbielle JC, et al: Fetal urinary insulin like growth factor 1 and binding protein 3 in bilateral obstructive uropathies. *Prenat Diagn* 15:1047, 1995.
- McLorie G, Farhat W, Klouvy A, et al: Outcome analysis of vesico-amniotic shunting in a comprehensive population. *J Urol* 166:1036, 2001.
- Makino Y, Kobayashi H, Kyono K, et al: Clinical results of fetal obstructive uropathy treated by vesico-amniotic shunting. *Urology* 55:118, 2000.
- Carr MC: Prenatal management of urogenital disorders. *Urol Clin N Am* 31:389, 2004.
- Blachar A, Blachar Y, Livne PM, et al: Clinical outcome and follow-up of prenatal hydronephrosis. *Prenat Diagn* 8:30, 1994.
- Yerkes EB, Adams MC, Pope JC, et al: Does every patient with prenatal hydronephrosis need voiding cystourethrography? *J Urol* 162:1218, 1999.
- Ismaili K, Avni FE, Hall M: Results of systematic voiding cystourethrography in infants with antenatally diagnosed renal pelvis dilatation. *J Pediatr* 141:21, 2002.
- Ismaili K, Avni FE, Wissing M, et al: Long-term clinical outcome of infants with mild and moderate pyelectasis: validation of neonatal ultrasound as a screening tool to detect significant nephro-uropathies. *J Pediatr* 144:759, 2004.



61. Upadhyay JU, McLorie GA, Bolduc S, et al: Natural history of neonatal reflux associated with prenatal hydronephrosis: long-term results of a prospective study. *J Urol* 169:1837, 2003.
62. Cheng AM, Phan V, Geary DF, et al: Outcome of isolated antenatal hydronephrosis. *Arch Pediatr Adolesc Med* 158:38, 2004.
63. Herndon CDA, McKenna PH, Kolon TF, et al: A multicenter outcome analysis of patients with neonatal reflux presenting with prenatal hydronephrosis. *J Urol* 162:1203, 1999.
64. Avni EF, Nicaise N, Hall M, et al: The role of MR imaging for the assessment of complicated duplex kidneys in children. *Pediatr Radiol* 31:215, 2001.
65. Onen A, Jayanthi VR, Koff SA: Long-term follow-up of prenatally detected severe bilateral newborn hydronephrosis initially managed nonoperatively. *J Urol* 168:1118, 2002.
66. Jaswon MS, Dibbie L, Puri S, et al: Prospective study of outcome in antenatally diagnosed renal pelvis dilatation. *Arch Dis Child Fetal Neonatal Ed* 80:F35, 1999.
67. John U, Kahler C, Schulz S, et al: The impact of fetal renal pelvic diameter on postnatal outcome. *Prenat Diagn* 24:591, 2004.
68. Chitty LS, Griffin DR, Johnson P, et al: The differential diagnosis of enlarged hyperechogenic kidneys with normal or increased liquor volume: report of five cases and review of the literature. *Ultrasound Obstet Gynecol* 1:115, 1991.
69. Carr MC, Benacerraf BR, Estroff JA, et al: Prenatally diagnosed bilateral hyperechoic kidneys with normal amniotic fluid: postnatal outcome. *J Urol* 153:442, 1995.
70. Slovis TL, Bernstein J, Gruskin A: Hyperechoic kidneys in the newborn and young infant. *Pediatr Nephrol* 7:294, 1993.
71. Estroff JA, Mandell J, Benacerraf BR: Increased renal parenchymal echogenicity in the fetus: importance and clinical outcome. *Radiology* 181:135, 1991.
72. Tsatsaris V, Gagnadoux MF, Aubry MC, et al: Prenatal diagnosis of bilateral isolated fetal hyperechogenic kidneys. Is it possible to predict long-term outcome? *BJOG* 109:1388, 2002.
73. Bernstein J: The multicystic kidney and hereditary renal dysplasia. *Am J Kidney Dis* 18:495, 1991.
74. de Bruyn R, Gordon I: Imaging in cystic renal disease. *Arch Dis Child* 83:401, 2000.
75. Kaplan BS, Kaplan P, Rosenberg H, et al: Polycystic kidney diseases in childhood. *J Pediatr* 115:867, 1989.
76. Blane CE, Barr M, DiPietro MA, et al: Renal obstructive dysplasia: ultrasound diagnosis and therapeutic implications. *Pediatr Radiol* 21:274, 1991.
77. Wilson PD: Polycystic kidney disease. *N Engl J Med* 350:151, 2004.
78. Zerres K, Muecher G, Becker J, et al: Prenatal diagnosis of autosomal recessive polycystic kidney disease (ARPKD): molecular genetics, clinical experience, and fetal morphology. *Am J Med Genet* 76:137, 1998.
79. Cassart M, Eurin D, Didier F, et al: Antenatal renal sonographic anomalies and postnatal follow-up of renal involvement in Bardet-Biedl syndrome. *Ultrasound Obstet Gynecol* 24:51, 2004.
80. Jain M, LeQuense GW, Bourne AJ, et al: High-resolution ultrasonography in the differential diagnosis of cystic diseases of the kidney in infancy and childhood: preliminary experience. *J Ultrasound Med* 16:235, 1997.
81. Avni EF, Granel L, Cassart M, et al: Perinatal assessment of hereditary cystic renal diseases: the contribution of US. *Pediatr Radiol* 36:458, 2006.
82. Barth RA, Guillot AP, Capeless EL, et al: Prenatal diagnosis of autosomal recessive polycystic kidney disease: Variable outcome within one family. *Am J Obstet Gynecol* 166:560, 1992.
83. Reuss A, Vladimiroff JW, Stewart PA, et al: Prenatal diagnosis by ultrasound in pregnancies at risk for autosomal recessive polycystic kidney disease. *Ultrasound Med Biol* 16:355, 1990.
84. Wisser J, Hebisch G, Froster U, et al: Prenatal sonographic diagnosis of autosomal recessive polycystic kidney disease (ARPKD) during the early second trimester. *Prenat Diagn* 15:868, 1995.
85. Lilford RJ, Irving HC, Allibone EB: A tale of two prior probabilities—avoiding the false positive antenatal diagnosis of autosomal recessive polycystic kidney disease. *Br J Obstet Gynaecol* 99:216, 1992.
86. Guay-Woodford LM, Desmond RA: Autosomal recessive polycystic kidney disease: the clinical experience in North America. *Pediatrics* 111:1072, 1992.
87. Bronshtein M, Bar-Hava I, Blumenfeld Z: Clues and pitfalls in the early prenatal diagnosis of "late onset" infantile polycystic kidney. *Prenat Diagn* 12:293, 1992.
88. Suranyi A, Retz C, Rigo J, et al: Fetal renal hyperechogenicity in intrauterine growth retardation: importance and outcome. *Pediatr Nephrol* 16:575, 2001.
89. Gabow PA: Autosomal dominant polycystic kidney disease. *N Engl J Med* 329:332, 1993.
90. Brun M, Maugey-Laulom B, Eurin D, et al: Prenatal sonographic patterns in autosomal dominant polycystic kidney disease: a multicenter study. *Ultrasound Obstet Gynecol* 24:55, 2004.
91. Michaud J, Russo P, Grignone A, et al: Autosomal dominant polycystic kidney disease in the fetus. *Am J Med Genet* 51:240, 1994.
92. Bernstein J: Glomerulocystic kidney disease—nosological considerations. *Pediatr Nephrol* 7:464, 1993.
93. Woolf AS, Feather SA, Bingham C: Recent insights into kidney diseases associated with glomerular cysts. *Pediatr Nephrol* 17:229, 2002.
94. Guay-Woodford LM, Galliani CA, Musulman-Mroczek E, et al: Diffuse renal cystic disease in children: morphologic and genetic correlations. *Pediatr Nephrol* 12:173, 1998.
95. Fick-Brosnahan GM, Tran ZV, Johnson AM, et al: Progression of autosomal-dominant polycystic kidney disease in children. *Kidney Int* 59:1654, 2001.
96. Demetriou K, Tziakouri C, Anninou K, et al: Autosomal dominant polycystic kidney disease - type 2. Ultrasound, genetic and clinical correlations. *Nephrol Dial Transplant* 15:205, 2000.
97. Avni EF, Guissard G, Hall M, et al: Hereditary polycystic kidney diseases in children. Changing US patterns in children. *Pediatr Radiol* 32:169, 2002.
98. Montemarano H, Bulas DI, Chandra R, et al: Prenatal diagnosis of glomerulocystic kidney disease in short-rib polydactyly syndrome type II, Majewski type. *Pediatr Radiol* 24:469, 1995.
99. Ickowicz V, Eurin D, Maugey-Laulom B, et al: Meckel Gruber syndrome: sonographic pathologic correlation. *Ultrasound Obstet Gynecol* 27:296, 2006.
100. Dar P, Sachs GS, Carter SM, et al: Prenatal diagnosis of Bardet-Biedl syndrome by targeted second-trimester sonography. *Ultrasound Obstet Gynecol* 17:354, 2001.
101. Dippell J, Varlam DE: Early sonographic aspects of kidney morphology in Bardet-Biedl syndrome. *Pediatr Nephrol* 12:559, 1998.
102. Gershoni-Baruch R, Nachlieli T, Leibo R, et al: Cystic kidney dysplasia and polydactyly in 3 sibs with Bardet-Biedl syndrome. *Am J Med Genet* 44:269, 1992.
103. Campos A, Figueroa ET, Gunasekaran S, et al: Early presentation of tuberous sclerosis as bilateral renal cysts. *J Urol* 149:1077, 1993.
104. Winyard P, Chitty L: Dysplastic and polycystic kidneys: diagnosis, associations and management. *Prenat Diagn* 21:924, 2001.
105. Rabelo EA, Oliveira EA, Silva GS, et al: Predictive factors of ultrasonographic involution of prenatally detected multicystic dysplastic kidney. *BJU Int* 95:868, 2005.
106. Rabelo EA, Oliveira EA, Diniz JS, et al: Natural history of multicystic kidney conservatively managed: a prospective study. *Pediatr Nephrol* 19:1102, 2004.
107. Oliveira EA, Diniz JS, Vilasboas AS, et al: Multicystic dysplastic kidney detected by fetal sonography: conservative management and follow-up. *Pediatr Surg Int* 17:54, 2001.
108. Matsell DG: Renal dysplasia: new approaches to an old problem. *Am J Kidney Dis* 32:535, 1998.
109. Blazer S, Zimmer EZ, Zelikovic I, et al: Natural history of fetal renal cysts detected in early pregnancy. *J Urol* 162:812, 1999.
110. McHugh K, Stringer DA, Hebert D, et al: Simple renal cysts in children: diagnosis and follow-up with US. *Radiology* 178:383, 1991.
111. Kolatsi-Joannou M, Bingham C, Ellard S, et al: Hepatocyte nuclear factor-1 $\beta$ : A new kindred with renal cysts and diabetes and gene expression in normal human development. *J Am Soc Nephrol* 12:2175, 2001.
112. Bingham C, Hattersley AT: Renal cysts and diabetes syndrome resulting from mutations in hepatocyte nuclear factor-1 $\beta$ . *Nephrol Dial Transplant* 19:2703, 2004.
113. Harker CP, Winter T III, Mack L: Prenatal diagnosis of Beckwith-Wiedemann Syndrome. *AJR* 168:520, 1997.
114. Herman TE, McAlister WH: Perlman syndrome: report of a case with additional radiographic findings. *Pediatr Radiol* 25:570, 1995.
115. Whitfield J, Hurst D, Bennett MJ, et al: Fetal polycystic kidney disease associated with glutaric aciduria type II: an inborn error of energy metabolism. *Am J Perinatol* 13:131, 1996.
116. Campagnola S, Fasoli L, Flessati P, et al: Congenital cystic mesoblastic nephroma. *Urol Int* 61:254, 1998.



117. Irsutti M, Puget C, Bauwin C, et al: Mesoblastic nephroma: prenatal US and MRI features. *Pediatr Radiol* 30:147, 2000.
118. Applegate KE, Ghei M, Perez Asayde AR: Prenatal detection of Wilm's tumor. *Pediatr Radiol* 29:65, 1999.
119. Bove KE: Wilm's tumor and related abnormalities in the fetus and newborn. *Semin Perinatol* 23:310, 1999.
120. Leclair MD, El Ghoneini A, Audry G, et al: The outcome of prenatally diagnosed renal tumors. *J Urol* 173:186, 2005.
121. Wright NB, Blanch G, Walkinshaw S, et al: Antenatal and neonatal renal vein thrombosis: new ultrasonic features with high frequency transducers. *Pediatr Radiol* 26:686, 1996.
122. Debiec H, Guigonis V, Mougenat B, et al: Antenatal membranous GN due to antineuronal endopeptidase antibodies. *N Engl J Med* 341:2053, 2002.
123. Wapren RJ, Jenkins TM, Silverman N, et al: Prenatal diagnosis of congenital nephrosis by in utero kidney biopsy. *Prenat Diagn* 21:256, 2001.
124. Koziell A, Pyer VK, Moghul NE, et al: Congenital nephrotic syndrome. *Pediatr Nephrol* 16:185, 2001.
125. Hofstaetter C, Neumann I, Lennert T, et al: Prenatal diagnosis of diffuse mesangial glomerulosclerosis by US. *Fetal Diagn Ther* 11:126, 1996.
126. Souka AP, Skeaton H, Geerts L, et al: Congenital nephrotic syndrome presenting with increased NT. *Prenat Diagn* 22:93, 2002.
127. McHugo J, Whittle M: Enlarged fetal bladders: aetiology, management and outcome. *Prenat Diagn* 21:958, 2001.
128. Anumba DO, Scott JE, Plant ND, et al: Diagnosis and outcome of fetal lower urinary tract obstruction in the Northern region of England. *Prenat Diagn* 25:7, 2005.
129. Stamm E, King G, Thickman D: Megacystic-Microcolon-Intestinal hypoperistalsis syndrome: prenatal identification in siblings. *J Ultrasound Med* 10:599, 1991.
130. Wilcox DT, Chitty LS: Non visualisations of the fetal bladder: aetiology and management. *Prenat Diagn* 21:577, 2001.
131. Gearhart JP, Ben Chaim J, Jeffs RD, et al: Criteria for the prenatal diagnosis of classic bladder exstrophy. *Obstet Gynecol* 85:961, 1995.
132. Goldstein I, Shale VE, Nisman D: The dilemma of prenatal diagnosis of bladder exstrophy: a case report and review. *Ultrasound Obstet Gynecol* 17:357, 2001.
133. Jaramillo D, Lebowitz RL, Hendren WH: The cloacal malformation: radiological findings and imaging recommendations. *Radiology* 177:441, 1990.
134. Austin PF, Homsy YL, Geahaut JP, et al: The prenatal diagnosis of cloacal exstrophy. *J Urol* 160:1179, 1998.
135. Stephens FD, Fortine DW: The pathogenesis of megalourethra. *J Urol* 149:1512, 1993.
136. Fisk NH, Dhillon HK, Ellis CE, et al: Antenatal diagnosis of megalourethra in a fetus with prune belly. *J Clin Ultrasound* 18:124, 1990.
137. Kilicdag EB, Kilicdag H, Bagis T, et al: Large pseudocyst of the umbilical cord associated with patent urachus. *J Obstet Gynecol Res* 30:444, 2004.
138. Anward J, Azar G, Soubra M: Sonographic diagnosis of a urachal cyst in utero. *Acta Obstet Gynecol Scand* 73:156, 1994.
139. Pajkci E, Chitty LS: Prenatal gender determination and the diagnosis of genital anomalies. *BJU Intern* 93:12(S), 2004.
140. Emerson DS, Felker E, Brown DL: The sagittal sign. *J Ultrasound Med* 8:293, 1989.
141. Shapiro E: The US appearance of normal and abnormal fetal genitalia. *J Urol* 162:530, 1999.
142. Soriano D, Lipitz S, Seidman DS, et al: Development of the fetal uterus between 19 and 38 weeks of gestation: in utero US measurements. *Hum Reprod* 14:215, 1998.
143. Chekhlard A, Luto D, Philippe-Chouette P, et al: How accurate is prenatal diagnosis of abnormal genitalia. *J Urol* 164:984, 2000.
144. Sivan E, Koch S, Reece A: US prenatal diagnosis of ambiguous genitalia. *Fetal Diagn Ther* 10: 311, 1995.
145. Mandell J, Browley B, Peeters CA, et al: Prenatal US detection of genital malformations. *J Urol* 153:1994, 1995.
146. Pinhas Hamiel O, Zalel Y, Smith E, et al: Prenatal diagnosis of sex differentiation disorders. *J Clin Endocr Metabol* 87:4547, 2002.
147. Chambrier ED, Heinrichs C, Avni FE: Adrenal hyperplasia in a fetus. *J Ultrasound Med* 21:97, 2002.
148. Bronshtein M, Riechler A, Zimmer EZ: Prenatal US signs of possible fetal genital anomalies. *Prenat Diagn* 15:215, 1995.
149. Smulian JC, Scorza WE, Guzman ER, et al: Prenatal diagnosis of midshaft hypospadias. *Prenat Diagn* 16:276, 1996.
150. Meizner I, Katz M, Zmora E, Insler V: In utero diagnosis of congenital hydrocele. *J Clin Ultrasound* 11:449, 1983.
151. Ring KS, Axelrod SL, Burbige KA, et al: Meconium hydrocele: an unusual etiology of a scrotal mass in the newborn. *J Urol* 141:1172, 1989.
152. Shipp TD, Benaceraff BR: Scrotal inguinal hernia in a fetus. *AJR Am J Roentgenol* 165:1494, 1995.
153. Tripp BJ, Homsy Y: Prenatal diagnosis of bilateral neonatal torsion: a case report. *J Urol* 153:1990, 1995.
154. Driver CP, Losty PD: Neonatal testicular torsion. *Br Urol* 82:855, 1998.
155. Comparetto C, Giudici S, Coccia ME, et al: Fetal and neonatal ovarian cysts: what's their real meaning? *Clin Exp Obstet Gynecol* 32:123, 2005.
156. Foley PT, Ford WD, McEwing R, et al: Is conservative management of prenatal and neonatal ovarian cysts justifiable? *Fetal Diagn Ther* 20:454, 2005.
157. Awad J, Azar G, Soubra M: US diagnosis of urachal cyst in utero. *Acta Obstet Gynecol Scand* 73:156, 1994.
158. Crombleholme TM, Craigo SD, Gaomal S, et al: Fetal ovarian cyst decompression to prevent torsion. *J Pediatr Surg* 32:1447, 1997.
159. D'Addario V, Vompe G, Kurjak A, et al: US diagnosis and perinatal management of complicated and uncomplicated fetal ovarian cyst. *J Perinat Med* 18:375, 1990.
160. Garcl L, Filiatrault D, Brandt M, et al: Antenatal diagnosis of ovarian cysts. *Pediatr Radiol* 21:182, 1991.
161. Hee-Jung L: Daughter cysts sign: a US finding of ovarian cyst in children. *AJR Am J Roentgenol* 174:1013, 2000.
162. Perrotin F, Roy F, Potin J, et al: US diagnosis and prenatal management of fetal ovarian cysts. *J Gynecol Obstet Biol Reprod* 29:161, 2000.
163. Geipel A, Berg C, Germer U, et al: Diagnostic and therapeutic problems in a case of prenatally detected fetal hydrocolpos. *Ultrasound Obstet Gynecol* 18:169, 2001.
164. Ogunyemi D: Prenatal sonographic diagnosis of bladder outlet obstruction caused by a ureteroceles associated with hydrocolpos and imperforate hymen. *Am J Perinatol* 18:15, 2001.
165. Manzella A, Filho PB: Hydrocolpos, uterus didelphys and septate vagina in association with ascites: antenatal sonographic detection. *J Ultrasound Med* 17:465, 1998.
166. Winderl LM, Silverman RK: Prenatal diagnosis of congenital imperforate hymen. *Obstet Gynecol* 85:857, 1995.
167. Brohnsstein M, Tsidomy D, Diamant M, et al: Transvaginal US measurement of the adrenal glands at 12 to 17 weeks of gestation. *Am J Obstet Gynecol* 169:1205, 1993.
168. Chang CH, Yu CH, Cheng FM, et al: Assessment of fetal adrenal gland volume using 3D-US. *Ultrasound Med Biol* 28:1383, 2002.
169. Saada J, Grebille AG, Aubry MC, et al: US in prenatal diagnosis of congenital adrenal hyperplasia. *Prenat Diagn* 24:627, 2004.
170. Cassart M, Massez A, Donner C, et al: US diagnosis of fetal adrenal hyperplasia. *Prenat Diagn* 25:1059, 2005.
171. Rubenstein SC, Benaceraff BR, Retik AB, et al: Fetal suprarenal masses: sonographic appearance and differential diagnosis. *Ultrasound Obstet Gynecol* 5:164, 1995.
172. Luca JL, Rousseau T, Durand C, et al: Diagnostic and therapeutic dilemma with large prenatally detected cystic adrenal masses. *Fetal Diagn Ther* 17:11, 2002.
173. Schwarzer P, Bernard JP, Senat MV, et al: Prenatal diagnosis of fetal adrenal masses: differentiation between hemorrhage and solid tumor by color Doppler sonography. *Ultrasound Obstet Gynecol* 13:351, 1999.
174. Gocmen R, Basaran C, Karcacalincaba M, et al: Bilateral hemorrhagic adrenal cysts in an incomplete form of Beckwith-Wiedemann syndrome: MRI and prenatal US findings. *Abdom Imaging* 30:786, 2005.
175. Yamagiwa I, Obata K, Saito H: Prenatally detected cystic neuroblastoma. *Pediatr Surg Int* 13:215, 1998.
176. Izbizky G, Elias D, Gallo A, et al: Prenatal diagnosis of fetal bilateral adrenal carcinoma. *Ultrasound Obstet Gynecol* 26:669, 2005.
177. Merrot T, Walz J, Anastasescu R, et al: Prenatally detected cystic adrenal mass associated with Beckwith-Wiedemann syndrome. *Fetal Diagn Ther* 19:465, 2004.
178. Hosoda Y, Miyano T, Kimura K, et al: Characteristics and management of patients with fetal neuroblastoma. *J Pediatr Surg* 27:623, 1992.
179. Lin JN, Lin CJ, Hung IJ, Hsueh C: Prenatally detected tumor mass in the adrenal gland. *J Pediatr Surg* 34:1620, 1999.

180. Haffa AJ, Many A, Hartoor J, et al: Prenatal US diagnosis of metastatic neuroblastoma. *Prenat Diagn* 13:73, 1993.
181. Liyanage IS, Katoch D: US prenatal diagnosis of liver metastases from adrenal neuroblastoma. *J Clin Ultrasound* 20:401, 1992.
182. Morganti VJ, Anderson NG: Simple adrenal cysts in fetus, resolving in neonate. *J Ultrasound Med* 10:521, 1991.
183. Patti G, Fiocca G, Latini T, et al: Prenatal diagnosis of bilateral adrenal cysts. *J Urol* 150:1189, 1993.
184. Saylor RL, Cohn SL, Morgan ER, et al: Prenatal detection of neuroblastoma by fetal US. *Am J Pediatr Hematol Oncol* 16:356, 1994.
185. Strouse PJ, Boweman RA, Schlenizer AE: Antenatal findings of fetal adrenal hemorrhage. *Clin Ultrasound* 23:442, 1995.
186. Daneman A, Baunin C, Lobo E, et al: Disappearing suprarenal masses in the fetus and neonate. *Pediatr Radiol* 27:675, 1997.



## ULTRASOUND EVALUATION OF HYDROPS FETALIS

Kenneth J. Moise, Jr., MD

### Definition of Hydrops

### Maternal Complications of Fetal Hydrops

### Immune Hydrops

Pathophysiology

Significance of Detection of Immune-Mediated Hydrops

Evaluation of the Sensitized Pregnancy

*Maternal Antibody Measurement*

*Fetal Antigen Testing*

Diagnosis of Fetal Anemia

*Amniocentesis*

*Middle Cerebral Artery Doppler*

*Choice of Surveillance Method*

Overall Management

Intrauterine Transfusion

### Method

The Patient With Recurrent Immune Hydrops Fetalis

Prognosis

### Nonimmune Hydrops

Incidence

Etiology

Pathophysiology

Evaluation

Treatment

Prognosis

### Conclusion

## DEFINITION OF HYDROPS

Hydrops fetalis is typically defined as the presence of Extracellular fluid in at least two fetal body compartments. These fluid collections include scalp and body wall edema, pericardial effusion, pleural effusions, and ascites (Figs. 17-1 to 17-8). This definition is more than academic. As is discussed below, in general, the prognosis for fetal hydrops is poor. Therefore, this term should only be used when the above criteria are met. The presence of ascites is often used to diagnose hydrops. Ascites may result from a variety of conditions, many of which should not be categorized as hydrops. For example, ascites may result from a unilateral high-grade ureteropelvic junction obstruction in which fornical rupture into the retroperitoneal and ultimately peritoneal space occurs. Although the kidney may not ultimately fare well, the prognosis for the fetus is usually excellent. The same is also true for a small amount of ascites resulting from a small bowel perforation, which may ultimately heal in utero. Therefore, hydrops fetalis should not be used to describe these conditions. It should be noted, however, that in those fetal conditions in which hydrops is a known outcome of progressive disease, a single accumulation of fluid in a body cavity may be enough to warrant referring to the condition as early hydrops. High cardiac output resulting from vascular abnormalities such as fetal sacrococcygeal teratoma and chorioangioma are examples of this situation. Some authors include polyhydramnios due to increased urine output, as well as placentomegaly as additional criteria for the diagnosis of hydrops fetalis.

Classically, the disease has been divided into two main entities based on etiology: immune (related to fetal anemia secondary to maternal alloimmunization to red cell antigens)

and nonimmune (related to a variety of other causes). Clearly, the advent of the widespread use of Rhesus immune globulin for the prevention of RhD alloimmunization has resulted in a shift in favor of the non-immune variety. In 1970, McAfee et al<sup>2</sup> reported that 82% of cases of fetal hydrops were immune mediated whereas in one recent series, 95% of cases of hydrops were classified as nonimmune.<sup>3</sup>

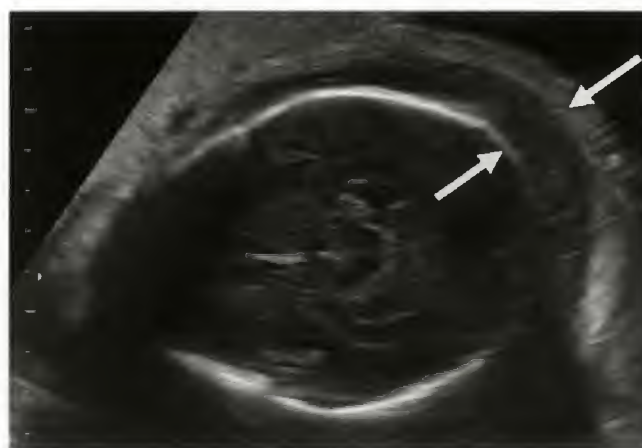


**FIGURE 17-1.** Scalp edema noted (between arrows) at 32 weeks' gestation. Etiology: idiopathic. (Courtesy of Anthony Swartz, BS, RT(R), RDMS.)



**FIGURE 17-2.** Cross-sectional view of the fetal thoracic cavity at 19 weeks' gestation. Note pericardial effusion (arrow). Also note the cardiomegaly. Etiology: maternal RhD alloimmunization and resulting hemolytic disease of the fetus/newborn.

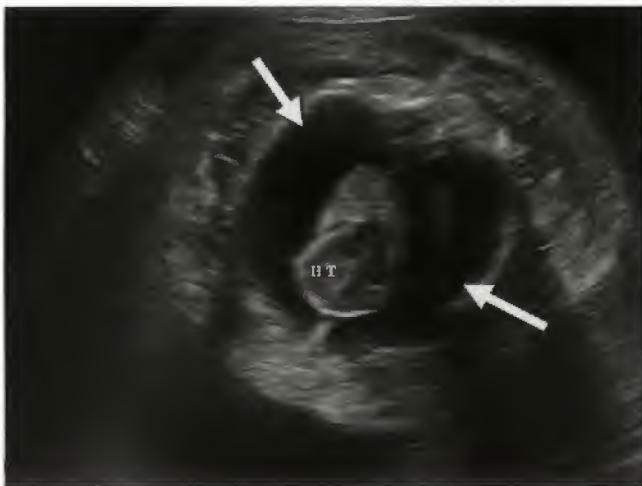


**FIGURE 17-3.** Bilateral pleural effusions (arrows) at 32 weeks' gestation. HT, midline fetal heart. Etiology: idiopathic. (Courtesy of Anthony Swartz, BS, RT(R), RDMS.)

## MATERNAL COMPLICATIONS OF FETAL HYDROPS

Fetal hydrops is often associated with polyhydramnios, leading to such maternal complications as supine hypotension syndrome, preterm labor, and preterm premature rupture of the membranes. If placental hydrops is significant, an additional life-threatening complication called Ballantyne syndrome (also known as mirror syndrome, triple edema, and pseudotoxemia) has been described.<sup>4</sup> The mirror syndrome is so named because the mother mirrors the hydropic state of the fetus. Although first described in association with immune hydrops, many subsequent case descriptions have been described in the literature secondary to nonimmune



**FIGURE 17-4.** Predominantly left-sided pleural effusion (large arrow) at 30 weeks' gestation. Fetal heart (asterisk) is displaced to the right side of the chest. Large left-sided pulmonary sequestration is noted (small arrow). Note extreme polyhydramnios as well. Etiology: intrathoracic mass with deviation of mediastinum. (Courtesy of Sharon Pinette, RDMS.)

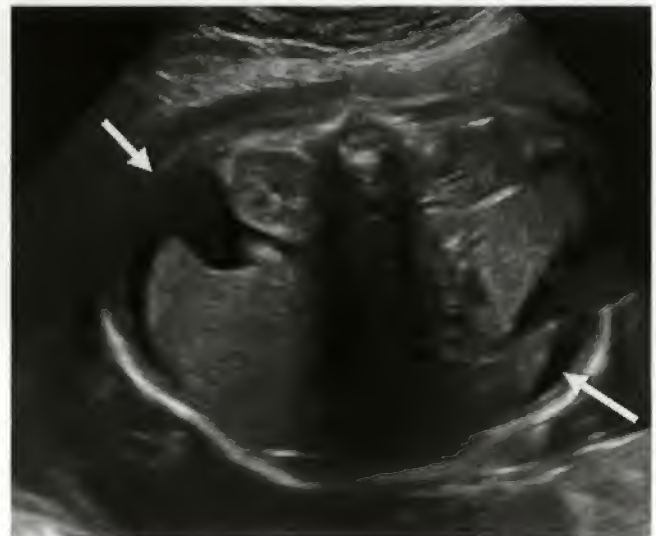


**FIGURE 17-5.** Cross-sectional view of the fetal abdomen at 32 weeks' gestation. Note ascites (arrows). Etiology: fetal cytomegalovirus infection.

hydrops fetalis (NIHF) due to a variety of etiologies. In this syndrome, maternal edema, rapid weight gain, mild proteinuria, and hypertension are noted. Although the condition shares many of the same clinical features of preeclampsia, the maternal intravascular volume appears to be expanded as opposed to the typical hemoconcentration seen with preeclampsia. Maternal hematocrit and albumin are low





**FIGURE 17-6.** Cross-sectional view of the fetal abdomen at 19 weeks' gestation. Note ascites (arrow). Etiology: trisomy 22. (Courtesy of Sharon Pinette, RDMS.)



**FIGURE 17-7.** Longitudinal section of the fetal abdomen (fetal head on left) at 19 weeks' gestation - same fetus as illustrated in Figure 17-6. Note ascites (arrow). Etiology: trisomy 22. (Courtesy of Sharon Pinette, RDMS.)

with minimal or no loss of urinary protein. Although the pathophysiology is unknown, hyperplacentosis is thought to be central to the cause. Reversal of maternal symptoms has been reported with the resolution of fetal hydrops after in utero treatment.<sup>5</sup> In other situations, the maternal condition worsens after correction of the hydropic fetal state owing to continued placentomegaly. In these cases, delivery is curative.



**FIGURE 17-8.** Longitudinal view of the fetal thorax and abdomen at 19 weeks' gestation (head on left of image). Note early ascites (arrows). Etiology: maternal RhD alloimmunization and resulting hemolytic disease of the fetus/newborn.

## IMMUNE HYDROPS

### Pathophysiology

The formation of maternal antibodies (red cell alloimmunization) to more than 40 different red cell antigens has been associated with severe fetal anemia (Table 17-1). The RhD (Rh<sub>0</sub>[D]) antigen is considered the most immunogenic of the antigens found on the surface of the human red blood cell.<sup>6</sup> In 1941, Levine, Katzin, and Burham<sup>7</sup> demonstrated that antibodies to the RhD antigen in pregnant women caused hemolysis and anemia in their offspring. Although this condition was originally called erythroblastosis fetalis secondary to the finding of a large number of immature red cells in the neonatal circulation, today it is known as hemolytic disease of the fetus and newborn (HDFN).

When RhD-positive fetal cells enter the maternal circulation as a result of pregnancy-related events such as miscarriage or delivery, anti-D antibody can be formed (Fig. 17-9). The administration of RhD immune globulin in these instances is effective in preventing the formation of anti-D antibody in more than 99% of cases. However, in rare cases, because of the inadvertent omission of the administration of immune globulin or improper dosing, the patient may become sensitized to the RhD antigen. Although the fetus that causes this alloimmunization is usually unaffected, transplacental passage of maternal anti-D antibodies in a subsequent pregnancy allows for their attachment to RhD-positive fetal red cells, resulting in the sequestration and destruction of these cells in the fetal spleen. Without treatment, this condition may lead to progressive anemia, excessive fluid collection in extracellular spaces (hydrops fetalis), and eventually fetal death. In milder cases, neonates may be born with only a minor degree of anemia, but the ongoing destruction of red cells results in hyperbilirubinemia. Unconjugated bilirubin then has the potential to enter the cerebral compartment and produce kernicterus.

Extramedullary hematopoietic sites are incorporated in the liver and spleen, resulting in enlargement of these organs.

**Table 17-1** Red Cell Antibodies and Associated Hemolytic Disease of the Fetus and Newborn

Antigen System	-Fy <sup>3</sup> Specific Antigen	Antigen System	-Jk <sup>3</sup> Specific Antigen	Antigen System	Specific Antigen
Frequently Associated With Severe Disease					
Rhesus	-D				
Kell	-K (K1)				
Infrequently Associated With Severe Disease					
Colton	-Co <sup>a</sup>	MNS	-Mr <sup>a</sup>	Rhesus	-HOFM
	-Co <sup>3</sup>		-MUT		-LOCR
Diego	-ELO		-Mur		-Riv
	-Di <sup>a</sup>		-M <sup>v</sup>		-Rh29
	-Di <sup>b</sup>		-s		-Rh32
	-Wr <sup>a</sup>		-s <sup>D</sup>		-Rh42
	-Wi <sup>b</sup>		-S		-Rh46
Duffy	-Fy <sup>a</sup>		-U		-STEM
Kell	-Js <sup>a</sup>	Rhesus	-Vw	Other Ags	-Tar
	-Js <sup>b</sup>		-Be <sup>a</sup>		-HJK
	-k (K2)		-C		-JFV
	-Kp <sup>a</sup>		-Ce		-JONES
	-Kp <sup>b</sup>		-C <sup>w</sup>		-Kg
	-K11		-C <sup>x</sup>		-MAM
	-K22		-ce		-REIT
	-Ku		-D <sup>w</sup>		-Rd
	-UI <sup>a</sup>		-E		
Kidd	-Jk <sup>a</sup>		-E <sup>w</sup>		
MNS	-En <sup>a</sup>		-Evans		
	-Far		-e		
	-Hil		-G		
	-Hut		-Go <sup>a</sup>		
	-M		-Hr		
	-Mi <sup>a</sup>		-Hr <sub>0</sub>		
	-Mit		-JAL		
Associated With Mild Disease					
Dombrock	-Do <sup>a</sup>	Gerbich	-Ge <sup>2</sup>	Scianna	-Sc2
	-Gy <sup>a</sup>		-Ge <sup>3</sup>	Other	-Vel
	-Hy		-Ge <sup>4</sup>		-Lan
	-Jo <sup>a</sup>		-Ls <sup>a</sup>		-At <sup>a</sup>
Duffy	-Fy <sup>b</sup>	Kidd	-Jk <sup>b</sup>		-Jr <sup>a</sup>

From Mari G, Deter RL, Carpenter RL, et al: Noninvasive diagnosis by Doppler ultrasonography of fetal anemia due to maternal red-cell alloimmunization. *N Engl J Med* 342:9, 2000.

Fetal hydrops does not occur until the fetal hemoglobin has fallen to below six standard deviations from the mean for gestational age.<sup>8</sup> In general, a small pericardial effusion represents the first extracellular compartment to exhibit excess fluid accumulation. This is followed by the onset of ascites and pleural effusions; scalp edema is a late manifestation. The early second trimester fetus may be severely anemic without demonstrating overt hydrops; rarely is the third trimester fetus anemic without hydrops being easily seen by ultrasound. This may be related to the significant reduction in normal fetal lymph flow that occurs with advancing gestational age.<sup>9</sup>

The exact mechanism of hydrops fetalis secondary to fetal anemia has not been well elucidated. Primary mechanisms that have been proposed include hypoproteinemia, myocardial failure, and lymphatic obstruction.

Hypoproteinemia has been suggested to occur owing to hepatic dysfunction with decreased production of serum proteins or owing to extravasation of proteins from the intravascular compartment secondary to endothelial damage. Iron overload due to hemolysis may contribute to free radical formation and endothelial dysfunction in HDFN.<sup>10</sup> De Groot et al<sup>11</sup> also noted decreased circulating levels of cGMP in fetuses with immune hydrops as compared to nonhydropic fetuses with only anemia. They proposed that this finding was related to endothelial cell damage in the hydropic fetuses. However, a study of 225 fetuses with HDFN noted that the serum albumin concentration was in the normal range in 71% of cases with hydrops.<sup>12</sup> The authors concluded that hypoalbuminemia is the unlikely cause of hydrops in immune-mediated cases. Moise et al<sup>13</sup> studied umbilical venous pressure as a surrogate for fetal



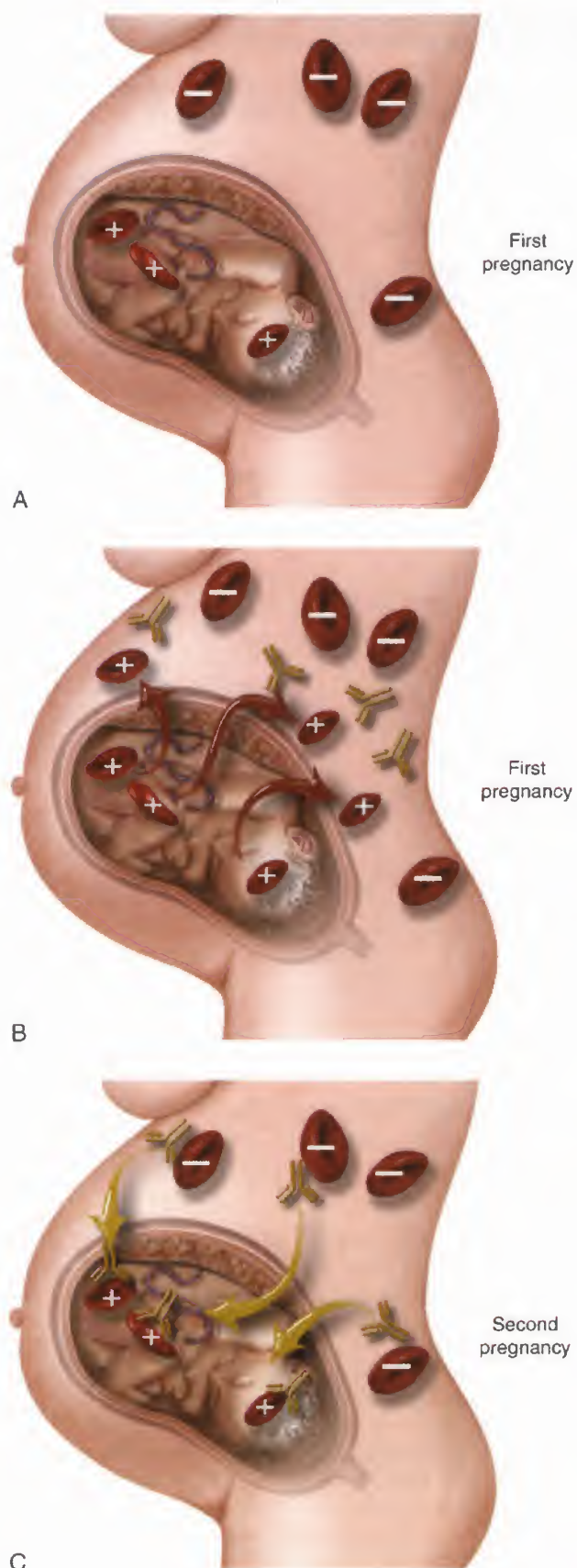


**FIGURE 17-9.** A. Initial pregnancy in which the mother is Rh negative and is carrying a fetus that is Rh positive. B. At the time of delivery, the fetal Rh positive red blood cells enter the maternal circulation and initiate an antibody response. C. In a subsequent pregnancy, antibodies enter the fetal circulation, attaching to the red blood cells and resulting in the sequestration and destruction of these cells. (Illustration by James A. Cooper, MD, San Diego, CA.)

central venous pressure (CVP) in cases of hydrops fetalis related to maternal red cell alloimmunization. They also evaluated colloid osmotic pressure (COP) at the time of the cordocentesis before intrauterine transfusion (IUT). These two important Starling forces that would contribute to the movement of fluid from the intravascular compartment to the extravascular space were therefore evaluated. Although the CVP-COP gradient was decreased in hydropic fetuses, a high venous pressure was the predominant abnormality. This led the authors to speculate that a high venous pressure was secondary to high-output cardiac failure in the anemic fetus. Such an increase in the venous pressure would cause a functional lymphatic blockade at the confluence of the right and left lymphatic duct systems and the corresponding brachiocephalic veins. Animal studies have indicated that for each 1-mm increase in venous pressure, there is a 17% reduction in lymphatic flow.<sup>14</sup> This theory is supported by the clinical observation that blood transfused into the peritoneal cavity of the hydropic fetus is not readily absorbed.<sup>15</sup>

### Significance of Detection of Immune-Mediated Hydrops

The fetus with hydrops fetalis secondary to maternal red cell alloimmunization represents a true challenge in perinatal management. Often this situation is the result of late entry into prenatal care; less commonly, it is secondary to late referral to perinatal centers experienced with the early detection of fetal anemia. The hydropic fetus represents end-stage disease in HDFN and is associated with a worse prognosis than if hydrops is absent. In one series of 213 fetuses undergoing 599 IUTs, the absence of hydrops or the presence of only mild hydrops was associated with a 98% rate of perinatal survival.<sup>16</sup> Severe hydrops was associated with a 55% survival rate. Clearly, the goal of optimal management of HDFN should be the early detection of fetal anemia before the advent of hydrops.

### Evaluation of the Sensitized Pregnancy

#### Maternal Antibody Measurement

The typical fetus becomes at risk for anemia once a maternal antibody screen (indirect Coombs) is determined to be positive for a red cell antibody that has been associated with HDFN. Maternal indirect Coombs titers are used to assess the degree of risk for fetal disease. Maternal antibody determinations are usually repeated at 4-week intervals in the first and second trimester and every 2 weeks in the third trimester. A critical value is considered the threshold level of antibody associated with fetal hydrops. Most centers use a titer value between 8 and 32 (dilution: 1:8 and 1:32) for both anti-D and other antibodies that cause HDFN as their definition of a critical value. The one notable exception to this is anti-K (Kell, K1) antibody. This particular antibody causes fetal anemia through two different mechanisms; sequestration of sensitized fetal red cells in the spleen and bone marrow suppression.<sup>17</sup> For this reason, a critical value of 8 (dilution 1:8) is often used for the Kell antibody. Once a patient is found to have a critical antibody titer, fetal testing is indicated.

### Fetal Antigen Testing

Paternal evaluation is the next step in management. If the patient's partner is negative for the particular red cell antigen involved and paternity is assured, then further evaluation of the fetus is unnecessary. In other cases, paternal phenotype testing using serology will reveal a heterozygous state. With the advent of the cloning of many of the genes responsible for the blood group antigens associated with HDFN, amniocentesis can be performed to obtain fetal DNA. Polymerase chain reaction (PCR) primers can then be used to determine the blood type of the fetus. This approach is now available for the D, C/c, E/e, and Kell (K1)/cellano (K2)/JK<sub>Fy</sub>/Fy<sub>M/N</sub>, S/s antigens. Typically, a reference laboratory will require a sample of maternal blood as a negative control and paternal blood as a positive control. If the fetus is noted to be negative for the involved red cell antigen, then no further testing is necessary. If the fetus is found to be positive, serial evaluation is needed (see later). Results of PCR testing on amniotic fluid that indicate an antigen-negative fetus should be viewed with some degree of suspicion when paternity is not assured or the patient's partner is not available for testing. In rare cases, a paternal gene rearrangement could lead to an incorrect correlation between fetal serology (phenotype) and PCR (genotype) results on amniotic fluid. In one review of 500 cases of amniotic fluid typing for the fetal RhD antigen, this rate of error was reported to be 1.3%.<sup>18</sup> Two fetuses died, one neonate required exchange transfusions, another neonate needed phototherapy in conjunction with a simple transfusion, and the remaining infant was lost to follow-up. Many laboratories have turned to the use of multiplex PCR in an effort to reduce this possibility for error. Another strategy that has been suggested when the fetus is determined to be antigen negative by PCR and paternity is in question is to repeat the maternal titer in 6 weeks. A rising maternal titer (more than a two-dilution increase) should make the fetal PCR typing suspect. Cordocentesis for direct acquisition of fetal blood for serologic typing should be considered in these cases.

Clearly, a noninvasive technique for determining the fetal red cell antigen status would negate the risk of fetal loss and enhanced maternal sensitization associated with amniocentesis. Lo et al<sup>19</sup> were the first to describe the use of free fetal DNA found in maternal plasma for fetal RhD typing. Several large series have confirmed the accuracy of this test.<sup>20,21</sup> Free DNA RhD typing is now routinely employed in clinical practice in the United Kingdom and Europe. Unfortunately, the test is not yet available for clinical use in the United States. Free DNA testing can currently only be used for fetal RhD typing. Assays for RhC and Kell typing are being developed.

### Diagnosis of Fetal Anemia

Once the fetus is determined to be antigen positive in association with a critical maternal titer, there are two approaches that are used to predict fetal anemia. The more traditional approach has been to employ serial amniocenteses to measure the bilirubin in the amniotic fluid through the  $\Delta OD_{450}$  assay. This approach has been virtually replaced by the use of serial assessments using Doppler ultrasound (discussed below).



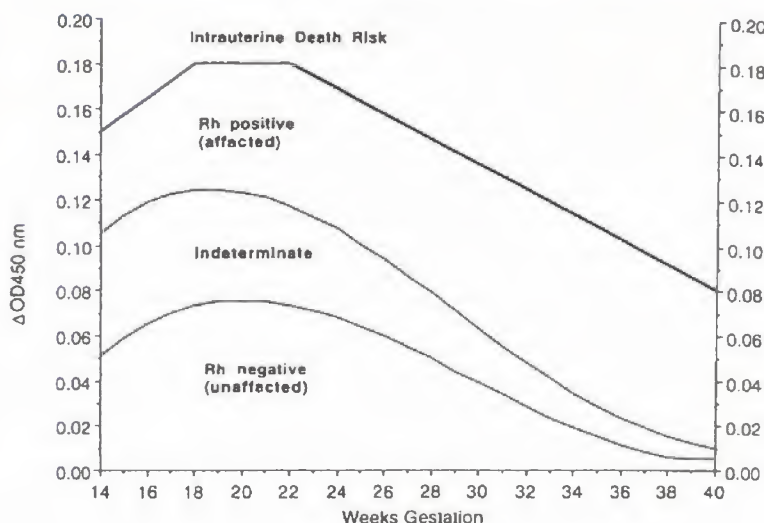


**FIGURE 17-10.** Queenan curve for  $\Delta OD_{450}$  between 14 and 40 weeks' gestation.

### Amniocentesis

Amniotic fluid bilirubin has been used for more than four decades as an indirect measure of the degree of fetal hemolysis. Immune-mediated red cell destruction results in the release of free hemoglobin into the fetal circulation. This is then metabolized to bilirubin, which gains access to the amniotic cavity predominantly through the egress of tracheal fluid. Fluid is analyzed by spectrophotometry and a baseline measurement is established between 365 and 550 nm. The peak of the optical density reading at 450 nm is then subtracted from this baseline to calculate the  $\Delta OD_{450}$ . This value is then plotted on a normative curve for gestations of greater than 27 weeks consisting of three zones known as the Liley curve.<sup>22</sup> Values in zone one are indicative of minimal fetal hemolytic disease, whereas values in zone 3 indicate severe disease with the potential for fetal death without intervention. Confidence was lost in this method when Nicolaides et al<sup>23</sup> reported that "modified" Liley curves extrapolated to gestational ages of less than 27 weeks missed 70% of anemic fetuses between 18 and 25 weeks' gestation. Queenan et al<sup>24</sup> subsequently published normal  $\Delta OD_{450}$  values between 14 and 40 weeks' gestation based on 520 unaffected pregnancies (Fig. 17-10). A recent study compared the Liley curve with that of Queenan and noted that the latter was associated with improved accuracy for the detection of severe fetal anemia.<sup>25</sup>

Amniocentesis can be initiated as early as 18 weeks' gestation using the Queenan curve. Procedures are repeated at 1- to 2-week intervals based on the initial value of the  $\Delta OD_{450}$  and subsequent trends. All attempts should be made to avoid a transplacental puncture so as to avert an anamnestic response and resultant worsening fetal hemolytic disease. Amniocenteses should be continued until fetal lung maturity is documented, at which time induction of labor would appear to be a more reasonable approach than continued amniocenteses. Cordocentesis should be undertaken with blood readied IUT when the  $\Delta OD_{450}$  value reaches the upper portion of the *Rh-positive, affected* zone.

### Middle Cerebral Artery Doppler

The peak systolic velocity of blood moving through various fetal vessels has been investigated as a method of determining when the fetus is developing anemia. This concept is based on animal data indicating that fetal blood velocities become elevated in response to an increase in cardiac output and a decline in blood viscosity when the fetus becomes anemic. Initial reports using such fetal vessels as the umbilical vein, descending thoracic aorta, and common carotid artery were disappointing in the prediction of fetal hematocrit.

Mari and coworkers<sup>26</sup> are credited with the first description of using the peak systolic velocity in the middle cerebral artery to detect fetal anemia. Because the normal peak systolic velocity in this vessel increases with advancing gestational age, the value in centimeters/second must be converted to multiples of the median (MoMs; Fig. 17-11 and Table 17-2). These authors established a normogram for fetal hemoglobin from 265 normal fetuses that had undergone cordocentesis for a variety of diagnostic indications. Mild anemia was defined as 0.84 to 0.65 MoM for gestational age, moderate anemia was 0.65 to 0.55 MoM, and severe anemia less than 0.55 MoM. One hundred eleven at-risk fetuses whose mothers were alloimmunized predominantly to RhD were then evaluated prospectively. An middle cerebral artery (MCA) velocity of greater than 1.50 MoMs detected all cases of moderate to severe anemia with a 10% false-positive rate. In a prospective study performed at 10 centers, Oepkes et al<sup>25</sup> followed 165 fetuses with both MCA Doppler and amniocentesis for  $\Delta OD_{450}$ . MCA Doppler was determined to be more accurate than amniocentesis in detecting severe fetal anemia (sensitivity: 88%, specificity: 82%).

Fetal MCA velocity determinations can be initiated as early as 18 weeks' gestation once the fetus is at risk for the development of anemia. Doppler studies are repeated every 1 to 2 weeks based on the trend in the data. The false-positive rate for the prediction of fetal anemia increases after 35 weeks' gestation.<sup>27</sup> Color flow or power Doppler is used

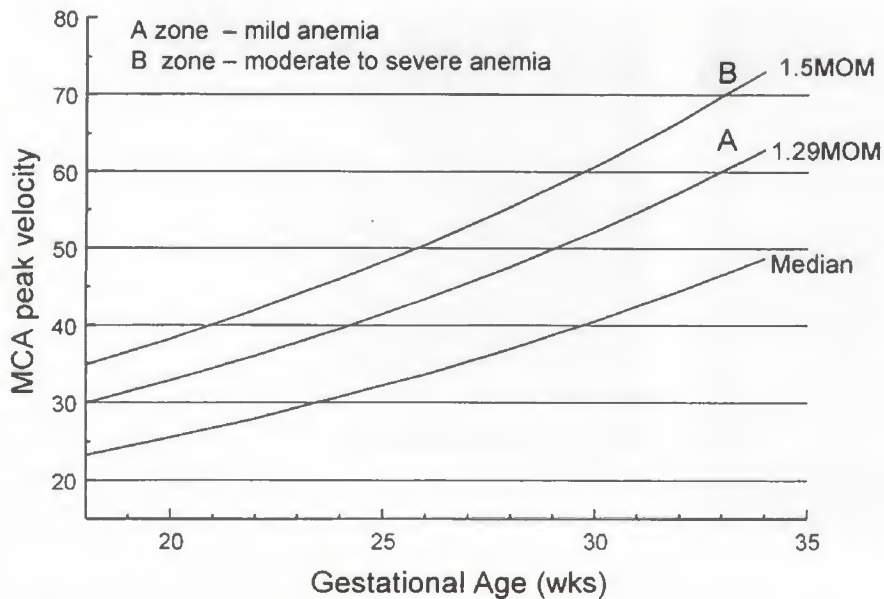


**FIGURE 17-11.** Normogram for mild anemia (1.29 MoMs) and moderate-severe anemia (1.5 MoMs). Zone A values, mild anemia; zone B values, moderate to severe anemia. MoM, multiple of median.

**Table 17-2**

**Expected Peak Velocity of Systolic Blood Flow in the Middle Cerebral Artery as a Function of Gestational Age**

Week of Gestation	Multiples of the Median			
	1.00 (Median)	1.29	1.50	1.55
Peak Velocity in cm/sec				
18	23.2	29.9	34.8	36.0
20	25.5	32.8	38.2	39.5
22	27.9	36.0	41.9	43.3
24	30.7	39.5	46.0	47.5
26	33.6	43.3	50.4	52.1
28	36.9	47.6	55.4	57.2
30	40.5	52.2	60.7	62.8
32	44.4	57.3	66.6	68.9
34	48.7	62.9	73.1	75.6
36	53.5	69.0	80.2	82.9
38	58.7	75.7	88.0	91.0
40	64.4	83.0	96.6	99.8

From Mari G, Deter RL, Carpenter RL, et al: Noninvasive diagnosis by Doppler ultrasonography of fetal anemia due to maternal red-cell alloimmunization. *N Engl J Med* 342:9, 2000.

to locate the MCA over the anterior wing of the fetal sphenoid bone (Figs. 17-12 and 17-13). All attempts are made to place the Doppler gate in the proximal portion of the MCA just distal to its origin from the carotid siphon. The angle of insonation is kept as close to zero as possible (i.e., the Doppler beam is “end-on” with the vessel); angle correction using computerized software is not used. The MCA closest to the ultrasound transducer is usually used because it is easier to visualize. However, the MCA in the far field has been shown to give equivalent results when the angle of insonation is minimal.<sup>28</sup> Doppler measurements should be undertaken during a period of fetal apnea and absent fetal movement. A manual measurement of the peak velocity is preferred over real-time software-based assessment

of the velocity. A value of greater than 1.5 MoMs is indicative of fetal anemia and warrants further investigation with cordocentesis to determine the fetal hematocrit.

### Choice of Surveillance Method

A growing body of evidence supports the use of serial MCA Doppler over amniocentesis for the detection of fetal anemia in the at-risk fetus. Previous experience has indicated that a significant learning curve exists for the accurate measurement of the MCA Doppler.<sup>29</sup> For this reason, referral centers should consider performing MCA Doppler scans in conjunction with serial amniocenteses for  $\Delta OD_{450}$  until expertise has been achieved. In addition, referral to a distant perinatal





**FIGURE 17-12.** Anterior and middle cerebral artery (arrow) using color flow Doppler for localization. (Courtesy of Anthony Swartz, BS, RT(R), RDMS.)



**FIGURE 17-13.** Middle cerebral artery assessment at 19 weeks' gestation. Top image illustrates power Doppler localization of the proximal MCA vessel. Note Doppler gate location. Peak systolic velocity on lower image was measured at 52.42 cm/sec; 1.87 MoMs for this gestational age. (Courtesy of Anthony Swartz, BS, RT(R), RDMS.)

center with experience in Doppler may not be practical for weekly testing. In such cases, serial amniocenteses may be a valid tool for following these pregnancies.<sup>6</sup>

## Overall Management

First sensitized pregnancy or pregnancy with a history of a minimally affected neonate (a pregnancy that was monitored with serial maternal titers, MCAs or amniocenteses and the fetus and neonate did not require transfusions) (Fig. 17-14):

- Follow maternal titers every 4 weeks up to 24 weeks' gestation; repeat every 2 weeks thereafter.
- Once a critical value is reached (usually 32; 8 for anti-Kell), begin serial MCA Doppler scans as early as 18 weeks' gestation. Alternatively, initiate amniocentesis every 10 days to 2 weeks for  $\Delta OD_{450}$  using the Queenan curve.
- In cases of a heterozygous paternal phenotype, perform amniocentesis by 24 weeks to determine the fetal antigen status. Send maternal and paternal blood samples with the amniotic fluid. If an antigen-negative fetus is found, no further testing is warranted.
- Begin antenatal testing at 32 weeks' gestation, with twice-weekly biophysical profiles.
- If the MCA Doppler is greater than 1.5 MoMs or the  $\Delta OD_{450}$  value enters the upper portion of the *Rh positive (affected)* zone of Queenan curve, perform cordocentesis with blood readied for IUT for a fetal hematocrit of less than 30%.
- If repeat MCA velocities remain less than 1.5 MoMs, consider induction at 37 to 38 weeks' gestation. If the MCA velocity is greater than 1.5 MoMs at more than 35 weeks' gestation, perform amniocentesis for  $\Delta OD_{450}$  and fetal lung maturity. If mature and the  $\Delta OD_{450}$  value is not in the upper, *Rh positive (affected)* zone, induce delivery in 2 weeks. If the fetal lungs are noted to be immature and the  $\Delta OD_{450}$  value is in the upper, *Rh positive (affected)*

zone, consider administering 7 days of maternal phenobarbital (30 mg PO TID) to enhance fetal hepatic maturity.<sup>30</sup> Induce labor in 1 week. If fetal lung immaturity is noted and the  $\Delta OD_{450}$  value is not in the upper, *Rh positive (affected)* zone, repeat the amniocentesis in 2 weeks.

- If using serial  $\Delta OD_{450}$  values and these remain below the *Rh positive (affected)* zone, perform the last amniocentesis at 37 weeks. If mature and the  $\Delta OD_{450}$  value is not in the upper, *Rh positive (affected)* zone, induce delivery in 1 to 2 weeks. If immature lungs and the  $\Delta OD_{450}$  value is in the upper, *Rh positive (affected)* zone, consider administering 7 days of maternal phenobarbital (30 mg PO TID) to enhance fetal hepatic maturity.<sup>30</sup> Induce labor in 1 week.
- *Previously affected fetus or infant (fetus needed IUTs or neonate required exchange transfusions)* (Fig. 17-15):
- Maternal titers are *not* helpful in predicting the onset of fetal anemia after the first affected gestation.
- In cases of a heterozygous paternal phenotype, perform amniocentesis at 15 weeks' gestation to determine the fetal RhD status. If an RhD-negative fetus is found, no further testing is warranted.
- Begin serial MCA Doppler assessment or amniocenteses for  $\Delta OD_{450}$  (Queenan curve) at 18 weeks' gestation. Repeat at 1- to 2-week intervals.
- Remainder of protocol is similar to the first affected pregnancy.

## Intrauterine Transfusion

### Method

The majority of IUTs are undertaken through ultrasound-directed needle puncture of the umbilical cord at its insertion into the placenta or by puncture of the intrahepatic portion of the umbilical vein. After an initial fetal blood sample is obtained to determine the hematocrit, an intravenous dose of a paralytic agent is administered to reduce

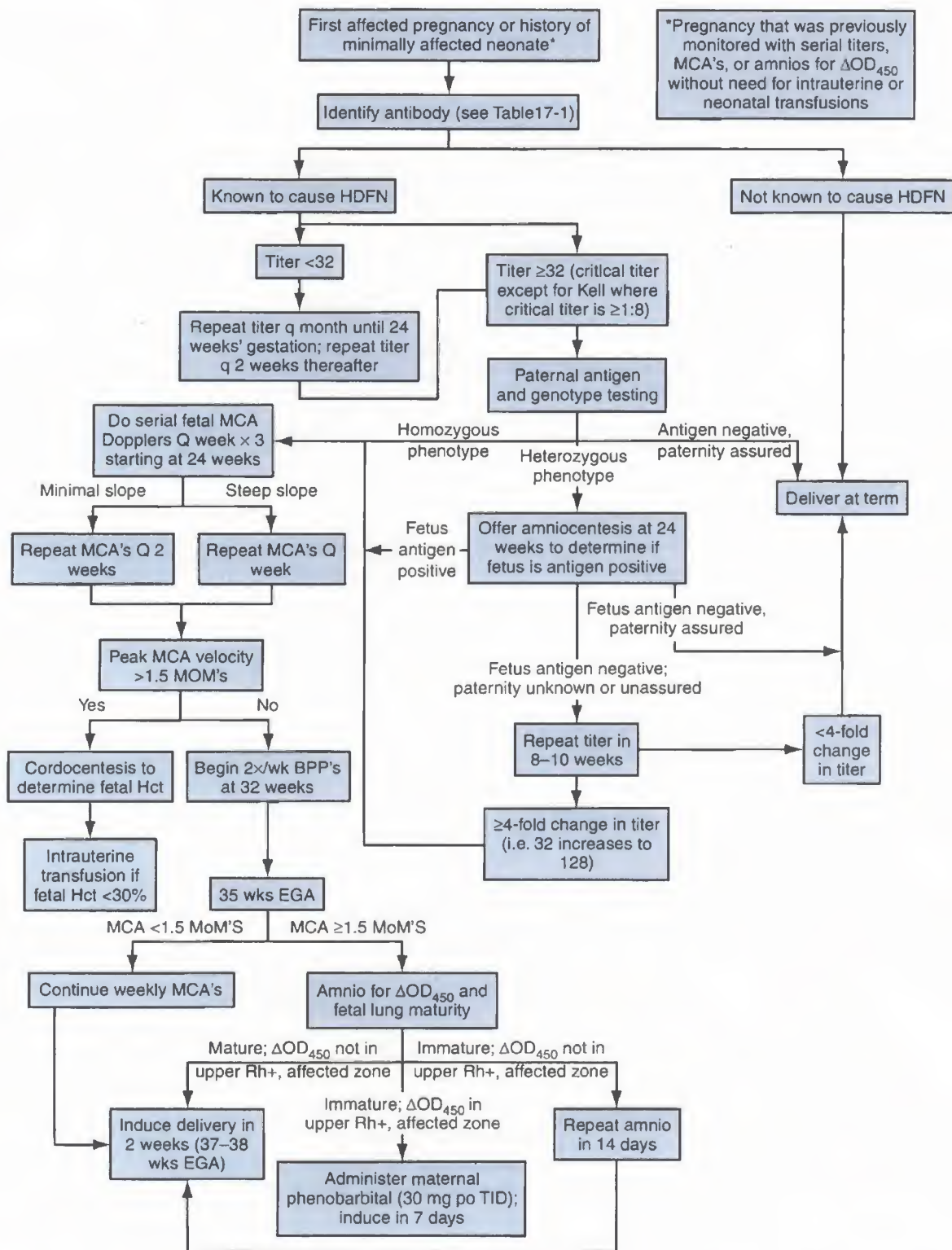


**FIGURE 17-14.** Algorithm for the management of the first affected pregnancy in a red blood cell alloimmunized patient. This algorithm can also be used in the patient with a previous alloimmunized pregnancy with a minimally affected neonate, that is, the pregnancy was followed with serial maternal antibody titers or serial amniocenteses for  $\Delta OD_{450}$  or middle cerebral artery Doppler scans. The fetus and neonate should not have required transfusion therapy.



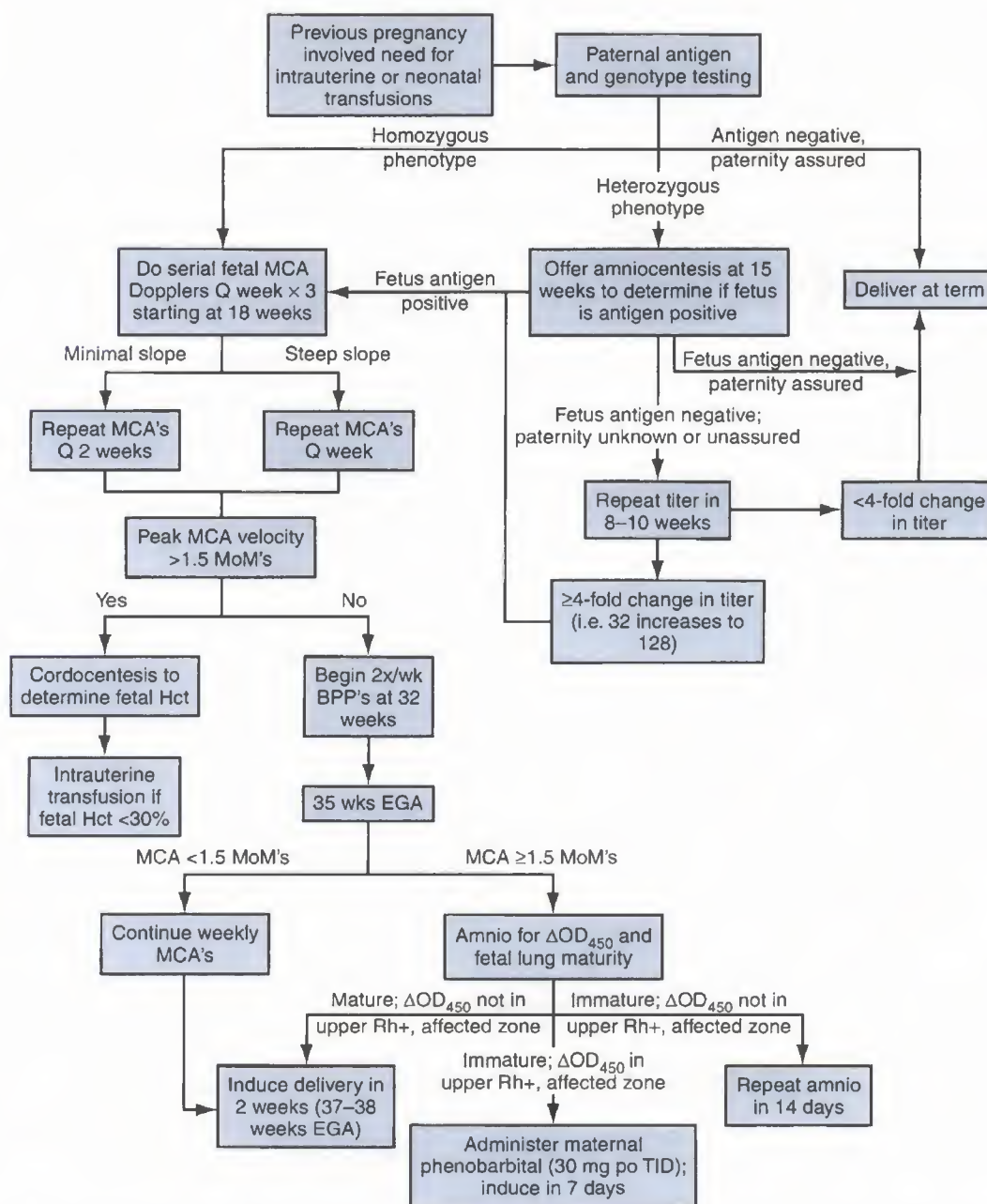


**FIGURE 17-15.** Algorithm for the management of a subsequent alloimmunized pregnancy when the previous fetus/infant required intrauterine and/or neonatal transfusions.



**FIGURE 17-16.** Packed red blood cells seen streaming in the fetal umbilical vein (arrow) at the time of an intravascular transfusion at 26 weeks' gestation. The cord insertion into the anterior placenta is located at the asterisk.

interference from fetal movement.<sup>31</sup> Tightly packed donor red cells (hematocrit 78% to 80%) are then infused. Streaming of the dense cells down the umbilical vein can be seen with real-time ultrasound (Fig. 17-16). Various formulas based on fetal weight estimated by ultrasound can be used to determine the volume of red cells to infuse. A final sample of blood is then submitted for fetal hematocrit.

A decline in fetal hematocrit of approximately 1% per day can be expected between procedures. In an effort to allow for a reasonable interval between IUTs, many centers transfuse to a final hematocrit value of 50% to 65%. Other centers employ an combined approach of first performing an intravascular transfusion (IVT), followed by an intraperitoneal infusion (IPT) of red cells.<sup>32</sup> The latter allows for slow absorption at a rate of approximately 10% per day and results in a more stable hematocrit between procedures. Subsequent IUTs are scheduled at 14-day intervals until suppression of fetal erythropoiesis is noted on Kleihauer-Betke stains. This usually occurs by the third IUT. Thereafter, the interval for repeat procedures can be determined based on the decline in hematocrit for the individual fetus, usually a 3- to 4-week interval.

When IPTs were used as the sole means of in utero therapy, fetuses were routinely delivered at 32 weeks' gestation. Hyaline membrane disease and the need for neonatal exchange transfusions for the treatment of hyperbilirubinemia were common. As experience with IVT became widespread, pregnancies were delivered at later gestational ages. It now appears reasonable to perform the final IUT as late as 35 weeks' gestation, with delivery anticipated at 37 to 38 weeks.<sup>33</sup> Maternal oral phenobarbital (30 mg TID) administered approximately 10 days before delivery can be given to enhance the neonate's ability to conjugate bilirubin and has negated the need for exchange transfusions after birth.<sup>30</sup>

The transfusion of the hydropic fetus requires several special considerations. It is generally accepted that hydrops fetalis is associated with poor absorption of red blood cells from the peritoneal cavity.<sup>15</sup> Harman et al<sup>34</sup> compared the experience at one referral center with IVT and IPT techniques for the treatment of the hydropic fetus using historic controls. Survival of the hydropic fetus was improved from 48% with IPT to 86% with IVT. Therefore, it would appear that IVT should be the primary modality for the management of the hydropic, anemic fetus. The severely anemic fetus in the early second trimester does not tolerate the acute correction of its hematocrit to normal values.<sup>35</sup> In these situations, the initial hematocrit should not be increased by more than fourfold at the time of the first procedure.<sup>36</sup> A repeat IVT is then performed within 48 hours to correct the fetal hematocrit into the normal range.

### The Patient With Recurrent Immune Hydrops Fetalis

The patient who presents with recurrent immune hydrops fetalis at less than 20 weeks' gestation represents a true perinatal challenge. Technical limitations make umbilical cord puncture difficult. On occasion, an intraperitoneal transfusion can be attempted before the overt development of hydrops; however, formulas for calculating the correct volume for transfusion do not exist. Plasmapheresis has been suggested as a modality that may have a role in the treatment of severe HDFN. Although acute declines in maternal antibody titer are achieved, a rebound to even higher antibody levels usually occurs. Intravenous immune globulin (IVIG) is another treatment modality that has generated extreme interest for the treatment of severe fetal hemolytic disease. Several mechanisms of action have been postulated including decrease of maternal antibody levels through anti-idiotypic suppression, blockade of the placental Fc receptor sites, and fetal reticuloendothelial blockade. Voto and coworkers<sup>37</sup> compared the outcome of 30 patients receiving IVIG before 20 weeks' gestation followed by IUTs after 20 weeks to a group of 39 patients treated with only IUTs between 20 and 25 weeks' gestation. Hydrops fetalis was less frequent in the IVIG/IUT group as compared with the IUT-only group (27% versus 74%; relative risk [RR], 0.36). In addition, the incidence of fetal death was markedly decreased with the addition of IVIG (20% versus 51%; RR, 0.39). These data would suggest that both plasmapheresis and IVIG could play a role in the prolongation of pregnancy until IUT can be initiated. Ruma et al<sup>38</sup> used a combined treatment program of plasmapheresis and IVIG in patients with a history of recurrent early second trimester hydrops fetalis or an extremely elevated maternal anti-red cell titer. Patients underwent a single-volume plasmapheresis every other day for three procedures at 10 to 12 weeks' gestation. After the third procedure, the first half of a 2-g/kg loading dose of IVIG was administered. The following day, the second half of the loading dose (1g/kg) of IVIG was given. The patients were then maintained on a weekly infusion of 1 g/kg of IVIG until 20 weeks' gestation. IUTs were initiated when an elevation in the MCA velocity was detected. All nine pregnancies resulted in a live-born infant. The authors concluded that their combined immunomodulation was



effective in prolonging gestation until successful IUTs could be undertaken in these select pregnancies.

## Prognosis

Serial intravascular IUTs inevitably result in fetal bone marrow suppression. Typically, these infants are born with a virtual absence of circulating reticulocytes with a red cell population consisting mainly of transfused red cells containing adult hemoglobin. Exchange neonatal transfusions for hyperbilirubinemia are rarely necessary allowing for significant maternal anti-red cell antibodies to remain in the neonatal circulation. Early neonatal reticulocytosis is therefore depressed and often by 4 to 6 weeks of age, these neonates require a "top-up" transfusion owing to symptoms associated with anemia. These infants should be followed with weekly hematocrits and reticulocyte counts. Most infants require only one transfusion, although the requirement for up to three transfusions has been reported.<sup>39</sup> Neonatal erythropoietin injections have met with mixed results because persistent maternal antibodies in the neonate probably are the major factor for the lack of circulating reticulocytes.<sup>40</sup> Supplemental iron is unnecessary because iron stores are elevated in these children as a result of in utero hemolysis and replacement of red cells with donor blood from serial IUTs.

Investigations regarding the long-term neurologic evaluation of infants that have been treated with IVTs are limited. Neurologic outcome in cases of hydrops fetalis is similar to that of the nonhydropic fetus.<sup>41</sup> Cerebral palsy and developmental delay are more common in fetuses with HDFN when compared with unaffected infants, although a normal outcome can be expected in more than 90% of cases.<sup>42</sup> A review of the cases of cerebral palsy reveals that the mean gestational age at delivery was 33.5 weeks; 80% of cases were delivered by emergency cesarean section. Sensorineural hearing loss is more frequent in infants affected by HDFN, probably because of their prolonged exposure to elevated levels of bilirubin and its toxic effect on the developing eighth cranial nerve.<sup>41</sup>

## NONIMMUNE HYDROPS

### Incidence

NIHF has been reported to occur in approximately 1 in 3000 pregnancies.<sup>43</sup>

### Etiology

More than 120 causes of NIHF have been reported (Table 17-3). In a review of almost 800 cases, Machin<sup>43</sup> noted that fetal cardiovascular disease was the leading cause of NIHF, accounting for one quarter of cases. This category included structural cardiac lesions, arrhythmias, and high-output failure related to large fetal tumors. The second highest category was chromosomal abnormalities (10% of cases), followed by thoracic lesions (9%), twin-to-twin transfusion (8%), nonimmune causes of fetal anemia (6%), and fetal infection (4%). A variety of other etiologies comprised the remaining 24% of cases; 22% of cases were considered idiopathic.

## Pathophysiology

Because the etiology of NIHF is so diverse, few studies have addressed the pathophysiology of this condition. Weiner<sup>44</sup> has proposed that three possible mechanisms may play a role—inadequate cardiac output, structural lymphatic obstruction, and hypoproteinemia. Decreased cardiac output can be the result of regurgitant intracardiac flows owing to the abnormal structure of valves (example: Ebstein anomaly), obstruction to preload or afterload based on intrathoracic lesions (example: chylothorax), or poor myocardial contractility (adenovirus-induced myocarditis). Structural lymphatic obstruction can occur in Turner or Noonan syndrome. Various congenital infections may lead to endothelial damage (increased capillary permeability) and loss of intravascular proteins (example: cytomegalovirus).

In a series of 20 fetuses with NIHF, umbilical venous pressure was elevated at the time of cordocentesis in 65% of the cases.<sup>44</sup> Correction of some of the lesions resulted in normalization of the venous pressure on subsequent measurements, which were accompanied by resolution of the hydrops. These authors concluded that an elevated umbilical venous pressure signaled inadequate cardiac output as the cause of the NIHF. Normalization of the venous pressure after correction of the fetal condition invariably resulted in perinatal survival.

## Evaluation

The initial diagnosis of hydrops fetalis is often made at the time of a routine ultrasound examination. Generalized skin edema is often the first feature of fetal hydrops revealed by ultrasound in early pregnancy.<sup>45</sup> Skin edema is best and most clearly observed at the level of the fetal head and more specifically at the back of the neck. This is the rationale for the measurement of the nuchal translucency. At other times, the patient complains of a decrease in fetal movement or a rapid increase in weight gain or abdominal girth, which are signs of significant polyhydramnios.

A comprehensive ultrasound examination should be undertaken. Special emphasis should be placed on evaluation of cardiac structures and rhythm. If necessary, a fetal echocardiogram should be undertaken. A decrease in cardiac output with right atrial overload is likely the primary cause in most cases of early hydrops fetalis. Inadequate cardiac output can be due to a major cardiac anomaly such as atrioventricular septal defect, fast ventricular rate with suboptimal filling of the ventricles, or cardiomyopathy.<sup>45</sup>

The sonographic finding of pericardial fluid has been somewhat controversial. Initially, the finding of any pericardial fluid was believed to be abnormal.<sup>46</sup> Subsequently, numerous investigators have evaluated pregnancies prospectively for this finding.<sup>47-49</sup> These investigators have determined that in the absence of cardiac structural or rhythm abnormalities, suspected anemia, viral infections, or suspected chromosomal abnormalities, the finding of 2 mm or less of pericardial fluid is a normal finding.

As was mentioned earlier, although ascites may be an early finding of hydrops in fetuses with conditions known to progress to hydrops (e.g., HDFN, sacroccoccygeal teratoma, and so on), the finding of ascites in the presence of urinary and gastrointestinal tract abnormalities should not be considered an early sign of hydrops.

**Table 17-3** Causes and Associations of Nonimmune Hydrops

Cause	Frequency*
Focal Abnormalities	
<i>Cranial</i>	
Fetal intracranial hemorrhage	Low
Vein of Galen aneurysm	Low
Cerebral tumor	Low
<i>Thorax</i>	
Cardiac structural defects	
AV septal defect, isolated or in association with Down syndrome	Low
AV septal defect in combination with heterotaxia syndrome (sinus ambiguous, left atrial isomerism, right atrial isomerism) and bradyarrhythmia	High
Tricuspid dysplasia and Ebstein's anomaly	Low
Severe obstruction of right ventricular outflow tract by pulmonary stenosis, pulmonary atresia, and premature obstruction of the ductus arteriosus (spontaneously or with indomethacin)	Low
Absent pulmonary valve syndrome (mostly combined with tetralogy of Fallot or agenesis of the ductus arteriosus)	Low
Truncus arteriosus communis with truncal valve insufficiency	Low
Premature closure of the foramen ovale	
Unknown	
Severe obstruction of left ventricular outflow tract by aortic stenosis and atresia leading to interatrial left-to-right shunt or premature closure of foramen ovale	Low
Cardiac tumors	
Rhabdomyoma often as part of tuberous sclerosis	Low
Hemangioma	
Hamartoma	
Intrapericardial teratoma	
Cardiomyopathy	
Dilated	
Restrictive	
Myocarditis	
Myocardial infarction	
Idiopathic arterial calcification	High
Arrhythmias	
Tachyarrhythmias	High
Supraventricular tachycardia	
Atrial flutter	
Ventricular tachycardia	
Bradyarrhythmias	
Sinus bradycardia	Low
Complete heart block	
Combined with atrial isomerism and structural defect (see above)	High
In presence of maternal autoimmune antibodies (anti-SSA, anti-SSB)	Low
Pulmonary and mediastinal	
Primary uni- or bilateral hydro-/chylothorax	High
CCAM	
Macrocytic CCAM	High
Microcystic CCAM	Low
Extralobar pulmonary sequestration	High
Laryngeal atresia (CHAOS)	
Mediastinal teratoma	
Fibrosarcoma	
Intrathoracic alimentary tract duplication cyst	
Diaphragmatic hernia	Low
Pulmonary lymphangioectasia	
<i>Gastrointestinal</i>	
Diaphragmatic hernia	Low
Meconium peritonitis caused by bowel perforation; spontaneous bowel obstruction (various types of atresia of the intestinal tract, volvulus), or infection	Low
Intestinal hemorrhage caused by bowel perforation	Low
Hepatitis	
Hepatic fibrosis	

Continued



**Table 17-3** Causes and Associations of Nonimmune Hydrops—cont'd

Cause	Frequency*
Hemachromatosis	
Cholestasis	
Cirrhosis with portal hypertension	
Congenital portal dysplasia	
Polycystic disease of liver	
Giant coli hepatitis	
Torsion of ovarian cyst	
<i>Renal</i>	
Congenital nephrosis (Finnish type)	Low
Urethral obstruction with rupture of bladder	Low
Polycystic kidney diseases (ARCKD, ADCKD)	Low
Renal vein thrombosis	
<i>Tumor and Vascular Disorders</i>	
Teratoma (sacroccocygeal, mediastinal, intracerebral, intrapericardial)	Low
Mediastinal fibrosarcoma	
Disseminated congenital neuroblastoma	
Hepatoblastoma	
Hamartoma	
Mesoblastic nephroma	
AVM	
Fetal hemangioma (liver, neck, chest)	Low
Diffuse neonatal hemangiomatosis	High
Klippel-Trenaunay-Weber syndrome	Low
Umbilical cord hemangioma	Low
Chorioangioma	Low
Vena cava inferior thrombosis	
Renal vein thrombosis	
Idiopathic arterial calcification	High
Generalized Abnormalities	
<i>Hematologic Disorders Causing Fetal Anemia</i>	
Excessive erythrocyte loss	
Intrinsic hemolysis or abnormal hemoglobins	
$\alpha$ Thalassemia	High
Erythrocyte enzyme disorders; glucose-6-phosphate dehydrogenase deficiency, pyruvate kinase deficiency, glucose phosphate isomerase deficiency	Low
Erythrocyte membrane disorders; abnormalities of spectrin	Low
Extrinsic hemolysis	
Kasabach-Merritt sequence (AVMs) and tumors	
Hemorrhage	
Fetomaternal hemorrhage	High
Fetal closed-space hemorrhage (bowel, intracranial, tumor)	Low
Twin-to-twin transfusion (including acardiac parasitic twin)	Low
Erythrocyte underproduction	
Liver and bone marrow replacement syndromes	
Transient myeloproliferative disorder	
Congenital leukemia	
Red cell aplasia and dyserythropoiesis	
Parvovirus B19 infection	High
Blackfan-Diamond syndrome	Low
Dyserythropoietic anemia (types I and II)	Low
<i>Infectious Causes</i>	
Parvovirus B19	High
Cytomegalovirus	Low
Syphilis	Low
Toxoplasmosis	Low
Herpes simplex virus	Low
Adenovirus	Low
Coxsackievirus	Low

Continued

**Table 17-3** Causes and Associations of Nonimmune Hydrops—cont'd

Cause	Frequency*
Varicella	Low
Hepatitis A	Low
Rubella	Low
Respiratory syncytial virus	Low
Listeriosis	Low
Chagas disease	Low
Leptospirosis	Low
<i>Skeletal Dysplasias</i>	Low
Achondrogenesis types I and IA	
Achondrogenesis, Langer-Saldino	
Short rib-polydactyly syndromes	
Salino-Noonan	
Majewski	
Verma-Naumoff	
Beemer	
Osteogenesis imperfecta type II	
Lethal osteopetrosis	
Asphyxiating thoracic dysplasia (Jeune syndrome)	
Achondroplasia	
Koide osteochondrodystrophy	
McGuire osteochondrodysplasia	
Intrauterine dwarfism with thin bones and fractures (Kozłowski-Kann syndrome)	
Greenberg-Rimoin chondrodystrophy	
Lethal chondrodysplasia with Dandy-Walker cyst and multiple congenital anomalies (Moerman-Vandenberghe-Fryns syndrome)	
Lethal Kniest-like dysplasia	
Chondrodysplasia punctata, Conradi-Hunermann variant	
Pyknoachondrogenesis	
Wegmann-Jones-Smith syndrome	
Boomerang skeletal dysplasia	
Lethal chondrodysplasia with advanced bone age (Blomstrand syndrome)	
Herva-Leisti-Kirkman syndrome (contractures, congenital lethal Finnish type)	
Congenital infantile cortical hyperostosis (Caffey syndrome)	
<i>Metabolic Disorders</i>	Low
Lysosomal storage disease	Low
Sphingolipidoses	
GM, gangliosidosis	
Galactosialidosis	
Farber disease	
Gaucher disease (glucocerebrosidase deficiency)	
Niemann-Pick disease type A	
Mucopolysaccharidoses	
Mucopolysaccharidosis type I (Hurler syndrome)	
Mucopolysaccharidosis type IVa (Morquio syndrome type A)	
Mucopolysaccharidosis type VII ( $\gamma$ -glucuronidase deficiency)	
Mucolipidoses	
Mucolipidosis type I (sialidosis)	
Mucolipidosis type II (I-cell disease)	
Transport defects	
Sialic acid storage disease	
Salla disease	
Niemann-Pick disease type C	
Other lysosomal storage diseases	
Wolman disease	
Carbohydrate-deficient glycoprotein syndrome	Low
Glycogen storage disease type II (Pompe syndrome)	Low
Cardiac glycogen storage disease with normal maltase activity	Low
Carnitine deficiency	Low
Erythrocyte enzyme disorders	
Glucose-6-phosphate dehydrogenase deficiency	Low
Pyruvate kinase deficiency	Low
Glucose phosphate isomerase deficiency	Low

Continued



**Table 17-3** Causes and Associations of Nonimmune Hydrops—cont'd

Cause	Frequency*
Fetal hyperthyroidism (maternal Graves disease)	Low
Fetal hypothyroidism	Low
<i>Syndromes</i>	Low
Autosomal-dominant inheritance	
G syndrome (Opitz-Frias syndrome)	
Congenital myotonic dystrophy	
Cornelia de Lange syndrome	
Noonan's syndrome	
Yellow nail syndrome	
Tuberous sclerosis (already in utero with rhabdomyomas)	
Autosomal-recessive inheritance	
Arthrogryposis multiplex congenita	
Pena-Shokeir syndrome	
Lethal multiple pterygium syndrome	
Neu-Laxova syndrome	
Recurrent isolated hydrops	
Cryptophthalmia-syndactyly syndrome (Fraser syndrome)	
Cumming syndrome	
Polysplenia syndrome (left atrial isomerism)	
Orofaciodigital syndrome type II (Mohr syndrome)	
Isolated recurrent cystic hygroma	
Elajalda syndrome	
Kaufman-McKusick syndrome	
Angio-osteohypertrophy syndrome (Klippel-Feil-Treuneunay syndrome)	Low
Beckwith-Wiedemann syndrome	Low
<i>Chromosomal Aberrations</i>	Low
Trisomy 13	
Trisomy 15	
Trisomy 16	
Turner syndrome	
Trisomy 18	
Trisomy 21	
Triploidy	
Tetraploidy	
Trisomy 10 mosaicism	
46, XX/XY mosaic	
49, XXXXY	
Partial duplication of chromosome 11	
Partial duplication of chromosomes 15 and 17	
Partial duplication of chromosome 18	
Partial deletion of short arm of chromosome 13	
Partial deletion of short arm of chromosome 18	
Rearrangement of long arm of chromosome 22	
<i>Placental and Umbilical Cord Anomalies</i>	Low
Chorioangioma	
Chorioangioma as part of Beckwith-Wiedemann syndrome	
Subchorial placental hematoma	
True knots of the cord	
Angiomyxoma of the umbilical cord	
Aneurysm of the umbilical artery	
Hemorrhagic endovascularitis of the placenta	
Chorionic vein thrombosis	
Placental and umbilical vein thrombosis	
Umbilical cord torsion	

ADCKD, autosomal-dominant cystic kidney disease; ARCKD, autosomal-recessive cystic kidney disease; AV, atrioventricular; AVM, arteriovenous malformation; CCAM, congenital cystic adenomatoid malformation; CHAOS, congenital high airway obstruction syndrome.

\*Rate of the occurrence of hydrops if the fetus has the respective disease. In the vast majority of causes and associations, the incidence are too low for giving reliable information.

Reprinted with permission from Tercanli S, Gembruch U, Holzgreve W: Nonimmune hydrops fetalis: Diagnosis and management. In Callen PW (ed): Ultrasonography in Obstetrics and Gynecology, 4th ed. Philadelphia, W. B. Saunders, 2000, p 553.

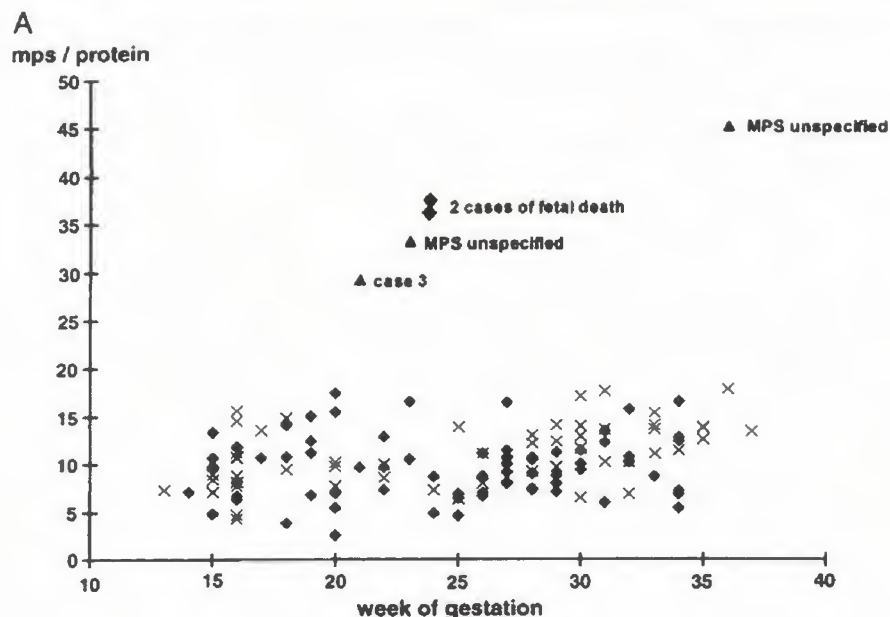


**FIGURE 17-17.** Normal values for amniotic fluid mucopolysaccharides corrected for total protein. Xs represent 40 normal control patients; ♦ represent 71 cases of nonimmune hydrops fetalis. Noted two cases of fetal death were found to have elevated levels of MPS, although cultured amniocytes for 21 different lysosomal enzymes were normal. Three abnormal cases are depicted. (Reprinted with permission from Kooper AJ, Janssens PM, de Groot AN, et al: Lysosomal storage diseases in non-immune hydrops fetalis pregnancies. *Clin Chim Acta* 371:176, 2006.)

Doppler evaluation of the middle cerebral artery should also be performed in these patients. An elevated value of the peak systolic velocity of the MCA has been associated with fetal anemia even in cases of NIHF.<sup>50</sup>

A careful maternal history should then be undertaken. This should include queries regarding exposure to children with *fifth disease* ("slapped cheek" disease) due to parvovirus B19. Maternal symptoms that would indicate subsequent infection include fever, arthralgia, and an exanthema on the upper body.<sup>51</sup> Parvovirus B19 is a small single-stranded DNA virus.<sup>51</sup> It is a potent inhibitor of hematopoiesis because it lytically infects erythroid precursor cells. The cellular receptor for parvovirus B19 is globoside, which is found on erythrocyte progenitor cells (erythroblasts and megakaryocytes) and also on erythrocytes, synovium, placental tissue, fetal myocardium and endothelial cells.<sup>51</sup> This explains the etiology of the maternal and fetal signs and symptoms affecting maternal joints and fetal red blood cells, placenta, and myocardium. Infection with parvovirus B19 usually takes place through respiratory droplets, but it can also be transmitted by blood and blood-derived products, and may also be transmitted vertically from mother to fetus. Vertical transmission does not occur if the mother is immune at the time of exposure. When maternal infection does occur, viremia in the mother reaches its peak approximately 1 week after infection. Maternal symptoms start approximately 10 to 14 days after infection in approximately 50% of infected women.<sup>51</sup> Parvovirus B19 IgM antibodies become detectable in maternal serum within 7 to 10 days after infection, peak at 10 to 14 days, and then decrease within 2 to 3 months. IgG antibodies rise more slowly and reach a plateau at 4 weeks after infection.<sup>51</sup> A previous obstetric history of stillbirth or a hydropic fetus should lead the investigator to contemplate lysosomal storage diseases. Similarly, a consanguineous relationship would also lead one to consider autosomal-recessive diseases as the etiology.

The next step in the diagnostic evaluation usually entails maternal venipuncture. Tests should include an antibody screen for anti-red cell antibodies, rapid test for syphilis, and a Kleihauer-Betke test or fetal cell stain by flow cytometry. Maternal serologies for toxoplasmosis, cytomegalovirus, and parvovirus should be considered but may not be diagnostic particularly with acute onset of fetal hydrops.

Although cordocentesis to sample fetal blood to perform rapid assays was commonly used in the past for the initial assessment of NIHF, fluorescent in situ hybridization for major chromosomal abnormalities, and PCR testing for viral infections have decreased the role of this procedure. Amniocentesis is warranted to complete the acute investigation. Samples should be sent for fluorescent in situ hybridization, PCR for toxoplasmosis, cytomegalovirus, parvovirus, adenovirus, and enteroviruses. Kooper et al<sup>52</sup> found that up to 8% of cases of NIHF may be related to lysosomal storage diseases. They recommend consideration of amniotic fluid analysis for mucopolysaccharides and neuraminic acid (Figs. 17-17 and 17-18). Cultured amniocytes should be analyzed for complete karyotype as well as enzymatic levels for the more common lysosomal disorders including  $\beta$ -glucuronidase,  $\beta$ -glucosidase, and  $\beta$ -galactosidase. Consideration for testing of other lysosomal diseases should be undertaken if warranted by maternal history. These would include Niemann-Pick types A and C, Wolman, Faber, Mucopolipidosis II, and multiple sulfatase deficiency.

## Treatment

A limited number of cases of NIHF can be treated in utero; however, these cases are based on an accurate determination of the specific etiology (Fig. 17-19).

Parvovirus has been associated with profound fetal anemia and hydrops fetalis when maternal infection occurs before 20 weeks' gestation.<sup>53</sup> In one series of 1019 pregnant



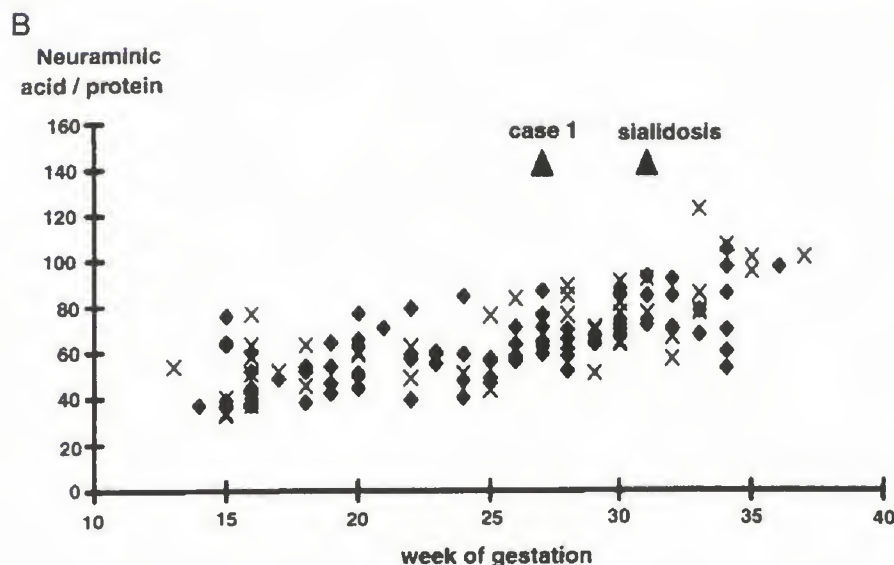


**FIGURE 17–18.** Normal values for amniotic fluid bound and free neuraminic acid corrected for total protein. Xs represent 40 normal control patients; ♦ represent 71 cases of NIHF. Two abnormal cases are depicted. (Reprinted with permission from Kooper AJ, Janssens PM, de Groot AN, et al: Lysosomal storage diseases in non-immune hydrops fetalis pregnancies. *Clin Chim Acta* 371:176, 2006.)

women with seroconversion, the risk for fetal hydrops was 3.9%. The peak incidence of parvovirus associated hydrops fetalis is between 17 and 24 weeks of gestation.<sup>47</sup> The MCA Doppler can be used in an analogous fashion to immune hydrops to confirm the anemia when there is an elevated systolic velocity of more than 1.5 MoMs. Although maternal serology (positive IgM or new presence of an IgG antibody in a patient that was previously seronegative) can be used to confirm some cases, amniocentesis for PCR determination of parvovirus usually is diagnostic in 24 to 48 hours. In one large series, one third of cases of fetal hydrops spontaneously resolved within 5 weeks; half of these cases occurred before 23 weeks' gestation.<sup>54</sup> In another series, IUT of packed red cells was associated with survival in approximately 85% of cases, whereas those cases with hydrops that were observed were universally fatal.<sup>53</sup> IUTs have also proved successful in cases of fetal hydrops secondary to fetomaternal hemorrhage.<sup>55</sup> If a recurrent decline in fetal hematocrit is detected due to a persistent fetomaternal bleed, abandonment of additional transfusions may be warranted.

Other bacterial and viral infections are associated with NIHF including cytomegalovirus, adenovirus, toxoplasmosis, and syphilis. Fetal cytomegalovirus infection has been treated with maternal and direct fetal administration of hyperimmune globulin; however, the few reported cases of NIHF have not resolved with this therapy.<sup>56</sup> Adenovirus can cause fetal myocarditis with resulting hydrops.<sup>57</sup> Maternal administration of digoxin has been successful in increasing fetal myocardial function resulting in resolution of the hydrops. NIHF related to fetal toxoplasmosis has resolved after maternal administration of pyrimethamine, sulphadiazine, and folinic acid with good short-term neurologic outcome.<sup>58</sup> Fetal infection with syphilis that results in NIHF can reverse with maternal treatment with penicillin however the overall prognosis due to cerebral complications remains high.<sup>59</sup>

Both fetal bradyarrhythmias and tachyarrhythmias have been associated with fetal hydrops. Ventricular rates of less

than 50 bpm due to structural cardiac lesions or inflammation secondary to maternal anti-Ro antibodies are not amenable to therapy. The administration of maternal betamimetics has not been successful at increasing the fetal heart rate. Attempts at direct fetal pacing have also failed.<sup>60</sup> Both fetal atrial flutter and supraventricular tachycardia are associated with NIHF. Parenteral administration of digoxin followed by the addition of flecanide or sotalol is usually successful in converting these to a sinus rhythm.<sup>61</sup>

Solid lesions of the chest and sacrococcygeal teratomas in association with NIHF have been treated with open fetal surgery with mixed results.<sup>62</sup> Referral to a center experienced in open fetal surgery should be considered if NIHF is noted before 26 weeks' gestation.

Unilateral pleural effusions or large, predominantly macrocystic cystic adenomatoid malformations of the fetal lung represent space-occupying lesions that can shift the mediastinum to the opposite side of the fetal chest. Therefore, these lesions can cause an obstruction to venous return as well as decreased cardiac output and subsequent development of NIHF. In the case of a large hydrothorax or macrocystic cystic adenomatoid malformation of the lung, thoracoamniotic shunt placement under ultrasound guidance has been successful in decreasing the size of the fluid or cyst resulting in a return of the mediastinum to its midline position.<sup>63</sup> Hydrops usually resolves within several weeks.

Twin-to-twin transfusion can present early in gestation with massive polyhydramnios in the "recipient" twin. Quintero<sup>64</sup> has proposed a staging system that describes various progressive ultrasound findings with stage IV disease defined as hydrops fetalis in one or both twins. Typically this occurs in the recipient of the twin pair. Untreated severe twin-to-twin transfusion at less than 24 to 26 weeks is associated with a 90% perinatal mortality.<sup>65</sup> Serial amnioreduction to remove the excess amniotic fluid or septostomy to allow for equilibration of the fluid between the amniotic compartments only marginally improves perinatal survival. In a large randomized trial, fetoscopic-directed laser ablation of

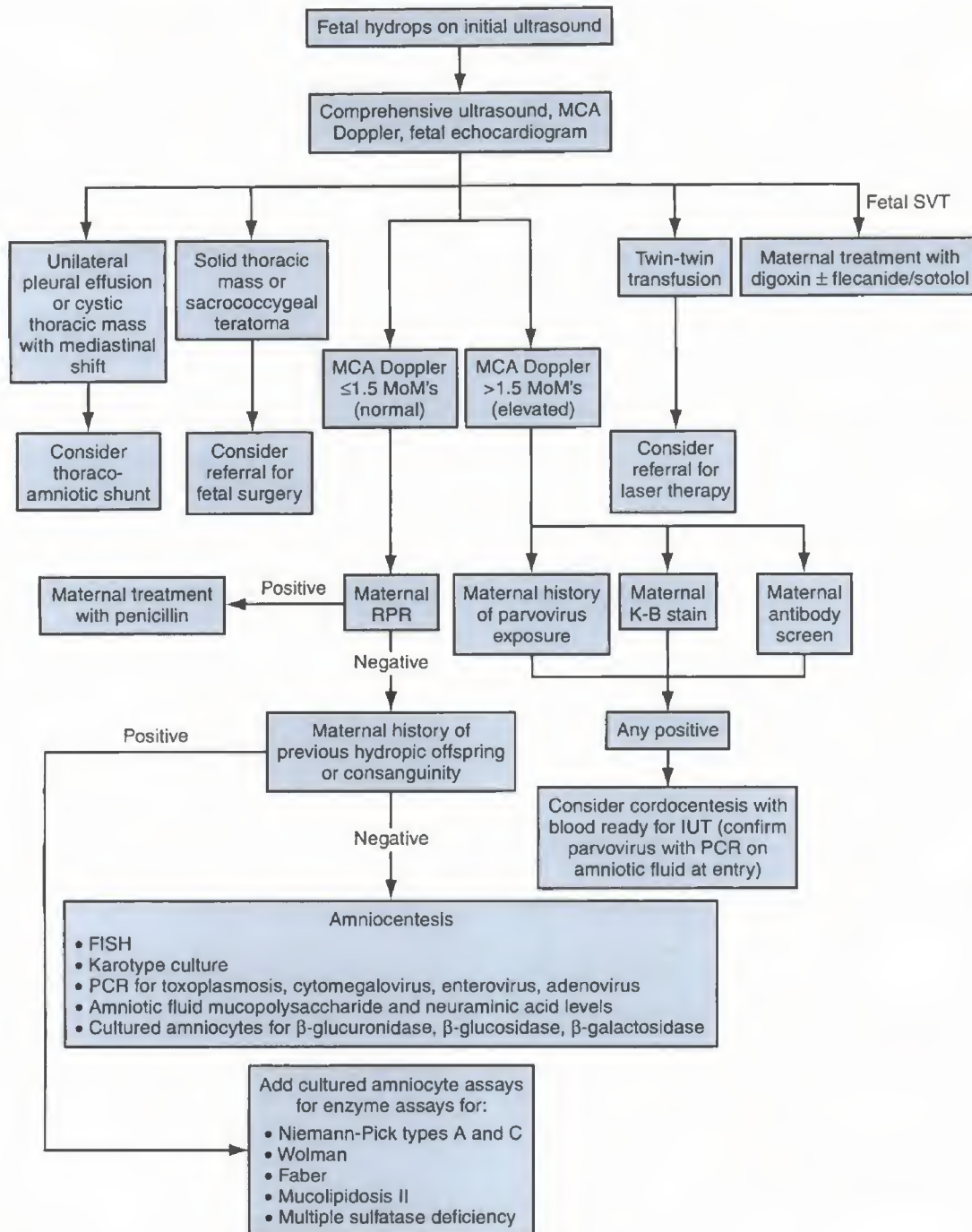


FIGURE 17-19. Algorithm for the management and treatment of nonimmune hydrops fetalis.

the anastomoses between the placental circulations of the twins resulted in an overall perinatal survival of 70%.<sup>66</sup> Laser therapy is now considered the standard of care in this condition.

## Prognosis

Perinatal survival for NIHF has improved modestly with advances in perinatal/neonatal medicine. Clearly, the etiology of the hydrops defines the ultimate outcome. New therapies

such as IUT for fetal anemia secondary to parvovirus infection and laser therapy for twin-to-twin transfusion have markedly improved the prognosis in these specific conditions.

Mortality rates as high as 98% were reported in some series in the early 1980s; more recent data would suggest a survival rate between 30% and 40%.<sup>67-69</sup> Several factors have been identified that predict a better prognosis. In one prospective series of 83 cases, the survival rate after exclusion of chromosomal abnormalities was 31% when NIHF was



detected before 24 weeks' gestation and 48% after this gestational age.<sup>3</sup> In another series, no infant with an Apgar score at 5 minutes of less than 5 survived the neonatal period.<sup>69</sup> The presence of major pleural effusions has also been associated with poor perinatal survival. Nakayama et al<sup>68</sup> reported a survival rate of 25% when pleural effusions were present as compared with 61% when they were absent. In addition, fetuses who developed pleural effusions after 29 weeks' gestation and who delivered after 31 weeks' gestation were more likely to survive. This is thought to be related to extrinsic compression of the fetal lungs with subsequent development of pulmonary hypoplasia.

Few studies on long-term outcome in NIHF have been reported. In one small series of 19 infants that survived to 1 year of age, 15% had severe psychomotor delay, whereas an additional 10% exhibited mild mental retardation.<sup>68</sup>

## CONCLUSION

Both immune hydrops fetalis and NIHF are signs of significant fetal disease with a guarded prognosis. Advances in prophylaxis and prenatal treatment have markedly changed the outcome for the fetus with immune hydrops. Some inroads in prenatal therapy have been achieved in certain conditions associated with NIHF such as fetal tachyarrhythmias, fetal parvovirus infection, and twin-to-twin transfusion syndrome. The majority of cases remain problematic because there is no effective treatment and the perinatal mortality rate remains high.

## References

1. Fleischer AC, Killam AP, Boehm FH, et al: Hydrops fetalis: sonographic evaluation and clinical implications. *Radiology* 141:163, 1981.
2. McAfee CAJ, Fortune DW, Beischer NA: Non-immunologic hydrops fetalis. *J Obstet Gynaecol Br Comm* 77:226, 1970.
3. Sohan K, Carroll SG, De La Fuente S, et al: Analysis of outcome in hydrops fetalis in relation to gestational age at diagnosis, cause and treatment. *Acta Obstet Gynecol Scand* 80:726, 2001.
4. Carbillon L, Oury JF, Guerin JM, et al: Clinical biological features of Ballantyne syndrome and the role of placental hydrops. *Obstet Gynecol Surv* 52:310, 1997.
5. Heyborne KD, Chism DM: Reversal of Ballantyne syndrome by selective second-trimester fetal termination. A case report. *J Reprod Med* 45:360, 2000.
6. Moise KJ Jr: Diagnosing hemolytic disease of the fetus—time to put the needles away? *N Engl J Med* 355:192, 2006.
7. Levine P, Katzin EM, Burham L: Isoimmunization in pregnancy: its possible bearing on etiology of erythroblastosis foetalis. *JAMA* 116:825, 1941.
8. Nicolaides KH, Thilaganathan B, Rodeck CH, et al: Erythroblastosis and reticulocytosis in anemic fetuses. *Am J Obstet Gynecol* 159:1063, 1988.
9. Brace RA: Thoracic duct lymph flow and its measurement in chronically catheterized sheep fetus. *Am J Physiol* 256:H16, 1989.
10. Berger HM, Lindeman JH, van Zoeren-Grobbe D, et al: Iron overload, free radical damage, and rhesus haemolytic disease. *Lancet* 335:933, 1990.
11. De Groot CJ, Oepkes D, Egberts J, et al: Evidence of endothelium involvement in the pathophysiology of hydrops fetalis? *Early Hum Dev* 57:205, 2000.
12. Pasman SA, Meerman RH, Vandenbussche FP, et al: Hypoalbuminemia: a cause of fetal hydrops? *Am J Obstet Gynecol* 194:972, 2006.
13. Moise KJ Jr, Carpenter RJ Jr, Hesketh DE: Do abnormal Starling forces cause fetal hydrops in red blood cell alloimmunization? *Am J Obstet Gynecol* 167:907, 1992.
14. Brace RA: Effects of outflow pressure on fetal lymph flow. *Am J Obstet Gynecol* 160:494, 1989.
15. Lewis M, Bowman JM, Pollock J, et al: Absorption of red cells from the peritoneal cavity of an hydropic twin. *Transfusion* 13:37, 1973.
16. van Kamp IL, Klumper FJ, Bakum RS, et al: The severity of immune fetal hydrops is predictive of fetal outcome after intrauterine treatment. *Am J Obstet Gynecol* 185:668, 2001.
17. Vaughan JI, Manning M, Warwick RM, et al: Inhibition of erythroid progenitor cells by anti-Kell antibodies in fetal alloimmune anemia [see comments]. *N Engl J Med* 338:798, 1998.
18. Van den Veyver IB, Moise KJ Jr: Fetal RhD typing by polymerase chain reaction in pregnancies complicated by rhesus alloimmunization. *Obstet Gynecol* 88:1061, 1996.
19. Lo YM, Hjelm NM, Fidler C, et al: Prenatal diagnosis of fetal RhD status by molecular analysis of maternal plasma. *N Engl J Med* 339:1734, 1998.
20. Daniels G, Finning K, Martín P, et al: Fetal blood group genotyping from DNA from maternal plasma: an important advance in the management and prevention of haemolytic disease of the fetus and newborn. *Vox Sang* 87:225, 2004.
21. Gaudier E, Benachi A, Giovannardi Y, et al: Fetal RHD genotyping by maternal serum analysis: a two-experience. *Am J Obstet Gynecol* 192:666, 2005.
22. Liley AW: Liquor amnii analysis in the management of pregnancy complicated by rhesus sensitization. *Am J Obstet Gynecol* 82:1359, 1961.
23. Nicolaides KH, Rodeck CH, Mibashan RS, et al: Have Liley charts outlived their usefulness? *Am J Obstet Gynecol* 155:90, 1986.
24. Queenan JT, Tomai TP, Ural SH, et al: Deviation in amniotic fluid optical density at a wavelength of 450 nm in Rh-immunized pregnancies from 14 to 40 weeks' gestation: a proposal for clinical management. *Am J Obstet Gynecol* 168:1370, 1993.
25. Oepkes D, Seaward PG, Vandenbussche FP, et al: Doppler ultrasonography versus amniocentesis to predict fetal anemia. *N Engl J Med* 355:156, 2006.
26. Mari G, Deter RL, Carpenter RL, et al: Noninvasive diagnosis by Doppler ultrasonography of fetal anemia due to maternal red-cell alloimmunization. *N Engl J Med* 342:9, 2000.
27. Zimmerman R, Carpenter RJ Jr, Durig P, et al: Longitudinal measurement of peak systolic velocity in the fetal middle cerebral artery for monitoring pregnancies complicated by red cell alloimmunization: a prospective multicentre trial with intention-to-treat. *Br J Obstet Gynecol* 109:746, 2002.
28. Abel DE, Grambow SC, Brancaccio LR, et al: Ultrasound assessment of the fetal middle cerebral artery peak systolic velocity: A comparison of the near-field versus far-field vessel. *Am J Obstet Gynecol* 189:986, 2003.
29. Mari G, Abuhamad AZ, Cosmi E, et al: Middle cerebral artery peak systolic velocity: technique and variability. *J Ultrasound Med* 24:425, 2005.
30. Trevett TN Jr, Dorman K, Lamvu G, et al: Antenatal maternal administration of phenobarbital for the prevention of exchange transfusion in neonates with hemolytic disease of the fetus and newborn. *Am J Obstet Gynecol* 192:478, 2005.
31. Moise KJ Jr, Deter RL, Kirshon B, et al: Intravenous pancuronium bromide for fetal neuromuscular blockade during intrauterine transfusion for red-cell alloimmunization. *Obstet Gynecol* 74:905, 1989.
32. Moise KJ Jr, Carpenter RJ Jr, Kirshon B, et al: Comparison of four types of intrauterine transfusion: effect on fetal hematocrit. *Fetal Ther* 4:126, 1989.
33. Klumper FJ, van Kamp IL, Vandenbussche FP, et al: Benefits and risks of fetal red-cell transfusion after 32 weeks gestation. *Eur J Obstet Gynecol Reprod Biol* 92:91, 2000.
34. Harman CR, Bowman JM, Manning FA, et al: Intrauterine transfusion—intraperitoneal versus intravascular approach: a case-control comparison. *Am J Obstet Gynecol* 162:1053, 1990.
35. Moise KJ Jr, Mari G, Fisher DJ, et al: Acute fetal hemodynamic alterations after intrauterine transfusion for treatment of severe red blood cell alloimmunization. *Am J Obstet Gynecol* 163:776, 1990.
36. Radunovic N, Lockwood CJ, Alvarez M, et al: The severely anemic and hydropic isoimmune fetus: changes in fetal hematocrit associated with intrauterine death. *Obstet Gynecol* 79:390, 1992.
37. Voto LS, Mathet ER, Zapaterio JL, et al: High-dose gammaglobulin (IVIG) followed by intrauterine transfusions (IUTs): a new alternative for the treatment of severe fetal hemolytic disease. *J Perinat Med* 25:85, 1997.
38. Ruma MS, Moise KJ Jr, Kim E, et al: Combined plasmapheresis and intravenous immune globulin for the treatment of red cell alloimmunization. *Am J Obstet Gynecol* 196:138e1, 2007.

39. Saade GR, Moise KJ, Belfort MA, et al: Fetal and neonatal hematologic parameters in red cell alloimmunization: predicting the need for late neonatal transfusions. *Fetal Diagn Ther* 8:161, 1993.
40. Ovali F, Samanci N, Dagoglu T: Management of late anemia in Rhesus hemolytic disease: use of recombinant human erythropoietin (a pilot study). *Pediatr Res* 39:831, 1996.
41. Hudon L, Moise KJ Jr, Hegemier SE, et al: Long-term neurodevelopmental outcome after intrauterine transfusion for the treatment of fetal hemolytic disease. *Am J Obstet Gynecol* 179:858, 1998.
42. Moise KJ, Whitecar PW: Antenatal therapy for haemolytic disease of the fetus and newborn. In Hadley A, Soothill P (eds): *Alloimmune disorders in pregnancy. Anaemia, thrombocytopenia and neutropenia in the fetus and newborn*, Vol 1, 1st ed. Cambridge, UK, Cambridge University Press, 2002, pp 173–202.
43. Machin GA: Hydrops revisited: literature review of 1,414 cases published in the 1980s. *Am J Med Genet* 34:366, 1989.
44. Weiner CP: Umbilical pressure measurement in the evaluation of nonimmune hydrops fetalis. *Am J Obstet Gynecol* 168:817, 1993.
45. Jauniaux E: Diagnosis and management of early non-immune hydrops fetalis. *Prenat Diagn* 17:1261, 1997.
46. Shenker L, Reed KL, Anderson CF, et al: Fetal pericardial effusion. *Am J Obstet Gynecol* 160:1505; discussion 1507, 1989.
47. Dizon-Townson DS, Dildy GA, Clark SL: A prospective evaluation of fetal pericardial fluid in 506 second-trimester low-risk pregnancies. *Obstet Gynecol* 90:958, 1997.
48. Jeanty P, Romero R, Hobbins JC: Fetal pericardial fluid: a normal finding of the second half of gestation. *Am J Obstet Gynecol* 149:529, 1984.
49. Yoo SJ, Min JY, Lee YH: Normal pericardial fluid in the fetus: color and spectral Doppler analysis. *Ultrasound Obstet Gynecol* 18:248, 2001.
50. Hernandez-Andrade E, Scheier M, Dezerega V, et al: Fetal middle cerebral artery peak systolic velocity in the investigation of non-immune hydrops. *Ultrasound Obstet Gynecol* 23:442, 2004.
51. de Jong EP, de Haan TR, Kroes ACM, et al: Parvovirus B19 infection in pregnancy: A review. *J Clin Virology* 36:1, 2006.
52. Kooper AJ, Janssens PM, de Groot AN, et al: Lysosomal storage diseases in non-immune hydrops fetalis pregnancies. *Clin Chim Acta* 371:176, 2006.
53. Enders M, Weidner A, Zoellner I, et al: Fetal morbidity and mortality after acute human parvovirus B19 infection in pregnancy: prospective evaluation of 1018 cases. *Prenat Diagn* 24:513, 2004.
54. Rodis JF, Borgida AF, Wilson M, et al: Management of parvovirus infection in pregnancy and outcomes of hydrops: a survey of members of the Society of Perinatal Obstetricians. *Am J Obstet Gynecol* 179:985, 1998.
55. Montgomery LD, Belfort MA, Adam K: Massive fetomaternal hemorrhage treated with serial combined intravascular and intraperitoneal fetal transfusions. *Am J Obstet Gynecol* 173:234, 1995.
56. Nigro G, Adler SP, La Torre R, et al: Passive immunization during pregnancy for congenital cytomegalovirus infection. *N Engl J Med* 353:1350, 2005.
57. Towbin JA, Griffin LD, Martin AB, et al: Intrauterine adenoviral myocarditis presenting as nonimmune hydrops fetalis: diagnosis by polymerase chain reaction. *Pediatr Infect Dis J* 13:144, 1994.
58. Friedman S, Ford-Jones LE, Toi A, et al: Congenital toxoplasmosis: prenatal diagnosis, treatment and postnatal outcome. *Prenat Diagn* 19:330, 1999.
59. Barton JR, Thorpe EM Jr, Shaver DC, et al: Nonimmune hydrops fetalis associated with maternal infection with syphilis. *Am J Obstet Gynecol* 167:56, 1992.
60. Carpenter RJ Jr, Strasburger JF, Garson A Jr, et al: Fetal ventricular pacing for hydrops secondary to complete atrioventricular block. *J Am Coll Cardiol* 8:1434, 1986.
61. Oudijk MA, Ruskamp JM, Ambachtsheer BE, et al: Drug treatment of fetal tachycardias. *Paediatr Drugs* 4:49, 2002.
62. Adzick NS, Kitano Y: Fetal surgery for lung lesions, congenital diaphragmatic hernia, and sacrococcygeal teratoma. *Semin Pediatr Surg* 12:154, 2003.
63. Wilson RD, Baxter JK, Johnson MP, et al: Thoracoamniotic shunts: fetal treatment of pleural effusions and congenital cystic adenomatoid malformations. *Fetal Diagn Ther* 19:413, 2004.
64. Quintero RA, Morales WJ, Allen MH, et al: Staging of twin-twin transfusion syndrome. *J Perinatol* 19:550, 1999.
65. Haverkamp F, Lex C, Hanisch C, et al: Neurodevelopmental risks in twin-to-twin transfusion syndrome: preliminary findings. *Eur J Paediatr Neurol* 5:21, 2001.
66. Senat MV, Deprest J, Boulvain M, et al: Endoscopic laser surgery versus serial amnioreduction for severe twin-to-twin transfusion syndrome. *N Engl J Med* 351:136, 2004.
67. Hutchison AA, Drew JH, Yu VY, et al: Nonimmunologic hydrops fetalis: a review of 61 cases. *Obstet Gynecol* 59:347, 1982.
68. Nakayama H, Kukita J, Hikino S, et al: Long-term outcome of 51 liveborn neonates with non-immune hydrops fetalis. *Acta Paediatr* 88:24, 1999.
69. Simpson JH, McDevitt H, Young D, et al: Severity of non-immune hydrops fetalis at birth continues to predict survival despite advances in perinatal care. *Fetal Diagn Ther* 21:380, 2006.



## ULTRASOUND EVALUATION OF THE CERVIX

Vincenzo Berghella, MD, and George Bega, MD

### Introduction

#### Ultrasound of the Cervix—Techniques

Transabdominal  
Translabial  
Transvaginal

#### Limitations and Pitfalls

Full Bladder  
Too Much Pressure  
Contraction  
Underdeveloped Lower Uterine Segment

#### Clinical Applications

Transvaginal Ultrasound Examination of the Cervix for Prediction of Preterm Birth  
*Screening Test*

#### What to Measure

Cervical Length  
Funneling  
Other Measurements

#### Dynamic Changes (Spontaneous or After Transfundal Pressure)

#### Normal Versus Abnormal

#### Best Gestational Age and Frequency of Examinations

#### Populations

Singleton Low Risk

Singleton High Risk

Twins

Triplets

Women With Cerclage

#### Three-Dimensional Transvaginal Ultrasound Examination of the Cervix

#### What Pathophysiologic Mechanisms Associate a Short Cervical Length With Preterm Birth?

#### Interventions for Preventing Preterm Birth if a Short Cervical Length is Identified in Asymptomatic Women

Ultrasound-Indicated Cerclage  
Indomethacin  
Antibiotics

#### Another Benefit of Transvaginal Ultrasound Screening in Asymptomatic Women: Avoiding Cerclage if Examination is Normal

#### Diagnosis and Management of Women With Suspected Preterm Labor

#### Predicting the Latency in Preterm Premature Rupture of the Membranes

#### Prediction of Start of Spontaneous Labor

#### Predicting the Success of Labor Induction and Mode of Delivery

#### Conclusions

## INTRODUCTION

Ultrasound of the cervix during pregnancy has been the focus of much research during the past decade. Significant advances have been made in understanding the proper role of this sonographic screening test. In this chapter we will review the technique of transvaginal cervical assessment and discuss its role in clinical practice.

## ULTRASOUND OF THE CERVIX—TECHNIQUES

### Transabdominal

In the 1970s, the first attempts at evaluating the cervix used transabdominal ultrasound (TAU). Unfortunately, this technique does not have sufficient reliability or validity, because of the following shortcomings: (1) the bladder often needs to be adequately filled to obtain a good image, resulting in elongation of the cervix and masking of any

funneling of the internal os; (2) fetal parts can obscure the cervix, especially after 20 weeks; and (3) the distance from the probe to the cervix results in degraded image quality.<sup>1</sup> Therefore, TAU should not be used for assessment of the cervix, even as a screening test, since its sensitivity for prediction of disease (e.g., increased risk for preterm birth [PTB]) is unacceptably low (8%),<sup>2</sup> much lower than the two other techniques described later.

### Translabial

Translabial (also known as transperineal) ultrasound (TLU) was first described in France in the early 1980s. This technique involves having the woman lie on table with the hips and knees flexed, while a gloved transducer in a sagittal orientation is positioned on the perineum between the labia majora (Fig. 18–1). Elevation of the woman's hips with a cushion can be used to improve visualization. Compared with TAU, this technique does not require bladder filling, is

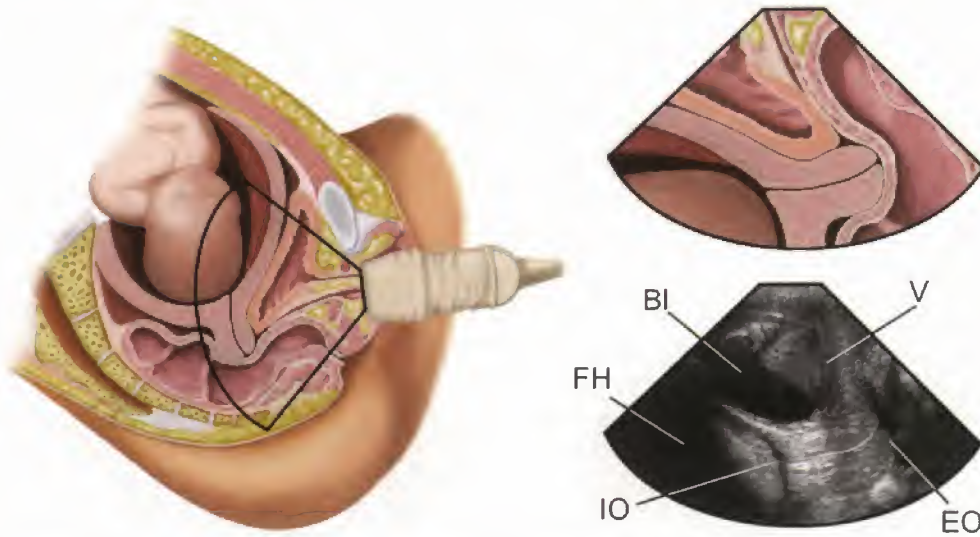


**FIGURE 18-1.** Diagrams and translabial sonogram of the female pelvis showing the transducer placed at the vaginal introitus and oriented in the direction of the vagina. BI, bladder; EO, external os; FH, fetal head; IO, internal os; V, vagina. (Illustration by James A. Cooper, MD, San Diego, CA.)

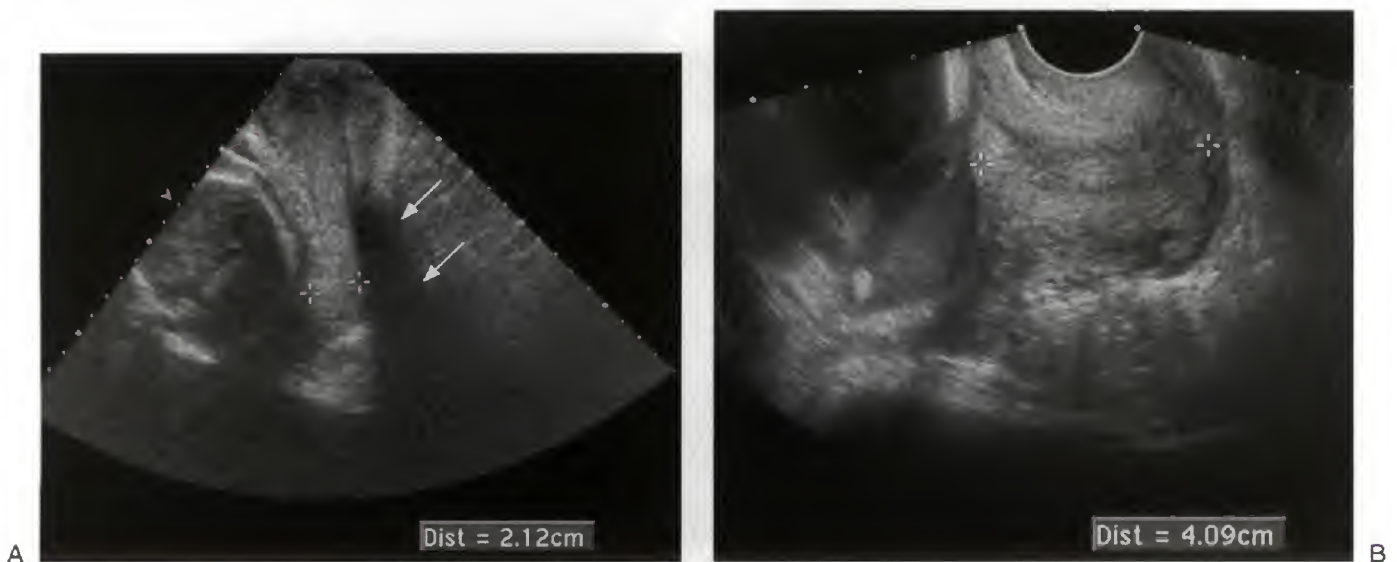


**FIGURE 18-2.** A. Translabial sonogram revealing an apparent cervical length of 2.12 cm. The true cervical length is partially obscured by rectal gas (arrows). B. Transvaginal sonogram from the same patient. The true cervical length of 4.09 cm is now clearly seen.

not impaired by obstruction by fetal parts, with the transducer closer to the cervix, achieving close to 100% visualization. Other advantages of this technique are the transducer does not enter the vagina (so no pressure can be exerted on the cervix), it does not require an additional transducer, and it is well accepted by most women. The main drawback of TLU is that gas in the rectum frequently can impede visualization of the cervix, especially the external os (Fig. 18-2). This technique is also a lot more difficult to master than transvaginal ultrasound and, therefore, is an unsatisfactory alternative to transvaginal ultrasound.<sup>3</sup>

## Transvaginal

The first studies of the human cervix using transvaginal ultrasound (TVU) are from the late 1980s. A clean transvaginal probe covered by a condom is inserted into the anterior fornix of the vagina (Fig. 18-3). The technique shares the advantages of translabial ultrasound; however, the probe is close to the cervix, without the problem of obscuring bowel gas. Thus, it has become the preferred gold standard method of evaluating the cervix in virtually all clinical settings (Fig. 18-4). Current recommendations for the performance of TVU of the cervix are shown in Table 18-1.<sup>1</sup>



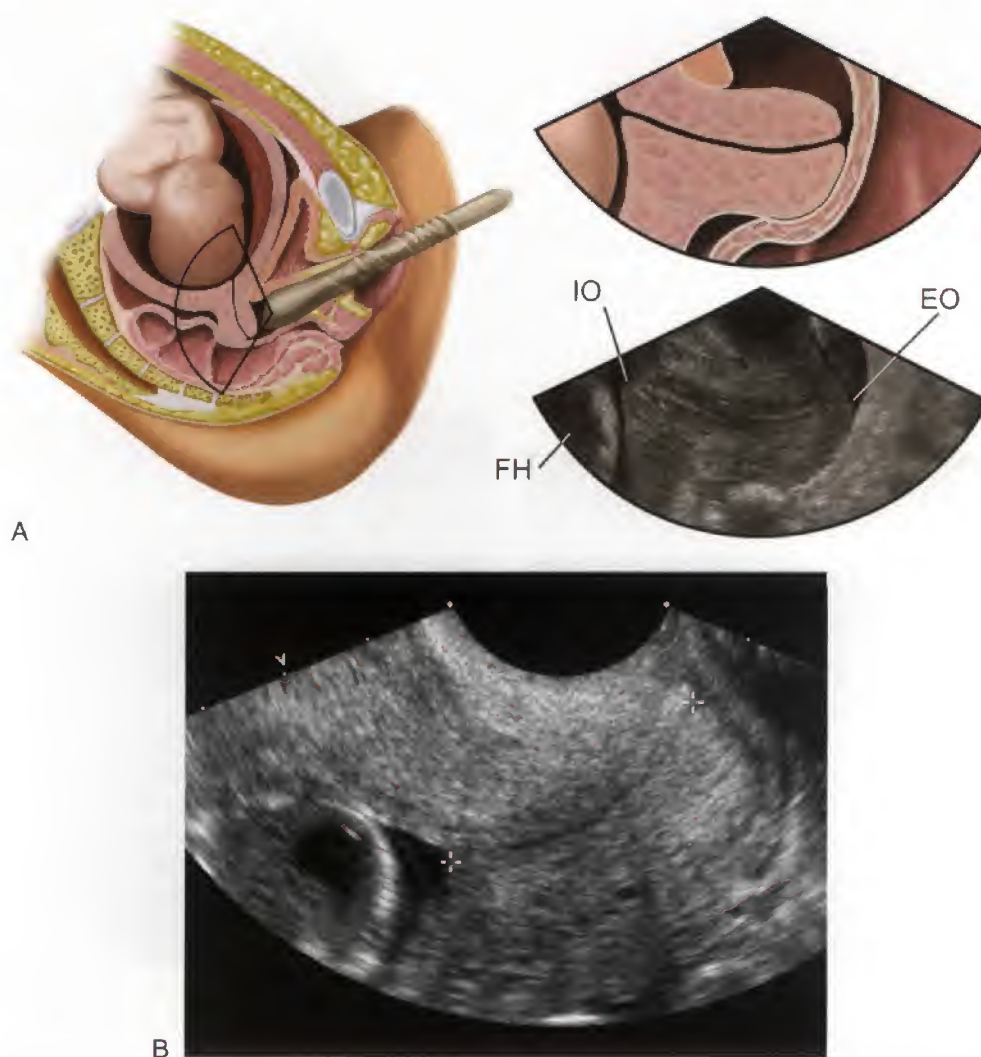


**FIGURE 18-3.** A. Diagrams and sonogram of the female pelvis demonstrating placement of the transvaginal transducer in the vagina. FH, fetal head; EO, external os; IO, internal os. (Illustration by James A. Cooper, M.D., San Diego, CA.) B. A two-dimensional ultrasound image of the cervix in its longest axis in the sagittal view. The internal and external os as well as the entire endocervical canal can be clearly seen, and the image is enlarged so that it occupies more than 75% of the screen.



**FIGURE 18-4.** Three methods of imaging the cervix. *A.* Transabdominal sonogram. The cervix, which is distant from the ultrasound transducer, is poorly seen and measures 1.62 cm. *B.* Translabial sonogram in the same patient. Although the cervix is seen somewhat better, shadowing from air in the rectum (arrows) obscures the true cervical length. *C.* Transvaginal sonogram. The true cervical length is now well seen and is virtually double the initial length measured.



The total time for a TVU of the cervix is approximately 5 minutes. For best results, the following criteria should be sought: the internal os should be either flat or at an isosceles angle with respect to the uterus, the whole length of the cervix should be visualized, a symmetric image of the external os should be obtained, the distance from the surface of the posterior lip to the cervical canal should be equal to the distance from the surface of the anterior lip to the cervical canal, and there should be no increased echogenicity in the cervix (a sign of excessive pressure).<sup>4</sup>

### LIMITATIONS AND PITFALLS

Although TVU of the cervix is usually straightforward, there can be an anatomic or technical difficulty that may be encountered in approximately one fourth of patients.<sup>5</sup>

### Full Bladder

A bladder that is not completely empty of urine can exert pressure on the cervix, and mask possible funneling or opening of the internal os.

### Too Much Pressure

Excessive pressure by the examiner can also mask funneling and/or opening of the internal os, and elongate the cervix. It can be easily identified by excessive echogenicity of the cervix (Fig. 18-5).

### Contraction

Uterine segment contractions may mimic the appearance of funneling of the internal cervical os. In such cases, there is



**Table 18-1** Recommendations for the Technical Performance of Transvaginal Ultrasound Examination of the Cervix

1. Have the woman empty her bladder;
2. Prepare the clean probe covered by a condom;
3. Insert the probe (probe can be inserted by the woman for more comfort);
4. Guide the probe in the anterior fornix of the vagina (Fig. 18-3A)
5. Obtain a sagittal long-axis view of endocervical canal, along its entire length;
6. Withdraw the probe until the image is blurred, and reapply just enough pressure to restore the image (to avoid excessive pressure on the cervix, which can elongate it);
7. Enlarge the image so that the cervix occupies at least two thirds of the image, and both external and internal os are well seen (Fig. 18-3B)
8. Measure the cervical length from the internal to the external os along the endocervical canal;
9. Obtain at least three measurements, and record the shortest best measurement in millimeters;
10. Apply transfundal pressure for 15 seconds, and record cervical length again.

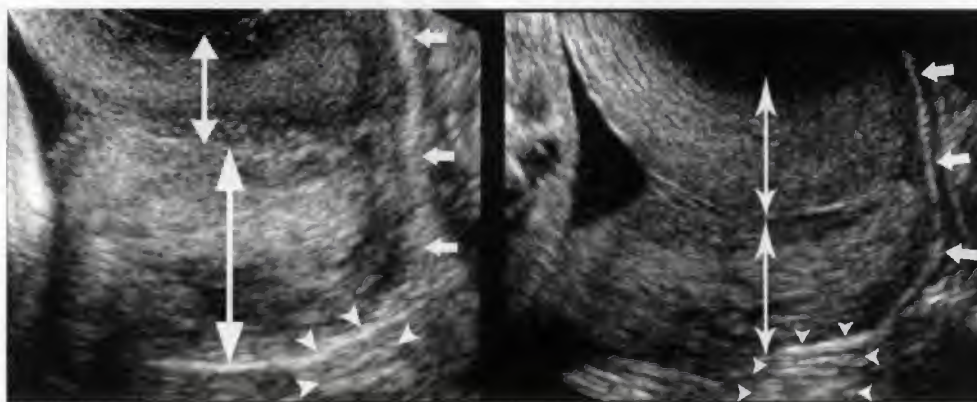


**FIGURE 18-5.** The ultrasound image on the left shows a cervix under excessive pressure from the vaginal probe. As a result, the anterior lip of the cervix is significantly thinner than the posterior lip of the cervix as shown by the double-headed arrows. The small triangular markers (*arrowheads*) show the increased echogenicity below the posterior lip of the cervix, a typical sign of excessive pressure. The image on the right shows that the anterior and posterior lips of the cervix are equal (as shown by the double-headed arrows) but still there is increased echogenicity below the posterior lip of the cervix. This demonstrates that there is still excessive pressure making the measurement of the cervix inadequate. The small short arrows in both images represent the vaginal mucosa that appears sonographically as a hyperechoic line. The vaginal mucosa is a reliable marker to identify the level where the external os should be seen (in difficult cases), and whether there is sliding between anterior and posterior lips of the cervix, which is another sign of excessive pressure.

rounded myometrium around the cervix, and a normal cervix distal to the contraction (Fig. 18-6).

### Underdeveloped Lower Uterine Segment

Often, before 14 weeks, the lower uterine segment is difficult to distinguish from the endocervical canal, because the gestational sac has not reached a sufficient size to completely expand the lower part of the uterus. Therefore, the measurement of the true cervical length (CL) is very difficult before 14 weeks. At other times, especially between 14 and 18 weeks, the presence of a contraction can also close the lower uterine segment, and make the distinction between this structure and the true CL difficult.

As is similarly done with other sonographic measurement techniques, such as the nuchal translucency measurement, some have recommended that a sonographer be supervised for his or her first 50 TVUs of the cervix to acquire sufficient expertise and ensure accuracy and reproducibility.

## CLINICAL APPLICATIONS

### Transvaginal Ultrasound Examination of the Cervix for Prediction of Preterm Birth

#### Screening Test

TVU of the cervix is often used in obstetrics as a screening test for the prediction of PTB.<sup>1</sup> To be clinically beneficial, a screening test must fulfill specific criteria.<sup>6</sup>

**Important and Prevalent Condition.** First, it must screen for a clinically important and prevalent condition. PTB occurs in 12% of births in the United States, or approximately 500,000 pregnancies per year in this nation alone.<sup>7</sup> It is the main cause of perinatal morbidity and mortality, and as such may be in fact the most important condition in obstetrics. In terms of years of life lost, PTB is one of the most important diseases in all of medicine.

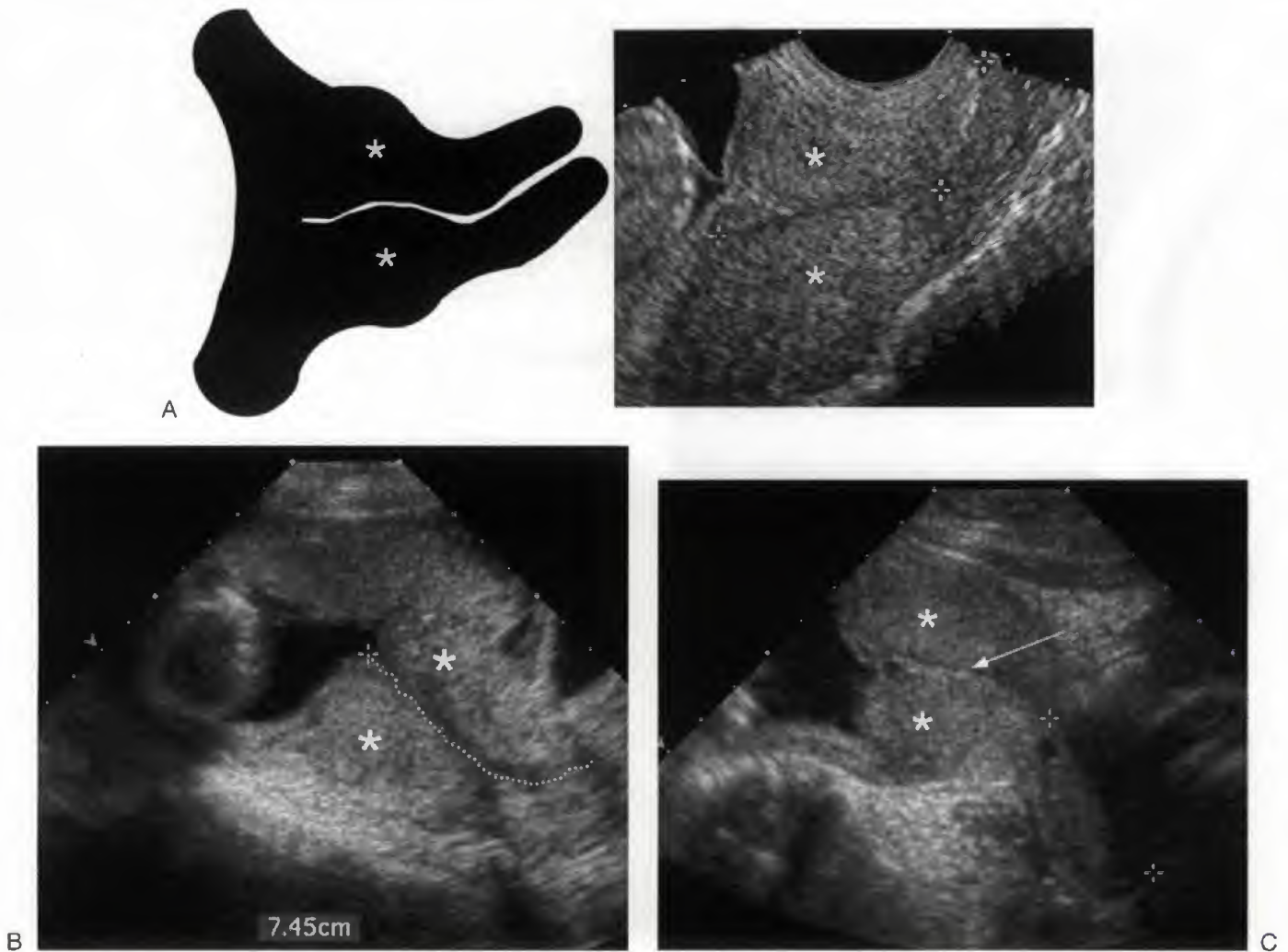


**FIGURE 18-8.** A. The diagram on the left and the ultrasound image on the right show a cervix with significant lower uterine segment contractions (asterisks). Lower uterine segment contractions should be considered whenever the cervical length measures more than 50 mm, the cervical canal assumes an S shape, and the lower uterine segments (either anteriorly or posteriorly or both) are thickened and asymmetric. The lower uterine segment contraction severely distorts the landmarks of the cervix and makes the measurement of cervical length inadequate. B. Lower uterine segment contractions (asterisks) seen on a transabdominal sonogram. The pseudocervical length measures more than 7 cm. This measurement alone should make one suspect of contractions. C. Although the cervix is not adequately visualized on this transabdominal sonogram, problems with adequate measurement are compounded by lower uterine segment contractions (asterisks). The reflection (arrow) between the contractions may simulate and can be misinterpreted as the endocervical canal.

**Technique Well Described.** The technique is well described (see Table 18-1).

**Safe and Acceptable.** TVU of the cervix is very safe. There is no inoculation of bacteria with TVU.<sup>8</sup> In a randomized trial comparing the use of TVU or the nonuse of TVU in the presence of premature preterm rupture of membranes (PPROM), there was no increased risk of infection for mother or fetus with TVU of the cervix compared with no TVU of the cervix.<sup>9</sup> TVU is also well accepted by pregnant women. Pain and severe discomfort is experienced by less than 2% of women undergoing TVU, and more than 99% of women would agree to a similar procedure in the future.<sup>10,11</sup>

**Reliable/Reproducible.** The interobserver and intraobserver variability of TVU are both less than 10%.<sup>12,13</sup> This low variability between operators is achieved only with strict adherence to proper technique as described earlier and after adequate training with supervised scans.

**Recognizable Early Asymptomatic Phase.** The changes of the cervix that ultimately lead to preterm or term labor have been demonstrated by TVU. These changes include initial opening of the internal os, progressive cervical shortening and widening along the endocervical canal from the internal to the external os, and ultimate opening of the external os. The earliest changes at the internal os are almost always asymptomatic and can only be detected by TVU.

**Valid (Accuracy of Prediction). Comparison With Manual Exam of the Cervix.** Cervical assessment by manual (digital) examination was a traditional method for prediction of PTB. Digital and TVU examinations of CL every 2 weeks from 14 to 30 weeks' gestation (with examiners blinded to the results of the alternate technique)<sup>12</sup> both independently predict PTB, but TVU has a much stronger association with PTB than manual examination of the cervix. The mean sonographic CL of the PTB group was significantly shorter



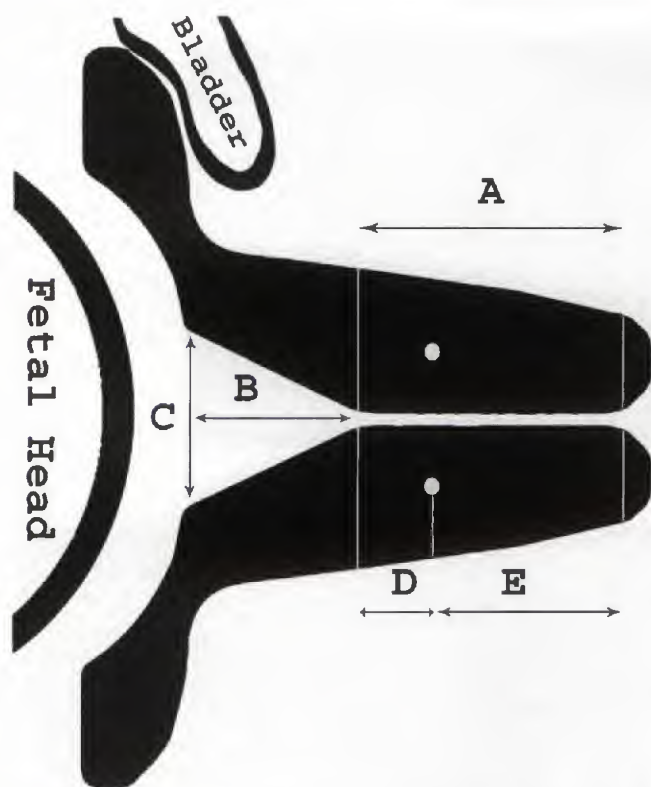


**FIGURE 18-7.** Diagram illustrating the major landmarks of the cervix and its surroundings. A is cervical length, B is funnel length, C is funnel width, D is the distance from internal os to the level of cerclage, E is the distance from the level of cerclage to the external os. Typically the fetal head is the presenting part seen adjacent to the level of the internal os or funnel. The maternal bladder is seen anteriorly above the anterior lower uterine segment.

than that of the term delivery group, whereas there was no difference in manual cervical measurements between the two groups.<sup>12</sup>

The relative lack of success of the digital exam in predicting PTB is probably due to the fact that it is subjective (interobserver variability of 52%),<sup>14</sup> not accurate for evaluating the internal os (the whole upper half of the cervix is not measurable by this method),<sup>15</sup> and nonspecific (15% to 16% of primiparous women and 17% to 35% of multiparous women who are delivered at term have cervixes that are 1 to 2 cm dilated by manual examination in the late second trimester).<sup>16</sup> Sonographic CL measurements are, on the average, 11 mm longer than manual estimations. The majority, about three fourths, of asymptomatic women with funneling of the internal os have a closed and at least 2-cm-long cervix on manual examination.<sup>13</sup> These data show that TVU is clearly superior to manual examination for evaluation of the cervix and prediction of PTB.

## WHAT TO MEASURE

### Cervical Length

Different cervical parameters have been evaluated as predictors of PTB (Fig. 18-7). CL, as measured from the

internal to the external os along the endocervical canal, is the most reproducible and reliable measurement (Figs. 18-3B and 18-8A and B). If the cervical canal is curved, the CL can be measured either as the sum of two straight lines that essentially follow the curve (when the deviation of the canal is > 5 mm), or by a straight line between internal and external os (Fig. 18-8C).<sup>17</sup> A short CL is usually straight, and the presence of a curved cervix generally signifies a CL greater than 25 mm and, therefore, is a reassuring finding. If the cervical canal is closed, CL is probably the only parameter that needs to be measured.

### Funneling

In about 10% of low-risk<sup>18</sup> and 25% to 33% of high-risk women,<sup>12,13,17</sup> the internal os is open (Fig. 18-9). In this case, the open portion of cervix (funnel length) and internal os diameter (funnel width) can be measured. Percent funneling is defined as funnel length divided by total CL. Total CL is equivalent to the sum of funnel length and functional CL. Functional CL in this case is the closed portion of the endocervical canal only. Functional CL is the sonographic CL used for calculations and predictions, and the term CL, if not otherwise specified, refers to the functional CL.

If funneling is present, the shape can be recorded. A continuous process of funneling has been described, going from a normal T shape, to Y, then V, and finally a U shape (Figs. 18-10 and 18-11).<sup>19</sup> It appears that U-shaped funneling is more likely to be associated with PTB compared with a V-shaped funnel<sup>20</sup>; however, these distinctions are somewhat subjective.

Careful evaluation of the apparent funneling with transvaginal ultrasound over several minutes (at least 5) should resolve any question of the morphology of the upper cervical canal. In some instances, the depth of a true funnel may be difficult to quantify, because the funneled portion may merge with the lower uterine segment and the characteristic shoulder that depicts the border between lower uterine segment and the true cervix may be flattened. Funneling has been reported to have higher interobserver variability among examiners and different centers than CL.<sup>18</sup>

In spite of these difficulties, funneling has been reported to have better or similar predictive accuracy for PTB than CL.<sup>12,13,18</sup> In one high-risk population, minimal funneling (< 25%) noted between 14 and 22 weeks was not associated with a significant increase in PTB, whereas moderate (25% to 50%) and severe funneling (> 50%) were associated with a 50% or more probability of PTB.<sup>13</sup> The fact that less than 25% funneling is not associated with an increased risk of PTB is important, because this is a common finding that should not raise alarm or result in intervention. Funneling has also been shown in all studies, not just high-risk ones, to predict PTB.<sup>12,13,17,18,21-26</sup> Almost always, if funneling is present, the CL is short (< 25 mm). In the presence of a short CL, the presence of funneling may<sup>18,22,25,26</sup> or may not<sup>17,21,23,24</sup> add to the prediction of PTB or adverse perinatal outcome. Compared with a CL less than 25 mm alone, adding funneling can increase the sensitivity for PTB (from 61% to 74%) without major changes in specificity, and positive and negative predictive values.<sup>22</sup> Also, the risk of PTB is higher if both a short CL and funneling are detected, compared with a short CL without funneling.<sup>26</sup> On the contrary, the presence

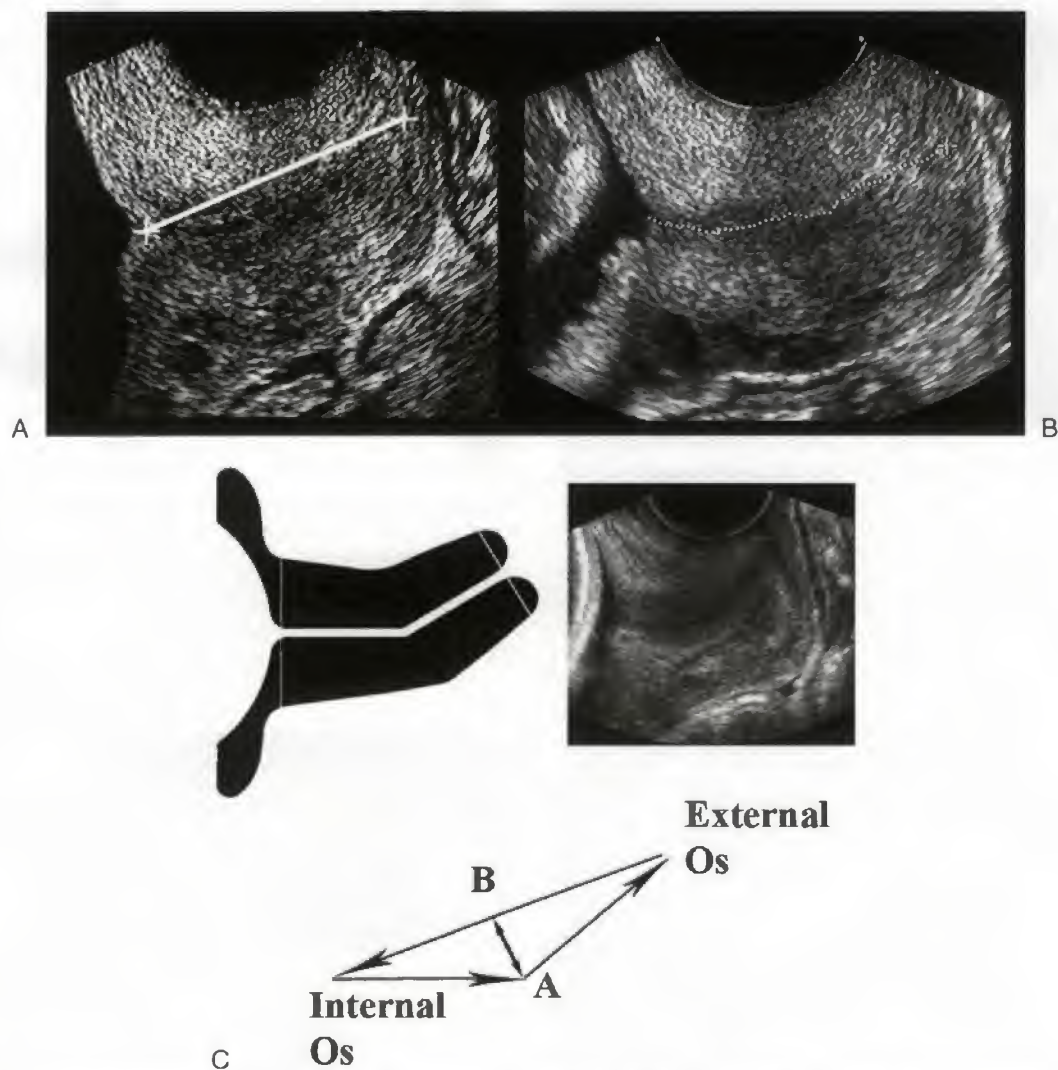


**FIGURE 18-8.** Measurement of the cervix using three techniques. *A.* The cervical length is measured in a straight fashion from the internal os to the external os because the cervical canal appears to be straight. *B.* The canal is measured with the manual draw feature of the equipment. As you can see, the draw feature will not properly draw the cervical canal and will overestimate the cervical length. *C.* The diagram and the ultrasound image illustrate the curved cervix and the decision-making process whether to measure the cervix in a straight line or in two steps. The curved cervix can be assessed by connecting the internal os to the level where the straight canal bends upward (A), then another line connects A to external os. The external os is connected with a line to the internal os. If the height of this triangle (distance A-B) is more than 5 mm, then the cervical canal should be measured in two steps.



of funneling in a woman with a normal ( $\geq 25$  mm) CL does not seem to increase her risk of PTB<sup>27</sup> (funnel Y in Fig. 18–10).

### Other Measurements

Many parameters other than CL and presence or absence of a funnel have been studied,<sup>28</sup> including funnel width, funnel

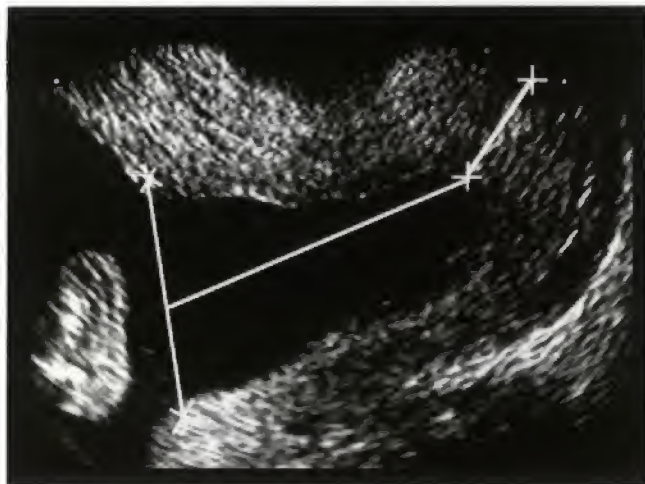


**FIGURE 18–9.** Sonogram in a patient with cervical funneling. Typically funnel width is measured by identifying the lower uterine segment notch (or genu) either anteriorly or posteriorly (or both), and a line perpendicular to the axis of the cervical canal connects to the opposite side. The funnel length is measured by connecting the middle of the funnel width with the tip of the funnel. Cervical length is measured from the tip of the funnel to external os.

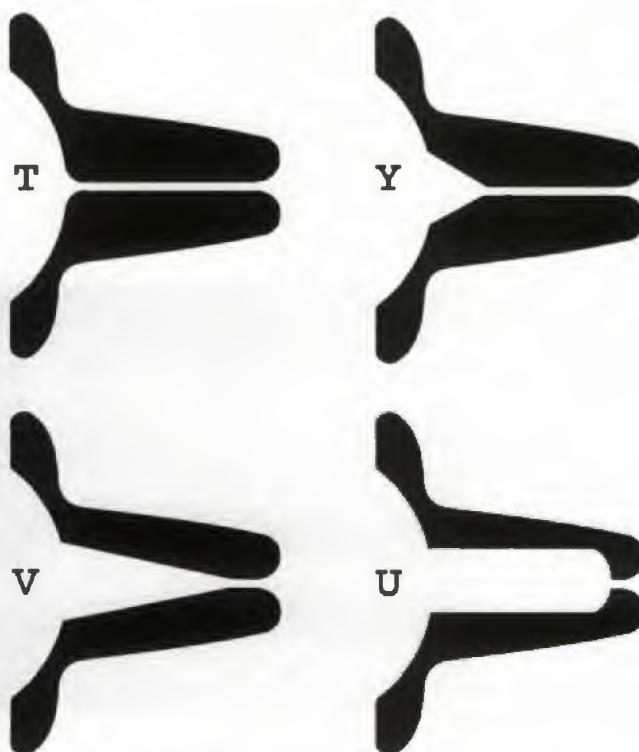


**FIGURE 18–10.** These diagrams show the typical shapes of the cervical funnels. T represents a closed normal cervix. Y represents a small funnel, which if less than 25%, with a cervical length  $\geq 25$  mm, may not be clinically significant. V represents a more significant funnel, closer to the external os. U represents the funnel of most concern; this is the clinical situation in which more often the cervix can be dilated by manual examination.

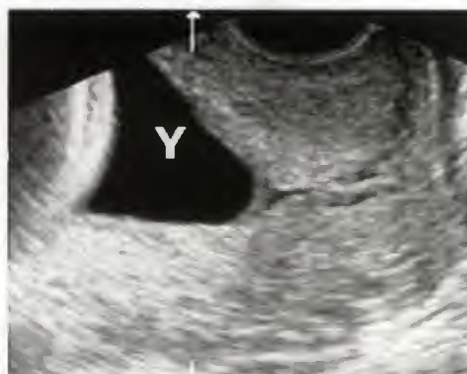
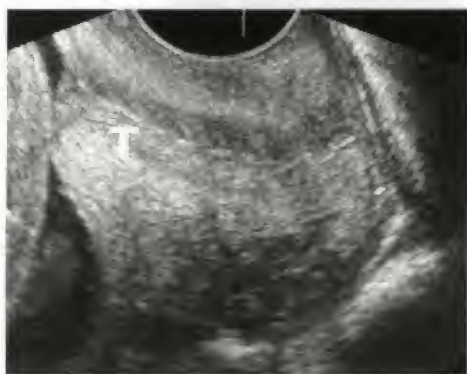


**FIGURE 18–11.** These ultrasound images show the respective funnel shapes, as depicted in Figure 18–10.

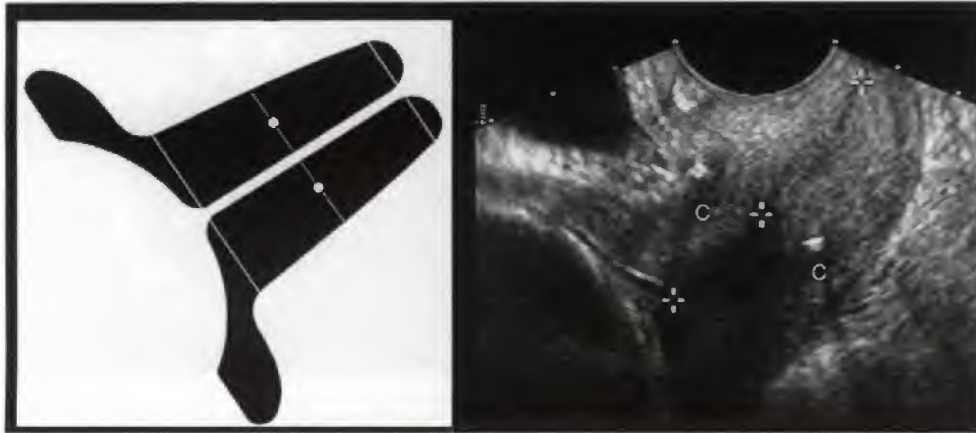


**FIGURE 18-12.** Diagram and an ultrasound image of a cervix with a cerclage in place. The cerclage (C) is seen as two bright spots seen in the anterior and posterior lips of the cervix. The measurement of the cervix in these cases is done from internal os to the level of cerclage, and from the level of cerclage to the external os. Note that the orientation of the cervix in this figure is not horizontal but vertical, a situation that usually makes the identification of the landmarks more difficult because the ultrasound beam does not hit the endocervical canal in a perpendicular fashion.

length, endocervical canal dilatation, cervical index (funnel length +1/functional length), anterior and posterior cervical width, cervical angle, cervical canal contour (straight versus curved), cervical position (horizontal versus vertical), lower uterine segment thickness, vascularity, visibility of chorion-amnion membranes at the internal os, presence of sludge,<sup>29</sup> cervical gland area,<sup>30</sup> quantitative tissue characterization,<sup>31</sup> and others. None of these parameters has proved more reliable or predictive than CL. Additionally, there is insufficient evidence to assess if the addition of any of these parameters improves the predictive accuracy already provided by CL. Several other measurements may be taken in the presence of a cerclage (Figs. 18-7 and 18-12 to 18-15). Although these measurements are predictive of PTB, again CL alone can be used with good predictive accuracy even in women with a cerclage in place.

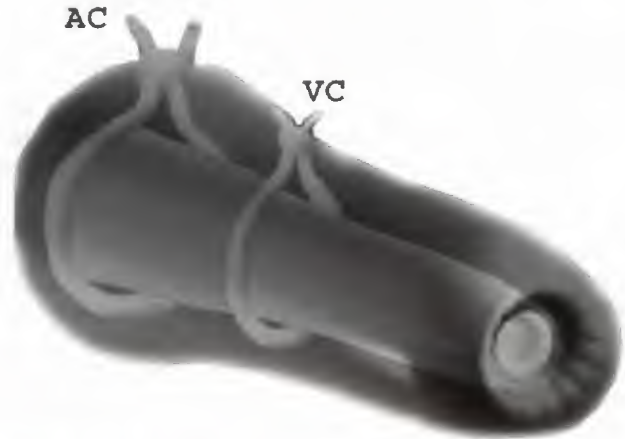


**FIGURE 18-13.** Three dimensional (3D) graphic of the cervix showing the usual locations of abdominal (AC) and vaginal (VC) cerclages. As seen in the image, the abdominal cerclage is high up and close to the level of the lower uterine segment, whereas the vaginal cerclage is placed usually somewhere in the middle of the cervical canal.



**FIGURE 18-14.** Three ultrasound images of vaginal cerclages. A. A two-dimensional ultrasound image of a cervix with a vaginal cerclage in which the cerclage sutures are seen only as two bright spots (arrows). B. A three-dimensional ultrasound derived image of a cervix with a vaginal cerclage in the axial plane in which the suture is depicted in its entirety (arrows). C. A three-dimensional ultrasound-derived image of a cervix with a vaginal cerclage (arrows) in the axial plane in which the suture has pulled through from the posterior lip of the cervix and can no longer be effective in preventing preterm birth.





**FIGURE 18-15.** Two ultrasound images of the cervix with an abdominal cerclage. *A.* A two-dimensional ultrasound image of a cervix with an abdominal cerclage in which the cerclage sutures (arrows) are seen only as two bright spots placed at the level of the internal os. *B.* A three-dimensional ultrasound-derived image of a cervix with an abdominal cerclage in the axial plane. Note the entire visualization of the suture (arrows).

### DYNAMIC CHANGES (SPONTANEOUS OR AFTER TRANSFUNDAL PRESSURE)

In less than 5% of TVU, CL may change dynamically during the course of a 5- to 10-minute examination, and in some cases, funneling of the upper cervical canal may appear and resolve. This usually happens if the woman is having contractions. Similarly, the cervix may shorten in response to transfundal pressure (TFP) in approximately 5% of cases.<sup>32</sup> When changes occur, the shortest CL should be recorded. In most of the cases in which the cervix shortens spontaneously or in response to TFP, it is already abnormal at baseline. There is conflicting evidence concerning whether TFP increases the screening potential of TVU. In one study, only one of nine patients with an initially normal cervix who had abnormalities after the application of TFP delivered preterm,<sup>12</sup> and adding response to TFP as a screening criteria for PTB did not significantly increase predictive accuracy. In contrast, in a larger study, dynamic changes, either spontaneous or after TFP, significantly improved the predictive accuracy of TVU for PTB.<sup>17</sup> Dynamic changes may indeed improve predictive accuracy; use the shortest best CL.

### NORMAL VERSUS ABNORMAL

A normal CL is 25 to 50 mm at 14 to approximately 30 weeks. Twenty-five millimeters is the 10% percentile for low-risk singletons<sup>18</sup> and approximately the 25% percentile for high-risk singletons.<sup>12,17</sup> A short CL is one less than 25 mm at these gestational ages, with the best prediction for PTB obtained at 16 to 24 weeks. **The shorter the CL, the higher the risk of PTB.**<sup>18</sup> A short CL is a better predictor of early PTB than later PTB.<sup>33</sup> A CL greater than 50 mm is also normal but often reflects a measurement that includes the lower uterine segment, as often happens before 16 weeks.

### BEST GESTATIONAL AGE AND FREQUENCY OF EXAMINATIONS

Almost all patients, even those at the highest risk, have a normal CL in the first and early second trimesters. Before 14 weeks, measuring CL may be predictive only in very high-risk women, such as those with a prior second trimester loss

or history of a large cervical cone biopsy. In a study of TVU of the cervix in high-risk women, only 5% had a CL greater than 25 mm between 10 and 14 weeks, and these women were indeed very high risk because of prior history.<sup>34</sup> Sensitivity for the prediction of PTB is very low in this time interval, because most women destined to deliver preterm have cervical shortening usually detected  $\geq 16$  weeks. An additional drawback of very early screening is that the lower uterine segment is difficult to distinguish from the true cervix in the late first and early second trimesters. After 30 weeks, the CL progressively shortens in preparation for term labor, so that a CL less than 25 mm, especially 15 to 24 mm, after 30 weeks can be physiologic and not associated with an increased risk of PTB in asymptomatic women. The most common gestational age when a short cervix or funneling develops is 18 to 22 weeks.<sup>12,13</sup> Therefore, if a screening program is to include only one CL assessment, it should be done in this time interval. High-risk patients destined to deliver preterm may have earlier cervical changes. **The earlier the short CL is detected, the higher the risk of PTB.** A cervix of less than 25 mm had a positive predictive value of 70% when detected between 14 and 18 weeks, and of 40% when detected between 18 and 22 weeks, in high-risk women.<sup>12</sup> Therefore, it may be that women with the highest risk of PTB (e.g., patients with classical histories of cervical incompetence, prior second trimester losses, or early PTBs) may benefit from early (i.e., 14–18 weeks) ultrasound examination to determine their need for intervention.

The benefit of repeated TVU examinations and the ideal interval for repeating TVU has not been clearly established. If a screening program were employed in relatively low-risk women, one TVU of the cervix at approximately 18 to 22 weeks would likely be most effective. It appears that one normal TVU CL assessment between 14 and 18 weeks and another between 18 and 22 weeks is reassuring in most high-risk women.<sup>22</sup> In women at very high risk for PTB, such as those with prior second trimester loss or very early spontaneous PTB, some have advocated TVU of the cervix every 2 weeks, at least between 14 and 24 weeks. The fact that TVU at 14 to 22 weeks is at least as predictive of PTB as TVU after 22 weeks is important, because interventions to

Table 18-2

## Prediction of Preterm Birth by Transvaginal Ultrasound Examination in Specific Populations of Pregnant Women

Author	n	PTB (%)	PTB Defined (wk)	GA Studied (wk)	CL Cut-off (mm)	% abn	Sens	Spec	PPV	NPV	RR
Asymptomatic											
Singleton: low risk (cross-sectional)											
<i>Iams</i> <sup>18</sup>	2915	4.3	<35	22–25	25	10	37	92	18	97	6.2*
Singleton: Prior preterm birth											
<i>Owen</i> <sup>17</sup>	183	26	<35	16–24	25	–	69	80	55	88	4.5
Singleton: Prior cone biopsy											
<i>Berghella</i> <sup>35</sup>	109	13	<35	16–24	<25	28	64	78	30	94	4.7
Singleton: Müllerian anomaly											
<i>Airolidi</i> <sup>36</sup>	64	11	<35	14–24	<25	16	71	91	50	96	13.5
Singleton: Prior D&E											
<i>Visintine</i> <sup>37</sup>	131	30	<35	14–24	<25	51	53	75	48	78	2.2
Twins											
<i>Goldenberg</i> <sup>38</sup>	147	32	<35	22–24	≤25	18	30	88	54	74	3.2
Triplets											
<i>Guzman</i> <sup>39</sup>	47	34	<32	15–20	≤25	<25	8.5	25	100	100	72
		NA									
Symptomatic											
Singletons with preterm labor											
<i>Venditelli</i> <sup>40</sup>	200	41	<37	19–36	<30	64	83	88	54	80	2.8

% abn, percent abnormal; CL, cervical length; D&E, dilation and evacuation; GA, gestational age; NPV, negative predictive value; PPV, positive predictive value; PTB%, incidence of preterm birth; RR, relative risk compared with those with normal CL, except\*. compared with values higher than the 75th percentile; sens, sensitivity; spec, specificity.

prevent PTB are most effective when changes leading to PTB are detected early in the process.

## POPULATIONS

There have been numerous studies evaluating the predictive accuracy of TVU CL for PTB in many different populations.<sup>1</sup> The populations screened include asymptomatic women with singleton, twin, and triplet pregnancies, and symptomatic women with preterm labor (PTL) or PPRM, as well as low-risk women, high-risk populations, and patients with a cerclage in place. Although the TVU technique in these studies is similar, study population (in particular, the incidence of prior PTB), gestational age at which TVU was done, frequency of TVU, cervical parameters studied, and outcomes vary. In reviewing the available studies, it is important to use those with the best design, that is, those that describe proper technique, blinding of managing physicians to ultrasound results, and the inclusion of large numbers of patients. In most studies, the cervical parameter found to have the best predictive accuracy, as determined by receiver operating characteristic curves, is a CL less than 25 mm. The screening interval is early in the second trimester, usually between 16 and 24 weeks. The most common primary outcome is spontaneous PTB at less than 35 weeks' gestation (Table 18-2).<sup>17,18,35–40</sup>

### Singleton Low Risk

Numerous studies have reported nomograms for CL in nonselected pregnant women with singleton gestations.<sup>18,41,42</sup>

In low-risk women, CL is a continuous variable, with a mean of 35 to 40 mm from 14 to 30 weeks, with the lower 10th percentile being 25 mm and the upper 10th (90th percentile) being 50 mm.<sup>18,42</sup> A progressive and natural shortening of CL is noticed after 30 weeks, even in patients destined to deliver at term.<sup>41</sup> There may be a very slight progressive linear reduction of CL even before 30 weeks.<sup>43</sup> There seems to be no difference in CL between nulliparous and multiparous women throughout pregnancy, whereas risk factors for PTB such as African origin, age younger than 20 years, low ponderal index, and prior miscarriage or PTB are associated with a shorter CL.<sup>43</sup>

In asymptomatic singleton gestations, as in all other groups, the shorter the cervix, the higher the risk of PTB.<sup>1</sup> Using different cutoffs for CL from 15 to 34 mm, the positive predictive values ranged from 6% to 44%.<sup>1</sup> These relatively low values are likely due at least in part to the low prevalence of PTB in this population (0.8% to 15%). In one of the better-designed, larger studies,<sup>18</sup> the sensitivity was only 37% and the positive predictive value only 18%. This means that the majority (63%) of the few such women without risk factors who delivered preterm were not identified by TVU screening, and that 82% of these low-risk patients who were found to have a short CL less than 25 mm at 24 weeks delivered at or after 35 weeks. Given this findings, routine screening with TVU CL is not recommended for all pregnant women.

### Singleton High Risk

Risk factors for PTB are numerous. Several studies have assessed the predictive value of TVU CL in women with



some of the most important of these risk factors, including a prior PTB,<sup>17</sup> cone biopsy,<sup>35</sup> two or more voluntary terminations,<sup>37</sup> or mullerian anomaly.<sup>36</sup> As Table 18-2 shows, TVU CL between 14 and 24 weeks is predictive of PTB in all of these high-risk populations. In fact, the worse the obstetric history, the shorter the cervix, because prematurity risk is a continuum.<sup>44</sup> A woman with clinical risk factors for PTB who has a normal ( $\geq 25$  mm) TVU CL between 18 and 22 weeks has a risk of PTB of less than 10%, which represents a significant reduction in risk and can prevent unnecessary interventions in these women. On the contrary, the sensitivity of TVU CL to detect which high-risk women will deliver preterm is often higher than 60%, much higher than in low-risk women. The prevalence of PTB less than 35 weeks is often greater than 50% when the additional risk factor of TVU CL less than 25 mm is discovered at less than 24 weeks in these women with historic risk factors for PTB. These positive predictive values are also much higher than those in low-risk women (see Table 18-2). PTB within 4 weeks of TVU occurs in about 13% of asymptomatic women with short CL, and in none of the pregnancies without such change; so steroid therapy for fetal maturity is rarely indicated, even in asymptomatic women with a short CL.<sup>22</sup> It is important to note that, at least in high-risk patients, PTB following the detection of a short CL is most often preceded by PPROM (48%–68%) instead of PTL.<sup>12,45</sup> A CL less than 10 mm in these women is particularly predictive of PPROM.<sup>46</sup> TVU in women with a prior PTB less than 32 weeks demonstrated that the best predictive accuracy is achieved with serial TVUs, including the shortest cervix seen after spontaneous or TFP-elicited changes.<sup>17</sup> The sensitivity and positive predictive value reached 69% and 55%, respectively. This was the only blinded multicenter study controlled for quality performed in women at high-risk for PTB and, therefore, contains the most reliable and valid predictive data in this population.<sup>17</sup>

## Twins

Despite the significant contribution of PTB to perinatal morbidity and mortality in twin pregnancies, the prediction of PTB in twins using traditional clinical means is limited. A CL of 25 mm or less at 24 weeks' gestation is the best of all the predictors of PTB evaluated in twins, including fetal fibronectin and bacterial vaginosis<sup>38</sup> (see Table 18-2). Compared with singleton pregnancies, twin pregnancies that deliver at term have been shown to have a similar TVU CL at 14 to 19 weeks but have a progressively much shorter cervix starting after 20 weeks' gestation.<sup>47</sup> Because cervical shortening can occur after 20 weeks' gestation even in some twin pregnancies destined to deliver at term,<sup>47</sup> TVU of the cervix before 20 to 24 weeks may lead to better prediction of PTB, but unfortunately, the predictive value of sonographic CL determination in twins between 24 and 34 weeks' gestation is low.<sup>48</sup> As with high-risk singletons, a short cervix is a good predictor of PTB in twins. The shorter the CL and the more severe the funneling, the higher the risk of PTB. Importantly, only less than 10% of twin pregnancies with a sonographic CL of greater than 35 mm between 18 and 26 weeks deliver before 35 weeks.<sup>49</sup> This finding should allow obstetricians to avoid bed rest and other interventions commonly used in twin pregnancies. Unfortunately,

sensitivity of TVU CL to predict which twin gestations will deliver preterm is only 30%. This is probably because multiple gestations deliver preterm not because of cervical insufficiency but because of rapid uterine expansion leading to contractions, a process not well screened by TVU CL.<sup>1</sup>

## Triplets

Few studies have reported on TVU of the cervix and its prediction of PTB in triplet pregnancies. As shown in Table 18-2, sensitivity of TVU CL to predict which triplet gestations will deliver preterm is low, as in twin gestations, making this screening test not very effective in general in multiple gestations.<sup>39</sup>

## Women With Cerclage

TVU of the cervix has been evaluated in women with history-indicated, ultrasound-indicated, or physical examination-indicated cerclage in place. Most studies have shown that transvaginal cerclage is placed in the middle part of the cervix in the vast majority of cases (see Figs. 18-13 and 18-14).<sup>50-52</sup> Transabdominal cerclage is instead placed at the internal os (see Figs. 18-13 and 18-15). It would be reasonable to believe that the higher (closer to the internal os) the cerclage suture is placed, the most effective is the prevention of PTB. Evaluation of pre- and post-cerclage TVU CL has shown that CL usually increases post-cerclage, and that an increase in CL is associated with a higher rate of term delivery.<sup>53,54</sup>

Studies that evaluated the accuracy of TVU for predicting PTB in patients with cerclage<sup>50-53</sup> all show that TVU cervical parameters are predictive of PTB. CL less than 25 mm and upper cervix (the closed portion above the cerclage, see Fig. 18-12) less than 10 mm are probably the two best predictive parameters.

## THREE-DIMENSIONAL TRANSVAGINAL ULTRASOUND EXAMINATION OF THE CERVIX

Recent developments in ultrasound technology make possible the acquisition of two-dimensional ultrasound data in a three-dimensional volume through dedicated ultrasound transducers. The three-dimensional volume data are presented in a variety of orthogonal multiplanar displays in which sagittal, axial, and coronal views of the cervix are shown simultaneously (Fig. 18-16). The multiplanar view makes possible visualization of anatomic planes that are simply impossible with two-dimensional ultrasound (i.e., planes that are perpendicular to the ultrasound beam such as the coronal plane of the cervix). In addition, the three-dimensional multiplanar display makes possible the visualization of the true midsagittal plane of the cervix by objectively selecting the midsagittal plane in the coronal view (Figs. 18-17 and 18-18). The coronal view of the cervix is a unique view that is obtained only with three-dimensional ultrasound and provides new information on the shape and dimensions of the endocervical canal. The visualization of the funnel is also improved by using three-dimensional ultrasound because the funnel can be evaluated in all three

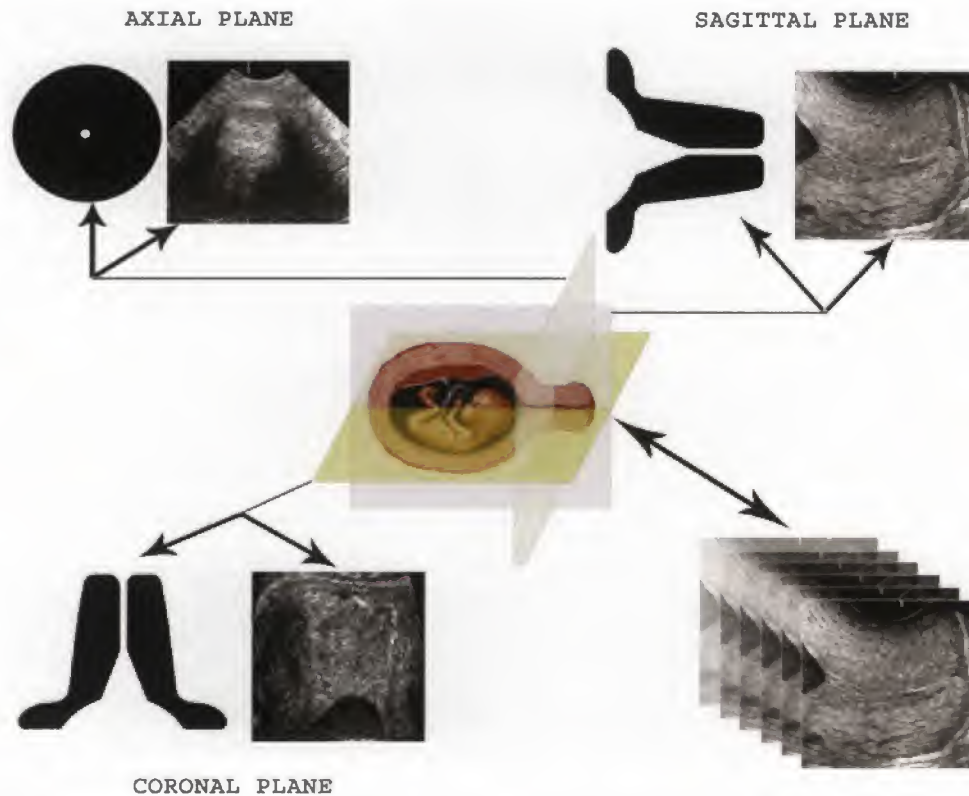


**FIGURE 18-16.** Diagram illustrating a three-dimensional volume acquisition of two-dimensional images of the cervix in the sagittal plane and the subsequent display of the cervix in three orthogonal planes (sagittal, axial, and coronal). Note that these three planes simultaneously shown (sagittal, axial, and coronal) are interactively linked to each other in a 90-degree (orthogonal) relationship. The evaluation of the cervix is not limited to the sagittal plane only but extends with the axial and coronal planes. Note that cervical length, and funnel length and width are shown both in sagittal and coronal planes. The coronal plane funnel width is the true funnel width, whereas what most people call funnel width in sagittal view is really the true funnel height.

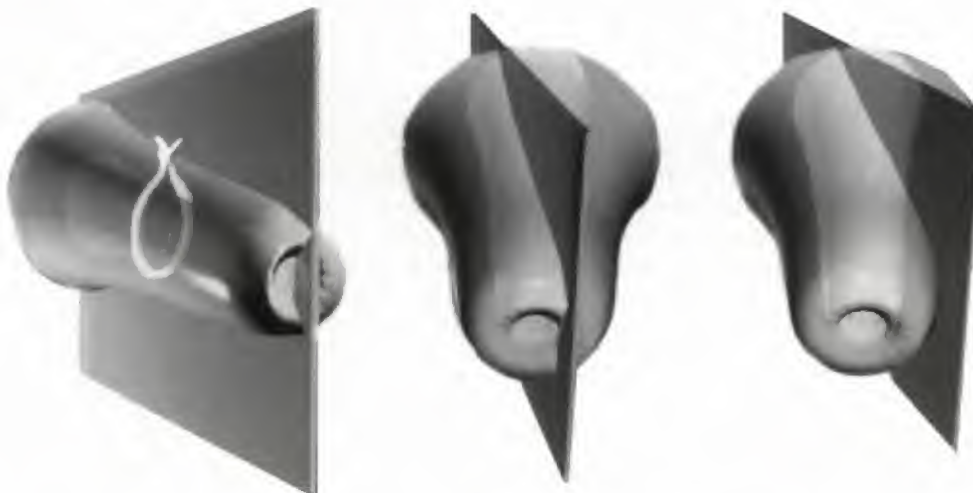


**FIGURE 18-17.** These diagrams illustrate the relationship between the ultrasound beam and the midsagittal axis of the endocervical canal. In the left diagram, the ultrasound beam is precisely lined up in the midsagittal axis of the endocervical canal, which theoretically is the right plane to estimate the cervical length. The diagram in the middle shows that the ultrasound beam is cutting the endocervical canal obliquely, somewhat overestimating its length. The diagram on the right shows the ultrasound beam cutting only part of the endocervical canal, thus significantly underestimating the cervical length. As the operator tries to blindly line up the ultrasound beam with the midsagittal plane of the endocervical canal, he typically observes small differences (1–3 mm) in the values from one measurement to the other.



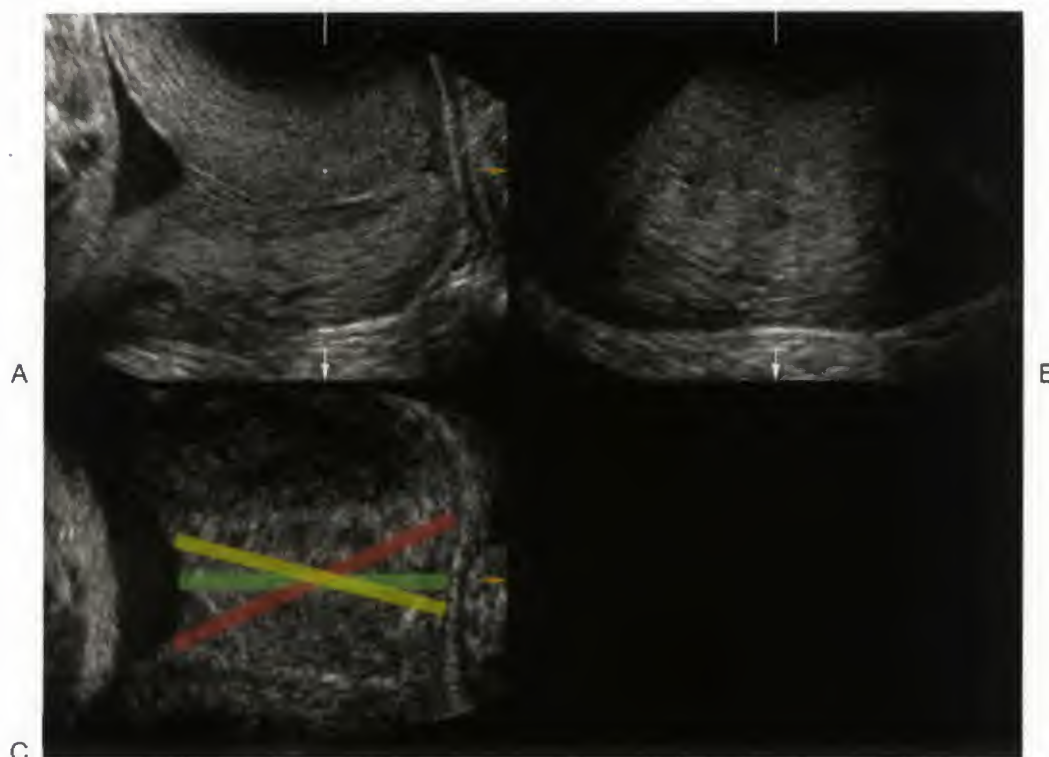


**FIGURE 18-18.** An ultrasound image of a normal cervix displayed in the multiplanar display. *A.* The sagittal plane of the cervix that corresponds to the acquisition plane of this volume. *B.* The computer-generated axial plane of the cervix cut precisely at the level of the cross-planar point (the orange dot) 90 degrees from the sagittal plane. *C.* The coronal plane of the cervix again precisely 90 degrees from the sagittal plane coronally. The green line in the coronal plane represents the true midsagittal plane of the cervical canal and is operator selectable. The green line illustrates the point the three-dimensional ultrasound objectively obtains the true midsagittal plane of the cervix. The red and yellow lines represent the parasagittal planes that commonly two-dimensional ultrasound operators take as they blindly try to line up the ultrasound beam to the midsagittal plane of the cervix.

planes: sagittal, axial, and coronal. The coronal funnel width is the true width of the funnel because the commonly known funnel width as seen with two-dimensional ultrasound represents the true funnel height (Fig. 18-19). The coronal funnel or endocervical canal widths are not necessarily the same value as their respective sagittal values and as such may provide additional, new and potentially useful information<sup>55</sup> (see Figs. 18-16 and 18-20 to 18-22). Three-dimensional ultrasound makes it possible to obtain an axial plane through the cervix at the level of the cerclage, demonstrating the entire stitch (see Figs. 18-14 and 18-15).<sup>55</sup> This view is not readily obtainable with conventional two-dimensional ultrasound. Whether three-dimensional ultrasound imaging will improve clinical management in patients with or without a cerclage in place is unknown. New display and acquisition methods enable the operator to view the cervix in multiple slices in operator-selectable distances such as computed tomography or magnetic resonance imaging-like displays or view the sagittal and coronal views of the cervix in real time such as with virtual contrast imaging (Figs. 18-23 to 18-25). Volume imaging methods of the cervix provide not only additional imaging views of the cervix but also assist in better standardizing the evaluation of the cervix by obtaining the important views of the cervix (i.e., the midsagittal view of the cervix) in a controlled fashion. Further research work is needed to evaluate whether this additional information has any impact in clinical management.

### WHAT PATHOPHYSIOLOGIC MECHANISMS ASSOCIATE A SHORT CERVICAL LENGTH WITH PRETERM BIRTH?

There are three main mechanisms that have been associated with the development of an asymptomatic short CL. First, the most obvious hypothesis is that a short CL is caused by an intrinsic weakness of the cervix, or cervical insufficiency (this term is preferred rather than cervical incompetence).<sup>56</sup> This cervical insufficiency is due in most cases to traumatic or surgical damage, or much more rarely, a congenital disorder or a connective tissue disease. It is interesting to note that almost no women, even the most high-risk, have a short CL in the first trimester.<sup>34</sup> This is probably because the pressure the growing gestational sac exerts on the cervix will be unlikely to open up even the weakest of cervixes. Second, another hypothesis is that a short CL is due to an inflammatory or infectious process. There is a strong association between a short CL on TVU and infection. High amniotic fluid Interleukin-6 (IL-6), later development of chorioamnionitis,<sup>57</sup> and acute inflammatory lesions of the placenta<sup>58</sup> have all been associated with a short CL on TVU. Women with both a short CL and bacterial vaginosis have a higher incidence of PTB than matched women with just a short CL but no bacterial vaginosis.<sup>59</sup> A short CL leading to PTB is often associated with PPROM instead of PTL, providing

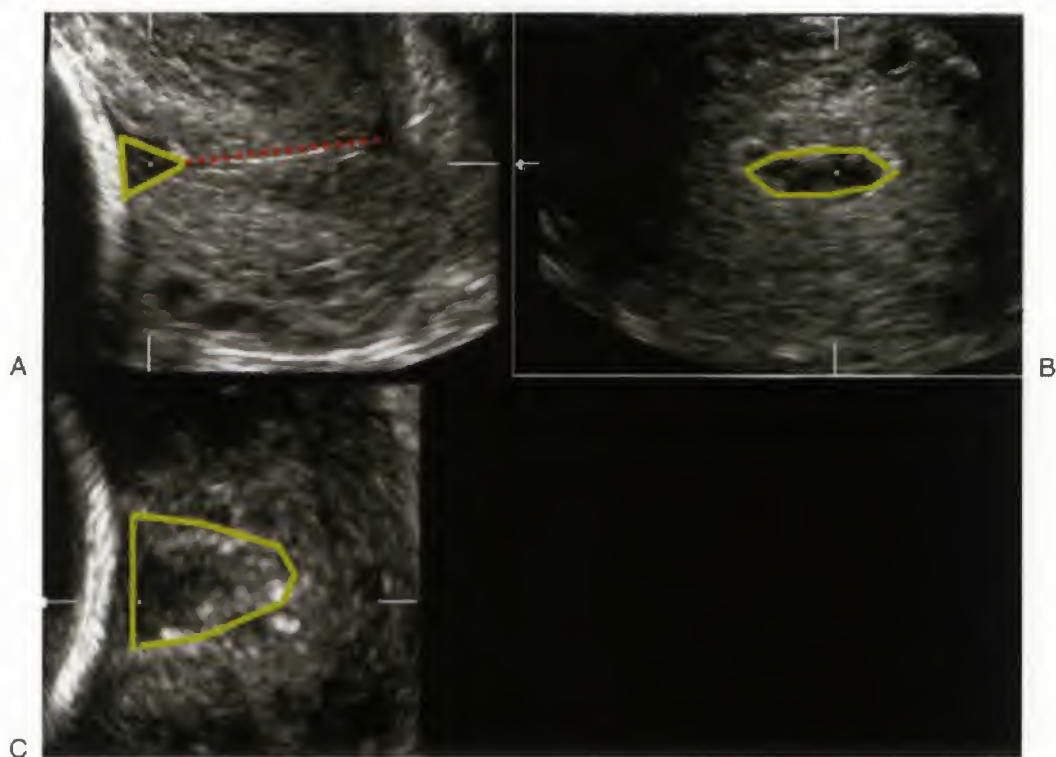


**FIGURE 18-19.** A multiplanar image of the cervix with minimal funneling (*yellow trace*) in the sagittal plane (*A*). In the axial plane (*B*) and the coronal plane (*C*), the funnel length and width are both seen significantly larger as compared with the sagittal plane.

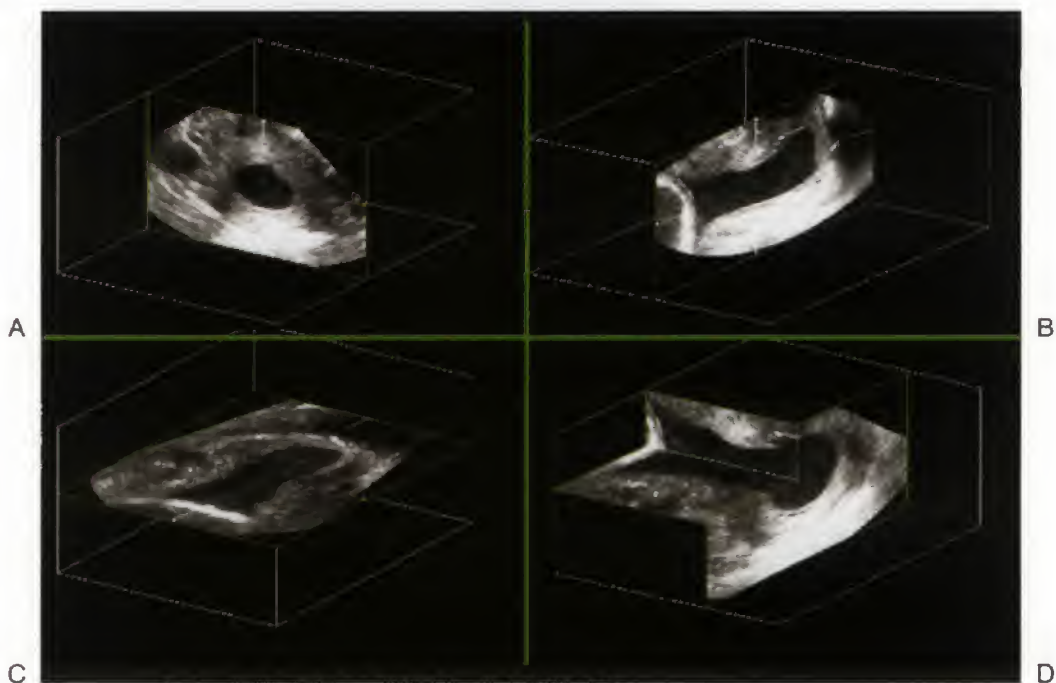


**FIGURE 18-20.** A composite image of a cervix with funnel shown in a multiplanar display (*A, B, C*) and in "Niche" mode (*D*) that shows all three planes intersecting with each other to create a three-dimensional relationship between the planes.





**FIGURE 18-21.** The three-dimensional ultrasound-derived coronal planes of six different cervixes depicting the cervical canal shape. Note the different shapes of each of these cervixes in the coronal plane.



**FIGURE 18-22.** A multiplanar display of the cervix (*A* is sagittal, *B* is axial, and *C* is coronal) with a significant funnel with "sludge" in it seen in *A* and *C*. Note that the "sludge" is better visualized in the coronal plane (*C*). Also, note that coronal plane of the funnel is more than twice as wide as is the height of the funnel.

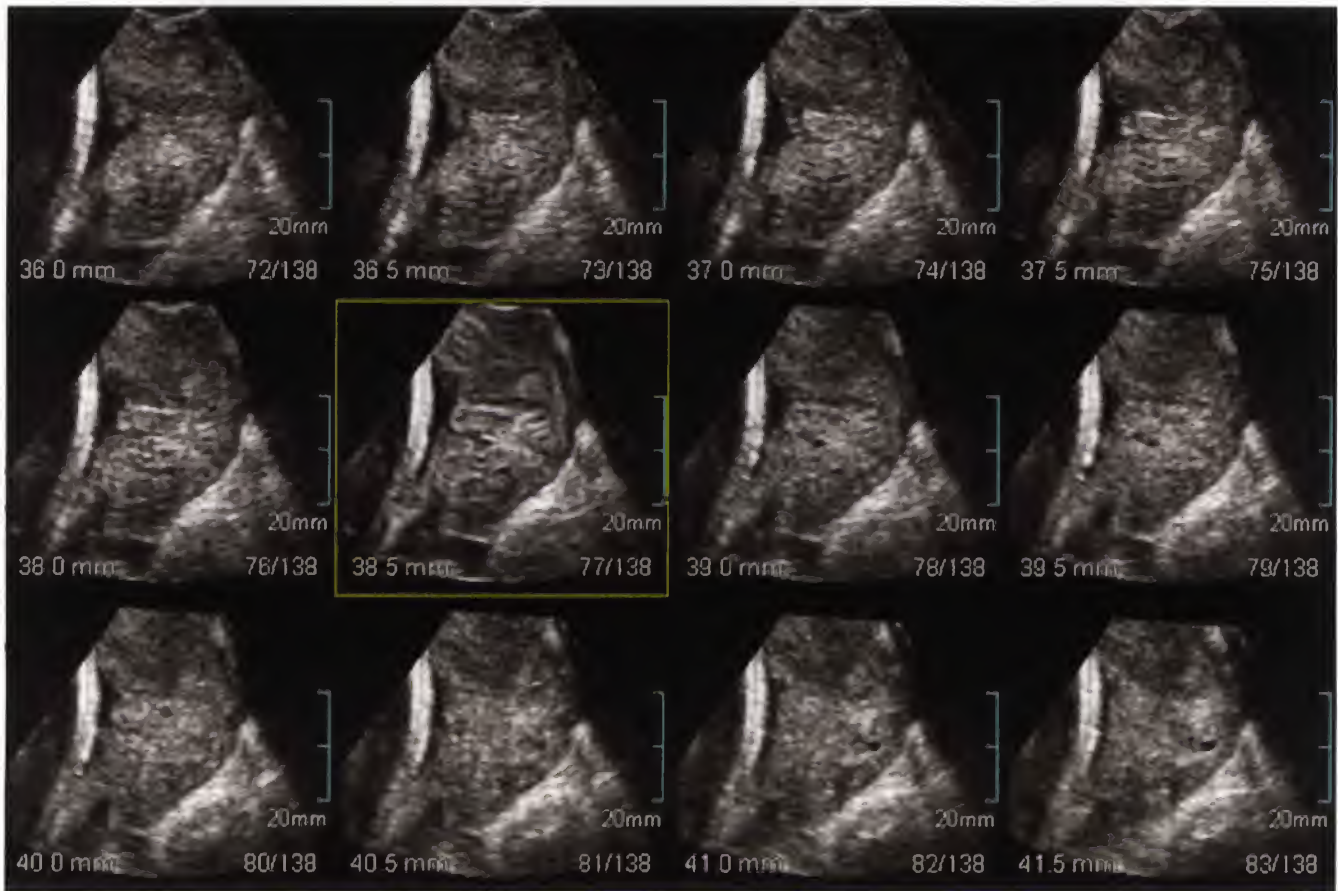


**FIGURE 18-23.** A relatively new way of presenting volume ultrasound data in a “CT and MRI like” display. The three-dimensional ultrasound volume of the cervix is shown here in multiple images of the cervix within the volume in the sagittal plane (the operator may select coronal and axial planes too) precisely 0.5 mm apart from each other. This display appears to be useful especially to understand volume ultrasound imaging of the cervix and better identify the image that represents the adequate plane to measure the cervical canal.

additional evidence for the role of infection in these women.<sup>45</sup> There is insufficient evidence thus far to discern if the infection causes the development of the short CL, or the association between infection and short CL occurs because the short CL allows ascending infection from the vagina. A short CL can provide easier access of potentially pathologic vaginal organisms into the intrauterine environment, leading to prolonged subclinical chorioamnionitis and subsequent PTB. Women with a normal CL have mechanical and immunologic protection against the ascent of lower vaginal organisms.

Third, recent studies have shown that the majority of asymptomatic women with CL less than 25 mm before 24 weeks have some contractions, more than controls with a normal cervix.<sup>60,61</sup> It is unclear whether contractions cause the short CL, are a result of the short cervix, or whether these two factors work synergistically.

Most probably, these three, as well as other mechanisms, often act synergistically in certain women to contribute, in each individual in different ways, to the development of a short CL.

### INTERVENTIONS FOR PREVENTING PRETERM BIRTH IF A SHORT CERVICAL LENGTH IS IDENTIFIED IN ASYMPTOMATIC WOMEN

Many investigators believe the high negative predictive value of TVU of the cervix is important because women with a normal CL can be reassured and interventions avoided. However, a high negative predictive value alone is not sufficient to validate that screening is beneficial. For TVU to be judged cost-effective, there must be an effective intervention to prevent PTB if the test is positive.

#### Ultrasound-Indicated Cerclage

Because cervical insufficiency is one of the leading hypotheses for short CL, cervical cerclage has been the first intervention postulated to be beneficial in this clinical situation. Randomized studies on history-indicated (previously called prophylactic, or elective) cerclage without the use of TVU have shown that this procedure does not prevent PTB in



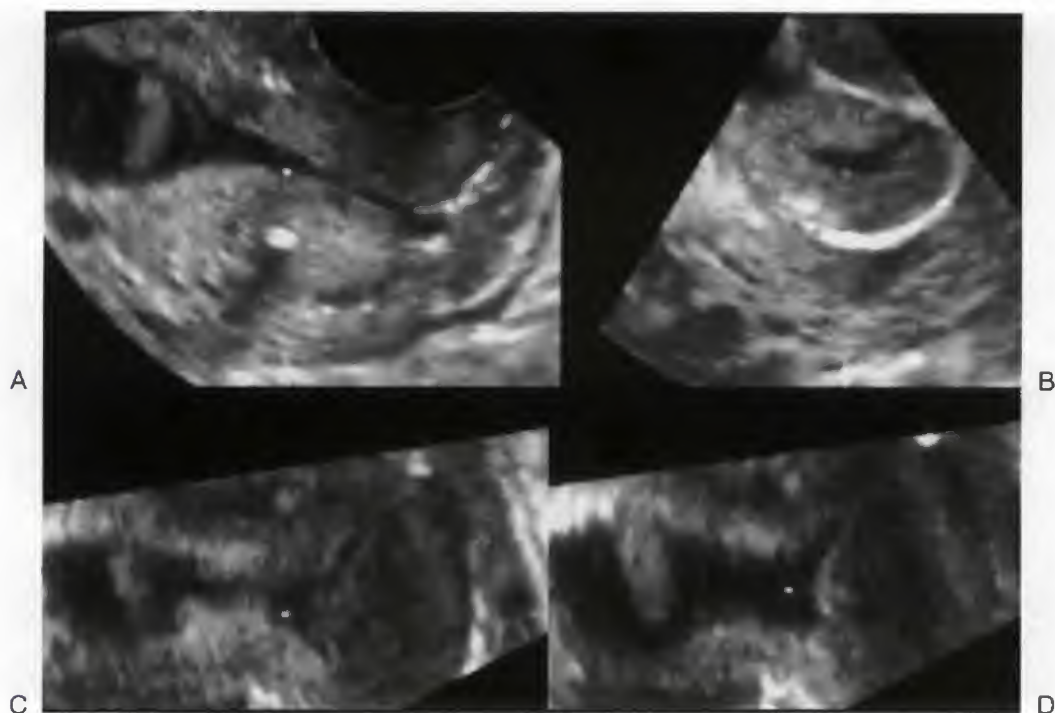


**FIGURE 18-24.** A, B, C. A four-dimensional multiplanar image of the cervix with a vaginal cerclage with funneling present before fundal pressure. D. The coronal plane of the funnel after 15 seconds of fundal pressure. Note that the funnel width is widened in the coronal plane after the fundal pressure, something that we simply cannot observe with two-dimensional ultrasound.

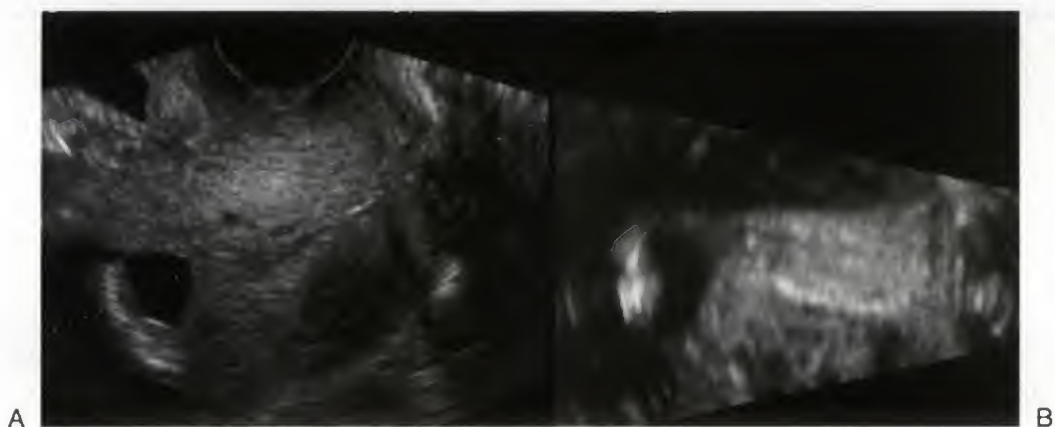


**FIGURE 18-25.** Virtual contrast imaging (VCI) of the cervix otherwise known as thin volume imaging. On the left (A), there is a two-dimensional ultrasound image of the cervix displayed simultaneously with a VCI derived image of the cervix in the coronal plane (B). This dual view enables the operator to evaluate the cervix real time not only in the sagittal plane but also in the true coronal plane by properly placing the dotted green line in the preferred plane in the two-dimensional image, as seen on the left.

high-risk singleton gestations,<sup>62,63</sup> except for the subgroup of women with three or more prior second trimester losses or PTBs,<sup>64</sup> and it is also not beneficial in twin gestations.<sup>65</sup> Given these disappointing results, researchers have hypothesized that a subgroup of women in whom a cerclage may be beneficial could be identified with TVU of the cervix. For asymptomatic women with a short CL, in fact the only intervention studied so far by randomized trials has been cervical cerclage. Cerclage was indeed devised more than 50 years ago for women with both a poor obstetric history

characterized by second trimester losses, and cervical changes in the current pregnancy.<sup>66,67</sup> The four randomized trials<sup>68-71</sup> on the efficacy of ultrasound-indicated cerclage have been analyzed in a meta-analysis,<sup>72</sup> which allowed not only larger numbers and more robust statistics but also careful analysis of different populations of women with a short CL. In fact, ultrasound-indicated cerclage has different effects in different populations (Table 18-3).<sup>72,73</sup> In women with a singleton gestation and a prior PTB or a second trimester loss, performing a cerclage if the TVU CL becomes

**Table 18-3** Efficacy of Ultrasound-Indicated Cerclage<sup>72,73</sup>

Population	Effect of Cerclage on PTB <35 Weeks
Singleton gestations	
Low-risk for PTB (no other risk factor)	24% decrease (nonsignificant)
Prior PTB 16-36 weeks	39% decrease (significant)
Prior second trimester loss	43% decrease (significant)
Twin gestations	215% increase (significant)

PTB, preterm birth.

less than 25 mm prior to 24 weeks prevents recurrent PTB. In women with a singleton gestation and either no risk factors, ultrasound-indicated cerclage was neither beneficial nor detrimental, with more studies needed to assess its efficacy. In women with twin gestations, ultrasound-indicated cerclage was detrimental. This last finding is not surprising, given the fact that TVU is not a good screening method for PTB in this population, who probably has PTB because of contractions and not a weak cervix.<sup>74</sup> Interestingly, cerclage for a short CL is efficacious both before and after 20 weeks, and both at the 25 and 15 mm cutoffs. Interestingly, the placement of a reinforcement (also called rescue) cerclage once a first cerclage seems to be failing is not associated with benefit, and this procedure should be avoided.<sup>75</sup>

### Indomethacin

The only randomized trial<sup>69</sup> that showed benefit from cerclage also gave indomethacin to these women, and not to the controls, raising the possibility that indomethacin may have contributed significantly to the prevention of PTB in that study. Analysis of the effect of indomethacin indeed reveals that it can prevent PTB less than 24 weeks and PPROM in women with a short CL.<sup>76</sup> Given that women with a short CL are often found to be having contractions,<sup>60,61</sup> it is possible that one of the most efficacious interventions is tocolytic therapy.

### Antibiotics

A short CL has also been associated with infection. Analysis of the effect of antibiotics reveals no effect of this therapy on prevention of PTB in women with a short CL.<sup>77</sup> Unfortunately antibiotics have often failed to prevent PTB when used for other risk factors for PTB, such as just a prior PTB,<sup>78</sup> positive fetal fibronectin,<sup>79</sup> or symptomatic PTL.<sup>80</sup> Other interventions such as bed rest, progesterone therapy, and others have not yet been adequately studied.

### ANOTHER BENEFIT OF TRANSVAGINAL ULTRASOUND SCREENING IN ASYMPTOMATIC WOMEN: AVOIDING CERCLAGE IF EXAMINATION IS NORMAL

There at least two major benefits to TVU screening. First, it identifies women who may benefit from cerclage (i.e., women with a prior PTB or second trimester loss who develop a short CL in the subsequent pregnancy at 14 to 24 weeks). Second, it can be used to avoid performing unneeded

interventions (e.g., cerclage) in women whose TVU CL remains normal. One randomized study<sup>81</sup> and three non-randomized studies<sup>82-84</sup> have evaluated whether women with suspected cervical insufficiency can be safely followed with TVU, with placement of a cerclage only in those who develop a short CL, compared with universal history-indicated cerclage. At least 60% of these high-risk women maintain a normal CL until after 24 weeks and deliver at term, and can be spared any intervention. Only about 40% develop a short CL and are at true risk of PTB, and can be offered intervention. Management of women with risk factors for PTB with serial TVU of the cervix appears to be a safe alternative to traditional history-indicated cerclage, but this finding should be confirmed by larger randomized trials.

### DIAGNOSIS AND MANAGEMENT OF WOMEN WITH SUSPECTED PRETERM LABOR

TVU of the cervix has been studied extensively as a predictor of PTB in women with symptoms of PTL (see Table 18-2). All studies have reported a statistically significant positive predictive accuracy of TVU CL for PTB.<sup>85</sup> The presence of sludge (see Fig. 18-22) in women with suspected PTL is associated with intramniotic infection and high risk for PTB.<sup>29</sup> TVU CL is indeed very helpful clinically in the management of women with suspected PTL. First, it helps in the diagnosis. The diagnosis of PTL was usually made between 20 and 36 weeks by regular contractions and documented cervical change by manual examination. Indeed, more than 70% of women with the diagnosis of PTL deliver at term, and would receive unnecessary interventions. Women with these findings but a TVU CL of  $\geq 30$  mm and negative fetal fibronectin, have less than a 1% chance of delivering within 1 week, and less than 10% chance of delivering before 35 weeks, and should not receive steroids for fetal maturity, tocolysis, or other interventions. The diagnosis of PTL should be confirmed by a TVU CL less than 20 mm and a positive fetal fibronectin, and only these women should receive interventions.<sup>85</sup> A randomized trial in our center is currently evaluating the benefit of such approach. Previously, a decrease in incidence of birth weight less than 2500 g was reported when TVU of the cervix was used to triage patients to bed rest and tocolysis only if the TVU CL was less than 30 mm compared with historic controls.<sup>86</sup> Using TVU in symptomatic women with suspected PTL for management has been shown to decrease the incidence of hospitalization and costs, but did not decrease PTB.<sup>87,88</sup> The shorter the CL is in women with PTL, the higher is the risk of intra-



amniotic infection, and this is also related to gestational age at presentation.<sup>89</sup> Women in PTL with a CL less than 10 mm at less than 28 weeks have a  $\geq 25\%$  incidence of intra-amniotic infection.

The possible utility of repeat measurement of CL after tocolysis for PTL predicts PTB, but not any better than the first measurement at presentation. The variation in CL between first and repeat CL seems not to be predictive of PTB, so that "to repeat ultrasonographic CL measurement after successful tocolysis [may be] useless."<sup>90</sup>

## PREDICTING THE LATENCY IN PRETERM PREMATURE RUPTURE OF THE MEMBRANES

Several studies have evaluated the utility of TVU of the cervix in women with PPROM. A randomized trial demonstrated the safety of performing TVU in this group, because women who had TVU had similar incidences of maternal and neonatal infections as controls who did not undergo TVU.<sup>9</sup> The latency to delivery is directly correlated with CL, with women with shorter CLs having the shorter latencies.<sup>91,92</sup> There are no studies to assess if this clinical knowledge affects outcomes.

## PREDICTION OF START OF SPONTANEOUS LABOR

TVU of the cervix can be useful in predicting the onset of labor in term women.<sup>93,94</sup> When the TVU CL is measured at 37 weeks, the mean of gestational age at delivery increased from 38 weeks for women with a CL of 10 mm to 41 weeks for women with a CL of 35 mm, with a 68% chance of delivering after 41 3/7 weeks if CL is greater than 40 mm (Fig. 18-26).<sup>94</sup>

## PREDICTING THE SUCCESS OF LABOR INDUCTION AND MODE OF DELIVERY

Several studies have evaluated the predictive accuracy of TVU of the cervix in term gravidas for length of induction and incidence of success (vaginal delivery). Short CL ( $<30$  mm,<sup>95</sup>  $<28$  mm,<sup>96</sup>  $<26$  mm,<sup>97</sup> or wedging<sup>98</sup>) is associated with a short duration of labor and a higher incidence of vaginal delivery compared with a longer cervix. Although some studies did not find that TVU of the cervix added significantly to the prediction obtained by dilatation of the cervix on manual examination,<sup>99,100</sup> most did find that TVU CL was a better predictor than any Bishop score parameter.<sup>94-97</sup> A recent randomized trial showed that the use of TVU CL instead of Bishop score for management of induction is associated with a decreased need for intracervical prostaglandin treatment without adverse effects on the success of the induction.<sup>101</sup> Additionally, women in spontaneous labor with a TVU of less than 20 mm have just a 4% incidence of cesarean delivery, whereas women with a TVU CL greater than 40 mm have a 12% chance of cesarean delivery.<sup>91</sup>

## CONCLUSIONS

TVU for cervical assessment is one of the best techniques for predicting PTB. The use of TVU of the cervix has been

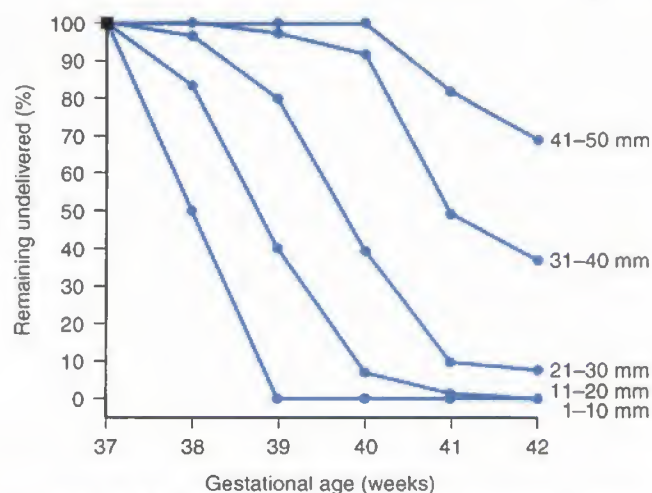


**FIGURE 18-26.** Survival curve estimates of percentages of women not delivered at different gestational ages, according to sonographically measured cervical length at 37 weeks. (Redrawn with permission from Ramanathan G, Yu C, Osei E, et al: *Ultrasound examination at 37 weeks' gestation in the prediction of pregnancy outcome: the value of cervical assessment.* *Ultrasound Obstet Gynecol* 22:598, 2003.)

found to be safe and acceptable to patients. A CL of less than 25 mm between 16 and 24 weeks has been shown to be the most reliable threshold for an increased risk of PTB. The shorter the cervix, the higher is the risk of PTB, and the earlier in gestational age the shortening occurs, the higher is the risk. The role of TVU of the cervix has been studied in a wide variety of settings and with different patient populations, always showing good prediction of PTB. Screening frequency should depend on severity of obstetric history, with serial TVUs of the cervix having a better predictive accuracy than a single evaluation, especially in high-risk populations. Women with a prior PTB or a second trimester loss who then develop a TVU CL less than 25 mm at 16 to 23 6/7 weeks while carrying a singleton gestation may benefit from ultrasound-indicated cerclage. There is accumulating evidence that this technique can be used to safely avoid cerclage placement unless or until cervical change occurs, but this management also needs to be confirmed by appropriate prospective trials. There are still limited data concerning whether TVU of the cervix is clinically useful in caring for women being evaluated for PTL or who experience PPROM, or for prediction of success of labor induction. Future research on all these clinical applications of TVU of the cervix has the potential to significantly improve the health outcomes of pregnant women and their babies.

## References

- Berghella V, Bega G, Tolosa J, et al: Ultrasound assessment of the cervix. *Clin Obstet Gynecol* 46:947, 2003.
- Hassan SS, Romero R, Berry S, et al: Patients with ultrasonographic cervical length  $\leq 15$  mm have a 50% risk of early spontaneous preterm delivery. *Am J Obstet Gynecol* 182:1458, 2000.
- Owen J, Neely C, Northern A: transperineal versus endovaginal ultrasonographic examination of the cervix in the midtrimester: a blinded comparison. *Am J Obstet Gynecol* 181:780, 1999.
- Burger M, Weber-Rössler T, Willman M: Measurement of the pregnant cervix by transvaginal sonography: an interobserver study and new standards to improve the interobserver variability. *Ultrasound Obstet Gynecol* 9:188, 1997.

5. Yost NP, Bloom SL, Twickler DM, et al: Pitfalls in ultrasonic cervical length measurement for predicting preterm birth. *Obstet Gynecol* 93:510, 1999.
6. Grimes DA: Understanding screening tests: the key to avoiding pitfalls in interpretation. *Contemp Obstet Gynecol* 6:46, 2000.
7. Hamilton BE, Martin JA, Ventura SJ, et al: Births: preliminary data for 2004. *Nat Vital Stat Rep* 54:1, 2005.
8. Krebs-Jimenez J, Neubert GA: The microbiological effects of endovaginal sonographic assessment of cervical length. *J Ultrasound Med* 21:727, 2002.
9. Carlan SJ, Richmond LB, O'Brien WF: Randomized trial of endovaginal ultrasound in preterm premature rupture of membranes. *Obstet Gynecol* 89:458, 1997.
10. Dutta RL, Economides DL: Patient acceptance of transvaginal sonography in the early pregnancy unit setting. *Ultrasound Obstet Gynecol* 22:503, 2003.
11. Clement S, Candy B, Heath V, et al: Transvaginal ultrasound in pregnancy: its acceptability to women and maternal psychological morbidity. *Ultrasound Obstet Gynecol* 22:508, 2003.
12. Berghella V, Tolosa JE, Kuhlman KA, et al: Cervical ultrasonography compared to manual examination as a predictor of preterm delivery. *Am J Obstet Gynecol* 177:723, 1997.
13. Berghella V, Kuhlman K, Weiner S, et al: Cervical funneling: sonographic criteria predictive of preterm delivery. *Ultrasound Obstet Gynecol* 10:161, 1997.
14. Phelps JV, Higby K, Smyth MH, et al: Accuracy and intraobserver variability of simulated cervical dilatation measurements. *Am J Obstet Gynecol* 173:942, 1995.
15. Michaels WH, Montgomery C, Karo J, et al: Ultrasound differentiation of the competent from the incompetent cervix: Prevention of preterm delivery. *Am J Obstet Gynecol* 154:537, 1986.
16. Floyd WS: Cervical dilatation in the mid-trimester of pregnancy. *Obstet Gynecol* 18:380, 1961.
17. Owen J, Yost N, Berghella V, et al: Mid-trimester endovaginal sonography in women at high risk for spontaneous preterm birth. *JAMA* 286:1340, 2001.
18. Iams JD, Goldenberg RL, Meis PJ, et al: The length of the cervix and the risk of spontaneous premature delivery. *N Engl J Med* 334:567, 1996.
19. Ziliani M, Azuaga A, Calderon F, et al: Transperineal sonography in second trimester to term pregnancy and early labor. *J Ultrasound Med* 10:481, 1991.
20. Berghella V: The natural history of cervical funneling in high-risk women. *Obstet Gynecol* 101:120, 2003.
21. Hasegawa I, Tanaka K, Takahashi K, et al: Transvaginal ultrasonographic cervical assessment for the prediction of preterm delivery. *J Mater Fetal Med* 5:305, 1996.
22. Berghella V, Daly SF, Tolosa JE, et al: Prediction of preterm delivery with transvaginal ultrasonography of the cervix in patients with high-risk pregnancies: Does cerclage prevent prematurity? *Am J Obstet Gynecol* 181:809, 1999.
23. To MS, Skentou C, Liao AW, et al: Cervical length and funneling at 23 weeks of gestation in the prediction of spontaneous early preterm delivery. *Ultrasound Obstet Gynecol* 3:200, 2001.
24. Guzman ER, Walters C, Ananth CV, et al: A comparison of sonographic cervical parameters in predicting spontaneous preterm birth in high-risk singleton gestations. *Ultrasound Obstet Gynecol* 18:204, 2001.
25. Andrews WW, Copper R, Hauth JC, et al: Second-trimester cervical ultrasound: Associations with increased risk for recurrent early spontaneous delivery. *Obstet Gynecol* 95:222, 2000.
26. Rust OA, Aulas RO, Kimmel S, et al: Does the presence of a funnel increase the risk of adverse perinatal outcome in a patient with a short cervix? *Am J Obstet Gynecol* 192:1060, 2005.
27. Berghella V, Roman A: Does funneling increase the incidence of preterm birth in women with normal cervical length? *Am J Obstet Gynecol* 193:147, 2005.
28. Yost NP, Owen J, Berghella V, et al: Second-trimester cervical sonography: Features other than cervical length to predict spontaneous preterm birth. *Obstet Gynecol* 103:457, 2004.
29. Espinoza J, Goncalves LF, Romero R, et al: The prevalence and clinical significance of amniotic fluid 'sludge' in patients with preterm labor and intact membranes. *Ultrasound Obstet Gynecol* 25:346, 2005.
30. Fukami T, Ishihara K, Sekira T, et al: Is transvaginal ultrasonography at midtrimester useful for predicting early spontaneous preterm birth? *J Nippon Med Sch* 70:135, 2003.
31. Tekesin I, Hellmeyer L, Heller G, et al: Evaluation of quantitative ultrasound tissue characterization of the cervix and cervical length in the prediction of premature delivery for patients with spontaneous preterm labor. *Am J Obstet Gynecol* 189:532, 2003.
32. Guzman ER, Rosenberg JC, Houlihan C, et al: A new method using vaginal ultrasound and transfundal pressure to evaluate the asymptomatic incompetent cervix. *Obstet Gynecol* 83:248, 1994.
33. Owen J, Yost N, Berghella V, et al, for the Maternal-Fetal Medicine Units Network, Bethesda, MD: Can shortened midtrimester cervical length predict very early spontaneous preterm birth? *Am J Obstet Gynecol* 191:298, 2004.
34. Berghella V, Talucci M, Desai A: Does transvaginal sonographic measurement of cervical length before 14 weeks predict preterm delivery in high-risk pregnancies? *Ultrasound Obstet Gynecol* 21:140, 2003.
35. Berghella V, Pereira L, Garipey A, et al: Prior cone biopsy: prediction of preterm birth by cervical ultrasound. *Am J Obstet Gynecol* 191:1393, 2004.
36. Airoidi J, Berghella V: Transvaginal ultrasound of the cervix to predict preterm birth in women with uterine anomalies. *Obstet Gynecol* 106:553, 2005.
37. Visintine JF, Baxter JK, Berghella V: The predictive value of cervical length by transvaginal ultrasound in women with multiple terminations. *Am J Obstet Gynecol* 2006 (in press).
38. Goldenberg RL, Iams J, Miodovnik M, et al: The preterm prediction study: Risk factors in twin gestation. *Am J Obstet Gynecol* 175:1047, 1996.
39. Guzman ER, Walters C, O'Reilly-Green C, et al: Use of cervical ultrasonography in prediction of spontaneous preterm birth in triplet gestations. *Am J Obstet Gynecol* 183:1108, 2000.
40. Venditelli F, Mamelle N, Munoz F, et al: Transvaginal ultrasonography of the uterine cervix in hospitalized women with preterm labor. *Internat J Gynecol Obstet* 72:117, 2001.
41. Andersen HF: Transvaginal and transabdominal ultrasonography of the uterine cervix during pregnancy. *J Clin Ultrasound* 19:77, 1991.
42. Andersen HF, Nugent CE, Wanty SD, et al: Prediction of risk for preterm delivery by ultrasonographic measurement of cervical length. *Am J Obstet Gynecol* 163:859, 1990.
43. Heath VCF, Southall TR, Souka AP, et al: Cervical length at 23 weeks of gestation: relation to demographic characteristics and previous obstetric history. *Ultrasound Obstet Gynecol* 12:304, 1998.
44. Iams JD, Johnson FF, Sonek J, et al: Cervical competence as a continuum: a study of ultrasonographic cervical length and obstetric performance. *Am J Obstet Gynecol* 172:1097, 1995.
45. Odibo AO, Berghella V, Reddy U, et al: Does transvaginal ultrasound of the cervix predict preterm premature rupture of membranes in a high-risk population? *Ultrasound Obstet Gynecol* 18:223, 2001.
46. Odibo AO, Talucci M, Berghella V: Prediction of preterm premature rupture of membranes by transvaginal ultrasound features and risk factors in a high-risk population. *Ultrasound Obstet Gynecol* 20:245, 2002.
47. Kushnir O, Izquierdo LA, Smith JF, et al: Transvaginal sonographic measurement of cervical length: Evaluation of twin pregnancies. *J Rep Med* 40:380, 1995.
48. Wennerholm UB, Holm B, Mautsby-Balzer I, et al: Fetal fibronectin, endotoxin, bacterial vaginosis and cervical length as predictors of preterm birth and neonatal morbidity in twin pregnancies. *Br J Obstet Gynecol* 104:1398, 1997.
49. Yang JH, Kuhlman K, Daly S, et al: Prediction of preterm birth by second trimester cervical sonography in twin pregnancies. *Ultrasound Obstet Gynecol* 15:288, 2000.
50. Quinn MJ: Vaginal ultrasound and cervical cerclage: a prospective study. *Ultrasound Obstet Gynecol* 2:410, 1992.
51. Andersen HF, Karimi A, Sakala EP, et al: Prediction of cervical cerclage outcome by endovaginal ultrasonography. *Am J Obstet Gynecol* 171:1102, 1994.
52. Berghella V, Davis G, Wapner RJ: Transvaginal ultrasound of the cervix in pregnancies with prophylactic cerclage. *Am J Obstet Gynecol* 180:173, 1999.
53. Guzman ER, Houlihan C, Vintzileos A, et al: The significance of transvaginal ultrasonographic evaluation of the cervix in women treated with emergency cerclage. *Am J Obstet Gynecol* 175:471, 1996.
54. Althuisius SM, Dekker GA, van Geijn HP, et al: The effect of therapeutic McDonald cerclage on cervical length as assessed by transvaginal ultrasonography. *Am J Obstet Gynecol* 180:366, 1999.



55. Bega G, Lev-Toaff A, Kuhlman K, et al: Three-dimensional multiplanar transvaginal ultrasound of the cervix in pregnancy. *Ultrasound Obstet Gynecol* 16:351, 2000.
56. ACOG Practice Bulletin: Clinical management guidelines for obstetrician-gynecologists. Cervical insufficiency. *Obstet Gynecol* 102:1901, 2003.
57. Althuisius SM, Barbe E, Dekker GA, et al: Short cervical length implies high risk of chorioamnionitis. *Am J Obstet Gynecol* 182:s20, 2000.
58. Guzman ER, Shen-Schwarz S, Benito C, et al: The relationship between placental histology and cervical ultrasonography in women at risk for pregnancy loss and spontaneous preterm birth. *Am J Obstet Gynecol* 181:793, 1999.
59. Dowd J, Permezel M, Garland S, et al: Is there an interaction between cervical length and cervical microbiology in the pathogenesis of preterm labour? *Aust N Z J Obstet Gynecol* 41:177, 2001.
60. Berghella V, for the NICHD MFMU Network: Frequency of uterine contractions in asymptomatic pregnant women with or without a short cervix on transvaginal ultrasound. *Am J Obstet Gynecol* 187:S127, 2003.
61. Lewis D, Pelham J, Sawhney H, et al: Most asymptomatic pregnant women with a short cervix on ultrasound are having uterine contractions. *Am J Obstet Gynecol* 185:S144, 2001.
62. Lazar P, Gueguen S: Multicentred controlled trial of cervical cerclage in women at moderate risk of preterm delivery. *Br J Obstet Gynecol* 91:731, 1984.
63. Rush RW, McPherson K, Jones L, et al: A randomized controlled trial of cervical cerclage in women at high risk of spontaneous preterm delivery. *Br J Obstet Gynecol* 91:724, 1984.
64. MRC/RCOG Working Party on Cervical Cerclage: Final report of the Medical Research Council/Royal College of Obstetricians and Gynaecologists multicentre randomized trial of cervical cerclage. *Br J Obstet Gynecol* 100:516, 1993.
65. Dor J, Shalev J, Mashlach S, et al: Elective cervical suture of twin pregnancies diagnosed ultrasonically in the first trimester following induced ovulation. *Gynecol Obstet Invest* 13:55, 1982.
66. Shirodkar VN: A new method of operative treatment for habitual abortions in the second trimester of pregnancy. *Antiseptic* 52:299, 1955.
67. McDonald IA: Suture of the cervix for inevitable miscarriage. *J Obstet Gynecol* 64:346, 1957.
68. Rust OA, Atlas RO, Reed J, et al: Revisiting the short cervix detected by transvaginal ultrasound in the second trimester: Why cerclage therapy may not help. *Am J Obstet Gynecol* 185:1098, 2001.
69. Althuisius SM, Dekker GA, Hummel P, et al: Final results of the cervical incompetence prevention randomized cerclage trial (CIPRACT): Therapeutic cerclage with bed rest versus bed rest alone. *Am J Obstet Gynecol* 185:1106, 2001.
70. To MS, Alfirevic Z, Heath VCF, et al: Cervical cerclage for prevention of preterm delivery in women with short cervix: randomized controlled trial. *Lancet* 363:1849, 2004.
71. Berghella V, Odibo AO, Tolosa JE: Cerclage for prevention of preterm birth in women with a short cervix found on transvaginal ultrasound examination: A randomized trial. *Am J Obstet Gynecol* 191:1311, 2004.
72. Berghella V, Odibo AO, To MS, et al: Cerclage for short cervix on ultrasound: Meta-analysis of trials using individual patient-level data. *Obstet Gynecol* 106:181, 2005.
73. Berghella V, Baxter J, Pereira L: Cerclage: should we be doing them? *Cont Obstet Gynecol* 12:34, 2005.
74. Roman AS, Rebarber A, Percira L, et al: Efficacy of ultrasound indicated cerclage in multiple gestations. *J Ultrasound Med* 24:763, 2005.
75. Baxter JK, Airolidi J, Berghella V: Short cervical length after history-indicated cerclage: is reinforcing cerclage beneficial? *Am J Obstet Gynecol* 193:1204, 2005.
76. Berghella V, Rust O, Althuisius S: Short cervix on ultrasound: Does indomethacin prevent preterm birth? *Am J Obstet Gynecol* 193:s48, 2005.
77. Berghella V, Rust O, Althuisius S, et al: Short cervix on ultrasound: Do antibiotics prevent preterm birth? *Am J Obstet Gynecol* 193:s48, 2005.
78. Gighangi PB, Ndinya-Achola JO, Ombete J, et al: Antimicrobial prophylaxis in pregnancy: a randomized, placebo-controlled trial with cefotamet-pivoxil in pregnant women with poor obstetrical history. *Am J Obstet Gynecol* 177:680, 1997.
79. Andrews WW, Sibai BM, Thom EA, et al: Randomized clinical trial of metronidazole plus erythromycin to prevent spontaneous preterm delivery in fetal-fibronectin-positive women. *Obstet Gynecol* 101:847, 2003.
80. King J, Flenady V: Prophylactic antibiotics for inhibiting preterm labour with intact membranes. *Cochrane Database of Systematic Reviews* 3, 2005.
81. Althuisius SM, Dekker GA, van Geijn HP, et al: Cervical incompetence prevention randomized cerclage trial (CIPRACT): Study design and preliminary results. *Am J Obstet Gynecol* 183:823, 2000.
82. To MS, Palaniappan V, Skentou C, et al: Elective cerclage vs. ultrasound-indicated cerclage in high-risk pregnancies. *Ultrasound Obstet Gynecol* 19:475, 2002.
83. Berghella V, Haas S, Chervoneva I, et al: Patients with prior second-trimester loss: Prophylactic cerclage or serial transvaginal sonograms? *Am J Obstet Gynecol* 187:747, 2002.
84. Kelly S, Pollock M, Maas B, et al: Early transvaginal ultrasonography versus early cerclage in women with an unclear history of incompetent cervix. *Am J Obstet Gynecol* 184:1097, 2001.
85. Berghella V, Ness A, Bega G, et al: Cervical sonography in women with symptoms of preterm labor. *Obstet Gynecol Clin N Am* 32:383, 2005.
86. Zalar RW: Transvaginal ultrasound and preterm prelabor: a nonrandomized intervention study. *Obstet Gynecol* 88:20, 1996.
87. Ragoth JC, Kernen B, Saurenmann E, et al: Premature contractions: possible influence of sonographic measurement of cervical length on clinical management. *Ultrasound Obstet Gynecol* 9:183, 1997.
88. Sanin-Blair J, Palachio M, Delgado J, et al: Impact of ultrasound cervical length assessment on duration of hospital stay in the clinical management of threatened preterm labor. *Ultrasound Obstet Gynecol* 24:756, 2004.
89. Gomez R, Romero R, Nien JK, et al: A short cervix in women with preterm labor and intact membranes: a risk factor for microbial invasion of the amniotic cavity. *Am J Obstet Gynecol* 192:678, 2005.
90. Rozenberg P, Rudant J, Chevrete S, et al: Repeat measurement of cervical length after successful tocolysis. *Obstet Gynecol* 104:995, 2004.
91. Rizzo G, Capponi A, Angeline E, et al: The value of transvaginal ultrasonographic examination of the uterine cervix in predicting preterm delivery in patients with preterm premature rupture of membranes. *Ultrasound Obstet Gynecol* 11:23, 1998.
92. Gire C, Faggianelli P, Nicaise C, et al: Ultrasonographic evaluation of cervical length in pregnancies complicated by preterm premature rupture of membranes. *Ultrasound Obstet Gynecol* 19:565, 2002.
93. Rozenberg P, Goffinet F, Hessabi M, et al: Comparison of the Bishop score, ultrasonographically measured cervical length, and fetal fibronectin assay in predicting time until delivery and type of delivery at term. *Am J Obstet Gynecol* 182:108, 2000.
94. Ramanathan G, Yu C, Osei E, et al: Ultrasound examination at 37 weeks' gestation in the prediction of pregnancy outcome: the value of cervical assessment. *Ultrasound Obstet Gynecol* 22:598, 2003.
95. Ware V, Raynor BD: Transvaginal ultrasonographic cervical measurement as a predictor of successful labor induction. *Am J Obstet Gynecol* 182:1030, 2000.
96. Pandis GK, Papageorgiou AT, Ramanathan VG, et al: Preinduction sonographic measurement of cervical length in the prediction of successful induction of labor. *Ultrasound Obstet Gynecol* 18:623, 2001.
97. Gabriel R, Darnaud T, Chalot F, et al: Transvaginal sonography of the uterine cervix prior to labor induction. *Ultrasound Obstet Gynecol* 19:254, 2002.
98. Boozarjomehri F, Timor-Tritsch E, Chao CR, et al: Transvaginal ultrasonographic evaluation of the cervix before labor: presence of cervical wedging is associated with shorter duration of induced labor. *Am J Obstet Gynecol* 171:1081, 1994.
99. Chandra S, Crane JMG, Hutchens D, et al: Transvaginal ultrasound and digital examination in predicting successful labor induction. *Obstet Gynecol* 98:2, 2001.
100. Watson WJ, Stevens D, Wleter S, et al: Factors predicting successful labor induction. *Obstet Gynecol* 88:990, 1996.
101. Bartha JL, Romero-Carmona R, Martinez-Del-Fresno P, et al: Bishop score and transvaginal ultrasound for preinduction cervical assessment: a randomized clinical trial. *Ultrasound Obstet Gynecol* 25:155, 2005.

# ULTRASOUND EVALUATION OF THE PLACENTA AND UMBILICAL CORD

Vickie A. Feldstein, MD, Robert D. Harris, MD, and Geoffrey A. Machin, MD, PhD

## Placenta

Normal Development and Anatomy  
 Placental Size/Shape  
 Circumvallate Placenta and Succenturiate Lobe  
 Placental Calcifications  
 Focal Cystic/Hypoechoic Lesions  
*Vascular Abnormalities*  
*Hematomas*  
 Placental Abruption  
 Placenta Previa  
 Vasa Previa  
 Placenta Accreta  
 Nontrophoblastic Placental Tumors  
 Placental Doppler

## Umbilical Cord

Embryology  
 Anatomy  
 Abnormalities of the Umbilical Cord  
*Single Umbilical Artery*  
*Length*  
*Nuchal Cord*  
*Coiling*  
*Insertion*  
*Anterior Abdominal Wall Defects*  
 Cord Cysts and Masses  
 Multiple Pregnancies

## PLACENTA

The placenta is a fascinating but often ignored organ that provides primary support for the developing fetus. In *The Diseases and Deformities of the Foetus* (1892), JW Ballantyne wrote

*A diseased foetus without its placenta is an imperfect specimen, and a description of a foetal malady, unless accompanied by a notice of the placental condition, is incomplete. Deductions drawn from such a case cannot be considered as conclusive, for in the missing placenta or cord may have existed the cause of the disease and death. During intrauterine life the foetus, the membranes, the cord and the placenta form an organic whole, and disease of any part must react upon and affect the others.<sup>21</sup>*

The same could be said in reference to sonography and the value of sonographic assessment of the placenta. Those who perform obstetric ultrasound (US) are encouraged to study this interesting, crucial structure because significant placental pathology may be found, often before the fetus is affected. Recognition of frequent anatomic variants and clinically important lesions of the placenta is highly valuable for optimal performance and interpretation of prenatal US.

This chapter reviews normal placental and umbilical cord development and anatomy, and presents common abnormalities of the placenta (including maternal and fetal processes) and cord, as shown by US, highlighted with pathologic correlation.

## Normal Development and Anatomy

The recently released ovum is normally fertilized in the fallopian tube and reaches the uterine cavity as the morula, which rapidly evolves into the blastocyst. The blastocyst, in turn, attaches to and implants in the endometrium on day 5 to 6 after fertilization.<sup>2</sup> The outer cell layer of the blastocyst, which will become the placenta, transforms to the trophoblastic cell mass that intermixes with endometrial cells (10th postovulatory day). The trophoblast shortly thereafter differentiates into the cytotrophoblast and syncytiotrophoblast. The latter cells erode into the endometrial glands and blood vessels.

Between 10 to 13 days after ovulation, lacunae or clefts appear among the rapidly proliferating trophoblastic cell mass. These spaces form the intervillous space, the wide channels where the transfer of gases and nutrients occurs between maternal and fetal circulations (Fig. 19-1). Early on, this proliferation of villi is characterized by a hyperechoic appearance on US, although a definitive placenta is only well seen after 10 to 12 weeks. Villi form from mesenchyme, and blood vessels that sprout into the primary villous stems, which then branch into secondary and tertiary villi. Around 8 weeks' gestation, the villi oriented toward the endometrium (now called the decidua) continue to divide and grow as the chorion frondosum. The villi toward the endometrial cavity atrophy and form a smooth surface, the chorion laeve. The chorion normally apposes with the amnion at approximately 12 to 16 weeks.



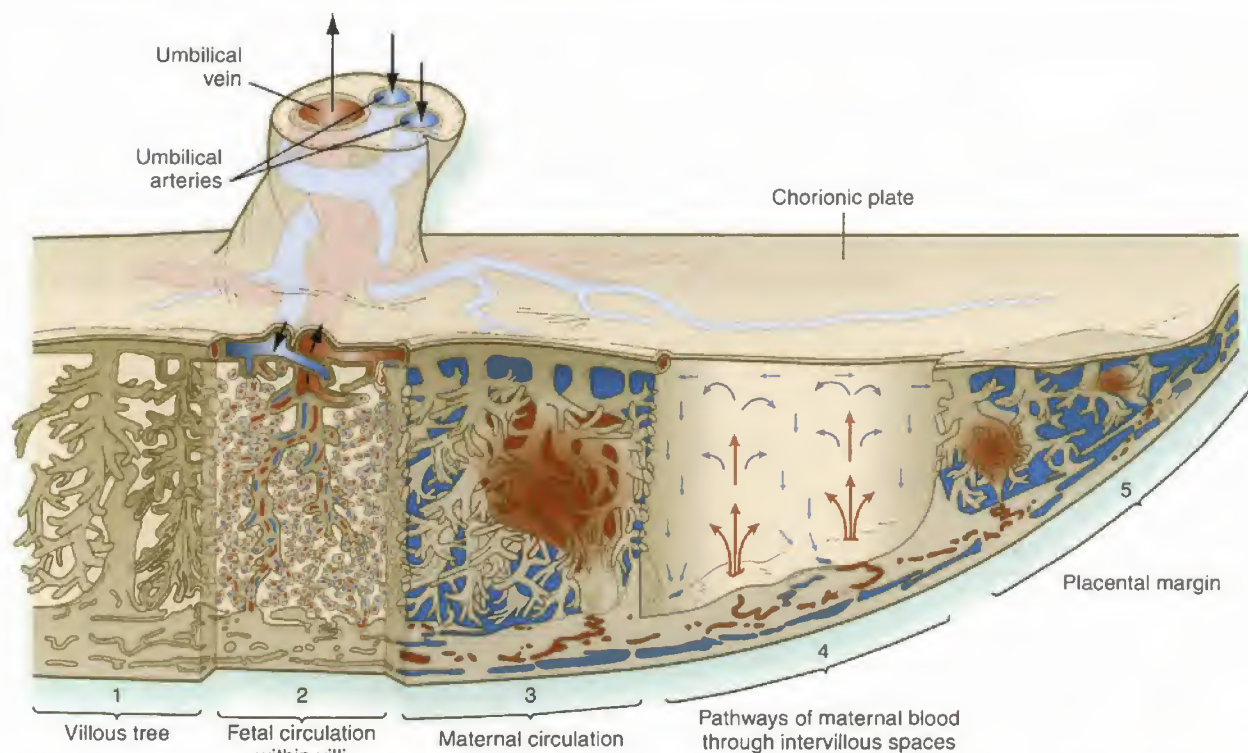


**FIGURE 19-1.** Schematic representation of placental structure delineating intervillous spaces, sites of exchange between maternal, and fetal circulations. (From Carlson BM (ed): *Human Embryology and Developmental Biology*. Philadelphia, Elsevier Ltd., 2004.)

True maternal blood flow is not established until 12 weeks of gestation; before then plasma (not blood) flow occurs in the intervillous space.<sup>2,3</sup> Uteroplacental circulation occurs when uterine spiral arterioles, dislodging the trophoblastic plugs, are transformed into flaccid, dilated uteroplacental arterioles, creating low-pressure, low-impedance blood flow to the intervillous space, thereby establishing an adequate reservoir of oxygen and nutrients for support of the early fetus. Investigators have described normal and abnormal early placental/villous circulation at 8 to 12 weeks.<sup>4</sup> Overall, there is a decrease in resistance to blood flow in the uterine circulation from early gestation to term in normal pregnancies.<sup>5</sup>

Sonographic evaluation of the placenta begins with localization. At US, the placenta may be visible as early as 10 weeks as a thickening of the hyperechoic rim of tissue around the gestational sac (Fig. 19-2). At 12 to 13 weeks, intervillous blood flow is easily demonstrable by color or power Doppler sonography. By 14 to 15 weeks, the placenta is well established and a prominent hypoechoic area, the retroplacental complex, composed of the decidua, myometrium, and uterine vessels, may be readily visualized (Fig. 19-3). At 16 to 18 weeks, small intraplacental arteries may be demonstrated with color or power Doppler US at low-flow settings. The third trimester placenta is a very vascular organ, and both retroplacental and intraplacental arteries are widely distributed and discernible at color or power Doppler imaging.



**FIGURE 19-2.** Transvaginal sonogram of first trimester pregnancy. At this stage, the placenta (PI) is recognized as focal thickening of hyperechogenic tissue adjacent to the gestational sac.

### Placental Size/Shape

US can be used to assess placental size, thickness, and echotexture. Because the placenta is primarily a fetal organ, its size is often a reflection of the health and size of the fetus. The normal term placenta measures 15 to 20 cm in diameter

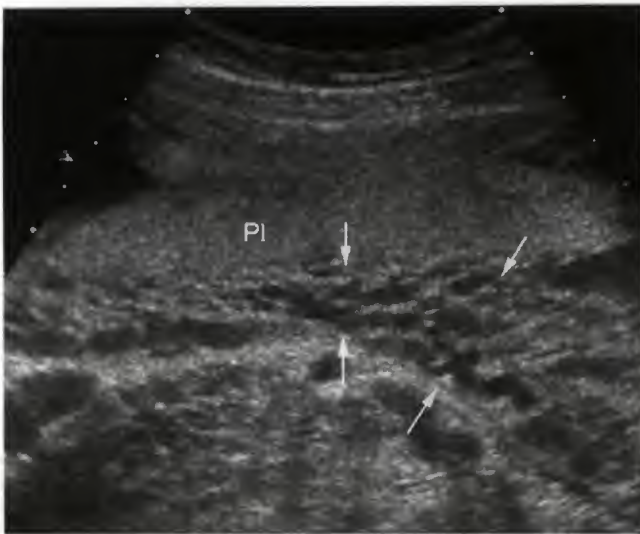


**FIGURE 19-3.** Retroplacental complex, which includes prominent vessels (arrows) and is relatively hypoechoic compared with adjacent placenta (PI), is demonstrated on this transabdominal ultrasound view.

with a volume of 400 to 600 mL.<sup>2</sup> Although there is a broad range, normal placental thickness is approximately 1 mm per week of gestation.<sup>6,7</sup> As a general rule, the placenta should be approximately equal in thickness (in millimeters) to the gestational age in weeks,  $\pm$  10 mm. The term placenta should generally not be thicker than 45 mm, although some exceptions occur.<sup>6</sup> Placental volume in the second trimester has been reported to be a predictor of abnormal fetal outcome, but the method of measurement is complex and not widely adopted.<sup>8-11</sup> A thin placenta may be a marker for a small-for-dates fetus or a sign of growth restriction. Marked polyhydramnios may cause thinning of the placenta (Fig. 19-4). In the presence of marked polyhydramnios, a normal size placenta may in fact be abnormally thickened.

Placentomegaly has many causes. A small area of attachment to the uterus may cause artifactual thickening of the placenta, but careful and complete scanning of the maternal surface and insertion site can make this apparent (Fig. 19-5). The causes of a truly thick placenta may generally be divided into two categories, based on sonographic morphology: homogeneous and heterogeneous echotexture. Common causes of homogeneous thickening are diabetes mellitus (DM; typically gestational-onset DM), anemia, hydrops, infection (villitis) and, rarely, aneuploidy (Fig. 19-6A and B). If multiple small cystic spaces are seen within a thickened placenta, the differential diagnosis would include: triploidy, placental hemorrhage, villitis, mesenchymal dysplasia,<sup>12</sup> and Beckwith-Wiedemann syndrome (Figs. 19-7 and 19-8).<sup>13</sup> Heterogeneous thickening may be seen with intraplacental hemorrhage, which is further discussed in a later section.

### Circumvallate Placenta and Succenturiate Lobe

Circumvallate placenta is an abnormality of placental shape whereby the membranes insert inward from the edge, toward the center of the placenta. The placenta is termed circummarginate if the fetal membrane insertion is flat. More often,



**FIGURE 19-4.** The anterior placenta (PI) is relatively thin in this third trimester pregnancy complicated by hydrops fetalis with polyhydramnios (amniotic fluid pocket measured by electronic calipers) and fetal pleural effusion.

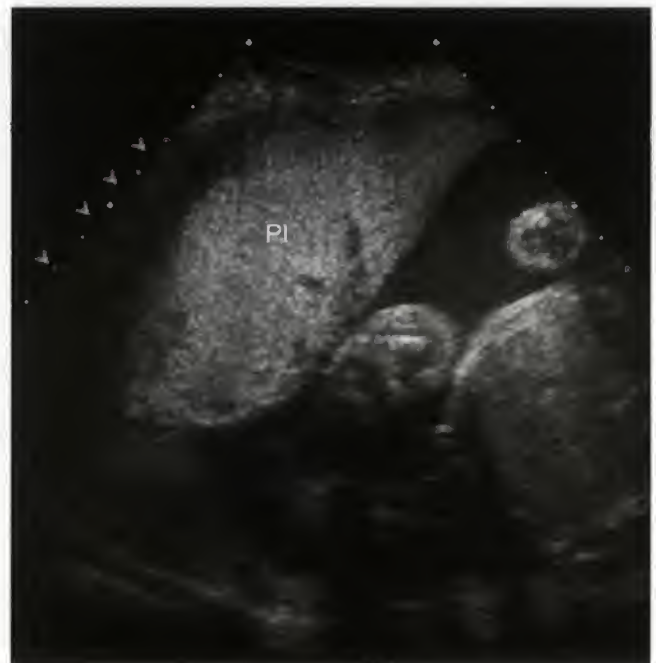
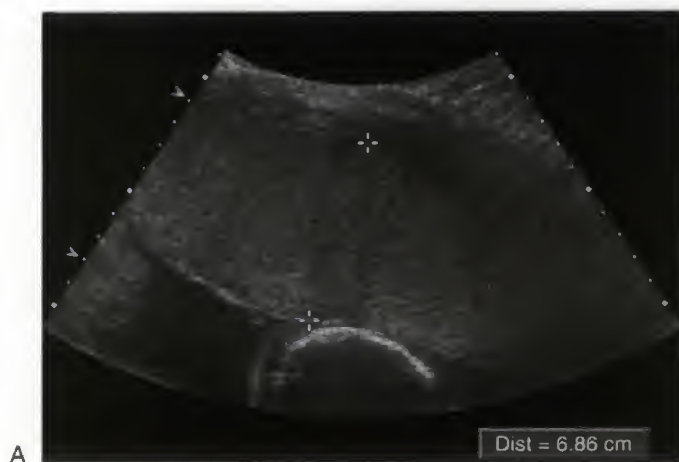


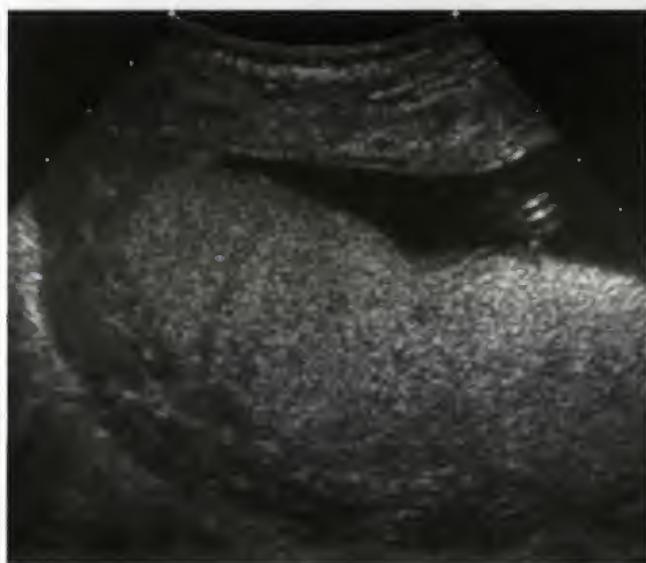
**FIGURE 19-5.** Apparently thick placenta (PI) due to short site of attachment to uterus.

the transition where the fetal vessels of the chorionic plate terminate has a raised or rolled edge, termed circumvallate.<sup>13,14</sup> Circumvallate placenta is characterized by thickened, rolled chorioamniotic membranes peripherally. This condition may be complete (involving 100%) or partial, when only a portion of the placental circumference is involved. In general,





A



B

**FIGURE 19-6.** A and B. Two sonograms of a homogenous thick placenta seen in a second trimester pregnancy complicated by hydrops. Note the smooth and homogeneous echotexture of the placenta.

circummarginate or partial circumvallate placentas are of no clinical (obstetric or fetal) significance. However, complete circumvallation has been associated with an increased risk of bleeding, low birth weight/intrauterine growth restriction (IUGR), oligohydramnios, preterm labor/delivery, placental abruption, and perinatal mortality. On US, an irregular placental edge with a heaped up appearance may be noted (Fig. 19-9).<sup>13,16</sup> The thickened ridge of peripheral tissue, often found at pathologic inspection to be accompanied by chronic placental hemorrhage or infarction, merits consideration because of its unusual but fairly characteristic sonographic appearance (Fig. 19-10A and B). Of note, the classic US feature of a rolled-up placental edge can appear on some views as a linear structure protruding into the fluid-filled amniotic cavity, and thus can potentially be misinterpreted as a uterine synechia (Figs. 19-11A and B, and 19-12).<sup>17</sup> It is possible to assess the degree of circumvallation sonographically by evaluating the entire placental edge over 360 degrees, with the transducer oriented radially to the placenta.



**FIGURE 19-7.** Thick heterogeneous placenta with small cystic areas demonstrated in a case of mesenchymal dysplasia.



**FIGURE 19-8.** Thick placenta with multiple cystic lesions shown by ultrasound. Images of the fetus revealed visceromegaly and macroglossia, with proven Beckwith-Wiedemann syndrome.

Succenturiate (or accessory) lobe of the placenta occurs in approximately 5% of pregnancies.<sup>14</sup> This is recognized on US as a distinct, apparently separate mass of placental tissue, without recognizable bridging tissue.<sup>18</sup> In these cases, there is a higher incidence of placental infarction and velamentous insertion of the umbilical cord. The most serious potential complication associated with this condition is when umbilical vessels supplying the succenturiate lobe cross the internal cervical os (vasa previa), to be covered in greater detail in a later section.

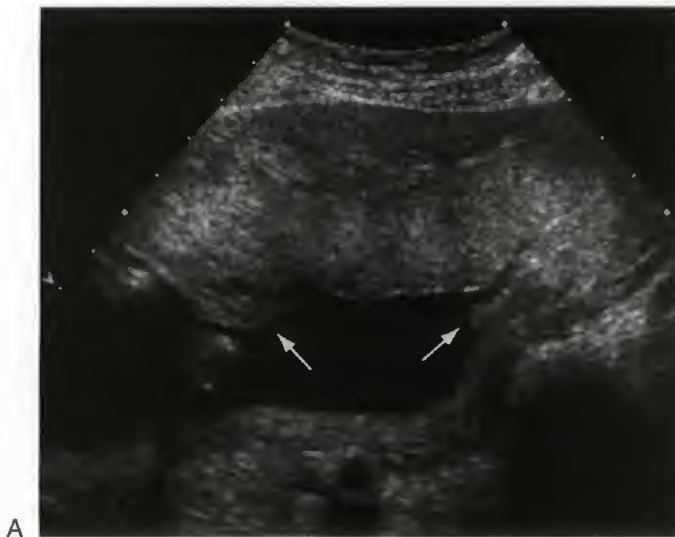


**FIGURE 19-9.** Characteristic appearance on ultrasound of circumvallate placenta. *A.* Curled peripheral edges (*arrows*) are seen in this anterior placenta. *B.* Curled peripheral edges (*arrows*) are shown in this pregnancy at 15 weeks' gestation. Note that at this stage, the amnion is not yet apposed to the chorion.



**FIGURE 19-10.** *A* and *B.* Two views of a complete circumvallate placenta in the second trimester with thick, curled peripheral ridge. This should not be confused with a uterine synechia.

## Placental Calcifications

It is known that the placenta can mature and calcify (recognized as the sonographic sign of aging) at a fairly reproducible rate. A sonographic classification system for grading placentas in utero according to maturational changes was developed by Grannum et al.<sup>19</sup> Extensive research attempted to correlate the placental maturity assessed by US with lung maturity in the 1970s and early 1980s.<sup>20</sup> Although early investigations were promising, it was later demonstrated that the US findings of placental maturation do not reliably predict fetal lung maturity. As a result, placental grading, which was in vogue for a time, is now rarely pursued because it is of little clinical value. Premature or accelerated placental calcification has been associated with several factors including chronic maternal hypertension, preeclampsia, IUGR, and maternal cigarette smoking (Fig. 19-13*A* and *B*).<sup>21</sup>

## Focal Cystic/Hypoechoic Lesions

Cystic or hypoechoic lesions are frequent placental abnormalities, commonly noted after 25 weeks' gestation. Although they may represent a variety of entities, small hypoechoic areas are often of no clinical significance (Fig. 19-14). They are more concerning if they are seen early in gestation, are numerous or large.<sup>22</sup> Although they represent a variety of pathologic entities, common etiologies for hypoechoic placental lesions include: intervillous thrombus, and decidual septal cysts. Intervillous thrombi (IVT) are usually 1 to 2 cm in diameter and consist of coagulated maternal blood in the intervillous space, often surrounded by compressed or infarcted villi (Fig. 19-15). They are very common, with reported incidence of 30% to 40%.<sup>23</sup> At times, IVT may appear as larger sonolucent lesions, which can cause some confusion and concern.



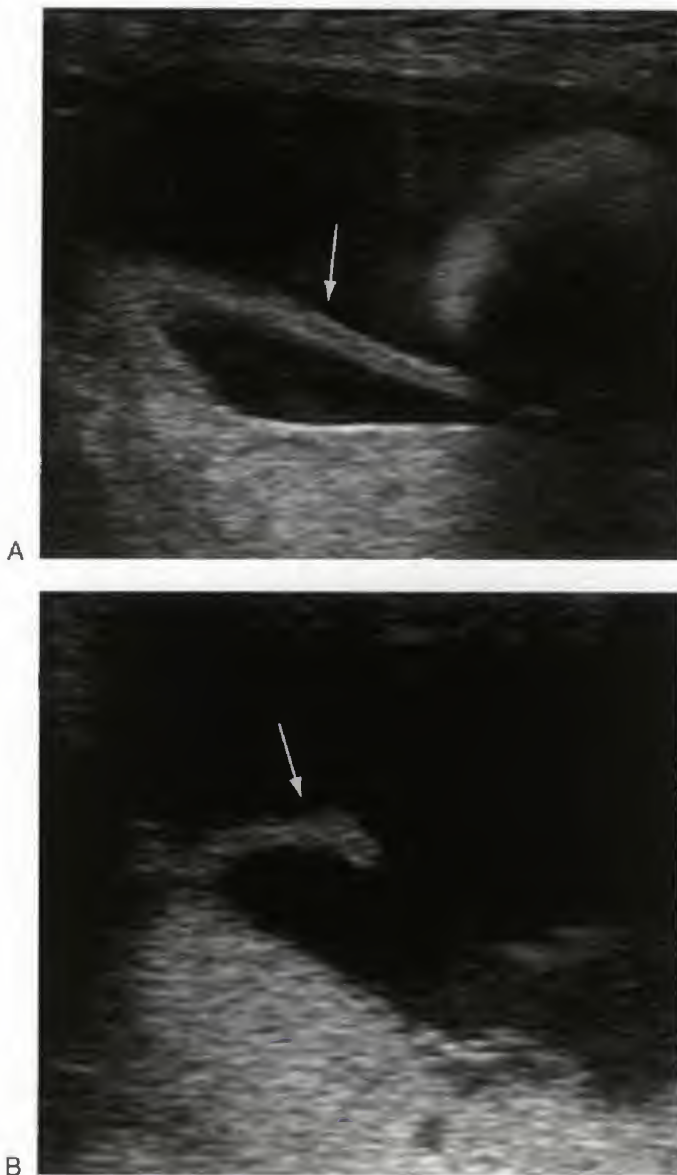


**FIGURE 19-11.** A. Linear structure shown protruding into fluid filled cavity (arrow) may be confused for other processes such as a uterine synechiae or amniotic band. B. An additional ultrasound view, perpendicular to the first, confirms that this represents the curled placental edge (arrow) of a circumvallate placenta.

Decidual septal cysts are usually less than 3 cm in diameter, with reported incidence of 20%. They usually occur near the subchorionic zone and result from degeneration of decidual cells within septa that extend from the decidual floor and support the placenta, resulting in cavities filled with homogeneous fibrinous fluid. Hemorrhage into the cavity may resemble IVT, and it is often difficult to distinguish these entities with US. Correct determination can be made at pathologic examination (Fig. 19-16).

Hypoechoic placental lesions may result from perivillous fibrin deposition, typically located at the periphery of the placenta, with macroscopically visible plaques occurring in 20% to 25% of uncomplicated pregnancies. Subchorionic fibrin deposition results in triangular or rectangular areas of

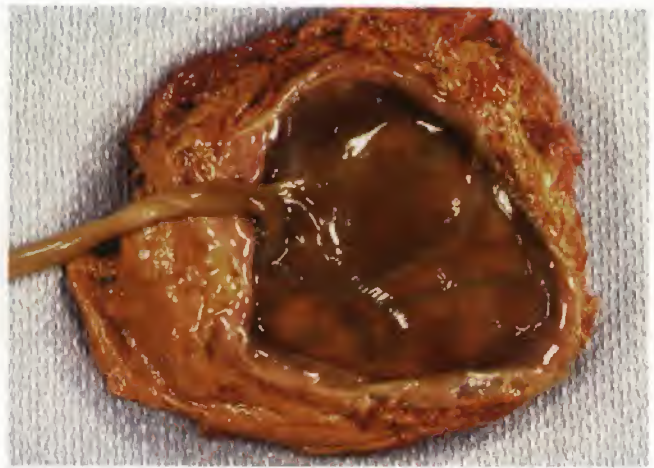


**FIGURE 19-12.** Gross pathologic specimen, viewed from the fetal surface, of a circumvallate placenta at term, with evidence of chronic hemorrhage peripherally.

fibrin deposited under the fetal surface of the placenta, with the base of the triangle along the chorion. At pathology, they are noted in approximately 20% of placentas. It has been observed that most placental surface cysts detected on sonography are related to cystic change in an area of subchorionic fibrin.<sup>24</sup> These entities are usually of no clinical significance because they are typically associated with normal pregnancy outcomes, and have no distinguishing sonographic appearance other than their characteristic locations.

The processes described likely account for the commonly reported sonographic finding of placental or venous lakes that appear as sonolucent intraplacental spaces. On US, swirling internal echoes can sometimes be observed and their shape may be modified with change in maternal position or uterine contractions.<sup>25</sup> Such hypoechoic cystic placental lesions, sometimes referred to as placental lakes, have variably been reported in association with maternal-fetal Rh incompatibility, elevated maternal serum alpha-fetoprotein levels, and edematous placentas (Fig. 19-17). They do not, however, appear to be of clinical concern because they have no proven effect on placental function or fetal health. Investigations into the clinical significance of these findings at routine obstetric US have revealed no associated risk of pregnancy complication or poor outcome.<sup>26</sup> In a report of placental lakes seen on US between 15 and 34 weeks' gestation in low-risk pregnancies, no significant difference in birth weight, gestational age at delivery, or adverse obstetric outcome was observed.<sup>27</sup>

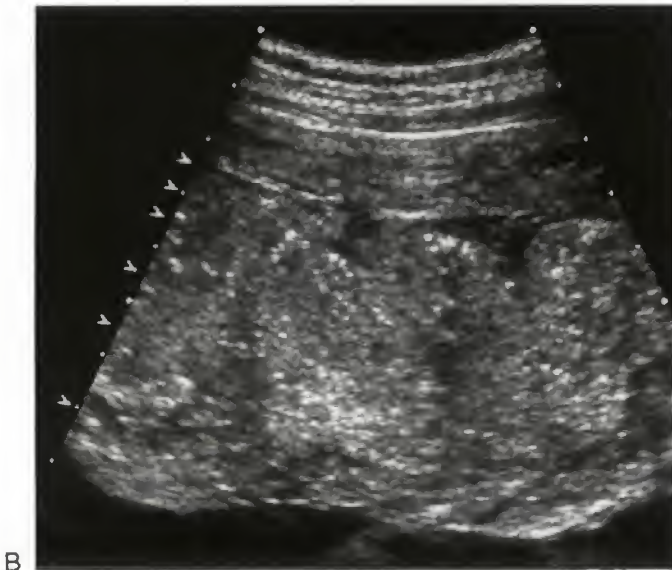
### Vascular Abnormalities

Placental infarction is a localized area of ischemic villous necrosis, resulting from interruption in maternal blood supply, more common at the periphery of the placenta. Most are roughly triangular in appearance at pathology, with the base of the triangle along the basal plate (Fig. 19-18). These have been associated with post-term pregnancies, maternal hypertension, and anticardiolipin antibodies. Most are due to thrombotic occlusion of an uteroplacental artery, less often from retroplacental hematoma stripping the placenta





A



B

**FIGURE 19-13.** A and B. Transabdominal ultrasound images in two different third trimester pregnancies showing placental calcifications (arrows) associated with preeclampsia.

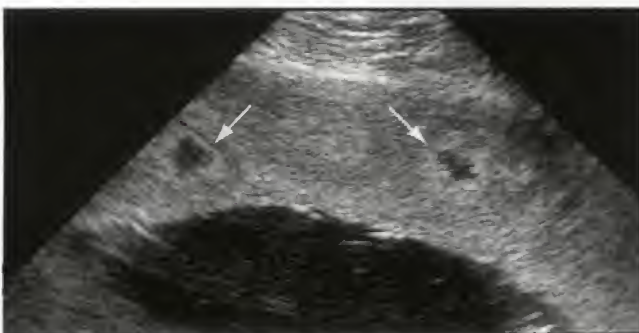


**FIGURE 19-14.** Incidental small hypoechoic areas (arrows) within the placenta in an uncomplicated third trimester pregnancy.



**FIGURE 19-15.** Transabdominal ultrasound image of an anterior placenta with hypoechoic lesions, which are nonspecific based on sonographic appearance and later proven to represent intervillous thrombi.



**FIGURE 19-16.** Gross pathologic specimen of a term placenta revealing a focus of coagulated blood within the intervillous space, called an intervillous thrombus.

away from its blood supply. Most placental infarction is not readily detectable by US because it is isoechoic with adjacent placental tissue,<sup>28</sup> unless there is associated hemorrhage in which case, the chronicity of the bleed will influence the echogenicity. In rare instances, acute placental infarction may be visible as a slightly hyperechoic region. Fortunately, most infarctions are small, affect less than 5% of the placenta, and are not clinically significant. When infarction occurs early, centrally or extensively (greater than 30% involvement of the placenta), it is strongly associated with pregnancy-induced hypertension, IUGR, preterm delivery and even fetal death.<sup>14,22</sup> Power Doppler US is being investigated as a means to detect areas of placental ischemia or infarction manifest as areas of diminished blood flow.

A separate and distinct process, which is of clinical consequence and has been diagnosed by prenatal US is *maternal floor infarction*. This rare but important, clinically relevant condition is worth understanding and recognizing





**FIGURE 19-17.** Focal hypoechoic cystic placental lesion. No other placental lesion or fetal abnormality seen in this pregnancy with a history of elevated maternal serum alpha-fetoprotein and normal outcome.



**FIGURE 19-18.** Serial sections from a gross pathologic specimen of a term placenta with multiple small sites of infarction.

because it is associated with significant fetal risk and has been reported to recur in subsequent pregnancies. This type of infarction is characterized histologically by massive deposition of fibrin in the basal plate of the placenta, encasing the villi which become avascular and necrotic (Fig. 19-19). The resulting impaired perfusion of the intervillous space by maternal blood is associated with a high incidence of fetal morbidity and mortality. In one series, fetal death occurred in 40% of cases, preterm birth in 60%, and IUGR in 54% of live births.<sup>29</sup> This condition has been diagnosed by prenatal US with hyperechoic areas corresponding to infarction, predominantly along the maternal surface, but extending through much of the placental tissue (Fig. 19-20*A* and *B*). Interspersed hypoechoic areas of varying dimensions and marked placental thickening have been



**FIGURE 19-19.** Gross pathologic placental specimen, viewed from the maternal surface, revealing maternal floor infarction with yellowish material representing excess fibrin deposition.

noted as well (Fig. 19-21*A* and *B*).<sup>30</sup> One hallmark on sonography is the typical basal location near the decidua (maternal surface), which is relatively unique to maternal floor infarction.

Fetal artery thrombosis results in a triangular region of injury, with the base of the triangle fused with the basal plate of placenta, as seen at gross pathology. The reported incidence is 5% in normal placentas, increased in cases of maternal DM. There is an association with maternal coagulation disorders, and they may serve as a marker for thrombosis elsewhere in the fetal vascular system. However, these lesions are not detectable by prenatal US.

### Hematomas

It is helpful to consider the location, etiology, sonographic appearance, and clinical impact when confronting blood collections related to the placenta (Fig. 19-22). Massive subchorionic thrombosis results from a large thrombus that strips the chorion away from villous tissue. This may result in a bulging protuberance that elevates and distorts the fetal surface of the placenta, sometimes referred to as a *Breus mole* (an unfortunate misnomer because this entity bears no relationship to a molar pregnancy or gestational trophoblastic disease). It is quite rare, with reported incidence of 0.05%. Its significance is controversial. In some cases, it may be associated with preterm delivery and spontaneous abortion, possibly due to venous compromise in the uteroplacental circulation.<sup>31</sup> Sonographically, it appears as a hypoechoic or cystic area along the fetal surface of the placenta<sup>32</sup> (Figs. 19-23*A* and *B*, and 19-24).

Subchorionic or marginal hematoma is a hematoma at the lateral margin of the placenta and has an incidence of 2% (Fig. 19-25). It occurs most often with placental implantation in the inferior uterus or lower uterine segment (LUS) and probably arises from rupture of uteroplacental veins. They can be associated with miscarriage and preterm labor but are generally of little significance. Rarely, prepla-



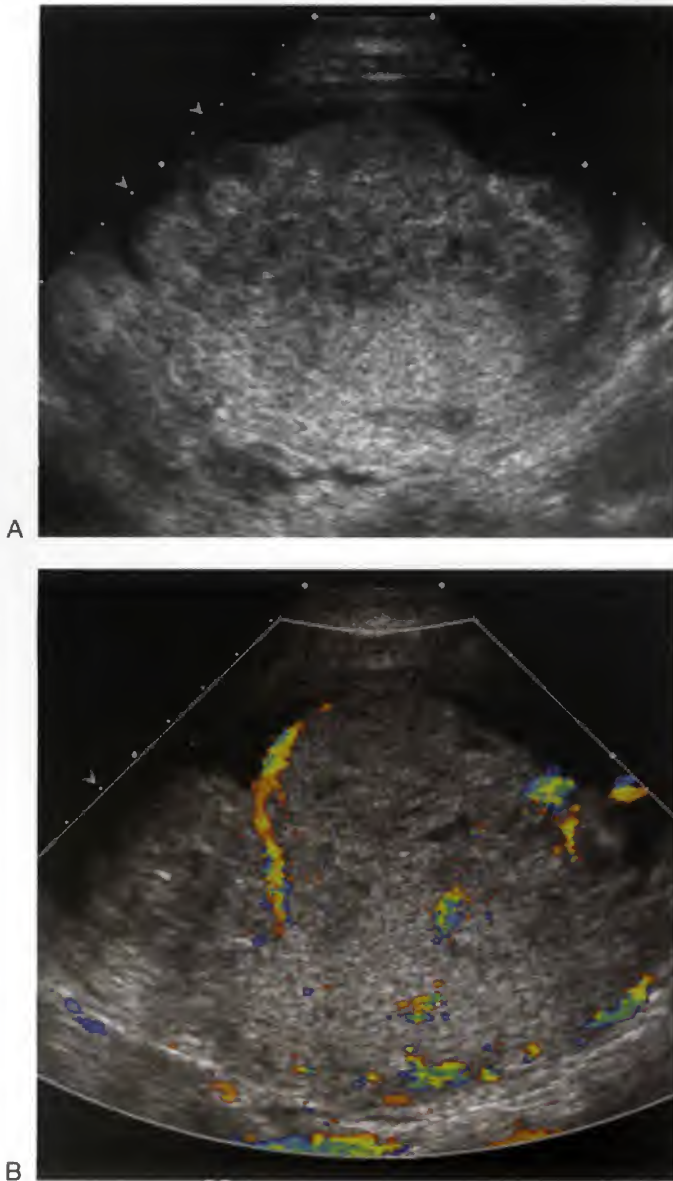


**FIGURE 19-20.** A. Transabdominal sonogram of an abnormally thick, heterogeneous placenta. B. Same patient demonstrated altered perfusion shown by color Doppler ultrasound. This was seen in association with intrauterine growth restriction and oligohydramnios. Maternal floor infarction was confirmed by pathologic inspection of the placenta postpartum.

central or subamniotic hematomas may be seen, although even large hematomas in this location tend to be of little consequence to the fetus. However, some data suggest that this lesion may be of significance in causing fetal growth restriction and fetomaternal hemorrhage in some cases.<sup>33</sup>

Retroplacental hematomas, which can manifest as the clinical condition of placental abruption, are of greatest clinical consequence. They are likely due to rupture of a decidual arteriole with bleeding separating the basal plate of the placenta from the uterine wall. The reported incidence at pathology is 5% with threefold increased risk in patients with preeclampsia. This lesion often leads to basal plate necrosis and villous infarction. The reported associations

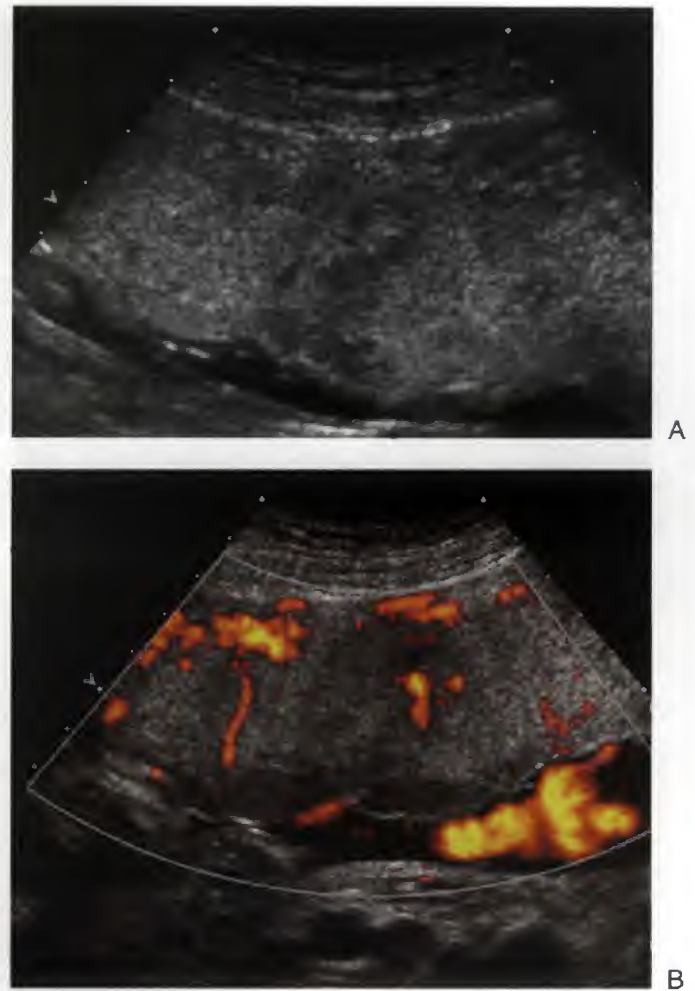


**FIGURE 19-21.** A and B. Another example of pathologically proven maternal floor infarction shown on grayscale and power Doppler ultrasound.

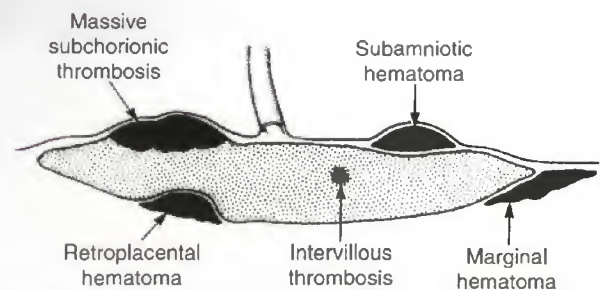


**FIGURE 19-22.** Diagrammatic representation of different sites of potential hemorrhage and abruption. (From Fox H: *Pathology of the Placenta*. London, WB Saunders, Philadelphia, 1978.)

include maternal hypertension/preeclampsia, obstruction of venous drainage of the placenta, cocaine abuse, cigarette smoking, anticardiolipin antibodies, blunt trauma, and chorioamnionitis. The clinical significance of such bleeds is related to the gestational age at onset and to their size: as expected, smaller hematomas have a larger impact on early



A



B



**FIGURE 19-23.** A. Grayscale sonogram revealing a subchorionic hematoma, also referred to as a Breus mole, which is hypoechoic relative to adjacent placental tissue, near the fetal surface of the anterior placenta. B. Power Doppler ultrasound image showing the absence of flow in the region of this hematoma.

(less than 20 wk) gestations, whereas large hematomas, which may cause significant infarction of villi, must strip more than 30% to 40% of placenta away from myometrium to have clinical implications.

When imaging the placenta, the retroplacental hypoechoic complex, composed of uteroplacental vessels (predominantly veins) and myometrium and measuring 1 to 2 cm in thickness (see Fig. 19-3), should be observed. When this region appears thicker, the possibility of retroplacental hemorrhage, focal myometrial contraction, or leiomyoma should be considered. Focal contractions are transient, typically changing in appearance during the examination and myomas are usually distinguishable by their round shape, attenuation and



**FIGURE 19-24.** Pathologic specimen revealing old subchorionic blood corresponding with the sonographic depiction of a Breus mole.



**FIGURE 19-25.** Hypoechoic collection deep to the lateral margin of the placenta, representing a subchorionic, or marginal hematoma (arrow) shown by ultrasound.

internal vascularity on Doppler interrogation, not present within hematomas.

## Placental Abruptio

Placental abruptio is characterized by spontaneous hemorrhage behind or within the placenta with premature separation of the normally implanted placenta from the uterus. The clinical condition (abruption) and the pathologic condition (hematoma) both refer to the abnormal accumulation of maternal blood within or beneath the placenta or membranes.<sup>34,35</sup> The incidence of placental abruptio is 0.5% to 1%.<sup>36,37</sup> It is one of the leading causes of perinatal mortality, accounting for 15% to 20% of all perinatal deaths.<sup>38</sup> If the bleeding is extensive, maternal cardiovascular shock and disseminated intravascular coagulopathy may develop. Associated maternal conditions linked with abruptio are hypertension, preeclampsia, abdominal trauma (especially





**FIGURE 19-26.** Hypoechoic collection (between calipers) deep to the placenta, near its lateral margin toward the maternal surface. This small retroplacental hematoma was of no clinical consequence.

anterior placentas), cocaine abuse, cigarette smoking (twofold increase), alcohol use and advanced maternal age.<sup>39–41</sup>

Occasionally, retroplacental or intraplacental hematomas are small and clinically silent (Fig. 19–26). Large hematomas are typically apparent and present clinically with classic features of sudden abdominal pain/cramping, vaginal bleeding, uterine tenderness and often with onset of labor. However, this reported classic presentation occurs in a minority of cases. It is important to remember that not all cases of abruption are identifiable as hemorrhage on US. The sensitivity of US in visualizing hemorrhage is reported to be approximately 50%, but the lack of a gold standard [pathology] limits this evaluation.<sup>42</sup> In one series, retroplacental blood clot was seen by US in only 15% of the cases.<sup>41</sup> Sonography of abruption may be relatively normal, non-contributory and potentially misleading because US may not be reflective of the gravity of the clinical situation. Given that US cannot always reliably identify this condition, particularly in the emergent setting, it may be ill-advised to perform a US examination and potentially delay management when there is a high clinical suspicion of placental abruption and urgent intervention is indicated.

Still, sonography, given its wide and quick availability, is the only reasonably accurate and practical method of evaluating placental abruption, when clinical circumstances allow.<sup>43,44</sup> Rarely, magnetic resonance imaging (MRI) may be used to show hemorrhage, particularly in cases of chronic abruption, but the expense and limited availability preclude its frequent use. If abnormal, US may show a hypoechoic, subchorionic thickened area at the margin of the placenta.<sup>45</sup> Doppler US can be useful in distinguishing acute hematoma from hypoechoic retroplacental uterine veins.

The most common site of separation is at the edge of the placenta, sometimes referred to as a marginal abruption or marginal hematoma, often with centrifugal extension away

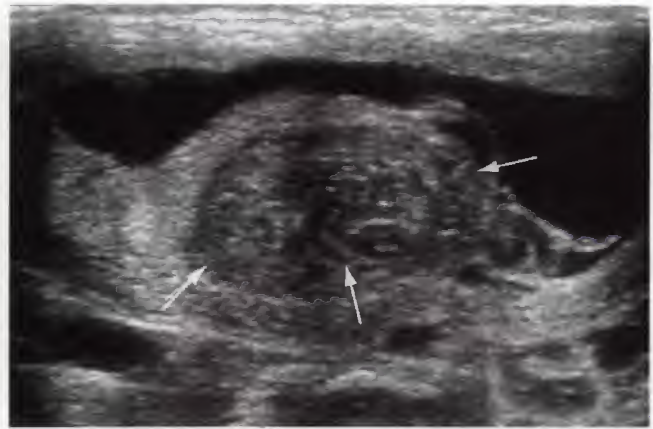


**FIGURE 19-27.** Large retroplacental hematoma (arrows) shown by ultrasound with significant elevation and detachment of the posterior placenta from the uterine wall in a patient who presented with clinical features typical of abruption.

from the placenta. Rarely, this subchorionic hemorrhage may be difficult to differentiate from unapposed chorion and amnion, which may be normal up to 18 weeks of gestational age. The gravest prognosis is for gestations complicated by retroplacental hemorrhage, in which a significant (>30%–40%) placental detachment from the myometrium not uncommonly results in IUGR or fetal demise.<sup>22,46</sup>

The extent of placental detachment and the volume (sonographic estimate =  $L \times W \times H/2$ ) and location of the bleed are the best predictors of pregnancy outcome. It seems fairly well documented that if a hemorrhage is visible at sonography, the patient is at higher risk than if no hematoma is seen in patients with vaginal bleeding.<sup>47</sup> Ball et al found that the presence of a sonographically visible subchorionic hemorrhage increased the risk of placental abruption 11-fold and the risk of miscarriage or stillbirth two- to fourfold.<sup>48,49</sup> In general, the worst outcomes are seen with retroplacental bleeds, hematomas larger than 50 mL, and greater than 50% placental detachment (Figs. 19–27 and 19–28).<sup>50–52</sup>

The sonographic appearance of retroplacental hemorrhage varies, depending on age and location of the bleed. Characteristically, hemorrhage may be acutely (0–48 h) hyperechoic, becoming isoechoic at 3 to 7 days, followed by hypoechoic echotexture at 1 to 2 weeks.<sup>45</sup> After 2 weeks, portions of the clot may become anechoic. Hematomas also tend to become smaller with age, although the rate of decrease is variable.

## Placenta Previa

A frequent US finding is an early diagnosis of placenta previa that appears to move (“migrate”) away from the internal cervical os during the latter half of pregnancy (Fig. 19–29A and B). The term placental migration has been used, but it is somewhat misleading. Rather than moving, it is suggested that the placenta is carried toward the fundus, away from the os because of elongation of the uterus with differential growth primarily in the LUS, as gestation advances. Thus the majority of cases of potential previa



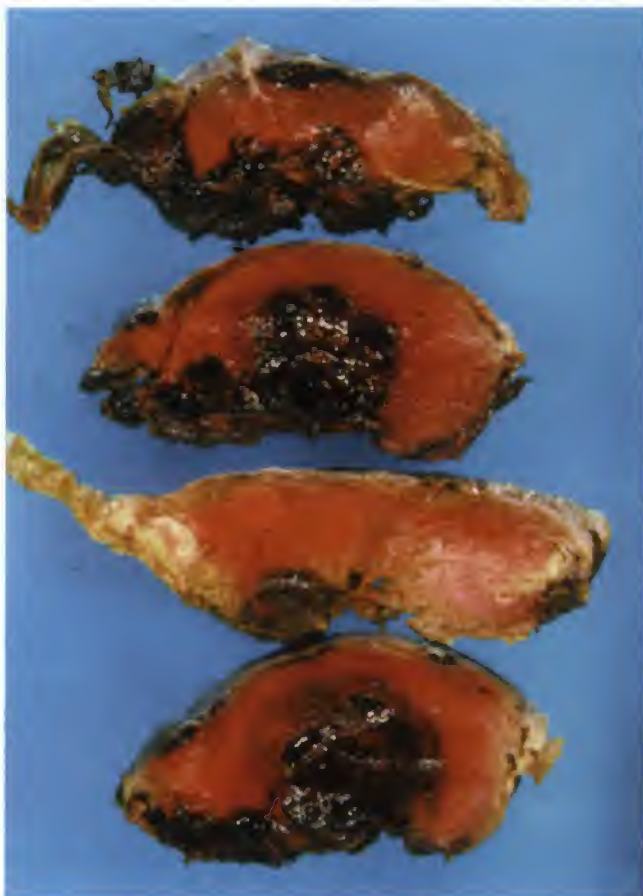


**FIGURE 19-28.** Gross pathologic specimen from a pregnancy complicated by abruption with large retroplacental hematomas, acute and subacute.

resolve before term (Fig. 19-30*A* and *B*). Although a fairly high incidence of apparent previa has been reported in the second trimester, few true previas persist at term.<sup>53-56</sup>

Placenta previa refers to a placenta that overlies or is proximate to the internal cervical os and is the most common cause of bleeding in the third trimester. The incidence of previa at term ranges from 0.5% to 1.0%, with greatly increased frequency in multiparous women, advanced maternal age, previous abortion, and prior cesarean section.<sup>13,39,57,58</sup> It is theorized that the increased incidence in multiparous women results from the depletion of normal decidua by each subsequent pregnancy, leaving the scantier decidua in the LUS for implantation. And, the higher incidence with prior cesarean sections is attributable to scarring in the LUS that renders its growth/elongation impaired; hence, the placenta is unable to migrate away from the internal os. The rate of migration of the placental edge away from the cervical os, which may occur progressively throughout the third trimester, has been measured and may be useful in predicting the eventual route of delivery.<sup>59</sup>

The terminology used to describe types of placenta previa is often confusing and variably understood (Fig. 19-31). Complete placenta previa, the condition in which a portion of the placenta completely covers the internal os, is straightforward and widely accepted (Fig. 19-32*A* and *B*). The term

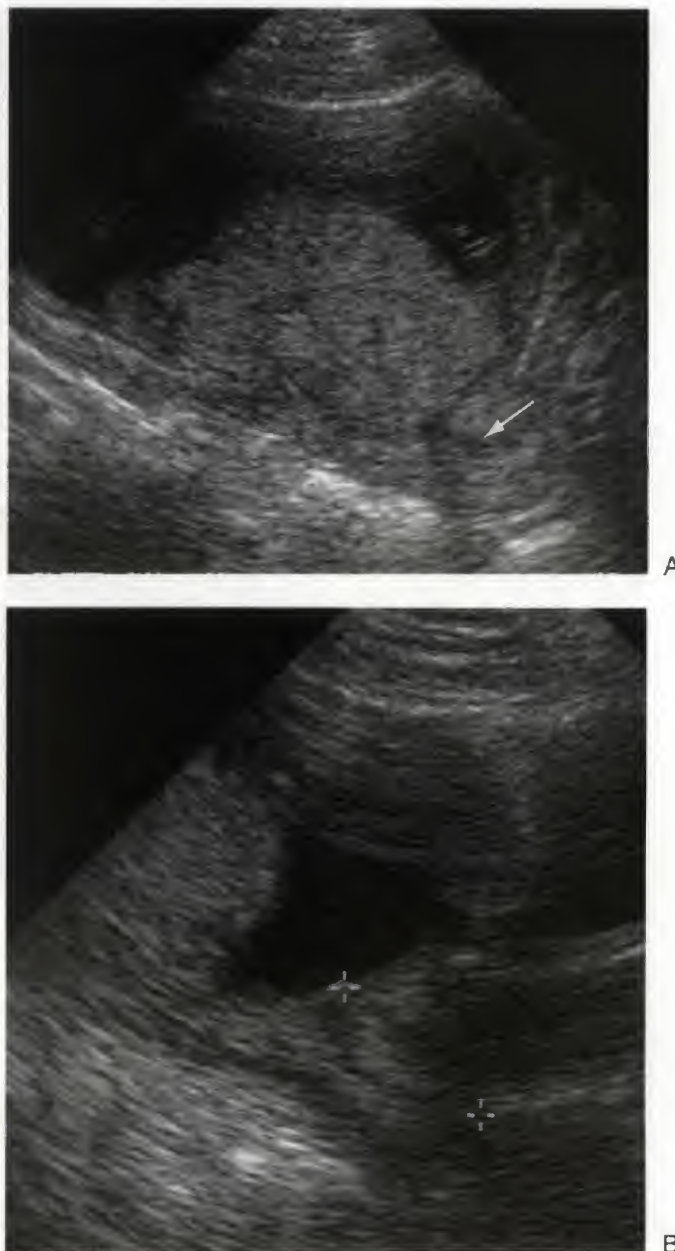


**FIGURE 19-29.** *A.* On initial second trimester sonogram, the posterior placenta overlies the region of the cervix (*arrow*), as seen on transabdominal ultrasound views. *B.* On follow-up third trimester examination, the placenta appears to have "migrated" without residual evidence of previa.

central previa is used when the midportion of the placenta, not just the edge, completely covers the os. Partial previa is used when the placenta partially covers the internal os, a condition that, strictly speaking, can only be applied when the internal os is dilated to some degree. Marginal previa describes placental tissue that reaches the edge, but does not cover the internal os. Confusion arises when describing a placenta shown to encroach upon cervical stroma but not reach or cover the os. Such forms of previa may be difficult to delineate sonographically and to convey with current terminology (Fig. 19-33*A* and *B*). Many investigators have



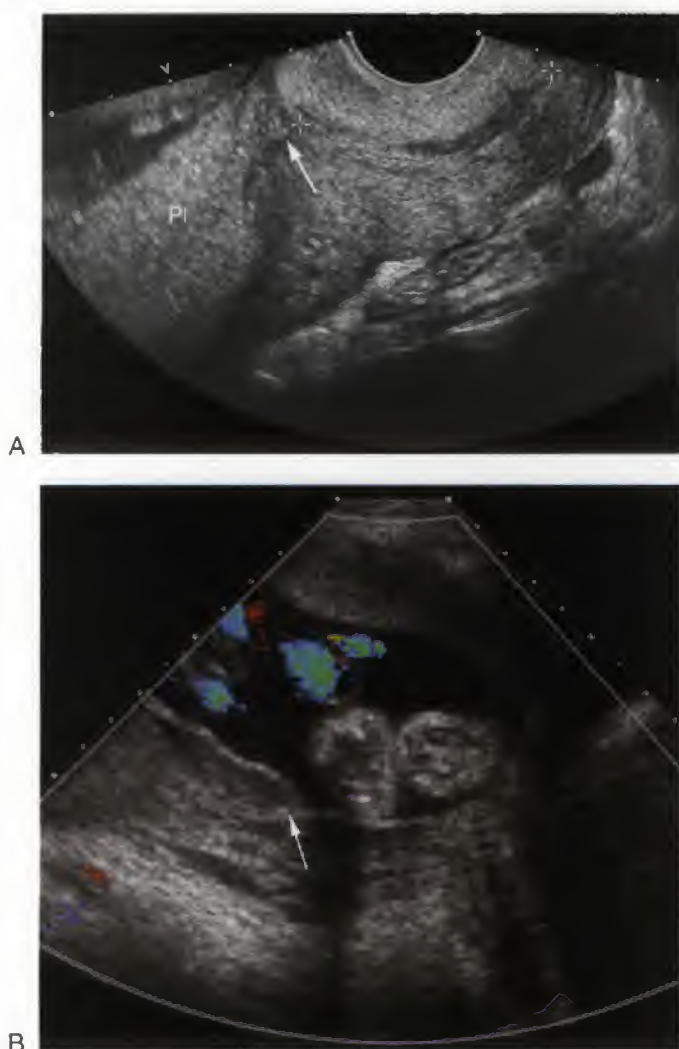


**FIGURE 19-30.** A. Transvaginal sonogram in the second trimester shows the inferior placental edge overlying the internal cervical os (arrow). Pl, placenta. B. Follow-up transabdominal sonogram with color Doppler in the third trimester of this pregnancy shows resolution without residual evidence of previa. Leading edge of the placenta (arrow).

chosen to use the term incomplete placenta previa and to report the measured distance from the placental edge to the internal os (Fig. 19-34A and B). Low-lying placenta refers to one that extends into the LUS, usually more than 2 cm from the internal os, and does not cover or reach it.

The problem of potential or possible previa is one that has stimulated much investigation. Placenta previa is eminently detectable with US. Complete previa, with placenta completely covering the internal os, is typically readily diagnosed sonographically. It is worth noting that an overly distended maternal bladder or a transient myometrial contraction of the LUS can potentially mimic a true placenta previa (Fig. 19-35A to C).<sup>60</sup> Awareness of these pitfalls can help avoid false-positive interpretations. The role and reliability of US in assessing previa has been particularly enhanced with the use of translabial and transvaginal techniques.<sup>53</sup> With translabial (also referred to as transperineal) imaging, the patient empties her bladder and assumes the



**FIGURE 19-31.** Illustration depicting different types of placenta previa. In cases of marginal previa and low-lying placenta, additional information regarding the distance from the leading edge of the placenta to the internal cervical os is often helpful. (Illustration by James A. Cooper, MD, San Diego, CA.)

lithotomy position. The sector transducer, with sterile cover and gel applied, is placed at the vaginal introitus affording a detailed, accurate, quick and well-tolerated view of the cervix to ascertain length and placental location relative to the internal os. The improved spatial and contrast resolution of transvaginal and translabial techniques compared with transabdominal US results from less interposed soft tissue and diminished acoustic attenuation (Fig. 19-36A and B). The safety and effectiveness of these approaches, which are now widely accepted and routinely used to assess the LUS, cervix, and placental location have been demonstrated.<sup>61,62</sup> Translabial US has been shown to be superior to transabdominal views in both diagnosis and exclusion of previa. In one series comparing translabial US findings with placental location determined at delivery, the sensitivity was 100% and specificity 70% if a distance of less than 2 cm was recorded from placenta to internal os. For a threshold of 1 cm, the sensitivity decreased slightly to 90% but the specificity increased to 95%.<sup>63</sup> It should be noted that when performing translabial scanning, shadowing from air within the rectum may obscure the true cervical length.

As mentioned earlier, the majority of placentas located in the LUS in the second trimester are found to not be in the region of the cervix by the time of delivery (Fig. 19-37A and B). Persistence of previa to term can be predicted based on gestational age at US detection of previa and on whether the



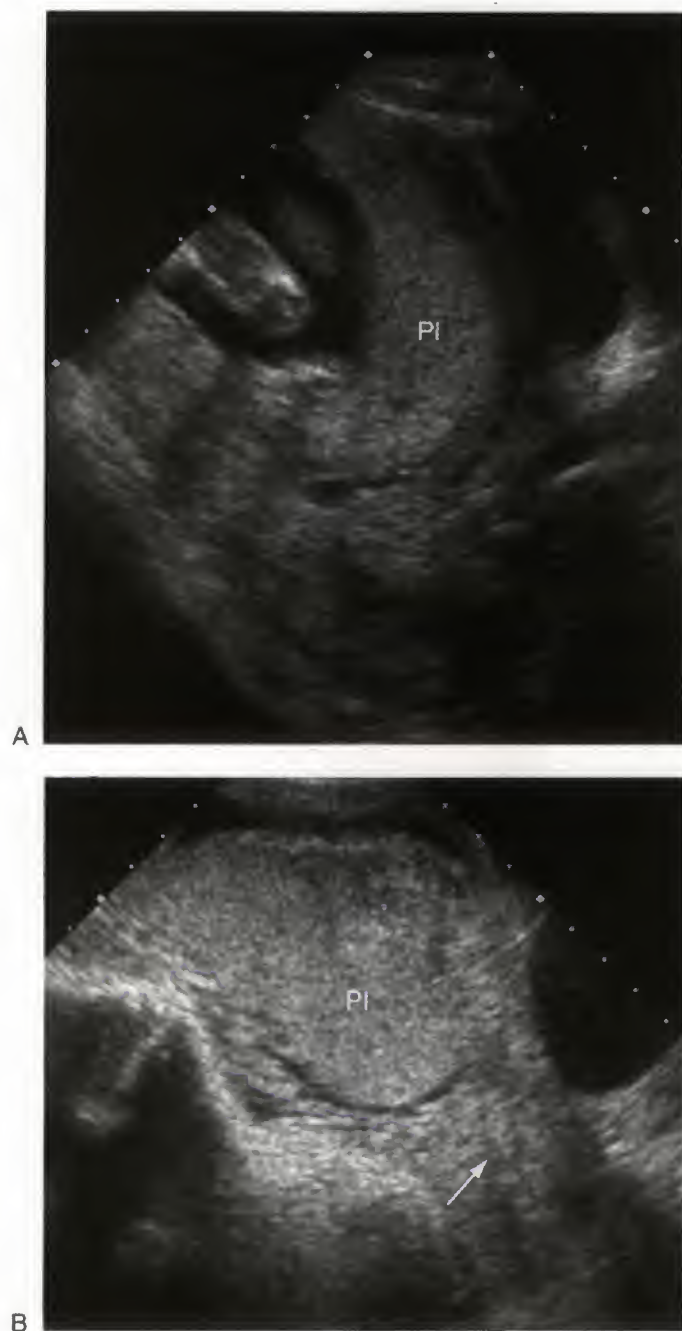


**FIGURE 19-32.** A and B. Two examples of complete central placenta previa shown by transabdominal ultrasound in the late second trimester. Placental tissue completely overlies the cervix. Pl, placenta. Cervix (arrow).

placenta overlaps the internal os in the second trimester and to what extent.<sup>64</sup> It should be noted that the precise definition of the term overlap used in several reports is unclear. It is likely that the authors refer to the apparent crossing and attachment of the placenta across the cervical os due to a rounded bulging of the placenta near the cervix. If there were true attachment across the cervical os, then focal infarction of the placental edge would be the only likely explanation as to why a placenta previa resolved on

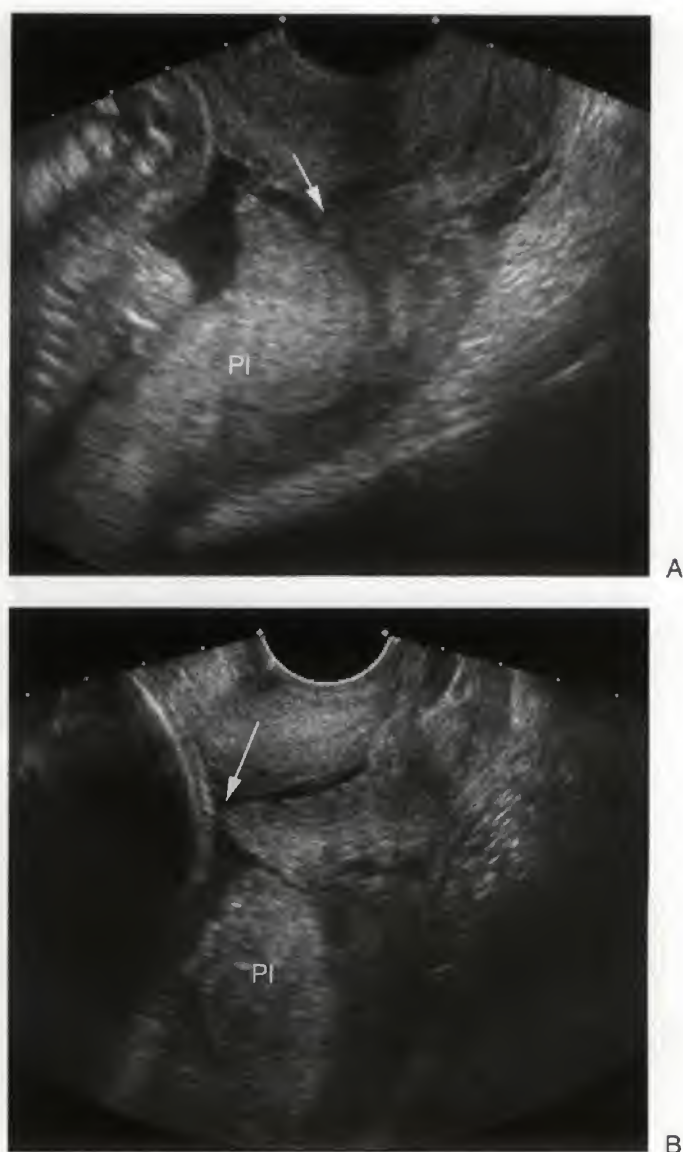


**FIGURE 19-33.** Transvaginal sonograms in the second trimester demonstrating different forms of placenta previa. A. The inferior placental edge (Pl) is shown to completely cover the internal cervical os (arrow), indicating complete previa. B. In this case, the inferior placental edge (Pl) is shown to encroach upon the posterior cervix but not reach or cover the internal cervical os (arrow).

subsequent sonographic scanning. It has been reported that the chance of a previa at term is 5% if the placenta extends more than 15 mm over the internal os at 12 to 16 weeks.<sup>65</sup> It is worthwhile to consider the corollary of this; 95% of such placentas will resolve without evidence of previa in the third trimester. Other investigators found that when the lower placental edge overlaps the internal cervical os by 23 mm, measured by transvaginal US at 11 to 14 weeks, the probability of placenta previa at term was 8% (sensitivity 83%, specificity 86%).<sup>66</sup> In another series using transvaginal US at 18 to 23 weeks, if the placental edge extended more than 15 mm over the os, the positive predictive value of previa at delivery was 19% with 100% sensitivity.<sup>67</sup> The advantage of

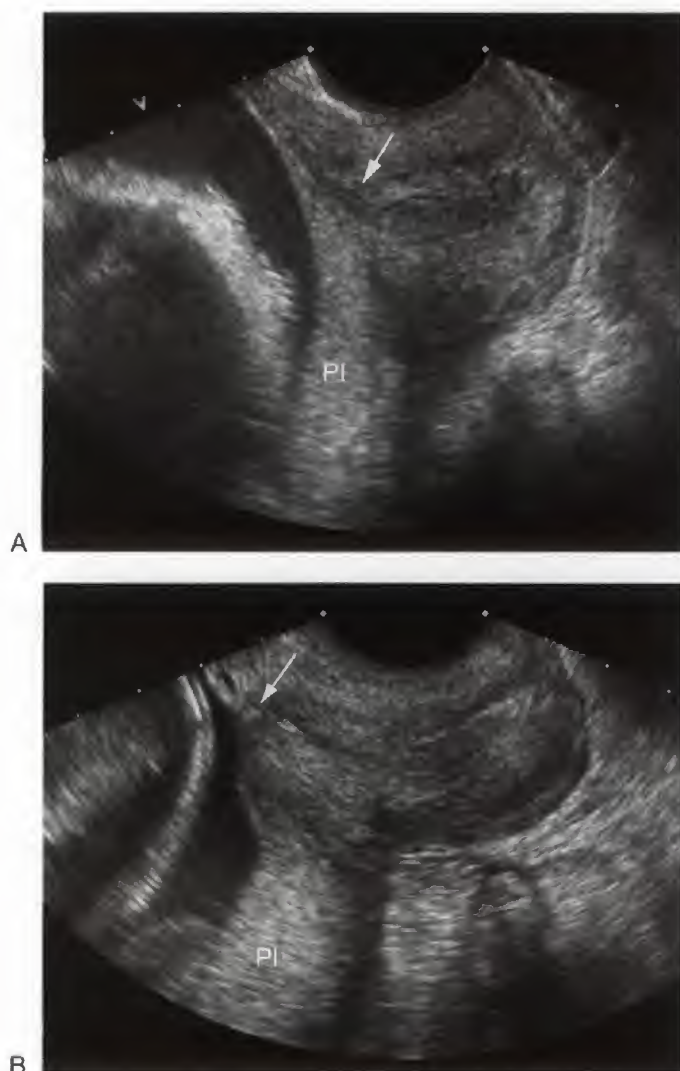


**FIGURE 19-34.** Additional examples of complete and incomplete previa demonstrated by transvaginal ultrasound. *A.* The thin inferior edge of the posterior placenta (PI) reaches and covers the internal os (arrow), extending onto anterior cervical tissue. *B.* In this case, the inferior placental edge (PI) extends onto the cervix posteriorly and is located approximately 1 cm from the internal cervical os (arrow).

determining placental position at 20 to 23 weeks is a lower false-positive rate of predicting previa compared with earlier stages of pregnancy (Fig. 19-38*A* to *C*). An overlap of the os by the placenta at this stage is associated with a high probability of previa at delivery, and in one series, no cases with measured overlap of more than 25 mm at this stage subsequently delivered vaginally.<sup>68</sup>

Studies have also addressed the correlation between placental edge to internal os distance, as seen by transvaginal US in the late third trimester, and the mode of delivery. As expected, the likelihood of vaginal delivery rose significantly as the edge to os distance increased (Fig. 19-39*A* and *B*).<sup>69</sup>

In summary, low-lying, incomplete or potential placenta previas are common in the second trimester, with only a small minority persisting into the late third trimester. If it is uncertain whether a placenta previa truly exists in the

second trimester examination, a translabial or transvaginal examination is suggested. Excluding a placenta previa early in gestation, rather than saying “cannot exclude placenta previa” will save the patient from unnecessary precautions that may be indicated in patients with true placenta previa. In cases in which a placenta previa is still suspected, follow-up third trimester US examinations to include targeted translabial or transvaginal imaging are suggested. These are safe, effective, well-tolerated means to avoid pitfalls, better image the region of the LUS, and are usually diagnostic. Also, in cases of incomplete placenta previa, measurement of the distance from internal cervical os to the placental edge, as seen by US, is a useful adjunct for predicting likelihood of safe vaginal delivery. Finding a placenta 2 cm or less from the internal os near term places the patient at risk and may require cesarean section for delivery.<sup>70</sup> It should also be remembered that many of these patients may also successfully deliver vaginally, with the fetal head tamponading the leading edge of the placenta at the time of delivery. Performing targeted translabial or transvaginal scans in patients at risk serves to precisely localize the placenta and aids in making the correct diagnosis of previa, which is essential for optimal obstetric management.

### Vasa Previa

Vasa previa is a rare but clinically important condition related to placenta previa in which fetal blood vessels are positioned between the presenting fetal part and the cervix. Fetal vessels run through the membranes over the cervix and under the presenting fetal part, unprotected by placenta. The estimated incidence of vasa previa is approximately 1 in 2500 deliveries.<sup>71</sup> Vasa previa occurs in the setting of either velamentous or membranous insertion of the cord (into the membranes rather than the placenta) or when umbilical vessels coursing between the placenta and a succenturiate lobe cross the internal os in the chorionic membranes (Fig. 19-40). The possible consequences of this condition, including hemorrhage and potential fetal exsanguination, are devastating. Reports of prenatal diagnosis of vasa previa by means of US with color Doppler techniques have been published.<sup>72,73</sup>

The importance and clinical impact of prenatal diagnosis of vasa previa with US is significant.<sup>74,75</sup> Improved outcomes depend on accurate prenatal diagnosis and delivery by cesarean section before rupture of membranes. In one retrospective study, when vasa previa was not recognized prenatally, it was associated with perinatal mortality of approximately 56%, whereas 97% of fetuses survived when the diagnosis was made prenatally (Fig. 19-41).<sup>76</sup>

On US, vasa previa may appear as linear echolucent structures overlying the cervix, but this is not always appreciated on grayscale images (Fig. 19-42*A* to *C*). The importance of using color or power Doppler US techniques for the prenatal diagnosis of vasa previa has been emphasized.<sup>77,78</sup> When these Doppler techniques are used, flow can be demonstrated within the vessels overlying the cervix and spectral Doppler may reveal fetal arterial waveforms (Fig. 19-43*A* to *E*). It is important to differentiate true vasa previa from a funic presentation, with umbilical cord positioned in front of the presenting fetal part, near the endocervical os. Funic presentation may temporarily simulate



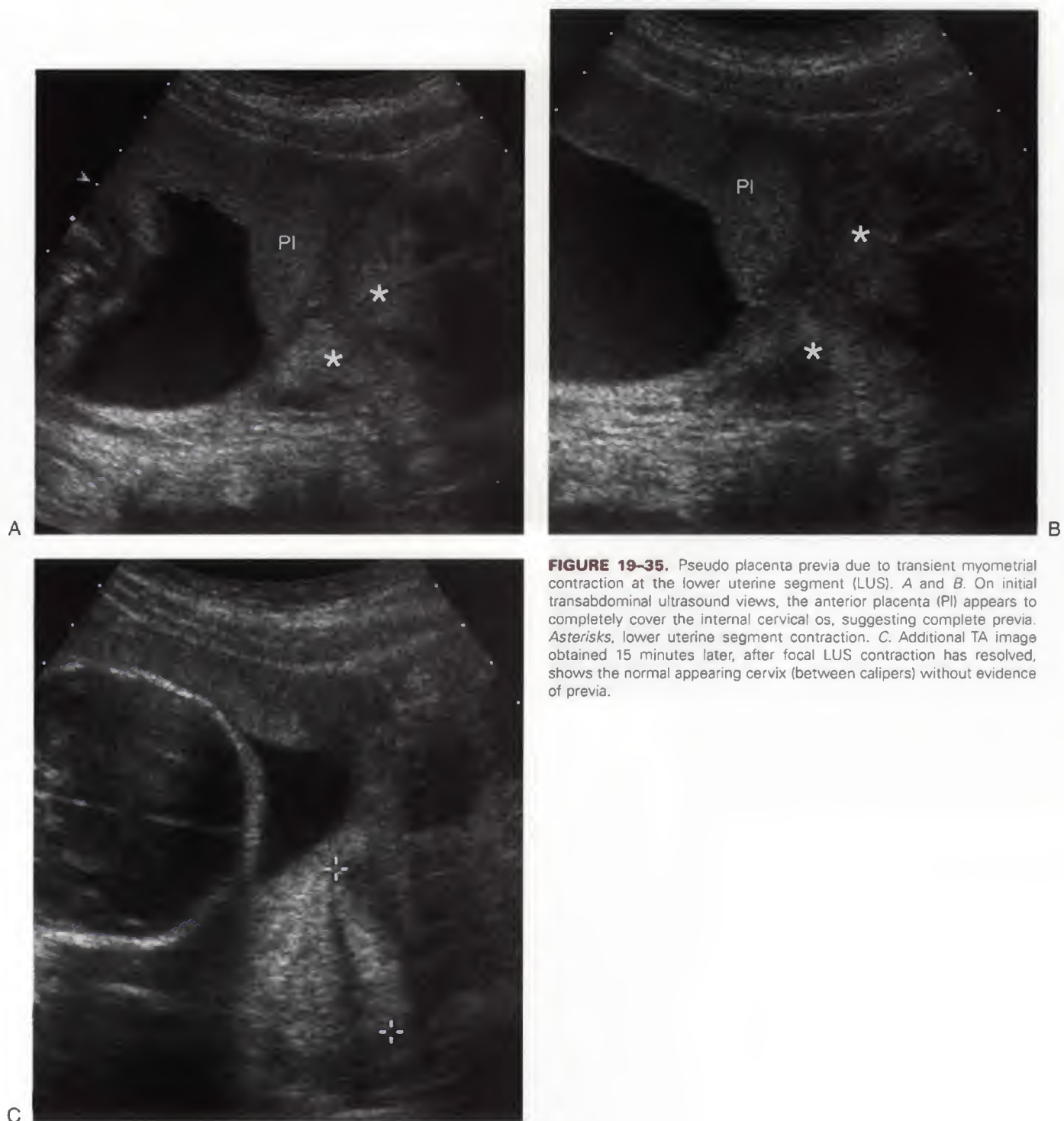


**FIGURE 19-35.** Pseudo placenta previa due to transient myometrial contraction at the lower uterine segment (LUS). *A* and *B*. On initial transabdominal ultrasound views, the anterior placenta (PI) appears to completely cover the internal cervical os, suggesting complete previa. *Asterisks*, lower uterine segment contraction. *C*. Additional TA image obtained 15 minutes later, after focal LUS contraction has resolved, shows the normal appearing cervix (between calipers) without evidence of previa.

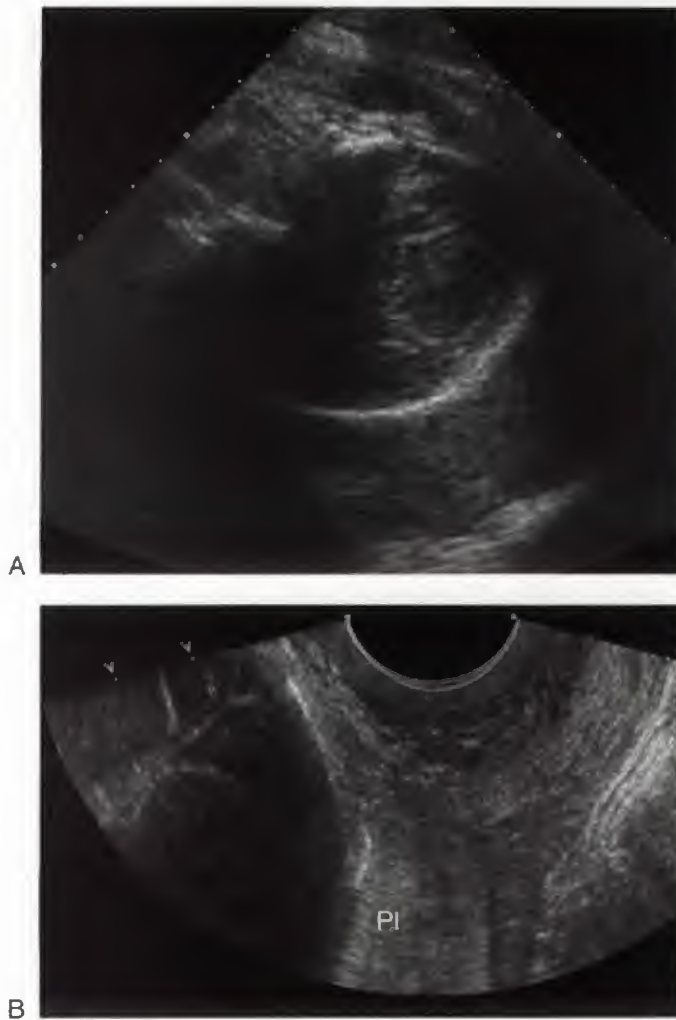


**FIGURE 19-36.** A. No evidence of previa was appreciated on this transabdominal (TA) view of the cervix in the third trimester. However, at this stage of gestation and with the fetus in cephalic presentation, the fetal head limits and often obscures the adequate visualization of the relationship of the cervix and placenta. B. Additional targeted transvaginal views were obtained revealing the presence of a complete previa. PI, placenta.

vasa previa but may be differentiated by re-examining the patient and observing moving vessels, a change in cord position, or a free-floating cord, falling away from the internal cervical os with change in maternal position. It may also be helpful to interrogate the placenta to demonstrate the site of umbilical cord insertion. Another point of clarification; vasa previa should be distinguished from the observation of a marginal vein or venous sinus at the inferior placental edge, near the internal cervical os, which is a form of placenta previa.

It has been shown that the majority of cases of vasa previa in asymptomatic women can be diagnosed with US by evaluating the cord insertion and by targeting the LUS, with transvaginal and color Doppler US, if the placental cord insertion cannot be identified or if there is a low-lying placenta or a suspected succenturiate lobe (Fig. 19-44A and B).<sup>74</sup> Most cases of vasa previa diagnosed by prenatal US are incidentally detected in women being evaluated for low-

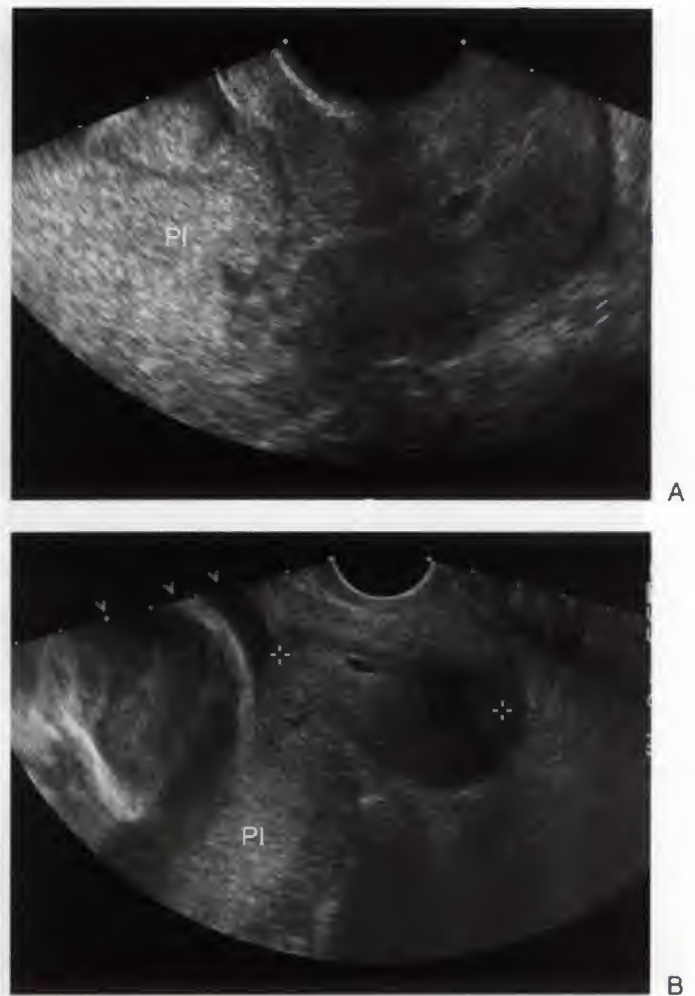


**FIGURE 19-37.** Two transvaginal sonograms assessing the cervix and placental position. A. On the initial study in the mid-second trimester, the placenta is shown to overlie the cervix consistent with complete previa. B. Follow-up study performed 6 weeks later shows the inferior edge of the posterior placenta abutting the posterior margin of the cervix but no longer extending to or covering the os. PI, placenta.

lying placentas. It has been shown that a second trimester low-lying placenta or previa is a significant risk factor for vasa previa, even if the low-lying placenta or previa appears to have resolved in the third trimester. In one series, 69% of vasa previa at delivery had a second trimester placenta previa as documented by midtrimester US compared with 4% of controls.<sup>79</sup> Therefore, it is strongly suggested that a third trimester scan performed to follow-up a low-lying placenta include targeted evaluation with Doppler to assess for possible vasa previa, given the dramatic impact on outcome when this condition is diagnosed prenatally, prompting appropriate, potentially life-saving perinatal management.

### Placenta Accreta

Placenta accreta refers to abnormal adherence of the placenta to the uterus with subsequent failure to separate



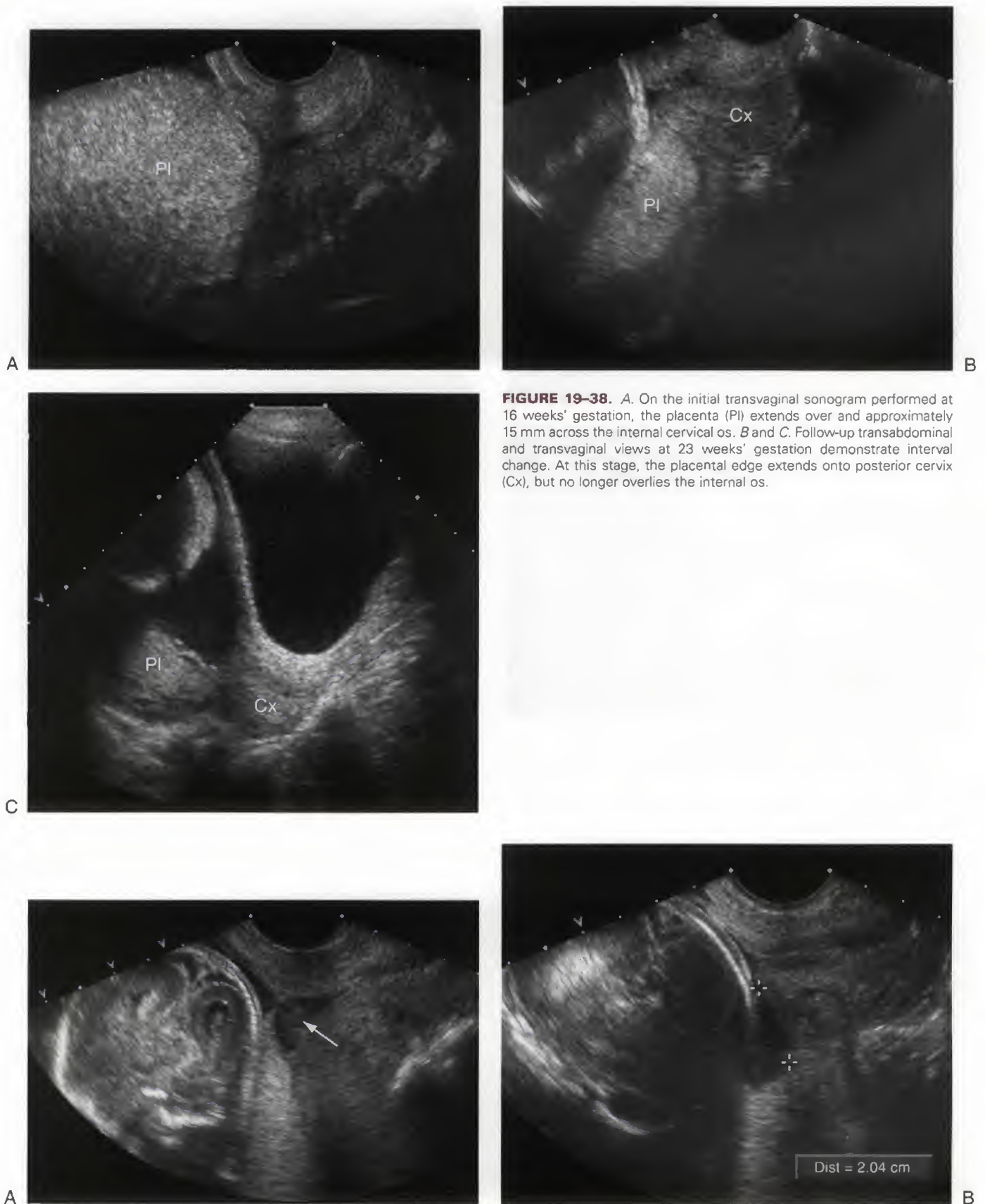


**FIGURE 19-38.** A. On the initial transvaginal sonogram performed at 16 weeks' gestation, the placenta (Pl) extends over and approximately 15 mm across the internal cervical os. B and C. Follow-up transabdominal and transvaginal views at 23 weeks' gestation demonstrate interval change. At this stage, the placental edge extends onto posterior cervix (Cx), but no longer overlies the internal os.

**FIGURE 19-39.** A. Second trimester transvaginal ultrasound reveals the inferior placental edge overlying posterior cervical tissue and extending to the internal os. The small amount of hypoechoic material within the upper cervical canal represents blood (arrow). B. On follow-up transvaginal ultrasound performed 1 month later, the os to inferior placental edge distance measures 2 cm. This patient subsequently delivered vaginally.



**FIGURE 19-40.** Illustration depicting abnormalities of umbilical cord insertion into the placenta. With a velamentous insertion of the umbilical cord into the membranes or with a succenturiate lobe, fetal vessels, within the chorionic membranes and unprotected by the placenta, may course across the cervix and result in a vasa previa. (Illustration by James A. Cooper, MD, San Diego, CA.)

after delivery of the fetus. Placental trophoblastic cells have tissue-invasive characteristics similar to malignant neoplastic cells. When trophoblastic villi burrow into an area of poorly developed or absent decidua, placenta accreta results (Fig. 19-45*A* and *B*). The type of accreta varies according to the depth of invasion. These abnormalities of placental attachment are defined as villi penetrate the decidua but not the myometrium (accreta); villi penetrate and invade into the myometrium but not the serosa (indecra); villi penetrate through the myometrium and may perforate the serosa, sometimes into adjacent organs (percreta) (Fig. 19-46).<sup>80</sup> The prevalence is estimated to be 1 in 2500 pregnancies, but in women with placenta previa, the prevalence is nearly 10%. The incidence of placenta accreta (often used interchangeably as a general term to describe all of these conditions) is increasing. The most frequent predisposing conditions are previous cesarean section and placenta previa. It has been found that in the setting of anterior placenta previa, the risk of placenta accreta increases from 24% in women with 1 prior cesarean delivery to 67% in women with three or more prior cesareans.<sup>57</sup>

Careful assessment of such at-risk pregnancies is warranted because this condition may lead to massive obstetric hemorrhage. Prenatal diagnosis allows effective delivery management planning to minimize morbidity. The diagnosis can be made by US, and the sonographic features of placenta accreta have been described. These include irregularly shaped placental lacunae (vascular spaces) with



**FIGURE 19-41.** Pathologic specimen with velamentous insertion of the umbilical cord and vasa previa, which was not recognized prenatally.

turbulent internal flow shown by Doppler, thinning of the myometrium overlying the placenta, loss of the retroplacental hypoechoic “clear” zone, absence of a decidual interface with normal placental echogenicity, interruption or increased vascularity of the uterine serosa-posterior bladder wall interface, and apparent bulging or protrusion of the placenta into the bladder (Fig. 19-47*A* and *B*). The prominent or multiple hypoechoic-anechoic irregular spaces (lacunae) in the placenta may result in a moth-eaten or Swiss cheese appearance of the placenta.<sup>81</sup> It has been reported that the presence of placental lacunae is the most predictive sonographic sign of accreta with a sensitivity of 79% in the 15- to 20-week range and sensitivity of 93% in the 15- to 40-week range.<sup>82</sup>

The appearance of the retroplacental hypoechoic space is of particular interest on US. The finding of obliteration of the retroplacental “clear space” is commonly thought to be associated with placenta accreta. In placenta accreta, this normally hypoechoic, 1- to 2-cm band is absent or markedly thinned (< 2 mm), and there may be loss of the normal decidual interface between the placenta and myometrium.<sup>83,84</sup> This observation is incompletely sensitive, and it may not always be a reliable diagnostic sign because false-positive results do occur.<sup>82</sup> Still, absence or thinning of this zone, particularly in a patient with a low-lying placenta or previa is suggestive and concerning. Doppler US techniques may be used to demonstrate turbulent flow within the placental lacunae. There may be marked periplacental vascularity on color Doppler.<sup>85-87</sup> Rarely, placental villous tissue may be visualized invading the bladder.<sup>88</sup>

The diagnosis of accreta should be carefully considered when a patient with risk factors (prior cesarean delivery or other uterine surgery, including myomectomy or hysterotomy) is shown by US to have placental implantation overlying the region of the uterine scar and manifests any of the described sonographic features associated with this condition. In addition to grayscale US findings, targeted Doppler assessment should be performed and, at times, MRI considered in this evaluation because it may provide additional diagnostic information in equivocal cases or when the placenta is



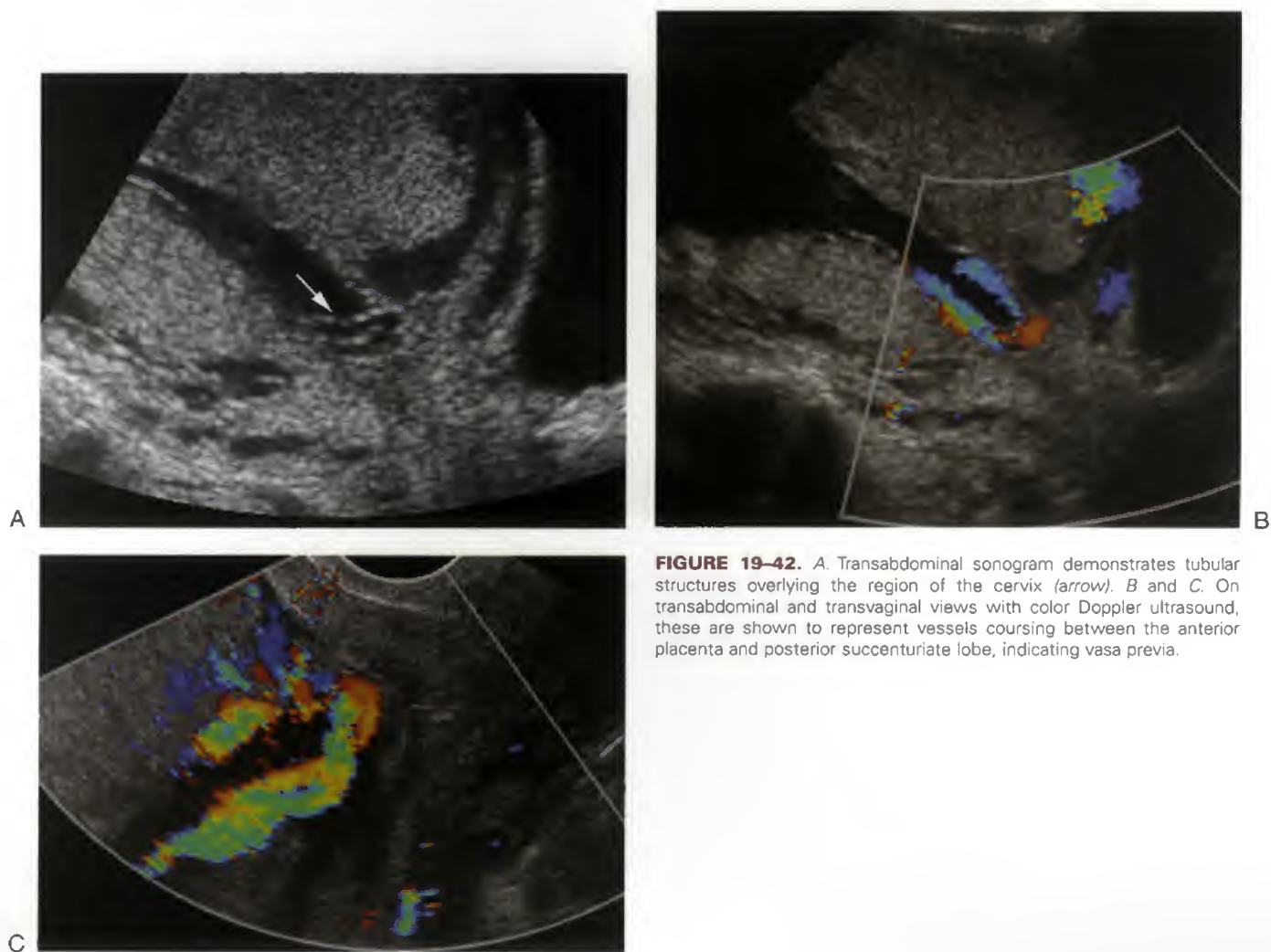


**FIGURE 19-42.** A. Transabdominal sonogram demonstrates tubular structures overlying the region of the cervix (*arrow*). B and C. On transabdominal and transvaginal views with color Doppler ultrasound, these are shown to represent vessels coursing between the anterior placenta and posterior succenturiate lobe, indicating vasa previa.

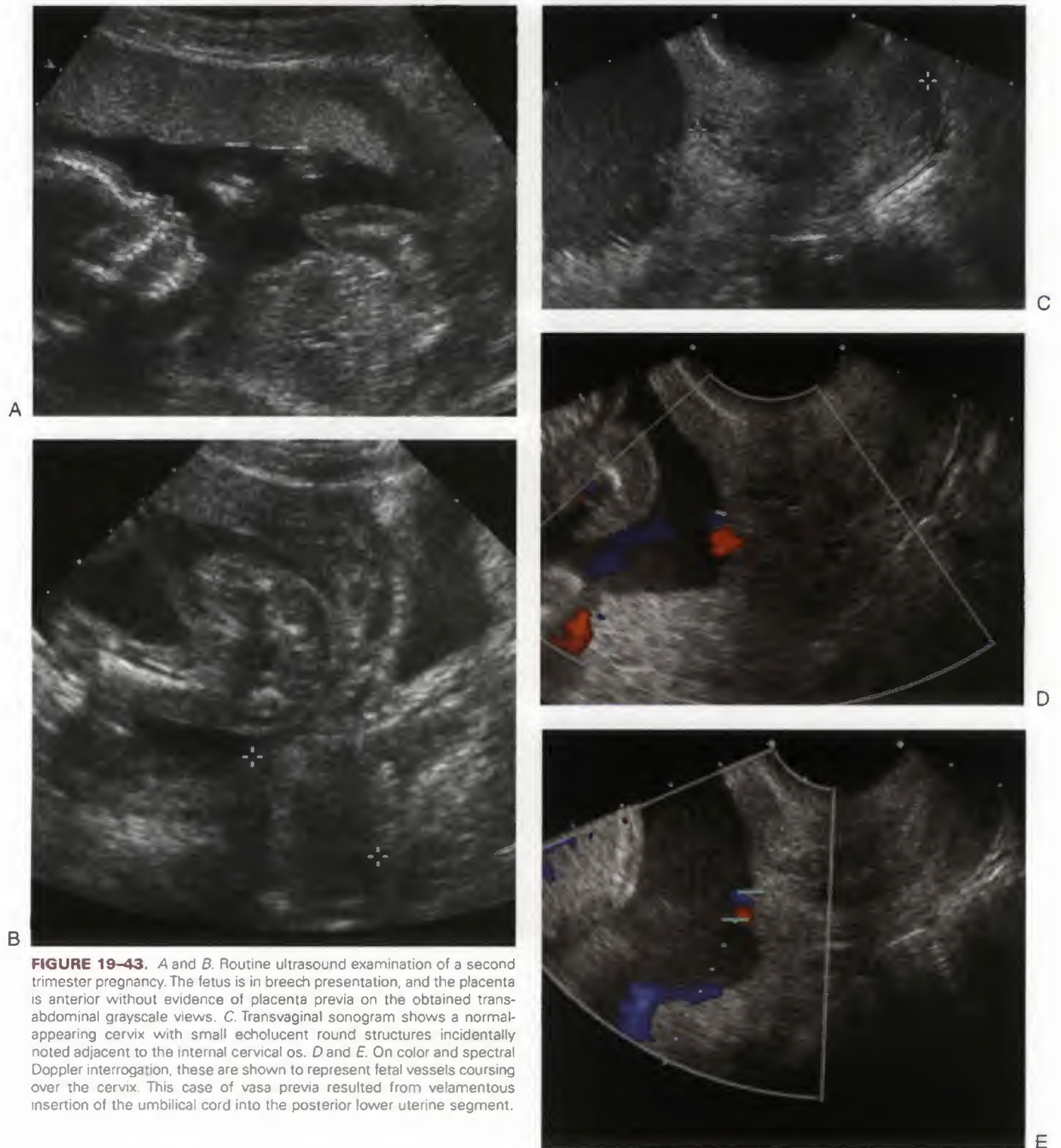


**FIGURE 19-43.** *A* and *B*. Routine ultrasound examination of a second trimester pregnancy. The fetus is in breech presentation, and the placenta is anterior without evidence of placenta previa on the obtained transabdominal grayscale views. *C*. Transvaginal sonogram shows a normal-appearing cervix with small echolucent round structures incidentally noted adjacent to the internal cervical os. *D* and *E*. On color and spectral Doppler interrogation, these are shown to represent fetal vessels coursing over the cervix. This case of vasa previa resulted from velamentous insertion of the umbilical cord into the posterior lower uterine segment.



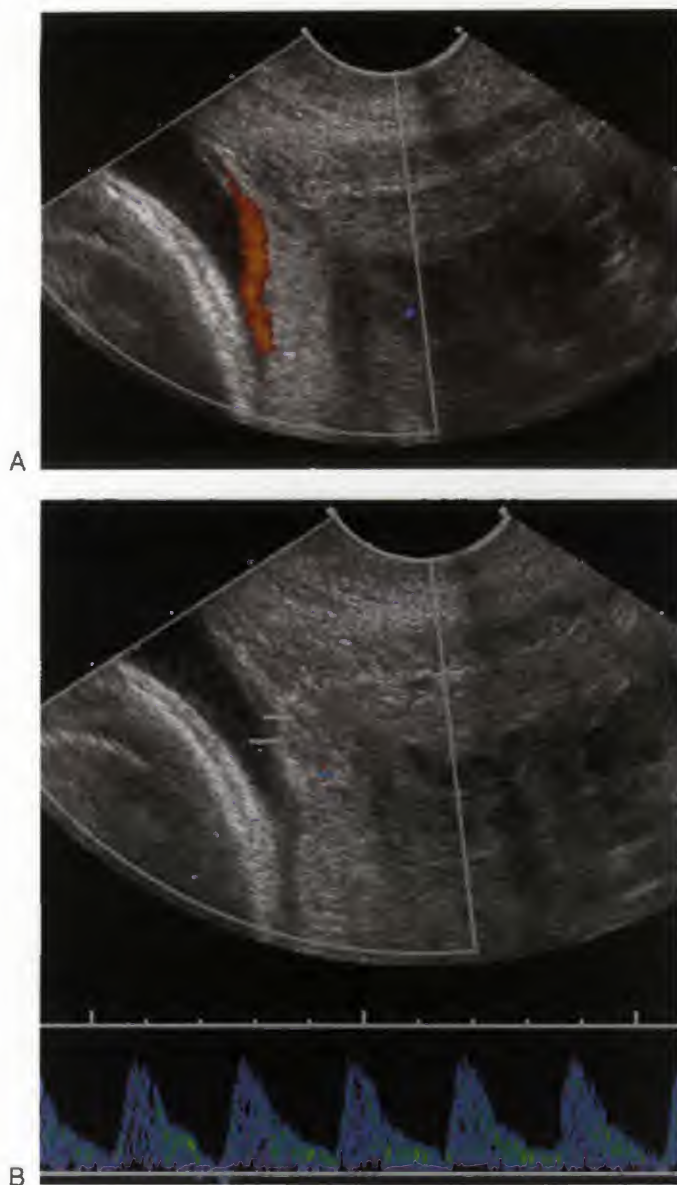


**FIGURE 19-44.** A and B. Vasa previa shown by transvaginal sonograms with color and spectral Doppler techniques.

posterior in location (Fig. 19-48A and B).<sup>84,89,90</sup> A two-stage imaging protocol to evaluate women at high risk for placenta accreta, using US first followed by MRI in cases with inconclusive US features, to optimize diagnostic accuracy has been proposed.<sup>91</sup> These efforts are warranted because prenatal diagnosis of accreta triggers appropriate preoperative and perioperative procedures, and helps reduce fetal and maternal morbidity.

### Nontrophoblastic Placental Tumors

Primary placental tumors are divided into trophoblastic and nontrophoblastic types. Trophoblastic disease is covered in detail elsewhere in this text (see Chapter 29). The majority of nontrophoblastic placental tumors are chorioangiomas.

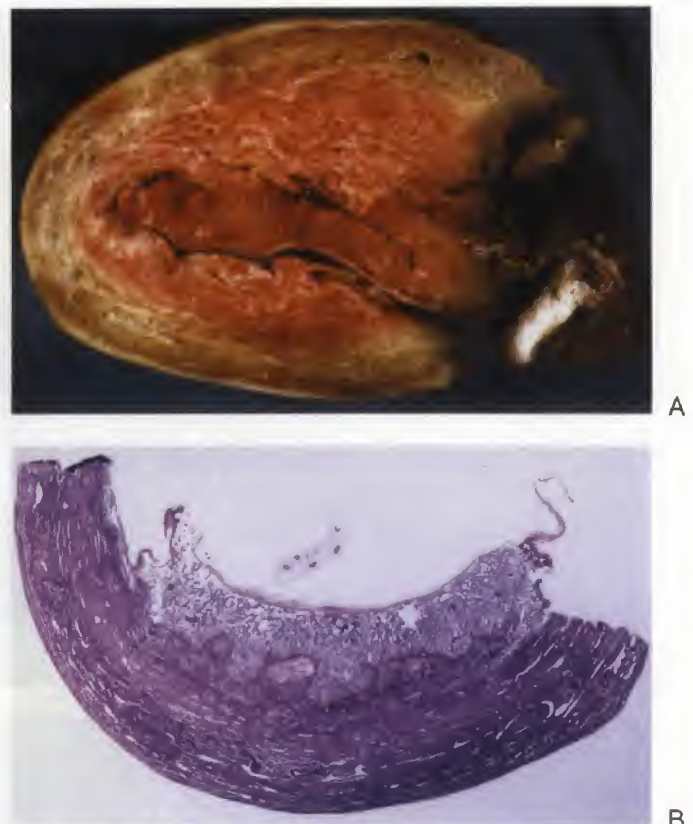


**FIGURE 19-45.** A and B. Pathologic specimens, gross and microscopic, revealing placenta accreta with invasion of the decidua by trophoblastic villi.

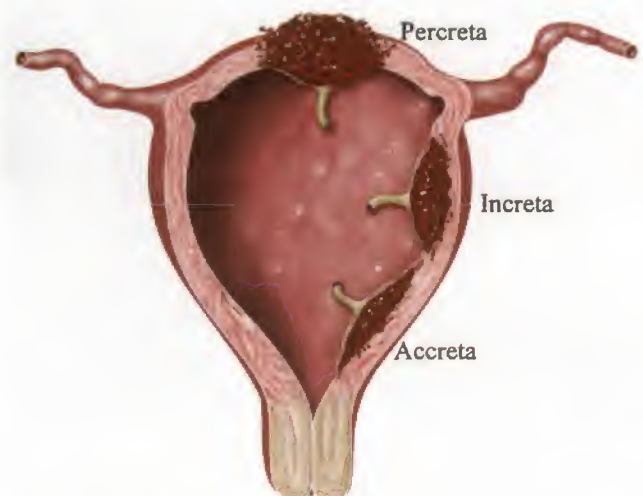


**FIGURE 19-46.** Illustration of types of placenta accreta. (Illustration by James A. Cooper, MD, San Diego, CA.)

Chorioangiomas are the most common benign neoplasm of the placenta, consisting of a vascular mass arising from chorionic tissue, similar to a hemangioma, although a few authors prefer to classify it as a hamartoma. The reported incidence of chorioangiomas at pathology is 1% (Fig. 19-49). Most are small and have no clinical significance or sequelae.

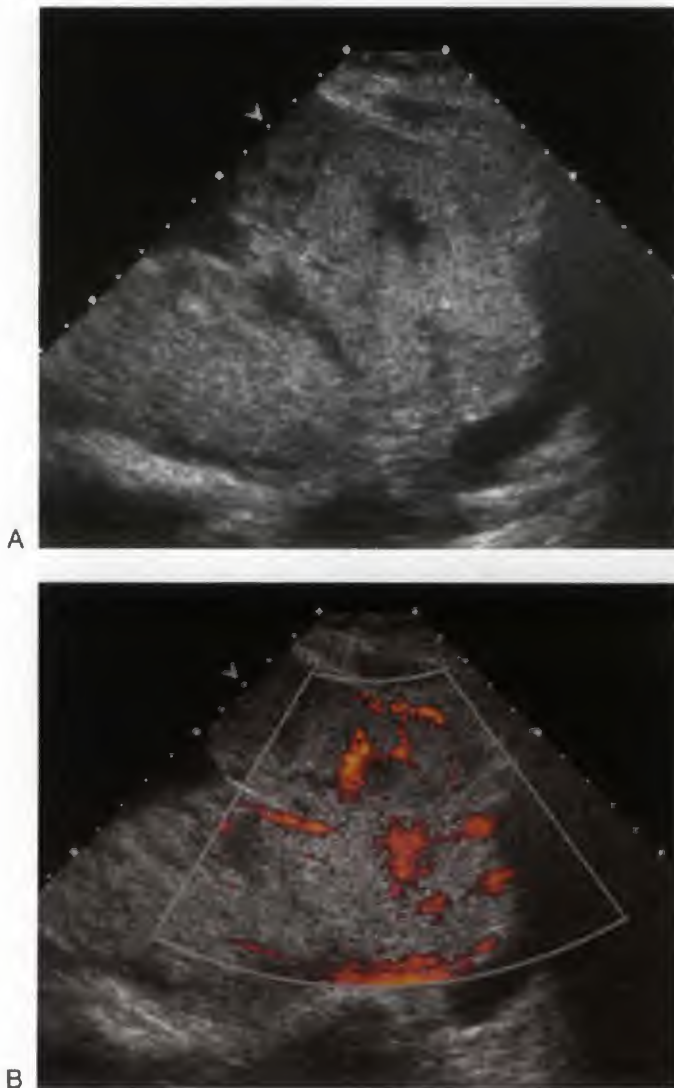


**FIGURE 19-47.** Grayscale (A) and power Doppler (B) ultrasound of placenta accreta. Complete placenta previa was identified in this patient with three prior cesarean deliveries who presented in the late third trimester with vaginal bleeding. On these views targeting the anterior lower uterine segment, the placenta appears heterogeneous with prominent vascular spaces. There is also loss of the retroplacental hypoechoic zone. Placenta increta was confirmed at cesarean hysterectomy.

Large chorioangiomas ( $> 5$  cm) range in frequency from 1:500-1:16,000 live births.<sup>92</sup> These lesions can be associated with fetal and maternal complications including polyhydramnios, hydrops, fetal cardiomegaly, thrombocytopenia, IUGR, preterm labor, preeclampsia, and elevated maternal serum alpha-fetoprotein.<sup>93,94</sup>

On US, chorioangiomas appear as well-circumscribed, round, hypoechoic or mixed echogenic masses that usually occur near the umbilical cord insertion site on the fetal surface of the placenta (Fig. 19-50A and B). They measure from 1 to 5 cm in diameter and often demonstrate moderate vascularity with Doppler interrogation. In one series reviewing US and Doppler flow characteristics, these lesions all showed abundant blood flow or a large feeding vessel

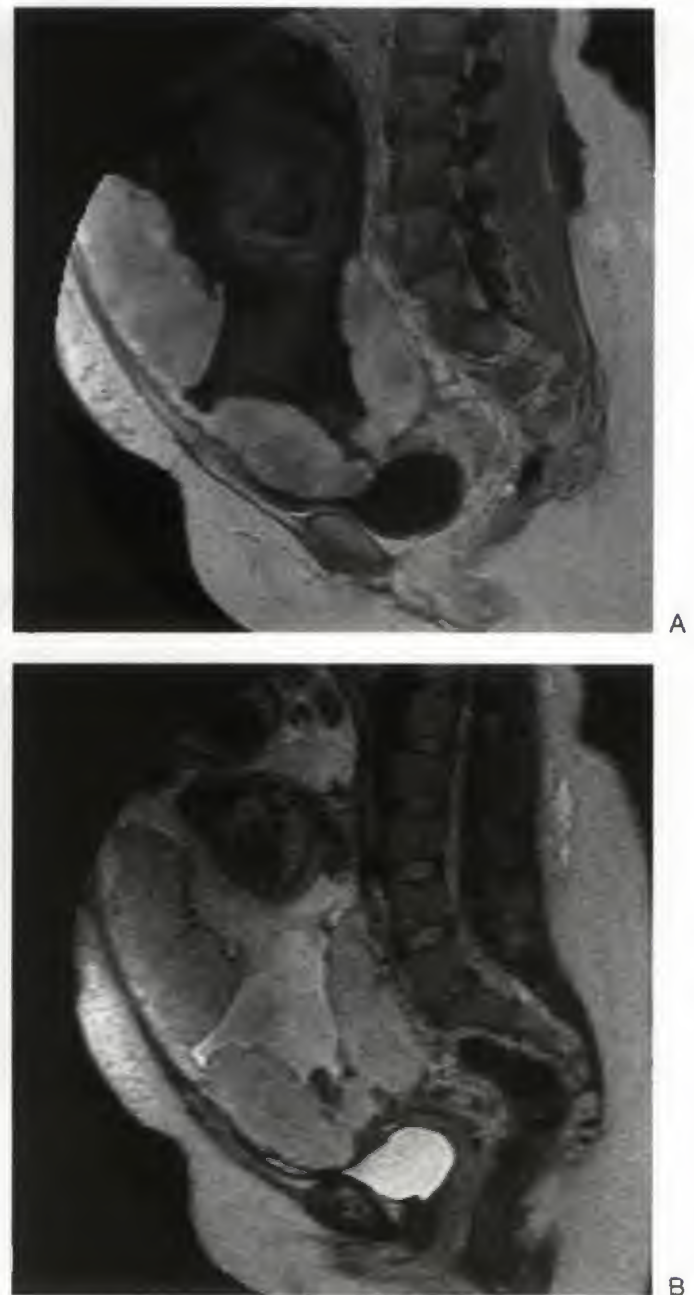


**FIGURE 19-48.** A and B. T1- and T2-weighted sagittal magnetic resonance imaging scans (MRIs) of the patient shown in Figure 19-47. MRI was used to confirm the diagnosis of placenta previa and accreta, to assist in delivery planning, and operative management. Invasion of the myometrium at the anterior lower uterine segment by placental tissue is revealed.

(Fig. 19-51A and B).<sup>93</sup> The prominent blood flow in these benign tumors, which poses a risk to the fetus, may be helpful in distinguishing chorioangioma from other placental processes such as hematoma, subchorionic fibrin deposition, hydropic degeneration, adjacent degenerating leiomyoma, or placental teratoma.<sup>95,96</sup> US can be used to assess and serially monitor the fetus in an effort to detect signs of volume overload with decompensation or hydrops. In utero



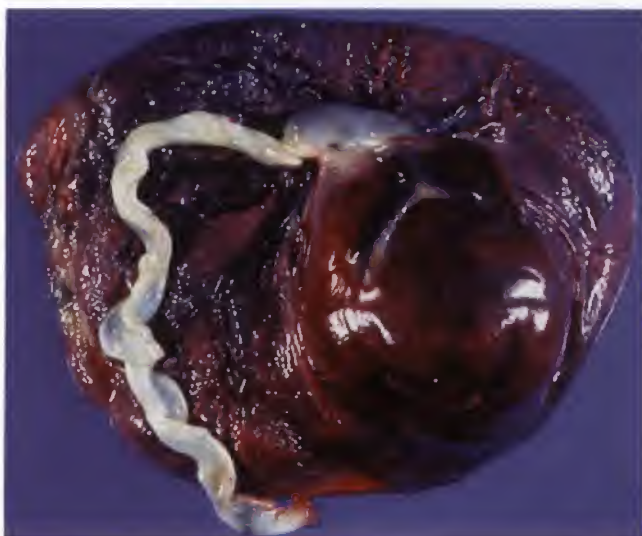


**FIGURE 19-49.** Gross pathologic specimen of a large chorioangioma, appearing as a smooth, round mass on the fetal surface of the placenta, located near the cord insertion site.

intervention with laser coagulation of placental chorioangioma blood supply has been described.<sup>97</sup>

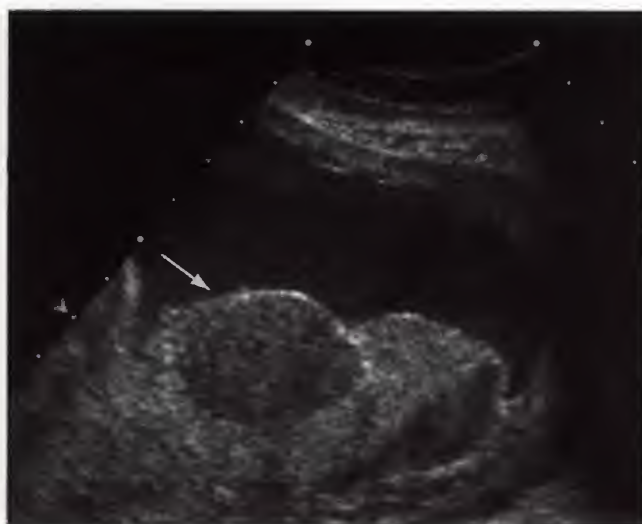
Placental teratoma is an exceedingly rare placental neoplasm.<sup>98</sup> Controversy exists over their origin as primary neoplasm or as abnormal fetus developing in a twin pregnancy. On US, they appear as cystic and solid masses with calcifications occurring in approximately 40%.

### Placental Doppler

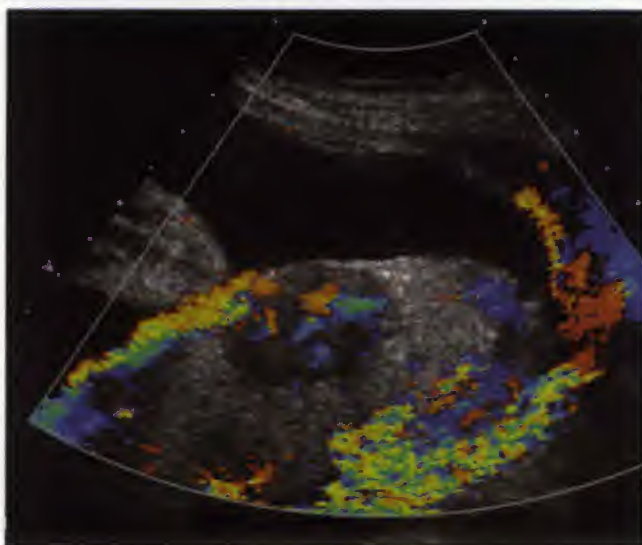
With the widespread application of spectral and color Doppler US imaging in the uteroplacental, umbilical, and fetal circulations, a potential extension is the interrogation of blood flow in the intraplacental arteries. There has been interest and investigation into the clinical significance and possible utility of Doppler measurements of placental perfusion. Use of placental Doppler in the first and early second trimester has not been generally successful or useful. One preliminary report characterized umbilical placental blood flow gradient during the early second trimester of normal pregnancy and established the presence of decreasing gradient.<sup>99</sup> Later in pregnancy, the use of intraplacental Doppler interrogation may be revealing.<sup>100-102</sup> However, this technique is still investigational and the role of intraplacental Doppler is not clearly established compared with uterine artery and other accepted and clinically applied Doppler measurement techniques, covered elsewhere in this text (see Chapter 22).

### UMBILICAL CORD

Many umbilical cord abnormalities can be detected sonographically and have important prognostic implications for perinatal morbidity and mortality. Abnormalities of the cord may be associated with fetal anomalies, chromosomal abnormalities, and potential complications during pregnancy. Several cord lesions are reported in association with adverse perinatal outcomes. Knowledge of normal umbilical cord



A



B

**FIGURE 19-50.** A. Sonogram from a 25-week-old gestation showing an incidental solid, relatively hypoechoic mass (arrow) at the fetal surface of the placenta. B. Blood flow is shown within this lesion on color Doppler ultrasound. This chorioangioma did not result in fetal compromise and was confirmed postnatally.

development and anatomy, and awareness of common abnormalities of the cord is therefore important for accurate prenatal diagnosis and assessment.<sup>103,104</sup>

### Embryology

In the fourth menstrual week, the blastocyst implants into the endometrium. The blastocyst contains the embryonic disc that is composed of two cell layers: the ectoderm and endoderm. The ectoderm forms the amniotic sac and the endoderm forms the yolk sac.<sup>104,105</sup> The embryonic disc, located between the two sacs, grows more rapidly along its dorsal than its ventral surface, causing the embryo to infold along its ventral surface in longitudinal and transverse directions. The dorsal surface flexes into and grows into the amniotic cavity. With infolding, the ventral surface engulfs a portion of the primary yolk sac and divides the yolk sac into



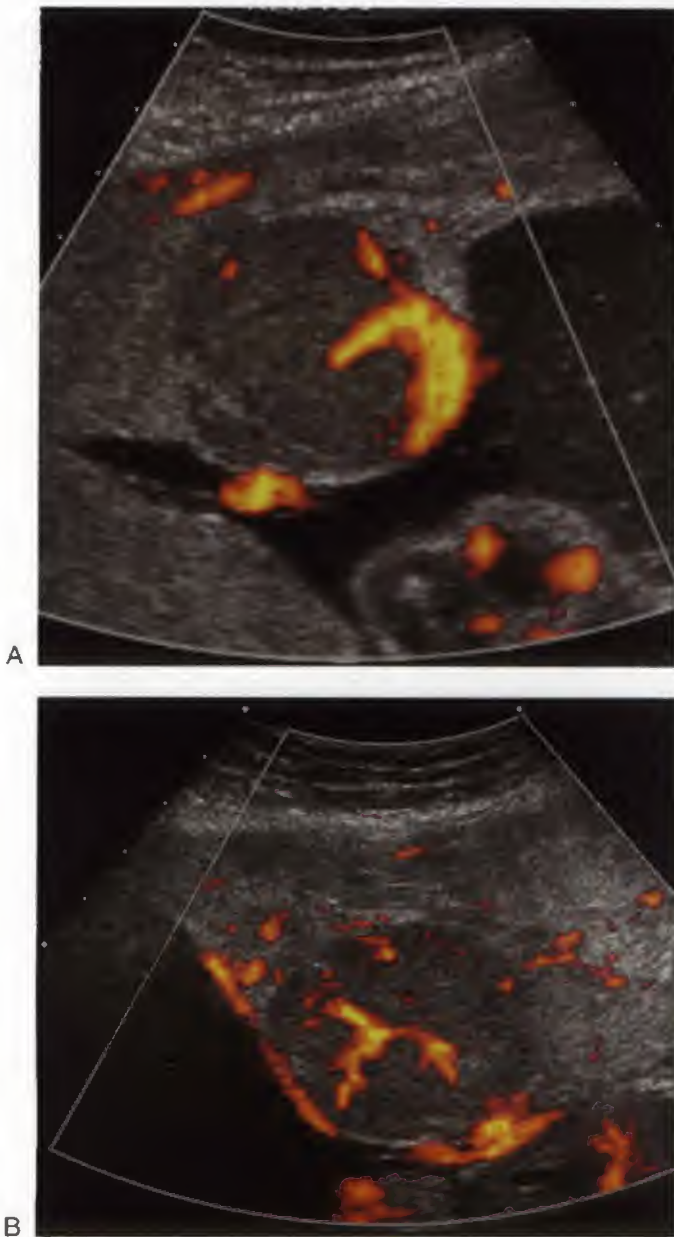


**FIGURE 19-51.** A and B. Transabdominal power Doppler images revealing prominent flow within this chorioangioma, noted along the fetal surface of the anterior placenta.

the intraembryonic portion, which becomes the primitive gut, and the extraembryonic portion, which becomes the omphalomesenteric duct. The proximal portion of the omphalomesenteric duct narrows and elongates, whereas the distal portion remains focally dilated and is known as the secondary yolk sac. The fetal end of the omphalomesenteric duct may persist as a Meckel diverticulum. The secondary yolk sac eventually disconnects from the omphalomesenteric duct and resides within the chorionic space. Sonographically, the secondary yolk sac may be seen at approximately 9 to 11 weeks, located between the unapposed amnion and chorion. At birth, the atrophic secondary yolk sac may be identified on the chorionic plate as a 3- to 5-mm disc.<sup>104</sup>



**FIGURE 19-52.** Ultrasound of a normal three-vessel umbilical cord with both arteries and a single vein seen in long axis.

The amnion rapidly expands and eventually apposes the chorion, usually by 12 to 16 weeks. As the amnion expands, the embryo and connecting stalk become covered with amniotic epithelium. The connecting stalk develops blood vessels and fuses with the omphalomesenteric duct at approximately 7 to 8 weeks to become the umbilical cord.

Toward the caudal end of the embryo, the allantois or urachus develops as a second outpouching from the primitive gut and projects into the connecting stalk. The allantois is connected to the urinary bladder and may persist as a patent urachus or urachal cyst. The blood vessels of the allantois develop into the vessels of the umbilical cord, and therefore, the umbilical arteries that course lateral to the urinary bladder are continuous with the iliac arteries within the pelvis.<sup>104,106</sup>

## Anatomy

The umbilical cord is first visualized by US at 8 weeks as a straight, rather thick structure. At this point, the length of the umbilical cord is approximately equal to the crown rump length. Although it is not possible to directly measure by US, the umbilical cord usually continues to be the same length as the fetus throughout pregnancy. The diameter of the umbilical cord is normally less than 2 cm.<sup>107</sup> The umbilical cord develops up to 40 spiral turns as it elongates during gestation.<sup>108</sup> The umbilical cord twists toward the left more frequently than to the right. Coiling is thought to aid in protecting the cord by resisting compression of the vessels.<sup>109</sup> The development of cord length and twist are also dependent upon tensile forces placed upon the cord by fetal movements. Therefore, there must be adequate fluid space and fetal activity to ensure normal length and coiling of the umbilical cord.<sup>104</sup>

Normally, the umbilical cord contains two arteries and one vein (Fig. 19-52). Although, early in development there



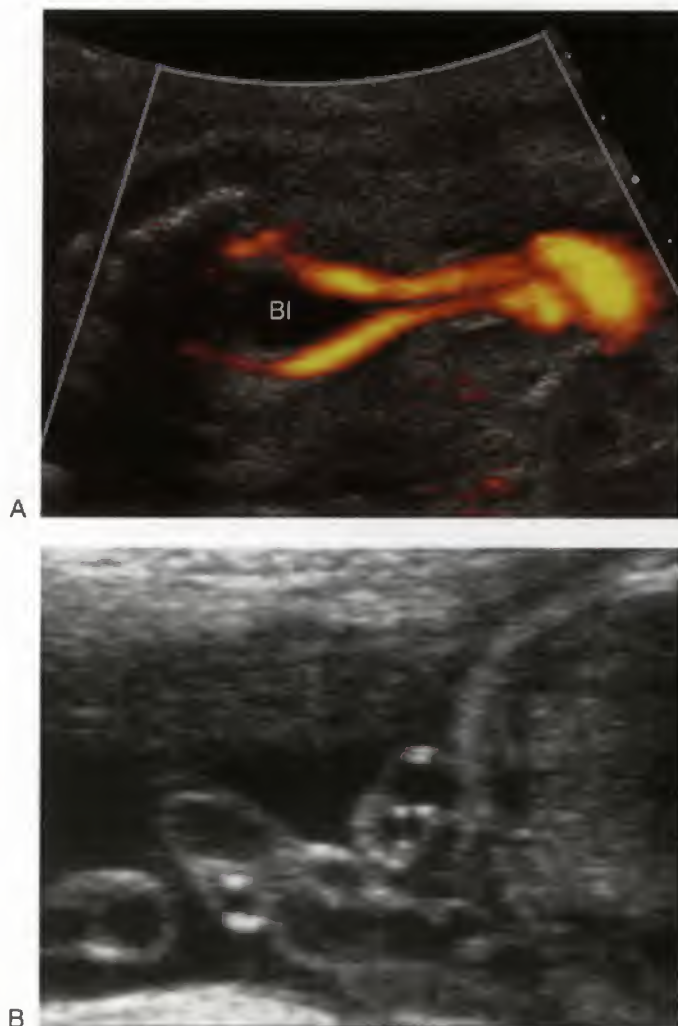


**FIGURE 19-53.** A. Color Doppler ultrasound showing two umbilical arteries flanking the fluid-filled fetal bladder (BI). B. In a separate case, a single umbilical artery is shown adjacent to the bladder.

are two umbilical veins, the right umbilical vein atrophies and the left umbilical vein persists. The umbilical vein carries oxygenated blood returning from the placenta and connects with the left portal vein in the liver. The umbilical arteries are continuous with the internal iliac arteries and carry deoxygenated blood from the fetus toward the placenta. The presence of two umbilical arteries may be confirmed by visualizing a short axis view of the umbilical cord and identifying two arteries and one vein or by visualizing vessels on each side, lateral to the fetal bladder on US (Fig. 19-53A and B). The vessels within the cord are surrounded by Wharton jelly, a gelatinous connective tissue that helps protect the umbilical vessels from compression.<sup>104</sup>

## Abnormalities of the Umbilical Cord

### Single Umbilical Artery

The most common abnormality of the umbilical cord is a single umbilical artery (SUA) seen in approximately 1% of

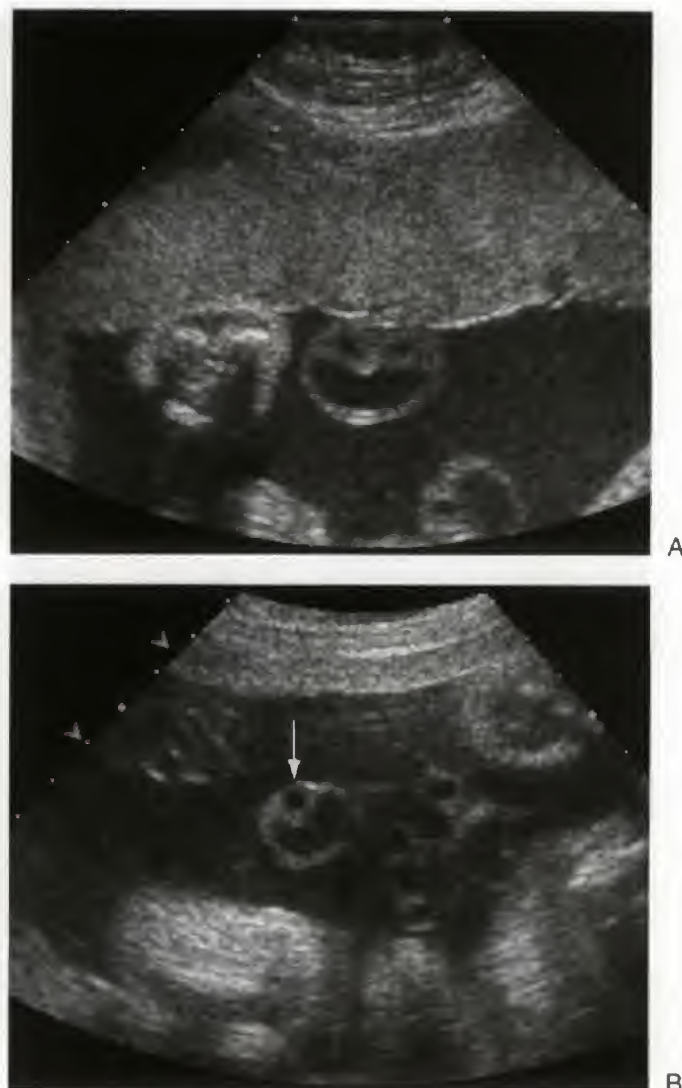


**FIGURE 19-54.** A. Transverse view showing a normal three-vessel umbilical cord (two arteries and one vein). B. An example of a single umbilical artery (arrow) with a two-vessel cord seen on this ultrasound image.

pregnancies (Fig. 19-54A and B).<sup>25</sup> Absence of one umbilical artery may occur as aplasia or as the consequence of atrophy of one artery secondary to thrombosis.<sup>104</sup> The presence of a SUA should be confirmed at the fetal end of the cord because it may represent a normal variant due to fusion of the two umbilical arteries at the placental end of the cord (Fig. 19-55A and B).<sup>104,110</sup> There has been great interest in the nature and significance of SUA regarding its association with fetal structural malformations, chromosomal abnormalities, and poor perinatal results.<sup>111</sup>

Increased incidence of fetal morphologic anomalies, including cardiac and genitourinary defects, in the setting of a SUA has been reported.<sup>104,112-115</sup> Currently, there is no definite correlation between SUA and any specific type or pattern of anomalies. SUA has been reported in association with malformations of all major organ systems and may also be seen with chromosomal abnormalities. In one series, 15%



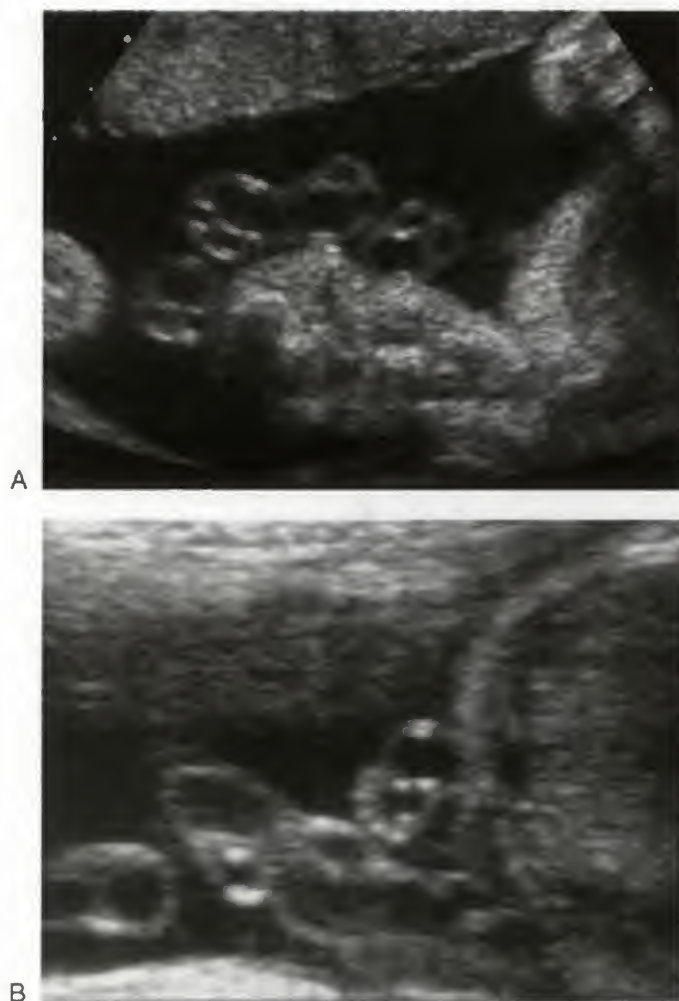


**FIGURE 19-55.** Transverse views through different portions of the umbilical cord showing (A) three vessels and (B) two vessels.

of cases with SUA, found by US at 20 weeks, had other malformations and/or chromosomal abnormalities confirmed at birth. Importantly, *no* aneuploidy was found in fetuses *without* other associated findings by US and *all* serious congenital malformations accompanying the SUA were recognized prenatally.<sup>116</sup> In another report, 72% of cases with antenatal diagnosis of SUA were isolated (no other anomalies identified by US). None of these fetuses had an abnormal echocardiogram. Of those fetuses with other anomalies, the four-chamber view of the heart accurately predicted all but one abnormal echocardiogram.<sup>117</sup>

Even in the absence of associated anomalies, there is an increased risk of IUGR in a fetus with SUA.<sup>118,119</sup> It has been proposed that, most likely SUA is either part of a constellation of multiple anomalies (which are typically more notable on US than SUA), not its cause, or it develops during pregnancy by atrophy and then may be related to restricted fetal growth.<sup>104</sup>

The discovery of a SUA on US warrants a meticulous search for any other associated detectable fetal malformation. In the absence of these, the risk of chromosomal abnormality or other major structural malformation is very low. Follow-



**FIGURE 19-56.** Pathologic specimen of a true knot of the umbilical cord, seen in a case of in utero fetal demise.

up US to assess fetal growth is also indicated when a SUA is observed. It should be remembered however that SUA is most often found in healthy, structurally normal fetuses.

The presence of more than one umbilical vein or more than two umbilical arteries is considered a multivessel cord. Multivessel cords are rare and have been reported in association with congenital anomalies and conjoined twins.<sup>120</sup>

### Length

Abnormally short umbilical cords can occur as a primary phenomenon secondary to failure of embryonic in-folding which is associated with limb body wall defects. Shortened umbilical cords can also occur secondarily when there is decreased fetal movement, as seen with underlying central nervous system or musculoskeletal abnormalities, or when there is limited space, as seen with oligohydramnios or multiple gestations.<sup>104</sup> Short cords have been reported in association with an increased incidence of congenital anomalies, in trisomy 21, oligohydramnios, and breech presentation. Shortened umbilical cords may lead to cord compression, placental abruption, or other difficulties associated with poor fetal descent during delivery.<sup>104,121,122</sup>

Although short cords have been associated with decreased fetal movement, the relationship between long cords and increased fetal movement is uncertain, and the etiology for elongated cords remains unclear. An abnormally long umbilical cord may predispose to cord knots, nuchal cord, and cord prolapse. These conditions may lead to cord compression and decreased perfusion secondary to obstruction of venous return.

Knots of the umbilical cord are classified as true and false. True knots occur in 1% of singleton pregnancies and can be a complication of monochorionic (MC) monoamniotic twin pregnancies (Fig. 19-56). They are rarely detected on prenatal US.<sup>123</sup> They may form as a result of torsion of the cord, forming a loop through which the fetus may slip, forming a knot.<sup>124</sup> The term false knots is a misnomer





**FIGURE 19-57.** Sonogram of a false knot of the umbilical cord, with focal redundancy of cord vessels.

because they represent a focal redundancy of the vessels that can appear sonographically as a vascular protuberance, simulating a knot (Fig. 19-57). The key feature is that the US appearance does not persist in all scanning planes.<sup>125</sup>

### Nuchal Cord

Nuchal cords, the term used to describe entanglement of the umbilical cord around the fetal neck, have been reported in approximately 25% of pregnancies, with an incidence ranging between 16% and 30%. They are frequently noted in many otherwise normal, uncomplicated pregnancies with uneventful deliveries in the vast majority of cases, and they are rarely associated with perinatal morbidity or mortality. But they have been considered worrisome for possible associated fetal injury, particularly when there are two or more tight loops around the fetal neck.<sup>104,126</sup> In one report, nuchal cords were implicated in the intrauterine deaths of three term fetuses who had presented with decreased fetal movements but with normal amniotic fluid volume, fetal size and umbilical artery Doppler findings before delivery.<sup>127</sup>

Nuchal cords may be recognized on prenatal US with many published reports of this observation.<sup>128</sup> They are recognized sonographically as two adjacent loops of cord in cross-section posterior to the neck on sagittal images and by visualizing cord circumferentially around the fetal neck on axial images, best appreciated with color Doppler interrogation (Fig. 19-58A and B).<sup>129</sup> A single loop of umbilical cord seen near the fetal neck is most often an incidental finding and not associated with fetal risk. Antenatal nuchal cords usually occur randomly, with increased frequency later in gestation.<sup>130</sup> It has been noted that nuchal cords seen by US early in pregnancy may spontaneously reduce during gestation.

The question of whether or not nuchal cords are associated with significantly increased adverse fetal outcome is rather controversial and remains unclear, despite many investigations. Furthermore, the question of whether the sonographic observation of a nuchal cord should be searched for at the time of an US examination and, if seen, should be reported has been debated.<sup>131</sup> It has been suggested that the

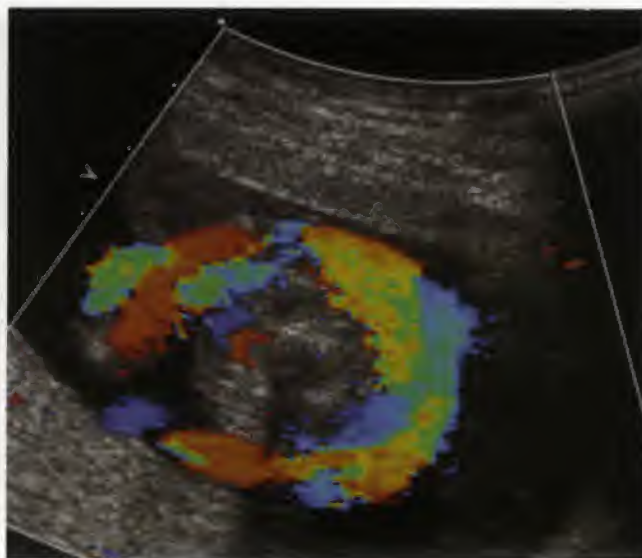


**FIGURE 19-58.** A and B. Two examples of nuchal cords shown by color Doppler ultrasound. In each case, cord vessels are shown circumferentially around the fetal neck.

observation of a nuchal cord is of greater concern when seen in association with other findings, specifically decreased amniotic fluid volume, growth restriction, post-dates, and especially decreased fetal movements.<sup>132</sup> These authors submit that nuchal cords should be sought for and reported, and their presence should, in some cases, prompt further evaluation with antenatal testing, close surveillance, and possible intervention (delivery).

Other investigators have found that antenatal nuchal cords found by US are rarely associated with perinatal complications.<sup>130,133</sup> A study of the utility of US in assessing for nuchal cords in term or post-term pregnancies at the time of induction found that the sensitivity of US in their detection was low, and fetal outcome and clinical management was not significantly altered by the information, arguing against searching for or reporting this finding.<sup>134</sup> In one series, nuchal cord was present at 18% of deliveries. The sensitivity of US in the diagnosis of nuchal cords was only



37.5% before induction of labor at term. Nuchal cord was not associated with increased risk of cesarean section or poor neonatal outcome and did not alter or influence clinical management at time of delivery.<sup>135</sup>

### Coiling

US assessment of the umbilical cord can reveal the direction of cord twists (left helix seven times more common than right) and the frequency of twists of the vessels (referred to as the coiling index) (Fig. 19–59). The normal umbilical cord coiling index (UCI) is calculated as the number of complete coils divided by the length of the cord in centimeters. In a series of 122 uncomplicated pregnancies and in a literature review dating back to 1966, the mean (SD) UCI was 0.17 ( $\pm 0.009$ ) coils/cm.<sup>136,137</sup> Investigators have reported the

frequency of and clinical correlation with abnormally coiled cords (Fig. 19–60).<sup>138</sup> Abnormal cord coiling (UCI < 10th centile (< 0.07) or greater than 90th centile (> 0.30) has been associated with adverse pregnancy outcome.

Undercoiled (< 0.07 coils/cm) and overcoiled (> 0.30 coils/cm) cords have been seen at all gestational ages. In one report, hypocoiling of the cord was associated with increased incidence of fetal demise, intrapartum fetal heart rate decelerations, operative delivery for fetal distress, structural and chromosomal abnormalities, and chorioamnionitis (Fig. 19–61*A* and *B*). Hypercoiling of the cord was associated with increased incidence of fetal growth restriction, intrapartum fetal heart rate decelerations, vascular thrombosis, and cord stenosis (Fig. 19–62). Of note, it is not clear to the investigators whether abnormal coiling was actually a cause of the pathology, or one of the sequelae, or both.<sup>137</sup>

Other reports describe abnormal cord coiling in association with fetal demise, fetal intolerance to labor, preterm delivery,

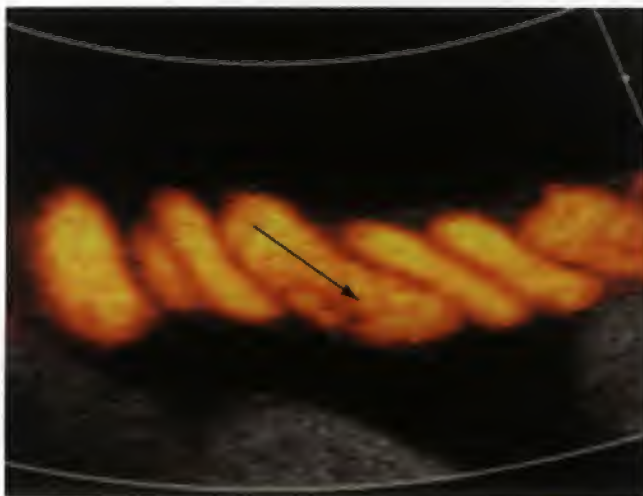


**FIGURE 19–59.** Power Doppler ultrasound of the umbilical cord with left helix (arrow). This direction of cord twists is much more common than right.



**FIGURE 19–60.** Pathologic specimens of 3 different umbilical cords with different degrees of coiling. The cord at the top is markedly overcoiled.

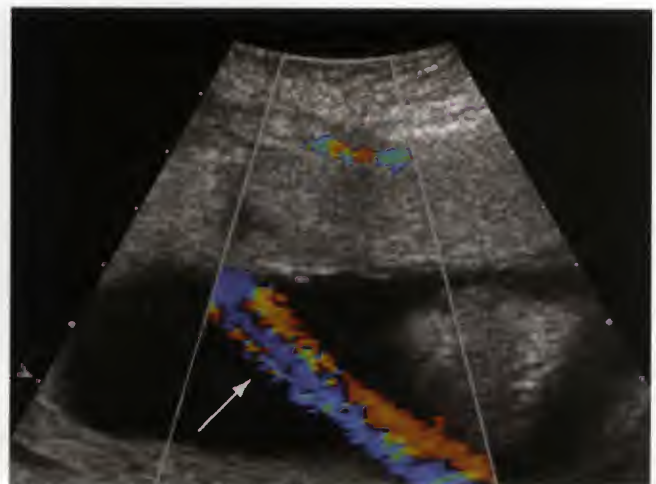
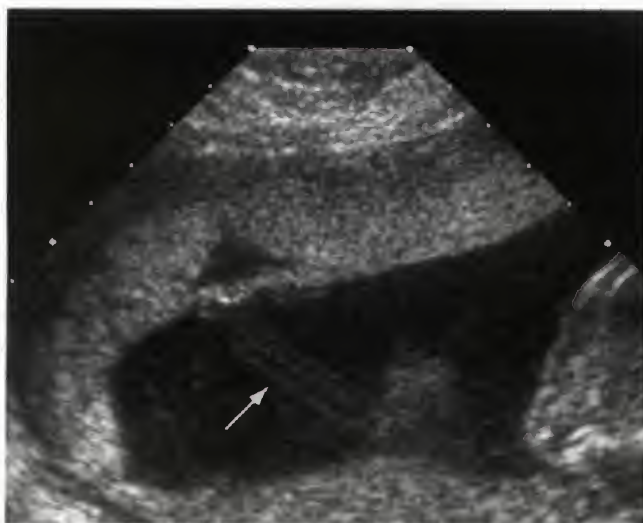


**FIGURE 19–61.** Undercoiled umbilical cord (arrow) demonstrated by (A) grayscale and (B) color Doppler ultrasound.





**FIGURE 19-62.** Sonogram of a markedly overcoiled cord.



**FIGURE 19-64.** Sonogram used to measure the umbilical cord coiling index. The distance between coils is demarcated by the calipers.



**FIGURE 19-63.** Pathologic specimen of singleton term placenta and markedly overcoiled umbilical cord. Thrombosis of chorionic plate (fetal placental) vessels was observed in this case.

fetal structural and chromosomal abnormalities, velamentous cord insertion, SUA, IUGR, and chorioamnionitis. Abnormal cord overcoiling has also been associated with thrombosis of chorionic plate (fetal placental) vessels and of the umbilical vein (Fig. 19-63).<sup>109,139,140</sup> Thus, it appears that abnormal cord coiling is a chronic state, established in early gestation, that may have chronic (growth restriction) and acute (fetal intolerance to labor and fetal demise) effects on the fetus. The underlying cause of abnormal cord coiling is not known, nor is it understood why the degree of coiling is of importance to fetal wellbeing.

Antenatal detection of abnormal cord coil index by US can be performed (Fig. 19-64).<sup>141</sup> The antenatal UCI can be calculated by measuring the distance between two pairs of coils as seen on longitudinal US images of the umbilical



**FIGURE 19-65.** Longitudinally cut umbilical cord specimens showing marked overcoiling (*top*) and undercoiling (*bottom*). Coiling index is calculated as the number of complete coils of the umbilical cord vessels divided by the length of cord (in centimeters).

cord. The sonographic evaluation of umbilical cord coiling in the second trimester was found to correlate with true UCI, obtained after birth (Fig. 19-65).<sup>142</sup> In one series, abnormal cord coiling detected at second trimester US was associated with a higher prevalence of SGA neonates and nonreassuring fetal status in labor.<sup>143</sup> Such investigations are of interest, although the impact on clinical decision making and potential for decreasing risk of adverse perinatal outcome is not yet determined. The cord coil index, the reliability of its detection by US in utero, and the impact on clinical outcome warrants further study and is under investigation.

### Insertion

Early in development, the embryo rotates such that the yolk sac and adjacent connecting stalk are positioned opposite





**FIGURE 19-66.** Normal central insertion of the umbilical cord into the anterior placenta, shown on color Doppler ultrasound.

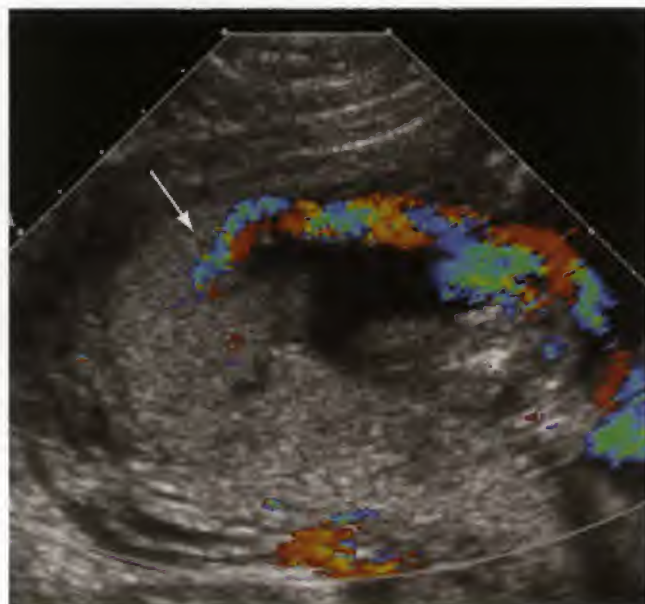
the implantation site. This allows the umbilical cord to insert centrally within the placenta (Fig. 19-66). As the placenta develops, it is believed to grow preferentially in areas of optimal myometrial perfusion and atrophy in areas of suboptimal blood supply. As a result, the cord insertion may become somewhat eccentric despite its initial central attachment. This process is referred to as trophotropism.<sup>101</sup>

**Marginal/Velamentous Insertion of the Cord.** An exaggerated form of eccentric insertion occurs in 7% of pregnancies, with insertion of the cord at the margin of the placenta (Fig. 19-67A and B). This is known as a battledore placenta. In 1% of pregnancies, the cord inserts beyond the placental edge into the free membranes of the placenta. This is known as velamentous insertion of the cord and may be complicated by rupture and thrombosis of the umbilical vessels because they are not protected by Wharton jelly.<sup>101</sup>

Pregnancies with velamentous cord insertion are at risk for the development of fetal growth restriction, prematurity, congenital anomalies, fetal bleeding, retained placenta, and fetal demise. Vasa previa, discussed previously, results from velamentous insertion of the cord with umbilical vessels crossing the cervical os. Such variations in placental insertion of the umbilical cord, including marginal and velamentous insertions can be detected by US.<sup>144-146</sup> In a study of the feasibility of identifying velamentous insertion of the cord using grayscale and color Doppler US, the placental cord insertion site was identified in 99% of cases and all cases of velamentous insertion confirmed after delivery were suspected by prenatal US (Fig. 19-68).<sup>147</sup> Assessment of placental cord insertion site on obstetric US potentially can identify pregnancies with velamentous insertion and, therefore, those at risk for obstetric complications including vasa previa. Velamentous insertion of the umbilical cord is also often seen in one fetus of a MC twin pregnancy.



A



B

**FIGURE 19-67.** Grayscale (A) and color Doppler (B) ultrasound views revealing marginal cord insertion into the placenta.

### Anterior Abdominal Wall Defects

Body stalk anomaly, omphalocele, and gastroschisis are abnormalities of anterior abdominal wall development that are related to the development of the umbilical cord. Body stalk anomaly and omphalocele are likely due to a failure of embryonic infolding.<sup>121,148</sup> Body stalk anomaly is far more severe than omphalocele because it involves longitudinal and lateral folds and is always fatal, whereas omphalocele results from abnormalities of transverse folds only. Failure of embryonic in-folding prevents normal development of the connecting stalk and therefore, the umbilical cord is absent or rudimentary.<sup>149</sup> Gastroschisis is an anterior abdominal wall defect that likely involves an abnormality of vascular



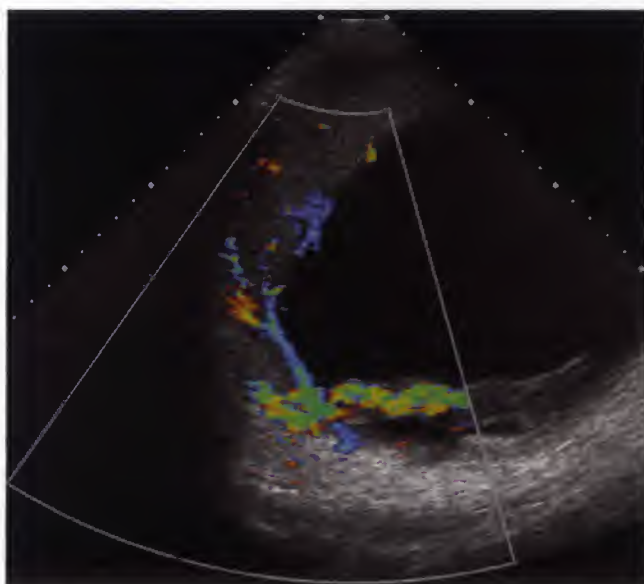


**FIGURE 19-68.** Color Doppler ultrasound of a velamentous cord insertion.

embryology rather than body wall folding.<sup>129</sup> It has been suggested that exaggeration of the normal regression of the right umbilical vein causes a defect in the anterior abdominal wall, through which fetal bowel segments protrude into the amniotic cavity. This defect is almost always seen to the right of an otherwise normal umbilical cord insertion.

### Cord Cysts and Masses

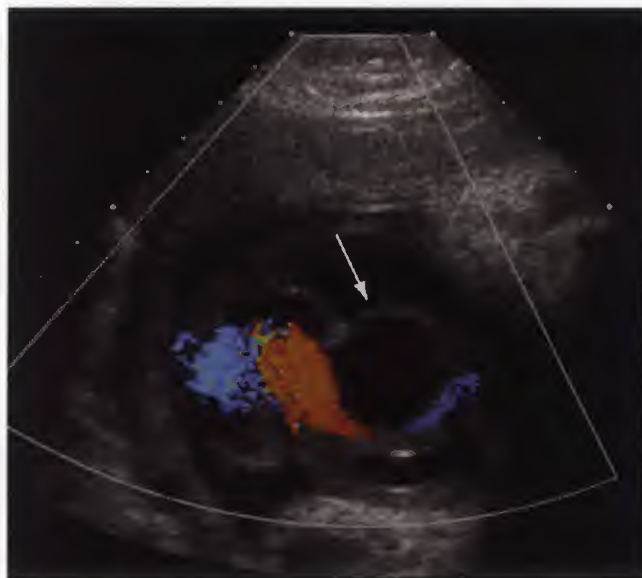
Focal abnormalities within the umbilical cord may be seen incidentally during routine sonography. Certain US characteristics may be helpful in assessing focal lesions of the umbilical cord and in guiding management. The presence of an umbilical cord mass warrants evaluation of flow within the vessels, to assess for vascular compromise resulting from compression or thrombosis.

Single or multiple cysts of the umbilical cord can be seen at sonography (Fig. 19-69). An association between second and third trimester umbilical cord cysts with fetal anomalies and aneuploidy has been reported.<sup>107,150-152</sup> Cysts of the umbilical cord seen in the first trimester more likely represent a normal finding.<sup>107</sup> True cysts of the umbilical cord are lined by epithelium and include remnants of the omphalomesenteric duct or allantoic duct. Amniotic inclusion cysts are lined by amniotic epithelium and develop when a portion of the amnion becomes entrapped in the formation of the umbilical cord. Omphalomesenteric and allantoic duct cysts are located toward the fetal end of the umbilical cord and may be seen in association with anomalies of the gastrointestinal and genitourinary tract, because they are developmentally related. Allantoic duct cysts have been reported in association with omphalocele, patent urachus, and possibly, obstructive uropathy.<sup>153,154</sup>

Pseudocysts, which are not lined by epithelium, result from focal edema within or focal absence of Wharton jelly,



A



B

**FIGURE 19-69.** Two patients with umbilical cord cysts. A. Small cyst (arrow). B. Large cyst (arrow).

secondary to degenerative changes. They are more common than true cysts, and they have also been reported in association with omphalocele.<sup>151</sup>

Focal masses of the cord include tumors, hematomas, varices, and aneurysms. Hemangiomas, although rare, are the most common tumors of the umbilical cord and may appear as a hyperechogenic or multicystic lesion, usually located near the cord insertion at the placenta. Hematomas of the cord are usually focal and typically result from invasive procedures, such as cordocentesis. They most often appear hyperechoic, but the echogenicity may vary depending upon the age of the blood. Rarely, they may develop spontaneously, owing to venous bleeding related to umbilical cord knots or torsion, and may be detected serendipitously or with the



**FIGURE 19-70.** Pathologic specimen of a monochorionic placenta, seen from the fetal surface, following injection of colored dyes into the umbilical vessels. The cord insertion sites into the shared placenta are labeled. The arteries are blue for both twins. The veins are yellow for twin A and red for twin B.

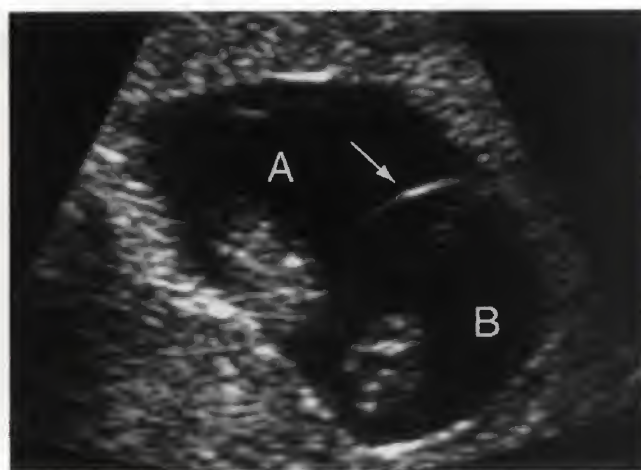
onset of fetal distress.<sup>155</sup> Hematomas are associated with 50% risk of fetal loss and therefore, this diagnosis should prompt fetal monitoring and possible emergency delivery.<sup>156</sup>

Umbilical vein varices may involve the intra-abdominal or extrafetal portion of the umbilical vein. Extrafetal varices can result in vascular compromise secondary to thrombosis. Cases of intra-abdominal umbilical vein varices associated with fetal anomalies and mortality have been reported; however, the significance of this finding remains uncertain.<sup>157,158</sup> Umbilical artery aneurysms are very rare lesions that may be complicated by rupture, dissection, or clot, resulting in vascular compromise.

## Multiple Pregnancies

Twin gestation is not the emphasis of this chapter and is covered in detail elsewhere in this text (see Chapter 8). It is worth noting here, however, that the high risks associated with some twin pregnancies is largely related to the placentas and umbilical cords, thus making the material covered in this chapter of particular relevance. Specifically, the risks associated with MC twin gestations are largely related to the shared placenta and its vascular anatomy. This anatomy has been carefully studied in postpartum placentas<sup>159,160</sup> (Fig. 19-70). More recent work has addressed the in utero sonographic assessment of these pregnancies, revealing the value of focused attention to the shared placenta, cord insertion sites and intertwin vascular connections.

The number of chorions (placentas) and amnions in a monozygotic (fertilization of a single ovum) twin pregnancy depends on when the fertilized ovum divides relative to differentiation of the chorion and amnion. Division between 4 and 8 days after fertilization results in an MC, diamniotic (DA) gestation and occurs in approximately 75% of monozygotic twin pregnancies. Sonographic detection of a MC, DA twin pregnancy and its differentiation from a dichorionic DA twin pregnancy is most accurate in the first trimester (Fig. 19-71). In the third trimester, it may be more difficult to assess true membrane thickness and, thus, chori-



A



B

**FIGURE 19-71.** A. First trimester sonogram of monochorionic twins. A thin membrane (arrow) is seen separating the two embryos, A and B, thus a monochorionic diamniotic twin pregnancy. B. First trimester sonogram of dichorionic twins. In addition to two gestational sacs each with an embryo, a thick intervening membrane is seen (arrow), thus a dichorionic diamniotic pregnancy.

onicity. If early comparison sonograms are not available at the time of a second or third trimester examination, the patient should be questioned as to whether a first trimester sonogram was performed and that sonogram should be evaluated to determine chorionicity.

One fairly common complication in MC twins is birth-weight discordance, which may result from unequal placental sharing. Unequal placental sharing is an abnormality of placentation. In singleton placentas, the site of placental implantation is theorized to determine the eventual cord insertion site. Factors that alter placenta parenchymal function or affect the area of the placenta available to each MC twin for nutrient delivery, gas exchange, and waste removal may affect fetal growth. MC placentas are frequently shared unequally, and when this occurs, discordance in



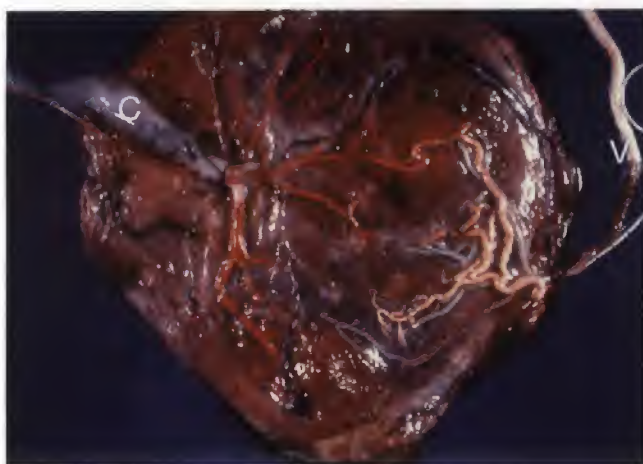


**FIGURE 19-72.** Pathologic specimen of an unequally shared monochorionic placenta with one central (c) and one velamentous (v) umbilical cord insertion. Significant (20%) birth-weight discordance was observed in this twin pair, with the velamentous cord belonging to the smaller twin.

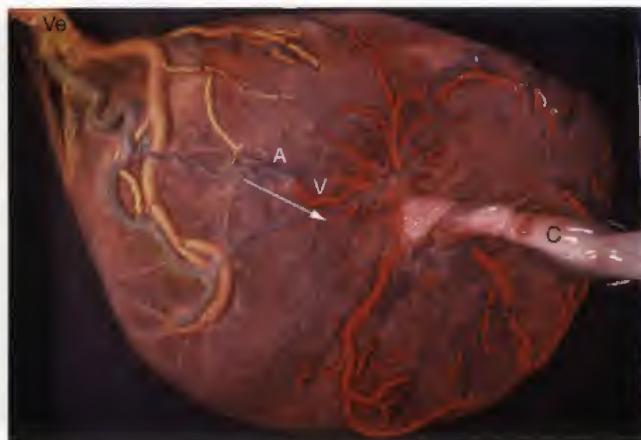


**FIGURE 19-73.** Monochorionic twin placenta with velamentous (Ve) and central (C) cord insertion sites. The feeding arterial limb (A) and draining venous limb (V) of an intertwin arteriovenous anastomosis is shown, with direction of flow indicated (arrow).

growth often results (Fig. 19-72).<sup>161,162</sup> Other unique features of MC placental vascular architecture such as the number, type, and caliber of intertwin vascular anastomoses and the distance between umbilical cord insertions likely also contribute to growth and birth weight discrepancy and to the risk of developing twin-to-twin transfusion syndrome (TTTS).

Velamentous cord insertions have been reported to occur in 13% to 45% of twin gestations, and have been associated with twin growth disorders. Although in the past umbilical cord insertion sites were not routinely examined by obstetric US, as mentioned in a previous section, it is worthwhile doing so to detect velamentous and marginal cord insertions that can be identified by US in singleton and twin gestations in the second trimester. Peripheral cord insertion in one twin of a MC pair is associated with an increased risk for unequal placental sharing and birth-weight discordance. It is possible that identification of cord insertion locations by prenatal US in MC twin pairs may be used as a proxy for identifying unequal placental sharing and is likely to correlate with both postpartum placental pathologic examination findings and with risk of growth and birth weight discordance. Identification of MC twin pairs with at least one peripheral cord insertion should prompt close surveillance with serial USs to assess fetal weight and growth.<sup>162</sup>

TTTS is the most common complication of MC twinning, reportedly occurring in approximately 10% to 20% of MC twin pregnancies. Through intertwin vascular connections on and within the placenta, blood is transfused from the donor (who can become growth-restricted and develop oligohydramnios, resulting in a "stuck" appearance) to the recipient, who can develop circulatory overload and respond with polyuria, resulting in polyhydramnios. There is significant variation in the manifestations of TTTS, including range in the gestational age and acuity of onset, probably reflecting the particular intertwin vascular anatomy (the number, size and character of connections) in the shared placenta, unique in each case.<sup>163,164</sup> (Fig. 19-73).

## References

- Ballantyne JW: The Diseases and Deformities of the Foetus, Vol I. Edinburgh, Oliver and Boyd, 1892.
- Fox H: The development and structure of the placenta. In Fox H (ed): Pathology of the Placenta, 2nd ed. London, WB Saunders Co. Ltd., 1997, pp 1-41.
- Jaffe R, Jauniaux E, Hustin J: Maternal circulation in the first-trimester human placenta—myth or reality? *Am J Obstet Gynecol* 176:695, 1997.
- Kurjak A, Kupesic S: Doppler assessment of the intervillous blood flow in normal and abnormal early pregnancy. *Obstet Gynecol* 89:252, 1997.
- Jauniaux E, Jurkovic D, Campbell S: Current topic: in vivo investigation of the placental circulations by Doppler echography. *Placenta* 16:323, 1995.
- Hoddick WK, Mahony BS, Callen PW, et al: Placental thickness. *J Ultrasound Med* 4:479, 1985.
- Tongsong T, Boonyanurak P: Placental thickness in the first half of pregnancy. *J Clin Ultrasound* 32:231, 2004.
- Wolf H, Oosting H, Treffers PE: Second-trimester placental volume measurement by ultrasound: prediction of fetal outcome. *Am J Obstet Gynecol* 160:121, 1989.
- Hafner E, Metznerbauer M, Hofinger D, et al: Placental growth from the first to the second trimester of pregnancy in SGA-foetuses and pre-eclamptic pregnancies compared to normal foetuses. *Placenta* 24:336, 2003.
- Hafner E, Schuchter K, van Leeuwen M, et al: Three-dimensional sonographic volumetry of the placenta and the fetus between weeks 15 and 17 of gestation. *Ultrasound Obstet Gynecol* 18:116, 2001.
- Thame M, Osmond C, Wilks R, et al: Second-trimester placental volume and infant size at birth. *Obstet Gynecol* 98:279, 2001.
- Jauniaux E, Nicolaides KH, Hustin J: Perinatal features associated with placental mesenchymal dysplasia. *Placenta* 18:701, 1997.
- Harris RD, Cho C, Wells WA: Sonography of the placenta with emphasis on pathological correlation. *Semin Ultrasound CT MR* 17:66, 1996.
- Benirschke K, Kaufmann P: Placental shape aberrations. In Benirschke K, Kaufmann P (eds): Pathology of the Human Placenta, 4th ed. New York, Springer-Verlag, 2000, pp 399-414.
- Bey M, Dott A, Miller JM Jr: The sonographic diagnosis of circumvallate placenta. *Obstet Gynecol* 78:515, 1991.
- Harris RD, Wells WA, Black WC, et al: Accuracy of prenatal sonography for detecting circumvallate placenta. *AJR Am J Roentgenol* 168:1603, 1997.
- McCarthy J, Thurmond AS, Jones MK, et al: Circumvallate placenta: sonographic diagnosis. *J Ultrasound Med* 14:21, 1995.



18. Jeanty P, Kirkpatrick C, Verhoogen C, et al: The succenturiate placenta. *J Ultrasound Med* 2:9, 1983.
19. Grannum PA, Berkowitz RL, Hobbins JC: The ultrasonic changes in the maturing placenta and their relation to fetal pulmonary maturity. *Am J Obstet Gynecol* 133:915, 1979.
20. Hopper KD, Komppa GH, Bice P, et al: A reevaluation of placental grading and its clinical significance. *J Ultrasound Med* 3:261, 1984.
21. Pinette MG, Loftus-Brault K, Nardi DA, et al: Maternal smoking and accelerated placental maturation. *Obstet Gynecol* 73:379, 1989.
22. Fox H: Macroscopic abnormalities of the placenta. In Fox H (ed): *Pathology of the Placenta*. London, WB Saunders Co. Ltd., 1997, pp 102-150.
23. Spirt BA, Gordon LP, Kagan EH: Intervillous thrombosis: sonographic and pathologic correlation. *Radiology* 147:197, 1983.
24. Brown DL, DiSalvo DN, Frates MC, et al: Placental surface cysts detected on sonography: histologic and clinical correlation. *J Ultrasound Med* 21:641; quiz 647, 2002.
25. Jauniaux E, Kingdom J: Clinical ultrasound and pathologic correlation of the placenta. In Lewis SH, Perrin E (eds): *Pathology of the Placenta*. New York, Churchill Livingstone, 1999.
26. Thompson MO, Vines SK, Aquilina J, et al: Are placental lakes of any clinical significance? *Placenta* 23:685, 2002.
27. Reis NS, Brizot ML, Schultz R, et al: Placental lakes on sonographic examination: correlation with obstetric outcome and pathologic findings. *J Clin Ultrasound* 33(2):67-71, 2005.
28. Harris RD, Simpson WA, Pet LR, et al: Placental hypoechoic-anechoic areas and infarction: sonographic-pathologic correlation. *Radiology* 176:75, 1990.
29. Andres RL, Kuypers W, Resnik R, et al: The association of maternal floor infarction of the placenta with adverse perinatal outcome. *Am J Obstet Gynecol* 163:935, 1990.
30. Mandsager NT, Bendon R, Mostello D, et al: Maternal floor infarction of the placenta: prenatal diagnosis and clinical significance. *Obstet Gynecol* 83:750, 1994.
31. Richards DS, Bennett BB: Prenatal ultrasound diagnosis of massive subchorionic thrombohematoma. *Ultrasound Obstet Gynecol* 11:364, 1998.
32. Thomas D, Makhoul J, Muller C: Fetal growth retardation due to massive subchorionic thrombohematoma: report of two cases. *J Ultrasound Med* 11:245, 1992.
33. Deans A, Jauniaux E: Prenatal diagnosis and outcome of subamniotic hematomas. *Ultrasound Obstet Gynecol* 11:319, 1998.
34. Nelson LH: *Ultrasonography of the Placenta—A Review*. Laurel, MD, American Institute for Ultrasound in Medicine, 1994.
35. Oyelese Y, Ananth CV: Placental abruption. *Obstet Gynecol* 108:1005, 2006.
36. Rasmussen S, Irgens LM, Bergsjø P, et al: The occurrence of placental abruption in Norway 1967-1991. *Acta Obstet Gynecol Scand* 75:222, 1996.
37. Abu-Heija A, al-Chalabi H, el-Iloubani N: Abruption placenta: risk factors and perinatal outcome. *J Obstet Gynaecol Res* 24:141, 1998.
38. Knab DR: Abruption placenta. An assessment of the time and method of delivery. *Obstet Gynecol* 52:625, 1978.
39. Ananth CV, Savitz DA, Luther ER: Maternal cigarette smoking as a risk factor for placental abruption, placenta previa, and uterine bleeding in pregnancy. *Am J Epidemiol* 144:881, 1996.
40. Kramer MS, Usher RH, Pollack R, et al: Etiologic determinants of abruption placenta. *Obstet Gynecol* 89:221, 1997.
41. Tikkanen M, Nuutila M, Hilesmaa V, et al: Clinical presentation and risk factors of placental abruption. *Acta Obstet Gynecol Scand* 85:700, 2006.
42. Sholl JS: Abruption placenta: clinical management in nonacute cases. *Am J Obstet Gynecol* 156:40, 1987.
43. Kikutani M, Ishihara K, Araki T: Value of ultrasonography in the diagnosis of placental abruption. *J Nippon Med Sch* 70:227, 2003.
44. Glantz C, Purnell L: Clinical utility of sonography in the diagnosis and treatment of placental abruption. *J Ultrasound Med* 21:837, 2002.
45. Nyberg DA, Cyr DR, Mack LA, et al: Sonographic spectrum of placental abruption. *AJR Am J Roentgenol* 148:161, 1987.
46. Toivonen S, Heinonen S, Anttila M, et al: Reproductive risk factors, Doppler findings, and outcome of affected births in placental abruption: a population-based analysis. *Am J Perinatol* 19:451, 2002.
47. Nagy S, Bush M, Stone J, et al: Clinical significance of subchorionic and retroplacental hematomas detected in the first trimester of pregnancy. *Obstet Gynecol* 102:94, 2003.
48. Ball RH, Ade CM, Schoenborn JA, et al: The clinical significance of ultrasonographically detected subchorionic hemorrhages. *Am J Obstet Gynecol* 174:996, 1996.
49. Manton M: Ultrasound signs in threatened abortion and their prognostic significance. *Obstet Gynecol* 65:471, 1985.
50. Nyberg DA, Mack LA, Benedetti TJ, et al: Placental abruption and placental hemorrhage: correlation of sonographic findings with fetal outcome. *Radiology* 164:357, 1987.
51. Manton M, Pedersen JF: Intrauterine haematoma. An ultrasonic study of threatened abortion. *Br J Obstet Gynaecol* 88:47, 1981.
52. Harris RD, Barth RA: Sonography of the gravid uterus and placenta: current concepts. *AJR Am J Roentgenol* 160:455, 1993.
53. Hertzberg BS, Bowie JD, Carroll BA, et al: Diagnosis of placenta previa during the third trimester: role of transperineal sonography. *AJR Am J Roentgenol* 159:83, 1992.
54. Gallagher P, Fagan CJ, Bedi DG, et al: Potential placenta previa: definition, frequency, and significance. *AJR Am J Roentgenol* 149:1013, 1987.
55. Oyelese Y, Smulian JC: Placenta previa, placenta accreta, and vasa previa. *Obstet Gynecol* 107:927, 2006.
56. Bhide A, Thilaganathan B: Recent advances in the management of placenta previa. *Curr Opin Obstet Gynecol* 16:447, 2004.
57. Clark SL, Koonings PP, Phelan JP: Placenta previa/accreta and prior cesarean section. *Obstet Gynecol* 66:89, 1985.
58. Taylor VM, Kramer MD, Vaughan TL, et al: Placenta previa and prior cesarean delivery: how strong is the association? *Obstet Gynecol* 84:55, 1994.
59. Oppenheimer L, Holmes P, Simpson N, et al: Diagnosis of low-lying placenta: can migration in the third trimester predict outcome? *Ultrasound Obstet Gynecol* 18:100, 2001.
60. Zemlyn S: The effect of the urinary bladder in obstetrical sonography. *Radiology* 128:169, 1978.
61. Timor-Tritsch IE, Yunis RA: Confirming the safety of transvaginal sonography in patients suspected of placenta previa. *Obstet Gynecol* 81:742, 1993.
62. Smith RS, Lauria MR, Comstock CH, et al: Transvaginal ultrasonography for all placentas that appear to be low-lying or over the internal cervical os. *Ultrasound Obstet Gynecol* 9:22, 1997.
63. Dawson WB, Dumas MD, Romano WM, et al: Translabial ultrasonography and placenta previa: does measurement of the os-placenta distance predict outcome? *J Ultrasound Med* 15:441, 1996.
64. Dashe JS, McInire DD, Ramus RM, et al: Persistence of placenta previa according to gestational age at ultrasound detection. *Obstet Gynecol* 99:692, 2002.
65. Taipale P, Hilesmaa V, Ylostalo P: Diagnosis of placenta previa by transvaginal sonographic screening at 12-16 weeks in a nonselected population. *Obstet Gynecol* 89:364, 1997.
66. Mustafa SA, Brizot ML, Carvalho MH, et al: Transvaginal ultrasonography in predicting placenta previa at delivery: a longitudinal study. *Ultrasound Obstet Gynecol* 20:356, 2002.
67. Taipale P, Hilesmaa V, Ylostalo P: Transvaginal ultrasonography at 18-23 weeks in predicting placenta previa at delivery. *Ultrasound Obstet Gynecol* 12:422, 1998.
68. Becker RH, Vonk R, Mendel BC, et al: The relevance of placental location at 20-23 gestational weeks for prediction of placenta previa at delivery: evaluation of 8650 cases. *Ultrasound Obstet Gynecol* 17:496, 2001.
69. Bhide A, Prefumo F, Moore J, et al: Placental edge to internal os distance in the late third trimester and mode of delivery in placenta praevia. *Br J Obstet Gynaecol* 110:860, 2003.
70. Oppenheimer LW, Farine D, Ritchie JW, et al: What is a low-lying placenta? *Am J Obstet Gynecol* 165:1036, 1991.
71. Oyelese KO, Turner M, Lees C, et al: Vasa previa: an avoidable obstetric tragedy. *Obstet Gynecol Surv* 54:138, 1999.
72. Harding JA, Lewis DF, Major CA, et al: Color flow Doppler—a useful instrument in the diagnosis of vasa previa. *Am J Obstet Gynecol* 163:1566, 1990.
73. Nomiya M, Toyota Y, Kawano H: Antenatal diagnosis of velamentous umbilical cord insertion and vasa previa with color Doppler imaging. *Ultrasound Obstet Gynecol* 12:426, 1998.
74. Lee W, Lee VL, Kirk JS, et al: Vasa previa: prenatal diagnosis, natural evolution, and clinical outcome. *Obstet Gynecol* 95:572, 2000.
75. Catanzarite V, Maida C, Thomas W, et al: Prenatal sonographic diagnosis of vasa previa: ultrasound findings and obstetric outcome in ten cases. *Ultrasound Obstet Gynecol* 18:109, 2001.



76. Oyelese Y, Catanzarite V, Prefumo F, et al: Vasa previa: the impact of prenatal diagnosis on outcomes. *Obstet Gynecol* 103:937, 2004.
77. Nelson LH, Melone PJ, King M: Diagnosis of vasa previa with transvaginal and color flow Doppler ultrasound. *Obstet Gynecol* 76:506, 1990.
78. Hsieh FJ, Chen HF, Ko TM, et al: Antenatal diagnosis of vasa previa by color-flow mapping. *J Ultrasound Med* 10:397, 1991.
79. Francois K, Mayer S, Harris C, et al: Association of vasa previa at delivery with a history of second-trimester placenta previa. *J Reprod Med* 48:771, 2003.
80. Fox H: Abnormalities of placentation. In Fox H (ed): *Pathology of the Placenta*. London, WB Saunders Co. Ltd., 1997, pp 54-76.
81. Comstock CH: Antenatal diagnosis of placenta accreta: a review. *Ultrasound Obstet Gynecol* 26:89, 2005.
82. Comstock CH, Love JJ Jr, Bronsteen RA, et al: Sonographic detection of placenta accreta in the second and third trimesters of pregnancy. *Am J Obstet Gynecol* 190:1135, 2004.
83. Cox SM, Carpenter RJ, Cotton DB: Placenta percreta: ultrasound diagnosis and conservative surgical management. *Obstet Gynecol* 71:454, 1988.
84. Levine D, Hulka CA, Ludmir J, et al: Placenta accreta: evaluation with color Doppler US, power Doppler US, and MR imaging. *Radiology* 205:773, 1997.
85. Hoffman-Trečin JC, Koenigsberg M, Rabin A, et al: Placenta accreta. Additional sonographic observations. *J Ultrasound Med* 11:29, 1992.
86. Jauniaux E, Toplis PJ, Nicolaides KH: Sonographic diagnosis of a non-previa placenta accreta. *Ultrasound Obstet Gynecol* 7:58, 1996.
87. Guy GP, Peisner DB, Timor-Tritsch IE: Ultrasonographic evaluation of uteroplacental blood flow patterns of abnormally located and adherent placentas. *Am J Obstet Gynecol* 163:723, 1990.
88. Finberg HJ, Williams JW: Placenta accreta: prospective sonographic diagnosis in patients with placenta previa and prior cesarean section. *J Ultrasound Med* 11:333, 1992.
89. Taipale P, Orden MR, Berg M, et al: Prenatal diagnosis of placenta accreta and percreta with ultrasonography, color Doppler, and magnetic resonance imaging. *Obstet Gynecol* 104:537, 2004.
90. Lam G, Kuller J, McMahon M: Use of magnetic resonance imaging and ultrasound in the antenatal diagnosis of placenta accreta. *J Soc Gynecol Invest* 9:37, 2002.
91. Warshak CR, Eskander R, Hull AD, et al: Accuracy of ultrasonography and magnetic resonance imaging in the diagnosis of placenta accreta. *Obstet Gynecol* 108:573, 2006.
92. Hadi HA, Finley J, Strickland D: Placental chorioangioma: prenatal diagnosis and clinical significance. *Am J Perinatol* 10:146, 1993.
93. Wallenberg H: Chorioangioma of the placenta. *Obstet Gynecol Surv* 26:411, 1971.
94. Zoppini C, Acaia B, Lucci G, et al: Varying clinical course of large placental chorioangiomas. Report of 3 cases. *Fetal Diagn Ther* 12:61, 1997.
95. Reinhart RD, Wells WA, Harris RD: Focal aneurysmal dilatation of subchorionic vessels simulating chorioangioma. *Ultrasound Obstet Gynecol* 13:147, 1999.
96. Bromley B, Benacerraf BR: Solid masses on the fetal surface of the placenta: differential diagnosis and clinical outcome. *J Ultrasound Med* 13:883, 1994.
97. Quarello E, Bernard JP, Leroy B, et al: Prenatal laser treatment of a placental chorioangioma. *Ultrasound Obstet Gynecol* 25:299, 2005.
98. Williams VL, Williams RA: Placental teratoma: prenatal ultrasonographic diagnosis. *J Ultrasound Med* 13:587, 1994.
99. Daniel-Spiegel E, Weiner Z, Weiner E, et al: Umbilical-placental blood flow gradient during the early second trimester of pregnancy. *J Matern Fetal Neonatal Med* 17:133, 2005.
100. Jaffe R, Woods JR: Doppler velocimetry of intraplacental fetal vessels in the second trimester: improving the prediction of pregnancy complications in high-risk patients. *Ultrasound Obstet Gynecol* 8:262, 1996.
101. Haberman S, Friedman ZM: Intraplacental spectral Doppler scanning: fetal growth classification based on Doppler velocimetry. *Gynecol Obstet Invest* 43:11, 1997.
102. Gudmundsson S, Korsun P, Olofsson P, et al: New score indicating placental vascular resistance. *Acta Obstet Gynecol Scand* 82:807, 2003.
103. Marino T: Ultrasound abnormalities of the amniotic fluid, membranes, umbilical cord, and placenta. *Obstet Gynecol Clin North Am* 31:177, 2004.
104. Benirschke K, Kaufmann P: Placental shape aberrations. In Benirschke K, Kaufmann P (eds): *Pathology of the Human Placenta*, 4th ed. New York, Springer-Verlag, 2000, pp 335, 363.
105. Sadler TW: *Langman's Medical Embryology*. 6th ed. Baltimore: Williams and Wilkins; 1990.
106. Yeh HC, Rabinowitz JG: Amniotic sac development: ultrasound features of early pregnancy—the double bleb sign. *Radiology* 166:97, 1988.
107. Weissman A, Jakobi P, Bronshtein M, et al: Sonographic measurements of the umbilical cord and vessels during normal pregnancies. *J Ultrasound Med* 13:11, 1994.
108. Ross JA, Jurkovic D, Zosmer N, et al: Umbilical cord cysts in early pregnancy. *Obstet Gynecol* 89:442, 1997.
109. Strong TH Jr, Elliott JP, Radin TG: Non-coiled umbilical blood vessels: a new marker for the fetus at risk. *Obstet Gynecol* 81:409, 1993.
110. Fujikura T: Fused umbilical arteries near placental cord insertion. *Am J Obstet Gynecol* 188:765, 2003.
111. Rembouskos G, Cicero S, Longo D, et al: Single umbilical artery at 11-14 weeks' gestation: relation to chromosomal defects. *Ultrasound Obstet Gynecol* 22:567, 2003.
112. Jassani MN, Brennan JN, Merkatz IR: Prenatal diagnosis of single umbilical artery by ultrasound. *J Clin Ultrasound* 8:447, 1980.
113. Persutte WH, Hobbins J: Single umbilical artery: a clinical enigma in modern prenatal diagnosis. *Ultrasound Obstet Gynecol* 6:216, 1995.
114. Prucka S, Clemens M, Craven C, et al: Single umbilical artery: what does it mean for the fetus? A case-control analysis of pathologically ascertained cases. *Genet Med* 6:54, 2004.
115. Johnson CW, Tennenbaum SY: Urologic anomalies and two-vessel umbilical cords: what are the implications? *Curr Urol Rep* 4:146, 2003.
116. Cristina MP, Ana G, Ines T, et al: Perinatal results following the prenatal ultrasound diagnosis of single umbilical artery. *Acta Obstet Gynecol Scand* 84:1068, 2005.
117. Gornall AS, Kurinczuk JJ, Konje JC: Antenatal detection of a single umbilical artery: does it matter? *Prenat Diagn* 23:117, 2003.
118. Heifetz SA: Single umbilical artery. A statistical analysis of 237 autopsy cases and review of the literature. *Perspect Pediatr Pathol* 8:345, 1984.
119. Leung AK, Robson WL: Single umbilical artery. A report of 159 cases. *Am J Dis Child* 143:108, 1989.
120. Cohen HL, Shapiro ML, Haller JO, et al: The multivessel umbilical cord: an antenatal indicator of possible conjoined twinning. *J Clin Ultrasound* 20:278, 1992.
121. Giacoia GP: Body stalk anomaly: congenital absence of the umbilical cord. *Obstet Gynecol* 80:527, 1992.
122. Rayburn WF, Beynen A, Brinkman DL: Umbilical cord length and intrapartum complications. *Obstet Gynecol* 57:450, 1981.
123. Jeanty P: Fetal and funicular vascular anomalies: identification with prenatal US. *Radiology* 173:367, 1989.
124. Collins JC, Muller RJ, Collins CL: Prenatal observation of umbilical cord abnormalities: a triple knot and torsion of the umbilical cord. *Am J Obstet Gynecol* 169:102, 1993.
125. Dudiak CM, Salomon CG, Posniak HV, et al: Sonography of the umbilical cord. *Radiographics* 15:1035, 1995.
126. Miser WF: Outcome of infants born with nuchal cords. *J Fam Pract* 34:441, 1992.
127. Jauniaux E, Ramsay B, Peellaerts C, et al: Perinatal features of pregnancies complicated by nuchal cord. *Am J Perinatol* 12:255, 1995.
128. Jouppila P, Kirkinen P: Ultrasonic diagnosis of nuchal encirclement by the umbilical cord: a case and methodological report. *J Clin Ultrasound* 10:59, 1982.
129. Finberg H: Umbilical cord and amniotic membranes. In McGahan JP, Goldberg BB (eds): *Diagnostic Ultrasound: A Logical Approach*. Philadelphia, Lippincott-Raven, 1998, pp 201-229.
130. Clapp JF 3rd, Stepanchak W, Hashimoto K, et al: The natural history of antenatal nuchal cords. *Am J Obstet Gynecol* 189:488, 2003.
131. Feinstein SJ, Lodeiro JG, Vintzileos AM, et al: Intrapartum ultrasound diagnosis of nuchal cord as a decisive factor in management. *Am J Obstet Gynecol* 153:308, 1985.
132. Sherer DM, Manning FA: Prenatal ultrasonographic diagnosis of nuchal cord(s): disregard, inform, monitor or intervene? *Ultrasound Obstet Gynecol* 14:1, 1999.
133. Gonzalez-Quintero VH, Tolaymat L, Muller AC, et al: Outcomes of pregnancies with sonographically detected nuchal cords remote from delivery. *J Ultrasound Med* 23:43, 2004.

134. Schaffer L, Burkhardt T, Zimmermann R, et al: Nuchal cords in term and postterm deliveries—do we need to know? *Obstet Gynecol* 106:23, 2005.
135. Peregrine E, O'Brien P, Jauniaux E: Ultrasound detection of nuchal cord prior to labor induction and the risk of Cesarean section. *Ultrasound Obstet Gynecol* 25:160, 2005.
136. van Diik CC, Franx A, de Laat MW, et al: The umbilical coiling index in normal pregnancy. *J Matern Fetal Neonatal Med* 11:280, 2002.
137. de Laat MW, Franx A, van Alderen ED, et al: The umbilical coiling index, a review of the literature. *J Matern Fetal Neonatal Med* 17:93, 2005.
138. Strong TH Jr, Jarles DL, Vega JS, et al: The umbilical coiling index. *Am J Obstet Gynecol* 170:29, 1994.
139. de Laat MW, Franx A, Bots ML, et al: Umbilical coiling index in normal and complicated pregnancies. *Obstet Gynecol* 107:1049, 2006.
140. Machin GA, Ackerman J, Gilbert-Barness E: Abnormal umbilical cord coiling is associated with adverse perinatal outcomes. *Pediatr Dev Pathol* 3:462, 2000.
141. Cromi A, Ghezzi F, Ducrig P, et al: Sonographic atypical vascular coiling of the umbilical cord. *Prenat Diagn* 25:1, 2005.
142. Predanic M, Perni SC, Chasen ST, et al: Assessment of umbilical cord coiling during the routine fetal sonographic anatomic survey in the second trimester. *J Ultrasound Med* 24:185; quiz 192, 2005.
143. Predanic M, Perni SC, Chasen ST, et al: Ultrasound evaluation of abnormal umbilical cord coiling in second trimester of gestation in association with adverse pregnancy outcome. *Am J Obstet Gynecol* 193:387, 2005.
144. Pretorius DH, Chau C, Poeltler DM, et al: Placental cord insertion visualization with prenatal ultrasonography. *J Ultrasound Med* 15:585, 1996.
145. Di Salvo DN, Benson CB, Laing FC, et al: Sonographic evaluation of the placental cord insertion site. *AJR Am J Roentgenol* 170:1295, 1998.
146. Liu CC, Pretorius DH, Scioscia AL, et al: Sonographic prenatal diagnosis of marginal placental cord insertion: clinical importance. *J Ultrasound Med* 21:627, 2002.
147. Sepulveda W, Rojas I, Robert JA, et al: Prenatal detection of velamentous insertion of the umbilical cord: a prospective color Doppler ultrasound study. *Ultrasound Obstet Gynecol* 21:564, 2003.
148. Ginsberg NE, Cadkin A, Strom C: Prenatal diagnosis of body stalk anomaly in the first trimester of pregnancy. *Ultrasound Obstet Gynecol* 10:419, 1997.
149. Daskalakis G, Sebire NJ, Jurkovic D, et al: Body stalk anomaly at 10-14 weeks of gestation. *Ultrasound Obstet Gynecol* 10:416, 1997.
150. Skibo LK, Lyons EA, Levi CS: First-trimester umbilical cord cysts. *Radiology* 182:719, 1992.
151. Ramirez P, Haberman S, Baxi L: Significance of prenatal diagnosis of umbilical cord cyst in a fetus with trisomy 18. *Am J Obstet Gynecol* 173:955, 1995.
152. Jauniaux E, Donner C, Thomas C, et al: Umbilical cord pseudocyst in trisomy 18. *Prenat Diagn* 8:557, 1988.
153. Fink IJ, Filly RA: Omphalocele associated with umbilical cord allantoic cyst: sonographic evaluation in utero. *Radiology* 149:473, 1983.
154. Frazier HA, Guerrieri JP, Thomas RL, et al: The detection of a patent urachus and allantoic cyst of the umbilical cord on prenatal ultrasonography. *J Ultrasound Med* 11:117, 1992.
155. Petrikovsky BM, Cooperman B, Kahn E, et al: Prenatal diagnosis of non-iatrogenic hematoma of the umbilical cord. *J Clin Ultrasound* 24:37, 1996.
156. Ballas S, Gitstein S, Kharasch J: Fetal heart rate variation with umbilical haematoma. *Postgrad Med J* 61:753, 1985.
157. Mahony BS, McGahan JP, Nyberg DA, et al: Varix of the fetal intra-abdominal umbilical vein: comparison with normal. *J Ultrasound Med* 11:73, 1992.
158. Estroff JA, Benacerraf BR: Fetal umbilical vein varix: sonographic appearance and postnatal outcome. *J Ultrasound Med* 11:69, 1992.
159. Machin G, Still K, Lalani T: Correlations of placental vascular anatomy and clinical outcomes in 69 monochorionic twin pregnancies. *Am J Med Genet* 61:229, 1996.
160. Machin G, Keith LG: *An Atlas of Multiple Pregnancy: Biology and Pathology*. New York, Parthenon Publishing Group, 1999.
161. Hanley ML, Ananth CV, Shen-Schwarz S, et al: Placental cord insertion and birth weight discordancy in twin gestations. *Obstet Gynecol* 99:477, 2002.
162. Fick AL, Feldstein VA, Norton ME, et al: Unequal placental sharing and birth weight discordance in monochorionic diamniotic twins. *Am J Obstet Gynecol* 195:178, 2006.
163. Denbow ML, Cox P, Taylor M, et al: Placental angioarchitecture in monochorionic twin pregnancies: relationship to fetal growth, fetofetal transfusion syndrome, and pregnancy outcome. *Am J Obstet Gynecol* 182:417, 2000.
164. Taylor MJ, Denbow ML, Duncan KR, et al: Antenatal factors at diagnosis that predict outcome in twin-twin transfusion syndrome. *Am J Obstet Gynecol* 183:1023, 2000.



# AMNIOTIC FLUID VOLUME: ITS ROLE IN FETAL HEALTH AND DISEASE

Peter W. Callen, MD

## Amniotic Fluid Physiology

Echogenic Amniotic Fluid

## Ultrasound and Amniotic Fluid Estimation

## Pitfalls in Amniotic Fluid Volume Estimation

## Commentary on Imaging Assessment of Amniotic Fluid Volume

## Oligohydramnios

## Intrauterine Growth Restriction

## Post-term Patients

## Pulmonary Hypoplasia

## Premature Rupture of Membranes

## Intrapartum Oligohydramnios in High-risk Patients

## Frequency of Amniotic Fluid Volume Assessments in the High-risk Patient

## Other Conditions Associated With or Causative of Oligohydramnios

## Oligohydramnios and Assessment of Fetal Weight and Malformations

## Polyhydramnios

## Polyhydramnios: Morbidity and Amnioreduction

## Imaging Considerations in Polyhydramnios

## Twins and Abnormalities in Amniotic Fluid Volume

The importance of amniotic fluid to fetal well-being cannot be overstated. Although once relegated to an afterthought during the sonographic examination, the evaluation of amniotic fluid is now considered an integral and important part of the sonographic evaluation of the gravid patient.

## AMNIOTIC FLUID PHYSIOLOGY

Amniotic fluid serves a number of important functions in the normal development of the embryo and fetus: it cushions the fetus against physical trauma, allows for growth of the fetus free from restriction or distortion by adjacent structures, provides for a thermally stable environment, allows the respiratory and gastrointestinal tracts and musculoskeletal system to develop normally, helps to prevent infection, and may provide a short-term source of fluid and nutrients to the developing embryo.<sup>1,2</sup>

A number of anatomic sites are involved in the regulation of amniotic fluid (Fig. 20-1). The volume of amniotic fluid at any moment represents a balance between those structures producing or allowing passage of fluid into the amniotic cavity: chorion frondosum and membranes, skin, urinary tract, and respiratory tract; and those involved in the removal of amniotic fluid: gastrointestinal tract, respiratory tract, and the amniotic-chorionic interface at the uterine wall.<sup>1-10</sup> Two additional pathways include the intramembranous and transmembranous routes. The more important intramembranous pathway includes transfers between amniotic fluid and fetal blood perfusing the fetal surface of the placenta, fetal skin, and umbilical cord. The transmembranous pathway involves exchange across the fetal mem-

branes between amniotic fluid and maternal blood within the wall of the uterus.<sup>1</sup> The importance of intra- and transmembranous pathways has been made clear, because the total amniotic fluid volume (AFV) cannot be accounted for on the basis of the fetal kidneys, lungs, and swallowing alone. Intramembranous flow reaches nearly 400 mL/day at term (Fig. 20-2).<sup>9</sup>

In early pregnancy, the chorioamnion acts almost as a molecular sieve, allowing for the free passage of water and solutes, electrolytes, creatinine, and urea. Little embryonic contribution to the amniotic fluid occurs at this time, as evidenced by the presence of chorioamniotic fluid both before and in the absence of a living embryo. In the mid-to-late first trimester, diffusion through the embryonic skin readily occurs because the skin is only four cell layers thick.<sup>11</sup> Diffusion across this permeable barrier continues until fetal keratinization at 24 to 26 weeks' gestation.<sup>2,11</sup>

In the latter half of gestation, the two primary sources of amniotic fluid are the fetal kidneys and lungs. The primary sources of amniotic fluid removal are the gastrointestinal tract (swallowing) and absorption into the fetal blood perfusing the surface of the placenta.<sup>1</sup> In the second and third trimesters, fetal urination plays an important role in the production of amniotic fluid. The excretion of hypotonic urine by the fetal kidneys has been reported as early as 12 weeks.<sup>12,13</sup> Confirmatory evidence of the kidneys' role in amniotic fluid production is based in part on the finding that, in the third trimester, concentrations of sodium and chloride in the fetal amniotic fluid and urine decrease, whereas the concentrations of urea and creatinine increase in both fluids.<sup>2</sup> Likewise, in the second trimester, sodium and potassium concentrations are significantly lower in amniotic

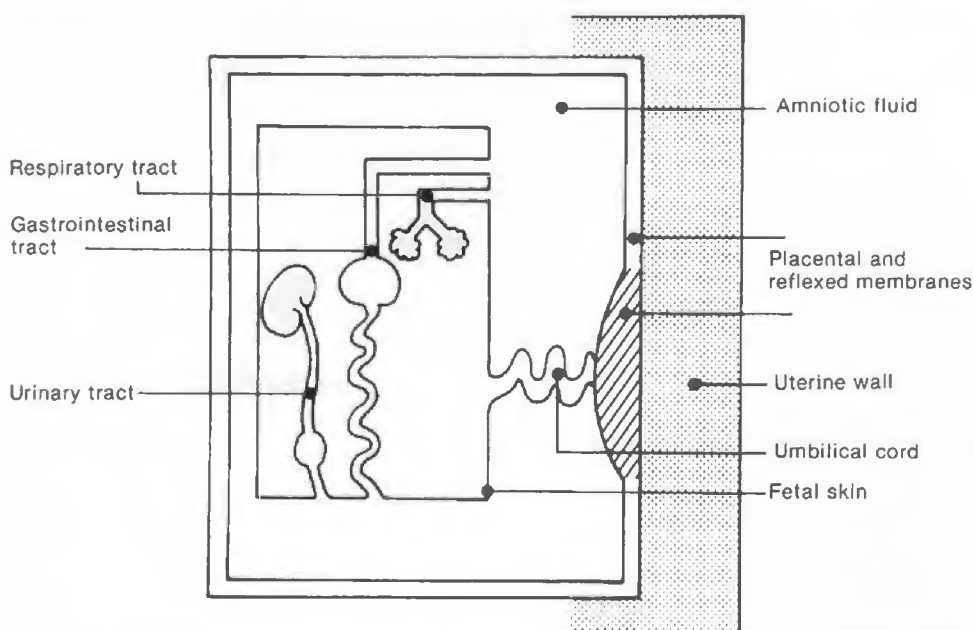


**FIGURE 20-1.** The major fetal and maternal amniotic structures involved in the formation and reabsorption of amniotic fluid. (From Wallenburg HCS: *The amniotic fluid*. *J Perinatol Med* 5:193, 1977.)

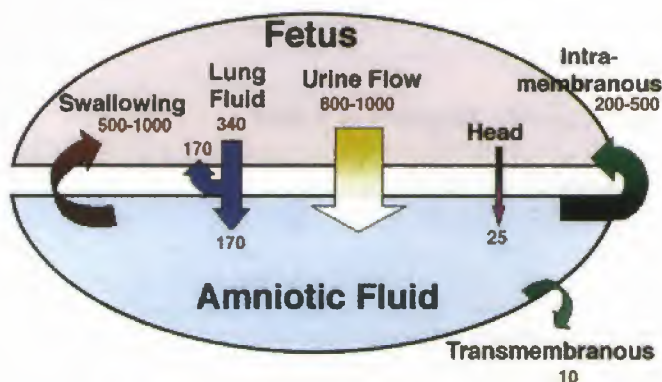


**FIGURE 20-2.** Summary of water flows into and out of the amniotic space in late gestation. (From Brace RA: *Physiology of amniotic fluid volume regulation*. *Clin Obstet Gynecol* 40:286, 1997.)

fluid compared with the maternal serum. This is in part due to small amounts of urine contributing to the amniotic fluid composition.<sup>7,14</sup> At 18 weeks' gestation, fetal urine production has been estimated to be between 7 and 17 mL/day and increases steadily throughout pregnancy (see Fig. 20-2).<sup>15</sup> It has been estimated that the volume of urine produced by the human fetus during the latter half of gestation is approximately 30% of body weight daily.<sup>1,16</sup> At term it is approximately 800 mL/day (range, 600 to 1200 mL/day), which approximates the total AFV at this stage.<sup>2,17</sup> The presence of normal AFV in the second and third trimesters implies that at least one functioning kidney must be present. A reduction in fetal renal arterial blood flow or an increase in renal tubular reabsorption from antidiuretic hormone (both a result of fetal hypoxemia) results in a diminution of AFV.

In addition to the fetal kidneys, the lungs also contribute to the total AFV (see Fig. 20-2). Although the exact amount of fluid secreted by the respiratory tract is not known, it is presumed to be in the range of 60 to 100 mL/kg/day of fetal weight near term.<sup>10,18</sup> Most of the fetal lung fluid leaves the trachea during episodes of fetal breathing.<sup>10,19</sup> According to Brace,<sup>1</sup> less than 1% of the secreted fluid is needed to expand the lungs with growth. Approximately half of the fluid that exits the trachea enters the amniotic fluid.<sup>20</sup> It has been wrongly assumed that the lungs provide a pathway for the absorption of fluid in the normal fetus. As Brace<sup>1</sup> stated, "only under conditions of fetal asphyxia or distress do the fetal lungs absorb fluid."

The removal of amniotic fluid throughout pregnancy is largely a result of fetal swallowing. Approximately one half of the daily urine produced is removed by fetal swallowing. Fetal swallowing has been estimated to be as low as 200 mL/day and as high as 1500 mL/day. Whereas at 20 weeks' gestation the percentage of AFV swallowed is small (approximately 5%), at term the fetus may swallow as much as 50% of the total AFV.<sup>21</sup> In their model of AFV dynamics, Mann, Nijland, and Ross<sup>9</sup> found that relatively low rates of swallowing in proportion to urine and lung fluid production account for the gradual increase in AFV in the first and second trimesters. They also found that increased swallowed AFV contributes to the reduction in AFV near term and possibly to the development of oligohydramnios in post-term patients. It is unlikely that fetal urination and swallowing can explain the total variation in AFV. As mentioned previously, intramembranous and, to a lesser degree, transmembranous flow between the amniotic space and mother and fetus are also likely to play a role in the fluctuations of AFV. Intramembranous flow reaches nearly 400 mL/day at term.<sup>9</sup>

A number of investigators calculated the volume of amniotic fluid throughout gestation. Weisman, Itskovitz-Eldor,



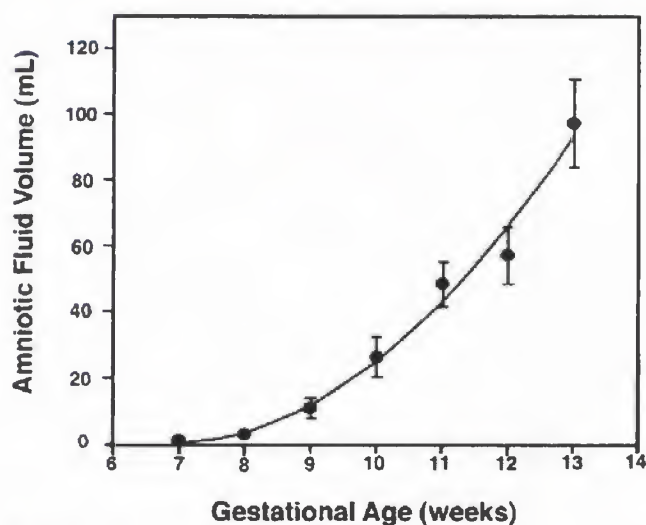


**FIGURE 20-3.** Amniotic fluid volume by gestational age. (From Weissman A, Itskovitz-Eldor J, Jakobi P: Sonographic measurement of amniotic fluid volume in the first trimester of pregnancy. *J Ultrasound Med* 15:772, 1996.)

and Jakobi<sup>22</sup> calculated the volume of amniotic fluid in the first trimester (Fig. 20-3). They found that the quantity of amniotic fluid increased from approximately 1 mL at 7 weeks to 25 mL at 10 weeks and 60 mL at 12 weeks. These authors made the interesting point that if an early amniocentesis is performed, removing 1 mL per gestational week, at 9 weeks, 72% of the AFV will be removed, whereas at 17 to 18 weeks, less than 10% of the total volume is removed. Brace and Wolf<sup>5</sup> found that the AFV progressively rises from 8 weeks' gestation, reaching its statistical maximum (variance analysis) at 22 weeks' gestation and remaining at this level (630 to 817 mL) through 39 weeks (Fig. 20-4). These authors calculated the mean changes in AFV on a weekly basis (based on a polynomial regression equation). At 8 weeks, the volume was increasing at 10 mL/week; at 13 weeks, it increased to 25 mL/week; and at 21 weeks, it reached a maximum of 60 mL/week. The weekly volume increment then decreased and reached zero at 33 weeks' gestation, at which point the mean volume reached its peak. After term, the AFV declines at a rate of approximately 8% per week. During the first half of pregnancy, AFV is closely correlated with fetal weight. The amniotic fluid–fetal volume ratio increases until about 30 weeks' gestation and then appears to decline. The late third trimester gestation fetus urinates and swallows a volume of amniotic fluid equal to 20% to 30% of its body weight per day, whereas an adult, in comparison, urinates and swallows approximately 2% to 3% of its body weight per day.

Although it has long been known that fetal metabolism and blood volume affect AFV, it is only in the last 2 decades that maternal effects, disease states, and hydration have been shown to affect fetal hydration, blood volume, and therefore, AFV.<sup>11,23</sup> Goodlin, Anderson, and Gallagher<sup>23</sup> in 1983 demonstrated the relationships between elevated maternal intravascular volume and polyhydramnios and between decreased maternal intravascular volume and oligohydramnios. Maternal hydration may increase AFV by improving

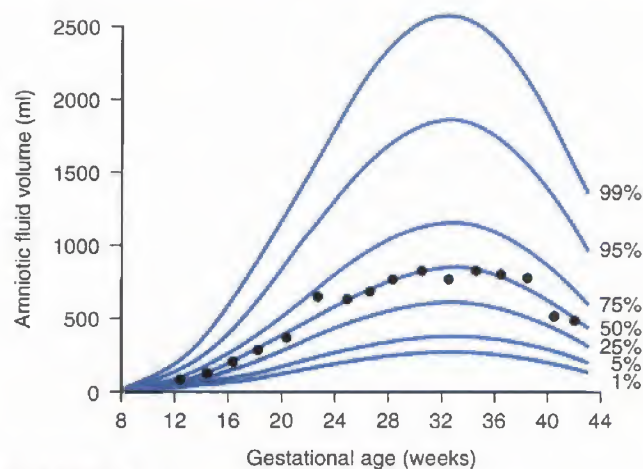


**FIGURE 20-4.** Nomogram shows amniotic fluid volumes as a function of gestational age on a linear scale. Dots are means for each 2-week interval. Percentiles are calculated from polynomial regression equation and standard deviation of residuals. Shaded area covers 95% confidence interval. (From Brace RA, Wolf EJ: Normal amniotic fluid volume changes throughout pregnancy. *Am J Obstet Gynecol* 161:386, 1989.)

uteroplacental blood flow or by bulk transfer of water across the placenta.<sup>24</sup> In a study of patients with normal AFV, Kilpatrick and Safford<sup>25</sup> found that both maternal serum and urinary osmolality significantly decreased after the ingestion of 2 L of water, whereas AFV increased.

### Echogenic Amniotic Fluid

In 1978, Bree<sup>26</sup> and subsequently Parulekar<sup>27</sup> in 1983, reported on the presence of echogenic 'particles' in amniotic fluid. Whereas initially this was believed to represent vernix, its appearance as early as 15 weeks makes this unlikely. Khaleghian<sup>28</sup> reported this finding and raised the possibility that these echoes were secondary to meconium. Whereas the cause of these echoes remains uncertain, they are unlikely to purely represent either meconium or vernix. More recently, Espinoza et al<sup>29</sup> have identified these echoes within the amniotic fluid near the cervix during transvaginal examinations and have termed these echoes *amniotic fluid sludge*. In their study, the prevalence of amniotic fluid sludge was 1% in patients with uncomplicated term pregnancies and 22.6% in those with preterm labor and intact membranes. Their conclusion was that "the presence of amniotic fluid 'sludge' in patients with preterm labor and intact membranes is a risk factor for microbial invasion of the amniotic cavity (MIAC), histological chorioamnionitis and impending preterm delivery." Another study by Mungen et al<sup>30</sup> found that in term patients, the presence of sonographically echogenic amniotic fluid was not associated with any adverse pregnancy outcome and "therefore should not alter routine pregnancy management."

### ULTRASOUND AND AMNIOTIC FLUID ESTIMATION

The recognition of the importance of amniotic fluid in fetal development made it imperative to develop methods of assessing the AFV throughout pregnancy. Although ultra-



**FIGURE 20-5.** Longitudinal sonogram in a second trimester gestation with normal amniotic fluid. Subjective evaluation of normal amniotic fluid depends on the relationship between amniotic fluid and the space occupied by the fetus and placenta.

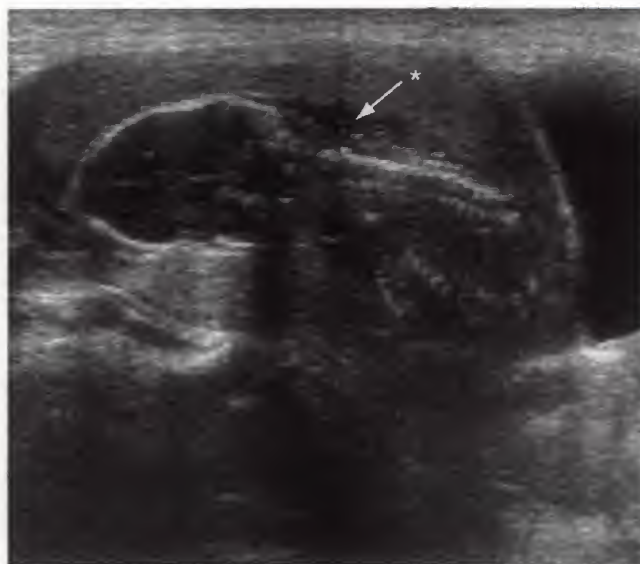


**FIGURE 20-6.** Sonogram of a fetus with renal agenesis. Virtually no amniotic fluid is seen. The fetus is "crowded" within the uterus. The only relatively anechoic space is occupied by the umbilical cord (*asterisk*).

sound has many advantages, not the least of which is its noninvasive nature, it also has inherent problems. The greatest difficulty relates to the tomographic nature of this modality. Sonographic scans across the gravid uterus are two-dimensional slices of the intrauterine contents. A decision about the amount of AFV requires that the examiner sum the individual pockets of amniotic fluid at the time of scanning or interpretation of the recorded films. Although most experienced sonologists are capable of making a subjective decision about the amount of fluid, the lack of objectivity is troublesome to some.

Although clinicians were readily able to recognize the development of an acute and severe excess of amniotic fluid in their patients, it was often difficult to recognize too little amniotic fluid. A noninvasive method of imaging marked reductions in AFV was needed. Sonography was, and is, well suited to this task. Sonographic assessment of oligohydramnios has been largely based in the past on the subjective judgment of the sonologist. The technique of subjective assessment of amniotic fluid involves comparing the echo-free fluid areas surrounding the fetus with the space occupied by the fetus and placenta (Fig. 20-5).<sup>31</sup> When too little fluid is present, the fetus appears crowded within the uterus (Fig. 20-6). In an interesting study, Halperin et al<sup>32</sup> evaluated inter- and intraobserver variability in the subjective assessment of AFV. In their study, experienced sonographers subjectively assigned patients to groups with normal, borderline-low, or reduced AFV. They found that more experienced sonographers had significantly higher intraobserver correlation scores ( $\kappa = 0.94$  versus  $0.63$ ).<sup>31</sup> In another study, Moore et al<sup>31</sup> demonstrated that well-trained observers could subjectively identify patients with oligohydramnios with an intraclass correlation coefficient of  $0.81$ .<sup>31</sup> Using a subjective assessment of AFV, Goldstein and Filly<sup>33</sup> reported intraobserver and interobserver agreements of  $84\%$  and  $96\%$ , respectively (Fig. 20-7).

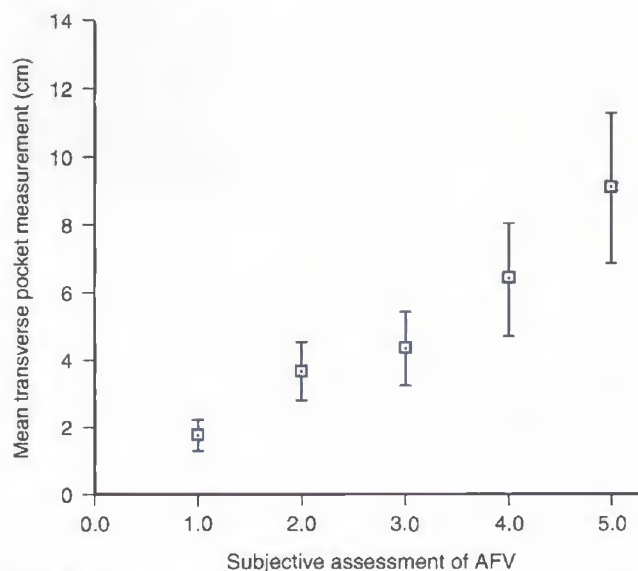


**FIGURE 20-7.** Mean of transverse measurements of the largest amniotic fluid pocket versus subjectively judged amniotic fluid volume (AFV). There is a good correlation between AFV estimates judged with pocket measurements and estimates judged subjectively. 1.0, oligohydramnios (little to no amniotic fluid, virtually no pocket free of umbilical cord, crowding of small parts); 2.0, somewhat decreased amniotic fluid (not frank oligohydramnios but subjectively less than expected AFV for gestational age); 3.0, normal (good fluid-fetal interface, especially about small parts, with fetus filling the anteroposterior diameter of the uterus); 4.0, somewhat increased (more fluid than expected around small parts, slight interface of fluid between fetus and uterine wall); 5.0, frank polyhydramnios (fetus does not fill the uterine cavity in the anteroposterior dimension and much more than expected fluid around both the fetal trunk and small parts). (From Goldstein RB, Filly RA: Sonographic estimation of amniotic fluid volume. *J Ultrasound Med* 7:363, 1988.)



Even though experienced sonologists and sonographers are capable of making such judgments, it is impossible to disseminate criteria for use by less experienced examiners. Furthermore, there is no method of ensuring that even the most experienced examiners use the same visual cues when attempting to diagnose too little fluid. Manning, Hill, and Platt<sup>34</sup> made an excellent step forward in visual evaluation in their description of a simple measurement to judge oligohydramnios. Their technique involves scanning the uterus to select the single deepest amniotic fluid pocket free of umbilical cord and fetal parts (Fig. 20–8). The greatest vertical dimension of this pocket is then measured with the ultrasound transducer perpendicular to the floor. This meas-

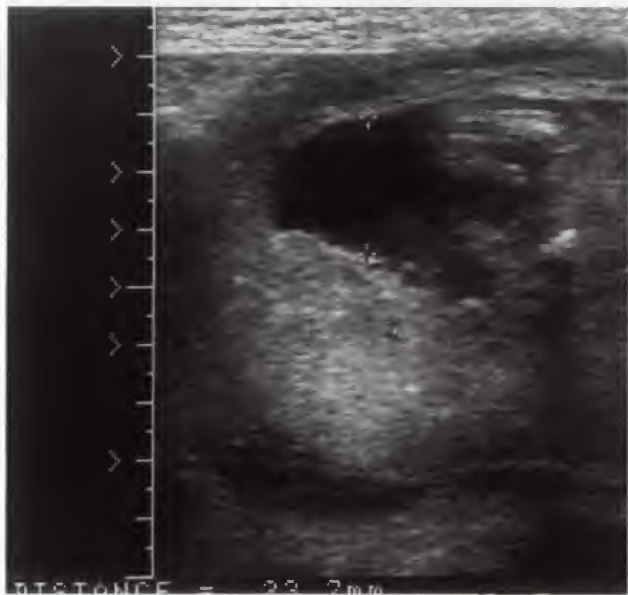


**FIGURE 20–8.** Normal amniotic fluid volume assessed by measurement of the largest single pocket of fluid. In this 22-week gestation, the largest vertical pocket of amniotic fluid, devoid of umbilical cord, is 24 mm.

urement has also been referred to as the maximum vertical pocket (MVP). At the time of their original study, a diagnosis of oligohydramnios was made when the single deepest pocket was less than 1 cm. This measurement has come to be known as the 1-cm rule. Although devised to assess pregnancies in which growth restriction was suspected, it was also used in the evaluation of post-term patients and in the fetal biophysical profile. The 1-cm rule originally described in the early 1980s was modified a number of times by others to increase as well as decrease the maximum allowable amniotic fluid pocket to define oligohydramnios, including measurements of 2 cm, 3 cm, and 0.5 cm (Table 20–1).<sup>35,36</sup> Unfortunately, this rule and others have subsequently proved too stringent to use. Bottoms et al<sup>37</sup> and others correctly noted that the absence of a fluid pocket at least 1 cm in depth was extremely rare and thus an insensitive marker for poor obstetric outcome.<sup>31</sup>

In 1987, Phelan et al<sup>38</sup> and subsequently Rutherford et al<sup>39,40</sup> and Moore and Cayle<sup>41</sup> developed a semiquantitative sonographic assessment of the AFV that has come to be known as the amniotic fluid index (AFI). This measurement is based on the division of the gravid uterus into four quadrants using the external maternal landmarks of the umbilicus and linea nigra (Fig. 20–9 and Table 20–2). The deepest amniotic fluid pocket in each quadrant, in a similar manner to the MVP, is measured. These four measurements are added together, and the sum is referred to as the AFI (Table 20–3). In a 1997 review, Hill<sup>11</sup> noted that Phelan et al's<sup>38</sup> original description of the AFI did not mention whether pockets of amniotic fluid containing umbilical cord should be included or excluded. Subsequently, Rutherford et al<sup>40</sup> stated that the umbilical cord or an extremity may traverse a pocket of measured amniotic fluid (Fig. 20–10).<sup>11</sup> However, when the pocket is almost entirely filled with either umbilical cord or extremities, it should not be included as one of the measured pockets (Fig. 20–11). It should be noted, however, that many sonologists include only pockets that are free of umbilical cord and extremities.<sup>11</sup>

Investigators and practitioners have used a variety of thresholds to define abnormalities in AFV. Moore and

Table 20–1 Definitions of Oligohydramnios		
Technique	Definition	Study
Dye dilution	200 mL	Horsager, Nathan, and Levenol <sup>58</sup>
Dye dilution	500 mL	Magann et al <sup>37</sup>
12 studies: Direct measurement or dye dilution	318 mL	Brace and Wolf <sup>5</sup>
Ultrasound	Single vertical pocket <0.5 cm	Mercer et al <sup>36</sup>
Ultrasound	Single vertical pocket <1.0 cm	Manning, Hill, and Platt <sup>68</sup>
Ultrasound	Single vertical pocket <2.0 cm	Manning et al <sup>58</sup>
Ultrasound	Single vertical pocket <3.0 cm	Halperin et al, <sup>32</sup> Crowley, O'Herlihy, and Boylan <sup>62</sup>
Ultrasound	Two diameter pocket (vertical × horizontal) <15.0 cm	Magann et al <sup>57</sup>
Ultrasound	Amniotic fluid index <fifth percentile for gestational age	Moore and Cayle <sup>41</sup>
Ultrasound	Amniotic fluid index <5.0 cm	Phelan et al <sup>38</sup>
Ultrasound	Amniotic fluid index <7.0 cm	Dizon-Townson et al <sup>159</sup>
Ultrasound	Amniotic fluid index <8.0 cm	Jeng et al <sup>160</sup>

From Hill LM: Oligohydramnios: Sonographic diagnosis and clinical implications. Clin Obstet Gynecol 40:314, 1997.

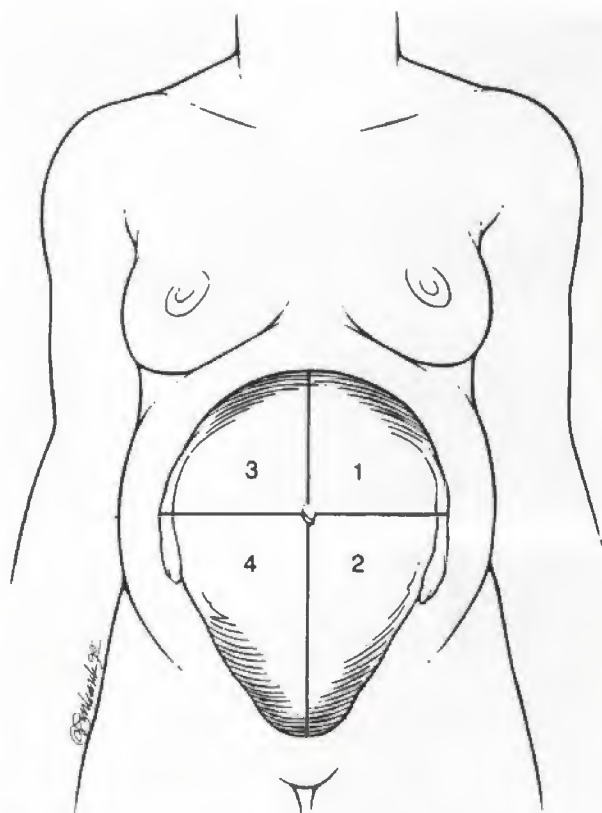


**FIGURE 20-9.** Diagram of the division of the uterus into four equal quadrants for determination of the amniotic fluid index. With the ultrasound transducer perpendicular to the table the vertical depth of the largest amniotic fluid pocket that is free of umbilical cord in each quadrant is measured. It should be noted that some examiners measure the pockets in millimeters and total the four quadrants, whereas others measure the pockets in centimeters. (From Gabbe SG, Niebyl JR, Simpson JL: *Obstetrics: Normal and Problem Pregnancies*, 2nd ed. New York, Churchill Livingstone, 1991.)

**Table 20-3**

**Amniotic Fluid Index Values in Normal Pregnancy**

Week	Amniotic Fluid Index Percentile					n
	2.5th	5th	50th	95th	97.5th	
16	73	79	121	185	201	32
17	77	83	127	194	211	26
18	80	87	133	202	220	17
19	83	90	137	207	225	14
20	86	93	141	212	230	25
21	88	95	143	214	233	14
22	89	97	145	216	235	14
23	90	98	146	218	237	14
24	90	98	147	219	238	23
25	89	97	147	221	240	12
26	89	97	147	223	242	11
27	85	95	146	226	245	17
28	86	94	146	228	249	25
29	84	92	145	231	254	12
30	82	90	145	234	258	17
31	79	88	144	238	263	26
32	77	86	144	242	269	25
33	74	83	143	245	274	30
34	72	81	142	248	278	31
35	70	79	140	249	279	27
36	68	77	138	249	279	39
37	66	75	135	244	275	36
38	65	73	132	239	269	27
39	64	72	127	226	255	12
40	63	71	123	214	240	64
41	63	70	116	194	216	162
42	63	69	110	175	192	30

Amniotic fluid index values are obtained by measuring the vertical depth of the largest clear amniotic fluid pocket in each of four equal uterine quadrants. The values from each quadrant are measured in millimeters and added together.

From Moore TR, Cayle JE: The amniotic fluid index in normal human pregnancy. *Am J Obstet Gynecol* 162:1168, 1990.

**Table 20-2** Amniotic Fluid Index Technique

Position patient supine.

A linear, curvilinear, or sector transducer can be used.

Divide the uterus into four quadrants using the maternal sagittal midline vertically, and arbitrary transverse line approximately halfway between the symphysis pubis and the upper edge of the uterine fundus.

The transducer must be kept parallel to the maternal sagittal plane and perpendicular to the maternal coronal plane throughout.

The deepest unobstructed and clear pocket of amniotic fluid is visualized, and the image frozen. The ultrasound calipers are manipulated to measure the pocket in a strictly vertical direction.

The process is repeated in each of four quadrants and the pocket measurements summed = AFI.

If the AFI is <8 cm, perform the four quadrant evaluation three times and average the values.

AFI, amniotic fluid index.

Adapted from Moore TR: Clinical assessment of amniotic fluid. *Clin Obstet Gynecol* 40:300, 1997.

Cayle<sup>41</sup> defined oligohydramnios when the AFI was less than the fifth percentile, which corresponded to an AFI of less than 7 to 8 cm. Rutherford et al<sup>39</sup> used 5 cm as a threshold to define oligohydramnios, a number that would be slightly less than the first percentile. Although controversy still exists as to which threshold values to use, values greater than 5 cm and less than 18 to 20 cm are considered by most examiners to be normal. Thus, the 1-cm rule has been replaced by the 5-cm rule.

Many studies found that the AFI more closely relates to the AFV based on dye-dilution studies and, in many cases, is more accurate than measuring a single pocket; however, this has not been true in all investigations. In one study comparing the AFI with dye-dilution methods, Dildy et al<sup>42</sup> found that the AFI overestimated the actual volume by as much as 88.7% at lower volumes and underestimated the actual volume by as much as 53.9% at higher volumes. In a dye-dilution study at the time of amniocentesis by Chauhan et al,<sup>43</sup> in which they correlated semiquantitative methods (AFI and two-diameter pocket measurements) with AFV, poor correlation was found. The authors concluded



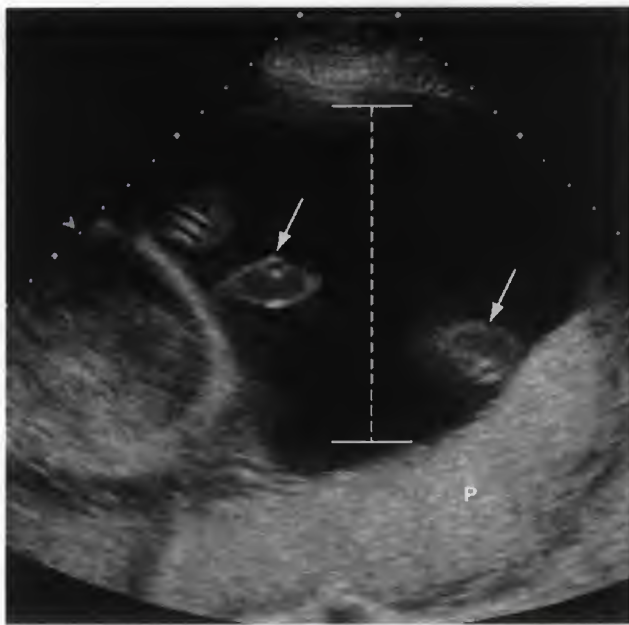
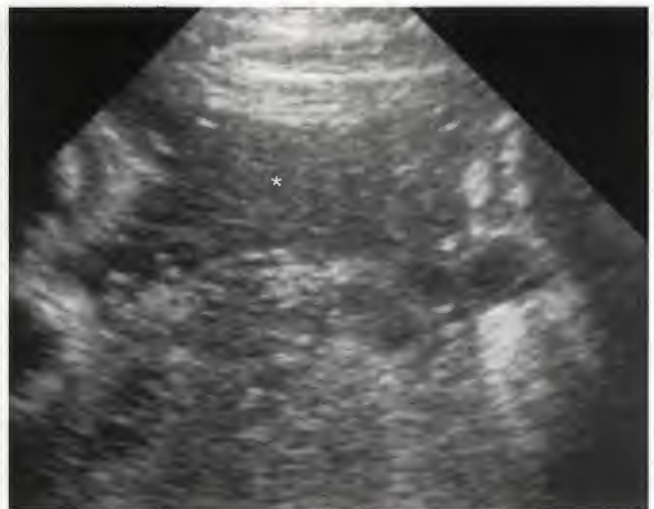


**FIGURE 20-10.** Sonogram of a pocket of amniotic fluid in a patient with hydrops fetalis and polyhydramnios. Two small segments of umbilical cord (arrows) are seen traversing the measured pocket of amniotic fluid. The placenta (P), which appears normal to prominent in this case, is, in fact, abnormally thickened.

that “for any specific AFI or two-diameter amniotic fluid pocket the 95% confidence range is so wide that ultrasonographic assessment is simply not a reasonable reflection of actual AFV. At a given AFI or two-diameter pocket measurement the prediction limits may include both conditions of oligohydramnios and polyhydramnios (that is, an AFI of 11 cm at the 95% range will vary from 141 to 1565 mL). A 95% confidence level that the actual AFV exceeds 500 mL (not oligohydramnios) requires that the AFI be greater than 30 cm (a measurement consistent with polyhydramnios).” Moore and Cayle,<sup>41</sup> in their original study, found the absolute error to be relatively constant at 10 mm regardless of the amount of fluid measured. However, they found that the percentage of error created during measurement of small volumes of amniotic fluid (less than 10 cm) was 20% or more. Likewise, although positive predictive accuracies are high for the group with AFI less than 5 cm, the sensitivities for the detection of oligohydramnios are poor: between 18% and 40%. A study by Baron, Morgan, and Garite<sup>44</sup> correlating the likelihood of abnormal fetal heart rate tracing and need for cesarean section for fetal distress found no difference in the group in which the AFI was between 5.1 and 8.0 and the group in which the AFI was between 8.0 cm and 20 cm.

Several groups tried to refine the results of the AFI to gain additional information. In one study, Myles and Strassner<sup>45</sup> examined the distribution of fluid between upper quadrants and lower quadrants. In two groups with the same AFI, those with greater fluid in the upper quadrants had a greater incidence of meconium staining, 1-minute Apgar scores less than 7, variable decelerations, late decelerations, cesarean section for fetal distress, and arterial pH less than 7.2 than did those in which the fluid in the lower quadrants



A



B

**FIGURE 20-11.** A. Apparent amniotic fluid pocket (asterisk) in a third trimester pregnancy. B. Color Doppler interrogation reveals that this pocket is entirely filled with umbilical cord.

was greater. The theory is that less fluid in the lower quadrants leads to head or umbilical cord compression during labor. In a similar 1998 study by Buckshee et al,<sup>46</sup> those with greater than 50% AFV distributed in the upper quadrants formed the “upper greater” group, whereas the rest of the patients constituted the “lower greater” group. The upper greater group had a higher incidence of cesarean section for nonreassuring fetal heart rate (40.74% versus 9.6%), persistent variable decelerations (14.8% versus 0%), and bradycardia (25.9% versus 4.1%). Interestingly, there was no statistically significant difference in the predictive value of perinatal outcome (Apgar, neonatal intensive care unit admissions). In another study, Sadovsky et al<sup>47</sup> evaluated additional cord containing amniotic fluid pockets in women in whom the AFI was less than 5 cm. In the subgroup in which the cord-containing pocket was greater than 5 cm (which would ordinarily be excluded), there was no evidence of an increase in poor outcome, normally seen in women with oligohydramnios. A 1998 report by Magann et al<sup>48</sup> found that using multiple assessments (that is, AFI plus deepest pocket) did not add to accuracy. In their report, the accuracy

of ultrasound estimates of abnormal AFV was relatively low (ranging from 12% to 53% correct).

## PITFALLS IN AMNIOTIC FLUID VOLUME ESTIMATION

Normally, it is easy to reach a conclusion as to the total AFV whether one uses subjective or objective methods of assessment. Studies demonstrated that fetal movement does not impact negatively the assessment of AFV.<sup>49</sup> The choice of either curvilinear or sector transducers does not have an effect on estimated AFV.<sup>50</sup> Measurements of AFV do not appear to be influenced by maternal position.<sup>51</sup> No difference in AFI measurement were noted when patients were in the supine or 45-degree elevated position. However, studies have shown that fetal position may influence amniotic fluid volume measurements. A study by Fok et al<sup>52</sup> studied the effect of fetal position on two of the measurements of the AFV, AFI, and the single deepest pocket (SDP). The AFI was on average 4.35 cm higher for fetuses lying centrally within the uterus compared with fetuses lying laterally inside the uterus. There was no difference for SDP measurements of fetuses lying laterally or centrally or for different orientations of the fetal trunk. Their conclusion was that SDP may be a more consistent parameter for the estimation of amniotic fluid volume.

Excessive maternal abdominal transducer pressure impacts AFI measurements. Flack et al<sup>53</sup> found that high pressure on the maternal abdomen resulted in a 21% decrease in AFI. Four additional potential pitfalls exist. First, as stated earlier, an umbilical cord-filled amniotic fluid pocket should not be used in the assessment of AFV. Color Doppler flow imaging often assists in identifying the umbilical cord (see Fig. 20-11). Second, fat tends to scatter the ultrasound

beam and as such may introduce artifactual echoes into the amniotic fluid. Obese patients may seem to have significantly reduced fluid because of these artifactual echoes (Fig. 20-12). Using a lower frequency transducer may often assist one in correctly assessing AFV in these patients. Third, in the third trimester, free-floating particles, perhaps resulting from vernix, may make the true amniotic space less conspicuous (Fig. 20-13). Fourth, a single large pocket of



**FIGURE 20-12.** Sonogram in a moderately obese patient. Artifactual echoes within the amniotic fluid make the actual amniotic fluid less apparent.

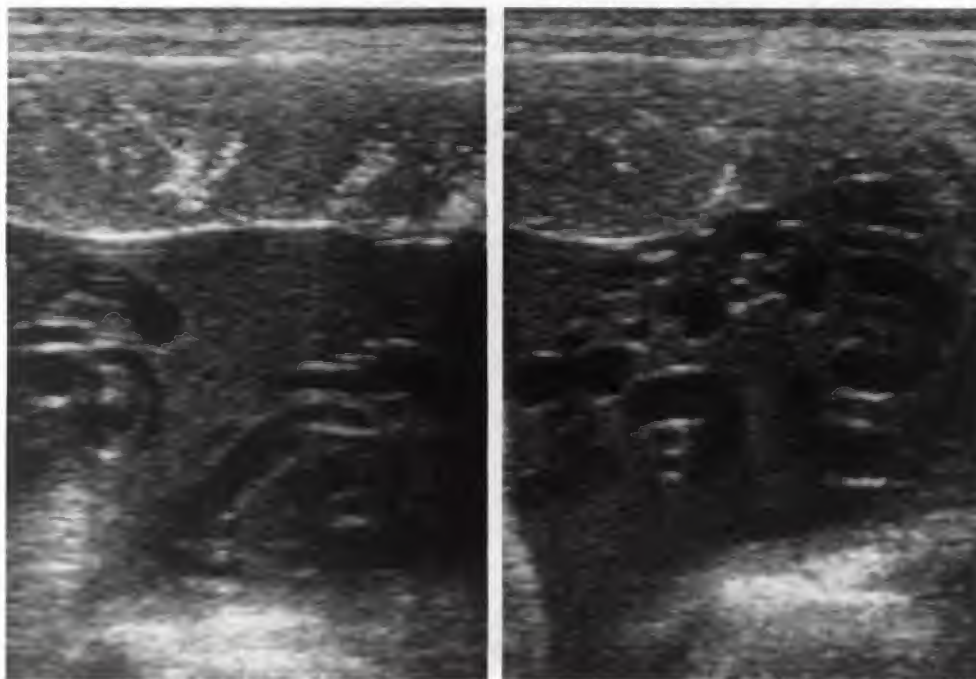


**FIGURE 20-13.** Two images of the amniotic fluid in a third trimester gestation. Highly echogenic fluid is seen surrounding the umbilical cord.



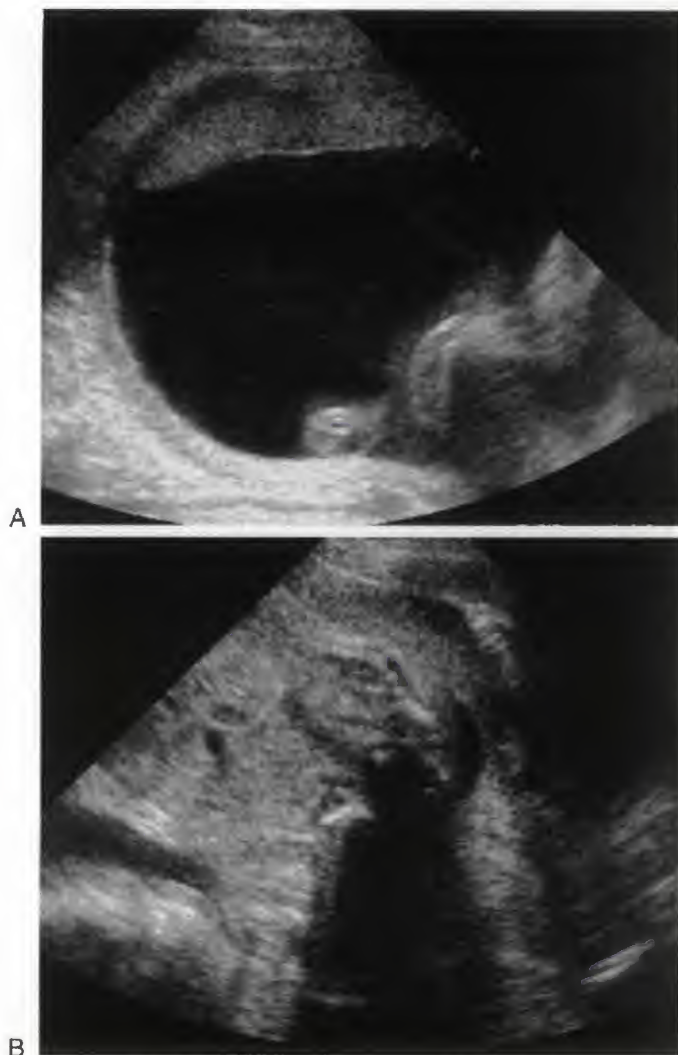


**FIGURE 20-14.** A. Sonogram of the fundic portion of the uterus in a second trimester pregnancy. Although this single large amniotic fluid pocket simulates polyhydramnios, it was the only area of amniotic fluid. B. Sonogram of the same patient in the mid- to lower uterine segment. No amniotic fluid is seen in this scan. If amniotic fluid volume had to be assessed on the basis of this image alone, it would be interpreted as oligohydramnios.

amniotic fluid seen on a static hard copy image may not be representative of the AFV in its entirety (Fig. 20-14).

As stated previously, color Doppler may prove useful in identifying an umbilical cord-filled pocket of what appears to be amniotic fluid in the patient with oligohydramnios. However, in the patient with otherwise normal amniotic fluid volume, it may underestimate AFV and lead to the false-positive diagnosis of oligohydramnios. A study of the use of color Doppler in the ultrasound estimate of AFV found that the use of color Doppler imaging resulted in the diagnosis of oligohydramnios in 21% of women who had normal AFVs.<sup>54</sup> The extremes of AFV did not seem to be impaired by the concurrent use of color Doppler with AFI and subjective evaluation of AFV.

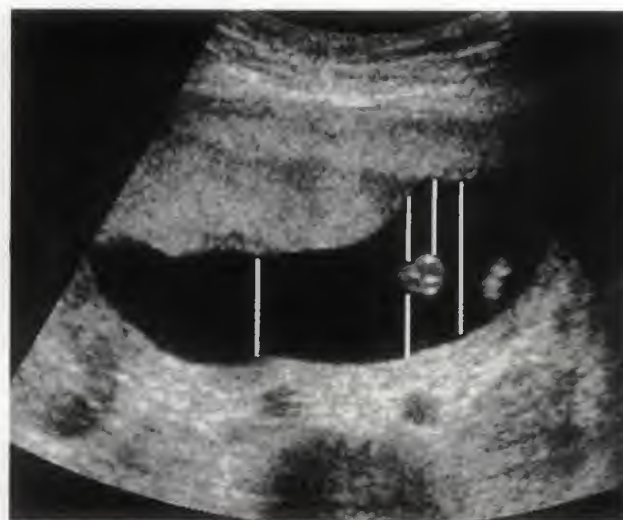


**FIGURE 20-15.** Sonogram of a second trimester pregnancy. Measurements of this amniotic fluid pocket might be made in a variety of locations by different examiners, and some examiners may choose not even to use this pocket for measurement.

### COMMENTARY ON IMAGING ASSESSMENT OF AMNIOTIC FLUID VOLUME

Even though sonographic assessment of AFV has been attempted for more than 2 decades, there is still no consensus as to the best method to report the status of AFV in an individual patient. There is a tendency to favor the assignment of an objective number to represent the AFV rather than rely on subjective descriptions of amniotic fluid. Somehow intertwined in this decision to use objective descriptors is the notion that assessments that result in a numeric value will be more accurate than those based on subjective descriptors. The reliance on fetal biometry rather than on the patient's last menstrual period to estimate gestational age in a fetus with intrauterine growth restriction (IUGR) is a perfect example of the problems with this sentiment. Likewise, there is an implied but never-stated view that these semiquantitative measurements are easier to acquire and require a less experienced sonographer or sonologist to perform than subjective estimations. Virtually every review of the sonographic imaging of AFV seems to have a statement similar to this one from this excellent review of the subject: "Subjective methods seem adequate to recognize abnormal AFV, but well-trained and experienced sonographers are necessary for clinically useful results. A disadvantage of the subjective technique is the lack of a numeric result that can be used to compare patients and to follow trends in AFV over time. Semiquantitative criteria for sonographic assessment of AFV have been developed to circumvent this limitation."<sup>55</sup> Is not a well-trained and experienced sonographer necessary to make objective assessments of AFV (that is, SDP or AFI)? To gain more insight into this issue, the reader should perform the following experiment. Photograph a single image of an amniotic fluid pocket that contains a small amount of umbilical cord or extremity or both (Fig. 20-15). Show this photograph to four different sonographers or sonologists with experience in performing



quantitative estimations of AFV, and ask them to measure this quadrant. It is highly likely that not only will some of the measurements vary from examiner to examiner but some individuals will choose not to use such an image in their calculations. Having a single well-trained and experienced examiner perform AFV estimations is the ideal solution, regardless of the method that is chosen.

Perhaps my major problem with the use of objective numeric values applied to AFVs is how the information is used in management decisions regarding the patient. I have attended management conferences in many centers throughout the country, and have repeatedly heard a similar discussion: "the AFI is 4.2 cm; therefore, the patient will be delivered immediately, whereas the patient in the next bed with an AFI of 5.2 cm and otherwise similar clinical findings will be sent home and return for follow-up monitoring." (There is no statistical difference in the AFI measurements in these hypothetical patients.) Again, because a numeric value is assigned to an interpretation does not make it any more accurate or useful than subjective assessments. The AFI is probably the best of the semiquantitative methods available for AFV assessment, but it should not be considered to be without its own inherent limitations. If subjective assessments of AFV are to be made, the person responsible for interpreting the examination should ideally scan the patient and not rely entirely on static images, particularly when AFVs are marginally abnormal.

## OLIGOHYDRAMNIOS

Oligohydramnios describes the condition in which the AFV is decreased relative to gestational age.<sup>55</sup> Quantitatively, oligohydramnios is defined as an AFV less than 300 to 500 mL after the midtrimester.<sup>5,55</sup> Subjectively, oligohydramnios is described by an obvious lack of fluid, poor fluid-fetal interface, and marked crowding of fetal parts (see Fig. 20-6).<sup>56</sup> Semiquantitatively, it is described by an MVP less than 1 to 2 cm, a two-diameter pocket of less than 15 cm,<sup>2</sup> and an AFI less than 5 cm (see Table 20-1).<sup>31,35,40,55,57</sup> As described previously, controversy exists as to the semiquantitative threshold that should be used to define oligohydramnios. Although most examiners use an AFI of 5 cm as the threshold, many use 5%. As Hill described, a single 3.2 × 2.2 cm pocket of amniotic fluid would be considered a normal AFV by Manning et al<sup>58</sup> but would be considered oligohydramnios by both Phelan et al<sup>38</sup> and Magann et al.<sup>11,57</sup>

Oligohydramnios may be due to a variety of conditions, including urinary tract abnormalities such as renal agenesis, bilateral renal obstruction, bilateral renal dysplasia, and posterior urethral valves or atresia; and prerenal abnormalities, including uteroplacental insufficiency leading to IUGR, preterm premature rupture of the membranes (PROM), and post-term pregnancy. Regardless of the cause, many investigators have noted increased perinatal morbidity and occasionally fetal or neonatal death in the presence of oligohydramnios.<sup>34-36,44,56,59-66</sup>

## INTRAUTERINE GROWTH RESTRICTION

The earliest sonographic evaluations of the potentially growth-restricted patient recognized the important role of amniotic fluid. The first use of sonographic evaluation of

decreased amniotic fluid was in the diagnosis of the growth-restricted fetus. Manning and Platt<sup>67</sup> and others recognized the high incidence of oligohydramnios in these patients. In 1980, Manning, Platt, and Sipos<sup>68</sup> used the MVP assessment of AFV in the fetal biophysical profile score. This assessment was termed the qualitative AFV (qAFV). For the purposes of the biophysical profile score, patients with less than a 1 cm pocket in both vertical and transverse diameters are designated as having decreased AFV and given a score of 0. Those with a largest vertical and transverse pocket ≥ 1.0 cm, but ≤ 2.0 cm in vertical diameter, and ≥ 1.0 cm in transverse diameter are designated as having marginal qAFV. If qAFV is greater than 2.0 cm but less than 8.0 cm in vertical diameter and ≥ 1.0 cm in transverse diameter, the patient is reported as having normal qAFV. In 1984, Chamberlain et al<sup>35</sup> performed a retrospective analysis of the impact of abnormal AFV and perinatal morbidity and mortality in a high-risk population. The perinatal mortality rate was increased 13-fold more than normal when AFV was sonographically marginal and increased 47-fold (187.5/1000) if severe oligohydramnios was present. Initially, the finding of a single largest amniotic fluid pocket no larger than 1 cm was found to be predictive of IUGR. Unfortunately, this criterion was too stringent and not sensitive enough to allow it alone to detect these patients. Although Chamberlain et al<sup>35</sup> and Manning et al<sup>68</sup> found that a qAFV of less than 1 cm was associated with IUGR in 78.8% to 89.6% of patients referred with clinically suspected IUGR, when qAFV is used as the sole criterion in a screening test for IUGR, the sensitivity reported by other investigators ranged from 4% to 15.8%.<sup>56,69</sup>

In theory, the hypoxemia resulting from poor placental perfusion results in a redistribution of cardiac output, so that the brain is protected with increased blood flow relative to the abdomen and kidneys. The decreased renal perfusion and increased antidiuretic hormone release from hypoxemia result in decreased urine output and oligohydramnios. In addition, in the presence of hypoxia, fetal lung resorption of fluid increases.<sup>1</sup> Opposing the diminution in AFV from uteroplacental insufficiency is the increased fluid that might result from hypoxic suppression of fetal swallowing.<sup>10</sup> Decreased fluid in the amniotic space can result in pressure against the umbilical cord and further complicate the already decreased perfusion to the fetus. Assessment of the AFV is now an important part of antenatal evaluation, along with the nonstress test in the fetus with suspected growth restriction.

In 1983, Miyazaki and Taylor,<sup>70</sup> and subsequently others, demonstrated an improvement in fetal heart rate patterns of patients with oligohydramnios after saline amnioinfusion into the amniotic sac.<sup>71-75</sup> A technique often used is as follows: A bolus of room temperature saline is given (~600 mL) over a 1-hour period by infusion pump, followed by infusion of saline at 200 mL/hr until the AFI is greater than 5 cm or 8 cm.<sup>24</sup> An excellent review of the controlled trials of amnioinfusion studies appeared in a report by Kilpatrick (Table 20-4).<sup>24</sup> Although a number of investigators reported relief of variable decelerations, none of the studies demonstrated an improvement in neonatal outcome based on Apgar scores or clinically significant cord gas results.<sup>24</sup> Another less invasive technique is that of maternal hydration. A study by Kilpatrick et al<sup>76</sup> demonstrated an increase in the AFI of 30% when women with oligohydramnios were treated with hydration of 2 L of water.



**Table 20-4****Prophylactic Amnioinfusion for Oligohydramnios**

Study	No. Cases	Decreased Cesarean Sections	Better Neonatal Outcome	Infection
Chauhan et al <sup>71</sup>	38	No	No	
Nageotte et al <sup>72</sup>	76	No	No	
Ogundipe, Spong, and Ross <sup>73</sup>	116	No	No	Yes*
Schrimmer, Macri, and Paul <sup>74</sup>	305	Yes	No	No†
Strong et al <sup>75</sup>	60	No	No	No‡

\*Maternal fever.

†Amnionitis, endometritis.

‡Maternal fever, neonatal sepsis.

From Kilpatrick SJ: Therapeutic interventions for oligohydramnios: Amnioinfusion and maternal hydration. Clin Obstet Gynecol 40:328, 1997.

**POST-TERM PATIENTS**

Post-term patients have increased morbidity with an increased risk of meconium aspiration, fetal postmaturity syndrome, and fetal death.<sup>65,77,78</sup> Amniotic fluid begins to decline near term and may do so precipitously in the post-term patient. Although the relationship between decreased amniotic fluid and perinatal morbidity is not known for certain, several theories have been proposed to explain this relationship. Perhaps the most popular is that placental insufficiency in these patients results in a redistribution of cardiac blood flow such that renal perfusion is decreased, resulting in oligohydramnios, whereas cerebral blood flow is increased. A report by Bar-Hava et al<sup>77</sup> showed that this mechanism is unlikely to play a major role in the post-term patient and that increased reabsorption in the fetal kidneys may be more important. An interesting 1999 report by Sylvester and Divon<sup>78</sup> examined the relationship among gestational age, birthweight, and AFV in 758 consecutive nondiabetic post-term patients ( $\geq 41$  weeks gestation). AFI was obtained within 3 days of delivery. The relationship between AFI and birthweight was best described as a linear equation, whereas that between AFI and gestational age was insignificant; regression analysis yielded a very wide scatterplot. In the small-for-gestational-age, appropriate-for-gestational-age, and large-for-gestational-age groups, the mean AFI (incidence of oligohydramnios) was 8.0 cm (28%), 10.5 cm (11%), and 11.8 cm (3%), respectively. In these same groups, the mean gestational age was 41.6 weeks, 41.6 weeks, and 41.5 weeks, respectively. The authors concluded that AFI is independent of gestational age and strongly dependent on birthweight. If confirmed, this would indicate that the progressive decrease in AFI seen in post-term patients is a pathologic rather than a physiologic process. Morris et al<sup>79</sup> evaluated the utility of the measurement of the amniotic fluid index and the single deepest pocket measurement in patients with prolonged pregnancy. They found that the

AFI is superior to a measure of the single deepest pocket as an assessment of the fetus at or after 40 weeks, but has a poor sensitivity for adverse pregnancy outcome. Their conclusion: "Routine use is likely to lead to increased obstetric intervention without improvement in perinatal outcomes."

**PULMONARY HYPOPLASIA**

Patients with prolonged oligohydramnios from any cause—whether renal, preterm PROM, and so on—are at increased risk for pulmonary hypoplasia, which is invariably fatal. It has long been known that amniotic fluid is an important factor in the normal development of the fetal lungs. What has been less clear is the manner in which oligohydramnios interferes with this normal developmental process. There are normally four stages of fetal lung development: embryonic, from conception to the 5th week; pseudoglandular, from the 5th to the 17th week; canalicular, from the 16th week to the 24th week; and terminal sac or alveolar period, from the 24th week to term and beyond. By the 16th week of gestation, all of the branches of the tracheobronchial tree up to the terminal bronchioles are established.<sup>80</sup> Oligohydramnios, resulting in pulmonary hypoplasia characterized by inadequate development of pulmonary acini and restricted vascularization, normally occurs during the canalicular stage of development. Several theories have been postulated in the past to explain pulmonary hypoplasia in patients with severe oligohydramnios: abnormal fetal breathing, increased pressure on the fetal thorax, and abnormal pulmonary fluid egress.<sup>80</sup> Abnormalities of fetal breathing are unlikely to be the cause because normal fetal breathing movements occur in animals as well as in humans with oligohydramnios-related pulmonary hypoplasia. Compression of the fetal thorax is also an unlikely cause because amniotic sac pressure in patients with oligohydramnios is low. Normally, the pressure in the amniotic space is between 1 and 14 mm Hg. When oligohydramnios is present and the membranes are intact, the intra-amniotic pressure is  $\leq 1$  mm Hg.<sup>11,81</sup> It has been postulated that fetal lung fluid acts as an internal stent for the developing surrounding lung.<sup>82</sup> Normally, the upper airways produce resistance to the egress of fluid out of the trachea. In the presence of oligohydramnios and low amniotic pressure, it is theorized that the pressure gradient results in the loss of this lung fluid.<sup>81</sup> In addition, interesting work by Harding, Hooper, and Dickson<sup>83</sup> in sheep showed that the rise in pulmonary airway pressure relative to amniotic sac pressure may also be caused by increased spinal flexion and resulting increased abdominal and thoracic pressure in the fetus with oligohydramnios. In this 1996 study, Kilbride, Yeast, and Thibeault<sup>84</sup> evaluated patients who experienced PROM less than 29 weeks' gestation. Most patients did not experience a change in amniotic fluid status over time; however, as many as 20% of patients did. Although the prognosis was dismal and the likelihood of pulmonary hypoplasia was great in the group in which the amniotic fluid pockets were less than 1 cm, there was no association between patients with moderate oligohydramnios (1 to 2 cm pockets) and pulmonary hypoplasia. Thus, on the basis of this study, it is inappropriate to group all patients with an AFI less than 5 cm together in an attempt to prognosticate the development of pulmonary hypoplasia.



## PREMATURE RUPTURE OF MEMBRANES

PROM is rupture of the amniotic sac before the onset of uterine contractions. This is reported to occur in approximately 10% of pregnancies at term and between 0.7% and 2.0% of pregnancies before 37 weeks.<sup>64,85</sup> PROM occurring at term is usually managed by induction of labor; however, preterm PROM is often treated conservatively. Although most patients at term will begin labor soon after membrane rupture, the earlier in gestation that membrane rupture occurs, the more likely it is that the latency period will be long.<sup>64</sup> Patients who experience rupture early in pregnancy have the added risk of pulmonary hypoplasia. Pulmonary hypoplasia has been reported in patients with PROM, particularly when the rupture occurs before 26 weeks and when the duration of the rupture is at least 2 weeks and often greater than 5 weeks.<sup>86</sup> As mentioned, a critical amount of amniotic fluid is necessary for normal lung development to occur. Lack of fluid, as might occur with PROM, results in a lack of the normal internal stenting force in the developing fetal lungs. The likelihood of pulmonary hypoplasia is dependent as much on the time of membrane rupture as the amount of residual fluid and duration of oligohydramnios.

Patients with preterm PROM are at increased risk for chorioamnionitis (between 25% and 46%), fetal morbidity, and death (between 37% and 78%).<sup>87</sup> The likelihood of these complications is dependent on the timing of membrane rupture, amount of residual amniotic fluid, and duration of persistent oligohydramnios. Hadi, Hodson, and Strickland<sup>63</sup> reported an overall survival rate of 55%. When delivery occurred before 25 weeks of gestation, 6.7% survived. For the cases delivered between 26 and 34 weeks of gestation, the survival rate was 89.4%. Although the prognosis is often poor when membrane rupture occurs early, it is not universally grave for all patients. Several series reported resealing of the leak, with reaccumulation of fluid and normal outcomes.<sup>88,89</sup> These events, although uncommon, must be considered at the time of counseling.

Aside from the issues of pulmonary hypoplasia, patients with PROM have a higher incidence of cesarean section for fetal distress than do patients with oligohydramnios from other causes. In Sarno, Ahn, and Phelan's<sup>90</sup> study, the cesarean section rate for fetal distress was 19% for PROM compared with less than 1% for other causes of oligohydramnios. Even when the evidence is overwhelming that PROM is the likely explanation for decreased fluid, the fetal urinary bladder should be identified to exclude renal agenesis as the primary cause.

## INTRAPARTUM OLIGOHYDRAMNIOS IN HIGH-RISK PATIENTS

In the past decade, a number of studies reported that oligohydramnios (defined as an AFI  $\leq 5$  cm) in laboring patients was associated with a poor peripartum outcome. As such, there are centers in which the results of the AFI are used to triage patients. However, an increasing number of reports have disputed the utility of a low AFI for predicting outcome. Chauhan et al<sup>91</sup> in 1997 found that the sensitivity and positive predictive values of an AFI less than the fifth percentile for gestational age to predict a pH less than 7.00

were 0.8% and 22%, respectively, and for an AFI less than or equal to 5.0 cm, 0.5% and 11%, respectively. In this study, "receiver-operator characteristic curves indicated that an AFI between 0 and 20 cannot predict accurately which patients will have cesarean sections for distress or be delivered of a newborn with a low Apgar score at 5 minutes or a pH less than 7.10." The patients in this study were high risk, with either medical or obstetric complications. In two studies, patients having an intrapartum assessment of AFI were significantly more likely to have abdominal delivery for presumed fetal distress without improving perinatal outcome.<sup>61,92</sup> In a randomized, controlled trial, Alfrevic et al<sup>93</sup> compared the impact of the AFI and maximum pool depth on the incidence of obstetric interventions in post-term pregnancies. Compared with maximum pool depth, the AFI led to more obstetric interventions without any impact on perinatal outcome. Recently, Ott<sup>94</sup> performed a study to assess the relationship of AFV and perinatal outcome. As he stated, "AFI is a weaker predictor of perinatal outcome than has been classically suggested. Although the AFI identification of polyhydramnios was helpful in identifying LGA fetuses and fetuses at risk for congenital abnormalities, oligohydramnios was a rather weak predictor of poor perinatal outcome. There was an increased risk of nonreassuring fetal heart rate patterns during labor for the oligohydramnios patient, but only in preterm patients." In his report, he summarized some of the studies showing similar findings. Garmel et al<sup>95</sup> studied 65 patients with oligohydramnios and found a higher incidence of premature delivery, but no increase in IUGR, perinatal death, or birth asphyxia. Kreiser et al<sup>96</sup> evaluated 150 low-risk patients and found no increase in poor perinatal outcome in cases of isolated oligohydramnios. Magann et al<sup>97</sup> studied 1001 high-risk patients and reported that oligohydramnios was a poor diagnostic test to predict poor outcome. Other investigators have found similar results.<sup>91,96,98-100</sup> In a meta-analysis of the relationship between AFI and perinatal outcome, Chauhan et al<sup>101</sup> came to the conclusion that there was an association between oligohydramnios and an increased incidence of cesarean delivery for nonreassuring fetal heart rate patterns and low Apgar score; however, insufficient data related it to neonatal acidosis, and called for further prospective studies with large enough numbers to properly evaluate the relationship. A large study by Morris et al<sup>79</sup> found that AFI has a poor sensitivity for adverse pregnancy outcome, and was likely to lead to increased obstetric intervention without improving outcome. To compound the controversy, a number of studies have compared AFI to actual AFV, determined by the dye-dilution technique, and found that the AFI was an unreliable technique for accurately estimating amniotic fluid.<sup>43,102</sup>

## FREQUENCY OF AMNIOTIC FLUID VOLUME ASSESSMENTS IN THE HIGH-RISK PATIENT

A final question that should be addressed is how frequently one should perform semiquantitative assessment of AFI during antepartum testing in the high-risk patient. Wing et al<sup>103</sup> and Lagrew et al<sup>104</sup> evaluated this issue. Wing et al concluded that, for patients at less than 41 weeks' of gestation undergoing antepartum testing, weekly assessment of AFI is



probably adequate if the initial measurement is in the normal range ( $\geq 8$  cm) because the risk of having oligohydramnios within 4 days is only 1.7% and within 7 days only 2.2%. As they stated in their report, "for patients at less than 41 weeks of gestation whose initial amniotic fluid index measurement is in the low-normal range (5 to 8 cm), twice-weekly assessment is justified on the basis of a higher risk for an amniotic fluid index  $\leq 5$  cm within 4 days (12.3%). For all patients at  $\geq 41$  weeks of gestation, twice-weekly amniotic fluid index assessments are recommended regardless of the initial measurement." In 1992, Lagrew et al<sup>104</sup> addressed the issue of frequency for amniotic volume assessment. They concluded that there is a minimal risk ( $< 0.5\%$ ) for oligohydramnios in the 4 days after a normal AFI; therefore, AFI measurements in patients less than 41 weeks of gestation should be performed weekly.

### OTHER CONDITIONS ASSOCIATED WITH OR CAUSATIVE OF OLIGOHYDRAMNIOS

There have been reports of oligohydramnios complicating chorionic villus sampling procedures. In a 1991 series by Cheng et al,<sup>105</sup> oligohydramnios developed in 2.7% of chromosomally normal pregnancies versus 0% in the control amniocentesis group. They theorized that chorionic villus sampling may cause a placental or endometrial injury that may result in perigestational hemorrhage. This, in turn, may result in altered fetoplacental perfusion. In their series, none of the patients in whom oligohydramnios developed survived.

Bronshtein and Zimmer<sup>106</sup> reported an association between oligohydramnios in the early second trimester, chorioamniotic separation, and fetal malformations. Nine patients with oligohydramnios and chorioamniotic separation were identified among 7000 women who underwent a transvaginal ultrasound examination at 15 to 16 weeks' gestation before any invasive procedure. Oligohydramnios was defined as a reduced amount of amniotic fluid, a distance of more than 1 cm between the chorion and amnion, and a good turgor of the amnion without floating membranes or intrauterine sheets. Fetal malformations were observed in all nine patients. In four of six fetuses for which chromosomal analysis was available, an abnormal karyotype was found (three cases of trisomy 18, one case of trisomy 21). They hypothesized that in malformed fetuses the secretion of fluid across the skin was reduced or that fetal malformations are associated with some defects in the structure of the amniotic membrane, which may lead to a reduced compliance or decrease in the ability to produce amniotic fluid. Another potential explanation may be leakage of amniotic fluid through a small hole in the amnion and accumulation of the fluid in the extra-amniotic space.

Prostaglandin inhibitors such as indomethacin can cause a dramatic reduction in the volume of amniotic fluid, probably as a result of decreased fetal urine production. The fetal kidneys are sensitive to indomethacin as early as 21 weeks' gestation and may respond to the drug's effects as early as 5 hours after administration. The effect is usually reversed after discontinuation of the drug. This side effect of the medication is used at times in patients with polyhydramnios to decrease the amniotic fluid through maternal ingestion.

### OLIGOHYDRAMNIOS AND ASSESSMENT OF FETAL WEIGHT AND MALFORMATIONS

Two other issues that should be discussed are the impact of oligohydramnios on estimation of fetal weight and the detection of congenital malformations. Barnhard, Bar-Hava, and Divon<sup>107</sup> reported clinical and sonographic intrapartum fetal weight estimates in singleton term patients with decreased amniotic fluid volume. In addition to standard biometry for estimation of gestational age and fetal weight, amniotic fluid was assessed. Oligohydramnios was defined as an AFI equal to 5 cm. The authors found that clinical and sonographic estimated fetal weights were significantly less accurate in patients with oligohydramnios than those derived from patients with normal amniotic fluid. The incidence of clinical and sonographic estimated fetal weights within  $\pm 10\%$  of the actual birthweight was 70.1% and 68.4%, respectively.

Levine et al<sup>108</sup> studied the effect of oligohydramnios on the detection of fetal anomalies with sonography. They evaluated a group of patients with ruptured membranes to determine the affect of oligohydramnios on the detection of anomalies and compared the results with those of a control group. Although anomalies were missed in both groups, they were of the type known to be difficult to diagnose antenatally and frequently missed on sonography (hand abnormalities and cardiac anomalies). The authors concluded that most "serious" noncardiac anomalies are detected even in the presence of oligohydramnios.

### POLYHYDRAMNIOS

Polyhydramnios is an excessive accumulation of amniotic fluid at some time during pregnancy. Its incidence varies from 0.2% to 3.3%<sup>109-112</sup> and depends on how this abnormality is defined (described later). The author prefers the use of the term *polyhydramnios* rather than *hydramnios*, which may often be used to describe the same condition. Pathologically and clinically, it is defined as an excess of amniotic fluid, greater than 1500 to 2000 mL.<sup>5,113</sup> Although a reasonably accurate assessment of excessive amniotic fluid can be made with dye-dilution studies, for many years the diagnosis was made and confirmed at delivery, a less than ideal way to estimate volume accurately. Before ultrasound, the diagnosis was made when the fundal height exceeded the patient's gestational age or there was difficulty in palpating fetal parts or auscultating the fetal heart.<sup>114</sup> In the past 20 years, ultrasound has played a pivotal role in correctly making this diagnosis in the patient who presents "large for dates." The methodology used to arrive at this diagnosis varies tremendously and is controversial. Most clinicians agree that ultrasound is the appropriate tool to estimate AFV. More than two decades ago, one of the first sonographic techniques used for the diagnosis of polyhydramnios was the total intrauterine volume.<sup>115,116</sup> The diagnosis of polyhydramnios was made if the total intrauterine volume exceeded 1 standard deviation above the mean volume for gestational age. This technique was cumbersome and was soon abandoned.<sup>114</sup> It became apparent to many sonologists that a subjective estimate of amniotic fluid (defining polyhydramnios when a fetus in the mid- to late second or third





**FIGURE 20-16.** Sonogram of a patient with marked polyhydramnios. The fetus is surrounded and virtually floating in the amniotic fluid.



**FIGURE 20-17.** Sonogram of a fetus with polyhydramnios resulting from gastrointestinal tract obstruction. A pocket of amniotic fluid larger than 8 cm is seen.

trimester appears to float in the amniotic fluid, displaced away from the anterior uterine wall or placenta) could be readily obtained (Fig. 20-16). Other sonologists measure the single deepest AFV pocket (defining polyhydramnios when the deepest pocket is greater than 8 cm), and still others use the AFI (a summation of the deepest pocket in four cord and extremity-free quadrants in the gravid uterus; here, polyhydramnios exists when the AFI is greater than 24 cm) (Fig. 20-17).<sup>33,117,118</sup> It is unlikely that any cases of true polyhydramnios escape detection when the AFV is analyzed subjectively by even a moderately experienced examiner. The greater problem is that too many false-positive diagnoses are likely when only subjective criteria are used. Many cases of normal pregnancies in the early second trimester may appear to have too much amniotic fluid. Care must be taken to avoid diagnosing polyhydramnios under this circumstance. Likewise, many cases of mild polyhydramnios occur in pregnancies with normal fetuses and normal pregnancy outcomes. For this reason, the author prefers to use the subjective assessment as a first line of screening and apply objective measurements such as the AFI when the amniotic fluid seems excessive.

An interesting study by Carlson et al<sup>119</sup> attempted to compare the utility of subjective estimation of the severity of polyhydramnios (mild, moderate, and severe) versus the AFI value of greater than 24 cm and assessment of the single deepest amniotic fluid pocket. Using the description of severe polyhydramnios, they found only 11 of 24 anomalies versus 22 of 24 anomalies using an AFI of greater than 24 cm. In their study, not only did an AFI of greater than 24 cm predict 49 of 50 cases of true polyhydramnios confirmed at delivery, but this measurement also included 92% of all anomalies and 100% of all trisomies and fetal and neonatal deaths. These results include seven patients in whom the AFI was less than 24 cm but one pocket of fluid that was greater than 8 cm. None of these fetuses or neonates had fetal anomalies, aneuploidy, perinatal death, neonatal intensive

care unit admission, or a diagnosis of polyhydramnios at delivery.

Polyhydramnios can result from a variety of maternal and neonatal disorders, and it may either be acute or chronic. Acute polyhydramnios, which may appear within days and is uncommon, usually occurs in the second trimester.<sup>55</sup> Chronic polyhydramnios occurs gradually, usually in the third trimester, and is often asymptomatic. Polyhydramnios often resolves spontaneously, and when it does, the pregnancy is not associated with increased morbidity and mortality.<sup>120,121</sup>

A variety of conditions, maternal and fetal, are known to be causative or associated with polyhydramnios (Table 20-5). Perhaps the most notable maternal disorder associated with polyhydramnios is diabetes mellitus. Most series mention diabetes mellitus as a common cause of increased amniotic fluid. These cases, under further examination, almost always involve patients with poor diabetic control and, as is discussed later, are associated with macrosomia. Erythroblastosis fetalis and associated hydrops may result in polyhydramnios. For that matter, fetal conditions resulting in hydrops often manifest polyhydramnios.

Fetal structural and chromosomal abnormalities are responsible for a significant number of polyhydramnios cases. The degree of polyhydramnios correlates with the probability that an anomaly will be detected. In Damato et al's<sup>122</sup> study of patients with sonographically documented polyhydramnios, in the lowest ranked group (MVP depth, 8 to 9.5 cm), 50% of fetuses manifested an anomaly, whereas in the highest rank (MVP, 16.0 cm or greater) 88% had anomalies. Central nervous system (CNS) abnormalities were once the most common cause for polyhydramnios resulting from fetal structural abnormalities. This is no longer true, perhaps in part because of recognition of severe CNS abnormalities in the second trimester resulting in termination before the development of polyhydramnios. Gastrointestinal tract abnormalities are now perhaps the most common structural cause; atresia or obstruction (that is, duodenal atresia or



**Table 20-5****Fetal Malformations Associated With Polyhydramnios****Central Nervous System**

Anencephaly  
Hydrocephaly  
Iniencephaly  
Hydranencephaly  
Encephalocele  
Microcephaly

**Gastrointestinal Tract**

Astomia  
Esophageal atresia  
Diaphragmatic hernia  
Duodenal stenosis  
Annular pancreas  
Gastroschisis  
Omphalocele  
Cleft palate

**Respiratory Tract**

Cystic adenomatoid malformation of the lung  
Chylothorax

**Genitourinary Tract**

Fetal renal hamartoma  
Unilateral ureteropelvic junction obstruction

**Cardiovascular System**

Valvular incompetence  
Valvular stenosis  
Ebstein's anomaly  
Arrhythmias  
Twin-to-twin transfusion syndrome

**Musculoskeletal System**

Skeletal dysplasia  
Myotonic dystrophy  
Pena-Shokeir syndrome  
Fetal akinesia/hypokinesia syndrome

From Larmon JE, Ross BS: Clinical utility of amniotic fluid assessment. *Obstet Gynecol Clin North Am* 25:652, 1998.

esophageal atresia) is the likely explanation (Fig. 20-18). These atresias, which are proximal to the distal large bowel and colon, interfere with the normal absorption of water and result in excessive amniotic fluid. Patients with these abnormalities may not manifest polyhydramnios either at all or not until the third trimester of pregnancy (absence of polyhydramnios should not exclude the diagnosis of gastrointestinal tract obstruction) (Fig. 20-19). In fetuses with esophageal atresia, polyhydramnios may develop in only 40% of cases.<sup>123</sup> In an animal study in which esophageal ligation was performed, Gilbert and Brace demonstrated that intramembranous absorption of amniotic fluid increased dramatically and thus may explain in part the failure for polyhydramnios to occur in those fetuses who are unable to swallow normally due to obstruction.<sup>123-125</sup>

Other fetal structural defects include cardiovascular, urinary tract abnormalities, and skeletal abnormalities. Two urinary tract abnormalities, congenital mesoblastic nephroma

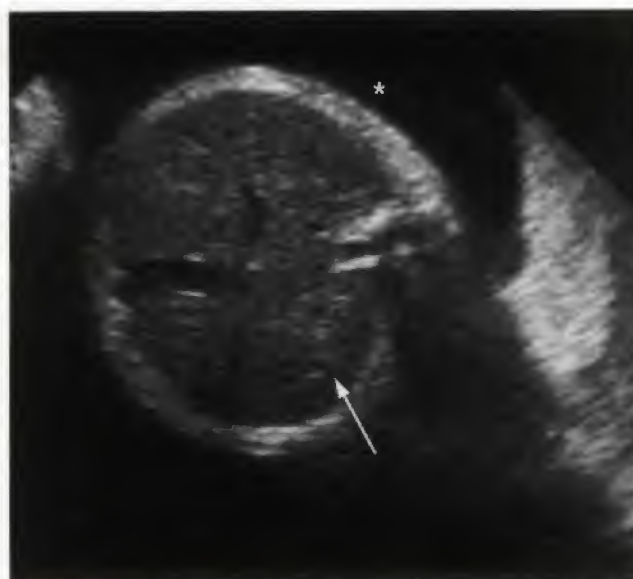


**FIGURE 20-18.** Sonogram of a patient with esophageal atresia and polyhydramnios. Absence of the fetal stomach (arrow) and increased amniotic fluid (asterisk) are seen.



**FIGURE 20-19.** Sonogram of a patient with duodenal atresia detected in the second trimester. A dilated stomach and proximal duodenum are seen; however, the amniotic fluid volume is normal. D, duodenum; S, stomach.

and unilateral ureteropelvic junction obstruction, may be associated with polyhydramnios (Fig. 20-20).<sup>126-128</sup> Although somewhat paradoxical, the polyhydramnios associated with ureteropelvic junction obstruction may be due to impairment of the concentrating ability of the kidney, resulting in high urine output. The association of lethal skeletal abnormalities with polyhydramnios is also interesting. Although no good explanation for this association has been presented,

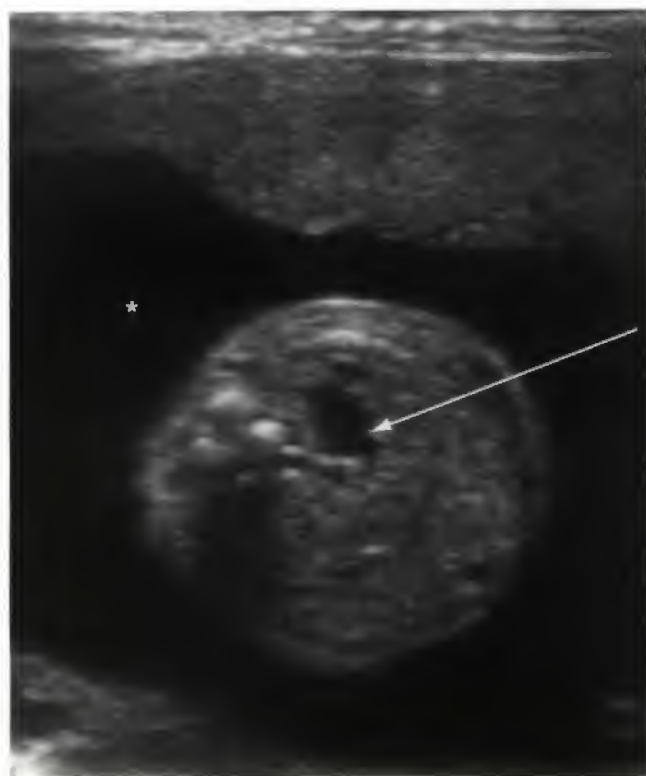


**FIGURE 20-20.** Sonogram demonstrating polyhydramnios (asterisk) in a patient with unilateral ureteropelvic junction obstruction (arrow).

there is no question that this association exists. Twin pregnancy, particularly monochorionic, can be associated with marked polyhydramnios owing to twin-to-twin transfusion syndrome. Movement disorders, akinesia, and hypokinesia may be associated with polyhydramnios.<sup>129</sup> Aberrant fetal movements with associated polyhydramnios have been reported in cases of myotonic dystrophy and congenital myasthenia gravis.<sup>130-132</sup> Maternal symptoms may be lacking, and these cases may appear normal sonographically. Medications may be associated with polyhydramnios. The ingestion of lithium is thought to cause polyhydramnios by causing fetal diabetes insipidus as well as cardiac decompensation.<sup>114,133</sup>

When no structural abnormalities are detected, polyhydramnios is said to be idiopathic. Before reaching this conclusion, two other entities should be considered: growth disturbances and chromosomal abnormalities. Studies comparing patients with normal AFV and those with polyhydramnios found a significantly higher incidence of fetuses with birth weights greater than 4000 g or greater than 90th percentile weight for gestational age in the polyhydramniotic group.<sup>134</sup> Benson, Coughlin, and Doubilet<sup>135</sup> evaluated the utility of AFV in the diagnosis of the large for gestational age fetus in nondiabetic patients. Polyhydramnios occurred more frequently in large for gestational age fetuses than in not large for gestational age fetuses (17% versus 8%) but had little effect on the positive predictive value of a fetal weight estimate above the 90th percentile. Of interest, the combination of oligohydramnios and a fetal weight estimate below

the 90th percentile virtually excluded the possibility of a large for gestational age fetus.

There is an increased incidence of chromosomal abnormalities when polyhydramnios is associated with morphologic fetal abnormalities. Brady et al,<sup>136</sup> Zahn, Hankin, and Yeomans,<sup>137</sup> Barnhard, Bar-Hava, and Divon,<sup>109</sup> and Sickler et al<sup>138</sup> demonstrated an increased incidence of karyotype abnormalities when polyhydramnios was present with either associated morphologic abnormalities or IUGR. In the absence of sonographically detected morphologic abnormalities, amniocentesis is not absolutely indicated.<sup>109</sup>

## POLYHYDRAMNIOS: MORBIDITY AND AMNIOREDUCTION

Aside from association with fetal and maternal abnormalities, polyhydramnios itself may result in perinatal morbidity. The reported prevalence of preterm births with polyhydramnios is between 11.1% and 29.4%.<sup>139</sup> In studies by Many et al,<sup>140,141</sup> the prevalence of prematurity was highest among those with malformations (39%) followed by those with diabetes mellitus (22.2%). In addition, abdominal pain and premature uterine contractions may lead to PROM and preterm delivery. Rupture of the membranes with sudden decompression of the uterus may lead to abruptio placentae.

In patients with severe polyhydramnios and difficulties with pain and breathing, therapeutic amniocenteses are often performed. The sonographic endpoint in patients having a therapeutic amniocentesis is either an AFI less than 24 cm or a maximal deepest pocket less than 8 cm.<sup>142</sup> Elliott et al<sup>142</sup> evaluated large volume fluid removal in patients with polyhydramnios. Ninety-four patients had 200 therapeutic amniocenteses for the following indications: twin-to-twin transfusion syndrome, 36 (38%); idiopathic, 24 (26%); diabetes mellitus, 11 (12%); fetal anomalies, 11 (12%); chromosomal anomalies, 5 (5%); twins (not twin-to-twin transfusion syndrome), 4 (4%); and other, 3 (3%). The mean AFV removed at each therapeutic amniocentesis was 1666 mL. The mean rate of fluid removed was 54 mL/minute. Patients with twin-to-twin transfusion syndrome required more repeat therapeutic amniocenteses (3.4 per patient) than other diagnoses (1.4 per patient). The mean gestational age at the time of the first therapeutic amniocentesis was 29 weeks 6 days. Indications for amnioreduction included either symptoms or acute abdominal distension. An 18-gauge spinal needle was used, with the tip in a cephalic direction. This allowed the needle to move up to 180 degrees as the uterus became smaller with decompression. Suction was used (1000 mL over 20 minutes). Delivery was delayed to a median gestational age of 37 weeks. There were complications in three patients: ruptured membranes occurring in one patient (1 day after her seventh amniocentesis), chorioamnionitis 18 hours after amniocentesis, and placental abruption. Although 33% of patients were given tocolytic drugs, there were no deliveries within 7 days of a procedure for "unstoppable" preterm labor. Leung et al<sup>143</sup> followed prospectively all patients with polyhydramnios treated with rapid amnioreduction under continuous ultrasound guidance using a vacuum wound-drainage system from 1995 to 2002 in a university teaching hospital. In the group of 70 patients with 130 procedures, there were four procedure-related complications representing a 3.1% complication rate.



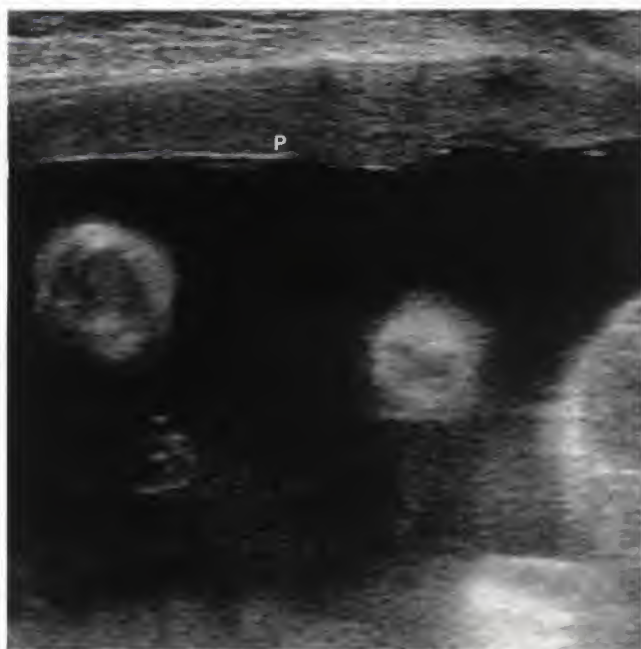


**FIGURE 20-21.** Sonogram in a patient with marked polyhydramnios. The placenta (P) becomes thin as the uterus expands from the increased amniotic fluid volume.

Because fluid often tends to reaccumulate rapidly, other noninvasive pharmacologic treatments of polyhydramnios have been sought. Currently, maternally ingested prostaglandin synthetase inhibitors such as indomethacin are used to treat polyhydramnios.<sup>144,145</sup> Indomethacin freely passes the placental barrier and can be detected in fetal blood within 15 minutes after administration. Its main mechanism of action is in the reduction of fetal urine output. Two potential ill effects of this treatment may be overtreatment with resultant oligohydramnios and premature closure of the ductus arteriosus. These may often reverse with cessation of treatment.

## IMAGING CONSIDERATIONS IN POLYHYDRAMNIOS

Patients with polyhydramnios present several diagnostic imaging challenges to the sonologist. Because the fetus has a large volume of fluid surrounding it, excessive movement may make attempts at interrogation of an organ or structure difficult. Likewise, the fetus may be positioned deep within the uterus, far from the ultrasound transducer and beyond ideal imaging zone ranges for an individual transducer. Occasionally, having the patient turn on her side may make imaging easier momentarily. As the uterus expands because of excessive fluid, placental thickness tends to decrease. A placenta that measures 35 mm in an anteroposterior dimension at 34 to 35 weeks gestation in a patient with hydrops fetalis and severe polyhydramnios may in fact be abnormally thickened (see Figs. 20-10 and 20-21). This is similar to the patient with chronic obstructive pulmonary disease and cardiac failure who has a large barrel chest with what appears to be a normal-sized heart. The heart may



**FIGURE 20-22.** Sonogram from a patient with a diamniotic dichorionic twin pregnancy. Subjective evaluation revealed normal amniotic fluid in each gestational sac on either side of the amniotic membrane (arrow).

be abnormally enlarged but appear normal because of elongation and compression by overdistended lungs.

## TWINS AND ABNORMALITIES IN AMNIOTIC FLUID VOLUME

Multiple gestations and twins in particular present a unique set of diagnostic difficulties with regard to amniotic fluid assessment. In the rare occurrence of monoamniotic twins, individual fluid compartments no longer exist; thus, standard subjective and semiquantitative assessments of AFV are more difficult. Although subjective evaluations of amniotic fluid in diamniotic pregnancies can be readily made, semiquantitative evaluation of AFV using the AFI can only be performed if modifications are made to the original protocol (Fig. 20-22). When a diamniotic twin pregnancy is evaluated sonographically, a question often asked is, "What is the normal expected amniotic fluid volume in each sac?" Magann et al<sup>146</sup> performed a dye-dilution study of 45 diamniotic twin pregnancies to determine the AFV. The AFV per amniotic sac ranged from 155 to 5430 mL, with a mean of 877 mL. This value is comparable to or slightly higher than the AFV reported for third trimester singletons. The AFV in individual amniotic cavities and the total of both cavities in the diamniotic twin pregnancies in their study were unchanged across the entire gestational age range (27 to 38 weeks). Several innovative semiquantitative methods have been attempted to assess AFV in twin gestations (that is, AFI of each sac or a modified AFI in which each sac is divided into two portions).<sup>147</sup> Watson et al<sup>148</sup> assessed AFI of the total volume of the uterus without regard for the amniotic membrane (Fig. 20-23). Magann et al<sup>149</sup> found that an additional method of performing a standard AFI measurement while disregarding the amniotic membrane is too inaccurate to be clinically useful.

In cases of monochorionic diamniotic twins, the ominous complication of twin-to-twin transfusion syndrome may

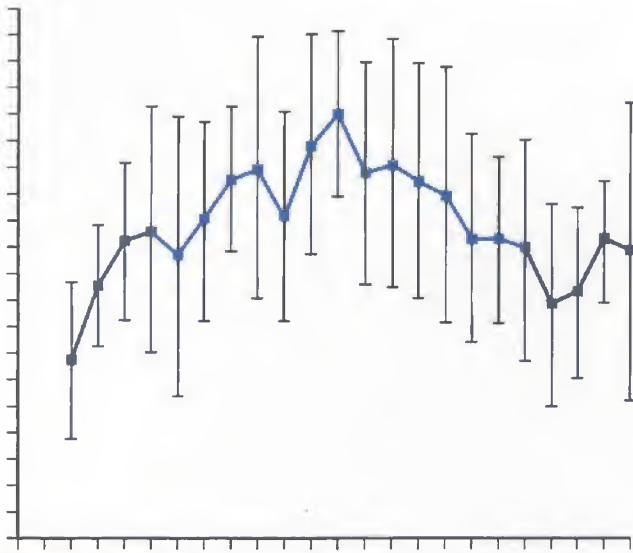


**FIGURE 20-23.** Amniotic fluid index values as a function of gestational age in 210 uncomplicated twin pregnancies (without regard for the intervening amniotic membrane). Dark squares indicate means, and bars indicate one standard deviation. (From Watson WJ, Harless FE, Menard MK, et al: *Sonographic assessment of amniotic fluid in normal twin pregnancy*. *Am J Perinatol* 12:123, 1995.)

develop. This occurs as a result of transplacental communication with vascular anastomoses between the circulations of the twins. The twins are often discordant in size; the recipient, larger twin resides within a polyhydramniotic sac and the donor, smaller growth-restricted twin within an oligohydramniotic sac (Fig. 20-24). Because the oligohydramnios may be severe (virtually no amniotic fluid) in the donor twin one must be careful not to assume that the fluid surrounding the donor is in the donor sac (Fig. 20-25A). More often than not, the fluid adjacent to the donor twin in a case of severe twin-to-twin transfusion syndrome is that of the recipient's sac. One visual clue that may be helpful is that the fluid in the donor sac may have a different echogenicity (often increased) compared with the recipient (Fig. 20-25B). Because of the high mortality for one or both twins (70% to 100%), a number of innovative interventional procedures have been attempted to alleviate this condition, including amnioreduction of the polyhydramniotic sac, laser occlusion of placental vessels, and amniotic septostomy.<sup>150,151</sup> Historically, the most widely used technique was serial amniocenteses of the polyhydramniotic sac. Numerous reports attested to the value of this technique in not only relieving excessive fluid but allowing a normalization of growth of both twins and a significant decrease in perinatal mortality.<sup>151-153</sup> In sites performing amnioreductions, real-time ultrasound guidance is used for entrance into the recipient's amniotic sac.<sup>154</sup> An effort is made to avoid the intertwin membrane and, thus, the gestational sac of the donor twin so as not to perform an unintentional septostomy. An 18-gauge needle is introduced into the amniotic cavity with polyhydramnios, and then connected to either wall suction or a syringe attached to extension tubing in an effort to actively drain the amniotic fluid, thereby reducing the total procedure time. Fluid is

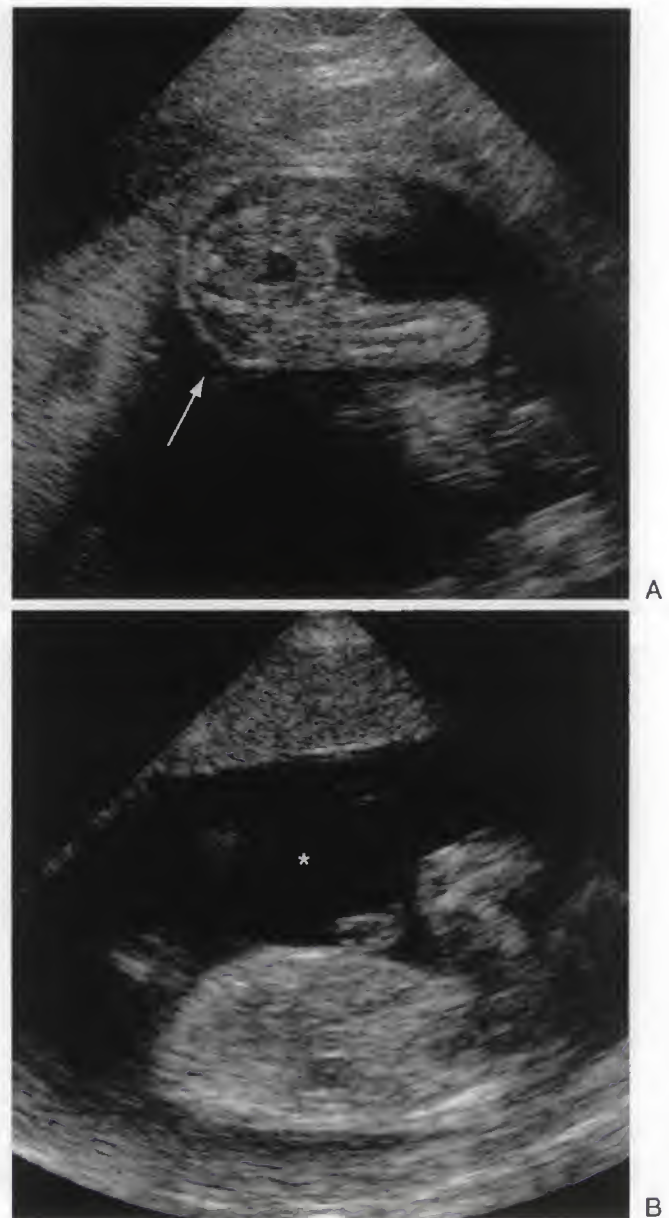


**FIGURE 20-24.** Sonogram of a patient with a monochorionic twin pregnancy with twin-to-twin transfusion syndrome. A. The donor fetus in the oligohydramniotic sac (arrow) is "stuck" to the anterior uterine wall. B. The recipient fetus is in a polyhydramniotic sac (asterisk). Often the dividing amniotic membrane cannot be identified.

removed until the deepest vertical pocket is less than or equal to 6 cm, or a total of 5 L is removed. Although the exact mechanism that improves this condition after amnioreduction is not known, it is likely due to relief of pressure on poorly supported vessels of a velamentous insertion or to improvement in blood flow of balanced vascular anastomoses.<sup>155,156</sup> Inadvertent or purposeful amniotic septostomy may also allow a normalization of amniotic fluid in both amniotic sacs.<sup>152</sup> This procedure is not without complications. Monoamniotic twins, umbilical cord entanglement, and fetal death have been reported after amniotic septostomy.<sup>157</sup>



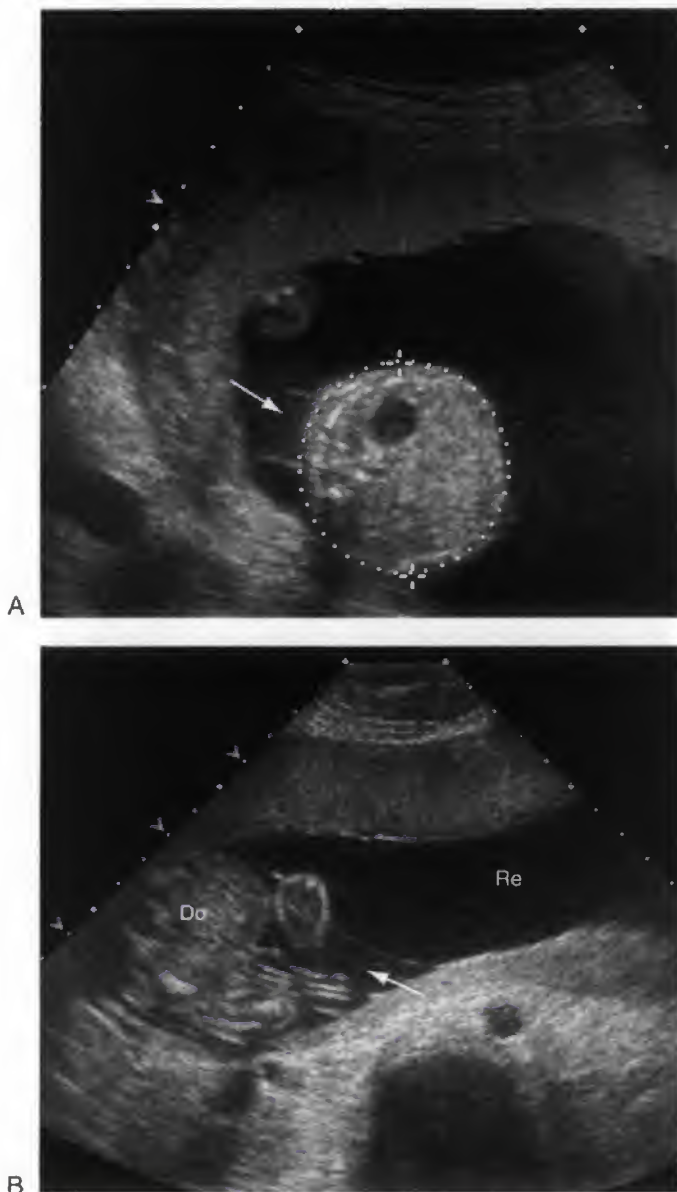


**FIGURE 20-25.** A. Sonogram of the fetal abdomen and surrounding amniotic fluid in a case of twin-to-twin transfusion syndrome. At first glance the fluid surrounding the donor abdomen appears to reside within its amniotic sac. In fact, there is only a small amount of hyperechogenic fluid (arrow) seen within the amniotic sac that enshrouds the fetus. B. Sonogram of the two amniotic sacs in a pregnancy with twin-to-twin transfusion syndrome. The amniotic fluid (arrow) surrounding the donor twin (Do) is more echogenic than the fluid in the recipient sac (Re).

## References

1. Brace RA: Physiology of amniotic fluid volume regulation. *Clin Obstet Gynecol* 40:280, 1997.
2. Wallenburg HC: The amniotic fluid I. Water and electrolyte homeostasis. *J Perinat Med* 5:193, 1977.
3. Brace RA: Fetal blood volume, urine flow, swallowing, and amniotic fluid volume responses to long-term intravascular infusions of saline. *Am J Obstet Gynecol* 161:1049, 1989.
4. Brace RA: Progress toward understanding the regulation of amniotic fluid volume: Water and solute fluxes in and through the fetal membranes. *Placenta* 16:1, 1995.
5. Brace RA, Wolf EJ: Normal amniotic fluid volume changes throughout pregnancy. *Am J Obstet Gynecol* 161:382, 1989.
6. Gilbert WM, Brace RA: Increase in fetal hydration during long-term intraamniotic isotonic saline infusion. *Am J Obstet Gynecol* 159:1413, 1988.
7. Jauniaux E, Gulbis B, Hyett J, et al: Biochemical analyses of mesenchymal fluid in early pregnancy. *Am J Obstet Gynecol* 178:765, 1998.
8. Jauniaux E, Jurkovic D, Gulbis B, et al: Biochemical composition of exocoelomic fluid in early human pregnancy. *Obstet Gynecol* 78:1124, 1991.
9. Mann SE, Nijland MJ, Ross MG: Mathematic modeling of human amniotic fluid dynamics. *Am J Obstet Gynecol* 175:937, 1996.
10. Ross MG, Nijland MJ: Fetal swallowing: Relation to amniotic fluid regulation. *Clin Obstet Gynecol* 40:352, 1997.
11. Hill LM: Oligohydramnios: Sonographic diagnosis and clinical implications. *Clin Obstet Gynecol* 40:314, 1997.
12. Moore K: The developing human: Clinically oriented embryology. In Moore KL, Persaud TVN, eds: *Before We Are Born: Essentials of Embryology and Birth Defects*. Philadelphia, WB Saunders, 1999, p 106.
13. Van Geuns H, Van Kessel H: Creatinine in amniotic fluid and fetal renal function. In Fairweather D, Eskes T, eds: *Amniotic Fluid: Research and Clinical Application*. Amsterdam, Excerpta Medica, 1978, p 81.
14. Lind T: The biochemistry of amniotic fluid. In Fairweather D, Eskes T, eds: *Amniotic Fluid: Research and Clinical Application*. Amsterdam, Excerpta Medica, 1978, p 59.
15. van Otterlo LC, Wladimiroff JW, Wallenburg HC: Relationship between fetal urine production and amniotic fluid volume in normal pregnancy and pregnancy complicated by diabetes. *Br J Obstet Gynaecol* 84:205, 1977.
16. Hedriana HL, Moore TR: Accuracy limits of ultrasonographic estimation of human fetal urinary flow rate. *Am J Obstet Gynecol* 171:989, 1994.
17. Gilbert WM, Moore TR, Brace RA: Amniotic fluid dynamics. *Fetal Med Review* 3:89, 1991.
18. Mescher EJ, Platzker AC, Ballard PL, et al: Ontogeny of tracheal fluid, pulmonary surfactant, and plasma corticoids in the fetal lamb. *J Appl Physiol* 39:1017, 1975.
19. Harding R, Sigger JN, Wickham PJ, et al: The regulation of flow of pulmonary fluid in fetal sheep. *Respir Physiol* 57:47, 1984.
20. Brace RA, Wlodck ME, Cock ML, et al: Swallowing of lung liquid and amniotic fluid by the ovine fetus under normoxic and hypoxic conditions. *Am J Obstet Gynecol* 171:764, 1994.
21. Pritchard JA: Fetal swallowing and amniotic fluid volume. *Obstet Gynecol* 28:606, 1966.
22. Weissman A, Itskovitz-Eldor J, Jakobi P: Sonographic measurement of amniotic fluid volume in the first trimester of pregnancy. *J Ultrasound Med* 15:771, 1996.
23. Goodlin RC, Anderson JC, Gallagher TF: Relationship between amniotic fluid volume and maternal plasma volume expansion. *Am J Obstet Gynecol* 146:505, 1983.
24. Kilpatrick SJ: Therapeutic interventions for oligohydramnios: Amnioinfusion and maternal hydration. *Clin Obstet Gynecol* 40:328, 1997.
25. Kilpatrick SJ, Safford KL: Maternal hydration increases amniotic fluid index in women with normal amniotic fluid. *Obstet Gynecol* 81:49, 1993.
26. Bree RL: Sonographic identification of fetal vernix in amniotic fluid. *J Clin Ultrasound* 6:269, 1978.
27. Parulekar SG: Ultrasonographic demonstration of floating particles in amniotic fluid. *J Ultrasound Med* 2:107, 1983.
28. Khaleghian R: Echogenic amniotic fluid in the second trimester: A new sign of fetal distress. *J Clin Ultrasound* 11:498, 1983.
29. Espinoza J, Goncalves LF, Romero R, et al: The prevalence and clinical significance of amniotic fluid 'sludge' in patients with preterm labor and intact membranes. *Ultrasound Obstet Gynecol* 25:346, 2005.
30. Mungen E, Tutuncu L, Muhcu M: Pregnancy outcome in women with echogenic amniotic fluid at term gestation. *Int J Gynaecol Obstet* 88:314, 2005.
31. Moore TR: Clinical assessment of amniotic fluid. *Clin Obstet Gynecol* 40:303, 1997.
32. Halperin ME, Fong KW, Zalev AH, et al: Reliability of amniotic fluid volume estimation from ultrasonograms: Intraobserver and interobserver variation before and after the establishment of criteria. *Am J Obstet Gynecol* 153:264, 1985.

33. Goldstein RB, Filly RA: Sonographic estimation of amniotic fluid volume. Subjective assessment versus pocket measurements. *J Ultrasound Med* 7:363, 1988.
34. Manning FA, Hill LM, Platt LD: Qualitative amniotic fluid volume determination by ultrasound: Antepartum detection of intrauterine growth retardation. *Am J Obstet Gynecol* 139:254, 1981.
35. Chamberlain PF, Manning FA, Morrison I, et al: Ultrasound evaluation of amniotic fluid volume. I. The relationship of marginal and decreased amniotic fluid volumes to perinatal outcome. *Am J Obstet Gynecol* 150:245, 1984.
36. Mercer LJ, Brown LG, Petres RE, et al: A survey of pregnancies complicated by decreased amniotic fluid. *Am J Obstet Gynecol* 149:355, 1984.
37. Bottoms SF, Welch RA, Zador IE, et al: Limitations of using maximum vertical pocket and other sonographic evaluations of amniotic fluid volume to predict fetal growth: Technical or physiologic? *Am J Obstet Gynecol* 155:154, 1986.
38. Phelan JP, Smith CV, Broussard P, et al: Amniotic fluid volume assessment with the four-quadrant technique at 36-42 weeks' gestation. *J Reprod Med* 32:540, 1987.
39. Rutherford SE, Phelan JP, Smith CV, et al: The four-quadrant assessment of amniotic fluid volume: An adjunct to antepartum fetal heart rate testing. *Obstet Gynecol* 70:353, 1987.
40. Rutherford SE, Smith CV, Phelan JP, et al: Four-quadrant assessment of amniotic fluid volume. Interobserver and intraobserver variation. *J Reprod Med* 32:587, 1987.
41. Moore TR, Cayle JE: The amniotic fluid index in normal human pregnancy. *Am J Obstet Gynecol* 162:1168, 1990.
42. Dildy GA 3rd, Lira N, Moise KJ Jr, et al: Amniotic fluid volume assessment: Comparison of ultrasonographic estimates versus direct measurements with a dye-dilution technique in human pregnancy. *Am J Obstet Gynecol* 167:986, 1992.
43. Chauhan SP, Magann EF, Morrison JC, et al: Ultrasonographic assessment of amniotic fluid does not reflect actual amniotic fluid volume. *Am J Obstet Gynecol* 177:291, 1997.
44. Baron C, Morgan MA, Garite TJ: The impact of amniotic fluid volume assessed intrapartum on perinatal outcome. *Am J Obstet Gynecol* 173:167, 1995.
45. Myles TD, Strassner HT: Amniotic fluid distribution in predicting perinatal outcome in patients with ruptured membranes. *Obstet Gynecol* 89:723, 1997.
46. Buckshee K, Deka D, Padmaja V, et al: Can amniotic fluid distribution predict fetal outcome? *Int J Gynaecol Obstet* 62:19, 1998.
47. Sadovsky Y, Christensen MW, Scheerer L, et al: Cord-containing amniotic fluid pocket: A useful measurement in the management of oligohydramnios. *Obstet Gynecol* 80:775, 1992.
48. Magann EF, Chauhan SP, Whitworth NS, et al: Do multiple measurements employing different ultrasonic techniques improve the accuracy of amniotic fluid volume assessment? *Aust N Z J Obstet Gynaecol* 38:172, 1998.
49. Wax JR, Costigan K, Callan NA, et al: Effect of fetal movement on the amniotic fluid index. *Am J Obstet Gynecol* 168:188, 1993.
50. Del Valle GO, Bateman L, Gaudier FL, et al: Comparison of three types of ultrasound transducers in evaluating the amniotic fluid index. *J Reprod Med* 39:869, 1994.
51. Tressler T, Bernazzoli M, Hole J, et al: The effects of maternal position on the amniotic fluid index. *J Ultrasound Med* 25:445, 2006.
52. Fok WY, Chan LY, Lau TK: The influence of fetal position on amniotic fluid index and single deepest pocket. *Ultrasound Obstet Gynecol* 28:162, 2006.
53. Flack NJ, Dore C, Southwell D, et al: The influence of operator transducer pressure on ultrasonographic measurements of amniotic fluid volume. *Am J Obstet Gynecol* 171:218, 1994.
54. Magann EF, Chauhan SP, Barrilleaux PS, et al: Ultrasound estimate of amniotic fluid volume: Color Doppler overdiagnosis of oligohydramnios. *Obstet Gynecol* 98:71, 2001.
55. Larmon JE, Ross BS: Clinical utility of amniotic fluid volume assessment. *Obstet Gynecol Clin North Am* 25:639, 1998.
56. Philipson EH, Sokol RJ, Williams T: Oligohydramnios: Clinical associations and predictive value for intrauterine growth retardation. *Am J Obstet Gynecol* 146:271, 1983.
57. Magann EF, Nolan TE, Hess LW, et al: Measurement of amniotic fluid volume: Accuracy of ultrasonography techniques. *Am J Obstet Gynecol* 167:1533, 1992.
58. Manning FA, Harman CR, Morrison I, et al: Fetal assessment based on fetal biophysical profile scoring. IV. An analysis of perinatal morbidity and mortality. *Am J Obstet Gynecol* 162:703, 1990.
59. Bar-Hava I, Scarpelli SA, Barnhard Y, et al: Amniotic fluid volume reflects recent glycemic status in gestational diabetes mellitus. *Am J Obstet Gynecol* 171:952, 1994.
60. Barss VA, Benacerraf BR, Frigoletto FD Jr: Second trimester oligohydramnios, a predictor of poor fetal outcome. *Obstet Gynecol* 64:608, 1984.
61. Chauhan SP, Washburne JF, Magann EF, et al: A randomized study to assess the efficacy of the amniotic fluid index as a fetal admission test. *Obstet Gynecol* 86:9, 1995.
62. Crowley P, O'Herlihy C, Boylan P: The value of ultrasound measurement of amniotic fluid volume in the management of prolonged pregnancies. *Br J Obstet Gynaecol* 91:444, 1984.
63. Hadi HA, Hodson CA, Strickland D: Premature rupture of the membranes between 20 and 25 weeks' gestation: Role of amniotic fluid volume in perinatal outcome. *Am J Obstet Gynecol* 170:1139, 1994.
64. King JC, Mitzner W, Butterfield AB, et al: Effect of induced oligohydramnios on fetal lung development. *Am J Obstet Gynecol* 154:823, 1986.
65. Marks AD, Divon MY: Longitudinal study of the amniotic fluid index in post-dates pregnancy. *Obstet Gynecol* 79:229, 1992.
66. Spong CY, McKindsey F, Ross MG: Amniotic fluid index predicts the relief of variable decelerations after amnioinfusion bolus. *Am J Obstet Gynecol* 175:1066, 1996.
67. Manning FA, Platt LD: Qualitative assessment of amniotic fluid volume: A rapid screen for detecting the small for gestational age fetus. 26th Annual Meeting of the Society for Gynecologic Investigation. San Diego, California, 1979.
68. Manning FA, Platt LD, Sipos L: Antepartum fetal evaluation: development of a fetal biophysical profile. *Am J Obstet Gynecol* 136:787, 1980.
69. Hoddick WK, Callen PW, Filly RA, et al: Ultrasonographic determination of qualitative amniotic fluid volume in intrauterine growth retardation: Reassessment of the 1 cm rule. *Am J Obstet Gynecol* 149:758, 1984.
70. Miyazaki ES, Taylor NA: Saline amnioinfusion for relief of variable or prolonged decelerations. A preliminary report. *Am J Obstet Gynecol* 146:670, 1983.
71. Chauhan SP, Rutherford SE, Hess LW, et al: Prophylactic intrapartum amnioinfusion for patients with oligohydramnios. A prospective randomized study. *J Reprod Med* 37:817, 1992.
72. Nageotte MP, Bertucci L, Towers CV, et al: Prophylactic amnioinfusion in pregnancies complicated by oligohydramnios: A prospective study. *Obstet Gynecol* 77:677, 1991.
73. Ogunidipe OA, Spong CY, Ross MG: Prophylactic amnioinfusion for oligohydramnios: A reevaluation. *Obstet Gynecol* 84:544, 1994.
74. Schrimmer DB, Macri CJ, Paul RH: Prophylactic amnioinfusion as a treatment for oligohydramnios in laboring patients: A prospective, randomized trial. *Am J Obstet Gynecol* 165:972, 1991.
75. Strong TH, Jr., Hetzler G, Sarno AP, et al: Prophylactic intrapartum amnioinfusion: A randomized clinical trial. *Am J Obstet Gynecol* 162:1370, 1990.
76. Kilpatrick SJ, Safford KL, Pomcroy T, et al: Maternal hydration increases amniotic fluid index. *Obstet Gynecol* 78:1098, 1991.
77. Bar-Hava I, Divon MY, Sardo M, et al: Is oligohydramnios in postterm pregnancy associated with redistribution of fetal blood flow? *Am J Obstet Gynecol* 173:519, 1995.
78. Sylvester SG, Divon MY: The pathophysiology of amniotic fluid volume in the post-term pregnancy. *Am J Obstet Gynecol* 180:523, 1999.
79. Morris JM, Thompson K, Smithy J, et al: The usefulness of ultrasound assessment of amniotic fluid in predicting adverse outcome in prolonged pregnancy: A prospective blinded observational study. *Br J Obstet Gynaecol* 110:989, 2003.
80. Lauria MR, Gonik B, Romero R: Pulmonary hypoplasia: Pathogenesis, diagnosis, and antenatal prediction. *Obstet Gynecol* 86:466, 1995.
81. Nicolini U, Fisk NM, Rodeck CH, et al: Low amniotic pressure in oligohydramnios—Is this the cause of pulmonary hypoplasia? *Am J Obstet Gynecol* 161:1098, 1989.
82. Adzick NS, Harrison MR, Glick PL, et al: Experimental pulmonary hypoplasia and oligohydramnios: Relative contributions of lung fluid and fetal breathing movements. *J Pediatr Surg* 19:658, 1984.
83. Harding R, Hooper SB, Dickson KA: A mechanism leading to reduced lung expansion and lung hypoplasia in fetal sheep during oligohydramnios. *Am J Obstet Gynecol* 163:1904, 1990.



84. Kilbride HW, Yeast J, Thibeault DW: Defining limits of survival: Lethal pulmonary hypoplasia after midtrimester premature rupture of membranes. *Am J Obstet Gynecol* 175:675, 1996.
85. Kitzmiller J: Preterm rupture of the membranes. In Fuchs F, Stubblefield P, eds: *Preterm Birth*. New York, Macmillan, 1984, p 298.
86. Nimrod C, Varela-Gittings F, Machin G, et al: The effect of very prolonged membrane rupture on fetal development. *Am J Obstet Gynecol* 148:540, 1984.
87. Bengtson JM, VanMarter LJ, Barss VA, et al: Pregnancy outcome after premature rupture of the membranes at or before 26 weeks' gestation. *Obstet Gynecol* 73:921, 1989.
88. Gold RB, Goyert GL, Schwartz DB, et al: Conservative management of second-trimester post-amniocentesis fluid leakage. *Obstet Gynecol* 74:745, 1989.
89. Johnson JW, Egerman RS, Moorhead J: Cases with ruptured membranes that "reseal." *Am J Obstet Gynecol* 163:1024, 1990.
90. Sarno AP Jr, Ahn MO, Phelan JP: Intrapartum amniotic fluid volume at term. Association of ruptured membranes, oligohydramnios and increased fetal risk. *J Reprod Med* 35:719, 1990.
91. Chauhan SP, Hendrix NW, Morrison JC, et al: Intrapartum oligohydramnios does not predict adverse peripartum outcome among high-risk parturients. *Am J Obstet Gynecol* 176:1130, 1997.
92. Chauhan SP, Cowan BD, Magann EF, et al: Intrapartum amniotic fluid index. A poor diagnostic test for adverse perinatal outcome. *J Reprod Med* 41:860, 1996.
93. Alfrevic Z, Luckas M, Walkinshaw SA, et al: A randomised comparison between amniotic fluid index and maximum pool depth in the monitoring of post-term pregnancy. *Br J Obstet Gynaecol* 104:207, 1997.
94. Ott WJ: Reevaluation of the relationship between amniotic fluid volume and perinatal outcome. *Am J Obstet Gynecol* 192:1803, 2005.
95. Garmel SH, Chelmon D, Sha SJ, et al: Oligohydramnios and the appropriately grown fetus. *Am J Perinatol* 14:359, 1997.
96. Kreiser D, el-Sayed YY, Sorell KA, et al: Decreased amniotic fluid index in low-risk pregnancy. *J Reprod Med* 46:743, 2001.
97. Magann EF, Chauhan SP, Kinsella MJ, et al: Antenatal testing among 1001 patients at high risk: The role of ultrasonographic estimate of amniotic fluid volume. *Am J Obstet Gynecol* 180:1330, 1999.
98. Magann EF, Chauhan SP, Doherty DA, et al: Predictability of intrapartum and neonatal outcomes with the amniotic fluid volume distribution: A reassessment using the amniotic fluid index, single deepest pocket, and a dye-determined amniotic fluid volume. *Am J Obstet Gynecol* 188:1523, 2003.
99. Magann EF, Kinsella MJ, Chauhan SP, et al: Does an amniotic fluid index of  $\leq 5$  cm necessitate delivery in high-risk pregnancies? A case-control study. *Am J Obstet Gynecol* 180:1354, 1999.
100. Williams K, Wittmann BK: The sensitivity and specificity of subjective and a semi-quantitative technique of amniotic fluid volume assessment in predicting intrapartum morbidity. *Ultrasound Obstet Gynecol* 3:180, 1993.
101. Chauhan SP, Sanderson M, Hendrix NW, et al: Perinatal outcome and amniotic fluid index in the antepartum and intrapartum periods: A meta-analysis. *Am J Obstet Gynecol* 181:1473, 1999.
102. Magann EF, Chauhan SP, Barrilleaux PS, et al: Amniotic fluid index and single deepest pocket: Weak indicators of abnormal amniotic volumes. *Obstet Gynecol* 96:737, 2000.
103. Wing DA, Fishman A, Gonzalez C, et al: How frequently should the amniotic fluid index be performed during the course of antepartum testing? *Am J Obstet Gynecol* 174:33, 1996.
104. Lagrew DC, Pircon RA, Nageotte M, et al: How frequently should the amniotic fluid index be repeated? *Am J Obstet Gynecol* 167:1129, 1992.
105. Cheng EY, Luthy DA, Hickok DE, et al: Transcervical chorionic villus sampling and midtrimester oligohydramnios. *Am J Obstet Gynecol* 165:1063, 1991.
106. Bronshtein M, Zimmer EZ: Oligohydramnios with amnio-chorionic separation at 15-16 weeks' gestation. *Prenat Diagn* 15:161, 1995.
107. Barnhard Y, Bar-Hava I, Divon MY: Accuracy of intrapartum estimates of fetal weight. Effect of oligohydramnios. *J Reprod Med* 41:907, 1996.
108. Levine D, Goldstein RB, Callen PW, et al: The effect of oligohydramnios on detection of fetal anomalies with sonography. *AJR Am J Roentgenol* 168:1609, 1997.
109. Barnhard Y, Bar-Hava I, Divon MY: Is polyhydramnios in an ultrasonographically normal fetus an indication for genetic evaluation? *Am J Obstet Gynecol* 173:1523, 1995.
110. Hill LM, Breckle R, Thomas ML, et al: Polyhydramnios: Ultrasonically detected prevalence and neonatal outcome. *Obstet Gynecol* 69:21, 1987.
111. Stoll CG, Alembik Y, Dott B: Study of 156 cases of polyhydramnios and congenital malformations in a series of 118,265 consecutive births. *Am J Obstet Gynecol* 165:586, 1991.
112. Wallenburg HC, Wladimiroff JW: The amniotic fluid. II. Polyhydramnios and oligohydramnios. *J Perinat Med* 5:233, 1977.
113. Magann EF, Morton ML, Nolan TE, et al: Comparative efficacy of two sonographic measurements for the detection of aberrations in the amniotic fluid volume and the effect of amniotic fluid volume on pregnancy outcome. *Obstet Gynecol* 83:959, 1994.
114. Rodriguez MH: Polyhydramnios: Does reducing the amniotic fluid volume decrease the incidence of prematurity? *Clin Perinatol* 19:359, 1992.
115. Gohari P, Berkowitz RL, Hobbins JC: Prediction of intrauterine growth retardation by determination of total intrauterine volume. *Am J Obstet Gynecol* 127:255, 1977.
116. Quinlan RW, Cruz AC, Martin M: Hydranios: Ultrasound diagnosis and its impact on perinatal management and pregnancy outcome. *Am J Obstet Gynecol* 145:306, 1983.
117. Bruner JP, Reed GW, Sarno AP Jr, et al: Intraobserver and interobserver variability of the amniotic fluid index. *Am J Obstet Gynecol* 168:1309, 1993.
118. Chamberlain PF, Manning FA, Morrison I, et al: Ultrasound evaluation of amniotic fluid volume. II. The relationship of increased amniotic fluid volume to perinatal outcome. *Am J Obstet Gynecol* 150:250, 1984.
119. Carlson DE, Platt LD, Medearis AL, et al: Quantifiable polyhydramnios: Diagnosis and management. *Obstet Gynecol* 75:989, 1990.
120. Glantz JC, Abramowicz JS, Sherer DM: Significance of idiopathic midtrimester polyhydramnios. *Am J Perinatol* 11:305, 1994.
121. Golan A, Wolman I, Sagi J, et al: Persistence of polyhydramnios during pregnancy—Its significance and correlation with maternal and fetal complications. *Gynecol Obstet Invest* 37:18, 1994.
122. Damato N, Filly RA, Goldstein RB, et al: Frequency of fetal anomalies in sonographically detected polyhydramnios. *J Ultrasound Med* 12:11, 1993.
123. Gilbert WM, Brace RA: Amniotic fluid volume and normal flows to and from the amniotic cavity. *Semin Perinatol* 17:150, 1993.
124. Sherer DM, Langer O: Oligohydramnios: Use and misuse in clinical management. *Ultrasound Obstet Gynecol* 18:411, 2001.
125. Gilbert WM, Brace RA: The missing link in amniotic fluid volume regulation: Intramembranous absorption. *Obstet Gynecol* 74:748, 1989.
126. Broecker BH, Redwine FO, Petres RE: Reversal of acute polyhydramnios after fetal renal decompression. *Urology* 31:60, 1988.
127. Ohmichi M, Tasaka K, Sugita N, et al: Hydranios associated with congenital mesoblastic nephroma: Case report. *Obstet Gynecol* 74:469, 1989.
128. Sanders R, Graham D: Twelve cases of hydronephrosis in utero diagnosed by ultrasonography. *J Ultrasound Med* 1:341, 1982.
129. Moise KJ Jr: Polyhydramnios. *Clin Obstet Gynecol* 40:266, 1997.
130. Esplin MS, Hallam S, Farrington PF, et al: Myotonic dystrophy is a significant cause of idiopathic polyhydramnios. *Am J Obstet Gynecol* 179:974, 1998.
131. Lidang Jensen M, Rix M, Schroder HD, et al: Fetal akinesia-hypokinesia deformation sequence (FADS) in 2 siblings with congenital myotonic dystrophy. *Clin Neuropathol* 14:105, 1995.
132. Verspyck E, Mandelbrot L, Dommergues M, et al: Myasthenia gravis with polyhydramnios in the fetus of an asymptomatic mother. *Prenat Diagn* 13:539, 1993.
133. Ang MS, Thorp JA, Parisi VM: Maternal lithium therapy and polyhydramnios. *Obstet Gynecol* 76:517, 1990.
134. Sohaey R, Nyberg DA, Sickler GK, et al: Idiopathic polyhydramnios: Association with fetal macrosomia. *Radiology* 190:393, 1994.
135. Benson CB, Coughlin BF, Doubilet PM: Amniotic fluid volume in large-for-gestational-age fetuses of nondiabetic mothers. *J Ultrasound Med* 10:149, 1991.
136. Brady K, Polzin WJ, Kopelman JN, et al: Risk of chromosomal abnormalities in patients with idiopathic polyhydramnios. *Obstet Gynecol* 79:234, 1992.

137. Zahn CM, Hankins GD, Yeomans ER: Karyotypic abnormalities and hydramnios. Role of amniocentesis. *J Reprod Med* 38:599, 1993.
138. Sickler GK, Nyberg DA, Sohay R, et al: Polyhydramnios and fetal intrauterine growth restriction: Ominous combination. *J Ultrasound Med* 16:609, 1997.
139. Phelan JP, Park YW, Ahn MO, et al: Polyhydramnios and perinatal outcome. *J Perinatol* 10:347, 1990.
140. Many A, Hill LM, Lazebnik N, et al: The association between polyhydramnios and preterm delivery. *Obstet Gynecol* 86:389, 1995.
141. Many A, Lazebnik N, Hill LM: The underlying cause of polyhydramnios determines prematurity. *Prenat Diagn* 16:55, 1996.
142. Elliott JP, Sawyer AT, Radin TG, et al: Large-volume therapeutic amniocentesis in the treatment of hydramnios. *Obstet Gynecol* 84:1025, 1994.
143. Leung WC, Jouannic JM, Hyett J, et al: Procedure-related complications of rapid amniodrainage in the treatment of polyhydramnios. *Ultrasound Obstet Gynecol* 23:154, 2004.
144. Kirshon B, Mari G, Moise KJ Jr: Indomethacin therapy in the treatment of symptomatic polyhydramnios. *Obstet Gynecol* 75:202, 1990.
145. Mamopoulos M, Assimakopoulos E, Reece EA, et al: Maternal indomethacin therapy in the treatment of polyhydramnios. *Am J Obstet Gynecol* 162:1225, 1990.
146. Magann EF, Chauhan SP, Martin JN Jr, et al: Ultrasonic assessment of the amniotic fluid volume in diamniotic twins. *J Soc Gynecol Investig* 2:609, 1995.
147. Gerson A, Free SM Jr, Russino J, et al: Amniotic fluid index in twin gestation. *Ultrasound Obstet Gynecol* 10:98, 1997.
148. Watson WJ, Harlass FE, Mcnard MK, et al: Sonographic assessment of amniotic fluid in normal twin pregnancy. *Am J Perinatol* 12:122, 1995.
149. Magann EF, Chauhan SP, Whitworth NS, et al: The accuracy of the summated amniotic fluid index in evaluating amniotic fluid volume in twin pregnancies. *Am J Obstet Gynecol* 177:1041, 1997.
150. De Lia JE, Cruikshank DP, Keye WR Jr: Fetoscopic neodymium: YAG laser occlusion of placental vessels in severe twin-twin transfusion syndrome. *Obstet Gynecol* 75:1046, 1990.
151. Mahony BS, Petty CN, Nyberg DA, et al: The "stuck twin" phenomenon: Ultrasonographic findings, pregnancy outcome, and management with serial amniocenteses. *Am J Obstet Gynecol* 163:1513, 1990.
152. Saade GR, Belfort MA, Berry DL, et al: Amniotic septostomy for the treatment of twin oligohydramnios-polyhydramnios sequence. *Fetal Diagn Ther* 13:86, 1998.
153. Wax JR, Henderson E: Effect of fetal movement on the amniotic fluid index in diamniotic twin gestations. *J Clin Ultrasound* 25:255, 1997.
154. Moise KJ Jr, Dorman K, Lamvu G, et al: A randomized trial of amnioreduction versus septostomy in the treatment of twin-twin transfusion syndrome. *Am J Obstet Gynecol* 193:701, 2005.
155. Blickstein I: The twin-twin transfusion syndrome. *Obstet Gynecol* 76:714, 1990.
156. Fries MH, Goldstein RB, Kilpatrick SJ, et al: The role of velamentous cord insertion in the etiology of twin-twin transfusion syndrome. *Obstet Gynecol* 81:569, 1993.
157. Suzuki S, Ishikawa G, Sawa R, et al: Iatrogenic monoamniotic twin gestation with progressive twin-twin transfusion syndrome. *Fetal Diagn Ther* 14:98, 1999.
158. Horsager R, Nathan L, Leveno KJ: Correlation of measured amniotic fluid volume and sonographic predictions of oligohydramnios. *Obstet Gynecol* 83:955, 1994.
159. Dizon-Townson D, Kennedy KA, Dildy GA, et al: Amniotic fluid index and perinatal morbidity. *Am J Perinatol* 13:231, 1996.
160. Jeng CJ, Jou TJ, Wang KG, et al: Amniotic fluid index measurement with the four-quadrant technique during pregnancy. *J Reprod Med* 35:674, 1990.



# ANTEPARTUM FETAL ASSESSMENT BY ULTRASONOGRAPHY: THE FETAL BIOPHYSICAL PROFILE

Martin R. Chavez, MD, Yinka Oyelese, MD, and Anthony M. Vintzileos, MD

## Technique for the Biophysical Profile

The Biophysical Profile: Original Findings  
Validation of the Biophysical Profile: Correlation With Perinatal Death

## Physiologic Basis for the Biophysical Profile

Appearance of the Components of the Biophysical Profile Across Gestational Age  
The Biophysical Profile and Fetal Acid-Base Status  
The Gradual Hypoxia Concept  
The Implications of the Gradual Hypoxia Concept on the Interpretation of the Biophysical Profile

The Effect of Preterm Premature Rupture of the Membranes on the Biophysical Profile

The Role of the Nonstress Test in the Biophysical Profile

The Biophysical Profile in the Management of High-Risk Pregnancy

A Proposed Algorithm for Using the Biophysical Profile in Clinical Practice

The Role of the Fetal Biophysical Profile in Detecting Intra-Amniotic Infection in Patients With Preterm Premature Rupture of the Membranes

The Effects of Medications on the Biophysical Profile

## Conclusion

In adult medicine, physical examination of the patient plays a crucial role in the assessment of health. The vital signs (heart rate, respiratory rate, temperature, urine output, state of alertness and activity) are universally used in the detection of health or disease. Similarly, the Apgar score for evaluation of the newborn assesses pulse rate, respiratory effort, appearance, tone, and responsiveness. The advent of real-time ultrasound has made it possible to perform a similar direct examination of the fetus in order to evaluate its state of health. In 1980, Manning and colleagues<sup>1</sup> introduced a biophysical profile (BPP) for evaluation of the fetus. This score consisted of five parameters: fetal breathing movements, gross fetal movements, fetal tone, fetal heart rate, and fetal urine output (amniotic fluid volume). This chapter reviews the role of the original BPP, and its modifications (Tables 21-1 and 21-2),<sup>1,2</sup> in the evaluation of fetal health. Importantly, we review the basic physiology and pathophysiology of the various components of the fetal BPP, and the role of each component or combination of components in predicting fetal asphyxia, and discuss the clinical applications of the BPP in high-risk patients.

The main objectives of any fetal surveillance modality are twofold: first, to identify fetuses at risk of intra- or extrauterine death or severe morbidity, and second, to identify these potential threats early enough to allow interventions to prevent adverse outcomes. In order to understand how to best evaluate the state of health of the fetus, it is important to realize that fetal disease may arise from a number of different pathways, and that tests of fetal well-being should be appropriate for the specific pathologic

condition that is proposed to put the fetus at risk. Thus, we recently presented an argument for condition-specific antenatal testing, because a form of surveillance that is ideal for one condition may be totally inappropriate for another.<sup>3</sup> Electronic fetal heart rate monitoring, in the form of the nonstress test (NST) is the most frequently used method for antepartum detection of fetal asphyxia. However, this method is limited because it relies solely on the fetal heart rate for determining the state of fetal health. And although a reactive NST is efficacious in determining that the fetus is not asphyxiated at the time of testing, it is associated with high false-positive rates (50%–75%).<sup>4–6</sup> Thus, an unacceptably high proportion of tested fetuses will be judged to have a nonreassuring status following an NST and may be subjected to unnecessary intervention. The BPP gives a more complete evaluation of the state of fetal health, and overcomes the problem of the high false-positive rates of the NST by assessing other parameters of fetal well-being, giving it improved diagnostic accuracy in the detection of antepartum fetal acidemia.

## TECHNIQUE FOR THE BIOPHYSICAL PROFILE

The first step in performing a BPP is performing a continuous fetal heart rate tracing, called an NST (Fig. 21-1). It is considered reactive, or reassuring, if there is a normal baseline of 110 to 160 beats per minute, and there are two or more accelerations over a period of 20 minutes. An acceleration is defined as an increase of the fetal heart rate

**Table 21-1** Fetal Biophysical Profile Scoring

Variable	Score 2	Score 0
Fetal breathing movements	Presence of at least 30 seconds of sustained fetal breathing movements in 30 minutes of observation	Less than 30 seconds of fetal breathing movements in 30 minutes
Fetal movements	Three or more gross body movements in 30 minutes of observation. Simultaneous limb and trunk movements are counted as a single movement	Two or less gross body movements in 30 minutes of observation
Fetal tone	At least one episode of motion of a limb from a position of flexion to extension and a rapid return to flexion	Fetus in a position of semi- or full-limb extension with no return to flexion with movement; absence of fetal movement is counted as absent tone.
Fetal reactivity	Presence of two or more fetal heart rate accelerations of at least 15 beats per minute and lasting at least 15 seconds and associated with fetal movement in 40 minutes	No acceleration or less than two accelerations of the fetal heart rate in 40 minutes of observation
Qualitative amniotic fluid volume	A pocket of amniotic fluid that measures at least 1 cm in two perpendicular planes	Largest pocket of amniotic fluid measures less than 1 cm in two perpendicular planes
Maximal score	10	
Minimal score		0

From Manning FA, Platt LD, Sipos L: Antepartum fetal evaluation: Development of a fetal biophysical profile score. *Am J Obstet Gynecol* 136:787, 1980.

**Table 21-2** Criteria for Scoring Biophysical Variables (Maximal Score 12, Minimal Score 0)

Score	Criteria
Nonstress Test	
2 (NST2)	Five or more fetal heart rate accelerations of at least 15 beats per minute in amplitude and at least 15 seconds duration associated with fetal movements in a 20-minute period
1 (NST1)	Two to four accelerations of at least 15 beats per minute in amplitude and at least 15 seconds duration associated with fetal movements in a 20-minute period
0 (NST0)	One or fewer accelerations in a 20-minute period
Fetal Movements	
2 (FM2)	At least three gross (trunk and limbs) episodes of fetal movements within 30 minutes; simultaneous limb and trunk movements were counted as a single movement
1 (FM1)	One or two fetal movements within 30 minutes
0 (FM0)	Absence of fetal movements within 30 minutes
Fetal Breathing Movements	
2 (FBM2)	At least one episode of fetal breathing of at least 60 seconds duration within a 30-minute observation period
1 (FBM1)	At least one episode of fetal breathing lasting 30 to 60 seconds within 30 minutes
0 (FBM0)	Absence of fetal breathing or breathing lasting less than 30 seconds within 30 minutes
Fetal Tone	
2 (FT2)	At least one episode of extension of extremities with return to position of flexion and also one episode of extension of spine with return to position of flexion
1 (FT1)	At least one episode of extension of extremities with return to position of flexion or one episode of extension of spine with return to flexion
0 (FT0)	Extremities in extension; fetal movements not followed by return to flexion; open hand
Amniotic Fluid Volume	
2 (AF2)	Fluid evident throughout the uterine cavity; a pocket that measures 2 cm or more in vertical diameter
1 (AF1)	A pocket that measures less than 2 cm but more than 1 cm in vertical diameter
0 (AF0)	Crowding of fetal small parts; largest pocket less than 1 cm in vertical diameter
Placental Grading	
2 (PL2)	Placental grading 0, 1, or 2
1 (PL1)	Placental posterior difficult to evaluate
0 (PL0)	Placental grading 3

From Vintzileos AM, Campbell WA, Ingardia CJ, et al: The fetal biophysical profile and its predictive value. *Obstet Gynecol* 62:271, 1983. Reprinted with permission from The American College of Obstetricians and Gynecologists.



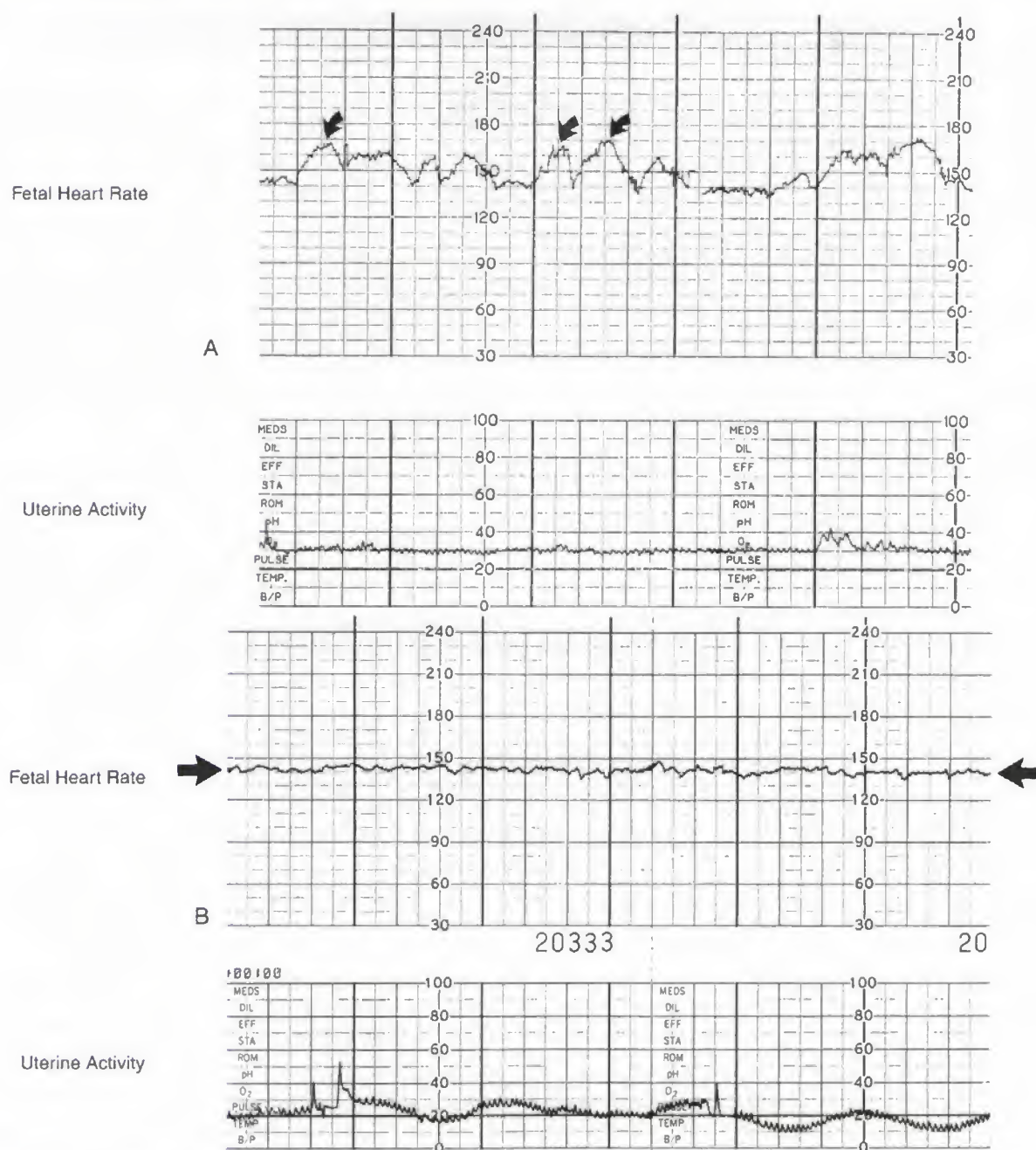


**FIGURE 21-1.** A. Reactive nonstress test. Fetal heart rate accelerations (curved arrows) of at least 15 beats per minute lasting 15 seconds or longer are readily identified in this patient. B. Nonreactive nonstress test. Lack of fetal heart rate acceleration (arrows). This pattern could indicate the effect of fetal sleep, medications, or hypoxia.

over the baseline of at least 15 beats per minute, and lasting at least 15 seconds.<sup>7</sup> Following the NST, real-time sonography is performed to evaluate the fetal biophysical activities (see Tables 21-1 and 21-2).<sup>1,2</sup> It is important that the examiner has adequate skill and experience and that appropriate technique is applied.<sup>8</sup> Amniotic fluid volume measurements should be performed only in cord loop-free pockets of amniotic fluid (Fig. 21-2).<sup>8</sup> Fetal breathing movements should be considered present only if they are continuous for at least 30 seconds, with breath-to-breath intervals of less

than 6 seconds.<sup>8</sup> The correct plane for assessing fetal breathing movements is shown in Figure 21-3. Similarly, gross fetal movements are only considered present if three or more rolling movements of the trunk are observed within 30 minutes.<sup>8</sup> Isolated limb movements do not meet the criteria for a normal score for gross fetal movements on a BPP. The examination is completed when a normal biophysical score (of 8/8 in the Manning BPP scoring system<sup>1</sup> or 12/12 in the scoring system described by Vintzileos et al<sup>2</sup>) has been achieved, or after 30 minutes of continuous real-time

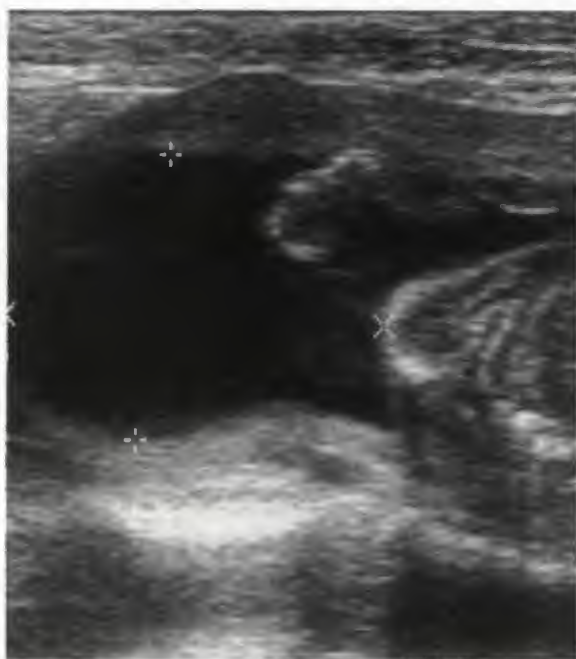


**FIGURE 21-2.** Sonogram demonstrating amniotic fluid measurement as part of the biophysical profile. The amniotic fluid pocket is measured in two perpendicular planes.

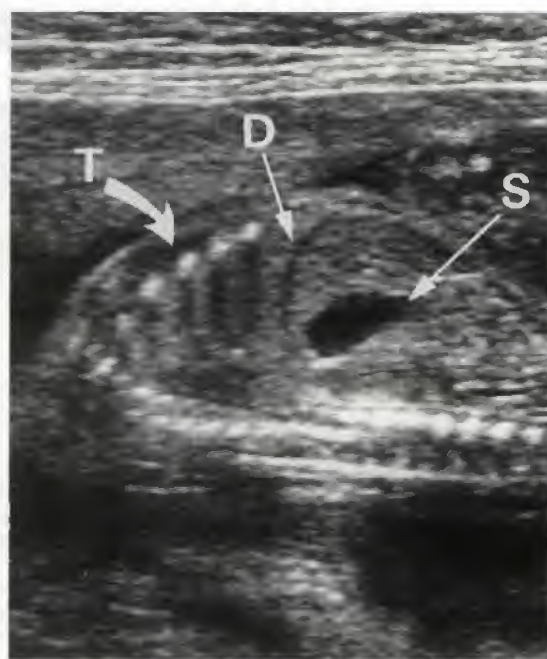


**FIGURE 21-3.** Longitudinal sonogram of a fetus demonstrating the recommended plane of section for evaluating fetal breathing movements. Downward movement of the fetal diaphragm (D) and abdomen and an inward, rocking motion of the fetal thorax (T) can be seen when fetal breathing is present. S, stomach.

sonographic examination (see Tables 21-1 and 21-2). More than 90% of tests that are normal are completed within the first 4 minutes, and the average testing time is less than 8 minutes.<sup>9</sup> Some have suggested using fetal acoustic stimulation to shorten the period for testing. Pinette and colleagues<sup>10</sup> used acoustic stimulation in 412 women if the biophysical score was not reassuring within 5 minutes of testing, and compared these with 458 control subjects in whom acoustic stimulation was not used. They found that the fetal acoustic stimulation group required less time for testing (3 minutes), had fewer nonreassuring tests (5%), and fewer tests with no fetal breathing movements.

The two scoring systems differ; in the original BPP described by Manning et al,<sup>1</sup> each of five parameters were either given a score of two when normal or zero, when abnormal, with no scores in between (see Table 21-1). As a result, a fetus who had some movements and tone, but did not meet the threshold for a score of two, was awarded a score of zero, the same score as a fetus demonstrating no movement or tone whatsoever. To deal with this limitation, Vintzileos et al<sup>2</sup> in 1983 proposed another scoring system (see Table 21-2), which gave intermediate scores, and also included placental grading as one of the biophysical variables. A normal biophysical score (of  $>8$ ) is considered predictive of a nonacidotic fetus. The presence of oligohydramnios in either scoring system is considered abnormal, because reduced amniotic fluid puts the fetus at risk of cord compression, death, or adverse perinatal outcomes, regardless of the scores of the other biophysical parameters. The value of the BPP is not the overall score per se, because different components of the BPP have different clinical implications.<sup>8,11</sup> This is discussed further in a later section.

### The Biophysical Profile: Original Findings

Before the development of the BPP, it had been noted that sonographic assessment of fetal breathing movements was as accurate a predictor of fetal well-being as the reactive NST, and that the combination of the NST with an assessment of breathing movements led to a lower rate of false-positive results.<sup>12</sup> This raised the prospect of using other forms of surveillance to complement fetal heart rate. In the original BPP study by Manning and co-workers,<sup>1</sup> which included 216 women with high-risk pregnancies, the NST was performed just before the ultrasound examination.<sup>1</sup> The patients were managed according to their NST results, and the physicians were blinded to the results of the other components of the BPP; therefore, these results did not influence outcomes. Although the patients were evaluated at different intervals, only the last observation was used in the assessment for the study, and in all cases, this was within a week of delivery. Outcomes assessed were the 5-minute Apgar score, incidence of fetal distress (defined as an abnormal fetal heart rate tracing necessitating emergency delivery), and perinatal mortality. The investigators found an association between abnormal biophysical scores and low 5-minute Apgar scores. They found that the absence of fetal breathing movements was most predictive of fetal distress in labor, even more so than a nonreactive NST. Importantly, no perinatal deaths occurred in fetuses with a BPP score of 10/10. The fetal death rate after a single normal test ranged from 6.1/1000 for fetuses with normal fetal tone, to 12.8/1000 for fetuses with a reactive NST.<sup>1</sup> This was statistically nonsignificant, but the incidence of fetal death



**Table 21-3** Fetal Central Nervous System Centers

Test	Center		
Fetal tone	Cortex (subcortical area ?)		
Fetal movements	Cortex nuclei		
Fetal breathing movement	Ventral surface of the fourth ventricle	Embryogenesis	↑ Hypoxia
Nonstress test	Posterior hypothalamus, medulla	↓	

From Vintzileos AM, Campbell WA, Ingardia CJ, et al: The fetal biophysical profile and its predictive value. *Obstet Gynecol* 62:271, 1983. Reprinted with permission from The American College of Obstetricians and Gynecologists.

after any single normal parameter was much lower than that in the general population. Conversely, fetuses with any abnormal parameter had a higher death rate than that in the general population, ranging from 58.8/1000 in fetuses with a nonreactive NST, to 142/1000 in the absence of fetal movements. A lack of fetal movements, therefore, was most predictive of fetal demise.

Vintzileos and colleagues<sup>2</sup> assessed 150 high-risk pregnancies using a modified BPP that included placental grading and assigned intermediate scores for fetuses that demonstrated some biophysical activity that was insufficient to meet the criteria used in the Manning study. These authors determined that this modification of the BPP was more accurate in the identification of the hypoxic fetus than any other alternative single method.

Thus, both the original and modified BPP, tested in observational studies, demonstrated an association between abnormal biophysical scores and adverse perinatal outcome. Conversely, it showed an inverse correlation between normal biophysical scores and adverse perinatal outcomes.

### Validation of the Biophysical Profile: Correlation With Perinatal Death

In 1981, Manning and colleagues<sup>13</sup> published the results of a prospective study of the BPP in 1184 high risk patients. Among these patients, six perinatal deaths occurred, giving a perinatal mortality rate of 5.06/1000. This was considerably less than the previously observed perinatal death rate of 65 per 1000 births observed in a similar high-risk population in the same region the previous year.

In 1984, Baskett and colleagues<sup>14</sup> published their findings in using the BPP in the management of 2485 high-risk pregnancies. The overall perinatal mortality was 9.2/1000. However, among those pregnancies with a normal BPP, the perinatal mortality was 1/1000. In the same year, Manning and colleagues<sup>15</sup> published the results of the first randomized controlled trial comparing the BPP (375 patients) with the NST (360 patients). They found that the BPP had higher prediction of low Apgar scores. Although the BPP had higher sensitivity, specificity, and accuracy than the NST, these differences were not statistically significant.

In a study of 29 fetuses with a biophysical score of 0/10, Manning and colleagues<sup>16</sup> found that almost half (48.3%) had a perinatal death. This fetal demise occurred as early as 30 minutes and as long as 11 days after the biophysical score of 0 was obtained. Although there was extremely high morbidity among fetuses with a BPP of zero, some did survive. Thus, a grossly abnormal biophysical score of zero

is not necessarily incompatible with survival after delivery; therefore, inaction based on the assumption that the prognosis is dismal is not justified. Manning et al<sup>17,18</sup> further explored the use of the fetal BPP in evaluating 12,620 high-risk patients. When the BPP score was 8 or more, the perinatal mortality was 0.652 per 1000 tests; and when the biophysical score was very abnormal (score 0), the perinatal mortality rose drastically to 187 per 1000 tests, demonstrating a direct correlation between the biophysical score and perinatal mortality. The corrected false-negative rate was 0.634 per 1000. A subsequent study by the same authors reporting 19,221 high-risk pregnancies<sup>18</sup> found that the incidence of intrauterine death after a normal biophysical score (8 or more) was only 0.726 per 1000. Manning et al,<sup>19</sup> in a study of 26,780 high-risk pregnancies, demonstrated a strong inverse linear correlation between the biophysical score and perinatal morbidity.

These studies, and several subsequent ones tested the BPP in fairly large groups of patients,<sup>20,21</sup> and provided strong evidence of its clinical usefulness, so that today the BPP is widely used in clinical practice.

### PHYSIOLOGIC BASIS FOR THE BIOPHYSICAL PROFILE

Aberrations of fetal health can be divided into those that are chronic and those of acute origin; the fetal BPP is designed to assess both of these. Fetal heart rate reactivity, breathing movements, gross movements, and tone evaluate the state of fetal well-being on an acute basis, whereas the amniotic fluid volume and placental grading evaluate chronic fetal threats to fetal health. For instance, impaired uteroplacental blood and placental dysfunction may lead to redistribution of the fetal cardiac output away from nonvital organs such as the kidney, resulting in decreased fetal urinary output with resultant oligohydramnios. Variable decelerations, on the other hand, most likely reflect acute cord compression.

The individual fetal biophysical activities are dependent on initiation and regulation by specific centers in the central nervous system (CNS) (Table 21-3).<sup>9</sup> Thus, the presence of any given biophysical activity implies intactness of the CNS center that regulates that activity.<sup>9</sup> These individual centers are sensitive to, and can be depressed by, varying degrees of fetal hypoxemia or acidemia.<sup>9</sup> Both animal and human data have demonstrated that these centers cease activity when subjected to hypoxemia at different thresholds for different centers.<sup>22</sup> These centers can also be depressed by medications, injury, or hemorrhage. In addition, biophysical activities are subject to physiologic periodicity, so the absence of a



**Table 21-4****Frequency of Individual Biophysical Variables and Biophysical Scoring of 8 or More in Pregnancies With Intact Membranes (N = 951)**

Biophysical Variable	Week 25-28		Week 29-32		Week 33-36		Week 37-40		Week 41-44
	n = 61 (6.4)	p	n = 192 (20.1)	p	n = 347 (36.4)	p	n = 257 (27.0)	p	n = 94 (9.8)
NST2	22 (36.0)	NS	82 (42.7)	<.01	223 (64.2)	NS	188 (73.1)	NS	77 (81.9)
NST1	19 (31.1)	NS	68 (35.4)	<.01	86 (24.7)	NS	44 (17.1)	NS	9 (9.5)
NST0	20 (32.7)	NS	42 (21.8)	<.01	38 (10.9)	NS	25 (9.7)	NS	8 (8.5)
FBM2	36 (59.0)	NS	143 (74.4)	NS	264 (76.0)	NS	181 (70.4)	<.05	52 (55.3)
FBM1	4 (6.5)	NS	15 (7.8)	NS	31 (8.9)	NS	20 (7.7)	NS	6 (6.3)
FBM0	21 (34.4)	NS	34 (17.7)	NS	52 (14.9)	NS	56 (21.7)	<.05	36 (38.3)
FM2	61 (100)	NS	188 (97.9)	NS	331 (95.3)	NS	242 (94.1)	NS	86 (91.4)
FM1	0	NS	4 (2.0)	NS	14 (4.0)	NS	12 (4.6)	NS	5 (5.3)
FM0	0	NS	0	NS	2 (0.5)	NS	3 (1.1)	NS	3 (3.1)
FT2	61 (100)	NS	182 (94.7)	NS	324 (93.3)	NS	232 (90.2)	NS	79 (84.0)
FT1	0	NS	9 (4.6)	NS	21 (6.0)	NS	24 (9.3)	NS	12 (12.7)
FT0	0	NS	1 (0.5)	NS	2 (0.5)	NS	1 (0.4)	NS	3 (3.1)
AF2	58 (95.0)	NS	189 (98.4)	NS	331 (95.3)	NS	231 (89.8)	<.01	70 (74.4)
AF1	1 (1.6)	NS	3 (1.5)	NS	11 (3.1)	NS	22 (8.5)	<.01	16 (17.0)
AF0	2 (3.2)	NS	0	NS	5 (1.4)	NS	4 (1.5)	<.01	8 (8.5)
PL2	61 (100)	NS	189 (98.4)	NS	321 (92.5)	NS	212 (82.4)	<.01	64 (68.0)
PL1	0	NS	3 (1.5)	NS	12 (3.4)	NS	10 (3.8)	<.01	13 (13.8)
PL0	0	NS	0	<.05	14 (4.0)	NS	35 (13.6)	<.01	17 (18.0)
						<0.01			
						1			
Total score 8 or more	61 (100)	NS	186 (96.8)	NS	341 (98.2)	NS	249 (96.8)	NS	83 (88.2)

AF, amniotic fluid volume; FBM, fetal breathing movements; FM, fetal movements; FT, fetal tone; NS, not significant; NST, nonstress test; PL, placental grading. From Vintzileos AM, Feinstein SJ, Lodeiro JC, et al: Fetal biophysical profile and the effect of premature rupture of the membranes. *Obstet Gynecol* 67:818, 1986. Reprinted with permission from The American College of Obstetricians and Gynecologists.

biophysical activity may not necessarily reflect a state of altered health. At term or near term, the fetus has cycles of periodicity of about 20 minutes; this has been likened to the circadian or diurnal cycle in adults. Thus, the duration of testing should be at least 30 minutes.

### Appearance of the Components of the Biophysical Profile Across Gestational Age

The CNS centers that control the individual biophysical activities start functioning at different times during gestation (see Tables 21-3 and 21-4).<sup>23</sup> For instance, tone, controlled by a center in the cortex-subcortical area, is the earliest biophysical activity to appear during intrauterine life, first being observed at a gestational age of approximately 8 weeks. The next biophysical activity to appear is fetal movement, regulated by a center in the cortex nuclei, appearing at about 9 weeks of gestation; thus, the sonographic observation of both fetal movements and tone are not affected by gestational age, as long as the sonogram is performed after the first trimester. Breathing movements are the next to appear at about 21 weeks. The fetal breathing center is located in the ventral surface of the fourth ventricle. The last of the fetal biophysical activities to appear is fetal heart rate reactivity; this appears late in the second trimester or early in the third trimester, and is regulated in the posterior hypothalamus and medulla. The variations in biophysical components throughout gestation have been described by

Vintzileos et al<sup>23</sup> (see Table 21-4). The frequency of reactive NSTs significantly increases after 32 weeks compared with earlier gestations. In later pregnancy, however, fetal breathing and amniotic fluid volume are decreased after 40 weeks compared with earlier gestations. Grade 3 placentas appear after 32 weeks.<sup>23</sup> In a large study of 11,012 BPPs in 5582 women with normal perinatal outcomes, Baskett and colleagues<sup>24</sup> found that NSTs and fetal breathing movements were likely to be abnormal at 26 to 33 weeks' gestation, compared to pregnancies at later gestations. Similarly, NSTs, amniotic fluid volumes, and fetal breathing movements and tone were more likely to be abnormal after 42 weeks compared with pregnancies at 37 to 41 weeks. Interestingly, Vintzileos et al<sup>23</sup> and Baskett and colleagues<sup>24</sup> found that the overall frequency of reassuring biophysical scores (8 or higher) was not altered by gestational age until 41 weeks, although many of the individual biophysical components changed across gestation.

### The Biophysical Profile and Fetal Acid-Base Status

In order to define the relationship between the BPP and fetal acid-base status, Vintzileos and colleagues<sup>25</sup> performed fetal BPPs on 124 nonlaboring pregnant patients at gestational ages ranging from 26 to 43 weeks immediately before cesarean delivery (Figs. 21-4 through Fig. 21-9). In all cases, umbilical arterial samples were taken for pH at delivery. This methodology avoided the long interval between



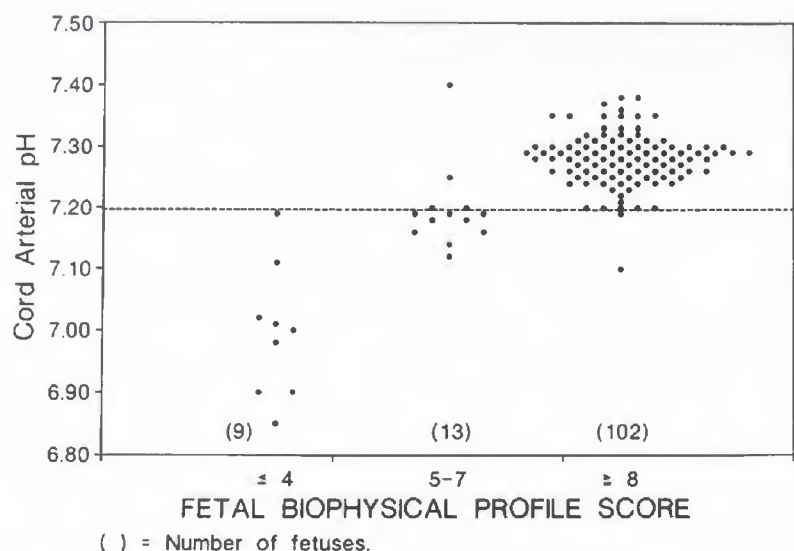


**FIGURE 21-4.** Relationship between the fetal biophysical profile score and cord arterial pH. (From Vintzileos AM, Gaffney SE, Salinger LM, et al: The relationship between fetal biophysical profile and cord pH in patients undergoing cesarean section before the onset of labor. *Obstet Gynecol* 70:196, 1987. Reprinted with permission from The American College of Obstetricians and Gynecology.)

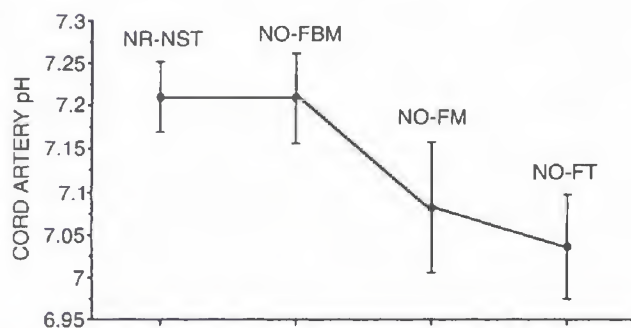


**FIGURE 21-5.** Relationship between cord artery pH and absent fetal biophysical activities. The pH tends to be lower in the absence of movements and/or tone compared with nonreactive nonstress testing or absence of breathing. Results are expressed in means (95% error bars). No FBM, absent fetal breathing; No FM, absent fetal movements; No FT, absent fetal tone; NR NST, nonreactive nonstress test. (From Vintzileos AM, Fleming AD, Scorza WE, et al: Relationship between fetal biophysical activities and umbilical cord blood gases. *Am J Obstet Gynecol* 165:707, 1991.)

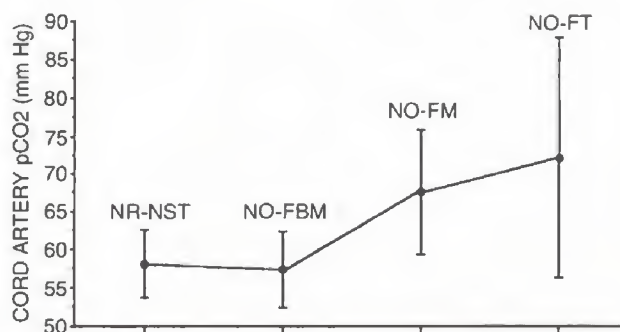


**FIGURE 21-7.** Relationship between cord artery carbon dioxide partial pressure ( $\text{PCO}_2$ ) and absent fetal biophysical activities. The  $\text{PCO}_2$  tends to be higher in the absence of movements or tone compared with nonreactive nonstress testing and absence of breathing. Results are means expressed in millimeters of mercury (95% error bars). No FBM, absent fetal breathing; No FM, absent fetal movements; No FT, absent fetal tone; NR NST, nonreactive nonstress test. (From Vintzileos AM, Fleming AD, Scorza WE, et al: Relationship between fetal biophysical activities and umbilical cord blood gases. *Am J Obstet Gynecol* 165:707, 1991.)

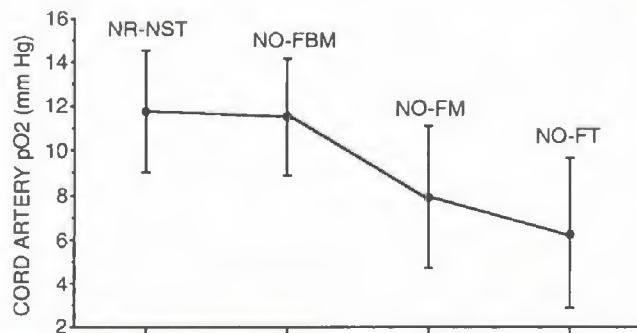


**FIGURE 21-6.** Relationship between cord artery oxygen partial pressure ( $\text{PO}_2$ ) and absent fetal biophysical activities. The  $\text{PO}_2$  tends to be lower in the absence of movements or tone compared with nonreactive nonstress testing and absence of breathing. Results are means expressed in millimeters of mercury (95% error bars). No FBM, absent fetal breathing; No FM, absent fetal movements; No FT, absent fetal tone; NR NST, nonreactive nonstress test. (From Vintzileos AM, Fleming AD, Scorza WE, et al: Relationship between fetal biophysical activities and umbilical cord blood gases. *Am J Obstet Gynecol* 165:707, 1991.)

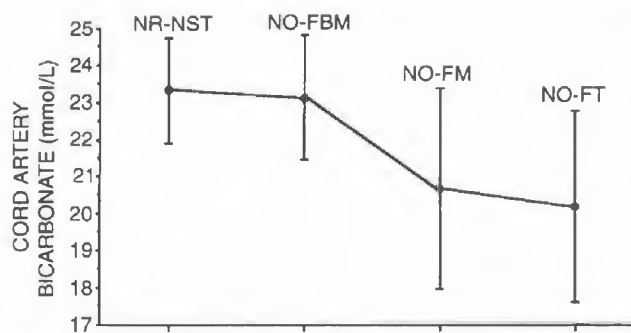


**FIGURE 21-8.** Relationship between cord artery bicarbonate level and absent fetal biophysical activities. The bicarbonate level tends to be lower in the absence of movements or tone compared with nonreactive nonstress testing and absence of breathing. Results are means expressed in millimoles per liter (95% error bars). No FBM, absent fetal breathing; No FM, absent fetal movements; No FT, absent fetal tone; NR NST, nonreactive nonstress test. (From Vintzileos AM, Fleming AD, Scorza WE, et al: Relationship between fetal biophysical activities and umbilical cord blood gases. *Am J Obstet Gynecol* 165:707, 1991.)

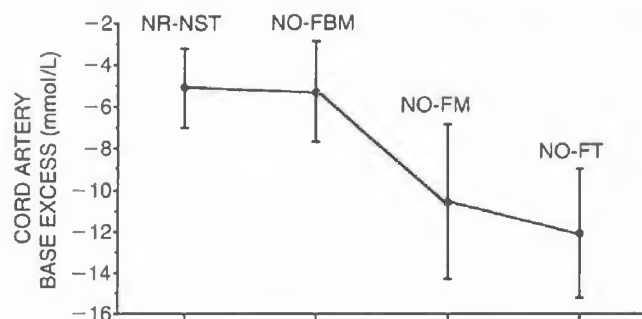


**FIGURE 21-9.** Relationship between cord artery base excess and absent fetal biophysical activities. The base excess tends to be lower in the absence of movements or tone compared with nonreactive nonstress testing and absence of breathing. Results are means expressed in millimoles per liter (95% error bars). No FBM, absent fetal breathing; No FM, absent fetal movements; No FT, absent fetal tone; NR NST, nonreactive nonstress test. (From Vintzileos AM, Fleming AD, Scorza WE, et al: Relationship between fetal biophysical activities and umbilical cord blood gases. *Am J Obstet Gynecol* 165:707, 1991.)

biophysical assessment and delivery observed in prior studies, eliminating the effect of labor and medications on neonatal status. These investigators found the sensitivity, specificity, and positive and negative predictive values of a BPP score of less than 8 for fetal acidemia (defined as an umbilical arterial pH of <7.2) to be 90%, 96%, 82%, and 98%, respectively.<sup>25</sup> Using a combination of only a nonreactive NST and absent fetal breathing movements, they found improved sensitivity, specificity, and positive and negative predictive values for fetal acidemia of 100%, 92%, 71%, and 100%, respectively.<sup>25</sup> When movements and tone were both absent (in seven fetuses), the mean cord pH was  $6.95 \pm 0.06$ . As the neonatal umbilical arterial pH values became lower, fetal biophysical activities disappeared sequentially (see Fig. 21-5).

## The Gradual Hypoxia Concept

Vintzileos and colleagues were the first to make the observation that the biophysical activities that appear first during fetal life are the last to disappear when there is fetal asphyxia or intra-amniotic infection.<sup>25</sup> They termed this the gradual hypoxia concept.<sup>8,25-27</sup> The first biophysical activities to become compromised in the presence of fetal acidemia are fetal heart rate reactivity and fetal breathing movements; these are the last biophysical activities to appear in intrauterine development (see Fig. 21-5). As fetal acidemia progresses, fetal body movements and then fetal tone sequentially become absent (see Fig. 21-5).<sup>27</sup> In fetuses with normal movements and tone but a nonreactive NST and no breathing, the incidence of acidemia was 59%, whereas fetuses with a nonreactive NST, no breathing movements, and compromised body movements and tone had an incidence of acidemia of 75%. This suggests that fetuses with no breathing movements and a nonreactive NST were more likely to be acidemic when there were no fetal movements and absent fetal tone.<sup>25</sup> These findings provide further support for the gradual hypoxia concept. All fetuses with the absence of all four biophysical activities had umbilical cord arterial pH values in the acidemic range.<sup>25</sup>

Thus, when the umbilical arterial pH drops below 7.20, fetal heart rate reactivity and fetal breathing movements are abolished (see Fig. 21-5). A pH value between 7.10 and 7.20 is associated with compromised fetal body movements and fetal tone, whereas pH values lower than 7.10 are associated with absent body movements and tone (see Fig. 21-5).<sup>25</sup> When, in addition to fetal heart rate nonreactivity and absence of fetal breathing, fetal body movements and tone were absent, perinatal mortality rose to 100%.<sup>2</sup> Thus, the presence of a given biophysical activity during sonography provides important information and implies absence of malfunction of the fetal CNS center that regulates that activity, thus indirectly ruling out fetal acidemia.

## The Implications of the Gradual Hypoxia Concept on the Interpretation of the Biophysical Profile

The gradual hypoxia concept brings into question the arbitrary assignment of equal weights of the individual activities in predicting fetal asphyxia in the fetal BPP. Because the individual components become compromised at different levels of fetal acidemia, it has been proposed that the overall score is less important than the results of the individual components. For instance, the presence of fetal breathing movements rules out fetal acidemia (pH <7.2). The absence of fetal movements and tone, when there are absent fetal breathing movements, if periodicity or other causes have been ruled out, suggest profound fetal compromise, and carry an increased risk of mortality or morbidity.

Manning and colleagues<sup>28</sup> also questioned the use of an equal score for each biophysical component. Perinatal morbidity outcomes of 525 fetuses were studied and compared with the last total abnormal biophysical score, as well as examining the individual score composition.<sup>28</sup> These investigators found that the accuracy of the score in predicting outcome depended primarily on the combination of the individual biophysical components rather than the total score. They found, as we had, that fetal heart rate reactivity (NST), amniotic fluid volume, and fetal breathing movements were the most powerful indicators of perinatal outcome.<sup>28</sup>

Several studies demonstrated a strong association between reduced amniotic fluid volume and an increased risk of adverse perinatal outcome in a dose-response fashion.<sup>1,2,29,30</sup> Chamberlain et al<sup>29</sup> found that patients with normal amniotic fluid volume (largest vertical pocket between 2 and 8 cm) had a perinatal mortality rate of 1.97 per 1000, whereas patients with marginal amniotic fluid volume (largest pocket 1 to 2 cm) and severe oligohydramnios (largest pocket <1 cm) had perinatal mortality rates of 37.7 per 1000 and 109.4 per 1000, respectively. Grade 3 placentas have been associated with an increased incidence of abnormal fetal heart rate patterns (44.4%) and abruptio placentae (14.8%) during labor.<sup>2</sup> Thus, placental grading is considered a chronic marker of fetal well-being, and some have included it in modifications of the BPP.<sup>2</sup>

In interpreting the BPP, however, it is important first to exclude normal periodicity or administration of medications that have a depressant effect on biophysical activities as



being responsible for the abnormal results. Thus, the diagnosis of acidemia should only be made after exclusion of other causes for the abnormal test.

### The Effect of Preterm Premature Rupture of the Membranes on the Biophysical Profile

Vintzileos et al<sup>23</sup> compared BPPs from 25 to 44 weeks between patients with intact membranes and patients with preterm premature rupture of the membranes (PPROM) of comparable gestational ages. Both groups had a similar frequency of reassuring biophysical scores (equal to 8) regardless of membrane status, suggesting that the same conclusions could be drawn from the BPP score regardless of whether or not the membranes were ruptured. However, as far as the individual BPP components were concerned, PPRM was associated with increased fetal heart rate reactivity when compared with gestations with intact membranes.<sup>23</sup> Conversely, gestations with PPRM had a decrease in fetal breathing movements, and amniotic fluid volume in comparison with those gestations without PPRM.<sup>23</sup> However, there was no significant difference in fetal body movements or fetal tone between the groups, nor was there any change in the overall biophysical score between both groups. It is important to be aware of these alterations in fetal biophysical activities in patients with PPRM to avoid inappropriate interpretation of BPP results and unnecessary interventions in these patients.

### The Role of the Nonstress Test in the Biophysical Profile

Manning and co-workers carried out a study evaluating only the ultrasound-monitored components of the BPP without including the NST, using the NST only if one or more of the ultrasound components were abnormal.<sup>31</sup> With this method, only 2.7% of 2712 tested patients required an NST, with no compromise in perinatal outcomes.<sup>31</sup> The practice of omitting the NST was subsequently challenged by Eden et al,<sup>32</sup> who found an increased incidence of abnormal perinatal outcome in fetuses with variable decelerations during NST testing despite normal ultrasound monitored biophysical components.<sup>32</sup> Mills and colleagues<sup>33</sup> evaluated 500 high-risk pregnancies with 2038 BPPs, and concluded no biophysical assessment was necessary when fetal growth was normal, but recommended twice-weekly NSTs and ultrasound assessment of fetal growth every 2 weeks in cases in which there was abnormal fetal growth. They suggested that the fetal BPP should be reserved for cases with abnormal or equivocal NST results. It is our practice to perform the NST as an integral part of our BPP.

### The Biophysical Profile in the Management of High-Risk Pregnancy

The BPP has been studied in the evaluation of several specific high-risk conditions including postdate pregnancy,<sup>34</sup> diabetes mellitus,<sup>35</sup> intrauterine growth restriction,<sup>36,37</sup> twin pregnancy,<sup>38</sup> and PPRM.<sup>39,40</sup> Johnson and colleagues<sup>34</sup> found, in a study of the BPP in 307 postdate patients, that a

normal biophysical score was associated with a higher rate of nonintervention and, therefore, increased rates of spontaneous onset of labor. This consequently resulted in a reduction in cesarean delivery rates (15% versus 42% for patients who underwent induction of labor).<sup>34</sup> In a later study of 238 diabetic pregnancies, the same group of investigators found that fetuses with abnormal BPP scores had higher rates of intensive care nursery admissions, cesarean section (50%), operative intervention, and neonatal morbidity.<sup>35</sup> Lodero et al,<sup>38</sup> evaluating high-risk twin pregnancies, found the sensitivity, specificity, and positive and negative predictive values of the biophysical score in predicting fetal distress to be 83.3%, 100%, 100%, and 97.7%, respectively. Data from Manning et al<sup>41</sup> suggest the incidence of cerebral palsy is lower in populations tested with the BPP, compared with populations in which BPP testing was not instituted. Although encouraging, these patients were monitored with other measures in addition to the BPP; therefore, the question still remains as to whether the decreased cerebral palsy rate was due solely to biophysical score assessment.<sup>41</sup>

The BPP is also a powerful tool in the evaluation of the growth-restricted fetus. Odibo and colleagues<sup>37</sup> evaluated the fetal surveillance modalities available for antepartum surveillance of the growth-restricted fetus, and concluded that the BPP was the optimal test. Ribbert and colleagues<sup>42,43</sup> examined the relationship between fetal BPP results and cord blood gases from cordocentesis. These investigators found that fetal heart rate reactivity was compromised when the difference between the expected and observed pH) was below 2 standard deviations (SD). Fetal breathing movements were compromised at pH values below 3 SD, and fetal body movements and fetal tone were both absent at pH values at or below 5 SD. The authors also concluded that fetal acidemia in initial stages causes fetal heart rate nonreactivity and abolishes fetal breathing movements, whereas absence of body movements and tone are late manifestations of fetal asphyxia. These findings are consistent with the gradual hypoxia concept.

### A Proposed Algorithm for Using the Biophysical Profile in Clinical Practice

We present a suggested algorithm for using the BPP based on the gradual hypoxia concept in Figure 21-10.

The modified BPP describes a testing scheme using the NST with an evaluation of the amniotic fluid. Thus, this modification assesses both the most sensitive acute marker (fetal heart rate tracing) and chronic marker (amniotic fluid volume) of fetal well-being. The perinatal morbidity and mortality of the modified BPP compares favorably with that of the complete BPP<sup>20,21</sup> (see Fig. 21-10). Of course, depending on the specific clinical situation, Doppler studies, including those of the uterine, umbilical, middle cerebral arteries, and the ductus venosus can also be helpful. The specific criteria used to define normal versus abnormal biophysical activities are illustrated in Table 21-5. Because fetal acidemia is ruled out when the NST is reactive, fetal examination should always start with an NST and evaluation of amniotic fluid volume. If, however, the NST is nonreactive for 40 minutes, real-time ultrasonography is performed. Because fetal breathing movements lasting more than



30 seconds are as accurate as a reactive NST in excluding fetal acidemia, once fetal breathing movements lasting more than 30 seconds are detected, the examination is terminated. If during a 30-minute real-time observation, however, all biophysical activities are absent, delivery should take place promptly. When the NST is nonreactive and there are no detectable fetal breathing movements or breathing movements lasting less than 30 seconds, extended testing is performed to differentiate between fetal asphyxia and fetal sleep. The amniotic fluid volume is always evaluated regardless of

the NST results. Oligohydramnios in term or near-term gestations, as well as in pregnancies complicated by intrauterine growth restriction is considered abnormal, and it is prudent to deliver women with oligohydramnios to avoid cord accident and in utero death. In very preterm gestations with oligohydramnios, however, delivery may be associated with high perinatal mortality due to prematurity. At gestational ages less than 26 weeks, each day of prolongation of gestation may be associated with increase in survival of 2% to 3%. Therefore, it is desirable to delay delivery as long as safely possible. In these cases, close fetal surveillance is mandatory with BPPs and fetal heart rate monitoring at least once a day. Doppler velocimetry of the uteroplacental circulation should be used in the management of preterm high-risk fetuses, especially those with intrauterine growth restriction. However, many fetuses at risk (that is, fetuses of diabetic mothers or postdate fetuses) do not suffer from reduced blood flow but from gas exchange disturbances at the trophoblastic membrane level; in these cases, it is unlikely that fetal Doppler velocimetry will be helpful.

Miller et al<sup>21</sup> evaluated the false-positive and false-negative rates of their antepartum testing results using the modified BPP. Over a 4-year period, they reported on 54,617 modified BPPs performed on 15,482 patients. The false-negative rate was 0.08%. The false-positive rate was 60%; however, intervention resulting from a false-positive test resulted in iatrogenic prematurity in only 1.5% of cases. Nageotte et al<sup>20</sup> compared the modified BPP with the contraction stress test. They evaluated the outcomes of high-risk patients who had a negative modified BPP with those whose last antepartum assessment was a negative contraction stress test. Patients managed by the modified BPP had a lower incidence of adverse perinatal outcomes after reassuring testing (5.1% versus 7.0%,  $p < .05$ ). In our experience using the modified BPP, intrauterine deaths of structurally normal fetuses occurring after a reassuring assessment is a rarity. In addition, this protocol has decreased the testing time, increased the number of tested patients, and, therefore, improved the efficiency of our unit. Management on the basis of the total BPP score rather than the individual biophysical components can result in misuse of this testing method. The most

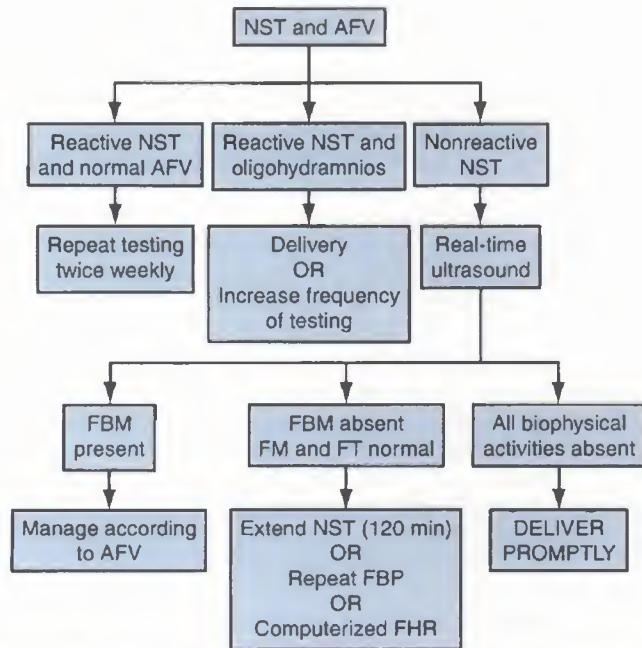


**FIGURE 21-10.** Modified fetal biophysical profile. AFV, amniotic fluid volume; FBM, fetal breathing movements; FM, fetal movements; FT, fetal tone; FHR, fetal heart rate; NST, nonstress test. (Redrawn with permission from Hanley ML, Vintzileos AM: *Antepartum and Intrapartum Surveillance of Fetal Well Being. Medicine of the Fetus and Mother*, 2nd ed, Philadelphia, J.B. Lippincott, 1988, p 793.)

**Table 21-5** Definition of Normal and Abnormal Biophysical Components

Component	Normal	Abnormal
Nonstress test accelerations	Two or more FHR accelerations (15 bpm for 15 seconds) in 20 minutes	One or fewer FHR in 20 minutes
FBM lasting	At least one episode of 30 seconds of confirmed breathing	Absence of FBM or FBM less than 30 seconds
FM	At least three trunk movements	Compromised: 1 to 2 FM
Absent: no FM		
Fetal tone	At least one episode of extensions of extremities with return to flexion and at least one episode of extension of spine with return to position of flexion	Compromised: only one episode of extension and flexion
Absent; absence of extension, flexion, open hand		
Amniotic fluid volume	Largest amniotic fluid pocket $\geq 2$ cm	Largest amniotic fluid less than 2 cm

FBM, fetal breathing movements; FHR, fetal heart rate; FM, fetal movements.

Reprinted with permission from Hanley ML, Vintzileos AM: Biophysical testing in premature rupture of the membranes. *Semin Perinatol* 20:418, 1996.



frequent errors in interpreting and applying fetal biophysical assessment data have been described in detail.<sup>8</sup>

### The Role of the Fetal Biophysical Profile in Detecting Intra-Amniotic Infection in Patients With Preterm Premature Rupture of the Membranes

PPROM is a leading cause of preterm birth and perinatal mortality and morbidity. When there is extreme prematurity, attempts are generally made for conservative management, prolonging gestation, with the hope of improving perinatal outcomes. However, there is often intra-amniotic infection, which jeopardizes the health of the fetus and mother. Intra-amniotic infection is an indication for delivery; yet, the commonly used modalities are imprecise in diagnosing intra-amniotic infection. Vintzileos et al<sup>44</sup> were the first to publish an association between abnormal fetal biophysical assessment and intra-amniotic infection in this group of patients. The initial study was observational, and the results from the biophysical assessment were not used for management.<sup>44</sup> Patients with PPRM were monitored with frequent (every 1 to 3 days) BPPs. None of the patients had any clinical signs of infection or labor at the time of ultrasound examination. The last BPP before delivery was correlated with the development of clinical infection. In the cases in which the interval between the last biophysical assessment and delivery was less than 24 hours, an abnormal BPP was associated with an overall infection rate of 93.7%; in contrast, a normal BPP was associated with an overall infection rate of 2.7%.<sup>44</sup> This strong correlation between BPP score and infectious morbidity did not exist when the testing-delivery interval was greater than 24 hours.<sup>44</sup> An interesting observation was that the earliest manifestations of intra-amniotic infection included a nonreactive NST and absence of fetal breathing, whereas advanced infection (fetuses that subsequently developed neonatal sepsis) was associated with compromise of both fetal body movements and tone.<sup>44</sup> There were no cord pH differences between infected and noninfected cases; thus, the diminished biophysical activities were attributed to infection and not acidemia. Further

studies by Vintzileos and colleagues<sup>39,40</sup> have demonstrated the use of the BPP in the management of PPRM.

At least 11 further studies, none of which were randomized or controlled, have evaluated the relationship between BPP assessment and infectious outcome in patients with PPRM.<sup>45-54</sup> There are summarized in Table 21-6. Eight of the 12 studies demonstrated an association between abnormal biophysical assessment and infectious outcomes. It is important to note that testing was done on a daily basis in those studies that demonstrated a correlation.

Five studies failed to demonstrate an association between abnormal biophysical assessment and infectious outcome. Miller et al<sup>45</sup> evaluated 47 patients with PPRM and did not find an association between clinical chorioamnionitis and the BPP performed within 2 days of delivery. There were no cases of fetal or neonatal sepsis in their study, and testing was performed at a frequency of 24 to 48 hours. Although it may be that clinical chorioamnionitis alone is not associated with abnormal BPP assessment, the testing frequency in this study was not optimal. Del Valle et al<sup>48</sup> evaluated the association between BPP assessment with regard to maternal amnionitis and neonatal sepsis. However, in this study, the frequency of testing was 48 to 72 hours, and the overall infection rate was low. In the third study by Carroll et al,<sup>53</sup> intra-amniotic infection as diagnosed by amniocentesis and cordocentesis was used as the outcome measure. They found no correlation between positive cultures and biophysical assessment. However, the majority of positive cultures were with *Mycoplasma* species.

In summary, the data suggest that the correlation between abnormal BPP and infectious perinatal outcome depends on the BPP being performed within 24 hours of delivery. In addition, colonization of the amniotic cavity with the *Mycoplasma* is not necessarily associated with an abnormal BPP evaluation.

We carried out a prospective study of 73 patients with PPRM, in which the BPP results were used for management.<sup>40</sup> Their outcomes were compared with two other historic groups, one managed without any invasive or fetal evaluation (control group) and the other managed with amniocentesis alone. We found that the group managed based on their BPP results developed significantly fewer

**Table 21-6 Fetal Biophysical Profile Studies in PROM**

Author (Year)	Outcome Measure	Frequency of Testing	Correlation
Vintzileos et al (1985) <sup>44</sup>	Clinical infection	Daily	Yes
Vintzileos et al (1986) <sup>39</sup>	Clinical infection	Daily	Yes
Roussis et al (1991) <sup>49</sup>	Clinical infection	Daily	Yes
Mercer et al (1991) <sup>54</sup>	Clinical infection	Daily × 5 days	Yes
Fleming et al (1991) <sup>47</sup>	Histologic chorioamnionitis	Daily	Yes
Goldstein et al (1988) <sup>51</sup>	IAI	Daily	Yes
Roberts et al (1991) <sup>52</sup>	IAI	Daily	Yes
Gauthier et al (1992) <sup>46</sup>	IAI	—	Yes
Miller et al (1990) <sup>45</sup>	Clinical infection	48 hours	No
Del Valle et al (1992) <sup>48</sup>	Clinical infection	48-72 hours	No
Carroll et al (1995) <sup>53</sup>	IAI	—	No
Ghidini et al (2000) <sup>50</sup>	Histologic chorioamnionitis	—	No



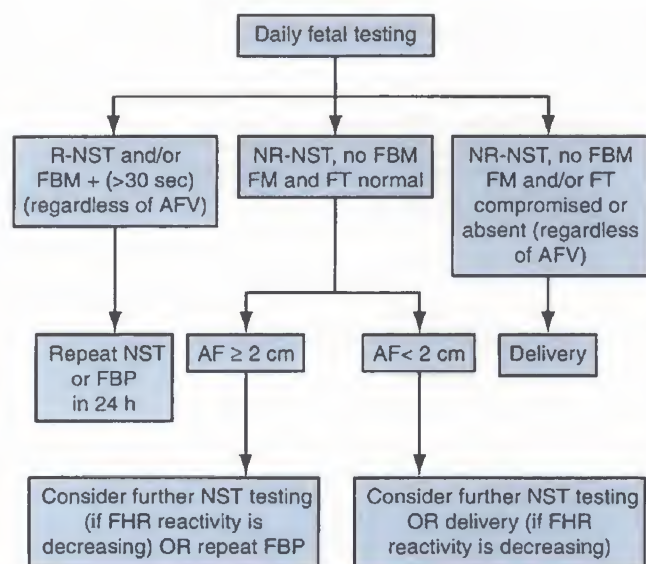


**FIGURE 21-11.** Fetal surveillance in premature rupture of the membranes. AF, amniotic fluid (largest vertical pocket); AFV, amniotic fluid volume; FBP, fetal biophysical profile; FBM +, fetal breathing present; FHR, fetal heart rate; FM, fetal movements; FT, fetal tone; NR-NST, nonreactive nonstress test; R-NST, reactive nonstress test. (Redrawn with permission from Hanley ML, Vintzileos AM: *Antepartum and Intrapartum Surveillance of Fetal Well Being*. Medicine of the Fetus and Mother, 2nd ed, Philadelphia, J.B. Lippincott, 1998, p 793.)

maternal and neonatal infections. Clinical amnionitis, possible neonatal sepsis, and neonatal sepsis occurred in 5.4%, 5.4%, and 1.4%, respectively, in the study group compared with 25.5%, 13.6%, and 9.5%, respectively, in the control group.<sup>40</sup> Neonatal sepsis was also less in the study group (1.3%) compared with the group managed by amniocentesis (12.3%). Figure 21-11 illustrates a protocol based on the individual biophysical components rather than on the total score for managing patients with PPROM. Again, the BPP or NST testing of these patients needs to be performed daily to predict infectious outcomes (see Fig. 21-11).

In a study of 53 patients with PPROM whose only indication for delivery was an abnormal biophysical assessment, only five of the 15 fetuses in whom neonatal sepsis subsequently developed were born acidemic.<sup>10</sup> The remaining 10 septic neonates as well as all 17 with possible neonatal sepsis were born with normal cord blood pH values, suggesting that acidemia does not play a major role in diminishing the fetal biophysical activities in the setting of intra-amniotic infection. It has been postulated that increased prostaglandin production from phospholipase A<sub>2</sub>-producing bacteria or cytokines such as interleukin or tumor necrosis factors may cause hemodynamic changes of the fetal placental unit through vasoconstriction of the umbilical and chorionic vessels.

## The Effects of Medications on the Biophysical Profile

A variety of medications that are commonly used in obstetric practice have significant effects on the BPP (Tables 21-7 through 21-10). The corticosteroids (dexamethasone

**Table 21-7**

### Studies on the Effects of Corticosteroids on Fetal Biophysical Activities

12/12 studies found decreased FHR reactivity (days 1 to 3)  
8/8 studies found decreased FBM (days 1 to 2)  
10/10 studies found decreased FM (days 1 to 2)  
3/3 studies found no change in FT  
1/4 studies found decreased BPP scores (days 1 to 3)  
4/4 studies found decreased BPP scores (days 1 to 3)  
BPP scores returned to baseline by day 4 (96 hours)  
Betamethasone had more pronounced fetal effects than dexamethasone

BPP, biophysical profile; FBM, fetal breathing movements; FHR, fetal heart rate; FM, fetal movements; FT, fetal tone.

**Table 21-8**

### Effects of Corticosteroids on Biophysical Activities\*

Fetal heart rate, reactivity ↓  
Fetal breathing movements ↓  
Fetal tone, no change  
Amniotic fluid volume, no change or ↓

\*Corticosteroids can cause false positive biophysical exams

**Table 21-9**

### Overall Effects of Magnesium Sulfate on Fetal Biophysical Activities

5 studies found clinically significant decreased FHR reactivity with magnesium levels 6–8 mg/dl in preterm fetuses  
2 studies found clinically insignificant decreased FHR reactivity with magnesium levels less than 6 mg/dl in term fetuses  
1 study found no effect on FHR reactivity  
2 studies found decreased FBM movements  
1 study found no effect on FBM  
3/3 studies found no effect on FM  
3/3 studies found no effect on FT  
2/2 studies found no effect on AF

AF, amniotic fluid volume; FBM, fetal breathing movements; FHR, fetal heart rate; FM, fetal movements; FT, fetal tone.

and betamethasone) are given in preterm gestations at risk of delivery, in order to promote fetal lung maturation. Reductions in fetal breathing, fetal heart rate reactivity/variability, and fetal movements are observed within 48 hours following steroid administration in at least one third of fetuses (see Tables 21-7 and 21-8).<sup>55–59</sup> Interestingly, Jackson and colleagues<sup>57</sup> found a reduction in amniotic fluid volume within 72 hours of steroid administration and attributed this to decreased fetal breathing movements. Our group studied the effects of magnesium sulfate, the tocolytic used most commonly in the United States, on the BPP in 25 fetuses and found that this medication did not significantly



**Table 21–10** Effects of Intravenous Magnesium Sulfate on Biophysical Activities\*

Fetal heart rate, reactivity ↓
Fetal breathing movements ↓
Fetal tone, no change
Amniotic fluid volume, no change

\*Magnesium sulfate can cause false-positive biophysical examinations.

alter the BPP.<sup>60</sup> Similarly, both Carlan<sup>61</sup> and Peaceman<sup>62,63</sup> and their coworkers found that although magnesium sulfate decreased fetal heart reactivity and breathing movements, it had no effects on the other sonographically monitored BPP parameters (see Tables 21–9 and 21–10). Hallak and coworkers<sup>63</sup> studied the effects of terbutaline and indomethacin, two other widely used tocolytics, on the BPP in 30 low-risk patients between 26 and 32 weeks of gestation with no signs of preterm labor. They found an increase in breathing movements, but no change in body movements. Studies evaluating the effects of magnesium sulfate on the BPP are summarized in Table 21–10.

If one is not aware of the effects of medications on the BPP, inappropriate interpretation of the results may occur resulting in the possibility of iatrogenic and unnecessary premature delivery. Conversely, it will help prevent erroneously attributing an abnormal BPP to administration of medications that do not affect the BPP.

## CONCLUSION

The BPP is a powerful tool in the evaluation of fetal well-being, and evaluates the intactness of the CNS centers responsible for the individual biophysical activities. The BPP assesses both acute and chronic markers of fetal well-being; understanding the pathophysiologic basis for the BPP, using proper technique in its performance, and correct interpretation and intervention based on the results are crucial to its accuracy in predicting fetal status and ensuring optimal perinatal outcomes. In the majority of cases, a modified BPP, assessing fetal heart rate reactivity, and amniotic fluid volume are adequate for assessment of the fetal status. The presence of fetal breathing movements essentially rules out fetal academia. Finally, it is not the absolute score per se but rather the individual components that determine outcomes.

## References

- Manning FA, Platt LD, Sipos L: Antepartum fetal evaluation: Development of a fetal biophysical profile. *Am J Obstet Gynecol* 136:787, 1980.
- Vintzileos AM, Campbell WA, Ingardia CJ, et al: The fetal biophysical profile and its predictive value. *Obstet Gynecol* 62:271, 1983.
- Kontopoulos EV, Vintzileos AM: Condition-specific antepartum fetal testing. *Am J Obstet Gynecol* 191:1546, 2004.
- Evertson LR, Gauthier RJ, Schiffrin BS, et al: Antepartum fetal heart rate testing. I. Evolution of the nonstress test. *Am J Obstet Gynecol* 133:29, 1979.
- Schiffrin BS, Guntz V, Gergely RC, et al: The role of real-time scanning in antenatal fetal surveillance. *Am J Obstet Gynecol* 140:525, 1981.
- Gauthier RJ, Evertson LR, Paul RH: Antepartum fetal heart rate testing. II. Intrapartum fetal heart rate observation and newborn outcome following a positive contraction stress test. *Am J Obstet Gynecol* 133:34, 1979.
- National Institute of Child Health and Human Development Research Planning Workshop. Electronic fetal heart rate monitoring: Research guidelines for interpretation. *Am J Obstet Gynecol* 177:1385, 1997.
- Vintzileos AM, Campbell WA, Nochimson DJ, et al: The use and misuse of the fetal biophysical profile. *Am J Obstet Gynecol* 156:527, 1987.
- Manning FA: Fetal biophysical profile. *Obstet Gynecol Clin North Am* 26:557, 1999.
- Pinette MG, Blackstone J, Wax JR, Cartin A: Using fetal acoustic stimulation to shorten the biophysical profile. *J Clin Ultrasound* 33:223, 2005.
- Manning FA: Assessment of fetal condition and risk: analysis of single and combined biophysical variable monitoring. *Semin Perinatol* 9:168, 1985.
- Manning FA, Platt LD, Sipos L, et al: Fetal breathing movements and the nonstress test in high-risk pregnancies. *Am J Obstet Gynecol* 179:135:511-5.
- Manning FA, Baskett TF, Morrison I, et al: Fetal biophysical profile scoring: A prospective study in 1,184 high-risk patients. *Am J Obstet Gynecol* 140:289, 1981.
- Baskett TF, Gray JH, Prewett SJ, et al: Antepartum fetal assessment using a fetal biophysical profile score. *Am J Obstet Gynecol* 148:630, 1984.
- Manning FA, Lange IR, Morrison I, et al: Fetal biophysical profile score and the nonstress test: a comparative trial. *Obstet Gynecol* 64:326, 1984.
- Manning FA, Harman CR, Morrison I, et al: Fetal assessment based on fetal biophysical profile scoring. III. Positive predictive accuracy of the very abnormal test (biophysical profile score = 0). *Am J Obstet Gynecol* 162:398, 1990.
- Manning FA, Morrison I, Lange IR, et al: Fetal assessment based on fetal biophysical profile scoring: experience in 12,620 referred high-risk pregnancies. I. Perinatal mortality by frequency and etiology. *Am J Obstet Gynecol* 151:343, 1985.
- Manning FA, Morrison I, Harman CR, et al: Fetal assessment based on fetal biophysical profile scoring: experience in 19,221 referred high-risk pregnancies. II. An analysis of false-negative fetal deaths. *Am J Obstet Gynecol* 157:880, 1987.
- Manning FA, Harman CR, Morrison I, et al: Fetal assessment based on fetal biophysical profile scoring. IV. An analysis of perinatal morbidity and mortality. *Am J Obstet Gynecol* 162:703, 1990.
- Nageotte MP, Towers CV, Asrat T, et al: Perinatal outcome with the modified biophysical profile. *Am J Obstet Gynecol* 170:1672, 1994.
- Miller DA, Rabello YA, Paul RH: The modified biophysical profile: Antepartum testing in the 1990s. *Am J Obstet Gynecol* 174:812, 1996.
- Dawes S, Fox H: Respiratory movements and paradoxical sleep in the fetal lamb. *J Physiol (London)* 210:47, 1970.
- Vintzileos AM, Feinstein SJ, Lodeiro JG, et al: Fetal biophysical profile and the effect of premature rupture of the membranes. *Obstet Gynecol* 67:818, 1986.
- Baskett TF: Gestational age and fetal biophysical assessment. *Am J Obstet Gynecol* 158:332, 1988.
- Vintzileos AM, Gaffney SE, Salinger LM, et al: The relationship between fetal biophysical profile and cord pH in patients undergoing cesarean section before the onset of labor. *Obstet Gynecol* 70:196, 1987.
- Vintzileos AM, Gaffney SE, Salinger LM, et al: The relationships among the fetal biophysical profile, umbilical cord pH, and Apgar scores. *Am J Obstet Gynecol* 157:627, 1987.
- Vintzileos AM, Fleming AD, Scorza WE, et al: Relationship between fetal biophysical activities and umbilical cord blood gas values. *Am J Obstet Gynecol* 165:707, 1991.
- Manning FA, Morrison I, Harman CR, et al: The abnormal fetal biophysical profile score. V. Predictive accuracy according to score composition. *Am J Obstet Gynecol* 162:918, 1990.
- Chamberlain PF, Manning FA, Morrison I, et al: Ultrasound evaluation of amniotic fluid volume. II. The relationship of increased amniotic fluid volume to perinatal outcome. *Am J Obstet Gynecol* 150:250, 1984.
- Vintzileos AM, Campbell WA, Nochimson DJ, et al: Degree of oligohydramnios and pregnancy outcome in patients with premature rupture of the membranes. *Obstet Gynecol* 66:162, 1985.

31. Manning FA, Morrison I, Lange IR, et al: Fetal biophysical profile scoring: Selective use of the nonstress test. *Am J Obstet Gynecol* 156:709, 1987.
32. Eden RD, Seifert LS, Kodack LD, et al: A modified biophysical profile for antenatal fetal surveillance. *Obstet Gynecol* 71:365, 1988.
33. Mills MS, James DK, Slade S: Two-tier approach to biophysical assessment of the fetus. *Am J Obstet Gynecol* 163:12, 1990.
34. Johnson JM, Harman CR, Lange IR, et al: Biophysical profile scoring in the management of the postterm pregnancy: An analysis of 307 patients. *Am J Obstet Gynecol* 154:269, 1986.
35. Johnson JM, Lange IR, Harman CR, et al: Biophysical profile scoring in the management of the diabetic pregnancy. *Obstet Gynecol* 72:841, 1988.
36. Habek D, Hodek B, Herman R, et al: Fetal biophysical profile and cerebro-umbilical ratio in assessment of perinatal outcome in growth-restricted fetuses. *Fetal Diagn Ther* 18:12, 2003.
37. Odibo AO, Quinones JN, Lawrence-Cleary K, et al: What antepartum fetal test should guide the timing of delivery of the preterm growth-restricted fetus? A decision-analysis. *Am J Obstet Gynecol* 191:1477, 2004.
38. Lodeiro JC, Vintzileos AM, Feinstein SJ, et al: Fetal biophysical profile in twin gestations. *Obstet Gynecol* 67:824, 1986.
39. Vintzileos AM, Campbell WA, Nochimson DJ, et al: Fetal biophysical profile versus amniocentesis in predicting infection in preterm premature rupture of the membranes. *Obstet Gynecol* 68:488, 1986.
40. Vintzileos AM, Bors-Koefoed R, Pelegano JF, et al: The use of fetal biophysical profile improves pregnancy outcome in premature rupture of the membranes. *Am J Obstet Gynecol* 157:236, 1987.
41. Manning FA, Bondagji N, Harman CR, et al: Fetal assessment based on the fetal biophysical profile score: Relationship of last BPS result to subsequent cerebral palsy. *J Gynecol Obstet Biol Reprod (Paris)* 26:720, 1997.
42. Ribbert LS, Nicolaides KH, Visser GH: Prediction of fetal acidemia in intrauterine growth retardation: Comparison of quantified fetal activity with biophysical profile score. *Br J Obstet Gynaecol* 100:653, 1993.
43. Ribbert LS, Stuinders RJ, Nicolaides KH, et al: Relationship of fetal biophysical profile and blood gas values at cordocentesis in severely growth-retarded fetuses. *Am J Obstet Gynecol* 163:569, 1990.
44. Vintzileos AM, Campbell WA, Nochimson DJ, et al: The fetal biophysical profile in patients with premature rupture of the membranes—An early predictor of fetal infection. *Am J Obstet Gynecol* 152:510, 1985.
45. Miller JM Jr, Kho MS, Brown HL, et al: Clinical chorioamnionitis is not predicted by an ultrasonic biophysical profile in patients with premature rupture of membranes. *Obstet Gynecol* 76:1051, 1990.
46. Gauthier DW, Meyer WJ, Bieniarz A: Biophysical profile as a predictor of amniotic fluid culture results. *Obstet Gynecol* 80:102, 1992.
47. Fleming AD, Salafia CM, Vintzileos AM, et al: The relationships among umbilical artery velocimetry, fetal biophysical profile, and placental inflammation in preterm premature rupture of the membranes. *Am J Obstet Gynecol* 164:38, 1991.
48. Del Valle GO, Joffe GM, Izquierdo LA, et al: The biophysical profile and the nonstress test: Poor predictors of chorioamnionitis and fetal infection in prolonged preterm premature rupture of membranes. *Obstet Gynecol* 80:106, 1992.
49. Roussis P, Rosemond RL, Glass C, et al: Preterm premature rupture of membranes: Detection of infection. *Am J Obstet Gynecol* 165:1099, 1991.
50. Ghidini A, Salafia CM, Kim V, et al: Biophysical profile in predicting acute ascending infection in preterm rupture of membranes before 32 weeks. *Obstet Gynecol* 96:201, 2000.
51. Goldstein I, Romero R, Merrill S, et al: Fetal body and breathing movements as predictors of intraamniotic infection in preterm premature rupture of membranes. *Am J Obstet Gynecol* 159:363, 1988.
52. Roberts AB, Goldstein I, Romero R, et al: Comparison of total fetal activity measurement with the biophysical profile in predicting intra-amniotic infection in preterm premature rupture of membranes. *Ultrasound Obstet Gynecol* 1:36, 1991.
53. Carroll SG, Papaioannou S, Nicolaides KH: Assessment of fetal activity and amniotic fluid volume in the prediction of intrauterine infection in preterm prelabor amniorrhexis. *Am J Obstet Gynecol* 172:1427, 1995.
54. Mercer B, Moretti M, LD S: Intensive antenatal testing for women with preterm premature rupture of the membranes (Abstract 420). Society of Perinatal Obstetricians. San Francisco, 1991.
55. Deren O, Karaer C, Onderoglu L, et al: The effect of steroids on the biophysical profile and Doppler indices of umbilical and middle cerebral arteries in healthy preterm fetuses. *Eur J Obstet Gynecol Reprod Biol* 99:72, 2001.
56. Rotmensch S, Liberati M, Celentano C, et al: The effect of betamethasone on fetal biophysical activities and Doppler velocimetry of umbilical and middle cerebral arteries. *Acta Obstet Gynecol Scand* 78:768, 1999.
57. Jackson JR, Kleeman S, Doerzbacher M, et al: The effect of glucocorticosteroid administration on fetal movements and biophysical profile scores in normal pregnancies. *J Matern Fetal Neonatal Med* 13:50, 2003.
58. Koenen SV, Mulder EJ, Wijnberger LD, et al: Transient loss of the diurnal rhythms of fetal movements, heart rate, and its variation after maternal betamethasone administration. *Pediatr Res* 57:662, 2005.
59. Mulder EJ, Koenen SV, Blom I, et al: The effects of antenatal betamethasone administration on fetal heart rate and behaviour depend on gestational age. *Early Hum Dev* 76:65, 2004.
60. Gray SE, Rodis JF, Lettieri L, et al: Effect of intravenous magnesium sulfate on the biophysical profile of the healthy preterm fetus. *Am J Obstet Gynecol* 170:1131, 1994.
61. Carlan SJ, O'Brien WF: The effect of magnesium sulfate on the biophysical profile of normal term fetuses. *Obstet Gynecol* 77:681, 1991.
62. Peaceman AM, Meyer BA, Thorp JA, et al: The effect of magnesium sulfate tocolysis on the fetal biophysical profile. *Am J Obstet Gynecol* 161:771, 1989.
63. Hallak M, Moise KJ Jr, Smith EO, et al: The effects of indomethacin and terbutaline on human fetal umbilical artery velocimetry: A randomized, double-blind study. *Am J Obstet Gynecol* 168:865, 1993.



## THE ROLE OF DOPPLER ULTRASOUND IN OBSTETRICS

Alfred Z. Abuhamad, MD

### Physical Principles

#### Fetal Arterial Doppler

Umbilical Artery

Middle Cerebral Artery

Uterine Artery

#### Fetal Venous Doppler

#### Fetal Cardiac Doppler

Optimizing Your Image

#### Fetal Doppler and Intrauterine Growth Restriction

### PHYSICAL PRINCIPLES

The Doppler effect, first reported by Christian Doppler in 1842,<sup>1</sup> describes the *apparent* variation in frequency of a light or a sound wave as the source of the wave approaches or moves away relative to an observer. The traditional example that is given to describe this physical phenomenon is the apparent change in sound level of a train as the train approaches and then departs a station. The sound seems higher in pitch as the train approaches the station and seems lower in pitch as the train departs the station. The actual sound of the train is constant, it is the apparent change in sound pitch to a stationary observer that describes the Doppler effect. This apparent change in sound pitch (Doppler effect), or what is also termed the frequency shift, is proportional to the speed of movement of the sound-emitting source. In clinical applications, when an ultrasound beam with a certain frequency is used to insonate a certain blood vessel, the reflected frequency or frequency shift is directly proportional to the speed with which the red blood cells are moving (blood flow velocity) within that particular vessel. This frequency shift of the returning signal is displayed in a graphic form as a time-dependent plot. In this display, the vertical axis represents the frequency shift and the horizontal axis represents the temporal change of this frequency shift as it relates to the events of the cardiac cycle (Fig. 22-1). This frequency shift is highest during systole, when the blood flow is at its fastest, and lowest during end-diastole, when the blood flow is at its slowest in the peripheral circulation. Given that the velocity of flow in a particular vascular bed is inversely proportional to the downstream impedance to flow, the frequency shift therefore derives information on the downstream impedance to flow of the vascular bed under study. The frequency shift is also dependent on the cosine of the angle that the ultrasound beam makes with the targeted blood vessel (see formula in Fig. 22-1). When the sound beam is parallel to the blood vessel of interest and thus

the moving red cells, the entire Doppler shift is measured. However, when an angle exists between the direction of flow and the sound beam, the measured velocity is less than the true velocity.<sup>2</sup> The degree to which the velocity is accurately measured depends on the angle of incidence (cosine  $\Theta$ ). At an angle of 0 degrees, the measured velocity is equal to the true velocity. When the sound beam is perpendicular to the direction of flow (90 degrees), the measured velocity is zero, because the cosine of 90 degrees is zero.<sup>2</sup> Thus, ideally, one wants to measure the velocity with as small an angle as possible.

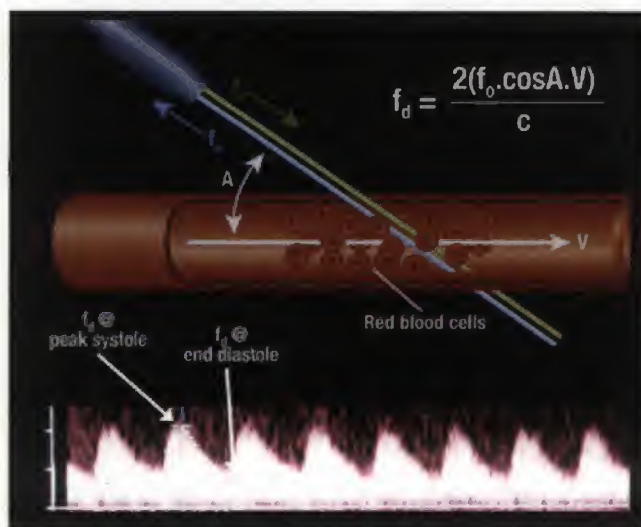


**FIGURE 22-1.** The Doppler effect ( $f_d$ ) is dependent on the initial frequency of the ultrasound transducer ( $f_0$ ), the velocity of flow ( $V$ ) of the blood within a vessel, and the cosine of the angle ( $A$ ) that the ultrasound beam makes with the direction of blood flow. The frequency shift ( $f_d$ ) is displayed as a time-dependent plot within a cardiac cycle.

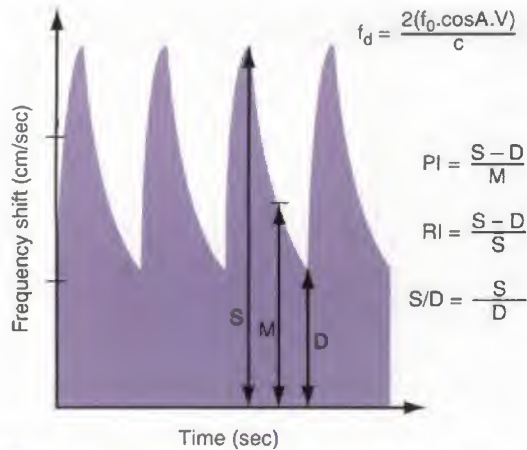


**FIGURE 22-2.** Doppler indices commonly used in obstetrical imaging. D, diastole; M, mean; PI, pulsatility index; RI, resistance index; S, systole.

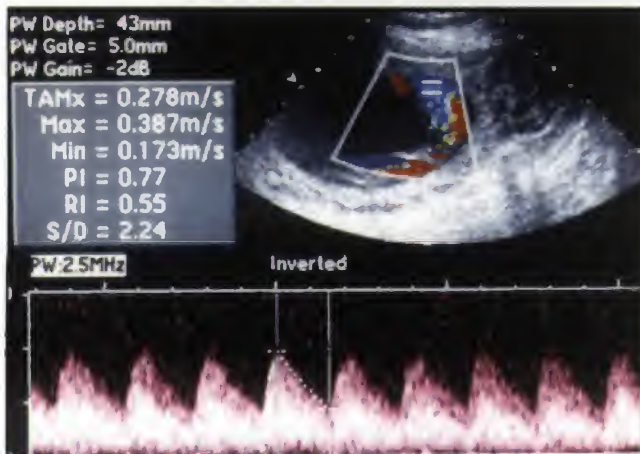


**FIGURE 22-3.** Doppler waveforms of the umbilical artery in a normal fetus in the third trimester of pregnancy. Note the increased end-diastolic velocity, consistent with a low impedance circulation.

Given that the insonating angle is difficult to measure in clinical practice, indices that rely on ratios of frequency shifts were developed to quantitate Doppler waveforms. By relying on ratios of frequency shifts, these Doppler indices are thus independent of the effects of the insonating angle of the ultrasound beam. Doppler indices that are commonly used in obstetric practice are shown in Figure 22-2.

## FETAL ARTERIAL DOPPLER

### Umbilical Artery

The umbilical arterial circulation is normally a low impedance circulation, with an increase in the amount of end-diastolic flow with advancing gestation.<sup>3,4</sup>

Umbilical arterial Doppler waveforms reflect the status of the placental circulation, and the increase in end-diastolic flow that is seen with advancing gestation is a direct result of an increase in the number of tertiary stem villi that takes place with placental maturation (Fig. 22-3).<sup>5,6</sup> Diseases that

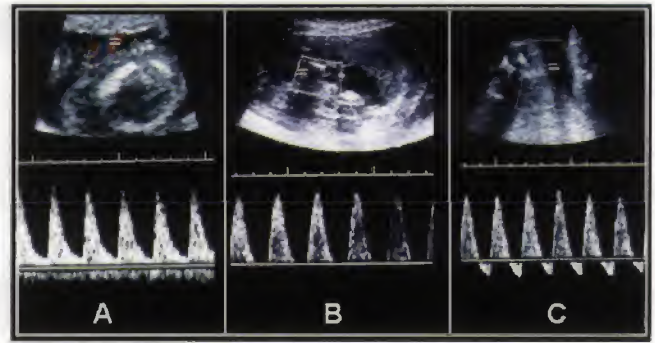


**FIGURE 22-4.** Abnormal umbilical artery waveforms; decreased end-diastolic velocity (A), absent end-diastolic velocity (B), reversed end-diastolic velocity (C).

obliterate small muscular arteries in placental tertiary stem villi result in a progressive decrease in end-diastolic flow in the umbilical arterial Doppler waveforms until absent and then reverse flow during diastole is noted (Fig. 22-4).<sup>7,8</sup> Reversed diastolic flow in the umbilical arterial circulation represents an advanced stage of placental compromise and is associated with more than 70% of placental arterial obliteration.<sup>9-12</sup> The notation of absent or reversed end-diastolic flow in the umbilical artery is commonly associated with severe intrauterine growth restriction (IUGR) and oligohydramnios.<sup>13,14</sup>

Doppler waveforms of the umbilical arteries can be obtained from any segment along the umbilical cord. Waveforms obtained from the placental end of the cord show more end-diastolic flow, thus lower ratio values (RI, S/D) than waveforms obtained from the abdominal cord insertion.<sup>15</sup> Differences in Doppler indices of arterial waveforms obtained from different anatomic locations of the same umbilical cord are generally minor and have no significance on clinical practice (Tables 22-1 to 22-3).<sup>3,4</sup>

### Middle Cerebral Artery

The middle cerebral artery is the most accessible cerebral vessel to ultrasound imaging in the fetus, and it carries more than 80% of cerebral blood flow.<sup>16</sup> The cerebral circulation is normally a high-impedance circulation with continuous forward flow throughout the cardiac cycle.<sup>17</sup> This is the reverse of flow within the umbilical cord toward the placenta. In the presence of fetal hypoxemia, central redistribution of blood flow occurs, resulting in an increased blood flow to the brain (Fig. 22-5), heart, and adrenals, and a reduction in flow to the peripheral and placental circulations. This blood flow redistribution is known as the brain-sparing reflex and plays a major role in fetal adaptation to oxygen deprivation.<sup>17-19</sup>

The right and left middle cerebral arteries represent major branches of the circle of Willis in the fetal brain. The circle of Willis, which is supplied by the internal carotids and vertebral arteries, can be imaged with color flow Doppler ultrasound in a transverse plane of the fetal head obtained at the base of the skull (Fig. 22-6). In this transverse plane, the proximal and distal middle cerebral arteries are seen in their long axis, with their course almost parallel to the ultrasound



**Table 22-1** Reference Values for Serial Measurements of the Umbilical Artery Systolic: Diastolic Ratio

Gestation (wk)	Percentile								
	2.5th	5th	10th	25th	50th	75th	90th	95th	97.5th
19	2.73	2.93	3.19	3.67	4.28	5.00	5.75	6.26	6.73
20	2.63	2.83	3.07	3.53	4.11	4.80	5.51	5.99	6.43
21	2.51	2.70	2.93	3.36	3.91	4.55	5.22	5.67	6.09
22	2.43	2.60	2.83	3.24	3.77	4.38	5.03	5.45	5.85
23	2.34	2.51	2.72	3.11	3.62	4.21	4.82	5.22	5.61
24	2.25	2.41	2.62	2.99	3.48	4.04	4.63	5.02	5.38
25	2.17	2.33	2.52	2.88	3.35	3.89	4.45	4.83	5.18
26	2.09	2.24	2.43	2.78	3.23	3.75	4.30	4.66	5.00
27	2.02	2.17	2.35	2.69	3.12	3.63	4.15	4.50	4.83
28	1.95	2.09	2.27	2.60	3.02	3.51	4.02	4.36	4.67
29	1.89	2.03	2.20	2.52	2.92	3.40	3.89	4.22	4.53
30	1.83	1.96	2.13	2.44	2.83	3.30	3.78	4.10	4.40
31	1.77	1.90	2.06	2.36	2.75	3.20	3.67	3.98	4.27
32	1.71	1.84	2.00	2.29	2.67	3.11	3.57	3.87	4.16
33	1.66	1.79	1.94	2.23	2.60	3.03	3.48	3.77	4.06
34	1.61	1.73	1.88	2.16	2.53	2.95	3.39	3.68	3.96
35	1.57	1.68	1.83	2.11	2.46	2.87	3.30	3.59	3.86
36	1.52	1.64	1.78	2.05	2.40	2.80	3.23	3.51	3.78
37	1.48	1.59	1.73	2.00	2.34	2.74	3.15	3.43	3.69
38	1.44	1.55	1.69	1.95	2.28	2.67	3.08	3.36	3.62
39	1.40	1.51	1.64	1.90	2.23	2.61	3.02	3.29	3.54
40	1.36	1.47	1.60	1.85	2.18	2.56	2.96	3.22	3.48
41	1.33	1.43	1.56	1.81	2.13	2.50	2.90	3.16	3.41

From Acharya G, Wilsgaard T, Bernstein GKR, et al: Reference ranges for serial measurements of umbilical artery Doppler indices in the second half of pregnancy. *Am J Obstet Gynecol* 192:937, 2005.

**Table 22-2** Resistance Index of the Umbilical Artery Between 20 and 40 Weeks of Gestation

Gestation (wks)	5th Percentile	50th Percentile	95th Percentile
20	0.567	0.690	0.802
21	0.557	0.680	0.793
22	0.548	0.671	0.784
23	0.539	0.663	0.776
24	0.530	0.655	0.768
25	0.522	0.646	0.760
26	0.514	0.639	0.752
27	0.506	0.631	0.745
28	0.498	0.623	0.737
29	0.490	0.615	0.730
30	0.482	0.608	0.723
31	0.474	0.600	0.715
32	0.465	0.592	0.707
33	0.457	0.584	0.700
34	0.449	0.576	0.692
35	0.440	0.567	0.684
36	0.431	0.559	0.675
37	0.422	0.550	0.667
38	0.412	0.540	0.657
39	0.402	0.530	0.648
40	0.390	0.519	0.637

From Merz E (ed): *Ultrasonography in Obstetrics and Gynecology*, vol 1. Stuttgart, New York, Thieme, 2005, pp 469–480, 614.

**Table 22-3** Pulsatility Index of the Umbilical Artery Between 20 and 40 Weeks of Gestation

Gestation (wks)	5th Percentile	50th Percentile	95th Percentile
20	0.940	1.216	1.505
21	0.913	1.189	1.476
22	0.890	1.165	1.450
23	0.869	1.142	1.427
24	0.849	1.122	1.405
25	0.831	1.102	1.385
26	0.813	1.084	1.365
27	0.798	1.065	1.346
28	0.780	1.048	1.327
29	0.764	1.031	1.308
30	0.748	1.014	1.290
31	0.732	0.997	1.272
32	0.716	0.980	1.254
33	0.700	0.963	1.236
34	0.684	0.946	1.218
35	0.668	0.928	1.199
36	0.651	0.910	1.180
37	0.634	0.891	1.160
38	0.615	0.872	1.139
39	0.595	0.851	1.117
40	0.573	0.828	1.093

From Merz E (ed): *Ultrasonography in Obstetrics and Gynecology*, vol 1. Stuttgart, New York, Thieme, 2005, pp 469–480, 614.

beam. As such, the insonating beam, which is parallel to the vessel and thus has a cosine of 0 degrees, will result in a measured velocity that accurately reflects the true velocity of blood in this vessel. Middle cerebral artery Doppler waveforms, obtained from the proximal portion of the vessel, immediately after its origin from the circle of Willis, have shown the best reproducibility (Tables 22-4 and 22-5 and Fig. 22-7).<sup>19</sup>

Although middle cerebral artery Doppler evaluation is often used to assess fetal well-being in the fetus with suspected IUGR (see later), more recently, middle cerebral artery velocity has been used in assessing the degree of anemia in fetuses with hemolytic disease due to Rh isoimmunization and parvovirus B19 infection (see Chapter 17) (Table 22-6).

## Uterine Artery

Pregnancy is associated with physiologic changes at the level of the uterine vasculature, resulting in a progressive decrease

in impedance with advancing gestation.<sup>20</sup> This maternal adaptation to pregnancy is thought to result from the trophoblastic invasion of the maternal spiral arterioles in the first half of pregnancy.<sup>21</sup> The invaded maternal spiral arterioles are rendered maximally dilated and minimally responsive to the sympathetic and parasympathetic systems. This adaptation is intended to ensure a sustained increase in blood flow to the uterus during pregnancy.

The uterine circulation can be assessed by Doppler velocimetry of the uterine arteries. Each uterine vessel can be demonstrated by color Doppler as it crosses over the hypogastric artery and vein just before it enters the uterus at the uterine-cervical junction (Fig. 22-8). Pulsed Doppler velocimetry of the uterine artery should be obtained immediately after the vessel crosses the hypogastric artery and before it divides into the uterine and cervical branches. The presence of a notch in the waveform and an increase in the impedance index after 22 weeks of gestation characterizes an abnormal uterine circulation (Fig. 22-9 and Tables 22-7 and 22-8).<sup>22</sup> A substantial risk of complication is noted in

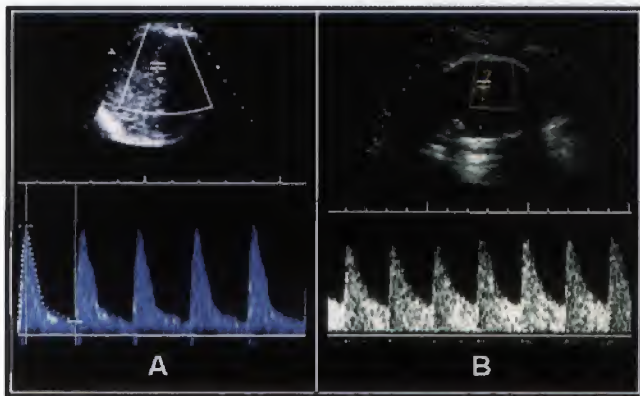


**FIGURE 22-5.** Doppler waveforms of the middle cerebral artery in a normal fetus (A) and in a hypoxemic fetus (B). Note the increase in end-diastolic velocity in fetus B resulting from a low impedance cerebral circulation as part of the brain-sparing reflex.

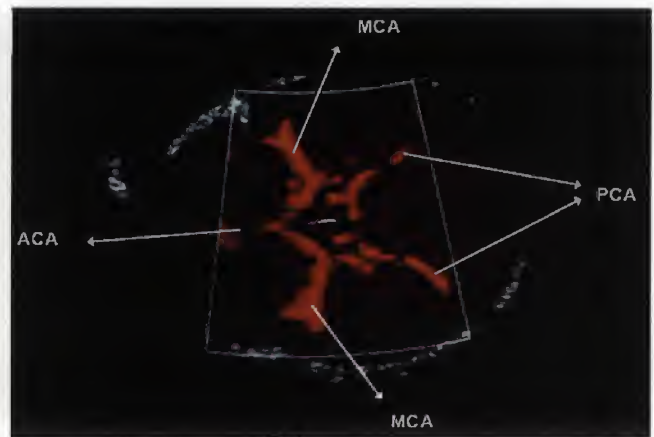


**FIGURE 22-6.** Circle of Willis shown on color Doppler imaging. ACA, anterior cerebral artery; MCA, middle cerebral artery; PCA, posterior cerebral artery.

**Table 22-4**

**Reference Values for the Resistance Index of the Middle Cerebral Artery**

Gestation (wks)	5th Percentile	50th Percentile	95th Percentile	Gestation (wks)	5th Percentile	50th Percentile	95th Percentile
18	0.544	0.687	0.787	31	0.652	0.798	0.907
19	0.574	0.708	0.808	32	0.645	0.792	0.902
20	0.592	0.727	0.828	33	0.636	0.783	0.894
21	0.608	0.744	0.846	34	0.625	0.773	0.885
22	0.622	0.758	0.861	35	0.612	0.761	0.873
23	0.633	0.771	0.874	36	0.597	0.747	0.86
24	0.643	0.782	0.886	37	0.579	0.73	0.844
25	0.651	0.79	0.895	38	0.56	0.712	0.826
26	0.656	0.796	0.902	39	0.539	0.692	0.807
27	0.659	0.801	0.907	40	0.515	0.669	0.785
28	0.661	0.803	0.91	41	0.489	0.644	0.761
29	0.66	0.803	0.911	42	0.462	0.618	0.735
30	0.657	0.801	0.91				



**Table 22-5****Reference Values for the Resistance Index of Umbilical and Middle Cerebral Arteries, as well as the UA/MCA Ratio**

Gestation (wks)	Umbilical Artery Resistance Index (UA RI)			Middle Cerebral Artery Resistance Index (MCA RI)			UA RI/MCA RI		
	5th Percentile	50th Percentile	95th Percentile	5th Percentile	50th Percentile	95th Percentile	5th Percentile	50th Percentile	95th Percentile
24	0.615	0.717	0.828	0.778	0.867	—	0.696	0.809	0.968
25	0.605	0.707	0.819	0.789	0.881	—	0.676	0.791	0.955
26	0.594	0.697	0.810	0.795	0.892	—	0.658	0.775	0.945
27	0.583	0.687	0.802	0.798	0.898	—	0.642	0.761	0.937
28	0.572	0.678	0.793	0.797	0.901	—	0.628	0.750	0.932
29	0.562	0.668	0.785	0.793	0.900	—	0.616	0.740	0.929
30	0.551	0.658	0.776	0.786	0.897	—	0.606	0.732	0.928
31	0.540	0.648	0.767	0.776	0.891	—	0.597	0.726	0.929
32	0.530	0.638	0.759	0.764	0.883	—	0.590	0.722	0.931
33	0.519	0.629	0.750	0.750	0.872	—	0.585	0.719	0.936
34	0.508	0.619	0.742	0.734	0.860	—	0.581	0.717	0.941
35	0.498	0.609	0.733	0.717	0.846	—	0.578	0.717	0.949
36	0.487	0.599	0.724	0.698	0.831	—	0.576	0.718	0.957
37	0.476	0.589	0.716	0.677	0.814	—	0.575	0.720	0.967
38	0.465	0.580	0.707	0.655	0.795	—	0.576	0.724	0.978
39	0.455	0.570	0.699	0.632	0.776	—	0.577	0.728	0.991
40	0.444	0.560	0.690	0.607	0.755	—	0.580	0.734	1.004
41	0.433	0.550	0.681	0.582	0.734	—	0.583	0.740	1.018
42	0.423	0.540	0.673	0.556	0.711	—	0.588	0.747	1.034

MCA, middle cerebral artery; RI, resistive index; UA, uterine artery.

From Kurmanavicius J, Florio I, Wisser J, et al: Reference resistance indices of the umbilical, fetal middle cerebral and uterine arteries at 24–42 weeks of gestation. *Ultrasound Obstet Gynecol* 10:112, 1997.

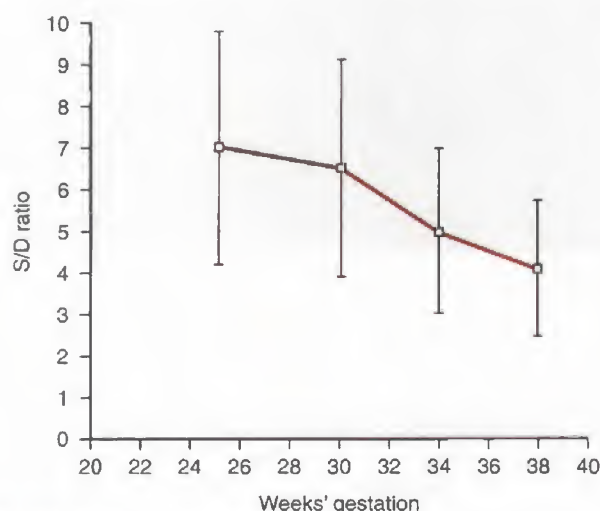


**FIGURE 22-7.** Middle cerebral artery Doppler systole/diastolic ratios. (Modified from Woo JSK, Liang ST, Chan FY, et al: Middle cerebral artery Doppler flow velocity. *Obstet Gynecol* 70:613, 1987. Reprinted with permission from the American College of Obstetricians and Gynecologists.)

pregnancies that show an abnormal uterine circulation in the late second and third trimester.<sup>23,24</sup> Pregnancy complications include fetal growth restriction, preeclampsia, preterm delivery and nonreassuring fetal status in labor.<sup>23,24</sup>

## FETAL VENOUS DOPPLER

Doppler waveforms obtained from the central venous circulation in the fetus, reflect the physiologic status of the

**Table 22-6****Threshold of Peak Velocity of Systolic Blood Flow in the Middle Cerebral Artery Above Which Mild, Moderate, and Severe Anemia Occurs**

Threshold of the Peak Velocity of the Middle Cerebral Artery (cm/sec) Above Which Degree of Anemia is Classified

Gestation (wks)	Mild Anemia	Moderate Anemia	Severe Anemia
18	29.9	34.8	36.0
20	32.8	38.2	39.5
22	36.0	41.9	43.3
24	39.5	46.0	47.5
26	43.3	50.4	52.1
28	47.6	55.4	57.2
30	52.2	60.7	62.8
32	57.3	66.6	68.9
34	62.9	73.1	75.6
36	69.0	80.2	82.9
38	75.7	88.0	91.0
40	83.0	96.6	99.8

From Mari G, Deter RL, Carpenter RL, et al: Non-invasive diagnosis by Doppler ultrasonography of fetal anemia due to maternal red-cell alloimmunization. Collaborative Group for Doppler Assessment of the Blood Velocity in Anemic Fetuses. *N Engl J Med* 342:9, 2000.

right ventricle. Specific information with regard to right ventricular preload, myocardial compliance, and right ventricular end-diastolic pressure can be derived from Doppler flow studies of the inferior vena cava and ductus venosus in the fetus.<sup>25–30</sup>



**FIGURE 22-8.** Color Doppler imaging in the lateral lower uterine segment showing the uterine artery (main) as it crosses over the hypogastric vessels (iliacs) before it enters the uterus and then divides into a uterine and a cervical branch.

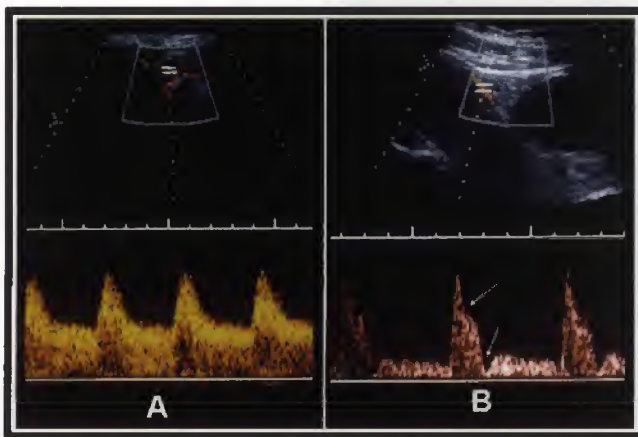


**FIGURE 22-9.** Doppler waveforms of the uterine artery obtained in the late second trimester of pregnancy showing a normal uterine circulation (A) with increased end-diastolic velocity implying a low impedance circulation and an abnormal uterine artery circulation (B) with a waveform notch and low end-diastolic velocity (high impedance).

Inferior vena cava Doppler waveforms can be obtained from a coronal plane of the chest and abdomen. In this view, the inferior vena cava can be imaged as it enters into the right atrium, joined by the ductus venosus and the left hepatic vein (Fig. 22-10). The inferior vena cava can be studied at two locations: at the inlet into the right atrium or in the segment between the entrance of the hepatic vein and the ductus venosus. A good correlation coefficient exists between these two measurement sites, and the location that provides the smallest angle of insonation with the blood flow should be chosen.<sup>29</sup> Inferior vena cava Doppler waveforms are triphasic in shape, with the first phase corresponding to ventricular systole, the second phase to early diastole, and the third phase to late diastole or the atrial kick (Fig. 22-11).

Ductus venosus Doppler waveforms can be easily obtained from a transverse view of the fetal abdomen at the same anatomic plane of the abdominal circumference (Fig. 22-12). By superimposing color flow Doppler to the grayscale image, the ductus venosus can be identified as it branches from the portal vein. High-velocity flow and

**Table 22-7** Resistance Index of the Uterine Artery

Gestation (wks)	5th Percentile	50th Percentile	95th Percentile
18	0.222	0.447	0.659
19	0.204	0.429	0.641
20	0.194	0.419	0.630
21	0.186	0.411	0.622
22	0.180	0.405	0.615
23	0.175	0.400	0.610
24	0.171	0.395	0.605
25	0.167	0.391	0.601
26	0.163	0.387	0.597
27	0.160	0.384	0.593
28	0.157	0.380	0.590
29	0.154	0.378	0.587
30	0.152	0.375	0.584
31	0.150	0.372	0.581
32	0.147	0.370	0.578
33	0.145	0.368	0.576
34	0.144	0.366	0.574
35	0.142	0.364	0.571
36	0.140	0.362	0.569
37	0.139	0.360	0.567
38	0.137	0.358	0.566
39	0.136	0.357	0.564
40	0.135	0.355	0.562

From Merz E (ed): *Ultrasonography in Obstetrics and Gynecology*, vol 1. Stuttgart, New York, Thieme, 2005, pp 469–480, 614.

**Table 22-8** Pulsatility Index of the Uterine Artery

Gestation (wks)	5th Percentile	50th Percentile	95th Percentile
18	0.509	0.888	1.407
19	0.460	0.838	1.356
20	0.436	0.812	1.328
21	0.420	0.795	1.309
22	0.407	0.781	1.293
23	0.397	0.769	1.280
24	0.388	0.759	1.268
25	0.381	0.751	1.258
26	0.374	0.743	1.248
27	0.369	0.736	1.239
28	0.363	0.729	1.230
29	0.358	0.722	1.222
30	0.354	0.716	1.214
31	0.349	0.711	1.207
32	0.345	0.705	1.199
33	0.341	0.700	1.192
34	0.337	0.695	1.185
35	0.333	0.690	1.178
36	0.330	0.684	1.171
37	0.326	0.679	1.164
38	0.322	0.674	1.157
39	0.318	0.669	1.150
40	0.313	0.663	1.143

From Merz E (ed): *Ultrasonography in Obstetrics and Gynecology*, vol 1. Stuttgart, New York, Thieme, 2005, pp 469–480, 614.



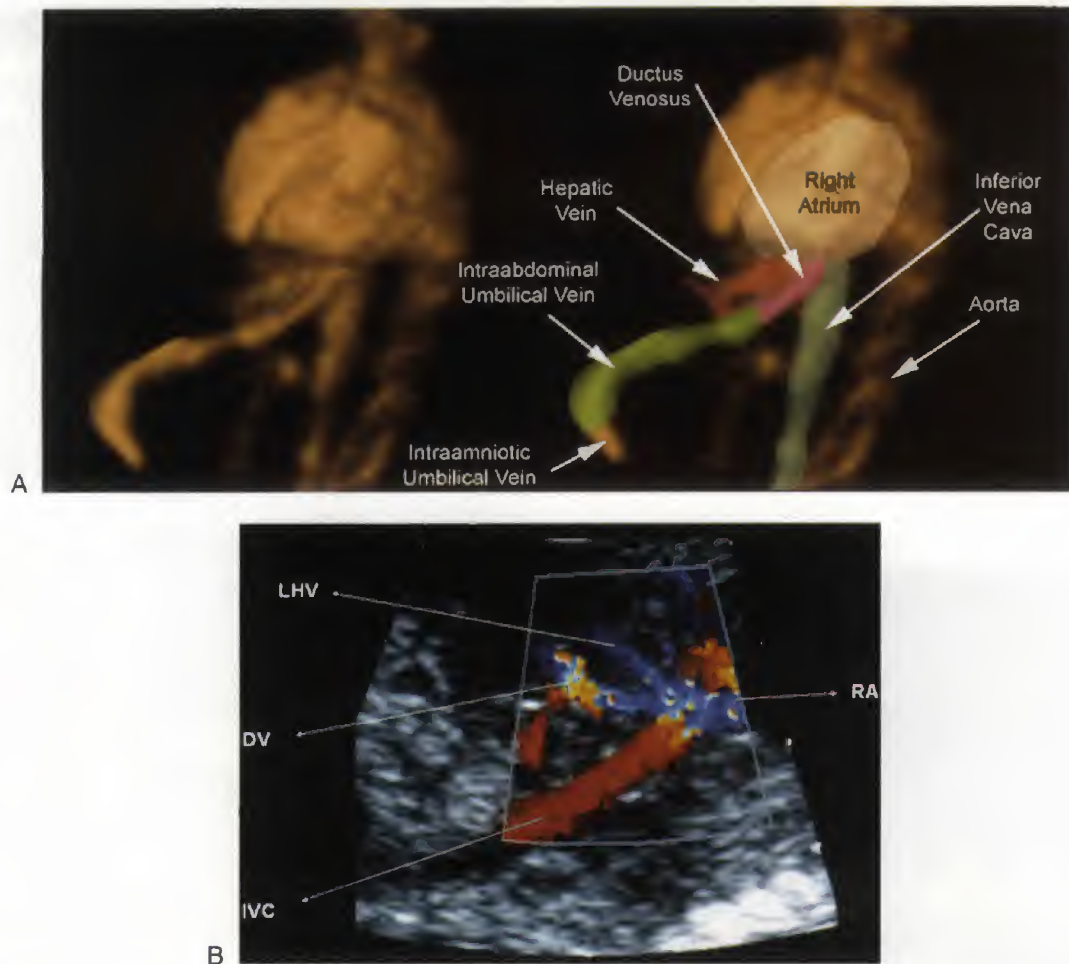


**FIGURE 22-10.** A. Three-dimensional B flow image from a 17-week-old fetus illustrating the relationships of the venous system, heart and aorta. B. Color Doppler ultrasound of a coronal plane of the fetal abdomen and chest showing the inferior vena cava (IVC), joined by the ductus venosus (DV) and the left hepatic vein (LHV) as it enters the right atrium (RA). (A from DeVore GR: *Pulsed Doppler examination of the fetal heart*. In Goldberg BB, McGahan JP [eds]: *Fetal Ductus Venosus in Atlas of Ultrasound Measurements*, 2nd ed. Philadelphia, Mosby Inc/Elsevier, 2006.)

turbulence is commonly seen within the ductus venosus given its narrow lumen. The presence of turbulence on color flow Doppler helps in identifying the ductus venosus in early gestations. Ductus venosus Doppler waveforms are biphasic in shape, with the first phase corresponding to ventricular systole, the second phase to early diastole, and the nadir of the second phase to late diastole or the atrial kick (Fig. 22-13 and Tables 22-9 to 22-12).

Blood flow through the umbilical vein carrying oxygenated blood to the fetus can be assessed either within its entrance into the fetal abdomen or adjacent to the fetus within the amniotic fluid (Table 22-13).

## FETAL CARDIAC DOPPLER

### Optimizing Your Image

Adequate imaging of the fetal heart is essential for accurate Doppler measurements. Several steps can improve ultrasound imaging when faced with suboptimal scanning conditions. Resort to the echocardiography settings on your

ultrasound equipment as the first step in optimizing your image. The echocardiography settings allow for enhanced image contrast, tissue characterization, and a faster frame rate which improve cardiac imaging. Other steps include minimizing the depth on the display monitor, insonating the heart through an angle that avoids shadowing by the fetal ribs and sternum, adjusting the focal zones to the area of interest, and most important, enlarging the area of interest (zoom), which allows visualization of details within the heart. These simple steps result in an adequate visualization of the fetal heart in most conditions. When adding color Doppler to your grayscale image, select high-velocity scales given that the velocity of cardiac blood flow is higher than the peripheral fetal circulation. By adjusting your filters to a high setting and by directing the angle of insonation of your ultrasound beam parallel to the direction of blood flow, the color Doppler image is optimized and wall motion artifact is significantly reduced.

Doppler indices in fetal echocardiography are quantitative parameters and, for the majority, are angle dependent. To obtain accurate Doppler indices in fetal echocardiography,

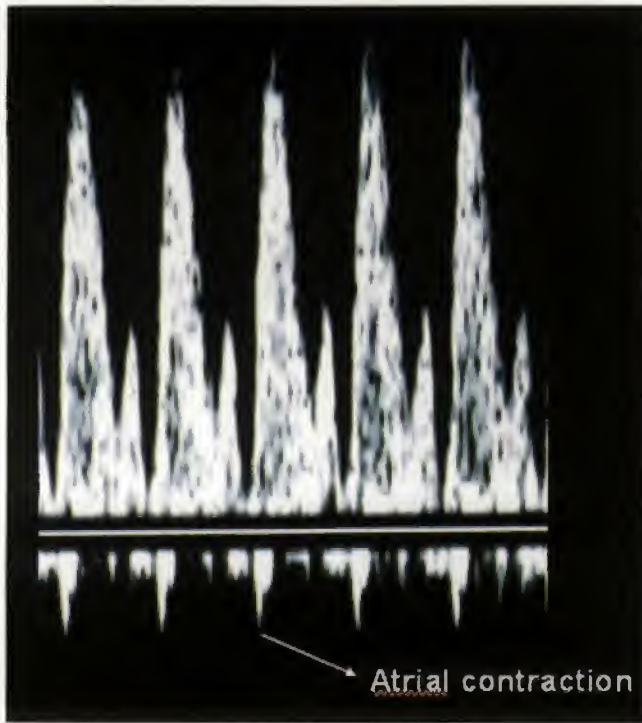


**FIGURE 22-11.** Doppler waveforms of the inferior vena cava in a normal fetus in the third trimester of pregnancy. Note the presence of reversed flow during the atrial contraction phase of diastole.

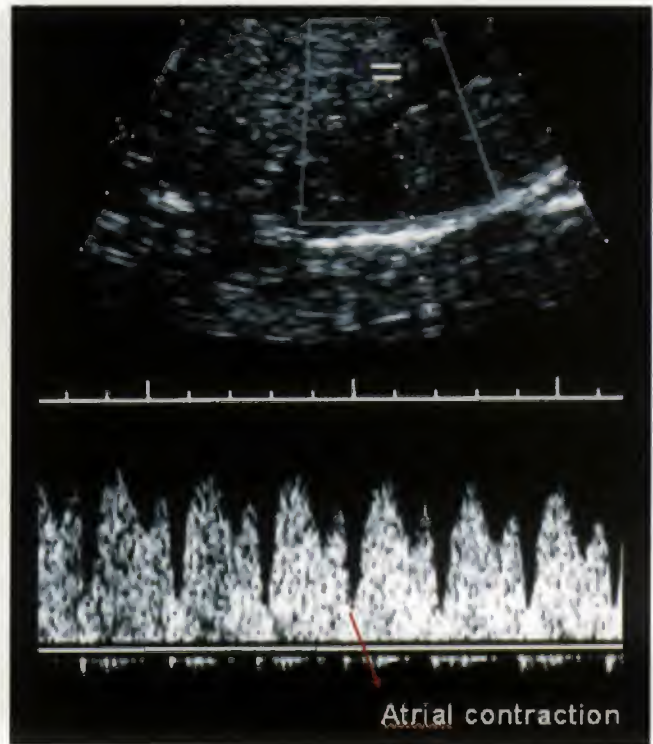


**FIGURE 22-13.** Doppler waveforms of the ductus venosus in a normal fetus in the third trimester of pregnancy. Note the presence of forward flow within the ductus venosus throughout the cardiac cycle.

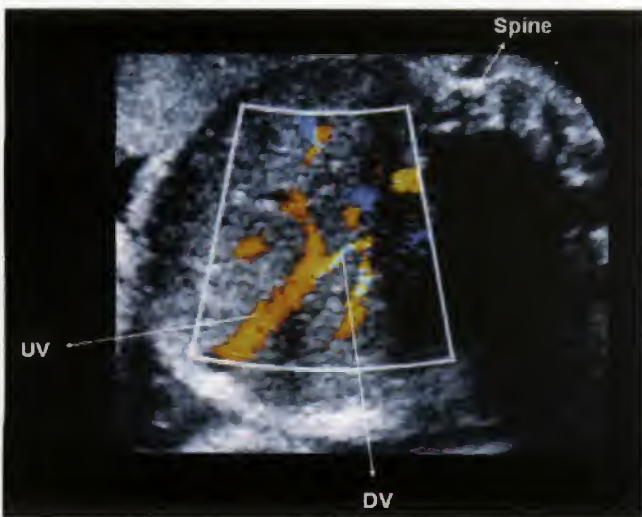


**FIGURE 22-12.** Color Doppler ultrasound of a transverse plane of the fetal abdomen showing the umbilical vein (UV) and the ductus venosus (DV). Note the presence of turbulence on color Doppler in the ductus venosus.

the sample volume is placed distal to the respective valves, the insonating angle should be within 15 to 20 degrees of the direction of blood flow, Doppler waveforms should be obtained during fetal apnea, and multiple measurements should be made. Color Doppler is used to direct placement of the sample volume; placing the sample volume at the

**Table 22-9** Ductus Venosus Preload Index (a/S)

Gestation (wks)	Preload Index (a/S)		
	5th Percentile	50th Percentile	95th Percentile
20	0.342	0.508	0.674
21	0.341	0.507	0.673
22	0.341	0.507	0.673
23	0.340	0.506	0.672
24	0.339	0.505	0.671
25	0.339	0.505	0.671
26	0.338	0.504	0.670
27	0.338	0.504	0.670
28	0.337	0.503	0.669
29	0.336	0.502	0.668
30	0.336	0.502	0.668
31	0.335	0.501	0.667
32	0.335	0.501	0.667
33	0.334	0.500	0.666
34	0.333	0.499	0.665
35	0.333	0.499	0.665
36	0.332	0.498	0.664
37	0.332	0.498	0.664
38	0.331	0.497	0.663
39	0.330	0.496	0.662
40	0.330	0.496	0.662

From Baschat AA: Relationship between placental blood flow resistance and precordial venous Doppler indices. *Ultrasound Obstet Gynecol* 22:561, 2003.



**Table 22-10****Ductus Venosus Peak Velocity Index (S-a)/D**

Gestation (wks)	Peak Velocity Index (S-a)/D		
	5th Percentile	50th Percentile	95th Percentile
20	0.381	0.580	0.779
21	0.380	0.579	0.779
22	0.380	0.579	0.778
23	0.379	0.578	0.777
24	0.678	0.578	0.777
25	0.378	0.577	0.776
26	0.377	0.576	0.776
27	0.377	0.576	0.775
28	0.376	0.575	0.774
29	0.375	0.575	0.774
30	0.375	0.574	0.773
31	0.374	0.573	0.773
32	0.374	0.573	0.772
33	0.373	0.572	0.771
34	0.372	0.572	0.771
35	0.372	0.571	0.770
36	0.371	0.570	0.770
37	0.371	0.570	0.769
38	0.370	0.569	0.768
39	0.369	0.569	0.768
40	0.369	0.568	0.767

From Baschat AA: Relationship between placental blood flow resistance and precordial venous Doppler indices. *Ultrasound Obstet Gynecol* 22:561, 2003.

**Table 22-11****Ductus Venosus Pulsatility Index (S-a)/Tamx**

Gestation (wks)	Pulsatility Index (S-a)/Tamx		
	5th Percentile	50th Percentile	95th Percentile
20	0.410	0.643	0.875
21	0.409	0.642	0.874
22	0.408	0.641	0.873
23	0.407	0.640	0.872
24	0.406	0.639	0.871
25	0.405	0.638	0.870
26	0.404	0.637	0.869
27	0.403	0.636	0.868
28	0.402	0.635	0.867
29	0.401	0.634	0.866
30	0.400	0.633	0.865
31	0.399	0.632	0.864
32	0.398	0.631	0.863
33	0.397	0.630	0.862
34	0.396	0.629	0.861
35	0.395	0.628	0.860
36	0.394	0.627	0.859
37	0.393	0.626	0.858
38	0.392	0.625	0.857
39	0.391	0.624	0.856
40	0.390	0.623	0.855

From Baschat AA: Relationship between placental blood flow resistance and precordial venous Doppler indices. *Ultrasound Obstet Gynecol* 22:561, 2003.

**Table 22-12****Ductus Venosus S/a**

Gestation (wks)	S/a		
	5th Percentile	50th Percentile	95th Percentile
20	1.331	2.161	2.991
21	1.329	2.159	2.989
22	1.327	2.157	2.987
23	1.324	2.154	2.984
24	1.322	2.152	2.982
25	1.320	2.150	2.980
26	1.318	2.148	2.978
27	1.315	2.145	2.975
28	1.313	2.143	2.973
29	1.311	2.141	2.971
30	1.308	2.138	2.968
31	1.306	2.136	2.966
32	1.304	2.134	2.964
33	1.301	2.131	2.961
34	1.299	2.129	2.959
35	1.297	2.127	2.957
36	1.295	2.125	2.955
37	1.292	2.122	2.952
38	1.290	2.120	2.950
39	1.288	2.118	2.948
40	1.285	2.115	2.945

From Baschat AA: Relationship between placental blood flow resistance and precordial venous Doppler indices. *Ultrasound Obstet Gynecol* 22:561, 2003.

brightest colors of the blood flow segment will ensure the best measurements. Figure 22-14 shows Doppler indices commonly used in fetal echocardiography.

The fetal circulation is different from the adult circulation in many aspects. The fetal circulation is in parallel rather than in series, and the right ventricular cardiac output is greater than the left ventricular cardiac output.<sup>31,32</sup> The progressive development of organs during gestation influence blood distribution and vascular impedance.<sup>31</sup> With advancing gestation, ventricular compliance is increased, total peripheral resistance is decreased, preload is increased, and combined cardiac output is increased.<sup>31</sup> Compliance of the left side of the fetal heart increases more rapidly than compliance of the right side of the fetal heart with advancing gestation.<sup>31</sup> The pulmonary vascular resistance is high in the fetus, and the pulmonary arterial pressure is almost systemic.<sup>33,34</sup> Flow to the pulmonary vascular bed is maintained at a low rate, with a noted increase toward the end of gestation.<sup>32,33</sup> Cardiac output in the fetus is mainly affected by preload and ventricular compliance.<sup>31</sup> The presence of right-to-left shunts at the level of the foramen ovale and ductus arteriosus have a significant impact on cardiac flow patterns and affect the distribution of blood and oxygen to various organs. Flow across the foramen ovale contributes to the majority of blood entering the left ventricle, and more than two thirds of right ventricular output is directed to the ductus arteriosus.<sup>32,35</sup> This shunting mechanism ensures the delivery of blood with high oxygen content to the coronary and cerebral circulations.

**Table 22-13** Umbilical Vein Mean Velocity (cm/sec)

Gestation (wks)	Mean Velocity (cm/sec)			Gestation (wks)	Mean Velocity (cm/sec)		
	5th Percentile	50th Percentile	95th Percentile		5th Percentile	50th Percentile	95th Percentile
20	5.70	7.90	10.70	31	7.04	9.67	13.02
21	5.82	8.06	10.91	32	7.17	9.83	13.23
22	5.94	8.22	11.12	33	7.29	9.99	13.44
23	6.07	8.38	11.33	34	7.41	10.16	13.66
24	6.19	8.54	11.54	35	7.53	10.32	13.87
25	6.31	8.71	11.76	36	7.65	10.48	14.08
26	6.43	8.87	11.97	37	7.78	10.64	14.29
27	6.56	9.03	12.18	38	7.90	10.80	14.50
28	6.68	9.19	12.39	39	8.02	10.96	14.71
29	6.80	9.35	12.60	40	8.14	11.12	14.92
30	6.92	9.51	12.81				

From Barbera A, Galan HL, Ferrazzi E, et al: Relationship of umbilical vein blood flow to growth parameters in the human fetus. *Am J Obstet Gynecol* 181:174, 1999.

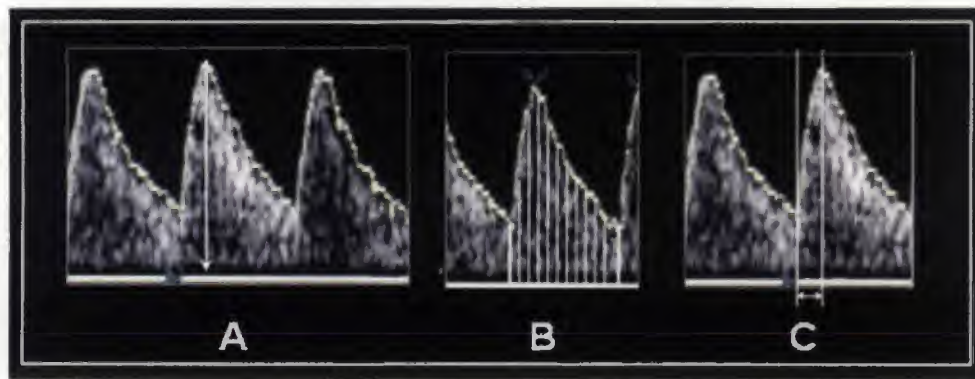


**FIGURE 22-14.** Doppler indices that are commonly used in fetal echocardiography. Peak-systolic velocity (A), time-velocity integral (B), and time-to-peak velocity (C).

Doppler waveforms across the atrioventricular valves are bicuspid in shape (Fig. 22-15). The first peak (E wave), corresponds to early ventricular filling of diastole, and the second peak (A wave) corresponds to atrial systole or the atrial kick. Unlike in postnatal life, the velocity of the A wave is higher than that of the E wave in the fetus.<sup>31,36</sup> This highlights the importance of the role that atrial systole plays in cardiac filling in the fetus. The E/A ratio increases with advancing gestation and reflects ventricular diastolic function.<sup>31,36</sup> E and A velocity peaks are higher in the right ventricle, and this right ventricular dominance is noted from the first trimester.<sup>31,36,37</sup> Shifting to left ventricular dominance starts in utero toward the end of gestation.<sup>31</sup> The E/A ratio is an index of ventricular preload and compliance (Table 22-14).<sup>31</sup>

Doppler waveforms across the semilunar valves are uniphasic in shape (Fig. 22-16). Indices most commonly used for the semilunar Doppler waveforms include the peak systolic velocity (PSV) and the time to peak velocity (TPV).

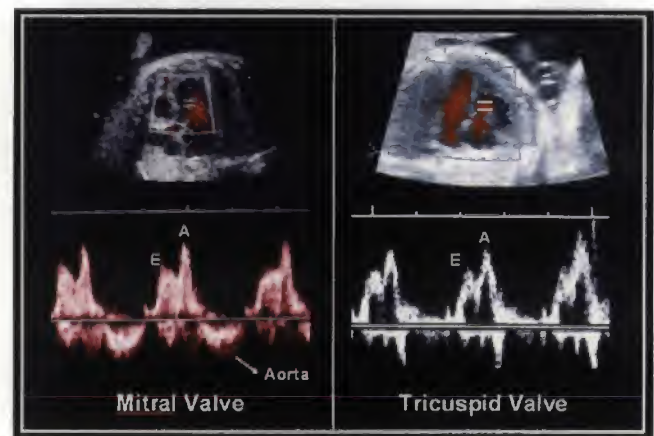


**FIGURE 22-15.** Doppler waveforms obtained across the mitral and tricuspid valves. Owing to the proximity of the mitral and aortic valves, a portion of the aortic outflow is noted during systole (arrow, aorta).



**Table 22-14** Mitral and Tricuspid Valve E/A Ratios

Gestation (wks)	Mitral Valve E/A Ratio			Tricuspid Valve E/A Ratio		
	2.5th Percentile	50th Percentile	97.5th Percentile	2.5th Percentile	50th Percentile	97.5th Percentile
20	0.40	0.59	0.77	0.47	0.65	0.83
21	0.42	0.60	0.79	0.49	0.66	0.84
22	0.43	0.62	0.80	0.50	0.68	0.85
23	0.45	0.63	0.82	0.52	0.69	0.86
24	0.46	0.65	0.83	0.53	0.70	0.87
25	0.48	0.66	0.84	0.54	0.71	0.88
26	0.49	0.68	0.86	0.55	0.72	0.89
27	0.50	0.69	0.87	0.56	0.73	0.90
28	0.52	0.70	0.88	0.57	0.74	0.90
29	0.53	0.71	0.89	0.58	0.74	0.91
30	0.54	0.73	0.90	0.58	0.75	0.91
31	0.55	0.74	0.91	0.59	0.75	0.92
32	0.56	0.75	0.92	0.59	0.76	0.92
33	0.57	0.76	0.93	0.60	0.76	0.92
34	0.58	0.76	0.93	0.60	0.76	0.92
35	0.59	0.77	0.94	0.60	0.76	0.92
36	0.59	0.78	0.95	0.60	0.76	0.92
37	0.60	0.79	0.95	0.60	0.76	0.92
38	0.61	0.79	0.96	0.60	0.76	0.92

From DeVore GR: Pulsed Doppler examination of the fetal heart. In Goldberg BB, McCahan JP (eds): Atlas of Ultrasound Measurements, 2nd ed. Philadelphia, Mosby Inc/Elsevier, 2006.

**FIGURE 22-16.** Doppler waveforms obtained across the aortic valve.

PSV and TPV increase with advancing gestation across the semilunar valves.<sup>31,35,38-41</sup> PSV is higher across the aorta than across the pulmonary artery owing to a decreased afterload and a smaller diameter across the aorta.<sup>31,35,38-41</sup> These Doppler indices reflect ventricular contractility, arterial pressures, and afterloads (Table 22-15).

### FETAL DOPPLER AND INTRAUTERINE GROWTH RESTRICTION

Arterial Doppler abnormalities, at the level of the umbilical and middle cerebral arteries (brain sparing reflex), confirm the presence of hypoxemia in the growth-restricted fetus and present early warning signs (see Table 22-5).<sup>42-45</sup> Once arterial centralization occurs, however, no clear trend is noted in the observational period, and thus, arterial redistribution may not be helpful for the timing of the delivery.<sup>42</sup> On the other hand, the presence of reversed end-diastolic flow in the umbilical arteries is a sign of advanced fetal compromise, and strong consideration should be given for delivery except for extreme prematurity. Cesarean delivery should be given preference in this setting because labor may cause further fetal compromise.

The current literature suggest that venous Doppler abnormalities in the inferior vena cava and ductus venosus and abnormal fetal heart rate monitoring, even in its computerized version, follow arterial Doppler abnormalities and are thus associated with a more advanced stage of fetal compromise.<sup>42-46</sup>

Furthermore, in the majority of severely growth-restricted fetuses, sequential deterioration of arterial and

**Table 22–15** Peak or Maximum Velocity of the Aorta and Main Pulmonary Artery

Gestation (wks)	Aorta Peak Velocity (cm/sec)			Pulmonary Artery Peak Velocity (cm/sec)		
	2.5th Percentile	50th Percentile	97.5th Percentile	2.5th Percentile	50th Percentile	97.5th Percentile
20	29	62	95	23	53	80
21	30	63	96	24	54	81
22	32	65	98	25	56	82
23	33	66	99	27	57	84
24	34	67	100	28	58	85
25	36	68	101	29	59	86
26	37	70	103	30	61	87
27	38	71	104	31	62	89
28	40	72	105	32	63	90
29	41	74	107	34	64	91
30	42	75	108	35	65	92
31	44	76	109	36	67	93
32	45	77	110	37	68	95
33	46	79	112	38	69	96
34	48	80	113	39	70	97
35	49	81	114	41	72	98
36	50	82	115	42	73	100
37	52	84	117	43	74	101
38	53	85	118	44	78	102

From DeVore GR: Pulsed Doppler examination of the fetal heart. In Goldberg BB, McGahan JP (eds): Atlas of Ultrasound Measurements, 2nd ed. Philadelphia, Mosby Inc/Elsevier, 2006.

venous Doppler precedes biophysical profile score deterioration.<sup>43</sup> At least one third of fetuses show early signs of circulatory deregulation 1 week before biophysical profile deterioration, and in most cases, Doppler deterioration preceded biophysical profile deterioration by 1 day.<sup>43</sup>

The occurrence of such abnormal late stage changes of vascular adaptation by the fetus IUGR appears to be the best predictor of perinatal death, independent of gestational age and weight.<sup>45</sup> In a longitudinal study on Doppler and IUGR fetuses, all intrauterine deaths and all neonatal deaths, with the exception of one case, had late Doppler changes at the time of delivery, whereas only a few of the surviving fetuses showed such changes.<sup>45</sup>

This sequential deterioration of the hypoxemic, growth-restricted fetus is rarely seen at gestations beyond 34 weeks.<sup>47,48</sup> Indeed, normal umbilical artery Doppler is common in growth-restricted fetuses in late gestations, and cerebroplacental ratios have poor correlation with outcome of IUGR fetuses at greater than 34 weeks of gestation.<sup>49</sup> Therefore, caution should be exercised when Doppler is used in the clinical management of fetuses with IUGR beyond 34 weeks of gestation.

The pathophysiology of fetal growth restriction has not been fully described because recent studies have highlighted the presence of significant variation in fetal adaptation to hypoxemia. The pattern of incremental deterioration of arterial Doppler abnormalities, followed by venous Doppler abnormalities, then followed by abnormal fetal heart tracings and biophysical profile abnormalities is not seen in approximately 20% of preterm fetuses.<sup>42</sup> Furthermore, only 70% of fetuses with IUGR show significant deterioration of all vascular beds by the time they were delivered and about 10% showed no significant circulatory change by delivery

time.<sup>43</sup> In a prospective, observational study, more than 50% of fetuses with IUGR delivered because of abnormal fetal heart rate tracings did not have venous Doppler abnormalities.<sup>45</sup> In view of these findings, the universal introduction of venous Doppler in the clinical management of the growth-restricted fetus should await the results of randomized trials on this subject.

IUGR is associated with several changes at the level of the fetal heart involving preload, afterload, ventricular compliance, and myocardial contractility. An increase in afterload is seen at the level of the right ventricle owing to increased placental impedance.<sup>50</sup> A decrease in afterload is noted at the level of the left ventricle owing to decreased cerebral impedance associated with the brain-sparing reflex.<sup>50</sup> These changes in afterload result in a redistribution of the cardiac output from right to left ventricle.<sup>50</sup> Preload is reduced at both atrioventricular valves owing to hypovolemia and decreased filling associated with IUGR.<sup>39,47,51,52</sup> This decrease in preload is reflected by a decrease in the E/A ratio, decreased atrial peak, and decreased time velocity integral at the mitral and tricuspid valves.<sup>39,51,52</sup>

Evidence of reduced myocardial contractility in the presence of severe IUGR has also been reported. Ventricular ejection force, an index of ventricular systolic function that is independent of preload and afterload is decreased at the level of the right and left ventricle in fetal growth restriction.<sup>53</sup> IUGR fetuses with reduced ventricular ejection force have a shorter time to delivery, a higher incidence of nonreassuring fetal heart rate tracing, and a lower pH at birth when compared with controls.<sup>53</sup> A significant correlation between the severity of fetal acidosis at cordocentesis and ventricular ejection force values validates the association of this index and the severity of fetal compromise.<sup>53</sup>



Myocardial cell damage, demonstrated by elevated levels of cardiac troponin T, is seen in some fetuses with severe growth restriction.<sup>50</sup> This advanced stage of fetal compromise is associated with signs of increased systemic venous pressure, a change in the distribution of cardiac output, a rise in right ventricle afterload, and a high incidence of tricuspid regurgitation.<sup>50</sup> These findings suggest that Doppler abnormalities in the proximal venous system of the growth-restricted fetus suggest fetal myocardial cell damage and increased systemic venous pressure.<sup>50</sup>

The fetal heart plays a central role in the adaptive mechanisms for hypoxemia and placental insufficiency. As discussed in this chapter, longitudinal data on the hemodynamic sequence of the natural history of fetal growth restriction show that the umbilical artery and middle cerebral artery are the first variables to become abnormal.<sup>54</sup> These arterial Doppler abnormalities are followed by abnormalities in the right cardiac diastolic indices, followed by the right cardiac systolic indices, and finally, by both left diastolic and systolic cardiac indices.<sup>54</sup> Preserving the left systolic function as the last variable to become abnormal ensures an adequate left ventricular output, which supplies the cerebral and coronary circulations.

Several of the Doppler changes seen in association with fetal IUGR in the peripheral circulation are directly related to the adaptation of the fetal heart. The current management of IUGR involves Doppler at the peripheral arterial circulation (middle cerebral and umbilical arteries), central venous vessels (ductus venosus and inferior vena cava), and cardiotocography. Adding cardiac Doppler may improve management of the fetus with IUGR, but studies are lacking on the prospective clinical evaluation of the IUGR fetus with cardiac Doppler. However, it is becoming more obvious that those changes in the central venous circulation reflect an advanced stage of fetal compromise, commonly associated with myocardial dysfunction and damage.

## References

- Doppler C: Über das farbige Licht der Dopplersterne und einiger anderer Gestirne des Himmels. [On the coloured light of double stars and certain other stars of the heavens]. Royal Bohemian Society 2:465, 1842.
- Edelman SK (ed): *Understanding Ultrasound Physics*, 3rd ed. Woodlands, Texas, Education for the Sonographic Professional, Inc. 2004.
- Fleischer A, Schulman H, Farmakides G, et al: Umbilical artery waveforms and intrauterine growth retardation. *Am J Obstet Gynecol* 151:502, 1985.
- Ott WJ: The diagnosis of altered fetal growth. *Obstet Gynecol Clin North Am* 15:237, 1988.
- Giles WB, Trudinger BJ, Baird PJ: Fetal umbilical artery flow velocity waveforms and placental resistance: Pathological correlation. *Br J Obstet Gynecol* 92:31, 1985.
- Manning FA: Intrauterine growth restriction. Diagnosis, prognostication, and management based on ultrasound methods. In Manning FA (ed): *Fetal Medicine: Principles and Practice*. Norwalk, CT, Appleton & Lange, 1995, pp 87–94.
- Hadlock FP, Deter RL, Harrist RB, et al: A date-independent predictor of intrauterine growth retardation: femur length/abdominal circumference ratio. *AJR Am J Roentgenol* 141:979, 1993.
- Trudinger BJ, Stevens D, Connelly A, et al: Umbilical artery flow velocity waveforms and placental resistance: The effect of embolizations of the umbilical circulation. *Am J Obstet Gynecol* 157:1443, 1987.
- Brown HL, Miller JM Jr, Gabert HA, et al: Ultrasonic recognition of the small-for-gestational-age fetus. *Obstet Gynecol* 69:631, 1987.
- Creasy RK, Resnick R: Intrauterine growth retardation. In Creasy RK, Resnick R (eds): *Maternal Fetal Medicine: Principles and Practice*. Philadelphia, WB Saunders, 1984.
- Kingdom JC, Burrell SJ, Kaufmann P: Pathology and clinical implications of abnormal umbilical artery Doppler waveforms. *Ultrasound Obstet Gynecol* 9:271, 1997.
- Morrow RJ, Adamson SL, Bull SB, et al: Effect of placental embolization on the umbilical arterial velocity waveform in fetal sheep. *Am J Obstet Gynecol* 161:1055, 1989.
- Bernstein IM, Horbar JD, Badger GJ, et al: Morbidity and mortality among very-low-birth weight neonates with intrauterine growth restriction. *Am J Obstet Gynecol* 182:198, 2000.
- Copel JA, Reed KL: *Doppler ultrasound in Obstetrics and Gynecology*. New York, Raven Press, 1995, pp 187–198.
- Trudinger BJ: Doppler ultrasonography and fetal well being. In Reece EA, Hobbins JC, Mahoney M (eds): *Medicine of the Fetus and Mother*. Philadelphia, JB Lippincott Co., 1992.
- Veille JC, Hanson R, Tatum K: Longitudinal quantitation of middle cerebral artery blood flow in normal human fetuses. *Am J Obstet Gynecol* 169:1393, 1993.
- Mari G, Deter RL: Middle cerebral artery flow velocity waveforms in normal and small-for-gestational age fetuses. *Am J Obstet Gynecol* 166:1262, 1992.
- Soothill PW, Ajayi RA, Campbell S, et al: Relationship between fetal acidemia at cordocentesis and subsequent neurodevelopment. *Ultrasound Obstet Gynecol* 2:80, 1992.
- Mari G, Abuhamad AZ, Brumfield J, et al: Doppler ultrasonography of the middle cerebral artery peak systolic velocity in the fetus: Reproducibility of measurement. *Am J Obstet Gynecol* 185:Abstract #669, 2001.
- Robertson WB, Brosens I, Dixon HG: Uteroplacental vascular pathology. *Eur J Obstet Gynecol Reprod Biol* 5:47, 1975.
- Pijnenborg R, Bland JM, Robertson WB, et al: Uteroplacental arterial changes related to interstitial trophoblast migration in early pregnancy. *Placenta* 4:397, 1983.
- Arduini D, Rizzo G, Boccolini MR, et al: Functional assessment of uteroplacental and fetal circulations by means of color doppler ultrasonography. *J Ultrasound Med* 9:249, 1990.
- Hernandez-Andrade E, Brodzki J, Lingman G, et al: Uterine artery score and perinatal outcome. *Ultrasound Obstet Gynecol* 19:438, 2002.
- Lees C, Parra M, Missfelder-Lobos H, et al: Individualized risk assessment for adverse pregnancy outcome by uterine artery Doppler at 23 weeks. *Obstet Gynecol* 98:369, 2001.
- Hecher K, Hackelöer B: Cardiotocogram compared to Doppler investigation of the fetal circulation in the premature growth-retarded fetus: longitudinal observations. *Ultrasound Obstet Gynecol* 9:152, 1997.
- Huisman TWA, Stewart PA, Wladimiroff JW: Flow velocity waveforms in the fetal inferior vena cava during the second half of normal pregnancy. *Ultrasound Med Biol* 17:679, 1991.
- Reed KL, Appleton CP, Anderson CF, et al: Doppler studies of vena cava flows in human fetuses: insights into normal and abnormal cardiac physiology. *Circulation* 81:498, 1990.
- Reuss ML, Rudolph AM, Dae MW: Phasic blood flow patterns in the superior and inferior venae cavae and umbilical vein of fetal sheep. *Am J Obstet Gynecol* 145:70, 1983.
- Rizzo G, Arduini D, Romanini C: Inferior vena cava flow velocity waveforms in appropriate and small-for-gestational-age fetuses. *Am J Obstet Gynecol* 166:1271, 1992.
- Rizzo G, Capponi A, Talone PE, et al: Doppler indices from inferior vena cava and ductus venosus in predicting pH and oxygen tension in umbilical blood at cordocentesis in growth-retarded fetuses. *Ultrasound Obstet Gynecol* 7:401, 1996.
- Chang CH, Chang FM, Yu CH, et al: Systemic assessment of fetal hemodynamics by Doppler ultrasound. *Ultrasound in Med and Biol* 26:777, 2000.
- Mielke G, Norbert B: Cardiac output and central distribution of blood flow in the human fetus. *Circulation* 103:1662, 2001.
- Mielke G, Benda N: Blood flow velocity waveforms of the fetal pulmonary artery and the ductus arteriosus: reference ranges from 13 weeks to term. *Ultrasound Obstet Gynecol* 15:213, 2000.
- Hong Y, Choi J: Doppler study on pulmonary venous flow in the human fetus. *Fetal Diagn Ther* 14: 86, 1999.
- Brezinka C: Fetal hemodynamics. *J Perinat Med* 29:371, 2001.
- Harada K, Rice MJ, Shiota T, et al: Gestational age and growth related alternations in fetal right and left ventricular diastolic filling patterns. *Am J Cardiol* 79:173, 1997.

37. Ben-Ami M, Peleg D, Haddad S, et al: Normal cardiac flow velocities at 14-16 weeks gestation measured by transvaginal ultrasound. *Ultrasound Obstet Gynecol* 19:47, 2002.
38. Severi FM, Rizzo G, Bocchi C, et al: Intrauterine growth retardation and fetal cardiac function. *Fetal Diagn Ther* 15:8, 2000.
39. Rizzo G, Arduini D, Romanini C: Doppler echocardiographic assessment of fetal cardiac function. *Ultrasound Obstet Gynecol* 2:434, 1992.
40. Groenenberg IAL, Stijnen T, Wladimiroff JW: Flow velocity waveforms in the fetal cardiac outflow tract as a measure of fetal well-being in intrauterine growth retardation. *Pediatr Res* 27:379, 1990.
41. Machado MVL, Chita SC, Allan LD: Acceleration time in the aorta and pulmonary artery measured by Doppler echocardiography in the midtrimester normal human fetus. *Br Heart J* 58:15, 1987.
42. Baschat AA, Gembruch U, Reiss I, et al: Relationship between arterial and venous Doppler and perinatal outcome in fetal growth restriction. *Ultrasound Obstet Gynecol* 16:407, 2000.
43. Baschat AA, Gembruch U, Harman CR: The sequence of changes in Doppler and biophysical parameters as severe fetal growth restriction worsens. *Ultrasound Obstet Gynecol* 18:571, 2001.
44. Hecher K, Bilardo CM, Stigter RH, et al: Monitoring of fetuses with intrauterine growth restriction: a longitudinal study. *Ultrasound Obstet Gynecol* 18:564, 2001.
45. Ferrazzi E, Bozzo M, Rigano S, et al: Temporal sequence of abnormal Doppler changes in the peripheral and central circulatory systems of the severely growth-restricted fetus. *Ultrasound Obstet Gynecol* 19:140, 2002.
46. Pardi G, Cetin I, Marconi AM, et al: Diagnostic value of blood sampling in fetuses with growth retardation. *N Engl J Med* 328:692, 1993.
47. Hecher K, Campbell S, Doyle P, et al: Assessment of fetal compromise by Doppler ultrasound investigation of the fetal circulation. Arterial, intracardiac, and venous blood flow velocity studies. *Circulation* 91:129, 1995.
48. Harrington K, Thompson MO, Carpenter RG, et al: Doppler fetal circulation in pregnancies complicated by pre-eclampsia or delivery of a small for gestational age baby: 2. Longitudinal analysis. *Br J Obstet Gynaecol* 106:453, 1999.
49. Bahado-Singh RO, Kovanci E, Jeffres A, et al: The Doppler cerebroplacental ratio and perinatal outcome in intrauterine growth restriction. *Am J Obstet Gynecol* 180:750, 1999.
50. Makikallio K, Vuolteenaho O, Jouppila P, et al: Ultrasonographic and biochemical marker of human fetal cardiac dysfunction in placental insufficiency. *Circulation* 105:2058, 2002.
51. Reed KI, Anderson CF, Shenker L: Changes in intracardiac Doppler blood flow velocities in fetuses with absent umbilical artery diastolic flow. *Am J Obstet Gynecol* 157:774, 1987.
52. Forouzan I, Graham E, Morgan MA: Reduction of right atrial peak systolic velocity in growth-restricted discordant twins. *Am J Obstet Gynecol* 175:1033, 1996.
53. Rizzo G, Capponi A, Rinaldo D, et al: Ventricular ejection force in growth-retarded fetuses. *Ultrasound Obstet Gynecol* 5:247, 1995.
54. Figueras F, Puerto B, Martinez JM, et al: Cardiac function monitoring of fetuses with growth restriction. *Eur J Obstet Gynecol Reprod Biol* 110:159, 2003.



## THE ROLE OF COMPUTED TOMOGRAPHY AND MAGNETIC RESONANCE IMAGING IN OBSTETRICS

Deborah Levine, MD

### Safety Issues

Safety of Computed Tomography in Pregnancy  
 Safety of Magnetic Resonance Imaging in Pregnancy  
*Fast Magnetic Resonance Imaging*  
*T2-Weighted Imaging*  
*T1-Weighted Imaging*  
*Maternal Imaging*  
*Pelvimetry*  
*Placental Evaluation*  
 Computed Tomographic Amniography  
*Fetal Imaging*  
*Real-Time Imaging*  
*Fetal Central Nervous System Anomalies*

### *The Fetal Surgery Patient*

### *Fetal Non-Central Nervous System Anomalies*

### *Screening for Anomalies*

Potential Pitfalls in Fetal Evaluation Using Fast Magnetic Resonance Imaging

### Imaging Beyond Anatomy

Diffusion-Weighted Imaging

Magnetic Resonance Spectroscopy

Oxygenation Imaging

Magnetic Resonance Volumetry

### Conclusion

Ultrasonography is the primary screening modality for obstetric imaging. When additional information is needed to care for pregnant patients, magnetic resonance imaging (MRI) can be used. This modality allows for visualization of maternal and fetal anatomy when sonography is insufficient to provide an adequate diagnosis. Because of radiation exposure, use of computed tomography (CT) is generally limited to evaluation of the acute maternal abdomen, when MRI is not available for this indication.

Because MRI provides superior contrast resolution compared with CT, uses no ionizing radiation, and permits imaging in more than one plane, it has been used in fetomaternal imaging. Traditionally, pelvic MRI has been used during pregnancy to evaluate maternal anatomy and abnormalities such as adnexal masses, which required further characterization beyond that available with ultrasound. Although adnexal structures can be visualized with conventional MRI techniques, fetal anatomy typically cannot be adequately assessed with conventional sequences because of degradation of image quality by fetal motion during the relatively long acquisition times.<sup>1-3</sup> Fast-scan techniques allow for imaging without maternal or fetal sedation and have markedly increased enthusiasm for use of this imaging tool to evaluate the obstetric patient and fetus. In this chapter, I address the use of CT and fast MRI in the evaluation of the pregnant patient and the fetus.

## SAFETY ISSUES

### Safety of Computed Tomography in Pregnancy

In general, because of the potential effects of radiation on the developing conceptus, we try to avoid the use of CT during pregnancy. The dose to the uterus from an abdominal CT is typically about 10 mGy (1 rad), and the dose to the uterus from an abdominal and pelvic CT is about 30 mGy (3 rads).<sup>4</sup> In the first trimester, this dose is sufficient to be associated with spontaneous abortion and growth restriction. In the second and third trimesters, these risks are decreased. However, there is a slight increased risk of childhood cancer with fetal irradiation.<sup>5,6</sup> The National Council on Radiation Protection and Measurements states that the risk of an abnormality caused by diagnostic radiation is considered to be negligible at 5 rads or less compared with the other risks of pregnancy.<sup>7</sup> Therefore, when the benefit of diagnosis supercedes the theoretic risk of radiation exposure to the fetus, it is worthwhile to perform diagnostic imaging with CT.

To minimize these risks, when performing a CT scan in a pregnant patient, it is important to have the scanner controls set in a manner to minimize radiation dose. Scans for evaluation of abdominopelvic disease should be performed with intravenous contrast to maximize the diagnostic

information obtained, and to limit the need for repeating the study if a noncontrast scan is insufficient for diagnosis.

### Safety of Magnetic Resonance Imaging in Pregnancy

There are no known biologic risks associated with MRI. No delayed sequelae from MRI examination have been encountered, and it is expected that the potential risk for any delayed sequelae is extremely small or nonexistent. The MRI procedure is not believed to be hazardous to the fetus.<sup>8-12</sup> In a survey of female MRI workers, no substantial increase in adverse pregnancy outcomes was found.<sup>9</sup> According to the Safety Committee of the Society for Magnetic Resonance Imaging,<sup>13</sup> MRI procedures are indicated for use in pregnant women if other nonionizing forms of diagnostic imaging are inadequate or if the examination provides important information that would otherwise require exposure to ionizing radiation (e.g., x-ray CT). It is required that pregnant patients be informed that, to date, although there is no indication that the use of clinical MRI procedures during pregnancy produces deleterious effects, according to the Food and Drug Administration,<sup>12</sup> the safety of MRI procedures during pregnancy has not been definitively proven. Also, it is well known that dividing cells, as in the case of the developing embryo during the first trimester, are susceptible to injury from a variety of physical agents. Because of limited data, we avoid MRI in the first trimester when feasible. However, if the MRI is being ordered for assessment of right lower quadrant pain, and the alternative imaging modality is CT (if MRI is not performed) then the risk of radiation exposure with CT must be weighed against the theoretic risk of MRI exposure. Because MRI is believed to be safe in pregnancy, the recent recommendation of Shellock and Cruess is that "in cases where the referring physician and attending radiologist can defend that the findings of the MR procedure have the potential to affect the care of the mother or fetus... the MR procedure may be performed... regardless of the trimester."<sup>14</sup> Note that this discussion regarding safety of MR in pregnancy is for imaging at 1.5 T or lower field strengths. Imaging at higher field strengths has not yet been proven safe in pregnancy.

Gadolinium is not recommended for use in pregnancy. Gadolinium has been shown to cross the placenta and appear within the fetal bladder only moments after intravenous administration.<sup>15</sup> From the fetal bladder, the contrast is excreted into the amniotic fluid, where it is then swallowed and potentially reabsorbed from the gastrointestinal tract. Because of this reabsorption, the half-life of gadolinium in the fetal circulation is not known.<sup>15</sup> Gadopentate dimeglumine has been shown to retard development slightly in rats when given in doses 2.5 times the human dose.<sup>16</sup> It is considered a pregnancy category C drug (meaning that it should be given only if potential benefit outweighs the risk) because animal studies revealed adverse effects, but no controlled studies have been performed in humans.<sup>16</sup>

### Fast Magnetic Resonance Imaging

Most of the MRI scans in this chapter from Beth Israel Deaconess Medical Center were obtained with a 1.5 T

superconducting system with four- or eight-element phased-array surface coils. The minimum gradient rise time is 600 microseconds (for a 25-mT peak gradient amplitude). The whole body specific absorption rate is less than 3.0 W/kg. Patients are positioned supine and feet first in the magnet to minimize claustrophobia. Images are acquired in axial, coronal, and sagittal planes of the fetus or orthogonal to the maternal pelvis depending on the indication for the examination. If patients are claustrophobic, sedation can be given with sublingual benzodiazepines. If the patient is uncomfortable lying supine, she can be imaged in the lateral decubitus position.

### T2-Weighted Imaging

Half Fourier single-shot RARE (*Rapid Acquisition with Relaxation Enhancement*) technique is used to obtain T2-weighted images. This is a turbo-spin echo technique in which the echo train length is approximately one half as long as a typical RARE sequence. The missing data are artificially created by computer to shorten acquisition time. A typical sequence for fetal imaging uses an echo spacing of 4.2 milliseconds, a TE of 60 milliseconds, an echo train length of 72, 1 acquisition, 4-mm section thickness, 24 × 24 cm field of view, and 192 × 256 acquisition matrix. A 130- to 150-degree refocusing pulse is used to minimize the amount of radio-frequency power deposition.

The acquisition time per image ranges from 400 to 800 milliseconds, depending on the imaging parameters. A 1-second delay between image acquisitions minimizes the specific absorption rate. Thus, the scan time for 13 slices acquired in a single sequence is 17 seconds. The highly T2-weighted RARE sequences provide excellent contrast resolution of the fetal tissues.<sup>17-21</sup> When using RARE imaging for evaluation of the fetus, it may be desirable to have contiguous sections because the fetus may move between sequences. However, for a better signal-noise ratio in fetuses for which motion is less of an issue, the acquisitions can be interleaved with an interslice gap equal to that of the slice thickness to minimize inadvertent radiofrequency excitation of adjacent sections.

Because the RARE sequence is a single-slice acquisition technique, it limits artifacts related to maternal and fetal motion<sup>18,21</sup>; only the slice in which the motion occurred will be affected. This will generally lead to nonvisualization of a portion of the fetal anatomy but may lead to repeated visualization of a fetal part.<sup>21</sup> For example, if the hand moves in plane with the sequence, it may be visualized more than once during the scan. Because fetal motion generally occurs throughout the examination, we have each acquisition serve as the scout for the subsequent acquisition when evaluating fetal anatomy.

### T1-Weighted Imaging

T1-weighted imaging of the fetus is more difficult than T2-weighted imaging, because there is less inherent soft tissue contrast. In addition, because most T1-weighted sequences are not single shot, the images are degraded by motion that occurs during the breath-hold. Our current favored technique is a TurboFLASH with repetition time (TR)/TE = 15.4/4.2, 6 mm slice thickness, 35 cm field of



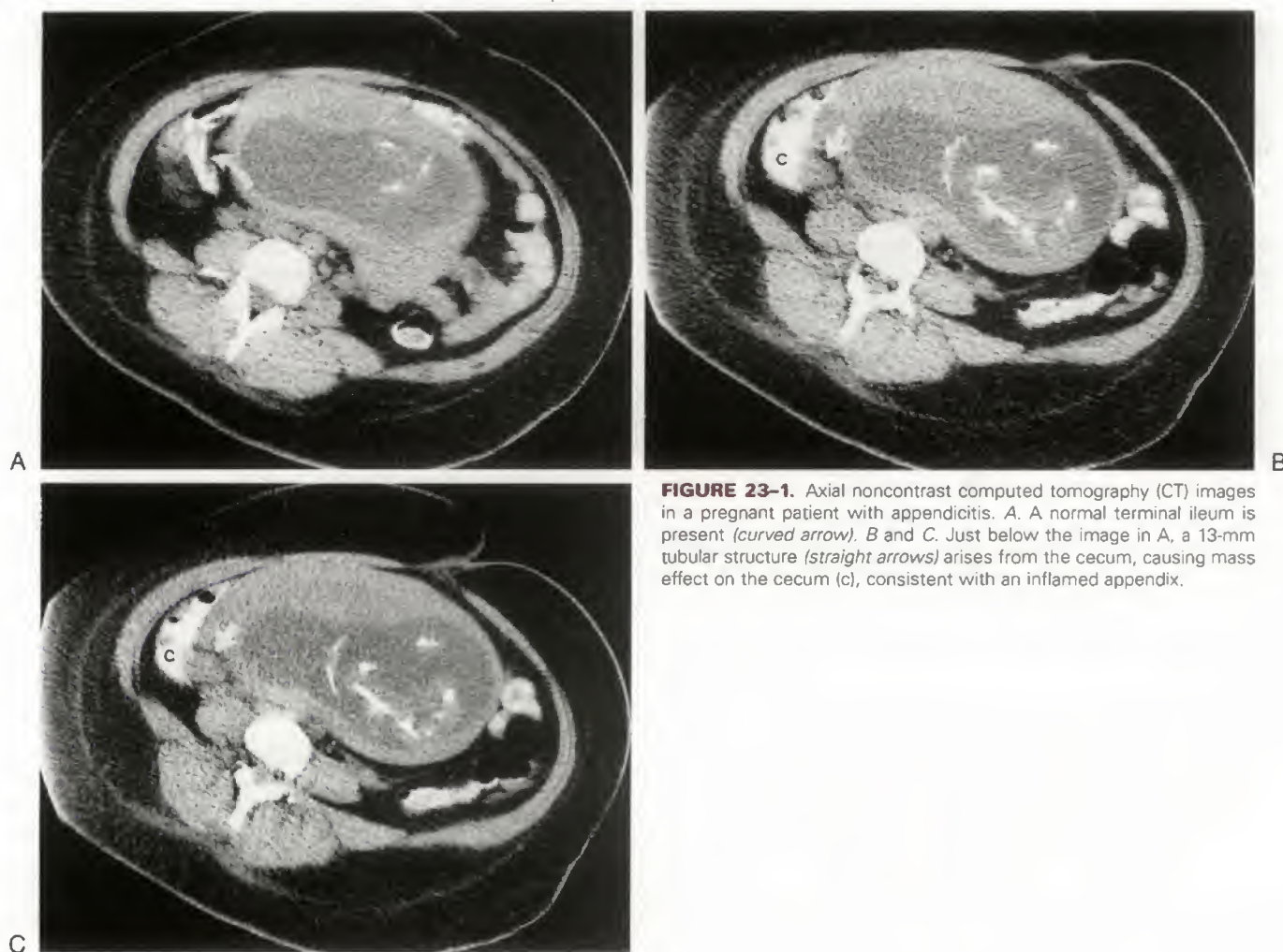


**FIGURE 23-1.** Axial noncontrast computed tomography (CT) images in a pregnant patient with appendicitis. A. A normal terminal ileum is present (*curved arrow*). B and C. Just below the image in A, a 13-mm tubular structure (*straight arrows*) arises from the cecum, causing mass effect on the cecum (c), consistent with an inflamed appendix.

view, and matrix of  $160 \times 256$ . T1-weighted images are useful for evaluating the maternal pelvis, confirming hemorrhage or fat in a lesion, and assessing the liver position in cases of congenital diaphragmatic hernia.

### Maternal Imaging

**Abdominal Pain.** Typically, evaluation of abdominal pain in a pregnant patient can be performed without a radiologic examination. The classic case necessitating a CT examination is a pregnant patient with right-sided pain in whom the diagnosis of appendicitis is uncertain, and for whom MRI for appendicitis is either contraindicated or not available (Fig. 23-1). Because, in pregnancy, the appendix is lifted out of the pelvis by the growing uterus, the clinical diagnosis of appendicitis is difficult. If the appendix is not visualized sonographically, it is reasonable to obtain additional imaging in patients in whom appendicitis is of concern. Pregnant patients have an increased incidence of perforation compared with nongravid patients with appendicitis. Similar to the nongravid patient, a mass may be seen focally indenting the cecum. Occasionally, CT may be performed for bowel obstruction or left-sided pain. These

cases should be interpreted in a manner similar to that of the nongravid patient.

MRI can be useful in the evaluation of abdominal pain in the pregnant patient without the need for ionizing radiation. Examples include evaluation for suspected appendicitis (Fig. 23-2, Table 23-1), abdominal pregnancies,<sup>24-26</sup> uterine rupture,<sup>27</sup> pelvic vein thrombosis,<sup>28</sup> biliary disease (Fig. 23-3A), and small bowel obstruction complicating pregnancy (Fig. 23-4).

**Hydronephrosis.** MRI also can be used in the evaluation of the maternal urinary tract. Physiologic hydronephrosis is the most common cause of dilatation of the urinary tract in pregnancy (Fig. 23-3B). However, renal colic also can occur secondary to stones in .03% to .24% of pregnant patients.<sup>29-31</sup> In physiologic hydroureteronephrosis, the dilatation extends to the sacral promontory, with tapering of the lower part of the dilated ureter. In obstruction caused by stones, an intrinsic ureteral mass is present. The traditional screening method for evaluating the pregnant patient with renal colic is ultrasound. Intravenous urography is performed in occasional cases. Some now advocate CT urograms because they are more sensitive for small stones. However, in CT urography the radiation dose to the uterus is about 3 rads. With the



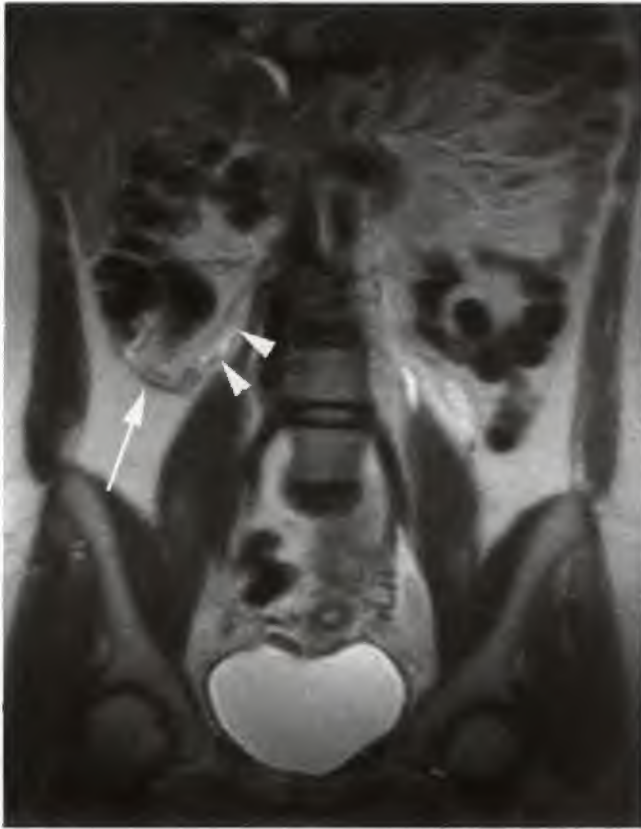


**FIGURE 23-2.** Mild acute appendicitis at 13 weeks' gestation. Coronal magnetic resonance image shows an enlarged fluid-filled appendix (arrow) measuring up to 9 mm in diameter. Note the increased signal intensity (arrowheads) in the mesoappendix consistent with inflammatory changes. Surgery and pathology confirmed the diagnosis. (From Eyvazzadeh A: MR imaging of right lower quadrant pain in pregnancy. *AJR Am J Roentgenol* 183:908, 2004.)

advent of MR urography, it is no longer necessary to expose the pregnant patient to the radiation and iodinated contrast media risks. Roy et al<sup>32</sup> showed that in 15 cases of hydro-ureteronephrosis in pregnancy, MR urography correctly identified 10 cases of physiologic dilatation, 4 cases of stones, and 1 case of ureteropelvic junction obstruction. Scans can be performed both with a thick slab heavily T2-weighted image and with thin slices in the maternal axial plane to assess for small filling defects.

**Adnexal Masses.** It is well established that MRI is useful in the pregnant patient for the evaluation of adnexal masses that cannot be fully characterized by ultrasound. As Weinreb et al<sup>33</sup> and Kier et al<sup>34</sup> found, in 7 of 16 (43%) patients and 8 of 17 (47%) patients studied respectively, MRI added additional information beyond that afforded by ultrasound (Fig. 23-5). Fast MRI techniques provide exquisite characterization of masses (Fig. 23-6) and should be considered when designing a protocol for these examinations. We have found MR to be particularly helpful in patients who have hyperstimulated ovaries, and in whom ovarian torsion is of concern due to pelvic pain. In these cases, torsion can be present, even with normal flow on Doppler examination. MRI can show edematous ovarian

stroma, associated with intermittent or partial torsion (see Fig. 23-6).

### Pelvimetry

Although pelvimetry is no longer commonly performed, it is beneficial in patients who desire a trial of labor when the fetus is in breech presentation.<sup>35-37</sup> When pelvimetry is requested, MRI offers the benefit of accurate measurement of the bony structures in the pelvis without ionizing radiation. When MRI is not available, CT pelvimetry has been shown to be as reliable as conventional radiographic pelvimetry.

Using the protocol for CT pelvimetry as described by Federle et al,<sup>38</sup> the radiation exposure is much less than that using conventional x-ray pelvimetry. Dose estimates using low-exposure (40 mA) technique demonstrate a maximal dose to the fetus of 0.23 rad. In this protocol, anteroposterior (AP) and lateral scout digital views are obtained, and one transverse axial section is obtained through the foresh of the femoral heads (Fig. 23-7). The AP pelvic inlet diameter (from the sacral promontory to the posterosuperior margin of the pubic symphysis) and transverse pelvic inlet diameter (between the arcuate lines of the iliac bones) are measured directly on scout views, using electronic calipers. The interspinous diameter is measured between the ischial spines on the axial image.

For MRI pelvimetry, gradient-echo techniques are used, with scan times of less than 5 minutes.<sup>36,39</sup> A midline sagittal view is obtained for assessment of the fetal presentation and for measurement of the anteroposterior pelvic inlet diameter (see Fig. 23-7D). Oblique coronal views (parallel to the AP pelvic inlet) are obtained for measurement of the pelvic inlet (maximum distance between the arcuate lines of the iliac bones on either side) and bispinous diameter.<sup>36</sup>

Using acceptable values of greater than 11.0 cm for the anteroposterior pelvic inlet, greater than 9.5 cm for the transverse midpelvic distance (interspinous distance), and greater than 11.0 cm for the pelvic outlet, van Loon et al<sup>36</sup> showed that, although use of MRI pelvimetry in breech presentation at term did not reduce the overall cesarean section rate, it allowed better selection of the delivery route with a significantly lower emergency cesarean section rate.

### Placental Evaluation

In patients with suspected placenta previa, a sagittal MRI sequence oriented in the plane of the cervix is used to assess the placental margin.<sup>3,40,41</sup> Given widespread use of transvaginal and translabial ultrasound, this is unlikely to be a common indication for an MRI examination. However, the placental edge is easily identified with fast-scan techniques (Fig. 23-8). Unusual placental abnormalities, such as succenturiate lobe, are readily assessed with MRI.<sup>1</sup> MRI also has been advocated in the evaluation of placental masses such as chorioangioma.<sup>42</sup>

A number of case reports recommended MRI for the evaluation of placenta accreta.<sup>43-46</sup> Placenta accreta, including its variants placenta increta and percreta, is a disorder that results in significant intrapartum morbidity and mortality. Uncontrollable bleeding frequently leads to hysterectomy. Abnormalities of placental attachment may



**Table 23-1** MR Imaging Protocol for Pregnant Patients with Acute Right Lower Quadrant Pain

Parameters	Pulse Sequences*					
	Coronal Single-Shot Fast SE	Axial Single-Shot Fast SE	Sagittal Single-Shot Fast SE	Axial 2D FS Single-Shot Fast SE	IP and OP 2D T1W GRE	2D TOF
Sequence type	Single shot	Single shot	Single shot	Single shot	GRE	GRE
Repetition time (msec)	800–1100	800–1100	800–1100	800–1100	205	5500
Echo time (msec)	60	60	60	60	2.2/4.5	100
Flip angle (degrees)	130–155	130–155	130–155	130–155	80	45
No. of signals acquired	1	1	1	1	1	1
2D or 3D	2D	2D	2D	2D	2D	2D
Section thickness (mm)	4	4	4	4	5	3
Gap (mm)	1	1	1	1	2	1
Field of view (mm)	350	350	350	350	350	350
No. of partitions or sections	20	20	20	20	32	24
Orientation	Coronal	Axial	Sagittal	Axial	Axial	Axial
Phase × frequency steps	192 × 256	192 × 256	192 × 256	192 × 256	160 × 256	128 × 256
Rectangular field of view	No	0.75	0.75	0.75	0.75	0.75
Fat suppression	No	No	No	Yes	No	No
Zero fill section	No	No	No	No	No	No
Partial Fourier	Yes	Yes	Yes	Yes	No	No
No. of measurements or repeats	1	1	1	1	1	1
Single or multiple shots	Single	Single	Single	Single	Multiple	Multiple
Echo train length	...	...	...	...	...	...
Bandwidth (kHz) <sup>†</sup>	62.5	62.5	62.5	62.5	62.5	31.25
Parallel imaging	No	No	No	No	No	No
Breath hold	Yes	Yes	Yes	Yes	Yes	Yes

From Pedrosa I, Zeikus EA, Levine D, Rofsky NM: MR imaging of acute right lower quadrant pain in pregnant and nonpregnant patients. *Radiographics* 27:721, 2007.

Note: An eight-channel torso phased-array coil is used.

\*FS, fat-saturated, IP, in-phase, OP, opposed-phase, TOF, time of flight, T1W, T1-weighted.

<sup>†</sup>62.5 kHz = 488 Hz/pixel, 31.25 kHz = 244 Hz/pixel.

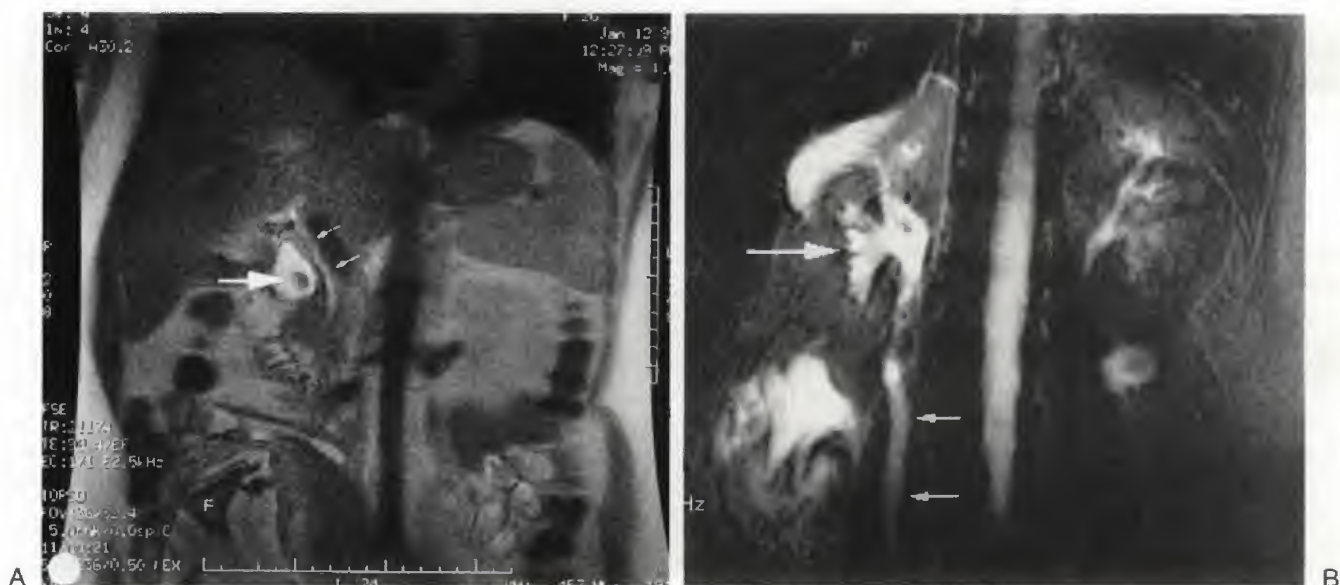


**FIGURE 23-3.** Coronal magnetic resonance image of pregnant patient with right upper quadrant pain. A. A gallstone is seen within the gallbladder (large arrow). The common duct is nondilated without evidence of choledocholithiasis (small arrows). A fetal foot (F) is seen within the gravid uterus. TE = 99.4, FOV 36 × 32, matrix 512 × 256, 5 mm thick, one acquisition. B. Coronal image shows mild right hydroureteronephrosis within normal limits for gestational age. TE = 776, FOV 40 × 36, matrix 512 × 256, 20 mm thick, one acquisition. (Photos courtesy of Randy Ernst, MD, LBJ Hospital, Houston, TX.)

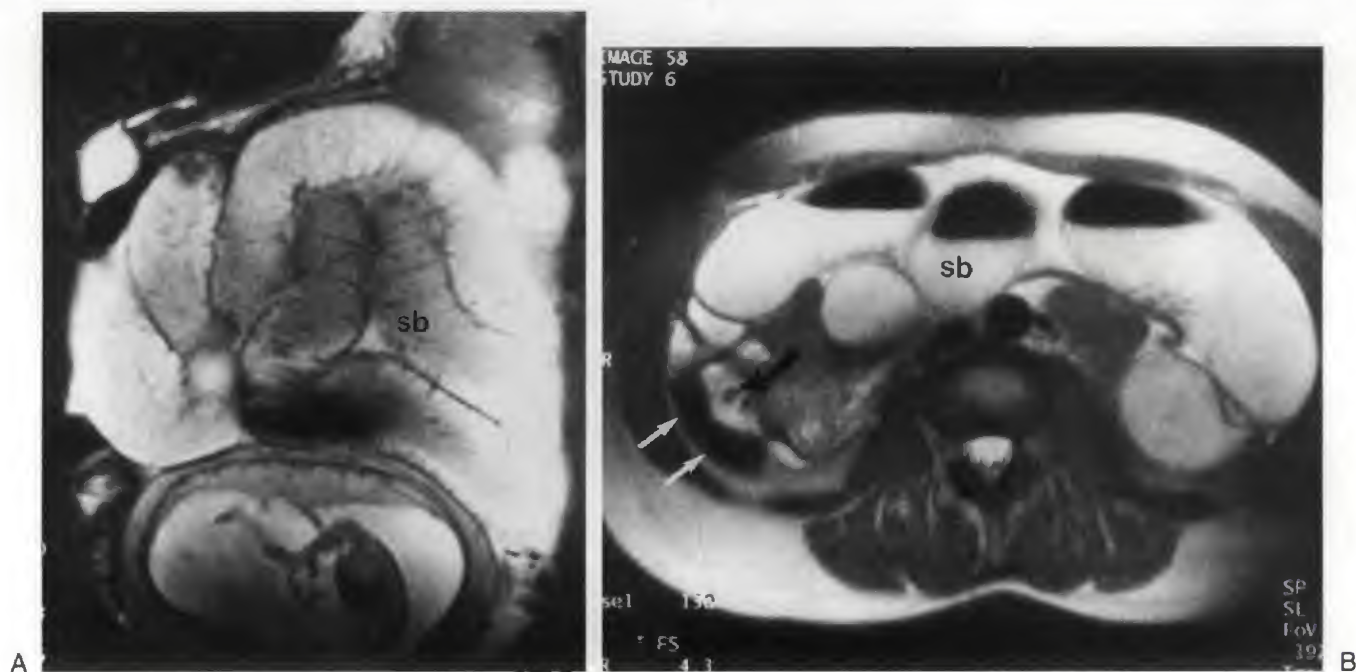


**FIGURE 23-4.** Distal small bowel obstruction in pregnant patient with prior abdominal surgery and adhesions. Coronal (A) and axial (B) single-shot RARE images demonstrate dilated small bowel (sb) with nondilated small bowel loop in the right lower quadrant (curved arrow) and with nondilated colon (straight arrows). (From Levine D: State of the art: Obstetric MR imaging. *Radiology* 211:609, 1999.)

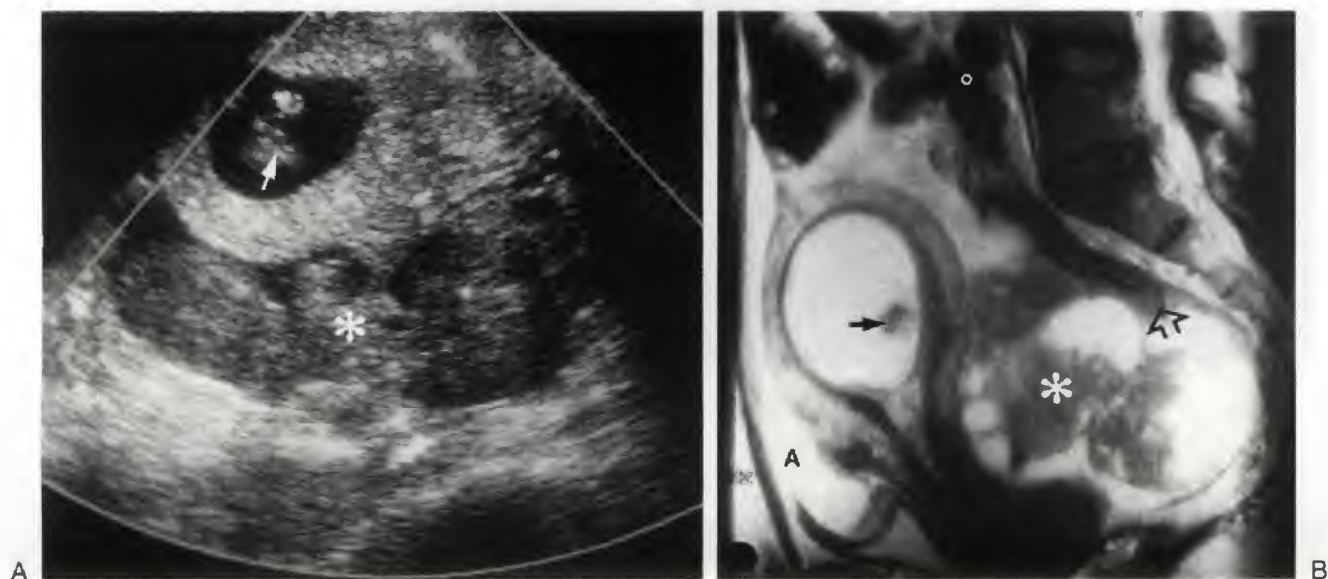


**FIGURE 23-5.** Ovarian neoplasm identified during pregnancy. A. Transvaginal sonogram showing an early intrauterine gestation with an identifiable embryo (arrow). Lobulated soft tissue mass (\*) and fluid are seen within the cul-de-sac. B. Sagittal T2-weighted image. The full extent of the large solid and cystic mass (\*), posterior to the gravid uterus and embryo (arrow), is clearly evident. There is evidence of invasion of the sigmoid colon (open arrow) and ascites (A). The appearance on magnetic resonance imaging is indicative of an ovarian malignancy. (Case courtesy of V. A. Feldstein, MD, San Francisco, CA.)



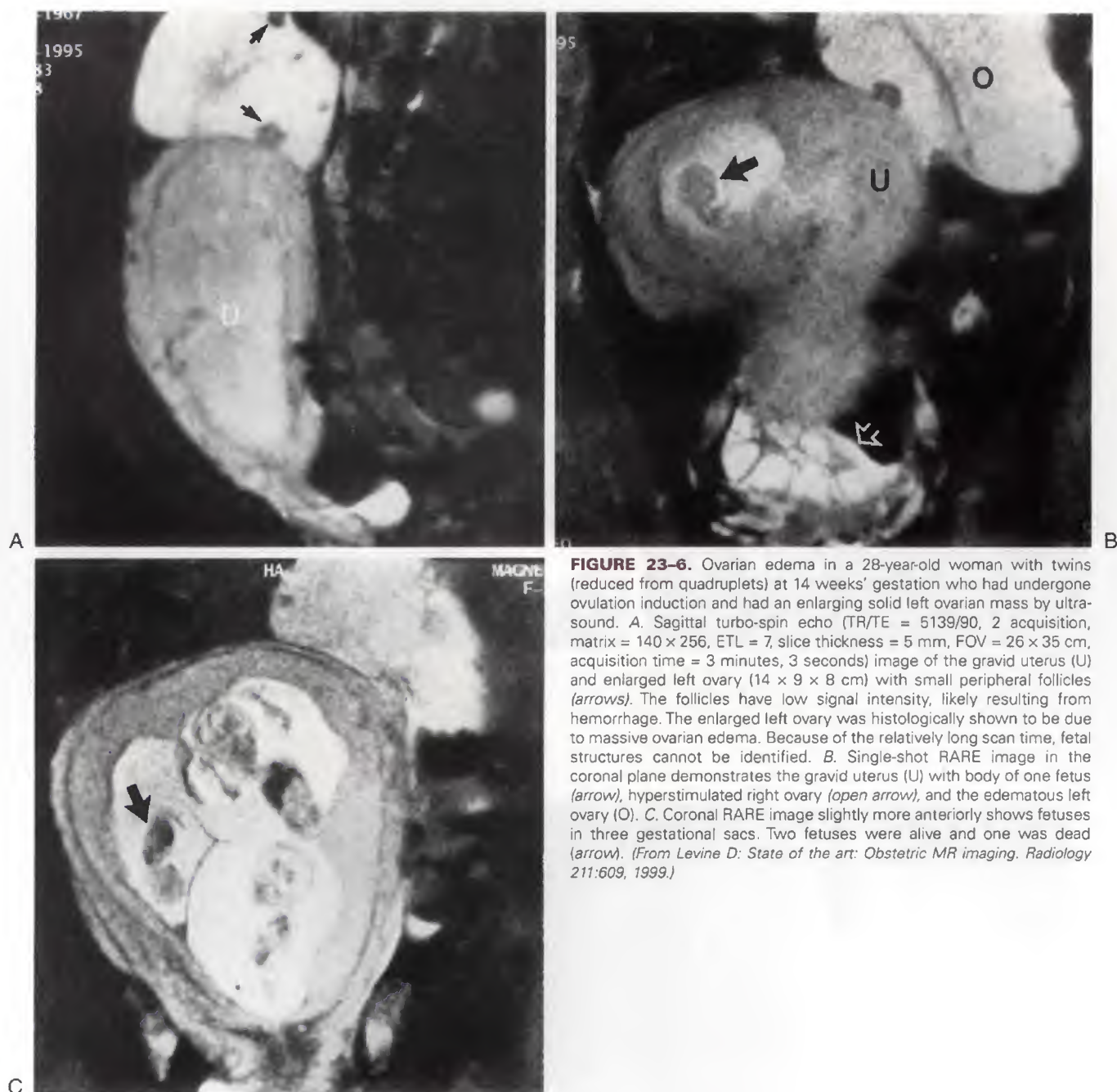


**FIGURE 23-6.** Ovarian edema in a 28-year-old woman with twins (reduced from quadruplets) at 14 weeks' gestation who had undergone ovulation induction and had an enlarging solid left ovarian mass by ultrasound. **A.** Sagittal turbo-spin echo (TR/TE = 5139/90, 2 acquisition, matrix =  $140 \times 256$ , ETL = 7, slice thickness = 5 mm, FOV =  $26 \times 35$  cm, acquisition time = 3 minutes, 3 seconds) image of the gravid uterus (U) and enlarged left ovary ( $14 \times 9 \times 8$  cm) with small peripheral follicles (arrows). The follicles have low signal intensity, likely resulting from hemorrhage. The enlarged left ovary was histologically shown to be due to massive ovarian edema. Because of the relatively long scan time, fetal structures cannot be identified. **B.** Single-shot RARE image in the coronal plane demonstrates the gravid uterus (U) with body of one fetus (arrow), hyperstimulated right ovary (open arrow), and the edematous left ovary (O). **C.** Coronal RARE image slightly more anteriorly shows fetuses in three gestational sacs. Two fetuses were alive and one was dead (arrow). (From Levine D: *State of the art: Obstetric MR imaging*. Radiology 211:609, 1999.)

result in the placenta attaching directly onto the myometrium (placenta accreta), extending more deeply into the myometrium (placenta increta), or invading through the uterine serosa (placenta percreta). These conditions occur in 5% of patients with placenta previa, in up to 10% of patients after four or more cesarean sections, and in 67% of patients who have both placenta previa and four or more cesarean sections.<sup>47</sup>

A study from our laboratory<sup>48</sup> found that transvaginal ultrasound with a partially full bladder was most beneficial in the evaluation of placenta accreta occurring in the lower uterine segment. However, in 1 of 17 cases, the placenta

accreta was identified only by the MRI examination because of a posterior placenta occurring over a region of a previous myomectomy (Fig. 23-9). We recommend that transvaginal ultrasound with a partially full bladder be the method of choice for the evaluation of placenta accreta. For patients with a history of myomectomy and posterior placenta, MRI should be considered.

### Computed Tomographic Amniography

In rare cases in which ultrasound is not sufficient to diagnose monoamniotic twins, amniography may be used.<sup>49-51</sup> For

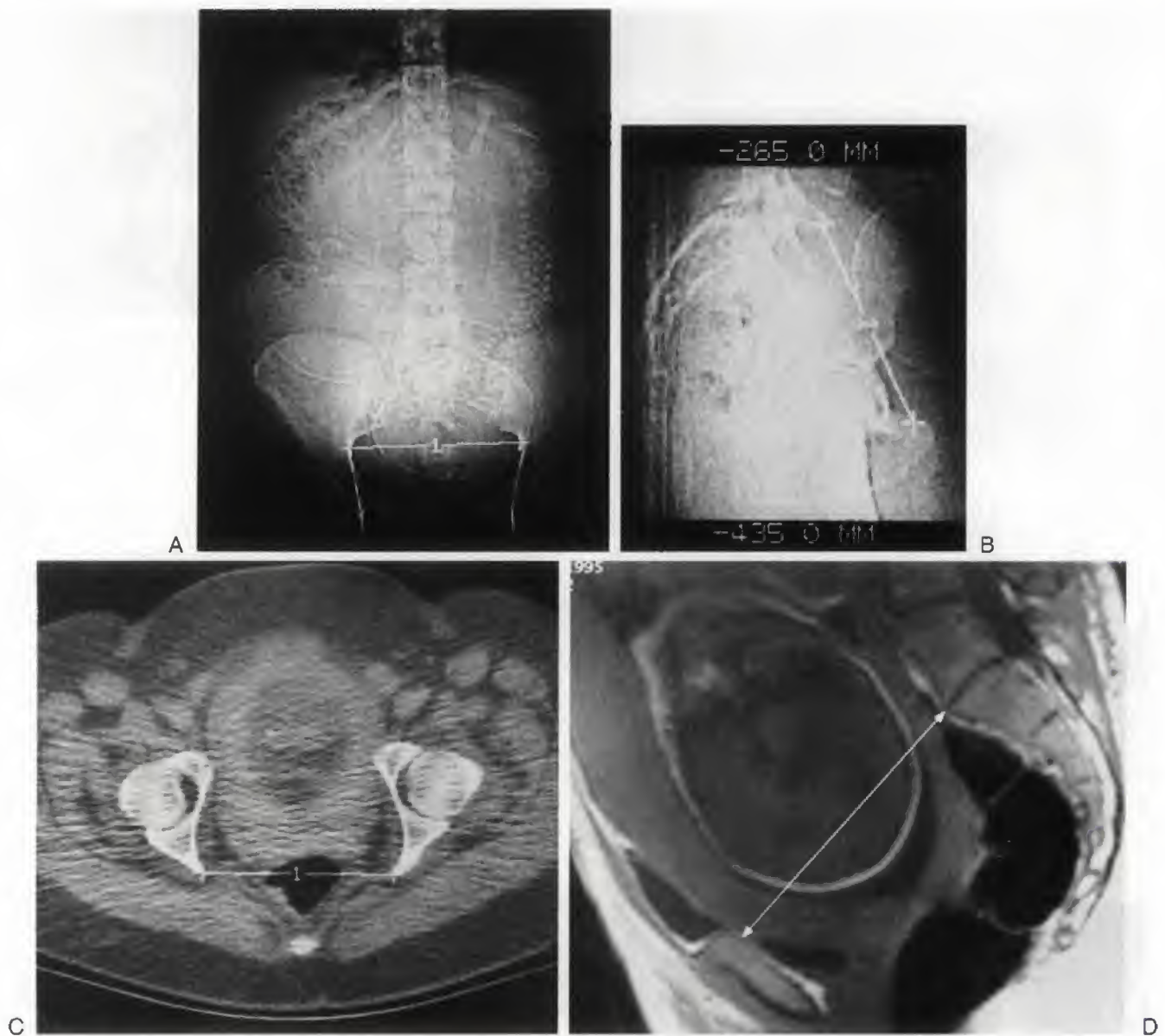


**FIGURE 23-7.** Computed tomography (CT) (A-C) and magnetic resonance imaging (MRI) (D) pelvimetry. A. Anteroposterior scout view demonstrating the transverse pelvic inlet, measured with electronic cursors. B. Lateral scout view demonstrating the obstetric conjugate measurement of the anteroposterior pelvic inlet. C. Transverse CT section through the ischial spines demonstrating the bispinous or transverse diameter. D. MRI pelvimetry. T1-weighted sagittal view of the pelvis demonstrates the pelvic inlet (arrows). This view is used as a scout for subsequent sequences.

CT amniography, sonography is used to select a transverse plane of section and this location is marked. A single transverse axial precontrast CT may be obtained at this level. Using sonographic guidance, the amniotic sac is punctured and water-soluble iodinated contrast material is instilled. When a contrast agent with a concentration of 300 mg of iodine per millimeter of solution is used, 1 mL per 100 mL of anticipated amniotic fluid volume provides adequate opacification. Typically, 8 to 10 mL of contrast agent is used in a third trimester twin pregnancy with normal amniotic fluid volume. A postcontrast transverse CT scan is obtained (Fig. 23-10). Monoamniocity is indicated by the presence of contrast material completely surrounding each twin, although rarely this appearance may be mimicked by a

diamniotic pregnancy with a stuck twin. Finberg and Clewell<sup>50</sup> reported that the presence of contrast material within the gastrointestinal tract of both twins, after a delay of approximately 4 hours, is a reliable, unambiguous sign of monoamniocity.

### Fetal Imaging

Early studies using MRI in the evaluation of fetal morphology were hindered by fetal motion. Recommendations were made to limit imaging to late pregnancy or to cases of oligohydramnios because fetal motion is lessened in these situations.<sup>35,52</sup> Garden et al<sup>53</sup> described gradient-echo images for the evaluation of fetal anatomy. Images were





**FIGURE 23-8.** Partial placenta previa in a 29-week pregnancy. Sagittal magnetic resonance imaging of the cervix shows placenta tip (arrow) partially covering the internal os of the cervix. (From Levine D: *State of the art: Obstetric MR imaging*. *Radiology* 211:609, 1999.)

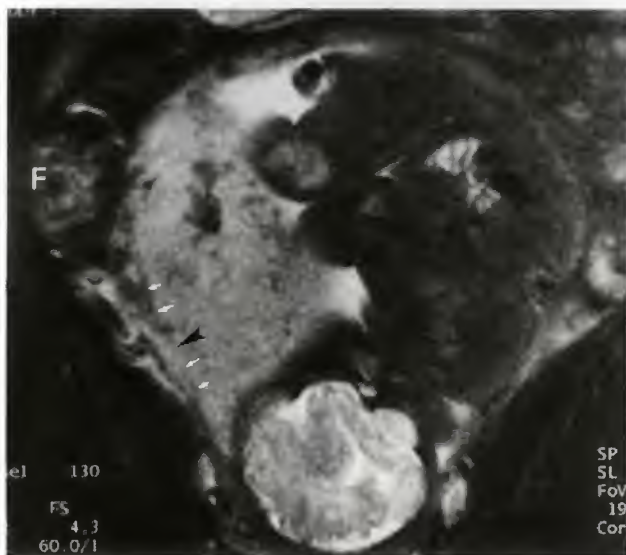


**FIGURE 23-9.** Placenta accreta diagnosed with magnetic resonance imaging (MRI) in a patient with a previous posterior myomectomy. Coronal RARE MRI shows an absent myometrial-placental interface in a posterolateral location (arrowhead) surrounded by normal myometrial-placental interface (small white arrows). This region was not well evaluated with ultrasound. A fibroid (F) is present in the right lateral aspect of the uterus. (From Levine D: *Placenta accreta: Evaluation with color Doppler, power Doppler and fast MRI*. *Radiology* 205:773, 1997.)

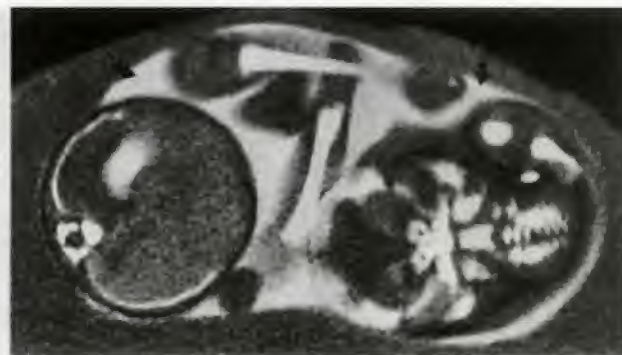


**FIGURE 23-10.** Computed tomography (CT) amniogram. Transverse CT section obtained after contrast instillation showing opacified amniotic fluid (arrows) completely surrounding both fetuses, confirming monoamnicity.

obtained in 3 to 14 seconds that reduced artifact from fetal motion but were compromised by low signal-to-noise ratio. Other investigators used benzodiazepines to sedate the pregnant patient or curarization by direct fetal injection to decrease fetal motion.<sup>1,3,54-58</sup> Subsequently, echo planar imaging was advocated for obstetric MRI because its short (100 milliseconds) scan time makes fetal paralysis unnecessary.<sup>6,59</sup> However, echo planar imaging has several disadvantages, including susceptibility artifacts, chemical shift artifacts, and limited availability as a result of special hardware requirements.<sup>60</sup> Despite these limitations, fetal MRI has been suggested as an important technique to evaluate anomalous fetuses.<sup>61-63</sup>

Fast MRI sequences with subsecond image acquisitions, such as single-shot RARE MRI, allow for excellent visualization of fetal anatomy.<sup>21</sup> In fetuses less than 20 weeks' gestational age, obtaining images with respect to fetal anatomy is important. In older gestational age groups, this is less of an issue. For ease of image interpretation, we attempt to align our acquisition planes orthogonal to fetal anatomy. However, if the fetus moves and the planes are slightly nonorthogonal, the acquisitions are not repeated, unless a particular question cannot be answered with the acquired images.

### Real-Time Imaging

We have recently begun using real-time imaging for improved assessment of specific areas of fetal anatomy. Using this technique, single images are repeated until they are obtained in the appropriate fetal orientation in order to best display the fetal anatomy.<sup>64,65</sup> We have found this to be particularly helpful to illustrate the normal fetal corpus callosum and to demonstrate the secondary palate in fetuses at risk for cleft palate (Fig. 23-11).<sup>66,67</sup>

### Fetal Central Nervous System Anomalies

One area in which MRI has proven to be especially beneficial is in the evaluation of the fetal central nervous system (CNS). Sonographic evaluation of the fetal CNS is limited by the nonspecific appearance of some anomalies; by



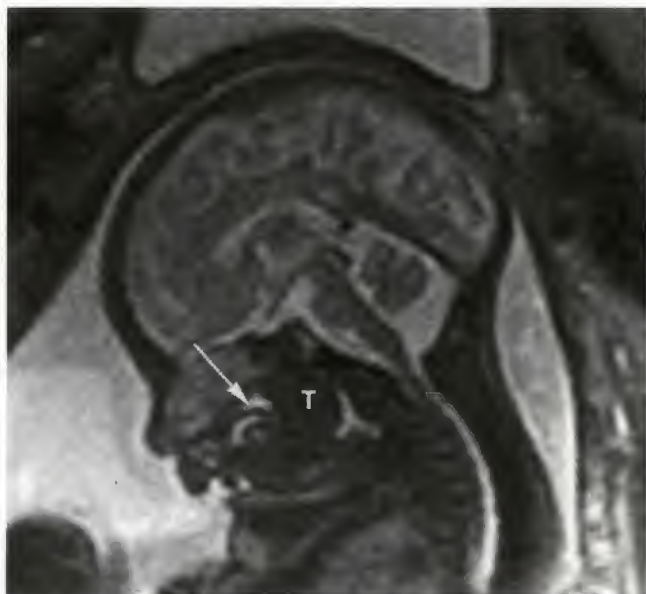


**FIGURE 23-11.** Fetus with micrognathia at 35 weeks, with soft palate defect seen on midline MR image obtained with real-time sequences. Real-time was helpful in obtaining images during fetal swallowing that allowed for outlining of the palate abnormality. Image shows an intact anterior palate (arrow), however the tongue (T) rides above the palatal shelf posteriorly, consistent with a cleft soft palate. Postnatal diagnosis was cleft soft palate with Robin sequence. The neonate required a tongue-lip adhesion to control his airway and permit feeding.

technical factors that limit resolution of the side of the brain near the transducer; by ossification, which obscures visualization of posterior fossa structures; and by subtle parenchymal abnormalities, which frequently cannot be visualized with ultrasound.<sup>68</sup> Multiplanar views can be difficult to obtain with sonography because of fetal position or advanced gestational age. MRI can be used to obtain multiplanar views. In addition, MRI allows for direct visualization of the brain parenchyma and, thus, detailed evaluation of the CNS anatomy in a manner not possible with sonography.<sup>69</sup> Many case reports and series reports detail the potential of MRI to improve on the sonographic diagnosis of CNS anomalies.<sup>63,70-81</sup>

Results from our study demonstrated that of 124 fetuses with CNS anomalies confirmed at our institution, there were 86 changes in counseling, 49 major changes in diagnosis, and 27 clear changes in management.<sup>81</sup> MRI findings not visualized by ultrasound include porencephaly (Fig. 23-12), dysgenesis of the corpus callosum, cortical gyral abnormalities (Fig. 23-13), tethered cord, cortical clefts, midbrain abnormalities (Fig. 23-14), dysgenesis of the septi pellucidi, holoprosencephaly, cerebellar hypoplasia, subependymal (Fig. 23-15) and cortical tubers, vascular malformation, subdural and intratentorial hemorrhage (Fig. 23-16), and vermian cysts. Abnormalities better defined by MRI than ultrasound include encephaloceles (Fig. 23-17), arteriovenous malformations, distal neural tube defects, and the mass effect of arachnoid cysts (Fig. 23-18).<sup>69,81,82</sup> We found that MRI was least helpful in patients with a normal confirmatory sonogram and myelomeningocele.

The information provided by MRI allows for improved patient counseling, which may be used to assist patients in the decision to continue or discontinue a pregnancy, or to facilitate planning the mode of delivery and perinatal care. The types of management changes were correlated with gestational age, with decisions to terminate/continue a pregnancy at early gestational ages, and decisions regarding mode of delivery, location of delivery, and perinatal care made late in gestation.<sup>81</sup> At times, MRI in the third trimester can obviate the need for postnatal MRI (which may require neonatal sedation and its associated risks).

We have found MRI to be especially useful in fetuses with ventriculomegaly (see Figs. 23-12 and 23-14). The degree of ventriculomegaly, the cause of ventriculomegaly, and any associated findings are important in providing a management plan and prognosis for the fetus.<sup>83-86</sup> MRI has been beneficial in establishing the presence of a normal corpus callosum in fetuses with suspected callosal agenesis,<sup>79</sup> and it has been helpful in diagnosing callosal dysgenesis in fetuses when sonography shows only ventriculomegaly.<sup>69,87</sup>

MRI has aided our understanding of rare CNS anomalies such as an intratentorial hematoma (see Fig. 23-16). These lesions differ from arachnoid cysts in that they are adjacent to bone instead of adjacent to the brain. Other areas of hemorrhage can be seen. These lesions may regress and not be evident at birth.<sup>88</sup>

Evaluation of neural tube defects can also be performed with MRI. MRI examination is very helpful in visualizing caudal neural tube defects that may be difficult to visualize with sonography. MRI is also useful in visualizing posterior fossa structures in cases of Chiari type II malformation, and this information is helpful in pre- and postoperative assessment of patients undergoing in utero therapy of spinal neural tube defect.<sup>89,90</sup> However, for the majority of sonographically well-visualized spinal neural tube defects in which fetal surgery is not being performed, MRI has limited potential to influence care.<sup>92</sup>

We have also evaluated fetal cerebral cortical development in relation to gestational age compared with norms based on anatomic specimens.<sup>91</sup> We found that cortical development by MRI follows a predictable course and lags slightly compared with that described in anatomic specimens. Cortical development is often further delayed in fetuses with mild ventriculomegaly or other CNS abnormalities. The time course of the appearance of normal cortical landmarks is important in screening for fetuses with suspected migrational disorders such as lissencephaly. In addition, if the cortical development is markedly delayed compared with the gestational age and the fetus has an otherwise normal-appearing brain, these neonates may benefit from early intervention postnatally.

### **The Fetal Surgery Patient**

A rapidly expanding area for MRI is in the evaluation of fetuses that potentially will undergo in utero surgery and in fetuses being assessed for potential ex utero intrapartum treatment (EXIT) procedure. In the EXIT procedure, the fetus is partially delivered, and while still attached to the umbilical circulation, diagnostic and therapeutic maneuvers are undertaken to ensure that the baby will be able to breathe and adequately oxygenate once the cord is clamped





**FIGURE 23-12.** Mild ventriculomegaly with multifocal hemorrhage and cortical destruction in 16-week gestational age fetus. *A.* Coronal sonogram demonstrated mild ventriculomegaly with slightly irregular margins of one of the ventricles. *B* and *C.* Coronal RARE images show destruction of brain tissue in right frontal lobe (arrows on *B*) and focal area of low signal intensity (open arrow on *C*). *D.* Axial fast T1-weighted magnetic resonance imaging reveals extra-axial high and low signal intensity (curved arrow) consistent with blood products. This image was acquired in 15 seconds. Note the degradation in image quality due to fetal motion during image acquisition. This illustrates the inherent problem of fetal motion in obstetric imaging when sequences longer than 1 second are used. (From Levine D: *Fetal CNS anomalies depicted with ultrafast MR imaging*. *AJR Am J Roentgenol* 172:813, 1999.)

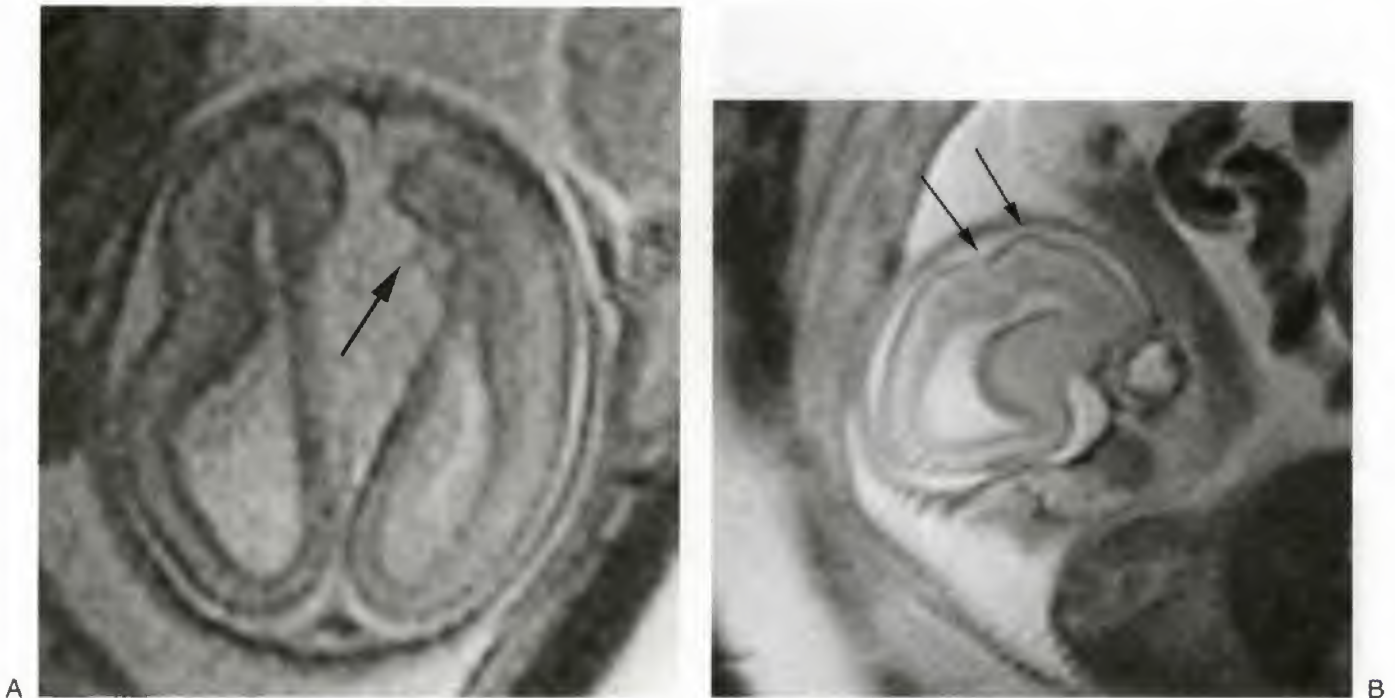


**FIGURE 23-13.** Fetus at 22 weeks' gestational age with agenesis of the corpus callosum and migrational abnormality. *A.* Axial image shows non-dilated ventricles with colpocephaly appearance with slit-like frontal horns. The hemispheres are splayed apart by an interhemispheric cyst that was better visualized sonographically (not shown). A region of abnormal gyral pattern is marked with an arrow. *B.* Sagittal image again shows the abnormal parenchyma with abnormality of both the cortical gyral pattern and the signal intensity of the white matter (arrows). This parenchymal abnormality was not evident sonographically. This type of information is important when counseling patients because the associated abnormalities help predict prognosis in fetuses with callosal dysgenesis.

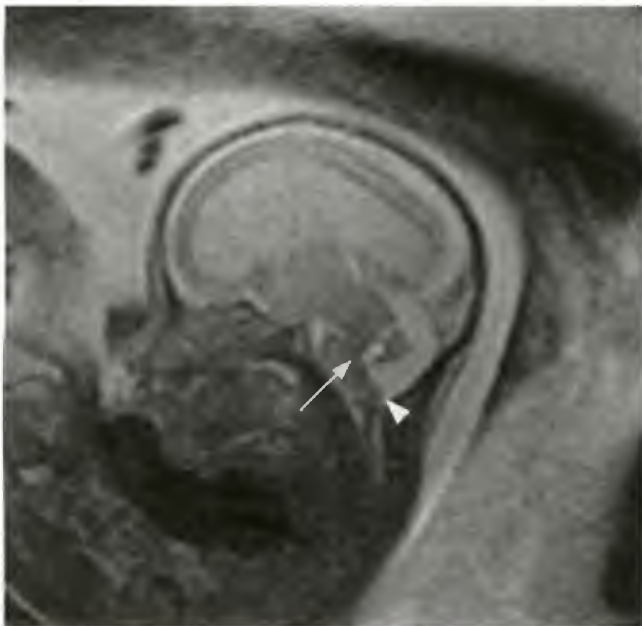


**FIGURE 23-14.** Ventriculomegaly at 19 weeks' gestational age by ultrasound with kinked midbrain by MRI. Sagittal T2-weighted MR shows marked ventriculomegaly and an abnormal configuration of the brainstem with a posterior kink (arrowhead) at the pontomesencephalic junction and an anterior kink (arrow) at the level of the fourth ventricle. The cerebellar vermis is hypoplastic. This type of abnormality is important because it indicates an early severe insult to the brain.

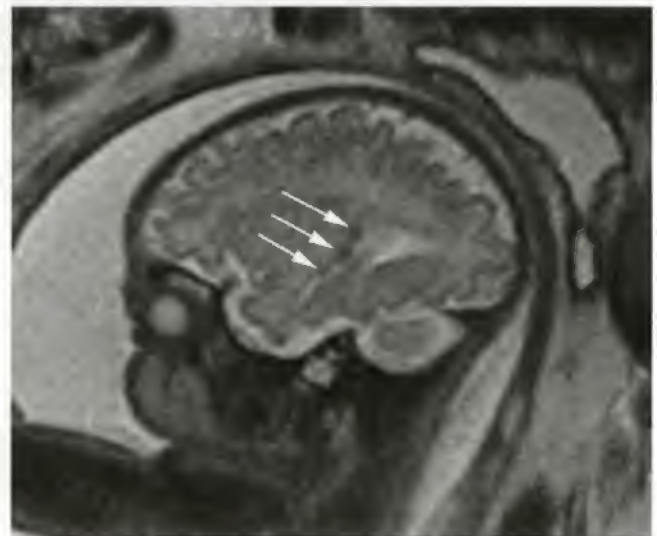


**FIGURE 23-15.** Fetus at 35 weeks' gestational age at risk for tuberous sclerosis due to sonographic findings of cardiac rhabdomyomas. Sagittal magnetic resonance image shows subependymal tubers (arrows), which were not visible sonographically. This allows for improved counseling of the patients at risk for tuberous sclerosis.



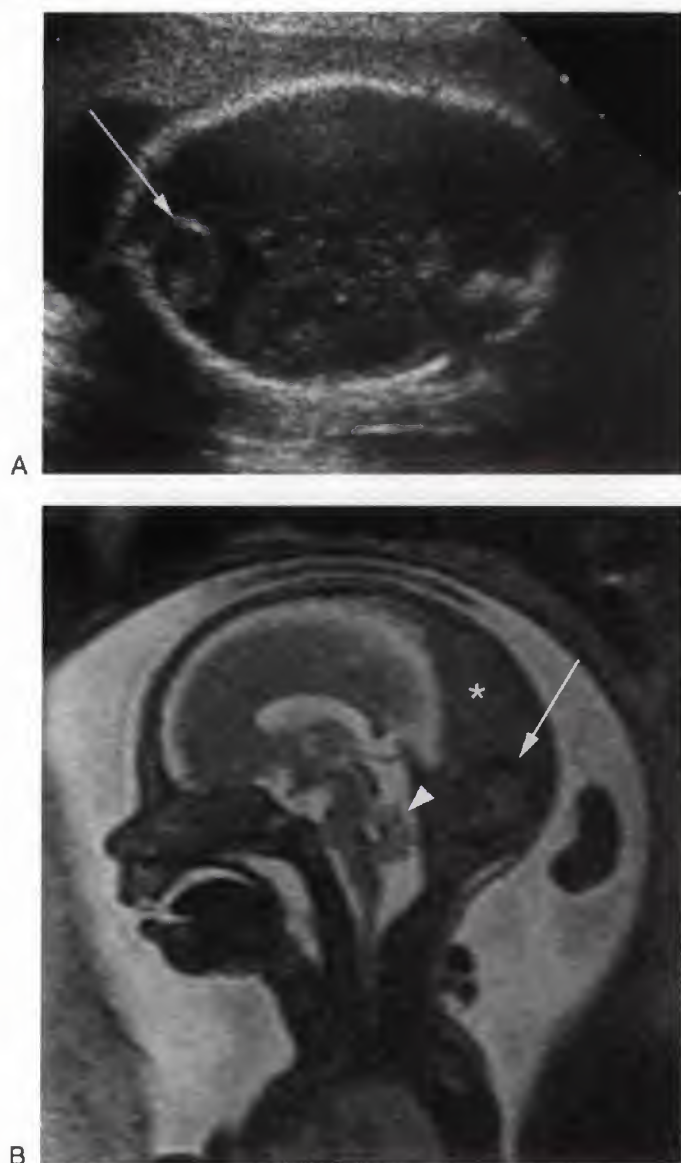


**FIGURE 23-16.** Intratentorial hematoma. *A.* Axial sonogram at 22 weeks' gestation shows a fluid collection in the posterior fossa with an hyperechogenic area (*arrow*) in a dependent location, suggesting focal calcification. A mass effect is shown as a slight flattened appearance to the cerebellar hemispheres. *B.* Sagittal MR shows a fluid collection adjacent to bone (*asterisk*), of intermediate signal intensity, lower than surrounding cerebrospinal and amniotic fluid, suggesting blood products. The fluid collection deviates the cerebellum anteriorly (*arrowhead*). The area that was hyperechogenic on ultrasound is of low signal on MR (*arrow*). This should be distinguished from an arachnoid cyst that would be adjacent to brain rather than conforming to bone. At 30 weeks, a similar appearance (not shown) was seen. At birth, a head ultrasound was normal. (Case courtesy of Robert Barr, MD, North Carolina).

(or to place the fetus on extracorporeal membrane oxygenation before clamping the cord).

For the fetal surgery patient, MRI is very helpful to ensure that unexpected anomalies are not present before undertaking the morbidity of fetal surgery.<sup>92,93</sup> In addition, MRI is helpful in the documentation of liver position in fetuses with congenital diaphragmatic hernia (CDH,

Fig. 23-19).<sup>93,94</sup> The liver position is important for prognosis because in cases of isolated CDH, the presence or absence of liver in the fetal chest is associated with respective mortalities of 57% and 7%.<sup>95,96</sup> This difference in mortality is believed in part to be due to the size of the hernia and the associated pulmonary hypoplasia. MRI is also helpful in fetuses with CDH in the assessment of the amount of normal-appearing lung remaining because the lung is poorly visualized with sonography but is well depicted on MRI.<sup>94</sup> In patients undergoing surgery for neural tube defects, MRI is helpful in characterizing the Chiari malformation, because the amount of cerebellar herniation is easily followed on serial MRI examinations.

In patients being evaluated for fetal procedures, MR is helpful for visualizing the potential airway obstruction (Figs. 23-20 and 23-21) and in planning for intervention at the time of delivery.<sup>97,98</sup>

### **Fetal Non-Central Nervous System Anomalies**

In the fetal lung, MRI has been shown to be helpful in accurately depicting the type of lung mass.<sup>99</sup> MR volumetry is also being established as an accurate method for measuring lung volume, to predict pulmonary hypoplasia.<sup>100,101</sup>

MRI contributes to the definition of fetal abdominal and pelvic masses<sup>97,102</sup> (Figs. 23-22 and 23-23). In a case from our series, fetal ultrasound showed an hyperechogenic abdominal mass suggestive of a meconium pseudocyst. MRI showed that the mass was more likely to be a gastric duplication cyst, which was confirmed with postnatal imaging (see Fig. 23-22). We demonstrated other anomalies by MRI, including omphalocele, gastroschisis, and cloacal malformation (see Fig. 23-23). Further studies are needed to assess how additional information from MRI affects patient management and outcome.

### **Screening for Anomalies**

MRI also has the potential to aid in genetic counseling and screening for disease processes for which limited prenatal diagnosis is available. Examples of this are tuberous sclerosis (see Fig. 23-15) in which subependymal tubers have been visualized with MR as early as 21 weeks' gestational age,<sup>103</sup> hemochromatosis,<sup>93</sup> and polymicrogyria or lissencephaly.<sup>82</sup> The sensitivity and specificity of prenatal MR for evaluation of these anomalies remains to be determined.

### **Potential Pitfalls in Fetal Evaluation Using Fast Magnetic Resonance Imaging**

As for all patients, there are absolute contraindications to MRI in pregnant patients (e.g., a ferromagnetic cerebral aneurysm clip), and some patients are too claustrophobic to undergo the examination. Use of short-bore magnets makes claustrophobia less of a concern, but if a patient is shorter than 5 feet 4 inches in height, her head will likely be within the magnet bore, even using a short bore magnet. An additional problem is that pregnant patients may have difficulty lying on their backs, especially in the third trimester. If a patient cannot lie on her back, she can be scanned in the decubitus position.



**FIGURE 23-17.** Posterior encephalocele in a fetus at 20 weeks' (A and B) and 32 weeks' gestational age (C). A. Axial sonogram shows a posterior encephalocele. A small amount of tissue is seen within the sac (arrow). B. Axial magnetic resonance image shows that the structures of the posterior fossa appear normal. A portion of the encephalocele is seen posteriorly (arrowheads). The information that the majority of the brain appeared normal was helpful to the patient in deciding to continue the pregnancy. C. In the same fetus at 32 weeks' gestational age, a sagittal image demonstrates that only a small portion of posterior cortex (arrow) is tented toward the encephalocele (E). At surgery, the encephalocele was removed and a small portion of cortex was pushed back into the cranial vault without difficulty. Postnatally, a meningocele sac was excised and the neural content returned to the posterior fossa. The infant is doing well at 1 year of age. (A and B from Levine D: *State of the art: Obstetric MR imaging*. *Radiology* 211:609, 1999. C from Levine D: *Fetal CNS anomalies depicted with ultrafast MR imaging*. *AJR Am J Roentgenol* 172:813, 1999.)



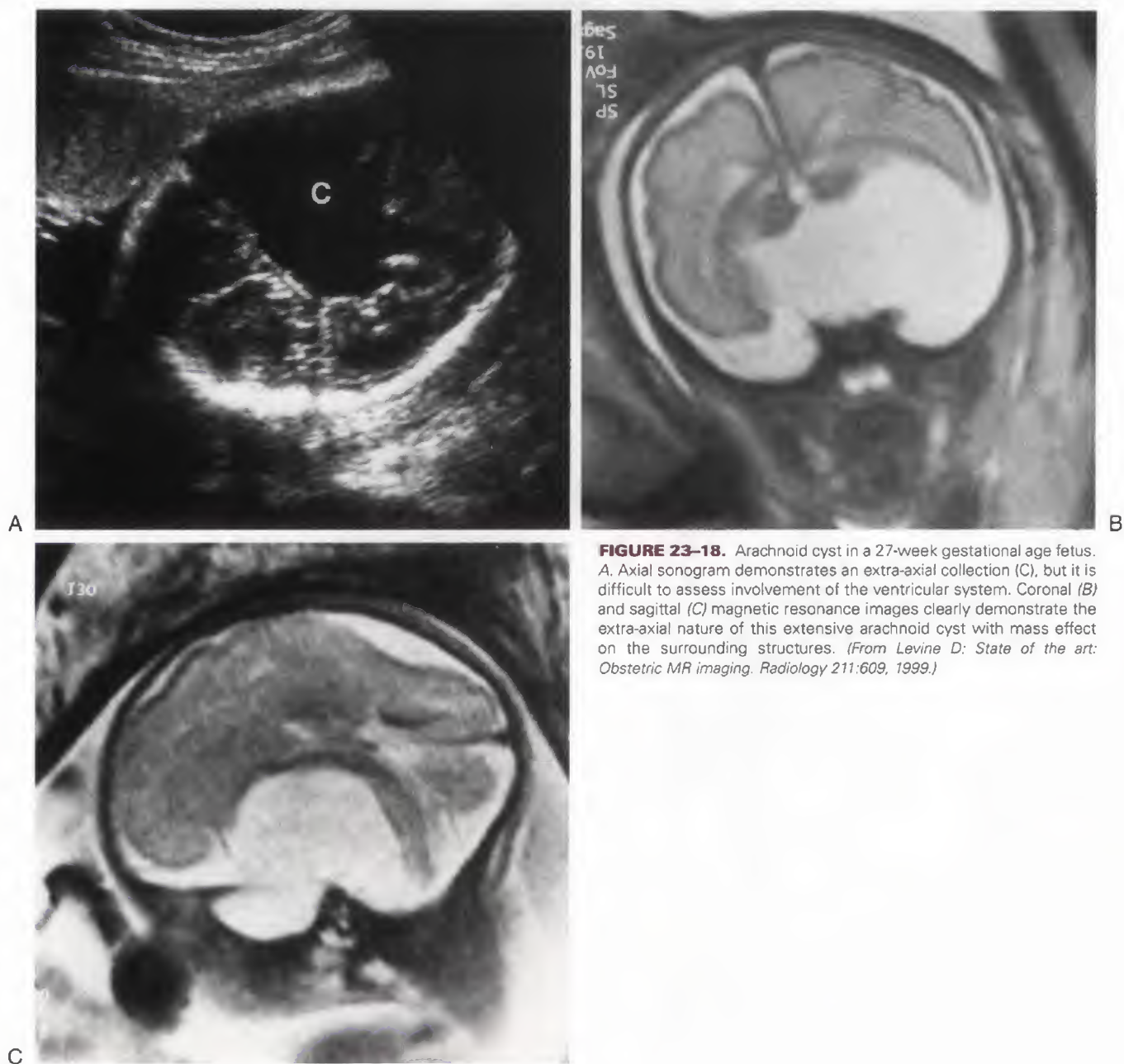


**FIGURE 23-18.** Arachnoid cyst in a 27-week gestational age fetus. A. Axial sonogram demonstrates an extra-axial collection (C), but it is difficult to assess involvement of the ventricular system. Coronal (B) and sagittal (C) magnetic resonance images clearly demonstrate the extra-axial nature of this extensive arachnoid cyst with mass effect on the surrounding structures. (From Levine D: *State of the art: Obstetric MR imaging*. *Radiology* 211:609, 1999.)

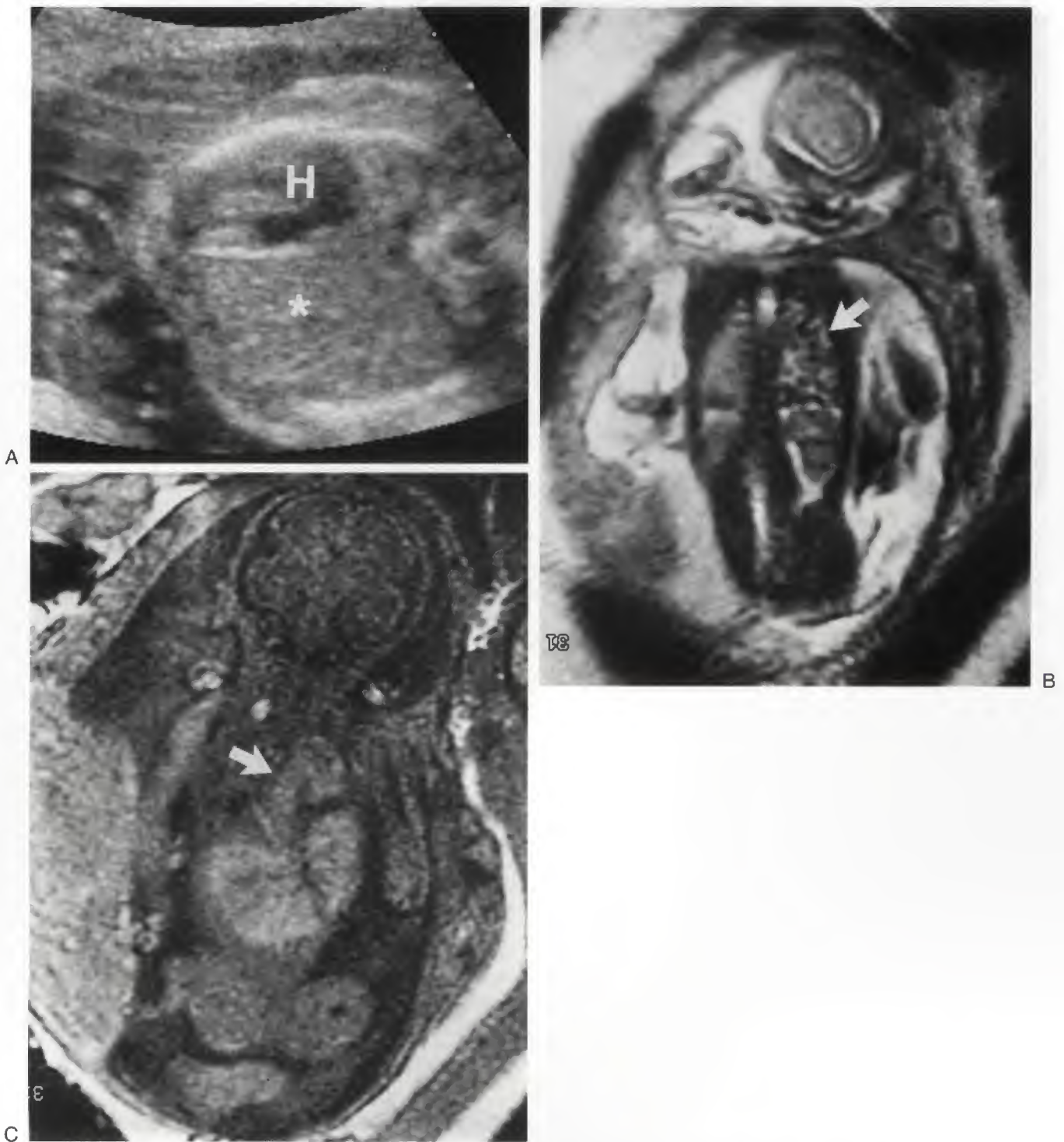


**FIGURE 23-19.** Sonogram and magnetic resonance imaging (MRI) of fetal congenital diaphragmatic hernia (CDH) in a 32-year-old woman at 25 weeks gestation. **A.** Transverse axial sonogram demonstrates herniated bowel and liver within the fetal thorax (*asterisk*). Distinction between fetal bowel and liver is not possible on this image. The heart (H) is displaced to the right by the herniated contents. **B.** Single-shot fast-spin echo T2-weighted (TE of 100 milliseconds) coronal section through the fetal thorax, demonstrating multiple bowel loops (*arrow*) in the left side of the chest. This confirms the presence of a left-sided CDH. The compressed right lung is visible. The left lung is not seen. **C.** Spoiled gradient-echo T1-weighted (flip angle of 70 degrees, and TR/TE of 120/4.2 milliseconds) coronal section through the fetal thorax, at a level more anterior to the section in **B**. The liver is of relatively high signal on this sequence, facilitating identification of hepatic position. Herniation of the left hepatic lobe (*arrow*) into the left side of the chest is seen. (MRI courtesy of Fergus Coakley, MD, University of California at San Francisco.)



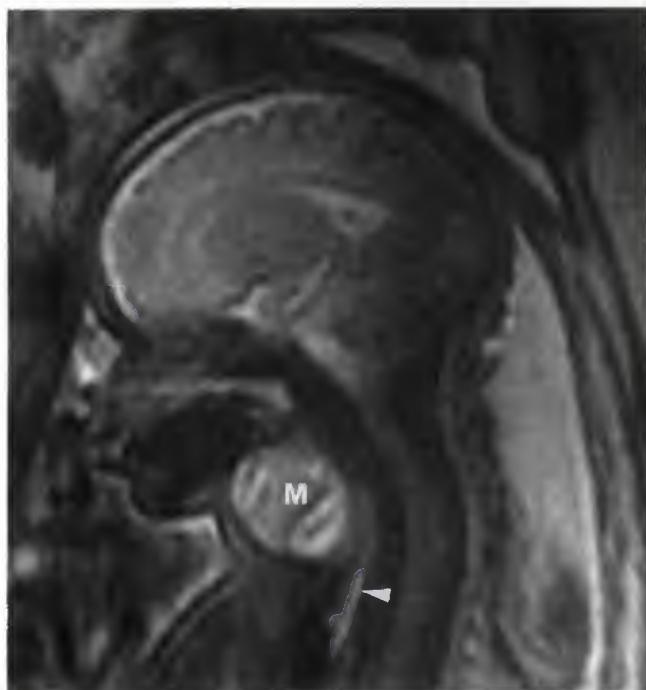


**FIGURE 23-20.** MR in planning for EXIT procedure. Sagittal MRI of fetus with neck mass. The MR showed the heterogeneous neck mass (M). Sequential images showed the trachea (arrowhead) to be patent but narrowed and deviated in the region of the mass. Because of concerns regarding ability to intubate at delivery, an EXIT procedure was performed. After partial delivery, while still attached to the umbilical cord, the fetus was intubated. After the intubation the umbilical cord was ligated.

Although artifacts from fetal motion are minimized using fast-scan techniques, if the fetus moves continuously during a sequence, reduced image quality is inevitable. This movement can be accommodated by repeated sequence acquisition if the anatomy has not been well visualized, or with use of real-time imaging, which allows for specific image slices to be obtained, until the pertinent anatomy is documented. In some cases when MR is undertaken for fetal indications, fetal movement that occurs after the scout acquisitions are obtained or between imaging sequences makes it difficult to obtain specific image planes. This is especially true in the evaluation of the distal extremities. When motion is not a problem, sequential images allow for assessment of the hands and feet. However, even small amounts of motion limit viewing of the extremities in their entirety. When the entire fetus moves, the region of interest may not be in the image plane at all. Because of signal-to-noise limitations, small fetal structures may be difficult to identify and evaluate. Thin structures surrounded by fluid can be difficult to visualize as a result of partial volume averaging occurring over the thickness of the slice. Examples include the membranous sac of a neural tube defect, the wall of an arachnoid cyst, and the forming corpus callosum in the second trimester.

## IMAGING BEYOND ANATOMY

MRI has the potential to give a wealth of information beyond anatomic images. Diffusion-weighted imaging, MR spectroscopy, and oxygenation imaging are all examples of the type of additional information that can be provided by MRI. In addition, MR volumetry can be used to potentially affect care of the pregnant patient.

### Diffusion-Weighted Imaging

Echo-planar diffusion-weighted imaging is being increasingly performed to assess for early brain damage.<sup>104,105</sup> Use of this technique can demonstrate hypoxic ischemic injury before anatomic abnormalities are seen on the more standard T1- and T2-weighted images. The apparent diffusion coefficient decreases with an acute injury.<sup>106</sup> Restricted diffusion can also be seen in areas of increased cellularity and advanced myelination,<sup>107</sup> and can be used to assess normal and abnormal myelination patterns. Diffusion-weighted imaging also can be performed to characterize cystic lesions in utero and distinguish them from the bulky mobile amniotic fluid.<sup>108</sup> It is also possible that diffusion measurements may be useful in assessing lung maturation.<sup>109</sup>

### Magnetic Resonance Spectroscopy

MR spectroscopy has the potential to show changes in composition of tissues and fluids in the fetus, potentially allowing for assessment of phospholipids in amniotic fluid<sup>110</sup> and normal development<sup>111,112</sup> and ischemia of the brain in the third trimester.<sup>104</sup> However, this tool is still being developed for use clinically in the fetus. Problems with use of MR spectroscopy are the relatively long scan times that allow for fetal motion to occur and the potential for partial volume averaging of small structures.

### Oxygenation Imaging

Placental oxygenation imaging may allow for early detection of growth restriction.<sup>113</sup> In a sheep study, Wedegartner et al<sup>114</sup> described the use of blood oxygen level-dependent MRI to provide assessment of fetal brain, liver, heart, lung, and placental oxygenation in sheep with hypoxia, and showed the strongest changes in T2\* values in the liver and heart (both organs with high blood flow in utero), with smaller changes in the brain, placenta, and lungs. It is anticipated that use of functional imaging studies like this will allow for improved distinction between the normal but small for gestational age fetus from a growth-restricted fetus.

### Magnetic Resonance Volumetry

Three-dimensional volumetry is easily performed on fetal MRI. Potential applications include (1) assessment of lung volumes in cases of chest masses and hernias; (2) better assessment of fetal weight (for example in diabetics with macrosomia, potentially allowing for decreased cesarean section rate or, in differentiating between the growth-restricted fetus from the normal but small for gestational age fetus); and (3) cerebral parenchymal volumes in cases of ventriculomegaly to better predict outcomes.

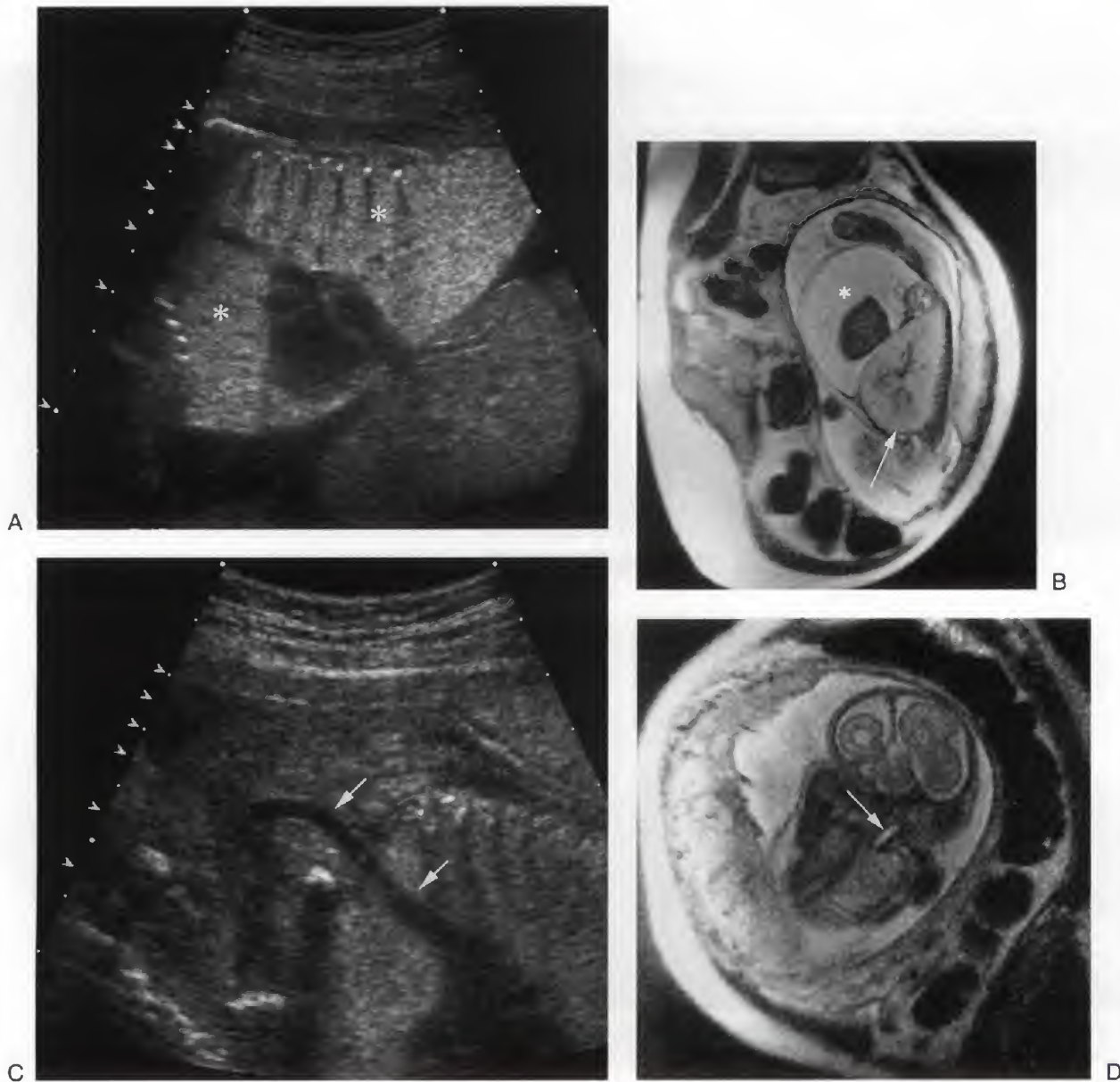


**FIGURE 23-21.** Sonograms and magnetic resonance imaging from a fetus with laryngeal atresia. *A.* Coronal plane of section demonstrates markedly enlarged and hyperechogenic lungs bilaterally (*asterisks*). *B.* Single-shot fast-spin echo (effective TE 100 milliseconds) demonstrates enlarged fetal lung (*arrow*). Marked ascites is also seen (*asterisk*). *C.* Coronal plane of section sonogram demonstrates the dilated fluid filled trachea (*arrows*) in this fetus. *D.* Single-shot fast-spin echo (effective TE 100 milliseconds) demonstrates the trachea (*arrow*) as a high intensity structure. (MRI courtesy of Fergus Coakley, MD, University of California at San Francisco.)



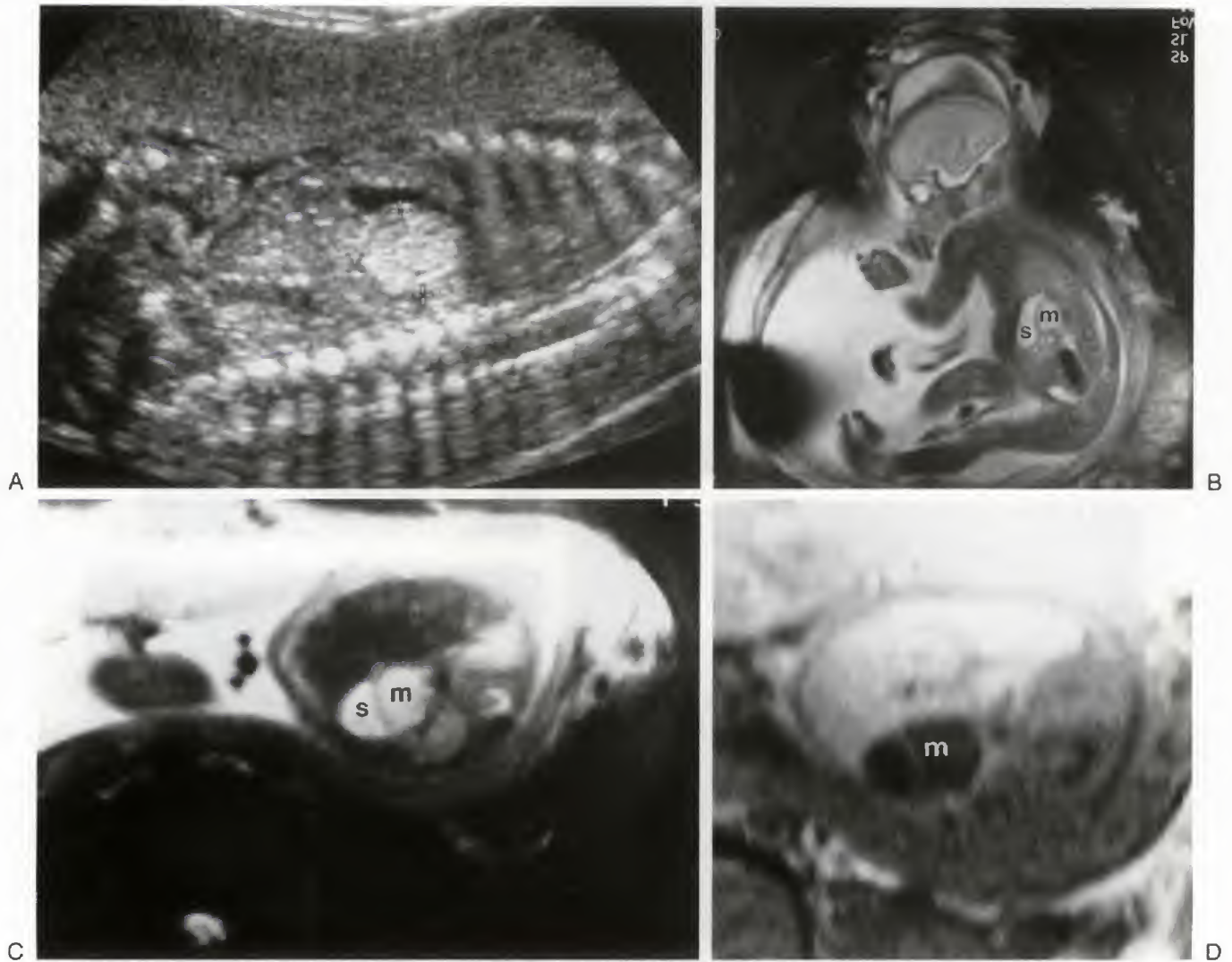


**FIGURE 23-22.** Gastric duplication cyst in a 28-week gestational age fetus. *A.* Oblique coronal ultrasound shows an hyperechogenic mass in the abdomen (calipers), suggestive of a meconium pseudocyst. *B.* Sagittal RARE image demonstrates the mass (m) impressing on the stomach (s). The mass is of slightly lower signal intensity than the stomach on this T2-weighted image. *C.* Axial RARE image shows similar findings to *B.* *D.* Axial T1-weighted image (TR/TE = 126/4; flip angle = 80 degrees; FOV = 24 × 32 cm; matrix = 96 × 256; 5-mm slice thickness; one signal acquired; section thickness, 5 mm) shows that the mass (m) has slightly higher signal than adjacent stomach. The appearance of the mass suggests a duplication cyst, which was confirmed postnatally. (From Levine D: State of the art: Obstetric MR imaging. *Radiology* 211:609, 1999.)

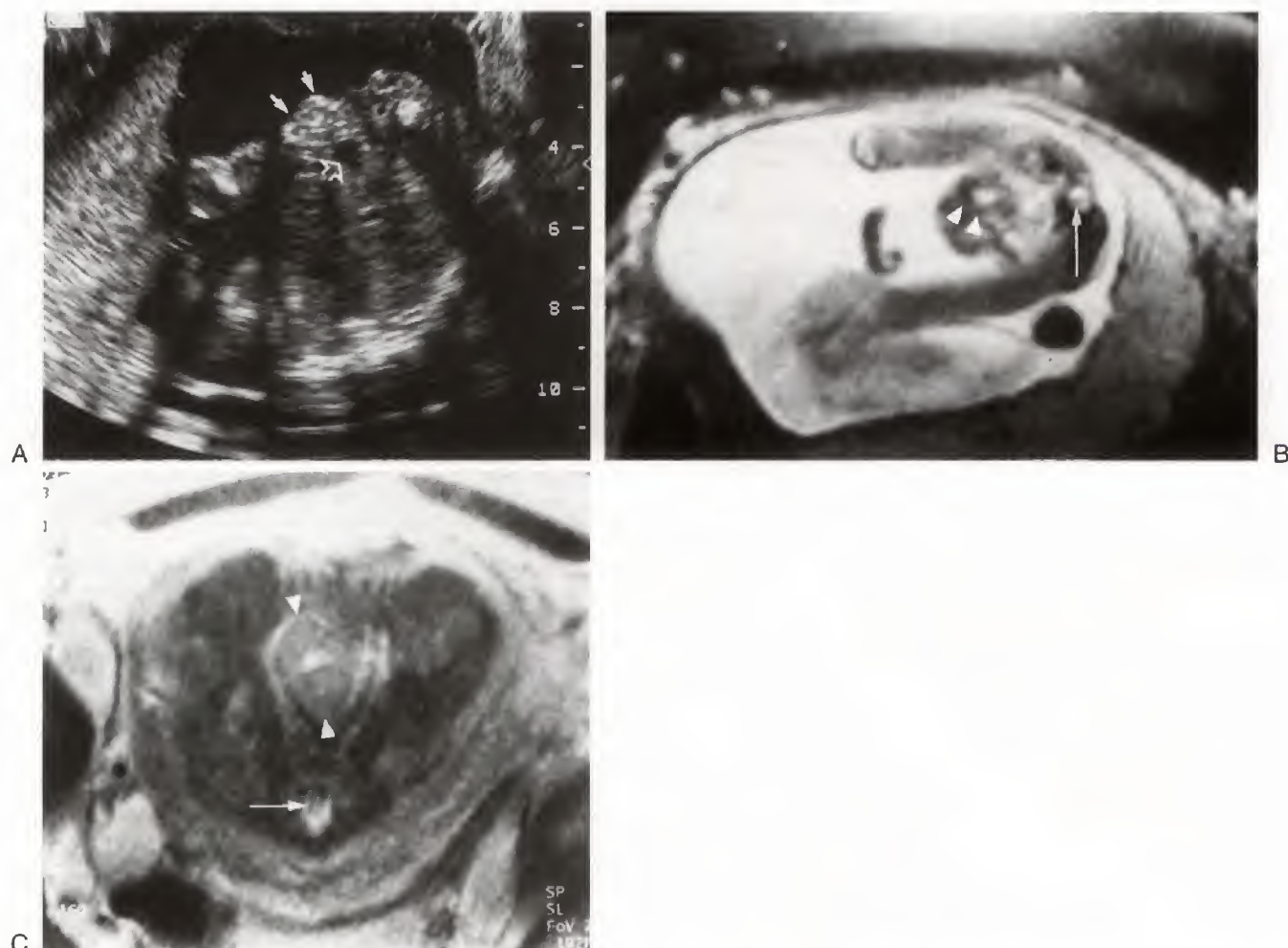


**FIGURE 23-23.** Cloacal exstrophy in a 20-week gestational age fetus. A. Sagittal ultrasound image demonstrates a low anterior abdominal wall defect (arrows). A fluid collection is seen in the pelvis suggestive of a deformed bladder (open arrow); however, a bladder should not be seen in a case of exstrophy. The kidneys were not visualized. B. Axial magnetic resonance image (MRI) at 20 weeks shows a pelvic kidney (arrowheads) in the region of the fluid collection seen by ultrasound. The spinal cord is seen at this level (thin white arrow) consistent with a tethered cord. C. Axial MRI at 38 weeks again shows the pelvic kidney (arrowheads) and tethered cord (arrow). These diagnoses were made prospectively after discussion with specialists in pediatric surgery and pediatric radiology. One of the benefits of fetal MRI is that specialists who are not accustomed to obstetric sonography may be better able to understand MRI with which they are more familiar. (From Levine D: State of the art: Obstetric MR imaging. *Radiology* 211:609, 1999.)

## CONCLUSION

Ultrasound continues to be the screening modality of choice in the evaluation of the maternal pelvis and fetus because of its relatively low cost and real-time capability. However, there are many cases in which alternative imaging is useful as an adjunct to ultrasound. The use of CT is typically limited to patients with abdominal pain at risk for appendicitis, but MRI use is increasing. Indications for fetal MRI include evaluation of adnexal masses, hydroureteronephrosis of pregnancy, and fetal anomalies. As our experience with fast MRI techniques increases, we will continue to identify patients in whom MRI contributes to patient evaluation.

## References

1. Angtuaco TL, Shah HR, Mattison DR, et al: MR imaging in high-risk obstetric patients: a valuable complement to US. *Radiographics* 12:91, 1992.
2. Powell MC, Worthington BS, Buckley JM, et al: Magnetic resonance imaging (MRI) in obstetrics. II. Fetal anatomy. *Br J Obstet Gynaecol* 95:38, 1988.
3. Weinreb JC, Lowe TW, Santos-Ramos R, et al: Magnetic resonance imaging in obstetric diagnosis. *Radiology* 154:157, 1985.
4. Wagner LK, Lester RG, Saldana LR: Exposure of the Pregnant Patient to Diagnostic Radiations. Madison, WI, Medical Physics Publishing, 1997.
5. Bithell JF, Stiller CA: A new calculation of the carcinogenic risk of obstetric x-raying. *Stat Med* 7:857, 1988.



6. Mole RH: Childhood cancer after prenatal exposure to diagnostic x-ray examination in Britain. *Br J Cancer* 62:152, 1990.
7. National Council on Radiology Protection and Measurements: Medical Radiation Exposure of Pregnant and Potentially Pregnant Women. Bethesda, MD, NCRPM, 1977.
8. Baker PN, Johnson IR, Harvey PR, et al: A three-year follow-up of children imaged in utero with echo-planar magnetic resonance. *Am J Obstet Gynecol* 170:32, 1994.
9. Kanal E, Gillen J, Evans JA, et al: Survey of reproductive health among female MR workers. *Radiology* 187:395, 1993.
10. Schwartz JL, Crooks LE: NMR imaging produces no observable mutations or cytotoxicity in mammalian cells. *AJR Am J Roentgenol* 139:583, 1982.
11. Wolff S, Crooks LE, Brown P, et al: Tests for DNA and chromosomal damage induced by nuclear magnetic resonance imaging. *Radiology* 136:707, 1980.
12. United States Food and Drug Administration: Guidelines for Content and Review of a Magnetic Resonance Diagnostic Device 510 (k) Application. Washington, D.C., USFDA, 1988.
13. Shellock FG, Kanal E: Policies, guidelines, and recommendations for MR imaging safety and patient management. SMRI Safety Committee. *J Magn Reson Imaging* 1:97, 1991.
14. Shellock FG, Cruess JV: MR procedures: biologic effects, safety, and patient care. *Radiology* 232:635, 2004.
15. Shellock FG: Biological effects and safety aspects of magnetic resonance imaging. *Magn Reson Q* 5:243, 1989.
16. Magnevist Product Information. Wayne, NJ, Berlex Laboratories, 1994.
17. Levine D, Edelman RR: Fast MRI and its application in obstetrics. *Abdom Imaging* 22:589, 1997.
18. Levine D, Hatabu H, Gaa J, et al: Fetal anatomy revealed with fast MR sequences. *AJR Am J Roentgenol* 167:905, 1996.
19. Levine D, Keedy J, Hatabu H, et al: Obstetrical magnetic resonance imaging with HASTE. *Proceedings of the International Society for Magnetic Resonance in Medicine* 1:159, 1996.
20. Yamashita Y, Namimoto T, Abe Y, et al: MR imaging of the fetus by a HASTE sequence. *AJR Am J Roentgenol* 168:513, 1997.
21. Levine D, Barnes PD, Sher S, et al: Fetal fast MR imaging: reproducibility, technical quality, and conspicuity of anatomy. *Radiology* 206:549, 1998.
22. Eyvazzadeh AD, Pedrosa I, Rofsky NM, et al: MRI of right-sided abdominal pain in pregnancy. *AJR Am J Roentgenol* 183:907, 2004.
23. Pedrosa I, Levine D, Eyvazzadeh AD, et al: MRI evaluation of suspected acute appendicitis in pregnancy. *Radiology* 238:891, 2006.
24. Cohen JM, Weinreb JC, Lowe TW, et al: MR imaging of a viable full-term abdominal pregnancy. *AJR Am J Roentgenol* 145:407, 1985.
25. Hage ML, Wall LL, Killam A: Expectant management of abdominal pregnancy. *J Reprod Med* 33:407, 1988.
26. Harris MB, Anguaco T, Frazier CN, Mattison DR: Diagnosis of a viable abdominal pregnancy by magnetic resonance imaging. *Am J Obstet Gynecol* 159:150, 1988.
27. Hamrick-Turner JE, Cranston PE, Lantrip BS: Gravid uterine dehiscence: MR findings. *Abdom Imaging* 20:486, 1995.
28. Spritzer CE, Evans AC, Kay HH: Magnetic resonance imaging of deep venous thrombosis in pregnant women with lower extremity edema. *Obstet Gynecol* 85:603, 1995.
29. Horowitz E, Schmidt JD: Renal calculi in pregnancy. *Clin Obstet Gynecol* 28:324, 1985.
30. Klein EA: Urologic problems of pregnancy. *Obstet Gynecol Surv* 39:605, 1984.
31. Stothers L, Lee LM: Renal colic in pregnancy. *J Urol* 148:1383, 1992.
32. Roy C, Saussine C, Jahn C, et al: Fast imaging MR assessment of ureterohydronephrosis during pregnancy. *Magn Reson Imaging* 13:767, 1995.
33. Weinreb JC, Browth CE, Lower TW, et al: Pelvic masses in pregnant patients: MR and US imaging. *Radiology* 159:717, 1986.
34. Kier R, McCarthy SM, Scoutt LM, et al: Pelvic masses in pregnancy: MR imaging. *Radiology* 176:709, 1990.
35. Stark DD, McCarthy SM, Filly RA, et al: Pelvimetry by magnetic resonance imaging. *AJR Am J Roentgenol* 144:947, 1985.
36. van Loon AJ, Mantingh A, Serlier EK, et al: HJ. Randomised controlled trial of magnetic-resonance pelvimetry in breech presentation at term. *Lancet* 350:1799, 1997.
37. van Loon AJ, Mantingh A, Thijn CJ, et al: Pelvimetry by magnetic resonance imaging in breech presentation. *Am J Obstet Gynecol* 163:1256, 1990.
38. Federle MP, Cohen HA, Rosenwein MF, et al: Pelvimetry by digital radiography: a low-dose examination. *Radiology* 143:733, 1982.
39. Wright AR, Cameron HM, Lind T: Magnetic resonance imaging pelvimetry: a useful adjunct in the management of the obese patient. *Br J Obstet Gynaecol* 99:852, 1992.
40. McCarthy SM, Stark DD, Filly RA, et al: Obstetrical magnetic resonance imaging: maternal anatomy. *Radiology* 154:421, 1985.
41. Powell MC, Buckley J, Price H, et al: Magnetic resonance imaging and placenta previa. *Am J Obstet Gynecol* 154:565, 1986.
42. Mochizuki T, Nishiguchi T, Ito I, et al: Case report. Antenatal diagnosis of chorioangioma of the placenta: MR features. *J Comput Assist Tomogr* 20:413, 1996.
43. Feigin MD, Rosen DJ, Ben-Nun I, et al: Ultrasonic and magnetic resonance imaging diagnosis of placenta accreta managed conservatively. *J Perinat Med* 21:165, 1993.
44. Ha TP, Li KC: Placenta accreta: MRI antenatal diagnosis and surgical correlation. *J Magn Reson Imaging* 8:748, 1998.
45. Kirkinen P, Helin-Martikainen HL, Vanninen R, et al: Placenta accreta: imaging by gray-scale and contrast-enhanced color Doppler sonography and magnetic resonance imaging. *J Clin Ultrasound* 26:90, 1998.
46. Thorp JM Jr, Councell RB, Sandridge DA, et al: Antepartum diagnosis of placenta previa percreta by magnetic resonance imaging. *Obstet Gynecol* 80:506, 1992.
47. Finberg HJ, Williams JW: Placenta accreta: prospective sonographic diagnosis in patients with placenta previa and prior cesarean section. *J Ultrasound Med* 11:333, 1992.
48. Levine D, Hulka CA, Ludmir J, et al: Placenta accreta: evaluation with color Doppler US, power Doppler US, and MR imaging. *Radiology* 205:773, 1997.
49. Carlan SJ, Angel JL, Sawai SK, et al: Late diagnosis of nonconjoined monoamniotic twins using computed tomographic imaging: a case report. *Obstet Gynecol* 76:504, 1990.
50. Finberg HJ, Clewell WH: Definitive prenatal diagnosis of monoamniotic twins, swallowed amniotic contrast agent detected in both twins on sonographically selected CT images. *J Ultrasound Med* 10:513, 1991.
51. Sargent SK, Young W, Crow P, et al: CT amniography: Value in detecting a monoamniotic pair in a triplet pregnancy. *AJR Am J Roentgenol* 156:559, 1991.
52. Johnson IR, Symonds EM, Kean DM, et al: Imaging the pregnant human uterus with nuclear magnetic resonance. *Am J Obstet Gynecol* 148:1136, 1984.
53. Garden AS, Griffiths RD, Weindling AM, et al: Fast-scan magnetic resonance imaging in fetal visualization. *Am J Obstet Gynecol* 164:1190, 1991.
54. Daffos F, Forestier F, Mac Aleese J, et al: Fetal curarization for prenatal magnetic resonance imaging. *Prenat Diagn* 8:312, 1988.
55. Horvath L, Seeds JW: Temporary arrest of fetal movement with pancuronium bromide to enable antenatal magnetic resonance imaging of holoprosencephaly. *Am J Perinatol* 6:418, 1989.
56. Lenke RR, Persutte WH, Nemes JM: Use of pancuronium bromide to inhibit fetal movement during magnetic resonance imaging. A case report. *J Reprod Med* 34:315, 1989.
57. Toma P, Lucigrai G, Dodero P, et al: Prenatal detection of an abdominal mass by MR imaging performed while the fetus is immobilized with pancuronium bromide. *AJR Am J Roentgenol* 154:1049, 1990.
58. Williamson RA, Weiner CP, Yuh WT, et al: Magnetic resonance imaging of anomalous fetuses. *Obstet Gynecol* 73:952, 1989.
59. Mansfield P, Stehling MK, Ordidge RJ, et al: Echo planar imaging of the human fetus in utero at 0.5 T. *Br J Radiol* 63:833, 1990.
60. Edelman RR, Wielopolski PA (eds): Fast MRI, 2nd ed. Philadelphia, PA, WB Saunders, 1996, pp 302-352.
61. Reiss I, Gortner L, Moller J, et al: Fetal intracerebral hemorrhage in the second trimester: diagnosis by sonography and magnetic resonance imaging. *Ultrasound Obstet Gynecol* 7:49, 1996.
62. Smith FW, Adam AH, Phillips WD: NMR imaging in pregnancy. *Lancet* 1:61, 1983.
63. Thickman D, Mintz M, Mennuti M, et al: MR imaging of cerebral abnormalities in utero. *J Comput Assist Tomogr* 8:1058, 1984.
64. Busse RF, Riederer SJ, Fletcher JC, et al: Interactive fast spin-echo imaging. *Magn Reson Med* 44:339, 2000.
65. Busse RF, Carrillo A, Vigneron DB, et al: Interactive fetal imaging with real-time SSFSE. *Radiology* 225:434, 2002.



66. Kazan-Tannus JF, Levine D, McKenzie C, et al: Real-time MR imaging aids prenatal diagnosis of isolated cleft palate. *J Ultrasound Med* 24:1533, 2005.
67. Levine D, Cavazos C, Kazan-Tannus JF, et al: An evaluation of real-time MR single shot fast spin echo imaging in visualization of fetal midline corpus callosum and secondary palate. *AJR Am J Roentgenol* 187:1505, 2006.
68. Filly RA, Goldstein RB, Callen PW: Fetal ventricle: importance in routine obstetric sonography. *Radiology* 181:1, 1991.
69. Levine D, Barnes PD, Madsen JR, et al: Fetal CNS anomalies revealed on ultrafast MR imaging. *AJR Am J Roentgenol* 172:813, 1999.
70. Campi A, Scotti G, Filippi M, et al: Antenatal diagnosis of vein of Galen aneurysmal malformation: MR study of fetal brain and postnatal follow-up. *Neuroradiology* 38:87, 1996.
71. Dinh DH, Wright RM, Hanigan WC: The use of magnetic resonance imaging for the diagnosis of fetal intracranial anomalies. *Childs Nerv Syst* 6:212, 1990.
72. Fusch C, Ozdoba C, Kuhn P, et al: Perinatal ultrasonography and magnetic resonance imaging findings in congenital hydrocephalus associated with fetal intraventricular hemorrhage. *Am J Obstet Gynecol* 177:512, 1997.
73. Guibaud L, Champion F, Buenerd A, et al: Fetal intraventricular glioblastoma: ultrasonographic, magnetic resonance imaging, and pathologic findings. *J Ultrasound Med* 16:285, 1997.
74. Koga Y, Tahara Y, Kida T, et al: Prenatal diagnosis of congenital unilateral hydrocephalus. *Pediatr Radiol* 27:319, 1997.
75. Kultursay N, Gelal F, Mutluer S, et al: Antenatally diagnosed neonatal craniopharyngioma. *J Perinatol* 15:426, 1995.
76. Reid A, Smith FW, Hutchinson JM: Nuclear magnetic resonance imaging and its safety implications; follow-up of 181 patients. *Br J Radiol* 55:784, 1982.
77. Rypens F, Sonigo P, Aubry MC, et al: Prenatal MR diagnosis of a thick corpus callosum. *AJNR Am J Neuroradiol* 17:1918, 1996.
78. Sonigo PC, Rypens FF, Carteret M, et al: MR imaging of fetal cerebral anomalies. *Pediatr Radiol* 28:212, 1998.
79. Glenn OA, Goldstein RB, Li KC, et al: Fetal magnetic resonance imaging in the evaluation of fetuses referred for sonographically suspected abnormalities of the corpus callosum. *J Ultrasound Med* 24:791, 2005.
80. Twickler DM, Magee KP, Caire J, et al: Second-opinion magnetic resonance imaging for suspected fetal central nervous system abnormalities. *Am J Obstet Gynecol* 188:492, 2003.
81. Levine D, Barnes PD, Robertson RR, et al: Fast MR imaging of fetal central nervous system abnormalities. *Radiology* 229:51, 2003.
82. Levine D, Barnes PD, Madsen JR, et al: Central nervous system abnormalities assessed with prenatal magnetic resonance imaging. *Obstet Gynecol* 94:1011, 1999.
83. Bloom SL, Bloom DD, Dellanebbia C, et al: The developmental outcome of children with antenatal mild isolated ventriculomegaly. *Obstet Gynecol* 90:93, 1997.
84. Nicolaides KH, Berry S, Snijders RJ, et al: Fetal lateral cerebral ventriculomegaly: associated malformations and chromosomal defects. *Fetal Diagn Ther* 5:5, 1990.
85. Patel MD, Filly AL, Hersch DR, et al: Isolated mild fetal cerebral ventriculomegaly: clinical course and outcome. *Radiology* 192:759, 1994.
86. Vergani P, Locatelli A, Strobelt N, et al: Clinical outcome of mild fetal ventriculomegaly. *Am J Obstet Gynecol* 178:218, 1998.
87. Levine D, Barnes PD, Madsen JR, et al: Fetal central nervous system anomalies: MR imaging augments sonographic diagnosis. *Radiology* 204:635, 1997.
88. Folkerth RD, McLaughlin ME, Levine D: Organizing posterior fossa hematomas simulating developmental cysts on prenatal imaging: report of 3 cases. *J Ultrasound Med* 20:1233, 2001.
89. Aaronson OS, Hernanz-Schulman M, Bruner JP, et al: Myelomeningocele: prenatal evaluation—comparison between transabdominal US and MR imaging. *Radiology* 227:839, 2003.
90. Mangels KJ, Tulipan N, Tsao LY, et al: Fetal MRI in the evaluation of intrauterine myelomeningocele. *Pediatr Neurosurg* 32:124, 2000.
91. Levine D, Barnes PD: Cortical maturation in normal and abnormal fetuses as assessed with prenatal MR imaging. *Radiology* 210:751, 1999.
92. Coakley FV: Role of magnetic resonance imaging in fetal surgery. *Top Magn Reson Imaging* 12:39, 2001.
93. Coakley FV, Hricak H, Filly RA, et al: Complex fetal disorders: effect of MR imaging on management—preliminary clinical experience. *Radiology* 213:691, 1999.
94. Leung JW, Coakley FV, Hricak H, et al: Prenatal MR imaging of congenital diaphragmatic hernia. *AJR Am J Roentgenol* 174:1607, 2000.
95. Adzick NS, Harrison MR, Glück PL, et al: Diaphragmatic hernia in the fetus: prenatal diagnosis and outcome in 94 cases. *J Pediatr Surg* 20:357, 1985.
96. Metkus AP, Filly RA, Stringer MD, et al: Sonographic predictors of survival in fetal diaphragmatic hernia. *J Pediatr Surg* 31:148; discussion 151, 1996.
97. Quinn TM, Hubbard AM, Adzick NS: Prenatal magnetic resonance imaging enhances fetal diagnosis. *J Pediatr Surg* 33:553, 1998.
98. Levine D, Jennings R, Barnewolt C, et al: Progressive fetal bronchial obstruction caused by a bronchogenic cyst diagnosed using prenatal MR imaging. *AJR Am J Roentgenol* 176:49, 2001.
99. Hubbard AM, Adzick NS, Crombleholme TM, et al: Congenital chest lesions: diagnosis and characterization with prenatal MR imaging. *Radiology* 212:43, 1999.
100. Coakley FV, Lopoo JB, Lu Y, et al: Normal and hypoplastic fetal lungs: volumetric assessment with prenatal single-shot rapid acquisition with relaxation enhancement MR imaging. *Radiology* 216:107, 2000.
101. Williams G, Coakley FV, Qayyum A, et al: Fetal Relative Lung Volume: Quantification by Using Prenatal MR Imaging Lung Volumetry. *Radiology* 233:457, 2004.
102. Levine D, Barnes PD, Edelman RR: Obstetric MR imaging. *Radiology* 211:609, 1999.
103. Levine D, Barnes PB, Korf B, et al: Tuberous sclerosis in the fetus: second-trimester diagnosis of subependymal tubers with ultrafast MR imaging. *Am J Roentgenol* 175:1067, 2000.
104. Borowska-Matwiejczuk K, Lemancewicz A, Tarasow E, et al: Assessment of fetal distress based on magnetic resonance examinations: preliminary report. *Acad Radiol* 10:1274, 2003.
105. Baldoli C, Righini A, Parazzini C, et al: Demonstration of acute ischemic lesions in the fetal brain by diffusion magnetic resonance imaging. *Ann Neurol* 52:243, 2002.
106. Huppi PS: Advances in postnatal neuroimaging: relevance to pathogenesis and treatment of brain injury. *Clin Perinatol* 29:827, 2002.
107. Agid R, Lieberman S, Nadjari M, et al: Prenatal MR diffusion-weighted imaging in a fetus with hemimegalencephaly. *Pediatr Radiol* 36:138, 2006.
108. Amano Y, Hayashi T, Takahama K, et al: MR imaging of umbilical cord urachal (allantoic) cyst in utero. *AJR Am J Roentgenol* 180:1181, 2003.
109. Moore RJ, Strachan B, Tyler DJ, et al: In vivo diffusion measurements as an indication of fetal lung maturation using echo planar imaging at 0.5T. *Magn Reson Med* 45:247, 2001.
110. Fenton BW, Lin CS, Ascher S, et al: Magnetic resonance spectroscopy to detect lecithin in amniotic fluid and fetal lung. *Obstet Gynecol* 95:457, 2000.
111. Kok RD, van den Bergh AJ, Heerschap A, et al: Metabolic information from the human fetal brain obtained with proton magnetic resonance spectroscopy. *Am J Obstet Gynecol* 185:1011, 2001.
112. Kok RD, van den Berg PP, van den Bergh AJ, et al: Maturation of the human fetal brain as observed by 1H MR spectroscopy. *Magn Reson Med* 48:611, 2002.
113. Spellacy WN: Fetal Growth retardation. In Scott JR, DiSaia PJ, Hammond B, et al (eds): *Danforth's Obstetrics and Gynecology*, 7th ed. Philadelphia, JB Lippincott Company, 1994.
114. Wedegartner U, Tchirikov M, Shafer S, et al: Functional MRI at 3T: Comparison of BOLD signal changes in fetal organs with fetal and maternal oxyhemoglobin saturation during hypoxia in a sheep model. *Radiology* 237:919, 2005.



# THE ROLE OF THREE-DIMENSIONAL ULTRASOUND IN THE EVALUATION OF THE FETUS

Beryl R. Benacerraf, MD

## Basic Principles

### Applications of Three-dimensional Ultrasound

#### Improving the Efficiency of Ultrasound Practice With Three-dimensional Ultrasound

#### Evaluation of Congenital Abnormalities With Three-dimensional Ultrasound

The Fetal Face

The Fetal Skeleton and Extremities

The First Trimester of Pregnancy

The Fetal Heart

### Evaluation of Volume Measurements

#### Artifacts

#### Parental-fetal Bonding

#### Conclusion

Two-dimensional (2D) ultrasound has been the mainstay of sonography for the past 30 years. Although technologic advances have improved image resolution, the technique of taking one 2D image at a time while spending extended periods of time one-on-one with a patient did not change until recently. As three-dimensional (3D) ultrasound emerges, the ability to acquire an entire volume of ultrasound information and then display any plane within the volume after the patient has left the premises opens a huge number of display possibilities that ultrasound had never enjoyed.

3D volume imaging is not new. Computed tomography (CT) and magnetic resonance imaging (MRI) have used 3D volume acquisition, followed by 2D reconstruction of many different types, surpassing ultrasound in these imaging display capabilities. Now that ultrasound has acquired this ability to obtain 3D volumes and display them in numerous new ways, many more opportunities have been opened in sonography. These opportunities are explored in this chapter.

The ability to think in three dimensions while scanning in two dimensions has always distinguished ultrasound practitioners from members of other disciplines. The ability now to display these 3D images digitally, heretofore available only in the mind's eye, represents an enormous advance in the field of ultrasound in obstetrics and gynecology.

## BASIC PRINCIPLES

There are two basic methods for producing a 3D volume data set. One of these methods involves free-hand acquisition, manually sweeping a 2D ultrasound transducer across the patient to produce a volume ultimately digitally saved. Although the addition of a position-sensing device to the transducer may standardize the sweep, the free-hand sweep still has the inherent limitations of the differences in individual operators' sweep techniques and speed. This manual acquisition technique has been largely abandoned.

The more current method of acquiring volumes involves an automated acquisition, still done with a 2D sweep, now housed within a mechanical volume probe. This allows the volume to be acquired at a constant speed, resulting in a reproducible volume that permits measuring in all planes. In the future, nonmechanical matrix-array transducers will likely allow for far more rapid volume acquisitions, resulting in real-time volume imaging. Four-dimensional (4D) ultrasound is defined as 3D ultrasound that is displayed over time, or real-time 3D (the fourth dimension being the time dimension).

Once the volume is acquired in a standardized fashion using an automated acquisition transducer, there are many important displays available to the sonologist to demonstrate the anatomy within the volume. The following five types of displays represent the most common and most useful methods of obtaining anatomic images from a volume acquisition.<sup>1-9</sup>

1. Multiplanar reconstruction allows viewing of three simultaneous orthogonal planes, with a single dot representing the point of intersection of all three planes. Using the tools provided by the manufacturer, we can navigate through this volume by moving either the dot or the individual planes to display any tomographic plane as well as the corresponding images that are perpendicular to that plane of section. This kind of manipulation gives us complete control over the volume and enables us to display any plane in any orientation from within the volume. Of the three displayed perpendicular planes (A, B, and C), the C plane is the one that can never be acquired by scanning the patient directly (Figs. 24-1 and 24-2). Although planes A and B are perpendicular to each other, and can be acquired from the patient using 2D ultrasound, the ability to reconstruct the C plane is what makes this technique unique.<sup>4,6,8</sup>

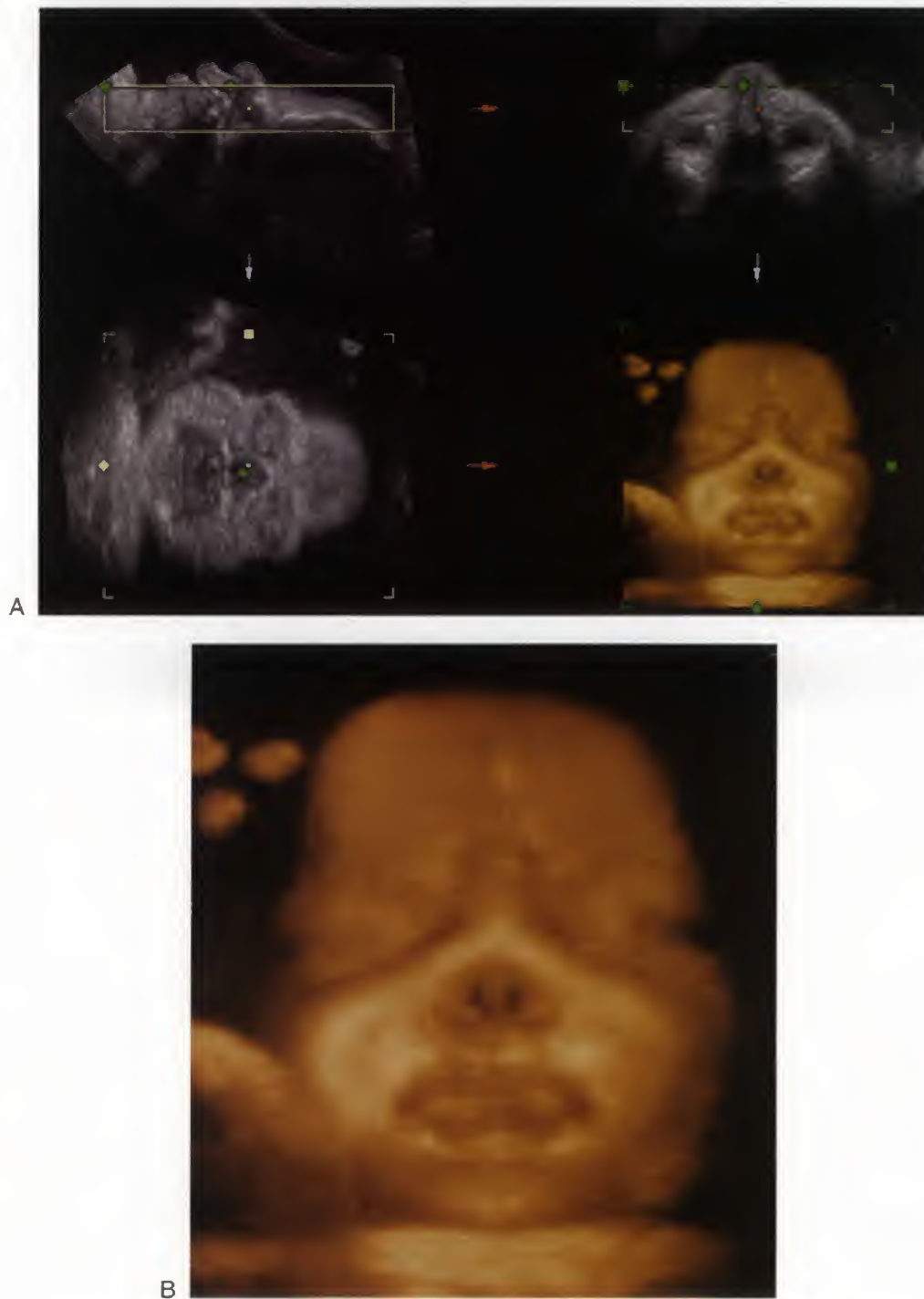


**FIGURE 24-1.** A. Multiplanar reconstruction of a fetal face showing the A plane as a profile, the B plane as transverse view through the orbits, and the C plane as a coronal view through the face. Also shown in the right lower quadrant of the image is a surface reconstruction emphasizing the midface. B. Close-up of the surface rendering on the same case, emphasizing the region of the maxilla, nose and nasal septum, and lips.



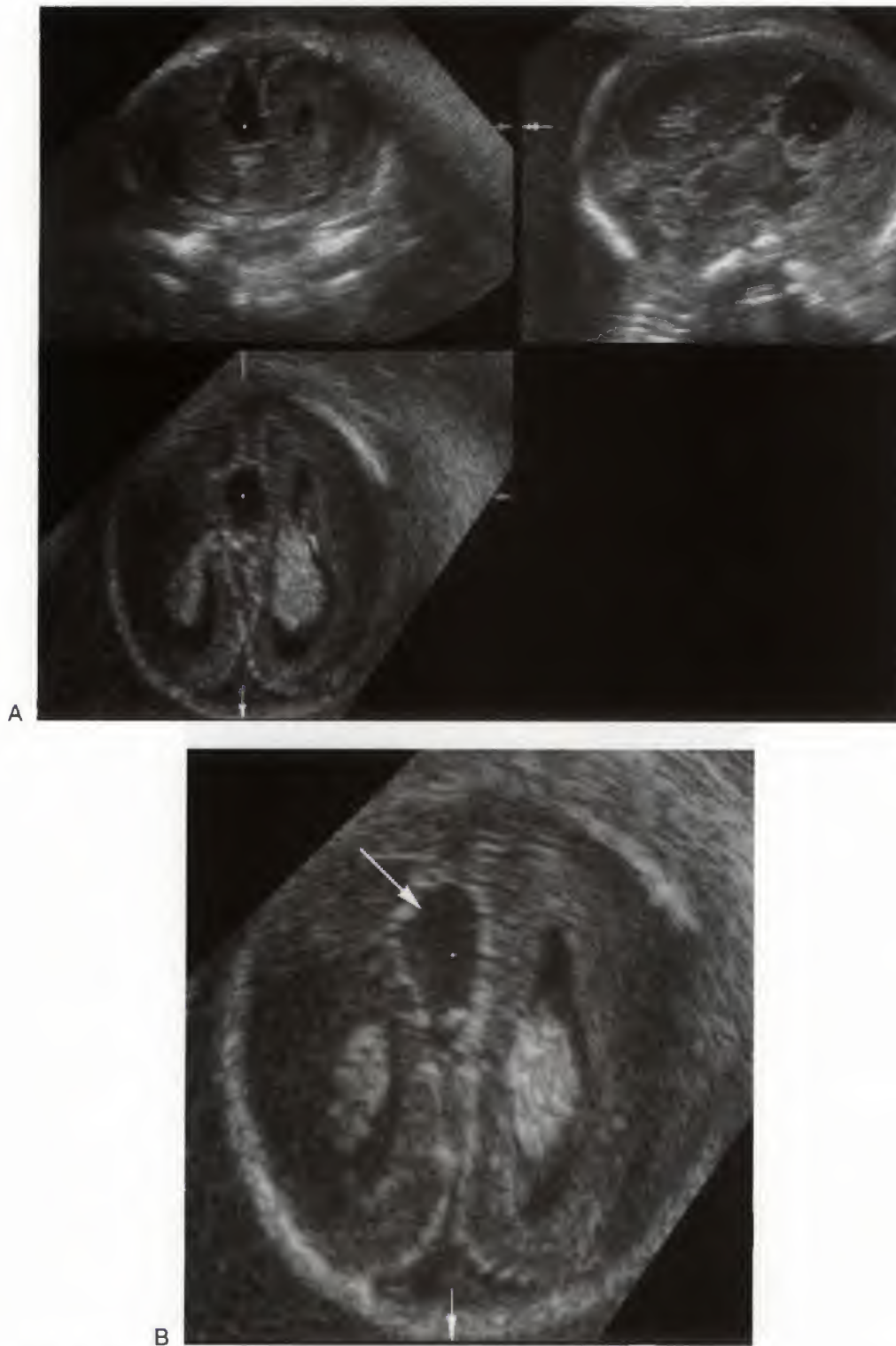


**FIGURE 24-2.** A. Multiplanar reconstruction of the fetal head in a fetus who has agenesis of the corpus callosum as well as an interhemispheric cyst. Note that the reconstructed plane (plane C) in the left lower quadrant of the image shows this plane akin to a CT plane of section. B. Plane C view shows the parallel orientation of the lateral ventricles and the cyst (*arrow*).

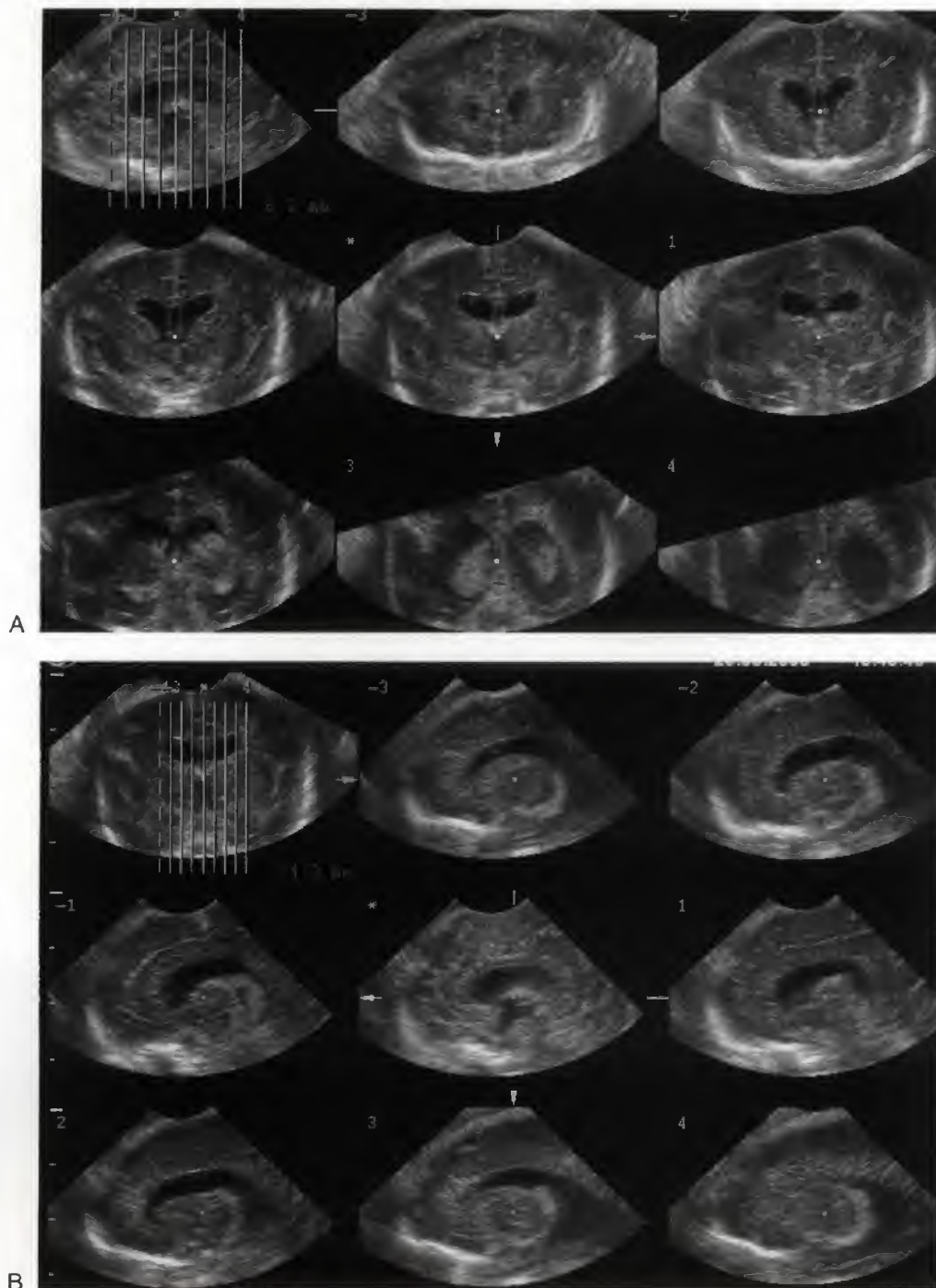


**FIGURE 24-3.** This figure shows three sets of images taken at right angles to each other, displaying parallel slices through the volume in each of the three orthogonal planes. Note that this fetus, who has mild ventriculomegaly, can be viewed in any reconstructed plane, regardless of the way the image was obtained. All of these images were obtained from a single volume acquisition. *A.* Coronal planes of section displayed from a sagittally obtained plane. *B.* Sagittal planes of section displayed from a coronally obtained plane. *Continued*

2. The volume can also be displayed in 8 to 10 parallel tomographic slices, similar to the displays used by CT and MRI. We can choose the distance between the individual slices and the number of slices displayed. These multiple parallel slices can be demonstrated in any of the three orthogonal planes chosen, thus showing the parallel slices in either plane A, plane B, or plane C

(Fig. 24-3). Without having to actively navigate throughout the volume, one can interrogate the entire volume in multiple slices and multiple planes.<sup>10</sup>

3. The surface-rendering mode is the display method that has been publicized in the lay press, often showing baby faces in utero (Fig. 24-4). This rendering requires a fluid interface in front of the area being imaged.<sup>5,11,12</sup> We can



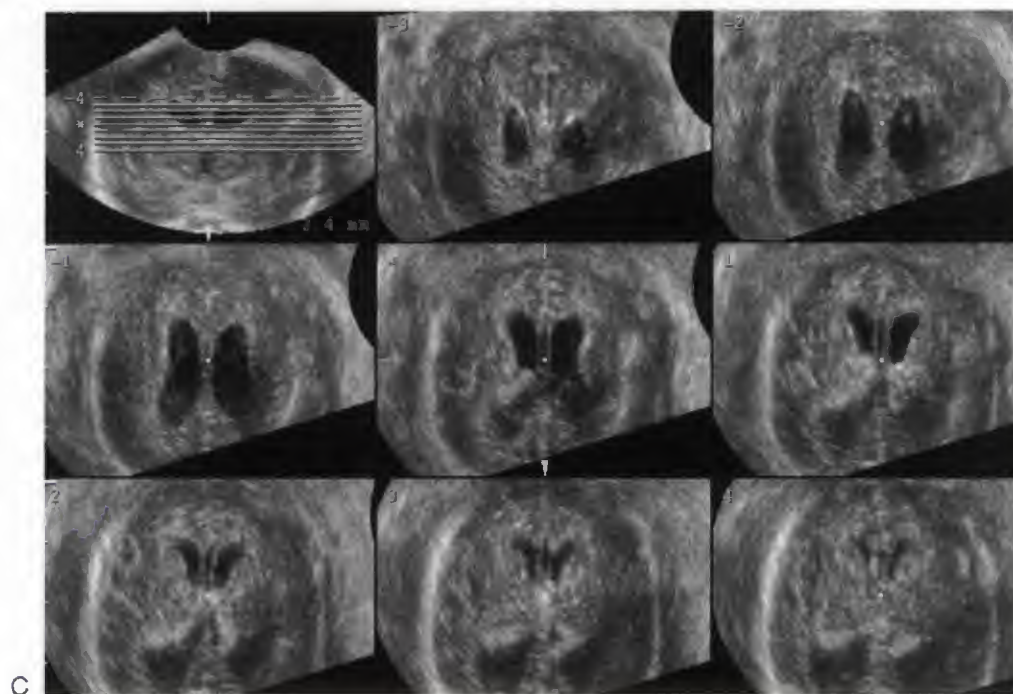


**FIGURE 24-3, cont'd.** C. Transverse axial planes of section displayed from a coronally obtained plane.



**FIGURE 24-4.** A and B. Surface rendering of the fetal face of two different fetuses in the third trimester. Note the detail of the facial features of these two fetuses.



**FIGURE 24-5.** A. A fetal face using the soft tissue rendering technique showing the surface of the face, nose, lips, and chin. B. The same fetus imaged using a bony window and in profile, demonstrating that the maxilla is more echogenic than the surrounding soft tissues of the nose and lips. These two images were obtained from the same volume but displayed with different post-processing settings.

turn the object around, looking at various aspects of its surface, as well as slice through the object and looking at cut surfaces of the volume.

One can then select one of the many postprocessing techniques to display either the soft tissue surface or the skeleton of the fetus (Figs. 24-5 to 24-7). There is also a transparent mode, which allows the color Doppler display to shine through a transparent fetal body<sup>13,14</sup> (Fig. 24-8). Finally, one can further evaluate the anatomy by using an electronic scalpel to cut away parts of the image, eliminating areas that are not part of the anatomy being sought, hence accentuating the area of interest (Fig. 24-9). The electronic scalpel has been shown to be very important in the evaluation of fetal malformations.<sup>15</sup>

4. The inverse mode is a rendering technique of the entire volume in which all of the cystic areas within the volume become digitally opaque and all of the solid areas become transparent (Figs. 24-10 to 24-12). This technique allows us to visualize all of the cystic areas that are otherwise hidden inside the volume. Surface rendering techniques do not permit us to visualize the cystic areas contained within a volume, and the multislice and the three orthogonal planes techniques allow us to see a only thin slice of the cystic areas at one time. The inverse mode is the only way to see, in a bird's eye view, all of the cystic areas otherwise hidden within the volume. We then can use our electronic scalpel to further slice the volume in order to concentrate on a particular area within it.<sup>16-19</sup>

5. Because mechanical sweeps are too slow to render adequate real-time images of the heart, an alternate method is often used called spatiotemporal image correlation (STIC). This is a cardiac gating technique that interrogates an entire cardiac cycle and plays it back, allowing us to see the anatomy of the heart in real time.<sup>20-23</sup> One then can display this real-time volume in three orthogonal views, in inverse mode, or any other type of display necessary. Such volumes can be manipulated to display the four chambers of the heart, the great vessels, or any other portion of the cardiac anatomy within the sample volume (Fig. 24-13).

The most important benefit of using volume imaging, however, is the ability to save entire volumes, containing all of the patient's sonographic information. Volumes can then be manipulated, reinterrogated, and reconstructed into different displays, either in 3D or 2D display modes, well after the patient has left the examining area. This allows the ultrasound examination to be far less operator dependent, because it no longer is completely reliant on the skill and eyes of the sonographer or sonologist holding the probe. If an image was not taken at the time of the original scan, or if the fetus was not in a perfect position, these additional images can be reconstructed and viewed after the patient has finished her examination.<sup>24-26</sup> Measurements also can be made within the volume—measurements that were perhaps inadvertently omitted at the time of the scan or measurements



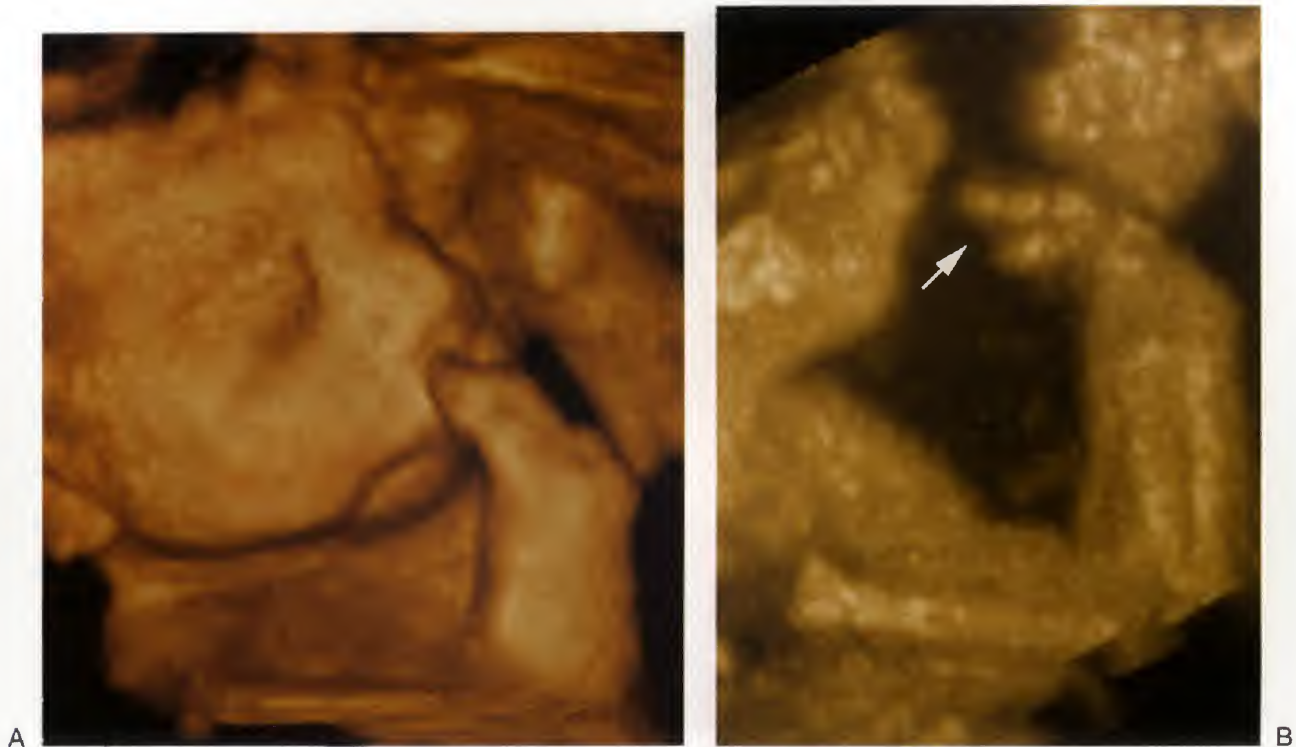


**FIGURE 24-6.** A. A distal limb abnormality of the upper extremity with a transverse limb defect involving the wrist and hand is shown. The hand appears to be missing on this surface rendering view using soft tissue settings. B. The same volume is shown with a bone window, demonstrating that there are two digits (*arrow*) within the distal portion of the amputated wrist. The ability to see the bones or the soft tissue settings using the same volume is an advantage of 3D, which enables the practitioner to evaluate different aspects of the abnormality without having to return to the patient.



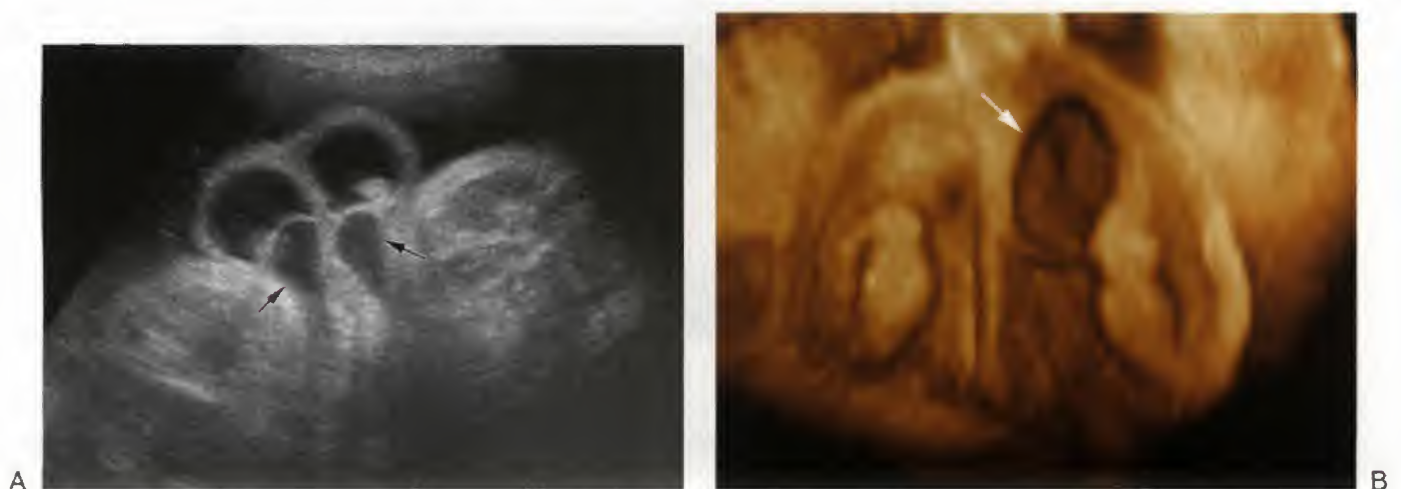
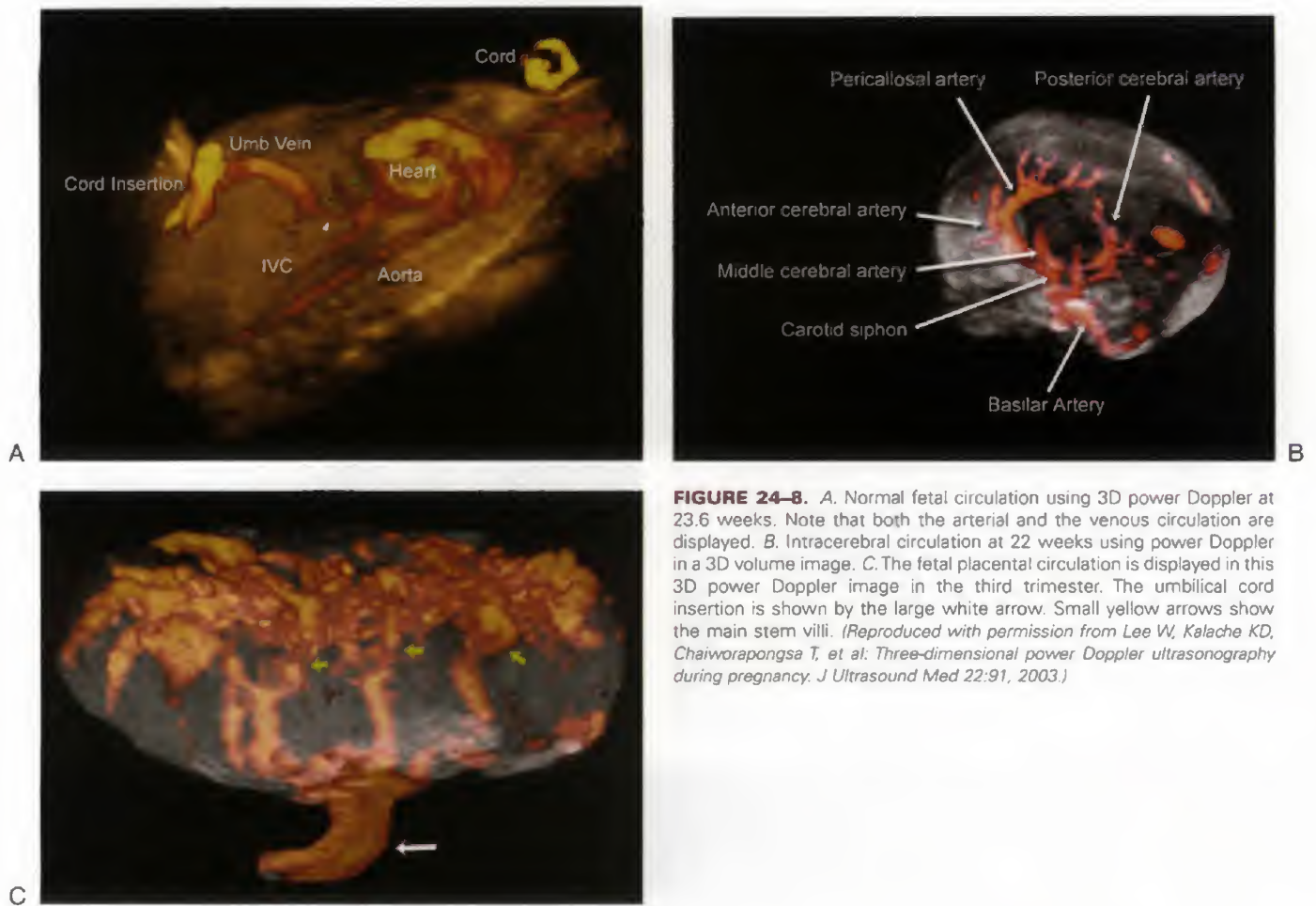
**FIGURE 24-7.** The bony window is used to demonstrate the fetal face. Note that the maxilla is particularly well seen using this maximum intensity window.

that can only be achieved in reconstructed planes. Last, one can transmit the entire data to other centers for review and virtual rescan for tertiary consultations or merely as an educational tool.<sup>26,27</sup> These capabilities make 3D volume imaging incredibly powerful in the field of sonography.

## APPLICATIONS OF THREE-DIMENSIONAL ULTRASOUND

The applications of 3D sonography are multifaceted and include the ability to perform the entire scan using a few rapidly obtained 3D volumes. This technique could replace the tedious 2D image acquisition, allowing the entire scan to be reconstructed virtually from a few volumes that contain an infinite number of image slices.<sup>24,25</sup> 3D sonography is also helpful in evaluating further those malformations seen in 2D that can be more extensively examined using surface rendering or multiple reconstructed planes. There are also many applications for imaging the heart and the face, performing volumetric measurements of many fetal organs, evaluating the first trimester fetus, and looking at the fetus using Doppler within the 3D displays. All of these are discussed in detail later in the chapter.

First, the overall importance of using volume imaging relates to the ability to save all of the sonographic information in a few volumes, to display any view or any plane long after the patient has left. This was first presented by Nelson et al,<sup>26</sup> who evaluated the feasibility of performing 3D ultrasound studies and transmitting them to another center across the country, for offline review at this remote location. This study showed that 3D sonography could produce images of diagnostic quality, which could be transmitted and reconstructed to produce images similar to the original images obtained during the patient's 2D scan. Although the quality of the reconstructed images was inferior to the original 2D images obtained directly from the





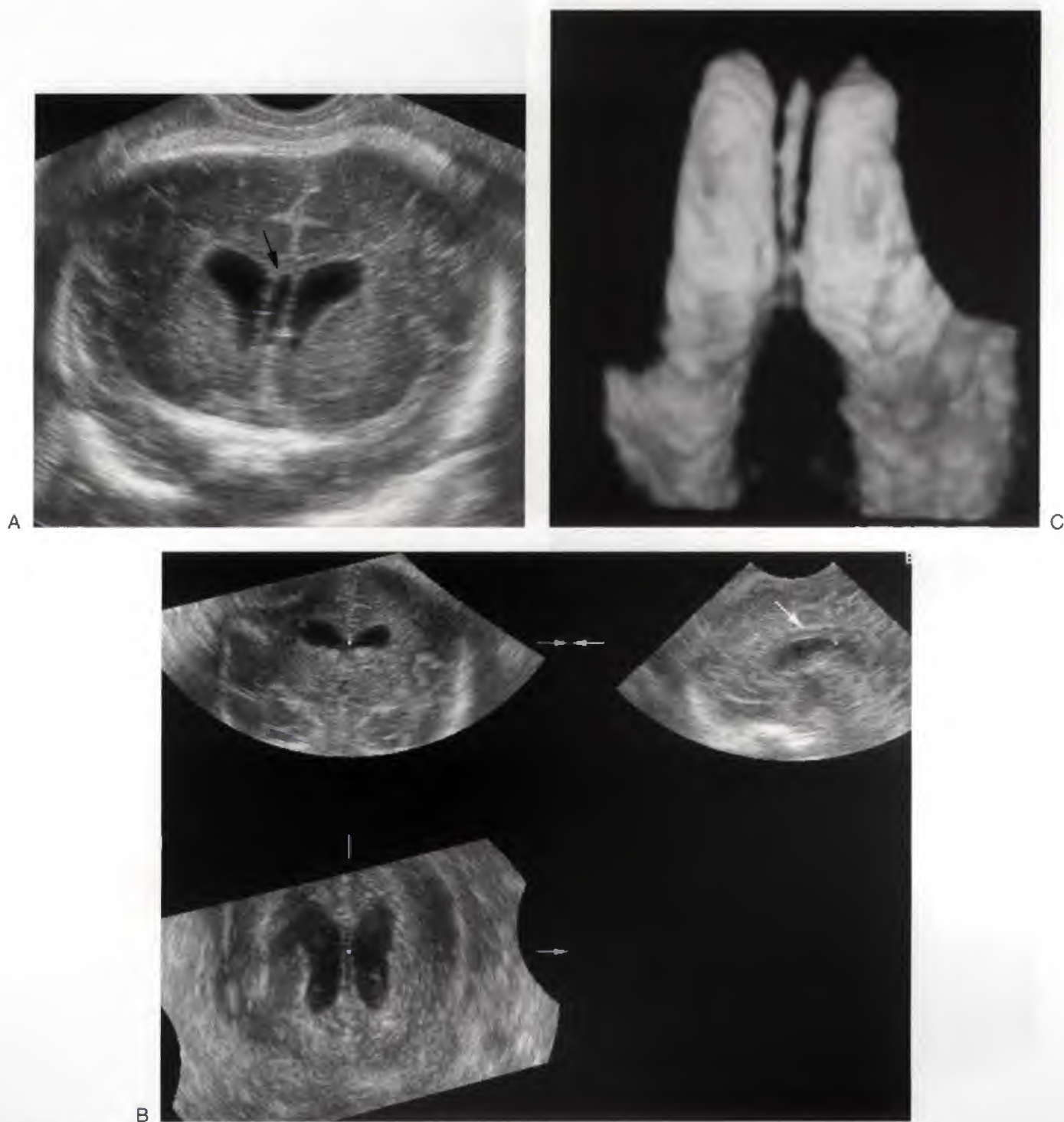


**FIGURE 24-10.** A. A coronal view through the fetal frontal horns in a fetus with mild ventriculomegaly. Note the presence of the cavum septum pellucidum (arrow) in between the frontal horns. B. Multiplanar reconstruction of the same fetus, demonstrating the presence of an intact corpus callosum (arrow). The third plane in the left lower corner of the image shows a transverse section through the atria of the lateral ventricles in a completely reconstructed view not obtainable in conventional 2D scanning. C. The inverse mode of the same case, showing a cast of the lateral ventricles and cavum septum pellucidum between the two frontal horns.

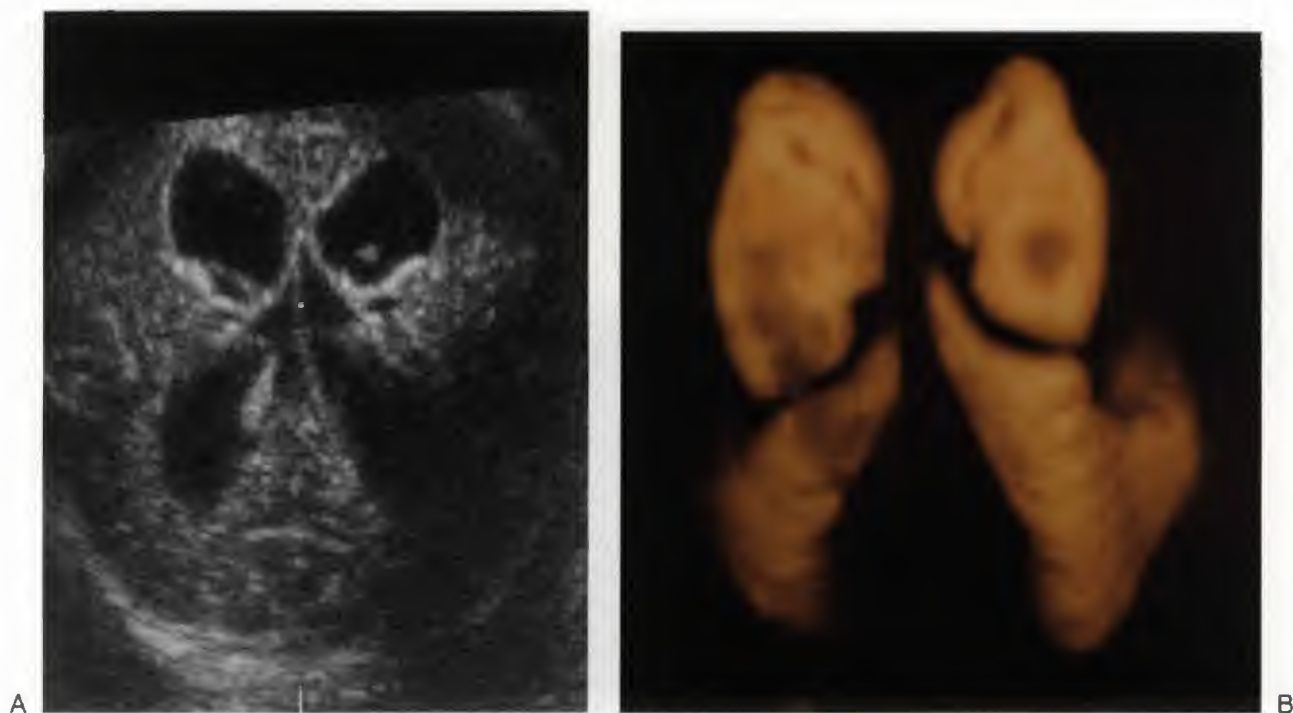


**FIGURE 24-11.** A. A reconstructed transverse view through the fetal head of a fetus with hydrocephalus and round cystic areas associated with the frontal horns. B. The inverse mode is shown, demonstrating a cast of the dilated lateral ventricles and frontal cystic areas.

patient, this study showed that it was clinically feasible to acquire 3D volume data at one site and display the data at another with reasonable clinical quality.<sup>26</sup>

### IMPROVING THE EFFICIENCY OF ULTRASOUND PRACTICE WITH THREE-DIMENSIONAL ULTRASOUND

There is no doubt that 3D volume imaging can be used to display all of the information that normally is obtained using 2D ultrasound, plus much more, in a very short time frame (Fig. 24-14).

In a pilot study of 25 cases, we first investigated the concept that five 3D volume sweeps could be used to produce all of the images necessary for a complete second trimester sonographic fetal survey. We demonstrated that the five volume data sets, designed to encompass all of the fetal anatomy (focused on the head, face, chest, abdomen, and lower extremities), could be saved and reviewed virtually on a review station, to produce the complete fetal survey, displaying fetal anatomy, as well as the biparietal diameter and femur-length measurements.<sup>24</sup> A complete structural survey was accomplished in 20 of the 25 fetuses, with most of the incomplete surveys due to the lack of complete visualization of a hand. Most importantly, however, the five volume acquisitions were accomplished in 1 minute and the review of the five volumes was done offline in only 5 minutes, resulting in a total scan time of 6 minutes compared with approximately 14 minutes per scan for performing the same examination in standard 2D imaging. This volume data set approach to the screening second trimester structural

surveys could markedly improve efficiency in ultrasound departments, because the scan could be performed in less than half the time spent performing a standard 2D fetal sonogram.

This study was expanded further using 50 patients, comparing the ability of three independent physicians to review the volumes.<sup>25</sup> The traditional 2D scan time was 19.6 minutes per scan, compared with 1.8 minutes for the acquisition of the five volumes by the sonographer. The review of the volumes, including the offline measurement of the biparietal diameter and femur, varied between 4.79 and 5.53 minutes for the three interpreting physicians. At least 90% of all anatomic landmarks were identified successfully on virtual 3D reconstruction, compared with 2D. All three physicians were equally successful at reconstructing the images as well as identifying the fetuses with abnormalities. This also indicates a marked time savings in performing the standard fetal anatomic survey, which was performed in less than 2 minutes of actual scanning time.<sup>25</sup> This application of 3D ultrasound is likely to become important in our attempt to improve the efficiency of our ultrasound departments.

The review and rescan of sonographic volumes is also crucial in allowing ultrasound to gain some of the standardization and flexibility enjoyed by CT and MRI. This application of volume sonography is likely to decrease operator dependency, which has plagued ultrasound for so long. The 3D virtual examination also is well suited for echocardiography, in which volumes can be obtained and sent to centers that can further evaluate the entire cardiac data set. This concept of volume scanning with offline interpretation would be particularly helpful for patients scanned



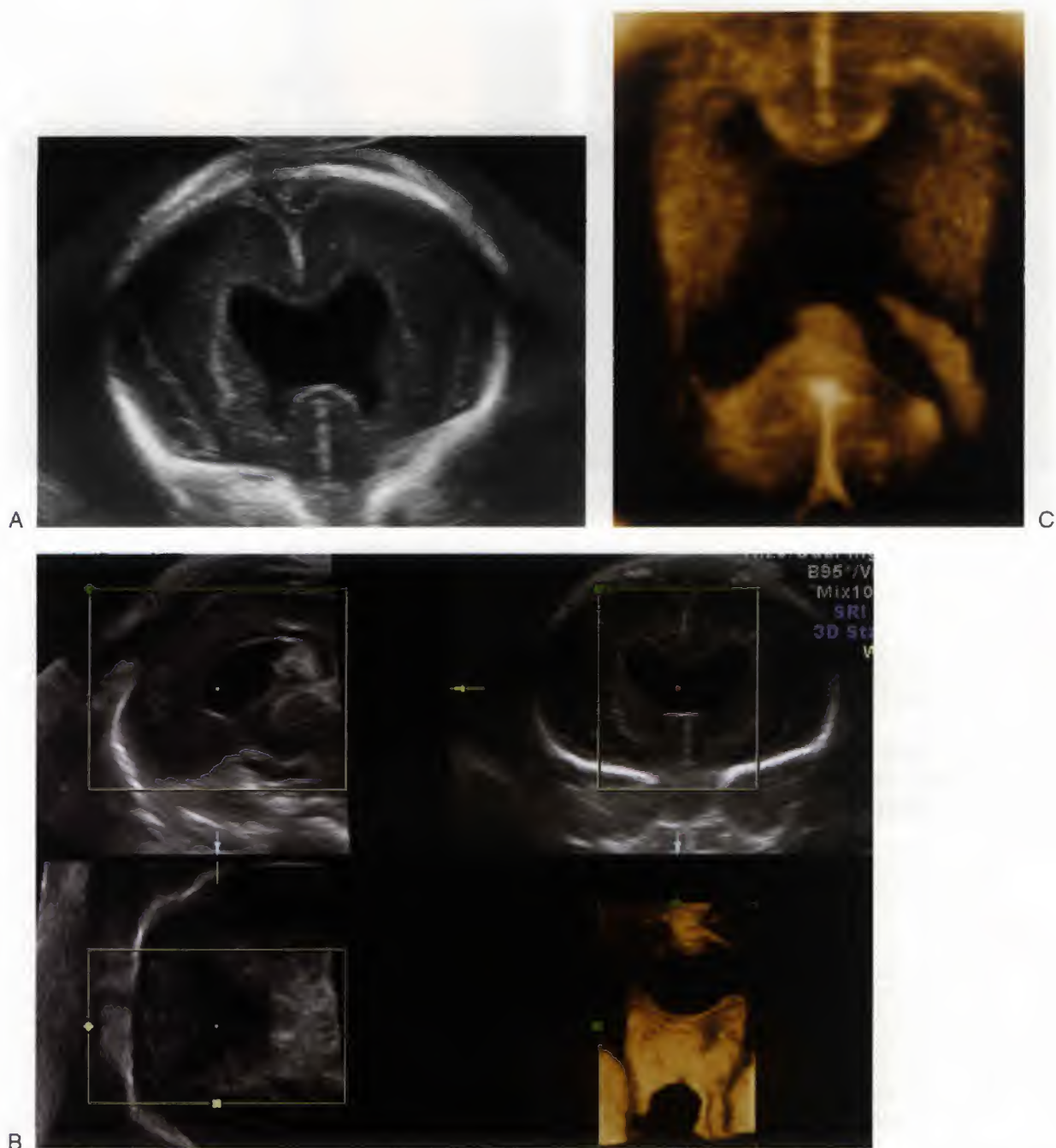


**FIGURE 24-12.** Lobar holoprosencephaly demonstrating absence of the cavum septum pellucidum and fusion of the frontal horns across the midline. *A.* A coronal view of the region of the frontal horns showing absence of the cavum septum pellucidum and connecting frontal horns. *B.* Multiplanar reconstruction of the three orthogonal planes. The defect is shown by the dot (top right, bottom left), which is located in the region where the cavum septum pellucidum should be. Also note that the inverse mode is shown in the lower right quadrant box, demonstrating a cast of the ventricles. *C.* A rendered image of the inside of the lateral ventricles right at the fusion between the lateral ventricles. *Continued*

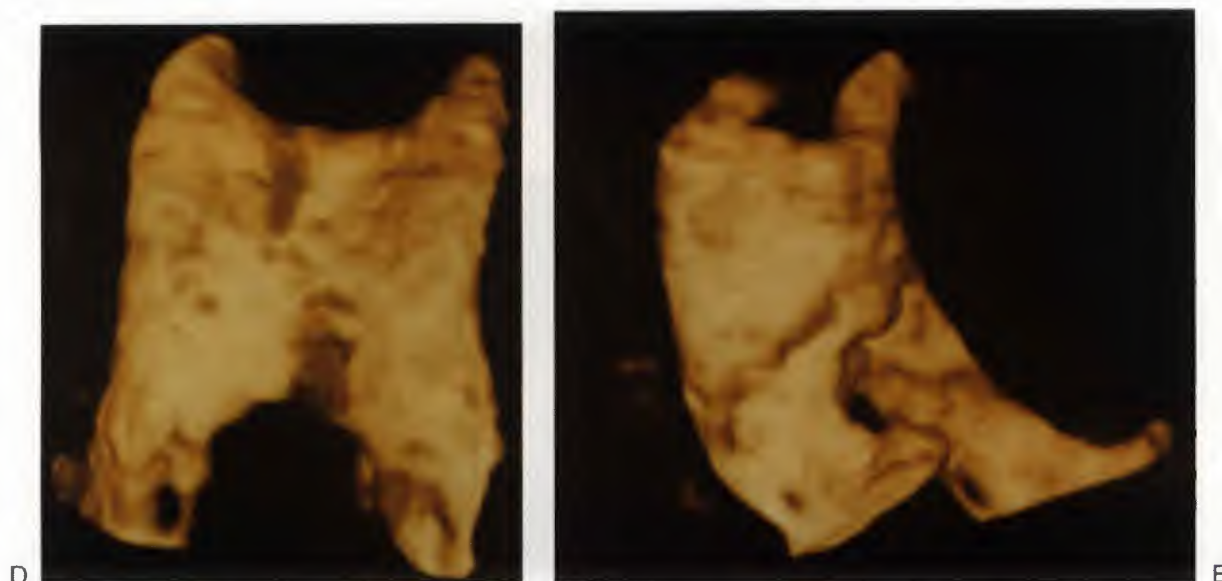


**FIGURE 24-12, cont'd.** D, E. The inverse mode demonstrating a cast of the lateral ventricles and the connection between them.

in remote locations where tertiary care expertise may not be easily obtainable. In particular, in areas where fetal heart expertise may not be available, practitioners would have the option to obtain assistance by forwarding these data sets to cardiac centers.<sup>28,29</sup>

### EVALUATION OF CONGENITAL ABNORMALITIES WITH THREE-DIMENSIONAL ULTRASOUND

Investigators have compared the use of 3D and 2D ultrasound in the assessment of fetal malformations identified originally by 2D ultrasound.<sup>30-37</sup> Much of this research has shown that volume imaging can add value to the standard 2D ultrasound in evaluating fetuses with malformations.<sup>32,34,35,37</sup> The largest studies were reported by Merz and his group,<sup>37</sup> who studied 906 anomalous fetuses and demonstrated that 3D sonography proved advantageous, providing additional information in 60.8% of cases when compared with 2D ultrasound alone. This additional information was derived from tomographic multiplanar reconstruction in most cases, although in some patients, the surface-rendering mode best displayed the malformation. Dyson et al<sup>34</sup> studied 63 patients with 103 anomalies using both 2D and 3D ultrasound. The investigators found that 3D images provided additional information in 51% of the anomalies, was equivalent in 45% of anomalies, and disadvantageous in 4% when compared with 2D ultrasound alone. Although half of the patients benefited from 3D ultrasound, there was only one patient whose management was actually affected by the 3D information. The type of anomalies in which 3-D imaging was helpful included facial defects, limb abnormalities, and neural tube defects. The additional benefit of 3D ultrasound was derived largely from the ability to reconstruct multiplanar slices from the 3D ultrasound volume data sets. These authors, as did Mertz et al, concluded that 3D

ultrasound should be used as an adjunct to 2D imaging for providing comprehensive evaluation of congenital fetal abnormalities.<sup>34,37</sup>

Other investigators, however, found that 3D ultrasound imaging did not provide significant additional information compared with what could be accomplished using 2D ultrasound. Although some of the malformations may be better visualized using 3D reconstruction, these authors believed that 3D ultrasound did not provide significant additional information that would change management in these anomalous cases.<sup>35</sup>

### The Fetal Face

Evaluation of the fetal face with 3-D ultrasound has received much attention in the literature as a complimentary technique to 2D sonography, once a fetal malformation is identified. A volume acquisition of the fetal face can be reoriented such that a true midline sagittal plane can be derived from a fetus who is not in a favorable position (Fig. 24-15). If a fetus is not in an ideal position to evaluate the profile, the true midsagittal plane can be reconstructed from a volume of a fetal face, thus optimizing the detection of fetal facial anomalies such as micrognathia.<sup>38</sup> Surface rendering views also can be helpful to evaluate the fetal lip and chin, and multiplanar views can be used to evaluate the fetal palate in cases of suspected cleft palate (Figs. 24-15 to 24-21).<sup>39-43</sup>

3D reconstruction of the fetal facial surface is one of the first applications made popular in the lay press, owing to the exquisite and life-like appearance of the fetal face this technology produces (see Fig. 24-4). A volume acquisition of the fetal face can allow the operator to reconstruct any plane throughout the entire volume, not only in three orthogonal planes but also in parallel tomographic slices as well as surface rendering.<sup>39-42,44</sup> This concept has led many investigators to study the addition of 3D ultrasound imaging to the



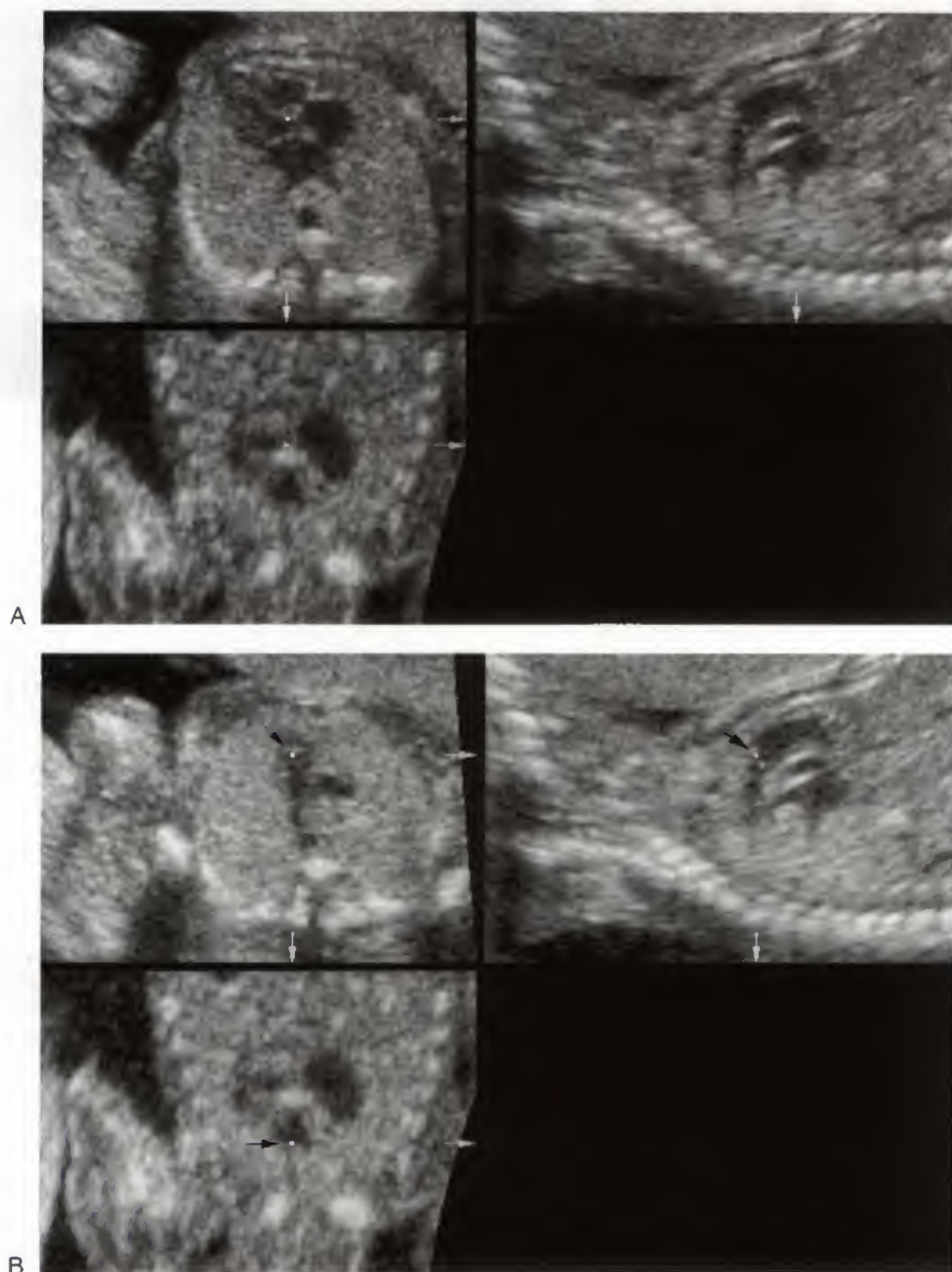


**FIGURE 24-13.** A. Multiplanar reconstruction of a normal second trimester heart. The four-chamber view is in the left upper quadrant, and the reconstructed view of the pulmonary artery is shown in the right upper quadrant of the image (plane B). B. The pulmonary outflow tract indicated by the dot (arrow) in the acquisition plane (plane A). The pulmonary artery is also seen in the reconstructed view on the other two planes and the dot (arrow) indicates a single point in space that represents the pulmonary outflow tract. *Continued*



**FIGURE 24-13, cont'd. C.** An inverse mode of the fetal heart showing a cast of the ventricles and great vessels. Note that the anterior-most ventricle is the right ventricle, giving rise to the pulmonary artery, which courses underneath the aortic arch.

standard 2D ultrasound study, to determine the additional benefit of using 3D imaging in facial anomalies.

Many studies have suggested that the evaluation of the fetal face using the multiple displays available from a volume have improved diagnostic accuracy for the detection of cleft lip and palate, and micrognathia, as well as orbital abnormalities and nasal bone dysplasia.<sup>38,41,42,45</sup> Gonçalves et al<sup>30</sup> have shown, in an elegant review of the literature, that among 11 studies that evaluated the addition of 3D to 2D ultrasound for the evaluation of the fetal face, seven concluded that there was additional information provided.<sup>38,46-51</sup> Four suggested that no additional useful information was provided.<sup>52-55</sup>

Several investigators, including Pretorius et al<sup>41,52</sup> and Mertz et al,<sup>38</sup> have suggested that 3D ultrasound confirmed facial abnormalities more frequently than did 2D ultrasound, and Mertz et al found an additional anomaly in a 3D ultrasound examination that had not been identified previously in 2D examination.

The main area of interest has been evaluating the fetal palate, which remains elusive using 2D ultrasound alone (see Fig. 24-18). Campbell et al<sup>56,57</sup> found that the most accurate imaging of the palate could be accomplished by using a 3D reverse-face view, in which the 3D rendering surface is adjusted to optimize the face from the inside of the skull. This image is obtained by performing a 3D surface rendering of the fetal face with a frontal-view display, and then rotating the volume 180 degrees along the Y or vertical axis, such that the back of the face is visible, showing the palate area, nasal cavity, and orbits from the back. The window of the surface-rendering area then is placed from

back to front, and the inside of the maxilla is demonstrated in this 3D reverse-face view. According to Campbell et al, this improves the visualization of the palate area (Fig. 24-22).

Chmait et al<sup>43</sup> studied more than 50 patients and also found that 3D ultrasound was better than 2D in evaluating clefts of the palate in particular. Mittermayer et al<sup>54</sup> found a greater accuracy of 3D ultrasound for the detection of cleft palate. A larger study, however, by Rotten and Levailant,<sup>58,59</sup> looked at combining 2D and 3D ultrasound examinations for the best diagnosis of facial clefts. They studied 96 fetuses with facial clefting at a mean gestational age of 28 weeks and found that the anatomic defect was correctly identified in 97.5% of their affected cases. In 8.3% of cases, the facial clefts were missed or underestimated, and in 4.1% of cases, the facial clefts were overestimated as having a palatal component. Hata et al<sup>47</sup> studied 94 healthy fetuses and showed that both 2D and 3D ultrasound showed normal anatomy with equal accuracy.

Looking at other aspects of the fetal face, Lee et al<sup>60</sup> showed that 3D multiplanar imaging has a very high likelihood of producing a true midline sagittal view of the fetal profile, which is very useful for detecting micrognathia regardless of the fetal position. Mertz et al<sup>38</sup> evaluated 618 patients and found that the true midsagittal profile was obtainable using 2D in only 69% of cases. 3D reconstruction allowed for the evaluation of the profile in all cases. Among the 25 cases of facial abnormalities, five cases had additional features identified using 3D ultrasound. Mangione<sup>55</sup> evaluated the use of 3D ultrasound to detect facial dysmorphism in a study of 41 patients. He found that 3D imaging performed better than 2D ultrasound in 20 cases, and that 2D imaging was more accurate in two cases, with the remaining cases having no detectable difference between the information derived from 2D and 3D ultrasound. It is important to note, however, that in seven cases, the 3D images could not be technically obtained, indicating some technical limitations of 3D ultrasound. These authors concluded that the evaluation of craniofacial dysmorphism, particularly the study of the fetal ears, was helpful in their patients (Figs. 24-23 and 24-24).

Others have evaluated fetal cranial sutures and fontanels using 3D ultrasound, and surface rendering of the fetal volume has been particularly helpful in this set of patients.<sup>61-64</sup> Although gestational age influenced the visibility of the sutures and fontanels, 3D ultrasound was a reliable technique for viewing most of the fetal sutures and fontanels during the second half of pregnancy (Fig. 24-25). This has an impact when evaluating fetuses for cranial synostosis and related syndromes.<sup>65</sup>

Another benefit of 3D ultrasound evaluation of the face is the ability to demonstrate to the patient and the plastic surgeon the extent of the lesion. Although practitioners who are trained in ultrasound can mentally reconstruct the extent of the abnormality based on standard 2D images, our non-scanning colleagues and the patients benefit greatly from seeing the face displayed in a traditional and less abstract way.<sup>66</sup>

The imaging of the fetal brain is one of the areas in which 3D multiplanar imaging has been studied in great detail and is most helpful. Imaging the brain through the fetal fontanel allows us to obtain an excellent volume of the entire brain, which subsequently can be reconstructed in any plane.<sup>67-69</sup>



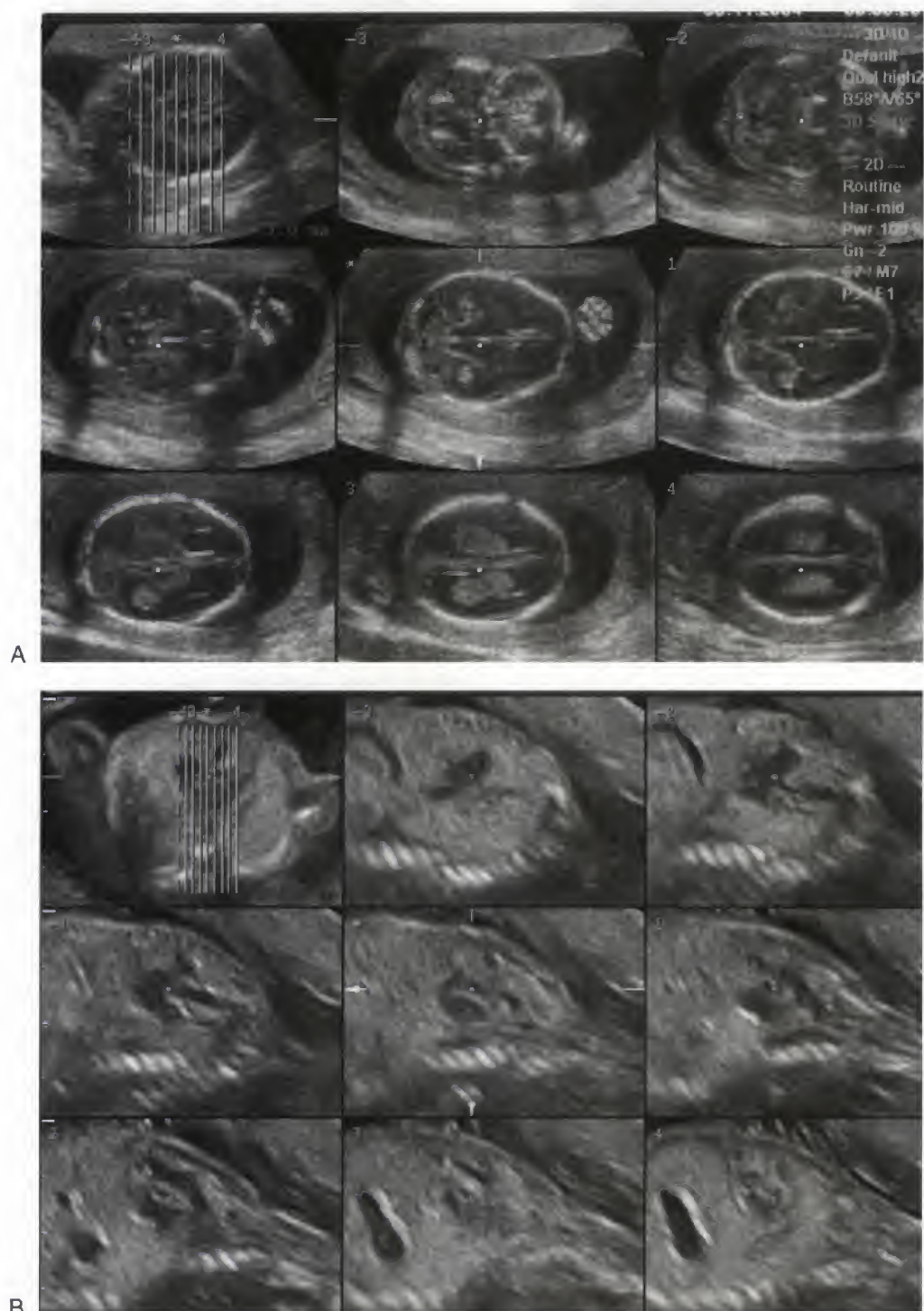
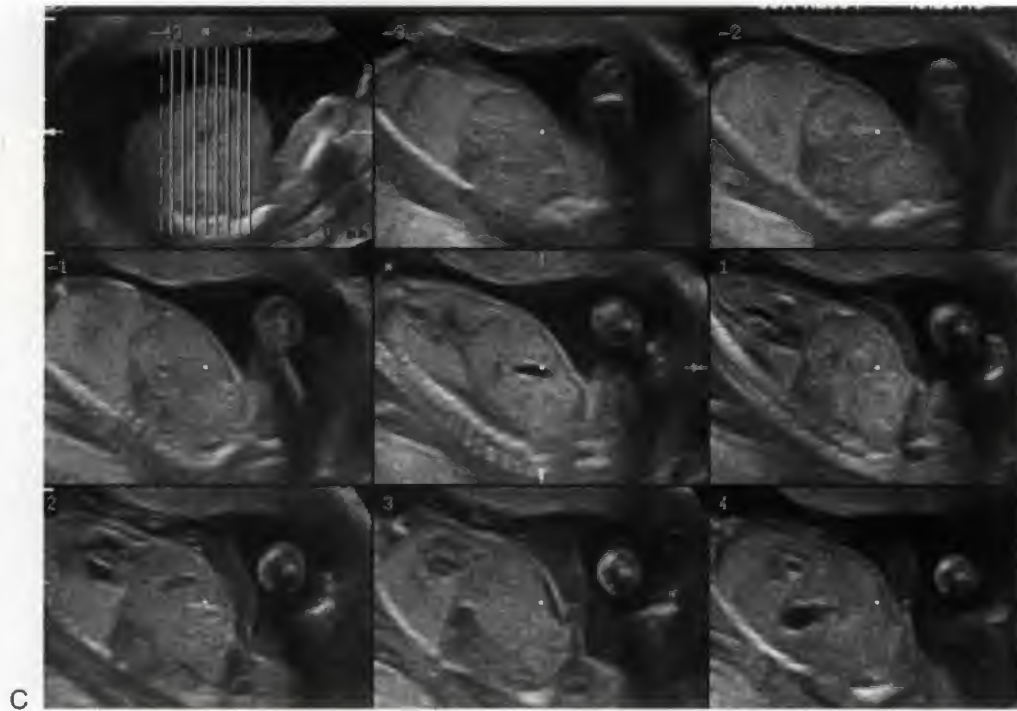


**FIGURE 24-14.** A. Tomographic imaging display of a normal second trimester fetal head, demonstrating that one can obtain views of the lateral ventricles, choroid plexus, posterior fossa and nuchal fold using the same single volume displayed in this way. B. A similar tomographic display through the fetal chest. Note that the entire heart is well displayed, demonstrating both the aorta and the pulmonary artery, as well as the fetal stomach underneath the heart using these multiple parallel slices. *Continued*



C

**FIGURE 24-14, cont'd. C.** The interface of the fetal lung and liver with multiple parallel sections taken from a single volume through the fetal chest and abdomen. The anatomy of the fetal chest, heart and abdomen can be displayed in its entirety using this single volume.

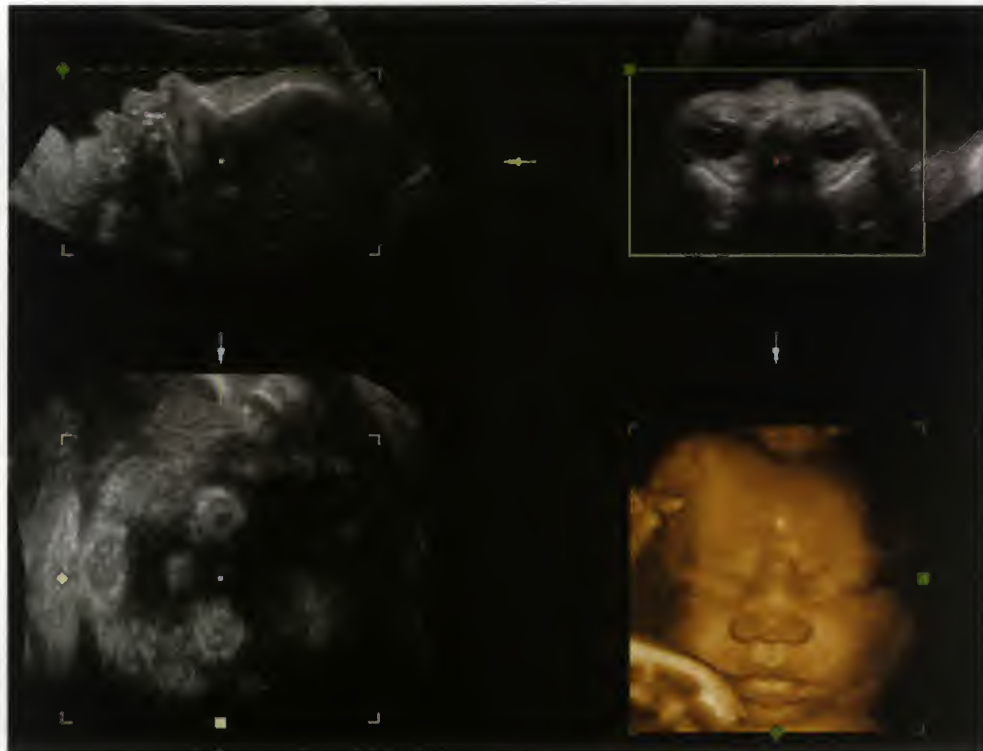


**FIGURE 24-15.** Multiplanar reconstruction of the fetal profile in the third trimester demonstrating that one can orient the fetal face such that a profile can appear in the left upper image (acquisition plane A), a transverse view through the orbits is seen in plane B, and plane C shows the coronal reconstructed view through both lenses of the orbits, a view that cannot be obtained by scanning the patient directly.



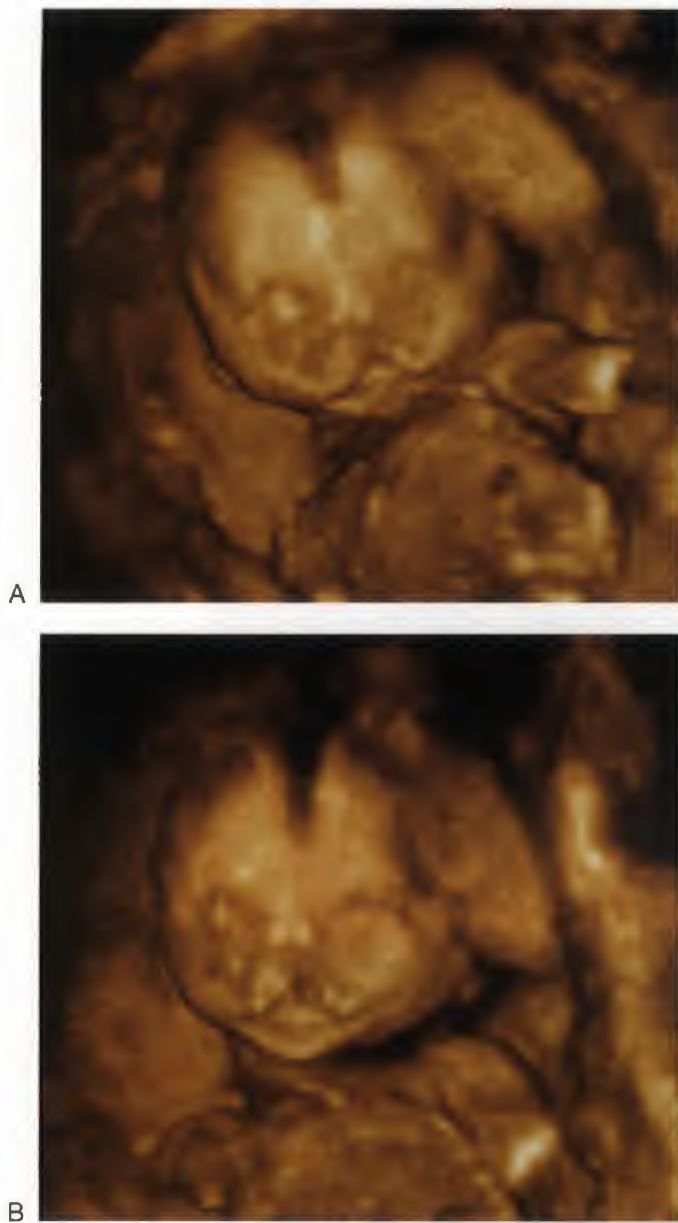


**FIGURE 24-16.** A and B. Two views of a fetus in the second trimester with a cleft lip and palate demonstrating the surface rendering of the defect.

This allows the visualization of the corpus callosum, which is not usually seen in the standard 2D fetal imaging planes (Fig. 24-26).<sup>70,71</sup> Monteagudo et al<sup>69</sup> have shown the versatility of 3D volume imaging in demonstrating many views and a multitude of planes of the fetal brain. A rapid sweep of the entire neuroanatomy of the brain can be accomplished within seconds and demonstrated using all of the different display modalities offline (Figs. 24-27 and 24-28). This is similar to what can be achieved with CT and MR. Monteagudo et al<sup>69</sup> have demonstrated that the practitioner can navigate through the volume using the marker dot showing the exact location of structures throughout the brain in many orientations different from the usual scanning



**FIGURE 24-17.** Profile of a fetus with a bilateral complete cleft lip and palate showing the anterior displacement of the inner maxillary segment.



**FIGURE 24-18.** Surface rendering of an incomplete cleft lip, without a cleft palate (although this is not imaged in this view). Note the subtle linear defect in the upper lip (arrow).



**FIGURE 24-19.** Third trimester fetus with a bilateral cleft lip and palate. *A.* A surface rendering of the fetal face, demonstrating that the cleft (*arrow*) extends into the floor of the nasal cavity. *B.* A section further into the maxilla, displaying the bilateral cleft which involves the hard palate. Note the nasal septum and the defects in the floor of both nostrils.



**FIGURE 24-20.** Central facial cleft in a fetus with trisomy 13. Note that the inner maxillary segment is absent and the central cleft involves the maxilla with the absence of the nose. Also note that this fetus has polydactyly.



**FIGURE 24-21.** Surface rendering of a second trimester fetus with micrognathia and polydactyly.





**FIGURE 24-22.** Reverse view of a fetus with a cleft lip and palate. Note that the surface rendering window has been rotated around the Y axis providing a view point from inside the mouth. The defect in the palate is seen from the back.

planes. For example, one can evaluate the brain using the three-horned view, which depicts the anterior, posterior, and inferior horns on the same image.<sup>72</sup> Fetal brain volume also can be measured by 3D ultrasound and correlated to fetal growth.<sup>73</sup> The use of Doppler flow imaging for assessing fetal brain flow can be done using power Doppler within a 3D volume<sup>74</sup> (see Fig. 24-8). Mueller et al<sup>53</sup> found 3D ultrasound beneficial in evaluating fetal central nervous system abnormalities: Among 11 fetuses, one case of spina bifida was recognized by 3D ultrasound and not by 2D, and one case of encephalocele was more accurately depicted using 3D ultrasound (Fig. 24-29). The benefit of 3D imaging in the brain, however, resides in the better visualization of the intracranial midline, in particular, the corpus callosum (see Fig. 24-26).

The remainder of the neural tube, particularly in cases of spina bifida, has also been studied using 3D (Fig. 24-30). The spine can be laid out using the maximum mode skeletal settings to evaluate one vertebra and one level at a time (Figs. 24-31 and 24-32).<sup>75-79</sup> Lee et al<sup>76</sup> studied nine fetuses with both 2D and 3D ultrasound and found that 2D ultrasound agreed with the postnatal vertebral segment level of the defect in six of nine cases of spina bifida. Using 3D ultrasound in the same cases resulted in agreement to within one level of spinal segment in eight out of nine infants, and the meningeal sac could be rendered in five out of nine cases. These authors concluded that the 3D approach improved the characterization of spina bifida by adding important diagnostic information to what already was accomplished with 2D ultrasound.<sup>76</sup>



**FIGURE 24-23.** Severely dysmorphic fetus with excessive hair on the forehead, severe micrognathia, flat facies, and abnormal ears.

## The Fetal Skeleton and Extremities

Nelson and Pretorius<sup>80</sup> first showed that 3D imaging could be applied to the skeleton, with good visualization of the bones and vertebral bodies. Using the maximum intensity mode (skeletal setting), the skeleton becomes more echogenic and easier to evaluate (see Figs. 24-5, 24-6, and 24-33). 3D volume imaging has demonstrated several skeletal dysplasias, including thanatophoric dysplasia, achondrogenesis, achondroplasia, chondrodysplasia punctata, and Apert syndrome.<sup>81-88</sup> Generally, the correct diagnosis is made using 2D imaging; however, according to Krakow et al,<sup>89</sup> 3D imaging confirms the diagnosis and can provide improved visualization of the abnormalities. Multiple case reports and short case series in the literature emphasize the specific features that 3D ultrasound can identify better than 2D ultrasound can. These include additional facial anomalies such as micrognathia and dysmorphic low-set ears, as well as the scapular anomaly in campomelic dysplasia, depressed nasal bridge and frontal bossing in thanatophoric dysplasia, abnormal vertebral bodies and absence of ribs in Jarcho-Levin syndrome, and low-set ears and midface hypoplasia in Larsen's syndrome, just to name a few.<sup>73,86-88,90-95</sup> Ruano et al<sup>91</sup> evaluated the contribution of 3D volume imaging in the depiction of skeletal dysplasias in six cases. Among three cases of achondroplasia, two cases of osteogenesis imperfecta and one case of chondrodysplasia punctata, 2D ultrasound was used to make the correct diagnosis in four cases, whereas 3D ultrasound achieved the correct diagnosis in all six. These authors indicated that 3D ultrasound had an advantage over 2D ultrasound in that the entire fetus could be imaged within a volume, as opposed to only one portion of the fetus using single, 2D ultrasound slices. Therefore, 3D ultrasound seemed to be a complimentary method to 2D



**FIGURE 24-24.** Severely dysmorphic fetus with micrognathia and a protuberant and elongated upper lip.



**FIGURE 24-25.** Normal second trimester fetus. Use of the bony window demonstrates the fontanel and sutures.

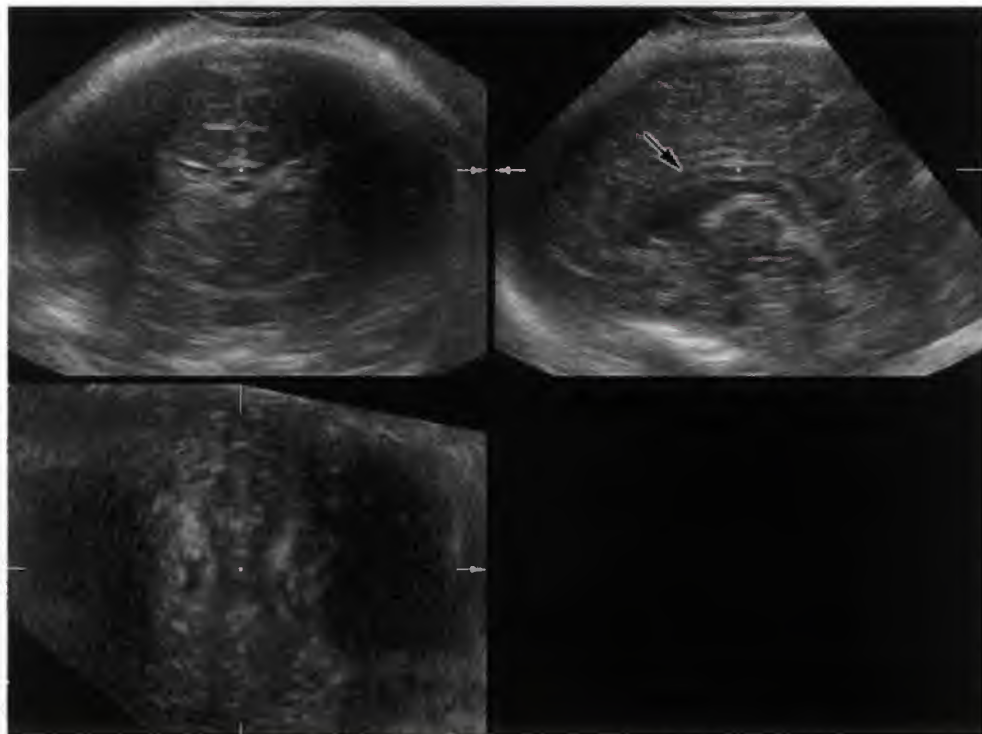


**FIGURE 24-26.** Third trimester normal fetal brain shown in three orthogonal views. Note that the corpus callosum (arrow) is well seen in plane B.





**FIGURE 24-27.** A. Multiplanar reconstructed view of an interhemispheric cyst in a third trimester fetus. Note the central cyst, which is associated with agenesis of the corpus callosum. B. A close-up of the reconstructed view showing the shape and configuration of the cyst.

ultrasound in providing the exact skeletal diagnosis. Opinions that 3D volume imaging provides valuable diagnostic information above and beyond 2D ultrasound remain restricted to relatively small case studies (Figs. 24-34 to 24-36).

There have been several attempts to use 3D ultrasound to aid in the detection of fetuses with Down syndrome (Fig. 24-37). Lee et al<sup>94</sup> studied the ability of 3D to provide fetal iliac angle measurements and showed that a standardized iliac angle could be acquired more easily from a volume of the fetal pelvis than from the 2D single-slice technique. These authors demonstrated a significantly

narrower fetal iliac angle (79 degrees) in normal fetuses, compared with those with Down syndrome (87.7 degrees),  $P < 0.001$ . The multiplanar view made it easy for different examiners to obtain reliable measurements, making the interobserver and intraobserver reliability of this angle measurement acceptable. For a false-positive rate of 5%, the iliac angle threshold of 87 degrees correctly identified 56% of fetuses with Down syndrome.

Several investigators have also studied the nasal bone in fetuses with Down syndrome in the second and third trimesters, using 3D imaging.<sup>95-97</sup> Lee et al<sup>95</sup> studied 40

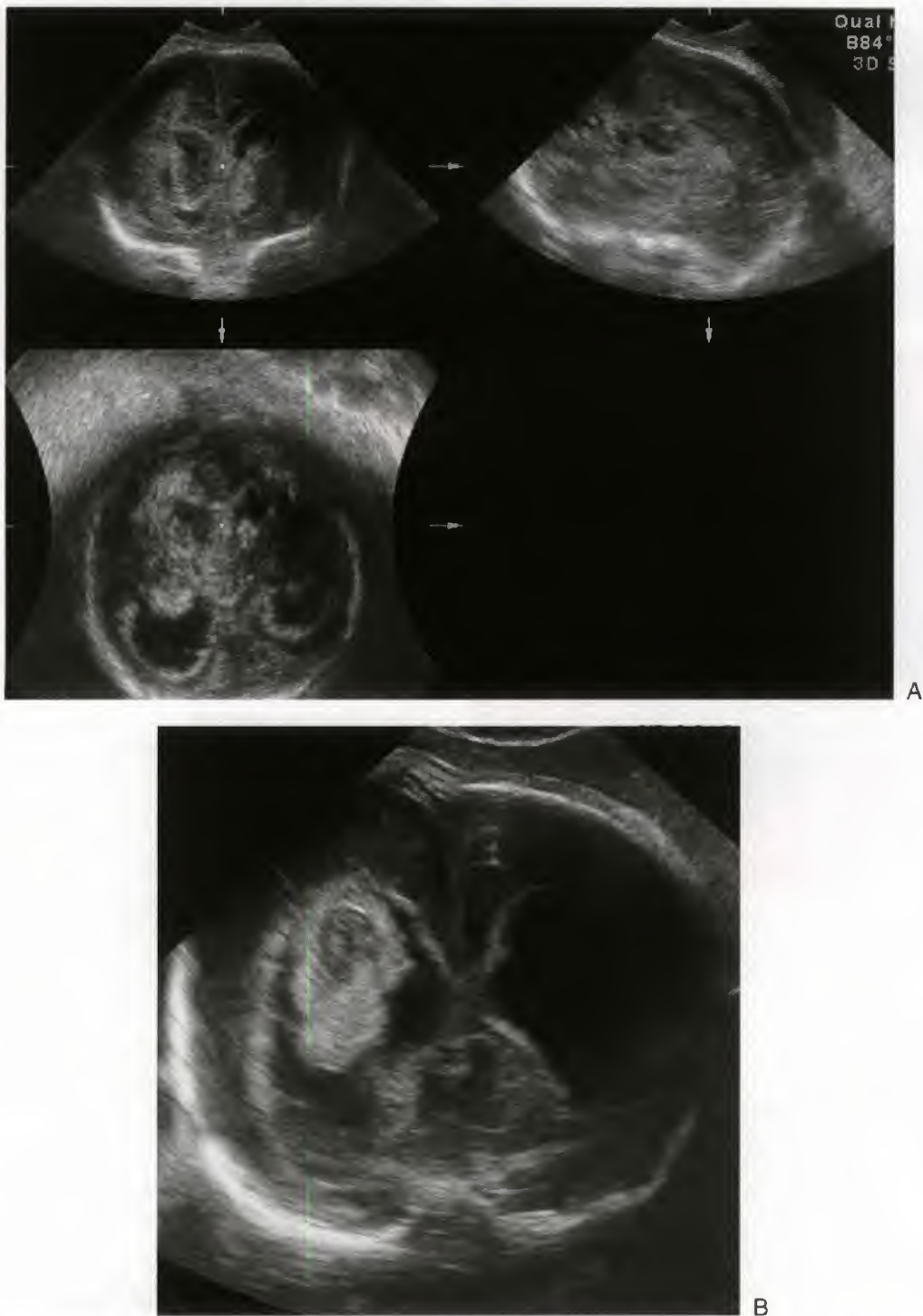


**FIGURE 24-28.** A. Intracranial hemorrhage in the third trimester shown in multiplanar reconstruction. Note that the information within the volume is displayed in all three perpendicular planes, allowing this single volume to generate any plane within the fetal head after the patient is gone. B. The reconstructed plane.





A



B

**FIGURE 24-29.** A. Longitudinal view of a fetus with an encephalocele in the first trimester. Note the small cystic area emanating from the top of the head. B. The 3D surface rendering of the same fetus with the defect in the posterior occipital aspect of the skull.

fetuses, including 20 with Down syndrome, and found that there was substantial agreement between two independent examiners in determining whether the fetal nasal bone was ossified. This study demonstrated that 3D ultrasound could be used to evaluate the nasal bone with good interobserver agreement. These investigators reported that nonvisualization of the nasal bone identified up to 45% of fetuses with Down syndrome. Several studies evaluated the use of 3D ultrasound to assess the fetal nasal bone ossification,<sup>97</sup> including Peralta et al,<sup>98</sup> who examined 450 fetuses using 3D ultrasound immediately after 2D evaluation of the nasal bone in screening for chromosomal abnormalities between 11 and 14 weeks. In 93.6% of cases, they found that the nasal bone was visualized using 2D ultrasound; 29 fetuses (6.4%) had apparent absence of the nasal bone. Assessing these 29 fetuses with 3D ultrasound in more detail, there was absence



**FIGURE 24-30.** Surface rendering of a neural tube defect (arrow) in the lumbosacral region of a second trimester fetus.

of both nasal bones in 25 of the 29 cases (86.2%) and absence of just one nasal bone in four of 29 (13.8%) of the cases. There was absence of one or both nasal bones in 0.7% of the chromosomally normal fetuses in this study, 61.3% of fetuses with trisomy 21, and 46.7% of those with other chromosomal abnormalities. 3D ultrasound in this study showed that there is a gap between the two nasal bones in about 20% of fetuses, which may lead to an erroneous diagnosis of absent nasal bone in the perfect midsagittal plane.<sup>98</sup> Benoit et al<sup>97</sup> demonstrated that the best way to evaluate the nasal bone in the early fetus is to use the maximum mode rendering to evaluate the skeleton in the frontal view of the rendered image, to evaluate the presence of one or both nasal bones. This differs from the sagittal views used by other practitioners. It must be stressed, however, that when obtaining a volume for the purpose of evaluating nasal bone ossification, the ultrasound beam must be at the proper angle with respect to the fetus. With an angle of 30 to 60 degrees, a good volume of the fetal profile will provide visualization of the nasal bone area with good quality on reconstructed images. The quality of the volume obtained will determine the final quality of the image rendered.<sup>99</sup>

### The First Trimester of Pregnancy

3D ultrasound in the first trimester is a very exciting area of active research. Using a high frequency transvaginal transducer, Blaas displayed images of the primitive brain, revealing that adequate images of very small structures could be demonstrated and accurately reconstructed using 3D volume imaging (sonoembryology) (Figs. 24-38 and 24-39).<sup>100-103</sup>

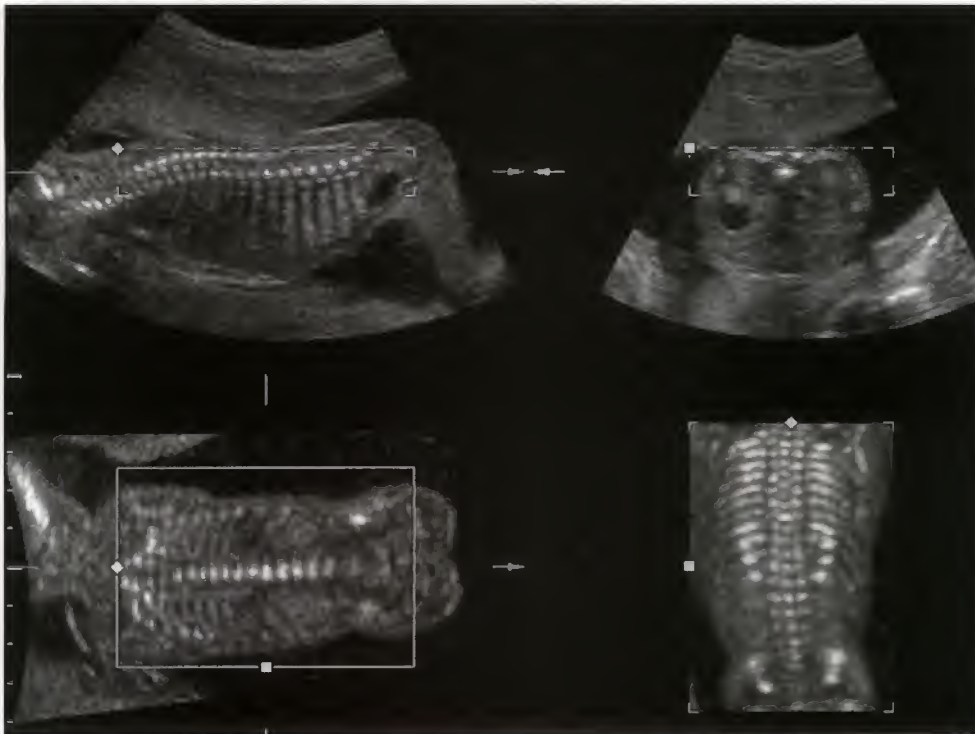


**FIGURE 24-31.** Multiplanar reconstruction of the normal fetal spine in the second trimester, using a bone window to enhance the appearance of the skeleton.



**FIGURE 24-32.** Close-up of an early third trimester fetal lumbar spine using the bone window. Note the detail of the vertebral bodies and the posterior aspect of the lower ribs.

It also is possible to use 3D imaging multiplanar reconstruction techniques to evaluate the nuchal translucency in fetuses who are not in an adequate position for the standard 2D measurement. Several studies have shown that there is excellent agreement between the standard 2D nuchal translucency measurements and the sagittal images obtained from volumes of the same fetuses by reslicing the sagittal 3D volumes.<sup>104-110</sup> Paul et al<sup>109</sup> demonstrated that if the 3D acquisition was performed with the fetus in an appropriate position for the nuchal translucency measurement, clear visualization of the nuchal membrane was achieved in 38 out of 40 fetuses, compared with 24 out of 40 when the fetus was in a random position when the acquisition was taken. Clearly, the agreement between the standard 2D nuchal translucency measurement and the 3D reconstructed measurement was far worse for volumes acquired randomly. Other practitioners have found that there was overestimation of the nuchal translucency measurements by transabdominal and transvaginal 3D reconstruction techniques when the nuchal translucency was less than 3 mm; when it was greater than 3 mm, the nuchal translucency was underestimated by 3D reconstruction.<sup>110</sup> Therefore, because of these widely differing opinions, nuchal translucency measurements on reconstructed planes have not been adopted fully at this time.

Other approaches to 3D evaluation of the first trimester of pregnancy include anatomic imaging of the fetus such as evaluation of the heart, brain, and extremities, as well as the placenta, and yolk sac. Success rates for evaluating overall fetal anatomy were higher using 3D ultrasound compared





A



B

**FIGURE 24-33.** A second trimester fetus with a vertebral body abnormality at the level of T11. Note the scoliosis produced by the vertebral body abnormality seen on the standard 2D image. *B.* The 3D reconstruction of this fetal skeleton using the bone window. This view demonstrates that there is unilateral absence of a rib at T10 (arrow), with a normal rib on the opposite side. The rib abnormality was not appreciated on the initial 2D scan, but was first seen on the 3D reconstruction.

with 2D (78.8% versus 47.5%), including better rates of visualization of the cerebral ventricles, choroid plexus, stomach, and so on.<sup>111-113</sup> In the study by Hull, it was also noted that the scanning time was significantly shorter when using 3D volume imaging compared with 2D ultrasound in first trimester scans. In that study, the nuchal translucency thickness was measured successfully in 96.6% of fetuses using 3D, compared with 37.5% of fetuses using 2D ultrasound.<sup>111</sup>

Another area of interest as an application of 3D imaging is the measurement of the gestational sac, placenta, and fetal volumes in the first trimester, and the relationship of these volumes to the presence of major chromosomal abnormalities.<sup>113-119</sup> In a study by Falcon et al<sup>117</sup> on 417 normal



**FIGURE 24-34.** Third trimester fetus with a unilateral clubfoot shown in surface-rendering mode.



**FIGURE 24-35.** Second trimester fetus with arthrogryposis, showing bilateral clenched hands with overlapping index fingers seen with surface rendering.

pregnancies and 83 pregnancies with major chromosomal abnormalities, the mean gestational sac volume was smaller in fetuses with trisomy 13 and triploidy, and the placental volumes were smaller in pregnancies with trisomies 13 and 18. The degree of fetal growth restriction may be more



**FIGURE 24-36.** Second trimester fetus with arthrogryposis, showing the contractures of both lower and upper extremities. Note the unusual posture of this fetus, indicating fixed positioning of the limbs. An advantage to 3D reconstruction is the wide field of view available to see the overall positioning of the fetus in utero.

accurately measured using volume imaging as opposed to standard 2D ultrasound.

### The Fetal Heart

There is much research activity concerning the 3D and 4D evaluations of the fetal heart.<sup>120-133</sup> Goncalves et al<sup>30</sup> presents an excellent summary of the studies that have occurred to date. In general, when comparing 2D and 3D imaging, 2D imaging has a better success rate in identifying the four chambers and the great vessels of the heart.<sup>30</sup> Unfortunately, owing to the fast movement of the heart, the 4D and 3D images produced are blurred by the cardiac cycle motion. The resultant lack of resolution has limited the ability of volume ultrasound to have clear enough imaging to compete. This is likely to change when matrix transducers become generally available for fetal imaging.

Some practitioners have used volume imaging to transmit data to another site, and such remote visualization of the heart has been relatively successful in some of these settings. One study reports a complete heart evaluation in 76% of cases in which the data set was transmitted to observers who were not involved in the image acquisition.<sup>137</sup>

More recently, the STIC acquisition technique, using current slow frame rates, has been proposed to try to improve the resolution of standard 4D imaging of the heart. This technique is a method by which the complete cardiac cycle is displayed in motion using a 3D cine loop.<sup>21-23,28,138-140</sup> This cine loop sequence is the result of a slow single sweep



**FIGURE 24-37.** A and B. Second trimester fetus with Down syndrome showing the rounded face, small low set ear, flat facies, and somewhat thickened soft tissues of the neck.





**FIGURE 24-38.** A. Eight and one-half week fetus shown in multiplanar reconstruction, demonstrating the normally developing fetal brain. B. The longitudinal view of the developing brain is shown in more detail. C. The cystic areas within the developing brain can be inverted with 3D rendering demonstrating the developing ventricular system as a cast. Note the two lateral ventricles and the third ventricle as well as the normally large fourth ventricle at this gestational age.



**FIGURE 24-39.** *A.* Nine-week-old fetus showing surface rendering detail of the fetal face, the presence of the fetal ear, the limb buds and cord insertion. *B.* A later first trimester fetus (11 weeks) imaged from the back, demonstrating the location of the fetal ear as well as detail of the extremities and back. *C.* The fetal ears again are noted at 13 weeks on a reconstructed surface image, which also shows details of the fetal face and insertion of the cord on the placenta.



recording of an entire 3D data set, from which the information regarding cardiac activity is averaged into one cycle. The fetus must remain motionless during the entire acquisition for this technique to be successful. This results in a higher resolution of the cardiac anatomy compared with standard 4D imaging, which is blurred owing to the fast cardiac activity. Vinals et al<sup>140</sup> studied 50 patients and uploaded acquired volume data sets using the Internet. The data sets were acquired by two sonographers with limited experience in cardiac imaging and received by an experienced cardiac investigator, who reviewed the cardiac cycles and achieved a complete cardiac examination in 86% and 95% of these cases sent by the two respective sonographers. In another study, four reviewers studied a single cardiac volume from each of 18 fetuses, seven of which had congenital heart disease. Ninety-three percent of the cases of congenital heart disease were correctly identified, with only one case missed by two of the four observers.<sup>141</sup> There were a few cases, however, in which adequate imaging was not possible, and therefore, the specificity for identifying congenital heart disease was only 45%, owing to the many artifacts and inadequate views. Using the STIC technique, Goncalves et al<sup>22</sup> studied 69 fetuses, half of whom were normal and half of whom had abnormalities. They demonstrated that volumes could be manipulated interactively, and the anomalies could be displayed in 4D to show the extents of the defects.

Several other types of settings have been used to better visualize the cardiac structures. These include several different postprocessing programs, such as the minimum projection mode, which emphasizes the cystic areas within the volume, as well as a free-hand acquisition of 3D volume.<sup>142,143</sup> Chaoui et al<sup>144</sup> have used color in the STIC technique. Three planes could be demonstrated in 24 of 27 fetuses with congenital heart disease, and in 31 of 35 fetuses with normal hearts. In the four normal fetuses with inadequate visualization using color Doppler STIC, the region of interest was at right angles to the ultrasound beam. Although this is a promising technique, there remain limitations to this type of imaging and artifacts to be overcome. DeVore et al<sup>124</sup> demonstrated the spin technique, in which the volume can be displayed in three-orthogonal planes of the heart, allowing the practitioner to spin around the dot in plane A using simple techniques of rotating around the X and Y axes to obtain standard cardiac views (see Fig. 24–13). Much work is being done to take this concept even further and automate the ability to find the various cardiac views from inside a volume using standardization of volume imaging. This would require that the volume be obtained and then standardized in the three orthogonal planes such that the four-chamber view would be located in the A plane.<sup>145,146</sup> A preset algorithm then could be applied to the volume to enable the automatic display of the great vessels and arches.

Yet another attempt to visualize the fetal heart uses the inverse mode, such that an echogenic cast is made of the heart, similar to an angiogram<sup>147</sup> (see Fig. 24–13). The solid areas usually seen by ultrasound as hyperechogenic fade away and become transparent, so that the cast of the fetal heart can be seen in its entirety. This also can be done using the STIC technique, so that the cast is seen to pulsate. There is no doubt that in the future, the matrix probe will result in

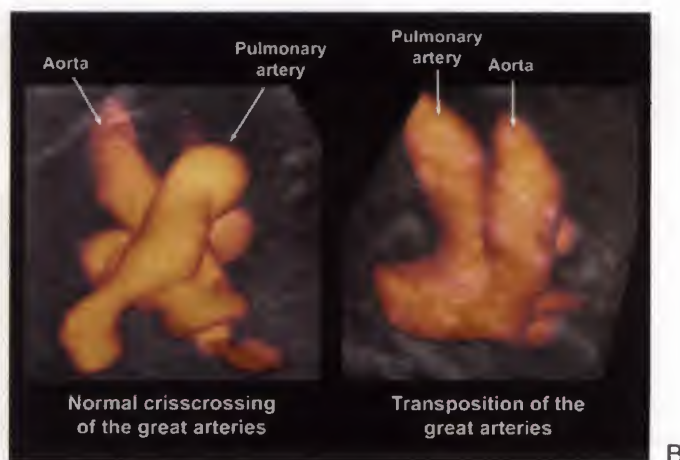


**FIGURE 24-40.** A. Normal fetal heart showing the normal great vessel crossover seen with power Doppler in a rendered image. B. Similar view of the great vessels of a fetus with transposition of the great arteries. Note the parallel course of the vessels in this rendered power Doppler volume image. (Reproduced with permission from Goncalves LF, Espinoza J, Romero R, et al: A systematic approach to prenatal diagnosis of transposition of the great arteries using 4-dimensional ultrasonography with spatiotemporal image correlation. *J Ultrasound Med* 23:1225, 2004.)

much higher frame rates enabling true real-time 4D ultrasound of the heart rather than a cine loop of one reconstructed cycle. Such probes already exist for adult and pediatric cardiac work; however, these have not yet been fully adapted for fetal imaging. Although there still are limitations to the image quality produced by the matrix array transducers today, it is likely that these probes will be sufficiently improved to allow a true real-time cardiac examination using volume technology.

The evaluation of the vascular system of the fetus has been studied using 3D power Doppler (Fig. 24–40). This involves not only the evaluation of the heart using Doppler, but also the study of the blood vessels throughout the fetal body and the placenta (see Fig. 24–8). Chaoui et al<sup>123</sup> have shown images of the fetal vascular system, stressing the importance of optimizing the power Doppler image before the 3D application. The reconstruction of satisfactory images, however, was possible in only 64% of pregnancies with abnormal vascular anatomy. The problems this group encountered included difficult fetal position, fetal movement, and overlapping signals from neighboring vessels. Specific areas of study using power Doppler in 3D imaging includes assessment of fetal renal blood flow, as well as normal fetal liver blood flow, showing the normal liver vascularization and changes in flow with advancing gestational age.<sup>148–150</sup> In a prospective study, Kalache et al<sup>150</sup> examined 390 fetuses, of whom eight had vascular anomalies including an absent ductus venosus, direct connection between the umbilical vein and the right atrium, and direct connection between the umbilical vein and the inferior vena cava. They found that 3D power Doppler was very helpful in mapping the course of the umbilical vein and the portal systemic circulation, as well as the ductus venosus, in these patients. 3D power Doppler was also used to evaluate the vasculature in



a case of pulmonary sequestration, adequately demonstrating the abnormal blood supply.<sup>151</sup>

## EVALUATION OF VOLUME MEASUREMENTS

An important clinical application of 3D volume imaging is the ability to measure volumes more easily and accurately, compared with using 2D imaging. Several practitioners have demonstrated that 3D sonographic methods provide a more accurate volume measurement than the usual multiple 2D images, regardless of the shape and regularity of objects.<sup>152-155</sup> Specific areas that have been studied include the fetal lung and the prenatal diagnosis of pulmonary hypoplasia, particularly in cases of diaphragmatic hernia.<sup>153-165</sup> There also have been volume measurements reported of the kidneys, liver, spine, thigh, and other extremities, as well as fetal weight.<sup>169-185</sup> Fetal brain volumes have been calculated using 3D volume imaging, with excellent success and good intraobserver and interobserver variability.<sup>73,185</sup> 3D fractional limb volumes have been investigated as a way to predict birth weight and overall fetal growth and nutrition during gestation.<sup>174-180</sup> Lee et al<sup>180</sup> have studied fractional limb volume, including both the upper arm and the thigh, in 100 fetuses at a mean of 39 weeks' menstrual age. The best prediction, which included abdominal circumference and fractional thigh volume, deviated by only  $-0.025\% \pm 7.8\%$  from actual birth weight. Thirty additional fetuses were tested prospectively, and the 3D method predicted 20 of 30 fetal weights to within 5% of the true birth weight, compared with the traditional 2D method, which predicted only six of 30 weights with the same accuracy. Other investigators also have studied thigh volume and have found that this measurement has promise as a useful reference in evaluating fetal growth and nutritional status in utero.<sup>177,179,180</sup> Song et al<sup>179</sup> also found that 3D ultrasound thigh volume measurements were simple to perform and were more accurate than 2D ultrasound methods for predicting estimated weight during the third trimester.

Several investigators have studied the volume and appearance of the placenta in an attempt to quantify fetal growth and well-being.<sup>187,188</sup> The volume measurement of the placenta, however, was not an accurate technique for predicting growth-restricted fetuses.<sup>187</sup>

Volumetric evaluation of the fetal lungs also has spurred a large amount of study using the 3D technique called virtual organ computer-aided analysis (VOCAL, GE Healthcare).<sup>153-165</sup> Kalache et al<sup>161,162</sup> also studied 32 fetuses at risk for pulmonary hypoplasia and found that both 3D multiplanar reconstruction and 3D VOCAL methods could be used to obtain accurate measurements of fetal lung volumes. VOCAL does have the advantage of being able to trace out irregular areas of lung parenchymas, such as in cases of diaphragmatic hernia compressing the lung. Volume sweeps are best performed with the fetus in transverse section. The ability to measure lung volume with 3D ultrasound has resulted in new nomograms for the normal fetal lung volume at different gestational ages. This method could be an alternative to MRI in imaging the fetal lungs. Sabogal et al<sup>168</sup> studied 75 patients at 20 to 30 weeks with 182 volumes, showing that 3D sonography-derived measurements were reliable and reproducible within that

window of gestational age. 3D assessment of fetal lungs was also studied as a prognostic factor for isolated diaphragmatic hernia. The observed-to-expected fetal lung-volume ratio was significantly lower in the group of fetuses with congenital diaphragmatic hernia, compared with the control group.<sup>164</sup> The distribution of this ratio was particularly low in patients with congenital diaphragmatic hernia who did not survive compared with those who survived.

## ARTIFACTS

The artifacts that occur as a result of volume imaging can be different from those that are familiar in 2D ultrasound.<sup>189-191</sup> The usual artifacts, such as shadowing and through-transmission, are present in any kind of ultrasound examination, but there also are new artifacts inherent to 3D reconstruction of images (Figs. 24-41 to 24-44). These include motion artifacts, such as fetal movement and cardiac motion. It also is important to recognize acoustic shadowing, because it is unlikely to be in the expected location in a reconstructed image. Shadowing is understandable based on the acquisition image, but as different planes are reconstructed, the shadow may no longer make sense and may be misinterpreted for pathology. Acoustic enhancement behind a cystic structure is also a finding that is an obvious part of a standard ultrasound image but that can be practically unrecognizable in a reconstructed image. The cystic area that has generated the through transmission is unlikely to be located in the usual proximity to the enhanced area in a reconstructed image and may not even appear in the image at all. Other artifacts can be produced, such as apparent limb or facial defects, based on the position of the acquiring data box within the image. It is important to learn about the appearances of these new artifacts in order to recognize them when they occur.

## PARENTAL-FETAL BONDING

Seeing the fetus in such a real-life form as 3D surface rendering may arouse many emotions from the mother and father, and family members (Figs. 24-45 and 24-46). This type of parental-fetal bonding can sometimes lead to altered behaviors of lifestyle, such as cessation of smoking or cessation of alcohol usage by the mother. There are several studies that compare the effects of 2D ultrasound with 3D and 4D ultrasound scanning on maternal emotional status and bonding.<sup>192-194</sup> Rustico et al<sup>193</sup> studied 52 women randomly assigned to 2D or 2D followed by 4D imaging. The patients who were examined with 4D ultrasound were more likely to see facial expressions of their fetuses, and hand-to-mouth movements compared with patients who were examined with 2D ultrasound. However, in this randomized study, the addition of 4D ultrasound did not change the antenatal emotional attachment of the mother, compared with patients undergoing conventional 2D ultrasound alone. On the other hand, Ji et al<sup>192</sup> studied 50 mothers who received 3D ultrasound and 50 who received standard 2D ultrasound scans. The 3D ultrasound patients appeared more positively influenced and showed their ultrasound images to greater numbers of people within their family and friends compared with those who had 2D ultrasounds alone. This study suggested that 3D ultrasound



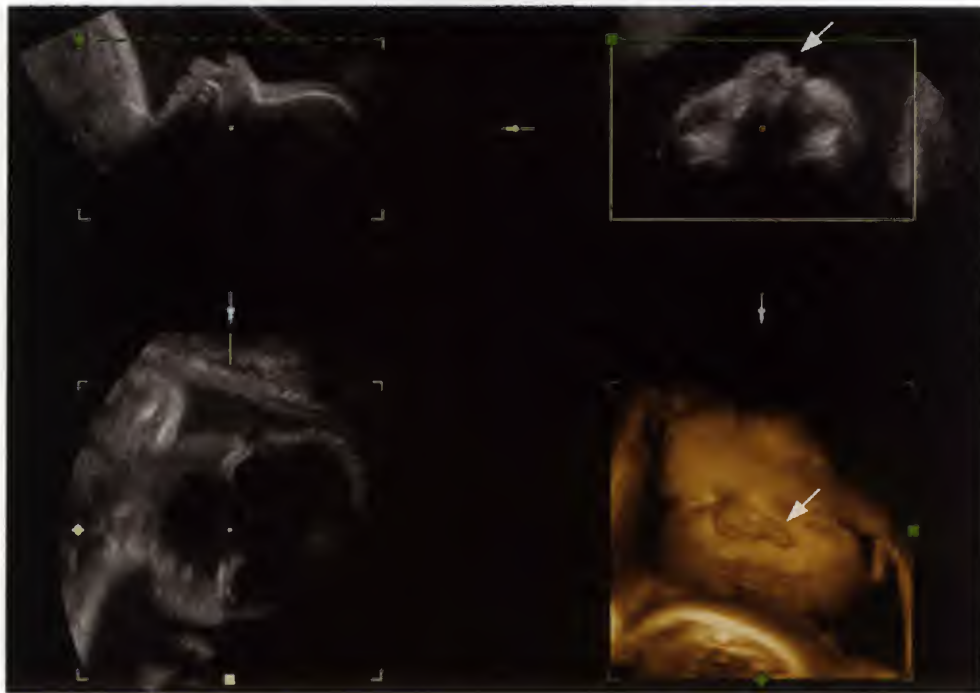


**FIGURE 24-41.** Multiplanar reconstruction of a third trimester fetal face showing an artifact due to fetal movement. There is an indentation in the nose on one side best seen in multiplanar plane B (*arrow*) and transmitted to the surface rendering as an elongated nose on one side (*arrow*). This is an artifact due to fetal movement during the acquisition and appears on all reconstructed views.



**FIGURE 24-42.** Third trimester fetal face showing the shadow from the digits of the hand that is located in front of the face. The hand itself is not seen owing to the position of the surface-rendering window, but the shadow of the digits is visualized as an artifact on the face.

may have a greater impact on the maternal-fetal bonding process. As we can see, there is controversy concerning whether the addition of 3D and 4D ultrasound increases the maternal or parental bonding to the fetus. At present, there are a number of organizations in business that provide entertainment ultrasound, which is mostly 3D imaging that



**FIGURE 24-43.** First trimester pregnancy at 6 weeks showing a gestational sac with a yolk sac. Note the shape of an intrauterine device (IUD) (*arrow*) located below the level of the gestational sac. This is actually the shadow of the IUD, which is located in a different plane. Such a shadow is an artifact, which is reconstructed in a plane different from the location of the IUD itself.



**FIGURE 24-44.** Multiplanar reconstruction and surface rendering of a late first trimester fetus showing that the entire fetus is located within the rendering box. Note that the rendered image shows the entire fetus, complete with extremities. **A.** Example of what happens if the fetus is moved partly out of the render box. **B.** Both the skull and the lower extremities are moved out, resulting in the rendered image that appears to have the fetal lower leg cut (arrow) off just above the knee. This is an artifact, which is dependent on the placement of the render box.





**FIGURE 24-45.** Late first trimester fetus showing upper extremities and face in a very life-like position.



**FIGURE 24-46.** Third trimester fetus yawning, which is easily recognizable by family members viewing the scan.

is done in many cases by nonmedical personnel. The ultrasound community and the major national ultrasound societies have condemned these nonmedical facilities.

## CONCLUSION

3D ultrasound is in its infancy and is one of the most exciting advances in sonography in the last decade. It started out as a problem-solving tool as an adjunct to 2D imaging in selected circumstances, but it has become increasingly a part of sonography in obstetrics and gynecology. One of the most important features of volume ultrasound is the ability to save an entire volume data set of sonographic information, which can be displayed and rescanned in ways similar to those used in CT and MRI. Such displays provide ultrasound with an opportunity to be as efficient, versatile, and standardized as these other cross-sectional imaging techniques. As the resolution of reconstructed volume sonographic images improves, and as the frame rate of real-time or 4D ultrasound increases, the potential of volume imaging in ultrasound will be far-reaching and may well reshape the way that ultrasound is practiced today.

## References

1. Nelson TR, Pretorius DH: Management of three-dimensional ultrasound patient data via networks. *Ultrasound Rev Obstet Gynecol* 1:184, 2001.
2. Lee A: Four-dimensional ultrasound in prenatal diagnosis: leading edge in imaging technology. *Ultrasound Rev Obstet Gynecol* 1:144, 2001.
3. Nelson TR, Pretorius DH, Lev-Toaff AR, et al: Feasibility of performing a virtual patient examination using three-dimensional ultrasonographic data acquired at remote locations. *J Ultrasound Med* 20:941, 2001.
4. Benacerraf BR: Three-dimensional fetal sonography: use and misuse. *J Ultrasound Med* 21:1063, 2002.
5. Nelson TR, Pretorius DH: Three-dimensional ultrasound of fetal surface features. *Ultrasound Obstet Gynecol* 2:166, 1992.
6. Merz E, Bahlmann F, Weber G: Volume scanning in the evaluation of fetal malformations: a new dimension in prenatal diagnosis. *Ultrasound Obstet Gynecol* 5:222, 1995.
7. Leung KY, Ngai CS, Chan BC, et al: Three-dimensional extended imaging: a new display modality for three-dimensional ultrasound examination. *Ultrasound Obstet Gynecol* 26:244, 2005.
8. Pretorius DH, Nelson TR: Three-dimensional ultrasound. *Ultrasound Obstet Gynecol* 5:219, 1995.
9. Bega G, Lev-Toaff A, Kuhlman K, et al: Three-dimensional ultrasonographic imaging in obstetrics. *J Ultrasound Med* 20:391, 2001.
10. Devore GR, Polanko B: Tomographic ultrasound imaging of the fetal heart. *J Ultrasound Med* 24:1685, 2005.
11. Pretorius DH, Borok NN, Coffer MS, et al: Three-dimensional ultrasound in obstetrics and gynecology. *Radiol Clin North Am* 39:499, 2001.
12. Riccabona M, Pretorius DH, Nelson TR, et al: Three-dimensional ultrasound: display modalities in obstetrics. *J Clin Ultrasound* 25:157, 1997.
13. Pooh RK, Pooh KH: The assessment of fetal brain morphology and circulation by transvaginal 3D sonography and power Doppler. *J Perinat Med* 30:48, 2002.
14. Chang CH, Yu CH, Ko HC, et al: Three-dimensional power Doppler ultrasound for the assessment of the fetal brain blood flow in normal gestation. *Ultrasound Med Biol* 29:1273, 2003.
15. Merz E, Miric-Tesanic D, Welter C: Value of the electronic scalpel (cut mode) in the evaluation of the fetal face. *Ultrasound Obstet Gynecol* 16:564, 2000.
16. Lee W, Goncalves LF, Espinoza J, Romero R: Inversion mode: a new volume analysis tool for 3-dimensional ultrasonography. *J Ultrasound Med* 24:201, 2005.
17. Espinoza J, Goncalves LF, Lee W, et al: A novel method to improve prenatal diagnosis of abnormal systemic venous connections using



- three- and four-dimensional ultrasonography and 'inversion mode.' *Ultrasound Obstet Gynecol* 25:428, 2005.
18. Benacerraf BR: Inversion mode display of 3D sonography: Applications in obstetric and gynecologic imaging. *AJR Am J Roentgenol* 187:965, 2006.
19. Timor-Tritsch IE, Monteagudo A, Tsymbal T, et al: Three dimensional inversion rendering. *J Ultrasound Med* 24:681, 2005.
20. DeVore GR, Falkensammer P, Sklansky MS, et al: Spatio-temporal image correlation (STIC): new technology for evaluation of the fetal heart. *Ultrasound Obstet Gynecol* 22:380, 2003.
21. Vinals F, Poblete P, Giuliano A: Spatio-temporal image correlation (STIC): a new tool for the prenatal screening of congenital heart defects. *Ultrasound Obstet Gynecol* 22:388, 2003.
22. Gonçalves LF, Lee W, Chaiworapongsa T, et al: Four-dimensional ultrasonography of the fetal heart with spatiotemporal image correlation. *Am J Obstet Gynecol* 189:1792, 2003.
23. Vinals F, Mandujano L, Vargas G, et al: Prenatal diagnosis of congenital heart disease using four-dimensional spatio-temporal image correlation (STIC) telemedicine via an Internet link: a pilot study. *Ultrasound Obstet Gynecol* 25:25, 2005.
24. Benacerraf BR, Shipp TD, Bromley B: How sonographic tomography will change the face of obstetric sonography: a pilot study. *J Ultrasound Med* 24:371, 2005.
25. Benacerraf BR, Shipp TD, Bromley B: 3D ultrasound of the fetus: volume imaging. *Radiology* 238:988, 2006.
26. Nelson TR, Pretorius DH, Lev-Toaff A, et al: Feasibility of performing a virtual patient examination using three-dimensional ultrasonographic data acquired at remote locations. *J Ultrasound Med* 20:941, 2001.
27. Johnson DD, Pretorius DH, Riccabona M, et al: Three-dimensional ultrasound of the fetal spine. *Obstet Gynecol* 89:434, 1997.
28. Gonçalves LF, Espinoza J, Romero R, et al: Four-dimensional fetal echocardiography with spatiotemporal image correlation (STIC): a systematic study of standard cardiac views assessed by different observers. *J Matern Fetal Neonatal Med* 17:323, 2005.
29. Michailidis GD, Simpson JM, Karidas C, et al: Detailed three dimensional fetal echocardiography facilitated by an Internet link. *Ultrasound Obstet Gynecol* 18:325, 2001.
30. Gonçalves LF, Lee W, Espinoza J, et al: Three- and 4-dimensional ultrasound in obstetric practice: does it help? *J Ultrasound Med* 24:1599, 2005.
31. Merz E, Bahlmann F, Weber G, et al: Three-dimensional ultrasonography in prenatal diagnosis. *J Perinat Med* 23:213, 1995.
32. Platt LD, Santulli T Jr, Carlson DE, et al: Three-dimensional ultrasonography in obstetrics and gynecology: preliminary experience. *Am J Obstet Gynecol* 178:1199, 1998.
33. Baba K, Okai T, Kozuma S, et al: Fetal abnormalities: evaluation with real-time-processible three-dimensional US—preliminary report. *Radiology* 211:441, 1999.
34. Dyson RL, Pretorius DH, Budorick NE, et al: Three-dimensional ultrasound in the evaluation of fetal anomalies. *Ultrasound Obstet Gynecol* 16:321, 2000.
35. Scharf A, Ghazwiny MF, Steinborn A, et al: Evaluation of two-dimensional versus three-dimensional ultrasound in obstetric diagnostics: a prospective study. *Fetal Diagn Ther* 16:333, 2001.
36. Xu HX, Zhang QP, Lu MD, et al: Comparison of two-dimensional and three-dimensional sonography in evaluating fetal malformations. *J Clin Ultrasound* 30:515, 2002.
37. Merz E, Welter C: 2D and 3D Ultrasound in the evaluation of normal and abnormal fetal anatomy in the second and third trimesters in a level III center. *Ultraschall Med* 26:9, 2005.
38. Merz E, Weber G, Bahlmann F, et al: Application of transvaginal and abdominal three-dimensional ultrasound for the detection or exclusion of malformations of the fetal face. *Ultrasound Obstet Gynecol* 9:237, 1997.
39. Kozuma S, Baba K, Okai T, et al: Dynamic observation of the fetal face by three-dimensional ultrasound. *Ultrasound Obstet Gynecol* 13:283, 1999.
40. Kuno A, Akiyama M, Yamashiro C, et al: Three-dimensional sonographic assessment of fetal behavior in the early second trimester of pregnancy. *J Ultrasound Med* 20:1271, 2001.
41. Pretorius DH, Nelson TR: Fetal face visualization using three-dimensional ultrasonography. *J Ultrasound Med* 14:349, 1995.
42. Lee W, Kirk JS, Shaheen KW, et al: Fetal cleft lip and palate detection by three-dimensional ultrasonography. *Ultrasound Obstet Gynecol* 16:314, 2000.
43. Chmait R, Pretorius D, Jones M, et al: Prenatal evaluation of facial clefts with two-dimensional and adjunctive three-dimensional ultrasonography: a prospective trial. *Am J Obstet Gynecol* 187:946, 2002.
44. Campbell S: 4D, or not 4D: that is the question. *Ultrasound Obstet Gynecol* 19:1, 2002.
45. Ulm MR, Kratochwil A, Ulm B, et al: Three-dimensional ultrasound evaluation of fetal tooth germs. *Ultrasound Obstet Gynecol* 12:240, 1998.
46. Devonald KJ, Ellwood DA, Griffiths KA, et al: Volume imaging: three-dimensional appreciation of the fetal head and face. *J Ultrasound Med* 14:919, 1995.
47. Hata T, Yonehara T, Aoki S, et al: Three-dimensional sonographic visualization of the fetal face. *AJR Am J Roentgenol* 170:481, 1998.
48. Ulm MR, Kratochwil A, Ulm B, et al: Three-dimensional ultrasonographic imaging of fetal tooth buds for characterization of facial clefts. *Early Hum Dev* 55:67, 1999.
49. Johnson DD, Pretorius DH, Budorick NE, et al: Fetal lip and primary palate: three-dimensional versus two-dimensional US. *Radiology* 217:236, 2000.
50. Chen ML, Chang CH, Yu CH, et al: Prenatal diagnosis of cleft palate by three-dimensional ultrasound. *Ultrasound Med Biol* 27:1017, 2001.
51. Rotten D, Levallant JM, Martinez H, et al: The fetal mandible: a 2D and 3D sonographic approach to the diagnosis of retrognathia and micrognathia. *Ultrasound Obstet Gynecol* 19:122, 2002.
52. Pretorius DH, House M, Nelson TR, et al: Evaluation of normal and abnormal lips in fetuses: comparison between three- and two-dimensional sonography. *AJR Am J Roentgenol* 165:1233, 1995.
53. Mueller GM, Weiner CP, Yankowitz J: Three-dimensional ultrasound in the evaluation of fetal head and spine anomalies. *Obstet Gynecol* 88:372, 1996.
54. Mittenmayer C, Blaicher W, Brugger PC, et al: Foetal facial clefts: prenatal evaluation of lip and primary palate by 2D and 3D ultrasound. *Ultraschall Med* 25:120, 2004.
55. Mangione R, Lacombe D, Carles D, et al: Craniofacial dysmorphism and three-dimensional ultrasound: A prospective study on practicability for prenatal diagnosis. *Prenat Diagn* 23:810, 2003.
56. Campbell S, Lees CC: The three-dimensional reverse face (3D RF) view for the diagnosis of cleft palate. *Ultrasound Obstet Gynecol* 22:552, 2003.
57. Campbell S, Lees C, Moscoso G, et al: Ultrasound antenatal diagnosis of cleft palate by a new technique: the 3D "reverse face" view. *Ultrasound Obstet Gynecol* 25:128, 2005.
58. Rotten D, Levallant JM: Two- and three-dimensional sonographic assessment of the fetal face. 1. A systematic analysis of the normal face. *Ultrasound Obstet Gynecol* 23:224, 2004.
59. Rotten D, Levallant JM: Two- and three-dimensional sonographic assessment of the fetal face. 2. Analysis of cleft lip, alveolus and palate. *Ultrasound Obstet Gynecol* 24:402, 2004.
60. Lee W, McNie B, Chaiworapongsa T, et al: 3D ultrasound presentation of micrognathia. *J Ultrasound Med* 21:775, 2002.
61. Pretorius DH, Nelson TR: Prenatal visualization of cranial sutures and fontanelles with three-dimensional ultrasonography. *J Ultrasound Med* 13:871, 1994.
62. Dikkeboom CM, Roelfsema NM, Van Adrichem LN, et al: The role of three-dimensional ultrasound in visualizing the fetal cranial sutures and fontanelles during the second half of pregnancy. *Ultrasound Obstet Gynecol* 24:412, 2004.
63. Ginath S, Debby A, Malinger G: Demonstration of cranial sutures and fontanelles at 15 to 16 weeks of gestation: a comparison between two-dimensional and three-dimensional ultrasonography. *Prenat Diagn* 24:812, 2004.
64. Mangione R, Lacombe D, Carles D, et al: Craniofacial dysmorphism and three-dimensional ultrasound: a prospective study on practicability for prenatal diagnosis. *Prenat Diagn* 23:810, 2003.
65. Benacerraf BR, Spiro R, Mitchell A: Using 3-D ultrasound to detect craniosynostosis in a fetus with Pfeiffer syndrome. *Ultrasound Obstet Gynecol* 20:290, 2002.
66. Mulliken JB, Benacerraf BR: Prenatal Diagnosis of cleft lip—what the sonologist needs to tell the surgeon. *J Ultrasound Med* 20:1159, 2001.
67. Lai TH, Chang CH, Yu CH, et al: Prenatal diagnosis of alobar holoprosencephaly by two-dimensional and three-dimensional ultrasound. *Prenat Diagn* 20:400, 2000.
68. Hata T, Yanagihara T, Matsumoto M, et al: Three-dimensional sonographic features of fetal central nervous system anomaly. *Acta Obstet Gynecol Scand* 79:635, 2000.



69. Monteagudo A, Timor-Tritsch IE, Mayberry P: Three-dimensional transvaginal neurosonography of the fetal brain: 'navigating' in the volume scan. *Ultrasound Obstet Gynecol* 16:307, 2000.
70. Wang PH, Ying TH, Wang PC, et al: Obstetrical three-dimensional ultrasound in the visualization of the intracranial midline and corpus callosum of fetuses with cephalic position. *Prenat Diagn* 20:518, 2000.
71. Pooh RK, Pooh K, Nakagawa Y, et al: Clinical application of three-dimensional ultrasound in fetal brain assessment. *Croat Med J* 41:245, 2000.
72. Timor-Tritsch IE, Monteagudo A, Mayberry P: Three-dimensional ultrasound evaluation of the fetal brain: the three horn view. *Ultrasound Obstet Gynecol* 16:302, 2000.
73. Roelofsma NM, Hop WC, Boito SM, et al: 3D sonographic measurement of the normal fetal brain volume during the second half of pregnancy. *Am J Obstet Gynecol* 190:275, 2004.
74. Pooh RK, Pooh KH: The assessment of fetal brain morphology and circulation by transvaginal 3D sonography and power Doppler. *J Perinat Med* 30:48, 2002.
75. Budorick NE, Pretorius DH, Nelson TR: Sonography of the fetal spine: technique, imaging findings, and clinical implications. *AJR Am J Roentgenol* 164:421, 1995.
76. Lee W, Chaiworapongsa T, Romero R, et al: A diagnostic approach for the evaluation of spina bifida by three-dimensional ultrasonography. *J Ultrasound Med* 21:619, 2002.
77. Schild RL, Wallny T, Fimmers R, et al: Fetal lumbar spine volumetry by three-dimensional ultrasound. *Ultrasound Obstet Gynecol* 13:335, 1999.
78. Ulm MR, Kratochwil A, Oberhucmer U, et al: Ultrasound evaluation of fetal spine length between 14 and 24 weeks of gestation. *Prenat Diagn* 19:637, 1999.
79. Schild RL, Wallny T, Fimmers R, et al: The size of the fetal thoracolumbar spine: a three-dimensional ultrasound study. *Ultrasound Obstet Gynecol* 16:468, 2000.
80. Nelson TR, Pretorius DH: Visualization of the fetal thoracic skeleton with three-dimensional sonography: a preliminary report. *AJR Am J Roentgenol* 164:1485, 1995.
81. Yanagihara T, Hata T: Three-dimensional sonographic visualization of fetal skeleton in the second trimester of pregnancy. *Gynecol Obstet Invest* 49:12, 2000.
82. Benoit B: The value of three-dimensional ultrasonography in the screening of the fetal skeleton. *Childs Nerv Syst* 19:403, 2003.
83. Steiner H, Spitzer D, Weiss-Wichert PH, et al: Three-dimensional ultrasound in prenatal diagnosis of skeletal dysplasia. *Prenat Diagn* 15:373, 1995.
84. Garjian KV, Pretorius DH, Budorick NE, et al: Fetal skeletal dysplasia: three-dimensional US—initial experience. *Radiology* 214:717, 2000.
85. Chen CP, Chern SR, Shih JC, et al: Prenatal diagnosis and genetic analysis of type I and type II thanatophoric dysplasia. *Prenat Diagn* 21:89, 2001.
86. Machado LE, Bonilla-Musoles F, Osborne NG: Thanatophoric dysplasia. *Ultrasound Obstet Gynecol* 18:85, 2001.
87. Moeglin D, Benoit B: Three-dimensional sonographic aspects in the antenatal diagnosis of achondroplasia. *Ultrasound Obstet Gynecol* 18:81, 2001.
88. Viora E, Sciarone A, Bastonero S, et al: Three-dimensional ultrasound evaluation of short-rib polydactyly syndrome type II in the second trimester: a case report. *Ultrasound Obstet Gynecol* 19:88, 2002.
89. Krakow D, Williams J 3rd, Poehl M, et al: Use of 3D ultrasound imaging in the diagnosis of prenatal onset skeletal dysplasias. *Obstet Gynecol* 21:467, 2003.
90. Clementschitsch G, Hasenohrl G, Steiner H, et al: [Early diagnosis of a fetal skeletal dysplasia associated with increased nuchal translucency with 2D and 3D ultrasound]. *Ultraschall Med* 24:349, 2003.
91. Ruano R, Molho M, Roume J, et al: Prenatal diagnosis of fetal skeletal dysplasias by combining two-dimensional and three-dimensional ultrasound and intrauterine three-dimensional helical computer tomography. *Ultrasound Obstet Gynecol* 24:134, 2004.
92. Seow KM, Huang LW, Lin YH, et al: Prenatal three-dimensional ultrasound diagnosis of a camptomelic dysplasia. *Arch Gynecol Obstet* 269:142, 2004.
93. Shih JC, Peng SS, Hsiao SM, et al: Three-dimensional ultrasound diagnosis of Larsen syndrome with further characterization of neurological sequelae. *Ultrasound Obstet Gynecol* 24:89, 2004.
94. Lee W, Blanckaert K, Bronsteen RA, et al: Fetal iliac angle measurements by 3D sonography. *Ultrasound Obstet Gynecol* 18:150, 2001.
95. Lee W, DeVore GR, Comstock CH, et al: Nasal bone evaluation in fetuses with Down syndrome during the second and third trimesters of pregnancy. *J Ultrasound Med* 22:55, 2003.
96. Goncalves LF, Espinoza J, Lee W, et al: Phenotypic characteristics of absent and hypoplastic nasal bones in fetuses with Down syndrome: description by 3-dimensional ultrasonography and clinical significance. *J Ultrasound Med* 23:1619, 2004.
97. Benoit B, Chaoui R: Three-dimensional ultrasound with maximal mode rendering: a novel technique for the diagnosis of bilateral or unilateral absence or hypoplasia of nasal bones in second-trimester screening for Down syndrome. *Ultrasound Obstet Gynecol* 25:19, 2005.
98. Peralta CFA, Falcon P, Wegrzyn P, et al: Assessment of the gap between nasal bones at 11-13 +6 weeks gestation by 3D ultrasound. *Ultrasound Obstet Gynecol* 25:464, 2005.
99. Rembouskos G, Cicero S, Longo D, et al: Assessment of the fetal nasal bone at 11-14 weeks of gestation by 3D ultrasound. *Ultrasound Obstet Gynecol* 23:232, 2004.
100. Blaas HG, Eik-Nes SH, Kiserud T, et al: Three-dimensional imaging of the brain cavities in human embryos. *Ultrasound Obstet Gynecol* 5:228, 1995.
101. Hata T, Aoki S, Manabe A, et al: Three-dimensional ultrasonography in the first trimester of human pregnancy. *Hum Reprod* 12:1800, 1997.
102. Blaas HG, Eik-Nes SH, Berg S, et al: In-vivo three-dimensional ultrasound reconstructions of embryos and early fetuses. *Lancet* 352:1182, 1998.
103. Benoit B, Hafner T, Kurjak A, et al: Three-dimensional sonoembryology. *J Perinat Med* 30:63, 2002.
104. Shipp TD, Bromley B, Benacerraf BR: Is 3-dimensional volume sonography an effective alternative method to the standard 2-dimensional technique of measuring the nuchal translucency? *J Clin Ultrasound* 34:118, 2006.
105. Chung BL, Kim HJ, Lee KH: The application of three-dimensional ultrasound to nuchal translucency measurement in early pregnancy (10-14 weeks): a preliminary study. *Ultrasound Obstet Gynecol* 15:122, 2000.
106. Clementschitsch G, Hasenohrl G, Schaffer H, et al: Comparison between two- and three-dimensional ultrasound measurements of nuchal translucency. *Ultrasound Obstet Gynecol* 18:475, 2001.
107. Czekierdowski A, Cholubek G, Sadowski K, et al: [Three dimensional sonography in nuchal translucency measurements between 10th and 14th weeks of gestation]. *Ginekol Pol* 72:961, 2001.
108. Eppel W, Worda C, Frigo P, et al: Three- versus two-dimensional ultrasound for nuchal translucency thickness measurements: comparison of feasibility and levels of agreement. *Prenat Diagn* 21:596, 2001.
109. Paul C, Krampfl E, Skentou C, et al: Measurement of fetal nuchal translucency thickness by three-dimensional ultrasound. *Ultrasound Obstet Gynecol* 18:481, 2001.
110. Worda C, Radner G, Lee A, et al: Three-dimensional ultrasound for nuchal translucency thickness measurements: comparison of transabdominal and transvaginal ultrasound. *J Soc Gynecol Investig* 10:361, 2003.
111. Hull AD, James G, Salerno CC, et al: Three-dimensional ultrasonography and assessment of the first-trimester fetus. *J Ultrasound Med* 20:287, 2001.
112. Bonilla-Musoles F, Raga F, Villalobos A, et al: First-trimester neck abnormalities: three-dimensional evaluation. *J Ultrasound Med* 17:419, 1998.
113. Kupesic S, Kurjak A, Ivancic-Kosuta M: Volume and vascularity of the yolk sac studied by three-dimensional ultrasound and color Doppler. *J Perinat Med* 27:91, 1999.
114. Falcon O, Peralta CF, Cavoretto P, et al: Fetal trunk and head volume measured by three-dimensional ultrasound at 11 + 0 to 13 + 6 weeks of gestation in chromosomally normal pregnancies. *Ultrasound Obstet Gynecol* 26:263, 2005.
115. Aviram R, Shpan DK, Markovitch O, et al: Three-dimensional first trimester fetal volumetry: comparison with crown rump length. *Early Hum Dev* 80:1, 2004.
116. Wegrzyn P, Faro C, Falcon O, et al: Placental volume measured by three-dimensional ultrasound at 11 to 13 + 6 weeks of gestation: relation to chromosomal defects. *Ultrasound Obstet Gynecol* 26:28, 2005.
117. Falcon O, Peralta CF, Cavoretto P, et al: Fetal trunk and head volume in chromosomally abnormal fetuses at 11 + 0 to 13 + 6 weeks of gestation. *Ultrasound Obstet Gynecol* 26:263, 2005.



118. Falcon O, Wegrzyn P, Faro C, et al: Gestational sac volume measured by three-dimensional ultrasound at 11 to 13 + 6 weeks of gestation: relation to chromosomal defects. *Ultrasound Obstet Gynecol* 25:546, 2005.
119. Metznerbauer M, Hafner E, Schuchter K, et al: First-trimester placental volume as a marker for chromosomal anomalies: preliminary results from an unselected population. *Ultrasound Obstet Gynecol* 19:240, 2002.
120. Nelson TR, Pretorius DH, Sklansky M, et al: Three-dimensional echocardiographic evaluation of fetal heart anatomy and function: acquisition, analysis, and display. *J Ultrasound Med* 15:1, 1996.
121. Goncalves LF, Espinoza J, Lee W, et al: A new approach to fetal echocardiography: digital casts of the fetal cardiac chambers and great vessels for detection of congenital heart disease. *J Ultrasound Med* 24:415, 2005.
122. Chaoui R, Kalache KD: Three-dimensional power Doppler ultrasound of the fetal great vessels. *Ultrasound Obstet Gynecol* 17:455, 2001.
123. Chaoui R, Kalache KD, Hartung J: Application of three-dimensional power Doppler ultrasound in prenatal diagnosis. *Ultrasound Obstet Gynecol* 17:22, 2001.
124. DeVore GR, Polanco B, Sklansky MS, et al: The 'spin' technique: a new method for examination of the fetal outflow tracts using three-dimensional ultrasound. *Ultrasound Obstet Gynecol* 24:72, 2004.
125. Bhat AH, Corbett VN, Liu R, et al: Validation of volume and mass assessments for human fetal heart imaging by 4-dimensional spatiotemporal image correlation echocardiography: in vitro balloon model experiments. *J Ultrasound Med* 23:1151, 2004.
126. Chang FM, Hsu KF, Ko HC, et al: Fetal heart volume assessment by three-dimensional ultrasound. *Ultrasound Obstet Gynecol* 9:42, 1997.
127. Zosmer N, Jurkovic D, Jauniaux E, et al: Selection and identification of standard cardiac views from three-dimensional volume scans of the fetal thorax. *J Ultrasound Med* 15:25, 1996.
128. Bhat AH, Corbett V, Carpenter N, et al: Fetal ventricular mass determination on three-dimensional echocardiography: studies in normal fetuses and validation experiments. *Circulation* 110:1054, 2004.
129. Levental M, Pretorius DH, Sklansky MS, et al: Three-dimensional ultrasonography of normal fetal heart: comparison with two-dimensional imaging. *J Ultrasound Med* 17:341, 1998.
130. Meyer-Wittkopf M, Rappe N, Sierra F, et al: Three-dimensional (3-D) ultrasonography for obtaining the four and five-chamber view: comparison with cross-sectional (2-D) fetal sonographic screening. *Ultrasound Obstet Gynecol* 15:397, 2000.
131. Bega G, Kuhlman K, Lev-Toaff A, et al: Application of three-dimensional ultrasonography in the evaluation of the fetal heart. *J Ultrasound Med* 20:307, 2001.
132. Sklansky MS, Nelson T, Strachan M, et al: Real-time three-dimensional fetal echocardiography: initial feasibility study. *J Ultrasound Med* 18:745, 1999.
133. Sklansky MS, DeVore GR, Wong PC: Real-time 3-dimensional fetal echocardiography with an instantaneous volume-rendered display: Early description and pictorial essay. *J Ultrasound Med* 23:283, 2004.
134. Meyer-Wittkopf M, Rappe N, Sierra F, et al: Three-dimensional (3-D) ultrasonography for obtaining the four and five-chamber view: comparison with cross-sectional (2-D) fetal sonographic screening. *Ultrasound Obstet Gynecol* 15:397, 2000.
135. Bega G, Kuhlman K, Lev-Toaff A, et al: Application of three-dimensional ultrasonography in the evaluation of the fetal heart. *J Ultrasound Med* 20:307, 2001.
136. Sklansky MS, Nelson T, Strachan M, et al: Real-time three-dimensional fetal echocardiography: initial feasibility study. *J Ultrasound Med* 18:745, 1999.
137. Michailidis GD, Simpson JM, Karidas C, et al: Detailed three-dimensional fetal echocardiography facilitated by an Internet link. *Ultrasound Obstet Gynecol* 18:325, 2001.
138. Goncalves LF, Espinoza J, Romero R, et al: A systematic approach to prenatal diagnosis of transposition of the great arteries using 4-dimensional ultrasonography with spatiotemporal image correlation. *J Ultrasound Med* 23:1225, 2004.
139. Goncalves LF, Romero R, Espinoza J, et al: Four-dimensional ultrasonography of the fetal heart using color Doppler spatiotemporal image correlation. *J Ultrasound Med* 23:473, 2004.
140. Vinals F, Mandujano L, Vargas G, et al: Prenatal diagnosis of congenital heart disease using 4D spatio-temporal image correlation (STIC) telemedicine via an internet link: a pilot study. *Ultrasound Obstet Gynecol* 25:25, 2005.
141. Sklansky M, Miller D, Devore G, et al: Prenatal screening for congenital heart disease using real-time three-dimensional echocardiography and a novel 'sweep volume' acquisition technique. *Ultrasound Obstet Gynecol* 25:435, 2005.
142. Espinoza J, Goncalves LF, Lee W, et al: The use of minimum projection mode in 4-D examination of the fetal heart with spatiotemporal image correlation. *J Ultrasound Med* 23:1227, 2004.
143. Esh-Broder E, Ushakov FB, Imbar T, et al: Application of free-hand three-dimensional echocardiography in the evaluation of fetal cardiac ejection fraction: a preliminary study. *Ultrasound Obstet Gynecol* 23:546, 2004.
144. Chaoui R, Hoffmann J, Heling KS: 3D and 4D color Doppler fetal echocardiography using spatio-temporal image correlation (STIC). *Ultrasound Obstet Gynecol* 23:535, 2004.
145. Abuhamad A: Automated multiplanar imaging: a novel approach to ultrasonography. *J Ultrasound Med* 23:573, 2004.
146. Abuhamad AZ: Standardization of 3-dimensional volumes in obstetric sonography: a required step for training and automation. *J Ultrasound Med* 24:397, 2005.
147. Goncalves LF, Espinoza J, Lee W, et al: Three- and four-dimensional reconstruction of the aortic and ductal arches using inversion mode: a new rendering algorithm for visualization of fluid-filled anatomical structures. *Ultrasound Obstet Gynecol* 24:696, 2004.
148. Chang CH, Yu CH, Ko HC, et al: Assessment of normal liver blood flow using quantitative 3D power Doppler ultrasound. *Ultrasound Med Biol* 29:943, 2003.
149. Chang CH, Yu CH, Ko HC, et al: Quantitative 3D power Doppler sonography for assessment of the fetal renal blood flow in normal gestation. *Ultrasound Med Biol* 29:929, 2004.
150. Kalache K, Romero R, Goncalves LF, et al: 3D color power imaging of the hepatic circulation. *Am J Obstet Gynecol* 189:1401, 2003.
151. Ruano R, Benachi A, Aubry MC, et al: Prenatal diagnosis of pulmonary sequestration using 3D power Doppler ultrasound. *Ultrasound Obstet Gynecol* 25:128, 2005.
152. Brinkley JF, McCallum WD, Muramatsu SK, et al: Fetal weight estimation from ultrasonic three-dimensional head and trunk reconstructions: evaluation in vitro. *Am J Obstet Gynecol* 144:715, 1982.
153. Favre R, Nisand G, Bettahar K, et al: Measurement of limb circumferences with three-dimensional ultrasound for fetal weight estimation. *Ultrasound Obstet Gynecol* 3:176, 1993.
154. Steiner H, Gregg AR, Bogner G, et al: First trimester three-dimensional ultrasound volumetry of the gestational sac. *Arch Gynecol Obstet* 255:165, 1994.
155. Hughes SW, D'Arcy TJ, Maxwell DJ, et al: Volume estimation from multiplanar 2D ultrasound images using a remote electromagnetic position and orientation sensor. *Ultrasound Med Biol* 22:561, 1996.
156. Lee A, Kratochwil A, Stumpflen I, et al: Fetal lung volume determination by three-dimensional ultrasonography. *Am J Obstet Gynecol* 175:588, 1996.
157. Laudy JA, Janssen MM, Struyk PC, et al: Three-dimensional ultrasonography of normal fetal lung volume: a preliminary study. *Ultrasound Obstet Gynecol* 11:13, 1998.
158. Pohls UG, Rempen A: Fetal lung volumetry by three-dimensional ultrasound. *Ultrasound Obstet Gynecol* 11:6, 1998.
159. Bahmaic A, Hughes SW, Clark T, et al: Serial fetal lung volume measurement using three-dimensional ultrasound. *Ultrasound Obstet Gynecol* 16:154, 2000.
160. Osada H, Iitsuka Y, Masuda K, et al: Application of lung volume measurement by three-dimensional ultrasonography for clinical assessment of fetal lung development. *J Ultrasound Med* 21:841, 2002.
161. Kalache KD, Espinoza J, Chaiworapongsa T, et al: Three-dimensional ultrasound fetal lung volume measurement: a systematic study comparing the multiplanar method with the rotational (VOCAL) technique. *Ultrasound Obstet Gynecol* 21:111, 2003.
162. Kalache KD, Espinoza J, Chaiworapongsa T, et al: Three-dimensional reconstructed fetal lung using VOCAL. *Ultrasound Obstet Gynecol* 21:205, 2003.
163. Ruano R, Benachi A, Martinovic J, et al: Can three-dimensional ultrasound be used for the assessment of the fetal lung volume in cases of congenital diaphragmatic hernia? *Fetal Diagn Ther* 19:87, 2004.
164. Ruano R, Joubin L, Sonigo P, et al: Fetal lung volume estimated by 3-dimensional ultrasonography and magnetic resonance imaging in cases with isolated congenital diaphragmatic hernia. *J Ultrasound Med* 23:353, 2004.



165. Ruano R, Benachi A, Joubin L, et al: Three-dimensional ultrasonographic assessment of fetal lung volume as prognostic factor in isolated congenital diaphragmatic hernia. *Br J Obstet Gynaecol* 111:423, 2004.
166. Moeglin D, Talmant C, Duyme M, et al: Fetal lung volumetry using two- and three-dimensional ultrasound. *Ultrasound Obstet Gynecol* 25:119, 2005.
167. Chang CH, Yu CH, Chang FM, et al: Volumetric assessment of normal fetal lungs using three-dimensional ultrasound. *Ultrasound Med Biol* 29:935, 2003.
168. Sabogal JC, Becker E, Bega G, et al: Reproducibility of fetal lung volume measurements with 3-dimensional ultrasonography. *J Ultrasound Med* 23:347, 2004.
169. Schild RL, Wallny T, Fimmers R, et al: The size of the fetal thoracolumbar spine: a three-dimensional ultrasound study. *Ultrasound Obstet Gynecol* 16:468, 2000.
170. Schild RL, Wallny T, Fimmers R, et al: Fetal lumbar spine volumetry by three-dimensional ultrasound. *Ultrasound Obstet Gynecol* 13:335, 1999.
171. Hsieh YY, Chang CC, Lee CC, et al: Fetal renal volume assessment by three-dimensional ultrasonography. *Am J Obstet Gynecol* 182:377, 2000.
172. Laudy JAM, Janssen MMM, Struyk PC, et al: Fetal liver volume measurement by three-dimensional ultrasonography: a preliminary study. *Ultrasound Obstet Gynecol* 12:93, 1998.
173. Kuno A, Hayashi Y, Akiyama M, et al: Three-dimensional sonographic measurement of liver volume in the small-for-dates. *J Ultrasound Med* 21:361, 2002.
174. Riccabona M, Nelson TR, Pretorius DH: Three-dimensional ultrasound: accuracy of distance and volume measurements. *Ultrasound Obstet Gynecol* 7:429, 1996.
175. Jeanty P, Romero R, Hobbins JC: Fetal limb volume: a new parameter to assess fetal growth and nutrition. *J Ultrasound Med* 4:273, 1985.
176. Favre R, Bader AM, Nisand G: Prospective study on fetal weight estimation using limb circumferences obtained by three-dimensional ultrasound. *Ultrasound Obstet Gynecol* 6:140, 1995.
177. Chang FM, Liang RI, Ko HC, et al: Three-dimensional ultrasound-assessed fetal thigh volumetry in predicting birth weight. *Obstet Gynecol* 90:331, 1997.
178. Liang RI, Chang FM, Yao BL, et al: Predicting birth weight by fetal upper-arm volume with use of three-dimensional ultrasonography. *Am J Obstet Gynecol* 177:632, 1997.
179. Song TB, Moore TR, Lee JI, et al: Fetal weight prediction by thigh volume measurement with three-dimensional ultrasonography. *Obstet Gynecol* 96:157, 2000.
180. Lee W, Deter RL, Ebersole JD, et al: Birth weight prediction by three-dimensional ultrasonography: fractional limb volume. *J Ultrasound Med* 20:1283, 2001.
181. Schild RL, Fimmers R, Hansmann M: Fetal weight estimation by three-dimensional ultrasound. *Ultrasound Obstet Gynecol* 16:445, 2000.
182. Hadlock FP, Harrist RB, Sharman RS, et al: Estimation of fetal weight with the use of head, body, and femur measurements—a prospective study. *Am J Obstet Gynecol* 151:333, 1985.
183. Lee W, Deter RL, McNie B, et al: Individualized growth assessment of fetal soft tissue using fractional thigh volume. *Ultrasound Obstet Gynecol* 24:766, 2004.
184. Lee W, Deter RL, McNie B, et al: The fetal arm: individualized growth assessment in normal pregnancies. *J Ultrasound Med* 24:817, 2005.
185. Deter RL, Rossavik IK: A simplified method for determining individual growth curve standards. *Obstet Gynecol* 70:801, 1987.
186. Endres LK, Cohen L: Reliability and validity of three-dimensional fetal brain volumes. *J Ultrasound Med* 20:1265, 2001.
187. Hafner E, Philipp K, Schuchter K, et al: Second-trimester measurements of placental volume by three-dimensional ultrasound to predict small-for-gestational-age infants. *Ultrasound Obstet Gynecol* 12:97, 1998.
188. Hull AD, Salerno CC, Sacnz CC, et al: Three-dimensional ultrasonography and diagnosis of placenta percreta with bladder involvement. *J Ultrasound Med* 18:853, 1999.
189. Hull AD, Pretorius DH, Lev-Toaff A, et al: Artifacts and the visualization of fetal distal extremities using three-dimensional ultrasound. *Ultrasound Obstet Gynecol* 16:341, 2000.
190. Nelson TR, Pretorius DH, Hull A, et al: Sources and impact of artifacts on clinical three-dimensional ultrasound imaging. *Ultrasound Obstet Gynecol* 16:374, 2000.
191. Bailey JE, Bude RO, Tuthill T: US artifacts: effects on out-of-plane US images reconstructed from three-dimensional data sets. *Radiology* 218:592, 2001.
192. Ji EK, Pretorius DH, Newton R, et al: Effects of ultrasound on maternal-fetal bonding: a comparison of two- and three-dimensional imaging. *Ultrasound Obstet Gynecol* 25:473, 2005.
193. Rustico MA, Mastromatteo C, Grigio M, et al: Two-dimensional vs. two- plus four-dimensional ultrasound in pregnancy and the effect on maternal emotional status: a randomized study. *Ultrasound Obstet Gynecol* 25:468, 2005.
194. Righetti PL, Dell'Avanzo M, Grigio M, et al: Maternal/paternal antenatal attachment and fourth-dimensional ultrasound technique: a preliminary report. *Br J Psychol* 96:129, 2005.

# THE PRENATAL MANAGEMENT OF THE FETUS WITH A CORRECTABLE DEFECT

Robert H. Ball, MD and Jan Deprest, MD, PhD

## Introduction

### Hysterotomy

Risks

Procedure

### Fetoscopy

Risks

Procedure

### Shunts and Radiofrequency Ablation

Risks

Procedure

## Disease Entities

Monochorionic Twin Problems

*Twin-Twin Transfusion Syndrome*

*Discordant Monochorionic Twins*

*Twin-Reversed-Arterial-Perfusion or Acardiac Twinning*

Congenital Diaphragmatic Hernia

Congenital Cystic Adenomatoid Malformation

Sacroccygeal Teratoma

Myelomeningocele

Lower Urinary Tract Obstruction

Pleural Effusions

Fetal Cardiac Interventions

## INTRODUCTION

The potential for the field of fetal surgery would never even have been considered without the existence of prenatal ultrasound diagnosis. This makes the discussion of these interventions particularly pertinent to a textbook dedicated to ultrasound in obstetrics and gynecology.

Most malformations considered for fetal surgery may be initially detected as abnormal on routine screening but may not be accurately identified until a targeted examination is performed. It is self-evident that an accurate diagnosis is critical to determining the appropriateness of a fetal surgical intervention. Fetal malformations that are not isolated or are associated with aneuploidy or a syndrome have always been excluded as candidates for intervention. This is because the risk-benefit ratio, given that all procedures involve some maternal risk, is not acceptable. Therefore, great effort should be made to confirm both the accurate diagnosis of a malformation and the fact that it is truly isolated. Ancillary techniques to ensure full and accurate assessment include fetal echocardiography, magnetic resonance imaging (MRI), and karyotyping, depending on what additional problems the fetus is most at risk. Regardless, one must always counsel patients regarding the fallibility of the process and that abnormalities initially that are believed to be isolated may not ultimately prove to be so in the final analysis.

The indications for fetal surgical interventions have expanded, as has the total number of procedures performed, the sites at which they are performed, and the number of physicians performing them. However, overall these procedures remain very limited when compared with the number of pregnancies and even the number of fetuses with malformations. One of the responsibilities of physicians with an

interest in prenatal diagnosis and intervention, in the future, is to determine training needs and oversight for operators and centers involved in this field. It is unclear how many centers would be needed given the rarity of malformations and the even smaller proportion of those with a malformation that may need fetal intervention. A decision will need to be made if ease of accessibility is a substitute for volume of procedures performed. Certainly with access to the World Wide Web, patients in our experience have become savvy consumers who are readily able to establish contact and provide information necessary to make a preliminary assessment regarding their fetus's diagnosis. This, together with the increasing ease of large volume electronic transfer of information, has made geographic proximity less important.

Over the past decade technologic advances have allowed a transition toward less invasive procedures. Initial fetal surgical procedures at the University of California, San Francisco (UCSF) involved maternal laparotomy and hysterotomy. This approach evolved into laparotomy and uterine endoscopy, and most recently, into percutaneous procedures using laparoscopic devices with diameters at times of 3 mm or less. Our experience suggests that the less invasive approaches are associated with a less complicated post-operative recovery for the mothers but does not entirely eliminate morbidity<sup>1</sup> (Table 25-1). Each one of these approaches is discussed in detail.

## HYSTEROTOMY

The feasibility of performing a hysterotomy and subsequent closure of the gravid human uterus was tested in the primate



**Table 25-1****Maternal Morbidity and Mortality for 178 Interventions at UCSF With Postoperative Continuing Pregnancy and Divided into Operative Subgroups**

Operative Technique	Open Hysterotomy	Endoscopy FETENDO/ Lap-FETENDO	Percutaneous FIGS/ Lap-FIGS	All Interventions
Patients with postop continuing pregnancy	79	68	31	178
Gestational age at surgery [wk]	25.1	24.5	21.1	24.2
Range [wk]	17.6–30.4	17.9–32.1	17.0–26.6	17.0–32.1
Gestational age at delivery [wk]	30.1	30.4	32.7	30.7
Range [wk]	21.6–36.7	19.6–39.3	21.7–40.4	19.6–40.4
Interval surgery to delivery [wk]	4.9	6.0	11.6	6.5
Range [wk]	0–16	0–19	0.3–21.4	0–21.4
Pulmonary edema	22/79 (27.8%)	17/68 (25.0%)	0/31 (0%)	39/178 (21.9%)
Bleeding requiring blood transfusion	11/87 (12.6%)	2/69 (2.9%)	0/31 (0%)	13/187 (7.0%)
PTL leading to delivery	26/79 (32.9%)	18/68 (26.5%)	4/31 (12.9%)	48/178 (27.0%)
Preterm premature rupture of membranes (PPROM)	41/79 (51.9%)	30/68 (44.1%)	8/31 (25.8%)	79/178 (44.4%)
Chorioamnionitis	7/79 (8.9%)	1/68 (1.5%)	0/31 (0%)	8/178 (4.5%)

FETENDO, fetal endoscopic procedure; FIGS, fetal image-guided surgery; Lap-FETENDO, laparotomy and fetal endoscopic procedure; Lap-FIGS, laparotomy and fetal image-guided surgery; UCSF, University of California, San Francisco.



**FIGURE 25-1.** Photograph of operative laparotomy and hysterotomy in a Rhesus monkey. This early work paved the way for the ability to perform such procedures safely in the mother carrying a fetus with a variety of malformations.

(Fig. 25-1). The reason for using the primate model is that other gravid large animal models such as the sheep, are much more forgiving. The sheep uterus is more thin walled and has a multicotyledonary placenta. Closure is more straightforward, and preterm labor is rarely a significant problem. The safety profile in this series of primate fetal surgeries was reassuring, including subsequent fertility.<sup>2</sup> The human experience is now extensive, both from UCSF and others,<sup>1,3,4</sup> primarily associated with the large numbers of fetal spina bifida repairs. We currently reserve maternal laparotomy/hysterotomy procedures for repair of spina bifida, resection of sacrococcygeal teratoma and other tumors, and lobectomy for congenital cystic adenomatoid malformation (CCAM) of the lung.

## Risks

We have recently reviewed our experience at UCSF with maternal hysterotomy<sup>1</sup> (see Table 25-1). Eighty-seven hysterotomies were performed between 1989 and 2003. There were significant immediate postoperative complications. In the early experience, pulmonary edema related to multiple tocolytic use, particularly nitroglycerin, and aggressive fluid management was a significant problem.<sup>5</sup> Thirteen percent required transfusion for intraoperative blood loss. Pregnancy outcomes were also significantly affected by a preterm premature rupture of membrane (PPROM) rate of 52%, and 33% having preterm labor refractory to maximal tocolytic management leading to delivery. The mean time from hysterotomy to delivery was 4.9 weeks (range 0 to 16 weeks). The mean gestational age at the time of delivery was 30.1 weeks (range 21.6 to 36.7 weeks). Others<sup>6,7</sup> have similar experiences with respect to an increased risk of preterm delivery following hysterotomy. Most of the morbidity associated with hysterotomy has decreased with experience. Significant pulmonary edema or blood loss is rare, and the mean gestational age at the time of delivery for repair of myelomeningocele (MMC) is now around 34 weeks.

## Procedure

The practical aspects of hysterotomy and postoperative management have evolved since the initial years of experience. The following is a description of our current approach. Lengthy discussions regarding the risks, benefits, and alternatives of the procedure are important, including the experimental nature of the surgery. We generally differentiate the risks to the mother, the fetus, and the pregnancy in our counseling. The risks to the mother are similar to any major abdominal surgery, although in this case, there is no direct physical benefit to her. In addition there are the risks associated with aggressive tocolytic therapy and bed rest in



a hypercoagulable state. The risks to the fetus are primarily vascular instability and hypoperfusion intraoperatively leading to organ injury or death, and prematurity due to postoperative complications. The risks to the pregnancy are primarily preterm labor and premature rupture of membranes and preterm delivery. Infectious complications are rare, except when premature rupture leads to prolonged latency. An important additional discussion point is that all subsequent deliveries, including the index pregnancy, must be by cesarean section. Data regarding future fertility are reassuring, with no increased incidence of infertility in the UCSF experience in those patients attempting pregnancy.<sup>8</sup> Experience from Children's Hospital of Pennsylvania (CHOP) suggests a concerning risk for uterine rupture/dehiscence in subsequent pregnancies that may be as high as 6% to 12%,<sup>9</sup> which would be considerably higher than the risk after previous low transverse cesarean section (1% or less)<sup>10</sup> or classic cesarean section (5% to 10%).<sup>11</sup> Another potential risk in subsequent pregnancies is placenta accreta. The reason for this risk is that the site of a hysterotomy performed in the second trimester is never in the same area as a cesarean section entry. There is an increased risk of placenta accreta in any case in which implantation is in an area of uterine scarring. Multiple incisions increase the likelihood of implantation in such an area. To our knowledge, there has not been a case of accreta in a fetal surgical patient of ours in a subsequent pregnancy.

Ultrasound is used for guidance before the hysterotomy procedure. Once the patient has had general anesthesia and intubation initiated, and the sterile field is established, ultrasound is used to establish fetal lie, its location within the uterus, and the position of the placenta. Transabdominal manipulation with ultrasound guidance is used to position the fetus such that the fetal surgical site is near the fundus. Depending on the maternal body habitus and fetal size and position, this may be challenging. Laparotomy is then performed, and the ultrasound transducer, covered in a sterile sleeve, is placed directly on the surface of the uterus. The edge of the placenta is identified, because this information is critical in deciding where to perform the uterine entry. Generally, one wants to make the uterine incision centered as far from the placental edge as possible. The reason for this is that once the incision is made, and the amniotic fluid leaves the confines of the uterus, the uterus shrinks. One is generally surprised at how close the incision is to the edge of the placenta regardless of one's efforts. The reason proximity to the placental edge is so critical is because of the risk of bleeding and abruption, which cannot readily be controlled and, if significant, will usually necessitate immediate delivery for maternal safety.

Ultrasound is also used to identify the specific position of the fetus within the uterus. Generally the incision in the uterus will have been made so as to have optimal access to the fetal part to be surgically addressed. Ultrasound is also used for transuterine monitoring of the fetal heart during the procedure. Following completion of the fetal intervention, the membranes and myometrium are closed with several layers of suture. A catheter is left in the uterine cavity to allow lactated Ringer's solution to be infused together with antibiotics. Ultrasound determines the volume of "amniotic" fluid, which is generally at a low-normal level to minimize stress on the suture line.

Post-operative management generally involves 24 hours of intravenous tocolysis with magnesium sulfate as well as maintenance with oral indomethacin for a total of 48 hours. Long-term tocolytic maintenance with nifedipine is continued basically until delivery. Antibiotic "prophylaxis" is continued for 24 hours. Ultrasound monitoring to evaluate fetal health, amniotic fluid volume, cervical length, and ductal patency is performed at least daily. Hospital discharge generally occurs 4 to 5 days after surgery. If all goes well, long-term monitoring with ultrasound continues at a weekly frequency.

## FETOSCOPY

The growing popularity of videoendoscopic surgery in the 1990s, combined with earlier experience with fetoscopy, paved the way for the concept of endoscopic fetal surgery. The rationale was that a tiny puncture of the amniotic cavity would overcome some of the limiting steps in fetal surgery: (1) preterm labor, which was believed to be triggered by the large uterine incision of open fetal surgery; and (2) significant maternal morbidity associated with a large laparotomy. The ultimate hope was that fetoscopic interventions would be possible by a percutaneous approach. Animal models were developed to test the new instruments and techniques. The ovine model is very resistant to postoperative preterm contractions, as mentioned earlier, and therefore not ideal to study the hypothesis that endoscopic access to the uterine cavity was associated with less uterine activity than after hysterotomy. We studied that aspect in midtrimester Rhesus monkeys (*Macaca mulatta*) who underwent triple cannulation of the amniotic cavity during 60 minutes. No significant postoperative premature contractions could be demonstrated, in contrast to uterine irritability following hysterotomy.<sup>12</sup> Use of this higher species is limited by ethical and financial constraints, but today, the model is still in use for study on healing of the fetal membranes after fetoscopic cannulation.

## Risks

The risks of fetoscopy are associated with the uterine puncture as well as the specific procedure that is being treated. In some cases, adverse outcomes may be inherent to the severity of the disease being treated, such as in twin-to-twin transfusion syndrome (TTTS). In the UCSF experience,<sup>1</sup> the morbidities were in some cases similar to the more invasive procedure of hysterotomy and in some cases much more akin to the pattern seen in the so-called fetal image-guided surgery (FIGS). One reason for this is that the initial UCSF approach was "macroinvasive" endoscopy including laparotomy, uterine exteriorization and general anesthesia. Current risk profiles with a percutaneous approach and smaller instruments demonstrate less morbidity.<sup>13</sup> This includes a much lower rate of preterm labor and even PPROM. Length of hospitalization and time of return to normal maternal activity are also much improved.

## Procedure

Patients are generally premedicated with a tocolytic agent, often indomethacin, and given prophylactic intravenous



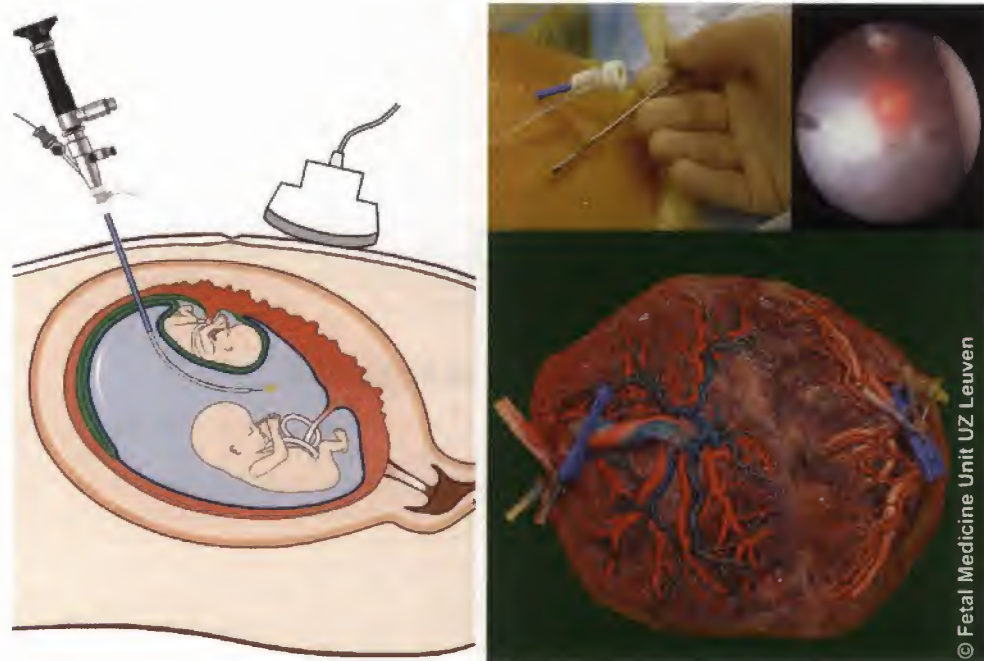


**FIGURE 25-2.** Schematic drawing of a percutaneous fetoscopic laser coagulation procedure for TTTS. (Reprinted with permission from Group TE: *The Eurofoetus Group*. In Deprest J, Ville Y, Barki G, et al [eds]: *Endoscopy in Fetal Medicine*. Tübingen, Germany, Endopress, 2004, pp 1–58.) Inserts, clockwise from top left: Percutaneously inserted 10 Fr cannula; fetoscopic view of arteriovenous anastomosis being coagulated. Bottom: injected placenta after procedure, demonstrating ablated vessels.

(IV) antibiotics. The procedures are performed under local or regional anesthesia. Depending on the gestational age and the tradition of the center, the surgery may be performed in the surgical operating rooms, labor and delivery, or the ultrasound suite. Cannulas, instruments, and particularly, endoscopes have undergone a tremendous evolution in the past 10 years, based on prototypes developed in animal models. Operative fetoscopy is a sonoendoscopic enterprise that has evolved so that the surgical team can see the ultrasound and fetoscopic images simultaneously. Purpose-designed embryo- or fetoscopes typically have remote eyepieces, to reduce weight and facilitate precise movements. Nearly all are bendable fiber-endoscopes rather than conventional rod lens scopes, and as the number of pixels increases over time, image quality improves. Typical diameters are between 1.0 and 2.0 mm. Thin-walled semiflexible plastic cannulas (10f Check-flo introducers, Cook Medical, Bloomington, IN) are used to create amniotic access, so that instrument changes are possible. Sharp trocars have been developed to accommodate the wide range of diameters used for different operations (Karl Storz, Germany). Alternatively, one introduces the endoscope sheath loaded with a sharp obturator (Fig. 25–2). Specifics can be reviewed in several texts.<sup>14,15</sup> Basically, however, ultrasound is used to identify an appropriate entry point and then is used to direct the trocar into the amniotic cavity, avoiding the placenta and the fetus, and obviously maternal organs such as bowel and bladder. One group has documented the safety, in their hands, of a transplacental approach.<sup>16</sup> Despite this experience, most operators still attempt to avoid the placenta. The trocar is then replaced by the fetoscope. Ultrasound is still used to direct the scope within the uterus, because its field

and depth of view can be relatively limited. These procedures are “sono-endoscopic.” For cases of TTTS, the endoscope is in the sac of the recipient twin, the one with the polyhydramnios. The entry point is determined by the factors noted earlier, but also to allow good visualization of the vascular equator of the twins. The whole equator is then explored, and any unpaired vessels consistent with abnormal communications are ablated using the laser fiber that is advanced through the operating channel of the endoscope sleeve. After successful ablation, the endoscope is withdrawn and the polyhydramnios drained through the cannula under ultrasound guidance. Once the fluid has reached a normal level (deepest vertical pocket of around 5 to 6 cm) the cannula is removed. This amnioreduction reduces the risk of port-site leaking and amniotic fluid irritation of the peritoneal cavity, which may be painful. It may also improve placental perfusion, but regardless, makes the patient more comfortable. In many cases, little or no tocolytic medication is needed, and patients are generally discharged within 24 hours or less of the procedure.

## SHUNTS AND RADIOFREQUENCY ABLATION

Shunts are used for chronic drainage of fluid-filled fetal cavities, organs, and cysts. The first shunt was developed by Harrison at UCSF in the early 1980s.<sup>17</sup> This is basically a double pigtail shunt that is introduced through a 14-gauge introducer (Cook Medical, Bloomington, IN). The Rodeck shunt was developed during a similar time period in the United Kingdom. It is also a double pigtail shunt but is longer and has a greater diameter (Rocket Medical, UK).



Obviously it uses a larger diameter introducer.<sup>18</sup> These catheters are used for draining obstructed bladders, pleural effusions, and large macrocystic CCAMs.

Radiofrequency ablation (RFA) is most commonly used in the nonobstetric patient for the destruction of tumor tissue in solid organs such as the liver. The group at the UCSF Fetal Treatment Center was first to use it for the application of localized cautery of vascular communications. Initially, it was used for ablating the feeding vessels to the anomalous fetus in twin-reversed-arterial perfusion (TRAP).<sup>19</sup> Since that time, we have used it for selective reduction in monochorionic twin gestations discordant for severe anomalies and in patients with severe TTTS without hope for salvage of one of the twins.

## Risks

The risks of complication of shunt placement and RFA are lower than for the more invasive fetal surgical interventions such as hysterotomy. Obviously by definition, all invasive procedures involve a risk of hemorrhage and infection. However, in our experience, these adverse events occur at a much lower frequency (see Table 25-1).<sup>1</sup> The triggering of preterm delivery by these procedures is also quite unusual, although the risk of PPROM remains. There is also the risk of fetal injury, which in cases of monochorionic twins, generally is related to hypotension from acute hypovolemia in the normal co-twin secondary to exsanguination into the placental vascular bed and the other fetus.

## Procedure

As we have become more comfortable with these procedures, the length of hospitalization, complexity of perioperative management, and type of anesthesia have changed. In many cases, they can be performed as an outpatient procedure. Tocolytic prophylaxis is given as a single dose of indomethacin. Routine preoperative antibiotic prophylaxis is given. These procedures are performed completely under ultrasound guidance (FIGS). We perform these procedures using either spinal or local anesthesia. For shunts, a small incision is made in the maternal skin, and then the introducer with the trochar in place is advanced into the amniotic cavity. Care is used to evaluate the myometrium that will be traversed, with a high frequency transducer and color flow Doppler with low flow settings, to avoid large veins. We generally avoid a transplacental approach as well. The trochar and introducer are then advanced into the area where the shunt will be placed. Once in position, the trochar is removed and care taken to not allow the fluid to be drained and escape by placing one's finger over the end. The shunt is then loaded into the introducer and advanced using a internal pushing device. These pushers either are of a certain length or have marks on them to advance just the internal coil of the catheter stent out of the introducer. It is critical to image this with ultrasound as well. Once the inner coils of the catheter stent are appropriately positioned, the introducer is carefully withdrawn, while at the same time advancing the shunt further, so that the outer coil is positioned on the skin of the fetus, within the amniotic cavity. Care must be taken to have enough of a fluid gap between the fetus and the wall of the uterus to minimize the risk of

the outer end of the shunt being stuck in the myometrium or maternal abdominal wall, with the risk of an amnioperitoneal shunt. Given the ready access to these shunts, and the fact that physicians feel capable of performing the procedure because of their comfort with image-guided procedures such as amniocentesis, this may be the most frequently and widely performed fetal surgical intervention. Unfortunately, this experience and associated outcomes are not documented in the scientific literature.

Postoperative management involves maternal and fetal monitoring. Further tocolytic management is tailored based on contraction activity. Frequently, no further medication is necessary. Maternal vital signs should be followed carefully because direct observation of the uterine puncture is not possible to determine hemostasis because of the percutaneous approach. One benefit of not needing tocolysis is that the hemostatic mechanism of the uterus in response to a puncture is a localized contraction. Ultrasound is obviously critical to fetal follow-up.

The RFA device that we currently use at UCSF includes a 17-g needle device (RITA Medical, Fremont, CA). The perioperative management is identical to that discussed earlier with shunts, except that local anesthesia alone is generally used. In the case of TRAP, the instrument is guided into the tissue of the acardiac twin at the level of the cord insertion. The prongs are deployed, and energy transmission to the device initiated. Because of the heat generation, there is outgassing that is readily visible with ultrasound. The procedure is considered completed when there is no evidence of flow in the acardiac twin or the cord leading to it on color and pulsed Doppler imaging. The prongs are then retracted and the device withdrawn. Postoperative monitoring is similar to shunt placement, and further tocolytic management is rarely necessary. The patients can generally be discharged within hours of the procedure.

## DISEASE ENTITIES

### Monochorionic Twin Problems

#### *Twin-Twin Transfusion Syndrome*

In an estimated 15% of monochorionic (MC) twins, there is a chronic imbalance in the net flow of blood across the vascular anastomoses, resulting in TTTS. The condition is usually explained by the combination of transfusion from the donor, leading to hypovolemia, oliguria, and oligohydramnios in the donor twin (so-called stuck twin) and hypervolemia, polyuria, and polyhydramnios in the recipient twin. The recipient twin often develops circulatory volume overload and hydrops. The condition coincides with specific patterns of vascular anastomoses. This forms the basis for the surgical approach to this condition. Fetal vessels run on the surface of the placenta, where they can be documented by fetoscopic inspection, and ablated (see Fig. 25-2). Although several types of anastomoses exist, knowledge about their nature (either by Doppler studies or by fetoscopy) does not play a role in TTTS: all intertwin anastomoses should be ablated as to functionally "bichorionize" the placenta (see Fig. 25-2).

The diagnosis of TTTS is based on ultrasound documentation of very specifically discrepant amniotic fluid levels.



**Table 25-2** Staging of Twin to Twin Transfusion Syndrome

Stage	Polyhydramnios/Oligohydramnios*	Persistently Empty Bladder in Donor	Abnormal Doppler†	Hydrops	Demise
I	X				
II	X	X			
III	X	X	X		
IV				X	
V					X

\*Polyhydramnios = deepest vertical pocket  $\geq 8$  cm, Oligohydramnios = deepest vertical pocket  $< 2$  cm

†At least one of the following: 1) umbilical artery absent/reserved end diastolic flow, 2) absent/reversed end diastolic flow in the ductus venosus, and 3) pulsatile umbilical venous flow

Modified from Quintero RA, Morales WJ, Allen MH, et al: Staging of twin-twin transfusion syndrome. *J Perinatol* 19:550, 1999; and Taylor MJO, Jolly M, Wee L, et al: Validation of the Quintero staging system for twin-twin transfusion syndrome. *Obstet Gynecol* 100:1257, 2002.

It requires the presence of oligouric oligohydramnios (deepest vertical pool [DVP]  $< 2$  cm), together with polyuric polyhydramnios (8 cm DVP  $< 20$  weeks;  $\geq 10$  cm  $\geq 20$  weeks; criteria based on the Eurofoetus trial). Intrauterine growth restriction may be part of the clinical picture but is *not* a criterion for establishing the diagnosis or an indication for therapy. The natural history of TTTS is not clearly defined yet, but in a number of cases, it may be progressive, with development of abnormal Doppler patterns in the umbilical artery of the donor fetus or abnormal venous Doppler patterns in the recipient, and ultimately fetal hydrops or fetal death. The latter signs form the basis of the ultrasound-based Quintero stages<sup>20</sup> (Table 25-2). However, cases may occasionally progress acutely from having discrepant fluids (stage I or II) directly to the stage of fetal death (stage V). This staging also does not necessarily determine management based on currently available data.

If left untreated, perinatal loss is more than 80% in severe TTTS; therefore, therapy is mandatory and fetoscopic laser has the best pathophysiologic basis. In addition, the Eurofoetus randomized trial demonstrated better outcomes after fetoscopic laser than after serial amnioreduction.<sup>21</sup> The median gestational age at delivery was significantly higher in the laser-treated group compared with the amnioreduction group. Survival of at least one twin to 6 months was higher following laser therapy. Amnioreduction more often leads to demise of both twins. Survival chances were similar for donors and recipients. It is important to stress that laser coagulation is more effective than amnioreduction for a given stage. It is true that survival decreases according to stage; however, even for stage IV, survival of the hydropic recipient is 50%.<sup>22</sup> Therefore, this does not justify promoting selective fetocide based purely on the stage of the disease at presentation. Preoperative measurement of the cervix can assess the risk for premature delivery.<sup>23</sup> With a cervix less than 30 mm, the risk for delivery before 34 weeks is about 74%. If the cervix is less than 20 mm, the vast majority of patients miscarry. The risk for PPROM is estimated to be around 10% or less; the risk for abruption is 1% to 2% but relates to the amnioreduction part of the procedure. Other uncommon complications are chorioamnionitis and hemorrhage. Post-laser fetal anemia and recurrent or persistent TTTS should be screened for and may suggest incomplete division of the placenta. Recent injection studies have demonstrated that this might be more often the case than expected, and that it does not always lead to clinical

problems.<sup>24</sup> Cardiac abnormalities can develop as well and require postnatal follow-up by a pediatric cardiologist. Therefore, it should be clear that compulsive postoperative ultrasound follow-up by experienced fetal medicine specialists is a critical component of successful therapy.

In the Eurofoetus trial,<sup>21</sup> a higher percentage of infants were alive without major neurologic morbidity at age 6 months or greater in the laser group (Table 25-3). The long-term follow-up of these patients is now pending. Until that time, counseling can be based on the detailed follow-up studies of Hecher's group,<sup>25</sup> with a 6% rate of severe handicap compared with 20% to 25%, which is the rate commonly associated with amnioreduction.

As noted earlier, TTTS predisposes to right ventricular outlet tract obstruction (pulmonary stenosis) in 8% of ex-recipients. Of these patients, half needed balloon dilatation.<sup>26</sup> Other pre-laser in utero signs of cardiac decompensation resolved and were undetectable postnatally. Normal renal function was also documented in former donors.<sup>27</sup>

Fetoscopic laser coagulation is the most frequently performed obstetric endoscopic procedure, with more than 1500 procedures performed by the Eurofoetus centers alone. Single center series reported better results than in the randomized trial. Experience, case selection, and probably closer postoperative management may play a role in this difference. Additional centers have started offering this operation with comparable results. The benefits and disadvantages of the growing number of centers, and the potential dilution of experience is a point of healthy discussion.

### Discordant Monochorionic Twins

Most MC twins are indeed very similar in appearance, but major discordances in structural and even in chromosomal anomalies can occur. Abnormalities associated with twins include those of the neural tube, brain, face, gastrointestinal tract, anterior abdominal wall and heart, with more than 80% being discordant. MC twins can also be discordant for aneuploidy (trisomy 13 or 21, monosomy 45,X). Counseling issues may be very challenging in heterokaryotypic twins, because it is not possible to exclude hidden but phenotypically important mosaicism and microchimerism in the twin with normal karyotype.<sup>28</sup> Options for MC twin pregnancies discordant for structural and chromosomal anomalies are essentially expectant management, selective fetocide, or



**Table 25-3** Randomized Controlled Trial of Fetoscopic Laser Surgery Versus Serial Amniodrainage

	Laser n=72	Amnioreduction n=70	P value
Gestation age at randomization (weeks)	20.6 (2.4)	20.9 (2.5)	ns
Quintero stage at randomization			
Stage 1	6 (8.3%)	5 (7.1%)	ns
Stage 2	31 (43.1%)	31 (44.3%)	ns
Stage 3	34 (47.2%)	33 (47.1%)	ns
Stage 4	1 (1.4%)	1 (1.4%)	ns
Number of procedures	1*	2.6 (1.9)	—
AFV drained per procedure (mL) in total overall amniodrainages	1725 (500–5500)	2000 (243–4000)	ns
median (range)		3800 (600–18000)	<0.001
Pregnancy loss at or within 7 days of the initial procedure	8 (11.6%)	2 (2.9%)	0.10
Premature rupture of membranes at or within 7 days of the first procedure	4 (5.8%)	1 (1.5%)	0.37
Premature rupture of membranes at or within 28 days of the first procedure	6 (8.7%)	6 (8.8%)	0.98
Intrauterine death $\leq 7$ days of the first procedure <sup>†</sup>	16/138 (11.6%)	9/136 (6.6%)	0.23
At least one survivor at 6 months of life	55 (76.4%)	36 (51.4%)	0.002
No survivors	17 (23.6%)	34 (48.6%)	
One survivor	29 (40.3%)	18 (25.7%)	
Two survivors	26 (36.1%)	18 (25.7%)	
At least one survivor at 6 months stratified by stage			
Quintero stages I and II	32/37 (86.5%)	21/36 (58.3%)	0.007
Quintero stages III and IV	23/35 (65.7%)	15/34 (44.1%)	0.07
Gestational age at delivery—median (interquartile range)	33.3 (26.1–35.6)	29.0 (25.6–33.3)	0.004
Neonatal and infant death	12 (8.3%)	41 (29.3%)	
Intraventricular hemorrhage (grades III–IV) <sup>‡</sup>	12 (1.4%)	8 (5.7%)	0.10
Donor	2 (2.8%)	2 (2.9%)	1.0
Recipient	0 (0%)	6 (8.6%)	0.02
Cystic periventricular leukomalacia <sup>§</sup>	8 (5.6%)	20 (14.3%)	0.02*
Donor	2/72 (2.8%)	5/70 (7.1%)	0.27
Recipient	6/72 (8.3%)	15/70 (21.4%)	0.03

AFV, amniotic fluid volume; ns, not significant.

Baseline characteristics according to group, results reported as number of pregnancies (n(percent)), means (SD).

\*Two patients had 2 laser procedures.

<sup>†</sup>With number of fetuses as denominator (P value adjusted for clustering).<sup>‡</sup>Severe intraventricular hemorrhage was defined as ventricular bleeding with dilatation of the cerebral ventricles (grade III) or parenchymal hemorrhage (grade IV).<sup>§</sup>Cystic periventricular leukomalacia was defined as periventricular densities evolving into extensive cystic lesions (grade III) or extending into the deep white matter evolving into cystic lesions (grade IV).

termination of the entire pregnancy. There is no ethical dilemma as to selective fetocide when there is a nonviable co-twin, for example, in TRAP sequence (see later), or even in complicated TTTS with associated severe irreversible anomalies. Also, when there is a high risk of fetal demise of one twin in the previable period, fetocide may prevent complications to the co-twin at the moment of demise. In other situations, the ethical dilemma is more complex. In the rare event of discordant chromosomal, or more commonly, structural or acquired anomalies, there is no immediate, or in some cases, even remote risk of demise of the anomalous fetus, and therefore no serious threat to the co-twin. In such situations, the poor quality of life for the abnormal twin may not be acceptable to the parents. In those situations, selective fetocide may be a more appropriate option than termination of the entire pregnancy. The situation becomes even more complex when some of these anomalies are diagnosed very early in pregnancy, at a time when it is difficult to reliably predict the natural history of the disease.

Conventional fetocide by intracardiac potassium chloride injection cannot be used because it could affect the co-twin

through the anastomoses, or post-mortem fetofetal haemorrhage might occur. Therefore, it is recommended to arrest both arterial and venous flow in the cord of the target fetus. Initially this was achieved by fetoscopic cord ligation, but today, most use bipolar cord coagulation.<sup>29</sup> Alternative minimally invasive techniques include the use of (interstitial as well as noncontact) laser, monopolar, or radiofrequency energy. It is difficult to compare results with different energy modalities because they may include patients with different conditions, gestational age at treatment, and experience of the operators.

There are two studies in the current literature reporting a significant case series experience. One is from the group of Robyr et al.<sup>30</sup> We published a prospective follow-up study on 80 consecutive cord occlusions (87 fetuses), mainly with bipolar coagulation.<sup>31</sup> The survival rate was 83%. Half of the in utero losses were in the immediate postoperative period, potentially related to incomplete occlusion (which was more likely after laser coagulation). The other losses were thought to be due to cord complications, raising the possibility that intertwin septostomy during the procedure



Table 25-4

## Larger Follow-Up Series on Cord Occlusion

	Lewi et al, 2005 (n=87)*	Robyr et al, 2005 (n=46)
GA at procedure	21 (15–29.5)	20 (16–35)
Prenatal loss	11%	17.5% <sup>†</sup>
PPROM		
<28 wk	6%	9%
<34 wk	20%	23%
Delivery		
<28 wk	8%	13%
>32 wk	79%	63%
Survival to discharge	84% (86% <sup>‡</sup> )	78%

GA, gestational age; IUFD, intrauterine fetal demise; PPRM, preterm premature rupture of the membranes.

\*Number of fetuses; 80 coagulations.

<sup>†</sup>Including triplets.

<sup>‡</sup>13% IUFD and 4% termination.

should be avoided. PPRM is the most common complication and is responsible for all perinatal deaths. Ninety-three percent of survivors were neurodevelopmentally normal at 1 year or older. Those with neurodevelopmental abnormalities generally delivered prematurely often after PPRM. There was a clear effect of experience, with a dramatic decrease in PPRM and intact survival in the first versus subsequent 40 procedures. Therefore, we recommend that the procedures are performed by an experienced operator and whenever possible late in gestation so as to minimize the consequences of PPRM. However, this may not be an option because of legal and/or ethical constraints (Table 25-4).

### Twin-Reversed-Arterial-Perfusion or Acardiac Twinning

The TRAP sequence is a very rare occurrence, affecting 1% of monozygotic twin pregnancies, or 1 in 35,000 pregnancies. The pathophysiology is based on a vascular communication on the surface of the placenta between the cord insertion of a normal fetus, known as the “pump twin” and the cord insertion of an acardiac twin. The acardiac twin can develop to a varying degree with skeletal development of the lower extremities, and pelvis and abdomen. In some cases, there is development of a cranium. As the name suggests, a pumping heart in this twin is exceedingly rare. The mass can be large because of cystic hygromas or lymphatic distension of the integument. The perfusion of this mass/fetus is in a reversed fashion, driven by the heart of the normal pump twin. The blood flow is toward the acardiac in the artery or arteries (acardiac fetuses often have single umbilical arteries) and returns through the vein. This was documented initially with Doppler ultrasound by Benson et al.<sup>32</sup> The acardiac twin is obviously nonviable; however, the normal pump twin can be adversely affected by the increased cardiac output required to perfuse the additional tissue. In addition, the blood returning to the pump twin will be “twice used,” which may have an adverse effect. The natural history of this sequence includes

development of polyhydramnios in the sac of the pump twin related to increased cardiac output and renal perfusion and urine output. This predisposes to preterm labor and delivery. In addition, if the condition is progressive, the high output state can lead to hydrops and death. The perinatal mortality in one large series was 55%.<sup>33</sup> In some cases, fetal demise can precede hydrops possibly related to a predisposition to arrhythmia or embolism, related to the sluggish circulation through the acardiac twin. Moore et al<sup>33</sup> correlated the relative size of the acardiac twin with adverse outcome. If the acardiac twin was 70% or more of the calculated weight of the normal twin, the rate of preterm delivery was 90%; polyhydramnios, 40%; and congestive heart failure, 30%. This compares with rates of 75%, 30%, and 10%, respectively, if the weight ratio was less than 70%. Dashe et al<sup>34</sup> correlated diastolic flow in the cord to the acardiac twin to flow toward the placenta and found that a larger discrepancy in resistive index was associated with a better outcome in their six cases.

As the morbidity and mortality for the pump twin appear directly related to the degree of perfusion of the acardiac twin, it seems evident that any decrease or interruption of blood flow to this tissue will have a beneficial therapeutic effect. A variety of techniques have been used to achieve this with varying success. These techniques include fetoscopic laser ablation of the vessels in the cord to the acardiac twin,<sup>35</sup> fetoscopic cord ligation,<sup>36</sup> intravascular alcohol injection to sclerose the vessel,<sup>37</sup> hysterotomy to remove the acardiac twin,<sup>38</sup> bipolar cord coagulation,<sup>39</sup> and RFA.<sup>19</sup> The therapies most commonly used currently are laser, bipolar coagulation, and RFA. A recent series of the former two techniques<sup>40</sup> in 60 patients resulted in an 80% survival rate, with two thirds of the patients delivering after 36 weeks. The procedures were performed at a median gestational age of 18 weeks. The most recent experience with RFA<sup>41</sup> recorded a survival of 92%, with a mean delivery gestational age of 35.6 weeks. The results in monoamniotic gestations were not comparable, with only one of four surviving. It is possible that this is related to the length of cord from the placenta to the acardiac twin in monoamniotic gestations complicated by TRAP. In the three cases of nonsurvivors, the umbilical cord was short compared with the one that had a longer cord, which is more similar to that seen in diamniotic gestations. This may predispose the pump twin either to clot propagation in a retrograde fashion into its circulation, or secondary hemorrhage into the acardiac twin.

### Congenital Diaphragmatic Hernia

The natural history of babies with isolated congenital diaphragmatic hernia (CDH) is determined by the degree of lung development at delivery. CDH babies have smaller and less compliant lungs with fewer airway branches and abnormal pulmonary vessels than normal neonates. Hypoplasia is lethal in 30% to 40% of prenatally diagnosed and live-born cases.<sup>42–44</sup> Initially, a variety of indirect measures were used to assess the prognosis of fetuses with left CDH. More recently, with left-sided lesions, in addition to herniation of liver into the thorax, the area of the remaining right lung and its relationship to the head circumference, the lung-to-head ratio (LHR) has been assessed to determine prognosis in these patients (Fig. 25-3). The presence of herniation of part

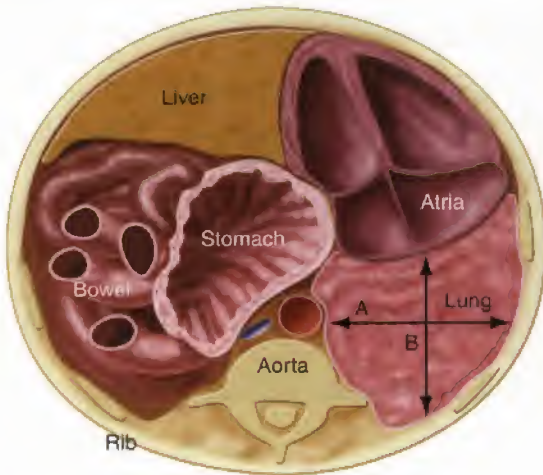
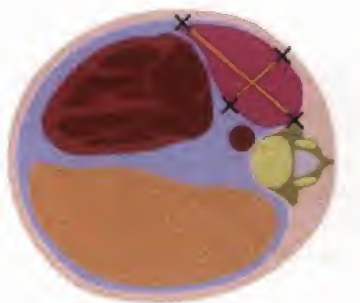
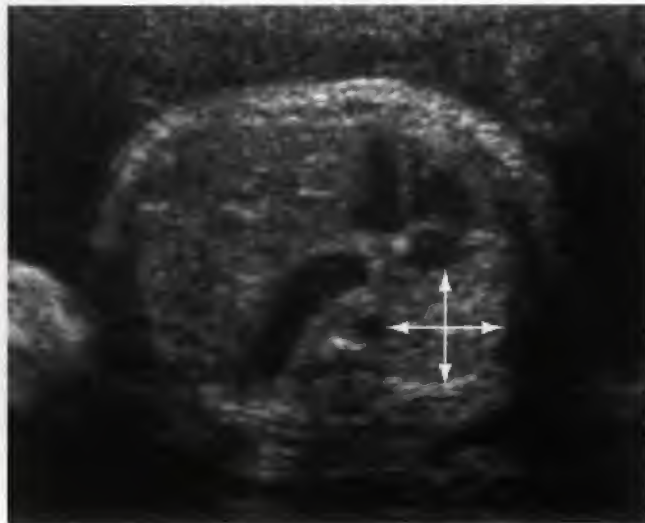


**FIGURE 25-3.** Two somewhat different measuring techniques for assessing the lung-to-head ratio (LHR) have been used. **A.** Illustration of the method for measuring the LHR in a fetus with congenital diaphragmatic hernia. The measurement of the right lung (in the typical left congenital diaphragmatic hernia) uses a transverse axial plane of section of the fetal thorax at the level of the four-chamber view of the fetal heart. The plane of section should be symmetric so that a single rib is seen on each side. A measurement in millimeters is made from the thoracic aorta to the lateral inner chest wall (A). Another measurement, also in millimeters, is made in a plane perpendicular to the first measurement from the outer wall of the atrium to the inner aspect of the posterior chest wall (B). These two measurements are multiplied by one another and divided by the measurement of the head circumference also in mm. Method of Roy A. Filly, MD, San Francisco. (Illustration by James A. Cooper, MD, San Diego, CA.) **B.** Measurement of the LHR: A transverse section of the chest is taken at the level of the four-chamber view. The contralateral lung is measured: The longest axis is measured and multiplied by the longest measurement perpendicular to it. This is shown on a drawing (top left) and ultrasound image (right). This is placed over the head circumference, which is measured at the standard biparietal view, typically showing two equal hemispheres, the septum cavum pellucidum, one third of the way from the front to the back, and the posterior horns of the lateral ventricles (schematic drawing at bottom left). (From Deprest J, Jania J, Van Schoubroeck D, et al: Current consequences of prenatal diagnosis of congenital diaphragmatic hernia. *J Pediatr Surg* 41:423, 2006.)

$$\text{LHR} = \frac{A \times B \text{ (mm)}}{\text{HC (mm)}}$$



**A** Head circumference



**B**





**Table 25-5** Neonatal Outcome as a Function of Preoperative LHR in Fetuses with L-CDH and Liver Herniation

Clinical Category	LHR	N	Expectant Management	LHR	N	FETO
Extreme hypoplasia	0.4–0.5	2	0 (0%)	0.4–0.5	6	1 (16.7%)
Severe hypoplasia	0.6–0.7	6	0 (0%)	0.6–0.7	13	8 (61.5%)
	0.8–0.9	19	3 (15.8%)	0.8–0.9	9	7 (77.8%)
	<i>LHR &lt; 1.0</i>	27	3 (11.1%)	<i>LHR &lt; 1.0</i>	28	16 (57.1%)
Intermediate hypoplasia	1.0–1.1	23	14 (60.9%)	1.0–1.1		na
	1.2–1.3	19	13 (68.4%)	1.2–1.3		na
Mild hypoplasia	1.4–1.5	11	8 (72.7%)	1.4–1.5		na
	≥1.6	6	5 (83.3%)	≥1.6		na
	<i>total</i>	86	43 (50%)			

FETO, fetal endoscopic tracheal occlusion; LHR, lung-to-head ratio; N, number, n.a., not applicable.

From Jani J, Keller RL, Benachi A, et al: Prenatal prediction of survival in isolated left-sided diaphragmatic hernia. *Ultrasound Obstet Gynecol* 27:18, 2006.

of the liver into the thorax and a low LHR during midgestation are validated indicators of poor outcome<sup>45,46</sup> (Table 25-5). In a multicenter study of 86 fetuses with left-sided CDH and liver herniation, that were managed expectantly and live born after 30 weeks of gestation, survival increased from 0% for those with an LHR of 0.4 to 0.7 to about 15% for an LHR of 0.8 to 0.9, 65% for an LHR of 1.0 to 1.5, and 83% for an LHR higher than 1.5. In other words, in the subgroup with an LHR of less than 1.0 and liver herniation, approximately 90% will succumb to the consequences of severe pulmonary hypoplasia. Because this problem cannot be solved by any currently available postnatal therapy, it makes sense to consider interventions in these pregnancies that stimulate lung growth prenatally.<sup>47</sup> Initially, surgeons emulated postnatal interventions for CDH, that is, *anatomic* repair of the diaphragm. The procedure was shown to be feasible, except when the liver was herniated. Acute reduction of the liver into the abdomen causes kinking of the ductus venosus, thereby blocking venous blood from the umbilical vein. Therefore, fetuses with the liver up, that is, those that are the target group, cannot benefit from in utero anatomic repair.

As an alternative, the use of fetal tracheal occlusion (TO) was explored. The concept for this treatment came after recognition of the pathophysiology of fetuses with congenital high airway obstruction, in which lung overgrowth was virtually always present. TO prevents egress of lung liquid, leading to increased pulmonary stretch and accelerated growth of airways and pulmonary vessels. The timing and duration of the occlusion are crucial for the quality and response of airways and pulmonary vessels and the subject of intense debate.<sup>48</sup> Sustained TO leads to a decreased number of type II alveolar cells, the surfactant producing cell in the lung. In sheep, TO in the late *canalicular* phase of lung development with prenatal *reversal* (plug-unplug sequence or *temporary* TO) is associated with in utero recovery of the type II alveolar cell population.<sup>49</sup> Clinically, occlusion by tracheal clipping was first performed through hysterotomy and later through laparotomy and multiple uterine ports.<sup>50</sup> However, fetoscopic tracheal dissection caused frequent local complications.<sup>51,52</sup> In the early surgical treatment of fetuses with CDH in which tracheal occlusion by ligature or clipping was used, fetuses were delivered with maintenance of the placental-umbilical circulation while



**FIGURE 25-4.** Photograph of a neonate status post reversal of tracheal occlusion procedure during intubation, while the placental umbilical circulation is still maintained.

the tracheal occlusion was reversed, the so-called *ex utero* intrapartum treatment (EXIT) procedure (Fig. 25-4).

Today it seems that TO can be best achieved by (1) percutaneous (rather than via laparotomy) access and (2) by tracheoscopic balloon occlusion (rather than external clipping)<sup>53</sup> (Fig. 25-5). This makes fetal surgery more acceptable to the mother and avoids the risks of neck dissection in the fetus. Occlusion with an expandable balloon accommodates the needs of tracheal growth. It also makes the occlusion more easily reversible, which presently is done at the transition of the saccular to alveolar phase of lung development. In utero restoration of the airways makes vaginal delivery possible in the referring tertiary center, rather than forcing patients to stay at a fetal surgery center far from home in addition to the benefit for lung development.<sup>54</sup>

The fetal endoscopic tracheal occlusion (FETO) task group (Leuven, London and Barcelona) has gathered considerable experience with the following protocol. Singleton pregnancies complicated by CDH in an otherwise anatomically and chromosomally normal fetus are eligible

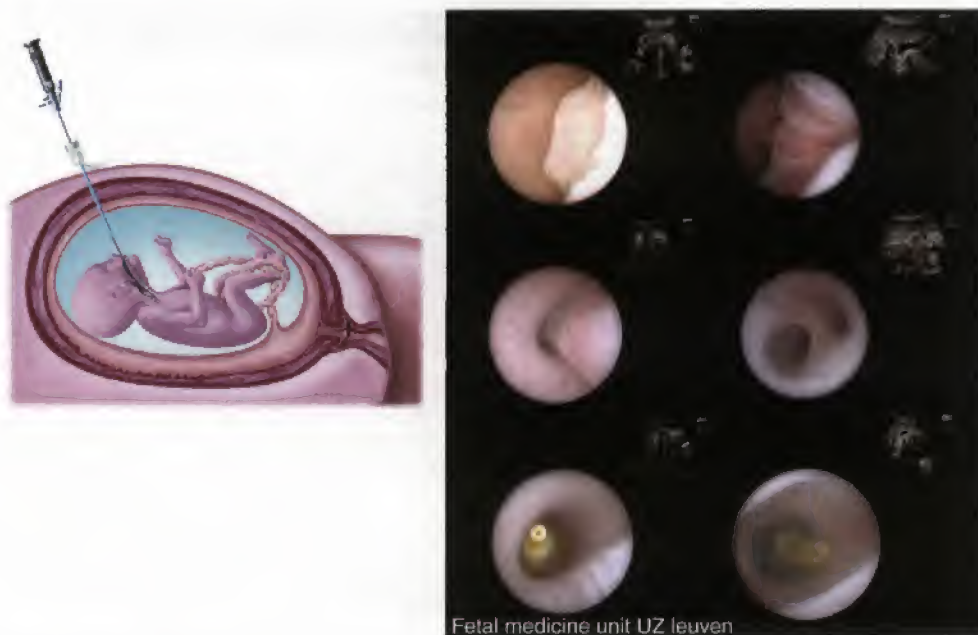


**FIGURE 25-5.** Schematic drawing of percutaneous FETO and fetoscopic images of landmarks during percutaneous FETO. (Reprinted with permission from ISUOG, John Wiley & Sons, Ltd and the authors.) From top left to right bottom: epiglottis, vocal cords, trachea, carina, inflated and detached balloon, vocal cords about to close over the balloon. Not all images are from the same patient. (Reprinted with permission from Nelson S, Cameron A, Deprest J: Fetoscopic surgery for in utero management of congenital diaphragmatic hernia. *Fetal Matern Med Rev* 17:69, 2006.)

for fetal therapy if there is intrathoracic herniation of the liver and the LHR is less than 1.0. Although these criteria are actually only truly validated for left-sided cases, the same ones are used for right-sided CDH. FETO is performed at 26 to 28 weeks, and whenever possible, removal of the balloon is performed at 34 weeks. Essentially, a 1.2-mm endoscope within a 3.0-mm sheath (Karl Storz, Tuttlingen, Germany) is introduced into the trachea to position, and later, retrieve a detachable balloon between the carina and vocal cords. FETO as well as fetoscopic removal are typically performed after prophylactic tocolytics, epidural maternal anesthesia, and fetal analgesia and paralysis have been administered. Patients are routinely admitted for 2 postoperative days. Ultrasound examination is performed every 1 to 2 weeks to confirm the endotracheal presence of the inflated balloon and to monitor lung growth (Fig. 25-6). Whenever preterm delivery is anticipated, active tocolysis is attempted unless contraindicated and a course of corticosteroids is administered when time allows.

In a report on 35 cases occluded at 26 to 28 weeks, mean operation time was 22 minutes. The survival rate was 55%, compared with 8% in contemporary controls treated by postnatal therapy. Pulmonary morbidity is lower than expected for severe cases, and survivors are not neurologically impaired at the age of 1 year. The limiting factor of the procedure is PPROM before 32 weeks, which still occurs in 35% of cases and leads to preterm delivery in 30% (<37 weeks). This compares favorably with the randomized trial from UCSF, in which the procedure was done through laparotomy and 5-mm transuterine ports (Table 25-6).

The growing experience yields some important trends. First, the rate as well as the consequences of iatrogenic

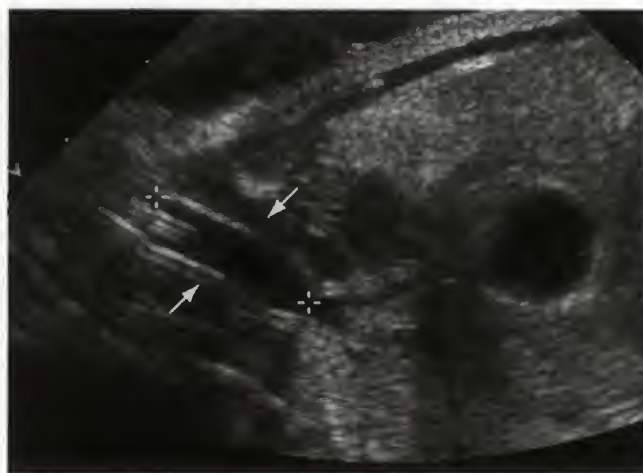


**FIGURE 25-6.** Sonogram of a fetus after placement of a tracheal occluding balloon. The balloon is seen between the calipers and arrows, distending and occluding the trachea.

PPROM have been improving. The incidence decreases with increasing experience.<sup>55</sup> The rate of delivery at less than 32 weeks is now 11% in our entire experience. For instance, in our last 20 cases, the mean gestation at delivery following FETO with in utero reversal at 34 weeks is now 37 weeks compared to 34 weeks initially. Survival rates are greater than 50% in a homogenous group of 43 consecutive left-sided CDH cases.<sup>48</sup> Prenatal balloon removal improves survival (33% without versus 66% with prenatal removal).<sup>54</sup>



**Table 25-6** Comparison of Recent Series of Fetoscopic Tracheal Occlusion

Criteria (left sided)	RCT Harrison <sup>52</sup>		Deprest <sup>53</sup>
	Liver up and LHR<1.4		Liver up and LHR<1.0
	Standard neonatal care – n=13 3 (23%)	Fetoscopic clip (n=2) or balloon (n=9) 11 (100%)	FETO n=20
PPROM		Not specified	7 (35%) <32 wk
<32 wk		11 (100%) < 34 wk	10 (50%) <34 wk
Gestational age at delivery (range; wk)	37.0±1.5 (34.0–39.0)	30.8±2.0 (28.0–34.0)	33.2 (27.0–38.5)
Birthweight (kg)	3.03±0.48	1.49±0.36	2.12±0.66
Survival n (%)	8/11 (73%) at 90 d	10/13 (77%) at 90 d	10/20 (50%) at discharge

FETO, fetal endoscopic tracheal occlusion; LHR, lung-to-head ratio; PPRM, preterm premature rupture of the membranes; RCT, randomized controlled trial. Data from Harrison MR, Sydorak RM, Farrell JA, et al: Fetoscopic temporary tracheal occlusion for congenital diaphragmatic hernia: prelude to a randomized, controlled trial. *J Pediatr Surg* 38:1012, 2003; and Deprest J, Gratacos E, Nicolaides KH: Fetoscopic tracheal occlusion (FETO) for severe congenital diaphragmatic hernia: evolution of a technique and preliminary results. *Ultrasound Obstet Gynecol* 24:121, 2004.

Survival after FETO is highly dependent on the LHR measured at the end of second trimester (see Table 25-5 and Fig. 25-3). It increased from 17% for an LHR of 0.4 to 0.5 to 62% for an LHR of 0.6 to 0.7 and 78% for an LHR of 0.8 to 0.9. This has prompted the proposal to classify cases and stratify prenatal therapy for cases with isolated (left-sided) CDH and liver up, based on LHR in this fashion:

1. Fetuses with an LHR that is greater or equal to 0.6 and less than 1.0 are considered to have *severe hypoplasia*. They have a predicted survival rate of greater than 60% following and less than 15% without FETO, respectively. A randomized study of FETO at 26 to 28 weeks with in utero reversal at greater than 34 weeks versus standard postnatal care is proposed.
2. Fetuses with an LHR of less than 0.6 have extreme hypoplasia because their predicted survival rate is 0% and this can increased to only 17% with FETO at 26 to 28 weeks. An alternative approach to consider is very early (<24 weeks) occlusion.
3. Fetuses with intermediate lung hypoplasia (an LHR greater or equal to 1.0 and less than 1.3) thus far have not been considered to be candidates for fetal surgery. However, in Europe, they have an anticipated survival of about 60%. This is considerably lower than the greater than 90% survival rate observed in fetuses with an LHR less than or equal to 0.8 and less than 1.0 treated by FETO. These fetuses have a larger lung surface area and, as a consequence, a larger lung liquid production. Therefore, a good response to TO can be anticipated. They might be the patients who would benefit from the greater growth rate later in pregnancy, and thus, FETO could be carried out later (e.g., in the sacular phase), reducing the consequences of iatrogenic PPRM, when that might occur.<sup>48</sup> Again, in this group, a randomized study comparing late TO versus expectant management is proposed.

### Congenital Cystic Adenomatoid Malformation

CCAM is a lung hamartoma that consists of abnormal proliferation of terminal bronchioles. Pathologically, these

are classified based on the postnatal experience into types I through III. Type I are unilocular large cysts of varying size, type II are a mixture of macrocystic and microcystic lesions, and type III are microcystic lesions. The vast majority of CCAMs are clinically benign prenatally and postnatally, although they are generally resected at some point owing to the risk of infection and a very low risk of malignant transformation. Management consists of appropriate counseling and ensuring that the relevant specialists are involved in the postnatal evaluation and treatment.

In contrast, some CCAMs, generally type III, are large enough and cause a degree of mediastinal shift, leading to hydrops secondary to cardiac compression and compromise to venous return, or secondary to raised intrathoracic pressure and lymphatic obstruction. In cases of fetal hydrops, typically presenting as fetal ascites, pleuropericardial effusions and subcutaneous edema, intervention is needed to prevent in utero fetal demise. If the hydrops is severe enough, the mother may also be at risk, from “mirror” or Ballantyne syndrome, particularly in the presence of placentomegaly. This manifests itself as a severe preeclampsia-like situation. In an attempt to be able to predict which patients with CCAM are at risk of developing hydrops, the use of the proportion of the mass of the lesion divided by the head circumference (CCAM Volume Ratio [CVR]) has been proposed.<sup>56</sup> When the CVR is higher than 1.6, there is a 80% risk for fetal hydrops. Hydropic fetuses greater than 32 weeks’ gestational age should be delivered. When hydrops is found earlier than 32 weeks in utero, intervention can be life saving. In type III CCAMs with hydrops, administration of a course of betamethasone, identical to that used for acceleration of lung maturity, has been associated with resolution of the hydrops and survival.<sup>57</sup> Short case series have also described different surgical interventions. In some cases, percutaneous puncture and thoracoamniotic shunting of type I macrocystic masses may be successful.<sup>58</sup> Others have proposed to use this approach more liberally. Laser and RFA coagulation of the masses have been attempted, but these methods can cause thermal damage to surrounding structures. They can also worsen fetal hydrops, leading to in utero death.

The most successful radical intervention is excision of the diseased lobes (Fig. 25-7). Fetal lobectomy is done using



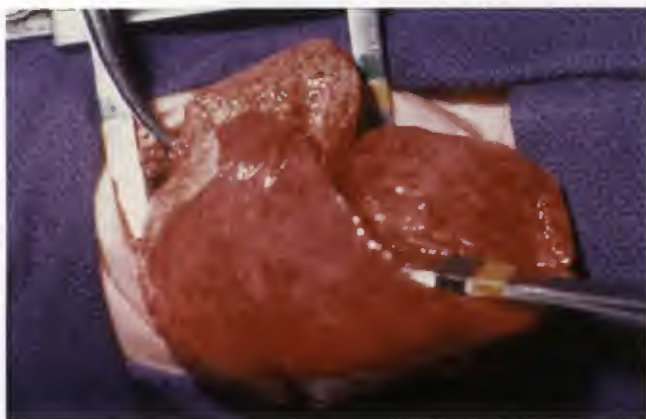


**FIGURE 25-7.** Photograph of in utero resection of congenital cystic adenomatoid malformation (CCAM) of the lung. The instrument on the right is on top of the affected part of the lung.

open fetal surgery with quite high survival rates in cases in which hydrops resolves postsurgically. In a series of 22 cases operated on between 21 and 31 weeks, there were 11 long-term survivors who were developmentally normal (up to 12 years of age).<sup>59</sup>

Hydrops resolved in 1 to 2 weeks, followed by reversal of mediastinal shift. Causes of fetal death despite fetal surgery were termination of pregnancy for “mirror” syndrome ( $n=1$ ), preterm labor or chorioamnionitis ( $n=2$ ), and fetal hemodynamic compromise leading to intraoperative death in six fetuses and postoperative death in another two cases. To reduce the risk of intraoperative deaths due to hypovolemia and hypotension, means of resuscitation, including direct access to the fetal circulation and appropriate fetal monitoring techniques, are now part of these open procedures.

### Sacroccocygeal Teratoma

Sacroccocygeal teratomas (SCTs) are exophytic cystic and solid tumors arising from the area of the coccyx. The cases of SCT that are relevant to the discussion of fetal surgery are giant, solid and highly vascularized. The amount of blood flow through SCTs can lead to high-output cardiac overload, hydrops, and death. Attempts have been made to either perform a definitive resection or simply devascularize the tumor in hopes of allowing cardiac recovery.<sup>60</sup> In the largest reported series from Children’s Hospital of Philadelphia (CHOP), even in the most experienced hands, the outcomes are poor. In the small group that advanced to fetal resection, the survival was encouraging (3/4), however the morbidity was significant (Fig. 25-8). These included one maternal and one fetal transfusion, and a fetal cardiac arrest with successful resuscitation. In addition, these fetuses delivered very preterm (mean 29 weeks) and remained in the hospital for up to 34 weeks’ gestation. Postnatally, there was one neonatal death, one embolic event leading to loss of one kidney and bowel injury, and one case of chronic lung disease. The long-term maternal sequelae of a hysterotomy have been discussed previously. Clearly, attempts at a less invasive approach to tackling this problem are important,



**FIGURE 25-8.** Photograph of in utero surgery before resection of a large sacroccocygeal teratoma.

although overall, the cases that truly need fetal rather than neonatal intervention are exceedingly rare.

### Myelomeningocele

The premise of fetal surgery for spina bifida is the “two-hit” hypothesis (correcting abnormalities of the brain and spine). The suggestion is that although the lack of closure of the neural tube leads to neurologic deficit, this is worsened by the ongoing injury to the placode from exposure to the amniotic fluid and trauma from impact with the uterine wall.<sup>61</sup> Additional work with animal models suggested that the cerebellar herniation associated with Arnold-Chiari II malformation was caused secondarily by the open neural tube, and might be reversible.<sup>61</sup> Preliminary experience at Vanderbilt and CHOP did show that intrauterine microsurgical closure of myelomeningocele improves outcome.<sup>4,62</sup> Both studies showed a decreased shunting rate for hydrocephalus, in part due to reversal of cerebellar herniation, which is a component of the Arnold-Chiari II malformation. Shunt status affects cognitive functioning in later life and therefore is a surrogate marker for long-term sequelae. Another important co-determinant of long-term outcome is the upper level of the lesion.<sup>63</sup> The higher the vertebral level, the higher the likelihood of needing a shunt. The gestational age at repair is also important: The shunt rate drops significantly from 71% to 39% when fetal surgery is done before 25 weeks. These findings were taken into account when designing the Management of Myelomeningocele Study (MOMS). This is a multicenter National Institute of Health (NIH)-funded randomized trial comparing maternal-fetal surgery to routine postnatal management of spina bifida ([www.spinabifidamoms.com](http://www.spinabifidamoms.com)). Inclusion criteria for this trial are a gestational age of less than 26 weeks at the time of randomization, a normal karyotype, no additional fetal malformations, and the willingness to relocate to one of the study sites (e.g., UCSF, Vanderbilt, or CHOP) until after delivery, if randomized to prenatal surgery, or to return there for delivery if randomized to postnatal management.



The myelomeningocele repair is done with techniques similar to those used postnatally (Fig. 25–9). In the United States, no fetal surgery for spina bifida is available outside the trial. From an obstetric viewpoint, Table 25–7 summarizes some important outcome variables from published experience. Open fetal surgery today has a definite but acceptable maternal risk. Pulmonary edema has been an issue, but may be reduced by refining tocolytic regimens. Transfusions are rare (2.2% in the Vanderbilt experience), and bowel obstruction happened in a single case. Preterm labor leading to preterm delivery at less than 30 weeks occurs in about 10% to 15%. Oligohydramnios is not uncommon but usually is without significant clinical consequences. An occasional case of lethal lung hypoplasia has been observed, however. This raises the critical issue of fetal risk, that is, an inherent iatrogenic risk of perinatal death (at the time of surgery or preterm delivery), which in these studies, was 3% to 6%. This is a risk the fetus would not be exposed to with routine management for a problem that is not life-threatening in utero. With fetal surgery for spina bifida, this is the first time that such radical surgery has been used to decrease long-term morbidity rather than prenatal/neonatal mortality. This alters the risk-benefit equation significantly.

### Lower Urinary Tract Obstruction

The sequelae of lower urinary tract obstruction (LUTO) have been documented in several animal models.<sup>64–66</sup> This closely mirrors the natural history as it is observed in the human fetus, with obstruction due to posterior urethral valves or less commonly urethral atresia. Complete obstruction leads to progressively severe oligohydramnios and then anhydramnios. Depending on the gestational age that this occurs, pulmonary hypoplasia results. In addition, the reflux and elevated back pressure on the renal parenchyma leads to cystic dysplasia and renal failure. In these studies, this led to shunting of the obstructed distended bladders, allowing

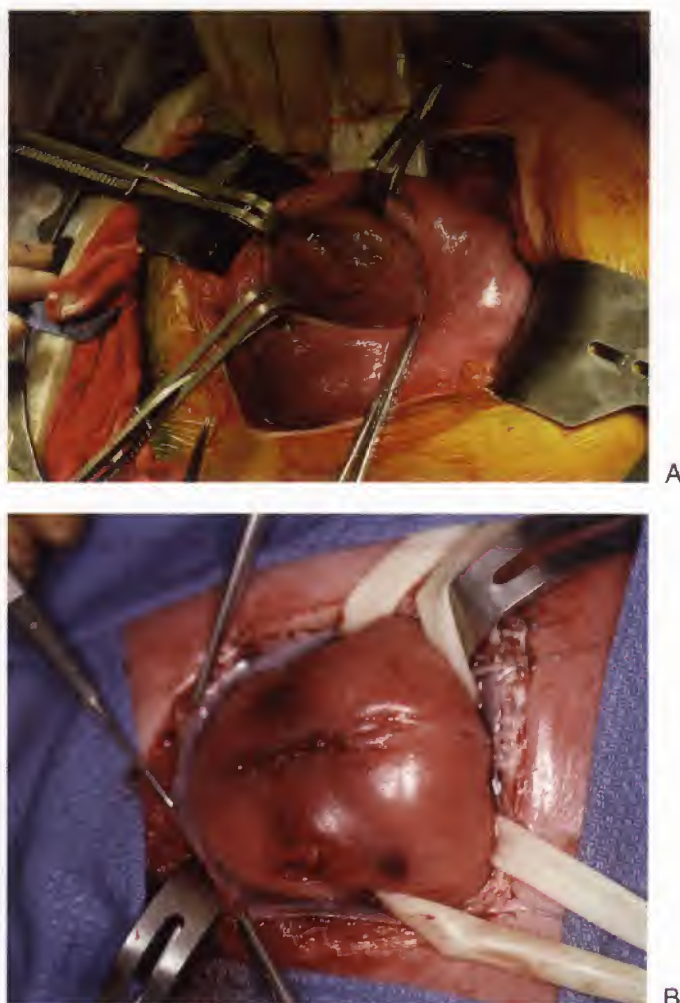


**FIGURE 25-9.** Photograph of a lumbar myelomeningocele before (A) and after (B) in utero repair.

**Table 25–7** Obstetric and Short-Term Outcomes in the CHOP and VUMC Series on MMC Repair

	CHOP (Johnson <sup>4</sup> ; n=51)	VUMC (Bruner <sup>63</sup> ; n=178)
Gestation at surgery (wks)	23+0 (20+0-25+4)	(19-30); later <26 wks
Gestation at delivery (wks)	34+4 (25+4-37)*	33+5 (25-38)
Chiari malformation		
Before (moderate/severe)	14%/86%	
After	100%/0%	7%/0%
Postnatal shunt (postnatal age)	46% (21 wks)	46% (12 wks)
Perinatal losses	3/51 (prematurity)	5/178 (2.8%) (not specified)
Length of hospital stay	4 days	3.3 days (3-7)
Oligohydramnios		25% early on
		30% readmission rate
Delivery <30 wks	5/47 (10.6%) <sup>†</sup>	11.8%
Delivery >32 wks	(40/47) 85% <sup>†</sup>	(not specified)
Maternal complications	None reported, including dehiscence or rupture; one amniotic fluid leak through hysterotomy	9(5.1%) mild pulmonary edema
		1 bowel obstruction
		4(2.2%) dehiscence, asymptomatic in three

CHOP, Children's Hospital of Pennsylvania; MMC, myelomeningocele; VUMC, Vanderbilt University Medical Center.

\*Includes all patients.

<sup>†</sup>Denominator is survivors only.

Data from Johnson MP, Sutton LN, Rintoul N, et al: Fetal myelomeningocele repair: short-term clinical outcomes. *Am J Obstet Gynecol* 189:482, 2003; and Bruner JP, Tulipan N: Intrauterine repair of spina bifida. *Clin Obstet Gynecol* 48:942, 2005.



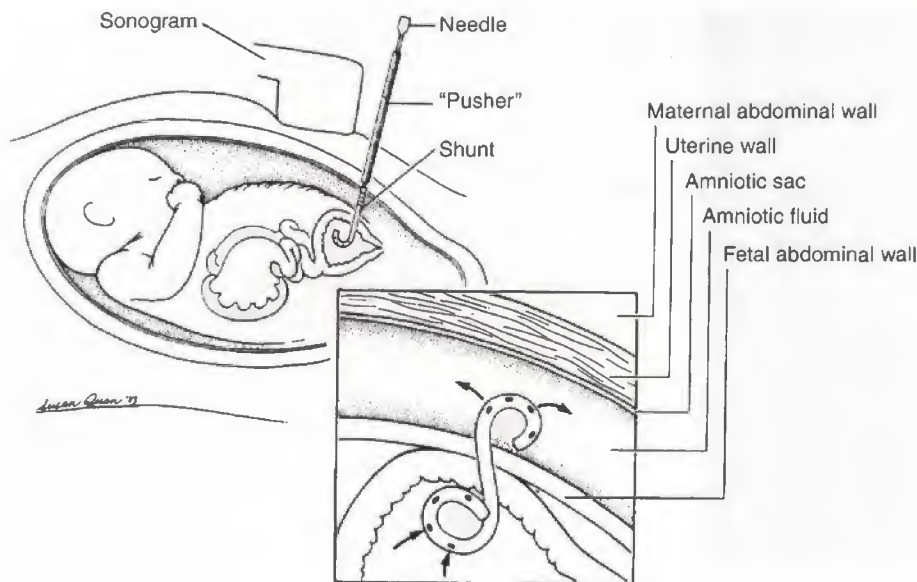


**FIGURE 25-10.** Placement of a fetal bladder shunt depicted schematically. The double pigtail catheter is pushed off the needle so that one end is in the bladder and the other end is in the amniotic space. (From Adzick NS, Flake AW, Harrison MR: *Recent advances in prenatal diagnosis and treatment*. *Pediatr Clin North Am* 32:1103, 1985.)

**Table 25-8 Fetal Urine Prognostic Thresholds\***

	Good Prognosis	Poor Prognosis
Sodium	<90 mmol/L	>100 mmol/L
Chloride	<90 mmol/L	>100 mmol/L
Osmolality	<180 mOsm/L	>200 mOsm/L
Total protein	<20 mg/dL	>40 mg/dL
Beta-2 microglobulin	<6 mg/L	>10 mg/L

\*Thresholds are based on urine obtained between 18–24 weeks' estimated gestational age. Values that fall between good and poor prognosis are considered 'gray zone', with expectation for moderate or greater postnatal renal impairment, but potential for postnatal pulmonary survival. (Johnson MP, personal communication.)

reaccumulation of amniotic fluid<sup>67</sup> (Fig. 25-10). As experience increased, it became clear that case selection was critical. In some cases with irreversible renal damage, pulmonary growth could be salvaged, but the terrible morbidity of neonatal renal failure and anticipation of long-term dialysis with later transplantation had to be confronted. This led to attempts to be able to predict fetal and thus neonatal renal function to avoid the above-mentioned scenario. It made sense that the best evaluation of renal function would be to sample fetal urine and analyze urinary electrolytes and other analytes. Evaluation of urinary electrolytes remains the most predictive when two sequential vesicocentesis are performed several days apart, in cases in which there is refilling of the bladder and sonographically normal-appearing renal parenchyma<sup>68</sup> (Table 25-8). Following this management algorithm, a recent series has documented variable success. Although the children that had follow-up at around 5 years of age were neurodevelopmentally normal, many were lagging in growth and had persistent pulmonary issues. In the 18 survivors, six had acceptable renal function, four mild insufficiency and six required dialysis and transplantation.<sup>69</sup> Similar experience

is mirrored by other centers,<sup>70,71</sup> with chronic renal insufficiency in half to two thirds of survivors, despite all having favorable fetal urine profiles as a prerequisite for in utero intervention.

Therefore, the approach to obstructive uropathy may need to be changed to lead to improved outcomes. This is critical because the long-term morbidity of neonatal renal impairment is so high. One newer approach is to perform fetal cystoscopy. The endoscopes available now are the same size as some of the trochars used to place the bladder shunts. Therefore, fetal and maternal postoperative complications should be similar. With cystoscopy, there is a potential to correct the obstructive problem completely and allow normal bladder cycling for the remainder of the pregnancy. The results are not consistent, but in those with success, the outcomes are remarkably promising, suggesting that this is an avenue worth pursuing.<sup>72,73</sup>

## Pleural Effusions

Fetal pleural effusions are rare; however, when they are large and cause a severe mediastinal shift, they can secondarily lead to hydrops and stillbirth. They are almost always lymphatic in origin. There is a significant association with aneuploidy and fetal karyotyping should be considered.<sup>74</sup> When bilateral pleural effusions of similar size are identified, the diagnosis of diffuse congenital pulmonary lymphangiectasia needs to be considered.<sup>75</sup> The significance of this is that even with successful drainage, there is generally neonatal respiratory failure because of abnormal lymphatics affecting gas exchange in the alveoli. This needs to be taken into account when counseling patients about possible interventions. The option of shunt drainage of pleural effusions is considered when progression to hydrops is documented. This is particularly the case when fetal echocardiography documents abnormal ventricular filling.<sup>76</sup> Recent series of cases with shunting document technical success. However, a residual risk of prematurity and neonatal mortality, potentially



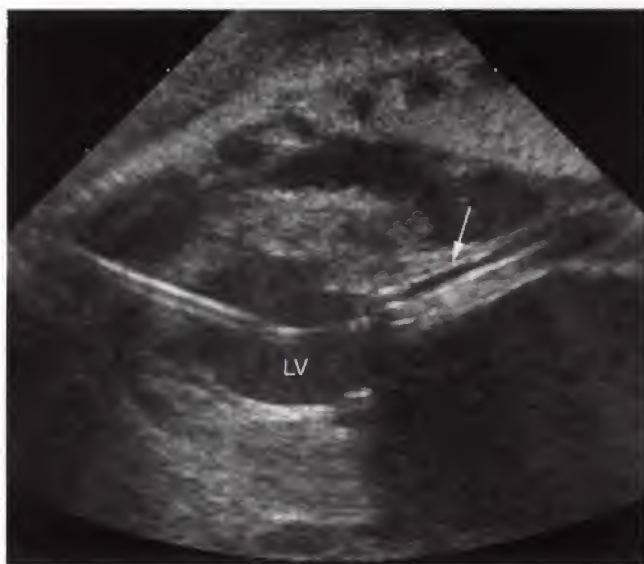


**FIGURE 25-11.** In utero repair of aortic stenosis. After needle puncture of the left ventricle (LV), a balloon catheter (arrow) is advanced into the aorta and the balloon is inflated to dilate the aorta.

related to the underlying pathology rather than the pleural effusion itself, remains.<sup>58,77</sup>

## Fetal Cardiac Interventions

One of the most exciting fields in the field of minimally invasive fetal therapy is the treatment of congenital heart defects (CHDs). Some defects are structurally simple, but because of the dynamic situation during fetal life, a progressively abnormal development of the great vessels and ventricles ensues. This then results in a poorly functioning heart after birth. An example of this is progressive critical aortic stenosis that may progress to hypoplastic left-sided heart syndrome (HLHS). It has been speculated that in utero reversal of the stenosis can reverse progression to ventricular hypoplasia. At present, the standard postnatal treatment for a single-ventricle heart (HLHS) is a staged palliative surgery (Norwood operation, followed by a Fontan procedure). The same principle may apply to critical pulmonary stenosis with intact ventricular septum, which leads to hypoplasia of the right side of the heart.

There is increasing experience with ultrasound-guided fetal heart catheterization and valvular balloon dilatation. In many cases, this can be done by a percutaneous approach (Fig. 25-11). The largest experience by far resides with the group at Boston Children's/Brigham and Women's Hospital.<sup>78</sup> In more than 50% of cases, the valvular dilatation is successful, but in about 20% of these, progression to hypoplasia cannot be reversed. Experience with HLHS with restrictive or intact atrial septum is more limited, as is that with pulmonary atresia or stenosis with intact ventricular septum. However, further research will determine optimal patient selection, timing, and technique for the different types of correctable heart defects. As noted earlier, these procedures can be percutaneous and involve needles that are smaller than fetoscopes or shunt trochars. Therefore, the

maternal and pregnancy risk profile is relatively low. This should allow a lower threshold for innovative intervention and may expand the indications, even if the success rate is variable.

## References

1. Golombek K, Ball RH, Lee H, et al: Maternal morbidity after maternal-fetal surgery. *Am J Obstet Gynecol* 194:834, 2006.
2. Adzick NS, Harrison MR, Glick PL, et al: Fetal surgery in the primate. III. Maternal outcome after fetal surgery. *J Pediatr Surg* 21:477, 1986.
3. Bruner JP, Tulipan N, Reed G, et al: Intrauterine repair of spina bifida: preoperative predictors of shunt-dependent hydrocephalus. *Am J Obstet Gynecol* 190:1305, 2004.
4. Johnson MP, Sutton LN, Rintoul N, et al: Fetal myelomeningocele repair: short-term clinical outcomes. *Am J Obstet Gynecol* 189:482, 2003.
5. DiFederico EM, Burlingame JM, Kilpatrick SJ, et al: Pulmonary edema in obstetric patients is rapidly resolved except in the presence of infection or of nitroglycerin tocolysis after open fetal surgery. *Am J Obstet Gynecol* 179:925, 1998.
6. Bruner JP, Tulipan NB, Richards WO, et al: In utero repair of myelomeningocele: a comparison of endoscopy and hysterotomy. *Fetal Diagn Ther* 15:83, 2000.
7. Wilson RD, Johnson MP, Crombleholme TM, et al: Chorioamniotic membrane separation following open fetal surgery: pregnancy outcome. *Fetal Diagn Ther* 18:314, 2003.
8. Farrell JA, Albanese CT, Jennings RW, et al: Maternal fertility is not affected by fetal surgery. *Fetal Diagn Ther* 4:190, 1999.
9. Wilson RD, Johnson MP, Flake AW, et al: Reproductive outcomes after pregnancy complicated by maternal-fetal surgery. *Am J Obstet Gynecol* 191:1430, 2004.
10. Macones GA, Peipert J, Nelson DB, et al: Maternal complications with vaginal birth after cesarean delivery: a multicenter study. *Am J Obstet Gynecol* 193:1656, 2005.
11. McMahon MJ: Vaginal birth after cesarean. *Clin Obstet Gynecol* 41:369, 1998.
12. van der Wildt B, Luks FI, Steegers EA, et al: Absence of electrical uterine activity after endoscopic access for fetal surgery in the rhesus monkey. *Eur J Obstet Gynecol Reprod Biol* 58:213, 1995.
13. Gratacos E, Deprest J: Current experience with fetoscopy and the Eurofoetus registry for fetoscopic procedures. *Eur J Obstet Gynecol Reprod Biol* 92:151, 2000.
14. Group TE: The Eurofoetus Group. In Deprest J, Ville Y, Barki G, et al (eds): *Endoscopy in Fetal Medicine*. Tuttlingen, Germany, Endopress, 2004, pp 1-58.
15. Deprest J, Barki G, Lewi L, et al: Fetoscopic instrumentation and techniques. In Van Vught J, Schulman L (eds): *Fetal Medicine*. New York, Marcel Dekker, 2006, pp 473-491.
16. Yamamoto M, El Murr L, Robyr R, et al: Incidence and impact of perioperative complications in 175 fetoscopy-guided laser coagulations of chorionic plate anastomoses in fetofetal transfusion syndrome before 26 weeks of gestation. *Am J Obstet Gynecol* 193:1110, 2005.
17. Harrison MR, Golbus MS, Filly RA, et al: Management of the fetus with congenital hydronephrosis. *J Pediatr Surg* 17:728, 1982.
18. Nicolini U, Rodeck CH, Fisk NM: Shunt treatment for fetal obstructive uropathy. *Lancet* 2:1338, 1987.
19. Tsao K, Feldstein VA, Albanese CT, et al: Selective reduction of acardiac twin by radiofrequency ablation. *Am J Obstet Gynecol* 187:635, 2002.
20. Quintero RA, Morales WJ, Allen MH, et al: Staging of twin-twin transfusion syndrome. *J Perinatol* 19:550, 1999.
21. Senat MV, Deprest J, Boulvain M, et al: Endoscopic laser surgery versus serial amnioreduction for severe twin-to-twin transfusion syndrome. *N Engl J Med* 351:136, 2004.
22. Huber A, Diehl W, Bregenzner T, et al: Stage-related outcome in twin-twin transfusion syndrome treated by fetoscopic laser coagulation. *Obstet Gynecol* 108:333, 2006.
23. Robyr R, Boulvain M, Lewi L, et al: Cervical length as a prognostic factor for preterm delivery in twin-to-twin transfusion syndrome treated by fetoscopic laser coagulation of chorionic plate anastomoses. *Ultrasound Obstet Gynecol* 25:37, 2005.
24. Lewi L, Jani J, Cannie M, et al: Intertwin anastomoses in mono-chorionic placentas after fetoscopic laser coagulation for twin-to-twin



- transfusion syndrome: is there more than meets the eye? *Am J Obstet Gynecol* 194:790, 2006.
25. Graef C, Ellenrieder B, Hecher K, et al: Long-term neurodevelopmental outcome of 167 children after intrauterine laser treatment for severe twin-twin transfusion syndrome. *Am J Obstet Gynecol* 194:303, 2006.
  26. Herberg U, Gross W, Bartmann P, et al: Long term cardiac follow up of severe twin to twin transfusion syndrome after intrauterine laser coagulation. *Heart* 92:95, 2006.
  27. Beck M, Graf C, Ellenrieder B, et al: Long-term outcome of kidney function after twin-twin transfusion syndrome treated by intrauterine laser coagulation. *Pediatr Nephrol* 20:1657, 2005.
  28. Lewi L, Blickstein I, Van Schoubroeck D, et al: Diagnosis and management of heterokaryotypic monochorionic twins. *Am J Med Genet A* 140:272, 2006.
  29. Deprest JA, Van Ballaer PP, Evrard VA, et al: Experience with fetoscopic cord ligation. *Eur J Obstet Gynecol Reprod Biol* 81:157, 1998.
  30. Robyr R, Yamamoto M, Ville Y: Selective feticide in complicated monochorionic twin pregnancies using ultrasound-guided bipolar cord coagulation. *Br J Obstet Gynaecol* 112:1344, 2005.
  31. Lewi L, Gratacos E, Oribus E, et al: Pregnancy and infant outcome of 80 consecutive cord coagulations in complicated monochorionic multiple pregnancies. *Am J Obstet Gynecol* 194:782, 2006.
  32. Benson CB, Bieber FR, Genest DR, et al: Doppler demonstration of reversed umbilical blood flow in an acardiac twin. *J Clin Ultrasound* 17:291, 1989.
  33. Moore TR, Gale S, Benirschke K: Perinatal outcome of forty-nine pregnancies complicated by acardiac twinning. *Am J Obstet Gynecol* 163:907, 1990.
  34. Dashe JS, Fernandez CO, Twickler DM: Utility of Doppler velocimetry in predicting outcome in twin reversed-arterial perfusion sequence. *Am J Obstet Gynecol* 185:135, 2001.
  35. Ville Y, Hyett JA, Vandenbussche FP, et al: Endoscopic laser coagulation of umbilical cord vessels in twin reversed arterial perfusion sequence. *Ultrasound Obstet Gynecol* 4:396, 1994.
  36. Quintero R, Munoz H, Hasbun J, et al: [Fetal endoscopic surgery in a case of twin pregnancy complicated by reversed arterial perfusion sequence (TRAP sequence)]. *Rev Chil Obstet Ginecol* 60:112; discussion 116, 1995.
  37. Sepulveda W, Bower S, Hassan J, et al: Ablation of acardiac twin by alcohol injection into the intra-abdominal umbilical artery. *Obstet Gynecol* 86:680, 1995.
  38. Fries MH, Goldberg JD, Golbus MS: Treatment of acardiac-acephalus twin gestations by hysterotomy and selective delivery. *Obstet Gynecol* 79:601, 1992.
  39. Deprest JA, Audibert F, Van Schoubroeck D, et al: Bipolar coagulation of the umbilical cord in complicated monochorionic twin pregnancy. *Am J Obstet Gynecol* 182:340, 2000.
  40. Hecher K, Lewi L, Gratacos E, et al: Twin reversed arterial perfusion: fetoscopic laser coagulation of placental anastomoses or the umbilical cord. *Ultrasound Obstet Gynecol* 28:688, 2006.
  41. Lee H, Wagner AM, Sy E, et al: Efficacy of radiofrequency ablation for twin-reversed arterial perfusion sequence. *Am J Obstet Gynecol* 196:459, 2007.
  42. Stege G, Fenton A, Jaffray B: Nihilism in the 1990s: the true mortality of congenital diaphragmatic hernia. *Pediatrics* 112:532, 2003.
  43. Colvin J, Bower C, Dickinson JE, et al: Outcomes of congenital diaphragmatic hernia: a population-based study in Western Australia. *Pediatrics* 116:e356, 2005.
  44. Gallot D, Coste K, Francannet C, et al: Antenatal detection and impact on outcome of congenital diaphragmatic hernia: a 12-year experience in Auvergne, France. *Eur J Obstet Gynecol Reprod Biol* 125:202, 2006.
  45. Metkus AP, Filly RA, Stringer MD, et al: Sonographic predictors of survival in fetal diaphragmatic hernia. *J Pediatr Surg* 31:148; discussion 151, 1996.
  46. Jani J, Keller RL, Benachi A, et al: Prenatal prediction of survival in isolated left-sided diaphragmatic hernia. *Ultrasound Obstet Gynecol* 27:18, 2006.
  47. Deprest J, Jani J, Clannie M, et al: Prenatal intervention for isolated congenital diaphragmatic hernia. *Curr Opin Obstet Gynecol* 18:355, 2006.
  48. Deprest J, Jani J, Gratacos E, et al: Deliberately delayed and shortened fetoscopic tracheal occlusion- A different strategy after prenatal diagnosis of life-threatening congenital diaphragmatic hernias. *J Pediatr Surg* 41:1345, 2006.
  49. Flageole H, Evrard VA, Piedboeuf B, et al: The plug-unplug sequence: an important step to achieve type II pneumocyte maturation in the fetal lamb model. *J Pediatr Surg* 33:299, 1998.
  50. Flake AW, Crombleholme TM, Johnson MP, et al: Treatment of severe congenital diaphragmatic hernia by fetal tracheal occlusion: clinical experience with fifteen cases. *Am J Obstet Gynecol* 183:1059, 2000.
  51. Harrison MR, Mychaliska GB, Albanese CT, et al: Correction of congenital diaphragmatic hernia in utero IX: fetuses with poor prognosis (liver herniation and low lung-to-head ratio) can be saved by fetoscopic temporary tracheal occlusion. *J Pediatr Surg* 33:1017; discussion 1022, 1998.
  52. Harrison MR, Sydorak RM, Farrell JA, et al: Fetoscopic temporary tracheal occlusion for congenital diaphragmatic hernia: prelude to a randomized, controlled trial. *J Pediatr Surg* 38:1012, 2003.
  53. Deprest J, Gratacos E, Nicolaides KH: Fetoscopic tracheal occlusion (FETO) for severe congenital diaphragmatic hernia: evolution of a technique and preliminary results. *Ultrasound Obstet Gynecol* 24:121, 2004.
  54. Jani J, Gratacos E, Greenough A, et al: Percutaneous fetal endoscopic tracheal occlusion (FETO) for severe left-sided congenital diaphragmatic hernia. *Clin Obstet Gynecol* 48:910, 2005.
  55. Deprest J, Jani J, Gratacos E, et al: Fetal intervention for congenital diaphragmatic hernia: the European experience. *Semin Perinatol* 29:94, 2005.
  56. Crombleholme TM, Coleman B, Hedrick H, et al: Cystic adenomatoid malformation volume ratio predicts outcome in prenatally diagnosed cystic adenomatoid malformation of the lung. *J Pediatr Surg* 37:331, 2002.
  57. Tsao K, Hawgood S, Vu L, et al: Resolution of hydrops fetalis in congenital cystic adenomatoid malformation after prenatal steroid therapy. *J Pediatr Surg* 38:508, 2003.
  58. Wilson RD, Baxter JK, Johnson MP, et al: Thoracoamniotic shunts: fetal treatment of pleural effusions and congenital cystic adenomatoid malformations. *Fetal Diagn Ther* 19:413, 2004.
  59. Adzick NS: Management of fetal lung lesions. *Clin Perinatol* 30:481, 2003.
  60. Hedrick HL, Flake AW, Crombleholme TM, et al: Sacrococcygeal teratoma: prenatal assessment, fetal intervention, and outcome. *J Pediatr Surg* 39:430; discussion 430, 2004.
  61. Meuli M, Meuli-Simmen C, Hutchins GM, et al: In utero surgery rescues neurological function at birth in sheep with spina bifida. *Nat Med* 1:342, 1995.
  62. Bruner JP, Tulipan N, Paschall RL, et al: Fetal surgery for myelomeningocele and the incidence of shunt-dependent hydrocephalus. *JAMA* 282:1819, 1999.
  63. Bruner JP, Tulipan N: Intrauterine repair of spina bifida. *Clin Obstet Gynecol* 48:942, 2005.
  64. Glick PL, Harrison MR, Noall RA, et al: Correction of congenital hydronephrosis in utero III. Early mid-trimester ureteral obstruction produces renal dysplasia. *J Pediatr Surg* 18:681, 1983.
  65. Harrison MR, Ross N, Noall R, et al: Correction of congenital hydronephrosis in utero. I. The model: fetal urethral obstruction produces hydronephrosis and pulmonary hypoplasia in fetal lambs. *J Pediatr Surg* 18:247, 1983.
  66. Nakayama DK, Glick PL, Harrison MR, et al: Experimental pulmonary hypoplasia due to oligohydramnios and its reversal by relieving thoracic compression. *J Pediatr Surg* 18:347, 1983.
  67. Manning FA, Harman CR, Lange IR, et al: Antepartum chronic fetal vesicoamniotic shunts for obstructive uropathy: A report of two cases. *Am J Obstet Gynecol* 145:819, 1983.
  68. Johnson MP, Bukowski TP, Reileman C, et al: In utero surgical treatment of fetal obstructive uropathy: a new comprehensive approach to identify appropriate candidates for vesicoamniotic shunt therapy. *Am J Obstet Gynecol* 170:1770; discussion 1776, 1994.
  69. Biard JM, Johnson MP, Carr MC, et al: Long-term outcomes in children treated by prenatal vesicoamniotic shunting for lower urinary tract obstruction. *Obstet Gynecol* 106:503, 2005.
  70. Holmes N, Harrison MR, Baskin LS: Fetal surgery for posterior urethral valves: long-term postnatal outcomes. *Pediatrics* 108:E7, 2001.
  71. McLorie G, Farhat W, Khoury A, et al: Outcome analysis of vesicoamniotic shunting in a comprehensive population. *J Urol* 166:1036, 2001.
  72. Welsh A, Agarwal S, Kumar S, et al: Fetal cystoscopy in the management of fetal obstructive uropathy: experience in a single European centre. *Prenat Diagn* 23:1033, 2003.



73. Clifton MS, Harrison M, Ball RH, et al: FetURP (fetoscopic trans-uterine release of posterior urethral valves): A new technique. *Fetal Diagn Ther* 2007 (in press).
74. Waller K, Chaithongwongwatthana S, Yamasmit W, et al: Chromosomal abnormalities among 246 fetuses with pleural effusions detected on prenatal ultrasound examination: factors associated with an increased risk of aneuploidy. *Genet Med* 7:417, 2005.
75. Wilson RD, Pawel B, Bebbington M, et al: Congenital pulmonary lymphangiectasis sequence: a rare, heterogeneous, and lethal etiology for prenatal pleural effusion. *Prenat Diagn* 26:1058, 2006.
76. Yonemoto H, Itoh S, Nakamura Y, et al: Hemodynamic evaluation of a prenatal thoracoamniotic shunt for fetal pleural effusion. *Early Hum Dev* 82:411, 2006.
77. Picone O, Benachi A, Mandelbrot L, et al: [Emergency thoraco amniotic shunting in cases with compressive pleural effusion with hydrops: a retrospective study of 60 cases.]. *J Gynecol Obstet Biol Reprod (Paris)* 35:652, 2006.
78. Makikallio K, McElhinney DB, Levine JC, et al: Fetal aortic valve stenosis and the evolution of hypoplastic left heart syndrome: patient selection for fetal intervention. *Circulation* 113:1401, 2006.



# GYNECOLOGIC ULTRASOUND

## Section Contents

Normal Anatomy of the Female Pelvis and Transvaginal Sonography .....	887	Ultrasonographic Imaging in Infertility .....	986
Ultrasound Evaluation of the Uterus .....	919	Ectopic Pregnancy .....	1020
Abnormal Uterine Bleeding: The Role of Ultrasound .....	942	The Role of Magnetic Resonance Imaging in the Evaluation of Gynecologic Disease .....	1048
Gestational Trophoblastic Neoplasia .....	951	Ultrasound of the Breast .....	1077
Ultrasound Evaluation of the Adnexa (Ovary and Fallopian Tubes) .....	968	Artifacts, Pitfalls, and Normal Variants .....	1098





## NORMAL ANATOMY OF THE FEMALE PELVIS AND TRANSVAGINAL SONOGRAPHY

Clifford S. Levi, MD, Edward A. Lyons, MD, Susan C. Holt, MD, and Sidney M. Dashefsky, MD

### Transvaginal Sonography

Indications  
Patient Preparation  
Probe Preparation  
Examination Technique  
Safety

### True and False Pelves

### Pelvic Musculature, Fascial Planes, Ligamentous Attachments

### Vascular Anatomy

### The Uterus and Vagina

### The Ovaries

### The Uterine (Fallopian) Tube

### Vestigial Structures

### The Ureters

### The Urinary Bladder

### The Rectosigmoid Colon

Transrectal Scanning

High-resolution transvaginal sonography (TVS) has been widely available since the mid-1980s and has gained acceptance as an integral part of gynecologic and early obstetric sonographic examinations.<sup>1</sup> In many ultrasound laboratories, the standard examination of the female pelvis is composed of the traditional transvesical/transabdominal approach (TAS) combined with TVS and, in some cases, transvaginal color flow Doppler (TVCFD).<sup>2,3</sup>

TAS is performed through the full urinary bladder and provides a wider field of view than the transvaginal approach. The transvesical approach provides better visualization of superficial structures and structures remote from the vagina than the transvaginal approach. The transvaginal approach bypasses attenuating tissue and allows a high frequency probe to be placed close to the "target organs." TVS demonstrates anatomic detail of the uterus, ovaries, and adnexa, which cannot be duplicated by TAS. The normal sonographic anatomy described in this chapter reflects a combined transvesical and transvaginal approach and is weighted, as in clinical practice, to use the positive attributes of both TVS and TAS.

As with all ultrasound applications, it is standard practice to use the highest possible transducer frequency, which allows visualization of the target organs. Using TAS, visualization of the pelvic organs is limited by body habitus owing to sonic attenuation of the intervening anterior abdominal wall, subcutaneous and properitoneal fat, and fat in the mesentery and omentum. As a result of this attenuation and the distance of the area of interest from the anterior abdominal wall, it is often not possible to use high frequency transducers and benefit from their inherent enhanced axial and lateral resolution. Differences in sonic attenuation among patients results in the need to use different transducers and different transducer frequencies in multifrequency broad-

band probes. It should be noted, however, that even with careful scanning technique in the optimal patient, 5- and 6-MHz transvaginal transducers may not provide resolution adequate for use in early pregnancy. Before applying data from the literature, it is advisable to confirm its reproducibility in one's own laboratory.<sup>4</sup>

## TRANSVAGINAL SONOGRAPHY

### Indications

As noted earlier, TVS provides diagnostic information that cannot be obtained with TAS. TVS should be incorporated into the examination in all situations in which it will provide additional clinically useful diagnostic information. Indications for TVS include

- Gynecologic sonography.
- Early first trimester obstetric sonography.
- Obstetric applications later in pregnancy when enhanced visualization of structures adjacent to the cervix is necessary based on TAS findings, including placenta previa, evaluation of the fetal lumbosacral spine in breech fetuses, evaluation of the fetal intracranial contents in cephalic fetuses, and evaluation of the fetal nuchal region before 14 weeks' gestation.
- Suspected ectopic pregnancy.
- Patients with suspected lower abdominal disease in whom a diagnosis has not been made with TAS (e.g., suspected diverticulitis).
- Follicle monitoring.
- Monitoring for assisted reproductive techniques.

In general, TAS is performed first, and then TVS is performed after the patient empties the urinary bladder. In urgent or



emergent situations when the patient arrives with an empty or incompletely filled urinary bladder, after a quick survey to assess the degree of bladder distention and the presence of obvious, large pelvic masses, a transvaginal examination is performed. In patients with significant free intraperitoneal fluid demonstrated with TVS, the hepatorenal space (Morrison's pouch) and paracolic gutters are examined with TAS for a volumetric estimate of free fluid.<sup>5</sup> Patients who are being assessed on a serial basis for specific targeted examinations such as follicle monitoring are usually examined with TVS only.

The diagnostic information available from TAS and TVS is often complementary. Although TVS provides enhanced resolution, and may visualize the ovaries and adnexal structures when they are obscured on TAS by acoustic shadowing from bowel gas,<sup>6</sup> TAS may visualize high or laterally positioned ovaries or pelvic masses not seen with TVS.<sup>7</sup> TAS may show the size and location of a mass, which can then be better characterized with TVS.

There are clearly situations in which TVS cannot or should not be performed. Contraindications include

- Premenarchal or virginal patients.
- Any patient who does not willingly consent to vaginal examination.

Patients with a narrow introitus or vagina may experience discomfort at the time of attempted probe insertion, which should result in immediate termination of the transvaginal portion of the examination. In general, TVS should be considered in any patient in whom bimanual examination is appropriate. In fact, it is our experience that in the older patient population and in patients with severe vaginal or pelvic pain, TVS is more easily accepted than the bimanual examination.<sup>6</sup>

## Patient Preparation

There is no specific preparation for TVS, except that the patient should void before the examination so that the urinary bladder is empty or almost completely empty. As with any other ultrasound examination, the sonologist or sonographer should obtain pertinent historic information from the patient before the examination. An adequate explanation of the procedure is essential, and consent must be obtained before the examination. In our practice, verbal consent is considered to be adequate.

Many patients are apprehensive at any mention of an "internal" examination, and most patients equate a TVS scan with a bimanual internal examination until the procedure is adequately explained. In the explanation, it is important to note why it is necessary to perform the TVS and to stress that the examination is a simple, usually painless procedure and that only part of the probe is inserted. In our institution, the majority of the transvaginal examinations are performed by sonographers. If a male examiner (sonologist or sonographer) is to perform the examination, a female staff member (an aide, nurse, or other staff member) is brought into the room for the entire transvaginal examination to act as a chaperone.

In any diagnostic examination, it is important to introduce all staff members who are in the examination room to the patient. This is even more critical in TVS. To maintain

patient dignity, the patient is appropriately covered with a sheet and placed in the supine position with the knees bent and the feet flat on the table, approximately shoulder width apart. The head and shoulders are slightly elevated with a pillow and, if possible, the patient is placed in a slightly reversed Trendelenburg position so that free intraperitoneal fluid can gravitate to the posterior cul-de-sac.

When only TVS examinations are performed or when TVS is being used to guide an invasive procedure, it is often desirable to use an examination table with leg supports so that the probe can be moved freely in all directions and the examiner is in a position to insert and remove instrumentation without constraint. When using an examination bed, it is sometimes not possible to angle the probe anteriorly because that handle of the probe is obstructed by the bed. Under those circumstances, one can place a foam wedge or a few folded towels behind the patient's hips. If anterior structures are still out of the field of view, it may be necessary to ask the patient to flex her hips and bring her knees up toward her chest.

## Probe Preparation

Probe preparation before TVS must take into consideration the following potential adverse effects:

1. Spread of infectious disease
2. Chemical irritation of the vagina
3. Latex allergy
4. Deleterious effect of the lubricant on sperm motility

To prevent the spread of infectious disease, the probe should be soaked in disinfectant between uses and a disposable cover, usually a latex condom, should be placed over the probe for the examination. If the patient has an allergy to latex, an alternate nonlatex cover should be used, which is often available from the probe manufacturer.

Many types of disinfectants are available. Most are glutaraldehyde based. We currently use Metricide (Metric Research Corp, Parker, CO) in our laboratory. Other brands include Sporidicin (Sporidicin International, Rockville, MD) and Cidex (Surgikos, Arlington, TX). The probe manufacturers usually recommend brands for their instruments and may also specify a limit to the maximum time that a probe may be immersed in disinfectant without damaging the probe or voiding the warranty. It is advisable to contact the probe manufacturer if information regarding the type of disinfectant and immersion time limit is not provided in the manual.

As indicated on the product label, disinfectants are toxic and caustic chemicals and should be treated with caution to safeguard the patient and staff members. Follow the instructions on the product label. Staff members must wear gloves when using a disinfectant or when touching a probe that has been immersed in disinfectant. Some manufacturers recommend the use of safety goggles. Emergency eyewash stations should be available on site. Care should be taken to rinse the probe with water or alcohol before covering the probe with a disposable cover. A wide range of probe covers are available, ranging from commercially available covers designed specifically for ultrasound probes to latex condoms. Having stated the need to follow the necessary precautions, we have used disinfectants for many years without incident.



Between examinations, we keep the probe immersed for 20 minutes in disinfectant in a reservoir inside a ductless fume system (PCimedical, Deep River, CT) on a cart situated beside the scanner. This cart also holds the other paraphernalia needed on an ongoing basis by the sonographer. If the condom breaks or tears, then more complete probe sterilization is necessary before reusing the probe. All ultrasound probes that come in contact with blood or body fluids should be covered, cleaned, and disinfected appropriately.

Once the probe has been disinfected and wiped clean, a small amount of transducer coupling gel is placed inside the tip of the condom (or other probe cover), and the condom is pulled over the shaft of the probe. The coupling gel should eliminate any air from the beam path. If there are air bubbles over the transducer face, the condom or probe cover should be readjusted. The final step in the process of probe preparation is to lubricate the tip of the covered probe with a sterile lubricant such as Muko (Ingram & Bell Medical, Don Mills, Ontario, Canada) to facilitate probe insertion. If the procedure is being performed as part of an infertility study, it is recommended that water or saline be used as a lubricant because some of the more commonly used lubricants may have an adverse effect on sperm motility.<sup>8</sup> The sonographer must wear gloves while preparing the probe and performing the examination.

## Examination Technique

Once the patient and transducer have been prepared, an 8- to 10-cm depth of field is selected to ensure that the transducer's position can be monitored during insertion. Once the probe has been inserted into the introitus, the operator should watch the screen and monitor the position of the probe continuously. This is critical to patient safety and to prevent inadvertent positioning of the probe in the posterior vaginal fornix, where the operator will see only bowel if the uterus is anteverted and will be unable to identify any anatomic landmarks. The probe is inserted into the vagina, and the scan generally performed through the anterior vaginal wall, anterior vaginal fornix, or lateral fornices. Probe position is determined by the site of optimal visualization of specific pelvic viscera.

The orientation of the probe is controlled by probe rotation and angulation. Three basic scanning maneuvers are performed to achieve appropriate orientation:

1. The probe can be rotated from 0 to 90 degrees about its long axis to obtain any plane of scan from sagittal to coronal (Figs. 26-1 and 26-2).
2. The probe can be angled or pointed in any direction (within the limitations of vaginal discomfort) to direct the plane of section (see Fig. 26-2C).
3. The probe can be advanced or withdrawn, which will move adjacent pelvic viscera and displace bowel, and allow structures to be placed in the focal zone of the transducer or out of regions of near-field artifact.

During insertion of the probe, the orientation of the transducer can be assessed by noting the position of the urinary bladder, which usually contains a small residual amount of urine. The normally consistent position of the angle of the bladder relative to the more variable positions of the uterus and ovaries makes it a good landmark to use when initially

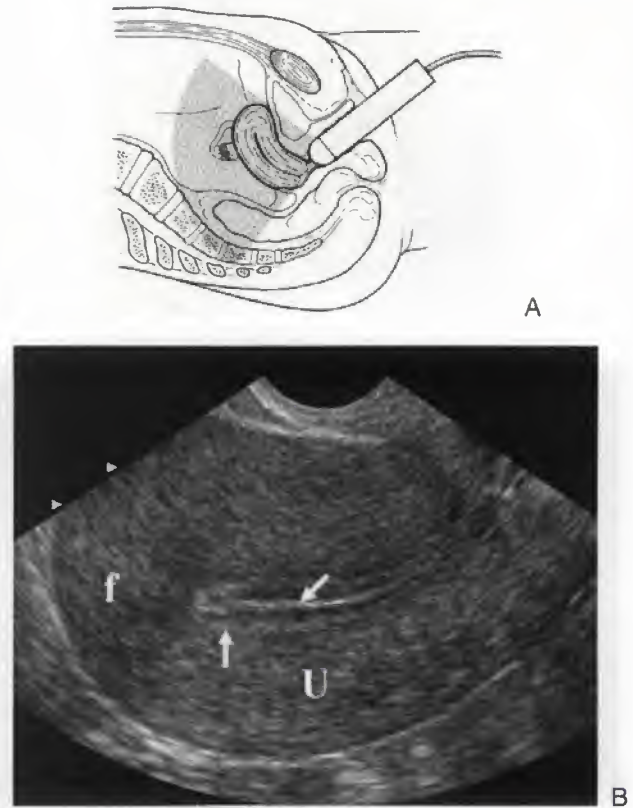


**FIGURE 26-1.** A. Diagram of sagittal transvaginal scan plane. (From Lyons EA, Gratton D, Harrington C: *Transvaginal sonography of normal pelvic anatomy*. *Radiol Clin North Am* 30:663, 1992.) B. Transvaginal sonogram in the sagittal plane showing the corpus (U) and fundus (f) of the uterus. Endometrial canal (vertical arrow) basal layer of the endometrium (oblique arrow).

assessing transducer position and orientation. Rotating the probe 90 degrees into the coronal plane permits visualization of both the uterus and adnexa. Before recording any images, a complete pelvic survey should be performed. This survey is performed by slowly sweeping the beam in a sagittal plane from the midline through both adnexa to the lateral pelvic side walls. The probe is then rotated to the coronal plane, and the beam swept from the cervix to the fundus of the uterus. The survey quickly ascertains the relative positions of the uterus and ovaries and identify any obvious masses.

After the survey, standard views are obtained. In our institution these include

Sagittal plane: (1) cervix, endocervical canal, posterior cul-de-sac, (2) uterus and endometrium, (3) right ovary and adnexa, and (4) left ovary and adnexa.

Coronal plane: (1) vagina, (2) cervix and posterior cul-de-sac, (3) uterine corpus and endometrium, (4) uterine fundus and endometrium, (5) right ovary and adnexa, and (6) left ovary and adnexa.



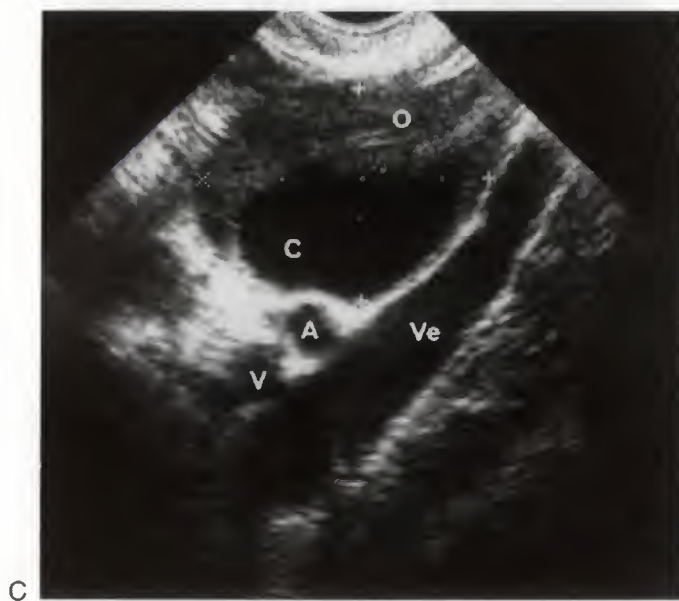
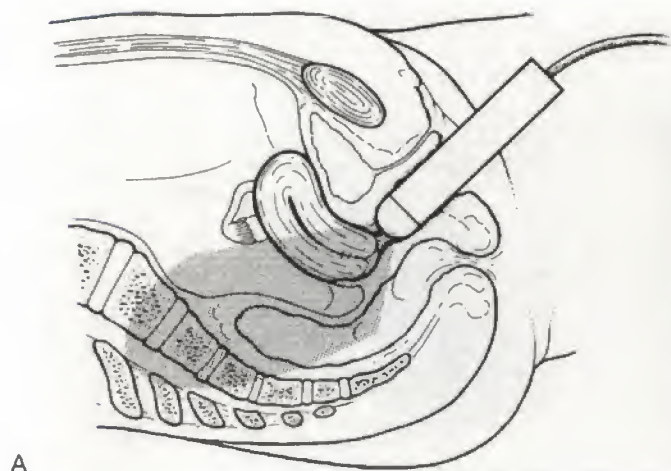


**FIGURE 26-2.** A. Diagram of coronal transvaginal scan plane. (From Lyons EA, Gratton D, Harrington C: *Transvaginal sonography of normal pelvic anatomy*. *Radiol Clin North Am* 30:663, 1992.) B. Transvaginal sonogram in the coronal plane through the corpus (U) of the uterus. Endometrium (open arrow). Serosal surface of the uterus (arrows). C. Transvaginal sonogram in the coronal oblique plane angled toward the left ovary demonstrating the left ovary (O), the external iliac vein (Ve), and the internal iliac artery (A) and vein (V). C, cyst.

Although these standard images are obtained, they are by no means the complete examination. Obtaining these images indicates that the entire organ or region imaged has been carefully assessed at real time in two orthogonal planes. Any pathology or variant of normal must be assessed and appropriate images recorded. Color flow Doppler, power Doppler, and pulsed Doppler are added to the examination depending on the clinical situation and pathology demonstrated on grayscale imaging.

Using three-dimensional ultrasound, a true coronal view of the uterus can be obtained that displays the entire endometrial canal in a view not otherwise available.

As noted previously, the angle of the bladder is a relatively constant landmark. It is noted later (see "The Uterus and Vagina") that the cervix is bound to the angle of the bladder by the parametrium. By locating the cervix, the position and location of the uterus can then be determined. Visualization of the ovaries may be more difficult and often requires significant angulation of the probe.

When the uterus is anteverted, a helpful technique for locating the ovary is to first obtain a coronal image of the uterine fundus and then to angle the probe out to the cornua and broad ligament. Once this region is identified, the ovary can usually be identified by slowly sweeping the beam anteriorly and posteriorly. If the ovary is positioned high in the pelvis or if the uterus is markedly anteverted, raising or flexing the patient's hips may help visualize the ovary. Another more common maneuver for the "high ovary" is to apply pressure of the anterior abdominal wall laterally by flexing the fingers, indenting the wall and drawing the mobile ovary or a mass down into the field of view of the transvaginal probe.

The capability to use the probe tip to assess pelvic structures for tenderness is an added advantage of TVS. By applying gentle pressure with the transducer tip to pelvic structures, it is possible to localize a region of tenderness with greater specificity than with TAS or bimanual examination. Moreover, a region of tenderness that has been



identified on bimanual examination can be investigated with TVS to determine which pelvic structure produces the same response.

In response to gentle pressure with the transvaginal probe, pelvic organs should normally slide over one another. Zimmer, Timor-Tritsch, and Rottem<sup>9</sup> described this effect, which is referred to as the sliding organ sign. A restriction to normal motion may indicate the presence of adhesions. Sometimes the organ of origin of a mass may not be obvious from grayscale and color Doppler findings. Motion of the mass with probe pressure may help to determine the organ of origin.

## Safety

The American Institute of Ultrasound in Medicine (AIUM) Bioeffects Committee identified an ultrasound intensity (free-field spatial peak, temporal average [SPTA]) of 100 mW/cm<sup>2</sup> as the intensity below which no significant biologic effects in mammalian tissues exposed *in vivo* have been confirmed.<sup>10,11</sup> The Food and Drug Administration set the acoustic output limit (SPTA) for fetal imaging at 94 mW/cm<sup>2</sup>. Manufacturers now have the option to market systems that exceed the previously allowed application-specific intensity levels provided that the exposure levels are displayed on screen so that the level can be monitored by the operator. In 1992, the National Electrical Manufacturer's Association and the AIUM agreed on voluntary output display standards, which consist of the thermal index (TI) and mechanical index (MI). These indexes provide a more accurate estimate of biologic exposure than do intensity levels, allowing operators to apply the ALARA principle for ultrasound exposure (as low as reasonably achievable). The AIUM guidelines conclude that no independently confirmed experimental evidence indicates damage in animal models below certain prescribed levels (TI < 2, and MI < 0.3).<sup>11</sup> The AIUM further states and reaffirmed as of March 26, 1997 that "There are no confirmed biological effects on patients or instrument operators caused by exposures from present diagnostic ultrasound instruments. Although the possibility exists that such biological effects may be identified in the future, current data indicate that the benefits to patients of the prudent use of diagnostic ultrasound outweigh the risks, if any, that may be present."<sup>12</sup> Because TVS is often used in early pregnancy during organogenesis, prudent use of the technology dictates that the transducer output be kept at the lowest level necessary to obtain appropriate diagnostic information. The operator should apply the ALARA principle in ultrasound scanning and, moreover, should keep the TI and MI at safe levels. In particular, sonographers and sonologists should be cognizant that ultrasound exposure levels with pulsed Doppler may frequently exceed the prescribed levels and pay close attention to the TI and MI. Pulsed Doppler should be used for as brief a period as possible to obtain necessary, clinically relevant information.

## TRUE AND FALSE PELVES

The pelvis is arbitrarily divided into two structurally continuous compartments: the true and false pelves. The division is defined by the sacral promontory and the linea terminalis. The linea terminalis is the arcuate line of the

ilium, the iliopectineal line, and the crest of the pubis. The false pelvis is bounded by the flanged portions of the iliac bones, the base of the sacrum posteriorly, and the abdominal wall anteriorly and laterally. The true pelvis is bounded anteriorly by the pubis and pubic rami, posteriorly by the sacrum and coccyx, laterally by the fused ilium and ischium, and inferiorly by the muscles of the pelvic floor.

In the absence of masses in the nongravid patient, the uterus, ovaries, and adnexa are situated in the true pelvis. The urinary bladder and loops of small bowel are situated anterior to the uterus and adnexal structures in the true pelvis. As the urinary bladder fills, the dome of the bladder extends into the false pelvis and displaces the loops of small bowel, providing a sonic window (Fig. 26-3) for TAS.<sup>5</sup> Intracavitary probes (transvaginal and transrectal) allow visualization of pelvic viscera from within the true pelvis. Translabial sonography views the true pelvis from the pelvic floor.<sup>13</sup>

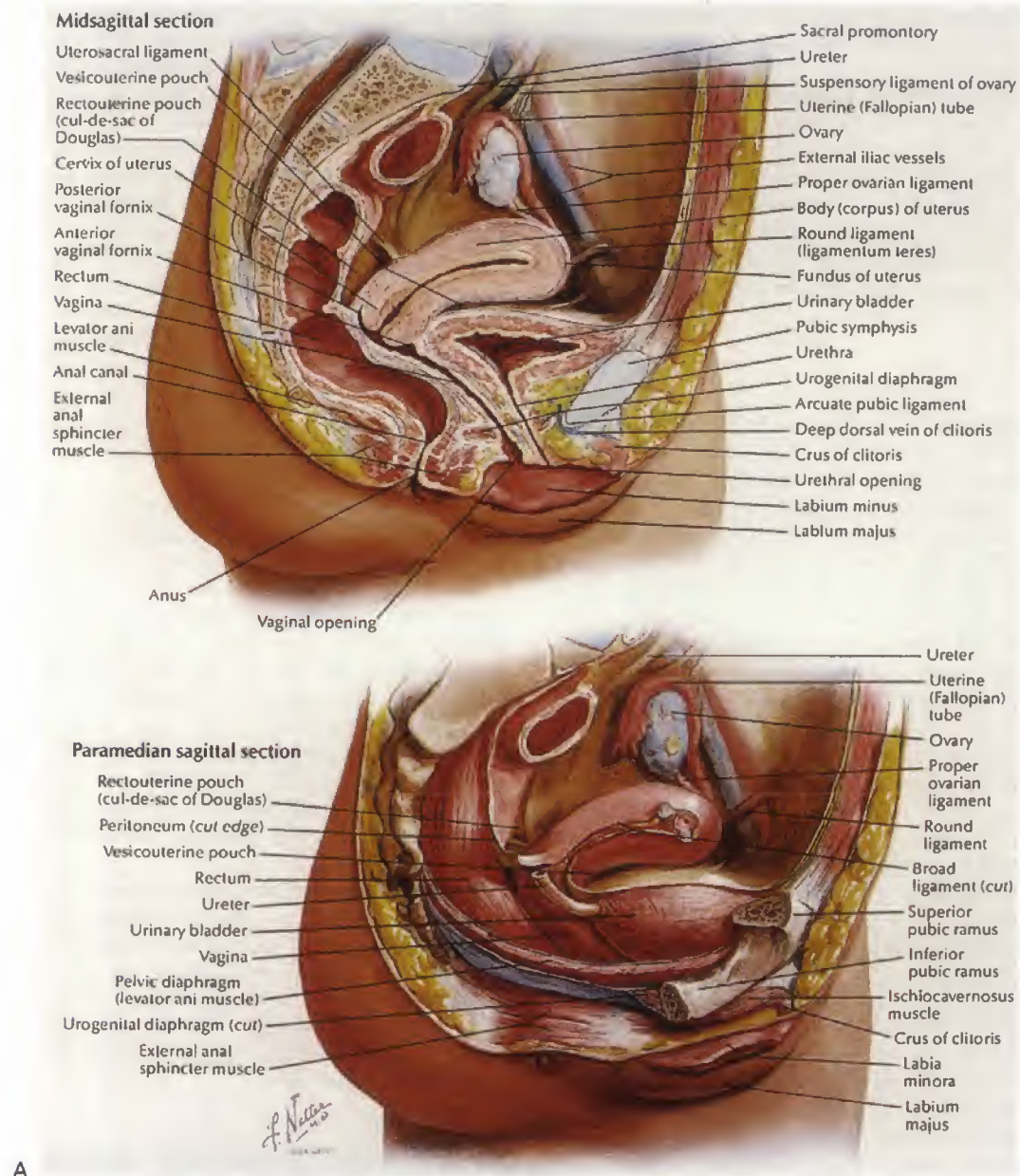
The disadvantages of TVS compared with TAS include a limited field of view and an inability to examine the false pelvis adequately. The full urinary bladder in TAS provides a window to examine the true pelvis by displacement of bowel but may also inadvertently displace pathologic structures into the false pelvis. A quick scan of the true and false pelves at the end of the study after the patient has voided is part of a routine examination. It will allow one to detect large masses that have been displaced by the full bladder and masses that mimic a full bladder (Figs. 26-4 and 26-5). On the postvoid examination, it is often necessary to use compression to displace gas in loops of small bowel and colon, especially when searching for a small mass in the false pelvis.

When TVS is used, free fluid is often demonstrated in the posterior cul-de-sac in normal patients (Figs. 26-6 and 26-7). The presence of fluid in the anterior cul-de-sac or lateral pelvic recesses or a large amount of fluid in the posterior cul-de-sac suggests a large intraperitoneal fluid collection (Figs. 26-8 and 26-9). The volume of fluid may be estimated by examining the hepatorenal space (Morrison's pouch) (see Fig. 26-9B).

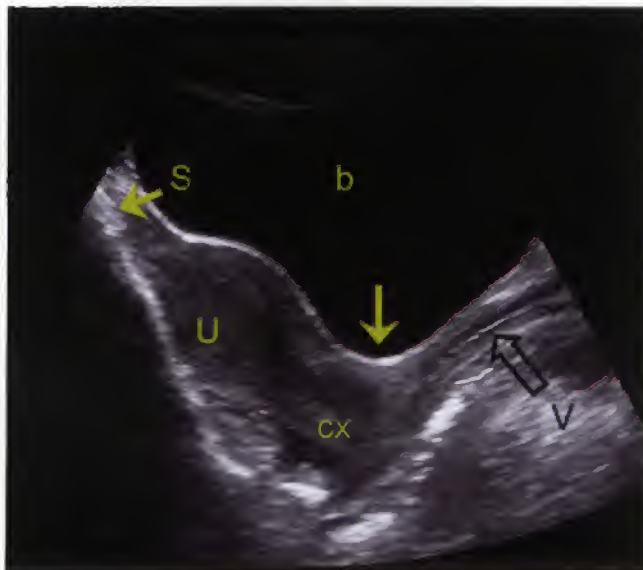
## PELVIC MUSCULATURE, FASCIAL PLANES, LIGAMENTOUS ATTACHMENTS

The superficial or subcutaneous fascia is areolar in texture and contains varying amounts of fat. The subcutaneous fascia is continuous with the superficial fascia of the thigh, labia majora, and perineum. The anterior and lateral walls of the false pelvis are the anterior and lateral muscles of the abdominal wall. Laterally, these muscles include the external and internal obliques and the transversus abdominis, which is the inner muscle layer<sup>14,15</sup> (Fig. 26-10). The rectus abdominis muscles are paired paramedian muscles oriented longitudinally on either side of the linea alba (see Figs. 26-10 and 26-11). The pelvic attachment of the rectus abdominis muscles is the crest of the pubis. The aponeuroses of the external and internal obliques and transversus muscles fuse with the anterior rectus abdominis fascia to form the linea alba in the midline. It should be noted that the anatomy of the rectus sheath is different above and below the arcuate





A



B

**FIGURE 26-3.** A. Midsagittal section diagram of the female pelvis demonstrating the relationship of the uterus, urinary bladder, rectum, and adnexal structures. (Copyright 1954 Novartis. From Netter FH: *The CIBA Collection of Medical Illustrations*, Volume 2, Reproductive System, Section VI, Plate 1. Summit, NJ, CIBA-Geigy Co, 1954. All rights reserved.) B. Transvesical sonogram in the midsagittal plane displaying the uterus (U). Angle of bladder (arrow). b, urinary bladder; cx, cervix; s, sacral promontory; v, vagina.

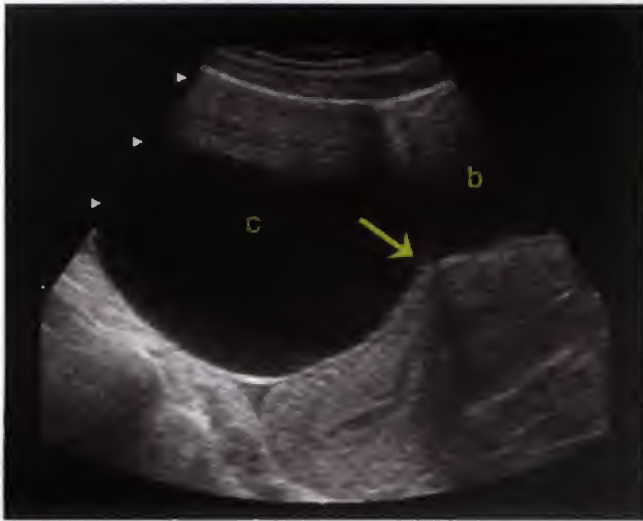


**FIGURE 26-4.** Midline longitudinal sonogram of a large serous cystadenoma (c) anterior to the uterus, mimicking a full urinary bladder. The partially full urinary bladder (b) is visualized as a triangle-shaped structure. The angle of the bladder is in contact with the cervix (arrow).

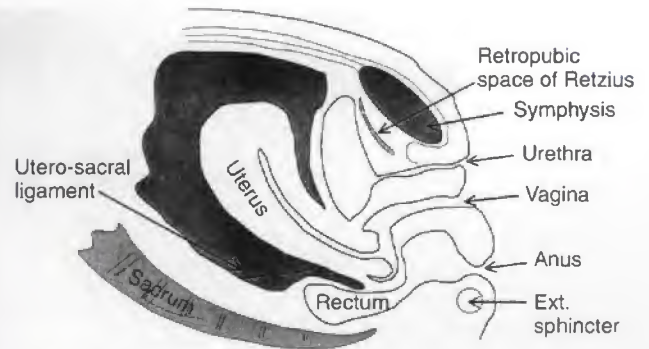


**FIGURE 26-6.** Diagram of a midline sagittal section through the pelvis showing the peritoneal reflections including the anterior cul-de-sac (vesicouterine recess) and the posterior cul-de-sac (rectouterine recess). The posterior cul-de-sac is closely related to the posterior fornix of the vagina.

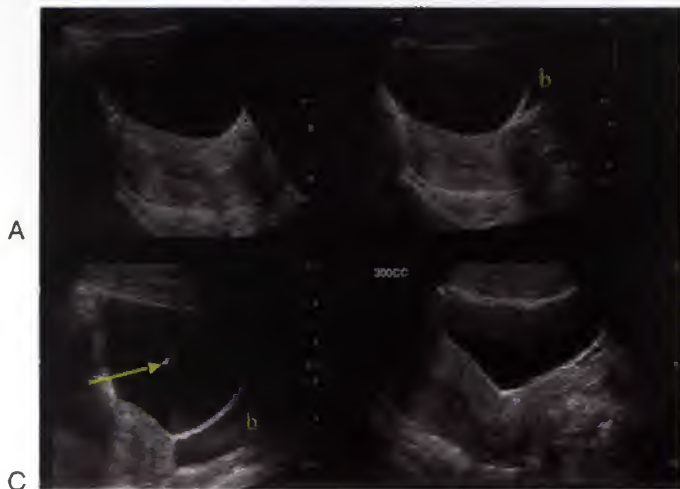


**FIGURE 26-5.** Ovarian cyst mistaken for the urinary bladder. A. Longitudinal midline scan. At the time of the examination, a large ovarian cyst (c) was missed because it was interpreted to be the urinary bladder. B. The bladder (b) was identified only when the transducer was angled caudad. C. Longitudinal midline scan of the cyst being aspirated. The tip of the needle is seen in the middle of the cyst (arrow). The bladder (b) is filling and is now better visualized. D. After 300 mL of clear serous fluid was aspirated, only the bladder lies anterior to the uterus. Note that scans A and D look identical.



**FIGURE 26-7.** Free fluid in the posterior cul-de-sac. Transvaginal sonogram in the sagittal plane demonstrating a small amount of free fluid in the posterior cul-de-sac (horizontal arrow). The endometrium is in the late proliferative phase. The functional zone of the endometrium (f) is hypoechoic compared with the echogenic basal layer (oblique arrows).

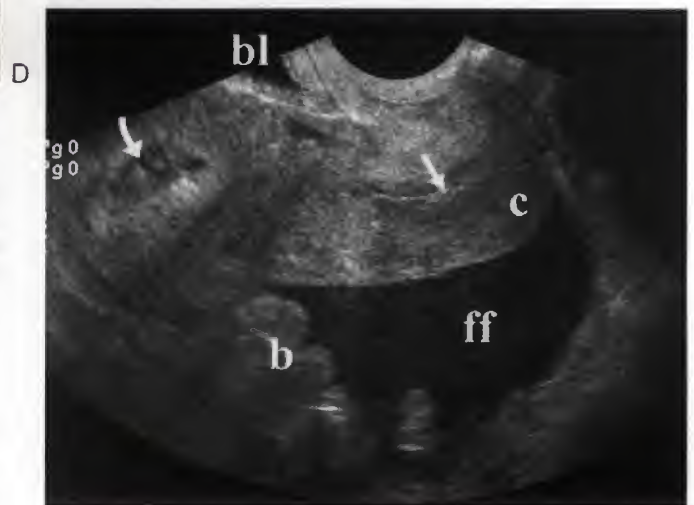


**FIGURE 26-8.** Ectopic pregnancy with blood in the posterior cul-de-sac. Debris-filled fluid (ff) is present in the posterior cul-de-sac in this patient with a ruptured ectopic pregnancy. The posterior cul-de-sac extends to the inferior aspect of the posterior lip of the cervix (c) and is in contact with the posterior vaginal fornix. Endocervical canal (oblique arrow); decidua cast (curved arrow). b, bowel; bl, partially full bladder.

line.<sup>14</sup> Below the arcuate line, a rectus sheath hematoma may extend across the midline and displace the bladder posteriorly.<sup>16</sup> Above the arcuate line, however, a hematoma will be confined and not cross the midline. Without careful evaluation of the abdominal wall and the epicenter of the mass, a hematoma of the rectus sheath may be mistaken for a mass of pelvic origin.

Masses in the space of Retzius (also known as the prevesical or retropubic space) may also be confused with



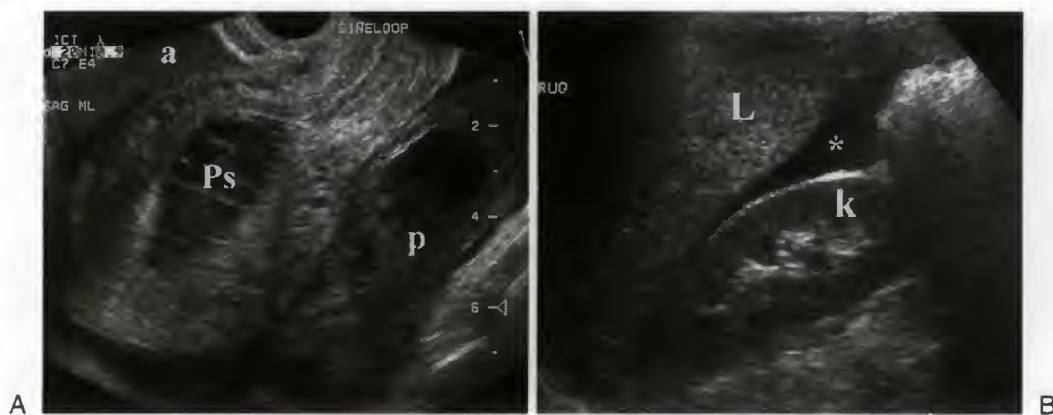


**FIGURE 26-9.** Ectopic pregnancy with blood in the anterior cul-de-sac, posterior cul-de-sac, and Morrison's pouch (hepatorenal space). *A.* Transvaginal sonogram in the sagittal plane demonstrating free fluid with internal debris in the anterior cul-de-sac (*a*) and posterior cul-de-sac (*p*). *Ps*, pseudogestational sac. *B.* Coronal scan of the right upper quadrant of the abdomen demonstrating free fluid (\*) in Morrison's pouch. *L*, liver; *k*, right kidney.

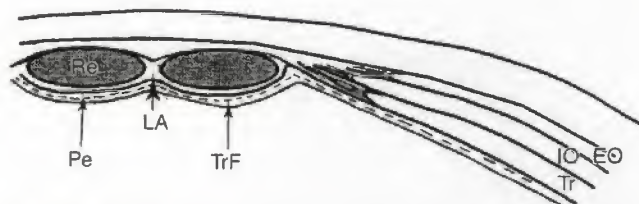


**FIGURE 26-10.** Diagram of a transverse section through the anterior abdominal wall, inferior to the arcuate line. *EO*, external oblique; *IO*, internal oblique; *LA*, linea alba; *Pe*, peritoneum; *Re*, rectus abdominis; *Tr*, transversus abdominis; *TrF*, transversalis fascia.



**FIGURE 26-11.** Transverse sonogram of the anterior abdominal wall showing the anterior (*open arrow*) and posterior (*solid arrow*) rectus sheath. *R*, rectus abdominis muscle; *B*, bowel loops in the peritoneal cavity.

masses arising from the pelvic viscera. The space of Retzius is situated between the transversalis fascia and the extraperitoneal fascia<sup>14,15</sup> (see Figs. 26-6 and 26-10). The transversalis fascia is a thin layer of connective tissue separating the transversus abdominis from the extraperitoneal fascia (see Fig. 26-10). Below the umbilicus, the extraperitoneal fascia presents two well-defined layers. The umbilical vesical fascia is the deeper of the two and is continuous with the vesical fascia. The umbilical prevesical fascia lies between the transversalis and umbilical vesical fasciae and is fused to the latter. It is also fused to the transversalis fascia along the medial umbilical ligaments and at the umbilicus. The

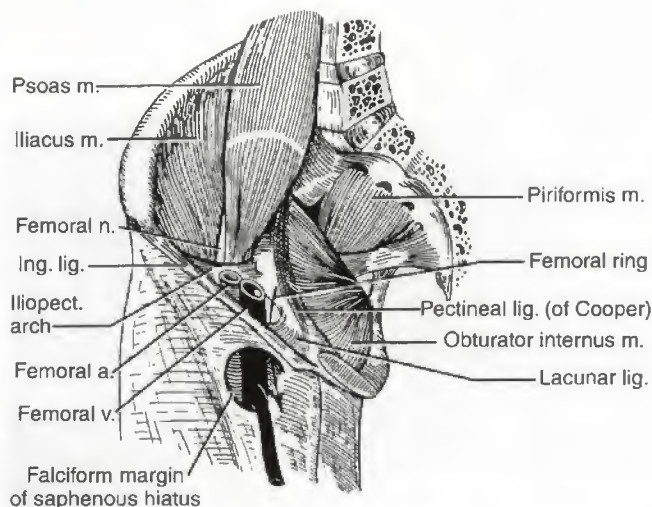


**FIGURE 26-12.** Diagram of the pelvic musculature. (From Pansky *B: Review of Gross Anatomy*, 5th ed. New York, Macmillan, 1987.)

resultant space between the transversalis fascia and the umbilical prevesical fascia is the space of Retzius. Sonographically, masses in the space of Retzius (usually hematomas or abscesses) displace the bladder posteriorly.<sup>17</sup> Posterior displacement of the urinary bladder is a characteristic feature of masses in the space of Retzius, which allows differentiation from pelvic or abdominal masses that displace the bladder inferiorly or anteriorly.

Muscles of the pelvis include those of the lower limb (psoas major, iliacus, piriformis, obturator internus) and the pelvic diaphragm (levator ani, coccygeus).<sup>15,18</sup> The psoas major is a large triangular muscle that arises from the lumbar transverse processes and the vertebral bodies and the disks of T-12 to L-2. It descends through the false pelvis on the pelvic side wall anteriorly and exits posterior to the inguinal ligament (Fig. 26-12). It converges with the iliacus to form a tendon that inserts on the lesser trochanter of the femur. The iliacus arises from the concavity of the upper two thirds



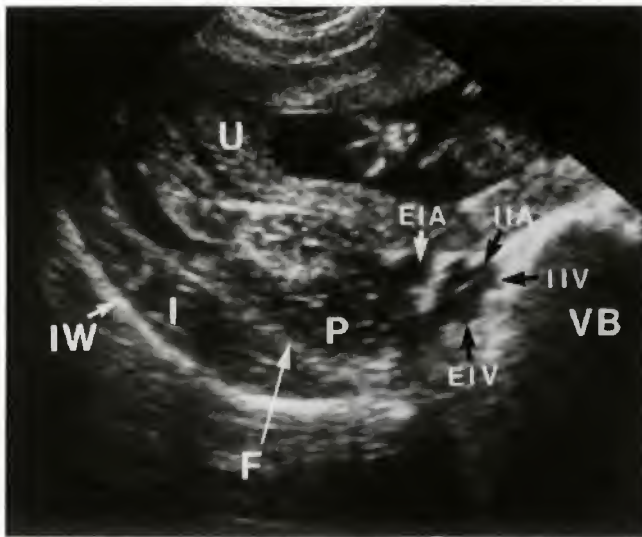


**FIGURE 26-13.** Transverse sonogram through the right iliac fossa, using the gravid uterus (U) as a sonic window, showing the relative positions of the iliacus (I) and psoas major (P) muscles separated by a fascial plane (F) in the false pelvis. The iliac vessels are medial to the psoas. EIA, external iliac artery; EIV, external iliac vein; IIA, internal iliac artery; IIV, internal iliac vein; IW, iliac wing; VB, vertebral body.

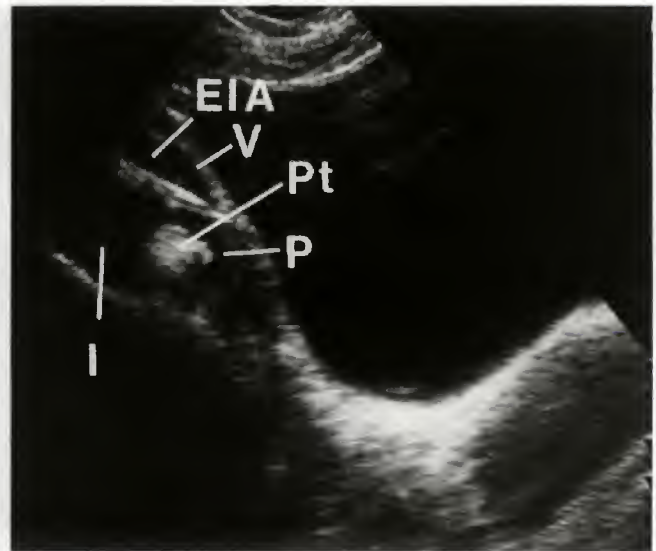


**FIGURE 26-14.** Transverse sonogram through the pelvic side wall angled to the right to visualize the psoas major (P), the iliacus muscle (I), and the psoas tendon (Pt). The external iliac artery (EIA) and vein (V) are anterior to the iliopsoas muscle bundle.

of the iliac fossa, the ventral surface of the sacroiliac and iliolumbar ligaments, and the lateral aspect of the upper part of the sacrum.<sup>18</sup>

Sonographically, the psoas is seen in the lower abdomen in a paravertebral position. In a transverse sonogram of the lower abdomen, the psoas is rounded and hypoechoic. Because the transducer is angled inferiorly, the psoas muscles diverge laterally and, in the false pelvis, assume a position medial and slightly anterior to the iliacus muscle (see Figs. 26-12 and 26-13). In the false pelvis, the iliac wings are identified as brightly echogenic linear structures with loss of distal sonic information (see Fig. 26-13). More inferiorly, within the true pelvis the iliacus/psoas muscle is seen as a hypoechoic, discretely margined muscle; its two component muscles are separated by a brightly echogenic line, which represents interposed fascia continuous with the psoas tendon (Fig. 26-14). The psoas may be demonstrated in its long axis by scanning in a longitudinal oblique plane (Fig. 26-15). In thin patients, the fasciculi of the psoas muscle may be identified (see Fig. 26-15). Movement of the normal psoas muscle may be seen with flexion of the hip.

The piriformis muscle arises from the sacrum between the pelvic sacral foramina and from the gluteal surface of the ilium<sup>14,15</sup> (Fig. 26-16). On pelvic sonography, the piriformis can be identified posteriorly within the pelvis until it passes through the greater sciatic notch (Fig. 26-17) to insert onto the greater trochanter of the femur. The obturator internus muscle arises from the anterolateral pelvic wall surrounding the obturator foramen and passes through the lesser sciatic foramen to insert on the greater trochanter of the femur (Fig. 26-18).

The pelvic diaphragm is formed by the levator ani and coccygeus muscles. This is the most caudal structure of the pelvic cavity and can be routinely identified on TAS when

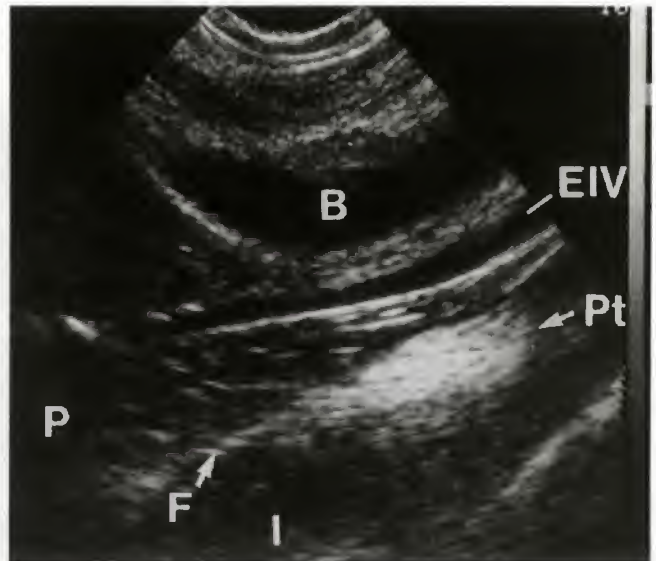


**FIGURE 26-15.** Coronal sonogram through the distended urinary bladder (B), with the transducer situated medially and angled laterally to visualize the psoas major (P) and the iliacus muscles (I) in their long axes. EIV, external iliac vein; F, iliopsoas fascial plane; Pt, psoas tendon.

the transducer is angled inferiorly (Fig. 26-19). The perineal body is situated between the anus and vagina. It is formed by the median raphe of the levator ani and the central tendon of the perineum on which converge the bulbocavernosus and superficial transverse perineal muscles and the external anal sphincter.<sup>14</sup> The perineal body provides much of the support for the perineum.<sup>19</sup> The right and left broad ligaments are folds of peritoneum, which extend from the



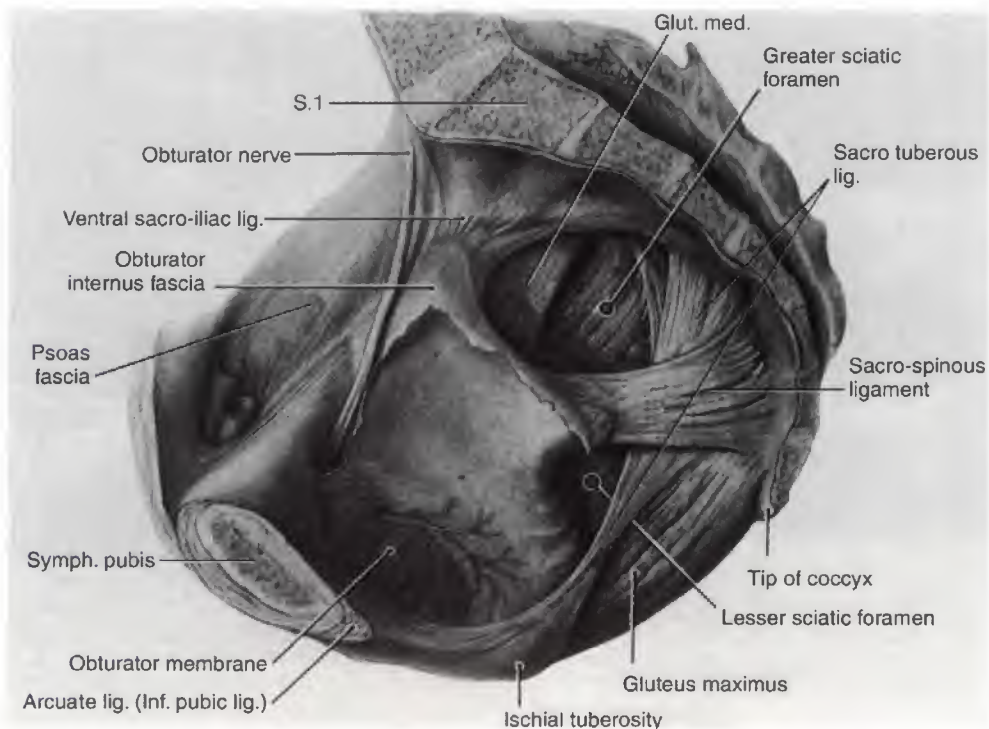


**FIGURE 26-16.** The muscles and ligaments of the lateral pelvic wall as viewed from the pelvis. (From Grant JCB: *Grant's Atlas of Anatomy*, 5th ed. Baltimore, Williams & Wilkins, 1962, p 217. Copyright, Williams & Wilkins Company.)

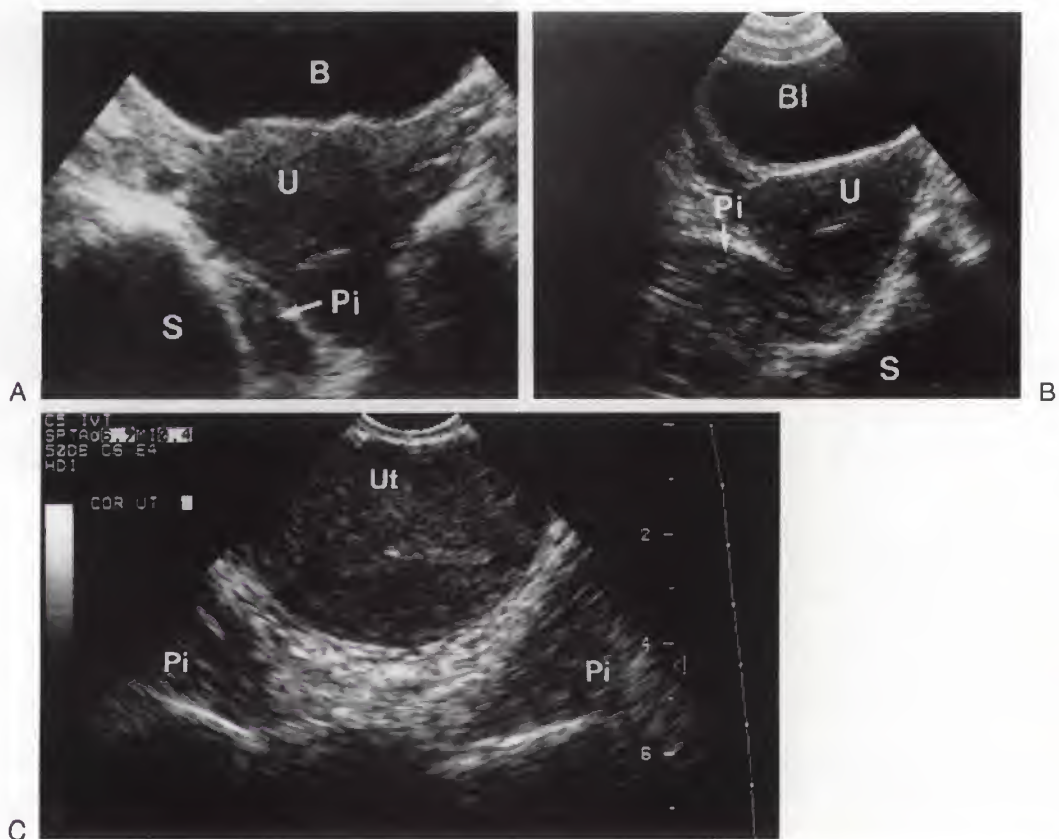


**FIGURE 26-17.** A. Longitudinal sonogram to the right of the midline through the bladder (B), showing the right piriformis muscle (Pi) in cross-section. B. Transverse sonogram through the bladder (Bl), angled to the right, showing the right piriformis muscle (Pi) in its length. S, sacrum, U, uterus. C. Transvaginal coronal sonogram of the uterus anterior to the paired piriformis muscles.

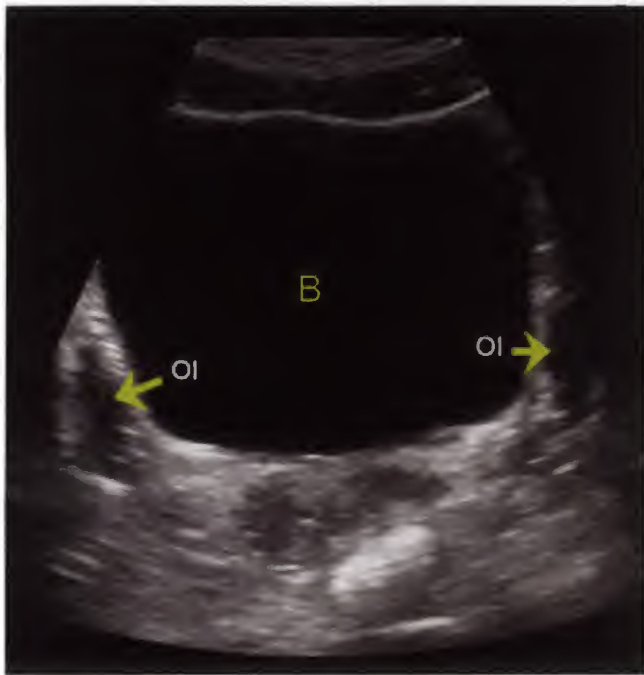


**FIGURE 26-18.** Transverse sonogram through the caudal aspect of the bladder (B) showing the obturator internus muscles (OI) laterally.

lateral aspects of the uterus to the lateral pelvic side walls (Fig. 26-20) and divide the pelvic cavity into anterior and posterior compartments. The free border of the broad ligament contains the uterine (fallopian) tube.<sup>15,20</sup>

The broad ligaments may be identified sonographically when they are outlined by free intraperitoneal fluid (Fig. 26-21) or when the uterus is retroverted. The ovary is

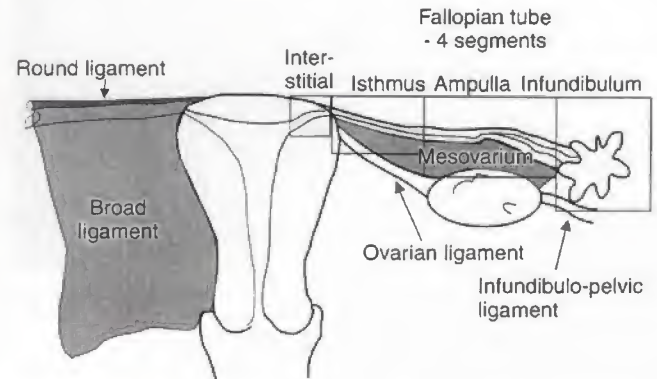


**FIGURE 26-20.** Diagram of the ovary, uterus, and adjacent peritoneal reflection and ligaments.

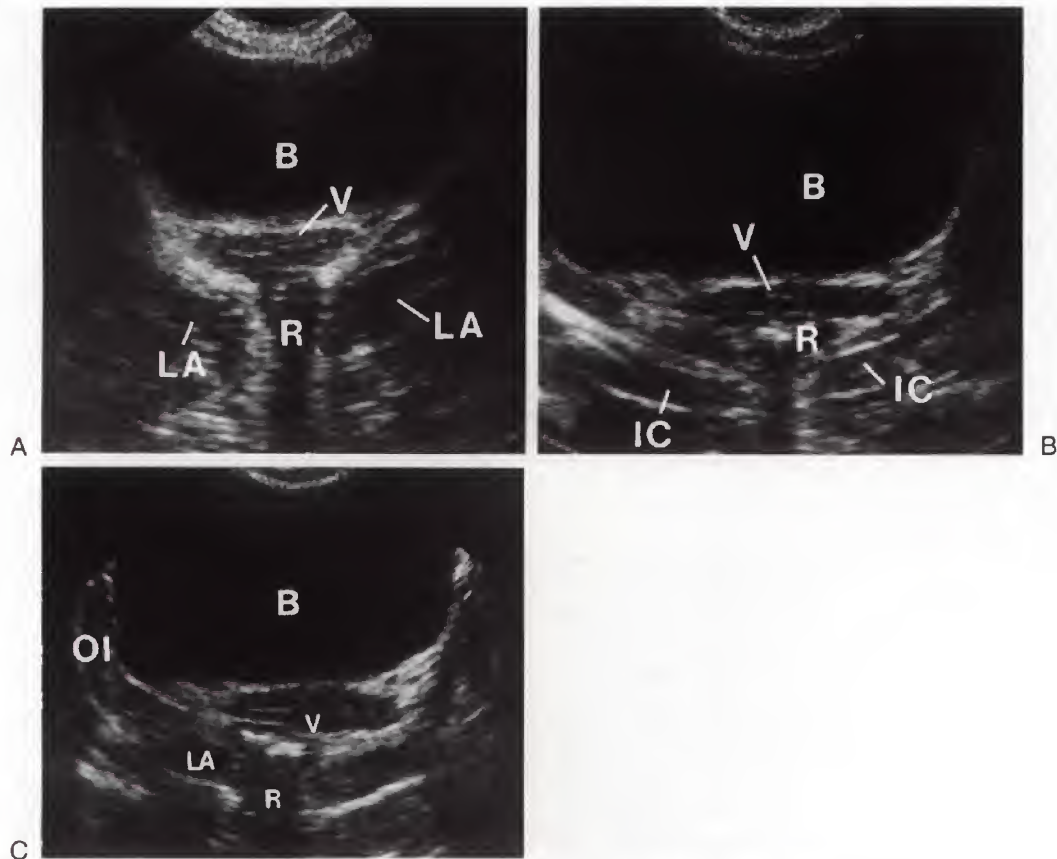


**FIGURE 26-19.** A and B. Transverse sonogram through the bladder (B) angled caudally, showing the levator ani (LA) and iliococcygeus (IC) muscles. C. Transverse sonogram with slightly less caudal angulation than in A or B, showing the obturator internus (OI) and levator ani (LA) muscles. R, rectum; V, vagina.





**FIGURE 26-21.** Transverse sonogram in a patient with gross ascites (A). The broad ligament (arrow) is well visualized.

attached to the posterior layer of the broad ligament by reflections of peritoneum referred to as the mesovarium (Fig. 26-22). The superior margin of the portion of the broad ligament containing the fallopian tube is referred to as the mesosalpinx. The superior margin of the broad ligament lateral to the fimbriated end of the fallopian tube is the suspensory ligament of the ovary (infundibulopelvic ligament) through which course the ovarian vessels and nerves<sup>20</sup> (see Fig. 26-22).

The round ligaments arise in the uterine cornua, anterior to the fallopian tubes in the broad ligaments, and extend anterolaterally to run beneath the inguinal ligament and insert into the fascia of the labia majora.<sup>20</sup> The ovarian (uteroovarian) ligaments arise from the uterine cornua posterior to the uterine tubes and attach to the inferior extremity of the ovary. In the absence of free intraperitoneal fluid, the mesovarium, mesosalpinx, ovarian, and round ligaments are not identified sonographically. The suspensory ligament of the ovary is usually not seen. The ovarian artery within the suspensory ligament of the ovary, however, is often identified with TAS or TVS. According to Kurjak and Zalud,<sup>21</sup> the ovarian artery can be identified within the suspensory ligament in approximately 21% of women in the reproductive age group and in 4% of postmenopausal women.

The base of the lateral margin of the broad ligament is continuous with dense connective tissue of the pelvic floor, which is united with the supravaginal portion of the cervix. The lower medial margin of the broad ligament is widely attached to the connective tissues adjacent to the cervix known as the parametrium.<sup>19</sup> The uterosacral ligaments (see Figs. 26-3 and 26-22) extend posterolaterally from the supravaginal cervix, encircle the rectum, and insert into the fascia over the sacrum. The uterosacral ligaments form the lateral boundaries of the rectouterine pouch.

## VASCULAR ANATOMY

The common iliac arteries course anteriorly and medially to the psoas muscles (see Fig. 26-22).<sup>22,23</sup> The right common iliac vein ascends posteriorly and then laterally to the right common iliac artery. The left common iliac vein ascends medially and then posteriorly to the left common iliac artery. The common iliac arteries bifurcate to form the external and internal iliac arteries. The external iliac arteries supply most of the lower limbs. The internal iliac arteries supply the pelvic viscera, walls of the pelvis, perineum, and gluteal regions (Fig. 26-23).

The external iliac arteries course through the false pelvis without entering the true pelvis. In the nongravid state, the caliber of the external iliac arteries is greater than that of the internal iliac arteries. The external iliac arteries assume a course adjacent to the medial psoas border and exit the pelvis through the femoral canals at the level of the inguinal ligaments (see Figs. 26-12, 26-13, and 26-22). The right external iliac vein ascends medially and then posteriorly to the right external iliac artery. The left external iliac vein is medial to the left external iliac artery.

The internal iliac arteries arise at the bifurcation of the common iliac arteries at the level of the L-5/S-1 disk immediately anterior to the sacroiliac joints and course approximately 4 cm posteriorly to the superior margin of the greater sciatic foramen. The internal iliac arteries then divide into anterior and posterior trunks, which pass posteriorly into the greater sciatic foramina. The anterior division divides into the following branches: (1) umbilical and superior vesicle; (2) inferior vesicle; (3) uterine; (4) vaginal; (5) middle rectal; (6) obturator; (7) internal pudendal; and (8) inferior gluteal. The posterior division divides into the iliolumbar, lateral sacral, and superior gluteal (see Fig. 26-23). High-velocity, high-impedance flow is the characteristic Doppler signal of the internal and external iliac arteries (Fig. 26-24). Anterior to the internal iliac arteries are the ureters, ovaries, and fimbriated ends of the fallopian tubes (see Fig. 26-22). The internal iliac veins are posterior to their respective arteries.

In patients in the reproductive age group, TVCFD can demonstrate the internal iliac arteries (Fig. 26-25) in 99% of patients and the external iliac arteries in 95% of patients.<sup>24</sup> In postmenopausal patients, the internal and external iliac arteries are demonstrated in 82% and 78% of patients, respectively. Occasionally, the division of the internal iliac artery into the anterior and posterior branches can be seen on TVS.

The uterine artery runs medially on the levator ani to the cervix. Approximately 2 cm from the cervix, it crosses superior and anterior to the ureter (Fig. 26-26). The uterine artery ascends in a tortuous course lateral to the uterus in the broad ligament to the junction of the fallopian tubes and the uterus. From the cornua of the uterus, the uterine artery courses laterally to reach the hilum of the ovary, and it ends by joining with the ovarian artery. The uterine artery supplies the cervix. Branches of the cervical branch of the uterine artery anastomose with branches of the vaginal artery to form the azygos arteries of the vagina, one of which is anterior to and the other posterior to the vagina.<sup>15,22</sup> The uterine arteries provide the main arterial supply to the uterus. Although the uterine arteries anastomose with the ovarian and vaginal arteries, the predominance of uterine blood supply from the uterine arteries is underscored by the fact

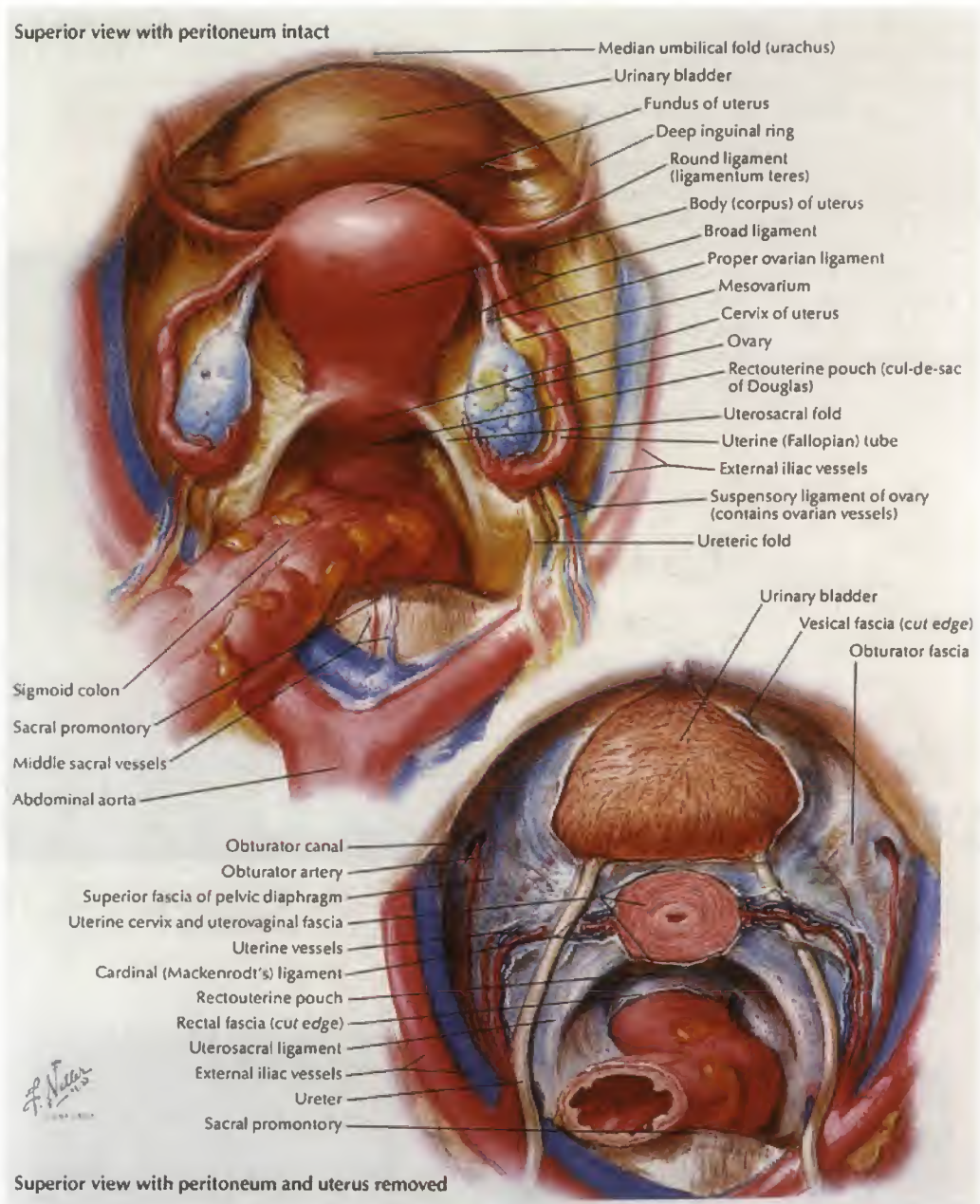


**FIGURE 26-22.** Diagram of the female pelvis (superior view). (Copyright 1954 Novartis. From Netter FH: *The CIBA Collection of Medical Illustrations*, Volume 2, Reproductive System. Section VI, Plate 7. Summit, NJ, CIBA-Geigy Co, 1954. All rights reserved.)



that the uterine arteries undergo marked hypertrophy in pregnancy, whereas the other vessels do not.<sup>19</sup> As they ascend lateral to the uterus, the uterine arteries produce multiple branches that pierce the uterine wall and then divide into the anterior and posterior arcuate arteries, which anastomose extensively with each other across the midline between the middle and outer layers of the myometrium<sup>20</sup> (see Figs. 26-22 and 26-27). The radial arteries arise as multiple branches from the arcuate arteries and travel centrally to supply the rich capillary network in the deeper layers of the myometrium and the endometrium (Fig. 26-28). Before entering the endometrium, the radial arteries give rise to the straight and spiral arteries of the endometrium. The straight arteries supply the basal layer of the endometrium. The muscular spiral arteries supply the superficial two thirds of the endometrium and become longer and more tortuous in the secretory phase of the menstrual cycle.

Sonographic visualization of pelvic vascular structures with TAS and TVCFD depends on the sensitivity of the equipment, and will change as equipment improves and new technical developments are introduced. The following discussion of flow in pelvic vasculature is based on the current literature but may become dated as newer data become available.

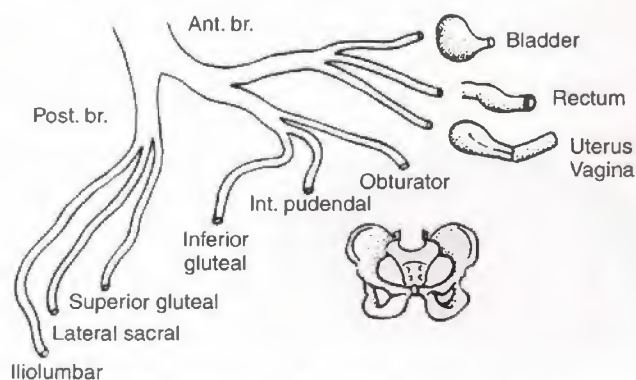


**FIGURE 26-23.** Branches of the internal iliac arteries and the pelvic viscera that they supply.

The resistive index (RI) and the pulsatility index (PI) are commonly used as Doppler indexes of vascular impedance. To prevent confusion, only RI values have been presented in this review. Much of the infertility literature, however, uses the PI as a predictor of vascular impedance. Readers are referred to reference articles in the literature for PI values.<sup>25-30</sup> In addition, peak systolic velocities and RI values vary from one study to another. These numbers are provided only as a rough guide and should not be used as absolutes.

Using color flow Doppler (TVS or TAS), the uterine arteries can be identified lateral to the cervix at the level of the cervicocorporeal junction in virtually all patients in the reproductive age group and in 80% of postmenopausal

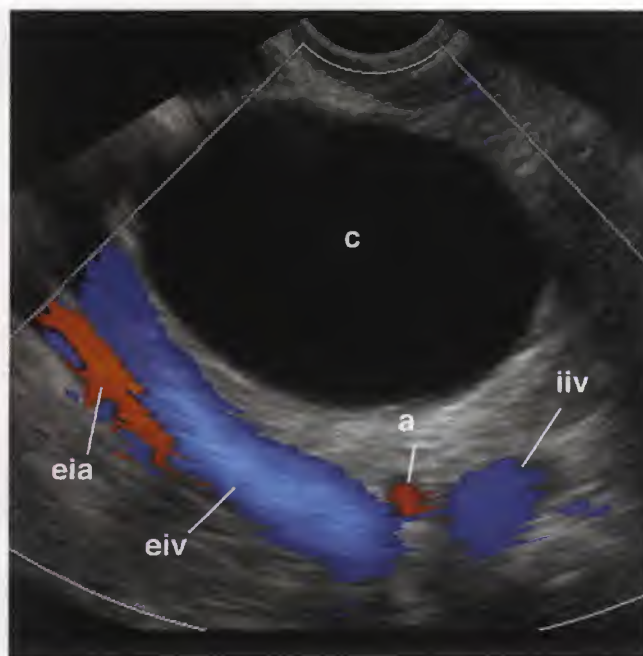


**FIGURE 26-25.** Coronal oblique sonogram through a right ovarian cyst (c) demonstrating the right external iliac vein (eiv) and artery (eia) and the internal iliac vein (iiv) and artery (a) in cross-section.

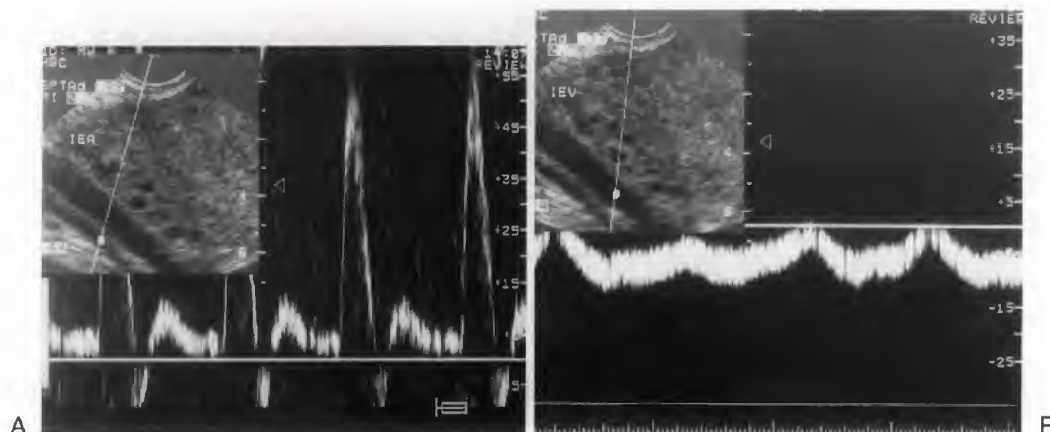


**FIGURE 26-24.** Doppler waveform of the external iliac artery and vein. Transvaginal sonogram in the coronal oblique plane through the right ovary. A. High-resistance flow in the external iliac artery. B. Venous flow with respiratory variation in the external iliac vein.



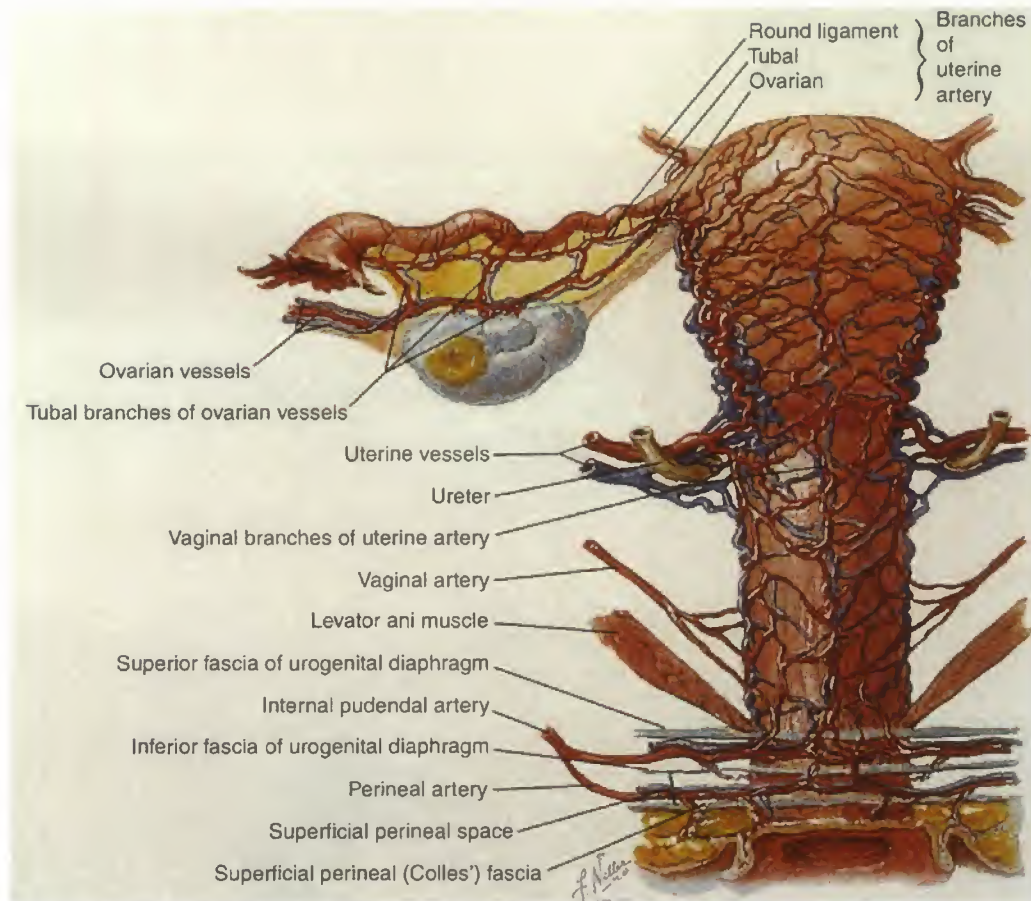


**FIGURE 26-26.** Diagram of the ovarian, uterine, and vaginal arteries and veins and the ipsilateral ureter. (Copyright 1995 Novartis. From Netter FH: *Interactive Atlas of Human Anatomy*. Plate 379B. Summit, NJ, CIBA-Geigy Co, 1995. Copyright 1981, 1990, 1965 & 1998. Novartis. Reprinted with permission from *Clinical Symposia*, Vol. 33/1; 42/2; *Netter Collection*, Vol. 2 & *Interactive Atlas*, illustrated by Frank H. Netter, M.D. & John A. Craig, M.D. All rights reserved.)

patients.<sup>24</sup> The uterine artery can be visualized with color flow Doppler as it ascends lateral to the uterus in the broad ligament to the junction of the fallopian tubes and the uterus. The pulsed Doppler waveform of the uterine artery demonstrates moderate- to high-velocity/high-resistance flow. The RI of the uterine arteries varies, possibly in part because of increased uterine flow associated with estrogen. Postmenopausal women have a statistically higher RI ( $0.89 \pm 0.06$ ) than women in the reproductive age group ( $0.86 \pm 0.04$ ). Kurjak and Kupesic<sup>31</sup> demonstrated that the RI of the uterine arteries of postmenopausal women increases with years after menopause. In patients in the reproductive age group, the RI is statistically higher in the proliferative phase of the menstrual cycle ( $0.88 \pm 0.05$ ) than in the luteal phase ( $0.84 \pm 0.06$ ).<sup>24,31,32</sup> During the proliferative phase, the RI decreases 1 to 2 days before ovulation and then increases 24 hours before ovulation.<sup>1,24</sup> There is generally no significant difference in RI between the right and left uterine arteries irrespective of the side of ovulation.<sup>24</sup> The uterine artery RI decreases significantly in pregnancy.<sup>24</sup>

In the radial arteries, the mean peak systolic flow velocity is approximately 23 cm/second (range, 9 to 44 cm/second), with a mean RI of 0.74 in the follicular phase dropping to 0.68 in the luteal phase.<sup>31-33</sup> The range of radial artery RI is

approximately 0.59 to 0.86.<sup>33</sup> Visualization of the radial arteries becomes more difficult with advancing years after menopause. In Kurjak and Kupesic's study,<sup>31</sup> only 33% of women more than 16 years postmenopause had sonographically demonstrable radial arteries.

Visualization of endometrial (spiral artery) blood flow (Fig. 26-29) is generally possible in the periovulatory period, occurring as early as day 8 of the menstrual cycle.<sup>31-37</sup> Using TVCFD, the spiral arteries can be visualized in the functional zone of the endometrium during this period.<sup>37</sup> The RI of the spiral arteries decreases from approximately 0.64 in the follicular phase to 0.50 in the luteal phase.<sup>31</sup> In women 1 to 5 years postmenopause, Kurjak and Kupesic<sup>31</sup> demonstrated a mean RI in the spiral arteries of 0.72. They were able to demonstrate the spiral arteries in only 30% of women 1 to 5 years postmenopause and in no women who were more than 5 years postmenopause. Failure to visualize the spiral arteries in the subendometrial region and within the functional zone may be associated with infertility and may be predictive of outcome in in vitro fertilization.<sup>38</sup>

Uterine venous channels follow a course similar to that of the arteries.<sup>20</sup> The arcuate venous plexus accompanies the arcuate arteries, passing circumferentially within the myometrium (Figs. 26-30 and 26-31). The venous plexus is



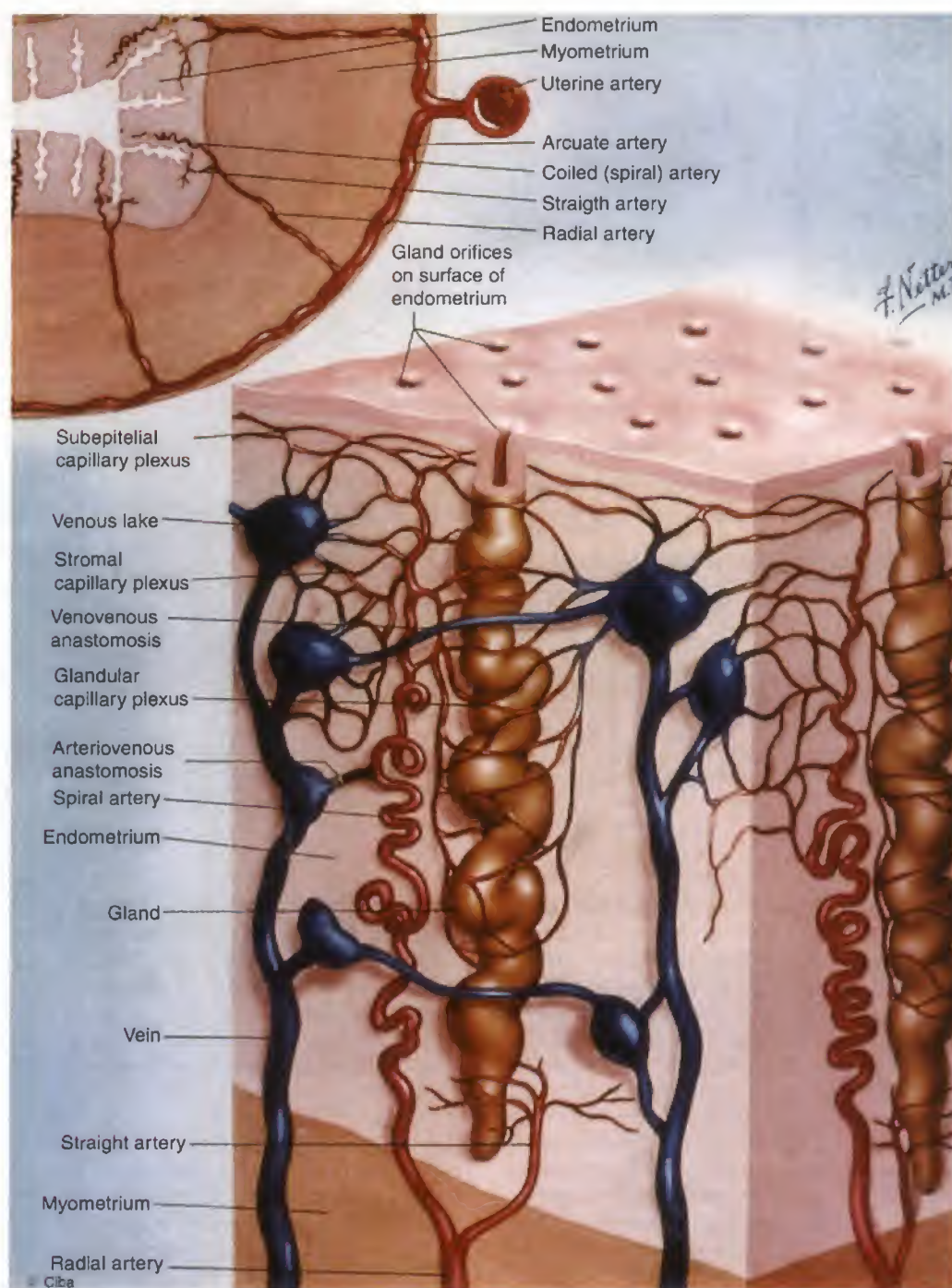


**FIGURE 26-27.** Diagram of a uterine cross-section and deep section showing the uterine artery, arcuate plexus, radial, straight, and spiral arteries. (Copyright 1954 Novartis. From Netter FH: *The CIBA Collection of Medical Illustrations*, Volume 2, Reproductive System. Section VI, Plate 23. Summit, NJ, CIBA-Geigy Co, 1954. Copyright 1981, 1990, 1965 & 1998. Novartis. Reprinted with permission from *Clinical Symposia*, Vol. 33/1; 42/2; *Netter Collection*, Vol. 2 & *Interactive Atlas*, illustrated by Frank H. Netter, M.D. & John A. Craig, M.D. All rights reserved.)





**FIGURE 26-28.** Uterine radial artery. Transvaginal sonogram in the sagittal plane in a patient with a retroverted uterus. A radial artery (arrow) is demonstrated coursing from the arcuate arterial plexus toward the endometrium.

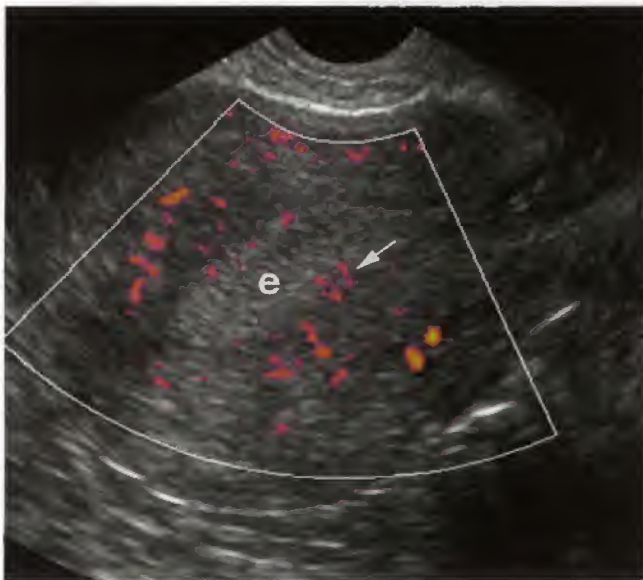


**FIGURE 26-29.** Spiral artery. Transvaginal sonogram in the sagittal plane demonstrating flow within a spiral artery (arrow) in the endometrium (e).

larger than the associated arterial channels and is frequently identified sonographically by both the transabdominal and transvaginal approaches.

The ovarian arteries arise from the lateral margin of the aorta at a level slightly inferior to the renal arteries. At the pelvic brim, they cross the external iliac artery and vein and course medially within the suspensory (infundibulopelvic) ligament of the ovary (see Figs. 26-21 and 26-32). The ovarian artery passes posteriorly in the mesovarium and breaks up into branches.

Ovarian arterial blood flow varies according to the stage of the menstrual cycle. Before formation of the dominant

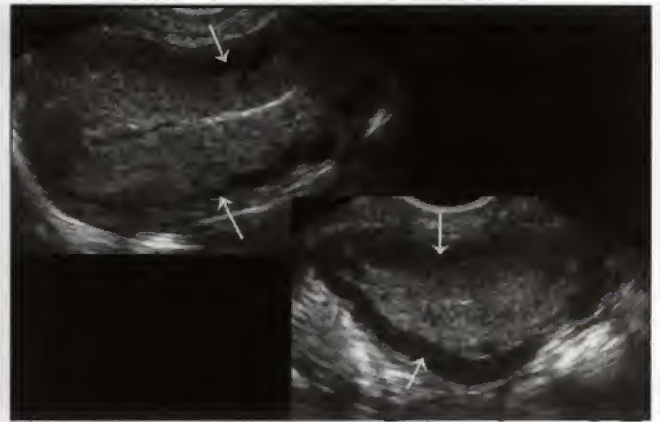
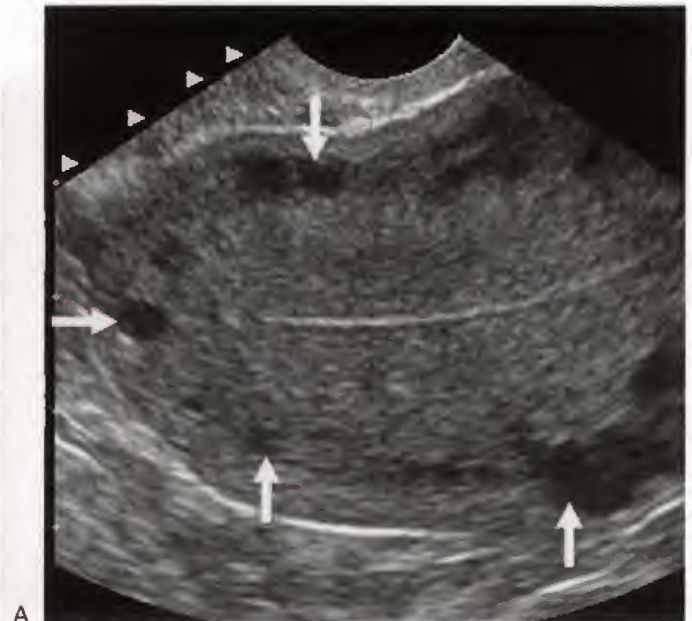


**FIGURE 26-30.** Arcuate venous plexus. Transvaginal sonogram in the sagittal (A) and coronal (B) planes demonstrating a prominent arcuate venous plexus (arrows).



A



B

**FIGURE 26-31.** Arcuate venous plexus-power Doppler. A. Transvaginal sonogram in the coronal plane demonstrating a prominent arcuate venous plexus (arrows). B. Power Doppler image of the same patient demonstrating blood flow within the venous plexus.





**FIGURE 26-32.** Ovarian artery. A. Transabdominal sagittal oblique sonogram through the right ovary (Ov) demonstrating the right ovarian artery. B. Similar scan plane with pulsed Doppler showing a peak systolic velocity of 100 cms/sec.

follicle, flow is often low velocity and high resistance. Diastolic flow is low or absent,<sup>1-3</sup> and the mean RI is approximately  $0.92 \pm 0.08$ ,<sup>31</sup> with a peak velocity in the 10 to 40 cm/second range.<sup>39</sup> The peak systolic velocity remains relatively constant in the ovarian arteries bilaterally irrespective of the side of ovulation.<sup>39</sup> The impedance drops dramatically in the ovarian artery on the side with the dominant follicle in the periovulatory period and luteal phase. The RI of the ovarian artery on the side with the dominant follicle drops in the late follicular phase (days 12 to 14) to a mean RI of  $0.86 \pm 0.04$  and by the early luteal phase flow is low resistance,<sup>1-3</sup> most obvious by day 21, when the mean RI is approximately  $0.83 \pm 0.04$ .<sup>31</sup> The RI rises during the late luteal phase.<sup>3</sup> The changes in RI are thought to be due to hormone-mediated changes in vessel wall compliance, allowing increased blood flow to the ovary in the late follicular and early luteal phases.<sup>3</sup> The nondominant ovary does not show cyclic changes, and the waveform remains high resistance throughout the cycle.

In postmenopausal women, the mean ovarian arterial RI is approximately 0.94 in the first 5 years postmenopause. In women 11 years or greater postmenopause, there is absent diastolic flow corresponding to an RI of 1.0.<sup>31</sup>

Intrafollicular (flow in the wall of the follicle) arterial flow velocity increases approximately 29 hours before follicle rupture, and the rise continues until approximately 72 hours after the formation of the corpus hemorrhagicum<sup>40</sup> (Fig. 26-33). The RI in the late follicular phase is approximately  $0.54 \pm 0.04$ .<sup>41</sup> The corpus luteum becomes highly vascularized within a few days after ovulation to provide a conduit for the delivery of luteal steroids to the general circulation.<sup>39</sup> The waveform of the corpus luteum is low resistance, with an RI in the early luteal phase of approximately  $0.44 \pm 0.4$ , rising in the late luteal phase to approximately  $0.50 \pm 0.04$ .<sup>41</sup>

Intraovarian arterial flow can be visualized within the stroma of the ovary using TVCFD and power Doppler<sup>42</sup>

(Fig. 26-34). Visualization of intraovarian flow can be observed more frequently in the luteal phase than in the early follicular or periovulatory phases.<sup>27</sup> In Kurjak and Kupesic's series,<sup>31</sup> it was not possible to detect intraovarian flow in postmenopausal patients.

Veins emerge from the hilum of the ovary forming the pampiniform plexus. These veins join together to form the ovarian vein, which ascends out of the pelvis adjacent to the ovarian artery.<sup>20</sup> The right ovarian vein empties into the inferior vena cava just below the renal vein. The left ovarian vein empties into the left renal vein. The ovarian veins, unlike the ovarian arteries, may become enlarged in pregnancy.<sup>20</sup>

The lymph nodes and lymphatic channels are not normally visualized by sonography. However, knowledge of the location of the major lymph node groups is important to recognize them when they are pathologically enlarged. The main groups are (1) the common iliac lymph nodes that accompany the common iliac artery; (2) the external iliac lymph nodes that are situated in the false pelvis and pelvic side wall lateral to the bladder and are associated with the external iliac artery and vein; and (3) the internal iliac lymph nodes that surround the internal iliac vessels. Outlying groups include the sacral and obturator nodes.

The lymphatic drainage of the pelvic viscera is variable. The following is a general guideline to drainage of specific viscera, which is important in assessing nodal spread in neoplasia:

1. Ovaries: the lymphatic channels ascend along the ovarian arteries to the lateral aortic and periaortic nodes at the level of the renal hila.
2. Cervix: the lymphatic channels course lateral in the parametrium to the external iliac nodes, posterolateral to the internal iliac nodes, and posterior to the rectal or sacral nodes.

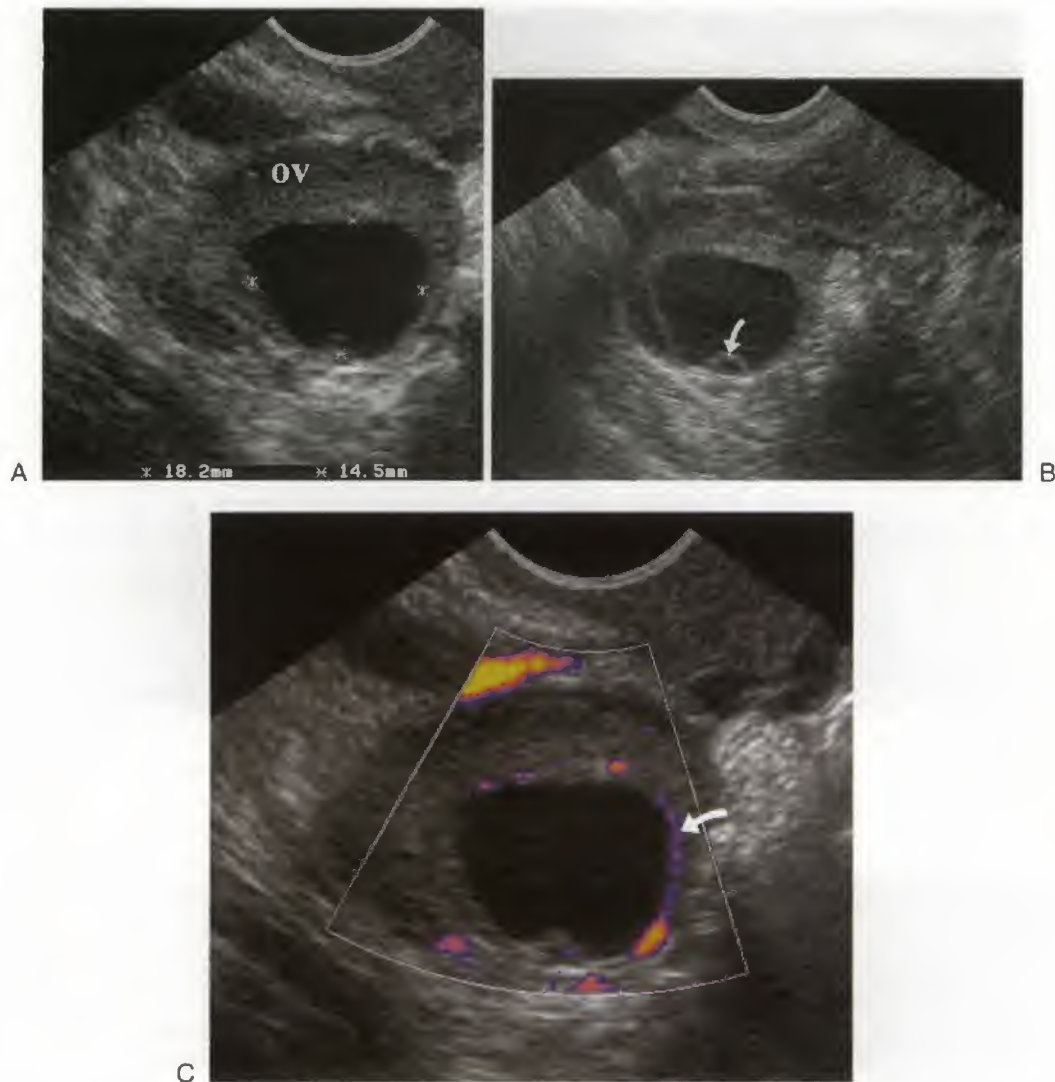


**FIGURE 26-33.** Intrafollicular flow. *A.* Transvaginal coronal oblique sonogram through the right ovary (OV) demonstrating a follicle measuring approximately 1.8 cm in maximal diameter. *B.* The cumulus oophorus (arrow) within the follicle. *C.* Power Doppler image demonstrating flow (arrow) in the wall of the follicle.

3. Uterus, lower corpus: the lymphatics course lateral to the external iliacs through the parametrium.
4. Uterus, lower corpus, fundus, and tube: the lymphatics accompany the ovarian channels.
5. Vagina: the lymphatics of the upper vagina accompany the uterine artery to the internal and external iliac lymph nodes, whereas those of the midvagina accompany the vaginal artery to the internal iliac lymph nodes. The vagina external to the hymen drains to the superficial inguinal nodes. This reflects the embryologic origin of the vagina, in which the fibromuscular wall of the upper two thirds of the vagina arises from the paramesonephric (müllerian) duct, which also gives rise to the uterus and fallopian tubes. The lower one third of the vagina arises from the urogenital sinus and, therefore, shares the lymphatic drainage with the external genitalia.

## THE UTERUS AND VAGINA

The uterus is located in the true pelvis between the urinary bladder anteriorly and the rectosigmoid posteriorly. The anterior surface of the uterus is covered with peritoneum to the level of the junction between the uterine corpus and cervix. The peritoneal space anterior to the uterus is the vesicouterine pouch or anterior cul-de-sac (see Figs. 26-3 and 26-6 to 26-9). This space is usually empty but may contain loops of small bowel. Posteriorly, the peritoneal reflection extends to the posterior fornix of the vagina (Fig. 26-35), forming the posterior cul-de-sac. Laterally, the peritoneal reflection forms the broad ligaments.

The uterus consists of two major parts: the body, or corpus, and the cervix, which is the lower cylindrical portion that projects into the vagina (Fig. 26-36). The isthmus is a narrow portion of the uterus that corresponds to the



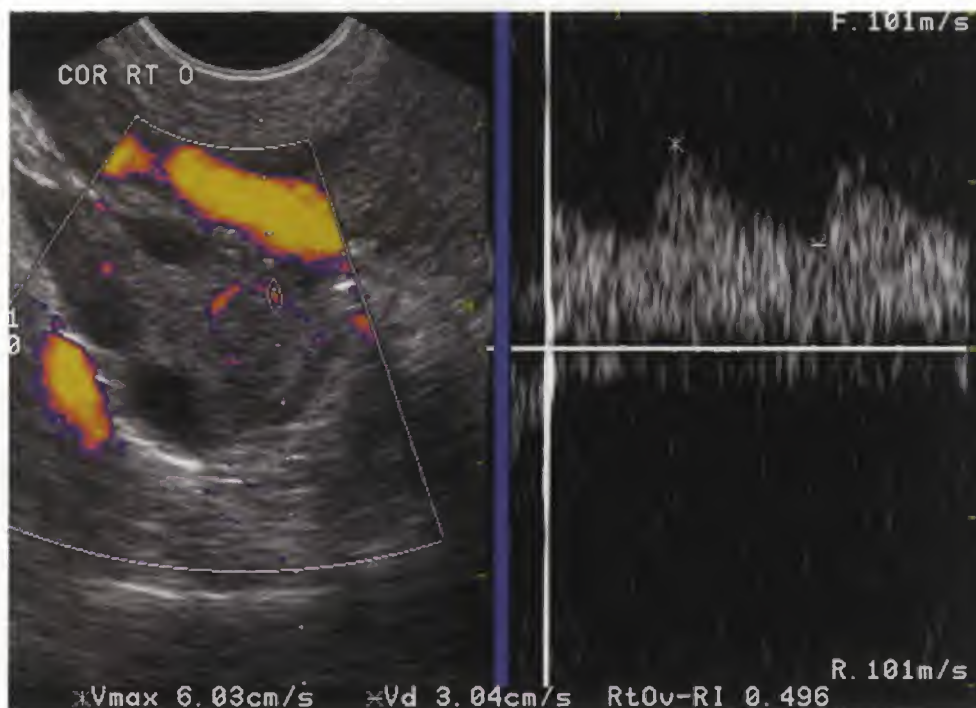


**FIGURE 26-34.** Intraovarian arterial flow. Transvaginal sonogram in the coronal oblique plane through the right ovary demonstrating arterial flow.



**FIGURE 26-35.** Posterior cul-de-sac/posterior vaginal fornix. Transvaginal sonogram in the sagittal plane through the uterine cervix with bowel (B) in the posterior cul-de-sac. The posterior wall of the vagina (arrows) is seen merging with the posterior lip of the cervix (P). The posterior fornix is demonstrated by a thin echogenic line (curved arrow). The external cervical os is seen at the end of the echogenic endocervical canal (short arrow).

approximate position of the internal os and is the separation between the corpus and cervix.<sup>43</sup> The anterior surface of the corpus is almost flat, whereas the posterior surface is convex. The uterine fallopian tubes emerge from the cone-shaped cornua of the uterus, which are situated at the junction between the superior and lateral uterine margins. The fundus of the uterus is the superior portion of the uterus between the insertion of the uterine fallopian tubes.<sup>19,43</sup> The

ratio of the length of the body and fundus varies with age. Before menarche, the corpus is approximately one half the length of the cervix; in nulliparous women, the corpus and cervix are of approximately equal length; and in multiparous women, the corpus is about twice the length of the cervix.<sup>19,43</sup> The corpus is predominantly muscular, whereas the cervix is composed predominantly of collagenous and elastic tissue; the proportion of smooth muscle is only about 10%.<sup>19,43</sup>

The size of the uterus is variable. In adults of reproductive age, the uterus measures approximately 6 to 8.5 cm in length in nulliparous women and 8 to 10.5 cm in length in multiparous women.<sup>19,44-46</sup> The width of the corpus measures approximately 3 to 5 cm in nulliparous women and 4 to 6 cm in multiparas. The anteroposterior (AP) diameter is 2 to 4 cm in nulliparas and 3 to 5 cm in multiparas.<sup>46</sup>

After menopause, the uterus atrophies. In women who are more than 5 years postmenopause, the uterus measures 3.5 to 7.5 cm in length,<sup>45,46</sup> 2 to 4 cm in width, and 1.7 to 3.3 cm in AP dimension.<sup>46</sup>

The prepubertal uterus measures approximately 2.0 to 4.4 cm in length.<sup>47,48</sup> Uterine length in neonates is similar, but the endometrium is thicker and more echogenic than in the prepubertal uterus, likely on the basis of high maternal estrogen levels resulting from placental estrogen production.<sup>48</sup> Uterine growth begins at approximately age 7 to 8 years, accelerates during puberty, and continues until approximately 20 years of age.<sup>49</sup>

Uterine position is highly variable and changes with varying degrees of bladder and rectal distention. The cervix can be identified sonographically in the sagittal plane as that portion of the uterus immediately posterior to the angle of

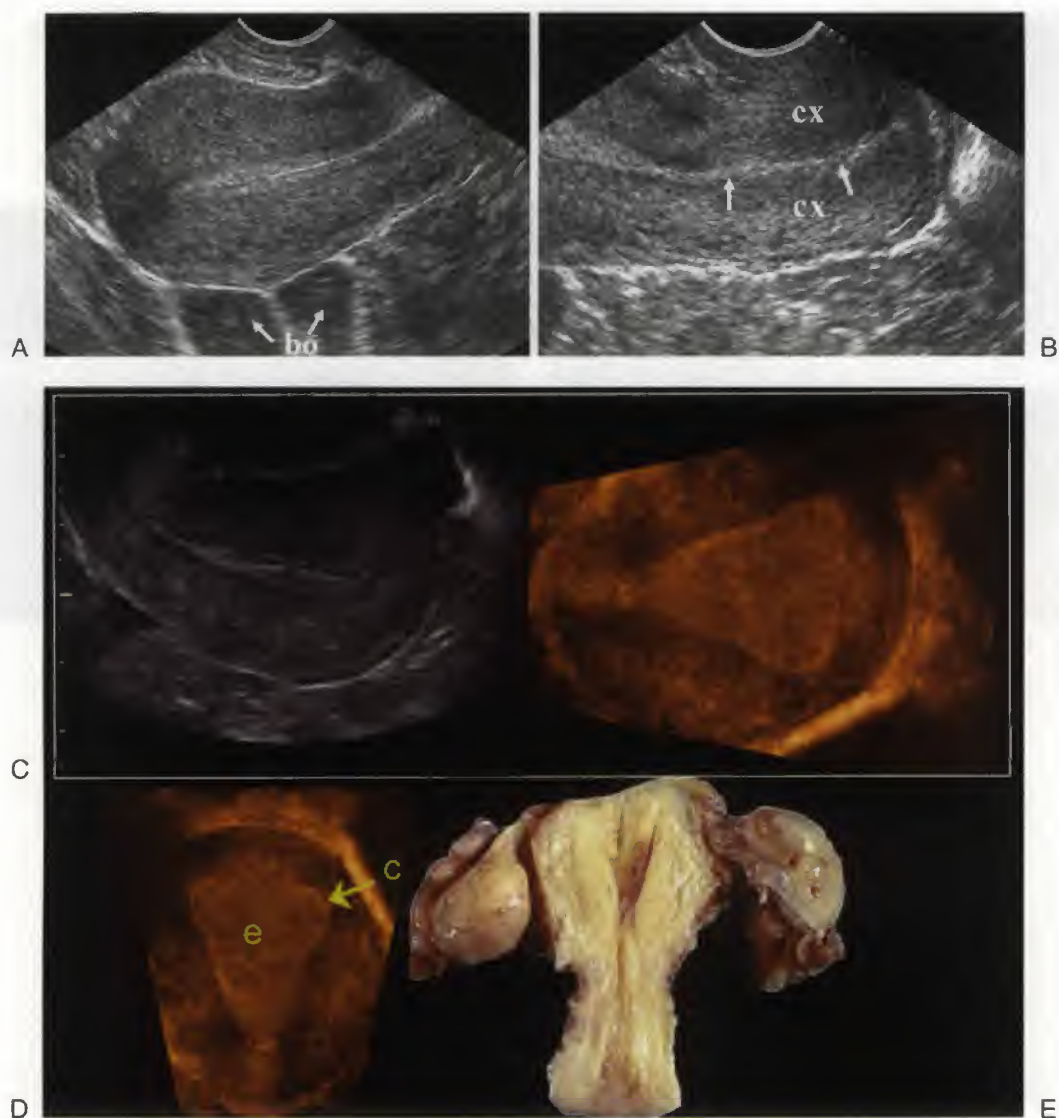


**FIGURE 26-36.** A. Transvaginal sonogram in the sagittal plane demonstrating the corpus of the uterus. bo, bowel. B. Inferior angulation of the probe demonstrates the cervix (cx) and the endocervical canal (arrows). C. This two-image set is a typical two-dimensional sagittal image of the uterus (on the left) with the three-dimensional rendered image in the coronal plane (on the right). D. The three-dimensional coronal view has been rotated showing the triangular shaped echogenic endometrial canal (e). The fallopian tubes and ovaries are not seen in this case. E. A postoperative specimen of the uterus, tubes, and ovaries from a different patient showing an appearance comparable to the coronal image in D.

the bladder (see Fig. 26-3). The cervix is anchored at the angle of the bladder by the parametrium and is less freely movable than the corpus and fundus. The cervix and the vagina form a 90-degree angle, a condition referred to as anteversion (Fig. 26-37). The more movable corpus is usually flexed anteriorly on the cervix (anteflexed). Filling of the bladder usually straightens out the uterus so that on TAS the uterus does not appear anteflexed (see Fig. 26-3B) and the angle between the cervix and vagina is greater than 90 degrees. Retroversion (see Fig. 26-28), retroflexion (Fig. 26-38), and tilting of the uterus to the right or the left are considered to be normal variants in position unless the uterus is displaced by pelvic pathology.<sup>43</sup> Retroversion of the uterus can result in poor visualization of the endometrial canal on TAS and widening of the adnexa because of

visualization of the broad ligaments. In addition, as a result of attenuation of sound by the uterus, the fundus of a retroverted uterus may be “echo poor” in appearance. This “dropout” phenomenon may simulate the appearance of a fundal fibroid. The differentiation between the fundal fibroid and dropout of sound may be made by the lack of displacement of the endometrial canal and the lack of a contour abnormality of the latter. Alternatively, dropout in the fundus of a retroverted uterus is usually not a problem in TVS. The transvaginal approach is used to better assess the myometrium and endometrial canal and to detect the presence of a fibroid or other myometrial pathology. The retroverted uterus may also be difficult to assess with the TAS because the endometrial canal may be parallel to the sound beam and not be resolved (Fig. 26-39). When the



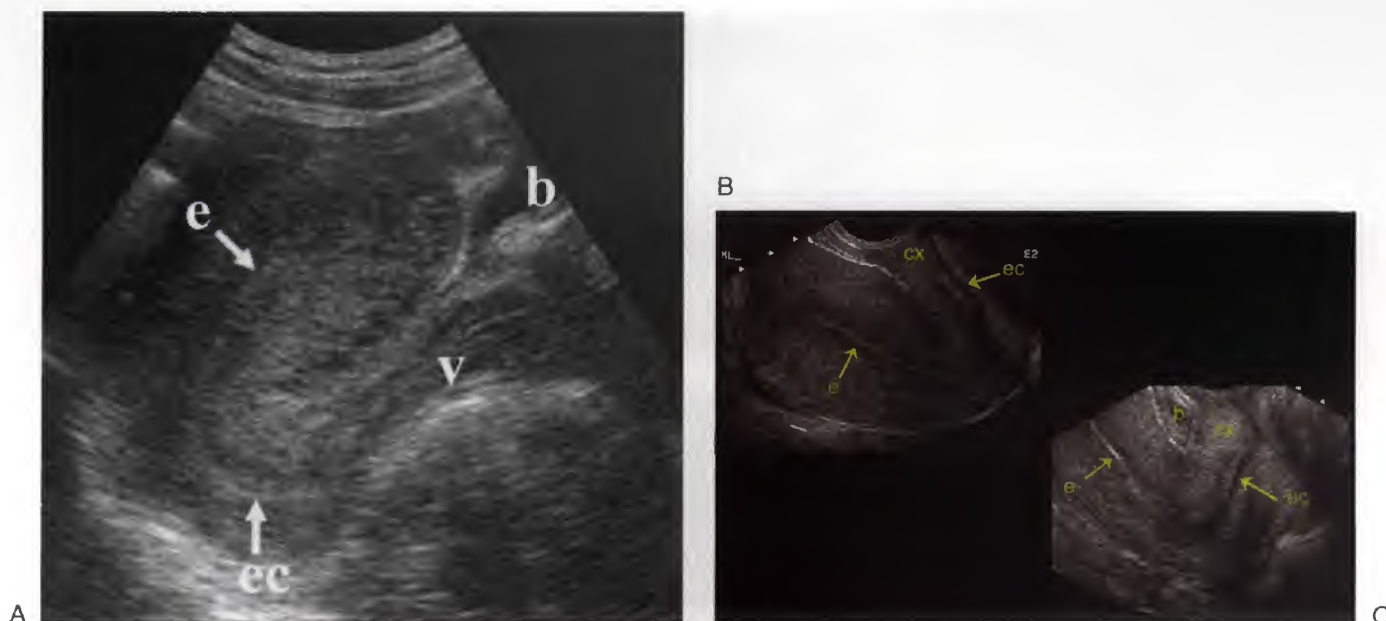


**FIGURE 26-37.** Anteflexed uterus. A. Transabdominal sonogram in the midline sagittal plane through the uterus. The bladder (b) is almost completely empty. v, vagina. B. Transvaginal midsagittal scan of an anteflexed uterus. C. Transvaginal scan of the cervix and lower uterine segment. The bladder (b) is almost empty. The endocervical canal (ec) and endometrial canals (e) form an angle of approximately 90 degrees in all three images.

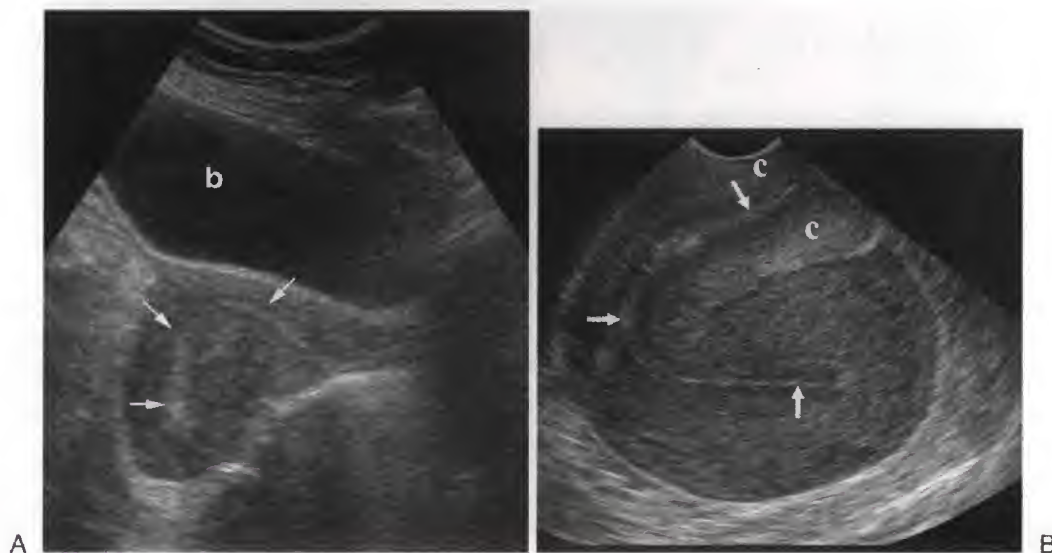


**FIGURE 26-38.** Retroflexed uterus. Transabdominal (A) and transvaginal (B) sonograms in the midline sagittal plane through the uterus demonstrating a retroflexed uterus. Endometrial and endocervical canals (arrows). b, bladder; c, cervix.

uterus is retroflexed, the cervix may be interposed between the probe and the body of the uterus, making assessment of the myometrium difficult (Fig. 26-39B). To improve uterine visualization with the transvaginal probe, one must move the probe around the cervix. In this situation, move it posteriorly so that the probe now lies immediately adjacent to the body and fundus of the uterus (Fig. 26-39C). In this position, the person scanning can also use the probe to “palpate” the uterus and detect the presence of tenderness, which is seen in adenomyosis and endometritis.

The muscular layer of the uterus (myometrium) is composed of three distinct layers that can be differentiated sonographically.<sup>6</sup> The outer layer of the myometrium consists of longitudinally oriented fibers that course over the fundus and converge at the cervix and cornua. The outer layer is separated from the intermediate layer by the arcuate vessels and is hypoechoic compared with the intermediate layer (Fig. 26-40). The intermediate layer is the thickest of the three layers. The muscle fibers consist of spiral bands extending from cornua to cervix, which interdigitate in the

midsagittal plane. The intermediate layer is considerably more echogenic than the inner layer and slightly more echogenic than the outer layer (see Fig. 26–40). The inner layer consists of longitudinal and circular fibers. The sonographic appearance is that of a thin hypoechoic halo surrounding the endometrium (see Fig. 26–40).

Contraction waves of the myometrium can be demonstrated sonographically. These waves are most apparent on videotapes or cine loops of real-time images played back at five times regular speed. The myometrial contractions result in a transmitted stripping motion of the endometrium typically beginning at the cervix and extending to the uterine fundus. The contractions increase in frequency in the periovulatory phase and are reversed in the menstrual phase.<sup>50</sup>

Contraction waves of the inner layer of the myometrium may play a role in sperm transport, implantation, and

maintenance of pregnancy. Disordered and reversed contractions may be seen in some infertile patients. Waves arising from the cervix and extending to the fundus are seen less frequently in patients on oral contraceptives than in a matched control group.

The endometrium is a thin echogenic strip composed of a superficial layer (zona functionalis) and a deep basal layer. The thickness and sonographic appearance of the endometrium change cyclically with the menstrual cycle. In the menstrual phase, the endometrium is thin and brightly echogenic as the superficial layer is shed. During the early proliferative phase (days 5 to 9), the endometrium is a thin, brightly echogenic line (see Figs. 26–30 and 26–31). In the late proliferative phase (days 10 to 14), the functional zone of the endometrium increases in thickness under the influence of estrogen. During the late proliferative phase, the functional zone is thick and hypoechoic compared with the basal layer (see Figs. 26–7, 26–28, and 26–40). During the secretory phase (days 15 to 28), the functional layer becomes thickened, soft, and edematous under the influence of progesterone (Fig. 26–41). A glycogen-rich fluid is secreted by



**FIGURE 26–39.** A. Longitudinal transvesical sonogram of a retroverted uterus. The endometrial canal (arrow) in the body is not seen as it lies parallel to the ultrasound beam. b, bladder. B. Transvaginal sonogram in the sagittal plane of a retroverted uterus. The cervix (c) is interposed between the transvaginal probe and the body of the uterus. This gives suboptimal visualization of the myometrium and endometrial canal. C. Transvaginal sonogram of the body and fundus with the probe situated immediately adjacent to the uterus. There is better visualization of the endometrium (arrow).



**FIGURE 26–41.** Secretory endometrium. Transvaginal sonogram in the sagittal plane on day 19 of the menstrual cycle. The functional zone of the endometrium (f) has become isoechoic with the basal layer (b).

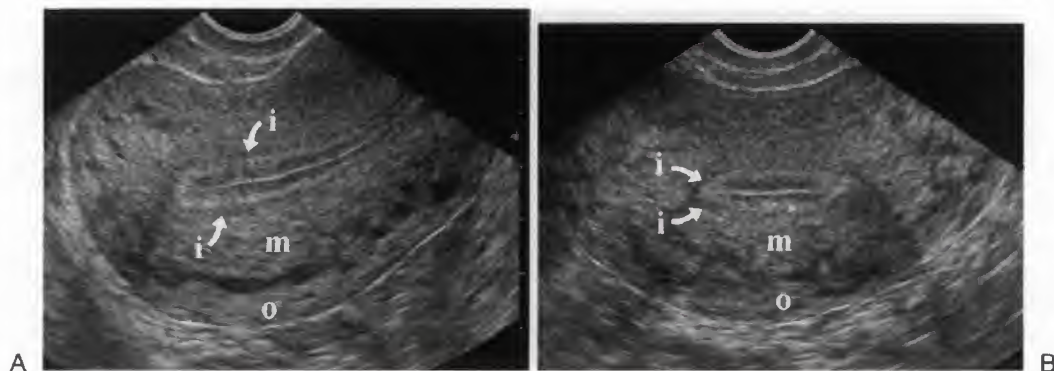


**FIGURE 26–40.** Myometrial layers. Transvaginal sonogram in the (A) sagittal and (B) coronal planes demonstrating the inner (i), middle (m), and outer (o) layers of myometrium.



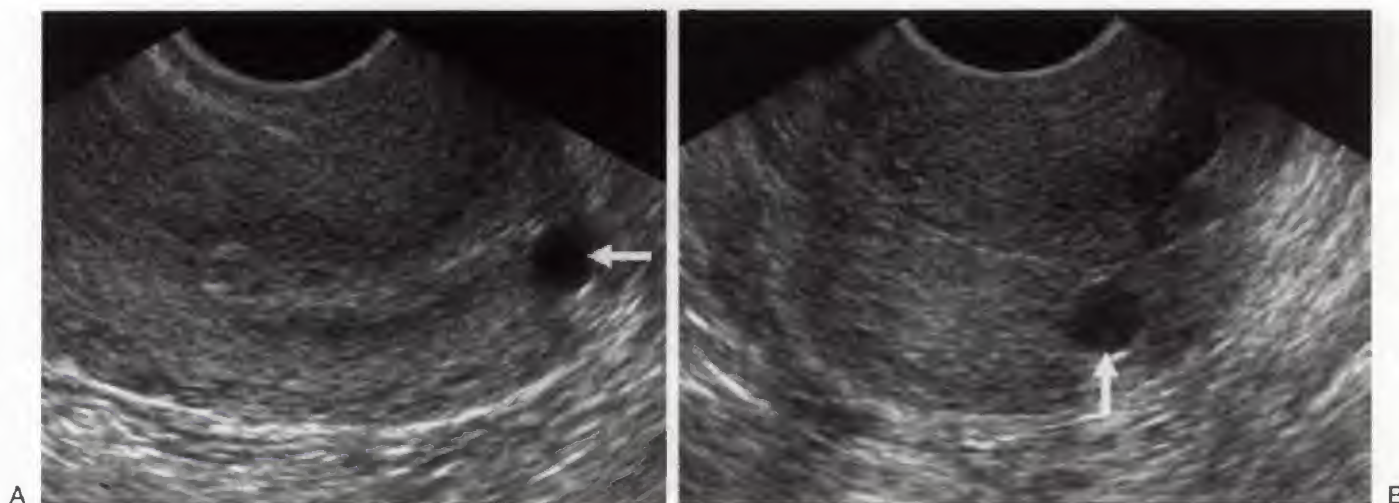


**FIGURE 26-42.** Nabothian cyst. Transvaginal sonogram in the (A) sagittal and (B) coronal planes through the uterine cervix demonstrating a nabothian cyst (arrow).

the glandular epithelium, and the spiral arteries become tortuous. The resultant effect is that the functional layer increases in echogenicity to become isoechoic to the basal layer.<sup>6</sup>

Measurement of the endometrial thickness should be performed in the sagittal plane of the uterus and should include both the anterior and posterior portions of the endometrium (i.e., the endometrial layers anterior and posterior to the endometrial canal). This is often referred to as the “double-layer” thickness. The hypoechoic halo (inner layer of the myometrium) should not be included in the measurement.

The endometrial thickness is normally 4 to 8 mm in the proliferative phase, 6 to 10 mm in the periovulatory period, and 7 to 14 mm in the secretory phase.<sup>6</sup> In postmenopausal women, the endometrium should measure less than 8 mm.<sup>51</sup> Eighty-one percent of postmenopausal women have an endometrial thickness of less than 8 mm. It should be remembered that this measurement is for normal asymptomatic patients. Patients with postmenopausal bleeding and an endometrial double-layer thickness of 5 mm or more should have further evaluation. Patients receiving hormone replacement therapy have a wider range of endometrial thickness than those receiving no exogenous hormones.<sup>51</sup>

The endometrial canal is best visualized with three-dimensional sonography using the rendered coronal image (see Fig. 26-36). The triangular shaped canal is seen on the coronal view with the upper angles being the cornual portions of the canal (c). They will be contiguous with the intramural portion of the fallopian tube (see Fig. 26-36B). This view is also the best, if not the only view that one can use to confidently diagnose a congenital uterine anomaly. In particular are the anomalies resulting from a lack of fusion of the two müllerian or paramesonephric ducts of the primitive uterus. Complete failure of fusion results in two fallopian tubes, two uteri, and even two vaginas. Partial failure will give a bicornuate uterus, which is difficult to differentiate with conventional scans from a uterine septum. This differentiation is important because there is a different treatment for each condition.

The cervix is best visualized transvaginally, with the tip of the probe about 2 to 3 cm from it, depending on the focal zone of the transducer. The endocervical canal is a continuation of the endometrial canal, appearing as a thin, echogenic stripe (see Fig. 26-36B). Fluid is sometimes seen in the endocervical canal, particularly in the preovulatory period. Occasionally, air can be seen in the vaginal fornices surrounding the cervix.

Numerous cervical glands extend from the endocervical mucosa into the adjacent connective tissue of the cervix. Occlusion of the cervical glands results in the formation of retention cysts, known as nabothian cysts<sup>19</sup> (Fig. 26-42).

The vagina is seen as a hypoechoic tubular structure with an echogenic lumen that curves inferiorly over the muscular perineal body at the introitus<sup>19,20</sup> (see Fig. 26-37). The bladder, trigone, and urethra are anterior to the vagina, and the rectum is posterior. The distal ureters are lateral to the upper vagina and pass anteriorly to enter the bladder. The cervix projects through the anterior vaginal wall, separating the vagina into the anterior, posterior, and two lateral fornices. The posterior fornix of the vagina is closely related to the rectouterine recess of the peritoneal cavity (posterior cul-de-sac) and is separated by the thickness of the vaginal wall and peritoneal membrane<sup>20</sup> (see Fig. 26-35).

## THE OVARIES

The ovaries are ellipsoid; the long axis is usually oriented vertically when the bladder is empty. Ovarian location is variable, especially in women who have been pregnant. In the nulliparous female, the ovaries are situated in the ovarian fossa (also known as the fossa of Waldeyer)<sup>20</sup> (see Fig. 26-2C). The ovarian fossa is situated on the lateral pelvic wall and is bounded by the obliterated umbilical artery anteriorly, the ureter and internal iliac artery posteriorly, and the external iliac vein superiorly.<sup>20</sup> One of the finger-like mucosal folds or fimbria, at the end of the fallopian tube is longer than the rest and is referred to as the ovarian fimbria. The ovarian fimbria and the suspensory (infundibulopelvic) ligament of the ovary are attached on the superior surface of





**FIGURE 26-43.** Three sectional views of the right ovary with multiple small follicles in a 34-year-old woman early in a normal menstrual cycle. A volume data set is collected and presented in three orthogonal views: transverse (A), sagittal (B), and coronal (C). The dimensions of the ovary are recorded using the electronic calipers, and the results are displayed in the image.

the ovary (see Fig. 26-20). The suspensory ligament of the ovary is a fold of peritoneum that arises from the pelvic side wall and contains the ovarian vessels and nerves. The inferior extremity of the ovary is slightly smaller than the superior (tubal) extremity. The inferior extremity is bound to the uterine cornua by the ovarian ligament, which lies within the broad ligament.<sup>20</sup> The lateral surface of the ovary is in contact with the parietal peritoneum lining the ovarian fossa, and most of the medial surface is covered by the uterine fallopian tube. The anterior border of the ovary is attached to the mesovarium. The hilus of the ovary, through which the vascular channels and nerves pass, is situated on the anterior border.<sup>15,20</sup>

Ovarian size varies depending on age, menstrual status, pregnancy status, body habitus, and phase of the menstrual cycle.<sup>52</sup> Cohen, Tice, and Mandel<sup>53</sup> measured ovarian volumes in premenarchal, menstruating, and postmenopausal subjects. In menstruating subjects, the mean ovarian volume was 9.8 mL, with 5% and 95% confidence intervals of 2.5 and 21.9 mL. For premenarchal girls, the mean was 3.0 mL, with 5% and 95% confidence intervals of 0.2 and 9.1 mL, and for postmenopausal patients 5.8 mL, with confidence intervals of 1.2 and 14.9 mL. Minor cyclic changes in volume were also identified, with highest volumes in the preovulatory phase and lowest volumes in the luteal phase.

Recruitment of follicles begins before the onset of menses. As fluid accumulates in the follicular antrum, the follicles increase in size and become sonographically visible. By the time the follicular size is 1 to 2 mm, they can be visualized with TVS. By day 5 to 7, multiple follicles are visible within the ovary<sup>54</sup> (Fig. 26-43). By day 8 to 12, one or more dominant follicles can be recognized (Fig. 26-44). Approximately 5% to 10% of patients have two dominant follicles. Up to 80% of patients have a second nondominant follicle that becomes almost as large as the dominant follicle. Nondominant follicles are usually smaller than 14 mm mean diameter.<sup>54</sup> For 4 to 5 days before ovulation, the dominant follicle grows

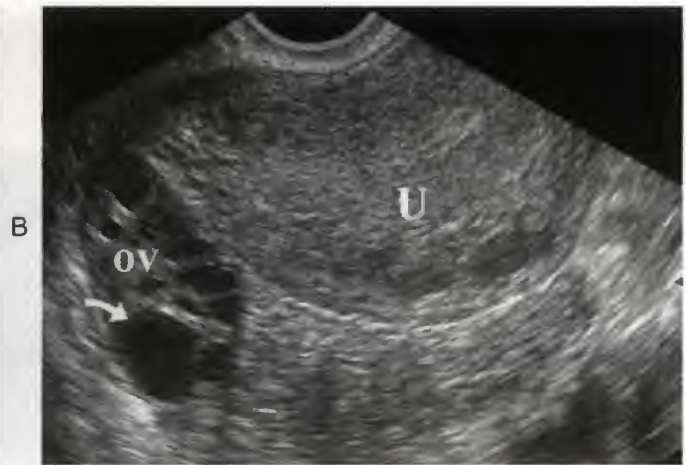


**FIGURE 26-44.** Dominant follicle. Transvaginal sonogram in the coronal oblique plane through the right ovary demonstrating a dominant follicle (arrow). ov, right ovary; U, uterus.

at a rate of 2 to 3 mm/day to reach a maximum mean diameter of approximately 20 mm (range, 16 to 28 mm).<sup>54</sup> Approximately 24 hours before ovulation, the granulosa layer separates from the theca layer, resulting in a hypoechoic ring. The cumulus oophorus (see Fig. 26-33) may occasionally be seen at this time.

Bleeding occurs into the follicle at the time of ovulation (corpus hemorrhagicum). The follicle decreases in size and may become echogenic or filled with echogenic debris or may be sonolucent if no internal bleeding has occurred. The corpus luteum may retain fluid over the next 4 to 5 days and increase in size to 2 to 3 cm<sup>54</sup> (Fig. 26-45). If pregnancy does not occur, the corpus luteum gradually involutes and atrophies to become the corpus albicans, which is not sonographically identifiable.

## THE UTERINE (FALLOPIAN) TUBE

The uterine fallopian tubes are variable in length, measuring approximately 7 to 12 cm.<sup>43</sup> Each tube is situated in the superior free margin of the broad ligament and is covered by peritoneum. The uterine fallopian tube is narrowest in the interstitial or intramural portion, which is contained within the muscular wall of the uterus. The interstitial portion of the uterine fallopian tube measures approximately 1 cm in length and can be visualized with TVS in the superior right and left lateral corpus of the uterus. The sonographic appearance is that of a fine, echogenic line arising from the endometrial canal and extending through the uterine wall (Fig. 26-46). Using three-dimensional ultrasound, one can obtain a superior image with the coronal view of the endometrial canal and interstitial portion of the fallopian tube (see Fig. 26-46C).

The isthmus is the narrow segment of the tube adjacent to the uterine wall. It is round and cord-like. The tube widens laterally, forming the ampullary and infundibular regions (see Fig. 26-20). The infundibulum is funnel shaped, terminates as the fimbriated end of the tube, and opens into the peritoneal cavity.<sup>43</sup> The peritoneal ostium of the uterine tube is approximately 3 mm in diameter. The isthmus,



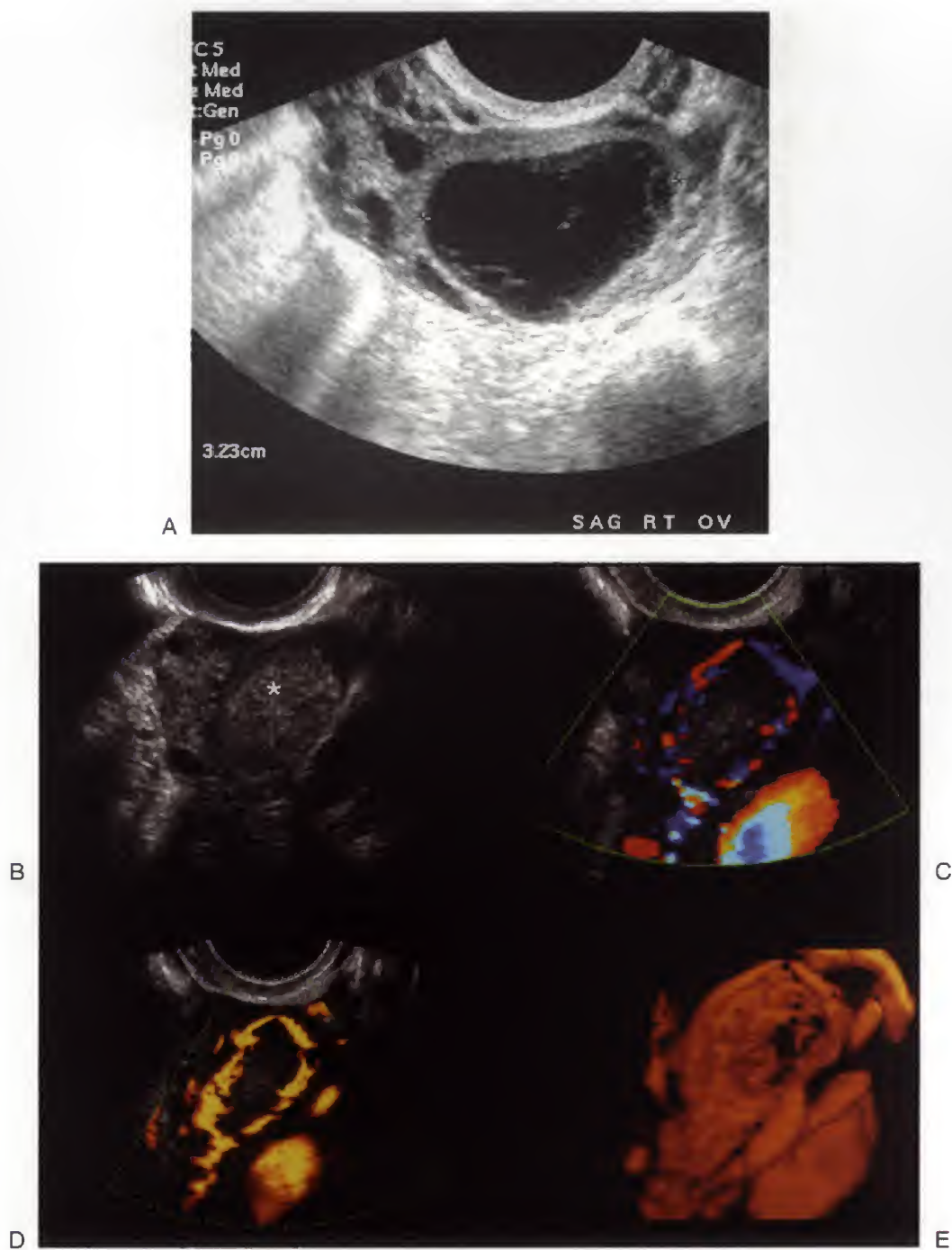


**FIGURE 26-45.** Corpus luteum cyst. *A.* Transvaginal sonogram in a parasagittal oblique plane through the right ovary demonstrating a hemorrhagic corpus luteum cyst measuring 3.23 cm in maximal diameter (calipers). *B.* The corpus luteum (\*) of another patient is filled with fresh echogenic blood and difficult to distinguish from normal ovarian tissue. *C.* Color flow Doppler surrounds the corpus luteum. *D.* Power Doppler of the corpus luteum. *E.* Three-dimensional power Doppler scan of the vasculature of the corpus luteum.

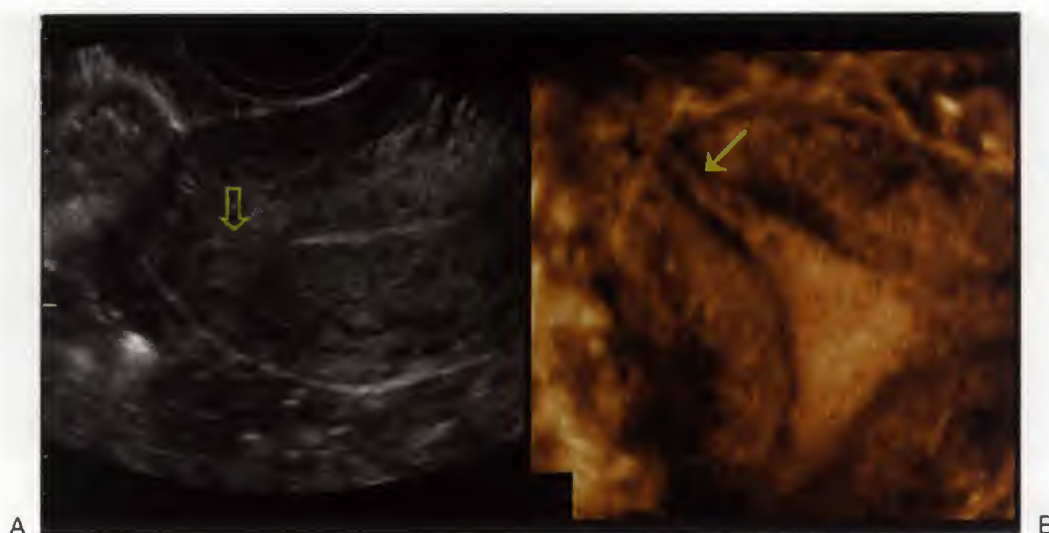


**FIGURE 26-46.** Interstitial portion of the fallopian tube. *A.* Transverse transvaginal scan of the uterine fundus showing the thin interstitial portion of the fallopian tube (*open arrow*). *B.* Three-dimensional coronal view of the uterine fundus showing the echogenic, triangular shaped endometrial canal and the interstitial portion of one tube (*arrow*) extending to the serosal surface. On three-dimensional ultrasound, this portion of the tube appears thicker than its true size.

ampulla, and infundibulum are usually not demonstrated with TAS or TVS unless there is tubal pathology or free fluid in the lateral pelvic recesses.

The vascular supply of the uterine tube comes from the vascular arch formed by the anastomosis of the uterine and ovarian arteries. Branches from this arch pass through the mesosalpinx to reach the uterine tube.<sup>43</sup>

## VESTIGIAL STRUCTURES

Part of the cranial end of the paramesonephric duct (which normally forms the uterus, uterine fallopian tube, and fibromuscular wall of the vagina) may persist as a vesicular appendage to the uterine fallopian tube referred to as a hydatid of Morgagni.<sup>55</sup> Hydatids of Morgagni may be visualized sonographically in the presence of free fluid (Fig. 26-47). Sonographically, they appear as small, unilocular, spheric, thin-walled cysts surrounded by the free intraperitoneal fluid.

The mesonephric ducts form the efferent ductules, epididymis, ductus deferens, seminal vesicles, and ejaculatory ducts in male fetuses. In female fetuses, the mesonephric ducts may persist as rudimentary, blind tubules in the parovarium, which is loose connective tissue in the mesosalpinx. Closer to the uterus, the mesonephric duct may persist as the duct of Gartner, which lies along the lateral wall of the uterus and vagina superior to the hymen.<sup>19,56</sup> Mesonephric duct remnants may persist as parovarian and Gartner duct cysts.

## THE URETERS

The ureters<sup>57</sup> are muscular tubes that measure 25 to 30 cm in length in the adult. In the pelvis, the ureters course within the extraperitoneal areolar tissue. In the true pelvis, the ureter begins anterior to the internal iliac artery and posterior to the ovary (Fig. 26-48). From there, it courses

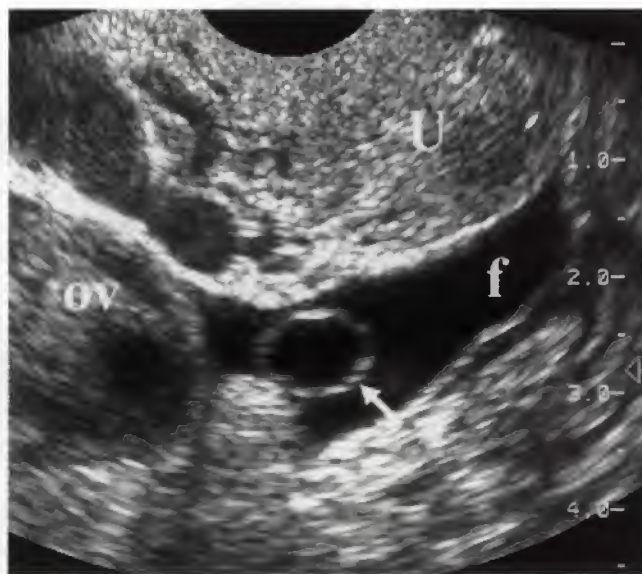


**FIGURE 26-47.** Hydatid of Morgagni. Transvaginal sonogram in the coronal plane demonstrating a hydatid of Morgagni (*arrow*) surrounded by free fluid (*f*) in the left lateral pelvic recess. *ov*, left ovary; *U*, uterus.

anteriorly and medially to lie within the inferior medial portion of the broad ligament, where it is in close proximity to the uterine artery. The ureter then runs anterior, situated in front of the lateral fornices of the vagina, about 2 cm lateral to the supravaginal cervix, and then passes medially to enter the trigone of the bladder anterior to the vagina (Fig. 26-49). The relationships of the ureter to the ovary, cervix, uterine artery, and vagina are of clinical importance because pelvic pathology may result in secondary hydronephrosis resulting from ureteric obstruction (Fig. 26-50). As a result, if a pelvic mass is present, we evaluate the kidneys after the postvoid examination during gynecologic sonography. This is done to confirm the presence





**FIGURE 26-48.** Longitudinal transabdominal sonogram of the right ovary (O) with a dilated ureter (U) demonstrated immediately posterior. B, bladder.

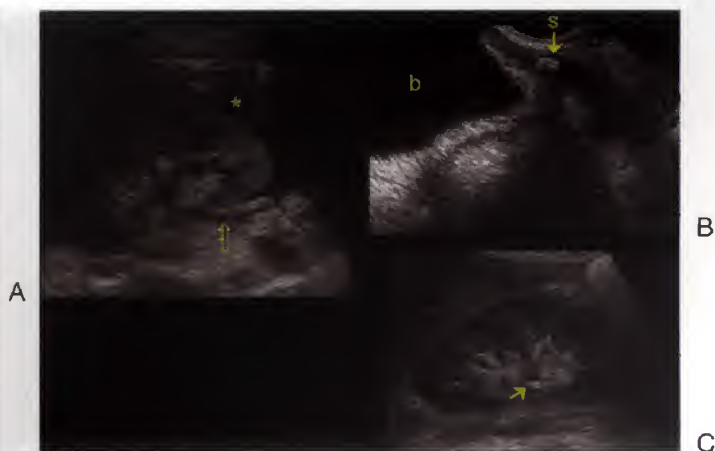


**FIGURE 26-50.** A. Longitudinal sonogram of the right kidney. There is mild hydronephrosis and dilatation of the proximal ureter (*open arrow*). After a calyx had ruptured, there was urine (\*) around the lower pole of the kidney. B. Transvaginal scan of the distal right ureter with a stone (s) or stones causing obstruction. b, bladder. C. Longitudinal sonogram of the right kidney with no hydronephrosis after insertion of a ureteric stent (*arrow*).

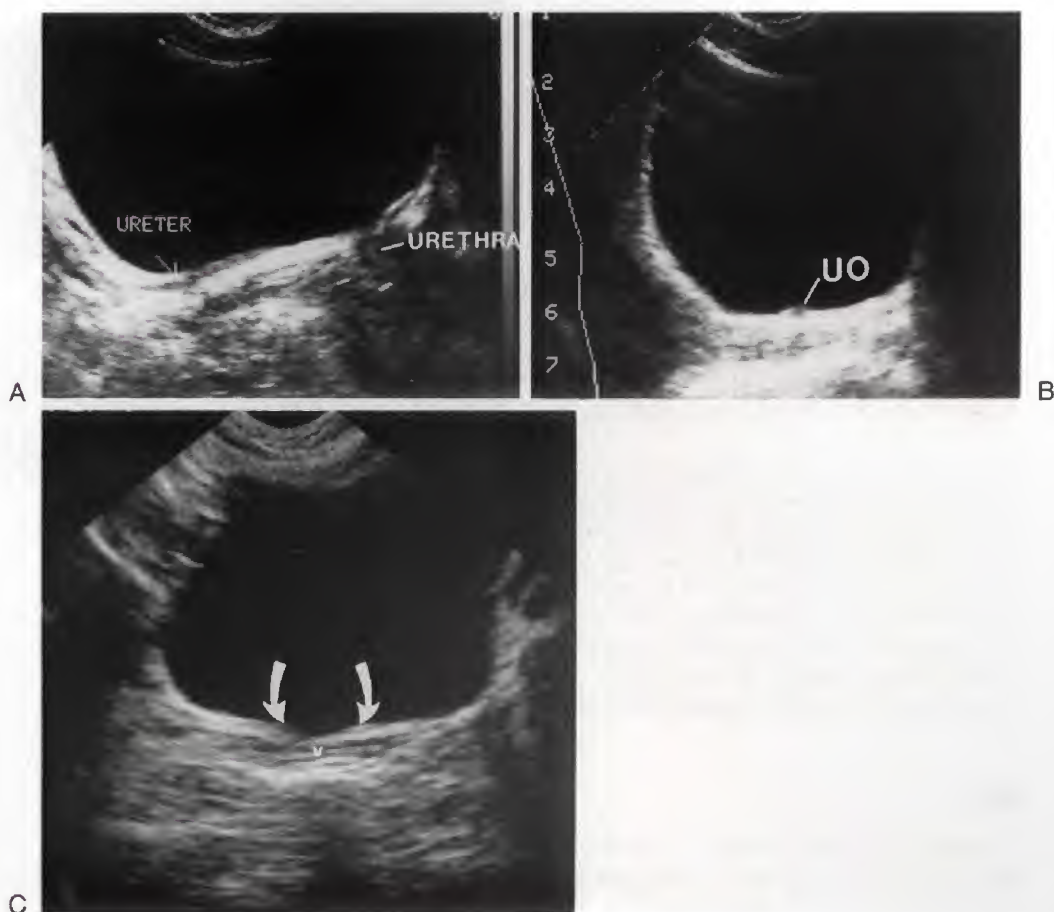


**FIGURE 26-49.** A. Longitudinal transabdominal sonogram of the right ureter and urethra. B. Longitudinal transabdominal sonogram of the right ureteric orifice (UO). C. Transverse transabdominal sonogram of both ureteric orifices (*curved arrows*). v, vagina.

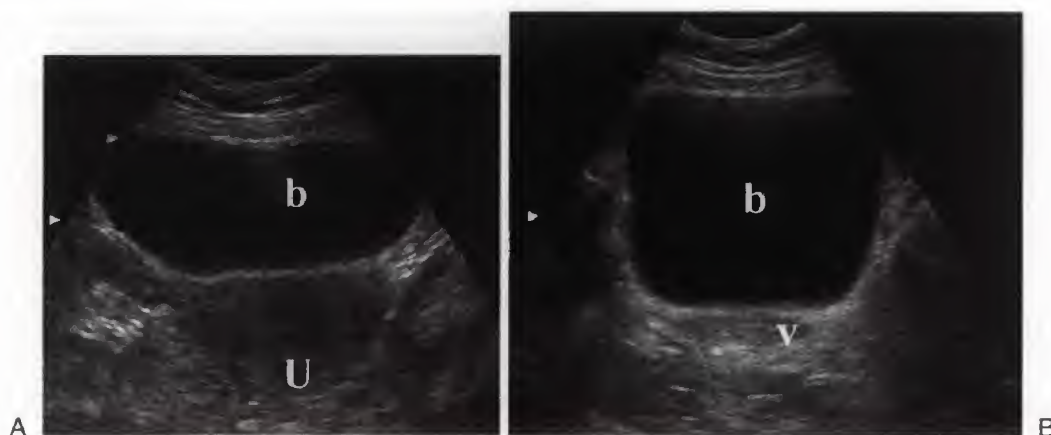


**FIGURE 26-51.** A. Transverse transabdominal sonogram of the urinary bladder at the level of the corpus of the uterus (U). At this level, the bladder (b) has a rounded or oval configuration. B. Transverse transabdominal sonogram of the urinary bladder at the level of the vagina (v). At this level, the bladder (b) has a square configuration.

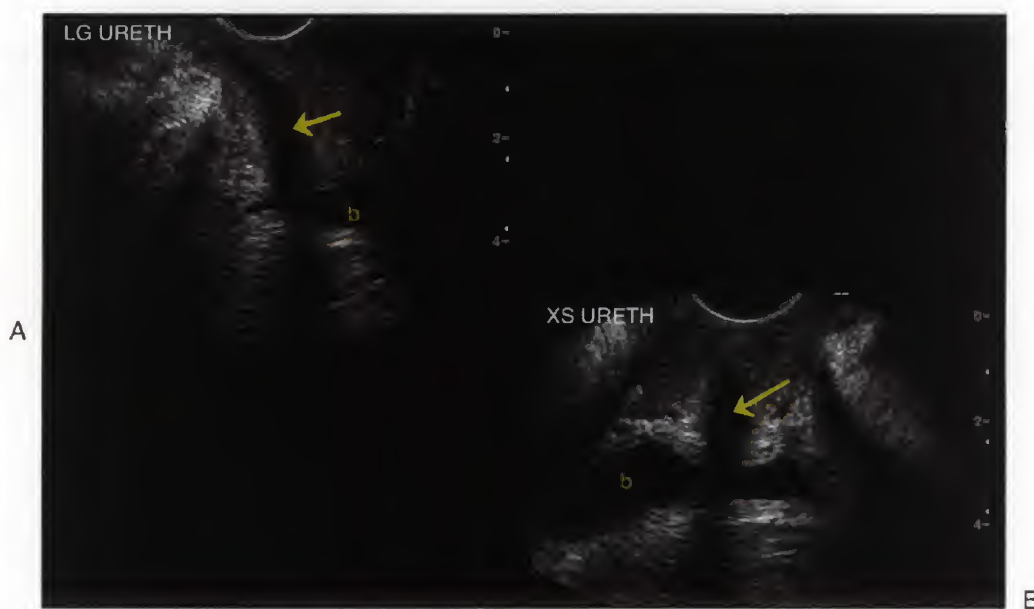


**FIGURE 26-52.** A. Longitudinal transvaginal scan of the urethra and bladder (b) outlet. The hypoechoic tubular structure (arrow) is the smooth muscle portion of the urethra. The central faint echogenic line is the collapsed urethral lumen the muscle is thickest anteriorly and in the mid portion of the urethra. B. Transverse transvaginal scan of the proximal portion of the urethra showing the hypoechoic smooth muscle portion (arrow). The walls of the urethra are collapsed. The urinary bladder (b) in this patient is almost empty.

of two kidneys, assess their position, and identify any degree of obstructive uropathy.

## THE URINARY BLADDER

The bladder is a distensible reservoir for urine. Its shape depends on the degree of distention of itself and neighboring viscera. The bladder is fixed inferiorly at the urethral orifice, base, and angle; and as it fills, the remainder of the walls displace movable viscera and conform to the space available within the confines of the true pelvis.<sup>57</sup> A transverse scan through the bladder superiorly gives it a rounded appearance. More inferiorly, the pelvic musculature and bones cause the bladder to appear square in the transverse plane (Fig. 26-51). The bladder wall is echogenic and should be of uniform thickness.

Transvaginal scanning enables better visualization of the trigone, posterior wall, and urethra. The ureteric and urethral orifices are visualized at the base and neck of the bladder, respectively.

The urethra can be seen throughout its length by translabial or better still, by transvaginal scanning (Fig. 26-52). The probe is placed at the introitus or just partially inserted into the vagina and directed upward. Around the inner layer of mucosa, there is a layer of smooth muscle and then an outer sheath of striated muscle. The longitudinally oriented smooth muscle is sonographically hypoechoic and is thicker on the anterior wall in the middle third of the urethra. The paraurethral glands of Skene lie posterior to the urethra near the urethrovaginal junction and empty through the paraurethral duct near the external urethral orifice. Urethral diverticula are distended urethral



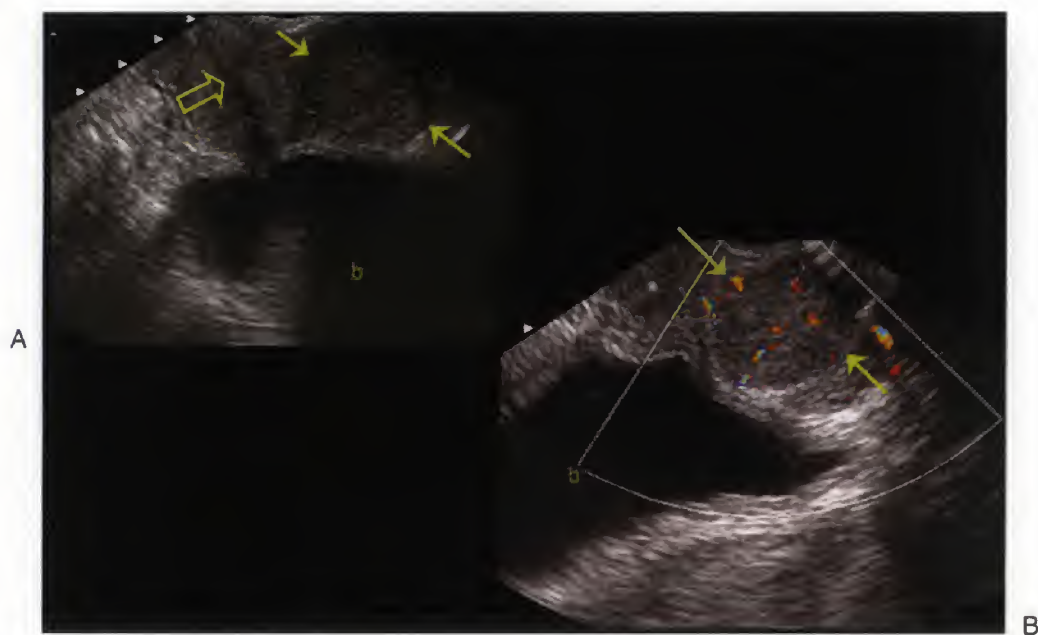


**FIGURE 26-53.** A. A longitudinal transvaginal scan of the urethra (open arrow) and bladder (b). The solid echogenic neoplasm is seen between the arrows at the base of the urethra posteriorly. B. Transvaginal scan with color Doppler shows some internal vascularity to the solid mass (between the arrows).

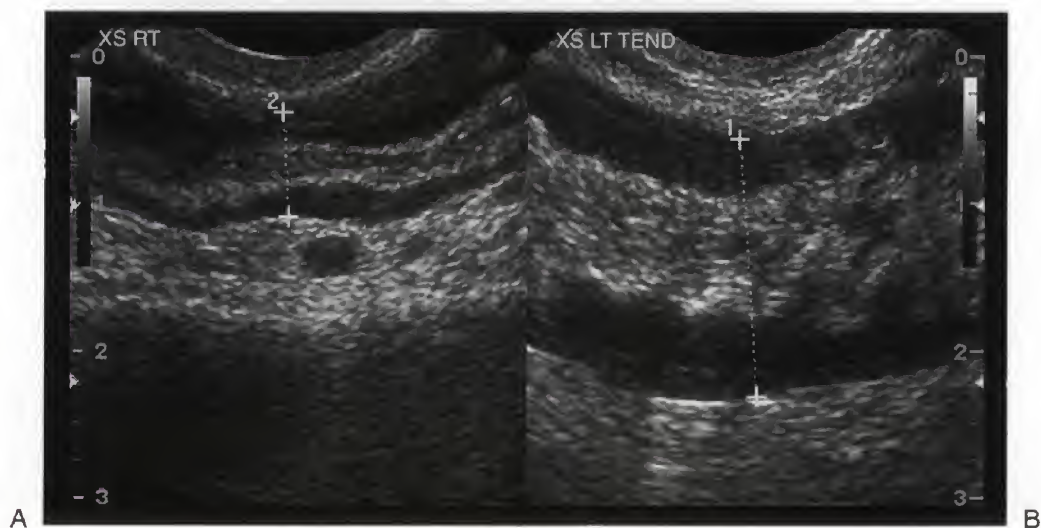


**FIGURE 26-54.** A. This transverse transvaginal scan through a section of normal sigmoid colon to the right of the midline. The overall thickness is 0.71 mm (calipers 2) compared with the abnormal segment in B. B. A scan in a similar plane but to the left of the midline showing a thick walled loop of bowel. The overall thickness is 1.7 cm. The muscularis layer (hypoechoic) and the submucosa (echogenic) is thicker in the abnormal, inflamed segment than in the normal segment. The inflamed segment was also focally tender when depressed with the transvaginal probe.

mucous glands and are found posterior and lateral to the urethra anywhere along its length. They may be a source of pelvic pain and recurrent urinary tract infection, and should be looked for in the appropriate clinical situation. Infected debris within a diverticulum may be seen as layering out of echogenic material within the cystic diverticular sac.

A neoplasm of the Skene gland may also be seen posterior to the urethra as a solid mass (Fig. 26-53).

## THE RECTOSIGMOID COLON

The sigmoid colon begins at the inlet of the true pelvis and is extremely variable in length. It has a mesentery, and its

course is variable, looping either to the left or right before ascending on the left to join the descending colon. The rectum begins at the third sacral vertebra and is fixed in position.<sup>15</sup> The rectosigmoid colon usually contains gas and fecal material that cast an acoustic shadow and may make identification or differentiation from pelvic masses difficult. Often, the differentiation between a pelvic mass and the rectosigmoid colon can be made by real-time imaging if peristalsis can be visualized or if the characteristic appearance of bowel wall can be identified (Fig. 26-54). Differentiation between bowel contents and a mass is not usually a problem if the transvaginal approach is used (see Figs. 26-8 and 26-36A). The sigmoid is best imaged with the

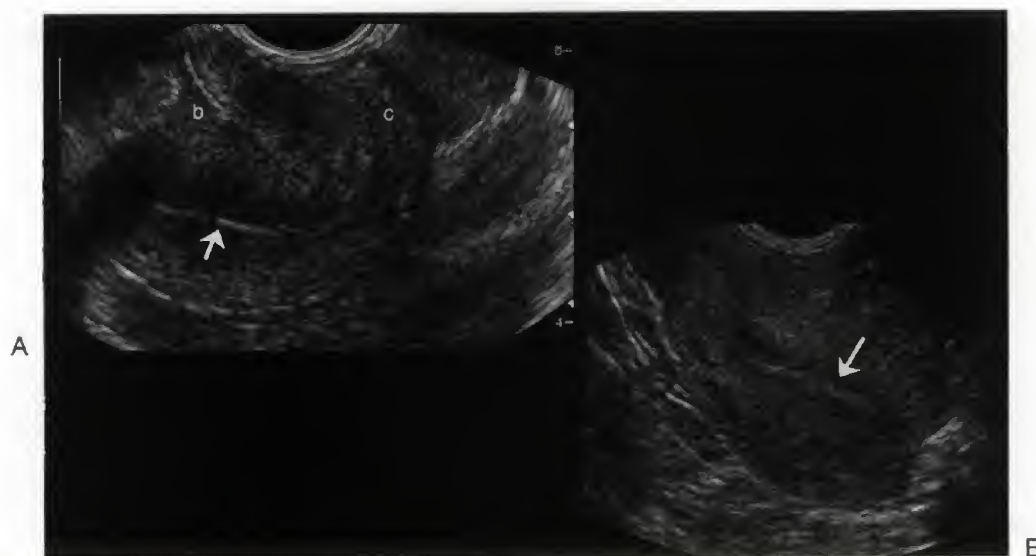


**FIGURE 26-55.** Longitudinal transrectal scan of an (A) anteverted and (B) retroverted uterus. The bladder (b) is almost empty. The endometrium is thin (arrow). c, cervix.

transvaginal probe that is directed posterior to the adnexa and gently pushed deeper into the pelvis. The sigmoid should be examined in each patient if the patient's symptoms cannot be explained by examination of the rest of the pelvic organs.

### Transrectal Scanning

Patients in whom a transvaginal scan is not possible can be scanned through the rectum. Using a conventional transvaginal probe, one can obtain superior images of the uterus, ovaries, and adnexa compared with the transvesical approach (Fig. 26-55). This is not commonly used but should be considered in the appropriate patient and with appropriate verbal consent and adequate lubrication. The study is not uncomfortable because the only discomfort is felt when the probe passes through the anal canal.

### References

- Freimanis MG, Jones AF: Transvaginal ultrasound. *Radiol Clin North Am* 30:955, 1992.
- Fleischer AC, Kepple DM, Vasquez J: Conventional and colour Doppler transvaginal sonography in gynecologic infertility. *Radiol Clin North Am* 30:693, 1992.
- Schiller VL, Grant EG: Doppler ultrasonography of the pelvis. *Radiol Clin North Am* 30:735, 1992.
- Levi CS: Prediction of early pregnancy failure on the basis of mean gestational sac size and absence of a sonographically demonstrable yolk sac [Letter]. *Radiology* 195:873, 1995.
- Levi CS, Lyons EA, Schollenberg J, et al: The value of post void scans in the diagnosis of ruptured ectopic pregnancy. *J Ultrasound Med* 1:253, 1982.
- Lyons EA, Gratton D, Hamington C: Transvaginal sonography of normal pelvic anatomy. *Radiol Clin North Am* 30:663, 1992.
- Coleman BG: Transvaginal sonography of adnexal masses. *Radiol Clin North Am* 30:677, 1992.
- Schwimmer SR, Rothman CM, Lebovic J, et al: The effect of ultrasound coupling gels on sperm motility in vitro. *Fertil Steril* 42:946, 1984.
- Zimmer EZ, Timor-Tritsch IE, Rottem S: The technique of transvaginal sonography. In Timor-Tritsch IE, Rottem S (eds): *Transvaginal Sonography*, 2nd ed. New York, Elsevier, 1991, p 61.
- Lee W: How to interpret the ultrasound output display standard for higher acoustic output diagnostic ultrasound devices. *J Ultrasound Med* 17:535, 1998.
- Fowlkes JB, Holland CK: Biologic effects and safety. In Rumack CM, Wilson SR, Charboneau JW (eds): *Diagnostic Ultrasound*, 2nd ed. St. Louis, CV Mosby, 1998, p 35.
- AIUM website Official statements on Clinical safety. <http://www.aium.org/publications/statements/statements.asp>
- Levi CS, Lyons EA, Lindsay DJ, et al: Transvaginal and translabial ultrasound in pregnancy. *Curr Opin Radiol* 4:85, 1992.
- Myology: Fasciae and muscles of the trunk. In Williams PM, Warwick R (eds): *Gray's Anatomy*, 36th ed. Edinburgh, Churchill Livingstone, 1980, p 551.
- Gardner E, Gray DJ, O'Rahilly R: The pelvis. In Gardner ED (ed): *Anatomy: A Regional Study of Human Structure*, 5th ed. Philadelphia, WB Saunders, 1986, p 445.
- Benson MP: Rectus sheath haematomas simulating pelvic pathology: The ultrasound appearances. *Clin Radiol* 33:651, 1982.
- Spring DB, Deshon GE Jr, Babu S: The sonographic appearance of fluid in the prevesical space. *Radiology* 147:205, 1983.
- Myology: Fasciae and muscles of the lower limb. In Williams PM, Warwick R (eds): *Gray's Anatomy*, 36th ed. Edinburgh, Churchill Livingstone, 1980, p 593.
- Cunningham FG, MacDonald PC, Gant NF, et al: Anatomy of the reproductive tract in women. In Williams Obstetrics, 19th ed. Norwalk, CT, Appleton & Lange, 1993, p 57.
- Splanchnology: Reproductive organs of the female. In Williams PM, Warwick R (eds): *Gray's Anatomy*, 36th ed. Edinburgh, Churchill Livingstone, 1980, p 1423.
- Kurjak A, Zalud I: Normal pelvic blood flow. In Kurjak A (ed): *Transvaginal colour Doppler*. Park Ridge, NJ, Parthenon, 1991, p 25.
- Angiology: The iliac arterial system. In Williams PM, Warwick R (eds): *Gray's Anatomy*, 36th ed. Edinburgh, Churchill Livingstone, 1980, p 719.
- Angiology: Veins of the abdomen and pelvis. In Williams PM, Warwick R (eds): *Gray's Anatomy*, 36th ed. Edinburgh, Churchill Livingstone, 1980, p 759.
- Kurjak A, Zalud I: Normal pelvic blood flow. In Kurjak A (ed): *Transvaginal colour Doppler*. Park Ridge, NJ, Parthenon, 1991, p 25.
- Collins W, Jurkovic D, Bourne T, et al: Ovarian morphology, endocrine function and intra-follicular blood flow during the periovulatory period. *Hum Reprod* 6:319, 1991.
- Weiner Z, Thaler I, Levron J, et al: Assessment of ovarian and uterine blood flow by transvaginal color Doppler in ovarian stimulated women: Correlation with the number of follicles and steroid hormone levels. *Fertil Steril* 59:743, 1993.



27. Lunenfeld E, Schwartz I, Meizner I, et al: Comparison of uterine blood flow characteristics between spontaneous and stimulated cycles before embryo transfer. *Hum Reprod* 11:364, 1996.
28. Steer CV, Campbell S, Pampiglione JS, et al: Transvaginal colour flow imaging of the uterine arteries during the ovarian and menstrual cycles. *Hum Reprod* 5:391, 1990.
29. Sladkevicius P, Valentin L, Marsal K: Transvaginal gray-scale and Doppler ultrasound examinations of the uterus and ovaries in healthy postmenopausal women. *Ultrasound Obstet Gynecol* 6:81, 1995.
30. Sladkevicius P, Valentin L, Marsal K: Blood flow velocity in the uterine and ovarian arteries during the normal menstrual cycle. *Ultrasound Obstet Gynecol* 3:199, 1993.
31. Kurjak A, Kupesic S: Ovarian senescence and its significance on uterine and ovarian perfusion. *Fertil Steril* 64:532, 1995.
32. Kupesic S, Kurjak A: Uterine and ovarian perfusion during the periovulatory period assessed by transvaginal color Doppler. *Fertil Steril* 60:439, 1993.
33. Huang MW, Muradali D, Thurston WA, et al: Uterine arteriovenous malformations: Gray-scale and Doppler US features with MR imaging correlation. *Radiology* 206:115, 1998.
34. Applebaum M: Normal endometrial signals at color and spectral Doppler US. *Radiology* 208:832, 1998.
35. Applebaum M: The "steel" or "Teflon" endometrium: Ultrasound visualization of endometrial vascularity in IVF patients and outcome. In *The Third World Congress of Ultrasound in Obstetrics and Gynecology*. London, Parthenon, 1993, p 10.
36. Applebaum M: Ultrasound visualization of endometrial vascularity in normal pre-menopausal women. In *The Third World Congress of Ultrasound in Obstetrics and Gynecology*. London, Parthenon, 1993, p 11.
37. Applebaum M: The uterine biophysical profile. *Ultrasound Obstet Gynecol* 5:67, 1995.
38. Zaidi J, Campbell S, Pitroff R, et al: Endometrial thickness, morphology, vascular penetration and velocimetry in predicting implantation in an in vitro fertilization program. *Ultrasound Obstet Gynecol* 6:191, 1995.
39. Miyazaki T, Tanaka M, Miyakoshi K, et al: Power and colour Doppler ultrasonography for the evaluation of the vasculature of the human corpus luteum. *Hum Reprod* 13:2836, 1998.
40. Campbell S, Bourne TH, Waterstone J, et al: Transvaginal color blood flow imaging of the periovulatory follicle. *Fertil Steril* 60:433, 1993.
41. Kurjak A, Kupesic-Urek S, Schulman H, et al: Transvaginal color flow Doppler in the assessment of ovarian and uterine blood flow in infertile women. *Fertil Steril* 56:870, 1991.
42. Zaidi J, Barber J, Kyei-Mensah A, et al: Relationship of ovarian stromal blood at the baseline ultrasound scan to subsequent follicular response in an in vitro fertilization program. *Obstet Gynecol* 88:779, 1996.
43. Burnett LS: Anatomy. In Jones HW III, Wentz AC, Burnett LS (eds): *Novak's Textbook of Gynecology*, 11th ed. Baltimore, Williams & Wilkins, 1988, p 40.
44. Platt JF, Bree RL, Davidson D: Ultrasound of the normal non-gravid uterus: Correlation with gross and histopathology. *J Clin Ultrasound* 18:15, 1990.
45. Miller EI, Thomas RH, Lines P: The atrophic postmenopausal uterus. *J Clin Ultrasound* 5:261, 1977.
46. Merz E, Mirio-Tesanic D, Bahlmann F, et al: Sonographic size of uterus and ovaries in pre- and postmenopausal women. *Ultrasound Obstet Gynecol* 7:38, 1996.
47. Orsini LF, Salardi S, Pili G, et al: Pelvic organs in premenarcheal girls: Real-time ultrasonography. *Radiology* 153:113, 1984.
48. Nussbaum AR, Sanders RC, Jones MD: Neonatal uterine morphology as seen on real-time US. *Radiology* 160:641, 1986.
49. Holm K, Laursen EM, Brocks V, et al: Pubertal maturation of the internal genitalia: An ultrasound evaluation of 166 healthy girls. *Ultrasound Obstet Gynecol* 6:175, 1995.
50. Lyons EA, Taylor PJ, Zheng XH, et al: Characterization of subendometrial myometrial contraction throughout the menstrual cycle in normal fertile women. *Fertil Steril* 55:771, 1991.
51. Lin MC, Gosink BB, Wolf SI, et al: Endometrial thickness after menopause: Effect of hormone replacement. *Radiology* 180:427, 1992.
52. Fleischer AC, McKee MS, Gordon AN, et al: Transvaginal sonography of post-menopausal ovaries with pathologic correlation. *J Ultrasound Med* 9:637, 1990.
53. Cohen HL, Tice HM, Mandel FS: Ovarian volumes measured by US: Bigger than we think. *Radiology* 177:189, 1990.
54. Wiseman DA, Greene CA, Pierson RA: Infertility. In Rumack CM, Wilson SR, Charbonneau JW (eds): *Diagnostic Ultrasound*, 2nd ed. St. Louis, CV Mosby, 1998, p 1407.
55. Schiebler ML, Dotters D, Baudoin L, et al: Sonographic diagnosis of hydatids of Morgagni of the fallopian tube. *J Ultrasound Med* 11:115, 1992.
56. Moore KL: The urogenital system: The urinary and genital systems. In *The Developing Human*, 3rd ed. Philadelphia, WB Saunders, 1982, p 255.
57. Splanchnology: The urinary organs. In Williams PM, Warwick R (eds): *Gray's Anatomy*, 36th ed. Edinburgh, Churchill Livingstone, 1980, p 1387.

## ULTRASOUND EVALUATION OF THE UTERUS

Liina Pöder, MD

### Imaging

Techniques

### Anatomy

Congenital Malformations

### Benign Uterine Conditions

Adenomyosis

Leiomyoma (Fibroids)

Lipomatous Uterine Tumors

### Malignant Conditions

Sarcomas

### Other Iatrogenic Processes

Arteriovenous Malformations

Intrauterine Contraceptive Devices

Ultrasound Evaluation of the Postpartum and Postabortive Uterus

Ultrasound is clearly the modality of choice for imaging the female pelvis, including the uterus and adnexal structures such as the ovaries and fallopian tubes. The endometrium, likewise, can be readily evaluated in the pre- and postmenopausal patient. In our clinical laboratory, a combination of transabdominal (transvesical) scanning as well as transvaginal examination are performed in most patients. This allows the examiner to evaluate the true pelvis in its entirety with a wide field of view, as well as using high-resolution interrogation of specific structures. Primary imaging with ultrasound in conjunction with clinical information guides optimal further imaging. When ultrasound fails to provide adequate information or does not answer the clinical question, further evaluation with magnetic resonance imaging (MRI) can be performed. This is discussed in detail in the chapter dedicated to the MRI of the uterus.

In this chapter, we discuss ultrasound evaluation of the normal uterus, anatomic variants, and its benign and malignant conditions. A discussion of the normal and abnormal endometrium in the patient that presents with abnormal uterine bleeding is presented in the following chapter.

### IMAGING

The American Institute of Ultrasound in Medicine (AIUM) guidelines for imaging of the uterus have been developed to assist sonologists in performing sonographic studies of the female pelvis.<sup>1</sup> Knowing the potential but also the limitations of ultrasound helps us to maximize the probability of detecting most significant abnormalities. As with any clinical test, ultrasound of the pelvis should be performed only if there is a valid clinical reason. Following the AIUM guidelines, the indications for pelvic sonography include, but are not limited to

1. Pelvic pain
2. Dysmenorrhea (painful menses)
3. Menorrhagia (excessive menstrual bleeding)

4. Metrorrhagia (irregular uterine bleeding)
5. Menometrorrhagia (excessive bleeding irregularly)
6. Follow-up on previously detected abnormality (that is, hemorrhagic cyst)
7. Evaluation or monitoring of infertile patients
8. Delayed menses or precocious puberty
9. Postmenopausal bleeding
10. Abnormal pelvic examination
11. Evaluation of congenital anomalies
12. Localization of intrauterine contraceptive device
13. Screening for malignancy in patients with an increased risk<sup>1</sup>

### Techniques

All relevant anatomic structures in the pelvis should be identified first by transabdominal technique, and then, more detailed evaluation of the deep pelvic structures should be performed by transvaginal technique. In specific situations in which transvaginal evaluation cannot be performed or tolerated, transrectal or transperineal evaluation can be very useful.

The transducer should be selected to operate at the highest clinically appropriate frequency that will allow adequate visualization of deep pelvic structures. For transabdominal evaluation, a 3.5-MHz or higher transducer is employed. Curved linear array, as well as sector, transducers with a smaller footprint are often employed. For transabdominal evaluation, the bladder should be adequately distended to displace bowel superiorly out of the true pelvis and provide an acoustic window to visualize the uterus and adnexa (Fig. 27-1).

For transvaginal evaluation, the urinary bladder should be emptied and the patient in comfortable position but with her pelvis tilted either with the use of stirrups or with an elevation under the hips. The patient or the sonographer, depending on the patient's preference, may introduce the vaginal transducer with real-time monitoring. For transvaginal



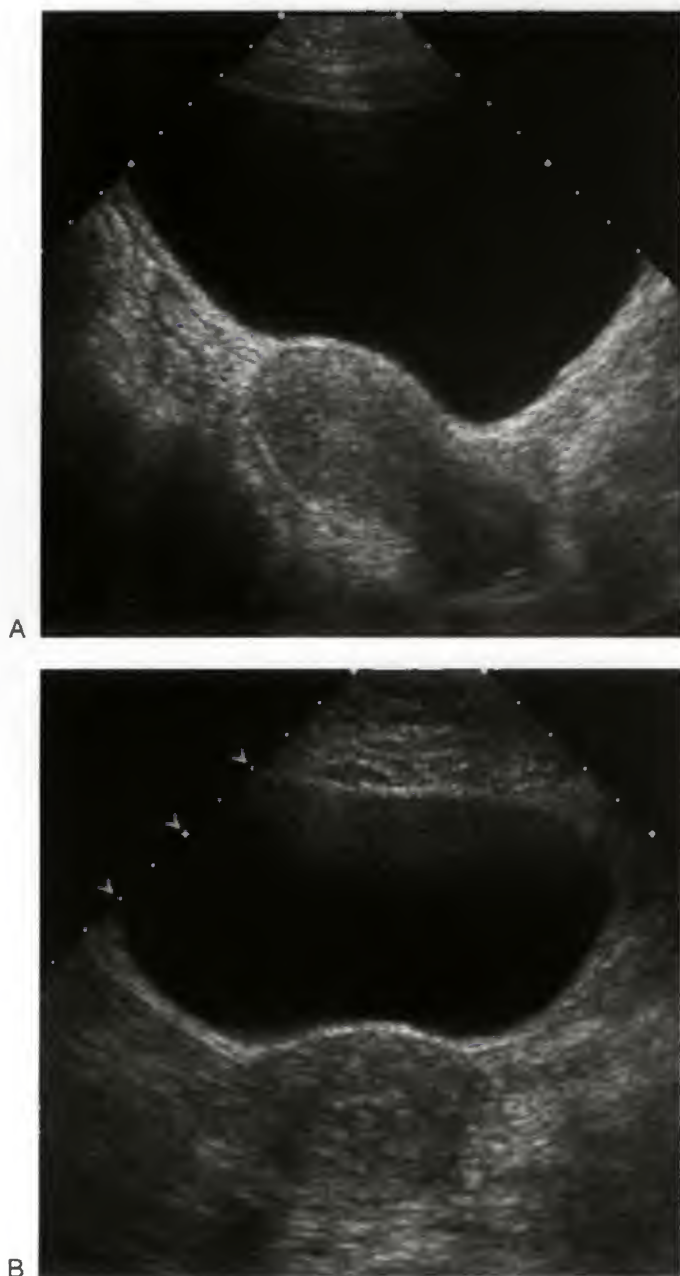


**FIGURE 27-1.** A. Sagittal-transabdominal view of the normal uterus. B. Transverse-transabdominal view of the normal uterus. Notice the acoustic window provided by the distended urinary bladder.

evaluation, the AIUM recommends using probes of 5 MHz or higher (Fig. 27-2). If a male sonologist is performing the examination, a female member of the staff should be present as a chaperone.

The vagina, uterus, and the urinary bladder are used as reference points for identification of the remaining normal and abnormal pelvic structures. The uterine size, shape, and orientation should be identified and documented in sagittal and transverse axial planes. The endometrium, myometrium, and cervix should be carefully evaluated, and their appearance documented. The uterine length is measured in long

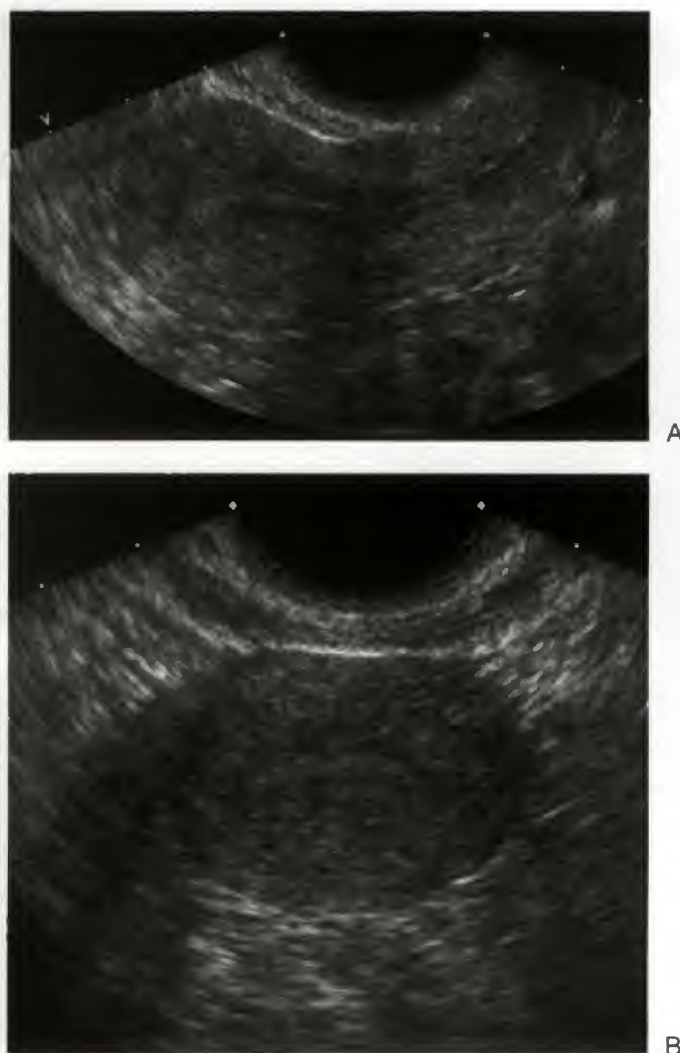


**FIGURE 27-2.** A. Sagittal-transvaginal view of the normal uterus. B. Transverse-transvaginal view of the normal uterus.

axis from the fundus to the cervix, and the anteroposterior dimension is measured on the same image perpendicular to the length. The width is to be measured on a separate image on either a transaxial or coronal plane of section. If the volume of the uterine corpus is assessed the cervical component should be excluded.<sup>1</sup>

Assessment of the endometrium is performed in a sagittal plane. Variations of the appearance of the endometrium with different phases of the menstrual cycle and with hormonal supplementation should be considered (Fig. 27-3). Myometrial masses and contour abnormalities should be recorded in two different planes and their locations recorded.<sup>1</sup> Doppler evaluation of the uterus and endometrium can be of added value.

Saline infused sonography (SIS) or, as it is often referred to, sonohysterography, is an innovative technique to evaluate a variety of endometrial and myometrial processes, which involve the endometrial canal. The most common indications for SIS are abnormal uterine bleeding in both pre- and postmenopausal women. Other indications include

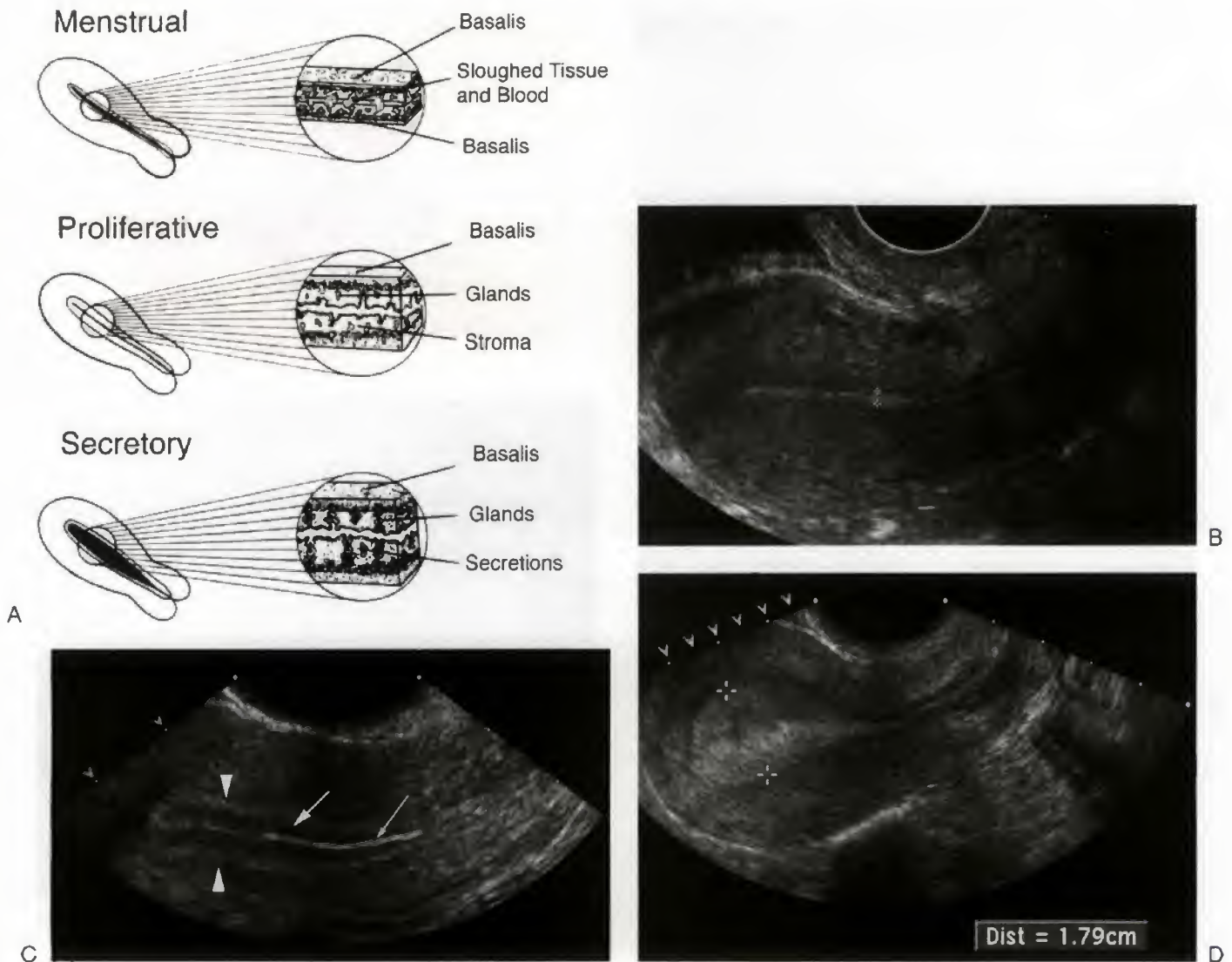


**FIGURE 27-3.** A. Diagram showing development of the endometrium during the menstrual, proliferative, and secretory phases. In the menstrual phase, the endometrium appears as a thin, irregular interface. The central echogenicity probably arises from sloughed tissue and blood. In the proliferative phase, the endometrium is relatively hypoechoic, likely a reflection of the straight and orderly arrangement of the glandular elements. The central thin, echogenic line is likely a specular reflection from the endometrial surfaces. In the secretory phase, the endometrium achieves its maximum thickness and echogenicity. This appearance is from the distended and tortuous glands, which contain secretions. (From Fleischer AC, Kalemeris GC, Entman SS: *Sonographic depiction of the endometrium during normal cycles*. *Ultrasound Med Biol* 12:271, 1986, Pergamon Journals Ltd. Reprinted by permission of Elsevier Science. Copyright 1986 by World Federation of Ultrasound in Medicine and Biology.) B. Postmenstrual, early proliferative endometrium. C. Periovulatory endometrium. A three-layered endometrium is seen: the collapsed endometrial lumen is demonstrated by the central echogenic line (thin arrow). A hypoechoic layer representing the edematous endometrium functionalis (thick arrow) and an outer hyperechoic layer representing the endometrium basalis (arrowheads) is seen. D. Secretory endometrium.

1. Infertility and habitual abortion
2. Congenital abnormalities or anatomic variants of uterine cavity.
3. Preoperative and postoperative evaluation of uterine cavity, especially with regard to uterine myomas, polyps, and cysts
4. Suspected uterine cavity synechiae
5. Further evaluation of suspected abnormalities as seen on transvaginal sonography, including focal or diffuse endometrial thickening or debris
6. Inadequate imaging of endometrium by transvaginal sonography

SIS is contraindicated in women who could be pregnant or have an active infection. Because the normal secretory endometrium may be thick and simulate endometrial disease, the examination should be scheduled in the follicular phase of the cycle, after menstrual flow has ceased but prior to ovulation, no later than the 10th day of the menstrual cycle. Active vaginal bleeding is not generally a contraindication but can make imaging challenging or even nondiagnostic.<sup>2</sup>

At our institution, we perform a preliminary transabdominal and transvaginal sonogram before SIS. After the procedure is explained to the patient, the external os is cleansed before catheterization of the cervical canal using



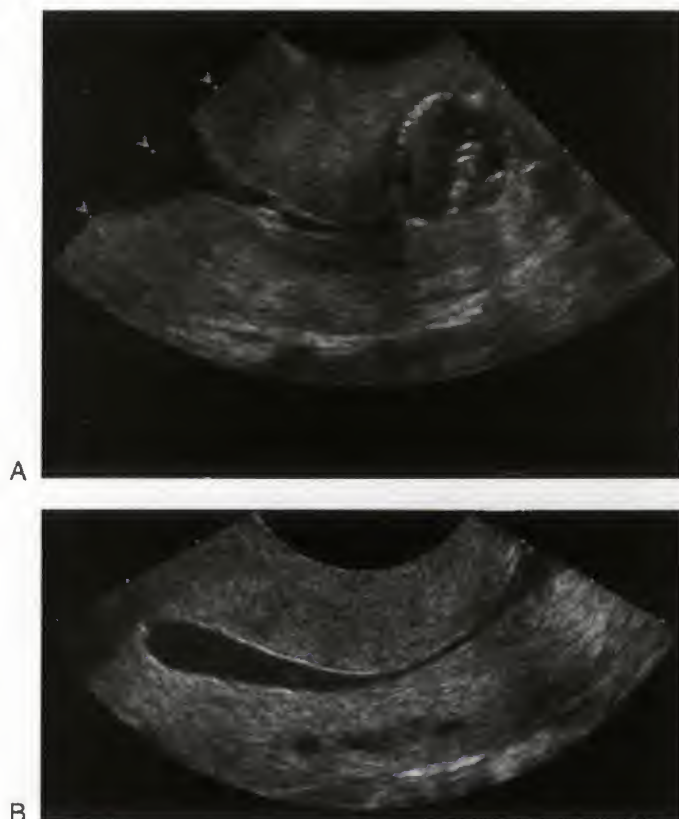


**FIGURE 27-4.** A. Sagittal-transvaginal image of balloon positioning in the cervix. B. Sagittal-transvaginal image after saline infusion. The normal thin endometrium is well seen.

aseptic technique. A sonohysterography catheter (flushed with saline to remove any air bubbles) is then advanced into the endometrial canal. Once in the endometrial canal, the balloon is inflated so that the catheter does not become dislodged. The speculum is removed, and the transvaginal probe is reinserted adjacent to the catheter. Under ultrasound guidance, the balloon is gently retracted to occlude the internal os. Sterile saline should be administered under real-time sonography. The amount of saline one introduces is variable, often between 5 and 30 mL. Normal anatomy and abnormal findings should be documented in two separate planes using the high-frequency transvaginal (TV) probe extending from one cornua to the other (Fig. 27-4).

## ANATOMY

The uterus is a hollow organ in which the myometrium is firmly adherent to a thin internal layer of endometrium. Externally the uterus is imbedded between the two layers of the broad ligament. Anatomically, the uterus lies between the bladder anteriorly and the rectosigmoid colon posteriorly. The uterus is divided into two major parts, the body and cervix. The most superior aspect of the uterus is referred to as the fundus, and the entrance of the fallopian tubes into the uterus are referred to as the cornua. Anterior to the origin of the fallopian tubes are the round ligaments, one on each side, which extend anterolaterally, coursing through

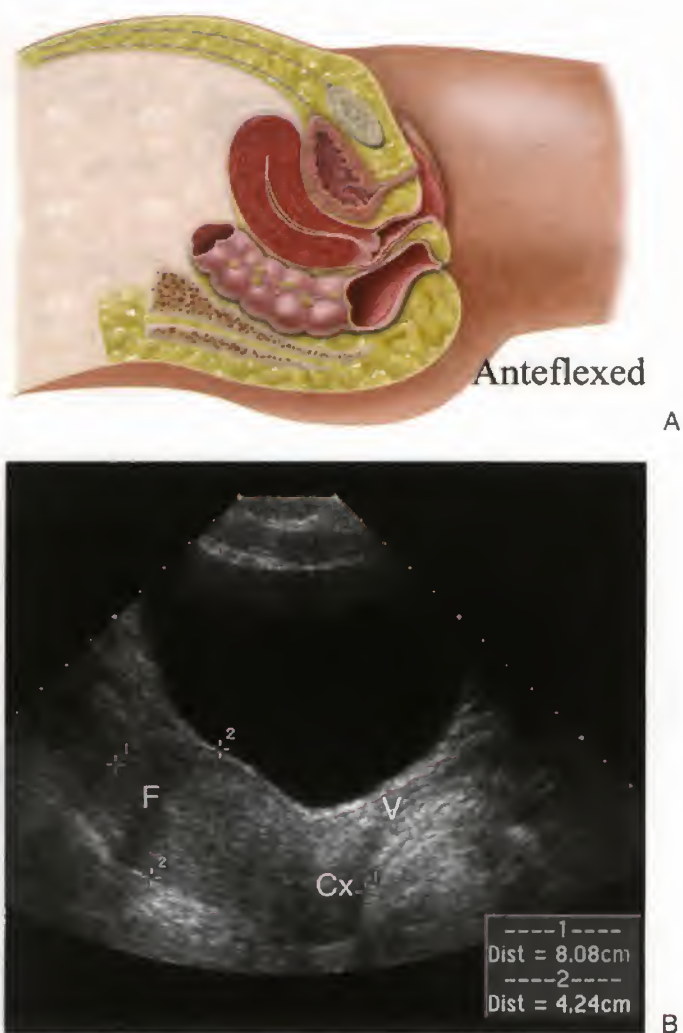


**FIGURE 27-5.** A. Illustration demonstrating an anteverted, anteverted normal uterus. (Illustration by James A. Cooper, MD, San Diego, CA.) B. Midline sagittal sonogram demonstrating anteversion (cervix [Cx] to the vagina [V]) and anteversion (fundus [F] to cervix). A distended urinary bladder slightly displaces the fundus posteriorly.

the inguinal canals and inserting onto the fascia of the labia majora. The uterus has a dual blood supply. The majority of blood supply is from the uterine arteries arising from the internal iliac arteries and a minor blood supply is from the ovarian arteries.

The uterus is physiologically most often anteverted and anteverted (Fig. 27-5) but may also be retroverted (Fig. 27-6) or retroverted (Fig. 27-7). The cervix of the uterus is fixed in the midline but the body of the uterus can be mobile, and may change with varying degrees of bladder and rectal distention. Descriptions of flexion refer to the relationship of the body of the uterus to the cervix (usually the angle is about 270 degrees), whereas version refers to the cervical relationship to the vagina.

Retroversion and retroflexion are not infrequent in the nonpregnant state. In these cases the fundus of the uterus is positioned in the sacral hollow. During pregnancy, by the 14th to 16th week of gestation, the uterus enlarges and physiologically undergoes reduction. The fundus and uterus

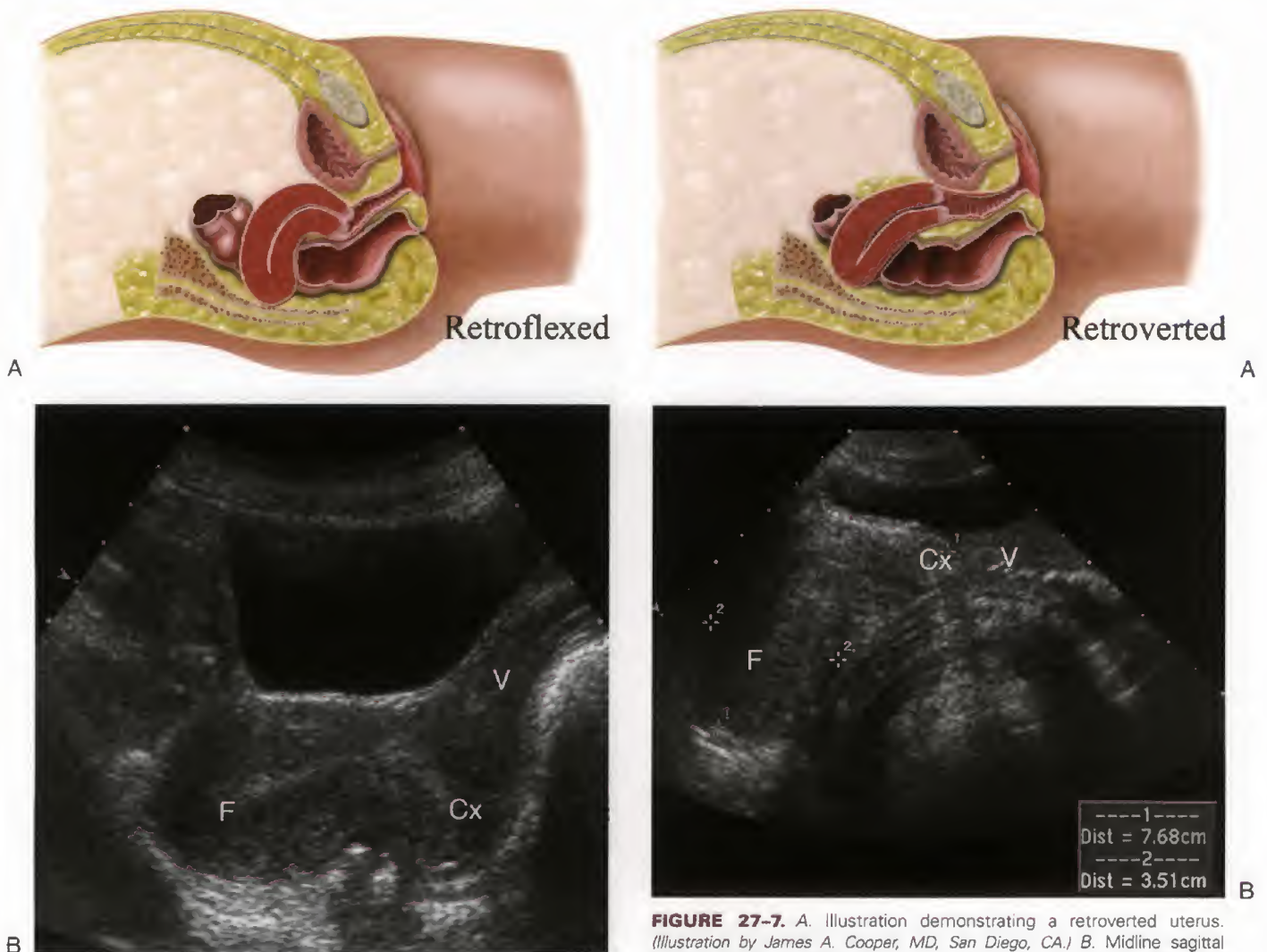


**FIGURE 27-6.** A. Illustration demonstrating an anteverted, retroflexed uterus. (Illustration by James A. Cooper, MD, San Diego, CA.) B. Midline sagittal sonogram demonstrating uterine retroflexion. The relationship of the cervix (Cx) to the vagina (V) is normal, but the fundus (F) is angled posteriorly.

**FIGURE 27-7.** A. Illustration demonstrating a retroverted uterus. (Illustration by James A. Cooper, MD, San Diego, CA.) B. Midline sagittal sonogram demonstrating retroversion. The cervix (Cx) is almost parallel to the vagina (V). There is often mild concomitant retroflexion as well. F, fundus.

then rise into the false pelvis. If this fails to happen, the uterus becomes “trapped” in the sacral hollow, often referred to as “incarcerated.” As the gestation evolves, the cervix is drawn upward either against or above the symphysis pubis, resulting in distortion of bladder and urethra. The posteriorly positioned fundus can cause pressure on the rectum. Usually, patients present between 13th to 17th week of pregnancy with symptoms of bladder outlet obstruction. A history of multiple trips to the emergency room for bladder outlet obstruction should raise suspicion. A constellation of three findings on sonography is diagnostic of an incarcerated uterus. First, the pregnancy is deep within the cul-de-sac. Second, the maternal urinary bladder lies anteriorly rather than inferiorly to the uterus and marked bladder distention is noted. Third, a soft tissue structure (the cervix) is seen between the bladder and pregnancy. This appearance can be misconstrued as an empty uterus associated with an

ectopic or abdominal pregnancy. Failure to recognize an incarcerated uterus can result in compromise of the uterine circulation, leading to spontaneous abortion or even uterine rupture. If recognized early, manual uterine repositioning usually is accomplished (Fig. 27-8).

The shape and size of the uterus varies throughout life, affected mostly by hormonal status. The mean measurement of a prepubertal uterus is 2.8 cm in length and 0.8 cm in maximum anteroposterior dimensions, with the cervix accounting for two thirds of the total length and contributing to the pear-shaped appearance (Fig. 27-9).<sup>3</sup> It is important to remember that in the immediate postdelivery state, the neonatal uterus can be slightly larger owing to the effects of residual maternal hormones. For the same reason, the echogenic endometrium is well seen and a small amount of fluid can be present in the endometrial cavity.

From birth until 4 years of age, the uterus decreases in size. At approximately 8 years of age the uterus starts to grow preferentially in the fundus. The uterus continues to



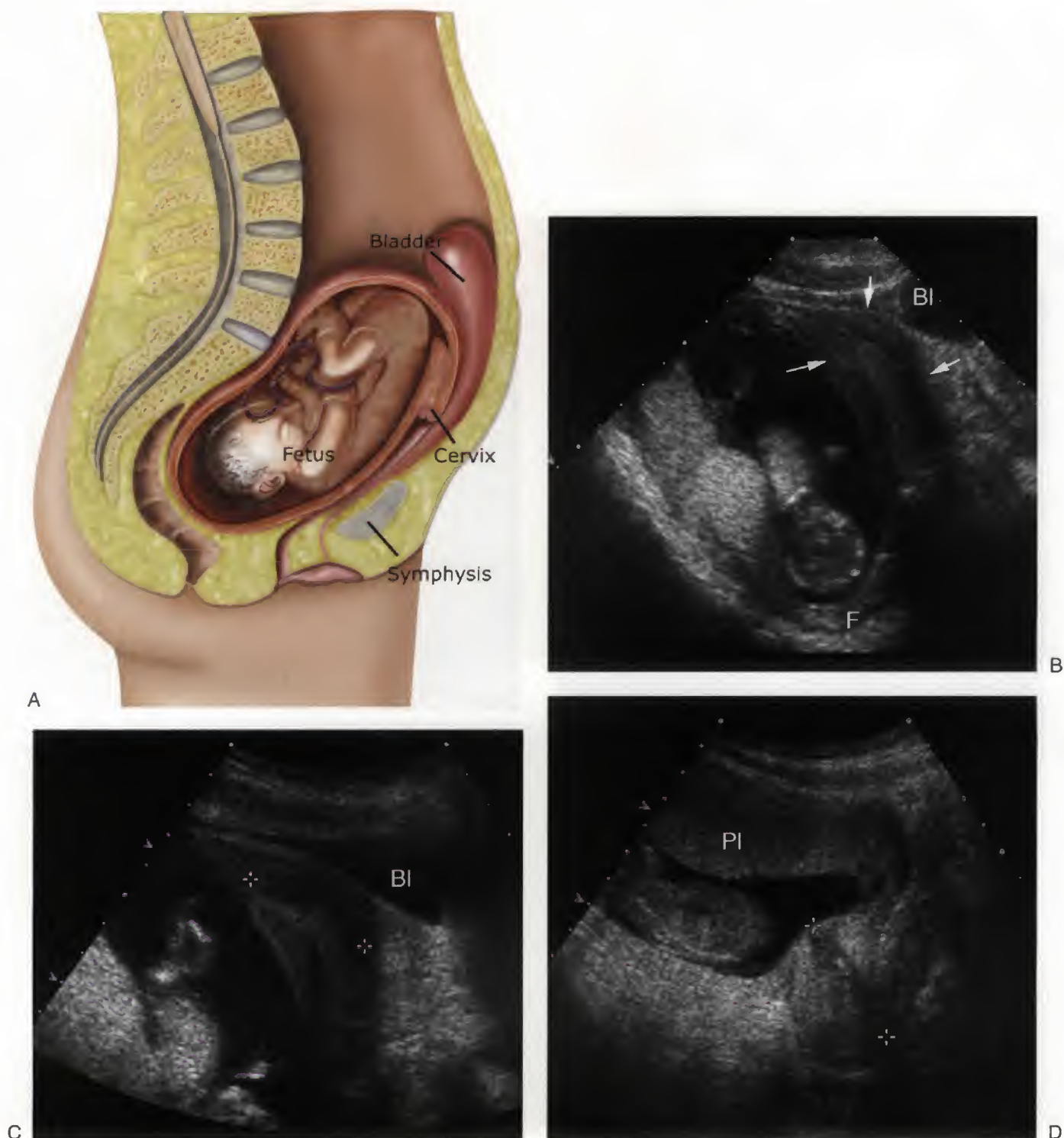


**FIGURE 27-8.** A. Incarcerated uterus. (Illustration by James A. Cooper, MD, San Diego, CA.) B. Sonogram of 14-week-old gestation. Patient presented with inability to empty urinary bladder. Sagittal-transabdominal images of an incarcerated uterus. The uterine fundus (F) is trapped in the sacral hollow. The cervix (arrows) is drawn anteriorly and superiorly, and can be misconstrued as an empty uterus with an ectopic or transabdominal pregnancy. C. Sagittal view of the same patient demonstrating the degree to which the bladder (BI) is drawn superiorly. D. Postmanual reduction view demonstrates physiologic relationship of the uterus and cervix (calipers). Note the normal anteriorly positioned placenta (PI) that appeared posterior when the uterus was incarcerated.

grow for several years after menarche until it reaches the mean dimensions of a reproductive age uterus, which are approximately 7 cm long and 4 cm wide.

Parity increases the size of the uterus, with a multiparous uterus measuring approximately 8.5 cm by 5.5 cm.<sup>4</sup>

The postmenopausal uterus is often small. The decrease in size is related to years passed after menopause,<sup>4</sup> although

the reduction in size is believed to be most rapid during the first decade after menopause. The range can be from 3.5 to 6.5 cm in length and 1.2 to 1.8 cm in anteroposterior dimensions.<sup>5</sup>

The normal myometrium is composed of three layers. The innermost layer is the thinnest, relatively hypovascular and hypoechoic when compared with the adjacent echogenic endometrium. This appearance is often referred to as the subendometrial halo. The next layer is the intermediate layer, which is the thickest layer and demonstrates uniform echotexture in a normal uterus. The outer layer is thin again and slightly less echogenic. The arcuate vessels separate the outer layer from the intermediate layer. The arcuate arteries branch into radial arteries that penetrate the intermediate layer and reach the level of inner layer. The arcuate vessels (particularly the veins) can be prominent and mimic cystic changes. This potential misinterpretation can easily be clarified by using color Doppler imaging (Fig. 27-10).

The arcuate arteries can calcify in postmenopausal women; this process can be seen earlier in diabetic patients. This is considered part of normal aging process (Fig. 27-11). Sometimes, small hyperechoic foci are seen in inner myometrium (usually a few millimeters and nonshadowing in appearance), which are thought to represent dystrophic calcifications due to previous intrauterine instrumentation and have no clinical significance.

### Congenital Malformations

The incidence of congenital müllerian duct anomalies is estimated to be approximately 0.5%. They are often diagnosed during workup for infertility, frequent miscarriages, or menstrual disorders. As one might remember from the embryology, the two paired müllerian ducts ultimately develop into fallopian tubes, uterus, cervix, and the upper two thirds of the vagina. The lower two thirds of the vagina and the ovaries have a separate origin. Uterine malformations

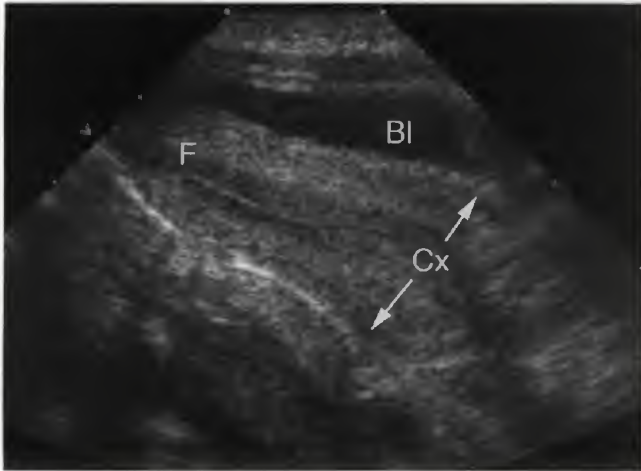


**FIGURE 27-9.** Sagittal-transabdominal view of the normal prepubertal uterus. Notice that the cervix (Cx) is significantly more prominent than the body or fundus (F). Bl, bladder.

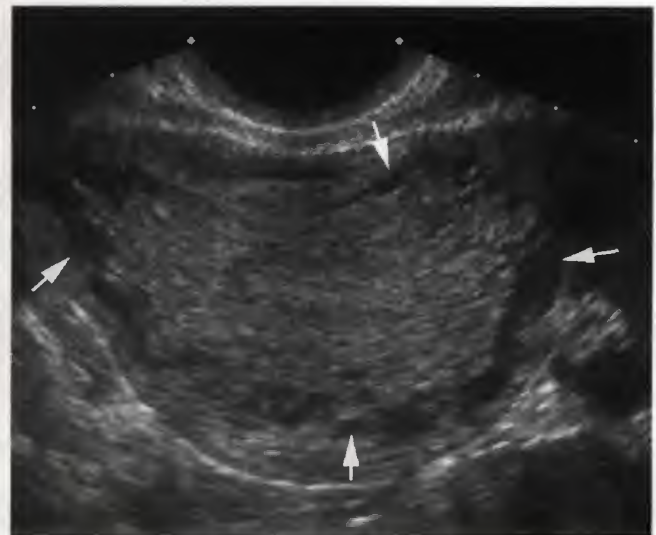
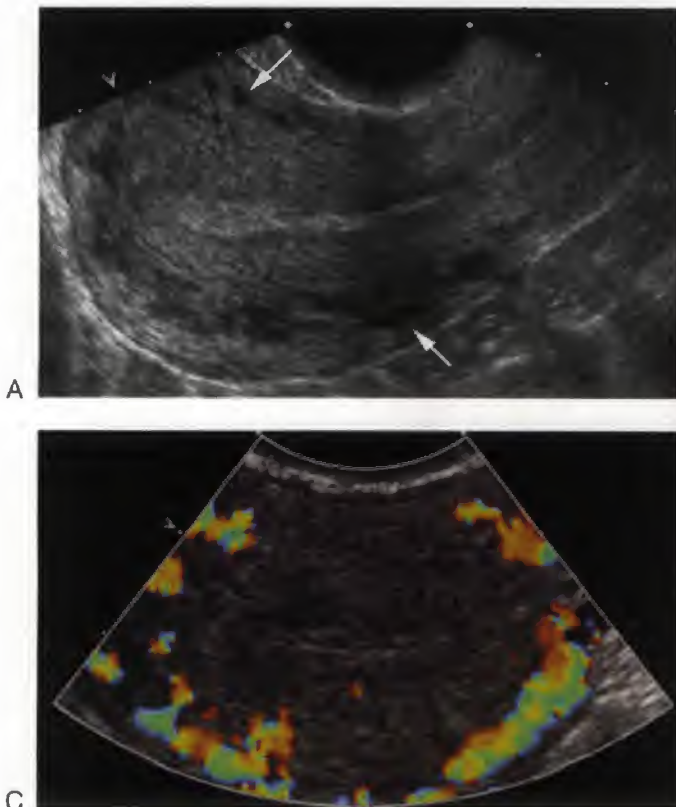


**FIGURE 27-10.** Sagittal (A) and transverse sonograms (B) of the uterus with prominent arcuate vessels (arrows) that can mimic cystic changes. C. These cystic appearing spaces are confirmed to be arcuate vessels by applying color Doppler.



arise from three different causes: arrested development of müllerian ducts, failure of fusion of the müllerian ducts, or failure of resorption of the median septum.

The arrested development of the müllerian ducts causes uterine agenesis or hypoplasia. This may present as vaginal, cervical, fundal, tubal, or combined agenesis or hypoplasia (Fig. 27-12).

Agenesis of a unilateral müllerian duct leads to a unicornuate uterus with a single fallopian tube.<sup>6</sup> In some cases, a rudimentary horn on the opposite side can be seen. This rudimentary horn may not communicate with the

normal side, which leads to retrograde menstruation and endometriosis, and makes resection necessary.

The poorest fetal survival among all uterine anomalies has been reported with a unicornuate uterus. Spontaneous abortion and preterm labor may occur.<sup>6</sup> The unicornuate uterus seems to be most difficult to confidently diagnose on sonography, because it can be confused as a small uterus. Looking for the contralateral rudimentary horn, which can be filled with blood, can sometimes help. The rudimentary horn may have a distended and dystrophic appearance, and should not be mistaken for an adnexal mass. MRI is the study of choice in resolving these complicated situations.

Complete failure of fusion of the müllerian ducts leads to uterus didelphys, which is two uteri each with its own cervix. A sagittal vaginal septum is usually but not always present. This anomaly is associated with a successful pregnancy.<sup>6</sup> The two uterine cavities and separate cervices can be identified on ultrasound, but the vaginal septum is better evaluated on physical examination and with computed tomography and/or MRI (Fig. 27-13).

Partial fusion of the two müllerian ducts leads to formation of a bicornuate uterus and a single cervix. The fundal portion is concave and horns divergent (MRI criteria based on this appearance: intercornual distance  $> 4$  cm, cleft depth at least 1 cm).<sup>6</sup> Sonographically, in a bicornuate uterus, the cavities are widely separated, and a deep indentation in the fundal contour is obvious. This should be distinguished from a uterine didelphys, and a single cervix should be confirmed in the bicornuate uterus (Fig. 27-14).

Failure of resorption of the septum after complete fusion of the müllerian ducts leads to formation of septate uterus (MRI is best at separating this from a bicornuate uterus, although this can be diagnosed with ultrasound). The fundal contour is flat or indented less than 1 cm. Many patients with septate uterus experience repeated abortions. Confirming this type of anomaly is clinically important because metroplasty is reported to improve fetal survival.<sup>6,7</sup> On sonography,



**FIGURE 27-11.** Sagittal-transvaginal view of the uterus demonstrates arcuate artery calcifications (arrows).

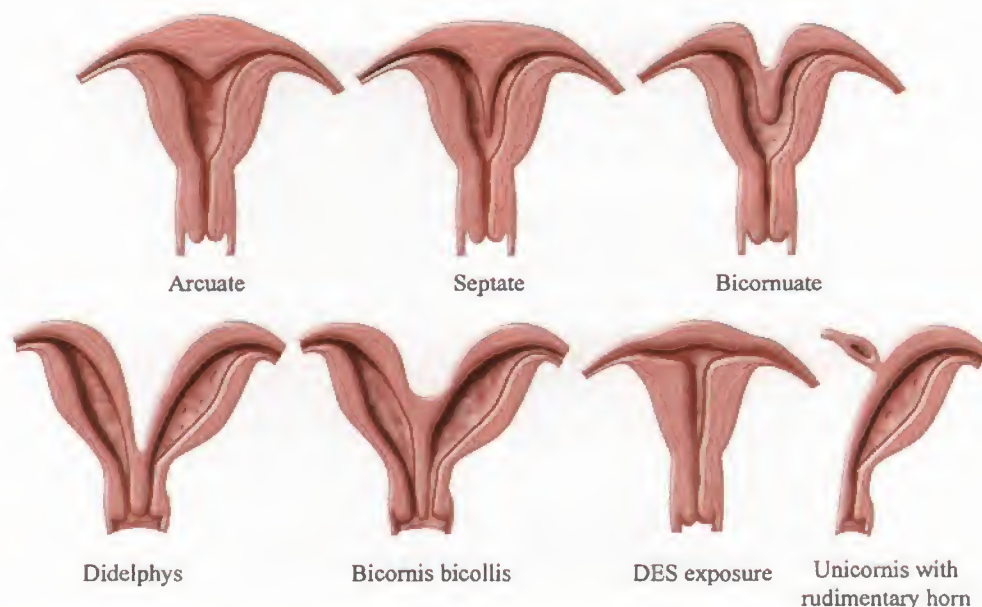


**FIGURE 27-12.** The more commonly diagnosed uterine anomalies. (Illustration by James A. Cooper, MD, San Diego, CA.)

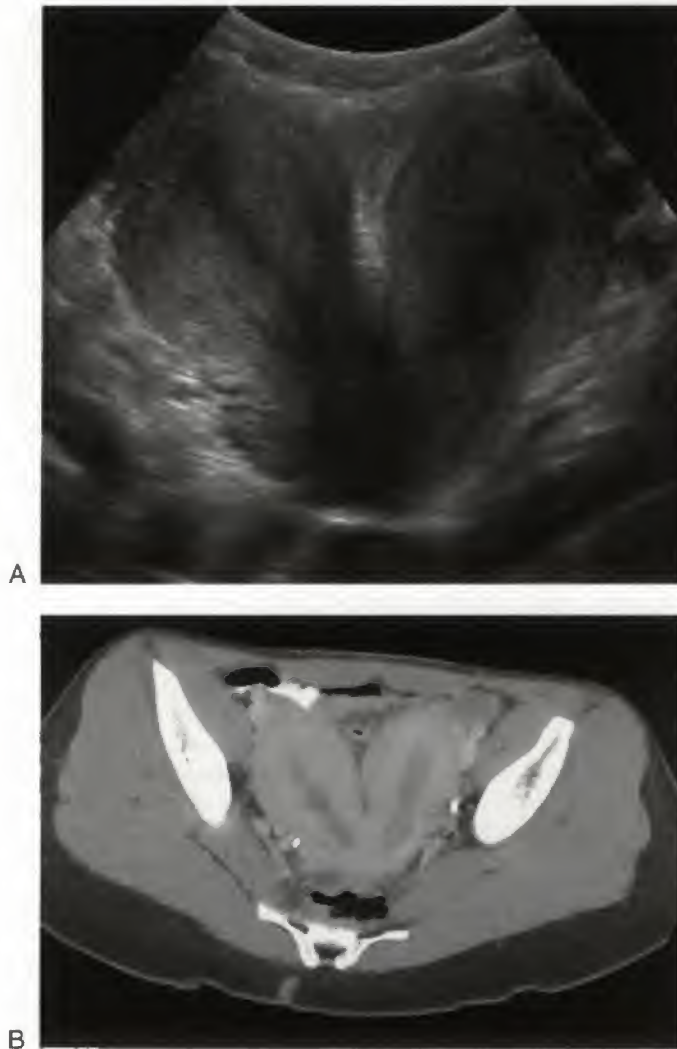


**FIGURE 27-13.** A. Coronal transvaginal view of a didelphys uterus with completely separate right and left cavities. B. Computed tomography scan of the same patient demonstrating a uterine didelphys.

the smooth fundal contour is diagnostic, with close endometrial cavities separated by a very thin septum (Fig. 27-15).

Arcuate uterus is a normal variant with a thickened fundal portion of the uterus slightly indenting the endometrial canal (Fig. 27-16). The external contour of the uterus is normal. There is a single uterine cavity, and as such, there is no associated pregnancy loss.

Diethylstilbestrol, used in 1940 to 1970, has been reported to result in uterine anomalies in the female fetus, specifically a T-shaped uterus. Patients with this anomaly have increased risk for spontaneous abortions, preterm deliveries, and ectopic pregnancies.<sup>6</sup> Sonography can reveal a small uterus with an irregular T-shaped appearance to the uterine cavity. Three-dimensional sonography with multiplanar capabilities can be of assistance in evaluation of the internal and external contours in these cases. Transvaginal sonography remains the primary imaging modality, although MRI is used as a problem-solving technique in more challenging cases.<sup>8</sup>



**FIGURE 27-14.** A three-dimensional image that demonstrates a heart-shaped bicornuate uterus. Fundal indentation is well seen (arrow), as well as the widely divergent horns (asterisks) with a single cervix (arrowhead). (Courtesy of Beryl R. Benacerraf, Boston, MA.)

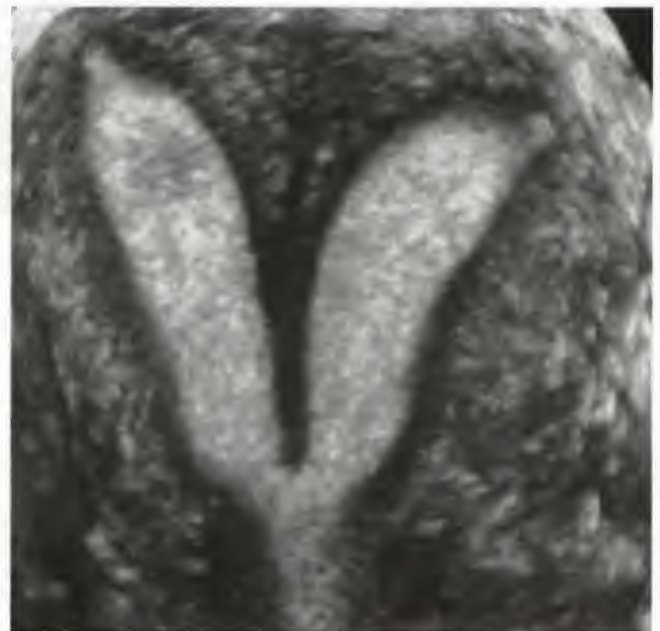


**FIGURE 27-15.** Coronal three-dimensional image of septate uterus. Two separate but close cavities, fibrous septum, and smooth-appearing fundal contour. (Courtesy of Beryl R. Benacerraf, Boston, MA.)

## BENIGN UTERINE CONDITIONS

### Adenomyosis

Adenomyosis is a common condition, although it is often overlooked. It is found in 70% of hysterectomy specimens. Adenomyosis is characterized by migration of endometrial





**FIGURE 27-16.** Transvaginal view of arcuate uterus with a small indentation in the fundal endometrium (*large arrow*). The outer contour of the uterus is smooth and normal appearing (*small arrows*).

glands from the stratum basale into the myometrium. This often occurs with reactive hyperplasia of the smooth muscle. The ectopic glands tend to be at least 2 to 3 mm below the endometrial-myometrial junction. Two widely accepted theories for the cause of adenomyosis are that it results from a defect or absence of the basement membrane at the endometrial-myometrial junction, or that it is related to endometrial migration by lymphatic or vascular channels. Possible risk factors include uterine trauma such as childbirth, uterine instrumentation, chronic endometritis, and hyperestrogenism.<sup>3,4,9,10</sup>

Adenomyosis is most prevalent among mature reproductive age patients and is much less commonly seen in nulliparous or postmenopausal patients. Presenting symptoms are usually uterine tenderness, dysmenorrhea, menorrhagia, and uterine enlargement. These symptoms are very similar to the symptoms seen in patients with uterine fibroids, pelvic congestion syndrome, endometriosis, endometrial polyps, and endometrial carcinoma. Given the differences in clinical treatment, the imaging diagnosis is important. These symptoms can be extremely debilitating, and misdiagnosis can prolong appropriate care. Specific therapy such as gonadotropin-releasing hormone inhibitors, oral contraceptives, nonsteroidal anti-inflammatory drugs, oral contraceptives, and endometrial ablation are available.<sup>3,4,9,10</sup>

One of the recently emerging therapies for adenomyosis is uterine artery embolization, but results for this treatment are controversial at this time. The only definitive treatment at this time is hysterectomy.<sup>11</sup>

Sonography and MRI play an important role in the diagnosis and proper management of these patients. Imaging is also used to evaluate response to treatment, and progression of the disease. For optimal diagnosis, transvaginal ultrasound should be performed at high frequencies, between 5 to 10 MHz. The reported sensitivity and specificity of

transvaginal ultrasound for identifying adenomyosis ranges from 53% to 89% and 67% to 98%, respectively, and overall accuracy of 68% to 86%. MRI sensitivity ranges from 78% to 88% and specificity 67% to 93%.<sup>4,10</sup> Although MRI and sonography are reported to have similar accuracy in diagnosing this condition, ultrasound is most often the first imaging study obtained in patients with the above-described symptoms.<sup>3,4,9</sup> MRI is considered to have better accuracy in women with associated disorders.<sup>12</sup> It is also important to know that oftentimes leiomyomas and adenomyosis coexist (> 60%).

The imaging appearance of adenomyosis is based on ectopic glands that are surrounded by a stromal reaction of densely packed smooth muscle cells. This process often leads to the globular appearance of the uterus, which is defined as rounded enlargement of the uterus without a discrete mass or contour deformity. Although a focal adenomyoma can be seen, they are unlikely to cause a contour abnormality, as leiomyomas often do.

Transvaginal ultrasound can demonstrate the zonal anatomy, which is often altered with adenomyosis. Abnormal heterogeneous myometrium is observed with areas of increased or decreased echogenicity. Hypoechoic striations usually radiate throughout the involved parenchyma, believed to be edge shadows due to extreme smooth muscle hypertrophy. Even though this is very similar to shadowing caused by leiomyomas, the lack of distinct margins and mass effect make this finding more characteristic of adenomyosis. Sonographically, anechoic/cystic areas are seen, which on pathology, correspond to dilated glands. Hyperechoic foci representing endometrial tissue can also be seen (Fig. 27-17). Poor definition of the endometrial-myometrial junction with pseudo-widening of the endometrial echo is caused by heterotopic endometrial tissue extending from stratum basale.

Color Doppler examination has been helpful to differentiate adenomyosis from fibroid change. In adenomyosis there is often diffuse hypervascularity throughout the lesions when compared to the typical peripheral flow noted with fibroids.

Focal adenomyosis presents with a more atypical appearance (see Fig. 27-17). It is defined as focal mass with poorly defined margins in contrast with leiomyomas with distinct margins. Again, it is important to differentiate between those two. Surgically, leiomyomas can often be easily separated and removed from the adjacent endometrium, whereas adenomyomas are not often easily separated from the surrounding myometrium. When difficulties arise in sonographic diagnosis, MRI can be very helpful in achieving a more definitive diagnosis. Focal adenomyomas may be difficult to differentiate with both imaging modalities.<sup>4,10</sup>

Sonography has reported sensitivity of 80% to 87% and specificity of 94% to 98% in differentiating between these two entities. The exceptions would be those rare occasions when an adenomyoma is protruding into the endometrial cavity and has an appearance identical to an intracavitary polyp versus leiomyoma. Some authors consider polypoid adenomyomas a separate entity from adenomyosis.<sup>13</sup>

Endometrial abnormalities such as hyperplasia and carcinoma are reported to occur more often in patients with adenomyosis.<sup>3,9</sup> An adenocarcinoma has reported to rarely arise from adenomyosis. This would be very difficult to distinguish from typical adenomyosis without malignancy

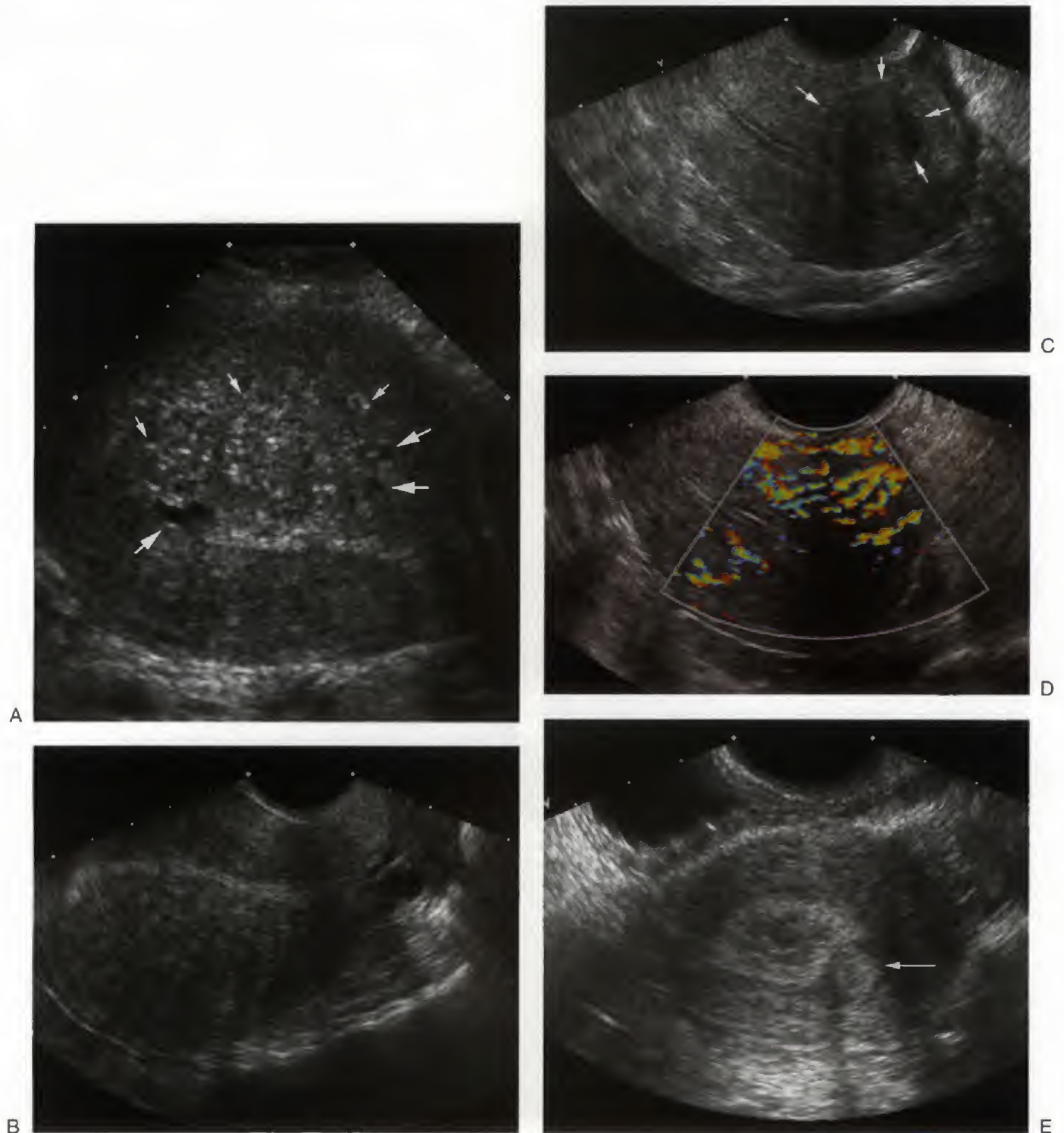


**FIGURE 27-17.** Adenomyosis: spectrum of appearances. **A.** Enlarged uterus with typical features of adenomyosis. Multiple bright echogenic foci are seen throughout the myometrium (*small arrows*) in addition to numerous subendometrial and myometrial cysts (*large arrows*). **B.** Longitudinal sonogram demonstrating numerous hypoechoic, 'venetian blind' striations in the posterior myometrium. Although these striations may be seen in myomatous disease, the absence of a focal myoma and the presence of other features make this more characteristic of adenomyosis. **C.** Transvaginal sonogram in a patient with a focal adenomyoma (*arrows*). **D.** Color Doppler image of the same patient in **C**, demonstrating increased vascularity within the adenomyoma. **E.** Another patient with an adenomyoma. In this case the adenomyoma is hyperechoic (*arrow*) and indenting but separate from the endometrium.

*Continued*



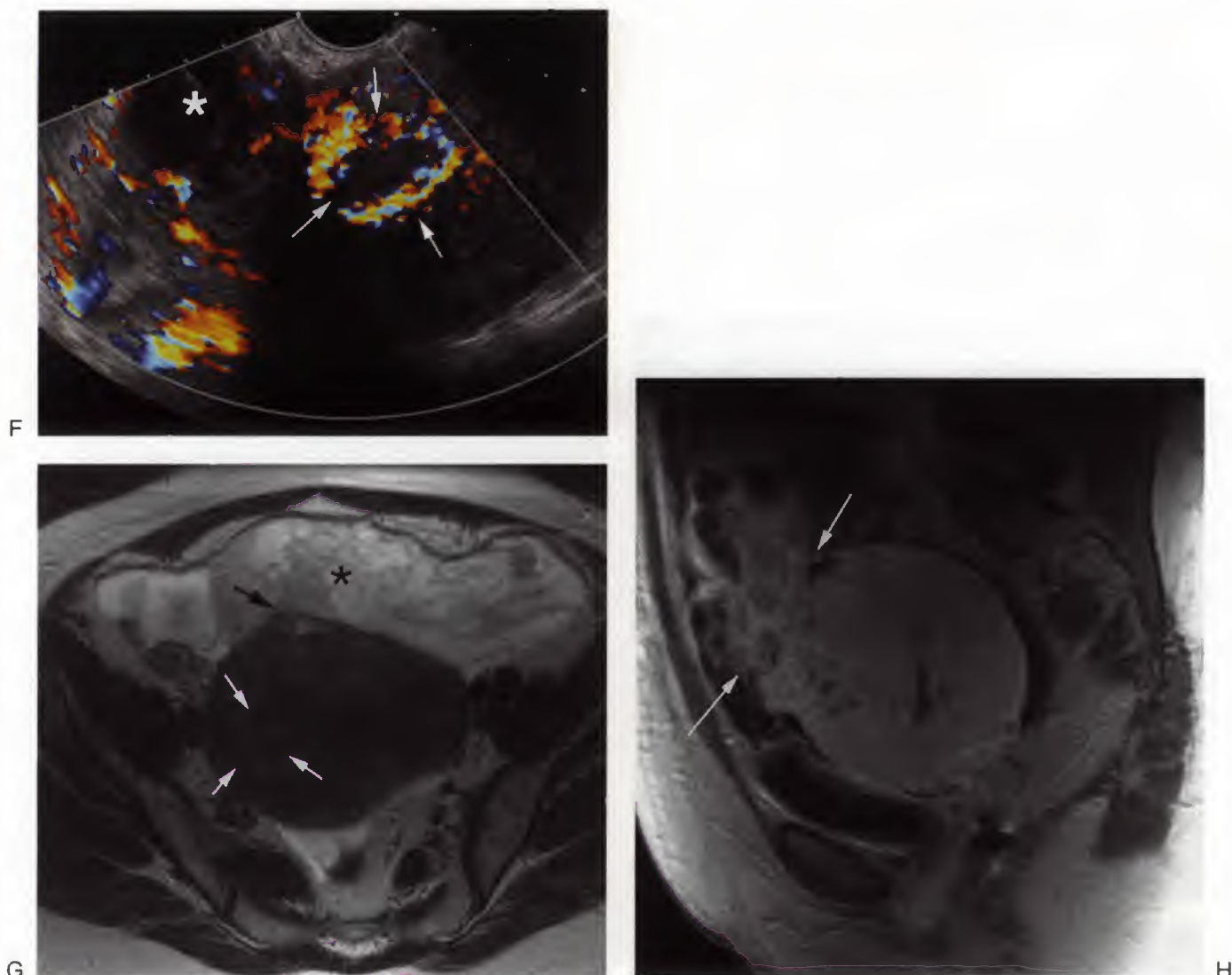


**FIGURE 27-17, cont'd.** *F.* Adenosarcoma arising in the background of adenomyosis with sarcomatous overgrowth. Transvaginal sonogram with color Doppler flow imaging. A focal vascular adenomyoma (*arrows*) is seen in the background of diffuse adenomyosis. A large cystic and solid mass (*asterisk*) is seen, which was thought to be of ovarian origin. *G.* MRI axial T2 image demonstrates better the extent of adenomyosis, and a more focal adenomyoma (*arrows*). A small subtle area of serosal breakthrough is noted (*black arrow*), which represents "expelling" of the adenosarcoma, high T2-signal heterogeneous mass noted anteriorly (*asterisk*). *H.* Sagittal postcontrast image demonstrates tumor extension from the uterine wall into the anterior pelvis (*arrows*). The final pathology demonstrated, endometrial stromal sarcoma with heterogeneous differentiation, FIGO: III.

(see Fig. 27-17). A more common scenario would be an endometrial carcinoma extending into foci of adenomyosis. In cases in which the adenomyosis coexist with endometrial cancer, it is very difficult to distinguish whether the cancer is insinuating into preexisting areas of adenomyosis or areas of true myometrial cancer invasion are present. Differentiation is crucial because myometrial invasion is an important prognostic indicator. This kind of differentiation is not achieved on imaging and can be even very difficult on histopathology (Table 27-1).<sup>14</sup>

### Leiomyoma (Fibroids)

Leiomyomas (fibroids) are the most common neoplasms of the uterus and are reported to occur in 20% to 30% of women older than 30 years of age. These tumors are usually

**Table 27-1** Features of Adenomyosis

#### Diffusely globular uterus but smooth external uterine contour

- Asymmetric globularity
- Myometrial cystic areas/echogenic foci
- Pseudothickening of the endometrium
- Diffuse increased internal vascularity
- Striated edge shadows/"Venetian blinds" without a discrete mass
- Focal ill-defined mass

#### Features that help to differentiate from leiomyomas

- Smooth external contour
- Minimal mass effect on serosa/endometrium relative to the size of the lesion
- Lack of calcification

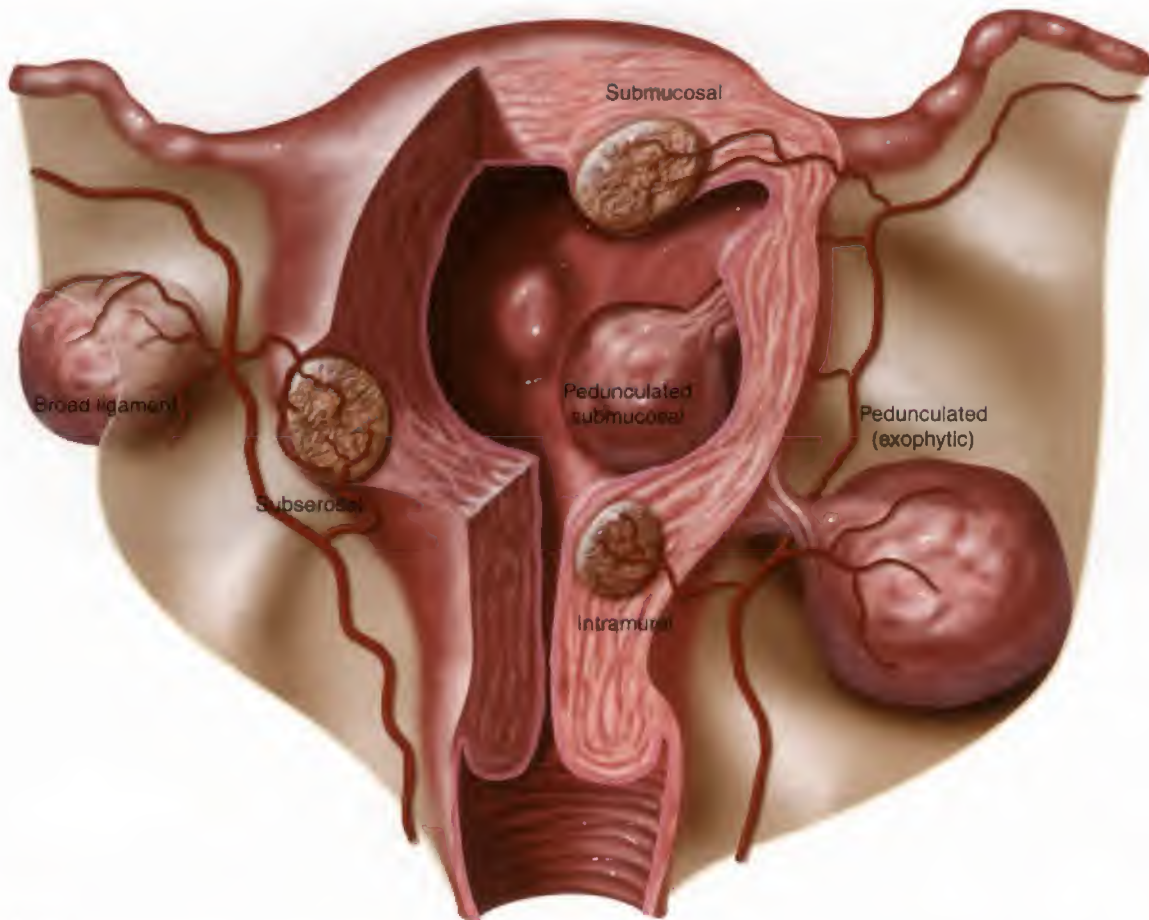


**FIGURE 27-18.** Common locations of leiomyomas. (Illustration by James A. Cooper, MD, San Diego, CA.)

multiple, causing enlargement of the uterus and surface lobularity unlike adenomyosis, which causes globular but smooth-contoured uterine enlargement. Leiomyomas most commonly present as palpable pelvic masses, uterine enlargement, or as causes for pelvic pain and dysfunctional uterine bleeding. Leiomyomas can be intra-transmural, submucosal, subserosal, intracavitary, or exophytic or pedunculated (Fig. 27-18). On rare occasions, the exophytic fibroids can project into the broad ligament (intraligamentous). In these instances, the fibroid may clinically and radiologically simulate an ovarian mass (Fig. 27-19). They can be located in the cervix rather than in myometrium. An unusual form of a fibroid is the parasitic leiomyoma, a pedunculated subserosal myoma, which, if it is in close contact with an adjacent structure, can parasitize the blood supply and even become detached from the uterus. This classification of leiomyomas is relevant because symptoms and treatment vary according to their location and subtype.<sup>15</sup>

The growth of fibroids is dependent on estrogen levels. Rapid growth may occur during pregnancy but only in about 50% of patients (Fig. 27-20). Leiomyomas are associated with increased risk of early pregnancy failure, especially with multiple gestations.<sup>16</sup> Cervical and lower uterine segment fibroids can interfere with delivery and should be monitored during pregnancy. As the estrogen level declines, the leiomyomas may regress and thus are rarely symptomatic in postmenopausal patients.<sup>15</sup>



**FIGURE 27-19.** Transverse abdominal sonogram. A left adnexal solid mass (asterisk) is seen. Although the location would make one think of an ovarian mass, it was in fact a broad ligament myoma. Ut, uterus.

Histologically, leiomyomas are composed of smooth muscle with varying amounts of fibrous connective tissue. The surrounding myometrium can become compressed and form a pseudocapsule, which can be readily identified on ultrasound and MRI imaging (Fig. 27-21). When rapidly





**FIGURE 27-20.** Longitudinal sonogram in a pregnant patient at 18 weeks' gestational age. An anterior lower uterine segment fibroid (arrows) is seen. It does not obstruct the cervix (demarcated by calipers). Bl, bladder.



**FIGURE 27-21.** Large uterine myoma demarcated by the calipers. A pseudocapsule can be seen from surrounding compressed myometrium (arrows).

growing, the leiomyomas can outgrow their blood supply, resulting in degeneration.<sup>15</sup>

Leiomyomas are usually readily recognized on sonography, often with a variable appearance. The uterus may be heterogeneous and globular in contour, which overlaps with the appearance of adenomyosis. Focal leiomyomas are usually heterogeneous but mostly hypoechoic when compared with the surrounding myometrium. The heterogeneity increases as the leiomyomas evolve through various changes such as growth, increased fibrosis, degeneration, and calcification (Fig. 27-22).

As leiomyomas increase in size, they tend to outgrow their blood supply, which leads to degeneration: hyaline, myxoid, calcification, cystic, and hemorrhagic (Fig. 27-23). This can give a more atypical appearance on sonography and on MRI (Fig. 27-24).<sup>15,16</sup> Many leiomyomas demonstrate areas of characteristic acoustic attenuation. This may not always be secondary to calcification. This attenuation is believed to be caused by the transitional zone between apposed tissues such as fibrous tissue and smooth muscle, the margins of the leiomyoma with adjacent normal myometrium, and the edges of whorls and bundles of smooth muscle.<sup>17</sup> This characteristic shadowing is very helpful in differentiating an exophytic leiomyoma from an adnexal/ovarian mass. Whereas this finding used to be very characteristic and specific of fibroids, it is currently recognized that adenomyosis with smooth muscle hypertrophy may produce a similar appearance (Fig. 27-25). Dystrophic calcification occurs predominantly in postmenopausal patients. The calcifications are curvilinear, with dense shadowing. Degeneration may produce cystic change, or edema with small multiple cystic spaces.

Submucosal fibroids may have varying degrees of intracavitary extension. The degree to which the fibroid projects into the endometrial cavity will help determine the

likelihood of hysteroscopic resection. Until recently, sonohysterography has been the best modality to determine the degree of intracavitary extension of the fibroid (Fig. 27-26). More recently, three-dimensional ultrasound has proved useful as well (Fig. 27-27). Transvaginal imaging may be limited if the fibroids are large. In this situation, transabdominal imaging may improve visualization. MRI is a valuable modality to evaluate large or atypical fibroids. The multiplanar capability and larger field of view is of great assistance.

## Lipomatous Uterine Tumors

Lipomatous tumors of the uterus are rare benign conditions but are readily recognized on ultrasound. Sonographically, the characteristic appearance is a highly echogenic mass within the myometrium without any demonstrable Doppler flow. They are usually asymptomatic and do not require surgery. The histology can reveal a spectrum including pure lipomas, lipoleiomyomas, fibrolipomas, and myolipomas (Fig. 27-28).<sup>18</sup>

## MALIGNANT CONDITIONS

### Sarcomas

Although leiomyomas are benign, rapid growth in peri- and postmenopausal patients raises the possibility of sarcomatous change. Most leiomyosarcomas arise independently rather than from a preexisting leiomyoma although it does occur.<sup>19</sup> It is commonly accepted that uterine sarcomas are extremely aggressive with poor prognosis. Early diagnosis can improve the survival rates, and therefore, attention to imaging clues is crucial. Usually there is no significant sonographic difference from rapidly growing or degenerating myoma

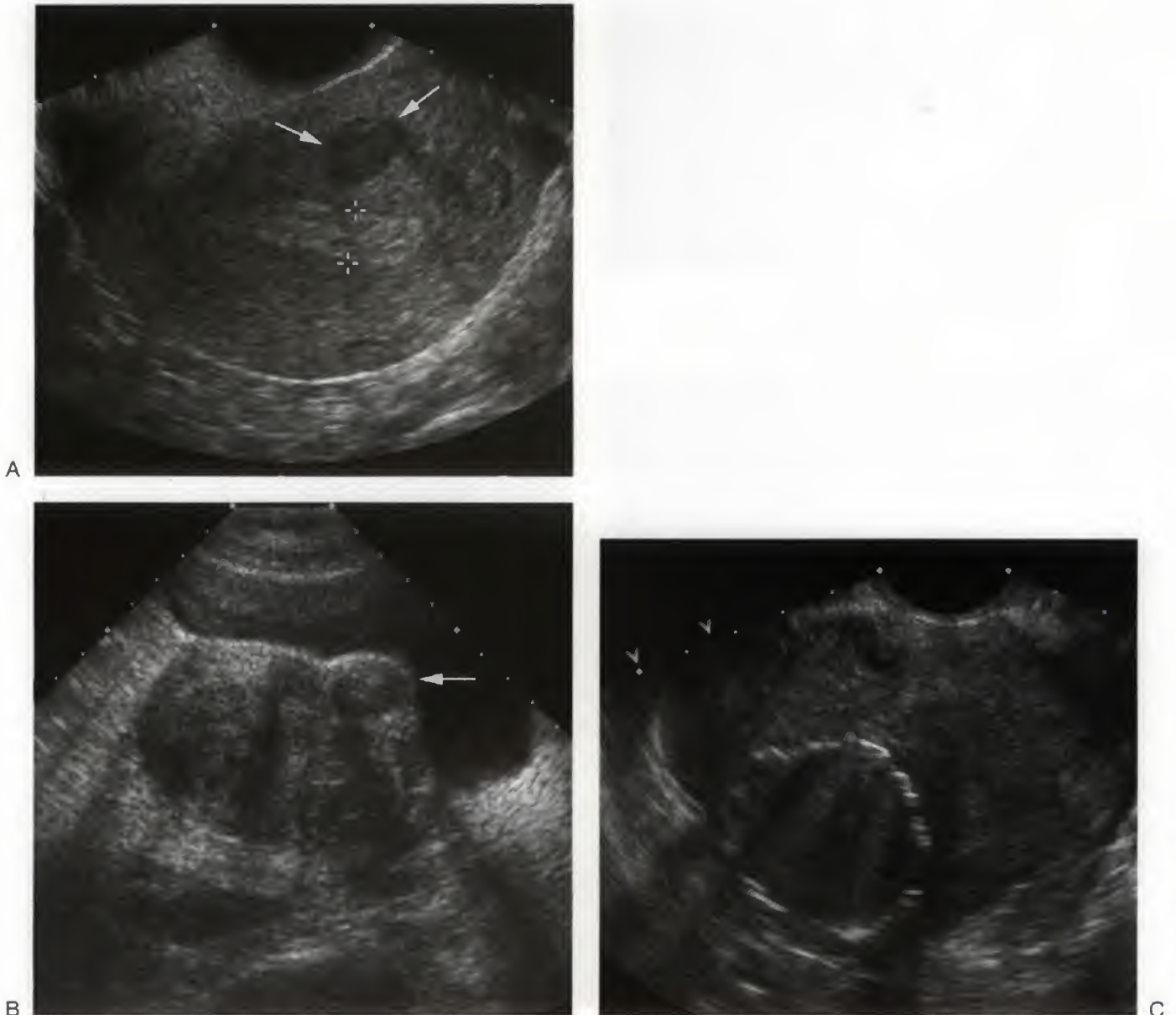


**FIGURE 27-22.** Variable appearance of uterine fibroids. *A.* Small intramural fibroid appearing as a round hypoechoic mass (*arrows*). *B.* Longitudinal sonogram in a patient with multiple uterine fibroids. The normal morphology of the uterus is markedly distorted. The endometrium could not be identified. An anterior subserosal fibroid (*arrow*) is projecting into the urinary bladder. *C.* Sonogram of a fibroid demonstrating peripheral calcification.



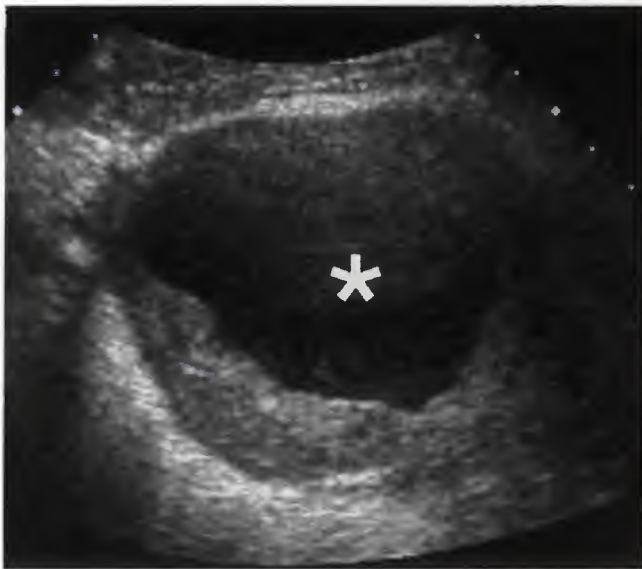


**FIGURE 27-23.** Marked cystic degeneration (*asterisk*) of a large intramural fibroid.

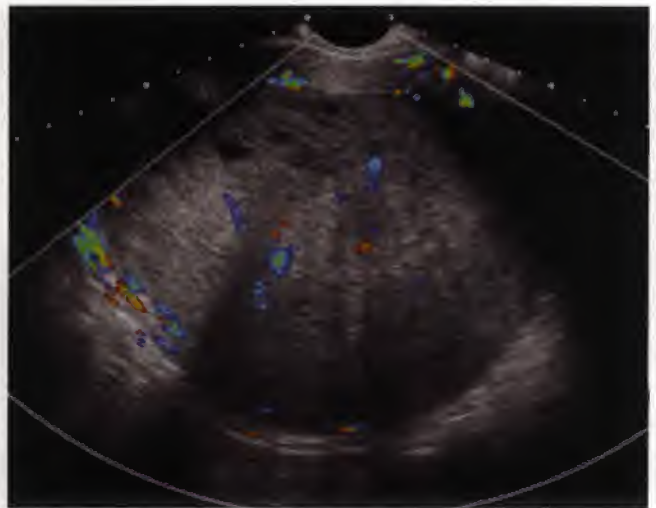


**FIGURE 27-25.** Large fibroid demonstrating areas of cystic change as well as shadowing (*venetian blind shadowing*). Both of these features are quite similar to the changes seen in adenomyosis.

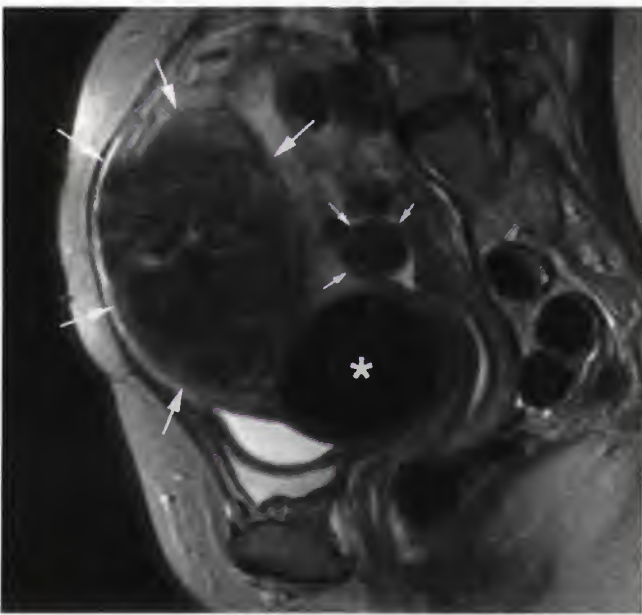


**FIGURE 27-24.** Sagittal T2 MRI image demonstrating various different but common appearances of fibroids: Small submucosal fibroid impressing the endometrial canal with typical low T2 signal (*small arrows*), large anterior fibroid with internal edema and/or degeneration (*large arrows*), anterior lower uterine segment fibroid with very low T2 signal consistent with internal blood products/hemosiderin from "red degeneration" (*asterisk*).

and a sarcoma. In instances of degenerating myomas there can be change in the internal architecture and, an increase in solid components rather than progressive degeneration. The increased solid components can be appreciated if previous studies are available for comparison. MRI can be obtained to confirm the avid enhancement of those solid components. If there are no baseline or previous studies, it is very difficult to determine if solid portions of the



A



B

**FIGURE 27-26.** Sonohysterography in two patients with submucosal, predominantly intracavitary fibroids. A. Sonohysterogram in which the myoma is projecting into the uterine cavity. This was resected hysteroscopically. B. Sonohysterogram of a patient with a submucosal fibroid projecting into the uterine cavity. The distended balloon (*arrow*) is seen as well in this image.

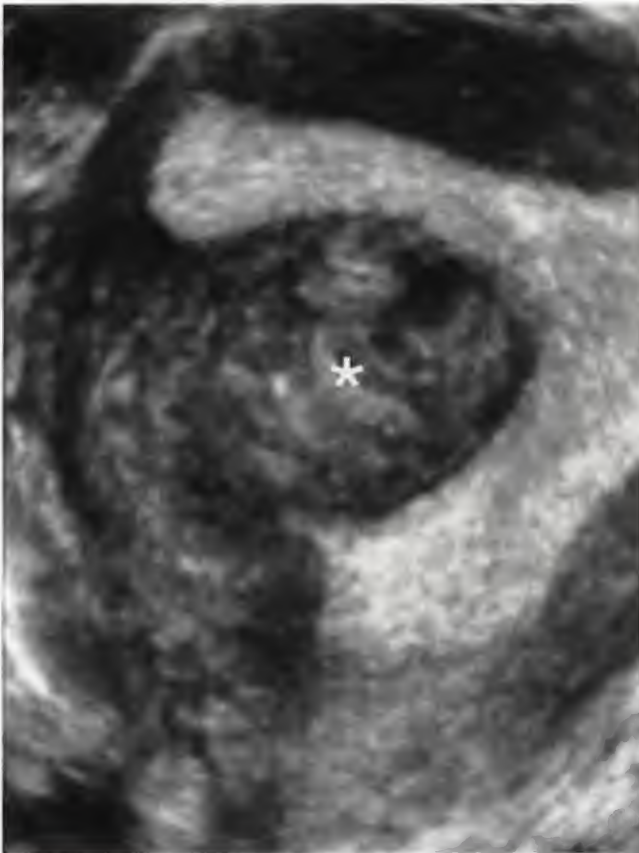


**FIGURE 27-27.** Three-dimensional image of a submucosal intracavitary fibroid (asterisk). (Courtesy of Beryl R. Benacerraf, Boston, MA.)

degenerated myoma are residual viable leiomyoma versus new developing leiomyosarcoma. The other signs of leiomyosarcoma include local invasion and distant metastases, which are detected on MRI or computed tomography (Fig. 27-29).

## OTHER IATROGENIC PROCESSES

### Arteriovenous Malformations

Arteriovenous malformations (AVMs) are multiple communications between the arterial and venous system without an intervening capillary network. These lesions can be congenital or more often iatrogenic due to intrauterine instrumentation. Acquired AVMs are more like multiple small arteriovenous fistulas. They can be secondary to trauma, malignancy, or infection. Specific etiologies include miscarriage, therapeutic abortion, dilation and curettage, cesarean delivery, carcinoma of the cervix or endometrium, uterine infection, trophoblastic disease, fibroids, endometriosis, and uterine surgery.<sup>20</sup> Sonography is often the first imaging study performed when the patient presents with a history of dysfunctional uterine bleeding. Color and duplex Doppler sonography have very characteristic findings. Serpiginous cystic areas and a vascular tangle of blood vessels can be seen in grayscale,

which fills with avid flow on color Doppler and demonstrate high-velocity, low-resistance flow on duplex Doppler (Fig. 27-30).<sup>21,22</sup> The Doppler characteristics may be similar to cases of gestational trophoblastic disease. Therefore, when these imaging findings are seen, gestational trophoblastic disease should always be excluded by serum  $\beta$ -human chorionic gonadotropin levels, which would be negative in the cases of AVM.

Pseudoaneurysms are also reported to occur as a complication after intrauterine procedures. These can be distinguished from AVMs by color and duplex Doppler imaging. Pseudoaneurysms appear as a blood-filled cystic structure with swirling arterial blood flow.<sup>21</sup>

Knowing that uterine curettage or surgical trauma can cause uterine vascular abnormalities such as arteriovenous fistulas, pseudoaneurysms, and arteriovenous fistulas is useful when imaging patients with such clinical history and bleeding. Recognizing these lesions on imaging is important because treatment is quite different than for other causes of dysfunctional uterine bleeding. These abnormalities can be treated safely with transcatheter arterial embolization and may be worsened by uterine curettage. Acquired arteriovenous fistulas are reported to be much easier to treat than the congenital lesions because they only have single or bilateral feeding arteries, and typically are not fed by extrauterine vessels and lack a nidus, unlike congenital lesions.<sup>21</sup>

### Intrauterine Contraceptive Devices

Contemporary intrauterine contraceptive devices (IUCDs), are easily visualized with transabdominal and transvaginal sonography. The brightly echogenic device with intense sound beam attenuation is well seen. Transvaginal sonography is commonly used to evaluate placement. Location and complications such as migration into the myometrium.<sup>23</sup> Three-dimensional ultrasound has been used with great success to improve visibility in technically challenging situations, as well as in confirming the specific type of the IUCD (Fig. 27-31).<sup>24</sup>

If an IUCD is not seen on sonography and history confirms placement, a plain radiograph should be obtained to exclude a perforation and expulsion into the peritoneal cavity. Blood products as well as products of conception can obscure the visualization of the IUCD. There are occasions when an intrauterine contraceptive device is seen associated with an intrauterine pregnancy. Although IUCDs can be easily identified during the first trimester, they are rarely visualized in the second or third trimester of pregnancy. If removal is being considered, the relationship of the IUCD to the gestational sac becomes important (superior or inferior to the sac).

### Ultrasound Evaluation of the Postpartum and Postabortive Uterus

Not infrequently, the sonologist is asked to evaluate the patient who has bleeding or pain after delivery or therapeutic abortion. The question most commonly asked is whether there are retained products of conception (RPOC) or a large hematoma within the uterine cavity. A basic knowledge of the normal postpartum uterus is necessary to accurately diagnose pathological conditions.



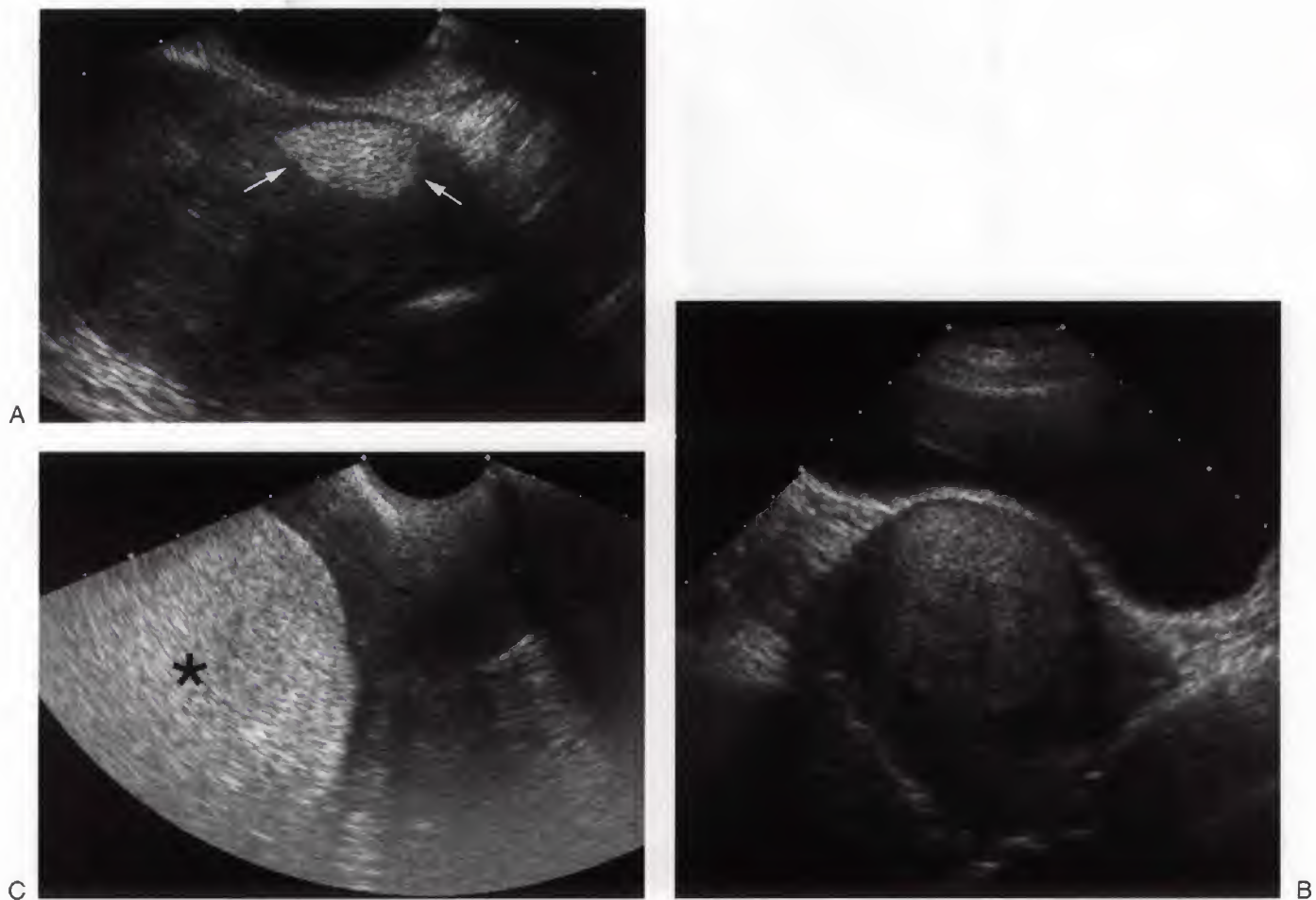


**FIGURE 27-28.** Spectrum of lipomatous uterine tumors. *A.* Sonogram in which a 1.5-cm focal hyperechogenic mass is seen in the uterus (*arrows*). This was a lipoleiomyoma. *B.* Transabdominal sonogram demonstrating a large 5-cm lipoleiomyoma. *C.* Transvaginal sonogram of a very large 7-cm hyperechogenic mass (*asterisk*). This was also a lipoleiomyoma.

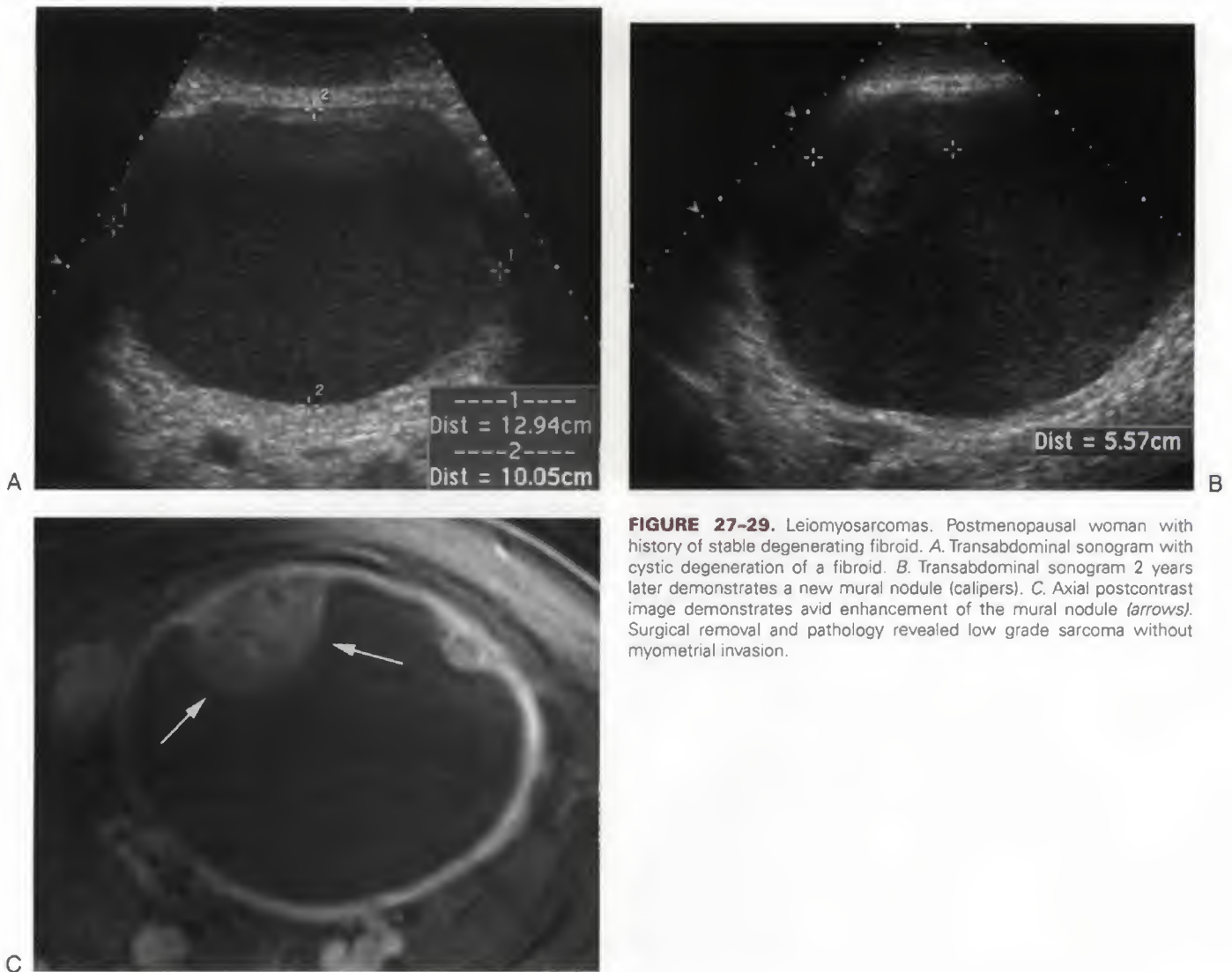


**FIGURE 27-29.** Leiomyosarcomas. Postmenopausal woman with history of stable degenerating fibroid. *A.* Transabdominal sonogram with cystic degeneration of a fibroid. *B.* Transabdominal sonogram 2 years later demonstrates a new mural nodule (calipers). *C.* Axial postcontrast image demonstrates avid enhancement of the mural nodule (arrows). Surgical removal and pathology revealed low grade sarcoma without myometrial invasion.

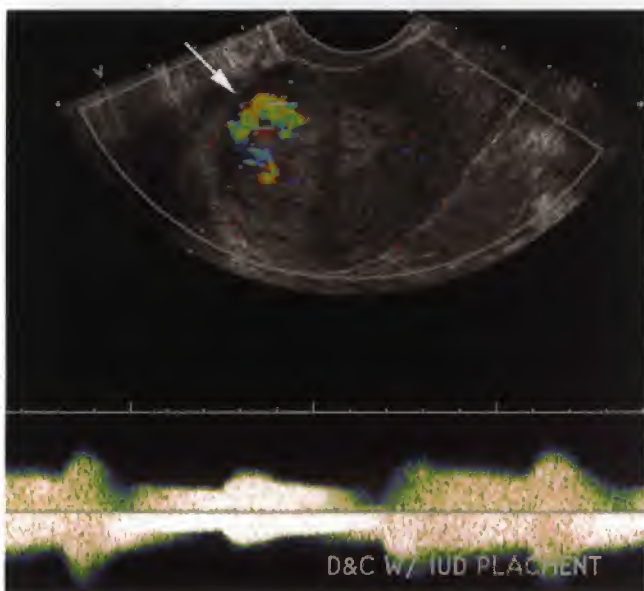


**FIGURE 27-30.** Iatrogenic AVMs. This patient presented after dilatation and curettage and intrauterine device placement with prolonged heavy bleeding for 1 week. This transvaginal image with Doppler demonstrates a large fundal iatrogenic AVM (arrow) with characteristic very low resistance arterial flow pattern. Gestational trophoblastic disease was excluded by negative  $\beta$ -human chorionic gonadotropin levels.



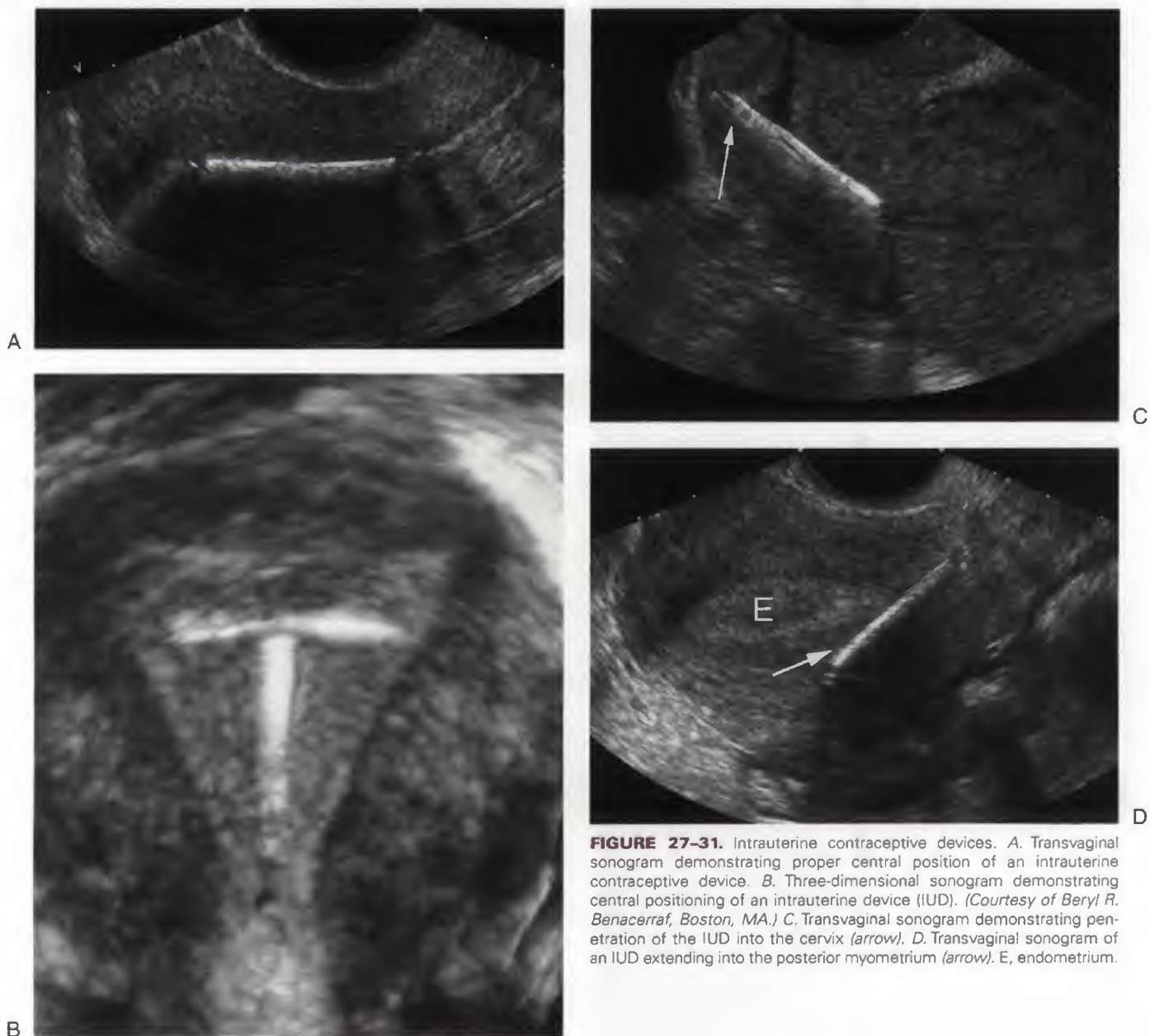


**FIGURE 27-31.** Intrauterine contraceptive devices. *A.* Transvaginal sonogram demonstrating proper central position of an intrauterine contraceptive device. *B.* Three-dimensional sonogram demonstrating central positioning of an intrauterine device (IUD). (Courtesy of Beryl R. Benacerraf, Boston, MA.) *C.* Transvaginal sonogram demonstrating penetration of the IUD into the cervix (arrow). *D.* Transvaginal sonogram of an IUD extending into the posterior myometrium (arrow). *E.* Endometrium.

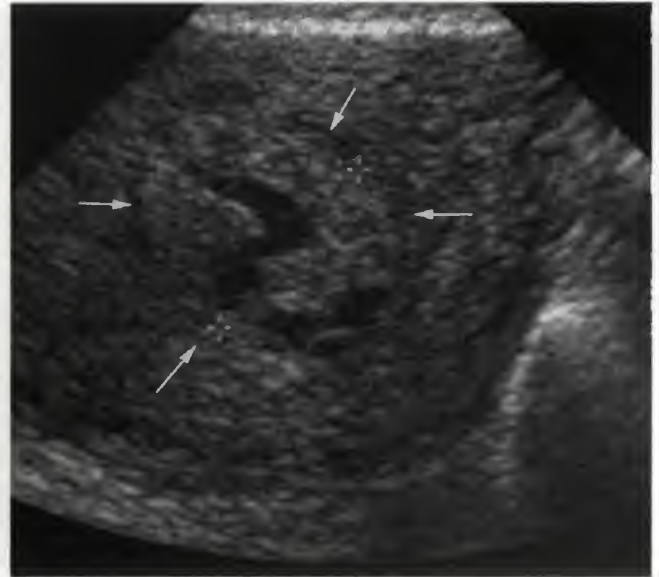


**FIGURE 27-32.** Longitudinal sonogram in a patient 3 days postpartum. Fluid and tissue (arrows) are seen in the uterine cavity. There was no evidence of retained products of conception.



**FIGURE 27-33.** Longitudinal sonogram in a patient 1 week after cesarean section. Residual air (arrow) is seen within the uterine cavity. The endometrium was thin and normal.

The normally enlarged gravid uterus begins to decrease in size several days after delivery.<sup>25</sup> The uterus rapidly decreases in size during the first 1 to 2 postpartum weeks and is usually back to its nongravid size by 6 to 8 weeks' postpartum.<sup>25-27</sup> The endometrium returns to its pregravid state by 3 to 6 weeks' postpartum.<sup>25</sup> Small amounts of fluid and echogenic material (likely representing blood clot) may be seen in the normal postpartum uterus (Fig. 27-32).<sup>25,28</sup> Bright hyperechogenic foci, likely secondary to air, can also be seen within the endometrial cavity and persist for several weeks postpartum (Fig. 27-33).<sup>25,29</sup>



A



B

**FIGURE 27-34.** A. Sonogram from a patient who had persistent bleeding after a first trimester therapeutic abortion. Tissue and fluid (arrows) representing retained products of conception are seen within the uterus. B. Doppler imaging of the same patient demonstrates markedly increased vascularity within the tissue.

The thickness of the postpartum endometrium is variable, ranging in one study from a mean value of 15.8 mm on day 1 to a mean of 5.5 mm on day 28.<sup>30</sup>

Several studies have evaluated the endometrial thickness as a sign of RPOC.<sup>25,31-38</sup> Although there does not appear to be a cutoff value above which RPOC are certain, if the endometrium is extremely thin it is unlikely that there are RPOC. One study found that in the absence of an endometrial mass or when the endometrial thickness was less than 10 mm, RPOC was extremely unlikely.<sup>25,38</sup> Thus, ultrasound appears to be more useful to exclude the diagnosis than to accurately make the correct diagnosis. A focal echogenic mass is suggestive of RPOC (Fig. 27-34).<sup>25,31,39</sup> This, however, is not a specific or reliable sign, because a hematoma may have a similar appearance.<sup>25</sup> Doppler ultrasound has proved useful in some cases to assist in the diagnosis of RPOC.<sup>25,40</sup> Whereas flow within a focal intracavitary mass is suggestive





**FIGURE 27-35.** A. A patient presented with bleeding 1 week postpartum. Tissue (arrows) was seen within the endometrial cavity. B. Doppler imaging demonstrated no evidence of blood flow within the tissue (arrows). This represented blood clots without retained products of conception.

of RPOC, the absence of flow does not exclude the diagnosis.<sup>25,38</sup> Placental tissue may persist for months after delivery and be a source of persistent hemorrhage (Fig. 27-35).

In all cases of vaginal bleeding, in the postgravida state, in which tissue is seen within the uterine cavity, the diagnoses of gestational trophoblastic disease and ectopic pregnancy should be considered (Fig. 27-36). Clinical correlation as well as correlation with  $\beta$ -human chorionic gonadotrophic levels is often helpful in excluding these conditions.

## References

1. AIUM. AIUM Practice guideline for the Performance of the Ultrasound Examination of the Female pelvis: AIUM; 2006.
2. AIUM Standard for the Performance of Saline Infusion Sonohysterography. 2002.
3. Sample WF, Lippe BM, Gyepes MT: Gray-scale ultrasonography of the normal female pelvis. *Radiology* 125:477, 1977.

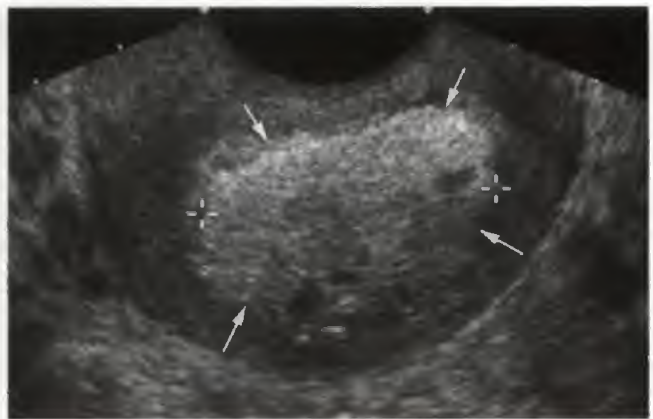


**FIGURE 27-36.** A patient presented with vaginal bleeding continuing 2 months after delivery. A hyperechoic soft tissue mass (arrows) was seen within the uterus. This was retained placental tissue.

4. Merz E, Miric-Tesanic D, Bahlmann F, et al: Sonographic size of uterus and ovaries in pre-and postmenopausal women. *Ultrasound Obstet Gynecol* 7:38, 1996.
5. Miller EI, Thomas RH, Lincs P: The atrophic postmenopausal uterus. *J Clin Ultrasound* 5:261, 1977.
6. Imaoka I, Wada A, Matsuo M, et al: MRI imaging of disorders associated with female infertility: Use in diagnosis, treatment and management. *Radiographics* 23:1401, 2003.
7. Daly DC, Maier D, Soto-Albers C: Hysteroscopic metroplasty: Six years' experience. *Obstet Gynecol* 73:201, 1989.
8. Kubik-Huch RA: Female pelvis. *Eur Radiol* 9:1715, 1999.
9. Andreotti RF: The sonographic diagnosis of adenomyosis. *Ultrasound Q* 213:167, 2005.
10. Chopra S, Lev-Toaff AS, Ors F, Bergin D: Adenomyosis: Common and uncommon manifestations on sonography and magnetic resonance imaging. *J Ultrasound Med* 25:617, 2006.
11. Kuligowska E: Pelvic pain: Overlooked and underdiagnosed gynecologic conditions. *Radiographics* 25:3, 2005.
12. Bazot M: Ultrasonography compared with magnetic resonance imaging for the diagnosis of adenomyosis: Correlation with histopathology. *Human Reprod* 16:2427, 2001.
13. Lee EJ: Sonographic findings of uterine polypoid adenomyomas. *Ultrasound Q* 20:2, 2004.
14. Tamai K: MRI imaging findings of adenomyosis: Correlation with histopathologic features and diagnostic pitfalls. *Radiographics* 25:21, 2005.
15. Murase E, Siegelman ES, Outwater EK, et al: Uterine leiomyomas: Histopathologic features, MR imaging findings, differential diagnosis, and treatment. *Radiographics* 19:1179, 1999.
16. Benson CB, Chow JS, Chang-Lee W, et al: Outcome of pregnancies in women with uterine leiomyomas identified by sonography in the first trimester. *J Clin Ultrasound* 29:261, 2001.
17. Klicwer MA, Hertzberg BS, George Y, et al: Acoustic shadowing from uterine leiomyomas: Sonographic-pathologic correlation. *Radiology* 196:99, 1995.
18. Serafini G, Marinoli C, Quadri P, et al: Lipomatous tumors of the uterus: Ultrasonographic findings in 11 cases. *J Ultrasound Med* 15:195, 1996.
19. Prayson RA, Hart WR: Pathologic considerations of uterine smooth muscle tumors. *Obstet Gynecol Clin North Am* 22:637, 1995.
20. Castro-Aragon I, Aragon I, Urcuyo R, et al: Conservative management of a uterine arteriovenous malformation diagnosed in pregnancy. *J Ultrasound Med* 23:1101, 2004.
21. Kwon JH, Kim GS: Obstetric iatrogenic arterial injuries of the uterus: Diagnosis with US and treatment with transcatheter arterial embolization. *Radiographics* 22:35, 2002.
22. Polat P, Suma S, Kantarcy M, et al: Color Doppler US in the evaluation of uterine vascular abnormalities. *Radiographics* 22:47, 2002.
23. Mogavero G, Sheth S, Hamper UM: Endovaginal sonography of the nonpregnant uterus. *Radiographics* 13:969, 1993.

24. Valsky DV, Cohen SM, Hochner-Celnikier D, et al: The shadow of the intrauterine device. *J Ultrasound Med* 25:613, 2006.
25. Brown DL: Pelvic ultrasound in the postabortion and postpartum patient. *Ultrasound Q* 21:27, 2005.
26. Wachsberg RH, Kurtz AB, Levine CD, et al: Real-time ultrasonographic analysis of the normal postpartum uterus: Technique, variability, and measurements. *J Ultrasound Med* 13:215, 1994.
27. Lavery JP, Shaw LA: Sonography of the puerperal uterus. *J Ultrasound Med* 8:481, 1989.
28. Edwards A, Ellwood DA: Ultrasonographic evaluation of the postpartum uterus. *Ultrasound Obstet Gynecol* 16:640, 2000.
29. Wachsberg RH, Kurtz AB: Gas within the endometrial cavity at postpartum US: A normal finding after spontaneous vaginal delivery. *Radiology* 183:431, 1992.
30. Mulic-Lutvica A, Bekuretsion M, Bakos O, et al: Ultrasonic evaluation of the uterus and uterine cavity after normal, vaginal delivery. *Ultrasound Obstet Gynecol* 18:491, 2001.
31. Cetin A, Cetin M: Diagnostic and therapeutic decision-making with transvaginal sonography for first trimester spontaneous abortion, clinically thought to be incomplete or complete. *Contraception* 57:393, 1998.
32. Alcazar JL, Baldonado C, Laparte C: The reliability of transvaginal ultrasonography to detect retained tissue after spontaneous first-trimester abortion, clinically thought to be complete. *Ultrasound Obstet Gynecol* 6:126, 1995.
33. Rulin MC, Bornstein SG, Campbell JD: The reliability of ultrasonography in the management of spontaneous abortion, clinically thought to be complete: A prospective study. *Am J Obstet Gynecol* 168:12, 1993.
34. Wong SF, Lam MH, Ho LC: Transvaginal sonography in the detection of retained products of conception after first-trimester spontaneous abortion. *J Clin Ultrasound* 30:428, 2002.
35. Nielsen S, Hahlin M: Expectant management of first-trimester spontaneous abortion. *Lancet* 345:84, 1995.
36. Nielsen S, Hahlin M, Oden A: Using a logistic model to identify women with first-trimester spontaneous abortion suitable for expectant management. *Br J Obstet Gynaecol* 103:1230, 1996.
37. Sadan O, Golan A, Girtler O, et al: Role of sonography in the diagnosis of retained products of conception. *J Ultrasound Med* 23:371, 2004.
38. Durfee SM, Frates MC, Luong A, et al: The sonographic and color Doppler features of retained products of conception. *J Ultrasound Med* 24:1181, 2005.
39. Achiron R, Goldenberg M, Lipitz S, et al: Transvaginal duplex Doppler ultrasonography in bleeding patients suspected of having residual trophoblastic tissue. *Obstet Gynecol* 81:507, 1993.
40. Keogan MT, Hertzberg BS, Kliever MA: Low resistance Doppler waveforms with retained products of conception: Potential for diagnostic confusion with gestational trophoblastic disease. *Eur J Radiol* 21:109, 1995.



## ABNORMAL UTERINE BLEEDING: THE ROLE OF ULTRASOUND

Steven R. Goldstein, MD

### Evolution of Endometrial Assessment

Transvaginal Ultrasound  
Saline Infusion Sonohysterography  
Technique  
Saline Infusion Sonohysterography—Technical Considerations  
*Timing of the Procedure*  
Difficulty Threading the Catheter  
Anesthesia/Analgesia

Risk of Infection

Concern About Spreading Adenocarcinoma into the Peritoneal Cavity  
Inadequate Distension of the Cavity  
Saline Infusion Sonohysterography—Pathology  
Abnormal Uterine Bleeding—An Algorithm  
Selective Estrogen Receptor Modulators—Tamoxifen

### Summary

Abnormal uterine bleeding accounts for up to 20% of gynecologic visits.<sup>1</sup> Obviously, any pregnancy event must first be excluded. Cheap, rapid, and monoclonal antibody urine  $\beta$ -human chorionic gonadotropin tests, now even readily available over the counter to our patients, make this a relatively simple maneuver. If a pregnancy event has been excluded, then the most likely cause of bleeding is dysfunctional anovulatory bleeding; what we often tell patients is hormone imbalance. However, as women get older, organic pathology such as polyps, submucous myomas, hyperplasias, and even frank carcinoma become more likely. The Surveillance Epidemiology and End Results (SEER) database<sup>2</sup> reports that the incidence of endometrial carcinoma in women 30 to 34 years of age is 2.3/100,000, and it increases to 6.1/100,000 between 35 to 40 years of age, and then rises dramatically to 36.2/100,000 in women 40 to 49 years of age. In postmenopausal women on no hormonal replacement therapy any bleeding is considered cancer until proven otherwise, although the incidence of malignancy in such patients ranges from 2% to 10%, depending on risk factors.<sup>3</sup>

The role of the clinician in a patient who presents with bleeding is twofold: first, in women over 40 years of age, it is to exclude endometrial carcinoma,<sup>4</sup> and second, to identify the source of bleeding so it can be stopped or managed.

The vast majority of patients with abnormal bleeding will have dysfunctional uterine bleeding in association with episodes of anovulation that can best be managed hormonally or expectantly with reassurance (premenopausal), or endometrial atrophy (postmenopausal). The value of an approach to distinguish such patients from those with organic pathologic conditions in a safe, painless, and convenient manner is obvious.

### EVOLUTION OF ENDOMETRIAL ASSESSMENT

Initially, curettage was the gold standard. First described in 1843,<sup>5</sup> its performance in the hospital became the most common operation performed on women in the world. As early as the 1950s, a review of 6907 curettage procedures<sup>6</sup> found the technique missed endometrial lesions in 10% of cases; of these, 80% were polyps.

In the 1970s, vacuum-suction curettage devices allowed sampling without anesthesia in an office setting. The most popular was the Vabra aspirator (Berkeley Medevices, Berkeley, CA). This was found to be 86% accurate in the diagnosis of cancer.<sup>7</sup> Subsequently, cheaper, smaller, and less painful plastic catheters with their own internal pistons to generate suction became popular. One of these, the Pipelle device (Unimar, Wilton, CT), was found to have similar efficacy but better patient acceptance when compared with the Vabra.<sup>8</sup>

A number of studies have evaluated the efficacy of endometrial sampling with the Pipelle catheter. Rodriguez et al<sup>9</sup> did a pathologic study of 25 hysterectomy specimens. The percentage of endometrial surface sampled by the Pipelle device was 4% versus 41% for the Vabra aspirator. In one widely publicized study,<sup>10</sup> the Pipelle had a 97.5% sensitivity to detect endometrial cancer in 40 patients undergoing hysterectomy. The shortcoming of that study was that the diagnosis of malignancy was known before the performance of the specimen collection. Finally, in yet another study, Guido et al<sup>11</sup> also studied the Pipelle biopsy in patients with known carcinoma undergoing hysterectomy. Among 65 patients, a Pipelle biopsy provided tissue adequate for



analysis in 63 (97%). Malignancy was detected in only 54 patients (83%). Of the 11 with false-negative results, five (8%) had disease confined to endometrial polyps, and three (5%) had tumor localized to less than 5% of the surface area of the cavity. The surface area of the endometrial involvement in that study was less than or equal to 5% of the cavity in three of 65 (5%); 5% to 25% of the cavity in 12 of 65 (18%), of which the Pipelle missed four; 26% to 50% of the cavity in 20 of 65 (31%), of which the Pipelle missed four; and greater than 50% of the cavity in 30 of 65 patients (46%), of which the Pipelle missed none. These results provide great insight about the way endometrial carcinoma can be distributed over the endometrial surface or confined to a polyp. Because tumors localized in a polyp or a small area of endometrium may go undetected, the authors in that study concluded that the "Pipelle is excellent for detecting global processes in the endometrium."

From these data it seems that undirected sampling, whether through curettage or various types of suction aspiration, is often fraught with error, especially in cases in which the abnormality is not global but focal (polyps, focal hyperplasia, or carcinoma involving small areas of the uterine cavity).

## Transvaginal Ultrasound

Introduced in the mid 1980s, the vaginal probe uses high frequency transducers in close proximity to the structure being studied. It yields a degree of image magnification that has been dubbed sonomicroscopy.<sup>12</sup> In the early 1990s it was used in women with postmenopausal bleeding to see if it could predict which patients lacked significant tissue and could avoid dilatation and curettage or endometrial biopsy and its discomfort, expense, and risk.<sup>13,14</sup> Consistently, the finding of a thin distinct endometrial echo less than 4 to 5 mm has been shown to effectively exclude significant tissue in women with bleeding. Thus, the value and contribution of ultrasound in this setting lies in its high-negative predictive value, which is its ability to tell us who lacks significant tissue and can reliably avoid any endometrial sampling. If some physicians thought this was only possible in the hands of luminaries, the endometrial surveillance arm of the Postmenopausal Estrogen/Progestin Interventions (PEPI) Study<sup>15</sup> went a long way to show that, in a multicentered trial with various investigators, visualization of a thin, distinct, endometrial echo had tremendous reliability. In that study an endometrial echo less than 5 mm had a 99% negative predictive value to exclude cancer (Fig. 28-1). Still, realizing that saying an endometrial echo 5 mm or less has a 99% negative predictive value is not remotely the same as saying that an endometrial echo greater than 5 mm is pathologic. In that study, the positive predictive value for disease of an endometrial echo greater than 5 mm was 9%, and if restricted to serious disease (cancer or atypical hyperplasia), the positive predictive value was merely 4%! In addition, that was a surveillance study; that is, the scans were not being performed for clinical history of bleeding. In my experience, many clinicians have inappropriately used a thick endometrial echo on ultrasound as an indicator of pathology. Such inappropriate application of transvaginal ultrasound is especially worrisome in patients with no bleeding in whom the finding is incidental.



**FIGURE 28-1.** Long axis transvaginal ultrasound image of a postmenopausal patient with uterine bleeding. A thin linear distinct endometrial echo here has a negative predictive value of 99%.



**FIGURE 28-2.** Long axis transvaginal ultrasound of a postmenopausal patient with an endometrial fluid collection. Note that the endometrium surrounding the fluid is thin. This picture is typical of inactive atrophic endometrium. Presumably the fluid collection is transudate and secondary to cervical stenosis in such a patient.

Endometrial thickness should be measured on a sagittal (long axis) image of the uterus and the measurement should be performed on the thickest portion of the endometrium, excluding the hypoechoic inner myometrium. It is a double thickness measurement from basalis to basalis. If fluid is present it is usually associated with cervical stenosis and atrophy (Fig. 28-2).<sup>16</sup> In these cases, the endometrial layers are measured separately and should be symmetric (Fig. 28-3). Remember that the endometrial cavity is a three-dimensional structure and attempts must be made to image the entire cavity. Recognizing the potentially pivotal role of transvaginal ultrasound in diagnostic evaluation, a statement should be included in the report regarding the technical adequacy of the scan. A well-defined endometrial echo should be seen emanating from the endocervical canal. The endometrial echo should be distinct. Often fibroids, previous surgery, marked obesity, or a tipped uterus may make visualization suboptimal. If so, it is perfectly acceptable, and in fact appropriate, to conclude endometrial echo is not well visualized.





**FIGURE 28-3.** Long axis transvaginal ultrasound of a postmenopausal patient with endometrial fluid collection. The tissue surrounding the fluid is thick and irregular measuring 6.2 and 7.7 mm respectively (calipers). Histopathology in this patient revealed endometrial hyperplasia with atypia.

In these cases, ultrasound cannot be relied upon to exclude disease. The next step for such patients with bleeding should be either hysteroscopy or saline infusion sonohysterography, depending on the skill set and preference of the physician and patient.

### Saline Infusion Sonohysterography

Although the use of fluid enhancement was described with abdominal ultrasound both for uterine and tubal observations,<sup>17</sup> the use of fluid to better evaluate the endometrium never gained widespread use. The introduction of the vaginal probe has changed that considerably.<sup>18,19</sup> The use of fluid instillation into the uterus coupled with such high-resolution transvaginal probes allows tremendous diagnostic enhancement with an inexpensive, simple, and well-tolerated office procedure.

### Technique

A palpatory bimanual examination is performed. As with any type of uterine instrumentation, absolute knowledge of whether the uterus is anteverted or retroverted and, if so, how sharply, only serves to enhance one's success and safety. Often, uterine version can be appreciated by the skilled sonographer. The clinician in obstetrics and gynecology should also be concerned about the presence of uterine tenderness or decreased mobility. The speculum is inserted. The cervix is cleansed with an antiseptic solution (10% iodine based solution). A catheter is inserted into the cervix. This is done by grasping it with a ring forceps and gently feeding it through the cervical os. Sterile saline has been flushed through the catheter to rid it of small amounts of air, which when first injected will cause a very echogenic artifactual appearance (Fig. 28-4). The speculum is removed carefully so as not to dislodge the catheter. The vaginal probe is then reinserted. A 10 mL syringe (being careful to rid it of any air bubble) is attached to the catheter. Scanning



**FIGURE 28-4.** Saline infusion sonohysterogram in which air has been allowed to enter the uterine cavity. Notice the echogenicity (arrow) and acoustic shadowing that results. This artifact can be avoided by flushing air out of the catheter and being sure there is no air bubble in the syringe.

in a long axis projection, fluid is instilled while watching the video monitor. In that long axis projection, the transducer is moved from side to side (that is, from cornua to cornua). The amount of fluid instilled is variable and depends on the image that one is producing on the ultrasound screen. When the uterus has been completely surveyed from cornua to cornua in a long axis projection, the transducer is then rotated 90 degrees into a coronal plane and further fluid is instilled while fanning down toward the endocervical canal and up toward the uterine fundus.

### Saline Infusion Sonohysterography—Technical Considerations

#### Timing of the Procedure

The uterus is an organ that has often had multiple procedures in many women including dilatation and curettages, childbirth, myomectomy, Cesarean sections, abortion, and so forth. As the endometrium proliferates it is not always a smooth homogeneous layer. Sonohysterography is best performed as soon as possible after the bleeding cycle has ended when the endometrium is as thin as it is going to be all month long. Otherwise, focal irregularities in the contour of the endometrium may be mistaken for small polyps or focal areas of endometrial hyperplasia (Fig. 28-5). This was supported in a prospective blinded study by Wolman et al<sup>20</sup> in which there was a 27% false positive rate in sonohysterography performed from day 16 to 28, whereas there were none when the procedure was performed before day 10.

Sometimes, the patient has such irregular bleeding that she cannot tell what is an actual menses. It may be helpful in such cases to use an empiric course of a progestogen such as medroxyprogesterone acetate 10 mg daily for 10 days as a medical curettage and then time the ultrasound evaluation to the withdrawal bleed.



**FIGURE 28-5.** Transvaginal pelvic scan of a patient 19 days since her last episode of bleeding. The endometrial surface is irregular. They measure 3.8 and 4.0 mm respectively. The irregular surface is not unusual especially in patients who have had previous dilatation and curettages, myomectomies, childbirth, and so forth. The irregular surface to the endometrium here identified as moguls can be misleading. Performing the procedure this long after the last bleeding episode can be fraught with error and should be avoided.

### Difficulty Threading the Catheter

Occasionally, there will be difficulty in threading the catheter into its desired position. Using the other hand to change the position of the speculum will often modify the angle of the cervix with the fundus sufficiently to allow successful completion. Use of a tenaculum is a last resort. A cervical stabilizer will be less painful, less traumatic, and does not cause bleeding from the cervix.

### Anesthesia/Analgesia

Anesthesia or analgesia is not required. In more than 1000 cases, I have seen three cases of a vasovagal response reminiscent of those occasionally seen with a plastic intrauterine device insertion in a nulliparous patient. The sonohysterography catheter is 1.8 mm in diameter and is remarkably painless in its insertion. The procedure is extremely well tolerated with no pain in the overwhelming majority of patients and minimal cramping in a very few.

### Risk of Infection

Sonohysterography should be handled similarly to traditional hysterosalpinography. Thus, the decision about whether to obtain gonorrhea or chlamydia cultures as well as whether to use antibiotics depends very much on the patient population with which the physician normally deals. In my experience, I have not routinely obtained cultures for sexually-transmitted diseases nor have prophylactic antibiotics been used. In more than 1000 cases, I have not experienced any infectious morbidity. Of 1153 procedures performed<sup>21</sup> the incidence of infectious complications that require surgical resolution was 0.7%, which is similar to diagnostic hysteroscopy<sup>22</sup> but less than hysterosalpingography.<sup>23</sup>

### Concern About Spreading Adenocarcinoma into the Peritoneal Cavity

Concern about spreading adenocarcinoma is a question of the benefit outweighing any theoretical risk. It is no longer standard practice to tie the fallopian tubes with silk before a total abdominal hysterectomy and bilateral salpingo-oophorectomy for endometrial carcinoma. Furthermore, hysteroscopy with saline or other distending media would have the same theoretical concern. Survival rates of patients with endometrial carcinoma who underwent standard hysterosalpinography were not different between patients who demonstrated intraperitoneal spill of the contrast medium and those who did not.<sup>24</sup> Alcazar<sup>25</sup> performed sonohysterography on 14 consecutive patients with stage I adenocarcinoma of the endometrium. It was done at the time of laparotomy, just when the abdomen was opened but before the start of the surgical procedure. All 14 readily spilled saline from the fallopian tubes. The fluid was analyzed as were cell washings. Only one patient (7%) had malignant cells in the spilled fluid causing the authors to conclude that the risk of malignant cell dissemination exists but is small.

### Inadequate Distension of the Cavity

In some patients, a patulous cervix results in a great deal of fluid running out transcervically. Other patients will have fluid going out through fallopian tubes even with slow injection and minimal pressure. As in hysteroscopy, some cavities are more difficult to distend than others. The position of the catheter should be checked, looking for its acoustic shadow in its entirety to the uterine fundus. However, unlike hysteroscopy (which requires distension for visualization), this procedure requires very little fluid to outline the cavity. Even a small ribbon of fluid acts as a sufficient interface to distinguish anterior and posterior endometrial surfaces and outline endometrial pathology.

### Saline Infusion Sonohysterography-Pathology

In a prospective pilot study, saline infusion sonohysterography was performed in 21 women with abnormal perimenopausal uterine bleeding.<sup>26</sup> Of the 21 patients, eight had obvious polypoid lesions (Fig. 28-6) and were triaged for operative hysteroscopic removal. The pathology report confirmed benign polyps in all eight patients. Three patients had submucous myomas. Two had wire loop resectoscopic excision (Fig. 28-7A and B). The third, with a submucous myoma that extended to the serosal edge of the uterus, received expectant management. Nine patients had no obvious anatomic lesion, and the endometrial thickness of either the anterior or posterior wall was a maximum of 3.2 mm. The studies were purposely performed on days 4 to 6 of the bleeding cycle when early proliferative change would be expected if, in fact, no anatomic abnormality existed. Biopsy in all nine of these patients revealed early proliferative endometrium. Thus, these patients had dysfunctional (that is, anovulatory) uterine bleeding and were successfully treated with progestational agents. One





**FIGURE 28-6.** Saline infusion sonohysterogram of a patient with abnormal uterine bleeding. In this coronal view of the uterus, a polyp measuring  $8.2 \times 12.3$  mm (calipers) is seen emanating from the posterior wall.

patient had an endometrial thickness along the anterior wall of 7.6 mm, although the posterior wall was thin (2.3 mm). Curettage with hysteroscopy revealed simple hyperplasia without atypia, and this patient was also treated with progestational agents. Thus, the conclusion was that endometrial fluid instillation (sonohysterogram) to enhance vaginal ultrasonography in perimenopausal women could reliably distinguish between patients with minimal tissue (3 mm or less single-layer measurements) whose bleeding is anovulatory and best treated hormonally from those patients with significant tissue (3 mm or more single-layer thickness) in need of formal curettage and hysteroscopy. Furthermore, polyps can be distinguished from submucous myomas. This allows appropriate triage for *operative* hysteroscopy in terms of skill required and length of time and equipment needed. Furthermore, this eliminates the need for diagnostic hysteroscopy in patients whose bleeding is dysfunctional.

As determined in this pilot study, the addition of saline infusion sonohysterography can reliably distinguish perimenopausal patients with dysfunctional abnormal bleeding (no anatomic abnormality) from those with globally thickened endometria or those with focal abnormalities.

### Abnormal Uterine Bleeding—An Algorithm

A clinical algorithm was proposed and studied in a large prospective trial of perimenopausal women with abnormal bleeding, using unenhanced transvaginal ultrasonography, followed by saline infusion sonohysterography for selected patients, and then either no endometrial sampling, undirected endometrial sampling, or visually directed endometrial sampling, depending on whether the ultrasonographically-based triage revealed no anatomic abnormality, globally thickened endometrium, or focal abnormalities, respectively (Fig. 28-8).<sup>27</sup> In that study, 280 patients (65%) displayed a thin, distinct, and symmetric endometrial echo less than 5 mm on day 4 to 6, and dysfunctional uterine bleeding was



**FIGURE 28-7.** A. Long axis view of a patient with abnormal uterine bleeding. There is a central thickened uterine echo which measures  $20.6 \times 29.8$  mm. B. Saline infusion sonohysterogram of the patient shown in A. The endoluminal mass ( $24.9 \times 24.7$  mm) outlined by calipers represents an intraluminal myoma. Note the acoustic shadowing emanating from the myoma. Furthermore, note the endometrial cavity itself is lined with thin endometrium compatible with the early proliferative phase in this perimenopausal patient.

diagnosed. One hundred fifty-three (35%) had saline infusion sonohysterography. Of these procedures, 44 (29%) were performed because of the inability to adequately characterize and measure the endometrium (Fig. 28-9A and B), and 109 (71%) were done for endometrial measurement greater than 5 mm. 61 of those patients then had both anterior and posterior endometrial thickness that was symmetric and less than 3 mm, compatible with dysfunctional uterine bleeding. Fifty-eight patients (13%) had focal polypoid masses

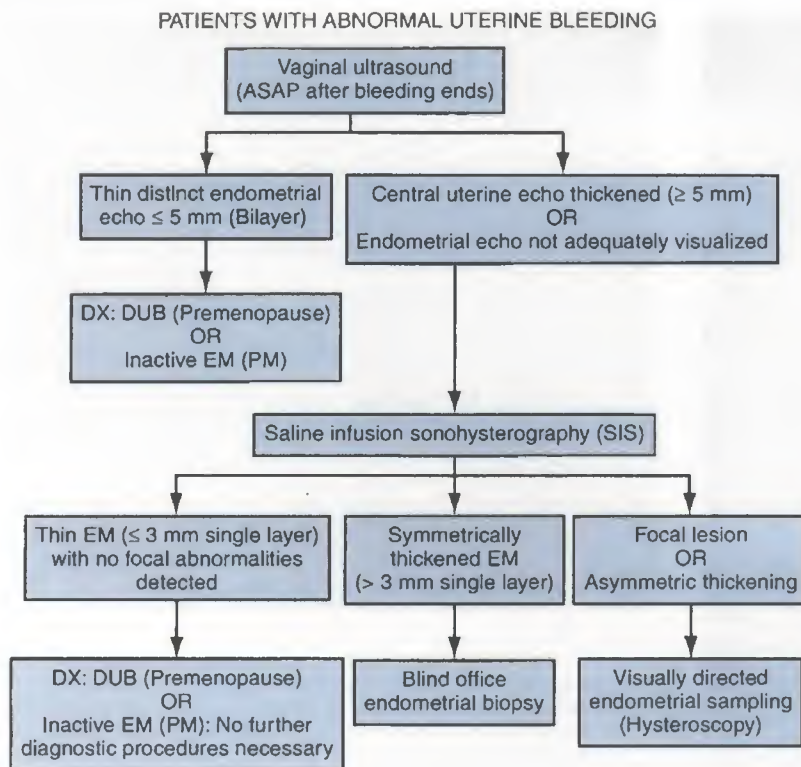


**FIGURE 28-8.** Clinical algorithm for patients with abnormal uterine bleeding. DUB, dysfunctional uterine bleeding.



**FIGURE 28-9.** A. Transvaginal scan in a long axis view of a perimenopausal patient with abnormal uterine bleeding. The endometrial echo is not sufficiently seen along its entirety to make an accurate diagnosis. B. Same patient as scanned in Figure 9A. Saline infusion sonohysterography reveals a lack of any endoluminal mass. The anterior and posterior endometrium measure 1.5 and 2.0 mm (calipers) respectively.

(Fig. 28-10A and B) that were removed hysteroscopically and confirmed pathologically. Twenty-two patients (5%) had submucous myomas, although 148 patients (34%) had clinical and ultrasonographic evidence of fibroids. Ten patients had symmetrical single-layer measurements of endometrium at saline infusion sonohysterography greater than 3 mm (range 3 mm–9 mm). Of these, the histologic type was proliferative endometrium in 5 patients and hyperplastic endometrium in 5 patients. Saline infusion

sonohysterography was technically inadequate in 2 patients who then underwent hysteroscopy with curettage. Undirected office biopsy alone without imaging potentially would have missed the diagnosis of focal lesions such as polyps, submucous myomas, and focal hyperplasia in up to 80 patients (18%).

Based on these results, it seems apparent that any blind endometrial sampling should be preceded by a fluid instillation sonohysterogram. A process must be shown to be



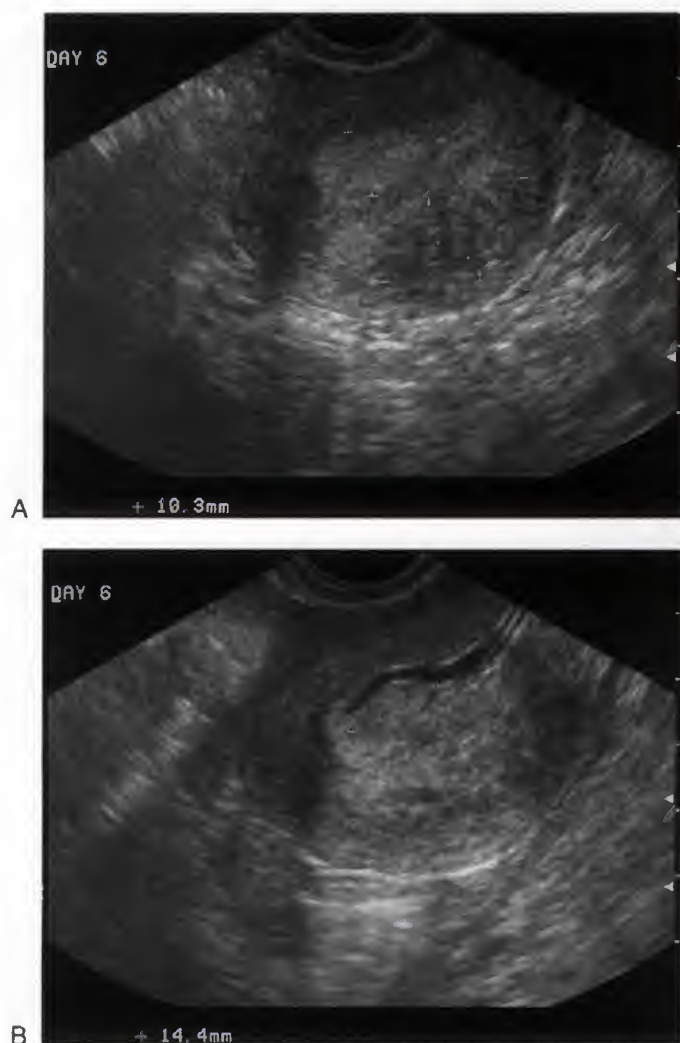


**FIGURE 28-10.** A. Long axis transvaginal ultrasound view of a perimenopausal patient with abnormal uterine bleeding. This is taken on day 6 just as the bleeding cycle has ended. The central uterine echoes are thickened and measure 10.3 mm. B. Saline infusion sonohysterogram of the patient shown in A. Note the presence of the catheter in the lower uterine segment. A polypoid lesion is seen extending from the fundal region. This measures 14.4 mm in its longest dimension. At the time of dilatation and curettage and hysteroscopy, a polyp was identified that was confirmed by pathology.

symmetrically “pan uterine” or global to justify a blind procedure. When changes are focal (that is, polyps, some hyperplasias, or some carcinomas), they can be appreciated as such with fluid instillation sonohysterography, and then directed biopsies must be carried out.

In the pilot study,<sup>26</sup> although nine of 21 patients had obvious sonographic and clinical evidence of fibroids, only three had a submucous component. Six of 21 had intramural-subserosal myomas coexisting with dysfunctional uterine bleeding. This was also true in the large prospective study,<sup>27</sup> when although 148/433 women had myomas only 22 had a submucous component.

Usually polyps are clearly discernable, as are submucous myomas. However, sometimes a broad-based polyp is difficult



**FIGURE 28-11.** Long axis view of the uterus in a patient with abnormal uterine bleeding. Saline infusion reveals a polypoid lesion emanating from the fundus. Color flow Doppler clearly identifies a central feeder vessel. Presence of such a feeder vessel can be used to make the diagnosis of a polyp even in the absence of saline infusion.

to distinguish from a submucosal myoma. This may be important for preoperative triage, in that a truly pedunculated submucous myoma will behave more like a polyp in terms of skill and equipment required for its removal in the operating room whereas a broad-based polyp may behave more like a myoma and require resectoscopic capability.

A reliable assessment with ultrasonography requires that the endometrial echo be homogeneous, surrounded by an intact hypoechoic junctional zone, and that the operator constantly remembers that the endometrial cavity is a three-dimensional structure. This may account for why Dijkhuizen et al<sup>28</sup> had 4 cases that supposedly measured less than 10 mm (some as little as 2 mm), and yet at hysteroscopy displayed polyps. Such cases underscore the importance of the three-dimensional character of the endometrial cavity and the occasional propensity of the ultrasonographic operator to obtain a limited number of two-dimensional views and assume that these represent the entire endometrial cavity. Any one frozen ultrasonographic image is nothing more than a two-dimensional snapshot, and failure to meticulously recreate three-dimensional anatomy will result in error. New three-dimensional ultrasound equipment will eliminate errors that may occur if the operator does not pay meticulous attention to mentally recreating three-dimensional anatomy.

Furthermore, the use of color flow or power Doppler to identify the central feeder vessel pathognomonic of an endometrial polyp is an alternative to sonohysterography in the diagnosis of polyps (Fig. 28-11). This had a positive predictive value of 81.3% in the study by Timmerman et al.<sup>29</sup>



**FIGURE 28–12.** Saline infusion sonohysterogram in a patient who had been taking tamoxifen for 1 and one half years. A polypoid mass with multiple microcysts is seen in the uterine cavity.

### Selective Estrogen Receptor Modulators–Tamoxifen

Tamoxifen, the first clinically available selective estrogen receptor modulator, was developed in 1966 and approved by the United States Food and Drug Administration in 1978.<sup>30</sup> It is the most prescribed antineoplastic drug in the world, with approximately 10 million women-use-years of experience. Tamoxifen has proved efficacious in all settings of breast cancer. However, in the mid-to-late 1980s, a series of letters to the editor and case reports announced an association between tamoxifen therapy in women with breast cancer and the development of endometrial carcinoma.<sup>31–35</sup> The published data demonstrating an association between tamoxifen and the development of benign as well as malignant endometrial lesions appeared to suggest a need for routine screening for endometrial neoplasms in women taking this drug.

Controversy existed about the extent of uterine surveillance, if any, that women on tamoxifen therapy require. We employed a regimen of transvaginal ultrasound and saline infusion sonohysterography when the image generated by an initial transvaginal ultrasound is of poor, indistinct quality, or suggestive of thickening of the endometrial wall. With the introduction of saline infusion sonohysterography<sup>36</sup> came the first reports of microcystic changes on ultrasound. Such changes represent glandular cystic atrophy and can be present in the basalis of the endometrium, in the proximal myometrium, or even within polyps (Fig. 28–12). Recent data seem to point to a high- and a low-risk group that can be identified before treatment with tamoxifen by screening with transvaginal ultrasound. Patients with no uterine abnormalities on transvaginal ultrasound appear to be at very low risk of developing atypical hyperplasia. However, patients with any lesions on the initial screen (although most are usually benign polyps) appear to have an 18-fold increased risk and, even if asymptomatic, may be appropriate candidates for ongoing surveillance, whereas low risk patients may be left alone unless they experience bleeding.

### SUMMARY

Abnormal uterine bleeding, whether in perimenopausal or postmenopausal patients, is an important clinical concern and accounts for much medical intervention. When bleeding occurs in women over 40 years of age as well as any postmenopausal women, endometrial assessment is mandatory. In the past and present, many clinicians prefer to begin such assessment with blind endometrial sampling. This chapter has presented an ultrasound-based approach to such patients. When present, a thin distinct endometrial echo excludes significant pathology, assuming it is performed at an appropriate time if the patient is, in fact, cycling. When a thin distinct endometrial echo is not visualized (inadequate visualization or presence of thickened echo) then saline infusion sonohysterography can help to triage patients to no anatomic pathology, globally thickened anatomic pathology that may then be evaluated with blind endometrial sampling, and focal abnormalities that must be evaluated under direct vision. Such an ultrasound-based approach will not only help to exclude endometrial carcinoma, but also to identify the source of any bleeding for better clinical management.

### References

1. Awwad JT, Toth TL, Schiff I: Abnormal uterine bleeding in the perimenopause. *Int J Fertil* 38:261, 1993.
2. SEER cancer statistics review, 1873-1996 (serial online). Available at [http://seer.cancer.gov/csr/1973\\_1996/index.html](http://seer.cancer.gov/csr/1973_1996/index.html).
3. Iatrakis G, Diakakis I, Kourounis G, et al: Postmenopausal uterine bleeding. *Clin Exp Obstet Gynecol* 24:157, 1997.
4. ACOG practice bulletin: Management of anovulatory bleeding. ACOG Committee on Practice Bulletins–Gynecology. American College of Obstetricians and Gynecologists. *Int J Gynaecol Obstet* 72:263, 2001.
5. Ricci JV: Gynaecologic surgery and instruments of the nineteenth century prior to the antiseptic age. In: *The Development of Gynaecological Surgery and Instruments*. Philadelphia, Blakiston, 1949, pp 326–328.
6. Word B, Gravlee LC, Widemon GL: The fallacy of simple uterine curettage. *Obstet Gynecol* 12:642, 1958.
7. Vuopala S: Diagnostic accuracy and clinical applicability of cytological and histological methods for investigating endometrial carcinoma. *Acta Obstet Gynecol Scand* 70:1, 1997.
8. Kaunitz AM, Masciello AS, Ostrovsky M, et al: Comparison of endometrial Pipelle and Vabra aspirator. *J Reprod Med* 33:427, 1988.
9. Rodriguez MJ, Platt LD, Medearis AL, et al: The use of transvaginal sonography for evaluation of postmenopausal size and morphology. *Am J Obstet Gynecol* 159:810, 1988.
10. Stovall TG, Photopoulos GJ, Poston WM, et al: Pipelle endometrial sampling in patients with known endometrial cancer. *Obstet Gynecol* 77:954, 1991.
11. Guido RS, Kanbour A, Ruhn M, et al: Pipelle endometrial sampling sensitivity in the detection of endometrial cancer. *J Reprod Med* 40:553, 1995.
12. Goldstein SR: *Endovaginal Ultrasound*, 2nd ed. New York, Wiley Liss, 1991.
13. Goldstein SR, Nachtigall M, Snyder JR, et al: Endometrial assessment by vaginal ultrasonography before endometrial sampling in patients with postmenopausal bleeding. *Am J Obstet Gynecol* 163:119, 1990.
14. Granberg S, Wiklund M, Karlsson B, et al: Endometrial thickness as measured by endovaginal ultrasound ultrasonography for identifying endometrial abnormality. *Am J Obstet Gynecol* 164:47, 1991.
15. Langer RD, Pierce JJ, O'Hanlan KA, et al: Transvaginal ultrasonography compared with endometrial biopsy for the detection of endometrial disease. *N Engl J Med* 337:1792, 1997.
16. Goldstein SR: Postmenopausal endometrial fluid collections revisited: Look at the doughnut rather than the hole. *Obstet Gynecol* 83:738, 1994.
17. Randolph JR, Ying YK, Maier DB, et al: Comparison of realtime ultrasonography, hysterosalpingography, and laparoscopy/hysteroscopy



- in evaluation of uterine abnormalities and tubal patency. *Fertil Steril* 46:828, 1986.
18. Parsons AK, Lense JJ: Sonohysterography for endometrial abnormalities: Preliminary results. *J Clin Ultrasound* 21:87, 1993.
  19. Syrop C, Sahakian V: Transvaginal sonographic detection of endometrial polyps with fluid contrast augmentation. *Obstet Gynecol* 79:1041, 1992.
  20. Wolman I, Groutz A, Gordon D, et al: Timing of sonohysterography in menstruating women. *Gynecol Obstet Invest* 48:254, 1999.
  21. Dessole S, Farina M, Rubattu G, et al: Side effects and complications of sonohysterosalpingography. *Fertil Steril* 80:620, 2003.
  22. Cooper JM, Brady RM: Intraoperative and early postoperative complications of operative hysteroscopy. *Obstet Gynecol Clin North Am* 27:347, 2000.
  23. Tuveng JM, Vold I, Jerve F, et al: Hysterosalpingography: Value in estimating tubal function, and risk of infectious complications. *Acta Eur Fertil* 16:125, 1985.
  24. DeVore GR, Schwartz PE, Morris J: Hysterography: A 5-year follow-up in patients with endometrial carcinoma. *Obstet Gynecol* 60:369, 1982.
  25. Alcazar JL, Errasti R, Zornoza A: Saline infusion sonohysterography in endometrial cancer: Assessment of malignant cells dissemination risk. *Acta Obstet Gynecol Scand* 79:321, 2000.
  26. Goldstein SR: Use of ultrasonohysterography for triage of perimenopausal patients with unexplained uterine bleeding. *Am J Obstet Gynecol* 170:565, 1994.
  27. Goldstein SR, Zelzter I, Horan CK, et al: Ultrasonography-based triage for perimenopausal patients with abnormal uterine bleeding. *Am J Obstet Gynecol* 177:102, 1997.
  28. Dijkhuizen FPHJ, Brolmann HAM, Potters AE, et al: The accuracy of transvaginal ultrasonography in the diagnosis of endometrial abnormalities. *Obstet Gynecol* 87:345, 1996.
  29. Timmerman D, Verguts J, Konstantinovic ML, et al: The pedicle artery sign based on sonography with color Doppler imaging can replace second-stage tests in women with abnormal vaginal bleeding. *Ultrasound Obstet Gynecol* 22:166, 2003.
  30. Goldstein SR: The effect of SERMs on the endometrium. *Ann N Y Acad Sci* 949:237, 2001.
  31. Killackey MA, Hakes TB, Pierce VK: Endometrial adenocarcinoma in breast cancer patients receiving antiestrogens. *Cancer Treat Rep* 69:237, 1985.
  32. Hardell L: Tamoxifen as risk factor for carcinoma of corpus uteri [letter]. *Lancet* 2:563, 1998.
  33. Jordan VC: Tamoxifen and endometrial cancer [letter]. *Lancet* 2:117, 1989.
  34. Mathew A, Chabon AB, Kabakow B, et al: Endometrial carcinoma in five patients with breast cancer on tamoxifen therapy. *N Y J Med* 90:207, 1990.
  35. Atlanta G, Pozzi M, Vincenzoni C, et al: Four case reports presenting new acquisitions on the association between breast and endometrial carcinoma. *Gynecol Oncol* 37:378, 1990.
  36. Anteby E, Yagel S, Zacut D, et al: False sonographic appearance of endometrial neoplasia in postmenopausal women treated with tamoxifen. *Lancet* 340:433, 1992.

# GESTATIONAL TROPHOBLASTIC NEOPLASIA

Neil J. Sebire, MB, MD

## Introduction

### Hydatidiform Molar Pregnancy

- Changes in the Epidemiology of the Diagnosis of Hydatidiform Mole
- Ultrasound in the Detection of Hydatidiform Mole
- Management of Hydatidiform Mole
- Persistent Gestational Trophoblastic Neoplasia
- Treatment of Persistent Gestational Trophoblastic Neoplasia

### Coexistent Hydatidiform Mole and Normal Fetus

- Partial Hydatidiform Mole

- Dichorionic Twin Pregnancy With Normal Fetus and Coexisting Complete Hydatidiform Mole
- Placental Mosaicism for Complete Hydatidiform Mole
- Placental Mesenchymal Dysplasia

### Invasive Hydatidiform Mole

- Ectopic Hydatidiform Mole

### Choriocarcinoma

### Placental Site Trophoblastic Tumor

### Epithelioid Trophoblastic Tumor

- Breus Mole

## INTRODUCTION

The term gestational trophoblastic neoplasia (GTN) encompasses a range of entities including the more common complete (CHM) and partial (PHM) hydatidiform mole, invasive mole (IM), coexistent complete mole and live fetus, and the rarer malignant entities choriocarcinoma (CC) and placental site trophoblastic tumor (PSTT). The major clinical significance of the diagnosis of CHM or PHM is the associated increased risk of development of subsequent persistent gestational trophoblastic neoplasia (pGTN), in the form of any of the other subtypes<sup>1</sup> (Fig. 29-1). However, in many cases in clinical practice, the strict distinction between these entities is often artificial. Following a suspected or proven diagnosis of a molar pregnancy, surveillance is usually instituted with serum and urine human chorionic gonadotropin (hCG) measurements and patients in whom the hCG levels either rise or fail to return to normal are considered as having pGTN and may be treated with chemotherapy without a further specific histologic tissue diagnosis having been made. The management of complications of GTN is most often performed in specialist tertiary referral centers. The aim of this chapter is not to provide a thorough dissertation on all aspects of GTN, but rather to discuss an overview of the important issues and to specifically highlight the use of ultrasound examination in the diagnosis and management of these conditions. For purposes of simplicity, the chapter is broadly divided into two sections, focusing on hydatidiform mole (HM) in the first instance and then pGTD and gestational trophoblastic tumors.

## HYDATIDIFORM MOLAR PREGNANCY

Hydatidiform moles essentially represent an abnormality of placental development as a consequence of overexpression of paternally derived genes and are therefore examples of

abnormalities of imprinting. They are associated with structural placental abnormalities and fetal developmental defects, and are characterized pathologically from nonmolar pregnancies by the presence of abnormal trophoblast hyperplasia. They are simply divided into two major subtypes, CHM and PHM according to pathologic and genetic features.<sup>2</sup>

CHMs are almost always diploid, but in most cases, all genetic material is of paternal origin, either as a consequence of genomic endoreduplication following monospermic fertilization of an anucleate oocyte or, more rarely, dispermic fertilization of an anucleate oocyte (Fig. 29-2). In rare cases, it has now been recognized that an unusual genetic variant of CHM, termed biparental CHM exists, in which the karyotype appears to be normal diploid with compliments from both parents, but the phenotype is identical to classic CHM, the defect appearing to be a result of abnormalities of imprinting with subsequent overexpression of the paternal genome.<sup>3</sup>

Partial hydatidiform moles are almost always triploid, with the additional set of genetic material also being paternally derived, almost always due to dispermic fertilization of an apparently normal oocyte. In PHM, the presence of a maternal genome is associated with less trophoblastic hyperplasia and a greater degree of fetal development. Thus, overexpression of paternally transcribed genes is likely to play a role in the development of PHM, whereas CHMs reflect both overexpression of paternally transcribed and loss of maternally transcribed genes. All HM are associated with increased risk of development of pGTN, which is about 15% post CHM and 0.5% post PHM.<sup>4</sup>

Classically, these entities are clinically, as well as genetically, distinct, with PHM being associated with the presence of a fetus and coexistent patchy hydatidiform change of the placenta, whereas CHMs are not associated



## SPECTRUM OF GESTATIONAL TROPHOBLASTIC NEOPLASIA

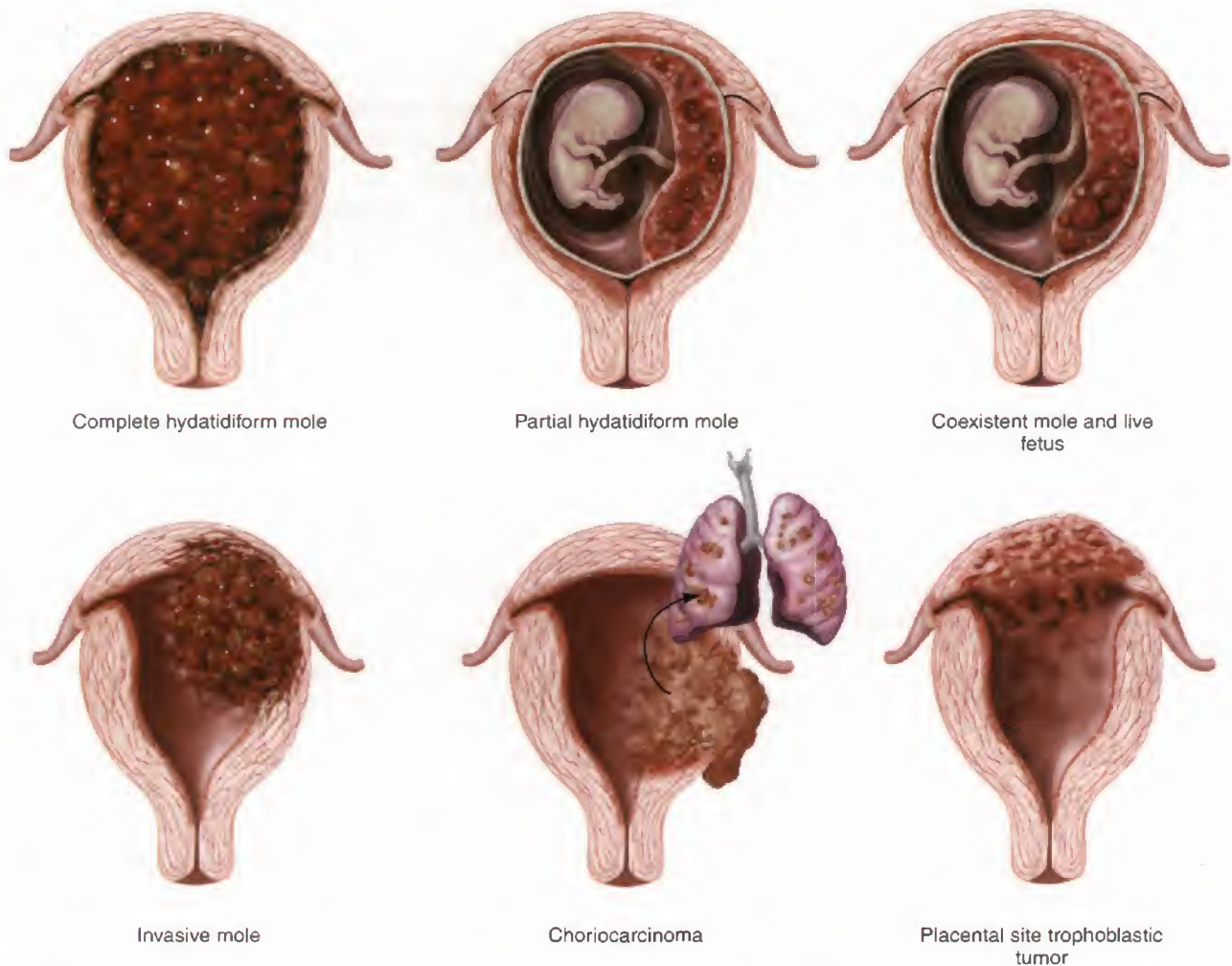


**FIGURE 29-1.** Illustration demonstrating the various subtypes of gestational trophoblastic disease and persistent gestational trophoblastic disease. Complete hydatidiform mole in which numerous vesicles, representing hydropic chorionic villi, are seen filling the uterus. Partial hydatidiform mole in which a fetus is seen associated with patchy cystic, hydatidiform change of the placenta. Dichorionic twin pregnancy with a normal fetus and coexisting complete hydatidiform mole. In these cases, the sonogram demonstrates a normal-appearing placenta associated with the fetus, as well as tissue that has the characteristic appearance of a complete hydatidiform mole. Invasive mole in which penetration of molar villi, usually from a complete hydatidiform mole, occurs in the myometrium. Choriocarcinoma in which trophoblastic invasion, in the absence of chorionic villus structures, may extend into and beyond the myometrium, with the potential of metastases (in this case, the lung). PSTT in which the myometrium is infiltrated by trophoblastic cells, which may extend beyond the uterus. (Illustration by James A. Cooper, MD, San Diego, CA.)

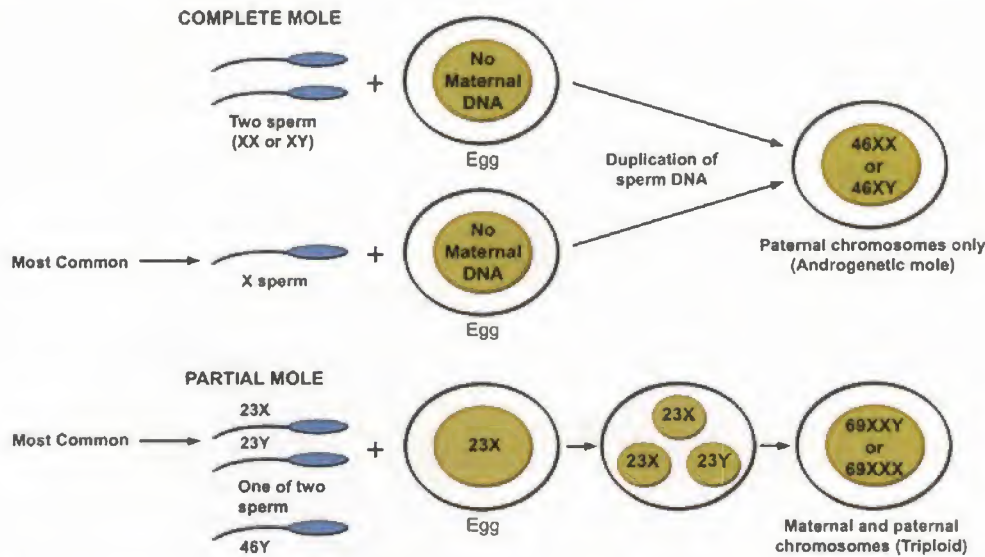


**FIGURE 29-2.** Patterns of fertilization to account for chromosomal origin of complete (46, XX) and triploid partial moles (XXY). In a complete mole, one or two sperm fertilize an egg that has lost its chromosomes. Partial moles are due to fertilization of an egg by one diploid, or two haploid sperm, depicted in this example as one 23,X and one 23,Y. Rarely, biparental complete moles are described, which are thought to be related to an imprinting defect. (Modified with permission from Crum CP: *The female genital tract*. In Kumar V, Robbins SL, Cotran RS [eds]: *Pathologic Basis of Disease*, 7th ed. Philadelphia, WB Saunders, 2005. Copyright © 2005 Saunders, An Imprint of Elsevier.)

with fetal development and demonstrate diffuse placental change (see Fig. 29-1). However, with increasing understanding of these pathologies, in combination with changes in the management of early pregnancy complications, such simplistic distinctions are no longer correct, because it is now recognized that histologic evidence of early fetal-type development can sometimes be identified in cases of CHM,<sup>5</sup> whereas the majority of cases of PHM are associated with early pregnancy failure in the absence of an identifiable fetus.<sup>6</sup> Therefore, it is important to emphasize that the classic clinical, sonographic and histopathologic descriptions of these conditions are now outdated in the era of current gynecologic management, and revised and updated criteria for their diagnosis are required.

The gold standard for the definitive diagnosis, and subtyping, of HM is histopathologic examination by a specialist pathologist, because both CHM and PHM have distinctive histologic characteristics even in the first trimester.<sup>7-9</sup> In the normal placenta, cytotrophoblast, syncytiotrophoblast, and intermediate trophoblast are present during placental development. Villus trophoblast covers chorionic villi and consists predominantly of cytotrophoblast and syncytiotrophoblast, cytotrophoblast being the proliferating component while syncytiotrophoblast differentiates from fusion of cytotrophoblast, composed of multinucleated cells with abundant dense cytoplasm and secretion of hCG. The diagnostic pathologic features of molar pregnancies are essentially characterized by abnormal proliferation of villus trophoblast (Fig. 29-3). Intermediate trophoblast, of various subtypes, is also present, and although of prime importance in implantation and placental site trophoblastic tumors, is not a major component of the diagnostic criteria for molar pregnancies.

In the classic, although now rarely seen, second trimester CHM, there is marked villus hydrops with extensive

circumferential villus trophoblast hyperplasia and central villus cistern formation (Figs. 29-3 and 29-4). However, in the first trimester, such features are not yet developed, the diagnostic features being abnormally distributed villus trophoblast hyperplasia, relative lack of villus hydrops, sheets of pleomorphic extravillous trophoblast, collapsed villus blood vessels and marked stromal karyorrhectic debris in association with characteristic abnormal budding villus architecture. In addition, extravillous trophoblast invasion may be abnormal in CHM, with absence of normal controlled endovascular trophoblast plugging of decidual vessels, instead showing florid interstitial trophoblast invasion, sometimes resulting in interstitial hemorrhage.<sup>7-10</sup>

PHMs also exhibit nonpolar trophoblast hyperplasia, but in first trimester PHMs, this may be patchy and mild. Other features include patchy mild villus hydrops with focal cistern formation, numerous villus vessels containing nucleated fetal red cells, angiomatoid change, abnormally shaped scalloped or dentate villi, with trophoblastic pseudoinclusions and villus stromal fibrosis. Fetal tissue may also be present. The main diagnostic histopathologic features of CM, PM, and non-molar hydropic abortion (HA) in products of conception evacuated in the first trimester are summarized in Table 29-1 (see Fig. 29-3).

It should be noted that although in most cases histopathologic diagnosis is easy, in some cases, a definite diagnosis may not be possible, particularly in cases with only limited material submitted for examination, and conceptions affected by other aneuploidies that may appear histologically similar to PHM. In such cases, ancillary diagnostic techniques may be required, including p57<sup>K112</sup> immunohistochemistry<sup>11,12</sup> (absent staining in CHM, positive nuclear staining in other diagnoses), assessment of ploidy using in situ hybridization or flow cytometry,<sup>13</sup> and microsatellite polymorphism analysis.<sup>14</sup>



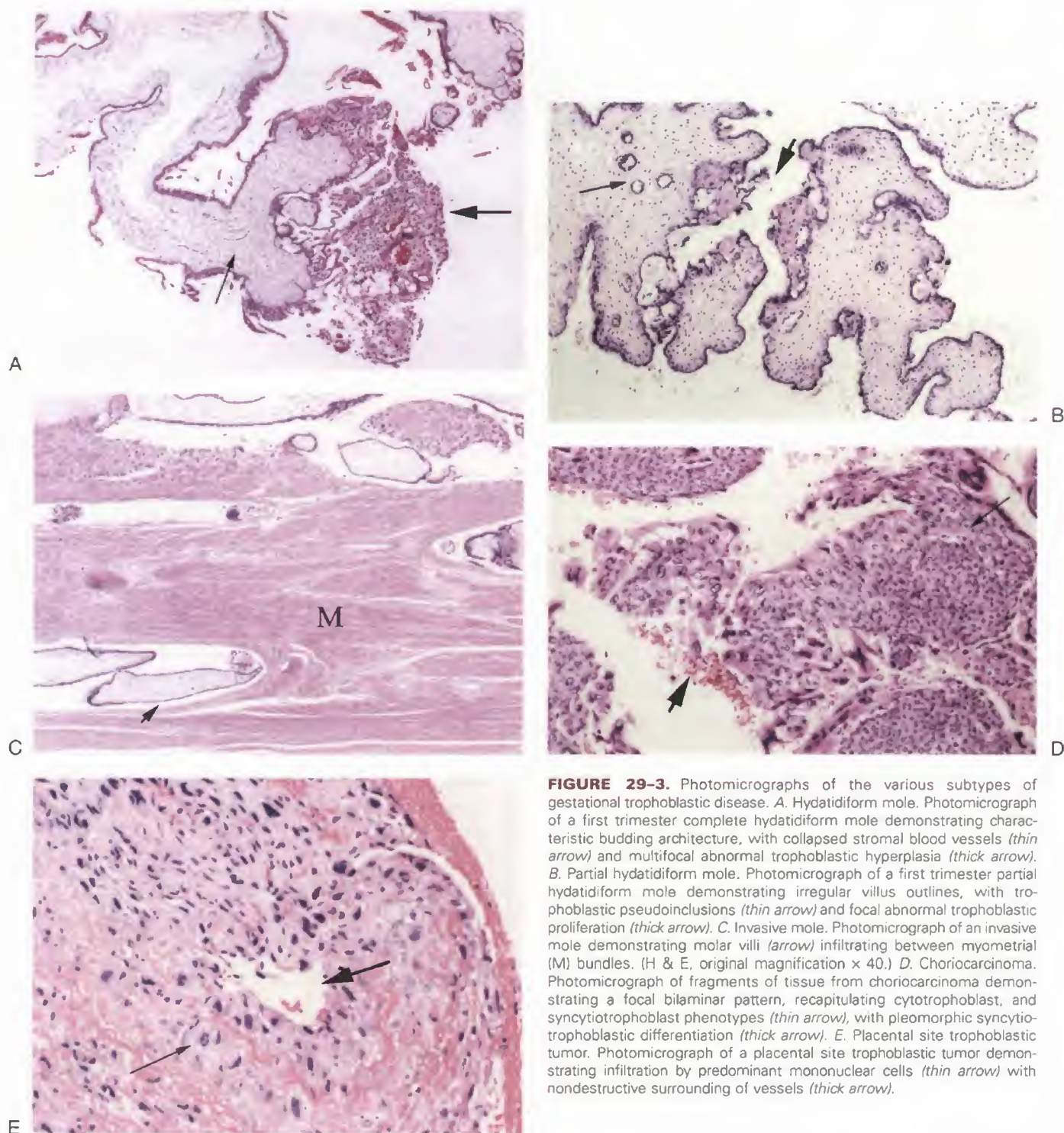


**FIGURE 29-3.** Photomicrographs of the various subtypes of gestational trophoblastic disease. **A.** Hydatidiform mole. Photomicrograph of a first trimester complete hydatidiform mole demonstrating characteristic budding architecture, with collapsed stromal blood vessels (*thin arrow*) and multifocal abnormal trophoblastic hyperplasia (*thick arrow*). **B.** Partial hydatidiform mole. Photomicrograph of a first trimester partial hydatidiform mole demonstrating irregular villus outlines, with trophoblastic pseudoinclusions (*thin arrow*) and focal abnormal trophoblastic proliferation (*thick arrow*). **C.** Invasive mole. Photomicrograph of an invasive mole demonstrating molar villi (*arrow*) infiltrating between myometrial (M) bundles. (H & E, original magnification  $\times 40$ .) **D.** Choriocarcinoma. Photomicrograph of fragments of tissue from choriocarcinoma demonstrating a focal bilaminar pattern, recapitulating cytotrophoblast, and syncytiotrophoblast phenotypes (*thin arrow*), with pleomorphic syncytiotrophoblastic differentiation (*thick arrow*). **E.** Placental site trophoblastic tumor. Photomicrograph of a placental site trophoblastic tumor demonstrating infiltration by predominant mononuclear cells (*thin arrow*) with nondestructive surrounding of vessels (*thick arrow*).



## Changes in the Epidemiology of the Diagnosis of Hydatidiform Mole

Classically, patients with singleton CHM present with vaginal bleeding, uterine enlargement greater than expected for gestational age, and abnormally high levels of serum hCG levels with passage of vesicles per vagina (see Figs. 29–3 and



**FIGURE 29–4.** Pathologic specimen of the vesicles in a patient with a complete hydatidiform mole. (Courtesy of Jonathan Carter, MD, The University of Sydney, Sydney, Australia.)

29–4). Medical complications include pregnancy-induced hypertension, hyperthyroidism, hyperemesis, anemia, and development of ovarian theca-lutein cysts, which may even occasionally lead to ovarian torsion or cyst rupture<sup>15</sup> (Fig. 29–5). This classic presentation now is highly unusual,<sup>16</sup> because the majority of uncomplicated pregnancies, and all those presenting with first-trimester vaginal bleeding, now undergo routine ultrasound examination, at which time either molar change or missed abortion is diagnosed, both of which lead to evacuation of the uterus. This has resulted in



**FIGURE 29–5.** Intraoperative photograph of bilateral theca lutein cysts in a patient with gestational trophoblastic disease. (Courtesy of C. Michael Peterson, MD, Department of Obstetrics & Gynecology, University of Utah Health Sciences Center.)

**Table 29–1**

**Diagnostic Histopathologic Features of Complete Mole (CHM), Partial Mole (PHM), and Nonmolar Hydropic Abortion (HA), in Products of Conception Evacuated in the First Trimester**

	CHM	PHM	HA
Villous size	Moderate variation	Marked variation	Uniform
Villous outline	Budding	Irregular	Smooth*
Villous stroma	Mucoid/myxoid	Fibrotic	Hypocellular
Villous hydrops	Varied	Varied	Uniform
Cistern formation	Varied	Varied	Scanty
Stromal karyorrhectic debris	Present	Absent	Absent
Villous vessels	Absent/collapsed	Present	Absent/collapsed
Nucleated red blood cells	Very rare	Present	Present
Trophoblast pseudoinclusions	Present	Present	Rare*
Trophoblast hyperplasia	Present, moderate	Present, mild†	Absent
Extravillous trophoblast	Pleomorphic	Present	Absent
Implantation site	Florid‡	Normal	Normal
Fetal parts/amnion	Absent	Present	Present

\*Cases of nonmolar fetal aneuploidy may demonstrate irregular, hydropic villi with pseudoinclusions but no abnormal trophoblast hyperplasia is present.

†Abnormal trophoblast hyperplasia may be focal and demonstrate a lace-like pattern around the villus.

‡Extravillous interstitial trophoblast invasion may appear florid, but there is reduced normal endovascular trophoblast plugging and interstitial hemorrhage may be seen.

Modified from Sebire NJ, Fisher RA, Rees HC: Histopathological diagnosis of partial and complete hydatidiform mole in the first trimester of pregnancy. *Pediatr Dev Pathol* 6:69, 2003.



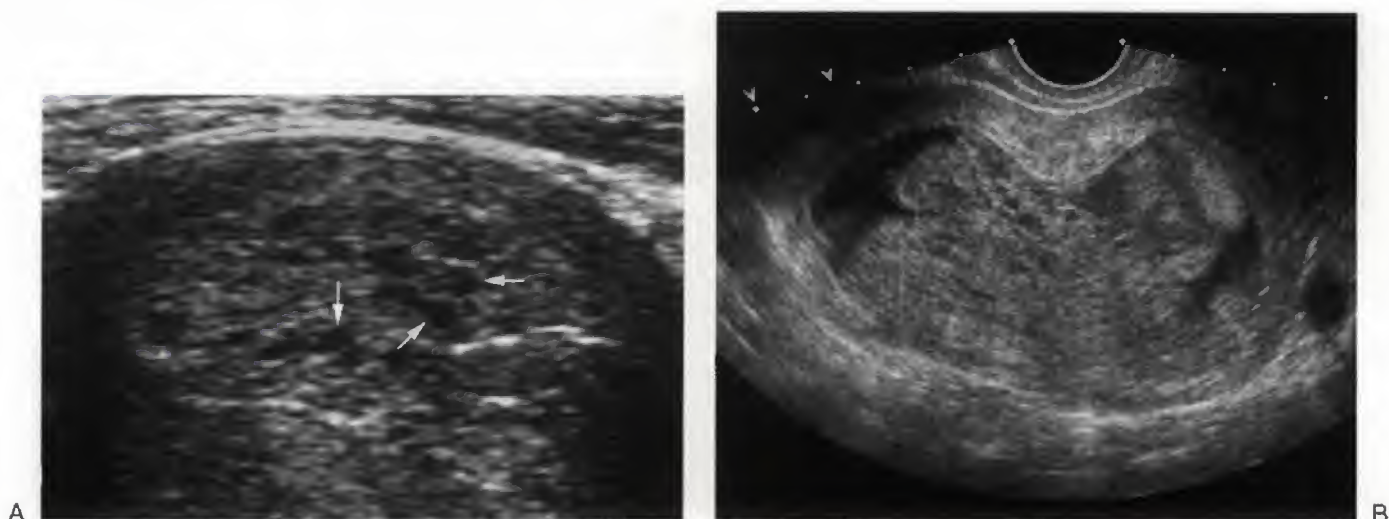


**FIGURE 29-6.** Two patients with a second trimester hydatidiform mole. *A.* A large moderately echogenic mass with numerous cystic spaces (arrows) is seen filling the central uterine cavity. The cystic spaces likely represent the markedly hydropic chorionic villi. *B.* A large moderately echogenic mass is seen filling the uterine cavity. In addition to the typical cystic hydatidiform molar tissue, large areas of hemorrhage are seen.

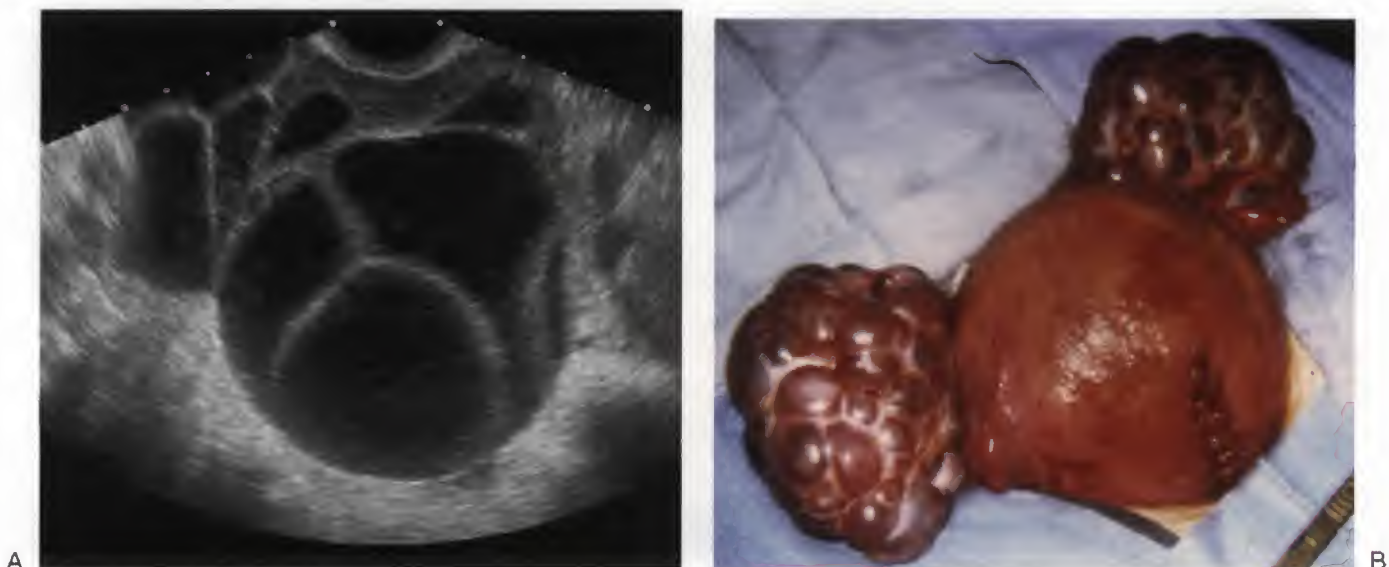


**FIGURE 29-7.** *A.* Sonogram from a patient with bilateral theca lutein cysts. The typical multilocular appearance is noted in the left ovary. *B.* Intraoperative photograph of the postgravid uterus and ovaries in a patient with coexistent mole and live pregnancy. Bilateral theca lutein cysts are identified. The characteristic multilocular appearance is seen. (From Yee B, Tu B, Platt LD: Coexisting hydatidiform mole with a live fetus presenting as a placenta previa on ultrasound. *Am J Obstet Gynecol* 144:726, 1982.)

a marked reduction in the number of molar pregnancies presenting with the symptoms and signs of overgrowth of trophoblast and excessive hCG secretion, and most cases are now evacuated in the late first trimester, the average gestation at diagnosis in the United Kingdom now being approximately 10 weeks.<sup>17</sup> It should be noted at this point, that ultrasound examination leads to earlier uterine evacuation in most cases following diagnosis of a failed pregnancy rather than identification of molar change (see later). In one recent study of patients with CHM, 40% were asymptomatic, the condition detected by routine sonographic examination, while 60% presented with vaginal bleeding; only 2% reported hyperemesis, and none had any other systemic manifestations.<sup>18</sup>

### Ultrasound in the Detection of Hydatidiform Mole

HMs have been recognized by ultrasound examination for many years, but much of the literature refers to ongoing pregnancies with second trimester moles. The typical features reported include a uterine cavity filled with central heterogeneous mass with anechoic spaces of varying size and shape, a snowstorm-like appearance in the early days of ultrasound, without associated fetal development (see Figs. 29-1 and 29-6).<sup>19,20</sup> In addition, theca lutein cysts secondary to the high hCG levels were reported, producing either soap-bubble or spoke-wheel appearance of the ovaries, which are enlarged (see Figs. 29-5 and 29-7). Doppler

ultrasound examination in this scenario almost always demonstrates high velocities and low resistance to flow in the uterine arterial circulation and low resistance flow from trophoblastic tissue (Fig. 29-8). In cases of invasive mole, in addition to the central uterine lesion, myometrial invasion is present, with choriocarcinoma (CC) appearing as a mass enlarging the uterus, with a heterogeneity corresponding to areas of necrosis and hemorrhage<sup>21</sup> (Fig. 29-9).

However, in an analogous manner to the changing clinical aspects, such sonographic presentations are also now only rarely encountered, with most cases being evacuated in the first trimester, when ultrasound demonstration of hydatidiform changes is much less readily apparent.

Several studies have now reported on the use of ultrasonography for detection of HM in early pregnancy<sup>22,23</sup> (Fig. 29-10). Fine et al<sup>24</sup> reported on the sonographic features of 22 PHMs compared with nonmolar abortions and suggested that cystic changes and increased placental echogenicity may be useful diagnostic features. Lazarus et al<sup>25</sup> examined 21 CHMs in the first and second trimester (4-18 weeks) and reported that correct pre-evacuation

diagnosis of HM could be made in about half; in no cases were theca lutein cysts present (Fig. 29-11). More recently, Benson et al<sup>26</sup> described 24 CHMs examined sonographically in a specialist center and reported that molar pregnancy was suspected by ultrasound in almost 80%, suggesting, as with all sonographic techniques, that experienced operators may achieve a higher rate of diagnostic accuracy. Jauniaux et al<sup>27</sup> reported that 10 of 11 pregnancies with sonographic features suggestive of HM at 10 to 14 weeks of gestation were pathologically proven HMs, indicating that specificity of sonographic diagnosis is high, but allowing no comment on sensitivity. Furthermore, Lindholm et al<sup>28</sup> reported that, on the basis of sonography and macroscopic examination of products of conception for molar change, about 80% of complete moles and 30% of partial moles could be detected, but it was noted that in several cases, macroscopic examination following uterine evacuation rather than the sonogram

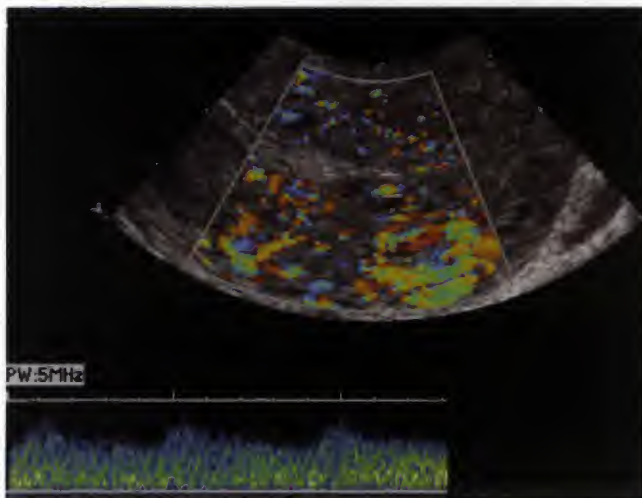


**FIGURE 29-8.** Doppler spectral analysis from trophoblastic tissue in a patient with an invasive mole demonstrating flow velocity waveforms with low resistance.

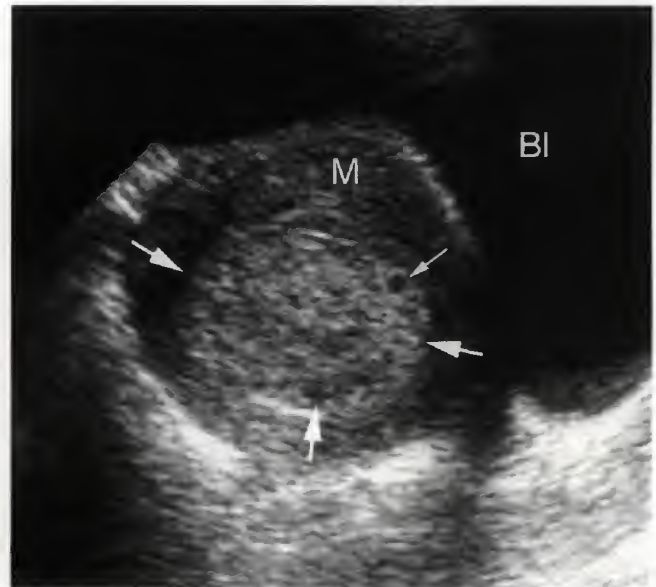


**FIGURE 29-10.** Sagittal sonogram from a patient with a first trimester hydatidiform mole. In this case, an echogenic mass (*large arrows*) is seen filling the uterine cavity. Except for one small cyst (*small arrow*), there are virtually none of the cystic spaces that are characteristically seen in more advanced molar pregnancies. Bl, bladder; M, myometrium.

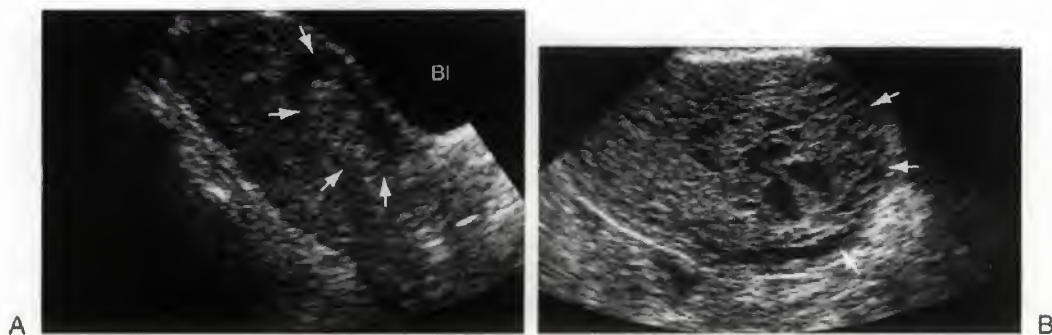


**FIGURE 29-9.** A and B. Extension of an invasive mole (*arrows*) into the myometrium in two patients with markedly elevated hCG levels. Bl, bladder.



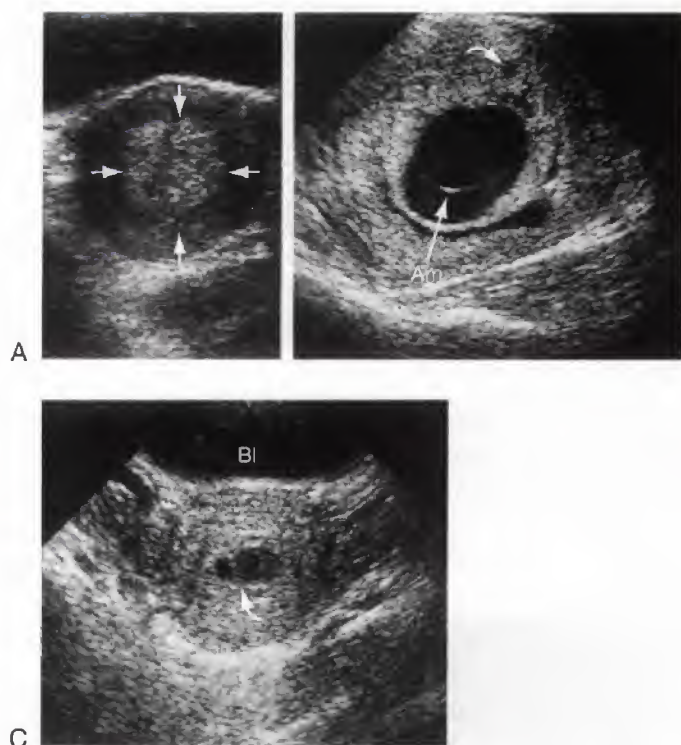


**FIGURE 29-11.** Three patients presented with vaginal bleeding and positive pregnancy tests. *A.* This patient has a hyperechogenic mass (arrows) filling the uterine cavity. The appearance is similar to that of a first trimester hydatidiform mole (compare with Fig. 29-10). This was a nonviable pregnancy (missed abortion). *B.* Sonogram in a patient with early pregnancy and vaginal bleeding. This pregnancy was nonviable. A small cystic area, likely representing hydropic change (arrow), is seen. Am, amnion. *C.* In this patient, an irregular fluid collection (arrow) was seen in the uterine cavity. This has the appearance of a nonviable gestation. At pathologic evaluation, there was evidence of trophoblastic proliferation consistent with a first trimester hydatidiform mole. Bl, bladder.

raised the first clue to the diagnosis (Fig. 29-12). In most cases of both PHM and CHM reported in which the diagnosis was not suspected before evacuation, the initial sonographic diagnosis was that of missed miscarriage/anembryonic pregnancy.<sup>29</sup> Two larger, recent studies have reported that correct pre-evacuation identification of molar pregnancy by ultrasound in the first and early second trimester is achieved in around 40% to 60% of cases.<sup>17,30</sup> The largest study by far to specifically address this issue examined the accuracy of routine ultrasound examination in 1,053 consecutive patients referred to a UK Regional trophoblastic disease unit for histologic review for possible or probable HM<sup>17</sup>; because all cases of GTN, suspected clinically, sonographically, or on the basis of histopathologic findings, are registered at the center, this allowed the highest possible ascertainment. The median gestational age in this study was only 10 weeks (range 5–27 weeks; Fig. 29-13). The final review diagnosis was HM in 859 (82%) cases, including 253 (29%) CHM and 606 (71%) PHM. Nonmolar hydropic miscarriage was diagnosed following histologic review in 194 (18%). Overall, around 40% of HM cases had a pre-evacuation ultrasound diagnosis suggesting molar pregnancy, including about 80% of CHM and 30% of PHM, the remainder of cases appearing sonographically simply as a missed miscarriage (Fig. 29-14).



**FIGURE 29-12.** Sonogram of a patient with a partial hydatidiform mole. Multiple cystic spaces are seen within the placenta. Triploidy was confirmed at pathologic examination. Embryo (arrow).

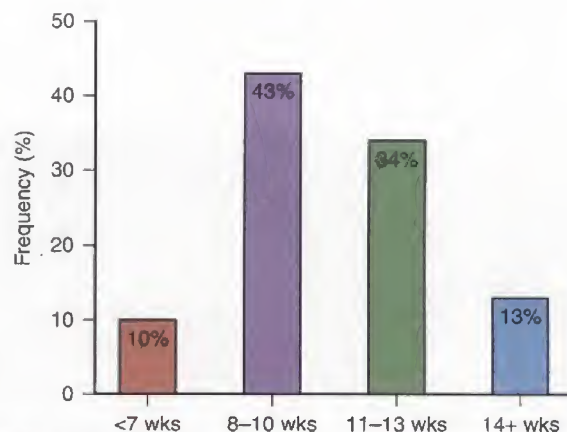


**FIGURE 29-13.** Gestational age distribution at evacuation of products of conception referred with suspected diagnosis of complete or partial hydatidiform mole to a regional center in 2004. The median gestational age at evacuation is 10 weeks (range: 5–27 weeks).<sup>17</sup>

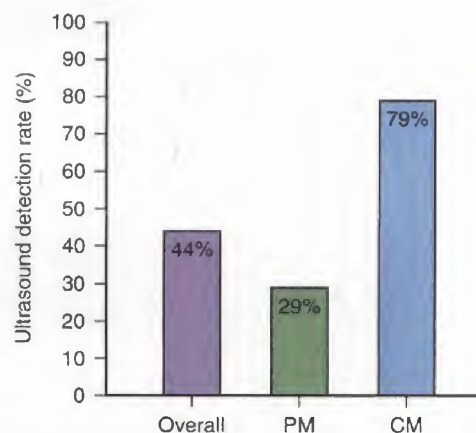


**FIGURE 29-14.** Pre-evacuation detection rates of complete (CM) and partial (PM) hydatidiform molar pregnancies following routine sonographic examination. Less than half of all hydatidiform moles (overall) in whom an ultrasound examination had been carried out were identified as molar pre-evacuation, the detection of complete moles being significantly better than for partial moles.



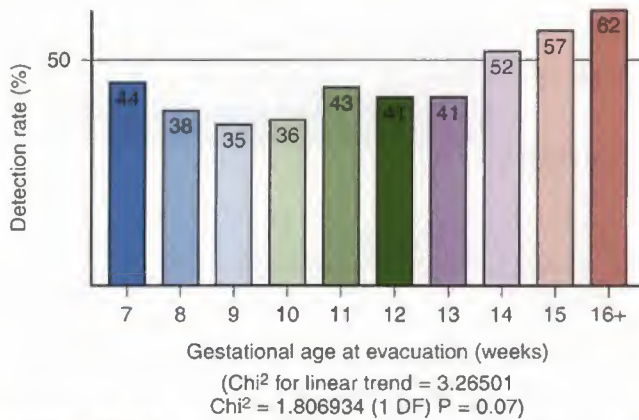


**FIGURE 29-15.** Pre-evacuation detection rates of hydatidiform molar pregnancies by gestational age. There is no significant difference in detection rates across the age range, but there is a clear trend toward improved detection rates at 14 weeks' gestation and beyond.

There was a trend toward increasing ultrasound detection rate with increasing gestational age; sonographic features of HM were reported in 35% of cases before 14 weeks of gestation compared with around 60% after this time (Fig. 29-15). It should also be noted that more than 10% of the cases identified as molar on ultrasound examination were in fact nonmolar hydropic miscarriage on histologic review. The sensitivity, specificity, positive and negative predictive values for routine pre-evacuation ultrasound examination for HM therefore are 44%, 74%, 88%, and 23%, respectively. These data compare favorably with a similar, smaller, study reporting on cases from 5 years previously in which the overall pre-evacuation ultrasound detection rate was approximately 30%.<sup>6</sup> This improvement is presumably as a consequence of increasing specialization of obstetric sonographers, increasing experience in the recognition of such pregnancies, and improved ultrasound technologies. It is likely that some further improvements will occur, but there are pathophysiologic reasons limiting the proportion of HMI, especially PHM, that will demonstrate sonographically detectable features in the first trimester.<sup>8,9</sup>

Therefore, with current gynecologic care, the majority of HMs present both clinically and sonographically as early pregnancy failure. Improved pre-evacuation detection of HM has potential important consequences for provision of medical care, because it could result in reduced numbers of products of conception undergoing histologic review and a reduced number of women undergoing follow-up for equivocal histologic findings, and would allow a safe increase in the proportion of nonmolar miscarriages that could be appropriately managed medically rather than with surgical evacuation of the uterus. In the United Kingdom, current Royal College of Obstetrics and Gynecology guidelines state that medical management of miscarriage is acceptable but medical methods of uterine evacuation are not recommended for suspected HM.<sup>1,31</sup> Because medical management of miscarriage does not usually result in tissue being submitted for histologic examination, such cases need to be accurately preselected to minimize the risk of missing an undiagnosed HM, which may present later with pGTN. There are convincing data, based on cases of GTN following terminations

of pregnancy, that women presenting with clinical pGTN have significantly more complications, morbidity, and requirements for radical surgery and combination chemotherapy compared with women identified by hCG surveillance protocols.<sup>32</sup>

Preliminary data suggest that the combination of ultrasound examination and maternal serum hCG measurement may provide a significantly improved method of pre-evacuation risk assessment for GTN, especially in those presenting with early pregnancy failure, although at present, no large scale studies of this combination have been performed. In molar pregnancies, maternal hCG concentrations are usually raised with associated low maternal serum alpha-fetoprotein (MSAFP) concentrations.<sup>33</sup> An hCG level more than two standard deviations above the mean, in combination with sonography, has been suggested as a way to identify up to 90% of cases,<sup>34</sup> and with the use of appropriate normal ranges for failed pregnancies, rather than ongoing pregnancies, this is likely to improve. In one recent study of 46 HMs examined at an early pregnancy assessment unit, in 33, HM was suspected sonographically, and in 15 cases for whom hCG results were available, nine were greater than two multiples of the median.<sup>30</sup> Further research in this area is likely to lead to significantly improved detection rates in the first trimester.

## Management of Hydatidiform Mole

In many cases (see earlier), the diagnosis of HM is not suspected until a uterine curettage has been performed and the products of conception examined by the pathologist. In cases suspected sonographically, uterine evacuation is also required as the initial management because the pregnancy will not be continued. This should be carried out by suction evacuation rather than sharp curettage to minimize the risk of uterine perforation. Generally, repeated evacuations should not be carried out because there is an increased risk of uterine perforation, and if persistent molar tissue is present, it may be deeply invasive and will likely require chemotherapy.<sup>35</sup> Ultrasound examination, either real-time grayscale imaging or combined with color Doppler flow assessment is useful to ensure completeness of uterine evacuation and identify residual trophoblastic tissue.<sup>36-41</sup>

Following uterine evacuation and histologic confirmation of the diagnosis, all patients should be followed up with serial hCG measurements for the early detection of pGTN, ideally by a centralized or regional service. The precise protocol of surveillance varies from country to country, but essentially women should be followed up until their hCG levels have been normal for at least 6 months. In addition, patients should be counseled that once they have had a molar pregnancy, there is increased risk of both a subsequent HM and pGTN development following any future pregnancy, even if it is nonmolar, owing to reactivation of latent trophoblast. Therefore, hCG levels must also be checked 6 and 10 weeks following any future pregnancies, regardless of its outcome. During the initial follow-up period, use of contraception is suggested because a subsequent pregnancy complicates the interpretation of a rising hCG level in this setting and because the hormonal effects of pregnancy may reactivate latent trophoblastic disease. There is controversy regarding the use of the combined oral



**Table 29-2****International Federation of Gynecology and Obstetrics (FIGO) Staging System for Gestational Trophoblastic Neoplasia (GTN)<sup>44</sup>**

Stage	Criteria
Stage I	Disease confined to the uterus
Stage II	GTN extends outside the uterus but is limited to the genital structures (adnexa, vagina, broad ligament)
Stage III	GTN extends to the lungs with or without genital tract involvement
Stage IV	All other metastatic sites

contraceptive pill (OCP) in this setting, but it appears that OCP use has no adverse effect in those women in whom there is spontaneous fall of hCG levels to normal within 8 weeks of evacuation, whereas cases in which the hCG remains slightly raised may represent a subpopulation in whom there may be a risk of stimulating GTN growth by administered exogenous hormones. Therefore, most centers would at least recommend avoidance of the OCP until hCG levels have clearly returned to normal.<sup>35</sup>

### Persistent Gestational Trophoblastic Neoplasia

A subgroup of women following a molar pregnancy, and some patients following a nonmolar pregnancy, develop pGTN. This condition may be associated either with symptoms due to localized or metastatic disease or, because the majority follow HM, it may be detected by hCG surveillance. pGTN complicates about 15% of CHMs and about 0.5% PHMs, and is rare, although well reported, following nonmolar gestations.<sup>4</sup>

The criteria for diagnosing pGTN are slightly different between countries, with the United Kingdom, for example, having a more conservative approach. Nevertheless, the principles remain the same. pGTN either presents with clinically apparent disease (uncommon) or on hCG surveillance (common), when it is manifest as either plateauing or rising hCG concentrations. Following the identification of pGTN, further investigations are required to stage the disease, including uterine and liver ultrasound, and additional staging investigations such as chest radiograph, computed tomography, or magnetic resonance imaging as indicated. The results of these studies are used to determine the stage and prognosis score in order to assign patients to high-risk or low-risk groups.<sup>42</sup>

There are many historical staging systems for GTN,<sup>43</sup> but now a more unified worldwide system has been agreed to allow comparison of outcome and treatment data across centers, the International Federation of Gynecology & Obstetrics (FIGO) 2000 Staging and Risk Factor Scoring System for GTN<sup>44</sup> (Tables 29-2 and 29-3). According to this system, the criteria for the diagnosis of post-HM pGTN are

1. Plateauing hCG for four measurements over a 3-week period or longer.

**Table 29-3****International Federation of Gynecology and Obstetrics (FIGO) Risk Scoring System for Gestational Trophoblastic Neoplasia (GTN)<sup>44</sup>**

FIGO SCORE	0	1	2	4
<i>Criteria</i>				
Age	<40	≥40	–	–
Antecedent pregnancy	Mole	Miscarriage	Term	–
Interval from index pregnancy (months)	<4	4–7	7–13	≥13
Pretreatment serum hCG (IU/L)	<10 <sup>3</sup>	10 <sup>3</sup> –10 <sup>4</sup>	10 <sup>4</sup> –10 <sup>5</sup>	≥10 <sup>5</sup>
Largest tumor size (cm)	<3	3–5	≥5	–
Site of metastases	Lung	Spleen, kidney	Gastro-intestinal	Liver, brain
Number of metastases	–	1–4	5–8	>8
Previous failed chemotherapy	–	–	Single agent	Multi agent

hCG, human chorionic gonadotropin.

For individual patients, a score is assigned for each variable and the scores summed to provide an overall score. The final result is expressed as the stage (roman numeral), then the score (Arabic numeral). An overall score of 6 or less equals low risk and 7 or higher equals high risk.

2. Rising hCG on three consecutive weekly measurements over a period of 2 weeks or longer.
3. Histologic evidence of choriocarcinoma.
4. hCG level remaining elevated for 6 months or more after evacuation.

Therefore, imaging techniques, including ultrasound, play an integral role in the initial assessment of a patient with pGTN. However, although genital tract lesions may be identified by sonography, this is most commonly in those cases with relatively high hCG levels; in those with lower hCG levels, although chemotherapy remains indicated, the uterine lesion, especially if intramyometrial, may not be visualized sonographically and, conversely, myometrial abnormalities may persist even after the tumor resolves.<sup>45</sup> In one series of more than 350 cases of GTN of varying types, initial sonography demonstrated molar tissue confined to the endometrial cavity in all cases of CHM, whereas in cases of IM and CC, myometrial invasion was correctly identified.<sup>46</sup> Doppler studies of the uterine vasculature in HM usually demonstrate significantly increased flow and reduced flow resistance, which, following evacuation, returns to normal in parallel with the serum hCG concentration, with a correlation between hCG levels and Doppler indices throughout.<sup>47</sup> Some data suggest that uterine artery resistance may be lower at presentation in cases of GTN subsequently requiring chemotherapy, compared with those requiring uterine evacuation alone and, hence, may provide additional risk stratification at presentation.<sup>46,48</sup>

## Treatment of Persistent Gestational Trophoblastic Neoplasia

Treatment of low-risk patients is with single-agent chemotherapy usually methotrexate with folinic acid. With such treatment, the overall survival in these patients is essentially now 100%, of which around 70% are cured with methotrexate alone, the remainder being resistant and requiring additional second agent or multiagent chemotherapy. In patients with high-risk pGTN, multidrug chemotherapy is administered, usually now based around weekly EMA-CO protocols (etoposide + methotrexate + dactinomycin and vincristine + cyclophosphamide).<sup>42</sup> The overall survival rate in this group remains optimistic at around 90%, and the majority of deaths are in fact due to late presentation with advanced disease rather than true treatment failure. In relapsed disease, cisplatin-based agents are added to the protocol. Surgery usually plays little role in the initial management of most cases of pGTN but a major role in the management of PSTT (see below), because this is a less chemosensitive tumor and surgery may be curative. There are also specific modified protocols for specific clinical scenarios, such as central nervous system disease, which is not covered here. Following successful treatment, patients are followed up with hCG measurements until they have been normal for at least 12 months.<sup>42</sup>

There are now numerous publications reporting on the use of sonographic examination, usually including color Doppler assessment of uterine blood flow, for both prediction and surveillance of response to chemotherapy in pGTN. Most of these reports describe similar features of GTN being associated with increased blood flow and reduced flow resistance, and there being a crude correlation between the Doppler indices and serum hCG levels.<sup>46,49–75</sup> It should be noted that abnormal hCG levels in association with normal uterine sonography may indicate the presence of new or residual extrauterine disease. In clinical practice, however, although ultrasound examination, including Doppler studies, may provide some information regarding disease extent and response, the fact that serum hCG is such a sensitive and specific marker in this context means that serum hCG levels provide the most sensitive and simplest measure of disease extent. Therefore, this is the most important clinical parameter used to monitor disease response.<sup>76</sup>

Occasionally there may be residual uterine vascular malformations following pGTN treatment, which may require embolization or even hysterectomy to control bleeding. Doppler studies may be useful to plan treatment and assess response but do not seem to predict success of embolization.<sup>77,78</sup>

## COEXISTENT HYDATIDIFORM MOLE AND NORMAL FETUS

This is a clinical scenario that may cause much confusion regarding the underlying pathology and appropriate management. The setting is usually that of a routine ultrasound examination demonstrating the presence of a morphologically normal fetus in association with apparent molar change of the placenta, often in the second or early third trimester. There are several possible explanations for this finding.

## Partial Hydatidiform Mole

A theoretical possibility is that the pregnancy simply represents a PHM, but this is in reality highly unlikely, because triploid PHMs rarely progress through pregnancy and the fetus is almost never structurally normal. Potentially, the exceedingly uncommon mosaic PHM could result in such a clinical presentation and is associated with patchy diffuse placental molar change.<sup>79</sup>

## Dichorionic Twin Pregnancy With Normal Fetus and Coexisting Complete Hydatidiform Mole

A dichorionic twin pregnancy with a CHM and a normal co-twin, is well-reported, usually presenting on ultrasound examination as an apparently structurally normal fetus with a corresponding sonographically normal placenta, adjacent to which is a mass of placental tissue demonstrating molar change (Fig. 29–16). Initial small studies and case reports suggested that such pregnancies may be associated with increased risk of maternal complications and pGTN. Recently, the outcome of pregnancies with a histologically confirmed CHM and a normal co-twin has been examined in a series of 77 well-described cases from a tertiary center. In this large series, the risk of pGTN was no greater than that reported following a singleton CHM, and furthermore, the risk of pGTN was not increased by continuing the pregnancy. However, in cases in which pregnancy continuation was attempted, several complications may develop. About half will result in spontaneous fetal loss before 24 weeks' gestation, and of those that reach potential viability, 25% end in intrauterine death and 40% deliver severely preterm at less than 32 weeks' gestation. In this the largest series, severe pre-eclampsia was an unusual complication (<10%). Therefore, patients can be counseled that the overall take-home-baby rate in those opting for continuation is around 30%, with a 15% to 20% chance of pGTN development and an increased risk of pregnancy complications requiring intense obstetric surveillance.<sup>80</sup>

## Placental Mosaicism for Complete Hydatidiform Mole

A single well-documented, genetically proven, case of mosaicism for CHM has now been reported presenting with an apparently normal fetus at midgestation in association with patchy but diffuse molar change of the placenta. The pregnancy resulted in the live birth of a karyotypically and phenotypically normal infant with the placenta demonstrating admixed areas of CHM and normal villi, both confirmed to be derived from the same sperm by microsatellite typing.<sup>81</sup>

## Placental Mesenchymal Dysplasia

Diffuse cystic molar changes of the placenta in association with an apparently normal fetus in the third trimester is usually due to placental mesenchymal dysplasia (PMD) rather than any type of GTN. Cases now recognized as PMD have previously been reported under a variety of names including placental vascular anomaly with diffuse





**FIGURE 29-16.** Coexistent mole and live fetus. *A.* Sonogram of the gravid uterus during the second trimester. Numerous cystic spaces are seen, apparently within the placenta. The presence of a living fetus virtually excludes the diagnosis of a complete hydatidiform mole. *B.* A slightly more lateral plane of section from the same patient reveals that in addition to the molar tissue (*asterisk*), a normal-appearing placenta (PI) is seen. In fact, this is a twin pregnancy, with a normal pregnancy and placenta, and a twin abnormal molar pregnancy.

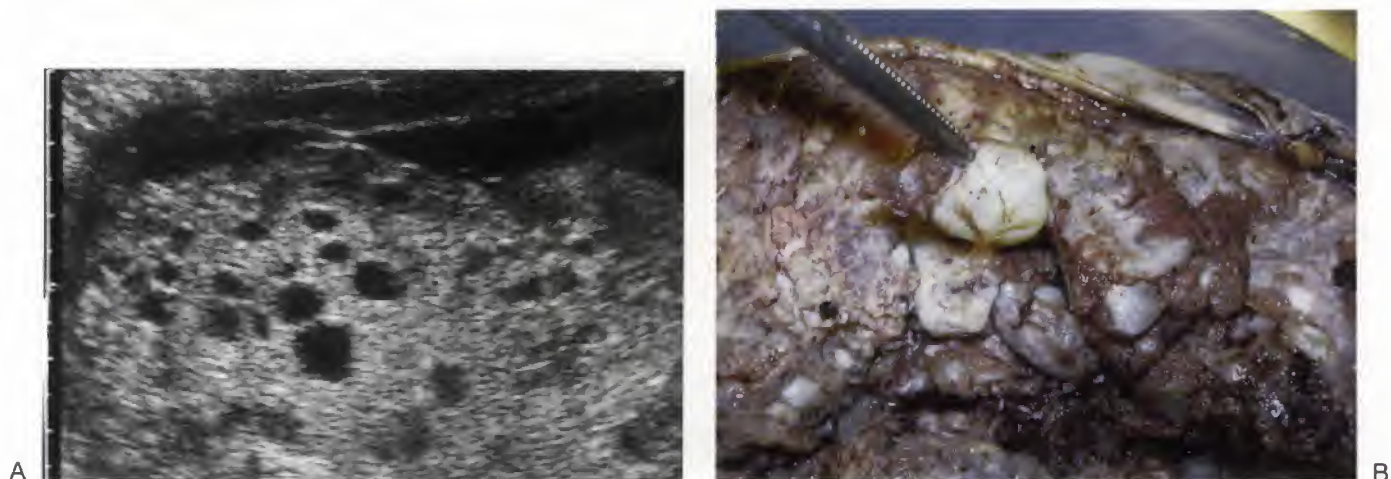


**FIGURE 29-17.** Placental mesenchymal dysplasia. *A.* Ultrasound at 22 weeks' gestation demonstrating multiple cysts resembling molar tissue, involving the entire placenta. *B.* Photograph of the placenta in the same case. A close-up view of one of the numerous cyst-like villi, seen on and beneath the maternal surface of the placenta. (Reproduced with permission from Cohen MC, Roper EC, Sebire NJ, et al: Placental mesenchymal dysplasia associated with fetal aneuploidy. *Prenat Diagn* 25:187, 2005.)

stem villous hyperplasia,<sup>82</sup> placentomegaly with massive hydrops of placental stem villi,<sup>83,84</sup> angiomatous malformation of placental chorionic stem vessels,<sup>85</sup> placental vascular malformation with mesenchymal hyperplasia and a localized chorioangioma,<sup>86</sup> diffuse cystic placental change<sup>87</sup> and pseudopartial mole.<sup>85,88</sup> There have now been around 70 well-documented cases of PMD reported,<sup>82-100</sup> the prevalence appearing to be around 1 in 4,000 to 5,000 pregnancies.<sup>92</sup>

PMD appears as diffuse molar change sonographically and often has a characteristic macroscopic appearance of the delivered placenta, which is enlarged with multiple cystic structures affecting the parenchyma and prominent, dilated

and tortuous chorionic vessels<sup>82,85</sup> (Fig. 29-17). Histologic findings are diagnostic, demonstrating normal terminal villi mixed with hydropic stem villi, without trophoblast hyperplasia.<sup>82,83,85,88,91,93</sup>

In addition to the sonographic identification of cystic placental changes, maternal serum levels of hCG are raised in about 40% and MSAFP is raised in all cases in which it has been recorded.<sup>93,99</sup> Pregnancy complications are common, including preterm delivery in 75%, intrauterine growth restriction in 20% and intrauterine fetal death in 30%. In addition, approximately 20% of reported cases of PMD are associated with fetal Beckwith-Wiedemann syndrome with a



marked predominance (80%) of female fetuses suggesting a possible defect in imprinting.<sup>99</sup> Recent data suggest that placental tissue-specific androgenetic-biparental mosaicism may be the underlying cause of the condition.<sup>100</sup>

## INVASIVE HYDATIDIFORM MOLE

An invasive mole is defined as the penetration of molar villi from a CHM or PHM (although in practice almost always a CHM), into the myometrium or the uterine vasculature. Rarely, such molar tissue can penetrate the full thickness of the myometrium (percreta), leading to uterine perforation or local pelvic extension. In contrast to choriocarcinoma, invasive mole contains distinct molar chorionic villi, and usually becomes clinically apparent as pGTN following initial evacuation of a molar pregnancy, with persistent heavy vaginal bleeding and elevated hCG levels (see Figs. 29-1,

29-3, 29-9, and 29-18). The tumor appears sonographically as focal areas of increased echogenicity within the myometrium,<sup>101</sup> which may appear similar to those of PSTT but occur concurrently or soon after a proven molar gestation. The lesion is usually heterogeneous, containing small fluid-filled cavities, and Doppler color flow mapping of the abnormal area can be used to evaluate the extent of the lesion and its subsequent response to chemotherapy.<sup>102-104</sup> Treatment is usually with standard chemotherapy protocols or surgery, but adjunctive local ultrasound-guided injection of methotrexate has also been described.<sup>105</sup>

## Ectopic Hydatidiform Mole

Primary molar pregnancies outside of the uterine cavity, most often in a fallopian tubes, may occur but are very rare.<sup>106-108</sup> There is a tendency for nonspecialist pathologists to over diagnose tubal moles following salpingectomy because nonmolar early gestation sac specimens demonstrate abundant polar and extravillous trophoblast around the trophoblastic shell.<sup>109</sup> Criteria for diagnosis of CHMs or PHMs are identical to HMs present within the uterine cavity. Such patients present sonographically with a tubal ectopic pregnancy.

## CHORIOCARCINOMA

This is a malignant neoplasm in which differentiation toward villous cytotrophoblast and syncytiotrophoblast is seen in the absence of chorionic villus structures. It can occur after CHM, PHM, normal pregnancy, stillbirth, miscarriage or ectopic pregnancy, but the incidence after CHM is about 1,000-fold greater than following a nonmolar pregnancy. CC either presents as pGTN in patients on hCG surveillance or as clinically apparent, often metastatic, disease in other patients. Uterine CC appears as a hemorrhagic nodule, which may be in communication with the uterine cavity or may be within the myometrium (see Figs. 29-1, 29-3, and 29-19). Microscopically, viable tumor



**FIGURE 29-18.** Invasive mole. Macroscopic photograph of a hysterectomy specimen containing an invasive mole. The uterine cavity is filled with vesicles (*thin arrow*), with multifocal myometrial invasion (*one area highlighted with thick arrow*).

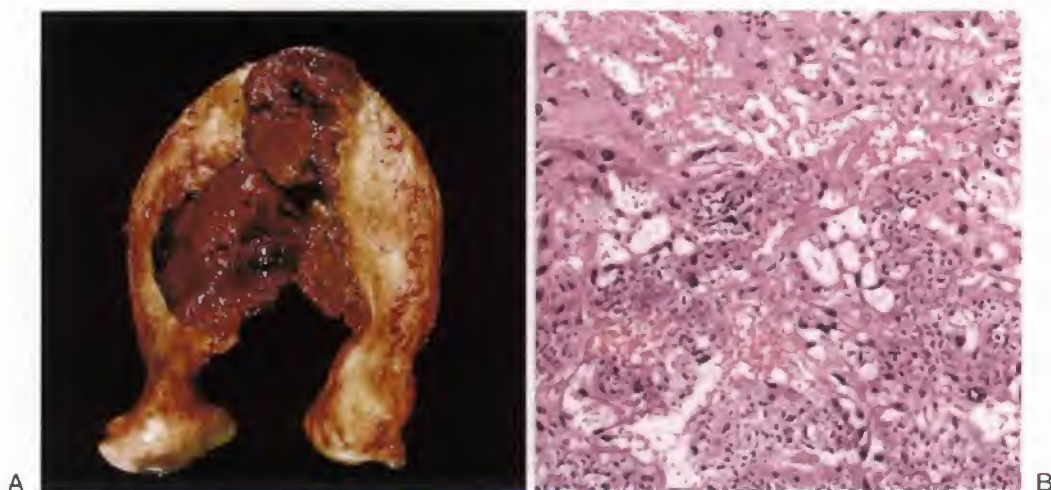


**FIGURE 29-19.** Choriocarcinoma. A. Choriocarcinoma presenting as a bulky hemorrhagic mass invading the uterine wall. B. Photomicrograph of choriocarcinoma illustrating both neoplastic cytotrophoblast and syncytiotrophoblast. (Courtesy of Dr. David R. Genest, Brigham and Women's Hospital, Boston, MA. Reproduced with permission from Crum CP: *The female genital tract*. In Kumar V, Robbins SL, Cotran RS [eds]: *Pathologic Basis of Disease*, 7th ed. Philadelphia, WB Saunders, 2005. Copyright © 2005 Saunders, An Imprint of Elsevier.)



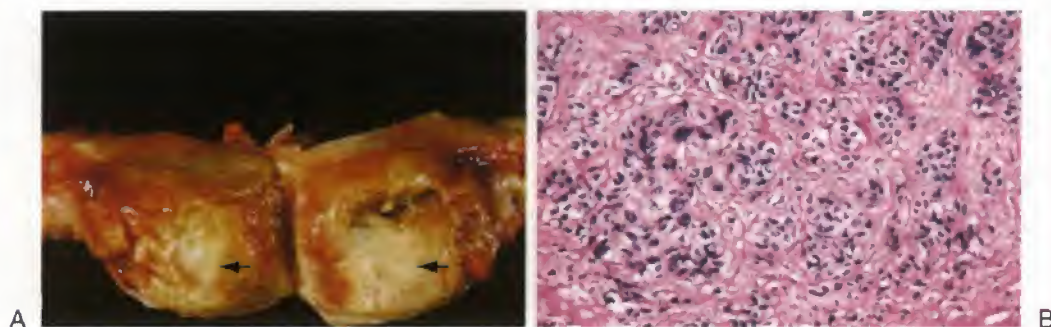


**FIGURE 29-20.** Placental site trophoblastic tumor. A, Placental site trophoblastic tumor, presenting as a discrete mass in the myometrium. B, Histology of placental site trophoblastic tumor. (Courtesy of Dr. Bradley J. Quade, Brigham and Women's Hospital, Boston, MA. Reproduced with permission from Crum CP: *The female genital tract*. In Kumar V, Robbins SL, Cotran RS [eds]: *Pathologic Basis of Disease*, 7th ed. Philadelphia, WB Saunders, 2005. Copyright © 2005 Saunders, An Imprint of Elsevier.)

is usually seen only at the periphery of the nodule and within vascular spaces in adjacent myometrium. In most patients, a bilaminar appearance can be identified, but some, especially post-treatment cases, may be predominantly composed of mainly mononuclear cytotrophoblast. CC metastasizes early and secondary nodules may be present in the cervix or vagina, or distant sites, at presentation. Unexplained intracerebral hemorrhage or acute cor pulmonale in a woman of childbearing age should always raise suspicion of CC. CC following a normal term pregnancy is presumably the result of metastatic intraplacental choriocarcinoma, such primary tumors being well reported but often microscopic and so they are not detected sonographically or at the time of delivery.<sup>110,111</sup>

## PLACENTAL SITE TROPHOBLASTIC TUMOR

This is a subtype of malignant GTN in which the predominant differentiation is toward intermediate extravillous, rather than villous, trophoblast. PSTTs usually present with amenorrhea or irregular vaginal bleeding many months or even years after the last known pregnancy, and their origin from both HM and nonmolar pregnancies have been demonstrated.<sup>112,113</sup> The average interval from the last pregnancy is 3 to 4 years, in contrast to weeks or months for other types of pGTN. The uterus in PSTT is usually enlarged, and the hCG level is only mildly elevated. Diagnosis is usually made on the basis of curettage, which demonstrates myometrium infiltrated by trophoblastic cells with eosinophilic cytoplasm- and nuclear pleomorphism-forming clusters, which infiltrate between muscle fibers. PSTT can infiltrate relentlessly and extend into adjacent organs such as the ovary, parametrium, rectum or bladder, and distant metastases can occur, although much less commonly than for CC<sup>110</sup> (see Figs. 29-1, 29-3, and 29-20).

PSTT has a lesser metastasizing potential, making it treatable with surgery. However, it is much more resistant to chemotherapy; therefore, hysterectomy is usually the treatment of choice, with chemotherapy indicated for patients

with metastases or residual disease. The mortality rate is approximately 20% and appears to be associated with the presence of lung metastases and presentation greater than 4 years from the previous pregnancy.<sup>114</sup> Sonographically, there are no specific features to reliably distinguish diagnose PSTT, but in conjunction with the history, an irregular, usually localized, uterine mass lesion may be identified.

## EPITHELIOID TROPHOBLASTIC TUMOR

This is the most recently described and rarest subtype of trophoblastic tumor, and it is essentially a variant of PSTT. It is also composed of trophoblast with an intermediate phenotype that often presents with a longer interval from the last pregnancy, around 6 to 7 years. Microscopically, it demonstrates a characteristic nodular, expansive growth pattern positive immunostaining with placental alkaline phosphatase. Behavior and treatment appears similar to PSTT.<sup>115</sup>

## Breus Mole

This is an antiquated and misleading term, which should no longer be used, to describe a large subchorionic thrombus that lies between the chorionic plate and the underlying villous tissue. There is no relationship with any type of hydatidiform mole. Such lesions are usually lobulated and elevate the fetal surface of the placenta, bulging into the amniotic cavity; prenatal ultrasonic diagnosis is well reported<sup>116-121</sup> (Fig. 29-21). Pathologically, the lesion consists solely of laminated thrombus. It was initially thought to be associated with miscarriage,<sup>122</sup> but such massive subchorionic thrombi have been demonstrated in placentas from live-born infants. It is probable that lesions of this type are due to sudden, marked slowing of blood flow in the intervillous space. The causes of this condition remain uncertain, but cases have now been reported following thrombolytic therapy in pregnant patients with prosthetic heart valves<sup>123</sup> and in women with thrombophilic conditions.<sup>124</sup>



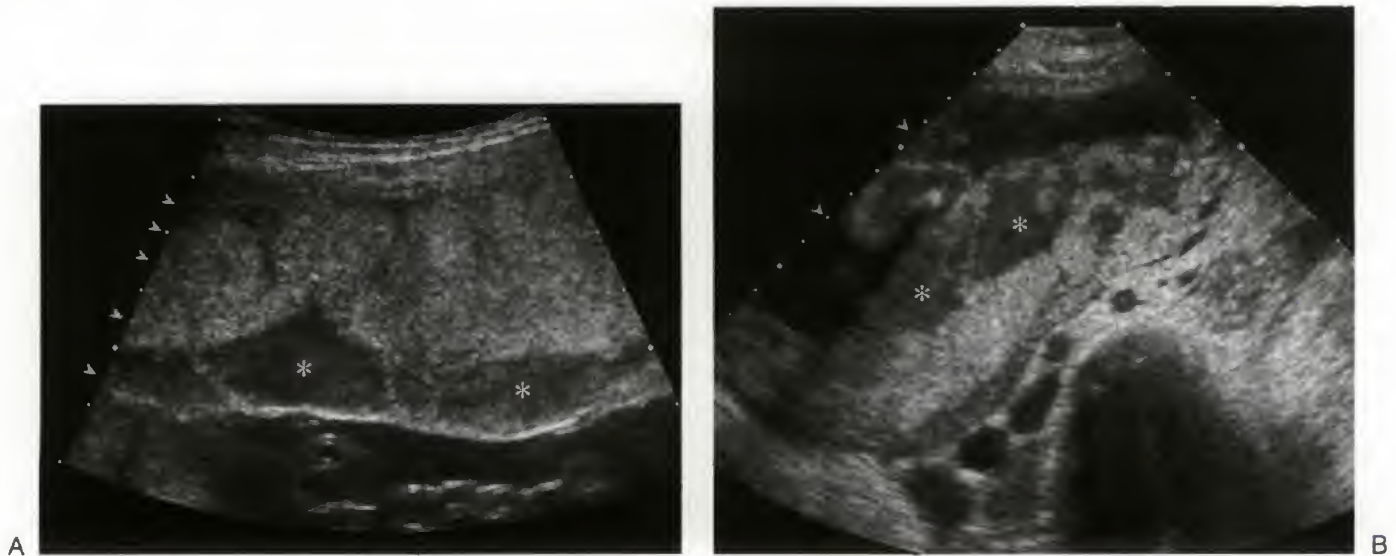


**FIGURE 29-21.** A and B. Breus mole. Two patients scanned in the second trimester of pregnancy with a subchorionic thrombohematoma. A hypoechoic area (asterisk) beneath the amniotic side of the placenta is seen in both patients. Although this lesion was initially thought to carry a poor prognosis, both fetuses delivered at term and were normal at birth.

## References

1. Tidy JA, Hancock BW, Newlands ES: The Management of Gestational Trophoblastic Neoplasia. Royal College of Obstetricians and Gynaecologists (RCOG) Clinical Guideline No. 38. London, UK, RCOG Press: Feb 2004.
2. Fisher RA: Genetics. In Hancock BW, Newlands ES, Berkowitz RS, et al (eds): *Gestational Trophoblastic Disease*, 2nd ed. New York, International Society for the Study of Trophoblastic Diseases, 2003. [www.isstid.org/gtd/contents/chapter2](http://www.isstid.org/gtd/contents/chapter2).
3. Fisher RA, Khatoun R, Paradinas FJ, et al: Repetitive complete hydatidiform mole can be biparental in origin and either male or female. *Hum Reprod* 15:594, 2000.
4. Seckl MJ, Fisher RA, Salerno G, et al: Choriocarcinoma and partial hydatidiform moles. *Lancet* 356:36, 2000.
5. Paradinas FJ, Fisher RA, Browne P, et al: Diploid hydatidiform moles with fetal red blood cells in molar villi. 1. Pathology, incidence, and prognosis. *J Pathol* 181:183, 1997.
6. Sebire NJ, Rees H, Paradinas F, et al: The diagnostic implications of routine ultrasound examination in histologically confirmed early molar pregnancies. *Ultrasound Obstet Gynecol* 18:662, 2001.
7. Sebire NJ, Fisher RA, Rees HC: Histopathological diagnosis of partial and complete hydatidiform mole in the first trimester of pregnancy. *Pediatr Dev Pathol* 6:69, 2003.
8. Sebire NJ, Makrydimas G, Agnantis NJ, et al: Updated diagnostic criteria for partial and complete hydatidiform moles in early pregnancy. *Anticancer Res* 23:1723, 2003.
9. Sebire NJ, Rees H: Diagnosis of gestational trophoblastic disease in early pregnancy. *Cur Diagn Pathol* 8:430, 2003.
10. Sebire NJ, Rees H, Paradinas F, et al: Extravillous endovascular implantation site trophoblast invasion is abnormal in complete versus partial molar pregnancies. *Placenta* 22:725, 2001.
11. Fisher RA, Hodges MD, Rees HC, et al: The maternally transcribed gene p57(KIP2) (CDKN1C) is abnormally expressed in both androgenetic and biparental complete hydatidiform moles. *Hum Mol Genet* 11:3267, 2002.
12. Castrillon DH, Sun D, Weremowicz S, et al: Discrimination of complete hydatidiform mole from its mimics by immunohistochemistry of the paternally imprinted gene product p57<sup>KIP2</sup>. *Am J Surg Pathol* 25:1225, 2001.
13. Berezowsky J, Zbieranowski I, Demers J, et al: DNA ploidy of hydatidiform moles and nonmolar conceptuses: a study using flow and tissue section image cytometry. *Mod Pathol* 8:775, 1995.
14. Fisher RA, Newlands ES: Gestational trophoblastic disease. Molecular and genetic studies. *J Reprod Med* 43:87, 1998.
15. Evans AC, Soper JT, Hammond CB: Clinical features of molar pregnancies and gestational trophoblastic tumors. In Hancock BW, Newlands ES, Berkowitz RS, et al (eds): *Gestational Trophoblastic Disease*, 2nd ed. New York, International Society for the Study of Trophoblastic Diseases, 2003. [www.isstid.org/gtd/contents/chapter8](http://www.isstid.org/gtd/contents/chapter8).
16. Paradinas FJ, Browne P, Fisher RA, et al: A clinical, histopathological and flow cytometric study of 149 complete moles, 146 partial moles and 107 non-molar hydropic abortions. *Histopathology* 28:101, 1996.
17. Fowler DJ, Lindsay I, Seckl MJ, et al: Routine pre-evacuation ultrasound diagnosis of hydatidiform mole: experience of >1,000 cases from a regional referral centre. *Ultrasound Obstet Gynecol* 27:56, 2006.
18. Gerner O, Segal S, Kopmar A, et al: The current clinical presentation of complete molar pregnancy. *Arch Gynecol Obstet* 264:33, 2000.
19. Reid MH, McGahan JP, Oi R: Sonographic evaluation of hydatidiform mole and its look-alikes. *AJR Am J Roentgenol* 140:307, 1983.
20. Santos-Ramos R, Fornay JP, Schwarz BE: Sonographic findings and clinical correlations in molar pregnancy. *Obstet Gynecol* 56:186, 1980.
21. Wagner BJ, Woodward PJ, Dickey GE: From the archives of the AFIP. Gestational trophoblastic disease: radiologic-pathologic correlation. *Radiographics* 16:131, 1996.
22. Crade M, Weber PR: Appearance of molar pregnancy 9.5 weeks after conception. Use of transvaginal ultrasound for early diagnosis. *J Ultrasound Med* 10:473, 1991.
23. Sherer DM, Allen T, Woods J: Transvaginal sonographic diagnosis of a hydatidiform mole occurring two weeks after curettage for an incomplete abortion. *J Clin Ultrasound* 19:224, 1991.
24. Fine C, Bundy AL, Berkowitz RS, et al: Sonographic diagnosis of partial hydatidiform mole. *Obstet Gynecol* 73:414, 1989.
25. Lazarus E, Hulka C, Siewert B, et al: Sonographic appearance of early complete molar pregnancies. *J Ultrasound Med* 18:589, 1999.
26. Benson CB, Genest DR, Bernstein MR, et al: Sonographic appearance of first trimester complete hydatidiform moles. *Ultrasound Obstet Gynecol* 16:188, 2000.
27. Jauniaux E, Nicolaides KH: Early ultrasound diagnosis and follow-up of molar pregnancies. *Ultrasound Obstet Gynecol* 9:17, 1997.
28. Lindholm H, Flam F: The diagnosis of molar pregnancy by sonography and gross morphology. *Acta Obstet Gynecol Scand* 78:6, 1999.
29. Woo JS, Wong LC, Hsu C, et al: Sonographic appearances of the partial hydatidiform mole. *J Ultrasound Med* 2:261, 1983.
30. Johns JN, Greenwold S, Buckley E, et al: A prospective study of ultrasound screening for molar pregnancies in missed miscarriages. *Ultrasound Obstet Gynecol* 25:493, 2005.



31. The Management of Early Pregnancy Loss. Clinical Guideline No. 25. London, UK, Royal College of Obstetricians and Gynaecologists (RCOG) RCOG press, 2000.
32. Seckl MJ, Gillmore R, Foskett M, et al: Routine terminations of pregnancy—should we screen for gestational trophoblastic neoplasia? *Lancet* 364:705, 2004.
33. Jannioux E, Brown R, Snijders RJM, et al: Early prenatal diagnosis of triploidy. *Am J Obstet Gynecol* 176:550, 1997.
34. Romero R, Horgan JG, Kohorn EI, et al: New criteria for the diagnosis of gestational trophoblastic disease. *Obstet Gynecol* 66:553, 1985.
35. Berkowitz RS, Goldstein DP: Presentation and management of molar pregnancy. In Hancock BW, Newlands ES, Berkowitz RS, et al (eds): *Gestational Trophoblastic Disease*, 2nd ed. New York, International Society for the Study of Trophoblastic Diseases, 2003. [www.isstd.org/gtd/contents/chapter9](http://www.isstd.org/gtd/contents/chapter9).
36. Achiron R, Goldenberg M, Lipitz S, et al: Transvaginal duplex Doppler ultrasonography in bleeding patients suspected of having residual trophoblastic tissue. *Obstet Gynecol* 81:507, 1993.
37. Alcazar JL: Transvaginal ultrasonography combined with color velocity imaging and pulsed Doppler to detect residual trophoblastic tissue. *Ultrasound Obstet Gynecol* 11:54, 1998.
38. Ben-Ami I, Schneider D, Maymon R, et al: Sonographic versus clinical evaluation as predictors of residual trophoblastic tissue. *Hum Reprod* 20:1107, 2005.
39. Wolman I, Jaffa AJ, Pauzner D, et al: Transvaginal sonohysterography: a new aid in the diagnosis of residual trophoblastic tissue. *J Clin Ultrasound* 24:257, 1996.
40. Wolman I, Hartoov J, Pauzner D, et al: Transvaginal sonohysterography for the early diagnosis of residual trophoblastic tissue. *J Ultrasound Med* 16: 257, 1997.
41. Zalc Y, Gamzu R, Lidor A, et al: Color Doppler imaging in the sonohysterographic diagnosis of residual trophoblastic tissue. *J Clin Ultrasound* 30:222, 2002.
42. Newlands ES: Presentation and management of persistent gestational trophoblastic disease (GTD) and gestational trophoblastic tumours (GTT) in the United Kingdom. In Hancock BW, Newlands ES, Berkowitz RS, et al (eds): *Gestational Trophoblastic Disease*, 2nd ed. New York, International Society for the Study of Trophoblastic Diseases, 2003. [www.isstd.org/gtd/contents/chapter10](http://www.isstd.org/gtd/contents/chapter10).
43. Ngan H, Wong LC, Ma HK: Staging and classification systems. In Hancock BW, Newlands ES, Berkowitz RS, et al (eds): *Gestational Trophoblastic Disease*, 2nd ed. New York, International Society for the Study of Trophoblastic Diseases, 2003. [www.isstd.org/gtd/contents/chapter6](http://www.isstd.org/gtd/contents/chapter6).
44. Kohorn IE: The FIGO 2000 staging and risk factor scoring system for gestational trophoblastic neoplasia. In Hancock BW, Newlands ES, Berkowitz RS, et al (eds): *Gestational Trophoblastic Disease*, 2nd ed. New York, International Society for the Study of Trophoblastic Diseases, 2003. [www.isstd.org/gtd/contents/chapter7](http://www.isstd.org/gtd/contents/chapter7).
45. Kohorn EI, McCarthy SM, Taylor KJ: Nonmetastatic gestational trophoblastic neoplasia. Role of ultrasonography and magnetic resonance imaging. *J Reprod Med* 43:14, 1998.
46. Zhou Q, Lei XY, Xie Q, Cardoza JD: Sonographic and Doppler imaging in the diagnosis and treatment of gestational trophoblastic disease: a 12-year experience. *J Ultrasound Med* 24:15, 2005.
47. Abd El Aal DE, El Senosy ED, et al: Uterine artery Doppler blood flow in cases of hydatidiform mole and its correlation with beta-hCG. *Eur J Obstet Gynecol Reprod Biol* 111:129, 2003.
48. Gungor T, Ekin M, Dumanli H, et al: Color Doppler ultrasonography in the earlier differentiation of benign molehydatidiforms from malignant gestational trophoblastic disease. *Acta Obstet Gynecol Scand* 77:860, 1998.
49. Berkowitz RS, Birmholz J, Goldstein DP, et al: Pelvic ultrasonography and the management of gestational trophoblastic disease. *Gynecol Oncol* 15:403, 1983.
50. Taylor KJ, Schwartz PE, Kohorn EI: Gestational trophoblastic neoplasia: diagnosis with Doppler US. *Radiology* 165:445, 1987.
51. Murao F, Takamori H, Aoki S, et al: Ultrasonic evaluation of trophoblastic disease and the response to chemotherapy. *Nippon Sanka Fujinka Gakkai Zasshi* 39:1137, 1987.
52. Long MG, Boulton JE, Begent RH, et al: Preliminary Doppler studies on the uterine artery and myometrium in trophoblastic tumours requiring chemotherapy. *Br J Obstet Gynaecol* 97:686, 1990.
53. Dobkin GR, Berkowitz RS, Goldstein DP, et al: Duplex ultrasonography for persistent gestational trophoblastic tumor. *J Reprod Med* 36:14, 1991.
54. Desai RK, Desberg AL: Diagnosis of gestational trophoblastic disease: value of endovaginal color flow Doppler sonography. *AJR Am J Roentgenol* 157:787, 1991.
55. Flam F, Lindholm H, Bui TH, et al: Color Doppler studies in trophoblastic tumors: a preliminary report. *Ultrasound Obstet Gynecol* 1:349, 1991.
56. Long MG, Boulton JE, Langley R, et al: Doppler assessment of the uterine circulation and the clinical behaviour of gestational trophoblastic tumours requiring chemotherapy. *Br J Cancer* 66:883, 1992.
57. Carter J, Carlson J, Hartenbach E, et al: Persistent postmolar gestational trophoblastic disease: use of transvaginal sonography and colour flow Doppler. *Aust NZ J Obstet Gynaecol* 33:417, 1993.
58. Mangili G, Spagnolo D, Valsecchi L, et al: Transvaginal ultrasonography in persistent trophoblastic tumor. *Am J Obstet Gynecol* 169:1218, 1993.
59. Park YW, Kim DK, Cho JS, et al: The utilization of Doppler ultrasonography with color flow mapping in the diagnosis and evaluation of malignant trophoblastic tumors. *Yonsei Med J* 35:329, 1994.
60. Hsieh FJ, Wu CC, Chen CA, et al: Correlation of uterine hemodynamics with chemotherapy response in gestational trophoblastic tumors. *Obstet Gynecol* 83:1021, 1994.
61. Hsieh FJ, Wu CC, Lee CN, et al: Vascular patterns of gestational trophoblastic tumors by color Doppler ultrasound. *Cancer* 74:2361, 1994.
62. Flam F: Colour flow Doppler for gestational trophoblastic neoplasia. *Eur J Gynaecol Oncol* 15:443, 1994.
63. Chan FY, Chau MT, Pun TC, et al: A comparison of colour Doppler sonography and the pelvic arteriogram in assessment of patients with gestational trophoblastic disease. *Br J Obstet Gynaecol* 102:720, 1995.
64. Kawano M, Masuzaki H, Ishimaru T: Transvaginal color Doppler studies in gestational trophoblastic disease. *Ultrasound Obstet Gynecol* 7:197, 1996.
65. Maymon R, Schneider D, Shulman A, et al: Serial color Doppler flow of uterine vasculature combined with serum beta-hCG measurements for improved monitoring of patients with gestational trophoblastic disease. A preliminary report. *Gynecol Obstet Invest* 42:201, 1996.
66. Chan FY, Pun TC, Chau MT, et al: The role of Doppler sonography in assessment of malignant trophoblastic disease. *Eur J Obstet Gynecol Reprod Biol* 68:123, 1996.
67. Zanetta G, Lissone A, Colombo M, et al: Detection of abnormal intrauterine vascularization by color Doppler imaging: a possible additional aid for the follow up of patients with gestational trophoblastic tumors. *Ultrasound Obstet Gynecol* 7:32, 1996.
68. Honigl W, Reich O, Ranner G, et al: Choriocarcinoma of the uterus after term pregnancy: imaging by vaginal color Doppler ultrasound. *Ultraschall Med* 18:165, 1997.
69. Bettencourt E, Pinto E, Abraul E, et al: Placental site trophoblastic tumour: the value of transvaginal colour and pulsed Doppler sonography (TV-CDS) in its diagnosis: case report. *Eur J Gynaecol Oncol* 18:461, 1997.
70. Bidzinski M, Lemieczek B, Drabik M: The assessment of value of transvaginal ultrasound for monitoring of gestational trophoblastic disease treatment. *Eur J Gynaecol Oncol* 18:541, 1997.
71. Xiang Y, Yang X, Yang N, et al: A comparative study of transvaginal ultrasonography and pelvic arteriogram in assessment of patients with gestational trophoblastic tumour. *Chin Med Sci J* 13:45, 1998.
72. Xie H, Hata K, Lu M, et al: Color Doppler energy and related quantitative analysis of gestational trophoblastic tumors. *Int J Gynaecol Obstet* 65:281, 1999.
73. Yalcin OT, Ozalp SS, Tanir HM: Assessment of gestational trophoblastic disease by Doppler ultrasonography. *Eur J Obstet Gynecol Reprod Biol* 103:83, 2002.
74. Agarwal R, Strickland S, McNeish IA, et al: Doppler ultrasonography of the uterine artery and the response to chemotherapy in patients with gestational trophoblastic tumors. *Clin Cancer Res* 8:1142, 2002.
75. Oguz S, Sargin A, Aytan H, et al: Doppler study of myometrium in invasive gestational trophoblastic disease. *Int J Gynecol Cancer* 14:972, 2004.
76. Cole LA: Human chorionic gonadotropin (hCG) assay. In Hancock BW, Newlands ES, Berkowitz RS, et al (eds): *Gestational Trophoblastic Disease*, 2nd ed. New York, International Society for the Study of Trophoblastic Diseases, 2003. [www.isstd.org/gtd/contents/chapter5](http://www.isstd.org/gtd/contents/chapter5).



77. Lim AK, Agarwal R, Seckl MJ, et al: Embolization of bleeding residual uterine vascular malformations in patients with treated gestational trophoblastic tumors. *Radiology* 222:640, 2002.
78. Ichikawa Y, Nakauchi T, Sato T, et al: Ultrasound diagnosis of uterine arteriovenous fistula associated with placental site trophoblastic tumor. *Ultrasound Obstet Gynecol* 21:606, 2003.
79. Daniel A, Wu Z, Bennetts B, et al: Karyotype, phenotype and parental origin in 19 cases of triploidy. *Prenat Diagn* 21:1034, 2001.
80. Sebire NJ, Foksett M, Paradinas FJ, et al: Outcome of twin pregnancies with complete hydatidiform mole and healthy co-twin. *Lancet* 359:2165, 2002.
81. Makrydimas G, Sebire NJ, Thornton SE, et al: Complete hydatidiform mole and normal live birth: a novel case of confined placental mosaicism: case report. *Hum Reprod* 17:2459, 2002.
82. Moscoso G, Jauniaux E, Hustin J: Placental vascular anomaly with diffuse mesenchymal stem villous hyperplasia. A new clinicopathological entity? *Pathol Res Pract* 187:324, 1991.
83. Lage JM: Placentomegaly with massive hydrops of placental stem villi, diploid DNA content, and fetal omphalocele: Possible association with Beckwith-Wiedemann syndrome. *Hum Pathol* 22:591, 1991.
84. Pridmore BR, Khong TY, Wells WA: Ultrasound placental cysts associated with massive placental stem villous hydrops, diploid DNA content, and exomphalos. *Am J Perinatol* 11:14, 1994.
85. Sander CM: Angiomatous malformation of placental chorionic stem vessels and pseudo-partial molar placenta: Report of five cases. *Pediatr Pathol* 13:621, 1993.
86. Hojberg KE, Aagaard J, Henriques U, et al: Placental vascular malformation with mesenchymal hyperplasia and a localized chorioangioma. *Pathol Res Pract* 190:808, 1994.
87. Uemura N, Kobayashi F, Korita D, et al: Diffuse cystic change of a term placenta with a normal newborn. *J Obstet Gynaecol Res* 23:433, 1997.
88. Paradinas FJ, Sebire NJ, Fisher RA, et al: Pseudo-partial moles: placental stem vessel hydrops and the association with Beckwith-Wiedemann syndrome and complete moles. *Histopathology* 39:447, 2001.
89. Lee, GK, Chi JG, Cha KS: An unusual venous anomaly of the placenta. *Am J Clin Pathol* 95:48, 1991.
90. McCowan LME, Becroft DMO: Beckwith-Wiedemann syndrome, placental abnormalities, and gestational proteinuric hypertension. *Obstet Gynecol* 83:813, 1994.
91. Hillstrom MM, Brown DL, Wilkins-Haug L, et al: Sonographic appearance of placental villous hydrops associated with Beckwith-Wiedemann syndrome. *J Ultrasound Med* 14:61, 1995.
92. Chen CP, Chern SR, Wang TY, et al: Pregnancy with concomitant chorangioma and placental vascular malformation with mesenchymal hyperplasia. *Hum Reprod* 12:2553, 1997.
93. Jauniaux E, Nicolaides KH, Hustin J: Perinatal features associated with placental mesenchymal dysplasia. *Placenta* 18:701, 1997.
94. Furuhashi M, Oda H, Nakashima T: Hydrops of placental stem villi complicated with fetal congenital adrenal hyperplasia. *Arch Gynecol Obstet* 264:101, 2000.
95. Ohya M, Kojyo T, Gotoda H, et al: Mesenchymal dysplasia of the placenta. *Pathol Intern* 50:759, 2000.
96. Arizawa M, Nakayama M: Suspected involvement of the X chromosome in placental mesenchymal dysplasia. *Congenit Anom* 42:309, 2002.
97. Chan YF, Sampson A: Placental mesenchymal dysplasia: a report of four cases with differentiation from partial hydatidiform mole. *Aust N Z J Obstet Gynaecol* 43:475, 2003.
98. Matsui H, Iitsuka Y, Yamazawa K, et al: Placental mesenchymal dysplasia initially diagnosed as partial mole. *Pathol Intern* 53:810, 2003.
99. Cohen MC, Roper EC, Sebire NJ, et al: Placental mesenchymal dysplasia associated with fetal aneuploidy. *Prenat Diagn* 25:187, 2005.
100. Kaiser-Rogers KA, McFadden DE, Livasy CA, et al: Androgenetic/biparental mosaicism causes placental mesenchymal dysplasia. *J Med Genet* 2005, epub ahead of print.
101. Aoki S, Hata T, Hata K, et al: Doppler color flow mapping of an invasive mole. *Gynecol Obstet Invest* 27:52, 1989.
102. Munyer TP, Callen PW, Filly RA, et al: Further observation on the sonographic spectrum of gestational trophoblastic disease of complete hydatidiform moles. *J Clin Ultrasound* 9:349, 1981.
103. Caspi B, Elchalal U, Dgani R, et al: Invasive mole and placental site trophoblastic tumor: Two entities of gestational trophoblastic disease with a common ultrasonographic appearance. *J Ultrasound Med* 10:517, 1991.
104. Chau MT, Chan FY, Pun TC, et al: Perforation of the uterus by an invasive mole using color Doppler ultrasound: Case report. *Ultrasound Obstet Gynecol* 3:51, 1993.
105. Tsukihara S, Harada T, Terakawa N: Ultrasound-guided local injection of methotrexate to treat an invasive hydatidiform mole. *J Obstet Gynaecol Res* 30:202, 2004.
106. Kika K, Matuda I: Primary tubal hydatidiform mole: report of a case. *Obstet Gynecol* 9:224, 1975.
107. Burton JL, Lidbury AE, Gillespie AM: Overdiagnosis of hydatidiform mole in early tubal ectopic pregnancy. *Histopathology* 38:409, 2001.
108. Rees HC, Paradinas FJ: The diagnosis of hydatidiform mole in early tubal ectopic pregnancy. *Histopathology* 39:320, 2001.
109. Sebire NJ, Lindsay I, Fisher RA, et al: Overdiagnosis of complete and partial hydatidiform mole in tubal ectopic pregnancies. *Int J Gynecol Pathol* 24:260, 2005.
110. Paradinas F, Sebire NJ, Rees HC: Pathology. In Hancock BW, Newlands ES, Berkowitz RS, et al (eds): *Gestational Trophoblastic Disease*, 2nd ed. New York, International Society for the Study of Trophoblastic Diseases, 2003. [www.isstg.org/gtd/contents/chapter4](http://www.isstg.org/gtd/contents/chapter4).
111. Sebire NJ, Lindsay I, Fisher RA, et al: Intraplacental choriocarcinoma: experience from a tertiary referral center and relationship with infarile choriocarcinoma. *Fetal Pediatr Pathol* 24:21, 2005.
112. Fisher RA, Paradinas FJ, Newlands ES, et al: Genetic evidence that placental site trophoblastic tumours can originate from a hydatidiform mole or a normal conceptus. *Br J Cancer* 65:355, 1992.
113. Bower M, Paradinas FJ, Fisher RA, et al: Placental site trophoblastic tumor: molecular analysis and clinical experience. *Clin Cancer Res* 2:897, 1996.
114. Papadopoulos AJ, Foksett M, Seckl MJ, et al: Twenty-five years' clinical experience with placental site trophoblastic tumors. *J Reprod Med* 47:460, 2002.
115. Shih IM, Kurman R: Epithelioid trophoblastic tumour: a neoplasm distinct from choriocarcinoma and placental site trophoblastic tumour simulating carcinoma. *Am J Surg Pathol* 22:1393, 1998.
116. Thomas D, Makhoul J, Muller C: Fetal growth retardation due to massive subchorionic thrombohematoma: report of two cases. *J Ultrasound Med* 11:245, 1992.
117. Tam WH, Fung HY, Fung TY, et al: Intra-uterine growth retardation and transverse lie due to massive subchorionic thrombohematoma and overlying large subchorionic cyst. *Acta Obstet Gynecol Scand* 76:381, 1997.
118. Richards DS, Bennett BB: Prenatal ultrasound diagnosis of massive subchorionic thrombohematoma. *Ultrasound Obstet Gynecol* 11:364, 1998.
119. Nishida N, Suzuki S, Hamamura Y, et al: Massive subchorionic hematoma (Breus' mole) complicated by intrauterine growth retardation. *J Nippon Med Sch* 68:54, 2001.
120. Nishijima K, Shukunami K, Tsuyoshi H, et al: Massive subchorionic hematoma: peculiar prenatal images and review of the literature. *Fetal Diagn Ther* 20:23, 2005.
121. Fisteag-Kiprono L, Foster K, McKenna D, et al: Antenatal sonographic diagnosis of massive subchorionic hematoma: report of a case. *J Reprod Med* 50:219, 2005.
122. Breus C: *Das Tuberoe Subchoriale-Hamatome der Decidua*. Leipzig, Franz Deuticke, 1892.
123. Usta IM, Abdallah M, El Hajj M, et al: Massive subchorionic hematomas following thrombolytic therapy in pregnancy. *Obstet Gynecol* 103:1079, 2004.
124. Heller DS, Rush DS, Baergen RN: Subchorionic hematoma associated with thrombophilia: report of three cases. *Pediatr Dev Pathol* 6:261, 2003.



## ULTRASOUND EVALUATION OF THE ADNEXA (OVARY AND FALLOPIAN TUBES)\*

Lil Valentin, MD, PhD and Peter W. Callen, MD

### Ultrasound Morphology for Discrimination Between Benign and Malignant Extrauterine Pelvic Masses

### The Role of Doppler Ultrasound for Discrimination Between Benign and Malignant Masses

### Ultrasound Morphology for Making a Specific Diagnosis in an Extrauterine Pelvic Mass

### Ultrasound Characteristics of Mature Cystic Teratomas (Dermoid Cysts)

### Ultrasound Characteristics of Benign, Hemorrhagic and Inflammatory Cysts

Ultrasound Characteristics of Endometriomas

Ultrasound Characteristics of Hemorrhagic Corpus Luteum Cysts

Ultrasound Characteristics of Pelvic Inflammatory Disease

(Hydro-Pyo-Hemato-Salpinx)

Ultrasound Characteristics of Paraovarian Cysts

Ultrasound Characteristics of Peritoneal Pseudocysts

Ultrasound Characteristics of Ovarian Fibromas, Fibrothecomas, Thecomas, Brenner Tumors, and Other Benign Solid Ovarian Tumors

Ultrasound Characteristics of Ovarian Serous Cystadenomas, Mucinous Cystadenomas, and Adenofibromas

Ovarian Masses in the Pregnant Patient

### Ultrasound in the Diagnosis of Adnexal Torsion

### Summary

### Practice Points

Before the ultrasound era, any persistent palpable adnexal mass had to be removed surgically, because that was the only way of excluding malignancy. Today, we can make a fairly confident diagnosis of a pelvic mass on the basis of its ultrasound image.<sup>1-13</sup> This possibility allows us to offer individual and, it is hoped, optimal treatment of women with a palpable pelvic mass. Some masses are almost certainly best treated expectantly, certainly if they are not causing any symptoms (e.g., functional cysts, hydrosalpinx, and uterine myomas), others might be best treated by cyst puncture (e.g., peritoneal inclusion cysts),<sup>14,15</sup> and yet others by surgery (e.g., borderline tumors and invasive malignancies). If surgery is judged to be the best treatment, then the ultrasound diagnosis may be important when choosing the optimal time and method of surgery: Many benign tumors can be removed laparoscopically by a gynecologist,<sup>16</sup> whereas malignant masses require open surgery by an oncologic surgeon. No doubt, transvaginal ultrasound examination is an excellent tool for solving clinical problems in women with symptoms suggesting the presence of an adnexal mass. However, today's liberal use of transvaginal ultrasound also presents many problems to the clinicians. Many adnexal masses that would almost certainly have remained undetected before the

ultrasound era are now found incidentally at transvaginal ultrasound examination of women without symptoms of an adnexal tumor. The natural history of incidentally detected pelvic masses with benign ultrasound morphology is not known. We do not know how often such tumors will cause problems in the future (e.g., torsion, pain, infertility). We do not know if there is a risk of some of them becoming malignant or the magnitude of any such a risk. In one study, 86 asymptomatic women (72 premenopausal and 14 postmenopausal) with an adnexal mass with sonographic morphology compatible with a mature cystic teratoma (dermoid cyst) not larger than 6 cm, were managed expectantly. The women were followed up for a mean of 3 years. Torsion or other complications did not occur. Twenty-eight women who desired pregnancy became pregnant and had one or more uncomplicated pregnancies during follow-up. Growth rate of the mature cystic teratomas was very low.<sup>17</sup> Hundreds of postmenopausal women with adnexal cysts—most of the cysts being simple cysts  $\leq 5$  cm in diameter—have been managed expectantly for up to 9 years without any adverse effects being noted.<sup>18-25</sup> It is by no means obvious that adnexal masses with benign ultrasound morphology incidentally detected at ultrasound examination should be surgically removed. Surgery is associated with risks. In published studies, the intraoperative and postoperative complication rate associated with adnexal surgery varies between 0.3% and 8%.<sup>26-31</sup> The mortality rate associated with adnexal surgery is difficult to estimate, but the mortality rate associated with gynecologic laparoscopic procedures may be 1 per 25,000.<sup>32</sup> Long-term complications after gynecologic surgery include adhesion formation.<sup>33</sup>

\*Portions of this chapter are reprinted from

(1) BEST PRACTICE & RESEARCH CLINICAL OBSTETRICS & GYNAECOLOGY, V18(1): 105-123, Okaro E & Valentin L: The role of ultrasound in the management of women with acute and chronic pelvic pain © 2004 Elsevier Ltd.

(2) BEST PRACTICE & RESEARCH CLINICAL OBSTETRICS & GYNAECOLOGY, V18(1): 71-89, Valentin L: Use of morphology to characterize and manage common adnexal masses. © 2004 Elsevier Ltd.



These adhesions, in turn, may cause infertility or bowel obstruction.<sup>33-35</sup> I have found no published information on the incidence of small bowel obstruction after adnexal surgery, but one may expect one death due to postoperative small bowel obstruction per 625 hysterectomies (my own calculations made on the basis of information from references 33 and 36). To determine if surgical removal of adnexal masses with benign ultrasound morphology incidentally detected at ultrasound examination in asymptomatic women is beneficial, it would be necessary to conduct a randomized controlled trial comparing surgery with expectant management. However, it would probably be difficult to conduct such a trial. Experts in gynecologic ultrasound would have to perform all ultrasound examinations, because confusion of benign and malignant tumors resulting in inclusion of malignancies in the trial would be unacceptable. Moreover, the primary endpoint of such a trial is not obvious, follow-up time would need to be very long, the trial would need to be large, and individual preferences of women might make it difficult to recruit patients. My personal opinion is that one should not examine asymptomatic women with ultrasound (or with gynecological palpation), because there is no evidence that detection of pelvic masses that do not cause symptoms is beneficial. This is true even of malignant masses. We have to await the results of ongoing randomized trials evaluating ultrasound screening for ovarian cancer before we will know if detection of ovarian cancer at an asymptomatic stage improves the prognosis.<sup>37</sup>

## ULTRASOUND MORPHOLOGY FOR DISCRIMINATION BETWEEN BENIGN AND MALIGNANT EXTRAUTERINE PELVIC MASSES

Subjective evaluation of the grayscale ultrasound image, that is, pattern recognition, for discrimination between benign and malignant tumors can almost certainly be learned by anyone performing gynecologic ultrasound examinations on a regular basis, but diagnostic accuracy increases with increasing experience.<sup>3</sup> An experienced ultrasound examiner can very confidently discriminate between benign and malignant pelvic tumors in the adnexal region using pattern recognition, the reported sensitivity of pattern recognition varying between 88% and 100% and the reported specificity between 62% and 96%.<sup>2,38-44</sup> Pattern recognition has been shown to be superior to all other ultrasound methods (e.g., simple classification systems, scoring systems, mathematical models for calculating the risk of malignancy) for discrimination between benign and malignant extrauterine pelvic masses.<sup>2,43</sup> Adding Doppler ultrasound examination to subjective evaluation of the grayscale ultrasound image does not seem to yield much improvement in diagnostic precision,<sup>2,38,39,42</sup> but it may increase the confidence with which a correct diagnosis of benignity or malignancy is made<sup>2,38</sup> (see later).

My personal experience is that absence of solid components and absence of irregularities in an adnexal mass at ultrasound examination suggests benignity, whereas any irregularity—be it in the outline, the cyst wall, or in the echogenicity of a tumor—suggests malignancy. I consider unilocular and multilocular cysts without solid components

to be benign, even though some cysts with an extremely large number of locules may be borderline mucinous cystadenomas of intestinal type,<sup>45</sup> even in the absence of irregularities or unequivocal solid components. In cystic tumors with solid components, the larger and more irregular the solid components are, the greater the risk of malignancy. In solid tumors, the more irregular the outline and echogenicity of the tumor, the greater the risk of malignancy. Using these simple rules, my detection rate (sensitivity) of malignant tumors including borderline tumors was 88% (21/24), with a specificity of 96% (143/149) in one series of patients undergoing preoperative ultrasound examination.<sup>2</sup> In a later series they were 83% (30/36) and 91% (91/100).<sup>43</sup> In these two series, all but two of the nine malignancies that were misdiagnosed as more likely to be benign than malignant were borderline tumors, the other two being a tubal cancer and a dysgerminoma.

Papillary projections—for example, a solid projection into a cyst cavity from the cyst wall of more than 3 mm in height<sup>46</sup>—are a strong sign of malignancy.<sup>47-52</sup> In one of my own series, they seemed to be more common in borderline ovarian tumors (5/12, 42%) than in benign ovarian tumors (20/100, 20%) and primary invasive ovarian tumors (3/12, 25%) (unpublished data from reference 43). This has been confirmed by Romanini and coworkers.<sup>53</sup> Papillary projections seem to be particularly common in ovarian adenofibromas (5/7, 70%), but they are also often seen in serous cystadenomas (4/11, 37%) and mucinous cystadenomas (3/14, 21%) (unpublished data from reference 43). Papillary projections in benign tumors explain many false-positive ultrasound diagnoses of malignancy. Many false-positive and false-negative diagnoses with regard to malignancy are also explained by mucinous cystadenomas/mucinous borderline tumors because of their overlapping ultrasound morphology.

Ultrasound images representative of benign and malignant extrauterine pelvic tumors are shown in Figure 30-1. The difficulty of correctly classifying tumors with papillary projections is illustrated in Figure 30-2, and the overlapping ultrasound morphology of mucinous cystadenomas and mucinous borderline tumors (of intestinal type) is shown in Figure 30-3.

## THE ROLE OF DOPPLER ULTRASOUND FOR DISCRIMINATION BETWEEN BENIGN AND MALIGNANT MASSES

Based on the results of prospective studies, there is little to support an important role of Doppler examination in the differential diagnosis of adnexal masses.<sup>1,2,38,39,42</sup> In most cases, a correct diagnosis can be made on the basis of the grayscale ultrasound image alone. A comprehensive description of the use of (color) Doppler ultrasound examination in the diagnosis of adnexal masses is given in reference 54. In summary, pulsatility index and resistance index seem to be the *least suitable* Doppler variables for discrimination between benign and malignant adnexal masses. They have been claimed to be lower in malignant than in benign adnexal tumors, but there is substantial overlap in results between the two categories. Subjective evaluation of the color content of the tumor scan or measurement of time-averaged



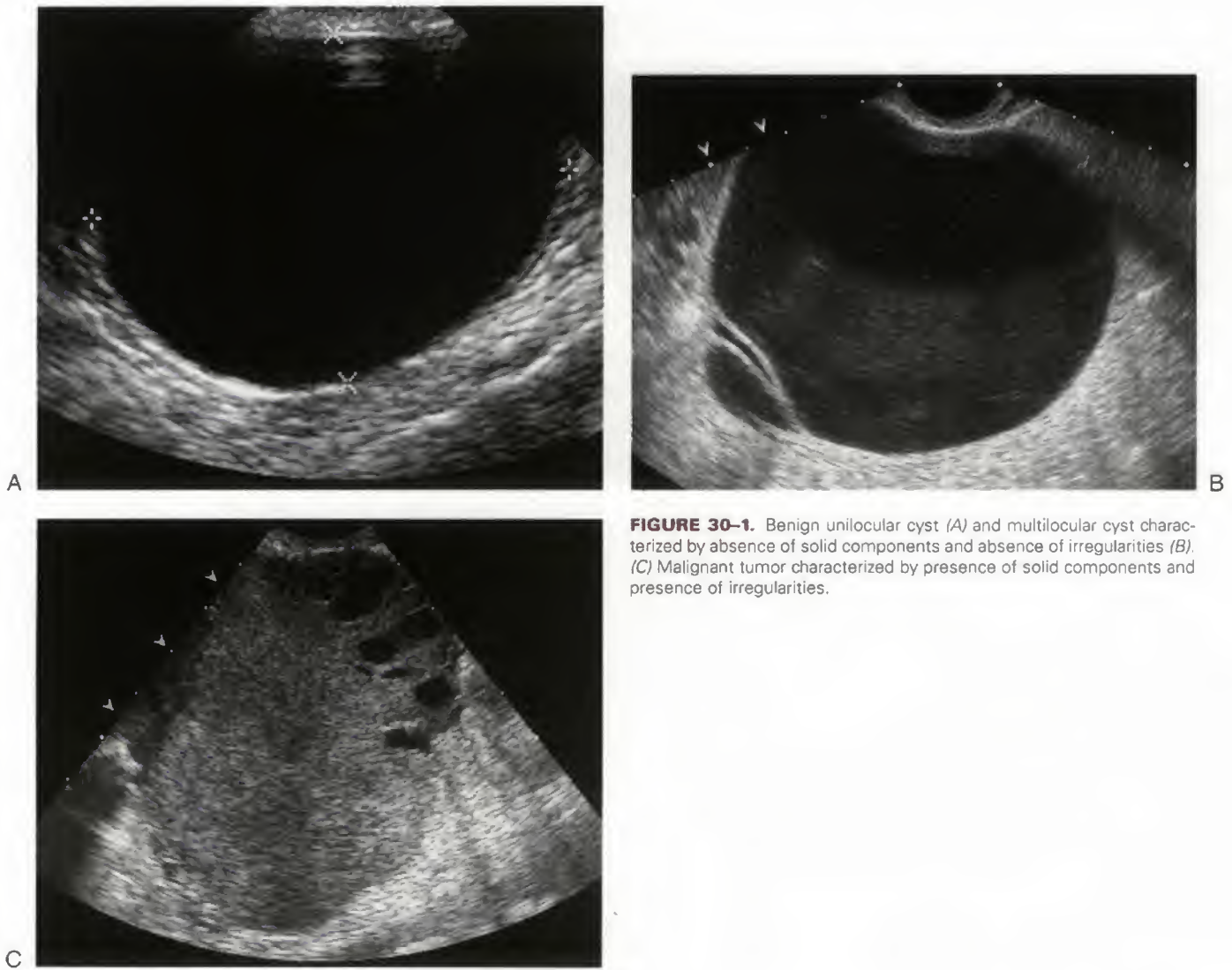


**FIGURE 30-1.** Benign unilocular cyst (A) and multilocular cyst characterized by absence of solid components and absence of irregularities (B). (C) Malignant tumor characterized by presence of solid components and presence of irregularities.

maximum velocity in tumor vessels are probably better; a high level of color content in the tumor scan and high blood flow velocity in tumor vessels support the presence of malignancy. If measurement of blood flow velocity is to be used, it is the highest time-averaged maximum velocity recorded from tumor vessels that should be used to characterize the tumor. However, the color content of the tumor scan probably reflects tumor vascularity better than any other Doppler variable. It might be said to give an overall impression of tumor vascularization in that it probably reflects both the number and size of tumor vessels and their functional capacity. The international ovarian tumor analysis group have suggested the use of a color score (color score 1, no detectable vascularization; color score 2, minimal vascularization; color score 3, moderate vascularization; color score 4, abundant vascularization).<sup>46</sup> Despite evaluation of the color Doppler image being entirely subjective, results have been shown to be reproducible enough for clinical use.<sup>55</sup>

### ULTRASOUND MORPHOLOGY FOR MAKING A SPECIFIC DIAGNOSIS IN AN EXTRAUTERINE PELVIC MASS

Some types of tumor (e.g., endometriomas, mature cystic teratomas (dermoid cysts), hydro- pyo- and hemato-salpinx, peritoneal pseudocysts, paraovarian cysts, hemorrhagic corpus luteum cysts, myomas, abscesses and ovarian fibromas, thecomas, and Brenner tumours) may manifest a characteristic appearance at grayscale imaging.<sup>1,9,10,36-67</sup> Therefore, an experienced ultrasound examiner can often make a correct specific diagnosis based on the grayscale ultrasound image by pattern recognition.<sup>1,38,39,63,64</sup> In some cases, however, diagnosis may be confusing. For example, ovarian endometrioma may be difficult to distinguish from tubo-ovarian abscess, mature cystic teratoma (dermoid cyst), mucinous cystadenoma, and hemorrhagic cyst,<sup>5</sup> as may pedunculated uterine leiomyoma from ovarian fibroma.<sup>58</sup> Doppler ultrasound examination does not contribute much to a correct specific diagnosis of an adnexal mass.<sup>1</sup>

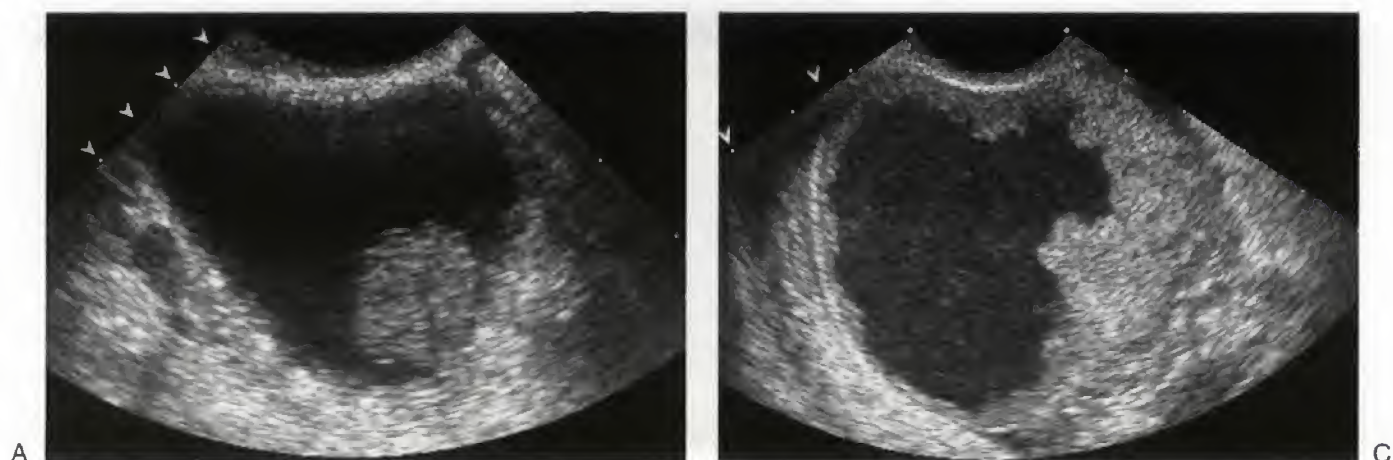


**FIGURE 30-2.** Papillary projections in (A) benign cyst, (B) borderline tumor, and (C) primary invasive ovarian cancer. Note the overlapping ultrasound characteristics between benign and borderline tumors with papillary projections.

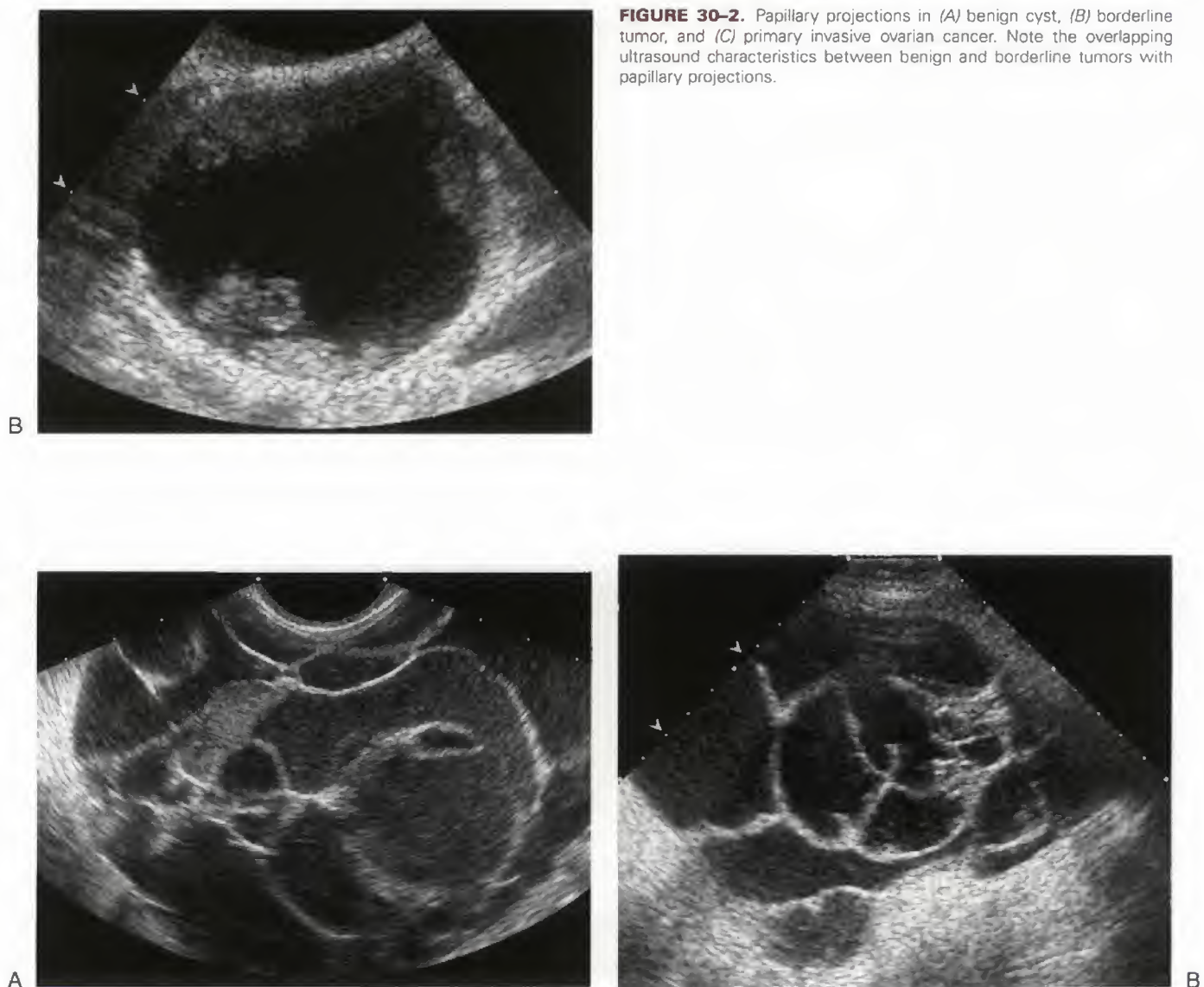


**FIGURE 30-3.** Overlapping ultrasound features of (A) benign mucinous cystadenoma and (B) intestinal type borderline mucinous tumor.



**Table 30-1**

**Sensitivity and Specificity of Subjective Evaluation of the Grayscale Ultrasound Image ('Pattern Recognition') for Discrimination Between Benign and Malignant Pelvic Masses and for Making a Specific Diagnosis**

Diagnosis	My Own Series <sup>1</sup>		Other Series <sup>6-13, 38-42, 113</sup>	
	Sensitivity	Specificity	Sensitivity	Specificity
Malignancy	88 (21/24) <sup>a</sup>	96 (143/149)	77-100	62-95
Dermoid cyst	90 (18/20) <sup>b</sup>	98 (150/153)	53-100	94-100
Endometrioma	92 (24/26)	97 (143/147)	43-84	89-100
Corpus luteum cyst	-	-	Not reported	Not reported
Hydro-, pyo-, or haemato-salpinx	100 (8/8)	100 (165/165)	83, 93	73, 90
Paraovarian or paratubal cyst	83 (5/6) <sup>c</sup>	99 (166/167)	10-97	Not reported
Peritoneal pseudocyst	100 (3/3)	99 (169/170)	Not reported	Not reported
Ovarian fibroma or fibrothecoma	56 (5/9)	100 (164/164)	Not reported	Not reported
Myoma	86 (6/7)	99 (165/166)	93	98

<sup>a</sup>All malignancies missed were borderline tumors.

<sup>b</sup>No specific diagnosis was suggested in the two cases missed (false-negative results). The two cysts were seen to contain sonolucent fluid, a few septae, and minor solid components not resembling fat or hair.

<sup>c</sup>No specific diagnosis was suggested in the case missed (false-negative).

From Valentin L: Use of morphology to characterize and manage common adnexal masses. *Best Pract Res Clin Obstet Gynaecol* 18:71, 2004

The sensitivity and specificity of pattern recognition in the diagnosis of some common specific diagnoses are shown in Table 30-1. It is important to emphasize that the ability to make a correct specific diagnosis in a series of pelvic tumors is highly dependent on the types of tumor in the tumor series studied. My own series<sup>1</sup> consists of a consecutive series of pelvic tumors removed at surgery. It contains a mixture of different types of tumor that in all likelihood is fairly representative of the types of pelvic tumor currently considered appropriate to operate.

## ULTRASOUND CHARACTERISTICS OF MATURE CYSTIC TERATOMAS (DERMOID CYSTS)

Germ cell tumors constitute the second largest group of ovarian neoplasms (approximately 20%). Ovarian teratomas are the most common germ cell tumor and are derived from several histologic types, all of which contain mature or immature tissues of germ cell (pluripotential) origin.<sup>68</sup> These include the mature cystic teratoma (dermoid cyst); the monodermal teratoma, that is, a teratoma composed predominantly of one tissue element, the most common being mature thyroid tissue (struma ovarii) and immature teratoma.

Mature cystic teratoma or ovarian cystic teratoma are more appropriate terms than the more commonly used term dermoid cysts. These cystic tumors are the most common of the ovarian teratomas. They typically contain mature tissues of ectodermal (skin, brain), mesodermal (muscle, fat), and endodermal (mucinous or ciliated epithelium) origin.<sup>68</sup> They affect a younger age group (mean patient age, 30 years) than epithelial ovarian neoplasms<sup>69</sup> and are the most common ovarian masses in children.<sup>70</sup> Most mature cystic teratomas are asymptomatic.<sup>68</sup>

Owing to the slow growth rate of mature cystic teratomas, with an average rate of 1.8 mm each year, some investigators advocate nonsurgical management of smaller (<6 cm)

tumors.<sup>71</sup> Mature cystic teratomas requiring removal can be treated with simple cystectomy. The tumors are bilateral in about 10% of cases.<sup>68,72</sup>

On gross pathologic examination, mature cystic teratomas are often (about 90%) unilocular and filled with sebaceous material, which is liquid at body temperature and semisolid at room temperature.<sup>68,72</sup> Squamous epithelium lines the wall of the cyst, and compressed, often hyalinized, ovarian stroma covers the external surface.<sup>73,74</sup> Hair follicles, skin glands, muscle, and other tissues are found within the wall. There is usually a raised protuberance projecting into the cyst cavity known as the Rokitansky nodule. Most of the hair typically arises from this protuberance,<sup>68</sup> as do bone or teeth when they are present.<sup>75</sup> Ectodermal tissue (skin derivatives and neural tissue) is invariably present.<sup>72,73,75</sup> Mesodermal tissue (fat, bone, cartilage, muscle) is present in more than 90% of cases, and endodermal tissue (e.g., gastrointestinal and bronchial epithelium, thyroid tissue) is seen in most cases.<sup>72</sup> Adipose tissue is present in 67% to 75% of cases, and teeth are seen in 31%.<sup>68,72,73,75</sup>

Most mature cystic teratomas are easily recognized at grayscale imaging because of their fat and hair content.<sup>61,65</sup> However, as many as 9% (1/11)<sup>11</sup> or even 18% (7/89)<sup>65</sup> of mature cystic teratomas may manifest a predominantly cystic echo pattern indistinguishable from other cystic masses. The most characteristic ultrasound features of a mature cystic teratoma are the presence of (1) a white ball (corresponding to hair and sebum), sometimes occupying the entire cystic tumor (Fig. 30-4A), (2) long, echogenic (white) lines and prominent echogenic dots in cyst fluid (corresponding to hair floating freely in non fatty fluid; see Fig. 30-4B), and (3) shadowing<sup>61,65,76</sup> (see Fig. 30-4C). Shadowing often makes it difficult or impossible to correctly measure the size of mature cystic teratomas. The Rokitansky nodule or dermoid plug is hyperechogenic with shadowing due to adipose tissue, hair, or calcifications (see Fig. 30-4D). Mature teratomas may be small and not deform the shape of the ovary (see Fig. 30-4E). Intracystic nondependent spheres of lipid material can



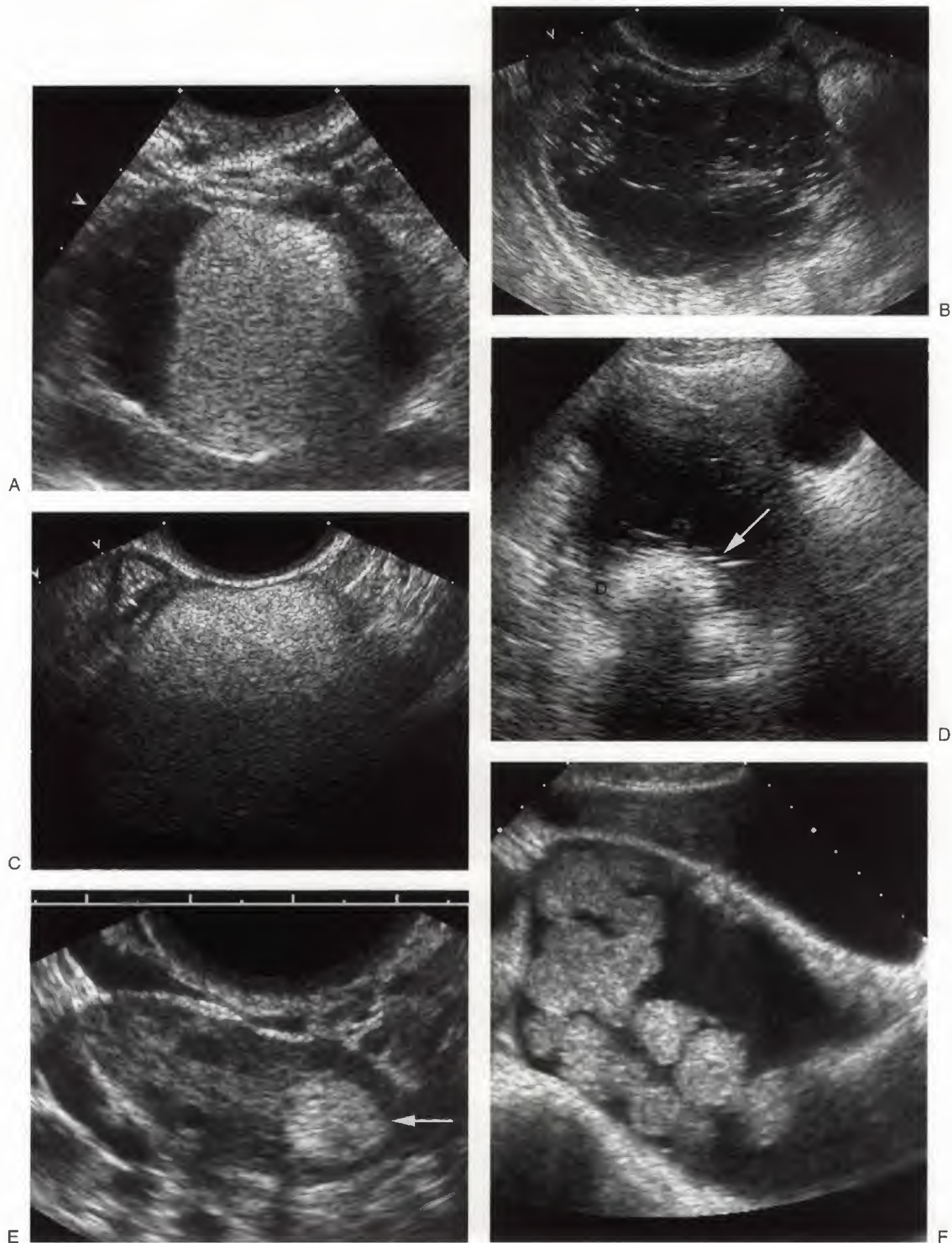


**FIGURE 30-4.** Mature cystic teratoma with (A) typical white (hyperechogenic) ball; (B) typical long hyperechogenic lines and bright prominent spots representing hair in fluid; (C) typical shadowing, making it difficult to determine the true boundaries of the teratoma; (D) Rokitansky nodule or dermoid plug (arrow) with posterior acoustic shadowing; (E) small mature teratoma within the ovary (arrow); (F) intracystic nondependent spheres in a patient with a mature cystic teratoma.



occasionally be identified in mature cystic teratomas, producing a dramatic appearance (see Fig. 30-4F).

Some mature cystic teratomas are impossible to detect, even when they are clearly palpable, because their echogenicity is similar to surrounding bowel (personal experience). Confusion of mature cystic teratomas with endometriomas, mucinous cystadenomas, struma ovarii, serous cystadenomas, cystadenofibromas, and Brenner tumors have been reported.<sup>1,5,9,11,13,60,61</sup>

## ULTRASOUND CHARACTERISTICS OF BENIGN, HEMORRHAGIC AND INFLAMMATORY CYSTS

### Ultrasound Characteristics of Endometriomas

Endometriomas are known to manifest typical ground glass appearance at gray scale imaging<sup>9,56,60,77</sup> (Fig. 30-5A). Quite often, one or more solid masses are seen to protrude from the cyst wall into the cyst lumen (see Fig. 30-5B). According to Patel and co-workers, such protrusions (wall nodularity) are seen in 20% of endometriomas.<sup>77</sup> By definition, these protruding masses should be classified as solid papillary projections, but they probably represent blood clots or fibrin (my own speculation). Patel and colleagues<sup>77</sup> reported that hyperechoic wall foci were much more common in endometriomas than in other types of adnexal pathology (35% versus 6%), a finding that has not been reported by others (see Fig. 30-5C). Endometriomas may be unilateral or bilateral and may have slightly different echogenicity of the internal content, if bilateral (see Fig. 30-5D). At grayscale imaging, endometriomas may be confused with mature teratomas (dermoid cysts), abscesses, ovarian adenofibromas, ovarian fibromas, unspecified benign ovarian cysts, mucinous and serous cystadenomas, and hemorrhagic cysts.<sup>1,5,9,11,12,13,77</sup>

### Ultrasound Characteristics of Hemorrhagic Corpus Luteum Cysts

A hemorrhagic corpus luteum cyst is a cyst that typically contains spiderweb-like material.<sup>56,77</sup> Bizarre blood clots may also be seen<sup>56,77</sup> (Fig. 30-6A and B). Even an experienced ultrasound examiner may confuse such clots with papillary projections or solid components (see Fig. 30-6C). This explains why there is a risk of misclassifying corpus luteum cysts as malignant tumors. Doppler ultrasound examination may help to discriminate between a clot (no Doppler signals detectable) and a solid component (Doppler signals detectable) (personal experience). When in doubt, follow up with ultrasound after 6 to 12 weeks. However, some hemorrhagic cysts may take up to 4 months to regress (personal experience).

### Ultrasound Characteristics of Pelvic Inflammatory Disease (Hydro-Pyo-Hemato-Salpinx)

Pelvic inflammatory disease (PID) usually occurs as a result of ascending spread of microorganisms from the vagina and cervix through the endometrial cavity, through the endometrium into the fallopian tubes.<sup>78</sup> The clinical

presentation often includes fever, pelvic pain, and a purulent vaginal discharge; however, a substantial amount of PID goes unrecognized because it is atypical or silent. The commonest causative organisms are *Chlamydia trachomatis* (which may run an indolent course) and *Neisseria gonorrhoeae*. Ultrasound is the imaging modality of choice in women with suspected pelvic inflammatory disease.

The normal fallopian tube is 10 cm long and is rarely visible on transvaginal sonography.<sup>78</sup> In most cases, a fluid-filled diseased tube is easily distinguishable from other types of adnexal masses at grayscale ultrasound examination (Fig. 30-7A). The most characteristic ultrasound features are (1) a fluid-filled sausage-shaped cystic structure, (2) the presence of incomplete septa, that is, septa that are not seen to reach the opposite wall of the cystic structure (see Fig. 30-7B), (3) on a transverse section of a fluid-filled tube, mucosal folds are seen to protrude into the lumen, resulting in cogwheel appearance (see Fig. 30-7C) if the tube is swollen and in beads-on-a-string appearance (see Fig. 30-7D) if it is not.<sup>4,79</sup> When the acutely inflamed tube has a lumen filled with hyperechoic material corresponding to pus it is called a pyosalpinx. The acute process may resolve spontaneously or with antibiotic therapy. However, it may progress to the development of a tubo-ovarian complex in which the tube and ovary are seen distinctly but are not separable with the transvaginal probe. This may progress to a tubo-ovarian abscess with the loss of architectural definition between one or both of the adnexa with the formation of a conglomerate in which neither the ovary nor the tube can be separately recognized as such (see Fig. 30-7E). If the tube becomes blocked at the fimbrial or cornual end, it becomes convoluted and incomplete septa are visible, thus assuming a retort-shape. This is called a hydrosalpinx (see Fig. 30-7B). The process may lead to a chronic phase with fluid accumulation in the blocked tube and distention of the wall, which is rendered thin. The endosalpingeal folds disappear or are flattened; in the transverse plane, the tubal wall is thin, with echogenic remnants of the endosalpingeal folds (usually 2 to 3 mm), and is described as the beads-on-a-string appearance (see Fig. 30-7D).

The ultrasound morphology of a tubo-ovarian abscess may be that of a unilocular cystic structure, or that of complex multicystic structure with thick walls and thick septae, filled with homogeneously echogenic material (ground glass appearance). Given the complex and varied echogenicity of tubo-ovarian abscesses, it is not surprising that they may be confused with a variety of other conditions, such as endometriomas or malignancies.<sup>1,4,80,81</sup> It is not always possible to distinguish a tubo-ovarian abscess from a pelvic abscess of another origin, such as a periappendiceal or diverticular abscess.<sup>4</sup> Knowledge of the patient's history and clinical findings is a prerequisite for making a correct diagnosis. For a detailed description of the ultrasound morphology of different types of pelvic inflammatory disease, the reader is referred to references 79, 82, and 83.

### Ultrasound Characteristics of Paraovarian Cysts

Paraovarian cysts may arise from embryonic ducts and are usually located between the tube and the ovary.<sup>53</sup> They may be of mesothelial, mesonephric, or paramesonephric



**FIGURE 30-5.** A. Endometrioma with homogeneously echogenic cyst fluid representing old blood. Ut, uterus. B. Wall nodularity (arrow), which likely represents blood clot. C. Endometrioma with calcification (arrows) in the wall. D. Bilateral endometriomas. U, uterus.



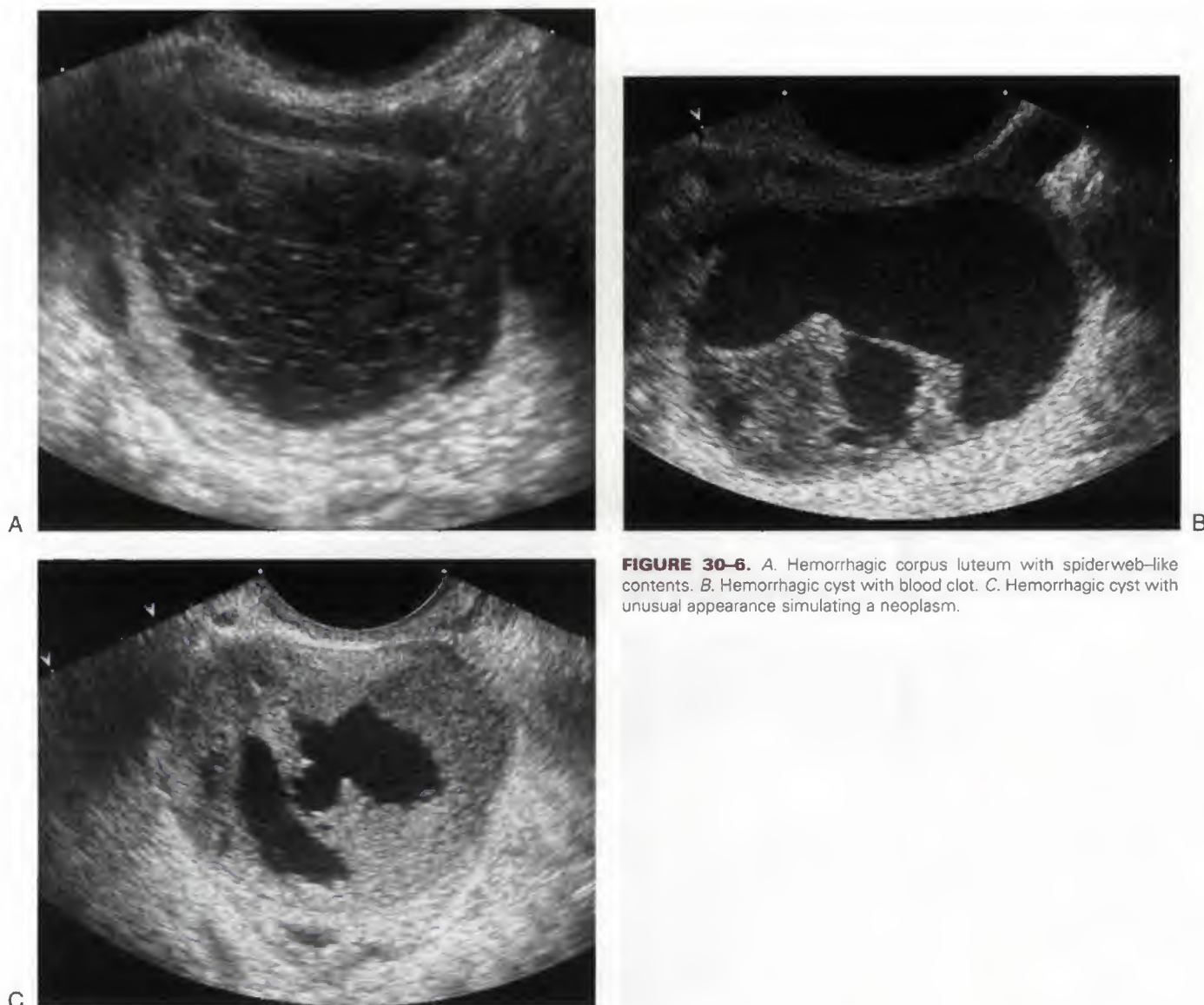


**FIGURE 30-6.** A. Hemorrhagic corpus luteum with spiderweb-like contents. B. Hemorrhagic cyst with blood clot. C. Hemorrhagic cyst with unusual appearance simulating a neoplasm.

origin.<sup>84,85</sup> At ultrasound examination, a paraovarian cyst may be seen as a cyst clearly separate from a normal ovary (Fig. 30-8A). Sometimes it is difficult to distinguish an ovarian cyst from a paraovarian cyst,<sup>56</sup> and if no ovary is seen separately from the cyst, it may be impossible (see Fig. 30-8B). The cyst fluid may be anechoic or echogenic.<sup>56</sup> Papillary projections and septa may be present.<sup>86</sup> Malignancy may develop in a paraovarian cyst, border-line tumors probably being more common than invasive cancers, with malignancy being found most often in paraovarian cysts larger than 5 cm with papillary projections.<sup>56,84,87,88</sup>

### Ultrasound Characteristics of Peritoneal Pseudocysts

Peritoneal pseudocysts are fluid collections among adhesions occurring after an inflammatory process in the peritoneal cavity or after an operation. The typical ultrasound

morphology of a peritoneal pseudocyst is that of a cystic mass following the contours of the pelvis (even though pseudocysts may also be oval or round), with a deformed ovary suspended amongst adhesions centrally or peripherally in the cyst (Fig. 30-9). The cyst fluid may be anechoic or echoic, and the cyst may contain both septa and papillary projections.<sup>15,56,89-91</sup>

### Ultrasound Characteristics of Ovarian Fibromas, Fibrothecomas, Thecofibromas, Thecomas, Brenner Tumors, and Other Benign Solid Ovarian Tumors

Fibromas and fibrothecomas usually yield an echo pattern indistinguishable from that of pedunculated myomas, that is, they are solid, round, or oval tumors with a smooth outline and a regular striped echogenicity. Different types of solid

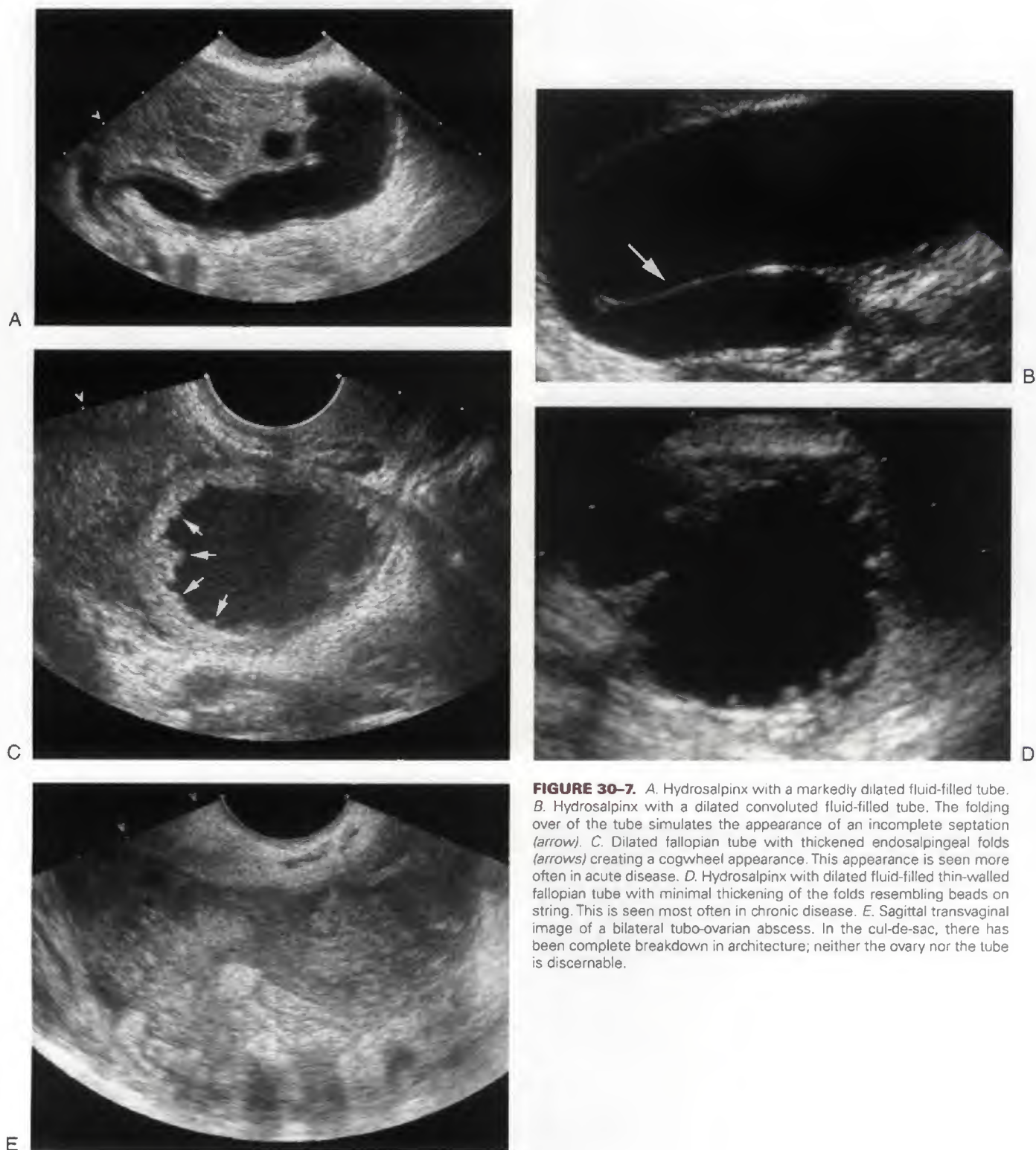


**FIGURE 30-7.** *A.* Hydrosalpinx with a markedly dilated fluid-filled tube. *B.* Hydrosalpinx with a dilated convoluted fluid-filled tube. The folding over of the tube simulates the appearance of an incomplete septation (arrow). *C.* Dilated fallopian tube with thickened endosalpingeal folds (arrows) creating a cogwheel appearance. This appearance is seen more often in acute disease. *D.* Hydrosalpinx with dilated fluid-filled thin-walled fallopian tube with minimal thickening of the folds resembling beads on string. This is seen most often in chronic disease. *E.* Sagittal transvaginal image of a bilateral tubo-ovarian abscess. In the cul-de-sac, there has been complete breakdown in architecture; neither the ovary nor the tube is discernable.



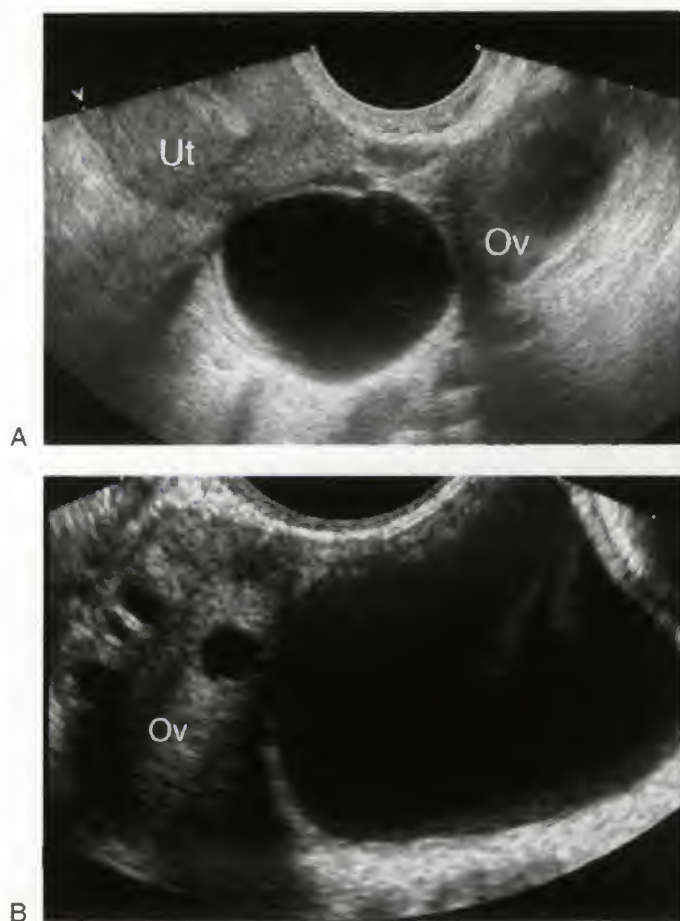


**FIGURE 30-8.** Paraovarian cyst. *A.* The cyst is separate from a normal ovary (Ov) and uterus (Ut). *B.* In this case, it is difficult to discriminate between a paraovarian cyst and an superficial ovarian cyst. O, ovary.

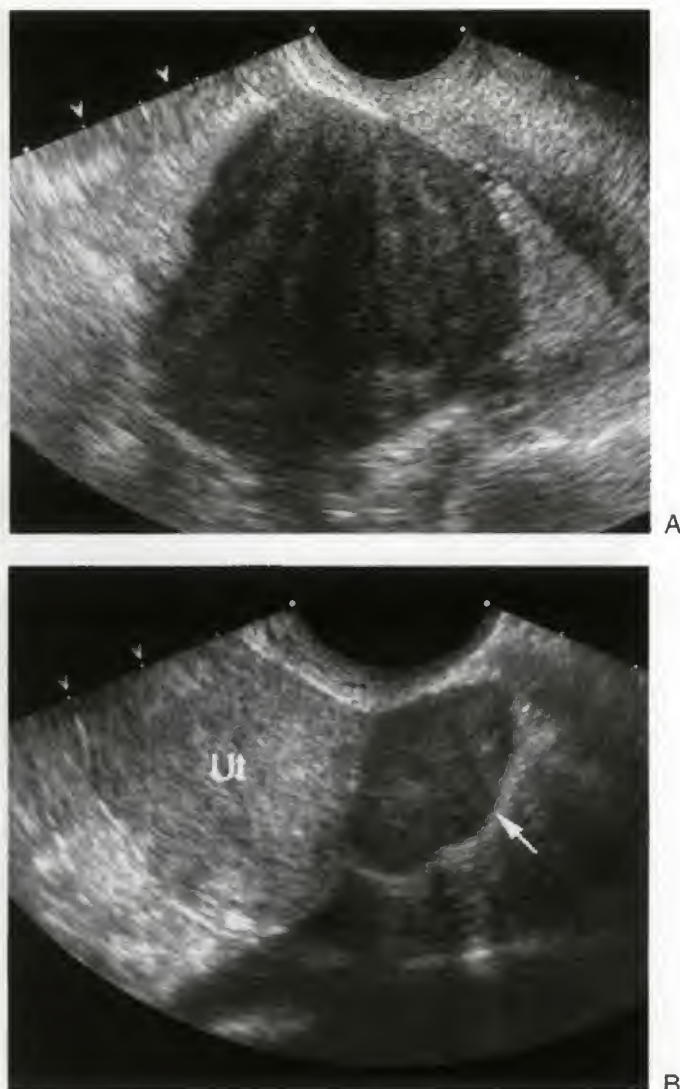


**FIGURE 30-10.** A benign solid ovarian tumor may be confused with a uterine myoma if no connection is seen between the myoma and the uterus (e.g., in case of a pedunculated myoma). *A.* Ovarian fibroma. *B.* Exophytic uterine leiomyoma (arrow). Ut, uterus.



**FIGURE 30-9.** Peritoneal inclusion pseudocyst. Note the ovary (Ov) suspended amongst adhesions in the periphery of the pseudocyst.

benign ovarian tumors, such as fibroma, thecoma, fibrothecoma, and Brenner tumor, may manifest similar echogenicity at grayscale sonography.<sup>56,59,66,67</sup> However, it is my impression that the echogenicity of fibromas does differ from that of other benign solid ovarian tumors, such as thecomas and thecofibromas. I find the echogenicity of fibromas to be virtually identical to that of myomas, whereas thecomas and thecofibromas often manifest more lobular contours and slightly more irregular echogenicity (Fig. 30-10*A* and *B*). However, these diagnostic criteria did not perform well when tested prospectively.<sup>1</sup> On the other hand, it is probably sufficient from a clinical point of view to merely suggest a diagnosis of benign solid ovarian tumor, and to refrain from attempting to suggest a more specific diagnosis. Guerriero and coworkers<sup>9</sup> reported confusion of ovarian endometrioma and fibroma at grayscale sonography, and such confusion also occurred in one of my own series.<sup>1</sup>



## Ultrasound Characteristics of Ovarian Serous Cystadenomas, Mucinous Cystadenomas, and Adenofibromas

In my experience the grayscale ultrasound images of serous cyst (aden)oma, mucinous cyst(aden)oma, and adenofibroma manifest overlapping characteristics. Therefore, I virtually never suggest any of these specific diagnoses on the basis of an ultrasound image. Overlapping characteristics have also found by others.<sup>59</sup> However, Fleischer and co-workers,<sup>7</sup> Buy and colleagues,<sup>63</sup> and Guerriero and colleagues<sup>8</sup> did find it possible to diagnose serous and mucinous cyst (aden)omas with grayscale sonography. Buy and co-workers<sup>63</sup> considered the characteristic features of a serous cystadenoma to be "a unilocular or bilocular cystic mass with homogenous water echogenicity, thin regular wall, thin regular septum (when present) and no vegetations," and those of a mucinous cystadenoma to be "a multilocular cyst containing fluid of different echogenicities, with regular wall and septa, and no vegetations." Using these criteria, they diagnosed serous cystadenomas with a sensitivity of 70% and a specificity of 98%, and mucinous cystadenomas with a sensitivity of 50% and a specificity of 96%. Fleischer and colleagues<sup>7</sup> and Guerriero and co-workers<sup>8</sup> found the sensitivity of grayscale imaging for diagnosing serous cystadenoma to be 75% and 78%, respectively, and the specificity to be 75% and 96%, respectively. The sensitivity and specificity of grayscale imaging for diagnosing mucinous cystadenomas were reported by Fleischer and co-workers to be 95% and 99%, respectively.<sup>7</sup>

The overlapping ultrasound features of serous and mucinous cystadenomas are shown in Figure 30-11.

## Ovarian Masses in the Pregnant Patient

As a result of the widespread use of diagnostic ultrasound in the pregnant patient, adnexal masses are being recognized with increasing frequency. An excellent recent review analyzed the scope of the problem when ovarian masses are detected, as well as management issues.<sup>92</sup> Before the routine use of obstetric ultrasound, adnexal masses were most often recognized either during a physical examination or when they became symptomatic. The prevalence of adnexal masses in the pregnant patient is reported to be between 1% and 2%.<sup>93-95</sup>

Of the adnexal masses detected, functional cysts are the most common in pregnancy.<sup>92</sup> The relative frequency of all other nonfunctional ovarian tumors is most often a reflection of the patient's age.<sup>92</sup> In descending order, the most common ovarian tumors found during pregnancy include functional ovarian cysts (follicular, corpus luteum, and theca-lutein), benign mature cystic teratomas, serous cystadenomas, paraovarian cysts, mucinous cystadenomas, endometriomas, and malignant tumors<sup>92,93,95-99</sup> (Table 30-2 and Fig. 30-12). The timing of detection of an adnexal mass during pregnancy influences the likely etiology of the mass. Cystic adnexal masses less than 5 cm that are detected in the first 16 weeks are usually functional and almost always resolve spontaneously.<sup>94</sup> However, ovarian tumors that persist beyond 16 weeks are more likely to be neoplastic and, therefore, are more likely to result in surgical intervention.<sup>92</sup> Ovarian malignancy is estimated to occur in approximately

2% to 3% of the masses identified during pregnancy,<sup>93,95-98,100,101</sup> but the frequency reported varies substantially between studies.<sup>92</sup> Ovarian tumors of low malignant potential (LMP) or borderline ovarian tumors are usually included in the category of ovarian malignancies.<sup>92</sup>

Leiserowitz et al<sup>102</sup> recently investigated the frequency of ovarian masses during pregnancy combining several California databases and analyzed the risk of ovarian malignancy during pregnancy. The California statistics suggested an occurrence of one malignancy for every 54,644 deliveries. Notably, the majority of the ovarian malignancies were actually LMP tumors. Ninety-five percent of the LMP tumors and 83.8% of the ovarian invasive malignancies were stage I. Nearly 40% of the ovarian invasive malignancies were germ cell tumors, which is typical for women in their reproductive years.<sup>92,102</sup> The finding that most ovarian malignancies are low stage and low grade is consistent with previous reports.<sup>103,104</sup> Most germ cell tumors are dysgerminomas, which are predominantly low stage.<sup>93,103</sup> Consequently, the overall prognosis of pregnant patients with either an LMP tumor or an invasive ovarian malignancy is highly favorable. These findings should strongly influence the management of adnexal masses during pregnancy.<sup>92</sup>

Zanetta et al<sup>105</sup> used US criteria to develop the following categories: simple cyst, endometriosis, or corpus luteum-like, dermoid-like, complex benign, borderline-like, and suspicious. They used their system to triage pregnant patients with adnexal masses into those who warranted surgical intervention (suspicious masses) versus those who were candidates for expectant management (all the other categories). In the limited number of patients who had adnexal surgery either antepartum or postpartum, the final pathology generally matched well with their US diagnoses. Magnetic resonance imaging can add additional diagnostic information in certain situations, particularly when the ultrasound examination is equivocal.<sup>106</sup>

## ULTRASOUND IN THE DIAGNOSIS OF ADNEXAL TORSION

Adnexal torsion is a serious condition that may be painful to varying degrees. It is the fifth most common gynecologic surgical emergency, with a prevalence of 2.7%.<sup>107</sup> Torsion may involve twisting of the ovary, fallopian tube, or both structures (Fig. 30-13A). Torsion usually occurs in the adnexa containing a lesion, for example, an ovarian cyst or a hydrosalpinx, but it may also occur in normal adnexa, especially in prepubertal girls.<sup>108</sup> Although there are some ultrasound findings suggestive of adnexal torsion, adnexal torsion can neither be 100% confirmed nor 100% excluded by ultrasound examination, not even using Doppler evaluation. Indeed, ultrasound findings are sometimes inconspicuous (Fig. 30-13A and B). In adnexal torsion, various degrees of arterial, venous, and lymphatic occlusion occur. This causes massive congestion and edema. Later hemorrhagic infarction may occur. This pathophysiology explains the ultrasound findings in cases of adnexal torsion. If a normal ovary is involved in the torsion, the edema causes enlargement of the ovary, and the ovary usually loses its oval shape and becomes round or globular. Another feature reported to be typical of ovarian torsion, especially in adolescent girls, is the



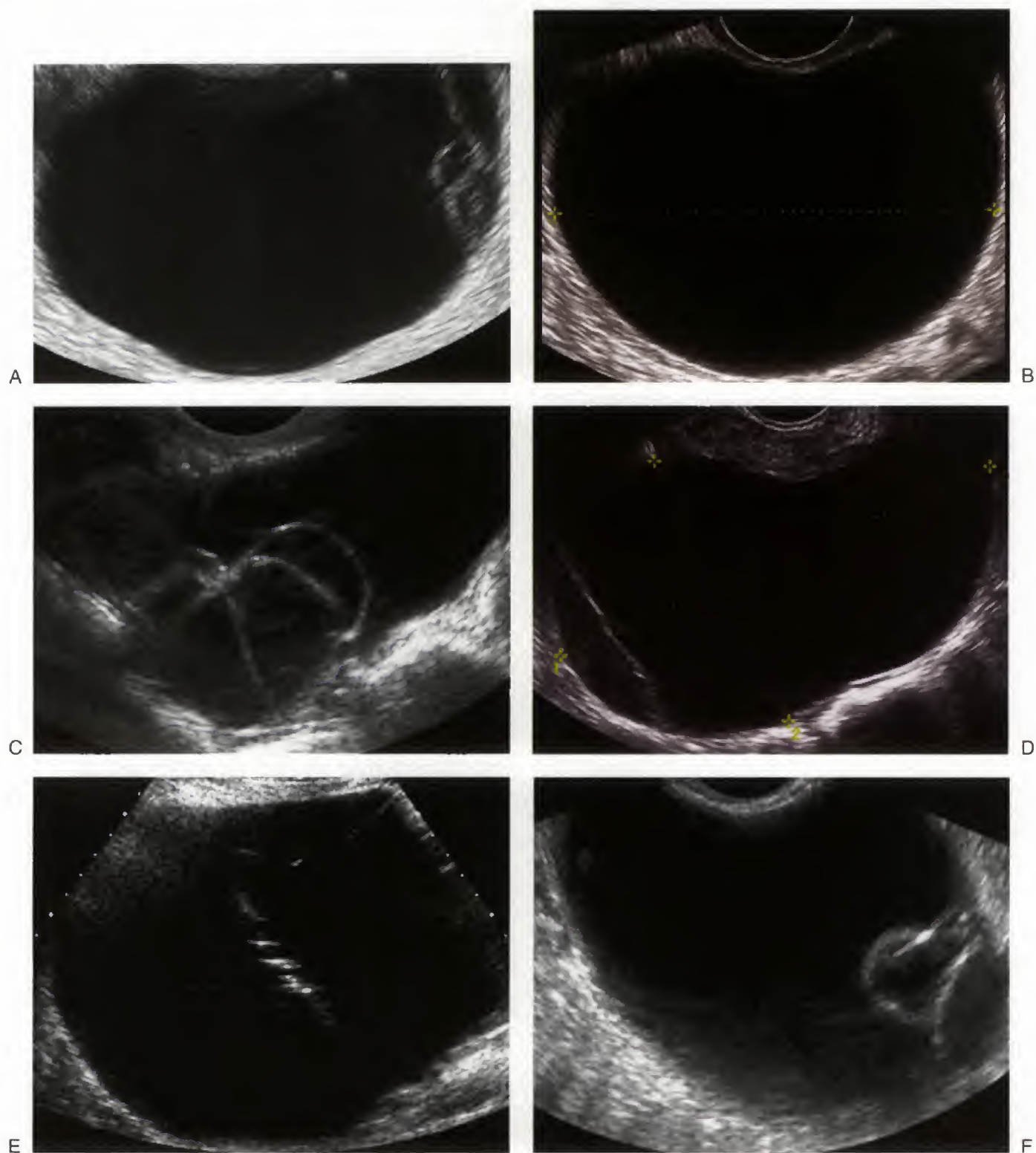


**FIGURE 30-11.** Grayscale ultrasound images of serous cyst(aden)oma and mucinous cyst(aden)oma manifest overlapping characteristics. *A, B, and C.* Serous cystadenomas. *D, E, and F.* Mucinous cystadenomas.

**Table 30-2****Etiology of Ovarian Tumors During Pregnancy**

Benign Tumors	Malignant Tumors
Functional cysts	Borderline ovarian tumors
Follicular cysts	Malignant epithelial tumors
Corpus luteum cysts	Malignant germ cell tumors
Theca-lutein cysts	Sex cord/stromal tumors
Hemorrhagic cysts	Granulosa cell tumor
Paraovarian cysts	Cancer metastatic to the ovary
Benign cystic teratomas	Krukenberg tumors
Serous cystadenoma	Pseudomyxoma peritonei
Mucinous cystadenoma	
Endometriomas	

From Leiserowitz GS: Managing ovarian masses during pregnancy. CME Review Article. *Obstet Gynecol Surv* 16:463, 2006.

presence of several round small cysts up to 25 mm in diameter at the periphery of the enlarged ovary.<sup>109</sup> Thus, torsion of a normal ovary in an adolescent girl is characterized by unilateral ovarian enlargement with peripheral, dilated cysts<sup>109</sup> (see Fig. 30-13D). If torsion occurs in a hyperstimulated ovary after ovulation induction, the main ultrasound characteristic is a very swollen ovarian parenchyma, which makes the diseased ovary look distinctly different from the contralateral one.<sup>109</sup> If torsion occurs in an ovarian cyst or a hydrosalpinx, the wall, mucosal folds, and septa of the cyst look swollen at ultrasound examination<sup>109-111</sup> (see Fig. 30-13A). If hemorrhagic infarction has occurred, echogenic fluid may be seen in cystic spaces in the tumor. Some fluid, often hyperechogenic and corresponding to blood, in the pouch of Douglas is also a common finding.<sup>109</sup> It may be difficult to detect ultrasound signs of torsion in an ovary containing a mature cystic teratoma, because of the shadowing typical of these tumors. Doppler ultrasound examination does not seem to play a decisive role in the diagnosis of adnexal torsion. Color Doppler signals can be detected either peripherally or centrally in a substantial proportion of twisted adnexa<sup>112</sup> (see Fig. 30-13C). Doppler findings probably parallel the vascular changes. Persistent arterial flow is compatible with less complete stages of torsion. Therefore, detection of flow using the Doppler technique does not exclude adnexal torsion.

## SUMMARY

Pattern recognition is superior to all other ultrasound methods (e.g., simple classification systems, scoring systems, mathematical models for calculating the risk of malignancy) for discrimination between benign and malignant extrauterine pelvic masses. Pattern recognition for discrimination between benign and malignant tumors can almost certainly be learned by anyone performing gynaecologic ultrasound examinations on a regular basis, but diagnostic accuracy increases with increasing experience. Using pattern recognition a fairly confident specific diagnosis can be made of mature cystic teratoma, endometrioma, haemorrhagic corpus luteum cyst, hydrosalpinx, paraovarian cyst, and peritoneal pseudocyst. However, based on pattern recognition, pelvic abscesses are often confused with a variety of other

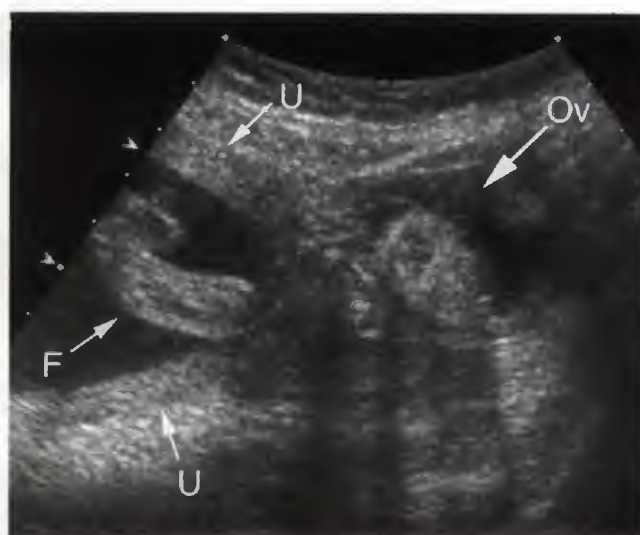


**FIGURE 30-12.** Second trimester pregnancy with left adnexal mass. An ovarian mature cystic teratoma (Ov) is seen adjacent to the uterus (U). F, fetal foot.

conditions. It is usually not possible to confidently discriminate between a solid benign ovarian tumor and a pedunculated uterine leiomyoma, or among ovarian fibroma, fibrothecoma, thecofibroma, and thecoma. Doppler ultrasound examination contributes little to a correct diagnosis of an adnexal mass, because in most cases, the grayscale ultrasound image contains sufficient diagnostic information. Ultrasound examination plays an important role when deciding how to treat extrauterine pelvic masses that cause symptoms: expectantly (e.g., hemorrhagic corpus luteum cysts), with puncture (e.g., peritoneal pseudocysts), or with surgery. Moreover, it allows choice of optimal time and method of operation (e.g., choice of laparoscopic surgery for benign lesions), if surgery is judged to be necessary. Optimal management of incidentally detected extrauterine pelvic masses with benign ultrasound morphology is unknown.

## PRACTICE POINTS

The most characteristic ultrasound features of

- benign tumors: absence of solid components and no irregularity.
- malignant tumors: presence of solid components and irregularity.
- mature cystic teratoma (dermoid cyst): white ball, long, echogenic (white) lines, and prominent echogenic dots in cyst fluid, shadowing.
- endometrioma: ground glass appearance of cyst contents, wall nodularities.
- haemorrhagic corpus luteum cyst: spiderweb-like contents, bizarre blood clots.
- hydro-pyo-hematosalpinx: fluid-filled sausage-shaped cystic structure, incomplete septa, cogwheel appearance, beads-on-a-string appearance.
- paraovarian cyst: cyst clearly separate from a normal ovary.



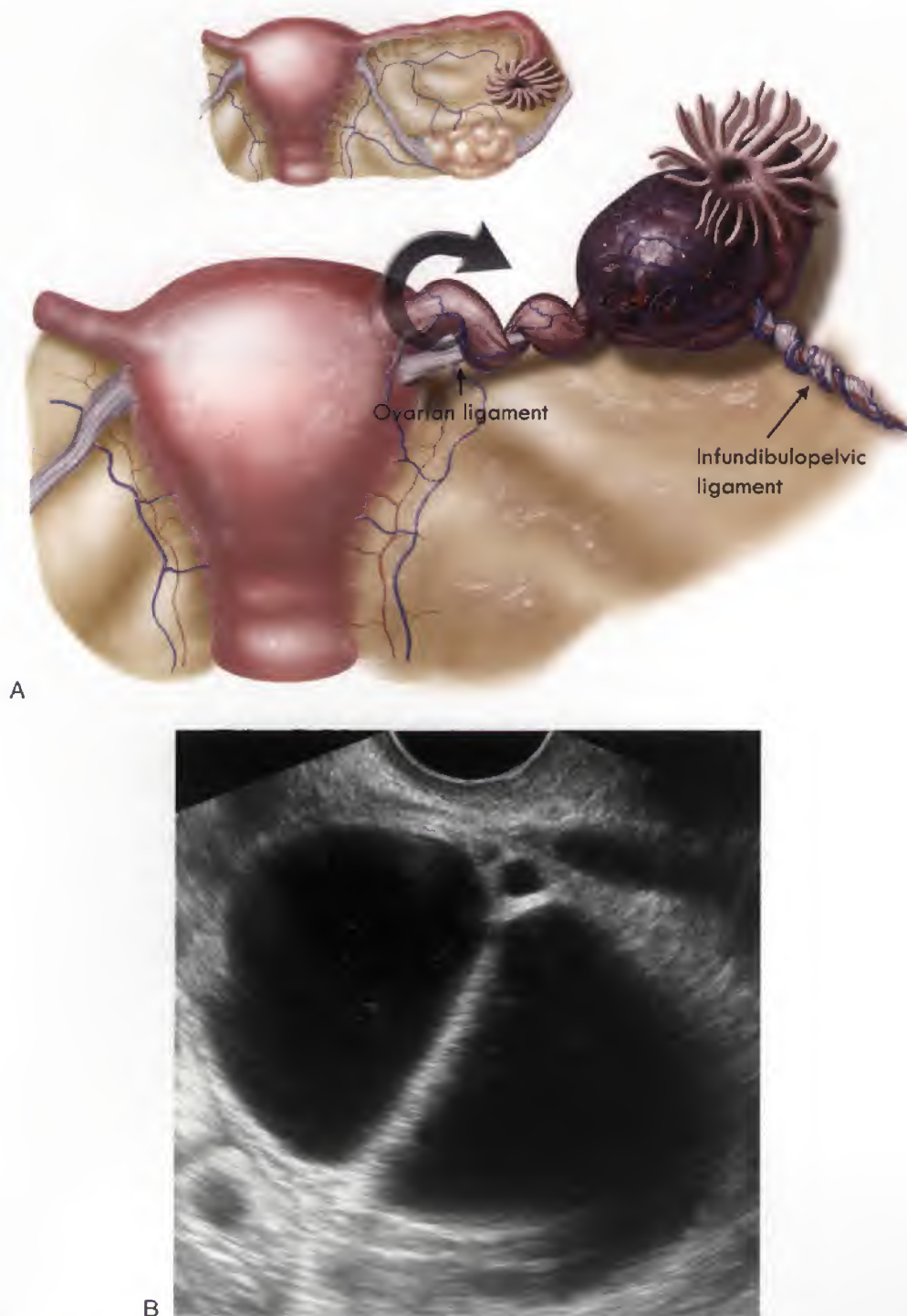


**FIGURE 30-13.** Ultrasound images of adnexal torsion. *A.* Illustration demonstrating adnexal torsion. Ovarian torsion results in twisting of suspensory ligaments and vascular pedicles resulting in venous occlusion and congestion. *B.* Twisted benign cyst; the only ultrasound feature suggesting torsion is the swollen cyst walls. (Illustration by James A. Cooper, MD, San Diego, CA.) *Continued*

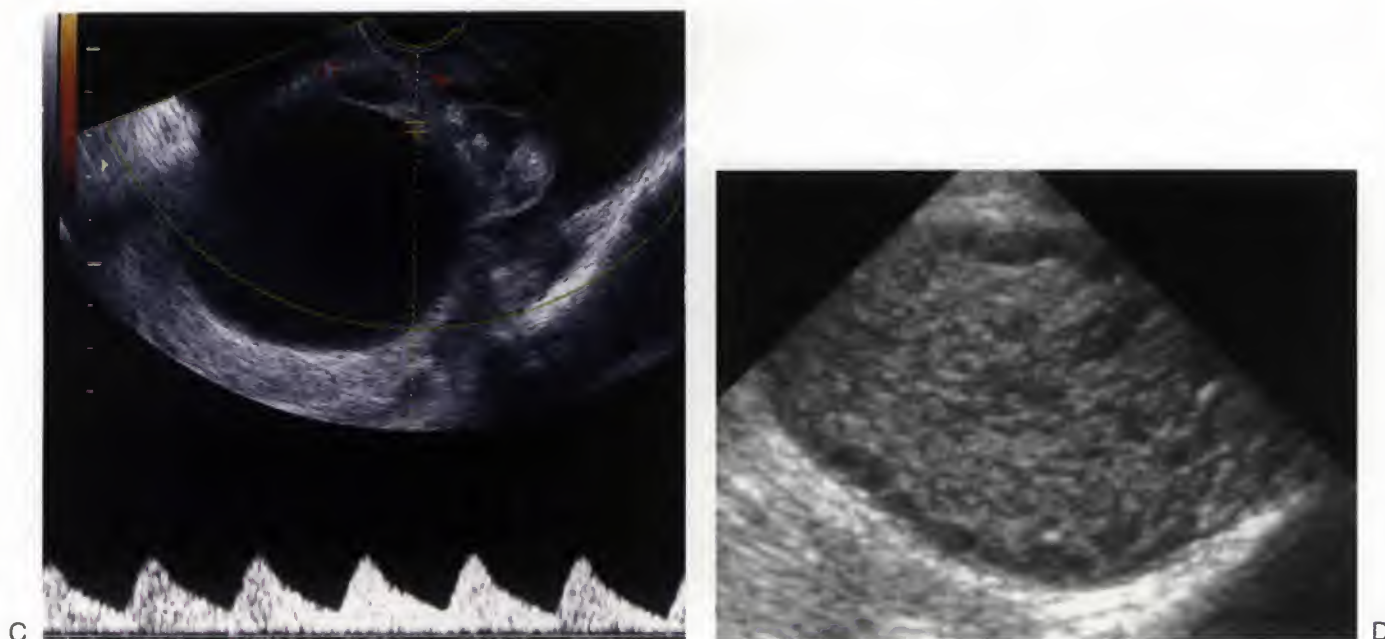


**FIGURE 30-13, cont'd** C. Twisted ovarian cyst with vascularization detectable at Doppler ultrasound examination. Despite ovarian torsion, arterial flow is still visible. D. Ovarian torsion in a prepubertal girl. The ovary is more round than normal and has multiple peripheral cysts.

- peritoneal pseudocyst: cystic mass following the contours of the pelvis and with an ovary, often deformed, suspended amongst adhesions centrally or peripherally in the cyst.
- fibroma, fibrothecoma: echo pattern indistinguishable from that of a pedunculated myoma, that is, a solid, round, lobular, or oval tumor with a smooth outline and a regular stripy echogenicity.
- tubo-ovarian abscess; unilocular cystic structure, or complex multicystic structure with thick walls and thick septae, filled with homogeneously echogenic material (ground glass appearance).
- adnexal torsion; the walls and any septa of the twisted lesion may look swollen at ultrasound examination; there may be fluid in the pouch of Douglas; the presence of color and spectral Doppler signals in the lesion does not exclude torsion.

## Acknowledgments

The studies from my institution were supported by grants from the Malmö General Hospital Cancer Foundation, Funds administered by the Malmö Health Care Administration, the Faculty of Medicine of Lund University, the Anna-Lisa och Sven-Erik Lundgren Foundation for Medical Research, the Ingabritt and Arne Lundberg Research Foundation, and the Swedish Medical Research Council (grant nos. B96-17X-11605-01A, K98-17X-11605-03A, K2001-72X-11605-06A, K2006-73X-11605-11-3).

## References

1. Valentin L: Pattern recognition of pelvic masses by gray-scale ultrasound imaging: the contribution of Doppler ultrasound. *Ultrasound Obstet Gynecol* 15:338, 1999.
2. Valentin L: Prospective cross-validation of Doppler ultrasound examination and gray-scale ultrasound imaging for discrimination of benign and malignant pelvic masses. *Ultrasound Obstet Gynecol* 14:273, 1999.
3. Timmerman D, Schwarzler P, Collins WP, et al: Subjective assessment of adnexal masses with the use of ultrasonography: an analysis of interobserver variability and experience. *Ultrasound Obstet Gynecol* 13:11, 1999.
4. Patten RM: The fallopian tube and pelvic inflammatory disease. In Nyberg DA, Hill LM, Böhm-Velez M, et al (eds): *Transvaginal Ultrasound*. St Louis, Mosby Year Book, 1992, pp 209-221.
5. Kurjak A, Kupesic S: Scoring system for prediction of ovarian endometriosis based on transvaginal color Doppler sonography. *Fertil Steril* 62:81, 1994.
6. Benacerraf BR, Finkler NJ, Wojciechowski C, et al: Sonographic accuracy in the diagnosis of ovarian masses. *J Reprod Med* 35:491, 1990.
7. Fleisher AC, James AE, Millis JB, et al: Differential diagnosis of pelvic masses by grey scale sonography. *Am J Radiol* 131:469, 1978.
8. Guerriero S, Mallarini G, Ajossa A, et al: Transvaginal ultrasound and computed tomography combined with clinical parameters and CA-125 determinations in the differential diagnosis of persistent ovarian cysts in premenopausal women. *Ultrasound Obstet Gynecol* 9:339, 1997.
9. Guerriero S, Mais V, Ajossa S, et al: The role of endovaginal ultrasound in differentiating endometriomas from other ovarian cysts. *Clin Exp Obstet Gynecol* 22:20, 1995.
10. Kim JS, Woo SK, Suh SJ, et al: Sonographic diagnosis of paraovarian cysts: value of detecting a separate ipsilateral ovary. *Am J Radiol* 164:1441, 1995.
11. Mais V, Guerriero S, Ajossa S, et al: Transvaginal sonography in the diagnosis of cystic teratoma. *Obstet Gynecol* 85:48, 1995.
12. Guerriero S, Mais V, Ajossa S, et al: Transvaginal ultrasonography combined with Ca-125 plasma levels in the diagnosis of endometrioma. *Fertil Steril* 65:293, 1996.
13. Mais V, Guerriero S, Ajossa S, et al: The efficiency of transvaginal ultrasonography in the diagnosis of endometrioma. *Fertil Steril* 60:776, 1993.
14. Tsai CC, Shen CC, Changchien CC, et al: Ultrasound-guided transvaginal cyst aspiration for the management of pelvic pseudocyst: a preliminary experience. *Chang Gung Medical Journal* 25:751, 2002.
15. Jain KA: Imaging of peritoneal inclusion cysts. *AJR Am J Roentgenol* 174:1559, 2000.



16. Yuen PM, Yu KM, Yip SK, et al: A randomized prospective study of laparoscopy and laparotomy in the management of benign ovarian masses. *Am J Obstet Gynecol* 177:109, 1997.
17. Caspi B, Appelman Z, Rabinerson D, et al: The growth pattern of ovarian dermoid cysts: a prospective study in premenopausal and postmenopausal women. *Fertil Steril* 68:501, 1997.
18. Levine D, Gosink BB, Wolf SI, et al: Simple adnexal cyst: the natural history in postmenopausal women. *Radiology* 184:653, 1992.
19. Kroon E, Andolf E: Diagnosis and follow-up of simple ovarian cysts detected by ultrasound in postmenopausal women. *Obstet Gynecol* 85:211, 1995.
20. Andolf E, Jorgensen C: Simple adnexal cysts diagnosed by ultrasound in postmenopausal women. *J Clin Ultrasound* 16:301, 1988.
21. Aubert JM, Rombaut C, Argacha P, et al: Simple adnexal cysts in postmenopausal women: conservative management. *Maturitas* 30:51, 1998.
22. Goldstein SR, Subramanyam B, Snyder JR, et al: The postmenopausal cystic adnexal mass: the potential role of ultrasound in conservative management. *Obstet Gynecol* 73:8, 1989.
23. Auslender R, Atlas I, Lissak A, et al: Follow-up of small, postmenopausal ovarian cysts using vaginal ultrasound and CA-125 antigen. *J Clin Ultrasound* 24:175, 1996.
24. Bailey CL, Ueland FR, Land GL, et al: The malignant potential of small cystic ovarian tumors in women over 50 years of age. *Gynecol Oncol* 69:3, 1998.
25. Conway C, Zalud I, Dilena M, et al: Simple cysts in the postmenopausal patient: detection and management. *J Ultrasound Med* 17:369-372, 1998.
26. Minelli L: Ovarian cysts. *Eur J Obstet Gynecol Reprod Biol* 65:81, 1996.
27. Canis M, Mage G, Pouly JL, et al: Laparoscopic diagnosis of adnexal cystic masses: a 12-year experience with long-term follow-up. *Obstet Gynecol* 83:707, 1994.
28. Yuen PM, Rogers MS: Laparoscopic management of ovarian masses: the initial experience and learning curve. *Aust N Z J Obstet Gynaecol* 34:191, 1994.
29. Reich H, Johns DA, Davis G, et al: Laparoscopic oophorectomy. *J Reprod Med* 38:497, 1993.
30. Daniell JF, Kurtz BR, Lee JY: Laparoscopic oophorectomy: comparative study of ligatures, bipolar coagulation, and automatic stapling devices. *Obstet Gynecol* 80:325, 1992.
31. Mage G, Wattiez A, Canis M, et al: Apport de la coelioscopie dans le diagnostic precoce des cancers ovariens. [Contribution of celioscopy in the early diagnosis of ovarian cancers]. *Ann Chir* 45:525, 1991.
32. Chapron C, Querleu D, Bruhat MA, et al: Surgical complications of diagnostic and operative gynecological laparoscopy: a series of 29,966 cases. *Hum Reprod* 13:867, 1998.
33. Al-Took S, Platt R, Tulandi T: Adhesion-related small-bowel obstruction after gynecologic operations. *Am J Obstet Gynecol* 180:313, 1999.
34. Toaff R, Toaff ME, Peyser MR: Infertility following wedge resection of the ovaries. *Am J Obstet Gynecol* 124:92, 1976.
35. Weinstein D, Polishuk WZ: The role of wedge resection of the ovary as a cause for mechanical sterility. *Surg Gynecol Obstet* 141:417, 1975.
36. Fevang BT, Fevang J, Stangland L, et al: Complications and death after surgical treatment of small bowel obstruction: A 35-year institutional experience. *Ann Surg* 231:529, 2000.
37. Lewis S, Menon U: Screening for ovarian cancer. *Exp Rev Anticancer Ther* 3:55, 2003.
38. Jain KA: Prospective evaluation of adnexal masses with endovaginal grey-scale and duplex and color Doppler US: Correlation with pathologic findings. *Radiology* 191:63, 1994.
39. Buy JN, Ghossain MA, Hugol D, et al: Characterization of adnexal masses: Combination of color Doppler and conventional sonography compared with spectral Doppler analysis alone and conventional sonography alone. *Am J Radiol* 166:385, 1996.
40. Levine D, Feldstein VA, Bahcook CJ, et al: Sonography of ovarian masses: Poor sensitivity of resistive index for identifying malignant lesions. *Am J Radiol* 162:1355, 1994.
41. Salem S, White LM, Lai J: Doppler sonography of adnexal masses: The predictive value of the pulsatility index in benign and malignant disease. *Am J Radiol* 163:1147, 1994.
42. Stein SM, Leifer-Narin S, Johnson MB, et al: Differentiation of benign and malignant adnexal masses: relative value of grey-scale, color Doppler, and spectral Doppler sonography. *Am J Radiol* 164:381, 1995.
43. Valentin L, Hagen B, Tingulstad S, et al: Comparison of 'pattern recognition' and logistic regression models for discrimination between benign and malignant pelvic masses. A prospective cross-validation. *Ultrasound Obstet Gynecol* 18:357, 2001.
44. Guerriero S, Ajossa S, Risalvato A, et al: Diagnosis of adnexal malignancies by using color Doppler energy imaging as a secondary test in persistent masses. *Ultrasound Obstet Gynecol* 11:277, 1998.
45. Fruscella E, Testa AC, Ferrandina G, et al: Ultrasound features of different histopathological subtypes of borderline ovarian tumors. *Ultrasound Obstet Gynecol* 26:644, 2005.
46. Timmerman D, Valentin L, Bourne TH, et al: Terms, definitions and measurements to describe the sonographic features of adnexal tumors: a consensus opinion from the International Ovarian Tumor Analysis (IOTA) group. *Ultrasound Obstet Gynecol* 16:500, 2000.
47. Granberg S, Wikland M, Jansson I: Macroscopic characterization of ovarian tumors and the relation to the histological diagnosis: criteria to be used for ultrasound evaluation. *Gynecol Oncol* 35:139, 1989.
48. Granberg S, Norström A, Wikland M: Tumors in the lower pelvis as imaged by vaginal sonography. *Gynecol Oncol* 37:224, 1990.
49. Tailor A, Jurkovic D, Bourne TH, et al: Sonographic prediction of malignancy in adnexal masses using multivariate logistic regression analysis. *Ultrasound Obstet Gynecol* 10:41, 1997.
50. Timmerman D, Bourne TH, Tailor A, et al: A comparison of methods for preoperative discrimination between malignant and benign adnexal masses: the development of a new logistic regression model. *Am J Obstet Gynecol* 181:57, 1999.
51. Marret H, Ecochard R, Giraudeau B, et al: Color Doppler energy prediction of malignancy in adnexal masses using logistic regression models. *Ultrasound Obstet Gynecol* 20:597, 2002.
52. Alcazar JL, Merce LT, Laparte C, et al: A new scoring system to differentiate benign from malignant adnexal masses. *Am J Obstet Gynecol* 188:685, 2003.
53. Romanini ME, Exacoustos C, Carusotti C, et al: Low malignant potential tumors: role of sonographic diagnostic criteria. *Ultrasound Obstet Gynecol* 22 (Suppl 1):69, 2003.
54. Valentin L: Ovarian masses: Color Doppler. In Timmerman D, Deprest J, Bourne T (eds): *Ultrasound and Endoscopic Surgery in Obstetrics and Gynaecology*. London, Springer-Verlag, 2002.
55. Sladkevicius P, Valentin L: Interobserver agreement in the results of Doppler examinations of extrauterine pelvic tumors. *Ultrasound Obstet Gynecol* 6:91, 1995.
56. Grant EG: Benign conditions of the ovary. In Nyberg DA, Hill LM, Böhm-Velez M, et al (eds): *Transvaginal Ultrasound*. St Louis, Mosby Year Book, 1992, pp 187-208.
57. Fleischer AC, Kepple DM: Benign conditions of the uterus, cervix, and endometrium. In Nyberg DA, Hill LM, Böhm-Velez M, et al (eds): *Transvaginal Ultrasound*. St Louis, Mosby Year Book, 1992, pp 21-41.
58. Bazot M, Ghossain MA, Buy JN, et al: Fibrothecomas of the ovary: CT and US findings. *J Comput Assist Tomogr* 17: 754, 1993.
59. Carter JR, Carson LF, Twiggs LB: Gynecologic oncology. In Nyberg DA, Hill LM, Böhm-Velez M, et al (eds): *Transvaginal Ultrasound*. St Louis, Mosby Year Book, 1992, pp 241-265.
60. Kupfer MC, Schwimer SR, Lebovic J: Transvaginal sonographic appearance of endometriomas: spectrum of findings. *J Ultrasound Med* 11:129-133, 1992.
61. Caspi B, Appelman Z, Rabinerson D, et al: Pathognomonic echo patterns of benign cystic teratomas of the ovary: classification, incidence and accuracy rate of sonographic diagnosis. *Ultrasound Obstet Gynecol* 7:275, 1996.
62. Sohaey R, Gardner TL, Woodward PJ, et al: Sonographic diagnosis of peritoneal inclusion cysts. *J Ultrasound Med* 14:913, 1995.
63. Buy JN, Ghossain MA, Sciote C, et al: Epithelial tumours of the ovary: CT findings and correlation with US. *Radiology* 178:811, 1991.
64. Jain KA, Frigman DL, Pettinger TW, et al: Adnexal masses: comparison of specificity of endovaginal US and pelvic MR imaging. *Radiology* 186:697, 1993.
65. Cohen L, Sabbagha R: Echo patterns of benign cystic teratomas by transvaginal ultrasound. *Ultrasound Obstet Gynecol* 3:120, 1993.
66. Athey PA, Malone RS: Sonography of ovarian fibromas/thecomas. *J Ultrasound Med* 6:431, 1987.
67. Athey PA, Siegel MF: Sonographic features of Brenner tumour of the ovary. *J Ultrasound Med* 6:367, 1987.
68. Outwater EK, Siegelman, Hunt JK: Ovarian teratomas: Tumor types and imaging characteristics. *RadioGraphics* 21:475, 2001.

69. Comerci JT Jr, Licciardi F, Bergh PA, et al: Mature cystic teratoma: a clinicopathologic evaluation of 517 cases and review of the literature. *Obstet Gynecol* 84:22, 1994.
70. Brown MF, Hcra S, McGeehin K, Ross AJ III: Ovarian masses in children: a review of 91 cases of malignant and benign masses. *J Pediatric Surg* 28:930, 1993.
71. Caspi B, Appleman Z, Rabinerson D, et al: The growth pattern of ovarian dermoid cysts: A prospective study in premenopausal and postmenopausal women. *Fertil Steril* 68:501, 1997.
72. Caruso PA, Marsh MR, Minkowitz S, et al: An intense clinicopathologic study of 305 teratomas of the ovary. *Cancer* 27:343, 1971.
73. Blackwell WJ, Dockerty MB, Mason JC, et al: Dermoid cysts of the ovary: their clinical and pathological significance. *Am J Obstet Gynecol* 51:151, 1946.
74. Talerman A: Germ cell tumors of the ovary. In Kurman RJ (eds): *Blaustein's pathology of the female genital tract*, 4th ed. New York, Springer-Verlag, 1994, pp 849-914.
75. Matz MH: Benign cystic teratomas of the ovary. *Obstet Gynecol Surv* 16:591, 1961.
76. Bronshtein M, Yoffe N, Brandes JM, et al: Hair as a sonographic marker of ovarian teratomas: improved identification using transvaginal sonography and simulation model. *J Clin Ultrasound* 19:351, 1991.
77. Patel MD, Feldstein VA, Chen DC, et al: Endometriomas: diagnostic performance of US. *Radiology* 210:739, 1999.
78. Okaro E, Valentin L: The role of ultrasound in the management of women with acute and chronic pelvic pain. *Best Pract Res Clin Obstet Gynaecol* 18:105, 2004.
79. Timor-Tritsch IE, Lerner JP, Monteagudo A, et al: Transvaginal sonographic markers of tubal inflammatory disease. *Ultrasound Obstet Gynecol* 12:56, 1998.
80. Hata K, Hata T, Aoki S, et al: Ultrasonographic evaluation of pelvic inflammatory disease. *Nippon Sanka Fujinka Gakkai Zasshi* 41:895, 1989.
81. Varras M, Polyzos D, Perouli E, et al: Tubo-ovarian abscesses: spectrum of sonographic findings with surgical and pathological correlations. *Clin Exp Obstet Gynecol* 30:117, 2003.
82. Molander P, Sjöberg J, Paavonen J, et al: Transvaginal power Doppler findings in laparoscopically proven acute pelvic inflammatory disease. *Ultrasound Obstet Gynecol* 17:233, 2001.
83. Taipale P, Tarjanne H, Ylostalo P: Transvaginal sonography in suspected pelvic inflammatory disease. *Ultrasound Obstet Gynecol* 6:430, 1995.
84. Genadry R, Parmley T, Woodruff JD: The origin and clinical behavior of the paraovarian tumor. *Am J Obstet Gynecol* 129:873, 1977.
85. Gardner GH, Greene RR, Peckham BM: Normal and cystic structures of the broad ligament. *Am J Obstet Gynecol* 55:917, 1948.
86. Korbin CD, Brown DL, Welch WR: Paraovarian cystadenomas and cystadenofibromas: sonographic characteristics in 14 cases. *Radiology* 208:459, 1998.
87. Stein AL, Koonings PP, Schlaerth JB, et al: Relative frequency of malignant paraovarian tumors: should paraovarian tumors be aspirated? *Obstet Gynecol* 75:1029, 1990.
88. Clark JE, Wood H, Jaffurs WJ, et al: Endometrioid-type cystadenocarcinoma arising in the mesosalpinx. *Obstet Gynecol* 54:656, 1979.
89. Hoffer FA, Kozakewich H, Colodny A, et al: Peritoneal inclusion cysts: ovarian fluid in peritoneal adhesions. *Radiology* 169:189, 1988.
90. McFadden DE, Clement PB: Peritoneal inclusion cysts with mural mesothelial proliferation. A clinicopathological analysis of six cases. *Am J Surg Pathol* 10:844, 1986.
91. Kim JS, Lee HJ, Woo SK, et al: Peritoneal inclusion cysts and their relationship to the ovaries: evaluation with sonography. *Radiology* 204:481, 1997.
92. Leiserowitz GS: Managing ovarian masses during pregnancy. *CME Review Article. Obstet Gynecol Surv* 16:463, 2006.
93. Goff BA, Paley PJ, Koh W-J, et al: Cancer in the pregnant patient. In Hoskins WJ, Perez CA, Young RC (eds): *Principles and Practice of Gynecologic Oncology*, 3rd ed. Philadelphia, Lippincott Williams & Wilkins, 2001, pp 501-528.
94. Bernhard LM, Klebba PK, Gray DL, et al: Predictors of persistence of adnexal masses in pregnancy. *Obstet Gynecol* 93:585, 1999.
95. Marino T, Craig SF: Managing adnexal masses in pregnancy. *Contemp Obstet Gynecol* 45:140, 2000.
96. Hermans RH, Fischer DC, van der Putten HW, et al: Adnexal masses in pregnancy. *Onkologie* 25:167, 2003.
97. Usui R, Minakami H, Kosuge S, et al: A retrospective survey of clinical, pathologic, and prognostic features of adnexal masses operated on during pregnancy. *J Obstet Gynecol Res* 26:89, 2000.
98. Whitecar MP, Turner S, Higby MK: Adnexal masses in pregnancy: a review of 130 cases undergoing surgical management. *Am J Obstet Gynecol* 181:19, 1999.
99. Struyk AP, Treffers PE: Ovarian tumors in pregnancy. *Acta Obstet Gynecol Scand* 63:421, 1984.
100. Agarwal N, Parul, Kiplani A, et al: Management and outcome of pregnancies complicated with adnexal masses. *Arch Gynecol Obstet* 267:148, 2003.
101. Ueda M, Ueki M: Ovarian tumors associated with pregnancy. *Int J Gynaecol Obstet* 55:59, 1996.
102. Leiserowitz GS, Xing G, Cress R, et al: Adnexal masses in pregnancy: how often are they malignant? *Gynecol Oncol* 101:315, 2005.
103. Boulay R, Podczaski E: Ovarian cancer complicating pregnancy. *Obstet Gynecol Clin North Am* 25:385, 1998.
104. Dgani R, Shoham Z, Altar E, et al: Ovarian carcinoma during pregnancy: a study of 23 cases in Israel between the years of 1960 and 1984. *Gynecol Oncol* 33:326, 1989.
105. Zanetta G, Mariani E, Lissoni A, et al: A prospective study of the role of ultrasound in the management of adnexal masses in pregnancy. *Br J Obstet Gynecol* 110:576, 2003.
106. Kier R, McCarthy SM, Scoutt LM, et al: Pelvic masses in pregnancy: MR imaging. *Radiology* 176:709, 1990.
107. Bayer AL, Wiskind AK: Adnexal torsion: can the adnexa be saved? *Am J Obstet Gynecol* 171:1506, 1994.
108. Nichols DH, Juhlin PJ: Torsion of the adnexa. *Clin Obstet Gynecol* 28:375, 1985.
109. Graif M, Shalev J, Strauss J, et al: Torsion in the ovary: sonographic features. *AJR Am J Roentgenol* 143:133, 1984.
110. Caspi B, Ben-Galim P, Weissman A, et al: The engorged fallopian tube: A new sonographic sign for adnexal torsion. *J Clin Ultrasound* 23:505, 1995.
111. Stark JE, Siegel MJ: Ovarian torsion in prepubertal and pubertal girls: sonographic findings. *AJR Am J Roentgenol* 163:1479, 1994.
112. Quillin CP, Siegel MJ: Transabdominal color Doppler ultrasonography of the painful adolescent ovary. *J Ultrasound Med* 13:549, 1994.
113. Barloon TJ, Brown BP, Abu-Yousef MM, et al: Paraovarian and paratubal cysts: preoperative diagnosis using transabdominal and transvaginal sonography. *J Clin Ultrasound* 24:117, 1996.



## ULTRASONOGRAPHIC IMAGING IN INFERTILITY

Roger A. Pierson, MS, PhD

### Diagnostic Use of Ultrasonography in Infertility

#### Ovary

*Assessment of Ovarian Follicular Development*  
*A Wave Model for Ovarian Folliculogenesis*  
*Preovulatory Follicles*  
*Ovarian Endometriomas*  
*Assessing Ovarian Reserve*  
*Determining Optimal Timing for Insemination*  
*Ovarian Vascular Flow*

#### Ovulation

*Ovulation Failure*

#### Corpus Luteum

#### Polycystic Ovary Syndrome

*Definition of Polycystic Ovary Syndrome Morphology by Ultrasonography*  
*Ovulation Induction in Women With Polycystic Ovary Syndrome*

#### Oviduct (Fallopian Tube)

*Oviductal Pathology*

#### Uterus

*Measuring the Endometrium*  
*Myometrium*

#### Uterine Abnormalities

*Fibroids (Leiomyomata)*

*Adenomyosis*

*Gartner Duct Cysts*

*Nabothian Cysts*

#### Hysterosalpingosonography

*Sonohysterographic Technique*

*Contrast-Enhanced Hysterosalpingosonography*

### Ultrasonography in Assisted Reproductive Technology Therapy

Monitoring the Course of Ovarian Stimulation

Ovarian Hyperstimulation Syndrome

Ultrasound-Guided Oocyte Retrieval

Endometrial Assessment at the Time of Embryo Transfer

*Spectral Doppler and Color Flow Doppler Ultrasonography*

*Imaging-Based Uterine Scoring System*

*Three-Dimensional Imaging of the Endometrium*

*Motion Analysis*

Ultrasound-Guided Embryo Transfer

### Concluding Remarks

Infertility is a medical condition revolving around a couple's inability to conceive after 1 year of unprotected intercourse. It is also an area of medicine that is overly imbued with emotion and misinformation. Our goal in this chapter is to provide medical practitioners with a broad overview of the role of ultrasonography in the diagnosis of root causes of infertility in women and describe its role in increasing the quality of care provided in the assisted reproductive technologies aimed at ameliorating infertility.

In North America, approximately 8% to 15% of couples in which the female partner is 15 to 45 years of age experience some form of infertility,<sup>1,2</sup> that is, they have not conceived after 12 months of unprotected sexual intercourse.<sup>3</sup> Normal fertility is considered to be between 20% to 22% per cycle, and approximately 50% after three cycles. Therefore, in a normal population, approximately 60% of women will become pregnant within 6 months, 80% within 12 months, and 90% within 18 months. In a "fertility-focused intercourse" study pregnancy was achieved in 76%, 90%, and 98% of cases by the first, third, and sixth cycles, respectively.<sup>4</sup> The age of the female partner is of paramount importance in making decisions about when to begin investigations.<sup>5</sup> In couples in which the woman is younger than 35 years of age,

it is generally accepted that infertility investigations be initiated after 12 to 18 months of unprotected intercourse. However, if the female partner is older than 35 years of age, has menstrual abnormalities, a history of pelvic disease or surgery, earlier initiation of the infertility work-up may be considered. It is important to remember that infertility is a couple's issue, and each couple will present with a different level of desire to pursue infertility investigations and therapy. Evaluation and management of infertility diagnosis and therapy will typically involve several members of a multidisciplinary team. Consensus documents outlining the optimal work-up of couples who present with infertility and optimal evaluation of the infertile female are available from the Canadian Fertility and Andrology Society and the American Society for Reproductive Medicine.<sup>6,7</sup> These guidelines should be consulted for best practices in determining the sequence of diagnostic investigation and therapeutic intervention.

Ultrasonography is an integral and essential part of both the diagnostic and therapeutic steps in ameliorating infertility. Although the causes of infertility may have only female factors, only male factors, a combination of issues from each partner, or are idiopathic in nature, the steps taken toward

resolution of the couple's inability to conceive are shared. Each step in the diagnostic or therapeutic process should entail clear communication and involve education and counseling so that the couple understands the reasons for each test, is involved in each decision at each stage of therapy, and has realistic expectations of the therapeutic interventions. An ultrasound examination may be routinely included in the physical examination during the initial infertility consultation in clinics where ultrasonography is an integral part of clinical practice. There is a tremendous amount of information to be gained using ultrasonography early in infertility investigations. We believe that imaging has become the de facto standard for obtaining information once thought to be the purview of more conventional tests and should now be considered as a standard in infertility studies. Uterine and ovarian abnormalities such as cysts, tumors, fibroids, endometriomas, hydrosalpinx, and congenital abnormalities may be instantly visualized and appropriate action taken.<sup>8</sup> In addition, a conceptus may be visualized very early in gestation.<sup>9-11</sup>

The overall goal of imaging in infertility is to assist clinicians in accurate, timely diagnoses of the causes underlying a couple's inability to conceive and to play a role in the delivery of safe, effective treatment that will lead to a high probability of conception. It is sound clinical technical skill in creating and interpreting the images and timely, accurate decision-making following acquisition of the knowledge made possible by the images, and visualization of our tools during treatment procedures that allows ultrasonography to shine as a truly indispensable tool. Each member of the team providing clinical care has a role to play in the provision of the treatment plan and must also be able to respond to the emotional needs of the infertile couple regardless of the pregnancy outcome. Much of the reward that we receive as providers of reproductive health care comes from helping to establish a healthy pregnancy and monitoring the early development of the new life. Noninvasive imaging has provided the eyes that have facilitated the incredible increase in our knowledge of basic human reproductive processes. This new knowledge has, in turn, allowed us to increase our knowledge of the conditions that underlie reproductive failure and design safer, more effective treatments.

## DIAGNOSTIC USE OF ULTRASONOGRAPHY IN INFERTILITY

### Ovary

#### *Assessment of Ovarian Follicular Development*

Our notions of human folliculogenesis have been radically altered in the recent past.<sup>12,13</sup> For the past 50 years, it has become generally accepted that a cohort of follicles is recruited to grow in the late luteal phase of the menstrual cycle, a single follicle is selected for preferential growth in the mid-follicular phase, with ovulation at mid-cycle and limited follicle development during luteal phase.<sup>14-17</sup> It has been generally accepted that a single follicle grew by chance during a hormonally privileged period of the cycle in women referred to as the "Propitious Moment Theory."<sup>18</sup> According



**FIGURE 31-1.** Normal ovary during a natural menstrual cycle demonstrating normal follicle population and distribution on day 12 after menstruation. A dominant follicle is visualized in the central portion of the image, and several subordinate follicles are observed in the left lateral aspect of the ovary.

to the theory, antral follicles were recruited and grew continuously until conditions were right for a gonadotropin surge, which stimulated ovulation of the follicles that just happened to be mature at exactly the right point in the cycle<sup>19-21</sup> (Fig. 31-1).

### **A Wave Model for Ovarian Folliculogenesis**

High-resolution transvaginal ultrasonographic evaluation of the numbers and diameters of antral follicles during the menstrual cycle resulted in the documentation of ovarian follicular waves in normal healthy women of reproductive age. Follicle waves are defined as the synchronous growth of a group of follicles that occur at regular intervals during the ovarian cycle.<sup>12</sup> Emergence of follicle waves occurs at regular intervals throughout the estrous cycle and is preceded by a rise in follicle-stimulating hormone (FSH) regardless of the species.<sup>12,19,20,22,23</sup> The dominant follicle appears to be identifiable on the basis of size at approximately day 7 postmenstruation and grows at a rate of approximately 2 mm per day.<sup>13,24,25</sup> The final wave of the human ovarian cycle was ovulatory, although all previous waves were anovulatory.<sup>12,13</sup> Major waves were defined as those in which a dominant follicle was selected for preferential growth over subordinate follicles, and minor waves were those in which dominance was not manifest. Sixty-eight percent of 50 women evaluated exhibited two waves of follicle development during their ovarian cycles, whereas 32% exhibited three waves.<sup>13</sup> Of the women with two follicle waves, 85% exhibited a minor wave-major wave pattern and the remaining 15% exhibited a major-major pattern. In the women with three follicle waves, 63% exhibited a minor-minor-major wave pattern, 19% exhibited a minor-major-major pattern, and the remaining 19% exhibited a major-major-major wave pattern.<sup>12</sup>



Waves of follicular development in women occur in association with changes in circulating concentrations of reproductively active hormones during the menstrual cycle. Regardless of when during the cycle the wave starts, all waves are preceded by a rise in serum FSH,<sup>12,22,23</sup> as documented in domestic animals.<sup>19,20,22,23,26,27</sup> The dominant ovulatory follicle in women with two versus three follicle waves emerges earlier and is associated with an earlier rise in serum estradiol levels in the mid-late follicular phase, earlier preovulatory surges in estradiol, luteinizing hormone (LH) and FSH, and a shorter interovulatory interval (IOI).<sup>12</sup>

Late antral follicle development in the luteal phase of normal menstrual cycles was not believed to occur in women owing to an inhibitory effect of luteal progesterone, estradiol, and inhibin on FSH and LH secretion.<sup>28-34</sup> However, in the early 1950s, two periods of increased follicular growth were described during the sexual cycle.<sup>35</sup> The first wave of development occurred early in the cycle under the influence of FSH. From this wave, an ovulatory follicle developed. The second wave of development occurred in the early luteal phase. Follicles that grew more than 5 mm within the second wave in the mid-late luteal phase were believed to be atretic. More follicles were seen to grow during the postovulatory phase; however, follicles grew to a larger diameter in the preovulatory phase. Similarly, two waves of follicular development were reported in two women with 30- to 35-day cycles in the early days of ultrasound.<sup>36</sup> The follicular phase was reportedly long (>19 days), the luteal phase was short (<10 days), and follicular growth was associated with a rise in estradiol. An increase in the number of ultrasonographically detected follicles in both the early follicular and luteal phases was reported during the menstrual cycle.<sup>37</sup> A biphasic pattern of reproductively active hormones was also documented.<sup>38</sup> LH pulse frequency rose in the early luteal phase (~20 pulses per day) and early follicular phase (~20 pulses per day), compared with the mid-luteal phase (~5 pulses per day).<sup>38</sup> It is interesting that biphasic patterns of follicle growth and endocrine levels supported the notion of the development of ovarian follicular waves in women; however, the development of ovarian follicles during the luteal phase was considered to be an abnormal physiologic event in the early literature and up until the recent ultrasound based discoveries.

### Preovulatory Follicles

A successful ovarian follicle is one that escapes the overwhelming odds of atresia and ovulates, releasing its oocyte into an environment where it has the potential to be fertilized. In natural cycles, the follicle destined to ovulate is physiologically selected for preferential development and eventual ovulation, whereas other follicles in its cohort are condemned to atresia by a mechanism that we are only beginning to understand<sup>39,40</sup> (Fig. 31-2*A* and *B*). The current concepts regarding physiologic selection of the dominant follicle in women and nonhuman primates have been critically evaluated, and it has been determined that physiologic selection is completed only during the ovarian cycle in which the individual ovulation occurs.<sup>21,40-42</sup> This notion is reinforced by our current best practices in ovarian stimulation in which the selection mechanism is overwhelmed and multiple follicles develop before oocyte collection.

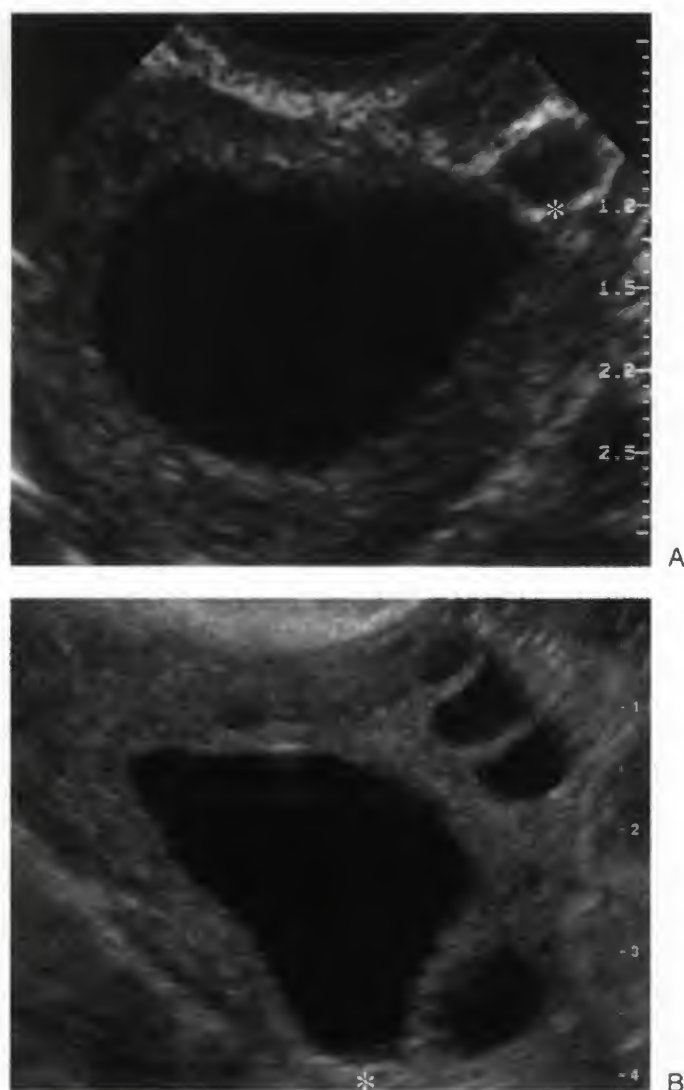


**FIGURE 31-2.** Imminently preovulatory follicles recorded during natural menstrual cycles (*A, B*). Note the stigma development on the right aspects of the follicles as the time follicular rupture approaches. The stigma (*asterisk*) is the portion of the follicle that protrudes from the surface of the ovary and its apex represents the location of impending follicular rupture.

Preovulatory follicles physiologically differ from subordinate follicles in their cohort in that they have a more extensive and permeable capillary network.<sup>43-45</sup> The vascular development surrounding the dominant follicle presumably facilitates accumulation of more circulating gonadotropins and achieves preferential development, whereas other follicles in the cohort are committed to atresia (Fig. 31-3*A* and *B*). The patterns and changes in blood flow around preovulatory follicles and, during ovulation, have been demonstrated by color flow Doppler ultrasonography in natural cycles and assisted reproductive technology (ART) cycles.<sup>46-48</sup> Follicles imaged after the LH surge and before ovulation showed pronounced changes in their peripheral vascular flow. There was increased flow at the base of the follicles and concomitant flow at the apex of the follicles, consistent with histologic and ultrasonographic studies of preovulatory follicles.<sup>44,49</sup> It appears that there is a very gradual decrease in impedance to blood flow in the vessels

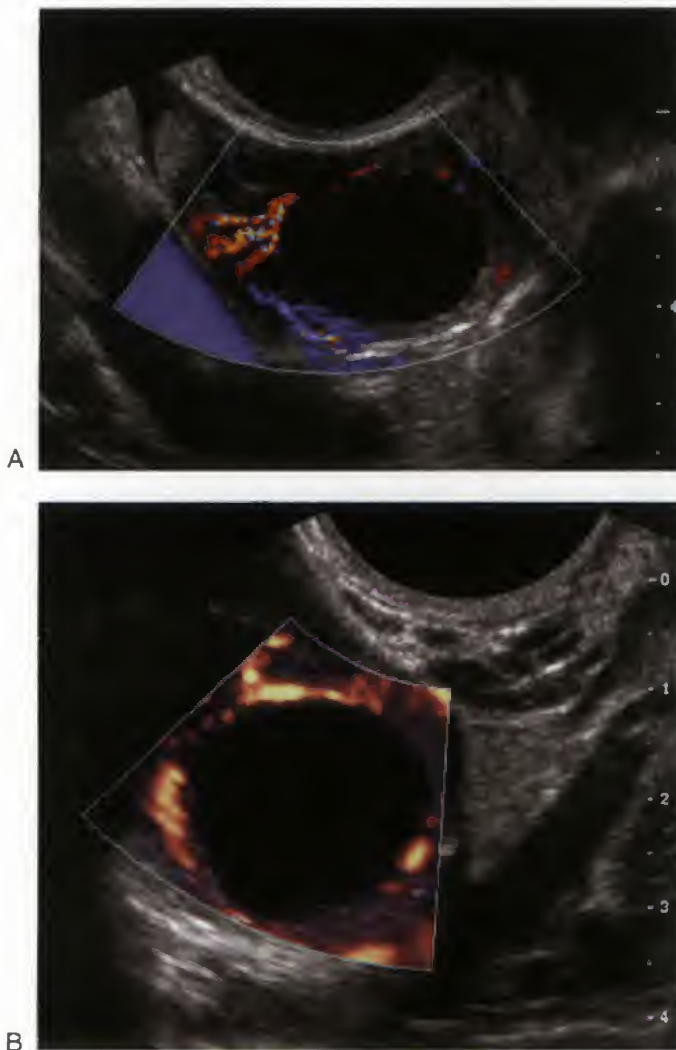


**FIGURE 31-3.** Color flow and power Doppler images demonstrating perfollicular vascularity in imminently preovulatory follicles (A,B). Visualization of full vascular flow around the follicle is challenging owing to the tortuous path of the vascular supply to the dominant follicle.

immediately surrounding the follicle as the interval to ovulation decreases. Immediately before ovulation, the perfollicular vessels are easily identified and spectral Doppler flow wave forms may be generated. It remains unclear whether the enhanced vascularity in dominant follicles is a cause or reflection of selection or has any utility in predicting the quality of the oocyte it may contain in humans. It has been proposed that Doppler investigation of individual follicles may provide a direct indication of the health of the follicle and developmental competence of the oocyte.<sup>50</sup> In addition, there is a preliminary indication in an animal model that computer-assisted image analysis may be useful in assessing the probability of a follicle containing a competent oocyte.<sup>51</sup> Assessment of perfollicular vascularity is beginning to be used in clinical ART settings.<sup>50,52</sup> The clinical utility of assessing perfollicular vascularity appears to be controversial at present. Some studies have demonstrated a relationship between perfollicular vascularity and pregnancy rates;

however, others have not found a positive indication for incorporating this endpoint into assessment of the follicles in clinical ART at present.<sup>52,53</sup> Similarly, there were no differences found in perfollicular vascularity of poor responders versus normal responders to ovarian stimulation in clinical IVF cycles.<sup>54</sup> New three-dimensional power Doppler imaging is able to generate outstanding images of the follicles before oocyte retrieval; however, their interpretation and clinical utility remain elusive.

Clinically, serial ultrasonography and assessment of circulating estrogen levels have potential in the isolation and identification of the root causes of follicular phase defects. Follicles may develop, and circulating estradiol concentrations appear to be within clinically normal limits for the follicular phase of the cycle; however, ultrasound examination may reveal the absence of a dominant follicle of preovulatory diameter. Alternatively, ultrasound examination during the late follicular phase of a spontaneous menstrual cycle may reveal a follicle of preovulatory diameter (e.g., 22 mm), yet the patient may exhibit clinically low estradiol concentrations. Follicles with this pattern of growth and regression have an thin, atretic appearance of the follicle wall, seem flaccid, fail to ovulate and subsequently regress<sup>55</sup> (Fig. 31-4A). When combined with our new knowledge of follicle wave patterns in women, serial ultrasonography and assessment of circulating hormone levels might be used to identify subtle defects in follicular recruitment, development, physiologic selection, final maturation, and ovulation. It seems reasonable that disturbances in the continuum of folliculogenesis may be responsible for much infertility previously classified as idiopathic.

### Ovarian Endometriomas

Endometriosis is probably the most common benign gynecologic disease and has been estimated to be present in 10% to 25% of women with gynecologic disease and is detected in approximately 40% of women presenting with infertility.<sup>56</sup> Endometriosis is broadly defined as the presence of functional endometrial tissue outside the uterine cavity. There are several types of deposits, including plaques, implants, nodules and endometriomas. An endometrioma is a cystic structure that is lined with endometrial epithelium. Although most types of diffuse endometriosis may not be identified with ultrasonography, endometriomas are easily identified structures associated with infertility. Endometriomas are typically hypoechoic, multiple or single, cystic-appearing lesions that vary in size and have a low amplitude uniform echotexture in the cavity of the cyst. They appear to compromise normal ovarian function by disrupting folliculogenesis, ovulation, and normal ovulation (see Fig. 31-4B and C).

Ultrasonography is now being used as a part of therapy to ameliorate the effects of endometriomas when they are diagnosed. The technique involves ultrasound guided drainage of the endometriomas followed by treatment with a recombinant interleukin-2 under chronic administration of gonadotropin-releasing hormone (GnRH) analogs to suppress the response of endometrial tissue.<sup>57</sup> Results of this new therapeutic intervention appear promising.

Dermoid cysts (ovarian cystic teratomas) are the most common ovarian pathology in young women of reproductive age.<sup>58-60</sup> The ultrasound appearance is broad; however,



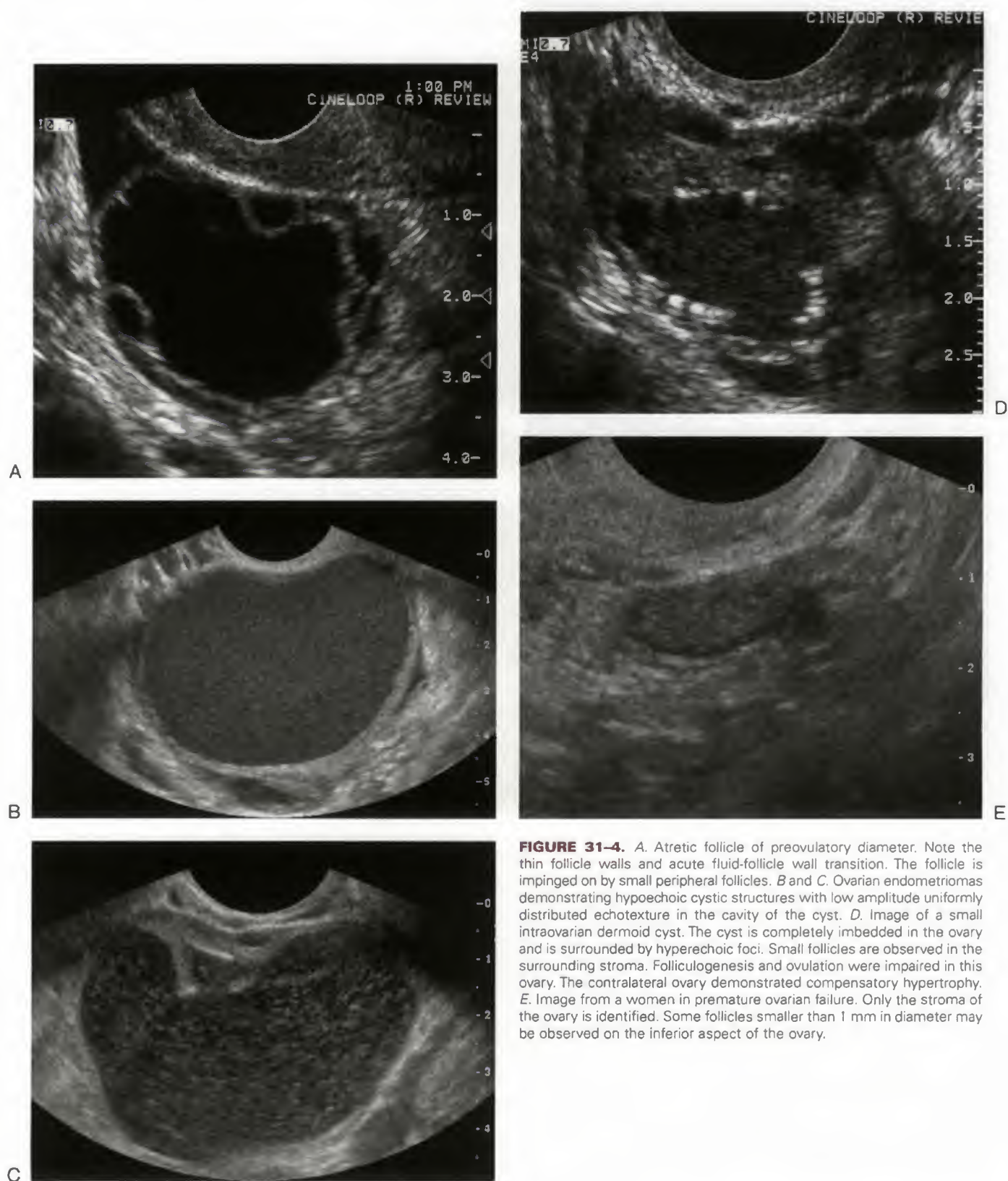


**FIGURE 31-4.** A. Atriotic follicle of preovulatory diameter. Note the thin follicle walls and acute fluid-follicle wall transition. The follicle is impinged on by small peripheral follicles. B and C. Ovarian endometriomas demonstrating hypoechoic cystic structures with low amplitude uniformly distributed echotexture in the cavity of the cyst. D. Image of a small intraovarian dermoid cyst. The cyst is completely imbedded in the ovary and is surrounded by hyperechoic foci. Small follicles are observed in the surrounding stroma. Folliculogenesis and ovulation were impaired in this ovary. The contralateral ovary demonstrated compensatory hypertrophy. E. Image from a woman in premature ovarian failure. Only the stroma of the ovary is identified. Some follicles smaller than 1 mm in diameter may be observed on the inferior aspect of the ovary.

most have evidence of hyperechoic tissues in a loosely organized mass.<sup>59–61</sup> In many cases, the dermoid mass may be completely imbedded in the ovary and not be detectable on laparoscopy (see Fig. 31–4D). Doppler flow characteristics of dermoid cysts are interesting in that vascular flow was detected in only approximately 24% of women in which they had been diagnosed.<sup>62</sup>

### Assessing Ovarian Reserve

Changes in demographic trends in the age at first pregnancy in our society have combined to yield more and more women wishing to conceive when they are older and less fertile.<sup>63–66</sup> Numerous studies in recent years have demonstrated that fertility declines progressively as age advances. In ART, the main focus in determining the starting dose of gonadotropin for ovarian stimulation and prediction of the ovarian response is an assessment of what is termed the ovarian reserve. Ultrasonography is now being used to investigate follicular dynamics in aging women, as are detailed endocrine based tests.<sup>67–70</sup> One focal point currently rests on day 3 antral follicle counts and FSH levels; however, the notion of day 3 follicle counts may need to be reconsidered in light of our new understanding of normal folliculogenesis.<sup>9,13</sup> Decreased ovarian reserve, or number of follicles capable of being stimulated, is a primary reason for poor response to ovarian stimulation.<sup>71</sup> The role of decreased numbers of antral follicles as women age relative to the capacity of the oocyte to be fertilized remains unclear.<sup>70–72</sup> The ovarian response to exogenous gonadotropin stimulation does decrease with age, but the range of individual variation is wide and age is only one part of the rough estimate of ovarian reserve and ovarian stimulation response.<sup>68,70–73</sup>

There are several tests of “ovarian reserve” that include clomiphene citrate challenge and the GnRH agonist stimulation tests.<sup>67–70,74,75</sup> Ovarian biopsy is also an option, although its use remains controversial.<sup>69,76</sup> The endocrine tests offer prognostic information valuable in the counselling of aging infertile women.<sup>70</sup> However, there is accumulating evidence to suggest that ultrasonography may be used to estimate the number of antral follicles at specific times of the menstrual cycle and provide additional useful information of clinical relevance.<sup>67,77–79</sup> Ultrasound assessments take place using antral follicle counts or measurement of ovarian volume. Antral follicle counts, typically done on days 3 to 7 after menstruation, may be used to predict the number of follicles likely to develop during ovarian stimulation.<sup>79–83</sup> Women having fewer than five follicles smaller than 10 mm in diameter before ovarian stimulation have a greater chance of a poor ovarian response.<sup>82</sup> The extent to which antral follicle counts correlate with endocrinologic measures of ovarian reserve (e.g., cycle day 3 FSH and estradiol concentrations) remains to be widely confirmed.<sup>67,68,73,78,84</sup>

Ovarian volume assessments are based on the presumption that there is a significant correlation between the population of primordial follicles remaining in the ovary and the volume of the ovary, measured using either 2- or 3-dimensional ultrasonography.<sup>68,73,77,80</sup> A very clear relationship between decreased ovarian volume and antral follicle counts and advancing age combined with increased FSH has been demonstrated.<sup>70,78</sup> The ovaries in women with premature

ovarian failure have the characteristic appearance of women in menopause. The ovaries are small and show no evidence of follicular activity other than what might be perceived as follicles smaller than 1 mm around the periphery of the cortex (see Fig. 31–4E).

Although ultrasonography remains an important aspect of ovarian reserve estimation, understanding folliculogenesis in older women and attempts to predict the probability of a successful ovarian stimulation cycle, it is important to note that a recent study did not support the routine clinical use of any of the current ovarian reserve tests.<sup>68,72,73,82,84,85</sup>

### Determining Optimal Timing for Insemination

Ultrasound monitoring of dominant follicular development is being used to more precisely define the time of ovulation and estimate the optimum time to schedule intercourse or perform IUI, when indicated, in both spontaneous and stimulated cycles. Ultrasonography is far superior to simple monitoring of basal body temperature (BBT) or urinary LH excretion. Our ability to estimate the interval to ovulation is based upon detailed ultrasound based studies of preovulatory follicle growth from different diameters and detailed knowledge of follicle growth rates.<sup>12,25,86,87</sup> During natural menstrual cycles, preovulatory follicles grow at approximately 1.6 mm per day and the mean diameter on the day before ovulation is 21.7 mm. In ovarian stimulation cycles, follicles grow slightly faster 1.8 mm per day, but the diameter on the day before ovulation is similar.<sup>24</sup> Given the relatively brief interval for which sperm remain functionally viable after IUI and the considerable costs involved, including ovarian ultrasonography is helpful in maximizing the effectiveness and efficiency of even the less invasive ART treatments. Definitive studies in humans have apparently not been done; however, in the equine animal model, ultrasonography is highly effective in estimating the interval to ovulation. Taken together, the data from detailed human studies and evidence from experimental animals would presume that accurate estimates may be easily calculated.<sup>13,23–25,88</sup>

### Ovarian Vascular Flow

The ovarian vessels may be visualized as they enter the ovarian hilus, and the intraovarian vascular supply also may be visualized. The ovary bearing the preovulatory follicle or corpus luteum exhibits lower resistance to blood flow than the vessels of the contralateral ovary based on spectral Doppler studies. The lowest impedance to blood flow occurs on the day of the LH peak while highest resistance to blood flow was observed on day 1 of menses.<sup>89</sup> However, a clear relationship between estradiol, progesterone, and other circulating hormones and the vascular indices of the ovarian and uterine arteries was not identified in a subsequent study.<sup>90</sup> Research is just beginning on the assessment of echotextural characteristics and vascular patterns of individual preovulatory follicles to evaluate the probability of ovulation or containing biologically competent oocytes.<sup>50,51,91</sup>

Color flow and power flow Doppler ultrasonography in two and three dimensions has been used to evaluate ovarian blood flow during ovarian stimulation before oocyte



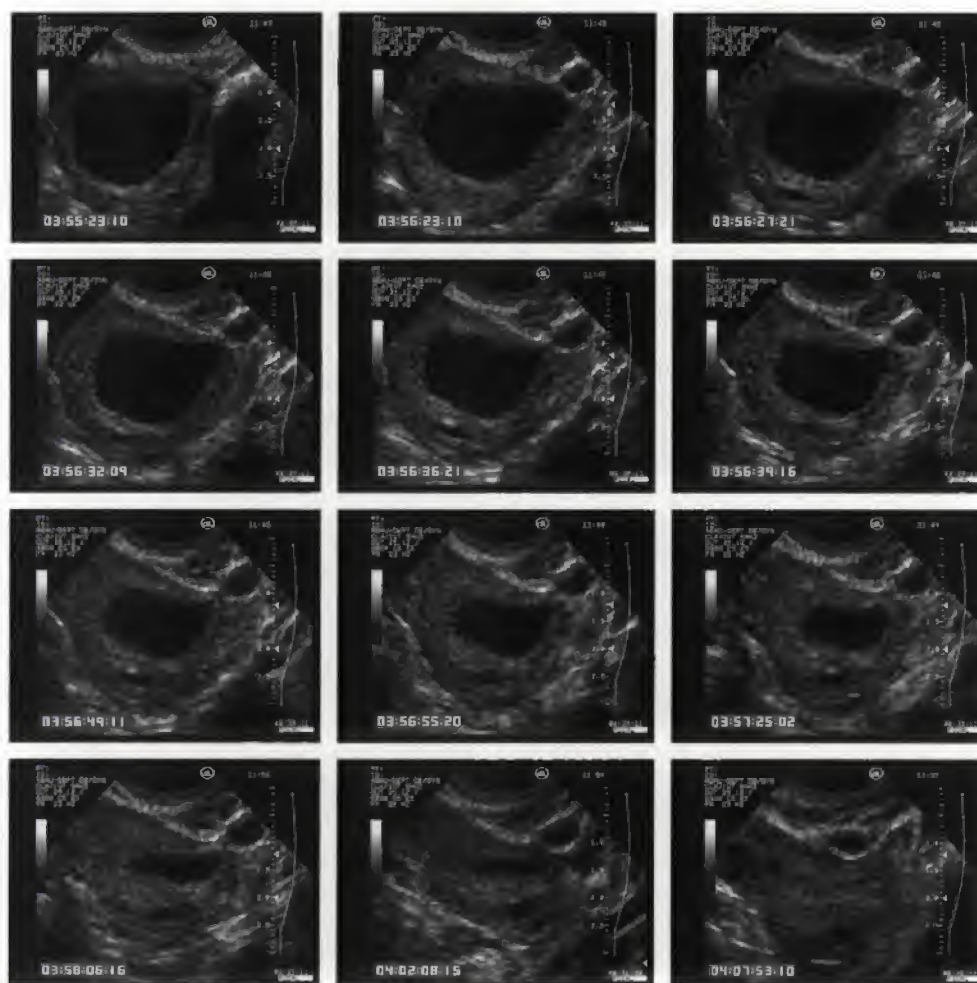


**FIGURE 31-5.** Sequence of images of ovulation. This ovulation occurred over 11 minutes and 30 seconds from the first detected fluid leakage to complete apposition of the follicle walls. Images range from 1 minute before the onset of ovulation to complete follicular evacuation. Time-code values are shown in the lower left corner of each image displaying hours, minutes, seconds, and frame number. (Reprinted with permission from Hanna MD, Chizen DR, Pierson RA: Characteristics of follicular evacuation during human ovulation. *J Ultrasound Obstet Gynaecol* 4:488, 1994.)

retrieval for in vitro fertilization (IVF) and an attempt has been made to associate ovarian vascular indices with IVF outcomes.<sup>50,92-95</sup> In an initial study, peak velocity measurements and resistive indices decreased as the diameter of the follicles increased, consistent with the idea that the vascularity of the follicles increases as the interval to ovulation decreases. However, the ovarian vascular indices were not useful for predicting the outcome of IVF cycles.<sup>93</sup> Later studies reached the conclusion that there is indeed a physiologic relationship between follicular vascular indices and the clinical outcomes of assisted reproduction cycles.<sup>50,94,95</sup> A strong correlation has been observed between oocyte recovery rates and the level of follicular vascularity, and it has been proposed that perifollicular blood flow may be indicative of the appropriate time for human chorionic gonadotropin (hCG) administration for optimal recovery rates.<sup>48,95-97</sup>

## Ovulation

Ovulation occurs on approximately day 14 after menstruation in a classically described textbook 28-day menstrual

cycle.<sup>21,44,98,99</sup> The first uses of ultrasound scanning in gynecology revolved around trying to understand ovarian function and ovulation.<sup>36</sup> Transabdominal ultrasound scanning has been used for many years to detect ovulation in women. Visualization of follicle rupture and evacuation of the follicular fluid and cumulus/oocyte complex has only recently been demonstrated by ultrasonography<sup>100,101</sup> (Fig. 31-5). The time required for ovulation appeared to vary from less than 1 minute to more than 20 minutes from the time that the first fluid leakage was observed until the walls of the former follicle were completely apposed. On average, follicular evacuation appeared to take approximately 10 minutes. However, the site of follicular evacuation/new corpus luteum was immediately detectable. The point of follicular rupture from the surface of the ovary was recognised for up to a week and the corpus luteum typically remains identifiable until the subsequent ovulatory cycle.<sup>100,102</sup>

Following ovulation in normal cycles, the corpus luteum develops. Evaluation of the ovulations and period of early luteogenesis in normative control patients and patients referred for idiopathic infertility is revealing previously

unknown information regarding normal luteal function and undescribed flaws in the ovulation and luteogenesis.<sup>100,102-105</sup>

### Ovulation Failure

Failure of ovulation most probably occurs by one of two mechanisms, although several more mechanisms probably exist. The luteinized, unruptured follicle syndrome (LUF) has been debated; however, transvaginal ultrasound has been used for detailed descriptions.<sup>46,49,106</sup> In ovulatory failure, dominant follicles attain preovulatory diameter and fail to rupture and extrude oocyte/cumulus complex. The oocyte/cumulus complex appears to remain within the lumen, the walls of the follicle thicken and acquire image attributes suggestive of luteal tissue (Fig. 31-6). The follicle wall-follicle fluid acquires hazy, indistinct borders. The LUF remains identifiable for the duration of the menstrual cycle and regresses typically by the subsequent menses. Basal body temperature charts and mid-cycle progesterone concentrations are typically within low clinically normal limits. Menses may be normal or somewhat lighter than normal for individual patients.

Alternative mechanisms for ovulatory failure involve the growth of the dominant follicle to a larger-than-usual diameter without ovulation.<sup>106</sup> In some cases, the capillaries in the follicle wall appear to fenestrate and extravasate blood into the follicular lumen. This is referred to as a hemorrhagic anovulatory follicle (HAF) (Fig. 31-7*A* and *B*). The follicular fluid of other anovulatory follicles remains clear and the fluid-follicle interface becomes acute (see Fig. 31-7*C*). There apparently is no luteinization of the follicular wall, which appears thin and highly echoic. In some cases, the granulosa cells around the interior of the follicles delaminate and float in the follicular lumen as the follicle regresses (see Fig. 31-7*D* and *E*). Mid-cycle progesterone values are below clinically normal. These types of anovulatory follicles typically remain static for one to several days and then begin to regress. The rates of follicular regression are to be highly variable. Menstrual periods following this type of ovulatory failure typically occur within a normal cycle length, although the amount of flow appears variable.

The use of ultrasonography to monitor follicular growth and confirm the occurrence of ovulation or ovulatory failure is becoming clinically useful. When considered along with well-timed circulating hormone levels, ultrasound offers answers to subtle problems in ovulatory dysfunction by the practicing clinician.

### Corpus Luteum

The corpus luteum (CL) is a dynamic endocrine gland within the ovary that plays an integral role in regulation of the menstrual cycle and early pregnancy. The CL forms from cells of the ovarian follicle wall just before, during, and after ovulation. The precise origin of the cells that comprise the luteal gland remains controversial. However, it is believed that luteal cells originate from the theca and granulosa cells following breakdown of the basal lamina immediately before follicle rupture.<sup>107</sup> The CL undergoes profound neoangiogenesis during its development, is dependent on vascular flow for normal function, and exhibits degradation of the vascular supply during regression if the woman does not

conceive or during the late stages of gestation in pregnant women.<sup>107,108</sup> The cyclic and temporary nature of the CL, its profound vascularity and its critical physiologic role regulating folliculogenesis, and the establishment and maintenance of pregnancy all make the luteal gland a primary target for assessment in infertility investigations.<sup>104</sup>

The human CL was first studied in the 1950s using histologic evaluation of ovaries following hysterectomy and salpingo-oophorectomy.<sup>109</sup> Ultrasonography has since become an invaluable tool for evaluating the CL in vivo. It has been reported that the CL grows to a maximum diameter of 25 to 40 mm during the luteal phase, as determined by transabdominal ultrasonography.<sup>110,111</sup> Some CL were reported to exhibit a "cystic cavity," whereas others did not.<sup>110-112</sup> Histologic evaluation of the CL revealed that there was fresh bleeding into the central cavity following follicle rupture.<sup>109</sup> The blood-filled CL is referred to as the 'corpus hemorrhagicum.' Growth of the CL is associated with an increase in luteal blood flow and serum progesterone concentrations.<sup>112-115</sup> Peak luteal vascularity appears to occur 7 days after ovulation, the approximate day of maximal progesterone secretion.<sup>115</sup>

Ultrasonographic detection of the CL following ovulation has been reported to occur in only 50% to 80% of natural menstrual cycles in the earliest studies.<sup>110,112,116</sup> However, later studies designed to visualize ovulation and study folliculogenesis have shown that the CL may be detected on the day of ovulation and throughout the luteal phase<sup>13,100,102,117</sup> (Fig. 31-8). Immediately following follicular evacuation, the walls of the former follicle become highly vascularized in the first 48 to 72 hours. Blood and lymphatic vessels colonize the developing CL, and there is typically a pronounced ring of vascularity, which appears to follow the path of the vascular supply surrounding the former preovulatory follicle. The vascular ring becomes more apparent as the corpus luteum matures and is visually spectacular color or power flow Doppler interrogation (Fig. 31-9). The grayscale values for the CL follow the vascular perfusion of the gland.<sup>102,114,118</sup> The luteal tissues are dark during luteogenesis and become progressively lighter shades of gray during luteal regression. Resistance to vascular flow is usually low as would be expected of an active endocrine tissue during the period of active progesterone secretion during the estrous cycle and during early pregnancy.

Two morphologic types of luteal glands were observed following ovulation: those with, and those without, a central fluid-filled cavity.<sup>102</sup> Most CLs contained a fluid-filled cavity at some time during their life span. Central fluid-filled cavities were attributed to the leakage of blood into the follicular lumen following follicle rupture. The cavities were most likely to be observed immediately following ovulation and then subsequently declined. Therefore, the detection of a fluid-filled cavity in the CL was interpreted to be a normal physiologic event during the menstrual cycle resulting either from vascular leakage into the developing CL or extravasation of blood during luteogenesis. The corpus albicans may typically be visualized following luteal regression at least until the time of subsequent ovulation.<sup>102</sup> Several corpora albicantia from previous cycles may occasionally be observed in the ovaries; however, visualization of these small structures may be dependent on the location of small follicles surrounding the regressing structures (Fig. 31-10).



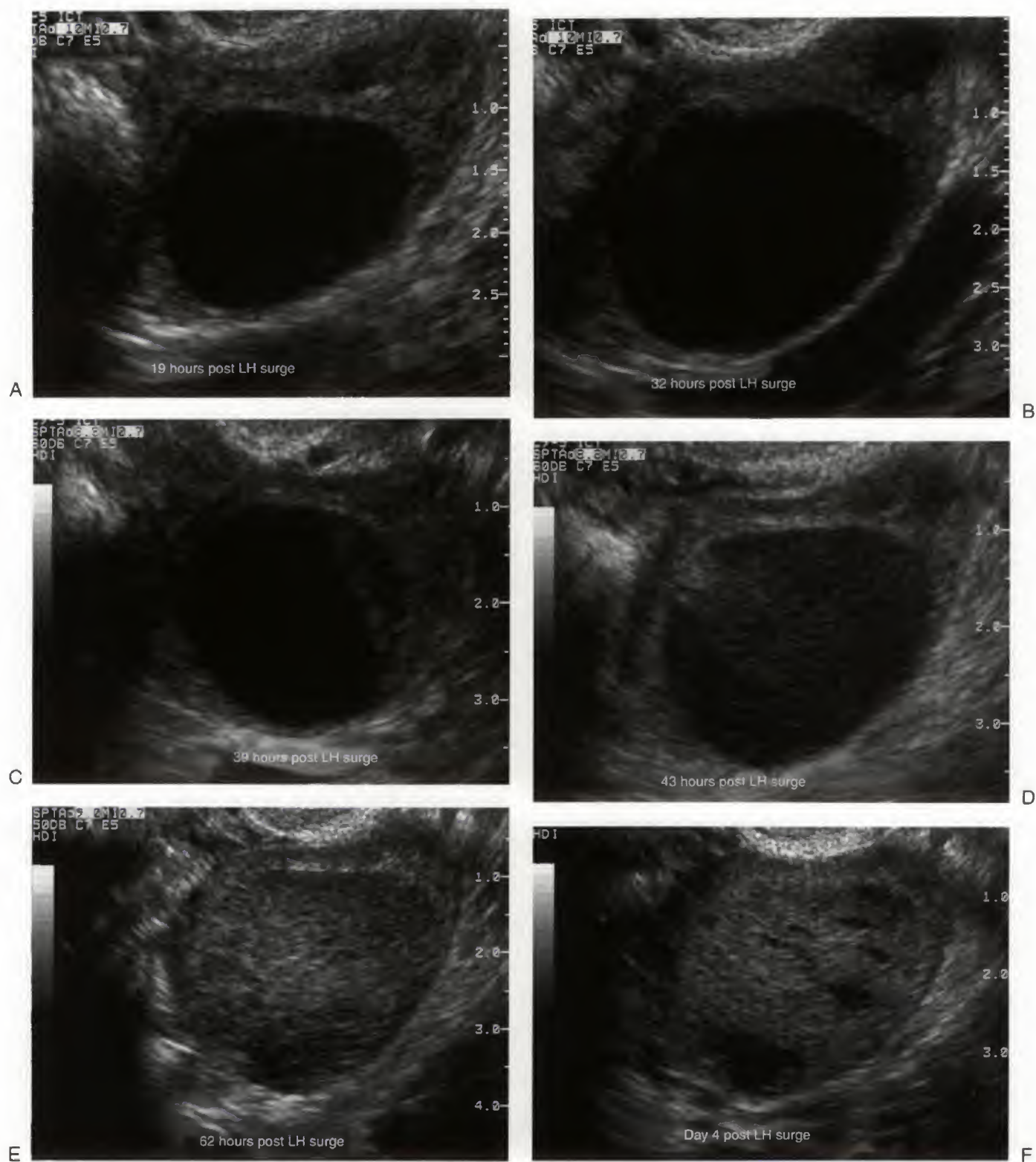


**FIGURE 31-6.** A to F Sequence of images of luteinized unruptured follicle (LUF) development. The woman was participating in a study of ovulation and its relationship to the LH surge. Images here were recorded at 19 hours, 32 hours, 39 hours, 43 hours, 62 hours, and 96 hours after the LH surge, respectively.

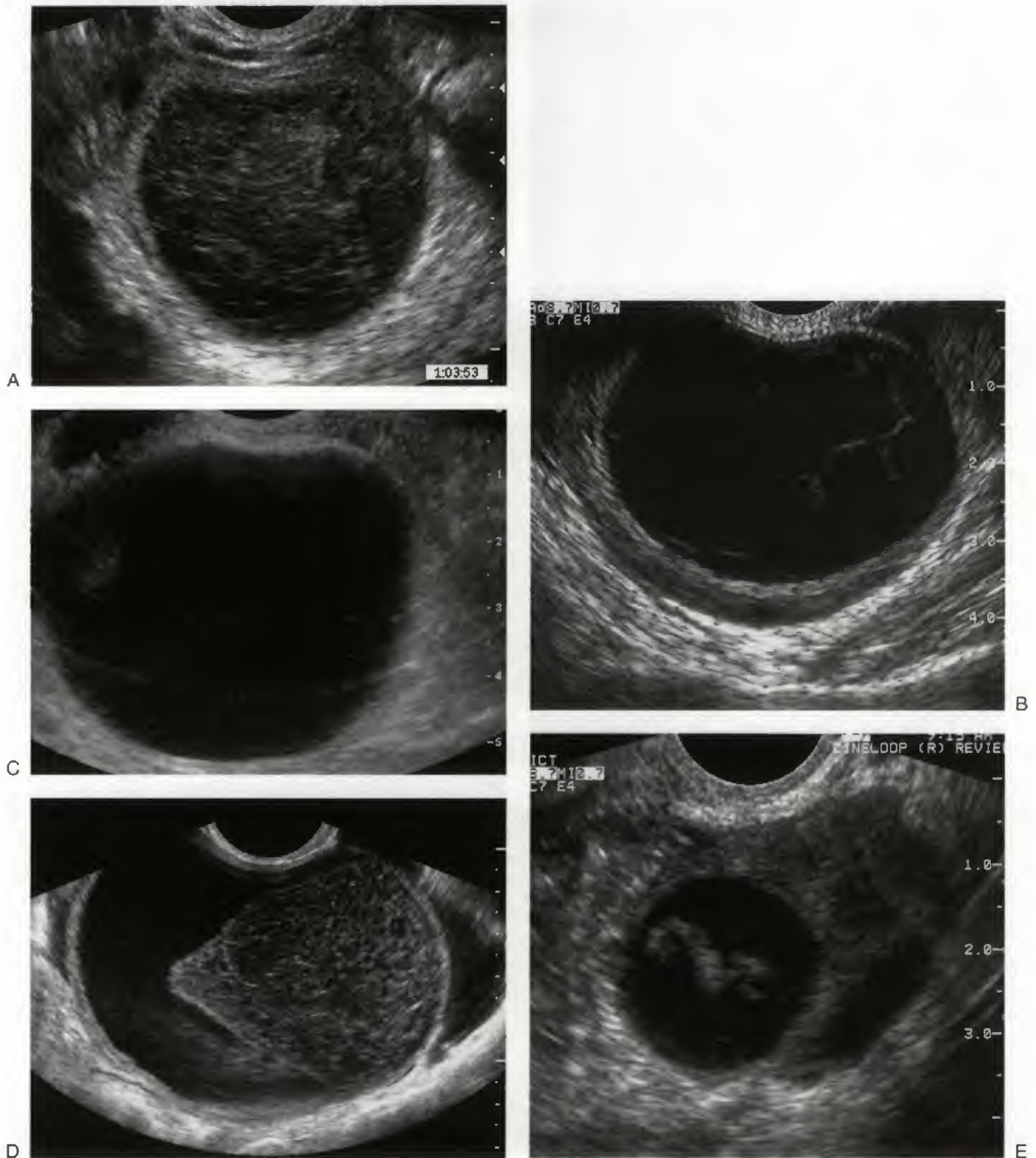


**FIGURE 31-7.** A and B. Images from two women who developed hemorrhagic anovulatory follicles during a study of natural cycle folliculogenesis and ovulation. There is evidence of extravasated blood in the lumen of the structures, and the walls did not develop any visual evidence of luteinization. Progesterone levels were less than those accepted as clinically normal. C. Failure of ovulation and development of "cystic" follicle. Thin follicle walls are observed and small flecks of particulate matter are frequently seen in the lumen. D and E. In some cases of ovulatory failure, the granulosa cell layer delaminates and floats within the follicular lumen. Different types of cellular debris and epithelial sheets are frequently observed.



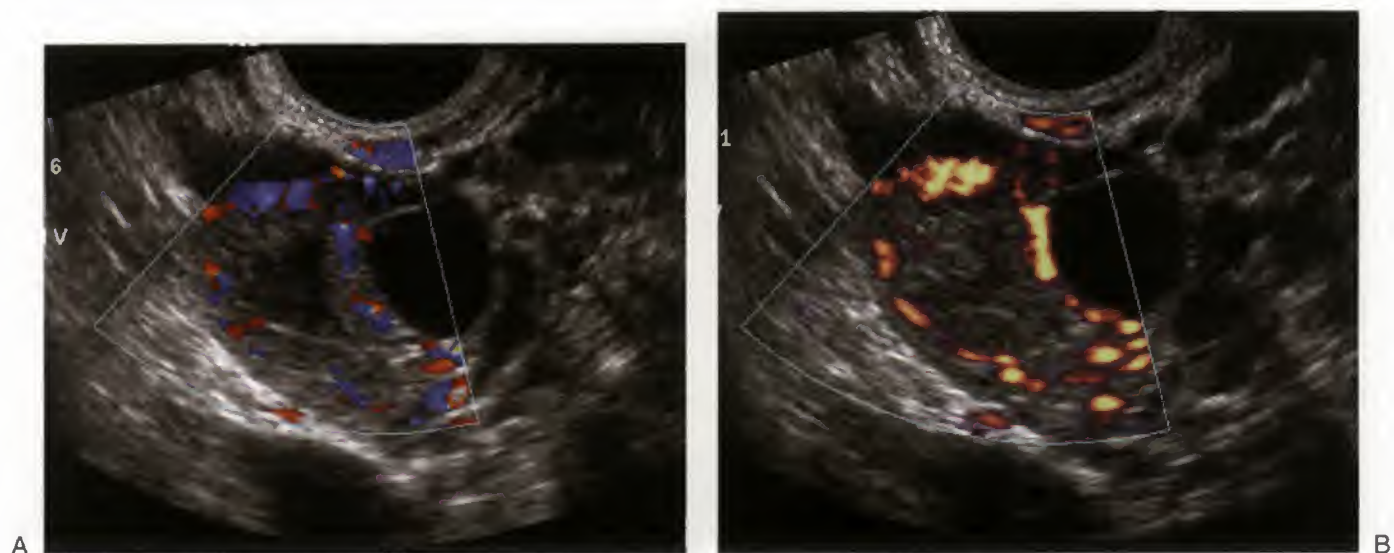


**FIGURE 31-8.** A and B. Color flow and power Doppler images of luteal glands visualized on the day of ovulation.

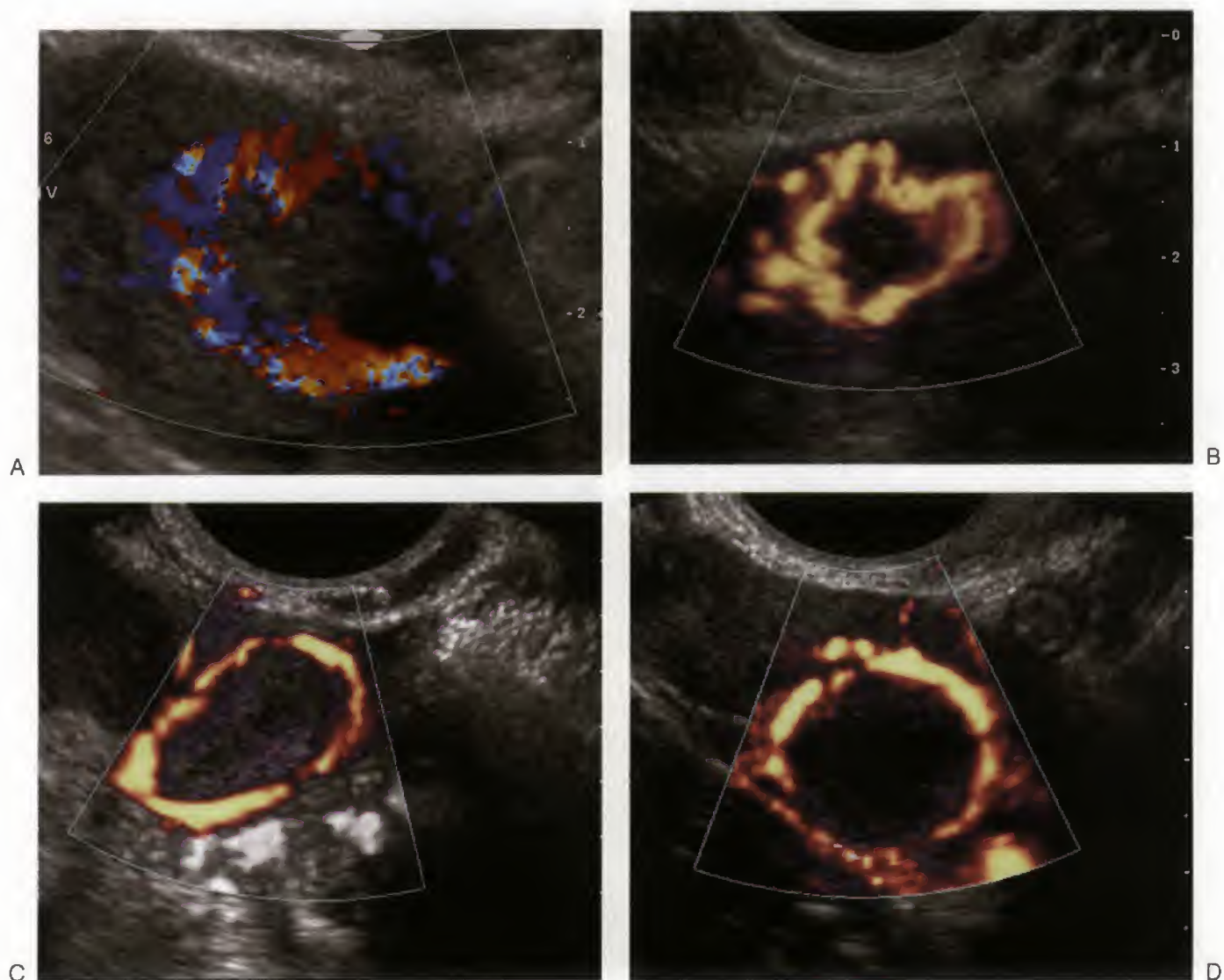


**FIGURE 31-9.** A to D. Color flow (A) and power Doppler images of new corpus luteum CL (B) and mature, mid-cycle luteal glands (C, D). Note the convolutions of the luteal wall in the power Doppler image of the developing CL.



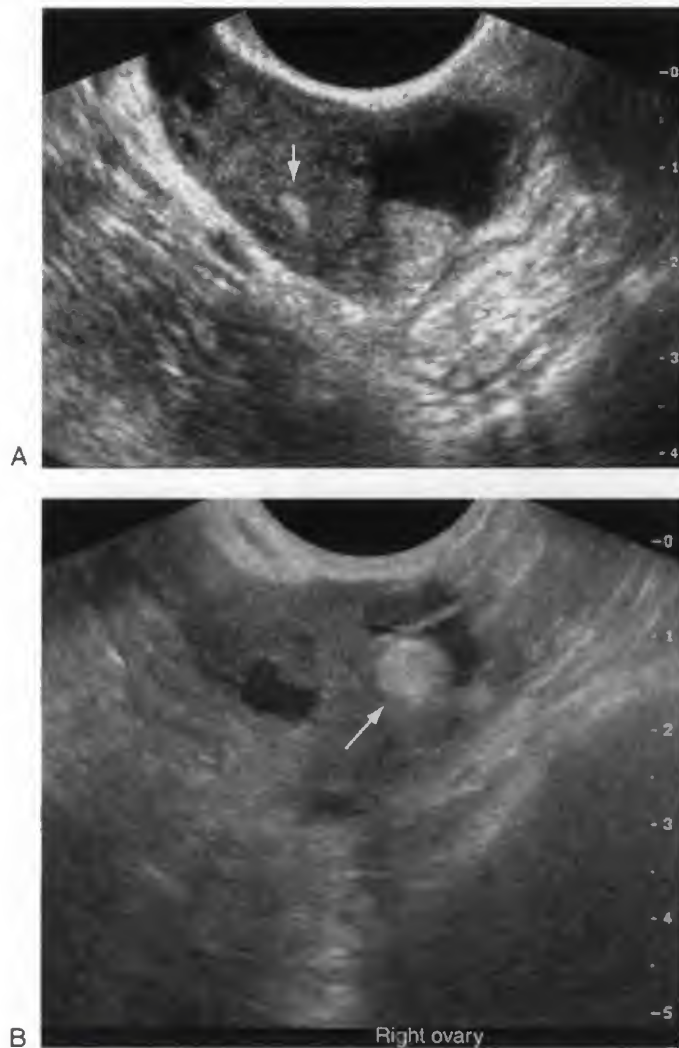


**FIGURE 31-10.** A and B. Images of corpora albicantia (CA) from previous cycles. CA are visualized as hyperechoic structures (arrows) within the ovary.

Limited information on the serial characterization and correlation of luteal morphology and endocrinologic function during spontaneous menstrual cycles is available; however, luteal area, progesterone concentration, and estradiol concentration increased for approximately the first 6 days following ovulation, followed by a subsequent decline.<sup>102,103,114</sup> The period of peak indicators was well correlated with the approximate time of maternal recognition of pregnancy. The vascular flow characteristics follow the decrease in luteal area and volume and decreasing progesterone levels as luteal regression ensues. The color flow mapping patterns become much less pronounced, and increased resistance to flow is observed. Definitive studies of the vascular dynamics within the corpus luteum have apparently not yet been performed; however, this is a promising research area with profound ramifications to infertility assessments, maternal recognition of pregnancy and etiology of early embryonic loss.<sup>103,104,114,118-122</sup>

Color Doppler imaging combined with high-resolution grayscale ultrasonography in two and three dimensions now

allows evaluation of the functional development of luteal gland,<sup>102,104,111,115</sup> Doppler imaging lends us the ability to visualize blood flow in very small vessels and assess the resistance to flow as an indicator of physiologic function.<sup>114,115</sup>

## Polycystic Ovary Syndrome

Polycystic ovary syndrome (PCOS) is a broad-spectrum metabolic disorder that commonly results in oligomenorrhea and anovulation.<sup>123</sup> In many women, it is also a cause of infertility.<sup>124-126</sup> Many of the women present with hyperandrogenism and menstrual disorders, and it is interesting to note that many women do not appear to have a diagnosis of PCOS until they are referred to a reproductive endocrinologist for infertility; however, the disorder has many personal health consequences that should be addressed well in advance of an infertility referral.<sup>125-132</sup> Ovarian function in women with PCOS is poorly understood.<sup>133</sup> The patterns of follicular turnover, initiation of follicular growth, and physiologic selection of a dominant follicle differ markedly from women with normal folliculogenesis and menstrual function.<sup>129</sup>

The diagnosis of PCOS is traditionally made on clinical history and endocrine assessment, and there is now an ongoing discussion on the merits of classifying women with the disorder on the basis of endocrine and metabolic criteria versus ovarian ultrasound based criteria.<sup>124,126,134,135</sup> The classic "string-of-pearls" ultrasonographic appearance of the ovaries of a PCOS patient strongly supports the clinical diagnosis. In many cases, PCOS may be identified solely on the ultrasonographic morphology of the ovaries; however, the metabolic disorder may be present in a woman with normal-appearing ovaries, and women with ovaries profoundly suggestive of PCOS on ultrasound examination may appear to be phenotypically normal.<sup>125,134</sup>

The ultrasonographic morphology of PCOS ovaries has been described and the attributes of PCOS morphology are being constantly updated as subtle differences in endocrine profiles are elucidated.<sup>124-126,129,134</sup> (Fig. 31-11). PCOS is emerging as one of the most active areas of research in reproductive endocrinology, and the literature is literally exploding as research and clinical experience with the condition increase.<sup>136</sup> Ultrasonography is considered the gold standard for the detection of polycystic ovaries, but there is considerable challenge in developing a standardized definition of the ovarian appearance of PCOS ovaries.<sup>133</sup> Several definitions for the ultrasound definition of PCOS were considered before 2002.<sup>134,137</sup> Increased stromal echogenicity appeared to be the most consistent finding among polycystic ovaries; however, evolving definitions have primarily focused on ovarian volume and follicle numbers, which are considered less subjective than stromal echogenicity in their appraisal.

## Definition of Polycystic Ovary Syndrome Morphology by Ultrasonography

A clear, working definition of PCOS ovarian morphology has emerged from a series of studies leading to a consensus definition. A set of diagnostic criteria was developed in 2000 which was somewhat more intermediate than that previously reported.<sup>134</sup> The criteria included an ovarian volume greater



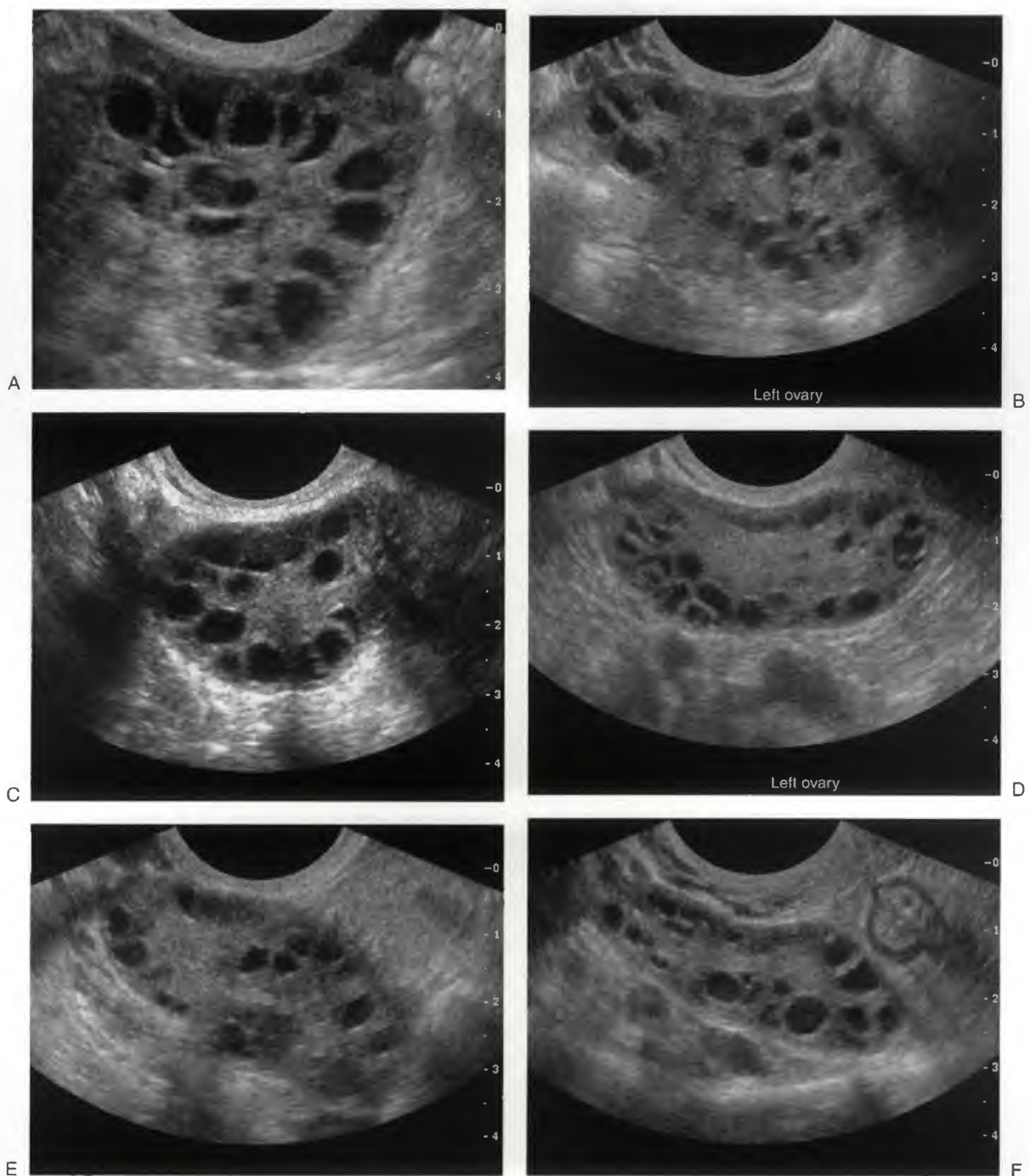


**FIGURE 31-11.** A to F. Images from women with differing expressions of the metabolic syndrome associated with polycystic ovary syndrome (PCOS). There are differing ultrasonographic appearances in the size and distribution of follicles within PCOS ovaries.

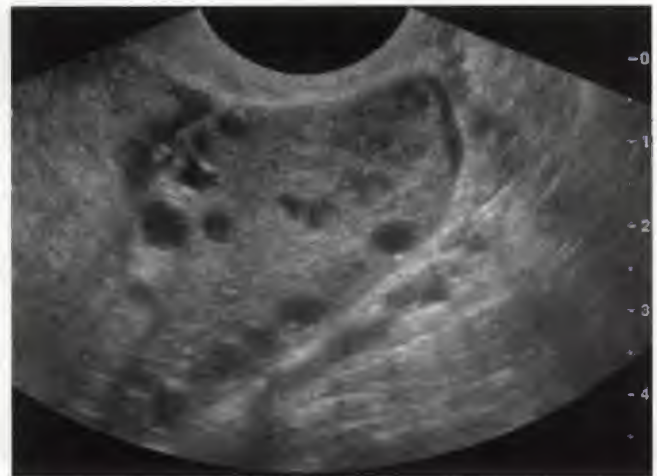
than 9 cm<sup>3</sup>, more than 10 follicles between 2 and 8 mm, and increased stromal echogenicity. Subsequently, a new set of criteria were developed that have become widely accepted.<sup>138</sup> This definition of the PCOS ovary includes increased ovarian stroma of greater than 5.5 cm<sup>2</sup> or a volume greater than 11 cm<sup>3</sup> and detection of more than 12 follicles between 2 and 9 mm in diameter (mean of both ovaries). At present, the Rotterdam consensus workshop on PCOS definitions represents our best means of defining PCOS on ultrasound examination.<sup>139</sup> The consensus committee has abbreviated the 2003 definition of PCOS ovaries to having 12 or more follicles measuring 2 to 9 mm and an ovarian volume greater than 10 cm<sup>3</sup>.<sup>139</sup>

### **Ovulation Induction in Women With Polycystic Ovary Syndrome**

Ovulation induction in women with PCOS is challenging owing to the range of metabolic disorders with which patients present. Some women attain menstrual regularity and ovulatory function with the administration of metformin, an insulin-sensitizing drug, but others are nonresponsive<sup>140–146</sup> (Fig. 31–12A and B). Restoration of menstrual cyclicity and ovulation induction strategies must be designed with the particular phenotype in mind.<sup>125,126,144,147,148</sup> Ovulation induction with mild or more potent ovulation inducing agents, such as clomiphene citrate or recombinant follicle-stimulating hormone, respectively, are typically used and may or may not be followed by administration of low-dose recombinant human chorionic gonadotropin (rhCG) to initiate ovulation.<sup>147,149,150</sup> GnRH agonists also may be used to help ameliorate the possibility of ovarian hyperstimulation syndrome (OHSS).<sup>151</sup> The ovarian response varies as widely as the metabolic disorder.<sup>147</sup> Some women with PCOS are refractory to clomiphene citrate, and others exhibit an exaggerated response to even the smallest doses of rFSH.<sup>129,147,152</sup> Regardless of the ovulation induction strategy employed, serial transvaginal ultrasonography is an extremely important adjunct in assessment of the ovarian response to the pharmaceutical agents used in ovulation induction of women with PCOS due to the heightened risk of OHSS.<sup>147</sup>

### **Oviduct (Fallopian Tube)**

The oviduct is difficult to visualize under normal circumstances because of the surrounding bowel and the similarities in tissue characteristics. However, it is possible to identify the oviduct from the uterine cornu, through the broad ligament, to the infundibulum in most patients (Fig. 31–13). The entire length of the oviduct is identifiable following hysterosalpingography (HSG) in women with patent oviducts. Similarly, visualization of the fimbria is more easily done following ovulation when collections of free fluid in the cul-de-sac help to outline the delicate fimbrial ends floating in the fluid (Fig. 31–14). Women with severely retroverted uteri or distended bowel present the most difficulty in imaging of the oviduct. The physical location of the uterus in the pelvis or having the oviduct surrounded by bowel containing gas pockets may render it nearly impossible to visualize. It is important to be able to develop the skill to visualize the entire oviduct from the uterus to the fimbria adjacent to the ovary consistently because transvaginal ultrasonography is



A



B

**FIGURE 31–12.** A and B. Images from patients with PCOS demonstrating recent corpus lutea. The patients' ovulatory and menstrual functions were restored with the administration of metformin.

the standard technique used to search for and evaluate early ectopic pregnancies.

### **Oviductal Pathology**

Hydrosalpinx is easily diagnosed using transvaginal ultrasound.<sup>153</sup> Fluid accumulation in the oviduct appears as anechoic areas within the defined contours of the oviduct (Fig. 31–15). If hydrosalpinx is diagnosed, there are really only two treatment options available for the patient. Surgical repair of the distal oviduct is a delicate operation and is appropriate only for patients whose mucosa remains intact. IVF appears to be the option of choice; however, the rates of implantation and clinical pregnancy are generally lower in patients with ultrasonographically visible hydrosalpinges undergoing IVF and embryo transfer. Such patients may be appropriately treated before undergoing ART. In a randomized controlled clinical trial, patients who had prophylactic salpingectomy before IVF had significantly increased pregnancy and live birth rates.<sup>154,155</sup> Typically, the dilated infundibulum and ampulla, apparently contiguous with the ovary, are seen. Small, nonpathologic aggregates of fluid



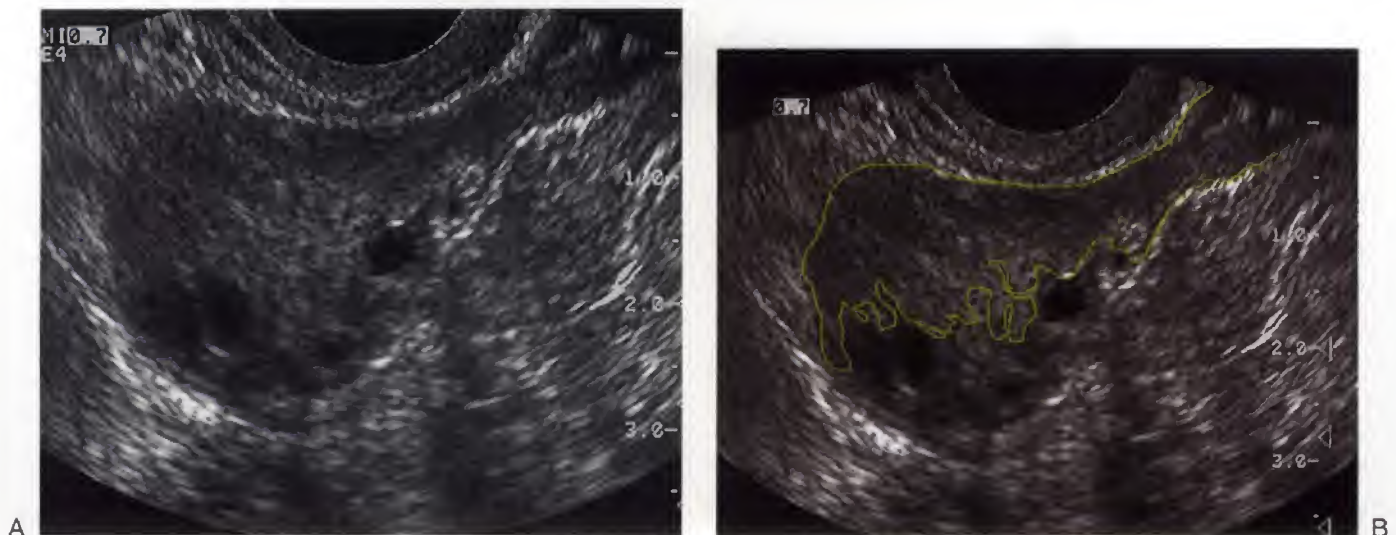


**FIGURE 31-13.** A. Image of the oviduct from the uterine cornu to the fimbria. B. The ampulla, infundibulum, and very fine interfaces representing the fimbria may be appreciated on the superior aspects of the ovaries (outline).

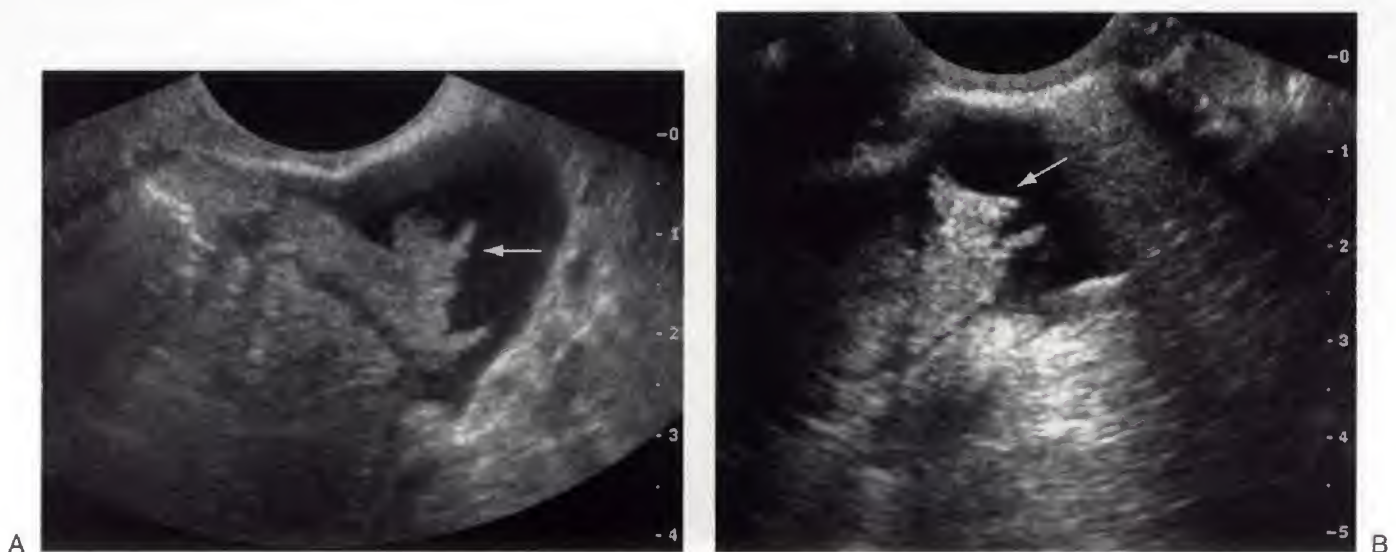


**FIGURE 31-14.** A and B. The fimbriated ends of the oviduct (arrow) are clearly visualized in free fluid surrounding the ovary following ovulation or hysterosalpingography.

may also be identified in the oviduct immediately following ovulation, intrauterine insemination, or saline-enhanced ultrasound examination.

If sufficient free fluid is present in the cul-de-sac, peritubal and periovarian adhesions may be visualized as hyperechoic foci or filmy strands when outlined by the fluid. Tubal lesions may be appreciated as irregularities, or swellings, on the otherwise smooth surface of the oviduct. In one case report, an oviductal torsion was identified preoperatively and followed allowing an appreciation of the ultrasound features associated with this rare condition.<sup>156</sup>

## Uterus

The endometrium undergoes dramatic morphologic changes mirroring the changes in ovarian follicular development and

luteal function in the ovaries during normal menstrual cycles. The endometrial detail that may be appreciated with high-resolution transvaginal ultrasonography is striking. The inner and outer strata of the endometrium may be clearly identified. The changes in echotexture of the stratum spongiosum during the follicular and luteal phases of the menstrual cycle are directly related to the circulating concentrations of estrogen and progesterone, and may be used as a bioassay from which to infer ovarian function<sup>157-161</sup> (Fig. 31-16).

The endometrium appears ultrasonographically as a thin, simple hyperechoic single stripe immediately following menses (A pattern). The stratum functionalis and basalis layers can be visually differentiated as the endometrium develops during the mid-late follicular phase (B pattern). A pronounced triple-line echotextural pattern, reflective of the

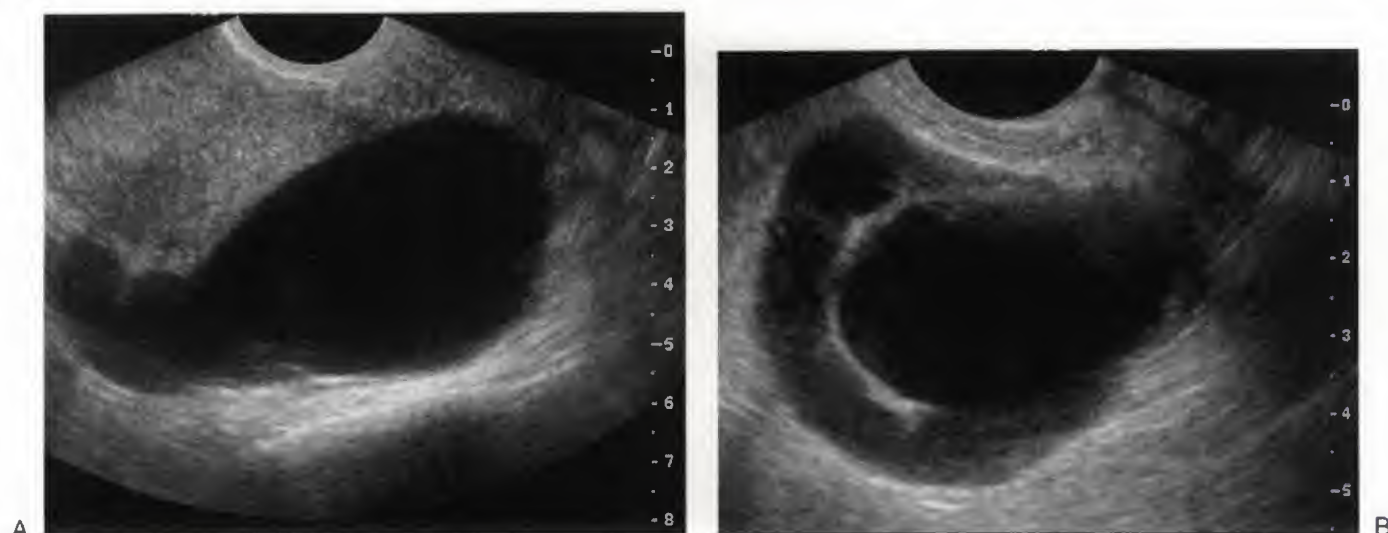


**FIGURE 31-15.** A and B. Hydrosalpinx is usually easily diagnosed as well-constrained fluid accumulation in the adnexae. In some cases, adhesions between the oviduct and ovary are visualized.

separation of the stratum basalis and functionalis layers, is observed in the periovulatory period in association with rising estradiol levels (C pattern). The triple-line pattern disappears after ovulation. After ovulation, the endometrium becomes progressively thicker and increases in echogenicity and a more homogeneous hyperechoic endometrium is observed as endometrial glands branch and expand under the influence of luteal progesterone in the secretory phase (D pattern). Visualization of active menstrual flow is indicative of menses (M pattern).<sup>157,161,162</sup> The changes in echotexture of the endometrium are well correlated to the plasma estradiol levels and defined morphologic criteria, providing an instant bioassay of its functionality.

The degree of synchronicity between the ovaries and uterus may be indicative of subtle defects in reproductive hormone production or action.<sup>161,162</sup> The presence of dominant follicles of preovulatory diameter combined with a thin, hyperechoic uterus would indicate potentially low levels of circulating estradiol. Similarly, endometrial hypertrophy in the absence of appropriate ovarian structures may be indicative of other clinical problems. The accuracy of ultrasonographic staging of the endometrium is 76% to 93% when compared with classic histologic dating.<sup>162</sup> It is important to remember to integrate the findings of the ovarian and uterine examinations; full luteal function is expected when the endometrium is at least 11 mm in thickness during the mid-luteal phase.

### Measuring the Endometrium

One highly variable endpoint in measuring the thickness of the endometrium appears to be the locations at which the measurement were taken and clear knowledge of exactly which layers to be measured. To clarify this issue, endometrial measurements should be taken using a line drawn from the endometrial-myometrial interface, on the superior to inferior aspects of the endometrial cavity, within 5 to 10 mm of the fundal aspect of the endometrium.<sup>161</sup>

Using this clearly defined location, endometrial thickness changes for the menstrual cycle in clinically normal women are demonstrable and are clearly responsive to the circulating levels of reproductively active hormones.<sup>161,163,164</sup>

### Myometrium

The myometrium apparently does not exhibit easily identifiable changes during the menstrual cycle. The echotexture appears homogenous throughout the body of the uterus. The vasculature of the uterus is distinct, especially at the interface with the broad ligament. Blood vessels in women who have previously been pregnant are demonstrably larger than those of nulligravida women and should be noted in women experiencing secondary infertility.

### Uterine Abnormalities

The American Society for Reproductive Medicine has a standardized classification scheme for müllerian anomalies that serves as the starting point for characterizing the broad spectrum of anomalies seen in clinical practice (Fig. 31-17). Congenital abnormalities in the uterine cavity may be diagnosed using high-resolution transvaginal ultrasonography and may contribute to infertility by repeated early pregnancy loss.<sup>165,166</sup> Although HSG is the usual infertility investigation dedicated to the diagnosis of uterine cavity abnormalities, it is possible to screen for anomalies such as an arcuate, unicornuate, bicornuate, or septate uterus using transvaginal ultrasonography at the time of initial referral.<sup>165-169</sup> (Fig. 31-18). Differentiation between a septate and bicornuate uterus is challenging in two-dimensional ultrasonography. However, it is important to establish the exact nature of the anomaly because the septate and bicornuate uteri are able to be repaired; however, they require two different surgical approaches.<sup>170,171</sup> (Fig. 31-19). Uterus didelphys may also be visualized as complete separation of the uterus and oviducts.<sup>170</sup>



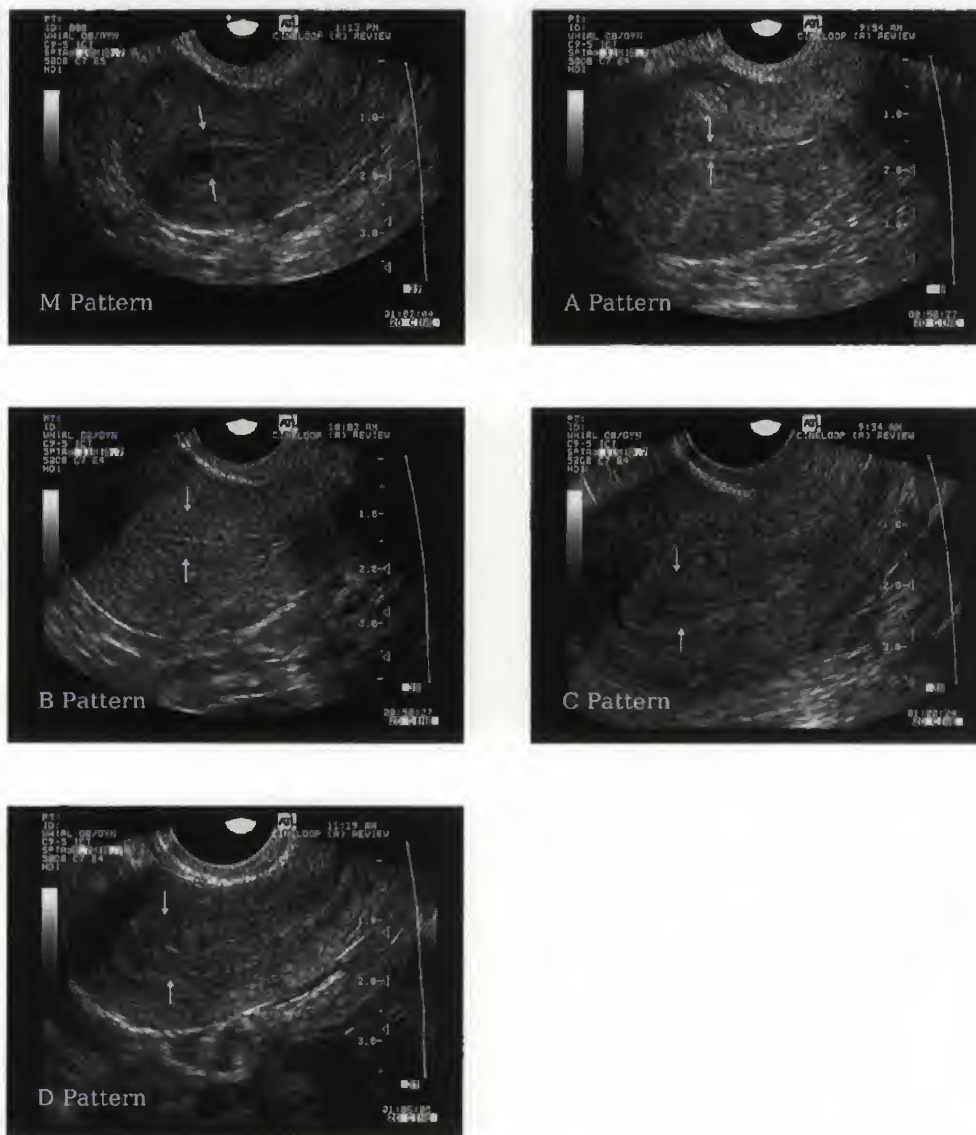


**FIGURE 31-16.** Ultrasound images of the uterus taken in the mid-sagittal plane showing the five primary patterns of endometrial development (M, A to D). For orientation, the cervix is located just out of the image to the right of the image and the fundus is seen to the left of the image. Evidence of active menstrual bleeding is observed within the uterine lumen (M). A thin, simple hyperechoic single stripe seen immediately following menstruation (A). Early follicular phase triple-line pattern indicative of increasing estradiol levels (B). Late follicular phase pronounced triple-line pattern with distinct separation of the stratum basalis and stratum functionalis observed with the high estradiol levels associated with the periovulatory period (C). Postovulation heterogenous, fully secretory endometrial pattern indicative of luteinization and exposure of the endometrial tissues to progesterone (D). Arrows identify the stratum basalis-myometrium interface. (Reprinted with permission from Baerwald AR, Pierson RA: Endometrial development in association with ovarian follicular waves during the menstrual cycle. *Ultrasound Obstet Gynecol* 24:453, 2004.)

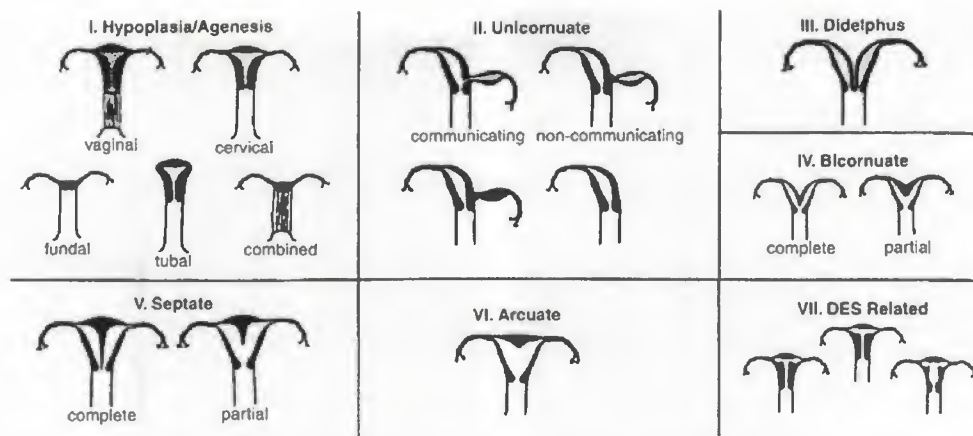


**FIGURE 31-17.** American Society for Reproductive Medicine classification scheme for müllerian anomalies. (Reprinted with permission from the American Society for Reproductive Medicine.)

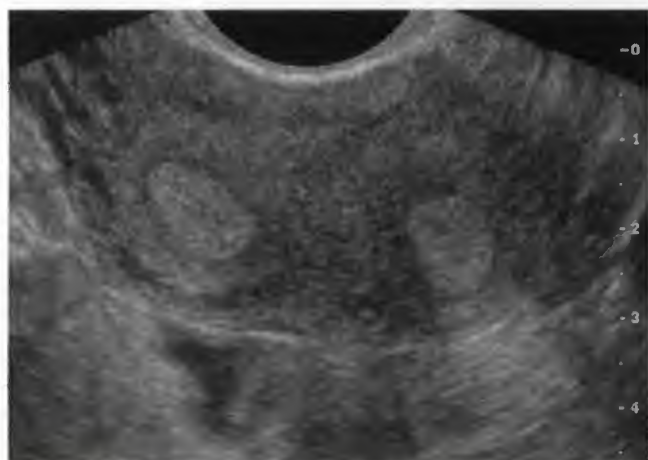


**FIGURE 31-18.** Transverse image of a bicornuate uterus identified at an ultrasound examination done at the first infertility referral visit.



**FIGURE 31-20.** Saline enhanced ultrasonographic image of a bicornuate uterus in transverse plane.



**FIGURE 31-19.** Profound bicornuate uterus with a pregnancy established in the right uterine horn. Indentation of the serosal surface is clearly visualized.

If an anomaly is suspected following ultrasonographic examination, definitive HSG or MRI may be performed. The advantages of this approach are that ultrasonography is noninvasive, is performed without contrast dye or ionizing radiation, and reduces the potential chance of infection. MRI may subsequently be used to add anatomic detail that is not currently possible with ultrasonography (Fig. 31-20). Saline-enhanced ultrasonography or hysterosalpingo-contrast sonography may provide additional diagnostic information regarding intrauterine morphology and recognition of abnormalities such as septae, polyps, synechiae, adhesions, or submucous myomas. In addition, a color flow Doppler investigation may be used to identify the vascular supply to various portions of the uterus, and it may be valuable to map vascular areas of a septum before resection.



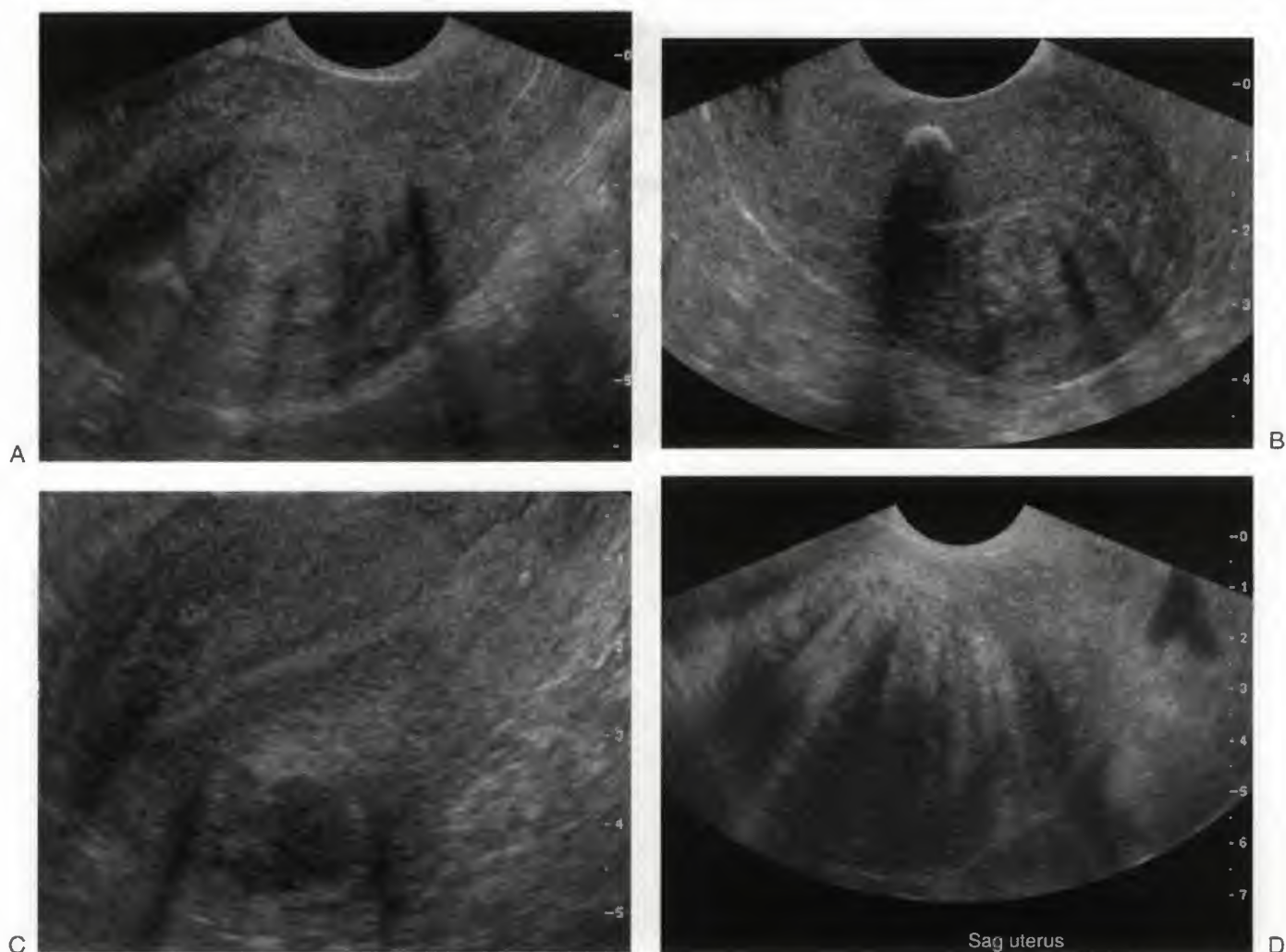


**FIGURE 31-21.** A to D. Intramural leiomyomata are frequently visualized. Examples of fibroids that compromise the contours of the endometrial cavity are shown.

### **Fibroids (Leiomyomata)**

Imaging uterine lesions has been greatly enhanced with the use of transvaginal ultrasonography.<sup>165,169,172</sup> Leiomyomata are frequently diagnosed in the myometrium, and their location and size may be mapped. The location of each fibroid and its relationship to the endometrial cavity are important considerations in infertility investigation (Fig. 31-21). Leiomyomata located in the cornu may exert pressure and effectively occlude the intramural portion of the oviduct. Similarly, fibroids that significantly alter the contour of the uterine cavity may affect the ability of an embryo to implant. Changes in the diameter and echotexture of leiomyomata in consecutive examinations may be assessed following surgical removal or GnRHa analog therapy to reduce their size. Although correlations between the presence of leiomyomata with infertility or repeated embryo loss are not clear, ultrasonography may help in elucidating putative mechanisms for the root causes of reproductive failure. It would also appear to be useful to establish a uterine map for localization of leiomyomata, especially concentrating on color flow Doppler evaluation of the vascular supply before

surgical excision. Similarly, it seems reasonable to use ultrasonographic evaluation in the decision-making process when medical treatment for size reduction is used prior to surgical removal.

### **Adenomyosis**

Tremendous strides have been made using ultrasound in the diagnosis of adenomyosis, although definitive diagnosis probably still remains within the MRI realm.<sup>173-177</sup> A combined approach of HSG and transabdominal ultrasonography has not been successful; however, adenomyosis has been successfully evaluated using transvaginal ultrasonography.<sup>172,178</sup> Uteri that demonstrate marked heterogeneity that used to be considered myomatous are now often noted to demonstrate the typical findings of adenomyosis, including small cystic change as well as hyperechogenic areas and “venetian blind” shadowing in the myometrium. Color flow mapping with transvaginal ultrasonography may be useful in the assessment of adenomyosis in some specialized centers, although it remains out of the realm of routine evaluation.<sup>179-184</sup>

### Gartner Duct Cysts

Gartner duct cysts range from 2 mm to 10 cm and are typically remnants of the embryologic wolffian duct system. Segmental failure of complete resolution of the mesonephric ducts during gestation may present in adults in the broad ligament as pockets of well circumscribed fluid along the cervix at the level of the vaginal wall. The ultrasound appearance is typically single or multiple roughly spheric hypoechoic structures along the lateral margins of the cervix and uterus.

### Nabothian Cysts

Nabothian cysts of various diameters are frequently noted at the external cervical os. The presence of these cysts is probably not noteworthy; however, the correlation of these small cystic structures with any aspects of infertility is not known.

### Hysterosalpingosonography

Assessment of tubal patency and evaluation of the uterine cavity are a basic part of an optimal infertility assessment.<sup>7</sup> Implantation failure, spontaneous abortion, or complications in the third trimester of pregnancy such as preterm labor, premature rupture of membranes, or malpresentation all may be caused by structural abnormalities or anatomic distortion of the uterus and endometrial cavity.<sup>185</sup> One estimate is that up to 10% of infertility may be related to uterine abnormalities and up to a 32% incidence has been reported in women with secondary infertility.<sup>186,187</sup> The increased incidence most likely arises from acquired uterine abnormalities following first trimester abortion or operative delivery.

It is likely that hysterosalpingosonography will replace standard HSG in the evaluation of infertility for initial assessment of the uterine cavity and tubal patency. The accuracy of sonohysterography (SHSG) versus standard HSG for uterine cavity assessment has been evaluated in several studies.<sup>188,189</sup> It is also now more frequently used in women being evaluated for abnormal uterine bleeding and recurrent pregnancy loss.<sup>190</sup> Overall, the sensitivity of SHSG is superior to that of HSG for diagnosing intrauterine abnormalities.<sup>191</sup>

### Sonohysterographic Technique

SHSG is performed by instillation of physiologic saline into the uterine cavity through a catheter such as a specially designed SHSG catheter, pediatric feeding tube, or pediatric Foley catheter and visualization of the uterus with concurrent transvaginal ultrasonography.<sup>192,193</sup> A pediatric Foley catheter is considerably less expensive but is less rigid than the SHSG catheter. SHSG performed with the Foley catheter usually requires the use of a tenaculum on the anterior cervix to ease transcervical catheter insertion. Catheters designed for SHSG can usually be inserted without using a tenaculum, which is typically more comfortable for the patient. An experienced transvaginal ultrasonographer is also an important component of a successful SHSG.

Saline is a negative (hypoechoic) contrast medium and is used to distend the cavity and outline the endometrial lumen

while the cavity is evaluated. SHSG is best performed in the follicular phase of the menstrual cycle, after menstruation, but before ovulation.<sup>194</sup> Scheduling SHSG at this time obviates the possibility of dislodging an early pregnancy and reduces false-positive results due to endometrial sloughing or blood clots that may occur in the late luteal phase of the cycle.

SHSG is best performed with the patient in a semi-upright lithotomy position. A speculum is first inserted into the vagina, and the cervix is visualized and washed with an antiseptic solution. The SHSG catheter is inserted approximately 3 to 4 cm beyond the distal aspect of the insufflation balloon, which is generally adequate to ensure that the balloon is just beyond the internal cervical os. The balloon is inflated with approximately 1 mL of normal saline to stabilize the catheter and prevent leakage of fluid back through the cervix. Care should be taken at this step to ensure that air is not introduced into the balloon. Air will create significant reflection artifacts in the image. The speculum is then removed, and the catheter left in place.

The transvaginal ultrasound probe is then gently inserted into the vagina, and the catheter balloon placement confirmed just above the internal cervical os in a sagittal plane. Normal saline (processed for intravenous use) is slowly instilled while the cavity is examined in both sagittal and transverse planes (Fig. 31–22). Documentation of findings is done either by print images or electronic acquisition and storage of digital images.

Tubal distention with normal saline and flow from the fimbriated end should be observed directly in women with patent oviducts.<sup>192,195</sup> Fluid collection in the cul-de-sac is also indicative of at least one tube being patent. Agitation of the saline before infusion can enhance visualization; the bubbles in the fluid makes it appear hyperechoic.<sup>196</sup> Saline agitation should only be done after the uterine cavity has been assessed because the reflectivity caused by the bubbles will make imaging detail much more difficult to visualize. Color flow Doppler in two- or three-dimensions may be added to the scanning protocol to assist in visualization of the movement of fluid through, and its exit from, the oviduct.<sup>197,198</sup>

One of the advantages of SHSG is that it allows evaluation of the size, shape, and contour of the uterine cavity in both the sagittal and transverse planes, and concurrent examination of the ovaries and other pelvic anatomy. This allows both identification and localization of filling defects such as polyps, fibroids, and adhesions (Fig. 31–23). The ability to evaluate the exterior uterine surface with concurrent ultrasonography helps to differentiate between septate and bicornuate uteri, two of the most commonly identified abnormalities.<sup>171</sup> The thickness of the septum and its relationship to the fundal myometrium can be measured when uterine septae are identified. The application of color flow or power Doppler interrogation helps assess the relative vascularity of the septum before resection. SHSG appears to be fully capable of replacing HSG for assessment of the uterine cavity, and a normal SHSG finding is almost as reliable as a diagnostic hysteroscopy.<sup>186,191,192,199,200</sup> Endometrial polyps or adhesions measuring less than 2mm may be difficult to identify on SHSG; however, these are likely clinically insignificant.<sup>201</sup> Three-dimensional SHSG is also an option with the new generation of ultrasound



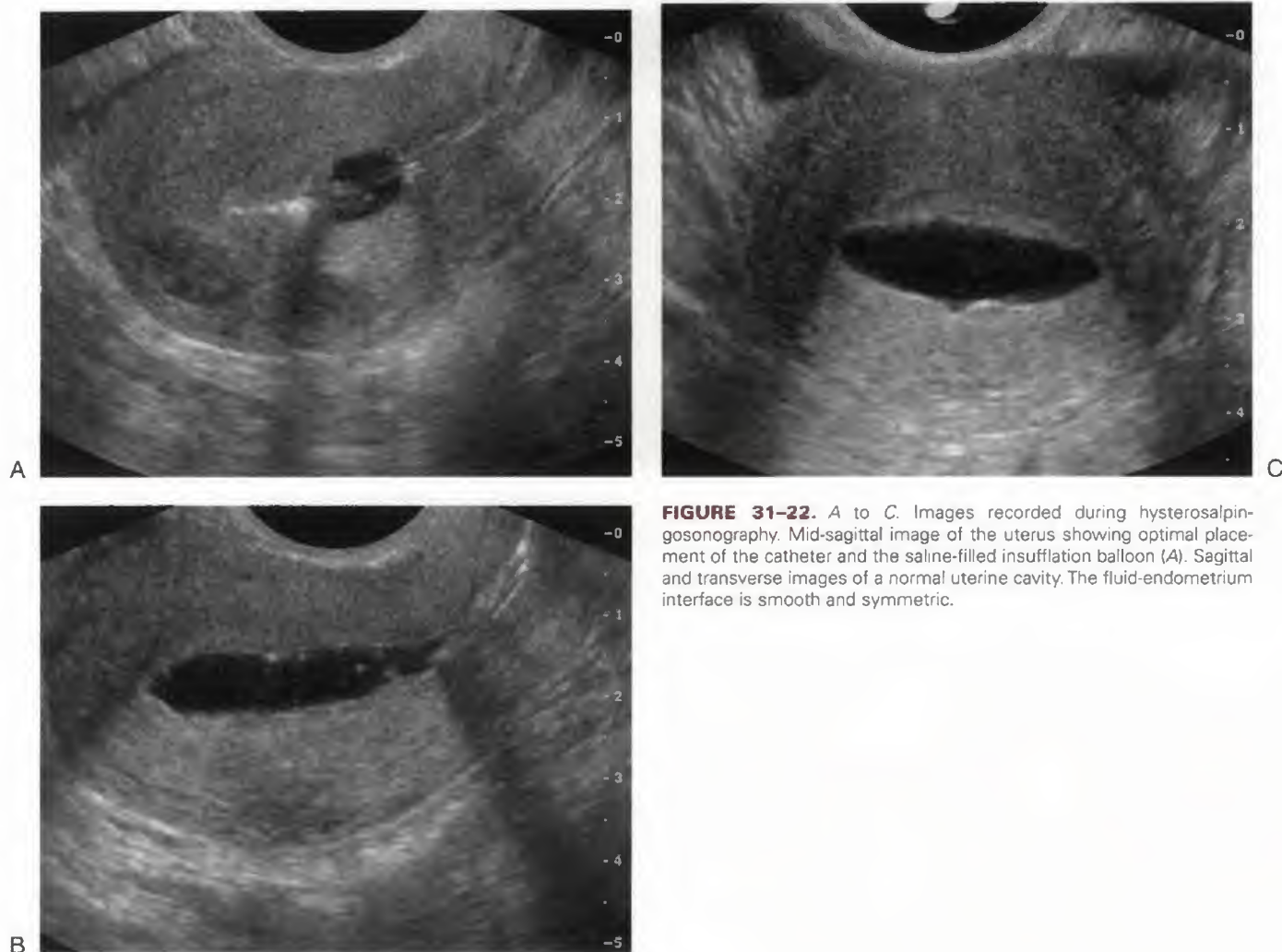


**FIGURE 31-22.** A to C. Images recorded during hysterosalpingosonography. Mid-sagittal image of the uterus showing optimal placement of the catheter and the saline-filled insufflation balloon (A). Sagittal and transverse images of a normal uterine cavity. The fluid-endometrium interface is smooth and symmetric.

instruments and add the ability to reinterrogate the volumetric data in many planes.<sup>202</sup> Coronal planes appeared to provide the most useful information in identifying relationships between lesions and the uterine cavity.

### **Contrast-Enhanced Hysterosalpingosonography**

If tubal assessment with saline alone is unsatisfactory, a contrast medium such as Echovist can be used.<sup>203</sup> Echovist is a positive contrast media that consists of a stabilized mixture of microbubbles mixed with microparticles of galactose that are highly echoic. The purpose of contrast agents is to increase the delineation and identification of anatomic structures in the ultrasonographic image by enhancing visualization of the fluid that is used.<sup>168</sup> Contrast agents also enhance the visualization of flow from the fimbrial end of the oviduct because perturbation of the contrast media creates easily visualized swirls on the ultrasound image as it exits the oviduct.

## **ULTRASONOGRAPHY IN ASSISTED REPRODUCTIVE TECHNOLOGY THERAPY**

### **Monitoring the Course of Ovarian Stimulation**

Ovarian stimulation protocols vary tremendously and have evolved from fairly simplistic administration of exogenous hormones derived from urinary sources to quite sophisticated blends of GnRH analogs, recombinant FSH, and LH and other compounds. Ultrasonography is used to determine the direct effects of the stimulatory drugs on the ovaries in all ovarian stimulation protocols. Ovarian stimulation protocols are changing constantly as new knowledge is incorporated into clinical practice; however, the goal of each is to override the physiologic mechanism of selection of a single dominant follicle and facilitate the development of many follicles so that properly matured oocytes may be retrieved for use in the ART. Ultrasonography is essential in determining the

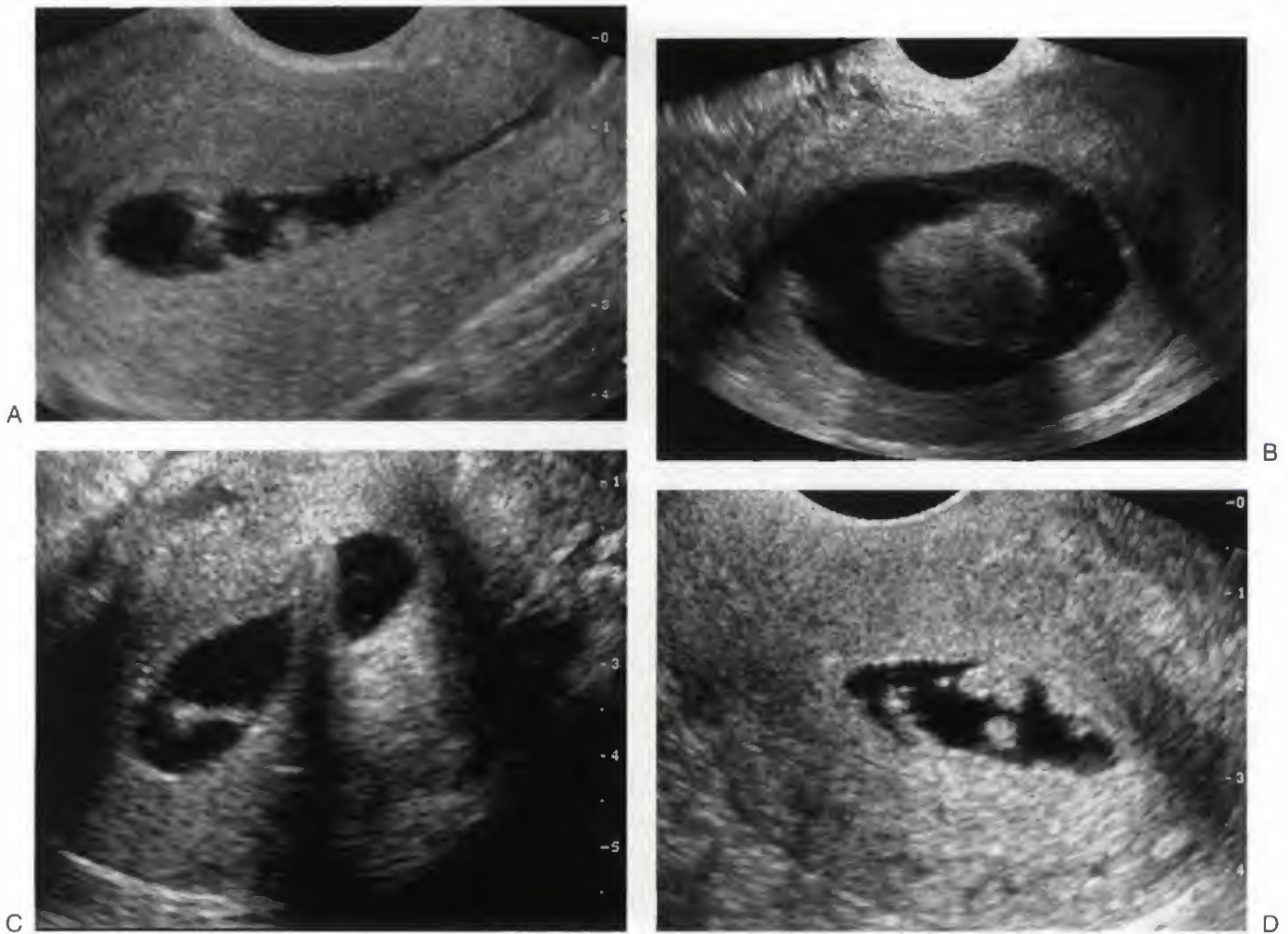


**FIGURE 31-23.** A to D. Images of endometrial polyps and adhesions recorded during hysterosalpingosonography. Sonohysterography is very helpful in identifying small and large lesions that are difficult to appreciate on unenhanced ultrasonography.

numbers and fates of individual follicles stimulated by exogenous gonadotropin at each step. It is essential to tailor the ovarian response of each woman to the stimulation protocol and the number of oocytes desired and balanced against clinical assessment of the risk of ovarian hyperstimulation. The daily doses of gonadotropins may be increased or decreased depending on the patient's response. The relationships between circulating estradiol concentrations and follicular diameter that we may infer from natural cycle studies often do not exist during ovarian stimulation. We understand that not all follicles probably contribute equally to estradiol concentrations in the systemic circulation and that not all follicles will give rise to physiologically competent oocytes.

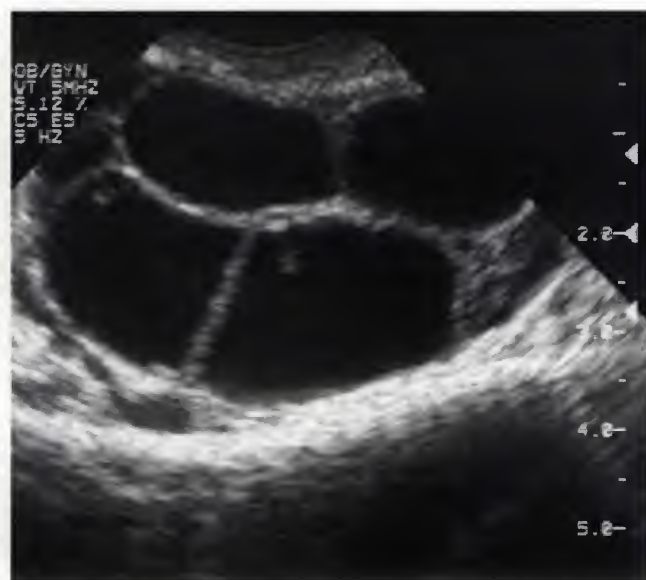
In all of the ART ovarian stimulation protocols, regardless of their technical complexity in the laboratory, the timing of hCG or recombinant LH administration is critical to establish a time for oocyte retrieval which will yield the highest quality of oocytes in the proper stage of development with the highest probability of fertilization. Although transabdominal ultrasonography has been used historically,

transvaginal ultrasonography is now the standard that we have for monitoring the course of follicular growth and development.<sup>204</sup> With ultrasonography, we have a rapid, noninvasive, and highly visual approach to following the fates of individual follicles and cohorts of follicles. When we combine our knowledge of natural ovarian physiology with concomitant assessment of circulating estradiol concentrations and oocyte development, we use this information to predict optimal timing for induction of the final stages of folliculogenesis and oogenesis and oocyte retrieval<sup>50,52,205-207</sup> (Fig. 31-24A and B).

The final phases of follicular maturation before oocyte retrieval are typically triggered using hCG in its native or a recombinant form when the largest follicle attains a predetermined diameter (e.g., 18 to 20 mm). The timing of hCG administrations varies based upon the attending physician's feel for the patient's stimulation cycle and the logistics imposed by the embryology laboratory. A dose of 10,000 IU of hCG is most commonly administered, and oocyte retrieval is scheduled 30 to 34 hours thereafter. In centers that do ovarian stimulations followed by ovulation



A



B

C



**FIGURE 31-24.** A and B. Images recorded at the end of ovarian stimulation protocols. Four large follicles may be identified within the ovary; however, only one follicle is observed in its largest dimension (A). The other follicles are seen only in glancing section. Expanded cumulus-oocyte complexes are observed still attached to the follicle wall (B). C. Multiple ovulation sites may be visualized following ovarian stimulation and ovulation induction. In this image, four distinct sites of follicular rupture are visualized.

induction and intrauterine insemination, the fates of the follicles should be determined. The number of ovulations and ovulation failures are important to document in each stimulation cycle (Fig. 31-24C). Many programs use only ultrasonographic monitoring to determine the course of ovarian stimulation, and it has been demonstrated that including estradiol monitoring during the stimulation protocol seldom changed the timing of hCG administration and did not affect pregnancy rates or the risks of ovarian hyperstimulation syndrome (OHSS).<sup>208</sup> Volumetric ultrasound has been employed to help identify patients at risk for OHSS based on new developments in three-dimensional ultrasonography. There was a significant correlation between three-dimensional volume of the ovary on the first day of ovarian stimulation and the subsequent occurrence of OHSS.<sup>209</sup>

The relationships between follicle size and oocyte maturity remain mysterious. Follicle size remains the best way to estimate oocyte maturity, and oocyte maturity is clearly an

influence on the probability of conception and the ability of an embryo to develop into a successful pregnancy.<sup>48,50,52,210-213</sup> Although we know that mature oocytes yield the highest fertilization rates, through recent developments in the embryo laboratory, we know that in vitro maturation (IVM) and fertilization are viable ideas in ART practice.<sup>214,215</sup> The role of ultrasonography in IVM-IVF protocols will very definitely revolve around the optimal timing of oocyte retrieval for optimal fertilization and cleavage rates.<sup>215-218</sup> Ovulation has been reported from follicles as small as 14 mm, and oocytes collected from small follicles are certainly capable of being fertilized. In a recent study, oocytes from follicles less than 10 mm in diameter and IVM were used to increase the number of transferable embryos.<sup>219</sup>

Power Doppler ultrasonography assessments of perifollicular vascularity are beginning to show promise in the prediction of ART cycle outcomes.<sup>48,50,52</sup> When combined with knowledge obtained through research in animal models, we know that there is a correlation between computer-

assisted ultrasound image attributes of follicles and the ability of the oocyte to fertilize; however, similar studies in humans have apparently not yet been completed.<sup>51</sup>

Examination of growth rates for individual follicles may be useful in predicting the number of follicles that may develop as a result of ovarian stimulation. This information is equally important when assessing the risks of OHSS.<sup>220,221</sup> In the past, follicular growth rates during induced cycles were observed to be faster than those of natural cycles.<sup>222</sup> Growth rates of follicles in spontaneous cycles were similar to those recruited by hMG therapy in a report based on a mathematical equation developed to equate follicular growth rate to follicular age.<sup>223</sup> Reduced follicle growth rates were observed in cycles in which a pregnancy was established and it was concluded that growth rate was a more useful characteristic for prediction of ovulation than follicular diameter.<sup>224</sup> Follow-up work does not appear to have been done.

It will be logistically challenging to combine daily detailed ultrasound measurements of individually mapped follicles with per follicle fertilization and conception outcomes from the embryo laboratory and final pregnancy outcomes. However, the rationale that follicular growth rates may be more accurate in predicting the actual maturity of the ova is intriguing. Recent detailed studies on follicular growth have shown that follicles grow at approximately 1.5 mm per day regardless of whether they developed during natural menstrual cycles, oral contraceptive cycles, or during ovarian stimulation.<sup>24,25</sup> These data fit well with a new mathematical model developed to predict the response to ovarian stimulation based on daily data on follicular growth rates.<sup>12,24,25,91,225</sup>

## Ovarian Hyperstimulation Syndrome

OHSS is a potentially serious complication of ovarian stimulation that is primarily iatrogenic, although spontaneous OHSS is possible.<sup>220,226–229</sup> Ultrasonography in women with OHSS typically shows grossly enlarged ovaries containing numerous large follicular cysts with thin, highly echogenic borders, and dramatically increased local blood flow<sup>55</sup> (Fig. 31–25). The ovaries may enlarge to diameters in excess of 10 cm, and echotexture interpreted as intrafollicular hemorrhage in some of the large cysts frequently may be observed. If a pregnancy is established, OHSS is exacerbated.<sup>221,226,227</sup> Extreme cases may require abdominal paracentesis and result in drainage of several liters of ascitic fluid.

Serial ultrasound examinations during ovarian stimulation cycles and careful tailoring of the dose of exogenous gonadotrophins has helped to limit the risk of OHSS.<sup>53,208,209,230,231</sup> Clinicians may take an active role in the prevention of OHSS by aborting the treatment cycle altogether, or “coasting” the final days of the treatment cycle.<sup>209,232–234</sup> Coasting refers to continuing to allow follicular development but withholding administration of additional gonadotropins and performing oocyte aspiration after 1 to 3 days of unstimulated development.<sup>233–235</sup> If oocyte aspiration is performed when excessive numbers of pre-ovulatory follicles develop in association with markedly elevated serum estradiol concentrations and the risk of OHSS is high, single-embryo transfer may be done, or all embryos may be cryopreserved and single embryos replaced



**FIGURE 31–25.** Transvaginal ultrasound image of a woman with moderate ovarian hyperstimulation syndrome. Both ovaries are observed in the posterior cul-de-sac. The ovaries are in close contact and displace the uterus anteriorly. Both ovaries contain several large unruptured follicles.

in a subsequent cycle when the danger of establishing a pregnancy has passed.<sup>230–232,234,236,237</sup> If OHSS occurs, transvaginal ultrasound-guided aspiration of the ascitic fluid may be performed.<sup>221,236</sup> If torsion of an enlarged OHSS ovary is suspected, color flow Doppler imaging can help to establish an early and accurate diagnosis.<sup>221–233,235,238–240</sup>

## Ultrasound-Guided Oocyte Retrieval

The most visible use of ultrasound imaging in IVF has been the tremendous advance facilitated by transvaginal retrieval of oocytes.<sup>241–251</sup> Oocyte retrieval was a procedure-limiting step when IVF was first done. Retrievals were done laparoscopically or using ultrasound guidance from transurethral, transvesicular, or transabdominal approaches.<sup>244,247,251–254</sup> The advent of transvaginal transducers and concerted efforts to develop effective, accurate tracking of the needles used for follicle aspiration was probably the single most important step in making IVF as safe and effective as it is today.<sup>241,249–251,255–259</sup>

Retrieval of oocytes in IVF cycles is now routinely performed under ultrasound guidance.<sup>245</sup> An aspiration needle introduced through a guide attached to a transvaginal probe is inserted into first one ovary, then the other, through the vaginal fornices (Fig. 31–26). Almost all aspiration needles now in common use have a small band of highly reflective surface near the tip of the needle. The needle tip can be observed directly as it is guided into the ovaries and maneuvered into each follicle. The follicular fluid containing the oocyte/cumulus complex is then aspirated by application of gentle suction. The walls of the follicle collapse as the fluid is aspirated and the needle moved within the follicle to ensure that all of the follicular fluid is withdrawn. The path of the needle also may be estimated accurately by biopsy guide lines imposed on the ultrasound screen.



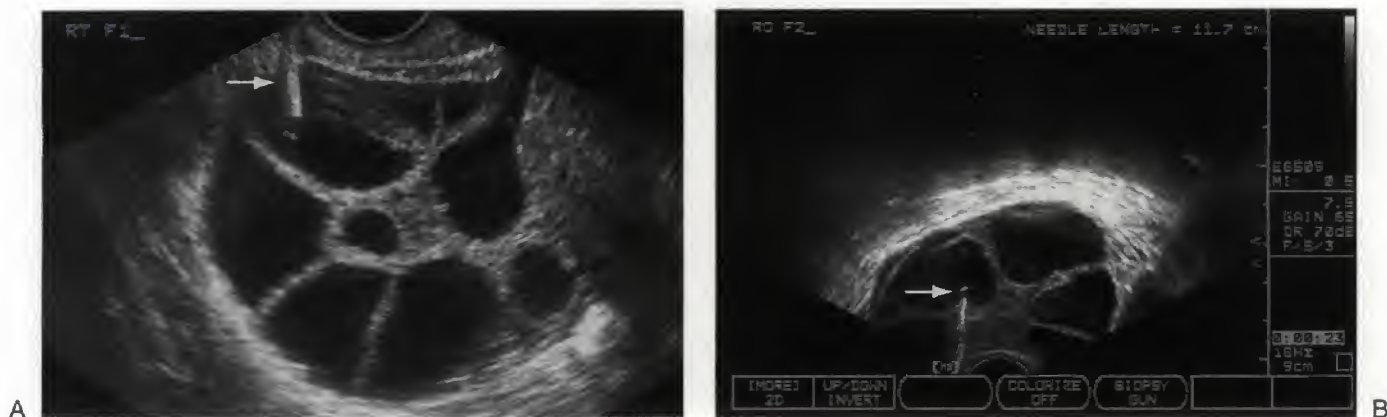


**FIGURE 31-26.** A and B. Ultrasound-guided oocyte retrieval. In both images, the oocyte collection needle may be visualized entering into a large follicle (arrow). The hyperechoic ring around the tip of the needle enhances its visualization. Image A is presented in the standard medical imaging orientation. Many assisted reproductive technology clinicians prefer the more gynecologically oriented image, as presented in B. (Images courtesy of Roger Stronell, MD.)

There are two main types of aspiration needles used for oocyte retrieval, single- and double-lumen needles. Single-lumen needles typically have a smaller diameter and tend to cause less discomfort.<sup>245</sup> The double-lumen needles were developed for a technique involving constant infusion of oocyte collection media into the follicle at the same time as the follicular fluid is being removed. The double-lumen flushing technique is thought to increase the turbulence within the follicle, assist in dislodging the oocyte-cumulus complex from the follicle wall, and increase the chances of oocyte collection. In many, if not most, IVF centers, follicle aspirations are performed using single-lumen needles and no follicle flushing. All of the follicular fluid is first aspirated from the follicle then the follicle is then refilled with collection medium and reaspirated. A gentle back-and-forth motion on the plunger of the infusion syringe may be used to increase the turbulence of flow, which helps to increase the rate of oocyte retrieval. Swirling of the medium within the follicle may be easily visualized on the ultrasound screen. A prospective, randomized trial and a retrospective examination of 2378 cases comparing flushing techniques with no flushing demonstrated no significant differences in the number of oocytes retrieved; however, the overall time required for retrieval in women whose follicles were flushed was increased.<sup>245,260,261</sup> The complication rates of oocyte retrieval are reportedly extremely low and almost all procedures are performed under conscious sedation on an outpatient basis.<sup>248,256,257,262-267</sup>

Unsuccessful oocyte retrieval following apparently normal ovarian stimulation reportedly occurs in 1% to 7% of cycles—the so-called “empty follicle syndrome.” The etiology appears to be multifactorial and may involve both technical and biological mechanisms.<sup>245,268</sup> Technical aspects of failure to retrieve oocytes include errors in administration of the hCG used to trigger the final phases of follicular maturation or difficulties with the quality of hCG used. In other patients, unsuccessful oocyte retrieval may be due to ovarian dysfunction underlying the root cause of the infertility.<sup>268</sup>

## Endometrial Assessment at the Time of Embryo Transfer

Correlation of the probability of implantation with the thickness of the endometrium when fertilized ova are transferred into the uterus following IVF has been addressed in several studies.<sup>269</sup> Ultrasonographic evaluation of the endometrium may have predictive value for the outcome of treatments to ameliorate infertility; however, the literature is diverse and, in many cases, contradictory. Definitive studies allowing us to draw decisive conclusions are required before we can apply predictive analysis of the endometrium to routine clinical care of infertile women.

## Spectral Doppler and Color Flow Doppler Ultrasonography

Doppler ultrasonography of the uterine arteries has had a confusing history in the literature at least partially because of lack of differentiation between spectral Doppler and color flow Doppler imaging. Early studies tended to be based upon spectral Doppler examinations, that may be used to evaluate the resistance to blood flow by measuring the pulsatility index (PI), resistance index (RI),  $V_{max}$ , or the systolic to diastolic ratio (S/D ratio).<sup>270</sup> Color flow Doppler imaging detects directional motion of blood flow either toward or away from the transducer (Fig. 31-27). Power Doppler imaging is used to turn motion in any direction into a visually discernable color overlay on the two- or three-dimensional ultrasound image.<sup>270,271</sup>

Initial attempts to determine if evaluation of blood flow in the uterine arteries could be useful were based on RI calculations to look for differences in uterine receptivity. In a small study, no differences were found between women who conceived and those who did not.<sup>272</sup> Grouping data into low, medium, and high categories of PI of the uterine arteries was not useful in distinguishing between conception and nonconception cycles; however, no pregnancies were established in the women with high PI values.<sup>273</sup> Elevated

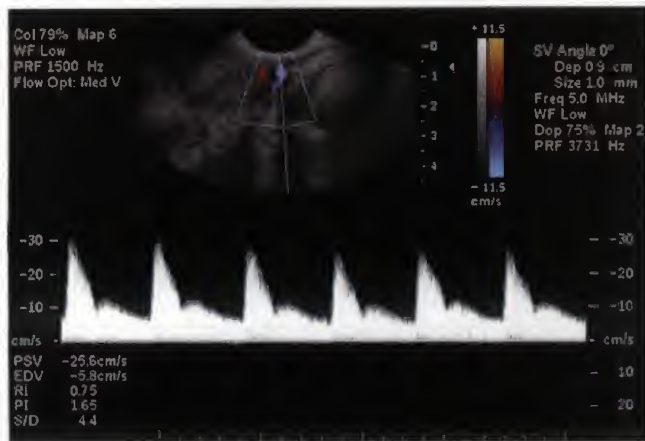


**FIGURE 31-27.** Combined color flow and spectral Doppler image demonstrating placement of the Doppler gate directly into the path of the uterine artery. The spectral Doppler trace is represented by the waveform just below it. Vascular indices representing resistance to flow are calculated automatically and displayed on the lower left aspect of the image.

PI, as a measure of impedance to vascular flow in the uterine artery, was associated with a significantly lower pregnancy rate.<sup>274</sup> Assessing the uterine artery RI was inconclusive, except that absent or low diastolic flow was associated with failure to conceive and PI in women undergoing cryopreserved embryo transfer cycles were lower in women who became pregnant than those who did not conceive.<sup>275</sup> Uterine artery vascular impedance measured by RI was not found to be useful for predicting the probability of pregnancy, but if the PI was greater than 0.79 before hCG administration, poor uterine vascular perfusion was assumed.<sup>276</sup> No further reports on this speculation were found. PI and RI in the uterine arteries were reported to be lower in conception cycles, although there was overlap in the confidence intervals. It was suggested that a PI greater than 3.3 and an RI greater than 0.95 before embryo transfer were associated with a low probability of conception.<sup>277</sup> However, these conditions were met in only 9% of the cycles in the study.<sup>277</sup> Furthermore, a study of women undergoing cycles to produce embryos using intracytoplasmic sperm, reported no differences in the PI on the day of embryo transfer between conception and nonconception cycles.<sup>278</sup>

In a critical review of the literature prior to 1996, some ultrasonographically detectable criteria were associated with negative pregnancy outcomes, although no prognostic value was observed in any measurement of vascular perfusion.<sup>279</sup> A more recent study seems to confirm the results that women who conceived exhibited lower PI than those who did not.<sup>280</sup>

Endometrial perfusion studies on the day of hCG administration consistently reported that values for PI and  $V_{max}$  were not different regardless of whether or not conception occurred. However, when only the color flow data were examined, absence of detectable subendometrial vascular flow, indicative of poor vascular penetration, was associated with failure of implantation.<sup>281</sup> Subendometrial

or intraendometrial vascular flow on the day of embryo transfer appears to be an indicator for maintaining a pregnancy.<sup>282,283</sup> Intraendometrial flow estimates in a study using power Doppler imaging to examine only women with an endometrial thickness greater than 10 mm demonstrated that women with color areas less than 5 mm<sup>2</sup>, based upon calculation of the maximal area that showed evidence of motion, to be associated with a lower pregnancy rate.<sup>283</sup> More recently, spiral arterial flow and uterine artery flow were not demonstrably different between pregnant and nonpregnant women; however, if spiral arterial flow could not be detected, conception did not occur.<sup>284</sup>

### Imaging-Based Uterine Scoring System

An imaging-based scoring system to predict uterine sensitivity was proposed in the mid 1990s, which appears to have been based upon an earlier uterine biophysical profile system.<sup>285,286</sup> The scoring system was designed by assigning “points” for various criteria and then adding the cumulative columns. Comparisons of uterine scores in women who conceived and those who did not were not different in any of the criteria evaluated, including endometrial thickness, endometrial pattern, PI, RI, color Doppler, and other vascular indices. Development of the scoring system appears to have ceased.

### Three-Dimensional Imaging of the Endometrium

Three-dimensional ultrasonography first became available in the late 1990s, and it is now a part of almost all high-end imaging systems. There are several methods used to provide three-dimensional information, and there do not appear to be any studies comparing the same endpoints with different imaging systems or different three-dimensional imaging techniques.<sup>287</sup> Prediction of the probability of implantation in ART programs has now extended into three-dimensional exploration of endometrial receptivity.<sup>288</sup> Conclusive indicators have not been determined.

Pregnancy and implantation rates were significantly lower in women with endometrial volumes of less than 2 mL when compared among women who conceived and those who did not. Yet, no pregnancies were established when endometrial volumes were less than 1 mL. No relationship between three-dimensional volume of the endometrium and conception was found in a contemporary study.<sup>288,289</sup> Similarly, no correlation was found among estradiol levels, endometrial thickness, or endometrial volume, leading to the conclusion that there was no predictive value in assessing endometrial volume. Endometrial thickness and endometrial volumes were not correlated with probability of pregnancy; however, three-dimensional power flow Doppler indices used to measure endometrial perfusion may have some predictive value.<sup>271,284,290,291</sup> Spiral artery blood flow measurements in three dimensions had positive predictive value when performed on the first day of ovarian stimulation, whereas women who became pregnant had lower RI and a higher three-dimensional flow index than those who did not.<sup>271,284</sup> Taken together, these observations provide a rationale for further investigation, although it is clear that a predictive index is beyond the limits of our current understanding.



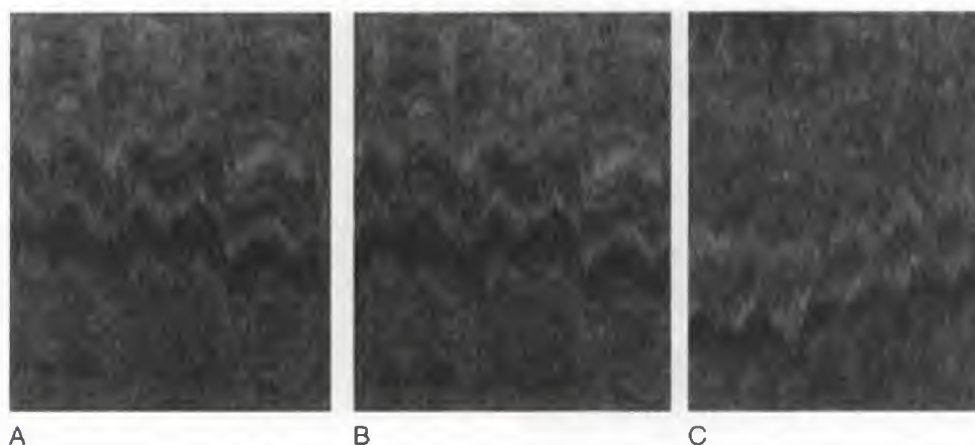


**FIGURE 31-28.** A to C. Motion analysis graph demonstrating endometrial contractility over time. Each image represents 1.5 minutes. Women with slow (A; three contractions per minute), medium (B; five contractions per minute), and fast (C; seven to eight contractions per minute) uterine contractions are shown. The amplitude and frequency of the contractions may be easily visualized and measured.

### Motion Analysis

Direct measurement of subendometrial contractions is a method of assessing endometrial function based on the observation that the uterus and endometrium are in constant motion.<sup>292-299</sup> Objective assessment of subendometrial contractions applied to ART cycles for prediction of successful pregnancy has yielded some interesting results.<sup>300-302</sup> To conduct motion analysis, a computer is interfaced with the ultrasound scanner, digital image frames are acquired, and the pixels comprising the area of interest on the endometrial image along a single line are isolated. A line is serially acquired from images taken one or two times per second over a 5- to 10-minute period, the pixel data from the line are concatenated and the result is displayed as a graph of the velocity and amplitude of endometrial contractions (Fig. 31-28). Conceptually, this technique is similar to a high resolution version of M-mode ultrasound.

Assessment of subendometrial contractions may have a predictive effect on the probability of pregnancy.<sup>296,301</sup> Women with a higher frequency of uterine contractions had lower pregnancy rates.<sup>301</sup> However, contradictory evidence has been reported.<sup>303</sup> Exogenous progesterone administration on the day of embryo transfer reduced uterine contractility, and it has been hypothesized that progesterone supplementation before embryo transfer may improve the probability of pregnancy by reducing the possibility that the contractions may expel the embryos.<sup>302,304,305</sup> The biologic effects of progesterone on uterine contractions were demonstrated by the observation that higher progesterone concentrations correlated with lower amplitude and frequency uterine contractions.<sup>297,305</sup> It has been suggested that progesterone could be administered prophylactically to reduce the frequency and amplitude of endometrial contractions. Progesterone intervention may have a positive impact on pregnancy rates, although this hypothesis does not appear to have been critically tested.<sup>306</sup> Endometrial contractions at the time of blastocyst transfer were lower and reached a nadir 7 days after hCG administration in IVF cycles. The slightly later time of blastocyst transfer was



**FIGURE 31-29.** Embryo transfer is enhanced by the use of ultrasound guidance to place the embryos at the optimal uterine location. Small hyperechoic areas (arrows) represent microbubbles of air expelled from the transfer pipette and serve to visualize embryo placement. (Image courtesy of Roger Stronell, MD.)

hypothesized to coincide with lower amplitude and frequency of contractions, thus facilitating implantation.<sup>306</sup>

### Ultrasound-Guided Embryo Transfer

Optimal embryo placement in the uterine cavity is increasingly important in enhancing the probability of a successful pregnancy.<sup>307-317</sup> Ultrasonography is now routinely used to guide placement of the embryo transfer catheter to increase pregnancy rates (Fig. 31-29). Transabdominal ultrasound guidance is a more common means of directing embryo transfer catheter placement; however, transvaginal scanning may also be used.<sup>314,318</sup> Ultrasound guidance of embryo replacement does not prevent the establishment of an ectopic gestation.<sup>319</sup> This observation may be interpreted to mean that the early human embryo may be mobile within the uterus before attachment and nidation. Three-dimensional

ultrasonography has opened new inquiries into the three-dimensional guidance of the embryo transfer catheter.<sup>316,320</sup> Three-dimensional imaging may prove to be an advantage in identifying the optimal site for embryo placement.

Clinical and laboratory preparations for embryo transfer are the same, regardless of whether the transfer is to be ultrasound guided or not. Patients are placed in a lithotomy position, and a bivalve speculum is used to visualize the cervix. After mucus and secretions are removed by cleansing with culture media, the tip of the transfer catheter is introduced into the cervix. A 3- to 4-MHz large aperture transabdominal transducer is placed on the lower abdomen and pelvis in a sagittal plane, and the uterus and cervix are imaged through a full bladder window.<sup>313,321,322</sup> Most embryo transfer catheters are easily visualized as a pair of highly echogenic lines within the endocervical canal. A transfer catheter system has been developed to increase the ease of imaging if the clinician has difficulty visualizing the standard catheters.<sup>323</sup> Once the catheter has been identified, the tip is carefully guided through the uterine lumen using real-time imaging. Once the clinician attains the optimal place within the uterus, the embryos are gently expelled.<sup>324</sup> The fluid droplet containing the embryos is visualized as a very small hypoechoic reflection deposited at the tip of the transfer catheter. Transvaginal ultrasound guidance is done similarly, except that a probe designed for intracavitary use is introduced through the speculum and placed into contact with the anterior vaginal fornix.<sup>314,318</sup> The transfer catheter is visualized, and the tip is guided to the uterine location selected by the clinician. There is varied opinion on exactly what optimal embryo placement means.<sup>325-328</sup>

The usefulness of ultrasonographic guidance during embryo transfer versus nonvisually guided clinical touch remains controversial.<sup>311,317,321,327,329-334</sup> Some clinicians prefer to rely on ultrasound guidance for mock transfers in cycles before IVF and embryo transfer and clinical touch in the actual procedure. Other practitioners use ultrasound guidance for all procedures, and still others make a decision regarding its use based on whether or not the transfer is likely to be classified as easy or difficult.<sup>317,322,335</sup> Two recent meta-analyses and a subsequent randomized controlled trial were interpreted to mean that transabdominal ultrasound guidance versus clinical touch for embryo transfer significantly increased pregnancy rates although the rates of miscarriage, ectopic pregnancy and multiple pregnancy were not affected.<sup>333,336-338</sup>

## CONCLUDING REMARKS

Ultrasonography has critical roles in our ability to increase our understanding of normal reproductive processes, diagnose the root causes of many different aspects of infertility, and act as our eyes in administering therapy to ameliorate the inability to conceive. It is difficult to imagine where our knowledge of how to best help couples suffering from infertility would be without the diagnostic information and ability to intervene in a world in which ultrasonography did not exist. The techniques for understanding changes in the reproductive organs over time have allowed us unprecedented depth in understanding folliculogenesis, ovulation, luteal function, endometrial response, conception, and implantation. We believe that ultrasonography is the most profound tool

that we have yet acquired to understand human reproduction and that advanced imaging technology, as it continues to evolve, will be indispensable in exploring the deepest reaches of our reproductive biology.

## References

1. Baird P: Proceed with Care: Final Report of the Royal Commission on New Reproductive Technologies, Vol 1. Ottawa, Ontario, Canada Communications Corporation; 1993.
2. Mosher W, Pratt W: Fecundity and infertility in the United States: Incidence and trends. *Fertil Steril* 56:1517, 1991.
3. Wilcox AJ, Weinberg CR, Baird DD: Timing of sexual intercourse in relation to ovulation. Effects on the probability of conception, survival of the pregnancy, and sex of the baby. *N Engl J Med* 333:1517, 1995.
4. Hilgers TW, Daly KD, Prebil AM, et al: Cumulative pregnancy rates in patients with apparently normal fertility and fertility-focused intercourse. *J Reprod Med* 37:864, 1992.
5. te Velde EE, Pearson P: Female Reproductive Aging. London, Taylor & Francis, 2000.
6. Belisle S, Pierson RAE: CFAS Consensus Document for the Investigation of Infertility. Montreal, Quebec, Canadian Fertility and Andrology Society, 2002.
7. Practice Committee of the American Society for Reproductive Medicine: Optimal Evaluation of the Infertile Female. *Fertil Steril* 82(Suppl 1):S169, 2004.
8. Timor-Tritsch I, Ruttem S: Transvaginal ultrasonography in the management of infertility. In Kurjak A (ed): *Ultrasound and Infertility*. Boca Raton, FL, CRC Press, 1989.
9. Goldstein S, Snyder JR, Watson C, et al: Very early pregnancy detection with endovaginal ultrasound. *Obstet Gynecol* 72:200, 1988.
10. Fossum G, Davajan V, Kletzky O: Early detection of pregnancy with transvaginal ultrasound. *Fertil Steril* 49:788, 1988.
11. Rempen A: Diagnosis of viability in early pregnancy with vaginal sonography. *J Ultrasound Med* 9:711, 1990.
12. Baerwald AR, Adams GP, Pierson RA: Characterization of ovarian follicular wave dynamics in women. *Biol Reprod* 69:1023, 2003.
13. Baerwald AR, Adams GP, Pierson RA: A new model for ovarian follicular development during the human menstrual cycle. *Fertil Steril* 80:116, 2003.
14. Gougeon A: Dynamics of human follicular growth: a morphologic perspective. In Adashi E, Leung P (eds): *Comprehensive Endocrinology: The Ovary*. New York, Raven Press, 1993, pp 21-39.
15. Gougeon A, Lefevre B: Evolution of the diameters of the largest healthy and atretic follicles during the human menstrual cycle. *Reprod Fertil* 69:497, 1983.
16. McGee E, Hsueh A: Initial and cyclic recruitment of ovarian follicles. *Endocr Rev* 21:200, 2000.
17. Pellicer A, Gaitin P, Neuspiller F, et al: Ovarian follicular dynamics: from basic science to clinical practice. *J Reprod Immunol* 39:29, 1998.
18. Gougeon A: Qualitative changes in medium and large antral follicles in the human ovary during the menstrual cycle. *Ann Biol Anim Bioch Biophys* 19:1464, 1979.
19. Adams GP, Pierson RA: Bovine model for study of ovarian follicular dynamics in humans. *Theriogenology* 43:113, 1995.
20. Adams GP, Matteri RL, Kastelic JP, et al: Association between surges of follicle-stimulating hormone and the emergence of follicular waves in heifers. *J Reprod Fertil* 94:177, 1992.
21. Baird DT: A model for follicular selection and ovulation: Lessons from superovulation. *J Steroid Biochem* 27:15, 1987.
22. Ginther OJ, Beg MA, Gastal EL, et al: Systemic concentrations of hormones during the development of follicular waves in mares and women: a comparative study. *Reproduction* 130:379, 2005.
23. Ginther OJ, Gastal EL, Gastal MO, et al: Comparative study of the dynamics of follicular waves in mares and women. *Biol Reprod* 71:1195, 2004.
24. Baerwald AR, Walker RA, Pierson RA: Growth Rates of Ovarian Follicles During Natural Menstrual Cycles and Ovarian Stimulation Cycles. Proceedings of the 50th Annual Conference of the Canadian Fertility and Andrology Society 68, 2004.
25. Baerwald AR, Walker RA, Pierson RA: Growth and Regression Rates of Ovarian Follicles During Natural Menstrual Cycles and Oral Contraception Cycles. Proceedings of the International Federation



- of Fertility Societies 18th World Congress on Fertility and Sterility, Abstracts:115, 2004.
26. Ginther OJ: Major and minor follicular waves during the equine estrous cycle. *Journal of Equine Veterinary Science* 13:18, 1993.
  27. Ginther OJ, Kastelic JP, Knopf L: Composition and characteristics of follicular waves during the bovine estrous cycle. *Anim Reprod Sci* 20:187, 1989.
  28. Chikazawa K, Araki S, Tamada T: Morphological and endocrinological studies on follicular development during the human menstrual cycle. *J Clin Endocrinol Metab* 62:305, 1986.
  29. Wiele RLV, Bogumil J, Dyrenfurth I, et al: Mechanisms regulating the menstrual cycle in women. *Recent Prog Horm Res* 26:63, 1970.
  30. McNatty KP, Hillier SG, Boogaard AMVD, et al: Follicular development during the luteal phase of the human menstrual cycle. *J Clin Endocrinol Metab* 56:1022, 1983.
  31. Baird D, Fraser IS: Concentration of oestrone and oestradiol in follicular fluid and ovarian venous blood of women. *Clin Endocrinol* 4:259, 1975.
  32. Toner SA, Zerega GSD: Intragonadal regulation of follicular maturation. *Endocr Rev* 10:205, 1989.
  33. DiZerega GS, Hodgen GD: Cessation of folliculogenesis during the primate luteal phase. *J Clin Endocrinol Metab* 51:158, 1980.
  34. Zeleznik AJ: Follicle selection in primates: "many are called but few are chosen." *Biol Reprod* 65:655, 2001.
  35. Block E: Quantitative morphological investigations of the follicular system in women: variations at different ages. *Acta Anat* 14:108, 1952.
  36. Hackelöer BJ, Fleming R, Robinson HP, et al: Correlation of ultrasonic and endocrinologic assessment of human follicular development. *Am J Obstet Gynecol* 135:122, 1979.
  37. Gore M: Prediction of ovarian cycle outcome by follicular characteristics, stage 1. *Hum Reprod* 10:2313, 1995.
  38. Yen SSC, Vanderberg G, Tsai CC, et al: *Biorhythms and Human Reproduction*. New York, John Wiley and Sons, 1974.
  39. Ginther OJ: Selection of the dominant follicle in cattle and horses. *Anim Reprod Sci* 60-61:61, 2000.
  40. Ginther OJ, Beg MA, Bergfelt DR, et al: Follicle selection in monovular species. *Biol Reprod* 65:638, 2001.
  41. Gougeon A: Dynamics of follicular growth in the human: A model from preliminary results. *Hum Reprod* 1:81, 1986.
  42. Greenwald GS, Terranova PF: Follicular selection and its control. In Knobil E, Neill J (eds): *The Physiology of Reproduction*. New York, Raven Press, 1988, pp 387-446.
  43. Carson R, Findlay J, Mattner P, et al: Relative levels of thecal blood flow in atretic and non-atretic ovarian follicles of the conscious sheep. *Aust J Exper Biol Med Sci* 64:381, 1986.
  44. Guraya SS: *Biology of Ovarian Follicles in Mammals*. New York, Springer-Verlag, 1985.
  45. Moor RM, Seamark RF: Cell signalling, permeability, and microvascular changes during follicle development in mammals. *J Dairy Sci* 69:927, 1986.
  46. Brannstrom M, Zackrisson U, Hagstrom HG, et al: Preovulatory changes of blood flow in different regions of the human follicle. *Fertil Steril* 69:435, 1998.
  47. Pierson RA: From ovulation to implantation. In Jaffe R, Warsof S (eds): *Color Doppler Imaging in Obstetrics and Gynecology*. New York, McGraw Hill, 1992, pp 35-60.
  48. Shrestha SM, Costello MF, Sjoblom P, et al: Power Doppler ultrasound assessment of follicular vascularity in the early follicular phase and its relationship with outcome of in vitro fertilization. *J Assist Reprod Genet* 23:161, 2006.
  49. Marinkuk SD, Chizen DR, Pierson RA: Ultrasonographic morphology of the human preovulatory follicle wall prior to ovulation. *Clin Anat* 5:1, 1992.
  50. Van Blerkom J, Antezak M, Schrader R: The developmental potential of the human oocyte is related to the dissolved oxygen content of follicular fluid: association with vascular endothelial growth factor levels and perifollicular blood flow characteristics. *Hum Reprod* 12:1047, 1997.
  51. Vassena R, Adams GP, Mapletoft RJ, et al: Ultrasound image characteristics of ovarian follicles in relation to oocyte competence and follicular status in cattle. *Anim Reprod Sci* 76:25, 2003.
  52. Van Blerkom J: Intrafollicular influences on human oocyte developmental competence: perifollicular vascularity, oocyte metabolism and mitochondrial function. *Hum Reprod* 15(Suppl 2):173, 2000.
  53. Palomba S, Russo T, Falbo A, et al: Clinical use of the perifollicular vascularity assessment in IVF cycles: a pilot study. *Hum Reprod* 21:1055, 2006.
  54. Kan A, Ng EH, Yeung WS, et al: Perifollicular vascularity in poor ovarian responders during IVF. *Hum Reprod* 21:1539, 2006.
  55. Pierson RA, Chizen DR, Olatunbosun OA: Ultrasonographic assessment of ovulation induction. In Jaffe R, Pierson RA, Abramowicz JA (eds): *Imaging in Infertility and Reproductive Endocrinology*. Philadelphia, J.B. Lippincott, 1994, pp 155-166.
  56. Kinkel K, Frei KA, Balleyguier C, et al: Diagnosis of endometriosis with imaging: a review. *Eur Radiol* 16:285, 2006.
  57. Acien P, Perez-Albert G, Quereda FJ, et al: Treatment of endometriosis with transvaginal ultrasound-guided drainage under GnRH analogues and recombinant interleukin-2 left in the cysts. *Gynecol Obstet Invest* 60:224, 2005.
  58. de Silva KS, Kanumakala S, Grover SR, et al: Ovarian lesions in children and adolescents—an 11-year review. *J Pediatr Endocrinol Metab* 17:951, 2004.
  59. Jerny K, Luise C, Bourne T: The characterization of common ovarian cysts in premenopausal women. *Ultrasound Obstet Gynecol* 17:140, 2001.
  60. Caspi B, Appelman Z, Rabinerson D, et al: The growth pattern of ovarian dermoid cysts: a prospective study in premenopausal and postmenopausal women. *Fertil Steril* 68:501, 1997.
  61. Caspi B, Elchalal U, Dgani R, et al: Preoperative sonography in detecting small benign cystic teratomas. *Int J Gynaecol Obstet* 48:75, 1995.
  62. Zalel Y, Caspi B, Tepper R: Doppler flow characteristics of dermoid cysts: unique appearance of struma ovarii. *J Ultrasound Med* 16:355, 1997.
  63. Rowe T: Fertility and a woman's age. *J Reprod Med* 51:157, 2006.
  64. Allen VM, Wilson RD, Cheung A: Pregnancy outcomes after assisted reproductive technology. *J Obstet Gynaecol Can* 28:220, 2006.
  65. Swanton A, Child T: Reproduction and ovarian ageing. *J Br Menopause Soc* 11:126, 2005.
  66. Pinnelli A, Di Cesare M: Human fertility: sociodemographic aspects. *Contraception* 72:303, 2005.
  67. Tufan E, Elter K, Durmusoglu F: Assessment of reproductive ageing patterns by hormonal and ultrasonographic ovarian reserve tests. *Hum Reprod* 19:2484, 2004.
  68. Wallace WH, Kelsey TW: Ovarian reserve and reproductive age may be determined from measurement of ovarian volume by transvaginal sonography. *Hum Reprod* 19:1612, 2004.
  69. Bukulmez O, Arici A: Assessment of ovarian reserve. *Curr Opin Obstet Gynecol* 16:231, 2004.
  70. Bukman A, Heineman MJ: Ovarian reserve testing and the use of prognostic models in patients with subfertility. *Hum Reprod Update* 7:581, 2001.
  71. Derman SG, Seifer DB: In vitro fertilization in the older patient. *Curr Womens Health Rep* 3:375, 2003.
  72. Tarlatzis BC, Zepiridis L: Perimenopausal conception. *Ann N Y Acad Sci* 997:93, 2003.
  73. Erdem M, Erdem A, Biberoglu K, et al: Age-related changes in ovarian volume, antral follicle counts and basal follicle stimulating hormone levels: comparison between fertile and infertile women. *Gynecol Endocrinol* 17:199, 2003.
  74. Broekmans FJ, Scheffer GJ, Bancsi LF, et al: Ovarian reserve tests in infertility practice and normal fertile women. *Maturitas* 30:205, 1998.
  75. Erdem M, Erdem A, Gursoy R, et al: Comparison of basal and clomiphene citrate induced FSH and inhibin B, ovarian volume and antral follicle counts as ovarian reserve tests and predictors of poor ovarian response in IVF. *J Assist Reprod Genet* 21:37, 2004.
  76. Lass A: Assessment of ovarian reserve—is there a role for ovarian biopsy? *Hum Reprod* 16:1055, 2001.
  77. Syrop CH, Dawson JD, Husman KJ, et al: Ovarian volume may predict assisted reproductive outcomes better than follicle stimulating hormone concentration on day 3. *Hum Reprod* 14:1752, 1999.
  78. Erdem A, Erdem M, Biberoglu K, et al: Age-related changes in ovarian volume, antral follicle counts and basal FSH in women with normal reproductive health. *J Reprod Med* 47:835, 2002.
  79. Bancsi LF, Broekmans FJ, Eijkemans MJ, et al: Predictors of poor ovarian response in in vitro fertilization: a prospective study comparing basal markers of ovarian reserve. *Fertil Steril* 77:328, 2002.
  80. Lass A, Skull J, McVeigh E, et al: Measurement of ovarian volume by transvaginal sonography before ovulation induction with human

- menopausal gonadotrophin for in vitro fertilization can predict poor response. *Hum Reprod* 12:294, 1997.
81. Durmusoglu F, Elter K, Yoruk P, et al: Combining cycle day 7 follicle count with the basal antral follicle count improves the prediction of ovarian response. *Fertil Steril* 81:1073, 2004.
  82. Hendriks DJ, Mol BW, Bancsi LF, et al: Antral follicle count in the prediction of poor ovarian response and pregnancy after in vitro fertilization: a meta-analysis and comparison with basal follicle-stimulating hormone level. *Fertil Steril* 83:291, 2005.
  83. Vladimirov IK, Tacheva DM, Kalinov KB, et al: Prognostic value of some ovarian reserve tests in poor responders. *Arch Gynecol Obstet* 272:74, 2005.
  84. Hansen KR, Thyer AC, Sluss PM, et al: Reproductive ageing and ovarian function: is the early follicular phase FSH rise necessary to maintain adequate secretory function in older ovulatory women? *Hum Reprod* 20:89, 2005.
  85. Broekmans FJ, Kwee J, Hendriks DJ, et al: A systematic review of tests predicting ovarian reserve and IVF outcome. *Hum Reprod Update* 12:685, 2006.
  86. Bomsel-Helmreich O: Ultrasound and the preovulatory human follicle. *Oxford Rev Reprod Biol* 7:1, 1985.
  87. Baerwald AR, Pierson RA: Ovarian follicular development during the use of oral contraception: a review. *J Obstet Gynaecol Can* 26:19, 2004.
  88. Carnevale E, Checure C, Coutino da Silva M, et al: The Use of Computer-Assisted Image Analysis to Determine the Interval Before and After Ovulation in Mares. Paper presented at: 48th Annual Conference of the American Association of Equine Practitioners, Orlando, FL, 2002.
  89. Collins W, Jurkovic D, Bourne T, et al: Ovarian morphology, endocrine function and intra-follicular blood flow during the peri-ovulatory period. *Hum Reprod* 6:319, 1991.
  90. Tinkanen H, Kujansuu E, Laippala P: The association between hormone levels and vascular resistance in uterine and ovarian arteries in spontaneous menstrual cycles—a Doppler ultrasound study. *Acta Obstet Gynecol Scand* 74:297, 1995.
  91. Singh J, Adams GP, Pierson RA: Promise of new imaging technologies for assessing ovarian function. *Animal Reproduction Sci* 78:371, 2003.
  92. Lovrec VG, Vlaisavljevic V, Reljic M: Dependence of the in-vitro fertilization capacity of the oocyte on perifollicular flow in the preovulatory period of unstimulated cycles. *Wien Klin Wochenschr* 113(Suppl 3):21, 2001.
  93. Balakier H, Stronell RD: Color Doppler assessment of folliculogenesis in in vitro fertilization patients. *Fertil Steril* 62:1211, 1994.
  94. Nargund G, Bourne T, Doyle P, et al: Associations between ultrasound indices of follicular blood flow, oocyte recovery and preimplantation embryo quality. *Hum Reprod* 11:109, 1996.
  95. Oyesanya OA, Parsons JH, Collins WP, et al: Prediction of oocyte recovery rate by transvaginal ultrasonography and color Doppler imaging before human chorionic gonadotropin administration in in vitro fertilization cycles. *Fertil Steril* 65:806, 1996.
  96. Altundag M, Levi R, Adakan S, et al: Intraovarian stromal artery Doppler indices in predicting ovarian response. *J Reprod Med* 47:886, 2002.
  97. Shrestha SM, Costello MF, Sjoblom P, et al: Longitudinal assessment of ovarian perifollicular and endometrial vascularity by power Doppler ultrasound in pregnant and non-pregnant cycles in the IVF setting. *J Assist Reprod Genet* 21:387, 2004.
  98. Bomsel-Helmreich O: Ultrasound and the preovulatory human follicle. *Oxf Rev Reprod Biol* 7:1, 1985.
  99. Leerentveld RA, VanGent I, DerStoop M, et al: Ultrasonographic assessment of Graafian follicle growth under monofollicular and multifollicular conditions in clomiphene citrate stimulated cycles. *Fertil Steril* 40:461, 1985.
  100. Hanna MD, Chizen DR, Pierson RA: Characteristics of follicular evacuation during human ovulation. *J Ultrasound Obstet Gynaecol* 4:488, 1994.
  101. Pierson R, Martinuk S, Chizen D, et al: Ultrasonographic visualization of human ovulation. Paper presented at: 7th Reinier de Graaf Symposium, Maastricht, Netherlands, 1990.
  102. Baerwald AR, Adams GP, Pierson RA: Form and function of the corpus luteum during the human menstrual cycle. *Ultrasound Obstet Gynecol* 25:498, 2005.
  103. Guerriero S, Ajossa S, Melis GB: Luteal dynamics during the human menstrual cycle: new insight from imaging. *Ultrasound Obstet Gynecol* 25:425, 2005.
  104. Parsons AK: Imaging the human corpus luteum. *J Ultrasound Med* 20:811, 2001.
  105. Swire MN, Castro-Aragon I, Levine D: Various sonographic appearances of the hemorrhagic corpus luteum cyst. *Ultrasound Q* 20:45, 2004.
  106. Pierson R, Chizen D: Ultrasonography of normal and aberrant ovulation. In Jaffe R, Pierson R, Abramowicz J (eds): *Imaging in Infertility and Reproductive Endocrinology*. Philadelphia, J.B. Lippincott, 1994, pp 155.
  107. Stouffer R: *Corpus Luteum Formation and Demise*. Philadelphia, Lippincott-Raven, 1996, pp 251–269.
  108. Hagstrom HG, Hahlin M, Bennegard-Eden B, et al: Regulation of corpus luteum function in early human pregnancy. *Fertil Steril* 65:81, 1996.
  109. Corner GW Jr: The histological dating of the human corpus luteum of menstruation. *Am J Anat* 98:377, 1956.
  110. Qurenan JT, O'Brien GD, Bains LM, et al: Ultrasound scanning of ovaries to detect ovulation in women. *Fertil Steril* 34:99, 1980.
  111. Geisthoel F, Skubisch U, Zabel G, et al: Ultrasonographic and endocrinological studies of ovarian function. *Ultrasound Med Biol* 2(Suppl 2):603, 1983.
  112. Lenz S: Ultrasonic study of follicular maturation, ovulation and development of corpus luteum during normal menstrual cycles. *Acta Obstet Gynecol Scand* 64:15, 1985.
  113. Zalud I, Kurjak A: The assessment of luteal blood flow in pregnant and non-pregnant women by transvaginal color Doppler. *J Perinat Med* 18:215, 1990.
  114. Bourne TH, Hagstrom H, Hahlin M, et al: Ultrasound studies of vascular and morphological changes in the human corpus luteum during the menstrual cycle. *Fertil Steril* 65:753, 1996.
  115. Miyazaki T, Tanaka M, Miyakoshi K, et al: Power and colour Doppler ultrasonography for the evaluation of the vasculature of the human corpus luteum. *Hum Reprod* 13:2836, 1998.
  116. Nitschke-Dabelstein S, Hackelöer B: Ovulation and corpus luteum formation observed by ultrasonography. *Ultrasound Med Biol* 1:33, 1980.
  117. Pierson RA, Martinuk SD, Chizen DR, et al: Ultrasonographic visualization of human ovulation. Paper presented at: From Ovulation to Implantation. Proceedings of the VIIth Reinier de Graaf Symposium, Maastricht, the Netherlands, 1990.
  118. Ortander U, Solensten NG, Bergh A, et al: Intraovarian blood flow measured with color doppler ultrasonography inversely correlates with vascular density in the human corpus luteum of the menstrual cycle. *Fertil Steril* 81:154, 2004.
  119. Frates MC, Doubilet PM, Durfee SM, et al: Sonographic and Doppler characteristics of the corpus luteum: can they predict pregnancy outcome? *J Ultrasound Med* 20:821, 2001.
  120. Tailor A, Jurkovic D, Bourne TH, et al: Comparison of transvaginal color Doppler imaging and color Doppler energy for assessment of intraovarian blood flow. *Obstet Gynecol* 91:561, 1998.
  121. Glock JL, Brumsted JR: Color flow pulsed Doppler ultrasound in diagnosing luteal phase defect. *Fertil Steril* 64:500, 1995.
  122. Ginsburg KA: Luteal phase defect. Etiology, diagnosis, and management. *Endocrinol Metab Clin North Am* 21:85, 1992.
  123. Goodarzi MO, Azziz R: Diagnosis, epidemiology, and genetics of the polycystic ovary syndrome. *Best Pract Res Clin Endocrinol Metab* 20:193, 2006.
  124. Pache TD, Hop WC, Wladimiroff JW, et al: Transvaginal sonography and abnormal ovarian appearance in menstrual cycle disturbances. *Ultrasound Med Biol* 17:589, 1991.
  125. Chang WY, Knochenhauer ES, Bartolucci AA, et al: Phenotypic spectrum of polycystic ovary syndrome: clinical and biochemical characterization of the three major clinical subgroups. *Fertil Steril* 83:1717, 2005.
  126. Dewailly D, Duhamel A, Robert Y, et al: Interrelationship between ultrasonography and biology in the diagnosis of polycystic ovarian syndrome. *Ann NY Acad Sci* 687:206, 1993.
  127. Goodarzi MO, Korenman SG: The importance of insulin resistance in polycystic ovary syndrome. *Fertil Steril* 80:255, 2003.
  128. Goodarzi MO, Erickson S, Port SC, et al: Relative impact of insulin resistance and obesity on cardiovascular risk factors in polycystic ovary syndrome. *Metabolism* 52:713, 2003.
  129. Chizen D, Pierson R: A New Approach to the Transvaginal Ultrasonography Diagnosis of Polycystic Ovary Syndrome (PCOS): A Pilot Study. Paper presented at: International Federation of Fertility Societies 18th World Congress on Fertility and Sterility. Montreal, Quebec, 2004.



130. Stoesser K: Treatment of polycystic ovary syndrome in adolescents. *Am Fam Physician* 70:447, 2004.
131. Salmi DJ, Zisser HC, Jovanovic L: Screening for and treatment of polycystic ovary syndrome in teenagers. *Exp Biol Med* (Maywood) 229:369, 2004.
132. Ibanez L, Ferrer A, Ong K, et al: Insulin sensitization early after menarche prevents progression from precocious pubarche to polycystic ovary syndrome. *J Pediatr* 144:23, 2004.
133. Pache TD, Wladimiroff JW, Hop WC, et al: How to discriminate between normal and polycystic ovaries: transvaginal US study. *Radiology* 183:421, 1992.
134. Atiomo WU, Pearson S, Shaw S, et al: Ultrasound criteria in the diagnosis of polycystic ovary syndrome (PCOS). *Ultrasound Med Biol* 26:977, 2000.
135. Glueck CJ, Papanna R, Wang P, et al: Incidence and treatment of metabolic syndrome in newly referred women with confirmed polycystic ovarian syndrome. *Metabolism* 52:908, 2003.
136. Tsilchorozidou T, Prelevic GM: The role of metformin in the management of polycystic ovary syndrome. *Curr Opin Obstet Gynecol* 15:483, 2003.
137. Lakhani K, Seifalian AM, Atiomo WU, et al: Polycystic ovaries. *Br J Radiol* 75:9, 2002.
138. Jonard S, Robert Y, Cortet-Rudelli C, et al: Ultrasound examination of polycystic ovaries: is it worth counting the follicles? *Hum Reprod* 18:598, 2003.
139. Balen AH, Laven JS, Tan SL, et al: Ultrasound assessment of the polycystic ovary: international consensus definitions. *Hum Reprod Update* 9:505, 2003.
140. Hahn S, Benson S, Elsenbruch S, et al: Metformin treatment of polycystic ovary syndrome improves health-related quality-of-life, emotional distress and sexuality. *Hum Reprod* 7:1925, 2006.
141. Barbieri RL: Metformin for the treatment of polycystic ovary syndrome. *Obstet Gynecol* 101:785, 2003.
142. Haas DA, Carr BR, Attia GR: Effects of metformin on body mass index, menstrual cyclicity, and ovulation induction in women with polycystic ovary syndrome. *Fertil Steril* 79:469, 2003.
143. Baillargeon JP, Luorno MJ, Nesler JE: Insulin sensitizers for polycystic ovary syndrome. *Clin Obstet Gynecol* 46:325, 2003.
144. Tasdemir S, Ficioglu C, Yalti S, et al: The effect of metformin treatment to ovarian response in cases with PCOS. *Arch Gynecol Obstet* 269:121, 2004.
145. Lord JM, Flight IH, Norman RJ: Metformin in polycystic ovary syndrome: systematic review and meta-analysis. *Br Med J* 327:951, 2003.
146. Sel E, Duleba AJ: Treatment of PCOS with metformin and other insulin-sensitizing agents. *Curr Diab Rep* 4:69, 2004.
147. Balen A: Ovulation induction for polycystic ovary syndrome. *Hum Fertil (Camb)* 3:106, 2000.
148. Balen A: Ovulation induction—optimizing results and minimizing risks. *Hum Fertil (Camb)* 6(Suppl):S42, 2003.
149. Sovino H, Sir-Petermann T, Devoto L: Clomiphene citrate and ovulation induction. *Reprod Biomed Online* 4:303, 2002.
150. Qublan HS, Malkawi HY: Metformin in the treatment of clomiphene citrate-resistant women with high BMI and primary infertility: clinical results and reproductive outcome. *J Obstet Gynaecol* 25:55, 2005.
151. Cardone VS: GnRH antagonists for treatment of polycystic ovarian syndrome. *Fertil Steril* 80(Suppl 1):S25; discussion S32, 2003.
152. Amin M, Abdel-Kareem O, Takekida S, et al: Minireview: Up-date management of non responder to clomiphene citrate in polycystic ovary syndrome. *Kobe J Med Sci* 49:59-73, 2003.
153. Tessler FN, Perrella RR, Fleischer AC, Grant EG: Endovaginal sonographic diagnosis of dilated fallopian tubes. *AJR Am J Roentgenol* 153:523, 1989.
154. Strandell A, Lindhard A, Waldenstrom U, et al: Hydrosalpinx and IVF outcome: cumulative results after salpingectomy in a randomized controlled trial. *Hum Reprod* 16:2403, 2001.
155. Sabatini L, Davis C: The management of hydrosalpinges: tubal surgery or salpingectomy? *Curr Opin Obstet Gynecol* 17:323, 2005.
156. Richard HM 3rd, Parsons RB, Broadman KF, et al: Torsion of the fallopian tube: progression of sonographic features. *J Clin Ultrasound* 26:374, 1998.
157. Fleischer AC, Kaleris GC, Entman SS: Sonographic depiction of the endometrium during normal cycles. *Ultrasound Med Biol* 12:271, 1986.
158. Forrest TS, Elyaderani MK, Muilenburg MI, et al: Cyclic endometrial changes: US assessment with histologic correlation. *Radiology* 167:233, 1988.
159. Persad RJ: Ultrasonographic assessment of endometrial thickness: a review. *J Obstet Gynaecol Can* 24:131, 2002.
160. Fleischer AC, Herbert CM, Sacks GA, et al: Sonography of the endometrium during conception and nonconception cycles of in vitro fertilization and embryo transfer. *Fertil Steril* 46:442, 1986.
161. Baerwald AR, Pierson RA: Endometrial development in association with ovarian follicular waves during the menstrual cycle. *Ultrasound Obstet Gynecol* 24:453, 2004.
162. Lindenberg A: Ultrasonographic assessment of the endometrium during the normal menstrual cycle. In Jaffe R, Pierson RA, Abramowicz JA (eds): *Imaging in Infertility and Reproductive Endocrinology*. Philadelphia, J.B. Lippincott, 1994, pp 47-61.
163. Pierson R: Imaging the endometrium: are there predictors of endometrial receptivity? *J Obstet Gynecol Can* 25:360, 2003.
164. Fleischer AC: Optimizing the accuracy of transvaginal ultrasonography of the endometrium. *N Engl J Med* 337:1839, 1997.
165. Malini S, Valdes C, Malinak LR: Sonographic diagnosis and classification of anomalies of the female genital tract. *J Ultrasound Med* 3:397, 1984.
166. Daya A: Ultrasonographic Evaluation of Uterine Anomalies. In Jaffe R, Pierson RA, Abramowicz JA (eds): *Imaging in Infertility and Reproductive Endocrinology*. Philadelphia, J.B. Lippincott, 1994, pp 63-94.
167. Chizen DR, Pierson RA: Transvaginal Ultrasonography at First Consultation Assists Management of Infertility. Paper presented at: International Federation of Fertility Societies 18th World Congress on Fertility and Sterility, Montreal, Quebec, 2004.
168. Salle B, Sergeant P, Gaucherand P, et al: Transvaginal hysterosonographic evaluation of septate uteri: a preliminary report. *Hum Reprod* 11:1004, 1996.
169. Valdes C, Malini S, Malinak LR: Ultrasound evaluation of female genital tract anomalies: a review of 64 cases. *Am J Obstet Gynecol* 149:285, 1984.
170. Reuter KL, Daly DC, Cohen SM: Septate versus bicornuate uteri: errors in imaging diagnosis. *Radiology* 172:749, 1989.
171. Braun P, Grau FV, Pons RM, et al: Is hysterosalpingography able to diagnose all uterine malformations correctly? A retrospective study. *Eur J Radiol* 53:274, 2005.
172. Siedler D, Laing FC, Jeffrey RB Jr, et al: Uterine adenomyosis. A difficult sonographic diagnosis. *J Ultrasound Med* 6:345, 1987.
173. Bromley B, Shipp TD, Benacerraf B: Adenomyosis: sonographic findings and diagnostic accuracy. *J Ultrasound Med* 19:529; quiz 535, 2000.
174. Atzori E: Sonography for the diagnosis of adenomyosis. *Ultrasound Obstet Gynecol* 21:626, 2003.
175. Andreotti RF, Fleischer AC: The sonographic diagnosis of adenomyosis. *Ultrasound Q* 21:167, 2005.
176. Dueholm M: Transvaginal ultrasound for diagnosis of adenomyosis: a review. *Best Pract Res Clin Obstet Gynaecol* 20:569, 2006.
177. Atri M, Reinhold C, Mehio AR, et al: Adenomyosis: US features with histologic correlation in an in-vitro study. *Radiology* 215:783, 2000.
178. Lone FW, Balogun M, Khan KS: Adenomyosis: not such an elusive diagnosis any longer. *J Obstet Gynaecol* 26:225, 2006.
179. Hata T, Hata K, Senoh D, et al: Transvaginal Doppler color flow mapping. *Gynecol Obstet Invest* 27:217, 1989.
180. Vercellini P, Vigano P, Somigliana E, et al: Adenomyosis: epidemiological factors. *Best Pract Res Clin Obstet Gynaecol* 20:465, 2006.
181. Harmanli OH, Bevilacqua SA, Dandolu V, et al: Adenomyosis interferes with accurate ultrasonographic detection of uterine leiomyomas. *Arch Gynecol Obstet* 273:146, 2005.
182. Lee EJ, Han JH, Ryu HS: Polypoid adenomyomas: sonohysterographic and color Doppler findings with histopathologic correlation. *J Ultrasound Med* 23:1421; quiz 1431, 2004.
183. Ascher SM, Jha RC, Reinhold C: Benign myometrial conditions: leiomyomas and adenomyosis. *Top Magn Reson Imaging* 14:281, 2003.
184. Hulka CA, Hall DA, McCarthy K, et al: Sonographic findings in patients with adenomyosis: can sonography assist in predicting extent of disease? *AJR Am J Roentgenol* 179:379, 2002.
185. Grimbizis G, Camus M, Tarlatzis B, et al: Clinical implications of uterine malformations and hysteroscopic treatment results. *Hum Reprod Update* 7:161, 2001.

186. Alatas C, Aksoy E, Akarasu C, et al: Evaluation of intrauterine abnormalities in infertile patients by sonohysterography. *Hum Reprod Update* 12:487, 1997.
187. Collins JT, Woodward PJ: Radiological evaluation of infertility. *Semin Ultrasound CT MR* 16:304, 1995.
188. Simpson WL Jr, Beitia LG, Mester J: Hysterosalpingography: a reemerging study. *Radiographics* 26:419, 2006.
189. Roma Delfo A, Ubeda B, Ubeda A, et al: Diagnostic value of hysterosalpingography in the detection of intrauterine abnormalities: a comparison with hysteroscopy. *AJR Am J Roentgenol* 183:1405, 2004.
190. Hamilton JA, Larson AJ, Lower AM, et al: Routine use of saline hysterosonography in 500 consecutive, unselected, infertile women. *Hum Reprod* 13:2463, 1998.
191. Soares SR, Barbosa dos Reis MM, Camargos AF: Diagnostic accuracy of sonohysterography, transvaginal sonography, and hysterosalpingography in patients with uterine cavity diseases. *Fertil Steril* 73:406, 2000.
192. Fleischer A, Cullinan J, Parsons A: Special procedures in gynecology: Sonohysterography and Sonohysterosalpingography. New York, Lippincott, Williams & Williams, 1997.
193. Dessole S, Farina M, Capobianco G, et al: Determining the best catheter for sonohysterography. *Fertil Steril* 76:605, 2001.
194. Wolman I, Grouz A, Gordon D, et al: Timing of sonohysterography in menstruating women. *Gynecol Obstet Invest* 48:254, 1999.
195. Schwarzer P, Concin H, Bosch H, et al: An evaluation of sonohysterography and diagnostic hysteroscopy for the assessment of intrauterine pathology. *Ultrasound Obstet Gynecol* 11:337, 1998.
196. Exacoustos C, Zupi E, Carusotti C, et al: Hysterosalpingo-contrast sonography compared with hysterosalpingography and laparoscopic dye perturbation to evaluate tubal patency. *J Am Assoc Gynecol Laparosc* 10:367, 2003.
197. Zalc Y, Soriano D, Lipitz S, et al: Contribution of color Doppler flow to the ultrasonographic diagnosis of tubal abnormalities. *J Ultrasound Med* 19:645, 2000.
198. Sladkevicius P, Ojha K, Campbell S, et al: Three-dimensional power Doppler imaging in the assessment of Fallopian tube patency. *Ultrasound Obstet Gynecol* 16:644, 2000.
199. Chenia F, Hofmeyr GJ, Moolia S, et al: Sonographic hydrotubation using agitated saline: a new technique for improving fallopian tube visualization. *Br J Radiol* 70:833, 1997.
200. Volpe E, Zuccaro G, Patriarca A, et al: Transvaginal sonographic tubal patency testing using air and saline solution as contrast media in a routine infertility clinic setting. *J Ultrasound Obstet Gynecol* 7:43, 1996.
201. Brown S, Clodding C, Schnorr J, et al: Evaluation of outpatient hysteroscopy, saline infusion hysterosonography, and hysterosalpingography in infertile women: a prospective, randomized study. *Fertil Steril* 74:1029, 2000.
202. Lev-Toaff AS, Pinheiro LW, Bega G, et al: Three-dimensional multiplanar sonohysterography: comparison with conventional two-dimensional sonohysterography and X-ray hysterosalpingography. *J Ultrasound Med* 20:295, 2001.
203. Dietrich M, Suren A, Hinney B, et al: Evaluation of tubal patency by hysterocontrast sonography (HyCoSy, Echovist) and its correlation with laparoscopic findings. *J Clin Ultrasound* 24:523, 1996.
204. Tarlatzis BC, Laufer N, DeCherney AH: The use of ovarian ultrasonography in monitoring ovulation induction. *J In Vitro Fert Embryo Transf* 1:226, 1984.
205. Witmaack FM, Kreger DO, Blasco L, et al: Effect of follicular size on oocyte retrieval, fertilization, cleavage, and embryo quality in in vitro fertilization cycles: a 6-year data collection. *Fertil Steril* 62:1205, 1994.
206. Nagai S, Yasumizu T, Kasai T, et al: Effect of oocyte retrieval from a small leading follicle in fixed-schedule in vitro fertilization program. *J Obstet Gynaecol Res* 23:165, 1997.
207. Requena A, Neupiller F, Cobo AC, et al: Endocrinological and ultrasonographic variations after immature oocyte retrieval in a natural cycle. *Hum Reprod* 16:1833, 2001.
208. Lass A: Monitoring of in vitro fertilization-embryo transfer cycles by ultrasound versus by ultrasound and hormonal levels: a prospective, multicenter, randomized study. *Fertil Steril* 80:80, 2003.
209. Danninger B, Brunner M, Obruca A, et al: Prediction of ovarian hyperstimulation syndrome by ultrasound volumetric assessment [corrected] of baseline ovarian volume prior to stimulation. *Hum Reprod* 11:1597, 1996.
210. Huang FJ, Huang HW, Lan KC, et al: The maturity of human cumulus-free oocytes is positively related to blastocyst development and viability. *J Assist Reprod Genet* 19:555, 2002.
211. Kitai H, Inagaki N, Kimura H, et al: A study on the correlation between maturation and quality of human oocytes. *Hum Cell* 10:263, 1997.
212. Salha O, Nugent D, Dada T, et al: The relationship between follicular fluid aspirate volume and oocyte maturity in in-vitro fertilization cycles. *Hum Reprod* 13:1901, 1998.
213. Merce LT, Bau S, Barco MJ, et al: Assessment of the ovarian volume, number and volume of follicles and ovarian vascularity by three-dimensional ultrasonography and power Doppler angiography on the hCG day to predict the outcome in IVF/ICSI cycles. *Hum Reprod* 21:1218, 2006.
214. Lin YC, Chang SY, Lan KC, et al: Human oocyte maturity in vivo determines the outcome of blastocyst development in vitro. *J Assist Reprod Genet* 20:506, 2003.
215. Pictet HM, Danfour MA, Harris SE, et al: Growth and maturation of oocytes in vitro. *Reprod Suppl* 61:445, 2003.
216. Russell JB: Immature oocyte retrieval combined with in-vitro oocyte maturation. *Hum Reprod* 13(Suppl 3):63; discussion 71, 1998.
217. Russell JB: Immature oocyte retrieval with in-vitro oocyte maturation. *Curr Opin Obstet Gynecol* 11:289, 1999.
218. Thornton MH, Francis MM, Paulson RJ: Immature oocyte retrieval: lessons from unstimulated IVF cycles. *Fertil Steril* 70:647, 1998.
219. Triwitayakorn A, Suwajanakorn S, Pruksananonda K, et al: Correlation between human follicular diameter and oocyte outcomes in an ICSI program. *J Assist Reprod Genet* 20:143, 2003.
220. Delbaere A, Smits G, Olatunbosun O, et al: New insights into the pathophysiology of ovarian hyperstimulation syndrome. What makes the difference between spontaneous and iatrogenic syndrome? *Hum Reprod* 19:486, 2004.
221. Al-Shawaf T, Grudzinski JG: Prevention and treatment of ovarian hyperstimulation syndrome. *Best Pract Res Clin Obstet Gynaecol* 17:249, 2003.
222. DeCherney AH, Laufer N: The monitoring of ovulation induction using ultrasound and estrogen. *Clin Obstet Gynecol* 27:993, 1984.
223. Rossavik IK, Gibbons WE: Variability of ovarian follicular growth in natural menstrual cycles. *Fertil Steril* 44:195, 1985.
224. Zegers-Hochschild F, Gomez Lira C, Parada M, et al: A comparative study of the follicular growth profile in conception and nonconception cycles. *Fertil Steril* 41:244, 1984.
225. Sarty GE, Pierson RA: Mathematical modelling of ovarian follicle growth for the prediction of ovarian response to superstimulation. *Math Biosci* 198:80, 2005.
226. Avelillas JF, Falcone T, Arroliga AC: Ovarian hyperstimulation syndrome. *Crit Care Clin* 20:679, 2004.
227. Budev MM, Arroliga AC, Falcone T: Ovarian hyperstimulation syndrome. *Crit Care Med* 33(Suppl):S301, 2005.
228. Smits G, Olatunbosun O, Delbaere A, et al: Ovarian hyperstimulation syndrome due to a mutation in the follicle-stimulating hormone receptor. *N Engl J Med* 349:760, 2003.
229. Delbaere A, Smits G, De Leener A, et al: Understanding ovarian hyperstimulation syndrome. *Endocrine* 26:285, 2005.
230. Orvieto R: Can we eliminate severe ovarian hyperstimulation syndrome? *Hum Reprod* 20:320, 2005.
231. Delvigne A, Rozenberg S: Review of clinical course and treatment of ovarian hyperstimulation syndrome (OHSS). *Hum Reprod Update* 9:77, 2003.
232. Mansour R, Aboulghar M, Serour G, et al: Criteria of a successful coasting protocol for the prevention of severe ovarian hyperstimulation syndrome. *Hum Reprod* 20:3167, 2005.
233. D'Angelo A, Amso N: "Coasting" (withholding gonadotrophins) for preventing ovarian hyperstimulation syndrome. *Cochrane Database Syst Rev* CD002811, 2002.
234. Garcia-Velasco JA, Isaza V, Quea G, et al: Coasting for the prevention of ovarian hyperstimulation syndrome: much ado about nothing? *Fertil Steril* 85:547, 2006.
235. Chen D, Burmeister L, Goldschlag D, et al: Ovarian hyperstimulation syndrome: strategies for prevention. *Reprod Biomed Online* 7:43, 2003.
236. Fukaya T, Chida S, Terada Y, et al: Treatment of severe ovarian hyperstimulation syndrome by ultrafiltration and reinfusion of ascitic fluid. *Fertil Steril* 61:561, 1994.
237. D'Angelo A, Amso NN: Embryo freezing for preventing ovarian hyperstimulation syndrome: a Cochrane review. *Hum Reprod* 17:2787, 2002.



238. Ben-Ami M, Perlitz Y, Haddad S: The effectiveness of spectral and color Doppler in predicting ovarian torsion. A prospective study. *Eur J Obstet Gynecol Reprod Biol* 104:64, 2002.
239. Auslender R, Lavie O, Kaufman Y, et al: Coiling of the ovarian vessels: a color Doppler sign for adnexal torsion without strangulation. *Ultrasound Obstet Gynecol* 20:96, 2002.
240. Cobellis L, Pecori E, Stradella L, et al: Ovarian hyperstimulation syndrome: distinction between local and systemic disease. *Gynecol Endocrinol* 17:95, 2003.
241. Russell JB, DeCherney AH, Hobbins JC: A new transvaginal probe and biopsy guide for oocyte retrieval. *Fertil Steril* 47:350, 1987.
242. Cohen J, Debache C, Pez JP, et al: Transvaginal sonographically controlled ovarian puncture for oocyte retrieval for in vitro fertilization. *J In Vitro Fert Embryo Transf* 3:309, 1986.
243. Dellenbach P, Nisand I, Moreau L, et al: Transvaginal sonographically controlled follicle puncture for oocyte retrieval. *Fertil Steril* 44:656, 1985.
244. Hamberger L, Wikland M, Enk L, et al: Laparoscopy versus ultrasound guided puncture for oocyte retrieval. *Acta Eur Fertil* 17:195, 1986.
245. Feichtinger W: Current technology of oocyte retrieval. *Curr Opin Obstet Gynecol* 4:697, 1992.
246. Gembruch U, Diedrich K, Welker B, et al: Transvaginal sonographically guided oocyte retrieval for in-vitro fertilization. *Hum Reprod* 3(Suppl 2):59, 1988.
247. Feldberg D, Goldman JA, Ashkenazi J, et al: Transvaginal oocyte retrieval controlled by vaginal probe for in vitro fertilization: a comparative study. *J Ultrasound Med* 7:339, 1988.
248. Schulman JD, Dorfmann AD, Jones SL, et al: Outpatient in vitro fertilization using transvaginal ultrasound-guided oocyte retrieval. *Obstet Gynecol* 69:665, 1987.
249. Hammarberg K, Enk L, Nilsson L, et al: Oocyte retrieval under the guidance of a vaginal transducer: evaluation of patient acceptance. *Hum Reprod* 2:487, 1987.
250. Wikland M, Enk L, Hammarberg K, et al: Oocyte retrieval under the guidance of a vaginal transducer. *Ann N Y Acad Sci* 541:103, 1988.
251. Wiseman DA, Short WB, Pattinson HA, et al: Oocyte retrieval in an in vitro fertilization-embryo transfer program: comparison of four methods. *Radiology* 173:99, 1989.
252. Diedrich K, Van der Ven H, Al-Hasani S, et al: Oocyte retrieval for in vitro fertilization. *Ann Biol Clin (Paris)* 45:351, 1987.
253. Padilla SL, Butler WJ, Boldt JP, et al: Transurethral ultrasound-guided oocyte retrieval for in vitro fertilization. *Am J Obstet Gynecol* 157:622, 1987.
254. Parsons J, Riddle A, Booker M, et al: Oocyte retrieval for in-vitro fertilisation by ultrasonically guided needle aspiration via the urethra. *Lancet* 1:1076, 1985.
255. Kemeter P, Feichtinger W: Trans-vaginal oocyte retrieval using a trans-vaginal sector scan probe combined with an automated puncture device. *Hum Reprod* 1:21, 1986.
256. Schulman JD, Dorfmann A, Jones S, et al: Outpatient in vitro fertilization using transvaginal oocyte retrieval and local anesthesia. *N Engl J Med* 312:1639, 1985.
257. Sterzik K, Jonatha W, Keckstein G, et al: Ultrasonically guided follicle aspiration for oocyte retrieval in an in vitro fertilization program: further simplification. *Int J Gynaecol Obstet* 25:309, 1987.
258. Yuzpe AA, Brown SE, Casper RF, et al: Transvaginal, ultrasound-guided oocyte retrieval for in vitro fertilization. *J Reprod Med* 34:937, 1989.
259. Ragni G, Lombroso GC, De Lauretis L, et al: Echoguided transvaginal oocyte retrieval: effective and easy to learn technique. *Acta Eur Fertil* 22:89, 1991.
260. Kingsland CR, Taylor CT, Aziz N, et al: Is follicular flushing necessary for oocyte retrieval? A randomized trial. *Hum Reprod* 6:382, 1991.
261. Knight DC, Tyler JP, Driscoll GL: Follicular flushing at oocyte retrieval: a reappraisal. *Aust N Z J Obstet Gynaecol* 41:210, 2001.
262. Barak Y, Lessing JB, Amit A, et al: The development of an efficient ambulatory in vitro fertilization (IVF) and embryo transfer (ET) program using ultrasonically guided oocyte retrieval. *Acta Obstet Gynecol Scand* 67:585, 1988.
263. Tureck RW, Garcia CR, Blasco L, et al: Perioperative complications arising after transvaginal oocyte retrieval. *Obstet Gynecol* 81:590, 1993.
264. Christiaens F, Janssenswillen C, Van Steirteghem AC, et al: Comparison of assisted reproductive technology performance after oocyte retrieval under general anaesthesia (propofol) versus paracervical local anaesthetic block: a case-controlled study. *Hum Reprod* 13:2456, 1998.
265. El-Shawarby S, Margara R, Trew G, et al: A review of complications following transvaginal oocyte retrieval for in-vitro fertilization. *Hum Fertil (Camb)* 7:127, 2004.
266. Ng EH, Miao B, Ho PC: Anxiolytic premedication reduces preoperative anxiety and pain during oocyte retrieval. A randomized double-blinded placebo-controlled trial. *Hum Reprod* 17:1233, 2002.
267. Tummon I, Newton C, Lee C, et al: Lidocaine vaginal gel versus lidocaine paracervical block for analgesia during oocyte retrieval. *Hum Reprod* 19:1116, 2004.
268. Bustillo M: Unsuccessful oocyte retrieval: technical artefact or genuine 'empty follicle syndrome'? *Reprod Biomed Online* 8:59, 2004.
269. Pierson RA: Imaging the endometrium: are there predictors of uterine receptivity? *J Obstet Gynaecol Can* 25:360, 2003.
270. Zagzebski J: *Essentials of Ultrasound Physics*. St. Louis, Mosby, Incorporated, 1996.
271. Kupesic S, Bekavac I, Bjelos D, et al: Assessment of endometrial receptivity by transvaginal color Doppler and three-dimensional power Doppler ultrasonography in patients undergoing in vitro fertilization procedures. *J Ultrasound Med* 20:125, 2001.
272. Sterzik K, Grab D, Sasse V, et al: Doppler sonographic findings and their correlation with implantation in an in vitro fertilization program. *Fertil Steril* 52:825, 1989.
273. Steer CV, Campbell S, Tan SL, et al: The use of transvaginal color flow imaging after in vitro fertilization to identify optimum uterine conditions before embryo transfer. *Fertil Steril* 57:372, 1992.
274. Scerifini P, Barzofin J, Nelson J, et al: Sonographic uterine predictors of pregnancy in women undergoing ovulation induction for assisted reproductive treatments. *Fertil Steril* 62:815, 1994.
275. Tekay A, Martikainen H, Jouppila P: Blood flow changes in uterine and ovarian vasculature, and predictive value of transvaginal pulsed colour Doppler ultrasonography in an in-vitro fertilization programme. *Hum Reprod* 10:688, 1995.
276. Basil S, Magritte JP, Roth J, et al: Uterine vascularity during stimulation and its correlation with implantation in in-vitro fertilization. *Hum Reprod* 10:1497, 1995.
277. Cacciatori B, Simberg N, Fusaro P, et al: Transvaginal Doppler study of uterine artery blood flow in in vitro fertilization-embryo transfer cycles. *Fertil Steril* 66:130, 1996.
278. Aytöz A, Ubaldi F, Tournaye H, et al: The predictive value of uterine artery blood flow measurements for uterine receptivity in an intracytoplasmic sperm injection program. *Fertil Steril* 68:935, 1997.
279. Friedler S, Schenker JG, Herman A, et al: The role of ultrasonography in the evaluation of endometrial receptivity following assisted reproductive treatments: a critical review. *Hum Reprod Update* 2:323, 1996.
280. Yokota A, Nakai A, Oya A, et al: Changes in uterine and ovarian arterial impedance during the periovulatory period in conception and nonconception cycles. *J Obstet Gynaecol Res* 26:435, 2000.
281. Zaidi J, Campbell S, Pitroff R, et al: Endometrial thickness, morphology, vascular penetration and velocimetry in predicting implantation in an in vitro fertilization program. *Ultrasound Obstet Gynecol* 6:191, 1995.
282. Maugey-Laulom B, Commenges-Ducos M, Jullien V, et al: Endometrial vascularity and ongoing pregnancy after IVF. *Eur J Obstet Gynecol Reprod Biol* 104:137, 2002.
283. Yang J, Wu M, Chen C, et al: Association of endometrial blood flow as determined by a modified colour Doppler technique with subsequent outcome of in-vitro fertilization. *Hum Reprod* 14:361, 1999.
284. Schild RL, Knobloch C, Dorn C, et al: Endometrial receptivity in an in vitro fertilization program as assessed by spiral artery blood flow, endometrial thickness, endometrial volume, and uterine artery blood flow. *Fertil Steril* 75:361, 2001.
285. Applebaum M: The uterine biophysical profile. *Ultrasound Obstet Gynecol* 5(1):67, 1995.
286. Salle B, Bied-Damon V, Benchaib M, et al: Preliminary report of an ultrasonography and colour Doppler uterine score to predict uterine receptivity in an in-vitro fertilization programme. *Hum Reprod* 13:1669, 1998.
287. Pierson RA: Three-dimensional ultrasonography of the embryo and fetus. In Jaffe R, Bui TH (eds): *Fetal and Neonatal Ultrasonography*. New York, Parthenon Publishing Group, 1999, pp 317-326.
288. Raga F, Bonilla-Musoles F, Casan EM, et al: Assessment of endometrial volume by three-dimensional ultrasound prior to embryo

- transfer: clues to endometrial receptivity. *Hum Reprod* 14:2851, 1999.
289. Schild RL, Indefrei D, Eschweiler S, et al: Three-dimensional endometrial volume calculation and pregnancy rate in an in-vitro fertilization programme. *Hum Reprod* 14:1255, 1999.
  290. Schild RL, Holthaus S, d'Alquen J, et al: Quantitative assessment of subendometrial blood flow by three-dimensional-ultrasound is an important predictive factor of implantation in an in-vitro fertilization programme. *Hum Reprod* 15:89, 2000.
  291. Wu HM, Chiang CH, Huang HY, et al: Detection of the subendometrial vascularization flow index by three-dimensional ultrasound may be useful for predicting the pregnancy rate for patients undergoing in vitro fertilization-embryo transfer. *Fertil Steril* 79:507, 2003.
  292. Martínez-Gaudio M, Yoshida T, Bengtsson LP: Propagated and nonpropagated myometrial contractions in normal menstrual cycles. *Am J Obstet Gynecol* 115:107, 1973.
  293. de Vries K, Lyons EA, Ballard G, et al: Contractions of the inner third of the myometrium. *Am J Obstet Gynecol* 162:679, 1990.
  294. Lyons EA, Taylor PJ, Zheng XH, et al: Characterization of subendometrial myometrial contractions throughout the menstrual cycle in normal fertile women. *Fertil Steril* 55:771, 1991.
  295. Ijland MM, Evers JL, Dunselman GA, et al: Endometrial wavelike movements during the menstrual cycle. *Fertil Steril* 65:746, 1996.
  296. Fanchin R, Ayoubi JM, Olivennes F, et al: Hormonal influence on the uterine contractility during ovarian stimulation. *Hum Reprod* 15(Suppl 1):90, 2000.
  297. Ijland MM, Evers JL, Dunselman GA, et al: Relation between endometrial wavelike activity and fecundability in spontaneous cycles. *Fertil Steril* 67:492, 1997.
  298. van Gestel I, Ijland MM, Hoogland HJ, et al: Endometrial wave-like activity in the non-pregnant uterus. *Hum Reprod Update* 9:131, 2003.
  299. Lesny P, Killick SR: The junctional zone of the uterus and its contractions. *Br J Obstet Gynaecol* 111:1182, 2004.
  300. Lesny P, Killick SR, Tedlow RL, et al: Uterine junctional zone contractions during assisted reproduction cycles. *Hum Reprod Update* 4:440, 1998.
  301. Fanchin R, Righini C, Olivennes F, et al: Uterine contractions at the time of embryo transfer alter pregnancy rates after in-vitro fertilization. *Hum Reprod* 13:1968, 1998.
  302. Fanchin R, Righini C, de Ziegler D, et al: Effects of vaginal progesterone administration on uterine contractility at the time of embryo transfer. *Fertil Steril* 75:1136, 2001.
  303. Vlaisavljevic V, Reljic M, Gavric-Lovrec V, et al: Subendometrial contractility is not predictive for in vitro fertilization (IVF) outcome. *Ultrasound Obstet Gynecol* 17:239, 2001.
  304. Baruffi R, Mauri AL, Petersen CG, et al: Effects of vaginal progesterone administration starting on the day of oocyte retrieval on pregnancy rates. *J Assist Reprod Genet* 20:517, 2003.
  305. Bullett C, de Ziegler D: Uterine contractility and embryo implantation. *Curr Opin Obstet Gynecol* 17:265, 2005.
  306. Fanchin R, Ayoubi JM, Righini C, et al: Uterine contractility decreases at the time of blastocyst transfers. *Hum Reprod* 16:1115, 2001.
  307. Strickler RC, Christianson C, Crane JP, et al: Ultrasound guidance for human embryo transfer. *Fertil Steril* 43:54, 1985.
  308. Leong M, Leung C, Tucker M, et al: Ultrasound-assisted embryo transfer. *J In Vitro Fertil Embryo Transf* 3:383, 1986.
  309. al-Shawaf T, Dave R, Harper J, et al: Transfer of embryos into the uterus: how much do technical factors affect pregnancy rates? *J Assist Reprod Genet* 10:31, 1993.
  310. al-Shawaf T, Yang D, al-Magid Y, et al: Ultrasonic monitoring during replacement of frozen/thawed embryos in natural and hormone replacement cycles. *Hum Reprod* 8:2068, 1993.
  311. Kan AK, Abdalla HI, Gafar AH, et al: Embryo transfer: ultrasound-guided versus clinical touch. *Hum Reprod* 14:1259, 1999.
  312. Coroleu B, Carreras O, Veiga A, et al: Embryo transfer under ultrasound guidance improves pregnancy rates after in-vitro fertilization. *Hum Reprod* 15:616, 2000.
  313. Rijnders RJ, Mol BW, Broekmans FJ: Use of ultrasound guidance during embryo transfer. *Hum Reprod* 15:2449, 2000.
  314. Anderson RE, Nugent NL, Gregg AT, et al: Transvaginal ultrasound-guided embryo transfer improves outcome in patients with previous failed in vitro fertilization cycles. *Fertil Steril* 77:769, 2002.
  315. Biervliet FP, Lesny P, Maguiness SD, et al: Transmyometrial embryo transfer and junctional zone contractions. *Hum Reprod* 17:347, 2002.
  316. Baba K, Ishihara O, Hayashi N, et al: Three-dimensional ultrasound in embryo transfer. *Ultrasound Obstet Gynecol* 16:372, 2000.
  317. de Camargo Martins AM, Baruffi RL, Mauri AL, et al: Ultrasound guidance is not necessary during easy embryo transfers. *J Assist Reprod Genet* 21:421, 2004.
  318. Kojima K, Nomiya M, Kumamoto T, et al: Transvaginal ultrasound-guided embryo transfer improves pregnancy and implantation rates after IVF. *Hum Reprod* 16:2578, 2001.
  319. Sieck UV, Jaroudi KA, Hollanders JM, et al: Ultrasound guided embryo transfer does not prevent ectopic pregnancies after in-vitro fertilization. *Hum Reprod* 12:2081, 1997.
  320. Leterie GS: Three-dimensional ultrasound-guided embryo transfer: a preliminary study. *Am J Obstet Gynecol* 192:1983; discussion 1987, 2005.
  321. Tang OS, Ng EH, So WW, et al: Ultrasound-guided embryo transfer: a prospective randomized controlled trial. *Hum Reprod* 16:2310, 2001.
  322. Matarras R, Urquijo E, Mendoza R, et al: Ultrasound-guided embryo transfer improves pregnancy rates and increases the frequency of easy transfers. *Hum Reprod* 17:1762, 2002.
  323. Leterie GS, Marshall L, Angle M: A new coaxial catheter system with an echodense tip for ultrasonographically guided embryo transfer. *Fertil Steril* 72:266, 1999.
  324. Mansour RT, Aboulghar MA: Optimizing the embryo transfer technique. *Hum Reprod* 17:1149, 2002.
  325. Hale L: Embryo transfer: how to ensure correct placement in utero. *Reprod Fertil Dev* 13:95, 2001.
  326. Schoolcraft WB, Surrey ES, Gardner DK: Embryo transfer: techniques and variables affecting success. *Fertil Steril* 76:863, 2001.
  327. Coroleu B, Barri PN, Carreras O, et al: The influence of the depth of embryo replacement into the uterine cavity on implantation rates after IVF: a controlled, ultrasound-guided study. *Hum Reprod* 17:341, 2002.
  328. Pope CS, Cook EK, Arny M, et al: Influence of embryo transfer depth on in vitro fertilization and embryo transfer outcomes. *Fertil Steril* 81:51, 2004.
  329. Wood EG, Batzer FR, Go KJ, et al: Ultrasound-guided soft catheter embryo transfers will improve pregnancy rates in in-vitro fertilization. *Hum Reprod* 15:107, 2000.
  330. Lindheim SR, Cohen MA, Sauer MV: Ultrasound guided embryo transfer significantly improves pregnancy rates in women undergoing oocyte donation. *Int J Gynaecol Obstet* 66:281, 1999.
  331. Prapas Y, Prapas N, Hatziparasidou A, et al: Ultrasound-guided embryo transfer maximizes the IVF results on day 3 and day 4 embryo transfer but has no impact on day 5. *Hum Reprod* 16:1904, 2001.
  332. Garcia-Velasco JA, Isaza V, Martinez-Salazar J, et al: Transabdominal ultrasound-guided embryo transfer does not increase pregnancy rates in oocyte recipients. *Fertil Steril* 78:534, 2002.
  333. Sallam HN: Should embryo transfer always be performed under ultrasound guidance? *Ultrasound Obstet Gynecol* 24:383, 2004.
  334. Shamonki MI, Spandorfer SD, Rosenwaks Z: Ultrasound-guided embryo transfer and the accuracy of trial embryo transfer. *Hum Reprod* 20:709, 2005.
  335. Shamonki MI, Schattman GL, Spandorfer SD, et al: Ultrasound-guided trial transfer may be beneficial in preparation for an IVF cycle. *Hum Reprod* 20:2844, 2005.
  336. Buckett WM: A meta-analysis of ultrasound-guided versus clinical touch embryo transfer. *Fertil Steril* 80:1037, 2003.
  337. Sallam HN, Sadek SS: Ultrasound-guided embryo transfer: a meta-analysis of randomized controlled trials. *Fertil Steril* 80:1042, 2003.
  338. Li R, Lu L, Hao G, et al: Abdominal ultrasound-guided embryo transfer improves clinical pregnancy rates after in vitro fertilization: experiences from 330 clinical investigations. *J Assist Reprod Genet* 22:3, 2005.



## ECTOPIC PREGNANCY

Deborah Levine, MD

### Introduction

### Clinical Presentation of Ectopic Pregnancy

### Risk Factors for Ectopic Pregnancy

### Pregnancy Testing

### Diagnosis of Ectopic Pregnancy

### Sonography of Normal Early Intrauterine Pregnancy Versus Ectopic Pregnancy

- Early Intrauterine Pregnancy
- Abnormal Intrauterine Pregnancy

### Scanning Technique

- Transabdominal Scan
- Transvaginal Scan
- Assessment of the Adnexa
- Assessment of the Cul-De-Sac

### Sonographic Findings in Ectopic Pregnancy

- Adnexal Mass
- Endometrial Findings
- Free Fluid

### The Normal Sonogram

- Mimics of Ectopic Pregnancy
- Role of Doppler Sonography

### Rare Forms of Ectopic Pregnancy

- Interstitial Pregnancy
- Cervical Pregnancy
- Scar Pregnancy
- Abdominal Pregnancy
- Heterotopic Pregnancy

### Role of Magnetic Resonance Imaging in the Diagnosis of Ectopic Pregnancy

### Management

- Surgery
- Methotrexate
- Sonographically Guided Percutaneous Treatment
- Expectant Management

### Fertility After Ectopic Pregnancy

### Conclusion

## INTRODUCTION

In the United States, ectopic pregnancy is the leading cause of pregnancy-related deaths during the first trimester.<sup>1</sup> In 1992 ectopic pregnancies accounted for approximately 2% of reported pregnancies, and ectopic pregnancy-related deaths accounted for 9% of all pregnancy-related deaths.<sup>2</sup> The incidence of ectopic pregnancy has been increasing since the 1970s (Fig. 32-1).<sup>3</sup> This increase in ectopic pregnancy diagnosis is multifactorial, owing to both a true increase in the disease, related to increased numbers of patients at risk for the disease (Table 32-1), and earlier diagnosis of cases that otherwise would have spontaneously resolved.

Before sensitive pregnancy tests and sonography, ectopic pregnancy was frequently a life-threatening diagnosis. In 1970 Breen<sup>4</sup> reviewed 654 cases of ectopic pregnancy and found that in 49% of cases, the patients were admitted in shock. Because of this, surgery was performed as soon as the diagnosis was made. Today more sensitive tests for human chorionic gonadotropin (hCG) and the use of high-resolution ultrasonography allow earlier diagnosis of previously unsuspected cases. This has led to a shift from inpatient surgical therapy of ectopic pregnancy to selective outpatient management.<sup>3</sup>

In addition to earlier diagnosis of cases, several factors have led to an increased incidence of ectopic pregnancy:

1. The treatment of salpingitis has improved, leading to an increased number of patients with scarred but patent fallopian tubes.
2. Patients with scarred tubes who undergo tuboplasty are now able to get pregnant.
3. Expectant management is thought to increase the number of women who had ectopic pregnancies who are now able to conceive again.<sup>5,6</sup>
4. Increased numbers of women are undergoing ovulation induction and other assisted reproduction techniques; the techniques themselves increase the incidence of ectopic pregnancy.

Currently, sonography and, more specifically, transvaginal sonography is used not only to diagnose ectopic pregnancy in symptomatic patients but to screen women at high risk; to guide decisions as to the most appropriate mode of therapy; and to monitor patients diagnosed with ectopic pregnancy who can be managed without surgery (either expectantly or with methotrexate). Thus, ultrasonography plays a role not only in the early diagnosis but also in our understanding of the natural history of ectopic pregnancy. This chapter illustrates the role of ultrasonography in the diagnosis and management of ectopic pregnancy.

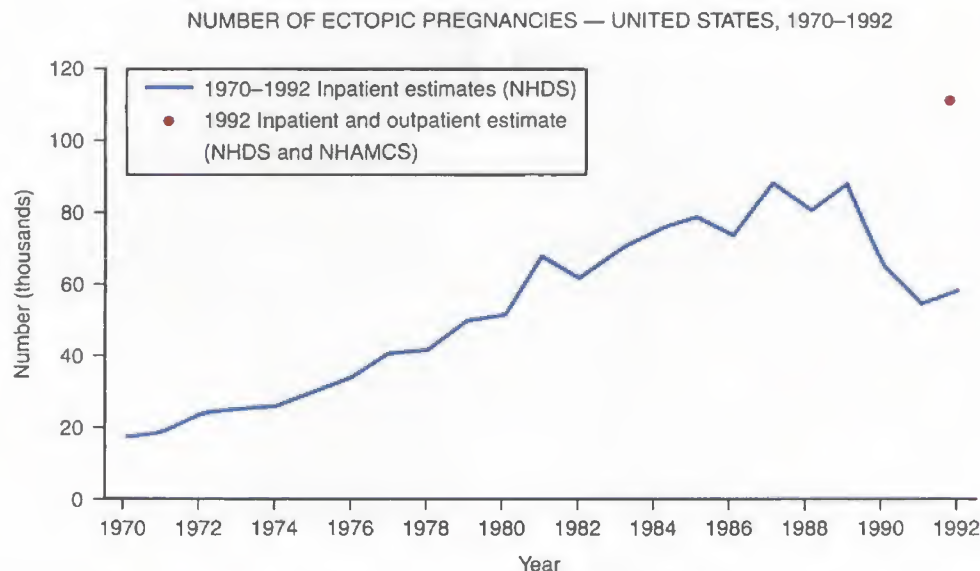


**FIGURE 32-1.** Incidence of ectopic pregnancies—United States, 1970 to 1992. NHDS, National Hospital Discharge Survey; NHAMCS, National Hospital Ambulatory Medical Care Survey.

**Table 32-1** Risk Factors for Ectopic Pregnancy

Risk Factor	Odds Ratio*
<b>High Risk</b>	
Tubal surgery	21.0
Sterilization	9.3
Previous ectopic pregnancy	8.3
In utero exposure to diethylstilbestrol	5.6
Use of intrauterine device	4.2–45.0
Documented tubal disease	3.8–21.0
<b>Moderate Risk</b>	
Infertility	2.5–21.0
Previous genital infections	2.5–3.7
Multiple sexual partners	2.1
<b>Slight Risk</b>	
Previous pelvic/abdominal surgery	0.9–3.8
Cigarette smoking	2.3–2.5
Vaginal douching	1.1–3.1
Early age at first intercourse (<18 years)	1.6

\*Single values, common odds ratio from homogeneous studies; point estimates, range of values from heterogeneous studies from Mol et al.<sup>9</sup> and Ankum et al.<sup>126</sup>

Reproduced with permission from Pisarka M, Carson SA, Buster JE: Ectopic pregnancy. *Lancet* 351:1115, 1998. Copyright by The Lancet Ltd.

## CLINICAL PRESENTATION OF ECTOPIC PREGNANCY

Clinical suspicion of ectopic pregnancy is raised when a patient has a positive pregnancy test, pain, bleeding, and an adnexal mass. However, the clinical triad of pain, bleeding, and adnexal mass is present in only 45% of patients.<sup>7</sup> Further complicating matters is that this clinical triad is not specific

for ectopic pregnancy. In a study by Schwartz and DiPietro,<sup>7</sup> only 14% of patients with clinically suspected ectopic pregnancy actually had this as their final diagnosis. Other diagnoses were symptomatic ovarian cysts (27%), pelvic inflammatory disease (PID) (15%), dysfunctional uterine bleeding (4%), and spontaneous abortions (5%). Obviously, this breakdown of patients will vary with individual hCG levels and risk factors (see Table 32-1).

Neither type of pain nor location of pain is specific for establishing the location of an ectopic pregnancy. In Breen's<sup>4</sup> 1970 study, the location of the pain varied as follows: shoulder (11%, all of whom had ruptured ectopic pregnancies), generalized abdominal (13%), lower abdominal (74%), lower quadrant ipsilateral to ectopic (51%), lower quadrant contralateral to ectopic (9%, perhaps secondary to contralateral corpus luteum cyst), back (6%), and vaginal (0.9%).<sup>4</sup>

Patients typically present at approximately 5 to 6 weeks' gestational age. However, because menstrual dates are often inaccurate, an early gestational age by dates should not influence the diligence with which one seeks an ectopic pregnancy.

## RISK FACTORS FOR ECTOPIC PREGNANCY

Patients with a history of ectopic pregnancy have a 12.6% chance of having a repeat ectopic pregnancy because risk factors contributing to the first episode are still present, along with further scarring of the fallopian tube as a result of the prior ectopic pregnancy. For patients with a history of PID and ectopic pregnancy, this risk is as high as 27%.<sup>8</sup> Other important risk factors are tubal ligation and use of an intrauterine contraceptive device. Both of these methods of contraception effectively prevent pregnancy. However, if pregnancy does occur, an ectopic location should be strongly suspected (Fig. 32-2).<sup>9</sup> A risk factor that is increasing in prevalence is that of women undergoing in vitro fertilization.



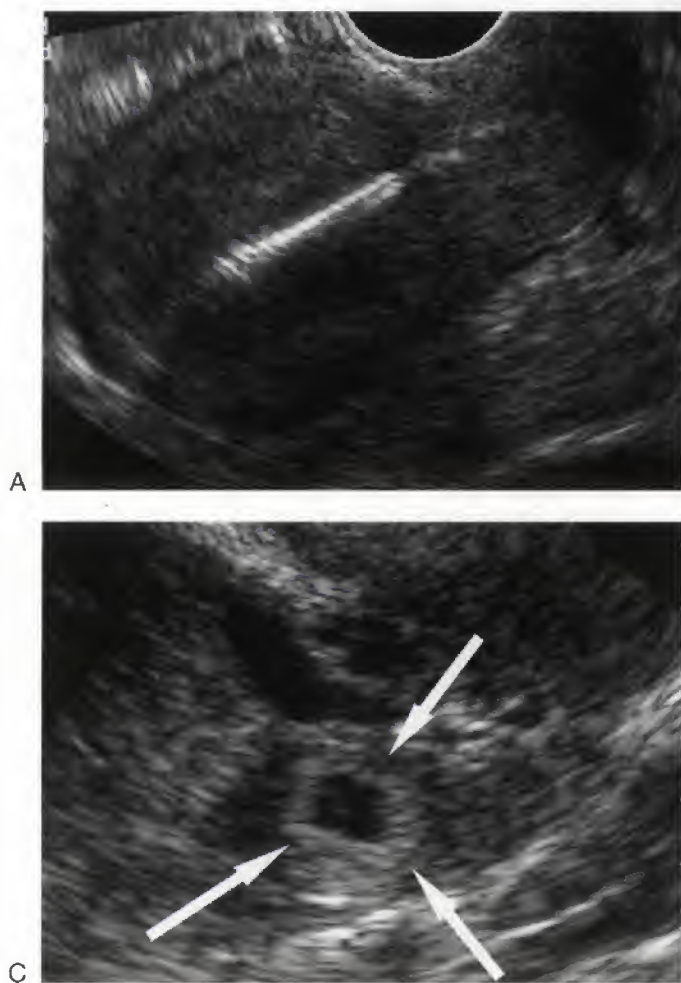


**FIGURE 32-2.** Ectopic pregnancy in a patient with intrauterine device (IUD). The patient presented with positive human chorionic gonadotropin (hCG) and abdominal pain. **A.** Transvaginal sagittal view of the uterus shows the IUD in appropriate position. No intrauterine pregnancy is visualized. **B.** Transvaginal transverse view shows the IUD in the uterine cavity and normal left ovary (calipers) with two cysts. **C.** Transvaginal sagittal view of the adnexa shows a tubal ring (arrows) with yolk sac. Because IUDs prevent implantation in the uterus, patients who become pregnant with an IUD in place have a high likelihood of ectopic pregnancy. The patient was treated surgically. (From Dialani V, Levine D: *Ectopic pregnancy: A review. Ultrasound Q* 20:105, 2004.)

The incidence of tubal pregnancy after oocyte retrieval/embryo transfer is as high as 4.5% (Fig. 32-3).<sup>10</sup> This increased rate is the result of risk factors for ectopic pregnancy overlapping those for infertility, use of superovulating agents, which may alter tubal motility, and embryo transfer with retrograde embryo migration into diseased tubes.<sup>11,12</sup> Even though identification of women at increased risk for ectopic pregnancy is helpful, because ectopic pregnancy is so common, it should be remembered that “a woman who is capable of conceiving is capable of having a pregnancy in a location other than the uterine cavity.”<sup>14</sup>

## PREGNANCY TESTING

The role of quantification of serum beta-hCG correlation with the clinical scenario and sonographic findings cannot be overemphasized in the diagnosis of ectopic pregnancy. A negative hCG essentially excludes the diagnosis of a live pregnancy, although a chronic ectopic pregnancy may be present. Sensitive radioimmunoassays are widely available, which become positive at approximately 23 menstrual days (9 days after conception). This is before the first missed menstrual period and before a gestational sac can be seen with transvaginal sonography.

When reviewing the literature or evaluating guidelines in clinical practice, it is important to know which standard of hCG is being used in the referring clinician’s laboratory. In the 1960s, the Second International Standard (IS) was introduced. Later, a purer standard, the International Reference Preparation (IRP) was introduced and is the main standard in use today. Correlation between the second IS and IRP can be performed by multiplying by a factor of 1.8 (second IS  $\times$  1.8 = IRP). Throughout the rest of this chapter, the hCG levels are corrected to IRP.

Early studies on gestational sac visualization evaluated normal early pregnancy and documented the presence of a sac when the hCG was 1000 to 2000 mIU/mL (IRP).<sup>13-19</sup> It must be emphasized that the majority of these studies evaluated normal early pregnancies and described an intrauterine gestational sac as any collection of fluid in the endometrial cavity. Small fluid collections of 2 mm (without a decidual reaction) were considered sufficient to describe an early gestational sac. As discussed later in this chapter, this type of fluid collection can be due to the pseudogestational sac of an ectopic pregnancy or a decidual cyst and may not represent an intrauterine pregnancy (IUP). Therefore, a fluid collection without a surrounding hyperechogenic rim is not sufficient to exclude the diagnosis of an ectopic pregnancy. However,

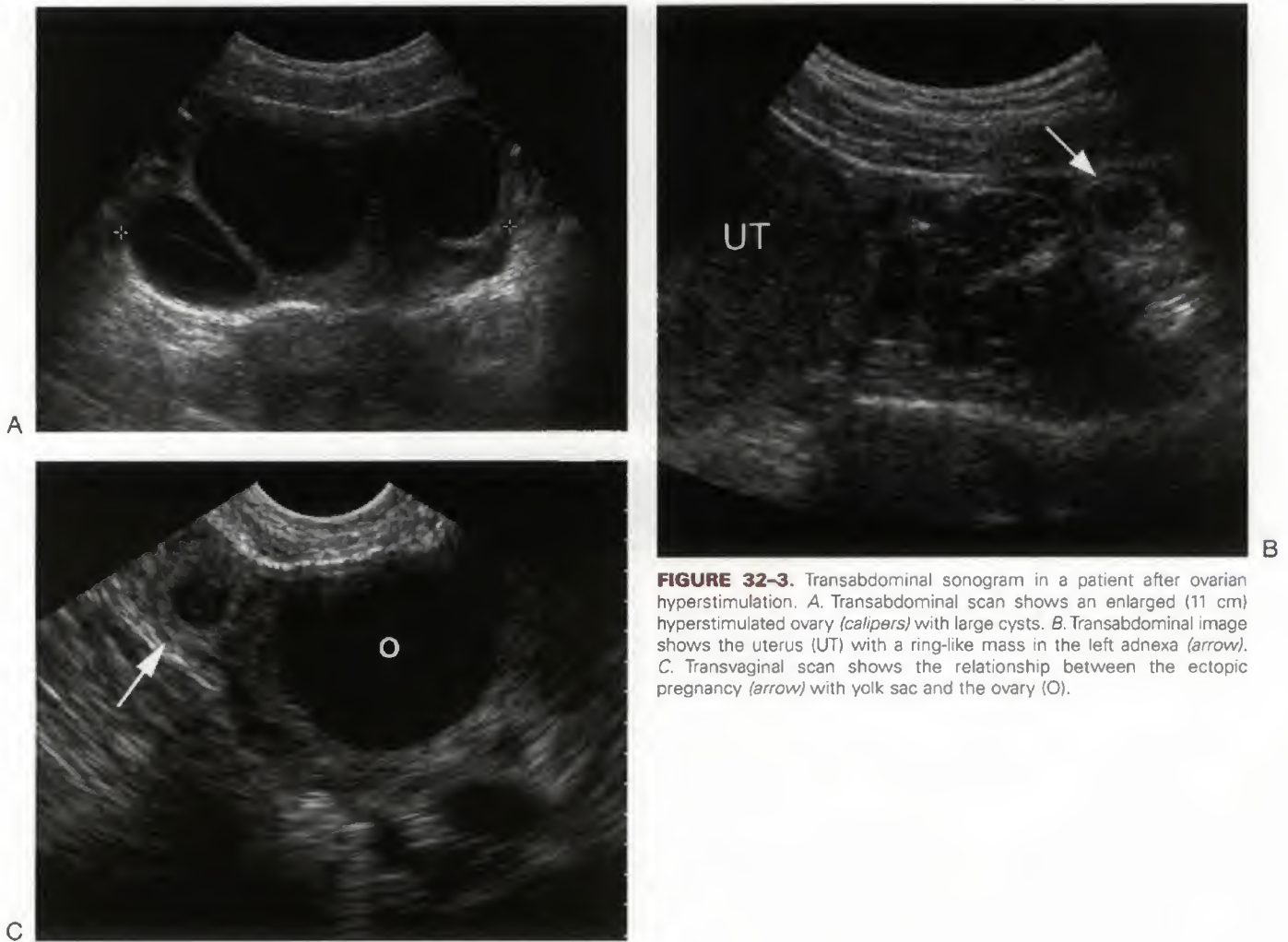


**FIGURE 32-3.** Transabdominal sonogram in a patient after ovarian hyperstimulation. *A.* Transabdominal scan shows an enlarged (11 cm) hyperstimulated ovary (*calipers*) with large cysts. *B.* Transabdominal image shows the uterus (UT) with a ring-like mass in the left adnexa (*arrow*). *C.* Transvaginal scan shows the relationship between the ectopic pregnancy (*arrow*) with yolk sac and the ovary (O).

these values of hCG are helpful in triaging patients. When hCG is below the discriminatory zone (2000 mIU/mL, IRP) and no intrauterine gestation is visualized, the diagnosis could be an early IUP, a miscarriage, or an ectopic pregnancy, and therefore, close follow-up is indicated, rather than treatment.<sup>20</sup> When the hCG value is above the discriminatory zone, one can expect to see an intrauterine gestational sac; however, even without visualization of a sac, there could still be a very early normal IUP.

In a study by Mehta,<sup>20</sup> 676 patients with symptoms suggestive of ectopic pregnancy were evaluated. Of 128 patients without a definite IUP on sonography, 51 had hCG values of greater than 2000, and 17 of these (33%) had an IUP on follow-up. Technical quality, presence of fibroids, intrauterine contraceptive devices, large hemorrhage, and multiple gestations have been described as factors in non-visualization of an early gestational sac with respect to a discriminatory level of hCG.<sup>14,18,20</sup> However, in Mehta's<sup>20</sup> study, none of these factors could be identified in 9 of 17 cases. The rate of indeterminate scans in this study (19%) was similar to that seen by Braffman et al,<sup>15</sup> who used an hCG threshold of 1500 mIU/mL. Braffman et al found fluid collections without an intradecidual sign in 40 of 90 patients. This emphasizes that if an hCG level of 2000 is used to treat

patients for ectopic pregnancy, then it is possible those women with early intrauterine pregnancies will be inappropriately treated and will lose an otherwise normal pregnancy. Therefore, it is recommended that if a patient presents with any symptoms suggestive of ectopic pregnancy, for example, bleeding, pain, and a pelvic sonogram that appears normal (without a fluid collection or gestational sac) the report should indicate that "although the pelvic sonogram appears normal, an ectopic pregnancy or a normal IUP too early to be seen sonographically cannot be excluded."

In the past, most patients suspected to have ectopic pregnancy were treated with laparotomy or laparoscopy. Currently, watchful waiting or treatment with methotrexate can be used for stable patients. However, it should be noted that, in many of these patients, the diagnosis of ectopic pregnancy is not confirmed. If patients are treated merely because of a single elevated hCG value, it is possible that normal early pregnancies will be improperly treated. In clinical practice, the discriminatory zone level of hCG should be taken as a guideline rather than an absolute. This raises the issue of whether the "discriminatory zone" for diagnosis of ectopic pregnancy should be raised. This is problematic in that any increase in the discriminatory zone, while increasing sensitivity for normal early pregnancy, will



decrease the already low sensitivity for early ectopic pregnancy. An hCG of 2000 is the level at which a sac will be seen in most, but not all, normal early pregnancies.

The important concept to understand is that there is a gray zone of hCG levels in which sonography is frequently indeterminate. When a patient is in an indeterminate group and is stable and reliable, we recommend serial hCG levels or repeat sonography, or both. Unstable patients should be treated as clinically indicated.

A normal IUP demonstrates an hCG doubling time of 2 days (range, 1.2 to 2.2 days).<sup>21</sup> In ectopic pregnancy, this doubling time is increased. If the hCG levels are rising abnormally (<60% increase over at least 48 hours and not steadily declining), the patient is presumed to have an ectopic pregnancy. Even small gestational sacs should grow 0.8 mm per day; therefore, a repeat exam in 2 to 3 days will show a definite change.

It should be recognized that 21% of ectopic pregnancies have an hCG rise that mimics an IUP.<sup>22</sup>

Several studies demonstrated that ectopic and abnormal IUPs have a lower mean level of serum progesterone compared with normal pregnancies.<sup>23-28</sup> A low progesterone level of less than 5 ng/mL can exclude a normal pregnancy with 99.8% accuracy.<sup>22</sup> It has been suggested that this test is most helpful in patients who have an hCG below a discriminatory threshold when sonographic findings are nonspecific.<sup>23</sup> However, a prospective study by Condous et al<sup>29</sup> showed that a single visit strategy with ultrasound and progesterone is not sufficient to exclude ectopic pregnancy.

## DIAGNOSIS OF ECTOPIC PREGNANCY

Diagnostic laparoscopy is considered the gold standard for the diagnosis of ectopic pregnancy, although this invasive approach has a false-negative rate of 3% to 4% and a false-positive rate of 5%.<sup>30</sup> The combined use of serum hCG testing and transvaginal sonography is the current non-invasive approach. Because of more sensitive laboratory tests and improved resolution with ultrasound, we are now able to detect ectopic pregnancies at an earlier stage compared with that possible in the 1970s.<sup>30</sup> It is, therefore, possible to have a more elective approach to management in stable patients. In addition, early diagnosis of ectopic pregnancy allows for screening of high-risk patients. Cacciatore, Stenman, and Ylostalo<sup>31</sup> in 1994 screened 225 women with risk factors of prior ectopic pregnancy and PID and found that 24% had ectopic pregnancies, 84% of which were diagnosed at first screening (37 days of gestation). They suggested that such early diagnosis prevents tubal rupture, substantial hemorrhage, and the need for emergent care.

If a firm diagnosis is not established at the time of initial scanning, follow-up sonography is important. As mentioned previously, gestational sacs grow at a rate of 0.8 mm per day; therefore, follow-up sonography in 2 to 3 days will demonstrate growth in normal pregnancy. Ectopic pregnancies also grow and hemorrhage, and therefore may become more apparent on follow-up. Among patients diagnosed to have ectopic pregnancy, 5% to 18% are detected or confidently diagnosed only at a repeat ultrasound.<sup>31</sup>

## SONOGRAPHY OF NORMAL EARLY INTRAUTERINE PREGNANCY VERSUS ECTOPIC PREGNANCY

In the work-up of ectopic pregnancy, the visualization of a normal early pregnancy dramatically reduces the likelihood of an ectopic pregnancy. Quoted risks for heterotopic pregnancies (concurrent pregnancies located both within the uterus and in an ectopic location) range from 1/30,000 to 1/2100 (Fig. 32-4).<sup>32-35</sup> The 1/30,000 figure was obtained by multiplying the incidence of ectopic pregnancy and dizygotic twinning.<sup>34</sup> However, the incidence of heterotopic pregnancies is increasing, especially in women undergoing ovulation induction, in whom the risk for heterotopic pregnancy is as high as 2.9%. This high incidence results from the high prevalence of tubal damage among in vitro fertilization patients and the use of superovulation and multiple embryo transfer, which predispose patients to the condition.

However, in general, the finding of an IUP excludes the diagnosis of ectopic pregnancy, except for patients at high risk. Therefore, attention to the uterine contents and understanding of normal early pregnancy are important in the management of patients at risk for ectopic pregnancy. Because transvaginal sonography allows for earlier diagnosis of an IUP than does transabdominal scanning, it is the preferred modality for evaluation of patients at risk for ectopic pregnancy. However, transabdominal views are important to screen for hemoperitoneum (Fig. 32-5) and to visualize ectopic pregnancies beyond the range of the vaginal probe.

### Early Intrauterine Pregnancy

The earliest sign of IUP is a small fluid collection in the endometrium. Sacs as small as 2 mm can be visualized with transvaginal sonography. However, because of the overlap with the decidual cysts and pseudogestational sacs of ectopic pregnancy, specificity for early IUP can be increased if a thin rim of echogenic material around the sac is visualized (Fig. 32-6). The sac should be eccentric to the endometrial cavity. This intradecidual sign was described by Yeh et al<sup>36</sup> in 1986 and appears at 4.5 menstrual weeks (2.5 weeks after conception). However, even among experienced radiologists, the accuracy of this finding is as low as 38%.<sup>37,38</sup> Laing et al<sup>38</sup> found that the intradecidual sac sign has a sensitivity and specificity of 48% and 66%, respectively. In a study by Bateman et al,<sup>14</sup> when sacs were less than 5 mm, only one third had a well-defined echogenic rim. This low sensitivity was due to the large number of indeterminate scans. However, in a study by Chiang et al<sup>39</sup> sensitivity and specificity of the intradecidual sign was found to be 60% to 68%, and 97% to 100%, respectively. In this study, Chiang and colleagues showed the importance of seeing the echogenic rim around the sac in more than one plane and assessing for lack of change in the appearance (Fig. 32-7). Owing to the possibility that a decidual cyst could be mistaken for a very early IUP, the prudent course is to follow up symptomatic patients with either hCG or sonography, or both.

The double decidual sac (DSS) sign (Fig. 32-8) is a more reliable indicator of an IUP,<sup>40</sup> but it is present slightly later than the intradecidual sign. The DSS sign is caused by the inner rim of chorionic villi surrounded by a thin crescent of fluid in the endometrial cavity, which, in turn, is surrounded

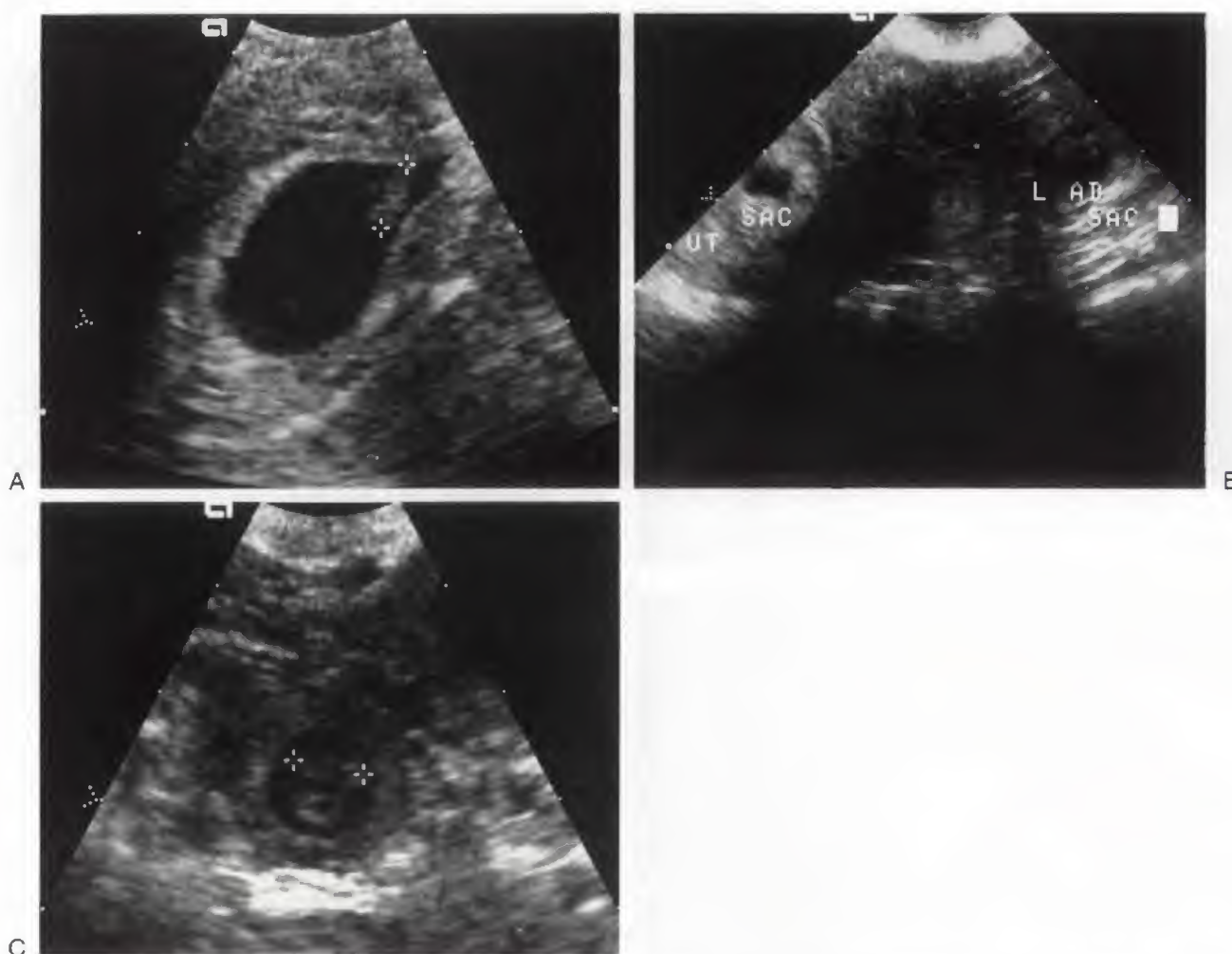


**FIGURE 32-4.** Transvaginal sonograms of patient with simultaneous intrauterine and extrauterine gestations. A. Sagittal view of the uterus demonstrates an intrauterine gestational sac with embryo (*calipers*). B. Transverse view toward the left shows intrauterine gestational sac (UT SAC) and left adnexal sac (L AD SAC). C. Magnified view of the left adnexa shows the extrauterine gestational sac with embryo (*calipers*) and yolk sac. Both embryos demonstrated cardiac activity. Heterotopic pregnancies are becoming more common with the use of ovulation induction agents. In patients with a history of ovulation induction, increased attention should be paid to the adnexa, even after an intrauterine pregnancy has been identified. This patient was not taking ovulation induction agents; this is a rare case of spontaneous heterotopic pregnancy.

by the outer echogenic rim of the decidua vera. This sign is highly reliable for the diagnosis of an intrauterine gestational sac. However, the DSS sign does not absolutely exclude a pseudogestational sac.<sup>41</sup> The presence of the yolk sac (Fig. 32-9) and the embryo (Fig. 32-10) further increase confidence in the diagnosis of an early IUP.

As mentioned earlier, although the finding of an IUP markedly decreases the risk of ectopic pregnancy, all patients should have evaluation of the adnexa. The importance of this evaluation is emphasized in women who have undergone in vitro fertilization. In these women, even visualization of one ectopic pregnancy should not decrease vigilance to identify other gestations, because a patient with twin ectopic pregnancies with simultaneous live triplet intrauterine pregnancies has been reported.<sup>42</sup>

### Abnormal Intrauterine Pregnancy

One of the difficult tasks in evaluating for ectopic pregnancy is distinguishing an abnormal IUP from the pseudogestational sac of ectopic pregnancy. This frequently is not possible. The diagnostic criteria for abnormal IUP are discussed in detail in Chapter 6. If an intrauterine sac is seen with a diameter exceeding that at which a yolk sac should be seen (i.e., mean sac diameter greater than 10 mm without visualization of a yolk sac) (Fig. 32-11) and the patient's history is suggestive of ectopic pregnancy, a dilatation and curettage can be performed. If this documents the presence of villi, then a nonviable gestation is present, and the patient's risk for an extrauterine gestation is effectively eliminated. If villi are not detected, the patient is still at risk for ectopic



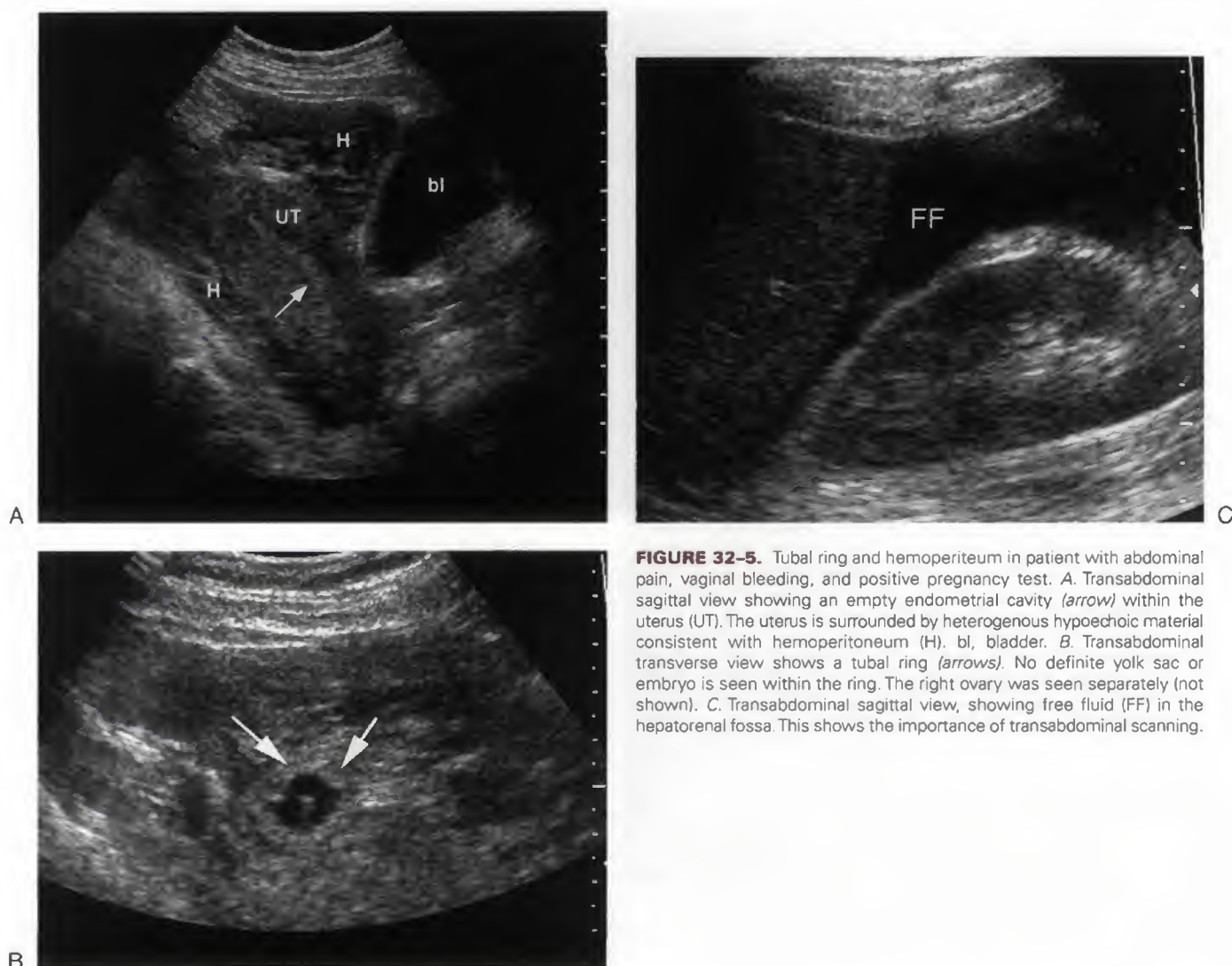


**FIGURE 32-5.** Tubal ring and hemoperitoneum in patient with abdominal pain, vaginal bleeding, and positive pregnancy test. A. Transabdominal sagittal view showing an empty endometrial cavity (*arrow*) within the uterus (UT). The uterus is surrounded by heterogenous hypoechoic material consistent with hemoperitoneum (H). bl, bladder. B. Transabdominal transverse view shows a tubal ring (*arrows*). No definite yolk sac or embryo is seen within the ring. The right ovary was seen separately (not shown). C. Transabdominal sagittal view, showing free fluid (FF) in the hepatorenal fossa. This shows the importance of transabdominal scanning.

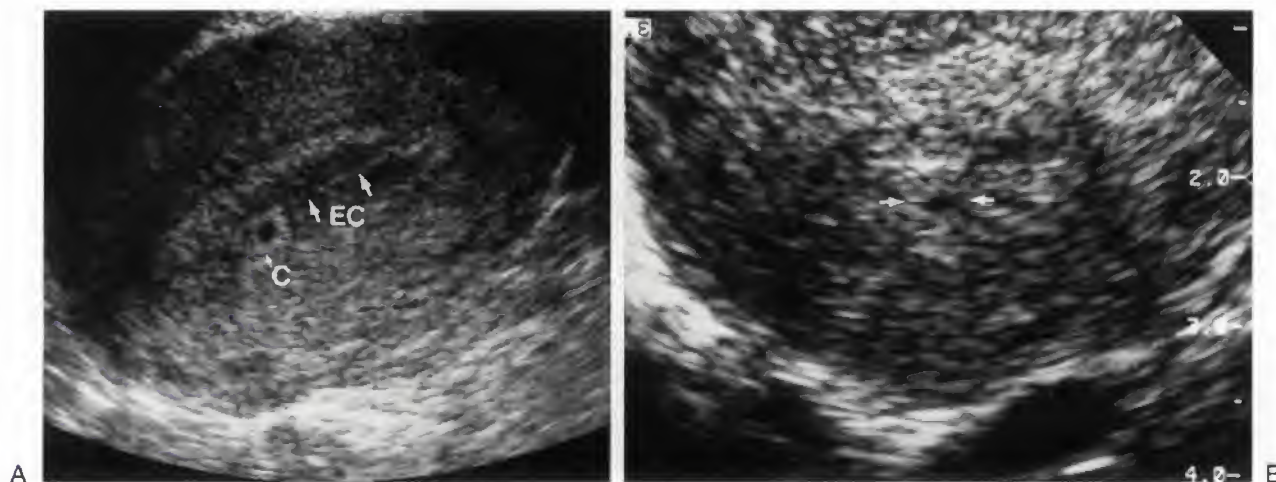


**FIGURE 32-6.** Transvaginal sonogram of very early intrauterine pregnancies. A. Sagittal sonogram demonstrates intradecidual sign, with an echogenic ring formed by chorionic villi (C) located eccentric to the endometrial cavity (EC). B. Transvaginal transverse view of a very early intrauterine pregnancy. A 2-mm sac is present. Although there is the suggestion of a decidual reaction (*arrows*) because of the echogenic surrounding endometrium, it is not sufficient to represent definitely an early intrauterine pregnancy. For this patient, a follow-up sonogram or serial human chorionic gonadotropin levels (hCGs) should be obtained to guide clinical management if an ectopic pregnancy is suspected.

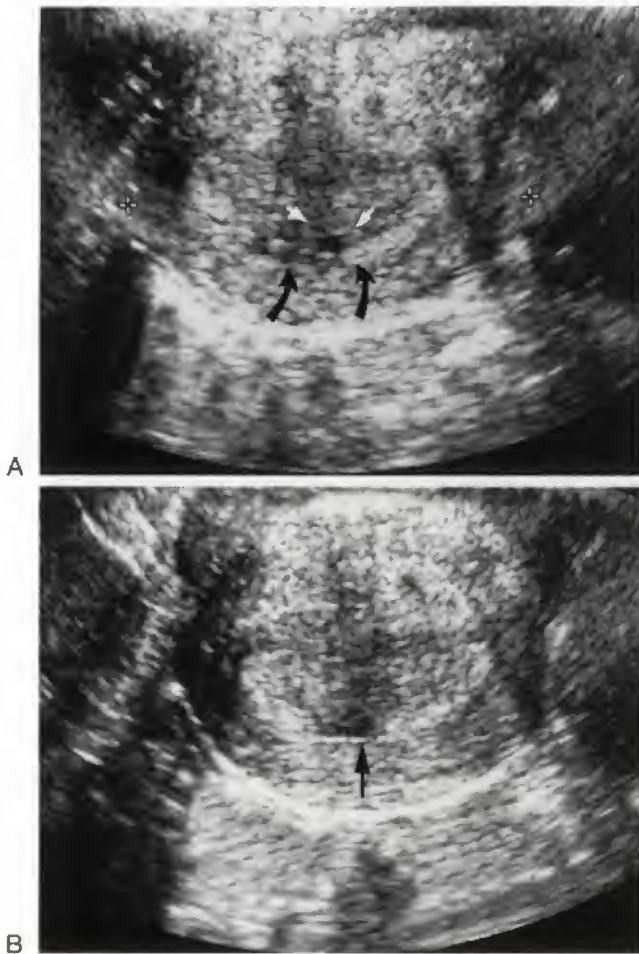


**FIGURE 32-7.** Pitfall in use of intradecidual sign. Transverse transvaginal scan in a patient suspected of harboring an ectopic pregnancy. *A.* Initial image demonstrates a 2-mm sac with mildly echogenic rim (arrows), eccentric to the endometrial stripe (curved arrows) suggestive of an intradecidual sign of normal early pregnancy. *B.* Image obtained 15 seconds after that in Figure 32-7A shows that the configuration of the fluid collection (arrow) has changed and the echogenic rim is no longer present. Small fluid collections in the endometrial cavity may show such changes. This change in appearance is consistent with blood in the endometrial cavity rather than an intrauterine gestational sac.



**FIGURE 32-8.** Transvaginal sonogram of an early pregnancy. This sonogram demonstrates the double decidual sac sign. The gestational sac is measured with calipers. The inner ring is formed by the echogenic chorionic villi. The outer ring is the deeper layer of decidua vera (D). The separating lucent zone is the more superficial decidua vera.



**FIGURE 32-9.** Sagittal transvaginal sonogram demonstrates the double decidual sac sign but also the more reliable feature of a yolk sac.

pregnancy. If the patient is stable, interval change in hCG levels can be monitored.

## SCANNING TECHNIQUE

### Transabdominal Scan

The sonographic evaluation of ectopic pregnancy should begin with a transabdominal scan to assess for any masses that might be out of the plane of the vaginal transducer. If the bladder is empty at the time of the initial examination, the examination can begin with transvaginal study; however, it must be emphasized that if the adnexal regions are not well evaluated, a transabdominal study through a full bladder should be performed. Cases have been reported of ectopic pregnancies visualized transabdominally that were

missed on vaginal scanning alone,<sup>43,44</sup> especially in patients with pelvic masses such as fibroids.<sup>44</sup> In some cases in which only vaginal scanning is used, either the ectopic pregnancy will not be identified or the ectopic pregnancy will be misinterpreted as intrauterine. The renal regions are evaluated for free fluid in the abdomen (see Fig. 32-5).

### Transvaginal Scan

Transvaginal sonography should then be performed. Multiple studies have shown that vaginal sonography provides additional clinically useful information above that available with transabdominal sonography for patients with suspected ectopic pregnancy.<sup>43,45-49</sup> The uterine contents are closely evaluated for signs of early IUP. As mentioned earlier, the documentation of an IUP greatly diminishes the likelihood of ectopic pregnancy.



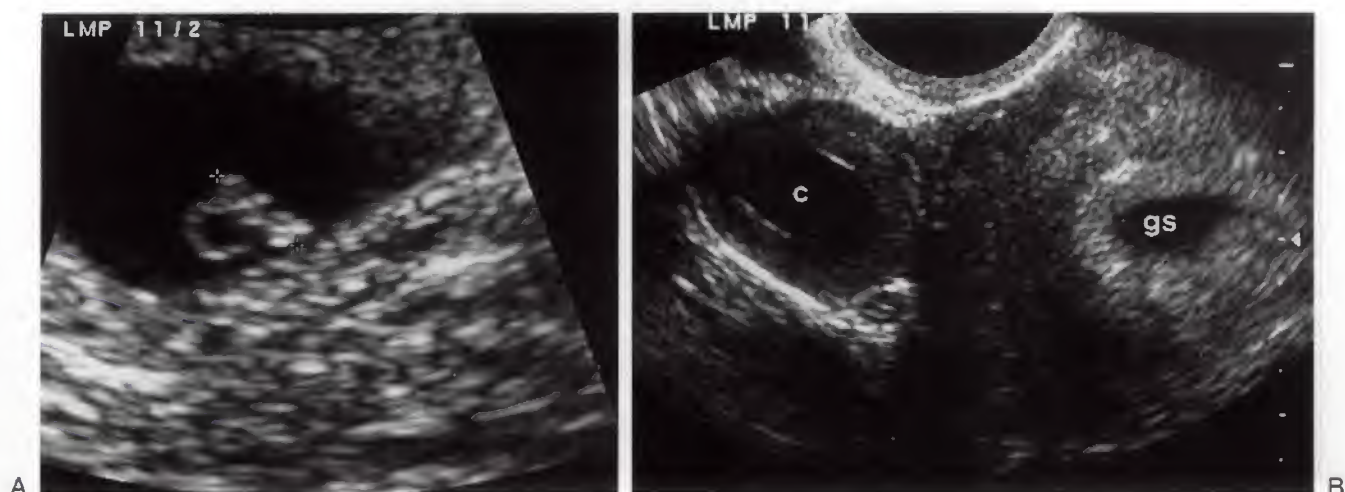


**FIGURE 32-10.** A. Sagittal transvaginal sonogram demonstrates an intrauterine gestational sac with an early embryo (*calipers*) with a crown-rump length of 6 mm. B. Transverse view of the left adnexa shows the intrauterine gestational sac (gs) and a thick-walled left adnexal cyst (c). Although adnexal cysts in patients with intrauterine pregnancy should be examined to exclude ectopic pregnancy, once an intrauterine pregnancy is visualized, a cyst such as this most likely represents a corpus luteum.

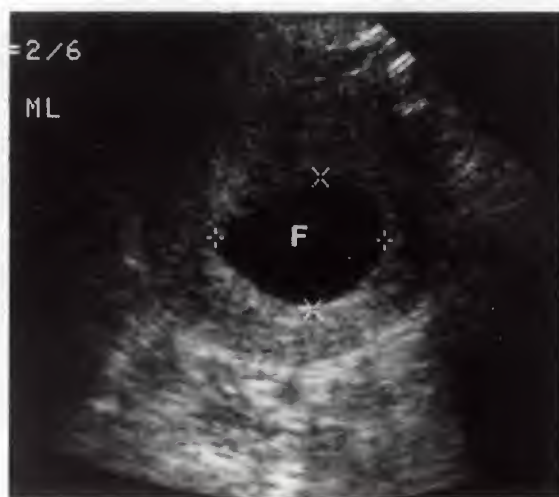


**FIGURE 32-11.** Transvaginal scan in a pregnant patient with bleeding. Sagittal view of the uterus shows an irregular fluid (F) collection in the uterus. No double decidual sac sign, yolk sac, or embryo is seen; therefore, an intrauterine pregnancy cannot be diagnosed. The mean sac diameter is 29 mm. Because of the large sac size, it can be concluded that if this is an intrauterine pregnancy, it is not viable (see Chapter 6). Therefore, the uterus can be safely evacuated and the products examined for chorionic villi. If chorionic villi are found, an abnormal intrauterine pregnancy is established and the patient's risk for extrauterine gestation is effectively eliminated.

### Assessment of the Adnexa

As shown in Figure 32-12, common locations of ectopic pregnancies are 75% to 80% in the ampullary portion of the fallopian tube, 10% in the isthmic portion, 5% in the fimbrial end, 2% to 4% in the interstitial end (sometimes called cornual ectopic), and 0.5% in the ovary.<sup>4</sup> Abdominal and cervical pregnancies are very rare.

Because the tube is the most common location for ectopic pregnancies, it is important to scan above and below the ovaries and between the uterus and ovaries to exclude an adnexal mass (see Figs. 32-3 and 32-13 to 32-15). The location of the corpus luteum is not helpful in directing the examination because contralateral implantation occurs in up to one third of cases (Fig. 32-16).<sup>50</sup> When an adnexal mass is visualized, it should be examined for yolk sac, embryo, and heartbeat (Figs. 32-17 to 32-19). If a heartbeat is visualized, this likely will influence the mode of treatment, because methotrexate has a lower success rate in cases of ectopic pregnancy with cardiac activity. However, finding cardiac activity in an ectopic pregnancy occurs only about 10% of the time. A hyperechogenic ring is a fairly specific finding for ectopic pregnancy; but this is easily confused with a normal corpus luteum cyst (see Figs. 32-16, 32-20, and 32-21).

An anechoic cyst is unlikely to be an ectopic pregnancy. Even a complex cyst in the ovary is much more likely to be the corpus luteum than an ectopic pregnancy because ovarian ectopics represent less than 1% of all ectopic pregnancies.<sup>4</sup> If a thick-walled cyst is seen, care should be taken to distinguish whether this is intraovarian (and, therefore, most likely the corpus luteum) or extraovarian (and, therefore, most likely an ectopic pregnancy) (see Figs. 32-16, and 32-20 to 32-22). If it is difficult to distinguish the corpus luteum cyst from a tubal mass, it may be helpful to palpate the abdomen over the region of the mass to determine whether it is tubal (moves separately from the ovary) or ovarian (moves with the ovary).<sup>51</sup>

### Assessment of the Cul-De-Sac

The cul-de-sac should be examined for free fluid. Fluid, when present, should be characterized as simple or complex. Complex fluid is suggestive of blood and, therefore, ectopic pregnancy (see Figs. 32-5 and 32-23). When echogenic fluid

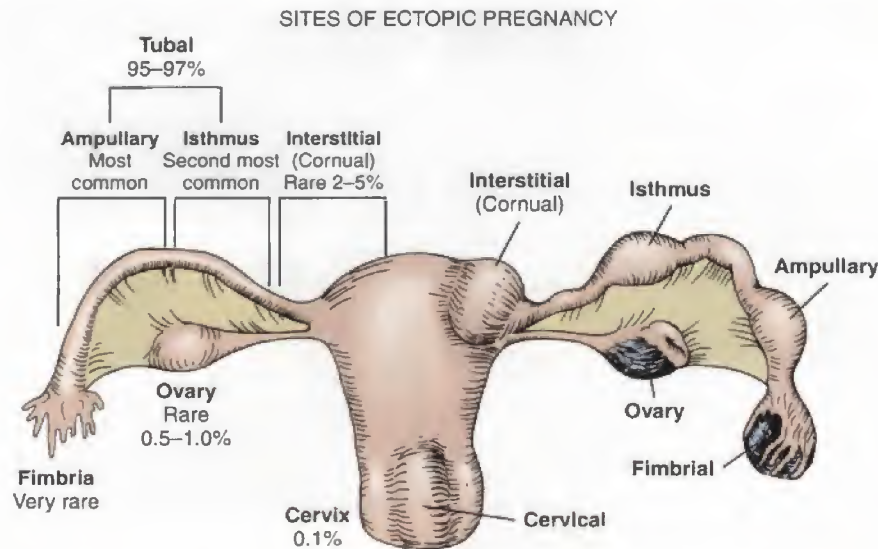


**FIGURE 32-12.** Common locations of ectopic pregnancy. Note that 95% to 97% of ectopic pregnancies occur somewhere along the course of the fallopian tube. (Modified from Benson RC: *Handbook of Obstetrics & Gynecology*, 8th ed. Los Altos, CA, Lange Medical Publications, 1983; and Schoenbaum S, Rosendorf L, Kappelman N, et al: *Gray-scale ultrasound in tubal pregnancy*. *Radiology* 127:757, 1978.)

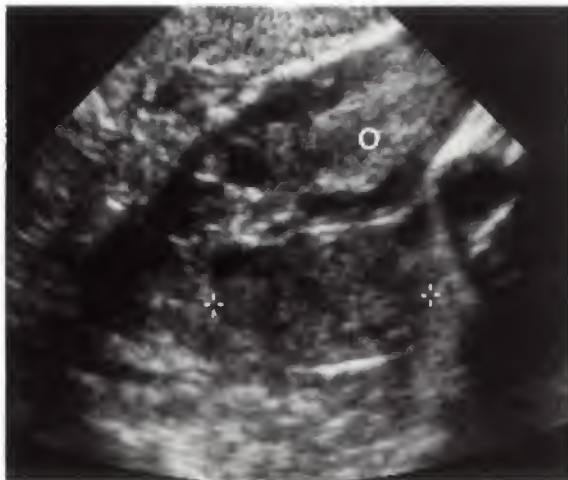


**FIGURE 32-13.** Transvaginal sonogram of a patient suspected of harboring an ectopic pregnancy. Transverse view of the left adnexa shows a hypoechoic mass (*calipers*) adjacent to the left ovary (O). No intrauterine pregnancy was visualized. A patient who fails to demonstrate an intrauterine pregnancy and also demonstrates a mass separate from the ovary is worrisome for ectopic pregnancy. A mass of this type generally represents a hematosalpinx.



**FIGURE 32-14.** Tubal ring in a patient suspected of harboring an ectopic pregnancy. Transverse transvaginal scan shows a left tubal ring (*arrowheads*) adjacent to the ovary (*arrow*) with a corpus luteum cyst. Note the trace free fluid (f) adjacent to the ovary. These findings are consistent with ectopic pregnancy.

is visualized in a patient with positive hCG results this has a positive predictive value (86% to 93%) in the diagnosis of ectopic pregnancy,<sup>52</sup> and may be the only transvaginal sonographic finding.<sup>53</sup> When free fluid is documented in the pelvis, it is helpful to obtain images of the kidneys in order to assess whether a large amount of hemoperitoneum is present (see Fig. 32-5).

## SONOGRAPHIC FINDINGS IN ECTOPIC PREGNANCY

### Adnexal Mass

Criteria for diagnosis of ectopic pregnancy are listed in Table 32-2. The most specific finding is of an extrauterine live embryo (see Figs. 32-18 and 32-19). Because of a lack



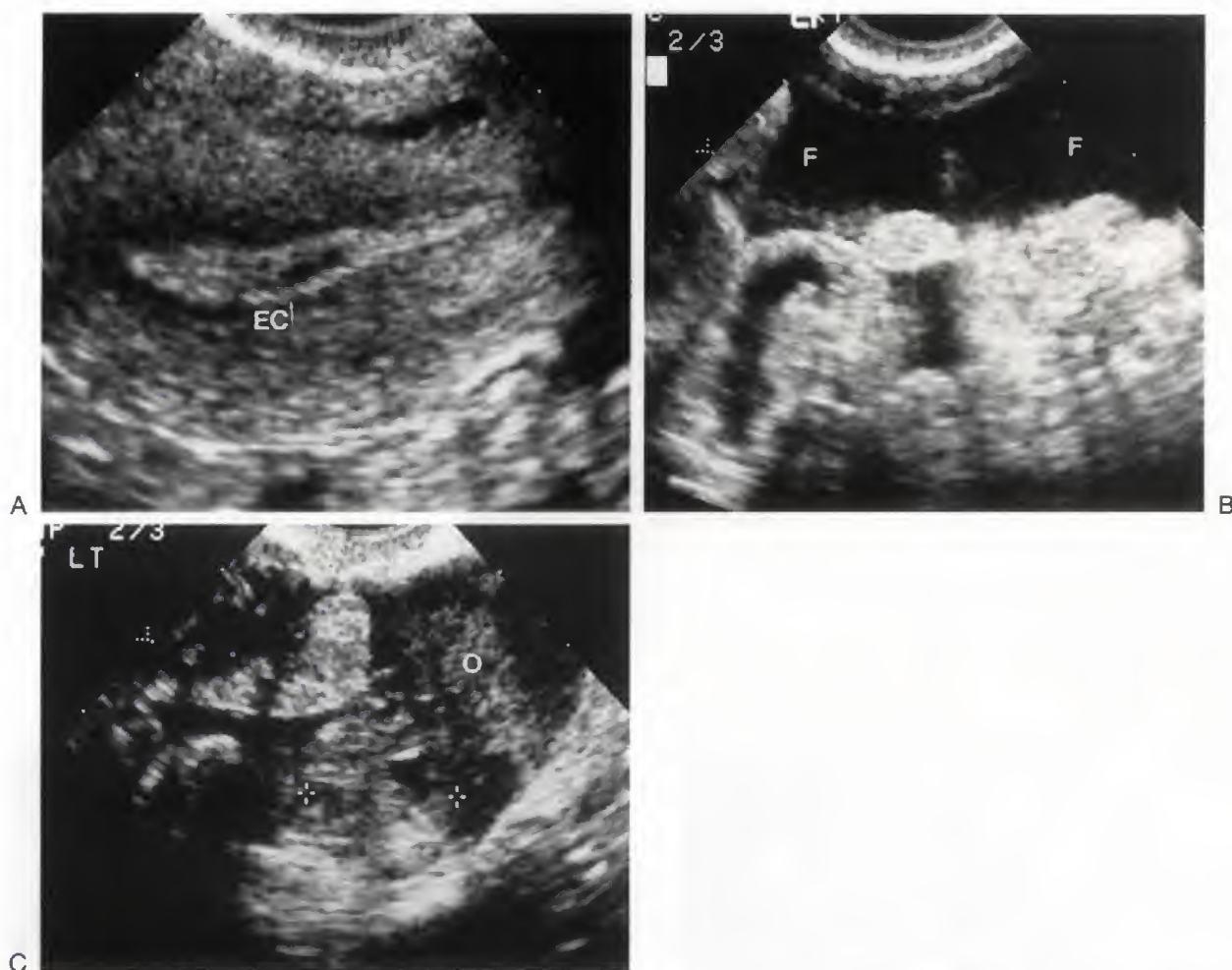


**FIGURE 32-15.** Transvaginal scan in a patient suspected of harboring an ectopic pregnancy. *A.* Sagittal view of the uterus shows a small amount of fluid in the endometrial cavity (EC). No pregnancy is seen. *B.* Transverse view of the cul-de-sac reveals complex fluid (F) consistent with blood. *C.* Transverse view of the left adnexa shows an echogenic tubal ring (*calipers*) medial to the left ovary (O). The combination of moderate fluid, a ring-like mass, and absence of an intrauterine pregnancy virtually confirms the presence of an ectopic pregnancy.

of sensitivity of this finding, most physicians use the criterion of an extraovarian adnexal mass. This finding has a specificity of up to 100% depending on the patient population selected (i.e., the discriminatory level of hCG for inclusion into the study). Most of the enlargement of the fallopian tube is caused by bleeding into the wall and lumen rather than from the products of conception.

As previously mentioned, it is important to distinguish between a tubal mass and an ovarian cyst. Sonographic findings that can help distinguish the corpus luteum from the adnexal ring of an ectopic pregnancy include a corpus luteum wall that is less echogenic compared with the wall of the tubal ring associated with the ectopic, and a corpus luteum wall that is less echogenic than the endometrium.<sup>54,55</sup> If the diagnosis of an adherent ectopic pregnancy or exophytic ovarian cyst cannot be confirmed and the patient is stable, a follow-up examination can be performed (see Fig. 32-20). The rapid change in the appearance of the ovarian cyst frequently allows differentiation of the two conditions.<sup>51</sup>

## Endometrial Findings

The endometrium may have a pseudogestational sac in ectopic pregnancy (see Figs. 32-16 and 32-24). The hormonal changes associated with ectopic pregnancy can cause fluid collections in the endometrial cavity, which mimic a gestational sac. In addition, blood products from an ectopic pregnancy can collect in the endometrium, leading to the appearance of a gestational sac. A pseudogestational sac is visualized in approximately 20% of patients with ectopic pregnancy.<sup>56</sup> This pseudogestational sac must be distinguished from the gestational sac of normal early IUP. Differentiating features are listed in Table 32-3.

There are no classic endometrial findings in ectopic pregnancy. The endometrial thickness in ectopic pregnancy varies from a thin to thick endometrium (Fig. 32-25).<sup>57</sup> Thin-walled, simple-appearing decidual cysts, usually at the junction of the endometrium and myometrium, are associated with ectopic pregnancy.<sup>58</sup> However, as mentioned earlier, decidual cysts are also seen with normal IUP and in

A



B



C



**FIGURE 32-16.** Transabdominal and transvaginal scans in a patient suspected of harboring an ectopic pregnancy. *A.* Transabdominal scan shows fluid centrally located within the endometrial cavity. *B.* Transvaginal sagittal image of the right ovary shows a thick-walled corpus luteal cyst. *C.* Transvaginal transverse image of the left adnexa shows the tubal ring (arrow) inferior to the left ovary. This case illustrates many features of ectopic pregnancy. A pseudosac can simulate a gestational sac. The corpus luteum can be contralateral to the ectopic pregnancy. The ring of the ectopic pregnancy is more echogenic than the ring around the corpus luteum. The ring of the ectopic pregnancy is adjacent to the ovary and not located within the ovary.

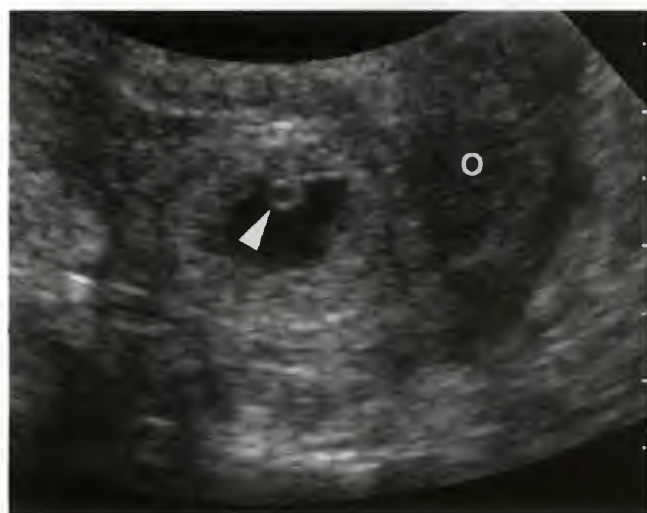


**FIGURE 32-17.** Transverse transvaginal sonogram of the left adnexa in a patient with an ectopic pregnancy. There is an adnexal ring containing a yolk sac (arrowhead) adjacent to the ovary (O). Just as a yolk sac within an intraendometrial fluid collection confirms an intrauterine pregnancy, a yolk sac within an adnexal mass confirms an extrauterine pregnancy.

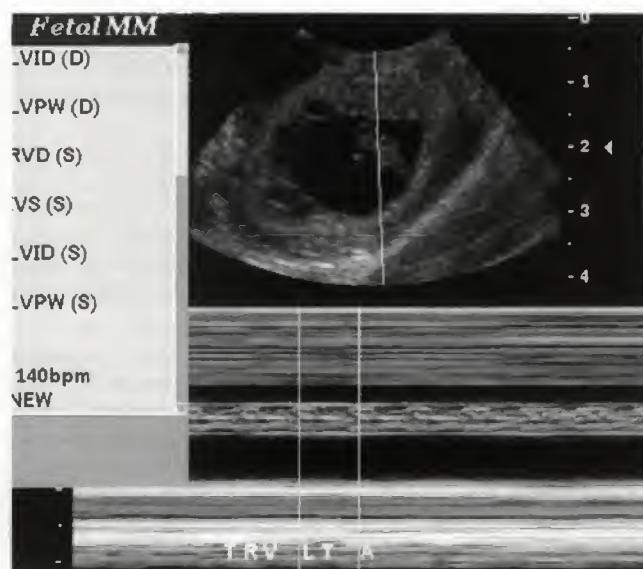


**FIGURE 32-18.** Transverse transvaginal scan of the right adnexa in a patient with an ectopic pregnancy reveals an echogenic ring with embryo. M-mode demonstrates cardiac activity. Only about 10% of ectopic pregnancies will demonstrate a heartbeat at the time of diagnosis.



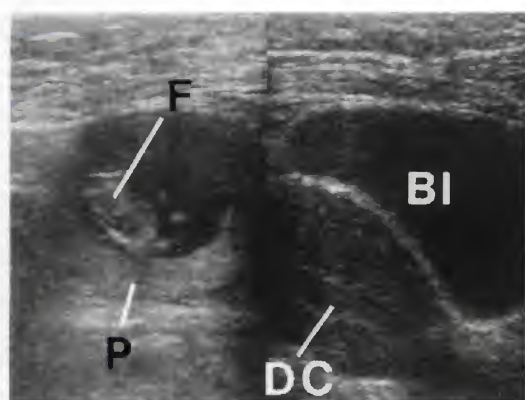


**FIGURE 32-19.** Composite linear array transabdominal sonogram of a patient suspected of harboring an ectopic pregnancy. A large ectopic gestation is located superior to the fundus of the uterus. A fetus (F) whose biparietal diameter was easily measured can be identified. Additionally, there is a well-developed placenta (p). Only a decidual cast (DC) is seen within the uterus. Although large and easily seen, such ectopic pregnancies may be misdiagnosed as intrauterine if the sonologist fails to observe the line of demarcation between the ectopic gestation and the uterine fundus. When this separation is not noted, the ectopic gestation is mistakenly incorporated into the uterine fundus. This error can be devastating to the patient. Bl, bladder.

nonpregnant patients (Fig. 32-26).<sup>58,59</sup> These decidual cysts differ from a pseudogestational sac in that they are removed from the endometrial cavity. Decidual cysts are distinguished from the intradecidual sign of normal early pregnancy in that they do not have an echogenic rim.

When a patient is seen with an indeterminate fluid collection in the endometrium, clinical judgment influences patient care. In stable patients at risk for ectopic pregnancy in whom no adnexal mass is demonstrable, it is prudent to perform a follow-up ultrasound.

## Free Fluid

Free fluid is a nonspecific finding, although a large amount of fluid is suggestive of an ectopic pregnancy (see Fig. 32-5). Complex fluid is consistent with hemoperitoneum (see Figs. 32-5 and 32-23). This is associated with ectopic pregnancy but does not necessarily signify tubal rupture, because a ruptured hemorrhagic corpus luteum cyst can also result in hemoperitoneum.<sup>60,61</sup> A small amount of fluid can be seen in both normal and abnormal pregnancies. However, large amounts of fluid or complex fluid increase the likelihood of ectopic pregnancy.<sup>53</sup> If the patient is clinically unstable, differentiating between a ruptured ectopic and a ruptured hemorrhagic corpus luteum is unimportant, because in either case, a laparotomy is indicated. In unstable patients with demonstration of hemoperitoneum, the sonographic examination can be terminated without demonstrating an ectopic pregnancy. In the clinically stable patient, it is more important to carefully examine the adnexa to determine if an ectopic pregnancy is present. Transvaginal sonography has been shown to be more sensitive than culdocentesis for the detection of hemoperitoneum and has a higher negative predictive value.<sup>62</sup> Therefore, vaginal sonography has almost completely replaced culdocentesis in the evaluation of ectopic pregnancy.



**FIGURE 32-20.** Transvaginal scan in a patient suspected of harboring an ectopic pregnancy. A. Sagittal transvaginal color Doppler image of a 2-cm thick-walled hemorrhagic cyst. Note the central fibrin strand mimicking a yolk sac (arrow). Note the ring of fire appearance to the cyst. B. Transverse, transvaginal image shows that the mass (arrows) is located within the ovary (arrowheads). Additional images (not shown) demonstrated an intrauterine gestational sac with yolk sac. Even in a patient with no visualized intrauterine pregnancy, an ovarian mass is more likely to represent a hemorrhagic corpus luteal cyst than an ovarian ectopic. In this case, the hemorrhagic cyst resolved on follow-up. (From Swire MN, Castro-Aragon I, Levine D: Various sonographic appearances of the hemorrhagic corpus luteum cyst. *Ultrasound Q* 20:49, 2004.)

## The Normal Sonogram

When a patient is pregnant and has no identifiable intrauterine gestational sac, one of three possibilities exists: an early IUP that is too small for definite identification, a recent spontaneous abortion, or an ectopic pregnancy. Because 15% to 35% of ectopic pregnancies will not demonstrate an identifiable extrauterine mass on transvaginal sonography,<sup>52,53,61</sup> an ectopic pregnancy cannot be excluded when no mass is seen. In up to 26% of patients with ectopic pregnancy, the sonogram may be completely normal (see

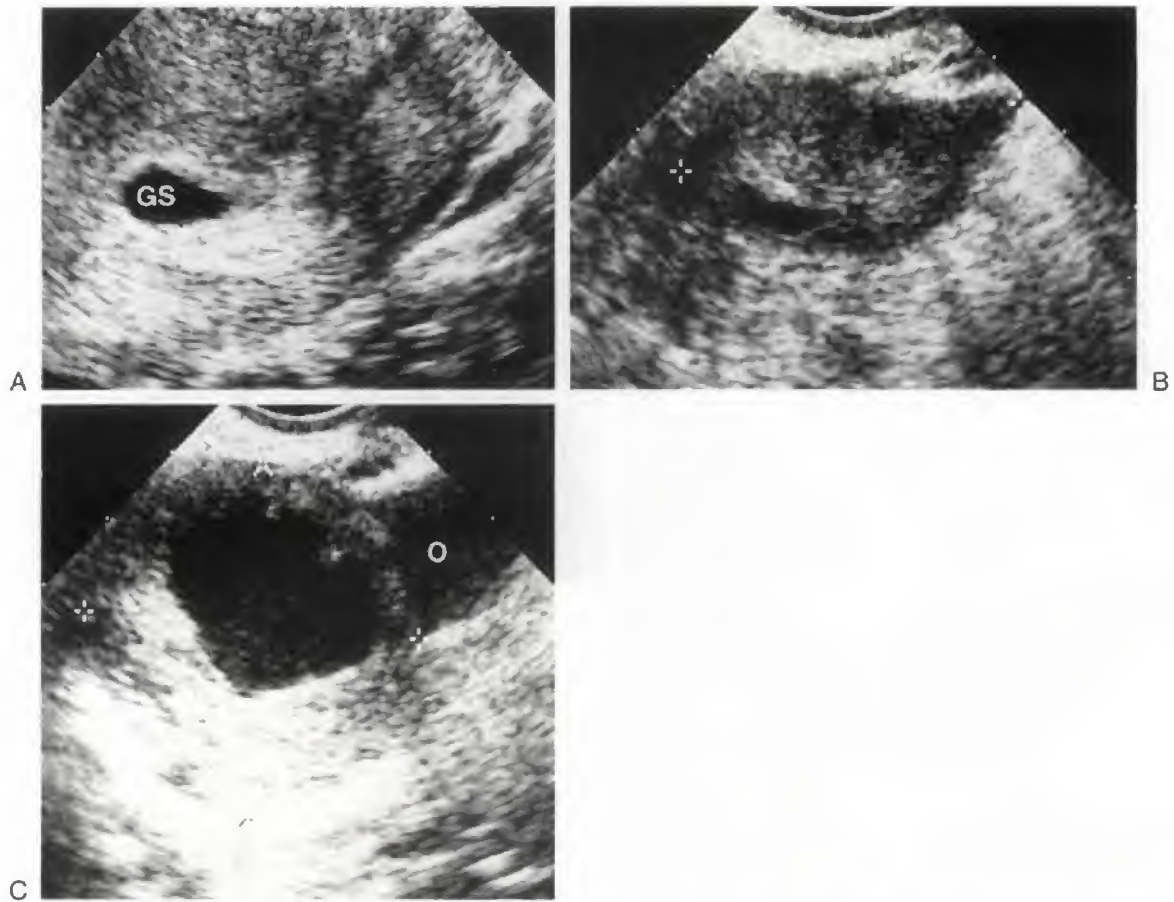


**FIGURE 32-21.** Transvaginal scans in a patient 6 weeks pregnant with bleeding and pain. *A.* Sagittal view of the uterus shows an intrauterine gestational sac (GS) with mean sac diameter of 12 mm. No yolk sac or embryo was identified. *B.* Sagittal view to the left shows a normal left ovary. *C.* Just lateral to the image in Figure 32-21*B*, adjacent to the left ovary (O), is a thick-walled cyst (*calipers*). The patient likely had a spontaneous abortion and an exophytic corpus luteum cyst. Because of atypical appearance of the adnexa, follow-up with human chorionic gonadotropin (hCG) and sonograms were obtained. The hCG levels declined normally. Within 4 weeks, the pelvic ultrasound was normal. This mass was believed to represent a hemorrhagic corpus luteum cyst.

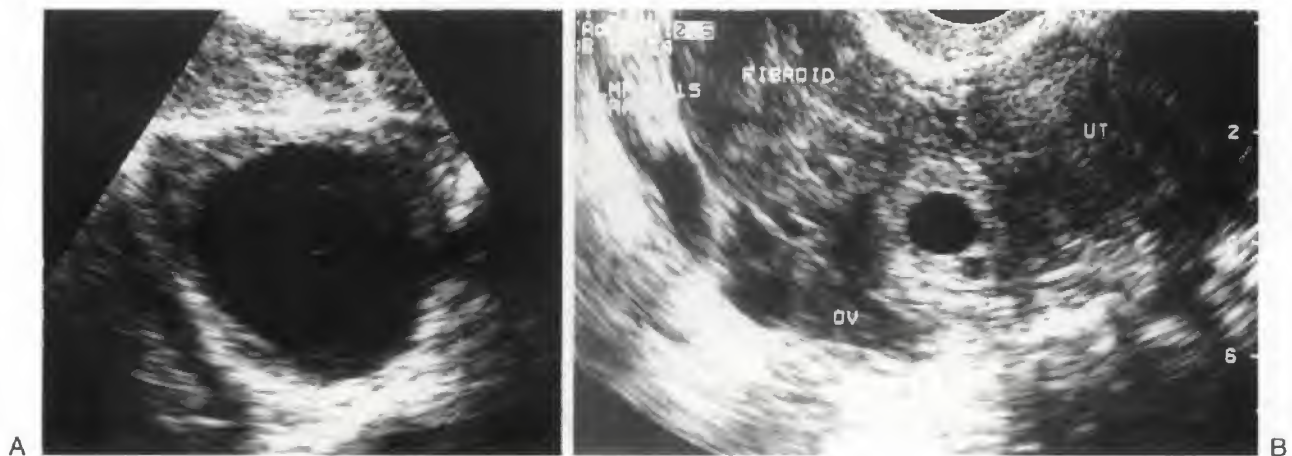


**FIGURE 32-22.** Transvaginal scan in a patient with exophytic fibroid and corpus luteum cyst ipsilateral to an ectopic pregnancy. *A.* Transverse view of the right ovary shows a 2 cm cyst with strands of internal hemorrhage consistent with a hemorrhagic corpus luteum cyst. *B.* Transverse view of the right pelvis shows a pedunculated fibroid to the right of the uterus and an echogenic ring representing the ectopic pregnancy (EP) between the fibroid, uterus (UT), and ovary (OV). Fibroids can make the examination for ectopic pregnancy difficult, but as demonstrated in this case, ectopic gestational sacs can still be visualized in these complicated cases.



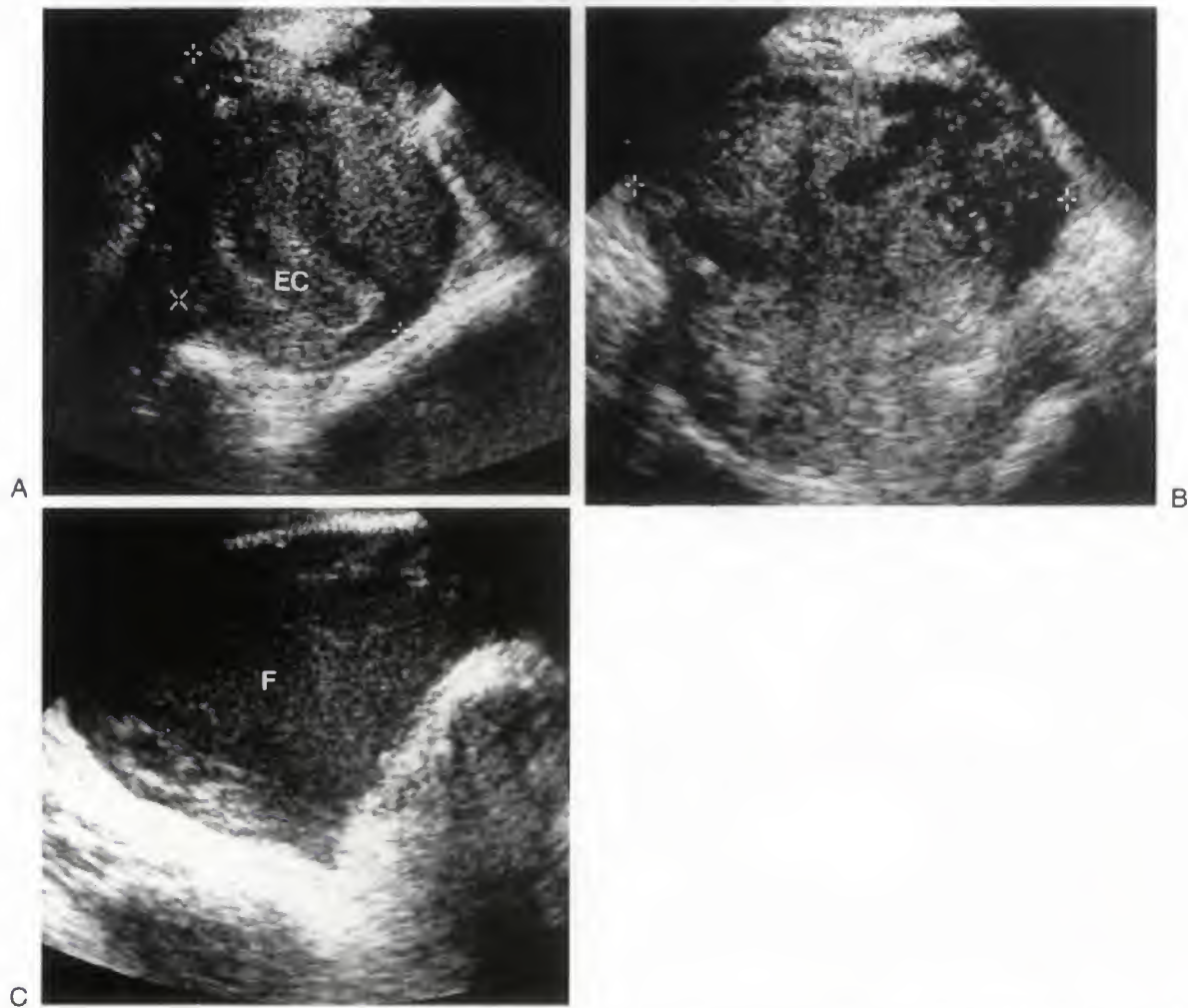


**FIGURE 32-23.** Transvaginal sonogram in a patient with ectopic pregnancy. A. Sagittal view of the uterus shows complex fluid in endometrial cavity (EC). B. Transverse view of the right adnexa shows 4-cm mass (*calipers*). C. Transverse view in the cul-de-sac shows echogenic fluid (F). Any free fluid seen in a patient without a demonstrable intrauterine pregnancy is worrisome for ectopic pregnancy. However, echogenic fluid is even more suggestive. In this patient with an adnexal mass and echogenic fluid, the diagnosis is almost certain.

Table 32-2	Criteria for Diagnosis of Ectopic Pregnancy		
Criteria*		Sensitivity (%)	Specificity (%)
Extrauterine gestational sac with yolk sac or embryo (with or without heartbeat)		8–34	100
Adnexal ring		40–68	100
Complex adnexal mass separate from ovary		89–100	92–99
Any fluid		46–75	69–83
Moderate to large amount of free fluid		29–63	21–96
Echogenic fluid		56	96
Decidual cyst		21	92

\*In patients with positive pregnancy test and no intrauterine pregnancy.  
 Data compiled from Cacciatore<sup>17</sup>; Bateman et al<sup>14</sup>; Nyberg et al<sup>19</sup>; Braffman et al<sup>15</sup>; Cacciatore, Stenman, and Ylostalo<sup>31</sup>; Dashefsky et al<sup>16</sup>; Thorsen et al<sup>18</sup>; Cacciatore, Stenman, and Ylostalo<sup>45</sup>; Kivikoski, Martin, and Smeltzer<sup>47</sup>; Nyberg et al<sup>55</sup>; Frates et al<sup>61</sup>; Russell, Filly, and Damato<sup>52</sup>; Ackerman et al<sup>58</sup>; Fleischer et al<sup>71</sup>; Ari et al<sup>105</sup>; Brown and Doubilet<sup>128</sup>; Nyberg et al<sup>129</sup>; DiMarchi, Kosasa, and Hale<sup>130</sup>; Süller, Haynes de Regt, and Blair<sup>151</sup>; Pennell et al<sup>132</sup>; Filly<sup>133</sup>; Cacciatore, Stenman, and Ylostalo<sup>144</sup>; Rempen<sup>145</sup>; Timor-Trisch.<sup>146</sup>

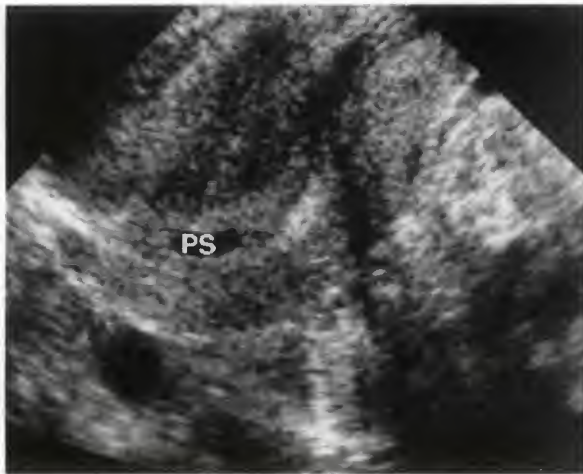


**FIGURE 32-24.** Pseudosac (PS) of ectopic pregnancy. Transvaginal sagittal view of the uterus shows a fluid collection centrally located in the endometrial cavity in a patient with an ectopic pregnancy.

**Table 32-3**

**Differentiating Features of the Pseudogestational Sac of Ectopic Pregnancy and Normal Early Intrauterine Pregnancy (IUP)**

Classic Sonographic Features	Early IUP	Pseudosac
Shape	Round	Ovoid
Location with respect to endometrial cavity	Eccentric	Central
Margins	Well defined	Poorly defined
Decidual reaction	Well defined	Absent
Single or double sac	May show double decidual sac sign	Single decidual layer

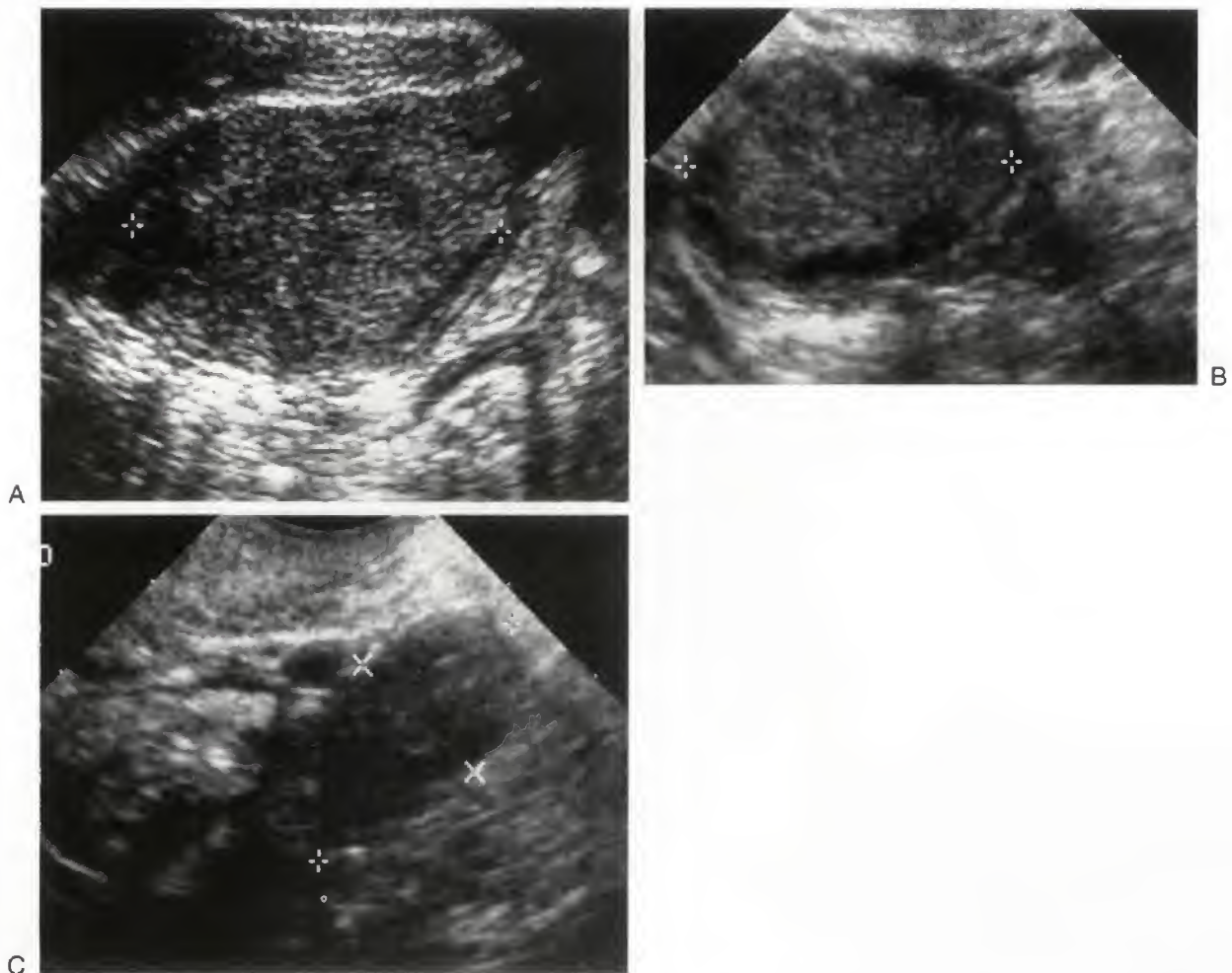


**FIGURE 32-25.** Normal pelvic sonogram in a patient suspected of harboring an ectopic pregnancy. *A*. Transvaginal transverse view of the uterus shows no intrauterine pregnancy. *B* and *C*. Transverse views of the adnexa are normal. Both ovaries are clearly identified. At real time, no abnormal masses were visualized. There is no free fluid in the cul-de-sac. Despite the normal appearance of this pelvis, there is an ectopic pregnancy. It is essential to remember that a normal pelvic sonogram does not exclude an ectopic pregnancy. Because of abnormally rising human chorionic gonadotropin levels (hCGs), the patient was treated with methotrexate (see Fig. 32-36).





**FIGURE 32-26.** Decidual cyst in a patient with an ectopic pregnancy. Transvaginal sagittal view of the uterus in a patient with ectopic pregnancy. A decidual cyst (arrow) is typically located at the endometrial-myometrial junction. These small cysts are associated with ectopic pregnancy but also can be present in a patient with an intrauterine pregnancy.

Fig. 32-25).<sup>52</sup> Therefore, it is important to obtain clinical follow-up with repeat sonography if hCG continues to rise.

### Mimics of Ectopic Pregnancy

False-positive findings of hematosalpinx can be due to an exophytic or ruptured corpus luteum cyst, pedunculated fibroids, ovarian torsion, retrograde flow of blood from a spontaneous abortion, a tuboovarian abscess, tubal cysts, or adjacent bowel (Fig. 32-27).<sup>51</sup>

### Role of Doppler Sonography

Color and pulsed Doppler have been advocated to improve the diagnosis of ectopic pregnancy.<sup>63-65</sup> Normal intrauterine pregnancies have low-impedance, high-diastolic flow at the placental implantation site. Because of low resistance, the area of color flow will appear continuous or nearly continuous during real-time examination. This is visualized in normal intrauterine pregnancies but not in the pseudogestational sac of an ectopic pregnancy.<sup>41,63,66</sup> When an indeterminate intrauterine sac is visualized, color Doppler can be helpful in showing a color flash beneath the implantation site. However, the effects of Doppler's high-energy output focused on the small developing normal pregnancy should be considered. Therefore, use of this technique should be limited to cases in which the results of a color study will potentially affect management.

Similar to intrauterine pregnancies, ectopic pregnancies can have low-impedance and high-diastolic flow (Fig. 32-28). Color Doppler is most helpful when an extraovarian mass has not yet been found, because use of Doppler may allow for detection of an ectopic surrounded by loops of bowel. In a study by Pellerito et al,<sup>65</sup> 1 of 65 cases of ectopic pregnancy was identified by color Doppler when no mass was



**FIGURE 32-27.** Bowel mimicking ectopic pregnancy. Transvaginal image shows an echogenic ring-like mass adjacent to the ovary. During the scan, this mass was noted to peristaltic, showing that it was bowel, and not an ectopic pregnancy.

visualized by grayscale. However, the normal corpus luteum also has low-impedance flow. Care should be taken to ensure that a mass is extraovarian before analyzing the color flow. Resistive index has also been advocated to distinguish between ectopic pregnancy and corpus luteum cysts. However, there is considerable overlap between the resistive index of ectopic pregnancy and corpus luteum.<sup>30,65</sup>

Although the presence of abnormal flow may indicate an ectopic pregnancy, the absence of color Doppler signal cannot be used to exclude ectopic pregnancy because early and dead ectopics can have absent flow.<sup>65</sup>

One possible use of color Doppler is to identify tissue that is nonviable, which would then be more apt to respond to nonsurgical or expectant management<sup>30,67</sup> or to monitor response to treatment.<sup>67</sup>

### RARE FORMS OF ECTOPIC PREGNANCY

As discussed earlier, approximately 95% of ectopic pregnancies occur in the ampullary or isthmic portion of the fallopian tube. The next most common site is in the interstitium of the tube (2% to 4%, Figs. 32-29 and 32-30), where it traverses the wall of the uterus to enter into the endometrial cavity. Ovarian, cervical (Figs. 32-31 and 32-32), and abdominal pregnancies are rare. Even less common are pregnancies occurring in a uterine scar (Fig. 32-33).<sup>68</sup> It is also important to assess for heterotopic pregnancy. When a pregnant patient presents with pelvic pain, and an IUP is visualized, care should still be taken to carefully assess the adnexa for additional gestational sacs.

### Interstitial Pregnancy

Interstitial pregnancies (often called cornual) represent 2% to 4% of all ectopic pregnancies<sup>69</sup> but have a higher rate of morbidity and mortality because of later presentation and massive hemorrhage.<sup>70</sup> In this location, myometrium surrounds a portion of the expanding gestational sac, allowing it to enlarge painlessly for a relatively long time. The diagnosis is suggested when an IUP is visualized high in the fundus

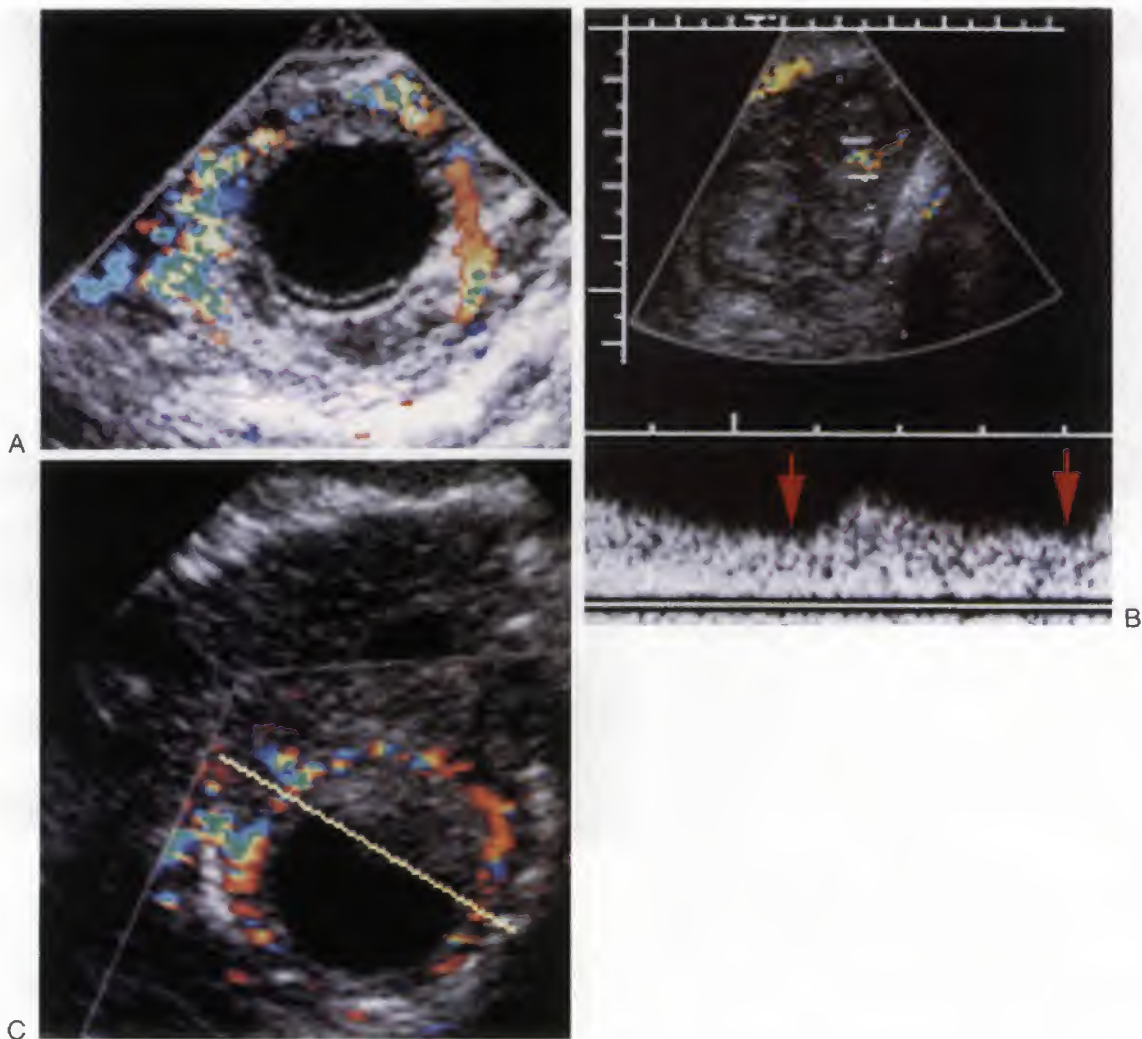


**FIGURE 32-28.** Color Doppler of ectopic pregnancy. A. Transvaginal sonogram of a highly suspicious tubal ring shows peritrophoblastic flow. B. Pulsed Doppler shows low-impedance, high-diastolic flow. Arrows point to end diastole. C. In another patient, increased vascularity is seen around a corpus luteum cyst. Visualization of flow around an adnexal mass is frequently misleading because corpus luteum cysts show low-impedance, high-diastolic flow. Care should be taken to verify that a mass is extraovarian to raise the suspicion of ectopic pregnancy.

that is not surrounded in all planes by 5 mm of myometrium (see Fig. 32-29).<sup>71</sup> The specificity of this 5-mm threshold has not been investigated. It should be remembered that the diagnosis of interstitial ectopic pregnancy can be difficult sonographically. It may be difficult to differentiate an eccentric normal IUP from an interstitial pregnancy (see Fig. 32-30D). True cornual pregnancies are those located in the horn of a bicornuate uterus. Previously therapy was by laparotomy. New therapies include systemic methotrexate<sup>72</sup> or transvaginal sonographically guided injection of potassium chloride.<sup>73</sup>

### Cervical Pregnancy

Cervical pregnancies represent less than 1% of all ectopic pregnancies.<sup>74,75</sup> Risk factors include multiparity, prior abortion, or instrumentation of the cervix or endometrial cavity. The sonographic diagnosis is made when a gestational sac with peritrophoblastic flow or a live embryo is identified

within the cervix. When a gestational sac with a yolk sac and embryo is seen within the cervix without a heartbeat, the differential diagnosis includes spontaneous abortion and cervical ectopic (see Figs. 32-31 and 32-32). In cases of spontaneous abortion, the sac shape and location should change on serial imaging. In cases of cervical ectopic pregnancy, the sac will be more round or hourglass shaped and should have trophoblastic flow on color Doppler.<sup>76</sup> However, increased flow in the cervix also can be seen around a spontaneous abortion.<sup>77</sup>

Because the cervix is composed predominantly of fibrous tissue, patients may bleed profusely. In the past, as a result of life-threatening hemorrhage, the diagnosis of a cervical ectopic pregnancy frequently led to hysterectomy. At present, conservative treatments are possible with the hope of preserving future reproductive potential, including sonographically guided local potassium chloride injection,<sup>78,79</sup> systemic or local methotrexate,<sup>76,78,80,81</sup> or preoperative uterine artery embolization<sup>78,82</sup> before dilatation and evacuation.



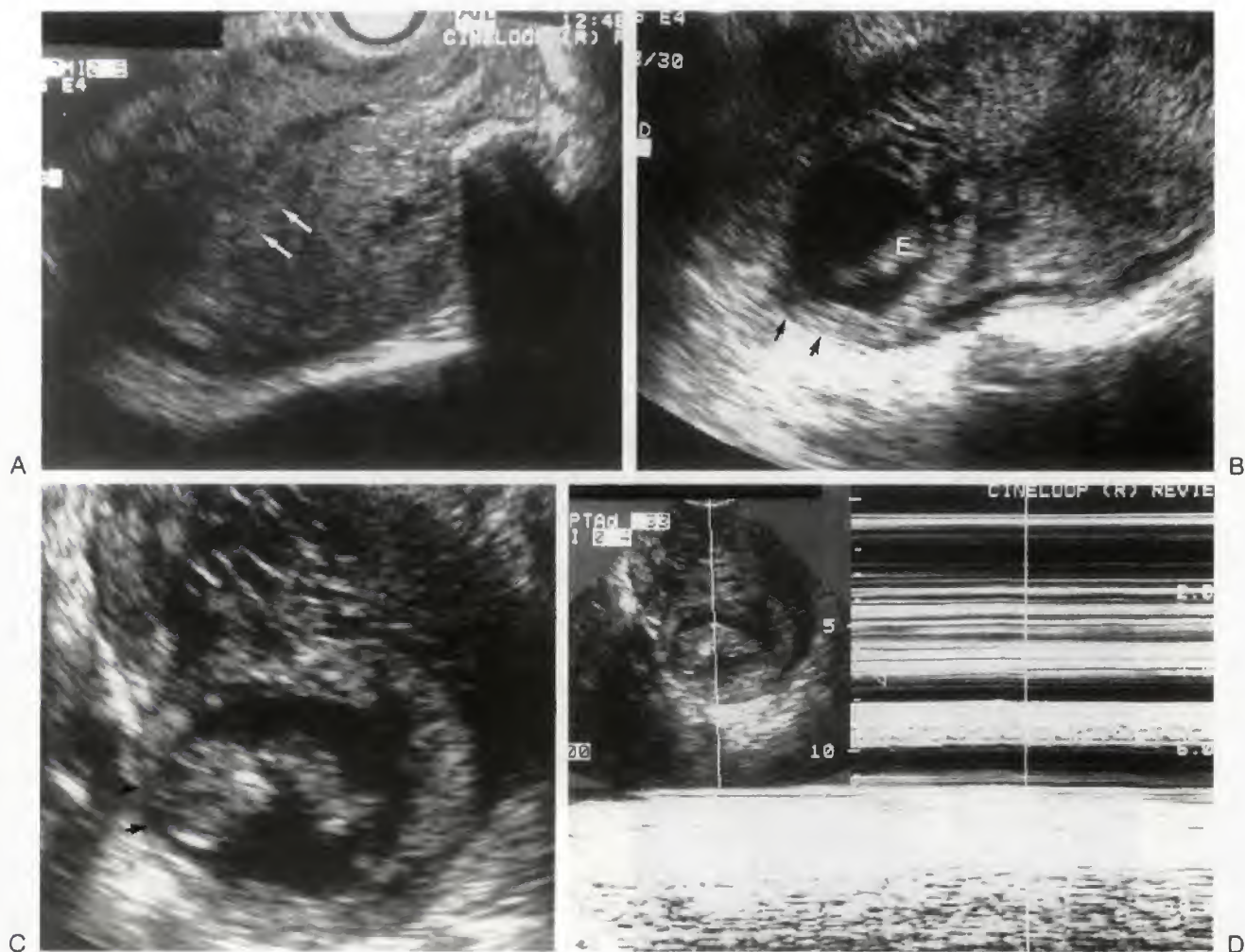


**FIGURE 32-29.** Live interstitial ectopic pregnancy. *A.* Transvaginal sagittal midline view of the uterus in a patient suspected of harboring an ectopic pregnancy shows no gestational sac in the endometrial cavity (white arrows). *B.* Transvaginal oblique transverse view shows a gestational sac high in the fundal region with an embryo (E). The crown rump length was consistent with 10 weeks. There is a paucity of myometrium laterally (black arrows). *C.* Magnified view shows no myometrium around the lateral aspect of the gestational sac (black arrows). *D.* M-mode demonstrates cardiac activity. It is common for interstitial ectopic pregnancies to present at a more advanced gestational age than ectopic pregnancies in other portions of the tube because the interstitial region dilates relatively painlessly.

## Scar Pregnancy

Once an extremely rare entity, cesarean section scar pregnancy is being increasingly reported.<sup>83</sup> The hypothesis is that the conceptus enters the myometrium through a microscopic dehiscence tract or defect in the cesarean section scar.<sup>84</sup> There is complete embedding of the gestational sac in the myometrium. The myometrium between the bladder and the sac becomes thinner or disappears owing to distention of the sac. Only the thin, serosal layer is apparent. Criteria used for diagnosis are an empty uterus, empty cervical canal, development of the sac in the anterior part of the lower uterine segment, and an absence of healthy myometrium between the bladder wall and the gestational sac (see Fig. 32-33).<sup>85</sup> Current non- and minimally invasive treatments include sonographically guided methotrexate or potassium chloride injection,<sup>73,86</sup> or intramuscular methotrexate.<sup>87</sup> Definitive treatment of a cesarean scar

pregnancy is by laparotomy and hysterotomy, with repair of the accompanying uterine scar dehiscence.<sup>84</sup> Other procedures that scar the uterus put the patient at increased risk for scar pregnancy. For example, a pregnancy can implant in a myomectomy scar.<sup>88</sup>

## Abdominal Pregnancy

Abdominal pregnancies are rare. The pregnancy typically develops in the ligaments of the ovary, usually the broad ligament. It can then obtain blood supply from the omentum and abdominal organs. Sonographically the pregnancy is seen separate from the uterus, adnexa, and ovaries (Fig. 32-34). Treatment is by laparotomy or laparoscopy.<sup>89</sup> Although abdominal pregnancy can result in a life-threatening emergency if diagnosed late, a viable pregnancy can result.



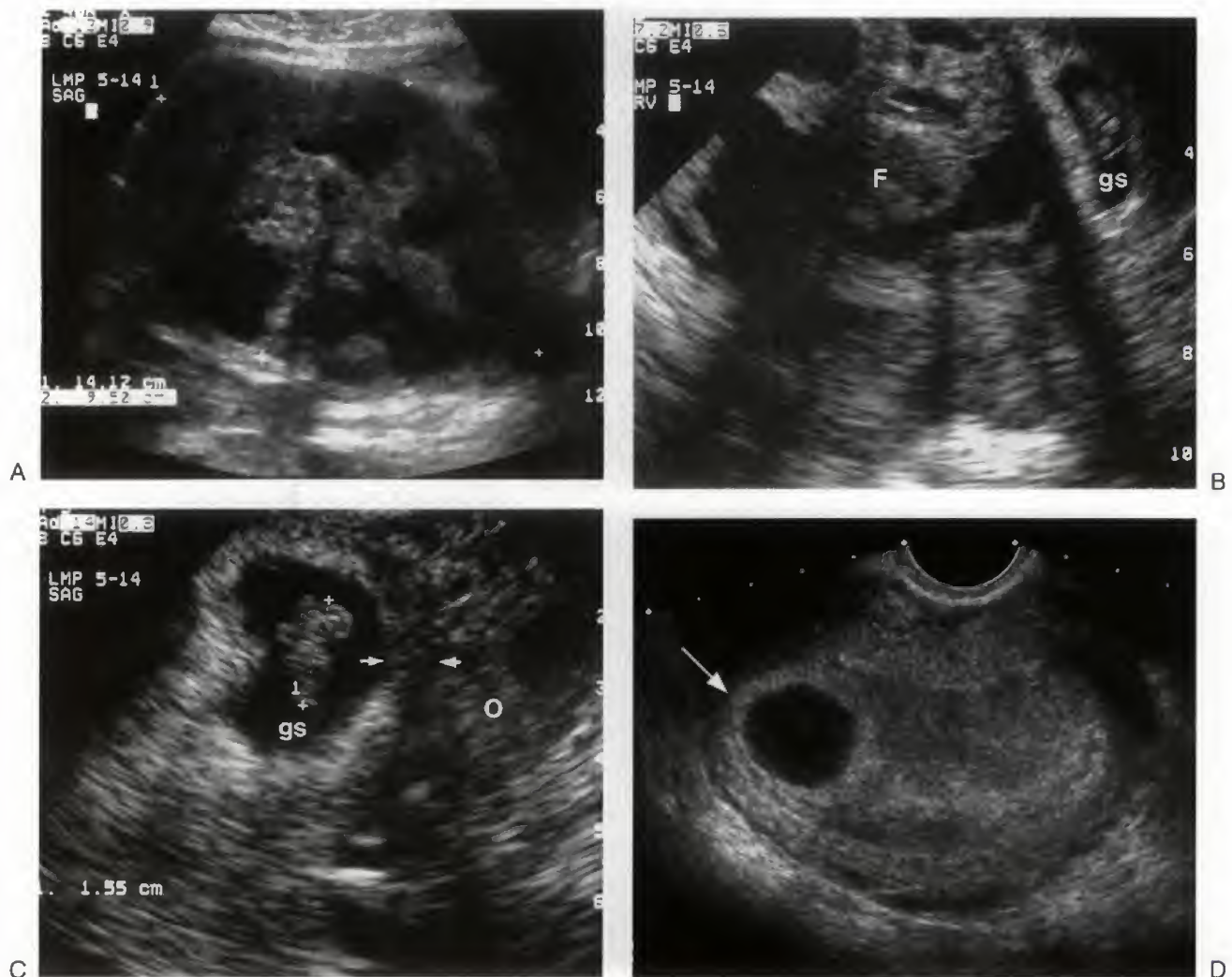


**FIGURE 32-30.** Pitfalls in the diagnosis of interstitial pregnancy. *A.* Transabdominal view of a patient suspected of having an ectopic pregnancy. A large partially necrotic fibroid is seen in the midline. *B.* Transverse transvaginal view shows the fibroid (F) in the midline with a gestational sac (gs) located to the far left of the uterus. *C.* Magnified view of the gestational sac shows a thick band of myometrium (arrows) around the gestational sac (gs), between the sac and the adjacent ovary (O). This is a normal intrauterine pregnancy in a sac deviated by a large fibroid. *D.* In another patient who presented with pelvic pain and a positive pregnancy test, a coronal transvaginal sonogram demonstrates a markedly eccentric gestational sac (arrow) on the right side of the uterus, suggesting the presence of an interstitial pregnancy. Follow-up sonograms demonstrated a more central location of the intrauterine gestational sac and a normally developing pregnancy.

## Heterotopic Pregnancy

The occurrence of heterotopic pregnancies is increasing owing to ovulation induction, in vitro fertilization, embryo transfer, previous pelvic surgery, and history of previous ectopic pregnancy managed conservatively and by salpingostomy.<sup>90</sup> In such high-risk patients, the presence of an intrauterine gestation sac should not negate the need for careful evaluation of the adnexa and follow-up sonography in symptomatic patients (see Figs. 32-4 and 32-35).<sup>91</sup> Hyperstimulated ovaries may make visualization of an ectopic pregnancy difficult.<sup>92</sup> In these cases, transabdominal scanning often shows the ectopic pregnancy, which may not be in the range of the transvaginal probe owing to a large ovarian size. A greater level of suspicion may allow early laparoscopic intervention before life-threatening intra-abdominal bleeding occurs.<sup>92</sup>

## ROLE OF MAGNETIC RESONANCE IMAGING IN THE DIAGNOSIS OF ECTOPIC PREGNANCY

Ultrasound is the method of choice for imaging pregnant patients. However, magnetic resonance imaging (MRI) is being increasingly used in complicated patients in whom the diagnosis is unclear. MRI is helpful in known abdominal pregnancy in order to plan the surgical approach (see Fig. 32-34).<sup>93</sup> MRI can be used to diagnose tubal ectopic pregnancy in cases in which the sonogram is equivocal.<sup>94,95</sup>

## MANAGEMENT

Because ectopic pregnancy is now being diagnosed earlier and more frequently than in prior decades, management has shifted from emergency laparotomy to laparoscopy to even



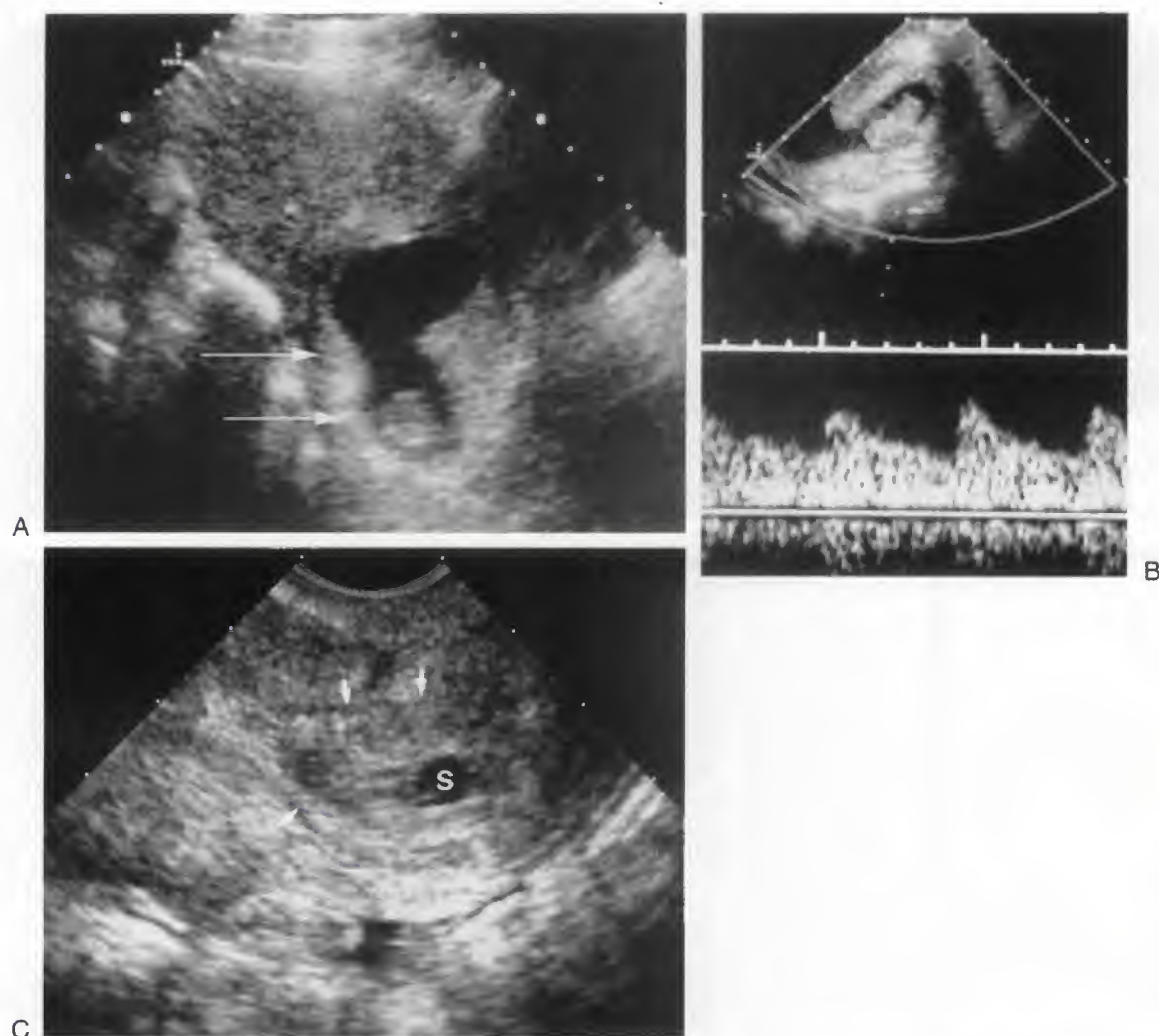


**FIGURE 32-31.** Cervical ectopic pregnancy versus inevitable abortion. **A.** Sagittal transabdominal scan in a pregnant patient shows a sac in the lower uterine segment and cervix. The placenta is present in the cervical area and lower uterine segment (*arrows*). A yolk sac is present within the cervical portion of the gestational sac. **B.** Pulsed Doppler examination shows low-impedance flow. Flow around a gestational sac in the cervical region (or embryonic cardiac activity) differentiates a cervical ectopic from a spontaneous inevitable abortion. **C.** In another patient, a gestational sac (S) or sacs are seen within the cervix. The dilated endocervical canal is indicated with *arrows*. Color Doppler (not shown) demonstrated no flow around the cervical sac, which is consistent with an aborting gestation.

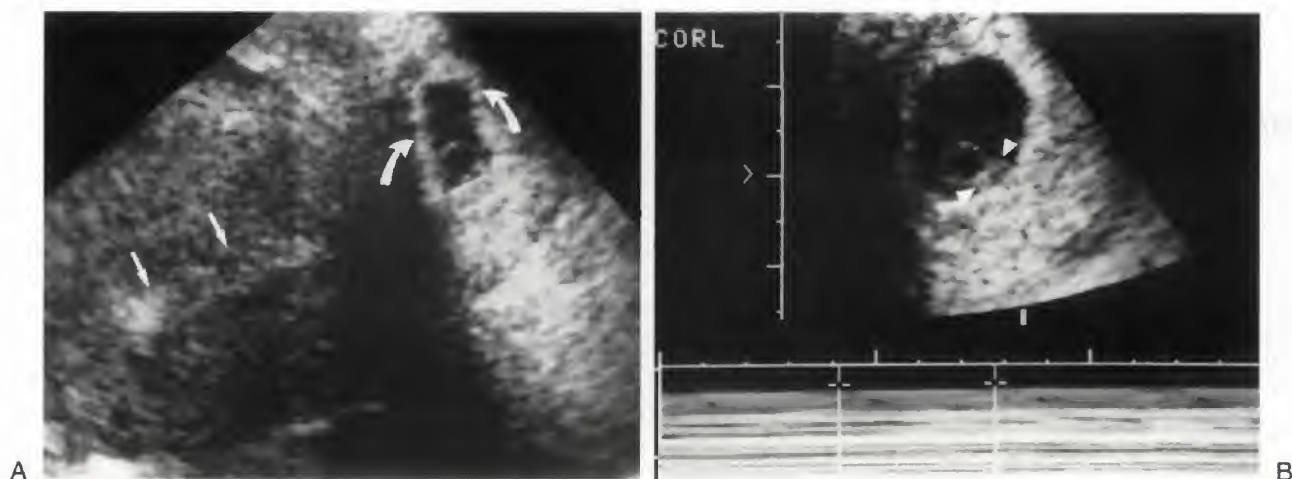


**FIGURE 32-32.** **A.** Transvaginal sagittal view of the uterus in a patient with cervical ectopic pregnancy. No gestational sac is present within the endometrial cavity (*straight arrows*), and an intact gestational sac (*curved arrows*) containing a yolk sac is present in the cervix. Gestational age is 6.2 weeks. A gestational sac with yolk sac is present in the cervix. **B.** Magnified view of the gestational sac shows an embryonic pole with cardiac activity, documented with M-mode tracing. Arrowheads mark the fetal pole. (From Frates M, Benson CB, Doubilet PM, et al: Cervical ectopic pregnancy: Results of conservative treatment. *Radiology* 191:773, 1994.)

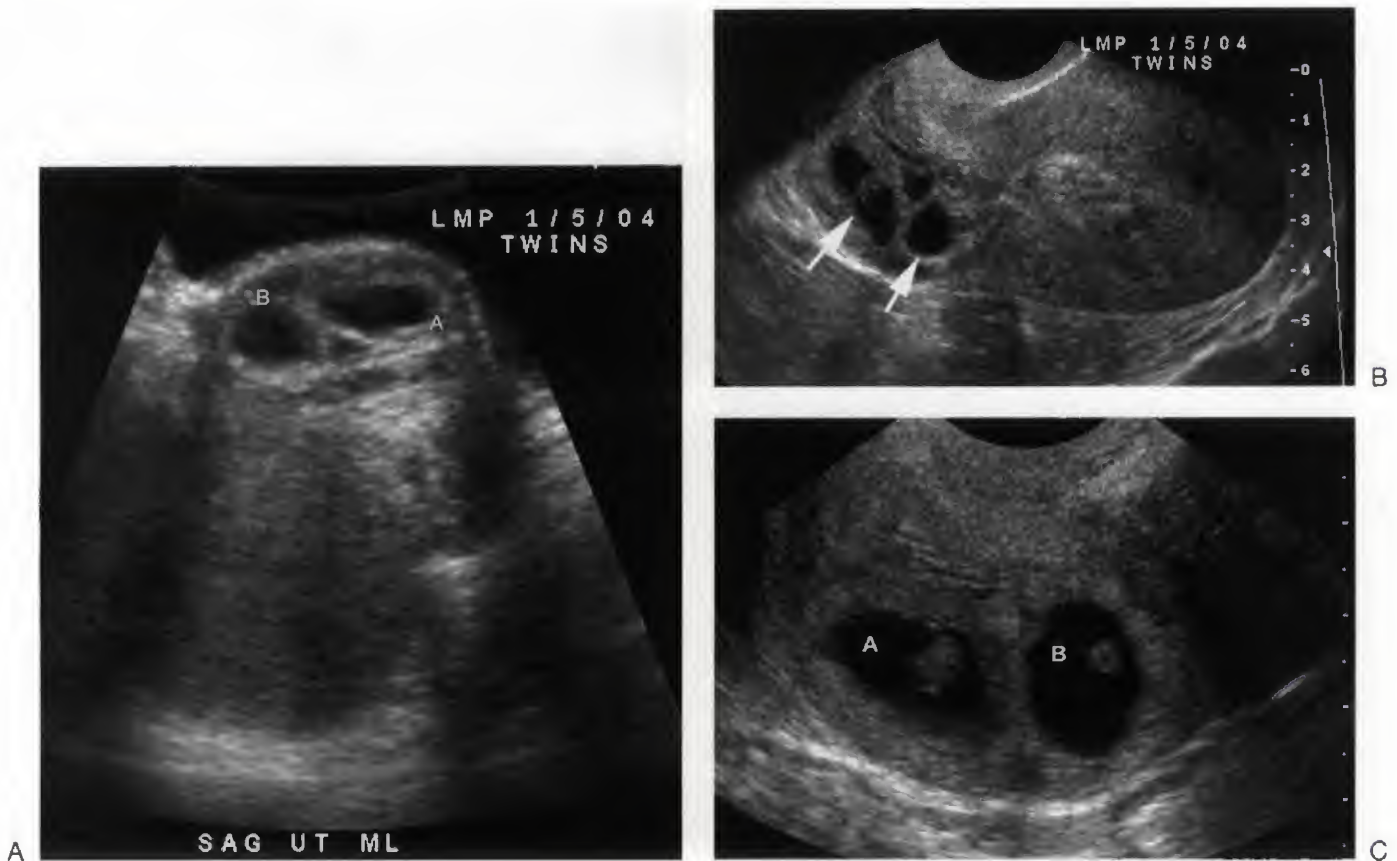


**FIGURE 32-33.** Cesarean section scar pregnancy in patient after in vitro fertilization. A. Transabdominal image shows a retroflexed uterus with gestational sacs (A, B) in the lower uterine segment, clearly not in the body of the uterus. B. Transvaginal image shows the two sacs (arrows) located in the anterior lower uterine segment, in the expected location of a cesarean section scar. C. Transvaginal image shows yolk sac and embryo.

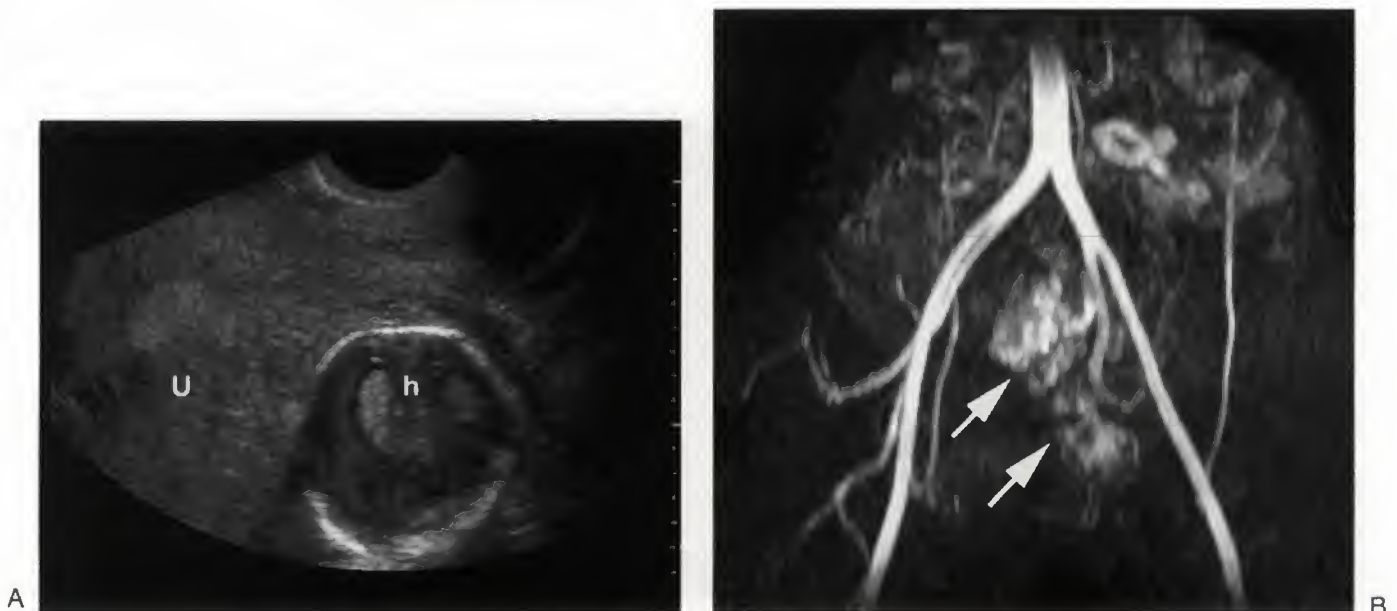


**FIGURE 32-34.** Abdominal ectopic pregnancy. A. Sagittal transvaginal image shows the fetal head (h) in the cul-de-sac, posterior to the uterus (U). B. Coronal gadolinium-enhanced image shows blood flow to the ectopic pregnancy (arrows). Note that gadolinium is not typically used during pregnancy but was in this case for surgical planning, because it was known that the pregnancy was nonviable.



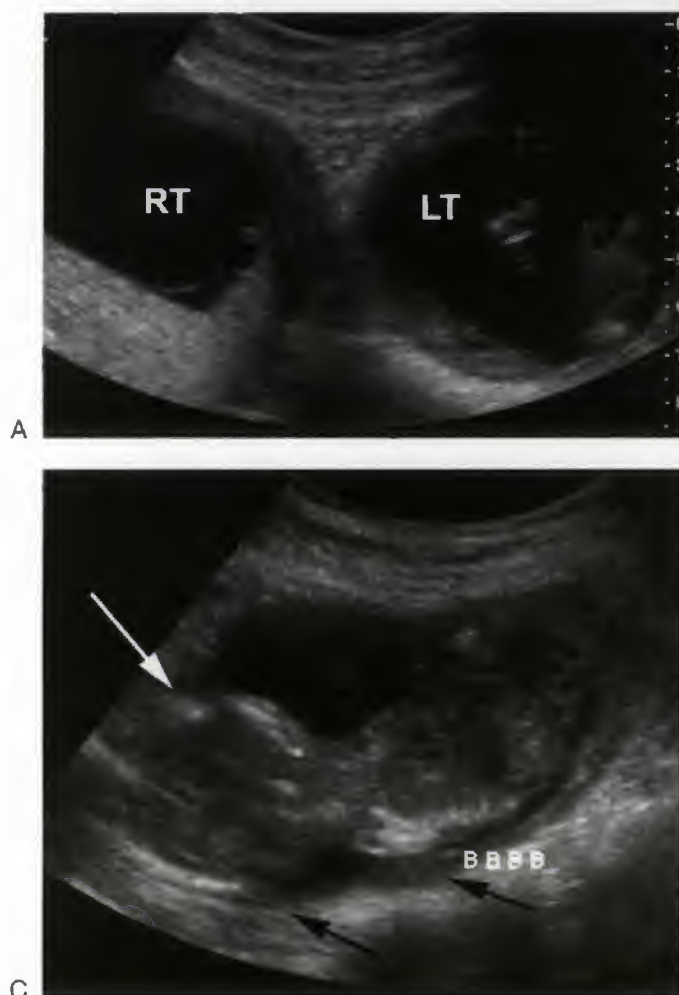


**FIGURE 32-35.** Transabdominal images of twin heterotopic pregnancy in a patient after in vitro fertilization at 15 weeks' gestational age. A. Transverse image shows two gestational sacs (RT, LT). At first glance, these appear to each lie within a uterine horn; however, as shown in images B and C. The sac on the left does not have surrounding myometrium (arrows) consistent with a heterotopic pregnancy. At surgery, this was found to be an abdominal heterotopic pregnancy.

more conservative management in select cases. Benefits of noninvasive approaches include preservation of fertility with decreased morbidity and decreased cost.<sup>96</sup>

## Surgery

When a patient is unstable, has a live ectopic pregnancy (meaning cardiac activity is visualized), a relatively large adnexal mass ( $> 4$  cm), or desires sterilization, surgery is the treatment of choice. Surgery is also performed when criteria are not met for expectant management or methotrexate therapy or if the patient may not be followed adequately after treatment.<sup>97</sup>

## Methotrexate

Methotrexate, a folate antagonist, is usually used for the treatment of ectopic pregnancy. This may be given as 50 mg/m<sup>2</sup> intramuscular (single dose regimen, without leucovorin, can be repeated on day 7 if hCG value did not decline 15% between days 4 and 7); or as 1 mg/kg intramuscular

(up to four doses with 0.1 mg/kg of leucovorin, with monitoring of hCG levels on alternate days until it declines 15% from previous value).<sup>98,99</sup> Criteria for medical treatment vary between institutions. Relative contraindications according to the American College of Obstetricians and Gynecologists are a gestational sac of 3.5 cm or greater and embryonic cardiac motion.<sup>100</sup> Medical treatment is the preferred option if the patient has already undergone previous surgeries, has extensive pelvic adhesions, has a contraindication for general anesthesia, and after failure of conservative laparoscopic treatment.<sup>97</sup> Methotrexate is successful in 70% to 97% of cases and has demonstrated that fertility is preserved equally well compared with laparoscopy.<sup>81,101,102</sup> Although most studies excluded ectopic pregnancies with cardiac activity, a 1998 report by Lipscomb et al<sup>103</sup> showed that 35 of 44 (79.5%) ectopic pregnancies of less than 3.5 cm in diameter with cardiac activity were successfully treated with methotrexate.

The most important predictor of treatment success with methotrexate is the hCG value. Tawfiq et al<sup>104</sup> found that only 7.5% of patients failed single-dose treatment when the

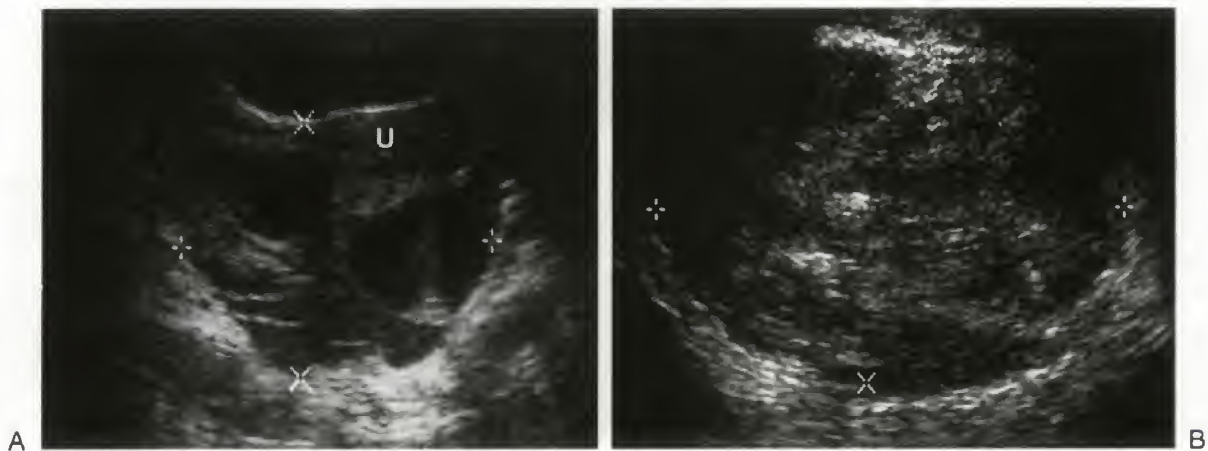


**FIGURE 32-36.** Two patients with tubal masses after treatment with methotrexate. *A.* Transverse transabdominal scan in a patient 10 days after treatment with methotrexate shows a complex cystic mass surrounding the uterus (U). This is a hematosalpinx, which had increased in size compared with that seen on scans before treatment. *B.* In another patient (see Fig. 32-25) in whom no ectopic pregnancy was seen sonographically but whose human chorionic gonadotropin levels (hCGs) were rising, a complex mass is seen in the region of the left tube. Both of these cases show the worrisome appearance of ectopic pregnancies after treatment with methotrexate. However, the hemorrhage into the tube with resulting enlarging mass does not indicate failure of treatment.

hCG level was less than 4000 IU/L compared to 65% when the level was greater than 4000 IU/L.

Ultrasonography after methotrexate is indicated only in cases in which rupture is suspected. Sonography of patients treated with methotrexate is complicated because most patients show a worsening appearance, with increased hemorrhage around the ectopic (Fig. 32-36). There may be an initial increase in size of the tubal mass after methotrexate treatment (see Fig. 32-36), and an adnexal mass may be visible up to 3 months after treatment.<sup>105,106</sup> The increase in tubal size and vascularity, in spite of the falling hCG level, represents a healing process and should not cause concern unless the patient is clinically unstable or has persistent symptoms.<sup>105</sup>

### Sonographically Guided Percutaneous Treatment

Sonographically guided intra-amniotic injection of potassium chloride or methotrexate are newer methods of treating ectopic pregnancy, especially unusual ectopic pregnancies.<sup>73,107,108</sup> This is less frequently a choice in tubal pregnancies, in which intramuscular methotrexate is an effective and less invasive alternative. However intra-amniotic injection is the method of choice in cervical, interstitial, heterotopic, and cesarean scar pregnancies.<sup>73</sup> One mg/kg of methotrexate,<sup>109</sup> or 1 to 3 mL of potassium chloride at a concentration of 2 mEq/mL is injected directly into the gestational sac or the embryo, if the embryo is greater than 5 mm in length.<sup>73</sup> The advantages of this procedure are they ablate the ectopic pregnancy, permit normal continuation of a concomitant pregnancy, and preserve the uterus for subsequent pregnancies.

### Expectant Management

One risk with methotrexate treatment in patients with unproven ectopic pregnancy is that some patients with

either early spontaneous abortion or very early IUP will be needlessly treated. In addition, many small ectopic pregnancies that previously went undiagnosed are now known to resolve spontaneously. These issues have led to increased interest in expectant management of ectopic pregnancy.

Lund<sup>110</sup> reported expectant management as early as 1955. Multiple studies of minimally symptomatic women with declining or stable hCG levels and small adnexal masses (less than 4 cm) can be safely monitored without treatment.<sup>111-113</sup> Patients must be willing to undergo close monitoring. About 25% of patients diagnosed with ectopic pregnancy fit this description.<sup>111,114</sup> In a study by Cacciatore et al,<sup>114,115</sup> no further treatment was needed in 69% of patients, however 31% of patients required laparoscopy at an average of 9 days after diagnosis owing to worsening clinical symptoms.

Fernandez et al<sup>112</sup> monitored spontaneous resolution of laproscopically confirmed ectopic pregnancies managed conservatively in 14 patients and concluded that there is a high probability of spontaneous resolution of the pregnancy when the serum hCG level at diagnosis is less than 1000 mIU/mL. In a study by Korhonen, Stenman, and Ylostalo,<sup>116</sup> the success rate for spontaneous resolution of ectopic pregnancy was 88% when the initial hCG level was less than 200 IU/L but only 25% at levels greater than 2,000 IU/L. In the 77 patients with a spontaneous resolution, the initial median hCG concentration was 374 IU/L (range, 20 to 10,762 IU/L), and it decreased to normal in 4 to 67 days (mean, 20 days). In this study, laparoscopy was performed in two thirds of the patients with a serum hCG level greater than 64% of the initial value after 7 days of follow-up.

In a different study by Korhonen, Stenman, and Ylostalo,<sup>117</sup> low-dose oral methotrexate was compared with placebo in patients with an ectopic pregnancy smaller than 4 cm in greatest diameter, no signs of bleeding, and an hCG increase less than 50% in 2 days and found no difference in the groups. In each group, 77% of patients required no further treatment.



In a study by Elson,<sup>118</sup> expectant management was 96% successful if the hCG was less than 175 IU/L, 66% successful if the hCG was 175 to 1500 IU/L, and 21% successful if hCG was greater than 1500 IU/L. There was 0% success rate if hCG was less than 1500 and the patient was more than 42 days pregnant.

In monitoring ectopic pregnancies, Atri et al<sup>105,111</sup> demonstrated that patients receiving methotrexate and expectant management could have increased size or increased vascularity on follow-up. The long resolution time of the ectopic pregnancy is a drawback of medical treatment. In the series by Atri et al,<sup>105</sup> the tubal mass took up to 147 days to resolve completely.

Thus, the mass of the ectopic pregnancy can persist long after the hCG levels normalize. The benefit of expectant management is the avoidance of surgery or drugs. Disadvantages of expectant management include cost of serial hCG measurements and transvaginal sonograms, anxiety associated with waiting to decide whether other treatment is necessary, and the possibility of emergent laparotomy. It is possible that falling hCG levels can occur followed by rupture of the ectopic.<sup>119,120</sup>

Tubal rupture, historically treated surgically, is an important issue with the trend toward nonsurgical management. Some investigators suggested that sonography can be used to determine whether the tubes are intact. The appearance of the adnexal mass,<sup>17</sup> and the type and amount of intraperitoneal fluid<sup>71</sup> have been suggested as predictors of tubal rupture. Although one report suggested that a tubal ring is associated with an intact tube,<sup>17</sup> this has not been substantiated in more recent reports.<sup>37,52,60,61</sup> Therefore, sonography should not be considered accurate in the characterization of fallopian tube status.

## FERTILITY AFTER ECTOPIC PREGNANCY

Approximately 60% of surgically treated patients subsequently experience term pregnancy. A randomized study by Hajenius et al<sup>121</sup> showed similar rates of tubal patency in patients treated with methotrexate compared with those treated with salpingostomy. Other studies showed ipsilateral tubal patency rates of 53% to 84%<sup>113,122–125</sup> with subsequent pregnancy rates of 27% to 80%.<sup>122,124,125</sup> Although patient numbers are smaller in the follow-up of patients treated expectantly, subsequent pregnancy has been found in 86% of these patients.

## CONCLUSION

Sonography and serum hCG guide the diagnosis and management of patients with ectopic pregnancy. An intrauterine gestational sac is typically seen when the hCG value is greater than 2000 mIU/mL (IRP). Knowledge of the variety of appearances of ectopic pregnancy will aid in diagnosis. Expectant medical and percutaneous management have decreased the number of patients needing laparoscopy/laparotomy. With these conservative treatments, there is an increased role for sonography in the appropriate triage and follow-up of patients with ectopic pregnancy. An algorithm for the workup of ectopic pregnancy is presented (Fig. 32–37).

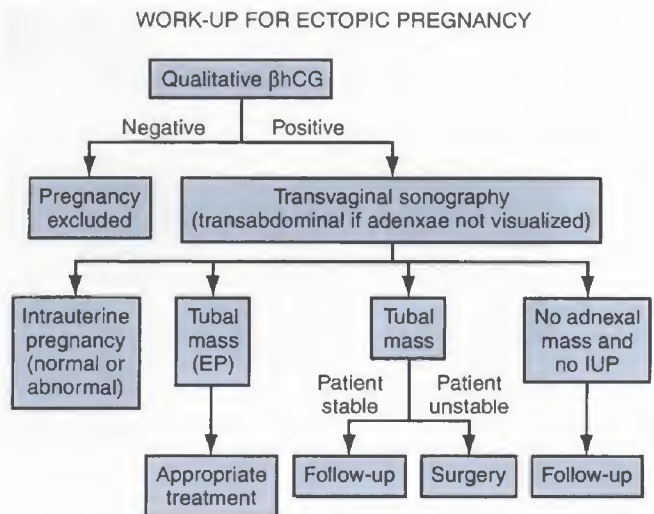


**FIGURE 32–37.** Algorithm for work-up of ectopic pregnancy. (Modified from Mehta TS, Levine D, Beckwith B: Treatment of ectopic pregnancy: is a human chorionic gonadotropin level of 2,000 mIU/mL a reasonable threshold? *Radiology* 205:569-573, 1997.)

## References

- Goldner TE, Lawson HW, Xia Z, et al: Surveillance for ectopic pregnancy—United States, 1970–1989. *MMWR CDC Surveill Summ* 42:73, 1993.
- NCHS: Advanced Report of Final Mortality Statistics, 1992. Hyattsville MD, U.S. Department of Health and Human Services (ed): Volume Report No. 43: Public Health Service, 1994.
- Ectopic pregnancy—United States, 1990–1992. *MMWR Morb Mortal Wkly Rep* 44:46, 1995.
- Breen JL: A 21 year survey of 654 ectopic pregnancies. *Am J Obstet Gynecol* 106:1004, 1970.
- Mitchell DE, McSwain HF, Peterson HB: Fertility after ectopic pregnancy. *Am J Obstet Gynecol* 161:576, 1989.
- Mueller BA, Daling JR, Weiss NS, et al: Tubal pregnancy and the risk of subsequent infertility. *Obstet Gynecol* 69:722, 1987.
- Schwartz RO, Di Pietro DL: Beta-hCG as a diagnostic aid for suspected ectopic pregnancy. *Obstet Gynecol* 56:197, 1980.
- Nagamani M, London S, Amand PS: Factors influencing fertility after ectopic pregnancy. *Am J Obstet Gynecol* 149:533, 1984.
- Mol BW, Ankum WM, Bossuyt PM, et al: Contraception and the risk of ectopic pregnancy: a meta-analysis. *Contraception* 52:337, 1995.
- Maymon R, Shulman A: Controversies and problems in the current management of tubal pregnancy. *Hum Reprod Update* 2:541, 1996.
- Herman A, Ron-El R, Golan A, et al: The role of tubal pathology and other parameters in ectopic pregnancies occurring in in vitro fertilization and embryo transfer. *Fertil Steril* 54:864, 1990.
- Nazari A, Askari HA, Check JH, et al: Embryo transfer technique as a cause of ectopic pregnancy in in vitro fertilization. *Fertil Steril* 60:919, 1993.
- Barnhart K, Mennuti MT, Benjamin I, et al: Prompt diagnosis of ectopic pregnancy in an emergency department setting. *Obstet Gynecol* 84:1010, 1994.
- Bateman BG, Nunley WC, Kolp LA, et al: Vaginal sonography findings and hCG dynamics of early intrauterine and tubal pregnancies. *Obstet Gynecol* 75:421, 1990.
- Braffman BH, Coleman BG, Ramchandani P, et al: Emergency department screening for ectopic pregnancy: a prospective US study. *Radiology* 190:797, 1994.
- Bree RL, Bohm-Velez M, Beyler S, et al: Transvaginal sonography in the evaluation of normal early pregnancy: correlation with hCG level. *AJR Am J Roentgenol* 153:75, 1989.
- Cacciatore B: Can the status of tubal pregnancy be predicted with transvaginal sonography? A prospective comparison of sonographic, surgical, and serum hCG findings. *Radiology* 177:481, 1990.



18. Goldstein SR, Snyder JR, Watson C, et al: Very early pregnancy detection with endovaginal ultrasound. *Obstet Gynecol* 72:200, 1988.
19. Nyberg DA, Mack LA, Laing FC, et al: Early pregnancy complications: endovaginal sonographic findings correlated with human chorionic gonadotropin levels. *Radiology* 167:619, 1988.
20. Mehta TS, Levine D, Beckwith B: Treatment of ectopic pregnancy: is a human chorionic gonadotropin level of 2,000 mIU/mL a reasonable threshold? *Radiology* 205:569, 1997.
21. Barzer R: Guidelines for choosing a pregnancy test. *Contemp Obstet Gynecol* 30:57, 1985.
22. Seiber BE, Barnhart KT: Suspected ectopic pregnancy. *Obstet Gynecol* 107:399, 2006.
23. Dart R, Dart L, Segal M, et al: The ability of a single serum progesterone value to identify abnormal pregnancies in patients with beta-human chorionic gonadotropin values less than 1,000 mIU/mL. *Acad Emerg Med* 5:304, 1998.
24. Grosskinsky CM, Hage ML, Tyrey L, et al: hCG, progesterone, alpha-fetoprotein, and estradiol in the identification of ectopic pregnancy. *Obstet Gynecol* 81:705, 1993.
25. Matthews CP, Coulson PB, Wild RA: Serum progesterone levels as an aid in the diagnosis of ectopic pregnancy. *Obstet Gynecol* 68:390, 1986.
26. Radwanska E, Frankenberg J, Allen EI: Plasma progesterone levels in normal and abnormal early human pregnancy. *Fertil Steril* 30:398, 1978.
27. Stovall TG, Ling FW, Carson SA, et al: Serum progesterone and uterine curettage in differential diagnosis of ectopic pregnancy. *Fertil Steril* 57:456, 1992.
28. Valley VT, Mateer JR, Aiman EJ, et al: Serum progesterone and endovaginal sonography by emergency physicians in the evaluation of ectopic pregnancy. *Acad Emerg Med* 5:309, 1998.
29. Condous G, Okaro E, Khalid A, et al: A prospective evaluation of a single-visit strategy to manage pregnancies of unknown location. *Hum Reprod* 20:1398, 2005.
30. Taylor KJ, Ramos IM, Feyock AL, et al: Ectopic pregnancy: duplex Doppler evaluation. *Radiology* 173:93, 1989.
31. Cacciatore B, Stenman UH, Ylostalo P: Early screening for ectopic pregnancy in high-risk symptom-free women. *Lancet* 343:517, 1994.
32. Bello GV, Schonholz D, Moshirpur J, et al: Combined pregnancy: the Mount Sinai experience. *Obstet Gynecol Surv* 41:603, 1986.
33. Berger MJ, Taymor ML: Simultaneous intrauterine and tubal pregnancies following ovulation induction. *Am J Obstet Gynecol* 113:812, 1972.
34. DeVoe RW, Pratt JH: Simultaneous intra- and extrauterine pregnancy. *Am J Obstet Gynecol* 56:1119, 1948.
35. Richards SR, Stempel LE, Carlton BD: Heterotopic pregnancy: reappraisal of incidence. *Am J Obstet Gynecol* 142:928, 1982.
36. Yeh HC, Goodman JD, Carr L, et al: Intradecidual sign: a US criterion of early intrauterine pregnancy. *Radiology* 161:463, 1986.
37. Laing FC: Sonographic determination of tubal rupture in patients with ectopic pregnancy: is it feasible? [editorial; comment]. *Radiology* 177:330, 1990.
38. Laing FC, Brown DL, Price JF, et al: Intradecidual sign: is it effective in diagnosis of an early intrauterine pregnancy? *Radiology* 204:655, 1997.
39. Chiang G, Levine D, Swire M, et al: The intradecidual sign: is it reliable for diagnosis of early intrauterine pregnancy? *AJR Am J Roentgenol* 183:725, 2004.
40. Bradley WG, Fiske CE, Filly RA: The double sac sign of early intrauterine pregnancy: use in exclusion of ectopic pregnancy. *Radiology* 143:223, 1982.
41. Parvey HR, Dubinsky TJ, Johnston DA, et al: The chorionic rim and low-impedance intrauterine arterial flow in the diagnosis of early intrauterine pregnancy: evaluation of efficacy. *AJR Am J Roentgenol* 167:1479, 1996.
42. Fisher AM, Goldberg BB: Unusual case of heterotopic pregnancies in an in vitro fertilization-Embryo transfer patient. *J Ultrasound Med* 16:703, 1997.
43. Nyberg DA, Mack LA, Jeffrey RB Jr, et al: Endovaginal sonographic evaluation of ectopic pregnancy: a prospective study. *AJR Am J Roentgenol* 149:1181, 1987.
44. Zinn HL, Cohen HL, Zinn DL: Ultrasonographic diagnosis of ectopic pregnancy: importance of transabdominal imaging. *J Ultrasound Med* 16:603, 1997.
45. Cacciatore B, Stenman UH, Ylostalo P: Comparison of abdominal and vaginal sonography in suspected ectopic pregnancy. *Obstet Gynecol* 73:770, 1989.
46. Dashefsky SM, Lyons EA, Levi CS, et al: Suspected ectopic pregnancy: endovaginal and transvesical US. *Radiology* 169:181, 1988.
47. Kivikoski AI, Martin CM, Smeltzer JS: Transabdominal and transvaginal ultrasonography in the diagnosis of ectopic pregnancy: a comparative study. *Am J Obstet Gynecol* 163:123, 1990.
48. Thorsen MK, Lawson TL, Aiman EJ, et al: Diagnosis of ectopic pregnancy: endovaginal vs transabdominal sonography. *AJR Am J Roentgenol* 155:307, 1990.
49. Timor-Tritsch IE, Yeh MN, Peisner DB, et al: The use of transvaginal ultrasonography in the diagnosis of ectopic pregnancy [see comments]. *Am J Obstet Gynecol* 161:157, 1989.
50. Berry SM, Coulam CB, Hill LM, et al: Evidence of contralateral ovulation in ectopic pregnancy. *J Ultrasound Med* 4:293, 1985.
51. Atri M, Leduc C, Gillett P, et al: Role of endovaginal sonography in the diagnosis and management of ectopic pregnancy. *Radiographics* 16:755; discussion 775, 1996.
52. Russell SA, Filly RA, Damato N: Sonographic diagnosis of ectopic pregnancy with endovaginal probes: what really has changed? *J Ultrasound Med* 12:145, 1993.
53. Nyberg DA, Hughes MP, Mack LA, et al: Extrauterine findings of ectopic pregnancy of transvaginal US: importance of echogenic fluid. *Radiology* 178:823, 1991.
54. Frates MC, Visweswaran A, Laing FC: Comparison of tubal ring and corpus luteum echogenicities: a useful differentiating characteristic. *J Ultrasound Med* 20:27; quiz 33, 2001.
55. Stein MW, Ricci ZJ, Novak L, et al: Sonographic comparison of the tubal ring of ectopic pregnancy with the corpus luteum. *J Ultrasound Med* 23:57, 2004.
56. Marks WM, Filly RA, Callen PW, Laing FC: The decidual cast of ectopic pregnancy: a confusing ultrasonographic appearance. *Radiology* 133:451, 1979.
57. Mehta TS, Levine D, McArdle CR: Lack of sensitivity of endometrial thickness in predicting the presence of an ectopic pregnancy. *J Ultrasound Med* 18:117; quiz 123, 1999.
58. Ackerman TE, Levi CS, Lyons EA, et al: Decidual cyst: endovaginal sonographic sign of ectopic pregnancy. *Radiology* 189:727, 1993.
59. Frates MC, Laing FC: Sonographic evaluation of ectopic pregnancy: an update. *AJR Am J Roentgenol* 165:251, 1995.
60. Atri M, de Stempel J, Bret PM: Accuracy of transvaginal ultrasonography for detection of hematosalpinx in ectopic pregnancy. *J Clin Ultrasound* 20:255, 1992.
61. Frates MC, Brown DL, Doubilet PM, et al: Tubal rupture in patients with ectopic pregnancy: diagnosis with transvaginal US. *Radiology* 191:769, 1994.
62. Chen PC, Sickler GK, Dubinsky TJ, et al: Sonographic detection of echogenic fluid and correlation with culdocentesis in the evaluation of ectopic pregnancy. *AJR Am J Roentgenol* 170:1299, 1998.
63. Emerson DS, Cartier MS, Altieri LA, et al: Diagnostic efficacy of endovaginal color Doppler flow imaging in an ectopic pregnancy screening program. *Radiology* 183:413, 1992.
64. Kurjak A, Zalud I, Schulman H: Ectopic pregnancy: transvaginal color Doppler of trophoblastic flow in questionable adnexa. *J Ultrasound Med* 10:685, 1991.
65. Pellcruto JS, Taylor KJ, Quedens-Case C, et al: Ectopic pregnancy: evaluation with endovaginal color flow imaging. *Radiology* 183:407, 1992.
66. Dillon EH, Feyock AL, Taylor KJ: Pseudogestational sacs: Doppler US differentiation from normal or abnormal intrauterine pregnancies. *Radiology* 176:359, 1990.
67. Tekay A, Martikainen H, Heikkinen H, et al: Disappearance of the trophoblastic blood flow in tubal pregnancy after methotrexate injection. *J Ultrasound Med* 12:615, 1992.
68. Valley MT, Pierce JG, Caniel TB, et al: Cesarean scan pregnancy: imaging and treatment with conservative surgery. *Obstet Gynecol* 91:838, 1998.
69. Bouyer J, Coste J, Fernandez H, et al: Sites of ectopic pregnancy: a 10 year population-based study of 1800 cases. *Hum Reprod* 17:3224, 2002.
70. Jafri SZ, Loginsky SJ, Bouffard JA, et al: Sonographic detection of interstitial pregnancy. *J Clin Ultrasound* 15:253, 1987.
71. Fleischer AC, Pennell RG, McKee MS, et al: Ectopic pregnancy: features at transvaginal sonography. *Radiology* 174:375, 1990.



72. Fernandez H, De Ziegler D, Bourget P, et al: The place of methotrexate in the management of interstitial pregnancy. *Hum Reprod* 6:302, 1991.
73. Doubilet PM, Benson CB, Frates MC, et al: Sonographically guided minimally invasive treatment of unusual ectopic pregnancies. *J Ultrasound Med* 23:359, 2004.
74. Celik C, Bala A, Acar A, et al: Methotrexate for cervical pregnancy. A case report. *J Reprod Med* 48:130, 2003.
75. Ushakov FB, Elchalal U, Aceman RJ, et al: Cervical pregnancy: past and future. *Obstet Gynecol Surv* 52:45, 1997.
76. Jurkovic D, Hackett E, Campbell S: Diagnosis and treatment of early cervical pregnancy: a review and a report of two cases treated conservatively. *Ultrasound Obstet Gynecol* 8:373, 1996.
77. Benson CB, Doubilet PM: Strategies for the conservative treatment of cervical ectopic pregnancy. *Ultrasound Obstet Gynecol* 8:371, 1996.
78. Frates MC, Benson CB, Doubilet PM, et al: Cervical ectopic pregnancy: results of conservative treatment. *Radiology* 191:773, 1994.
79. Monteagudo A, Tarricone NJ, Timor-Tritsch IE, et al: Successful transvaginal ultrasound-guided puncture and injection of a cervical pregnancy in a patient with simultaneous intrauterine pregnancy and a history of a previous cervical pregnancy. *Ultrasound Obstet Gynecol* 8:381, 1996.
80. Sherer DM, Abramowicz JS, Thompson HO, et al: Comparison of transabdominal and endovaginal sonographic approaches in the diagnosis of a case of cervical pregnancy successfully treated with methotrexate. *J Ultrasound Med* 10:409, 1991.
81. Stovall TG, Ling FW: Ectopic pregnancy. Diagnostic and therapeutic algorithms minimizing surgical intervention. *J Reprod Med* 38:807, 1993.
82. Meyerovitz MF, Lobel SM, Harrington DP, et al: Preoperative uterine artery embolization in cervical pregnancy. *J Vasc Interv Radiol* 2:95, 1991.
83. Jurkovic D, Hillaby K, Woelfer B, et al: First-trimester diagnosis and management of pregnancies implanted into the lower uterine segment Cesarean section scar. *Ultrasound Obstet Gynecol* 21:220, 2003.
84. Fylstra DL: Ectopic pregnancy within a cesarean scar: a review. *Obstet Gynecol Surv* 57:537, 2002.
85. Li SP, Wang W, Tang XL, Wang Y: Cesarean scar pregnancy: a case report. *Chin Med J (Engl)* 117:316, 2004.
86. Seow KM, Huang LW, Lin YH, et al: Cesarean scar pregnancy: issues in management. *Ultrasound Obstet Gynecol* 23:247, 2004.
87. Haimov-Kochman R, Sciaky-Tamir Y, Yanai N, et al: Conservative management of two ectopic pregnancies implanted in previous uterine scars. *Ultrasound Obstet Gynecol* 19:616, 2002.
88. Dialani V, Levine D: Ectopic pregnancy: a review. *Ultrasound Q* 20:105, 2004.
89. Siow A, Chern B, Soong Y: Successful laparoscopic treatment of an abdominal pregnancy in the broad ligament. *Singapore Med J* 45:88, 2004.
90. Ludwig M, Kaisi M, Bauer O, et al: Heterotopic pregnancy in a spontaneous cycle: do not forget about it! *Eur J Obstet Gynecol Reprod Biol* 87:91, 1999.
91. Raccuia JS, Neckles S, Butler D, et al: Synchronous intrauterine and ectopic pregnancy associated with clomiphene citrate. *Surg Gynecol Obstet* 168:417, 1989.
92. Soriano D, Shrim A, Seidman DS, et al: Diagnosis and treatment of heterotopic pregnancy compared with ectopic pregnancy. *J Am Assoc Gynecol Laparosc* 9:552, 2002.
93. Beddock R, Naepels P, Gondry C, et al: [Diagnosis and current concepts of management of advanced abdominal pregnancy]. *Gynecol Obstet Fertil* 32:55, 2004.
94. Angtuaco TL, Shah HR, Mattison DR, et al: MR imaging in high-risk obstetric patients: a valuable complement to US. *Radiographics* 12:91; discussion 110, 1992.
95. Smolders D, Deckers F, Pouillon M, et al: Ectopic pregnancy within a rudimentary horn in a case of unicornuate uterus. *Eur Radiol* 12:121, 2002.
96. Yao M, Tulandi T, Falcone T: Treatment of ectopic pregnancy by systemic methotrexate, transvaginal methotrexate, and operative laparoscopy. *Int J Fertil Menopausal Stud* 41:470, 1996.
97. Canis M, Savary D, Pouly JL, et al: [Ectopic pregnancy: criteria to decide between medical and conservative surgical treatment?]. *J Gynecol Obstet Biol Reprod (Paris)* 32:S54, 2003.
98. Barnhart K, Coutifaris C, Esposito M: The pharmacology of methotrexate. *Expert Opin Pharmacother* 2:409, 2001.
99. Barnhart KT, Gosman G, Ashby R, et al: The medical management of ectopic pregnancy: a meta-analysis comparing "single dose" and "multidose" regimens. *Obstet Gynecol* 101:778, 2003.
100. American College of Obstetricians and Gynecologists: Medical management of tubal pregnancy. *ACOG Practice Bulletin* 3 1998.
101. Feng W, Cao B, Li Q: [Advances in diagnosis and treatment of ectopic pregnancy during the past ten years]. *Zhonghua Fu Chan Ke Za Zhi* 35:408, 2000.
102. Pansky M, Bukovsky I, Golan A, et al: Local methotrexate injection: a nonsurgical treatment of ectopic pregnancy. *Am J Obstet Gynecol* 161:393, 1989.
103. Lipscomb GH, Bran D, McCord ML, et al: Analysis of three hundred fifteen ectopic pregnancies treated with single-dose methotrexate. *Am J Obstet Gynecol* 178:1354, 1998.
104. Tawfiq A, Agameya AF, Claman P: Predictors of treatment failure for ectopic pregnancy treated with single-dose methotrexate. *Fertil Steril* 74:877, 2000.
105. Atri M, Bret PM, Tulandi T, et al: Ectopic pregnancy: evolution after treatment with transvaginal methotrexate. *Radiology* 185:749, 1992.
106. Brown DL, Felker RE, Stovall TG, et al: Serial endovaginal sonography of ectopic pregnancies treated with methotrexate. *Obstet Gynecol* 77:406, 1991.
107. Fernandez H, Pauthier S, Doumerc S, et al: Ultrasound-guided injection of methotrexate versus laparoscopic salpingotomy in ectopic pregnancy. *Fertil Steril* 63:25, 1995.
108. Menard A, Crequat J, Mandelbrot L, et al: Treatment of unruptured tubal pregnancy by local injection of methotrexate under transvaginal sonographic control. *Fertil Steril* 54:47, 1990.
109. Fernandez H, Benifla JL, Lelaidier C, et al: Methotrexate treatment of ectopic pregnancy: 100 cases treated by primary transvaginal injection under sonographic control. *Fertil Steril* 59:773, 1993.
110. Lund J: Early ectopic pregnancy treated nonsurgically. *J Obstet Br Empire* 62:70, 1955.
111. Atri M, Bret PM, Tulandi T: Spontaneous resolution of ectopic pregnancy: initial appearance and evolution at transvaginal US. *Radiology* 186:83, 1993.
112. Fernandez H, Rainhorn JD, Papiernik E, et al: Spontaneous resolution of ectopic pregnancy. *Obstet Gynecol* 71:171, 1988.
113. Sauer MV, Gorrill MJ, Rodi IA, et al: Nonsurgical management of unruptured ectopic pregnancy: an extended clinical trial. *Fertil Steril* 48:752, 1987.
114. Cacciatore B, Korhonen J, Stenman UH, et al: Transvaginal sonography and serum hCG in monitoring of presumed ectopic pregnancies selected for expectant management. *Ultrasound Obstet Gynecol* 5:297, 1995.
115. Ylostalo P, Cacciatore B, Korhonen J, et al: Expectant management of ectopic pregnancy. *Eur J Obstet Gynecol Reprod Biol* 49:83, 1993.
116. Korhonen J, Stenman UH, Ylostalo P: Serum human chorionic gonadotropin dynamics during spontaneous resolution of ectopic pregnancy. *Fertil Steril* 61:632, 1994.
117. Korhonen J, Stenman UH, Ylostalo P: Low-dose oral methotrexate with expectant management of ectopic pregnancy. *Obstet Gynecol* 88:775, 1996.
118. Elson J, Taylor A, Banerjee S, et al: Expectant management of tubal ectopic pregnancy: prediction of successful outcome using decision tree analysis. *Ultrasound Obstet Gynecol* 23:552, 2004.
119. Gretz E, Quagliarello J: Declining serum concentrations of the beta-subunit of human chorionic gonadotropin and ruptured ectopic pregnancy. *Am J Obstet Gynecol* 156:940, 1987.
120. Kim PY, de La Vallee C: Isthmic ectopic gestation: a contraindication to methotrexate therapy? *Am J Obstet Gynecol* 176:711, 1997.
121. Hajenius PJ, Engelsbel S, Mol BW, et al: Randomised trial of systemic methotrexate versus laparoscopy salpingostomy in tubal pregnancy. *Lancet* 350:774, 1997.
122. Glock JL, Johnson JV, Brumsted JR: Efficacy and safety of single-dose systemic methotrexate in the treatment of ectopic pregnancy. *Fertil Steril* 62:716, 1994.
123. Ichinoe K, Wake N, Shinkai N, et al: Nonsurgical therapy to preserve oviduct function in patients with tubal pregnancies. *Am J Obstet Gynecol* 156:484, 1987.
124. Stovall TG, Ling FW: Single-dose methotrexate: an expanded clinical trial [see comments]. *Am J Obstet Gynecol* 168:1759; discussion 1762, 1993.
125. Stovall TG, Ling FW, Gray LA, et al: Methotrexate treatment of unruptured ectopic pregnancy: a report of 100 cases. *Obstet Gynecol* 77:749, 1991.

126. Ankum WM, Mol BW, Van der Veen F, et al: Risk factors for ectopic pregnancy: a meta-analysis [see comments]. *Fertil Steril* 65:1093, 1996.
127. Pisarska MD, Carson SA, Buster JE: Ectopic pregnancy. *Lancet* 351:1115, 1998.
128. Brown DL, Doubilet PM: Transvaginal sonography for diagnosing ectopic pregnancy: positivity criteria and performance characteristics. *J Ultrasound Med* 13:259, 1994.
129. Nyberg DA, Filly RA, Laing FC, et al: Ectopic pregnancy. Diagnosis by sonography correlated with quantitative HCG levels. *J Ultrasound Med* 6:145, 1987.
130. DiMarchi JM, Kosasa TS, Hale RW: What is the significance of the human chorionic gonadotropin value in ectopic pregnancy? *Obstet Gynecol* 74:851, 1989.
131. Stiller RJ, Haynes de Regt R, Blair E: Transvaginal ultrasonography in patients at risk for ectopic pregnancy. *Am J Obstet Gynecol* 161:930, 1989.
132. Pennell RG, Baltarowich OH, Kurtz AB, et al: Complicated first-trimester pregnancies: evaluation with endovaginal US versus transabdominal technique. *Radiology* 165:79, 1987.
133. Filly RA: Ectopic pregnancy: the role of sonography. *Radiology* 162:661, 1987.
134. Cacciatore B, Ulf-hakan S, Ylostalo P: Diagnosis of ectopic pregnancy by vaginal ultrasonography in combination with a discriminatory serum hCG level of 1000 IU/l (TRP). *Br J Obstet Gynaecol* 97:904, 1990.
135. Rempen A: Vaginal sonography in ectopic pregnancy. A prospective evaluation. *J Ultrasound Med* 7:381, 1988.
136. Timor-Tritsch I: Transvaginal ultrasonographic findings in surgically verified ectopic pregnancy. *Am J Obstet Gynecol* 170:1205, 1994.



# THE ROLE OF MAGNETIC RESONANCE IMAGING IN THE EVALUATION OF GYNECOLOGIC DISEASE

Antonio C. Westphalen, MD and Aliya Qayyum, MD, MBBS

## Imaging Techniques

### Anatomy and Physiology

Uterus  
Ovaries

### Congenital Anomalies

Müllerian Duct Anomalies  
*Agenesis/Hypoplasia*  
*Unicornuate Uterus*  
*Uterus Didelphys*  
*Bicornuate Uterus*  
*Septated Uterus*  
*Arcuate Uterus*  
*Diethylstilbestrol Exposure*

Vaginal Anomalies  
Ovarian Anomalies

### Leiomyomas

Definition and Epidemiology  
Clinical Aspects  
Pathophysiology  
Treatment  
Diagnosis  
Imaging Characteristics

### Adenomyosis

Definition and Epidemiology

## Clinical Aspects

Pathophysiology  
Diagnosis  
Imaging Characteristics

### Endometriosis

Definition and Epidemiology  
Etiology  
Clinicopathologic Aspects  
Imaging

### Cervical Cancer

Epidemiology and Clinical Presentation  
Histopathology  
Diagnosis  
Treatment  
Clinical Staging  
Imaging

*Early Stage Disease*  
*Parametrial Extension*  
*Stage III Disease*  
*Stage IV Disease*  
*Tumor Size Assessment*  
*Lymph Node Assessment*

### Endometrial Cancer

Epidemiology and Clinical Presentation  
Histopathology  
Diagnosis  
Treatment  
Staging  
Imaging

### Adnexal Masses

Epidemiology and Clinical Significance  
Imaging Diagnosis and the Role of Magnetic Resonance Imaging  
Differentiation of Benign and Malignant Lesions  
Specific Diagnosis Based on Magnetic Resonance Imaging Findings

*Adnexal Masses With Distinctive Imaging Features (Fat, Blood, and Fibrous Tissue)*

*Cystic, Benign-Appearing Lesions*  
*Cystic, Malignant-Appearing Lesions*  
*Predominantly Solid Lesions*

Preoperative Staging

This chapter describes the main indications of magnetic resonance imaging (MRI) for the evaluation of nonobstetric gynecologic diseases. In the first two sections, the normal anatomy of the female pelvis and common congenital anomalies are discussed. In subsequent sections, the use of MRI in the setting of common benign pathologies, namely leiomyomas, adenomyosis, and endometriosis is outlined, and finally, the role of MRI in patients with malignant neoplasms of the reproductive organs is discussed. The main clinical and epidemiologic aspects are presented, in addition to imaging features in order to emphasize a practical clinical approach to the diagnostic question.

## IMAGING TECHNIQUES

A detailed discussion of imaging techniques and protocols used in MRI is beyond the scope of this chapter. There are,

however, a few basic concepts with regard to imaging techniques that may make the images easier to understand to those not familiar with MRI.

T2-weighted images are the mainstream of MRI of the female pelvis. These images are used for evaluation of the normal anatomy and detection of most uterine and adnexal abnormalities. T1-weighted images, especially when used in conjunction with fat suppression, are helpful in characterizing the content of adnexal lesions, namely blood and fat. When used after the administration of intravenous gadolinium, T1-weighted images assist in the characterization of some benign and malignant tumors. As a general rule, on T1-weighted images, fat-containing lesions are bright. Water, such as the urine in the bladder, is dark. However, water is bright on T2-weighted images. Therefore, tissues with higher amounts of water, such as tumors and cysts, have high signal intensity on T2-weighted images. Gadolinium is

the main component of the most commonly used intravenous contrast media in MRI. Tissues that are impregnated by gadolinium show an increase in signal intensity on T1-weighted images when compared with images acquired before its administration. It is used to increase the contrast between normal and abnormal tissues in the body. For instance, many neoplastic processes enhance more avidly than the adjacent tissues and become more easily visible. In addition, it is used to improve visualization of vascular structures.

## ANATOMY AND PHYSIOLOGY

Although it is not within the scope of this chapter to discuss the anatomy of the female pelvis, a few words on specific features of MRI are important. A basic concept that must be kept in mind is that the patient's hormonal status affect imaging features of the female gynecologic organs, irrespective of the imaging modality.<sup>1-3</sup>

### Uterus

The uterus typically measures from 6 to 9 cm in length in women of reproductive age, the cervix accounting for approximately 30% to 50% of the total, being proportionally larger in size before the menarche. Its anatomic features are best visualized using T2-weighted images, usually acquired in the axial and sagittal planes. T2-weighted sequences clearly depict the uterine zonal anatomy, which may be described considering two separate regions, the cervix and the uterine body.

The cervical anatomy is divided in three zones on T2-weighted sequences: the endocervical mucosa, which demonstrates high-signal intensity due to the presence of mucus glands; the cervical stroma, which demonstrates low signal intensity owing to the presence of fibrous connective tissue; and the peripherally located smooth muscle, which demonstrates intermediate signal intensity (Fig. 33-1). Varying amounts of mucus may be seen within the endocervical canal, which has a very high signal intensity similar to fluid.<sup>2-4</sup>

The zonal anatomy of the body of the uterus also consists of three distinct regions on T2-weighted sequences: centrally, the endometrium demonstrates a very high signal intensity; adjacent to the endometrium, the junctional zone (inner myometrial layer) demonstrates low signal intensity; and the outer myometrium, which demonstrates intermediate signal intensity (Fig. 33-2). At its inferior aspect, the junctional zone is continuous with the low signal intensity cervical stroma.<sup>4-6</sup>

Identification of the junctional zone is extremely important when evaluating the uterine magnetic resonance zonal anatomy. Studies have shown that the appearance of the zonal anatomy, in particular the ability to distinguish the junctional zone, is influenced by female hormones.<sup>1-3</sup> Normally, the junctional zone should not measure more than 11 mm in thickness in women of reproductive age. In postmenopausal women, women taking oral contraceptives, or in girls before menarche, the zonal anatomy is frequently indistinct and the junctional zone may be very thin.<sup>4</sup>

The MRI appearance of the endometrium is also hormonally influenced and varies with the menstrual cycle.

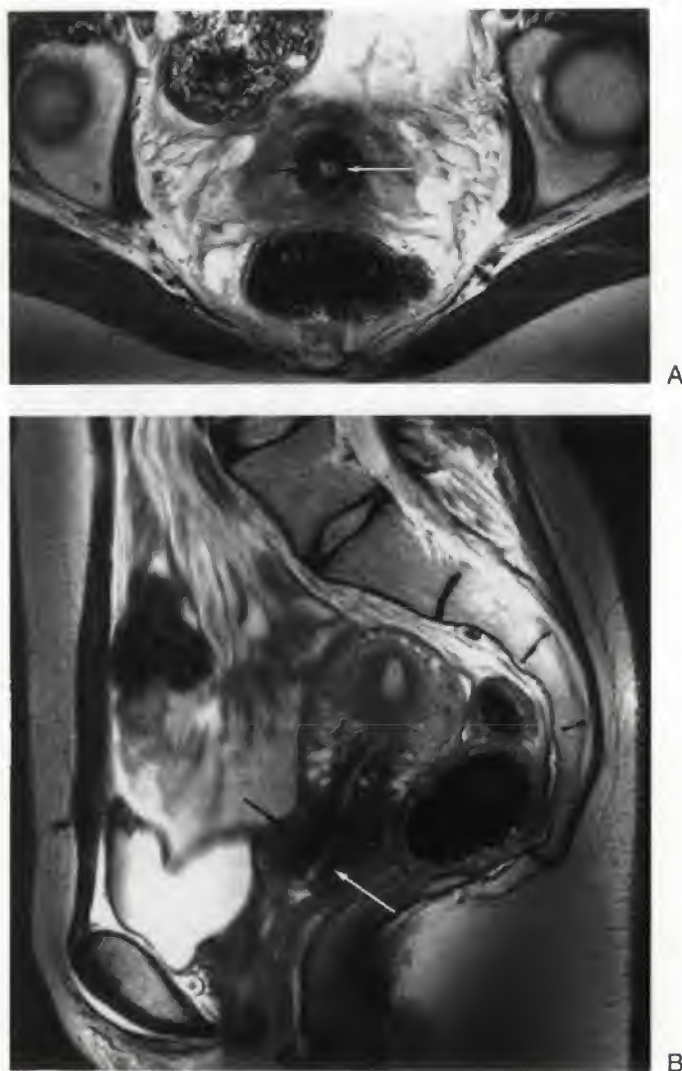


**FIGURE 33-1.** Normal cervix. Axial (A) and sagittal (B) T2-weighted image demonstrate the normal zonal anatomy of the cervix, composed of an external rim of smooth muscle (short arrow on A and B) with intermediate signal intensity, a dark ring of fibrous stroma (long arrow on A and B), and the endocervical mucosa (asterisk on A).

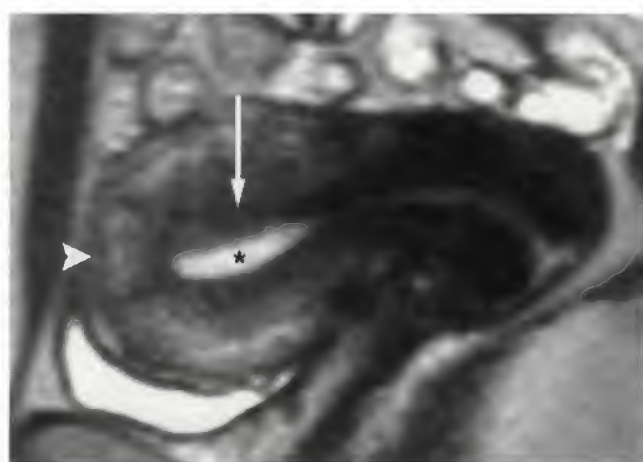


**FIGURE 33-2.** Normal uterus. Sagittal T2-weighted image demonstrates the high signal intensity of the endometrium (asterisk) and zonal anatomy of the uterus, characterized by a dark transitional zone (arrow) and intermediate signal intensity of the outer myometrium (arrowhead).



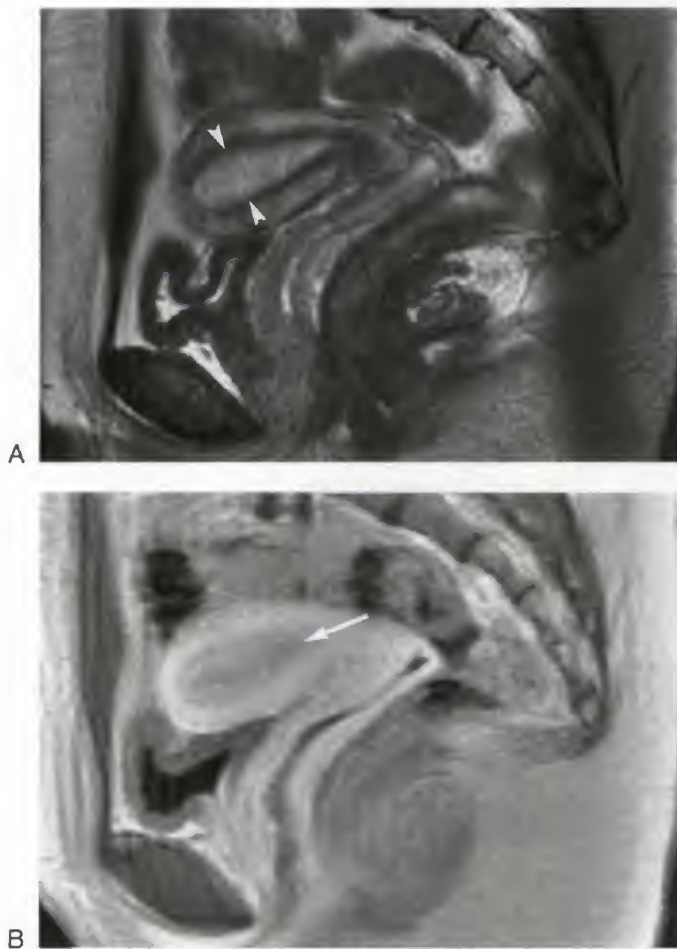


**FIGURE 33-3.** Apparent endometrial thickening. Sagittal T2-weighted (A) and enhanced T1-weighted (B) images. Apparent thickening of the endometrium is seen on the T2-weighted image (arrowheads); however, after enhancement of the endometrium, fluid within the cavity becomes evident (arrow).

The endometrium becomes progressively thicker between the early follicular (proliferative) phase and ovulation, measuring from 1 or 3 mm to an average of 8 or 9 mm. The endometrium should not measure more than 15 mm in thickness in women of menstrual age, and typically measures 11 mm or less in postmenopausal women who are not on hormonal replacement therapy.<sup>7,8</sup> The endometrium has its highest signal intensity during the luteal (secretory) phase.<sup>1,3,4</sup> It is imperative to remember that the use of T2-weighted images for evaluation of the thickness of the endometrium using may result in overestimation, because fluid within the endometrial cavity also has high signal intensity (Fig. 33-3).

Unlike the uterine corpus, the cervical zonal anatomy does not demonstrate significant changes during the menstrual cycle. In addition, because the cervix is composed largely of fibrous elastic tissue, the enhancement of the cervix is different from the uterine corpus. The uterine body is a very vascular structure when compared with the cervix and enhances more avidly and earlier than the cervix

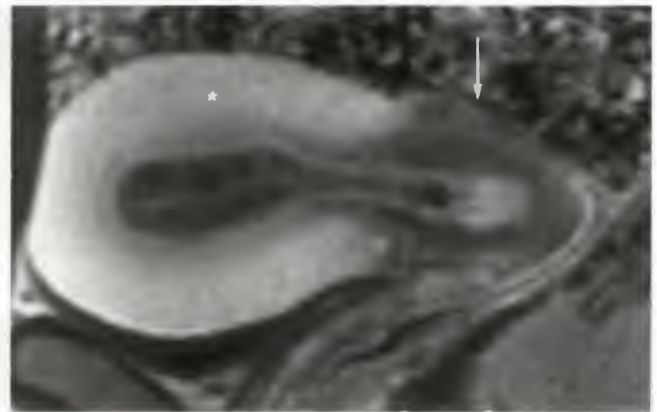


**FIGURE 33-4.** Normal uterus. Gadolinium-enhanced sagittal T1-weighted image demonstrate the normal difference between the enhancement of the myometrium (asterisk) and cervical stroma (arrow).

(Fig. 33-4). This is important because the difference in enhancement may give the appearance of a pseudomass and lead to a misdiagnosis of cervical cancer in the unwary.

## Ovaries

Normal ovaries have homogeneous intermediate T1 signal intensity; however, they are characterized by an outer high-signal-intensity cortex and a hypointense central medulla when imaged using T2-weighted sequences.<sup>9-12</sup> The ovaries measure approximately 2 cm × 2 cm × 3 cm; however, their size fluctuates according to the hormonal status, especially because of follicle production and enlargement. The ovaries are most readily identified in women of reproductive age by the presence of such follicles, which are seen as small cysts of high signal intensity on T2-weighted sequences and low signal intensity on T1-weighted sequences (Fig. 33-5). Primordial follicles are usually smaller, measuring up to 9 mm in diameter, whereas stimulated graafian follicles may reach up to 3 cm or 5 cm.<sup>9</sup> Other features of these physiologic cysts seen on T2-weighted sequences include imperceptible or thin walls (less than 3 mm), and an absence of mural nodules (see Fig. 33-5).<sup>9-12</sup> Ovarian follicles are seen in only about 22% to 40% of postmenopausal patients.<sup>10</sup> Ovarian stroma enhances after intravenous contrast administration and the use of fat-suppressed sequences help with the identification of ovaries when follicles are not visible.<sup>9</sup>

The normal fallopian tubes are not visualized on MRIs.<sup>11,12</sup>

## CONGENITAL ANOMALIES

MRI is the method of choice for evaluation of congenital anomalies. Advantages of the method include its noninvasiveness, lack of ionizing radiation, multiplanar capability enabling interrogation of the fundal contour of the uterus, and excellent soft tissue characterization. The use of MRI may reduce the number of invasive procedures and related costs by guiding management decisions.<sup>13,14</sup>

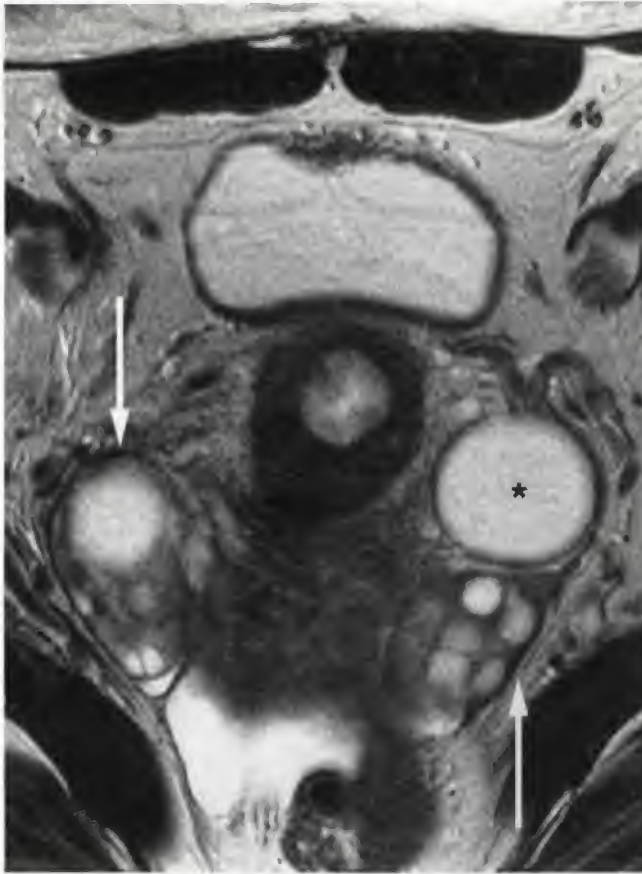


**FIGURE 33-5.** Normal ovaries. Axial T2-weighted image demonstrates the presence of multiple hyperintense follicles in both ovaries (arrows), one of which represents the dominant follicle (asterisk).

## Müllerian Duct Anomalies

Müllerian ducts are paired embryologic structures that normally fuse between the 6th and 11th weeks of gestation, forming the uterus, fallopian tubes, cervix, and most of the upper vagina.<sup>15</sup> However, in 0.1% to 10.0% of the general population, either fusion fails to occur or the ducts do not have normal development, resulting in one of multiple anomalies.<sup>9,16-19</sup> Although müllerian duct anomalies may be asymptomatic, they are more often associated with primary amenorrhea, infertility, obstetric complications, and endometriosis.<sup>15,17,20,21</sup> It is estimated that about 15% of women who present with recurrent miscarriages have müllerian duct anomalies.<sup>22</sup> In addition, 30% to 50% of these women have concurrent renal anomalies, which include agenesis, ectopia, fusion, malrotation, and duplication.<sup>9,15,20</sup> Patients suspected of having müllerian duct anomalies are often initially investigated with transvaginal ultrasound, because it is widely available and has a relatively low cost. Although multiple studies have demonstrated the usefulness of MRI for the evaluation of müllerian duct anomalies,<sup>23-29</sup> it is frequently reserved for indeterminate cases or cases in which further information is needed. T2-weighted sequences are the most useful because zonal anatomy identification is necessary. In addition, the study must include an oblique coronal and axial plane to ensure adequate visualization of the contour of the uterine fundus.

There are many different classifications of müllerian duct anomalies, the American Society for Reproductive Medicine classification perhaps being the most used and well-known (Fig. 33-6).<sup>30</sup>

## Agenesis/Hypoplasia

The anomalies within this group result from bilateral nondevelopment or arrested development of the müllerian ducts. Agenesis of the upper vagina and uterus is the most

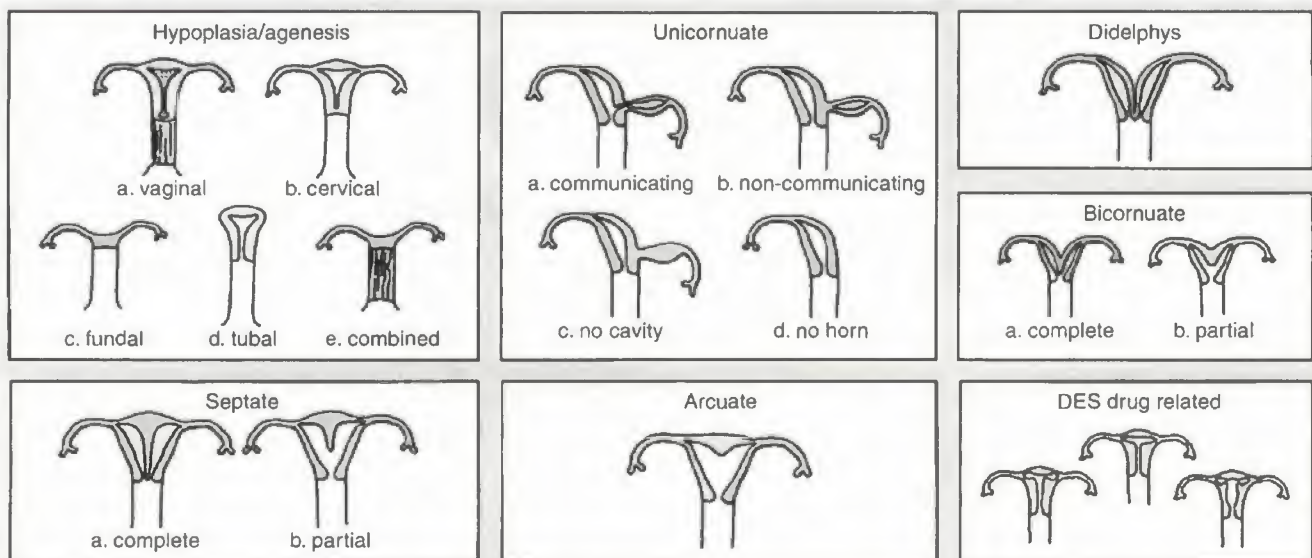


**FIGURE 33-6.** Graphic representation of multiple müllerian duct anomalies. American Society for Reproductive Medicine classification.





**FIGURE 33-7.** Uterus didelphys. Axial T2-weighted images of the pelvis (A and B) and coronal T1-weighted image of the abdomen (C) demonstrate two separate uteri (asterisks on A and arrows on C) and cervixes (black arrow on A), as well as two separate vaginas (white arrows on B). The right kidney was congenitally absent (C).

common anomaly in this group and part of the spectrum of the Mayer-Rokitansky-Küster-Hauser syndrome. Patients with this syndrome may present with an atrophic uterus, however, and vaginal abnormalities can range from hypoplasia to agenesis. Urinary system malformations are sometimes associated with Mayer-Rokitansky-Küster-Hauser syndrome. The second most common anomaly in this class is segmental vaginal agenesis. Isolated agenesis or hypoplasia of the uterus is very rare. In complete uterine agenesis, MRI demonstrates a short blind-ending vagina only, whereas in cases of uterine hypoplasia, the uterus is small and the intercornual diameter of the endometrial cavity is reduced, measuring less than 2.0 cm.

### Unicornuate Uterus

A unicornuate uterus is the consequence of complete arrest or partial development of one müllerian duct. In 90% of cases, there is partial development of the duct, resulting in a rudimentary horn, which may contain functioning endometrium. The rudimentary horn may be obstructed or communicate with the main uterine cavity. Clinical associations include a very high rate of spontaneous

miscarriage, obstetric complications, and endometriosis. A unicornuate uterus has normal zonal anatomy and a characteristic banana-shaped configuration. A rudimentary horn can be seen as a soft tissue mass of similar signal intensity as the myometrium; and if obstructed, it may be distended with blood products, resulting in high signal intensity on T1-weighted sequences.

### Uterus Didelphys

The uterus didelphys results from nonfusion of the müllerian ducts and is characterized by the presence of two separate uteri and cervixes, with a vertical septum in the upper vagina. Very rarely, two completely separated vaginas and vaginal orifices may be seen. Patients are usually asymptomatic, but hematometrocolpos may occur if an obstructing transverse hemivaginal septum is present. Clinical complications are similar to those associated with a unicornuate uterus. MRI demonstrates two widely separated fusiform uterine horns and two cervixes (Fig. 33-7). The zonal anatomy is preserved. Vaginal septa may not be detected with MRI and physical examination may be necessary for confirmation and distinction from a bicornuate bicollis uterus.





**FIGURE 33-8.** Bicornuate unicollis uterus. Axial T2-weighted image demonstrates a clefted fundus (white double-headed arrow) and single cervix (black arrow).

### Bicornuate Uterus

This anomaly is the result of partial failure of fusion of the müllerian ducts. It is characterized by an increased intercornual distance, typically measuring larger than 4 cm; a concave external contour of the fundus, measuring more than 1 cm in depth; and a fibrous-muscular septa separating the endometrial cavity in two. The septa may be incomplete, partially dividing the uterine cavity (bicornuate unicollis [Fig. 33-8]), or complete, extending all the way to the external cervical os (bicornuate bicollis). The vagina has normal development. Images obtained in the oblique coronal plane, along the long axis of the uterus, are useful in assessing the fundal contour. The dividing septum often exhibits signal characteristics of myometrium, but may be of low signal intensity inferiorly when fibrous tissue is present.

### Septated Uterus

This is the most common müllerian duct anomaly and the result of failure of resorption of a fibrous septum in later stages of development.<sup>15</sup> The resultant divided endometrial cavity may be small, and the septum may be partial or extend to the external cervical os. Reproductive complications are greatest in this class of müllerian duct anomaly. MRI features (Fig. 33-9), which distinguish a septated uterus from a bicornuate uterus, include a nonclefted fundal contour; a normal intercornual distance of less than 4 cm; and a thin, dividing, often fibrous septum of low T1- and T2-signal intensity.

### Arcuate Uterus

This anomaly consists of mild indentation affecting only the fundal aspect of the endometrium because of minimally incomplete resorption of the uterovaginal septum. It is classified separately because it is a benign variant without clinical significance. On MRI, the arcuate uterus has a single endometrial cavity associated a small fundal cleft measuring less than 1.0 cm in depth.

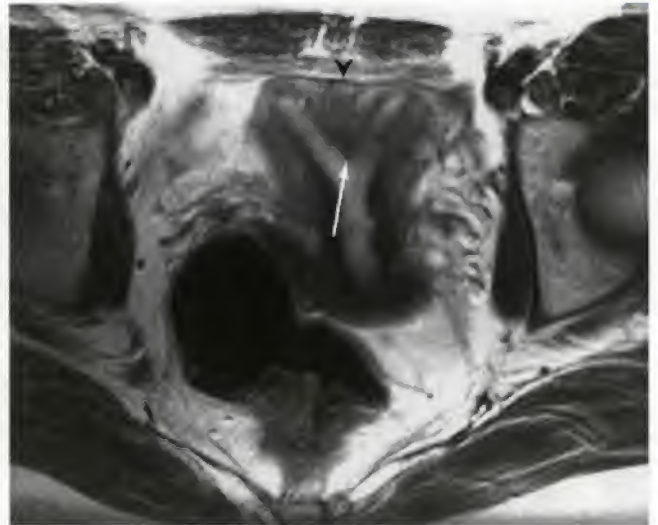


**FIGURE 33-9.** Septated uterus. Axial T2-weighted image demonstrates a partial septum dividing the endometrial cavity (arrow) and a nonclefted uterine fundus (arrowhead).

### Diethylstilbestrol Exposure

Diethylstilbestrol is a synthetic estrogen that was used in the past, up to 1971, to prevent miscarriages. It is estimated that approximately two thirds of the patients who were exposed to it in utero have uterine anomalies. The most common of these anomalies is the classic hypoplastic T-shaped uterus, but other deformities of the uterine horns and endometrial cavity may be identified.

### Vaginal Anomalies

The lower third of the vagina originates from the urogenital sinus. Developmental failure of the urogenital sinus results either in the absence of the distal vagina or the presence of a transverse membrane, mimicking an imperforated hymen. In both cases, obstruction results in fluid distention of the vagina and uterus. The upper vagina presents with very thin walls, whereas the uterus may have thin or thick myometrium (Fig. 33-10). Hematometocolpos is identified as a heterogeneous collection with high T1- and T2-signal intensity.

### Ovarian Anomalies

The ovaries are derived from primitive germ cells, which migrate to the embryonic gonadal ridge and subsequently descend into the pelvis. Congenital anomalies of the ovaries are habitually associated with chromosomal disease and represent gonadal dysgenesis. Turner syndrome (45X0 karyotype) and Turner syndrome mosaic (45X0/46XX karyotype) are common causes. The ovaries of patients with gonadal dysgenesis are absent or seen as fibrous streaks. The fat-suppressed T2-weighted and gadolinium-enhanced T1-weighted sequences are most helpful in the identification of ovaries.



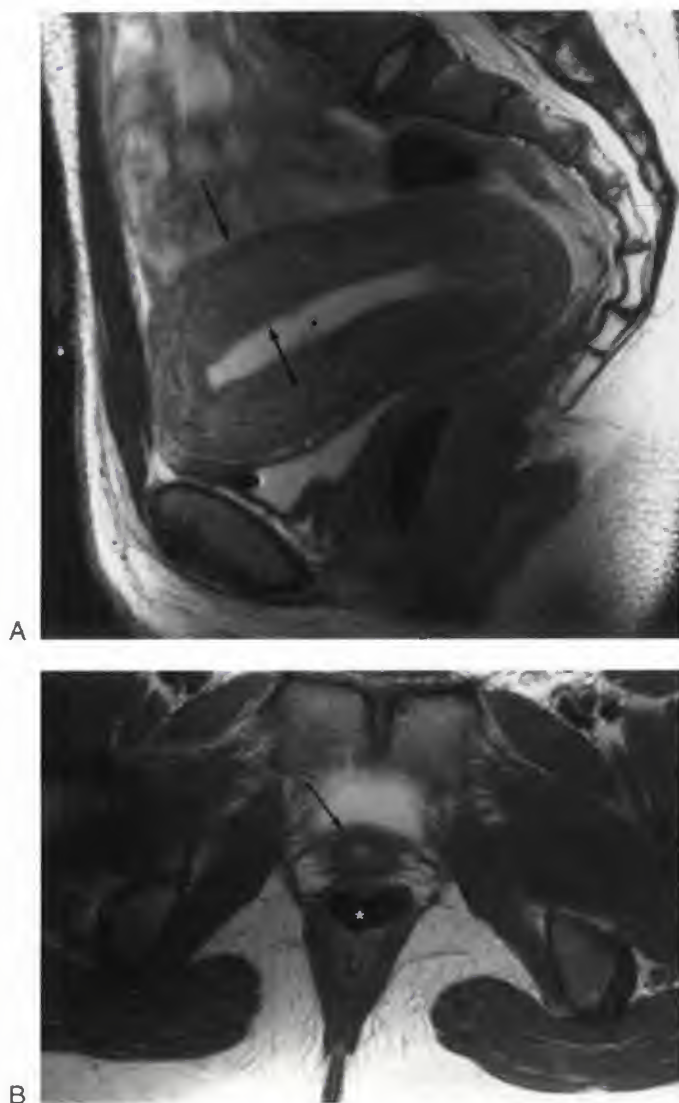


**FIGURE 33-10.** Vaginal agenesis. Sagittal T2-weighted (A) and axial T2-weighted (B) images demonstrate mild distension of the uterine cavity (asterisk on A) and thickening of the myometrium (arrows on A), as well as absence of the vagina between the normal urethra (arrow on B) and rectum (asterisk on B).

## LEIOMYOMAS

### Definition and Epidemiology

Leiomyomas are benign tumors arising from uterine smooth muscle cells with a prevalence ranging from 25% to up to 77%.<sup>31</sup> Leiomyomas are more often seen in women older than 30 to 35 years of age, and are 2 to 3 times more common in black women.<sup>32–34</sup> Leiomyomas have a significant impact on public health, accounting for at least one third of the 600,000 hysterectomies performed each year in the United States.<sup>35</sup>

### Clinical Aspects

Most patients with leiomyomas are asymptomatic.<sup>31</sup> Clinical symptoms associated with leiomyomas include dysfunctional

uterine bleeding, pelvic pressure, and pelvic pain. In addition, there is an association with impaired reproductive function, which may be related to impaired implantation, tubal obstruction, increased miscarriage, and preterm labor.<sup>36,37</sup>

Symptoms are largely related to the location of the leiomyoma. Approximately 90% occur in the uterus, but about 5% to 10% are cervical in location. In pregnant patients, these may grow and cause dystocia.<sup>42,43</sup> A minority of leiomyomas are seen in the round and broad ligaments (Fig. 33-11) or adnexa.

Uterine leiomyomas are classified as submucosal, intramural, or subserosal (Fig. 33-12). Approximately 5% of leiomyomas are submucosal in location (Fig. 33-13),<sup>43</sup> and typically present with menorrhagia. Clinically, the submucosal location is considered to be a cause of infertility, and can be treated with hysteroscopic resection. Submucosal leiomyomas are distinguished from large intramural leiomyomas by an endometrial location of the core or center of the lesion; and adjacent myometrium encircling the lesion by less than 180 degrees.

Subserosal leiomyomas account for approximately 10% to 20% of uterine leiomyomas, are located just under the uterine serosa, and may be pedunculated or sessile (see Figs. 32-13 and 33-14). Symptoms are associated with a large size or torsion of a pedunculated lesion. The bridging vascular sign (vascular vessels originating from the uterus and feeding a pelvic mass) is seen in approximately 77% of exophytic leiomyomas and is helpful in the differentiation from adnexal masses.<sup>44</sup> Another feature on imaging that may be useful to make the distinction between a subserosal leiomyoma and an ovarian mass is the identification of an ovarian vascular pedicle. The ovarian vascular pedicle is characterized by drainage of a pelvic mass by a gonadal vein. This pedicle is seen in 92% of the ovarian masses and 13% of pedunculated subserosal leiomyomas.<sup>45</sup>

### Pathophysiology

The pathophysiology of leiomyomas is unknown; however, genetic predisposition and hormonal status are involved in tumor development and growth.<sup>31</sup> Because these tumors respond to hormonal stimulation, frequently they are noted to enlarge during pregnancy and involute after menopause. They may undergo various types of degeneration, the most frequent types being hyaline (seen in at least 60% of leiomyomas), cystic, myxoid, fatty, and hemorrhagic (Fig. 33-15).<sup>38</sup> In most cases, the distinction of different kinds of degeneration is not possible solely based on imaging findings; however, there are some features that may suggest one or another type. Degeneration may make the diagnosis difficult with ultrasound, and MRI characteristics may be used to identify a degenerating leiomyoma.<sup>39,40</sup>

In addition, leiomyomas may present in unusual ways, such as metastasizing leiomyomas, intravenous leiomyomas, diffuse leiomyomatosis, and peritoneal disseminated leiomyomatosis. Although these uncommon presentations may seem to suggest a malignant behavior, they are essentially a variation in the growth pattern of this benign lesion.<sup>38</sup> Uterine leiomyosarcomas have been reported to

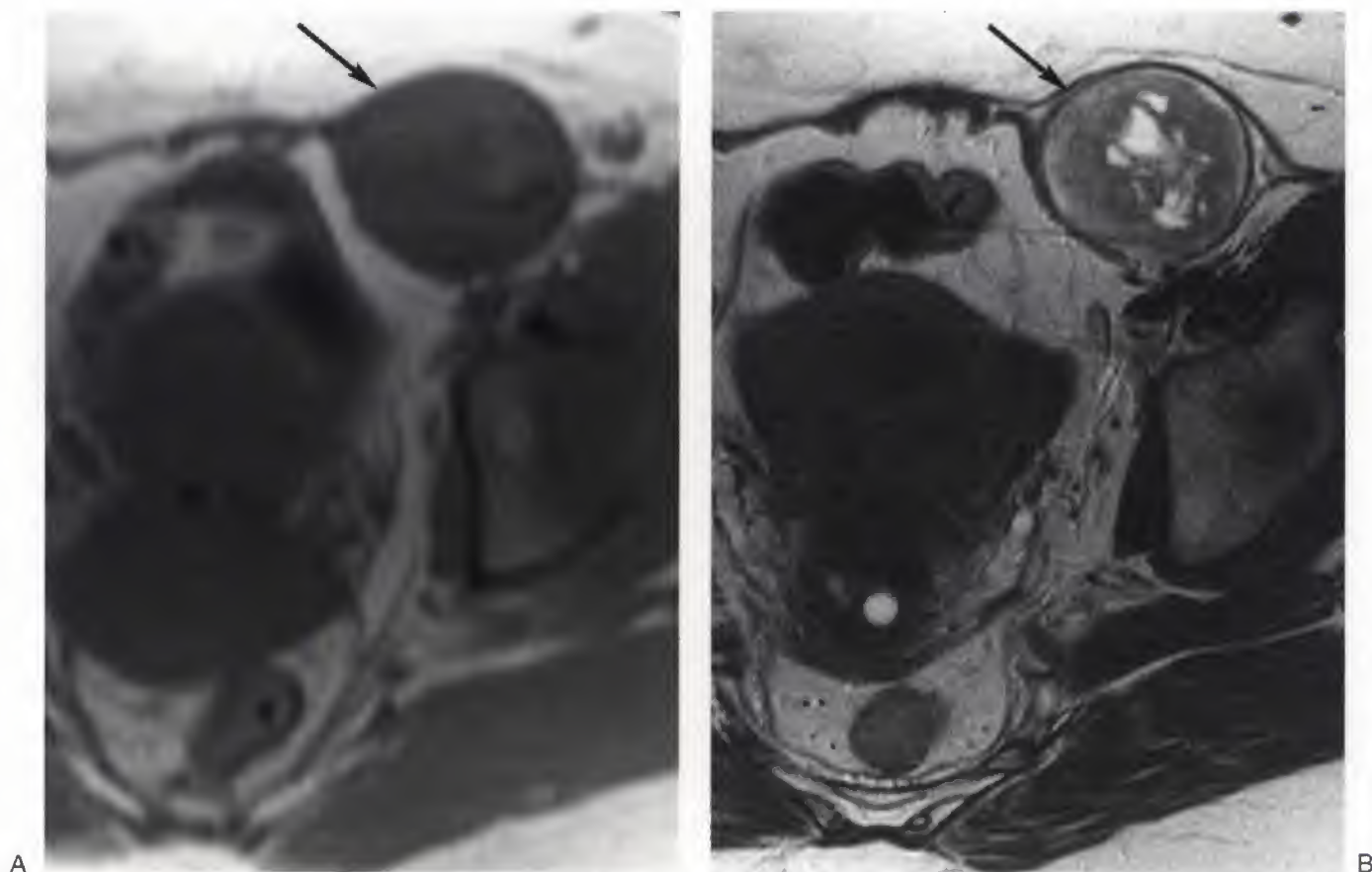


**FIGURE 33-11.** Round ligament leiomyoma. Axial T1-weighted (A) and T2-weighted (B) images demonstrate a round mass with the typical appearance of a degenerating leiomyoma (arrows), but separate from the uterus and herniated into the left inguinal canal. This was surgically proven to be a leiomyoma of the round ligament.

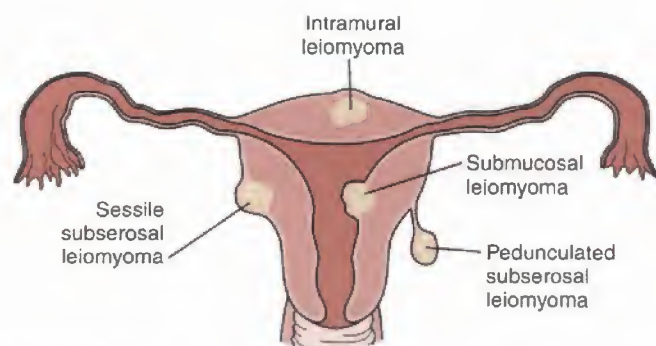


**FIGURE 33-12.** Graphical representation of a sessile subserosal leiomyoma (S), a pedunculated subserosal leiomyoma (P), an intramural leiomyoma (I), and a submucosal leiomyoma (M).

occur in association with leiomyomas,<sup>41</sup> however, genetic studies suggest that these are two different entities arising from separate pathways.<sup>31</sup> Sometimes, the distinction between a leiomyoma and a leiomyosarcoma cannot be reliably made based on MRI characteristics of the primary lesion; however, rapid growth, evidence of extrauterine

extension, lymphadenopathy, and metastases indicate malignancy (Fig. 33-16).

## Treatment

The treatment of choice of a leiomyoma depends on its size and location, as well as on the clinical presentation. The most common options are hysterectomy, myomectomy (transabdominal, laparoscopic, and hysteroscopic), myolysis, and uterine artery embolization.<sup>31,37</sup> Hysterectomy is usually performed in women who have completed childbearing and do not wish to preserve the uterus. Myomectomy is usually the choice of treatment for those patients who wish to preserve the uterus. In these cases, an abdominal approach is used for multiple large leiomyomas; the laparoscopic approach is appropriate for the resection of subserosal and pedunculated lesions, whereas the hysteroscopic technique is preferred for patients who have submucosal tumors. Uterine fibroid embolization is a safe and effective technique with the potential to become the first choice for treatment of symptomatic uterine fibroids.<sup>46</sup> Most patients are candidates for uterine embolization, as long as contraindications, such as active pelvic infection, renal insufficiency, and contrast allergy, are excluded. The main advantage of uterine fibroid embolization is the decreased morbidity when compared with other treatment options.





**FIGURE 33-13.** Myomatous uterus. Sagittal T2-weighted image demonstrates a small submucosal leiomyoma (white arrow) and distention of the endometrial cavity, which was due to blood (asterisk). Amongst others, a subserosal leiomyoma is identified in the fundus of the uterus (black arrow).

## Diagnosis

The purpose of imaging these patients is to determine size and location of leiomyomas, as well as the presence of necrosis or hemorrhage; all of these factors are essential for selection of appropriate management. The diagnosis of a leiomyoma is typically confirmed and monitored by transvaginal ultrasound. Nonetheless, ultrasound evaluation may be limited when the uterus is retroverted or retroflexed, enlarged to an extent that prevents its complete visualization, in the presence of a pedunculated subserosal leiomyoma (when differentiation from an adnexal mass may be difficult), and when lesions present atypical imaging features. MRI is a problem-solving tool reserved for these cases, as well as for those in which conservative treatment is being contemplated. Although overall MRI and ultrasound have similar sensitivity (99% and 99%, respectively) and specificity (86% and 91%, respectively) to establish the presence of uterine leiomyomas, MRI is better to identify and determine the total number of lesions.<sup>47</sup> The advantages of MRI over ultrasound are likely related to its large field of view and multiplanar capabilities.<sup>47</sup> An additional benefit of MRI is the ability to distinguish leiomyomas from focal adenomyosis, which is

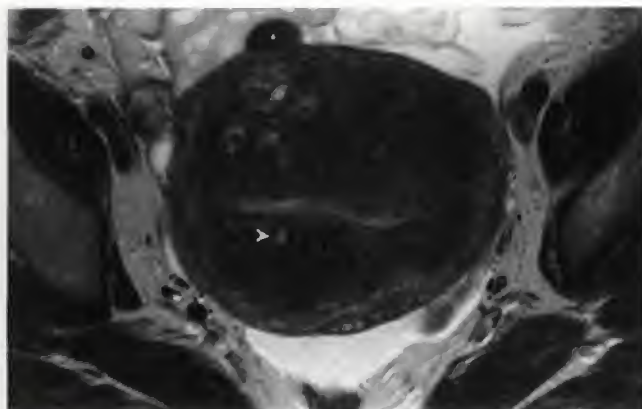


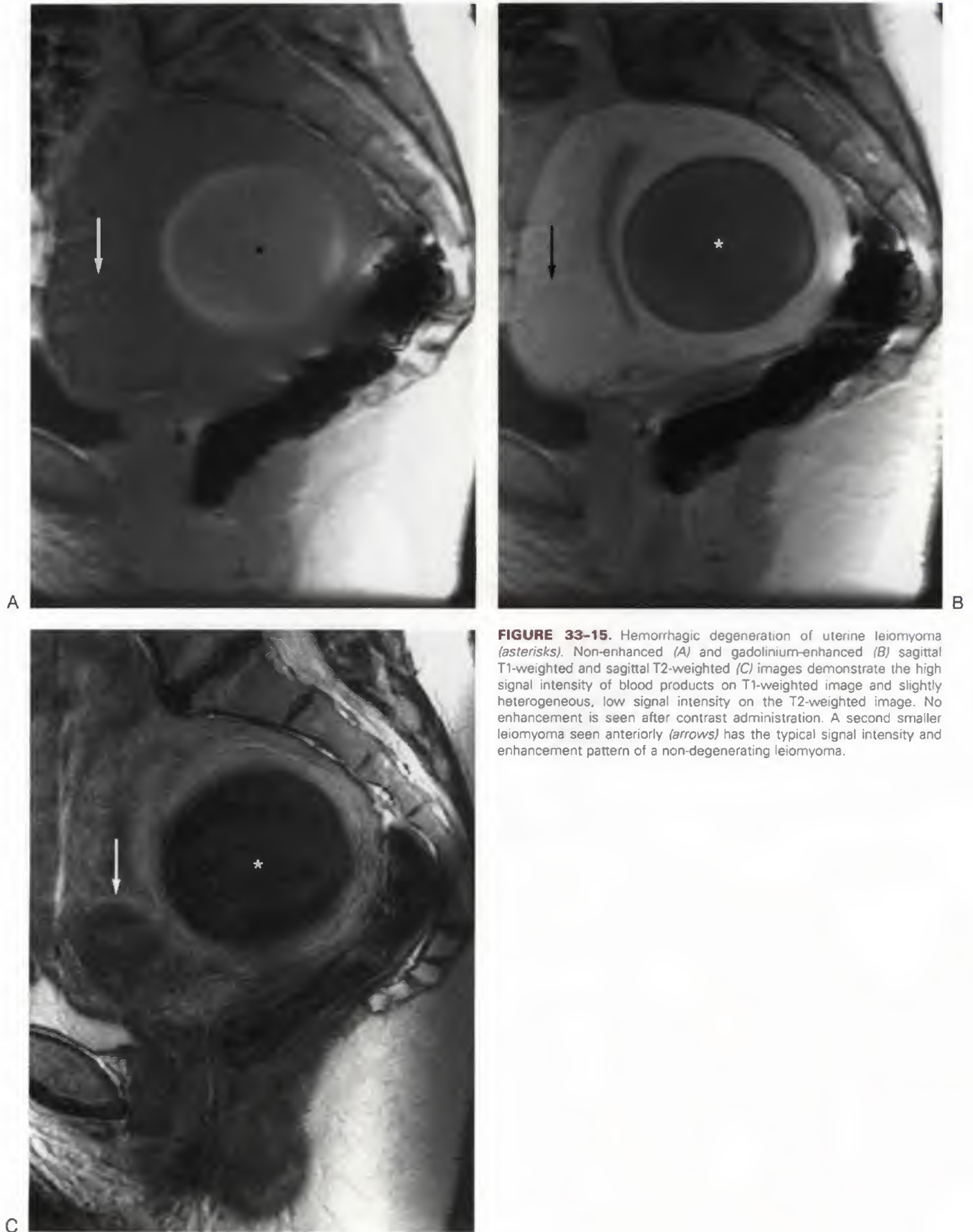
**FIGURE 33-14.** Leiomyoma and adenomyosis. Axial T2-weighted image demonstrates a small subserosal leiomyoma anteriorly (asterisk). The junctional zone is thickened and has indistinct margins. Multiple punctate foci with high signal intensity (starry sky appearance) (arrowhead), characteristic of adenomyosis, are seen.

clinically important because the treatment of these two entities may differ significantly if uterine preservation is necessary.<sup>48,49</sup> Finally, MRI also has a role in predicting and monitoring treatment response, especially uterine artery embolization.<sup>50-52</sup> Factors reported to predict good response to treatment are a submucosal location, smaller baseline size, and high T2-signal intensity before embolization. On the other hand, the presence of hemorrhagic degeneration before embolization often predicts a poor response. Successful uterine artery embolization results in a reduction in size of both uterus and leiomyomas, and development of hemorrhagic infarction.<sup>50,51,53</sup>

## Imaging Characteristics

On MRI, a simple nondegenerating leiomyoma is seen as a well-circumscribed, round nodule or mass with low signal intensity on both T1- and T2-weighted sequences (see Fig. 33-15).<sup>43</sup> Intramural leiomyomas may demonstrate a high-signal-intensity pseudocapsule on T2-weighted sequences, which is thought to represent edema and vascular congestion of the surrounding myometrium (Fig. 33-17).<sup>54</sup> Calcifications may be seen as signal void areas, but may not be well visualized with MRI. Leiomyomas typically show marked enhancement after gadolinium administration, but the use of contrast material is only necessary to evaluate vascularity when embolization is being considered (see Fig. 33-15).

As mentioned previously, imaging characteristics of degeneration are nonspecific, but some magnetic resonance features may suggest specific types. Leiomyomas with cystic degeneration present with very high signal intensity on T2-weighted sequences (Fig. 33-18).<sup>43</sup> Low T2-signal intensity and a cobblestone appearance in a leiomyoma is usually due to hyaline degeneration.<sup>38,43</sup> Hemorrhagic degeneration of leiomyomata are usually the result of rapid enlargement, as seen during pregnancy or after uterine artery embolization. Hemorrhagic degeneration characteristically has high signal intensity on T1-weighted sequences due to the high





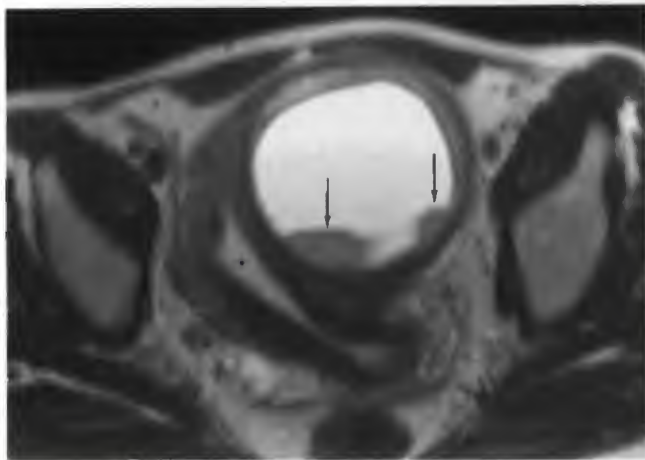


**FIGURE 33-16.** Uterine sarcoma. Axial T2-weighted image. The endometrial cavity (*asterisk*) is displaced by a large cystic mass that contains mural nodules (*arrows*), a pathologically proven uterine sarcoma.



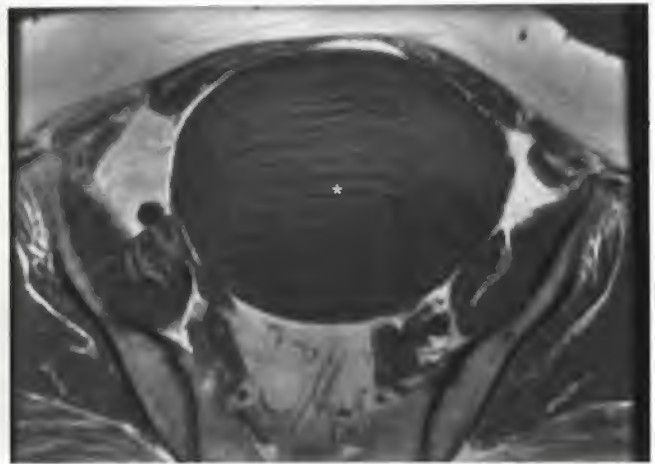
**FIGURE 33-17.** Leiomyomas and adenomyosis. Sagittal T2-weighted image demonstrate a diagnostic pseudocapsule of high signal intensity around a well-delimited leiomyoma (*arrow*). The junctional zone is diffusely thickened and has the characteristic starry sky appearance of adenomyosis (*arrowheads*). *Asterisk*, Nabothian cyst.

proteinaceous content of blood or the presence of methemoglobin (see Fig. 33-15).<sup>38,43</sup> The lesion may exhibit a rim of low signal intensity on T2 and high signal intensity on T1-weighted sequences, which represents obstructed veins around the lesion.<sup>43</sup> Myxoid degeneration is usually characterized by the presence of multiple areas of cystic change and very high T2-signal intensity.<sup>38,43</sup>

## ADENOMYOSIS

### Definition and Epidemiology

Adenomyosis refers to the presence of intramyometrial endometrial mucosa (glands and stroma) surrounded by



A



B

**FIGURE 33-18.** Cystic degeneration of uterine leiomyoma (*asterisks*). Axial T1-weighted (*A*) and sagittal T2-weighted (*B*) images demonstrate a well-circumscribed mass arising from the uterus. The lesion has cystic signal intensity characteristics (low and high T1-weighted and T2-weighted signal intensity, respectively). A few thin septations are seen. This was pathologically proven to be cystic degeneration of a leiomyoma.

hypertrophic myometrium. It is a common disorder; however, its exact prevalence is difficult to determine. The reported prevalence varies in both autopsy (20% to 67%)<sup>55</sup> and clinical studies (10% to 88%)<sup>56-59</sup>; this is likely the reflection of several factors, including inconsistent pathological definition of adenomyosis, different uterine specimen

processing, and varied patient inclusion criteria. Typically, adenomyosis is diagnosed in a multiparous woman in the 4th or 5th decade of life.

## Clinical Aspects

The classic clinical scenario is that of a patient who presents with menorrhagia, dysmenorrhea, and metrorrhagia accompanied by an enlarged, soft uterus that is tender on examination. However, one third of patients with adenomyosis are asymptomatic. It is important to note that the frequency and severity of symptoms appear to correlate with the extent and depth of adenomyosis.<sup>55,60,61</sup>

## Pathophysiology

Adenomyosis causes globular and cystic enlargement of the uterus with some cysts filled with degraded red blood cells. It may be described as focal, diffuse, or both, depending on its distribution in the myometrium. Irrespective of presentation and unlike leiomyomas, the lesions have poorly defined margins.<sup>55</sup>

There are three hypotheses that attempt to explain the development of adenomyosis.<sup>55</sup> Two of the hypotheses suggest a process of invagination of the basalis layer of the endometrial mucosa, either in between muscle fibers or along the intramyometrial lymphatic system. The third theory suggests adenomyosis develops as a result of metaplasia from de novo ectopic intramyometrial endometrial tissue.

In up to 80% of the cases, there is an additional uterine pathology, most commonly leiomyomas, but also endometrial polyps, endometrial hyperplasia, and endometrial adenocarcinoma.<sup>55</sup>

## Diagnosis

Although the typical clinical presentation may strongly suggest adenomyosis, the clinical diagnosis is not accurate and imaging is often used prior to treatment selection.

## Imaging Characteristics

Transvaginal ultrasound is probably the first choice of imaging modality in patients with adenomyosis. It is widely available, and has low cost and good accuracy, similar to that reported to MRI. Its sensitivity ranges from 57% to 89% and the specificity from 65% to 98%.<sup>62-67</sup> However, it is a technique that is operator dependent, and the best results are obtained with experienced examiners. In addition, the accuracy of the method decreases in patients who present with large uteri and associated leiomyomas. The reported sensitivity and specificity of MRI range from 70% to 86% and 86% to 93%, respectively,<sup>62-64</sup> and MRI is generally used if ultrasound results are equivocal or when additional information is needed, especially for treatment planning.

The diagnosis of adenomyosis on MRI is made based on findings identified on T2-weighted sequences. Typical adenomyosis is characterized by the presence of focal or diffuse widening of the junctional zone (inner myometrium), or an ill-defined, hypointense, myometrial mass (see Figs. 33-14 and 33-17). The normal junctional zone in



**FIGURE 33-19.** Focal adenomyosis. Sagittal T2-weighted image demonstrate a region of thickened junctional zone (arrow) with indistinct margins.

premenopausal women appears as a band of low signal intensity between the endometrium and outer myometrium. Based on the study of Reinhold et al,<sup>62</sup> identification of a junctional zone with 12 mm or more is diagnostic of adenomyosis, whereas a width of 8 mm or less reliably excludes the disease. For patients that fall in the indeterminate category (junctional zone measuring between 9 mm and 11 mm), secondary findings may help to establish the diagnosis. Such secondary findings include hyperintense punctate foci on T2-weighted images; hyperintense parallel lines radiating out from the endometrium, also on T2-weighted images; and ill-defined margins (see Fig. 33-14).<sup>49,63,68</sup> The high-signal punctate foci are thought to be dilated endometrial glands, whereas the striations may represent endometrial invasion into the myometrium.<sup>68</sup> One of the greatest challenges for both ultrasound and MRI can be the differentiation between focal adenomyosis and a leiomyoma, the main differential diagnosis on MRI, because both lesions have low signal intensity on T2-weighted sequences and are concomitantly seen in 35% to 55% of the subjects.<sup>55</sup> The distinction is important because leiomyomas are often treated conservatively, whereas adenomyosis may require hysterectomy. Imaging features that suggest the diagnosis of focal adenomyosis are an ovoid rather than round shape; indistinct margins without a pseudocapsule; minimal mass effect; and continuation with the junctional zone (Fig. 33-19).<sup>68,69</sup> Although small hyperintense areas



of hemorrhage are occasionally identified on T1-weighted sequences,<sup>68</sup> the T1-weighted images, with or without contrast enhancement, are not generally helpful in the diagnosis. It should be remembered, however, that focal adenomyosis or adenomyoma may not always be differentiated from a leiomyoma based on imaging findings.<sup>62,64</sup>

## ENDOMETRIOSIS

### Definition and Epidemiology

Endometriosis refers to ectopic functional endometrial tissue, which may proliferate in response to hormonal secretion. White women between 25 and 40 years of age are more commonly affected by this process.<sup>70</sup> Endometriosis is identified in 5% to 15% of all premenopausal women, but in up to 50% of infertile patients.<sup>70–72</sup> The overall incidence of endometriosis is 298/100,000 person-years; however, the incidence is five times greater if there is a history of infertility, especially if due to Müllerian duct anomalies.<sup>70</sup>

### Etiology

The etiology of endometriosis remains unclear; however, proposed theories include peritoneal seeding from retrograde transport of endometrial cells through the fallopian tubes, development from müllerian remnants, and peritoneal epithelium metaplasia. The suggested etiologic mechanisms may be complementary, although at present, the theory of retrograde transport of cells seems favored.<sup>73</sup>

### Clinicopathologic Aspects

Typical symptoms of endometriosis include dysmenorrhea, dyspareunia, chronic pelvic pain, and infertility. Although most frequently identified within the pelvis, endometriosis has been described in multiple locations, including the lungs, abdominal wall, and central nervous system.<sup>74–76</sup> Within the pelvis, the sites of involvement in order of decreasing frequency are the ovaries (endometriomas), uterine ligaments, pouch of Douglas, and pelvic peritoneal surfaces. Ovarian involvement is bilateral in 30% to 50% cases.<sup>77</sup>

Endometriomas are one of the most common blood-containing ovarian lesions and are usually seen in association with more extensive endometriosis. The ovarian tissue may be partially or completely replaced by the ectopic endometrial tissue, with glands and stroma seen lining the wall of the lesion. A thick and dense fibrous capsule is almost always present around the endometrioma. Although the endometrioma usually contains old degraded blood, fresh hemorrhage and clots are also identified. Adhesions to surrounding structures and internal septations are common and may lead to the misdiagnosis of an ovarian malignancy at ultrasound.

### Imaging

MRI is usually reserved for cases in which ultrasound is inconclusive or when there is failure of regression of an ovarian mass seen in the context of endometriosis. Although there are MRI features that suggest the diagnosis of endometrioma, differentiation from a hemorrhagic cyst is

not always possible based on imaging criteria alone however, patients have typically undergone multiple ultrasound examinations before MRI and the persistence of a hemorrhagic adnexal mass favors the diagnosis of endometriosis.<sup>78</sup>

The main advantage MRI has over ultrasound is its ability to confirm the presence of blood within the mass. Blood products demonstrate high signal intensity on T1-weighted images, which is characteristically persists with the application of fat suppression (Fig. 33–20).<sup>79</sup> On T2-weighted sequences, the contents of an endometrioma typically demonstrate low or intermediate signal intensity, depending on the concentration of methemoglobin and other iron products.<sup>80</sup> Layering of these low-signal-intensity blood products within the cyst is a frequently identified sign of endometriomas called T2-shading (Fig. 33–21).<sup>81</sup> A black rim surrounding the lesion is another feature that has been described; however, it is not specific of endometriomas (see Fig. 33–21).<sup>78</sup> This rim is caused by the presence of iron within the mass, secondary to blood degradation. The fibrous wall of endometriomas typically has low signal intensity on both T1- and T2-weighted sequences and may show contrast enhancement.<sup>82</sup> Although uncommon, cancer has been reported in association with endometriosis and should be suspected in the presence of an enhancing solid nodule or mass within the lesion (Fig. 33–22).<sup>83</sup> In a study by Brinton et al,<sup>41</sup> patients with a long-standing history of ovarian endometriosis had increased risk of ovarian cancer (standardized incidence ratio of 4.2, ranging from 2.0 to 7.7).

In some instances, ultrasound may fail to correctly identify an obstructed, blood-filled, and dilated fallopian tube, which often occurs in endometriosis. The diagnostic dilemma may be resolved with MRI, owing to its large field-of-view and multiplanar capabilities. Endometrial implants are usually hyperintense on both T1- and T2-weighted images (Fig. 33–23); however, small endometrial implants ranging from 2 to 3 mm in diameter are often not detected by any imaging modality. MRI does appear to be fairly accurate for the detection of lesions greater than 1 cm in diameter, and the use of fat-suppressed T1 images reportedly increases the detection of smaller implants.<sup>84,85</sup> Stratton et al<sup>86</sup> reported a sensitivity and specificity of 69% and 75%, respectively for MRI detection of endometriosis using laparoscopy as a standard of reference. Another study reported similar results comparing MRI to laparoscopy; MRI had a diagnostic accuracy of approximately 77%. In addition, statistical analysis demonstrated excellent agreement between disease stages attributed by the two methods ( $\kappa = 0.916$ ,  $p < 0.001$ ).<sup>86</sup> MRI appears to be especially useful for the evaluation of deep pelvic endometriosis and cul-de-sac obliteration with sensitivities and specificities ranging from 68% to 94% and 76% to 100%, respectively.<sup>87–89</sup>

## CERVICAL CANCER

### Epidemiology and Clinical Presentation

Cervical carcinoma represents the third most common gynecologic malignancy in the United States. It is diagnosed in one in every 135 American women over their lifetime, with approximately 9710 new cases and 3700 deaths estimated to occur in 2006.<sup>90</sup> Patients typically present

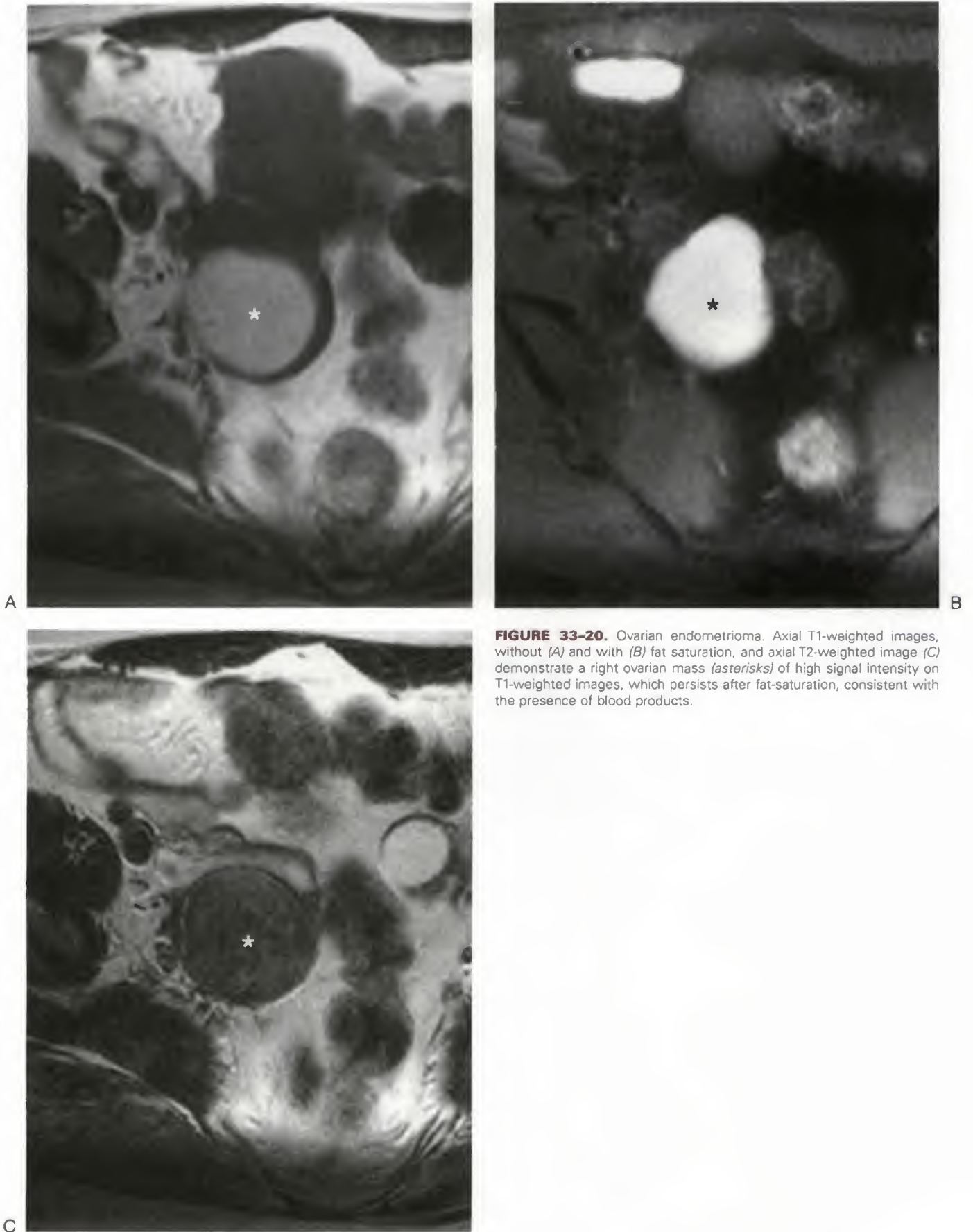


**FIGURE 33-20.** Ovarian endometrioma. Axial T1-weighted images, without (A) and with (B) fat saturation, and axial T2-weighted image (C) demonstrate a right ovarian mass (asterisks) of high signal intensity on T1-weighted images, which persists after fat-saturation, consistent with the presence of blood products.



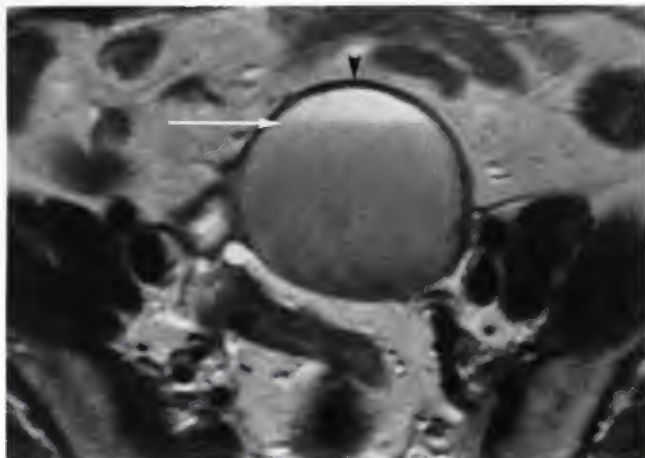


**FIGURE 33-21.** Ovarian endometrioma. Axial T2-weighted image demonstrating layering of low-signal-intensity blood products within the endometrioma, also known as T2-shading sign (*arrow*). Another common finding is a very dark peripheral rim (*arrowhead*), due to hemosiderin deposition, which is also the result of blood degradation.

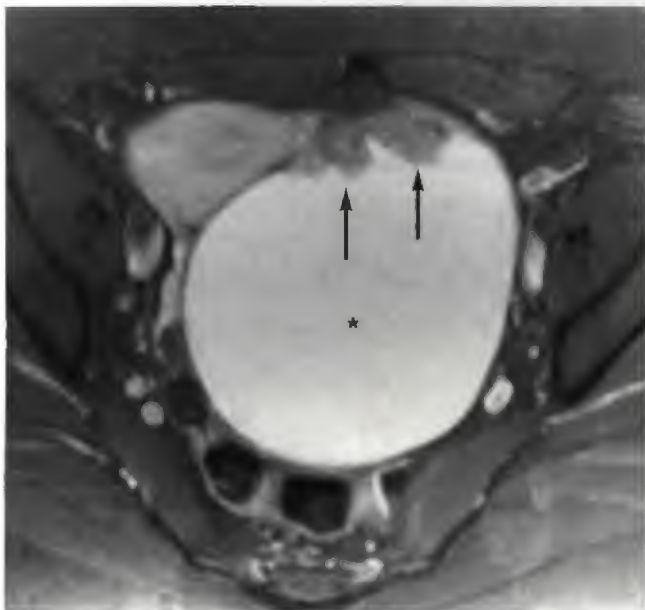


**FIGURE 33-22.** Clear cell carcinoma. Gadolinium-enhanced T1-weighted image with fat-saturation. A large cystic mass that contains fluid with high signal intensity after fat-saturation (*asterisk*), consistent with blood, is seen within the pelvis. Mural nodules (*arrows*) are suggestive of malignancy and the lesion was pathologically proven to be a clear cell carcinoma within an endometrioma.

between the third and fourth decades. Most noninvasive cervical cancers are asymptomatic and detected only by the Papanicolaou's (Pap) smear. Patients with invasive cancer in general have a history of intermenstrual or postcoital bleeding but may also be asymptomatic.

The most significant risk factor for development of cervical cancer is infection by human papilloma virus (HPV),

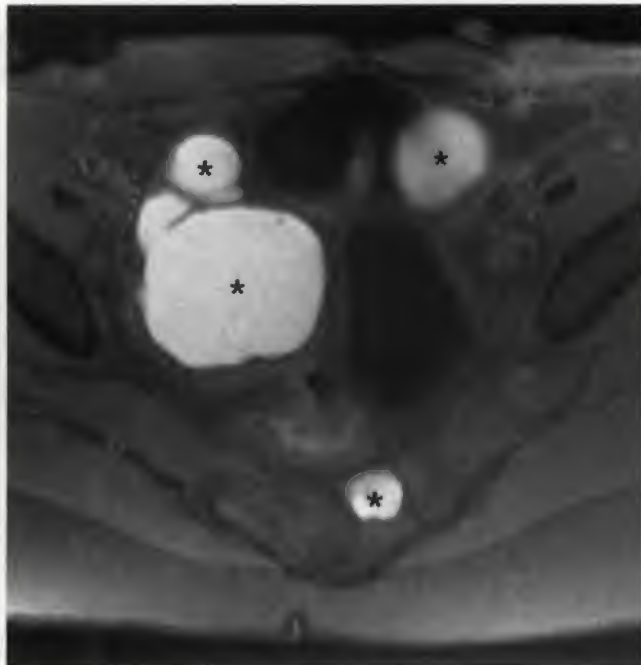


**FIGURE 33-23.** Endometriosis. Axial fat-saturated T1-weighted image demonstrates multiple masses of high signal intensity (*asterisks*), consistent with endometriosis.

especially types 16 and 18, among another 13 types also classified as high-risk viruses. More than a risk factor, it is likely that infection by HPV has causal effect. Several other risk factors have been reported, including an early sexual life, multiplicity of sexual partners, low socioeconomic status, smoking, and use of oral contraceptives; however, it is unclear if they represent independent factors or are directly or indirectly related to HPV infection.<sup>91</sup>

## Histopathology

The vast majority are squamous cell carcinomas arising from foci of dysplasia and atypia at the squamocolumnar junction. The remaining 10% to 15% are adenocarcinomas that originate in the endocervical glands.<sup>92,93</sup> Adenoma malignum is a very rare subtype of cervical adenocarcinoma (3%). It is a multicystic lesion associated with copious watery vaginal discharge and is diagnosed only with deep biopsies of the cervix. Although histologically, it is a well-differentiated lesion, in reality, it has very poor prognosis and response to therapy. The MRI appearance of adenoma malignum may be indistinguishable from a nabothian cyst. It is important to remember that this cancer is exceedingly uncommon and should not be diagnosed based on imaging findings alone.<sup>94</sup> A few other rare tumors, such as villoglandular tumors, may be seen in the uterine cervix.<sup>95</sup>

There are three patterns of spread of squamous cell carcinoma of the cervix: direct invasion of adjacent organs, the most common; lymphatic dissemination to pelvic and para-aortic lymphnodes; and rarely, hematogenous spread to the lungs and bones.<sup>96</sup>

**Table 33-1****Carcinoma of the Uterine Cervix—Federation of Gynecology and Obstetrics Staging**

Stage	Description	5-year Survival
0	Carcinoma in situ	
I	Confined to the uterus	
IA	Microscopically invasive	> 93%
IB1	Clinically visible < 4 cm	90%
IB2	Clinically visible > 4 cm	80%–95%
II A/B	Beyond the uterus, to the upper vagina (A) or parametrial invasion (B)	75%–78%
III A/B	Extension to lower vagina (A) or to pelvic sidewall and/or hydronephrosis (B)	47%–50%
IV A/B	Bladder/rectum invasion (A) or distant metastasis (B)	20%–30%

Data from Ueda M, Ueki M: Ovarian tumors associated with pregnancy. *Int J Gynaecol Obstet* 55:59, 1996; and Leiserowitz GS, Xing C, Cress R, et al: Adnexal masses in pregnancy: how often are they malignant? *Gynecol Oncol* 101:315, 2005.

References: (101, 102)

## Diagnosis

Imaging has no role in the diagnosis of cervical cancer. In the majority of cases, the cancer is detected through Pap smear, or exfoliative cytology. The effective use of screening has caused a decline in incidence and mortality from invasive squamous cell carcinomas but a relative increase in incidence of adenocarcinomas.<sup>97–99</sup>

## Treatment

Treatment of cervical cancer largely depends on the stage of disease.<sup>92,100</sup> Patients with microinvasive (stage IA) and early macroinvasive disease (stage IB1, IIA < 4 cm) are usually offered curative surgery—total hysterectomy, with or without lymphadenectomy. If fertility is desired, patients with microinvasive cervical cancer can be treated with cone biopsy. Primary radiotherapy is another alternative for early macroinvasive disease. For more advanced cases, treatment is usually a combination of surgery, radiotherapy, and chemotherapy.

## Clinical Staging

Staging of cervical cancer aims at assessing tumor resectability and is currently based on the International Federation of Gynecology and Obstetrics (FIGO) classification system (Table 33-1). The FIGO classification is a clinical approach based on findings from physical examination, which may be performed under anesthesia. Nonetheless, staging is usually complemented by a combination of colposcopy, biopsy, chest radiography, intravenous excretory urography, barium enema, cystoscopy, or proctosigmoidoscopy. Although some studies have already shown the value of cross-sectional imaging,<sup>103–107</sup> it has not yet been included in the FIGO staging system.<sup>101,102</sup>

The FIGO staging system is used as a predictor of patient survival<sup>101,102</sup> but has limitations. Studies have shown a

poor correlation between the clinical stage and surgical-pathologic findings. Errors in staging have been reported to reach 30% for stage I tumors, 50% for stage II, and 75% for stage III.<sup>93,108,109</sup> These limitations relate particularly to a failure in the accurate estimation of tumor size, and the detection of parametrial, pelvic sidewall, bladder and rectal wall invasion, as well as metastases to distant organs.<sup>93</sup> In addition, nodal status, known to be one of the most important prognostic factors, is not included in the staging system.<sup>93,96,108,110</sup>

Accurate staging influences clinical management. Current FIGO and International Gynecologic Cancer Society<sup>96</sup> guidelines suggest surgical treatment or radiotherapy alone for patients with early disease, stages IA, IB1, and IIA with tumor size less than or equal to 4 cm. Patients who have more extensive early disease, stages IB2 and IIA with tumor size greater than 4 cm, may require radiation and/or chemotherapy. Furthermore, stage IIB (limited extrauterine extension to the parametrium) disease or greater precludes curative surgical treatment.

## Imaging

MRI is highly accurate for staging cervical cancer, surpassing clinical staging when only stage IIA or greater are considered (53% versus 73%–81%). The T2-weighted sequences are most valuable in the evaluation of cervical cancer. It is identified as a mass of intermediate signal intensity disrupting the normally low-signal-intensity cervical stroma.<sup>42,93</sup> Dynamic gadolinium-enhanced T1-weighted imaging has been shown to improve detection of cervical cancer and may be especially useful for the evaluation of depth of stromal invasion, parametrial involvement, and bladder wall invasion.<sup>93,107,111</sup> However, the use of single-phase contrast enhanced T1-weighted images may result in overestimation of disease.<sup>93,106</sup>

## Early Stage Disease

Microinvasive carcinoma (stage IA) cannot be detected by MRI; however, macroinvasive disease (stage IB) can be detected, with an accuracy of 91%.<sup>42,93</sup> In addition, MRI may be used to determine the depth of stromal invasion.<sup>107</sup> In stage IB disease the cervical stromal ring completely surrounds the tumor (Fig. 33-24).<sup>42,93</sup> Stage II disease is characterized by local extension of tumor beyond the uterus. Stage IIA indicates invasion of the upper two-thirds of the vagina and stage IIB indicates parametrial extension. Vaginal wall extension is best evaluated in the sagittal plane on MRI. Invasion of the vagina should only be diagnosed in the presence of vaginal wall thickening and an increase in the signal intensity of the normally low-signal-intensity vaginal wall on T2-weighted sequences.<sup>42,93</sup>

## Parametrial Extension

Axial T2-weighted images are used to determine parametrial invasion. Parametrial extension (stage IIB disease) is diagnosed in the presence of partial or complete disruption of the dark ring of cervical stroma, associated with an irregular interface between the cervix and adjacent fat (Fig. 33-25). The presence of a definite bulge of asymmetric





**FIGURE 33-24.** Stage IB cervical cancer. Axial T2-weighted image. A large hyperintense cervical cancer (asterisk) expands the cervix but does not extend beyond the low signal intensity ring of cervical stroma (arrows).

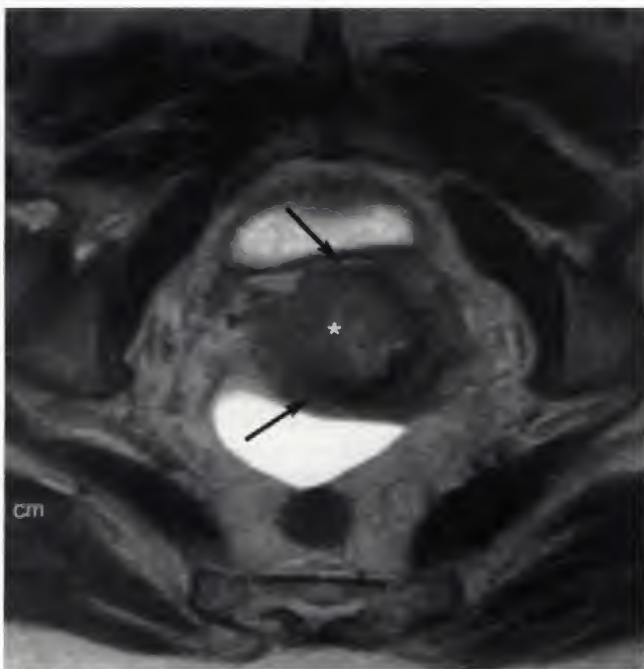


**FIGURE 33-25.** Stage IIB cervical cancer. Axial T2-weighted image. There is interruption (arrows) of the hypointense ring of cervical stroma by a large hyperintense cervical mass (asterisk) that bulges into the adjacent fat.

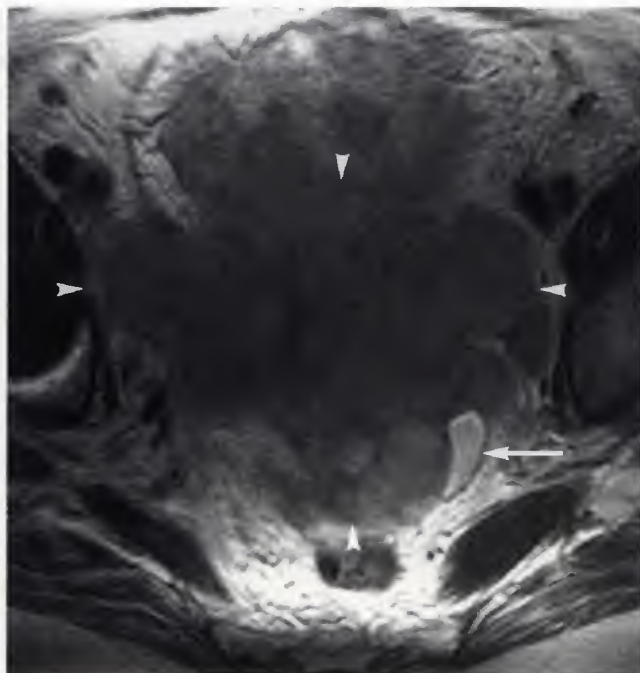


**FIGURE 33-26.** Stage IIIB cervical cancer. Axial T2-weighted image demonstrates a large cervical cancer extending to the pelvic sidewalls (arrowheads). A dilated left ureter (arrow) is present.

high signal tissue is a more specific finding of parametrial invasion. Occasionally, encasement of parametrial vessels may also be seen. Parametrial invasion is demonstrated with an accuracy of 68% to 96% on MRI.<sup>93,105,109</sup> More important, MRI has a high negative predictive value for parametrial invasion—ranging from 79% to 100%.<sup>93,109,110,112</sup> The positive predictive value of MRI for parametrial invasion is low, because MRI cannot accurately differentiate benign reactive changes seen adjacent to the cervix from actual tumor invasion.

### Stage III Disease

Invasion of the lower third of the vagina (IIIA) and pelvic sidewall invasion (IIIB) characterizes stage III disease. Pelvic sidewall invasion (stage IIIB) is demonstrated by the loss of fat planes between the tumor and iliac blood vessels and muscles of the pelvic sidewall.<sup>93</sup> The increased signal intensity of these muscles may also be observed on T2-weighted sequences.<sup>93</sup> An important indicator of pelvic sidewall invasion is the presence of hydronephrosis; therefore, MRI evaluation must include imaging of the upper abdomen, more specifically the kidneys, for assessment of hydronephrosis.<sup>42,93</sup> MRI has an accuracy of approximately 95% to characterize stage III disease (Fig. 33-26).<sup>112</sup>

### Stage IV Disease

Bladder and rectal invasion are also characterized by loss of fat planes between the organs and the tumor, as well as by increased T2 signal intensity, enhancement, thickening and

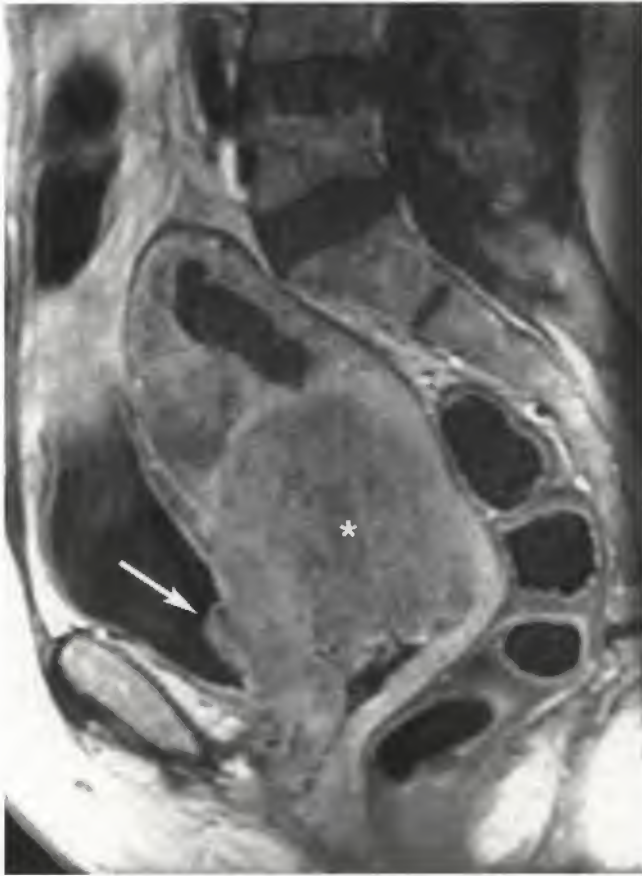


**FIGURE 33-27.** Stage IVA cervical cancer. Gadolinium-enhanced sagittal T1-weighted image. An enhancing mass (arrow) is seen in the posterior bladder wall representing bladder invasion by the large cervical cancer (asterisk).

irregularity of the bladder and rectum walls (Fig. 33-27).<sup>42,93</sup> MRI is 96% accurate in making the diagnosis of bladder and rectal invasion, respectively.<sup>112</sup>

### Tumor Size Assessment

Tumor size has been shown to be a significant prognostic factor and several studies have demonstrated that MRI is an accurate technique for assessing tumor size.<sup>93,103,108,110,112</sup> MRI measurements are within 0.5 cm of the surgical in 70% to 90% of the cases.<sup>93</sup>

### Lymph Node Assessment

The FIGO staging of cervical cancer does not include the evaluation of lymph nodes, although it has been shown that lymph node metastases carry significant prognostic information. For instance, in patients undergoing surgery for stage IB and IIA disease, survival decreases from 85% to 90% and to 50% to 55% if lymph nodes are positive. MRI determination of lymph node involvement is largely dependent on size criteria in current practice. A threshold of 1 cm diameter in the short-axis is generally accepted as indicative of metastatic involvement.<sup>113-115</sup> However, enlarged lymph nodes may represent reactive, hyperplastic change in patients with malignancy, and small nodes may

contain microscopic foci of metastatic disease. An exciting new development in the detection of metastatic lymph node disease is the use of ultra-small superparamagnetic iron oxide-enhanced MRI. Initial studies have consistently reported excellent results for detection of pelvic lymph nodes in a variety of cancers.<sup>113-115</sup> The reported specificities and negative predictive values range from 80% to 99% and 98% to 100%, respectively. The sensitivity of the method was shown to range widely, from 25% to 100%.

## ENDOMETRIAL CANCER

### Epidemiology and Clinical Presentation

Endometrial carcinoma is the fourth most common cancer in women, and the most common of the gynecologic malignancies. In 2006, 41,200 new cases and 7350 deaths are expected to occur.<sup>90</sup> Despite the high incidence of cases as compared with other gynecologic malignancies, endometrial cancer is associated with the best prognosis, and most patients with newly diagnosed disease are cured by surgery alone or in combination with adjuvant radiation therapy.<sup>116</sup> Endometrial cancer occurs more frequently in whites and typically presents during the 6th and 7th decades with painless postmenopausal bleeding.<sup>117,118</sup> Many risk factors have been described, most directly or indirectly related to estrogen exposure, including early menarche, late menopause, nulliparity, Stein-Leventhal syndrome (polycystic ovary syndrome), diabetes, and obesity. In addition, a higher incidence of endometrial cancer is associated with adenomatous polyps, breast cancer and the use of unopposed estrogen therapy.<sup>117-120</sup>

### Histopathology

More than 80% of endometrial cancers are of the endometrioid type, which refers to the presence of endometrial type glands of varying differentiation. These are subdivided into two groups, type 1 (low grade) and type 2 (high grade). Type 1 endometrial cancers are related to long-term unopposed estrogen therapy; they originate from endometrial hyperplasia and have a more favorable prognosis. Type 2 cancers represent 10% of endometrial cancers; they are most often seen in association with atrophic endometrium, and have a poorer prognosis. Other histologic types include serous and clear cell carcinomas. Approximately 8% of patients with endometrial cancer present with a synchronous ovarian carcinoma of the same histology.<sup>117</sup>

Endometrial carcinoma may present as a localized endometrial lesion, mimicking a polyp, or as diffuse thickening of the endometrium. Tumor spread initially occurs by direct myometrial or cervical extension. Lymphatic invasion is usually limited to the pelvis but may extend to periaortic and aortocaval nodes.<sup>117</sup> Transtubal peritoneal seeding and hematogenous dissemination to the lungs or other sites may occur.<sup>121,122</sup>

### Diagnosis

The diagnosis of endometrial cancer is based on histologic evaluation of endometrial biopsy specimens, which is highly



accurate, especially in symptomatic postmenopausal women. The two most common diagnostic pathways are biopsy or transvaginal ultrasound, followed by biopsy.<sup>117</sup> An estimation of the risk of cancer following ultrasound in a postmenopausal woman depends on the presence or absence of vaginal bleeding and on the thickness of the endometrial stripe. In patients with vaginal bleeding, an endometrium measuring more than 4 to 5 mm translates to a risk of approximately 7.3%, whereas in the absence of bleeding, a similar risk (6.7%) is seen if the endometrium measures 11 mm or more in thickness.<sup>8</sup> In these two situations, biopsy is warranted. MRI has no role in diagnosing the disease and is usually reserved as an aid for pretreatment planning.

## Treatment

The primary treatment modality of endometrial cancer is total hysterectomy with bilateral salpingo-oophorectomy, and peritoneal fluid aspiration and washings. In selected cases, omentectomy and retroperitoneal lymph node dissection are performed.<sup>117</sup> Radiation therapy is generally prescribed as an adjuvant treatment, targeting microscopic lymphadenopathy. In patients who are medically inoperable, it may be used with curative purposes. Systemic adjuvant chemotherapy seems to have results similar to those obtained with radiation therapy but with greater toxicity. In patients with more advanced disease, its use is palliative.<sup>117</sup>

## Staging

Patients with endometrial cancer are staged surgically, usually using the system proposed by FIGO (Table 33-2)<sup>123</sup> or the American Joint Committee on Cancer.<sup>124</sup> Staging provides prognostic information, but it is also important for making treatment selection.

A poorer prognosis is expected in patients who present with deep myometrial invasion (> 50%, stage IC), cervical extension (stage II), and nodal involvement (stage IIIC). Other important prognostic factors are positive peritoneal

cytology, poorly differentiated cancer, serous papillary tumor, and clear cell tumors.

Depth of myometrial invasion was found to be the single most important predictor of survival at 5 and 10 years, in a series of 1566 women with endometrial carcinoma.<sup>126</sup> Women with superficial myometrial invasion (less than 50% of myometrial wall thickness) have a 3% to 9% incidence of lymph node metastases and a survival rate of 85% at 5 years. Deep myometrial invasion (> 50% of myometrial wall thickness) is associated with a 20% to 40% risk of nodal disease and a survival rate of 63% at 5 years.<sup>126</sup> Besides providing prognostic information, staging is also important for treatment selection. For instance, there is evidence that radiation therapy is not indicated in low or intermediate risk stage I disease (stage IA and IB), but may be beneficial for patients with more advanced disease and higher risk.<sup>123</sup> Similarly, surgical treatment is dictated by staging, and patients with stage IA or IB disease do not require radical lymphadenectomy.<sup>123</sup>

MRI is an accurate tool for endometrial cancer staging, with an overall staging accuracy of approximately 85%.<sup>106,127</sup> The use of gadolinium is an important part of the study. It has been shown to increase the accuracy of the method.<sup>106,128-130</sup> Many studies have demonstrated that MRI is particularly accurate for assessment of myometrial invasion. Reported accuracy for the identification of deep myometrial invasion varies from 74% to 95%,<sup>127, 137</sup> compared with 68% to 73% for transvaginal ultrasonography.<sup>128,138</sup> However, MRI can overestimate myometrial invasion, especially when bulky disease stretches and thins the myometrium.<sup>134,135</sup> Finally, MRI can also assess cervical extension of tumor (stage II) and extrauterine disease (stages III and IV).

Although the evaluation of nodal metastasis with imaging modalities typically has not been as good as the surgical approach due to the limited accuracy of the size criteria used, results of studies applying ultra-small particles of iron oxide or ultra-small superparamagnetic iron oxide (unavailable in the United States, as its use is not yet approved by the Food and Drug Administration) have been promising. Rockall<sup>114</sup> reported excellent sensitivity and specificity for the detection of nodal metastasis on analysis performed per node and per patient, ranging from 82% to 100% and 87% to 97%. The negative predictive value varied between 96% and 100%.

## Imaging

As mentioned previously, MRI is not used for the diagnosis of endometrial carcinoma, but it is an established part of patient evaluation when locally extensive disease is suspected or when physical examination is limited.

Endometrial carcinoma is usually seen as an endometrial mass, which is iso- or hypointense to normal endometrium on T1-weighted sequences, and slightly hyperintense or heterogeneous on T2-weighted sequences. After contrast administration, tumor enhancement is variable, depending on histologic type and temporal resolution. Endometrial carcinoma is usually hypointense to the myometrium on early phase images. The administration of gadolinium allows tumors to be distinguished from debris or fluid in the endometrial and endocervical cavities. In addition, as the

**Table 33-2** Carcinoma of the Endometrium—Federation of Gynecology and Obstetrics Staging

Stage	Description	5-year Survival
0	Carcinoma in situ	
I	Confined to the uterine body	85%
IA	Endometrium only	
IB	Myometrial invasion < 50%	
IC	Myometrial invasion > 50%*	
II A/B	Extends to the cervix, without (A) or with (B) invasion of the cervical stroma	75%
III	Local and/or regional spread to serosa and/or adnexa (A), vagina (B), pelvic and/or para-aortic lymph nodes (C)	45%
A/B/C		
IV A/B	Bladder/rectum invasion (A) or distant metastasis (B)	25%

\*20%-40% incidence of lymph node metastases

References: (117, 125)





**FIGURE 33-28.** Stage IB endometrial cancer. Gadolinium-enhanced sagittal T1-weighted image demonstrating expansion of the endometrial cavity by an enhancing mass (asterisk) and associated focal superficial invasion of the myometrium anteriorly (arrow).

zonal anatomy may not be clearly defined in postmenopausal women, dynamic gadolinium enhancement facilitates the visualization of the junctional zone and the tumor-myometrium interface.

Superficial myometrial invasion (stage IB) is suspected in the presence of interruption of the dark junctional zone on T2-weighted sequences or subendometrial band of enhancement after contrast administration (Fig. 33-28).<sup>127,128,137</sup> Deep myometrial invasion (stage IC) is characterized if tumor is seen extending into more than 50% of the myometrial thickness, with an intact outer rim (Fig. 33-29).

Cervical extension of tumor (stage II) is best evaluated using sagittal T2-weighted or contrast-enhanced images and may appear as a mass expanding the cervical canal. Stage III disease is characterized by extension of tumor beyond the serosa, to the adnexa and parametrium, positive peritoneal cytology, invasion of the vagina, and metastatic pelvic and para-aortic lymph nodes (Fig. 33-30). Stage IV is defined as bladder or rectal invasion and distant metastases. Invasion of the bladder and rectum is suggested by the loss of normal tissue planes, especially fat planes, associated with an increase in signal intensity and thickness of bladder or rectal walls on T2-weighted images. Contrast administration is also useful to make this diagnosis.

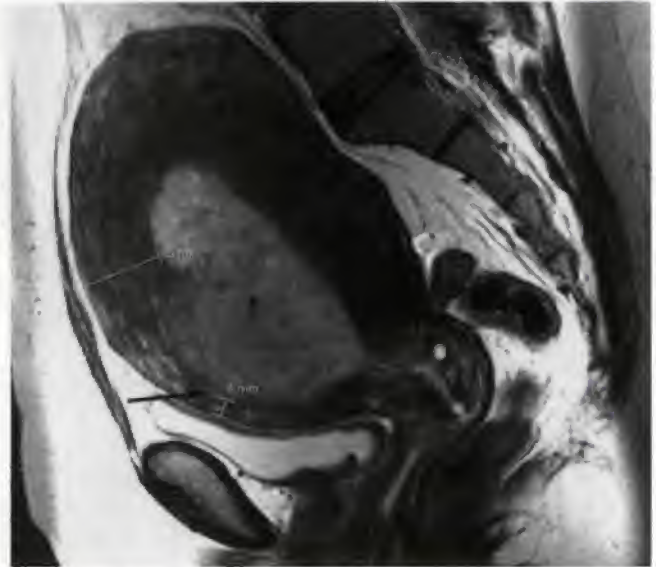


**FIGURE 33-29.** Stage IC endometrial cancer. Sagittal T2-weighted image demonstrating a large hyperintense mass (asterisk) invading more than 50% of the myometrium in the anterior uterine wall (arrow).

## ADNEXAL MASSES

### Epidemiology and Clinical Significance

Every woman, pre- and post-menopausal, develops an adnexal mass in her lifetime. In the vast majority of cases these are functional cysts that are involute and remain undiagnosed; however, about 1.5% of women develop a malignant ovarian tumor.<sup>1</sup> For the year 2006, 20,180 new cases of ovarian cancer and 15,310 deaths are expected to occur.<sup>90</sup> Adnexal masses, irrespective of the diagnosis and aggressiveness status, represent a major indication for gynecologic surgery. Approximately 5% to 10% of women in the United States undergo surgery because of a suspected ovarian mass. Imaging plays an important role in staging patients and planning treatment.<sup>139</sup>

Many factors must be taken into account when imaging work-up is being considered. These include the patient's age and menopausal status, cancer antigen 125 levels, and clinical history. A precise diagnosis of a benign lesion is crucial, as further unnecessary work-up is then avoided, resulting in reduction of overall costs, morbidity, and patient's anxiety. Conversely, if resection of a benign lesion is warranted, less invasive approaches, such as laparoscopic surgery, may be used. Furthermore, patients who have malignant lesions should be referred to a gynecologic oncologist, as specialized management has been shown to result in improved survival.<sup>140</sup>

### Imaging Diagnosis and the Role of Magnetic Resonance Imaging

The primary imaging modality for the evaluation of an adnexal mass is ultrasound. It has a sensitivity and specificity for differentiating benign from malignant adnexal masses



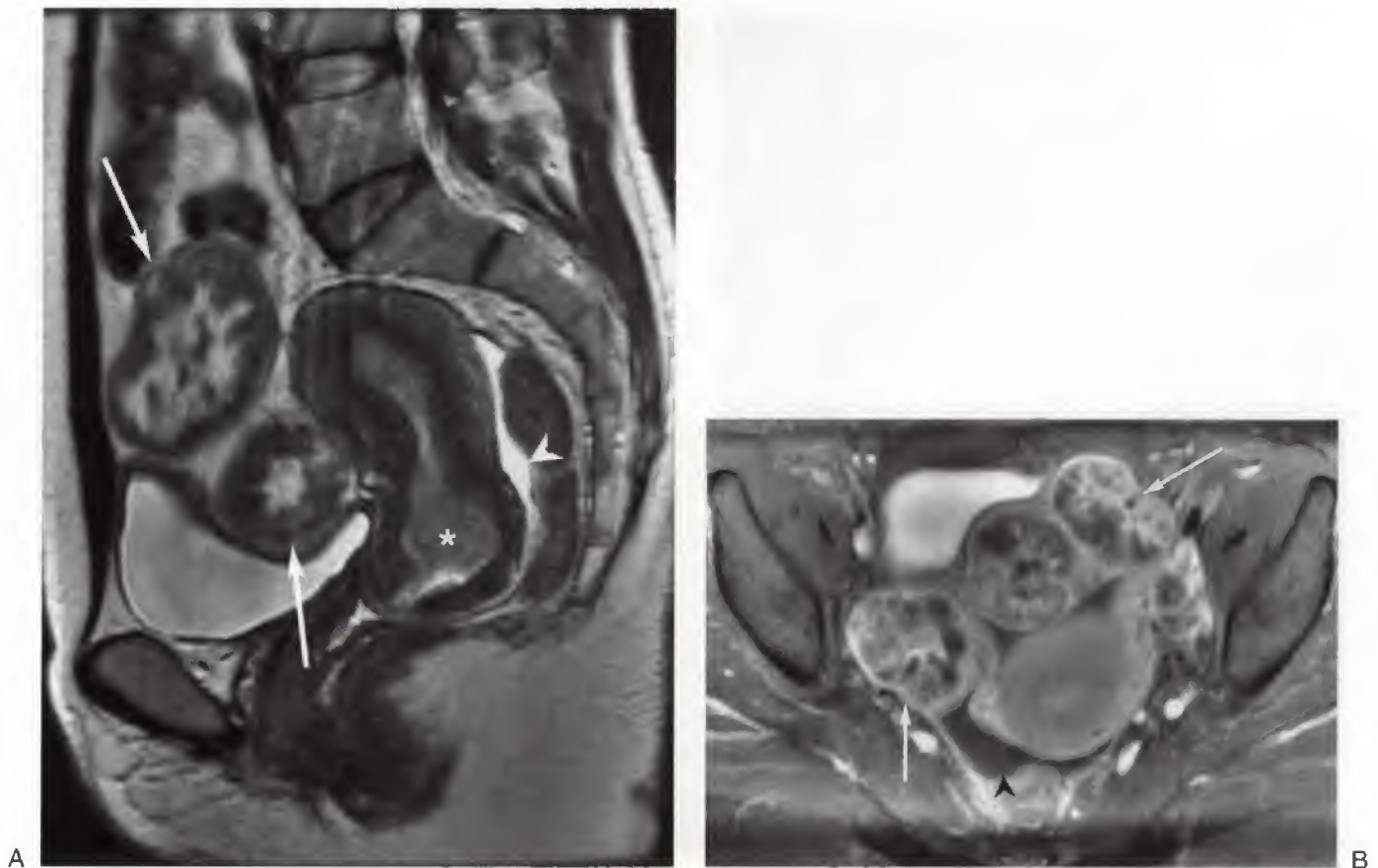


**FIGURE 33-30.** Stage IIIA endometrial cancer. Sagittal T2-weighted (A) and gadolinium-enhanced axial T1-weighted (B) images. The sagittal image demonstrates extension of the endometrial tumor to the cervix (asterisk) and bilateral solid and cystic ovarian masses that represent metastases (arrows). The axial T1-weighted gadolinium-enhanced image shows enhancement of the tumor invading the ovaries and bilateral enhancing solid and cystic ovarian masses that represent metastases (arrows). A small amount of free fluid is seen in the cul-de-sac (arrowheads).

that range from 50% to 100% and 46% to 100%, and is particularly useful in distinguishing simple cysts from complex cystic or solid lesions. MRI is sometimes an option, especially for women who have sonographically indeterminate lesions and a low risk for malignancy. Advantages of MRI over ultrasound relate to its ability to better depict information on the composition of soft tissue masses, using differences in tissue relaxation times. MRI typically is not a first-line modality because it is expensive and ultrasound more often than not provides all additional information necessary to guide management. However, it is a good tool to differentiate a benign from a malignant lesion, with an accuracy of 88% to 93%.<sup>141-144</sup> The Radiology Diagnostic Oncology Group study showed that MRI was the most accurate technique in the preoperative assessment of adnexal masses for possible ovarian malignancy, whereas there was no significant difference between ultrasound and computed tomography.<sup>144</sup> The authors also noted that malignancies were seldom subtle and peritoneal spread was often present at the time of imaging.

### Differentiation of Benign and Malignant Lesions

As a general rule, benign masses are cystic and have thin walls and septa (less than 3 mm); however, there are exceptions to this rule, as shown subsequently.

Malignant adnexal masses are classically said to have internal complexity, a somewhat indeterminate term to describe the presence of mural nodules, thick septa, solid components, and necrosis. Another feature that also favors malignancy is bilateralism.<sup>82</sup> Malignant tumors are rarely subtle lesions, and frequently, peritoneal spread is identified at the time of imaging.<sup>144</sup> Although lesion size has been reported to be a useful attribute to differentiate a benign from a malignant lesion,<sup>145,146</sup> it is important to remember that even very large tumors are more often benign.

Although a solid adnexal mass is suggestive of malignancy, especially metastasis, not all solid tumors are malignant,<sup>147</sup> and MRI can diagnose some benign entities with enough accuracy to avoid further work-up.

A good diagnostic approach is to categorize the adnexal masses into one of the following groups: lesions with distinctive features (fat, blood, and fibrous tissue) and a specific diagnosis; cystic, benign-appearing lesions; cystic, malignant appearing lesions; and predominantly solid lesions.

## Specific Diagnosis Based on Magnetic Resonance Imaging Findings

### *Adnexal Masses With Distinctive Imaging Features (Fat, Blood, and Fibrous Tissue)*

Dermoid cysts, also known as benign mature teratoma, are hamartomas composed of hair, teeth, fat, and mural nodules.<sup>82,142,148,149</sup> Usually identified during the first three decades of life, these lesions are not uncommon but may be missed in up to 27% of cases on ultrasound examination.<sup>148</sup> A possible explanation for this is that the echogenicity of fat in the dermoid cyst on ultrasound may simulate surrounding normal structures. In contrast, because of fat, these tumors are identified on MRI without difficulty, because the high signal intensity of fat on T1-weighted images is lost after fat suppression techniques are applied (Fig. 33–31).<sup>82,142</sup>

The two most common adnexal lesions that contain blood are hemorrhagic cysts and endometriomas. Endometriomas have been extensively discussed earlier in this chapter. Imaging of hemorrhagic cyst with MRI is not as common, as these usually resolve after one or two menstrual cycles and follow-up is completed with ultrasound only. Herein, it suffices to say that if MRI confirms blood within an endometrial cyst, no further diagnostic tests are unnecessary.

Fibromas are the most common sex cord tumors and represent 4% of all ovarian neoplasms. Because of their solid appearance, they can be misdiagnosed as a malignant lesion at ultrasound; however, on MRI fibromas have a very characteristic appearance. Fibromas are composed of bundles of spindle cells resembling fibroblasts, collagen, and hyalinized fibrous tissue and demonstrate low signal intensity on both T2- and T1-weighted sequences and only slight enhancement after gadolinium administration (Fig. 33–32). Ascites may be present in up to 40% of cases, more often when the lesion is large. Meig syndrome refers to its association with pleural effusions.<sup>82,142,150,151</sup> Its malignant potential is reported to be less than one percent. Two other lesions that characteristically present with foci of low signal intensity on both T2- and T1-weighted sequences are the fibrothecoma and the cystadenofibroma. The fibrothecoma is a variant of the fibroma that has a small population of thecal cells containing intracellular lipid. It is similar in appearance on MRI but may be hormonally active or be associated with endometrial polyps and hyperplasia.<sup>82,142,150,151</sup> The cystadenofibroma is a variant of a serous cystadenoma with very low malignant potential. In most cases it presents as a multiseptated mass.<sup>82,142</sup>

### *Cystic, Benign-Appearing Lesions*

This group is composed of various entities, the most frequently identified ones being physiologic cysts, including follicular and corpus luteum cysts; theca-lutein cysts;

paraovarian cysts; hydrosalpinx; peritoneal inclusion cysts; and cystadenomas. In the vast majority of patients, ultrasound correctly diagnoses and classifies the cysts as benign. However, MRI may provide additional diagnostic information in an occasional case complicated by infection or hemorrhage.

### *Cystic, Malignant-Appearing Lesions*

Epithelial tumors represent the most common primary ovarian cancers<sup>82,152</sup>; therefore, they are the most common malignant appearing cystic adnexal masses. Histologically, these tumors are classified as serous, mucinous, endometrioid, and mesonephroid (clear cell). Typically they are cystadenocarcinomas or borderline tumors. Distinguishing these two entities can be difficult, because both present with similar imaging features, namely, thick walls or septations and some solid component (Figs. 33–33 and 33–34).<sup>82</sup> The absence of invasion or metastatic disease favors the diagnosis of a borderline tumor. Ascites is frequently considered a sign of more aggressive disease. In addition, extensive calcifications usually indicate malignancy, especially in the case of serous tumors. The T1 and T2 signal intensity of the cystic areas of a mucinous tumor is variable, owing to different amounts of mucin within locules.<sup>82</sup>

### *Predominantly Solid Lesions*

Predominantly solid lesions of the adnexa may represent primary ovarian lesions, leiomyomas, and nonovarian tumors, such as metastases and lymphoma.

The ovaries are the most common sites of metastasis to the female genital tract. Primary tumors commonly spreading to the ovaries are the endometrial, cervical, gastric, colorectal, and breast cancers.<sup>153</sup> Ovarian metastases have no specific appearance, but are commonly bilateral and strongly enhancing masses. They can be predominantly cystic and with necrotic areas (see Fig. 32–30). The primary tumor is usually clinically overt.<sup>153–156</sup> Although exceptionally rare, ovarian lymphoma may be suspected in the presence of extensive lymphadenopathy associated with nonobstructive vessel encasement.<sup>157</sup>

Primary ovarian tumors can also present as predominantly solid masses; examples are the dysgerminomas, granulosa cell tumors, and Sertoli-Leydig tumors, also known as androblastomas and arrhenoblastomas. All three types are uncommon tumors without specific imaging features and all may present with associated cystic areas (Fig. 33–35). They are most frequently diagnosed in patients younger than 30 years of age, although granulosa cell tumors also have a peak incidence in postmenopausal women. Dysgerminomas are responsible for one third of all ovarian tumors during pregnancy and disproportionate amount of adenopathy, relative to the size and appearance of the ovarian lesion, is sometimes noted.<sup>96</sup> Granulosa cell tumors and Sertoli-Leydig cell tumors are hormonally active, the former producing estrogen and the latter androgen.<sup>150,158,159</sup> Hormonal secretion helps building up a clinical differential diagnosis.

A pedunculated leiomyoma, or a leiomyoma of the broad ligament and adnexa may be misdiagnosed as solid ovarian lesion at ultrasound, especially because the origin of the lesion is hard to determine. In this situation, MRI may



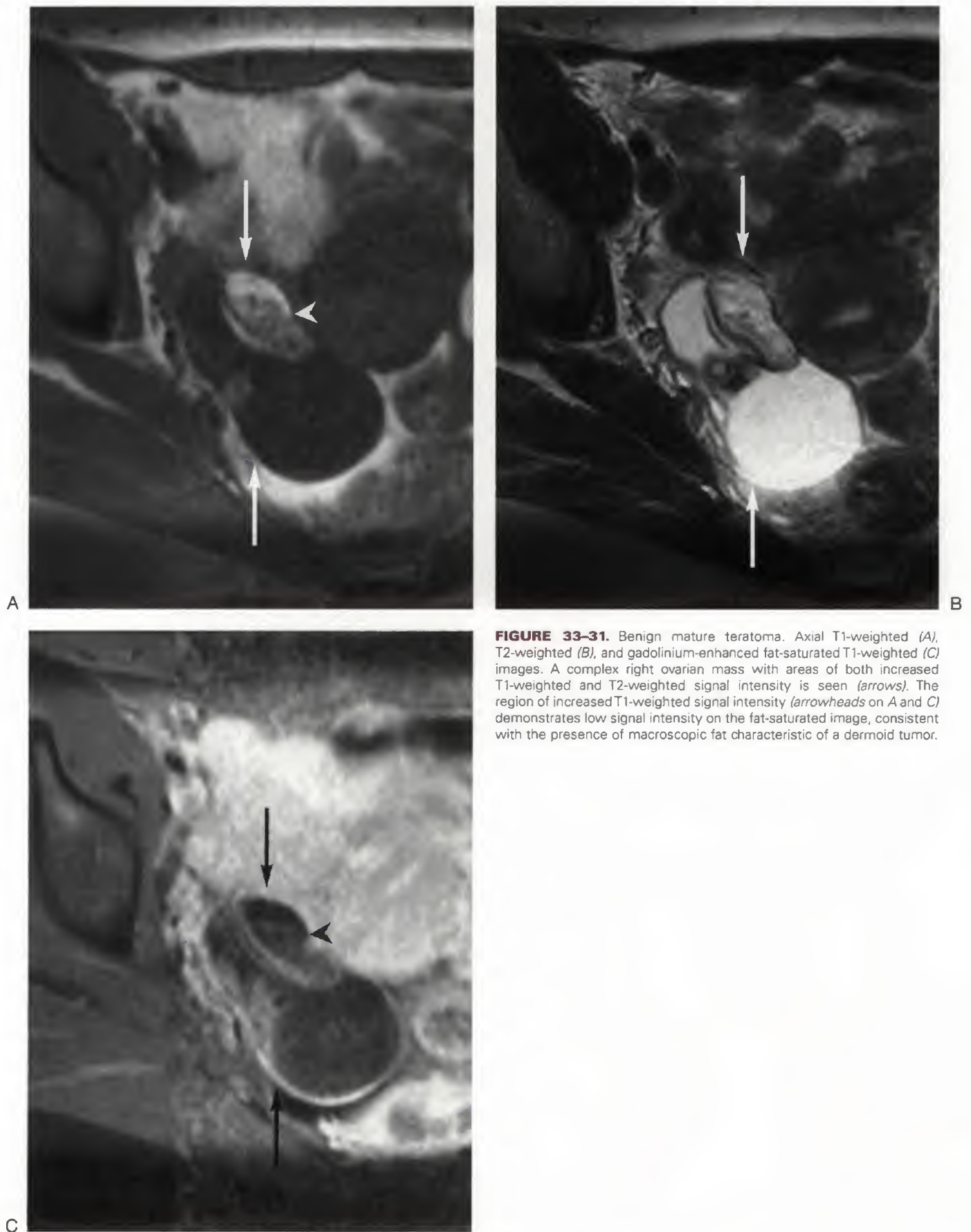


**FIGURE 33-31.** Benign mature teratoma. Axial T1-weighted (A), T2-weighted (B), and gadolinium-enhanced fat-saturated T1-weighted (C) images. A complex right ovarian mass with areas of both increased T1-weighted and T2-weighted signal intensity is seen (arrows). The region of increased T1-weighted signal intensity (arrowheads on A and C) demonstrates low signal intensity on the fat-saturated image, consistent with the presence of macroscopic fat characteristic of a dermoid tumor.

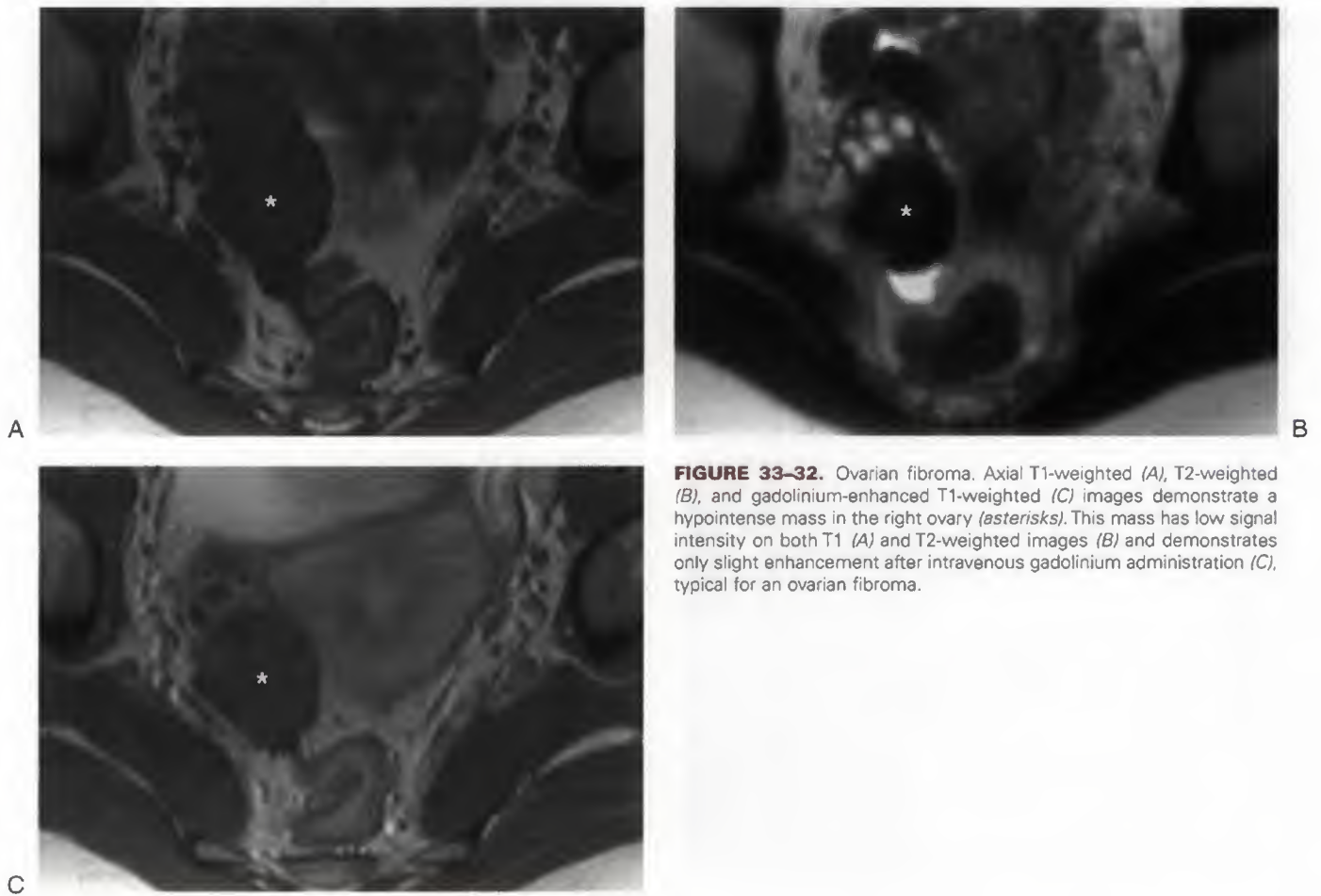
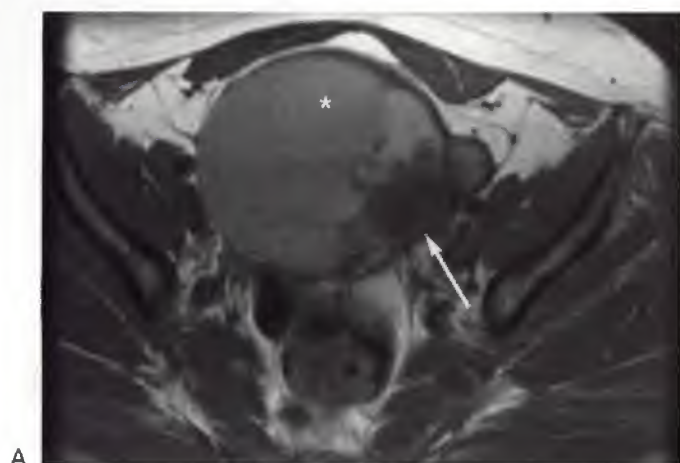
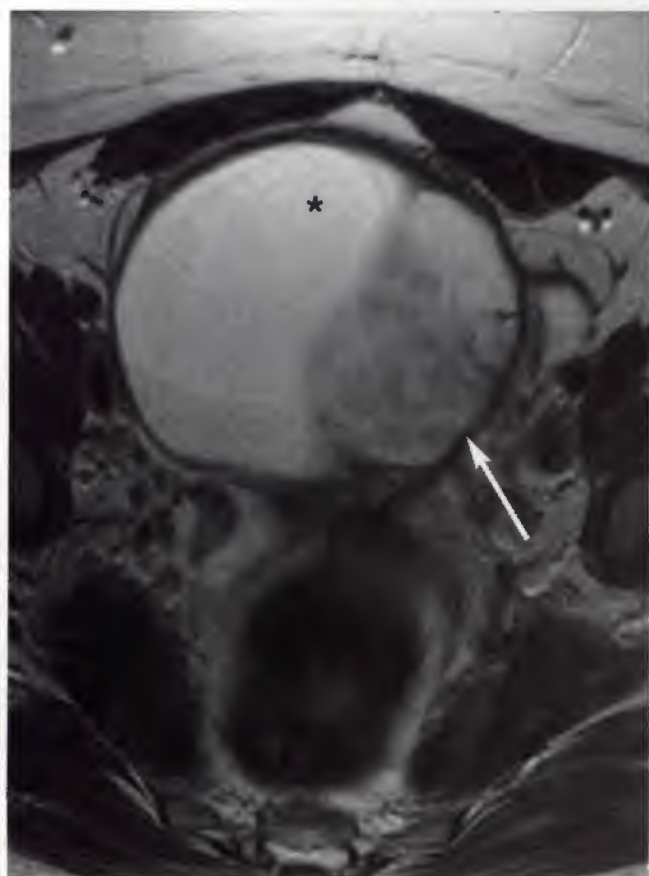


**FIGURE 33-32.** Ovarian fibroma. Axial T1-weighted (A), T2-weighted (B), and gadolinium-enhanced T1-weighted (C) images demonstrate a hypointense mass in the right ovary (asterisks). This mass has low signal intensity on both T1 (A) and T2-weighted images (B) and demonstrates only slight enhancement after intravenous gadolinium administration (C), typical for an ovarian fibroma.





A



B

**FIGURE 33-33.** Borderline epithelial ovarian tumor. Axial T1-weighted (A) and T2-weighted (B) images demonstrate a large ovarian mass with solid (arrows) and cystic (asterisks) components. The findings are consistent with a malignant neoplasm, but not specific for any particular histology. Histopathologic analysis diagnosed a borderline ovarian cancer.

prove to be very helpful making the correct diagnosis. As mentioned previously, leiomyomas have very typical appearance on MRI.<sup>38,43,54</sup>

### Preoperative Staging

Ovarian cancers most often present at an advanced stage with widespread intraperitoneal metastases. The disease is

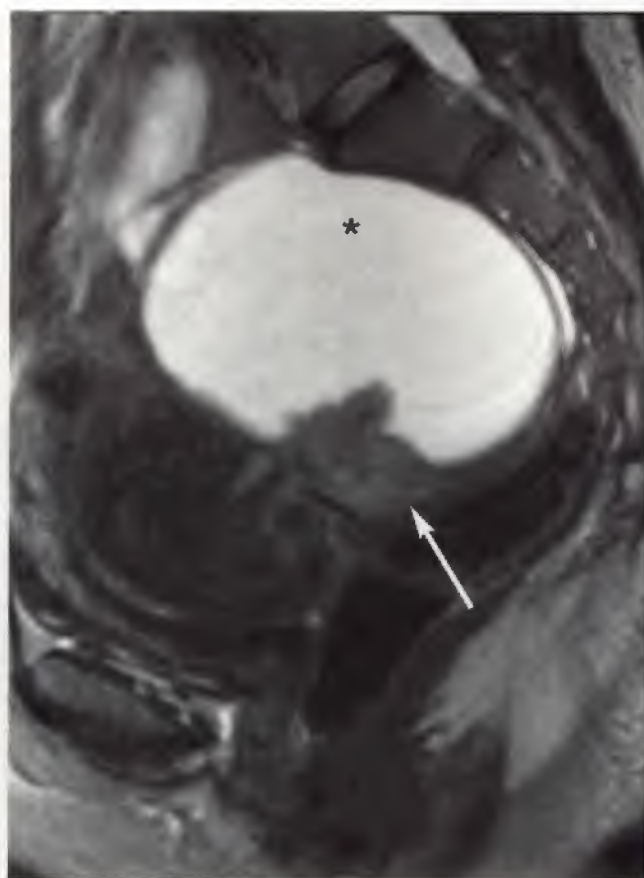


**FIGURE 33-34.** Ovarian serous cystadenocarcinoma. Sagittal T2-weighted image demonstrate a large ovarian mass with solid (arrow) and cystic (asterisk) components. The findings are consistent with a malignant neoplasm, but not specific for any particular histology. This tumor is indistinguishable from a borderline tumor (see Fig. 32-33) based on radiologic findings in the absence of metastatic disease. Histopathologic analysis diagnosed a serous adenocarcinoma.

surgically and pathologically staged; the surgical procedure characterized by a laparotomy including total abdominal hysterectomy, bilateral salpingo-oophorectomy, and omentectomy. In addition, biopsy of multiple frequently involved sites is recommended, including the mesentery, diaphragm, peritoneal surfaces, pelvic nodes, and para-aortic nodes.

Although final staging usually results from postoperative histologic findings, this may be modified after imaging analysis. Besides detecting and characterizing adnexal masses as likely malignant, imaging is used to demonstrate metastases, thus preventing understaging. CT and MRI can often detect specific sites of disease that may be unresectable. As such, neoadjuvant chemotherapy with interval debulking rather than primary debulking with adjuvant chemotherapy may be utilized.<sup>160</sup> Qayyum et al<sup>161</sup> found that preoperative computed tomography and MRI were equally accurate in the detection of inoperable tumor and prediction of suboptimal debulking in newly diagnosed epithelial ovarian cancer. Imaging sensitivity, specificity, positive predictive value, and negative predictive value were 76%, 99%, 94%, and 96%, respectively.

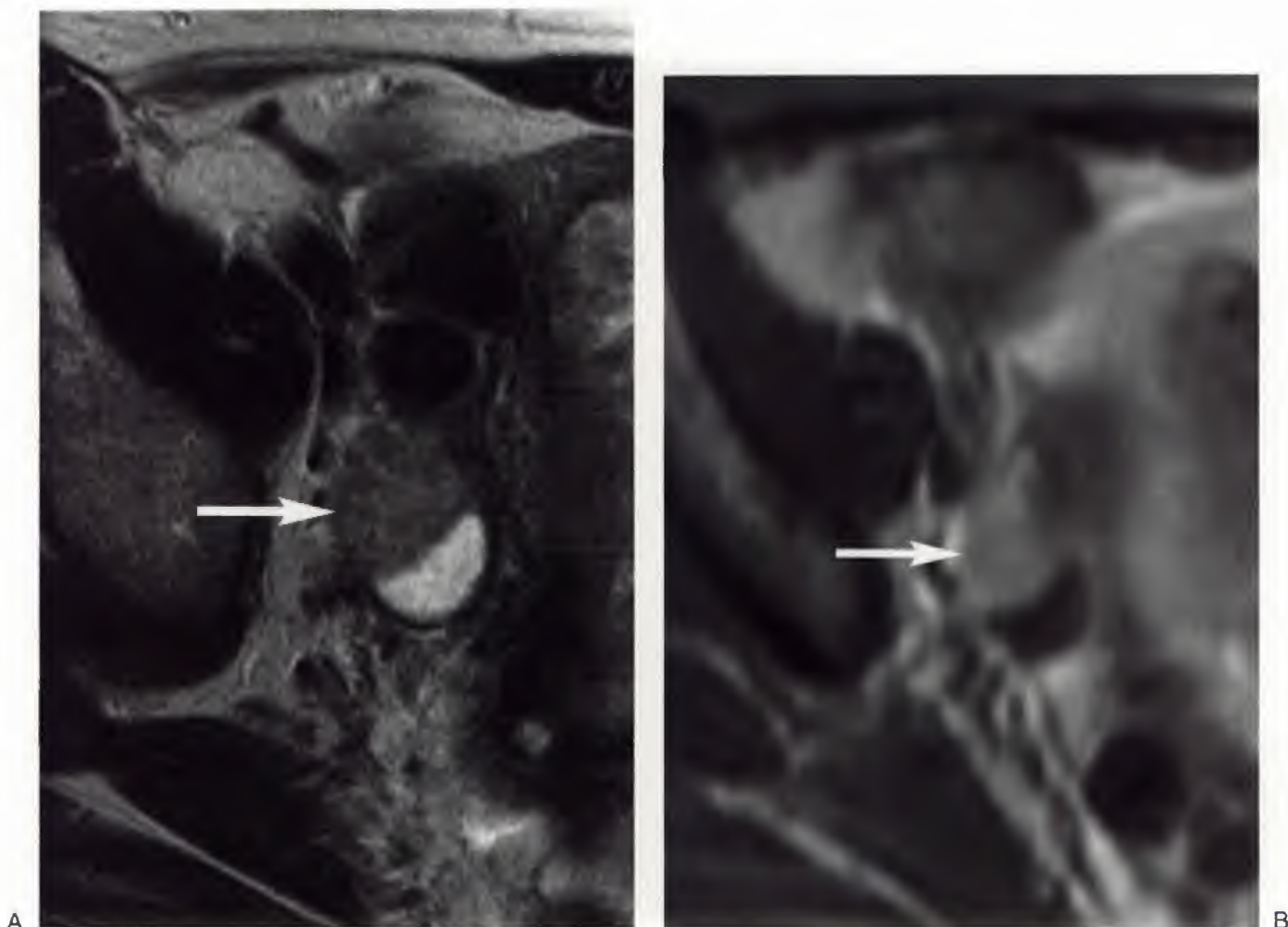


**FIGURE 33-35.** Granulosa cell tumor. Axial T2-weighted (A) and gadolinium-enhanced T1-weighted (B) images. The small enhancing solid mass (B) with low T2 signal (A) (arrows) was proven to be a granulosa cell tumor on histopathologic analysis.

Both computed tomography and MRI have been shown to accurately identify foci of small peritoneal implants, with sensitivities of 95% and 92%, respectively.<sup>162</sup> Similar results were obtained by the Radiology Diagnostic Oncology Group, investigating and comparing the use of Doppler and conventional ultrasound, computed tomography, and MRI for staging of ovarian cancer. In this study, for differentiating nonadvanced disease (benign lesions, stage I and II cancers) from advanced malignancy (stage III and IV cancers), the specificity of MRI was 88% and the sensitivity 98%. Ultrasound had the highest specificity (96%), but the lowest sensitivity (75%); whereas computed tomography results were similar to MRI (specificity equal to 89% and sensitivity equal to 92%).<sup>144</sup>

## References

- Hoad CL, Raine-Fenning NJ, Fulford J, et al: Uterine tissue development in healthy women during the normal menstrual cycle and investigations with magnetic resonance imaging. *Am J Obstet Gynecol* 192:648, 2005.
- Kido A, Togashi K, Nakai A, et al: Oral contraceptives and uterine peristalsis: Evaluation with MRI. *J Magn Reson Imaging* 22:265, 2005.
- Togashi K, Nakai A, Sugimura K: Anatomy and physiology of the female pelvis: MR imaging revisited. *J Magn Reson Imaging* 13:842, 2001.
- Fielding JR: MR imaging of the female pelvis. *Radiol Clin North Am* 41:179, 2003.
- Brown HK, Stoll BS, Nicosia SV, et al: Uterine junctional zone: Correlation between histologic findings and MR imaging. *Radiology* 179:409, 1991.
- Scoutt LM, Flynn SD, Luthringer DJ, et al: Junctional zone of the uterus: Correlation of MR imaging and histologic examination of hysterectomy specimens. *Radiology* 179:403, 1991.
- Goldstein RB, Bree RL, Benson CB, et al: Evaluation of the woman with postmenopausal bleeding: Society of Radiologists in Ultrasound-Sponsored Consensus Conference statement. *J Ultrasound Med* 20:1025, 2001.
- Smith-Bindman R, Weiss E, Feldstein V: How thick is too thick? When endometrial thickness should prompt biopsy in postmenopausal women without vaginal bleeding. *Ultrasound Obstet Gynecol* 24:558, 2004.
- Siegel MJ: Magnetic resonance imaging of the adolescent female pelvis. *Magn Reson Imaging Clin N Am* 10:303, 2002.
- Ourwater EK, Mitchell DG: Normal ovaries and functional cysts: MR appearance. *Radiology* 198:397, 1996.
- Ourwater EK, Talerman A, Dunton C: Normal adnexa uteri specimens: Anatomic basis of MR imaging features. *Radiology* 201:751, 1996.
- Togashi K: MR imaging of the ovaries: Normal appearance and benign disease. *Radiol Clin North Am* 41:799, 2003.



13. Fielding JR: MR imaging of Mullerian anomalies: Impact on therapy. *AJR Am J Roentgenol* 167:1491, 1996.
14. Schwartz LB, Panageas E, Lange R, et al: Female pelvis: Impact of MR imaging on treatment decisions and net cost analysis. *Radiology* 192:55, 1994.
15. Troiano RN, McCarthy SM: Mullerian duct anomalies: Imaging and clinical issues. *Radiology* 233:19, 2004.
16. Byrne J, Nussbaum-Blask A, Taylor WS, et al: Prevalence of Mullerian duct anomalies detected at ultrasound. *Am J Med Genet* 94:9, 2000.
17. Manceschi F, Zupi E, Marconi D, et al: Hysteroscopically detected asymptomatic mullerian anomalies. Prevalence and reproductive implications. *J Reprod Med* 40:684, 1995.
18. Stampe Sorensen S: Estimated prevalence of mullerian anomalies. *Acta Obstet Gynecol Scand* 67:441, 1988.
19. Raga F, Bauser C, Remohi J, et al: Reproductive impact of congenital Mullerian anomalies. *Hum Reprod* 12:2277, 1997.
20. Li S, Qayyum A, Coakley FV, et al: Association of renal agenesis and mullerian duct anomalies. *J Comput Assist Tomogr* 24:829, 2000.
21. Qayyum A, Hricak H: Imaging in infertility. *Références en Gynécologie Obstétrique* 6:305, 1999.
22. Devi Wold AS, Pham N, Arici A: Anatomic factors in recurrent pregnancy loss. *Semin Reprod Med* 24:25, 2006.
23. Carrington BM, Hricak H, Nuruddin RN, et al: Mullerian duct anomalies: MR imaging evaluation. *Radiology* 176:715, 1990.
24. Fedele L, Dorta M, Brioschi D, et al: Magnetic resonance imaging in Mayer-Rokitansky-Kuster-Hauser syndrome. *Obstet Gynecol* 76:593, 1990.
25. Fedele L, Dorta M, Brioschi D, et al: Magnetic resonance evaluation of double uteri. *Obstet Gynecol* 74:844, 1989.
26. Minto CL, Hollings N, Hall-Craggs M, et al: Magnetic resonance imaging in the assessment of complex Mullerian anomalies. *BJog* 108:791, 2001.
27. Mintz MC, Grumbach K: Imaging of congenital uterine anomalies. *Semin Ultrasound CT MR* 9:167, 1988.
28. Mintz MC, Thickman DI, Gussman D, et al: MR evaluation of uterine anomalies. *AJR Am J Roentgenol* 148:287, 1987.
29. Pellerito JS, McCarthy SM, Doyle MB, et al: Diagnosis of uterine anomalies: Relative accuracy of MR imaging, endovaginal sonography, and hysterosalpingography. *Radiology* 183:795, 1992.
30. Allen S, Feste JR: Pelvic disease classifications. *Fertil Steril* 51:199, 1989.
31. Stewart EA: Uterine fibroids. *Lancet* 357:293, 2001.
32. Marshall LM, Spiegelman D, Barbieri RL, et al: Variation in the incidence of uterine leiomyoma among premenopausal women by age and race. *Obstet Gynecol* 90:967, 1997.
33. Wise LA, Palmer JR, Stewart EA, et al: Age-specific incidence rates for self-reported uterine leiomyomata in the Black Women's Health Study. *Obstet Gynecol* 105:563, 2005.
34. Kjerulff KH, Langenberg P, Seidman JD, et al: Uterine leiomyomas. Racial differences in severity, symptoms and age at diagnosis. *J Reprod Med* 41:483, 1996.
35. Keshavarz H, Hillis SD, Kieke BA, et al: Hysterectomy Surveillance—United States, 1994–1999. *MMWR Surveillance Summaries* 2002:1, 2002.
36. Qidwai GI, Caughey AB, Jacoby AF: Obstetric outcomes in women with sonographically identified uterine leiomyomata. *Obstet Gynecol* 107:376, 2006.
37. Manyonda I, Sinthamoney E, Belli AM: Controversies and challenges in the modern management of uterine fibroids. *BJog* 111:95, 2004.
38. Ueda H, Togashi K, Konishi I, et al: Unusual appearances of uterine leiomyomas: MR imaging findings and their histopathologic backgrounds. *Radiographics* 19:S131, 1999.
39. Inoue H, Aizawa N, Mizuno T, et al: A large degenerated subserous leiomyoma of the uterus: Uncommon scintigraphic and ultrasonographic findings. *Ann Nucl Med* 3:55, 1989.
40. Reddy NM, Jain KA, Gerscovich EO: A degenerating cystic uterine fibroid mimicking an endometrioma on sonography. *J Ultrasound Med* 22:973, 2003.
41. Brinton LA, Sakoda LC, Sherman ME, et al: Relationship of benign gynecologic diseases to subsequent risk of ovarian and uterine tumors. *Cancer Epidemiol Biomarkers Prev* 14:2929, 2005.
42. Okamoto Y, Tanaka YO, Nishida M, et al: MR imaging of the uterine cervix: Imaging-pathologic correlation. *Radiographics* 23:425, 2003.
43. Murase E, Siegelman ES, Outwater EK, et al: Uterine leiomyomas: Histopathologic features, MR imaging findings, differential diagnosis, and treatment. *Radiographics* 19:1179, 1999.
44. Kim JC, Kim SS, Park JY: "Bridging vascular sign" in the MR diagnosis of exophytic uterine leiomyoma. *J Comput Assist Tomogr* 24:57, 2000.
45. Lee JH, Jeong YK, Park JK, et al: "Ovarian vascular pedicle" sign revealing organ of origin of a pelvic mass lesion on helical CT. *AJR Am J Roentgenol* 181:131, 2003.
46. Stavropoulos SW, Shlansky-Goldberg R: Embolization of Uterine Fibroids: Patient Selection and Results of Treatment. *J Womens Imaging* 3:153, 2001.
47. Dueholm M, Lundorf E, Hansen ES, et al: Accuracy of magnetic resonance imaging and transvaginal ultrasonography in the diagnosis, mapping, and measurement of uterine myomas. *Am J Obstet Gynecol* 186:409, 2002.
48. Togashi K, Ozasa H, Konishi I, et al: Enlarged uterus: Differentiation between adenomyosis and leiomyoma with MR imaging. *Radiology* 171:531, 1989.
49. Togashi K, Nishimura K, Itoh K, et al: Adenomyosis: Diagnosis with MR imaging. *Radiology* 166:111, 1988.
50. Jha RC, Ascher SM, Imaoka I, et al: Symptomatic fibroid leiomyomata: MR imaging of the uterus before and after uterine arterial embolization. *Radiology* 217:228, 2000.
51. Spies JB, Roth AR, Jha RC, et al: Leiomyomata treated with uterine artery embolization: Factors associated with successful symptom and imaging outcome. *Radiology* 222:45, 2002.
52. Kitamura Y, Ascher SM, Cooper C, et al: Imaging manifestations of complications associated with uterine artery embolization. *Radiographics* 25:S119, 2005.
53. Burn PR, McCall JM, Chinn RJ, et al: Uterine fibroleiomyoma: MR imaging appearances before and after embolization of uterine arteries. *Radiology* 214:729, 2000.
54. Mittle RL, Jr., Yeh IT, Kressel HY: High-signal-intensity rim surrounding uterine leiomyomas on MR images: Pathologic correlation. *Radiology* 180:81, 1991.
55. Bergeron C, Amant F, Ferenczy A: Pathology and physiopathology of adenomyosis. *Best Pract Res Clin Obstet Gynaecol* 20:511, 2006.
56. Seidman JD, Kjerulff KH: Pathologic findings from the Maryland Women's Health Study: Practice patterns in the diagnosis of adenomyosis. *Int J Gynecol Pathol* 15:217, 1996.
57. Curtis KM, Hillis SD, Marchbanks PA, et al: Disruption of the endometrial-myometrial border during pregnancy as a risk factor for adenomyosis. *Am J Obstet Gynecol* 187:543, 2002.
58. Bergholt T, Eriksen L, Berendt N, et al: Prevalence and risk factors of adenomyosis at hysterectomy. *Hum Reprod* 16:2418, 2001.
59. Vercellini P, Parazzini F, Oldani S, et al: Adenomyosis at hysterectomy: A study on frequency distribution and patient characteristics. *Hum Reprod* 10:1160, 1995.
60. Nishida M: Relationship between the onset of dysmenorrhea and histologic findings in adenomyosis. *Am J Obstet Gynecol* 165:229, 1991.
61. Goswami A, Khemani M, Logani KB, et al: Adenomyosis: Diagnosis by hysteroscopic endomyometrial biopsy, correlation of incidence and severity with menorrhagia. *J Obstet Gynaecol Res* 24:281, 1998.
62. Reinhold C, McCarthy S, Bret PM, et al: Diffuse adenomyosis: Comparison of endovaginal US and MR imaging with histopathologic correlation. *Radiology* 199:151, 1996.
63. Bazot M, Cortez A, Darai E, et al: Ultrasonography compared with magnetic resonance imaging for the diagnosis of adenomyosis: Correlation with histopathology. *Hum Reprod* 16:2427, 2001.
64. Dueholm M, Lundorf E, Hansen ES, et al: Magnetic resonance imaging and transvaginal ultrasonography for the diagnosis of adenomyosis. *Fertil Steril* 76:588, 2001.
65. Bazot M, Darai E, Rouger J, et al: Limitations of transvaginal sonography for the diagnosis of adenomyosis, with histopathological correlation. *Ultrasound Obstet Gynecol* 20:605, 2002.
66. Atzori E, Tronci C, Sionis L: Transvaginal ultrasound in the diagnosis of diffuse adenomyosis. *Gynecol Obstet Invest* 42:39, 1996.
67. Vercellini P, Cortesi I, De Giorgi O, et al: Transvaginal ultrasonography versus uterine needle biopsy in the diagnosis of diffuse adenomyosis. *Hum Reprod* 13:2884, 1998.
68. Reinhold C, Tafazoli F, Mehio A, et al: Uterine adenomyosis: Endovaginal US and MR imaging features with histopathologic correlation. *Radiographics* 19:S147, 1999.
69. Hricak H, Finck S, Honda G, et al: MR imaging in the evaluation of benign uterine masses: Value of gadopentetate dimeglumine-enhanced T1-weighted images. *AJR Am J Roentgenol* 158:1043, 1992.



70. Missmer SA, Hankinson SE, Spiegelman D, et al: Incidence of laparoscopically confirmed endometriosis by demographic, anthropometric, and lifestyle factors. *Am J Epidemiol* 160:784, 2004.
71. Missmer SA, Cramer DW: The epidemiology of endometriosis. *Obstet Gynecol Clin North Am* 30:1, 2003.
72. Endometriosis and infertility. The Practice Committee at the American Society of Reproductive Medicine. *Fertil Steril* 81:1441, 2004.
73. Vinauer D, Orazi G, Cosson M, et al: Theories of endometriosis. *Eur J Obstet Gynecol Reprod Biol* 96:21, 2001.
74. Chung SY, Kim SJ, Kim TH, et al: Computed tomography findings of pathologically confirmed pulmonary parenchymal endometriosis. *J Comput Assist Tomogr* 29:815, 2005.
75. Dwivedi AJ, Agrawal SN, Silva YJ: Abdominal wall endometriomas. *Dig Dis Sci* 47:456, 2002.
76. Thibodeau LL, Prioleau GR, Manuelidis EE, et al: Cerebral endometriosis. Case report. *J Neurosurg* 66:609, 1987.
77. Carbognin G, Guarise A, Minelli L, et al: Pelvic endometriosis: US and MRI features. *Abdom Imaging* 29:609, 2004.
78. Outwater E, Schiebler ML, Owen RS, et al: Characterization of hemorrhagic adnexal lesions with MR imaging: blinded reader study. *Radiology* 186:489, 1993.
79. Kier R, Smith RC, McCarthy SM: Value of lipid- and water-suppression MR images in distinguishing between blood and lipid within ovarian masses. *AJR Am J Roentgenol* 58:321, 1992.
80. Sugimura K, Takemori M, Sugiyama M, et al: The value of magnetic resonance relaxation time in staging ovarian endometrial cysts. *Br J Radiol* 65:502, 1992.
81. Glastonbury CM: The shading sign. *Radiology* 224:199, 2002.
82. Jeong YY, Outwater EK, Kang HK: Imaging evaluation of ovarian masses. *Radiographics* 20:1445, 2000.
83. Wu TT, Coakley FV, Qayyum A, et al: Magnetic resonance imaging of ovarian cancer arising in endometriomas. *J Comput Assist Tomogr* 28:836, 2004.
84. Sugimura K, Okizuka H, Imaoka I, et al: Pelvic endometriosis: Detection and diagnosis with chemical shift MR imaging. *Radiology* 188:435, 1993.
85. Takahashi K, Okada S, Ozaki T, et al: Diagnosis of pelvic endometriosis by magnetic resonance imaging using "fat-saturation" technique. *Fertil Steril* 62:973, 1994.
86. Zanardi R, Del Frate C, Zuiani C, et al: Staging of pelvic endometriosis based on MRI findings versus laparoscopic classification according to the American Fertility Society. *Abdom Imaging* 28:733, 2003.
87. Bazot M, Darai E, Hourani R, et al: Deep pelvic endometriosis: MR imaging for diagnosis and prediction of extension of disease. *Radiology* 232:379, 2004.
88. Kataoka ML, Togashi K, Yamaoka T, et al: Posterior cul-de-sac obliteration associated with endometriosis: MR imaging evaluation. *Radiology* 234:815, 2005.
89. Takeuchi H, Kuwatsuru R, Kitade M, et al: A novel technique using magnetic resonance imaging jelly for evaluation of rectovaginal endometriosis. *Fertil Steril* 83:442, 2005.
90. Estimated New Cancer Cases and Deaths by Sex for All Sites, U.S., 2006. In: *Cancer Facts and Figures 2006*. Atlanta, American Cancer Society, 2006.
91. Tjalma WA, Van Waas TR, Van den Eeden LE, et al: Role of human papillomavirus in the carcinogenesis of squamous cell carcinoma and adenocarcinoma of the cervix. *Best Pract Res Clin Obstet Gynaecol* 19:469, 2005.
92. National Cancer Institute. Cervical Cancer (PDQ®): Treatment. Bethesda, MD, National Cancer Institute, 2006. <http://www.cancer.gov/cancertopics/pdq/treatment/cervical/healthprofessional>
93. Kaur H, Silverman PM, Iyer RB, et al: Diagnosis, staging, and surveillance of cervical carcinoma. *AJR Am J Roentgenol* 180:1621, 2003.
94. Yamashita Y, Takahashi M, Katayuchi H, et al: Adenoma malignum: MR appearances mimicking nabothian cysts. *AJR Am J Roentgenol* 162:649, 1994.
95. Matthews-Greer J, Dominguez-Malagon H, Herrera GA, et al: Human papillomavirus typing of rare cervical carcinomas. *Arch Pathol Lab Med* 128:553, 2004.
96. Takemori M, Ichimura T, Nishimura R, et al: Ovarian dysgerminoma with massive metastases to para-aortic lymph nodes. *Gynecol Obstet Invers* 49:211, 2000.
97. Kyndi M, Frederiksen K, Kruger Kjaer S: Cervical cancer incidence in Denmark over six decades (1943-2002). *Acta Obstet Gynecol Scand* 85:106, 2006.
98. Vizcaino AP, Moreno V, Bosch FX, et al: International trends in incidence of cervical cancer: II. Squamous-cell carcinoma. *Int J Cancer* 86:429, 2000.
99. Vizcaino AP, Moreno V, Bosch FX, et al: International trends in the incidence of cervical cancer: I. Adenocarcinoma and adenosquamous cell carcinomas. *Int J Cancer* 75:536, 1998.
100. Cancer of the Cervix Uteri. In: Benedet JL, Hacker NF, Ngan HY, eds. Staging classifications and clinical practice guidelines of gynaecologic cancers. FIGO Committee on Gynecologic Oncology and International Gynecologic Cancer Society. 2nd ed: Philadelphia, Elsevier, 2000, pp 36-58.
101. Benedet JL, Odicino F, Maisonneuve P, et al: Carcinoma of the cervix uteri. *J Epidemiol Biostat* 6:7, 2001.
102. Benedet JL, Odicino F, Maisonneuve P, et al: Carcinoma of the cervix uteri. *Int J Gynaecol Obstet* 83:41, 2003.
103. Subak LL, Hricak H, Powell CB, et al: Cervical carcinoma: computed tomography and magnetic resonance imaging for preoperative staging. *Obstet Gynecol* 86:43, 1995.
104. Kim SH, Choi BI, Han JK, et al: Preoperative staging of uterine cervical carcinoma: Comparison of CT and MRI in 99 patients. *J Comput Assist Tomogr* 17:633, 1993.
105. Park W, Park YJ, Huh SJ, et al: The usefulness of MRI and PET imaging for the detection of parametrial involvement and lymph node metastasis in patients with cervical cancer. *Jpn J Clin Oncol* 35:260, 2005.
106. Hricak H, Hamm B, Semelka RC, et al: Carcinoma of the uterus: Use of gadopentetate dimeglumine in MR imaging. *Radiology* 181:95, 1991.
107. Seki H, Azumi R, Kimura M, et al: Stromal invasion by carcinoma of the cervix: Assessment with dynamic MR imaging. *AJR Am J Roentgenol* 168:1579, 1997; 1585.
108. Narayan K: Arguments for a magnetic resonance imaging-assisted FIGO staging system for cervical cancer. *Int J Gynecol Cancer* 15:573, 2005.
109. Hricak H, Gatsonis C, Chi DS, et al: Role of imaging in pretreatment evaluation of early invasive cervical cancer: Results of the intergroup study American College of Radiology Imaging Network 6651: Gynecologic Oncology Group 183. *J Clin Oncol* 23:9329, 2005.
110. Folcn M, Levenback CF, Iyer RB, et al: Imaging in cervical cancer. *Cancer* 98:2028, 2003.
111. Yamashita Y, Takahashi M, Sawada T, et al: Carcinoma of the cervix: Dynamic MR imaging. *Radiology* 182:643, 1992.
112. Hricak H, Lacey CG, Sandles LG, et al: Invasive cervical carcinoma: Comparison of MR imaging and surgical findings. *Radiology* 166:623, 1988.
113. Keller TM, Michel SC, Fröhlich J, et al: USPIO-enhanced MRI for preoperative staging of gynecological pelvic tumors: preliminary results. *Eur Radiol* 14:937, 2004.
114. Rockall AG, Sohaib SA, Harisinghani MG, et al: Diagnostic performance of nanoparticle-enhanced magnetic resonance imaging in the diagnosis of lymph node metastases in patients with endometrial and cervical cancer. *J Clin Oncol* 23:2813, 2005.
115. Harisinghani MG, Barentsz J, Hahn PF, et al: Noninvasive detection of clinically occult lymph-node metastases in prostate cancer. *N Engl J Med* 348:2491, 2003.
116. National Cancer Institute. Endometrial Cancer (PDQ®): Treatment. Bethesda, MD, National Cancer Institute, 2006. <http://www.cancer.gov/cancertopics/pdq/treatment/endometrial/healthprofessional>
117. Amant F, Moerman P, Neven P, et al: Endometrial cancer. *Lancet* 366:491, 2005.
118. Purdie DM, Green AC: Epidemiology of endometrial cancer. *Best Pract Res Clin Obstet Gynaecol* 15:341, 2001.
119. Swerdlow AJ, Jones ME: Tamoxifen treatment for breast cancer and risk of endometrial cancer: A case-control study. *J Natl Cancer Inst* 97:375, 2005.
120. Lacey JV Jr, Brinton LA, Lubin JH, et al: Endometrial carcinoma risks among menopausal estrogen plus progestin and unopposed estrogen users in a cohort of postmenopausal women. *Cancer Epidemiol Biomarkers Prev* 14:1724, 2005.
121. Nagele F, Wieser F, Decry A, et al: Endometrial cell dissemination at diagnostic hysteroscopy: A prospective randomized cross-over comparison of normal saline and carbon dioxide uterine distension. *Hum Reprod* 14:2739, 1999.
122. Tangitgamol S, Levenback CF, Beller U, et al: Role of surgical resection for lung, liver, and central nervous system metastases in patients with gynecological cancer: A literature review. *Int J Gynecol Cancer* 14:399, 2004.



123. Cancer of the Corpus Uteri. In: Benedet JL, Hacker NF, Ngan HY, eds. Staging classifications and clinical practice guidelines of gynaecologic cancers. FIGO Committee on Gynecologic Oncology and International Gynecologic Cancer Society. 2nd ed: Philadelphia, Elsevier, 2000, pp 36–58.
124. Corpus uteri. In: Greene FL, Fritz AG, Balch CM, et al, eds. American Joint Committee on Cancer: AJCC Cancer Staging Manual, 6th ed. New York, Springer-Verlag, 2002.
125. American Cancer Society. Cancer Facts and Figures 2006. Atlanta, American Cancer Society, 2006. [http://www.cancer.org/docroot/STT/content/STT\\_1x\\_Cancer\\_Facts\\_Figures\\_2006.asp](http://www.cancer.org/docroot/STT/content/STT_1x_Cancer_Facts_Figures_2006.asp)
126. Abeler VM, Kjørstad KE: Endometrial adenocarcinoma in Norway. A study of a total population. *Cancer* 67:3093, 1991.
127. Hricak H, Rubinstein LV, Gherman GM, et al: MR imaging evaluation of endometrial carcinoma: Results of an NCI cooperative study. *Radiology* 179:829, 1991.
128. Yamashita Y, Mizutani H, Torashima M, et al: Assessment of myometrial invasion by endometrial carcinoma: Transvaginal sonography vs contrast-enhanced MR imaging. *AJR Am J Roentgenol* 161:595, 1993.
129. Sironi S, Colombo E, Villa G, et al: Myometrial invasion by endometrial carcinoma: Assessment with plain and gadolinium-enhanced MR imaging. *Radiology* 185:207, 1992.
130. Nasi F, Fiocchi F, Pecchi A, et al: MRI evaluation of myometrial invasion by endometrial carcinoma. Comparison between fast-spin-echo T2w and coronal-FMPSPGR Gadolinium-Dota-enhanced sequences. *Radiol Med (Torino)* 110:199, 2005.
131. Harrill CD, Kopecky KK, Weaver SR, et al: Magnetic resonance imaging in the preoperative assessment of clinical stage I endometrial carcinoma. *Comput Med Imaging Graph* 14:191, 1990.
132. Belloni C, Vigano R, del Maschio A, et al: Magnetic resonance imaging in endometrial carcinoma staging. *Gynecol Oncol* 37:172, 1990.
133. Chen SS, Rumancik WM, Spiegel G: Magnetic resonance imaging in stage I endometrial carcinoma. *Obstet Gynecol* 75:274, 1990.
134. Lien HH, Blomlie V, Trope C, et al: Cancer of the endometrium: Value of MR imaging in determining depth of invasion into the myometrium. *AJR Am J Roentgenol* 157:1221, 1991.
135. Sironi S, Taccagni G, Garancini P, et al: Myometrial invasion by endometrial carcinoma: Assessment by MR imaging. *AJR Am J Roentgenol* 158:565, 1992.
136. Tsuda H, Murata K, Kawabata M, et al: Preoperative assessment of myometrial invasion of endometrial cancer by MR imaging and intrauterine ultrasonography with a high-frequency probe: Preliminary study. *J Ultrasound Med* 16:545, 1997.
137. Ito K, Matsumoto T, Nakada T, et al: Assessing myometrial invasion by endometrial carcinoma with dynamic MRI. *J Comput Assist Tomogr* 18:77, 1994.
138. Arko D, Takac I: High frequency transvaginal ultrasonography in preoperative assessment of myometrial invasion in endometrial cancer. *J Ultrasound Med* 19:639, 2000.
139. Ovarian Cancer: Screening, Treatment, and Follow-up. In: NIH Consensus Statement: Online [accessed 2005 December 20] 1994; pp 1–30.
140. Engelen MJ, Kos HE, Willemse PH, et al: Surgery by consultant gynecologic oncologists improves survival in patients with ovarian carcinoma. *Cancer* 106:589, 2006.
141. Sohaib SA, Mills TD, Sahdev A, et al: The role of magnetic resonance imaging and ultrasound in patients with adnexal masses. *Clin Radiol* 60:340, 2005.
142. Saini A, Dina R, McIndoe GA, et al: Characterization of adnexal masses with MRI. *AJR Am J Roentgenol* 184:1004, 2005.
143. Rieber A, Nussle K, Stohr I, et al: Preoperative diagnosis of ovarian tumors with MR imaging: Comparison with transvaginal sonography, positron emission tomography, and histologic findings. *AJR Am J Roentgenol* 177:1232001.
144. Kurtz AB, Tsimikas JV, Tempany CM, et al: Diagnosis and staging of ovarian cancer: Comparative values of Doppler and conventional US, CT, and MR imaging correlated with surgery and histopathologic analysis—Report of the Radiology Diagnostic Oncology Group. *Radiology* 212:19, 1999.
145. DePriest PD, Shenson D, Fried A, et al: A morphology index based on sonographic findings in ovarian cancer. *Gynecol Oncol* 51:7, 1993.
146. Granberg S, Wikland M, Jansson I: Macroscopic characterization of ovarian tumors and the relation to the histological diagnosis: Criteria to be used for ultrasound evaluation. *Gynecol Oncol* 35:139, 1989.
147. Chang WC, Meux MD, Yeh BM, et al: CT and MRI of adnexal masses in patients with primary nonovarian malignancy. *AJR Am J Roentgenol* 186:1039, 2006.
148. Bloomfield TH: Benign cystic teratomas of the ovary: A review of seventy-two cases. *Eur J Obstet Gynecol Reprod Biol* 25:231, 1987.
149. Comerici JT, Licciardi F, Bergh PA, et al: Mature cystic teratoma: A clinicopathologic evaluation of 517 cases and review of the literature. *Obstet Gynecol* 84:22, 1994.
150. Jung SE, Rha SE, Lee JM, et al: CT and MRI findings of sex cord-stromal tumor of the ovary. *AJR Am J Roentgenol* 185:207, 2005.
151. Troiano RN, Lazzarini KM, Scoutt LM, et al: Fibroma and fibrothecoma of the ovary: MR imaging findings. *Radiology* 204:795, 1997.
152. Zhang J, Ugnat AM, Clarke K, et al: Ovarian cancer histology—Specific incidence trends in Canada 1969–1993: Age-period-cohort analyses. *Br J Cancer* 81:152, 1999.
153. McCluggage WG, Wilkinson N: Metastatic neoplasms involving the ovary: A review with an emphasis on morphological and immunohistochemical features. *Histopathology* 47:231, 2005.
154. Ha HK, Back SY, Kim SH, et al: Krukenberg's tumor of the ovary: MR imaging features. *AJR Am J Roentgenol* 164:1435, 1995.
155. Hann LE, Lui DM, Shi W, et al: Adnexal masses in women with breast cancer: US findings with clinical and histopathologic correlation. *Radiology* 216:242, 2000.
156. Kim SH, Kim WH, Park KJ, et al: CT and MR findings of Krukenberg tumors: Comparison with primary ovarian tumors. *J Comput Assist Tomogr* 20:393, 1996.
157. Ferrozzi F, Tognini G, Bova D, et al: Non-Hodgkin lymphomas of the ovaries: MR findings. *J Comput Assist Tomogr* 24:416, 2000.
158. Schumer ST, Cannistra SA: Granulosa cell tumor of the ovary. *J Clin Oncol* 21:1180, 2003.
159. Kim SH, Kim SH: Granulosa cell tumor of the ovary: Common findings and unusual appearances on CT and MR. *J Comput Assist Tomogr* 26:756, 2002.
160. Coakley FV: Staging ovarian cancer: role of imaging. *Radiol Clin North Am* 40:609, 2002.
161. Qayyum A, Coakley FV, Westphalen AC, et al: Role of CT and MR imaging in predicting optimal cytoreduction of newly diagnosed primary epithelial ovarian cancer. *Gynecol Oncol* 96:301, 2005.
162. Tempany CM, Zou KH, Silverman SG, et al: Staging of advanced ovarian cancer: Comparison of imaging modalities—Report from the Radiological Diagnostic Oncology Group. *Radiology* 215:761, 2000.

## ULTRASOUND OF THE BREAST

Ellen B. Mendelson, MD, FACR

### Introduction

Equipment and Technique  
The Breast Ultrasound Examination  
Anatomy  
Lesion Feature Analysis and Interpretation

### Indications for Breast Ultrasound

Palpable and Nonpalpable Abnormalities  
*Density of Breast Tissue*  
Calcifications  
Inflammatory Processes Including Inflammatory Carcinoma  
Fatty Breast: Need for Ultrasound?  
Negative Predictive Value of Ultrasound and Mammography

### Ultrasound Guidance of Interventional Procedures

#### Evaluating Problems With Breast Implants

The Postsurgical Breast and Treatment Planning for Radiation Therapy

### Young, Pregnant, and Lactating Patients

Controversial or Evolving Applications of Breast Ultrasound in Problem Solving

#### Characterizing Multiple Masses

For Extent of Disease Bilaterally, Including Axillary Evaluation, in Breast Cancer Patients

Staging

### Summary and Conclusions

## INTRODUCTION

Major advances in breast ultrasound (US) have occurred in the last decade in diagnostic breast imaging services. For many years, technical inadequacies, focus on mammography, and inexperience with US may have prevented broadening of the accepted indications for breast US and limited some of its potential uses for problem solving from being realized. US analysis of masses was allowed only for cyst versus solid characterization and not for differentiation of benign from malignant solid masses.<sup>1</sup> More recently, transducer developments, systems improvements, and user experience have advanced US depiction of masses sufficiently to attempt classifying solid masses into categories defined by likelihood of malignancy.<sup>2-6</sup> Currently, the US evaluation of palpable breast masses and those seen on mammograms has become standard of care in the United States. Although x-ray mammography is the only imaging technique for breast cancer screening established by randomized controlled trials to reduce mortality, the contributions of other imaging methods in the completion of the problem-solving process have been recognized. Among the other methods for imaging breast tissue, US is second to mammography because of its use for many years, its accessibility and relatively low cost, and the unique opportunity it affords for real-time guidance of needle biopsy and other interventional procedures.

### Equipment and Technique

Compared with mammography, a summative modality, breast US performed with high-resolution handheld probes is a tomographic imaging technique with synthesis during real-time scanning of the very thin slices within a small rectangular or square field of view (FOV) of 4 to 5 cm

dimensions. Real-time scanning enables tracing of ductal anatomy, perception of architectural distortion, and differentiation of a mass from normal anatomic components.

Important technical progress has been made. High frequency linear broad bandwidth transducers enable scanning to be performed with high resolution in superficial tissues and without compromise of penetration deeper in the FOV, up to 5 cm. These transducers are available for use with all high-end systems as well as more modestly priced US scanners designed primarily for breast imaging and US-guided interventional procedures. Typical bandwidth ranges of these linear transducers are 5 to 10 MHz, 5 to 12 MHz, 8 to 15 MHz, and more recently, 5 to 17 MHz and 8 to 17 MHz. Center frequencies are equal to or greater than 8 MHz, and the footprints vary from 38 mm to more than 50 mm, enabling efficient survey scanning. Linear transducers are excellent for real-time guidance of the needle in breast interventional procedures. However, transducer footprints greater than 60 mm are too large for use on the average size breast, with loss of contact likely to occur at either end of the transducer face.

Several manufacturers have developed spatial compounding.<sup>7-8</sup> Spatial compounding is produced by the intersection of three to nine angulated beams within tissue. This mode diminishes acoustic speckle to enable clear and confident perception of marginal detail when a mass is centered within the FOV. The greatest smoothing occurs with the intersection of nine beams, but the tradeoff is reduction in frame rate, which may become too slow for scanning in real time. The use of spatial compounding with three intersecting beams achieves image improvement with an adequate frame rate. Because of the angulated beams, posterior acoustic features—shadowing or enhancement—of a mass centered





**FIGURE 34-1.** Spatial compounding: invasive ductal carcinoma. A. On a conventional scan an irregularly shaped hypoechoic carcinoma, marred by speckle, is seen in the center of image (*arrow*). B. Spatial compounding in reducing noise enables feature analysis to be applied more confidently. Irregular shape, indistinct margins, and orientation not parallel to the skin suggest malignancy. The posterior aspect of the mass (*arrow*) is unobscured in the center of image. C. Mammogram with spot compression correlating well with size and shape of carcinoma (*arrow*) as depicted with ultrasound.

within the FOV may be less apparent or appear triangular with the apex of the triangle facing the deepest part of the image. In my view, the opportunity afforded by spatial compounding for better perception of marginal features and better depiction of the posterior aspect of a mass, which may be obscured by intense shadowing, is sufficient compensation for diminishing imaging of posterior features. These are less significant than shape, margin, and orientation in assessing likelihood of malignancy of the mass (Fig. 34-1).

Newer US systems have broad dynamic ranges that, at the high end, can be used to optimize the grayscale for breast imaging—different types of tissues should be represented in shades of gray rather than two-toned in black and white.

The older contrast settings may have been responsible in part for serious misinterpretation of a cancer as a cyst (Fig. 34-2). The dynamic range and image presets should not eliminate contrast to achieve a broad grayscale. If the image is adjusted in this way, it will appear washed out, and differences between structures of similar echogenicity, such as fat lobules and some fibroadenomas, may not be perceptible.

Intraoperative curved linear or straight linear probes with short footprints of approximately 18 mm ranging from 15 to 17 (or higher) MHz at the high end of their bandwidths are beneficial in breast imaging. These high-resolution, small “hockey stick” transducers are often useful for scanning the skin and very superficial subcutaneous tissues to identify and

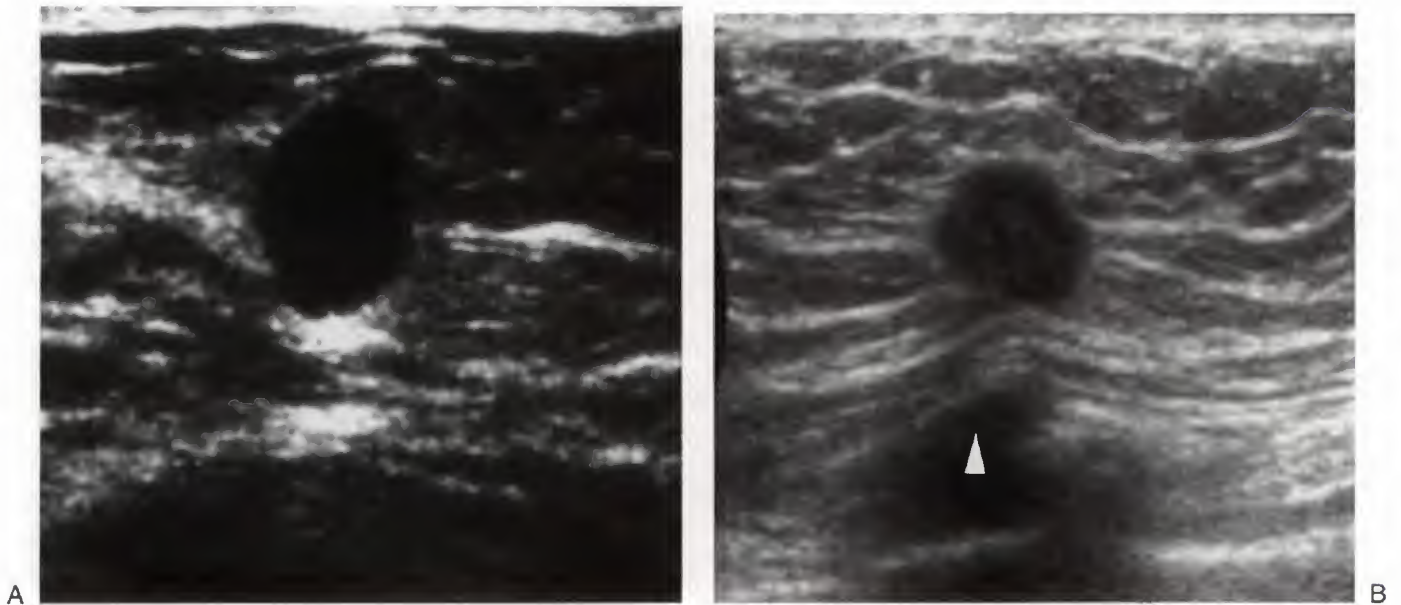


**FIGURE 34-2.** High contrast versus broad grayscale: invasive ductal carcinoma. *A.* This sonographic image is bright black and white which impairs ability to perceive echoes in the mass or its indistinct anterior margin. Strong enhancement and near-anechogenicity suggest erroneously that the mass is a simple cyst. *B.* Sonographic image of a mass in a different patient with the same diagnosis, poorly differentiated invasive ductal carcinoma, is easier to interpret. Its broad grayscale enables recognition of marginal detail and differences in the echogenicity of normal tissues and abnormalities. The cancer is just anterior to the pectoral muscle layer. US is unreliable in determining involvement; pectoral muscle enhancement on MRI is more reliable. Deep to the pectoral muscle, a portion of rib (*arrowhead*) can be seen.

characterize lesions located in the skin, such as sebaceous or epidermal inclusion cysts. A thin offset pad or mound of gel must still be used to bring the skin into focus. The tissue posterior to the nipple-areolar complex may also be difficult to image because of shadowing from the crevices of the nipple. The small-footprint probes can be angulated into this area and depict the ducts and fibroglandular tissue without artifact.

Other developments suited for breast imaging may include tissue harmonic imaging that heightens contrast and may aid in distinguishing similar-appearing hypoechoic structures from one another, such as fat lobules and fibroadenomas (Fig. 34-3).<sup>9,10</sup>

Although elastography has been studied for more than a decade, several manufacturers have recently begun to market transducers adapted for clinical use. The principle of elastography is that tissue compression produces strain (displacement) within the tissue, and the strain is smaller in harder tissue than in softer tissue. Thus, by measuring the tissue strain produced by compression, one can estimate tissue hardness, which could be useful in diagnosing breast cancer.<sup>11</sup> Through color-coding, brightness-darkness, and lesion size on compression, the degree of compressibility of malignant and benign masses can be used as another feature along with morphologic characteristics in differentiating benign from malignant masses.<sup>11-13</sup> Results of research in the usefulness of elasticity imaging and ways to measure mass compressibility will be forthcoming in the next few years.

Except for some niche applications, color and power Doppler imaging have not significantly increased the specificity of mass characterization above and beyond that of morphologic assessment. For circumscribed hypoechoic masses thought possibly to be cysts, power Doppler can

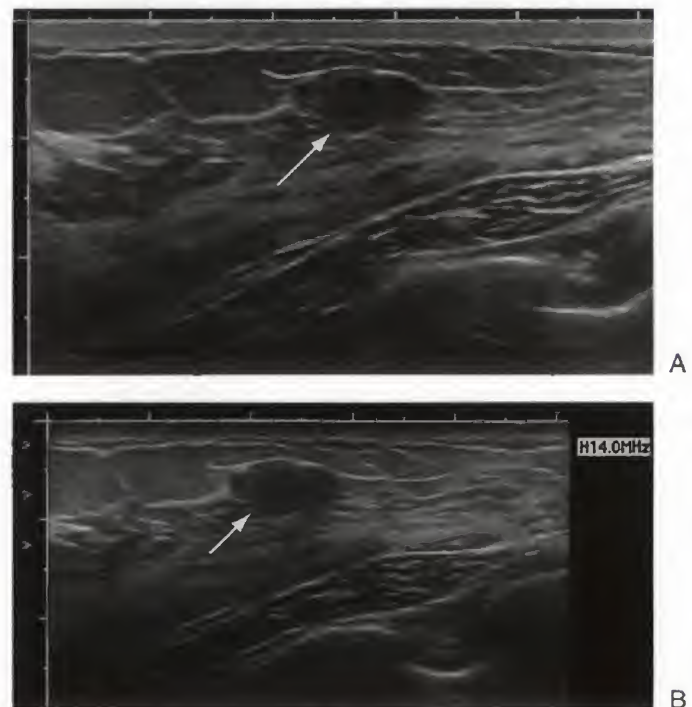


**FIGURE 34-3.** Spatial compounding and tissue harmonic imaging. *A.* Biopsy-proven hypoechoic fibroadenoma (*arrow*) is in an interlocking pattern with surrounding fat lobules. The mass could be mistaken for a fat lobule. Spatial compounding reduces speckle. *B.* With tissue harmonic imaging added to spatial compounding, the heightened contrast increases conspicuity of the fibroadenoma. The fibroadenoma (*arrow*) lies at the junction of the hypoechoic zone of fat lobules and the more echogenic fibroglandular tissue. Hypoechoic ducts of normal caliber, some branching, can be seen within the fibroglandular tissue.



excite motion of particles within thick fluid. Color Doppler can be used to show absence of internal flow with demonstration of some vascularity at the rim or tissue surrounding the lesion. For Doppler imaging, scanning pressure should be very light, enough only to maintain contact so that the blood vessels are not occluded by compression of the tissue. Although research using intravenous contrast materials has been performed in Europe, the United States Food and Drug Administration has not yet approved contrast medium for breast US.

## The Breast Ultrasound Examination

For optimal, high-resolution scanning of the breast with high frequency probes, a basic principle is to minimize the thickness of tissue to be traversed by the acoustic beam. The breast is a cooperative organ in its mobility: For the outer breast, a patient can be positioned obliquely to her opposite side with a bolster or wedge to support her back and shoulder. The breast tissue falls contralaterally and the thickness of the outer half reduced compared with a fully supine or upright position. For most women, the preponderance of fibroglandular tissue is in the upper outer quadrant. Most of the pathology resides there as well. Similarly, for the medial breast, the bulk of the breast tissue falls laterally when the patient is fully supine, decreasing the skin-to-pectoral muscle distance in the inner half of the breast.

Mammography, US, and the clinical picture should be brought together and US adapted to answer the questions raised in an individual case. As an example, if the patient best feels a mass in her breast when she is seated or standing, the sonogram can be performed with her in the position she best feels the mass. For each patient and for each breast lesion being studied with US, the focal zones and gain settings should be adjusted and image presets selected to ensure both an adequate grayscale as well as sufficient contrast to identify a mass of slightly different echogenicity compared with adjacent normal tissue. For establishing the location of a mass on or within the skin, a thin offset pad or mound of gel should be used to place the superficial mass within the focal zones of the transducer.

The images should be labelled with the patient's name and an identifying number (medical record number, birth date, and so forth), name and location of the facility, initials or other identifier of the person performing the study, breast laterality (right or left), clock-face notation, distance from the nipple in centimeters, and view, such as transverse, longitudinal or sagittal, oblique, radial (as in hands of a clock rotating 360° around the nipple), and the orthogonal, antiradial projection.

For survey breast US, quadrant-by-quadrant systematic scanning in overlapping views in two projections, including the retroareolar area and axillary regions will result in complete evaluations. The recording of images is controversial, and there is no consensus; some breast imagers record a radial view of each quadrant if no abnormality is present, and others will record only patient demographics for documentation that a scan had been performed.

If a mass or other abnormality is found on either targeted or survey scanning, images should be recorded in two projections, the first being the longest dimension found and the second a view perpendicular to the first. The naming of

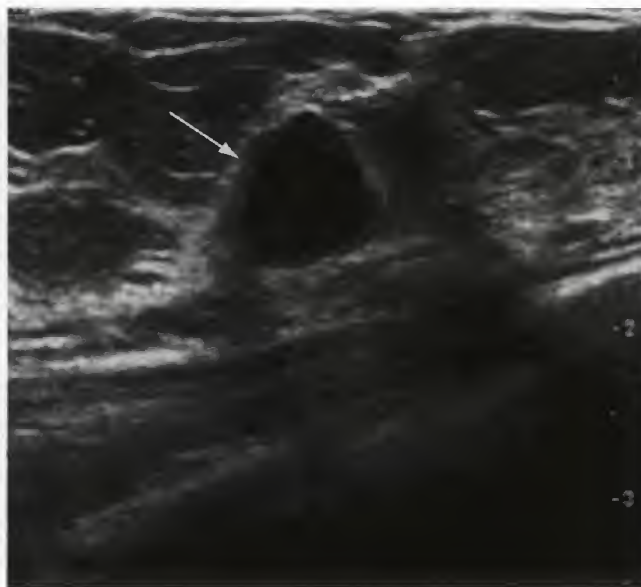


**FIGURE 34-4.** Staging carcinomas: measurement of size. Invasive ductal carcinoma is predominantly hypoechoic, but the mass is indistinctly separated from the echogenic halo (arrow) that surrounds it. The halo may or may not contain tumor cells, but two measurements, one of the hypoechoic area alone and a second, the diameter of the hypoechoic component plus the echogenic rim, could be reported.

these projections should reflect the position of the transducer against the breast in the recorded images. Although some masses may develop along planes defined by the ductal segments, such as radial, many masses do not. Scars, abscesses, and many cancers are not oriented radially, and transducer orientation might accurately be labelled oblique.

Measuring masses can be problematic. The longest axis of a mass should be located, recorded, and measured at its boundary. When the mass is circumscribed, the edge of the mass is easy to recognize. When the borders of a mass are indistinct and there is no abrupt transition between the mass and the tissue surrounding it, as is the case in many carcinomas, it is more difficult to know where to place the calipers. Remember that the size of a cancer is important in its staging. Perhaps the best recommendation is to measure the hypoechoic portion in three dimensions and then to measure the hypoechoic portion along with the echogenic halo surrounding the lesion (Fig. 34-4). The halo may or may not contain tumor cells or just reflect desmoplastic response or compression of the fibroglandular parenchyma.

## Anatomy

The breast is a modified sweat gland located between two layers of superficial pectoral fascia on the anterior thorax between the second and sixth ribs. The posterior layer of pectoral fascia lies anterior to the pectoral muscle and the anterior layer of this fascia lies just beneath the skin. Portions of the anterior layer are sometimes seen on sonograms as curved echogenic lines just posterior to the deeper of the two layers of skin (Fig. 34-5). Cooper ligaments, the connective tissue suspensory ligaments supporting the breast, straddle



**FIGURE 34-5.** Skin. Normal skin of the breast is a 2-mm complex (arrow) composed of two echogenic lines with a thin hypoechoic layer sandwiched between. The complex can have slight increased thickness at the areola and in the lower breast. An offset pad or mound of gel is needed to bring the skin into focus.

the two fascial layers and can also be identified on both mammograms and sonograms.

With considerable individual variation, 12 to 20 duct segments comprise the breast, along with fat and stroma. The duct segments end in puncta at the nipple, a contractile protuberance surrounded by the pigmented areola, widely variable in its width. In the areola are sebaceous glands of Montgomery, some of which may communicate with lactiferous ducts. Normal ducts vary in caliber ranging from less than 1 mm in diameter in the central breast to more than 5 to 8 mm near the nipple. As the ducts arborize, they become smaller and smaller, eventually ending in lobules, similar to leaves emanating from twigs. The lobules are approximately 3 mm in greatest dimension. The significant anatomic structure in the breast is the terminal duct-lobular unit, where cancers arise as well as cysts and fibroadenomas. Acini within the lobules may distend with fluid, forming microcysts (Fig. 34-6). Lobules are not present in the vestigial male breast, and unless a man has been receiving estrogenic therapy for prostate carcinoma or if he has an XXY chromosome (Klinefelter syndrome), one would not expect a breast mass to be either a fibroadenoma or cyst. In many women, a cone of fibroglandular parenchyma, flanked on either side by subcutaneous fat can be seen, with ducts passing through it on their way to the nipple (Fig. 34-7).

A premammary layer of subcutaneous fat is identifiable on US images. The fat lobules that comprise this layer are larger than those in the posterior fat layer that is found anterior to the pectoral muscle. These fat lobules often are oval in one view and outlined by a thin, echogenic layer of connective tissue (Fig. 34-8). Fat, hypoechoic in the breast compared with elsewhere in the body, is the reference tissue for echogenicity, not fibroglandular tissue, which is more echogenic. The fat-fibroglandular-fat layers can be homogeneous within their layers, or the breast composition can be heterogeneous with an admixture of fat and fibroglandular tissue throughout.

The arterial blood supply to the breast is axillary artery to thoracoacromial, lateral thoracic, and subscapular arteries, as well as subclavian to internal mammary artery. A venous plexus lies beneath the nipple with drainage to intercostal, axillary, and internal thoracic veins.



**FIGURE 34-6.** Microcysts are fluid-containing dilated lobular acini, and these contain milk of calcium layering in the dependent portion of the tiny cysts (arrows). Groups of microcysts can be considered probably benign (Breast Imaging Reporting and Data System category 3, for short interval follow-up, most commonly 6 months) but must be scanned carefully to exclude a solid component. Biopsy is advised for microcysts seen in conjunction with a solid mass or tissue focus.

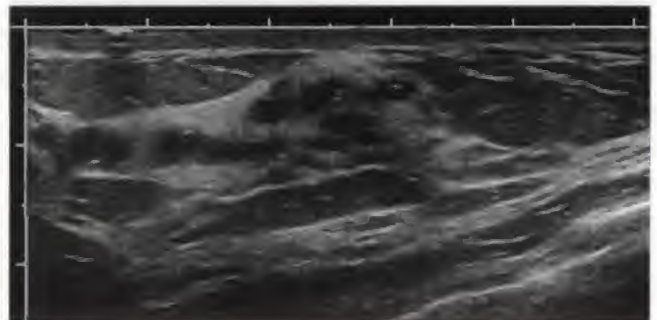


**FIGURE 34-7.** Retroareolar anatomy. In scanning this region of the breast, a central cone of echogenicity through which ducts converge toward the nipple is flanked by hypoechoic fat. Angling the probe from the side of the nipple about 45 degrees accomplishes visualization without shadowing artifact from the uneven surfaces of the nipple. Other techniques include moving the nipple-areolar complex to one side and scanning directly as well as using a small-footprint, high-frequency linear probe.

More than 90% of the lymphatic drainage of the breast is to the ipsilateral axilla, including lymphatics from the subareolar lymphatic plexus and medial lymphatics. A small percentage of lymphatics drain to the contralateral axilla, accounting for crossover metastases, or into the internal mammary chain. Lymph nodes resembling miniature kidneys on US can be identified within the breast and provide the identity of a mammographically-visible nodule when its radiolucent hilus is obscured (Fig. 34-9). Intramammary lymph nodes are usually seen in the upper, posterior two



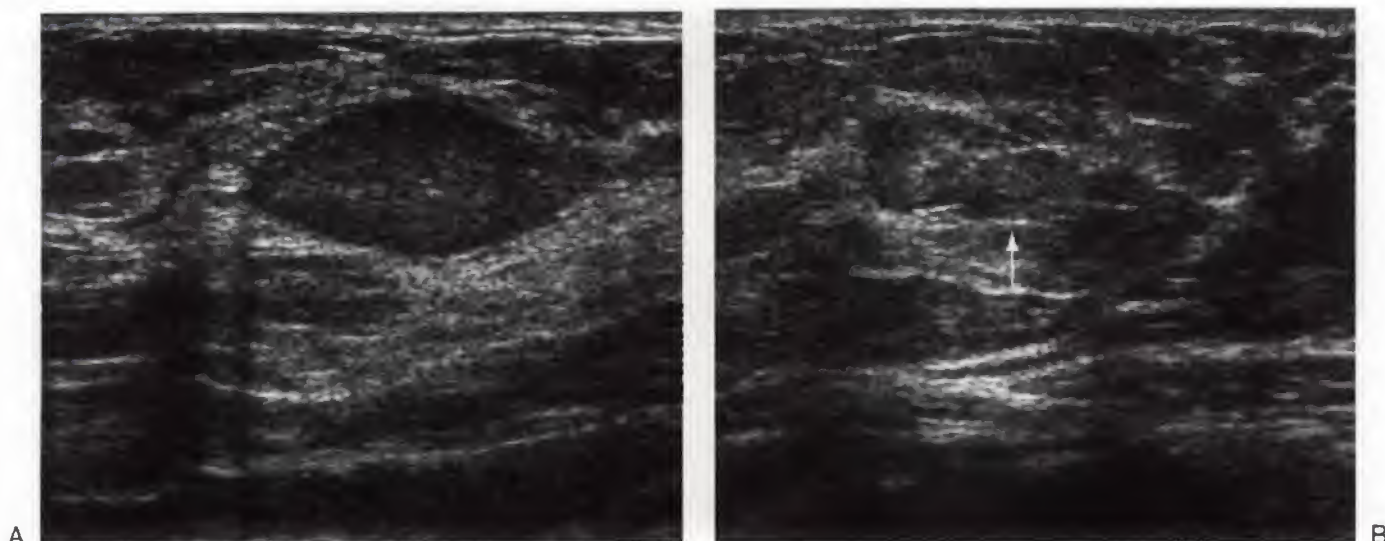


**FIGURE 34-8.** A. Fat lobules in the breast are discrete, may mimic fibroadenomas, and are bound by thin connective tissue capsules. B. Orthogonal view can demonstrate elongation and interconnection of the fat lobules (arrow), excluding a mass.

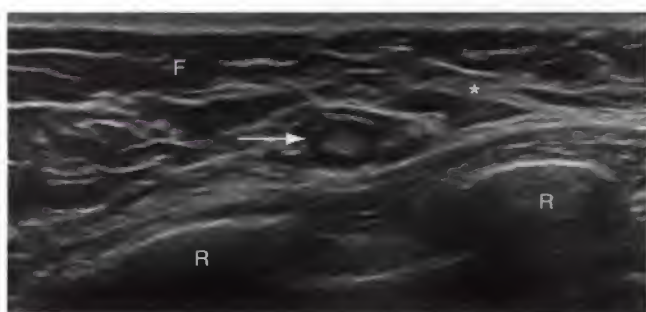


**FIGURE 34-9.** Normal intramammary lymph node resembles a miniature kidney in the center of the image (arrow). The cortex should measure less than 3 mm and be hypoechoic compared with fat. Fat in the hilus of the node is isoechoic with fibroglandular tissue and far more echogenic than breast fat lobules. Rib (R), fat lobule (F), fibroglandular tissue (asterisk).

thirds of the breast, but are found also, but less commonly, in medial locations.

Normal axillary lymph nodes can range in size from less than a centimeter to several centimeters if the node is dominated by fat and has only a very thin cortical rim. To determine whether or not the axilla will be dissected, most breast surgeons currently perform sentinel node imaging at the time of lumpectomy or mastectomy. Injected isosulfan blue dye, technetium sulfur colloid, or both are used, and the affected node or nodes, hot or blue, that appear to drain the tumor are removed. If no metastatic tumor is found within the node, the axilla is spared surgical exploration. If an abnormal lymph node with a cortical bulge containing a focal area of increased or decreased echogenicity, or an abnormally large, dense, rounded node is found on mammography, US can be used to direct sampling of the abnormal-appearing portion of the lymph either with fine

needle or core biopsy (Figs. 34-10 and 34-11). If metastatic involvement is confirmed, the sentinel node procedure is unnecessary and the surgeon will remove axillary nodes.

An US probe angled between the second and fifth ribs from a parasternal vantage point can be used to identify internal mammary lymph nodes, but many breast oncologic surgeons do not harvest these nodes. Unless there is some action attendant upon identification of internal mammary nodes, it is unnecessary to look for them.

The skin of the breast is thin, and with US, seen as a complex of two echogenic lines separated by a narrow hypoechoic band, that measures 2 mm or less, except at the areola and in the lower posterior breast near the inframammary fold.

## Lesion Feature Analysis and Interpretation

Just as systematization of descriptors for mammography has provided a framework for assessment, management, and reporting, a set of feature categories for US and a lexicon of descriptors within these categories formalizes pattern recognition and makes possible the consistent classification of breast lesions.<sup>2,4-6</sup> No one feature alone can be relied upon for diagnosis, and using combinations of features to analyze a mass, breast imagers can be more confident in classifying solid masses seen on US as benign, indeterminate, or malignant (Table 34-1, American College of Radiology Breast Imaging Reporting and Data System [BI-RADS] Lexicon). Final assessment categories similar to those used for mammography can be applied to US and multimodality breast imaging assessments. The phrases accompanying the final assessment categories are required by Federal law (the Mammography Quality Standards Act of 1992) to be given in any diagnostic mammography report unless additional imaging (category 0 or Incomplete) is recommended. In the last edition of BI-RADS, integrated reporting of

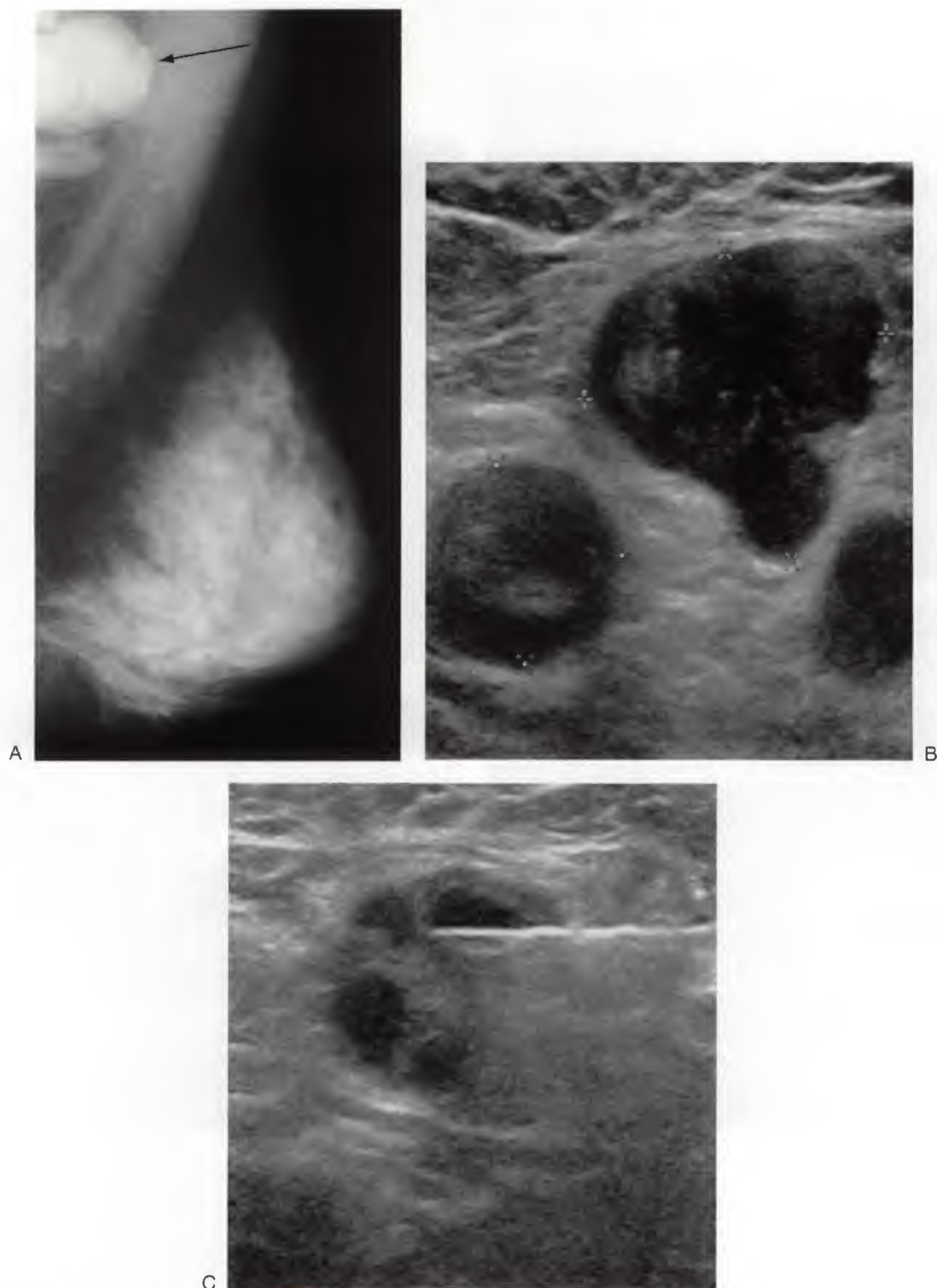


**FIGURE 34-10.** Abnormal lymph nodes: tuberculosis. *A.* Mediolateral oblique mammogram shows dense, enlarged lymph node in the left axilla (*arrow*) of a woman 32 years of age. No abnormality is seen in the breast. *B.* Sonogram of axillary nodes shows cortex to be markedly thickened to 1 cm and containing hypoechoic foci. Biopsy is required to differentiate between metastatic and benign reactive lymph nodes. *C.* Ultrasound-guided core biopsy performed with ultrasound guidance demonstrating the needle directed into one of the hypoechoic areas in nodal cortex. Pathology revealed caseating granulomas with culture of acid-fast bacilli consistent with tuberculosis.



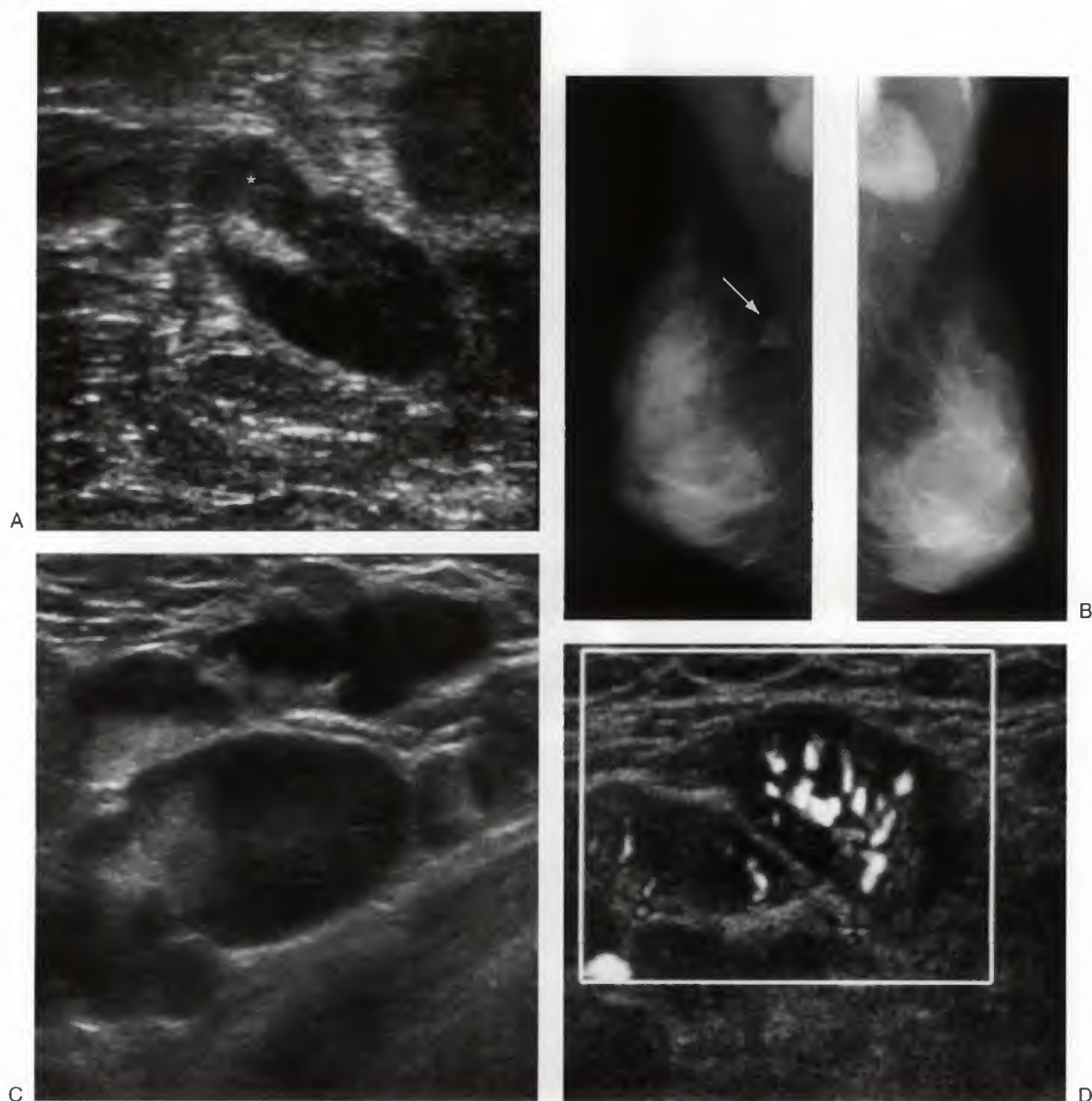


**FIGURE 34-11.** Abnormal lymph nodes. **A.** Metastatic breast cancer in lymph node. A woman 57 years of age with invasive ductal carcinoma. Lymph node was detected during survey scan performed to evaluate extent of disease. Although the node is only slightly enlarged, the upper anterior cortex (*asterisk*) is thickened, lobulated, and hyperechoic. Presence of hilar fat is not a reliable sign of benign etiology, and biopsy is indicated. **B.** Chronic lymphocytic leukemia. Mediolateral oblique mammograms show massive bilateral lymph nodal enlargement, a hallmark of chronic lymphocytic leukemia. Note enlargement also of low axillary or intramammary lymph node (*arrow*), right breast. **C.** Chronic lymphocytic leukemia ultrasound (US) of right axilla shows group of bulky lymph nodes correlating with mammographic findings. The border between the hilar fat and cortex of these nodes is blurred, and the cortex is extremely thick. Similar findings were present in US examination of the left axilla. **D.** Color Doppler sonogram of right axillary lymph nodes in a patient with chronic lymphocytic leukemia showing flow in hilus of node. US can be used to guide the needle's path toward the thick area of cortex and away from the vascular hilus.

**Table 34-1****ACR BI-RADS-Ultrasound Lexicon  
Classification Form**

A. Masses: A mass occupies space and should be seen in two different projections.

<i>Shape</i>	<i>Posterior Acoustic Features</i>
Oval	None
Round	Enhancement
Irregular	Shadowing
	Combined pattern
<i>Orientation</i>	<i>Surrounding Tissue</i>
Parallel	Identifiable effect
Not parallel	Duct changes
<i>Margin</i>	<i>Cooper ligament changes</i>
Circumscribed	
Not circumscribed	
Indistinct	
Angular	
Microlobulated	
Spiculated	
<i>Lesion Boundary</i>	<i>Edema</i>
Abrupt interface	Architectural distortion
Echogenic halo	Skin thickening
<i>Echo Pattern</i>	<i>Skin reaction/irregularity</i>
Anechoic	
Hyperechoic	
Complex	
Hypoechoic	
Isoechoic	

B. Calcifications: Calcifications are poorly characterized with ultrasound but can be recognized particularly in a mass.

Macrocalcifications  
Microcalcifications out of mass  
Microcalcifications in mass

C. Special Cases: Special cases are those with a unique diagnosis or finding.

Clustered microcysts  
Complicated cysts  
Mass in or on skin  
Foreign body  
Lymph nodes – intramammary  
Lymph nodes – axillary

D. Vascularity

Not present or not assessed  
Present in lesion  
Present immediately adjacent to lesion  
Diffusely increased vascularity in surrounding tissue

Assessment Category

**Category 0 – Incomplete**

*Final Assessment*

**Category 1 – Negative**

**Category 2 – Benign finding**

**Category 3 – Probably benign finding**

**Category 4 – Suspicious abnormality**

**Category 5 – Highly suggestive of malignancy**

**Category 6 – Known cancer**

mammography and US is recommended and, if magnetic resonance imaging (MRI) was performed, inclusion also of its findings.<sup>3,4</sup> Although the equivalent US criteria for probably benign mammographic lesions (BI-RADS category 3, less than 2% likelihood of malignancy), remain to be validated by multicenter data, the fibroadenoma, an oval or macrolobulated, circumscribed, hypoechoic mass with orientation parallel to the skin (Fig. 34-12) has become the prototype of the probably benign mass through common use.<sup>2,4,14,15</sup> It is hoped that analysis of breast lesions reported in the American College of Radiology Imaging Network (ACRIN 6666, [www.acrin.org](http://www.acrin.org)) research study of US for breast cancer screening in women of high risk with mammographically dense breasts will provide additional support.

## INDICATIONS FOR BREAST ULTRASOUND

The indications listed in the American College of Radiology practice guideline for the performance of the breast US examination summarize most of the ways that US is currently used to solve diagnostic problems and include the following list.<sup>16</sup> Breast cancer screening, the province of mammography, is not among the indications.

1. Identification and characterization of palpable and nonpalpable abnormalities and the further evaluation of clinical and mammographic findings.
2. Guidance of interventional procedures.
3. Evaluating problems associated with breast implants.
4. The postsurgical breast including treatment planning for radiation therapy.
5. Initial imaging technique for young (younger than 30 years of age), lactating, and pregnant women.

## Palpable and Nonpalpable Abnormalities

### Density of Breast Tissue

When a patient complains of a mass or thickening of the breast, or is referred for evaluation of a palpable finding on clinical examination, in general, mammography is the initial examination if the patient is older than 30 to 35 years of age. The usefulness of US in problem solving depends in part on the overall mammographic breast density.<sup>17,18</sup> In women with heterogeneously or extremely dense breasts, because of lack of contrast between the mass and the breast tissue around it, a mass that might explain the physical finding can be overlooked or imperceptible (white on white) on a mammogram (Fig. 34-13).

US is indicated for evaluating a palpable mass or one suspected in, or partially obscured by, dense fibroglandular tissue. The mammographic evaluation may include a view tangential to the mass or thickening, on which a small, radiopaque skin marker should be placed. This view may allow the convex anterior border of a mass to be silhouetted in the subcutaneous fat (Fig. 34-14). A well-exposed mammogram in dense breast tissue can depict calcifications in or near the mass, and the standard of care would be violated if mammography were not performed, but an endless number



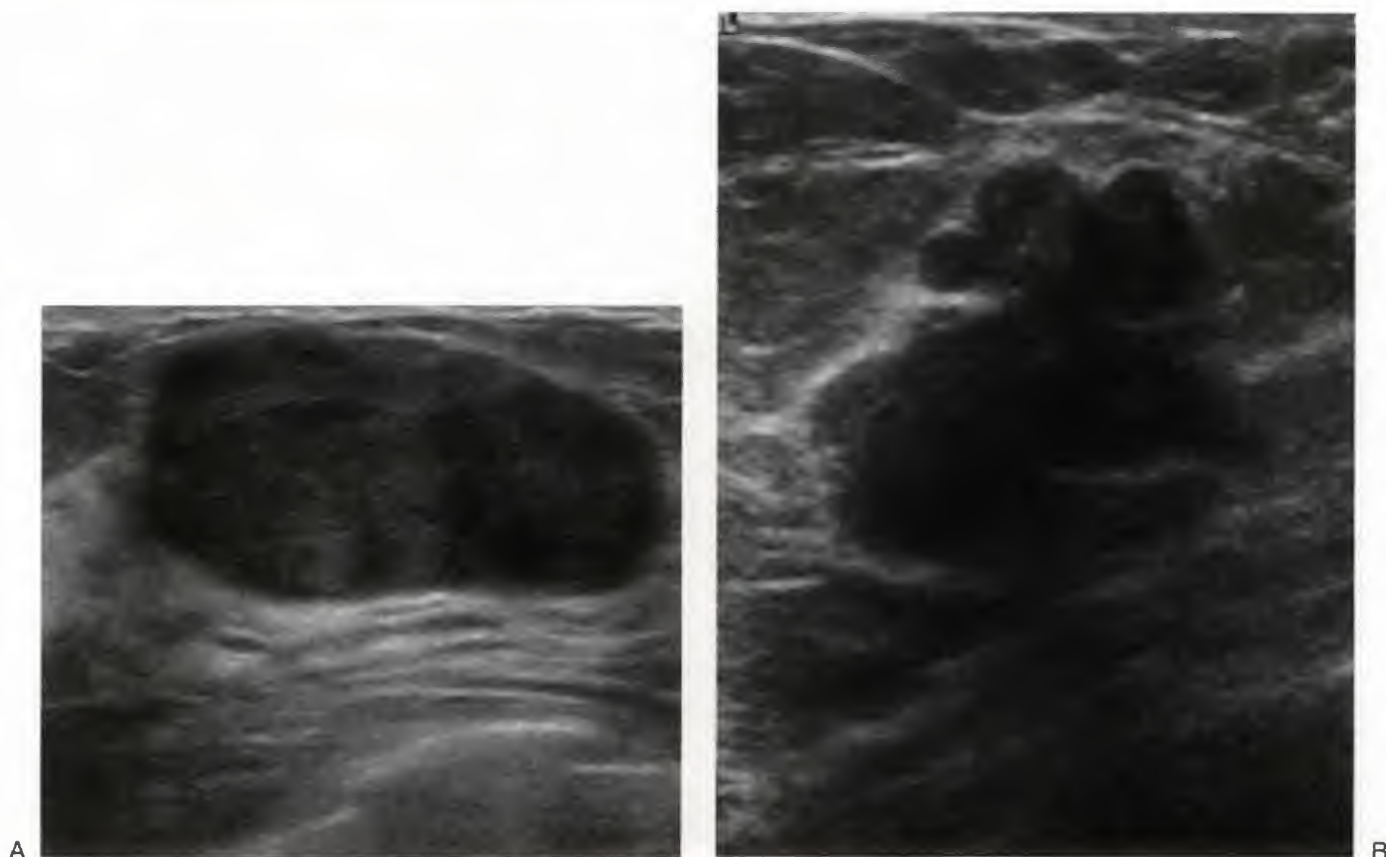


**FIGURE 34-12.** Fibroadenomas. A. Typical fibroadenoma, prototype of the Breast Imaging Reporting and Data System 3 category; probably benign finding. Noteworthy features are oval shape, circumscribed margin, and parallel to the skin. Mass is more hypoechoic than adjacent fat lobules. B. Grouping of fibroadenomas. The micro- and macrolobulation of this aggregate of masses may make it reasonable to biopsy, as in this case.

of additional views that contribute only to the radiation dose without profiling the mass should be avoided. US has the triple function of lesion identification, characterization, and guidance for biopsy, if indicated.

### Calcifications

Additionally, if US is directed to an area of calcifications, an associated mass may be seen (Fig. 34-15). The mass may increase the likelihood of invasive disease, although rarely ductal carcinoma in situ can present as a mass,<sup>18</sup> and US can be used as the imaging guide for tissue sampling (with radiography of the cores to confirm calcifications within the specimens). This application of US is becoming common in current practice.

### Inflammatory Processes Including Inflammatory Carcinoma

When the pathologic process itself contributes to overall breast density significantly enough to limit mammography, US is indicated. An example is an inflammatory process, such as mastitis. In this case, US can be used to identify and guide drainage of an underlying abscess. When inflammatory carcinoma is suspected, tumor masses that are hidden in

dense, edematous breast tissue may be found with ultrasound or MRI (Fig. 34-16).

### Fatty Breast: Need for Ultrasound?

Less clear is the need for US in a site of clinical concern when the mammogram in two views shows the area to be fatty. Although US may not be indicated in these cases and the standard of care does not require it, in the author's experience, US has at times provided specific answers when mammography has been negative but unhelpful, the tissue fatty, and a mass distinctly palpable.

### Negative Predictive Value of Ultrasound and Mammography

In their evaluation of palpable masses, Soo et al<sup>19</sup> studied 420 patients with 455 palpable masses and found that when mammography is negative and targeted US is also negative, the negative predictive value for cancer is high (99.8%). A 99.9% negative predictive value of a negative clinical examination, mammography, and US was also reported for 3516 patients studied by investigators from The Netherlands.<sup>20</sup> If US is performed to confirm or to characterize a mass suspected on mammograms, and if no mass is found, the

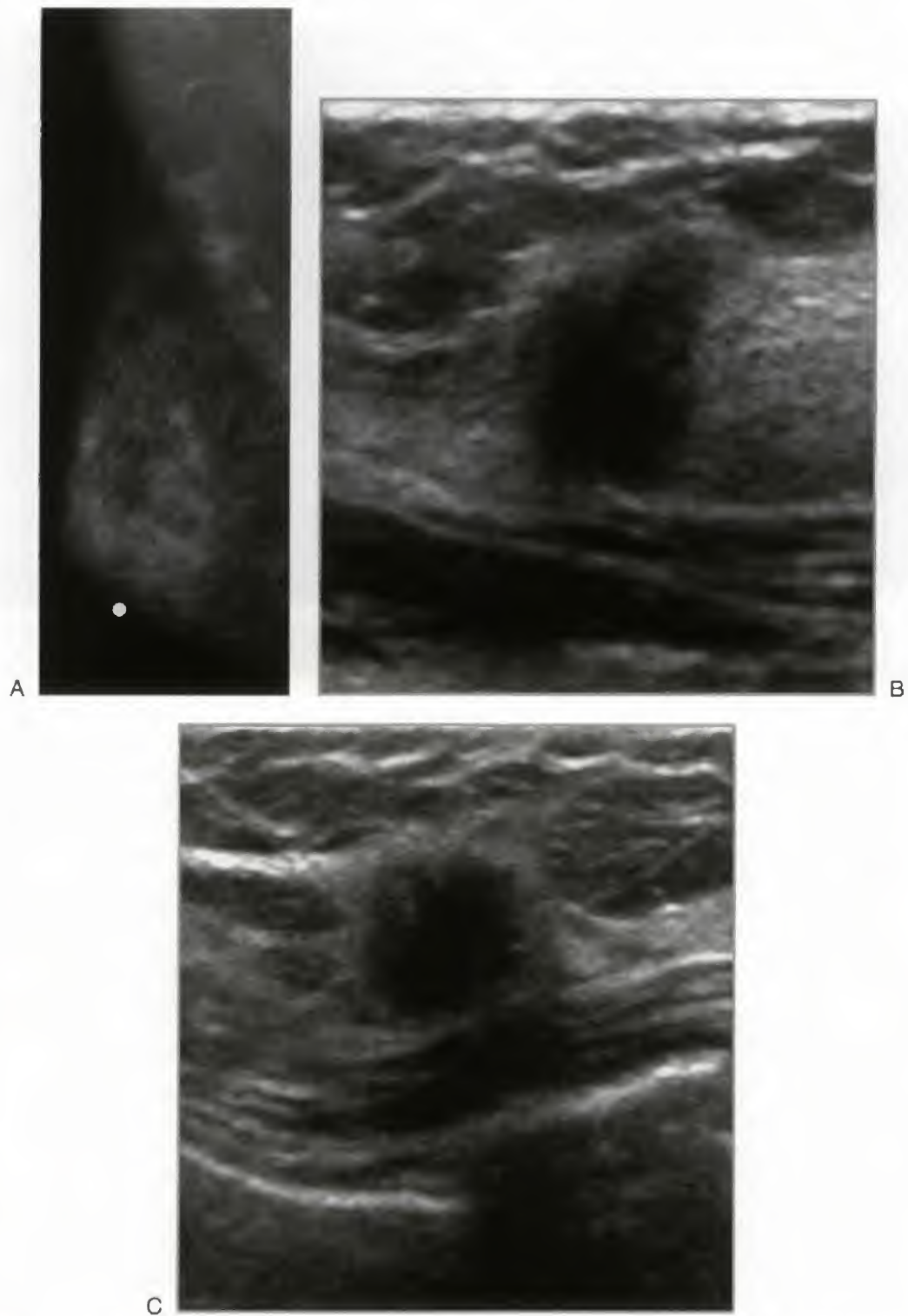


**FIGURE 34-13.** Decreased sensitivity of mammography in dense fibroglandular tissue: role of ultrasound. *A.* Mediolateral oblique mammogram of heterogeneously dense breast. Mass palpable in lower breast (•), is invisible in a background of dense, white fibroglandular tissue on the mammogram. *B.* Ultrasound unmasks a hypoechoic, irregularly shaped, spiculated mass. *C.* On subsequent ultrasound survey, a second abnormal area was identified on the sonogram.



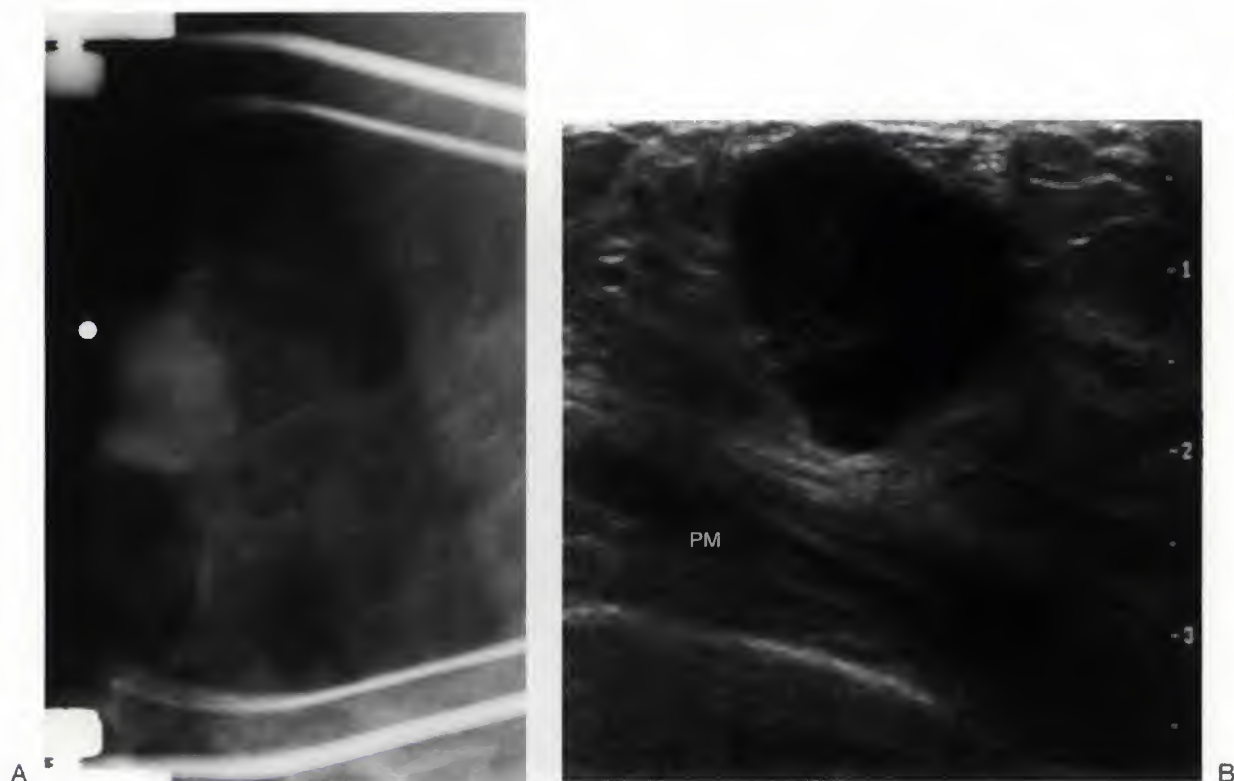


**FIGURE 34-14.** A. Spot compression mammographic view with x-ray beam tangential to mass (♦) frames anterior border of mass in subcutaneous fat. B. Ultrasound shows mass just anterior to pectoral muscle (PM) to be solid, irregularly shaped, and indistinctly margined. As in this case, posterior acoustic enhancement, rather than shadowing, is associated with many poorly differentiated invasive ductal carcinomas.

parenchymal focus that might explain the mammographic findings can be correlated with the shape, size, and anatomic arrangement of fat and fibroglandular tissue on US, accounting also for changes in a patient's position (upright in mammography and supine or supine oblique in US). This correlation supports US exclusion of an abnormality and should be helpful to the referring clinician, but to direct patient management, particularly if a mass or thickening is palpated, a biopsy may be performed if warranted by clinical suspicion.

When mammography is negative but US confirms a mass as the cause of a palpable finding, BI-RADS feature analysis is applied to assess its likelihood of malignancy. Currently, when sonography determines that a palpable mass is solid, many breast imagers and clinicians will recommend or perform biopsy, although the imaging assessment of the mass is benign or probably benign. There have been a few studies reporting on the safety of basing management recommendations on sonographic features of palpable masses.<sup>19,21,22</sup> Each of these methods substantiates the safety of short-term follow-up, commonly in 6 months, if the palpable mass has not been imaged previously. This management protocol is for masses that have benign sonographic features, such as a fibroadenoma: oval shape, circumscribed margin, and orientation parallel to the skin. When a mass has these features but is hyperechoic to fat and isoechoic to fibroglandular tissue, such as a lipoma, its assessment is benign (Fig. 34-17). The follow-up recommendation is for 1 year, and biopsy is unnecessary.<sup>2</sup> The difficulty in arriving at

management recommendations is accentuated when the mass is new or newly palpated, and there is no history of weight loss (accounting for new palpability of a mass that may or may not have been present previously) or change in physician. If the mass is new and not definitively benign by mammographic or sonographic criteria, as lipomas and hamartomas would be, the standard of care would require biopsy, preferably image-guided percutaneous large-needle biopsy for histology rather than an open surgical procedure.

A second scenario in evolving management strategies concerns the use of survey US examinations, unilateral or bilateral, when the patient complains of one palpable mass and US depicts several in one or both breasts. If these masses all look alike and have no sonographic features that are associated with malignancy, why biopsy the palpable one or the largest one? Logic would call for all or none to be biopsied, although many breast imagers defend biopsy of the largest mass or one that is palpable. The dilemma arises commonly when young women with palpable masses are sent by their physicians for breast evaluation, and the palpable mass identifiable with US as a probable fibroadenoma and others may be seen if survey scanning is performed.

### **Ultrasound Guidance of Interventional Procedures**

Of all of the imaging techniques used to evaluate breast abnormalities and guide interventions for tissue sampling or surgical excision, US is the only one to be performed in real

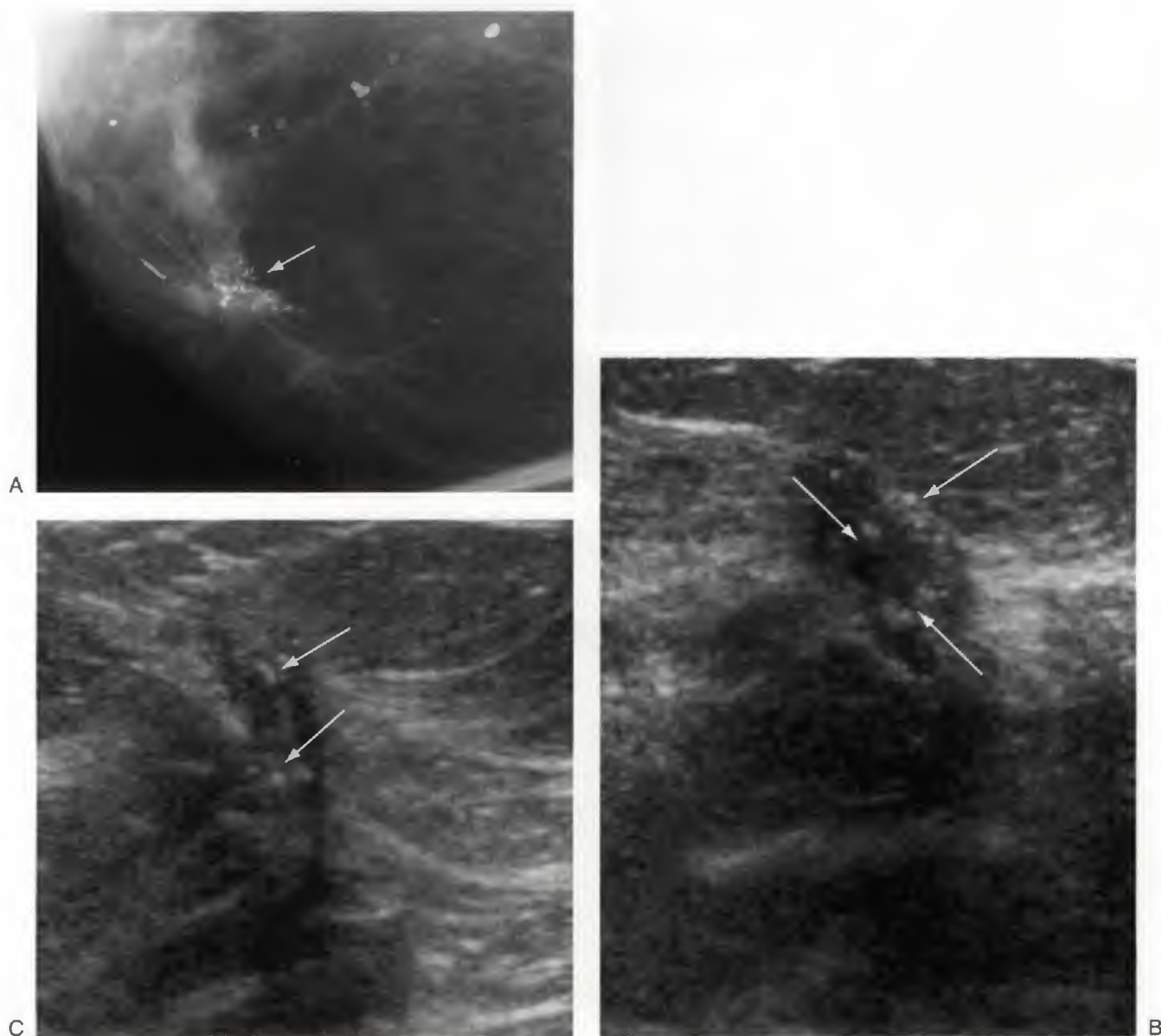


**FIGURE 34-15.** Recurrent carcinoma. *A.* Invasive and intraductal carcinoma. A woman 59 years of age had been treated for high-grade ductal carcinoma in situ with lumpectomy and radiation therapy 4 years earlier. Mammographic view with magnification shows new microcalcifications at lumpectomy site (*arrow*). Linear marker placed on skin denotes surgical incision site for the lumpectomy. *B* and *C.* Ultrasound images show hypoechoic mass containing microcalcifications (*arrows*) in a background of postsurgical architectural distortion correlating with the mammographic finding. Tiny, echogenic foci, the microcalcifications, which measure 0.1 to 0.5 cm in diameter, will not cause posterior acoustic shadowing. The uneven, concentrated distribution of these particles allows differentiation from speckle.



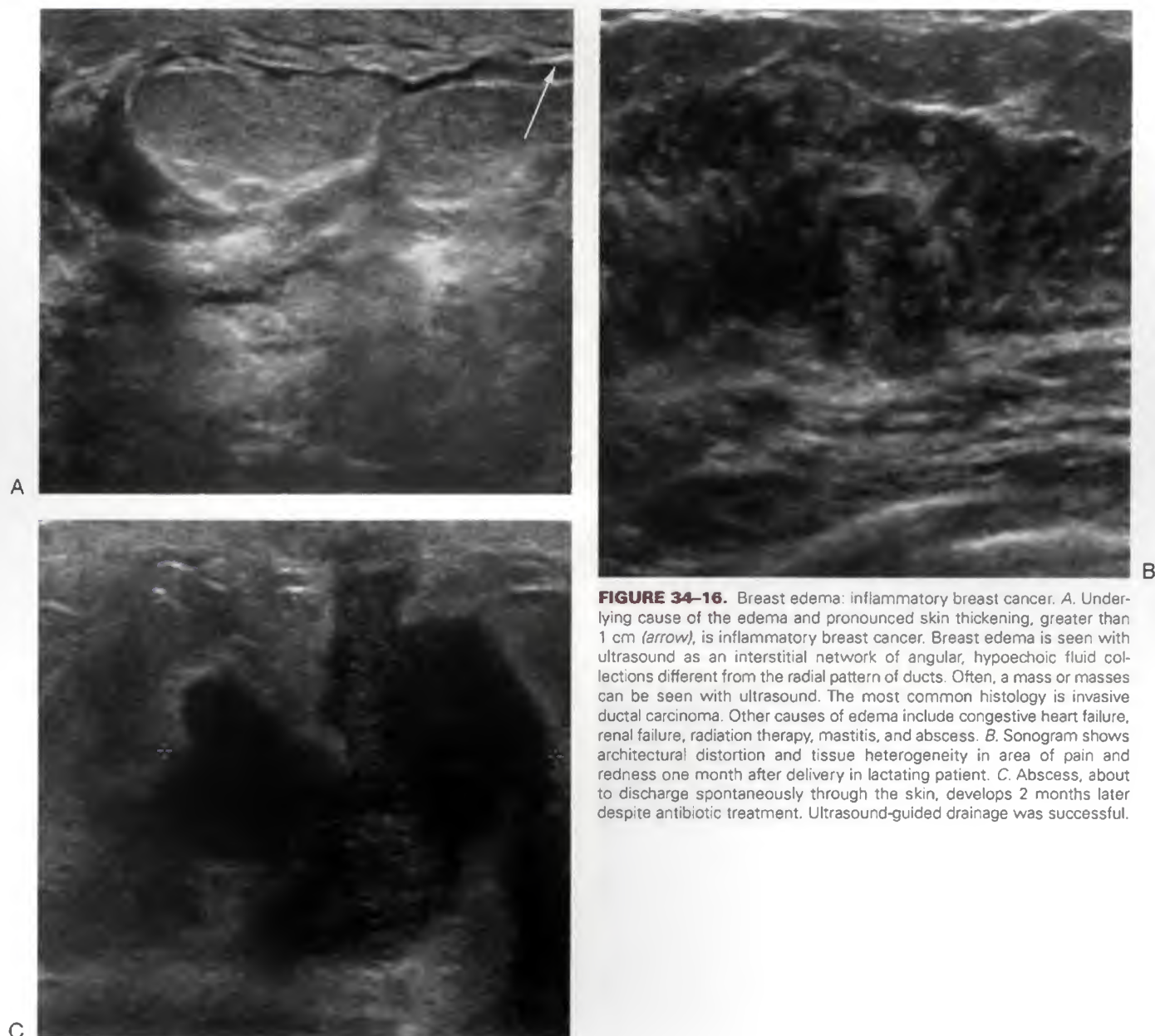


**FIGURE 34-16.** Breast edema: inflammatory breast cancer. *A.* Underlying cause of the edema and pronounced skin thickening, greater than 1 cm (*arrow*), is inflammatory breast cancer. Breast edema is seen with ultrasound as an interstitial network of angular, hypoechoic fluid collections different from the radial pattern of ducts. Often, a mass or masses can be seen with ultrasound. The most common histology is invasive ductal carcinoma. Other causes of edema include congestive heart failure, renal failure, radiation therapy, mastitis, and abscess. *B.* Sonogram shows architectural distortion and tissue heterogeneity in area of pain and redness one month after delivery in lactating patient. *C.* Abscess, about to discharge spontaneously through the skin, develops 2 months later despite antibiotic treatment. Ultrasound-guided drainage was successful.

time. Patients and physicians prefer US guidance for its rapidity, comfort (the patient is supine or supine-oblique rather than prone as she would be for stereotactically or MRI-guided biopsies), reliability, and accuracy. US is the choice for biopsy of solid masses with either spring-activated devices using 12- or 14-gauge needles or with vacuum-assisted devices that yield larger specimens obtained with needles ranging from 8 to 12 gauge, as well as biopsy devices using other mechanisms. If US rather than stereotactic guidance is elected for a mass containing microcalcifications or for microcalcifications identified with US that are not associated with a mass, specimen radiography should be performed to confirm microcalcifications in the biopsy specimens. US is also an excellent imaging guide for pre-surgical localization as well as for aspiration of cysts and drainage of abscesses.

The management recommendations for BI-RADS assessments 4 (suspicious for malignancy) and 5 (highly suggestive of malignancy) are tissue sampling, and image-guided percutaneous biopsies are replacing surgical biopsies in current practice. Probably benign lesions, such as fibroadenomas, are often biopsied as well if requested by the patient or her referring physician, but short-interval follow-up is the suggested management.

In the past, category 5 lesions—those for which cancer is the diagnosis in more than 95%—went directly to surgical excision, frozen section (not reliable for microcalcifications) providing the histologic documentation. It was thought unnecessary to perform needle biopsies before surgical excision. Currently, sentinel node imaging and biopsy are nearing standard of care, and histologic diagnosis of invasive tumor is required beforehand. Image-guided core biopsy

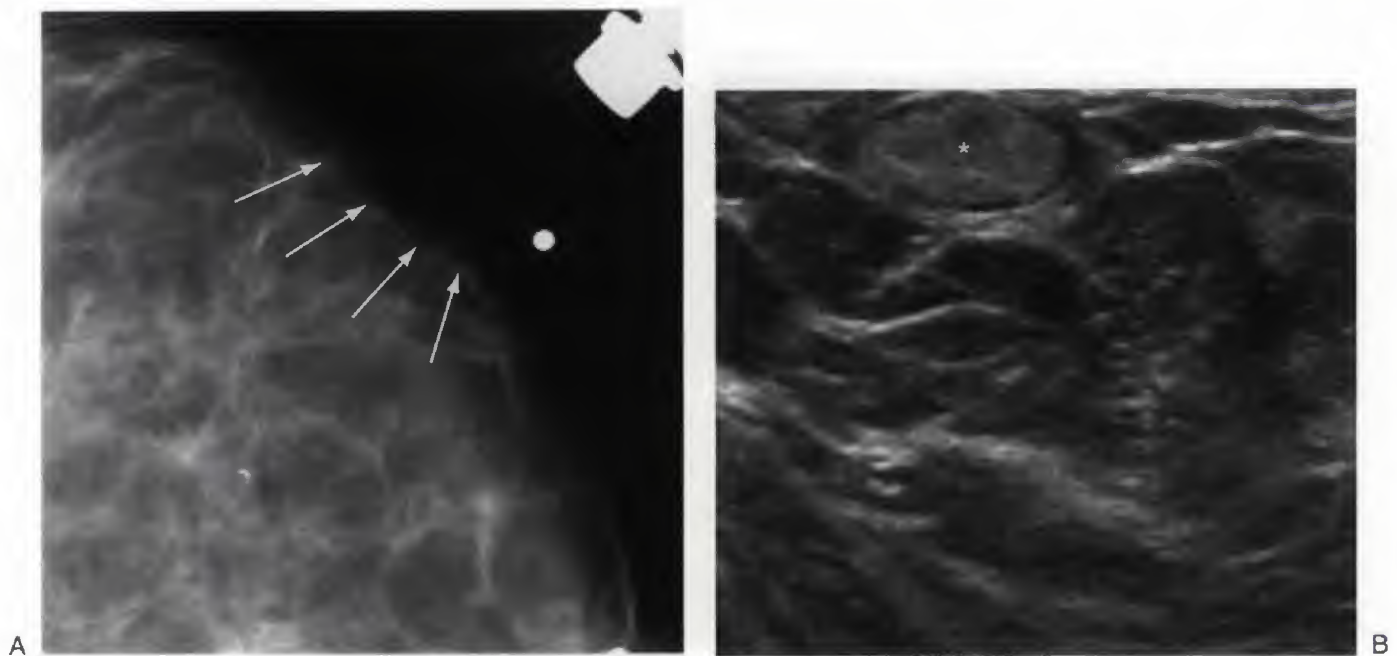


**FIGURE 34-17.** Lipoma. *A.* Spot compression mammographic view tangential to palpable mass, which is marked by metallic BB on skin. Area of fat density lies beneath the marker, arrows outlining its posterior aspect. *B.* Ultrasound image shows encapsulated subcutaneous mass, more echogenic than the fat lobules surrounding it. This represents a lipoma (*asterisk*), correlating with the benign mammographic assessment but providing a specific diagnosis.

specimens can also be used to determine the estrogen and progesterone receptor status, along with other prognostic factors. Most patients with masses and calcifications thought possibly to be malignant are biopsied with imaging guidance before surgery, using US wherever possible.

The biopsy technique calls for written informed consent, sterile draping of the cleansed area of the breast to be biopsied, preparation according to the manufacturer's recommendations of the same high-resolution linear broadband width probe used for scanning (Cidex or glutaraldehyde followed by a sterile water rinse are two ways to prepare the probe), and the entire procedure performed with direct US visualization. The area is anesthetized with 10 mL or more of 1% lidocaine (with epinephrine for hemostasis if vacuum assisted devices are used with 8- to 11-gauge needles), a small incision—a few millimeters—is made in the skin, and approximately five passes are made into the lesion if a spring-activated device and 14-gauge needle are used. The needle is advanced into tissue in alignment with the middle of the short end of the transducer and passes along the long axis of the probe, parallel to the face of the transducer and perpendicular to the expected path of the beam. The more horizontal the entry, the better the entire needle shaft is seen. Most devices that fire will have throws between 2 and 2.3 cm. If the mass is small, less than a centimeter in greatest dimension, to prevent overshooting the target, one should stop short of the targeted lesion by about 1 cm and fire. Specimens are placed in formalin jars, but the needle should never be immersed in formalin and then re-enter the breast.

At the conclusion of the procedure, for small masses that may be obscured by the biopsy procedure itself or large malignant-appearing masses that may be treated with several cycles of neoadjuvant chemotherapy prior to surgery,

tiny marker clips should be placed within or adjacent to the biopsied lesion. The marker clips of titanium, stainless steel, or ceramic are preloaded into needles and once the biopsy location has been verified with US, the clips can be deployed. Lateral and craniocaudal mammographic views should be taken after clip placement for correlation of mammographic and sonographic findings as well as to document the proximity of the clip to the lesion or biopsy site (Fig. 34-18).

If image-guided biopsy services are provided for patients, it is the responsibility of the breast imager who has performed the biopsy to receive the histopathology interpretation, make certain that it is concordant with the prebiopsy assessment, and notify the patient or referring physician with the biopsy results and a management recommendation.

With increasingly frequent use of contrast-enhanced MRI for evaluation of the extent of disease in newly diagnosed breast cancer patients as well as for screening of high-risk women, especially those who have breast cancer (BRCA) 1 and 2 genetic abnormalities, second-look US is commonly performed to locate a mass that correlates with an enhancing lesion seen on MRI. Biopsy can then be guided with US and accomplished more rapidly, in real time, and more comfortably for the patient than an MRI-guided biopsy, in which the patient is prone and requires intravenous administration of gadolinium for lesion visualization, breast compression for lesion targeting, and several MRI sequences to confirm accuracy.

### Evaluating Problems With Breast Implants

Indications for breast US in women with augmented breasts are the same as those for women without breast prostheses, with the additional application of US to determine the



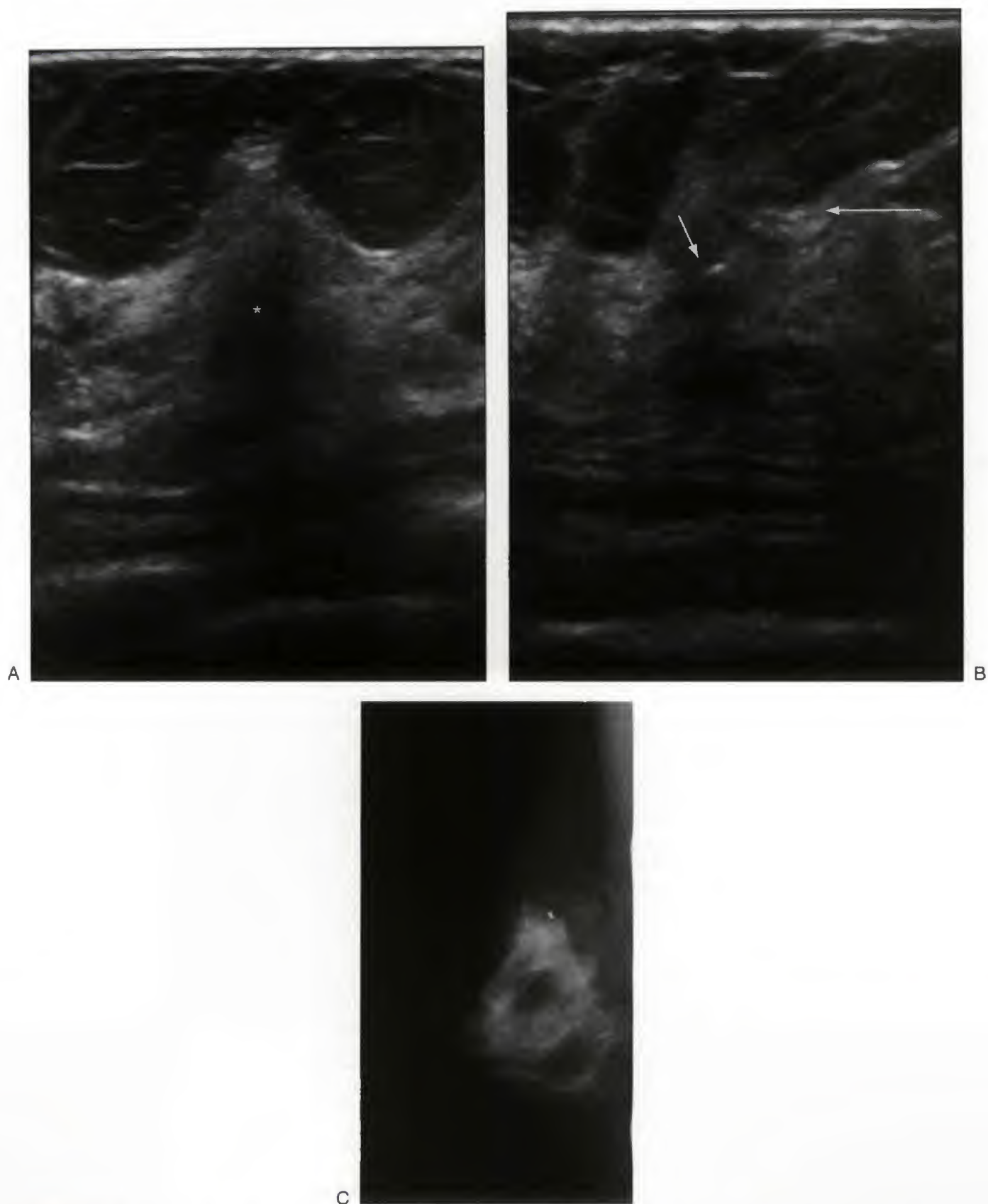


**FIGURE 34-18.** Marker clip. A. Small indistinctly margined mass (*asterisk*) before ultrasound-guided core needle biopsy. B. After biopsy, with ultrasound guidance, a small marker clip (*short arrow*) was placed within the mass. Microcalcifications are present adjacent to the mass (*large arrow*). After marker clip placement, it is important to obtain lateral and craniocaudal mammograms that can be used later to guide presurgical localization and to detect clip migration should it have occurred. C. Mediolateral oblique mammogram confirms clip placement within a small, low-density mass, a mixed invasive ductal and lobular carcinoma. Clip can be used as target for needle-wire placement for presurgical localization before excision.

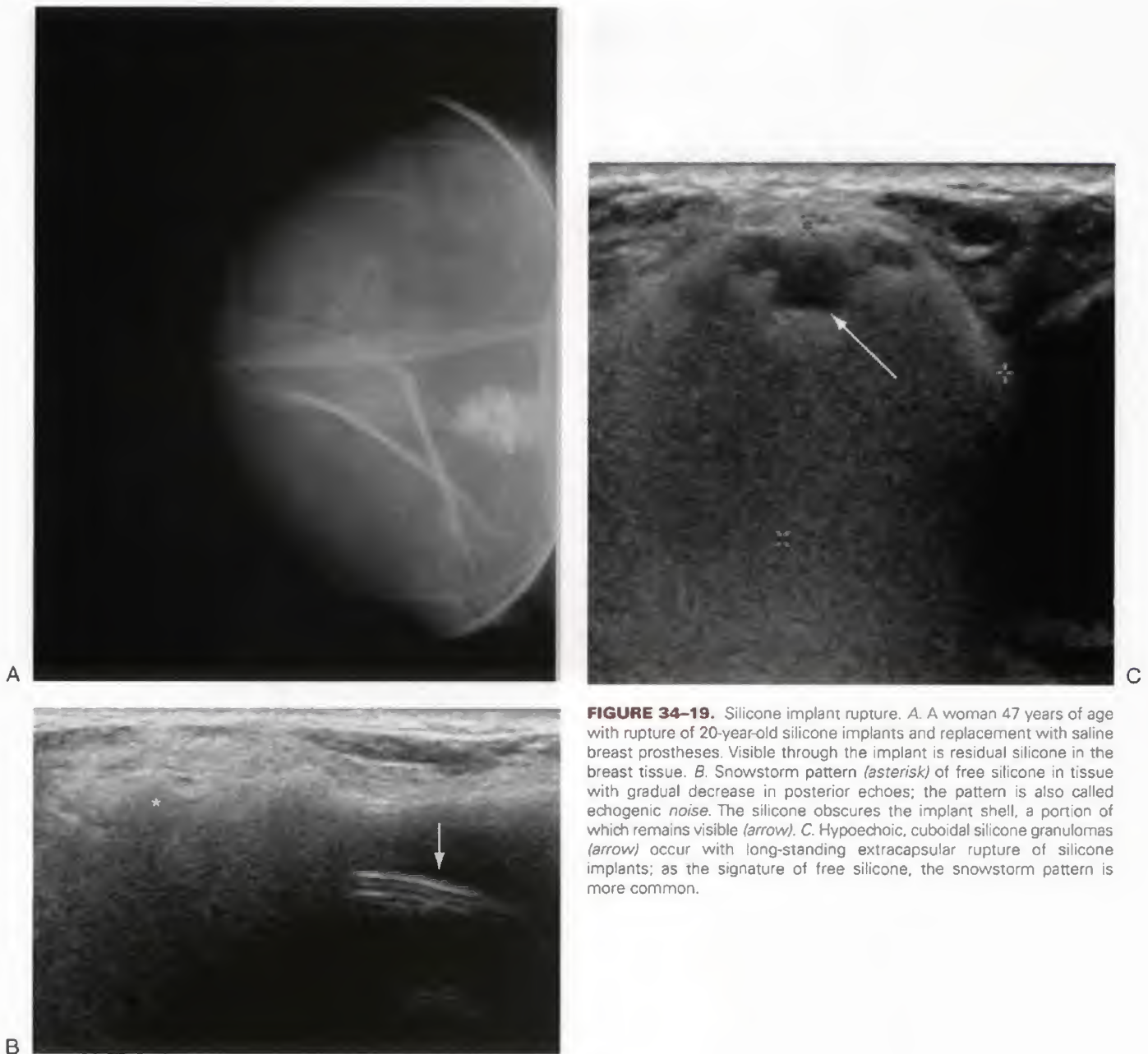


**FIGURE 34-19.** Silicone implant rupture. **A.** A woman 47 years of age with rupture of 20-year-old silicone implants and replacement with saline breast prostheses. Visible through the implant is residual silicone in the breast tissue. **B.** Snowstorm pattern (*asterisk*) of free silicone in tissue with gradual decrease in posterior echoes; the pattern is also called *echogenic noise*. The silicone obscures the implant shell, a portion of which remains visible (*arrow*). **C.** Hypoechoic, cuboidal silicone granulomas (*arrow*) occur with long-standing extracapsular rupture of silicone implants; as the signature of free silicone, the snowstorm pattern is more common.

nature of palpable masses as either originating in the breast, as a breast lesion, free silicone or silicone granuloma, or related to the implant as a wrinkle, fold, or shell irregularity. Although MRI has been found to be more sensitive and specific in identifying intracapsular and extracapsular rupture of silicone implants, the “snowstorm” or “echogenic noise” US signature of extravasated silicone is characteristic (Fig. 34-19).<sup>24-27</sup> US can also suggest intracapsular rupture, whatever its clinical significance, by depicting shreds of implant shell floating within the silicone gel and producing a stepladder of echogenic lines or wavy echogenic bands. For evaluating a palpable mass, before recommending MRI, US should be used as a lower cost, more rapid, reliable method of making the important distinction of the origin of a mass

within the breast rather than as related to the implant. At the same time, if the mass is of breast origin, it can be characterized as cystic or solid, and its features analyzed using BI-RADS to assign a level of suspicion of malignancy. For saline implants, the use of either MRI or US is unnecessary to confirm rupture of clinically apparent deflation.

### The Postsurgical Breast and Treatment Planning for Radiation Therapy

After the surgical excision of a breast malignancy, a seroma nearly always develops at the lumpectomy site. Septa or clumps of echogenic material may be present within the



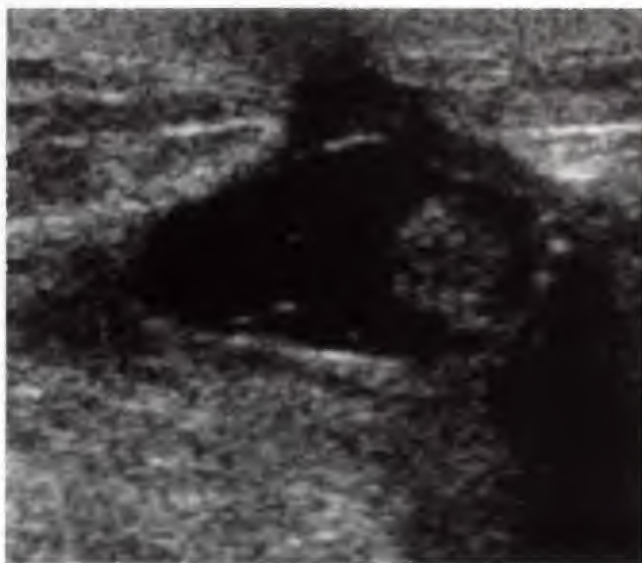


**FIGURE 34-20.** Postsurgical fluid collection after lumpectomy for carcinoma. Nearly all lumpectomy patients have seromas that may last for weeks or months after the surgical procedures. The collections are not drained unless there are clinical signs of abscess formation. The skin is focally thickened at the incision site, and fluid collects within the tract made by the scalpel. As the fluid is gradually resorbed, scarring develops at the lumpectomy site, the circumscribed margins of the fluid collection replaced by spiculation as a manifestation of scarring. Sequential studies that track these changes over time can help exclude recurrence.

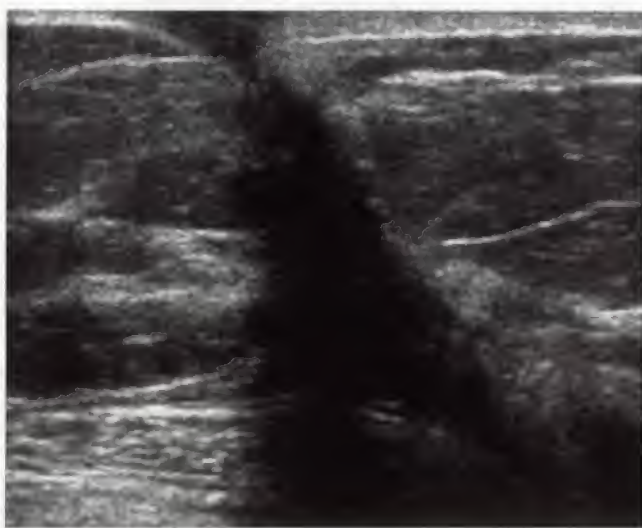
fluid collection, but unless the patient shows signs of abscess, the fluid collection should not be aspirated (Fig. 34-20). Abscess formation is unusual, and the gradual resorption of fluid over a period of months is thought to promote cosmesis by preserving the normal contours of the breast rather than creating a crater in the breast by draining the fluid collection. Unless significant mass remains in the breast after lumpectomy, neither mammography nor US can be relied upon to show the residual tumor; here, contrast-enhanced MRI may show clumped enhancement at the involved tumor margin.

After 6 to 12 months have elapsed, the seroma will have been resorbed gradually and replaced by scarring with imaging features similar to those of malignancy. The margins of the scar are spiculated and indistinct, and posterior acoustic shadowing replaces the seroma's enhancement. Knowledge of the marginal status at excision, sequential studies, and the ability to follow the path of the scalpel from the skin, where there is focal thickening in a V pattern, down to the tumor bed helps in excluding recurrence (Fig. 34-21). As with mammography, a new mass or other interval change at or near the lumpectomy site can signal recurrence. The average time to local recurrence after lumpectomy and radiation therapy is 3 years, and between 3 and 7 years, recurrent tumor is most likely to be found within a few centimeters of the lumpectomy site.<sup>27-29</sup>

There are various methods of demarcating a lumpectomy site for radiation therapy. Computed tomography (CT) can be used, and some surgeons mark the boundaries of the lumpectomy site with surgical clips to facilitate radiation treatment planning. US can provide the shortest distance from the skin to a carcinoma for presurgical needle-wire



A



B

**FIGURE 34-21.** Changes after breast conserving therapy. A. Scar after lumpectomy and radiation therapy. Tangential mammographic view shows focally thickened skin 5 years after breast conservation for carcinoma. The focal thickening does not resolve, and wisps of scar around the tumor bed are expected findings. B. US shows findings similar to those seen on the mammogram: a "V" at the skin incision site, with focal thickening, and intense scarring along the scalpel tract extending from the skin to the tumor bed just anterior to the pectoral muscle. Recurrence, not present, would be evident as a new mass or microcalcifications adjacent to the scar or a bulbous enlargement within the tumor bed after the site has been stable for a year or more. Average time to local recurrence is 3 years.

localization of a nonpalpable mass, once the excision has been performed. Likewise, the target area for radiation therapy can be mapped with US more directly using its real-time capabilities, although radiation oncologists more commonly use CT simulation for treatment planning.<sup>27,28</sup> For whole breast irradiation with a boost, the depth of the tumor bed from the skin surface can be shown, the dimensions and shape of the fluid collection can be depicted on orthogonal views, and its volume calculated from dimensions in these views.

More recently, another application of US in radiation treatment planning for breast cancer has been identified. Partial breast irradiation, a brachytherapy procedure with radioactive seeds (Iridium 192) delivered to the lumpectomy

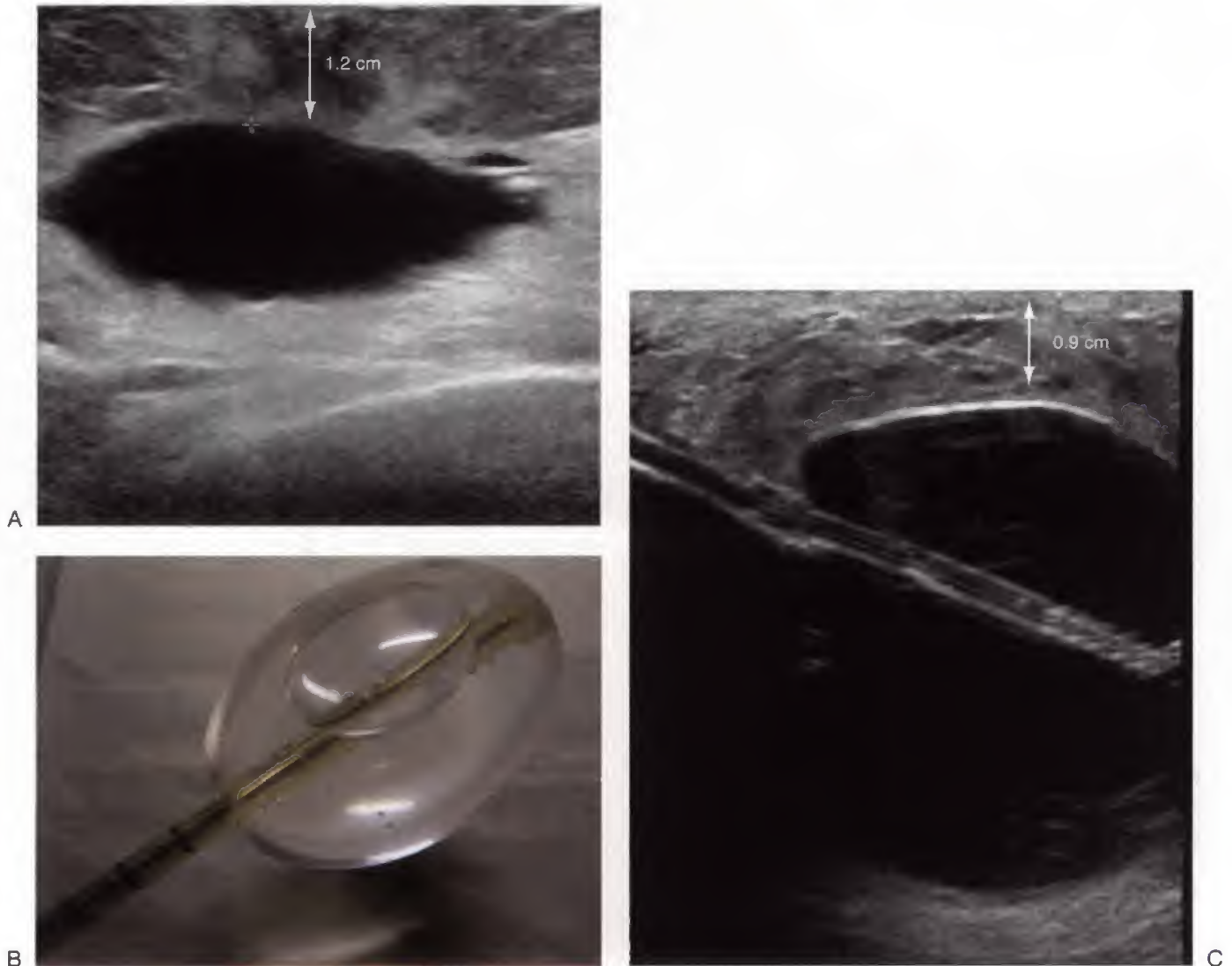


**FIGURE 34-22.** Ultrasound guidance for device for partial breast irradiation. *A.* Ultrasound scan confirms eligibility: seroma is ample and tissue thickness between skin and top of seroma, which must be at least 0.6 cm, is 1.2 cm. *B.* The fully inflated balloon shown filled with saline during preplacement testing. *C.* Balloon catheter placement is successful. The fully inflated balloon occupies the entire lumpectomy cavity, and the remeasured skin-to-balloon surface distance remains acceptable.

site through a balloon catheter (MammoSite, Cytac Corporation, Marlborough, MA) or several other techniques, has become an option for some women with small invasive or in situ tumors. High-dose radiotherapy is delivered twice a day through these catheters, which can be placed either surgically at time of lumpectomy or percutaneously with US guidance. Some protocols, such as National Surgical Adjuvant Breast and Bowel Project B-39 (A Randomized Phase III Study of Conventional Whole Breast Irradiation Versus Partial Breast Irradiation for Women with Stage 0, I, or II Breast Cancer), call for histologically free margins of resection, which may take 24 hours or more to establish. If the device is to be placed with US guidance within the first weeks following surgical excision of the tumor, US is used to determine eligibility. The seroma should be oval or round, and at least 3 cm in one of its dimensions. The key measurement is the distance from the skin to the top of the seroma, a tissue thickness of at least 0.6 cm to prevent injury to the

skin and ensure even and equal radiation throughout the field (Fig. 34-22).<sup>28,29</sup> Although many surgeons are learning the use of US to place these catheters into the lumpectomy site, breast radiologists experienced in image-guided interventions may be preferred for safe, percutaneous insertion of these relatively large devices into the tumor bed with direct US visualization.

### YOUNG, PREGNANT, AND LACTATING PATIENTS

The American College of Radiology Practice Guideline for the Performance of the Breast Ultrasound Examination (2002) suggests that US be the initial imaging technique for women 30 years of age and younger.<sup>16</sup> Most women younger than 30 years of age have come to clinical attention because of palpable masses, pain, or signs of mastitis and abscess. Exceptions to this include women at high risk of breast



cancer such as those who have breast cancer 1 or 2 genetic abnormalities or strong familial breast cancer patterns for whom mammographic screening is recommended to commence approximately 10 years before the age at which the first-degree relative (mother, sister, daughter) was diagnosed. If the US findings suggest malignancy, bilateral mammography is indicated for assessing extent of disease before any intervention.<sup>22,23</sup> For example, mammography might reveal microcalcifications not seen or suspected at US or an area of architectural distortion not appreciated sonographically. In addition, if US demonstrates no abnormality, bilateral mammography or bilateral mediolateral oblique mammographic views may help to exclude pathology.<sup>22</sup>

Fear of radiation exposure is unjustified; radiation exposure to a fetus or to the nongravid pelvic organs from mammography, a highly collimated examination, is near zero.<sup>30</sup> When mammography might show significant abnormalities not seen at US, the benefits of mammography outweigh any perceived negatives of an x-ray study.

When US of a palpable mass in a young patient, most commonly a fibroadenoma, shows a solid lesion with typical benign features, such as oval shape, circumscribed margins, and orientation parallel to the skin, mammography may be unnecessary.<sup>31,32</sup> Management of the mass may include clinical or US follow-up; tissue sampling if the patient or physician requests it; or excision of the mass for abatement of pain. In general, there is no consensus concerning the need for mammography in a patient younger than 30 years of age when an initial US examination is negative.

## Controversial or Evolving Applications of Breast Ultrasound in Problem Solving

### Characterizing Multiple Masses

A rule of multiplicity is often invoked in evaluating and managing multiple masses.<sup>33</sup> This dictum states that multiple masses with similar, mammographically benign features need not be characterized with US; the recommendation is for annual mammographic follow-up.<sup>33</sup> Others believe that the capability for increasing interpretive accuracy is promoted with a supplemental US examination.<sup>34</sup> Additionally and anecdotally, many breast imagers will relate, and some have reported their experiences in finding an unsuspected cancer adjacent to cysts or benign solid masses as they scan to characterize masses observed on mammograms. US is time consuming, and its acknowledged operator dependence arouses skepticism in using US to follow-up masses after their initial characterization. The use of US in continued patient follow-up of multiple masses is variable, although improvement in interpretive consistency has been noted recently.<sup>35</sup> There is no established standard to suggest follow-up intervals or guide patient management in these cases. Most management recommendations are extrapolated from those applicable to mammography.

If the breasts are fatty, soft tissue density masses are more conspicuous against the gray background of fat. Once a mass has been diagnosed with US as a simple cyst, it is not difficult to follow its increase or decrease mammographically. If breast tissue is heterogeneously or extremely dense, confident mammographic follow-up may be more difficult and,

in this scenario, US may be used. Recognition of similar pattern of anatomy surrounding the mass compared with a previous study will aid in comparability of size and appearance. Any new mass that is either palpable or evident on the mammograms should be characterized with US.<sup>16,34</sup>

## For Extent of Disease Bilaterally, Including Axillary Evaluation, in Breast Cancer Patients

When establishing a candidate's eligibility for breast conservation when the breast tissue is dense and the index carcinoma was seen best with US, there has been increasing use of US to survey the entire affected breast and the contralateral breast for additional foci.<sup>35-39</sup> Although these independent reports have suggested efficacy, the effectiveness of this approach, however, may be substantiated by additional data from the ACRIN 6666 multicenter trial, screening breast ultrasound in high-risk women, currently closed to accrual, and whose third follow-up round of mammography and US will also offer participants contrast-enhanced MRI at some sites.

The US assessment of extent of disease should include the axillae, or at least the axilla of the affected breast. In scanning the axilla, if lymph nodes are seen to have cortical contour bulges or masses (see Fig. 34-11), US-guided percutaneous core or fine-needle biopsy can confirm metastatic involvement, obviating the need for a sentinel node procedure.<sup>40</sup>

## Staging

Establishment of multicentricity can alter treatment decisions, as is becoming recognized with increasing incorporation of MRI in the evaluations of breast cancer patients. With detection of additional cancers in breast quadrants other than that in which the cancer was originally found, plans for conservation have been changed to mastectomy. Both US and MRI are being used, sometimes competitively, in this way for assessing extent of disease in newly diagnosed breast cancer patients. Hlawatsch et al<sup>41</sup> found that a combination of mammography and whole breast US was adequate in most cases and certainly less costly. Berg<sup>39</sup> reported 93% accuracy of mammography, physical examination, and US compared with the accuracy of MRI, mammography, and physical examination at 99%. Data are accumulating in support of the efficacy of MRI to assess extent of disease, and MRI bested clinical examination, mammography, and US in breast cancer detection in those very high-risk women with breast cancer 1 and 2.<sup>42</sup> If CE-MRI is planned for evaluating a newly diagnosed breast cancer patient, it would be unnecessary to start out with bilateral survey US. Handheld small FOV screening breast US is time consuming, and completeness of the study is difficult to ensure. Anticipating increasing need, automated scanners, older versions of which became extinct in the early 1990s, are in development by several of the manufacturers of US equipment. Some of these automated systems are designed to acquire images using mammographic-like positioning for greater certainty in correlating with findings on mammography. These systems, whose efficacy remains to be



validated, could offer answers to the challenges of follow-up of solid masses, interobserver inconsistency and other operator dependence issues. Determining the order of and most cost-effective imaging methods for judging extent of cancer involvement is an area of active research.

## SUMMARY AND CONCLUSIONS

In recent years, technical advances, increasing familiarity with breast anatomy as depicted sonographically, and a standardized approach to interpretation have broadened the clinical applications of breast US. With mammography and physical examination, breast US makes important contributions to problem solving. The accepted indications for using US to examine the breasts include evaluation of palpable and mammographic masses; guiding interventional procedures, evaluating implant problems; the postsurgical breast and radiation treatment planning; and as the initial imaging technique in young (30 years of age and younger), pregnant, and lactating patients.<sup>16</sup> Newer or controversial applications are also discussed, including use of US to look for an associated mass in an area of microcalcifications seen on mammograms; initial evaluation and follow-up of patients with multiple similar, benign-appearing masses; and survey US for extent of disease and treatment planning for patients with at least one established focus of breast cancer. Although much progress has been made in breast US, it should be kept in mind that US is to be used *with* mammography and not as a substitute for mammographic screening.

## References

- Jackson VP: The role of US in breast imaging. *Radiology* 177:305, 1990.
- Stavros AT, Thickman D, Rapp CL, et al: Solid breast nodules: Use of sonography to distinguish between benign and malignant lesions. *Radiology* 196:123, 1995.
- D'Orsi CJ, Bassett LW, Berg WA, et al: BI-RADS, Breast Imaging Reporting and Data System, 4th ed. Reston, VA, American College of Radiology, 2003.
- Mendelson EB, Berg WA, Merritt CR: Toward a standardized breast ultrasound lexicon, BI-RADS: Ultrasound. *Semin Roentgenol* 36:217, 2001.
- Rahbar G, Sie AC, Hansen GC, et al: Benign versus malignant solid breast masses: US differentiation. *Radiology* 213:889, 1999.
- Baker JA, Kornguth PJ, Soo MS, et al: Sonography of solid breast lesions: Observer variability of lesion description and assessment. *AJR Am J Roentgenol* 172:1621, 1999.
- Entrekin RR, Porter BA, Sillesen HH, et al: Real-time spatial compound imaging: Application to breast, vascular, and musculoskeletal ultrasound. *Semin Ultrasound CT MR* 22:50, 2001.
- Kwak JY, Kim EK, Keun KJ: Variable breast conditions-comparison of conventional and real-time compound ultrasonography. *J Ultrasound Med* 23:85, 2004.
- Rosen EL, Soo MS: Tissue harmonic imaging sonography of breast lesions. *Clin Imaging* 25:379, 2001.
- Szopinski KT, Pajk AM, Wysocki M, et al: Tissue harmonic imaging: Utility in breast sonography. *J Ultrasound Med* 22:479, 2003.
- Garra BS, Cespedes EI, Ophir J, et al: Elastography of breast lesions: Initial clinical results. *Radiology* 202:79, 1997.
- Itoh A, Ueno E, Tohno E, et al: Breast disease: Clinical application of US elastography for diagnosis. *Radiology* 239:341, 2006.
- Ophir J, Alam SK, Garra B, et al: Elastography: Ultrasonic estimation and imaging of the elastic properties of tissues. *Proc Inst Mech Eng [H]* 213:203, 1999.
- Sickles EA: Periodic mammographic follow-up of probably benign lesions: Results in 3,184 consecutive cases. *Radiology* 179:463, 1991.
- Sickles EA: Probably benign breast lesions: When should follow-up be recommended and what is the optimal follow-up protocol? *Radiology* 213:11, 1999.
- American College of Radiology: Standard for the performance of the breast ultrasound examination. Reston, VA, American College of Radiology, 2002.
- Kolb TM, Lichy J, Newhouse JH: Occult cancer in women with dense breasts: Detection with screening US-diagnostic yield and tumor characteristics. *Radiology* 207:191, 1998.
- Ikedo DM: Ductal carcinoma in situ: Atypical mammographic appearances. *Radiology* 172:661, 1989.
- Soo MS, Rosen EL, Baker JA, et al: Negative predictive value of sonography with mammography in patients with palpable breast lesions. *AJR Am J Roentgenol* 177:1167, 2001.
- Flobbe K, Bosch AM, Kessels AG, et al: The additional diagnostic value of ultrasonography in the diagnosis of breast cancer. *Arch Intern Med* 163:1194, 2003.
- Dennis MA, Parker SH, Klaus AJ: Breast biopsy avoidance: The value of normal mammograms and normal sonograms in the setting of a palpable lump. *Radiology* 219:186, 2001.
- Mainiero MM, Goldkamo A, Lazarus E: Characterization of breast masses with sonography: Can biopsy of some solid masses be deferred? *J Ultrasound Med* 24:161, 2005.
- Shetty MK, Shah YP, Sharnan RS: Prospective evaluation of combined mammographic and sonographic assessment in patients with palpable abnormalities of the breast. *J Ultrasound Med* 22:263, 2003.
- Harris KM, Ganott MA, Shestak KC, et al: Silicone implant rupture: Detection with US. *Radiology* 187:761, 1993.
- Mund DF, Farria DM, Gorczyca DP, et al: MR imaging of the breast in patients with silicone-gel implants: Spectrum of findings. *AJR Am J Roentgenol* 161:773, 1993.
- DeBruhl ND, Gorczyca DP, Ahn CY, et al: Silicone breast implants: US evaluation. *Radiology* 189:95, 1993.
- Smitt MC, Birdwell RL, Goffinet DR: Breast electron boost planning: Comparison of CT and US. *Radiology* 219:203, 2001.
- Leonard C, Harlow CL, Coffin C: Use of US to guide radiation boost planning following lumpectomy for carcinoma of the breast. *Int J Radiat Oncol Biol Phys* 27:1193, 1993.
- Mendelson EB: Radiation changes in the breast. *Semin Roentgenol* 28:344, 1993.
- Kopans DB: Mammography and radiation risk. In Janower ML, Linton OW, eds: *Radiation Risk: A Primer*. Reston, VA, American College of Radiology, 1996, p 12.
- Appropriateness Criteria ACR: Imaging work-up of palpable breast masses. Reston, VA, American College of Radiology, 2003.
- Mendelson EB: The development and meaning of appropriateness guidelines. *Radiol Clin North Am* 33:1081, 1995.
- Leung JW, Sickles EA: Multiple bilateral masses detected on screening mammography: Assessment of need for recall imaging. *AJR Am J Roentgenol* 175:23, 2000.
- Skaane P, Engedal K, Skjennald A: Interobserver variation in the interpretation of breast imaging: Comparison of mammography, ultrasonography, and both combined in the interpretation of palpable noncalcified breast masses. *Acta Radiol* 38:497, 1997.
- Bosch AM, Kessels AG, Boets GL, et al: Interexamination variation of whole breast ultrasound. *Br J Radiol* 76:328, 2003.
- Gordon PB, Goldenberg SL: Malignant breast masses detected only by ultrasound: A retrospective review. *Cancer* 76:626, 1995.
- Buchberger W, Nichoff A, Obrist P, et al: Clinically and mammographically occult breast lesions: Detection and classification with high-resolution sonography. *Semin Ultrasound CT MR* 21:325, 2000.
- Kaplan SS: Clinical utility of bilateral whole-breast US in the evaluation of women with dense breast tissue. *Radiology* 221:641, 2001.
- Berg WA, Gilbreath PL: Multicentric and multifocal cancer: Whole-breast US in preoperative evaluation. *Radiology* 214:59, 2000.
- Deurloo EE, Tanis PJ, Gilhuijs KG, et al: Reduction in the number of sentinel lymph node procedures by preoperative ultrasonography of the axilla in breast cancer. *Eur J Cancer* 39:1068, 2003.
- Hlawatsch A, Teifke A, Schmidt M, Thelen M: Preoperative assessment of breast cancer: Sonography versus MR imaging. *AJR Am J Roentgenol* 179:1493, 2002.
- Kriege M, Brekelmans C, Boetes C, et al: Efficacy of MRI and mammography for breast cancer screening in women with a familial or genetic predisposition. *N Engl J Med* 351:427, 2004.



## ARTIFACTS, PITFALLS, AND NORMAL VARIANTS

Peter W. Callen, MD

**Pelvis, Gravid, and Nongravid Uterus**

**The First Trimester**

**The Fetal Head and Neck**

**The Fetal Thorax**

**The Fetal Abdomen**

**Amniotic Fluid and Membranes**

**The Fetal Skeleton**

**Multiple Gestations**

**Artifacts**

**Breast Ultrasound**

**The End**

When I began my involvement with diagnostic ultrasonography three decades ago, this chapter would have been considered ludicrous. Virtually all of ultrasonography was considered to be either an artifact or a pitfall. Clinicians did not take this modality seriously, and few critical decisions were ever based on the results of the ultrasound examination alone. With time, improvements in both technology and our understanding of normal and abnormal findings made this a useful clinical diagnostic modality. It did not take long for important clinical decisions to be based solely on the results of the ultrasound examination, for example, surgery, early delivery of the fetus, or even termination of the pregnancy. This evolution, although welcomed by many, has placed a large responsibility on the sonographer. The phrase “primum non nocere,” or first do no harm, has never proven more true.

This chapter is not an attempt to explain the physical principles of ultrasound or artifact production. It is also unlikely that such a chapter could ever be all-inclusive. I have attempted to find examples of pitfalls, the diagnostic dilemmas that have the potential to lead us to the wrong diagnosis. I have tried to cover both basic potential pitfalls and some of the more esoteric normal variants. Undoubtedly, some readers will find examples here that are so basic as to seem almost insulting. I apologize in advance and will only respond that this chapter is meant to appeal to a wide audience of beginners and “well-seasoned” experts. I also do not attempt to give an overly detailed explanation for each example but try to offer what is theorized at the time.

If I am able to avoid one false-positive diagnosis and prevent unnecessary surgery, termination of a pregnancy, or even 20 weeks of an emotional roller coaster for the parents, I have fulfilled my goal.

### PELVIS, GRAVID, AND NONGRAVID UTERUS

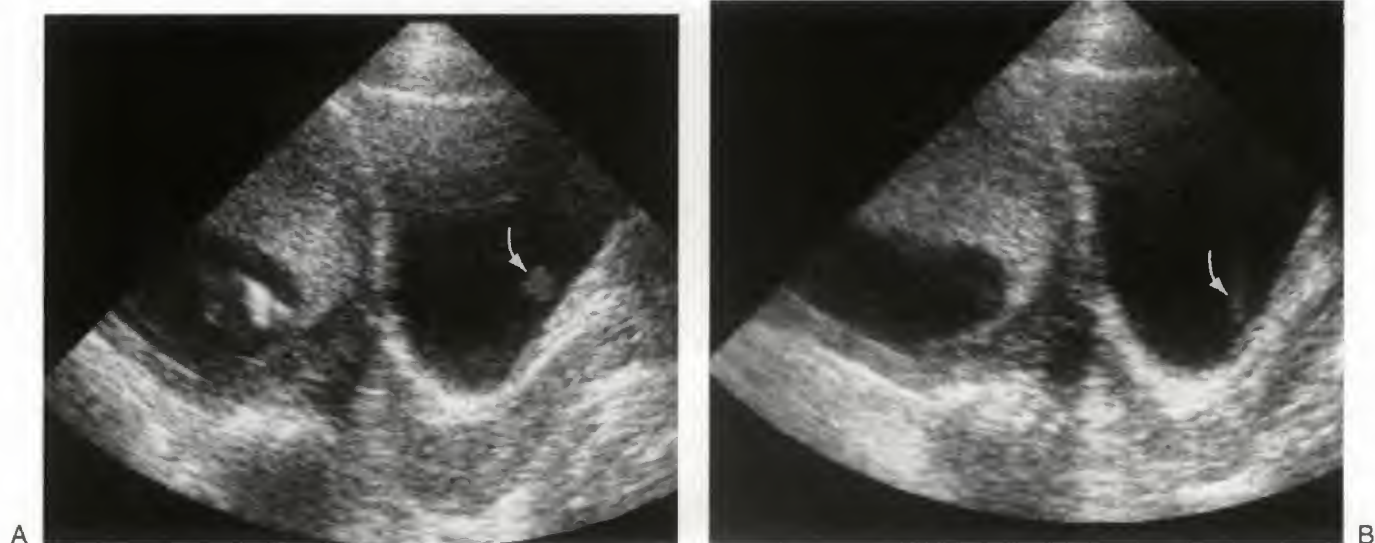


**FIGURE 35-1.** Longitudinal sonograms demonstrating the maternal urinary bladder and the gravid uterus. A. An apparent soft tissue mass is seen in the urinary bladder (arrow). B. In fact, this is the stream of urine entering the bladder through the ureteral orifice.

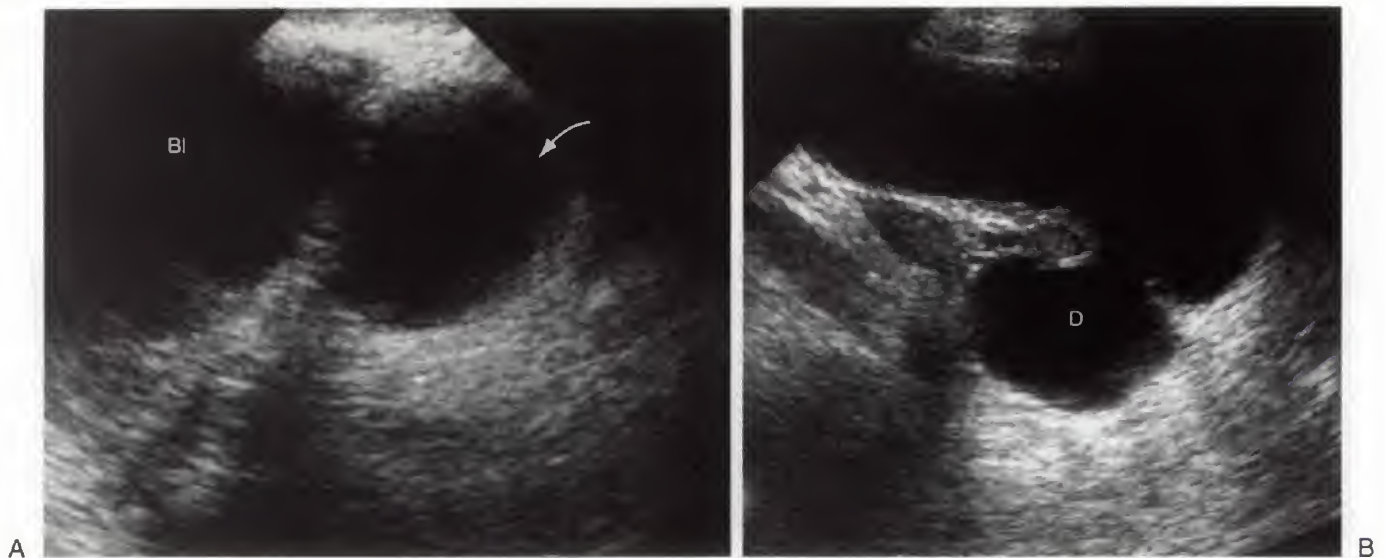


**FIGURE 35-2.** A. What appears to be a large pelvic cyst is seen in this patient (arrow). Bl, bladder. B. Although the connection to the bladder was not seen in A, this bladder diverticulum (D) is clearly seen in another plane of section.

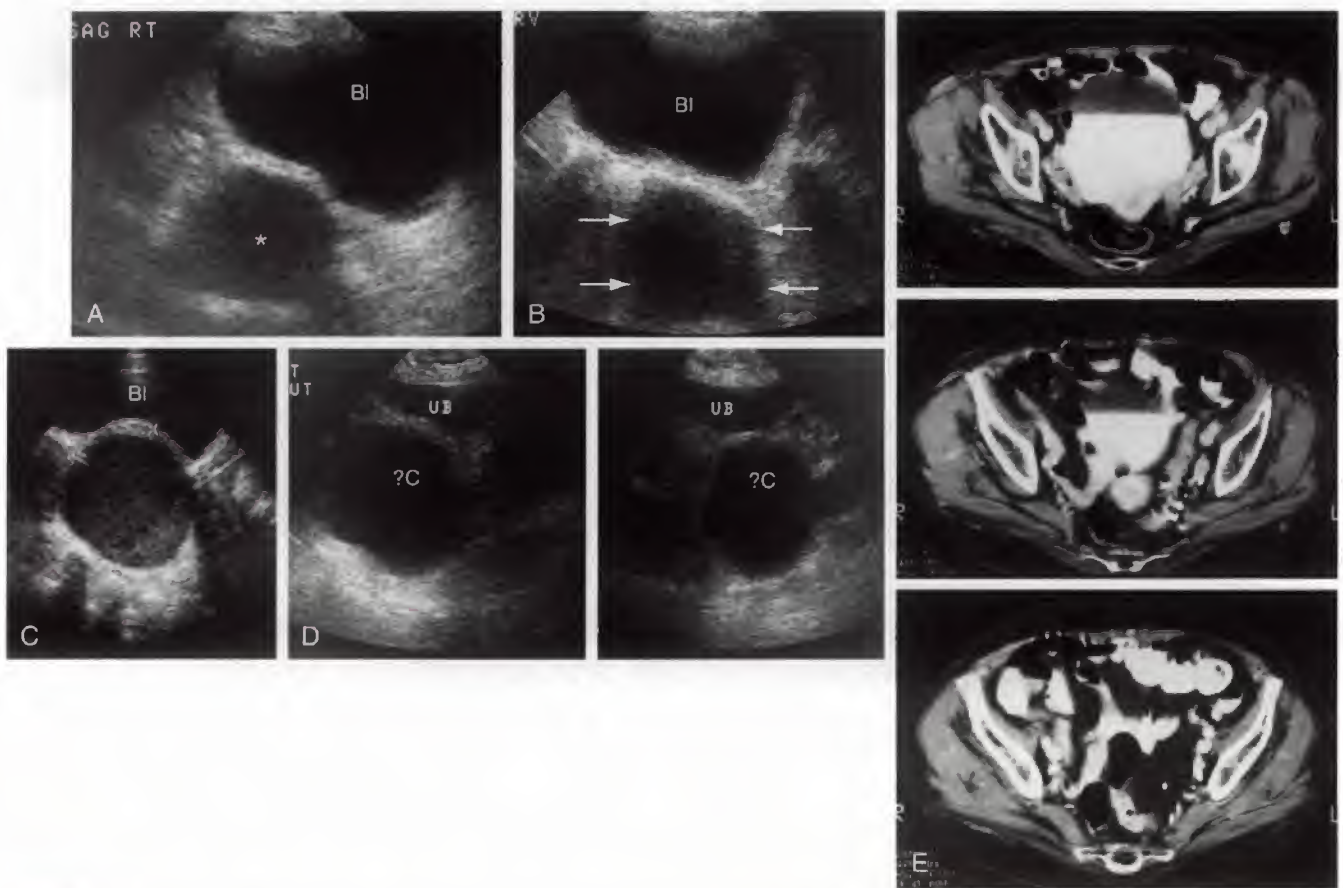


**FIGURE 35-3.** Bowel within the pelvis can masquerade as ovarian cysts. A. In this patient, bowel gas and its shadowing create the appearance of a mass (asterisk). Bl, bladder. B. The strong reflection adjacent to the urinary bladder (Bl) or the "squared" appearance (arrows) to the "cyst" should make one suspicious that bowel gas artifact is causing this appearance. C. In a different patient, a true ovarian cyst (cursors) has borders on nearly every side and has enhanced through-sound transmission and internal echoes. Bl, bladder. D. In another patient, two different planes of section demonstrate what appears to be a large pelvic cyst (?C). In fact, this was due to bowel gas artifact. UB, bladder. E. Because this appearance was virtually indistinguishable from a pelvic cyst, a computed tomographic scan was performed immediately after the sonogram, confirming the artifactual nature of this "cyst." The scans were normal without evidence of a pelvic mass.



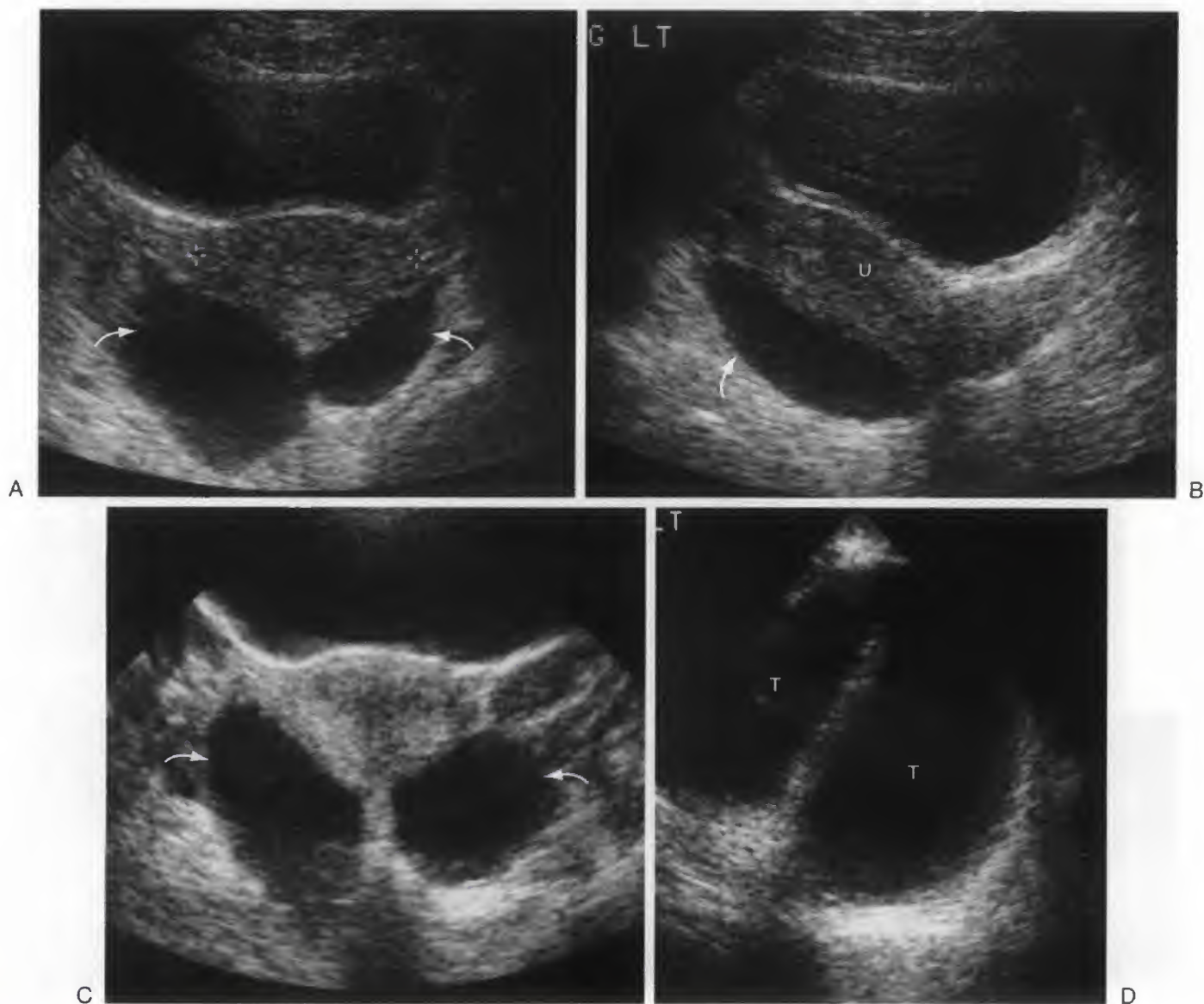


**FIGURE 35-4.** Dilated fallopian tubes simulating ovarian cysts. *A.* A transverse sonogram in this patient demonstrates what appear to be two ovarian cysts (arrows) posterior to the uterus (cursors). *B.* A longitudinal sonogram displays the elongated tubular nature of this fluid collection (arrow), which is more compatible with a dilated fallopian tube. U, uterus. *C.* In another patient, two large, rounded fluid collections are seen (arrows) simulating ovarian cysts. *D.* A longitudinal plane of section through one of these collections demonstrates the tubular (T) retort nature of these dilated fallopian tubes.

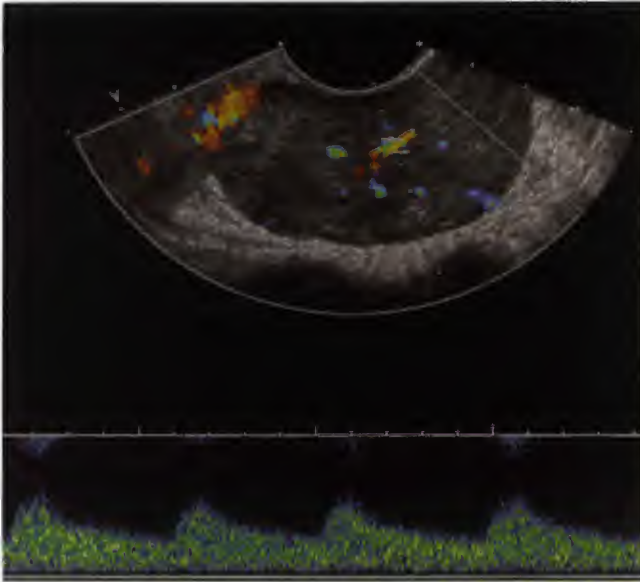


**FIGURE 35-5.** A 19-year-old woman presented with severe pelvic pain. She had been in an emergency room 1 month earlier with the same symptoms. A pelvic sonogram demonstrates an enlarged ovary with arterial and venous blood flow. Three hours later, an avascular necrotic ovary from ovarian torsion was removed at surgery. Do not be reassured by an apparently normal sonogram when ovarian torsion is suspected.



**FIGURE 35-7.** Two round and oval structures are seen in the right adnexa. Although they might be mistaken for abnormal ovaries or paraovarian masses they represent normal prominent bowel. Typical hypoechoic muscularis (arrows) is seen.

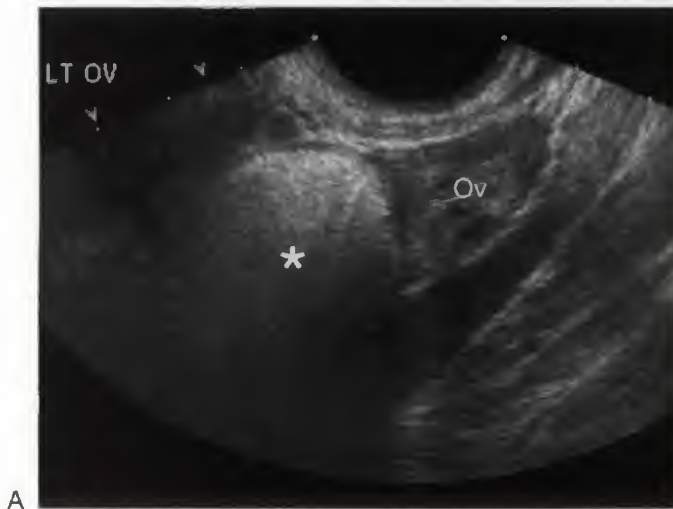


**FIGURE 35-6.** Bowel simulating an ovarian cystic teratoma (dermoid). *A.* A large shadowing mass (asterisk) is seen adjacent to or possibly emanating from the ovary (Ov). *B.* Minutes later the normal ovary and adnexal structures are well seen. The bowel, which was the cause of the shadowing, was not seen.



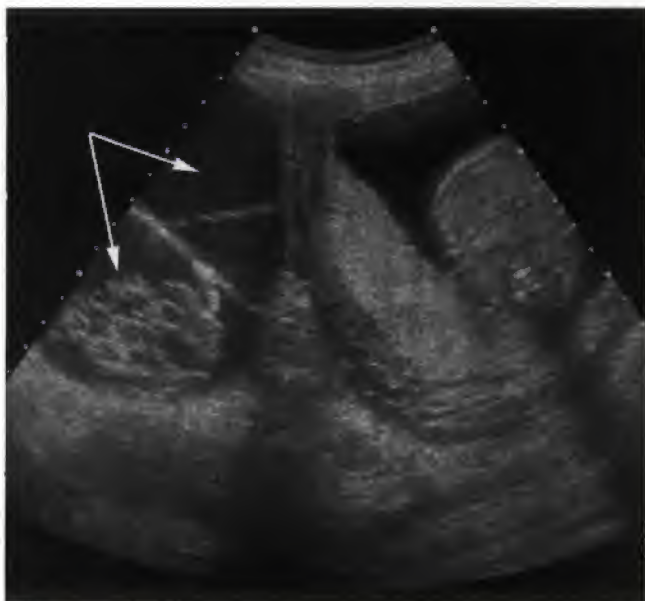


**FIGURE 35-8.** Pregnancy with coexistent ovarian carcinoma. Unfortunately, just because a patient is pregnant does not mean that she cannot have a concomitant ovarian cancer. A multilocular cystic mass (arrows) with solid components is seen adjacent to the gravid uterus.

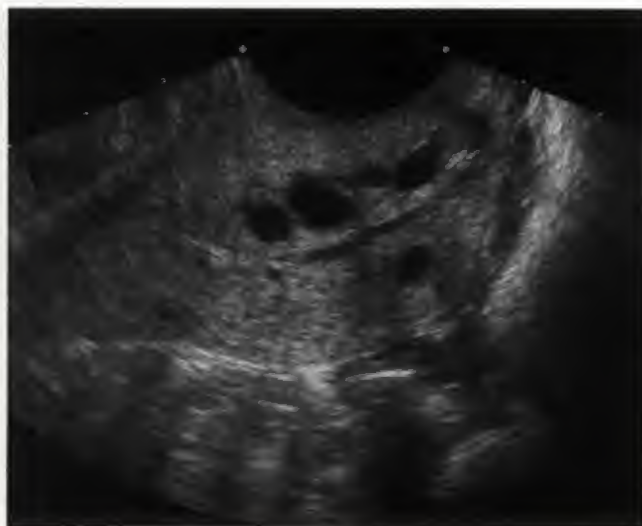


**FIGURE 35-10.** Longitudinal scan through the cervix of a gravid uterus. Multiple nabothian cysts are seen in the cervix. These retention cysts are common and should not be confused with low-implanted gestational sacs or other pathology.

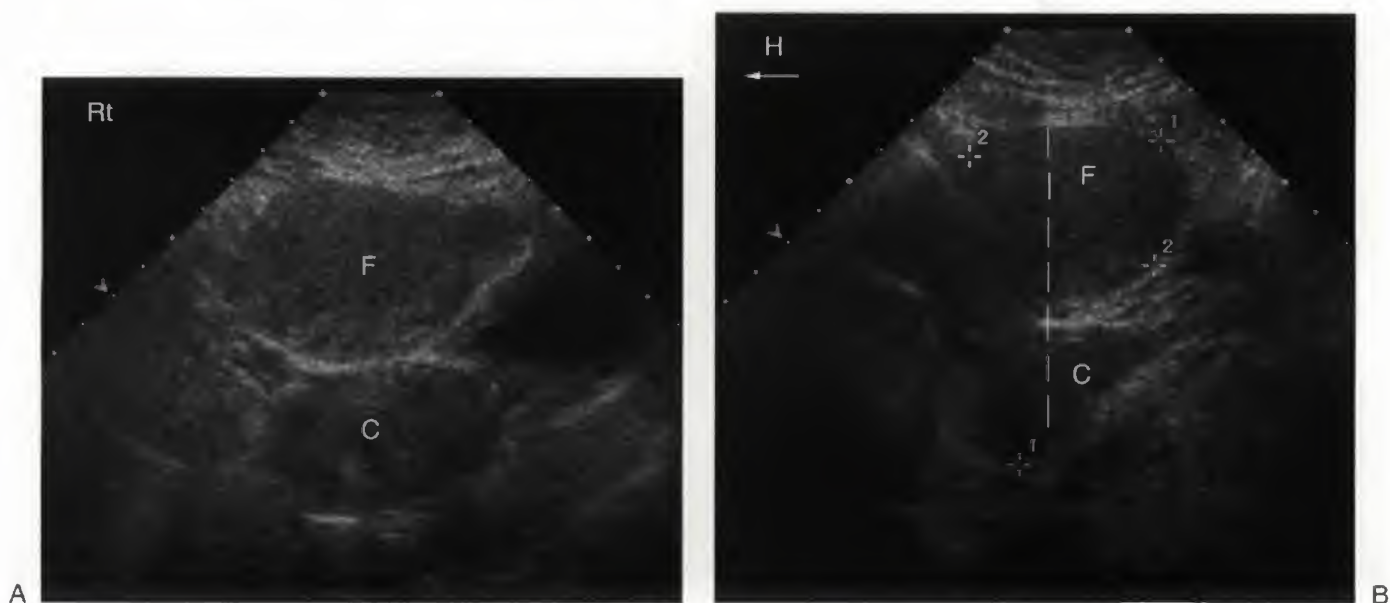


**FIGURE 35-9.** A. Transverse axial sonogram of the pelvis in a non gravid patient. There appears to be either a duplication of the uterus or the uterus and an adjacent mass (C, F). Rt, right. B. A sagittal scan demonstrates that what was seen in the transverse scan was the cervix (C) and fundus (F) of an anteverted uterus. The dashed line represents the plane of section in A. H, head.



**FIGURE 35-11.** In this patient, the uterus is markedly enlarged and lobular with numerous small cystic areas (*arrows*) throughout. Although this has an appearance similar to a hydatidiform mole, in fact, the serum hCG was zero and the mass was due to myomatous disease. Bl, bladder.



**FIGURE 35-13.** Sonogram of a gravid uterus in the second trimester demonstrating a circumvallate placenta (*arrow*). The infolding of the edge of the placenta should not be confused with a uterine synechiae.



**FIGURE 35-12.** Transverse scan through the gravid uterus demonstrates a uterine synechiae (*arrow*) crossing the uterine cavity from the anterior to the posterior wall. The fetus moved freely around the synechiae. This should not be confused with an amniotic band.



**FIGURE 35-14.** Transverse scan of the pelvis demonstrating a left adnexal solid mass (*asterisk*). Although the anatomic position might suggest an ovarian lesion, the solid nature of the mass should suggest the possibility of a broad ligament myoma, which was ultimately demonstrated on a magnetic resonance imaging scan. U, uterus; R, right.





**FIGURE 35-15.** A myometrial contraction (M) is common in first and second trimester sonograms. This should not be confused with a myoma. Two features help make this distinction: First, in general, myometrial contractions tend to bulge inwardly without affecting the outer contour of the uterus. Uterine fibroids tend to bulge inward and outward. Second, myometrial contractions may resolve during the time of scanning.



**FIGURE 35-17.** Marked overdistention of the urinary bladder results in the appearance of a markedly elongated cervix (*between calipers*). One is visualizing not only the cervix but the apposed anterior and posterior walls of the lower uterine segment.



**FIGURE 35-16.** A myometrial contraction (M) in this second trimester pregnancy simulates a myoma. This should not be confused with a succenturiate lobe of the placenta. P, placenta.



**FIGURE 35-18.** A distended urinary bladder has caused the anterior and posterior walls of the lower uterine segment (*arrows*) to come near one another. The trapped amniotic fluid gives the appearance of an incompetent cervix. The cervix was normal in this case.

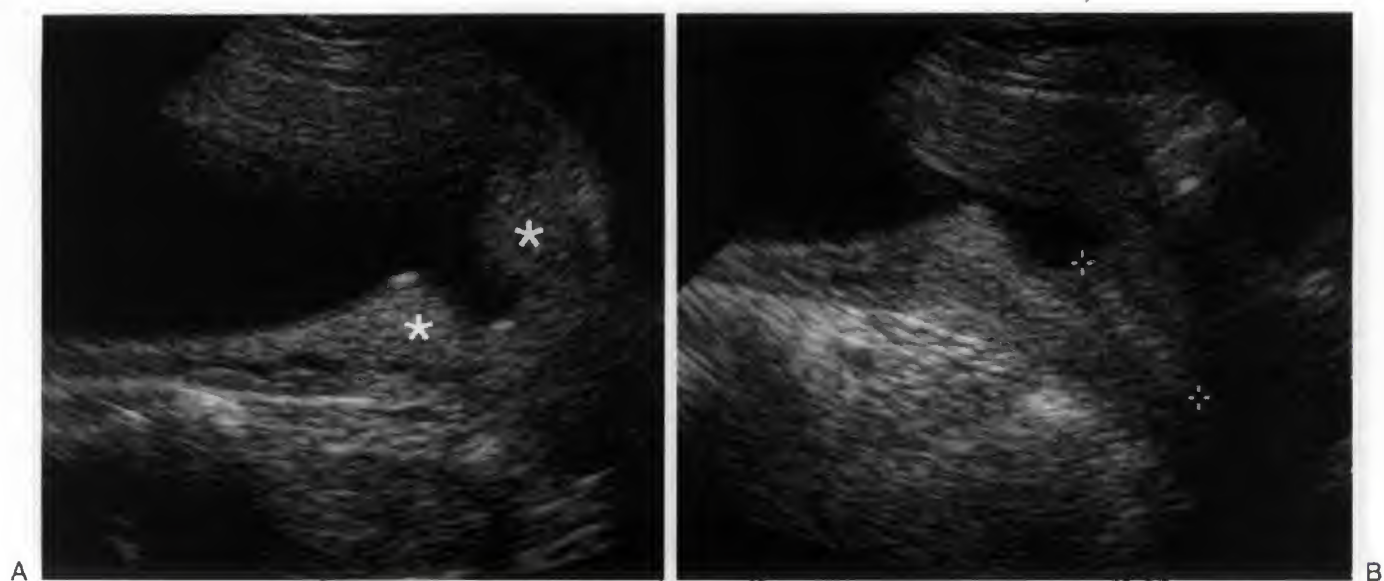


**FIGURE 35-19.** Myometrial contractions of the lower uterine segment are common and may often touch one another. *A.* In this case the contractions (*asterisks*) of the lower uterine segment simulate an open and incompetent cervix. *B.* The normal-appearing cervix, in fact, is well seen (*calipers*) caudal to this contraction.



**FIGURE 35-20.** Myometrial contractions of the lower uterine segment may often touch one another (*asterisks*). These have been referred to as “kissing contractions.” Bl, bladder.



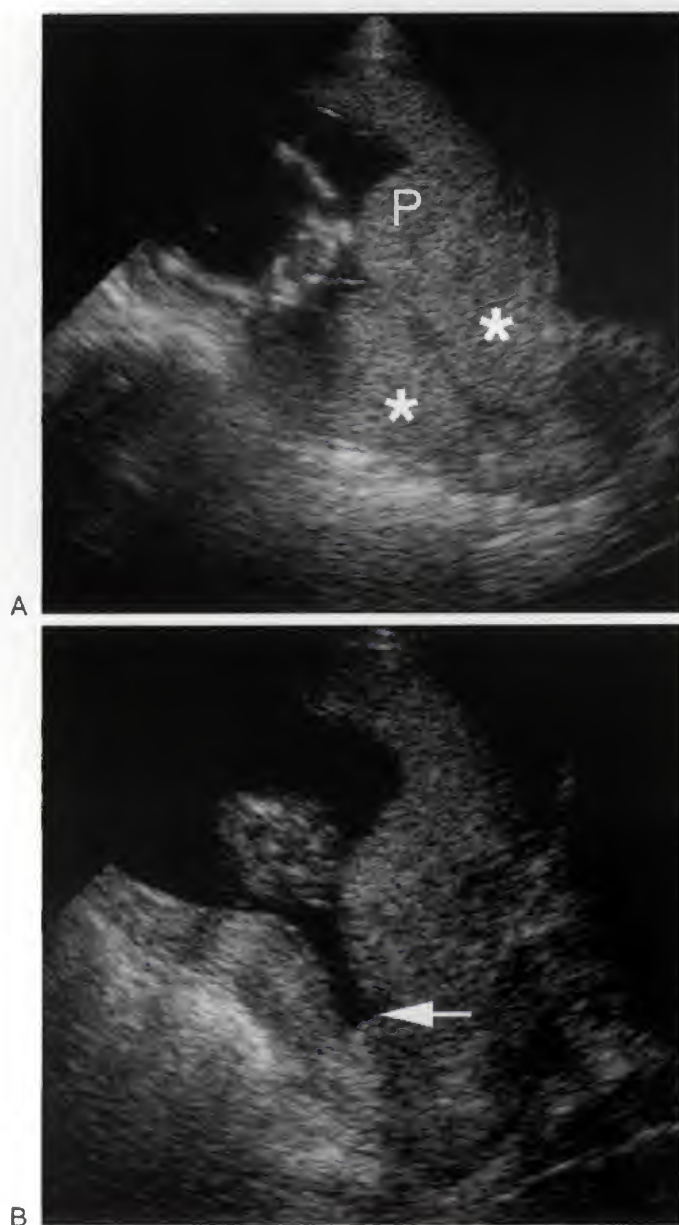


**FIGURE 35-21.** A. “Kissing contractions” of the lower uterine segment (*asterisks*). The caudal end of the placenta rests at the junction of these contractions. These contractions should not be confused with the cervix and mistakenly called a placenta previa. P, placenta. B. With time, there was resolution of the anterior contraction, so that the internal cervical os could be identified (*arrow*).

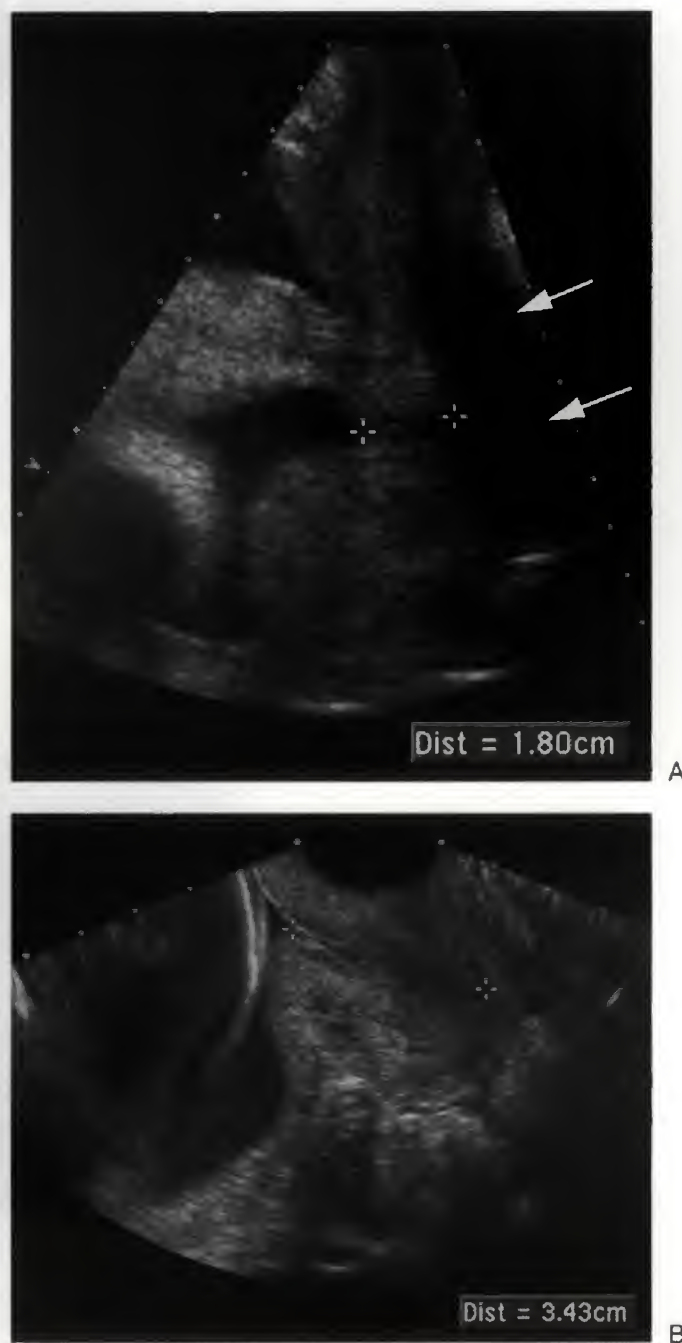


**FIGURE 35-22.** Artifactual short cervix. A. Transperineal scan demonstrates a short cervix (*between calipers*) measuring 1.8 cm. Shadowing (*arrows*) from the rectum obscures the remainder of the cervix. B. A transvaginal scan in the same patient demonstrates a normal length to the cervix (*between calipers*) of 3.43 cm.



**FIGURE 35-23.** Dynamic changes of cervix. Three transvaginal scans of the cervix (A to C) taken minutes apart, demonstrate progressive dilatation of the cervix with fluid entering the endocervical canal. This finding should be reported to the referring obstetrician and the residual shortened closed length of the cervix should be reported, as well as the total cervical length.



**FIGURE 35-24.** A. A slightly oblique longitudinal scan through the uterus. A small area of placental tissue (*asterisk*) is separate from the major portion of the placenta (P). This appears to be a succenturiate lobe of the placenta. B. When the scan plane is aligned along the major long axis of the placenta, the area in A can be seen to be continuous with the remainder of the placenta.



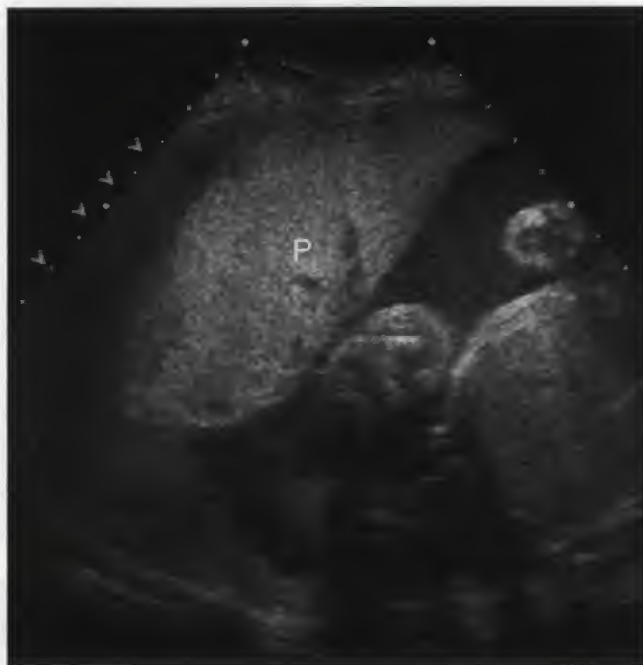


**FIGURE 35-25.** In some patients, the surface area over which the placenta implants may be small. This short insertion site may create the false appearance of a thickened hydropic placenta (P).



**FIGURE 35-26.** Changing placenta previa. *A.* A transvaginal scan in a patient at 17 weeks demonstrates a complete placenta previa. The leading edge (arrow) of the posterior placenta (P) extends across the internal cervical os. *B.* Six weeks later at 23 weeks, the leading edge of the placenta extends to but not beyond the internal cervical os.

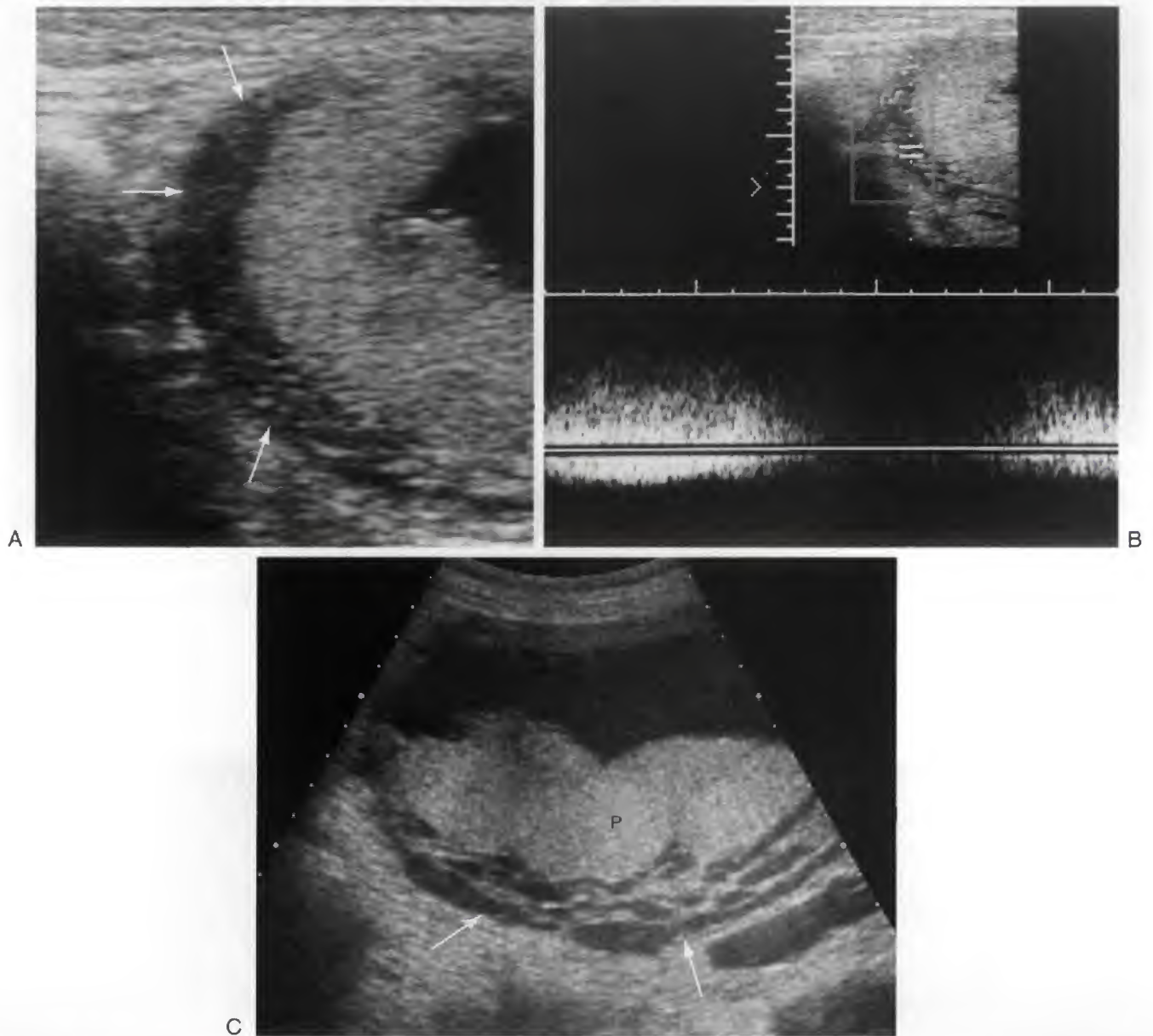


**FIGURE 35-27.** A. Veins present in the decidua basalis and myometrium contribute to a hypoechoic region beneath the placenta (*arrows*). This should not be misinterpreted as an abruption. B. Doppler interrogation of this region will often confirm the venous nature of this area. C. In this case, the veins (*arrows*) deep to the placenta (P) are clearly seen.





**FIGURE 35-28.** A hypoechoic area (*asterisk*) behind the placenta (P) simulates a placental abruption. It is in fact a myometrial contraction that resolved during the examination.

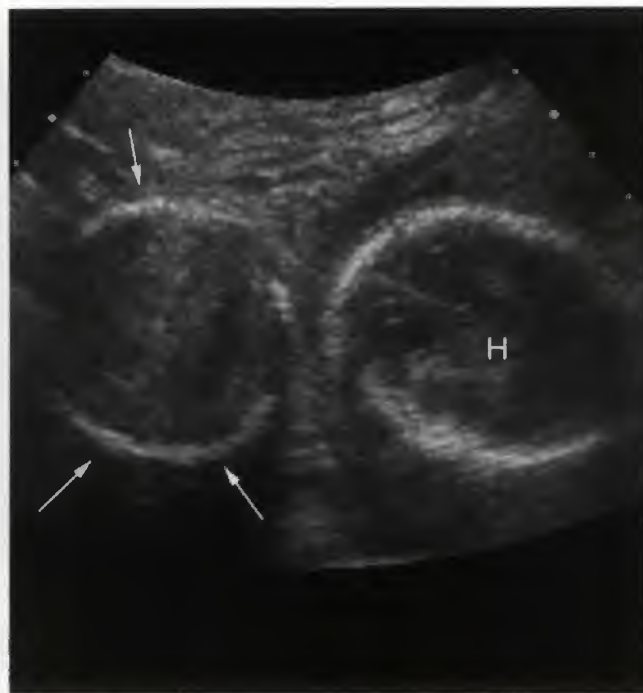


**FIGURE 35-30.** Transverse scan of the gravid uterus demonstrates the fetal head (H). A calcified structure (*arrows*) is seen adjacent to the fetal head. At first glance, this appears to be another fetus but in fact represents a calcified myoma.



**FIGURE 35-29.** Prominent vessels (*arrows*) at the periphery of the uterus. These are common in the uterus and should not be mistaken as a precursor to an abruption or as trophoblastic disease. *A.* In this patient, the arcuate vessels (*arrows*) at the periphery of the uterus are quite prominent. *B.* With color Doppler flow imaging, the vascular nature of these structures is well seen.

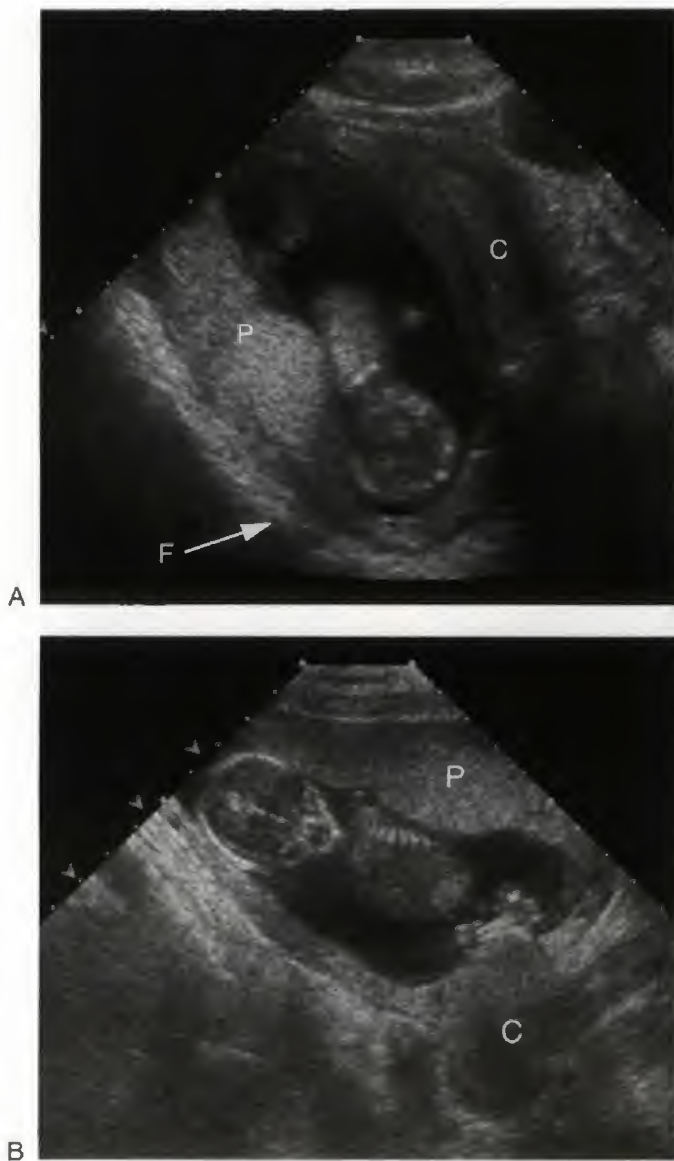


**FIGURE 35-31.** Incarcerated uterus. A persistently retroflexed or retroverted uterus may become 'trapped' within the sacral hollow. *A.* Longitudinal scan demonstrating an incarcerated uterus in the early second trimester. What appears to be the lower uterine segment is in fact the fundus (F) that is stuck within the sacral hollow. The cervix (C) is drawn anteriorly and superiorly. The urethra often becomes obstructed, and these patients are often seen in the emergency room with urinary obstruction. P, placenta. *B.* After manual reduction, the cervix (C) and uterus now have a more normal appearance. The placenta (P), which appeared to be posterior in the prereduction scan, is now seen anteriorly.

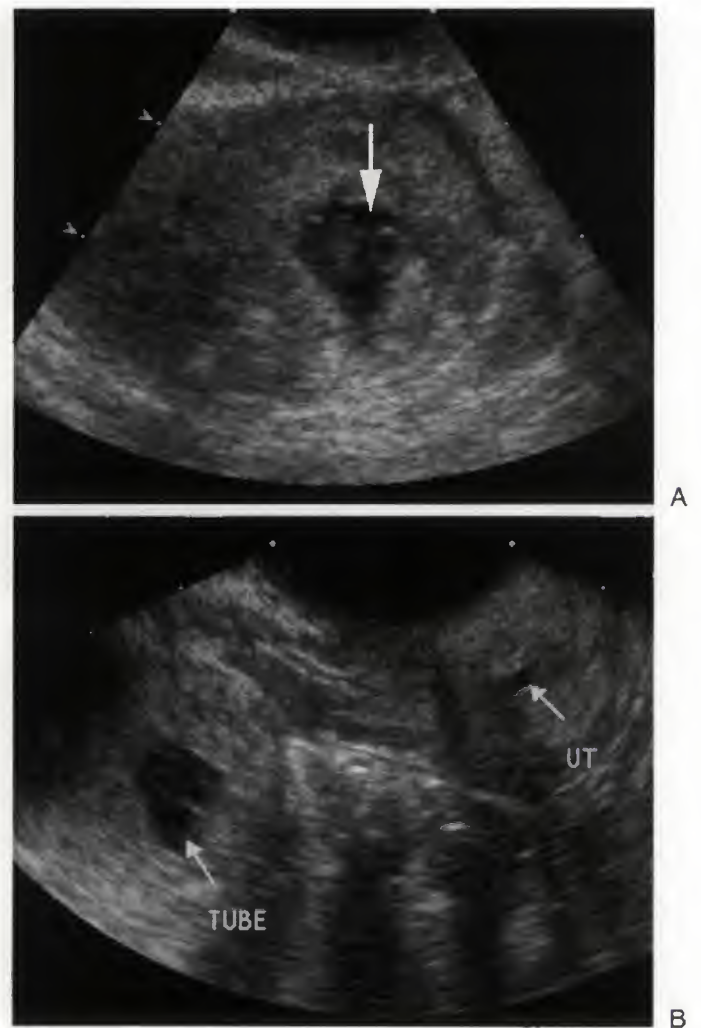


**FIGURE 35-32.** *A.* A transvaginal sonogram demonstrates an embryo and yolk sac (arrow) centrally positioned in what appears to be the uterus. *B.* A transabdominal sonogram of the same patient demonstrates that the pregnancy was in the fallopian tube (TUBE). A small fluid collection representing fluid within the endometrial cavity (decidual cast) of the uterus (UT) is seen. The patient had an ectopic pregnancy.



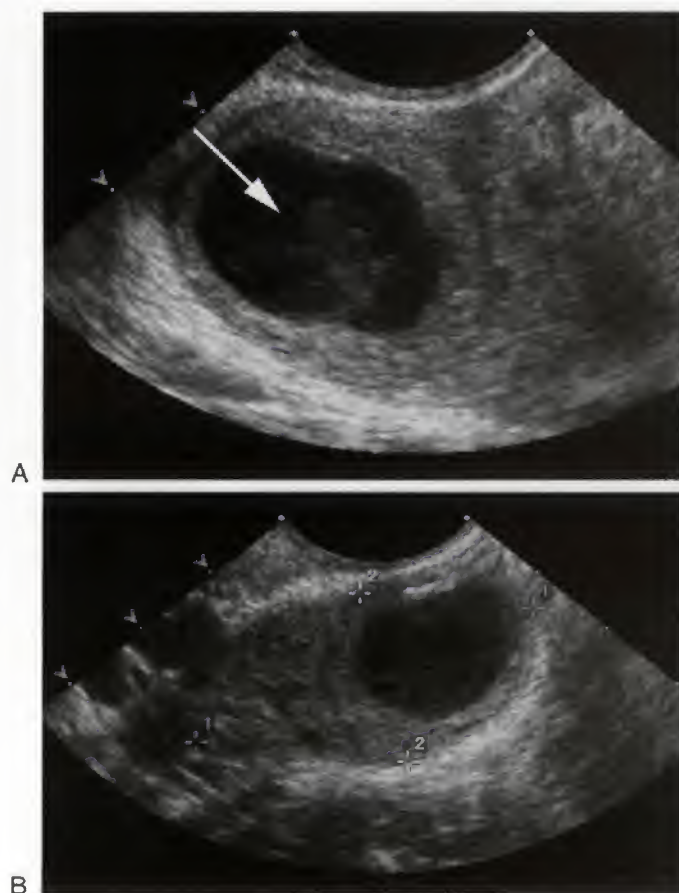


**FIGURE 35-33.** A. A transvaginal sonogram demonstrates an ill-defined soft tissue mass (*arrow*) in a cystic fluid collection within the ovary. The uniformly thick wall of the cyst simulates a decidual reaction. This has the appearance of a disorganized embryo within a gestational sac. B. An additional scan of the same adnexa demonstrates a more characteristic "fishnet" appearance of hemorrhage within an ovarian cyst.

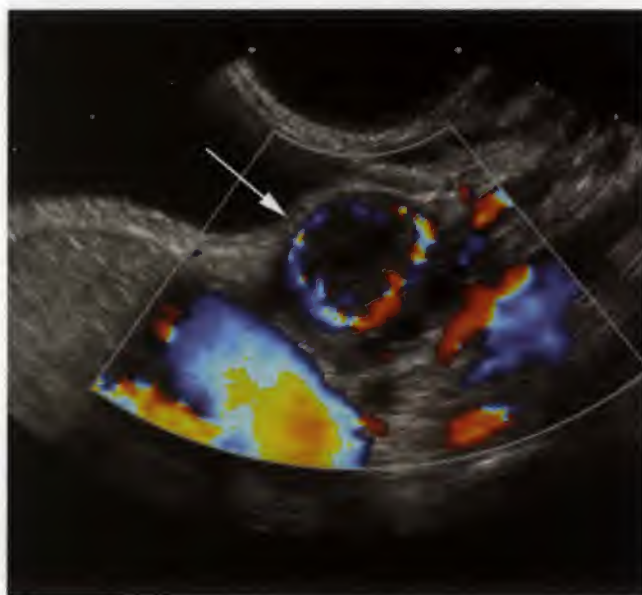


**FIGURE 35-34.** A vascular ring (*arrow*) is seen around a cyst within the adnexa. Although this "ring of fire" was once thought to be characteristic of an ectopic pregnancy, it is recognized that a corpus luteum cyst, as in this case, may produce a similar appearance.

## THE FIRST TRIMESTER

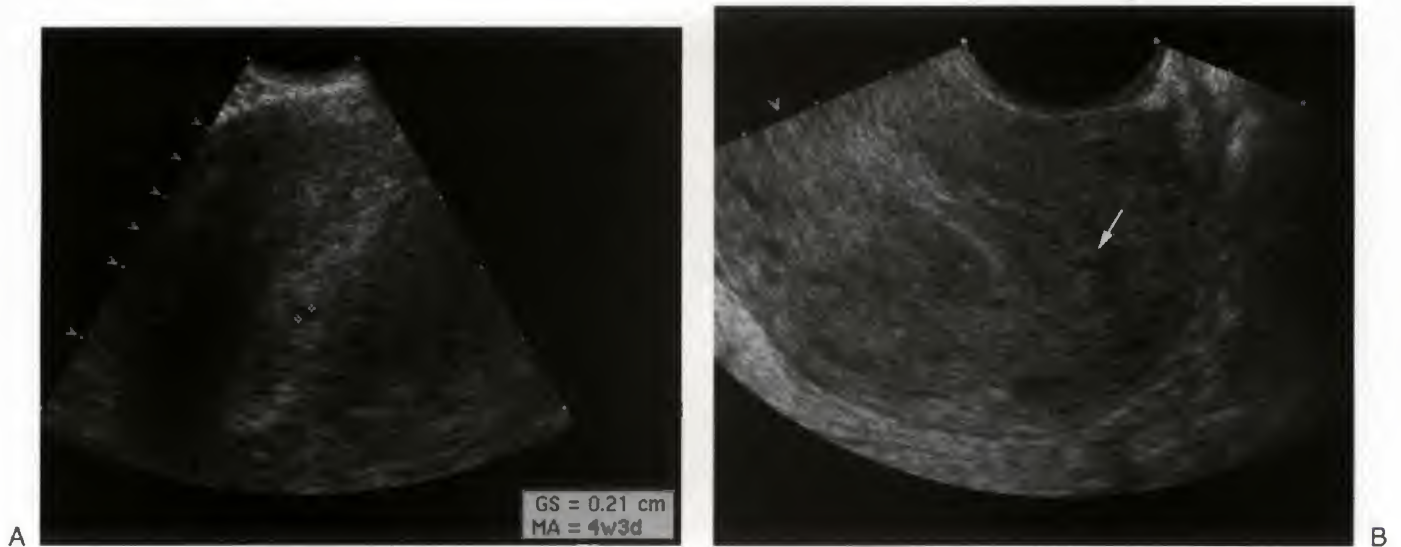
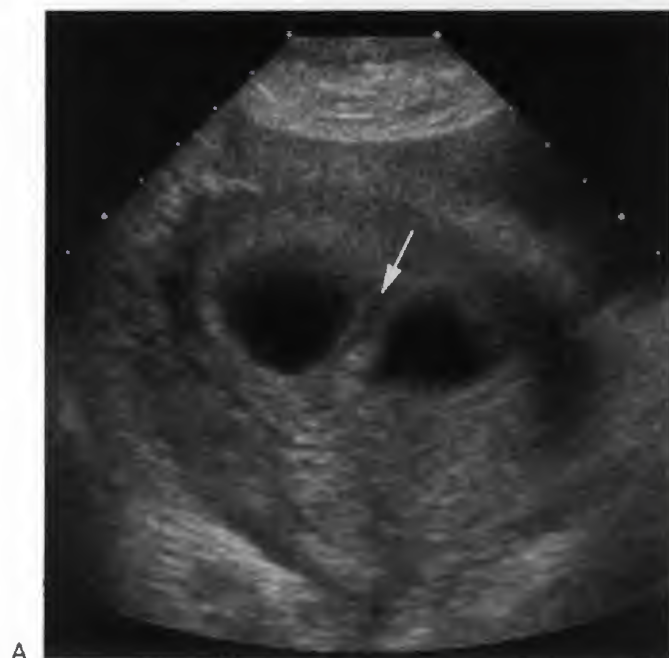


**FIGURE 35-35.** *A.* Small gestational sac, seen too early to characterize, is seen within the decidualized endometrium. A normal intrauterine pregnancy resulted. *B.* Small cystic structure (*arrow*) is seen in the periphery of the endometrium. Although the structure is similar to a small gestational sac as seen in *A*, this was a decidual cyst of an ectopic pregnancy.



**FIGURE 35-36.** Transverse scan of an early gravid uterus. Although there appears to be two gestational sacs (*arrows*), in fact, there was only one. Moving the transducer slightly over to one side demonstrated the single gestational sac. This effect is believed to be due to the refraction of sound at the interface between the abdominal musculature and fat.





A



B

**FIGURE 35-37.** A. A sonogram of the gravid uterus in the first trimester demonstrates what appears to be two gestational sacs divided by a thick intertwin membrane (*arrow*). B. With slight angulation one can see that the structure dividing the gestational sac was a uterine synechiae (*arrow*). E, embryo.



**FIGURE 35-38.** Transvaginal sonogram of an early intrauterine pregnancy and intrauterine device (IUD). The linear structure (*arrow*) seen in the lower uterine segment is an IUD. The relationship of the IUD and the gestational sac should be reported.



**FIGURE 35-39.** The yolk sac (*arrow*) is commonly identified in first trimester pregnancies. This should not be included in the measurement of the embryonic crown rump length or mistakenly called a twin gestation.

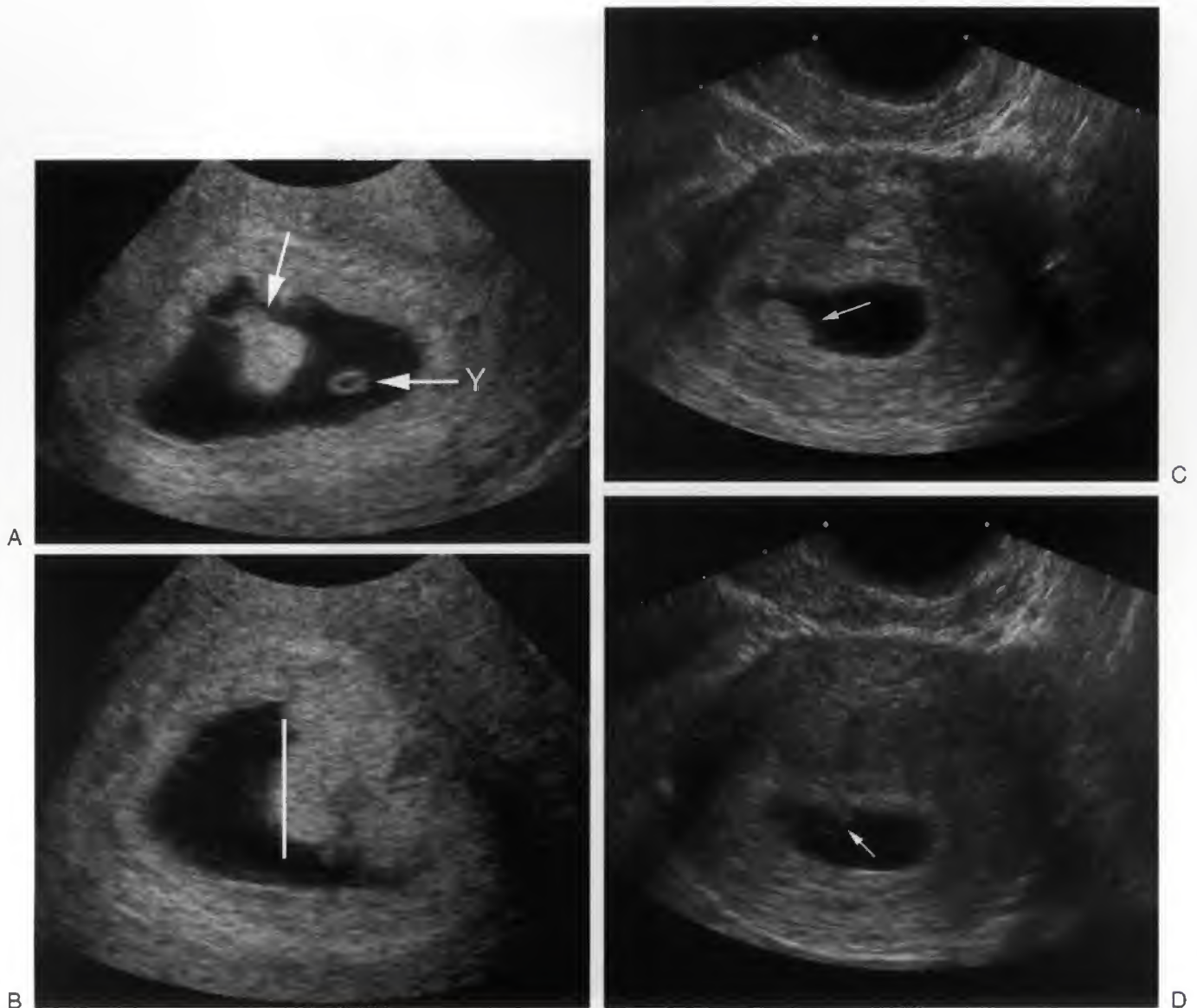


**FIGURE 35-40.** A. Longitudinal section through the uterus of a patient presenting with vaginal bleeding during early pregnancy. A yolk sac (Y) is seen in addition to what appears to be an abnormal embryo (arrow). B. A transverse scan reveals that no embryo is present and that the tissue seen in A was due to partial volume through the developing placenta (line). This was a case of early pregnancy failure. C. Sonogram of another patient with a first trimester pregnancy at 6 weeks and 2 days. A soft tissue area is seen apparently within the gestational sac simulating a nonviable embryo (arrow). D. On the opposite side of the gestational sac, a yolk sac and embryo are seen (arrow). The patient's pregnancy was subsequently uneventful, and she delivered a normal infant. The structure seen in (C) was a lobular portion of the placenta referred to recently as the "chorionic bump." (See Harris RD, Couto C, Karpovsky C, et al. The chorionic bump: A first-trimester pregnancy sonographic finding associated with a guarded prognosis. *J Ultrasound Med* 25:757, 2006.)



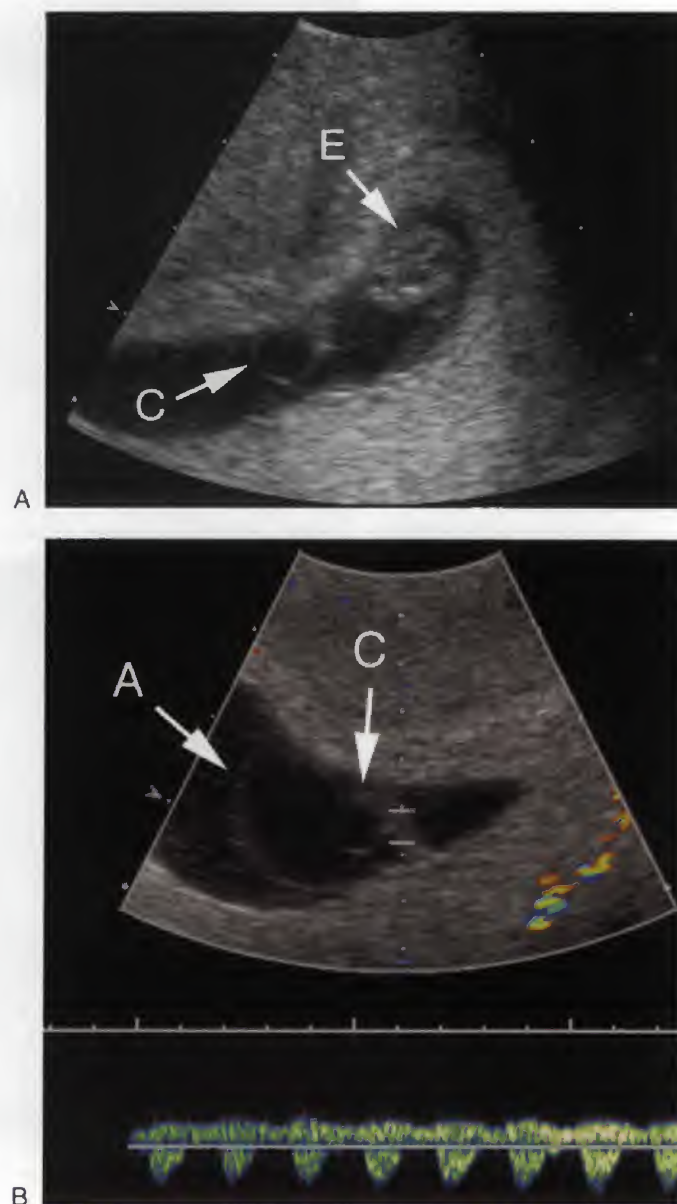


**FIGURE 35-41.** A. An umbilical cord cyst (C) is seen in this first trimester pregnancy separate from the embryo (E). B. Doppler interrogation of the umbilical cord demonstrates that the cyst (C) is associated with the umbilical cord. A, amnion.

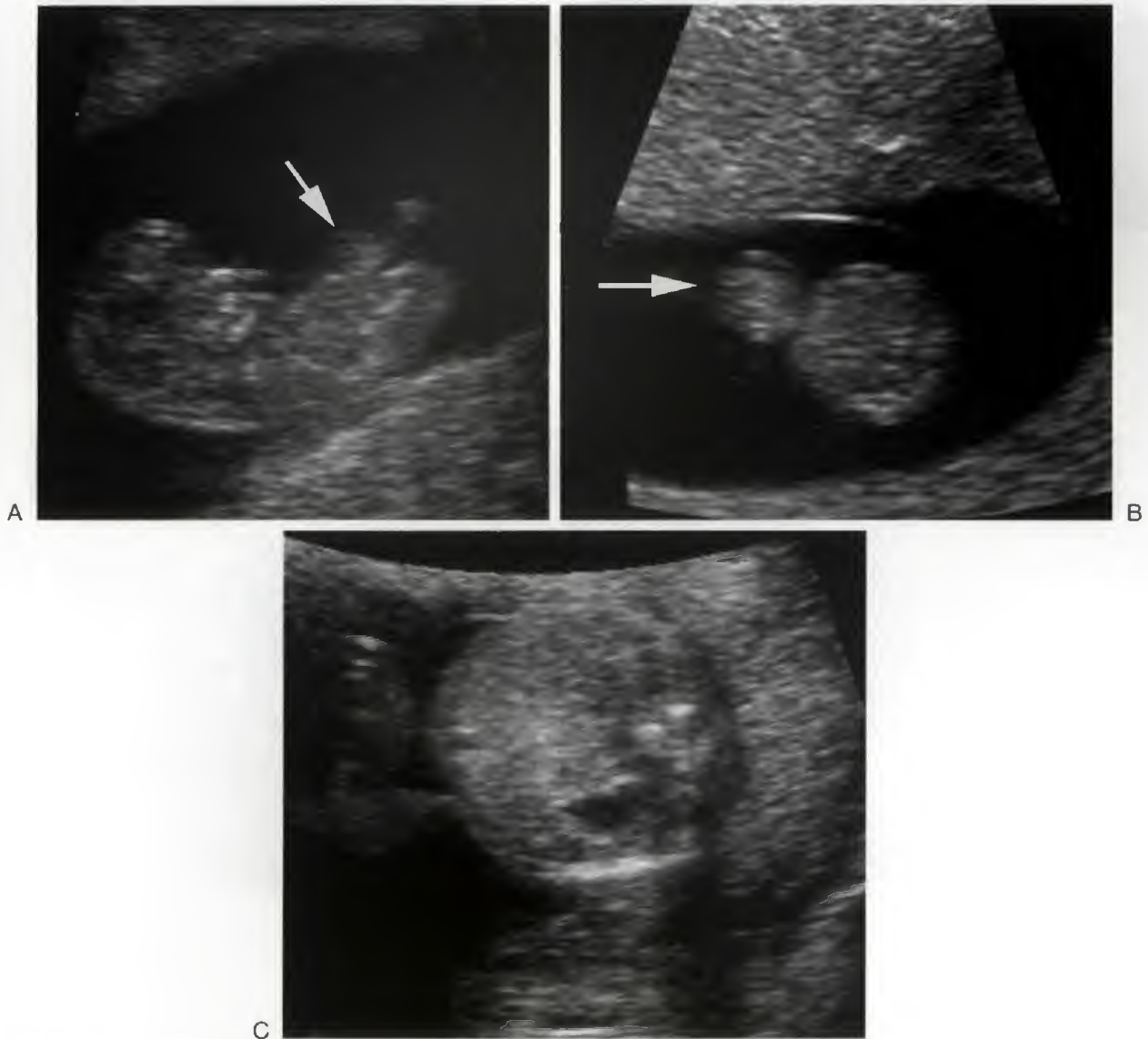


**FIGURE 35-42.** A. Sonogram of an embryo demonstrates normal herniation of bowel (*arrow*) into the umbilical cord adjacent to the anterior abdominal wall. B. Sonogram of another embryo demonstrates an even larger but normal appearance to the herniated bowel (*arrow*). C. A follow-up scan of the patient in B demonstrates a normal anterior abdominal wall without evidence of an anterior abdominal wall defect. If there is any question, a follow-up scan, as was done in this case, should be performed.





**FIGURE 35-43.** The amnion (*arrow*) is frequently identified in first trimester gestations. It apposes the chorion between 12 and 16 weeks' gestation. It should not be mistaken for amniotic band syndrome.



**FIGURE 35-44.** A prominent fluid-filled intracranial area (*arrow*) can be seen in the cranium of the embryo particularly with transvaginal sonography. This represents the developing rhombencephalon and should not be mistaken for either hydrocephalus or holoprosencephaly.



A



B

**FIGURE 35-45.** A. A transabdominal sonogram of the gravid uterus demonstrated what appeared to be a normal embryo. B. A transvaginal sonogram of the same patient done at the time of chorionic villus sampling demonstrates a large monoventricular cavity (*arrows*) consistent with holoprosencephaly. Trisomy 13 was detected.



A



B

**FIGURE 35-46.** Although the diagnosis of anencephaly is certainly possible in the first trimester, the likelihood of a false-negative diagnosis is high. The angiomatous stroma (A, *arrow*) in a case of anencephaly simulates the normal brain in another case (B, *arrow*).

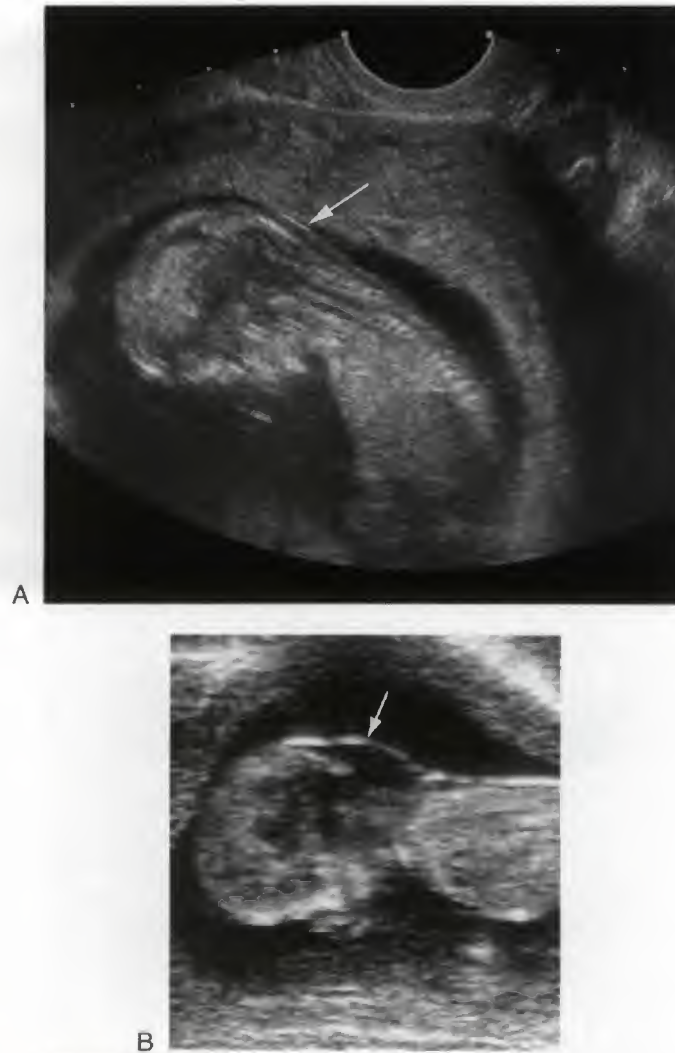


**FIGURE 35-47.** A. Normal integument (nuchal translucency) (*arrow*) in an early second trimester fetus. B. Normally, the nuchal translucency is measured to determine if it is abnormally increased in thickness. In this fetus, the large rounded configuration to the nuchal translucency (*arrow*) can readily be determined to be abnormal subjectively.



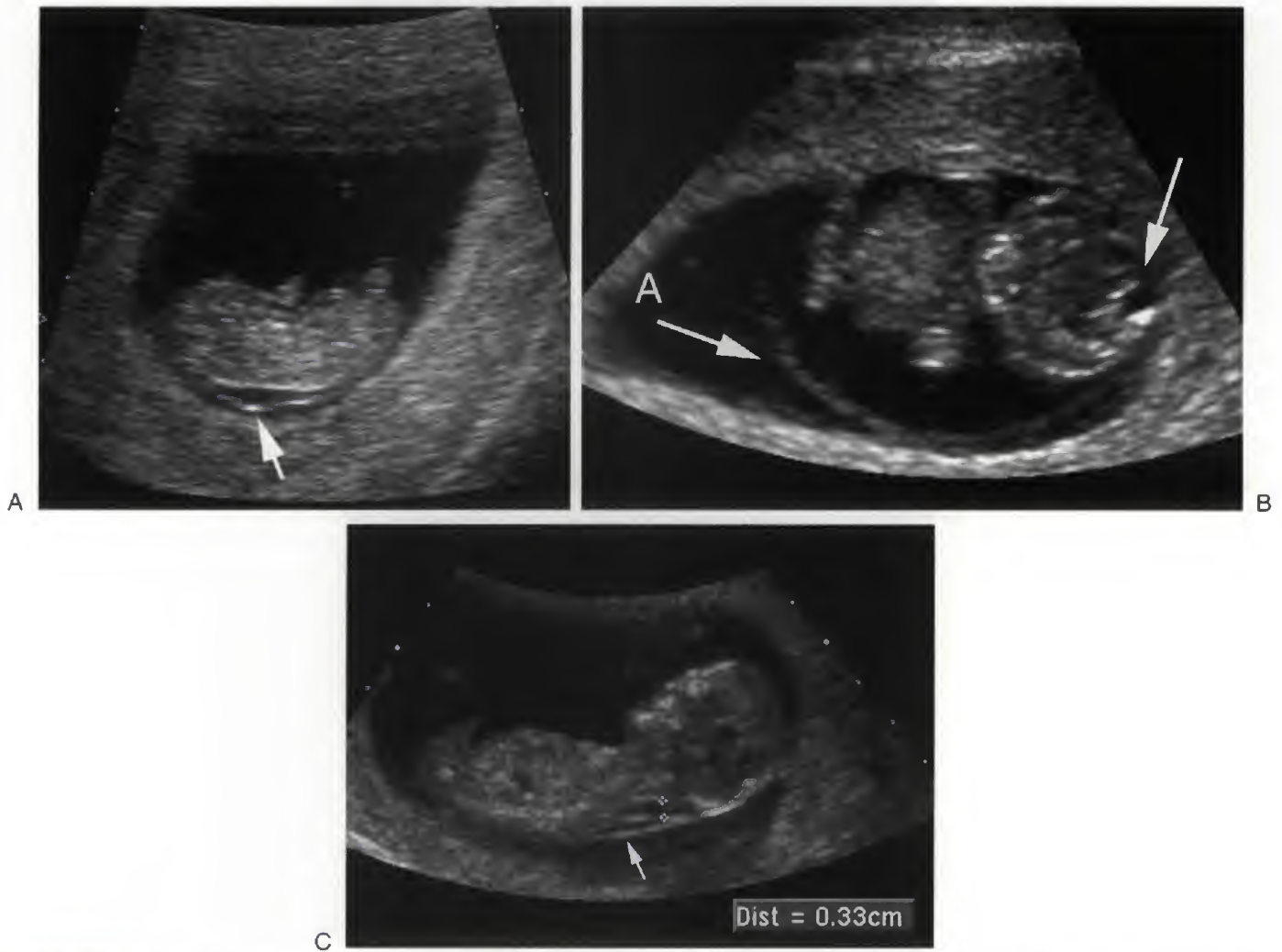


**FIGURE 35-48.** *A.* In this case of an abnormally increased nuchal translucency, there is the potential to misinterpret the outermost reflection of integument (*arrow*) as representing amnion. *B.* In another plane of section, the amnion (*A*) can be seen distinct from the integumentary edema (*arrows*). *C.* In this fetus, the abnormally increased nuchal translucency can be readily distinguished from the adjacent amnion (*arrow*).

## THE FETAL HEAD AND NECK

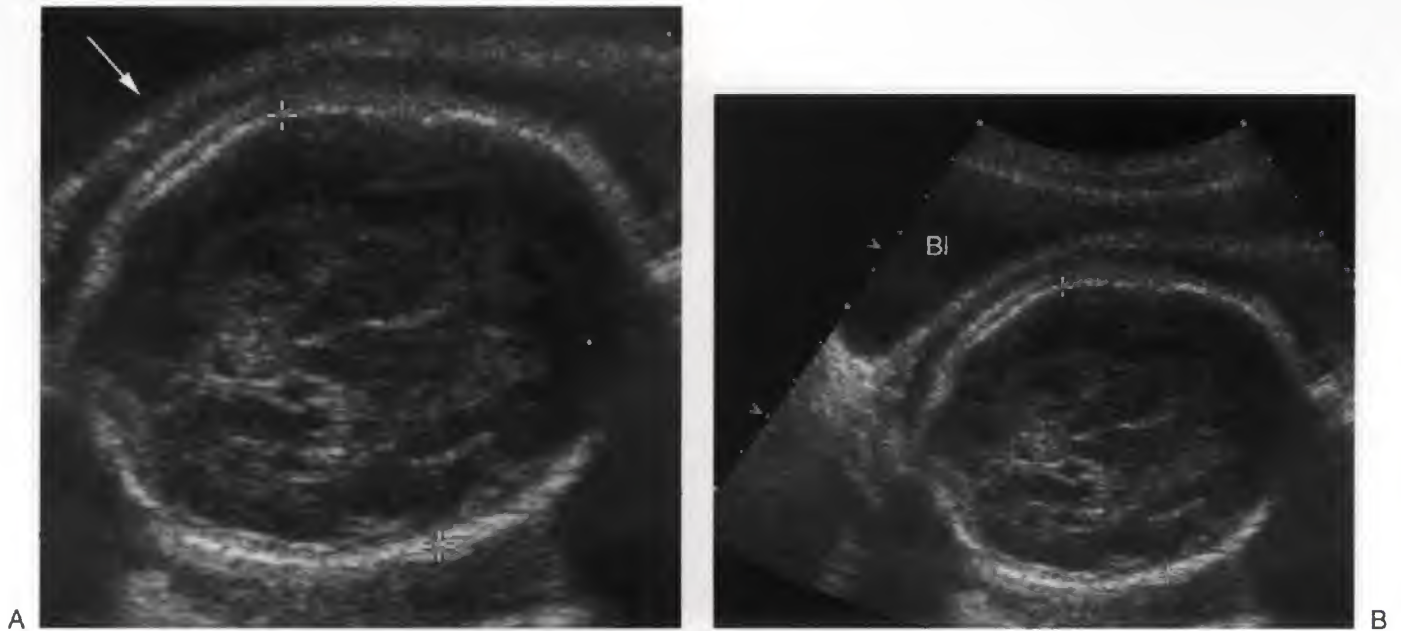


**FIGURE 35-49.** *A.* Sonogram of a third trimester fetus demonstrates what appears to be scalp thickening (*arrow*). *B.* In a slightly wider field of view, it can be clearly seen that what appeared to be fetal scalp was in fact the wall of the maternal urinary bladder. Bl, bladder.

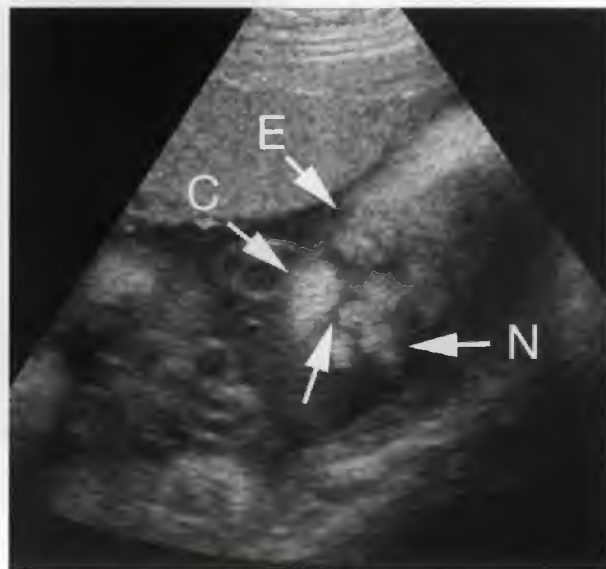


**FIGURE 35-50.** Pseudocleft of the face. The space (*arrow*) between the fetal nose (N) and cheek (C) should not be misinterpreted as a cleft. E, eye.



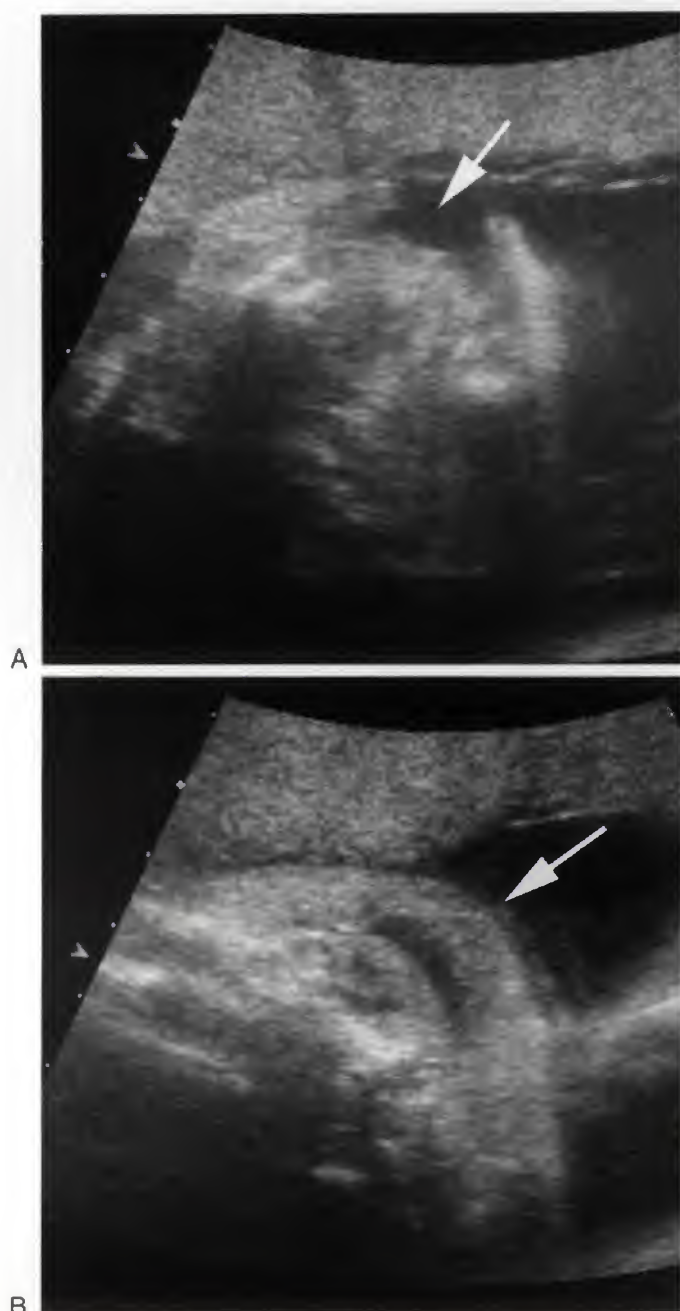


**FIGURE 35-51.** Pseudocleft lip. *A.* An angled "oblique" view of the face demonstrates what appears to be a gap in the lip (*arrow*). *B.* Normal-appearing lip (*arrow*) obtained on a slightly different plane of section.



**FIGURE 35-52.** *A.* Coronal plane of section of the fetal face. Because of a slight compression of the fetal face, the upper lip creates the appearance of a mass (*arrow*). *B.* As the mouth opens wider, the upper lip (*arrow*) appears normal.

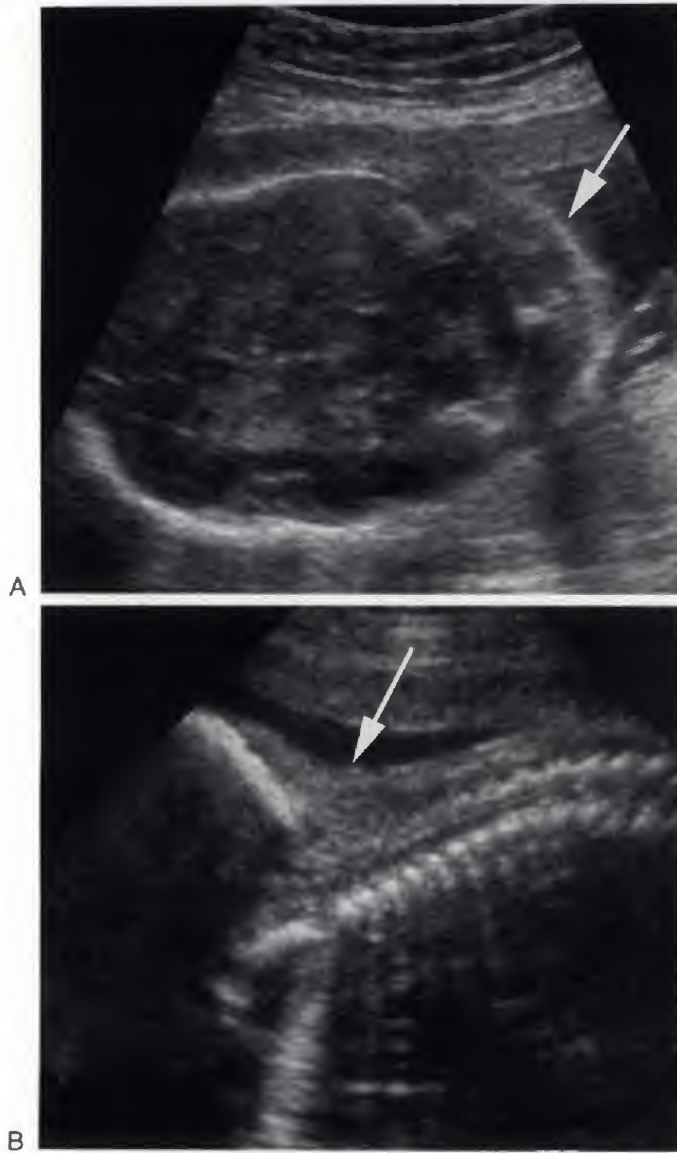


**FIGURE 35-53.** A. A steep oblique transverse plane of section of the fetal head demonstrates what appears to be marked nuchal thickening (*arrow*). B. A longitudinal plane of section demonstrates that the nuchal integument (*arrow*) is prominent as a result of extension of the fetal head on the neck. As expected, the neonate was normal.



**FIGURE 35-54.** Normal fetal hair (*arrows*) may be seen commonly in third trimester fetuses. This should not be mistaken for a calvarial mass or scalp edema.



**FIGURE 35-55.** Sonogram of the fetal head commonly used for measurement of the biparietal diameter and head circumference. This case has a common variation referred to as dolichocephaly. The importance is that measurement of the biparietal diameter in such fetuses will tend to underestimate gestational age. Dolichocephaly may also be seen in cases of breech presentation, oligohydramnios, and fetuses with myelomeningoceles.



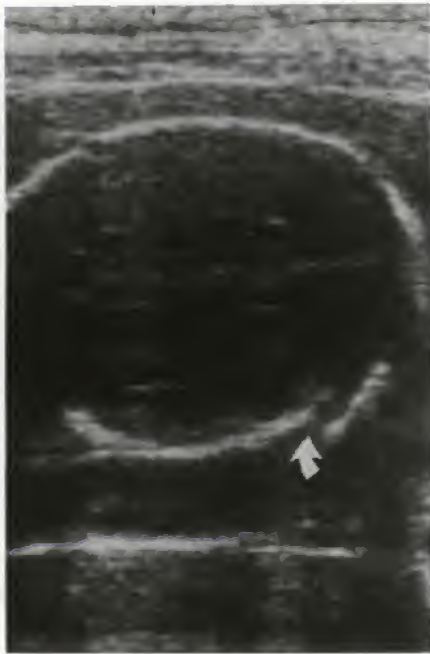


**FIGURE 35-56.** Interaction of the sound beam with the curved surface of the calvarium produces troubling appearances. This fetus appears to have overlapping sutures (arrow). In fact, this was an artifact related to refraction of the sound beam. The fetal calvarium was normal when the transducer angle was changed.



**FIGURE 35-57.** Frontal concave scalloping (arrows), the so-called lemon sign, has been described in patients with a myelomeningocele. This may also be a normal finding, as it was in this case.



**FIGURE 35-58.** A transverse axial plane of section demonstrates an echogenic mass (arrow), which appears to be within the fetal brain. This is due to a slightly oblique scan in which projection of the petrous ridge at the same level of the normal brain on the opposite side is seen.

**FIGURE 35-59.** Projections from the fetal cranium can often be disturbing. In cases of polyhydramnios, the fetal ear (E) can be seen perpendicular to the fetal skull and may simulate an encephalocele, which would be uncommon in this location.



**FIGURE 35-60.** Amniotic fluid (*arrow*) is “trapped” between the posterior fetal neck and the myometrium. This may simulate such pathology as a cystic hygroma. Identification of structures within the fluid, such as umbilical cord, as in this case, or displacing the fetus away from the uterine wall will often reveal this to be “artifactual.” H, head.

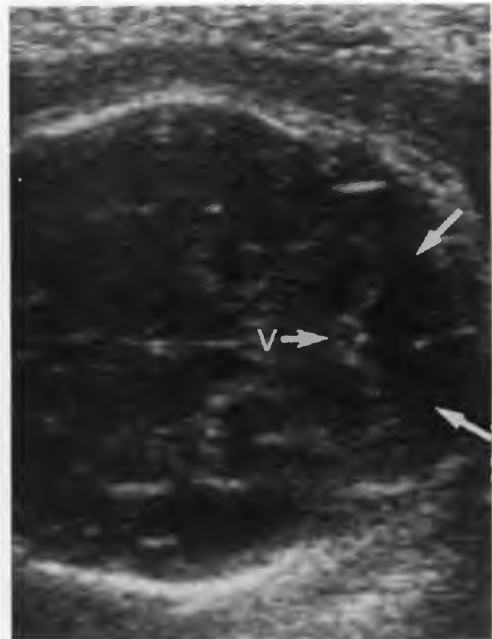
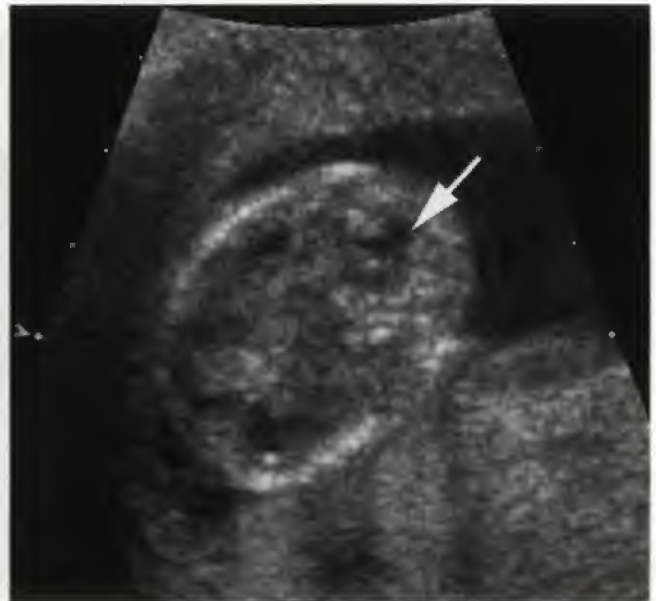


**FIGURE 35-62.** The cisterna magna (*arrows*) may be normally prominent. Controversy exists regarding the significance of a prominent cisterna magna in the absence of ventricular dilation. It is my belief that if the cisterna magna is prominent, the cerebellar vermis (v) is normal, the ventricles are normal, and no other malformations are detected, then the overwhelming likelihood is that this is a normal variant.



A



B

**FIGURE 35-61.** A and B. Two slightly angled transverse axial scans of the fetal head at 14 weeks' gestation demonstrate what appears to be vermian agenesis (*arrow*). It should be remembered that development of the posterior fossa anatomy is usually not complete until the middle of the second trimester. This fetus developed normally.





**FIGURE 35-63.** Steep transverse scan through the posterior fossa may contribute to a pitfall. The normal space (arrow) between the cerebellar hemispheres (vallecula) may appear overly prominent and simulate vermian agenesis.

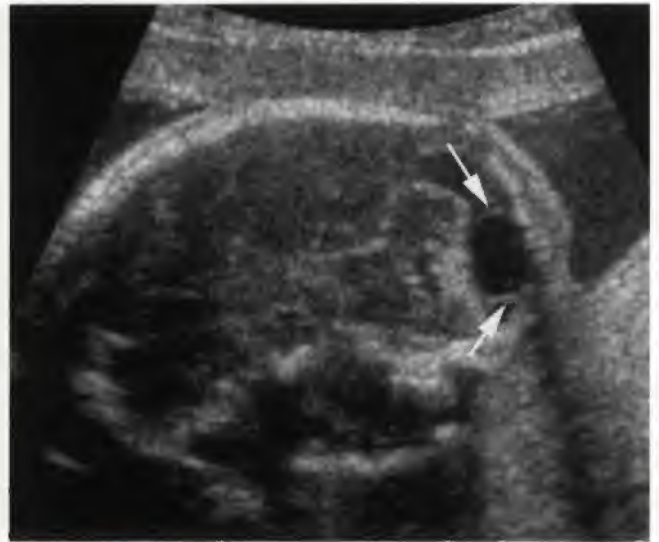


**FIGURE 35-64.** Linear echoes (arrows) seen in the region of the cisterna magna should not be mistaken for either an arachnoid cyst or a dilated sinus. The exact etiology is controversial, although a recent hypothesis is that these may represent the vestigial remnants of Blake's pouch. (From Robinson AJ, Goldstein R: The cisterna magna septa: Vestigial remnants of Blake's pouch and a potential new marker for normal development of the rhombencephalon. *J Ultrasound Med* 26:83, 2007)



A



B

**FIGURE 35-65.** A and B. The choroid plexus cyst (arrow) is a normal variant that has been the subject of much controversy during the past several years. Although most cases are simply normal variants that will resolve by 24 to 26 weeks' gestation, some cases may be associated with other anomalies and trisomy 18.

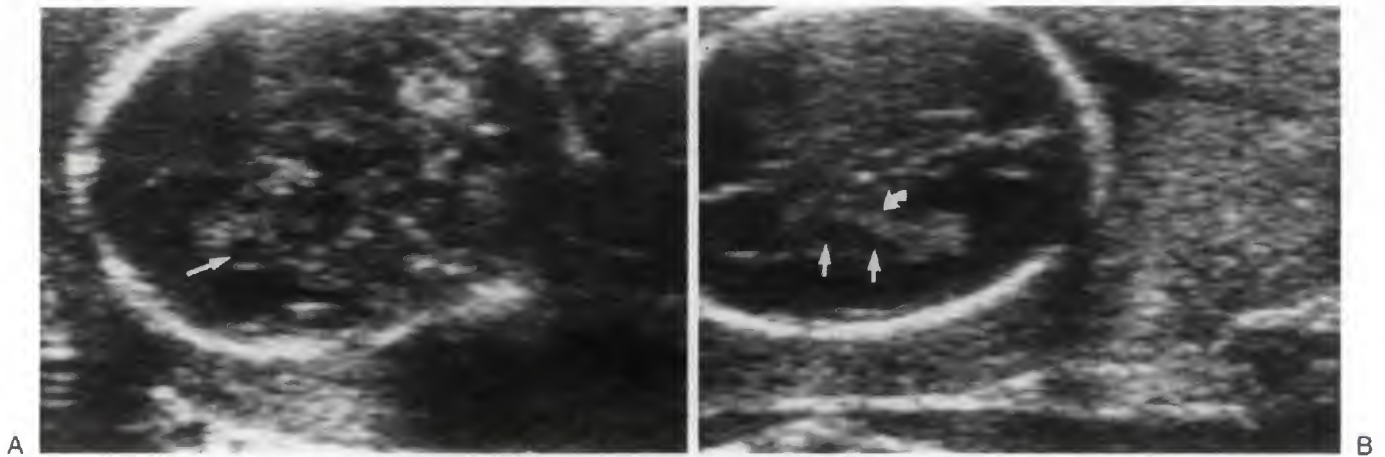


**FIGURE 35-66.** *A.* This patient has what appears to be a choroid plexus cyst (arrow) on this somewhat oblique scan of the fetal head. *B.* On a more conventional transverse axial plane of section, this “pseudocyst” elongates (arrows), proving to indent rather than be within the substance of the choroid plexus. Although the exact cause of this is uncertain, it may represent the corpus striatum.

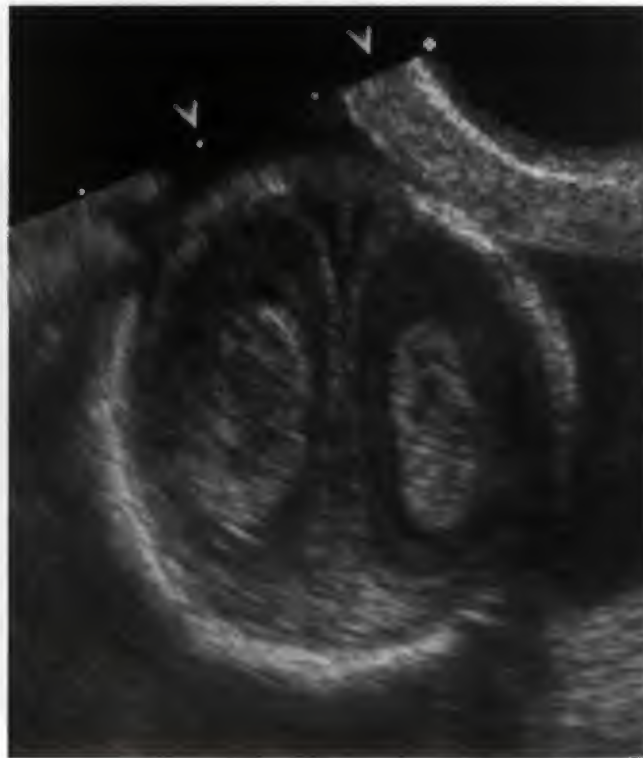


**FIGURE 35-67.** Heterogeneous choroid plexus bilaterally. No defined cysts were seen. The fetus and neonate developed normally.



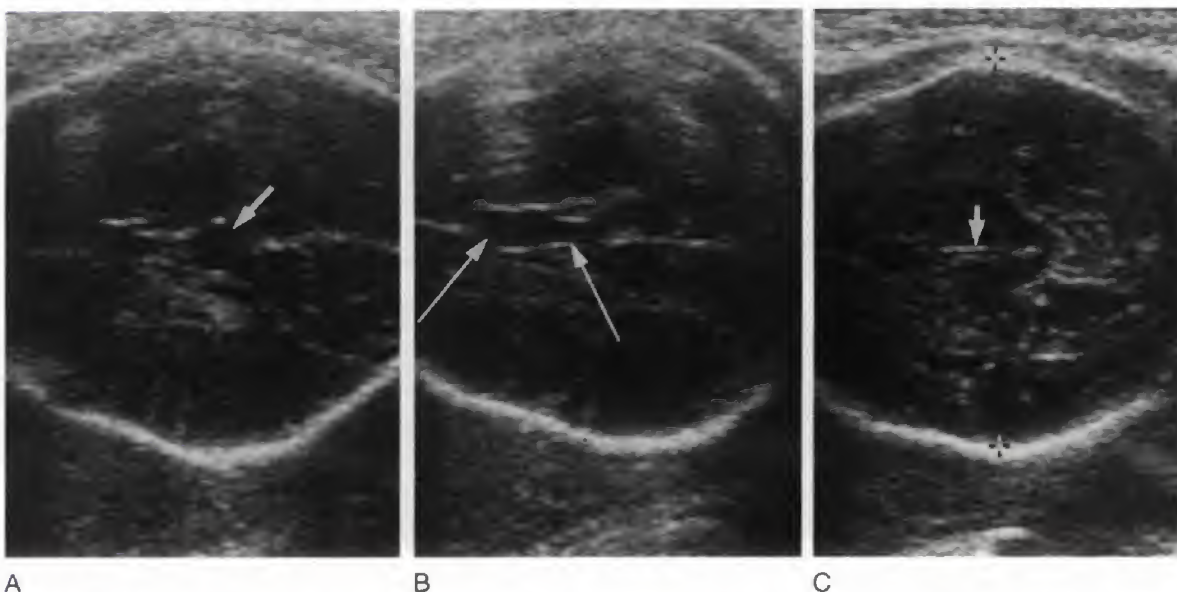


**FIGURE 35-68.** The cavum septi pellucidi is normally seen in scans of the second trimester fetal brain. At times, a prominent but normal posterior continuation, referred to as the cavum vergae, can be seen. *A* and *B*. Portions of the cavum (arrows) may simulate either an arachnoid cyst or a dilated third ventricle. *C*. The normal third ventricle (arrow) is easily identified in this case.

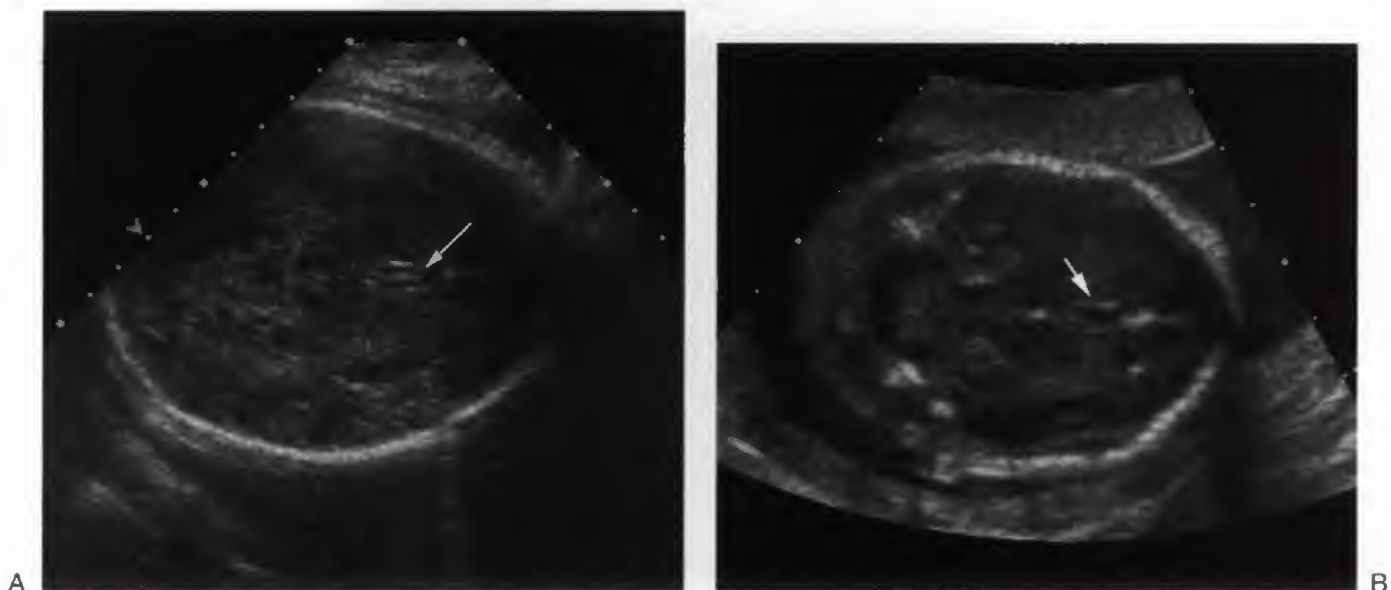


**FIGURE 35-69.** *A*. Transverse axial sonogram of the fetal head. In the expected position of the cavum septum pellucidum, a trilinear structure is seen (arrow). This represents the columns of the fornix and should not be mistaken for the cavum septum pellucidum, which is at a slightly more rostral level. *B*. At a slightly more rostral level, the normal cavum septum pellucidum is seen (arrow). The normal cavum is filled with fluid and has a box-like appearance.

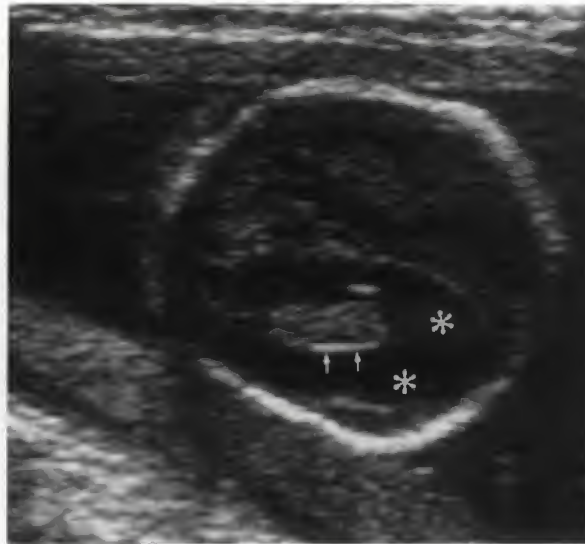


**FIGURE 35-70.** The normal fetal brain is sonolucent (*asterisks*) and may simulate cerebrospinal fluid. This may incorrectly lead to the diagnosis of hydrocephalus. Identification of the lateral ventricular walls (*arrows*) and the choroid plexus within will help resolve this confusion.



A

B

**FIGURE 35-71.** A. Transverse axial scan in which both choroids plexi are seen (*asterisks*). B. In this angulated scan, the choroid plexi (*arrows*) simulate bilateral subependymal hemorrhages. This fetus was normal on subsequent scans and on neurosonograms at birth.



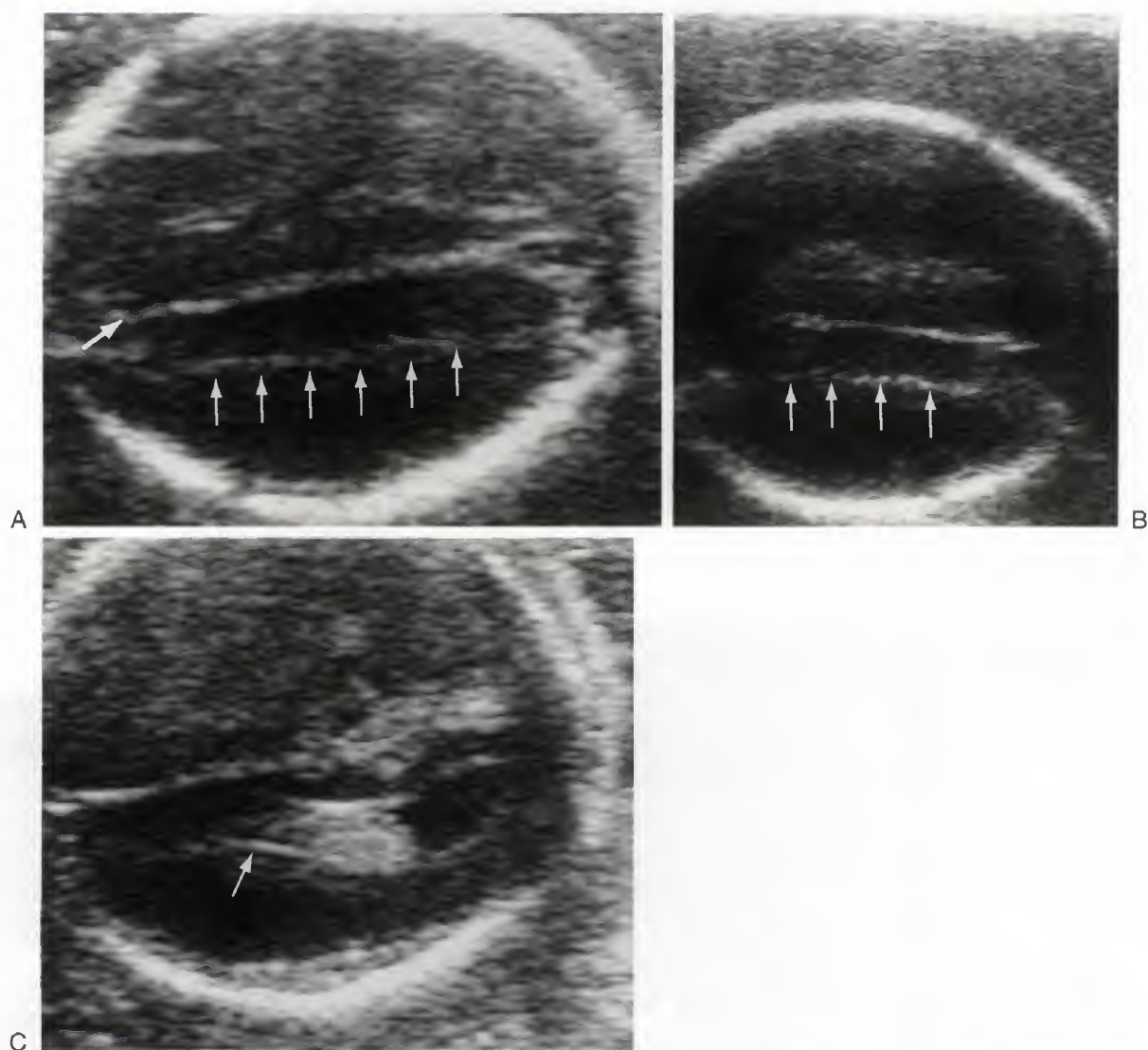


**FIGURE 35-72.** *A and B.* Transverse axial plane of section in two normal patients. The paramedian lines (*small arrows*) (paralleling the midline interhemispheric fissure echo [*large arrow*]) are due to deep cerebral medullary white matter veins and not the lateral wall of the lateral ventricle. *C.* The lateral wall of the lateral ventricle (*arrow*) is seen at a slightly more basal level and angling laterally away from the midline.



**FIGURE 35-73.** Shadowing (*arrow*) from the iliac wing (*curved arrow*) may simulate a gap or fluid-filled cystic space (i.e., myelomeningocele) of the lumbar spine.



**FIGURE 35-75.** The hyaloid artery (*arrow*) and a branch of the ophthalmic artery can be seen in this sonogram. This vessel often degenerates during the third trimester.

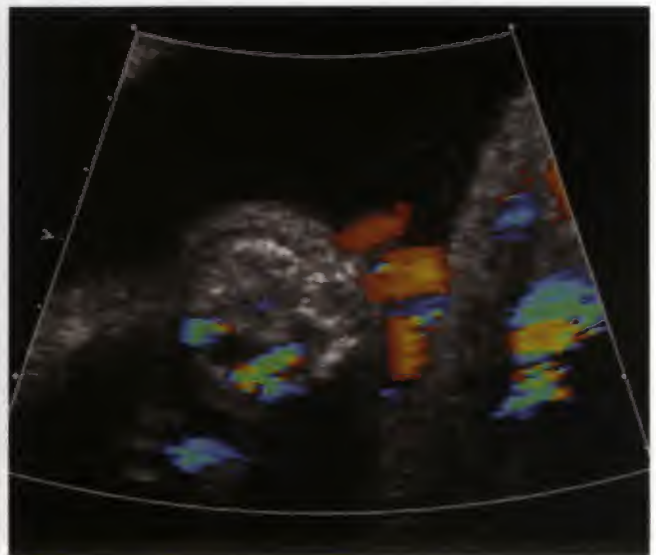
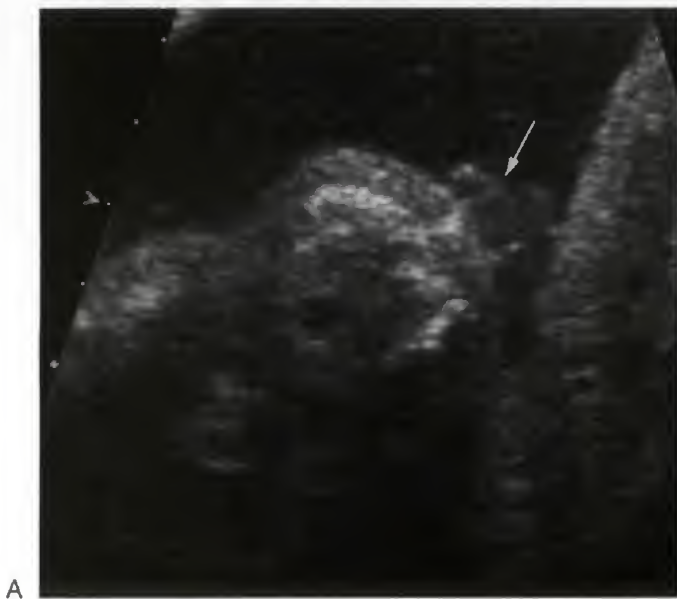


**FIGURE 35-74.** A. A sac-like structure is seen just posterior and adjacent to the lumbosacral spine (*arrow*). This has the appearance of a myelomeningocele sac. B. Color Doppler imaging demonstrates that this structure is the umbilical cord.



## THE FETAL THORAX



**FIGURE 35-76.** The fetal hypopharynx (*arrow*) may be prominent. It may be seen to fill and empty with fluid during the examination. This should not be mistaken as representing esophageal obstruction.

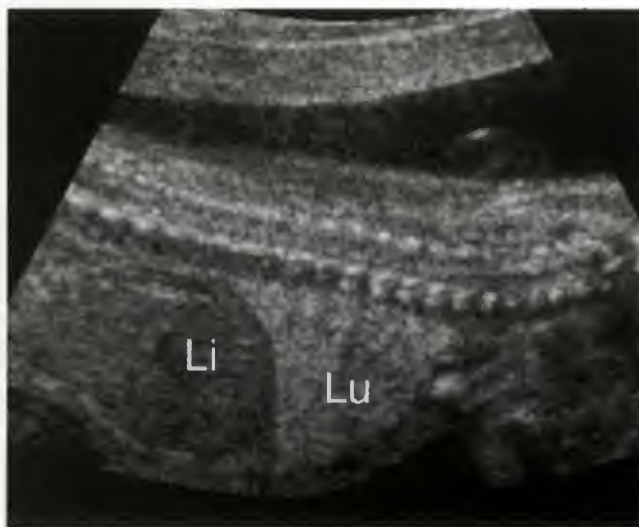


**FIGURE 35-77.** The echogenicity of the fetal lung (Lu) may often be misleading. The lung in this oblique coronal scan appears brightly echogenic compared with the liver (Li); however, this fetus neither is mature nor has lung pathology.

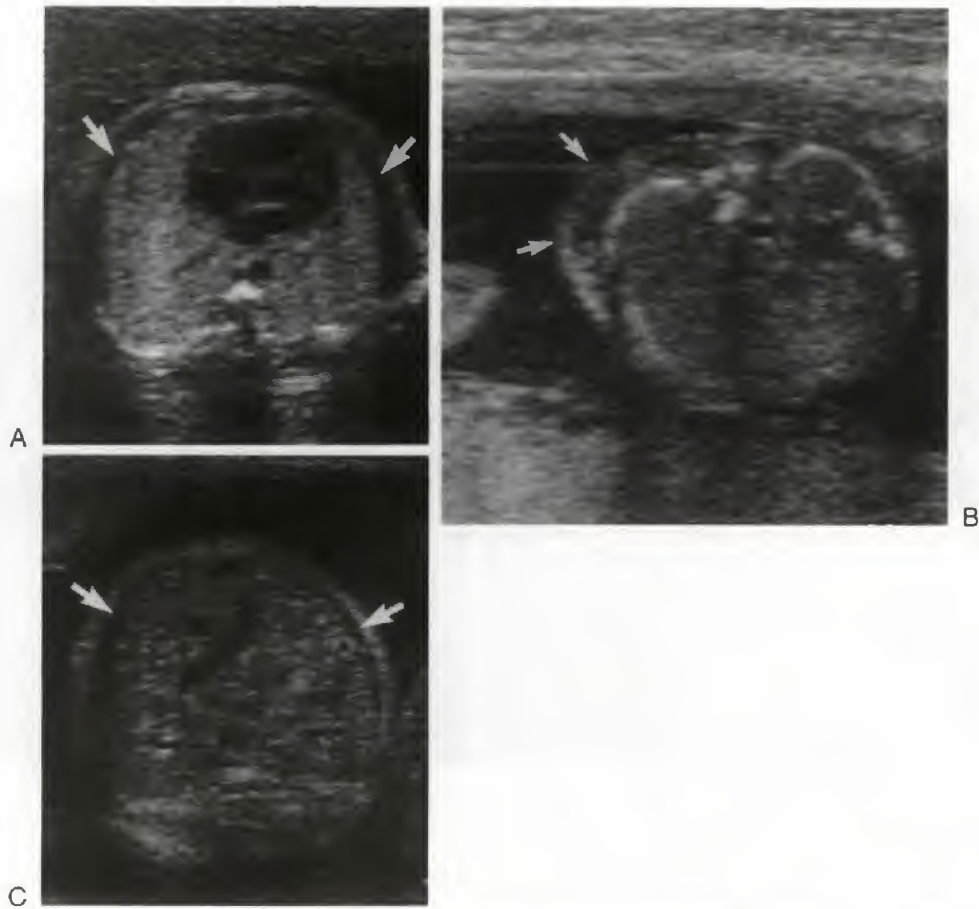


A



B

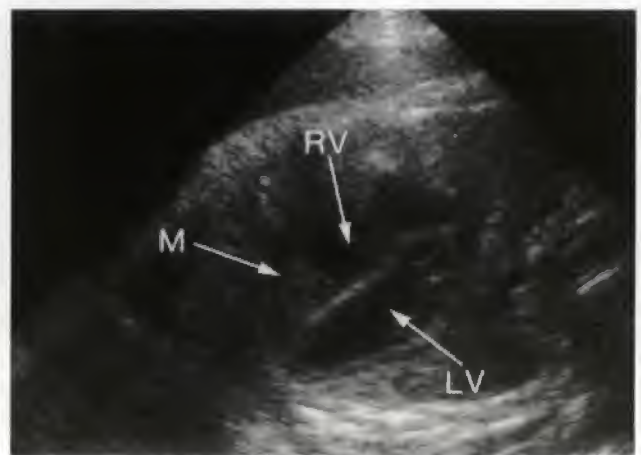
**FIGURE 35-78.** *A.* Angled transverse axial plane of section at the level of the fetal heart (H). The fetal stomach (S) is seen at the same level as the heart, raising the possibility of a diaphragmatic hernia. *B.* This sagittal plane of section from the same patient reminds us that the diaphragms (*arrow*) are curved, and a slightly angled transverse plane of section will portray what appears to be a diaphragmatic hernia, although the stomach (S) is, in fact, below the diaphragm.



**FIGURE 35-79.** Pseudoskin thickening and pseudoascites. *A.* The sonolucent region (*arrows*) at the level of the thorax does not represent integumentary edema but rather the normal thoracic musculature. *B.* At a slightly lower plane of section, the same appearance is seen (*arrows*) simulating ascites. *C.* In another patient, this appearance is also noted at the region of the scapula (*arrows*), where it is often most prominent.

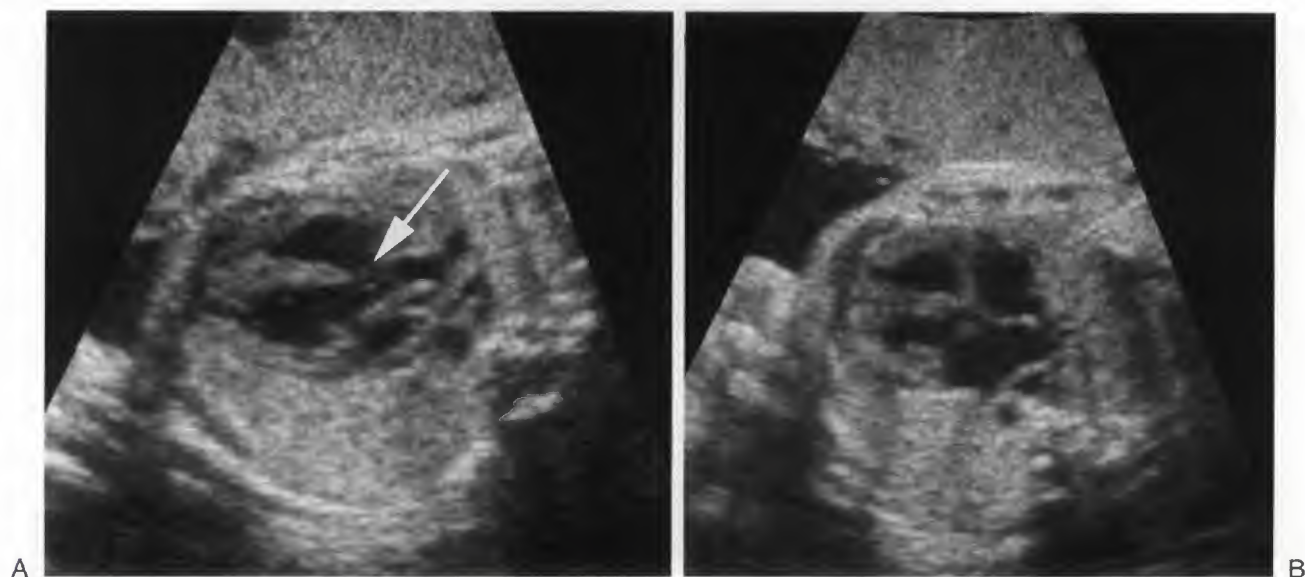


**FIGURE 35-80.** A high-amplitude echo (*short arrow*) with shadowing is seen possibly involving the pericardium. This is the normal rib seen along its short axis. The contralateral rib (*long arrow*) is somewhat more elongated.

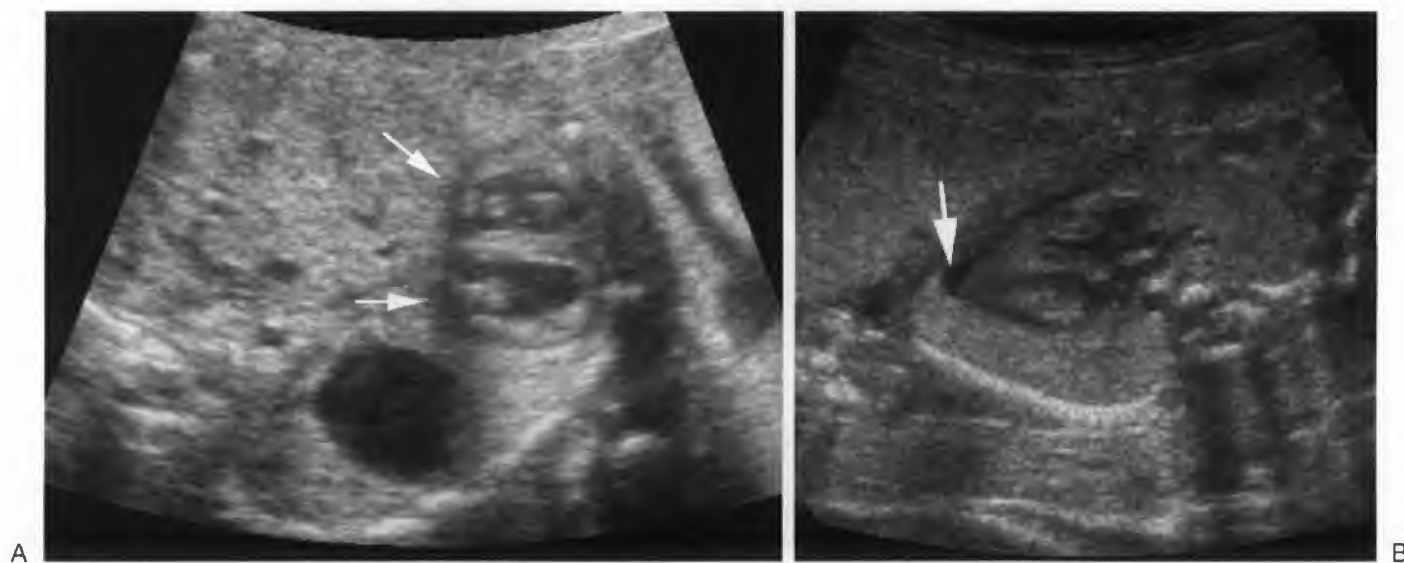


**FIGURE 35-81.** Soft tissue seen within the ventricle is always worrisome for either thrombus or neoplasm. In this patient, the normal but prominent moderator band of the right ventricle (*M*) is seen. RV, right ventricle; LV, left ventricle.

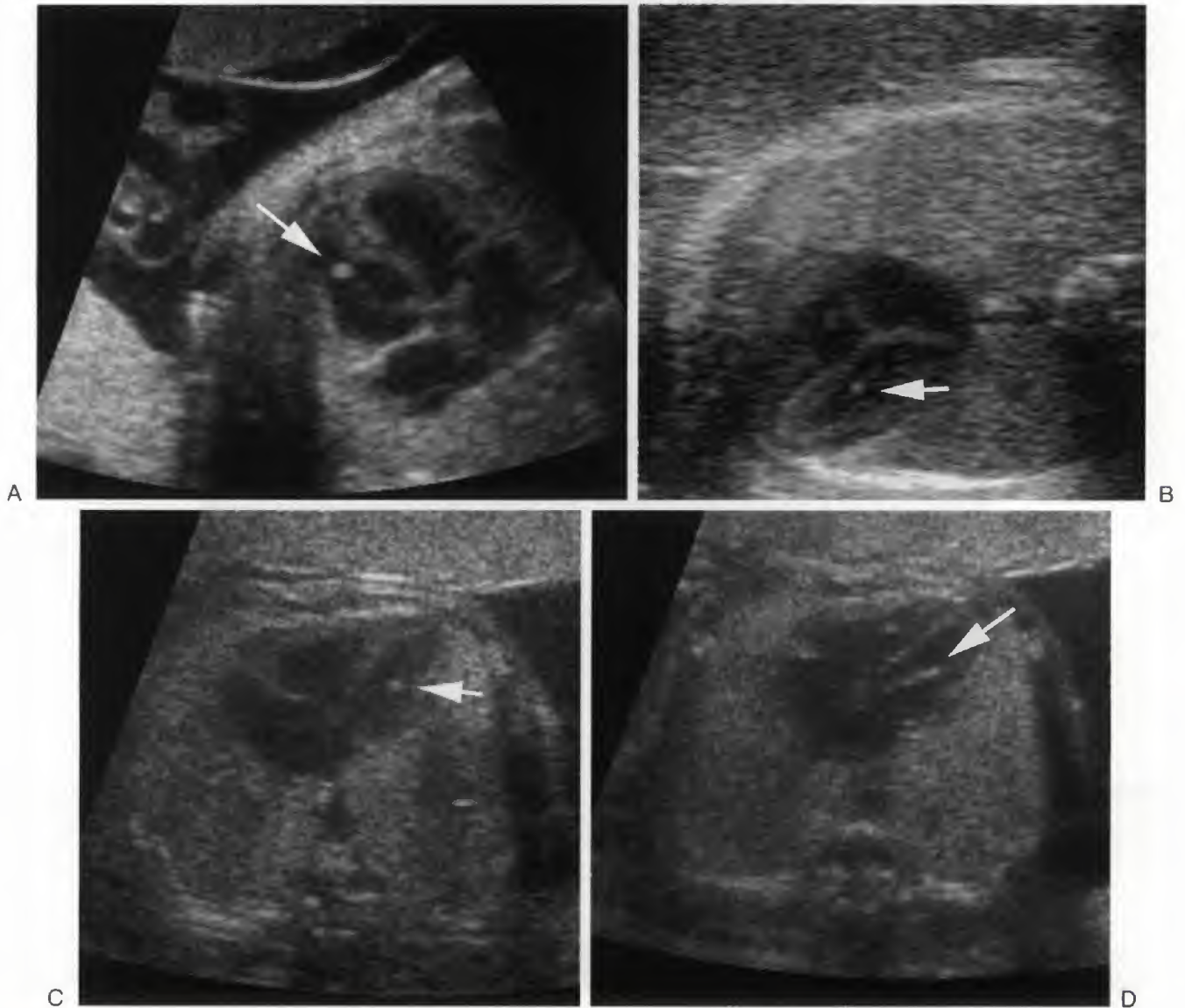




**FIGURE 35-82.** A. An apparent defect in the ventricular septum (*arrow*) is seen. This may be due to the origin of the aortic root and the thin membranous septum. B. Slight change of the transducer position demonstrates a normal-appearing septum.

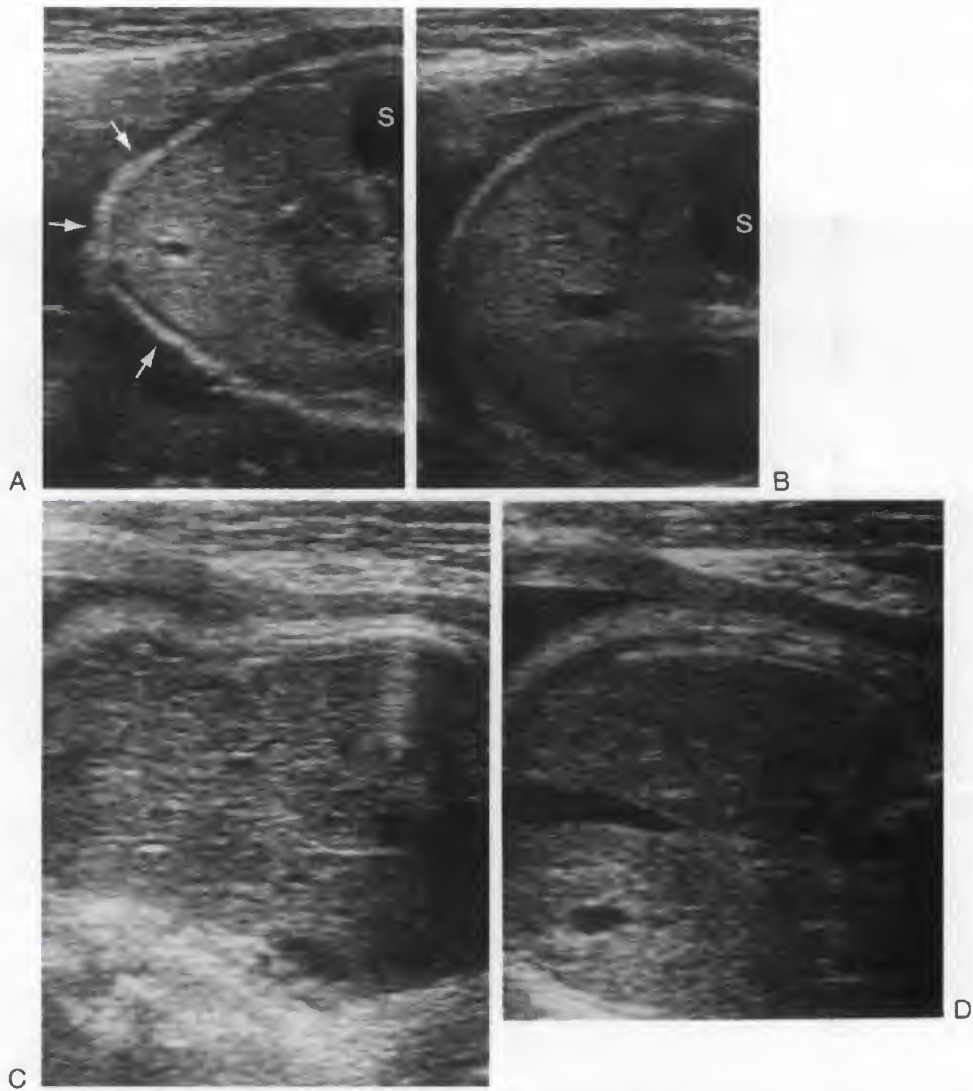


**FIGURE 35-83.** A. The poorly echogenic myocardium (*arrows*) may simulate pericardial fluid. The observation that this area blends imperceptibly with the intraventricular septum should alert one that this is a normal cardiac structure and not pericardial fluid. B. The case in A should be contrasted with real pericardial fluid (*arrow*), which contains no echoes.



**FIGURE 35-84.** Echogenic intracardiac focus. *A.* A high-amplitude echo (*arrow*) is seen in the left ventricle in this patient. This appearance is believed to be due to reflection from calcification in the papillary muscle. In this case, the echogenic structure was fairly large. The significance of this finding is controversial; in some cases, it is associated with karyotype abnormalities. *B.* A smaller echogenic intracardiac focus (*arrow*) is seen in another patient. *C.* In this patient, a reflection (*arrow*) from the atrioventricular valve is seen. It appears similar to an echogenic intracardiac focus. *D.* The reflection from the surface of the valve (*arrow*) is better seen in another plane of section.



**THE FETAL ABDOMEN**

**FIGURE 35-85.** Pseudo-omphalocele in two patients. *A* and *C*. Excessive pressure with the linear array transducer causes deformation of the abdominal wall, simulating an abdominal wall defect. Identification of the normal skin covering this protuberance (*arrows*) and less pressure on the maternal abdomen will usually resolve the confusion. *B* and *D*. Same patients demonstrating normal anterior abdominal wall with light pressure on the maternal abdomen. S, stomach.



**FIGURE 35-86.** Pseudogastroschisis caused by an extremity (E) adjacent to the umbilical cord insertion site (*arrow*).



**FIGURE 35-87.** Gastroschisis in a second trimester pregnancy. Multiple loops of bowel are seen adjacent to the fetal abdomen within the amniotic fluid. What appears to be dilated bowel is normal colon (*arrow*), which may appear to be prominent although nondilated.



A



B



C

**FIGURE 35-88.** A. Pseudoascites resulting from the poorly echogenic appearance of the normal integument (*arrows*). B and C. A small amount of real ascites is identified in this patient. Notice that the fluid invaginates between the viscera on the right side (*arrows*).





**FIGURE 35-89.** Debris within the fetal stomach (*arrow*). Although occasionally the cause may be known (i.e., swallowed blood from an intrauterine transfusion), most often it is unknown. This is almost always an innocuous finding.

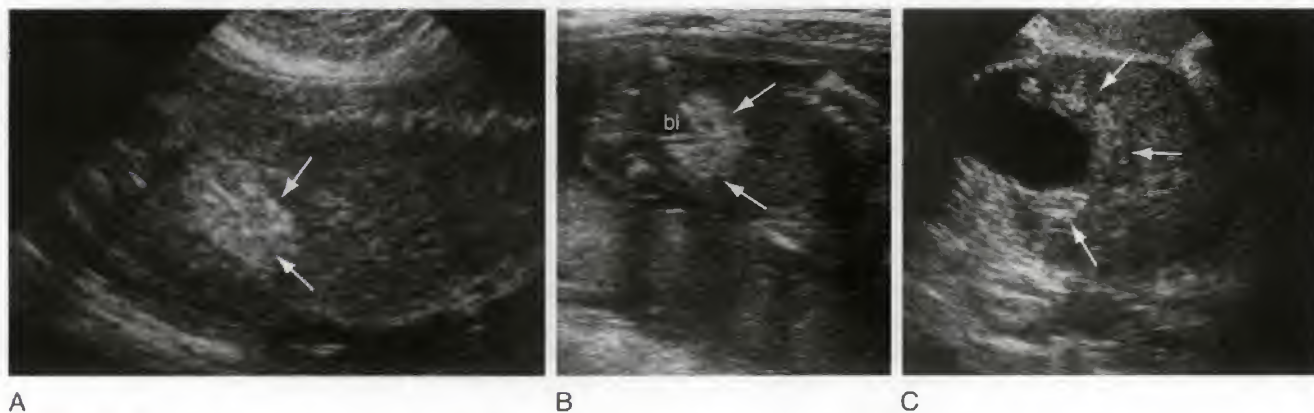


**FIGURE 35-90.** Hyperechogenicity within the fetal abdomen (*arrows*). This finding has received recent attention in the literature as a possible clue to the diagnosis of either cystic fibrosis or aneuploidy. The problem is in differentiating normal from abnormal. *A* and *B*. Normal chromosomes and no evidence of cystic fibrosis. *bl*, bladder. *C*. A case of meconium ileus and cystic fibrosis at birth (*arrows*). To be called "echogenic bowel" the echogenicity of the bowel should be similar to adjacent bone.

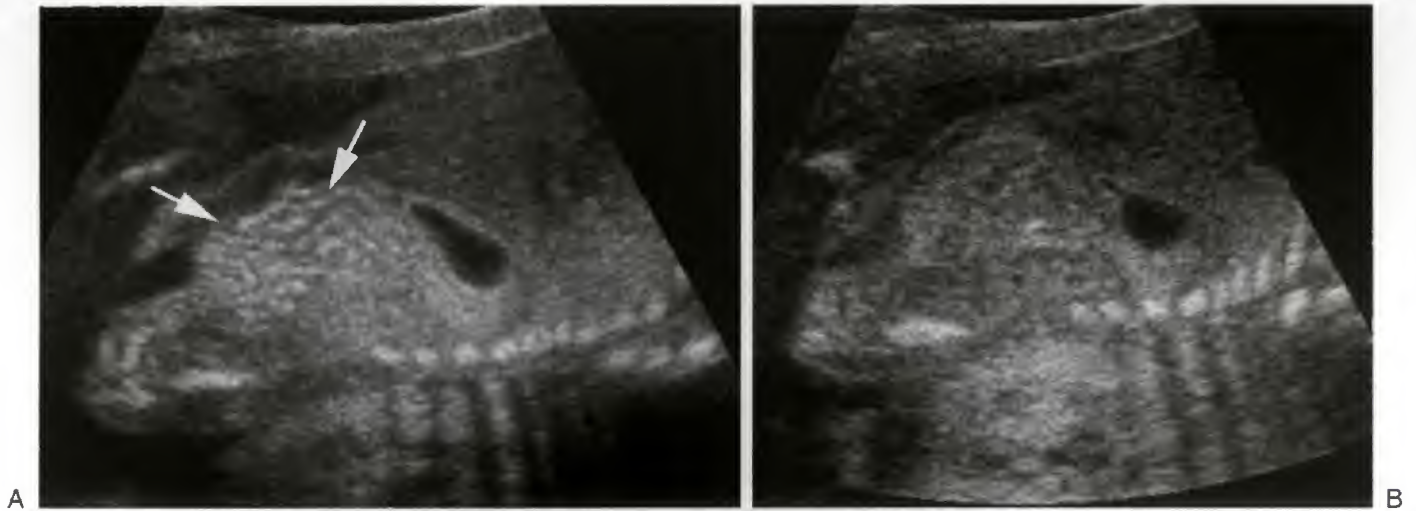


**FIGURE 35-91.** Pseudohyperechoic fetal bowel. *A.* Sonogram of the fetal abdomen obtained with an 8-MHz frequency transducer demonstrates hyperechoic fetal bowel (*arrows*). The bowel wall is accentuated at this frequency. *B.* Sonogram of the same patient obtained with a 5-MHz frequency transducer appears more normal in appearance. This is a common phenomenon, and the sonologist should be aware of the effect of transducer frequency on bowel echogenicity before declaring the bowel echogenicity abnormal and proceeding to invasive testing.



**FIGURE 35-92.** *A* and *B.* Fetal gallstones (*arrows*) seen in two third trimester fetuses. In both cases, the fetus was otherwise normal. This finding does not indicate biliary pathology and may resolve before birth.



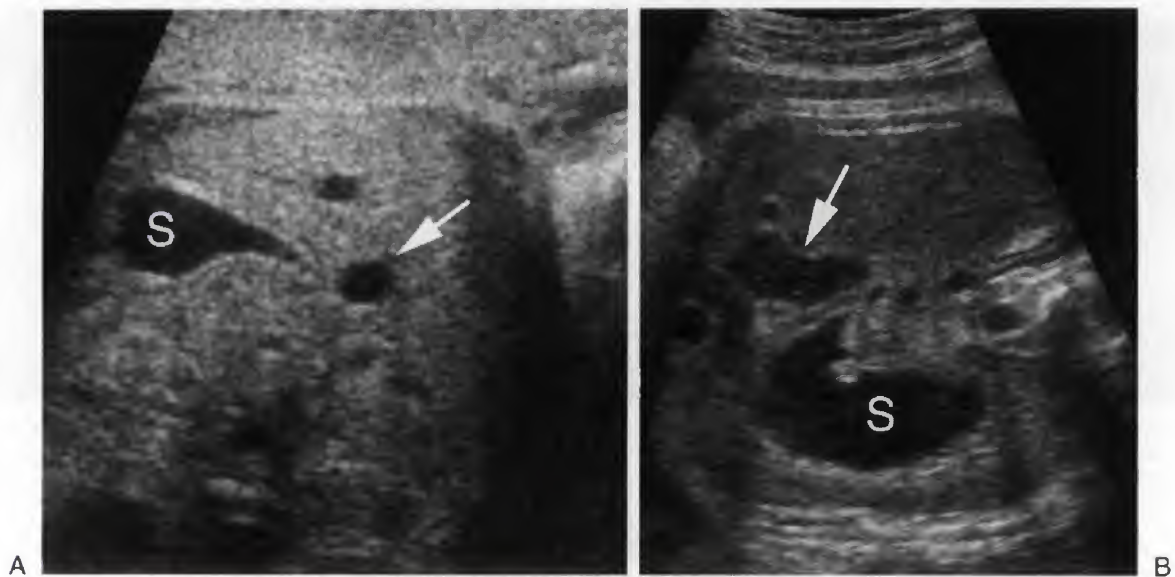


**FIGURE 35-93.** Pseudo-double bubble sign. The double bubble may be seen in cases of duodenal obstruction and has been associated with trisomy 21. *A.* In this case, the fluid-filled structure adjacent to the stomach (S) is the gallbladder (*arrow*) and not the duodenum. *B.* A sonogram of the fetal abdomen in the third trimester demonstrates a prominent segment of colon (*arrow*) adjacent to the fetal stomach (S) and should not be misinterpreted as dilated duodenum.

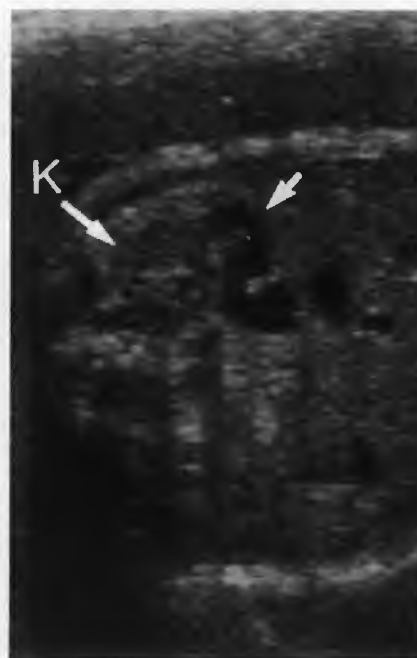


**FIGURE 35-94.** The fetal intestine (*arrow*) may simulate other nonintestinal structures such as a dilated ureter. This is especially true in the second trimester, when the meconium-filled distal small bowel and colon are sonolucent. K, kidney.

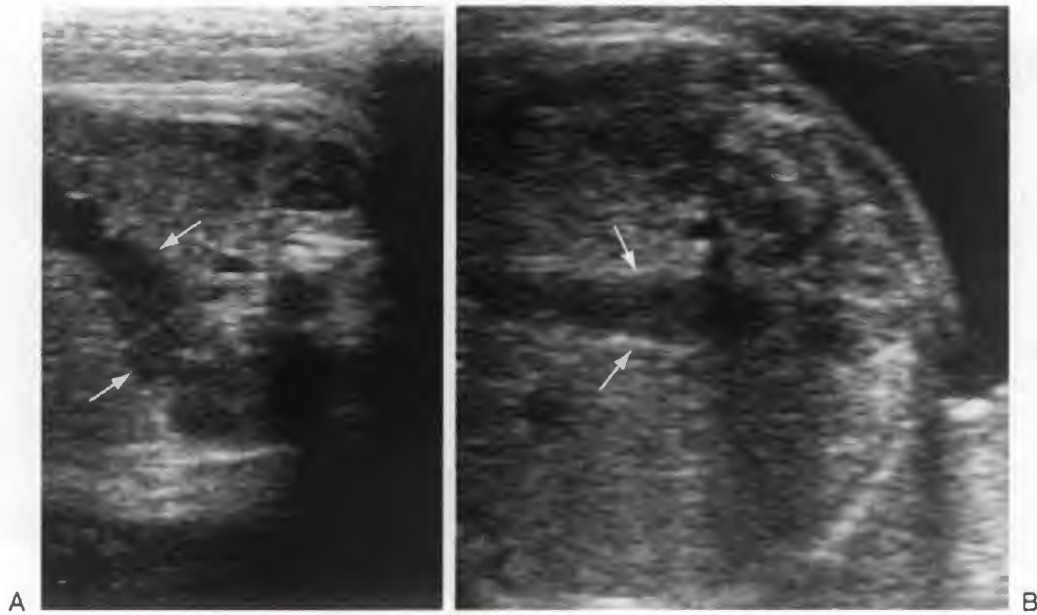


**FIGURE 35-95.** A and B. The fetal colon may be prominent in the third trimester fetus. Normal colon in two fetuses in the third trimester. The colon (arrows) is prominent but normal in both of these patients.

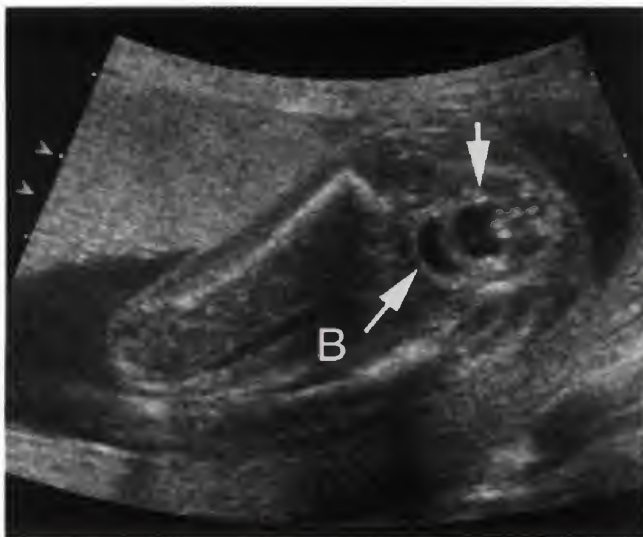


**FIGURE 35-96.** The normal rectum (arrow) can occasionally be seen in the second and third trimester fetus. This should not be mistaken for a myelomeningocele or other intrapelvic pathology. B, bladder.



**FIGURE 35-97.** In the presence of fetal ascites (A), fluid may enter the lesser sac and result in outlining of the greater omentum (arrow). This should not be mistaken for a dilated loop of intestine. L, liver.



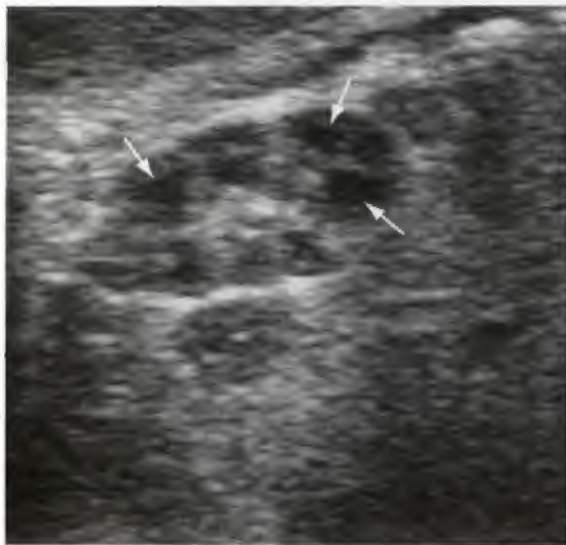


**FIGURE 35-98.** The normal fetal renal pyramids may be sonolucent (*arrows*) and simulate hydronephrosis. This appearance is normal and should be seen as a normal and expected finding. Failure to identify a dilated medial renal pelvis should reassure the interpreter.

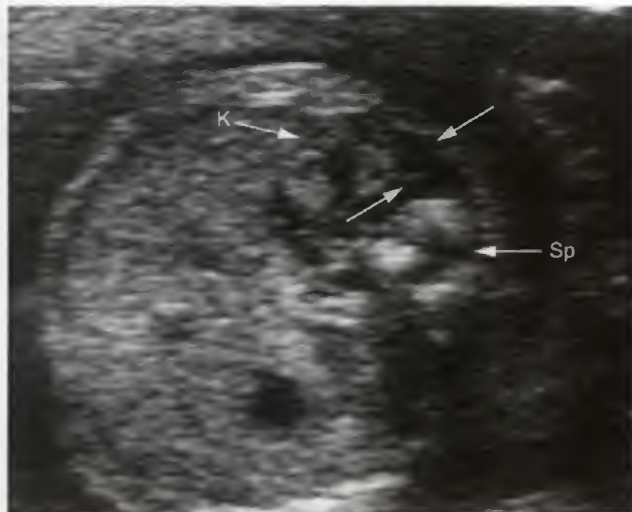


**FIGURE 35-100.** The normal poorly echogenic pararenal musculature (quadratus lumborum and psoas) (*arrows*) may simulate fluid around the kidney (K). Sp, spine.

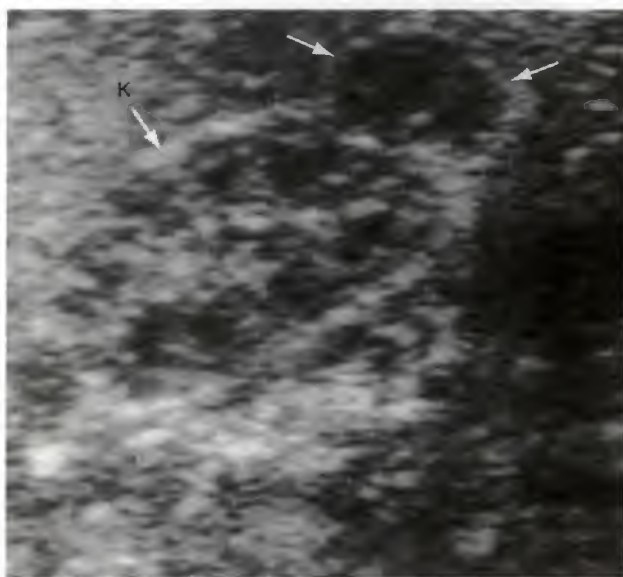
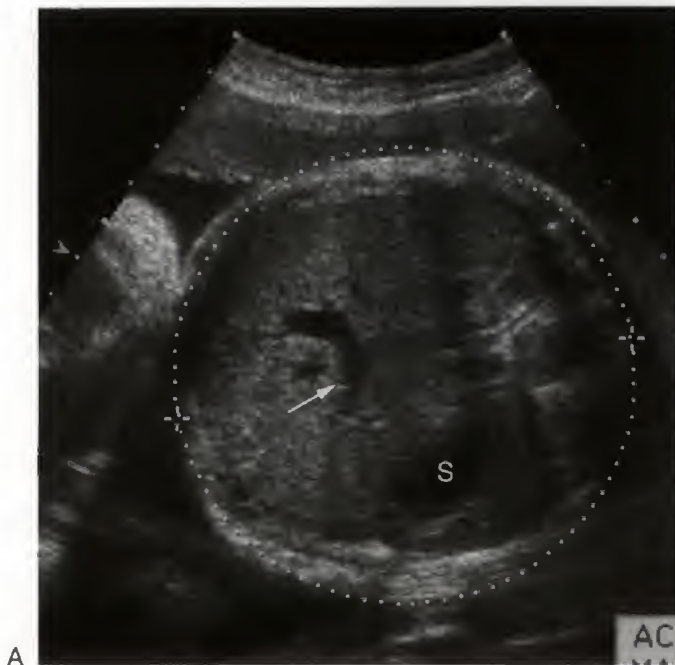


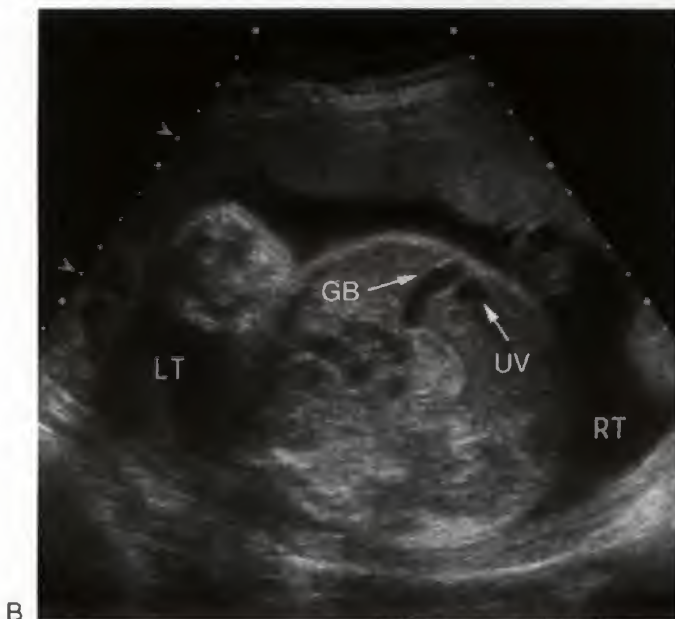
**FIGURE 35-99.** The non-fluid-filled colon (*arrows*) is seen adjacent to the kidney (K) in this patient. This should not be misinterpreted as a renal mass.



**FIGURE 35-101.** An oval paraspinal soft tissue structure is seen simulating the fetal kidney (*arrow*). This structure is the normal adrenal gland, which often is quite prominent in the fetus. The hyperechoic medulla and hypoechoic cortex are well seen.



A



B

**FIGURE 35-102.** Persistent right umbilical vein. *A.* In this transverse axial scan, the portal vein (*arrow*) is curving toward, rather than away from the stomach (s). This is a case of persistent right umbilical vein. No other anomalies were detected. *B.* In another case of persistent right umbilical vein, the umbilical vein (*arrow*) is to the right rather than the left of the gallbladder (GB).



A



B

**FIGURE 35-103.** Umbilical vein varix. Initially it was thought that the prognosis in cases of umbilical vein varix was uniformly poor. If there are no associated abnormalities, most cases do well. *A.* Umbilical vein varix (*arrow*) seen adjacent to the anterior abdominal wall and the urinary bladder (Bl). *B.* Color Doppler imaging of an umbilical vein varix (*arrow*). In neither case was there associated abnormalities, and the outcome was normal in both cases.



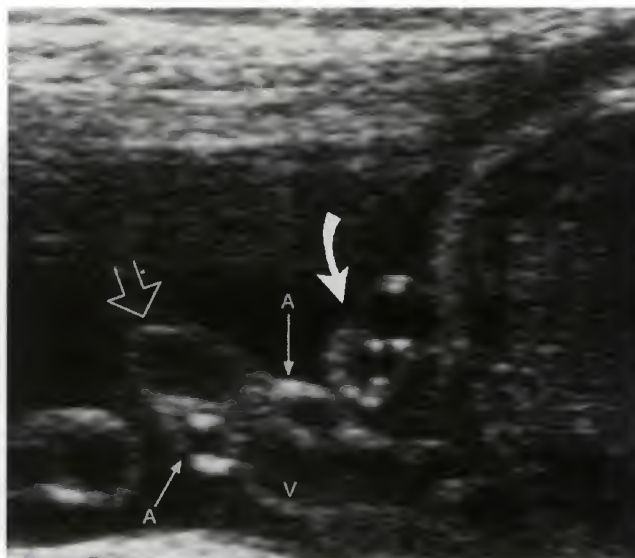
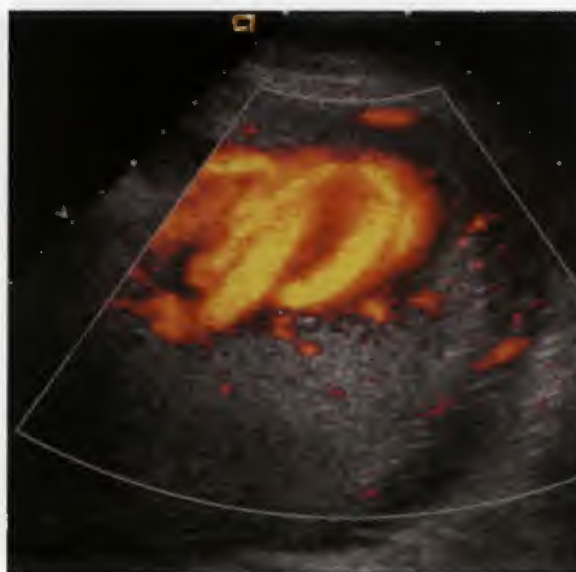


**FIGURE 35-104.** A short-axis view of the umbilical cord should always be obtained when attempting to identify the number of vessels. In this case, the long-axis view (*open arrow*) appears to show two umbilical arteries (A) and one vein (V). In the short-axis view (*curved arrow*), the correct interpretation of a single umbilical artery in a two-vessel cord can be made.

## AMNIOTIC FLUID AND MEMBRANES



A



B

**FIGURE 35-105.** When amniotic fluid volume is assessed, the “pocket” of fluid should be free of umbilical cord. A. In this patient, there appears to be a 3-cm pocket of amniotic fluid (*calipers*). B. Doppler evaluation of this area revealed that this “pocket” was not amniotic fluid but all umbilical cord.

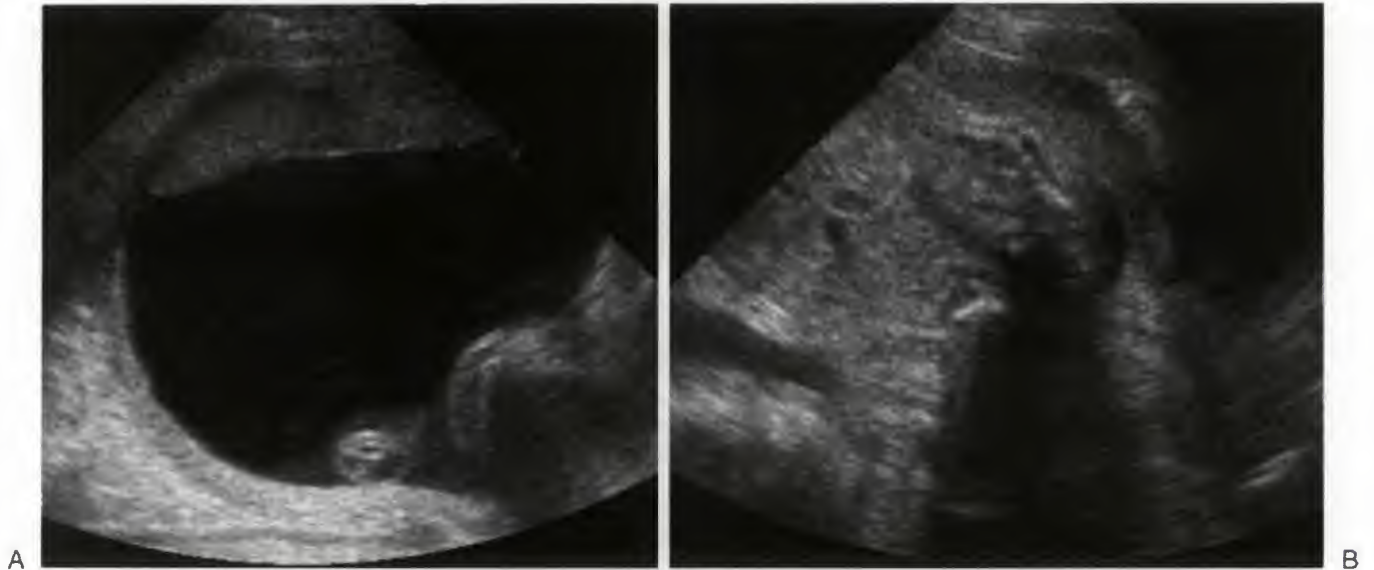


**FIGURE 35-106.** *A.* In this scan of a second trimester pregnancy, a large amniotic fluid pocket is seen, suggesting polyhydramnios. *B.* Little amniotic fluid is seen in a scan near the lower portion of the uterus. The total volume of amniotic fluid was normal. Thus, single views of the gravid uterus may be misleading as to the correct volume of amniotic fluid.

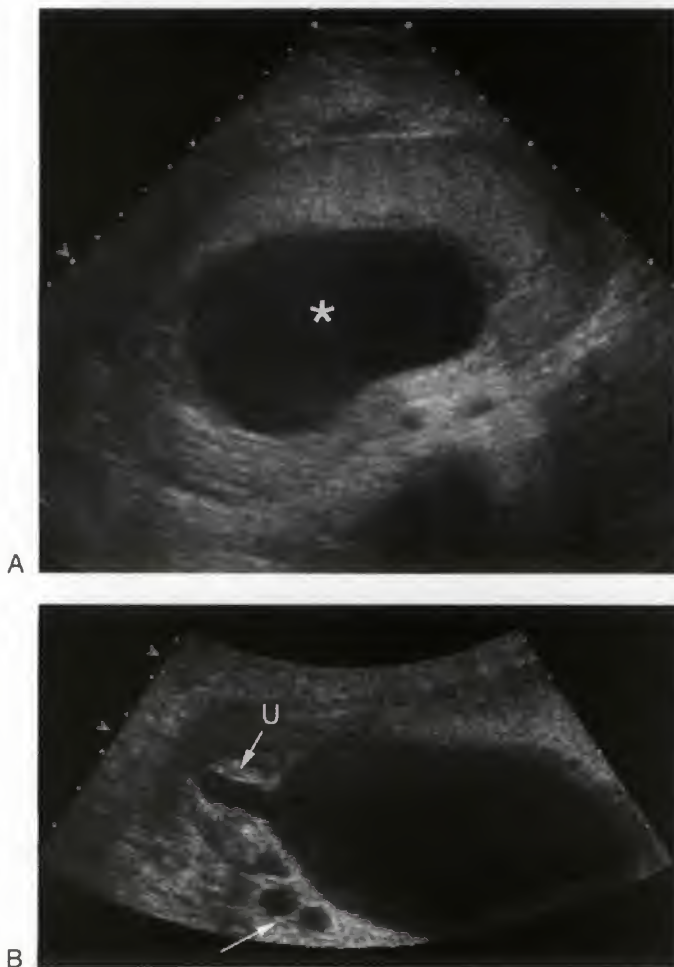


**FIGURE 35-107.** *A.* Large fluid collection (*asterisk*) appears to be amniotic fluid; however, it represents a markedly dilated urinary bladder in a patient with posterior urethral valves. In fact, there was virtually no amniotic fluid. *B.* Another sonogram in the same case demonstrates a dilated posterior urethra (*U*) and dilated ureters (*arrow*) in addition to the dilated urinary bladder.



**FIGURE 35-108.** In this early second trimester fetus, the amnion (*arrows*) is seen slightly separated from the chorion. This is normal until the 12th to 14th week of gestation, at which time the two membranes appose one another.





**FIGURE 35-109.** Pseudochorioamniotic separation. *A.* Apparent chorioamniotic separation is seen with an unapposed amniotic membrane (*arrows*). *B.* Color Doppler imaging reveals that the structure thought to represent membrane was, in fact, umbilical cord.

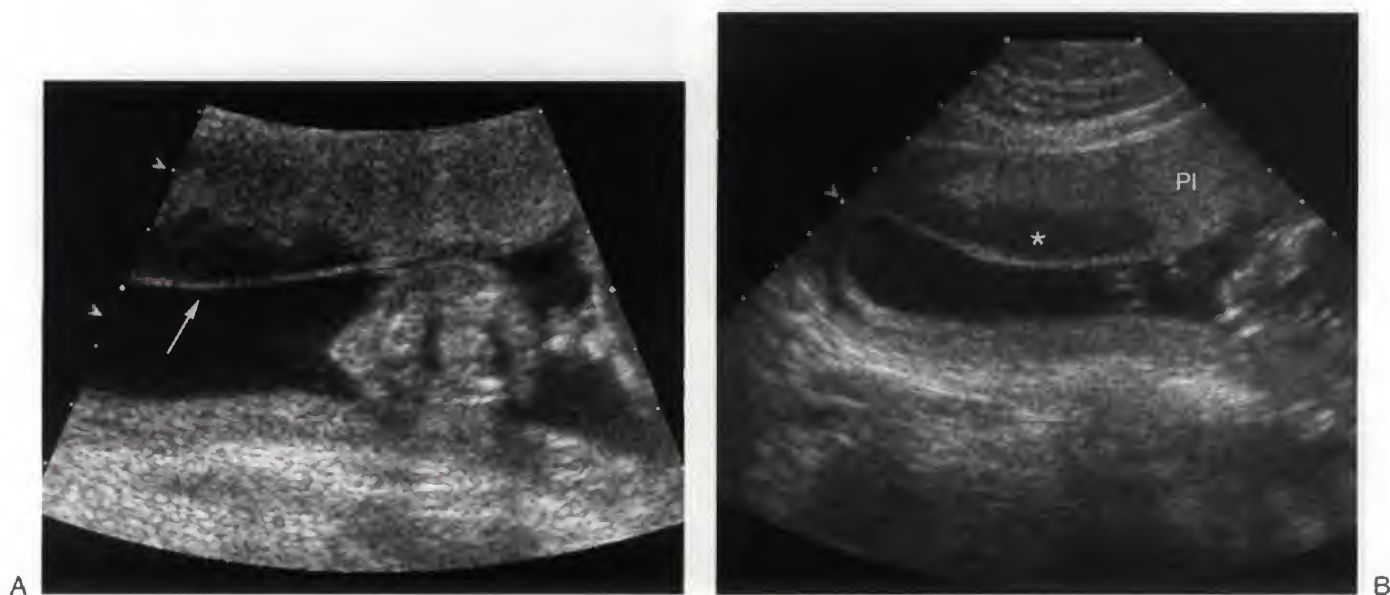


**FIGURE 35-110.** *A.* A linear structure (*arrow*) is seen anteriorly adjacent to the fetal head and placenta. It has the appearance of a free-floating amniotic membrane. *B.* With a larger field of view, the membrane is seen to represent the surface of the placenta, under which is a hypoechoic area (*asterisk*) likely representing a subchorionic plate hematoma.

## THE FETAL SKELETON



**FIGURE 35-111.** A. The normal fetal femur has a medial curve to the metadiaphyseal region. This is seen in the femur farthest from the transducer (arrow). The femur closest to the transducer (*cursors*) will demonstrate a straight appearance because the lateral aspect is reflecting the sound and the medial aspect is within its shadow. B. Radiograph of a normal neonatal femur demonstrating the normal curved appearance of its medial aspect (arrow).

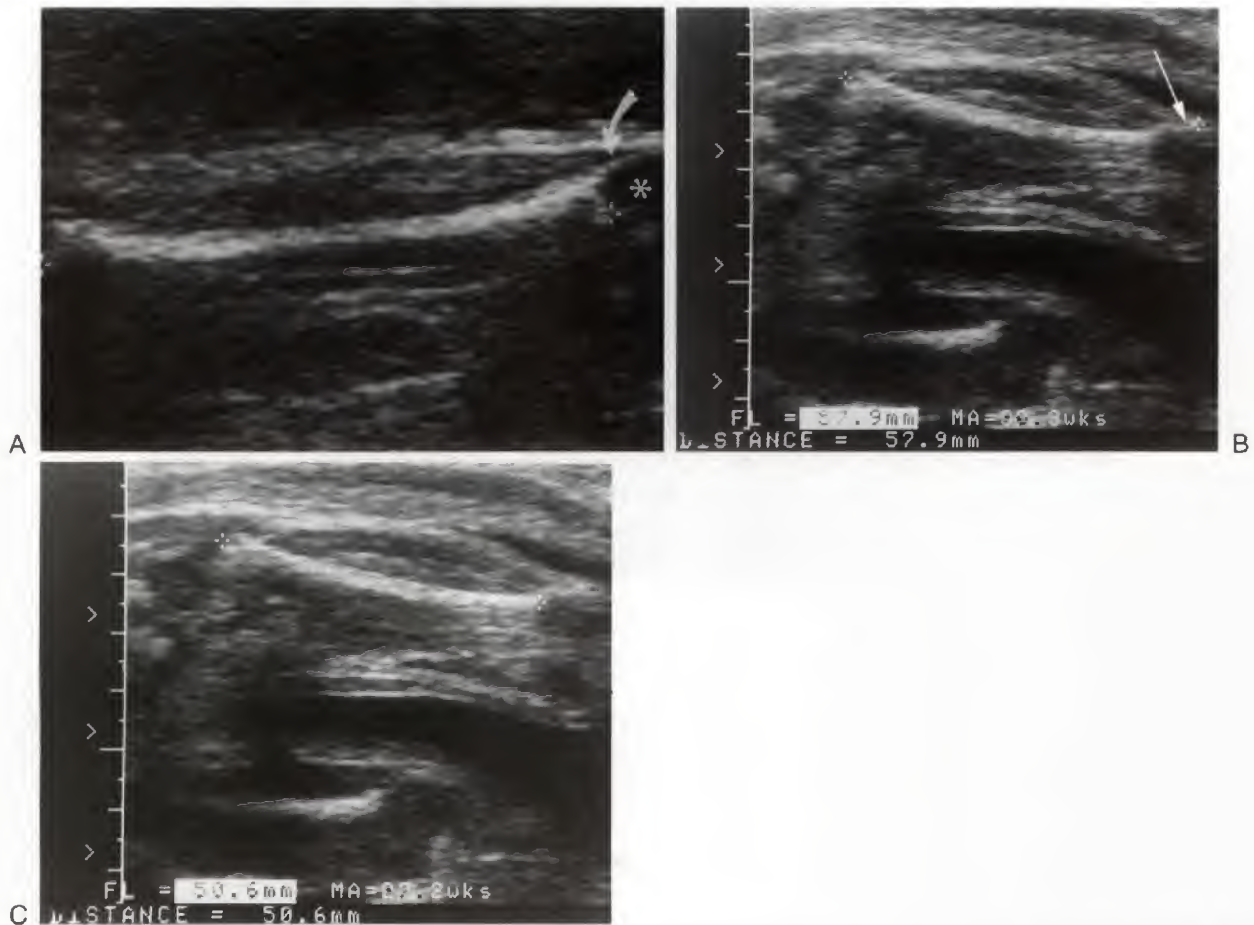


**FIGURE 35-112.** Scans of the fetal femur often demonstrate a linear projection from the distal end. A. This projection (arrow) is a specular reflection from the distal epiphyseal cartilage (asterisk). B. The measurement of the femur should not include this reflection (arrow). C. The measurement should include only the calcified bone. Inclusion of this reflection would have overestimated the gestational age by as much as 3 weeks.



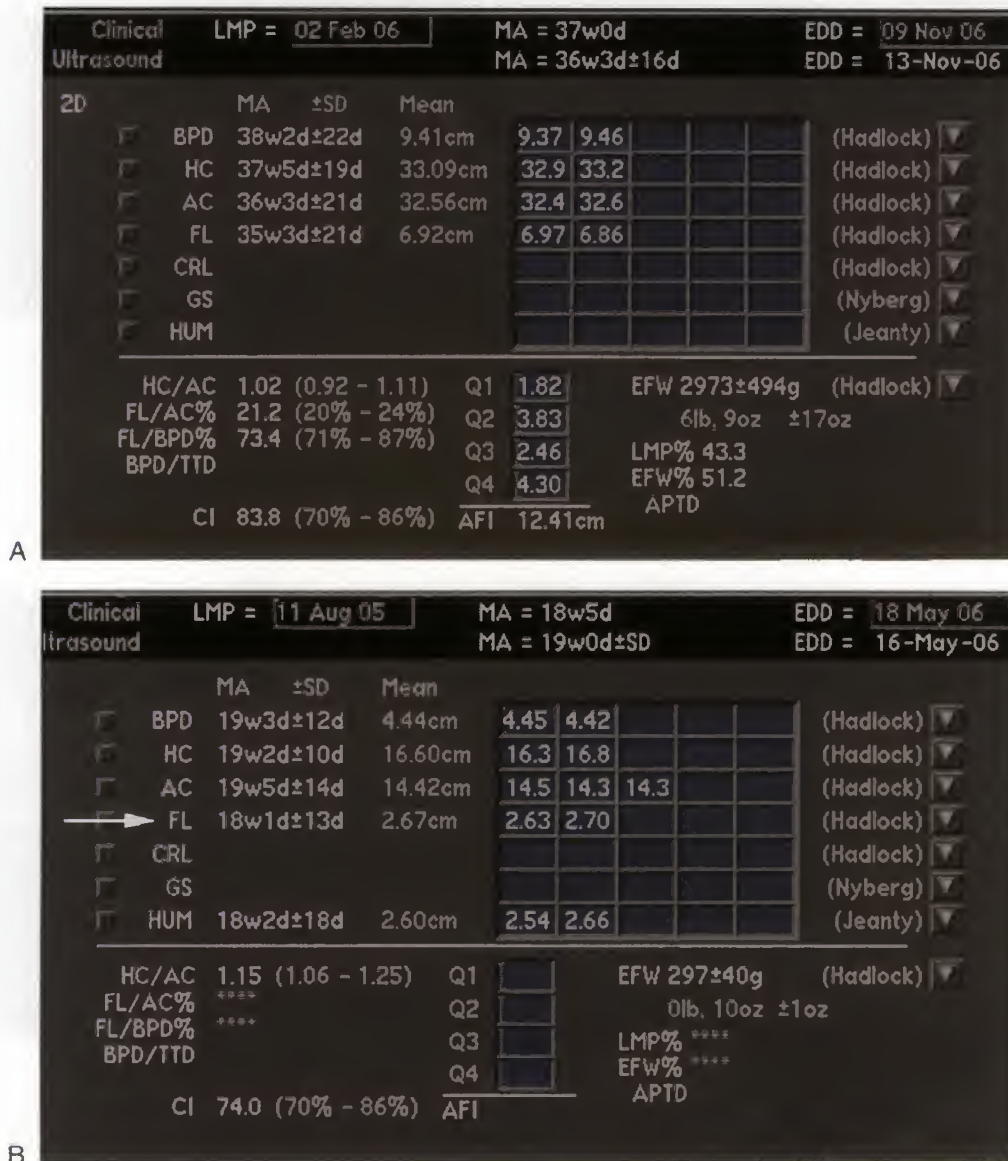


**FIGURE 35-113.** Significance of short femoral length. **A.** In the mid to late third trimester, it is not unusual for the femur to be significantly shorter than the other measurements used to estimate gestational age. In this case, the femur is approximately 2 weeks less than the head circumference and menstrual age. The etiology of this is uncertain, and is often attributed to biologic variation and or ethnicity. If the bones appear normal morphologically and no anomalies are seen, it is likely a normal variant. This fetus was from white parents of normal height and middle socioeconomic status. **B.** Although the femur can be smaller than other measurements in the third trimester, it is not acceptable for it to be greater than one week less than the other measurements in the late first and early to mid second trimester, as it was in this case (arrow). Although this may be nothing more than a temporary growth lag or normal variation at this stage, it may also be a sign of trisomy 21 or an early manifestation of a short-limb skeletal dysplasia. This was a case of trisomy 21. One should not take comfort in comparing the femur measurement to the estimated gestational age by ultrasound. Remember, that unless excluded, the femur measurement is included in the sonographic estimation of gestational age.

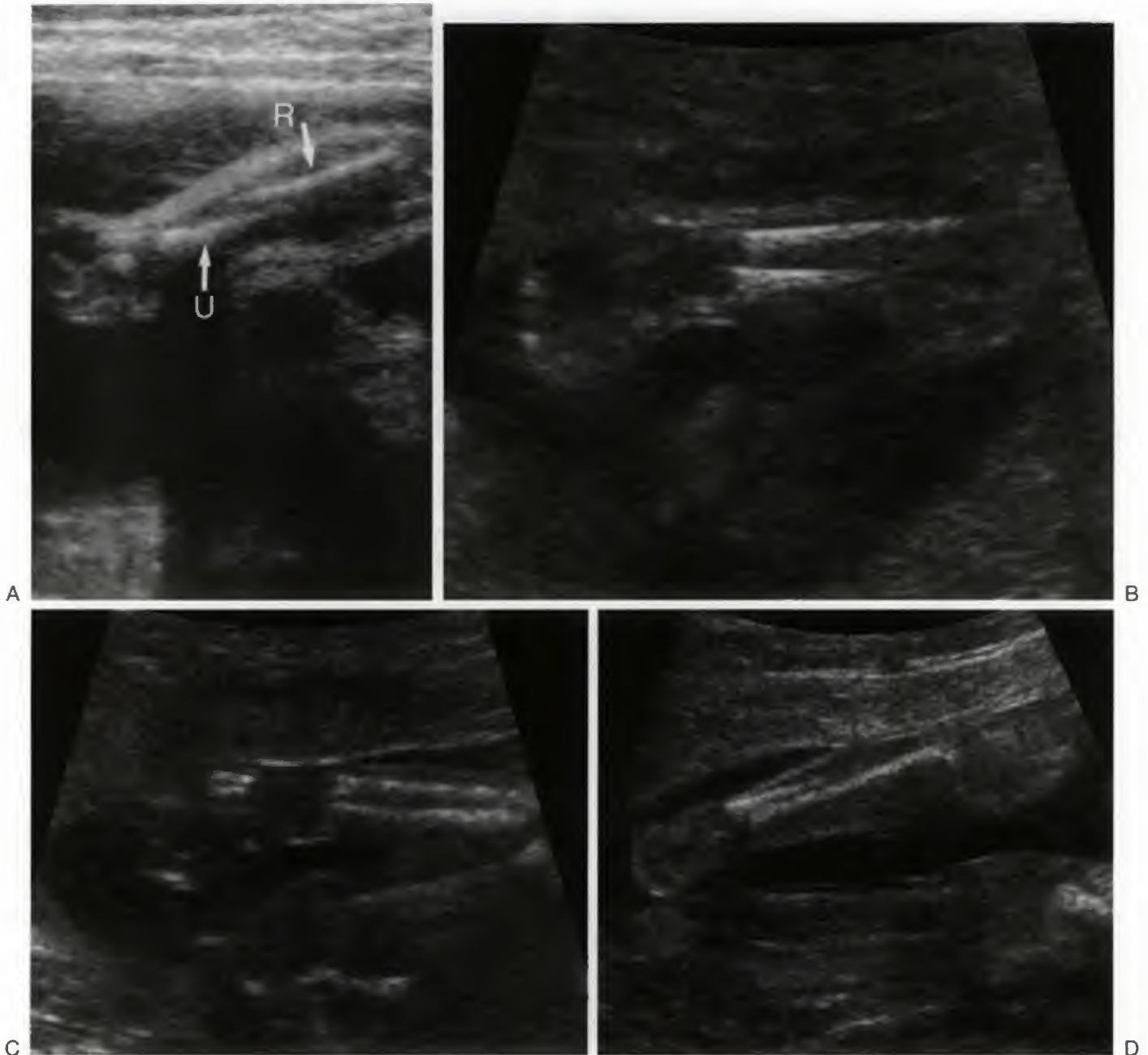


**FIGURE 35-114.** Pseudolimb reduction. *A.* Pronation and supination of the forearm may create the appearance that the radius (R) or the ulna (U) is abnormally short (limb reduction abnormality). When both bones are “short” at opposite ends in the same scan, one should be suspicious that this is a technical rather than a real abnormality. *B.* Partial volume of the proximal forearm makes it appear as though the radius and ulna are hypoplastic. *C.* Slight change in transducer angulation reveals that both bones of the forearm are present and normal. *D.* Again, a tomographic plane of section demonstrating only part of the fibula. Both bones of the leg were present and normal.



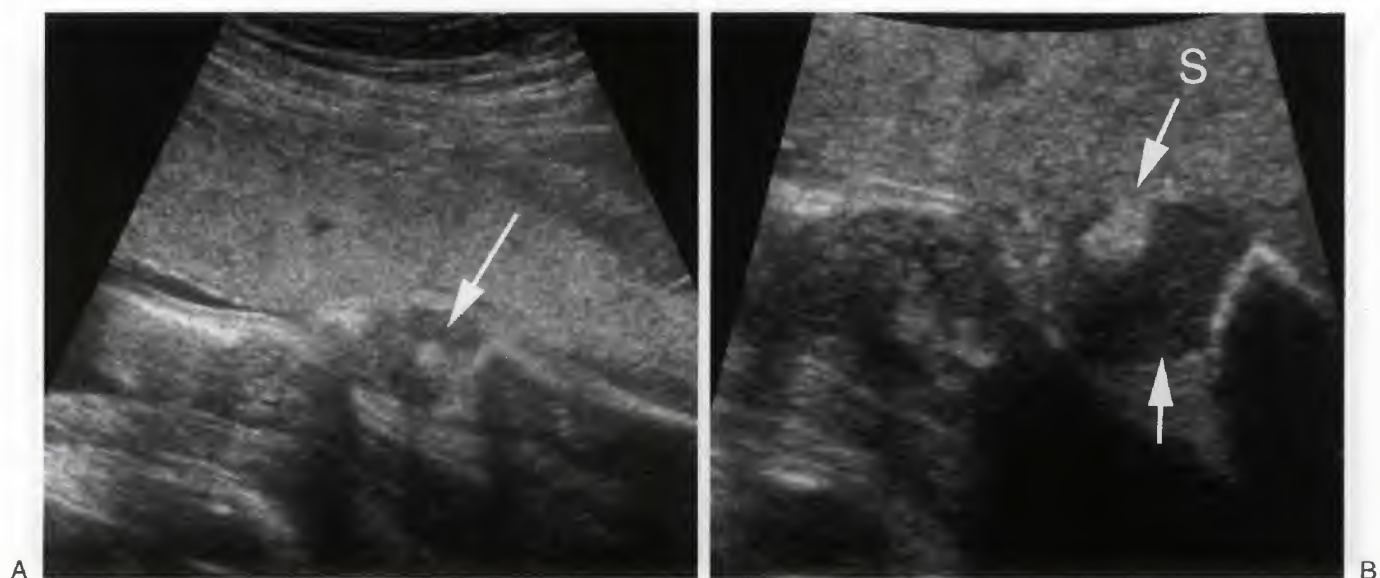


**FIGURE 35-115.** The appearance of the epiphyseal ossification centers is helpful in assessing gestational age. *A.* The synovial tissue is echogenic (*arrow*) and may simulate the appearance of one of these centers, as in this case. The real epiphyseal center would be slightly more proximal. *B.* Synovial tissue (*S*) is well seen in the same case, without evidence of calcification within the epiphyseal center (*arrow*).

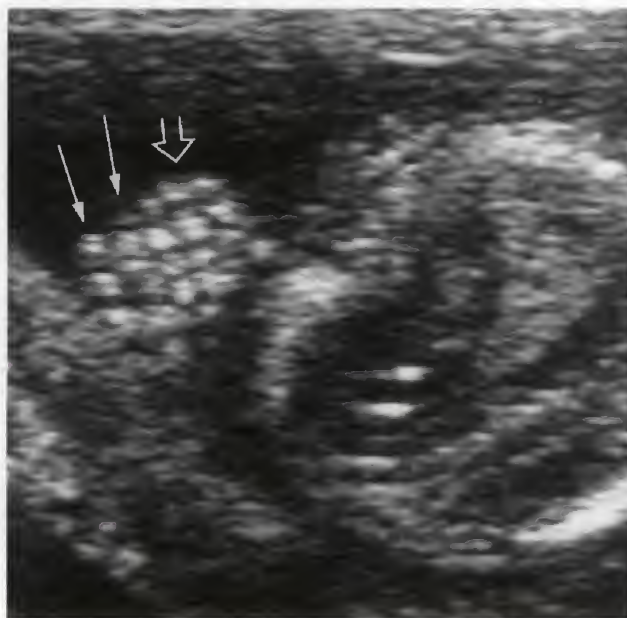


**FIGURE 35-116.** In this case, both hands of the fetus are adjacent to one another. The fingers (*arrows*) from one hand and the fingers (*open arrow*) from the other simulate the appearance of polydactyly.

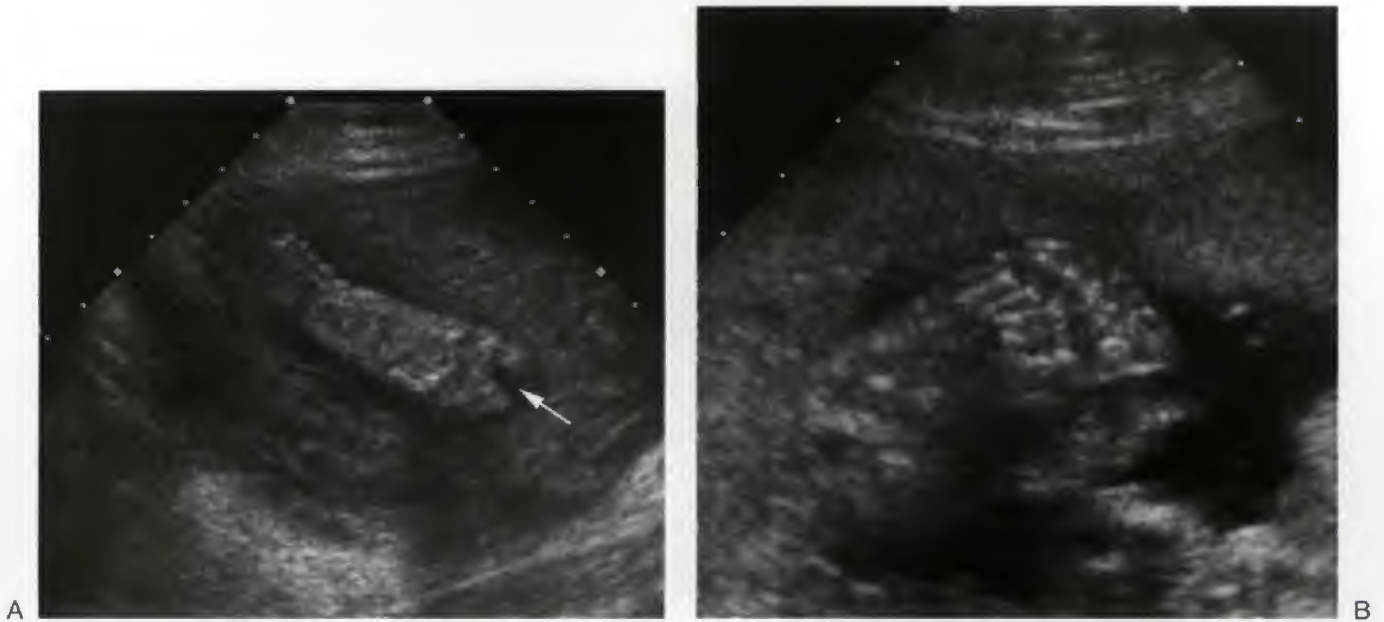


**FIGURE 35-117.** *A.* Separation of the first and second toe (arrow) referred to as a sandal gap deformity. This abnormality has been described in some fetuses and neonates with trisomy 21; however, it may also be a positional abnormality and normal variant. *B.* A scan performed later demonstrated normal appearance of the foot. No other abnormalities were seen, and the neonate was normal at birth.

## MULTIPLE GESTATIONS

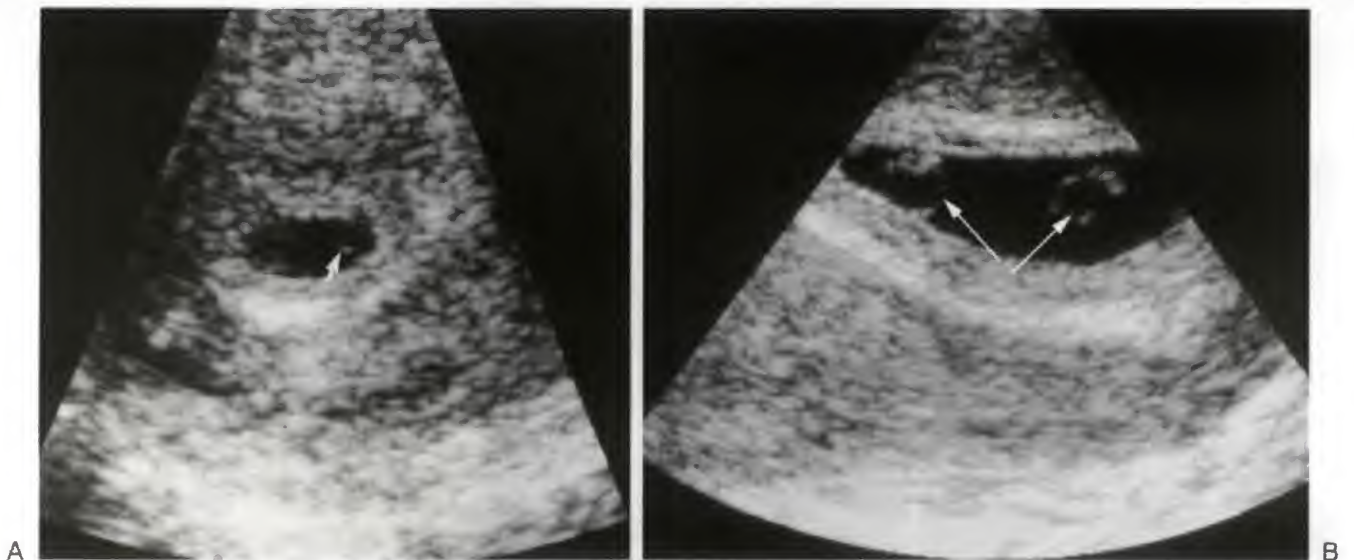


**FIGURE 35-118.** Although ideally multiple gestation pregnancies should never be missed, it is my experience that when cases are missed, it is usually in the first trimester, even with transvaginal scanning. *A.* A transvaginal sonogram done for vaginal bleeding revealed a yolk sac (arrow), with cardiac activity noted at the edge of the yolk sac. *B.* Because of continued spotting, the patient returned the following week. At this time, two yolk sacs (arrows) were identified in this monochorionic pregnancy.



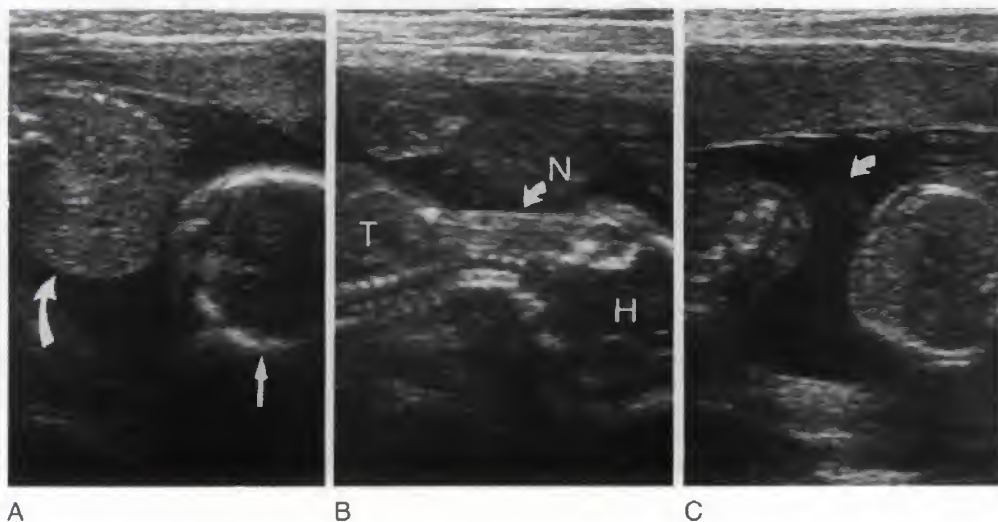


**FIGURE 35-119.** The false-negative diagnosis of twins is unusual in the second trimester. If this occurs, it likely results from not “connecting” the fetal head to its body during routine scanning. *A.* In this patient, the fetal head (*straight arrow*) and body (*curved arrow*) are seen in this longitudinal plane of section. Unfortunately, these structures are from different fetuses in this twin pregnancy. *B.* The only way to be absolutely sure of the relation of the head (H) to the body is to demonstrate both structures on the same scan connected to one another through the neck (N) (T, thorax). *C.* The dividing membrane (*arrow*) is seen on another plane of section clearly dividing the two fetuses.

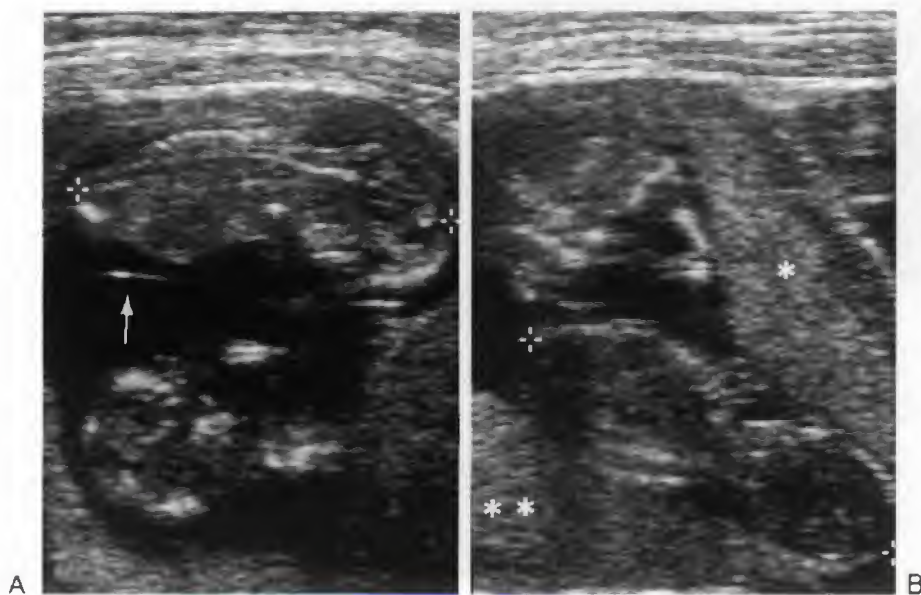


**FIGURE 35-120.** Membrane thickness is often useful in differentiating between monochorionic twins (thin membrane) and dichorionic twins (thick membrane). This method is not always successful, however. *A.* In this twin pregnancy, a scan at 14 weeks' gestation demonstrates a thin membrane (*arrow*) dividing the two gestational sacs. This implies monochorionicity. *B.* A longitudinal plane of section at the same time reveals both an anterior placenta (*asterisk*) and a posterior placenta (*double asterisks*).



**FIGURE 35-121.** In this twin gestation, one of the twins was noted to be fixed to the anterior uterine wall. It was initially assumed that this was a monoamniotic twin gestation. Careful inspection reveals that the membrane (*arrow*) dividing the twins can be seen. The anterior fetus is in an oligohydramniotic sac and is smaller than the other twin. This was a case of twin-to-twin transfusion syndrome.



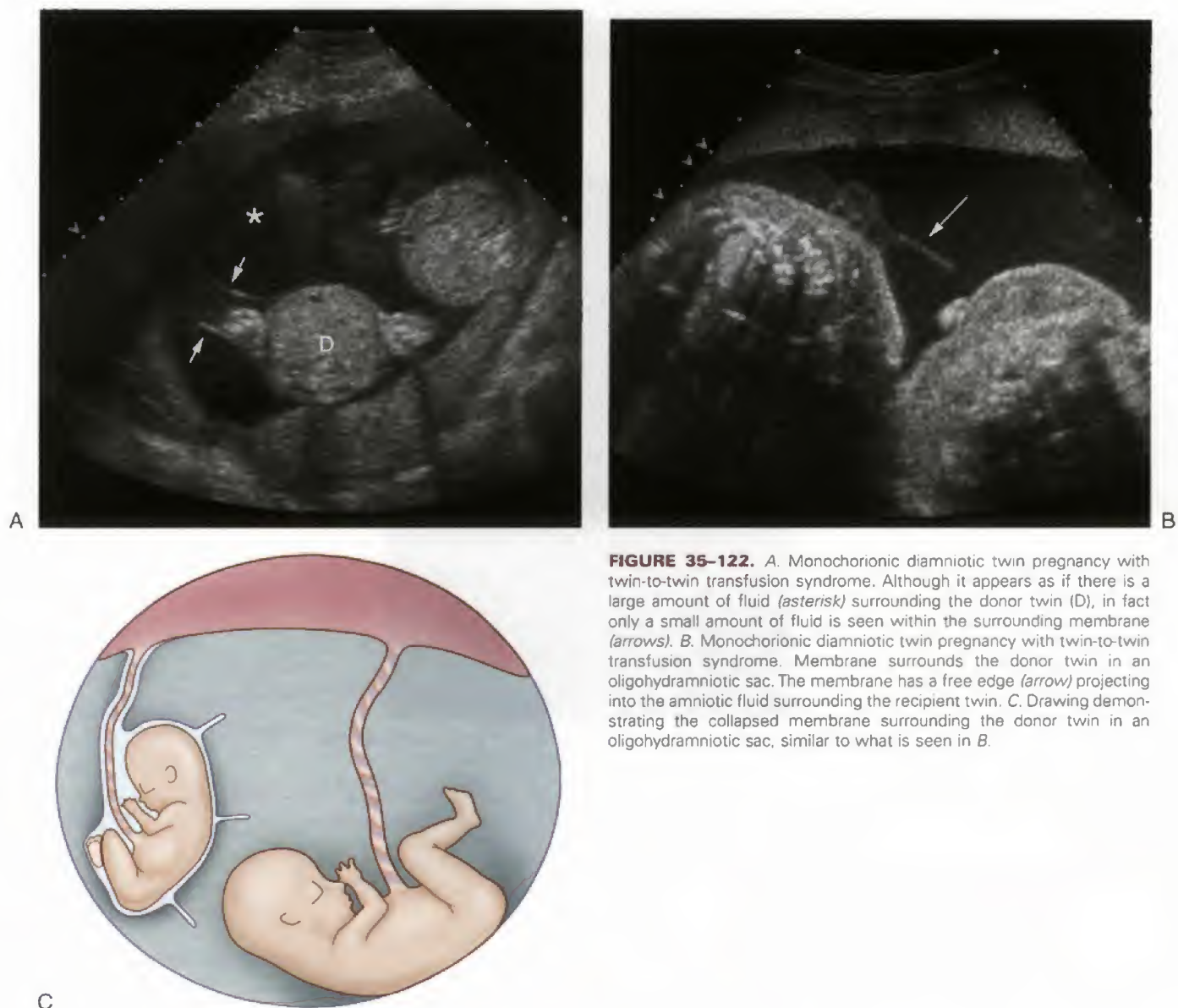


**FIGURE 35-122.** A. Monochorionic diamniotic twin pregnancy with twin-to-twin transfusion syndrome. Although it appears as if there is a large amount of fluid (*asterisk*) surrounding the donor twin (D), in fact only a small amount of fluid is seen within the surrounding membrane (*arrows*). B. Monochorionic diamniotic twin pregnancy with twin-to-twin transfusion syndrome. Membrane surrounds the donor twin in an oligohydramniotic sac. The membrane has a free edge (*arrow*) projecting into the amniotic fluid surrounding the recipient twin. C. Drawing demonstrating the collapsed membrane surrounding the donor twin in an oligohydramniotic sac, similar to what is seen in B.

## ARTIFACTS

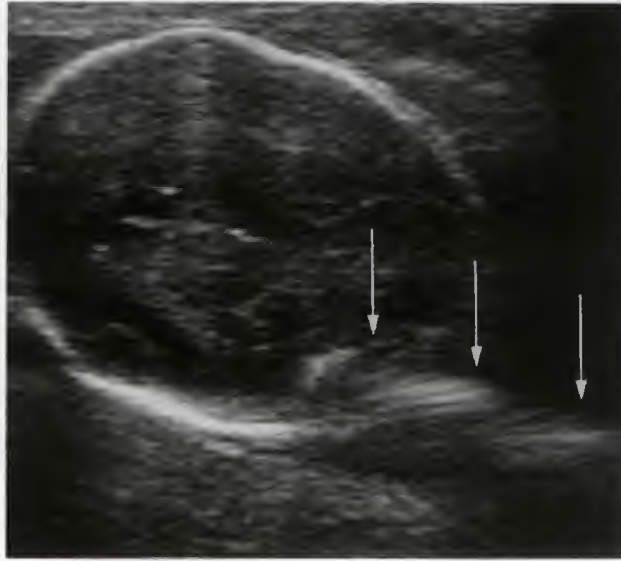


**FIGURE 35-123.** Side lobe (gradient) artifact can occur with even the most sophisticated ultrasound scanning equipment. In this case, a side lobe artifact is seen overlying the fetal head (*arrows*). The artifactual nature of these echoes can be confirmed by noting that these echoes are not confined to the head but extend beyond its confines. In addition, changing the scan plane orientation will show the region to be normal.

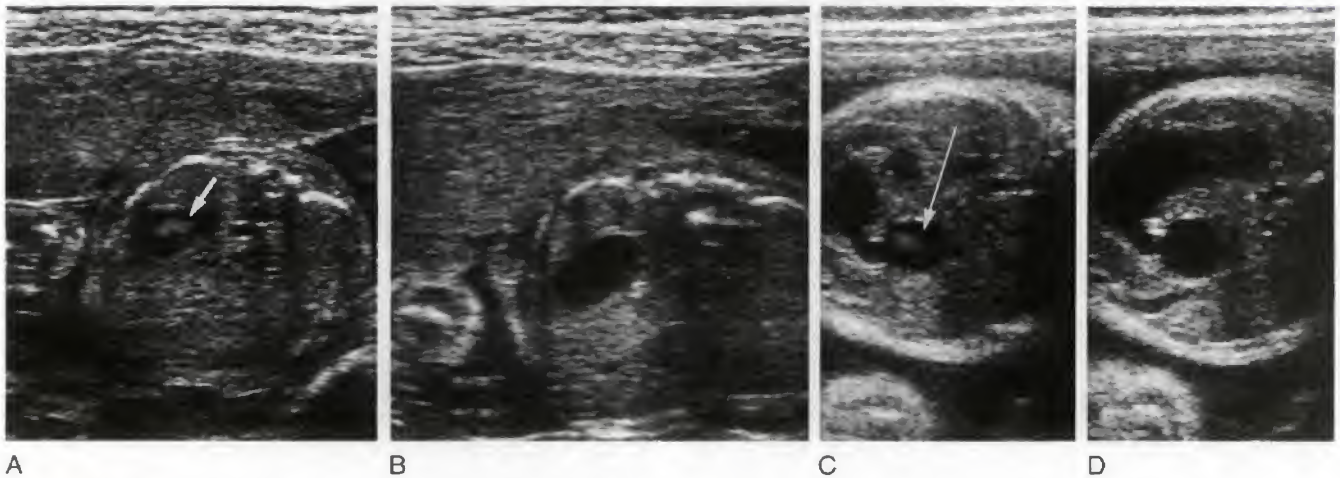


**FIGURE 35-124.** A and C. Two cases of artifact (*arrow*) appear in the fetal stomach and duodenum. B and D. If one changes the scanning plane, these echoes will disappear from the area of concern.



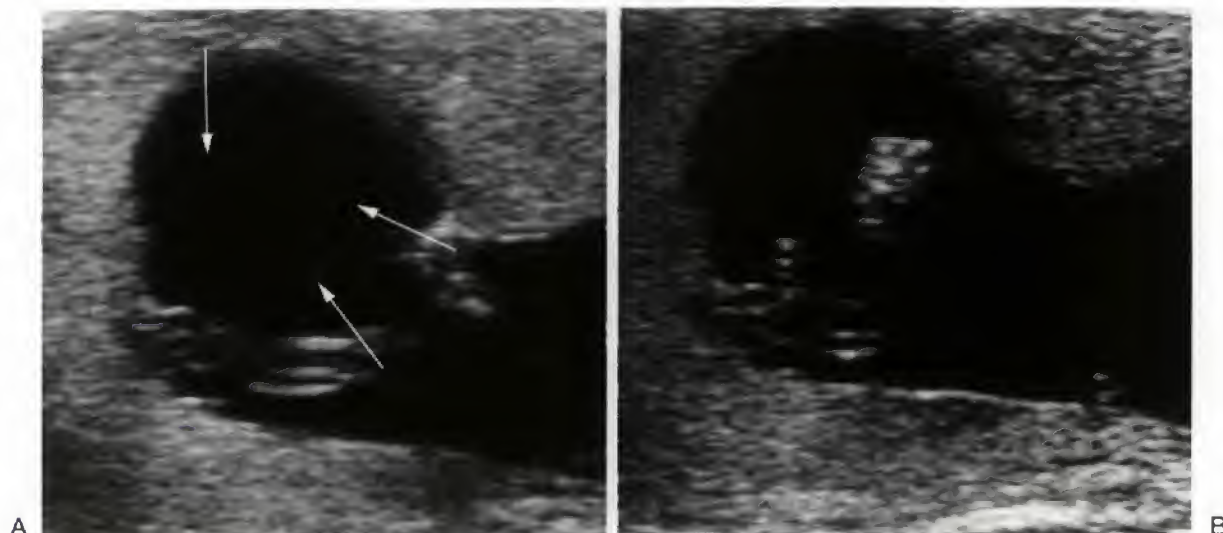


**FIGURE 35-125.** The differentiation of real from artifactual echoes is often problematic during sonographic scanning. A common misconception is that changing to a lower frequency transducer and decreasing the overall system gain or just reducing the system gain will only cause the artifactual echoes alone to disappear. Although it is true that artifactual echoes will not be displayed with these maneuvers, it should be remembered that the real echoes will not be displayed either. *A.* In this patient, numerous low-level echoes (*arrows*) were seen swirling in the amniotic fluid during real-time scanning. Although the origin of the echoes is not known, they may represent shed fetal epithelial cells. *B.* When the system gain was decreased, these real echoes virtually disappeared. Although the hard copy images do not resolve this dilemma, the echoes were clearly seen to be moving and real when the sonologist was performing the scan.

## BREAST ULTRASOUND

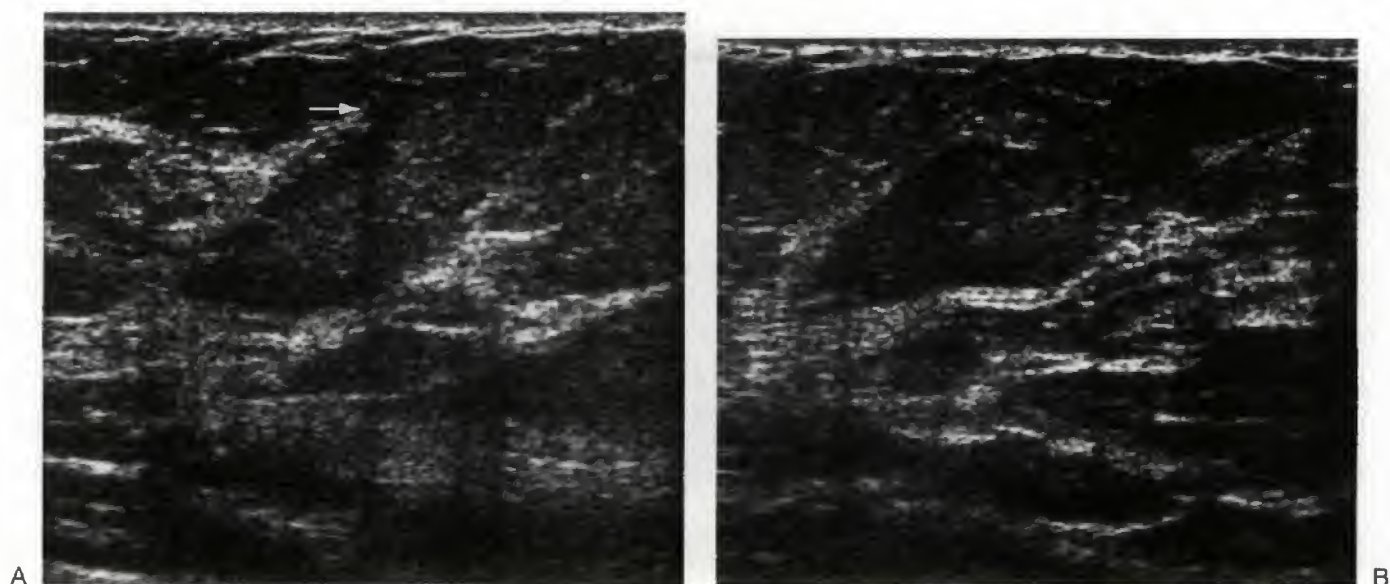


**FIGURE 35-126.** Cancer or artifact? *A.* Is small, hypoechoic suspicious mass or refraction at edges of curved surfaces (*arrow*) cause of the shadowing? *B.* Slight change in patient position, probe angulation, or amount of compression applied by transducer can often provide resolution. (Images courtesy of E. Mendelson, MD.)

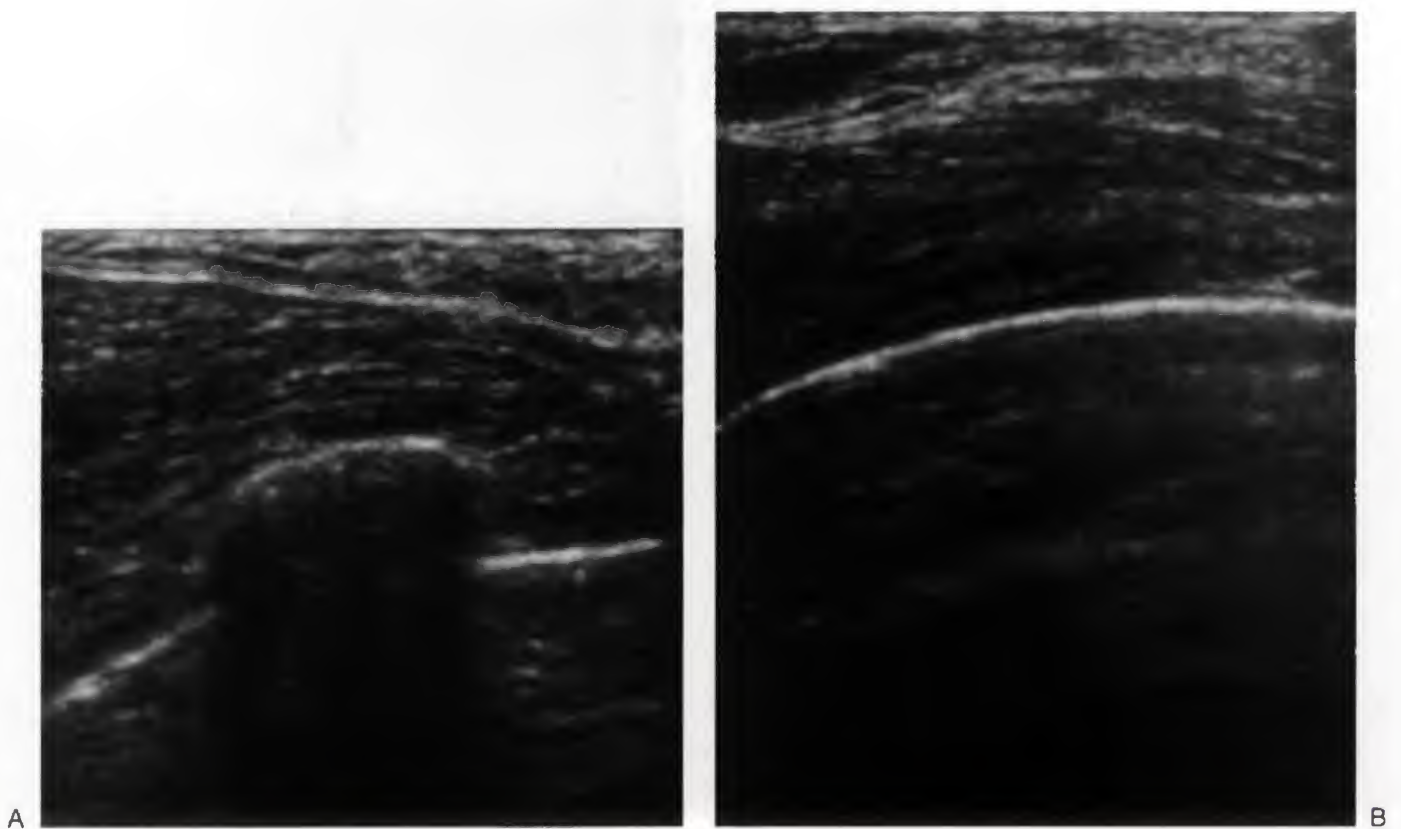


**FIGURE 35-127.** Orthogonal imaging. A. Hypoechoic mass with posterior acoustic shadowing is recommended for ultrasound-guided biopsy. B. The “mass” is a rib sitting in normal location behind muscle. Orthogonal imaging and knowledge of US breast anatomy are essential to avoid misdiagnosis. (Images courtesy of E. Mendelson, MD.)

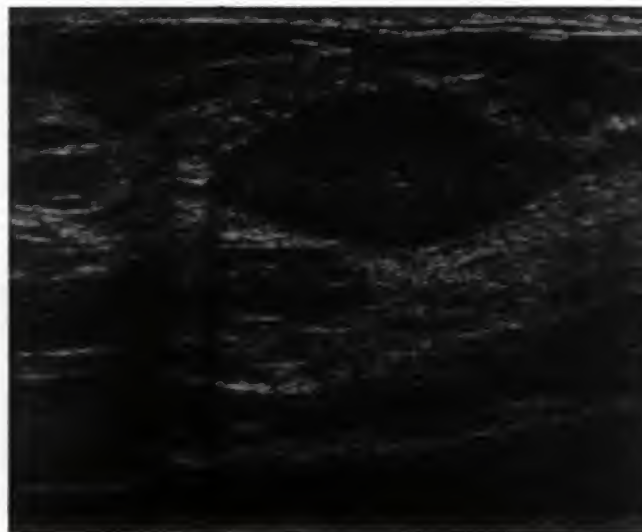


**FIGURE 35-128.** Fat lobules in the breast, as in this case, are discrete and may mimic fibroadenomas, and are bound by thin connective tissue capsules. (Image courtesy of E. Mendelson, MD.)



**'THE END'**

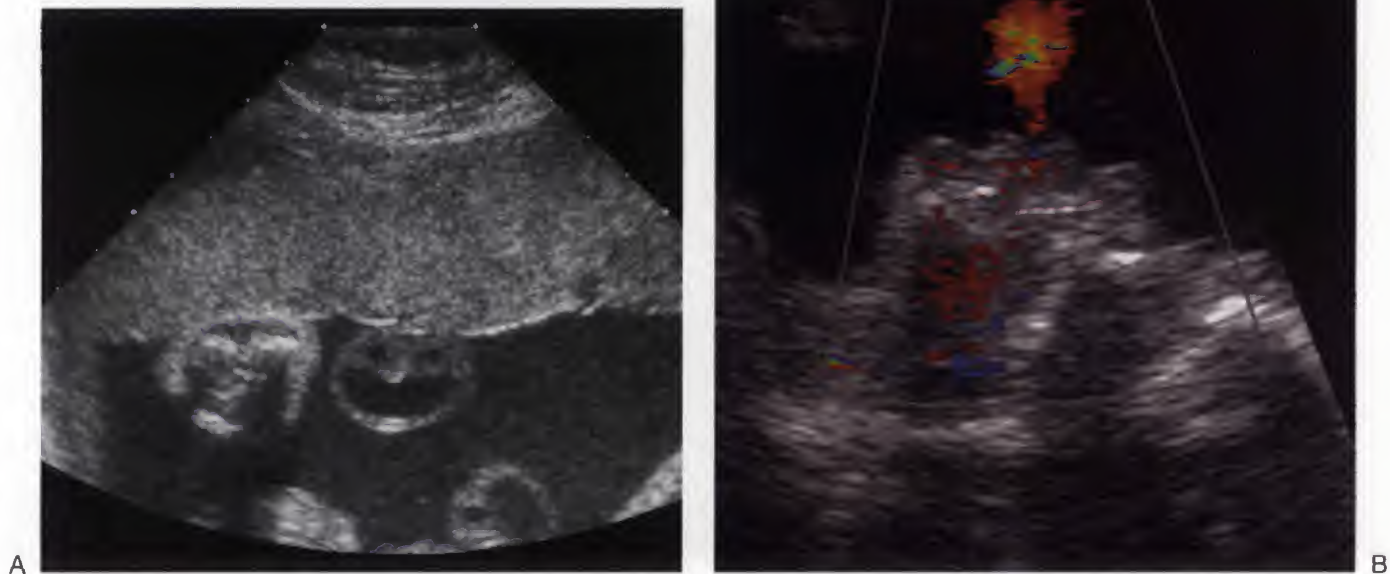


**FIGURE 35-129.** After viewing so many artifacts, pitfalls, and normal variants, you wonder whether: *A.* The umbilical cord is smiling back at you. *B.* The fetus is blowing bubbles.

# APPENDIX A

## Measurements Frequently Used to Estimate Gestational Age and Fetal Biometry

**Table A-1** Methods for Determining Menstrual Age

Clinical or Sonographic Parameter	Variability Estimate (2 SD)
In vitro fertilization*	±1 day
Ovulation induction*	±3 days
Artificial insemination*	±3 days
Single intercourse record*	±3 days
Basal body temperature record*	±4 days
First trimester physical examination	±2 weeks
Second trimester physical examination	±4 weeks
Third trimester physical examination	±6 weeks
First trimester sonographic examination (CRL)	±8% of the estimate
Second trimester sonographic examination (HC, FL)	±8% of the estimate
Third trimester sonographic examination (HC, FL)	±8% of the estimate

CRL, crown rump length; FL, femur length; HC, head circumference.

\*These are indicators of conceptual age (menstrual age = conceptual age + 14 days).

Adapted from Frank P. Hadlock, MD, and James D. Bowie, MD.

**Table A-2** Variability in Predicting Menstrual Age from Sonographic Measurements (14–20 Weeks)

Parameter	Variability (2 SD)			
	Hadlock et al <sup>*</sup>	Rossavik and Fishburne <sup>†</sup>	Persson and Weldner <sup>‡</sup>	Benson and Doubilet <sup>§</sup>
BPD	0.94 wk	1.02 wk	0.92 wk	1.40 wk
HC	0.84 wk	0.92 wk	ND	1.20 wk
AC	1.04 wk	1.12 wk	ND	2.10 wk
FL	0.96 wk	ND	0.98 wk	1.40 wk
BPD, FL	0.80 wk	ND	0.78 wk	ND
HC, FL	0.76 wk	ND	ND	ND

AC, abdominal circumference; BPD, biparietal diameter; FL, femur length; HC, head circumference; ND, no data.

<sup>\*</sup>Data from Hadlock FP, Harrist RB, Martínez-Poyer J: How accurate is second trimester fetal dating? *J Ultrasound Med* 10:557, 1992.

<sup>†</sup>Data from Rossavik IK, Fishburne JI: Conceptual age, menstrual age, and ultrasound age: A second trimester comparison of pregnancies of known conception date with pregnancies dated from the last menstrual period. *Obstet Gynecol* 73:243, 1989.

<sup>‡</sup>Data from Persson PH, Weldner BM: Reliability of ultrasound fetometry in estimating gestational age in the second trimester. *Acta Obstet Gynecol Scand* 65:481, 1986.

<sup>§</sup>Data from Benson CB, Doubilet PM: Sonographic prediction of gestational age: Accuracy of second and third trimester fetal measurements. *Am J Roentgenol* 157:1275, 1991.



**Table A-3** Variability in Predicting Menstrual Age in the Second Half of Pregnancy (14–42 Weeks)

Parameter	Variability in Weeks ( $\pm 2$ SD)			
	14–20 Weeks	20–26 Weeks	26–32 Weeks	32–42 Weeks
BPD	1.4	2.1	3.8	4.1
Corrected BPD	1.2	1.9	3.3	3.8
HC	1.2	1.9	3.4	3.8
AC	2.1	3.7	3.0	4.5
FL	1.4	2.5	3.1	3.5

AC, abdominal circumference; BPD, biparietal diameter; FL, femur length; HC, head circumference.

Adapted from Benson CB, Doubilet PM: Sonographic prediction of gestational age: Accuracy of second and third trimester fetal measurements. *Am J Roentgenol* 157:1275, 1991.

**Table A-4** Variability Estimates for Secondary Biometric Parameters

Parameter	Variability in Weeks ( $\pm 2$ SD)				
	12–18 Weeks	18–24 Weeks	24–30 Weeks	30–36 Weeks	36–42 Weeks
Binocular distance*	1.8	2.4	3.0	4.0	4.0
Cerebellar diameter†	1.0	1.8	2.0	2.4	3.2
Clavicle length‡	6.5	6.5	6.5	6.5	6.5
Radius length§	1.8	2.2	2.9	3.5	4.1
Ulna length	3.6	3.6	3.6	3.6	3.6
Tibia length	3.5	3.5	3.5	3.5	3.5
Foot length¶	1.2	1.7	2.2	2.6	3.1

\*Data from Jeanty P, Cantraine F, Cousaert E, et al: The binocular distance: A new way to estimate fetal age. *J Ultrasound Med* 3:241, 1984.

†Data from Hill LM: Transverse cerebellar diameter as a predictor of menstrual age. *Obstet Gynecol* 75:983, 1990.

‡Data from Yarkoni S, Schmidt W, Jeanty P, et al: Clavicular measurement: A new biometric parameter for fetal evaluation. *J Ultrasound Med* 4:467, 1985.

§Data from Hill LM, Guzik D, Thomas ML, et al: Fetal radius length: A critical evaluation of race as a factor in gestational age assessment. *Am J Obstet Gynecol* 161:193, 1989.

||Data from Jeanty P, Rodesch F, Delbeke D: Estimation of fetal age by long bone measurements. *J Ultrasound Med* 3:75, 1984.

¶Data from Mercer BM, Sklar S, Shariatmadar A, et al: Fetal foot length as a predictor of gestational age. *Am J Obstet Gynecol* 15:350, 1987.

**Table A-5** Gestational Sac Measurement

Mean Predicted Gestational Sac (cm)	Gestational Age (wk)	Mean Predicted Gestational Sac (cm)	Gestational Age (wk)
1.0	5.0	3.6	8.8
1.1	5.2	3.7	8.9
1.2	5.3	3.8	9.0
1.3	5.5	3.9	9.2
1.4	5.6	4.0	9.3
1.5	5.8	4.1	9.5
1.6	5.9	4.2	9.6
1.7	6.0	4.3	9.7
1.8	6.2	4.4	9.9
1.9	6.3	4.5	10.0
2.0	6.5	4.6	10.2
2.1	6.6	4.7	10.3
2.2	6.8	4.8	10.5
2.3	6.9	4.9	10.6
2.4	7.0	5.0	10.7
2.5	7.2	5.1	10.9
2.6	7.3	5.2	11.0
2.7	7.5	5.3	11.2
2.8	7.6	5.4	11.3
2.9	7.8	5.5	11.5
3.0	7.9	5.6	11.6
3.1	8.0	5.7	11.7
3.2	8.2	5.8	11.9
3.3	8.3	5.9	12.0
3.4	8.5	6.0	12.2
3.5	8.6		

From Hellman LM, Kobayashi M, Fillisti L, et al: Growth and development of the human fetus prior to the twentieth week of gestation. *Am J Obstet Gynecol* 103:789, 1969.

**Table A-6** Mean Diameter of Gestational Sac and Corresponding Estimates of Gestational Age

Mean Sac Diameter (mm)	Mean Gestational Age (wk)	Gestational Age (Days)	
		Mean	95% Confidence Interval
2	5.0	34.9	34.3–35.5
3	5.1	35.8	35.2–36.3
4	5.2	36.6	36.1–37.2
5	5.4	37.5	37.0–38.0
6	5.5	38.4	37.9–38.9
7	5.6	39.4	38.9–39.7
8	5.7	40.2	39.8–40.6
9	5.9	41.1	40.7–41.4
10	6.0	41.9	41.6–42.3
11	6.1	42.8	42.5–43.2
12	6.2	43.7	43.4–44.0
13	6.4	44.6	44.3–44.9
14	6.5	45.5	45.2–45.8
15	6.6	46.3	46.0–46.6
16	6.7	47.2	46.9–47.5
17	6.9	48.1	47.8–48.4
18	7.0	49.0	48.6–49.4
19	7.1	49.9	49.5–50.3
20	7.3	50.8	50.3–51.2
21	7.4	51.6	51.2–52.1
22	7.5	52.5	52.0–53.0
23	7.6	53.4	52.9–53.9
24	7.8	54.3	53.7–54.8
25	7.9	55.2	54.6–55.7
26	8.0	56.0	55.4–56.7
27	8.1	56.9	56.3–57.6
28	8.3	57.8	57.1–58.5
29	8.4	58.7	58.0–59.4
30	8.5	59.6	58.8–60.4

From Daya S, Woods S, Ward S, et al: Early pregnancy assessment with transvaginal ultrasound scanning. *Can Med Assoc J* 144:441, 1991.



**Table A-7** Combined Data Comparing Menstrual Age With Mean Gestational Sac Diameter, Crown Rump Length, and HCG Levels\*

Menstrual Age (days)	Menstrual Age (weeks)	Gestational Sac Size (mm)	Crown Rump Length (cm)	HCG Level (First IRP) Mean (U/L)	HCG Level (First IRP) Range (U/L)
30	4.3				
31	4.4				
32	4.6	3		1710	(1050-2800)
33	4.7	4		2320	(1440-3760)
34	4.9	5		3100	(1940-4980)
35	5.0	5.5		4090	(2580-6530)
36	5.1	6		5340	(3400-8450)
37	5.3	7		6880	(4420-10,810)
38	5.4	8		8770	(5680-13,660)
39	5.6	9		11,040	(7220-17,050)
40	5.7	10	0.2	13,730	(9050-21,040)
41	5.9	11	0.3	15,300	(10,140-23,340)
42	6.0	12	0.35	16,870	(11,230-25,640)
43	6.1	13	0.4	20,480	(13,750-30,880)
44	6.3	14	0.5	24,560	(16,650-36,750)
45	6.4	15	0.6	29,110	(19,910-43,220)
46	6.6	16	0.7	34,100	(25,530-50,210)
47	6.7	17	0.8	39,460	(27,470-57,640)
48	6.9	18	0.9	45,120	(31,700-65,380)
49	7.0	19	0.95	50,970	(36,130-73,280)
50	7.1	20	1.0	56,900	(40,700-81,150)
51	7.3	21	1.1	62,760	(45,300-88,790)
52	7.4	22	1.2	68,390	(49,810-95,990)
53	7.6	23	1.3	73,640	(54,120-102,540)
54	7.7	24	1.4	78,350	(58,100-108,230)
55	7.9	25	1.5	82,370	(61,640-112,870)
56	8.0	26	1.6	85,560	(64,600-116,310)
57	8.1	26.5	1.7		
58	8.3	27	1.8		
59	8.4	28	1.9		
60	8.6	29	2.0		
61	8.7	30	2.1		
62	8.9	31	2.2		
63	9.0	32	2.3		
64	9.1	33	2.4		
65	9.3	34	2.5		
66	9.4	35	2.6		
67	9.6	36	2.8		
68	9.7	37	2.9		
69	9.9	38	3.0		
70	10.0	39	3.1		
71	10.1	40	3.2		
72	10.3	41	3.4		
73	10.4	42	3.5		
74	10.6	43	3.7		
75	10.7	44	3.8		
76	10.9	45	4.0		
77	11.0	46	4.1		
78	11.1	47	4.2		
79	11.3	48	4.4		
80	11.4	49	4.6		
81	11.6	50	4.8		
82	11.7	51	5.0		
83	11.9	52	5.2		
84	12.0	53	5.4		

IRP, International Reference Preparation; U/L, units/liter.

\*Data from Daya S, Woods S: Transvaginal ultrasound scanning in early pregnancy and correlation with human chorionic gonadotropin levels. *J Clin Ultrasound* 19:139, 1991; Hadlock FP, Shah YP, Kanon DJ, et al: Fetal crown rump length: Reevaluation of relation to menstrual age (5-18 weeks) with high-resolution real-time US. *Radiology* 182:501, 1992; and Robinson HP: "Gestation sac" volumes as determined by sonar in the first trimester of pregnancy. *Br J Obstet Gynaecol* 82:100, 1975.

Table appears in this form in Nyberg DA, Hill LM, Bohm-Velez M, et al: *Transvaginal Ultrasound*. St. Louis, Mosby-Year Book, 1992.

**Table A-8**

**Predicted Menstrual Age (MA) in Weeks  
From Crown Rump Length (CRL)  
Measurements (CM)\***

CRL	MA	CRL	MA	CRL	MA
0.2	5.7	4.2	11.1	8.2	14.2
0.3	5.9	4.3	11.2	8.3	14.2
0.4	6.1	4.4	11.2	8.4	14.3
0.5	6.2	4.5	11.3	8.5	14.4
0.6	6.4	4.6	11.4	8.6	14.5
0.7	6.6	4.7	11.5	8.7	14.6
0.8	6.7	4.8	11.6	8.8	14.7
0.9	6.9	4.9	11.7	8.9	14.8
1.0	7.2	5.0	11.7	9.0	14.9
1.1	7.2	5.1	11.8	9.1	15.0
1.2	7.4	5.2	11.9	9.2	15.1
1.3	7.5	5.3	12.0	9.3	15.2
1.4	7.7	5.4	12.0	9.4	15.3
1.5	7.9	5.5	12.1	9.5	15.3
1.6	8.0	5.6	12.2	9.6	15.4
1.7	8.1	5.7	12.3	9.7	15.5
1.8	8.3	5.8	12.3	9.8	15.6
1.9	8.4	5.9	12.4	9.9	15.7
2.0	8.6	6.0	12.5	10.0	15.9
2.1	8.7	6.1	12.6	10.1	16.0
2.2	8.9	6.2	12.6	10.2	16.1
2.3	9.0	6.3	12.7	10.3	16.2
2.4	9.1	6.4	12.8	10.4	16.3
2.5	9.2	6.5	12.8	10.5	16.4
2.6	9.4	6.6	12.9	10.6	16.5
2.7	9.5	6.7	13.0	10.7	16.6
2.8	9.6	6.8	13.1	10.8	16.7
2.9	9.7	6.9	13.1	10.9	16.8
3.0	9.9	7.0	13.2	11.0	16.9
3.1	10.0	7.1	13.3	11.1	17.0
3.2	10.1	7.2	13.4	11.2	17.1
3.3	10.2	7.3	13.4	11.3	17.2
3.4	10.3	7.4	13.5	11.4	17.3
3.5	10.4	7.5	13.6	11.5	17.4
3.6	10.5	7.6	13.7	11.6	17.5
3.7	10.6	7.7	13.8	11.7	17.6
3.8	10.7	7.8	13.8	11.8	17.7
3.9	10.8	7.9	13.9	11.9	17.8
4.0	10.9	8.0	14.0	12.0	17.9
4.1	11.0	8.1	14.1	12.1	18.0

\*The 95% confidence interval is  $\pm 8\%$  of the predicted age.  
From Hadlock FP, Shah YP, Kanon DJ, et al: Fetal crown-rump length:  
Reevaluation of relation to menstrual age (5–18 weeks) with high-resolution  
real-time US. Radiology 182:501, 1992.

**Table A-9**

**Gestational Age (GA) Prediction Based on  
Head Measurements**

BPD or BPDC* (mm)	Predicted GA (wk)	BPD or BPDC* (mm)	Predicted GA (wk)
20	13.2	59	23.8
21	13.4	60	24.2
22	13.6	61	24.5
23	13.8	62	24.9
24	14	63	25.3
25	14.3	64	25.7
26	14.5	65	26.1
27	14.7	66	26.5
28	14.9	67	26.9
29	15.1	68	27.3
30	15.4	69	27.7
31	15.6	70	28.1
32	15.8	71	28.5
33	16.1	72	29
34	16.3	73	29.4
35	16.6	74	29.9
36	16.8	75	30.3
37	17.1	76	30.8
38	17.3	77	31.2
39	17.6	78	31.7
40	17.9	79	32.2
41	18.1	80	32.7
42	18.4	81	33.2
43	18.7	82	33.7
44	19	83	34.2
45	19.3	84	34.7
46	19.6	85	35.2
47	19.9	86	35.8
48	20.2	87	36.3
49	20.5	88	36.9
50	20.8	89	37.4
51	21.1	90	38
52	21.4	91	38.6
53	21.7	92	39.2
54	22.1	93	39.8
55	22.4	94	40.4
56	22.8	95	41
57	23.1	96	41.6
58	23.5	≥97	42

\*BPDC = corrected BPD =  $\sqrt{(\text{BPD} \times \text{OFD})/1.265}$

From Doubilet PM, Benson CB: Improved prediction of gestational age in the  
late third trimester. J Ultrasound Med 12:647, 1993.



**Table A-10****Predicted Menstrual Age for Head Circumference Measurements (8.5–36.0 cm)**

Head Circumference (cm)	Menstrual Age (wk)	Head Circumference (cm)	Menstrual Age (wk)
8.5	13.7	22.5	24.4
9.0	14.0	23.0	24.9
9.5	14.3	23.5	25.4
10.0	14.6	24.0	25.9
10.5	15.0	24.5	26.4
11.0	15.3	25.0	26.9
11.5	15.6	25.5	27.5
12.0	15.9	26.0	28.0
12.5	16.3	26.5	28.6
13.0	16.6	27.0	29.2
13.5	17.0	27.5	29.8
14.0	17.3	28.0	30.3
14.5	17.7	28.5	31.0
15.0	18.1	29.0	31.6
15.5	18.4	29.5	32.2
16.0	18.8	30.0	32.8
16.5	19.2	30.5	33.5
17.0	19.6	31.0	34.2
17.5	20.0	31.5	34.9
18.0	20.4	32.0	35.5
18.5	20.8	32.5	36.3
19.0	21.2	33.0	37.0
19.5	21.6	33.5	37.7
20.0	22.1	34.0	38.5
20.5	22.5	34.5	39.2
21.0	23.0	35.0	40.0
21.5	23.4	35.5	40.8
22.0	23.9	36.0	41.6

**Variability Estimates ( $\pm 2$  SD)**

12–18 wk	$\pm 1.3$ wk
18–24 wk	$\pm 1.6$ wk
24–30 wk	$\pm 2.3$ wk
30–36 wk	$\pm 2.7$ wk
34–42 wk	$\pm 3.4$ wk

From Hadlock FP, Deter RL, Harrist RB, et al: Fetal head circumference: Relation to menstrual age. *AJR Am J Roentgenol* 138:649, 1982.

**Table A-11****Percentile Values for Fetal Head Circumference**

Menstrual Weeks	Head Circumference (cm)				
	3rd	10th	50th	90th	97th
14	8.8	9.1	9.7	10.3	10.6
15	10.0	10.4	11.0	11.6	12.0
16	11.3	11.7	12.4	13.1	13.5
17	12.6	13.0	13.8	14.6	15.0
18	13.7	14.2	15.1	16.0	16.5
19	14.9	15.5	16.4	17.4	17.9
20	16.1	16.7	17.7	18.7	19.3
21	17.2	17.8	18.9	20.0	20.6
22	18.3	18.9	20.1	21.3	21.9
23	19.4	20.1	21.3	22.5	23.2
24	20.4	21.1	22.4	23.7	24.3
25	21.4	22.2	23.5	24.9	25.6
26	22.4	23.2	24.6	26.0	26.8
27	23.3	24.1	25.6	27.1	27.9
28	24.2	25.1	26.6	28.1	29.0
29	25.0	25.9	27.5	29.1	30.0
30	25.8	26.8	28.4	30.0	31.0
31	26.7	27.6	29.3	31.0	31.9
32	27.4	28.4	30.1	31.8	32.8
33	28.0	29.0	30.8	32.6	33.6
34	28.7	29.7	31.5	33.3	34.3
35	29.3	30.4	32.2	34.1	35.1
36	29.9	30.9	32.8	34.7	35.8
37	30.3	31.4	33.3	35.2	36.3
38	30.8	31.9	33.8	35.8	36.8
39	31.1	32.2	34.2	36.2	37.3
40	31.5	32.6	34.6	36.6	37.7

Adapted from Hadlock FP, Deter RL, Harrist RB, et al: Estimating fetal age: Computer-assisted analysis of multiple fetal growth parameters. *Radiology* 152:497, 1984.

**Table A-12****Predicted Menstrual Age for Abdominal Circumference Measurements (10–36 cm)**

Abdominal Circumference (cm)	Menstrual Age (wk)	Abdominal Circumference (cm)	Menstrual Age (wk)
10.0	15.6	23.5	27.7
10.5	16.1	24.0	28.2
11.0	16.5	24.5	28.7
11.5	16.9	25.0	29.2
12.0	17.3	25.5	29.7
12.5	17.8	26.0	30.1
13.0	18.2	26.5	30.6
13.5	18.6	27.0	31.1
14.0	19.1	27.5	31.6
14.5	19.5	28.0	32.1
15.0	20.0	28.5	32.6
15.5	20.4	29.0	33.1
16.0	20.8	29.5	33.6
16.5	21.3	30.0	34.1
17.0	21.7	30.5	34.6
17.5	22.2	31.0	35.1
18.0	22.6	31.5	35.6
18.5	23.1	32.0	36.1
19.0	23.6	32.5	36.6
19.5	24.0	33.0	37.1
20.0	24.5	33.5	37.6
20.5	24.9	34.0	38.1
21.0	25.4	34.5	38.7
21.5	25.9	35.0	39.2
22.0	26.3	35.5	39.7
22.5	26.8	36.0	40.2
23.0	27.3		

**Variability Estimates ( $\pm 2$  SD)**

12–18 wk	$\pm 1.9$ wk
18–24 wk	$\pm 2.0$ wk
24–30 wk	$\pm 2.2$ wk
30–36 wk	$\pm 3.0$ wk
36–42 wk	$\pm 2.5$ wk

From Hadlock FP, Deter RL, Harrist RB, et al: Fetal abdominal circumference as a predictor of menstrual age. *AJR Am J Roentgenol* 139:367, 1982.

**Table A-13****Percentile Values for Fetal Abdominal Circumference**

Menstrual Weeks	Abdominal Circumference (cm)				
	3rd	10th	50th	90th	97th
14	6.4	6.7	7.3	7.9	8.3
15	7.5	7.9	8.6	9.3	9.7
16	8.6	9.1	9.9	10.7	11.2
17	9.7	10.3	11.2	12.1	12.7
18	10.9	11.5	12.5	13.5	14.1
19	11.9	12.6	13.7	14.8	15.5
20	13.1	13.8	15.0	16.3	17.0
21	14.1	14.9	16.2	17.6	18.3
22	15.1	16.0	17.4	18.8	19.7
23	16.1	17.0	18.5	20.0	20.9
24	17.1	18.1	19.7	21.3	22.3
25	18.1	19.1	20.8	22.5	23.5
26	19.1	20.1	21.9	23.7	24.8
27	20.0	21.1	23.0	24.9	26.0
28	20.9	22.0	24.0	26.0	27.1
29	21.8	23.0	25.1	27.2	28.4
30	22.7	23.9	26.1	28.3	29.5
31	23.6	24.9	27.1	29.4	30.6
32	24.5	25.8	28.1	30.4	31.8
33	25.3	26.7	29.1	31.5	32.9
34	26.1	27.5	30.0	32.5	33.9
35	26.9	28.3	30.9	33.5	34.9
36	27.7	29.2	31.8	34.4	35.9
37	28.5	30.0	32.7	35.4	37.0
38	29.2	30.8	33.6	36.4	38.0
39	29.9	31.6	34.4	37.3	38.9
40	30.7	32.4	35.3	38.2	39.9

Adapted from Hadlock FP, Deter RL, Harrist RB, et al: Estimating fetal age: Computer-assisted analysis of multiple fetal growth parameters. *Radiology* 152:497, 1984.

**Table A-14****A Comparison of Abdominal Circumference Percentiles Using Sonography**

Percentile Menstrual Weeks	Abdominal Circumference (cm)					
	10th Percentile			90th Percentile		
	Jeanty et al <sup>*</sup>	Hadlock et al <sup>†</sup>	Tamura and Sabbagha <sup>‡</sup>	Jeanty et al <sup>*</sup>	Hadlock et al <sup>†</sup>	Tamura and Sabbagha <sup>‡</sup>
18	10.2	11.5	11.7	13.6	13.5	12.0
20	12.4	13.7	14.2	15.8	16.3	16.7
22	14.6	16.0	14.7	18.0	18.8	19.7
24	16.7	18.1	18.9	20.1	21.3	22.8
26	18.8	20.1	19.8	22.2	23.7	26.7
28	20.8	22.0	23.1	24.2	26.0	27.2
30	22.7	23.9	24.4	26.1	28.3	30.1
32	24.5	25.8	26.7	27.9	30.4	32.4
34	26.2	27.5	28.6	29.6	32.5	33.6
36	27.6	29.2	31.0	31.0	34.4	37.8
38	28.9	30.8	32.8	32.3	36.4	38.5
40	29.9	32.4	33.3	33.3	38.2	41.2

<sup>\*</sup>Adapted from Jeanty P, Coussaert E, Cantraine F: Normal growth of the abdominal perimeter. *Am J Perinatol* 1:129, 1984.

<sup>†</sup>Adapted from Hadlock FP, Deter RL, Harrist RB, et al: Estimating fetal age: Computer-assisted analysis of multiple fetal growth parameters. *Radiology* 152:497, 1984.

<sup>‡</sup>Adapted from Tamura RK, Sabbagha RE: Percentile ranks of sonar fetal abdominal circumference measurements. *Am J Obstet Gynecol* 138:475, 1980.



**Table A-15** GA Prediction Based on Femur Length (FL)

FL (mm)	Predicted GA (wk)	FL (mm)	Predicted GA (wk)
10	13.7	45	24.5
11	13.9	46	24.9
12	14.2	47	25.3
13	14.4	48	25.7
14	14.6	49	26.2
15	14.9	50	26.6
16	15.1	51	27.0
17	15.4	52	27.5
18	15.6	53	28.0
19	15.9	54	28.4
20	16.2	55	28.9
21	16.4	56	29.4
22	16.7	57	29.9
23	17.0	58	30.4
24	17.3	59	30.9
25	17.6	60	31.4
26	17.9	61	31.9
27	18.2	62	32.5
28	18.5	63	33.0
29	18.8	64	33.6
30	19.1	65	34.1
31	19.4	66	34.7
32	19.7	67	35.3
33	20.1	68	35.9
34	20.4	69	36.5
35	20.7	70	37.1
36	21.1	71	37.7
37	21.4	72	38.3
38	21.8	73	39.0
39	22.2	74	39.6
40	22.5	75	40.3
41	22.9	76	40.9
42	23.3	77	41.6
43	23.7	≥78	42.0
44	24.1		

GA, gestational age.

From Doubilet PM, Benson CB: Improved prediction of gestational age in the late third trimester. *J Ultrasound Med* 12:647, 1993.**Table A-16** Percentile Values for Fetal Femur Length

Menstrual Weeks	Femur Length (cm)				
	3rd	10th	50th	90th	97th
14	1.2	1.3	1.4	1.5	1.6
15	1.5	1.6	1.7	1.9	1.9
16	1.7	1.8	2.0	2.2	2.3
17	2.1	2.2	2.4	2.6	2.7
18	2.3	2.5	2.7	2.9	3.1
19	2.6	2.7	3.0	3.3	3.4
20	2.8	3.0	3.3	3.6	3.8
21	3.0	3.2	3.5	3.8	4.0
22	3.3	3.5	3.8	4.1	4.3
23	3.5	3.7	4.1	4.5	4.7
24	3.8	4.0	4.4	4.8	5.0
25	4.0	4.2	4.6	5.0	5.2
26	4.2	4.5	4.9	5.3	5.6
27	4.4	4.6	5.1	5.6	5.8
28	4.6	4.9	5.4	5.9	6.2
29	4.8	5.1	5.6	6.1	6.4
30	5.0	5.3	5.8	6.3	6.6
31	5.2	5.5	6.0	6.5	6.8
32	5.3	5.6	6.2	6.8	7.1
33	5.5	5.8	6.4	7.0	7.3
34	5.7	6.0	6.6	7.2	7.5
35	5.9	6.2	6.8	7.4	7.8
36	6.0	6.4	7.0	7.6	8.0
37	6.2	6.6	7.2	7.9	8.2
38	6.4	6.7	7.4	8.1	8.4
39	6.5	6.8	7.5	8.2	8.6
40	6.6	7.0	7.7	8.4	8.8

Adapted from Hadlock FP, Deter RL, Harrist RB, et al: Estimating fetal age: Computer-assisted analysis of multiple fetal growth parameters. *Radiology* 152:497, 1984.

**Table A-17** Length of Fetal Long Bones (mm)

Week No.	Humerus Percentile			Ulna Percentile			Radius Percentile			Femur Percentile			Tibia Percentile			Fibula Percentile		
	5	50	95	5	50	95	5	50	95	5	50	95	5	50	95	5	50	95
11	—	6	—	—	5	—	—	5	—	—	6	—	—	4	—	—	2	—
12	3	9	10	—	8	—	—	7	—	—	9	—	—	7	—	—	5	—
13	5	13	20	3	11	18	—	10	—	6	12	19	4	10	17	—	8	—
14	5	16	20	4	13	17	8	13	12	5	15	19	2	13	19	6	11	10
15	11	18	26	10	16	22	12	15	19	11	19	26	5	16	27	10	14	18
16	12	21	25	8	19	24	9	18	21	13	22	24	7	19	25	6	17	22
17	19	24	29	11	21	32	11	20	29	20	25	29	15	22	29	7	19	31
18	18	27	30	13	24	30	14	22	26	19	28	31	14	24	29	10	22	28
19	22	29	36	20	26	32	20	24	29	23	31	38	19	27	35	18	24	30
20	23	32	36	21	29	32	21	27	28	22	33	39	19	29	35	18	27	30
21	28	34	40	25	31	36	25	29	32	27	36	45	24	32	39	24	29	34
22	28	36	40	24	33	37	24	31	34	29	39	44	25	34	39	21	31	37
23	32	38	45	27	35	43	26	32	39	35	41	48	30	36	43	23	33	44
24	31	41	46	29	37	41	27	34	38	34	44	49	28	39	45	26	35	41
25	35	43	51	34	39	44	31	36	40	38	46	54	31	41	50	33	37	42
26	36	45	49	34	41	44	30	37	41	39	49	53	33	43	49	32	39	43
27	42	46	51	37	43	48	33	39	45	45	51	57	39	45	51	35	41	47
28	41	48	52	37	44	48	33	40	45	45	53	57	38	47	52	36	43	47
29	44	50	56	40	46	51	36	42	47	49	56	62	40	49	57	40	45	50
30	44	52	56	38	47	54	34	43	49	49	58	62	41	51	56	38	47	52
31	47	53	59	39	49	59	34	44	53	53	60	67	46	52	58	40	48	57
32	47	55	59	40	50	58	37	45	51	53	62	67	46	54	59	40	50	56
33	50	56	62	43	52	60	41	46	51	56	64	71	49	56	62	43	51	59
34	50	57	62	44	53	59	39	47	53	57	65	70	47	57	64	46	52	56
35	52	58	65	47	54	61	38	48	57	61	67	73	48	59	69	51	54	57
36	53	60	63	47	55	61	41	48	54	61	69	74	49	60	68	51	55	56
37	57	61	64	49	56	62	45	49	53	64	71	77	52	61	71	55	56	58
38	55	61	66	48	57	63	45	49	53	62	72	79	54	62	69	54	57	59
39	56	62	69	49	57	66	46	50	54	64	74	83	58	64	69	55	58	62
40	56	63	69	50	58	65	46	50	54	66	75	81	58	65	69	54	59	62

From Jeanty P: Fetal limb biometry. (Letter) Radiology 147:602, 1983.



**Table A-18** Reference Values of Major Long Bones

GA (wk)	Humerus (mm) <sup>d</sup>			Radius (mm) <sup>e</sup>			Ulna (mm) <sup>f</sup>		
	Percentiles			Percentiles			Percentiles		
	5th	50th	95th	5th	50th	95th	5th	50th	95th
12	4.8	8.6	12.3	3.0	6.9	10.8	2.9	6.8	10.7
13	7.6	11.4	15.1	5.6	9.5	13.4	5.8	9.7	13.7
14	10.3	14.1	17.9	8.1	12.0	16.0	8.6	12.6	16.6
15	13.1	16.9	20.7	10.5	14.5	18.5	11.4	15.4	19.4
16	15.8	19.7	23.5	12.9	16.9	20.9	14.1	18.1	22.1
17	18.5	22.4	26.3	15.2	19.3	23.3	16.7	20.8	24.8
18	21.2	25.1	29.0	17.5	21.5	25.6	19.3	23.3	27.4
19	23.8	27.7	31.6	19.7	23.8	27.9	21.8	25.8	29.9
20	26.3	30.3	34.2	21.8	25.9	30.0	24.2	28.3	32.4
21	28.8	32.8	36.7	23.9	28.0	32.2	26.5	30.6	34.8
22	31.2	35.2	39.2	25.9	30.1	34.2	28.7	32.9	37.1
23	33.5	37.5	41.6	27.9	32.0	36.2	30.9	35.1	39.3
24	35.7	39.8	43.8	29.7	34.0	38.2	33.0	37.2	41.5
25	37.9	41.9	46.0	31.6	35.8	40.0	35.1	39.3	43.5
26	39.9	44.0	48.1	33.3	37.6	41.9	37.0	41.3	45.6
27	41.9	46.0	50.1	35.0	39.3	43.6	38.9	43.2	47.5
28	43.7	47.9	52.0	36.7	41.0	45.3	40.7	45.0	49.3
29	45.5	49.7	53.9	38.3	42.6	46.9	42.5	46.8	51.1
30	47.2	51.4	55.6	39.8	44.1	48.5	44.1	48.5	52.8
31	48.9	53.1	57.3	41.2	45.6	50.0	45.7	50.1	54.5
32	50.4	54.7	58.9	42.6	47.0	51.4	47.2	51.6	56.1
33	52.0	56.2	60.5	44.0	48.4	52.8	48.7	53.1	57.5
34	53.4	57.7	62.0	45.2	49.7	54.1	50.0	54.5	59.0
35	54.8	59.2	63.5	46.4	50.9	55.4	51.3	55.8	60.3
36	56.2	60.6	64.9	47.6	52.1	56.6	52.6	57.1	61.6
37	57.6	62.0	66.4	48.7	53.2	57.7	53.7	58.2	62.8
38	59.0	63.4	67.8	49.7	54.2	58.8	54.8	59.3	63.9
39	60.4	64.8	69.3	50.6	55.2	59.8	55.8	60.4	64.9
40	61.9	66.3	70.8	51.5	56.2	60.8	56.7	61.3	65.9

GA, gestational age.

\*Femur (mean) =  $-25.252 + 2.555 \times \text{GA} + 0.027566 \times \text{GA}^2 - 0.00073286 \times \text{GA}^3$  (Jeanty et al., 1984).\*Tibia (mean) =  $5.555 - 0.915554 \times \text{GA} + 0.23359 \times \text{GA}^2 - 0.00638 \times \text{GA}^3 + 0.000055801 \times \text{GA}^4$  (Jeanty et al., 1984).\*Fibula (mean) =  $36.563 + 3.963 \times \text{GA} - 0.037 \times \text{GA}^2$  (Exacoustos et al., 1991).\*Humerus (mean) =  $-16.24 + 0.76315 \times \text{GA} + 0.1683 \times \text{GA}^2 - 0.0056212 \times \text{GA}^3 + 0.000055666 \times \text{GA}^4$ .\*Radius (mean) =  $-29.09 + 3.371 \times \text{GA} - 0.031 \times \text{GA}^2$  (Exacoustos et al., 1991).\*Ulna (mean) =  $-34.313 + 3.8685 \times \text{GA} - 0.036949 \times \text{GA}^2$  (Jeanty et al., 1984).

Derived from compilation of data: Jeanty P, Coussaert E, Cantraine F, et al. A longitudinal study of fetal limb growth. *Am J Perinatol* 1:136, 1984; Merz E, Grubner A, Kern F: Mathematical modeling of fetal limb growth. *J Clin Ultrasound* 17:179, 1989; and Exacoustos C, Rosaù P, Rizzo C, Arduini D: Ultrasound measurements of fetal limb bones. *Ultrasound Obstet Gynecol* 1:325, 1991.

From Nyberg DA, McCahan JP, Pretorius DH, Pilu G: *Diagnostic Imaging of Fetal Anomalies*. Philadelphia, Lippincott Williams & Wilkins, 2003.

**Table A-19** Gestational Age for Clavicle Length

Clavicle Length (mm)	Gestational Age (Weeks and Days) Percentile		
	5th	50th	95th
11	8 + 3	13 + 6	17 + 2
12	9 + 1	14 + 4	18 + 1
13	10 + 0	14 + 3	19 + 6
14	11 + 6	15 + 2	20 + 5
15	12 + 5	16 + 1	21 + 4
16	12 + 3	18 + 0	21 + 3
17	13 + 2	18 + 5	22 + 2
18	14 + 1	19 + 4	23 + 0
19	16 + 0	19 + 3	24 + 6
20	16 + 6	20 + 2	25 + 5
21	17 + 4	21 + 1	26 + 4
22	17 + 3	22 + 6	26 + 2
23	18 + 2	23 + 5	27 + 1
24	19 + 1	24 + 4	28 + 0
25	21 + 0	24 + 3	29 + 6
26	21 + 5	25 + 1	30 + 5
27	22 + 4	26 + 0	30 + 3
28	22 + 3	27 + 6	31 + 2
29	23 + 2	28 + 5	32 + 1
30	24 + 0	29 + 4	34 + 0
31	25 + 6	29 + 2	34 + 6
32	26 + 5	30 + 1	35 + 4
33	27 + 4	31 + 0	35 + 3
34	27 + 3	32 + 6	36 + 2
35	28 + 1	33 + 5	37 + 1
36	29 + 0	33 + 3	39 + 0
37	30 + 6	34 + 2	39 + 5
38	31 + 5	35 + 1	40 + 4
39	32 + 4	37 + 0	40 + 3
40	32 + 2	37 + 6	41 + 2
41	33 + 1	38 + 4	42 + 0
42	35 + 0	38 + 3	43 + 6
43	35 + 6	39 + 2	44 + 5
44	36 + 5	40 + 1	45 + 4
45	36 + 3	41 + 6	45 + 3

From Yarkoni S, Schmidt W, Jeanty P, et al: Clavicular measurement: A new biometric parameter for fetal evaluation. *J Ultrasound Med* 4:467, 1985.

**Table A-20**

Comparison of Mean Postpartum and Ultrasonographic Foot Length With Streeter's Pathologic Data (1920)

Gestation Week	Streeter's Data (mm)	Ultrasonographic Foot Length (mm)	Postpartum Foot Length (mm)
11	7	8	
12	9	9	
13	11	10	
14	14	16	
15	17	16	
16	20	21	
17	23	24	
18	27	27	
19	31	28	
20	33	33	33
21	35	35	
22	40	38	
23	42	42	
24	45	44	
25	48	47	48
26	50	51	
27	53	54	52
28	55	58	
29	57	57	57
30	59	61	60
31	61	62	60
32	63	63	66
33	65	67	68
34	68	68	71
35	71	71	72
36	74	74	74
37	77	75	78
38	79	78	78
39	81	78	80
40	83	82	81
41			82
42			82
43			84

From Mercer BM, Sklar S, Shariatmadar A, et al: Fetal foot length as a predictor of gestational age. *Am J Obstet Gynecol* 156:350, 1987.



**Table A-21** Fetal Foot Length Percentiles by Menstrual Age\*

Menstrual Age (wk)	Fetal Foot Length Percentiles (Smoothed)						
	N	CV (%)	5th	10th	50th	90th	95th
15	18	12.7	1.4	1.5	1.8	2.2	2.3
16	146	10.4	1.6	1.7	2.1	2.5	2.6
17	375	9.7	1.9	2.0	2.4	2.8	2.9
18	613	9.8	2.2	2.3	2.7	3.1	3.2
19	1160	8.9	2.5	2.6	3.0	3.3	3.4
20	929	9.3	2.8	2.9	3.2	3.6	3.7
21	552	8.5	3.1	3.2	3.5	3.9	4.0
22	360	8.9	3.4	3.5	3.9	4.2	4.3
23	222	8.1	3.7	3.8	4.2	4.6	4.7
24	177	7.0	4.0	4.1	4.5	4.9	5.0
25	125	7.1	4.3	4.4	4.8	5.1	5.2
26	123	7.0	4.6	4.7	5.1	5.4	5.5
27	108	6.3	4.8	4.9	5.3	5.7	5.8
28	74	5.4	5.1	5.2	5.6	5.9	6.0
29	66	6.2	5.3	5.4	5.8	6.2	6.3
30	65	5.2	5.6	5.7	6.1	6.4	6.5
31	62	5.7	5.8	5.9	6.3	6.7	6.8
32	65	5.3	6.0	6.1	6.5	6.9	7.0
33	39	4.4	6.3	6.4	6.8	7.1	7.2
34	37	6.8	6.5	6.6	7.0	7.4	7.5
35	24	6.2	6.8	6.9	7.3	7.6	7.7
36	15	5.5	7.0	7.1	7.5	7.9	8.0
37	17	5.3	7.3	7.4	7.7	8.1	8.2

CV, coefficient of variation; N, number of fetuses.

\*Values for percentiles are in centimeters.

From Mcirowitz NB, Ananth CV, Smulian JC, et al: Foot length in fetuses with abnormal growth. J Ultrasound Med 19:201, 2000.

**Table A-22****Predicted Menstrual Ages for Transverse Cerebellar Diameters of 14 to 56 mm**

Cerebellum Diameter (mm)	Menstrual Age (wk)	Cerebellum Diameter (mm)	Menstrual Age (wk)
14	15.2	35	29.4
15	15.8	36	30.0
16	16.5	37	30.6
17	17.2	38	31.2
18	17.9	39	31.8
19	18.6	40	32.3
20	19.3	41	32.8
21	20.0	42	33.4
22	20.7	43	33.9
23	21.4	44	34.4
24	22.1	45	34.8
25	22.8	46	35.3
26	23.5	47	35.7
27	24.2	48	36.1
28	24.9	49	36.5
29	25.5	50	36.8
30	26.2	51	37.2
31	26.9	52	37.5
32	27.5	54	38.0
33	28.1	55	38.3
34	28.8	56	38.5

Variability Estimates ( $\pm 2$ SD)	
12–18 wk	$\pm 1.0$ wk
18–24 wk	$\pm 1.8$ wk
24–30 wk	$\pm 2.0$ wk
30–36 wk	$\pm 2.4$ wk
36–42 wk	$\pm 3.2$ wk

From Hill LM, Guzick D, Fries J, et al: The transverse cerebellar diameter in estimating gestational age in the large-for-gestational-age fetus. *Obstet Gynecol* 75:983, 1990. Reprinted with permission from the American College of Obstetricians and Gynecologists.

**Table A-23****Nomogram of the Transverse Cerebellar Diameter According to Percentile Distribution**

Gestational Age (wk)	Cerebellum Diameter (mm)				
	10	25	50	75	90
15	10	12	14	15	16
16	14	16	16	16	17
17	16	17	17	18	18
18	17	18	18	19	19
19	18	18	19	19	22
20	18	19	20	20	22
21	19	20	22	23	24
22	21	23	23	24	24
23	22	23	24	25	26
24	22	24	25	27	28
25	23	21.5	28	28	29
26	25	28	29	30	32
27	26	28.5	30	31	32
28	27	30	31	32	34
29	29	32	34	36	38
30	31	32	35	37	40
31	32	35	38	39	43
32	33	36	38	40	42
33	32	36	40	43	44
34	33	38	40	41	44
35	31	37	40.5	43	47
36	36	29	43	52	55
37	37	37	45	52	55
38	40	40	48.5	52	55
39	52	52	52	55	55

From Goldstein I, Reece A, Pilu G, et al: Cerebellar measurements with ultrasonography in the evaluation of fetal growth and development. *Am J Obstet Gynecol* 156:1065, 1987.



**Table A-24****Predicted Biparietal Diameter (BPD) and Weeks' Gestation From the Inner (IOD) and Outer (OOD) Orbital Distances**

BPD (cm)	Gestation (wk)	IOD (cm)	OOD (cm)	BPD (cm)	Gestation (wk)	IOD (cm)	OOD (cm)
1.9	11.6	0.5	1.3	5.8	24.3	1.6	4.1
2.0	11.6	0.5	1.4	5.9	24.3	1.6	4.2
2.1	12.1	0.6	1.5	6.0	24.7	1.6	4.3
2.2	12.6	0.6	1.6	6.1	25.2	1.6	4.3
2.3	12.6	0.6	1.7	6.2	25.2	1.6	4.4
2.4	13.1	0.7	1.7	6.3	25.7	1.7	4.4
2.5	13.6	0.7	1.8	6.4	26.2	1.7	4.5
2.6	13.6	0.7	1.9	6.5	26.2	1.7	4.5
2.7	14.1	0.8	2.0	6.6	26.7	1.7	4.6
2.8	14.6	0.8	2.1	6.7	27.2	1.7	4.6
2.9	14.6	0.8	2.1	6.8	27.6	1.7	4.7
3.0	15.0	0.9	2.2	6.9	28.1	1.7	4.7
3.1	15.5	0.9	2.3	7.0	28.6	1.8	4.8
3.2	15.5	0.9	2.4	7.1	29.1	1.8	4.8
3.3	16.0	1.0	2.5	7.3	29.6	1.8	4.9
3.4	16.5	1.0	2.5	7.4	30.0	1.8	5.0
3.5	16.5	1.0	2.6	7.5	30.6	1.8	5.0
3.6	17.0	1.0	2.7	7.6	31.0	1.8	5.1
3.7	17.5	1.1	2.7	7.7	31.5	1.8	5.1
3.8	17.9	1.1	2.8	7.8	32.0	1.8	5.2
4.0	18.4	1.2	3.0	7.9	32.5	1.9	5.2
4.2	18.9	1.2	3.1	8.0	33.0	1.9	5.3
4.3	19.4	1.2	3.2	8.2	33.5	1.9	5.4
4.4	19.4	1.3	3.2	8.3	34.0	1.9	5.4
4.5	19.9	1.3	3.3	8.4	34.4	1.9	5.4
4.6	20.4	1.3	3.4	8.5	35.0	1.9	5.5
4.7	20.4	1.3	3.4	8.6	35.4	1.9	5.5
4.8	20.9	1.4	3.5	8.8	35.9	1.9	5.6
4.9	21.3	1.4	3.6	8.9	36.4	1.9	5.6
5.0	21.3	1.4	3.6	9.0	36.9	1.9	5.7
5.1	21.8	1.4	3.7	9.1	37.3	1.9	5.7
5.2	22.3	1.4	3.8	9.2	37.8	1.9	5.8
5.3	22.3	1.5	3.8	9.3	38.3	1.9	5.8
5.4	22.8	1.5	3.9	9.4	38.8	1.9	5.8
5.5	23.3	1.5	4.0	9.6	39.3	1.9	5.9
5.6	23.3	1.5	4.0	9.7	39.8	1.9	5.9
5.7	23.8	1.5	4.1				

From Mayden KL, Tortora M, Berkowitz RL, et al: Orbital diameters: A new parameter for prenatal diagnosis and dating. *Am J Obstet Gynecol* 144:289, 1982.

**Table A-25** Fetal Thoracic Circumference Measurements\*

Gestational Age (wk)	No.	Predictive Percentiles								
		2.5	5	10	25	50	75	90	95	97.5
16	6	5.9	6.4	7.0	8.0	9.1	10.3	11.3	11.9	12.4
17	22	6.8	7.3	7.9	8.9	10.0	11.2	12.2	12.8	13.3
18	31	7.7	8.2	8.8	9.8	11.0	12.1	13.1	13.7	14.2
19	21	8.6	9.1	9.7	10.7	11.9	13.0	14.0	14.6	15.1
20	20	9.5	10.0	10.6	11.7	12.8	13.9	15.0	15.5	16.0
21	30	10.4	11.0	11.6	12.6	13.7	14.8	15.8	16.4	16.9
22	18	11.3	11.9	12.5	13.5	14.6	15.7	16.7	17.3	17.8
23	21	12.2	12.8	13.4	14.4	15.5	16.6	17.6	18.2	18.8
24	27	13.2	13.7	14.3	15.3	16.4	17.5	18.5	19.1	19.7
25	20	14.1	14.6	15.2	16.2	17.3	18.4	19.4	20.0	20.6
26	25	15.0	15.5	16.1	17.1	18.2	19.3	20.3	21.0	21.5
27	24	15.9	16.4	17.0	18.0	19.1	20.2	21.3	21.9	22.4
28	24	16.8	17.3	17.9	18.9	20.0	21.2	22.2	22.8	23.3
29	24	17.7	18.2	18.8	19.8	21.0	22.1	23.1	23.7	24.2
30	27	18.6	19.1	19.7	20.7	21.9	23.0	24.0	24.6	25.1
31	24	19.5	20.0	20.6	21.6	22.8	23.9	24.9	25.5	26.0
32	28	20.4	20.9	21.5	22.6	23.7	24.8	25.8	26.4	26.9
33	27	21.3	21.8	22.5	23.5	24.6	25.7	26.7	27.3	27.8
34	25	22.2	22.8	23.4	24.4	25.5	26.6	27.6	28.2	28.7
35	20	23.1	23.7	24.3	25.3	26.4	27.5	28.5	29.1	29.6
36	23	24.0	24.6	25.2	26.2	27.3	28.4	29.4	30.0	30.6
37	22	24.9	25.5	26.1	27.1	28.2	29.3	30.3	30.9	31.5
38	21	25.9	26.4	27.0	28.0	29.1	30.2	31.2	31.9	32.4
39	7	26.8	27.3	27.9	28.9	30.0	31.1	32.2	32.8	33.3
40	6	27.7	28.2	28.8	29.8	30.9	32.1	33.1	33.7	34.2

\*Measurements in centimeters.

From Chitkara U, Rosenberg J, Chervenak FA, et al: Prenatal sonographic assessment of the fetal thorax: Normal values. Am J Obstet Gynecol 156:1069, 1987.



## Measurements Used in Assessing Fetal Weight, Growth, and Body Proportions

**Table B-1** Equations for the Estimation of Fetal Weight

Source	Year	Equation
<b>AC equations</b>		
Campbell and Wilkin*	1975	$\text{Ln EFW} = -4.564 + 0.282 (\text{AC}) - 0.00331 (\text{AC})^2$
Hadlock et al	1984	$\text{Ln EFW} = 2.695 + 0.253 (\text{AC}) - 0.00275 (\text{AC})^2$
Jordaan	1983	$\text{Log}_{10} \text{EFW} = 0.6328 + 0.1881 (\text{AC}) - 0.0043 (\text{AC})^2 + 0.000036239 (\text{AC})^3$
Warsof et al*	1977	$\text{Log}_{10} \text{EFW} = -1.8367 + 0.092 (\text{AC}) - 0.000019 (\text{AC})^3$
Higginbottom et al	1975	$\text{EFW} = 0.0816 (\text{AC})^3$
<b>FL equation</b>		
Warsof et al	1986	$\text{Ln EFW} = 4.6914 + 0.151 (\text{FL})^2 - 0.0119 (\text{FL})^3$
<b>AC/FL equations</b>		
Hadlock et al	1985	$\text{Log}_{10} \text{EFW} = 1.304 + 0.05281 (\text{AC}) + 0.1938 (\text{FL}) - 0.004 (\text{AC}) (\text{FL})$
Warsof et al	1986	$\text{Ln EFW} = 2.792 + 1.08 (\text{FL}) + 0.0036 (\text{AC})^2 - 0.027 (\text{FL}) (\text{AC})$
Woo et al	1985	$\text{Log}_{10} \text{EFW} = 0.59 + 0.08 (\text{AC}) + 0.28 (\text{FL}) - 0.00716 (\text{AC}) (\text{FL})$
<b>AC/BPD equations</b>		
Warsof et al*	1977	$\text{Log}_{10} \text{EFW} = 1.599 + 0.144 (\text{BPD}) + 0.032 (\text{AC}) - 0.000111 (\text{BPD})^2 (\text{AC})$
Hadlock et al	1984	$\text{Log}_{10} \text{EFW} = 1.1134 + 0.05845 (\text{AC}) - 0.000604 (\text{AC})^2 - 0.007365 (\text{BPD})^2 + 0.000595 (\text{BPD}) (\text{AC}) + 0.1694 (\text{BPD})$
Jordaan*	1983	$\text{Log}_{10} \text{EFW} = -1.1683 + 0.0377 (\text{AC}) + 0.0950 (\text{BPD}) - 0.0015 (\text{BPD}) (\text{AC})$
Hsieh et al	1987	$\text{Log}_{10} \text{EFW} = 2.1315 + 0.0056541 (\text{AC}) (\text{BPD}) - 0.00015515 (\text{BPD}) (\text{AC})^2 + 0.000019782 (\text{AC})^3 + 0.052594 (\text{BPD})$
Woo et al	1985	$\text{Log}_{10} \text{EFW} = 1.63 + 0.16 (\text{BPD}) + 0.00111 (\text{AC})^2 - 0.0000859 (\text{BPD}) (\text{AC})^2$
Vintzileos et al	1987	$\text{Log}_{10} \text{EFW} = 1.879 + 0.084 (\text{BPD}) + 0.026 (\text{AC})$
Shepard et al*	1982	$\text{Log}_{10} \text{EFW} = -1.7492 + 0.166 (\text{BPD}) + 0.046 (\text{AC}) - 0.002546 (\text{BPD})$
<b>AC/BPD/FL equations</b>		
Woo et al	1985	$\text{Log}_{10} \text{EFW} = 1.54 + 0.15 (\text{BPD}) + 0.00111 (\text{AC})^2 - 0.0000764 (\text{BPD}) (\text{AC})^2 + 0.05 (\text{FL}) - 0.000992 (\text{FL}) (\text{AC})$
Shinozuka et al†	1987	$\text{EFW} = 0.23966 (\text{AC})^2 (\text{FL}) + 1.6230 (\text{BPD})^3$
Hadlock et al	1985	$\text{Log}_{10} \text{EFW} = 1.335 - 0.0034 (\text{AC}) (\text{FL}) + 0.0316 (\text{BPD}) + 0.0457 (\text{AC}) + 0.1623 (\text{FL})$
Hsieh et al	1987	$\text{Log}_{10} \text{EFW} = 2.7193 + 0.0094962 (\text{AC}) (\text{BPD}) - 0.1432 (\text{FL}) - 0.00076742 (\text{AC}) (\text{BPD})^2 + 0.001745 (\text{FL}) (\text{BPD})^2$

Continued

**Table B-1** Equations for the Estimation of Fetal Weight—Continued

Source	Year	Equation
<b>AC/HC/FL equations</b>		
Hadlock et al	1984	$\text{Log}_{10} \text{ EFW} = 1.326 - 0.00326 (\text{AC}) (\text{FL}) + 0.0107 (\text{HC}) + 0.0438 (\text{AC}) + 0.158 (\text{FL})$
Ott et al <sup>*</sup>	1986	$\text{Log}_{10} \text{ EFW} = 2.0661 + 0.04355 (\text{HC}) + 0.05394 (\text{AC}) 0.0008582 (\text{HC}) (\text{AC}) + 1.2594 (\text{FL}/\text{AC})$
Combs et al	1993	$\text{EFW} - 0.23718 (\text{AC})^2 (\text{FL}) + 0.03312 (\text{HC})^5$
<b>AC/HC/BPD/± FL equations</b>		
Jordaan	1983	$\text{Log}_{10} \text{ EFW} = 2.3231 + 0.02904 (\text{AC}) + 0.0079 (\text{HC}) 0.0058 (\text{BPD})$
Hadlock et al	1985	$\text{Log}_{10} \text{ EFW} = 1.3596 + 0.0064 (\text{HC}) + 0.0424 (\text{AC}) + 0.174 (\text{FL}) + 0.00061 (\text{BPD}) (\text{AC}) - 0.00386 (\text{AC}) (\text{FL})$
<b>Maternal characteristics equation</b>		
Nahum et al <sup>‡</sup>	2002	$\text{EFW} = \text{Gestational age (d)} \mu (9.38 = 0.264 \mu \text{ fetal sex}^{\S} + 0.000233 \times \text{maternal height [cm]} \times \text{maternal weight at 26.0 wks [kg]} + 4.62 \times \text{third-trimester maternal weight gain rate [kg/d]} \times [\text{parity} + 1])^{\parallel}$

Ln, Natural logarithm; EFW, estimated fetal weight (expressed in grams).

AC, FL, BPD, and HC are expressed in centimeters.

<sup>\*</sup>The estimated fetal weight for these six algorithms is expressed in kilograms rather than grams.

<sup>†</sup>The equation of Shinozuka et al has been modified from its original form to include the fetal AC instead of the fetal transverse and anteroposterior abdominal diameters, as were described in the original equation. (Shinozuka N, Okai T, Kohzuma S, et al: Formulas for fetal weight estimation by ultrasound measurements based on neonatal specific gravities and volumes. *J Obstet Gynecol* 157:1140, 1987 and Combs CA, Jackle RK, Rosenn B, et al: Sonographic estimation of fetal weight based on a model of fetal volume. *Obstet Gynecol* 82:365, 1993).

<sup>‡</sup>This equation applies only to healthy white mothers who carry term singleton pregnancies. Fetal weight estimates that use this equation should be adjusted systematically for (1) black maternal race (decrement by 161 g), (2) East Asian maternal race (decrement by 291 g), (3) chronic hypertension (decrement by 161 g), (4) pregnancy-induced hypertension/preeclampsia (decrement by 105 g), (5) maternal cigarette smoking (decrement by 17 g per cigarette smoked per day), and (6) high altitude (decrement by 102 g for every 1000 meters in altitude above sea level).

<sup>§</sup>Fetal sex independently explains approximately 1% of the variance in term fetal weight. It is a significant predictor of birth weight (F test,  $P < 0.001$ ), but it has little overall impact in birth weight predictions. When 0 is entered for fetal sex so that sex is ignored, the mean absolute prediction error does not change, and the median absolute prediction error increases only slightly by 10 g (0.2%). Thus fetal sex, although potentially useful if available, is nonessential for use of the maternal characteristics equation.

<sup>||</sup>Where fetal sex = +1 for male, -1 for female, and 0 when sex is not known; gestational age = days since the onset of the last normal period = the conception age (in days) + 14. (Wahum GG, Stanislaw H: Ultrasonographic prediction of term birth weight: How accurate is it? *Am J Obstet Gynecol* 188:566, 2003.)

From Hill LM: Fetal weight. In Goldberger BB, McGahan JP (eds): *Atlas of Ultrasound Measurements*, 2nd ed. Philadelphia, Mosby Inc/Elsevier, 2006.

**Table B-2** Neonatal Birth Weight Derived From Gestations Dated by Early Ultrasonography (Male and Female Subjects Combined)

Gestational Age (wk)*	Weight Percentile (g)						
	5th	10th	25th	50th	75th	90th	95th
25	450	490	564	660	772	889	968
26	523	568	652	760	885	1016	1103
27	609	660	754	875	1015	1160	1257
28	707	765	870	1005	1162	1322	1430
29	820	884	1003	1153	1327	1504	1623
30	947	1020	1151	1319	1511	1706	1836
31	1090	1171	1317	1502	1713	1928	2070
32	1249	1338	1499	1702	1933	2167	2321
33	1422	1519	1696	1918	2169	2421	2587
34	1608	1714	1906	2146	2416	2687	2865
35	1804	1919	2125	2383	2671	2959	3148
36	2006	2129	2349	2622	2927	3230	3428
37	2210	2340	2572	2859	3177	3493	3698
38	2409	2544	2786	3083	3412	3736	3947
39	2595	2735	2984	3288	3622	3952	4164
40	2762	2904	3155	3462	3798	4127	4340
41	2900	3042	3293	3597	3930	4254	4462
42	3002	3142	3388	3685	4008	4322	4523
43	3061	3195	3432	3717	4026	4324	4515

\*Age to the nearest week. Percentiles listed for 25 weeks, for example, apply to neonates aged 24.5 to 25.4 weeks.

From Doubilet PM, Benson CB, Nadel AS, et al: Improved birth weight table for neonates developed from gestations dated by early ultrasonography. *J Ultrasound Med* 16:241, 1997.



**Table B-3** Nomogram of Estimated Fetal Weight in Twin Gestations

Gestational Age (wk)	Estimated Fetal Weight (g) by Percentile				
	5th	25th	50th	75th	95th
16	132	141	154	189	207
17	173	194	215	239	249
18	214	248	276	289	291
19	223	253	300	333	412
20	232	259	324	378	534
21	275	355	432	482	705
22	319	452	540	586	876
23	347	497	598	684	880
24	376	543	656	783	885
25	549	677	793	916	1118
26	722	812	931	1049	1352
27	755	978	1087	1193	1563
28	789	1145	1244	1337	1774
29	900	1266	1395	1509	1883
30	1011	1387	1546	1682	1992
31	1198	1532	1693	1875	2392
32	1385	1677	1840	2068	2793
33	1491	1771	2032	2334	3000
34	1597	1866	2224	2601	3208
35	1703	2093	2427	2716	3336
36	1809	2321	2631	2832	3465
37	2239	2540	2824	3035	3679
38	2669	2760	3017	3239	3894

From Yarkoni S, Reece EA, Holford T, et al: Estimated fetal weight in the evaluation of growth in twin gestations: A prospective longitudinal study. *Obstet Gynecol* 69:636, 1987. Reprinted with permission from The American College of Obstetricians and Gynecologists.

**Table B-4** Growth Parameters in Triplets Generated From Regression Equations

Weeks	BPD	HC	Bicerebellar Diameter	Humerus Length	FL	Tibia Length	Fibula Length	AC
16	3.5	12.8	1.5	2.1	2.0	1.7	1.6	10.7
17	3.9	14.1	1.6	2.3	2.3	2.0	1.9	11.9
18	4.2	15.3	1.7	2.6	2.6	2.3	2.2	13.1
19	4.5	16.5	1.9	2.8	2.9	2.5	2.4	14.2
20	4.8	17.6	2.0	3.1	3.2	2.8	2.7	15.3
21	5.1	18.7	2.2	3.3	3.5	3.1	2.9	16.4
22	5.4	19.8	2.3	3.5	3.7	3.3	3.2	17.4
23	5.7	20.8	2.5	3.7	4.0	3.5	3.4	18.4
24	6.0	21.8	2.6	3.9	4.2	3.7	3.6	19.4
25	6.2	22.7	2.7	4.1	4.4	3.9	3.7	20.3
26	6.5	23.6	2.8	4.2	4.6	4.1	3.9	21.2
27	6.7	24.5	3.0	4.4	4.8	4.2	4.1	22.1
28	6.9	25.3	3.1	4.6	5.0	4.4	4.2	22.9
29	7.1	26.1	3.2	4.7	5.2	4.5	4.3	23.7
30	7.3	26.8	3.4	4.8	5.4	4.7	4.4	24.5
31	7.5	27.5	3.5	4.9	5.5	4.8	4.6	25.2
32	7.7	28.1	3.6	5.0	5.7	4.9	4.6	25.9
33	7.8	28.7	3.8	5.1	5.8	4.9	4.7	26.6
34	8.0	29.2	3.9	5.2	5.9	5.0	4.8	27.2
35	8.1	29.7	4.0	5.2	6.0	5.1	4.8	27.8

AC, abdominal circumference; BPD, biparietal diameter; FL, femur length; HC, head circumference.

From Rodis JF, Arky L, Egan JF, et al: Comprehensive fetal ultrasonographic growth measurements in triplet gestations. *Am J Obstet Gynecol* 181:1128, 1999.

**Table B-5** Estimates of Fetal Weight (g) Based on Abdominal Circumference and Femur Length

		Abdominal Circumference (cm)																					
		20.0	20.5	21.0	21.5	22.0	22.5	23.0	23.5	24.0	24.5	25.0	25.5	26.0	26.5	27.0	27.5	28.0	28.5	29.0	29.5	30.0	
Femur	4.0	663	691	720	751	783	816	851	887	925	964	1006	1048	1093	1139	1188	1239	1291	1346	1403	1463	1525	
	Length (cm)	4.1	680	709	738	769	802	836	871	907	946	986	1027	1070	1115	1162	1211	1262	1315	1371	1429	1489	1551
	4.2	697	726	757	788	821	855	891	928	967	1007	1049	1093	1138	1186	1235	1287	1340	1396	1454	1515	1578	
	4.3	715	745	776	808	841	875	912	949	988	1029	1071	1116	1162	1209	1259	1311	1365	1422	1480	1541	1605	
	4.4	734	764	795	827	861	896	933	971	1010	1051	1094	1139	1185	1234	1284	1336	1391	1448	1507	1568	1632	
	4.5	753	783	815	847	882	917	954	993	1033	1074	1118	1163	1210	1259	1309	1362	1417	1474	1534	1596	1660	
	4.6	772	803	835	868	903	939	976	1015	1056	1098	1142	1187	1235	1284	1335	1388	1444	1501	1561	1623	1688	
	4.7	792	823	856	889	924	961	999	1038	1079	1122	1166	1212	1260	1310	1361	1415	1471	1529	1589	1652	1717	
	4.8	812	844	877	911	947	984	1022	1062	1103	1146	1191	1237	1286	1336	1388	1442	1498	1557	1618	1681	1746	
	4.9	833	865	899	933	969	1007	1046	1086	1128	1171	1216	1263	1312	1363	1415	1470	1527	1585	1647	1710	1776	
	5.0	855	887	921	956	993	1031	1070	1111	1153	1197	1243	1290	1339	1390	1443	1498	1555	1615	1676	1740	1806	
	5.1	877	910	944	980	1016	1055	1095	1136	1179	1223	1269	1317	1367	1418	1471	1527	1584	1644	1706	1770	1837	
	5.2	899	933	967	1004	1041	1080	1120	1162	1205	1250	1296	1344	1395	1447	1500	1556	1614	1674	1737	1801	1868	
	5.3	922	956	992	1028	1066	1105	1146	1188	1232	1277	1324	1373	1423	1476	1530	1586	1645	1705	1768	1833	1900	
	5.4	946	981	1016	1053	1091	1131	1172	1215	1259	1305	1352	1401	1452	1505	1560	1617	1675	1736	1799	1865	1933	
	5.5	971	1005	1041	1079	1118	1158	1199	1242	1287	1333	1381	1431	1482	1535	1591	1648	1707	1768	1832	1897	1966	
	5.6	995	1031	1067	1105	1144	1185	1227	1271	1316	1362	1411	1461	1513	1566	1622	1679	1739	1801	1864	1931	1999	
	5.7	1021	1057	1094	1132	1172	1213	1255	1299	1345	1392	1441	1491	1544	1598	1654	1712	1772	1834	1898	1964	2033	
	5.8	1047	1084	1121	1160	1200	1242	1285	1329	1375	1422	1472	1523	1575	1630	1686	1744	1805	1867	1932	1999	2068	
	5.9	1074	1111	1149	1188	1229	1271	1314	1359	1406	1454	1503	1555	1608	1663	1719	1778	1839	1902	1966	2034	2103	
	6.0	1102	1139	1178	1217	1258	1301	1345	1390	1437	1485	1535	1587	1641	1696	1753	1812	1873	1936	2002	2069	2139	
	6.1	1130	1168	1207	1247	1289	1331	1376	1421	1469	1518	1568	1620	1674	1730	1788	1847	1908	1972	2038	2105	2175	
	6.2	1160	1198	1237	1278	1319	1363	1408	1454	1501	1551	1602	1654	1709	1765	1823	1882	1944	2008	2074	2142	2212	
	6.3	1189	1228	1268	1309	1351	1395	1440	1487	1535	1585	1636	1689	1744	1800	1858	1919	1981	2045	2111	2180	2250	
	6.4	1220	1259	1299	1341	1384	1428	1473	1520	1569	1619	1671	1724	1779	1836	1895	1956	2018	2082	2149	2218	2289	
	6.5	1251	1291	1332	1373	1417	1461	1507	1555	1604	1655	1707	1760	1816	1873	1932	1993	2056	2121	2188	2256	2328	
	6.6	1284	1324	1365	1407	1451	1496	1542	1590	1640	1691	1743	1797	1853	1911	1970	2031	2094	2160	2227	2296	2367	
	6.7	1317	1357	1399	1441	1486	1531	1578	1626	1676	1728	1780	1835	1891	1949	2009	2070	2134	2199	2267	2336	2408	
	6.8	1351	1391	1433	1477	1521	1567	1615	1663	1713	1765	1819	1873	1930	1988	2048	2110	2174	2240	2307	2377	2449	
	6.9	1385	1427	1469	1513	1558	1604	1652	1701	1752	1804	1857	1913	1970	2028	2089	2151	2215	2281	2348	2418	2490	
	7.0	1421	1463	1506	1550	1595	1642	1690	1740	1791	1843	1897	1953	2010	2069	2130	2192	2256	2322	2391	2461	2533	
	7.1	1458	1500	1543	1588	1633	1681	1729	1779	1830	1883	1938	1994	2051	2110	2171	2234	2299	2365	2433	2504	2576	
	7.2	1495	1538	1581	1626	1673	1720	1769	1819	1871	1924	1979	2035	2093	2153	2214	2277	2342	2408	2477	2547	2620	
	7.3	1534	1577	1621	1666	1713	1761	1810	1861	1913	1966	2021	2078	2136	2196	2258	2321	2386	2453	2521	2592	2665	
	7.4	1573	1616	1661	1707	1754	1802	1852	1903	1955	2009	2065	2122	2180	2240	2302	2365	2431	2498	2566	2637	2710	
	7.5	1614	1657	1702	1749	1796	1845	1895	1946	1999	2053	2109	2166	2225	2285	2347	2411	2476	2543	2612	2683	2756	
	7.6	1655	1699	1745	1791	1839	1888	1939	1990	2043	2098	2154	2211	2270	2331	2393	2457	2523	2590	2659	2730	2803	
	7.7	1698	1742	1788	1835	1883	1933	1983	2035	2089	2144	2200	2258	2317	2378	2440	2504	2570	2638	2707	2778	2851	
	7.8	1741	1786	1833	1880	1928	1978	2029	2082	2135	2191	2247	2305	2365	2426	2488	2553	2618	2686	2755	2827	2899	
	7.9	1786	1832	1878	1926	1975	2025	2076	2129	2183	2238	2295	2353	2413	2474	2537	2602	2668	2735	2805	2876	2949	
	8.0	1832	1878	1925	1973	2022	2073	2124	2177	2232	2287	2344	2403	2463	2524	2587	2652	2718	2785	2855	2926	2999	
	8.1	1879	1926	1973	2021	2071	2121	2173	2227	2281	2337	2394	2453	2513	2575	2638	2702	2769	2837	2906	2977	3050	
	8.2	1928	1974	2022	2070	2120	2171	2224	2277	2332	2388	2446	2504	2565	2626	2690	2754	2821	2889	2958	3029	3102	
	8.3	1978	2024	2072	2121	2171	2223	2275	2329	2384	2440	2498	2557	2617	2679	2743	2807	2874	2942	3011	3082	3155	

Continued



**Table B-5** Estimates of Fetal Weight (g) Based on Abdominal Circumference and Femur Length—Continued

		Abdominal Circumference (cm)																			
		30.5	31.0	31.5	32.0	32.5	33.0	33.5	34.0	34.5	35.0	35.5	36.0	36.5	37.0	37.5	38.0	38.5	39.0	39.5	40.0
Femur Length (cm)	4.0	1590	1658	1729	1802	1879	1959	2042	2129	2220	2314	2413	2515	2622	2734	2850	2972	3098	3230	3367	3511
	4.1	1617	1685	1756	1830	1907	1987	2071	2158	2249	2344	2442	2545	2652	2764	2880	3002	3128	3260	3397	3540
	4.2	1644	1712	1783	1858	1935	2016	2100	2187	2279	2373	2472	2575	2683	2794	2911	3032	3159	3290	3427	3570
	4.3	1671	1740	1812	1886	1964	2045	2129	2217	2308	2404	2503	2606	2713	2825	2942	3063	3189	3321	3458	3600
	4.4	1699	1768	1840	1915	1993	2075	2159	2247	2339	2434	2533	2637	2744	2856	2973	3094	3220	3352	3488	3630
	4.5	1727	1797	1869	1944	2023	2105	2189	2278	2370	2465	2565	2668	2776	2888	3004	3125	3251	3383	3519	3661
	4.6	1756	1826	1898	1974	2053	2135	2220	2309	2401	2497	2596	2700	2807	2919	3036	3157	3283	3414	3550	3692
	4.7	1785	1855	1928	2004	2084	2166	2251	2340	2432	2528	2628	2732	2840	2952	3068	3189	3315	3446	3582	3723
	4.8	1814	1885	1959	2035	2115	2197	2283	2372	2464	2560	2660	2764	2872	2984	3100	3221	3347	3478	3613	3754
	4.9	1845	1916	1990	2066	2146	2229	2315	2404	2497	2593	2693	2797	2905	3017	3133	3254	3380	3510	3645	3786
	5.0	1875	1947	2021	2098	2178	2261	2347	2437	2530	2626	2726	2830	2938	3050	3166	3287	3412	3542	3677	3818
	5.1	1906	1978	2053	2130	2210	2294	2380	2470	2563	2659	2760	2864	2972	3084	3200	3320	3445	3575	3710	3850
	5.2	1938	2010	2085	2163	2243	2327	2413	2503	2597	2693	2794	2898	3006	3117	3234	3354	3479	3608	3743	3882
	5.3	1970	2043	2118	2196	2277	2360	2447	2537	2631	2728	2828	2932	3040	3152	3268	3388	3513	3642	3776	3915
	5.4	2003	2076	2151	2229	2311	2395	2482	2572	2665	2762	2863	2967	3075	3186	3302	3422	3547	3676	3809	3948
	5.5	2036	2109	2185	2264	2345	2429	2516	2607	2700	2797	2898	3002	3110	3221	3337	3457	3581	3710	3843	3981
	5.6	2070	2143	2220	2298	2380	2464	2552	2642	2736	2833	2933	3038	3145	3257	3372	3492	3616	3744	3877	4015
	5.7	2104	2178	2254	2333	2415	2500	2587	2678	2772	2869	2970	3074	3181	3293	3408	3527	3651	3779	3911	4048
	5.8	2139	2213	2290	2369	2451	2536	2624	2714	2808	2905	3006	3110	3218	3329	3444	3563	3686	3814	3946	4082
	5.9	2175	2249	2326	2405	2488	2573	2660	2751	2845	2942	3043	3147	3254	3366	3480	3599	3722	3849	3981	4117
	6.0	2211	2286	2363	2442	2525	2610	2698	2789	2883	2980	3080	3184	3292	3403	3517	3636	3758	3885	4016	4151
	6.1	2248	2323	2400	2480	2562	2647	2736	2827	2921	3018	3118	3222	3329	3440	3554	3673	3795	3921	4052	4186
	6.2	2285	2360	2438	2518	2600	2686	2774	2865	2959	3056	3157	3260	3367	3478	3592	3710	3832	3957	4087	4222
	6.3	2323	2398	2476	2556	2639	2725	2813	2904	2998	3095	3195	3299	3406	3516	3630	3747	3869	3994	4124	4257
	6.4	2362	2437	2515	2595	2678	2764	2852	2943	3037	3134	3235	3338	3445	3555	3668	3785	3906	4031	4160	4293
	6.5	2401	2477	2555	2635	2718	2804	2892	2983	3077	3174	3274	3378	3484	3594	3707	3824	3944	4069	4197	4329
	6.6	2441	2517	2595	2675	2759	2844	2933	3024	3118	3215	3315	3418	3524	3633	3746	3863	3983	4106	4234	4366
	6.7	2481	2557	2636	2716	2800	2885	2974	3065	3159	3256	3355	3458	3564	3673	3786	3902	4021	4144	4271	4402
	6.8	2523	2599	2677	2758	2841	2927	3016	3107	3200	3297	3397	3499	3605	3714	3826	3941	4060	4183	4309	4439
	6.9	2564	2641	2719	2800	2884	2969	3058	3149	3242	3339	3438	3541	3646	3754	3866	3981	4100	4222	4347	4477
	7.0	2607	2683	2762	2843	2927	3012	3101	3192	3285	3381	3481	3583	3688	3796	3907	4022	4140	4261	4386	4514
	7.1	2650	2727	2806	2887	2970	3056	3144	3235	3328	3424	3523	3625	3730	3838	3948	4062	4180	4300	4425	4552
	7.2	2694	2771	2850	2931	3014	3100	3188	3279	3372	3468	3567	3668	3772	3880	3990	4104	4220	4340	4464	4591
	7.3	2739	2816	2895	2976	3059	3145	3233	3323	3416	3512	3610	3712	3816	3922	4032	4145	4261	4381	4503	4629
	7.4	2785	2861	2940	3021	3105	3190	3278	3369	3461	3557	3655	3756	3859	3966	4075	4187	4303	4421	4543	4668
	7.5	2831	2908	2987	3068	3151	3236	3324	3414	3507	3602	3700	3800	3903	4009	4118	4230	4344	4462	4583	4708
	7.6	2878	2955	3034	3115	3198	3283	3371	3461	3553	3648	3745	3845	3948	4053	4161	4272	4387	4504	4624	4747
	7.7	2926	3003	3081	3162	3245	3331	3418	3508	3600	3694	3791	3891	3993	4098	4205	4316	4429	4545	4665	4787
	7.8	2974	3051	3130	3211	3294	3379	3466	3555	3647	3741	3838	3937	4039	4143	4250	4360	4472	4588	4706	4827
	7.9	3024	3100	3179	3260	3343	3427	3514	3604	3695	3789	3885	3984	4085	4188	4295	4404	4515	4630	4748	4868
	8.0	3074	3151	3229	3310	3392	3477	3564	3653	3744	3837	3933	4031	4131	4234	4340	4448	4559	4673	4790	4909
	8.1	3125	3202	3280	3360	3443	3527	3614	3702	3793	3886	3981	4079	4179	4281	4386	4493	4604	4716	4832	4950
	8.2	3177	3253	3332	3412	3494	3578	3664	3752	3843	3935	4030	4127	4226	4328	4432	4539	4648	4760	4875	4992
	8.3	3230	3306	3384	3464	3546	3630	3716	3803	3893	3985	4080	4176	4275	4376	4479	4585	4693	4804	4918	5034

From Hadlock FP, Harrist RB, Carpenter RJ, et al: Sonographic estimation of fetal weight. Radiology 150:535, 1984.

**Table B-6** Normal Body Ratio Data (14 to 21 Wk)

Menstrual Week	Cephalic Index (SD = 3.7)*	Femur/BPD $\times$ 100 (SD = 4.0) <sup>†</sup>	Femur/HC $\times$ 100 (SD = 1.0) <sup>†</sup>	Femur/AC $\times$ 100 (SD = 1.3) <sup>‡</sup>
14	81.5	58.0	15.0	19.0
15	81.0	59.0	15.7	19.3
16	80.5	61.0	16.4	19.8
17	80.1	63.0	16.9	20.3
18	79.7	65.0	17.5	20.8
19	79.4	67.0	18.1	21.0
20	79.1	69.0	18.4	21.3
21	78.8	70.0	18.6	21.5

AC, abdominal circumference; BPD, biparietal diameter; HC, head circumference; SD, standard deviation.

\*Data from Gray DL, Songster GS, Parvin CA, et al: Cephalic index: A gestational age-dependent biometric parameter. *Obstet Gynecol* 74:600, 1989.

<sup>†</sup>Data from Hadlock FP, Harrist RB, Martinez-Poyer J: Fetal body ratios in second trimester: A useful tool for identifying chromosomal abnormalities? *J Ultrasound Med* 11:81, 1992.

**Table B-7** Normal Fetal Body Ratios (22 to 40 Wk)

Menstrual Week	Cephalic Index (SD = 4.4)*	Femur/BPD $\times$ 100 (SD = 5.0) <sup>†</sup>	Femur/HC $\times$ 100 (SD = 1.1) <sup>‡</sup>	Femur/AC $\times$ 100 (SD = 1.3) <sup>§</sup>
22	78.3	77.4	18.6	21.6
23	78.3	77.6	18.8	21.7
24	78.3	77.8	19.0	21.7
25	78.3	78.0	19.2	21.8
26	78.3	78.2	19.4	21.8
27	78.3	78.4	19.6	21.9
28	78.3	78.6	19.8	21.9
29	78.3	78.8	20.0	21.9
30	78.3	79.0	20.3	22.0
31	78.3	79.2	20.5	22.0
32	78.3	79.4	20.7	22.1
33	78.3	79.6	20.9	22.1
34	78.3	79.8	21.1	22.2
35	78.3	80.0	21.4	22.2
36	78.3	80.2	21.6	22.2
37	78.3	80.4	21.8	22.3
38	78.3	80.6	22.0	22.3
39	78.3	80.8	22.2	22.3
40	78.3	81.0	22.4	22.4

AC, abdominal circumference; BPD, biparietal diameter; HC, head circumference; SD, standard deviation.

\*Data from Hadlock FP, Deter RL, Carpenter RJ, et al: The effect of head shape on the accuracy of BPD in estimating fetal gestational age. *AJR* 137:83, 1981.

<sup>†</sup>Data from Hohler CW, Quetel TA: The relationship between fetal femur length and biparietal diameter in the last half of pregnancy. *Am J Obstet Gynecol* 141:759, 1981.

<sup>‡</sup>Data from Hadlock FP, Harrist RB, Shah YP, et al: The use of femur length/head circumference relation in obstetrical sonography. *J Ultrasound Med* 3:439, 1984.

<sup>§</sup>Data from Hadlock FP, Deter RL, Harrist RB, et al: A date-independent predictor of intrauterine growth retardation: Femur length/abdominal circumference ratio. *AJR* 141:979, 1983.



**Table B-8** Comparison of Fetal Parameters in LGA and AGA Fetuses

Parameter	AGA Group (mean $\pm$ SD)	LGA Group (mean $\pm$ SD)	p Value
BPD (cm)	9.2 $\pm$ 0.4	9.6 $\pm$ 0.4	<.0001
HC (cm)	33.7 $\pm$ 1.1	35.2 $\pm$ 1.3	<.0001
AC (cm)	33.6 $\pm$ 1.6	37.4 $\pm$ 1.3	<.0001
FL (cm)	7.4 $\pm$ 0.4	7.6 $\pm$ 0.3	<.0001
HC/AC	1.0 $\pm$ 0.05	0.94 $\pm$ 0.04	<.0001
FL/AC*	22.0 $\pm$ 1.0	20.5 $\pm$ 1.0	<.0001

AC, abdominal circumference; AGA, appropriate for gestational age; BPD, biparietal diameter; FL, femur length; HC, head circumference; LGA, large for gestational age.

\*FL/AC expressed as FL/AC  $\times$  100.

From Hadlock FP, Harrist RB, Fearnleyhough TC, et al: Use of femur length/abdominal circumference ratio in detecting the macrosomic fetus. Radiology 154:503, 1985.

**Table B-9** Conventional Sonographic Criteria for IUGR: Performance Characteristics

Criterion	Predictive Values (%) <sup>*†</sup>			
	Sensitivity (%) <sup>*</sup>	Specificity (%) <sup>*</sup>	Positive	Negative
Advanced placental grade	62	64	16	94
Elevated FL/AC	34–49	78–83	18–20	92–93
Low TIUV	57–80	72–76	21–24	92–97
Small BPD	24–88	62–94	21–44	92–98
Small BPD and advanced placental grade	59	86	32	95
Slow rate of BPD growth	75	84	35	97
Low EFW	89	88	45	99
Decreased AFV	24	98	55	92
Elevated HC/AC	82	94	62	98

AFV, amniotic fluid volume; BPD, biparietal diameter; EFW, estimated fetal weight; FL/AC, femur length/abdominal circumference ratio; HC/AC, head circumference/abdominal circumference ratio; IUGR, intrauterine growth restriction; TIUV, total intrauterine volume.

<sup>\*</sup>A range of values is given for a criterion when difference studies apply that criterion in two or more ways.

<sup>†</sup>Computed using Bayes' theorem and assuming an IUGR prevalence rate of 10%.

From Benson CB, Doubilet PM, Saltzman DH: Intrauterine growth retardation: Predictive value of US criteria for antenatal diagnosis. Radiology 160:415, 1986.

# APPENDIX C

## Measurements for Amniotic Fluid Assessment

**Table C-1**

**Amniotic Fluid Index Values in Normal Pregnancy**

Week	Amniotic Fluid Index Percentile Values (mm)				
	3rd	5th	50th	95th	97th
16	73	79	121	185	201
17	77	83	127	194	211
18	80	87	133	202	220
19	83	90	137	207	225
20	86	93	141	212	230
21	88	95	143	214	233
22	89	97	145	216	235
23	90	98	146	218	237
24	90	98	147	219	238
25	89	97	147	221	240
26	89	97	147	223	242
27	85	95	146	226	245
28	86	94	146	228	249
29	84	92	145	231	254
30	82	90	145	234	258
31	79	88	144	238	263
32	77	86	144	242	269
33	74	83	143	245	274
34	72	81	142	248	278
35	70	79	140	249	279
36	68	77	138	249	279
37	66	75	135	244	275
38	65	73	132	239	269
39	64	72	127	226	255
40	63	71	123	214	240
41	63	70	116	194	216
42	63	69	110	175	192

Adapted from Moore TR, Cayle JE: The amniotic fluid index in normal human pregnancy. *Am J Obstet Gynecol* 162:1168, 1990.



**Table C-2** Amniotic Fluid Index Values During Normal Pregnancy, From the 5th Through to the 95th Percentile

Menstrual Age (wk)	Amniotic Fluid Index (cm)						
	No.	5th Percentile	10th Percentile	50th Percentile	Mean	90th Percentile	95th Percentile
14	50	2.8	3.1	5.0	5.4	8.0	8.6
15	50	3.2	3.6	5.4	5.7	8.2	9.1
16	50	3.6	4.1	5.8	6.1	8.5	9.6
17	50	4.1	4.0	6.3	6.6	9.0	10.3
18	50	4.6	5.1	6.8	7.1	9.7	11.1
19	50	5.1	5.6	7.4	7.7	10.4	12.0
20	50	5.5	6.1	8.0	8.3	11.3	12.9
21	50	5.9	6.6	8.7	8.9	12.2	13.9
22	50	6.3	7.1	9.3	9.6	13.2	14.9
23	50	6.7	7.5	10.0	10.3	14.2	15.9
24	50	7.0	7.9	10.7	11.0	15.2	16.9
25	50	7.3	8.2	11.4	11.7	16.1	17.8
26	50	7.5	8.4	12.0	12.3	17.0	18.7
27	50	7.6	8.6	12.6	12.8	17.8	19.4
28	50	7.6	8.6	13.0	13.3	18.4	19.9
29	50	7.6	8.6	13.4	13.6	18.8	20.4
30	50	7.5	8.5	13.6	13.8	18.9	20.6
31	50	7.3	8.4	13.6	13.8	18.9	20.6
32	50	7.1	8.1	13.6	13.7	18.7	20.4
33	50	6.8	7.8	13.3	13.4	18.2	20.0
34	50	6.4	7.4	13.9	13.0	17.7	19.4
35	50	6.0	7.0	12.4	12.5	16.9	18.7
36	50	5.6	6.5	11.8	11.8	16.2	17.9
37	50	5.1	6.0	11.1	11.1	15.3	16.9
38	50	4.7	5.5	10.3	10.3	14.4	15.9
39	50	4.2	5.0	9.4	9.4	13.7	14.9
40	50	3.7	4.5	8.6	8.6	12.9	13.9
41	50	3.3	4.0	7.8	7.7	12.3	12.9

From Magann EF, Sanderson M, Martin JN Jr, et al: The amniotic fluid index, single deepest pocket and two diameter pocket in normal pregnancy. Am J Obstet Gynecol 182:1581, 2000.

**Table C-3****Single Deepest Pocket Values of Amniotic Fluid During Normal Pregnancy, From the 5th Through to the 95th Percentile**

Menstrual Age (wk)	Single Deepest Pocket (cm)						
	No.	5th Percentile	10th Percentile	50th Percentile	Mean	90th Percentile	95th Percentile
14	50	1.7	1.9	2.9	3.1	4.7	5.0
15	50	2.0	2.2	3.4	3.5	5.1	5.5
16	50	2.3	2.5	3.6	3.8	5.4	5.9
17	50	2.5	2.7	3.9	4.0	5.7	6.2
18	50	2.7	2.9	4.1	4.2	5.9	6.4
19	50	2.8	3.1	4.3	4.4	6.1	6.6
20	50	2.9	3.2	4.4	4.5	6.2	6.7
21	50	2.9	3.3	4.5	4.6	6.3	6.8
22	50	3.0	3.3	4.6	4.7	6.3	6.8
23	50	3.0	3.4	4.6	4.7	6.3	6.8
24	50	3.1	3.4	4.7	4.8	6.3	6.8
25	50	3.0	3.3	4.7	4.8	6.3	6.8
26	50	3.0	3.3	4.8	4.8	6.4	6.8
27	50	3.0	3.3	4.8	4.8	6.4	6.9
28	50	3.0	3.3	4.8	4.8	6.4	6.9
29	50	2.9	3.3	4.8	4.8	6.4	6.9
30	50	2.9	3.3	4.8	4.8	6.4	6.9
31	50	2.9	3.2	4.8	4.9	6.5	7.0
32	50	2.9	3.2	4.8	4.9	6.6	7.1
33	50	2.9	3.2	4.82	4.9	6.6	7.2
34	50	2.8	3.2	4.8	4.8	6.6	7.2
35	50	2.8	3.1	4.7	4.8	6.6	7.2
36	50	2.7	3.1	4.7	4.7	6.6	7.1
37	50	2.6	2.9	4.5	4.6	6.5	7.0
38	50	2.4	2.8	4.4	4.5	6.3	6.8
39	50	2.3	2.7	4.2	4.3	6.1	6.6
40	50	2.1	2.5	3.9	4.0	5.8	6.2
41	50	1.9	2.2	3.7	3.7	5.4	5.7

From Magann EF, Sanderson M, Martin JN Jr, et al: The amniotic fluid index, single deepest pocket and two diameter pocket in normal pregnancy. *Am J Obstet Gynecol* 182:1581, 2000.



## Fetal Doppler Assessment (Noncardiac)

**Table D-1 Resistance Index of the Uterine Artery**

Gestation (wk)	5th Percentile	50th Percentile	95th Percentile
18	0.222	0.447	0.659
19	0.204	0.429	0.641
20	0.194	0.419	0.630
21	0.186	0.411	0.622
22	0.180	0.405	0.615
23	0.175	0.400	0.610
24	0.171	0.395	0.605
25	0.167	0.391	0.601
26	0.163	0.387	0.597
27	0.160	0.384	0.593
28	0.157	0.380	0.590
29	0.154	0.378	0.587
30	0.152	0.375	0.584
31	0.150	0.372	0.581
32	0.147	0.370	0.578
33	0.145	0.368	0.576
34	0.144	0.366	0.574
35	0.142	0.364	0.571
36	0.140	0.362	0.569
37	0.139	0.360	0.567
38	0.137	0.358	0.566
39	0.136	0.357	0.564
40	0.135	0.355	0.562

From Merz E (ed): *Ultrasonography in Obstetrics and Gynecology*. Stuttgart, New York, Thieme, pp 469–480, 613, 614.

**Table D-3 Resistance Index of the Umbilical Artery Between 20 and 40 Weeks of Gestation**

Gestation (wk)	5th Percentile	50th Percentile	95th Percentile
20	0.567	0.690	0.802
21	0.557	0.680	0.793
22	0.548	0.671	0.784
23	0.539	0.663	0.776
24	0.530	0.655	0.768
25	0.522	0.646	0.760
26	0.514	0.639	0.752
27	0.506	0.631	0.745
28	0.498	0.623	0.737
29	0.490	0.615	0.730
30	0.482	0.608	0.723
31	0.474	0.600	0.715
32	0.465	0.592	0.707
33	0.457	0.584	0.700
34	0.449	0.576	0.692
35	0.440	0.567	0.684
36	0.431	0.559	0.675
37	0.422	0.550	0.667
38	0.412	0.540	0.657
39	0.402	0.530	0.648
40	0.390	0.519	0.637

From Merz E (ed): *Ultrasonography in Obstetrics and Gynecology*. Stuttgart, New York, Thieme, pp 469–480, 613, 614.

**Table D-2 Pulsatility Index of the Uterine Artery**

Gestation (wk)	5th Percentile	50th Percentile	95th Percentile
18	0.509	0.888	1.407
19	0.460	0.838	1.356
20	0.436	0.812	1.328
21	0.420	0.795	1.309
22	0.407	0.781	1.293
23	0.397	0.769	1.280
24	0.388	0.759	1.268
25	0.381	0.751	1.258
26	0.374	0.743	1.248
27	0.369	0.736	1.239
28	0.363	0.729	1.230
29	0.358	0.722	1.222
30	0.354	0.716	1.214
31	0.349	0.711	1.207
32	0.345	0.705	1.199
33	0.341	0.700	1.192
34	0.337	0.695	1.185
35	0.333	0.690	1.178
36	0.330	0.684	1.171
37	0.326	0.679	1.164
38	0.322	0.674	1.157
39	0.318	0.669	1.150
40	0.313	0.663	1.143

From Merz E (ed): *Ultrasonography in Obstetrics and Gynecology*. Stuttgart, New York, Thieme, pp 469–480, 613, 614.

**Table D-4 Pulsatility Index of the Umbilical Artery Between 20 and 40 Weeks of Gestation**

Gestation (wk)	5th Percentile	50th Percentile	95th Percentile
20	0.940	1.216	1.505
21	0.913	1.189	1.476
22	0.890	1.165	1.450
23	0.869	1.142	1.427
24	0.849	1.122	1.405
25	0.831	1.102	1.385
26	0.813	1.084	1.365
27	0.798	1.065	1.346
28	0.780	1.048	1.327
29	0.764	1.031	1.308
30	0.748	1.014	1.290
31	0.732	0.997	1.272
32	0.716	0.980	1.254
33	0.700	0.963	1.236
34	0.684	0.946	1.218
35	0.668	0.928	1.199
36	0.651	0.910	1.180
37	0.634	0.891	1.160
38	0.615	0.872	1.139
39	0.595	0.851	1.117
40	0.573	0.828	1.093

From Merz E (ed): *Ultrasonography in Obstetrics and Gynecology*. Stuttgart, New York, Thieme, pp 469–480, 613, 614.

**Table D-5****Reference Values for the Resistance Index of Umbilical and Middle Cerebral Arteries, as well as the UA/MCA Ratio**

Gestation (wk)	Umbilical Artery Resistance Index (UA RI)			Middle Cerebral Artery Resistance Index (MCA RI)			UA RI/MCA RI		
	5th Percentile	50th Percentile	95th Percentile	5th Percentile	50th Percentile	95th Percentile	5th Percentile	50th Percentile	95th Percentile
24	0.615	0.717	0.828	0.778	0.867	—	0.696	0.809	0.968
25	0.605	0.707	0.819	0.789	0.881	—	0.676	0.791	0.955
26	0.594	0.697	0.810	0.795	0.892	—	0.658	0.775	0.945
27	0.583	0.687	0.802	0.798	0.898	—	0.642	0.761	0.937
28	0.572	0.678	0.793	0.797	0.901	—	0.628	0.750	0.932
29	0.562	0.668	0.785	0.793	0.900	—	0.616	0.740	0.929
30	0.551	0.658	0.776	0.786	0.897	—	0.606	0.732	0.928
31	0.540	0.648	0.767	0.776	0.891	—	0.597	0.726	0.929
32	0.530	0.638	0.759	0.764	0.883	—	0.590	0.722	0.931
33	0.519	0.629	0.750	0.750	0.872	—	0.585	0.719	0.936
34	0.508	0.619	0.742	0.734	0.860	—	0.581	0.717	0.941
35	0.498	0.609	0.733	0.717	0.846	—	0.578	0.717	0.949
36	0.487	0.599	0.724	0.698	0.831	—	0.576	0.718	0.957
37	0.476	0.589	0.716	0.677	0.814	—	0.575	0.720	0.967
38	0.465	0.580	0.707	0.655	0.795	—	0.576	0.724	0.978
39	0.455	0.570	0.699	0.632	0.776	—	0.577	0.728	0.991
40	0.444	0.560	0.690	0.607	0.755	—	0.580	0.734	1.004
41	0.433	0.550	0.681	0.582	0.734	—	0.583	0.740	1.018
42	0.423	0.540	0.673	0.556	0.711	—	0.588	0.747	1.034

From Kurmanavicius J, Florio I, Wisser J, et al: Reference resistance indices of the umbilical, fetal middle cerebral and uterine arteries at 24–42 weeks of gestation. *Ultrasound Obstet Gynecol* 10:112, 1997.

**Table D-6****Umbilical Vein Mean Velocity (cm/sec)**

Gestation (wk)	Mean Velocity (cm/sec)			Weeks Gestation	Mean Velocity (cm/sec)		
	5th Percentile	50th Percentile	95th Percentile		5th Percentile	50th Percentile	95th Percentile
20	5.70	7.90	10.70	31	7.04	9.67	13.02
21	5.82	8.06	10.91	32	7.17	9.83	13.23
22	5.94	8.22	11.12	33	7.29	9.99	13.44
23	6.07	8.38	11.33	34	7.41	10.16	13.66
24	6.19	8.54	11.54	35	7.53	10.32	13.87
25	6.31	8.71	11.76	36	7.65	10.48	14.08
26	6.43	8.87	11.97	37	7.78	10.64	14.29
27	6.56	9.03	12.18	38	7.90	10.80	14.50
28	6.68	9.19	12.39	39	8.02	10.96	14.71
29	6.80	9.35	12.60	40	8.14	11.12	14.92
30	6.92	9.51	12.81				

From Barbera A, Galan HL, Ferrazzi E, et al: Relationship of umbilical vein blood flow to growth parameters in the human fetus. *Am J Obstet Gynecol* 181:174, 1999.



**Table D-7** Ductus Venosus Preload Index (a/S)

Pre-Load Index (a/S)			
Gestation (wk)	5th Percentile	50th Percentile	95th Percentile
20	0.342	0.508	0.674
21	0.341	0.507	0.673
22	0.341	0.507	0.673
23	0.340	0.506	0.672
24	0.339	0.505	0.671
25	0.339	0.505	0.671
26	0.338	0.504	0.670
27	0.338	0.504	0.670
28	0.337	0.503	0.669
29	0.336	0.502	0.668
30	0.336	0.502	0.668
31	0.335	0.501	0.667
32	0.335	0.501	0.667
33	0.334	0.500	0.666
34	0.333	0.499	0.665
35	0.333	0.499	0.665
36	0.332	0.498	0.664
37	0.332	0.498	0.664
38	0.331	0.497	0.663
39	0.330	0.496	0.662
40	0.330	0.496	0.662

From Baschat AA: Relationship between placental blood flow resistance and precordial venous Doppler indices. *Ultrasound Obstet Gynecol* 22:561, 2003.

**Table D-9** Ductus Venosus Pulsatility Index (S-a)/Tamx

Pulsatility Index (S-a)/Tamx			
Gestation (wk)	5th Percentile	50th Percentile	95th Percentile
20	0.410	0.643	0.875
21	0.409	0.642	0.874
22	0.408	0.641	0.873
23	0.407	0.640	0.872
24	0.406	0.639	0.871
25	0.405	0.638	0.870
26	0.404	0.637	0.869
27	0.403	0.636	0.868
28	0.402	0.635	0.867
29	0.401	0.634	0.866
30	0.400	0.633	0.865
31	0.399	0.632	0.864
32	0.398	0.631	0.863
33	0.397	0.630	0.862
34	0.396	0.629	0.861
35	0.395	0.628	0.860
36	0.394	0.627	0.859
37	0.393	0.626	0.858
38	0.392	0.625	0.857
39	0.391	0.624	0.856
40	0.390	0.623	0.855

From Baschat AA: Relationship between placental blood flow resistance and precordial venous Doppler indices. *Ultrasound Obstet Gynecol* 22:561, 2003.

**Table D-8** Ductus Venosus Peak Velocity Index (S-a)/D

Peak Velocity Index (S-a)/D			
Gestation (wk)	5th Percentile	50th Percentile	95th Percentile
20	0.381	0.580	0.779
21	0.380	0.579	0.779
22	0.380	0.579	0.778
23	0.379	0.578	0.777
24	0.378	0.578	0.777
25	0.378	0.577	0.776
26	0.377	0.576	0.776
27	0.377	0.576	0.775
28	0.376	0.575	0.774
29	0.375	0.575	0.774
30	0.375	0.574	0.773
31	0.374	0.573	0.773
32	0.374	0.573	0.772
33	0.373	0.572	0.771
34	0.372	0.572	0.771
35	0.372	0.571	0.770
36	0.371	0.570	0.770
37	0.371	0.570	0.769
38	0.370	0.569	0.768
39	0.369	0.569	0.768
40	0.369	0.568	0.767

From Baschat AA: Relationship between placental blood flow resistance and precordial venous Doppler indices. *Ultrasound Obstet Gynecol* 22:561, 2003.

**Table D-10** Ductus Venosus S/a

S/a			
Gestation (wk)	5th Percentile	50th Percentile	95th Percentile
20	1.331	2.161	2.991
21	1.329	2.159	2.989
22	1.327	2.157	2.987
23	1.324	2.154	2.984
24	1.322	2.152	2.982
25	1.320	2.150	2.980
26	1.318	2.148	2.978
27	1.315	2.145	2.975
28	1.313	2.143	2.973
29	1.311	2.141	2.971
30	1.308	2.138	2.968
31	1.306	2.136	2.966
32	1.304	2.134	2.964
33	1.301	2.131	2.961
34	1.299	2.129	2.959
35	1.297	2.127	2.957
36	1.295	2.125	2.955
37	1.292	2.122	2.952
38	1.290	2.120	2.950
39	1.288	2.118	2.948
40	1.285	2.115	2.945

From Baschat AA: Relationship between placental blood flow resistance and precordial venous Doppler indices. *Ultrasound Obstet Gynecol* 22:561, 2003.

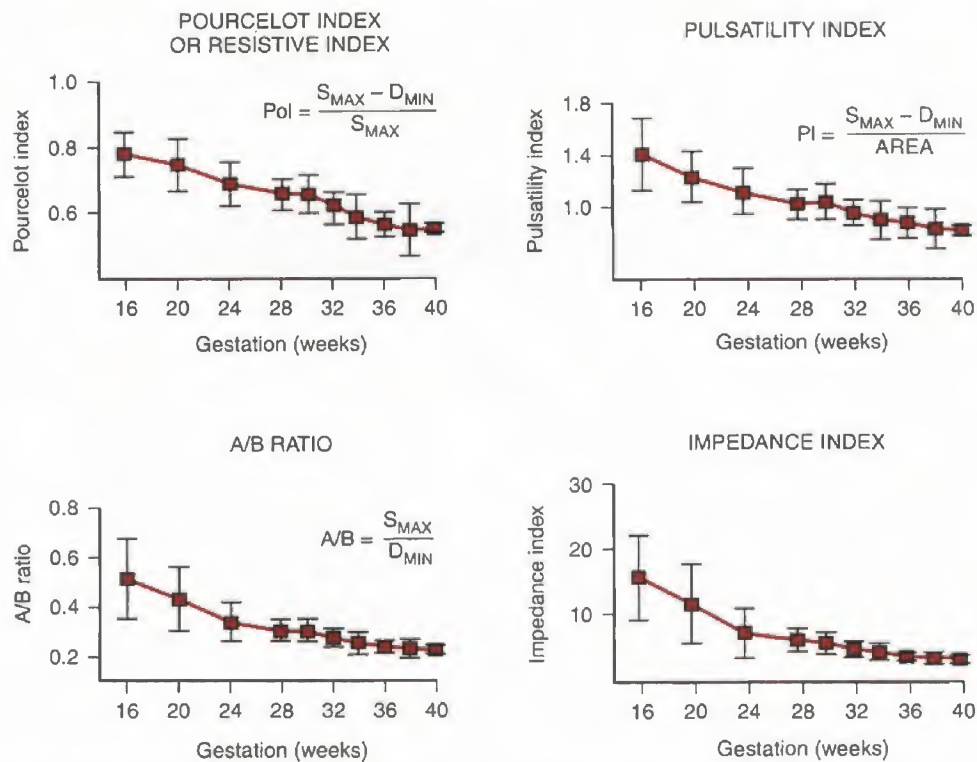


**FIGURE D-1.** Doppler waveform analysis of the fetal umbilical artery. With advancing gestation and increasing compliance of the placenta, there is a progressive decrease in the systolic/diastolic ratio, Pourcelot index (Pol), and pulsatility index (PI) of the umbilical artery that is a result of increased placental flow owing to decreased resistance. (Modified from Erskine RLA, Ritchie JWK: Umbilical artery blood flow characteristics in normal and growth retarded fetuses. *Br J Obstet Gynecol* 92:605, 1985.)

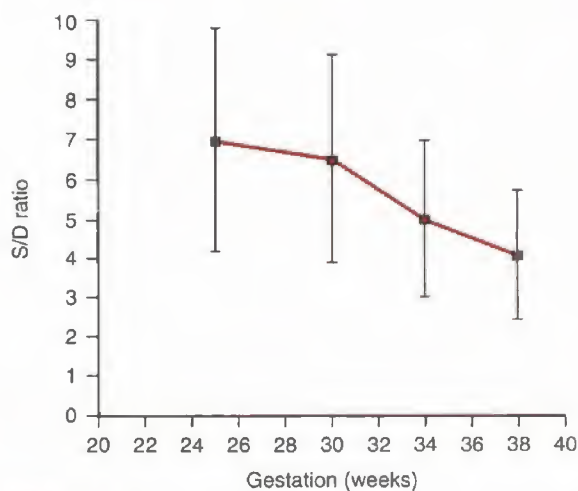


**FIGURE D-2.** Middle cerebral artery Doppler systolic/diastolic ratios. (Modified from Woo JSK, Liang ST, Lo RL, Chan FY: Middle cerebral artery Doppler flow velocity waveforms. *Obstet Gynecol* 70:613, 1987. Reprinted with permission from the American College of Obstetricians and Gynecologists.)



## Doppler of the Middle Cerebral Artery to Assess Fetal Anemia

**Table E-1**

**Threshold of Peak Velocity of Systolic Blood Flow in the Middle Cerebral Artery Above Which Mild, Moderate, and Severe Anemia Occurs**

Threshold of the Peak Velocity of the Middle Cerebral Artery (cm/sec) Above Which Degree of Anemia is Classified				
Gestation (wk)	1.00 (Median)	Mild Anemia (1.29 MoM)	Moderate Anemia (1.50 MoM)	Severe Anemia (1.55 MoM)
18	23.2	29.9	34.8	36.0
20	25.5	32.8	38.2	39.5
22	27.9	36.0	41.9	43.3
24	30.7	39.5	46.0	47.5
26	33.6	43.3	50.4	52.1
28	36.9	47.6	55.4	57.2
30	40.5	52.2	60.7	62.8
32	44.4	57.3	66.6	68.9
34	48.7	62.9	73.1	75.6
36	53.5	69.0	80.2	82.9
38	58.7	75.7	88.0	91.0
40	64.4	83.0	96.6	99.8

MoM, multiple of median.

From Mari G, Deter RL, Carpenter RL, et al: Non-invasive diagnosis by Doppler ultrasonography of fetal anemia due to maternal red-cell alloimmunization. Collaborative Group for Doppler Assessment of the Blood Velocity in Anemic Fetuses. *N Engl J Med* 342:9, 2000.

# APPENDIX F

## Fetal Cardiac Measurements and Doppler Assessment

**Table F-1** Mitral and Tricuspid Valve E/A Ratios

Gestation (wk)	Mitral Valve E/A Ratio			Tricuspid Valve E/A Ratio		
	2.5th Percentile	50th Percentile	97.5th Percentile	2.5th Percentile	50th Percentile	97.5th Percentile
20	0.40	0.59	0.77	0.47	0.65	0.83
21	0.42	0.60	0.79	0.49	0.66	0.84
22	0.43	0.62	0.80	0.50	0.68	0.85
23	0.45	0.63	0.82	0.52	0.69	0.86
24	0.46	0.65	0.83	0.53	0.70	0.87
25	0.48	0.66	0.84	0.54	0.71	0.88
26	0.49	0.68	0.86	0.55	0.72	0.89
27	0.50	0.69	0.87	0.56	0.73	0.90
28	0.52	0.70	0.88	0.57	0.74	0.90
29	0.53	0.71	0.89	0.58	0.74	0.91
30	0.54	0.73	0.90	0.58	0.75	0.91
31	0.55	0.74	0.91	0.59	0.75	0.92
32	0.56	0.75	0.92	0.59	0.76	0.92
33	0.57	0.76	0.93	0.60	0.76	0.92
34	0.58	0.76	0.93	0.60	0.76	0.92
35	0.59	0.77	0.94	0.60	0.76	0.92
36	0.59	0.78	0.95	0.60	0.76	0.92
37	0.60	0.79	0.95	0.60	0.76	0.92
38	0.61	0.79	0.96	0.60	0.76	0.92

From DeVore GR: Pulsed Doppler examination of the fetal heart. In Goldberg BB, McGahan JP (eds): Atlas of Ultrasound Measurements, 2nd ed. Philadelphia, Mosby Inc/Elsevier, 2006.

**Table F-2** Peak or Maximum Velocity of the Aorta and Main Pulmonary Artery

Gestation (wk)	Aorta Peak Velocity (cm/sec)			Pulmonary Artery Peak Velocity (cm/sec)		
	2.5th Percentile	50th Percentile	97.5th Percentile	2.5th Percentile	50th Percentile	97.5th Percentile
20	29	62	95	23	53	80
21	30	63	96	24	54	81
22	32	65	98	25	56	82
23	33	66	99	27	57	84
24	34	67	100	28	58	85
25	36	68	101	29	59	86
26	37	70	103	30	61	87
27	38	71	104	31	62	89
28	40	72	105	32	63	90
29	41	74	107	34	64	91
30	42	75	108	35	65	92
31	44	76	109	36	67	93
32	45	77	110	37	68	95
33	46	79	112	38	69	96
34	48	80	113	39	70	97
35	49	81	114	41	72	98
36	50	82	115	42	73	100
37	52	84	117	43	74	101
38	53	85	118	44	78	102

From DeVore GR: Pulsed Doppler examination of the fetal heart. In Goldberg BB, McGahan JP (eds): Atlas of Ultrasound Measurements, 2nd ed. Philadelphia, Mosby Inc/Elsevier, 2006.



**Table F-3****Longitudinal Reference Ranges for Peak Systolic Velocity in the Ductus Venosus (cm/s) Based on 547 Observations in 160 Low-Risk Pregnancies**

Gestational Age (wk)	Percentile								
	50th	2.5th	5th	10th	25th	75th	90th	95th	97.5th
21	59.3	46.2	48.0	50.2	54.3	65.1	70.9	74.8	78.5
22	61.8	48.3	50.1	52.4	56.6	67.6	73.7	77.7	81.4
23	63.9	50.1	52.0	54.3	58.6	69.9	76.1	80.1	83.9
24	65.7	51.6	53.5	55.9	60.3	71.9	78.2	82.3	86.2
25	67.2	52.8	54.8	57.2	61.7	73.5	79.9	84.2	88.1
26	68.5	53.8	55.8	58.3	62.8	74.9	81.4	85.7	89.7
27	69.5	54.5	56.6	59.1	63.8	76.0	82.7	87.1	91.1
28	70.3	55.1	57.2	59.7	64.4	76.9	83.7	88.1	92.3
29	70.8	55.4	57.6	60.2	64.9	77.6	84.5	89.0	93.2
30	71.2	55.6	57.7	60.4	65.2	78.0	85.0	89.7	94.0
31	71.4	55.6	57.8	60.5	65.3	78.3	85.4	90.1	94.5
32	71.4	55.5	57.7	60.4	65.3	78.5	85.7	90.4	94.9
33	71.4	55.3	57.5	60.2	65.2	78.5	85.8	90.6	95.1
34	71.2	55.0	57.2	59.9	64.9	78.3	85.7	90.6	95.2
35	70.8	54.6	56.8	59.5	64.5	78.1	85.5	90.5	95.1
36	70.4	54.1	56.3	59.1	64.1	77.7	85.2	90.3	94.9
37	70.0	53.6	55.8	58.6	63.6	77.3	84.9	89.9	94.7
38	69.4	53.0	55.2	58.0	63.0	76.8	84.4	89.5	94.3
39	68.8	52.4	54.6	57.4	62.4	76.2	83.9	89.0	93.8

From Kessler J, Rasmussen S, Hanson M, et al: Longitudinal reference ranges for ductus venosus flow velocities and waveform indices. *Ultrasound Obstet Gynecol* 28:890, 2006.

**Table F-4****Longitudinal Reference Ranges for End-Diastolic Velocity in the Ductus Venosus (cm/s) Based on 547 Observations in 160 Low-Risk Pregnancies**

Gestational Age (wk)	Percentile								
	50th	2.5th	5th	10th	25th	75th	90th	95th	97.5th
21	31.0	15.8	18.1	20.8	25.5	36.7	42.0	45.3	48.1
22	32.5	17.1	19.4	22.2	27.0	38.3	43.6	46.9	49.8
23	33.9	18.3	20.6	23.4	28.3	39.7	45.1	48.4	51.2
24	35.1	19.3	21.7	24.5	29.4	40.9	46.3	49.6	52.5
25	36.1	20.3	22.7	25.5	30.5	42.0	47.5	50.8	53.7
26	37.1	21.1	23.5	26.4	31.4	43.0	48.4	51.8	54.7
27	37.9	21.8	24.3	27.2	32.1	43.8	49.3	52.7	55.6
28	38.6	22.5	24.9	27.8	32.8	44.6	50.1	53.4	56.4
29	39.3	23.0	25.5	28.4	33.5	45.2	50.8	54.1	57.1
30	39.8	23.5	26.0	29.0	34.0	45.8	51.4	54.7	57.7
31	40.3	24.0	26.5	29.4	34.5	46.3	51.9	55.3	58.2
32	40.8	24.4	26.9	29.8	34.9	46.8	52.3	55.7	58.7
33	41.1	24.7	27.2	30.2	35.3	47.2	52.7	56.1	59.1
34	41.5	25.0	27.5	30.5	35.6	47.5	53.1	56.5	59.5
35	41.7	25.3	27.8	30.8	35.9	47.8	53.4	56.8	59.8
36	42.0	25.5	28.0	31.0	36.1	48.0	53.6	57.1	60.1
37	42.2	25.7	28.2	31.2	36.3	48.3	53.9	57.3	60.3
38	42.4	25.8	28.4	31.3	36.5	48.4	54.0	57.5	60.5
39	42.5	25.9	28.5	31.5	36.6	48.6	54.2	57.6	60.6

From Kessler J, Rasmussen S, Hanson M, et al: Longitudinal reference ranges for ductus venosus flow velocities and waveform indices. *Ultrasound Obstet Gynecol* 28:890, 2006.

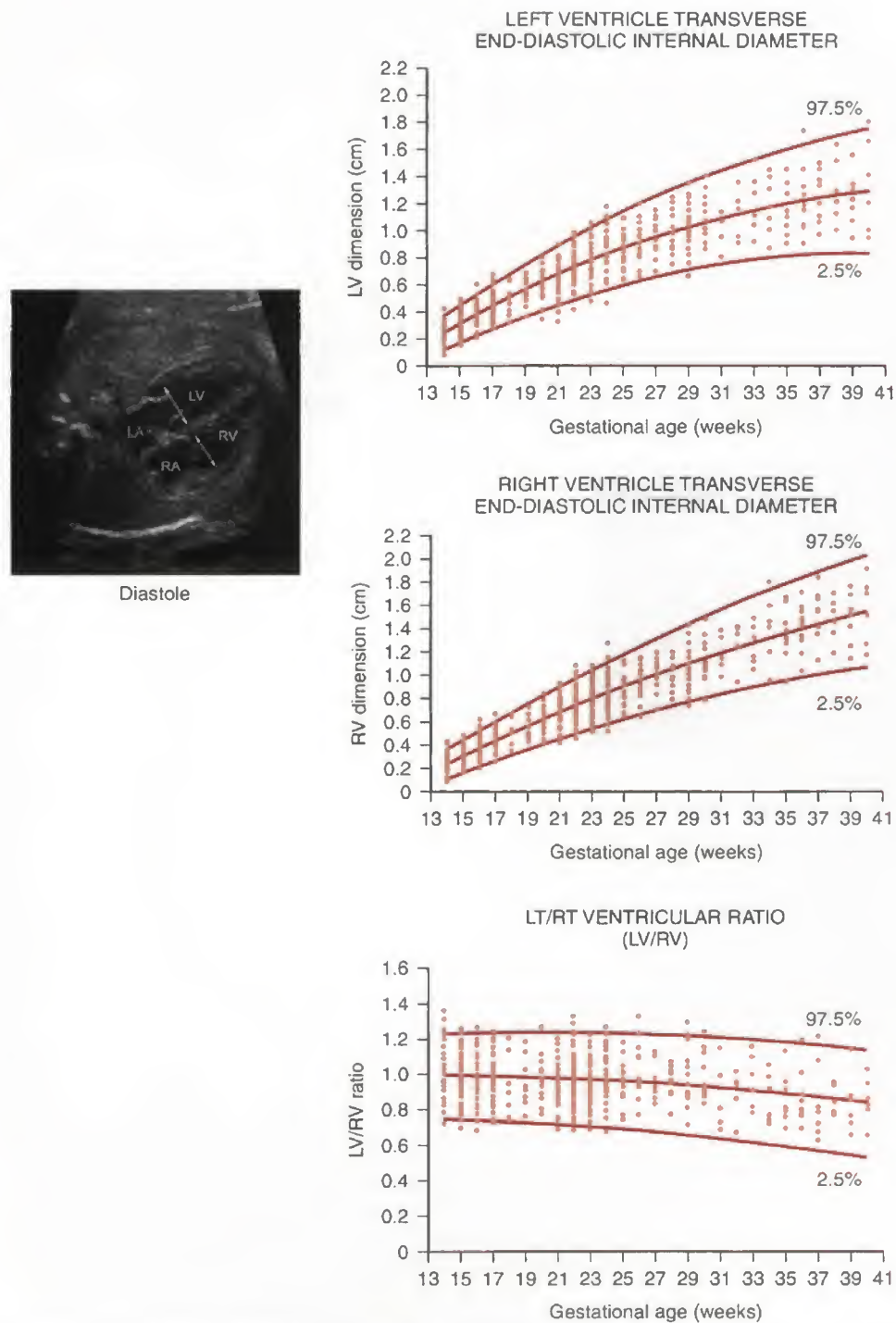


**FIGURE F-1.** Left ventricular (LV) and right ventricular (RV) dimensions and LV/RV ratio. Measurements should be taken from a diastolic four-chamber view. (Modified with permission from Shapiro I, Degani S, Leibovitz Z, et al: Fetal cardiac measurements derived by transvaginal and transabdominal cross-sectional echocardiography from 14 weeks of gestation to term. *Ultrasound Obstet Gynecol* 12:404, 1998.) (Figure by Shi-Joon Yoo, MD, Toronto, Canada.)



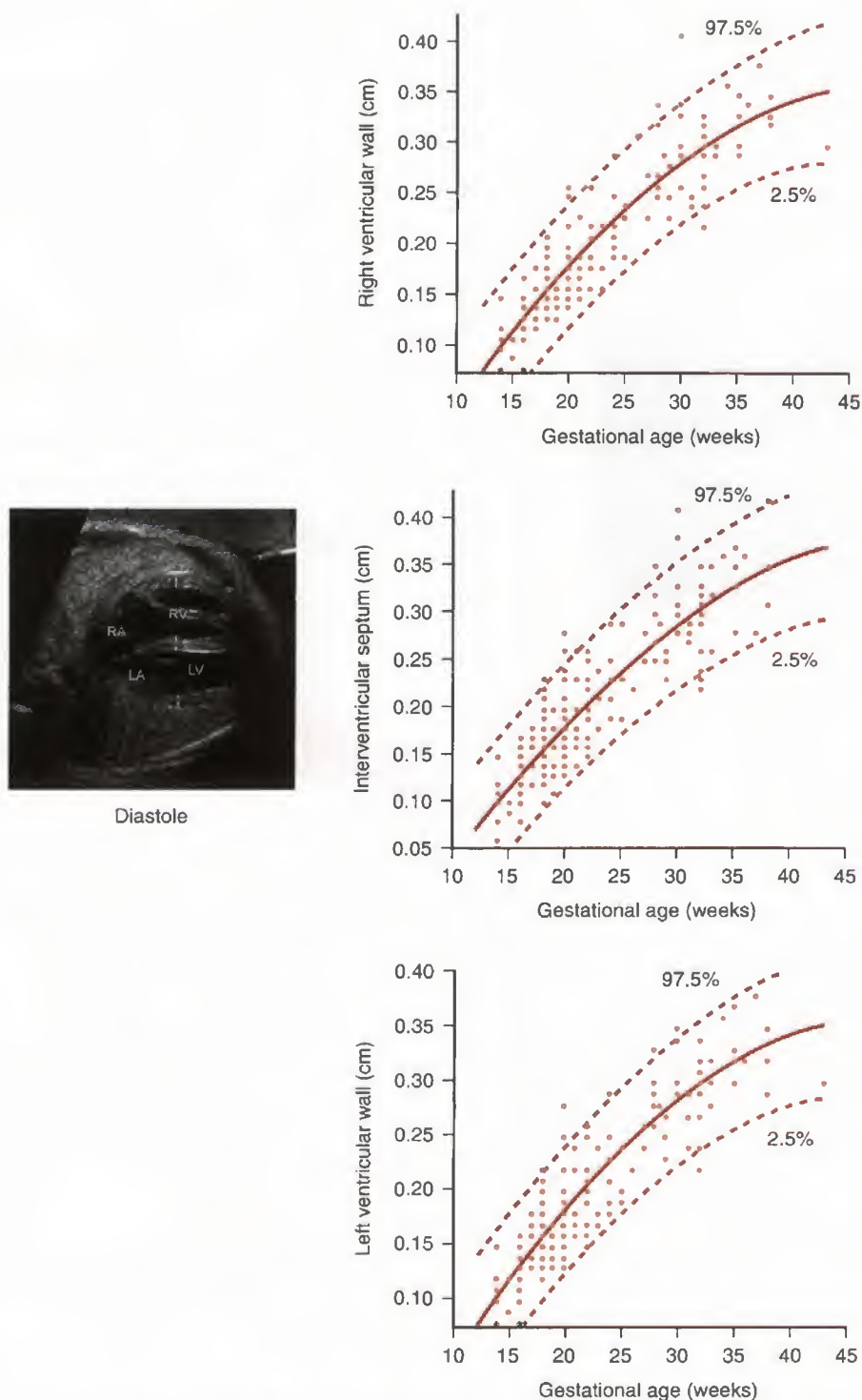


**FIGURE F-2.** Thicknesses of the right ventricular wall, interventricular septum and left ventricular wall. Measurements should be taken from a diastolic four-chamber view. (Modified with permission from Firpo C, Hoffman JL, Silverman NH: Evaluation of fetal heart dimensions from 12 weeks to term. *Am J Cardiol* 87:594, 2001.) (Figure by Shi-Joon Yoo, MD, Toronto, Canada.)

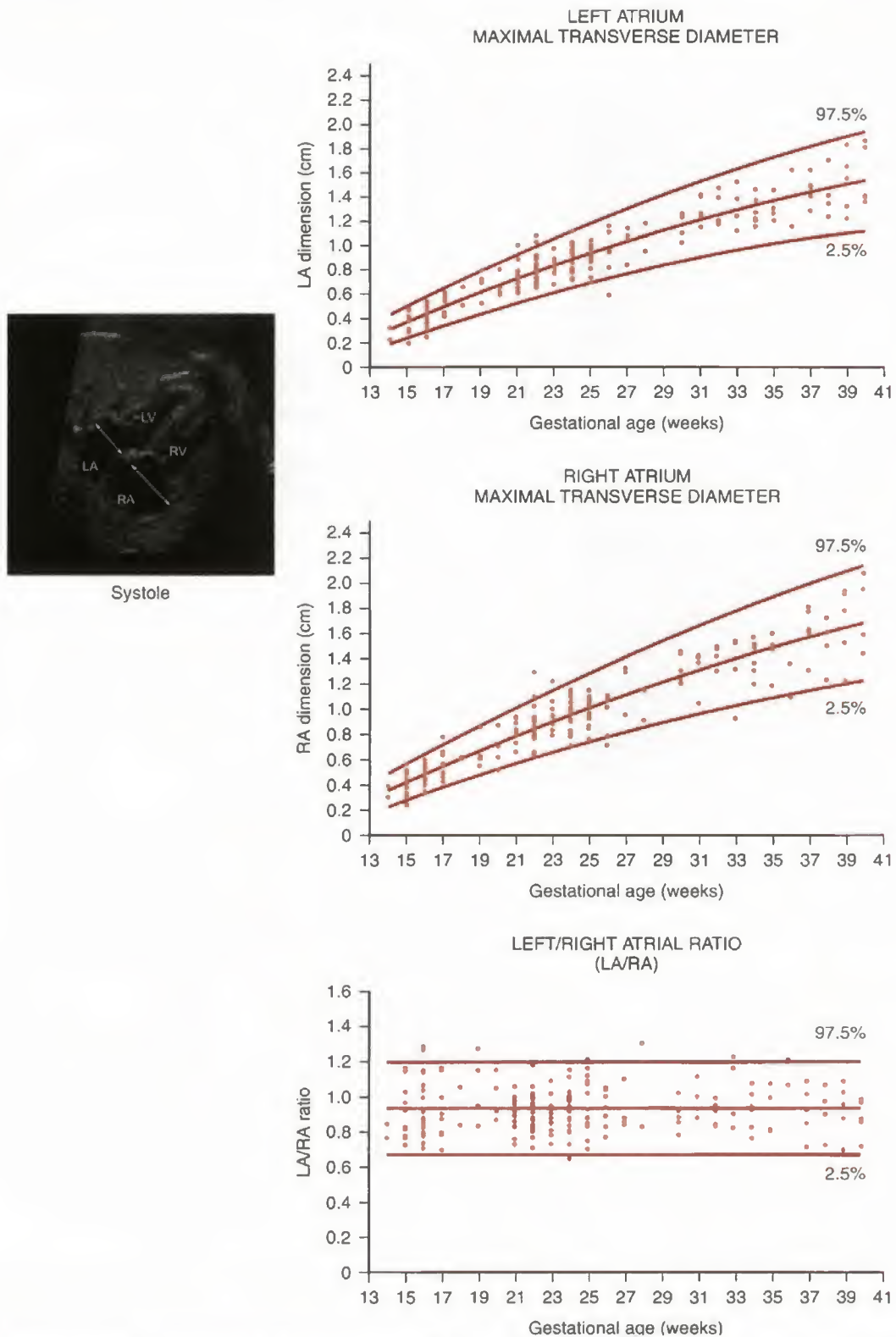


**FIGURE F-3.** Left atrial (LA) and right atrial (RA) dimensions and LA/RA ratio. Measurements should be taken from a systolic four-chamber view. (Modified with permission from Shapiro I, Degani S, Leibovitz Z, et al: Fetal cardiac measurements derived by transvaginal and transabdominal cross-sectional echocardiography from 14 weeks of gestation to term. *Ultrasound Obstet Gynecol* 12:404, 1998.) (Figure by Shi-Joon Yoo, MD, Toronto, Canada.)



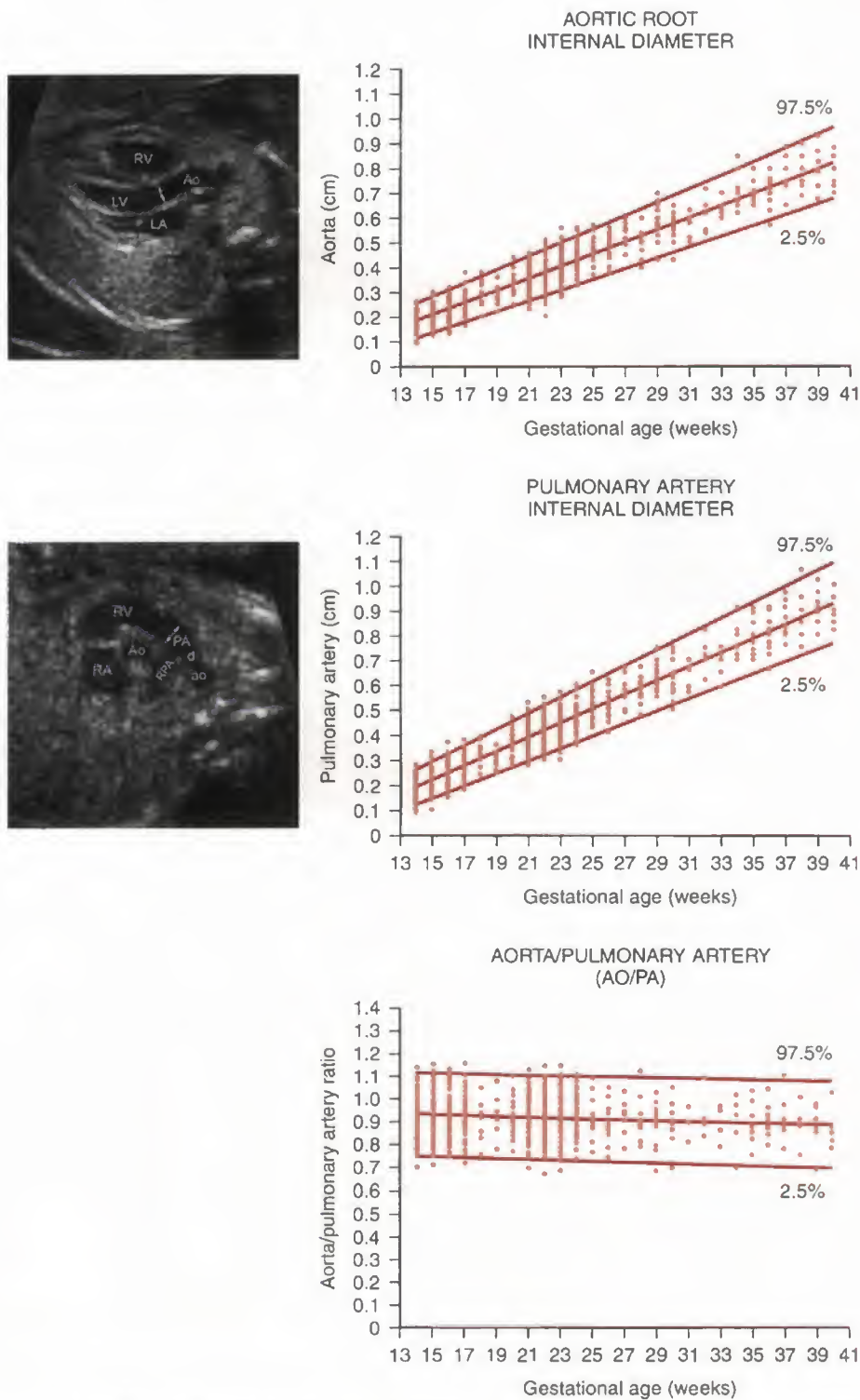


**FIGURE F-4.** Diameters of the ascending aorta (Ao) and main pulmonary trunk (PA) and aorta/pulmonary artery ratio. ao, descending aorta; d, ductus arteriosus; RA, right atrium; RPA, right pulmonary artery; RV, right ventricle. (Modified with permission from Shapiro I, Degani S, Leibovitz Z, et al: *Fetal cardiac measurements derived by transvaginal and transabdominal cross-sectional echocardiography from 14 weeks of gestation to term. Ultrasound Obstet Gynecol* 12:404, 1998.) (Figure by Shi-Joon Yoo, MD, Toronto, Canada.)

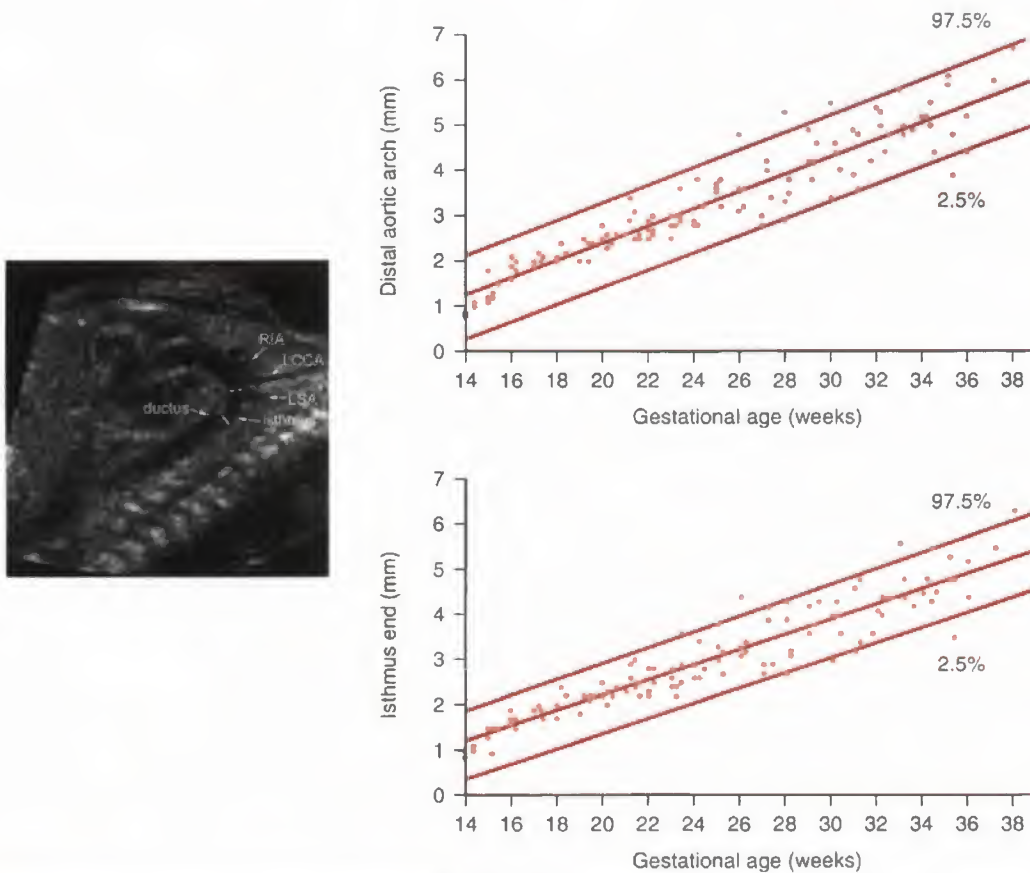


**FIGURE F-5.** Diameters of the distal aortic arch (upper double headed arrow) and distal end of the aortic isthmus (lower double headed arrow). LCCA, left common carotid artery; LSA, left subclavian artery; RIA, right innominate artery. (Modified with permission from Achiron R, Zimand S, Hegesh J, et al: Fetal aortic arch measurements between 14 and 38 weeks' gestation: in-utero ultrasonographic study. *Ultrasound Obstet Gynecol* 15:226, 2000.) (Figure by Shi-Joon Yoo, MD, Toronto, Canada.)



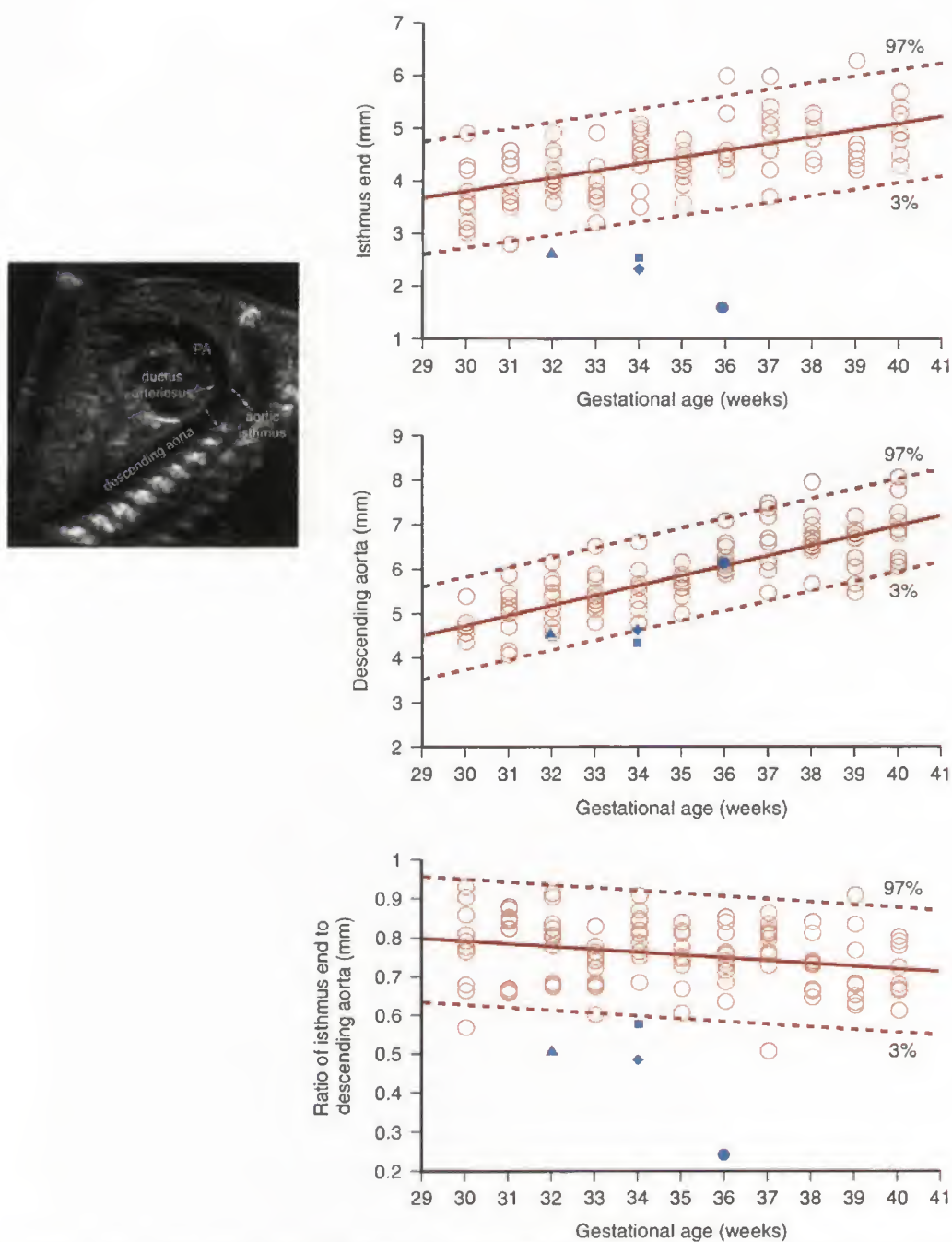


**FIGURE F-6.** Diameters of the distal end of the aortic isthmus and proximal descending aorta and isthmus/descending aorta ratio. PA, main pulmonary artery. (Modified with permission from Nomiya M, Ueda Y, Toyota Y, Kawano H: Fetal aortic isthmus growth and morphology in late gestation. *Ultrasound Obstet Gynecol* 19:153, 2002.) (Figure by Shi-Joon Yoo, MD, Toronto, Canada.)

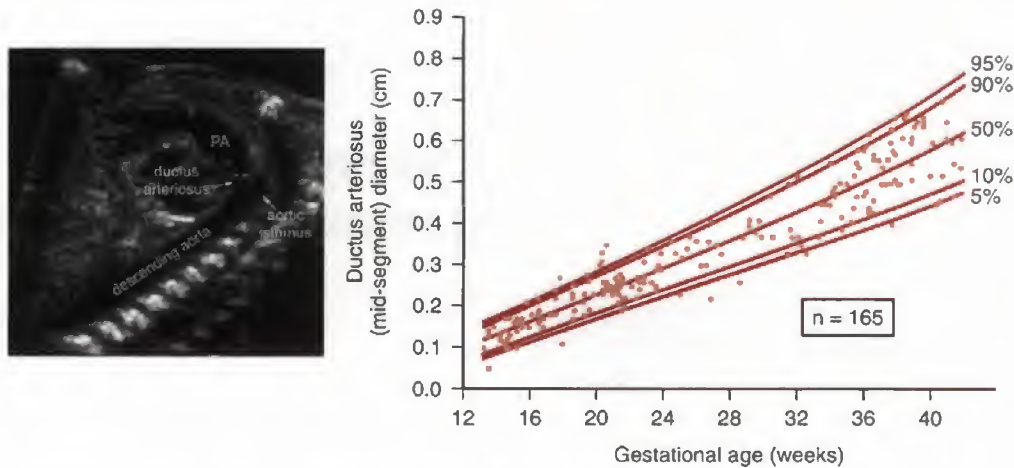


**FIGURE F-7.** Diameter of the mid-segment of the ductus arteriosus. PA, main pulmonary artery. (Modified with permission from Mielke G, Benda N: Reference ranges for two-dimensional echocardiographic examination of the fetal ductus arteriosus. *Ultrasound Obstet Gynecol* 15:219, 2000.) (Figure by Shi-Joon Yoo, MD, Toronto, Canada.)

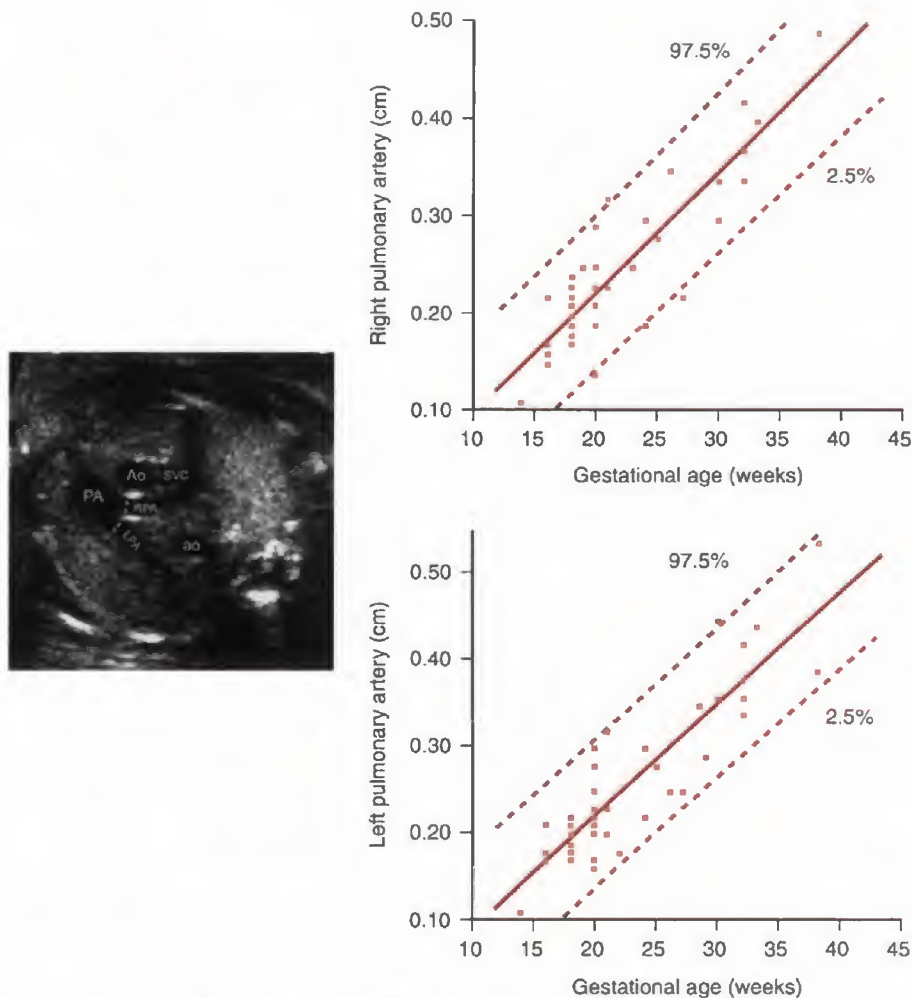


**FIGURE F-8.** Diameters of the right and left pulmonary arteries (RPA and LPA respectively). Ao, ascending aorta; ao, descending aorta; PA, main pulmonary artery; SVC, superior vena cava. (Modified with permission from Firpo C, Hoffman JL, Silverman NH: Evaluation of fetal heart dimensions from 12 weeks to term. *Am J Cardiol* 87:594, 2001.) (Figure by Shi-Joon Yoo, MD, Toronto, Canada.)



## Sonographic Detection of Chromosomal Abnormalities

**Table G-1**
**Reference Intervals for Nuchal Translucency (mm) by Days**

Days	Lower	Predicted	Upper
60	0.35650	1.03417	1.84865
61	0.36709	1.04690	1.86395
62	0.37940	1.06169	1.88174
63	0.39346	1.07858	1.90204
64	0.40927	1.09759	1.92488
65	0.42688	1.11875	1.95031
66	0.44629	1.14209	1.97836
67	0.46755	1.16764	2.00907
68	0.49069	1.19545	2.04249
69	0.51574	1.22555	2.07868
70	0.54274	1.25800	2.11768
71	0.57173	1.29285	2.15956
72	0.60276	1.33014	2.20438
73	0.63587	1.36994	2.25222
74	0.67113	1.41232	2.30315
75	0.70858	1.45733	2.35725
76	0.74829	1.50505	2.41461
77	0.79031	1.55557	2.47532
78	0.83473	1.60895	2.53948
79	0.88161	1.66529	2.60720
80	0.93102	1.72468	2.67858
81	0.98305	1.78722	2.75374
82	1.03780	1.85301	2.83282
83	1.09534	1.92217	2.91594
84	1.15578	1.99481	3.00325
85	1.21921	2.07106	3.09489
86	1.28577	2.15105	3.19103
87	1.35554	2.23491	3.29182
88	1.42867	2.32280	3.39746
89	1.50528	2.41488	3.50812
90	1.58550	2.51130	3.62401
91	1.66949	2.61224	3.74533
92	1.75739	2.71789	3.87231
93	1.84937	2.82844	4.00519
94	1.94560	2.94411	4.14420
95	2.04627	3.06509	4.28962
96	2.15156	3.19164	4.44171
97	2.26167	3.32399	4.60078
98	2.37683	3.46240	4.76713
99	2.49726	3.60713	4.94109
100	2.62319	3.75849	5.12301
101	2.75489	3.91678	5.31325
102	2.89261	4.08231	5.51220
103	3.03665	4.25543	5.72028
104	3.18730	4.43650	5.93790
105	3.34489	4.62590	6.16554

From Yagel S, Anteby EY, Rosen L, et al: Assessment of first-trimester nuchal translucency by daily reference intervals. *Ultrasound Obstet Gynecol* 11:262, 1998.

**Table G-2** Normal Percentile Ranges for Nasal Bone Lengths (mm) (n = 3537) for a Specific Menstrual Age (wk)

Gestational Age (wk)	Subjects (n)	Percentile				
		2.5th	5th	50th	95th	97.5th
11	16	1.3	1.4	2.3	3.3	3.4
12	54	1.7	1.8	2.8	4.2	4.3
13	59	2.2	2.3	3.1	4.6	4.8
14	82	2.2	2.5	3.8	5.3	5.7
15	103	2.8	3.0	4.3	5.7	6.0
16	134	3.2	3.4	4.7	6.2	6.2
17	203	3.7	4.0	5.3	6.6	6.9
18	252	4.0	4.3	5.7	7.0	7.3
19	388	4.6	5.0	6.3	7.9	8.2
20	440	5.0	5.2	6.7	8.3	8.6
21	322	5.1	5.6	7.1	9.0	9.3
22	208	5.6	5.8	7.5	9.3	10.2
23	157	6.0	6.4	7.9	9.6	9.9
24	121	6.6	6.8	9.3	10.0	10.3
25	123	6.3	6.5	8.5	10.7	10.8
26	96	6.8	7.4	8.9	10.9	11.3
27	80	7.0	7.5	9.2	11.3	11.6
28	103	7.2	7.6	9.8	12.1	13.4
29	95	7.2	7.7	9.8	11.8	12.3
30	104	7.3	7.9	10.0	12.6	13.2
31	92	7.9	8.2	10.4	12.6	13.2
32	66	8.1	8.6	10.5	13.6	13.7
33	54	8.6	8.7	10.8	12.8	13.0
34	41	9.0	9.1	10.9	12.8	13.5
35	37	7.5	8.5	11.0	14.1	15.0
36	40	7.3	7.8	10.8	12.8	13.6
37	36	8.4	8.7	11.4	14.5	15.0
38	13	9.2	9.3	11.7	15.7	16.6
39	12	9.1	9.2	10.9	14.0	14.8
40	6	10.3	10.4	12.1	14.5	14.7

From Sonck JD, McKenna D, Webb D, et al: Nasal bone length throughout gestation: normal ranges based on 3537 fetal ultrasound measurements. *Ultrasound Obstet Gynecol* 21:152, 2003.

**Table G-3** Observed Number of Trisomies 21, 18, and 13 in Relation to Fetal Nuchal Translucency Thickness and Expected Number of Trisomies on the Basis of Maternal Age

Nuchal Translucency Thickness (mm)	n	Observed			Expected by Age			Observed/Expected		
		21	18/13	21/18/13	21	18/13	21/18/13	21	18/13	21/18/13
3	383	16	7	23	4.20	1.81	6.01	3.8	3.9	3.8
4	67	16	5	21	0.71	0.31	1.02	22.5	16.0	20.6
5	41	13	7	20	0.53	0.23	0.76	24.5	30.0	26.3
≥6	69	16	22	38	0.65	0.28	0.93	24.6	78.6	40.9
Total	560	61	41	102	6.09	2.63	8.72	10.0	15.6	11.7

From Pandya PP, Beizot ML, Kuhn P, et al: First-trimester fetal nuchal translucency thickness and risk of trisomies. *Obstet Gynecol* 84:420, 1994.

**Table G-4** Nuchal Thickness at 14 to 24 Weeks' Gestation by Maternal Age

	Nuchal Skin Fold					
	5 mm		6 mm		7 mm	
	<35 y	≥35 y	<35 y	≥35 y	<35 y	≥35 y
Sensitivity	75% (6/8)	46% (11/24)	62% (5/8)	38% (9/24)	38% (3/8)	21% (5/24)
95% confidence interval	35%–97%	26%–68%	24%–91%	19%–59%	8%–75%	7%–42%
Specificity	92.3%	95.5%	98.8%	99.2%	99.7%	99.7%
Positive predictive value	1/168	1/42	1/34	1/11	1/14	1/7
Positive screens	7.8%	4.8%	1.3%	1.0%	0.3%	0.4%

From Grav DL, Crane JP: Optimal nuchal skin-fold thresholds based on gestational age for prenatal detection of Down syndrome. *Am J Obstet Gynecol* 171:1282, 1994.



**Table G-5****Maternal Age-Specific Odds (1:\_) of Fetal Down Syndrome During the Second Trimester Based on Nonstructural Findings**

Maternal Age (Years)	Pre-US Odds (1:_)	Normal US Scan (1:_)	Nuchal Thickness (1:_)	Echogenic Bowel (1:_)	Short Humerus (1:_)	Short Femur (1:_)	EIF (1:_)
20	1176	2939	64	215	512	471	589
21	1160	2899	63	212	505	465	581
22	1136	2839	62	207	494	455	569
23	1114	2784	61	203	485	446	558
24	1087	2716	59	198	473	435	544
25	1040	2599	57	190	453	417	521
26	990	2474	54	181	431	397	496
27	928	2319	51	170	404	372	465
28	855	2136	47	156	372	343	428
29	760	1899	42	139	331	305	381
30	690	1724	38	126	301	277	346
31	597	1491	33	109	260	239	299
32	508	1269	28	93	221	204	255
33	421	1051	24	77	184	169	211
34	342	854	19	63	149	137	172
35	274	684	16	51	120	110	138

EIF, echogenic intracardiac focus; US, ultrasound.

From Nyberg DA, Luthy DA, Resta RG, et al: Age-adjusted ultrasound risk assessment for fetal Down's syndrome during the second trimester: Description of the method and analysis of 142 cases. *Ultrasound Obstet Gynecol* 13:221, 1998.

# APPENDIX H

## Normal Measurements of the Uterus and Ovaries

**Table H-1** Ovarian Volume by Decade of Life

Decade	Mean Volume (cm <sup>3</sup> )	Standard Deviation	No. of Ovaries	95% Confidence Interval (cm <sup>3</sup> )*
1	1.7	1.4	19	0.2–4.9
2	7.8	4.4	83	1.7–18.5
3	10.2	6.2	308	2.6–23.1
4	9.5	5.4	358	2.6–20.7
5	9.0	5.8	206	2.1–20.9
6	6.2	3.6	57	1.6–14.2
7	6.0	3.8	44	1.0–15.0

\*Calculated on the basis of cube root values, then transformed back to cubic centimeters.

From Cohen HL, Tice HM, Mandel FS: Ovarian volumes measured by US: Bigger than we think. *Radiology* 177:189, 1990.

**Table H-2** Ovarian Volume by Menstrual Status

Group	Mean Volume (cm <sup>3</sup> )	Standard Deviation	95% No. of Ovaries	Confidence Interval (cm <sup>3</sup> )*
Premenarchal	3.0	2.3	32	0.2–9.1
Menstruating	9.8	5.8	866	2.5–21.9
Postmenopausal	5.8	3.6	100	1.2–14.1

\*Calculated on the basis of cube root values, then transformed back to cubic centimeters.

From Cohen HL, Tice HM, Mandel FS: Ovarian volumes measured by US: Bigger than we think. *Radiology* 177:189, 1990.

**Table H-3** Normal Uterine Diameters and Volume\*

Age (y)	No. of Patients	Uterine Diameters (mm)				Uterine Volume (cm <sup>3</sup> )	
		TUL	COAP	CEAP	COAP/CEAP	By Chronologic Age	By Bone Age
		Mean SD	Mean SD	Mean SD	Mean SD	Mean SD	Mean SD
2	7	33.1 ± 4.4	7.0 ± 3.4	8.3 ± 2.0	0.84 ± 0.29	1.98 ± 1.58	1.76 ± 0.72
3	8	32.4 ± 4.3	6.4 ± 1.3	7.6 ± 2.2	0.89 ± 0.29	1.63 ± 0.81	1.80 ± 0.74
4	15	32.9 ± 3.3	7.6 ± 1.8	8.6 ± 1.8	0.90 ± 0.22	2.10 ± 0.57	1.97 ± 0.74
5	7	33.1 ± 5.5	8.0 ± 2.8	8.4 ± 1.6	0.95 ± 0.28	2.36 ± 1.39	2.19 ± 1.16
6	9	33.2 ± 4.1	6.7 ± 2.9	7.5 ± 1.8	0.86 ± 0.18	1.80 ± 1.57	1.65 ± 0.93
7	9	32.3 ± 3.9	8.0 ± 2.2	7.7 ± 2.5	1.08 ± 0.26	2.32 ± 1.07	2.81 ± 1.44
8	11	35.8 ± 7.3	9.0 ± 2.8	8.4 ± 1.7	1.05 ± 0.20	3.12 ± 1.52	2.70 ± 1.43
9	11	37.1 ± 4.4	9.7 ± 3.0	8.8 ± 2.0	1.10 ± 0.24	3.70 ± 1.62	2.69 ± 1.83
10	13	40.3 ± 6.4	12.8 ± 5.3	10.7 ± 2.6	1.17 ± 0.31	6.54 ± 3.78	4.66 ± 3.03
11	13	42.2 ± 5.1	12.8 ± 3.1	10.7 ± 2.6	1.22 ± 0.26	6.66 ± 2.87	6.24 ± 3.07
12	6	54.3 ± 8.4	17.3 ± 5.3	14.3 ± 5.2	1.23 ± 0.16	16.18 ± 9.15	8.88 ± 3.65
13	5	53.8 ± 11.4	15.8 ± 4.5	15.0 ± 2.4	1.03 ± 0.15	13.18 ± 5.64	15.55 ± 5.98

CEAP, anteroposterior diameter of the cervix; COAP, anteroposterior diameter of the corpus; SD, standard deviation; TUL, total uterine length.

\*As determined by ultrasonography in 114 girls from age 2 to 13.

From Orsini LF: Pelvic organs in premenarcheal girls: Real-time ultrasonography. *Radiology* 153:113, 1984.



## Medications and Reported Associated Malformations

**Table I-1** Selected Medications and Reported Associated Malformations\*

Drug	Malformation
Acetazolamide	Sacroccygeal teratoma
Acyclovir	CDH, neural tube defect, cleft lip, clubfoot, transposition
Alprazolam	Umbilical hernia, clubfoot
Albuterol	Cleft palate, cranioschisis, cardiovascular defect, spina bifida, polydactyly, fetal tachycardia
Amantadine	Cardiac defects
Aminopterin	Neural tube defects, hydrocephalus, limb shortening, cleft lip/palate, clubfoot
<i>p</i> -Aminosalicylic acid	Ear deformity, limb deformity, hypospadias
Amiodarone	IUGR, ventricular septal defect, micrognathia
Amitriptyline	Limb reduction, micrognathia, hypospadias, cleft palate, thanatophoric dysplasia
Ampicillin	Transposition of the great vessels
Amobarbital	Anencephaly, cardiac defects, limb deformity, cleft lip/palate, polydactyly, genitourinary defects, clubfoot
Amphetamine	Cerebral injury in neonates
Aspirin	Intracranial hemorrhage, IUGR
Atenolol	Hypospadias, cardiovascular defects
Atropine	Polydactyly, limb reduction
Azatadine	Oral cleft, limb reduction
Baclofen	Spina bifida
Belladonna	Eye/ear malformations, hypospadias
Benztropine	Cardiovascular defects
Bromides	Polydactyly, gastrointestinal anomalies, clubfoot, IUGR
Busulfan	IUGR, cleft palate, neural tube defects
Captopril	Second-trimester hypocalvaria, oligohydramnios, renal dysfunction
Carbamazepine	Neural tube defects, cardiac defects
Carisoprodol	Oral clefts
Cephalexin	Cardiovascular defects, oral clefts
Cephradine	Cardiovascular defects
Chlorambucil	Renal agenesis, cardiac defects
Chlordiazepoxide	Microcephaly, duodenal atresia, cardiac defects
Chloroquine	Wilms tumor, hemihypertrophy, tetralogy of Fallot
Chlorothiazide	Fetal bradycardia
Chlorpheniramine	Polydactyly, gastrointestinal defects, hydrocephalus
Chlorpromazine	Microcephaly, syndactyly
Chlorpropamide	Microcephaly, hand anomalies
Ciprofloxacin	Hypospadias, cerebellar hypoplasia, cardiovascular defect, femoral aplasia
Clarithromycin	Craniofacial abnormalities, absent clavicles, spina bifida, cleft lip, pulmonary hypoplasia, coloboma, heart anomaly, choanal atresia, retardation (mental and somatic), genital and ear anomalies (CHARGE) association
Clomiphene	Microcephaly, neural tube defects, cleft lip/palate, cardiac defects, syndactyly, clubfoot, hypospadias
Clonazepam	Cardiovascular defects
Clorazepate	Bifid foot, absent scrotum, short femur, absent fibula, absent metacarpal bones, renal agenesis
Cloxacillin	Cardiovascular defects
Cocaine	Spontaneous abortion, placental abruption, cardiac defects, urinary tract and limb abnormalities, bowel atresias, IUGR
Codeine	Pulmonary and genitourinary defects, hydrocephalus, cleft lip/palate
Colchicine	Cardiac malformation, syndactyly, cleft palate
Cortisone	Cataracts, cyclopia, VSD, coarctation of the aorta, clubfoot, cleft lip, gastroschisis
Coumarin derivatives	Spontaneous abortion, IUGR, neural tube defects (open and closed) (dorsal midline dysplasia), cardiac defects, scoliosis, limb hypoplasia, cleft palate
Cyclophosphamide	Cleft palate, hand abnormalities, cardiac defects, IUGR
Cyclosporine	Limb hypoplasia, agenesis of the corpus callosum, anencephaly, IUGR

Continued

**Table 1-1** Selected Medications and Reported Associated Malformations\*—Continued

Drug	Malformation
Cyproheptadine	Cleft lip/palate, hypospadias
Cytarabine	Hand abnormalities (lobster claw deformity), lower limb defects, neural tube defects, cardiac defects
Dacarbazine	Limb reduction defects, cleft palate, encephalocele
Danazol	Ambiguous genitalia
Daunorubicin	IUGR
Dexfenfluramine	Hand malformation, anencephaly, vertebral abnormality
Diazepam	Cleft lip/palate, cardiac defects
Dicyclomine	Polydactyly
Dilantin	Microcephaly, hypertelorism, cleft lip/palate, hypoplasia of distal phalanges, short neck, broad nasal ridge
Diltiazem	Cardiovascular defects
Dimenhydrinate	Cardiovascular defects
Diphenhydramine	Cleft lip/palate, genitourinary defects, clubfoot, cardiac defects
Disulfiram	Clubfoot, vertebral defects, anal atresia, cardiac anomalies, tracheoesophageal fistula with esophageal atresia, renal anomalies, limb anomalies (VACTERL) syndrome, phocomelia
Doxepin	Oral clefts, polydactyly
Properidol	Hydrocephalus, cerebral hypoplasia
Enalapril	Hypocalvaria, renal defects
Ephedrine	Clubfoot
Ethanol (alcohol)	IUGR, microphthalmia, micrognathia, microcephaly, hypoplastic maxilla, cardiac defects, genitourinary defects, radioulnar synostosis, Klippel-Fell anomaly, diaphragmatic hernia
Ethioheptazine	Umbilical hernia, hip dislocation
Ethotoin	Cleft lip/palate, patent ductus arteriosus
Ethosuximide	Cleft lip/palate, hydrocephalus, patent ductus arteriosus, spontaneous hemorrhage in the neonate
Etretinate	Neural tube defects, facial dysmorphism, multiple synostoses, syndactylies, limb reduction
Fluconazole	Craniosynostosis, cleft palate, limb shortening
Fluorouracil	Radial aplasia, pulmonary hypoplasia, esophageal and duodenal atresia, cloacal malformation
Fluphenazine	Ocular hypertelorism, cleft lip/palate, imperforate anus
Furosemide	Hypospadias
Griseofulvin	Conjoined twins
Haloperidol	Limb reduction, aortic valve defect
Heparin	Cardiovascular defects
Heroin	IUGR, multiple and varied congenital malformations
Hydroxyprogesterone	Spina bifida, anencephaly, tetralogy of Fallot, truncus arteriosus, VSD
Hydroxyzine	Oral clefts
Hyoscyamine	Polydactyly, limb reduction
Ibuprofen	Oligohydramnios, premature closure of patent ductus arteriosus
Imipramine	Diaphragmatic hernia, cleft palate, exencephaly, renal cystic dysplasia, amelia
Indomethacin	Oligohydramnios, premature closure of patent ductus arteriosus, phocomelia, penile agenesis
Isoetharine	Clubfoot
Isotretinoin	Hydrocephalus, neural tube defects, microphthalmia, microcephaly, cardiac defects, limb abnormalities, cleft palate
Itraconazole	Limb defect
Ketoconazole	Limb defect
Ketolac	Constriction of the ductus arteriosus, fetal renal impairment
Levothyroxine	Cardiac defects, polydactyly
Lindane	Hypospadias
Lisinopril	Hypocalvaria, polydactyly, oligohydramnios
Lithium	Cardiac defects (Ebstein anomaly, VSD, coarctation, mitral atresia), neural tube defects
Lovastatin	Aortic hypoplasia, VSD, anal atresia, renal dysplasia, radial aplasia
Lysergic acid diethylamide	IUGR, limb reduction, neural tube defects, cardiac defects
Marijuana	IUGR, facial anomalies
Mechlorethamine	IUGR, oligodactyly, malformed kidneys
Medroxyprogesterone	Cardiovascular defect
Meclizine	Eye and ear defects, hypoplastic heart, respiratory defects
Mefenamic acid	Constriction of the ductus arteriosus
Melphalan	IUGR
Meprobamate	Cardiac defects, omphalocele, joint abnormalities
Mercaptopurine	Cleft palate, microphthalmia, IUGR
Metaproterenol	Polydactyly

Continued



**Table 1-1** Selected Medications and Reported Associated Malformations\*—Continued

Drug	Malformation
Methimazole	Patent urachus
Methotrexate	IUGR, hypertelorism, dextroposition of the heart, absent digits, absence of frontal bone
Methotrimeprazine	Hydrocephalus, cardiac defects
Metronidazole	Spontaneous abortion, limb, cardiac, urinary, and facial abnormalities
Mifepristone	Sirenomelia, caudal regression syndrome
Minoxidil	Omphalocele, clinodactyly, cardiac defects (VSD and transposition)
Misoprostol	Limb defects, hypocalvaria, cleft lip, clubfoot, gastroschisis
Norethindrone	Neural tube defects, hydrocephalus
Norethynodrel	Cardiac defects, hypospadias
Nortriptyline	Limb reduction
Ofloxacin	Myelomeningocele, hydrocephalus, hypospadias
Omeprazole	Anencephaly, hydranencephaly, clubfoot
Oxazepam	Neural tube defects, IUGR
Paramethadione	Spontaneous abortions, IUGR, cardiac defects
Penicillamine	Hydrocephalus, flexion deformities, perforated bowel
Pentoxifylline	Cardiac defects
Phenacetin	Craniosynostosis and atresia, musculoskeletal and urinary tract defects
Phenobarbital	Cardiovascular defects
Phensuximide	Ambiguous genitalia
Phenylephrine	Eye and ear abnormalities, syndactyly, clubfoot, musculoskeletal defects
Phenylpropanolamine	Eye and ear abnormalities, polydactyly, hypospadias
Phenytoin	Microcephaly, hypertelorism, cleft lip/palate, hypoplasia of distal phalanges, short neck, broad nasal ridge
Podophyllum	Limb reduction
Procarbazine	IUGR, cardiac defects, oligodactyly, malformed kidneys
Prochlorperazine	Cleft palate/micrognathia, cardiac defects, skeletal defects
Propoxyphene	Limb abnormalities, omphalocele, micrognathia, clubfoot, microcephaly
Quinacrine	Renal agenesis, neural tube defects
Quinine	Neural tube defects, hydrocephalus, limb defects, facial defects, cardiac defects, urogenital abnormalities, vertebral abnormality, gastrointestinal anomaly
Reserpine	Microcephaly, hydronephrosis
Retinoic acid	Hydrocephalus, neural tube defects, microphthalmia, microcephaly, cardiac defects, limb abnormalities, cleft palate
Rifampin	Anencephaly, hydrocephalus, limb malformation
Sodium iodide	Ablation of fetal thyroid gland
Sulfasalazine	Cleft lip/palate, hydrocephalus, cardiac defects, urinary tract abnormalities
Sulfonamides	Limb hypoplasia, urinary tract abnormalities
Sumatriptan	Phocomelia, tibial aplasia, clubfoot, cleft palate
Tamoxifen	Ambiguous genitalia
Tazarotene	Reduced skeletal ossification, hydrocephaly, spina bifida, cardiac defects
Temazepam	Oral clefts
Terfenadine	Polydactyly
Tetracycline	Hypospadias, limb hypoplasia
Thioguanine	Absent digits
Tolbutamide	Syndactyly, cardiac defects, clubfoot
Trifluoperazine	Phocomelia, transposition of the great vessels
Trimethadione	IUGR, microcephaly, cleft lip/palate, cardiac defects, malformed hand, clubfoot, ambiguous genitalia, esophageal atresia, tracheoesophageal fistula
Trimethoprim	Cardiovascular defects
Valproic acid	Neural tube defects, cardiac defects, facial dysmorphism, hypertelorism, protruding eyes, micrognathia, hydrocephalus, cleft lip/palate, microcephaly, limb reduction, scoliosis, renal hypoplasia, duodenal atresia, hand deformity
Zidovudine	Renal agenesis, microphthalmus, polydactyly, cleft lip/palate, clubfoot, VSD

CDH, congenital diaphragmatic hernia; IUGR, intrauterine growth restriction; VSD, ventricular septal defect.

\*This list represents selected medications and their possible associations with fetal structural abnormalities. Many of the listed associations are based on isolated case reports that have appeared in the medical literature for which the association is unproven or in animal studies where the dosage of medication far exceeded the normal clinical amount normally used. It is likely that in many cases the reported association was coincidental to, rather than resultant from, the medication.

This list is not intended for patient counseling regarding the likelihood of fetal malformations or abnormalities. The table should be used by the sonologist/sonographer as a guide for evaluating specific organ systems in addition to a thorough sonographic examination. In all cases of suspected teratogenic effects, a reproductive geneticist or teratologist and the drug manufacturer should be consulted.

Modified from Briggs GG, Freeman RK, Yaffe SJ: *Drugs in Pregnancy and Lactation*, 7th ed. Philadelphia, Lippincott Williams & Wilkins, 2005.

# APPENDIX J

## Estimated Radiation Exposure to the Fetus during Radiographic Examinations

**Table J-1**

**Estimated Fetal Dose for Single Radiographic Image of Abdomen or Pelvis With Fetus in Field of View**

Patient Body Thickness (cm)	Estimated Dose			
	Anteroposterior		Lateral	
	mSv	mrem	mSv	mrem
14-15	1.0	100	0.7	70
16-19	1.5	150	1.0	100
20-23	2.1	210	1.5	150
24-26	3.1	310	2.0	200
27-30	4.3	430	3.0	300
31-34	5.6	560	4.0	400

Note.—Fluoroscopy fetal dose =  $0.15 \times$  entrance skin dose;  
mSv = millisievert, mrem = millirem (roentgen equivalent man).

**Table J-2**

**Estimated Fetal Dose for CT of the Abdomen or Pelvis With Fetus in Field of View**

Multidetector CT (Four-Slice Scanner)				Single-Detector Helical CT			
Technique		Dose		Technique		Dose	
mAs	pitch	mSv	rem	mAs	pitch	mSv	rem
300	4.5	35	3.5	300	1.0	35	3.5
300	6.5	25	2.5	300	1.5	25	2.5
200	4.5	23	2.3	200	1.0	23	2.3
200	6.5	15	1.5	200	1.5	15	1.5
150	4.5	17.5	1.75	150	1.0	17.5	1.75
150	6.5	12.5	1.25	150	1.5	12.5	1.25

Note.—Calculations are based on 120 kVp and a slice thickness of  $\geq 5$  mm. Slice thickness is an acquisition parameter that refers to the width of the detector element along the long axis of the patient. The nominal beam width for a four-slice multidetector CT (MDCT) scanner with an acquisition slice thickness of 5 mm is 20 mm. Below 5 mm on MDCT systems, the penumbra of the X-ray beam results in increased dose. The increase for 3-mm slices is 10–20%, the increase for 1-mm slices is 30–40%, and the increase for 0.5-mm slices is 50–150% depending on manufacturer. mAs = milliamperes-second, mSv = millisievert, rem = roentgen equivalent man.

From El-Khoury GY, Madsen MT, Blake ME, Yankowitz J: A new pregnancy policy for a new era. *Am J Roentgenol* 181:335, 2003.



## MR Imaging Protocol for Pregnant Patients with Acute Right Lower Quadrant Pain

**Table K-1** MR Imaging Protocol for Pregnant Patients with Acute Right Lower Quadrant Pain

Parameters	Pulse Sequences*					
	Coronal Single-Shot Fast SE	Axial Single-Shot Fast SE	Sagittal Single-Shot Fast SE	Axial 2D FS Single-Shot Fast SE	IP and OP 2D T1W GRE	2D TOF
Sequence type	Single shot	Single shot	Single shot	Single shot	GRE	GRE
Repetition time (msec)	800–1100	800–1100	800–1100	800–1100	205	5500
Echo time (msec)	60	60	60	60	2.2/4.5	100
Flip angle (degrees)	130–155	130–155	130–155	130–155	80	45
No. of signals acquired	1	1	1	1	1	1
2D or 3D	2D	2D	2D	2D	2D	2D
Section thickness (mm)	4	4	4	4	5	3
Gap (mm)	1	1	1	1	2	1
Field of view (mm)	350	350	350	350	350	350
No. of partitions or sections	20	20	20	20	32	24
Orientation	Coronal	Axial	Sagittal	Axial	Axial	Axial
Phase × frequency steps	192 × 256	192 × 256	192 × 256	192 × 256	160 × 256	128 × 256
Rectangular field of view	No	0.75	0.75	0.75	0.75	0.75
Fat suppression	No	No	No	Yes	No	No
Zero fill section	No	No	No	No	No	No
Partial Fourier	Yes	Yes	Yes	Yes	No	No
No. of measurements or repeats	1	1	1	1	1	1
Single or multiple shots	Single	Single	Single	Single	Multiple	Multiple
Echo train length	...	...	...	...	...	...
Bandwidth (kHz) <sup>†</sup>	62.5	62.5	62.5	62.5	62.5	31.25
Parallel imaging	No	No	No	No	No	No
Breath hold	Yes	Yes	Yes	Yes	Yes	Yes

From Pedrosa I, Zeikus EA, Levine D, Rofsky NM: Imaging of acute right lower quadrant pain in pregnant and nonpregnant patients. *Radiographics* 27:721–743, 2007.

Note.—An eight-channel torso phased-array coil is used.

\*FS = fat-saturated, IP = in-phase, OP = opposed-phase, TOF = time of flight, T1W = T1-weighted.

<sup>†</sup>62.5 kHz = 488 Hz/pixel, 31.25 kHz = 244 Hz/pixel.

Note: Page numbers followed by "f" indicate figures; those followed by "t" indicate tables.

## A

Aase syndrome, 465, 467

Abdomen. *See also specific structures*

fetal

calcifications within, 602–603, 602f–604f, 613

idiopathic cysts within, 624–625, 625f

MRI evaluation of, 820, 826f–827f

ultrasound imaging of, 325, 326f

artifacts, pitfalls, and normal variants, 1136f–1144f

fetal position and, 300

portal circulation, 320–328, 327f–329f, 338

maternal

CT and MRI evaluation of pain in, 810, 810f–813f, 812t, 1206t

transverse view of upper abdomen, 514, 516f

abnormalities on, 523, 527t, 527–528, 528t, 529f–530f

neonatal, 297, 298f

Abdominal circumference (AC), 20, 227, 232, 514

fetal weight estimation based on and,

1177t–1178t

in gestational age estimation, 240, 242t, 1159t–1160t, 1165t

in large and small for gestational age fetuses, 1180t

in late third trimester, 239t, 240

intrauterine growth restriction and, 248

measurement of, 237f, 237–238, 241f

errors in, 240, 242f

relationship with other biometric parameters, 246, 246t

femur length, 1177t–1179t

kidney circumference, 342

thoracic-to-abdominal circumference ratio, 436, 494, 498f

Abdominal pregnancy, 1028, 1038, 1041f–1042f

Abdominal wall defects, fetal, 625–631

abnormal umbilical cord development and, 751–752

gastroschisis, 27, 43, 43f, 80, 218, 220f, 627–631, 630f–631f, 1137f

in pentalogy of Cantrell, 159–160, 160f

in prune-belly syndrome, 164–165, 165f

MRI imaging of, 820, 827f

omphalocele, 43, 43f, 75–76, 76f, 75–76, 76f, 126, 126f, 159–160, 160f, 218, 219f, 625–627, 626f–629f

physiologic midgut herniation, 625, 625f

vs. normal findings, 1117f, 1136f–1137f

Abdominal wall musculature

fetal, 320, 326f

maternal, 891–893, 894f

Abnormal uterine bleeding. *See* Uterine

bleeding, abnormal

Abortion, spontaneous

complete, 202t

due to chromosomal defects, 29, 70

first trimester risk factors for, 205–214

abnormal amnion development, 211, 212f–214f

gestational age, 205

heart rate irregularities, 206–207, 209f–210f

intrauterine blood, 205–206, 207f–208f

large yolk sac, 208–209, 210f–211f

maternal factors, 211–214

small sac size-growth delay, 207–208

in progress, 202t

incomplete, 202t

missed, 201

prevalence of, 200

recurrent, 211–214

related to prenatal diagnostic procedures, 50

in multiple gestations, 51

retained products of conception after, 202, 203f

threatened, 200–201, 202t

hCG levels in, 214

with abnormal gestational sac, 203–204, 203f–204f

with absent intrauterine sac, 201–202

with gestational sac but no cardiac activity, 205

with gestational sac without an embryo or yolk sac, 202

Abortion, therapeutic, retained products of

conception after, 935, 939f, 939–940

Abruptio placentae, 18, 207f, 730–731,

731f–732f, 729, 773

hyperechoic area behind placenta simulating, 1109f–1110f

Abscess

breast, 1090, 1090f, 1094

tubo-ovarian, 974

Absent pulmonary valve syndrome, 553

AC. *See* Abdominal circumference (AC)

Acalvaria, 369

ACC. *See* Agenesis of corpus callosum (ACC)

Acetylcholinesterase, amniotic fluid levels of, 44

Acheira, 462

Achciropodia, 462

Achondrogenesis, 113–115, 114f, 116, 320,

451–452, 452f, 453t, 452

genetics of, 452

nosology of, 429t

prevalence of, 424, 424t, 452

Achondrogenesis (*Continued*)

subtypes of, 113–115, 452, 453t

three-dimensional imaging in, 435t

Achondroplasia, 115–116, 115f–116f, 383, 447–449, 448f

femur length in, 436, 448–449

genetics of, 33, 34, 449

growth hormone treatment for, 449

heterozygous, 19, 449

homozygous, 448–449

prevalence of, 424, 424t, 447

severe, with developmental delay and

acanthosis nigricans, 449

three-dimensional imaging in, 435t, 848

Acid-base status, fetal biophysical profile and, 785–787, 786f–787f, 788

Acidemia, percutaneous umbilical cord blood sampling in, 252, 253

Acinar dysplasia, 501

ACOG (American College of Obstetricians and Gynecologists)

criteria for fetal lung maturity, 242

guidelines of, 7, 8, 9t–12t

Acoustic shadowing, 305

ACR. *See* American College of Radiology (ACR)

Acrania, 369

Acromelia, 425

Adams-Oliver syndrome, 464

Adenofibroma, ovarian, 979

Adenomyosis, 927–930, 1004, 1058–1060

clinical presentation of, 1059

definition of, 1058

diagnosis of, 1059

endometrial cancer and, 928–930, 930f

epidemiology of, 1058–1059

leiomyoma and, 1056f, 1058f

MRI of, 1056f, 1058f, 1059f, 1059–1060

pathophysiology of, 1059

prevalence of, 1058

sonographic appearance of, 928, 929f–930f

treatment of, 928

vs. leiomyomata, 928, 930t, 932, 934f, 1056

Adenosine, 576

Adenovirus infection, 694

Adhesion formation, postoperative, 968–969

Adnexa. *See also* Fallopian tube(s); Ovary(ies)

assessment in ectopic pregnancy, 1028,

1029f–1033f

torsion of, 968, 979–981, 982f–983f, 1101f

fetal, 811

ultrasound evaluation of, 14, 19, 968–983

Adnexal mass(es), 968–979, 1067–1073

artifacts, pitfalls and normal variants in

imaging of, 1100f–1101f, 1103f

clinical significance of, 1067



Adnexal mass(es) (*Continued*)

- cystic
  - benign-appearing lesions, 1069, 1072f
  - malignant-appearing lesions, 1069, 1072f
- discriminating between benign and malignant masses, 969–970
- Doppler imaging, 969–970
- MRI, 1068–1069
- ultrasound morphology, 969, 970f–971f, 972t
- due to ectopic pregnancy, 1021, 1029f, 1029–1030, 1031f–1032f, 1034f
- endometrioma, 974, 975f, 989, 990f, 1060, 1061f–1062f, 1069
- epidemiology of, 1067
- expectant management of, 968
- hemorrhagic corpus luteum cyst, 974, 976f
- imaging diagnosis of, 1067–1068
- in pelvic inflammatory disease, 974, 977f
- incidental ultrasound detection of, 968–969
- mature cystic teratoma, 968, 972–974, 973f, 981f, 989–991, 990f, 1069, 1070f
- bowel simulating, 1101f
- MRI of, 811, 813f–814f, 979, 1068–1073, 1070f–1073f
- ovarian fibroma, fibrothecoma, thecofibroma, thecoma, Brenner tumor, and other benign solid tumors, 976–978, 978f, 1069, 1071f
- ovarian masses in pregnant patient, 979, 981f
- ovarian serous cystadenoma, mucinous cystadenoma, and adenofibroma, 979, 980f
- paraovarian cyst, 974–976, 978f
- peritoneal pseudocyst, 976, 978f
- predominantly solid lesions, 1069
- preoperative staging of, 1072–1073
- surgical removal of, 968
- complications of, 968–969
- ultrasound morphology for making specific diagnosis of, 970–972, 972t
- with distinctive imaging features, 1069
- ADPKD (autosomal-dominant polycystic kidney disease), 654, 655t, 656–658, 657f–658f
- Adrenals
  - fetal, 326f, 344, 345f, 670f, 670–671, 1142f
  - calcifications in, 671, 671f
  - corticomedullary differentiation of, 670, 670f
  - lying down adrenal sign of renal agenesis, 644f, 670
  - masses in, 670–671, 671f, 671t
  - neonatal, 298f
- Adrenogenital syndrome (AGS), 666, 670, 670f
- AFI. *See* Amniotic fluid index (AFI)
- AFP. *See* Alpha-fetoprotein (AFP)
- AFV. *See* Amniotic fluid volume (AFV)
- Agenesis of corpus callosum (ACC), 78, 78f, 353, 355, 376–377
- complete, 376, 376f
- interhemispheric cysts and, 377, 850f
- lipomas and, 384, 385f
- MRI of, 376f, 819f
- partial, 376–377, 377f
- syndromes associated with, 377, 378t
- with absence of septum pellucidum, 377, 379f
- Aglossia-adactylia syndrome, 463
- AGS (adrenogenital syndrome), 666, 670, 670f
- Agyria, 151
- Aicardi syndrome, 34, 116–117, 377
- Airway obstruction
  - congenital high, 503, 504f–505f
  - due to micrognathia, 409
  - due to neck tumors, 415, 416
  - MRI evaluation of, 820, 824f–825f

- AIUM. *See* American Institute of Ultrasound in Medicine (AIUM)
- Alagille syndrome, 32t, 117f, 117–118
- Alcohol exposure, 39t, 131–133, 132f
- Alkaline phosphatase (ALP), 454–455
- Allantoic cyst, 665, 666f, 752
- Allantois, 634, 642, 745
- ALP (alkaline phosphatase), 454–455
- Alpha-fetoprotein (AFP), 7, 42–45
- amniotic fluid levels of, 42, 43f, 44, 45
- elevated maternal serum levels of, 42–44, 43f, 45t
- causes of, 44, 45t
- Down syndrome and, 43f, 45, 45t, 60, 60t, 67, 70–71
- neural tube defects and, 42–44, 43f, 45t, 60t, 369
- other defects and, 43f, 44–45
- perinatal outcome and, 47
- placental mesenchymal dysplasia and, 962
- trisomy 18 and, 45t, 46, 60t, 103
- fetal serum levels of, 42, 43f, 44
- gestational age and, 44
- Ambiguous genitalia, 666, 667f
- AMC (arthrogryposis multiplex congenita), 94, 123, 123f, 469–470, 470f, 469–470, 470f
- three-dimensional imaging of, 834f–855f
- Amelia, 462
- American College of Obstetricians and Gynecologists (ACOG)
  - criteria for fetal lung maturity, 242
  - guidelines of, 7, 8, 9t–12t
- American College of Radiology (ACR)
  - Breast Imaging Reporting and Data System, 1082, 1085t, 1088
  - guidelines of, 7, 8, 9t–12t
- Imaging Network research study of
  - ultrasound for breast cancer screening, 1085
- Practice Guideline for the Performance of the Breast Ultrasound Examination, 1095
- American Institute of Ultrasound in Medicine (AIUM), 919
- biometric measurements recommended by, 227
- guidelines of, 4, 7, 8, 9t–12t
- statement on ultrasound safety, 891
- American Joint Committee on Cancer, 1066
- American Society for Reproductive Medicine, 986, 1001
- Amiodarone, 576
- Amniocentesis, 49, 49f
- in diagnosis of Down syndrome, 98–99
- in diagnosis of fetal anemia, 682, 682f, 693
- in multiple gestations, 51
- in twin gestations, 290
- maternal age recommendations for, 98
- risks of, 50
- therapeutic, in twin-to-twin transfusion syndrome, 176, 283, 286, 773, 775, 872, 873t
- Amniography, CT, 814–815, 816f
- Amnion. *See* Amniotic membrane
- Amnionity, in twin gestations, 272–273, 273t, 274f
- Amnioreduction, in twin-to-twin transfusion syndrome, 176, 283, 286, 773, 775, 872, 873t
- Amniotic band syndrome, 27, 80, 118–119, 118f–119f, 218, 218f
- atypical facial clefts and, 403
- congenital amputations due to, 27, 462
- vs. normal amnion, 1118f
- Amniotic cavity, 185f, 190f, 196–198, 744
- enlarged relative to crown rump length, 211, 213f

- Amniotic fluid, 758–775, 1144f–1145f
- acetylcholinesterase levels in, 44
- alpha-fetoprotein levels in, 42, 43f, 44
- digestive enzymes in, 615
- echogenic, 760
- intramembranous flow of, 758, 759f
- mucopolysaccharides in, 693, 693f
- neuraminic acid in, 693, 694f
- physiology of, 758–760
- sludge in, 760
- sources of, 758
- transmembranous flow of, 758, 759f
- “trapped,” 1125f
- Amniotic fluid index (AFI), 762–765, 763f, 763t, 1181t–1183t
- birthweight and, 768
- frequency of assessments in high-risk patient, 769–770
- in polyhydramnios, 771
- in twin pregnancy, 774, 775f
- intrapartum, 769
- limitations of, 766–767
- normal values by gestational age, 763t
- sensitivity of, 763–764
- Amniotic fluid volume (AFV), 17, 758–775.
  - See also* Oligohydramnios; Polyhydramnios
- anatomic structures involved in regulation of, 758, 759f
- by gestational age, 759–760, 760f
- correlation with fetal weight, 760
- distribution in upper vs. lower quadrants, 764
- fetal swallowing and, 334, 759
- in biophysical profile, 781t, 782, 783f, 787
- in multiple gestations, 17
- in obese patients, 17
- in twin pregnancy, 774–775, 774f–775f
- twin-to-twin transfusion syndrome, 175–176, 280–281, 281f, 282f, 773, 775–776, 775f–776f, 871–872
- maternal intravascular volume, hydration and, 760
- medication effects on, 791–792, 791t–792t
- normal, 761f, 762f
- oligohydramnios, 767–770
- polyhydramnios, 770–774
- qualitative, 767
- role of kidneys in, 758–759
- role of lungs in, 759
- thresholds for abnormalities in, 762–763
- ultrasound estimation of, 760–767, 761f–764f
- amniotic fluid index, 762–765, 763f, 763t
- Doppler imaging, 766
- fetal position and, 765
- frequency of assessments in high-risk patient, 769–770
- in obese patient, 765, 765f
- inter- and intraobserver variation in, 761f, 761–762
- measurement of maximum vertical pocket, 762, 762f
- 1-cm rule, 762
- pitfalls in, 764f–766f, 765–766
- Amniotic membrane, 1145f–1146f
- development of, 185f–186f, 188f, 188–189, 190f, 745
- abnormalities of, 211, 212f–214f
- ultrasound detection of, 196–197, 199f
- vs. large yolk sac, 211, 214f
- with no embryo, 211, 213f
- Amniotic sac. *See* Gestational sac
- Amniotic septostomy, 775
- Amputations, congenital, 27, 462f, 462–463
- Anal atresia, 177, 177f, 468, 610f, 610–611
- Anembryonic pregnancy, 203–204

- Anemia, fetal  
 diagnosis of, 681–684  
   amniocentesis, 682, 682f  
   choice of surveillance method, 683–684  
   middle cerebral artery Doppler, 682–683, 683t, 683f–684f, 797, 798t, 1188f  
 due to hematologic disorders, 690t  
 intrauterine transfusion for, 684, 687, 687f  
 maternal red cell alloimmunization and, 678, 679t  
 mechanism of hydrops fetalis secondary to, 679
- Anencephaly, 344, 368–369, 370f  
 alpha-fetoprotein levels and, 43, 43f  
 first trimester diagnosis of, 216–217, 217f, 1118f  
 incidence of, 368t  
 malformations associated with, 368
- Aneuploidy, 29–32. *See also* Chromosomal abnormalities; *specific syndromes*  
 biochemical screening for, 45t, 45–47, 60t, 62–63  
 first trimester ultrasound screening for, 60–69  
 frequency of, 70  
 monochorionic twins discordant for, 872  
 nonimmune hydrops and, 74f, 74–75, 692t  
 prenatal sonographic features of, 71–97  
   agenesis of corpus callosum, 78, 78f  
   brachycephaly, 97, 97f  
   cardiac defects, 72, 73f, 74f  
   cerebellar abnormalities, 77f, 77–78  
   choroid plexus cysts, 86f, 86–88, 87t, 389  
   cleft lip/palate, 79, 80f  
   clubfoot, 92f, 92–93, 470  
   cystic hygroma, 63–64, 73–74, 74f, 414–415  
   diaphragmatic hernia, 75, 75f  
   duodenal atresia, 73, 74f  
   ear length, 91f, 91–92  
   echogenic intracardiac focus, 84–85, 84f–85f  
   extremity abnormalities, 92–95, 92f–96f  
   facial anomalies, 78–79, 79f, 80f  
   genitourinary anomalies, 80, 81f  
   holoprosencephaly, 78, 78f, 79f, 143–145, 144f, 144t  
   hydrocephalus, 76, 77f  
   hydrothorax, 75, 75f  
   hyperechoic bowel, 85f, 85–86  
   iliac wing angle, 90–91, 91f  
   in trisomy 13, 73t  
   in trisomy 18, 72t  
   in trisomy 21, 72t, 98  
   nasal bones, 64–65, 82, 88f, 88–90, 89f, 89t  
   nuchal fold, 60t, 61f–63f, 61–64, 81–82, 81f–82f  
   ocular anomalies, 79f, 80, 80f  
   omphalocele, 75–76, 76f, 626  
   placental thickening, 723  
   pyelectasis, 83f, 83–84  
   short long bones, 82t, 82–83, 83t  
   single umbilical artery, 95–97, 96f  
   spina bifida, 76, 77f  
   strawberry-shaped skull, 97, 97f  
   ventriculomegaly, 76, 76f  
 risk factors for, 71  
 screening in twin gestations, 288–290, 289t  
 second trimester ultrasound screening for, 98–106  
 sex chromosome, 31, 31t  
 soft markers for, 21, 71  
 techniques for prenatal diagnosis of, 54f, 54–55
- Aneurysm  
 ductus arteriosus, 557–558, 560f  
 umbilical artery, 753  
 vein of Galen, 386f, 386–387
- Angelman syndrome, 32t
- Angiotensin II antagonists, 646
- Angiotensin-converting enzyme inhibitors, 39t
- Ankle joint, 307, 309–311, 310f–311f, 316f
- Anomalous pulmonary venous connection, 534, 542f–543f
- Anophthalmia, 80, 407–408
- Anosteogenesis. *See* Achondrogenesis
- Anovulation, 993, 994f–995f
- Antiarrhythmic agents, 576
- Antibiotic prophylaxis  
 for fetoscopy, 869–870  
 for shunt placement, 871  
 to prevent preterm birth in women with short cervical length, 717
- Anticardiolipin antibodies, 726, 729
- Anticipation, genetic, 35–36
- Anti-La/SSB antibodies, 574, 576–577
- Anti-Ro/SSA antibodies, 574, 576–577
- Antithyroid medications, 416, 416f
- Antley-Bixler syndrome, 456
- Anus, 338f
- Anysospondyly, 456
- Aorta  
 abdominal, 326f, 328, 328f, 329, 330f, 332f  
   in situs abnormalities, 523  
 ascending  
   abnormal alignment of, 553f, 554  
   abnormal arrangement of, 554–555, 555f  
   dilatation of, 553–554  
   size in relation to main pulmonary artery, 552, 1194f  
   Doppler imaging of peak velocity of, 804, 805t, 1189t  
   measuring diameter of, 1194f–1196f  
   origin of branch pulmonary arteries from, 557, 558f  
   thoracic, 329, 330f, 341f
- Aortic arch, 332f  
 double, 558, 562f  
 interruption of, 565, 566f  
 measuring diameter of, 1195f  
 obstructive lesions of, 565  
 position relative to trachea, 516  
 positional abnormality of, 558, 561f  
 reversed flow in, 534, 538, 541f  
 tubular hypoplasia of, 565  
 V- or Y-confluence view of, 565
- Aortic arch view of fetal heart, 523, 525f–526f
- Abnormalities on, 527t, 565
- Aortic stenosis, in utero repair of, 882, 882f
- Aortic valve, 804f
- Apert syndrome, 37t, 119–121, 120f, 407, 411–412, 412f, 435t
- Apgar score, 780, 783
- Apodia, 462
- Appendicitis, maternal, 810, 810f–811f
- “Apple peel” atresia, 599
- Arachnoid cyst, 387–388, 388f  
 MRI of, 817, 822f  
 vs. vestigial remnants of Blake’s pouch, 1126f
- Arcuate artery(ies), 900, 902f, 925, 925f, 1110f  
 postmenopausal calcification of, 925, 926f
- Arcuate uterus, 926f, 927, 928f, 1001, 1003f, 1051f  
 MRI of, 1053
- Arcuate venous plexus, 901–902, 903f
- Arcola, 1081
- Arm, 311f
- Arnold-Chiari malformation, 121f, 121–123, 122t  
 frequency of brain and spine anomalies with, 372t  
 spina bifida and, 121, 122f, 370, 879
- ARPKD (autosomal-recessive polycystic kidney disease), 654, 655t, 655–656, 656f–657f
- Arrhythmias, fetal, 571–576, 572t  
 bradyarrhythmias, 573–575, 574f  
 embryonic bradycardia and, 207  
 nonimmune hydrops and, 688, 689t, 694  
 premature atrial contractions, 572–573  
 premature ventricular contractions, 573  
 tachyarrhythmias, 575–576, 575f–576f
- ART. *See* Assisted reproductive technology (ART)
- Arteriovenous anastomoses, in twin-to-twin transfusion syndrome, 281–283, 283f–284f
- Arteriovenous malformations (AVMs)  
 iatrogenic uterine, 935, 937f  
 vein of Galen aneurysm, 386f, 386–387
- Arthrogryposis multiplex congenita (AMC), 94, 123, 123f, 469–470, 470f  
 three-dimensional imaging of, 854f–855f
- Artifacts, 1155f–1156f  
 bowel gas, 1099f  
 calvarial reverberation, 347f, 358, 358f  
 in fetal stomach, 1155f  
 on three-dimensional ultrasonography, 859, 860f–861f  
 side lobe, 1155f
- Ascites, fetal, 75, 75f, 502f, 613, 1141f  
 congenital high airway obstruction and, 503  
 hydrops fetalis and, 676, 677f–678f, 679, 688  
 in cytomegalovirus infection, 133f, 134  
 in Fraser syndrome, 138f  
 urinary, 648, 649  
 vs. abdominal wall musculature, 320, 326f  
 vs. pseudoascites, 320, 1133f, 1137f
- Ashkenazi Jews, 41, 41t, 42
- Asphyxia, fetal, nonstress test for detection of, 780
- Asphyxiating thoracic dysplasia, 124, 124f, 457t, 457–458, 624, 624f
- Asplenia, heterotaxy with, 523, 527–528, 528t, 529f–530f
- Asplenia-polysplenia syndromes, 124f, 124–125, 125t
- Assisted reproductive technology (ART), 1006–1013. *See also* In vitro fertilization (IVF)  
 determining optimal timing for insemination, 991  
 endometrial assessment at time of embryo transfer, 1010–1012  
   Doppler imaging, 1010–1011, 1011f  
   imaging-based uterine scoring system, 1011  
   motion analysis, 1012, 1012f  
   three-dimensional imaging, 1011  
 in vitro maturation–in vitro fertilization protocols, 1008  
 multiple pregnancies and, 267, 268–269  
 ovarian stimulation protocols, 1006–1009, 1008f  
   ovarian hyperstimulation syndrome, 1008–1009, 1009f  
 perfollicular vascularity in preovulatory follicles and, 988–989, 1008  
 ultrasound-guided embryo transfer, 1012f, 1012–1013  
 ultrasound-guided oocyte retrieval, 1009–1010, 1010f
- Association, 113
- Astrocytoma, 384–385
- Atelosteogenesis, 451
- Atria of heart, 330f, 340f, 341f, 517f, 533f  
 measuring dimensions of, 1193f
- Atrial bigeminy, 573, 574f
- Atrial flutter, 572t, 576, 576f  
 nonimmune hydrops and, 694
- Atrial septum, 515, 517f
- Atrioventricular block, 572t, 573–575, 574f, 577
- Atrioventricular canal defect, in Down syndrome, 72, 73f



Atrioventricular connections, 528, 531–534  
     biventricular, 531–532, 534f  
     discordant, 531–532, 535f–536f  
     univentricular, 532, 534f, 538f  
 Atrioventricular septal defect, 548–551, 548f–551f  
 Atrioventricular septum, 515  
 Atrioventricular valves, 515, 518f, 577  
     Doppler imaging of, 803, 803f  
 Autosomal-dominant disorders, 33–34  
     paternal age and, 33, 33f  
     penetrance and variable expression of, 34  
 Autosomal-dominant polycystic kidney disease (ADPKD), 654, 655t, 656–658, 657f–658f  
 Autosomal-recessive disorders, 34  
 Autosomal-recessive polycystic kidney disease (ARPKD), 654, 655t, 655–656, 656f–657f  
 AV reentrant tachycardia, 575f, 575–576  
 AVMs (arteriovenous malformations)  
     iatrogenic uterine, 935, 937f  
     vein of Galen aneurysm, 386f, 386–387  
 Axillary lymph nodes, 1082  
     evaluation in breast cancer patients, 1096  
     in chronic lymphocytic leukemia, 1084f  
     metastatic breast cancer in, 1084f  
     tuberculosis in, 1083f  
 Axillary vessels, 1081

## B

Bacterial vaginosis, 712  
 Balanced translocations, 32  
 Ballantyne syndrome, 677–678, 878  
 Banana sign, 121, 121f, 370, 371f  
 Bardet-Biedl syndrome, 655, 659, 659f  
 Barker hypothesis, 250  
 Basal body temperature (BBT), 991, 993  
 Basal ganglia, 349  
 Basal short-axis view of fetal heart, 523, 524f  
     abnormalities on, 527t, 565  
 Basilar artery, 346  
 Battledore placenta, 751  
 BBT (basal body temperature), 991, 993  
 Beckwith-Wiedemann syndrome, 35, 126–127, 126f–127f, 383, 409, 409f, 568, 616, 646, 663, 671, 962  
     omphalocele in, 126, 126f, 627, 628f  
     placenta in, 723, 724f  
 Beemer-Langer syndrome, 457t, 458–459  
 Betamethasone  
     effect on fetal biophysical profile, 791, 791t  
     for atrioventricular block, 574  
     for congenital cystic adenomatoid malformation, 878  
 Biceps femoris muscle, 314f  
 Bicornuate uterus, 910, 926, 926f, 927f, 1001, 1003f, 1051f  
     MRI of, 1053, 1053f  
 Biliary atresia, extrahepatic, 621, 622f  
 Biliary cirrhosis, 458  
 Biliary disease, maternal, 810, 812f  
 Binder syndrome, 410, 411f  
 Binocular distance, 241, 1160t  
 Biochemical screening (Continued)  
     in second trimester, 70–71  
     pregnancy-associated plasma protein A, 60, 60t  
     quadruple screen, 45t, 46t, 60, 60t, 63, 63f, 67, 68, 71  
     third-trimester pregnancy complications after, 47  
     unconjugated estriol, 45t, 45–46, 47, 60, 60t  
 Biometric parameters, 13, 20, 226–227, 232–261  
     abdominal circumference, 20, 227, 232, 237f, 237–238, 240, 241f, 242f, 242t  
     biparietal diameter, 20, 227, 232–235, 233f–234f, 238t, 238–239, 239t, 1159t–1160t, 1172t  
     calculation of gestational age from, 245–247, 246t  
     clinical applications of, 247–260  
         accelerated fetal growth, 253–255, 258t  
         interval fetal growth and growth potential, 255–260, 259f  
         intrauterine growth restriction, 247–250, 258f  
     colonic echogenicity, 244–245  
     determining value of, 227  
     femur length, 13, 20, 227, 232, 235–237, 236f, 240–241  
     fetal weight estimation and, 247  
     foot length, 244, 1169t–1170t  
     head circumference, 13, 20, 227, 232, 234f, 234–235, 239–240, 240t, 1163t–1164t  
     in diagnosis of pulmonary hypoplasia, 435–436, 439f, 440t, 441t, 494, 498t, 498f–499f  
     in diagnosis of skeletal dysplasias, 425, 429, 432t, 433t  
     in first trimester, 232  
     in gestational age estimation, 226–227, 232–241, 1159t–1160t  
     in large and small for gestational age fetuses, 1180t  
     in second and third trimesters, 232, 238–239, 239t, 242, 1160t  
     inferior facial angle, 445, 445f  
     interpretation of, 23f  
     lung-to-head ratio, 494, 499f  
     mandible/maxilla ratio, 445, 446f  
     measurement of, 232–238  
         ocular, 241, 394t  
     placental grading, 244  
     relationships between, 246, 246t  
     secondary, 1160t  
     small intestinal peristalsis, 244  
     thoracic circumference, 440t, 494, 498t, 643  
     transition from crown rump length to, 232  
     transverse cerebellar diameter, 241–242, 243t, 244, 1160t, 1171t  
 Biophysical profile (BPP), 780–792  
     acute markers in, 784  
     advantages of, 780  
     algorithm for clinical use of, 788–790, 789f  
     amniotic fluid volume in, 781t, 782, 783f, 787, 789t  
     Apgar score and abnormal score on, 783  
     central nervous system centers for activities of, 784, 784t, 785  
     completion of examination for, 782–783  
     definition of normal and abnormal components of, 789t  
     duration of testing for, 783, 785  
     fetal acid-base status and, 785–787, 786f–787f, 788  
     fetal breathing movements in, 781t, 782, 783, 783f, 788–789, 789t  
     fetal movements in, 781t, 782, 789t  
     fetal reactivity in, 781t  
     fetal tone in, 781t, 789t  
 Biophysical profile (BPP) (Continued)  
     gradual hypoxia concept and, 787–788  
     in diabetic pregnancy, 788  
     in management of high-risk pregnancy, 788  
     in post-term pregnancy, 788  
     intrauterine growth restriction and, 788, 789  
     medication effects on, 791–792, 791t–792t  
     modified, 788–789, 789f  
     nonstress test in, 780–782, 782f, 783, 788–789, 789t  
     normal periodicity and, 784–785, 787  
     of growth-restricted fetus, 788  
     of twins, 788  
     oligohydramnios and, 783, 789  
     original findings for, 783–784  
     perinatal death and score on, 783–784  
     physiologic basis for, 784t, 784–785  
     placental grading and, 784, 787  
     preterm premature rupture of membranes and, 788, 790–791  
         to detect intra-amniotic infection, 790t, 790–791, 791f  
     scoring systems for, 781t, 782, 783, 787  
     technique for, 780–783  
     validation of, 784  
     variations by gestational age, 785, 785t  
     with acoustic stimulation, 783  
 Biopsy  
     breast, 1088–1091, 1092f, 1157f  
     endometrial, 942–943, 1065–1066  
 Biparietal diameter (BPD), 20, 227, 232–235, 238–239, 363  
     cephalic index and, 239  
     head shape—corrected, 239  
     in dolichocrphaly, 1123f  
     in first trimester, 230–232  
     in gestational age estimation, 238t, 238–239, 239t, 1159t–1160t, 1172t  
     in large and small for gestational age fetuses, 1180t  
     in late pregnancy, 238–239, 239t  
     in microcephaly, 382, 382t  
     in second trimester, 226, 238  
     long bone length and, 82t, 82–83  
     measurement of, 232–235, 233f–234f  
     errors in, 232–232, 233f, 235f, 238–239  
     head circumference and, 235  
     nasal bone length and, 90  
     relationship with other biometric parameters, 246, 246t  
     femur length, 1179t  
     widest, 233  
 BI-RADS (Breast Imaging Reporting and Data System), 1082, 1085t, 1088  
 Birth defects. *See* Congenital anomalies  
 Birth trauma, macrosomia and, 254  
 Birthweight, 1175t. *See also* Fetal weight  
     amniotic fluid index and, 768  
     association of prenatal ultrasound with, 4  
     maternal and fetal adverse events and, 254  
     percentiles at term, 258t  
     polyhydramnios and, 773  
 Bladder, fetal  
     development of, 641f, 642  
     enlargement of, 647, 647f, 664, 665, 666f  
     causes of, 649, 652t  
     exsufflation of, 665, 665f  
     filling and emptying of, 343, 642  
     imaging of, 299, 337f, 338f, 343–344, 344f, 608f, 642, 642f–643f, 664  
     in prune-belly syndrome, 164–165, 164f–165f  
     malformations of, 665  
     nonvisualization of, 664–665  
     pseudomegabladder, 642  
     relation of umbilical arteries to, 320, 328f, 344f, 642, 642f

- Bladder, fetal** (*Continued*)  
 responses to urinary tract dilatation, 649, 651f, 652f  
 volume of, 343–344
- Bladder, maternal**  
 anatomic relationships of, 891, 892f  
 with incarcerated uterus, 923  
 anatomy of, 915–916, 915f–916f  
 angle of, 891, 893f  
 artifacts, pitfalls, and normal variants in  
 imaging of, 1098f–1099f, 1104f  
 displacement by masses in space of Retzius, 894  
 diverticulum of, 1099f  
 filling for transabdominal sonography, 698, 887, 891  
 masses mimicking, 891, 893f  
 urine stream in, 1098f
- Bladder outlet obstruction (BOO)**, 80, 648, 649, 664, 665, 923
- Blake's pouch**  
 cyst of, 377, 378, 379, 381f  
 vestigial remnants of, 1126f
- Blastocyst**, 182t, 184–185, 184f–186f, 721, 744
- Bleeding, uterine**. *See* Uterine bleeding, abnormal
- Blighted ovum**, 201, 202t, 203
- Blood flow**. *See also* Circulation  
 corpus luteal, in first trimester, 214  
 fetoplacental, 249f  
 uteroplacental insufficiency and, 249  
 ovarian, 991–992  
 uteroplacental  
 development of, 185, 186–188, 188f  
 in first trimester, 191, 193f–194f, 214
- Blood type of fetus**, 681
- Body stalk anomaly**, 751
- Bone(s)**. *See also* Ossification; Skeletal dysplasias;  
*specific bones*  
 bowing of, 435  
 in campomelic dysplasia, 127–128, 128f, 435, 437f, 456  
 in thanatophoric dysplasia, 437f, 449  
 demineralization of, 435, 437f  
 determining degree of ossification of, 320  
 development of, 420–421, 420f–421f  
 intramembranous ossification, 421f, 421–422  
 endochondral, 421f, 421–422  
 imaging of, 305–320, 421  
 artifacts, pitfalls, and normal variants, 1147f–1151f  
 three-dimensional, 305  
 in osteogenesis imperfecta, 156f–157f, 156–158  
 long, 305, 308f  
 degree of curvature of, 435, 437f  
 degree of mineralization of, 435, 437f  
 fractures of, 435, 438f  
 identification of, 308–309  
 length of (*See also* Femur length (FL);  
 Humerus, length of)  
 gestational age and, 14, 242, 1166t–1168t  
 in achondroplasia, 115, 115f  
 in Down syndrome, 82t, 82–83, 83t  
 normal values for, 432t–433t  
 relationship with head circumference, 425, 433f  
 measurement of, 311, 434–435  
 compared with head circumference, 425, 433f  
 in diagnosis of skeletal dysplasias, 425, 429, 432t, 433t  
 metaphyseal flaring of, 435  
 visualizing cartilaginous ends of, 305, 308f–310f, 311  
 of neonate, 423f  
 ossification of, 421–422, 422f, 421–422, 421f–422f
- BOO** (bladder outlet obstruction), 80, 648, 649, 664, 665, 923
- Bowel**. *See also* Colon; Small intestine  
 fetal  
 gestational age and echogenicity of, 244–245  
 normal herniation into umbilical cord, 1117f  
 perforation of, 602–603, 602f–604f  
 pseudohyperechogenic, 1139f  
 maternal  
 bowel gas artifact vs. ovarian cyst, 1099f  
 simulating ovarian cystic teratoma, 1101f
- BPD**. *See* Biparietal diameter (BPD)
- BPP**. *See* Biophysical profile (BPP)
- BPS** (bronchopulmonary sequestration), 493, 502–503, 503f–504f
- Brachial plexus injury**, macrosomia and, 254
- Brachial vessels**, 329
- Brachiocephalic artery**, 329, 332f
- Brachycephaly**, 97, 97f, 411
- Brachydactyly**, 443, 443t  
 in fibula aplasia complex brachydactyly, 463
- Brachytherapy, breast**, 1094–1095
- Bradycardia**, 571, 573–575, 574f  
 embryonic, 207, 209f–210f, 212f  
 nonimmune hydrops and, 694  
 sinus, 573
- Brain**. *See also specific disorders*  
 abnormalities of  
 absence of septum pellucidum, 377, 379f  
 agenesis of corpus callosum, 78, 78f, 376–377, 376f–377f, 378t, 819f, 850f  
 anencephaly, 43, 43f, 216–217, 217f, 368–369, 370f, 1118f  
 arachnoid cyst, 387–388, 388f, 822f  
 Arnold-Chiari malformation, 121f, 121–123, 122f, 122t  
 brachycephaly, 97, 97f  
 choroid plexus cysts, 86f, 86–88, 87t, 1126f–1127f  
 cisterna magna enlargement, 77–78  
 cysts, 387–389, 388f  
 Dandy-Walker malformation, 77, 77f, 377–380, 379f–380f, 380t  
 dural sinus thrombosis, 387, 387f  
 encephalocele, 217, 217f, 821f  
 holoprosencephaly, 78, 78f, 79f, 143–145, 144f, 144t, 217, 217f, 373f–375f, 373–376, 1118f  
 hydranencephaly, 382  
 hydrocephalus, 76, 77f  
 hydrolethrus syndrome, 146–147  
 in Aicardi syndrome, 116  
 in Apert syndrome, 120  
 in chondroectodermal dysplasia, 460  
 in fetal toxoplasmosis syndrome, 135, 135f  
 in Jeune syndrome, 458  
 in Meckel syndrome, 153, 153f  
 in septo-optic dysplasia, 166–167, 167f  
 in thanatophoric dysplasia, 450  
 in tuberous sclerosis, 819f  
 in Walker-Warburg syndrome, 178, 178f  
 interhemispheric cyst, 850f  
 intracranial hemorrhage, 366, 380, 381f, 385, 851f  
 intratentorial hematoma, 820f  
 lissencephaly, 151–153, 152f  
 megalencephaly, 383, 384t  
 microcephaly, 382–383, 382t–383t, 384f  
 neuronal migration anomalies, 385–386, 386f, 819f  
 periventricular leukomalacia, 382, 382f  
 porencephaly, 380–382, 382f, 818f  
 prenatal diagnosis of, 344  
 pseudoporencephaly, 382  
 schizencephaly, 382, 382f  
 tumors, 383–385, 384t, 385f
- Brain** (*Continued*)  
 vein of Galen aneurysm, 386f, 386–387  
 ventriculomegaly, 76, 76f, 817, 818f, 819f  
 fetal, 299, 299f, 344–360, 345f–359f, 363, 364f–365f  
 artifacts, pitfalls, and normal variants in  
 imaging of, 1124f–1130f  
 basic scan of, 363  
 fissures and sulci of, 353, 355f, 357f  
 lateral ventricles of, 351–352  
 MRI of, 366, 367f, 816–817, 818f–822f  
 neurosonogram of, 363  
 normal developmental anatomy of, 345–346, 363, 364f–365f  
 relative echogenicity of structures of, 349–350  
 sonographic “skeleton” of, 350–351  
 three-dimensional imaging of, 363, 365f, 843–848, 844f, 849f–852f, 856f  
 transverse cerebellar diameter of, 241–242, 243t, 244, 363, 1160t, 1171t  
 of 6-month-old infant, 349f  
 of neonate, 297, 298f, 346
- Breast anatomy**, 1080–1082  
 blood supply, 1081  
 fat lobules, 1081, 1082f, 1157f  
 lymphatic drainage, 1081–1082, 1082f–1084f  
 microcysts, 1081, 1081f  
 retroareolar, 1081, 1081f  
 skin, 1080, 1081f, 1082
- Breast biopsy, ultrasound-guided**, 1088–1091, 1092f, 1157f
- Breast cancer**  
 ductal carcinoma in situ, 1086  
 establishing extent of disease bilaterally, 1096  
 inflammatory, 1086, 1090f  
 invasive ductal carcinoma, 1078f–1080f, 1088f  
 lumpectomy for  
 fluid collection at site of, 1093–1094, 1094f  
 planning radiation therapy after, 1094–1095, 1095f  
 recurrent carcinoma after, 1089f  
 scarring after, 1094, 1094f  
 MRI in, 1091, 1096  
 negative predictive value of ultrasound and  
 mammography for, 1086–1088  
 staging of, 1096–1097  
 ultrasound-guided biopsy in diagnosis of, 1088–1091, 1092f  
 vs. artifact, 1156f  
 with axillary node metastases, 1084f
- Breast Imaging Reporting and Data System (BI-RADS)**, 1082, 1085t, 1088
- Breast implant rupture**, 1091–1093, 1093f
- Breast ultrasound**, 1077–1097, 1156f–1157f  
 equipment and technique for, 1077–1080  
 Doppler imaging, 1079–1080  
 dynamic range, 1078, 1079f  
 elastography, 1079  
 orthogonal imaging, 1157f  
 spatial compounding, 1077–1078, 1078f, 1079f  
 tissue harmonic imaging, 1079, 1079f  
 transducers, 1077, 1078–1079  
 examination procedure, 1080  
 in chronic lymphocytic leukemia, 1084f  
 in tuberculosis, 1083f  
 indications for, 1085–1097  
 breast implant rupture, 1091–1093, 1093f  
 establishing extent of breast cancer  
 bilaterally, 1096  
 guidance of interventional procedures, 1088–1091, 1092f  
 multiple masses, 1096  
 palpable and nonpalpable abnormalities, 1085–1088



Breast ultrasound (*Continued*)

- indications for (*Continued*)
  - palpable and nonpalpable abnormalities (*Continued*)
    - calcifications, 1086, 1089f
    - density of breast tissue, 1085–1086, 1087f–1088f
    - fatty breast, 1086
    - inflammatory processes, 1086, 1090f
    - negative predictive value, 1086–1088
    - postsurgical breast and radiation therapy planning, 1093–1095, 1094f–1095f
    - staging, 1096–1097
    - young, pregnant, and lactating patients, 1095–1096
  - lesion feature analysis and interpretation, 1082, 1085, 1085t
  - mammography and, 1077, 1078f, 1080, 1097 (*See also* Mammography)
    - integrated reporting of, 1082, 1085
    - measuring masses detected by, 1080, 1080f
    - of abscess, 1090f
    - of fibroadenoma, 1079f, 1085, 1086f
    - of invasive ductal carcinoma, 1078f–1080f
    - of lipoma, 1088, 1091f
    - patient positioning for, 1080
- Breathing movements, fetal, 494
  - brain center for, 784t, 785
  - gradual hypoxia concept and, 787
  - in biophysical profile, 781t, 782, 783, 783f
  - medication effects on, 791–792, 791t–792t
  - variations by gestational age, 785
- Breech presentation, 14, 16f, 17f, 81
- Brenner tumor, 976–978
- Breus mole, 964, 965f
- Broad ligament, 895–898, 898f, 905, 922
  - myoma of, 1054, 1103f
- Bronchial arches, 493
- Bronchogenic cyst, 504, 505f
- Bronchopulmonary sequestration (BPS), 493, 502–503, 503f–504f
- BUN Trial, 62

**C**

- Calcaneus, 307, 310f–311f, 311, 316f
- Calcarine fissure, 353
- Calcification(s)
  - adrenal, 671, 671f
  - arcuate artery, 925, 926f
  - breast, 1085, 1086, 1089f
  - hepatic, 619, 619f
  - in papillary muscle, 84, 1135f
  - intrapertoneal, 602–603, 602f–604f, 613
  - of leiomyoma, 932, 933f, 1056, 1110f
  - placental, 725, 727f
- Calvarial reverberation artifact, 347f, 358, 358f
- Calvarium, 305, 314, 1124f. *See also* Skull
  - absence of, 369
  - nonossified, 320
  - ossification of, 358
- Campomelic dysplasia, 37t, 127–128, 128f, 435, 435t, 437f, 456–457, 848
- Canadian Fertility and Andrology Society, 986
- Carbamazepine, 37, 39t
- Cardiac activity, fetal. *See also* Heart rate, fetal
  - adaptations to uteroplacental insufficiency, 249, 251–252
  - in first trimester, 185, 194–195, 195t, 196f, 205
  - absence of, 205, 206f
- Cardiac axis, 528, 533f
- Cardiac cycle, 577, 579f
- Cardiac output, 579–580, 802
  - uteroplacental insufficiency and, 249, 252
- Cardiac rhythm, fetal, 569–577
  - abnormalities of, 571–576, 572t (*See also* Arrhythmias, fetal)
    - bradycardia, 573–575, 574f
    - irregular rhythm, 571–573
    - tachycardia, 575–576, 575f–576f
  - normal, 569–570
  - sonographic techniques for assessment of, 570–571
    - ECG, 571
    - M mode echocardiography, 570, 570f
    - pulsed wave Doppler, 570–571, 571f
    - tissue Doppler, 571, 572f
- Cardiac tumors, 567–569
  - fibroma, 567–568
  - hemangioma, 568–569, 569f
  - prognosis for, 569
  - rhabdomyomas, 173f, 173–174, 567, 569f
  - teratoma, 568
- Cardiomegaly, 532
- Cardiomyopathy, 581–582
  - dilated, 582
  - hypertrophic, 581–582
  - restrictive, 582
- Cardiovascular system, fetal, 511–582. *See also* Heart, fetal; *specific structures*
  - function of, 577–582, 578f
  - abnormal, 581f, 581–582
  - cardiac cycle, 577, 579f
  - cardiac output, 579–580
  - diastolic, 579f, 580–581, 581f
  - myocardial performance index, 581
  - shortening fraction, 579, 580f
  - techniques for assessment of, 577–579
  - imaging of, 320–329, 326f–333f
- Caroli disease, 617, 618f
- Carotid artery(ies), 329, 332f, 341f, 414
- Carpal bones, 307, 308f, 309–311, 313f
- Carrier (heterozygote) screening, 40–42, 41t
  - for cystic fibrosis, 41t, 41–42, 42f
  - for Tay-Sachs disease, 41
  - recommendations for, 41t
  - techniques for, 41
- Cartilage, 305, 308f–310f, 309, 318–320
  - destruction of, in diastrophic dysplasia, 455
  - development of, 420
- Cat eye syndrome, 32t
- Cataract, congenital, 408, 408f
- Caudal regression syndrome, 128–130, 129f
- Caudate nucleus, 351f, 355f, 358f
- CAVB (complete atrioventricular block), 572t, 573–575, 574f
- Cavitation, 4
- Cavum septi pellucidi/cavum vergae complex, 355–356, 356f, 1128f
- Cavum septum pellucidum, 838f, 1128f
  - absence of
    - agenesis of corpus callosum and, 78, 78f, 376f, 376–377, 379f
    - in septo-optic dysplasia, 166–167, 167f
    - lobar holoprosencephaly and, 373, 840f
  - syndromes associated with, 377
- CCAM. *See* Congenital cystic adenomatoid malformation (CCAM)
- CCAM volume ratio (CVR), 878
- CDH. *See* Congenital diaphragmatic hernia (CDH)
- Cebocephaly, 406f
- Celiac axis, 329, 332f
- Central nervous system (CNS), fetal. *See also* Brain; Spine; *specific structures*
  - aneuploidy and anomalies of, 76–78, 76f–79f
  - centers for biophysical profile activities, 784, 784t, 785

Central nervous system (CNS), fetal (*Continued*)

- MRI evaluation of, 366, 367f, 816–817, 818f–822f
  - normal sonographic anatomy of, 344–360, 345f–360f, 363–366, 364f–366f
  - polyhydramnios and anomalies of, 771, 772t
- Central venous pressure, hydrops and, 681
- Cephalic index, 239, 246t, 1179t
- Cephalic presentation, 14, 15f, 16f
- Cephalocele, 371–372
  - conditions associated with, 372t
  - in Walker-Warburg syndrome, 178, 178f
  - location of, 371
  - MRI of, 373f
  - occipital, in Meckel syndrome, 153f, 153–154
  - outcome of, 372
- Cephalocentesis, 368
- Cerebellar vermis, 354f, 356, 357f, 1125f–1126f
  - agenesis of, 77f, 77–78
  - hypoplastic, 378–379, 381f
  - MRI of, 819f
  - in Dandy-Walker malformation, 77, 77f, 377–378, 379f
  - in Joubert syndrome, 379, 381f
  - normal values by gestational age, 381t
- Cerebellum, 349, 351, 353f, 354f
  - abnormalities of, 77f, 77–78
  - aneuploidy and, 77f, 77–78
  - transverse cerebellar diameter, 241–242, 243t, 244, 363, 1160t, 1171t
- Cerebral artery(ies)
  - anterior, serpent crawling under the skull sign, 375, 375f
  - middle (MCA), 329, 346
    - Doppler evaluation of, 252, 256f, 795–797, 797f–798f, 797t–798t
    - in diagnosis of fetal anemia, 682–683, 683f–684f, 693
    - in intrauterine growth restriction, 804, 806
    - resistance index, 797t, 798t
    - gestational age and velocity of flow in, 683t
    - in uteroplacental insufficiency, 252, 256f
  - posterior, 346
  - three-dimensional imaging of, 837f, 848
- Cerebral hemispheres, 358
- Cerebral palsy
  - hemolytic disease of fetus and newborn and, 688
  - in multiple pregnancies, 266, 271–272
- Cerebral vesicles, 363, 364f
- Cerebrohepatorenal syndrome, 130, 130f
- Cerebrospinal fluid, 349, 352f, 1129f
- Cervical carcinoma, 1060–1065
  - clinical presentation of, 1060–1062
  - clinical staging of, 1063, 1063t
  - diagnosis of, 1063
  - epidemiology of, 1060
  - histopathology of, 1062
  - human papillomavirus and, 1062
  - lymph node assessment in, 1065
  - MRI of, 1063–1065, 1064f–1065f
  - treatment of, 1063
  - tumor size assessment in, 1065
- Cervical cerclage, 715–717
  - abdominal, 707f, 708f, 710
  - cervical measurements with, 707, 707f–708f, 710
  - efficacy in prevention of preterm birth, 715–716
  - ultrasound-indicated cerclage, 716–717, 717t
  - in twin gestations, 290–291, 716, 717, 717t
  - transvaginal ultrasound to safely avoid placement of, 717, 718
  - vaginal, 707f, 710
- Cervical index, 707
- Cervical length (CL)
  - abnormal, 708
  - after 30 weeks, 708

- Cervical length (CL)** (*Continued*)  
 before 14 weeks, 702, 708  
 dynamic changes in, 708, 1107f  
 functional, 704  
 in multiple pregnancies, 709t, 710  
 in preterm labor, 717–718  
 in singleton high-risk gestation, 709t, 709–710  
 in singleton low-risk gestation, 709, 709t  
 in triplet pregnancy, 709t, 710  
 in twin pregnancy, 290–291, 291t, 709t, 710  
 normal, 708  
 obscured by rectal gas, 699, 699f, 701f  
 preterm birth and, 290–291, 291t, 703–704, 708–710, 709t  
 infection and, 712, 715, 717–718  
 pathophysiology of, 712, 715  
 prevention of, 715–717  
 technique for measurement of, 704, 704f–705f  
 total, 704  
 with transfundal pressure, 708
- Cervical pregnancy**, 1028, 1029f, 1037, 1040f
- Cervical teratoma**, 415, 415f, 416
- Cervix**, 698–718  
 anatomy of, 905–907, 922, 1049, 1050  
 endometrial cancer extending to, 1067, 1068f  
 funneling of, 704–706, 706f  
 measuring length of, 704  
 measuring width of, 704, 706f  
 preterm birth and, 704–706  
 shapes of, 704, 706f  
 vs. lower uterine segment contractions, 701–702, 703f  
 insufficiency of, 712, 715  
 lymphatic drainage of, 904  
 manual examination of, 703–704  
 MRI of, 1049f, 1049–1050  
 other measurements of, 706–707  
 with cerclage in place, 707, 707f–708f, 710  
 ultrasound evaluation of  
 artifacts, pitfalls, and normal variants, 701–702, 702f–703f, 1104f–1107f  
 bladder filling for, 698  
 three-dimensional, 710–712, 711f–715f  
 transabdominal, 698, 701f  
 translabial, 698–699, 699f, 701f  
 transvaginal, 699–701, 700f–701f, 702t, 910  
 gestational age and frequency of, 708–709  
 in diagnosis and management of preterm labor, 717–718  
 safety of, 703  
 technique for, 702t  
 to predict onset of spontaneous labor, 718, 718f  
 to predict preterm birth, 702–710  
 to predict success of labor induction and mode of delivery, 718  
 to safely avoid cervical cerclage, 717, 718
- Cesarean delivery**  
 after hysterotomy, 869  
 after preterm premature rupture of membranes, 769  
 as risk factor for placenta accreta, 739, 743f  
 for placenta previa, 735  
 of monoamniotic twins, 277  
 scar pregnancy after, 1038, 1041f
- CF**. *See* Cystic fibrosis (CF)
- CHAOS** (congenital high airway obstruction), 503, 504f–505f
- CHARGE** association, 131, 131t
- Charlie M** syndrome, 463
- CHD**. *See* Congenital heart disease (CHD)
- Chemotherapy**  
 for endometrial cancer, 1066  
 for persistent gestational trophoblastic neoplasia, 961
- Chemotherapy** (*Continued*)  
 tamoxifen for abnormal uterine bleeding, 949  
 teratogenicity of, 39t
- Chest**. *See* Thorax
- Chiari** malformation. *See* Arnold-Chiari malformation
- CHILD** syndrome (congenital hemidysplasia with ichthyosiform erythroderma and limb defects), 162, 463
- Chloride** diarrhea, congenital, 605, 606f, 607t
- Choanal** atresia, 131, 131t
- Choledochal** cyst, 621–623, 622f–623f, 669f
- Chondrodysplasia**  
 platyspondylic lethal, 429t, 435t  
 punctata, 410, 429t, 435t
- Chondroectodermal** dysplasia, 446, 457t, 459–460, 459f–460f
- Chondrogenesis** imperfecta, 113
- Chorioamnionitis**  
 preterm premature rupture of membranes and, 769  
 biophysical profile for detection of, 790t, 790–791, 791f  
 short cervical length and, 712
- Chorioangioma**, 676, 742–744, 744f–745f
- Choriocarcinoma**, 951, 951f, 954f, 963f, 963–964
- Chorion** frondosum, 188, 721, 758
- Chorion** laeve, 185, 187f, 188f, 189, 721
- Chorionic** bump, 204, 204f, 1115f
- Chorionic** cavity, 187f  
 low-level echogenic material in, 198, 200f  
 ultrasound detection of, 198
- Chorionic** membrane, 188f
- Chorionic** sac, 227. *See also* Gestational sac
- Chorionic** villi, 185–186, 188, 187f, 188f, 190f, 227, 721
- Chorionic villus** sampling (CVS), 49f, 49–51  
 in multiple gestations, 51, 290  
 limb reduction deficits after, 50–51  
 nuchal translucency screening related to  
 availability of, 67  
 oligohydramnios and, 770  
 timing of, 67
- Chorionicity**, 19, 51  
 in twin gestations, 269, 270, 270f, 272  
 first trimester evaluation, 272–273, 273t, 274f  
 in second and third trimesters, 273  
 membrane layers, 275–276  
 membrane thickness, 274–275  
 monoamniotic twins, 276–279, 277f–278f  
 multiple sonographic markers for, 276  
 survival and, 271, 271f  
 “twin-peak” sign, 273–274, 275f–276f
- Choroid** plexus, 345f–348f, 349, 363, 1129f  
 dangling, 76, 77f  
 papilloma of, 385
- Choroid** plexus cyst(s), 86f, 86–88, 388f, 388–389  
 aneuploidy and, 87t, 87–88, 389  
 trisomy 18, 30, 87, 389  
 trisomy 21, 88  
 in normal fetus, 86–87, 1126f–1127f  
 vs. corpus striatum, 347f
- “Christmas tree” atresia, 599
- Chromosomal** abnormalities, 29–33. *See also* specific syndromes  
 congenital heart defects and, 53, 511  
 frequency of, 70, 215f  
 in abortuses, 29t  
 in twin gestations, 51  
 nonimmune hydrops and, 74f, 74–75, 692t  
 numeric, 29–32  
 aneuploidy, 29–31  
 frequency of, 29, 29t, 30t  
 maternal age and risk of, 29t, 30t  
 polyploidy, 29, 31–32
- Chromosomal** abnormalities (*Continued*)  
 polyhydramnios and, 773  
 pregnancy loss due to, 29, 70  
 prenatal diagnosis of, 54, 1198t–1200t  
 biochemical screening, 42–47, 60  
 first trimester ultrasound screening, 60–69  
 G banding, 53f, 54  
 second trimester ultrasound screening, 70–106  
 skeletal dysplasias and, 447  
 soft markers for, 21  
 structural, 29, 32–33  
 deletions, 32, 32t  
 duplications, 32  
 marker chromosomes, 32–33  
 translocations, 29, 32
- Chronic** lymphocytic leukemia, 1084f
- Chylothorax**, 75, 508
- Cine** clip technology, 299
- Cingulate** sulcus, 353, 357f
- CIFO** (congenital intestinal pseudo-obstruction), 604–605, 606f, 607t
- Circle** of Willis, 252, 255f, 329, 333f, 795
- Circulation**. *See also* Blood flow  
 fetal, 577, 578f, 802  
 hepatic, 616, 616f  
 portal, 252, 320–328, 327f–329f, 338  
 pulmonary, 329, 330f, 331f, 339–340, 341f, 493, 497f  
 uteroplacental  
 development of, 185, 186–188, 188f, 722  
 in first trimester, 191, 193f–194f, 214
- Circummarginate** placenta, 723, 724
- Circumvallate** placenta, 723–724, 725f–726f, 1103f  
 vs. uterine synechia, 724, 726f
- Cisterna** magna  
 cerebellar hypoplasia with enlargement of, 77–78  
 in Dandy-Walker malformation, 377–379, 379f–381f  
 prominent, as normal variant, 1125f
- Cisterns**, 349, 352f, 356, 358f
- CL**. *See* Cervical length (CL)
- Clavicle(s)**, 305, 307–308, 312f  
 in Jeune syndrome, 458  
 length of, 1160t, 1169t  
 ossification of, 422
- Cleft** lip/palate, 36, 397–401  
 aneuploidy and, 79, 80f  
 anomalies associated with, 399, 403t  
 bilateral, 399, 400f, 401t–402t, 403f–404f, 407f, 846f–847f  
 ectrodactyly ectodermal dysplasia-cleft lip/palate syndrome, 465  
 embryologic development and, 397–399, 398f–400f  
 imaging of, 333, 394, 399, 403f–405f, 1121f–1122f  
 three-dimensional, 404f–405f, 444, 843, 846f–848f  
 in Pierre Robin syndrome, 161  
 incomplete, 846f  
 median cleft lip, 402, 405f–406f  
 MRI of, 401, 405f  
 prognosis for, 401  
 recurrence risk for, 399, 401t  
 skeletal dysplasias with, 444, 445t  
 spectrum of severity of, 399, 400f, 401t–402t  
 unilateral, 399, 400f, 401t–402t, 403f–405f
- Cleidocranial** dysplasia, 435t, 460–461, 461f
- Clinodactyly**, 93f, 93–94, 425
- Clitoris**, 665–666
- Cloacal** dysgenesis sequence, 613, 615f
- Cloacal** exstrophy sequence, 631, 633f, 827f
- Cloacal** malformation, 665, 669f, 820, 827f



- Clomiphene citrate, 999
- Clubfoot, 28f, 470
- aneuploidy and, 92f, 92–93, 470
  - cleft lip/palate and, 399
  - in diastrophic dysplasia, 455
  - three-dimensional imaging of, 854f
- Clubhand, 465–470
- radial, 465–468, 466t
  - ulnar, 465, 467t, 468
- CMV infection. *See* Cytomegalovirus (CMV) infection, intrauterine
- CNS. *See* Central nervous system (CNS), fetal
- Coarctation of aorta, 528, 534, 538, 544f–545f, 565
- vein of Galen malformation with, 546, 547f
- Cocaine, 39t
- Coccygeus muscle, maternal, 895, 897f
- Collagenopathies, 456
- Colloid osmotic pressure, hydrops and, 681
- Colon
- fetal, 337, 337f, 338f, 605–606, 608f, 1141f, 605–606
  - duplication cyst of, 591
  - hausta of, 244, 605
  - in Hirschsprung disease, 607–609, 609f
  - nomograms of diameter of, 606, 607f–608f
  - peristalsis in, 606
  - vs. dilated small bowel, 337
  - maternal rectosigmoid, 916f, 916–917
- COM syndrome, 152
- Comparative genomic hybridization, 55, 55f, 56f
- Complete atrioventricular block (CAVB), 572t, 573–575, 574f
- Computed tomography (CT), 808
- amniography, 814–815, 816f
  - for maternal abdominal pain, 810
  - appendicitis, 810, 810f
  - for pelvimetry, 811, 815f
  - of maternal hydronephrosis, 810–811
  - radiation exposure from, 808, 1205t
  - safety in pregnancy, 808–809
  - three-dimensional helical, in skeletal dysplasias, 434, 436f
- Conceptional age, 225
- Conceptus period, 182t, 184–185, 189
- Confined placental mosaicism, 50
- Congenital adrenal hyperplasia, 47
- Congenital anomalies, 112–180. *See also specific structures and anomalies*
- aneuploidy and, 71–80, 73f–81f
  - association of prenatal ultrasound with, 4
  - associations, 113
  - causes of, 27, 27f, 215, 215f
  - classification of, 27, 28f, 112–113
  - counseling parents about, 21–22
  - craniofacial, 78–79, 392 (*See also* Craniofacial anomalies)
  - definition of, 27
  - deformations, 27, 28f, 112–113
  - developmental disorders, 27–29, 28f
  - diagnosis in first year of life, 18
  - disruptions, 27, 28f, 112–113
  - dysplasia, 112–113
  - embryonic susceptibility to teratogens, 37, 38f, 215, 215f
  - fetal surgery for, 867–882
  - gestational age and risk of, 215, 215f
  - health care costs associated with, 18
  - incidence of, 18
  - malformations, 27, 28f, 112–113
  - maternal serum alpha-fetoprotein and, 42–45, 43f, 45t
  - medications associated with, 38–40, 39t, 135, 1202t–1204t
  - monozygotic twins discordant for, 291–292, 872
- Congenital anomalies (*Continued*)
- mortality due to, 18
  - multifetal pregnancy reduction for twins discordant for, 291–292
  - of neural axis, 368–389
  - parental concerns about, 18
  - prenatal diagnosis of, 48–53
  - aneuploidy screening, 60–69
  - sonographic, 5–6
  - confirming accuracy of, 867
  - effect of oligohydramnios on, 770
  - fetal lie and, 14
  - in first trimester, 5t, 5–6, 6t, 13, 181–182, 215–218, 216f–220f
  - in second and third trimesters, 18–19
  - pitfalls in, 13, 216, 216f
  - three-dimensional, 841–862 (*See also* Three-dimensional ultrasonography)
  - testing, 53f, 53–55, 54f
  - recurrence risk for, 48
  - sequences, 27, 113
  - single gene disorders, 34–37
  - syndromes, 27, 113
  - teratogen-induced, 27, 37–40, 39t, 1202t–1204t
  - with complex inheritance, 36–37
- Congenital cystic adenomatoid malformation (CCAM), 493, 501–502, 501f–502f, 694
- CCAM volume ratio, 878
  - fetal surgery for repair of, 868, 878–879, 879f
  - hydrops and, 502, 502f, 878–879
  - pathological classification of, 878
- Congenital diaphragmatic hernia (CDH), 75, 75f, 500f, 505–507, 506f–508f
- anomalies associated with, 506
  - fetal tracheal occlusion for, 507, 874–878, 875f–877f, 876t, 878t
  - MRI evaluation for, 820, 823f
  - incidence of, 505
  - lung-to-head ratio and, 507, 874–876, 875f, 876t, 878, 878t
  - MRI of, 507, 508f, 820, 823f
  - prognosis for, 506, 507, 874, 876t, 878
  - pulmonary hypoplasia and, 506, 874–876, 876t
  - stomach location and, 506–507, 507f–508f, 594f, 1132f
- Congenital heart disease (CHD), 27, 36, 511–512, 514–567. *See also specific cardiac defects*
- clues to abnormality at each sonographic view, 523–565, 527t
  - aortic arch view, 527t, 565
  - basal short-axis view, 527t, 565
  - four-chamber view, 527t, 528, 531–551, 532t, 534f–551f
  - three-vessel view, 527t, 551–558, 552t, 553f–562f
  - transverse view of upper abdomen, 523, 527t, 527–528, 528t, 529f–530f
  - ventricular outflow tract views, 527t, 558–565, 563f–565f
  - conditions associated with, 511
  - asplenia-polysplenia syndromes, 125, 523, 527–528, 528t, 529f–530f
  - chondroectodermal dysplasia, 460
  - chromosomal abnormalities, 53, 72, 73f, 74f, 511
  - cleft lip/palate, 399
  - congenital diaphragmatic hernia, 506
  - Down syndrome, 30, 72, 73f
  - fetal rubella syndrome, 134
  - Goldenhar syndrome, 140
  - heterotaxy, 523, 527t, 527–528, 529f–531f, 531t
  - Holt-Oram syndrome, 145–146, 467
  - nonimmune hydrops, 688, 689t
  - Noonan syndrome, 155–156
- Congenital heart disease (CHD) (*Continued*)
- conditions associated with (*Continued*)
  - pentology of Cantrell, 159–160
  - polyhydramnios, 772t
  - single umbilical artery, 97
  - thrombocytopenia with absent radius syndrome, 467
  - 22q microdeletion syndrome, 32, 53, 53f, 558
  - VATER association, 468
  - Wolf-Hirschhorn syndrome, 179t
  - ductus-dependent, 566, 566t
  - fetal demise due to, 566
  - fetal screening examination for, 514–523
  - imaging technique and normal anatomy, 514–523, 516f–522f, 524f–526f
  - sequential segmental approach, 514, 514f
  - sonographic views, 514, 515f
  - incidence of, 511
  - nuchal translucency and, 60t
  - parental counseling about, 566
  - postoperative prognosis for, 567, 568t
  - prenatal diagnosis of, 53, 511–512
  - risk factors for, 512t
  - treatment of, 566–567
  - fetal surgery, 566, 882, 882f
- Congenital hemidysplasia with ichthyosiform erythroderma and limb defects (CHILD syndrome), 162, 463
- Congenital high airway obstruction (CHAOS), 503, 504f–505f
- Congenital intestinal pseudo-obstruction (CIPO), 604–605, 606f, 607t
- Congenital malformation sequence, 27
- Congenital pulmonary airway malformation (CPAM), 501
- Congenital pulmonary lymphangiectasia, 881
- Conjoined twins, 218, 220f
- Contractures
- in arthrogryposis multiplex congenita, 123, 123f, 469–470, 470f
  - in diastrophic dysplasia, 455
  - in lethal multiple pterygium syndrome, 151, 151f
  - in SC phocomelia syndrome, 464
  - in trisomy 18, 94, 95
- Contrast agents, 297
- Conus medullaris, fetal, 366, 366f
- Cooper ligaments, 1080–1081
- Coronary sinus, 515, 518f
- dilatation of, 534, 550f
- Corpus albicans, 184f, 911, 993, 997f
- Corpus callosum, 838f
- agenesis of, 78, 78f, 353, 355, 376–377
  - complete, 376, 376f
  - interhemispheric cysts and, 377, 850f
  - lipomas and, 384, 385f
  - MRI of, 376f, 819f
  - partial, 376–377, 377f
  - syndromes associated with, 377, 378t
  - with absence of septum pellucidum, 377, 379f
  - development of, 355
  - dysgenesis of, 353
  - imaging of, 355, 355f, 359f
  - three-dimensional, 846, 848, 849f
  - spina bifida and abnormalities of, 370
- Corpus hemorrhagicum, 911
- Corpus luteum, 182, 183f, 184f, 911, 992–997, 996f–997f
- fluid-filled cavity in, 993
  - growth of, 993
  - ultrasound detection of, 993
- Corpus luteum cyst, 911, 912f
- hemorrhagic, 974, 976f, 1032, 1033f
  - vs. ectopic pregnancy, 1028, 1030, 1031f–1033f, 1032, 1112f

- Corpus striatum, 347f
- Corticosteroids  
effect on fetal biophysical profile, 791, 791t  
for arioventricular block, 574–575  
for congenital cystic adenomatoid malformation, 878
- Coumarin anticoagulants, 39t
- Counseling  
about examination results, 21  
genetic, 48t, 48–49  
prescan, 18
- CPAM (congenital pulmonary airway malformation), 501
- Cranial fossae, 312
- Cranial meningocele, 371–372, 373f
- Cranial sutures, 411–412, 843, 849f
- Cranio cervical junction, 360, 360f
- Craniofacial anomalies, 78–79, 79f, 80f, 392  
conditions associated with  
achondroplasia, 447  
chondroectodermal dysplasia, 460  
cleidocranial dysplasia, 461  
congenital intracranial tumors, 384  
Down syndrome, 300  
fetal alcohol spectrum disorders, 132, 132f  
Fraser syndrome, 138  
Fryns syndrome, 139  
Goldenhar syndrome, 139–140, 140f  
holoprosencephaly, 143–144, 144f, 374, 402, 405f–406f  
Moebius sequence, 463  
Pallister-Killian syndrome, 158f, 158–159  
Pena-Shokeir syndrome, 159  
Pfeiffer syndrome, 161  
Prader-Willi syndrome, 163  
radial clubhand, 466t, 468  
Roberts syndrome, 166, 464  
SC phocomelia syndrome, 464  
Simpson-Colabi-Behmel syndrome, 167  
skeletal dysplasias, 443–445, 445f–446f, 445t–446t  
Smith-Lemli-Opitz syndrome, 169–170, 170t  
Wolf-Hirschhorn syndrome, 179t
- cranosynostosis, 410–412, 412f–413f
- facial clefts, 397–403  
atypical, 402–403, 405f–407f  
typical, 397–401, 398f–400f, 401t–403t, 403f–405f (See also Cleft lip/palate)
- facial dysmorphism, 410, 411f
- facial tumors, 409–410, 410f
- micrognathia, retrognathia, and macroglossia, 408–409, 409f
- MRI of, 397  
orbital and ocular defects, 407–408, 408f  
three-dimensional imaging of, 394–395
- Craniopharyngioma, 383, 385
- Craniosynostosis, 410–412, 412f–413f  
in Apert syndrome, 120f, 411–412, 412f  
in Crouzon syndrome, 411–412  
in Pfeiffer syndrome, 161, 412f, 413f
- Cri-du-chat syndrome, 32t
- CRL. See Crown rump length (CRL)
- Crouzon syndrome, 407, 411–412, 412f, 425
- Crown rump length (CRL), 13  
absent cardiac activity and, 205  
in first trimester, 185, 187f, 228–232, 230f  
amnion abnormalities and, 211, 213f  
biparietal diameter and, 230–232  
size for embryo detection, 228  
smaller than expected, 208  
in gestational age estimation, 200, 201t, 228–232, 230f, 231t, 1162t–1163t  
measurement of, 187f, 229, 230f  
of twins, 292–293  
transition to biometric parameters from, 232
- Cruciate ligaments of knee, 315f, 319f
- CT. See Computed tomography (CT)
- Cuboid, 310f, 311
- Cumulus oophorus, 905f, 911
- CVR (CCAM volume ratio), 878
- CVS. See Chorionic villus sampling (CVS)
- Cyclooxygenase inhibitors, 545
- Cyclopia, 79f, 80  
holoprosencephaly and, 143–144, 144f, 374, 406f
- Cyst(s)  
adrenal, 671, 671f  
allantoic, 665, 666f, 752  
arachnoid, 387–388, 388f, 817, 822f  
Blake's pouch, 377, 378, 379, 381f  
bronchogenic, 504, 505f  
choledochal, 621–623, 622f–623f, 669f  
choroid plexus, 86f, 86–88, 87t, 388f, 388–389, 1126f–1127f  
corpus luteum, 911, 912f, 1028, 1031f–1033f  
hemorrhagic, 974, 976f, 1032, 1033f  
decidual, 725, 1030–1032, 1036f  
dermoid, 968, 972–974, 973f, 981f, 989–991, 990f, 1069, 1070f  
enteric duplication, 591, 591f–592f, 595, 597, 597f  
Gartner duct, 913, 1005  
gliopendymal, 388  
idiopathic intra-abdominal, 624–625, 625f  
in congenital cystic adenomatoid malformation, 501–501, 501f–502f  
interhemispheric, with agenesis of corpus callosum, 377, 850f  
meconium, 603, 604f  
midabdominal, differential diagnosis of, 597–598  
nabothian, 910, 910f, 1005, 1102f  
neurenteric, 504, 506f, 591–592  
omphalomesenteric, 752  
ovarian, 668, 668f–669f, 970f–971f, 1112f  
theca lutein, 955, 955f, 956, 956f  
pancreatic, 624, 624f  
paraovarian, 974–976, 978f  
porencephalic, 380–382, 382f, 388  
renal (See Renal cystic diseases)  
splenic, 623  
transient hepatic, 616–617, 617f  
umbilical cord, 212f, 629f, 752, 752f, 1116f  
urachal, 665, 745  
vesicallantoic, 631–634, 634f  
vitelline duct, 209
- Cystadenocarcinoma, ovarian, 1069, 1072f
- Cystadenofibroma, 1069
- Cystadenoma  
mucinous, 971f, 979, 980f  
serous, 979, 980f, 1069
- Cystic fibrosis (CF), 41t, 41–42, 613  
carrier screening for, 41t, 41–42  
hyperechoic bowel in, 42, 42f, 86  
inheritance of, 34  
meconium ileus in, 601–602, 1138f  
nonvisualized gallbladder in, 621
- Cystic hygroma, 63f, 63–64, 73–74, 74f, 217, 218f, 414–415  
aneuploidy risk and, 63–64, 73–74, 414–415  
conditions associated with, 414–415  
acardiac twin, 287f  
Down syndrome, 73  
lethal multiple pterygium syndrome, 151, 151f  
Noonan syndrome, 155–156  
Turner syndrome, 64, 73, 74f, 154–155, 155f, 415  
development of, 414  
imaging of, 414f, 414–415  
nuchal translucency and, 63f, 63–64, 414
- Cystic hygroma (Continued)  
prognosis for, 415  
vs. cranial meningocele, 372  
vs. scalp hair, 302, 306f  
vs. “trapped” amniotic fluid, 372
- Cytomegalovirus (CMV) infection, intrauterine, 23f, 38, 39t, 133f, 133–134, 677f  
congenital brain lesions due to, 382  
hydrops and, 694  
renal, 663
- Cytotrophoblast, 185f, 721
- ## D
- Dacryocystocele, 408, 408f
- Dandy-Walker complex, 377, 378
- Dandy-Walker malformation, 77, 77f, 377–380, 379f–381f  
abnormalities associated with, 378, 380t  
distinguishing variants of, 377, 378, 379–380, 381f  
MRI of, 378, 379  
vs. arachnoid cyst, 388  
vs. Joubert syndrome, 379, 381f
- Dating a pregnancy. See Gestational age (GA)
- Daughter cyst sign, 668
- Decidua, 185, 721–722  
basalis, 185, 186, 187f, 188f  
capsularis, 185, 187f, 188, 189  
parietalis (vera), 185, 188f, 189, 189f
- Decidual cyst, 725  
in ectopic pregnancy, 1030–1032, 1036f
- Defecation, fetal, 606–607, 608f–609f
- Deformations, 27, 28f, 112–113. See also Congenital anomalies
- 7-Dehydrocholesterol, 169–170
- Dehydroepiandrosterone sulfate, 45
- Deletions, 32, 32t. See also Chromosomal abnormalities
- Delivery  
cesarean  
after hysterotomy, 869  
after preterm premature rupture of membranes, 769  
as risk factor for placenta accreta, 739, 743f  
for placenta previa, 735  
of monoamniotic twins, 277  
scar pregnancy after, 1038, 1041f  
transvaginal ultrasound of cervix to predict mode of, 718
- deMorsier syndrome, 377
- Dermatomyotome, 422
- Dermoid cyst, 968, 972–974, 973f, 981f, 989–991, 990f, 1069, 1070f  
bowel simulating, 1101f  
MRI of, 1069, 1070f
- Developmental disorders, 27–29, 28f
- Dexamethasone  
effect on fetal biophysical profile, 791, 791t  
for arioventricular block, 574–575
- Dextrocardia, 14, 528, 527t
- Diabetes mellitus, maternal, 40  
alpha-fetoprotein levels and, 44  
fetal biophysical profile and, 788  
macrosomia and, 254, 255, 771  
placental thickening and, 723  
polyhydramnios and, 771  
shoulder dystocia and, 255  
yolk sac diameter and, 208–209
- Diaphragm  
fetal, 341, 342f  
hernia of (See Congenital diaphragmatic hernia (CDH))  
normal development of, 505  
pelvic, 895



- Diaphysis, 305  
 femoral, 305, 309f, 310f
- Diarrhea, congenital chloride, 605, 606f, 607t
- Diastolic function, fetal, 579f, 580–581, 581f
- Diastrophic dysplasia, 116, 443, 455f, 455–456
- Didelphys uterus, 926, 926f, 927f, 1001, 1003f, 1051f
- MRI of, 1052, 1052f
- Diethylstilbestrol exposure, uterine anomalies and, 39t, 211, 926f, 927, 1003f, 1051f, 1053
- Diffusion-weighted imaging (MRI), 824
- DiGeorge sequence, 53, 54f
- Digital anomalies, 443  
 clinodactyly, 93f, 93–94, 425  
 in aglossia-adactylia syndrome, 463  
 in chondroectodermal dysplasia, 459, 459f–460f  
 in fibula aplasia complex brachydactyly, 463  
 in Fraser syndrome, 137–138, 138f  
 in Grebe syndrome, 464  
 in hydrolethrus syndrome, 146–147  
 in Jeune syndrome, 457–458  
 in Meckel syndrome, 153f, 153–154  
 in Pfeiffer syndrome, 161  
 in short rib–polydactyly syndromes, 429t, 439f, 459  
 in Smith-Lemli-Opitz syndrome, 169–170  
 in Yunis-Varon syndrome, 461  
 polydactyly, 95, 96f, 425  
 skeletal dysplasias associated with, 443, 443t  
 split hand and foot deformities, 465  
 syndactyly, 425  
 terminology for, 425
- Digoxin, 576
- Dilated cardiomyopathy, 582
- Disinfection of transvaginal probe, 888–889
- Disruptions, 27, 28f, 112–113. *See also* Congenital anomalies
- DNA  
 cell-free fetal, 55–56  
 mitochondrial, 36  
 techniques for analysis of, 54–55
- Documentation of ultrasound examination, 12t, 12–13
- Dolichocephaly, 1123f
- Doppler effect, 794, 794f
- Doppler ultrasonography, 250–253, 251f, 252t, 253f–257f, 794–806  
 in first trimester, 4, 214–215  
 absent cardiac activity on, 206f  
 of corpus luteal blood flow, 214  
 of gestational sac abnormalities, 204–205, 205f  
 of uteroplacental blood flow, 191, 193f, 214  
 temperature elevation due to, 4  
 of acardiac twin, 287, 287f  
 of adenomyosis, 928  
 of aorta, 804, 805t, 1189t  
 of arcuate venous plexus, 903f  
 of atrioventricular valves, 803, 803f  
 of axillary nodes in chronic lymphocytic leukemia, 1084f  
 of brachial vessels, 329  
 of breast, 1079–1080  
 of bronchopulmonary sequestration, 504f  
 of cerebral arteries, 252, 256f, 837f, 848  
 of circle of Willis, 333f, 795, 797f  
 of congenital cystic adenomatoid malformation, 501  
 of corpus luteum, 912f, 993, 996f, 997  
 hemorrhagic corpus luteum cyst, 974  
 of ductus venosus, 252, 256f–257f, 283, 285f, 327f, 799–800, 801f, 801t–802t, 1186t, 1190t  
 of dural sinus thrombosis, 387, 387f  
 of ectopic pregnancy, 204–205, 1032f, 1036, 1037f
- Doppler ultrasonography (*Continued*)  
 of endometrial polyps, 948, 948f  
 of fetal defecation, 607, 608f  
 of fetal venous circulation, 252, 256f, 798–800, 800f–801f, 801t–803t, 837f  
 of heart, 512, 513f, 800–804, 803f–804f, 804t–805t, 1189t  
 of hydatidiform mole, 957, 957f  
 of inferior vena cava, 799, 800f–801f  
 of intracranial vessels, 329  
 of intrafollicular flow, 905f  
 of intraovarian flow, 904, 906f  
 of intrauterine growth restriction, 251–253, 254f, 804–806  
 of lobar holoprosencephaly, 375, 375f  
 of middle cerebral artery, 252, 256f, 795–797, 797f–798f, 797t–798t, 1185t, 1187f  
 in diagnosis of fetal anemia, 682–683, 683f–684f, 693, 1188t  
 of mitral valve, 803, 803f, 804t, 1189t  
 of monoamniotic twins, 276–277, 277f, 278f  
 of ovarian artery, 904f  
 of ovarian blood flow, 991  
 of patent foramen ovale flow, 546, 547f  
 of pericardial fluid movement, 551  
 of perfollicular vascularity in preovulatory follicles, 988–989, 989f  
 of persistent gestational trophoblastic neoplasia, 961  
 of placenta, 744  
 chorioangioma, 743, 744f–745f  
 maternal floor infarction, 729f  
 placenta accreta, 739, 743f  
 placental abruption, 731  
 vasa previa, 735, 737, 740f–742f  
 of portal circulation, 252  
 of pulmonary artery and vein, 493, 497f, 515, 518f, 1189t  
 of pulmonary hypoplasia, 442, 500f, 500–501  
 of retained products of conception, 939, 939f  
 of semilunar valves, 803–804, 804f  
 of tracheal fluid flow, 442  
 of tricuspid regurgitation, 518f, 515–516  
 of tricuspid valve, 803, 803f, 804t, 1189t  
 of twin-to-twin transfusion syndrome, 281–283, 284f–285f, 872  
 of umbilical artery, 96, 251, 251f, 252t, 320, 327f, 344f, 642f, 795, 795f, 796t, 1184t–1185t, 1187f  
 of umbilical cord, 327f, 749f, 1146f  
 cyst, 1116f  
 entangled cords and galloping fetal heart rates, 277, 278f  
 velamentous cord insertion, 751, 752f  
 of umbilical vein, 252, 327f, 252, 327f, 800, 800f, 801f, 803t, 1185t  
 varix, 1143f  
 of uterine arteriovenous malformations, 935, 937f  
 of uterine artery, 251, 254f, 797–798, 799f, 799t, 900–901, 1184t  
 of uterus, 920  
 of vein of Galen aneurysm, 386, 386f  
 physical principles of, 794–795, 794f–795f  
 angle of insonation, 251, 253f, 794  
 commonly used indices, 795, 795f  
 three-dimensional, 835, 837f  
 to assess cardiac rhythm, 570–571, 571f  
 to discriminate between benign and malignant adnexal masses, 969–970  
 to estimate amniotic fluid volume, 766  
 transvaginal color flow, 887
- Dorsal sac, 144f, 373, 374f
- Double bleb sign, 211, 212f
- Double bubble sign, 73, 74f, 596, 597f, 624  
 transient, 597
- Double decidual sac (DSS) sign, 187f, 191, 192f, 228, 228f, 1024–1025, 1027f
- Double inlet left ventricle with discordant ventriculoarterial connection, 528, 536f, 556
- Double outlet left ventricle, 562
- Double outlet right ventricle, 554, 554f, 562, 565f
- Down syndrome, 30, 98. *See also* Trisomy 21  
 translocation, 30, 32
- Drash syndrome, 663, 664
- “Dropout” phenomenon, 907
- Drugs, teratogenic, 38–40, 39t, 135, 1202t–1204t
- DSS (double decidual sac) sign, 187f, 191, 192f, 228, 228f, 1024–1025, 1027f
- Du Pan syndrome, 463
- Duchenne muscular dystrophy, 33, 34, 34f
- Duct of Gartner, 913
- Ductal arch view of fetal heart, 523, 525f–526f  
 abnormalities on, 527t
- Ductus arteriosus, 329, 331f, 532, 802  
 absence of, 546  
 aneurysm of, 557–558, 560f  
 constriction of, 545–546, 546f, 557  
 ductus-dependent congenital heart diseases, 566, 566t  
 measuring diameter of, 1197f  
 neonatal treatment to maintain patency of, 566
- Ductus venosus, 322–325, 577, 616, 616f  
 Doppler evaluation of, 252, 256f, 327f, 799–800, 801f, 801t–802t, 1186t  
 in twin-to-twin transfusion syndrome, 283, 285f  
 in uteroplacental insufficiency, 252, 257f  
 peak velocity index, 802t, 1186t, 1190t  
 preload index, 801t, 1186t  
 pulsatility index, 802t, 1186t  
 S/a, 802t, 1186t  
 in first trimester, 65, 65f  
 right-to-left shunt at, 802
- Duodenal atresia, 19, 73, 74f, 596, 597f  
 esophageal atresia and, 591  
 polyhydramnios and, 771, 772f  
 trisomy 21 and, 30, 73, 74f, 596, 597
- Duodenum, fetal, 595, 596f, 1140f, 595–598  
 duplication cyst of, 591, 597, 597f  
 etiologies of dilatation of, 597, 598  
 obstruction of, 595–597  
 peristalsis in, 595, 596f
- Duplication cysts, enteric, 591, 591f–592f, 820, 826f
- Dura, 349, 360
- Dural sinus thrombosis, 387, 387f
- Dwarfism, thanatophoric. *See* Thanatophoric dysplasia
- Dysgerminoma, 1069
- Dysplasia, 112–113. *See also* Congenital anomalies
- Dyssegmental dysplasia, 456
- ## E
- E wave/A wave ratio  
 mitral valve, 803, 804t  
 tricuspid valve, 803, 804t
- E<sub>3</sub> (unconjugated estradiol), in aneuploidy screening, 45t, 45–46, 47, 60, 60t, 67, 71
- Ear, fetal, 300–302, 305f  
 anomalies of, 227  
 aneuploidy and, 91f, 91–92  
 in Beckwith-Wiedemann syndrome, 126f  
 in CHARGE association, 131, 131t  
 in fetal alcohol spectrum disorders, 132f  
 in Pallister-Killian syndrome, 158, 158f

- Ear, fetal (*Continued*)  
 anomalies of (*Continued*)  
   lateral facial clefts and, 402, 403  
   micrognathia/retrognathia and, 408  
   three-dimensional imaging of, 848, 848f, 857f
- Ear-head, 408
- Ebstein malformation, 528, 532, 538f  
   corrected transposition of great arteries with, 562, 565f
- ECG (electrocardiography), fetal, 571
- Echocardiography, fetal, 328–329, 330f–331f, 514–523, 1133f–1135f. *See also* Heart, fetal  
   clues to abnormality at each sonographic view, 523–565, 527t  
   aortic arch view, 527t, 565  
   basal short-axis view, 527t, 565  
   four-chamber view, 527t, 528, 531–551, 532t, 534f–551f  
   three-vessel view, 527t, 551–558, 552t, 553f–562f  
   transverse view of upper abdomen, 523, 527t, 527–528, 528t, 529f–530f  
   ventricular outflow tract views, 527t, 558–565, 563f–565f
- Doppler imaging, 512, 513f, 800–804, 803f–804f, 804t–805t  
   screening examination, 514–523  
     imaging technique and normal anatomy, 514–523, 516f–522f, 524f–526f  
     sequential segmental approach, 514, 514f  
     sonographic views, 514, 515f  
   three-dimensional, 512, 513f  
   to assess cardiac function, 577  
   to assess cardiac rhythm, 569–577
- Echogenic intracardiac focus (EIF), 84–85, 84f–85f
- Ectoderm, 744
- Ectopic hydatidiform mole, 963
- Ectopic pregnancy, 201, 1020–1044  
   abdominal, 1028, 1038, 1041f–1042f  
   algorithm for workup of, 1044f  
   assessment of adnexa in, 1028, 1029f–1033f  
   assessment of cul-de-sac in, 1026f, 1028–1029, 1034f  
   cervical, 1028, 1029f, 1037, 1040f  
   clinical presentation of, 1021  
   decidual cysts in, 1030–1032, 1036f  
   diagnosis of, 1024, 1034t  
   fertility after, 1044  
   hCG levels in, 214, 1022–1024, 1043–1044  
   in cesarean section scar, 1038, 1041f  
   in patient with intrauterine contraceptive device, 1021, 1022f  
   incidence of, 1020, 1021f  
   in vitro fertilization and, 1021–1022, 1023f  
   interstitial, 1028, 1029f, 1036–1037, 1038f–1039f  
   intrauterine pregnancy concurrent with, 1024, 1025f, 1039, 1042f  
   locations of, 1028, 1029f  
   management of, 1039, 1042–1044  
     expectant, 1043–1044  
     methotrexate, 1042–1043, 1043f  
     surgery, 1042  
     ultrasound-guided percutaneous treatment, 1043  
   mimics of, 1036, 1036f  
   mortality from, 1020  
   MRI in, 1039, 1041f  
   pseudogestational sac of, 189–191, 192f, 202, 204–205, 228, 1024–1027, 1025f–1028f, 1030, 1031f, 1035f  
   risk factors for, 1021t, 1021–1022  
   sonographic findings in, 1029–1036, 1034t  
     adnexal mass, 1021, 1029f, 1029–1030, 1031f–1032f, 1034f
- Ectopic pregnancy (*Continued*)  
   sonographic findings in (*Continued*)  
     artifacts, pitfalls, and normal variants, 1112f–1113f  
     Doppler imaging, 204–205, 1032f, 1036, 1037f  
     endometrium, 1030–1032, 1031f, 1035t, 1035f–1036f  
     free fluid, 983f–984f, 1026f, 1028–1029, 1029f–1031f, 1032, 1034f  
     normal sonogram, 1032, 1035f, 1036  
     transabdominal ultrasound in, 1026f, 1027  
     transvaginal ultrasound in, 1027  
     tubal, 1028, 1029f, 1111f  
   vs. abnormal early intrauterine pregnancy, 1025–1027, 1028f  
   vs. corpus luteum cyst, 1028, 1030, 1031f–1033f, 1032, 1112f  
   vs. incarcerated uterus, 923  
   vs. normal early intrauterine pregnancy, 1024–1025, 1025f–1028f
- Ectrodactyly, 465
- Ectrodactyly ectodermal dysplasia-cleft lip/palate syndrome, 465
- EDD (estimated date of delivery), 226, 227
- Edema  
   breast, 1086, 1090f  
   hereditary lymphedema, 141–142, 141f–142f  
   in Klippel-Trenaunay-Weber syndrome, 149f
- Edwards syndrome. *See* Trisomy 18
- EFW. *See* Estimated fetal weight (EFW)
- EIF (echogenic intracardiac focus), 84–85, 84f–85f
- Elastography, breast, 1079
- Elbow joint, 312f
- Electrocardiography (ECG), fetal, 571
- Electronic scalpel, 835, 837f
- Ellis-van Creveld syndrome, 446, 457t, 459–460, 459f–460f
- Embryo  
   detecting gestational sac without yolk sac or, 202, 228, 229f, 230  
   development in first trimester, 182t, 182–185, 184f–187f, 186t, 229, 231f  
   normal growth rate of, 200  
   sonographic detection of, 195t, 194–196, 195f–198f  
   susceptibility to teratogens, 37, 38f, 215, 215f
- Embryo transfer, 268–269  
   endometrial assessment at time of, 1010  
   progesterone on day of, 1012  
   ultrasound-guided, 1012f, 1012–1013
- Embryologic age, 181
- Embryonic demise, 201, 202t. *See also* Abortion, spontaneous  
   absent cardiac activity and, 205, 206f  
   gestational age and, 205  
   heart rate and, 206–207, 209f–210f  
   intrauterine blood and, 205–206, 207f–208f  
   large yolk sac and, 208–209, 209f–210f
- Embryonic disk, 189, 190f, 194, 195f, 196, 744
- Embryonic length, 200
- Embryonic number, 13
- Embryonic period, 8, 182t, 185  
   development during, 187f, 194–196, 196f–197f  
   safety of ultrasound during, 3–4
- Emphysema, congenital lobar, 504
- Encephalocele, 217, 217f, 371, 373f  
   MRI of, 821f  
   three-dimensional imaging of, 848, 852f  
   vs. fetal ear, 1124f  
   vs. scalp hair, 302
- Endocervical canal, 704, 705f
- Endoderm, 744
- Endometrial biopsy, 942–943, 1065–1066
- Endometrial canal, 907f, 910
- Endometrial carcinoma, 942, 1065–1067  
   adenomyosis and, 928–930  
   age-related incidence of, 942  
   clinical presentation of, 1065  
   diagnosis of, 1065–1066  
   epidemiology of, 1065  
   histopathology of, 1065  
   MRI of, 1066–1067, 1067f–1068f  
   prognosis for, 1065  
   risk factors for, 1065  
   staging of, 1066, 1066t  
   treatment of, 1066  
   with cervical extension, 1067, 1068f
- Endometrial curettage, 942
- Endometrial polyps, 945, 946f, 948f, 1005, 1007f
- Endometrioma, 974, 975f, 989, 990f  
   carcinoma within, 1060, 1062f  
   MRI of, 1060, 1061f–1062f
- Endometriosis, 926, 989, 1060  
   carcinoma and, 1060, 1062f  
   clinical features of, 1060  
   definition of, 1060  
   epidemiology of, 1060  
   etiology of, 1060  
   MRI of, 1060, 1061f–1062f  
   pathology of, 1060
- Endometrium, 922  
   anatomy of, 909f, 909–910  
   assessment at time of embryo transfer, 1010–1012  
   Doppler imaging, 1010–1011, 1011f  
   imaging-based uterine scoring system, 1011  
   motion analysis, 1012, 1012f  
   three-dimensional imaging, 1011  
   decidualized, blastocyst implantation into, 184, 185f  
   during menstrual cycle, 182–184, 183f, 189, 921f, 1000–1001, 1002f  
   in ectopic pregnancy, 1030–1032, 1031f, 1035f–1036f  
   MRI of, 1049–1050, 1049f–1050f  
   postpartum, 939, 939f  
   sonographic appearance in early pregnancy, 189  
   thickness of, 910, 1001, 1050, 1050f  
   retained products of conception and, 939  
   ultrasound evaluation of, 920, 1001
- Endoscopic fetal surgery. *See* Fetoscopy
- Enteric duplication cysts, 591, 591f–592f
- Environmental exposures, 27, 215, 215f  
   teratogens, 37–40  
     medications, 38–40, 39t, 135, 1202t–1204t
- Epiblast, 185f
- Epidermolysis bullosa, 594, 615
- Epiglottis, fetal, 339, 340f
- Epignathus, 409, 410f
- Epiphyses, 243–244, 244f, 245f, 305, 421, 1150f
- Epispadias, 666–668
- Epithelioid trophoblastic tumor, 964
- Equipment and technology, 8, 12, 12t, 297–299.  
   *See also* Transducers  
   for breast imaging, 1077–1080  
   for fetal cardiac examination, 512  
   for fetoscopy, 870  
   for radiofrequency ablation, 871  
   shunts, 870–871
- Erb-Duchenne palsy, 254
- Erythroblastosis fetalis, 678
- Esophageal atresia, 468, 589–591  
   anomalies associated with, 589  
   duodenal or pyloric atresia and, 591  
   incidence of, 589  
   outcome of, 589  
   polyhydramnios and, 590, 772, 772f  
   prenatal diagnosis of, 590, 590f  
   timing of diagnosis of, 590  
   types of, 589, 589f



- Esophagus, fetal, 333, 335f, 340f, 414, 588, 589f, 588-592  
 duplication cyst of, 591, 591f  
 laryngotracheoesophageal cleft, 591  
 motility patterns in, 598-599  
 pyloric atresia with dilatation of, 594, 595f  
 Estimated date of delivery (EDD), 226, 227  
 Estimated fetal weight (EFW), 14, 17, 19, 247, 255, 247, 255. *See also* Fetal weight  
 based on abdominal circumference and femur length, 1177t-1178t  
 equations for, 1174t-1175t  
 in intrauterine growth restriction, 248  
 in macrosomia, 254  
 in twin gestations, 1176t  
 of large for gestational age fetus, 254  
 oligohydramnios and, 770  
 Estriol, unconjugated (E<sub>3</sub>), in aneuploidy screening, 45t, 45-46, 47, 60, 60t, 67, 71  
 Estrogen, 182, 988  
 Ethmocephaly, 406f  
 Ex utero intrapartum treatment (EXIT), 817, 820. *See also* Fetal surgery  
 for neck mass, 416, 824f  
 for tracheal occlusion, 876, 876f  
 MRI evaluation for, 817, 824f  
 Exchange neonatal transfusion, for hyperbilirubinemia, 688  
 Exocoelomic cavity, 185f  
 Exocoelomic membrane, 185f  
 Exomphalos. *See* Omphalocele  
 Extraperitoneal fascia, 894  
 Eye, 312-314, 320f, 321f, 392  
 anomalies of, 79f, 80, 80f, 407-408  
 congenital cataract, 408, 408f  
 in cerebrohepato-renal syndrome, 130, 130f  
 in CHARGE association, 131, 131t  
 in fetal rubella syndrome, 134  
 in Jeune syndrome, 458  
 in Walker-Warburg syndrome, 178  
 microphthalmia, 407-408, 408f  
 nasolacrimal duct obstruction, 408, 408f  
 ocular biometry, 241, 394t
- F**  
 Face, 392-412  
 anomalies of, 78-79, 79f, 80f, 392, 397-  
 (See also Craniofacial anomalies)  
 atypical clefts, 402-403, 405f-407f  
 dysmorphism, 410, 411f  
 micrognathia, retrognathia, and  
 macroglossia, 408-409, 409f  
 orbital and ocular defects, 407-408, 408f  
 tumors, 409-410, 410f  
 typical clefts, 397-401, 398f-400f,  
 401t-403t, 403f-405f (See also Cleft  
 lip/palate)  
 imaging of, 300, 302f-304f, 392-397  
 artifacts, pitfalls, and normal variants,  
 1121f-1122f  
 growth of ocular parameters, 394t  
 musculature, 334f  
 planes for, 392-394, 393f, 393t-394t  
 reverse view, 396, 396f  
 three-dimensional, 300f, 392, 394-396,  
 395f-396f, 834f-836f, 841-843,  
 845f-849f, 857f, 860f, 862f  
 ossification of bones of, 422  
 Failed pregnancy, 200, 201. *See also* Abortion,  
 spontaneous  
 Fallopian tube(s), 922, 999-1000  
 adhesions around, 1000  
 anatomy of, 906, 911-913, 913f  
 dilated, vs. ovarian cyst, 1100f  
 Fallopian tube(s) (Continued)  
 fertilization in, 184  
 hydrosalpinx, 974, 977f, 999-1000, 1001f  
 lesions of, 1000  
 pregnancy in, 1028, 1029f, 1111f (See also  
 Ectopic pregnancy)  
 torsion of, 968, 979-981, 1000  
 ultrasound visualization of, 999, 1000f  
 vascular supply of, 913  
 Falx cerebri, 349, 357f  
 Fanconi anemia, 465, 466-467  
 Fanconi syndrome, 425  
 FAS (fetal alcohol syndrome), 39t, 131-133,  
 132f  
 Fascial planes of female pelvis, 891, 894  
 FASTER Trial, 62-63, 64, 67  
 Femoral vessels, superficial, 329  
 Femur, fetal, 305, 308, 309f, 310f, 311-312,  
 314f, 315f, 344f, 434f, 1147f  
 bowing of  
 in campomelic dysplasia, 127-128, 128f  
 "telephone receiver" femur in  
 thanatophoric dysplasia, 449, 450f  
 distal epiphysis of, 243-244, 244f, 245f, 308f,  
 309, 309f, 317f-319f, 421, 422f  
 distal femoral point, 311-312  
 head of, 314f, 344f  
 proximal femoral focal deficiency, 465f,  
 464-465  
 Femur length (FL), 13, 20, 227, 232, 240-241,  
 429  
 fetal weight estimation based on abdominal  
 circumference and, 1177t-1178t  
 in achondroplasia, 436, 448-449  
 in atelosteogenesis, 451  
 in Down syndrome, 13, 20, 82t, 82-83, 83t  
 in gestational age estimation, 240-241,  
 1159t-1160t, 1166t-1167t  
 in large and small for gestational age fetuses,  
 1180t  
 in skeletal dysplasias, 429  
 achondroplasia, 115, 115f, 429, 436  
 lethality and, 436  
 measurement of, 235-237, 236f, 240,  
 311-312, 318f, 1147f  
 normal values for, 432t  
 relationship with other biometric parameters,  
 246, 246t, 429, 1179t  
 foot length, 443, 444f  
 head circumference, 433f  
 significance of short length, 1148f  
 Fertilization, 184, 184f, 721  
 Fetal acid-base status, 785-787, 786f-787f  
 Fetal age, 8, 225  
 Fetal alcohol effects, 131-133  
 Fetal alcohol syndrome (FAS), 39t, 131-133,  
 132f  
 Fetal anatomy  
 MRI evaluation of, 815-816  
 ultrasound evaluation of, 297-360  
 cardiovascular system, 320-329, 326f-333f  
 central nervous system, 344-360,  
 345f-360f, 363-366, 364f-366f  
 gastrointestinal system, 333-339, 334f-339f  
 genitourinary system, 342-344, 343f-344f  
 musculoskeletal system, 305-320,  
 308f-326f  
 respiratory system, 339-341, 340f-342f  
 superficial structures, 300-305, 302f-307f  
 technique for, 297-300  
 Fetal breathing movements, 494  
 brain center for, 784t, 785  
 gradual hypoxia concept and, 787  
 in biophysical profile, 781t, 782, 783, 783f  
 medication effects on, 791-792, 791t-792t  
 variations by gestational age, 785  
 Fetal circulation, 577, 578f, 802  
 hepatic, 616, 616f  
 portal, 252, 320-328, 327f-329f, 338  
 pulmonary, 329, 330f, 331f, 339-340, 341f,  
 493, 497f  
 Fetal death  
 abnormal biophysical profile score and,  
 783-784  
 diagnosis of, 14  
 due to cardiac defects, 566  
 in twin gestations, 266, 270-272, 271f-273f  
 monoamniotic twins, 279  
 Fetal DNA, cell-free, 55-56  
 Fetal endoscopic tracheal occlusion (FETO),  
 876-878, 877f, 878t  
 Fetal growth. *See also* Fetal weight  
 accelerated, 253-255  
 biometric parameters for, 13, 20, 226-227,  
 232-247 (See also Biometric parameters)  
 estimated fetal weight, 247  
 in twin-to-twin transfusion syndrome, 248  
 interval growth assessment in high-risk  
 pregnancy, 255-260, 259f  
 intrauterine growth restriction, 247-253  
 large for gestational age fetus, 253-255  
 macrosomia, 253-255  
 of twins, 292f, 292-293  
 small for gestational age fetus, 247  
 symmetric vs. asymmetric abnormalities of,  
 248  
 ultrasound evaluation of, 6, 7  
 Fetal hydatinoin syndrome, 39t  
 Fetal image-guided surgery (FIGS), 868t, 869,  
 871. *See also* Fetal surgery  
 Fetal lie, 14, 15f-17f  
 of twins, 293  
 sonographic technique and, 299-300, 301f-302f  
 Fetal lung maturity, 494  
 criteria for, 242  
 of monoamniotic twins, 277  
 placental grading and, 244, 725  
 Fetal movements, 299, 469  
 brain center for, 784t, 785  
 decreased, short umbilical cord and, 747  
 disorders causing impairment of, 469t  
 in biophysical profile, 781t, 782  
 medication effects on, 791-792, 791t-792t  
 Fetal number. *See also* Multiple pregnancies;  
 Twins  
 determination of, 13, 14  
 Fetal origins of adult disease hypothesis, 250  
 Fetal pole, 8  
 Fetal position, 14, 15f-17f  
 sonographic technique and, 297, 299-300,  
 301f-302f  
 Fetal postmaturity syndrome, 17  
 Fetal presentation, 14, 15f-17f  
 malpresentation, 14  
 of twins, 293, 293f  
 sonographic technique and, 299-300, 301f-302f  
 Fetal reactivity, 781t  
 Fetal rubella syndrome, 37, 38, 39t, 134-135  
 Fetal safety of ultrasound, 3-4, 12t, 891  
 Fetal sex determination, 665-666  
 Fetal surgery, 867-882  
 confirming accuracy of diagnosis for, 867  
 for aortic stenosis, 882, 882f  
 for arrhythmias, 576  
 atrioventricular block, 574  
 bradycardia, 574-575  
 tachycardia, 576  
 for cardiac defects, 566, 882, 882f  
 for congenital cystic adenomatoid  
 malformation, 868, 878-879, 879f  
 for congenital diaphragmatic hernia, 507,  
 874-878, 875f-877f, 876t, 878t

Fetal surgery (*Continued*)

- for lower urinary tract obstruction, 649, 880-881, 881f, 881t
  - for monozygotic twin problems, 871-874
    - discordant monozygotic twins, 872-874, 874t
    - twin-reversed arterial perfusion (acardiac twinning), 874
    - twin-to-twin transfusion syndrome, 176, 869, 870, 870f, 871-872, 872t, 873t
  - for myelomeningocele, 370, 868, 879-880, 880f, 880t
  - for neck mass, 416, 824f
  - for nonimmune hydrops, 693-695
  - for ovarian cyst, 668
  - for pleural effusions, 881-882
  - for polyhydramnios, 773-774
  - for sacrococcygeal teratoma, 879, 879f
  - indications for, 867
  - intrauterine transfusion of hydropic, anemic fetus, 684, 687f, 687-688
  - MRI evaluation for, 817, 820, 823f-825f
  - procedures for, 867-871
    - fetoscopy, 869-870, 870f
    - hysterotomy, 867-869
    - radiofrequency ablation, 871
    - risks of, 868t
    - shunt placement, 870-871
    - technical advances in, 867
  - saline amnioinfusion for oligohydramnios, 767, 768t
  - training and oversight for, 867
- Fetal swallowing, 334, 759
- hypoxic suppression of, 767
- Fetal syndromes, 112-180. *See also* Congenital anomalies
- Fetal tone, 781t
- brain center for, 784t, 785
  - medication effects on, 791-792, 791t-792t
- Fetal toxoplasmosis syndrome, 38, 39t, 135f, 135-136
- Fetal urine production, 334, 343, 642, 758-759
- amount of, 759
  - lack of, 664
- Fetal viability, 8
- determination of, 13, 14
  - documentation of, 14
- Fetal warfarin syndrome, 39t
- Fetal weight. *See also* Birthweight; Fetal growth
- correlation with amniotic fluid volume, 760
  - estimation of, 14, 17, 19, 247, 255
    - based on abdominal circumference and femur length, 1177t-1178t
    - equations for, 1174t-1175t
    - in twin gestations, 1176t
  - in intrauterine growth restriction, 248
  - in macrosomia, 254-255
  - individualized growth curves, 259-260
  - menstrual age and, 17
  - normal range of, 259f
  - of large for gestational age fetus, 254
  - oligohydramnios and estimation of, 770
- FETO (fetal endoscopic tracheal occlusion), 876-878, 877f, 878t
- Fetoplacental blood flow, 249f, 320
- uteroplacental insufficiency and, 249
- Fetoscopy, 869-870
- animal studies of, 869
  - for tracheal occlusion, 876-878, 877f, 878t
  - in twin-to-twin transfusion syndrome, 870, 870f, 872, 873t
  - procedure for, 869-870
  - rationale for, 869
  - risks of, 868t, 869
- Fetus papyraceus, 271, 272f
- Fibrin deposition, subchorionic, 725

- Fibroadenoma of breast, 1079f, 1085, 1086f
- Fibroblast growth factor receptor gene mutations, 113, 116, 449, 451
- Fibroblast growth factors, in skeletogenesis, 420
- Fibrochondrogenesis, 451
- Fibroid(s), uterine. *See* Leiomyoma(ta), uterine
- Fibroma
- cardiac, 567-568
  - ovarian, 976-978, 978f, 1069, 1071f
- Fibrothecoma, ovarian, 976-978, 1069
- Fibula, 308-309, 434f
- in fibula aplasia complex brachydactyly, 463
  - length of, 432t, 1167t
  - proximal, 316f
- Fibula aplasia complex brachydactyly, 463
- FIGO (International Federation of Gynecology and Obstetrics)
- staging and risk scoring system for gestational trophoblastic neoplasia, 960, 960t
  - staging system for cervical cancer, 1063, 1063t
  - staging system for endometrial cancer, 1066, 1066t
- FIGS (fetal image-guided surgery), 868t, 869, 871. *See also* Fetal surgery
- Fingers, 309, 313f. *See also* Digital anomalies; Hand(s)
- First trimester
- amniotic membrane development in, 185f-186f, 188f, 188-189, 190f
  - complications in, 200-202
  - maternal physiology and embryo development in, 182t, 182-185, 183f-185f
  - placental development in, 185-186, 187f
  - risk factors for spontaneous abortion in, 205-214
    - abnormal amnion development, 211, 212f-214f
    - gestational age, 205
    - heart rate irregularities, 206-207, 209f-210f
    - intrauterine blood, 205-206, 207f-208f
    - large yolk sac, 208-209, 210f-211f
    - maternal factors, 211-214
    - small sac size-growth delay, 207-208
  - threatened abortion in, 200-201, 202t
  - uteroplacental circulation in, 185, 186-188, 188f
- First trimester ultrasound examination, 7, 13-14, 181-220
- artifacts, pitfalls, and normal variants on, 1113f-1120f
  - cost-benefit analysis of, 6
  - Doppler, 4, 214-215
  - embryonic effects of, 3-4
  - gestational sac abnormalities on, 202-205
    - absent sac, 201-202
    - criteria for, 203-204
    - Doppler evaluation of, 204-205, 205f
    - sac without an embryo or yolk sac, 202
    - small sac size-growth delay, 207-208
  - guidelines for, 9t-10t
  - indications for, 181
  - normal anatomy and landmarks, 189-198
    - blood flow, 191, 193f-194f
    - detection of embryo and cardiac activity, 194-196, 195t, 195f-198f
    - fetal membranes and placenta, 196-198, 199f-200f
    - gestational sac, 189-191, 191f-192f
    - yolk sac, 193-194, 194f-195f, 195t
  - of amniotic membrane, 211, 212f-214f
  - three-dimensional, 852-855, 856f-857f, 860f-861f
  - to ascertain site of placentation, 13
  - to detect fetal anomalies, 5t, 5-6, 6t, 13, 181-182, 215-218, 216f-220f

- First trimester ultrasound examination (*Continued*)
- to determine embryonic/fetal number, 13
  - to estimate gestational age, 13, 198-200, 200t, 227-232
    - biometric parameters, 232
    - crown rump length, 200, 201t, 228-232, 230f, 231t
    - mean sac diameter, 199-200, 227-228, 228t, 229f
  - to evaluate uterus and adnexa, 14
  - to evaluate yolk sac, 208-209, 210f-211f
  - to identify intrauterine pregnancy, 13
  - to screen for aneuploidy, 60-69, 181
    - ductus venosus blood flow, 65, 65f
    - informed consent for, 68-69
    - nasal bones, 64f, 64-65
    - nuchal translucency, 60t, 60-64, 61f-63f, 66-69, 181
    - tricuspid regurgitation, 65f, 65-66
    - transvaginal, 181, 182f
- Five-chamber view of fetal heart, 516, 518f
- FL. *See* Femur length (FL)
- Flattened profile, 79, 80f
- Flecainide, 576
- Fluorescence in situ hybridization, 32, 53, 54, 54f
- FOD (fronto-occipital diameter), 239
- Folic acid antagonists, 39t
- Folic acid levels, neural tube defects and, 37
- Follicle-stimulating hormone (FSH), 182, 183f, 987-988, 991
- recombinant, in polycystic ovary syndrome, 999
- Fontaine syndrome, 465
- Fontanels, 314, 322f, 347f, 358, 843, 849f
- Foot, 305-307, 309, 310f-311f
- abnormalities of, 443
    - clubfoot, 92f, 92-93, 470
    - in achondroplasia, 447
    - in diastrophic dysplasia, 455
    - in Fraser syndrome, 138, 138f
    - in Grebe syndrome, 464
    - in hereditary lymphedema, 141-142, 141f-142f
    - in phocomelia, 464
    - in sirenomelia, 168-169, 169f
    - in trisomy 18, 92-93, 93f, 94, 94f, 95
    - polydactyly, 95
    - rocker-bottom foot, 93, 93f
    - sandal gap deformity, 94, 94f, 1151f
    - split hand and foot deformities, 465
  - absence of, 462
  - gestational age related to length of, 244
  - length of, 244, 443t, 1160t, 1169t-1170t
  - relationship with femur length, 443, 444f
- Foramen ovale, 546-547, 802
- Forearm, 308, 308f, 313f, 319f
- pseudolimb reduction of, 1149f
- Foregut, 588, 588f
- Forehead, 392, 393t. *See also* Frontal bossing
- sloping, 78, 79f
- 48XXXX karyotype, 31
- 48XXXY karyotype, 31
- 45X karyotype. *See* Turner syndrome (45X)
- 47XXX syndrome, 30t, 31, 31t
- 47XXY karyotype (Klinefelter syndrome), 31, 31t, 76, 1081
- 47XYY syndrome, 30t, 31, 31t
- Fossa of Waldeyer, 911
- Fossa ovalis defect, 548
- 4p deletion syndrome, 179-180, 179t-180t
- Four-chamber view of fetal heart, 329, 330f, 514-516, 517f-518f
- abnormalities on, 527t, 528, 531-531, 532t, 534f-531f
- Four-dimensional ultrasonography, 196, 859, 862



Fractaro achondrogenesis, 452, 453f  
 Fractures, 435  
   in hypophosphatasia, 454  
   in osteogenesis imperfecta, 156f–157f, 156–158, 438f  
   rib, 438f  
 Fragile X syndrome, 34–35, 35f, 36  
 Fraser syndrome, 137–139  
 Free fetal DNA, 55–56  
 Freeman-Sheldon syndrome, 470  
 Frontal bossing, 300, 443  
   in achondroplasia, 115, 115f, 444f, 447  
   in Apert syndrome, 120f  
   in thanatophoric dysplasia, 171, 450, 450f, 848  
 Frontonasal dysplasia, 402  
 Fronto-occipital diameter (FOD), 239  
 Fryns syndrome, 139  
 FSH (follicle-stimulating hormone), 182, 183f, 987–988, 991  
   recombinant, in polycystic ovary syndrome, 999  
 Funneling, cervical, 704–706, 706f  
   measuring length of, 704  
   measuring width of, 704, 706f  
   preterm birth and, 704–706  
   shapes of, 704, 706f  
   vs. lower uterine segment contractions, 701–702, 703f

**G**  
 GA. *See* Gestational age (GA)  
 Gadolinium-based contrast agents, 809  
 Gallbladder, fetal, 326f, 333, 619–623  
   agenesis of, 619–621  
   embryology of, 619  
   in situs abnormalities, 523, 529f  
   late-onset disappearance of, 621  
   location of, 619, 620f  
   nonvisualization of, 619–621  
   size and shape of, 619, 620f  
   sludge in, 621, 621f  
 Gallstones  
   fetal, 621, 621f, 1139f  
   maternal, 810, 812f  
 Gartner duct cyst, 913, 1005  
 Gastric duplication cyst, 591, 592f, 595, 820, 826f  
   MRI of, 820, 826f  
 Gastric emptying cycles, 593  
 Gastrohepatic ligament, 324–325  
 Gastrointestinal system, fetal, 587–625  
   approach to suspected pathology of, 613–615  
   embryology of, 588, 588f  
   MRI of, 615, 820, 826f  
   nonimmune hydrops and abnormalities of, 689t–690t  
   polyhydramnios and anomalies of, 771–772, 772f, 772t  
   ultrasound imaging of, 333–339, 334f–339f  
   (See also specific structures)  
 Gastroschisis, 27, 80, 218, 220f, 627–631  
   abnormal umbilical cord development and, 751–752  
   alpha-fetoprotein levels and, 43, 43f  
   anomalies associated with, 627–629  
   definition of, 627  
   etiology of, 627  
   incidence of, 627  
   mode of delivery and, 629  
   prenatal diagnosis of, 629–631, 630f–631f  
   prognosis for, 629  
   vs. pseudogastroschisis, 1137f  
 Gastrulation, 185

Gender determination, 19, 302–305, 307f  
 Genetic counseling, 48–49  
   indications for, 48, 48t  
 Genetic screening, 40–47  
   alpha-fetoprotein, 42–45, 43f, 45t  
   biochemical markers and fetal chromosomal defects, 45, 45t  
   carrier (heterozygote), 40–42, 41t  
   for cystic fibrosis, 41t, 41–42, 42f  
   for Tay-Sachs disease, 41  
   recommendations for, 41t  
   techniques for, 41  
   for fetal aneuploidy, 45–46, 46t  
   for low estriol, 47  
   in multiple gestations, 46  
   maternal age and, 46–47  
   third-trimester complications after abnormal serum screening, 47  
 Genetics, 26–56  
   birth defects and, 27, 215f  
   chromosomal defects, 29t–32t, 29–33  
   developmental disorders, 27–29, 28f  
   future directions in, 55–56  
   cell-free fetal DNA, 55–56  
   quantitative fluorescent PCR and comparative genomic hybridization, 55, 55f, 56f  
   multifactorial disorders, 36t, 36–37  
   prenatal diagnosis of, 48–53, 49f, 50f  
   prenatal testing for congenital malformations, 53f, 53–55, 54f  
   prevalence of genetic diseases, 27, 27f  
   single gene disorders, 33–36  
   anticipation, 35–36  
   autosomal-dominant inheritance, 33f, 33–34  
   autosomal-recessive inheritance, 34  
   imprinting, 35, 36f  
   mitochondrial disorders, 36, 36t  
   X-linked inheritance, 34–35, 35f  
   syndromes due to disordered function of specific developmental genes, 37  
   teratology, 37–40  
 Genital tract, fetal, 665–668  
   ambiguous genitalia, 666, 667f  
   anomalies in female, 668  
   hydrocolpos-vaginal malformations, 668, 669f  
   ovarian cysts, 668, 668f–669f  
   anomalies in male, 666–668  
   hypospadias/epispadias, 666–668, 668f  
   scrotal, 668  
   normal genitalia, 302–305, 307f, 665–666  
   polyhydramnios and anomalies of, 772t  
 Genitourinary system, fetal, 640–671  
   adrenals, 670–671  
   conditions associated with anomalies of aneuploidy, 80, 81f  
   prune-belly syndrome, 164–165, 164f–165f  
   sirenomelia, 168–169, 169t  
   Smith-Lemli-Opitz syndrome, 169–170, 170t  
   VACTERL association, 177f, 177–178  
   Wolf-Hirschhorn syndrome, 179t  
   genital tract, 665–668  
   imaging of, 342–344, 343f–344f  
   urinary tract, 640–665  
 Genu recurvatum, 150, 150f  
 Germline mosaicism, 33  
 Gestational age (GA)  
   alpha-fetoprotein levels and, 44  
   amniotic fluid index by, 1181t–1183t  
   amniotic fluid volume by, 759–760, 760f  
   based on last menstrual period, 226, 227, 247  
   biophysical profile variations and, 785, 785t

Gestational age (GA) (*Continued*)  
   clinical importance of, 226  
   definition of, 8  
   determination of, 225–227  
   methods for, 226t, 1159t  
   embryo detection and, 194  
   embryogenesis and, 185, 187f, 186t  
   fetal growth and, 226  
   for biochemical screening, 226  
   gestational sac detection and, 189, 203, 227  
   heart rate and, 194, 195t, 196f, 206–207  
   large for, 253–254  
   menstrual age and, 8, 14, 181  
   pregnancy loss and, 205  
   small for, 247  
   susceptibility to teratogens related to, 37, 38f, 215, 215f  
   ultrasound estimation of, 6, 225–227  
   biometric parameters for, 226–227, 232–247  
     abdominal circumference, 240, 241f, 242t, 1165t  
     biparietal diameter, 238t, 238–239, 239t, 1159t–1160t, 1172t  
     clavicle length, 1160t, 1169t  
     colonic echogenicity, 244–245  
     femoral and tibial epiphyseal ossification centers, 243–244, 244f, 245f  
     femur length, 240–241, 1159t–1160t, 1166t–1167t  
     foot length, 244, 443t, 1160t, 1169t–1170t  
     GA calculation from, 245–247, 246t  
     head circumference, 239–240, 240t  
     long bone length, 14, 240, 1166t–1168t  
     placental grading, 244  
     relationships between, 246, 246t  
     small intestinal peristalsis, 244  
     thoracic circumference, 440t, 494, 498t, 643, 1173t  
     transverse cerebellar diameter, 241–242, 243t, 244, 1160t, 1171t  
     variability of, 1159t–1160t  
     crown rump length, 200, 201t, 228–232, 230f, 231t, 1162t–1163t  
   in first trimester, 13, 198–200, 200t, 227–232, 242  
   in late pregnancy, 242–245  
   in second and third trimesters, 14, 17, 242, 1160t  
   mean sac diameter, 199–200, 227–228, 228t, 229f, 1161t–1162t  
   reporting of, 227  
   umbilical artery Doppler waveform and, 251, 251f  
   visual estimates of, 230  
   yolk sac diameter and, 193, 195f, 195t, 208–209  
 Gestational sac, 185, 186f, 188f, 207, 744  
   abnormalities of, 203–204, 203f–204f  
   absence of, 201–202  
   artifacts, pitfalls, and normal variants in imaging of, 1113f–1114f  
   chorionic bump protruding into, 204, 204f, 1115f  
   Doppler evaluation of, 204–205, 205f  
   growth rate of, 203–204  
   mean sac diameter (MSD), 13, 189, 191f, 203  
   abnormal, 203, 204f, 207  
   abortion risk and, 207  
   crown rump length and, 228  
   hCG levels and, 214, 228t, 1162t  
   in gestational age estimation, 199–200, 227–228, 228t, 229f, 1161t  
   size of, 203, 204f, 207  
   three-dimensional imaging of, 854, 860f  
   trophoblastic appearance of, 204, 204f

**Gestational sac (Continued)**

- ultrasound detection of, 189–191, 191f–192f, 202, 227, 1113f
  - double decidual sac sign, 187f, 191, 192f, 228, 228f, 1024–1025, 1027f
  - gestational age and, 189, 203, 227
  - intradecidual sign, 189–191, 192f, 228, 229f, 1024, 1026f–1027f
  - vs. pseudogestational sac of ectopic pregnancy, 189–191, 192f, 202, 204–205, 227–228, 1024–1027, 1025f–1028f, 1030, 1031f, 1035f
  - without an embryo or yolk sac, 202, 203f, 228, 229f, 230
- Gestational trophoblastic neoplasia (GTN)**, 201, 951–964
- Breus mole and, 964, 965f
  - choriocarcinoma, 963f, 963–964
  - epithelioid trophoblastic tumor, 964
  - histopathology of, 954f, 955f, 955t
  - hydatidiform molar pregnancy, 951–963 (See also Hydatidiform mole)
  - persistent, 951, 960–961
    - treatment of, 961
  - placental site trophoblastic tumor, 964, 964f
  - risk scoring system for, 960, 960t
  - staging and risk scoring system for, 960, 960t
  - subtypes of, 951, 952f
- Gliopendymal cyst**, 388
- Glomerulocystic kidneys**, 654, 655t, 658, 658t, 659f
- Glomerulonephritis, fetal**, 663, 664f
- Glossopalatine ankylosis syndrome**, 463
- Glossoptosis**
- in Pierre Robin syndrome, 161f, 161–162
  - micrognathia/retrognathia and, 408
- Goiter, fetal**, 415–416, 416f
- Goldenhar syndrome**, 139–140, 140f, 408, 468
- Gonadal dysgenesis**, 1053
- Gonadotropin-releasing hormone (GnRH)**
- agonists, in polycystic ovary syndrome, 999
- Corlin syndrome**, 568
- Gradual hypoxia concept**, 787–788
- Granulosa cell tumor**, 1069, 1073f
- Graves' disease**, 416
- Gray matter heterotopias**, 385
- Grebe syndrome**, 464
- Growth hormone**, for achondroplasia, 449
- GTN**. See **Gestational trophoblastic neoplasia (GTN)**
- Gut tube, primitive**, 588, 588f, 745

**H**

- Hadlock formula for fetal weight estimation**, 247
- HAF (hemorrhagic anovulatory follicle)**, 993, 995f
- Hair**
- on forehead, 848f
  - scalp, 302, 306f, 1123f
- Hand(s)**, 305–307, 309, 312f, 313f, 319f
- abnormalities of**, 443
- clinodactyly, 93f, 93–94
  - clubhands, 465–470
  - in chondroectodermal dysplasia, 459, 459f–460f
  - in diastrophic dysplasia, 455, 455f
  - in fetal alcohol spectrum disorders, 132f
  - in Grebe syndrome, 464
  - in Jeune syndrome, 457–458
  - in phocomelia, 464
  - in short rib–polydactyly syndromes, 459
  - in trisomy 18, 94–95, 94f–95f
  - mitten hand deformity, 120, 120f
  - polydactyly, 95, 96f

**Hand(s) (Continued)**

- abnormalities of (Continued)
  - split hand and foot deformities, 465
  - trident hand in achondroplasia, 448, 448f
  - absence of, 462
  - clenched, 94–95, 94f–95f, 309
- Hanhart syndrome**, 463
- Hard-copy documentation of ultrasound**
- examination, 12t, 12–13
- HARD+/E syndrome**, 152
- HC**. See **Head circumference (HC)**
- hCG**. See **Human chorionic gonadotropin (hCG)**
- HDFN (hemolytic disease of fetus and newborn)**, 678f, 678–681, 688
- Head**, 346. See also **Brain**; **Face**; **Skull**; *specific structures*
- artifacts, pitfalls, and normal variants in imaging of, 1121f–1131f, 1155f
- Head circumference (HC)**, 13, 20, 227, 232, 239–240, 363
- in gestational age determination, 239–240, 240t, 1159t–1160t, 1163t–1164t
  - in large and small for gestational age fetuses, 1180t
  - in late pregnancy, 239t, 240
  - measurement of, 234f, 234–235, 239
  - biparietal diameter measurement and, 235
  - relationship with other biometric parameters, 246, 246t
  - femur length, 1179t
  - long bone length, 425, 433f
  - lung-to-head ratio, 494, 499f
  - thoracic-to-abdominal circumference ratio, 436
- Hearing loss, hemolytic disease of fetus and newborn and**, 688
- Heart, fetal**, 511–582. See also **Cardiac entries**
- conduction system of, 569
  - congenital defects of (See **Congenital heart disease (CHD)**)
  - echogenic intracardiac focus, 84–85, 84f–85f
  - function of, 577
  - imaging of, 328–329, 330f–331f, 514–523, 1133f–1135f
  - cardiac axis, 528, 533f
  - clues to abnormality at each sonographic view, 523–565, 527t
  - Doppler imaging, 512, 513f, 800–804, 803f–804f, 804t–805t, 1189t
  - sequential segmental approach, 514, 514f
  - sonographic views, 514, 515f
  - aortic and ductal arch views, 523, 525f–526f
  - basal short-axis view, 523, 524f
  - five-chamber view, 516, 518f
  - four-chamber view, 329, 330f, 514–516, 517f–518f
  - three-vessel view, 516, 519f–520f
  - transverse view of upper abdomen, 514, 516f
  - ventricular outflow tract views, 516, 521f–522f, 522–523
  - technique and normal anatomy, 514–523
  - three-dimensional, 512, 513f, 842f–843f, 855, 858f, 858–859
  - in intrauterine growth restriction, 805–806
  - malpositions of, 527t, 532t, 533f
  - measuring dimensions of, 439f, 1191f–1197f
  - normal position of, 528, 533f
  - prenatal examination of, 511–512
  - rhythm of, 569–577 (See also **Cardiac rhythm, fetal**)
  - tumors of, 567–569
  - fibroma, 567–568
  - hemangioma, 568–569, 569f
  - prognosis for, 569

**Heart, fetal (Continued)**

- tumors of (Continued)
  - rhabdomyomas, 173f, 173–174, 567, 569f
  - teratoma, 568
  - ventricular compliance of, 802
- Heart rate, fetal**, 569–577
- acceleration of, 782
  - bradycardia, 573–575, 574f
  - embryonic, 207, 209f–210f, 212f
  - gestational age and, 194, 195t, 196f, 206–207
  - in first trimester, 194–195, 195t, 196f
  - pregnancy outcome and irregularities of, 206–207, 209f–210f
  - irregular, 571–573
  - medication effects on, 791–792, 791t–792t
  - nonstress test for monitoring of, 780–782, 782f
  - normal, 569–570
  - tachycardia, 575–576, 575f–576f
- Heavy metal exposure**, 39t
- HELLP syndrome**, 140–141
- Hemangioma**
- cardiac, 568–569, 569f
  - hepatic, 618, 618f
  - in neck, 415
- Hematoma**
- intracranial, 817, 820f
  - intrauterine, pregnancy loss and, 205–206, 207f–208f
  - marginal, 728, 729f, 731
  - rectus sheath, 893
  - retroplacental, 206, 207f, 729f, 729–730, 731, 731f
  - with placental abruption, 730–731, 731f 732f
  - subamniotic, 729, 729f
  - subchorionic, 207f, 208f, 728–729, 729f–730f, 1146f
  - Breus mole, 964, 965f
  - umbilical cord, 752–753
- Hematometocolpos**, 1053
- Hemifacial microsomia**, 408
- Hemimelia**, 462
- Hemispheres, cerebral**, 358
- Hemivertebra**, 425, 432f, 445–446
- Hemochromatosis**, 820
- Hemolytic disease of fetus and newborn (HDFN)**, 678f, 678–681, 688
- Hemoperitoneum**, 1024, 1026f, 1029, 1030f, 1032
- Hemophilia A**, 33
- Hemorrhagic anovulatory follicle (HAF)**, 993, 995f
- Hepatic fibrosis, autosomal-recessive polycystic kidney disease and**, 655, 656
- Hepatic vein**, 323–324, 328, 327f–330f, 338f, 800f
- Hepatitis, cytomegalovirus**, 134
- Hepatoblastoma**, 618
- Hepatomegaly**, 616
- Hepatorenal space, free fluid collections in**, 891, 894f
- Hepatosplenomegaly**, 616, 616f
- Herpes simplex infection**, 143
- Heterotaxy**, 523, 527t, 527–528, 529f–530f
- congenital heart disease and, 528, 531f, 531t
- Heterotopic pregnancy**, 1024, 1025f, 1039, 1042f
- Hindgut**, 588, 588f
- Hip joint**, 308, 314f
- Hirschsprung disease**, 37t, 607–609, 609f
- HLHS (hypoplastic left heart syndrome)**, 72, 74f, 147f, 147–148, 528, 534, 540f–541f, 882
- Holoprosencephaly**, 78, 143–145, 373–376
- alobar, 78f, 79f, 143, 144f, 373–374, 374f
  - classification of, 143, 144t, 373, 373f
  - facial anomalies and, 144f, 374, 405, 406f
  - median cleft lip, 402, 405f–406f



- Holoprosencephaly** (*Continued*)  
 in trisomy 13, 78, 79f, 143–145, 144f, 144t, 217, 374, 1118f  
 lobar, 373, 374–375, 375f  
   three-dimensional imaging of, 840f–841f  
 middle interhemispheric variant of, 373, 374, 375f  
 prenatal diagnosis of, 374–375  
   in first trimester, 217, 217f  
 semilobar, 373, 374  
 vs. developing rhombencephalon, 1118f  
 with absence of cavum septum pellucidum, 373, 840f
- Holt-Oram syndrome**, 37t, 145–146, 145f–146f, 446, 465, 467
- Houston-Harris achondrogenesis**, 113–115, 452, 453t
- HPV (human papillomavirus) infection**, 1062
- Human chorionic gonadotropin (hCG)**  
 in aneuploidy screening, 45, 46, 60, 60t, 71, 181  
   Down syndrome, 60t, 62, 63f, 67, 68f, 71  
   in twin gestations, 288–290, 289t  
   perinatal outcome and, 47  
   trisomy 18, 103  
 in ectopic pregnancy, 214, 1022–1024, 1043–1044  
 in molar pregnancy, 951, 959  
 in ovarian stimulation protocols, 1007–1008  
 in placental mesenchymal dysplasia, 962  
 in pregnancy testing, 185, 942  
 mean sac diameter, menstrual age and, 214, 227, 228t  
 usefulness in first trimester evaluation, 214
- Human genome project**, 33
- Human papillomavirus (HPV) infection**, 1062
- Human placental lactogen**, in Down syndrome, 45
- Humerus**, 307, 311f, 312f  
 in atelostegocgenesis, 451  
 length of, 433t, 1167t–1168t  
   in Down syndrome, 82–83  
   relationship with head circumference, 433f  
   relationship with ulna length, 430f  
 proximal epiphyseal ossification center of, 309, 317f, 422f
- Hyaloid artery**, 1131f
- Hydantoin**, 39t
- Hydatid of Morgagni**, 913, 913f
- Hydatidiform mole**, 951–963  
 cause of, 951  
 clinical significance of, 951  
 complete, 951–953, 952f, 953f  
   asymptomatic, 956  
   biparental, 951  
   clinical presentations of, 955  
   complications of, 955  
   in second trimester, 951, 956f  
   placental mosaicism for, 961  
 ectopic, 963  
 histopathologic diagnosis of, 953, 954f, 955f, 955t  
 human chorionic gonadotropin levels and, 951  
 invasive, 951, 952f, 954f, 957f, 963, 963f  
 management of, 955–956, 959–960  
 partial, 951–953, 952f, 953f, 958f, 961  
 persistent gestational trophoblastic neoplasia and, 951  
 ultrasound detection of, 956–959, 956f–959f  
 vs. myomatous disease, 1103f  
 with coexistent normal fetus, 951, 952f, 961–963, 962f
- Hydranionos**. *See* Polyhydramnios
- Hydranencephaly**, 80, 382
- Hydrocele**, 666, 837f
- Hydrocephalus**, 76, 77f, 344  
 arachnoid cyst and, 388  
 Arnold-Chiari malformation and, 122f, 123  
 cephalocele and, 372  
 Dandy-Walker malformation and, 377  
 genetic implications of, 368  
 in VACTERL association, 178  
 in Walker-Warburg syndrome, 178  
 porencephaly and, 382  
 spina bifida and, 370  
 three-dimensional imaging of, 839f  
 vs. developing rhombencephalon, 1118f  
 vs. normal sonoluent brain, 1129f
- Hydrocolpos**, 668, 669f
- Hydrolethrus syndrome**, 146–147
- Hydronephrosis**  
 congenital, grading of, 653, 653f  
 maternal, 914f  
   CT and MRI evaluation of, 810–811, 812f
- Hydrops fetalis**, 676–696  
 acardiac twins and, 286–288, 287f  
 ascites and, 676, 677f–678f, 679, 688  
 congenital cystic adenomatoid malformation and, 502, 502f, 878–879  
 congenital intracranial tumors and, 384  
 definition of, 676  
 immune, 676, 678–688  
   diagnosis of fetal anemia, 681–684  
   amniocentesis, 682, 682f  
   choice of surveillance method, 683–684  
   middle cerebral artery Doppler, 682–683, 683t, 683f–684f  
   evaluation of sensitized pregnancy, 681  
   fetal antigen testing, 681  
   maternal antibody measurement, 681  
   management of, 684–688, 685f–686f  
   for recurrent immune hydrops, 687–688  
   intrauterine transfusion, 684, 687, 687f  
   pathophysiology of, 678–681, 679t, 680f  
   prognosis for, 688  
   significance of detection of, 681  
 intrauterine infections and, 690t–691t, 693–694  
 lethal multiple pterygium syndrome and, 151  
 maternal complications of, 677–678  
 mesenchymal hamartoma and, 618  
 nonimmune (NIHF), 676, 688–696  
   aneuploidy and, 74f, 74–75  
   causes of, 688, 689t–692t  
   evaluation of, 688, 693, 693f–694f  
   incidence of, 688  
   pathophysiology of, 688  
   prognosis for, 695–696  
   treatment of, 693–695, 695f  
 pericardial effusion and, 676, 677f, 679, 688  
 placental abnormalities and, 692t, 723, 723f, 724f  
 pleural effusions and, 74f, 74–75, 676, 677f, 679, 694, 696  
 skeletal dysplasias and, 691t  
 Turner syndrome and, 75  
 twin-reversed arterial perfusion sequence and, 874  
 twin-to-twin transfusion syndrome and, 175–176, 283, 694
- Hydrosalpinx**, 974, 977f, 999–1000, 1001f
- Hydrothorax**, congenital, 75, 75f, 507–508, 508f, 507–508, 508f, 694
- Hyperechoic bowel**, 85–86, 335–337, 611, 611f  
 differential diagnosis of, 85, 86  
   clinical causes, 612t  
   physical causes, 612t  
 grading of, 85  
 in cystic fibrosis, 42, 42f, 86  
 in Down syndrome, 85f, 85–86, 609  
 in meconium ileus, 602  
 poor perinatal outcome and, 86
- Hyperechoic kidneys**, 646, 653–654, 654t, 654f–655f
- Hypertelorism**, 80, 314, 402, 407
- Hypertension**, pregnancy-induced  
 HELLP syndrome and, 140–141  
 placental calcification and, 725, 727f  
 placental infarction and, 726, 727  
 retroplacental hematoma and, 729
- Hypertrophic cardiomyopathy**, 581–582
- Hypoalbuminemia**, 679
- Hypoblast**, 185f
- Hypochondrogenesis**, 113–115, 453, 453t
- Hypochondroplasia**, 451
- Hypognathia**, 300
- Hypopharynx**, fetal, 334f, 339, 340f, 1132f
- Hypophosphatasia**, 320, 429t, 447, 454–455
- Hypoplastic left heart syndrome (HLHS)**, 72, 74f, 147f, 147–148, 528, 534, 540f–541f, 882
- Hypospadias**, 666–668, 668f
- Hypotelorism**, 80, 80f, 312, 407
- Hypothyroidism**, congenital, 415–416, 416f
- Hysterectomy**  
 for adenomyosis, 928  
 for cervical cancer, 1063  
 for endometrial cancer, 1066  
 for leiomyomas, 1055
- Hysterosalpingosonography**, 1005
- Hysterotomy**, 867–869  
 animal studies of, 867–868, 868f  
 indications for, 868  
 procedure for, 868–869  
 risks of, 868t, 868–869
- I**
- ICH (intracranial hemorrhage)**, 366, 380, 381f  
 three-dimensional imaging of, 851f  
 vs. brain tumor, 385
- IGCs (individualized growth curves)**, 259–260
- Ileal atresia**, 599–601, 601t
- Ileum**, 598f
- Iliac artery(ies)**  
 fetal, 329, 332f  
 maternal, 898, 899f–900f, 922
- Iliac vein**  
 fetal, 329  
 maternal, 898
- Iliac wing angle**, 90–91, 91f  
 in Down syndrome, 90–91  
 measurement of, 91
- Iliacus muscle**, maternal, 894–895, 895f
- Ilium**, 314
- Implantation**, 184, 185f, 744
- Imprinting**, genetic, 35, 36f
- In vitro fertilization (IVF)**. *See* Assisted reproductive technology (ART)  
 ectopic pregnancy after, 1021–1022, 1023f  
 endometrial assessment at time of embryo transfer, 1010–1012  
   Doppler imaging, 1010–1011, 1011f  
   imaging-based uterine scoring system, 1011  
   motion analysis, 1012, 1012f  
   three-dimensional imaging, 1011  
 evaluation of ovarian blood flow for, 992–993  
 hydrosalpinx and, 999  
 in vitro maturation and, 1008  
 preimplantation genetic diagnosis for, 52f, 52–53  
 singleton births from higher order gestations, 270  
 ultrasound-guided embryo transfer, 1012f, 1012–1013  
 ultrasound-guided oocyte retrieval, 1009–1010, 1010f

- Incarcerated uterus, 923, 924f, 1111f  
 Incontinenti pigmenti, 34  
 Indirect Coombs titers, 681  
 Individualized growth curves (IGCs), 259–260  
 Indomethacin  
   for polyhydramnios, 770, 774  
   for tocolysis  
     during fetoscopy, 869  
     during shunt placement, 871  
     in women with short cervical length, 717  
 oligohydramnios due to, 770  
 prenatal exposure to, 545  
 Infant mortality  
   due to congenital heart defects, 511  
   in multiple gestations, 266, 270  
 Infarction  
   maternal floor, 727–728, 728f–729f  
   placental, 726–727, 728f  
 Infection  
   human papillomavirus, 1062  
   intrauterine, 38, 39t (*See also specific infections*)  
     cervical length, preterm birth and, 712, 715, 717–718  
     effect of antibiotics, 717  
     cytomegalovirus, 23f, 38, 39t, 133f, 133–134, 382  
     herpes simplex, 143  
     nonimmune hydrops and, 690t–691t, 693–694  
     rubella, 37, 38, 39t, 134–135  
     toxoplasmosis, 38, 39t, 135f, 135–136, 382  
     varicella zoster, 136–137, 137f  
   pelvic inflammatory disease, 974, 977f  
   tubo-ovarian abscess, 974  
 Inferior facial angle, 444–445, 445f  
 Inferior vena cava (IVC), 326f, 328, 328f, 329, 330f, 338, 340f  
   Doppler evaluation of, 799, 800f–801f  
   in situs abnormalities, 523, 527–528, 529f–531f  
 Infertility, 986–1013  
   consensus statements on work-up for, 986  
   diagnostic use of ultrasound in, 987–1006  
   corpus luteum, 993–997, 996f–997f  
   hysterosalpingography, 1005–1006, 1006f  
   ovary, 987–992  
     dermoid cyst, 989–991, 990f  
     determining optimal timing for insemination, 991  
     endometriomas, 989, 990f  
     follicular development, 987, 987f  
     ovarian reserve, 991  
     preovulatory follicles, 988–989, 988f–990f  
     vascular flow, 991–992  
     wave model for ovarian folliculogenesis, 987–988  
   oviduct, 999–1000, 1000f–1001f  
   ovulation, 992f, 992–993  
     failure of, 993, 994f–995f  
   polycystic ovary syndrome, 997–999, 998f–999f  
   uterus, 1000–1005, 1002f  
     abnormalities of, 1001–1003, 1003f  
     adenomyosis, 1004  
     endometrial thickness, 1001  
     Gartner duct cysts, 1005  
     leiomyomata, 1004, 1004f  
     myometrium, 1001  
     nabothian cysts, 1005  
   due to adhesions, 969  
   due to endometriosis, 989  
   goal of imaging in, 987  
   maternal age and, 986  
   prevalence of, 986  
 Infertility (*Continued*)  
   ultrasound in assisted reproductive technology therapy for, 1006–1013  
     endometrial assessment at time of embryo transfer, 1010–1012, 1011f–1012f  
     guiding embryo transfer, 1012f, 1012–1013  
     oocyte retrieval, 1009–1010, 1010f  
     ovarian hyperstimulation syndrome, 1009, 1009f  
     ovarian stimulation, 1006–1009, 1008f  
 Informed consent, for prenatal aneuploidy screening, 68–69  
 Infrapinnatus muscle, 312f  
 Infundibulopelvic ligament, 910–911, 982f  
 Inguinal hernia, 837f  
 Inhibin A, in aneuploidy screening, 45, 45t, 46, 60, 60t, 67, 71  
 Intercostal vein, 1081  
 Internal mammary artery, 1081  
 International Federation of Gynecology and Obstetrics (FIGO)  
   staging and risk scoring system for gestational trophoblastic neoplasia, 960, 960t  
   staging system for cervical cancer, 1063, 1063t  
   staging system for endometrial cancer, 1066, 1066t  
 International Gynecologic Cancer Society, 1063  
 International Nosology and Classification of Constitutional Disorders of Bone, 424–425  
 International Skeletal Dysplasia Registry, 446  
 International Skeletal Dysplasia Society, 424  
 Interorbital diameter, 241, 312  
 Interstitial pregnancy, 1028, 1029f, 1036–1037, 1038f–1039f  
 Intervillous space(s), 188, 188f, 721–722, 722f  
 Intervillous thrombosis (IVT), 725, 727f, 729f  
 Intestinal malrotation, 613, 614f–615f  
 Intestinal pseudo-obstruction, 604–605, 606f, 607t  
 Intestinal volvulus, 611–612, 612f  
 Intra-abdominal cyst, idiopathic, 624–625, 625f  
 Intracranial hemorrhage (ICH), 366, 380, 381f  
   three-dimensional imaging of, 851f  
   vs. brain tumor, 385  
 Intracranial tumors, congenital, 383–385, 384t  
 Intracardiac sign, 189–191, 192f, 228, 229f, 1024, 1026f–1027f  
 Intraorbital diameter, 241  
 Intraperitoneal calcifications, 602–603, 602f–604f, 613  
 Intrauterine contraceptive device (IUCD), 860f, 935, 938f  
   ectopic pregnancy and, 1021, 1022f  
   in early intrauterine pregnancy, 1114f  
 Intrauterine growth restriction (IUGR), 247–253, 767  
   abnormal biochemical screening and, 47  
   assessment of fetal status in, 250, 250f  
   biometric criteria for, 247–248  
   biophysical profile and, 788, 789  
   cardiac physiology in, 805–806  
   Doppler imaging in, 250–253, 254f, 804–806  
   early, 208  
   etiologies of, 248  
   in twin gestation, 266  
   in twin-to-twin transfusion syndrome, 872  
   management algorithm for, 258f  
   maternal floor infarction and, 728  
   oligohydramnios and, 767  
   pathophysiology of, 248–249, 249f, 805  
   placental calcification and, 725  
   placental infarction and, 727  
   retroplacental hemorrhage and, 731  
   short- and long-term sequelae of, 249–250  
   single umbilical artery and, 747  
   small for gestational age and, 247  
 Intrauterine growth restriction (IUGR) (*Continued*)  
   sonographic criteria for, 1180t  
   symmetric and asymmetric growth lag, 248  
   uteroplacental insufficiency and, 248–249, 767  
   villamentous cord insertion and, 751  
 Intrauterine insemination (IUI), 991  
 Intrauterine transfusion (IUT), 687–688  
   bone marrow suppression due to, 688  
   intravascular, 687  
   of hydropic, anemic fetus, 684, 687f, 687–688  
   via intraperitoneal infusion, 687  
 Intravenous immune globulin (IVIG), for recurrent immune hydrops fetalis, 687  
 Intussusception, intrauterine, 613  
 Iodide preparations, 416  
 Ischium, 314, 314f, 324f  
 Isotretinoin, 39t  
 IUCD (intrauterine contraceptive device), 860f, 935, 938f  
   ectopic pregnancy and, 1021, 1022f  
   in early intrauterine pregnancy, 1114f  
 IUGR. *See* Intrauterine growth restriction (IUGR)  
 IUI (intrauterine insemination), 991  
 IUT. *See* Intrauterine transfusion (IUT)  
 IVC (inferior vena cava), 326f, 328, 328f, 329, 330f, 338, 340f  
   Doppler evaluation of, 799, 800f–801f  
   in situs abnormalities, 523, 527–528, 529f–531f  
 Ivemark syndrome, 659, 660f  
 IVF. *See* In vitro fertilization (IVF)  
 IVIG (intravenous immune globulin), for recurrent immune hydrops fetalis, 687  
 IVT (intervillous thrombosis), 725, 727f, 729f
- J**  
 Jarcho-Levin syndrome, 97, 435t, 458f, 848  
 Jaw index, 444  
 Jejunioileal atresia, 596f, 599–601, 600f–602f, 601t  
 Jejunum, 598, 598f  
 Jeune syndrome, 457–458, 458f, 624  
 Joint contractures  
   in arthrogryposis multiplex congenita, 123, 123f, 469–470, 470f  
   in diastrophic dysplasia, 455  
   in lethal multiple pterygium syndrome, 151, 151f  
   in SC phocomelia syndrome, 464  
   in trisomy 18, 94, 95  
 Joint dislocations, in Larsen syndrome, 150, 150f  
 Joubert syndrome, 379, 381f  
 Jugular lymphatic sac, 414  
 Jugular vein(s), 329, 341f, 414
- K**  
 Kallman syndrome, 47  
 Karsch-Neugebauer syndrome, 465  
 Karyotype analysis, prenatal, 53f, 54, 54f. *See also* Prenatal diagnosis  
 Kidney(s), fetal, 300f, 342–343, 343f, 344f, 643, 643f, 1142f, 640–664. *See also* Renal entries  
   acquired pathologies of, 663  
   glomerulonephritis, 663, 664f  
   renal vein thrombosis, 663, 663f  
   agenesis of, 446, 644, 644f  
   amniotic fluid production by, 758–759  
   conditions associated with abnormalities of  
     cerebrohepatorenal syndrome, 130, 130f  
     chondroectodermal dysplasia, 460  
     Down syndrome, 83f, 83–84  
     Jeune syndrome, 457, 458  
     Meckel syndrome, 153f, 153–154  
     nonimmune hydrops, 690t



Kidney(s), fetal (*Continued*)

- conditions associated with abnormalities of (*Continued*)
  - sirenomelia, 168–169, 169t
  - trisomy 13, 105f
  - VACTERL association, 177
- congenital nephrotic syndrome, 664, 664f
- corticomedullary differentiation of, 643, 643f, 655
  - reversed, 655
- cystic diseases of, 654–663, 655t (*See also* Renal cystic diseases)
  - development of, 640–642, 641f
  - dilatation of renal pelvis, 646–653, 646f–653f, 648t
  - duplications of, 645, 645f, 649, 650f
  - ectopic, 645, 645f
  - enlarged, 646, 657t
  - growth of, 643
  - horseshoe, 645, 645f
  - hyperchole, 646, 653–654, 654t, 654f–655f
  - multicystic dysplastic, 80, 81f, 649
  - neonatal, 298f
  - pelvic, 645, 645f, 661f, 827f
  - responses to urinary tract dilatation, 648, 648f
  - size of, 342–343
  - small, 646
  - tumors of, 663, 663f

## Kidney(s), maternal, 913–915, 914f

## Klinefelter syndrome (47XXY), 31, 31t, 76, 108t

## Klippel-Feil syndrome, 148–149, 148f–149f, 463, 468, 470

## Klippel-Trenaunay-Weber syndrome, 149f, 149–150

## Knee joint, 308, 308f, 315f, 316f, 319f

## Kniest syndrome, 115, 429t, 456

## Kyphomelic dysplasia, 456

## Kyphosis, 425

**L**

## Labia majora and minora, 666, 667f, 922

## Labor

- induction of, transvaginal ultrasound of cervix to predict success of, 718
- preterm (*See also* Preterm birth (PTB))
  - amniotic fluid sludge and, 760
  - transvaginal ultrasound in diagnosis and management of, 717–718
  - transvaginal ultrasound of cervix to predict start of, 718, 718f

## Lambda (“twin-peak”) sign, 273–274, 275f–276f

## Langer-Saldino achondrogenesis, 113–115, 452, 453f

## Large for gestational age (LGA) fetus, 253–255

- biometric parameters in, 1180t
- polyhydramnios and, 773

## Larsen syndrome, 150, 150f, 435t, 848

## Laryngeal atresia, 503, 504f–505f, 825f

## Laryngotracheoesophageal cleft (L-TEC), 591

## Larynx, fetal, 334f, 339, 340f, 341f

## Laser photocoagulation of communicating vessels, in twin-to-twin transfusion syndrome, 283, 286, 286f, 694–695, 870, 870f, 872, 873t

## Last menstrual period (LMP), 226, 227, 247

## Lateral facial cleft, 402–403, 407f

## Lateral fissure, 353, 355f, 357f

## Lateral thoracic vessels, 1081

## Latissimus dorsi muscle, 311f

Left isomerisms, 528, 531f, 531t. *See also* Heterotaxy

## Leiomyoma(ta), uterine, 14, 930–932, 1004

- adenomyosis and, 1056f, 1058f
- calcification of, 932, 933f, 1056, 1110f

Leiomyoma(ta), uterine (*Continued*)

- clinical features of, 1054
- definition of, 1054
- degeneration of, 932, 934f, 1054, 1056–1058, 1057f–1058f
- diagnosis of, 1056
- ectopic pregnancy and, 1033
- epidemiology of, 1054
- in broad ligament, 1054, 1103f
- in pregnancy, 931, 932f
- in round ligament, 1054, 1055f
- infertility and, 1004
- intracavitary extension of, 932, 934f–935f
- intramural, 1054, 1055f, 1056
- intravenous, 1054
- locations of, 931, 931f, 1004
- malignant transformation of, 932–935, 937f
- metastasizing, 1054
- MRI of, 934f, 1055f–1058f, 1056–1058
- parasitic, 931
- pathophysiology of, 1054–1055
- spontaneous abortion and, 211
- submucosal, 1054, 1055f, 1056f
- subserosal, 1054, 1055f, 1056f
- treatment of, 1055
- ultrasound appearance of, 931f–935f, 932, 1004f
- unusual presentations of, 1054
- vs. adenomyosis, 928, 930t, 932, 934f, 1056
- vs. leiomyosarcoma, 1055, 1058f
- vs. myometrial contraction, 1104f
- vs. ovarian mass, 931, 931f, 1069, 1072
- fibroma, 978, 978f

## Leiomyomatosis, 1054

## Leiomyosarcoma, 932–935, 937f, 1054–1055, 1058f

## Lemon sign, 370, 371f, 1124f

## Leptomeninges, 348f, 349, 350, 355f, 360, 360f

## Lethal multiple pterygium syndrome, 151, 151f

## Levator ani muscle, maternal, 895, 897f, 901f

## Levodardia, 527t, 528, 533f

## Lewis upper limb–cardiovascular syndrome, 465, 467

LGA (large for gestational age) fetus, 253–255

- biometric parameters in, 1180t
- polyhydramnios and, 773

## LH (luteinizing hormone), 182, 183f, 988, 991

## LHR (lung-to-head ratio), 494, 499f

## congenital diaphragmatic hernia and, 507, 874–876, 875f, 876t, 878, 878t

## Ligaments of female pelvis, 895–898, 896f–897f

## Ligamentum teres hepatis, 323

## Ligamentum venosum, 325

## Limb reduction deficits, 28f, 94, 463–465

- after chorionic villus sampling, 50–51
- chromosomal abnormalities and, 463
- conditions associated with, 425, 430t, 463
  - Adams-Oliver syndrome, 464
  - aglossia-adactylia syndrome, 463
  - congenital hemidysplasia with ichthyosiform erythroderma and limb defects, 463
  - fibula aplasia complex brachydactyly, 463
  - Grebe syndrome, 464
  - Moebius sequence, 463
  - phocomelia, 464
  - proximal femoral focal deficiency, 465f, 464–465
  - Roberts syndrome, 464
  - SC phocomelia syndrome, 464
  - splenogonadal fusion syndrome, 463–464
  - thrombocytopenia with absent radius syndrome, 464
  - trisomy 18, 94, 94f
- limb deficiency or congenital amputations, 462f, 462–463

Limb reduction deficits (*Continued*)

- prenatal detection rate for, 462
- terminology for, 425, 430f, 462
- vs. pseudolimb reduction, 1149f

## Limb-body wall complex, 80

## Linea alba, 891

## Lip(s), 333, 392–394, 393f, 393t

- cleft (*See* Cleft lip/palate)
- in chondroectodermal dysplasia, 460
- micrognathia/retrognathia and, 408, 409f, 849f

## Lipoleiomyoma, 936f

## Lipoma(s)

- breast, 1088, 1091f
- closed spina bifida with, 370, 372f
- intracranial, 383–385, 385f
- uterine, 932, 936f

## Lissencephaly, 151–153, 152f, 178, 353, 820

## gestational age and diagnosis of, 385–386

## Lithium, 39t

## Little People of America, 116

## Liver, fetal, 333, 337–338, 339f, 340f, 615–619

- calcifications in, 619, 619f
- conditions associated with abnormalities of
  - cerebrohepatorenal syndrome, 130
  - congenital diaphragmatic hernia, 820, 823f, 874–876, 876t

## HELLP syndrome, 140–141

## Jeune syndrome, 457, 458

## situs abnormalities, 523, 529f

## cytomegalovirus infection of, 134

## echogenicity differences between lung and, 340–341, 342f, 493

## estimated volume of, 616

## hepatomegaly, 616, 616f

## herniation of, 506–507, 507f–508f

## masses in, 617–618

## hemangioma, 618, 618f

## hepatoblastoma, 618

## mesenchymal hamartoma, 617–618

## polycystic liver disease, 617, 618f

## transient idiopathic cysts in early pregnancy, 616–617, 617f

## venous circulation in, 616, 616f

## portal circulation, 320–328, 327f–329f, 338

## LMP (last menstrual period), 226, 227, 247

## Lobster-claw deformity, 465

## London Dysmorphology Database, 113

## Long QT syndrome, 573, 576

## Longitudinal lie, 14, 15f, 16f

## LTEC (laryngotracheoesophageal cleft), 591

## LUF (luteinized, unruptured follicle) syndrome, 993, 994f

## Lumpectomy for breast cancer

- fluid collection at site of, 1093–1094, 1094f
- recurrent carcinoma after, 1089f

## Lung(s), fetal, 340–341, 341f, 342f, 493–504

- abnormalities of
  - bronchogenic cyst, 504, 505f
  - bronchopulmonary sequestration, 493, 502–503, 503f–504f
  - classification of, 493
  - congenital cystic adenomatoid malformation, 493, 501–502, 501f–502f, 878–879, 879f
  - congenital high airway obstruction, 503, 504f–505f
  - congenital lobar emphysema, 504
  - in Fraser syndrome, 137–139, 138f
  - in Wolf-Hirschhorn syndrome, 179t
  - neurenteric cyst, 504, 506f
  - nonimmune hydrops and, 689t, 694
  - pulmonary hypoplasia, 435–442, 494–501 (*See also* Pulmonary hypoplasia)
- amniotic fluid production by, 759

**Lung(s), fetal (Continued)**

- biometric measurements of, 435–436, 439f, 440t, 441t, 494, 498t, 498f–499f
  - echogenicity differences between liver and, 340–341, 342f, 493, 1132f
  - estimating size of, 494
  - estimating volume of, 436–439, 494, 497
    - MRI, 439, 442, 494, 498, 500f, 820
    - three-dimensional ultrasound, 436–439, 442f, 494, 497, 498
  - growth of, 494
  - intrapulmonary fluid, 491
  - length of, 494
  - maturity of, 494
    - criteria for, 242
    - of monoamniotic twins, 277
    - placental grading and, 244, 725
  - MRI evaluation of masses of, 820
  - normal development of, 493–494, 494f–496f
  - pulmonary circulation, 329, 330f, 331f, 339–340, 341f, 493, 497f
- Lung-to-head ratio (LHR), 494, 499f**
- congenital diaphragmatic hernia and, 507, 874–876, 875f, 876t, 878, 878t
- Luteinized, unruptured follicle (LUF) syndrome, 993, 994f**
- Luteinizing hormone (LH), 182, 183f, 988, 991**
- Lymphangiectasia, 75, 217, 218f**
- congenital pulmonary, 881
- Lymphangioma, in neck, 415, 415f**
- Lymphatic drainage**
- of breast, 1081–1082, 1082f–1084f
  - of pelvis, 904–905
- Lymphatic obstruction sequence, cystic hygroma with, 414, 414f**
- Lymphedema, hereditary, 141–142, 141f–142f**
- Lyon hypothesis, 34**

**M****Macrocephaly**

- achondroplasia and, 447
- congenital intracranial tumors and, 384
- holoprosencephaly and, 373
- thanatophoric dysplasia and, 449

**Macroglossia, 409**

- in Beckwith-Wiedemann syndrome, 126, 127f, 409, 409f, 628f

**Macrosomia, 253–255**

- antenatal diagnosis of, 255
- birth trauma and, 254
- cesarean delivery and, 254, 255
- diabetes mellitus and, 254, 255, 771
- in Beckwith-Wiedemann syndrome, 126
- polyhydramnios and, 255, 771
- prevalence of, 254
- shoulder dystocia and, 254, 255

**Macrostomia, 402**

- Magnesium sulfate, effect on fetal biophysical profile, 791–792, 791t–792t

**Magnetic resonance imaging (MRI)**

- advantages of, 808
- blood oxygen level–dependent, 824
- contraindications in pregnancy, 820
- diffusion-weighted, 824
- fast, 809
  - pitfalls in fetal evaluation using, 820
- for evaluation of fetal anatomy, 815–816
- real-time imaging, 816, 817f
- screening for anomalies, 820
- for evaluation of fetal surgery patient, 817, 820, 823f–825f

**Magnetic resonance imaging (MRI) (Continued)**

- for maternal abdominal pain, 810, 812t, 1206t
  - appendicitis, 811f
  - biliary disease, 812f
  - small bowel obstruction, 813f
- for pelvimetry, 811, 815f
- gadolinium-based contrast agents for, 809, 1048–1049
  - in ectopic pregnancy, 1039, 1041f
  - in gynecologic disease, 1048–1073
  - in obstetrics, 808–827
  - in tuberous sclerosis, 819f, 820
- of adnexal masses, 811, 813f–814f, 979, 1068–1073, 1070f–1073f
- of breast cancer, 1091, 1096
- of breast implant rupture, 1093
- of cervical carcinoma, 1063–1065, 1064f–1065
- of cervix, 1049f, 1049–1050
- of endometrial carcinoma, 1066–1067, 1067f–1068f
- of endometriosis, 1060, 1061f–1062f
- of fetal airway obstruction, 820
  - laryngeal atresia, 825f
  - neck mass, 824f
- of fetal central nervous system, 366, 367f, 816–817, 818f–822f
  - agenesis of corpus callosum, 376f, 819f
  - arachnoid cyst, 822f
  - brain, 297, 366, 367f
  - cephalocele, 373f
  - closed spina bifida, 372f
  - cortical development, 817
  - Dandy-Walker malformation, 378, 379
  - dural sinus thrombosis, 387
  - encephalocele, 821f
  - hypoplastic cerebellar vermis, 819f
  - intracranial hemorrhage, 366
  - intratentorial hematoma, 817, 820f
  - lobar holoprosencephaly, 375f
  - neural tube defects, 817, 821f
  - neuronal migration anomalies, 385, 386f
  - patient counseling based on, 817
  - porencephaly, 818f
  - tuberous sclerosis, 819f
  - vein of Galen aneurysm, 386, 386f
  - ventriculomegaly, 817, 818f, 819f
- of fetal craniofacial anomalies, 397
  - clef lip/palate, 401, 405f
- of fetal gastrointestinal system, 615, 820
  - esophageal atresia, 590
  - gastric duplication cyst, 820, 826f
- of fetal thorax
  - bronchopulmonary sequestration, 503, 503f
  - congenital cystic adenomatoid malformation, 501
  - congenital diaphragmatic hernia, 507, 508f, 820, 823f
  - lung mass, 820
  - to estimate fetal lung volume, 439, 442, 498, 500f, 820
- of fetal urinary system
  - renal agenesis, 644
  - urinary tract dilatation, 652
- of hematometocolpos, 1053
- of maternal hydronephrosis, 810, 812f
- of ovaries, 1050, 1051f
  - anomalies, 1053
  - endometrioma, 1060, 1061f–1062f
- of placenta accreta, 742, 743f, 811, 814, 816f
- of placenta previa, 811, 816f
- of placental abruption, 731
- of uterus, 919, 1003, 1049–1050, 1049f–1050f
  - adenomyosis, 1056f, 1058f, 1059f, 1059–1060

**Magnetic resonance imaging (MRI) (Continued)**

- of uterus (Continued)
  - anomalies, 1051–1053, 1052f–1053f
  - endometrial carcinoma, 1066–1067, 1067f–1068f
  - leiomyomas, 934f, 1055f–1058f, 1056–1058
  - leiomyosarcoma, 934–935, 1054–1055, 1058f
  - of vaginal anomalies, 1053, 1054f
  - safety in pregnancy, 809, 820
  - T1-weighted, 809–810, 1048–1049
    - TurboFLASH technique, 809–810
  - T2-weighted, 809, 1048
    - rapid acquisition with relaxation enhancement technique, 809
  - techniques for, 809–810, 1048–1049
  - volumetric, 824
- Magnetic resonance spectroscopy, 824
- Majewski syndrome, 457t, 458–459
- Major aortopulmonary collateral arteries (MAPCA), 546
- Malformations, 27, 28f, 112–113. *See also*
  - Congenital anomalies
- Malleolus, medial, 316f
- Malpractice, 22
- Malrotation, intestinal, 613, 614f–615f
- Mammary lymph nodes, 1081–1082
- Mammography, 1077, 1078f
  - density of breast tissue and sensitivity of, 1085, 1087f–1088f
  - in chronic lymphocytic leukemia, 1084f
  - in tuberculosis, 1083f
  - in young, pregnant, or lactating patients, 1096
  - integrated reporting of sonography and, 1082, 1085
  - multiple masses on, 1096
  - negative predictive value of ultrasound and, 1086–1088
  - of breast implant rupture, 1093f
  - of calcifications, 1085
  - of fatty breast, 1086
  - of marker clip placement, 1092f
  - of recurrent carcinoma, 1089f
  - safety of, 1096
- Mammography Quality Standards Act of 1992, 1082
- Management of Myelomeningocele Study (MOMS), 879
- Mandible, 305, 314, 334f, 393t
  - hypoplasia of (*See* Micrognathia)
  - posterior displacement of (*See* Retrognathia)
- Mandible/maxilla (MD/MX) ratio, 445, 446f
- Mandibulofacial dysostosis, 463
- MAPCA (major aortopulmonary collateral arteries), 546
- Marginal hematoma, 728, 729f, 728, 729f, 731
- Marker chromosomes, 32–33
- Mastitis, 1086
- Maternal age
  - average, 288
  - Down syndrome and, 29, 29t, 30t, 46, 98–99
  - infertility investigation based on, 986
  - nuchal translucency and, 1199t
  - prenatal screening based on, 60
    - amniocentesis, 98–99
    - biochemical, 46–47
    - invasive, 60
    - spontaneous abortion and, 211
    - twin gestation and, 288
- Maternal floor infarction, 727–728, 728f–729f
- Mature cystic teratoma, 968, 972–974, 973f, 981f, 989–991, 990f
  - bowel simulating, 1101f
  - MRI of, 1069, 1070f
- Maxilla, 305, 314, 334f



- Maxillary pseudomass, cleft lip/palate and, 399, 404f
- Maxillonasal dysplasia, 410, 411f
- Maximum vertical pocket (MVP) of amniotic fluid, 762, 762f, 767. *See also* Amniotic fluid volume (AFV)
- Mayer-Rokitansky-Küster-Hauser syndrome, 1052
- MCA. *See* Middle cerebral artery (MCA)
- MCD (medullary cystic dysplasia), 654, 655t, 658–659, 659f
- McKusick-Kaufman syndrome, 400
- MDK (multicystic dysplastic kidney), 80, 81f, 649, 654, 655t, 660–661, 660f–662f
- MD/MX (mandible/maxilla) ratio, 445, 446f
- Mean sac diameter (MSD), 13, 189, 191f
- abnormal, 203, 204f, 207
- abortion risk and, 207
- crown rump length and, 228
- hCG levels and, 214, 228t
- to estimate gestational age, 199–200, 227–228, 228t, 229f
- Meckel diverticulum, 603, 605f–606f, 745
- Meckel syndrome (Meckel-Gruber syndrome), 97, 105, 153f, 153–154, 659
- Meconium cyst/pseudocyst, 603, 604f
- Meconium ileus, 335, 601–602, 1138f
- Meconium peritonitis, 602–603, 602f–604f, 668
- Median cleft face syndrome, 402, 405f–406f, 407, 444
- Medications, teratogenic, 38–40, 39t, 135, 1202t–1204t
- Medullary cystic dysplasia (MCD), 654, 655t, 658–659, 659f
- Megacisterna magna, in Dandy-Walker malformation, 377–379, 379f–381f
- Megacystis, 647, 647f, 664, 665, 666f
- causes of, 649, 652t
- Megacystis-megaureter association, 649, 652f
- Megalencephaly, unilateral, 385
- Megalourethra, 665, 666f
- Meig syndrome, 1069
- Meningocele, 370
- cranial, 371–372, 373f
- Menstrual age, 8, 14, 17, 181, 225. *See also* Gestational age (GA)
- Menstrual cycle, 182–184
- endometrium during, 182–184, 183f, 189, 921f, 1000–1001, 1002f
- follicular phase of, 226, 226f
- ovarian folliculogenesis during, 987–988
- ovaries during, 182, 911, 1201t
- ovulation in, 992f, 992–993
- Menstrual history in pregnancy dating, 226, 227
- Mercury exposure, 39t
- Mesenchymal hamartoma, hepatic, 617–618
- Mesenteric artery, superior, 329, 332f
- Mesoblastic nephroma, 663, 663f
- Mesocardia, 528
- Mesomelia, 425, 430f, 430t, 459
- Mesonephric duct, 913
- Mesonephros, 640, 641f
- Metabolic disorders, nonimmune hydrops and, 691t–692t, 693
- Metacarpals, 305–307, 311, 313f
- Metanephros, 640, 641f
- Metatarsals, 305–307, 308, 310f
- Metatropic dysplasia, lch2al, 429t
- Mcfornin, in polycystic ovary syndrome, 999
- Methotrexate
- for ectopic pregnancy, 1042–1043, 1043f
- for persistent gestational trophoblastic neoplasia, 961
- Meyer-Wiegert rule, 650f
- Microcephaly, 14, 382–383, 384f
- classification of, 383t
- diagnosis of, 382–383, 382t
- holoprosencephaly and, 373
- Microdeletion syndromes, 32, 32t
- Microgastria, congenital, 593
- Microglossia, 409
- Micrognathia, 78, 79f, 408–409, 409f, 817f
- in Moebius sequence, 463
- in Pierre Robin syndrome, 161–162
- mandible/maxilla ratio in diagnosis of, 445, 446f
- skeletal dysplasias with, 444, 445t
- three-dimensional imaging of, 841, 843, 847f–849f, 848
- Micromelia, 425, 430f, 430t
- in achondrogenesis, 114f, 452
- in achondroplasia, 115–116
- in atelosteogenesis, 451
- in diastrophic dysplasia, 455
- in fibrochondrogenesis, 451
- in short rib–polydactyly syndromes, 459, 459f
- in thanatophoric dysplasia, 449–450
- Microphthalmia, 80
- Microptalmia, 407–408, 408f
- Microsomia, hemifacial, 408
- Midbrain, 351, 351f, 353f
- Middle cerebral artery (MCA), 329, 346
- Doppler evaluation of, 252, 256f, 795–797, 797f–798f, 1187f
- in diagnosis of fetal anemia, 682–683, 683f–684f, 693, 797, 798t, 1188t
- in intrauterine growth restriction, 804, 806
- resistance index, 797t, 798t, 1185t
- gestational age and velocity of flow in, 683t
- in uteroplacental insufficiency, 252, 256f
- Midface hypoplasia, 300
- Midgut, 588, 588f
- physiologic herniation of, 625, 625f
- Midline disruption sequence, 631, 632f–633f, 633
- Miller-Dieker syndrome, 32t, 151–152, 152f
- Mirror syndrome, 677–678, 878, 879
- Miscarriage. *See* Abortion, spontaneous
- Misoprostol, 39t, 463
- Mitochondrial disorders, 36, 36t
- Mitral stenosis, 534, 540f
- Mitral valve, Doppler imaging of, 803, 803f, 804t, 1189t
- Mitten hand deformity, 120, 120f
- MMC. *See* Myelomeningocele (MMC)
- M-mode echocardiography, 570, 570f
- atrial bigeminy on, 574f
- atrial flutter on, 576f
- atrioventricular block on, 574f
- during cardiac cycle, 579, 579f–580f
- in ectopic pregnancy, 1031f
- tachycardia on, 575f
- Moderator band, 515, 517f
- Moebius sequence, 463
- Molar pregnancy. *See* Hydatidiform mole
- Molecular-Pathogenetic Classification of Genetic Disorders of the Skeleton, 425, 426t–428t
- MOMS (Management of Myelomeningocele Study), 879
- Monosomy, 29
- Monosomy X. *See* Turner syndrome (45X)
- Morphogenesis, errors in, 27–29, 28f
- Morrison's pouch, free fluid collections in, 891, 894f
- Morula, 182t, 184, 184f, 185f
- Mosaicism
- confined placental, 50
- germline, 33
- MRI. *See* Magnetic resonance imaging (MRI)
- MSD. *See* Mean sac diameter (MSD)
- MTHFR gene mutations, 37
- Mucinous cystadenoma, 971f, 979, 980f
- Mucopolysaccharides in amniotic fluid, 693, 693f
- Müllerian duct anomalies, 925–927, 1001–1003, 1003f, 1051f
- MRI of, 1051–1053, 1052f–1053f
- Multicystic dysplastic kidney (MDK), 80, 81f, 649, 654, 655t, 660–661, 660f–662f
- Multifetal pregnancy reduction, 51, 291–292, 873
- Multiple pregnancies, 266–293, 1151f–1154f. *See also* Triplets; Twins
- amniotic fluid volume in, 17
- assisted reproductive technologies and, 267, 268–269
- biochemical screening in, 46, 288–290, 289t
- cerebral palsy and, 266, 271–272
- chorionic villus sampling in, 51, 290
- complications of, 266, 271–272
- determination of
- in first trimester, 13, 1151f
- in second and third trimesters, 14, 1152f
- Down syndrome and, 66, 288–290, 289f, 289t, 290t
- fetal growth in, 1176t
- growth restriction in, 266
- incidence of, 266, 267f
- intrapartum ultrasound in, 293, 293f
- invasive testing in, 290
- maternal age and, 288
- multifetal pregnancy reduction in, 51, 291–292, 873
- methods for, 292
- when twins are discordant for anomalies, 291–292
- nuchal translucency screening in, 66
- perinatal loss in, 266, 270–272, 271f–273f
- prenatal diagnostic procedures in, 51
- preterm birth in, 271, 273f
- cervical length and, 290–291, 291t, 709t, 710
- selective termination in, 51
- Muscular dystrophy, 178
- Musculature, fetal
- abdominal wall, 320, 326f
- imaging of, 320 (*See also* specific muscles)
- Musculature, maternal pelvic, 891–895, 894f–897f
- Musculoskeletal system, fetal, 305–320, 419–470. *See also* Bone(s); specific structures
- clubfoot, 470
- clubhand, 465–470, 466t, 467t
- development of, 420–422, 420f–422f
- ectrodactyly ectodermal dysplasia-cleft lip/palate syndrome, 465
- polyhydramnios and anomalies of, 772t, 772–773
- skeletal dysplasias, 422–465
- split hand and foot deformities, 465
- three-dimensional imaging of, 848–852
- MVP (maximum vertical pocket) of amniotic fluid, 762, 762f, 767. *See also* Amniotic fluid volume (AFV)
- Myelomeningocele (MMC), 28f, 369–370, 371f
- Arnold-Chiari malformation and, 121, 122f, 370, 372t
- determining most cephalic level of, 360
- fetal surgery for repair of, 868, 879–880, 880f, 880t
- timing of evaluation for, 360
- vs. umbilical cord, 1131f
- Myoblastoma, 409
- Myocardial performance index, 581
- Myocarditis, fetal, 694
- Myonectomy, 1055

Myometrium, 922, 925, 1001  
 anatomy of, 908–909, 909f, 925  
 contraction waves of, 909  
 “kissing” contractions of, 1105f–1106f  
 ultrasound evaluation of, 920

## N

Nabothian cyst, 910, 910f, 1005, 1102f  
 Nasal bones, fetal, 300, 302f–304f, 393t  
   in Down syndrome, 64f, 64–65, 82, 88f, 88–90, 89f, 89t  
   length by gestational age, 1199t  
   three-dimensional imaging of, 90, 850–852  
 Nasolacrimal duct obstruction, 408, 408f  
 National Institutes of Health, 6  
 National Organization for Rare Disorders (NORD), 113  
 Naumoff syndrome, 457t, 458–459  
 Neck, fetal, 412–416  
   cystic hygroma of (*See* Cystic hygroma)  
   echolucent area at back of (*See* Nuchal translucency (NT))  
   MRI evaluation of masses of, 820, 824f  
   ultrasound imaging of, 340f, 341f, 412–414, 413f  
   webbed, 414  
 Neonate  
   Apgar score of, 780, 783  
   diagnosis of congenital anomalies in first year of life, 18  
   dural sinus thrombosis in, 387  
   evaluation for skeletal dysplasias, 446–447  
   exchange transfusion for hyperbilirubinemia, 688  
   maintaining ductus arteriosus patency in, 566  
   managing urinary tract dilatation in, 649–653, 652t, 653f  
   prenatal ultrasound and outcome of, 4  
   sequelae of intrauterine growth restriction in, 219–250  
   skeleton of, 423f  
   ultrasound evaluation of, 297, 298f  
   uterus of, 906  
   vein of Galen aneurysm in, 387  
 Nephroblastomatosis, 663  
 Nephron, development of, 640, 641f  
 Nephrotic syndrome, 664, 664f  
 Neu-Laxova syndrome, 152  
 Neural axis, fetal, 363–389  
   anomalies of neuronal migration, 385–386, 386f  
   artifacts, pitfalls, and normal variants in imaging of, 1124f–1131f  
   destructive cerebral lesions, 380–382  
   due to intrauterine cytomegalovirus infection, 382  
   hydranencephaly, 382  
   intracranial hemorrhage, 380, 381f  
   periventricular leukomalacia, 382, 382f  
   porencephaly, 380–382, 382f  
   pseudoporencephaly, 382  
   schizencephaly, 382, 382f  
   disorders of nerve cell proliferation, 382–385  
   intracranial tumors, 383–385, 384t, 385f  
   megalencephaly, 383, 384t  
   microcephaly, 382–383, 382t–383t, 384f  
   intracranial cysts, 387–389, 388f  
   midline anomalies, 373–380  
   absence of septum pellucidum, 377, 379f  
   agenesis of corpus callosum, 376–377, 376f–377f, 378t  
   Dandy-Walker malformation, 377–380, 379f–380f, 380t  
   holoprosencephaly, 373f–375f, 373–376

Neural axis, fetal (*Continued*)  
   MRI of brain, 366, 367f  
   neural tube defects, 368–372  
     anencephaly, 368–369, 370f  
     cephalocele, 371–372, 373f  
     spina bifida, 369–371, 371f–372f  
   normal sonographic anatomy of CNS, 344–360, 345f–360f, 363–366, 364f–366f  
   vascular abnormalities, 386–387  
     dural sinus thrombosis, 387, 387f  
     vein of Galen aneurysm, 386f, 386–387  
   ventriculomegaly, 366–368, 367f, 368f  
 Neural placode, 370  
 Neural tube defects (NTDs), 7, 368–372  
   alpha-fetoprotein levels and, 42–44, 43f, 45t  
   anencephaly, 368–369, 370f  
   aneuploidy and, 76, 77f  
   causes of, 369t  
   cephalocele, 371–372, 372f, 372t  
   congenital scoliosis and, 446  
   encephalocele, 848, 852f  
   incidence of, 363, 368, 368t, 369t  
   inheritance of, 36–37  
   locations of, 316  
   maternal folic acid levels and, 37  
   MRI of, 817, 821f  
   MTHFR gene mutations and, 37  
   prenatal diagnosis of, 314–316, 360  
   risk factors for, 369t  
   spina bifida, 369–371, 371f–372f  
     fetal surgery for repair of, 370, 868, 879–880, 880f, 880t  
     three-dimensional imaging of, 849, 852f  
   Neuraminic acid in amniotic fluid, 693, 694f  
   Neurenteric cyst, 504, 506f, 591–592  
   Neuroblastoma, 670–671, 671f  
   Neurofibromatosis, 33, 34, 383  
   Neuronal migration anomalies, 385–386, 386f, 819f  
   NIHF. *See* Hydrops fetalis, nonimmune (NIHF)  
 Nipple, 1081  
 Nonstress test (NST), 784t  
   false-positive, 780  
   gradual hypoxia concept and, 787  
   in biophysical profile, 780–782, 783, 788  
   reactive, 780, 782f  
   variations by gestational age, 785  
 Noonan syndrome, 155–156, 411f  
 NORD (National Organization for Rare Disorders), 113  
 Norman-Roberts syndrome, 151–152  
 Nose, 300, 302f–304f, 339, 392–394, 393t, 394t, 314  
   in Binder syndrome, 410, 411f  
   in Down syndrome, 64f, 64–65, 82, 88f, 88–90, 89f, 89t  
   nostril width, 227  
   three-dimensional imaging of, 90  
 NST. *See* Nonstress test (NST)  
 NT. *See* Nuchal translucency (NT)  
 NTDs. *See* Neural tube defects (NTDs)  
 Nuchal cord, 748f, 748–749  
 Nuchal translucency (NT), 61–64, 66–69, 181  
   aneuploidy and, 60t, 81, 1199t  
   causes of increase in, 62  
   congenital heart defect and, 60t  
   cystic hygroma and, 63f, 63–64, 414  
   definition of, 61  
   Down syndrome and, 60–63, 60t, 62f, 81–82, 81f–82f  
   serum marker screening and, 62–63, 63f  
   interpretation of, 66–69, 81–82, 1119f–1120f, 1123f, 1198t–1199t  
   availability of early prenatal diagnosis, 67  
   choosing correct combination of screening tests, 67–69, 68f

Nuchal translucency (NT) (*Continued*)  
   interpretation of (*Continued*)  
     cutoff values for normal, 66–67, 81  
     implications for second trimester serum screening, 67  
     implications for second trimester ultrasound, 67  
   maternal age and, 1199t  
   measurement of, 61f, 61–62, 81  
     in breech fetus, 81  
   Noonan syndrome and, 411f  
   quality control in screening of, 66  
   screening in multiple gestations, 66, 289, 289f, 289t, 290t  
   skeletal dysplasias and, 447, 447t  
   three-dimensional imaging of, 853

## O

Obesity, maternal  
   alpha-fetoprotein levels and, 44  
   amniotic fluid assessment and, 17, 765, 765f  
 Oblique abdominal muscles  
   fetal, 320  
   maternal, 891  
 Obstructive renal dysplasia, 661, 662f  
 Obturator internus muscle, maternal, 895, 897f  
 Ocular biometry, 241, 394t  
 Ocular defects, 407–408, 408f  
 Odontohypophosphatasia, 454–455  
 OEIS (omphalocele–exstrophy–imperforate anus) complex, 665  
 OHSS (ovarian hyperstimulation syndrome), 999, 1008–1009, 1009f  
 OI. *See* Osteogenesis imperfecta (OI)  
 Olecranon, 312f, 313f  
 Oligohydramnios, 767–770  
   abnormal biochemical screening and, 47  
   biophysical profile score and, 783, 789  
   conditions associated with, 767–770  
     absent or nonfunctioning kidneys, 664–665, 761f  
     autosomal-recessive polycystic kidney disease, 655  
     chorioamniotic separation and fetal malformations, 770  
     chorionic villus sampling, 770  
     intrauterine growth restriction, 767  
     post-term pregnancy, 768  
     premature rupture of membranes, 769  
     pulmonary hypoplasia, 768  
     small kidneys, 646  
     “stuck” twin, 280–281, 281f  
     twin-to-twin transfusion syndrome, 175, 281, 282f, 775, 775f–776f, 871–872  
     uteroplacental insufficiency, 249, 767  
   definitions of, 762t, 767  
   diagnosis of, 17  
   effect on estimation of fetal weight and malformations, 770  
   extrinsic and intrinsic causes of, 27  
   in first trimester, 207, 210f  
   intrapartum, in high-risk patients, 769  
   saline amnioinfusion for, 767, 768t  
   ultrasound estimation of, 761  
     amniotic fluid index, 762–765, 763f, 763t, 767  
     Doppler imaging, 766  
     5-cm rule, 763  
     frequency of assessments in high-risk patient, 769–770  
     inter- and intraobserver variation in, 761f, 761–762  
     maximum vertical pocket, 762, 762f, 767  
     1-cm rule, 762



- OMIM (*Online Mendelian Inheritance in Man*), 33, 113
- Omphalocoele, 218, 219f, 625–627  
abnormal umbilical cord development and, 751  
alpha-fetoprotein levels and, 43, 43f  
aneuploidy and, 75–76, 76f, 626  
anomalies associated with, 626  
definition of, 625  
differential diagnosis of, 629, 629f  
in Beckwith-Wiedemann syndrome, 126, 126f, 627, 628f  
in pentalogy of Cantrell, 159–160, 160f  
prenatal diagnosis of, 626, 626f  
prognosis for, 626  
transient, 626–627, 627f  
vs. pseudo-omphalocoele, 1135f  
with intracorporeal liver, 76, 76f
- Omphalocoele-exstrophy-imperforate anus (OEIS) complex, 665
- Omphalomesenteric duct, 195, 198f, 745  
cyst of, 752
- Online Mendelian Inheritance in Man* (OMIM), 33, 113
- Oocyte retrieval, ultrasound-guided, 1009–1010, 1010f
- Ophthalmic artery, 1131f
- Opitz syndrome, 37t
- Oral cavity, 333, 393t  
tumors arising from, 409–410
- Orbit(s), 312–314, 320f, 321f  
defects of, 407–408, 408f  
three-dimensional imaging of, 845f
- Orbital teratoma, 410, 410f
- Oropharynx, fetal, 333, 334f
- Ossification, 421–422, 421f–422f  
centers of, 421, 423f, 1150f  
calcaneal, 311f  
carpal, 307  
femoral, 243–244, 244f, 245f, 308f, 309, 309f, 317f, 421, 422f  
humeral, 309, 317f  
iliac, 314  
imaging of, 305  
ischial, 314, 314f, 324f  
metatarsal, 310f  
phalangeal, 310f, 313f  
primary, 421  
pubic, 324f  
secondary, 421  
talar, 311f  
tarsal, 307  
ribial, 243–244, 245f, 309, 317f, 422f  
vertebral, 314–316, 322f, 324f, 360, 445  
endochondral, 421f, 421–422  
intramembranous, 422
- Osteochondrodysplasias. *See* Skeletal dysplasias
- Osteogenesis imperfecta (OI), 156–158, 453–454  
birth prevalence of, 424, 424t  
classification of, 453–454, 454t  
fractures in, 156f–157f, 156–158, 438f  
genetics of, 454  
lethal, 33, 116, 320, 453  
nosology of, 429t  
skull in, 157, 157f, 358, 358f, 437f  
three-dimensional imaging in, 848
- Osteopenia, 320
- Osteopetrosis, 320
- Otocephaly, 408
- Ovarian artery(ies), 898, 901f, 903–904, 904f, 922
- Ovarian blood flow, 991–992
- Ovarian cyst, 970f–971f, 1112f  
corpus luteum, 911, 912f  
hemorrhagic, 974, 976f  
vs. ectopic pregnancy, 1028, 1030, 1031f–1033f, 1112f
- Ovarian cyst (*Continued*)  
fetal, 668, 668f–669f  
mimicking full bladder, 893f  
theca lutein, 955, 955f, 956, 956f  
twisted, 979–981, 982f–983f  
vs. bowel gas, 1099f  
vs. dilated fallopian tube, 1099f
- Ovarian cystic teratoma, 968, 972–974, 973f, 981f, 989–991, 990f  
MRI of, 1069, 1070f
- Ovarian fimbria, 910
- Ovarian follicle(s), 911, 987f, 987–988  
atretic (degenerating), 184f  
bleeding into, 911  
cumulus oophorus within, 905f, 911  
development of, 182, 183f, 987–988  
propitious moment theory of, 987  
wave model for, 987–988  
dominant, 911, 911f, 987f, 987–988  
hemorrhagic anovulatory, 993, 995f  
intrafollicular arterial flow velocity, 904  
luteinized, unruptured follicle syndrome, 993, 994f  
monitoring course of ovarian stimulation, 1005–1009, 1008f  
preovulatory, 988–989, 988f–990f  
primary, 184f  
ruptured, 184f  
secondary, 184f  
size of, 911  
oocyte maturity and, 1008  
sonographic visualization of, 911, 911f
- Ovarian fossa, 911
- Ovarian hyperstimulation syndrome (OHSS), 999, 1008–1009, 1009f
- Ovarian mass(es), 968–979, 1067–1073  
borderline epithelial tumor, 1069, 1072f  
cystadenocarcinoma, 1069, 1072f  
cystic  
benign-appearing lesions, 1069  
malignant-appearing lesions, 1069, 1072f  
discriminating between benign and malignant masses, 969–970  
Doppler imaging, 969–970  
MRI, 1068–1069  
ultrasound morphology, 969, 970f–971f, 972t  
endometrioma, 974, 975f, 989, 990f, 1060, 1061f–1062f, 1069  
fibroma, fibrothecoma, thecofibroma, thecoma, Brenner tumor, and other benign solid tumors, 976–978, 978f, 1069, 1071f  
granulosa cell tumor, 1069, 1073f  
in pregnant patient, 979, 981f  
incidental ultrasound detection of, 968–969  
mature cystic teratoma, 968, 972–974, 973f, 981f, 989–991, 990f, 1069, 1079f  
metastatic, 1068f, 1069  
MRI of, 811, 813f–814f, 979, 1068–1073, 1070f–1073f  
pregnancy with coexistent ovarian carcinoma, 1102f  
preoperative staging of, 1072–1073  
serous cystadenoma, mucinous cystadenoma, and adenofibroma, 979, 980f, 1069  
Sertoli-Leydig cell tumor, 1069  
surgical removal of, 968  
complications of, 968–969  
ultrasound morphology for making specific diagnosis of, 970–972, 972t  
vs. leiomyoma, 931, 931f, 1069, 1072
- Ovarian reserve, assessment of, 991
- Ovarian stimulation  
ectopic pregnancy after, 1022, 1023f  
monitoring course of, 1006–1009, 1008f
- Ovarian stimulation (*Continued*)  
ovarian hyperstimulation syndrome, 999, 1008–1009, 1009f  
ultrasound-guided oocyte retrieval after, 1009–1010, 1010f
- Ovarian torsion, 968, 979–981, 982f–983f, 1101f  
fetal, 811
- Ovarian vein, 904
- Ovary(ies), 914f  
anatomy of, 911–912  
artifacts, pitfalls, and normal variants in imaging of, 1099f–1102f  
during menstrual cycle, 182, 911, 1201t  
in polycystic ovary syndrome, 997–999, 998f–999f  
location of, 911  
lymphatic drainage of, 904  
metastases to, 1068f, 1069  
MRI of, 1050, 1051f  
size of, 912  
suspensory ligament of, 910–911  
synchronicity between uterus and, 1001  
ultrasound examination in infertility, 987–992  
dermoid cyst, 989–991, 990f  
determining optimal timing for insemination, 991  
endometriomas, 989, 990f  
follicular development, 987, 987f  
ovarian reserve, 991  
preovulatory follicles, 988–989, 988f–990f  
vascular flow, 991–992  
wave model for ovarian folliculogenesis, 987–988  
volume of, 1201t
- Ovary(ies), fetal, 344, 666  
edematous, 811, 814f  
MRI evaluation of masses of, 811, 813f–814f  
torsion of, 811  
tumor of, 813f
- Oviduct. *See* Fallopian tube(s)
- Ovulation, 182–184, 184f, 992f, 992–993  
failure of, 993, 994f  
induction of, in polycystic ovary syndrome, 999, 999f

## P

- Pachygyria, 151
- PACS (picture archiving and communication system), 12
- PACs (premature atrial contractions), 572t, 572–573
- Palate, fetal, 333, 393t, 394t, 396, 397f, 413  
cleft (*See* Cleft lip/palate)  
development of, 399, 399f  
cleft arising from, 409  
MRI evaluation of, 816, 817f
- Pallister-Hall syndrome, 468
- Pallister-Killian syndrome, 32t, 158f, 158–159
- Pampiniform plexus, 904
- Pancreas, fetal, 333, 338, 339f, 623–624, 624f, 623–625  
annular, 624  
cyst in, 624, 624f
- Pancreatoblastoma, 624, 625f
- Papillary muscle mineralization, 84, 1135f
- Papilloma, choroid plexus, 385
- PAPP-A (pregnancy-associated plasma protein A), 60, 60t, 62, 63f, 67, 68f, 181  
early growth restriction and, 208  
in twin gestations, 288–290, 289t
- Paramesonephric duct, 913
- Paraovarian cyst, 974–976, 978f
- Parental-fetal bonding, 859–862

- Parenti-Fraccaro achondrogenesis, 113–115, 452  
 Parieto-occipital fissure, 353, 355f, 357f  
 Parvovirus B19 infection, 693  
 Patau syndrome. *See* Trisomy 13  
 Patella, 308f, 309, 309f, 316f, 319f  
 Patent urachus, 631–634, 634f, 665, 745  
 Paternal age  
   autosomal-dominant disorders and, 33, 33f  
   osteogenesis imperfecta and, 453  
 PCOS (polycystic ovary syndrome), 997–999, 998f–999f  
 PCR (polymerase chain reaction), 55  
 Pectoral fascia, 1080  
 Pelvic diaphragm, 895  
 Pelvic inflammatory disease (PID), 974, 977f  
 Pelvimetry, CT and MRI, 811, 815f  
 Pelvis, fetal. *See also specific structures*  
   in achondrogenesis, 453t  
   in chondroectodermal dysplasia, 459  
   in Jeune syndrome, 458  
   MRI evaluation of, 820  
   ultrasound imaging of, 314, 332f, 344f  
 Pelvis, maternal, 887–917, 899f  
   anatomic relationships of, 891, 892f–893f  
   artifacts, pitfalls, and normal variants in  
     imaging of, 1098f–1112f  
   CT and MRI pelvimetry, 811, 815f  
   fallopian tubes, 906, 911–913  
   false, 891  
   fascial planes of, 891, 894, 894f  
   indications for pelvic sonography, 919  
   ligaments of, 895–898, 896f–898f  
   lymphatic drainage of, 904–905  
   masses in space of Retzius, 893–894  
   muscles of, 891–895, 894f–897f  
   ovaries, 910–911, 911f–912f  
   rectosigmoid colon, 916f, 916–917  
   transvaginal sonographic evaluation of,  
     887–891, 919–920  
   true, 891  
   ureters, 913–915, 914f  
   urinary bladder, 915–916, 915f–916f  
   uterus, 905–910, 907f–910f  
   vagina, 910  
   vascular anatomy of, 898–904, 900f–906f  
   vestigial structures, 913, 913f  
 Pena-Shokeir syndrome, 159  
 Penetrance, 34  
 Penis, 303–305, 307f, 665–666, 666f  
   hypospadias/epispadias, 666–668, 668f  
 Pentalogy of Cantrell, 159–160, 160f  
 PEPI (Postmenopausal Estrogen/Progestin  
   Interventions) study, 943  
 Percutaneous umbilical cord blood sampling  
   (PUBS), 320  
 Pericardial effusion, 72, 551, 1134f  
   hydrops fetalis and, 676, 677f, 679, 688  
   cardiac teratoma and, 568  
 Perinatal outcome. *See also* Abortion,  
   spontaneous; Fetal death  
   abnormal biophysical profile score and,  
     783–784  
   after abnormal biochemical screening, 47  
   after cord occlusion for fetal reduction,  
     873–874, 874t  
   after hysterotomy, 868  
   fetal hypercholeic bowel and, 86  
   in twin-reversed arterial perfusion sequence,  
     874  
   intrapartum oligohydramnios and, 769  
   nuchal cord and, 748–749  
   of multiple gestations, 266, 270–272, 271f–273f  
     monoamniotic twins, 277–279  
   placental abruption and, 730–731  
   polyhydramnios and, 773  
   preterm birth and, 702  
 Perinatal outcome (*Continued*)  
   preterm premature rupture of membranes  
     and, 769  
   skeletal dysplasia and, 424  
 Perineal artery, 901f  
 Perineal body, 895  
 Peristalsis, fetal, 613  
   in colon, 606  
   in small intestine, 244, 595, 596f, 598  
 Peritoneal pseudocyst, 976, 978f  
 Peritonitis, meconium, 602–603, 602f–604f, 668  
 Periventricular leukomalacia, 382, 382f  
 Perlman syndrome, 127, 663  
 Peroxisome biogenesis disorders, 130  
 Pfeiffer syndrome, 161, 407, 412, 412f, 413f  
 Phalanges, 305, 307, 308  
   of foot, 310t, 311f  
   of hand, 313f  
 Pharynx, fetal, 333, 339, 413  
 Phenobarbital, before delivery of hydropic fetus,  
   687  
 Phenylketonuria, 40  
 Phocomelia, 462, 464  
 PI. *See* Pulsatility index (PI)  
 Pia-arachnoid, 349, 351f, 353, 360f  
 Picture archiving and communication system  
   (PACS), 12  
 PID (pelvic inflammatory disease), 974, 977f  
 Pierre Robin syndrome, 161f, 161–162, 470  
 Piriform sinuses, 333, 339  
 Piriformis muscle, maternal, 895, 896f  
 Pitfalls, artifacts, and normal variants, 13, 216,  
   216f, 701–702, 702f–703f, 764f–766f,  
   765–766, 1098f–1158f  
 PITT syndrome, 179  
 Placenta, 721–744  
   abnormalities of  
     abnormal biochemical screening and, 47  
     hydrops and, 692f, 723, 723f, 724f  
     placenta accreta, 737–742, 742f–743f, 811,  
       814, 816f  
     placenta previa, 731–735, 732f–738f, 811,  
       816f  
     placental abruption, 18, 207f, 729, 730–731,  
       731f–732f  
   battledore, 751  
   calcifications of, 725, 727f  
   circummarginate, 723, 724  
   circumvallate, 723–724, 725f–726f, 1103f  
     vs. uterine synechia, 724, 726f  
   development and anatomy of, 185–186,  
     721–722, 722f, 723f  
   focal cystic or hypoechoic lesions of, 725–726  
   decidual septal cyst, 725  
   intervillous thrombus, 725, 727f  
   placental lakes, 725, 728f  
   subchorionic fibrin deposition, 725  
   grading of, 244, 725  
   biophysical profile and, 784, 787  
   hematomas of, 728–730, 729f–730f  
   in twin-to-twin transfusion syndrome, 283,  
     285f  
   inflammation of, short cervical length and,  
     712  
   low-lying, 733, 733f  
   vasa previa and, 737  
   MRI evaluation of, 811, 814, 816f  
   nontrophoblastic tumors of, 742–744  
   chorioangioma, 742–744, 744f–745f  
   teratoma, 744  
   size and shape of, 722–723, 723f–724f  
   succenturiate (accessory) lobe of, 724, 739f,  
     1107f  
   vasa previa and, 737, 740f  
   vs. myometrial contraction, 1104f  
   surface blood vessels of, 320  
 Placenta (*Continued*)  
   thickening of, 723, 723f–724f  
   ultrasound evaluation of, 198, 721, 722, 722f  
   artifacts, pitfalls, and normal variants,  
     1103f–1110f  
   in first trimester, 13  
   in second and third trimesters, 17–18  
   vascular abnormalities of, 726–728  
   fetal artery thrombosis, 728  
   maternal floor infarction, 727–728,  
     728f–729f  
   placental infarction, 726–727, 728f  
   vasculature of, 722  
   volume of, 723  
 Placenta accreta, 737–742, 742f–743f  
   incidence of, 739  
   MRI of, 742, 743f, 811, 814, 816f  
   prenatal diagnosis of, 739  
   risk in subsequent pregnancies after  
     hysterotomy, 869  
   types of, 739, 742f  
 Placenta increta, 742f  
 Placenta percreta, 742f  
 Placenta previa, 731–735, 732f–738f  
   central, 732, 734f  
   cesarean delivery due to, 735  
   complete, 732, 733, 733f–735f  
   definition of, 732  
   diagnosis of, 17–18  
   incidence of, 732  
   incomplete, 733, 734f–735f  
   marginal, 732, 733f  
   MRI of, 811, 816f  
   partial, 732  
   placenta accreta and, 739  
   types of, 732, 733f  
   ultrasound imaging of, 733, 1108f  
     predicting persistence to term, 733–735,  
       738f  
     translabial, 733, 735  
     transvaginal, 733, 734f–735f, 735, 737f–738f  
   vasa previa and, 735–737, 739f–742f  
   vs. contractions of lower uterine segment, 733,  
     736f, 1106f  
 Placental abruption, 18, 207f, 729, 730–731,  
   731f–732f, 773  
   hyperechoic area behind placenta simulating,  
     1109f–1110f  
 Placental infarction, 726–727, 728f  
 Placental lakes, 725, 728f  
 Placental mesenchymal dysplasia (PMD),  
   961–963, 962f  
 Placental migration, 731–732. *See also* Placenta  
   previa  
 Placental oxygenation imaging, 824  
 Placental resistance, 251, 252t, 254f  
 Placental site trophoblastic tumor (PSTT), 951,  
   952f, 954f, 964, 964f  
 Placentation  
   ascertaining site of, 13  
   in twin gestations, 267, 268f, 269, 272–279  
   chorionicity and amnionicity, 270f, 272  
   multiple sonographic markers for, 276  
   first trimester evaluation, 272–273, 273t,  
     274f  
   membrane layers, 275–276  
   membrane thickness, 274–275  
   monoamniotic twins, 276–279, 277f–278f  
   second and third trimester evaluation,  
     273  
   “twin-peak” sign, 273–274, 275f–276f  
   twin-to-twin transfusion syndrome and, 281  
 Placentomectomy, 676, 678, 723, 723f–724f  
 Plasmapheresis, for recurrent immune hydrops  
   fetalis, 687  
 Platyspondyly, 425, 431f, 446



- Pleural effusion(s), 75, 75f, 341, 507–508, 508f  
fetal interventions for, 881–882  
hydrops fetalis and, 74f, 74–75, 676, 677f, 679, 694, 696  
in congenital pulmonary lymphangiectasia, 881
- PMID (placental mesenchymal dysplasia), 961–963, 962f
- Poland syndrome, 162, 463, 468
- Polycystic kidney disease, 34, 654–658  
autosomal-dominant, 654, 655t, 656–658, 657f–658f  
autosomal-recessive, 654, 655t, 655–656, 656f–657f
- Polycystic liver disease, 617, 618f
- Polycystic ovary syndrome (PCOS), 997–999, 998f–999f
- Polydactyly, 95, 96f, 468–469, 1150f  
conditions associated with  
Bardet-Biedl syndrome, 659  
cleft lip/palate, 399, 847f  
Meckel syndrome, 153f, 153–154, 659  
skeletal dysplasias, 443, 443t, 457t  
chondroectodermal dysplasia, 459, 459f–460f  
Jeune syndrome, 457–458  
short rib polydactyly syndromes, 429t, 439f, 459  
Smith-Lemli-Opitz syndrome, 170  
definition of, 425  
preaxial, postaxial, and central, 425, 443f, 443t, 468, 469  
three-dimensional imaging of, 847f
- Polyhydramnios, 770–774  
amniotic fluid index in, 771  
birthweight and, 773  
conditions associated with, 771–773, 772t  
acardiac twins, 287–288  
anencephaly, 368  
chromosomal abnormalities, 773  
congenital diaphragmatic hernia, 506  
diabetes mellitus and macrosomia, 255, 771  
enlarged stomach, 594  
epignathus, 409  
esophageal atresia, 590, 772, 772f  
gastrointestinal obstruction, 596, 613–615  
goiter, 416  
hydrops fetalis, 677, 764f  
intracranial tumors, 384  
myoblastoma, 410  
“stuck” twin, 280–281, 281f  
twin-reversed arterial perfusion sequence, 874  
twin-to-twin transfusion syndrome, 175, 281, 282f, 775, 775f–776f, 871–872  
definition of, 770  
diagnosis of, 17  
idiopathic, 773  
imaging considerations in, 774, 774f  
incidence of, 770  
indomethacin for, 770  
management of, 773–774  
indomethacin, 770, 774  
therapeutic amnioreduction, 773  
perinatal morbidity and, 773  
placental thinning and, 723, 723f  
prenatal diagnosis of, 770  
preterm birth and, 773  
sonographic diagnosis of, 770–771, 771f–774f
- Polymerase chain reaction (PCR), 55
- Polymicrogyria, 385, 820
- Polyplody, 29, 31–32
- Polyps, endometrial, 945, 946f, 948f, 1005, 1007f
- Polysplenia, 124f, 124–125, 125t  
heterotaxy with, 523, 527–528, 528t, 529f–530f
- Pons, 351, 357f
- Popliteal vessels, 329
- Porencephaly, 27, 380–382, 382f, 388, 818f
- Portal circulation, fetal, 252, 320–328, 327f–329f, 338
- Portal hypertension, in Jeune syndrome, 458
- Posterior urethral valves (PUVs), 649, 651f, 665
- Postmenopausal Estrogen/Progestin Interventions (PEPI) study, 943
- Post-term pregnancy, 17  
biophysical profile in, 788  
oligohydramnios and, 768  
placental infarction in, 726
- Potassium chloride, intra-amniotic, for ectopic pregnancy, 1043
- Potter sequence, 27, 40, 446, 644
- Pouch sign of esophageal atresia, 590, 590f
- PPROM. *See* Preterm premature rupture of membranes (PPROM)
- Prader-Willi syndrome, 32t, 35, 162–163
- Preeclampsia  
HELLP syndrome and, 140–141  
placental calcification and, 725, 727f  
retroplacental hematoma and, 729
- Pregnancy dating. *See* Gestational age (GA)
- Pregnancy failure, 200, 201. *See also* Abortion, spontaneous
- Pregnancy loss. *See also* Abortion, spontaneous; Fetal death  
in twin gestations, 266, 270–272, 271f–273f  
Pregnancy outcome. *See* Perinatal outcome
- Pregnancy testing, 185, 942
- Pregnancy-associated plasma protein A (PAPP-A), 60, 60t, 62, 63f, 67, 68f, 181  
early growth restriction and, 208  
in twin gestations, 288–290, 289t
- Preimplantation genetic diagnosis, 52f, 52–53
- Premature atrial contractions (PACs), 572t, 572–573
- Premature ventricular contractions (PVCs), 572t, 573
- Prenatal diagnosis, 48–53  
biochemical screening, 42–47  
Down syndrome, 43f, 45, 45t, 60, 60t  
neural tube defects, 42–44, 43f  
first trimester ultrasound screening for aneuploidy, 60–69  
percutaneous umbilical blood sampling, 52  
preimplantation genetic diagnosis, 52f, 52–53  
procedures for, 48–51  
amniocentesis, 49, 49f  
chorionic villus sampling, 49f, 49–51  
genetic counseling before, 48–49  
in multiple gestations, 51  
pregnancy loss related to, 50  
techniques of genetic analysis, 54f, 54–55  
testing for congenital malformations, 53, 53f  
timing of, 48
- Preovulatory follicles, 988–989, 988f–990f
- Preterm birth (PTB)  
after fetal surgical procedures, 868t  
cord occlusion for fetal reduction, 874t  
hysterotomy, 868, 869  
spina bifida repair, 880  
hydrops fetalis and, 677  
incidence of, 702  
maternal floor infarction and, 728  
of twins, 271, 273f  
cervical length and, 290–291, 291t, 709t, 710  
in twin-reversed arterial perfusion sequence, 874  
polyhydramnios and, 773  
prevention of, 715–717 (*See also* Tocolysis)  
antibiotics, 717  
cervical cerclage, 715–717, 717t  
indomethacin, 717
- Preterm birth (PTB) (*Continued*)  
risk factors for, 709–710  
transvaginal ultrasound of cervix in prediction of, 702–710  
cervical funneling, 704–706  
dynamic changes in cervical length during, 708, 1107f  
gestational age and frequency of, 708–709  
in singleton high-risk gestation, 709t, 709–710  
in singleton low-risk gestation, 709, 709t  
in triplet pregnancy, 709t, 710  
in twin pregnancy, 709t, 710  
other cervical measurements, 706–707  
short cervical length, 290–291, 291t, 703–704, 708, 717  
pathophysiology of, 712, 715  
vs. manual examination, 703–704  
with cerclage in place, 707, 707f–708f, 710
- Preterm premature rupture of membranes (PPROM)  
after fetal surgical procedures, 868t  
cord occlusion, 874, 874t  
fetoscopy, 869  
for tracheal occlusion, 877–878, 878t  
hysterotomy, 868, 869  
shunt placement and radiofrequency ablation, 871  
biophysical profile and, 788, 790t, 790–791, 791f  
cervical length, preterm birth and, 712  
cesarean delivery after, 769  
chorioamnionitis and, 769  
biophysical profile for detection of, 790t, 790–791, 791f  
complications of, 769  
hydrops fetalis and, 677  
oligohydramnios and, 769  
predicting latency to delivery in, 718, 769  
survival rate after, 769  
transvaginal ultrasound of cervix in women with, 703, 718
- Procainamide, 576
- Proctodeum, 588
- Progesterone, 182, 988, 993  
on day of embryo transfer, 1012
- Pronephros, 640, 641f
- Propylthiouracil, 416, 416f
- Prostaglandin E1, to maintain ductus arteriosus patency, 566
- Proximal femoral focal deficiency, 465f, 464–465
- Prune-belly syndrome, 164–165, 164f–165f
- Pseudoascites, 320, 1133f, 1137f
- Pseudocyst  
meconium, 603  
peritoneal, 976, 978f
- Pseudo-double bubble sign, 1140f
- Pseudogastroschisis, 1137f
- Pseudogestational sac, 189–191, 192f, 202, 204–205, 228, 1024–1027, 1025f–1028f, 1030, 1031f, 1035f
- Pseudohypophosphatasia, 454
- Pseudolimb reduction, 1149f
- Pseudomegabladder, 642
- Pseudo-omphalocele, 1136f
- Pseudoporencephaly, 382
- Pseudotoxemia, 677
- Psoas muscle  
fetal, 328f, 1142f  
maternal, 894–895, 895f
- PSTT (placental site trophoblastic tumor), 951, 952f, 954f, 964, 964f
- PTB. *See* Preterm birth (PTB)

Pterygium  
 colli, 414  
 lethal multiple pterygium syndrome, 151, 151f  
 Pubis, 324f  
 PUBS (percutaneous umbilical cord blood sampling), 320  
 in acidemia, 252, 253  
 Pulmonary artery(ies), 329, 331f, 339–340, 493, 497f  
 branch  
 abnormalities of, 557t  
 absence or hypoplasia of, 556–557  
 dilatation of, 557  
 origin from aorta, 557, 558f  
 Doppler velocimetry of, 442, 500f, 500–501, 804, 805t, 1189t  
 in tetralogy of Fallot, 552–553, 553f  
 measuring diameters of, 1194f, 1197f  
 preferential flow into, 552  
 size in relation to ascending aorta, 552, 1194f  
 three-dimensional imaging of, 842f–843f  
 three-vessel view of, 516, 519f–520f  
 Pulmonary artery sling, 557, 558f  
 Pulmonary atresia, 532, 539f  
 tetralogy of Fallot with, 546, 556, 557, 559f  
 with major aortopulmonary collateral arteries, 546  
 with ventricular septal defect, 565  
 Pulmonary circulation, 329, 330f, 331f, 339–340, 341f, 493, 497f  
 Pulmonary hypoplasia, 494–501  
 congenital diaphragmatic hernia and, 506, 874–876, 876t, 878  
 congenital hydrothorax and, 508  
 definition of, 494  
 due to absence of branch pulmonary artery, 556  
 incidence of, 494  
 mortality due to, 494  
 oligohydramnios and, 768  
 prediction of, 435–442, 494–501  
 biometric parameters, 435–436, 439f, 440t, 441t, 494, 498t  
 Doppler assessment of tracheal fluid flow, 442  
 Doppler velocimetry of pulmonary arteries, 442, 500f, 500–501  
 MRI, 439, 442, 498, 500f  
 three-dimensional ultrasound, 436–439, 442f, 494, 497, 498  
 Pulmonary lymphangiectasia, 881  
 Pulmonary stenosis, twin-to-twin transfusion syndrome and, 872  
 Pulmonary vascular resistance, 494, 802  
 Pulmonary vein(s), 330f, 339–340, 341f, 493, 497f  
 anomalous pulmonary venous connection, 534, 542f–543f  
 on four-chamber view, 515, 517f  
 Pulsatility index (PI), 900  
 ductus venosus, 802t  
 pulmonary artery, 442  
 umbilical artery, 251, 796t, 1184t, 1187f  
 uterine artery, 799t, 1010–1011, 1184t  
 PUVs (posterior urethral valves), 649, 651f, 665  
 PVCs (premature ventricular contractions), 572t, 573  
 Pyelectasis, 647  
 in Down syndrome, 83f, 83–84  
 Pyloric atresia, 591, 594, 595f, 615

## Q

Quadratus lumborum muscle, 328f, 1142f  
 Quadriceps femoris muscle, 314f, 319f

Quadruple screen, 45t, 46t, 60, 60t, 63, 63f, 67, 68, 71  
 Quadruplets, 266, 267f. *See also* Multiple pregnancies  
 Quality assurance, 12t  
 in nuchal translucency screening, 66  
 Quantitative fluorescent polymerase chain reaction assays, 55

## R

Race/ethnicity  
 carrier screening and, 41, 41t  
 maternal alpha-fetoprotein levels and, 44  
 Radial artery(ies), 900, 901, 901f–902f, 925  
 Radial clubhand, 465–468, 466t  
 hematologic disorders and, 466–467  
 scoliosis and, 467–468  
 Radiation exposure  
 from CT, 808, 1205t  
 from mammography, 1096  
 teratogenicity of, 40  
 to fetus, 1205t  
 Radiation therapy  
 for breast cancer, 1094–1095, 1095f  
 for cervical cancer, 1063  
 for endometrial cancer, 1066  
 Radiofrequency ablation (RFA), 871, 874  
 Radius, 307, 308–309, 313f  
 aplasia of, 462f  
 in trisomy 18, 94, 94f  
 in atelosteogenesis, 451  
 length of, 433t, 1160t, 1167t–1168t  
 thrombocytopenia with absent radius syndrome, 464, 465, 467  
 RADIUS (Routine Antenatal Diagnostic Imaging with Ultrasound) study, 5  
 Rapid acquisition with relaxation enhancement (RARE) MRI technique, 809  
 Reciprocal translocations, 32  
 Rectum, fetal, 338f, 344f, 1141f  
 sonograms of diameter of, 606, 607f–608f  
 Rectus abdominis muscles, maternal, 891, 894f  
 Rectus sheath hematoma, 893  
 Red cell alloimmunization, 676, 678–681, 678f, 679t, 680f, 693  
 Red cell antibody measurement, maternal, 681  
 Red cell antigen testing, 681  
 Renal agenesis, 644, 644f  
 lying down adrenal sign of, 644f, 670  
 oligohydramnios and, 664–665, 761f  
 Renal artery(ies), 329  
 Renal cystic diseases, 654–663  
 classification of, 654–655, 655t  
 genetic, 655–659  
 autosomal-dominant polycystic kidney disease, 656–658, 657f–658f  
 autosomal-recessive polycystic kidney disease, 655–656, 656f–657f  
 glomerulocystic kidneys, 658, 658t, 659f  
 medullary cystic dysplasia, 658–659, 659f  
 unclassified cystic disease, 659, 660f  
 nongenetic, 660–661  
 multicystic dysplastic kidney, 660–661, 660f–662f  
 obstructive renal dysplasia, 661, 662f  
 simple renal cyst, 661, 662f  
 sonographic evaluation of, 655, 662t  
 work-up of, 661–663, 662t–663t  
 Renal duplications, 645, 645f, 649, 650f  
 Renal dysplasia, 654  
 Renal vein, 329  
 thrombosis of, 663, 663f

Resistance index (RI), 900  
 middle cerebral artery, 797t, 798t, 1185t  
 ovarian artery, 904  
 radial artery, 901  
 spiral artery, 901  
 umbilical artery, 251, 252t, 796t, 798t, 1184t–1185t, 1187f  
 uterine artery, 799t, 901, 1010–1011, 1184t  
 Respiratory distress syndrome, 242  
 Respiratory system, fetal. *See also* specific structures  
 imaging of, 339–341, 340f–342f, 493–498  
 polyhydramnios and anomalies of, 772t  
 Restrictive cardiomyopathy, 582  
 Retained products of conception (RPOC), 202, 203f, 935, 939–940, 939f–940f  
 Retinoblastoma, 32t, 34  
 Retrognathia, 79, 408–409  
 differentiating from micrognathia, 444–445  
 inferior facial angle in diagnosis of, 445, 445f  
 Retroplacental complex, 722, 723f  
 Retroplacental hematoma, 206, 207f, 729f, 729–730, 731, 731f  
 with placental abruption, 730–731, 731f–732f  
 Retropubic space, masses in, 893f, 893–894  
 Rett syndrome, 34  
 RFA (radiofrequency ablation), 871, 874  
 Rh immune globulin, 676  
 Rhabdomyoma, cardiac, 173f, 173–174, 567, 569f  
 RhD alloimmunization, 676, 678, 678f, 680f  
 management of, 684, 685f–686f  
 Rhizomelia, 425, 430f, 430t  
 in achondroplasia, 447  
 in thanatophoric dysplasia, 449  
 Rhombencephalon, vs. congenital anomaly, 216, 216f, 1118f  
 Rhomboid muscle, 312f  
 RI. *See* Resistance index (RI)  
 Rib(s), fetal, 312f, 314, 1133f  
 fractures of, 438f  
 in chondroectodermal dysplasia, 459  
 short rib–polydactyly syndromes, 429t, 439f, 457t, 458–459, 459f  
 thoracic vertebral anomalies and defects of, 446

Right isomerisms, 528, 531t  
 Roberts syndrome, 166, 464  
 Robertsonian translocations, 32  
 Robin anomaly, 408  
 Rocker-bottom foot, 93, 93f  
 Rodeck shunt, 870  
 Rolland-Desbuquois syndrome, 456  
 Round ligament(s), 898, 901f, 922  
 leiomyoma in, 1054, 1055f  
 Routine Antenatal Diagnostic Imaging with Ultrasound (RADIUS) study, 5  
 RPOC (retained products of conception), 202, 203f, 935, 939–940, 939f–940f  
 Rubella infection, intrauterine, 37, 38, 39t, 134–135  
 Rubenstein-Taybi syndrome, 32t, 37t

## S

Sacroccoccygeal teratoma (SCT), 676, 694  
 fetal surgery for repair of, 868, 879, 879f  
 SADDAN (severe achondroplasia with developmental delay and acanthosis nigricans), 449  
 Safety  
 of mammography, 1096  
 of prenatal CT, 808–809  
 of prenatal MRI, 809  
 of prenatal ultrasound, 3–5, 12t, 891  
 Saldino-Noonan syndrome, 457t, 458–459



- Saline infused sonography (SIS), 920–922, 922f  
 anesthesia/analgesia for, 945  
 concern about spreading adenocarcinoma with, 945  
 contrast-enhanced, 1006  
 difficulty threading catheter for, 945  
 during tamoxifen treatment, 949, 949f  
 in evaluation of uterine bleeding, 944–946, 944f–948f  
 in infertility evaluation, 1005–1006, 1006f  
 inadequate distention of cavity for, 945  
 of endometrial polyps, 945, 946f, 948f, 1005, 1007f  
 of leiomyomata, 932, 934f  
 pathology detected by, 945–946  
 risk of infection from, 945  
 technique for, 944, 1005–1006  
 Sandal gap deformity, 94, 94f, 1151f  
 Sarcoma(s), uterine, 932–935, 937f  
 SC phocomelia syndrome, 464  
 Scalp, fetal, 1121f  
   defect in Adams-Oliver syndrome, 464  
   edema of, 676, 676f, 679  
   hair on, 302, 306f, 1123f  
 Scaphocephaly, 411  
 Scapula, 307, 311f–312f  
 Scar pregnancy, 1038, 1041f  
 Schizencephaly, 382, 382f, 385, 388  
 Scimitar syndrome, 533f, 556  
 Sclerotome, 422  
 Scoliosis, 425, 431f, 445, 446  
   radial clubhand and, 467–468  
   three-dimensional imaging of, 431f, 854f  
 Scrotum, 303, 344, 666, 667f  
   abnormalities of, 668  
   split scrotum sign, 667f  
   three-dimensional imaging of, 837f  
 SCT (sacroccoccygeal teratoma), 676, 694  
   fetal surgery for repair of, 868, 879, 879f  
 Scathre-Chotzen craniosynostosis, 371  
 Second and third trimester ultrasound examination(s), 7, 14–19  
   biometry, 232  
   guidelines for, 10t–12t  
   Level I and Level 2, 7  
   prescan counseling for, 18  
   second trimester screening for aneuploidy, 70–106  
     biochemical screening and, 70–71  
     Down syndrome, 98–103  
     sonographic features, 71–97  
     trisomy 13, 104–105, 105f, 105t  
     trisomy 18, 103–104, 104t  
   to ascertain fetal life, 14  
   to assess amniotic fluid volume, 17  
   to assign gestational age and weight, 14, 17  
   to detect fetal anomalies, 18–19  
   to determine fetal number, 14  
   to determine fetal position, 14, 15f–17f  
   to evaluate placenta, 17–18  
   to evaluate uterus and adnexa, 19  
 Selective termination of multifetal pregnancies, 51, 291–292  
 Semilunar valves, Doppler imaging of, 803–804, 804f  
 Septate uterus, 211, 926–927, 926f–927f, 1001, 1003f, 1051f  
   MRI of, 1053, 1053f  
 Septo-optic dysplasia, 166–167, 167f  
 Sequence, 27, 113. *See also* Congenital anomalies  
 Serous cystadenoma, 979, 980f  
 Serpent crawling under the skull sign, 375, 375f  
 Sertoli-Leydig cell tumor, 1069  
 Severe achondroplasia with developmental delay and acanthosis nigricans (SADDAN), 449  
 Sex chromosome aneuploidy, 31, 31t  
 Sex determination, fetal, 665–666  
 SF (shortening fraction), 579, 580f  
 SGA (small for gestational age) fetus, 247  
   abnormal cord coiling in, 750  
   biometric parameters in, 1180t  
 Shepard formula for fetal weight estimation, 247  
 Shone syndrome, 534  
 Short rib–polydactyly syndromes, 429t, 439f, 457t, 458–459, 459f  
 Shortening fraction (SF), 579, 580f  
 Shoulder, 311f  
 Shoulder dystocia  
   gestational diabetes and, 255  
   macrosomia and, 254  
   prevalence of, 255  
 Shunts, 870–871  
   procedure for placement of, 871  
   risks of, 871  
   thoracoamniotic, 508, 878  
   vesicoamniotic, 649  
 Side lobe artifact, 1155f  
 Silicone breast implant rupture, 1093, 1093f  
 Silverman-Handmaker syndrome, 456  
 Simpson-Golabi-Behmel syndrome, 167–168  
 Single umbilical artery (SUA), 95–97, 96f, 468, 746–747, 746f–747f, 1144f  
 Sinus bradycardia, 573  
 Sinus tachycardia, 575  
 Sinus venosus defect, 548  
 Sirenomelia, 168–169, 169f, 169t  
 SIS. *See* Saline infused sonography (SIS)  
 Situs ambiguus, 523  
 Situs inversus, 523, 527t, 529f  
 Situs solitus, 523, 527t, 529f  
 Skeletal dysplasias, 422–465  
   birth prevalence of, 422–424, 424t  
   chromosomal abnormalities and, 447  
   classification of, 424–425, 426t–428t  
   clinical presentation of, 430–431  
   diagnostic approach to, 434–447  
     evaluation of fetal face, 443–445, 445f–446f, 445t–446t  
     evaluation of fetal hands and feet, 443, 443t, 444f  
     evaluation of fetal internal organs, 446  
     evaluation of fetal long bones, 434–435, 437f–438f  
     evaluation of fetal skull, 443, 444f, 445t  
     evaluation of fetal spine, 431f–432f, 445–446  
     newborn evaluation, 446–447  
     nuchal translucency, 447, 447t  
     prediction of pulmonary hypoplasia, 435–442, 438t, 439f, 440t, 441t, 442f  
   diagnostic imaging and prenatal diagnosis of, 431–434  
     accuracy of, 432, 434t  
     clinical importance of, 430–431  
     long bone biometry, 425, 429, 432t, 433t  
     three-dimensional helical CT, 434, 436f  
     three-dimensional ultrasound, 432–434, 434f, 435t, 437t, 848  
   lethal, 425, 429t, 447  
   nonimmune hydrops and, 691t  
   perinatal mortality and, 422–424  
   relative frequency of, 424, 424t  
   specific disorders, 447–465  
     achondrogenesis, 113–115, 114f, 451–452, 452f, 453t  
     achondroplasia, 115–116, 115f–116f, 447–449, 448f  
     Adams-Oliver syndrome, 464  
     aglossia-adactylia syndrome, 463  
     asphyxiating thoracic dysplasia, 124, 124f, 457t, 457–458  
     atclosteogenesis, 451  
     diastrophic dysplasia, 116, 455f, 455–456  
     dyssegmental dysplasia, 456  
     fibrochondrogenesis, 451  
     fibula aplasia complex brachydactyly, 463  
     Grebe syndrome, 464  
     hypochondroplasia, 451  
     hypophosphatasia, 454–455  
     Kniest syndrome, 115, 456  
     lethal, 429t  
     limb deficiency or congenital amputations, 462f, 462–463  
     limb reduction defects with other anomalies, 463–465, 465f  
     Moebius sequence, 463  
     osteogenesis imperfecta, 156f–157f, 156–158, 358f, 437f, 438f, 453–454, 454t  
     phocomelia, 464  
     proximal femoral focal deficiency, 465f, 464–465  
     Roberts syndrome, 166, 464  
     SC phocomelia syndrome, 464  
     short rib–polydactyly syndromes, 429f, 457t, 458–459, 459f  
     splenogonadal fusion syndrome, 463–464  
     thanatophoric dysplasia, 171–172, 171f–172f, 449–450, 450f  
     thrombocytopenia with absent radius syndrome, 464  
     with absent limbs and facial anomalies, 463  
     with predominant membranous bone involvement, 460–461, 461f  
     with thoracic hypoplasia, 457t, 457–460, 459f–460f  
   Yunis-Varon syndrome, 461  
   terminology for, 425, 430f  
 Skeletal imaging, 305–320. *See also* Bone(s)  
 Skeletogenesis, 420–421, 420f–421f  
 Skene gland, 915  
   neoplasm of, 916, 916f  
 Skull  
   abnormalities of  
     cloverleaf deformity, 443  
     in Pfeiffer syndrome, 161, 412f  
     in thanatophoric dysplasia, 171f, 171–172, 444f, 449  
     in achondrogenesis, 452, 453t  
     in cleidocranial dysplasia, 461, 461f  
     in craniosynostosis, 410–412, 412f–413f  
     in hypophosphatasia, 455  
     in osteogenesis imperfecta, 157, 157f, 358, 358f, 437f  
     in Wolf-Hirschhorn syndrome, 179t  
   skeletal dysplasias and, 443, 445t  
   strawberry-shaped skull, 97, 97f  
   absence of, 369  
   demineralization of, 435, 437f, 443  
   imaging of, 312, 314, 319f, 322f  
   artifacts, pitfalls, and normal variants, 1123f–1124f  
   three-dimensional, 396f, 461f, 843, 849f  
 Small for gestational age (SGA) fetus, 247  
   abnormal cord coiling in, 750  
   biometric parameters in, 1180t  
 Small intestinal obstruction, maternal, 810, 813f

- Small intestine, fetal, 335, 336f, 595, 596f, 598, 598f, 599f, 595-605. *See also* Bowel congenital intestinal pseudo-obstruction. 604-605, 606f  
 vs. chloride diarrhea, 605, 606f, 607t  
 duodenum, 595-597, 596f  
 obstruction of, 595-597, 596f-597f  
 duplication of, 604  
 fluid-containing, 334  
 idiopathic transient early intestinal fluid dilatation of, 598-599, 599f  
 jejunum and ileum, 598-602  
 jejunoileal atresia, 596f, 599-601, 600f-602f, 601t  
 Meckel diverticulum, 603, 605f-606f  
 meconium ileus, 335, 601-602  
 perforation of, 602-603, 602f-604f  
 peristalsis in, 244, 595, 596f, 598  
 physiologic herniation of, 216, 216f  
 vs. ventral wall defects, 218  
 pseudomass of, 335  
 Smith-Lemli-Opitz syndrome, 47, 113, 169-170, 170t  
 Smith-Magenis syndrome, 32t  
 Sodium iodide, 39t  
 Sonocmbryology, 196  
 Sonographers, 6, 8  
 Sonohysterography, 920-922, 922f  
 anesthesia/analgesia for, 945  
 concern about spreading adenocarcinoma with, 945  
 contrast-enhanced, 1006  
 difficulty threading catheter for, 945  
 during tamoxifen treatment, 949, 949f  
 in evaluation of uterine bleeding, 944-946, 944f-948f  
 in infertility evaluation, 1005-1006, 1006f  
 inadequate distention of cavity for, 945  
 of endometrial polyps, 945, 946f, 948f, 1005, 1007f  
 of leiomyomata, 932, 934f, 946f  
 pathology detected by, 945-946  
 risk of infection from, 945  
 technique for, 944, 1005-1006  
 Sonologists, 6, 8  
 Sotalol, 576  
 Space of Retzius, masses in, 893f, 893-894  
 Spatial compounding, in breast imaging, 1077-1078, 1078f, 1079f  
 Spina bifida, 27, 369-371. *See also* Neural tube defects (NTDs)  
 alpha-fetoprotein levels and, 43, 43f, 314, 369  
 aneuploidy and, 76, 77f  
 Arnold-Chiari malformation and, 121, 122f, 370, 372t, 879  
 closed, 369-370, 372f  
 fetal surgery for repair of, 370, 868, 879-880, 880f, 880t  
 hydrocephalus and, 370  
 incidence of, 368t  
 level of, 370  
 open, 360, 369, 370, 371f  
 outcome of, 370-371  
 prenatal diagnosis of, 314-316, 370, 371f-372f  
 three-dimensional imaging of, 848, 852f  
 Spinal abnormalities  
 conditions associated with  
 achondrogenesis, 114, 114f, 320, 452, 452f, 453t  
 achondroplasia, 116f  
 Alagille syndrome, 117  
 Arnold-Chiari malformation, 122t  
 caudal regression syndrome, 128-130, 129f  
 Goldenhar syndrome, 468  
 Klippel-Feil syndrome, 148-149, 148f-149f, 468  
 Spinal abnormalities (Continued)  
 conditions associated with (Continued)  
 Larsen syndrome, 150, 150f  
 skeletal dysplasias, 431f-432f, 445-446  
 thanatophoric dysplasia and platyspondyly, 171, 431f  
 VACTERL association, 177, 177f  
 Wolf-Hirschhorn syndrome, 179t  
 congenital scoliosis, 431f, 445, 446  
 hemivertebra, 425, 432f, 445-446  
 in diastrophic dysplasia, 455  
 in dyssegmental dysplasia, 455  
 platyspondyly, 425, 431f  
 split notochord syndrome, 591-592, 592f  
 terminology for, 425, 431f-432f  
 vertebral clefts, 446  
 Spinal cord, 360, 360f  
 tethered, 827f  
 Spine. *See also* Vertebra(e)  
 curvature of, 446  
 imaging of, 312f, 314-320, 322f-325f, 360, 360f, 363, 366, 366f  
 artifacts, pitfalls, and normal variants, 1131f  
 three-dimensional, 367f, 848, 852f-854f  
 lumbar, 323f, 325f, 853f  
 neurocentral synchondrosis of, 318-320  
 ossification of, 314-316  
 sacral, 323f-324f  
 Spiral endometrial artery(ies), 901, 902f-903f  
 in first trimester, 184, 186-188, 188f, 191, 193f, 722  
 Spleen, fetal, 329f, 333, 338-339, 623  
 cyst in, 623  
 splenomegaly, 623, 623f  
 visceral situs with asplenia or polysplenia, 523, 527-528, 528t, 529f-530f  
 Splenogonadal fusion syndrome, 463-464  
 Split hand and foot deformities, 465  
 Split notochord syndrome, 591-592, 592f  
 Split scrotum sign, 667f  
 Spondylocostal dysostosis, 425, 435t  
 Spondyloepiphyseal dysplasia, 115  
 Spotting, 200. *See also* Uterine bleeding, abnormal  
 Staging  
 of breast cancer, 1096-1097  
 of cervical carcinoma, 1063, 1063t  
 of endometrial carcinoma, 1066, 1066t  
 of gestational trophoblastic neoplasia, 960, 960t  
 of twin-to-twin transfusion syndrome, 283, 285t, 872, 872t  
 preoperative, of adnexal mass, 1072-1073  
 Sternocleidomastoid muscle, 341f  
 Steroid sulfatase deficiency, 47  
 Stomach, fetal, 592-595  
 abnormal location of, 590  
 congenital diaphragmatic hernia and, 506-507, 507f-508f, 594f  
 in situs abnormalities, 523, 529f  
 debris within, 1138f  
 duplications of, 591, 592f, 595  
 MRI of, 820, 826f  
 emptying cycles of, 593  
 esophageal atresia and abnormalities of, 590  
 fluid-containing, 334-335  
 imaging of, 326f, 328f, 329f, 333-335, 335f-337f, 592, 592f-593f  
 artifacts, 1155f  
 incisura angularis of, 335  
 intraluminal masses in, 594-595, 595f  
 nonvisualization of, 593  
 pyloric atresia, 591, 594, 595f  
 size of, 335, 593  
 congenital microgastria, 593  
 enlarged stomach with normal amount of amniotic fluid, 594, 594f  
 enlarged stomach with polyhydramnios, 594  
 Stomodeum, 588  
 "Stuck" twin, 175, 280-281, 281f  
 SUA (single umbilical artery), 95-97, 96f, 468, 746-747, 746f-747f, 1144f  
 Subamniotic hematoma, 729, 729f  
 Subarachnoid spaces, 349, 352f  
 Subchorionic hematoma, 207f, 208f, 728-729, 729f-730f, 1146f  
 Subclavian artery, 329, 332f, 1081  
 disruption sequences, 463  
 Subendometrial halo, 925  
 Subscapular artery, 1081  
 Subscapularis muscle, 312f  
 Substantia nigra, 351, 351f  
 Subtelomere deletions, 32  
 Sulci, gestational age and visibility of, 385-386  
 Superior vena cava (SVC), 329, 331f  
 bilateral, 550f, 556  
 dilatation of, 554  
 in situs abnormalities, 529f  
 Supine hypotension syndrome, hydrops fetalis and, 677  
 Supraspinatus muscle, 312f  
 Supraventricular tachycardia, 572t, 575f, 575-576  
 SURUSS trial, 67  
 Suspensory ligament of ovary, 910-911  
 Sutures, cranial, 411-412, 843, 849f. *See also* Craniosynostosis  
 SVC. *See* Superior vena cava (SVC)  
 Swallowing, fetal, 334, 759  
 hypoxic suppression of, 767  
 Syncytiotrophoblast, 185f, 721  
 Syndactyly  
 definition of, 425  
 in Apert syndrome, 120, 120f  
 in Fraser syndrome, 137-138, 138f  
 in Pfeiffer syndrome, 161  
 in Smith-Lemli-Opitz syndrome, 169-170  
 skeletal dysplasias associated with, 443, 443t  
 Syndromes, 27, 113. *See also* Congenital anomalies  
 Syphilis, intrauterine, 38, 39t
- T**  
 "T" sign, 273, 276f  
 Tachycardia, fetal, 571, 575-576, 575f-576f  
 atrial ectopic, 575  
 AV reentrant, 575f, 575-576  
 management of, 576  
 nonimmune hydrops and, 694  
 permanent junctional reciprocating, 575  
 prenatal treatment of, 576  
 sinus, 575  
 supraventricular, 572t, 575f, 575-576  
 ventricular, 572t, 576  
 Talipes equinovarus. *See* Clubfoot  
 Talus, 307, 311, 311f, 316f  
 Tamoxifen, for abnormal uterine bleeding, 949, 949f  
 TAR (thrombocytopenia with absent radius) syndrome, 464, 465, 467  
 Tarsal bones, 307, 309-311, 310f-311f  
 Tarsal navicular, 311, 311f  
 TAS. *See* Transabdominal sonography (TAS)  
 Tay-Sachs disease, 41  
 Technology and equipment, 8, 12, 12t, 297-299. *See also* Transducers  
 for breast imaging, 1077-1080  
 for fetoscopy, 870  
 for radiofrequency ablation, 871  
 shunts, 870-871  
 Teeth  
 in chondroectodermal dysplasia, 460  
 in odontohypophosphatasia, 454-455



- Tei index, 581  
 Telemedicine, 13  
 Temperature extremes, teratogenicity of, 40  
 Tentorium cerebelli, 349  
   in Dandy-Walker malformation, 378, 379f  
 Teratogens, 27, 37–40, 39t  
   embryonic susceptibility to, 37, 38f, 215, 215f  
   maternal factors, 40  
   maternal infections, 38  
   mechanical factors, 40  
   medications, 38–40, 39t, 135, 1202t–1204t  
   radiation, 40  
   temperature extremes, 40  
 Teratoma  
   cardiac, 568  
   cervical, 415, 415f, 416  
   epignathus, 409, 410f  
   intracranial, 383–385, 385f  
   orbital, 410, 410f  
   ovarian cystic, 968, 972–974, 973f, 981f, 989–991, 990f  
   placental, 744  
   acrococcygeal, 676, 694  
     fetal surgery for repair of, 868  
 Tessier cleft number 0, 402, 405f  
 Tessier cleft number 7, 402–403, 407f  
 Testis, 303, 344, 666, 667f  
   three-dimensional imaging of, 837f  
   torsion of, 668  
   undescended, 668  
 Tethered cord, 827f  
 Tetralogy of Fallot, 528, 533f, 552–554, 553f, 565  
   with absent pulmonary valve syndrome, 546, 556, 557, 559f  
 Tetraploidy, 31  
 Tetrasomy 12p, 158f, 158–159  
 Thalamus, fetal, 345f, 346, 355f  
 Thalidomide, 37, 39t, 40  
 Thanatophoric dysplasia, 37t, 116, 171–172, 171f–172f, 412, 431f, 437f, 439f, 449–450, 450f  
   birth prevalence of, 424, 424t  
   brain abnormalities in, 450  
   cloverleaf skull in, 171f, 171–172, 444f, 449  
   differential diagnosis of, 450  
   genetics of, 449  
   nosology of, 429t  
   subtypes of, 449  
   three-dimensional imaging in, 435t, 848  
 Theca lutein cyst, 955, 955f, 956, 956f  
 Thecofibroma, 976–978  
 Thecoma, 976–978  
 Thela choroidea, 373  
 Thermal index, 3–4  
 Thoracic circumference, 440t, 494, 498t, 643, 1173t  
 Thoracic-to-abdominal circumference ratio, 436, 494, 498f  
 Thoracoacromial artery, 1081  
 Thoracoamniotic shunting, 508, 878  
 Thorax, 493–508. *See also specific structures*  
   congenital hydrothorax, 507–508, 508f  
   diaphragm, 505–507  
   evaluating dimensions of, 435–436, 439f, 440t  
   thoracic circumference, 440t, 494, 498t  
   thoracic length, 440t  
   thoracic-to-abdominal circumference ratio, 436, 494, 498f  
   thoracic-to-head circumference ratio, 436  
   heart, 511–582  
   imaging of, 330f–332f, 341f, 342f  
     artifacts, pitfalls, and normal variants, 1132f–1135f  
     three-dimensional, 844f–845f  
   lateral thoracic expansion, 458  
   lung, 493–503  
   Thorax (*Continued*)  
     nonimmune hydrops and abnormalities of, 688, 689t  
     skeletal dysplasias with altered dimensions of, 435, 438t, 439f, 457t, 457–460  
       achondrogenesis, 453t  
       asphyxiating thoracic dysplasia, 457–458, 458f  
       chondroectodermal dysplasia, 459–460, 459f–460f  
       pulmonary hypoplasia and, 435–442  
       short rib–polydactyly syndromes, 458–459, 459f  
 Three-dimensional ultrasonography, 297, 299, 830–862  
   applications of, 836, 839  
   artifacts on, 859, 860f–861f  
   basic principles of, 830–836  
     inverse mode, 833, 838f–841f, 843f  
     multiplanar reconstruction, 830, 831f–832f, 842f  
     multiple parallel slices, 833, 833f–834f  
     spatiotemporal image correlation, 835, 842f  
     surface-rendering mode, 833–835, 834f–837f  
   for volume measurements, 859  
     brain volume, 859  
     fractional limb volume, 859  
     lung volume, 436–439, 442f, 494, 497, 498, 859  
     placental volume, 859  
   improving efficiency of ultrasound practice with, 839–841, 844f–845f  
   in Down syndrome, 850–852, 855f  
   in evaluation of congenital anomalies, 841  
   in first trimester, 852–855, 856f–857f, 860f–861f  
   of cervix, 710–712, 711f–715f  
     cerclage, 707f, 708f  
   of fetal brain, 363, 365f, 843–848, 844f, 849f–852f, 856f  
     encephalocele, 852f  
     holoprosencephaly, 840f–841f  
     hydrocephalus, 839f  
     interhemispheric cyst, 850f  
     intracranial hemorrhage, 851f  
     ventriculomegaly, 838f  
   of fetal chest, 844f–845f  
   of fetal face and neck, 300f, 392, 394–396, 395f–396f, 834f–836f, 841–843, 845f–849f, 857f, 860f, 862f  
     central facial cleft, 847f  
     cleft lip/palate, 404f–405f, 444, 843, 846f–848f  
     cystic hygroma, 414f  
     in Binder syndrome, 411f  
     in Pfeiffer syndrome, 413f  
     lateral facial cleft, 402, 407f  
     micrognathia, 841, 843, 847f–849f  
     nasal bones, 90  
   of fetal heart, 512, 513f, 842f–843f, 855, 858f, 858–859  
   of fetal neural tube defects, 848, 852f  
   of fetal scrotum, 837f  
   of fetal skeleton and extremities, 305, 848–852, 862f  
     arthrogryposis, 854f–855f  
     clubfoot, 854f  
     hand and wrist defect, 836f  
     in skeletal dysplasias, 432–434, 434f, 435t, 437t  
       osteogenesis imperfecta, 438f  
     polydactyly, 847f  
     skull, 396f, 461f, 843, 849f  
     spine, 367f, 853f  
       scoliosis, 431f, 854f  
 Three-dimensional ultrasonography (*Continued*)  
   of uterus, 907f, 910  
   endometrial assessment at time of embryo transfer, 1011  
   parental-fetal bonding and, 859–862  
 Three-vessel view of fetal heart, 516, 519f–520f  
   abnormalities on, 527t, 551–558, 552t, 553f–562f  
 Thrombocytopenia with absent radius (TAR) syndrome, 464, 465, 467  
 Thrombosis  
   fetal artery, 728  
   intervillous, 725, 727f, 729f  
   of chorionic plate, 750f  
   subchorionic, 728  
     Breus mole, 964, 965f  
 Thumb  
   hitchhiker, in diastrophic dysplasia, 455, 455f  
   in Aase syndrome, 467  
   in Holt–Oram syndrome, 467  
   in radial clubhand, 465  
 Thyroid gland, fetal, 341f  
   goiter, 415–416, 416f  
 Tibia, 308–309, 434f  
   distal, 311f, 316f  
   in atelosteogenesis, 451  
   length of, 432t, 1160t, 1167t  
   proximal, 243–244, 244f, 308f, 309, 315f, 316f, 317f, 319f, 422f  
 Tissue harmonic imaging of breast, 1079, 1079f  
 Tocolysis  
   effect of magnesium sulfate on fetal biophysical profile, 791–792, 791t–792t  
   for fetoscopy, 869–870  
   for hysterotomy, 868, 869  
   for radiofrequency ablation procedures, 871  
   for shunt placement, 871  
   indomethacin for, 717, 869, 871  
 Toes, 309, 310f–311f. *See also* Digital anomalies;  
   Foot  
   in trisomy 18, 95  
   sandal gap deformity of, 94, 94f, 1151f  
 Tongue, 333, 334f, 409, 413  
   anomalies of, 409, 409f  
   in aglossia-adactylia syndrome, 463  
   in micrognathia/retrognathia, 408  
 Tooth buds, 334f, 393f  
 Torcular Herophili, in Dandy-Walker malformation, 378, 379f  
 Toxoplasmosis, intrauterine, 38, 39t, 135f, 135–136, 382  
 Trachea, 339, 340f, 341f  
   Doppler assessment of fluid flow in, 442  
   fetal tracheal occlusion for congenital diaphragmatic hernia, 876–878, 876f–877f, 878t  
   position of aortic arch in relation to, 516  
 Tracheoesophageal fistula  
   esophageal atresia and, 590  
   gastric fluid due to, 334–335  
   in VACTERL association, 177, 468  
 Tracheoscopic balloon occlusion, 876–878, 877f, 878t  
 Transabdominal sonography (TAS), 887, 919, 920f  
   bladder filling for, 698, 887, 891  
   in ectopic pregnancy, 1026f, 1027  
   of cervix, 698, 701f  
   of placenta previa, 733, 734f, 736f–737f  
   of vasa previa, 740f  
   sonic attenuation and transducers for, 887, 919  
   to estimate volume of intraperitoneal fluid, 888  
   transvaginal sonography and, 888

- Transducers, 8, 12  
 for breast examination, 1077, 1078–1079  
 for fetal cardiac examination, 512  
 transabdominal, 887, 919  
 transvaginal, 13, 297, 699, 700f, 702t, 887–889, 920
- Transfusion  
 exchange neonatal, for hyperbilirubinemia, 688  
 intrauterine  
   bone marrow suppression due to, 688  
   intravascular, 687  
   of hydropic, anemic fetus, 684, 687f, 687–688  
   via intraperitoneal infusion, 687  
 twin-to-twin, 175f–176f, 175–177, 266, 281–286, 282f–286f
- Translabial ultrasound  
 of cervix, 698–699, 699f, 701f  
 of placenta previa, 733, 735
- Translocations, 29, 32. *See also* Chromosomal abnormalities
- Transposition of great arteries, 528, 554–555, 555f, 560–562, 858f  
 corrected, 555–556, 562, 565f
- Transrectal sonography, 917, 917f
- Transvaginal color flow Doppler, 887
- Transvaginal sonography (TVS), 12, 297, 299f, 887–891, 919–920, 920f  
 advantages of, 887  
 chaperone for, 888  
 contraindications to, 888  
 disadvantages of, 891  
 examination technique for, 889f–890f, 889–891  
 free fluid in posterior cul-de-sac in normal patients, 891, 893f  
 in adenomyosis, 928, 1004  
 in ectopic pregnancy, 1027  
 in evaluation of uterine bleeding, 943–944, 943f–944f  
 indications for, 887–888  
 large intraperitoneal fluid collections on, 891, 893f–894f  
 of adnexal masses, 968  
 of cervix, 699–701, 700f–701f  
   dynamic changes in cervical length during, 708, 1107f  
   gestational age and frequency of, 708–709  
   in diagnosis and management of preterm labor, 717–718  
   in specific populations, 709t, 709–710  
   in women with preterm premature rupture of membranes, 703, 718  
 limitations and pitfalls of, 701–702, 702f–703f  
 technique for, 702t  
 to predict preterm birth, 702–710, 709t  
 to predict start of spontaneous labor, 718, 718f  
 to predict success of labor induction and mode of delivery, 718  
 to safely avoid cervical cerclage, 717, 718  
 transducer placement for, 700f  
 of placenta previa, 733, 734f–735f, 735, 737f–738f  
 patient preparation for, 888, 919  
 safety of, 891  
 transabdominal sonography and, 888  
 transducers for, 13, 297, 699, 700f, 702t, 887, 920  
   preparation of, 888–889
- Transversalis fascia, maternal, 894, 894f
- Transverse cerebellar diameter, 241–242, 243t, 244, 363, 1160t, 1171t
- Transverse view of fetal upper abdomen, 514, 516f  
 abnormalities on, 523, 527t, 527–528, 528t, 529f–530f
- Transversus abdominis muscle  
 fetal, 320  
 maternal, 891
- TRAP (twin-reversed arterial perfusion) sequence, 287, 871, 873, 874
- Treacher Collins syndrome, 37t, 445
- Triceps muscle, 312f
- Tricuspid atresia, 532, 537f
- Tricuspid regurgitation, 65f, 65–66, 72, 515–516, 518f, 532–534, 538f, 545, 552
- Tricuspid valve, 515, 518f  
 Doppler imaging of, 803, 803f, 804t, 1189t
- Trigeminny, 573
- Trimethadione, 39t
- Triple edema, 677
- Triplets. *See also* Multiple pregnancies  
 cervical length and preterm birth of, 709t, 710  
 growth parameters for, 1176t  
 incidence of, 266, 267f
- Triploidy, 31–32  
 hydrocephalus, spina bifida and, 76  
 omphalocele and, 76
- Trisomy, 29
- Trisomy 1, 180
- Trisomy 8, 29, 78
- Trisomy 9, 79f, 93f
- Trisomy 13, 30, 30t, 70, 71, 104–105  
 clinical features of, 104  
 prenatal sonographic features of, 71, 73t, 104–105, 105t  
   agenesis of corpus callosum, 78  
   cleft lip/palate, 79, 847f  
   clubfoot, 92  
   cystic hygroma, 73  
   Dandy-Walker malformation, 77f  
   diaphragmatic hernia, 75  
   echogenic intracardiac focus, 84–85  
   genitourinary anomalies, 80  
   holoprosencephaly, 78, 79f, 143–145, 144f, 144t, 217, 374, 1118f  
   hydrocephalus and spina bifida, 76  
   nonimmune hydrops, 75  
   nuchal fold, 81, 1199t  
   omphalocele, 75  
   rocker-bottom foot, 93  
   short ear length, 91  
   ventriculomegaly, 76  
   prevalence of, 104  
   prognosis for, 104  
   recurrence risk for, 105  
   second trimester ultrasound screening for, 104–105, 105t  
   vs. Meckel-Gruber syndrome, 104
- Trisomy 16, 29
- Trisomy 18, 30, 30t, 70, 103–104  
 biochemical screening for, 45t, 46, 71, 103  
 clinical features of, 103  
 prenatal sonographic features of, 72t, 103–104, 104t  
   agenesis of corpus callosum, 78  
   cardiac defects, 72  
   choroid plexus cysts, 30, 87, 389  
   cleft lip/palate, 79  
   clenched hands, 94–95, 94f–95f  
   cystic hygroma, 64, 73  
   Dandy-Walker malformation, 77  
   diaphragmatic hernia, 75  
   enlarged cisterna magna, 77  
   facial anomalies, 79, 80f  
   foot abnormalities, 95  
   clubfoot, 92  
   rocker-bottom foot, 93
- Trisomy (Continued)  
 prenatal sonographic features of (Continued)  
   genitourinary anomalies, 80  
   hydrocephalus and spina bifida, 76  
   limb reduction deficits, 94, 94f  
   nonimmune hydrops, 75  
   nuchal fold, 60t, 64, 81, 1199t  
   oligohydramnios, 770  
   omphalocele, 75–76, 76f  
   short ear length, 91–92  
   single umbilical artery, 96  
   strawberry-shaped skull, 97, 97f  
   structural anomalies, 71  
 prevalence of, 103  
 prognosis for, 103  
 recurrence risk for, 104  
 second trimester ultrasound screening for, 103–104, 104t
- Trisomy 21, 14, 30, 98  
 age-adjusted ultrasound risk adjustment for, 102–103, 102t, 102–103  
 amniocentesis in diagnosis of, 98–99  
 biochemical screening for, 45t, 45–46, 46t  
   alpha-fetoprotein, 43f, 45, 45t, 60t, 70–71  
   combined with fetal nuchal translucency, 60t, 62–63, 63f, 67, 68f  
   in second trimester, 70–71  
   in twin gestations, 288–290, 289t  
   quadruple screen, 45t, 46t, 60, 60t, 63, 63f, 67, 68, 71  
   timing of, 71  
   triple screen, 46t, 71  
 choosing correct screening tests for, 67–69, 68f  
 clinical features of, 30, 98  
 first trimester ultrasound screening for, 60–69, 289  
 FISH in prenatal diagnosis of, 54, 54f  
 in twin gestations, 66, 288–290, 289f, 289t, 290t  
 maternal age, gestational age and, 29, 29t, 30t, 46, 98–99  
 mental retardation due to, 30, 98  
 prenatal sonographic features of, 72t, 99, 100, 100t  
   ascites, 75, 75f  
   brachycephaly, 97, 97f  
   cardiac defects, 30, 72, 73f  
   choroid plexus cysts, 88  
   clinodactyly, 93f, 93–94  
   cystic hygroma, 64, 73  
   diaphragmatic hernia, 75  
   duodenal atresia, 30, 73, 74f, 596, 597  
   echogenic intracardiac focus, 84–85  
   facial anomalies, 300  
   hepatosplenomegaly, 616, 616f  
   hydrothorax, 75  
   hyperechoic bowel, 85f, 85–86, 609  
   iliac wing angle, 90–91  
   nasal bone hypoplasia or absence, 64–65, 82, 88f, 88–90, 89f, 89t  
   nonimmune hydrops, 75  
   nuchal translucency, 60t, 60–63, 61f–63f, 81–82, 81f–82f, 1199t  
   in multiple gestations, 66  
   skeletal dysplasias and, 447  
   omphalocele, 75  
   pyelectasis, 83f, 83–84  
   sandal gap deformity, 94, 94f  
   short ear length, 91–92  
   short long bones, 82t, 82–83, 83t  
   structural anomalies, 71–72  
   tricuspid regurgitation, 66  
   ventriculomegaly, 76  
 prevalence of, 30, 30t, 98  
 recurrence risk for, 30, 98



Trisomy (*Continued*)

- second trimester ultrasound screening for, 70, 98-103
  - accuracy of, 99t, 99-101, 101t
  - aneuploidy markers of, 100, 100t
  - clinical practice guideline for, 101-102, 102f
  - cost effectiveness of, 103
  - in twin gestations, 289
  - indications for, 101
  - scoring index system for, 102
  - utilization of, 100, 100t
- soft markers for, 60
- three-dimensional imaging in, 850-852, 855f
- Trisomy 22, 678f
- Trisomy E. *See* Trisomy 18
- Trisomy rescue, 50, 50f
- Trophoblast, 184, 185, 185f, 186f, 721
- Truncus arteriosus, 528, 556, 556f, 562, 565
- TTTS. *See* Twin-to-twin transfusion syndrome (TTTS)
- Tuberous sclerosis, 34, 173-174, 174t, 383
  - cardiac rhabdomyomas in, 173f, 173-174, 567, 569f
  - MRI in, 819f, 820
  - renal macrocysts in, 659
- Tubo-ovarian abscess, 974
- Tumors
  - adnexal, 968-979, 1067-1073 (*See also* Adnexal mass(es))
  - cardiac, 567-569
    - fibroma, 567-568
    - hemangioma, 568-569, 569f
    - prognosis for, 569
    - rhabdomyomas, 173f, 173-174, 567, 569f
    - teratoma, 568
  - choriocarcinoma, 951, 951f, 954f, 963f, 963-964
  - facial, 409-410
    - epignathus, 409, 410f
    - myoblastoma, 410
    - orbital teratoma, 410, 410f
  - fetal surgery for, 868
  - hepatic, 617-618
    - hemangioma, 618, 618f
    - hepatoblastoma, 618
    - mesenchymal hamartoma, 617-618
  - in neck, 414-415
    - cervical teratoma, 415, 415f, 416
    - cystic hygroma, 63f, 63-64, 73-74, 74f, 217, 218f, 414f, 414-415
    - hemangioma, 415
    - lymphangioma, 415, 415f
  - intracranial, 383-385, 384t, 385f
  - neuroblastoma, 670-671, 671f
  - nonimmune hydrops and, 690t
  - ovarian, 813f
  - pancreatoblastoma, 624, 625f
  - placental
    - chorioangioma, 742-744, 744f-745f
    - teratoma, 744
  - placental site trophoblastic tumor, 951, 952f, 954f, 964, 964f
  - renal, 663
    - mesoblastic nephroma, 663, 663f
    - Wilms' tumor, 663, 664
  - sacroccygeal teratoma, 676, 694, 868, 879, 879f
  - umbilical cord, 752
  - uterine
    - leiomyomata, 930-932, 931f-935f, 1004, 1004f, 1054-1058, 1055f-1058f
    - lipomas, 932, 936f
    - sarcomas, 932-935, 937f, 1054-1055, 1058f

- Turner syndrome (45X), 30t, 31, 154-155, 155f, 303
  - chromosomal abnormalities in, 31
  - clinical features of, 31, 31t
  - ovarian anomalies in, 1053
  - prenatal sonographic features of
    - cystic hygroma, 64, 73, 74f, 154-155, 155f, 415
    - diaphragmatic hernia, 75
    - hydrothorax, 75
    - lymphangiectasia, 75
    - nonimmune hydrops, 75
    - nuchal fold, 81
    - omphalocele, 75
- Turner syndrome mosaic, 1053
- TVS. *See* Transvaginal sonography (TVS)
- 22q microdeletion syndrome, 32, 32t, 53, 53f, 558
- Twin embolization syndrome, 176
- "Twin-peak" ( $\lambda$ ) sign, 273-274, 275f-276f
- Twin-reversed arterial perfusion (TRAP) sequence, 287, 871, 873, 874
- Twins, 266-293, 1151f-1154f. *See also* Multiple pregnancies
  - acardiac, 286-288, 287f, 874
  - aneuploidy screening in, 288-290, 289t
  - "appearing," 270, 272-273
  - assisted reproductive technologies and, 267, 268-269
  - biochemical screening of, 46
  - biophysical profile of, 788
  - cerebral palsy in, 266, 271-272
  - chromosomal abnormalities in, 51
  - complications affecting, 266, 271-272
  - conjoined, 218, 220f, 279-280
    - detailed prenatal evaluation of, 280
    - first trimester diagnosis of, 280, 280f
    - pitfalls in diagnosis of, 279
    - prognosis for, 279, 280
    - types of, 279f, 279t, 280f
  - CT amniography of, 814-815, 816f
  - dichorionic, with normal fetus and coexisting complete hydatidiform mole, 961
  - discordant monochorionic, 291-292, 872-874
  - dizygotic, 267, 268f, 268-269, 270f
  - etiology of, 267-269, 268f-269f
  - false-negative diagnosis of, 1151f-1152f
  - fetal death rate for, 266
  - fetal weight estimation for, 1176t
  - gender determination for, 303
  - geographic rates of, 267, 269t
  - growth of, 292f, 292-293
  - growth restriction in, 266
  - identification of placentation, 267, 268f, 269, 272-279
    - chorionicity and amnionicity, 270f, 272
    - multiple sonographic markers for, 276
    - first trimester evaluation, 272-273, 273t, 274f
    - membrane layers, 275-276
    - membrane thickness, 274-275
    - monoamniotic twins, 276-279, 277f-278f
    - second and third trimester evaluation, 273
    - "twin-peak" sign, 273-274, 275f-276f
  - incidence of, 266, 267, 267f
  - intrapartum ultrasound for, 293, 293f
  - invasive testing of, 290
  - maternal age and, 288
  - monozygotic, 267, 268f-270f, 269t
  - multifetal pregnancy reduction, 51, 291-292, 873
    - methods for, 292, 873
    - when twins are discordant for anomalies, 291-292, 873
  - neonatal intensive care admission of, 266
  - perinatal loss of, 270-272, 271f-273f

Twins (*Continued*)

- placentation of, 267, 268f, 269
- prenatal diagnostic procedures in, 51
- preterm birth of, 271, 273f
  - cervical cerclage in prevention of, 290-291, 716, 717, 717t
  - cervical length and, 290-291, 291t, 709t, 710
- selective termination of, 51
- "stuck," 175, 280-281, 281f
- "surprise," 14
- twin-reversed arterial perfusion sequence, 287, 871, 873, 874
- ultrasound diagnosis of, 269-270
- umbilical cord abnormalities with, 276-277, 277f-278f, 747, 751, 753-754, 753f-754f
- "vanishing," 270, 271f
- yolk sacs of, 212f
- Twin-to-twin transfusion syndrome (TTTS), 175f-176f, 175-177, 266, 281-286, 282f-286f, 1153f-1154f
  - acardiac twin and, 286-288, 287f
  - amniotic fluid volume in, 175-176, 280-281, 281f, 282f, 773, 775-776, 775f-776f, 871-872
  - asymmetric fetal growth in, 248
  - diagnosis of, 871-872
  - differential diagnosis of, 176
  - Doppler imaging in, 281-283, 284f-285f, 872
  - hydrops and, 175-176, 283, 694
  - intrauterine growth restriction and, 872
  - management of, 176-177, 283-286, 871-872
    - amniotic septostomy, 775
    - laser photocoagulation of communicating vessels, 283, 286, 286f, 694-695, 870, 870f, 872, 873t
    - radiofrequency ablation, 871
    - therapeutic amniocentesis, 176, 283, 286, 773, 775, 872, 873t
  - natural history of, 872
  - pathophysiology of, 175-176, 281, 871
  - placenta in, 283, 285f
  - pulmonary stenosis due to, 872
  - second trimester screening for, 271
  - severe, 283
  - sonographic features of, 175f, 175-176, 281
  - staging of, 283, 285t, 872, 872t
  - "stuck" twin and, 281, 282f
  - umbilical cord abnormalities in, 754, 754f
  - vascular anastomoses in, 281-283, 283f-284f, 754, 871

## U

- UCI (umbilical cord coiling index), 749-750, 750f
- Ulrich-Turner syndrome. *See* Turner syndrome (45X)
- Ulna, 307, 308-309, 312f, 313f
  - in atelosteogenesis, 451
  - length of, 433t, 1160t, 1167t-1168t
  - relationship between humerus length and, 430f
- Ulnar clubhand, 465, 467t, 468
- Ultrasound examination, 3-24
  - artifacts, pitfalls, and normal variants in, 13, 216, 216f, 701-702, 702f-703f, 764f-766f, 765-766, 1098f-1158f
  - classification, 7
  - contrast for, 297, 299
  - cost-benefit analysis of, 6
  - detection rate for fetal anomalies, 5-6, 5t, 6t
  - discussing results with patient, 21-22, 24
  - documentation of, 12-13

- Ultrasound examination (Continued)**  
 Doppler (See Doppler ultrasonography)  
 equipment and technology for, 8, 12, 12t, 297-299  
 evaluating literature on, 22, 22t  
 fetal position and, 297, 299-300, 301f-302f  
 four-dimensional, 196, 859, 862  
 guidelines for, 7, 8, 9t-12t, 19  
 in first trimester (See First trimester ultrasound examination)  
 in second and third trimesters (See Second and third trimester ultrasound examination(s))  
 indications for, 5-7  
 interpretation of, 8, 19-20, 22, 23f  
 limited, 7  
 malpractice and, 22  
 minimizing exposure to, 4-5, 5f  
 normal fetal anatomy on, 297-360  
 of fetal movements, 299  
 reporting results of, 20-21  
 routine, 5  
 safety of, 3-5, 12t, 891  
 spatial resolution for, 297  
 specialized, 7-8  
 technique for, 297-300  
 terminology for, 7-8  
 thermal index in, 3-4  
 three-dimensional, 830-862 (See also Three-dimensional ultrasonography)  
 training for performance and interpretation of, 7, 8  
 transabdominal, 887  
 transducers for, 8, 12  
 transrectal, 917, 917f  
 transvaginal, 13, 297, 299f, 887-891, 889f-890f  
 who should perform, 6, 7-8
- Umbilical artery, 320, 328f, 332f, 745f, 745-746**  
 aneurysm of, 753  
 biophysical profile and pH of, 785-787, 786f-787f  
 Doppler evaluation of, 96, 251, 251f, 252t, 320, 327f, 344f, 642f, 795, 1184t-1185t, 1187f  
 absent or reversed end-diastolic velocity, 251, 253, 795, 795f  
 flow velocity waveform, 251, 251f  
 gestational age and, 251, 251f  
 impedance index, 1187f  
 in intrauterine growth restriction, 804, 806  
 in monoamniotic twins, 277, 278f  
 in twin-to-twin transfusion syndrome, 283, 285f  
 pulsatility index, 251, 796t, 1184t, 1187f  
 resistance index, 251, 252t, 796t, 798t, 1184t-1185t, 1187f  
 systolic:diastolic ratio, 251, 252t, 796t  
 relation to bladder, 320, 328f, 344f, 642, 642f  
 reverse flow in, 287, 795  
 single, 95-97, 96f, 468, 746-747, 746f-747f, 1144f
- Umbilical cord, 190f, 744-754**  
 abnormalities of, 744, 746-753  
 abdominal wall defects and, 751-752  
 abnormal coiling, 749-750, 749f-750f  
 cysts and masses, 212f, 629f, 752f, 752-753, 1116f  
 hematoma, 752-753  
 in twin pregnancy, 276-277, 277f-278f, 747, 751, 753-754, 753f-754f  
 knots, 747f, 747-748  
 marginal/vellamentous cord insertion, 725, 739f, 741f, 751, 751f-752f, 754, 754f  
 multivessel cord, 747  
 nuchal cord, 748f, 748-749  
 short cord, 747
- Umbilical cord (Continued)**  
 abnormalities of (Continued)  
 single umbilical artery, 95-97, 96f, 468, 746-747, 746f-747f, 1144f  
 anatomy of, 745-746, 745f-746f  
 coiling of, 326f, 745, 749f, 749-750  
 development of, 744-745  
 diameter of, 745  
 Doppler imaging of, 327f, 749f, 1146f  
 insertion of, 328f, 750-751, 751f  
 coalescing of fetal blood vessels at, 320  
 identification of, 320  
 marginal, 739f, 751, 751f  
 membranous, 725  
 physiologic bowel herniation at, 216, 216f  
 three-dimensional imaging of, 857f  
 velamentous, 725, 739f, 751, 752f, 754, 754f  
 vasa previa and, 725, 739f, 741f, 751  
 length of, 745  
 nonimmune hydrops and anomalies of, 692t  
 normal bowel herniation into, 1117f  
 normal three-vessel, 95, 320, 326f, 745-746, 745f-746f  
 occlusion of, for fetal reduction, 873-874, 874t  
 shortened, 747  
 ultrasound detection of, 745  
 vs. myelomeningocele, 1131f
- Umbilical cord blood sampling, percutaneous (PUBS), 320**  
 in acidemia, 252, 253
- Umbilical cord coiling index (UCI), 749-750, 750f**
- Umbilical cord cyst, 212f, 629f, 752, 752f, 1116f**
- Umbilical ligaments, 894**
- Umbilical prevesical fascia, maternal, 894**
- Umbilical vein, 320-323, 325, 326f, 745f, 745-746**  
 Doppler evaluation of, 252, 327f, 800, 800f-801f, 803t, 1185t  
 intraabdominal, 800f  
 intraamniotic, 800f  
 persistent right, 620f, 1143f  
 varices of, 753, 1143f
- Umbilical vesical fascia, maternal, 894**
- Unbalanced translocations, 32**
- Unconjugated estradiol (E<sub>2</sub>), in aneuploidy screening, 45t, 45-46, 47, 60, 60t, 67, 71**
- Unicornuate uterus, 926, 926f, 1001, 1003f, 1051f**  
 MRI of, 1052
- Uniparental disomy, 36f**  
 trisomy rescue and, 50, 50f
- Unsuccessful pregnancy, 201. See also Abortion, spontaneous**
- UPI. See Uteroplacental insufficiency (UPI)**
- UPJ (ureteropelvic junction) obstruction, 80, 646f-647f, 648-649**  
 polyhydramnios and, 772, 773f
- Upper respiratory atresia sequence, 503, 505f**
- Urachal cyst, 665**
- Urachus, 634, 642, 745**  
 patent, 631-634, 634f, 665, 745
- Ureter(s)**  
 fetal, 343, 641f  
 maternal, 913-915, 914f
- Ureteric bud, 640-642, 641f**
- Ureterocele, ectopic, 650f, 651**
- Ureteropelvic junction (UPJ) obstruction, 80, 646f-647f, 648-649**  
 polyhydramnios and, 772, 773f
- Ureterovesical junction (UVJ) obstruction, 648, 649**
- Urethra, fetal, 344**  
 atresia of, 647f, 649  
 development of, 642  
 megalourethra, 665, 666f  
 posterior urethral valves, 649, 651f, 665
- Urethra, maternal, 914f-915f, 915**  
 diverticula of, 915-916
- Urinary ascites, 648, 649**
- Urinary tract, fetal, 640-665**  
 bladder, 299, 337f, 338f, 343-344, 344f, 608f, 642, 642f-643f, 664-665  
 development of, 641f, 642  
 enlargement of, 647, 647f, 649, 652f, 664, 665, 666f  
 exstrophy of, 665, 665f  
 filling and emptying of, 343, 642  
 imaging of, 299, 337f, 338f, 343-344, 344f, 608f, 642, 642f-643f, 664  
 in prune-belly syndrome, 164-165, 164f-165f  
 malformations of, 665  
 nonvisualization of, 664-665  
 pseudomegabladder, 642  
 relation of umbilical arteries to, 320, 328f, 344f, 642, 642f  
 responses to urinary tract dilatation, 649, 651f, 652f  
 volume of, 343-344  
 dilatation of, 646-653  
 bladder responses to, 649, 651f, 652f  
 causes of, 648, 648t  
 nonobstructive dilatation, 649  
 posterior urethral valves, 649, 651f  
 renal duplications, 649, 650f  
 ureteropelvic junction obstruction, 646f-647f, 648-649  
 ureterovesical junction obstruction, 648, 649  
 definition of, 646-647  
 fetal surgery for, 649, 880-881, 881f, 881t  
 imaging of, 646f-647f, 647-649, 649f-652f  
 kidney responses to, 648, 648f  
 postnatal management of, 649-653, 652t, 653f  
 grading of congenital hydronephrosis, 653, 653f  
 prognosis for, 649, 652t  
 threshold measurement for, 646, 646f-647f, 648
- embryology of, 640-642, 641f**  
 evidence of normal functioning of, 643  
 kidneys, 300f, 342-343, 343f, 344f, 643, 643f, 643-664  
 abnormal size of, 646  
 acquired pathologies of, 663, 663f-664f  
 agenesis of, 644, 644f  
 congenital nephrotic syndrome, 664, 664f  
 cystic diseases of, 654-663, 655t  
 duplications of, 645, 645f, 649, 650f  
 ectopic, 645, 645f  
 hyperechoic, 653-654, 654t, 654f-655f  
 tumors of, 663, 663f  
 urinary tract dilatation, 646-653, 646f-653f, 648t  
 polyhydramnios and anomalies of, 772t
- Urinary tract, maternal**  
 CT and MRI evaluation of, 810-811, 812f  
 dilatation of, 810
- Urine, fetal**  
 electrolytes in, as prognostic factor in urinary tract dilatation, 649, 652t  
 fetal swallowing of, 759  
 production of, 334, 343, 642, 758-759  
 amount of, 759  
 lack of, 664
- Urinoma, 648-649, 649f, 651f**
- Urogenital sinus, 641f, 642**  
 persistence of, 665, 665f
- Urography, CT and MRI, 810-811**



- Uterine artery(ies)**, 186, 898–900, 901f–903f  
 Doppler imaging of, 251, 254f, 797–798, 799f, 900–901  
 at time of embryo transfer, 1010–1011, 1011f  
 diastolic notching, 251, 254f  
 pulsatility index, 799t, 1010–1011, 1184t  
 resistance index, 799t, 901, 1011–1011, 1184t  
 uteroplacental insufficiency and, 251–252  
 embolization of  
 for adenomyosis, 928  
 for leiomyomas, 1055  
 hypertrophy in pregnancy, 900  
 pregnancy outcome and resistance of, in first trimester, 214–215
- Uterine bleeding, abnormal**, 942–949  
 assessment of, 942–948  
 algorithm for, 946–948, 947f  
 curettage, 942  
 Pipelle biopsy, 942–943  
 saline infusion sonohysteroscopy, 944–946, 944f–948f  
 transvaginal ultrasound, 943–944, 943f–944f  
 causes of, 942  
 due to endometrial carcinoma, 942, 1065–1066  
 due to hydatidiform mole, 955, 956  
 due to retained products of conception, 939–940, 939f–940f  
 in ectopic pregnancy, 1021  
 in first trimester, 184, 200  
 pregnancy loss and, 205–206, 207f–208f  
 tamoxifen for, 949  
 uterine surveillance during treatment with, 949, 949f
- Uterine blood flow**, 186–188  
 in first trimester, 191, 193f–194f
- Uterine contractions**  
 lower segment  
 “kissing,” 1105f  
 vs. cervical funneling, 701–702, 703f  
 vs. myoma, 1104f  
 vs. placenta previa, 733, 736f, 1106f  
 short cervical length and, 715  
 subendometrial, motion analysis of, 1012, 1012f  
 vs. myoma, 1104f
- Uterine fibroids**. *See* Leiomyoma(ta), uterine
- Uterine synechiae**, 1103f, 1114f  
 vs. circumvallate placenta, 724, 726f
- Uteroplacental circulation**  
 development of, 185, 186–188, 188f, 722  
 in first trimester, 191, 193f–194f, 214
- Uteroplacental insufficiency (UPI)**, 248  
 Doppler velocimetry in, 251–253, 254f  
 etiologies of, 248  
 fetal adaptive responses to, 249, 249f, 252–253  
 fetal status and, 250, 250f  
 intrauterine growth restriction due to, 248–249, 767  
 oligohydramnios and, 249, 767
- Uterus**, 905–910, 919–940. *See also*  
 Endometrium; Myometrium  
 agenesis/hypoplasia of, 1051f, 1051–1052  
 anatomic relationships of, 892f, 922  
 anatomy of, 905–906, 907f, 922–925, 1049–1050  
 antelexion and anteversion of, 907, 907f, 917f, 922, 922f, 1102f  
 arcuate, 926f, 927, 928f, 1001, 1003f, 1051f, 1053  
 benign conditions of, 927–932  
 adenomyosis, 927–930, 929f–930f, 930t, 1004, 1056f, 1058f, 1058–1060, 1059f  
 leiomyomata, 907, 930–932, 931f–935f, 1004, 1004f, 1054–1058, 1055f–1058f  
 lipomatous tumors, 932, 936f
- Uterus (Continued)**  
 bicornis bicolis, 926f  
 bicornuate, 910, 926, 926f, 927f, 1001, 1003f, 1051f, 1053, 1053f  
 blood supply of, 922  
 cervix of (*See* Cervix)  
 changes during pregnancy, 922–923  
 congenital abnormalities of, 910, 925–927, 1001–1003, 1003f  
 diethylstilbestrol exposure and, 39t, 211, 926f, 927, 1003f, 1051f, 1053  
 infertility due to, 1005  
 MRI of, 1051–1053, 1052f–1053f  
 spontaneous abortion and, 211  
 cornua of, 922  
 diameters of, 1201t  
 didelphys, 926, 926f, 927f, 1001, 1003f, 1051f–1052f, 1052  
 early pregnancy loss and blood collections in, 205–206, 207f–208f  
 endometrium of, 909f, 909–910  
 fetal, 344, 666, 667f  
 fundus of, 906, 922  
 “dropout” of, 907  
 growth of, 906, 923–925  
 iatrogenic arteriovenous malformations of, 935, 937f  
 imaging of, 919–922  
 arifacts, pitfalls, and normal variants in, 1102f–1111f  
 in first trimester, 14  
 in second and third trimesters, 19  
 indications for pelvic sonography, 919  
 MRI, 919, 1003, 1049–1050, 1049f–1050f  
 saline infused sonography, 920–922, 922f  
 incarcerated, 923, 924f, 1111f  
 isthmus of, 905–906  
 lymphatic drainage of, 905  
 myometrium of, 908–909, 909f, 925, 1001  
 neonatal, 906  
 polyps in, 945, 946f, 948f, 1005, 1007f  
 position of, 906–908  
 postmenopausal, 906, 925  
 postpartum or postabortive, 935, 939–940, 939f–940f  
 prepubertal, 906, 923, 925f  
 retained products of conception within, 202, 203f, 935, 939–940, 939f–940f  
 retroversion and retroflexion of, 907–908, 908f, 917f, 922, 923f  
 risk of rupture in subsequent pregnancies after hysterotomy, 869  
 sarcomas of, 932–935, 937f, 1054–1055, 1058f  
 septate, 211, 926–927, 926f–927f, 1001, 1003f, 1051f, 1053, 1053f  
 size of, 906, 923–925, 1049  
 synchronicity between ovaries and, 1001  
 ultrasound examination in infertility, 1000–1005, 1002f–1004f  
 unicornuate, 926, 926f, 1001, 1003f, 1051f, 1052  
 visualizing contraceptive device within, 860f, 935, 938f, 1114f  
 volume of, 770, 1201t
- UVJ** (ureterovesical junction) obstruction, 648, 649
- V**  
**VACTERL/VATER association**, 97, 177f, 177–178, 468, 589, 591, 610
- Vagina**, 906f, 910  
 agenesis/hypoplasia of, 1051f, 1051–1052, 1054f  
 anatomy of, 910
- Vagina (Continued)**  
 azygos arteries of, 898  
 lymphatic drainage of, 905  
 Vaginal artery, 898, 901f  
 Vaginal bleeding. *See* Uterine bleeding, abnormal  
 Valproic acid, 37, 39t, 136  
 “Vanishing twin” phenomenon, 270, 271f  
 Varicella zoster virus infection, 39t, 136–137, 137f  
 Varices, umbilical vein, 753, 1143f  
 Vasa previa, 18, 735–737, 739f–742f  
 Doppler imaging of, 735, 737, 740f–742f  
 importance of prenatal diagnosis of, 735  
 incidence of, 735  
 succenturiate placenta and, 724, 737, 740f  
 vellamentous cord insertion and, 725, 739f, 741f, 751  
 vs. funic presentation, 735–737
- Vascular abnormalities**  
 anastomoses in twin-to-twin transfusion syndrome, 281–283, 283f–284f, 754, 871  
 dural sinus thrombosis, 387, 387f  
 fetal artery thrombosis, 728  
 iatrogenic uterine arteriovenous malformations, 935, 937f  
 maternal floor infarction, 727–728, 728f–729f  
 placental infarction, 726–727, 728f  
 umbilical artery aneurysm, 753  
 umbilical vein varices, 753, 1143f  
 vein of Galen aneurysm, 386f, 386–387
- VATER/VACTERL association**, 97, 177f, 177–178, 468, 589, 591, 610
- VCUG** (voiding cystourethrogram), 651–652
- Vein of Galen aneurysm**, 386f, 386–387, 554  
 with coarctation of aorta, 546, 547f
- Vellamentous**. *See* Umbilical cord
- Velocardiofacial syndrome**, 32t, 53
- Vena cava**  
 inferior (IVC), 326f, 328, 328f, 329, 330f, 338, 340f  
 Doppler evaluation of, 799, 800f–801f  
 in situs abnormalities, 523, 527–528, 529f–531f  
 superior (SVC), 329, 331f  
 bilateral, 550f, 556  
 dilatation of, 554  
 in situs abnormalities, 529f
- Venous lakes**, 191
- Ventricles of heart**  
 biventricular and univentricular repairs, 567, 567t  
 compliance of, 802  
 double inlet left ventricle with discordant ventriculoarterial connection, 528, 536f, 556  
 double outlet right ventricle, 554, 554f  
 double-outlet ventricle, 554, 554f, 562  
 filling characteristics of, 580  
 imaging of, 330f, 331f, 341f, 517f, 528–532, 533f, 1133f  
 measurements of, 1191f–1192f  
 ventricular discrepancy with right-sided dominance, 534, 544f–545f  
 ventricular disproportion with right-sided dominance, 532–534, 538t, 538f–540f
- Ventricular outflow tract(s)**  
 left, 518f  
 obstruction of, 534, 551, 560–562  
 right, 331f  
 obstruction of, 562
- Ventricular outflow tract views of fetal heart**, 516, 521f–522f, 522–523  
 abnormalities on, 527t, 558–565, 563f–565f
- Ventricular septal defect**, 551, 558–560, 563f, 1134f  
 double-outlet right ventricle and, 562, 565f  
 in Down syndrome, 72, 73f

Ventricular septal defect (*Continued*)  
 pulmonary atresia with, 565  
 transposition of great arteries with, 562  
 with single arterial trunk, 562, 565

Ventricular septum, 515

Ventricular tachycardia, 572t, 576

Ventriculoarterial connections, 560, 564f

Ventriculomegaly, 23f, 366–368  
 aneuploidy and, 76, 76f  
 as normal second trimester variant, 76  
 cephalocentesis for, 368  
 congenital intracranial tumors and, 384  
 mild, 367f, 368, 368f  
 moderate, 368  
 MRI of, 817, 818f, 819f  
 severe, 366, 367f, 368  
 three-dimensional ultrasonography of, 838f

Verma-Naumoff syndrome, 457t, 458–459

Vertebra(e). *See also* Spine  
 abnormalities of, 854f  
 in Klippel-Feil syndrome, 468  
 in skeletal dysplasias, 445–446  
 in VACTERL association, 177, 177f, 468

block, 445

butterfly, 117, 445

clefts in, 446

flattened (platyspondyly), 425, 431f, 446

hemivertebra, 425, 432f, 445–446

imaging of, 312f, 314–320, 322f–325f

in dyssegmental dysplasia, 456

ossification centers of, 314–316, 322f, 324f, 360, 445

Vertex presentation, 14

Vesicoallantoic cyst, 631–634, 634f

Vesicoamniotic shunting, 649

Vesicoureteric reflux (VUR), 647, 647f, 648, 649, 652

Vesicouterine pouch, 905

Viability. *See* Fetal viability

Visceral situs, 523, 527t, 527–528, 529f

Vitelline duct, 195, 198f  
 cyst of, 209

Voiding cystourethrogram (VCUG), 651–652

Volume imaging, 299, 305

Volvulus, 611–612, 612f

VUR (vesicoureteric reflux), 647, 647f, 648, 649, 652

## W

Waardenburg syndrome, 37t

WAGR syndrome, 32t

Walker-Warburg syndrome, 152, 178, 178f

Weyers acrofacial dysostosis, 460

Wharton jelly, 746, 751, 752

Whistler syndrome, 470

Williams syndrome, 32t

Wilms' tumor, 663, 664

Wolf-Hirschhorn syndrome, 32t, 179–180, 179t–180t

Wolman syndrome, 671, 671f

Wrist, 307, 308f, 309–311, 313f

## X

X-linked disorders, 34–35, 35f, 303

XXX karyotype, 31

XXY karyotype, 31

XXX karyotype, 31

## Y

Yolk sac, 182f, 184, 186f, 187f, 744  
 attachment to embryo, 195, 198f  
 detecting gestational sac without embryo or, 202, 203f, 228, 229f, 230  
 diameter in relation to gestational age, 193, 195f, 195t, 200, 208–209  
 early evaluation of, 208–209, 210f–211f  
 extraembryonic portion of, 745  
 intraembryonic portion of, 745  
 large  
 maternal diabetes and, 208–209  
 pregnancy outcome and, 209, 209f–211f  
 vs. amniotic membrane, 211, 213f–214f  
 secondary, 185, 190f, 745  
 sonographic detection of, 193–194, 194f–195f, 199f, 1114f–1115f  
 in twin gestations, 212f, 269f, 273

Yunis-Varon syndrome, 461

## Z

Zellweger syndrome, 127, 130, 130f

Zink finger syndrome, 180

Zona functionalis, 909, 909f

Zygote, 184, 184f



